2012

AMERICAN SOCIETY *of* BIOMECHANICS

36th Annual Meeting

AUGUST 15-18, 2012
GAINESVILLE, FL

UF | UNIVERSITY *of* FLORIDA

A SPECIAL THANK YOU TO OUR 2012 SPONSORS:

AMTI FORCE AND MOTION

ANYBODY TECHNOLOGY

ATI INDUSTRIAL AUTOMATION www.ati-ia.com

BERTEC

C-Motion

DELSYS®

FDA

footscan® usa

METRIA INNOVATION INC IMAGE-BASED SPATIAL MEASUREMENT

KISTLER

The Motion Monitor ...The Total Solution in Motion Capture®

NDI Northern Digital Inc. RESEARCH-GRADE MOTION CAPTURE

MotionAnalysis

NIBIB

NORAXON® EMG & Sensor Systems

POLHEMUS INNOVATION IN MOTION™

PKMAS Zeno

QUALISYS Motion Capture Systems

simi reality motion systems

novel

Tekscan

ViTRAK Systems Inc

VISION RESEARCH

Visit GAINESVILLE where nature and culture meet

Xcitex

VICON

AMETEK® MATERIALS ANALYSIS DIVISION

UF College of Public Health and Health Professions Physical Therapy UNIVERSITY of FLORIDA

UF Center for Exercise Science College of Health and Human Performance UNIVERSITY of FLORIDA

UF UNIVERSITY of FLORIDA College of Health & Human Performance

UF UNIVERSITY of FLORIDA College of Public Health and Health Professions

AMERICAN SOCIETY of BIOMECHANICS 2012

TABLE OF CONTENTS

HILTON GAINESVILLE | UF CONFERENCE CENTER - MAIN LEVEL

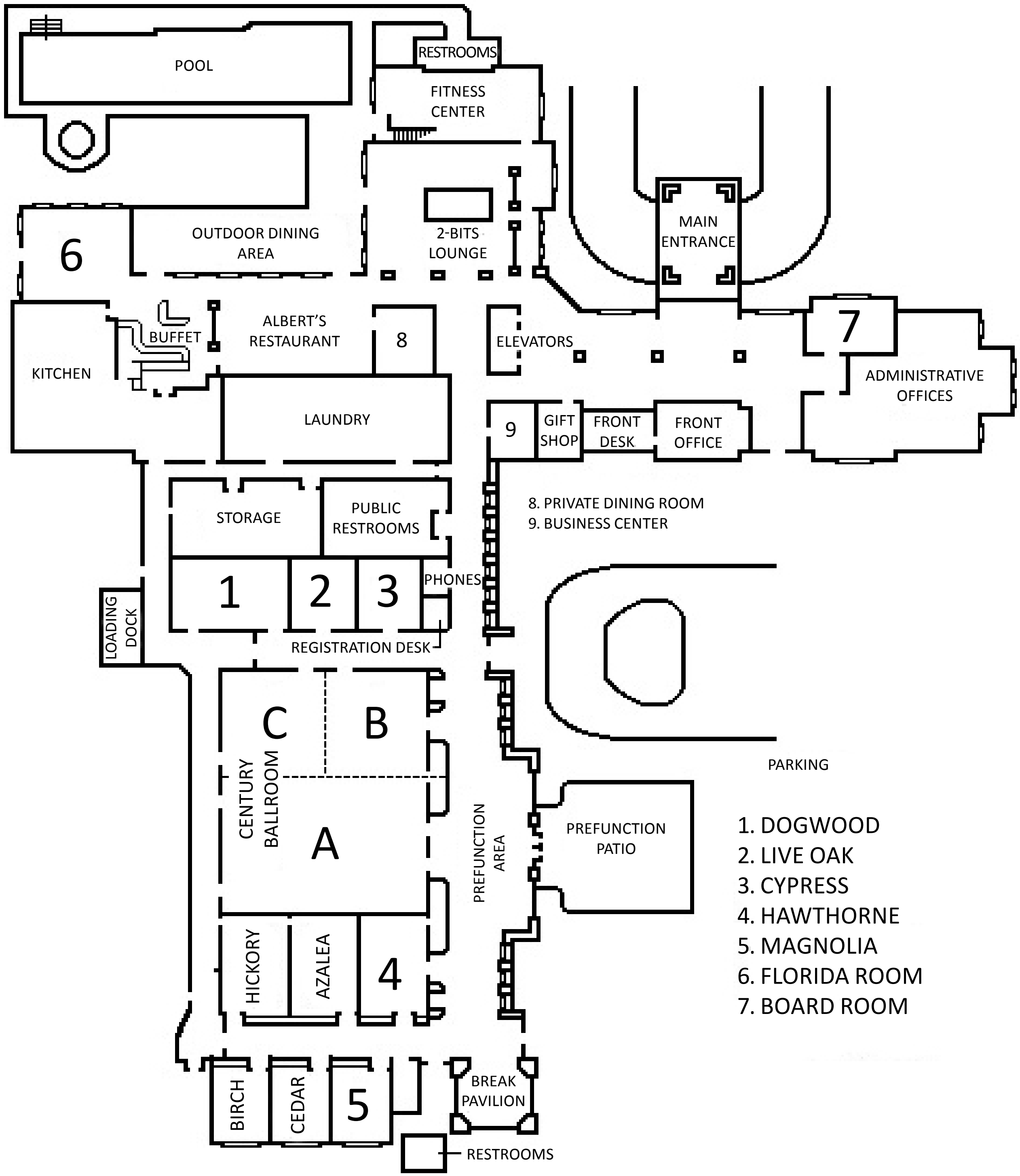

1. DOGWOOD
2. LIVE OAK
3. CYPRESS
4. HAWTHORNE
5. MAGNOLIA
6. FLORIDA ROOM
7. BOARD ROOM

MEETING SCHEDULE OVERVIEW

WEDNESDAY AUGUST 15

10:30 - 12:30
Lab Tour 1

12:30 - 2:30
Tutorial I (Century A)

2:00 - 5:00
ASB Executive Board Meeting (Board Room)

2:00 - 4:00
Lab Tour 2

2:40 - 3:10
Tutorial II (Century A)

3:20 - 4:20
Tutorial III (Century A)

4:30 - 5:30
Student Speakers (Century A)

5:45 - 7:45
Opening Reception
(Florida Museum of Natural History)

THURSDAY AUGUST 16

7:00 - 8:00
Breakfast (Open seating first floor);
Past Presidents' Breakfast (Albert's Dining Room)

7:45
Opening Remarks (Century A)

8:00 - 9:15
Oral Presentations
- Balance During Locomotion (Century A)
- Tissue Mechanics (Century B)
- Bone (Century C)
- Stroke - Thematic (Azalea)

9:45 - 11:00
Oral Presentations
- ASB Fellows Symposium (Century A)
- Ergonomics (Century B)
- Imaging: Knee (Century C)
- Obesity - Thematic (Azalea)

11:30 - 12:45
Oral Presentations
- Gait 1: Methods (Century A)
- Postural Control (Century B)
- Orthopedics (Century C)
- Journal Awards - Thematic (Azalea)

12:45 - 1:45
Lunch (Open seating first floor);
Diversity Lunch (Florida Room)

2:00 - 3:00
Keynote Lecture - Susan Harkema, Ph.D.
(Phillips Center for the Performing Arts)

3:30 - 6:30
Poster Session 1
(Century A, Dogwood, Hickory, Azalea)

7:00 - 10:00
Banquet & Induction of Fellows
(J. Wayne Reitz Union Grand Ballroom)

FRIDAY AUGUST 17

7:00 - 8:00
Breakfast (Open seating first floor);
Women in Science Breakfast (Two Bits Lounge)

8:00 - 11:00
Poster Session 2
(Century A, Dogwood, Hickory, Azalea)

11:15 - 12:15
Tribute to David Winter, Ph.D., P.Eng.
(Phillips Center for the Performing Arts)

12:30 - 1:30
Lunch (Open seating first floor)

1:30 - 3:15
Oral Presentations
- Aging & Gait Symposium (Century A)
- Motor Control (Century B)
- Muscle 1: Modeling & Behavior (Century C)
- Amputee Gait - Thematic (Azalea)

3:45 - 5:15
Oral Presentations
- Teaching Symposium (Century A)
- Comparative (Century B)
- Sports (Century C)
- Computational Biomechanics (Azalea)

5:30 - 6:30
Borelli Award Lecture - Carlo Deluca, Ph.D.
(Phillips Center for the Performing Arts)

6:30 - 7:30
APTA Networking (Florida Room)

SATURDAY AUGUST 18

7:00 - 8:00
Breakfast (Open seating first floor);
5K Fun Run through UF Campus

8:00 - 9:30
Oral Presentations
- Clinical Gait (Century A)
- Upper Extremity (Century B)
- Knee 1 (Century C)
- Seating Symposium - Thematic (Azalea)

10:00 - 11:15
Oral Presentations
- Gait 2: Analysis (Century A)
- Spine (Century B)
- Knee 2: ACL (Century C)
- Muscle 2: Imaging - Thematic (Azalea)

11:30 - 12:45
(Phillips Center for Performing Arts)
Young Scientist Predoctoral Award - Jacob Elkins; **Young Scientist Postdoctoral Award** - Metin Yavuz , Ph.D.; **James J. Hay Memorial Award Lecture** - Jesus Dapena, Ph.D.

1:00 - 2:00
Lunch (Open seating first floor);
ASB Business Meeting - Open to All (Century A)

2:00 - 3:30
Oral Presentations
- Falls (Century A)
- Computational Modeling (Century B)
- Running (Century C)
- Powered Exoskeleton & Prosthetics - Thematic (Azalea)

3:45 - 4:15
Closing Ceremony & Awards (Century A)

4:30 - 6:00
ASB Executive Board Meeting - Closed Meeting (Board Room)

WELCOME FELLOW BIOMECHANISTS!

On behalf of the ASB executive board, the University of Florida, and everyone who has contributed to the planning and execution of this meeting, we would like to enthusiastically welcome you to Gainesville, FL. We are excited for the opportunity to host the 36^{th} Annual Meeting of the American Society of Biomechanics.

We are pleased by the continued growth of the ASB annual meeting. In total, 536 abstracts were submitted to this year's meeting from across the United States and the world. Of the submitted abstracts, 169 were selected as presentations (podium and thematic posters) and 332 as traditional poster presentations. In addition, the meeting will feature informative tutorials and symposia, engaging keynote lectures, award presentations, networking opportunities, lab tours, and inaugural research studies with conference attendees. These opportunities will surely make for an enlightening, energizing and productive meeting for all attendees.

The ASB and its Annual Meeting are run exclusively by volunteers. Each year, the tireless efforts of many make it possible for attendees to enjoy a first-rate meeting experience. We would like to thank all of those who have contributed to the planning and implementation of this meeting. In particular, the ASB executive board and the representatives at the University of Florida provided critical guidance and assistance in the planning and organization of the meeting. Abstract reviewers carefully evaluated submissions and many student volunteers donated their time prior to and during the meeting. We greatly appreciate these efforts.

Furthermore, financial support for the meeting has been provided by the following institutions: UF College of Health and Human Performance, UF College of Public Health and Health Professions, UF Center for Exercise Science, Visit Gainesville, UF Center for Movement Disorders and Neurorestoration, Bob and Becky Allen, Institute of Biomedical Imaging and Bioengineering at the National Institutes of Health. And last, but certainly not least, we would like to thank you, the meeting participants, for making this event a worthwhile endeavor. We are confident you will enjoy Gainesville and the planned social activities. We are pleased to welcome you and wish you a wonderful stay.

Sincerely,

Chris Hass
Meeting Co-Chair

Mark Tillman
Meeting Co-Chair

Mark Bishop
Head Local Organizing Committee

Elizabeth Hsiao-Wecksler
Program Chair

ASB EXECUTIVE BOARD & COMMITTEES

ASB EXECUTIVE BOARD

President:
Donald D. Anderson
University of Iowa

President – Elect:
John Challis
Pennsylvania State University

Past-President:
Jill McNitt-Gray
University of Southern California

Treasurer:
Gary Heise
University of Northern Colorado

Secretary:
Michael Madigan
Virginia Tech

Education Committee Chair:
Gerald Smith
Utah State University

Communications Committee Chair:
Zong-Ming Li
Cleveland Clinic

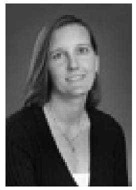

Newsletter Editor:
Michelle Sabick
Boise State University

Program Chair:
Elizabeth Hsiao-Wecksler
University of Illinois at Urbana-Champaign

Program Chair-Elect:
Rakie Cham
University of Pittsburgh

Meeting Co-Chair:
Chris Hass
University of Florida

Meeting Co-Chair:
Mark Tillman
University of Florida

Student Representative:
Meghan Vidt
Wake Forest University

ASB REVIEW COMMITTEE

Gordon Alderink
Kyle Allen
Dennis Anderson
Allison Arnold
Kurt Beschorner
Sanghita Bhattacharya
Mark Bishop
Timothy Brindle
Timothy Burkhart
Tamara Bush
John H. Challis
Rakie Cham
April Chambers
Young-Hui Chang
Steven Charles
Ajit Chaudhari
Li-Shan Chou
Evangelos Christou
Bryan Conrad
Bradley Davidson
John De Witt
Paul DeVita
Angela DiDomenico
Janet Dufek
Brent Edwards
Alejandro Espinoza Orias
Sue Ferguson
Glenn Fleisig
Kevin Ford
Emily Fox
Samir Ghadiali
Jinger Gottschall
Melissa Gross
Chris Hass
Daniel Herman
Walter Herzog
Pilwon Hur
Benjamin Infantolino
Hyun Gu Kang
Andy Karduna
Ata Kiapour
Rodger Kram
Laurel Kuxhaus
Zong-Ming Li
Arash Mahboobin
Denise McGrath
Jill McNitt-Gray
Chris Miller
Ross Miller
Matthew Moran
Melissa Morrow
Erika Nelson-Wong
Rick Neptune
Joe Nocera
Justus Ortega
Pranav Parikh
Michael Pavol
Sarah Ridge
Raziel Riemer
Stacie Ringleb
Mary Rodgers
Elizabeth Russell
Malisa Sarntinoranont
Anne Schmitz
Brian Schulz
Jason Scibek
Jae Kun Shim
K. Alex Shorter
Rob Siston
Kachun Siu
Cecile Smeesters
Joe Sommer
Elizabeth Stegemöller
Martin L. Tanaka
Karen Troy
Brian Umberger
Gangadhar Utturkar
Srikant Vallabhajosula
Dwight Waddell
Laura Wojcik
Ting Xia
Yawen Yu

ASB PROGRAM COMMITTEE

Kurt Beschorner; Rakie Cham; Glenn Fleisig; Mary Rodgers; Jae Kun Shim; Karen Troy; Brian Umberger

ASSISTANTS TO THE MEETING & PROGRAM CHAIRS

Special thanks to Morgan Boes, David Li, and Matt Petrucci. Special thanks also to Allison Vitt, Rusty Haskell, Curtis Weldon, Andrew Campbell, Jennifer Norse, Matt Denning and Iain Hunter for assistance with conference organization, program development and website construction and maintenance.

MEETING INFORMATION AT A GLANCE

MEETING LOCATIONS

All of the academic meeting events (podium oral presentations, posters, mentoring sessions, etc.) will be held at the Hilton University of Florida Conference Center. The Plenary and Award sessions will be held in the University of Florida Center for Performing Arts. The welcome reception will be at the University of Florida's Museum of Natural History and banquet will be held in the Grand Ballroom of the J.Wayne Reitz Union.

REGISTRATION

The registration desk is located in the lobby of the Hilton University of Florida Conference Center. The registration desk will be staffed on Wednesday from 12 pm to 6 pm, and Thursday and Friday from 7 am to 5 pm.

EXHIBITOR BOOTHS

Exhibitor booths will be located in the Prefunction Area and Hawthorne. See page 56.

ASB EXECUTIVE BOARD/EXHIBITOR'S RECEPTION

Wednesday, August 15, 2012, 4:45-5:30 pm, Two Bits Lounge
Attendance limited to ASB Executive Board, Exhibitor Representatives and Organizers of the 2012 and 2013 Annual Meetings of the ASB.

GENERAL OPENING RECEPTION

Wednesday, August 15, 2012, 5:45 - 7:45 pm, Florida Natural History Museum
Attendance is open to all meeting delegates, staff and exhibitor representatives. See Social Program for details.

POSTER PRESENTATIONS

At least one named author is required to be present at each poster during its designated poster session. Odd-numbered posters will be presented during the first 90 minutes of the session. Even-numbered posters will be presented during the second 90 minutes of the session. Posters can be a maximum of 36" wide x 48" tall (portrait format). Any posters not removed will be discarded. Posters will be mounted on free-standing poster boards or on walls with push pins, which will be provided. **There will be two formal poster sessions:**

POSTER SESSION 1:

THURSDAY, FROM 3:30 - 6:30 PM

(Posters must be mounted by 3:15 pm and removed by 6:45 pm.)
Azalea meeting room: Thematic posters from Stroke, Obesity and Journal Awards
Hickory meeting room: Bone (Posters 1-5); Cell & Tissue Mechanics (Posters 7-12); Muscle (Posters 13-16); and Imaging (17-24)
Dogwood meeting room: Orthopedics (Posters 25-36) and Computational Modeling (Posters 37-50)
Ballroom A: Methods (Posters 51-64); Motor Control (Posters 65-79); Ergonomics (Posters 80-90); Lower Extremity (Posters 91-102); Falls (Posters 103-113); Posture & Balance (Posters 114-133); Clinical (Posters 134-156); Rehabilitation (Posters 157-168); and Wheelchair Biomechanics (Posters 169-172)

POSTER SESSION 2:

FRIDAY, FROM 8:00 - 11:00 AM

(Posters must be mounted by 7:45 am and removed by 11:15 am.)
Azalea meeting room: Thematic posters from Amputee Gait and Computational biomechanics
Hickory meeting room: Upper Extremity (Posters 203-220)
Dogwood meeting room: Comparative (Posters 173-175); Knee (Posters 176-192); and Spine (Posters 193-202)
Ballroom A: Running (Posters 221-241); Sports (Posters 242-270); Instrumentation (Posters 271-276); Gait (Posters 277-313); Prosthetics and Orthotics (Posters 314-332); Thematic Posters from Seating, Muscle Imaging and Powered Exoskeleton.

PODIUM PRESENTATIONS

Presenters are allotted 10 minutes for the presentation and 5 minutes for discussion. **Speakers will not be allowed to use their own computers for podium presentations. Speakers must upload their presentation to the conference computer in their presentation room during the break prior to their presentation session.** Due to space constraints, we will also stream all talks in Ballroom B to the Cypress meeting room and talks in Ballroom C to the Live Oak meeting room.

THEMATIC POSTER PRESENTATIONS

Posters must be mounted by 8:00 am and removed by: 6:45 pm (Thurs.), 5:30 pm (Fri.) and 4:00 pm (Sat.). Thematic Poster sessions have been added for 2012. The first 15 minutes of each session are dedicated to viewing the posters for the session. Each poster will have a 5 minute formal presentation and a 10 minute discussion period. Thematic poster sessions are audience-centric, with the majority of the session being devoted to stimulate scientific discussion on the theme topic. (Podium presentations are presenter-centric, the majority of time devoted to presentation with only a few minutes for questions from the audience.) The discussion in a thematic poster session differs from a slide presentation in that it involves the entire audience. In fact, the ideal discussion is one in which the members of the audience engage in discussion with each other. Successful discussions should focus on the topic and not on the individual presentation or presenter. Participants should leave having both learned about the work presented, but also about how the work will be integrated into the field and what some next steps might be.

BREAKFAST & LUNCHES

Breakfast: Hot and cold breakfast options and fruit will be served daily beginning at 7:00 am. ***Lunches:*** A choice of prepared lunches and salads will be provided daily, including a vegetarian option.

BANQUET

7:00 – 10:00 pm, J. Wayne Reitz Union Grand Ballroom. The first bus will leave the Hilton at 6:15 pm. The last bus will leave the Reitz Union at 10 pm.

SPEAKER PRACTICE ROOM

Birch meeting room

INTERNET ACCESS

Free wireless internet access is available throughout the conference hotel. You are **strongly** encouraged to check and download updated meeting proceedings and abstracts from the ASB 2012 website prior to the presentation sessions. No electronic versions of the proceedings or abstracts (e.g. USB thumb drives or CDs) will be provided at the meeting.

SOCIAL PROGRAM

OPENING COCKTAIL RECEPTION

WEDNESDAY, AUGUST 15
5:45 - 7:45 PM
FLORIDA MUSEUM OF NATURAL HISTORY

The opening cocktail reception will be held in the Florida Museum of Natural History (http://www.flmnh.ufl.edu/), which is located on the campus of UF and is a short walk (7 minutes) from the conference venue at the UF-Hilton. The museum features the Butterfly Rainforest, a screened vivarium which houses subtropical and tropical plants and trees to support 55 to 65 different species and hundreds of free-flying butterflies. Guests can stroll through the Butterfly Rainforest on a winding path and relax to the sounds of cascading waterfalls.

BANQUET

THURSDAY, AUGUST 16
7:00 - 10:00 PM
REITZ GRAND BALLROOM

The banquet will be held in the Grand Ballroom of the J. Wayne Reitz Union on the UF campus. Buses will be available for transportation between the UF – Hilton and the Reitz Union. At the beginning of the banquet, the 2012 class of Fellows of the American Society of Biomechanics will be inducted. Be sure to take advantage of your discount coupons for souvenirs at the Reitz Union Bookstore prior to entering the Annual Banquet!

STUDENT NIGHT ON THE TOWN

FRIDAY, AUGUST 17
6:30 PM
GATOR'S DOCKSIDE

An informal opportunity for students to mix and mingle with other ASB student members. Please plan to join us at Gator's Dockside (just west of the UF campus: 3842 Newberry Road, Suite 1-A; (352) 338-4445) to meet fellow ASB students and casually network with one another. Students will be on their own for dinner and drinks this evening. You don't want to miss the chance to kick back and relax with your fellow students!

APTA SOCIAL

FRIDAY, AUGUST 17
6:30 - 7:30 PM
FLORIDA ROOM

The 2nd annual Networking Social of the American Physical Therapy Association (APTA) at the ASB annual meeting is an outreach for the Physical Therapy profession at the conference that provides a casual environment for professionals to talk about the integration of physical therapy in the biomechanics research setting, providing exposure for the profession and promotes collaborative research. Rehabilitation therapists, collaborators and students welcome! Light fare and beverages will be provided. The event is sponsored by The MotionMonitor®. Contact Margaret Finley, PT, Ph.D. (finleym@uindy.edu) if you have questions.

5K RUN THROUGH THE SWAMP

SATURDAY, AUGUST 18
7:00 - 8:00 AM
UF HILTON LOBBY

Meet in the Hilton lobby to join us in a 5K Fun Run around the UF campus.

NETWORKING & PROFESSIONAL DEVELOPMENT

STUDENT EVENT

WEDNESDAY, AUGUST 15
4:30 - 5:30 PM
BALLROOM A

The event will include tips and pointers on how you can excel as a student as you work toward your career. Irene Davis, Ph.D., Thomas Clanton, Ph.D., and Angela DiDomenico, Ph.D. will be leading discussions about how to effectively network while at the meeting, give pointers for writing a fellowship application that will stand out to reviewers, and share the ins and outs of working in the industry.

This will be an informative session for students, so you don't want to miss it! Open to student members of ASB.

DIVERSITY LUNCHEON

THURSDAY, AUGUST 16
12:45 - 1:45 PM
FLORIDA ROOM

The diversity luncheon will feature a discussion led by members of the ASB Diversity Task Force. During the discussion, we hope to identify ways in which ASB can better reach those of diverse backgrounds and further extend its reach to the academic community.

The luncheon is open to all meeting attendees. Due to room size constraints, reservations will be taken. Remaining seats will be open on a first-come, first-served basis. Please make plans to join us for this very important conversation!

Contact ASB Student Representative Meghan Vidt (mvidt@wakehealth.edu) to RSVP for this event if not done when registering for the conference.

WOMEN IN SCIENCE BREAKFAST

FRIDAY, AUGUST 17
7:00 - 8:00 AM
FLORIDA ROOM

The Women in Science Breakfast is a roundtable discussion between students and members of ASB. The informal atmosphere allows students and professionals to network and discuss the unique aspects of women pursuing a career in a scientific field.

This has been a very popular event in the past, so reservations will be required. Contact ASB Student Representative Meghan Vidt (mvidt@wakehealth.edu) to RSVP for this event if not done when registering for the conference.

TUTORIALS
WEDNESDAY, AUGUST 15

12:30 - 2:30 PM

CENTURY A

Filtering of Biomechanical Data

John H. Challis, Ph.D.;
Pennsylvania State University

This tutorial will review: frequency analysis, data acquisition, noise properties, recursive and non-recursive filters, filter types, splines, truncated Fourier series, data differentiation, selecting the degree of filtering, and conclude with some biomechanics-specific examples.

2:40 - 3:10 PM

CENTURY A

Overview of the Annual Grand Challenge Competition to Predict In Vivo Knee Loads

B.J. Fregly, Ph.D.;
University of Florida

This tutorial will provide an overview of an annual "Grand Challenge Competition to Predict In Vivo Knee Loads" being held each year at the ASME Summer Bioengineering Conference.

The goal of the competition is to encourage critical evaluation of musculoskeletal model estimates of contact and muscle forces during movement. Competing research teams predict in vivo medial and lateral knee contact forces in a blinded fashion using gait data collected from subjects implanted with a force-measuring knee replacement.

The tutorial will cover the goals of the competition, the accuracy of the blinded contact force predictions generated thus far, and plans for upcoming data distributions from these unique subjects.

3:20 - 4:20 PM

CENTURY A

Measuring 3D Skeletal Kinematics Using Radiographic Images

Scott A. Banks, PhD;
University of Florida
Shang Mu, PhD;
MAKO Surgical Corp

The purpose of this tutorial will be to introduce participants to the basic principles of skeletal kinematic measurement from radiographic images, and to show examples of how these techniques can be applied in a variety of different research contexts.

Examples of single- and stereo-projection imaging will be covered, as well as methods for performing measurements with natural bones, bones with implanted metallic markers, and with joint replacement implants.

LAB TOURS
WEDNESDAY, AUGUST 15

LAB TOUR 1: 10:30 AM - 12:30 PM
LAB TOUR 2: 2:00 - 4:00 PM

APPLIED NEUROMECHANICS LABORATORY

The Applied Neuromechanics Laboratory focuses on interactions between musculoskeletal biomechanics and sensorimotor control of lower extremity function with particular emphasis on the coordination of locomotion and balance. This lab applies biomechanical and neurophysiologic principles to understand aging and disease processes (Autism Spectrum Disorders, Progressive Supranuclear Palsy, Parkinson's disease, Essential tremor) to optimize behavioral and surgical interventions.

BIOMECHANICS LABORATORY

The Center for Exercise Science Biomechanics Lab, founded in 1995, focuses on analyzing human movement, specializing on the lower extremities. The lab studies the motion of the hip, knee and ankle during activities of daily living and fast-paced movements for different populations. Ongoing projects include investigation of the health benefits of a lever-drive wheelchair and effects of whole-body vibration on balance control.

NEUROMUSCULAR PHYSIOLOGY LABORATORY

The Neuromuscular Physiology Lab has the broad research interest of the lab in neuromuscular mechanisms that mediate acute perturbations (arousal, fatigue, and sleep) and chronic influences (aging, disease, training, and learning) to motor performance in humans. Currently, research in the lab involves identifying neural activation strategies from the single motor unit to the whole muscle level. The clinical significance of this work relates to populations that have increased tremor and impaired accuracy, such as in older adults and Parkinsonian patients.

BIOMECHANICS & MOTION ANALYSIS LABORATORY

The Biomechanics & Motion Analysis Lab in the Orthopaedics and Sports Medicine Institute contains one of the largest 3D motion analysis laboratories in the southeast. The lab is focused on clinical research across the spectrum of musculoskeletal disease including low back pain and osteoarthritis. The lab also has a strong history of research in sports medicine with a number of ongoing studies addressing sports performance and injury prevention.

HUMAN PERFORMANCE MOTION LABORATORY

The Human Performance Motion Lab (HPML) represents a collaboration between the Brain Rehabilitation Research Center at the VA Medical Center, and the Department of Physical Therapy, University of Florida. Projects ongoing at the HPML use neurophysiological and biomechanical approaches to understand the neural control of movement, mechanisms of disordered motor control in neuropathological conditions, and the capacity for motor recovery in adults following central nervous system injury.

LABORATORY FOR REHABILITATION NEUROSCIENCE

The Laboratory for Rehabilitation Neuroscience (LRN) is focused on developing an understanding of how the human brain is impaired in movement disorders and stroke, and developing interventions that mitigate the corresponding behavioral deficits. There are more than 3,000 square feet of space for laboratory data collection and analysis. Data collection devices include: Vicon motion analysis, 256 channel Biosemi EEG, Delsys EMG, Medoc pain stimulation system, and manipulanda for measuring force and movement from upper and lower limb joints. There is a fiber optic sensor laboratory where MRI-compatible sensors are manufactured. There is dedicated computer space for a full complement of neuroimaging techniques including voxel based morphometry, functional MRI, resting state fMRI, iron imaging and diffusion imaging.

PLENARY SESSIONS

THURSDAY, AUGUST 16

KEYNOTE ADDRESS

2:00 - 3:00 PM

PHILLIPS CENTER FOR THE PERFORMING ARTS

Functional recovery in individuals with chronic incomplete spinal cord injury with intensive activity-based rehabilitation

Susan J. Harkema, Ph.D.

Professor and Owsley B. Frazier Rehabilitation Chair, Department of Neurological Surgery, University of Louisville

ABOUT THE SPEAKER

Dr. Susan J. Harkema, Ph.D., is the Rehabilitation Research Director of the Kentucky Spinal Cord Injury Research Center at the University of Louisville. She is the Director of Research at Frazier Rehab Institute and is Director of the NeuroRecovery Network that provides standardized activity-based therapies for individuals with spinal cord injury at seven national rehabilitation centers in the United States. Her research focuses on neural plasticity of spinal networks and recovery of function after spinal cord injury.

In 2007, the National Spinal Cord Injury Association nominated her into the SCI Hall of Fame for Achievement in Research in Quality of Life, and most recently, Dr. Harkema was a co-recipient of the Reeve-Irvine Research Medal in 2009, awarded to individuals who have made critical contributions to promoting repair of the damaged spinal cord and recovery of function. In 2011, she received the Rick Hansen Foundation Difference Maker Award and Popular Mechanics Breakthrough Award.

FRIDAY, AUGUST 17

KEYNOTE ADDRESS

11:15 AM - 12:15 PM

PHILLIPS CENTER FOR THE PERFORMING ARTS

Memorial Tribute to Prof. David Winter, Ph.D., P.Eng

(June 16, 1930 – February 6, 2012)

Organizers:

Philip E. Martin, Ph.D., Iowa State University, and Erika Nelson-Wong, Ph.D., Regis University

ABOUT DR. WINTER

Dr. Winter had a long and impactful academic career in biomechanics, primarily at the University of Waterloo from 1974 through 2012, as an engineer, scientist, author, teacher and mentor. Trained in electrical engineering, physiology, and biophysics, Dr. Winter made many lasting contributions to our field. He authored four highly significant textbooks on the measurement, assessment, and interpretation of normal and pathological gait, posture, and balance; contributed numerous scientific publications to our research literature; trained a new generation of biomechanics scholars and educators; and was an internationally recognized leader in the development of biomechanics as a field of study.

Among his many distinctions, awards, and honors, he received the Career Investigators Award from the Canadian Society for Biomechanics, the Lifetime Achievement Award from the Gait and Clinical Movement Analysis Society, and the Muybridge Medal from the International Society of Biomechanics.

The purpose of this tribute session is to celebrate Dr. Winter's tremendous accomplishments in biomechanics and highlight the large impact that his work has had on most, if not all, of us. Presenters will provide four perspectives of his accomplishments and impact. Audience members will also have an opportunity to share additional memories of the effects Dr. Winter had on their careers and our field.

Presenters:

Philip Martin, Ph.D., Iowa State University. Walter Herzog, Ph.D., University of Calgary. John Yack, Ph.D., University of Iowa. Erika Nelson-Wong, Ph.D., Regis University.

FRIDAY, AUGUST 17

BORELLI AWARD LECTURE

5:30 - 6:30 PM | PHILLIPS CENTER FOR PERFORMING ARTS

Neural Control of Force: A Biomechanics Perspective

Carlo De Luca, Ph.D.

NeuroMuscular Research Center, Boston University

ABOUT THE SPEAKER

Carlo J. De Luca is a Biomedical Engineer who received his doctorate degree in 1972 from Queen's University in Canada, where he began his academic career. He was appointed to the faculties of MIT and Harvard Medical School simultaneously from 1974 to 1984. He then joined Boston University, where he currently holds the titles of: Professor of Biomedical Engineering, founding Director of the NeuroMuscular Research Center, Research Professor of Neurology, and Professor of Electrical and Computer Engineering. He served as Dean ad interim of the College of Engineering from 1986 to 1989.

Dr. De Luca has taught students in engineering and medical schools. He has trained 41 M.S. and Ph.D. students, in addition to 40 scientists from 14 countries. He is recognized for introducing engineering principles and concepts to the field of Electromyography; for introducing EMG signal decomposition technologies; for studies on the control of motor neurons during voluntary contractions; for assessment of muscle fatigue via the surface EMG signal; and for co-introducing the concept of open-loop /closed-loop control for posture.

His body of work includes: a book, Muscles Alive, 111 peer-reviewed articles, 20 book chapters, 17 peer-reviewed conference papers, and 15 patents. His writings have been cited over 12,000 times. He founded Delsys Inc., and continues to serve as its President and CEO. He is the founder and president of the Neuromuscular Research Foundation, established to recognize researchers in the field of Electromyography, and in the field of Biomechanics with emphasis on Motor Control.

He is a Founding Fellow of two Bioengineering societies (AIMBES and BMES), and a Life Fellow of the IEEE BMES. He served a term on the National Advisory Council for Biomedical Imaging and Bioengineering of NIH. Throughout his career he has received awards from scientific and philanthropic societies.

SATURDAY, AUGUST 18

YOUNG SCIENTIST PRE-DOC AWARD

11:30 - 11:45 AM | PHILLIPS CENTER FOR PERFORMING ARTS

JACOB ELKINS, University of Iowa:
Expedited Computational Analysis of Fracture of Ceramic THA Liners: Obesity and Stripe Wear Considerations

YOUNG SCIENTIST POST-DOC AWARD

11:45 AM - 12:00 PM | PHILLIPS CENTER FOR PERFORMING ARTS

METIN YAVUZ, PH.D. Ohio College of Podiatric Medicine:
Plantar Shear Stress and its Clinical Implications

JAMES J. HAY MEMORIAL AWARD LECTURE

12:00 - 12:45 PM | PHILLIPS CENTER FOR PERFORMING ARTS

Approaches to Research in Sports Biomechanics

Jesus Dapena, Ph.D.

Professor, Director of the Biomechanics Laboratory, Indiana University

ABOUT THE SPEAKER

Dr. Jesus Dapena received a Licenciado degree in biological sciences from the Universidad Complutense, Madrid in 1973, and a Ph.D. in biomechanics from the University of Iowa in 1979. From 1979 to 1982 he held an assistant professor position in the Department of Exercise Science at the University of Massachusetts, and since 1982 he has held associate and full professor positions in the Department of Kinesiology at Indiana University. He specializes in sports biomechanics. His research has focused on a variety of activities, including high jumping, discus throwing, hammer throwing, hurdling, flail-like motions, tennis serving and field hockey, among others.

In addition, Dr. Dapena has worked on the development of various tools for the analysis of human motion, including the calculation of angular momentum, computer simulation, and 3D movie/video analysis techniques. Between 1982 and 2007, Dr. Dapena was the scientist in charge of the biomechanical analysis of the high jump event for USA Track & Field, where he analyzed the techniques of the top American high jumpers and gave them advice for technique changes.

THURSDAY, AUGUST 16

ASB FELLOWS SYMPOSIA

9:45 - 11:00 AM | BALLROOM A

Organized by: Jill McNitt-Gray, University of Southern California

The inaugural 2012 ASB Fellows symposia will feature the research and perspectives of ASB Fellows pursuing diverse lines of research. Each presentation will focus on a particular area of interest, with reference to classic papers that influenced their approach, helped frame their working hypothesis, or provided perspective implications of their results. The last session will conclude with a panel discussion focusing on future directions and opportunities for cross-disciplinary collaborations.

Featured Speakers: Ted Gross, University of Washington; Melissa Gross, University of Michigan; Kenton Kaufman, Mayo Clinic; Peter Cavanagh, University of Washington.

FRIDAY, AUGUST 17

AGING AND GAIT SYMPOSIUM

1:30 - 3:15 PM | BALLROOM A

Organized by: Jason Franz and Roger Kram, University of Colorado Boulder

Sponsored by: UF Institute on Aging

Advanced age brings energetic and biomechanical changes that can negatively affect walking ability, independence and quality of life. Active research in this area continues to probe the pervasive consequences of aging on gait, including greater antagonist leg muscle coactivation, greater metabolic cost of movement, and the redistribution of leg muscle function. This symposium brings together leading researchers to share their latest scientific findings and identify future directions in aging research.

Featured Speakers: Justus Ortega, Humboldt State University; Kevin Conley, University of Washington; Paul DeVita, East Carolina University; Jason Franz, University of Colorado; Dennis Anderson, Beth Israel Deaconess Medical Center; Christopher Hurt, University of Illinois at Chicago.

FRIDAY, AUGUST 17

TEACHING BIOMECHANICS

3:45 - 5:15 AM | BALLROOM A

Organized by: Cecile Smeesters, Universite de Sherbrooke

This year's Teaching Biomechanics Symposium will examine the benefits and challenges of shifting from passive (lecture, reading, audio-visual, demonstration) to active (group discussion, practice, teaching others) teaching methods. Topics will include: lecture slide completeness, course design to promote learning, problem- and project-based learning, as well as teamwork for both students and teachers. Finally, to put into practice the just-in-time teaching skills learned in last year's symposium, attendees are invited to participate in a short questionnaire prior to this year's symposium: **http://www.surveymonkey.com/s/D85BDHH.**

Featured Speakers: Patrik Doucet, Université de Sherbrooke; Hyun Gu Kang, California State Polytechnic University; Erika Nelson-Wong, Regis University; Cécile Smeesters, Université de Sherbrooke.

SATURDAY, AUGUST 18

SEATING

8:00 - 9:30 AM | AZALEA

Organized by: Tammy Bush, Michigan State University

We are excited to include a symposium on seating mechanics this year at ASB. This session will include topics associated with the biomechanics of automotive and medical seating, as well as issues related to seating for cyclists. Research will highlight upper extremity loading in wheelchairs, tissue deformation of the buttocks, seating vibration, and changes in blood flow due to loading. These presentations will occur in the form of the newly added Thematic Poster Session where speakers will provide a brief podium presentation of their work and then time will be allowed for longer discussions with each speaker.

Featured Speakers: Abinand Manorama, Michigan State University; Timothy Craig, University of Kansas; Sharon Sonenblum, Georgia Institute of Technology; Philip Requejo, Rancho Los Amigos National Rehabilitation Center; Sujeeth Parthiban, University of Illinois at Chicago.

RESEARCH STUDIES

WEDNESDAY - SATURDAY

CEDAR MEETING ROOM:

Want to test proprioception? There's an app for that. (*PI: Andrew Karduna, PhD, University of Oregon)*

Help us evaluate the feasibility of using smart phone technology to assess proprioception. We only need 5 minutes of your time and one lucky participant will walk away from the conference with a iPod Touch.

MAGNOLIA MEETING ROOM:

Portable Concussion Assessment Using the iPad2 (*PI: Jay L. Alberts, PhD, Cleveland Clinic)*

Want to see how your cognitive and motor function, balance, and reaction time stack up? In about 15 minutes, we can test all this and more with a series of modules currently being piloted for use in assessing concussion at injury and during recovery – all on the Apple iPad. Stop by our booth for more information!

ORAL PRESENTATIONS | THURSDAY, AUGUST 16, 8:00 - 9:15 AM

	CENTURY A BALANCE DURING LOCOMOTION ***Session Chairs:*** *John Dingwell, Rick Neptune*	CENTURY B OVERFLOW CYPRESS TISSUE MECHANICS ***Session Chairs:*** *Kyle Allen, Thomas Angelini*	CENTURY C OVERFLOW LIVE OAK BONE ***Session Chairs:*** *Brent Edwards, Timothy Burkhart*	AZALEA THEMATIC POSTERS STROKE ***Session Chairs:*** *Margaret Finley, Carolyn Patten*
8:00 AM	Reduced Light Intensity Alters Spatiotemporal Gait Patterns During Treadmill Walking **Huang C, Chien J, Mukherjee M, Siu K** *Nebraska Biomechanics Core Facility; University of Nebraska Medical Center*	A Computational Model to Estimate Pre-Stress Between Brain Tissue and a Needle Used for Convection Enhanced Delivery **Casanova F, Carney P, Sarntinoranont M** *University of Florida*	Repeatability of Image Registration and Segmentation Procedures for CT Scans of the Human Distal Radius **Bhatia V, Edwards W, Troy K** *University of Illinois at Chicago*	Poster Viewing
8:15 AM	Active Control of Lateral Balance Varies Throughout a Step During Treadmill Walking **Sawers A, Hahn M** *University of Washington*	Correlations Between Temporo-mandibular Disc Damage and Bulk Shear Mechanics **Juran C, McFetridge P** *University of Florida*	Predicting Distal Radius Bone Strains and Injury in Response to Impacts to Failure Using Multi-Axial Accelerometers. **Burkhart T, Dunning C, Andrews D** *Western University*	Scapulohumeral Kinematics in Individuals with Upper Extremity Impairment from Stroke **Finley M, Combs S** *Krannert School of Physical Therapy University of Indianapolis*
8:30 AM	Whole-Body Angular Momentum During Stair Ascent and Descent **Silverman A, Neptune R, Sinitski E, Wilken J** *Colorado School of Mines*	A Novel High-Order Element for the Analysis of Heart Valve Leaflet Tissue Mechanics **Mohammadi H, Herzog W** *University of Calgary*	Tracking High-Speed Patella Motion Using Biplanar Videoradiography: An Accuracy Study **Rainbow M, Cheung R, Miranda D, Schwartz J, Crisco J, Davis I, Fleming B** *Harvard Medical School*	Gait Training with Visual and Proprioceptive Feedback Improves Overground Propulsive Forces in People Post-Stroke **Wutzke C, Michael L** *University of North Carolina at Chapel Hill*
8:45 AM	Balance Recovery Kinematics After a Lateral Perturbation in Patients with Transfemoral Amputations **Werner K, Linberg A, Wolf E** *Department of Orthopedics and Rehabilitation, Walter Reed National Military Medical Center*	Age-Related Changes in Dynamic Compressive Properties of Soft Tissues Over the Hip Region Measured by Forced Vibration **Choi W, Robinovitch S** *Simon Fraser University*	Storage and Loss Moduli of Bone in Osteogenesis Imperfecta **Albert C, Jameson J, Toth J, Smith P, Harris G** *Marquette University*	Comparison of Module Quality and Walking Performance of Hemiparetic Subjects Pre and Post Locomotor Rehabilitation Therapy **Routson R, Clark D, Bowden M, Kautz S, Neptune R** *Department of Mechanical Engineering, The University of Texas at Austin*
9:00 AM	Dynamic Stability of Individuals with and Without Unilateral Trans-Tibial Amputations Walking in Destabilizing Environments **Faust K, Terry K, Dingwell J, Wilken J** *Brooke Army Medical Center*	Influence of Scaling Assumptions on Tendon Stiffness Estimation **Walker E, Sandercock T, Perreault E** *Northwestern University*	Metaphyseal and Diaphyseal Bone Loss Following Transient Muscle Paralysis Are Distinct Osteoclastogenic Events **Ausk B, Gross T** *University of Washington*	Distinct Patterns of Recovery Following Therapeutic Intervention Post-Stroke: Responders vs. Non-Responders **Patil S, Patten C** *University of Florida*

ORAL PRESENTATIONS | THURSDAY, AUGUST 16, 9:45 - 11:00 AM

	CENTURY A ASB FELLOWS SYMPOSIUM *Session Chair:* *John Challis*	CENTURY B OVERFLOW CYPRESS ERGONOMICS *Session Chairs:* *Angela DiDominico, Bradley Davidson*	CENTURY C OVERFLOW LIVE OAK IMAGING-KNEE *Session Chairs:* *Zachary Domire, Ryan Breighner*	AZALEA THEMATIC POSTERS OBESITY *Session Chairs:* *Paul DeVita; Ray Browning*
9:45 AM	Can Muscle Atrophy Enable Bone Hypertrophy? **Gross T** *University of Washington*	Use of Marker-Less Motion Capture Approach for Construction Field Workers' Biomechanical Analysis **Li C, Lee S, Armstrong T** *University of Michigan*	Measuring 3D Tibiofemoral Kinematics and Contact Using Dynamic Volumetric Magnetic Resonance Imaging **Kaiser J, Bradford R, Johnson K, Wieben O, Thelen D** *University of Wisconsin*	Poster Viewing
10:00 AM	Why Feelings Matter: Emotions and Biomechanics in Health and Illness **Gross M** *University of Michigan*	What Causes Slips, Trips, and Falls on the Fireground? A Survey **Petrucci M, Harton B, Rosengren K, Horn G, Hsiao-Wecksler E** *University of Illinois at Urbana-Champaign*	3D-To-2D Registration for the EOS Biplanar Radiographic Imaging System **Kern A, Kang L, Baer T, Segal N, Anderson D** *University of Iowa*	The Issue of Tissue: A Comparison of Kinematic Models in Obese Adults **Board W, Haight D, Browning R** *Colorado State University*
10:15 AM	Use of Assistive Technology to Improve Mobility **Kaufman K** *Mayo Clinic*	Determining Stabilization Time Using a Negative Exponential Mathematical Model **DiDomenico A, McGorry R, Banks J** *Liberty Mutual*	Lateral Heel Wedge Affects the Tibiofemoral Kinematics in Knee OA Patients: A Preliminary Weight Bearing MRI Study **Wei F, Allen J, Gade V, Stolfi C, Cole J, Barrance P** *Kessler Foundation Research Center*	Changes in Gait Over a 30 Minute Walking Session in Obese Individuals Do Biomechanical Loads Increase in Pursuit of Weight Loss? **Singh B, Janz K, Yack H** *University of Iowa*
10:30 AM	Remote Monitoring of Human Movement **Cavanagh P** *University of Washington*	A Biomechanical Comparison of Three Backpack Frames During Treadmill Walking. **Higginson B, Mills K, Pribanic K, Hollins J, Heil D** *Gonzaga University*	Effect of ACL Reconstruction on Tibiofemoral Cartilage Contact During Downhill Running. **Thorhauer E, Anderst B, Tashman S** *University of Pittsburgh*	Impact of Obesity on the Function of Hip Knee and Ankle During Transition Between Level and Stair Walking **Umezaki K, Ramsey D** *University at Buffalo*
10:45 AM	Panel Discussion	Vertical Trajectory of Center of Mass is Maintained with Increased Vertical Stiffness while Carrying Load **Caron R, Wagenaar R, Lewis C, Saltzman E, Holt K** *Boston University, College of Health and Rehabilitation Sciences: Sargent*	The Influence of Concentric vs. Eccentric Muscle Control on 3D and Dynamic Patellofemoral Contact Kinematics **Borotikar B, Siddiqui A, Sheehan F** *National Institutes of Health, Bethesda, MD, USA*	Obesity Modifies Canine Gait **Brady R, Sidiropoulos A, Bennett H, Rider P, Domire Z, DeVita P** *East Carolina University*

ORAL PRESENTATIONS | THURSDAY, AUGUST 16, 11:30 AM - 12:45 PM

	CENTURY A **GAIT 1: METHODS** ***Session Chairs:*** *Jinger Gottschal, Greg Sawiki*	CENTURY B OVERFLOW CYPRESS **POSTURAL CONTROL** ***Session Chairs:*** *Hyun Gu Kang, Kimberly Bigelow*	CENTURY C OVERFLOW LIVE OAK **ORTHOPEDICS** ***Session Chairs:*** *Robert Siston, Steve Piazza*	AZALEA THEMATIC POSTERS **JOURNAL AWARDS** ***Session Chair:*** *Don Anderson*
11:30 AM	Simple Predictive Models Reveal Step-To-Step Control of Walking **Dingwell J, Bohnsack N, Cusumano J** *University of Texas at Austin*	Movement Strategy and Arm Use Redistribute Sit-To-Stand Joint Moments **Gillette J, Stevermer C, Hall M** *Iowa State University*	Scratch-Based Damage Quantification and Wear Prediction in Total Hip Arthroplasty **Kruger K, Tikekar N, Heiner A, Baer T, Lannutti J, Brown T** *University of Iowa*	Poster Viewing
11:45 AM	Are External Knee Load and EMG Measures Strong Indicators of Internal Knee Contact Forces During Gait? **Meyer A, D'Lima D, Banks S, Lloyd D, Besier T, Colwell C, Fregly B** *University of Florida*	Coherence Analysis Reveals Altered Postural Control During Standing in Persons with Multiple Sclerosis **Huisinga J, Mancini M, Veys C, Horak F** *University of Kansas Medical Center*	A PLLA Fabric System for Prevention of Hip Dislocation **Andersen L, M. Genin G, Brondsted P** *DTU wind energy*	Do Skeletal Muscle Properties Recover Following Repeat Botulinum Toxin Type-A Injections? **Fortuna R, Horisberger M, Vaz M, Herzog W** *University of Calgary*
12:00 PM	A Novel Methodology Using Principal Component Analysis to Quantify Global Bilateral Asymmetry of Human Gait **Hoerzer S, Maurer C, Federolf P.** *Human Performance Laboratory - University of Calgary*	Postural Sway Correlates of Perceived Comfort in Pointing Tasks **Solnik S, Coelho C, Pazin N, Latash M, Rosenbaum D, Zatsiorsky V** *Pennsylvania State University*	Comparison of Unicompartmental Knee Arthroplasty and Healthy Limb for Knee Moments Generated During Stair Ascent **Fu Y, Kinesy T, Mahoney O, Brown C, Simpson K** *University of Georgia*	Plantar Shear Stress Distributions in Diabetic Patients with and Without Neuropathy **Yavuz M, Franklin A, McGaha R, Prakash V, Rispoli J, Stuto J, Torrence G, Lowell D, Canales M** *Ohio College of Podiatric Medicine*
12:15 PM	Discriminating Between Knee Osteoarthritis Severity Levels in Walking Using Only Force Platform Data **Miller R, Brandon S, Deluzio K** *Queen's University*	A New Approach to Understand Postural Instability in Young Children with Autism Spectrum Disorders **Lee H, Amano S, Fournier K, Radonovich K, Hass C** *University of Florida*	Dynamic Cadaveric Robotic Gait Simulation of Pes Planus **Whittaker E, Roush G, Ledoux W** *VA Puget Sound*	Compressive Loading of the Distal Radius Improves Bone Structure in Young Women **Troy K, Bhatia V, Edwards W** *University of Illinois at Chicago*
12:30 PM	Determining the Inertial Properties of Running-Specific Prostheses **Baum B, Schultz M, Tian A, Hobara H, Kwon H, Shim J** *University of Maryland, College Park*	Flexible Framework for Testing Postural Control Models: Evidence for Intermittent Control? **Kang H, Murdock G** *California State Polytechnic University, Pomona*	Graft Material Properties Affect Supraspinatus Force-Generating Capacity in a Simulated Rotator Cuff Repair **Santago A, Weinschenk R, Mannava S, Saul K** *Virginia Tech - Wake Forest School for Biomedical Engineering and Sciences*	Simulation Predictions of Prosthetic Foot and Muscle Function in Response to Altered Foot Stiffness During Below-Knee Amputee Gait **Fey N, Klute G, Neptune R** *The University of Texas at Austin*

ORAL PRESENTATIONS | FRIDAY, AUGUST 17, 1:30 - 3:15 PM

	CENTURY A AGING AND GAIT SYMPOSIUM ***Session Chair:*** *Jason Franz, Roger Kram*	CENTURY B OVERFLOW CYPRESS MOTOR CONTROL ***Session Chairs:*** *Evangelos Christou, Mike Pavol*	CENTURY C OVERFLOW LIVE OAK MUSCLE 1: MODELING & BEHAVIOR ***Session Chairs:*** *Brian Umberger, Jonas Rubenson*	AZALEA THEMATIC POSTERS AMPUTEE GAIT ***Session Chairs:*** *Jae Kun Shim, Erik Wolf*
1:30 PM	The Determinants of Walking Enegetics in Elderly Adults **Ortega J** *Humboldt State University*	Motor Learning is Enhanced in Older Adults Following Training with a Less Difficult Task **Onushko T, Kim C, Christou E** *University of Florida*	How Do Lower Limb Muscles Scale Across Individuals? **Handsfield G, Sauer L, Hart J, Abel M, Meyer C, Blemker S** *University of Virginia Dept. of Biomedical Engineering*	Poster Viewing
1:45 PM	Exercise Efficiency and Mitochondrial Coupling in the Elderly **Conley K, Jubrias S** *Univ. of Washington*	Quantifying Increased Skill Using Measured Bicycle Kinematics As Riders Learn to Ride Bicycles **Cain S, Ulrich D, Perkins N** *University of Michigan*	A General Approach to Muscle Wrapping Over Multiple Surfaces **Stavness I, Sherman M, Delp S** *Stanford University*	Decreased Gait Transition Speeds in Unilateral, Transtibial Amputee Gait **Norman T, Chang Y** *Georgia Institute of Technology*
2:00 PM	Modulating Stride Length & Walking Velocity by Young & Old Adults **DeVita P, Rider P, Sidiropoulos A, Copple T, Domire Z, Hortobagyi T** *East Carolina University*	Modeling Intra-Trial Variability of a Redundant Planar Reaching Task **Nguyen H, Cusumano J, Dingwell J** *University of Texas Austin, Dept. of Mechanical Engineering*	Parameterizing and Validating a Three Compartment Muscle Fatigue Model for Isometric Tasks **Looft J, Frey Law L** *The University of Iowa*	Both Limbs in Unilateral Transtibial Amputees Display Increased Risk for Tripping **Wurdeman S, Yentes J, Myers S, Jacobsen A, Stergiou N** *Nebraska Biomechanics Core Facility*
2:15 PM	How Does Age Affect Individual Leg Mechanics During Uphill and Downhill Walking? How Does Age Affect Individual Leg Mechanics During Uphill and Downhill Walking? **Franz J, Kehler A, MacDonald L, Kram R** *University of Colorado Boulder*	Biomechanics Constrains Variability in Spatial Structure of Muscle Coordination for Endpoint Force Generation **Sohn M, McKay J, Ting L** *Georgia Institute of Technology*	Near-Infrared Light Therapy Delays the Onset of Skeletal Muscle Fatigue **Larkin K, Christou E, Baweja H, Moore M, Tillman M, George S, Borsa P** *University of Florida*	Comparison of Kinematic, Kinetic, and Mechanical Work Data Between Traditional and Bone Bridge Amputation Techniques During Fast Walking One Year Post Ambulation Without an Assistive Device **Kingsbury T, Thesing N, Collins J, Carney J, Wyatt M** *Naval Medical Center, San Diego, CA*
2:30 PM	Reduced Hip Extension Range of Motion and Plantar Flexion Strength Are Functionally Significant Impairments That Affect Gait in Older Adults **Anderson D, Madigan M** *Beth Israel Deaconess Medical Center Park*	Cortical Activations During a Joystick Pursuit Task with Modulated Spindle Afferents **Soltys J, Wilson S** *The University of Missouri Kansas City*	Immediate Application of Cyclic Compressive Loading Attenuates Secondary Hypoxic Injury Folowing Damaging Eccentric Exercise **Haas C, Abshire S, Butterfield T, Best T** *The Ohio State University*	Upper Body Kinematics of Bilateral Transtibial Prosthesis Users During Gait **Major M, Stine R, Hodgson M, Gard S** *Northwestern University Prosthetics-Orthotics Center*

	CENTURY A AGING AND GAIT SYMPOSIUM ***Session Chair:*** *Jason Franz, Roger Kram*	CENTURY B OVERFLOW CYPRESS MOTOR CONTROL ***Session Chairs:*** *Evangelos Christou, Mike Pavol*	CENTURY C OVERFLOW LIVE OAK MUSCLE 1: MODELING & BEHAVIOR ***Session Chairs:*** *Brian Umberger, Jonas Rubenson*	AZALEA THEMATIC POSTERS AMPUTEE GAIT ***Session Chairs:*** *Jae Kun Shim, Erik Wolf*
2:45 PM	Age-Related Differences in the Maintenance of Frontal Plane Dynamic Stability while Stepping to Targets **Hurt C, Grabiner M** *Universtiy of Illinois at Chicago*	Effect of Tactile Pertubation on Blindfolded Circular Path Navigation **Vallabhajosula S, Mukherjee M, Stergiou N** *Nebraska Biomechanics Core Facility, University of Nebraska at Omaha*	Force Enchancement: An Evolutionary Strategy to Reduce the Metabolic Cost of Muscle Contraction? **Joumaa V, Herzog W** *University of Calgary*	Net Efficiency of the Combined Ankle-Foot System in Normal Gait: Insights for Passive and Active Prosthetics **Takahashi K, Stanhope S** *University of Delaware*
3:00 PM	Panel Discussion	Vibration Impairs Proprioception During Active Cyclical Ankle Movements **Holmes T, Floyd L, Dean J** *Medical University of South Carolina*	Association Between Motor Unit Recruitment and the Rates of Strain, Force Rise and Relaxation **Lee S, de Boef-Miara M, Arnold A, Biewener A, Wakeling J** *Simon Fraser University*	Ground Reaction Force and Temporal-Spatial Adaptations to Running Velocity When Wearing Running-Specific Prostheses **Baum B, Tian A, Schultz M, Hobara H, Linberg A, Wolf E, Shim J** *University of Maryland, College Park*

ORAL PRESENTATIONS | FRIDAY, AUGUST 17, 3:45 - 5:15 PM

	CENTURY A TEACHING SYMPOSIUM ***Session Chairs:*** *Cecile Smeester, Erika Nelson-Wong*	CENTURY B OVERFLOW CYPRESS COMPARATIVE ***Session Chairs:*** *K. Alex Shorter, Raziel Riemer*	CENTURY C OVERFLOW LIVE OAK SPORTS ***Session Chairs:*** *Glen Fleiseg, Matt Seeley*	AZALEA THEMATIC POSTERS COMPUTATIONAL BIOMECHANICS ***Session Chairs:*** *Karen Troy, Silvia Blemker*
3:45 PM	Influence of Lecture Slide Completeness on Student Learning in a Biomechanics Course Within a Physical Therapy Curriculum **Nelson-Wong E, Eigsti H, Hammerich A, Marcisz N** *Regis University*	Mesozoic Speed Demons: Flight Performance of Anurognathid Pterosaurs **Habib M, Hall J** *University of Southern California*	The Relationship Between Leg Dominance and Knee Mechanics During the Cutting Maneuver **Brown S, Dickin C, Wang H** *Ball State University*	Poster Viewing
4:00 PM	Designing Biomechanics Courses for Significant Learning: Fink Model Applied at Cal Poly Pomona **Kang H** *California State Polytechnic University, Pomona*	Suction and Skin: The Effect of Vacuum Loading on the Skin of a Common Dolphin **Shorter K, Hurst T, Johnson M, Cramer S, Ketten D, Moore M** *University of Michigan*	The Influence of Prophylactic Ankle Braces on Lower Limb Mechanics During a 90° Side-Step Cutting Task **Yang H, Boros R, Davies B** *Texas Tech University*	Muscle Force Estimates During the Weight-Acceptance Phase of Single-Leg Jump Landing **Morgan K, Donnelly C, Reinbolt J** *University of Tennessee*
4:15 PM	Problem- and Project-Based Learning in Bioengineering: A Case Study **Smeesters C, Berube-Lauziere Y, Rancourt D, Langelier E, Balg F, Fontaine R** *Universite de Sherbrooke*	Control of the Cat Paw Trajectory During Walking on a Flat Surface and Horizontal Ladder **Klishko A, Farrell B, Beloozerova I, Latash M, Prilutsky B** *Georgia Institute of Technology*	Neuromuscular Asymmetries and Deficiencies of Active Adolescent Volleyball Players with Patello-femoral Pain **Di Stasi S, Myer G, Wertz J, Stammen K, Hewett T** *The Ohio State University, Sports Health and Performance Institute*	Peak and Nonuniform Fiber Stretch Increase in the Biceps Femoris Long Head Muscle at Faster Sprinting Speeds **Fiorentino N, Chumanov E, Thelen D, Blemker S** *University of Virginia*
4:30 PM	A Tool for Evaluating Individual Contribution in Teamwork **Doucet P** *Universite de Sherbrooke*	Muscle Activation Strategy in the Sand-Swimming Sandfish Lizard (Scincus Scincus) **Sharpe S, Goldman D** *Georgia Institute of Technology*	Lower Extremity Work is Associated with Club Head Velocity During the Golf Swing in Experienced Golfers **McNally M, Yontz N, Chaudhari A** *Ohio State University Wexner Medical Center*	Comparision of Patella Bone Stress Between Individuals with and Without Patellofemoral Pain **Ho K, Powers C** *University of Southern California*
4:45 PM	Intervention for Improving Project Teams **Doucet P** *Universite de Sherbrooke*	A Quadrupedal Postural Controller with Physiological Delays Reveals the Need for Multi-Level Stability **Bunderson N** *Georgia Institute of Technology*	Bilateral Analysis of the Shoulder Internal Rotation Passive Torque-Angle Relationship for Elite Pitchers with Glenohumeral Internal Rotation Deficit **Wight J, Grover G, Larkin K, Livingston B, Tillman M,** *University of North Florida*	The Influence of Increased DOF in the Knee Joint on Muscle Activation Timings and Forces in a Musculoskeletal Model **Roos P, Jonkers I, Button K, van Deursen R** *Cardiff University*

ORAL PRESENTATIONS | CONTINUED FROM PAGE 18

	CENTURY A **TEACHING SYMPOSIUM** ***Session Chairs:*** *Cecile Smeester, Erika Nelson-Wong*	CENTURY B OVERFLOW CYPRESS **COMPARATIVE** ***Session Chairs:*** *K. Alex Shorter, Raziel Riemer*	CENTURY C OVERFLOW LIVE OAK **SPORTS** ***Session Chairs:*** *Glen Fleiseg, Matt Seeley*	AZALEA THEMATIC POSTERS **COMPUTATIONAL BIOMECHANICS** ***Session Chairs:*** *Karen Troy, Silvia Blemker*
5:00 PM	Panel Discussion	Joint Kinematics in Chimpanzee and Human Bipedal Walking **Lee L, O'Neill M, Demes B, LaBoda M, Thompson N, Larson S, Stern J, Umberger B** *University of Massachusetts Amherst*	Batting Cage Performance of Various Youth Baseball Bats **Crisco J, Rainbow M, Wilcox B, Schwartz J** *Department of Orthopaedics, Warren Alpert Medical of Brown University and Rhode Island Hospital*	An Adaptive Tabu Search Optimization Algorithm for Generating Forward Dynamics Simulations of Human Movement **Vistamehr A, Neptune R** *Mechanical Engineering Department, The University of Texas, Austin*

ORAL PRESENTATIONS | SATURDAY, AUGUST 18, 8:00 - 9:30 AM

	CENTURY A **CLINICAL GAIT** ***Session Chair:*** *Cara Lewis, Mary Rodgers*	CENTURY B OVERFLOW CYPRESS **UPPER EXTREMITY** ***Session Chairs:*** *Steven Charles, Laurel Kaxhaus*	CENTURY C OVERFLOW LIVE OAK **KNEE 1** ***Session Chairs:*** *Li-Shan Chou, Ajit Chaudhari*	AZALEA THEMATIC POSTERS **SEATING** ***Session Chairs:*** *Tamara Bush, Stephen Sprigle*
8:00 AM	Development of a Dementia-Specific Gait Profile: Application of Signal Detection Theory **Karakostas T, Hsiang S, Davis B** *Rehabilitation Institute of Chicago*	Wrist Rotations Are Considerably Less Smooth than Reaching Movements **Salmond L, Charles S** *Brigham Young University*	Reliability of a Novel Proprioception Testing Device **Rojas J, Blackburn T, Dahners L, Olcott C, Weinhold P** *UNC Biomedical Engineering*	Poster Viewing
8:15 AM	Positive Ankle Work is Affected by Peripheral Arterial Disease **Yentes J, Wurdeman S, Pipinos I, Johanning J, McGrath D, Myers S** *Nebraska Biomechanics Core Facility*	Motions of the Thumb Carpometacarpal (CMC) Joint Are Coupled During the Initiation of Three Functional Tasks **Halilaj E, Rainbow M, Got C, Schwartz J, Ladd A, Weiss A, Moore D, Crisco J** *Brown University, Providence, RI*	Evidence of Medial Maltracking in Patellofemoral Pain **Behnam A, Boden B, Sheehan F** *National Institutes of Health*	Bicycle Riding, Arterial Compression and Erectile Dysfunction **Parthiban S, Yang C, Jones L, Baftiri A, Niederberger C** *University of Illinois at Chicago*

ORAL PRESENTATIONS | CONTINUED FROM PAGE 19

	CENTURY A **CLINICAL GAIT** ***Session Chair:*** *Cara Lewis, Mary Rodgers*	CENTURY B OVERFLOW CYPRESS **UPPER EXTREMITY** ***Session Chairs:*** *Steven Charles, Laurel Kaxhaus*	CENTURY C OVERFLOW LIVE OAK **KNEE 1** ***Session Chairs:*** *Li-Shan Chou, Ajit Chaudhari*	AZALEA THEMATIC POSTERS **SEATING** ***Session Chairs:*** *Tamara Bush, Stephen Sprigle*
8:30 AM	Is the Problem Really Foot-Drop? **Little V, McGuirk T, Patten C** *University of Florida*	An Iterative Learning Controller for an Elbow Simulator to Maintain Flexion Angle During Supination **Schimoler P, Vipperman J, Miller M** *University of Pittsburgh*	Sex Differences in Unconstrained Transverse Plane Kinematic Response Under Compression and Simulated Muscle Forces **Wordeman S, Quatman C, Kiapour A, Ditto R, Goel V, Demetropoulos C, Hewett T** *The Ohio State University*	Investigating the Etiology of Vibration-Induced Low Back Pain **Craig T, Soltys J, Wilson S** *University of Kansas*
8:45 AM	Forefoot Orientation Angle Determines Duration and Amplitude of Pronation During Walking **Monaghan G, Lewis C, Hsu W, Saltzman E, Hamill J, Holt K** *Boston University*	Anterior and Middle Deltoid Are Functionally Critical Targets for Nerve Transfer Following C5-C6 Root Avulsion Injury **Crouch D, Plate J, Li Z, Saul K** *Department of Biomedical Engineering, Wake Forest School of Medicine*	Changes in in Vivo Knee Contact Force Through Gait Modification **Hall A, Besier T, Silder A, Delp S, D'Lima D, Fregly B** *University of Florida*	Factors Associated with Pressure Ulcers: The Effects of Shear Loads on Blood Flow **Manorama A, Reid Bush T** *Michigan State University*
9:00 AM	Children with Cerebral Palsy Have Increased Variability in Their Stepping Pattern and Increased Cortical Activity During Gait **Arpin D, Wilson T, Kurz M** *University of Nebraska Medical Center*	A Scapulothoracic Joint Model for Fast and Accurate Simulations of Upper-Extremity Motion **Seth A, Matias R, Veloso A, Delp S** *Stanford University*	Increasing Running Step Rate Reduces Patellofemoral Joint Forces **Lenhart R, Wille C, Chumanov E, Heiderscheit B, Thelen D** *University of Wisconsin-Madison*	Tissue Deformation in the Seated Buttocks Model **Sonenblum S, Cathcart J, Winder J, Sprigle S** *Georgia Institute of Technology*
9:15 AM	Locomotor Adaptive Learning is Impaired in Persons with Parkinson's Disease **Roemmich R, Nocera J, Hass C** *University of Florida*	Kinematic Variability at the Shoulder is Not Related to Shoulder Pain During Manual Wheelchair Propulsion **Longworth J, Troy K** *University of Illinois at Chicago*	Toe-In Gait Reduces the First Peak in the Knee Adduction Moment During Walking in Knee Osteoarthritis Patients **Shull P, Shultz R, Silder A, Besier T, Cutkosky M, Delp S** *Stanford University Center*	Effect of Seat Position Modifications on Upper Extremity Mechanical Loading During Manual Wheelchair Propulsion **Requejo P, Mulroy S, Munaretto J, Mendoza Blanco M, Wagner E, Mc-NittGray J** *Rancho Los Amigos National Rehabilitation Center*

ORAL PRESENTATIONS | SATURDAY, AUGUST 18, 10:00 AM - 11:15 AM

	CENTURY A GAIT 2: ANALYSIS ***Session Chairs:*** *Rakie Cham, April Chambers*	CENTURY B OVERFLOW CYPRESS SPINE ***Session Chairs:*** *Dennis Anderson, Ting Xia*	CENTURY C OVERFLOW LIVE OAK KNEE 2: ACL ***Session Chairs:*** *Daniel Herman, Terese Chmielewski*	AZALEA THEMATIC POSTERS MUSCLE 2: IMAGING ***Session Chairs:*** *Ben Intantolino, Darryl Thelen*
10:00 AM	Task-Specific Differences in the Cortical Contribution to Walking Are Revealed by 30-60hz Oscillatory EMG Activity **Clark D, Kautz S, Bauer A, Chen Y, Christou E** *Malcom Randall VA Medical Center*	Viscoelastic Modeling of the Lumbar Spine: The Effect of Prolonged Flexion on Internal Loads **Toosizadeh N, Nussbaum M, Madigan M** *Virginia Tech*	Knee Articular Cartilage Pressure Distribution Under Single- and Multi-Axis Loading Conditions: Implications for ACL Injury Mechanism **Kiapour A, Quatman C, Goel V, Ditto R, Wordeman S, Levine J, Hewett T, Demetropoulos C** *University of Toledo*	Poster Viewing
10:15 AM	Effects of Fractional Anisotropy in the Corpus Callosum As Determined by Diffusion Tensor Imaging on Temporal Variability in Older Adults **Sukits A, Ledgerwood A, Haney J, Chambers A, Cham R, Aizenstein H, Nebes R** *University of Pittsburgh*	Forward Bending with Increased Erector Spinae Force Helps Reduce Disk Herniation Risk **Rundell S, Weaver B** *Armstrong Forensic Engineers*	On the Fatigue Life of the Anterior Cruciate Ligament During Simulated Pivot Landings **Lipps D, Wojtys E, Ashton-Miller J** *University of Michigan*	Comparison of Sarcomere Heterogeneity Measured in Passive Live and Fixed Muscle **Sandercock T, Cash A, Tresch M** *Northwestern University*
10:30 AM	Changes in Spatiotemporal Gait Characteristics When Anticipating Slippery Floors in Young and Older Adults **Chambers A, Cham R** *University of Pittsburgh*	Helical Axis Patterns of Motion for the Healthy to Severely Degenerated Lumbar Intervertebral Disc **Ellingson A, Nuckley D** *University of Minnesota*	Are Internal-External Rotational Moments in ACL Deficient Subjects Different than Those in Healthy Subjects? **Lanier A, MacLeod T, Manal K, Buchanan T** *University of Delaware*	Pennation Angle Variability in Human Whole Muscle **Infantolino B, Challis J** *Penn State Berks*
10:45 AM	Manipulation of the Structure of Gait Variability with Rhythmic Auditory Stimulus **Hunt N, Haworth J, McGrath D, Myers S, Stergiou N** *Nebraska Biomechanics Core Facility*	Characterization of Interlamellar Shear Properties of the Annulus Fibrosus **Han S, Chen C, Chen Y, Hsieh A** *University of Maryland*	Control of Coronal Plane Kinematics and Kinetics During a Single Leg Hop for Distance in Individuals with Anterior Cruciate Ligament Injury **Roos P, Button K, Rimmer P, van Deursen R** *Cardiff University*	Posture and Activation Dependent Variations in Shear Wave Speed in the Gastrocnemius Muscle and Aponeurosis **Chernak L, DeWall R, Thelen D** *University of Wisconsin-Madison*
11:00 AM	Age Differences in the Stabilization of Swing Foot Trajectory in the Frontal Plane **Krishnan V, Rosenblatt N, Latash M, Grabiner M** *University of Illinois, Chicago*	Associations of Costal Cartilage Calcification with Prevalent Vertebral Fractures in Older Adults **Anderson D, Allaire B, Bouxsein M** *Beth Israel Deaconess Medical Center*	Knee Joint Loading After ACL Reconstruction: Influence of Graft Type **Manal K, Gardinier E, Snyder-Mackler L, Buchanan T** *University of Delaware*	On the Ascent: The Soleus Operating Length is Conserved to the Ascending Limb of the Force-Length Curve Across Gait Mechanics in Humans **Rubenson J, Neville P, Heok L, Pinniger G, Shannon D** *The University of Western Australia*

AWARD PRESENTATIONS | SATURDAY, AUGUST 18, 11:30 AM - 12:00 PM

YOUNG SCIENTIST PRE-DOC AWARD
11:30 - 11:45 AM
PHILLIPS CENTER FOR PERFORMING ARTS

JACOB ELKINS, University of Iowa
Expedited Computational Analysis of Fracture of Ceramic THA Liners: Obesity and Stripe Wear Considerations

YOUNG SCIENTIST POST-DOC AWARD
11:45 AM - 12:00 PM
PHILLIPS CENTER FOR PERFORMING ARTS

METIN YAVUZ, PH.D., Ohio College of Podiatric Medicine
Plantar Shear Stress and its Clinical Implications

ORAL PRESENTATIONS | SATURDAY, AUGUST 18, 2:00 - 3:30 PM

	CENTURY A **FALLS** ***Session Chair:*** *Kurt Beschorner, Pilwon Hur*	CENTURY B OVERFLOW CYPRESS **COMPUTATIONAL MODELING** ***Session Chairs:*** *Sukyung Park, Melissa Morrow*	CENTURY C OVERFLOW LIVE OAK **RUNNING** ***Session Chair:*** *Irene Davis, Iain Hunter*	AZALEA THEMATIC POSTERS **POWERED EXOSKELETONS & PROSTHETICS** ***Session Chairs:*** *Liz Hsiao-Wecksler, Matthew Major*
2:00 PM	Momentum Control Strategies During Walking in Elderly Fallers **Fujimoto M, Chou L** *University of Oregon*	Computational Model of Maximum-Height Single-Joint Jumping Predicts Bouncing As an Optimal Strategy **van Werkhoven H, Piazza S** *Penn State University*	Tibial Stresses in Habitual and Converted Forefoot and Rearfoot Strike Runners **Derrick T, Edwards W, Rooney B** *Iowa State University*	Poster Viewing
2:15 PM	Effects of Age and Experience on Foot Clearance During Up and Down Stepping **Beschorner K, Milanowski A, Tomashek D, Smith R** *University of Wisconsin-Milwaukee*	Development of a Subject-Specific Vertical Ground Contact Force Model **Jackson J, Hass C, Fregly B** *University of Florida*	Comparison of Tibial Strains and Strain Rates in Barefoot and Shod Running **Altman A, Davis I** *Biomechanics and Movement Science, University of Delaware*	Magnitude and Time Course of Adaptation During Walking with a Passive Elastic Exoskeleton **Charalambous C, Dean J** *Medical University of South Carolina*
2:30 PM	Anterior, But Not Posterior Compensatory Stepping Thresholds, Are Reduced with Increasing Age **Crenshaw J, Grabiner M** *University of Illinois at Chicago*	Modeling of Head Injury Response for Translational and Rotational Impacts of Varying Directions and Magnitudes **Stitzel J, Weaver A, Danelson K** *Virginia Tech - Wake Forest University Center for Injury Biomechanics*	The Influence of Step Frequency on Muscle Activity During Downhill Running **Sheehan R, Lutz R, Gottschall J** *The Pennsylvania State University*	Biomechanical and Metabolic Implications of Wearing a Powered Exoskeleton to Carry a Backpack Load **Gregorczyk K, Adams A, O'Donovan M, Schiffman J, Bensel C, Brown M** *U.S. Army Natick Soldier Research, Development and Engineering Center*

	CENTURY A **FALLS** ***Session Chair:*** *Kurt Beschorner, Pilwon Hur*	CENTURY B OVERFLOW CYPRESS **COMPUTATIONAL MODELING** ***Session Chairs:*** *Sukyung Park, Melissa Morrow*	CENTURY C OVERFLOW LIVE OAK **RUNNING** ***Session Chair:*** *Irene Davis, Iain Hunter*	AZALEA THEMATIC POSTERS **POWERED EXOSKELETONS & PROSTHETICS** ***Session Chairs:*** *Liz Hsiao-Wecksler, Matthew Major*
2:45 PM	Effect of Age and Lean Direction on the Threshold of Balance Recovery in Younger, Middle-Aged and Older Adults **Carbonneau E, Smeesters C** *Universite de Sherbrooke*	Simple FE Models of the Forefoot for Use in the Design of Therapeutic Footwear for Diabetic Patients **Spirka T, Erdemir A, Cavanagh P** *University of Washington*	A Test of the Metabolic Cost of Cushioning Hypothesis in Barefoot and Shod Running **Tung K, Franz J, Kram R** *University of Colorado*	The Effects of Wearing a Spring-Loaded Ankle Exoskeleton on Soleus Muscle Mechanics During Two-Legged Hopping in Humans **Farris D, Sawicki G** *North Carolina State University & UNC-Chapel Hill*
3:00 PM	Kinematics, Kinetics and Muscle Activation Patterns of the Upper Extremity During Simulated Forward Falls. **Burkhart T, Clarke D, Andrews D** *Western University*	A Computational Model for Convection-Enhanced Delivery in a Hind Limb Tumor **Magdoom-Mohamed K, Pishko G, Sarntinoranont M** *University of Florida*	Vertical Load Distribution in the Metatarsals During Shod Running **Becker J, Howey R, Osternig L, James S, Chou L** *University of Oregon*	Gait Mode Recognition Using an Inertia Measurement Unit on a Powered Ankle-Foot-Orthosis **Li Y, Hsiao-Wecksler E** *University of Illinois at Urbana-Champaign*
3:15 PM	Clinical Balance Measures Are Associated with Variability of Inter-Joint Coordination During Walking in Elderly Adults **Chiu S, Chou L** *University of Oregon*	Is Push-Off Propulsion Energetically Optimal for Accelerated Gait? **Oh K, Baek J, Ryu J, Park S** *Korea Advanced Institute of Science and Technology (KAIST)*	Modulation of Stiffness on Impact Loadings During Running **Cheung R, Rainbow M, Altman A, Davis I** *Harvard Medical School*	Electromyographic Effects of Using a Powered Ankle-Foot Prosthesis **Williams M, Grabowski A, Herr H, D'Andrea S** *Center for Restorative and Regenerative Medicine, PVAMC*


simpleware
SIMPLEWARE RELEASE 5.0
OUT NOW!
We are delighted to announce that version 5.0 of our ScanIP+FE+CAD software package has been released. This latest release introduces some exciting new features that will help you accelerate the process of segmenting and meshing 3D data.
New and improved features of ScanIP+FE+CAD version 5.0 include:
• New Scripting Capability: automate repetitive tasks or write your own plugins
• Improved Grayscale Materials Assignment: easier to use and more interactive 3D visualization for better feedback
• New and Improved Tools and Exports: enhanced 2D and 3D view usability and new dedicated OpenFOAM export
• Parallelised Remeshing in +FE Free and New Fast Preview Modes: significantly improve the speed and performance of your operations
OpenFOAM
The Open Source CFD Toolbox
About Simpleware Ltd.
Simpleware develops world-leading software solutions for the conversion of 3D image data into high-quality CAD, Rapid Prototype, CFD and Finite Element models. Simpleware customers range from international blue chip corporations to research institutes and universities world-wide.
www.simpleware.com

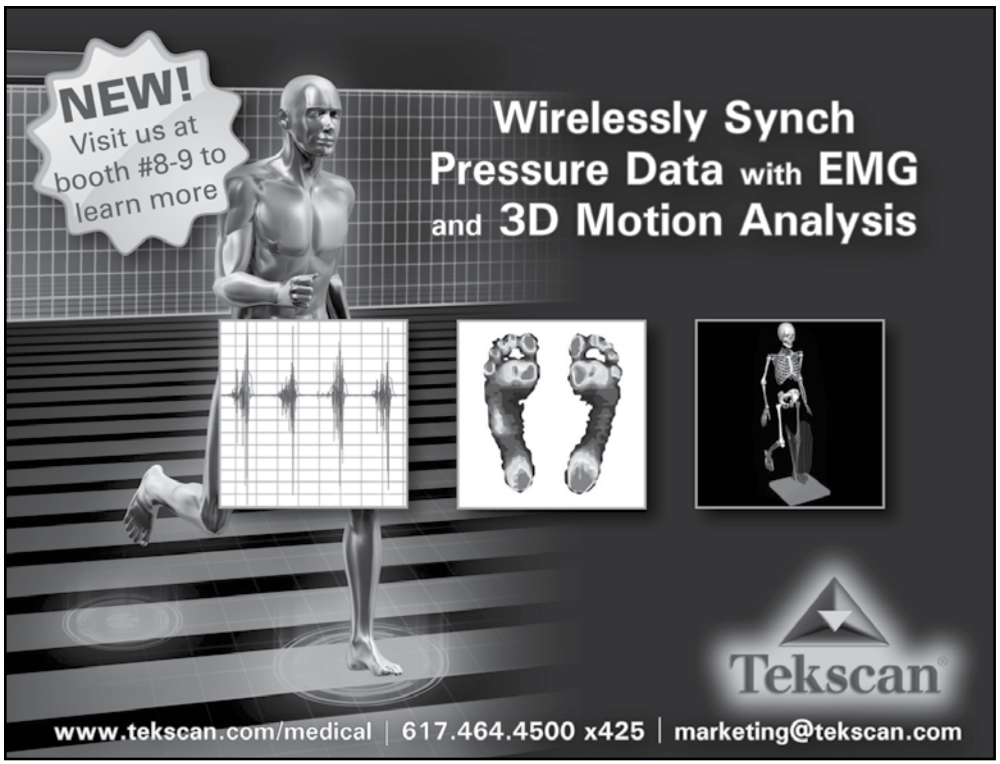
NEW!
Visit us at booth #8-9 to learn more
Wirelessly Synch
Pressure Data with EMG
and 3D Motion Analysis
Tekscan
www.tekscan.com/medical | 617.464.4500 x425 | marketing@tekscan.com

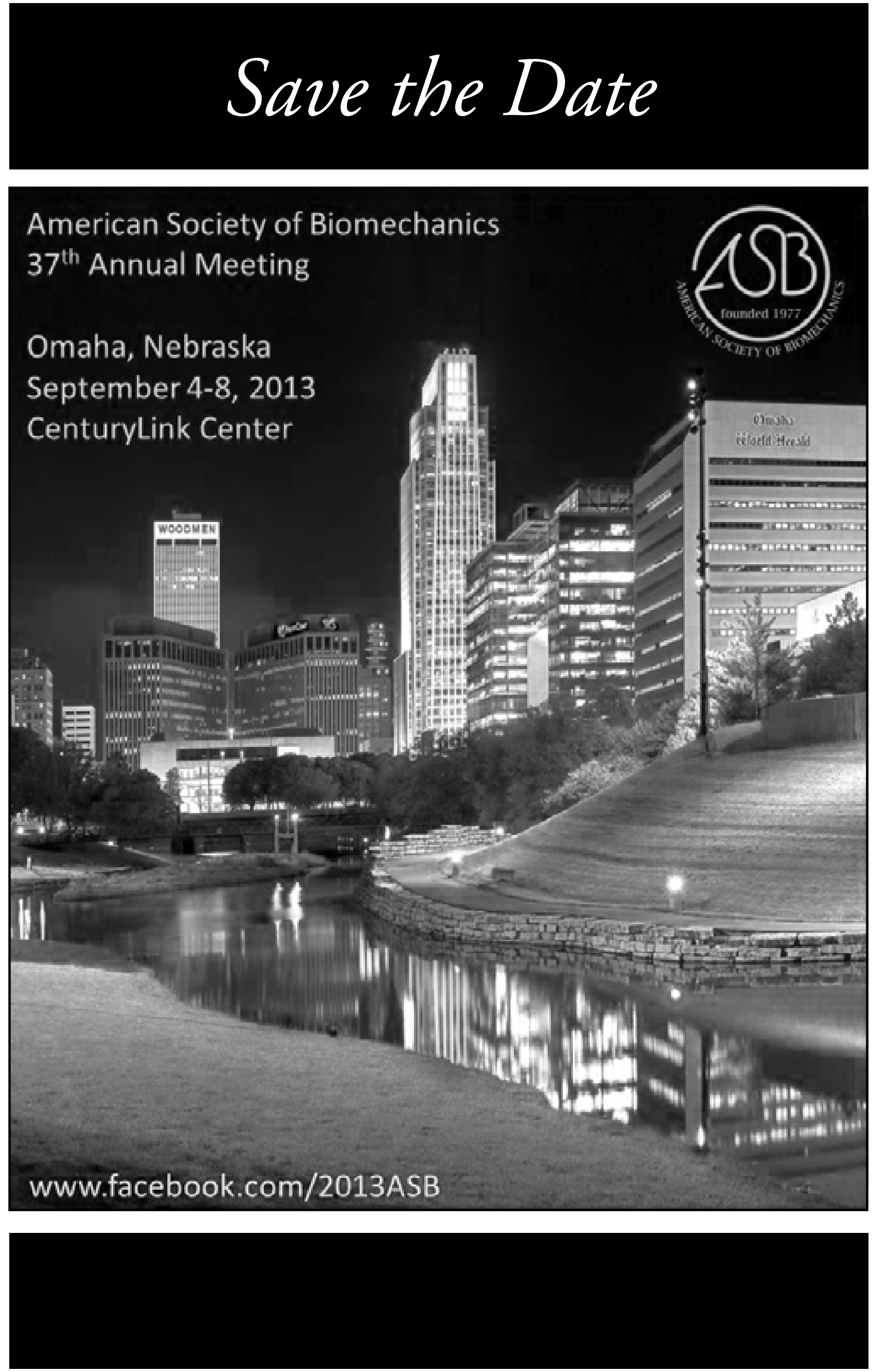
Save the Date
American Society of Biomechanics
37th Annual Meeting
Omaha, Nebraska
September 4-8, 2013
CenturyLink Center
ASB
founded 1977
AMERICAN SOCIETY OF BIOMECHANICS
WOODMEN
Omaha World-Herald
www.facebook.com/2013ASB

POSTER SESSION OVERVIEW & QUICK REFERENCE

POSTER PRESENTATIONS

At least one named author is required to be present at each poster during its designated poster session. **There will be two formal poster sessions:**

POSTER SESSION 1: THURSDAY, FROM 3:30 - 6:30 PM
POSTER SESSION 2: FRIDAY, FROM 8:00 - 11:00 AM

General posters must be mounted by 3:15 pm (Thursday) or 7:45 am (Friday) and removed by 6:45 pm (Thursday) and 11:15 am (Friday). Any poster not removed will be discarded. Posters from Thematic Poster Sessions will also be viewed during these general poster sessions. Odd-numbered posters will be presented during the first 90 minutes of the session. Even-numbered posters will be presented during the second 90 minutes of the session.

POSTER SESSION 1

TOPIC	POSTER #	LOCATION	PAGE
BONE	1-5	HICKORY	27
CELL & TISSUE MECHANICS	6-12	HICKORY	27
CLINICAL	134-156	BALLROOM A	37,38
COMPUTATIONAL MODELING	37-50	DOGWOOD	30
ERGONOMICS	80-90	BALLROOM A	33
FALLS	103-113	BALLROOM A	35
IMAGING	17-24	HICKORY	28
JOURNAL AWARDS	J1-J4	AZALEA	26
LOWER EXTREMITY	91-102	BALLROOM A	34
METHODS	51-64	BALLROOM A	31
MOTOR CONTROL	65-79	BALLROOM A	32
MUSCLE	13-16	HICKORY	28
OBESITY	O1-O4	AZALEA	26
ORTHOPEDICS	25-36	DOGWOOD	29
POSTURE & BALANCE	114-133	BALLROOM A	36,37
REHABILITATION	157-168	BALLROOM A	39
STROKE	S1-S4	AZALEA	26
WHEELCHAIR BIOMECHANICS	169-172	BALLROOM A	39

POSTER SESSION 2

TOPIC	POSTER #	LOCATION	PAGE
AMPUTEE GAIT	A1-A6	AZALEA	40
COMPARATIVE	173-175	DOGWOOD	41
COMPUTATIONAL BIOMECHANICS	C1-C5	AZALEA	40
GAIT	277-313	BALLROOM A	48-50
INSTRUMENTATION	271-276	BALLROOM A	48
KNEE	176-192	DOGWOOD	41,42
MUSCLE	M1-M4	BALLROOM A	53
POWERED EXOSKELETONS	P1-P5	BALLROOM A	53
PROSTHETICS & ORTHOTICS	314-332	BALLROOM A	51,52
RUNNING	221-241	BALLROOM A	44,45
SEATING	S1-S5	BALLROOM A	52
SPORTS	242-270	BALLROOM A	46,47
SPINE	193-202	DOGWOOD	42,43
UPPER EXTREMITY	203-220	HICKORY	43,44

POSTER SESSION 1 | THURSDAY, 3:30 - 6:30
AZALEA (THURSDAY THEMATIC POSTERS)

STROKE
ODD NUMBERS PRESENT 5:00 - 6:30

EVEN NUMBERS PRESENT 3:30 - 5:00

S1 Scapulohumeral Kinematics in Individuals with Upper Extremity Impairment from Stroke
Finley M, Combs S
Krannert School of Physical Therapy University of Indianapolis

S2 Gait Training with Visual and Proprioceptive Feedback Improves Overground Propulsive Forces in People Post-Stroke
Wutzke C, Michael L
University of North Carolina at Chapel Hill

S3 Comparison of Module Quality and Walking Performance of Hemiparetic Subjects Pre and Post Locomotor Rehabilitation Therapy
Routson R, Clark D, Bowden M, Kautz S, Neptune R
Department of Mechanical Engineering, The University of Texas at Austin

S4 Distinct Patterns of Recovery Following Therapeutic Intervention Post-Stroke: Responders vs. Non-Responders
Patil S, Patten C
University of Florida

OBESITY
ODD NUMBERS PRESENT 5:00 - 6:30

EVEN NUMBERS PRESENT 3:30 - 5:00

O1 The Issue of Tissue: A Comparison of Kinematic Models in Obese Adults
Board W, Haight D, Browning R
Colorado State University

O2 Changes in Gait Over a 30 Minute Walking Session in Obese Individuals Do Biomechanical Loads Increase in Pursuit of Weight Loss?
Singh B, Janz K, Yack H
University of Iowa

O3 Impact of Obesity on the Function of Hip Knee and Ankle During Transition Between Level and Stair Walking
Umezaki K, Ramsey D
University at Buffalo

O4 Obesity Modifies Canine Gait
Brady R, Sidiropoulos A, Bennett H, Rider P, Domire Z, DeVita P
East Carolina University

OBESITY
ODD NUMBERS PRESENT 5:00 - 6:30

EVEN NUMBERS PRESENT 3:30 - 5:00

J1 Do Skeletal Muscle Properties Recover Following Repeat Botulinum Toxin Type-A Injections?
Fortuna R, Horisberger M, Vaz M, Herzog W
University of Calgary

J2 Plantar Shear Stress Distributions in Diabetic Patients with and Without Neuropathy
Yavuz M, Franklin A, McGaha R, Prakash V, Rispoli J, Stuto J, Torrence G, Lowell D, Canales M
Ohio College of Podiatric Medicine

J3 Compressive Loading of the Distal Radius Improves Bone Structure in Young Women
Troy K, Bhatia V, Edwards W
University of Calgary University of Illinois at Chicago

J4 Simulation Predictions of Prosthetic Foot and Muscle Function in Response to Altered Foot Stiffness During Below-Knee Amputee Gait
Fey N, Klute G, Neptune R
The University of Texas at Austin

POSTER SESSION 1 | THURSDAY, 3:30 - 6:30

HICKORY

BONE

ODD NUMBERS PRESENT 5:00 - 6:30

1 A Linear Actuated Torsional Device to Replicate Clinically Relevant Spiral Fractures in Long Bone
Edwards W, Troy K
University of Illinois at Chicago

3 The Influence of Occlusal Splinting on the Trabecular Morphology in the Sagittal Plane of the Temporomandibular Joint
Zaylor W, Sindelar B, Cotton J
Ohio University, Mechanical Engineering

5 A Modeling Framework for Examining Changes in Femoral Strength due to Long Duration Bedrest
Genc K, Cavanagh P
Simpleware Ltd.

EVEN NUMBERS PRESENT 3:30 - 5:00

2 DXA Derived Measures of Bone Mineral Can Reliably Predict Mechanical Behavior of Proximal Tibias Loaded in Torsion
Edwards W, Troy K
University of Illinois at Chicago

4 Variability of Strain and Strain Rate in the Human Tibial Diaphysis During Walking
Rooks T, Leib D, Sasaki K, Dugan E
US Army Aeromedical Research Laboratory

CELL & TISSUE MECHANICS

ODD NUMBERS PRESENT 5:00 - 6:30

7 A Protocol to Assess the Contribution of the Components of Human Abdominal Wall to Its Biomechanical Reponse
Tran D, Mitton D, Voirin D, Guerin G, Turquier F, Beillas P
Universite de Lyon, France

9 Loading History of the Mechanical Properties of Human Heel Pads
Gales D, Challis J
Pennsylvania State University

11 Physiologically Modeled Shear Stress As a Function of Pulse Frequency: Driving Endothelial Cells Toward a Quiescent Phenotype
Uzarski J, McFetridge P
University of Florida

EVEN NUMBERS PRESENT 3:30 - 5:00

6 Mapping the Mechanical Topography of Healthy Tibial Cartilage
Deneweth J, Sylvia S, Newman K, McLean S, Arruda E
University of Michigan

8 A Micromechanical Analysis on Diffuse Axonal Injury for Heterogeneous Brain Tissue
Soheilypour M, Khorshidi M, Peyro M, Abolfathi N, Naei M
University of Tehran

10 Optically Based Indentation for Brain Tissue: A New Histological Approach
Canchi S
University of Florida

12 Boundary Conditions Affect Mechanical Behavior of In-Situ Chondrocytes
Moo E, Han S, Jinha A, Abusara Z, Abu Osman N, Pingguan-Murphy B, Herzog W
University of Malaya

POSTER SESSION 1 | THURSDAY, 3:30 - 6:30
HICKORY

MUSCLE
ODD NUMBERS PRESENT 5:00 - 6:30

13 Training Induced Changes in Quadriceps Activation During Maximal Eccentric Contractions
Voukelatos D, Pain M
School of Sport, Health and Exercise Sciences, Loughborough University

15 The Role of the Latissimus Dorsi Muscle in Pelvic Girdle and Trunk Rotations
Patel J, Sumner A, Fox J, Romer B, Rehm J, Campbell B, Weimar W
Auburn University

EVEN NUMBERS PRESENT 3:30 - 5:00

14 Aging is All Relative: Modeling the Relationship Between Strength and Fatigue on Endurance Time in Older Adults
Frey Law L, Avin K, Tumuluri A
The University of Iowa

16 Muscle Stiffness and Response to Exercise in Caloric Restricted and Ad Libitum-Fed Elderly Rats
Pauwels L, Dowling B, Okafor N, Breighner R, Domire Z
Texas Tech University

IMAGING
ODD NUMBERS PRESENT 5:00 - 6:30

17 Static Comparison of Subtalar Joint Neutral and Neutral Cushioning Running Shoes to Barefoot Stance Using Markerless Radiostereometric Analysis
Balsdon M, Bushey K, Dombroski C, Jenkyn T
University of Western Ontario

19 Geometric Accuracy of Physical and Surface Models Created from Medical Image Data
McCoy S, Piller G, Collins C, Sokn S, Ploeg H
University of Wisconsin Madison

21 Automated Analysis of 3D Glenoid Version
Ghafurian S, Galdi B, Tan V, Li K
Rutgers University

23 Reliability of Lumbar Vertebra Position and Orientation Measurement Using Weight-Bearing MRI
Simons C, Davidson B, Cobb L
University of Denver

EVEN NUMBERS PRESENT 3:30 - 5:00

18 A Framework for Visualizing Biomechanical Movement for Designers Within 3D Modeling Programs
Schwartz M, Viswanathan J
University of Michigan

20 Thalamic Projection Fiber Integrity in De Novo Parkinson's Disease
Planetta P, Schulze E, Geary E, Goldman J, Corcos D, Little D, Vaillancourt D
University of Florida

22 An MRI-Compatible Device for Obtaining Patient-Specific Plantar Soft Tissue Material Properties
Stebbins M, Fassbind M, Cavanagh P, Haynor D, Chu B, Ledoux W
VA Puget Sound

24 Measurement of MTPJ Cartilage Thickness Distribution Using 14T MRI
Kumar A, Lee D, Cavanagh P
Asian Institute of Tele-surgery

POSTER SESSION 1 | THURSDAY, 3:30 - 6:30
DOGWOOD

ORTHOPEDICS

ODD NUMBERS PRESENT 5:00 - 6:30

25 A Markov Chain Model Predicts Early Failure of Rotator Cuff Tear Repairs
Donnell D, Carpenter J, Miller B, Hughes R
University of Michigan Department of Orthopaedic Surgery

27 Is There a Gold Standard for Rotational Alignment of the Tibial Component During TKA?
Hutter E, Granger J, Beal M, Siston R
The Ohio State University

29 Does Interlimb Kinematic Symmetry Exist During Stair Ascent After Unicompartmental Knee Arthroplasty?
Simpson K, Fu Y, Kinsey T, Brown-Crowell C, Mahoney O
University of Georgia Biomechanics Laboratory

31 Loading Patterns During a Step-Up-And-Over Task in Individuals Following Total Knee Arthroplasty
Pozzi F, Alnhadi A, Zeni J, Snyder-Mackler L
University of Delaware

33 Asymmetric Morphology of the Hamstring Muscles Following ACL Autografts
Suydam S, Manal K, Buchanan T
University of Delaware

35 Computer Planning of Arthroscopic Femoroacetabular Impingement Surgery
Li J, Theiss M
Inova Fairfax Hospital

EVEN NUMBERS PRESENT 3:30 - 5:00

26 Design Study of Stability and Safety of Median Sternotomy Fixation
Price N, Kim N, Wilcox B, Hatcher B
University of Florida

28 Kinematical and Load Sharing Effect of a Novel Posterior Dynamic Stabiization System Implnated in Lumbar Spine
Erbulut D, Kiapour A, Oktenoglu T
Koc University

30 Biomechanical Effects of Component Alignment Variability in Total Knee Arthroplasty: A Computer Simulation Study of an Oxford Rig
Lemke S, Beal M, Piazza S, Siston R
The Ohio State University

32 Computer Navigation As an Investigational Tool for ACL Reconstruction
Drewniak-Watts E, Shalvoy R, D'Andrea S
Providence VA Medical Center; Alpert Medical School of Brown University

34 Comparison of Stress Distribution Patterns Within Trigonal, Quadrangle, and Hexagonal Srew Drive Designs of an ACL Interference Screw Using Finite Element Analysis
Flowers J, McCullough M
North Carolina A&T State University

36 Computer Methods for Designing Artificial Talus Bone in Ankle Joint
Islam K, Dobbe A, Adeeb S, El-Rich M, Duke K, Jomha N
University of Alberta

POSTER SESSION 1 | THURSDAY, 3:30 - 6:30

DOGWOOD

COMPUTATIONAL MODELING

ODD NUMBERS PRESENT 5:00 - 6:30

EVEN NUMBERS PRESENT 3:30 - 5:00

37 Comparison of Finger Interaction Matrix Computation Techniques
Martin J, Terekhov A, Latash M, Zatsiorsky V
Penn State

39 Development of an Efficient Fluid-Structure Interaction Solver for Applications to the Vascular System
Fernandez C, Berceli S, Garbey M, Kim N, Tran-Son-Tay R
University of Florida

41 Patient-Specific Musculoskeletal Modeling for Evaluating the Efficacy of Meniscus Transplantation
Zheng L, Aiyangar A, Carey R, Lippert C, Harner C, Zhang X
University of Pittsburgh

43 A Novel Statistical Method for EMG-To-Moment Estimation During Gait
Meyer A, Patten C, Fregly B
University of Florida

45 Residual Elimination Algorithm Improvements for Forward Dynamic Simulation of Gait
Jackson J, Hass C, Fregly B
University of Florida

47 Ulna Simulation Assesses Sensitivity to Bone Elastic Modulus Variations in a MRTA Test
Cotton J, Bowman L, Stroud C
Ohio University

49 Is Push-Off Propulsion Energetically Optimal for Accelerated Gait?
Oh K, Baek J, Ryu J, Park S
Mechanical Engineering dept. KAIST

38 Modeling the Demands of a Dance Jump: A Mismatch Between Mechanical Demands and Aesthetic Constraints
Jarvis D, Valero-Cuevas F
University of Southern California

40 Effects of Exercises for Prevention of Femoral Neck Fracture Based on Dynamics and Finite-Element Moel Simulation
Qian J, Zhang H, Li Z, Bian R, Zhang S
Nanjing Institute of Physical Education, Nanjing

42 Finite Element Modeling of Interaction of Implantable Cardiac Rhythm Devices During Frontal Motor Vehicle Deceleration Injuries
Belwadi A, Jacob S, Repalle T, Yang K
Biomedical Engineering Department, Wayne State University, Detroit, MI

44 A Phenomenological Human Energy Expenditure Model in Joint Space
Roberts D, Kim J
Polytechnic Institute of New York University

46 Hamstrings Weakness Increases ACL Loading During Sidestep Cutting
Weinhandl J, Earl-Boehm J, Ebersole K, Huddleston W, Armstrong B, O'Connor K
Old Dominion University

48 Highly Automated Methods for Subject-Specific, Population-Wide Investigations of Habitual Contact Stress Exposure in the Knee
Kern A, Segal N, Lynch J, Sharma L, Anderson D
University of Iowa

50 The Importance of Accounting for Knee Laxity When Simulating Gait
Schmitz A, Thelen D
University of Wisconsin-Madison

POSTER SESSION 1 | THURSDAY, 3:30 - 6:30

BALLROOM A

METHODS

ODD NUMBERS PRESENT 5:00 - 6:30

51 Statistically-Significant Contrasts Between EMG Waveforms Revealed Using Wavelet-Based Functional Anova
McKay J, Welch T, Vidakovic B, Ting L
Emory University and Georgia Institute of Technology

53 Inter-Segmental Coordination Variability During Locomotion - Do Different Analytical Approaches Tell the Same Story?
Armour Smith J, Gordon J, Kulig K
University of Southern California

55 EMG Normalization Techniques for Patients with Pain
Ettinger L, Weiss J, Karduna A
University of Oregon

57 A Robust Kinematic Based Event Detection Algorithm That Works for Walking and Running on Both Uphill and Downhill Surfaces
Sheehan R, Gottschall J
The Pennsylvania State University

59 Surgical Simulation Validating Methods to Improve Orthopaedic Resident Skills Competency
Ohrt G, Karam M, Thomas G, Kho J, Yehyawi T, Marsh J, Anderson D
University of Iowa

61 Quantification Impaction System for a Large Survival Model of Intraarticular Fracture
Diestelmeier B, Rudert M, Tochigi Y, Baer T, Fredericks D, Brown T
University of Iowa

63 Neural Networks Based Identification of Joint Moments Using Nonlinear Model of Sit-To-Stand
Abdulrahman A, Iqbal K
University of Arkansas at Little Rock

EVEN NUMBERS PRESENT 3:30 - 5:00

52 Study on Anthropometric Measurement on Korean Skeletal Systems Based on Cadaveric CT Images
Ko C, Cho D, Chun K
Gerontechnology R&D Group, Korea Institute of Industrial Technology (KITECH)

54 Designing Training Sample Size for Support Vector Machines Based on Kinematic Gait Data
Fukuchi R, Stirling L, Ferber R
University of Calgary

56 Inertial Estimate Errors for Female Arms and Legs from Different Body Models
Wicke J, Dumas G
William Paterson University

58 A Comparison of Position Measurement Accuracy Using Two Different Camera Arrangements
Denning W, Hunter I, Seeley M
Brigham Young University

60 Evaluating Knee Stability After Total Knee Arthroplasty Using Inertial Measurement Units
Roberts D, Khan H, Kim J, Slover J, Walker P
Polytechnic Institute of New York University

62 Empirical Plantar Pressure Insole Pose Estimation
Sinsel E, Lebiedowska M, Buczek F
NIOSH

64 Kinect Abnormal Involuntary Motion Assessment System: Increased Reliability of Testing for Tardive Dyskinesia
Szajnberg L, Roberts D, Karlin D
New York University

POSTER SESSION 1 | THURSDAY, 3:30 - 6:30
BALLROOM A

MOTOR CONTROL
ODD NUMBERS PRESENT 5:00 - 6:30

EVEN NUMBERS PRESENT 3:30 - 5:00

65 Adaptive Changes in Finger Force Variance in Response to Index Finger Fatigue in Unimanual and Bimanual Tasks
Singh T, Zatsiorsky V, Latash M
Pennsylvania State University

67 Performance Optimality and Variability Studied at the Level of Hypothetical Commands
Martin J, Terekhov A, Latash M, Zatsiorsky V
Penn State

69 Two-Weeks of Unloaded Precision Training Improves Motor Performance in Older Adults to the Level of Young Adults
Baweja H, Larkin K, Tanner E, Moore M, Christou E
University of Florida

71 The Effects of Visual Feedback and Aging on Force Oscillations Within 0-1 Hz
Fox E, Baweja H, Kim C, Vaillancourt D, Christou E
University of Florida

73 Impaired Endpoint Accuracy in Older Adults is Associated with Greater Time Variability
Kwon M, Chen Y, Reid J, Fox E, Christou E
University of Florida

75 Kinematics and Kinetics of Stair Ascent while Dual-Tasking
Vallabhajosula S, Tan C, Davidson A, Mukherjee M, Siu K, Yentes J, McGrath D, Myers S
Nebraska Biomechanics Core Facility, University of Nebraska at Omaha

77 Task Difficulty Exacerbates the Age Associated Differences in Force Control
Kim C, Onushko T, Christou E
Neuromuscular Physiology Lab, APK, HHP, University of Florida

79 Interhemispheric Inhibition and Motor Lateralization: Relationship to Age
Lodha N, Corti M, Triggs W, Patten C
University of Florida

66 Non-Negative Matrix Factorization Applied to a Feedback System
van Antwerp K, Burkholder T
Georgia Institute of Technology

68 Coupling of Oscillatory Motion: The Impact of Voluntary and Phsyiological Tremor on Posture
Morrison S, Cortes N, Kerr G, Newell K
Old Dominion University

70 Sensory Reweighting for Visually Induced Roll Tilt Perception Under Sensory Conflict Conditions
Lim H, Park H, Park S
KAIST

72 Endpoint Instructions Result in Higher Proprioceptive Acuity than Joint Angle Instructions
Hyler J, Karduna A
University of Oregon

74 Maximum Voluntary Force Production Changes with Visual Feedback Modulation During Multi-Finger Pressing
Karol S, Kwon H, Koh K, Shim J
University of Maryland, College Park

76 Older Adults Exhibit an Impaired Ability to Predict Movement Accuracy due to Greater Motor Output Variability
Chen Y, Kwon M, Reid J, Fox E, Christou E
University of Florida

78 Trial-To-Trial Control Dynamics in Redundant Reaching Tasks
Smallwood R, Cusumano J, Dingwell J
University of Texas at Austin

ERGONOMICS

ODD NUMBERS PRESENT 5:00 - 6:30

81 Study on Lumbar Morphological Measurements of Korean Adults and the Elderly
Lee E, Kang I, Park S, Yang J, Cho D, Ko C, Chun K
Korea University Guro Hospital

83 The Effects of Load Carriage and Fatigue on Frontal-Plane Knee Mechanics During Walking
Wang H, Frame J, Ozimek E, Leib D, Dugan E
Ball State University

85 Intersegmental Adaptation of Lumbar Spine on Different Load-Carrying Types
Shin J, Park Y, Kim Y, Kim Y
University of Kyung Hee

87 Lower Limb Coordination is Altered During Asymmetric Load Carrying while Walking on a Treadmill
Wang J, Roemmich R, Tillman M
University of Florida

89 A Nonlinear Hand-Arm Model for Interaction with Impulsive Forces
Ay H, Luscher A, Sommerich C, Berme N
The Ohio State University

EVEN NUMBERS PRESENT 3:30 - 5:00

80 Study on Wheelbase Design Parameters of a Shower Carrier Through Drivability Tests
Ko C, Cho D, Chun K
Gerontechnology R&D Group, Korea Institute of Industrial Technology (KITECH)

82 A Hybrid Model Simulating Hand Gripping on a Cylindrical Handle
Wu J, Dong R, Warren C, Welcome D, McDowell T
National Institute for Occupational Safety and Health (NIOSH)

84 The Effect of Extended Durations of Walking in Occupational Footwear on Balance
Chander H, Garner J, Wade C
Applied Biomechanics Laboratory, The University of Mississippi

86 Mimetic Jar Device Capable of Measuring Dynamic Opening Forces: Development and Validation
Ellingson A, Ferkul M, McGee C, Mathiowetz V, Nuckley D
University of Minnesota

88 Influence of Object Size and Hand Posture on Upper Limb Joint Loads During One-Handed Lifting Exertion
Zhou W, Armstrong T, Wegner D, Reed M
University of Michigan

90 Cervical and Masticatory Muscles Activity During a 30 Minutes Laptop Typing Task - a Preliminary Study
Barbara D, Edward H, Gadotti I
Florida International University

POSTER SESSION 1 | THURSDAY, 3:30 - 6:30
BALLROOM A

LOWER EXTREMITY
ODD NUMBERS PRESENT 5:00 - 6:30

EVEN NUMBERS PRESENT 3:30 - 5:00

91 A Potential Role of Eversion in Limiting Medial and High Ankle Sprains: A Parametric Study
Wei F, Haut R
Kessler Foundation Research Center

93 Validation of an Electrogoniometry System As a Measure of Knee Kinematics During Activities of Daily Living
Urwin S, Kader D, Caplan N, St Clair Gibson A, Stewart S
Northumbria University

95 Comparison of Hip Morphology in Femoroacetabular Impingement and Normal Patients
Weaver A, Rucker L, Urban J, Theivendran K, Stitzel J
Virginia Tech-Wake Forest University Center for Injury Biomechanics

97 Effects of Regional Foot Pain on Plantar Pressure and Loading
Riskowski J, Dufour A, Hagedorn T, Casey V, Hannan M
Institute for Aging Research / Harvard Medical School

99 The Effects of Leg Dominance, Neuromuscular Training, and Fatigue on Bilateral Lower Extremity Kinematics
Greska E, Cortes N, Ringleb S, Samaan M, Van Lunen B
Old Dominion University

101 Knee Kinematics During Sloped Walking and Running in Healthy Women with Knee Hyperextension
Teran-Yengle P, Bissig K, Paige A, Rogers A, Yack H
University of Iowa

92 Varying Foam Surface Thickness Does Not Affect Landing EMG Pre-Activation in Active Females
Lippa N, Krzeminski D, Goetz J, Piland S, Rawlins J, Gould T
University of Southern Mississippi

94 Muscle Activity Patterns of Lower Limb During Lateral (Frontal) Side Stepping Task Modulation from Different Heights
Bhatia D, Novo M, Munoz M, Bejarano T, Jung R, Brunt D
Adaptive Neural Systems Lab, Department of Biomedical Engineering, Florida International University, Miami

96 Effect of the Foot Toe-Out Angle on the Knee Adduction Moment During Walking and Running
Alcantara C, Castanharo R, Duarte M
Universidade de Sao Paulo

98 Effects of Volitional Preemptive Abdominal Contraction on Trunk and Lower Extremity Biomechanics and Neuromuscular Control During a Drop Vertical Jump
Haddas R, Hooper T, Sizer P, James R
Texas Tech University Health Sciences Center

100 Influence of Eccentric Body Weight on the Knee Balance of Obese Patients
Li J, MacMahon E, Theiss M
Inova Fairfax Hospital

102 The Influence of Prophylactic Ankle Braces on Lower Limb Mechanics During Single-Leg Hopping Tasks
Anderson A, Boros R, Stodden D, Yang H
Texas Tech University

POSTER SESSION 1 | THURSDAY, 3:30 - 6:30

BALLROOM A

FALLS

ODD NUMBERS PRESENT 5:00 - 6:30

EVEN NUMBERS PRESENT 3:30 - 5:00

103 Age-Related Redistribution of Hip and Knee Kinetics During Out-And-Back Stepping
Schulz B
VA HSR&D/RR&D Center of Excellence, Maximizing Rehabilitation Outcomes

105 Age-Related Differences in the Stepping Response to Laterally-Directed Disturbances
Hurt C, Grabiner M
Universtiy of Illinois at Chicago

107 Fall Detecting Using Inertial and Electromyographic Sensors
Yang B, Liao S
National Chiao Tung University

109 Strength, Power and Electromyographic Performance of Hip Musculature in Older Female Fallers and Non-Fallers
Zamfolini Hallal C, Morcelli M, Fernandes Crozara L, Ribeiro Marques N, Martineli Rossi D, LaRoche D, Goncalves M, Navega M
Sao Paulo State University

111 Common Head Acceleration Exposures in the Early Pediatric Population
Desautels D, Serina E
Talas Engineering, Inc.

113 Which Muscles Limit the Ability of Older Adults to Recover Balance?
Kadono N, Pavol M
University of Ottawa

104 Altered Movement Strategy During Sit-To-Walk in Elderly Adults with History of Falling
Chen T, Chou L
University of Oregon

106 Knee Joint Loading During a Compensatory Step: Preliminary Data for Observing Recovery Responses in Knee Osteoarthritic Patients
Hoops M, Rosenblatt N, Skoirchet A, Grabiner M
University of Illinois at Chicago

108 Association Between Strength, Kinematics, and the Energy Cost of Walking in Older, Female Fallers and Non-Fallers
Marques N, Hallal C, LaRoche D, Crozara L, Morcelli M, Karuka A, Navega M, Goncalves M
Sao Paulo State University

110 The Effects of Fatigue on Recovery from a Postural Perturbation
McClain M, Dickin C, Wang H
Ball State University

112 Investigating the Link Between Kinematic Deviations and Recovery Response to Unexpected Slips
Hur P, Beschorner K
University of Wisconsin-Milwaukee

POSTER SESSION 1 | THURSDAY, 3:30 - 6:30

BALLROOM A

POSTURE & BALANCE

ODD NUMBERS PRESENT 5:00 - 6:30

EVEN NUMBERS PRESENT 3:30 - 5:00

115 The Effect of Vibrotactile Stimulation on Long Range Correlation of Stride Interval Time Series Among Different Walking Speeds
Chien J, Huang C, Vallabhajosula S, Mukherjee M, Siu K, Stergiou N
Nebraska Biomechanics Core Facility, University of Nebraska at Omaha

---

117 Using Stationary and Non-Stationary Measures of Balance to Assess Handstand Performace
Blenkinsop G, Pain M, Hiley M
Loughborough University

---

119 Individuals with Diminished Hip Abductor Muscle Strength Exhibit Higher Moments & Neuromuscular Activation at the Ankle During Unipedal Balance Tasks
Lee S, Powers C
University of Southern California

---

121 Margin of Stability As a Metric for Balance Impairment in Multiple Sclerosis
Cutler E, Wurdeman S, McGrath D, Myers S, Stergiou N, Huisinga J
University of Nebraska at Omaha

---

123 Stabilogram Diffusion Analysis Applied to Dynamic Stability: One-Legged Landing from a Short Hop
Heise G, Smith J, Liu K
University of Northern Colorado

---

125 The Use of a Platform for Dynamic Simulation of Movement: Application to Balance Recovery
Mansouri M, Clark A, Reinbolt J
University of Tennessee

---

127 The Effect of Different Foams on Posturography Measures in Healthy and Impaired Populations
Petit D, Bigelow K
University of Dayton

---

114 Stability Radius As a Method for Comparing the Dynamics of Neuromechanical Systems
Bingham J, Ting L
Georgia Institute of Technology

---

116 Lingering Impairments in Postural Control, Despite Symptom Resolution, Following a Concussion.
Buckley T, Tapia-Lovler T, Munkasy B
Georgia Southern University

---

118 Response to Medio-Lateral Perturbations of Human Walking and Running
Qiao M, Hughes M, Jindrich D
Arizona State University

---

120 Validation and Calibration of the Wii Balance Board As an Inexpensive Force Plate
Bartlett H, Bingham J, Ting L
Georgia Institute of Technology

---

122 Children with Cerebral Palsy May Not Benefit from Stochastic Vibration When Developing Independent Sitting
Yu Y, Vallabhajosula S, Haworth J, Stergiou N, Harbourne R
Nebraska Biomechanics Core Facility, University of Nebraska at Omaha

---

124 Postural Sway Changes in Altered Sensory Environments Following Individualized Whole Body Vibration
Dickin D, Hubble R, Heath J, Beltran E, Haggerty M
Biomechanics Laboratory - Ball State University

---

126 Effect of Obesity and Overweight on Postural Balance in Children from 7 to 14-Years-Old
de David A, Barbacena M
University of Brasilia

POSTURE & BALANCE (CONTINUED)
ODD NUMBERS PRESENT 5:00 - 6:30

129 The Relationship Between Structural and Spatial Variability of Postural Control in Persons with Parkinson Disease
Amano S, Stegemöller E, Altmann L, Hass C
University of Florida

131 Effects of Multifocal Lens Glasses on Stepping Accuracy During Step Down
Beschorner K, Dyapa S, Moore C, Tomashek D, Keenan K
University of Wisconsin-Milwaukee

133 The Effect of Age and Movement Direction on Rapid and Targeted Center of Pressure Submovements while Crouching
Hernandez M, Ashton-Miller J, Alexander N
University of Michigan

EVEN NUMBERS PRESENT 3:30 - 5:00

128 The Influence of Repetitive Loads on Foot Sensitivity and Dynamic Balance
Hamilton S, Raisbeck L, Roemer K
Michigan Technological University

130 Impact of Dual-Tasking on Lower Joint Dynamics During Stair Ascension
Davidson A, Vallabhajosula S, Tan C, Mukherjee M, Siu K, Yentes J, McGrath D, Myers S
Nebraska Biomechanics Core Facility, University of Nebraska at Omaha

132 Postural Control Model of Spasticity in Persons with Multiple Sclerosis
Boes M, Hsiao-Wecksler E, Motl R, Sosnoff J
University of Illinois at Urbana-Champaign

CLINICAL
ODD NUMBERS PRESENT 5:00 - 6:30

135 The Gait Pattern of Children with Cerebral Palsy Has Greater Stochastic Features
Kurz M, Harbourne R
University of Nebraska Medical Center

137 Dual-Task Walking and Computerized Cognitive Tests in Assessing Concussed High School Athletes
Howell D, Osternig L, Chou L
University of Oregon

139 Emotion As a Gait Therapy in Parkinson's Patients: Affective Stimuli & Gait Pattern Variability
Beatty G, Roemmich R, Naugle K, Janelle C, Hass C
University of Florida

141 The Impact of Obesity on the Accuracy of Predicting Body Fat Percentage in Older Men
Parise E, Chambers A, McCrory J, Cham R
University of Pittsburgh

EVEN NUMBERS PRESENT 3:30 - 5:00

134 Children with Cerebral Palsy Do More Positive Mechanical Work After Gait Rehabilitation
Kurz M, Stuberg W, Arpin D, Gosselin M
University of Nebraska Medical Center

136 The Gait Variability Profile of Patients with Parkinson's Disease When Compared to Older Adults with Mobility Disability and a History of Falls.
Nocera J, Okun M, Skinner J, Hass C
1Department of Veterans Affairs

138 Effect of L-Dopa on Multi-Finger Synergies and Anticipatory Synergy Adjustments in Parkinson's Disease
Park J, Zatsiorsky V, Lewis M, Huang X, Latash M
Pennsylvania State University, University Park

140 Gait Compensations in a Rat Medial Meniscus Transection Model of Knee Osteoarthritis
Allen K, Mata B, Gabr M, Huebner J, Kraus V, Setton L
University of Florida

CLINICAL (CONTINUED)

ODD NUMBERS PRESENT 5:00 - 6:30

143 Distinct Features of Grip Force Characterize Parkinson's Disease and Atypical Parkisonian Disorders
Neely K, Planetta P, Prodoehl J, Corcos D, Comella C, Goetz C, Shannon K, Vaillancourt D
University of Florida

145 Changes in Muscle Co-Activation in Spinal Cord Injured Individuals After Body-Weight Supported Treadmill Training
Lee S, Pauhl K, Lam T, Wakeling J
Simon Fraser University

147 Computerized Gait Analysis and Lumbar Range of Motion Assessments in People with Lumbar Spinal Stenosis
Conrad B, Abbasi A, Vincent H, Seay A, Kennedy D
University of Florida

149 Using MRI-Based Muscle Volumes and Gait Analysis to Quantify Relative Muscle Effort in Children with Cerebral Palsy
Russell S, Handsfield G, Boyle M, Sauer L, Meyer C, Abel M, Blemker S
University of Virginia

151 Frequency Domain Analysis of Ground Reaction Force Does Not Differentiate Between Hyperkinetic and Hypokinetic Movement Disorders.
Skinner J, Roemmich R, Amano S, Stegemöller E, Altmann L, Hass C
University of Florida

153 The Effect of Anesthetic Hip Joint Injections on Gait
Kennedy D, Sun D, Vincent H, Seay A, Abbasi A, Conrad B
University of Florida

155 Altered Hip Movement in Females with Hip Pain During Single Leg Step Down
Lewis C
Boston University

EVEN NUMBERS PRESENT 3:30 - 5:00

142 The Influence of Merged Muscle Excitation Modules on Post-Stroke Hemiparetic Walking Performance
Allen J, Kautz S, Neptune R
The University of Texas at Austin

144 Differences in Repetitive Finger Movement Between the Most Effected and Least Effected Hand in Parkinson's Disease
Stegemöller E, MacKinnon C, Tillman M, Hass C
University of Florida

146 Walking Abnormalities in Patients with COPD
Yentes J, Rennard S, Stergiou N
Nebraska Biomechanics Core Facility

148 Spatiotemporal Gait Asymmetry is Related to Balance/Fall Risk in Individuals with Chronic Stroke
Bradley C, Wutzke C, Zinder S, Lewek M
University of North Carolina at Chapel Hill

150 The Relationship Between Lower Extremity Joint Power During Sit to Stand and Clinical Measures of Function Among Subjects Post Hip Fracture
Kneiss J, Houck J, Hilton T
MGH Institute of Health Professions

152 Patients with Peripheral Arterial Disease Exhibit Greater Toe Clearance than Healthy Controls
Rand T, Wurdeman S, Johanning J, Pipinos I, Myers S
Nebraska Biomechanics Core Facility

154 Pelvic Excursion During Walking Post-Stroke
Little V, McGuirk T, Perry L, Patten C
University of Florida

156 Mechanical Cueing Using a Portable Powered Ankle-Foot Orthosis
Petrucci M, MacKinnon C, Hsiao-Wecksler E
University of Illinois at Urbana-Champaign

REHABILITATION

ODD NUMBERS PRESENT 5:00 - 6:30

EVEN NUMBERS PRESENT 3:30 - 5:00

157 Biomechanical Analysis of Discrete Versus Cyclic Reaching in Survivors of Stroke
Massie C, Malcolm M, Greene D, Browning R
Colorado State University

158 Preliminary Study of Changes in Trunk Forward Bend Aberrant Patterns Post Core Stabilization Intervention
Wattananon P, Biely S, Sung W, Cannella M, Silfies S
Drexel University

159 Partnered Human-Robot Stepping Based on Interactive Forces at the Hand
Chen T, McKay J, Bhattacharjee T, Hackney M, Kemp C, Ting L
Georgia Institute of Technology

160 Gender Effects on Lower Extremity Biomechanics in Adolescent Patients Following ACL Reconstruction
Dai B, Butler R, Garrett W, Queen R
Duke University

161 The Effect of Kinesio Taping on Kinematics and Muscle Activity for Subjects with Neck Pain
Lee S, Chen G, Chou M, Su F
Department of Biomedical Engineering, National Cheng Kung University

162 Objective Evaluation of Chronic Ankle Instability and Balance Exercise Treatment
Jain T, Wauneka C, Liu W
University of Kansas Medical Center

163 A Novel Elastic Loading-Based Exercise Program Improves Both Strength Aand Power at the Ankle Joint
Carey J, Rand T, Myers S
University of Nebraska at Omaha

164 Sit to Stand Mechanics After Symmetry Training for Patients After Total Knee Arthroplasty
Abujaber S, Zeni J, Snyder-Mackler L
University of Delaware

165 Kinematic Analysis of Gesture in Aphasia
Osmanzada H, Ringleb S, Samaan M, Raymer A
Old Dominion University

166 Scapular and Clavicular Kinematics During Empty and Full Can Exercises in Subjects with Subacromial Impingement Syndrome
Timmons M, Grover M, Lopes-Albers A, Ericksen J, Michener L
Department of Veterans Affairs-Hunter Holmes McGuire VA Medical Center

167 Priming the Motor System: Passive and Active Movements Induce Distinct Gabaergic Effects
Guri A, Corti M, Patten C
University of Florida

168 Power Training Post-Stroke Engages Neural Circuits at Spinal and Supraspinal Levels
Corti M, Patten C
University of Florida

WHEELCHAIR BIOMECHANICS

ODD NUMBERS PRESENT 5:00 - 6:30

EVEN NUMBERS PRESENT 3:30 - 5:00

169 A Reanalysis of Wrist Jerk During Ergonomic Hand Drive Wheelchair Propulsion
Zukowski L, Roper J, Otzel D, Hovis P, Shechtman O, Tillman M
University of Florida

170 The Effect of Crank Position and Backrest Inclination on Shoulder Load During Handcycling
Arnet U, van Drongelen S, Schlussel M, Lay V, van der Woude L, Veeger D
Swiss Paraplegic Research

171 Correlation Analysis of Upper Extremity Kinematics for Manual Wheelchair Propulsion
Jayaraman C, Hsu I, Moon Y, Hsiao-Wecksler E, Rice I, Beck C, Sosnoff J
University of Illinois Urbana Champaign

172 Pain During Ergonomic Hand Drive Wheelchair Propulsion
Hovis P, Zukowski L, Roper J, Otzel D, Shechtman O, Bishop M, Tillman M
University of Florida

AZALEA (FRIDAY THEMATIC POSTERS)

GAIT

ODD NUMBERS PRESENT 9:30 - 11:00

EVEN NUMBERS PRESENT 8:00 - 9:30

A1 Decreased Gait Transition Speeds in Unilateral, Transtibial Amputee Gait
Norman T, Chang Y
Georgia Institute of Technology

A3 Comparison of Kinematic, Kinetic, and Mechanical Work Data Between Traditional and Bone Bridge Amputation Techniques During Fast Walking One Year Post Ambulation Without an Assistive Device
Kingsbury T, Thesing N, Collins J, Carney J, Wyatt M
Naval Medical Center, San Diego, CA

A5 Net Efficiency of the Combined Ankle-Foot System in Normal Gait: Insights for Passive and Active Prosthetics
Takahashi K, Stanhope S
University of Delaware

A2 Both Limbs in Unilateral Transtibial Amputees Display Increased Risk for Tripping
Wurdeman S, Yentes J, Myers S, Jacobsen A, Stergiou N
Nebraska Biomechanics Core Facility

A4 Upper Body Kinematics of Bilateral Transtibial Prosthesis Users During Gait
Major M, Stine R, Hodgson M, Gard S
Northwestern University Prosthetics-Orthotics Center

A6 Ground Reaction Force and Temporal-Spatial Adaptations to Running Velocity When Wearing Running-Specific Prostheses
Baum B, Tian A, Schultz M, Hobara H, Linberg A, Wolf E, Shim J
University of Maryland, College Park

COMPUTATIONAL BIOMECHANICS

ODD NUMBERS PRESENT 9:30 - 11:00

EVEN NUMBERS PRESENT 8:00 - 9:30

C1 Muscle Force Estimates During the Weight-Acceptance Phase of Single-Leg Jump Landing
Morgan K, Donnelly C, Reinbolt J
University of Tennessee

C3 Comparision of Patella Bone Stress Between Individuals with and Without Patellofemoral Pain
Ho K, Powers C
University of Southern

C5 An Adaptive Tabu Search Optimization Algorithm for Generating Forward Dynamics Simulations of Human Movement
Vistamehr A, Neptune R
Mechanical Engineering Department, The University of Texas, Austin

C2 Peak and Nonuniform Fiber Stretch Increase in the Biceps Femoris Long Head Muscle at Faster Sprinting Speeds
Fiorentino N, Chumanov E, Thelen D, Blemker S
University of Virginia

C4 The Influence of Increased DOF in the Knee Joint on Muscle Activation Timings and Forces in a Musculoskeletal Model
Roos P, Jonkers I, Button K, van Deursen R
Cardiff University

POSTER SESSION 2 | FRIDAY, 8:00 - 11:00 AM

DOGWOOD

COMPARATIVE

ODD NUMBERS PRESENT 9:30 - 11:00

EVEN NUMBERS PRESENT 8:00 - 9:30

173 A Laboratory Method for Evaluating Dynamic Properties of Equine Racetrack Surfaces
Setterbo J, Chau T, Fyhrie P, Hubbard M, Upadhyaya S, Stover S
University of California, Davis

175 Hindwing Function in Four-Winged Feathered Dinosaurs
Hall J, Habib M, Hone D, Chiappe L
Natural History Museum of Los Angeles County/University of Southern California

174 Breezing Racehorse Limb Kinematics on Different Race Surface Materials
Symons J, Garcia-Nolen T, Stover S
UCDavis

KNEE

ODD NUMBERS PRESENT 9:30 - 11:00

EVEN NUMBERS PRESENT 8:00 - 9:30

177 Real-Time Biofeedback for ACL Injury Prevention
Ford K, DiCesare C, Myer G, Hewett T
Cincinnati Children's Hospital

179 The Influence of Upper Body Stability on Peak Knee Loading During Sidestepping: Implications for Athlete Screening and ACL Injury Risk
Edmonds D, Lloyd D, Donnelly C
The University of Western Australia

181 Predicting in Vitro Articular Cartilage Wear in the Patellofemoral Joint Using Finite Element Modeling
Li L, Patil S, Steklov N, Bae W, D'Lima D, Sah R, Fregly B
Department of Mechanical and Aerospace Engineering, University of Florida

183 Tibiofemoral Joint Articular Surface Motion Gender Differences in Subject Specific and Generic Knee Models
Deusinger R, Zou D, Koleini M, Smith K, Hensley G, Machan T
Washington University School of Medicine

185 Correlation Between KT Arthrometer Data and ACL Strain Suggests Diagnostic Importance
Kiapour A, Quatman C, Wordeman S, Levine J, Ditto R, Paterno M, Goel V, Demetropoulos C, Hewett T
University of Toledo

176 Hop Performance in Individuals with Anterior Cruciate Ligament Injuries
Roos P, Button K, van Deursen R
Cardiff University

178 The Correlation Between Internal Skeletal Dimensions of Tibiofemoral Joint and External Body Measurements
Zou D, Deusinger R, Koleini M, Smith K, Hensley G, Machan T, Vasiljevic D
Washington University School of Medicine

180 Estimating ACL Force from Lower Extremity Kinematics and Kinetics
Dai B, Yu B
The University of North Carolina at Chapel Hill

182 A Novel Impaction System to Model Cartilage Injury in Living Rabbit Knees
Diestelmeier B, Tochigi Y, Rudert M, Fredericks D, Arunakul M, Brown T, McKinley T
University of Iowa

184 Latent Profile Analysis: Grouping Subjects by Biomechanical Predictors of Increased Kam & Potential Risk for ACL Injury
Hewett T, Ford K, Xu Y, Khoury J, Myer G
The Ohio State University, Cincinnati Children's Hospital Research Foundation

POSTER SESSION 2 | FRIDAY, 8:00 - 11:00 AM
DOGWOOD

KNEE (CONTINUED)
ODD NUMBERS PRESENT 9:30 - 11:00

187 Single Leg Hop Landing Biomechanics and Association with Symmetry Index Following Meniscectomy
Hsieh C, Chmielewski T
University of Florida

189 Tibial Slope and Knee Flexion Moderate Muscle Induced Strain in the Anterior Cruciate Ligament
Breighner R, Domire Z, Slauterbeck J, Hashemi J
Texas Tech University

191 Tibiofemoral Cartilage Thickness Following ACL Reconstruction
Thorhauer E, Tashman S
University of Pittsburgh

EVEN NUMBERS PRESENT 8:00 - 9:30

186 The Effect of Unilateral and Total Menisectomy on Posterior Cruciate Ligament Forces Under Femoral Anterior Drawer in Passive Human Knee at Full Extension.
El Sagheir S, Moglo K
Royal Military College of Canada

188 Knee Kinematics and Kinetics During Descent of a Navy Ship Ladder
Coulter J, Bawab S, Weinhandl J, Ringleb S
Old Dominion University

190 Effect of Enhanced Eccentric Resistance During the Squat Exercise on Lower Extremity Stability and Strength
Conrad B, David H, Barone T, Tang S, MacMillan M
University of Florida

192 Influence of Sex and Severity on the External Adduction Moment in Medial Compartment Knee Osteoarthritis
Morrow M, Kaufman K
Mayo Clinic

SPINE
ODD NUMBERS PRESENT 9:30 - 11:00

193 In Vivo Three-Dimensional Analysis of the Thoracic Spine in Trunk Rotation
Fujimori T, Iwasaki M, Ishii T, Kashii M, Murase T, Sugamoto K, Yoshikawa H
Department of Orthopedic Surgery, Osaka University Graduate School of Medicine

195 Quantification of Multi-Segmental Spine Movement During Gait
Breloff S, Chou L
University of Oregon

197 Biomechanical Loading of the Sacrum in Pre- and Post Operative Adolescents Idiopathic Scoliosis
Pasha S, Aubin C, Parent S, Labelle H, Mac-Thiong J
Ecole polytechnique de Montreal

EVEN NUMBERS PRESENT 8:00 - 9:30

194 The Effect of Thoracic Kyphosis and Sagittal Plane Alignment on Vertebral Compressive Loading
Bruno A, Anderson D, D'Agostino J, Bouxsein M
Harvard-MIT Health Sciences and Technology Program

196 Disturbances to Intrinsic Stiffness and Reflexive Muscle Responses Following Repeated Static Trunk Flexion
Muslim K, Hendershot B, Toosizadeh N, Nussbaum M, Bazrgari B, Madigan M
Virginia Tech

198 Loading Rate During Spinal Manipulation Has Minimal Effect on Lumbar Spine Peak Reaction Force and Spinal Stiffness: A Human Specimen Study
Xia T, Gudavalli R, Qin Y, Goel V, Ianuzzi-Morris A, Pickar J
Palmer College of Chiropractic

POSTER SESSION 2 | FRIDAY, 8:00 - 11:00 AM

DOGWOOD

SPINE (CONTINUED)

ODD NUMBERS PRESENT 9:30 - 11:00

199 Creating Physiologically Realistic Vertebral Fractures
Corbiere N, Lewicki K, Ferrucci L, Issen K, Kuxhaus L
Clarkson University

201 Anticipatory Activation of the Erector Spinae and Multifidus in Patients with and Without Low Back Pain
Currie S, Myers C, Davidson B, Enebo B
University of Denver

EVEN NUMBERS PRESENT 8:00 - 9:30

200 Analysis of the Biomechanical Characteristics of the Spinal Interspinous Implants
Choi D, Kim Y, Kim K
University of Kyung Hee

202 Impact of the Loading Type on the Biomechanics of the Cervical Spine
Mesfar W, Moglo K
Royal Military College of Canda

HICKORY

UPPER EXTREMITY

ODD NUMBERS PRESENT 9:30 - 11:00

203 Musculoskeletal Loading of the Thumb During Pipette Operation
Wu J, Sinsel E, Shroyer J, Warren C, Welcome D, Zhao K, An K, Buczek F
National Institute for Occupational Safety and Health (NIOSH)

205 Contact Stress Analysis of the Radial Head and the Radial Head Implants
Kim S, Miller M
University of Pittsburgh

207 Handgrip Force and Upper-Limb Kinetics During Handcycling
Griswold J, Sasaki K
Boise State University

209 The Effect of Arm Position on Bony Bankart Lesion: A Finite Element Study
Walia P, Miniaci A, Jones M, Fening S
Cleveland State University; Cleveland Clinic

211 Effects of Cortical Stimulation on Sensorimotor Functions of the Hand in Healthy Old Adults
Parikh P, Cole K
University of Iowa

EVEN NUMBERS PRESENT 8:00 - 9:30

204 Calculating Thumb and Index Finger Postures During Pinch with a Minimal Marker Set
Nataraj R, Li Z
Cleveland Clinic

206 Removal of Pain from Patients with Shoulder Impingement Results in Alterations in Shoulder Muscle Activity & Scapular Kinematics
Ettinger L, Shapiro M, Karduna A
University of Oregon

208 The Effect of Arm Position on Hill-Sachs Engagement: A Finite Element Study
Walia P, Miniaci A, Jones M, Fening S
Cleveland State University; Cleveland Clinic

210 Assessment of Functional Reaching Tasks in Older Adults
Vidt M, Daly M, Marsh A
Wake Forest School of Medicine, Department of Biomedical Engineering

212 The Effects of Upper Extremity Lymphedema on Dominant Limb 3-Dimensional Scapular Kinematics and Upper Extremity Function in Survivors of Breast Cancer
Biggers L, Rundquist P
Krannert School of Physical Therapy

HICKORY

UPPER EXTREMITY (CONTINUED)

ODD NUMBERS PRESENT 9:30 - 11:00

EVEN NUMBERS PRESENT 8:00 - 9:30

213 Development and Verification of an Elbow Stiffness Tester
Zeng S, Robinson C, Kuxhaus L
Clarkson University

215 Electromyographic and Kinematic Analysis of Medial Reverse Shoulder Arthroplasties During Functional Motions
Walker D, Struk A, Wright T, Banks S
University of Florida

217 Characterization of Coupled Wrist and Forearm Stiffness
Drake W, Charles S
Brigham Young University

219 Reliability and Precision of the Resistance Zone and Laxity Zone for Shoulder Internal and External Rotation
Livingston B, Wight J, Wikstrom E, Tillman M
University of North Florida

214 The Medial Ulnar Collateral Ligament Carries No Load During Passive Flexion and Extension
Muiuki M, Schimoler P, Campbell B, Vaccariello M, Snell E, Akhavan S, DeMeo P, Miller M
Allegheny General Hospital

216 Altered Scapulohumeral Coordination in Individuals with Scapular Dyskinesis
Spinelli B, Ebaugh D
Drexel University

218 Kinematic Coupling of Wrist and Forearm Movements
Anderton W, Charles S
Brigham Young University

220 Effects of Serratus Anterior Muscle Fatigue on Scapular Kinimatics
Costantini O, Dashottar A, Borstad J
The Ohio State University

BALLROOM A

RUNNING

ODD NUMBERS PRESENT 9:30 - 11:00

EVEN NUMBERS PRESENT 8:00 - 9:30

221 Mechanical Demand Distribution During Shod and Novice Barefoot Running
Hashish R, Samarawickrame S, Gaur K, Salem G
University of Southern California

223 Plantar Pressure Differences Between Rearfoot and Midfoot Striking Runners
Becker J, Howey R, Osternig L, James S, Chou L
University of Oregon

225 Age Related Changes in Running
Freedman Silvernail J, Rohr E, Brueggemann G, Hamill J
University of Massachusetts

222 Biomechanics of Retrospective Navicular Stress Fractures
Becker J, Osternig L, James S, Chou L
University of Oregon

224 Static Foot Structure and Knee Kinematics During Running
DiCesare C, Taylor-Haas J, Hickey K, Myer G, Hegedus E, Ford K
Cincinnati Children's Hospital

226 Trunk Flexion Angle is Associated with Patellofemoral Joint Stress During Overground Running
Teng H, Powers C
University of Southern California

RUNNING (CONTINUED)

ODD NUMBERS PRESENT 9:30 - 11:00

227 Predictors of Initial Impact Load and Loading Rates in Runners
Noehren B, Pohl M
University of Kentucky

229 Changing Step Width Alters Lower Extremity Kinematics During Running
Milner C, Brindle R, Zhang S, Fitzhugh E
University of Tennessee

231 Accuracy of Self-Reported Footstrike Paterns and Loading Rates Associated with Traditional and Minimalist Running Shoes
Goss D, Lewek M, Yu B, Gross M
University of North Carolina at Chapel Hill

233 Trunk Endurance Strength and Running Biomechanics After Iliotibial Band Syndrome
Foch E, Pfeiffer J, Milner C
University of Tennessee

235 Medial Longitudinal Arch Characteristics During Running
Forrester S
Loughborough University

237 Average Ankle Dynamic Joint Stiffness During Heel Strike Running
Razzook A, Gleason C, Willy R, Fellin R, Davis I, Stanhope S
University of Delaware

239 Differences in Running and Walking Gait Kinematics During Earth and Simulated Mars and Lunar Gravitational Environments: Preliminary Investigation
Shapiro R, Cunningham T, Wallace B, Norberg J, Phillips M, Miller M
University of Kentucky

241 Exertion Modulates Ankle Joint Co-Activation During Novel Barefoot and Post-Transition Barefoot Running Conditions
Samarawickrame S, Hashish R, Gaur K, Salem G
University of Southern California

EVEN NUMBERS PRESENT 8:00 - 9:30

228 EMG Activity while Alter-G Treadmill Running
Hunter I, Seeley M, Hopkins T, Franson J, Collins M
Brigham Young University

230 Lower Extremity Joint Moments During the Active Peak Vertical Ground Reaction Force in Three Different Running Conditions
Standifird T, Johnson W, Hunter I, Ridge S
Brigham Young University

232 Ground Reaction Forces During Treadmill Exercise on the International Space Station
De Witt J, Fincke R, Guilliams M, Ploutz-Snyder L
Wyle Science, Technology and Engineering Group/NASA JSC

234 Effect of Running Classes on Running Kinematics and Economy
Craighead D, Lehecka N, King D
Ithaca College

236 Computer Simulation Assists Gait Retraining Program, a Case Study
Beltran E, McClain M, Wang H
Ball State University

238 Sagittal Kinematics & Kinetics of Midfoot/Forefoot Running After 4 Weeks of Training
Boyer E, Derrick T
Iowa State University

240 Insights into the Footstrike Patterns of Women Distance Runners
Cavanagh P, Glauberman M, Manner K, Sawyer K, Devasia S
University of Washington

SPORTS

ODD NUMBERS PRESENT 9:30 - 11:00

243 The Effect of Load on Movement Coordination During Sled Towing
Lawrence M, Leib D, Masterson C, Hartigan E
University of New England

245 Biomechanical Analysis of Basketball Free Throw Shooting
Bradley S, Martin J
Penn State

247 Softball Windmill Pitch: Necessity of a Pitch Count
Postlmayr C, Wu T, Ashley J
Bridgewater State University

249 Deceleration: Relationship Between Body Position and Velocity
Havens K, Sigward S
University of Southern California

251 The Influence of Fatigue on Landing Mechanics in Youth Male Lacrosse Athletes
Cortes N, Greska E, Bamberg J, Ringleb S, Van Lunen B
George Mason University

253 Influence of Various Heights and Surfaces on Neuromuscular Strategies During Drop Landings
Esselman E, Carpenter A, Smith J, Heise G
University of Northern Colorado

255 Rate of Loading and Lower Extremity Sagittal Plane Biomechanics When Landing from a Drop-Jump: Shod and Barefoot Comparisions Between Genders
Cochrane R, McNeaney B, Lawrence M, Hartigan E
University of New England

257 Relationships Between Electromyography and Oxygen Consumption in Different Work Loads - Rowing Exercise
Hsu H, Hong W, Wang H
Department of Sports Medicine

EVEN NUMBERS PRESENT 8:00 - 9:30

242 The Effect of Pedal Crank Arm Length on Lower Limb Joint Angles in an Upright Cyling Position
Too D, Williams C
The College at Brockport

244 The Rotational Stiffness of Football Shoes May Affect the Location of a Potential Ankle Injury
Wei F, Meyer E, Braman J, Powell J, Haut R
Michigan State University

246 Between Landing Kinetic and Kinematic Differences in a Drop Vertical Jump
Bates N, Ford K, Myer G, Hewett T
University of Cincinnati

248 Batting Cage Performance of Various Youth Baseball Bats
Crisco J, Rainbow M, Wilcox B, Schwartz J
Department of Orthopaedics, Warren Alpert Medical of Brown University and Rhode Island Hospital

250 Latissimus Dorsi Anthropometry and Swimming
Weimar W, Campbell B
Auburn University

252 The Influence of Pedal Platform Height on Maximal Average Crank Power During Pedaling: A Simulation Study
Vistamehr A, Neptune R
Mechanical Engineering Department, The University of Texas, Austin

254 The Examination of Softball Pitching Fatigability in Lower Extremities.
Ashley J, Wu T, Postlmayr C
Bridgewater State University

256 Effects of a 6 Week Intervention Program on Lower Limb Joint Moment Asymmetry in Healthy Female Collegiate Athletes
Spencer R, St Jeanos A, Wynot M, Lawrence M, Hartigan E
University of New England

SPORTS (CONTINUED)

ODD NUMBERS PRESENT 9:30 - 11:00

259 The Effects of Neuromuscular Fatigue on Coordiation Variation
Samaan M, Cortes N, Hoch M, Ringleb S, Weinhandl J, Greska E, Lucci S, Quammen D, Bawab S
Old Dominion University

261 Comparison Between Squat Jump vs. Weighted Squat Jump: Simulation Study.
Cimadoro G, Minetti A, Pain M, Van Hoecke J, Alberti G, Babault N, Yeadon M
University of Milan, Department of Sport, Nutrition and Health Science, Milano, ITALY

263 Stride Length Compensations and Their Impacts on Brace-Transfer Ground Forces in Baseball Pitchers
Crotin R, Ramsey D
University at Buffalo

265 Muscle Activation Changes Across Three Different Skate Skiing Techniques.
Mills K, Heil D, Higginson B
Gonzaga University

267 Kinematic Analysis of Volleyball Spiking Maneuver
Dunbar N, Chmielewski T, Tillman S, Zheng N, Conrad B
University of Florida

269 Effects of Long-Term Use of Ankle Taping on Balance
McGregor S, Johnson S, Pavol M
Oregon State University

EVEN NUMBERS PRESENT 8:00 - 9:30

258 Joint Angles and Joint Moments Following Neuromuscular Fatigue in Futsal Players
Fukuchi R, Fukuchi C, Dinato M, Riani L, Duarte M
University of Calgary

260 A Comparison of Volleyball Blocking Techniques: Jumping Velocities and Effective Blocking Areas
Ficklin T, Schipper M, Lund R
University of Northern Iowa

262 Using Ankle Bracing Influences the Torque Ratio Among Ankle Stabilizers Muscles After Simulation Basketball Match-Play?
Marques N, Castro A, Milanezi F, Almeida A, Crozara L, Goncalves M
Sao Paulo State University

264 The Effects of Whole Body Vibration on the Wingate Test for Anaerobic Power When Applying Individualized Frequencies
Surowiec R, Wang H, Nagelkirk P, Frame J, Dickin D
Ball State University; Steadman Philippon Research Institute

266 A Comparison of Knee Moments During a Lateral Cutting Maneuver: Shod vs. Barefoot
Bisesti B, Cottle C, Lawrence M, Carlson L
University of New England

268 Common Control Strategies for Generating Angular Impulse in Forward and Backward Translating Tasks
Ramos C, Mathiyakom W, McNitt-Gray J
University of Southern California

270 Mechanisms Dancers Use to Maintain Balance and Regulate Reaction Forces When Turning
Zaferiou A, McNitt-Gray J
USC

POSTER SESSION 2 | FRIDAY, 8:00 - 11:00 AM
BALLROOM A

INSTRUMENTATION
ODD NUMBERS PRESENT 9:30 - 11:00

271 Comparing Metabolic Costs of Harvesting Biomechanical Energy from Human Motion Versus Carrying Batteries for the Same Energy Supply
Schertzer E, Riemer R
Ben-Gurion University

273 Estimating Peak Achilles Tendon Forces in Youth During Locomotion Using Hip Acceleration
Neugebauer J, Hawkins D
University of California - Davis

275 Robust Optical Sensor for Noninvasive Cardiac Monitoring
Sabick M, Johnson J
Boise State University

EVEN NUMBERS PRESENT 8:00 - 9:30

272 Posture and Activity Detection Using a Tri-Axial Accelerometer
Lugade V, Fortune E, Morrow M, Kaufman K
Mayo Clinic

274 Step Counts Using a Tri-Axial Accelerometer During Activity
Fortune E, Lugade V, Morrow M, Kaufman K
Mayo Clinic

276 Validation of a Commercial Wearable Sensor System for Accurately Measuring Gait on Uneven Terrain
Rigsby M, Edginton Bigelow K
University of Dayton

GAIT
ODD NUMBERS PRESENT 9:30 - 11:00

277 Concussion Alters Gait Termination Strategies
Wikstrom E, Tapia-Lovler T, Munkasy B, Buckley T
UNC Charlotte

279 Muscle Activations in Response to Achilles Tendon Rupture and Repair
Suydam S, Buchanan T, Manal K, Silbernagel K
University of Delaware

281 Torso Kinematics During Gait Differ Between Pregnant Fallers and Non-Fallers
McCrory J, Chambers A, Daftary A, Redfern M
West Virginia University

283 Six-Week Gait Retraining Program for Knee Osteoarthritis Patients: Learning Retention and Symptom Changes
Shull P, Silder A, Shultz R, Besier T, Delp S, Cutkosky M
Stanford University

EVEN NUMBERS PRESENT 8:00 - 9:30

278 Why Do Humans Walk the Way We Do? Evidence from Dynamic Simulations
Miller R
Queen's University

280 Metabolic Cost and Lower Extremity Muscle Activity During Constant Speed Walking at Different Stride Frequencies
Boynton A, Royer T
U.S. Army Research Laboratory/University of Delaware

282 Frontal Plane Mechanics Are Altered During Split Belt Treadmill Walking in Young Healthy Adults
Roper J, Roemmich R, Tillman M, Hass C
University of Florida

284 The Metabolic and Mechanical Costs of Step-Time Asymmetry in Walking
Ellis R, Howard K, Kram R
University of Colorado at Boulder

GAIT (CONTINUED)

ODD NUMBERS PRESENT 9:30 - 11:00

285 Comparisons of Flip-Flop, Sandal, Barefoot and Running Shoe in Walking
Zhang S, Zhang X, Paquette M
The University of Tennessee, Knoxville

287 Maximal Dynamic Stability of Walking Coincides with the Freely Adopted Speed and Stride Frequency
Russell D, Haworth J, Martinez-Garza C
Old Dominion University

289 Differences in Stride Interval Variability During Stair-Climbing and Treadmill Walking
Renz J, Vallabhajosula S, Hunt N, Chien J, Stergiou N
Nebraska Biomechanics Core Facility, University of Nebraska at Omaha, Omaha, NE

291 Spatiotemporal Parameters of Uphill, Level and Downhill Walking Are Similar Between Treadmill and Overground Surfaces
Fellin R, Seay J, Gregorczyk K, Hasselquist L
US Army Research Institute of Environmental Medicine

293 Influence of Stepping Rate on Stride Interval Variability of Stair-Climbing
Vallabhajosula S, Renz J, Chien J, Hunt N, Stergiou N
Nebraska Biomechanics Core Facility, University of Nebraska at Omaha, Omaha, NE

295 The Effect of Varying Cadences on Shod & Barefoot Gait Kinematics
Romer B, Fox J, Patel J, Rehm J, Weimar W
Auburn University

297 Comparison of First and Second Generation Rocker Bottom Shoes
Gardner J, Zhang S, Paquette M, Milner C, Foch E
University of Tennessee

299 A Gender Comparison of Lower Extremiy Ambultory Mechanics in Healthy Subjects with Excessive Varus Alignment
Barrios J, Bare D
University of Dayton

EVEN NUMBERS PRESENT 8:00 - 9:30

286 Maintaining a Constant Margin of Stability Across Dyamic Conditions May Rely on Different Control Strategies
Rosenblatt N, Hurt C, Grabiner M
University of Illinois at Chicago

288 Metabolic Cost of Maintaining Balance During a Perturbed Gait Task is Related to Gait Variability
McGrath D, Wurdeman S, Yentes J, Hunt N, Myers S, Stergiou N
Nebraska Biomechanics Core Facility

290 Lower Limb Muscle Coactivation in Younger and Older Adults During Dual-Task Gait
Hallal C, Ribeiro Marques N, Hebling Spinoso D, Brunt D, Vieira E, Goncalves M
Sao Paulo State University

292 Physiological Cost of Heavy Load Carriage
Bartlett J, Robusto K
Naval Health Research Center

294 The Effect of Knee Pain and Effusion on Vertical Ground Reaction Force During Walking
Seeley M, Park J, Hunter I, Francom D, Black B, Hopkins J
Brigham Young University

296 Altered Kinematics Between Flat and Curved Treadmills Do Not Cause Increased Energy Expenditure
Korgan W, Wurdeman S
University of Nebraska at Omaha

298 The Relationship Between Ambulatory Activity Patterns and Kinematic Variability
Hasenkamp R, Wurdeman S, Myers S
University of Nebraska at Omaha

GAIT (CONTINUED)

ODD NUMBERS PRESENT 9:30 - 11:00

301 Comparison of Tibial Torsion Measurements Using Motion Capture, Physical Therapy Evaluation, and Computed Tomography
Nguyen C, Mueske N, Wren T
University of Southern California

303 Adaptation of Plantarflexor Muscle Activity During Gait
Bunchman A, Wellinghoff M, Dean J
Medical University of South Carolina

305 Limb Force Variance is Structured to Stabilize the Step-To-Step Transitions of Dynamic Walking
Toney M, Chang Y
Georgia Institute of Technology

307 Gender Comparison of Trunk and Pelvis Kinematics During Walking and Running
Westlake C, Noehren B
University of Kentucky

309 Influence of Tai Chi on Kinematics During Multi-Directional Gait Initiation
Vallabhajosula S, Roberts B, Hass C
University of Nebraska at Omaha, Omaha, NE

311 Effects of a Biomechanical Energy Harvesting Ankle Device on Gait Kinetics
Gregory R, Zifchock R, Manuel S, Brechue W
U.S. Military Academy

313 Evaluation and Classification of Load Accomodation Strategies During Walking with Extremity-Carried Weights: A Pilot Study
Atkins L, Dufek J, James R
Texas Tech University Health Science Center

EVEN NUMBERS PRESENT 8:00 - 9:30

300 Effect of Ankle Load on Gait Patterns During Treadmill Walking
Wu J, Ajisafe T
Georgia State University

302 Walking Speed Overground and on a Feedback-Controlled Treadmill
Collins J, Sessoms P, Bartlett J
Naval Health Research Center

304 Natural Gait May Not Be Neutral: It All Depends on How You Feel
Kang G, Gross M
University of Michigan, Ann Arbor

306 Gait Initiation Impairments in Essential Tremor and Parkinson’s Disease
Fernandez K, Roemmich R, Stegemöller E, Nocera J, Hass C
University of Florida

308 Identifying Fallers and Non-Fallers Using Gait Variability Indicators Based on Methods Proposed for Heart Rate Assessment
Zamfolini Hallal C, RIbeiro Marques N, LaRoche D, Ramos Vieira E, Hebling Spinoso D, Fernandes Crozara L, Morcelli M, Goncalves M
Sao Paulo State University

310 Slow Uphill Walking: Better for the Knees of Obese Adults?
Haight D, Reynolds M, Board W, Connor T, Browning R
Colorado State University

312 Induced Alterations of Interlimb Coordination Caused by the Use of a Split-Belt Treadmill
Elrod J, Hoover B, Roemmich R, Hass C
Department of Applied Physiology & Kinesiology, University of Florida

PROSTHETICS & ORTHOTICS

ODD NUMBERS PRESENT 9:30 - 11:00

315 The Influence of Wedged Insoles on Knee and Ankle Moments and Angular Impulses During Walking.
Fukuchi C, Lewinson R, Worobets J, Stefanyshyn D
University of Calgary

317 Comparing Visual Perturbation Responsiveness in Individuals with and Without Trans-Tibial Amputation
Terry K, Faust K, Wilken J, Dingwell J
University of Texas at Austin

319 A Passive Elastic Exoskeleton Reduces the Metabolic Cost of Walking Using Controlled Energy Storage and Release
Wiggin B, Sawicki G
Joint Dept. of Biomedical Engineering, North Carolina State University and University of North Carolina

321 Metabolic Costs of Locomotion When Walking with and Without Ankle and Knee Braces
Smith J, Kievenaar C, Falgien V, Wilmes J
University of Northern Colorado

323 More is Not Always Better: Consequences of Exoskeleton Assistance in a Compliant Muscle-Tendon System
Robertson B, Sawicki G
UNC Chapel Hill/NC State Joint Dept of Biomedical Engineering

325 Muscle Contributions to Whole-Body Angular Momentum During Unilateral Below-Knee Amputee Walking
Silverman A, Neptune R
Colorado School of Mines

327 Trip Recovery Strategies in a Unilateral Transfemoral Amputee
Shirota C, Simon A, Kuiken T
Northwestern University

EVEN NUMBERS PRESENT 8:00 - 9:30

314 Kinematic Effects of Biomechanical Energy Harvest at the Ankle: Implications for Injury Susceptibility
Leemans A, Zifchock R, Gregory R, Brechue W
United States Military Academy

316 Reduced and Asymmetric Trunk Stiffness Among Unilateral Lower-Limb Amputees During Multi-Directional Trunk Perturbations
Hendershot B, Nussbaum M
Virginia Tech

318 Comparison of Powered and Unpowered Prostheses in Patients with Transtibial Amputation Walking on a Rock Surface
Gates D, Aldridge J, Wilken J
Brooke Army Medical Center

320 Transtibial Amputee Joint Motion Has Larger Lyapunov Exponents
Wurdeman S, Myers S, Stergiou N
Nebraska Biomechanics Core Facility

322 Biomechanical Design of Rolling Contact Knee Joint Prostheses
Slocum Jr A, Herder J, Varanasi K
MIT

324 The Effect of a New Microprocessor Controlled Prosthetic Knee on Stair Ascent Strategies in Patients with Unilateral Transfemoral Amputation
Aldridge J, Wolf E, Scoville C, Wilken J
Department of Orthopaedics and Rehabilitation, Center for the Intrepid, Brooke Army Medical Center

326 Spring-Mass Characteristics During Overground Running in Amputees Using Running Specific Prostheses
Hobara H, Baum B, Shim J
University of Maryland

328 Weight Bearing Asymmetries and Changes in COP Trajectories: Unilateral ERTL Amputees vs Non-Amputees
Carpenter A, Smith J, Christiansen C, Heise G
University of Northern Colorado

POSTER SESSION 2 | FRIDAY, 8:00 - 11:00 AM
BALLROOM A

PROSTHETICS & ORTHOTICS (CONTINUED)

ODD NUMBERS PRESENT 9:30 - 11:00

EVEN NUMBERS PRESENT 8:00 - 9:30

329 The Effects of Independent Variations in Rearfoot and Forefoot Prosthesis Stiffness on Amputee Gait
Adamczyk P, Roland M, Hahn M, Sawers A
Intelligent Prosthetic Systems, LLC

330 A Comparison of the Effect of Foam-Box Casted and Plaster-Casted Orthotics on the Normal Foot Population Using Bi-Planar X-Ray Fluoroscopy
Bushey K, Balsdon M, Dombroski C, Jenkyn T
University of Western Ontario

331 An Externally Powered and Controlled Ankle-Foot Prosthesis for Use in Push-Off Experiments
Caputo J, Collins S
Carnegie Mellon University

332 Two-Dimensional Parameter Study to Characterize Performance of Ankle-Foot Orthosis Joint Impedance Control
Eicholtz M, Collins S
Carnegie Mellon University

POSTER SESSION 2 | FRIDAY, 8:00 - 11:00 AM
BALLROOM A (SATURDAY THEMATIC POSTERS)

SEATING

ODD NUMBERS PRESENT 9:30 - 11:00

EVEN NUMBERS PRESENT 8:00 - 9:30

S1 Bicycle Riding, Arterial Compression and Erectile Dysfunction
Parthiban S, Yang C, Jones L, Baftiri A, Niederberger C
University of Illinois at Chicago

S2 Investigating the Etiology of Vibration-Induced Low Back Pain
Craig T, Soltys J, Wilson S
University of Kansas

S3 Factors Associated with Pressure Ulcers: The Effects of Shear Loads on Blood Flow
Manorama A, Reid Bush T
Michigan State University

S4 Tissue Deformation in the Seated Buttocks Model
Sonenblum S, Cathcart J, Winder J, Sprigle S
Georgia Institute of Technology

S5 Effect of Seat Position Modifications on Upper Extremity Mechanical Loading During Manual Wheelchair Propulsion
Requejo P, Mulroy S, Munaretto J, Mendoza Blanco M, Wagner E, McNittGray J
Rancho Los Amigos National Rehabilitation Center

POSTER SESSION 2 | FRIDAY, 8:00 - 11:00 AM
BALLROOM A (SATURDAY THEMATIC POSTERS)

MUSCLE
ODD NUMBERS PRESENT 9:30 - 11:00

EVEN NUMBERS PRESENT 8:00 - 9:30

M1 Comparison of Sarcomere Heterogeneity Measured in Passive Live and Fixed Muscle
Sandercock T, Cash A, Tresch M
Northwestern University

M3 Posture and Activation Dependent Variations in Shear Wave Speed in the Gastrocnemius Muscle and Aponeurosis
Chernak L, DeWall R, Thelen D
University of Wisconsin-Madison

M2 Pennation Angle Variability in Human Whole Muscle
Infantolino B, Challis J
Penn State Berks

M4 On the Ascent: The Soleus Operating Length is Conserved to the Ascending Limb of the Force-Length Curve Across Gait Mechanics in Humans
Rubenson J, Neville P, Heok L, Pinniger G, Shannon D
The University of Western Australia

OBESITY
ODD NUMBERS PRESENT 9:30 - 11:00

EVEN NUMBERS PRESENT 8:00 - 9:30

P1 Magnitude and Time Course of Adaptation During Walking with a Passive Elastic Exoskeleton
Charalambous C, Dean J
Medical University of South Carolina

P3 The Effects of Wearing a Spring-Loaded Ankle Exoskeleton on Soleus Muscle Mechanics During Two-Legged Hopping in Humans
Farris D, Sawicki G
North Carolina State University & UNC-Chapel Hill

P5 Electromyographic Effects of Using a Powered Ankle-Foot Prosthesis
Williams M, Grabowski A, Herr H, D'Andrea S
Center for Restorative and Regenerative Medicine, PVAMC

P2 Exoskeleton to Carry a Backpack Load
Gregorczyk K, Adams A, O'Donovan M, Schiffman J, Bensel C, Brown M
U.S. Army Natick Soldier Research, Development and Engineering Center

P4 Gait Mode Recognition Using an Inertia Measurement Unit on a Powered Ankle-Foot-Orthosis
Li Y, Hsiao-Wecksler E
University of Illinois at Urbana-Champaign

NOTES

NOTES

EXHIBITOR FLOORPLAN

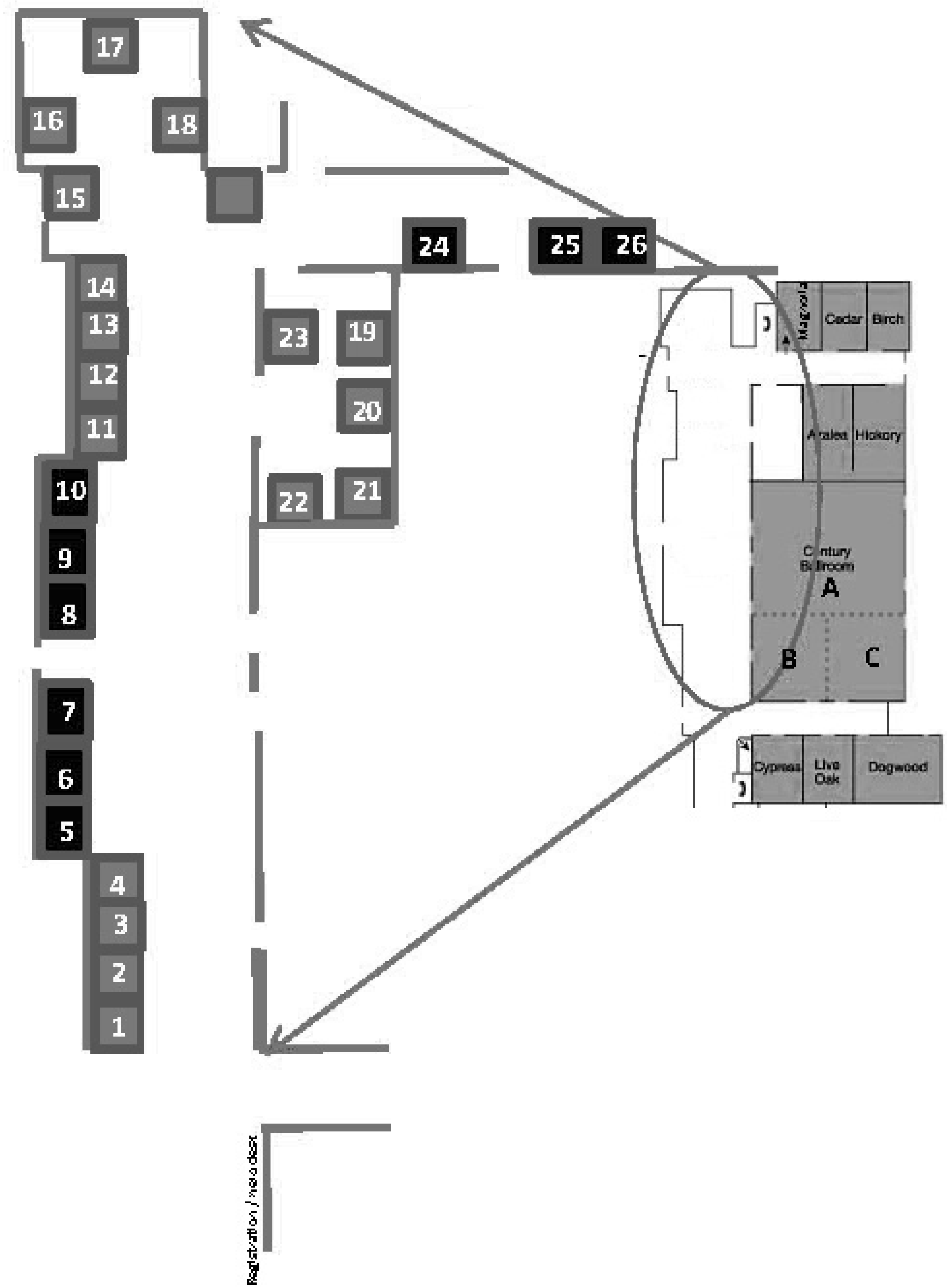

EXHIBITOR	BOOTH #
Noraxon USA Inc.	1
Simi Reality Motion Systems GmbH	2
AnyBody Technology	3
Delsys Inc.	4
C Motion	5
Vicon	6
Northern Digital	7
Tekscan Inc.	8, 9
Polhemus	10
Kistler Instrument Corporation	11
Novel	12
Xcitex	13
AMTI	14
The Motion Monitor	15
ATI, Industrial Automation	16
Motion Analysis Corporation	18
Qualysis	19
Bertec	20
Metria Innovation Inc	21
ViTRAK Systems Inc	22
Footscan	23
Vision Research, AMETEK	24
ProtoKinetics	25
FDA/CDRH/Office of Device Evaluation	26

UNIVERSITY OF FLORIDA CAMPUS MAP

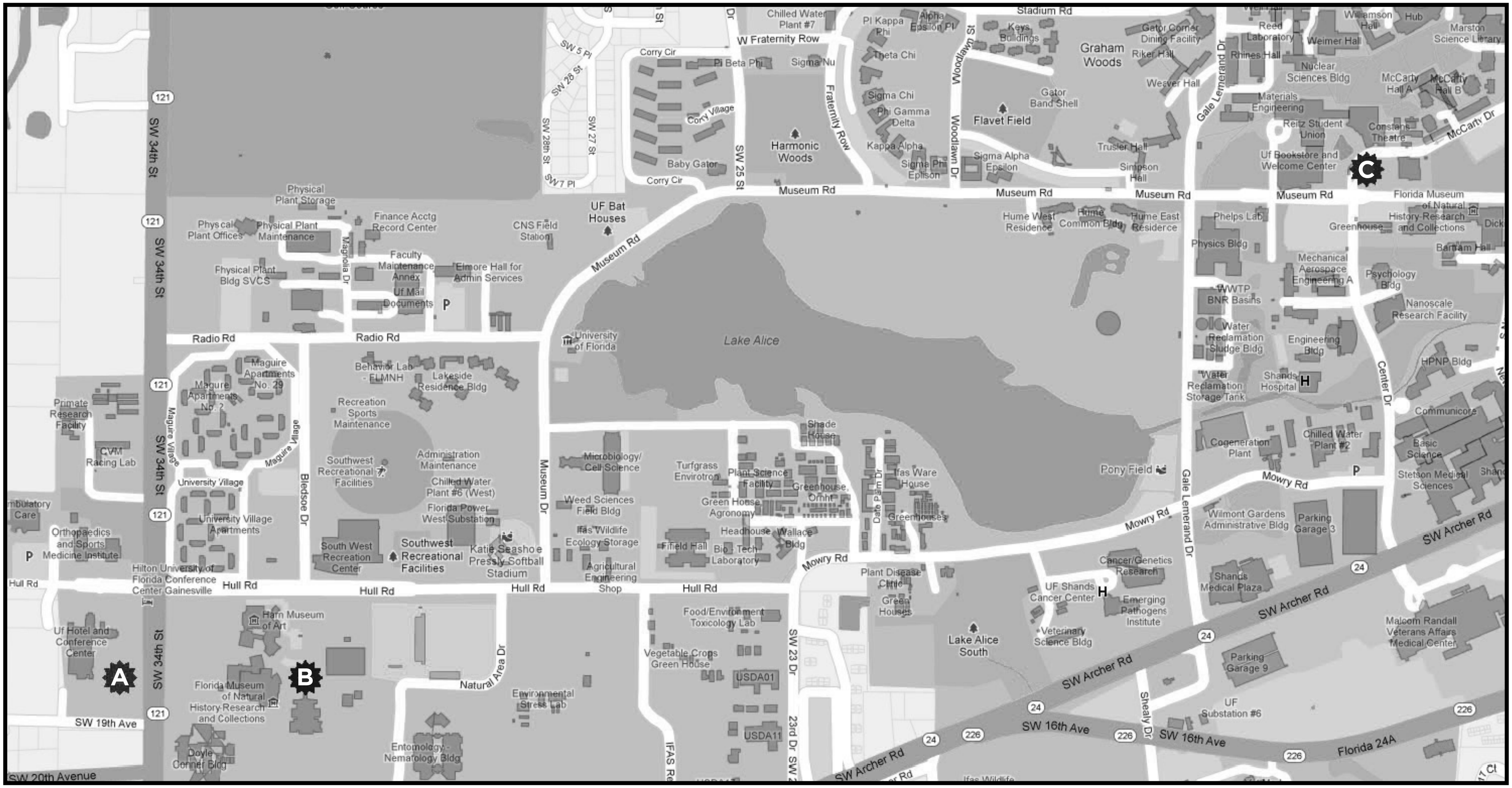

A. HILTON GAINESVILLE / UNIVERSITY OF FLORIDA CONFERENCE CENTER
B. UF CULTURAL PLAZA (PHILLIPS CENTER FOR THE PERFORMING ARTS: RECEPTION & KEYNOTES)
C. J. WAYNE REITZ UNION (BANQUET)

ASB MEETING SCHEDULE AT A GLANCE

Time slots: 7:00 – 8:00 (every 15 minutes)

WEDNESDAY, AUGUST 15

CENTURY A

- **LAB TOUR 1** (10:30 AM - 12:30 PM)
- TUTORIAL I (CHALLIS) 12:30 - 2:30
- TUTORIAL II (FREGLY) 2:40 - 3:10
- TUTORIAL III (BANKS/MU) 3:20 - 4:20
- STUDENT SPEAKERS (4:30 - 5:30)
- **QUICK RESEARCH STUDIES** (MAGNOLIA & CEDAR) **ONGOING** WEDS. - SAT.
- **ASB EXEC. BOARD MEETING** (BOARD ROOM) 2:00 - 5:00
- **LAB TOUR 2** (2:00 - 4:00 PM)
- EXEC. BOARD EXHIBITOR (2-BITS LOUNGE)
- **OPENING RECEPTION** (5:45 - 7:45 PM) FLORIDA MUSEUM OF NATURAL HISTORY

THURSDAY, AUGUST 16

CENTURY A | CENTURY B | CENTURY C | AZALEA

- **BREAKFAST 7:00 - 8:00** (OPEN SEATING ENTIRE FIRST FLOOR)
- **PAST PRES B'FAST** (ALBERT'S DINING ROOM)
- WELCOMING REMARKS (CENTURY A)
- **ORAL PRESENTATIONS (8:00 - 9:15 AM)**: BALANCE DURING LOCO-MOTION | TISSUE MECHANICS | BONE | STROKE (THEMATIC)
- **BREAK AND EXHIBITS**
- **ORAL PRESENTATIONS (9:45 - 11:00 AM)**: ASB FELLOWS SYMPOSIUM | ERGONOMICS | IMAGING: KNEE | OBESITY (THEMATIC)
- **BREAK AND EXHIBITS**
- **ORAL PRESENTATIONS (11:30 AM - 12:45 PM)**: GAIT 1: METHODS | POSTURAL CONTROL | ORTHOPEDICS | JOURNAL AWARDS (THEMATIC)
- **LUNCH** (OPEN SEATING ENTIRE FIRST FLOOR)
- **DIVERSITY LUNCH** (FLORIDA ROOM)
- **TRAVEL**
- **KEYNOTE LECTURE:** SUSAN HARKEMA, PH.D. (2:00 - 3:00 PM) PHILLIPS CENTER FOR PERFORMING ARTS
- **BREAK AND EXHIBITS/ SET UP POSTERS**
- **POSTER SESSION 1 WITH REFRESHMENTS** (3:30 - 6:30 PM) CENTURY A, DOGWOOD, HICKORY & AZALEA
- **TRAVEL VIA BUS**
- **BANQUET & INDUCTION OF FELLOWS** (7:00 - 10:00 PM) J. WAYNE REITZ UNION GRAND BALLROOM

FRIDAY, AUGUST 17

CENTURY A | CENTURY B | CENTURY C | AZALEA

- **BREAKFAST 7:00 - 8:00** (OPEN SEATING ENTIRE FIRST FLOOR)
- **WOMEN IN SCIENCE B'FAST** (FLORIDA ROOM)
- **POSTER SESSION 2 WITH REFRESHMENTS** (8:00 - 11:00 AM) CENTURY A, DOGWOOD, HICKORY & AZALEA
- **TRAVEL**
- **TRIBUTE TO DAVID WINTER, PH.D., P.ENG.** (11:15 AM - 12:15 PM) PHILLIPS CENTER FOR PERFORMING ARTS
- **TRAVEL**
- **LUNCH** (OPEN SEATING ENTIRE FIRST FLOOR)
- **ORAL PRESENTATIONS (1:30 - 3:15 PM)**: AGING AND GAIT SYMPOSIUM | MOTOR CONTROL | MUSCLE 1: MODELING & BEHAVIOR | AMPUTEE GAIT (THEMATIC)
- **BREAK AND EXHIBITS**
- **ORAL PRESENTATIONS (3:45 - 5:15 PM)**: TEACHING SYMPOSIUM | COMPARATIVE | SPORTS | COMPUTATIONAL BIOMECHANICS
- **TRAVEL**
- **BORELLI AWARD LECTURE:** CARLO DE LUCA, PH.D. (5:30 - 6:30 PM) PHILLIPS CENTER FOR PERFORMING ARTS
- **NIGHT ON THE TOWN**
- **APTA NETWORKING** (FLORIDA ROOM, 6:30 - 7:30 PM)

SATURDAY, AUGUST 18

CENTURY A | CENTURY B | CENTURY C | AZALEA

- **BREAKFAST 7:00 - 8:00** (OPEN SEATING ENTIRE FIRST FLOOR)
- **5K FUN RUN**
- **ORAL PRESENTATIONS (8:00 - 9:30 AM)**: CLINICAL GAIT | UPPER EXTREMITY | KNEE 1 | SEATING SYMPOSIUM (THEMATIC)
- **BREAK AND EXHIBITS**
- **ORAL PRESENTATIONS (10:00 - 11:15 AM)**: GAIT 2: ANALYSIS | SPINE | KNEE 2: ACL | MUSCLE 2: IMAGING (THEMATIC)
- **TRAVEL**
- (11:30 AM - 12:45 PM) **PRE & POST DOC AWARD TALKS, FOLLOWED BY**
- **JAMES J. HAY MEMORIAL AWARD LECTURE** (PHILLIPS CENTER FOR PERFORMING ARTS)
- **TRAVEL**
- **LUNCH** (OPEN SEATING ENTIRE FIRST FLOOR)
- **ASB BUSINESS MTG.** (OPEN TO ALL - CENTURY A)
- **ORAL PRESENTATIONS (2:00 - 3:30 PM)**: FALLS | COMPUTATIONAL MODELING | RUNNING | POWERED EXOSKELETON & PROSTHETICS (THEMATIC)
- **BREAK**
- **CLOSING CEREMONY & AWARDS** (CENTURY A)
- **BREAK**
- **ASB EXECUTIVE BOARD MEETING** (CLOSED MEETING - BOARD ROOM) 4:30 - 6:00 PM

2012 ASB Abstracts

Click on the First Author or Title to See Abstract

Baweja, Harsimran S.	Two-weeks Of Unloaded Precision Training Improves Motor Performance In Older Adults To The Level Of Young Adults
Beatty, Garrett F	Emotion As A Gait Therapy In Parkinson’s Patients: Affective Stimuli And Gait Pattern Variability
Becker, James	Plantar Pressure Differences Between Rearfoot And Midfoot Striking Runners During Shod Running
Becker, James	Biomechanics Of Retrospective Navicular Stress Fractures
Becker, James	Vertical Load Distribution In The Metatarsals During Shod Running
Behnam, Abrahm J.	Evidence Of Medial Maltracking In Patellofemoral Pain
Beltran, Eduardo	Computer Simulation Assists Gait Retraining Program A Case Study
Belwadi, Aditya	Finite Element Modeling Of Interaction Of Implantable Cardiac Rhythm Devices During Frontal Motor Vehicle Deceleration Injuries
Beschorner, Kurt E.	Effects Of Multifocal Lens Glasses On Stepping Accuracy During Step Down
Beschorner, Kurt E.	Effects Of Age And Experience On Foot Clearance During Up And Down Stepping
Bharadwaj, Shruthi S	Topographical Classification Of Normal And Tumorigenic Colonic Tissue
Bhatia, Dinesh	Muscle Activity Patterns of Lower Limb During Lateral (Frontal) Side Stepping Task Modulation from Different Heights
Bhatia, Varun A	Repeatability Of Image Registration And Segmentation Procedures For Ct Scans Of The Human Distal Radius
Biggers, Linda	The Effects Of Upper Extremity Lymphedema On Dominant Limb-dimensional Scapular Kinematics And Upper Extremity Function In Survivors Of Breast Cancer
Bingham, Jeffrey T.	Stability Radius As A Method For Comparing The Dynamics Of Neuromechanical Systems
Bisesti, Brianna	A Comparison Of Knee Moments During A Lateral Cutting Maneuver: Shod Vs. Barefoot
Blenkinsop, Glen	Using Stationary And Non-stationary Measures Of Balance To Assess Handstand Performace
Board, Wayne J.	The Issue Of Tissue: A Comparison Of Kinematic Models In Obese Adults
Boes, Morgan K.	Postural Control Model Of Spasticity In Persons With Multiple Sclerosis
Borotikar, Bhushan S.	The Influence Of Concentric Vs. Eccentric Muscle Control On D And Dynamic Patellofemoral Contact Kinematics
Bowley, Susan M.	Accurate Reconstruction Of Forensic Biomechanics Cases
Boyer, Elizabeth R	Sagittal Kinematics And Kinetics Of Midfoot-forefoot Running After Weeks Of Training
Boynton, Angela	Metabolic Cost And Lower Extremity Muscle Activity During Constant Speed Walking At Different Stride Frequencies
Bradley, Steve	Biomechanical Analysis Of Basketball Free Throw Shooting
Bradley, Claire E.	Spatiotemporal Gait Asymmetry Is Related To Balance-fall Risk In Individuals With Chronic Stroke
Brady, Robert	Obesity Modifies Canine Gait
Breighner, Ryan	Tibial Slope And Knee Flexion Moderate Muscle Induced Strain In The Anterior Cruciate Ligament
Breloff, Scott P.	Quantification Of Multi-segmental Spine Movement During Gait
Brewin, M.P.	Characterisation Of Agarose Gel As A Tissue Mimicking Material For Use In An Anthropomorphic Test Object Investigating The Acoustic Localisation Of Coronary Stenosis
Brown, Scott	The Relationship Between Leg Dominance And Knee Mechanics During The Cutting Maneuver

Brown, Geoffrey L.	Experiments And Theory For Curved Path Human Locomotion
Bruno, Alexander G.	The Effect Of Thoracic Kyphosis And Sagittal Plane Alignment On Vertebral Compressive Loading
Buckley, Thomas A.	Lingering Impairments In Postural Control Despite Symptom Resolution Following A Concussion
Bunchman, Alison M.	Adaptation Of Plantarflexor Muscle Activity During Gait
Bunderson, Nathan	A Quadrupedal Postural Controller With Physiological Delays Reveals The Need For Multi-level Stability
Burkhart, Timothy A.	Kinematics Kinetics And Muscle Activation Patterns Of The Upper Extremity During Simulated Forward Falls.
Burkhart, Timothy A.	Acknowledgements Nserc Predicting Distal Radius Bone Strains And Injury In Response To Impacts To Failure Using Multi-axial Accelerometers.
Bushey, Kristen M.	A Comparison Of The Effect Of Foam-box Casted And Plaster-casted Orthotics On The Normal Foot Population Using Bi-planar X-ray Fluoroscopy
Busquets, Albert	Sensory Reweighting During Postural Control In Adults With Different Sport Expertise: A Pilot Study
Cain, Stephen M.	Quantifying Increased Skill Using Measured Bicycle Kinematics As Riders Learn To Ride Bicycles
Canchi, Saranya	Optically Based Indentation For Brain Tissue: A New Histological Approach
Caputo, Joshua M.	An Externally Powered And Controlled Ankle-foot Prosthesis For Use In Push-off Experiments
Carbonneau, Evelyne	Effect Of Age And Lean Direction On The Threshold Of Balance Recovery In Younger Middle-aged And Older Adults
Carey, Jon D.	A Novel Elastic Loading-based Exercise Program Improves Both Strength And Power At The Ankle Joint
Caron, Robert R.	Vertical Trajectory Of Center Of Mass Is Maintained With Increased Vertical Stiffness While Carrying Load
Carpenter, Abigail L.	Weight Bearing Asymmetries And Changes In Cop Trajectories: Unilateral Ertl Amputees Vs Non-amputees
Casanova, Fernando	A Computational Model To Estimate Pre-stress Between Brain Tissue And A Needle Used For Convection Enhaced Delivery
Cavanagh, Peter R.	Insights Into The Footstrike Patterns Of Women Distance Runners
Chambers, April J.	Changes In Spatiotemporal Gait Characteristics When Anticipating Slippery Floors In Young And Older Adults
Chander, Harish	The Effect Of Extended Durations Of Walking In Occupational Footwear On Balance
Charalambous, Charalambos C.	Magnitude And Time Course Of Adaptation During Walking With A Passive Elastic Exoskeleton
Chen, Chien-Chih	A Method For Measuring D Kinematics Of The Mandible Using Modified Conebeam Computerized Tomography
Chen, Tiffany L.	Partnered Human-robot Stepping Based On Interactive Forces At The Hand
Chen, Tzurei	Altered Movement Strategy During Sit-to-walk In Elderly Adults With History Of Falling
Chen, Yen-Ting	Older Adults Exhibit An Impaired Ability To Predict Movement Accuracy Due To Greater Motor Output Variability
Chernak, Laura	Posture And Activation Dependent Variations In Shear Wave Speed In The Gastrocnemius Muscle And Aponeurosis
Chernak, Laura	Posture And Activation Dependent Variations In Shear Wave Speed In The Gastrocnemius Muscle And Aponeurosis
Cheung, Roy T.H.	Modulation Of Stiffness On Impact Loadings During Running
Chien, Jung Hung	Stride Interval Time Series Among Different Walking Speeds

Chiu, Shiu-Ling	Clinical Balance Measures Are Associated With Variability Of Interjoint Coordination During Walking In Elderly Adults
Choi, Dae Kyung	Analysis Of The Biomechanical Characteristics Of The Spinal Interspinous Implants
Choi, Woochol Joseph	Age-related Changes In Dynamic Compressive Properties Of Soft Tissues Over The Hip Region Measured By Forced Vibration
Cimadoro, Giuseppe	Comparison Between Squat Jump Vs Weighted Squat Jump: Simulation Study
Clark, David J.	Task Specific Differences In The Cortical Contribution To Walking Are Revealed By Thirty To Sixty Hz Oscillatory Activity
Cochrane, Robert	Rate Of Loading And Lower Extremity Sagittal Plane Biomechanics When Landing From A Drop-jump: Shod And Barefoot Comparisions Between Genders
Collins, John-David	Walking Speed Overground And On A Feedback-controlled Treadmill
Conley, Kevin E.	Exercise Efficiency And Mitochondrial Coupling In The Elderly
Conrad, Bryan P.	Computerized Gait Analysis And Lumbar Range Of Motion Assessments In People With Lumbar Spinal Stenosis
Conrad, Bryan P	Effectiveness Of Cervicothoracic Orthoses For Immobilizing An Unstable Cervicothoracic Junction Injury
Corbiere, Nicole C.	Creating Physiologically Realistic Vertebral Fractures
Cortes, Nelson	The Influence Of Fatigue On Landing Mechanics In Youth Male Lacrosse Athletes
Corti, Manuela	Power Training Post-stroke Engages Neural Circuits At Spinal And Supraspinal Levels
Costantini, Oren	Effects Of Serratus Anterior Muscle Fatigue On Scapular Kinimatics
Cotton, John R.	Ulna Simulation Assesses Sensitivity To Bone Elastic Modulus Variations In A Mrta Test
Coulter, Jonathan D.	Knee Kinematics And Kinetics During Descent Of A Navy Ship Ladder
Craig, Timothy D.	Investigating The Etiology Of Vibration-induced Low Back Pain
Craighead, Daniel	Effect Of Running Classes On Running Kinematics And Economy
Crenshaw, Jeremy R.	Anterior But Not Posterior Compensatory Stepping Thresholds Are Reduced With Age
Crisco, J.J.	Batting Cage Performance Of Various Youth Baseball Bats
Crotin, Ryan L.	Stride Length Compensations And Their Impacts On Brace-transfer Ground Forces In Baseball Pitchers
Crouch, Dustin L.	Anterior And Middle Deltoid Are Functionally Critical Targets For Nerve Transfer Following C-six Root Avulsion Injury
Currie, Stuart J.	Anticipatory Activation Of The Erector Spinae And Multifidus In Patients With And Without Low Back Pain
Cutler, Eric L.	Margin Of Stability As A Metric For Balance Impairment In Multiple Sclerosis
Dai, Boyi	Gender Effects On Lower Extremity Biomechanics In Adolescent Patients Following Acl Reconstruction
Dai, Boyi	Estimating Acl Force From Lower Extremity Kinematics And Kinetics
Davidson, Austin J.	Impact Of Dual-tasking On Lower Joint Dynamics During Stair Ascension
Barbacena, Ana de David Marcella	Effect Of Obesity And Overweight On Postural Balance In Children From Seven To Fourteen Years Old
Demirel, Aynur	Evaluation Of Shoulder Joint Arthtokinematics In Physically Disabled Athletes
Deneweth, Jessica M.	Mapping The Mechanical Topography Of Healthy Tibial Cartilage
Denning, Matt	A Comparison Of Position Measurement Accuracy Using Two Different Camera Arrangements

Derrick, Timothy R.	Tibial Stresses In Habitual And Converted Forefoot And Rearfoot Strike Runners
Desautels, Daniel M.	Common Head Acceleration Exposures In The Early Pediatric Population
Deusinger, Robert H.	Tibiofemoral Joint Articular Surface Motion Gender Differences In Subject Specific And Generic Knee Models
DeVita, P	Modulating Stride Length And Walking Velocity By Young And Old Adults
DeWitt, John K.	Ground Reaction Forces During Treadmill Exercise On The International Space Station
Diaz, Barbara	Cervical And Masticatory Muscles Activity During A Thirty Minute Laptop Typing Task: A Preliminary Study
DiCesare, Christopher A.	Static Foot Structure And Knee Kinematics During Running
Dickin, Clark	Postural Sway Changes In Altered Sensory Environments Following Individualized Whole Body Vibration
DiDomenico, Angela	Determining Stabilization Time Using A Negative Exponential Mathematical Model
Diestelmeier, B.W.	A Novel Impaction System To Model Cartilage Injury In Living Rabbit Knees
Dingwell, Jonathan B.	Simple Predictive Models Reveal Step-to-step Control Of Walking
DiStasi, Stephanie L	Neuromuscular Asymmetries And Deficiencies Of Active Adolescent Volleyball Players With Patellofemoral Pain
Donnell, Drew Michael S.	A Markov Chain Model Predicts Early Failure Of Rotator Cuff Tear Repairs
Doucet, Patrik	A Tool For Evaluating Individual Contribution In Teamwork
Doucet, Patrik	Intervention For Improving Project Teams
Drake, Will	Characterization Of Coupled Wrist And Forearm Stiffness
Drewniak-Watts, Elizabeth	Computer Navigation As An Investigational Tool For Acl Reconstruction
Dunbar, Nicholas	Kinematic Analysis Of Volleyball Spiking Maneuver
Edmonds, David W.	The Influence Of Upper Body Stability On Peak Knee Loading During Sidestepping: Implications For Athlete Screening And Acl Injury Risk
Edwards, Brent	A Linear Actuated Torsional Device To Replicate Clinically Relevant Spiral Fractures In Long Bone
Edwards, Brent	Dxa Derived Measures Of Bone Mineral Can Reliably Predict Mechanical Behavior Of Proximal Tibias Loaded In Torsion
Eicholtz, Matthew R.	Two-dimensional Parameter Study To Characterize Performance Of Ankle-foot Orthosis Joint Impedance Control
Elkins, Jacob M.	Expedited Computational Analysis Of Fracture Of Ceramic Tha Liners: Obesity And Stripe Wear Considerations
Ellingson, Arin M.	Mimetic Jar Device Capable Of Measuring Dynamic Opening Forces: Development And Validation
Ellingson, Arin M.	Helical Axis Patterns Of Motion For The Healthy To Severely Degenerated Lumbar Intervertebral Disc
Ellis, Richard	The Metabolic And Mechanical Costs Of Step-time Asymmetry In Walking
Elrod, Jonathan M.	Induced Alterations Of Interlimb Coordination Caused By The Use Of A Splitbelt Treadmill
Erbulut, D.U.	Kinematical And Load Sharing Effect Of A Novel Posterior Dynamic Stabiization System Implnated In Lumbar Spine
Esselman, Emily M.	Rsrr Dsdr Influence Of Various Heights And Surfaces On Neuromuscular Strategies During Drop Landings.
Ettinger, Luke R.	Removal Of Pain From Patients With Shoulder Impingement Results In Alterations In

	Shoulder Muscle Activity And Scapular Kinematics
Ettinger, Luke R.	Emg Normalization Techniques For Patients With Pain
Farris, Dominic	The Effects Of Wearing A Spring-loaded Ankle Exoskeleton On Soleus Muscle Mechanics During Two-legged Hopping In Humans
Faust, Kathryn A.	Dynamic Stability Of Individuals With And Without Unilateral Trans-tibial Amputations Walking In Destabilizing Environments
Fellin, Rebecca E.	Spatiotemporal Parameters Of Uphill Level And Downhill Walking Are Similar Between Treadmill And Overground Surfaces
Fernandez, Chessy	Development Of An Efficient Fluid-structure Interaction Solver For Applications To The Vascular System
Fernandez, Kristina	Gait Initiation Impairments In Essential Tremor And Parkinson’s Disease
Fey, Nicholas P.	Simulation Predictions Of Prosthetic Foot And Muscle Function In Response To Altered Foot Stiffness During Below-knee Amputee Gait
Ficklin, Travis	A Comparison Of Volleyball Blocking Techniques: Jumping Velocities And Effective Blocking Areas
Finley, Margaret A	Scapulohumeral Kinematics In Individuals With Upper Extremity Impairment From Stroke
Fiorentino, Niccolo	Peak And Nonuniform Fiber Stretch Increase In The Biceps Femoris Long Head Muscle At Faster Sprinting Speeds
Flowers, Jonquil R.	Comparison Of Stress Distribution Patterns Within Trigonal Quadradle And Hexagonal Screw Drive Designs Of An Acl Interference Screw Using Finite Element Analysis
Foch, Eric	Trunk Endurance Strength And Running Biomechanics After Iliotibial Band Syndrome
Ford, Kevin R.	Real-time Biofeedback For Acl Injury Prevention
Forrester, Steph	Medial Longitudinal Arch Characteristics During Running
Fortuna, Rafael	Do Skeletal Muscle Properties Recover Following Repeat Botulinum Toxin Type-a Injections?
Fortune, Emma	Step Counts Using A Tri-axial Accelerometer During Activity
Fox, Emily J.	The Effects Of Visual Feedback And Aging On Force Oscillations Within Zero To One Hz
Fox, John	Influence Of Shod And Barefoot Gait On Single Support And Double Support
Franz, Jason R.	How Does Age Affect Individual Leg Mechanics During Uphill And Downhill Walking?
Fu, Yang-Chieh	Comparison Of Unicompartmental Knee Arthroplasty And Healthy Limb For Knee Moments Generated During Stair Ascent
Fujimori, Takahito	In Vivo Three-dimensional Analysis Of The Thoracic Spine In Trunk Rotation
Fujimoto, Masahiro	Momentum Control Strategies During Walking In Elderly Fallers
Fukuchi, Reginaldo K	Designing Training Sample Size For Support Vector Machines Based On Kinematic Gait Data
Fukuchi, Claudiane A.	The Influence Of Wedged Insoles On Knee And Ankle Moments And Angular Impulses During Walking
Fukuchi, Reginaldo K	Joint Angles And Joint Moments Following Neuromuscular Fatigue In Futsal Players
Gales, Daniel J.	Loading History Of The Mechanical Properties Of Human Heel Pads
Gao, Fan	Investigation Of Prosthetic Socket Interface Pressure And Gait In Transtibial Amputees: Effects Of Suspension Types And Socket Alignment
Gardner, Jacob	Comparison Of First And Second Generation Rocker Bottom Shoes
Gates, Deanna H.	Comparison Of Powered And Unpowered Prostheses In Patients With Transtibial Amputation Walking On A Rock Surface
Genc, Kerim O.	A Modeling Framework For Examining Changes In Femoral Strength Due To Long Duration Bedrest

Ghafurian, Soheil	Automated Analysis Of D Glenoid Version
Gillette, Jason C.	Movement Strategy And Arm Use Redistribute Sit-to-stand Joint Moments
Goss, Donald L.	Accuracy Of Self-reported Footstrike Paterns And Loading Rates Associated With Traditional And Minimalist Running Shoes
Gregorczyk, Karen N.	Biomechanical And Metabolic Implications Of Wearing A Powered Exoskeleton To Carry A Backpack Load
Gregory, Robert	Effects Of A Biomechanical Energy Harversting Ankle Device On Gait Kinetics
Greska, Eric	The Effects Of Leg Dominance Neuromuscular Training And Fatigue On Bilateral Lower Extremity Kinematics
Griswold, Jason	Handgrip Force And Upper-limb Kinetics During Handcycling
Guri, Albina	Priming The Motor System Passive And Active Movements Induce Distinct Gabaergic Effects
Habib, Michael	Mesozoic Speed Demons: Flight Performance Of Anurognathid Pterosaurs
Haddas, R	Effects Of Volitional Preemptive Abdominal Contraction On Trunk And Lower Extremity Biomechanics And Neuromuscular Control During A Drop Vertical Jump
Hafer, Jocelyn F.	Correlations Between Running Cadence And Kinematics
Haight, Derek J.	Slow Uphill Walking: Better For The Knees Of Obese Adults?
Halilaj, Eni	Motions Of The Thumb Carpometacarpal Joint Are Coupled During The Initiation Of Three Functional Tasks
Hall, Allison L.	Changes In In Vivo Knee Contact Force Through Gait Modification
Hall, Justin T.	Hindwing Function In Four-winged Feathered Dinosaurs
Hallal, Camilla Zamfolini	Identifying Fallers And Non-fallers Using Gait Variability Indicators Based On Methods Proposed For Heart Rate Assessment
Hallal, Camilla Z.	Lower Limb Muscle Coactivation In Younger And Older Adults During Dual-task Gait
Hallal, Camilla Z.	Strength Power And Electromyographic Performance Of Hip Musculature In Older Female Fallers And Non-fallers
Hamilton, Stephanie	The Influence Of Repetitive Loads On Foot Sensitivity And Dynamic Balance
Han, Sang Kuy	Characterization Of Interlamellar Shear Properties Of The Annulus Fibrosus
Handsfield, Geoffrey	How Do Lower Limb Muscles Scale Across Individuals?
Harput, Gulcan	Comparison Between Nintendo Wii Fit And Conventional Rehabilitation On Functional Performance Outcomes After Hamstring Anterior Cruciate Ligament Reconstruction
Harput, Gulcan	Evaluation Of Ankle Muscular Activation During Selected Balance Exercises On Different Balance Platforms
Hasenkamp, Ryan M.	The Relationship Between Ambulatory Activity Patterns And Kinematic Variability
Hashish, Rami	Mechanical Demand Distribution During Shod And Novice Barefoot Running
Haas, Caroline	Immediate Application Of Cyclic Compressive Loading Attenuates Secondary Hypoxic Injury Folowing Damaging Eccentric Exercise
Havens, Kathryn L.	Deceleration: Relationship Between Body Position And Velocity
Heise, Gary D.	Stabilogram Diffusion Analysis Applied To Dynamic Stability: One-legged Landing From A Short Hop
Hendershot, Brad D.	Reduced And Asymmetric Trunk Stiffness Among Unilateral Lower-limb Amputees During Multi-directional Trunk Perturbations
Hernandez, Manuel E.	The Effect Of Age And Movement Direction On Rapid And Targeted Center Of Pressure Submovements While Crouching
Neugebauer, Jennifer	Estimating Peak Achilles Tendon Forces In Youth During Locomotion Using Hip Acceleration
Hewett, T.E.	Latent Profile Analysis: Grouping Subjects By Biomechanical Predictors Of Increased Kam

	And Potential Risk For Acl Injury
Higginson, Brian K.	A Biomechanical Comparison Of Three Backpack Frames During Treadmill Walking
Ho, Kai-Yu	Comparision Of Patella Bone Stress Between Individuals With And Without Patellofemoral Pain
Hobara, Hiroaki	Spring-mass Characteristics During Overground Running In Amputees Using Running Specific Prostheses
Hoerzer, Stefan	A Novel Methodology Using Principal Component Analysis To Quantify Global Bilateral Asymmetry Of Human Gait
Holmes, Taylor C.	Vibration Impairs Proprioception During Active Cyclical Ankle Movements
Holtz, Melissa	Design Of Suspended Load Backpacks For Young Urban Professionals
Hong, Yu	Development Of A Test System To Study Brain Tissue Damage Due To Cavitation
Hoops, Mackenzie L.	Knee Joint Loading During A Compensatory Step: Preliminary Data For Observing Reovery Responses In Knee Osteoarthritic Patients
Hovis, Patty	Pain During Ergonomic Hand Drive Wheelchair Propulsion
Howell, David	Dual-task Walking And Computerized Cognitive Tests In Assessing Concussed High School Athletes
Hsieh, Chao-Jung	Single Leg Hop Landing Biomechanics And Association With Symmetry Index Following Meniscectomy
Hsu, Hsiang Yi	Relationships Between Electromyography And Oxygen Consumption In Different Work Loads Rowing Exercise
Huang, Chun-Kai	Reduced Light Intensity Alters Spatiotemporal Gait Patterns During Treadmill Walking
Hughes, Richard E.	Experimental Design Using Particle Swarm Optimization
Huisinga, Jessie M.	Coherence Analysis Reveals Altered Postural Control During Standing In Persons With Multiple Sclerosis
Hunt, Nathaniel	Manipulation Of The Structure Of Gait Variability With Rhythmic Auditory Stimulus
Hunter, Iain	Emg Activity While Alter-g Treadmill Running
Hur, Pilwon	Investigating The Link Between Kinematic Deviations And Recovery Response To Unexpected Slips
Hurt, Christopher P.	Age-related Differences In The Stepping Response To Laterally-directed Disturbances
Hussain, Mozammil	Biomechanical Relationship Between The Properties Of Collagen Fibers In Different Regions Of Annulus Matrix And The Decompression Of Disc Tissues
Hutter, Erin E.	Is There A Gold Standard For Rotational Alignment Of The Tibial Component During
Hyler, Jacqlyn S.	Endpoint Instructions Result In Higher Proprioceptive Acuity Than Joint Angle Instructions
Infantolino, Benjamin W.	Pennation Angle Variability In Human Whole Muscle
Islam, Kamrul	Computer Methods For Designing Artificial Talus Bone In The Ankle Joint
Jackson, Jennifer N.	Development Of A Subject-specific Vertical Ground Contact Force Model
Jackson, Jennifer N.	Residual Elimination Algorithm Improvements For Forward Dynamic Simulation Of Gait
Jain, Tarang K.	Objective Evaluation Of Chronic Ankle Instability And Balance Exercise Treatment
Jarvis, Danielle N.	Modeling The Demands Of A Dance Jump: A Mismatch Between Mechanical Demands And Aesthetic Constraints
Jayaraman, Chandrasekaran	Correlation Analysis Of Upper Extremity Kinematics For Manual Wheelchair Propulsion
Joumaa, Venus	Force Enhancement: An Evolutionary Strategy To Reduce The Metabolic Cost Of Muscle Contraction?

Juran, Cassandra	Correlations Between Temporomandibular Disc Damage And Bulk Shear Mechanics
Kadono, Norio	Which Muscles Limit The Ability Of Older Adults To Recover Balance?
Kaiser, Jarred	Measuring D Tibiofemoral Kinematics And Contact Using Dynamic Volumetric Magnetic Resonance Imaging
Kang, Hyun Gu	Designing Biomechanics Courses For Significant Learning: Fink Model Applied At Cal Poly Pomona
Kang, Gu Eon	Natural Gait May Not Be Neutral: It All Depends On How You Feel
Kang, Hyun Gu	Flexible Framework For Testing Postural Control Models: Evidence For Intermittent Control?
Karakostas, Tasos	Development Of A Dementia-specific Gait Profile: Application Of Signal Detection Theory
Karol, Sohit	Step Disc Maximum Voluntary Force Production Changes With Visual Feedback Modulation During Multi-finger Pressing
Kennedy, David J.	The Effect Of Anesthetic Hip Joint Injections On Gait
Kern, Andrew M.	Highly Automated Methods For Subject-specific Population-wide Investigations Of Habitual Contact Stress Exposure In The Knee
Kern, Andrew M.	D-to-d Registration For The Eos Biplanar Radiographic Imaging System
Keshavarz, Roshanak	Effects Of Kinesio-tape On Pain And D Scapular Kinematics Inpatients With Shoulder Impingemenet Syndrome During Scaption: A Randomized Double Blinded Placebo-controlled Study
Kiapour, Ata M.	Correlation Between Kt Arthrometer Data And Acl Strain Suggests Diagnostic Importance
Kiapour, Ata M.	Knee Articular Cartilage Pressure Distribution Under Single- And Multi-axis Loading Conditions: Implications For Acl Injury Mechanism
Kim, Sunghwan	Contact Stress Analysis Of The Radial Head And Radial Head Implants
Kim, Changki	Task Difficulty Exacerbates The Age Associated Differences In Force Control
Kingsbury, Trevor	Comparison Of Kinematic Kinetic And Mechanical Work Data Between Traditional And Bone Bridge Amputation Techniques During Fast Walking One Year Post Ambulation Without An Assistive Device
Klishko, Alexander N.	Control Of The Cat Paw Trajectory During Walking On A Flat Surface And Horizontal Ladder
Kneiss, Janet A.	The Relationship Between Lower Extremity Joint Power During Sit To Stand And Clinical Measures Of Function Among Subjects Post Hip Fracture
Ko, Cheolwoong	Study On Anthropometric Measurement On Korean Skeletal Systems Based On Cadaveric Ct Images
Ko, Cheolwoong	Study On Wheelbase Design Parameters Of A Shower Carrier Through Drivability Tests
Korgan, Whitney	Altered Kinematics Between Flat And Curved Treadmills Do Not Cause Increased Energy Expenditure
Krishnan, Vennila	Age Differences In The Stabilization Of Swing Foot Trajectory In The Frontal Plane
Kruger, Karen	Scratch-based Damage Quantification And Wear Prediction In Total Hip Arthroplasty
Kruse, Carola	On The Potential Of Computational Mathematics In The Diagnosis Of Coronary Heart Disease
Kumar, Atul	Measurement Of Mtpj Cartilage Thickness Distribution Using T Mri
Kurz, Max J.	The Gait Pattern Of Children With Cerebral Palsy Has Greater Stochastic Features
Kurz, Max J.	Children With Cerebral Palsy Do More Positive Mechanical Work After Gait Rehabilitation
Kwon, Minhyuk	A. B. Impaired Endpoint Accuracy In Older Adults Is Associated With Greater Time Variability
Lanier, Amelia S.	Are Internal-external Rotational Moments In Acl Deficient Subjects Different Than Those In Healthy Subjects?
Larkin, Kelly A.	Near-infrared Light Therapy Delays The Onset Of Skeletal Muscle Fatigue
Law, Laura Frey	Aging Is All Relative: Modeling The Relationship Between Strength And Fatigue On Endurance Time In Older Adults

Lawrence, Michael	The Effect Of Load On Movement Coordination During Sled Towing
Lee, Su-Ya	The Effect Of Kinesio Taping On Kinematics And Muscle Activity For Subjects With Neck Pain
Lee, Hyokeun.	A New Approach To Understand Postural Instability In Young Children With Autism Spectrum Disorders
Lee, Sabrina S.M.	Associations Between Motor Unit Recruitment And The Rates Of Strain Force Rise And Relaxation
Lee, Sabrina S.M.	Changes In Muscle Co-activation In Spinal Cord Injured Individuals After Body-weight Supported Treadmill Training
Lee, Szu-Ping	Individuals With Diminished Hip Abductor Muscle Strength Exhibit Higher Moments And Neuromuscular Activation At The Ankle During Unipedal Balance Tasks
Lee, Euiseok	Study On Lumbar Morphological Measurements Of Korean Adults And The Elderly
Lee, Leng-Feng	Joint Kinematics In Chimpanzee And Human Bipedal Walking
Leemans, Adam	Kinematic Effects Of Biomechanical Energy Harvest At The Ankle: Implications For Injury Susceptibility
Lemke, Sean	Biomechanical Effects Of Component Alignment Variability In Total Knee Arthroplasty: A Computer Simulation Study Of An Oxford Rig
Lenhart, Rachel L.	Increasing Running Step Rate Reduces Patellofemoral Joint Forces
Lewis, Cara L.	Altered Hip Movement In Females With Hip Pain During Single Leg Step Down
Li, Jihui	Influence Of Eccentric Body Weight On The Knee Balance Of Obese Patients
Li, Yifan David	Gait Mode Recognition Using An Inertia Measurement Unit On A Powered Ankle-foot-orthosis
Li, Chunxia	Use Of Markerless Motion Capture Approach For Construction Field Workers Biomechanical Analysis
Li, Lingmin	Predicting In Vitro Articular Cartilage Wear In The Patellofemoral Joint Using Finite Element Modeling
Li, Jihui	Computer Planning Of Arthroscopic Femoroacetabular Impingement Surgery
Lim, Hyerim	Sensory Reweighting For Visually Induced Roll Tilt Perception Under Sensory Conflict Conditions
Lippa, Nadine M.	Varying Foam Surface Thickness Does Not Affect Landing Emg Preactivation In Active Females
Lipps, David B.	On The Fatigue Life Of The Anterior Cruciate Ligament During Simulated Pivot Landings
Little, Virginia L.	Pelvic Excursion During Walking Post-stroke
Little, Virginia L.	Is The Problem Really Foot-drop?
Livingston, Beven P.	Reliability And Precision Of The Resistance Zone And Laxity Zone For Shoulder Internal And External Rotation
Lodha, Neha	Interhemispheric Inhibition And Motor Lateralization: Relationship To Age
Longworth, Jessica	Kinematic Variability At The Shoulder Is Not Related To Shoulder Pain During Manual Wheelchair Propulsion
Looft, John M.	Parameterizing And Validating A Three Compartment Muscle Fatigue Model For Isometric Tasks
Lu, Tung-Wu	Inter-joint Coordination In Patients With Cervical Spondylosis During Obstacle-crossing
Lugade, Vipul	Posture And Activity Detection Using A Tri-axial Accelerometer
Magdoom-Mohamed, K.N.	A Computational Model For Convection-enhanced Delivery In A Hind Limb Tumor
Major, Matthew J.	Upper Body Kinematics Of Bilateral Transtibial Prosthesis Users During Gait
Manal, Kurt	Knee Joint Loading After Acl Reconstruction: Influence Of Graft Type
Manorama, Abinand	Factors Associated With Pressure Ulcers: The Effects Of Shear Loads On Blood Flow

Mansouri, Misagh	The Use Of A Platform For Dynamic Simulation Of Movement: Application To Balance Recovery
Marques, Nise R.	Association Between Strength Kinematics And The Energy Cost Of Walking In Older Female Fallers And Non-fallers
Marques, Nise R.	Using Ankle Bracing Influences The Torque Ratio Among Ankle Stabilizers Muscles After Simulation Basketball Match-play?
Martin, Joel R.	Performance Optimality And Variability Studied At The Level Of Hypothetical Commands
Martin, Joel	Comparison Of Finger Interaction Matrix Computation Techniques
Massie, Crystal L.	Biomechanical Analysis Of Discrete Versus Cyclic Reaching In Survivors Of Stroke
McClain, Matthew	The Effects Of Fatigue On The Recovery From A Postural Perturbation
McCrory, Jean L.	Torso Kinematics During Gait Differ Between Pregnant Fallers And Non-fallers
McGrath, Denise	Metabolic Cost Of Maintaining Balance During A Perturbed Gait Task Is Related To Gait Variability
McGregor, Stephanie F.	Effects Of Long-term Use Of Ankle Taping On Balance
McKay, Lucas	Statistically Significant Contrasts Between Emg Waveforms Revealed Using Wavelet Based Functional Anova
McNally, Michael P.	Lower Extremity Work Is Associated With Club Head Velocity During The Golf Swing In Experienced Golfers
Merrier, Nicholas	Fmvss Compliance Testing: Evaluation Of Lateral Acceleration And Brain Injury
Mesfar, Wissal	Impact Of The Loading Type On The Biomechanics Of The Cervical Spine
Meyer, Andrew J.	A Novel Statistical Method For Emg To Moment Estimation During Gait
Meyer, Andrew J.	Are External Knee Load And Emg Measures Strong Indicators Of Internal Knee Contact Forces During Gait?
Miller, Ross H.	Why Do Humans Walk The Way We Do? Evidence From Dynamic Simulations
Miller, Ross H.	Discriminating Between Knee Osteoarthritis Severity Levels In Walking Using Only Force Platform Data
Mills, Kaya L.	Muscle Activation Changes Across Three Different Skate Skiing Techniques
Milner, Clare E.	Changing Step Width Alters Lower Extremity Kinematics During Running
Mohammadi, Hadi	A Novel High-order Element For The Analysis Of Heart Valve Leaflet Tissue Mechanics
Monaghan, Gail	Forefoot Orientation Angle Determines Duration And Amplitude Of Pronation During Walking
Moo, E.K.	Boundary Conditions Affect Mechanical Behavior Of In-situ Chondrocytes.
Morgan, Kristin D.	Muscle Force Estimates During The Weight-acceptance Phase Of Single-leg Jump Landing
Morrison, S	Coupling Of Oscillatory Motion: The Impact Of Voluntary And Phsyiological Tremor On Posture
Morrow, Melissa M. B.	Influence Of Sex And Severity On The External Adduction Moment In Medial Compartment Knee Osteoarthritis
Muñoz, Juan C.	Ff Graphs And Ground Reaction Force
Muriuki, Muturi G	The Medial Ulnar Collateral Ligament Carries No Load During Passive Flexion And Extension
Muslim, Khoirul	Disturbances To Intrinsic Stiffness And Reflexive Muscle Responses Following Repeated Static Trunk Flexion
Nataraj, Raviraj	Calculating Thumb And Index Finger Postures During Pinch With A Minimal Marker Set
Neely, K.A.	Distinct Features Of Grip Force Characterize Parkinsons Disease And Atypical Parkisonian Disorders
Nelson-Wong, Erika	Influence Of Lecture Slide Completeness On Student Learning In A Biomechanics Course Within A Physical Therapy Curriculum

Nguyen, Cassie	Comparison Of Tibial Torsion Measurements Using Motion Capture Physical Therapy Evaluation And Computed Tomography
Nguyen, Hung P	Modeling Intra-trial Variability Of A Redudant Planar Reaching Task
Nocera, Joe R.	The Gait Variability Profile Of Patients With Parkinson's Disease When Compared To Older Adults With Mobility Disability And A History Of Falls.
Noehren, Brian	Predictors Of Initial Impact Load And Loading Rates In Runners
Norman, Tracy	Decreased Gait Transition Speeds In Unilateral Transtibial Amputee Gait
Oh, Keonyoung	Is Push-off Propulsion Energetically Optimal For Accelerated Gait?
Ohrt, Gary T.	Surgical Simulation: Validating Methods To Improve Orthopaedic Resident Skills Competency
Onushko, Tanya	Motor Learning Is Enhanced In Older Adults Following Training With A Less Difficult Task
Ordelt, Thomas A.	Lower-limb Acceleration During Sprint-start And Selected Power Exercises
Ortega, Justus D.	The Determinants Of Walking Enegetics In Elderly Adults
Osmanzada, Haroon	Kinematic Analysis Of Gesture In Aphasia
Parikh, Pranav J.	Effects Of Cortical Stimulation On Sensorimotor Functions Of The Hand In Healthy Old Adults
Parise, Erica	The Impact Of Obesity On The Accuracy Of Predicting Body Fat Percentage In Older Men
Park, Jaebum	Effect Of L-dopa On Multi-finger Synergies And Anticipatory Synergy Adjustments In Parkinson's Disease
Parthiban, Sujeeth	Bicycle Riding Arterial Compression And Erectile Dysfunction
Pasha, Saba	Biomechanical Loading Of The Sacrum In Pre- And Post Operative Adolescents Idiopathic Scoliosis
Patel, Jaynesh	The Role Of The Latissimus Dorsi Muscle In Pelvic Girdle And Trunk Rotations
Patil, Shilpa	Distinct Patterns Of Recovery Following Therapeutic Intervention Poststroke: Responders Vs. Non-responders
Pauwels, Laura L.	Muscle Stiffness And Response To Exercise In Caloric Restricted And Ad Libitum-fed Elderly Rats
Petit, Daniel J	The Effect Of Different Foams On Posturography Measures In Healthy And Impaired Populations
Petrucci, Matthew N.	What Causes Slips Trips And Falls On The Fireground? A Survey
Petrucci, Matthew N.	Mechanical Cueing Using A Portable Powered Ankle-foot Orthosis
Piller, Geoffrey	Geometric Accuracy Of Physical And Surface Models Created From Computed Tomography Data
Planetta, P.J.	Thalamic Projection Fiber Integrity In De Novo Parkinson's Disease
Postlmayr, Cara	Softball Windmill Pitch: Necessity Of A Pitch Count
Pozzi, Federico	Loading Patterns During A Step-up-and-over Task In Individuals Following Total Knee Arthroplasty
Price, Nathaniel	Design Study On Stability And Safety Of Median Sternotomy Fixation
Qian, Jing-Guang	Effects Of Exercises For Prevention Of Femoral Neck Fracture Based On Dynamics And Finite-element Moel Simulation
Qiao, Mu	Response To Medio-lateral Perturbations Of Human Walking And Running
Rainbow, Michael J.	Tracking High-speed Patella Motion Using Biplanar Videoradiography: An Accuracy Study
Ramos, Christopher R.	Common Control Strategies For Generating Angular Impulse In Forward And Backward Translating Tasks
Rand, Troy J	Patients With Peripheral Arterial Disease Exhibit Greater Toe Clearance Than Healthy

	Controls
Razzook, Alexander	Average Ankle Dynamic Joint Stiffness During Heel Strike Running
Rehm, Jared	The Effect Of Leg Dominance On Step Length In Shod And Barefoot Walking
Renz, Jessica J.	Differences In Stride Interval Variability During Stair-climbing And Treadmill Walking
Requejo, Philip S.	Effect of Seat Position Modifications on Upper Extremity Mechanical Loading During Manual Wheelchair Propulsion
Rigsby, Mark Tyler	Validation Of A Commercial Wearable Sensor System For Accurately Measuring Gait On Uneven Terrain
Riskowski, Jody L.	Effects Of Regional Foot Pain On Plantar Pressure And Loading
Roberts, Beverly L	Balance Control During Tai Chi Movements
Roberts, Dustyn P.	A Phenomenological Human Energy Expenditure Model In Joint Space
Roberts, Dustyn P.	Evaluating Knee Stability After Total Knee Arthroplasty Using Inertial Measurement Units
Robertson, Benjamin	More Is Not Always Better: Consequences Of Exoskeleton Assistance In A Compliant Muscle Tendon System
Roemmich, Ryan T.	Locomotor Adaptive Learning Is Impaired In Persons With Parkinson’s Disease
Roewer, Ben D.	The Influence Of Filtering Cutoff Frequency On Landing Biomechanics Measured During A Drop Vertical Jump
Rojas, Juan D.	Reliability Of A Novel Proprioception Testing Device
Romer, Braden	The Effect Of Varying Cadences On Shod And Barefoot Gait Kinematics
Rooks, Tyler	Variability Of Strain And Strain Rate In The Human Tibial Diaphysis During Walking
Roos, Paulien	Hop Performance In Individuals With Anterior Cruciate Ligament Injuries
Roos, Paulien	Control Of Coronal Plane Kinematics And Kinetics During A Single Leg Hop For Distance In Individuals With Anterior Cruciate Ligament Injury
Roper, Jaimie A	Frontal Plane Mechanics Are Altered During Split Belt Treadmill Walking In Young Healthy Adults
Rosenblatt, Noah J.	Maintaining A Constant Margin Of Stability Across Dyamic Conditions May Rely On Different Control Strategies
Routson, Rebecca L.	Comparison Of Module Quality And Walking Performance Of Hemiparetic Subjects Pre And Post Locomotor Rehabilitation Therapy
Rubenson, Jonas	On The Ascent: The Soleus Operating Length Is Conserved To The Ascending Limb Of The Force-length Curve Across Gait Mechanics In Humans
Rundell, Steven A.	Forward Bending With Increased Erector Spinae Force Helps Reduce Disk Herniation Risk
Russell, Elizabeth	Stretching With Applied Vibration Increases Triceps Surae Flexibility In Patients With Plantar Fasciitis
Russell, Daniel M.	Maximal Dynamic Stability Of Walking Coincides With The Freely Adopted Speed And Stride Frequency
Russell, Shawn	Using Mri-based Muscle Volumes And Gait Analysis To Quantify Relative Muscle Effort In Children With Cerebral Palsy
Sabick, Michelle	Robust Optical Sensor For Noninvasive Cardiac Monitoring
ElSagheir, Sohaila	The Effect Of Unilateral And Total Menisectomy On Posterior Cruciate Ligament Forces Under Femoral Anterior Drawer In Passive H The Effect Of Unilateral And Total Menisectomy On Posterior Cruciate Uman Knee At Full Extension
Salmond, Layne H.	Wrist Rotations Are Considerably Less Smooth Than Reaching Movements
Samaan, Michael	The Effects Of Neuromuscular Fatigue On Coordination Variation
Samarawickrame, Sachithra	Exertion Modulates Ankle Joint Co-activation During Novel Barefoot And Post-transition Barefoot Running Conditions
Sandercock,	Comparison Of Sarcomere Heterogeneity Measured In Passive Live And Fixed Muscle

Thomas G.	
Sanders, Ozell P.	Protocol To Assess Hyoid Bone Density For Prediction Of Fracture
Santago, Anthony C.	Graft Material Properties Affect Supraspinatus Force-generating Capacity In A Simulated Rotator Cuff Repair
Sawers, Andrew	Active Control Of Lateral Balance Varies Throughout A Step During Treadmill Walking
Scherzter, Eliran	Comparing Metabolic Costs Of Harvesting Biomechanical Energy From Human Motion Versus Carrying Batteries For The Same Energy Supply
Schimoler, Patrick J.	An Iterative Learning Controller For An Elbow Simulator To Maintain Flexion Angle During Supination
Schmitz, Anne	The Importance Of Accounting For Knee Laxity When Simulating Gait
Schulz, Brian W.	Age-related Redistribution Of Hip And Knee Kinetics During Out-and-back Stepping
Schwartz, Mathew	A Framework For Visualizing Biomechanical Movement For Designers Within D Modeling Programs
Seeley, Matthew K.	The Effect Of Knee Pain And Effusion On Vertical Ground Reaction Force During Walking
Seth, Ajay	A Scapulothoracic Joint Model For Fast And Accurate Simulations Of Upper-extremity Motion
Setterbo, Jacob J.	A Laboratory Method For Evaluating Dynamic Properties Of Equine Racetrack Surfaces
Shapiro, Robert	Differences In Running And Walking Gait Kinematics During Earth And Simulated Mars And Lunar Gravitational Environments: Preliminary Investigation
Sharpe, Sarah S	Muscle Activation Strategy In The Sand-swimming Sandfish Lizard
Sheehan, Riley C.	A Robust Kinematic Based Event Detection Algorithm That Works For Walking And Running On Both Uphill And Downhill Surfaces
Sheehan, Riley C.	The Influence Of Step Frequency On Muscle Activity During Downhill Running
Shin, Jun Ho	Intersegmental Adaptation Of Lumbar Spine On Different Load-carrying Types
Shirota, Camila	Trip Recovery Strategies In A Unilateral Transfemoral Amputee
Shorter, K Alex	Suction And Skin: The Effect Of Vacuum Loading On The Skin Of A Common Dolphin
Shull, Pete B.	Toe-in Gait Reduces The First Peak In The Knee Adduction Moment During Walking In Knee Osteoarthritis Patients
Shull, Pete B.	Six-week Gait Retraining Program For Knee Osteoarthritis Patients: Learning Retention And Symptom Changes
Silverman, Anne K.	Whole-body Angular Momentum During Stair Ascent And Descent
Silverman, Anne K.	Muscle Contributions To Whole-body Angular Momentum During Unilateral Below-knee Amputee Walking
Silvernail, Julia Freedman	Age Related Changes In Running
Simons, Craig J.	Reliability Of Lumbar Vertebra Position And Orientation Measurement Using Weight-bearing Mri
Simpson, Kathy J.	Does Interlimb Kinematic Symmetry Exist During Stair Ascent After Unicompartmental Knee Arthroplasty?
Singh, Tarkeshwar	Adaptive Changes In Finger Force Variance In Response To Index Finger Fatigue In Unimanual And Bimanual Tasks
Singh, Bhupinder	Changes In Gait Over A Thirty Minute Walking Session In Obese Individuals Do Biomechanical Loads Increase In Pursuit Of Weight Loss?
Sinsel, Erik W.	Empirical Plantar Pressure Insole Pose Estimation
Skinner, Jared W.	Frequency Domain Analysis Of Ground Reaction Force Does Not Differentiate Between Hyperkinetic And Hypokinetic Movement Disorders.
Slocum, Alexander H.	Biomechanical Design Of Rolling Contact Knee Joint Prostheses
Smallwood,	Trial-to-trial Control Dynamics In Redundant Reaching Tasks

Rachel F.	
Smeesters, Cécile	Problem- And Project-based Learning In Bioengineering: A Case Study
Smith, Jeremy D.	Metabolic Costs Of Locomotion When Walking With And Without Ankle And Knee Braces
Soheilypour, Mohammad	A Micromechanical Analysis On Diffuse Axonal Injury For Heterogeneous Brain Tissue
Sohn, Hongchul	Biomechanics Constrains Variability In Spatial Structure Of Muscle Coordination For Endpoint Force Generation
Solis, Fredy M.	Landing Technique Not Body Mass Or Quadriceps Strength Is Associated With Force During Jump-landing Task In Male Athletes
Solnik, Stanislaw	Postural Sway Correlates Of Perceived Comfort In Pointing Tasks
Soltys, Joseph	Cortical Activations During A Joystick Pursuit Task With Modulated Spindle Afferents
Sonenblum, Sharon Eve	Tissue Deformation In The Seated Buttocks Model
Spencer, Lee	Asymmetry In Healthy Female Collegiate Athletes
Spinelli, Bryan A	Altered Scapulohumeral Coordination In Individuals With Scapular Dyskinesis
Spirka, Thomas A.	Simple Fe Models Of The Forefoot For Use In The Design Of Therapeutic Footwear For Diabetic Patients
Standifird, Tyler	Lower Extremity Joint Moments During The Active Peak Vertical Ground Reaction Force In Three Different Running Conditions
Stavness, Ian	A General Approach To Muscle Wrapping Over Multiple Surfaces
Stebbins, Michael J.	An Mri-compatible Device For Obtaining Patient-specific Plantar Soft Tissue Material Properties
Stegemöller, Elizabeth	Differences In Repetitive Finger Movement Between The Most Effected And Least Effected Hand In Parkinson's Disease
Stitzel, Joel D.	Modeling Of Head Injury Response For Translational And Rotational Impacts Of Varying Directions And Magnitudes
Sukits, Alison L.	Effects Of Fractional Anisotropy In The Corpus Callosum As Determined By Diffusion Tensor Imaging On Temporal Variability In Older Adults
Surowiec, Rachel K.	The Effects Of Whole Body Vibration On The Wingate Test For Anaerobic Power When Applying Individualized Frequencies
Suydam, Stephen M	Muscle Activations In Response To Achilles Tendon Rupture And Repair
Suydam, Stephen M	Asymmetric Morphology Of The Hamstring Muscles Following Acl Autografts
Symons, Jennifer E.	Breezing Racehorse Limb Kinematics On Different Race Surface Materials
Szajnberg, Lily	Kinect Abnormal Involuntary Motion Assessment System: Increased Reliability Of Testing For Tardive Dyskinesia
Takahashi, Kota Z.	Net Efficiency Of The Combined Ankle-foot System In Normal Gait: Insights For Passive And Active Prosthetics
Teng, Hsiang-Ling Sharon	Trunk Flexion Angle Is Associated With Patellofemoral Joint Stress During Overground Running
Teran-Yengle, P	Knee Kinematics During Sloped Walking And Running In Healthy Women With Knee Hyperextension
Terry, Kevin	Comparing Visual Perturbation Responsiveness In Individuals With And Without Trans-tibial Amputation
Thorhauer, Eric	Effect Of Acl Reconstruction On Tibiofemoral Cartilage Contact During Downhill Running
Thorhauer, Eric	Tibiofemoral Cartilage Thickness Following Acl Reconstruction
Timmons, Mark	Scapular And Clavicular Kinematics During Empty And Full Can Exercises In Subjects With Subacromial Impingement Syndrome
Toney, Megan	Limb Force Variance Is Structured To Stabilize The Step-to-step Transitions Of Dynamic

	Walking
Too, Danny	Upright Cyling Position
Toosizadeh, Nima	Viscoelastic Modeling Of The Lumbar Spine: The Effect Of Prolonged Flexion On Internal Loads
Tran, D	A Protocol To Assess The Contribution Of The Components Of Human Abdominal Wall To Its Biomechanical Reponse
Troy, Karen L.	Compressive Loading Of The Distal Radius Improves Bone Structure In Young Women
Tung, Kryztopher D.	A Test Of The Metabolic Cost Of Cushioning Hypothesis In Barefoot And Shod Running
Umezaki, Kyoko	Impact Of Obesity On The Function Of Hip Knee And Ankle During Transition Between Level And Stair Walking
Urwin, Samuel G.	Validation Of An Electrogoniometry System As A Measure Of Knee Kinematics During Activities Of Daily Living
Uzarski, Joseph S.	Physiologically Modeled Shear Stress As A Function Of Pulse Frequency: Driving Endothelial Cells Toward A Quiescent Phenotype
Vallabhajosula, Srikant	Kinematics And Kinetics Of Stair Ascent While Dual-tasking
Vallabhajosula, Srikant	Effect Of Tactile Pertubation On Blindfolded Circular Path Navigation
Vallabhajosula, Srikant	Influence Of Stepping Rate On Stride Interval Variability Of Stair-climbing
Vallabhajosula, Srikant	Influence Of Tai Chi On Kinematics During Multi-directional Gait Initiation
vanAntwerp, Keith W.	Non-negative Matrix Factorization Applied To A Feedback System
Vidt, Meghan E.	Assessment Of Functional Reaching Tasks In Older Adults
Vistamehr, Arian	An Adaptive Tabu Search Optimization Algorithm For Generating Forward Dynamics Simulations Of Human Movement
Vistamehr, Arian	The Influence Of Pedal Platform Height On Maximal Average Crank Power During Pedaling: A Simulation Study
Voukelatos, Dimitrios	Training Induced Changes In Quadriceps Activation During Maximal Eccentric Contractions
Walia, Piyush	The Effect Of Arm Position On Hill-sachs Engagement: A Finite Element Study
Walia, Piyush	The Effect Of Arm Position On Bony Bankart Lesion: A Finite Element Study
Walker, D.R.	Electromyographic And Kinematic Analysis Of Medial Reverse Shoulder Arthroplasties During Functional Motions
Walker, D.R.	Scapulohumeral Rhythm Of Reverse Shoulder Arthroplasties During Weighted And Unweighted Shoulder Abduction
Walker, Elise	Influence Of Scaling Assumptions On Tendon Stiffness Estimation
Wang, He	The Effects Of Load Carriage And Fatigue On Frontal-plane Knee Mechanics During Walking
Wang, J.S.	Lower Limb Coordination Is Altered During Asymmetric Load Carrying While Walking On A Treadmill
Wattananon, Peemongkon	Preliminary Study Of Changes In Trunk Forward Bend Aberrant Patterns Post Core Stabilization Intervention
Weaver, Ashley A.	Comparison Of Hip Morphology In Femoroacetabular Impingement And Normal Patients
Wei, Feng	The Rotational Stiffness Of Football Shoes May Affect The Location Of A Potential Ankle Injury
Wei, Feng	A Potential Role Of Eversion In Limiting Medial And High Ankle Sprains: A Parametric Study
Wei, Feng	Lateral Heel Wedge Affects The Tibiofemoral Kinematics In Knee Oa Patients: A

	Preliminary Weight Bearing Mri Study
Weimar, Wendi H.	Latissimus Dorsi Anthropometry And Swimming
Weinhandl, Joshua T.	Hamstrings Weakness Increases Acl Loading During Sidestep Cutting
Weiss, K	The Effect Of Seating Surface Compliance On Trunk Motion
vanWerkhoven, Herman	Computational Model Of Maximum-height Single-joint Jumping Predicts Bouncing As An Optimal Strategy
Werner, Kathryn M	Balance Recovery Kinematics After A Lateral Perturbation In Patients With Transfemoral Amputations
Westlake, Carolyn G.	Gender Comparison Of Trunk And Pelvis Kinematics During Walking And Running
Whittaker, Eric C.	Dynamic Cadaveric Robotic Gait Simulation Of Pes Planus
Wicke, Jason	Inertial Estimate Errors For Female Arms And Legs From Different Body Models
Wiggin, Bruce	A Passive Elastic Exoskeleton Reduces The Metabolic Cost Of Walking Using Controled Energy Storage And Release
Wight, Jeff T.	Bilateral Analysis Of The Shoulder Internal Rotation Passive Torqueangle Relationship For Elite Pitchers With Glenohumeral Internal Rotation Deficit
Wight, Jeff T.	Does The Number Of Repetitions Achieved For The Bench Press Predict The Number Of Repetitions Achieved For Other Common Resistance Training Exercises?
Wikstrom, Erik A	Concussion Alters Gait Termination Strategies
Williams, Matthew R.	Electromyographic Effects Of Using A Powered Ankle-foot Prosthesis
Wordeman, Samuel C	Sex Differences In Unconstrained Transverse Plane Kinematic Response Under Compression And Simulated Muscle Forces
Wu, John Z.	A Hybrid Model Simulating Hand Gripping On A Cylindrical Handle
Wu, John Z.	Musculoskeletal Loading Of The Thumb During Pipette Operation
Wu, Jianhua	Effect Of Ankle Load On Gait Patterns During Treadmill Walking
Wurdeman, Shane R.	Transtibial Amputee Joint Motion Has Larger Lyapunov Exponents
Wurdeman, Shane R.	Both Limbs In Unilateral Transtibial Amputees Display Increased Risk For Tripping
Wutzke, Clinton J.	Gait Training With Visual And Proprioceptive Feedback Improves Overground Propulsive Forces In People Post-stroke
Xia, Ting	Loading Rate During Spinal Manipulation Has Minimal Effect On Lumbar Spine Peak Reaction Force And Spinal Stiffness: A Human Specimen Study
Yang, BingShiang	Fall Detecting Using Inertial And Electromyographic Sensors
Yang, Hyung Suk	The Influence Of Prophylactic Ankle Braces On Lower Limb Mechanics During A Ninety Deg Side-step Cutting Task
Yavuz, Metin	Plantar Shear Stress Distributions In Diabetic Patients With And Without Neuropathy
Yavuz, Metin	Plantar shear stress and its clinical implications (Post-doctoral awardee)
Yentes, Jennifer M.	Walking Abnormalities In Patients With Copd
Yentes, Jennifer M.	Positive Ankle Work Is Affected By Peripheral Arterial Disease
Yu, Yawen	Children With Cerebral Palsy May Not Benefit From Stochastic Vibration When Developing Independent Sitting
Zaferiou, Antonia M.	Mechanisms Dancers Use To Maintain Balance And Regulate Reaction Forces When Turning
Zaylor, William	The Influence Of Occlusal Splinting On The Trabecular Morphology In The Sagittal Plane Of The Temporomandibular Joint
Zeng, Sisi	Development And Verification Of An Elbow Joint Stiffness Tester

Zhang, Songning	Comparisons Of Flip-flop Sandal Barefoot And Running Shoe In Walking
Zheng, Liying	Patient-specific Musculoskeletal Modeling For Evaluating The Efficacy Of Meniscus Transplantation
Zhou, Wei	Influence Of Object Size And Hand Posture On Upper Limb Joint Loads During One-handed Lifting Exertion
Zobeck, Kyle	Quantifying The Stiffness Of Running Shoes
Zou, Dequan	The Correlation Between Internal Skeletal Dimensions Of Tibiofemoral Joint And External Body Measurements
Zukowski, Lisa A	A Reanalysis Of Wrist Jerk During Ergonomic Hand Drive Wheelchair Propulsion

THE EFFECT OF LUMBAR SPINE EPIDURAL ANESTHETIC INJECTIONS ON GAIT

Abdullah Abbasi, David J. Kennedy, Heather Vincent, Amanda Seay, and Bryan P. Conrad [1]

[1] University of Florida, Gainesville, FL, USA
Spine and Sports Interventional Center at Shands Rehabilitation Hospital
E-mail: bconrad@ufl.edu Web: http://www.ortho.ufl.edu/motion-lab

INTRODUCTION

Fluoroscopically guided lumbar transforaminal injections with a local anesthetic have been utilized for diagnostic purposes in patients with suspected lumbosacral radicular pain. From a diagnostic standpoint the injection of a local anesthetic should result in a profound rapid onset (although short term) decrease in pain if the injection site is indeed the primary pain generator. However diagnostic injections have been shown to have a significant placebo response when measuring pain scores only. We therefore proposed to study the immediate effects of fluoroscopically guided transforaminal epidural injection of local anesthetic in patients with suspected lumbosacral radicular pain on gait parameters. Our hypothesis is that immediately following an injection of a local anesthetic in the epidural space, gait function will be adversely affected o to impaired neural control of the lower limb muscles. This study provides novel information regarding the functional abilities of patients immediately after they receive an anesthetic injection.

METHODS

Twenty five patients who were receiving a fluoroscopically guided lumbar transforaminal epidural injection of local anesthetic for suspected symptomatic lumbar radicular pain. Before receiving the injection, each subject completed gait analysis using an instrumented walkway (GaitRite®; CIR Systems, Inc.; Havertown, PA). Immediately after the injection, gait analysis testing was repeated. Three trials of each subject walking at a self-selected pace were collected and averaged together for analysis. A repeated measures ANOVA was used to evaluate whether differences in gait (specifically stride length, cadence, base of support and velocity) were present after the injection.

RESULTS

The average age of the patients receiving a lumbar injection was 61±13 years, the average Oswestry Disability Score was 42±12. Immediately following injection, patients reported a significant decrease in VAS pain scores (from 6.2 to 1.6, $p < 0.0001$). There were no significant differences in gait function (stride length, cadence, base of support or velocity, Table 1, Figure 1) immediately following transforaminal injection of local anesthetic in the epidural space.

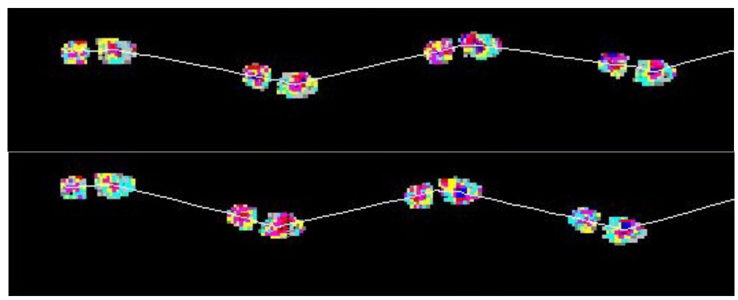

Figure 1. Gait recordings before (above) and after (below) lumbar epidural injection. No significant differences were detected

DISCUSSION

Our hypothesis, that gait would be negatively affected immediately following epidural injection was not supported by the data. Although the gait velocity and step length are lower for patients receiving an epidural injection compared to healthy age matched norms, it does not deteriorate following injection. These results have several implications on clinical practice, such as discharged instructions and post-injection care. Questions remain regarding the potential short term alterations of gait due to the administration of corticosteroids.

ACKNOWLEDGMENTS
We appreciate the assistance of the Spine and Sports Intervention Center at Shands Rehab Hospital, in particular Patti O'Steen, Angie Korab, Lisa Herber, Sharon , Shelly Hines.

DISCLOSURE STATEMENT
The authors have no conflicts of interest to report.

Table 1. Summary of gait parameters before and after injection. Significant Pre/Post differences are denoted with *.

Cohort	Time	Pain	Velocity (cm/s)	Stride Length (cm)	Base of Support (cm)	Cadence (steps/min)
Lumbar Spine	Pre-Injection	6.2	88 ± 30	106 ± 25	11 ± 3	98 ± 13
	Post-Injection	1.6*	91 ± 30	108 ± 26	11 ± 3	99 ± 15

NEURAL NETWORKS BASED IDENTIFICATION OF JOINT MOMENTS USING NONLINEAR MODEL OF SIT-TO-STAND

[1]Alaa Abdulrahman, [2]Kamran Iqbal

[1]University of Arkansas at Little Rock, Arkansas, AR, USA
[2]University of Arkansas at Little Rock, Arkansas, AR, USA
email: amabdulrahma@ualr.edu, kxiqbal@ualr.edu

INTRODUCTION

Artificial Neural Networks have been successfully used in parameter estimation and identification of joint moments during various human movements [1],[2]. These studies have commonly used EMG signals, in addition the kinematic data, for identification of joint moments using neural networks (NN) based identifiers. The estimation of joint moment was usually specific to a single joint. For example, Wang et al, [1], used adjusted back-propagation to train a four layer NN to estimate the required muscles activation underlying elbow joint moments using ten EMG muscles signals as inputs. The trained network was successful and the moment estimation was close to the measured values (at about 0.8%-3% average relative error). A dynamic identification scheme, NNARX (neural network autoregressive with exogenous input) has been utilized by Lee et al.,[2] to estimate the knee joint moment in sit-to-stand movement. Six EMG signals beside the joint angle and velocity were used as input to train the NN including regressions. The resulting estimation of knee joint moment was successful with a correlation of 0.97.

In this paper, compare the performance of Static Neural Network (SNN) and Dynamic Neural Network (DNN) structures in an identification system for estimation of joint (ankle, knee, and hip) moments during sit-to-stand (STS) and stand-to-sit (STTS). Both structures work with inverse dynamic model and use only the kinematic data (joints angles) as inputs. Moreover, the networks trained on STS were successfully tested for STTS without requiring further training. Since comparable results were obtained by the two networks, we discount use of regression and kinematic data involving velocity or acceleration as inputs to the network.

METHODS

The sagittal model used for identification was constructed from three rigid-body segments connected using revolute joints. The model thus had three degrees of freedom (DOF) defined as joint angles for ankle, knee and hip joints. Dynamics of the model were formulated using Lagrangian methods and are given as:

$$D(\theta)\cdot\begin{bmatrix}\ddot{\theta}_1\\ \ddot{\theta}_2\\ \ddot{\theta}_3\end{bmatrix}+C(\theta,\dot{\theta})\cdot\begin{bmatrix}\dot{\theta}_1\\ \dot{\theta}_2\\ \dot{\theta}_3\end{bmatrix}+G(\theta)=\begin{bmatrix}\tau_{Ankle}\\ \tau_{Knee}\\ \tau_{Hip}\end{bmatrix} \qquad (1)$$

where, D, C and G represent the inertia, coriolis and gravity terms, respectively. In this model, D and C are R^{3x3} and G is R^{3x1}; and, $\theta_i, \dot{\theta}_i, \ddot{\theta}_i$ represent the angles, velocities and accelerations of joint *i* (*i=1,2* and 3 representing ankle, knee and hip joints). The parameters used in this model were obtained from [3]. As seen from (1), each joint moment depends on the kinematic motion of all the other joints.

Kinematic data for the joint angles were collected from four participants (aged 25-40). Each participant performed 15 trials of STS and STTS movements. During trials, each subject was affixed with 5 markers and VICON motion cameras were used to capture marker trajectories. Data was captured at 100Hz (sampling time of 0.01 seconds). A difference algorithm was later used to extract the joint angles.

Feedforward Neural Network was used as an identifier to estimate the joint moments. The SNN identifier consisted of an input layer with 3 linear neurons, a hidden layer with 10 nonlinear *logsig* neurons, and an output layer with 3 linear neurons. Backpropagation method was used to train the identifier using Levenberg-Marquardt algorithm to minimize the mean square error between the identifier and the measurement (Figure 1). A DNN that included a time delay line in front of the identifier was similarly tested with the same data to compare with SNN and reveal how the system could be identified without the need for regression.

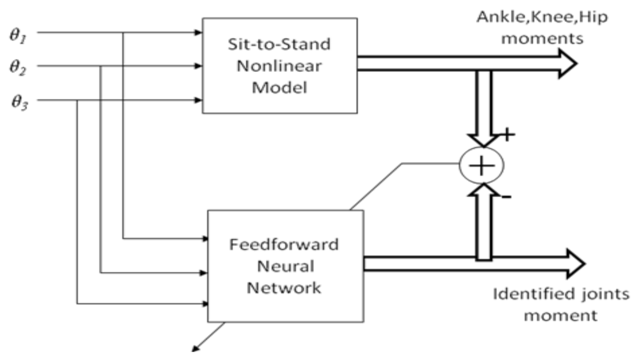

Figure 1: Identification system using SNN

RESULTS

Measured joint angles data was divided into two parts: part 1 was used for training and part 2 for testing. Part 1 data consisted of three participants and the first five trials of each participant; part 2 data consisted of the remaining participants and trials. Testing results for the 4th participant at trial 10 for STS and trial 11 for STTS are presented here. In each case, equation (1) was used to compute joint moments to train the NN identifier, initialized with random weights. Figure 2, shows model output and the SNN before training. Figure 3 reveals how the identifier was trained, and how the trained system could successfully estimate the tested data of both STS and STTS.

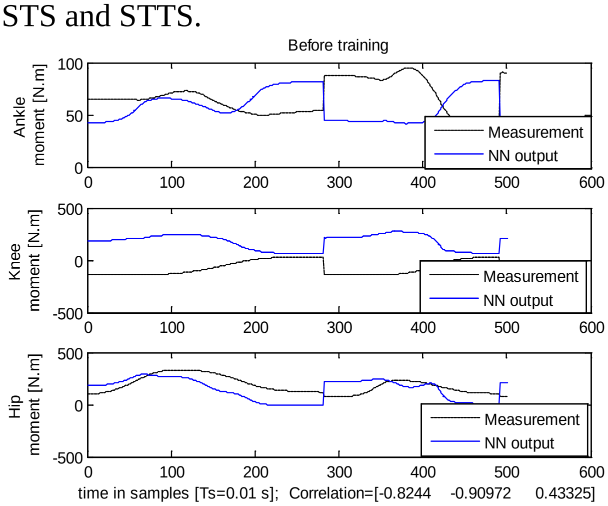

Figure 2: System outputs before training

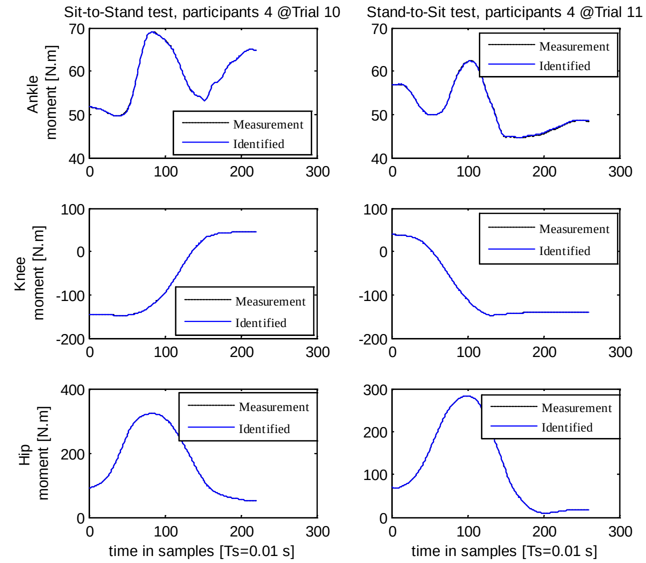

Figure 3: The SNN and measurement outputs are matched with correlation 0.99-1.

The correlation obtained between the trained network and the measurement outputs was 0.99 to 1, which shows almost an exact match. The same data was applied to the DNN which gave results comparable to the SNN. These results imply that input regressions were unnecessary for estimation.

CONCLUSIONS

Dynamic NN and Feedforward NN were successively utilized to identify the nonlinear inverse dynamics of STS movement. Exact identification matches were obtained for all joint moments using only the kinematic motion of angles. It reveals that using only kinematic data may be sufficient to train the inverse dynamic system. These results discount the need for EMG and other kinematic data for estimation of joint moments. Further, the system can be trained with a SNN with only three inputs, dispensing the need for regression and time delay line. Also use of fewer neurons leads to faster training.

REFERENCES

1. Wang L, et al. *IEEE T NSRE* **10**, **1**, 30-37, 2002.
2. Lee JK, et al. *Proceedings ICCASJ'08*,COEX, Seoul, Korea, 2008.
3. Iqbal K, et al. *J Biomech* **33**, 1619-1627, 2000.

SIT TO STAND MECHANICS AFTER SYMMETRY TRAINING FOR PATIENTS AFTER TOTAL KNEE ARTHROPLASTY

[1]Sumayeh B. Abujaber, [1] Joseph A. Zeni, [1]Lynn Snyder-Mackler
[1]University of Delaware, Newark, DE, USA

INTRODUCTION

Total knee arthroplasty (TKA) is one of the most common surgeries in the United States for end stage knee osteoarthritis (OA). TKA reduces pain and disabilities in this population; however, the patient's functional performance is not comparable to that in people without any knee problems 1 year after TKA [1]. After TKA, patients demonstrate functional improvement and more satisfaction with their functional abilities; however they still have marked impairments, functional limitations, quadriceps weakness and asymmetrical movement patterns [2, 3, and 4]. Quadriceps strength symmetry explains a small portion of symmetry in biomechanical variables [3] and even patients who participate in rehabilitation programs that focus on progressive strengthening after surgery demonstrate persistent kinetic and kinematic asymmetries [5]. During a sit to stand task (STS), subjects who underwent TKA demonstrated altered movement patterns that unloaded the operated limb and shifted the weight to the non-operated side [3,4,6] This altered movement pattern may lead to excessive loading in the non-operated limb, thus predisposing the joints of the non-operated limb to OA progression in the long term. Therefore, rehabilitation strategies for individuals after TKA may need to address impairments in movement symmetry in addition to progressive strengthening in order to maximize movement symmetry after TKA.

The purpose of this study is to evaluate the effectiveness of adding a symmetry training component into post-operative rehabilitation. Our first aim was to examine longitudinal changes in STS mechanics in subjects received symmetry training along with strengthening exercise after TKA. The second aim was to evaluate the biomechanical differences between subjects who received symmetry training and subjects who received standard of care alone after TKA.

METHODS

Eight subjects with primary unilateral TKA were recruited for this study. Four subjects received strengthening exercises plus symmetry training (2 women, Age 58 ± 4.2y) and the other four subjects underwent standard of care rehabilitation (2 women, Age 58.5±3.7). The standard of care protocol consisted of progressive quadriceps strengthening, functional retraining, appropriate manual therapy and modalities to reduce post-operative inflammation that began 3-4 weeks after TKA. The symmetry training consisted of the same protocol, but also includes a progressive symmetry retraining program that focused on improving symmetry of weight distribution between limbs during strengthening and functional retraining exercises.

All subjects underwent 3D motion analysis of STS task using an 8 camera infrared motion system (Vicon) and 2 force-plates (Bertec). Inverse dynamic techniques were used to calculate Joint angles and joint moments for each limb. Subjects in the symmetry group were tested before surgery, 3 months, and 6 months post-surgery while subjects in the other group were tested only 6 months after surgery. The outcome measures used were the symmetry ratio of peak sagittal knee moment (PSKM) during standing, peak vertical ground reaction force (PVGRF) during standing, during sitting and vertical ground reaction force (VGRF) while standing. Symmetry ratio was calculated by dividing the outcome value of operated side by that of the non-operated side. 3-month follow up was not obtained for one subject in symmetry group. Qualitative comparisons were made between time points and groups.

RESULTS AND DISCUSSION

For the first aim, subjects in symmetry group showed improvements in symmetry in all outcome variables across time. The ratio of PSKM increased by 11.3% from pre-operative to 3 months and 27.3% from 3 months to 6 months. Ratio of PVGRF during standing increased from pre-operative to 3 months by 2.1 % while increased by 10.3% from 3 months to 6 months. Symmetry in PVGRF during sitting increased from pre-operative to 3 months by 8.3 % while increased by 7.7% from 3 months to 6 months. While VGRF symmetry while standing increased from pre-operative to 3 months by 16.4 % while increased by 3.1% from 3 months to 6 months. Results for the second aim showed more symmetry in Symmetry group compared with standard of care group. Persons 6 months after TKA in symmetry group demonstrated more symmetry in all outcome variables. Symmetry subjects at 6 months after TKA showed more symmetry than the other group by 38.3%, 11.3%, 25.4%, and 16.5% in PSKM during standing, PVGRF during standing, PVGRF during sitting, and VGRF while standing respectively.

CONCLUSIONS

The improvements in biomechanical symmetry in the subjects who received symmetry training suggest the need to include elements beyond strengthening in the rehabilitation programs for patient after TKA. Although early post-operative strength deficits may resolve with training, this protocol may improve normal and symmetrical dynamic movement pattern. These protocols may provide a reduction in loading on the non-operative side and restore normal movement on the operated side. Most post-surgical rehabilitation regimes address muscular and functional deficits; however no regimens have been established to overcome the asymmetrical movement patterns that result in excessive loading on the uninvolved limb. In our sample, we also noticed a marked improvement between the 3 and 6 month time points and symmetry ratios at 6 months exceeded the standard of care group. It is possible that this improvement is attributable to continued use of a more asymmetrical movement pattern that promotes strength on the operated limb during daily tasks. We will continue to evaluate this novel symmetry protocol in a larger subject pool.

REFERENCES

1. Walsh M, et al. *Phys Ther*, **78**(3), 248-258, 1998.
2. Bade M J, et al. *J Orthop Sports Phys Ther*, **40**(9), 559-567, 2010.
3. Mizner RL, et al. *J Orthop Res*, **23**(5), 1083-1090, 2005.
4. Farquhar SJ, et al. *Phys Ther*, **88**(5), 567-579, 2008.
5. Alnahdi AH, et al. *J Orthop Res*, **29***(5)*, 647-652, 2011.
6. Christiansen CL, et. *Arch Phys Med Rehabil*, **92**(10), 1624-1629, 2011

ACKNOWLEDGEMENTS

NIH grants (K12 HD055931, P20RR016458)

Table 1: Sit to stand parameters [mean (standard deviation)]

	Symmetry Group			Standard care
Outcome measure	Pre-surgery	*3-months after TKA	6-months after TKA	6-months after TKA
PSKM Ratio	0.58 (0.2	0.64 (0.09)	0.82 (0.22)	0.59 (0.18)
PVGRF Ratio during standing	0.84 (0.15)	0.86 (0.19)	0.95 (0.14)	0.85 (0.14)
PVGRF Ratio during sitting	0.84 (0.14)	0.91 (0.09)	0.98 (0.15)	0.78 (0.1)
VGRF Ratio while standing	0.86 (0.12)	1.01 (0.08)	1.00 (0.13)	0.89 (0.1)

* This is the data of 3 subjects; one session couldn't be obtained for one subject.

The Effects of Independent Variations in Rearfoot and Forefoot Prosthesis Stiffness on Amputee Gait

[1]Peter G. Adamczyk, [2]Michelle Roland, [2]Andrew B. Sawers and [2,3]Michael E. Hahn

[1]Intelligent Prosthetic Systems, LLC, Ann Arbor, MI, USA
[2]Department of Veterans Affairs Rehabilitation R&D Center of Excellence, Seattle, WA, USA
[3]Department of Mechanical Engineering, University of Washington, Seattle, WA, USA
email: p.g.adamczyk@gmail.com

INTRODUCTION

Selection of a foot prosthesis for a lower-limb amputee involves trade-offs among many design parameters, including height, weight, shape, adjustability, damping and stiffness. Perhaps most important is stiffness [1,2], which exhibits a wide range of values in commercial products: roughly 27-68 $N{\cdot}mm^{-1}$ at the rearfoot [3] and 28-76 $N{\cdot}mm^{-1}$ at the forefoot [4]. Past studies have compared biomechanical outcomes from different feet and attributed changes to their different stiffness values. But, there are many differences between brands, making it difficult to conclusively determine how a single parameter influences gait. We designed an experimental multi-component foot to vary rearfoot and forefoot stiffness independently of other parameters. We measured walking with several stiffness values at several speeds, to determine what behaviors are attributable specifically to stiffness. We hypothesized that increasing rearfoot stiffness would lead to increases in limb loading rate, knee flexion angle and internal knee extension moment. We also hypothesized that increasing forefoot stiffness would lead to increases in late stance force (vertical and forward) and internal knee flexion moment. Finally, we hypothesized that for both rearfoot and forefoot, higher stiffness would lead to reduced prosthesis energy storage and return.

METHODS

The experimental multi-component foot (Fig. 1) consists of a main mounting rail with adjustable side blocks (Aluminum 7075 T6), and independent rearfoot and forefoot structural keels (Garolite G10/FR4 woven glass-epoxy composite). The mounting rail allows the anterior-posterior position of the keels and pylon to be adjusted in 10 mm and 14 mm increments, respectively. The side blocks allow angular adjustment of keel orientation in 5° increments. The interchangeable rearfoot and forefoot keels were machined to have linear stiffness ranges of 22-69 $N{\cdot}mm^{-1}$ [4] and 14-90 $N{\cdot}mm^{-1}$ [5], respectively. Stiffness was adjusted by tapering the thickness of the composite. The outline shape of all rearfoot keels was constant, with cantilever length 130 mm. Forefoot keels were made in two versions, similar in design but with lengths of 140 mm or 175 mm.

Subjects (n=3) walked at speeds 0.7, 0.9, 1.1, 1.3, and 1.5 $m{\cdot}s^{-1}$ on a split-belt instrumented treadmill, using a Nominal Stiffness configuration (**NS**, with foot length and stiffness chosen according to subject height and weight), and 5 configurations varying one parameter from NS: Compliant Rearfoot (**CR**), Stiff Rearfoot (**SR**), Compliant Forefoot (**CF**) and Stiff Forefoot (**SF**). "Compliant" and "Stiff" varied from nominal by about 15 N/mm. This two-parameter "t-shaped" design resulted in three variations each of rearfoot and forefoot stiffness. We collected ground reaction forces (GRF) and whole-body motion capture data, and used these to

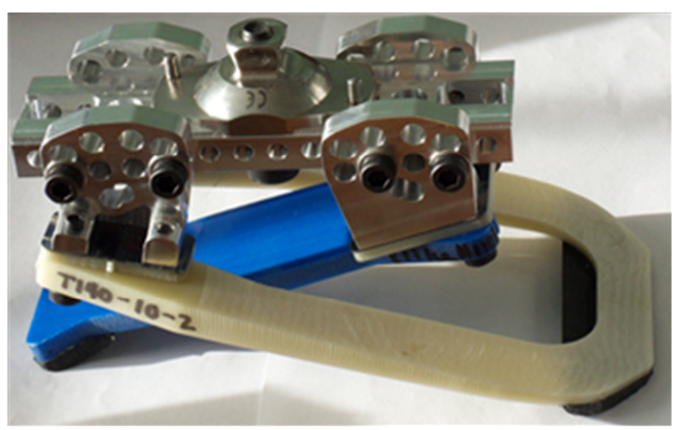

Figure 1: Experimental foot prosthesis. A standard pyramid adapter attaches to a main mounting rail. Side blocks hold separate rearfoot (left) and forefoot (right) keels, and adjust in position and angle. Keels are interchangeable, in stiffness increments of about 15 $N{\cdot}mm^{-1}$.

estimate center of mass mechanics and lower-body inverse dynamics. We computed outcome metrics from estimates of COM work rate; joint angle, moment and power output; and deformable-body work at the prosthetic ankle. Significance of trends was indicated by a two-factor linear regression of each metric across speed and stiffness category with slope significantly different from zero ($P < 0.05$).

RESULTS AND DISCUSSION

As predicted, increasing stiffness of the rearfoot keel led to higher loading rates (time derivative of vertical force) when the prosthesis first contacted the ground ($P < 0.001$). This effect may reflect passive landing dynamics of the prosthesis, similar to the transient "impact" peak of normal gait.

Increasing rearfoot stiffness also led to increased peak knee flexion during early stance ($P = 0.007$) and increased peak internal knee extension moment ($P = 0.006$). The higher loading rate of the stiffer rearfoot produces a higher or earlier external moment that tilts the shank forward, flexing the knee. It appears that a greater knee moment is produced in response, to maintain or restore an extended knee posture.

Increasing stiffness of the forefoot keel led to increased peak internal knee flexion moment slightly later in stance ($P < 0.001$). High toe stiffness may require that the knee produce a flexor moment to counteract the tendency of a ground force near the toe to hyperextend the knee.

Our hypothesis that the late-stance vertical force peak would increase with higher forefoot stiffness was not supported ($P = 0.47$). The force was constant across stiffness, perhaps because the foot must support body weight no matter what the stiffness is, leaving little room for changes.

Finally, estimates of total deformable-body energy stored and returned by the prosthesis (Fig. 2) decreased with higher stiffness at both the rearfoot (storage, $P = 0.01$; return, $P < 0.001$) and forefoot (storage and return, $P < 0.001$). Energy storage and return are maximized by the combination of high force with high displacement, rather than either

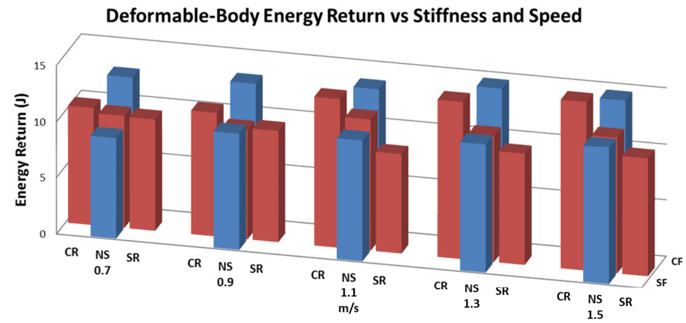

Figure 2: Deformable-body energy return from the prosthesis decreases as hindfoot (red) or forefoot (blue) stiffness increases. Groups are plotted for each speed, 0.7 to 1.5 $m{\cdot}s^{-1}$.

alone. A keel that is very stiff stores less energy than a more compliant keel that deflects further.

We also observed several other effects that we did not hypothesize. For example, increases in speed tended to introduce additional peaks in vertical and fore-aft ground reaction force during the landing phase, which fluctuated with rearfoot stiffness. Also, while the reported trends hold statistically, individuals exhibited substantial variation in walking strategy and outcome metrics. It may be that a short test battery similar to this protocol may yield more useful information for an individual than a population-based study.

CONCLUSIONS

Varying rearfoot and forefoot stiffness independently of other parameters provides the opportunity to study their effects directly, rather than inferring these effects from among several covariant properties. These two parameters have distinct effects on outcomes such as knee moment and elastic energy return. With this expanded understanding, it may be possible to better fit the properties of a prosthesis to each individual's needs.

REFERENCES

1. Klodd E, et al. *JRRD*, **47**, 899-910, 2010.
2. Ventura JD, et al. *Clin Biomech,* **26**, 298-303, 2010.
3. Klute GK, et al. *JRRD*, **41**, 535-546, 2004.
4. Geil M. *J Prosth Orth* **13**, 70, 2001.

ACKNOWLEDGEMENTS

Funded by VA Rehabilitation R&D Grant N7348R.

Axial and Transverse Compressive Properties of Human Vertebral Trabecular Bone

Ameet K. Aiyangar, Juan Vivanco, Anthony G. Au, Everett L. Smith and Heidi-Lynn Ploeg

University of Wisconsin-Madison USA
email: ameetaiyangar@gmail.com

INTRODUCTION

Obtaining bone mechanical properties from clinical resolution quantitative computed tomography (QCT)-derived localized apparent density presents the most attractive, available tool for developing subject-specific finite element (FE) bone models [1]. Human vertebral trabecular bone (HVTB) is mechanically heterogeneous, anisotropic and strongly influenced by architectural variations [2]. However, most studies investigating HVTB mechanical property-density relationships have only presented results for the superior-inferior, or "on-axis" direction [3].
The current study aims to quantify the empirical relationships between QCT-based apparent density of HVTB and its apparent compressive mechanical properties – elastic modulus, yield stress and strain – in both the superior-inferior (SI) and transverse (TR) directions for purposes of future FE modeling.

METHODS

Sixty-six cylindrical specimens (height(H)=5mm, diameter(D)=10mm) were cored from four L1 human lumbar cadaveric vertebrae. The low aspect-ratio (H/D=0.5) allowed extraction of multiple specimens from each vertebra. Vertebrae were scanned along with calibrated phantoms in a clinical resolution (voxel dimensions: 0.625x0.351x0.351 mm^3) CT scanner (GE Lightspeed 16, GE Medical System, Waukesha, WI) before and after specimen extraction to obtain QCT-based apparent density (ρ_{CT}). Specimens were tested in quasi-static compression in wet condition using the mechanical testing component of the *Zetos Bioreactor and Bone Loading* System, which has been designed to test low aspect-ratio specimens [4,5]. After discarding specimens damaged during preparation and handling, 33 and 18 specimens were tested in the SI and TR directions respectively.

RESULTS AND DISCUSSION

Apparent elastic modulus **(Figure 1)** and yield stress **(Figure 2)** were linearly related to the QCT-based apparent density in the superior-inferior direction [$E_{SI} = 1493.8*(\rho_{CT})$, $r = 0.77$, $p < 0.01$; $\sigma_{Y,SI} = 6.9*(\rho_{CT}) - 0.13$, r =0.76, p < 0.01].

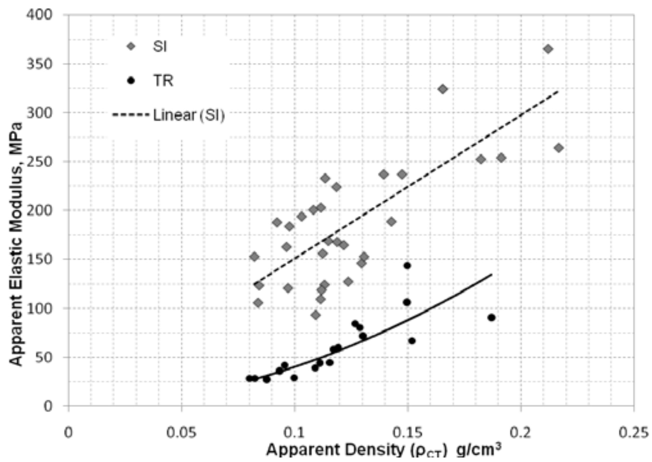

Figure 1: Variation of Elastic Modulus *(E)* with QCT-derived apparent density *(ρ_{CT})*.

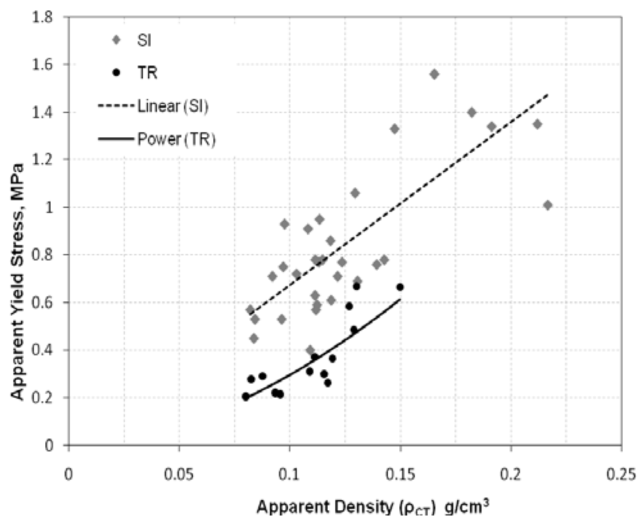

Figure 2: Variation of Apparent Yield stress *(σy)* with respect to CT-derived apparent density *(ρ_{CT})*.

A power law relation provided the best fit in the transverse direction [$E_{TR} = 3349.1*(\rho_{CT})^{1.94}$, $r = 0.89$, $p < 0.01$; $\sigma_{Y,TR} = 18.81*(\rho_{CT})^{1.83}$, $r = 0.83$, $p < 0.01$.]. Apparent elastic modulus and yield strength were greater in the axial direction compared to the transverse direction by a factor of 3.2 and 2.3 respectively, on average. Furthermore, the degree of anisotropy (anisotropic ratio) decreased in an exponential manner with increasing density **(Figure 3)**. Comparatively, and contrary to studies on higher density bones such as human and bovine femoral trabecular bone [6], yield strain exhibited a mild, but statistically significant ($p<0.001$) anisotropy: TR yield strains (mean = 0.9%) were larger than SI strains (mean = 0.67%) by 30%, on average.

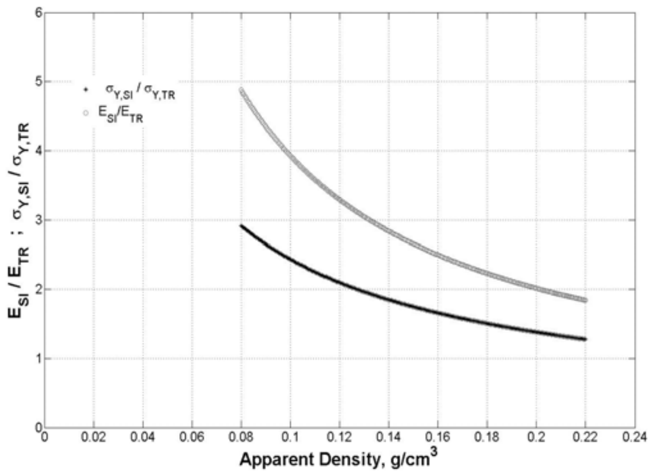

Figure 3: Anisotropic Ratio: Ratio of SI–to–TR elastic moduli (E_{SI}/E_{TR}) and yield stress (σ_{SI}/σ_{TR})

The current study contributes to the available literature with regard to mechanical properties of human vertebral trabecular bone.

Ability to map apparent mechanical properties in the transverse direction, in addition to the superior-inferior direction from clinical resolution QCT-based densitometric measures allows incorporation of important information regarding material orientation into FE models. This can partly offset the lack of information in clinical CT data regarding trabecular architectural variations, which have a strong influence on vertebral mechanical properties.

REFERENCES

1. Viceconti M. et al., J Biomech, **39**(7), 1169-1179, 2006.
2. Keaveny TM, et al., Ann Rev of Biomed. Eng, **3(1)**, 301-333, 2001.
3. Morgan EF, et al., J. Biomech., **34(5)**, 569-577, 2001.
4. Jones DB et al., Eur Cells Mat., **15**, 58-60, 2003.
5. Garcia-Rodrguez S., et al., J. Medical Devices., **2(1)**, 1-6, 2008.
6. Chang WCW, et al., J. Orthop. Res., **17(4)**, 582-585, 1999.

Acknowledgements

The authors gratefully acknowledge Geoff Piller, Yvonne Schumacher and Sarah McCoy for the assistance provided in bone specimen preparation. The authors are also grateful to Professor T.D. Crenshaw for allowing use of equipment for physical measurement of bone core densities and Debra Schneider for technical assistance with the same. Financial support for this project was received from the Natural Science and Engineering Research Council of Canada (NSERC) and the University of Wisconsin Graduate School.

STORAGE AND LOSS MODULI OF BONE IN OSTEOGENESIS IMPERFECTA (OI)

[1]Carolyne Albert, [1]John Jameson, [2]Jeffrey Toth, [3]Peter Smith, and [1,3]Gerald Harris

[1]Marquette University, Milwaukee, WI, USA
[2]Medical College of Wisconsin, Milwaukee, WI, USA
[3]Shriners Hospitals for Children, Chicago, IL, USA
e-mail: carolyne.albert@marquette.edu

INTRODUCTION

Osteogenesis imperfecta (OI), or brittle bone disease, is a genetic disorder of bone fragility affecting between 20,000 and 50,000 people in the United States [1]. Severity varies widely between individuals with OI. While the mildest form, type I OI, generally presents with few fractures, the most severe form in children surviving the perinatal period, type III OI, leads to multiple fractures and progressive skeletal deformities [2].

Bone fragility in OI results in part from a bone mass deficiency. Histomorphometric analysis of iliac crest biopsies has shown that children with OI have lower trabecular bone volume and thinner cortices than age-matched controls [3]. Impaired collagen network and abnormal mineralization have also been observed in OI bone [4], suggesting that compromised material properties may further contribute to bone fragility. Few studies have examined bone material properties in OI. Using nanoindentation, it was found that elastic bone modulus and hardness are higher in type III OI than in age-matched controls [5], while no significant differences were found between moderately severe (type IV) and severe OI (type III) [6]. These studies reported elastic moduli between 11 and 24 GPa for type III OI, and the reason for this wide range of values has not been explained. Finally, no studies have yet characterized bone material properties for the most common form of OI, type I.

The objectives of this study were to compare the storage (elastic) modulus, E', and loss (viscous) modulus, E'', of cortical bone between individuals with type I and type III OI, and to examine how these properties vary between osteonal and interstitial lamellar bone regions.

METHODS

Under an IRB approved protocol (HR-2167), osteotomy specimens were collected from the femur or tibia of ten individuals with OI during routine surgical procedures. The donors were between ages 7 and 16 years. Five had type I OI, and the other five type III. The bone specimens were stored in a freezer (-70°C) prior to testing.

The specimens were cross-sectioned with a diamond saw (IsoMet, Buehler, Lake Bluff, IL) with the cross-section surfaces being approximately perpendicular to the long bone axis. The specimens were then dehydrated in ethanol and embedded in resin (EpoThin, Buehler, Lake Bluff, IL). The cross-sections were polished with a grinder-polisher (Metaserv® 3000; Buehler, Lake Bluff, IL), and the polished cross-sections were indented using a nanoindenter (Nanoindenter XP, MTS, Eden Prairie, MN). A continuous stiffness measurement method was used, in which a low magnitude oscillating force was superimposed onto a quasistatic force ramp, at a frequency of 45 Hz, amplitude of 2 nm, and a strain rate of 0.05 s^{-1}. The measured moduli, E’ and E”, were averaged between indentation depths of 800 and 1600 nm, a range over which these measurements were found to be approximately constant.

Twenty indentations were performed in each specimen. Using a reflectance microscope, lamellar microstructure was observed at each indent site and classified as being located in either osteonal or interstitial lamellar bone regions (Figure 1). Indents that were in contact with voids or that were not easily identified as osteonal or interstitial were excluded from the study.

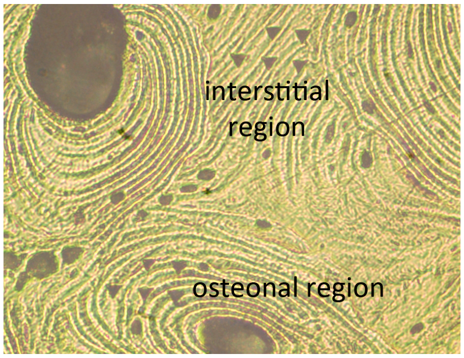

Figure 1: Typical nanoindentation sites (triangles): interstitial lamellar bone (top) and osteonal bone (bottom). This specimen was obtained from the femur of a 12 year-old female with type III OI.

A linear mixed effects model was used to assess the effects of OI severity (types I/III) and lamellar microstructure (osteonal/interstitial) on the moduli. Four covariates were explored: age, gender, site (femur/tibia), and history of bisphosphonate treatment (yes/no). Only covariates and interactions that were found to be significant ($p<0.05$) were included in the final statistical model.

RESULTS AND DISCUSSION

Anatomic site had a significant effect on E' only, therefore this covariate was included only in the final statistical model for E'. Other covariates and all interactions did not have significant effects and these were not included in either model. Results of the linear mixed models for E' and E" are shown in Tables 1 and 2.

Table 1: Linear mixed model results for E'.

	Coefficient (GPa)	SE	P value
(Intercept)	17.5	0.5	<0.001
Severity = OI type III	-1.5	0.6	0.01
Microstructure = Osteonal	-2.1	0.3	<0.001
Anatomic site = Tibia	1.2	0.6	0.04

Table 2: Linear mixed model results for E".

	Coefficient (GPa)	SE	P value
(Intercept)	0.82	0.02	<0.001
Severity = OI type III	-0.03	0.02	0.11
Microstructure = Osteonal	-0.05	0.01	<0.001

OI severity, microstructure and anatomic site had statistically significant effects on E' ($p<0.05$, Table 1). Only microstructure, however, had a significant effect on E" (Table 2). Mean E' was lower in individuals with type III OI than in those with type I by 1.5 GPa (9%). Mean E' and E" were lower in osteonal than in interstitial regions by 2.1 GPa (12%) and 0.05 GPa (6%), respectively. Finally, E' was higher in the tibia than the femur by 7%.

The results of the current study indicate that OI severity affects the ability of bone tissue to store energy under load, as denoted by E'. The ability of bone material to dissipate energy through viscous mechanisms, as denoted by E", however, does not appear to be affected by OI severity. The results also demonstrate that significant heterogeneity in material properties is present between regions of different lamellar structure, with osteonal regions having lower moduli than interstitial regions. This heterogeneity is likely attributed to variations in local degrees of mineralization between these regions.

Bisphosphonate treatment has become common in children with OI. In this study, patient history of such treatment did not have a significant effect on the moduli.

A limitation of this study is that nanoindentation does not provide fracture-related properties. Future research is therefore needed to determine how strength and toughness of bone tissue are affected in OI, and whether these properties are compromised by bisphosphonate treatment.

REFERENCES

1. National Institute of Arthritis and Musculoskeletal and Skin Disease, www.niams.nih.gov, 2009.
2. Sillence DO, et al. *Med Genet* **16**, 101-16, 1979.
3. Rauch F, et al. *Bone* **26**, 581-9, 2000.
4. Traub W, et al. *Matrix Biol* **14**, 337-45, 1994.
5. Weber M, et al. *Bone* **39**, 616-22, 2006.
6. Fan Z. et al., *Conn Tissue Res* **48**, 70-5, 2007.

ACKNOWLEDGEMENTS

This work was supported by U.S. Department of Education grants H133P080005 and H133E100007. The authors would like to thank Dr. Sergey Tarima for his assistance with the statistical analysis.

EFFECT OF THE FOOT TOE-OUT ANGLE ON THE KNEE ADDUCTION MOMENT DURING WALKING AND RUNNING

[1]Cristina Porto Alves Alcantara, [1]Raquel Castanharo and [2]Marcos Duarte

[1]University of Sao Paulo, Sao Paulo, SP, Brazil
[2]University Federal of ABC, Sao Paulo, SP, Brazil
email: cristina.alcantara@usp.br

INTRODUCTION

Several studies have demonstrated that the magnitude of the toe-out angle is inversely associated with the external knee adductor moment during the late-stance phase of walking [1-7]. In simple terms, presumably an increased toe out angle would lead the moment arm of the ground reaction force to be located closer to the knee joint center during the later part of stance and would thus result in a lower adduction moment [4,5]. It has been hypothesized that increasing the toe-out angle would then be a strategy to decrease the pressure on the medial compartment of the knee adopted by persons with osteoarthritis [2, 5].
To our knowledge, this relationship between toe-out angle and knee adduction moment has been observed only for walking and in this work we sought to verify whether a similar relationship is also observed during running.

METHODS

We analyzed nine healthy young adults (4 males and 5 females), with the following age, mass and height (mean ± standard deviation): 30±5 years, 62±9 Kg and 1.66±0.11 cm, respectively. The subjects performed two tasks (walking and running) at three different conditions (normal and with a self selected feet rotated externally (toe-out) or rotated internally (toe-in)). Each condition was executed 10 times along an 8m runway at a self-selected speed. All the subjects gave informed consent. We collected three-dimensional (3D) surface marker data using the Cleveland Clinic marker set at 150Hz with an eight-camera video-based motion analysis system (Motion Analysis Corporation, Santa Rosa, CA). Ground reaction forces and torques were measured at 600Hz by one force plate (Advanced Mechanical Technology, Inc). The raw kinematic and kinetic data were filtered using a low-pass Butterworth filter with a cutoff frequency of 6Hz and 100Hz respectively. We analyzed only the data for the right lower limb.
The data were analyzed with the Visual 3D software. The external moments were calculated in the frontal plane and normalized to each subject's body weight. The toe-out angle of each leg was computed as the angle formed by the intersection of the long axis of the foot and the direction of forward progression at the horizontal plane [2,7]. We analyzed the first and second peaks of the external knee adduction moment in the frontal plane during the stance phase of walk and the single peak during the stance phase of running.
Normality of the data was verified with Shapiro-Wilk test. Two-tailed paired t-tests were used to compare the different conditions, with Bonferroni correction for multiple comparisons. A significance level of 0.05 was used for all statistical tests.

RESULTS AND DISCUSSION

The three conditions had significant differences in the toe-out angle (normal foot, toe-out and toe-in) during the first and second knee adduction moment peak of walking and the single peak of running.
During walking, t-test revealed differences between the knee adduction moment values for all conditions for the first peak: normal foot/toe-out $t(5)=4.5$, $p<0.05$; normal foot/toe-in $t(8)=-10.8$, $p<0.05$; toe-in/toe-out $t(5)=11.1$, $p<0.05$ and just between normal foot and toe-out for the second peak $t(5)=-4.4$, $p<0.05$ ($p<0.05$). During running, no differences were observed.

The mean (±SD) of knee adduction moment peaks in the three conditions are shown in table 1 and are consistent with the literature [8,9].

The differences found in the second knee adduction moment peak between the normal and the toe-out conditions is confirmed by other studies [1, 4-7]. However, the relationship noted between the greater degree of toe-out angle and the peak knee adduction moment during early stance of the gait is still unclear in the literature. Lin et al. [6] found that this first peak increased when healthy teenagers walked with a 30° increase in their foot progression angle. On the other hand, Guo et al. [4] did not observe a similar effect when their subjects walked with a 15° increased in the toe-out angle, but these last authors concluded that is not possible to affirm if the different findings of their study and those of Lin et al. was due to subjects walking with different amounts of toe-out or because they were distinctly different populations.

In addition, the toe-in condition, that is not commonly tested in other studies, showed a significant difference in the first peak knee adduction moment during gait, but didn't appear to cause these differences during running and in the second knee adduction moment peak. Nevertheless, Fregly [10] noted that the decreased toe-out angle during gait had the most influence on the first peak (4 to 8% additional reductions) but increased the second one (0 to 3%). In contrast, increased toe out angle had the most influence on the second peak (5 to 9% additional reductions) while simultaneously decreasing the first one (0 to 4%).

The external knee adduction moment during walking exhibits two peaks during stance phase. The first peak is generally larger than the second, and it is highly correlated with increased disease severity, pain and rate of disease progression [11], as in individuals with medial compartment osteoarthritis [5] and meniscal lesions [3].

Recently, Walter et al. [11] studied an individual with a force-measuring knee implant and their findings suggest that reducing the peak external knee adduction moment does not necessarily guarantee a corresponding decrease in the medial-compartment contact force. Walter et al. showed that gait modifications can significantly reduce both peaks of the external knee adduction moment curve without producing corresponding significant reductions of the medial-compartment contact force. However, these results were obtained from one single subject and this issue is still under debate.

REFERENCES

1. Andrews M, et al. *Journal of Orthopaedic Research,* **14**, 289-295, 1996
2. Chang A, et al. *Ann Rheum Dis*, **66**, 1271-1275, 2007.
3. Davis-Tuck ML, et al. *Arthritis research & Therapy*, **10**, R58-R64, 2008.
4. Fregly BJ. *IEEE Trans Biomed Eng,* **55**, 2104-2106, 2008.
5. Guo M, et al. *Gait and Posture*, **26**, 436-441, 2007.
6. Hurwitz DE, et al. *Journal of Orthopaedic Research*, **20**, 101-107, 2002.
7. Teichtahl AJ, et al. *Journal of Science and Medicine in Sport,* **9**, 67-71, 2006.
8. Ferber R, et al. *Clinical Biomechanics*, **18**, 350-357, 2003.
9. Heiden TL, et al. *Clinical Biomechanics*, **24**, 833-841, 2009.
10. Lin C, et al. *Gait and Posture*, **14**, 85-91, 2001.
11. Walter JP, et al. *Journal of Orthopaedic Research,* **October**, 1348-1354, 2010.

ACKNOWLEDGEMENTS

The authors acknowledge funding from FAPESP.

Table 1: Mean (±SD) of knee adduction moment peaks and toe-out angles in the three conditions studied: normal, toe-out and toe-in during walking and running.

		Normal	Toe-out	Toe-in
Knee adduction moment (Nm/kg)	Walking – first peak	-0.32±0.13	-0.39±0.15	-0.14±0.12
	Walking – second peak	-0.31±0.05	-0.11±0.15	-0.39±0.15
	Running	-0.36±0.18	-0.39±0.26	-0.20±0.17
Toe-out Angle (°)	Walking – first peak	5.6±2.0	28.5±4.9	-13.5±9.2
	Walking – second peak	5.3±3.7	29.4±4.5	-14.1±10.7
	Running	13.0±10.5	30.7±6.6	-11.0±9.2

THE EFFECT OF A NEW MICRPROCESSOR CONTROLLED PROSTHETIC KNEE ON STAIR ASCENT STRATEGIES IN PATIENTS WITH UNILATERAL TRANSFEMORAL AMPUTATION

Jennifer M. Aldridge[1], Erik J. Wolf[2], Charles R. Scoville[2], and Jason M. Wilken[1]

[1]Department of Orthopaedics and Rehabilitation, Center for the Intrepid, Brooke Army Medical Center, Ft. Sam Houston, TX

[2]Department of Orthopaedics and Rehabilitation, Walter Reed National Military Medical Center, Bethesda, MD

email: Jennifer.Aldridge@us.army.mil

INTRODUCTION

Stair ambulation is a common activity of daily living, and is affected by lower limb amputation. Persons with transfemoral (above the knee) amputation commonly adopt a step-to-step strategy in which the intact limb is placed on the step and the prosthetic limb is then lifted to the same stair to account for the loss of knee joint function [1].

Some prosthetic users are able to ascend stairs in a step-over-step manner without the use of either a handrail or an intelligent prosthetic knee [2]. A step-over-step strategy can be accomplished by rapidly extending the hip and knee on the leading prosthetic limb, while the trailing intact ankle and knee are plantarflexed and extended. Hip extensor torque is used to rapidly extend the knee and prevent buckling as weight is transferred onto the limb. This method, however, is not easily accomplished by the majority of persons with transfemoral amputation.

A new microprocessor controlled prosthetic knee (X2, Ottobock, Duderstadt, Germany) was recently developed to allow patients with trans-femoral amputation to ascend stairs using a step-over-step technique without the use of rails. The X2 knee uses activity recognition and variable extension and flexion resistance to allow the prosthesis user to ascend stairs in a step-over-step manner.

The purpose of this study was to compare the self-selected stair ascent strategy and biomechanics of step-over-step stair ascent between the X2 knee and a conventional knee in persons with unilateral transfemoral amputation.

METHODS

11 male young adults with unilateral transfemoral amputation participated in the study. Participants were assessed 1) wearing their clinically prescribed prosthetic knee (CONV), and 2) wearing the X2. The two visits were separated by approximately 12 weeks and identical biomechanical testing was conducted during each visit.

Participants were instrumented with 57 reflective markers. A 26 camera optoelectronic motion capture system (120 Hz; Motion Analysis, Santa Rosa, CA) was used to track full-body movement. Ground reaction force data were collected using an “interlaced stairway” design (1200 Hz; AMTI Inc, Watertown, MA) that allowed for instrumentation of four steps using two force plates [3].

Participants were asked to ascend the 16-step staircase using a self-selected speed and strategy and then at a controlled cadence of 80 steps per minute using a step-over-step strategy. For each stair condition a minimum of five good force plate strikes were obtained for each limb.

A 2x2 repeated measures ANOVA (limb by device) was used to determine limb (prosthetic and intact) and device (CONV and X2) main effects for the step-over-step controlled cadence strategy. Pearson correlations were used to examine the association between hip moments and powers and resulting limb kinematics.

RESULTS AND DISCUSSION

While wearing the conventional knee, eight patients self-selected a step-to-step strategy, two a skip-step strategy, and one a step-over-step strategy. In contrast, while wearing the X2 device, one patient self-selected a step-to-step strategy, four a skip-step strategy, and six a step-over-step strategy. Nine patients were able to ascend the stairs in a step-over-step manner at the controlled cadence while using both their conventional knee and the X2. Only their data is included in the kinematic and kinetic analysis of stair ascent presented below.

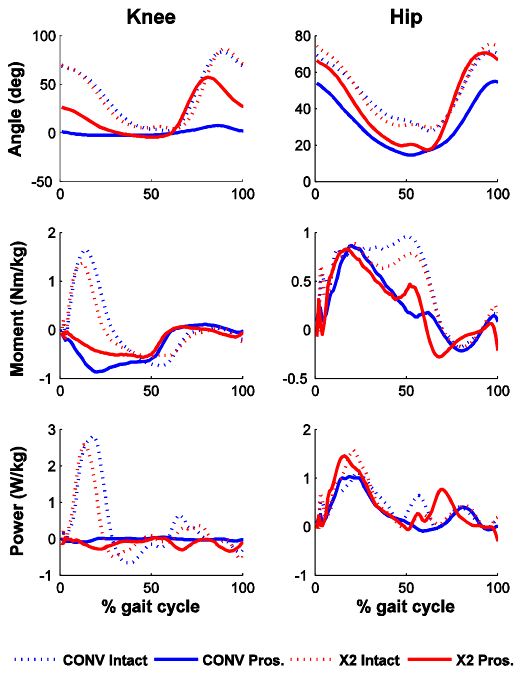

Figure 1: *Kinematics and kinetics of the knee and hip during stair ascent while using both CONV (blue) and X2 (red) knees for both the intact (dashed) and prosthetic limb (solid.)*

Patients had increased knee and hip flexion on the prosthetic limb at both heel strike and during swing ($p < 0.025$) while wearing the X2 compared to CONV (Figure 1, Table 1). The increase in knee and hip flexion during swing resulted in the restoration of between limb symmetry (Limb Effect: Knee - p = 0.089, Hip – p = 0.342). However, peak knee flexion during swing on the prosthetic limb was variable (SD 46°) indicating a large variation in stair ascent strategy. Additional analysis revealed a strong positive correlation between hip power generation during initial-swing and knee flexion during swing (Figure 2; $r^2 = 0.868$, $p < 0.001$). Greater hip power was associated with increased knee flexion. While wearing the X2 device patients had significantly greater hip power generation on their prosthetic side during initial-swing than with CONV ($p = 0.002$). It is likely that the added hip power aided in flexing the knee and pulling the leg through during swing.

CONCLUSIONS

In conclusion, the majority of patients self-selected a step-over-step method while using the X2 knee. The variable resistance of the knee allowed them to flex the knee during swing and initial contact. Increased hip power during initial-swing was used to initiate knee flexion during swing and place the foot on the next stair.

Further study is required to determine why specific individuals choose to initiate knee flexion, while others use a circumduction approach during step-over-step stair ascent. Potential factors include device specific training, balance confidence and joint specific muscle strength.

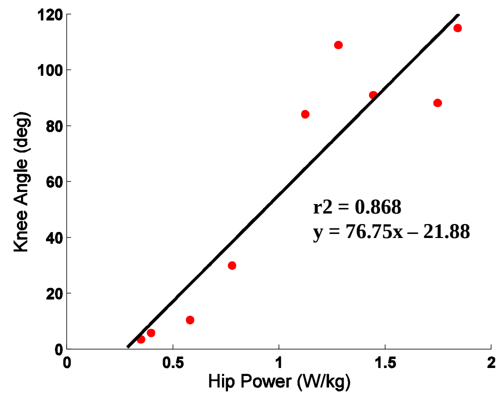

Figure 2: *The correlation between hip power during initial swing and knee flexion during swing. The positive correlation represents that greater hip power is associated with greater knee flexion.*

	CONV	X2
Knee Flex - IC (deg)	1.2 (3.5)	26.3 (25.3)
Knee Flex - SW (deg)	6.4 (3.3)	59.6 (46.4)
Hip Flex - IC (deg)	53.9 (3.0)	66.2 (11.6)
Hip Flex - SW (deg)	54.7 (2.6)	72.4 (14.3)
Hip Power - SW (W/kg)	0.48 (0.2)	1.06 (0.6)

Table 1: *Mean (SD) peak kinematic and kinetic values of interest for the prosthetic limb. (IC-Initial contact, SW – Swing)*

REFERENCES

1.Hafner BJ et al., *Arch. Phys. Med. Rehabil.* **88**, 2007.
2.Hobara H et al., *Prosthet. Orthot. Int.* **35**, 2011.
3.Sinitski EH et al., *J. Biomech.* **45**, 2012.

ACKNOWLEDGEMENTS

Support provided by the U.S. Army Telemedicine & Advanced Technology Research Center.

GAIT COMPENSATIONS IN A RAT MEDIAL MENISCUS TRANSECTION MODEL OF KNEE OSTEOARTHRITIS

[1]Kyle D. Allen, [2]Brian A. Mata, [2]Mostafa A. Gabr, [2]Janet L. Heubner, [2]Virginia B. Kraus, and [2]Lori A. Setton

[1] University of Florida, Gainesville, FL, USA
[2] Duke University and Duke University Medical Center, Durham, NC, USA
email: kyle.allen@bme.ufle.edu

INTRODUCTION

Osteoarthritis (OA) results in cartilage loss, bone remodeling, and up-regulation of inflammatory and catabolic mediators within a joint[1]. Despite a complex etiology, OA ultimately leads to pain and disability. Clinically, OA is diagnosed through physical exams and radiographs; however, OA assessments in the preclinical model focus on joint histology[2]. Behavioral analyses can be used to describe some symptomatic consequences of OA in the preclinical model[3-5]; however, these assays can have high variability and limited translation to the patient condition. Gait assessment provides a tool to evaluate the consequences of OA in both the preclinical model and the patient[6]. The objective of this study is to evaluate gait compensations, weight distribution imbalance, and limb sensitivity in a rat model post-traumatic OA.

METHODS

A medial collateral ligament transection (MCL sham, n=6) or a MCL and medial meniscus transection (MMT, n=6)[4-5,7] was performed in male Lewis rats (200-250g); 4 additional rats received neither anesthesia nor surgery (naïve, n=4). Weight bearing, limb sensitivity, and gait were evaluated on post-operative day 9, 16, and 23. Weight bearing was assessed on an scale that records left-right weight distribution during rearing (incapacitance meter, IITC, Inc)[3]. Paw withdrawal thresholds were evaluated using von Frey filaments (Stoelting)[8]. Spatiotemporal gait data were collected by manual digitization of five high-speed videos of each rat at each time point (200 fps, Phantom V4.2)[6]. Similarly, 3-component ground reaction forces were obtained on a Hall-effect force transducer (AMTI) for each rat at each time point[9]. On day 28, serum and knees were collected. Cytokine activity in the serum was assessed with a 10-plex cytokine panel (Invitrogen). Knees were sectioned, stained, and graded with the OARSI histopathology scheme[10]. Two-way analysis of variance or two-way generalized linear models that included a linear dependence on trial velocity were used to detect differences between groups.

RESULTS AND DISCUSSION

Gait cycles became progressively asymmetric in the MMT group (Fig. 1, top), indicating syncopations in the foot-strike sequence. Moreover, left and right limb stance time (ST) tended to be imbalanced in MMT rats (Fig. 1, bottom), indicating that MMT rats spent less time on their operated limb while walking. Differences in stride length, step width, and stride frequency were not observed.

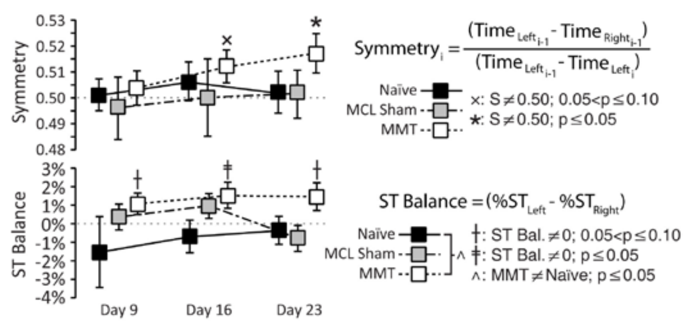

Figure 1: Temporal Gait Changes in MMT Rats

Ground reaction forces aligned with spatiotemporal changes. Peak vertical force and impulse were decreased in the operated limb of MMT rats (Fig. 2). Moreover, peak vertical force in the operated limb of MMT animals was lower than naïve controls (p=0.004) and vertical impulse in the operated limb of MMT animals was lower than MCL sham and naïve controls (p<0.02). Propulsive forces, but not braking forces, were altered in the hind limbs of MMT rats (p<0.05, not shown). Mediolateral forces did not vary amongst groups.

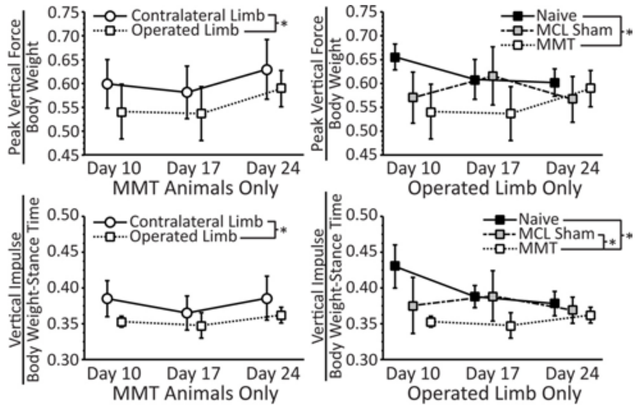

Fig 2. Shifts in Vertical Ground Reaction Forces resulting from MMT Surgery (*; p< 0.05, main effect)

While gait data revealed limb compensations, imbalanced weight distribution was not observed on the incapacitance meter. This incongruity is likely due to differences between tests; incapacitance meters measure weight distribution during rearing, while ground reaction forces measure limb use during locomotion.

MMT and MCL animals had heightened sensitivity (lower thresholds) in their operated limb relative to their contralateral limb ($p<0.05$) and tended to be more sensitive than naïve controls ($p=0.056$), indicating limb sensitivity can occur with both MCL and meniscal injuries in rats.

Rats with the MMT surgery had severe lesions on the medial tibial plateau (Fig 3), ranking as either OARSI grade 4 or 5 (erosion or denudation). Severe lesions were not observed in MCL sham, naïve, or within the contralateral limb of MMT rats.

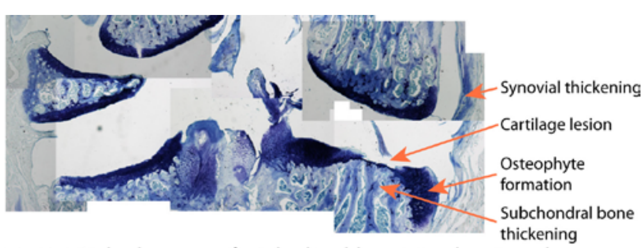

Fig. 3: Stitched images of a toluidine blue-stained section shows cartilage lesions, osteophyte formation, synovial thickening, and subchondral bone thickening in the rat MMT model at 4 weeks.

Serum cytokine concentrations were not different, though serum IL6 in MMT rats did tend to be higher than that of naïve controls ($p=0.072$, Fig 4).

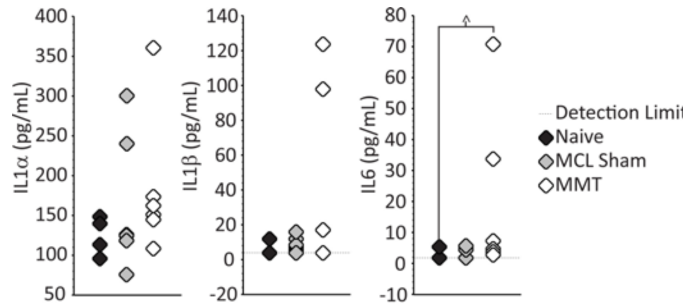

Fig 4: Serum Level Concentrations of IL1α, IL1β, and IL6 in MMT Rats

CONCLUSIONS

To our knowledge, this is the first study to describe gait compensations in the rat MMT model of OA. The data reported herein indicate that gait analyses are sensitive to knee joint remodeling. In particular, gait parameters yielded more robust comparisons of the affected and contralateral limb than the incapacitance meter. Moreover, gait symmetry demonstrated a tendency to increase as OA progressed; no other parameter, including established assays of limb sensitivity and weight-bearing, demonstrated this potential. Future work will focus on correlating joint degeneration, sera biomarkers, and behavioral assessments in this rat model of knee OA.

REFERENCES

[1]Buckwalter, IOS Press; 2007; [2]Bendele, J Musculoskelet Neuronal Interact 2001; [3]Bove, OA Cart 2003; [4]Bove, OA Cart 2004, [5]Fernihough, Pain 2004; [6]Allen, Tissue Eng Part B Rev 2010; [7]Janusz, OA Cart 2002; [8]Chaplan, J Neurosci Methods 1994; [9]Zumalt, J Biomech 2006; [10]Pritzker, OA Cart 2006;

ACKNOWLEDGEMENTS

This work was supported by NIH/NIAMS funding (P01AR050245, K99AR057426, R00AR057426)

	Naïve		*MCL Sham*		MMT	
	Left	Right	*Left*	*Right*	Left	Right
Day 9	17.4 ± 2.2	19.7 ± 3.4	*20.1 ± 4.8*	*14.3 ± 2.7*	17.8 ± 2.3	10.4 ± 2.7
Day 16	13.6 ± 3.2	11.8 ± 2.4	*12.3 ± 1.7*	*14.9 ± 2.0*	16.6 ± 4.4	13.6 ± 4.9
Day 23	12.5 ± 0.6	23.3 ± 6.7	*19.7 ± 4.1*	*8.3 ± 2.5*	22.8 ± 4.6	10.4 ± 1.9

Table 1: Paw Withdrawal Thresholds in MMT Rats

THE INFLUENCE OF MERGED MUSCLE EXCITATION MODULES ON POST-STROKE HEMIPARETIC WALKING PERFORMANCE

[1]Jessica L. Allen, [2]Steven A. Kautz and [1]Richard R. Neptune

[1]The University of Texas at Austin, TX, USA
[2]Medical University of South Carolina, Charleston, SC, USA
email: jessica.allen@utexas.edu, web: http://me.utexas.edu/~neptune

INTRODUCTION

A recent study found that muscle excitation patterns during non-impaired walking can be explained by a combination of four muscle excitation modules: (1) an *early stance* module with hip abductor and knee extensor activity, (2) a *late stance* module with plantarflexor activity, (3) an *early swing* module with dorsiflexor and biarticular knee extensor activity and (4) a *late swing and early stance* module with hamstrings activity [1]. However, many post-stroke hemiparetic subjects exhibit altered muscle excitation patterns due to their inability to independently activate these four modules. These subjects often utilize a reduced number of modules, with at least one module resembling a merging of multiple non-impaired modules [1]. Within those subjects who could independently activate three modules, two distinct types of modular organizations were found. The first group (Group A) appeared to merge non-impaired modules 1 and 2, with a prolonged stance module composed of plantarflexor, hip abductor and knee extensor activity. A second group (Group B) appeared to merge non-impaired modules 1 and 4, with a prolonged stance module composed of hip abductor, knee extensor and hamstring activity.

Previous modeling and simulation analyses have found that each non-impaired module has a distinct contribution to body support, forward propulsion and/or mediolateral (ML) acceleration [2, 3]. Merging any of these modules may adversely affect the generation of these subtasks and impair walking performance. The purpose of this study was to develop forward dynamics simulations of walking for hemiparetic (Groups A and B) and non-impaired control subjects to identify the influence of merged modules on post-stroke hemiparetic walking performance.

METHODS

Experimental kinematics, ground reaction forces (GRFs) and electromyography (EMG) were collected from 11 post-stroke hemiparetic and 14 non-impaired control subjects. Group average kinematic and GRF tracking data were generated for the hemiparetic (Group A, n=7; Group B, n=4) and control (n=14) subjects. Forward dynamics simulations of walking were then generated using a 3D musculoskeletal model (SIMM, MusculoGraphics, Inc.) and a simulated annealing algorithm that optimized the module-based excitation patterns to replicate the above experimental data [3]. Modules were previously identified from the EMG using a non-negative matrix factorization algorithm [1]. These module patterns were used to excite the muscles identified in each module, where each muscle received the same excitation timing while the magnitude was allowed to vary. All remaining muscles not associated with a module received a bimodal excitation pattern. The influence of the merged modules on walking performance was assessed by quantifying the potential of muscles within each module to contribute to the anterior-posterior (AP), vertical and ML GRFs using a perturbation analysis. First, muscle forces were perturbed 1N and a muscle's per unit force contribution was taken as the difference between the unperturbed and perturbed GRFs. Then, per unit force contributions were scaled by each muscle's respective module timing pattern.

RESULTS AND DISCUSSION

A consequence of merging non-impaired modules 1 and 2 in Group A was a reduced ability to generate forward propulsion (compare Fig. 1a and 1c, top and middle panels). This merged module excited soleus and gastrocnemius (SOL+GAS) earlier while gluteus medius (GMED), rectus femoris and vasti (RF+VAS) excitation was extended later into stance (Fig. 1d, top panel). Each of these muscles normally contributes to braking in early stance, and therefore the prolonged excitation increased overall braking. In addition, while the plantarflexors were a primary source for forward propulsion during late stance in the control simulation, they had minimal contributions to propulsion, likely due to differences in body segment kinematics. This is consistent with experimental data showing Group A had decreased paretic leg propulsion [1].

Conversely, when modules 1 and 4 were merged in Group B (Fig. 1d, bottom panel), only minimal differences existed in contributions to forward propulsion. Instead, body support and ML acceleration were altered (compare Fig. 1b and 1c, middle and bottom panels). In the control simulation, HAM contributed minimally to body support except during early stance. In Group B, however, HAM contributed negatively to body support (due to flexing the knee more than extending the hip). In addition, HAM's lateral acceleration was prolonged later in stance, opposing GMED's medial acceleration (Fig. 1b, bottom panel). While the actual magnitude of these contributions depends on the level each muscle is recruited by the merged module, these results highlight the potential for compromised body support and ML acceleration in the Group B subjects with merged modules 1 and 4.

This study highlights how altered coordination in hemiparetic subjects can influence walking performance and that the merging of specific modules has different functional consequences. Merging modules 1 and 2 resulted in poor forward propulsion while merging modules 1 and 4 influenced the generation of body support and ML acceleration. Future study is needed to examine module contributions to leg swing and power transfer among body segments, which are additional subtasks that are important in walking.

REFERENCES

1. Clark DJ, et al., *J Neurophysiol*. **103**, 884-57, 2010.
2. Neptune RR, et al., *J Biomech*. **42**, 1282-7, 2009.
3. Allen JL, et al., *Proceedings of ASB'11*, Long Beach, CA, USA, 2011

ACKNOWLEDGEMENTS

This work was supported by NIH Grant R01 HD46820 and the NSF GRFP. The contents are solely the responsibility of the authors and do not necessarily represent the official views of the NIH, NICHD or NSF.

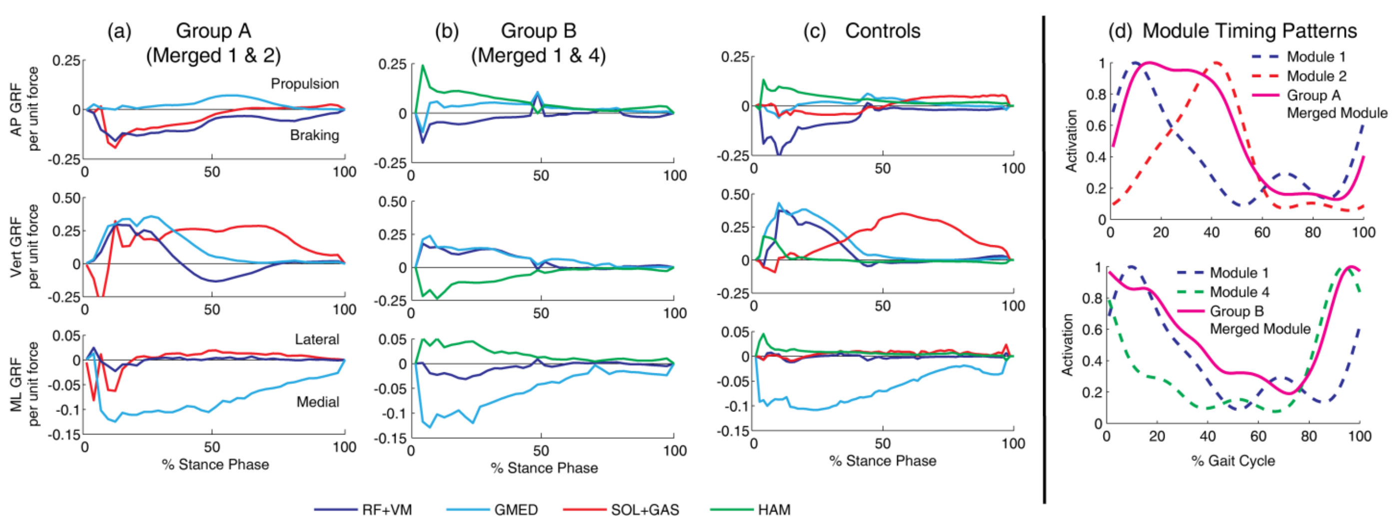

Figure 1: Per-unit-force muscle contributions (scaled by module excitation timing patterns) to forward propulsion (AP GRF), body support (Vert GRF) and ML acceleration (ML GRF) from (a) merged modules 1 and 2 in Group A, (b) merged modules 1 and 4 in Group B and (c) non-impaired Module 1 (RF+VM and GMED), Module 2 (SOL+GAS) and Module 4 (HAM). (d) Module timing patterns for merged modules in Group A (top panel) and Group B (bottom panel) compared to non-impaired module timings.

COMPARISON OF TIBIAL STRAINS AND STRAIN RATES IN BAREFOOT AND SHOD RUNNING

[1]Allison R. Altman, [2]Irene S. Davis

[1]Biomechanics & Movement Science, University of Delaware, Newark, DE, USA
[2]Spaulding National Running Center, Harvard Medical School, Cambridge, MA, USA
email: aaltman@udel.edu

INTRODUCTION

Runners with high impact loading have an increased risk for tibial stress fractures.[1] Stress fractures are one of the most serious running injuries. The risk of re-injury in this population can be especially problematic, since those who obtain a stress fracture are more likely to incur another.[2] However, converting from a rearfoot strike pattern to a forefoot or midfoot strike pattern reduces impact loading.[3] Barefoot runners, tend to adopt a forefoot strike pattern, which attenuates the impacts from landing, thus reducing their impact loading.[4] Anecdotal evidence suggests that barefoot runners sustain fewer injuries than shod runners, and a recent study concluded that forefoot strikers sustain fewer and less severe injuries than rearfoot strikers.[5]

However, it is unclear what affect these global reductions in impact loading have on the tibial bone tissue. The purpose of this study was to examine changes in tibial strains and strain rates between a shod rearfoot strike pattern, a shod forefoot strike pattern and barefoot running. We hypothesized that the peak strains and strain rates would be highest in rearfoot striking and similar in forefoot and barefoot conditions.

METHODS

Five healthy runners (2M, 3F, aged 22.8 (2.2) yrs) have been recruited to date. All were rearfoot strikers and ran 23.6 (15.6) mpw.

Each runner underwent a standard motion analysis data collection session. Shod rearfoot striking, shod forefoot striking, and barefoot running were collected during overground running at 3.5 m/s. Leg and torso kinematic data were sampled at 240 Hz. Ground reaction force, along with EMG data from the ankle plantar and dorsiflexors were sampled at 1200 Hz. Five trials were collected for each of the 3 conditions, and the trial which best represented the mean was used for analysis.

3D kinematics were calculated using inverse kinematics in Visual 3D (C-Motion, Rockville, MD), and exported into OpenSim (Simtk, Stanford, CA). Within OpenSim, the subject and segments were scaled according to the subject mass. Reduced residual analysis and computed muscle control were then used to calculate optimized kinematics and muscle forces used to drive the motion. Finally, the ankle joint contact force was calculated by combining the contributions from the ground reaction force and the muscle forces crossing the ankle joint.

A CT scan of the tibia of each subject's dominant limb was performed at Omega Imaging (Diagnostic Imaging Associates, Newark, DE). The tibia was extracted from the images using Mimics (Materialise, Leuven, Belgium) software to separate the bone from the surrounding tissues. A 3D mesh was generated using 8-node hexahedral elements. The elastic modulus was calculated for each voxel in the CT scan using relationships between Hounsfield units, bone density, and elastic modulus and applied to the respective elements in the mesh.[6]

This subject specific tibia mesh was imported into Abaqus (3DS Simula, Velizy, France) software for finite element analysis. Here, the joint contact force was applied to the center of the distal end of the tibia. A static step type analysis was used to ramp the joint contact force in the same pattern used during the first 50% of stance for each subject. The maximum and minimum principal strains were extracted from the midshaft region of the tibia for analysis. Peak and average strains and strain rates were analyzed descriptively due to the small sample size.

RESULTS AND DISCUSSION

The tensile and compressive strains were similar between the three conditions (Figures 1 & 2). The peak tended to occur around 50% of stance, reflecting the point where the joint contact force is highest. While peak strain can ultimately cause bone to fail at high magnitudes, it is also possible that the repeated high strain rates observed in running cause microfractures, which ultimately lead to stress fractures.[7]

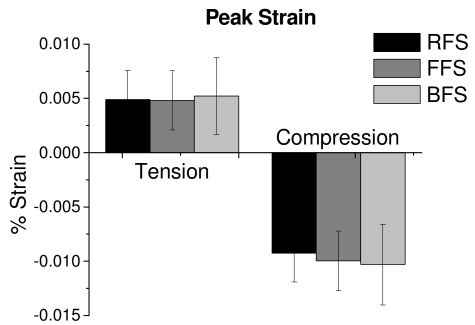

Figure 1: Peak strain shown for the rearfoot (RFS), forefoot (FFS) and barefoot (BFS) conditions in both tension and compression.

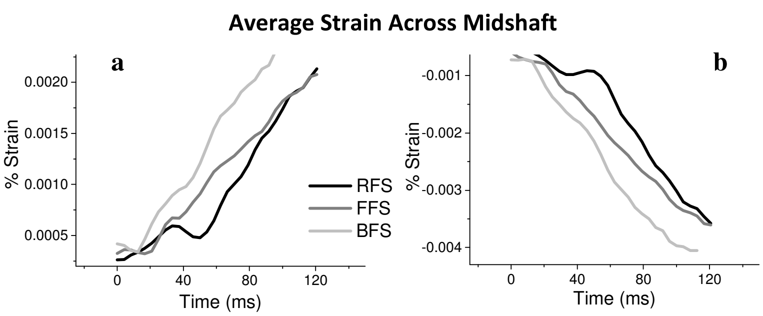

Figure 2: Average tensile (a) or compressive (b) strain from the all elements in the midshaft for a representative subject.

Strain rate was highest in the forefoot strike condition in both tension and compression (Figure 3). We expected the strain rate to be highest in the rearfoot strike condition due to the local maxima observed around the impact peak of the vertical ground reaction force (Figure 2). However, it is plausible that the increased strain seen in the forefoot strike may be a result of muscular contraction (Figure 4). The plantarflexors were producing more force in this condition, possibly to keep the heel raised. Compared to barefoot, participants are forced into a greater plantarflexed position in the shod forefoot condition due to the elevation of the cushioned heel. On average the plantarflexion angle at footstrike was 10.5° for the forefoot and 5.7° for the barefoot condition. This reduction was seen in all 5 subjects.

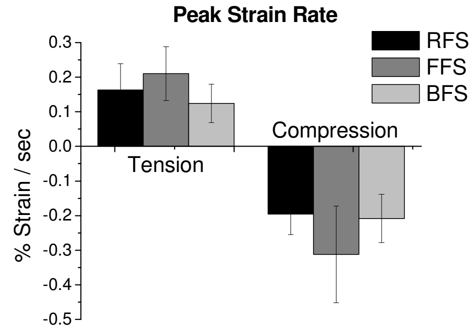

Figure 3: Peak strain rate for all conditions in both tension and compression.

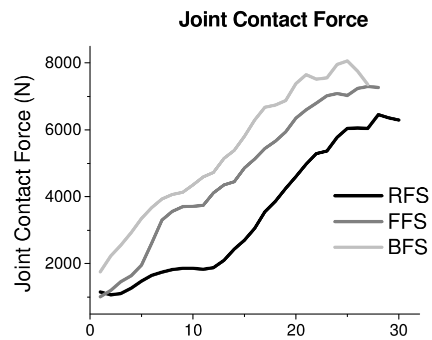

Figure 4: Joint contact forces for the first 50% of stance for all three conditions for a representative subject.

CONCLUSIONS

While peak strains were similar between conditions, strain rates were highest in the forefoot condition due to muscular contributions. It may be that barefoot running requires less muscle force than the shod forefoot condition due to the lower inclination angle of the foot at footstrike.

REFERENCES

1. Milner CE et al. *MSSE* **38(2)**, 323-328, 2006.
2. Almeida SA et al. *MSSE* **31(8)**, 1176-1182, 1999.
3. Altman AR, et al. *ASB'09,* State College, PA, USA, 2009.
4. Lieberman DE, et al. *Nature* **463**, 531-535, 2010.
5. Daoud AI et al. *MSSE* **epub**, 2012.
6. Austman *J Biomech* **41(15)**, 3171-3176, 2008.
7. Kulin et al., *J Mech Behav Biomed Mater* **4** 57-75, 2011.

ACKNOWLEDGEMENTS

Work supported by the ASB Student Grant-in-Aid

THE RELATIONSHIP BETWEEN STRUCTURUAL AND SPATIAL VARIABILITY OF POSTURAL CONTROL IN PERSONS WITH PARKINSON DISEASE.

Shinichi Amano, Elizabeth Stegemöller, Lori Altmann and Chris J. Hass

University of Florida, Gainesville, FL, USA
email: samano@ufl.edu

INTRODUCTION

Computerized posturography has been widely used in the laboratory setting to evaluate postural stability. To date, various outcome measures have been proposed and used, including the mean velocity of center of pressure (COP) and postural sway area, to evaluate postural stability in healthy adults and various pathological populations. However, these measures are summary statistics of COP movement and are not time-dependent. Given that postural stability must be maintained continuously in time-series, these summary statistics might not be sufficient to fully quantify and understand postural control abilities. Moreover, there is contradicting evidence regarding postural stability in persons with Parkinson disease (PD). Specifically, some previous studies stated that persons with PD exhibited more pronounced postural sway than age-matched healthy individuals, while the other studies have reported that persons with PD exhibit less variability, indicating postural inflexibility in persons with PD [1]. Thus, The time-dependent measures may give further insight into how persons with PD control posture. Recently, approximate entropy (ApEn) and Time-To-Boundary (TTB) have been used to assess subtle changes in postural stability across age and disease. Briefly, ApEn is the regularity statistic representing the complexity of a time-series physiological signal [2]. TTB, which is derived from instantaneous velocity and acceleration, predicts the time it would virtually take the COP to reach the limits of the base of support (BOS) [3]. Lower TTB measures are associated with greater postural instability.

To date, there is a lack of research evaluating how both spatial and time-dependent measures may be related with each other in persons with PD. Thus, the purpose of this study is to examine the relationship among summary, regularity, and frequency-related statistics during quiet standing in persons with PD.

METHODS

Twenty-nine people with idiopathic PD (mean age: 65.1±2.0 years, height: 164.7±6.0cm, mass: 77.3±3.4 kg) participated in this study. A written informed consent was obtained from each participant prior to participation. During testing, each participant was asked to stand as still as possible for 60 seconds on a force platform with their feet 10cm apart. The ground reaction forces under the feet were collected at 360Hz and low-pass filtered at 12.5 Hz using a second-order Butterworth filter. COP velocity (COPVEL), 95% confidence ellipse (Area95), ApEn and mean peak TTB ($pTTB_{mean}$) in both anteroposterior (AP) and mediolateral (ML) directions were calculated using the time-series COP data. The algorithms for these calculations were based on the previous literature [3,4]. To obtain 95% frequency range (95%FREQ), the raw time-series COP data was detrended, multiplied by a Hanning window, and then transformed to the frequency domain using a discrete Fourier Transformation (DFT) method. The power spectrum was then normalized so that the total power from 0 to 12.5 Hz was equal to 1. All dependent measures were computed using customized MATLAB software (The MathWorks, Inc, Natick, MA). Each participant completed three consecutive trials and all dependent measures were first computed for each trial and then averaged across trials. A Pearson correlation analysis was conducted to assess relationships among the dependent measures. The level of significance was set at α=0.05.

RESULTS

Area95 was not significantly related to any other dependent measures except COPVEL (r=0.53, *p*<.05). ApEn and TTB measure were significantly related. Specifically, ApEn in AP direction was negatively related to mean peak TTB in both directions ($pTTB_{mean}$-AP: r=-.67 and $pTTB_{mean}$-ML: r=-.48, both *p*<.05). The same pattern was also found in ApEn in ML direction ($pTTB_{mean}$ -AP: r=-.59 and $pTTB_{mean}$-ML: r=-.65, both *p*<.05). As for the relationship between ApEn and the frequency component, ApEn in ML direction was positively related to 95%FREQ only on ML direction (r=.79, both *p*<.05), while ApEn in AP direction was positively related to 95%FREQ on both directions (AP: r=.66, ML: r=.68, all *p*<.05). The $pTTB_{mean}$ on each direction was related to each other (r=.78, *p*<.05), but they were negatively correlated only with 95%FREQ in ML direction ($pTTB_{mean}$-AP: r=-.55, $pTTB_{mean}$-ML: r=-.56, both *p*<0.05), not in AP direction. The COPVEL was significantly related to both ApEn (AP: r=.47, ML: r=.51, both *p*<.05) and $pTTB_{mean}$ (AP: r=-.74, ML: r=.48, both *p*<.05) in both directions but not to frequency components.

DISCUSSION

The present study demonstrated that spatial measure (Area95) was not significantly related to any of the outcome measures, except COPVEL. This finding may be expected since Area95 only represents the magnitude of postural variability, and the other dependent measures (i.e., ApEn, TTB, 95%FREQ) assess the structure of its variability, which is indicative of time-dependent postural dynamics. Although sway magnitude has been widely used to evaluate postural control, our results indicate that evaluating only “magnitude” of postural fluctuation cannot fully capture an individual’s postural control ability. Indeed, some participants with PD who exhibited a small magnitude of COP (i.e., small Area95) swayed at higher frequency range and/or manifested lower $pTTB_{mean}$. Previous literature suggested that postural fluctuation at a higher frequency range is indicative of reliance on visual information and age-related balance deterioration [5]. It appears that our findings are contradicting, but may indicate postural inflexibility often observed in persons with PD, rather than good postural control ability.

The other intriguing finding is the positive relationship between ApEn and 95%FREQ. High ApEn values indicate lower regularity and high complexity of COP oscillation, and vice versa. Generally, reduction of afferent input leads to more predictable time-dependent postural dynamics, called the loss-of-complexity hypothesis [5,6]. However, we also found that our PD participants who manifested unpredictable (reduced regularity) COP oscillation tended to show COP patterns in the high frequency range. These conflicting results indicate that high ApEn may also be indicative of compromised postural abilities which may be a result of disease-related muscle co-contraction. High ApEn values may also be the consequence of high sway frequency that persons with PD chose to overcome their limitations, rather than the manifestation of high adaptability in postural control. The alternative explanation is that both parameters are measuring the same characteristic of postural control. Further investigations are needed to identify the relationship between complexity and frequency-related measures.

In conclusion, it is imperative to evaluate postural dynamics and instability from multiple perspectives, such as spatial magnitude, time-dependent structure, and frequency components of COP variability. Relying on only one aspect of postural control may be detrimental and may possibly lead to misinterpretation of true biological capabilities.

REFERENCES

1. Horak FB et al. *J Neurol Sci* **111-1**, 46-58, 1992.
2. Pincus SM. *Proc Natl Acad Sci*, **88**, 2297-2301, 1991.
3. Slobounov SM et al. *J Gerontol A Biol Sci Med Sci* **53A(1)**, B71-78, 1998
4. Rhea CK et al. *PLoS One*, **6(3)**, 2011
5. Maki BE et al. *J Gerontol*, **49(2)**, 72-84, 1994
6. Hong SL et al. *Neurosci Lett*, **423**, 104-108, 2007
7. Lipsitz LA et al. *J Am Med Assoc*, **267(13)**, 1806-1809, 1992

A PLLA FABRIC SYSTEM FOR PREVENTION OF HIP DISLOCATION

[1]Lonnie Andersen, [2]Guy M. Genin and [1]Povl Brøndsted

[1]DTU Wind Energy, Denmark
[2]Washington University in St Louis, MO, USA
email: loul@risoe.dtu.dk

INTRODUCTION

Early dislocation is a very common complication after total hip arthroplasty. In most Western countries between 0.5 and 1% of the population will require hip joint replacement surgery at some point, and of these approximately 3-5% will experience dislocation of the artificial hip during the approximately six month healing period following surgery [1]. The primary source of disclocations (60-70% over three months [2]) is instability associated with adduction beyond a critical level, as can occur, e.g., when exiting a car seat. The current standard of care is to instruct a patient to avoid such movements, or in certain cases to equip the patient with a hip dislocation brace. The objective of this study was design of an implantable, biocompatible, biodegradable device to guard against these dislocations. The strategy is to provide increased resistance to motion of the leg at distensions that approach those associated with dislocation and to provide a resistive and corrective force against extreme movements of the hip implant, without obstructing normal movement of the hip.

METHODS

A poly-L-lactic acid (PLLA) fabric in a conical shape was studied. The strategy was to attach the base of the cone with biodegradable staples around a modified acetabular cup, and the truncated tip around a modified femoral stem. The rationale for using PLLA is that PLLA is biocompatible and could be designed to retain its strength over the critical 6 month interval, then to biodegrade. The challenge addressed here was to design the fabric and the device to provide resistive and righting force over the desired range of motion.

Over the large range of motion associated with normal hip movement, the device should be highly compliant. Near the extreme of adduction at the end of this range, the device should engage with increased resistance. Beyond the critical point, the device should become stiff and simultaneously hold the hip implant in place. This critical point was defined by the angle between the femur and the pelvis, which should always be greater than 90° to ensure stability.

A 2D kinematic analysis was conducted to calculate the requisite shape of the strain versus angular displacement curve (Figure 1). The device in the neutral position (L0) contains a degree of slack that is drawn out after approximately 30° of adduction (L1). The device provides increasing resistance as it makes contact with the hip implant (L2). The device is then designed to lock in extreme flexion defined as approximately 90° from the neutral position (L3).

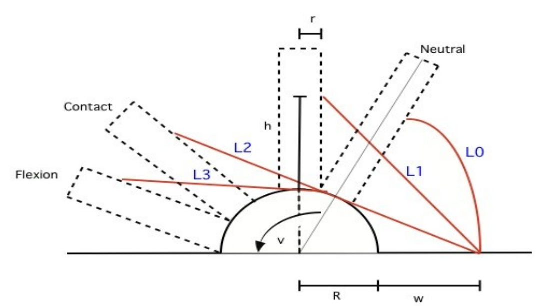

Figure 1: 2D model used of the hip implant (dashed lines corresponding to four different positions) and cross-section of the conical PLLA implant (red, shown in these same four positions) to determine the requisite character of the fabric material properties.

Uniaxial tensile tests were performed on PLLA yarns of the type under consideration, and it was determined that the shape of their stress-strain curves were inadequate to provide the specific range of motion required. Therefore, a fabric was considered as a means of modifying the mechanical response of the PLLA device structurally. A braided mesh fabric was investigated using a uniaxial tensile model developed by Kawabata, et al [3].

RESULTS AND DISCUSSION

The angle of distension versus nominal strain curve for the device was calculated using straightforward kinematic methods (Figure 2). This was used to identify the desired shape of the stress-strain curve for the PLLA fabric. The PLLA fabric requires a "toe region" with little resistance to deformation. In Figure 2 the dashed lines show the required toe-region using different mounting distances varying *h*, the height of the hip implant stem, and *w*, the width of the acetabular cup. Results show that to ensure normal hip movement the length of the toe region would have to be around 40% strain, and will depend on the mounting distances.

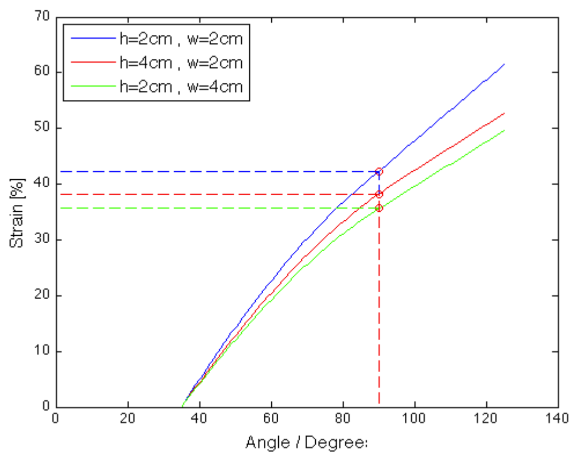

Figure 2: Strain versus angle used to determine the length requirement for the toe-region.

The stress-strain behavior of the PLLA yarns was inadequate on its own with a toe region of about 3% strain and a yield strain of about 5% (Figure 3). We therefore explored the design of a fabric constructed of these PLLA yarns.

The fabric model of Kawabata et al. [3] indicated that the yarns of Figure 3 could be woven into an orthogonal fabric with a toe region sufficiently large to meet the design requirements (Figure 4). The toe-region size was a strong function of the radii of fibers in the weft direction (loading direction, radius r_1) and warp direction (azimuthal direction of the cone, radius r_2). With a sufficiently large (>10) ratio of warp to weft diameter, a toe region of approximately 40% strain could be obtained. This would ensure normal hip movement, and establishes the feasibility of the approach. At yield, such a device less than 1mm thick could provide on the order of several hundred Newtons of restoring force, far more than adequate to resist dislocation [4].

While the basic feasibility is established by these calculations, testing is certainly required. Durability issues that the model of Kawabata et al. does not account for include effects of repeated loading and detailed analysis of the stresses of individual threads within yarns. Many more complicated fabric weaves exist that could overcome issues of this character should they arise, and to further tailor the device response.

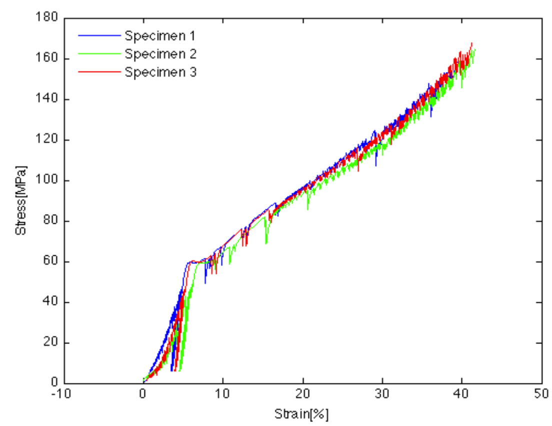

Figure 3: Measured stress versus strain response for a PLLA yarn.

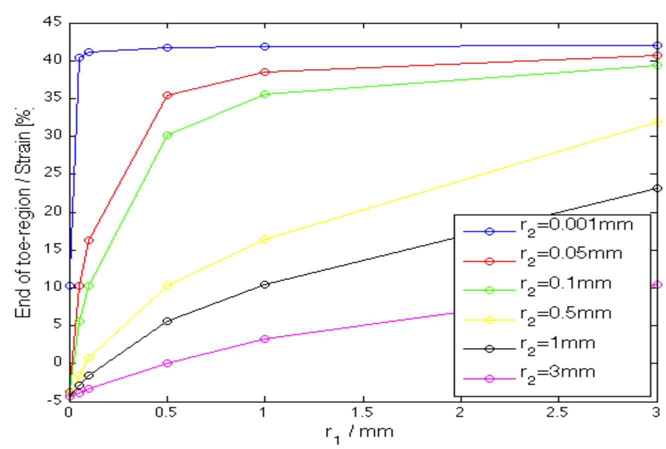

Figure 4: Toe-region obtained by using a simple braided structure with varying diameter of weft and warp yarns.

REFERENCES

1. Phillips CB, et al. *J Bone Joint Surg Am* **85,** 20-26, 2003.
2. Douglas AD. et al., *J Orth Surg,* 1998.
3. Kawabata S. et al. *J Textile Ins,* ***64***, 47-61, 1973.
4. Clarke, MT, et al., *J Bone Joint Surg Am* **85,** 650-654, 2003.

REDUCED HIP EXTENSION RANGE OF MOTION AND PLANTAR FLEXION STRENGTH ARE FUNCTIONALLY SIGNIFICANT IMPAIRMENTS THAT AFFECT GAIT IN OLDER ADULTS

[1]Dennis E. Anderson and [2]Michael L. Madigan

[1]Center for Advanced Orthopaedic Studies, Beth Israel Deaconess Medical Center, Boston, MA, USA
[2]Department of Engineering Science and Mechanics, Virginia Tech, Blacksburg, VA, USA
email: danders7@bidmc.harvard.edu

INTRODUCTION

Older adults have been found to have reduced ankle plantar flexion (PF) peak torque, angular impulse and power compared to young adults during gait [1-5]. This is thought to be due to reduced PF strength in older adults, and it has been suggested that increased hip extension (HE) power and work [1, 5] or alternatively increased hip flexion (HF) power [2] in older adults are adaptations to compensate for this. Older adults also walk with the hip more flexed than young adults [1, 3, 4], which may be due to reduced HE range of motion (ROM) in older adults [3]. However, while reduced PF strength and HE ROM may be impairments that affect gait in older adults, there has been little study of age-related differences in gait in conjunction with relevant measurements of functional capacity.

The purpose of this study was to examine age differences in kinematics, kinetics and the functional capacity utilized (FCU) during gait. We hypothesized that older adults would walk with the hip more flexed and lower ankle PF kinetics compared to young adults due to reduced functional capacity. We further hypothesized that older adults would exhibit higher HE kinetics than young adults to compensate for reduced PF function.

METHODS

Ten young and ten older healthy adults who could walk normally based on self-report participated in functional testing and gait testing. Maximum isometric joint torques (MT) for HE, HF and PF, as well as maximum HE and HF ROM were measured using a dynamometer. In gait testing, both speed and step length were controlled as gait kinetics are affected by speed [3, 4] and step length [6]. Slow and Fast conditions (target speeds 1.1 m/s and 1.5 m/s) were tested with a target step length of 0.65 m for both speeds. Ground reaction forces and marker position data were collected and inverse dynamics analyses performed. The study was approved by the Virginia Tech Institutional Review Board, and all participants provided written informed consent.

The outcomes of interest were HE and HF angular excursions (HEA and HFA) as well as HE, HF and ankle PF peak torques (HET, HFT and PFT) and angular impulses (HEI, HFI and PFI). FCU was evaluated for angular excursions and peak torques relative to ROM and MT measurements, with MTs adjusted for joint angles and angular velocities during gait [7]. Statistical analyses were performed in JMP (SAS Institute, Inc., Cary, NC) with overall significance of $\alpha=0.05$. Age differences in subject characteristics and functional measurements were tested with independent t-tests. Outcome variables were tested with two-factor (age and speed) mixed-model ANOVAs followed by t-tests for age and speed differences with a Bonferroni correction.

RESULTS AND DISCUSSION

Older adults were not different than young adults in body mass or height, but had lower HE ROM and MTs than young adults (Table 1). Older adults walked with less HEA and more HFA than young adults (Table 2), consistent with previous findings [1, 3, 4]. Older adults had higher HET and HEI (at slow speed), and lower PFT (at fast speed), consistent with previous reports of age differences in gait kinetics [1-5]. Older adults had higher FCU than young adults for HFA, HET and PFT at both speeds and HFT at fast speed. The highest FCUs in both groups were for PFT and HEA, and younger adults showed greater actual PFT (at fast speed) and

HEA than older adults. This supports the hypothesis that reduced PF strength and reduced HE ROM are specific impairments that affect gait in older adults.

Older adults appear to compensate for reduce HEA by increasing HFA. However, these results do not suggest that older adults compensate for reduced PF kinetics by increasing HE kinetics [1, 5], as age differences in HET and HEI were significant only in the slow condition when there were no age differences in PFT or PFI. Rather, it may be that higher HE kinetics are the result of larger HF angles in early stance in older adults, and thus due to reduced HE ROM. Older adults had higher HFT FCU at fast speed only, and increased HFI with speed while young adults did not, which may support the alternative that older adults increase HF kinetics to compensate for PF deficits [2].

CONCLUSIONS

This study indicates that reduced HE ROM and reduced PF strength are both functionally significant impairments that affect gait in older adults. However, increased HE kinetics in older adults do not appear to be a compensation for reduced PF strength, but rather may be the result of reduced HE ROM. Older adults may compensate for reduced PF strength by increasing HF kinetics.

REFERENCES

1. DeVita, P, et al. *J Appl Physiol* **88,** 1804-1811, 2000.
2. Judge, J, et al. *J Gerontol A Biol Sci Med Sci* **51A**, M303-M312, 1996.
3. Kerrigan, D, et al. *Arch Phys Med Rehabil* **79**, 317-322, 1998.
4. Monaco, V, et al. *Clin Biomech* **24**, 493-498, 2009.
5. Silder, A, et al. *J Biomech*, **41**, 1520-1527, 2008.
6. Allet, L, et al. *Gait Posture* **34**, 300-306, 2011.
7. Anderson, D, et al. *J Biomech* **40**, 3105-3113, 2007.

ACKNOWLEDGEMENTS

This work was supported by grants from the NIA (F31-AG030904; T32-AG023480)

Table 1: Mean (SD) subject characteristics, maximum hip ROMs and maximum isometric joint torques (normalized by body mass) by age group.

	Young	**Older**
Age (years)	23.9 (3.3)	80.3 (4.0) [a]
Body mass (kg)	61.7 (7.3)	65.2 (10.5)
Height (m)	1.65 (0.09)	1.63 (0.08)
HE ROM (°)	28 (8)	20 (5) [a]
HF ROM (°)	73.5 (8)	69 (11)
HE MT (N-m/kg)	4.51 (0.94)	3.02 (0.85) [a]
HF MT (N-m/kg)	2.67 (0.51)	1.76 (0.23) [a]
PF MT (N-m/kg)	2.64 (0.59)	2.12 (0.25) [a]

[a] Significant age difference ($p < 0.05$).

Table 2: Mean (SD) values of hip angular excursions, peak joint torques and angular impulses during gait by age group and gait condition, as well as percent of functional capacity utilized.

	Speed	**Young**	**Older**
HEA (°)	Slow	21 (3)	15 (3) [a]
	Fast	18 (4)	13 (5) [a]
HEA FCU (%)	Slow	78 (18)	82 (32)
	Fast	69 (19)	69 (40)
HFA (°)	Slow	23 (3)	31 (2) [a]
	Fast	25 (4) [s]	33 (3) [a,s]
HFA FCU (%)	Slow	32 (6)	46 (7) [a]
	Fast	34 (6) [s]	49 (8) [a,s]
HET* (N-m/kg)	Slow	0.59 (0.10)	0.79 (0.19) [a]
	Fast	0.85 (0.13) [s]	0.90 (0.17) [s]
HET FCU (%)	Slow	17 (5)	37 (13) [a]
	Fast	24 (6) [s]	43 (13) [a,s]
HEI* (N-m-s/kg)	Slow	0.11 (0.03)	0.16 (0.05) [a]
	Fast	0.13 (0.02)	0.14 (0.04)
HFT* (N-m/kg)	Slow	0.64 (0.13)	0.56 (0.10)
	Fast	0.89 (0.14) [s]	0.79 (0.15) [s]
HFT FCU (%)	Slow	25 (6)	33 (6)
	Fast	35 (8) [s]	46 (8) [a,s]
HFI* (N-m-s/kg)	Slow	0.14 (0.04)	0.11 (0.04)
	Fast	0.14 (0.03)	0.13 (0.04) [s]
PFT* (N-m/kg)	Slow	1.46 (0.14)	1.40 (0.08)
	Fast	1.53 (0.13) [s]	1.35 (0.14) [a]
PFT FCU (%)	Slow	67 (18)	90 (12) [a]
	Fast	71 (18)	92 (17) [a]
PFI* (N-m-s/kg)	Slow	0.41 (0.05)	0.39 (0.08)
	Fast	0.29 (0.05) [s]	0.27 (0.04) [s]

[a]Significant age difference within gait condition; [s]Significant speed difference within age group ($p < 0.025$ in all cases). *Normalized by body mass.

ASSOCIATIONS OF COSTAL CARTILAGE CALCIFICATION WITH PREVALENT VERTEBRAL FRACTURES IN OLDER ADULTS

[1,2]Dennis E. Anderson, [1]Brett T. Allaire and [1,2]Mary L. Bouxsein

[1]Center for Advanced Orthopaedic Studies, Beth Israel Deaconess Medical Center, Boston, MA, USA
[2]Department of Orthopedic Surgery, Harvard Medical School, Boston, MA, USA
email: danders7@bidmc.harvard.edu, web: http://www.bouxseinlab.org/

INTRODUCTION

Vertebral fractures (VFx) are the most common type of fracture in older adults, accounting for about 27% of all osteoporotic fractures [1]. Risk factors for incident VFx include advanced age, female sex, and low bone mineral density (BMD) [2]. However, the contributions of thoracic biomechanics to VFx risk are poorly understood. For example, VFx are most prevalent in mid-thoracic (around T7-T8) and thoraco-lumbar (around T12-L1) vertebrae [3], but the reasons for this pattern remain unclear. It has been proposed that the transition from the relatively stiff thoracic spine to the more mobile lumbar spine increases vertebral loading and thus fracture risk in the thoraco-lumbar region [3].

The costal cartilages provide a flexible connection between the bony ribs and the sternum. Costal cartilage calcification (CCC), as shown in Figure 1, increases significantly with age in both men and women, and is more prevalent in men than women [4]. A possible consequence of CCC is stiffer costal cartilage and a stiffer thorax, which could alter vertebral loading and the risk of VFx, but the biomechanical effects of CCC are not well studied. The purpose of this study was to examine CCC in a community-based sample of older adults, and to determine if CCC was significantly associated with prevalent VFx using a case-control design.

METHODS

We studied a subset of 196 adults ages 50 – 85 from 3,529 participants who received CT scans of the thorax and lumbar spine as part of the Framingham Heart Study Offspring and Third Generation Multidetector CT Study [5]. Cases included 20 men and 18 women diagnosed with moderate or severe prevalent VFx, and 30 men and 30 women diagnosed with mild prevalent VFx. Controls were 98 randomly selected individuals without VFx, age- and sex-matched with cases. This study was approved by the institutional review board of Beth Israel Deaconess Medical Center.

CT scans (e.g. Fig. 1) were viewed to evaluate the level of CCC present, and each subject was assigned a CCC score of 1 through 4, as defined in Table 1. This is similar to the scoring methods utilized in previous works [4, 6]. To evaluate scoring reliability, the two readers scored a subset of 15 scans two times each, and inter- and intra-reader

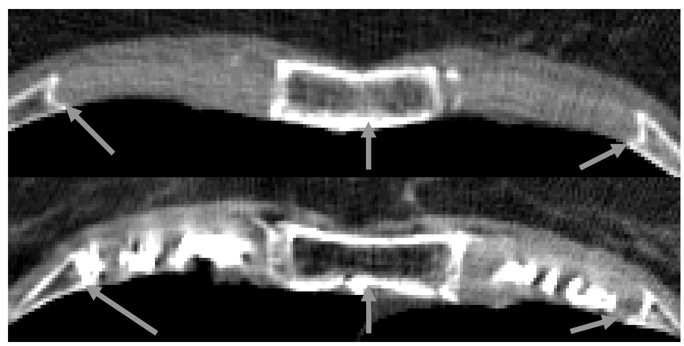

Figure 1: Examples of CT scans from two older women showing the costal cartilage connecting the sternum (center arrows) and the costochondral joints of the 4th ribs (left and right arrows). The upper image shows little CCC (Score = 1), while the lower image shows extensive CCC (Score = 4).

Table 1: Scoring criteria for level of CCC, based on amount present, and whether CCC appears to form structures along the length of the costal cartilage.

Score	Amount?	Structures?
1	Minimal	None
2	Moderate	None
3	Moderate-Large	May be present
4	Large	In many cartilages

reliability was determined. Each reader then scored half of the scans, randomly selected and blinded to subject age, sex, and fracture status.

Initially, the associations of age, sex and vertebral body BMD at L3 on CCC score were examined in controls using a multiple ordinal logistic regression analysis. Based on the results of this analysis, associations between CCC and prevalent fracture were examined separately in men and women, adjusting for age and BMD. Specifically, odds ratios for having any prevalent VFx at any location with high levels of CCC (score = 3 or 4) versus low levels of CCC (score = 1 or 2) were calculated. Odds ratios were also calculated when examining only subjects with moderate and severe fractures, as well as limiting fracture location to mid-thoracic (T4-T10) and thoraco-lumbar (T11-L4) regions.

RESULTS AND DISCUSSION

Intraclass correlation coefficients indicate good CCC scoring reliability within and between readers (intra-reader: 0.78 and 0.81; inter-reader: 0.87). In controls, mean ± SD CCC scores were 3.04 ± 0.92 and 2.42 ± 1.15 in men and women respectively, while in cases CCC scores were 2.76 ± 0.85 and 2.98 ± 1.06 in men and women respectively. In controls, higher CCC score was independently associated with increased age ($p < 0.001$), higher BMD ($p = 0.011$), and male sex ($p = 0.006$). This is consistent with previous reports that CCC is higher in men than women and increases with age [4].

Odd ratios (Table 2) indicated that women with high levels of CCC were more than twice as likely to have any prevalent VFx ($p = 0.038$), and more than five times more likely to have a prevalent VFx in the thoraco-lumbar region ($p = 0.011$), than women with low levels of CCC. In contrast, trends indicated that men with high levels of CCC were nearly three times less likely to have a moderate or severe VFx ($p = 0.083$), and nearly four times less likely to have a moderate or severe VFx in the mid-thoracic region ($p = 0.082$), than men with low levels of CCC.

Based on cross-sectional associations with prevalent VFx, high levels of CCC appear to increase the risk of thoraco-lumbar VFx in women, but may protect against mid-thoracic VFx in men. If CCC increases costal cartilage stiffness, that might increase load sharing by the rib cage and reduce vertebral loading and VFx risk in the thoracic spine. However, a stiffer thorax could also increase motion, compressive loading and VFx risk in the thoraco-lumbar spine. Thus, these results are consistent with the possible mechanical effects of CCC on vertebral loading, but it is unclear why CCC seems to affect the risk of VFx differently in men and women. Further studies are needed to determine how costal cartilage and CCC affect thoracic stiffness, vertebral loading and risk of VFx, including longitudinal studies of CCC and the risk of incident VFx.

Table 2: Odd ratios (95% Confidence Intervals) for prevalent VFx (by fracture Type and Location) with high levels of CCC, adjusted for age and L3 BMD.

Type	Loc.	Men	Women
Any	Any	0.65 (0.26-1.58)	**2.52 (1.07-6.16)***
MS	Any	0.34 (0.10-1.12)	3.43 (0.90-14.9)
Any	M-T	0.73 (0.27-1.92)	2.01 (0.79-5.26)
MS	M-T	0.27 (0.05-1.15)	2.83 (0.56-16.8)
Any	T-L	0.87 (0.27-2.92)	**5.63 (1.62-24.0)***
MS	T-L	0.60 (0.13-2.92)	5.62 (0.95-48.9)

* $p < 0.05$. MS = moderate/severe fracture; M-T =mid-thoracic; T-L = thoraco-lumbar

REFERENCES

1. Burge, R, et al. *J Bone Miner Res* **22**, 465-475, 2007.
2. Van der Klift, M, et al. *J Bone Miner Res* **17**, 1051-1056, 2002.
3. Ismail, AA, et al. *Osteoporos Int* **9**, 206-213, 1999.
4. Teale C, et al. *Age Ageing* **18**, 333-336, 1989.
5. Hoffmann U, et al. *Am J Cardiol*. **102**, 1136-1141, 2008.
6. Lau A, et al. *Acta Biomater* **4**, 97-103, 2008.

ACKNOWLEDGEMENTS

This work was supported by grants from NIAMS and NIA (R01-AR053986; R01-AR/AG041398; T32-AG023480), and by the NHLBI Framingham Heart Study (NIH/NHLBI Contract N01-HC-25195).

The Influence of Prophylactic Ankle Braces on Lower Limb Mechanics during Single-Leg Hopping Tasks

[1]Anthony Anderson, [1]Rhonda L. Boros, [1]David Stodden, [1]Hyung Suk Yang

[1]Texas Tech University, Lubbock, TX, USA
email: anthony.anderson@ttu.edu

INTRODUCTION

Prophylactic ankle braces are commonly used by athletes at a variety of skill levels as an injury prevention tactic. Past studies have focused on the effects of the ankle braces on ankle movement, joint proprioception, balance as well as performance. However, the influence of ankle braces on the mechanics of other joints is not clear, especially during maximal or near maximal single leg landing tasks as commonly occur during ballistic sporting activities. The restriction of ankle movement may create a kinematic change in landing or ground contact strategy, which could lead to an increased loading at the knee and increased knee injury (e.g. anterior cruciate ligament, ACL) potential during certain stressful landing activities.

Anterior cruciate ligament (ACL) injury is a relatively common knee injury in both male and female athletes. Athletes often have difficulties once they have sustained ACL injuries, and are at increased risk of developing knee osteoarthritis 10-15 years after the injury. The financial cost from surgical intervention [1] and loss of playing/practice time are additional burdens injured athletes must bear [2]. Thus, even though an ACL tear is not normally a career ending injury, it often has a lasting effect on the athlete.

A single-leg hop for distance was chosen as the movement for analysis because it is comparable with the high functional demands that are needed in sport [3]. Additionally, it is used as a highly reliable functional test for lower extremity stability [4] and it has been used to evaluate ACL-reconstructed patients.

The purpose of this study was to determine the effect of ankle bracing on lower limb mechanics during near maximal (90% effort) single leg hopping tasks. It is hypothesized that the ankle braces will change the kinematics during landing and lead to an increased torque at the knee.

METHODS

Eight subjects (N=4 male, 21.75±2.50 y, 82.27±6.2 kg, 1.82±0.08m; N=4 female, 21.5±0.58 y, 60.57±6.2 kg, 1.82±0.08 m) were recruited to participate in the study. Participants were free of injury, reasonably fit (BMI≤30) and physically active in sports exclusive of distance running at the time of testing. All methods were approved by the Texas Tech University Protection of Human Subjects Committee IRB. Subjects signed an informed consent prior to participation.

Subjects were required to complete a series of forward hop tasks off their right and left legs on to a force plate. Following a warm up protocol, subjects performed 3 forward hops for maximum distance off each of their right and left legs. The average of these maximum hops was taken and scaled down to 90%. The rationale was to make the hop landings challenging yet feasible to land on the force plate consistently. This distance was then measured from the edge of the force plate for each leg, and the subjects performed single leg hop trials off each leg at the 90% distance. For each distance condition, Subjects were required to complete 5 successful trials both with and without wearing ankle braces. A successful trial was defined as landing and recovering with the foot fully on a single force plate, without touchdown with the other foot.

Joint kinematics and kinetics were obtained using a six-camera motion analysis system (VICON Nexus, Denver, CO) sampling at 300Hz and ground reaction forces from an AMTI force plate (2000Hz, Watertown, MA). Kinematic markers were placed bilaterally on participants' lower body anatomy (sacrum, ASIS, thigh, knee, tibia ankle, heel, toe). Force plate data were time-synched with the VICON system. From the kinematic and force data, the following measures were determined and compared across condition: Peak VGRF (VGRF); Time to peak VGRF (tVGRF); Peak knee flexion moment (kMOM); Peak knee abduction moment (kABMOM); Knee flexion angle at contact (Kcon); Peak knee flexion angle (Kpk); Knee flexion angle at peak knee flexion moment (Kpkm); Knee abduction angle at peak knee flexion moment (KABpkm); Peak knee abduction angle (KABpk). Additionally, ankle range of motion (A-ROM) was monitored to establish that the ankle braces in fact restricted ankle motion.

Peak VGRF were normalized to each subject's body weight. Comparisons across brace condition were evaluated utilizing a repeated measures ANOVA, and significance level of 0.05.

RESULTS AND DISCUSSION

No statistically significant changes in knee mechanics were observed across the brace conditions during landings. Mean and standard deviation measures for all conditions are presented in Table 1. Results are consistent with previous work examining single leg hop for distance kinematics and kinetics which revealed no differences between dominant and non-dominant limbs [3].

While no statistically significant changes were observed, the braces did appear to reduce knee flexion and increase knee abduction slightly during landings. The ankle braces may have altered subjects landing strategy slightly. Some subjects may have adopted a more upright landing pattern while wearing the braces because the ankle was restricted. Alternatively, subjects may have utilized more ankle motion while not braced, landing onto a more outstretched and extended knee. Freedom of ankle motion without the brace likely allowed subjects to utilize more of an "ankle strategy" to absorb the impact and control the landing.

This study was the first of its kind to test the effects of prophylactic ankle braces knee motion during near maximal single leg landing tasks. Large standard deviations for nearly all measured variables were observed. Increasing the subject population and perhaps collecting data on more highly skilled or experienced athletes could likely decrease some of this variability, and help determine the consistency of these results.

CONCLUSION

This study examined the effects of wearing ankle braces on knee kinematics and kinetics during near maximal single leg hop landings. Results revealed virtually no change in knee motion or mechanics while wearing the ankle braces. Continued research is needed in order to establish whether or not ankle braces detrimentally hinder knee mechanics, and whether males and females adapt different landing strategies while wearing ankle braces.

REFERENCES

1. von Porat A et al. *Annals Rheum Dis*, **63**, 269-273, 2004.
2. Baier M & Hopf T. *Arch Physical Med Rehabil,* **79**, 939-944, 1998
3. van der Harst J et al. A. *Clin Biomech*, 22, 674-680, 2007.
4. Ageberg E, et al. *Scand. J Med Sci Sports*, **11**, 47-53. 2001.

Table 1: Comparison of ankle braces versus control

Condition	VGRF	tVGRF (s)	Kcon (º)	Kpk (º)	Kpkm (º)
Control	4.64 ± .93	.029 ± .03	4.47 ± 7.1	47.7 ± 14.4	18.8 ± 16.9
Braced	4.65 ± .77	.033 ± .03	4.42 ± 5.0	43.5 ± 11.9	18.9 ± 15.9

KINEMATIC COUPLING OF WRIST AND FOREARM MOVEMENTS

William Anderton[1] and Steven K. Charles[1,2]

[1]Department of Mechanical Engineering and [1,2]Neuroscience Center
Brigham Young University, Provo, UT
Email: skcharles@byu.edu

INTRODUCTION

Wrist stiffness dominates the dynamics of wrist rotations and has been shown to be anisotropic, with greater stiffness in radial-ulnar deviation than in flexion-extension [5, 6]. This anisotropy results in paths that require less torque than others and opens the opportunity for people to choose such paths when they have the choice (i.e. when there is redundancy). More specifically, we suspect that wrist and forearm rotations are often coordinated to avoid areas and paths of large stiffness and joint torques. The purpose of this study is to quantify the coordination and coupling of wrist and forearm rotations. Most previous studies of wrist kinematics have only measured the range of motion and centroids of wrist rotations [1, 2], but *how* the wrist moves within this range of motion (preferred orientations and pathways, coupling, etc.) is almost entirely unknown. In addition, previous studies have not investigated the interaction between wrist and forearm movements (pronation/supination).

Here we extend the previous findings of range of motion to include preferred orientations, pathways, and coupling, and we do so for both degrees of freedom (DOF) of the wrist and forearm rotation. Determining preferred areas and pathways is critical to establishing healthy wrist and forearm behavior, identifying potentially harmful behavior (leading to repetitive strain injury), and correctly re-training patients with wrist and forearm impairments.

METHODS

For this experiment, 10 young, healthy subjects (5 male, 5 female) performed 24 activities of daily living (ADL), with 5 repetitions each. Wrist and forearm angles were measured bi-laterally using motion sensors (trakSTAR 3-D guidance system by Ascension Technology). Joint angles and neutral position were defined in accordance with the guidelines for global movement set forth by the International Society of Biomechanics [4].

The 24 ADL were selected based on their use in previous studies [1, 2], with the inclusion of a few more modern tasks (e.g. typing on a keyboard, using a computer mouse). Subjects were instructed to perform each repetition of each task as naturally as possible.

To quantify movement preferences, we calculated the level of coupling between DOF using covariance. Preferred pathways are identified as common trajectory orientations. Finally, to extend the results of previous 2-DOF studies to the 3 DOF of the wrist and forearm, we calculated mean orientation and displacement (absolute and in terms of the range of motion of the wrist and forearm).

RESULTS

Mean and standard deviation of wrist and forearm orientation during ADL are shown in Table 1. Subjects' movements during ADL formed a cluster of paths within the space spanned by the 3 DOF of the wrist and forearm (Figure 1). Trends in these pathways are more easily discerned in an orthogonal projection such as the one shown in Figure 2.

Some of the degrees of freedom were found to exhibit considerable coupling. The mean Pearson Correlation Coefficient (with the mean offset removed) for flexion compared to ulnar deviation was 0.2903, meaning that flexion is often accompanied by ulnar deviation (and extension by radial deviation). The mean correlation coefficient for flexion compared to forearm pronation was -0.4256, meaning that flexion is often associated with supination (and extension with pronation). There was very little correlation between ulnar deviation and forearm pronation (R = -0.0105). We are currently investigating preferences in pathways.

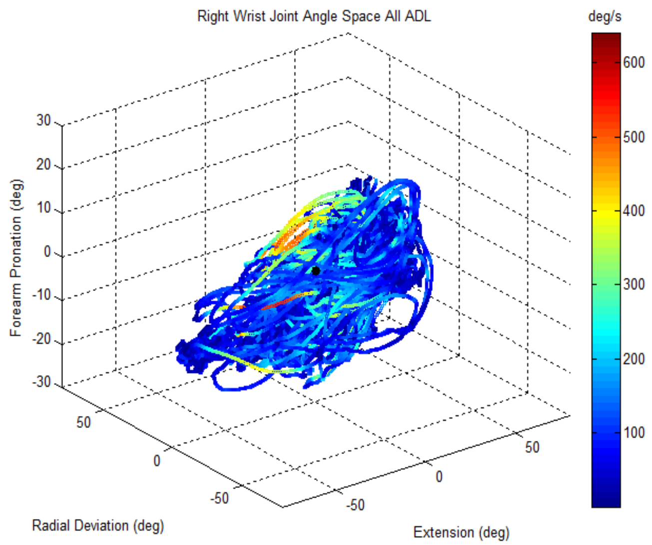

Figure 1: A subject's movement pathways plotted in FE, RUD, and PS. All 5 repetitions of all 24 ADL tasks are included. Movement speed is indicated by color according to the color bar (in deg/s). Negative extension is flexion, negative radial deviation is ulnar deviation, and negative pronation is supination.

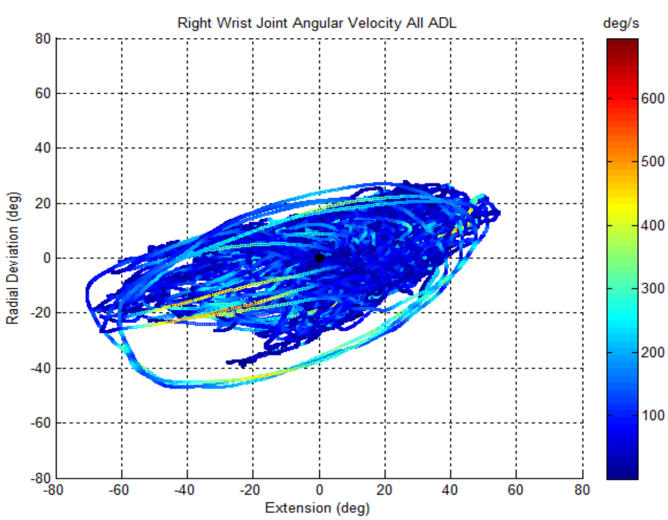

Figure 2: A projection of Figure 1 onto the FE-RUD plane. The range of motion of the wrist is represented by the surrounding traces to show how much of the range of motion is used during ADL

Mean Flexion	Standard Deviation	% ROM Flexion	%ROM Extension
-9.942	20.531	20.866	30.371

Mean Ulnar Dev.	Standard Deviation	%ROM Ulnar	%ROM Radial
3.27	11.621	24.109	27.475

Mean Pronation	Standard Deviation	%ROM Pronation	%ROM Supination
9.7626	25.851	43.248	35.735

Table 1: Measures characterizing the preferred orientations for all subjects. %ROM is the standard deviation of orientation in a DOF, expressed as a percentage of the total range of motion in that DOF (it describes how much range of motion subjects used with respect to their limits in each DOF). In the left column, negative flexion indicates extension.

DISCUSSION

Kinematics in FE, RUD, and PS are anisotropic (not the same in all directions) and coupled (Figure 1), indicating that range of motion and centroids are not adequate information to describe how healthy subjects move their wrists during ADL.

An understanding of preferred wrist and forearm kinematics is valuable for rehabilitation; valuable therapy time could be shifted away from less used areas/paths and instead spent retraining preferred areas/paths. Special emphasis could be placed on retraining preferred coupling between wrist and forearm rotations. Comparing patients' paths to those preferred by healthy subjects could provide a more sensitive measure of rehabilitation progress.

REFERENCES

1. Palmer, A.K. et al, *The Journal of Hand Surgery*, **10A**, No. 1 pp. 39-46, 1985.
2. Ryu, J. et al, *The Journal of Hand Surgery*, **16A** No. 3 pp. 409-419, 1991.
3. Charles, S.K., Hogan, N., *Experimental Brain Research*, **203** pp. 63-73, 2010.
4. Wu, G. et al, *The Journal of Biomechanics*, **38**, pp. 981-992, 2005.
5. Charles, S.K., Hogan, N., *The Journal of Biomechanics*, **44**, pp. 614-621, 2011.
6. Charles, S.K., Hogan, N., *The Journal of Neurophysiology*, **107**, pp. 1230-1240, 2012.

THE EFFECT OF CRANK POSITION AND BACKREST INCLINATION ON SHOULDER LOAD DURING HANDCYCLING

[1,2]Ursina Arnet, [1,2]Stefan van Drongelen, [1]Matthias Schlüssel, [1]Veronika Lay, [3] Lucas H. V. van der Woude and [2,4]DirkJan H. E. J. Veeger

[1] Swiss Paraplegic Research, Nottwil, Switzerland
[2] VU University Amsterdam, The Netherlands
[3] University of Groningen, Groningen, The Netherlands
[4] Delft University of Technology, Delft, The Netherlands
Email: ursina.arnet@paranet.ch

INTRODUCTION

Physical activity of the upper body is very important to increase the general health of persons with spinal cord injury. The negative consequences of increased physical activity are related to overload of the upper extremities, which could lead to overuse injuries and pain of the musculoskeletal system. Prevalence rates of 30 – 73% for shoulder pain [1] indicate that overload injuries to the musculoskeletal system are a serious long-term problem in persons with spinal cord injury [2].
The handbike, which is an alternative mobility device for outdoor training, has been shown to be preferable over the handrim wheelchair regarding shoulder load [3]. The optimal handbike-user interface with respect to shoulder load is yet not known. The aim of this study was to analyze whether the crank position or the backrest inclination influences the shoulder load during submaximal handcycling. Shoulder load was quantified by the glenohumeral contact force and the muscle forces of the rotator cuff since this muscle group is most prone to overuse injuries in persons with spinal cord injury.

METHODS

Thirteen handbike users (4 women, 9 men) with spinal cord injury participated. The handbike used in the experiments was a stationary handbike construction consisting of an attach-unit system attached with an adaptor to the rigid frame of a sports handbike. The handbike was fitted with a special purpose crank unit on the left hand side that recorded three-dimensional forces (Figure 1). The handbike was attached to an ergotrainer. For the analysis of the crank position, combinations of two crank distances (close: elbow angle 15°, distant: elbow angle 35°) and two crank heights (high: shoulder height (acromion), low: shoulder height - 15% of arm length) were studied, while keeping the backrest inclination constant. To analyze the influence of the backrest inclination, four inclinations were studied (60°, 45°, 30° and 15°), while keeping the distance of the crank constant.

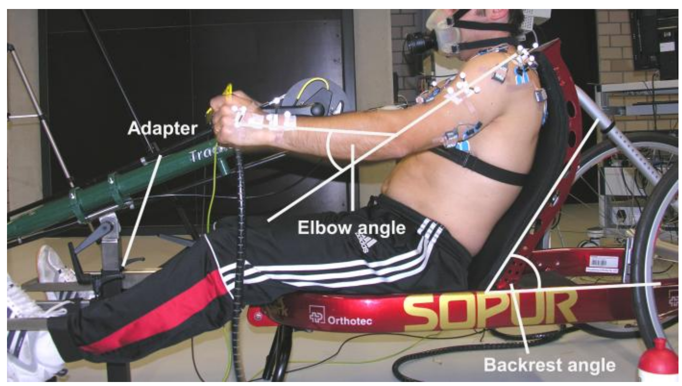

Figure 1: Handbike setup

The resistance of the ergotrainer and the cycling cadence (68 rpm) was constant for all subjects and trials. The trials with a duration of 3.5 min were conducted in a randomized order. During the trials the three-dimensional forces applied by the hand and the kinematics of the upper extremity were measured. Kinetics and kinematics were input to the Delft Shoulder and Elbow Model which is an inverse dynamic model that calculates the glenohumeral contact force and the muscle forces of the rotator cuff based on an energy cost function.

To quantify the effect of handbike setup, two series of linear mixed models were calculated with the backrest or the crank positions as fixed effect. Level of significance was set at $p < 0.05$.

RESULTS AND DISCUSSION

The analysis of the backrest inclination showed that more upright backrest positions resulted in lower glenohumeral contact forces (Figure 2). This force is seen as the closest estimate for internal load acting on the glenohumeral joint, because it comprises both the external forces due to handcycling, and the muscle forces which are needed to carry out the handcycling movement and to stabilize the shoulder joint. Higher mean, and especially higher peak glenohumeral contact forces, point to a higher risk for overuse injuries.

The rotator cuff consists of the four muscles supraspinatus, subscapularis, infraspinatus and teres minor. Besides their function of abduction, extension or axial rotation of the humerus, they assist in the stabilization of the shoulder joint. Muscle imbalance or chronic fatigue of the rotator cuff due to overloading could lead to displacement of the humeral head and thus to impingement, which is the most common cause of shoulder pain in persons with a spinal cord injury. In this context, an optimal setup of a handbike should strive to prevent overloading of the rotator cuff by reducing its activity. In the present study, the mean and peak relative muscle force of both the supraspinatus and the infraspinatus increased with lower backrest inclinations (Figure 2).

The best crank position could not be identified among the tested handbike setups. Except for the subscapularis there was no difference in shoulder load between the four crank positions (Figure 2). When comparing the close vs. the distant crank position, the latter resulted in lower relative muscle force of the subscapularis.

CONCLUSIONS

Handbike users, whose main interest is in improving health and physical capacity in a shoulder-friendly way should set up their handbike with a backrest inclination of 60° and a distant crank placement with an elbow flexion angle of 15°.

REFERENCES

1. Dyson-Hudson TA, et al. *J Spinal Cord Med* **27**, 4-17, 2004.
2. Pentland WE, et al. *Paraplegia* **32**,211-218,1994.
3. Arnet U, et al. *J Rehabil Med* **44**, 222-228, 2012.

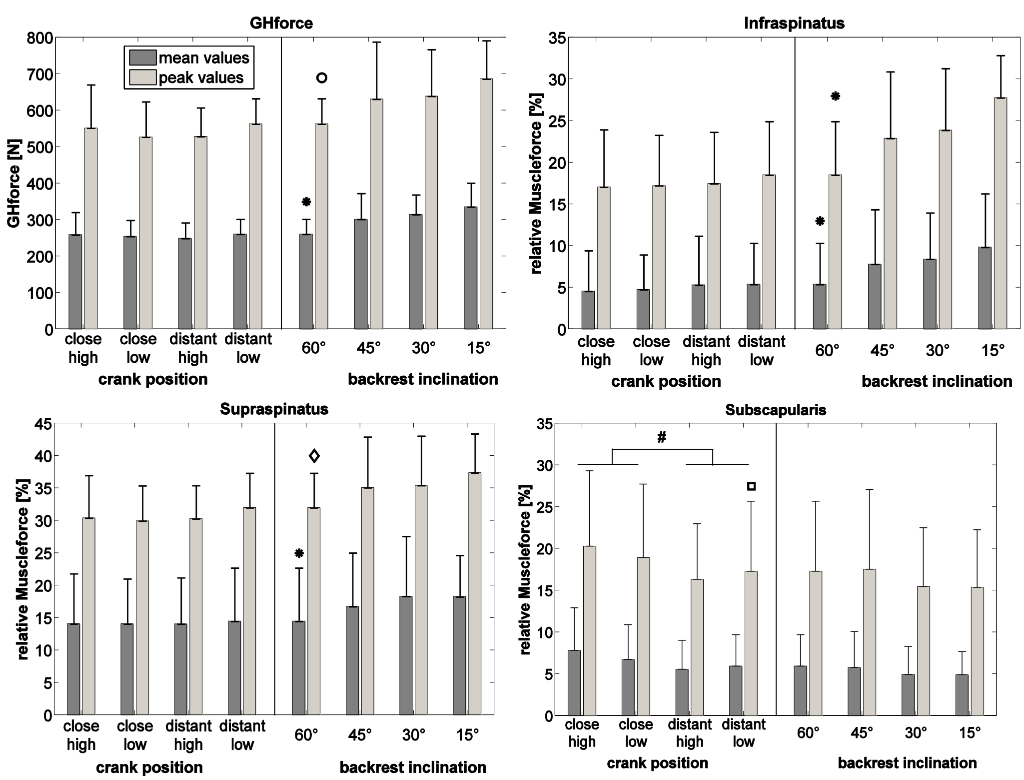

Figure 1: Mean and peak values with standard deviations for each setup. Significant differences ($p<0.05$):
* = 60° < 45°, 30° and 15°
o = 60° < 30° and 15°
◊= 60° < 15° °
□ = distant low < close high
= distant < close.

CHILDREN WITH CEREBRAL PALSY HAVE INCREASED VARIABILITY IN THEIR STEPPING PATTERN AND INCREASED CORTICAL ACTIVITY DURING GAIT

[1]David J. Arpin, [2]Tony W. Wilson & [1]Max J. Kurz

[1]Munroe-Meyer Institute, University of Nebraska Medical Center, Omaha, Nebraska
[2]College of Medicine, University of Nebraska Medical Center, Omaha, Nebraska
Email: mkurz@unmc.edu Web: http://www.unmc.edu/mmi/

INTRODUCTION

Children with cerebral palsy (CP) display balance and walking impairments that are commonly provoked by damage to the periventricular white matter during birth or shortly after. Although it has been previously shown that these children have an increased amount of variability in their stepping pattern [1], it is currently unknown if these variations are a result of an aberrant brain-body connection.

Due to recent computational and hardware advances in the technique of functional near-infrared spectroscopy (fNIRS), we are now able to quantify the amount and location of the cortical activation that occurs during gait [2]. Our recent fNIRS investigation has demonstrated that the amount of cortical activation is related to the difficulty of the walking task [2]. Moreover, we have shown that the amount of cortical activation is also positively related to the amount of variation present in the gait pattern of adults [2]. Based on these insights, we suspect that the increased variability seen in the gait pattern of children with CP will be reflected in their cortical activity during gait. The purpose of this investigation was three fold: 1) To further substantiate that children with CP have a more variable stepping pattern, 2) To determine if there is positive relationship between the amount of cortical activity and the variation in the gait patterns of children, 3) To determine if children with CP have an altered amount of activity across the cortical network during gait.

METHODS

Children with spastic diplegic CP (n= 4; Age = 11 $\pm$ 4 yrs.) who had a Gross Motor Function Classification Score (GMFCS) of II-III and TD children (n= 8; Age = 13.2 $\pm$ 3 years) participated in this investigation. A GMFCS of II indicates that the children have notable walking impairments but do not require an assistive mobility device to walk, while a GMFCS III indicates that the child requires an assistive mobility device (e.g., forearm crutches, wheeled walker) to walk.

The children walked on a programmable treadmill for two sessions that consisted of five alternating blocks of standing still for 30 seconds and 30 seconds of walking at 0.45 m/s. Cortical activation was measured using a 24-channel fNIRS system. fNIRS quantifies the concentration of deoxygenated and oxygenated hemoglobin (oxyHb) in the neural tissues beneath the array, which is closely linked to the amount of neuronal activity. We focused on oxyHb measurements in this study. The optodes of the system were positioned on the child's head using the International 10/20 system for EEG recording, with Cz located beneath the center of the front two rows of optodes (i.e., between channels 5-6). The full 24-channel array was separated into smaller 5-channel arrays that were located over the supplemental motor area (SMA), precentral gyrus, postcentral gyrus, and superior parietal lobe (SPL).

Concurrently, a two-dimensional sagittal plane video was collected at 60 Hz and was used to determine temporal kinematics. The respective stride, stance and swing times were determined from the video using the SIMI motion capture software. The coefficient of variation of the respective temporal kinematic measures was calculated to quantify the amount of variability present in the gait pattern.

RESULTS AND DISCUSSION

The children with CP had a greater amount of variability in their stance and stride times (Figures 1 A & B). The greater variability suggests that the children with CP had more errors in the execution of the stepping motor command. This result concurs with what has been previously reported for the over ground walking patterns of children with CP [1].

We additionally found positive correlations between the amount of variability in the temporal kinematics and the amount of cortical activation seen during the gait of the children. Specifically, strong positive correlations were found between the variability in the stride ($r=0.77$) and stance time intervals ($r=0.76$) and the SPL ($p<0.05$). We also found moderate correlations ($p<0.05$) between variability in the stride time intervals and the postcentral gyrus ($r=0.55$). Additionally, moderate correlations ($p<0.05$) were found between the stance time intervals and the precentral gyrus ($r=0.56$) and postcentral gyrus ($r=0.62$). These results further confirm that an increased amount of gait variability is associated with an increased amount of cortical activity [2].

Our results also showed that the amount of activation across the cortical network was higher for the children with CP (Figure 2). For children with CP, activity was significantly greater in the precentral gyrus, postcentral gyrus, and SPL ($p<0.05$). Conversely, activations in the SMA were not significantly different ($p>0.05$). These results infer that walking presents a greater burden on the cortical networks for children with CP than TD children. We suspect that the increased burden may be partly related to the damage present in the corticospinal and thalamocortical tracts of the children with CP [3]. Effectively, the damage may diminish the efficiency of the neuronal groups that are involved in the formulation and correction of the stepping motor command.

CONCLUSIONS

The results of our experiment are three fold: 1) Children with CP have greater variability, 2) Increased gait variability is associated with increased activity across the cortical network, 3) Children with CP have an increased amount of cortical activation during gait. These results are the first to evaluate the link between the brain and biomechanics in children with CP during walking. Further exploration of this connection will enhance our understanding of the movement impairments seen in children with CP, and may enhance our ability to assess the efficacy of therapeutic strategies that are directed at improving the motor control and learning of children with CP.

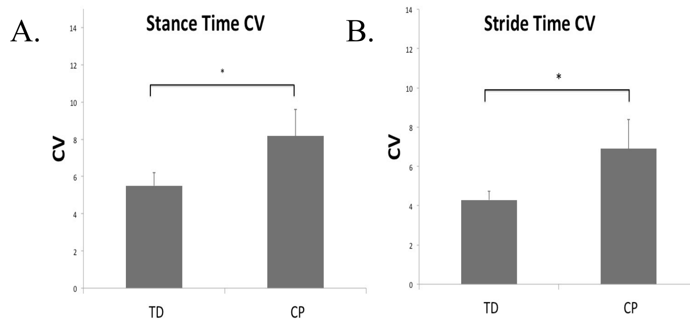

Figure 1. Coefficient of variation of the stance time intervals (A), and coefficient of variation of the stride time intervals (B). *p<0.05

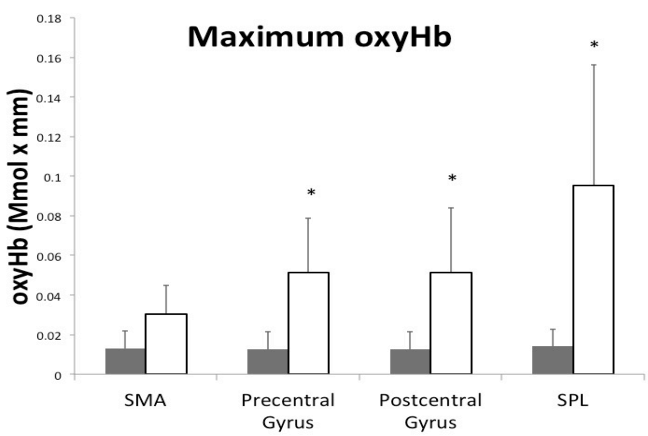

Figure 2. Maximum oxyHb in the respective cortical areas for children with CP (white) and TD children (gray). *p<0.05

REFERENCES

1. Katz-Leurer, et al. 2009 *Dev Neurorehab* **12**,100-105, 2009.
2. Kurz MJ, et al. *NeuroImage* **59**, 1602-1607, 2012.
3. Hoon AH, et al. *Dev Med Child Neurol* **51**, 697-704, 2009.

THE EXAMINATION OF SOFTBALL PITCHING FATIGABILITY IN LOWER EXTREMITIES

Jennifer Ashley, Tom Wu and Cara Postlmayr

Bridgewater State University, Bridgewater, MA, USA
email: jashley@bridgew.edu web: http://www.bridgew.edu

INTRODUCTION

Frenandez, Yard & Comstock (2005) report that 52% (2,298) of all reported serious injuries were lower extremities injuries [1]. Guido, Werner & Meister (2009) examined the throwing mechanics and the effects of ground reaction forces used to break the forward momentum unique to softball pitches. They found peak vertical ground reaction force, peak anterior force, and peak medial directed force averaged 139%, 24%, and 42% of body weight, respectively. The stride foot created force in three different directions to break the forward motion of the body during a pitch [2]. Oliver and Plummer (2010) noted the increase in ball velocity with increase in vertical ground reaction force requiring the lower extremities to work harder to compensate for this increase [3]. However, often times a fast pitch softball pitchers pitches an entire game, thus fatigability may alter the mechanics of pitching motion in the lower extremities, which can affect the pitching performance and increase the chances of injury. Therefore, the purpose of this study was to examine the fatigability of the lower extremities in fast pitch softball pitchers.

METHODS

Five university female softball pitchers between the ages of 20 and 25 participated in the study. Written consent forms were obtained from the pitchers prior to testing. Each pitcher had reflective markers placed on the right side of their body at the shoulder, hip, knee, ankle, and toe. After a warm up period, participants were asked to pitch seventy pitches. The number of pitches was consistent with a typical softball game. Participants were asked to only throw fastballs in attempt to control the influences on the joint mechanics from other types of pitch. Pitchers had a two-minute break after every ten pitches in order to allow the restoration of their ATP system. A team catcher caught all pitched balls, and a Sports Radar gun (Model: SRA3000) was positioned behind the catcher to record the speed of the ball.

A two-dimensional kinematic analysis was conducted with a Casio Camera (model: EX-FH25) capturing the movement at 120 frames per second with the use of 500W artificial light. Trials were recorded from pitches, #1-10 (beginning), #31-40 (middle) and #61-70 (end). These ten pitch increments were chosen so researchers could analyze the development of fatigue over time. Pitchers' lower limb joint angles and angular velocities at the instant of ball release were analyzed with APAS software, and the digital filter function was applied to data at 8Hz. A one-way repeated measure ANOVA statistical analysis was conducted at $\alpha = 0.05$, and followed by t-test with Bonferroni adjustment if a significant different was found. Pearson product moment correlation analyses were conducted to determine the relationship between the linear ball velocity and joint angular velocity. All statistical analyses were conducted with SPSS software.

RESULTS AND DISCUSSION

The results showed that there was no statistically significant difference from beginning to end intervals in hip, knee and ankle joint angles at the instance of ball release (Figure 1 & Table 1).

From the data analysis of beginning to end intervals, the participants showed an average hip joint angular velocities of 158 ± 350°, 236 ± 338° and 196 ± 168°, respectively. The average knee joint angular velocities were -218 ± 500°, -307 ± 501° and -286 ± 522°, respectively, and the average ankle joint angular velocities were -433 ± 586°, -392 ± 517° and -418 ± 573°, respectively, No statistical significant difference was found in all three lower limb joint angular velocities of hip, knee and ankle from beginning to end trial intervals.

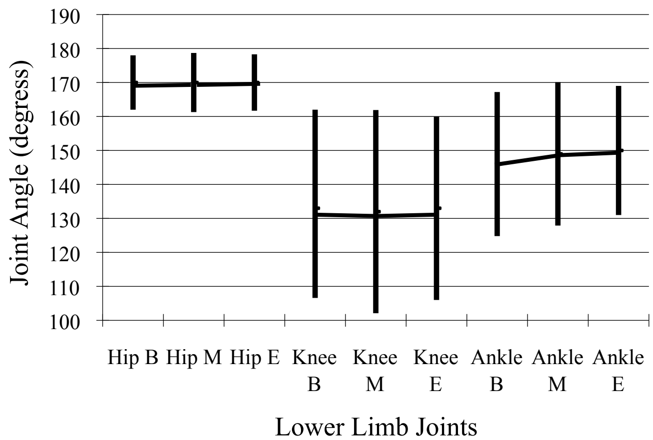

Figure 1: The three trial intervals (B-beginner, M-middle, and E-end) of the lower limb joints.

From the results of Pearson product moment correlation analyses, the hip and knee and ankle did not show significant correlation to the linear ball velocity across the three pitching intervals. However, a trend of increase in correlation from the beginning to the end interval was observed in the hip joint. This indicates that fatigability may influence the pitching mechanics in the hip joint, so a proper strengthening program should focus on the hip joint in the lower body.

This study measured the fatigability of the pitching mechanics in the lower body with a span of 70 pitches. Due to the limited number of pitches, the results of the study cannot be generalized to multiple games pitched in a competition weekend.

This study only examined the changes in pitching mechanics with fastball. In a real game situation, pitchers throw multiple types of pitch (i.e. curve, ball, change-up and riser), and the mixture of these different types of pitch may place a greater amount of stress on the lower body joints. Nonetheless, this study provides a preliminary understanding on how fatigue may influence the lower body joint mechanics.

CONCLUSIONS

The purpose of this study was to examine the fatigability of the lower extremities in fast pitch softball pitchers. Fatigue may alter the mechanics of pitching and increase the chances of injury. The findings of the study suggest the importance of strengthening the hip joint in training. Future studies are warranted with a greater number of pitches and sample size, and different types of pitch.

REFERENCES

1. Fernandez W, et al. *Acad Emerg Med* **14**(7):641-645, 2007.
2. Guido, JA, et al. *J Strength Cond Res* **23**(6), 1873-1876, 2009.
3. Oliver GD et al. *Proceedings of ISBS'10* Marquette, MI, USA, 2010.

Table 1: The three pitching intervals of the lower limb joint angles for fast pitch softball pitchers

Variables	**Beginning**	**Middle**	**End**	***p***
Hip (°)	170 ± 8.0	170 ± 8.7	170 ± 8.3	0.94
Knee (°)	133 ±26.4	132 ± 29.9	133 ± 27.0	0.90
Ankle (°)	146 ± 21.2	149 ± 21.1	150 ± 19.0	0.28

Table 2: Pearson product correlations between each joint angular velocity and linear ball velocity

Variables	**Beginning**	**Middle**	**End**
Hip	0.20	0.25	0.34
Knee	0.23	0.34	0.24
Ankle	0.01	0.17	0.05

Evaluation and Classification of Load Accommodation Strategies during Walking with Extremity-Carried Weights: A Pilot Study

Lee T. Atkins[1], Janet S. Dufek[2] and C. Roger James[1]

[1]Texas Tech University Health Science Center, Lubbock, TX, USA
[2]University of Nevada Las Vegas, Las Vegas, NV, USA
email: lee.atkins@ttuhsc.edu

INTRODUCTION

Mechanical loading provides a stimulus for maintaining tissue homeostasis [1]. Insufficient (e.g., osteoporosis) or excessive (e.g., stress fracture) loading can be detrimental to tissue health [1]. Movement control strategies can be used to alter the magnitude of the ground reaction force and subsequently the force acting on a tissue [2,3,4]. Load accommodation strategies may be elicited with the application of an external stressor during a dynamic activity, such as walking while carrying additional weight. Such load accommodation strategies have been identified for running and landing [5,6,7]. These strategies were classified using a load accommodation model based on observed vertical ground reaction force (vGRF) in relation to the magnitude of an external stressor [8]. Based on Newtonian mechanics the magnitude of the vGRF should be predictable and increase at an equal rate to the applied external stressor. However, when observed individually, some subjects demonstrate vGRF values greater or less than predicted. It is unknown if extreme load accommodation strategies during routine daily activities such as walking while carrying an object in the hands or walking with weights on the feet (e.g. winter boots, heavy occupational footwear), are present within the general population. The purpose of this pilot study was to evaluate and classify the load accommodation strategies that occur during walking with extremity-carried weights.

METHODS

Six healthy subjects (1 male, 5 female) walked on a treadmill at 1.34 m/s while carrying 0, 44.5, and 89 N weights attached to the wrists (Wr) or ankles (Ank). In the wrist weight conditions, subjects' arms were either unconstrained (U) or constrained (C) by clasping their hands in front of their bodies. Vertical GRF data were obtained using an instrumented treadmill (Kistler Gaitway; 100 Hz). Left side peak vGRF values during weight acceptance were extracted and averaged across 10 footfalls in each condition. Load accommodation strategies were evaluated by comparing the rate of change (regression line slope) of the observed vGRF with respect to the known increases in system weight. The strategy (slope) was calculated for each load carriage position resulting in three comparison conditions: WrU, WrC and Ank. The mean strategy across conditions also was calculated. The presence of a group strategy for a condition was evaluated by comparing the observed slope to the predicted slope (one N/N) using 95% Confidence Intervals. Strategy differences between conditions were determined using paired t-tests ($\alpha = 0.05$). Identified strategies were classified using the load accommodation model [8].

RESULTS AND DISCUSSION

Walking with extremity-carried weights elicited load accommodation strategies. The WrC and Ank conditions and the mean strategy were significantly ($p \leq 0.05$) greater than predicted as indicated by the 95% Confidence Intervals (Table 1). The observed strategies were classified as super-Newtonian strategies as defined by the load accommodation model [8].

The WrC and Ank conditions elicited greater strategies than WrU. WrC was significantly ($p \leq 0.05$) greater than WrU. Relative to WrU, Ank exhibited a large effect size (d=0.87), but was not significantly different because of low statistical power due to the small sample size. Descriptively, Ank exhibited a greater strategy than WrC, but this effect was not significant due to the large variability in the Ank condition. Subject three (Figure 1) exhibited a disproportionately large super-Newtonian response (Table 1).

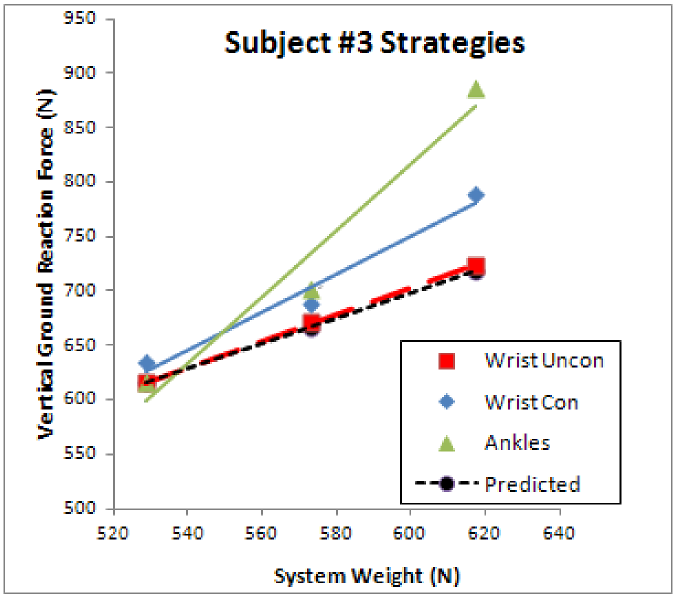

Figure 1: Example strategies (regression lines) for one subject. System weight = body weight + extremity carried weight.

CONCLUSIONS

The results of this pilot study indicate that walking with extremity carried weights elicits load accommodation strategies and that different extremity load carriage positions result in different strategies. Extreme load accommodation strategies may lead to abnormal tissue loading. Insufficient or excessive tissue loading may be detrimental to tissue health potentially leading to force-related pathologies. Future research should evaluate the relationships among load accommodation strategies and force-related pathologies.

REFERENCES

1. Mueller MJ, et al. *Phys Ther* **82**, 383-403, 2002.
2. Peterman MM, et al. *J Biomech* **34**, 693-698, 2001.
3. Reilly SM, et al. *J Exp Biol* **208,** 993-1009, 2005.
4. Scott SH, et al. *Med Sci Sports Exerc* **22**, 357-369, 1990.
5. Bates, B. T., et al. *5th edn, University of Ottawa*, 40-41, 1988.
6. Caster BL, et al. *Med.Sci.Sports Exerc.* **27**, 736-744, 1995.
7. Simpson KJ, et al. *Free University Press, Amsterdam*, 701-704, 1988.
8. James CR, et al. *J Appl Biomech*, **19,** 106-118, 2003.

Table 1: Load accommodation strategy (slope) by condition.

Subject	Wrist Weights, Arms Unconstrained (N/N)	Wrist Weights, Arms Constrained (N/N)	Ankles Weights (N/N)	Mean Strategy (N/N)
1	0.96	1.32	0.83	1.04
2	1.33	1.33	1.09	1.25
3	1.23	1.74	3.05	2.00
4	1.36	1.72	1.94	1.67
5	0.67	1.26	1.29	1.07
6	1.30	1.39	2.01	1.57
Mean (SD)	**1.14 (0.27)**	**1.46 (0.21)***	**1.70 (0.81)**	**1.43 (0.38)**
95% CI	**0.92 < PS < 1.36**	**PS < 1.29 < 1.63****	**PS < 0.1.05 < 2.35****	**PS < 1.13 < 1.74****

*Significantly ($p \leq 0.05$) different than the wrist weights, arms unconstrained.
PS is predicted slope (one); **Predicted slope lies outside of the 95% Confidence Interval ($p \leq 0.05$).

Metaphyseal and Diaphyseal Bone Loss Following Transient Muscle Paralysis are Distinct Osteoclastogenic Events

[1]Brandon J. Ausk and [1]Ted S. Gross
[1]University of Washington, Seattle, WA, USA; email: bjausk@u.washington.edu

INTRODUCTION

We have previously demonstrated that transient paralysis of the murine calf muscles causes profound degradation of trabecular and cortical bone in the adjacent tibia within 3 weeks, primarily a result of osteoclastic bone resorption [1]. In more recent studies, we have begun to identify the temporal and spatial nature of this bone loss through acute time course micro-CT (μCT) imaging of trabecular bone resorption (proximal tibia metaphysis) and endocortical bone resorption (tibia diaphysis, [2]). The timing and magnitude of bone resorption differs greatly between the two compartments. Within the metaphyseal region, significant trabecular bone resorption was identified by d.3 (-25.46% reduction in bone volume/total volume: *BV/TV)* and occurs at locations of high bone turnover nearest the growth plate, suggesting an enhancement of basal osteoclast activity is the initial cellular mechanism underlying trabecular bone loss following muscle paralysis [3]. Bone resorption in the tibia diaphysis, however, occurs much more slowly, with endocortical bone volume (E.Vol) expansion (indicating cortical bone resorption) first identified at d.12 [2].

Given the differences in timing and magnitude of acute bone resorption in the tibia metaphysis and diaphysis and the spatial distance between these compartments, we hypothesized that bone loss in the proximal tibia metaphysis and tibia diaphysis occur through distinct osteoclastogenic events.

METHODS

To assess our hypothesis, we performed two *in vivo* experiments. In the first study, six female C57B6 mice (16 wk) received IM injections of Botox (2.0 units/100 g) in the right calf immediately following a μCT scan. Additional *in vivo* μCT scans were obtained on d.6 and d.13, with a terminal scan obtained on d.20. The scan length was 6.3 mm beginning at the distal end of the proximal growth plate and continuing through the midshaft of the tibia. The scanning location and time points enabled determination of whether osteoclast activity temporally and spatially migrated from the metaphysis to the diaphysis or occurred in two distinct events as hypothesized. As the scan volume used encompassed both the highly trabecularized metaphyseal compartment and the diaphyseal compartment lacking trabecular bone, endocortical expansion was the primary outcome measure used to contrast osteoclast activity across these compartments. The scan volume was discretized into six discrete bins (each 1.05 mm) starting at the growth plate and E.Vol calculated within bins (Fig 1A). Alterations in E.Vol occurring between each μCT scan were integrated within each bin to assess temporal osteoclast activity.

In the second experiment we determined if the magnitude of bone loss initiation within the diaphysis was independent of the magnitude of bone loss initiation in the metaphysis following transient muscle paralysis. Previously, we reported that young mice (6 wk) demonstrated a rate of trabecular bone loss following calf paralysis that greatly exceeded that of adult mice [4]. Here, we examined the magnitude of endocortical bone resorption in the same specimens. Specifically, *ex vivo* scans of the tibia midshaft were obtained 14 days following transient muscle paralysis for experimental and contralateral tibias and alterations in the endocortical volume were calculated versus contralateral controls (previously shown to have no change in endocortical volume in contralateral limb following muscle paralysis, [1]).

In the first experiment, statistical significance in the metaphyseal and diaphyseal regions were analyzed separately ($p<0.05$). Specifically two-way ANOVAs, with bin location and scanning time periods being the main effects, were calculated for each compartment with TUKEY post-hoc analysis. In the second experiment, significant differences were determined using unpaired T-tests ($p<0.05$).

RESULTS AND DISCUSSION

Consistent with previous data in adult mice, osteoclast activity within 6 days of muscle paralysis was profound and occurred predominantly in the proximal tibia metaphysis nearest the growth plate (Fig 1B-black bars). Osteoclastic activity within this bone compartment was significantly reduced at later timepoints. In contrast, osteoclast activity in the diaphyseal region occurred almost entirely within the d.6 to d.13 time period, with significantly decreased bone resorption in the preceding and trailing time periods ($p<0.01$). Within this time period bone loss was not significantly different between bins.

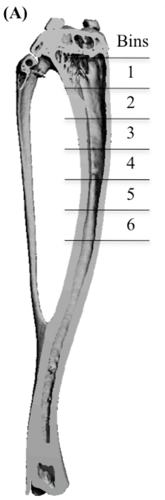

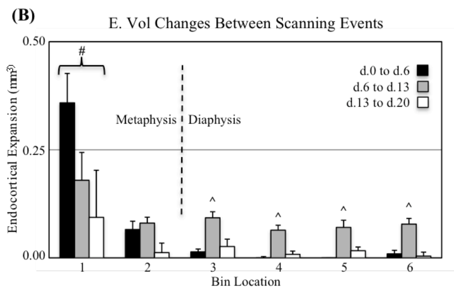

(C)

	% Change BV/TV (d.3 Metaphysis)	% Change E.Vol (d.12/d.14 Diaphysis)
Adult Mice	-25.46 ± 3.81 % *	6.72 ± 1.41 %
Young Mice	-64.15 ± 3.48 %	2.61 ± 3.65 %

Figure 1: Osteoclastic activity within the tibia following transient muscle paralysis was quantified in each of six discrete bins (A). Endocortical expansion (mean ± s.e.) in the metaphysis and diaphysis are distinctly different in both timing and magnitude (B; # significant difference between Bin 1 and 2; ^ significant difference between scanning time points; all $p<0.05$). A significant increase in metaphyseal bone loss initiation in young mice does not correlate with the magnitude of bone loss initiation within the diaphysis when compared to adult mice (C; mean ± s.e.; * $p<0.01$).

In young growing mice, the magnitude of bone resorption 3 days following muscle paralysis was significantly enhanced versus adult mice (significant decrease in BV/TV, Fig 1C). However, there was no significant difference in the magnitude of endocortical diaphysis expansion between young and adult mice (Fig 1C).

Taken together, these data suggest that two distinct osteoclastogenic events mediate bone loss in the metaphyseal and diaphyseal compartments. In contrast with metaphyseal bone loss, there was no effect of spatial location on bone loss magnitude in the diaphysis, suggesting osteoclast migration between the compartments did not occur. The young animal data in which increased metaphyseal bone loss did not correlate with increased diaphyseal resorption also supports this thesis. The timing and spatial homogeneity of bone resorption within the diaphyseal region suggests a distinct osteoclastogenic event from that driving acute trabecular resorption. Given that the timing of bone loss initiation in this compartment (d.6 at the earliest) correlates well with the amount of time required to form osteoclasts from monocyte/macrophage precursors *in vitro* and *in vivo* [5,6], one possible explanation for these data is that profound osteoclastogenesis within the marrow cavity drives a secondary wave of bone resorption.

CONCLUSIONS

Initial bone resorption following paralysis is achieved through an increase in basal osteoclast activity within the proximal tibia metaphysis, while profound *de novo* osteoclastogenesis within the bone marrow is the predominant mechanism driving resorption elsewhere. This data suggests the presence of two distinct osteoclastogenic pathways that may be targeted to prevent bone resorption in models of severe muscle dysfunction such as spinal cord injury or sarcopenia.

REFERENCES

1) Warner SW, et al. *Bone,* **38**(2): 257-64, 2006; 2) Poliachik SL, et al. *Bone*, **46**(1): 18-23, 2010 ; 3) Ausk BJ, et al. *2011 ORS Annual Meeting, Long Beach, CA*; 4) McNamara EA, et al. *2010 ORS Annual Meeting, New Orleans, LA; 5)* Tinkler SMB, et al. *J. Anat*, **133**(1): 91-97, 1981; 6) Collin-Osdoby P, et al. *Methods Mol Med*, **80**: 153-166, 2003.

ACKNOWLEDGEMENTS

This work supported in part by NIA (F31AG037287), NIAMS (AR060304) and the Sigvard T. Hansen, Jr. Endowed Chair.

A NONLINEAR HAND-ARM MODEL FOR INTERACTION WITH IMPULSIVE FORCES

Haluk Ay[1], Anthony F. Luscher[1], Carolyn M. Sommerich[2], Necip Berme[1,3]
[1] Department of Mechanical Engineering, The Ohio State University, Columbus, OH, USA
[2] Department of Integrated Systems Engineering, The Ohio State University, Columbus, OH, USA
[3] Bertec Corporation, Columbus, OH, USA

INTRODUCTION

Impulsive forces in the transverse plane are commonly encountered by operators in industry using powered torque tools [1]. Previous studies proposed linear hand-arm models for interaction with such forces [2-3]. However, it is likely that the linearity assumptions in these studies are limited to the range of tested input excitation conditions, because human hand-arm dynamics have adaptive characteristics [4]. We hypothesized that a nonlinear model would be necessary to accurately represent hand-arm dynamics in a broader range of input profiles. The goal of this study was to develop and validate a nonlinear model for the endpoint hand-arm dynamics subjected to impulsive forces. We conducted experiments with human subjects and compared the accuracy of nonlinear and linear models in terms of hand displacement.

METHODS

A novel tester bar assembly was developed, that consisted of head, middle, and handle sections affixed together (Fig. 1). The head section was connected to a rotational actuator mounted inside a configurable stand (Fig. 2). The handle was instrumented with a custom load cell to measure hand reaction force in the transverse plane and moment about the pivot. A rate gyro was also inserted in the load cell to measure the angular velocity of the tester bar.

Testing was conducted with 12 male and 10 female subjects (see Table 1 for descriptive information). The subjects were instructed to grasp the tester bar handle and provide resistance against a computer-controlled half-sine torque pulse applied by the actuator. Excitation torque, hand force, moment and angular velocity were sampled simultaneously. Vertical and horizontal positions of the tester bar were equal to each subjects' elbow height from floor and forearm length from the midpoint between ankle bones (Fig. 2), respectively. Two torque amplitude (20 and 30 Nm) and four duration (200, 360, 520, and 680 ms) levels were applied.

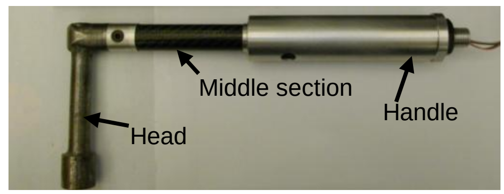

Figure 1: Tester bar assembly.

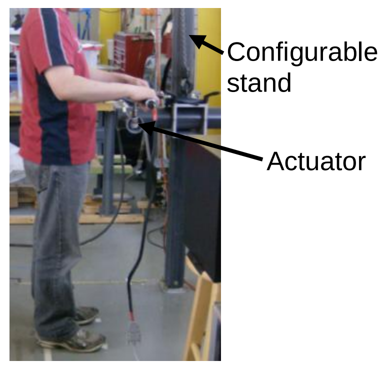

Figure 2: A test subject.

Table 1: Subjects' descriptive information.

	Female (n=10)		Male (n=12)	
	Mean	SD	Mean	SD
Height (cm)	162	6.1	177	7.0
Weight (kg)	57	9.1	80	10.9
Age (years)	30	9.5	28	7.0

The nonlinear hand-arm model during the application of the torque pulse (t_0 to t_f) was represented as a single degree-of-freedom (DOF) second-order system with stiffness (k_n), mass (m_n) and damping (c_n) parameters (Eqn 1a-b). The passive dynamics were lumped in constants m_n and c_n, whereas the active resistance modulation was modeled with k_n, a piecewise continuous function consisting of three regions. In region 1, $k_{n,1}(x)$ was assumed zero, representing muscle reflex and electromechanical delays. In regions 2 and 3, $k_{n,2}(x)$

and $k_{n,3}(x)$ were second degree polynomials in terms of hand displacement (x), which represented stiffness modulation with respect to x in eccentric and concentric muscle exertions, respectively. Model parameters were computed in the time domain with the least squares technique. The linear and nonlinear models were compared to each other in terms of estimated hand displacement error and displacement R^2 with respect to experimental measurements.

$$m_n, c_n = \text{constant},$$

1a-b
$$k_n(x,\dot{x},t) = \begin{cases} k_{n,1}(x), & t_0 \le t \le (t_0+t_1) \\ k_{n,2}(x), & (t_0+t_1) < t \text{ and } \dot{x} > 0 \\ k_{n,3}(x), & \dot{x} \le 0 \text{ and } t \le t_f \end{cases}$$

RESULTS AND DISCUSSION

Pulse amplitude had no significant effect on either of the models' accuracy. Pulse duration, on the other hand, had significant effects. Figure 3 shows sample results of experimental displacement profiles and nonlinear and linear model estimations based on simulation. The graphs suggest that the developed nonlinear model provided accurate estimation for both pulse durations, whereas the linear model's accuracy decreased for longer duration pulses. These observations were verified via statistical testing (results in Table 2). The nonlinear model had less displacement error ($p<0.001$) and greater displacement R^2 than the linear model for all pulse durations. Also, the SD of the nonlinear model displacement R^2 was less, by an order of magnitude, than that of the linear model for all pulse durations. Overall, the nonlinear model developed in this study consistently provided greater displacement accuracy compared to the linear model. In other terms, the nonlinear model was reliable over a broader range of input profiles when compared with the linear model.

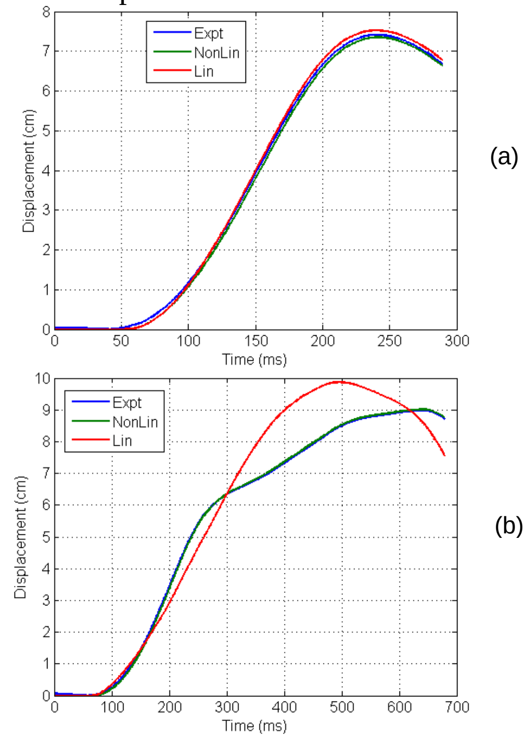

Figure 3: Sample results of model accuracy for (a) 200 ms, (b) 680 ms pulse durations. Experimental measurements (Expt, blue) are plotted with nonlinear (NonLin, green) and linear model (Lin, red) displacement estimations.

REFERENCES

1. Ku C-H, *et al.* Power hand tool kinetics associated with upper limb injuries in an automobile assembly plant. *Journal of Occupational and Environmental Hygiene*. 2007; 4: 391-399.
2. Lin J-H, *et al.* A single-degree-of-freedom dynamic model predicts the range of human responses to impulsive forces produced by power hand tools. *J Biomech*. 2003; 36: 1845-52.
3. Ay, H., *et al.*, 2010, Biodynamic modeling and physical capacity assessment of human arm response in experienced torque tool operators. *34th Annual Meeting of the ASB*, Providence.
4. Frolov A., *et al.* Adjustment of human arm viscoelastic properties to the direction of reaching. *Biol Cybern*. 2006; 94: 97-109.

Table 2: Displacement R^2 and peak displacement error of the nonlinear and linear models. The statistical significance of the mean difference in peak displacement error between the models was calculated with the paired t-test (* $p<0.001$).

Pulse Duration (ms)	Model	Mean (SD) Displacement R^2	Mean (SD) Peak Displacement Error (%)	Mean Difference in Peak Displacement Error (%)
200	Nonlinear	0.9974 (0.0028)	-0.82 (1.34)	-2.82*
	Linear	0.9781 (0.0445)	2.01 (1.29)	
360	Nonlinear	0.9984 (0.0046)	-0.05 (0.77)	-2.92*
	Linear	0.9523 (0.1055)	2.87 (5.29)	
520	Nonlinear	0.9988 (0.0033)	0.36 (0.35)	-3.74*
	Linear	0.8449 (0.2084)	4.11 (3.82)	
680	Nonlinear	0.9869 (0.0921)	0.26 (0.27)	-4.23*
	Linear	0.8209 (0.2346)	4.49 (5.04)	

MUSCLE ACTIVITY PATTERNS OF LOWER LIMB DURING LATERAL (FRONTAL) SIDE STEPPING TASK MODULATION FROM DIFFERENT HEIGHTS

[1]Dinesh Bhatia, [2]Mario Novo,[2]Marcos Munoz,[1]Tatiana Bejarano,[1]Ranu Jung and[2]Denis Brunt

[1]Adaptive Neural Systems Lab, Department of Biomedical Engineering, Florida International University, Miami, FL-33174, USA
[2]Department of Physical Therapy, Florida International University, Miami, FL-33199, USA
email: dinesh.bhatia@fiu.edu

INTRODUCTION

Different muscle groups function in synchrony and coordination to perform a given task, wherein the activity of one muscle group closely affects that of another [1,3]. Osteoarthritis (OA), a chronic joint disease, is the most common musculoskeletal complaint worldwide characterized by pain, disability and progressive loss of function. It is associated with significant health and welfare costs [2,7]. The knee is the most frequently affected lower limb joint and prevalence of knee OA increases with age [6]. Several studies have shown that muscle recruitment patterns and neuromuscular efficiency are different for patients with OA compared to normal controls during simple closed chain activities [4,5]. However, no studies have investigated frontal plane control or the modulation of control due to, for example, a change in time or distance in OA [5,6]. This paper reports the results of a pilot study with healthy subjects to determine muscle activation patterns (electromyogram, EMG), and modulation of these patterns, in a frontal plane step initiation task.

METHODS

Four subjects, age 23-32 years, mean height and weight 165 cm and 75 kg respectively, participated in the study. EMG for the support limb was recorded from rectus femoris (RF), vastus lateralis (VL), vastus medius (VM), biceps femoris (BF), semi membranous (SM), tibias anterior (TA), gastrocnemius (GAS), gluteus medius (GM), and gluteus maximus (GMax) while the subjects side stepped up (at a fixed interval with feet on separate force plates) on a 4 or 8 inch step (Figure 1).Subjects completed 3 successful trials. Muscle activity and ground reaction forces (GRF) were recorded employing an 8 channel EMG system (Motion Lab Corp.) and dual force plates (AMTI) respectively. The signals were sampled at 1000 Hz and band-pass filtered (20-500 Hz) with the EMG full-wave rectified [3]. The recorded EMG and GRF data were averaged across these trials for each subject. The GRF data were used to identify the phases of movement and matched with the corresponding EMG data in Visual 3D software.

RESULTS AND DISCUSSION

Three distinct phases for the step up task were identified as shown in figure 2 for the 8 inch step. These were from initiation to toe-off (1-2), toe-off to contact (2-3), contact to loading and stabilization (3-4). It was observed that for the 8 inch step, there was both an increase in slope and the peak of ground reaction force. For example, the slope of mediolateral GRF (figure 2B) for the 8 inch step increased by 200% over the 4 inch step. Subjects completed the 8 inch step in relatively less time duration. The GM and GMax were also found to be more active from initiation to end of the stabilization phase. The RF was active from beginning of initiation to end of contact phase. However, the activity of the SM and GAS was quite insignificant. In addition, the EMG amplitudes also greatly increased in 8 inch step up task. The mean integral values increased for most muscles (figure 2 C-E) by approximately -50%.

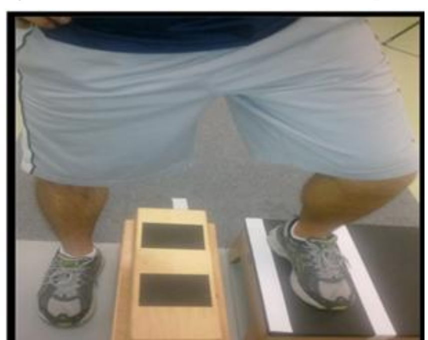

Figure 1: Lateral step up task from 8 inch step on force plate.

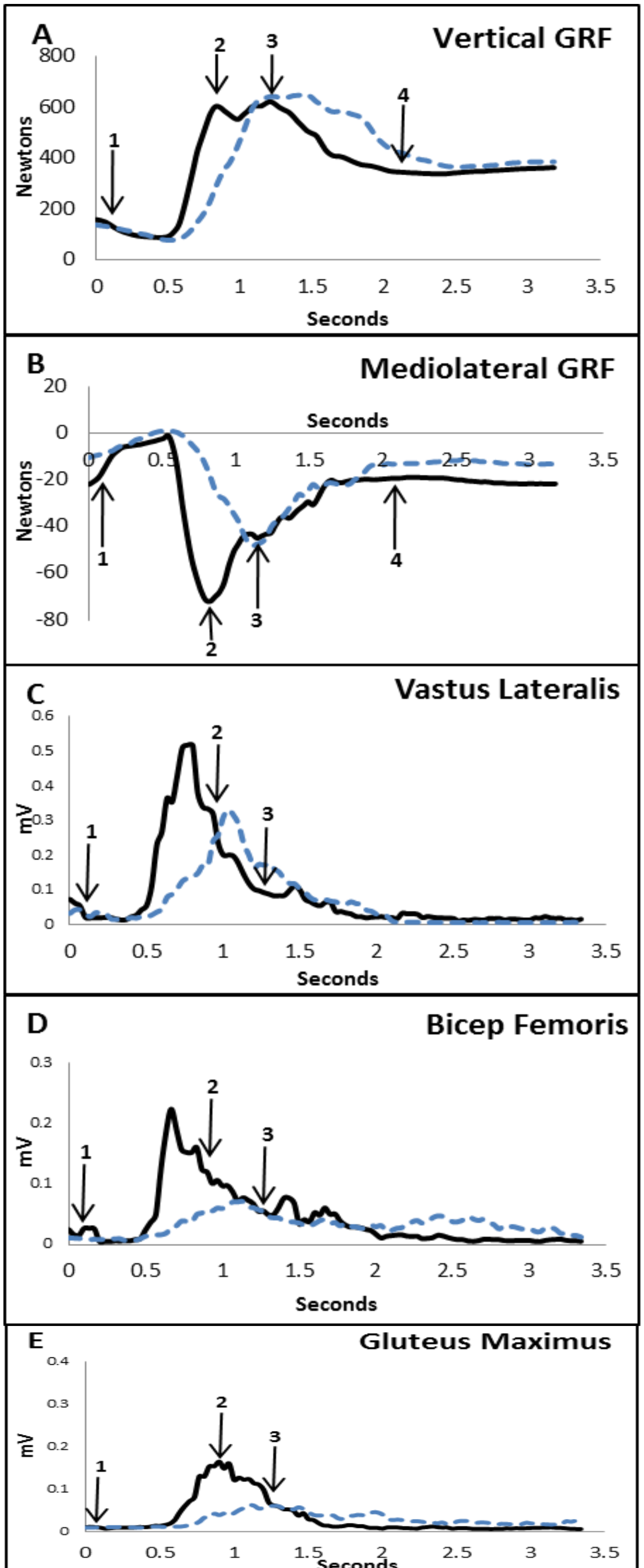

Figure 2: Comparison of 4 inch (dotted) and 8 inch (solid) step-up task phases:
1. Initiation, 2. Toe-off, 3. Contact, 4. Stability
A. Stability Leg (Z) GRF
B. Stability Leg (X) GRF
C. EMG Vastus Lateralis
D. EMG Biceps Femoris
E. EMG Gluteus Maximus

CONCLUSIONS

These results provide a baseline standard for understanding lower extremity muscle group patterns actively involved in performance of lateral side stepping tasks. These distinct phases in the step up task were found to be consistent for all subjects. The results illustrate coordination in the muscle activity patterns of different muscle groups during task modulation with prominent firing of the quadriceps, hamstrings and the hip abductor/extensor muscles for the side step up task. Future studies will examine OA subjects and determine if there is both a phase shift and amplitude change. This could be useful in defining kinematic and activation patterns for identifying early onset of the disease as well as rehabilitation protocols prior to surgery.

REFERENCES

1. Bhatia D., et al. "Coordination between lower limb muscles in different locomotion activities", *IJBET*, **6 (2)**, 23-30, 2011**.**
2. Childs J.D., et al. "Alterations in lower extremity movement and muscle activation patterns in individuals with knee osteoarthritis", *Clin. Biom.*, **19**, 44-49, 2004.
3. De Luca, C.J., "The use of surface electromyography in biomechanics", *Journal of App.Biom.*, **13 (2)**, 135–163, 1997.
4. Likivainio T., et al. "Physical function and properties of Quadriceps femoris muscle in men with knee Osteoarthritis", *A. Phys. Med.Rehabil*, **89**, 2185-2193, 2008.
5. Pai Y.C., et al. "Alteration in multijoint dynamics in patients with bilateral knee osteoarthritis", *Arthritis Rheum.*, **37 (9)**, 1297-304, 1994.
6. Rana S., et al. "Delayed onset of Quadriceps activity and altered knee joint kinematics during stair stepping in individuals with knee Osteoarthritis", *A.Phys Med. Rehab.*, **83**, 1080-1086, 2002.
7. Rana S. H., et al. "Hip Muscle Weakness in Individuals with Medial Knee Osteoarthritis", *Arthritis Care & Research*, **62 (8)**, 1190-1193, 2010.

Static Comparison of Subtalar Joint Neutral and Neutral Cushioning Running Shoes to Barefoot Stance using Markerless Radiostereometric Analysis

[1]Megan Balsdon, [1]Kristen Bushey, [2]Colin Dombroski and [1,3]Thomas R. Jenkyn

[1]Dept. of Mechanical and Materials Engineering, Faculty of Engineering, The University of Western Ontario, London, ON, Canada
[2]SoleScience, Fowler Kennedy Sport Clinic, The University of Western, Ontario
[3]School of Kinesiology, Faculty of Health Sciences, The University of Western Ontario
email: mbalsdon@uwo.ca

INTRODUCTION

The medial longitudinal arch (MLA) is a concave arch that is located along the medial aspect of the foot between the head of the first metatarsal and the calcaneal tuberosity – the highest part of the arch being the talonavicular and naviculocuneiform joints. The MLA is of considerable interest in recent research, as evidence suggests that arch structure can affect an individual's overall kinematics. Williams III et. al saw an increase in leg stiffness in high arch compared to low arch runners [1].

The multi-segment foot model using optical motion capture has previously measured foot kinematics and more specifically, the MLA angle in posterior tibialis tendon dysfunction [2]. In a study performed by Tome et. al, the researchers added a reflective marker on the navicular tuberosity to calculate a three dimensional angle using the dot product of two vectors from the navicular to both the metatarsal head and the posterior calcaneus. A similar angle calculation was used for this study using the medial process of the calcaneus. The location of the first metatarsal, navicular and calcaneus were tracked using fluoroscopic markerless radiostereometric analysis (fRSA), a process validated at the Wolf Orthopaedic Quantitative Imaging Laboratory [3,4].

The purpose of this study was to quantify the difference in angle of the MLA during weight-bearing barefoot stance, in subtalar joint neutral position and in neutral cushioning running shoes. It was hypothesized that the arch angle would decrease in both shoed feet and the subtalar joint neutral position compared with barefoot, with a greater angle decrease occurring in the subtalar neutral position – meaning the elongation of the arch of the foot will be restricted the most for this condition.

METHODS

Sixteen participants were recruited from the Fowler Kennedy Sports Medicine Clinic by a certified Canadian pedorthist – 6 normal, 5 pes planus (low arch) and 5 pes cavus (high arch). The clinician performed a comprehensive assessment of the participants' gait patterns as well as their foot function in all three planes (inversion/eversion, forefoot ab/adduction and ankle planter/dorsi flexion) in order to assure they fit the study criteria.

Participants were instructed to stand in quiet, full weight bearing stance as a static image was taken of the left foot. Three static conditions were looked at for this study – barefoot, neutral cushioning running shoe and the subtalar joint neutral (STN) position. For each trial, it was ensured that the calcaneus, navicular and the first metatarsal were visible in both fluoroscopes.

Two fluoroscopes (SIREMOBIL Compact (L); Siemens Medical Solutions USA Inc., Malvern, PA, USA) were set-up up at approximately 120° to one another. A wooden platform was designed to raise the participants to a level where their fields of view were positioned to get a sagittal plane, lateral view and an oblique anterior-posterior view of the left foot. The fluoroscopes were calibrated and corrected for distortion using custom MATLAB code [5] (MATLAB, The MathWorks, Natick, MA, USA). Additional algorithms were used to determine the remaining calibration parameters such as the x-ray source locations and both image plane orientations.

The experimental set up was then recreated in modeling software – Rhinoceros (Rhinoceros, Robert McNeel & Associates, Seattle, WA, USA) where a 3D model of the bones (calcaneus, navicular and first metatarsal) were imported to match the exact pose for each image separately. The locations of three bony landmarks of each bone were exported into a spreadsheet and run through MATLAB code to determine the MLA angle.

RESULTS

In barefoot static stance, the planus group had the greatest mean medial longitudinal arch (MLA) angle of 127.8° ± 13.7° and the smallest mean angle seen by the normal group at an angle of 98.7° ± 16.0° (Table 1).

Table 1: Absolute MLA angles in three groups during static images of barefoot stance.

	Absolute Angle (°)			
	Mean	**Maximum**	**Minimum**	**Range**
Normal	98.7	129.3	84.4	44.9
Planus	127.8	139.3	104.4	34.8
Cavus	110.9	128.3	88.3	40.0

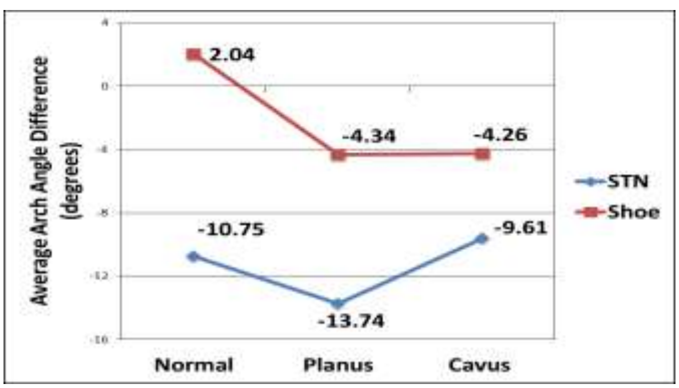

Figure 1: Average MLA angle differences of subtalar joint neutral and neutral cushioning running shoes compared to static barefoot stance.

The average angle differences within each patient group, normal, cavus and planus are shown in Figure 1. The largest difference occurred in the planus group, with an average angle decrease of -13.7° in the subtalar neutral position with respect to the barefoot condition. The average angle decreases were -10.8° and -9.61° in both the normal and pes cavus groups, respectively.

DISCUSSION

This study shows a fairly consistent decrease in arch angle across study volunteers when placed in the subtalar joint neutral (STN) position as compared with standing barefoot. As expected, the greatest change in angle occurred in the planus group as they have by definition the largest arch angle and therefore, should have the largest angle adjustment to the subtalar joint neutral position.

Both the planus and cavus groups showed a small decrease in MLA angle with the running shoes. This means that the MLA was restricted a bit less in shoes than in the subtalar neutral position. The normal group showed an increase in arch angle meaning the arch elongated, causing a greater MLA angle. Though the neutral running shoe may not provide as much support as a stability shoe, arch restriction was still expected, demonstrating additional support compared with no shoe.

Due to the nature of the extensive experimental protocol and time constraints of the study, only a small number of subjects in each group could be tested. Though participants may look and function as a pes cavus or a normal, their absolute arch angle may not reflect overall foot motion, causing slightly inconsistent angles. Further analysis would include comparing the subtalar joint neutral angle with the use of orthotics since the ultimate goal of orthotics are to restrict the MLA and maintain close to neutral position through flatfoot in gait.

REFERENCES

1. Williams III, D. S., et al. *Gait and Posture* **19**, 263-269, 2004.
2. Tome, J., et al. *J Ortho & Sports Phys Ther* **36** (9), 635-644, (2006).
3. Fox, A.-M, et al. *J Biomech* **44**, 2847-2850, 2011.
4. Allen, A.-M. Thesis - University of Western Ontario. London, ON, Canada. 2009.
5. Kedgley, A. & Jenkyn, T.R. *Medical physics* **36** (7), 3176-3180, 2009.

A GENDER COMPARISON OF LOWER EXTREMIY AMBULTORY MECHANICS IN HEALTHY SUBJECTS WITH EXCESSIVE VARUS ALIGNMENT

[1]Joaquin A. Barrios and [1]Danielle E. Bare
[1]University of Dayton, Dayton, OH, USA
email: jbarrios1@udayton.edu

INTRODUCTION

Frontal plane lower extremity alignment and gender are documented risk factors for osteoarthritis (OA). In regards to alignment, varus malalignment has been linked to incident and progressive medial knee OA (Brouwer, 2007). It is often suggested that the high dynamic knee joint loading associated with varus malalignment partly explains this disease link. In regards to gender, the prevalence of medial knee OA is greater in females (Srikanth, 2005). Interestingly, the interplay between malalignment, dynamic loading and gender has not been thoroughly explored in individuals at risk for developing disease. Therefore, we aimed to analyze the ambulatory mechanics of healthy and high-functioning males and females with excessive varus malalignment in an effort to explain gender-specific consequences to malalignment prior to the potential onset of pathology.

METHODS

Thirty total subjects with varus but otherwise healthy knees were recruited for the study. In an attempt to match the gender groups by degree of malalignment, we utilized the frontal plane mechanical axis of the tibia as measured using a caliper-inclinometer device (Barrios, 2009). A value of ≥ 10° from vertical was needed to qualify, as this value is 1.5 standard deviations from the mean of an in-house normative database of 175 volunteers. To confirm that subjects' knees were healthy, subjects completed the Sports and Recreational Activities subscale of the Knee Injury and Osteoarthritis Outcome Score Knee Survey. A score of ≤ 2/20 (where 20/20 means extreme symptoms) was needed to qualify. The more malaligned limb was chosen for analysis unless the limbs were symmetrical, in which case a limb was chosen at random.

Three-dimensional motion analysis was then conducted. A static standing and functional hip motion trial were collected. Level walking was then captured at a controlled speed at 1.46 m/s (± 2.5%) along a 23 m walkway. Marker trajectory data were captured using an 8-camera VICON motion analysis system (120 Hz), and kinetic data using a Bertec force platform (1080 Hz). Five usable trials were post-processed using Visual 3D. Custom Labview software was used to extract the discrete variables of interest. Specifically, we extracted discrete gait variables previously observed to be altered in the presence of knee OA. This included frontal and sagittal plane angles (XYZ Cardan sequence) and external moments (expressed in the distal coordinate system) for the hip and the knee. We also evaluated knee internal rotation, contralateral pelvic drop and rearfoot eversion angles. SPSS software was used to perform independent samples t-tests, with a predetermined alpha set to 0.05. As we matched the groups for tibial alignment in the frontal plane, we expected no differences in the frontal mechanics. However, as males have been found to exhibit greater lower extremity flexion in dynamic tasks in other studies, we hypothesized potential differences may be revealed in the sagittal data.

RESULTS AND DISCUSSION

15 female and 15 male subjects participated in the study (Table 1). There were no significant differences between the groups in age, BMI, KOOS-SR score, or TMA angulation.

Table 1: Subject demographics by gender

	Age (yrs)	BMI (kg/m^2)	KOOS-SR (0-20)	TMA (deg)
Males	22.8 (3.0)	23.1 (2.7)	0.3 (0.6)	11. (0.6)
Females	21.1 (2.5)	21.2 (3.0)	0.5 (0.8)	10.7 (0.8)
P-value	0.095	0.092	0.322	.228

Interestingly, we only observed differences in the frontal plane variables, while observing no differences in the sagittal or transverse plane joint mechanics. At the hip joint, we observed greater peak adduction angles and external adduction moments in the females (Figure 1). At the knee, the males exhibited greater peak knee adduction angles, but did not exhibit greater peak external adduction moments.

In general, and consistent with other studies, our results support the notion that there is no difference in lower extremity sagittal patterns during walking between genders. In comparing to other knee OA gait studies, these values suggest that the stiffer, more extended mechanics seen in OA patients is related to the onset of disease (Barrios, 2009).

Contrary to our hypotheses, we did observe frontal plane differences between genders. As we matched the groups for frontal plane tibial angulation, we suggest that the more adducted hip mechanics seen in the females may reflect anthropometric differences. To further support this notion, we did not observe differences in the frontal plane pelvic kinematics. Possibly, relative to height or femoral length, pelvic width may greater in females. While we did not collect pelvic width measures, this may be a focus of future investigation.

At the knee, the greater dynamic varus angles seem to suggest that thigh segment mechanics may have varied such the females exhibited more global thigh adduction, while the male thighs may have been more vertically oriented. Future analysis of segmental kinematics is warranted.

CONCLUSIONS

In summary, we evaluated 3D gait mechanics in varus-aligned but otherwise healthy males and females. The groups were matched by tibial angulation. Interestingly, the results revealed greater adduction mechanics at the hip in the females, suggest of underlying anthropometric differences. Future work in the area should include analysis of segmental thigh and shank mechanics, as well as evaluation of anthropometric measures such as pelvic width.

REFERENCES

1. Brouwer GM et al., (2007). Arthritis Rhuem 56:1204-1211.
2. Srikanth VK et al., (2005). Osteoarthritis Cartilage 13:769-781
3. Barrios JA et al., (2009). J Orthop Res 27:1414-1419.

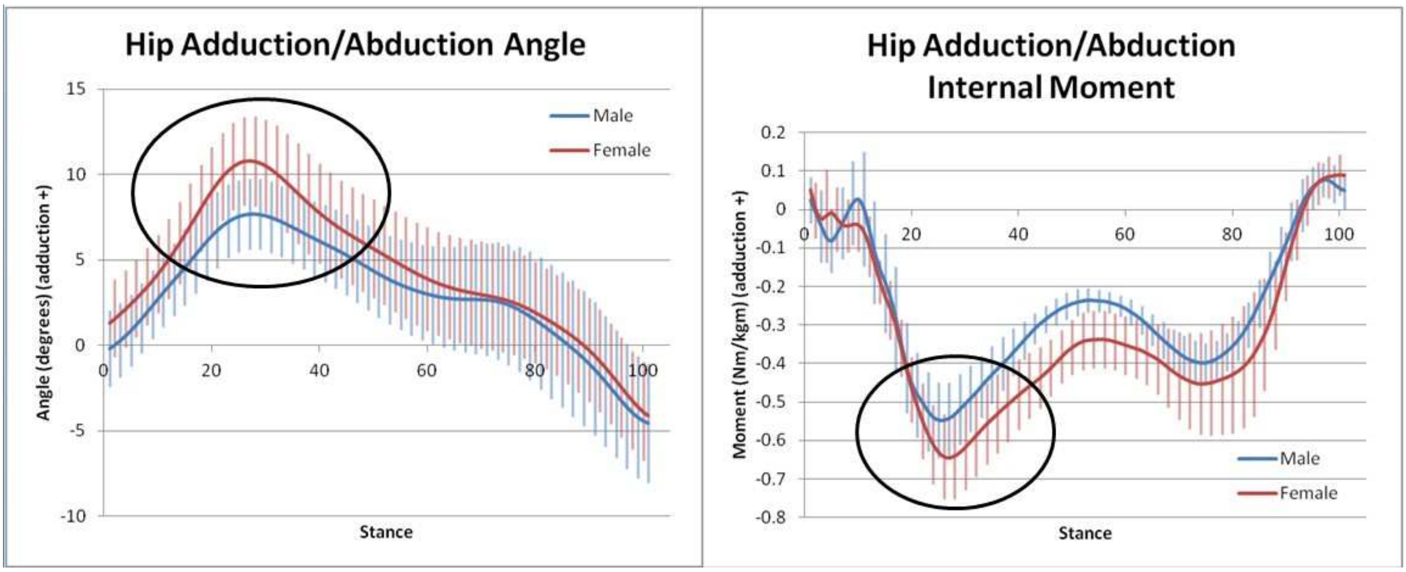

Figure 1. Greater hip adduction angles and moments were observed in the varus-aligned but otherwise healthy females

VALIDATION AND CALIBRATION OF THE WII BALANCE BOARD AS AN INEXPENSIVE FORCE PLATE

[1]Harrison Bartlett, [1]Jeff Bingham and [1,2]Lena H. Ting

[1]Georgia Institute of Technology, Atlanta, GA, USA
[2]Emory University, Atlanta, GA, USA
email: hbartlett3@gatech.edu

INTRODUCTION

Integral to the study of balance and movement is the ability to quantitatively measure it. However, current methods of quantifying balance used in research studies require expensive force plates and complex instrumentation that is inaccessible to the public. Inexpensive solutions may be achieved by appropriating current advances in video game technology, allowing a broader range of investigators to take quantitative balance measurements [1,2,3,4].

Some researchers have begun using interactive video games with the Nintendo Wii Balance Board (WBB) to aid in balance rehabilitation [3]. Similarly, researchers have developed custom games using the WBB to reduce fear of falling in elderly populations [4]. Inherent to these games is the use of the WBB as a measurement device.

Thus, the WBB also has potential to be an inexpensive (<$100) and readily accessible force plate. However, the accuracy and reliability of the device has not been documented. Previous validation attempts have compared center-of-pressure (COP) path length measured during standing balance using the WBB versus laboratory grade force plates [1]. These results offered qualitative evidence that the WBB provides accurate COP measurements, but did not quantify the device's measurement uncertainty.

METHODS

Here we tested the accuracy of the individual vertical force sensors used in the WBB, as well as the accuracy of the computed COP location.

Data collection
Data from the WBB was collected through Bluetooth using a custom Matlab interface. The data stream from the WBB was un-calibrated digital data from each of the four force sensors of the WBB. In addition to this data stream, the WBB was polled to recover internally stored calibration values that related the raw data stream for each sensor to kilogram values (a three-point calibration at 0, 17, and 34 kg).

Calibration of individual force sensors
Each individual sensor of the WBB was tested in the original enclosure 5 times with 20 different weights in a range of 0-29.3 kg. Weight increments were applied directly to each foot, with the WBB top surface face down, in increasing then decreasing value.

Calibration of COP
The entire WBB was tested 5 times by placing 2 different magnitudes (approximately 15kg and 45kg) of weight at 30 different locations across the WBB top surface (Figure 1). Weights were placed on the board using a vertical pole with a rounded tip so that weight was applied at a single point. The pole was then stabilized to ensure only downward force on the WBB. COP was calculated using the center of the board as the origin to utilize information from all four sensors instead of the corner of the board, which requires only two sensors and would increase uncertainty. The formulas below use the following nomenclature (L = long x-dimension, W = short y-dimension, TR = top right, BR = bottom right, TL = top left, BL = bottom left).

$$COPx = \frac{L}{2}\frac{((TR+BR)-(TL+BL))}{TR+BR+TL+BL}$$

$$COPy = \frac{W}{2}\frac{((TR+TL)-(BR+BL))}{TR+BR+TL+BL}$$

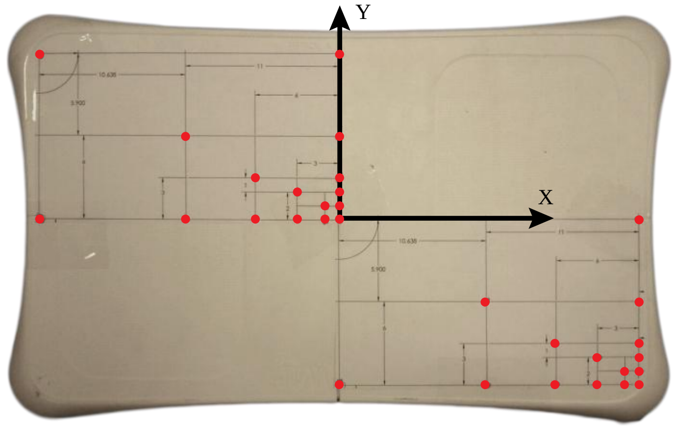

Figure 1: Top surface of the WBB. Filled dots represent locations where COP was tested.

Data analysis

Raw force data from the WBB was calibrated using both the internally stored calibration values and the validated weights used in the experiment. Weight uncertainty was calculated based on data errors of hysteresis (e_H), linearity (e_L) and repeatability (e_R) with t-values appropriately selected from the student-t distribution.

$$U_c = \sqrt{t_H e_H{}^2 + t_L e_L{}^2 + t_R e_R{}^2}$$

COP uncertainty was calculated based on data errors of linearity (e_L) and repeatability (e_R).

$$U_c = \sqrt{t_L e_L{}^2 + t_R e_R{}^2}$$

The accuracy for each data condition was a combination of uncertainty (U_c), resolution (r) and standard deviation (σ)of a measurement.

$$U_N = \sqrt{(U_c)^2 + (\frac{r}{2})^2 + (t_{v\_95}\sigma)^2}$$

RESULTS AND DISCUSSION

The internal calibration values stored in the WBB were found to be within 1.1% of those determined experimentally. Therefore, further analyses were computed using only the internal calibration.

Individual WBB weight sensors were found to have an accuracy of ±0.61 kg with a resolution of 0.1g, hysteresis error of ±0.12 kg, linearity error of ±0.83 kg and repeatability error of ±0.52 kg. The uncertainty of weight measurements for the combined sensors was ±1.4 kg.

COP from the WBB was found to have uncertainties of ±0.8 cm in the long dimension (COPx) and ±0.9cm in the short dimension (COPy). COPx had errors in linearity of ±0.7 cm and repeatability of ±0.4 cm. COPy had errors in linearity of ±0.5 cm and repeatability of ±0.3 cm.

Table 1: Accuracy of the WBB using internally stored calibration values and for a laboratory grade force plate AMTI OPT464508HF-1000 [5].

	Mass	COPx	COPy
	g	mm	mm
WBB	±1400	±80	±90
AMTI	±20	±2	±2

CONCLUSIONS

Our WBB calibration shows that this device may be an inexpensive force plate substitute to quantify balance. The uncertainty in the WBB is 45 times more than the uncertainty in scientific force plates (WBB=90 mm vs AMTI=2 mm), but with a cost of 200 times less (WBB=$100 vs AMTI= $20000).

The WBB can reliable differentiate COP location differences greater than 1 cm, which may be useful in distinguishing healthy from impaired populations during standing balance [2]. There may be greater resolving power in cases of repeated measures experiments, since repeatability errors of the WBB are <0.5 cm.

Finally, the WBB can be used for measuring static vertical forces with uncertainties on the order of a kilogram. However, the dynamic characteristics of the WBB remain untested, which will require further validation.

REFERENCES

1. Clark, R. A., et al. *Gait & Posture*, ***31*(3)**, 307-310. 2010.
2. Fox, Z. G., et al. *Journal of Athletic Training*, ***43*(5)**, 456-463. 2008.
3. Gil-Gómez, et al.. *Journal of NeuroEngineering & Rehabilitation (JNER)*, ***8*(1)**, 30-39. 2011.
4. Kwok, B., et al. (2011). *Trials*, ***12*(1)**, 155. 2011.
5. AMTI Data Sheet. http://amti.biz. Accessed Feb 27, 2012.

PHYSIOLOGICAL COST OF HEAVY LOAD CARRIAGE

[1]Jamie L. Bartlett and [2]Kristi Robusto

[1]Naval Health Research Center, San Diego, CA, USA
[2]Pacific Science & Engineering Group, Inc., San Diego, CA, USA
e-mail: jamie.bartlett@med.navy.mil

INTRODUCTION

It is well known that carrying heavy loads has a negative effect on physical and cognitive measures of human performance. Most of the previous literature has primarily examined loads under 100 pounds. In modern military engagements, infantry warfighters carry between 97–167 lbs [1]. Tactical considerations require warfighters to carry a minimal amount of equipment, weaponry, and sustenance to meet mission goals. Commanders understand that heavy loads can have negative consequences on the health and performance of their warfighters. However without detailed knowledge of these effects, mission requirements take priority.

METHODS

Subjects. As part of a larger study on heavy load carriage, we recruited 29 US Marine Corps infantrymen from the USMC School of Infantry West at Camp Pendleton, CA. Table 1 summarizes subject demographics. Currently, no females actively participate in the USMC infantry and were therefore excluded from the study. Seventeen volunteers completed all study sessions. Eleven participants did not complete all of the sessions and missed one or more due to the following: illness (n=1), previous injury (n=1), discomfort (n=3), exceeded physiological stop criteria of a heart rate (HR) >90% age-predicted max heart rate (n=2), did not show up (n=2), or session was canceled or data were missing due to other reasons (n=3). Participant ranks included 14 privates, 13 privates first class, and 2 lance corporals. Volunteers gave written and informed consent in accordance with the Institutional Review Board at the Naval Health Research Center.

Table 1. Subject Characteristics (N=17)

Age (yr)	Height (in)	Weight (lbs)
19, 18–24	70.05, 63.0–76.0	165.8, 130–221

Values are listed as mean, range.

Pretest. Each testing day consisted of a 3-hour session on consecutive days. The initial session also included equipment and treadmill familiarization. We measured urine specific gravity (USG) to determine adequate hydration for the session. A USG <1.028 was required for participation. If the participant surpassed this criterion, we asked him to hydrate and then retested until the criterion was met. At the beginning of each session, we measured pretesting weight (gym shorts and T-shirt) and a total weight (uniform, hydration pack, and pack load).

Test Conditions. For each weight condition (0, 98, 135 lbs), participants walked on the treadmill for 120 minutes with a 5-minute rest at the 60-minute mark. This simulates a typical Marine march procedure of resting every 60 minutes. We standardized carriage weight based on typical operational requirements: no load, assault load (98 lbs), and approach load (135 lbs). During the no load condition, subjects wore their battle dress uniform, boots, and hydration pack. For the loaded conditions, subjects additionally wore their standard-issue military pack, a Kevlar helmet, and carried a simulated M16 rifle. Bags of sand were placed in the pack to obtain the proper load of 98 or 135 pounds. Treadmill speed was set at 2.0 mph and 0% grade. Metabolic cost was assessed via indirect calorimetry (TrueOne 2400, ParvoMedics, Sandy, UT) at rest and at four time periods during each session. At the same intervals, we recorded HR (Garmin Forerunner 50) and ratings of perceived exertion (RPE) using the 6-20 Borg scale [2].

RESULTS AND DISCUSSION

Table 2. Heart Rate and Perceived Exertion

Load (lbs)	HR (beats/min)	RPE
0	88.4 ± 11.6 Range: 83–94	6.6 ± 0.2 Range: 6–7
98	110.1 ± 13.1 Range: 104–116	11.5 ± 0.6 Range: 10–13
135	130.8 ± 10.4 Range: 126–136	15.4 ± 0.6 Range: 14–17

Values are listed as mean ± standard deviation.

Table 2 summarizes the results for HR and RPE at each load condition. A one-way repeated-measures analysis of variance was used to compare variables across load. HR, RPE, and net metabolic power significantly increased as load carriage weight increased (all $p<0.001$). Net metabolic power (Figure 1) is calculated from the difference in metabolic rate during exercise and rest [3].

For the two loading conditions (98 and 135 lbs) subjects were on average walking at 58 and 80% of their total body weight. However, this percentage ranged from 44 and 61% for the heaviest subject (221 lbs) to 69 and 95% for the lightest subject (142 lbs).

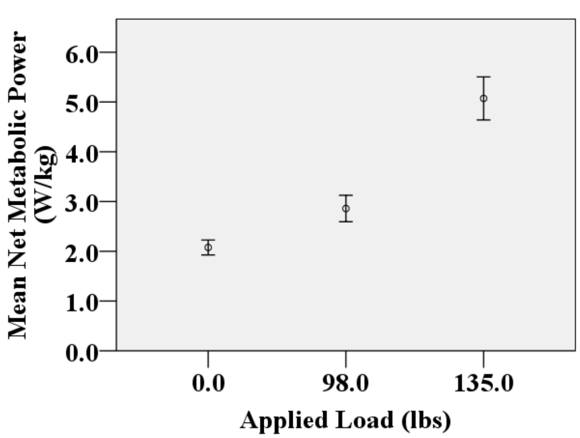

Figure 1. Mean (n=17) net metabolic power (Watts) per kg of body weight for the unloaded (0 lb) and loaded (98.0, 135.0 lb) conditions. The plot includes mean values and standard deviations.

CONCLUSIONS

Not surprisingly, carrying heavy loads increased the HR, RPE, and metabolic work of every subject. For some subjects, the heaviest loading condition required carrying over 90% of their body weight. This extreme condition is not uncommon during typical field movements while training or on deployment. While the physiological demand notably increased with heavy loading, maximal heart rates only reached approximately 65% of the age-predicted max. This demonstrates that the typical infantryman can maintain a high level of physical demand over time. However, the long-term physiological and biomechanical effects of heavy load carriage are unknown.

REFERENCES

1. Bachkosky J, et al. *Naval Research Advisory Committee Report*. NRAC 07-02, 2007.
2. Borg E, et al. *Scand J Med Sci Sports* 16:57-69, 2006.
3. Brockway JM, *Hum Nutr Clin Nutr* 41(6):463-471, 1987.

ACKNOWLEDGMENTS

We would like to acknowledge Pacific Science and Engineering Group, Inc., for the assistance with data collection and subject recruitment.

This work was supported by Office of Naval Research under work unit no. N00014-07-C-0459. The views expressed are those of the authors and do not reflect the official policy or position of the Department of the Navy, Department of Defense, or the U.S. Government. Approved for public release; distribution is unlimited. This research was conducted in compliance with all applicable federal regulations governing the protection of human subjects (Protocol NHRC.2008.0021).

BETWEEN LANDING KINETIC AND KINEMATIC DIFFERENCES IN A DROP VERTICAL JUMP

Nathaniel A. Bates[1], Kevin R. Ford[1,2], Greg D. Myer[1,2], Timothy E. Hewett[1,2,3]

[1]University of Cincinnati, Cincinnati, OH, USA
[2]Cincinnati Children's Hospital Medical Center, Cincinnati, OH, USA
[3]Ohio State University, Columbus, OH, USA
email: batesna@mail.uc.edu website: http://cincinnatichildrens.org/sportsmed

INTRODUCTION

ACL ruptures are catastrophic injuries that are debilitating to athletes. Specific kinematic and kinetic variables observed in landing and cutting are associated with increased ACL injury risk. The drop vertical jump (DVJ) test has been established as an ideal task to evaluate neuromuscular control and simulate motions and moments that place athletes at risk for ACL injuries. [1] Each DVJ involves athletes landing from a 31 cm drop and a subsequent landing following the maximal vertical jump. Though this second landing represents a more realistic simulation of in-game motion, to our knowledge it has not previously undergone biomechanical evaluation. This study aimed to examine kinetic and kinematic differences between the first and second landing of a DVJ. It was hypothesized that the second landing would be represented by less joint flexion and greater frontal plane moments at the knee and hip.

METHODS

The subject population consisted of 239 middle and high school female basketball athletes. Subjects performed three DVJ trials, which involved dropping from a 31 cm box, landing on dual force platforms, an immediate maximal vertical jump, and a second landing on the force platforms. The first landing was controlled with instructions for both feet to simultaneously make contact on separate force platforms, while no directions were given for the second landing. Trials in which a subject failed to fully contact both force platforms during the second landing were excluded. Motion data was collected on each DVJ with at 10-camera motion analysis system and the dual force platforms. Landing data was processed through Visual 3D and analyzed with custom MATALB scripts. [2] Landing stance time was used for analysis and defined as the time between initial contact with the platform and lowest calculated position of the center of gravity. Accepted trials were averaged into individual subject means and ANOVA evaluated differences between landings, while symmetry index calculated side-to-side asymmetry.

RESULTS AND DISCUSSION

Sagittal plane angular differences were present in all joints (Table 1) between the first and second landing. Subjects exhibited greater maximum extension at initial contact and less maximum flexion in all joints during the second landing relative to the first (Figure 1). When moving proximally up the kinematic chain, differences in flexion and extension angles between landings increased at each joint. Thus, differences between the tasks were most evident at the proximal joints.

Table 1: Mean maximum joint angles (degrees) for each landing phase and their statistical differences.

Joint	Angle	1st Land	2nd Land	p-value
Trunk	Extension	-12.1	13.4	< 0.001*
	Flexion	-21.3	-0.1	< 0.001*
Hip	Extension	26.8	8.7	< 0.001*
	Flexion	60.1	31.8	< 0.001*
	Adduction	0.1	-1.2	< 0.001*
	Internal	0.8	1.6	0.089
	External	-9.3	-8.6	0.091
Knee	Extension	-23.6	-14.9	< 0.001*
	Flexion	-85.1	-66.6	< 0.001*
	Abduction	-10.3	-8.6	< 0.001*
	Internal	7.2	8.2	< 0.001*
	External	-2.9	-1.5	< 0.001*
Ankle	Extension	-24.6	-27.8	< 0.001*
	Flexion	30.8	26.3	< 0.001*

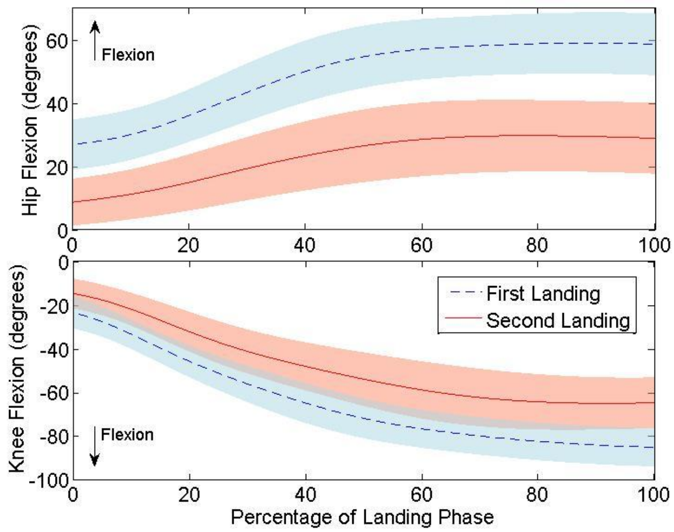

Figure 1: Graphic depiction of hip and knee flexion through stance phase of the both landings.

Table 2: Mean maximum joint torques (N*m) for each landing phase and their statistical difference.

Joint	Moment	1st	2nd	p-value
Hip	Flexion	68.0	29.9	< 0.000*
	Adduction	28.6	27.4	0.234
	Internal	12.3	10.6	< 0.000*
	External	7.7	9.7	< 0.000*
Knee	Flexion	114.0	99.4	< 0.000*
	Abduction	17.8	16.2	0.017*
	Internal	2.5	3.1	0.032*
	External	7.7	6.0	< 0.000*
Ankle	Flexion	76.4	85.4	< 0.000*

Frontal plane differences existed in knee abduction and hip adduction between each of the movements. Frontal plane joint angles were equivalent at intial contact and diverted through landing stance time. Hip adduction and knee abduction decreased in magnitude on the second landing, which may be indicative of the reduced flexion maganitudes as stiffer sagittal plane kinematics may restrict frontal plane range of motion. Transverse plane rotations only showed differences at the knee. Again, initial contact poitions were equivalent and disparity progressed through landing. Subjects demonstrated increased knee internal and hip external rotation during the second landing.

Sagittal plane kinetics decreased in hip and knee flexion moment and increased in ankle moment in the second landing (Table 2). The frontal plane exhibited greater knee abduction moments, but no differences were observed in hip adduction in the second relative to the first landing. Transverse kinetics had elevated hip external and knee internal moments for the second landing phase.

Maximum GRFs between first and second landings of DVJ task were consistent, while minimum center of gravity differences were observed during the second landing. [3] The observed differences in joint flexion may influence a more erect posture which verifies a higher center of gravity. Less sagittal plane flexion during the DVJ may be an associated characteristic of decreased neuromuscular control and increased ACL injury risk. [1] Placing athletes in more strenuous situations enhances a clinician's ability to evaluate injury risk patterns as neuromechanical deficits may be exacerbated during higher level complex tasks in athletes with deficient control. [4] Thus, restrictive flexion in the second landing may serve as a better sagittal plane screening tool, while excessive abduction in the first landing may prove optimal to assess frontal plane control and injury risk.

CONCLUSIONS

The second landing had decreased flexion angles in all joints as hypothesized. The second landing showed a lower maximum knee abduction moment and angle, but no difference in hip adduction moment. Differences between landings indicated that the second landing may provide a superior evaluation of neuromuscular control in the sagittal plane relative to the initial landing of a DVJ.

REFERENCES

1. Hewett TE, et al. *Am J Sport Med.* **33**, 492-501. 2005.
2. Ford KR, et al. *Med Sci Sport Ex.* **42**, 1923-1931. 2010.
3. Bates NA, et al. *Proceedings of UC 2012 GPF.* Cincinnati, OH, USA, 2012.
4. Ford KR, et al. *J App Bio.* **27**, 215-222. 2010.

ACKNOWLEDGEMENTS

Funding supported by NIH Grants R01-AR049735, R01-AR055563, R01-AR056259, and R03-057551.

GROUND REACTION FORCE AND TEMPORAL-SPATIAL ADAPTATIONS TO RUNNING VELOCITY WHEN WEARING RUNNING-SPECIFIC PROSTHESES

[1]Brian S. Baum, [1]Andrea Tian, [1]Melanie P. Schultz, [1]Hiroaki Hobara, [1,2]Alison Linberg, [2]Erik J. Wolf, [1]Jae Kun Shim

[1]University of Maryland, College Park, MD, USA
[2]Walter Reed National Military Medical Center, Bethesda, MD, USA
email: brianbaum1@gmail.com

INTRODUCTION

Great interest exists in whether running-specific prostheses (RSPs) provide a performance advantage to individuals with lower extremity amputations (ILEA); however little attention has been given to adaptations that ILEA must make when exercising and running with RSPs at sub-maximal velocities. Runners can modulate a large number of factors including temporal-spatial parameters to adjust velocity which will affect ground reaction forces (GRFs). Able-bodied runners tend to increase step length at lower velocities, and step frequency at greater velocities [1]. However, literature differs in how ILEA increase their running speed by either predominantly increasing step frequency [2], or primarily increasing step length [3]. In a previous study, ILEA that ran with RSPs showed similar increases between limbs in average vertical GRFs with increasing velocity [4], but the antero-posterior (AP) forces were not examined. The aim of this study was to quantify temporal-spatial and GRF adaptations to different running velocities when running with a passive RSP. It was hypothesized that ILEA running with RSPs would exhibit different temporal-spatial and AP GRF outcomes than able-bodied controls indicating altered strategies to increase running velocity.

METHODS

Eight male subjects with unilateral transtibial amputations who wear RSPs and eight male control subjects volunteered to run around a 100m long track at constant, prescribed velocities (2.5 m/s, 3.0 m/s, and 3.5 m/s ±0.2m/s) administered randomly. Ten force platforms embedded in the track collected GRF at 1000 Hz. Ten motion capture cameras collected temporal-spatial data at 200 Hz. Six sets of laser sensors evenly spaced around the track monitored velocity in real time. Variables of interest included step length, step frequency, stance time, swing time, peak AP braking and propulsive GRFs, and AP braking and propulsive impulses (GRF time integrals). GRF data were normalized to body weight. A 2x2x3 (leg x group x velocity) repeated measures ANOVA with Bonferroni-adjusted post-hoc analyses determined differences with $\alpha=0.05$.

RESULTS and DISCUSSION

All subjects achieved the target velocities. No differences existed between the left and right control limbs for any variable, so these data were averaged for presentation in tables and figures. Table 1 shows the average values of temporal-spatial parameters for the prosthetic, intact, and control limbs across all tested running velocities. ILEA intact limb step lengths, pushing off with the prosthetic limb, were significantly shorter than the prosthetic and control limb step lengths at all velocities ($p<0.001$). To compensate for shorter intact limb step lengths, ILEA used greater step frequencies ($p\leq0.011$) than the able-bodied subjects at all velocities. No swing time differences existed between any limb. However, both prosthetic and intact limbs in ILEA had significantly shorter stance times than controls indicating an adaptation which may be used to match running velocities of able-bodied runners. ILEA increased both step frequency and step length to achieve greater velocities. This contrasts previous literature that suggested ILEA predominantly rely on increasing only one of these variables [2, 3]. With increasing velocity, stance time decreased for both ILEA and control subjects, but swing time did not change for either group or for any limb. Since ILEA limbs had shorter step times than the control group, decreasing step time also appears to be an adaptive mechanism that ILEA use to increase velocity.

Peak AP propulsive forces were lowest in the prosthetic limb at 3.0 m/s and 3.5 m/s ($p=0.044$) (Fig. 1A). However, prosthetic limb propulsive impulses were comparable to the intact and control limbs (Fig. 1B). These similar impulses were generated by having an earlier onset and longer period of positive propulsive force. Significant velocity effects were evident for the peak braking and propulsive GRF ($p<0.020$ for all) and braking and propulsive impulse for the intact and control limbs ($p\leq0.040$). Prosthetic limb braking and propulsive impulses did not change with velocity ($p=0.403$ and 0.079, respectively). Significant leg x speed interactions were identified for the peak AP propulsive GRF ($p=0.042$) and braking impulse ($p=0.002$) where the intact limb magnitudes increased at a greater rate with velocity than the prosthetic limb. The intact and control limbs had a greater braking impulse than the prosthetic limb at each velocity ($p\leq0.003$). These data indicate that ILEA use the intact limb to a greater extent than the prosthetic limb to brake and propel at faster velocities, but not more than the control limbs.

CONCLUSIONS

ILEA wearing RSPs increase running velocity by increasing step length and step frequency. Reducing stance time appears to be an adaptation that ILEA wearing RSPs use to match running velocities of able-bodied runners and to increase their velocity. Despite lower prosthetic limb peak AP propulsive GRFs, ILEA compensated by prolonging this limb's propulsive force period to generate similar propulsive impulses to the intact and control limbs.

REFERENCES

1. Keller TS et al. *Clin Biomech* **11,** 253-9, 1996.
2. Enoka RM et al. Am *J Phys Med* **61,** 66-84, 1982.
3. Sanderson D, Martin P. *Arch Phys Med Rehabil* **77**, 1279-1285, 1996.
4. Grabowski A et al. *Biol Letters* **6**, 201-204, 2010.

ACKNOWLEDGEMENTS

Funding by the Univ. of Maryland Dept. of Kinesiology Graduate Research Initiative Fund.

Table 1. Average values (±SD) of temporal-spatial parameters for the prosthetic, intact, and control limbs across the tested running velocities.

	Stance Time[vg] (s)			**Swing Time (s)**			**Step Length[vg] (m)**			**Step Frequency[vg] (steps/min)**		
Velocity:	***2.5 m/s***	***3.0 m/s***	***3.5 m/s***	***2.5 m/s***	***3.0 m/s***	***3.5 m/s***	***2.5 m/s***	***3.0 m/s***	***3.5 m/s***	***2.5 m/s***	***3.0 m/s***	***3.5 m/s***
Prosthetic Limb	0.27[a] (0.03)	0.24[a] (0.02)	0.22[a] (0.02)	0.46 (0.04)	0.48 (0.04)	0.47 (0.03)	1.04[a] (0.09)	1.20[a] (0.10)	1.31[a] (0.10)	163.5[a] (10.74)	165.9[ab] (9.17)	174.3[a] (8.92)
Intact Limb	0.27[a] (0.02)	0.25[a] (0.01)	0.23[b] (0.02)	0.46 (0.04)	0.47 (0.03)	0.46 (0.03)	0.86[b] (0.08)	1.00[b] (0.07)	1.11[b] (0.08)	164.4[a] (8.51)	167.7[a] (8.66)	176.2[a] (9.16)
Control Limbs	0.32[b] (0.03)	0.28[b] (0.02)	0.26[c] (0.02)	0.47 (0.02)	0.47 (0.02)	0.48 (0.02)	1.04[a] (0.02)	1.20[a] (0.05)	1.32[a] (0.06)	151.8[b] (7.16)	157.9[b] (6.51)	163.2[b] (7.36)

[v] indicates significant velocity effects for each limb.
[g] indicates significant group effects between the ILEA and control subjects.
[a, b, c] indicate subgroups for limb differences within a velocity where group members are significantly different from non-group members.

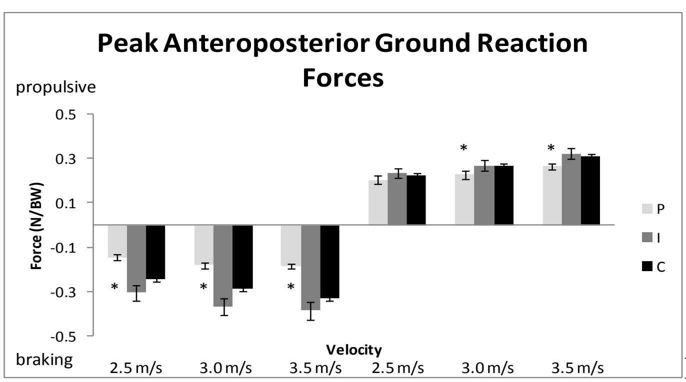

A)

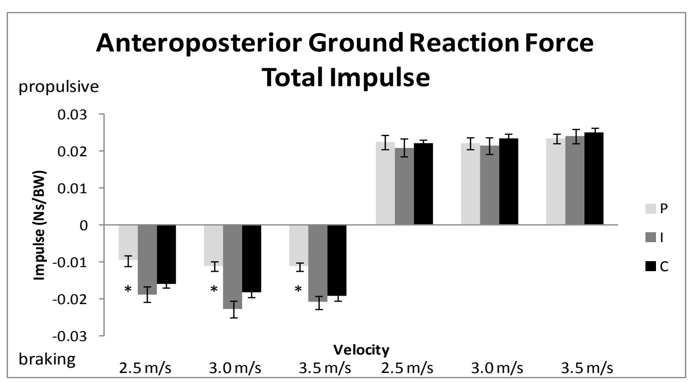

B)

Figure 1. Anteroposterior (AP) peak GRFs (A) and total impulses (B) for the prosthetic (P), intact (I), and averaged control (C) limbs for each velocity. Error bars represent ±1 standard error. * indicates the prosthetic limb is significantly different ($p<0.05$) from the intact and control limbs. The intact and control limbs did not significantly differ for these data.

DETERMINING THE INERTIAL PROPERTIES OF RUNNING-SPECIFIC PROSTHESES

Brian S. Baum, Melanie P. Schultz, Andrea Tian, Hiroaki Hobara, Hyun-Joon Kwon, Jae Kun Shim

University of Maryland, College Park, USA
Email: brianbaum1@gmail.com

INTRODUCTION

Body segment inertial properties, i.e. mass, center of mass position, and moment of inertia, affect the joint kinetics and subsequent limb control during ambulation. Accurate segment inertial property measurements are necessary to accurately calculate kinetic parameters. For amputees, prosthesis inertial properties can influence gait mechanics [1]. To our knowledge, only one study to date [2] has reported inertial property values for a running-specific prosthesis (RSP), so limited information exists on the inertial properties of different RSP designs, different stiffness categories within a design, and methods to measure these properties. The purpose of this study was to determine the inertial properties for four commercially available RSPs across three stiffness categories for each model. Use of a trifilar pendulum is described to measure these values along with errors associated with the measurements.

METHODS

RSPs included the Freedom Innovations Nitro, Ossur Cheetah, Ossur Flex-Run, and Otto Bock 1E90. Prosthesis masses were measured using a standard laboratory scale. The center of mass (COM) for each prostheses in the sagittal plane (x-z plane) was measured using a reaction board [3]. Equation 1 was then established to calculate the COM of an RSP in the absence of available equipment to directly measure this quantity. The COM relates to the RSP head and toe via:

$$COM = r|\vec{T}| * \begin{bmatrix} cos\theta & 0 & sin\theta \\ 0 & 1 & 0 \\ -sin\theta & 0 & cos\theta \end{bmatrix} \begin{bmatrix} u_{Tx} \\ u_{Ty} \\ u_{Tz} \end{bmatrix} \quad (1)$$

$|\vec{T}|$ is the head-toe vector magnitude, r is the ratio of the head-COM ($|\overrightarrow{CM}|$) and $|\vec{T}|$ vector magnitudes, θ is the angle between $\vec{T}$ and $\overrightarrow{CM}$ vectors, and u_T describes the x, y, and z components of the $\vec{T}$ unit vector. Fig. 1 shows a schematic of these variables.

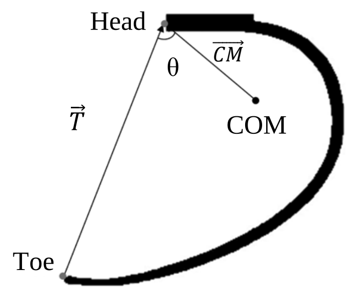

Figure 1: Relationship between the center of mass (COM), Head, and Toe of an RSP.

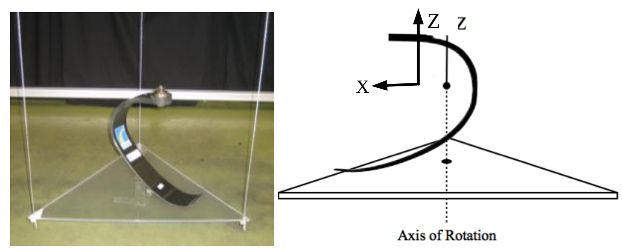

Figure 2. Trifilar pendulum with an RSP. RSP primary axes of rotation (z-axis shown) are aligned with the platform's axis of rotation.

The inertial properties of all prostheses along their principal axes were calculated by placing them on a trifilar pendulum (Fig. 2) and measuring the periods of oscillation [4]. The pendulum consisted of a rigid equilateral plexiglass triangle with its corners suspended from a custom built frame by equidistant wires. Periods of oscillation were measured with a background suppression reflective photoelectric sensor. The local coordinate system of each prosthesis was defined to originate at the COM. Prostheses COM were aligned with that of the triangular platform, determined to be the centroid of the triangle. Each principal axis of each prosthesis was aligned with vertical (Fig. 2). The platform-prosthesis system was then oscillated about each primary axis of rotation. The moment of inertia about each axis was calculated via Equation 2 [4]:

$$I_{Ozz} = \frac{R^2 g \tau^2}{4\pi^2 L}(m_P + m_O) - I_{Pzz} \quad (2)$$

where R is the distance from each wire connection to the center of rotation, g is gravity, τ is period of oscillation, L is wire length, m_p is platform mass, m_o

is object mass (RSP), and I_{pzz} is moment of inertia of the platform about its rotational axis.

System Validation: The pendulum's accuracy was determined by measuring moments of inertia of an aluminum block with known values. Errors induced by linear (1-10cm in 1cm increments) and rotational (±5°) misalignment of the object's and platform's COM and axes of rotation were also examined.

RESULTS and DISCUSSION

Mass, center of mass position, and moment of inertia varied by less than 0.134kg, 0.04m, and 0.0038 $kg{\cdot}m^2$, respectively, between stiffness categories within any RSP design, but varied more substantially between different RSP designs. Table 1 presents inertial property measurements for the middle stiffness category of each RSP along with the predicted COM positions using Equation 1. Predicted COM values for all RSPs and stiffness categories ranged in error from 0.1-2.8 cm with a majority of errors less than one centimeter along the x- and z-axes. Intact limb center of mass predictions are shown to vary by greater than 2 cm when using different predictive equations [5]. This suggests that center of mass predictions within the range reported in this study are within error rates commonly accepted in gait studies.

Moment of inertia errors were -6.21 $x10^{-5}$ $kg{\cdot}m^2$ for the horizontal and -2.65 x 10^{-6} $kg{\cdot}m^2$ for the vertical axes of the aluminum block, which represent a 1% and 0.1% error in the results, respectively. Misalignments of object and platform COM positions ≤ 5cm produced errors less than 0.002 $kg{\cdot}m^2$, which is lower than differences in intact foot moments of inertia due to measurement technique differences [5]. This indicates that using a trifilar pendulum to estimate moments of inertia of prosthetic components will yield errors less than those currently accepted in the literature for intact limbs, as long as the prosthesis center of mass is aligned within 5cm of the pendulum's center of mass. Angular misalignment of ±5° from neutral resulted in errors of less than 8.55 $x10^{-4}$ $kg{\cdot}m^2$ for the x- and z-axes. A limitation of this study is that inertial property measurements only included RSP keels. Inertial properties for sockets and connecting pylons were not investigated.

CONCLUSIONS

Inertial properties and a predictive equation to determine the COM of RSPs were presented. These data may be used for predicting inertial parameters of similar RSP designs. The predictive equation and pendulum method measured inertial properties with errors equal to or less than those found in commonly used predictive methods for intact limb inertial parameters.

REFERENCES

1. Mattes SJ et al. *Arch Phys Med Rehab* **81**, 561-568, 2000.
2. Bruggemann GP et al. *Sports Tech* **1**, 220-227, 2009.
3. Hay JG. *The Biomechanics of Sports Techniques*. Englewood Cliffs, NJ, USA, 1985.
4. du Bois JL et al. *Exp Mechanics* **49**, 533-540, 2008.
5. Rao G et al. *J Biomech* **39**, 1531-1536, 2006.

ACKNOWLEDGEMENTS

Funding by the DOD Deployment Related Medical Research Program Grant #W81XWH-09-2-0067 and the University of Maryland Department of Kinesiology Graduate Research Initiative Fund.

Table 1. Inertial properties of each tested prosthesis for the middle stiffness category.

Prosthesis	Cat	Mass (kg)	Moment of Inertia ($kg{\cdot}m^2$)			Measured COM (m)		Predicted COM (m)		COM Error (m)	
			x-axis	y-axis	z-axis	x	z	x	z	x	z
Flex-Run	5	0.437	0.0037	0.0051	0.0017	-0.065	-0.079	-0.059	-0.079	-0.006	0.001
Nitro	6	0.349	0.0024	0.0033	0.0012	-0.051	-0.069	-0.063	-0.053	0.012	-0.016
Cheetah	5	0.511	0.0127	0.0143	0.0023	0.019	-0.304	0.022	-0.286	-0.003	-0.018
1E90	185lb	0.605	0.0131	0.0152	0.0035	0.029	-0.278	0.037	-0.287	-0.008	0.009

Cat = stiffness category; Error = difference between measured and predicted COM positions

TWO-WEEKS OF UNLOADED PRECISION TRAINING IMPROVES MOTOR PERFORMANCE IN OLDER ADULTS TO THE LEVEL OF YOUNG ADULTS

Harsimran S. Baweja, Kelly A. Larkin, Erica P. Tanner, Molly A. Moore and Evangelos A. Christou

University of Florida, Gainesville, FL, USA
email: eachristou@hhp.ufl.edu, web: http://hhp.ufl.edu/apk/ces/affil/npl/Home.htm

INTRODUCTION

Normal aging influences the ability of older individuals to perform tasks smoothly and accurately. There is evidence that training that emphasizes muscle coordination or precision can improve motor performance in older adults. For example, training interventions that emphasize muscle coordination with unloaded movements demonstrate a significant improvement in the motor performance of older adults [1, 2]. Furthermore, training interventions that emphasize precision with light loads are superior to strength training in improving performance in older adults due to changes in agonist muscle activity [3, 4]. A methodological limitation with all of these studies is the absence of a proper control group. The improvements in performance, therefore, cannot entirely be attributed to the effects of training. Furthermore, it is unclear whether unloaded training interventions that emphasize precision improve motor performance in older adults to the level of young adults. The purpose of this study was to determine whether two weeks of unloaded precision training improves performance of ankle movements in older adults to the level of young adults.

METHODS

Thirty older (71.7 ± 6.2 years; 16 women) and ten young adults (23.8 ± 5 years; 5 women) participated in the study involving dorsi-plantar flexion of the non-dominant ankle. Subjects were divided into one training (20 older adults) and two control groups (10 young & 10 older). The training group practiced unloaded ankle dorsi-plantar flexion movements for 5 sessions (x 60 trials) over 2 weeks. Maximal voluntary contraction (MVC) and agonist muscle activity from the tibialis anterior (TA) was recorded at the beginning (Day 1) and end (Day 14) of the training.

Movement of the foot was produced by the dorsi-plantar flexion of the left ankle over a 10° range of motion (90-110°). TA muscle activity was recorded with a pair of surface electrodes (8mm diameter). The target was provided as a red sinusoidal line (0.6 Hz) in the middle of the screen and the movement of the subjects in blue progressing with time from left to right. Subjects were asked to match the sinusoidal target as accurately and smoothly as possible. Each trial lasted 35 s. Movement error was quantified as the root mean squared error (RMSE) between the target and the tracking performance of the subject, whereas movement variability was quantified as the standard deviation (SD) of the detrended movement trajectory. Neural activation was quantified as the wavelet power spectrum of the TA interference EMG signals from 5-300 Hz.

RESULTS AND DISCUSSION

Before training, older adults exhibited significantly greater movement error and variability than young adults (Figure 1). The older adults who participated in the 5 session training intervention reduced their ankle movement errors ($P<0.01$) and variability ($P<0.01$) to the level of young adults (Figure 1). The older control group did not change. Furthermore, the older adults who participated in the low-intensity training exhibited an increase from 30-60 Hz in the EMG activity of the tibialis anterior muscle ($P<0.01$; Figure 2). All subjects exhibited similar MVCs pre and post training indicating there were no strength gains over the 2 week period and any changes in movement error or variability were not associated with changes in the strength of the subjects.

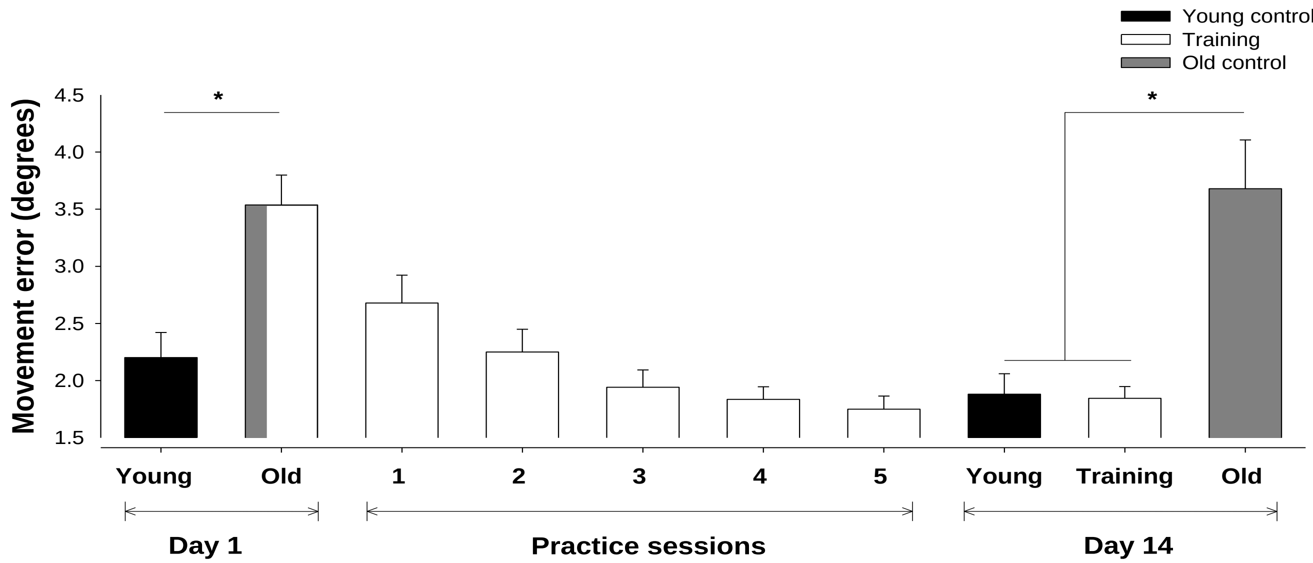

Figure 1: Movement error across practice sessions for the three groups.

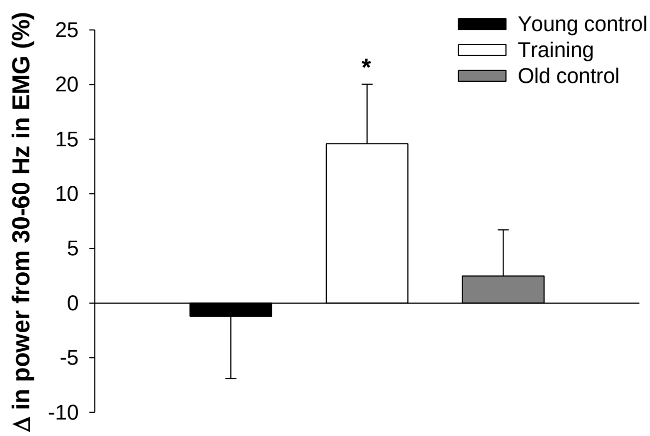

Figure 2: Change in TA wavelet power from 30-60 Hz for the three groups from day 1 to 14.

Our findings support and extend previous studies of the effect of precision training on older adults. Specifically, we demonstrate the following novel findings: 1) Unloaded precision training in older adults can improve their motor performance; 2) In this study, we incorporate a young and an older control group that, in the absence of training, did not show any changes in motor performance; 3) Following 2 weeks of unloaded precision training the motor performance of older adults improved to the level of young adults; 4) The training-induced improvements in motor performance in older adults may be due to changes in the modulation of the primary agonist muscle but not due to changes in muscle strength.

CONCLUSIONS

We demonstrate that the aging nervous system has remarkable plasticity and improvements in motor performance can occur within a few practice sessions. These improvements in motor performance can occur with very low-intensity training, which can be safer for older adults. These findings may have important implications in designing rehabilitation protocols for older adults.

REFERENCES

1. Ranganathan VK, et al. *J Gerontol A Biol Sci Med Sci*. **56**, 8:M518-522, 2001
2. Christou EA, et al. *J Gerontol A Biol Sci Med Sci*. **58**, 8:763-6, 2003
3. Darling WG, et al. **10** *Neurobiol Aging.* 149-157, 1989.
4. Kornatz KW, et al. *J Appl Physiol.* **98**, 6:2072-2080, 2005.

ACKNOWLEDGEMENTS

This study was supported by National Institutes of Health R01 AG031769 to Evangelos A. Christou.

EMOTION AS A GAIT THERAPY IN PARKINSON'S PATIENTS: AFFECTIVE STIMULI & GAIT PATTERN VARIABILITY

[1]Garrett F. Beatty, [1]Ryan T. Roemmich, [1]Kelly M. Naugle, [1]Christopher M. Janelle, and [1]Chris J. Hass

[1]University of Florida, Gainesville, FL, USA
email: gbeatty@hhp.ufl.edu

INTRODUCTION

Parkinson's disease (PD), a disease of the basal ganglia (BG), is characterized by progressive debilitation of the motor system. PD patients often suffer from postural instability and gait dysfunction. Treatment interventions targeted at improving gait and preventing falls among PD patients will benefit from novel recommendations to complement existing behavioral and pharmacological treatments. Emotion manipulations may hold promise for augmenting existing rehabilitation protocols. Naugle, Hass, Bowers, and Janelle [1] found that pleasant emotional states facilitate the anticipatory postural adjustments and the velocity of the first step during gait initiation in PD patients. They concluded that manipulation of emotional states may prove a beneficial strategy for *optimizing gait initiation* in PD patients. While emotional manipulations show promise as a viable therapeutic strategy, little is known regarding the role that affective stimuli might have on increasing *variability in gait* parameters (step length, stride length, and step velocity). Importantly, Roemmich et al. [2] found that PD patients exhibit more variability in gait compared to healthy cohorts. Such variability increases the likelihood of injurious and potentially catastrophic falls. Prior to implementing emotional manipulations in therapeutic strategies, it is important to identify how emotional states impact stepping variability. Our aim, therefore, was to determine how emotional manipulations affect gait variability in PD patients and age-matched controls.

We hypothesized that PD patients would exhibit greater variability in step length, stride length, and stride velocity, than the age-matched healthy controls. While no studies exist examining the role of emotion on gait variability, Coombes, Gamble, Cauraugh, and Janelle [3] found that emotional states do not impact the variability of sustained pinch force in healthy young adults. Considering these findings as well as those from Roemmich et al. [2] we hypothesized that emotional state would not impact gait variability in control participants, but speculated that emotional state might increase gait variability in PD participants.

METHODS

Following completion of informed consent, seventeen idiopathic PD patients (female = 3) and seventeen age-matched (±4 years) controls (female = 3) were fitted with retro-reflective markers on the lower body. Participants were positioned on a force platform (Bertec, Columbus, Ohio, model 4060) 6m in front of a 3.3 x 2m screen. During each trial, participants were presented with a fixation cross (2s) followed by a randomized picture stimulus (2-4s) at a resolution of 1024 x 768 pixels and a size of 127 x 91cm. Participants were instructed to begin walking and continue walking for several steps (approximately 4m) immediately following picture offset. Picture stimuli represented exemplars from the categories of attack, mutilation, contamination, erotica, happy people, and neutral objects and were selected from the International Affective Picture System (IAPS) [4]. Participants completed five trials per affective category. Kinematic data were sampled at 120Hz using a ten-camera Optical Motion Capture system (Vicon Peak, Oxford, U.K.).

RESULTS

Within subject variability of step length, stride length, and step velocity were calculated as the coefficient of variation $(CV = \frac{\sigma}{\mu} * 100\%)$ [2]. A 2 (group: PD, control) x 6 (category: attack, mutilation, contamination, erotica, happy people, and neutral objects) ANOVA with repeated measures on the second factor was run for each of the five dependent measures (variability of step 1 length, step 2 length, stride length, step 1 velocity, and step 2 velocity). Analyses revealed significant differences in variability of the length of step 2 ($p=0.020$), stride length ($p=0.012$), velocity of step 1 ($p=0.010$), and velocity of step 2 ($p=0.002$) with greater variability in the PD group. Tests revealed no significant differences across valence categories and no significant group by valence interaction for any of the dependent measures.

DISCUSSION & CONCLUSION

Our hypothesis that PD patients would exhibit greater variability during gait than healthy controls was confirmed in all dependent measures except for variability of length of the first step. Additionally, our speculative hypothesis that emotional states would not influence variability in healthy controls was confirmed. However, emotional states did not increase gait variability in PD patients.

Combined, results provide additional support for the inclusion of emotional state manipulations in gait therapy within PD populations. Because gait variability did not increase as a function of manipulated emotional states, inclusion of emotional manipulations during gait therapy will likely enhance gait initiation performance [1] while not increasing the risk of gait instability or falls.

REFERENCES

1. Naugle, K.M., et al. (2012). Emotional state affects gait initiation in individuals with Parkinson's disease. *Cognitive, affective & behavioral neuroscience* **12**, 207-219.
2. Roemmich, R.T., et al. (in press). Spatiotemporal variability during gait initiation in Parkinson's disease. *Gait & Posture*.
3. Coombes, S.A., et al. (2008). Emotional states alter force control during a feedback occluded motor task. *Emotion* **8**, 104-113.
4. Lang, P.J., et al. (2008). *International affective picture system (IAPS): Affective ratings of pictures and instruction manual (Tech. Rep. A-8)*. University of Florida: Gainesville, Fl.

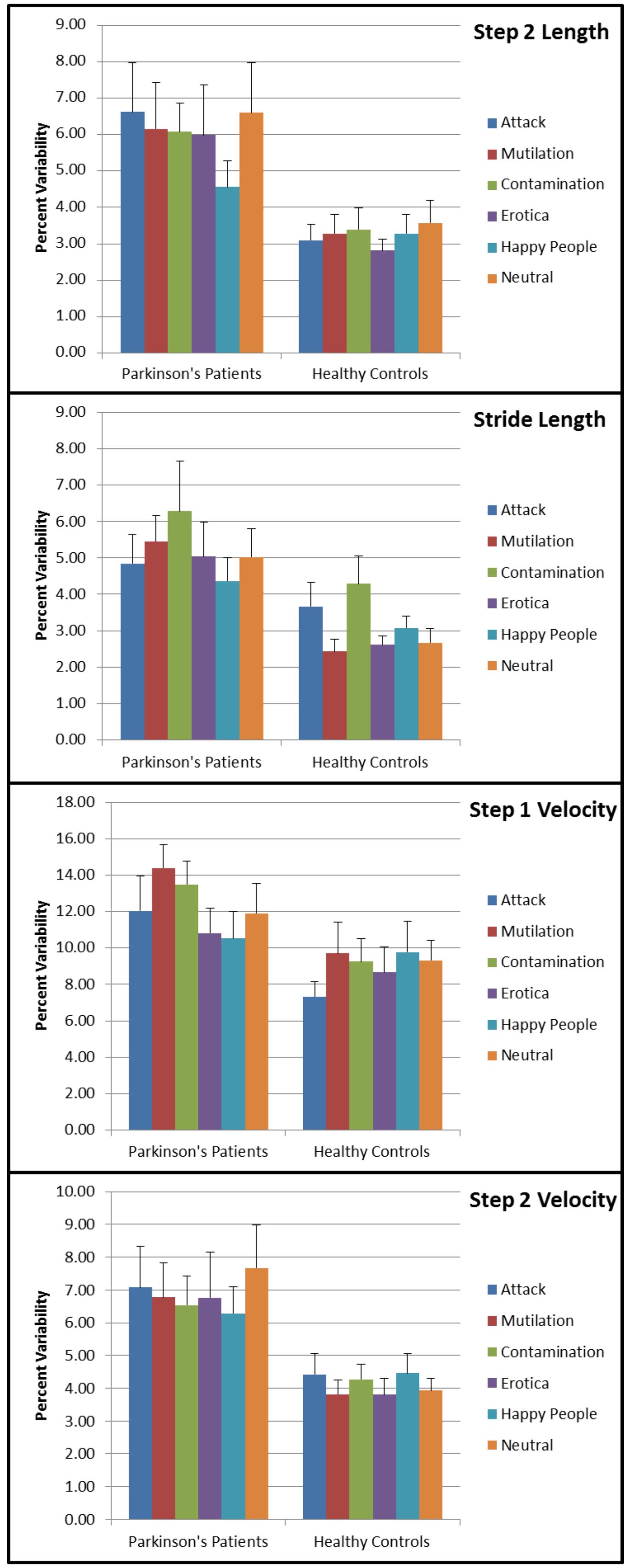

Figure 1: Mean variability percentages for dependent variables by group and valence category

PLANTAR PRESSURE DIFFERENCES BETWEEN REARFOOT AND MIDFOOT STRIKING RUNNERS DURING SHOD RUNNING

[1]James Becker, [1]R.J. Howey, [1]Louis Osternig, [2]Stan James, and [1]Li-Shan Chou

[1]Motion Analysis Laboratory, Department of Human Physiology, University of Oregon, Eugene, OR, USA
[2]Slocum Center for Orthopedics and Sports Medicine, Eugene, OR, USA
email: chou@uoregon.edu, web: http://biomechanics.uoregon.edu/MAL/index.html

INTRODUCTION

Up to 74% of all runners sustain an injury in any given year [1]. Due to such a high injury rate it is important for runners to consider adaptive strategies which may reduce their risk of injury. One such strategy is switching from using a rearfoot strike (RFS) to a midfoot strike (MFS) pattern, the most commonly proposed benefits of which are reductions in external impact peak forces and loading rates [2,3]. However, while switching foot strike patterns may reduce injury risk from one mechanism, it may simultaneously increase injury risk from a different mechanism.

Plantar pressure distribution under the foot is one risk factor which may be particularly affected by changing foot strike patterns. It has been hypothesized that increased pressure under the metatarsals may increase risk for stress fractures, especially in the presence of fatigue [4]. Compared to a RFS, a MFS should result in less of the foot's plantar surface in contact with the ground. Theoretically, this will increase pressures under various regions of the foot, even without fatigue being present. However, it is currently unknown to what extent plantar pressures differ in healthy, non-fatigued runners who naturally use a RFS or a MFS. Therefore, the purpose of this study was to determine if there are differences in plantar pressure between RFS and MFS runners.

METHODS

Ten runners who habitually used a RFS (age: 32.4 ± 13.4 years; weekly mileage: 50.0 ± 19.7 miles) and ten runners who habitually used a MFS (age: 28.9 ± 10.3 years; weekly mileage: 52.5 ± 19.3 miles) participated in this study. All subjects were injury at the time of testing. Plantar pressure data was collected using an F-Scan VersaTek wireless system (TekScan, Inc. South Boston, MA) while subjects ran on a treadmill at self selected speed (RFS: 3.47 ± 0.31 m/s; MFS: 3.56 ± 0.28 m/s). Prior to data collection an FScan insole (model: 3000E; resolution: 3.9 sensors/cm^2) was trimmed to fit the insole from each subject's running shoes. Subjects wore their own running shoes. Sensors were calibrated using a step calibration and data was collected with the system sampling at 100 Hz.

Data were analyzed using the F-Scan Mobile Research software. For each foot, 30 consecutive steps were averaged and ten regions were defined for analysis (Figure 1). Dependent variables included the overall contact time, and the peak pressure (PP), time to peak pressure (TTPP), pressure time integral (PTI), maximum force (MF), time to maximum force (TTMF), and force time integral (FTI) in each region.

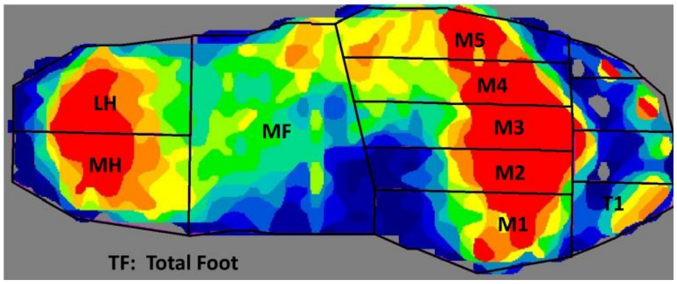

Figure 1. Regions selected for analysis. MH: medial heel, LH: lateral heel, MF: midfoot, M1-5: metatarsals 1-5, T1: hallux.

For each variable, differences between RFS and MFS were examined using an ANCOVA with running speed entered as a covariate. Significance level of $p < 0.05$ was used for all tests.

RESULTS AND DISCUSSION

Contact time was not different between foot strike patterns (RFS: 238.5 ± 28.14 ms, MFS: 228.2 ± 39.27 ms; p = 0.521). Compared to the MFS runners, the RFS runners demonstrated higher peak pressures and forces and shorter time to peak pressures and forces in the heel and midfoot regions (Figure 2). While the MFS group demonstrated higher pressures and forces in some metatarsal regions, they had lower time to peak pressure and force in all metatarsal regions (Figure 2). Regions with significant differences in pressure time integral are shown in Table 1. For the force-time integral, the heel and midfoot were the only regions where significant differences were observed, with RFS runners having larger values than MFS runners.

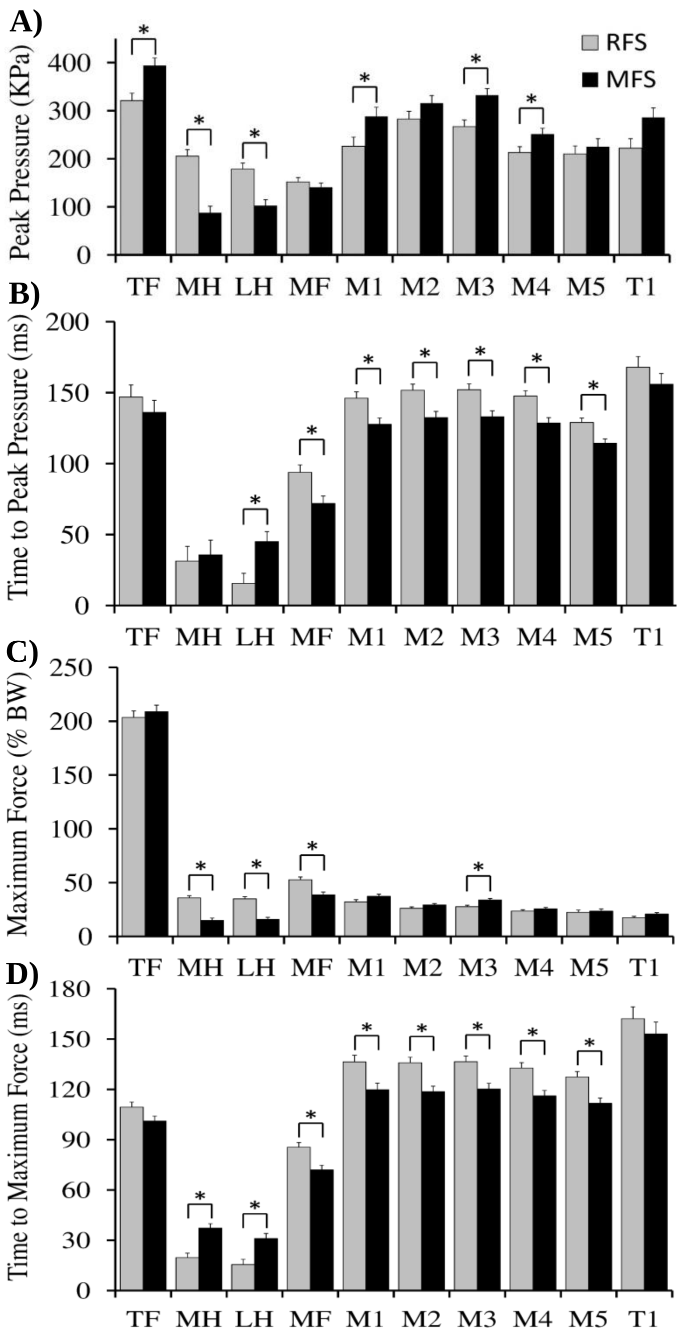

Figure 2. Peak pressure (A), time to peak pressure (B), maximum force (C), and time to maximum force (D) for the twelve regions analyzed.

Table 1. Pressure-time integrals in regions with significant difference between strike patterns. Units are KPa*s.

	RFS	MFS	p
Medial heel	11.84 (±7.92)	1.33 (±2.41)	0.002
Lateral heel	9.92 (±3.29)	6.83 (±2.45)	0.003
1st Met	17.04 (±7.11)	21.48 (±4.98)	0.011
2nd Met	20.63 (±7.29)	24.91 (±3.16)	0.006
3rd Met	21.19 (±6.31)	27.57 (±4.72)	0.001
4th Met	18.40 (±4.92)	22.45 (±5.30)	0.004

CONCLUSIONS

The results of this study suggest overall loading of the metatarsals is greater in individuals who naturally use a MFS compared to those who naturally use a RFS. It is unknown whether these differences would still be present in individuals who convert from a RFS to a MFS. However, the authors hypothesize these differences likely will still exist, as it has previously been reported that individuals using a converted foot strike pattern closely replicate kinematics and kinetics of individuals who naturally use that foot strike pattern [5]. Thus, while individuals who convert their foot strike pattern may obtain lower impact forces and loading rates in the vertical ground reaction force, these reductions may come at the trade off of higher loading of the metatarsals. How this may influence injury rates requires further investigation.

REFERENCES

1. Van Ghent, RN *Br J Sports Med* **41**, 469-480, 2007
2. Cheung, RT, et al. *J Orthop Sports Phys Ther* **41**, 914-919, 2011.
3. Daoud, AI, et al. *Med Sci Sport Exerc.* **epub ahead of print**, 2012.
4. Nagel, A, et al. *Gait & Posture* **27**, 152-155, 2008.
5. Williams, DS, et al. *J Applied Biomech*, **16**, 210-218, 2000.

BIOMECHANICS OF RETROSPECTIVE NAVICULAR STRESS FRACTURES

[1]James Becker, [1]Louis Osternig, [2]Stan James, and [1]Li-Shan Chou

[1]Motion Analysis Laboratory, Department of Human Physiology, University of Oregon, Eugene, OR, USA
[2]Slocum Center for Orthopedics and Sports Medicine, Eugene, OR, USA
email: chou@uoregon.edu, web: http://biomechanics.uoregon.edu/MAL/index.html

INTRODUCTION

Navicular stress fractures (NSF) account for approximately 14% of all stress fractures [1], with track and field athletes in particular, sustaining a large percentage of these injuries [2]. Given the importance of the navicular bone for maintaining normal foot function, early detection and treatment of these high risk stress fractures is paramount. However, there is a distinct lack of literature documenting anatomical or biomechanical factors which may contribute to the development of this injury. The limited studies which do exist suggest greater amounts of foot pronation and pronation velocities, pes cavus foot structure, and limited ankle or subtalar range of motion as potential factors [1,3] as these conditions theoretically increase stress on the navicular bone during stance. However, no study has demonstrated statistical significance in any of these factors. Therefore, the purpose of this study was to examine whether differences exist in anatomic, clinical, or biomechanical measures between individuals who retrospectively sustained a NSF and healthy control subjects without a history of this injury.

METHODS

Four subjects with a history of NSF (sex: 3M, 1F; age: 24 ± 3.5 years; weekly mileage: 70 ± 4.08 miles) and four matching control subjects (sex: 3M, 1F; age: 22 ± 0.82 years; weekly mileage 66.25 ± 7.5 miles) participated in this study. All subjects were elite distance runners who used a midfoot strike pattern and all were symptom free and had resumed normal training at the time of testing.

A clinical exam assessing lower limb alignment, flexibility, and joint mobility was performed on all subjects. Detailed descriptions of the exam have been published previously [4]. Subjects then completed a three-dimensional running gait analysis where they ran continuous laps at self selected speed around a short track in the laboratory. Whole body motion was recorded at 200 Hz using a 10 camera motion capture system (Motion Analysis Corp.) while ground reaction forces were recorded at 1000 Hz with three force plates (AMTI). Holes were cut in the subject's shoes allowing placement of retro-reflective markers directly on the skin. Foot kinematics were quantified using a multi-segment foot model consisting of rearfoot and forefoot segments.

Joint and segment angles were calculated using custom LabView (National Instruments, Austin TX) software. Joint angles were used to calculate excursions, average and maximal instantaneous velocities, and time to peak excursions for forefoot abduction and rearfoot eversion, respectively. Segment angles were used to calculate tibia varus and toe out angles at foot contact. Average and maximal instantaneous loading rates were calculated from the vertical ground reaction force over the initial 15% of stance.

In addition to the discrete variables, coordination of movement between the forefoot and rearfoot segments was examined using a modified vector coding method [5]. Forefoot transverse plane segment angles were plotted against rearfoot frontal plane segment angles. A coupling angle was defined by calculating as the angle between a vector joining two successive time points and the right horizontal [5].

A minimum of ten trials per foot per subject were analyzed. For the discrete kinematic and kinetic variables, comparisons were made between the involved and non-involved limbs within the NSF subjects, and between the involved limbs of the NSF subjects and the matching limbs of the control subjects. Forefoot-rearfoot joint coupling was evaluated qualitatively by plotting the coupling angles on a polar plot.

RESULTS AND DISCUSSION

There were no differences in any of the clinical exam measures between the involved and non-involved limbs within the NSF group or between the involved limbs of the NSF group and the matching limbs of control subjects (all measures $p > 0.05$).

Of the twelve discrete variables examined, only four were significantly different between the involved and non-involved limbs of the NSF subjects (Table 1). However, these values were not significantly different between the involved limbs of the NSF subjects and the matching limbs of the control subjects.

The joint coupling results (Figure 1) indicated the NSF subjects and the control subjects had distinctly different forefoot-rearfoot coupling patterns. The non-involved limb of the NSF subjects (Figure 1A) showed a smooth progression of coupling angles across stance, while the involved limb demonstrated an abrupt change in coupling angles. Interestingly, the control subjects also demonstrated this abrupt change in coupling patterns. However, the control subjects were symmetric between left and right limbs whereas the NSF subjects demonstrated

Table 1. Variables which were significantly different between involved and non-involved limbs in the NSF subjects. * $p < .05$

	Involved Limb	Non-Involved Limb
Forefoot abduction excursion (°)	1.82 (± 0.38)	2.79 * (± 0.29)
Rearfoot eversion excursion (°)	12.59 (± 3.32)	10.29 * (± 3.42)
Average eversion velocity (°/s)	268.99 (± 78.12)	211.10 * (± 79.85)
Maximal eversion velocity (°/s)	388.75 (± 102.82)	314.66 * (± 110.14)

substantial asymmetry in forefoot-rearfoot coupling between involved and non-involved limbs.

CONCLUSIONS

The reduced forefoot abduction, higher amounts of rearfoot eversion, and higher eversion velocities in the involved limb of the NSF subjects supports theories that atypical foot pronation may be related to the development of NSF. However, since these values were not different than those found in the control subjects, it may be that higher values are only problematic when present in conjunction with asymmetric forefoot-rearfoot coupling.

REFERENCES

1. Coris, E, et al. *Am Fam Physician* **67**, 85-90, 2003
2. Brukner, P, et al. *Clin J Sports Med* **6**, 85-89, 1996
3. Ting, A, et al. *Clin Sports Med* **7**, 89-101, 1988
4. Stergiou, N et al. *Med Sci Sport Exer* **31**, 1645-1655, 1999.
5. Chang, R et al. *J Biomech* **41**, 3101-3105, 2008

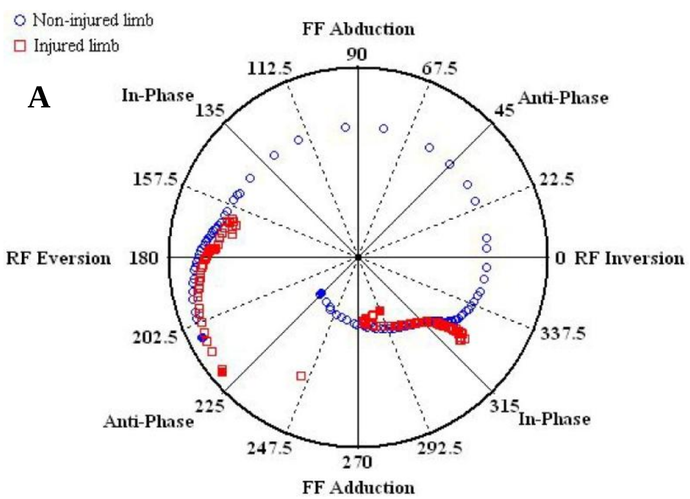

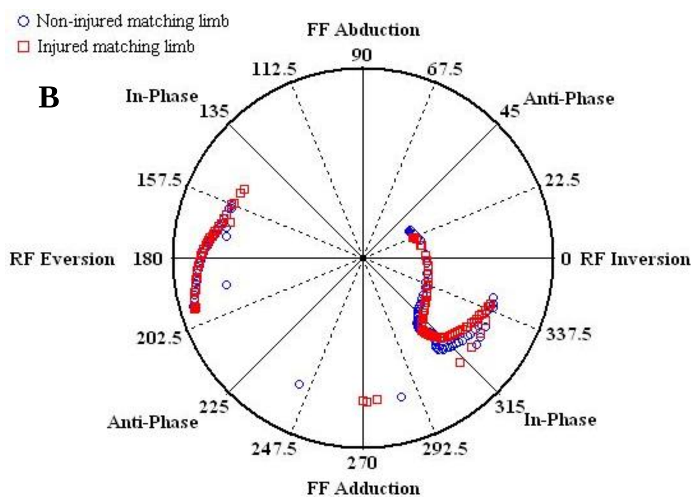

Figure 1. Polar plots showing forefoot-rearfoot joint coupling angles across stance phase for involved and non-involved limbs of the NSF subjects (A) and left and right limbs of the control subjects (B).

VERTICAL LOAD DISTRIBUTION IN THE METATARSALS DURING SHOD RUNNING

[1]James Becker, [1]R.J. Howey, [1]Louis Osternig, [2]Stan James, and [1]Li-Shan Chou

[1]Motion Analysis Laboratory, Department of Human Physiology, University of Oregon, Eugene, OR, USA
[2]Slocum Center for Orthopedics and Sports Medicine, Eugene, OR, USA
email: chou@uoregon.edu, web: http://biomechanics.uoregon.edu/MAL/index.html

INTRODUCTION

The metatarsals are one of the most common sites for stress fracture injuries among runners [1]. Though exact mechanisms responsible for these injuries are not clear, alterations in loading across the metatarsals has been hypothesized as one potential factor [2]. Anecdotal evidence from our laboratory suggests individuals with a history of metatarsal stress fracture demonstrate “hotspots” of pressure focused under specific metatarsals (Figure 1). In theory, such loading concentrations may help explain the recurrent injuries these individual have sustained. Thus, examining plantar pressure patterns for such concentrations may be a useful tool to help identify those at heightened risk for metatarsal stress fracture injuries.

However, using abnormal load distribution among the metatarsals in any diagnostic capacity first requires clarification of normal load distribution patterns in healthy individuals. While this information has been reported for walking [3,4], it has not been reported for running. Therefore, the purpose of this study was to describe the vertical load distribution among the metatarsals in healthy shod runners. A secondary purpose was to determine if there are any differences in load distribution between runners who use a rearfoot (RFS) or midfoot (MFS) strike.

METHODS

Nine runners who habitually used a RFS (age: 33.7 ± 13.4 years; weekly mileage: 50.0 ± 20.91 miles) and six runners who habitually used a MFS (age: 31.66 ± 12.6 years; weekly mileage: 45.83 ± 28.833 miles) participated in this study. All subjects were injury free at the time of testing and no subject had a history of metatarsal stress fractures. Plantar pressure data was collected using an F-Scan VersaTek wireless system (TekScan, Inc. South Boston, MA) while subjects ran on a treadmill at self selected speed. Prior to data collection an FScan insole (model: 3000E; resolution: 3.9 sensors/cm^2) was trimmed to fit the insole from each subject’s running shoes. Subjects wore their own running shoes. Sensors were calibrated using a step calibration and data was collected with the system sampling at 100 Hz.

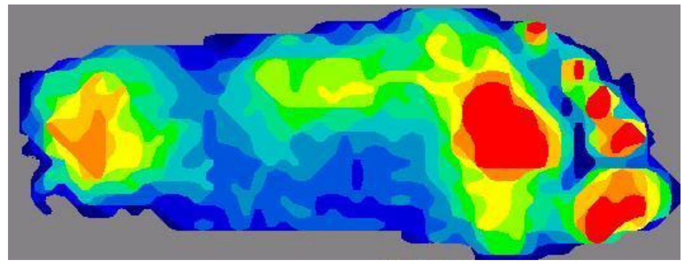

Figure 1. Plantar pressure images from an individual with a history of multiple metatarsal stress fractures.

Data were analyzed using the F-Scan Mobile Research (TekScan, Inc.) software. For each foot, 30 consecutive steps were averaged. Each individual metatarsal region was defined and total vertical force across all metatarsals (TMF) was calculated at every 1% of stance by summing the vertical forces in each individual metatarsal region. All forces were normalized to percent body weight. The maximum total force and percent stance at which this maximum occurred were then identified. At the instant of maximum TMF, the relative load carried by each metatarsal was identified by calculating what percentage of the total force was found under each metatarsal. Lastly, the percent TMF carried by each individual metatarsal was also calculated across the entire stance phase.

For each variable, differences between RFS and MFS were examined using an ANCOVA with running speed entered as a covariate. Significance level of $p < 0.05$ was used for all tests.

RESULTS AND DISCUSSION

TMF was not different between foot strike patterns (RFS: 1.31 ± 19.21 BW; MFS: 1.44 ± 28.12 BW; p = .121). However, maximal TMF occurred earlier in subjects who used a MFS (p = 0.002; Figure 2).

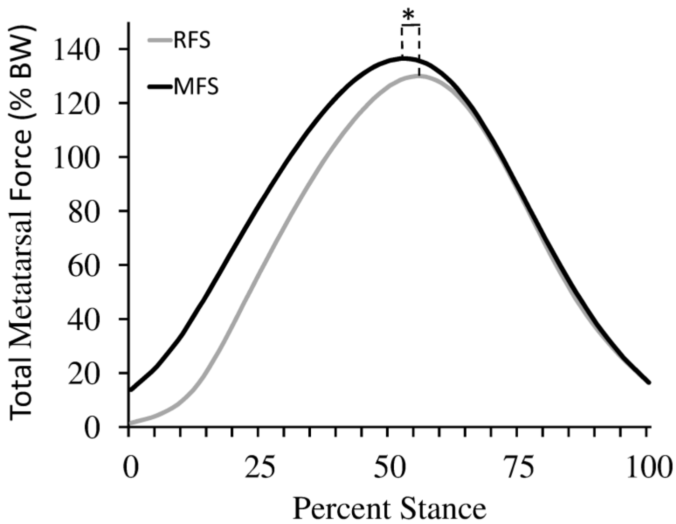

Figure 2. Total force in the metatarsals. * indicates peak force occurs earlier in subjects with a MFS compared to those with a RFS.

The distribution of load among the metatarsals at the instant of maximal TMF is shown in Figure 3. There were small, but statistically significant, differences in the percent load carried by the 3rd and 5th metatarsals. Since there were only small differences between RFS and MFS runners, these

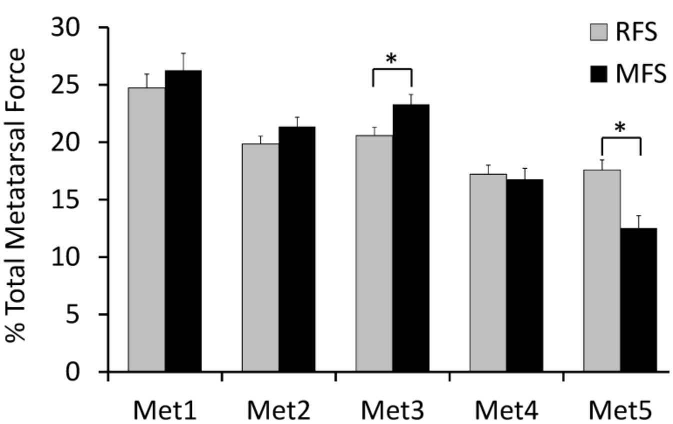

Figure 3. Percentage of force carried by each metatarsal at the instant of maximal TMF for both RFS and MFS runners. * indicates significant difference between foot strike patterns ($p < 0.05$).

two groups were pooled together and load carried in each individual metatarsal across stance was plotted along with the total load in the metatarsals (Figure 4).

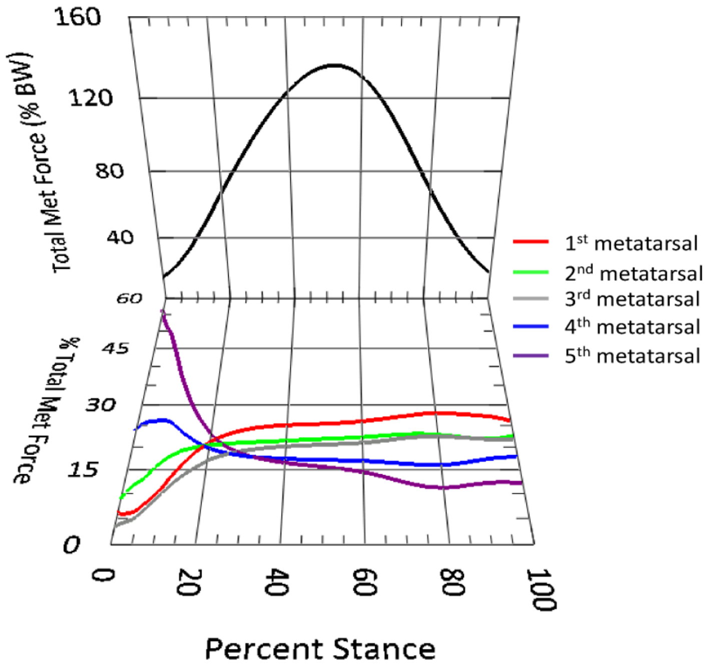

Figure 4. Force in each individual metatarsal across stance expressed as a percentage of total force in the metatarsals.

CONCLUSIONS

In general, the metatarsals are subjected to vertical loads around 130% body weight during the stance phase of shod running. At the time of maximal metatarsal loading the first metatarsal carries approximately 25% of the load with the remaining 75% being evenly distributed among metatarsals two through four. However, early during stance, the 4th and 5th metatarsals carry much higher percentages of the total load. It appears that there are small differences in load distribution between runners who utilize a RFS and those who utilize a MFS. Future studies examining if load distribution differs in individuals with a history of metatarsal stress fracture appear warranted.

REFERENCES

1. Matheson, GO et al, *Am J Sports Med*, **15**, 46-58, 1987.
2. Queen, RM, et al. *Am J Sports Med*, **37**, 390-395, 2009.
3. Ledoux, WR, et al. *Gait & Posture*, **15**, 1-9, 2002.
4. Stokes, IF, et al. *J Anat*, **129**, 579-590, 1979.

EVIDENCE OF MEDIAL MALTRACKING IN PATELLOFEMORAL PAIN

[1]Abrahm J. Behnam, [2]Barry P. Boden and [1]Frances T. Sheehan

[1]Functional and Applied Biomechanics, Dept. of Rehabilitation Medicine, NIH, Bethesda, MD, USA
[2]The Orthopaedic Center, Rockville, MD, USA
email: gavellif@cc.nih.gov, web: http://pdb.cc.nih.gov/

INTRODUCTION

Although chronic idiopathic patellofemoral pain (PFP) is highly prevalent and debilitating in the young, active population, the exact etiology of this pain remains unknown. The most common theory is that lateral patellofemoral (PF) malalignment and/or maltracking results in PFP through either an overloading of the subchondral bone or through shortening of the lateral retinaculum (leading to secondary nerve changes). However, a review [1] suggests that symptomatic patellae do not consistently demonstrate lateral PF malalignment/ matracking. In agreement, our previous work [2] identified a subgroup of patients with PFP that did not exhibit excessive lateral shift/tilt, but instead trended towards excessive medial shift. Yet, significant medial maltracking was not found, likely due to insufficient power. Thus, the purpose of this study was to determine if significant medial maltracking in a subgroup of individuals with PFP could be identified using a much larger study cohort. Such a finding would have profound ramifications in terms of patient-specific treatments.

METHODS

In this case-control study, data were acquired from a database that has been under development since 2000. Based solely on previously published criteria [2], 80 datasets from able-bodied volunteers (50F/30M, 26.4±8.1years, 169.3±10.4cm, 66.5± 15.3kg) and 70 datasets from individuals clinically diagnosed with PFP (55F/15M, 25.2+10.9 years, 165.9+8.0cm, 61.3+11.9kg) were accepted into the IRB-approved study.

After providing informed consent, each subject was asked to lay supine within a 1.5T (GE Medical Systems, Milwaukee, WI, USA) or 3.0T (Philips Medical Systems, Best, NL) MRI unit. *In vivo* 3D PF kinematics were derived during volitional leg extension using cine-PC MRI. The accuracy of acquiring these kinematics on both the 1.5T and 3.0T platforms has been demonstrated to be quite similar (<0.5mm & <0.3mm [4]). Although a range of knee motion (53° flexion to full extension) was evaluated, not all subjects were able to reach this full range due to the limited MR bore diameter. Therefore, comparisons focused on 10° knee flexion, as this was the angle closest to full extension with all subjects represented.

The PFP cohort was divided into two subgroups based on average PF medial-lateral displacement of the control cohort, as was done previously [2]. Individuals in the PFP cohort with a value of medial-lateral PF displacement greater than the current asymptomatic average (-0.5mm) were assigned to the medial subgroup (n = 30). All others were assigned to the lateral subgroup (n = 40). Differences between the subgroups and the control cohort were evaluated using an analysis of variance. A p-value of < 0.05 was considered significant.

RESULTS AND DISCUSSION

A medial maltracking group displaying excessive **medial** shift (2.0mm) and **medial** tilt (3.4°), along with flexion (3.1°) and valgus rotation (-1.5°), as compared to the control group, was identified. This finding is opposite to the long-standing belief that the only casual pathway to PFP begins with excessive lateral shift and tilt. One potential explanation for this medial maltracking pattern is weakness in the patellar medial stabilizers combined with a high lateral femoral sulcus, which has been documented in this subgroup [3]. Medial weakness would likely cause a lateral shift in the patella. The presence of a high femoral sulcus would limit lateral translation and potentially redirect the lateral-patellar edge anteriorly, resulting in the observed medial tilt. This theory is supported by recent work demonstrating both lateral and medial tilt in response to a loss of vasti medialis strength in healthy controls [5]. In comparing the medial and lateral PFP subgroups, it would appear that the medial subgroup has a hypo-mobile, as opposed to a hyper-mobile patella in the lateral subgroup. Thus, the pathway to pain is likely unique in each subgroup.

These results provide new insights and guidance into the treatment of PFP. Specifically, 43% of the current population demonstrated medialized, not lateralized, maltracking. Therefore, the majority of current treatment modalities designed to target lateral PF tilt and translation (lateral release, VMO strengthening, McConnell taping, and/or patellar medialization), may actually be harmful rather than helpful for a patient with medialized maltracking. Further, the existence of a medial maltracking subgroup may partially explain the discrepancies in results between previous 3D kinematic studies focused on PFP. These studies have been limited by small population sizes (e.g., 40PFP/ 20 controls [6], 9PFP/ 10controls [7], 30PFP/37 controls [2]), in which the representation of subgroups may have created biased results. Specifically, in the current PFP cohort, PF tilt did not differ from controls, yet when seen through the lens of PF maltracking subgroups, there were significant differences.

CONCLUSIONS

This study confirms the presence of a unique PFP medial maltracking subgroup and provides an alternative pathway to pain outside of the long standing theory of excessive lateral tracking. It is critical to clinically recognize this subgroup since the conventional treatment modalities may be potentially harmful instead of beneficial. Further research is necessary to develop clinical diagnostic tools and appropriate treatments for this subgroup.

REFERENCES

1. Chen-Yi S, et al. *PT in Sport* **12**, 140-147, 2011.
2. Sheehan FT, et al. *JOR Res* **27**, 561-70, 2009.
3. Harbaugh CM, et al. *JOR* **28**, 865-872, 2010
4. Behnam AJ, et al. *JOB* **44**, 193-197, 2011.
5. Sheehan FT, et al. *Clin Biomech*, 2012
6. Macintyre NJ, et al. *JBJS Am* **88**, 2596-605.
7. Wilson NA, et al. *JBJS Am* **91**, 558-6

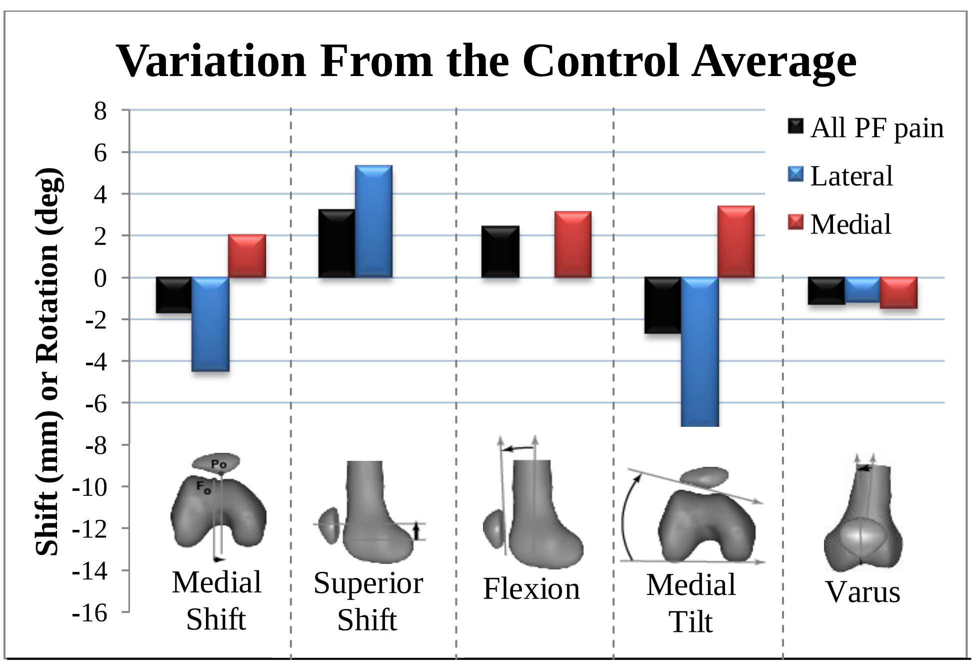

Figure 1: Kinematic variations of PFP cohort (n=70), the lateral subgroup (n=40), and the medial subgroup (n=30) relative to the control cohort (n=80). A medial and superior translation is in the positive direction, as is flexion, medial tilt and varus rotation.

COMPUTER SIMULATION ASSISTS GAIT RETRAINING PROGRAM, A CASE STUDY

Eduardo Beltran, Matthew McClain, Henry Wang
Ball State University, Muncie, IN, USA
email: ejbeltran@bsu.edu, web: http://www.bsu.edu/biomechanics

INTRODUCTION

Despite the benefits from running, a majority of runners experience overuse injuries. Knee pain depicts a common type of running-related injury with higher prevalence in women. Abnormal frontal plane mechanics have been associated with higher joint stress and, thusly, pain in the knee. Improvement of such factors at early onset may reduce the development of more severe conditions, such as osteoarthritis, in the future [1].

The gluteus medius (GM) muscle serves an important role in running: stabilizing the pelvis during the stance phase of running [2]. During running, GM weakness may cause increased hip adduction and high, pain-causing, loading moments in the knees. The wider pelvis featured in females may explain their increased risk for such ailment.

Common interventions have included lower body muscle strengthening and gait retraining; two strategies which have been used in exclusivity. While strong evidence exists about improved mechanics and reduction of pain from these interventions, research is lacking on the effect of the combination of these interventions. Furthermore, while motion capture has become standard for kinematic and kinetic assessment, recent studies have shown the benefits of using musculoskeletal simulation as a noninvasive means of determining internal variables, such as muscle forces, during gait [3,4].

The purposes of this study were to reduce the knee pain in a subject by means of a gait retraining program that included muscle strengthening and to quantify the effectiveness of this subject-specific training intervention via motion capture and musculoskeletal simulation technologies. It was expected that running mechanics would improve as a result of the retraining program and, most importantly, that pain would diminish.

METHODS

The subject was a 14-year old female cross-country runner with 3 years of competitive experience. She had reported occasional knee pain for the past 5-6 months. She also mentioned that she was prone to tripping herself when she ran.

Static pose and gait analysis on the first visit was used for determining the intervention method. During the initial gait analysis, the subject ran on an instrumented treadmill (AMTI, Watertown, MA, USA) at a self-selected pace of 2.78 m/s and motion capture data was collected with Vicon Workstation v5.0(VICON, Oxford, UK). Running variables were calculated with Visual 3D v4.9 (C-Motion, Germantown, MD, USA). Initial analysis confirmed abnormal mechanics associated with her overlapping step pattern possibly caused or perpetuated by hip abductor weakness.

A gait retraining and exercise program was prescribed for the runner to be performed for 8 weeks, six of which were during her cross-country season. Gait retraining focused on increasing step width (SW) as well as reducing impact vertical ground reaction forces (VGRF). The exercise regimen consisted of a series of open kinetic chain exercises aimed at strengthening the GM muscles. After 8 weeks, the subject came in for a second visit where motion capture was recorded while she ran at the speed selected during the first visit. Motion data and force plate data were imported into LifeMod (Lifemodelor Inc., Santa Clemente, CA, USA). Forward dynamic simulation was performed to evaluate the GM muscle forces.

RESULTS AND DISCUSSION

Motion capture data and simulation data are depicted in Table 1 and Figure 1, respectively. From the second visit, step width had shown an increase to a positive, normal range. Vertical impact forces decreased, knee abduction moment discrepancy decreased, and peak hip abductor moment increased by 8.2%, 59.6%, and 8.4%, respectively. Finally, a decrease in gluteus medius muscle force discrepancy of 63.6% was observed after the gait retraining program.

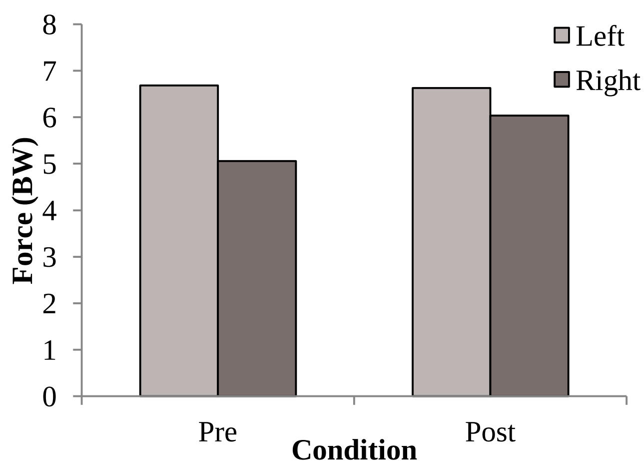

Figure 1: Average peak gluteus medius muscle force data.

Finally, the runner experienced no pain during the 8-week program and even set a personal record running time during a 10K race.

CONCLUSIONS

The runner's knee pain experienced during the past spring training season may have been caused by high impact forces and asymmetrical frontal-plane knee joint moments. This, in turn, may have been caused, or perpetuated, by uneven hip abductor strength.

Authors were successfully able to improve running mechanics with validation from motion capture and simulation technologies. Most importantly, the goal of knee pain reduction was achieved. The use of a gait retraining program by computer simulation and biomechanical analysis served as an effective tool against running-related injuries.

REFERENCES

1. Willy R, et al. *Proceedings of ASB'10*, Providence, RI, USA, 2010.
2. Presswood L, et al. *Strength Cond J* **30**, 41-53, 2008.
3. Miller RH, Hamill J. *Proceedings of NACOB'08*, Ann Arbor, MI, USA, 2008.
4. Russell SD, et al. *Proceedings of ASB'10*, Providence, RI, USA, 2010

	Step Width (cm)	***Impact VGRF (BW)***	***Knee Mom. Discrepancy (N*m/kg)***	***Peak Hip Add. Moment (N*m/kg)***
Pre	-3.44	1.34	.22	1.79
Post	4.81	1.23	.09	1.94

Table 1: Motion capture analysis data

FINITE ELEMENT MODELING OF INTERACTION OF IMPLANTABLE CARDIAC RHYTHM DEVICES DURING FRONTAL MOTOR VEHICLE DECELERATION INJURIES

Aditya Belwadi PhD[1], Sony Jacob MD[2], Teja Repalle MS[1], King H. Yang PhD[1]

[1]Biomedical Engineering Department, Wayne State University, Detroit, Michigan
[2]Division of Cardiology/Electrophysiology, Department of Internal Medicine, School of Medicine, Wayne State University, Detroit, Michigan
email: belwadia@email.chop.edu

INTRODUCTION

Traffic accidents causes high rate of mortality and morbidity. Compulsory seat belt use had successfully reduced the severity of trauma in car crash accidents largely (Traffic safety facts, 2009). Among all the seat belt users, a large number of occupants are embedded with Implantable Cardiac Devices (ICDs). Therefore, more patients with ICD's involve in car crash accidents while wearing seat belt. The role of seat belt in causing injury to the ICD implanted patients during motor accident has been widely documented; however, incidences of these injuries following seat belt-ICD interaction during and after the traffic accident have never taken seriously either by manufacturer or by the National Highway Traffic Safety Administration (NHTSA). The injuries may cause dislodgement of lead or as severe as disabling the device following an accident which can be fatal to life.

The study objective is to validate the interaction of a seat belt with an implanted ICD (with sutures) using a combination of a finite element (FE) model of the human body and a FE model of an ICD. Further, radiographs from one thousand patients were reviewed to obtain the optimum site of ICD placement during modeling. A questionnaire based anonymous study (based on accepted IRB protocol) was carried out on 450 patients to populate the number of patients who prefer not to wear their seatbelts after an ICD implantation.

METHODS

The second version of Wayne State Human Body Model (WSHBM) is a detailed FE model validated for frontal and lateral automotive impacts. The model has been developed to be used with a dynamic explicit FE solver; LS-DYNA v. 970 (LSTC Corporation, Livermore, CA). The WSHBM is a 50th percentile adult male model with 79,471 nodes and 94,484 elements with a mass of 75.6 kilograms. Additional details on its construction and validation can be found in Shah et al. (2007).

A FE model of a Medtronic ICD was developed by converting surfaces obtained from a 3D laser scanner (eScan3D, 3D Digital Corporation, CT) into solid hexahedral elements. The base was modeled as bio grade Titanium and the header as polyurethane. The ICD model was placed sub-pectorals in the quadrant obtained from the review of X-rays from 1000 patients implanted with ICDs.

A standard three-point seatbelt system with retractors and pretensioner was modeled and the entire setup was positioned on a surrogate seat for the sake of simplicity. Fig.1 shows the placement of the WSHBM along with the ICD and seatbelt in the surrogate seat setup.

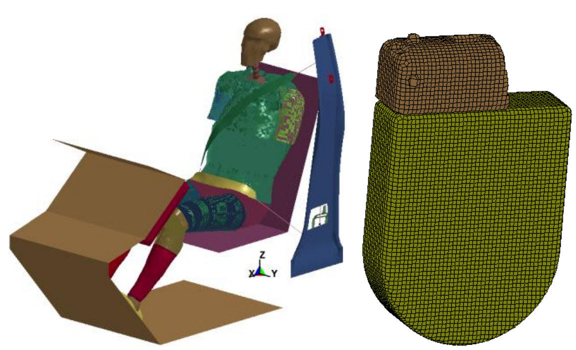

(a) **(b)**

Figure 1: (a) WSHBM with the 3-point seatbelt in a simulated buck (b) Pacemaker with the base and header

Loading and boundary conditions for the FE model. Based on the "X-Ray" analysis and patient survey it was seen that in 84% of patients after implantation of pacemaker, seatbelt were not worn. In order to study the interaction of seatbelt and ICD in frontal automotive crashes, four cases with, and without a seatbelt; and with single and double suture as a means of countermeasure were simulated. The model was simulated with an initial velocity of 20 mph (and 30mph) and the retractor was set to fire 2 ms into the event.

RESULTS AND DISCUSSION

Table 1 outlines the simulation configuration setup.

Table 1: Simulation matrix

Run # 20 mph, 30 mph	Suture	Seatbelt
1,5(Sham)	Single	Not Modeled
2,6	Single	Modeled
3,7(Sham)	Double	Not Modeled
4,8	Double	Modeled

Fig.2 through Fig. 4 shows the position of the ICD for run #1 with respect to the seatbelt and the pectoralis. The red lines on the ICD track the motion through the time steps.

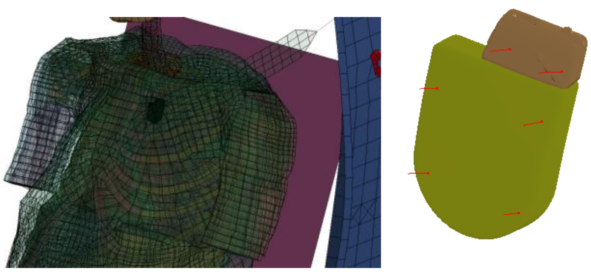

Figure 2: ICD Trace – 18 ms

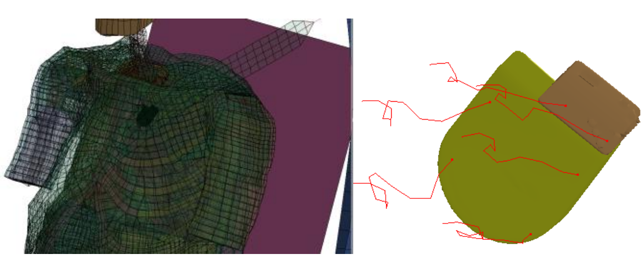

Figure 3: ICD Trace – 50 ms

From Fig. 3 we observe that as the seatbelt starts to engage the ICD, the ICD rotates clockwise in the coronal plane and then assumes a 2 o'clock position until the end of the simulation (Fig. 4).

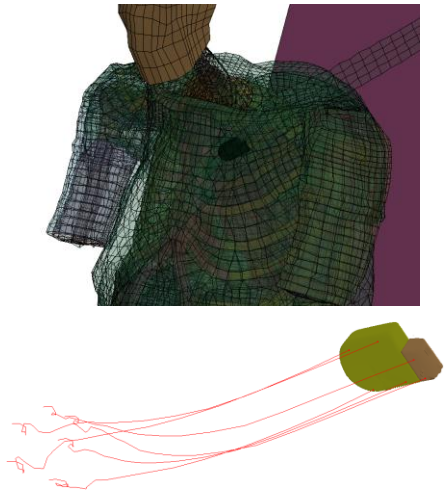

Figure 4: ICD Trace – 80 ms

Comparing run #1 and #2 we observe that the introduction of 3-point seatbelt significantly affects the kinematics of the ICD. A similar trend was seen between run #3 and #4. It was found that the addition of a second suture (Run #4) to the ICD drastically reduced the initial rotation (Fig. 3) of the ICD. It was seen that stabilizing the ICD during seatbelt interaction greatly reduced the risk of lead pullout both at the site of origin and insertion.

CONCLUSIONS

Eight finite element based simulations with a Medtronic ICD and the second version of the Wayne State Human Body Model were simulated. The models were simulated with seatbelt (with and without) and sutures (single and double) as design factors. It was observed from kinematic data that the ICD rotated in the counterclockwise direction (when looking at the anterior aspect of the WSHBM) while interacting with the seatbelt in a frontal 20 mph crash with a single suture. With the addition of the second suture, the initial rotation of the ICD decreased significantly. It was seen that the addition of the second suture decreased the probability of lead pullout both from the ICD and at the point of insertion into the cardiac wall.

REFERENCES

1. Shah, C.S., et al., Development of a computer model to predict aortic rupture due to impact loading. *Stapp Car Crash J*, 2001. 45: p. 161-82.

EFFECTS OF MULTIFOCAL LENS GLASSES ON STEPPING ACCURACY DURING STEP DOWN

[1]Kurt E. Beschorner, [1]Swathi Dyapa, [1]Caitlin M. Strobel, [1]Dennis Tomashek and [1]Kevin Keenan

[1]University of Wisconsin-Milwaukee, Milwaukee, WI, USA
email: beschorn@uwm.edu, web: http://www4.uwm.edu/gabl/

INTRODUCTION

Multifocal lens (MfL) glasses including bifocal or progressive lens glasses are commonly prescribed to people requiring different prescriptions for near and distance viewing. Distortion of ground level objects, caused by MfL glasses, are associated with increased fall rates [1]. Blur and visual distortions during step up and step down tasks are known to change stepping patterns including toe clearance [2], approach step distance [2], time to step down [3] and weight transfer during step down [3]. Johnson et al. suggested that participants with single lens glasses had better stepping accuracy based on observations that the intra-participant variability in approach step distance was lower in the single lens group [2]. This study, however, did not directly measure stepping accuracy. Foot placement when stepping to a specific location (such as a narrow step) or avoiding a hazard (like a puddle) may be particularly relevant to fall prevention. This study examines the effects of multifocal lens glasses on stepping accuracy and other relevant stepping variables during a step down task.

METHODS

A sample of nine participants (8F, 1M Ages 19-29) was recruited to participate in a two-hour testing session. The protocol was approved by the University of Wisconsin-Milwaukee Institutional Review Board. Participants were asked to step off of a 150 mm step onto one of three targets that were projected onto a force plate. The targets were located centrally in the medial/lateral direction and at distances 310 mm, 480 mm and 650 mm from the edge of the step. Trials alternated between stepping down from static standing and stepping down during gait and target location was randomized in order to minimize the learning effect from repeated trials. Participants donned four different types of glasses (single lens and multifocal lens with a lower add region of 1.75, 2.75 and 3.75). The order of glasses was randomized

Stepping accuracy was calculated as the anterior/ posterior distance between center of pressure and the target location when the vertical force first exceeded 20% of body weight. The average neck flexion angle was calculated using markers placed on the torso (right and left acromion process, c7 and suprasternal notch) and head (4 markers on the anterior/posterior and medial/lateral "corners" of the head). Flexion angle was determined as the rotation about the medial-lateral torso axis using segments and rotation sequence as recommended by ISB [4]. Head angle was averaged from toe off to heel contact of the stepping foot to determine if lens strength caused participants to flex their necks more in order to shift the target location into the upper lens region. Lastly, the time to step down was also analyzed to determine if the stepping cadence changed with different lens strength.

ANOVA analyses were used to determine which of the independent variables (e.g.,lens strength, standing vs. walking, target location and the first-order interactions) affected the dependent variables (e.g.,step placement, average neck flexion angle and step time). Participant was treated as a random-independent variable. Within-participant ANOVA analyses were also performed to determine if the effects were participant-specific. Independent effects were the same as the previous ANOVA with the exception of participant. Learning effect was analyzed by using trial number and lens order as independent variables in separate analyses.

RESULTS AND DISCUSSION

Lens strength was the only significant variable to affect step placement ($p<0.05$) (Fig. 1). Higher strength lenses caused a more anterior foot placement. Lens strength was also the only significant variable that affected the neck flexion angle ($p<0.05$) with higher lens strengths being associated with more neck flexion. Target location was the only variable that affected the step time ($p<0.01$). The farthest target required the longest amount of step time. No trial number or lens order effect was found for any of the measures.

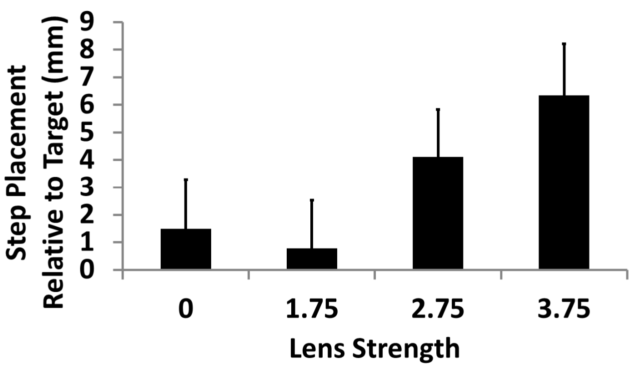

Fig. 1 Effect of lens strength on step placement. Vertical bars represent standard error.

Within-participant analyses revealed variation across participants in the response to the glasses (Table 1). Six of the nine participants had a statistically significant positive correlation of head flexion with increasing lens strength. Of the six that had increasing head flexion with lens strength, three participants showed a significant correlation with foot placement and lens strength. The three participants who did not have a significant correlation between head flexion and lens strength also did not have a significant correlation between foot placement and lens strength.

Changes in the lens strength of the lower regions of multifocal lens glasses produced changes in step placement and neck flexion angle during stepping, although this effect varied greatly across participants. Because many of the same participants demonstrated responses in both neck flexion and step placement, flexing the neck during stepping may not be an effective compensatory strategy. The variations in effect size across participants suggest that certain individuals may be more sensitive to multifocal lens glasses than other individuals. Modest fall reductions have been attained by replacing multifocal lens glasses with single lens glasses when walking [5]. The effectiveness of this intervention may be improved by identifying individuals who are most sensitive to visual distortion and focusing interventions on those individuals.

Table 1: Intra-participant analysis of lens strength on step placement and neck flexion. Significance levels of: *p<0.05, **p<0.01, ***p<0.001.

Participant	Step Placement	Neck Flexion
1	**	*
2	*	
3	***	*
4	***	
5	***	
6		
7		
8		
9	***	**

Future studies could improve on a few of the limitations of this study. First, the participants used in this study were a convenience sample of non-multifocal lens glasses wearers who were primarily young and healthy adults. Differences may be found with an older population. Secondly, while the results were statistically significant, the effect size of step placement was relatively modest. Therefore, changes in the protocol that could make the visual component more challenging such as a secondary task may improve the sensitivity of the protocol in identifying sensitive individuals. Lastly, studies are needed to determine if the measures in this study are associated with actual falls.

REFERENCES

1. Lord, S.R. et al. *J. Am. Geriatr. Soc.* **50**, p. 1760-1766, 2002.
2. Johnson, L. et al. *J. Am. Geriatr. Soc.* **56**, p. 178-80, 2008.
3. Buckley, JG et al. *Gait Posture* **21**, p.65-71, 2005.
4. Wu & Cavanagh, *J. Biomch* **28**, 1257-72, 1995.
5. Haran, MJ et al. Br Med J **340**, 2010.

ACKNOWLEDGEMENTS

This study was funded by a UWM College of Health Sciences SEED grant

EFFECTS OF AGE AND EXPERIENCE ON FOOT CLEARANCE DURING UP AND DOWN STEPPING

[1]Kurt E. Beschorner, Autumn Milanowski, Dennis Tomashek and Roger O. Smith

University of Wisconsin-Milwaukee, Milwaukee, WI, USA
[1]email: beschorn@uwm.edu web: http://www4.uwm.edu/gabl

INTRODUCTION

Multifocal (MfL) lens glasses, a commonly prescribed solution to presbyopia, have been shown to increase fall risk [1]. One way in which MfL glasses may cause falls is by distorting the apparent location and shape of steps (Fig. 1). Differences in toe clearance and approach step distance occur when wearing MfL glasses compared with single lens (SL) glasses [2]. While MfL glasses are known to modify gait parameters during step-up (e.g. approach step distance, toe clearance, step distance) [2], the effects of these glasses during step down is not as well understood. When stepping down from a standing posture, participants respond to blurred vision with caution by slowing stepping speed and reducing weight transfer indicating that visual feedback is important to stepping down [3]. Additionally, there is a paucity of research on novice wearers, who may be at the most risk of falling while they are learning to adapt to the distortion. The participant pools of other research have been primarily been elderly population [2-3] and therefore the effects of aging have not been teased out from the effects of the lenses alone. This study aims to examine the effects of multifocal lens glasses, age and experience during step up and step down tasks.

Figure 1: Appearance of step through MfL glasses

METHODS

Fifteen younger novice (YN: 24.3 (18-28) y.o., 10 F, 5M), seven older novice (ON: 52.4 (48-56) y.o., 4F, 3M) and five older experienced MfL glasses wearers (OE: 51 (45-58) y.o., 2F, 3M) were recruited for a single 1.5 hour testing session. “Younger” and “older” terms refer to the relative ages of the participants and not age categories. Novice wearers eye sight was corrected with contact lenses if necessary. The protocol was approved by the UWM Institutional Review Board. Participants experienced three trials for five walking conditions in random order: level walking, walking up a ramp then down a 75 mm step, walking up a ramp then down a 150 mm step, a 75 mm step up then a ramp down and a 150 mm step up then a ramp down. Participants did this set of trials while wearing both SL and progressive MfL glasses in random order. MfL glasses for novice wearers had no upper lens region correction, and an “add” of +2.75 diopters in the lower region for the novice wearers. Experienced wearers wore glasses with their current prescription for the MfL condition and single lens glasses with their upper prescription for the SL condition.

Toe clearance during step up and heel clearance during step down were calculated as the minimum distance between the edge of the step and a marker placed on the front of the toe and back of the heel, respectively. In addition, the distance between a marker placed on the toe of the non-stepping leg, a marker placed at the heel of the stepping leg and the step were also calculated.

The effects of the independent variables: lens type, step height, group (YN, ON, or OE) and the first order interactions; were evaluated on the dependent variables: toe clearance during step up and heel clearance during step down. Correlation analyses between step up toe clearance and step down heel clearance were performed with the trailing leg toe to step distance and the stepping leg heel to step distance. This analysis aimed to identify if changes in toe clearance might be due to step placement.

RESULTS AND DISCUSSION

Toe clearance during step up was greater in the MfL glasses condition than the SL condition ($p<0.001$). The type of lens affected the different participants group differently (lens * group effect: $p<0.01$). Experienced MfL wearers demonstrated little difference in toe clearance between the single lens and MfL glasses, while both the other novice groups increased toe clearance during the MfL condition as opposed to the single lens (Table 1). Both the distance from the toe to the step of the non-stepping leg ($p<0.001$, $R^2=0.15$) and the heel to the step of the stepping leg ($p<0.001$, $R^2 = 0.06$) were significantly correlated with the toe clearance.

Heel clearance during step down was higher with single lens glasses than MfL glasses ($p<0.05$, Table 1). Other significant effects for heel clearance included step height (more clearance for high step height, $p<0.05$), group (older novice group had lowest heel clearance, $p<0.05$), group * height interaction (older experienced had higher clearance with the low step than high step while other groups had higher heel clearance with the high step, $p<0.01$). The heel clearance during step down was correlated with the toe to step distance of the non-stepping leg ($p<0.01$, $R^2 = 0.06$) and the heel to step distance of the stepping leg ($p<0.001$, $R^2 = 0.10$).

Novice participants (both younger and older) responded to MfL glasses with large increases in toe clearance when stepping up, while older experienced wearers used a similar stepping technique for both types of glasses. This indicates that experienced wearers have adapted to the MfL glasses and no longer alter their stepping pattern when wearing MfL glasses. Increase in toe clearance may be a compensatory response by novice users to prevent tripping as they first start to learn how to navigate using the glasses. Heel clearance, however, was found to decrease during MfL glasses compared with single lens glasses during step down, indicating a greater potential for tripping. No interaction effect was observed between the glasses worn and the group during step down, indicating that the same adaptation may not be present during step down task. Because of the extra burden of absorbing the potential energy during a step down task, an increase in trip risk during step down (as indicated by lower heel clearance) may be responsible for severe falls. Step placement seemed to contribute partially to the heel and toe clearance.

Novice wearers may automatically compensate during step up by increasing toe clearance thus reducing the need for interventions for that task. Yet stepping down may be a more challenging activity and it is unclear what, if any, protective adaptations are used by novice wearers. Therefore, future research may wish to determine if stepping down variables such as heel clearance, approach step distance or stepping foot placement are associated with fall risk and if interventions can improve these outcomes. In addition, older novice wearers responded to MfL glasses similarly to younger wearers, indicating that convenience sampling of young participants may be an appropriate group to pilot test interventions. Because the "older" group was relatively young and healthy, the results would likely vary for higher age groups including elderly adults.

REFERENCES

1.Lord S et al. *J. Am. Geriatr. Soc.* **58***,* 1760-6, '02.
2.Johnson, L. et al. *J. Am. Geriatr. Soc.* **56**, p. 178-80, 2008.
3.Buckley JK et al. *Gait & Posture* **21***,* 65-71, 2005.

Table 1: Toe clearance and heel clearance mean values (standard deviation).

Variable	Lens	Older Experienced	Older Novice	Younger Novice	Lens	Group	Lens x Group
Toe Clearance Step Up (mm)	MfL	102.3 (26.2)	131.1 (28.8)	117.6 (33.6)	p<0.001		p<0.01
	SL	103.7 (20.1)	108.9 (22.6)	92.0 (26.8)			
Heel Clearance Step Down (mm)	MfL	82.5 (25.8)	65.7 (23.0)	89.8 (21.8)	p<0.05	p<0.05	
	SL	89.4 (34.9)	72.1 (16.2)	90.7 (26.3)			

Topographical Classification of Normal and Tumorigenic Colonic Tissue

[1,2]Shruthi S Bharadwaj and [2]Sarah C. Glover

[1]Department of Biomedical Engineering, University of Florida, Gainesville, FL, USA
[2]Department of Medicine, University of Florida, Gainesville, FL, USA
email: sbharadwaj@ufl.edu or sarah.glover@medicine.ufl.edu

INTRODUCTION

Colon cancer is the third most commonly diagnosed cancer and the third leading cause of cancer death in both men and women in the U.S. [1, 2]. In the event of colon cancer, the integrity of colonic tissue is significantly compromised. Specific patterns have been identified as being unique to tumorigenic tissue.

The purpose of this project is to recognize these both nano as well as micro-scaled patterns and classify these as normal or tumorigenic. The classification will be done via data mining - a process of automatic classification of cases based on data patterns obtained from a dataset [3].

METHODS

Tissue sample Isolation: 15 normal as well as 15 tumorigenic colonic tissue samples will be obtained and kept frozen until ready to be imaged.

Scanning Electron Microscopy (SEM): The extracellular matrix of colonic epithelia will be prepared for scanning electron microscopy as previously described [4]. Frozen tissue samples will be thawed fixed with Trump's fixative for at least 1 hour. Samples will then be washed with distilled water and prepared for SEM by alcohol dehydration. Samples will finally be dried using hexamethyldisilazane (HMDS). Uncoated specimens will be glued onto metal stubs with carbon-coated tabs. SEM images will be obtained using a Hitachi S-3000N scanning electron microscope at 20 kV in variable pressure mode at 10 Pa.

Roughness Profile: Roughness parameters will be directly calculated using the MeX software. Briefly, stereopair images will be obtained at 0 and +10 º from the horizontal and input into the MeX image analysis software program (Alicona Imaging, Graz, Austria). The tilt angle along with the working distance and the size of image pixels will also be input for proper calibration. Reconstruction will then be performed in two steps. First, corresponding points will be extracted from the stereoscopic images. Secondly, metrically correct 3D points will be calculated using the geometric relationships from the SEM images obtained previously.

Classification: To recognize and classify topographical differences seen in colonic tissue, support vector machine (SVM) will be used. Briefly, it is a kernel-based algorithm where each parameter will be identified and classified as being tumorigenic or not.

RESULTS AND DISCUSSION

ECM topography underlying normal, well, and poorly differentiated colon cancer cells were evaluated. Scanning electron microscopy (SEM) was used to characterize colonic epithelial tissue of normal, well differentiated and poorly differentiated tissue (**Figure 1**). The pore sizes in the tissue were

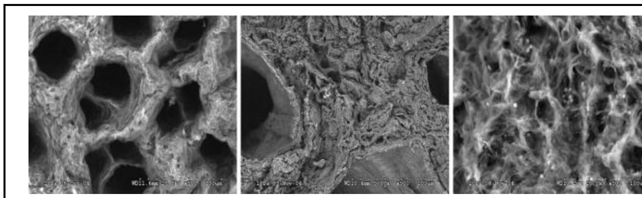

Figure 1: Scanning electron micrographs of the extracellular matrix underlying normal colonic epithelia (a), well differentiated (b), and poorly differentiated colon cancer cells (c). Tumors processed as described in Materials and Methods, fixed in Trump's fixative, air dried using HMDS, and imaged using a Hitachi S-3000N VP-SEM. Note that the microtopography in (a) is trough-like whereas that in (c) is peak-like. Scale bars = 100 μm.

significantly different in well and poorly differentiated when compared to the normal colonic tissue. Roughness parameters (**Table 1**) from SEM images were generated using MeX software. The normal colonic tissue had significantly lower roughness parameter values when compared to the tumorigenic colonic tissue (**Figure 2**). Using the Roughness parameter values, a SVM classifier was built using MATLAB (**Table 2**).

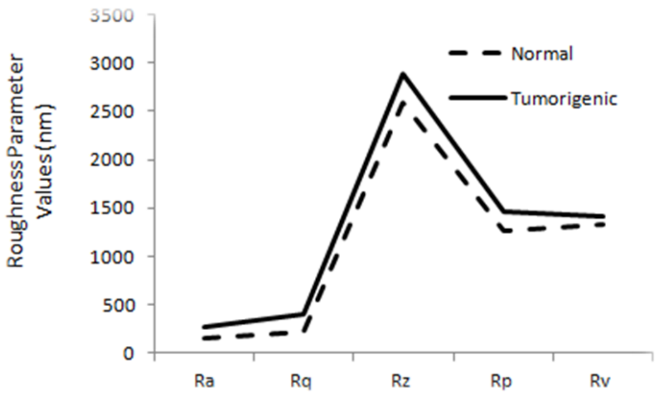

Figure 2: Roughness parameters values of normal (dashed line) and tumorigenic (solid line) of colonic tissue. Roughness parameter values were obtained by MeX software.

CONCLUSIONS

We have presented a method to analyze topographical features observed in the event of colon cancer using SVM. Classification of tissue surface is essential in early diagnosis of colon cancer. Although current optical modalities are emerging, these lack quantifiable proof of diagnosis. The classification of tissue based on topographical features, as shown in this project, will provide the sensitivity and the specificity that these modalities lack.

REFERENCES

1. Jemal A, Bray F, Center MM, Ferlay J, Ward E, Forman D: **Global cancer statistics.** *CA: a cancer journal for clinicians* 2011, **61:**69-90.
2. Siegel R, Ward E, Brawley O, Jemal A: **Cancer statistics, 2011: the impact of eliminating socioeconomic and racial disparities on premature cancer deaths.** *CA: a cancer journal for clinicians* 2011, **61:**212-236.
3. Fung G and Stoeckel J (2007). **SVM feature selection for classification of SPECT images of Alzheimer's disease using spatial information**. *Knowl Inf Syst* 11(2): 243–258
4. Howat WJ, Barabas T, Holmes JA, Holgate ST, Lackie PM: **Distribution of basement membrane pores in bronchus revealed by microscopy following epithelial removal.** *Journal of structural biology* 2002, 139**:**137-145.

Table 1: Roughness Parameter Values for Normal and Tumorigenic Colonic Tissue

Parameters		***Approximate value for normal colonic tissue (nm)***	***Approximate value for tumorigenic colonic tissue (nm)***
R_a	Average roughness of profile	157	270
R_q	Root-Mean-Square roughness of profile	220	402
R_z	Maximum height of roughness profile	2592	2880
R_p	Maximum peak height of roughness profile	1257	1460
R_v	Maximum valley depth of roughness profile	1336	1420
R_{sk}	Skewness of roughness profile	-0.339	-0.238
R_{dq}	Root-Mean-Square slope of roughness profile	0.573	1.296
R_L	Ratio between true length and projected length of roughness profile	1.125	1.415

Table 2: Normal and Tumorigenic tissue classified using SVM

Sample	***Features***	***Normal Misclassified***	***Tumor Misclassified***
30 colon samples	250	6	4

REPEATABILITY OF IMAGE REGISTRATION AND SEGMENTATION PROCEDURES FOR CT SCANS OF THE HUMAN DISTAL RADIUS

[1] Varun A. Bhatia, [2] W. Brent Edwards, [1,2] Karen L. Troy
[1]Bioengineering Department, University of Illinois at Chicago
[2]Department of Kinesiology and Nutrition, University of Illinois at Chicago
email: vbhati2@uic.edu, web: http://www.uic.edu/ahs/biomechanics

INTRODUCTION

Serial CT scans are often used to quantify changes in bone resulting from disease or intervention. For meaningful comparisons between time points, it is imperative that scans are accurately registered and consistently segmented for analyses. Our purpose was to test the accuracy and precision of semi-automated protocols to align, register, and segment bone from serial CT scans of the distal radius.

METHODS

Accuracy and precision of the image registration and segmentation procedure were calculated by registering randomly rotated images back into their respective original alignments.

Native Image Alignment and Segmentation
Six distal radii were imaged with a clinical CT scanner (GE Brightspeed, GE Medical, Milwaukee, WI) as part of a larger study. Each scan contained a calibration phantom to convert CT attenuation in Hounsfield units (HU) to hydroxyapatite equivalent density. Native images were manually aligned along the long axis of the radius using Mimics (Materialise, Leuven, Belgium). The periosteal surface of the radius was segmented from the scans using a density threshold of 0.175 g/cm^3. Bony regions missed by the thresholding procedure were manually identified. Stereo-lithographic (STL) models of the segmented aligned radii were created.

Registration Accuracy
Aligned images were randomly rotated about the three orthogonal axes based on a random numbers generator that was constrained between angles of ±15° corresponding to a “worst case” positioning error scenario. This procedure was performed three times for each of the six aligned images. These rotated images were segmented and their corresponding STL models exported to Matlab (MathWorks, Natick, MA). ICP-FINITE [1], an iterative closest point registration algorithm for 3D point clouds, available through Matlab Central File Exchange, was used to rigidly register STL models from the randomly rotated radii into their respective STL models from the aligned radii (Fig 1). The Cardan angles were back calculated from the resulting rotation matrices and compared to the corresponding (known) random rotations for a measure of image registration accuracy.

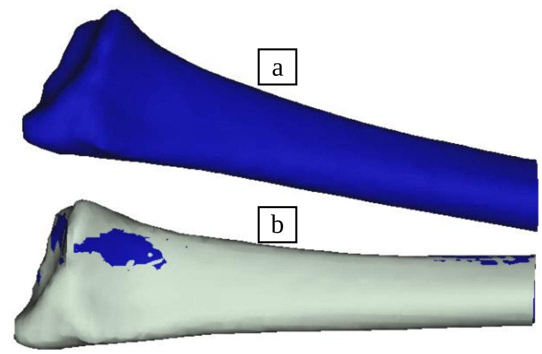

Figure 1: a) Rotated and b) registered STL models.

QCT Mineral Analysis
Cardan angles were used to register rotated radii back into the aligned coordinate system and images were segmented as described earlier. Measurements of bone mineral and strength were computed for a 45 mm region immediately proximal to the subchondral plate of the distal radius. The subchondral plate was automatically determined and corresponded to the largest cross-sectional area of the radius (Fig. 2). A 15 mm section proximal to the subchondral plate was selected as the ultra-distal (UD) region, while a 30 mm section proximal to the UD region was selected as the mid-radius (MID) region. Mineral content (BMC; g), density (BMD; g/cm^3), cross-sectional area (CSA; cm^2), compressive strength index (CSI; g^2/cm^4), and bending strength index (BSI; cm^3) were determined for both the UD and MID regions. Strength measures CSI and BSI are functions of both mineral density and structure [2].

Data Analysis
Registration accuracy was calculated as the absolute difference between the random (known) and corresponding calculated (from registration)

rotations. Precision for each outcome measure was assessed using the root-mean-square coefficient of variation (RMS CV) [3].

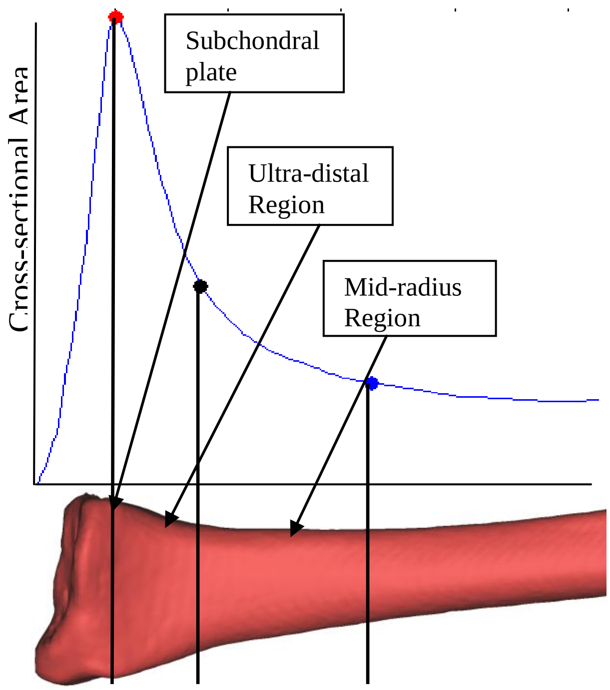

Figure 2: Identification of subchondral plate, Ultra-distal region and Mid-radius region.

RESULTS AND DISCUSSION

The aim of this study was to develop, and test the repeatability of registration and segmentation procedures used to analyze serial CT scans of the distal radius. The image registration procedure was highly accurate. Absolute errors for rotations about the anatomic anterior-posterior and medial-lateral axes were 0º (SD 0º), while that for the longitudinal axis was 0.67º (SD 0.69º). The error about the longitudinal axis may be explained by the presence of local minima in the iterative optimization scheme used for registration. The bone mineral distribution is quite uniform about this axis and adjusting the registration tolerance may eliminate this error. However, because mineral analyses are calculated along transverse sections, registration error about the longitudinal axis would not be expected to influence outcome measures.

The image registration and segmentation procedure were highly repeatable. The RMS CV was less than 1.47% for all the outcome measures (Table 1). The CV was larger in the UD region compared to the MID region. Rotating images often requires interpolation techniques that can act as a low pass filter. This could result in minor changes in the actual density values that would depend on the gradient of the image and the degree of rotations. As the UD region is comprised predominately of trabecular bone it may be more sensitive to image rotation than the predominately cortical MID region.

The RMS CV was larger for strength measures (0.98%) compared to the mineral measures (0.71%). This is likely because mineral measures are a function of bone density, while strength measures are a function of both density and shape.

The methods described here are semi-automated at best. Some amount of manual adjustment is needed for accurate segmentation of the bone, which adds subjectivity to the process. Additionally, Mimics only allows angular rotations of whole numbers (not fractions), which adds error to the registration technique. Given these limitations, this study suggests that the current registration and segmentation procedure is highly reliable and can be used to analyze serial CT scans of the distal radius with sufficient accuracy and repeatability.

Table 1: Percent RMS coefficient of variance for bone mineral and strength outcome measures.

Mineral Prameters	Percent RMS CV	Strength Parameters	Percent RMS CV
UD BMC	0.98	UD CSA	1.47
UD BMD	0.97	UD CSI	1.19
MID BMC	0.32	UD BSI	1.31
MID BMD	0.65	MID CSA	0.77
Total BMC	0.53	MID CSI	0.66
Total BMD	0.84	MID BSI	0.46

REFERENCES

[1] ICP-FINITE, Matlab central file exchange (http://www.mathworks.com/matlabcentral/fileexchange/24301-finite-iterative-closest-point) Last accessed 03/01/2012.
[2] Lang T, J Bone Miner Res, 2004:19, 1006-1012.
[3] Glüer CC, *Osteoporos Int*, 1995: 5, 262-270

MUSCLE ACTIVITY PATTERNS OF LOWER LIMB DURING LATERAL (FRONTAL) SIDE STEPPING TASK MODULATION FROM DIFFERENT HEIGHTS

[1]Dinesh Bhatia, [2]Mario Novo,[2]Marcos Munoz,[1]Tatiana Bejarano,[1]Ranu Jung and[2]Denis Brunt

[1]Adaptive Neural Systems Lab, Department of Biomedical Engineering, Florida International University, Miami, FL-33174, USA
[2]Department of Physical Therapy, Florida International University, Miami, FL-33199, USA
email: dinesh.bhatia@fiu.edu

INTRODUCTION

Different muscle groups function in synchrony and coordination to perform a given task, wherein the activity of one muscle group closely affects that of another [1,3]. Osteoarthritis (OA), a chronic joint disease, is the most common musculoskeletal complaint worldwide characterized by pain, disability and progressive loss of function. It is associated with significant health and welfare costs [2,7]. The knee is the most frequently affected lower limb joint and prevalence of knee OA increases with age [6]. Several studies have shown that muscle recruitment patterns and neuromuscular efficiency are different for patients with OA compared to normal controls during simple closed chain activities [4,5]. However, no studies have investigated frontal plane control or the modulation of control due to, for example, a change in time or distance in OA [5,6]. This paper reports the results of a pilot study with healthy subjects to determine muscle activation patterns (electromyogram, EMG), and modulation of these patterns, in a frontal plane step initiation task.

METHODS

Four subjects, age 23-32 years, mean height and weight 165 cm and 75 kg respectively, participated in the study. EMG for the support limb was recorded from rectus femoris (RF), vastus lateralis (VL), vastus medius (VM), biceps femoris (BF), semi membranous (SM), tibias anterior (TA), gastrocnemius (GAS), gluteus medius (GM), and gluteus maximus (GMax) while the subjects side stepped up (at a fixed interval with feet on separate force plates) on a 4 or 8 inch step (Figure 1).Subjects completed 3 successful trials. Muscle activity and ground reaction forces (GRF) were recorded employing an 8 channel EMG system (Motion Lab Corp.) and dual force plates (AMTI) respectively. The signals were sampled at 1000 Hz and band-pass filtered (20-500 Hz) with the EMG full-wave rectified [3]. The recorded EMG and GRF data were averaged across these trials for each subject. The GRF data were used to identify the phases of movement and matched with the corresponding EMG data in Visual 3D software.

RESULTS AND DISCUSSION

Three distinct phases for the step up task were identified as shown in figure 2 for the 8 inch step. These were from initiation to toe-off (1-2), toe-off to contact (2-3), contact to loading and stabilization (3-4). It was observed that for the 8 inch step, there was both an increase in slope and the peak of ground reaction force. For example, the slope of mediolateral GRF (figure 2B) for the 8 inch step increased by 200% over the 4 inch step. Subjects completed the 8 inch step in relatively less time duration. The GM and GMax were also found to be more active from initiation to end of the stabilization phase. The RF was active from beginning of initiation to end of contact phase. However, the activity of the SM and GAS was quite insignificant. In addition, the EMG amplitudes also greatly increased in 8 inch step up task. The mean integral values increased for most muscles (figure 2 C-E) by approximately -50%.

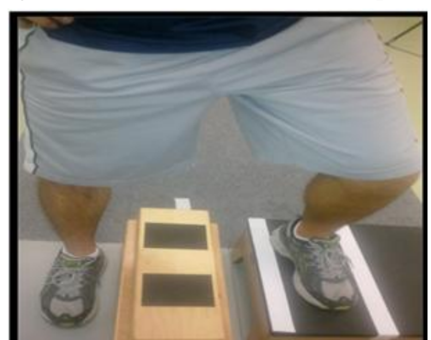

Figure 1: Lateral step up task from 8 inch step on force plate.

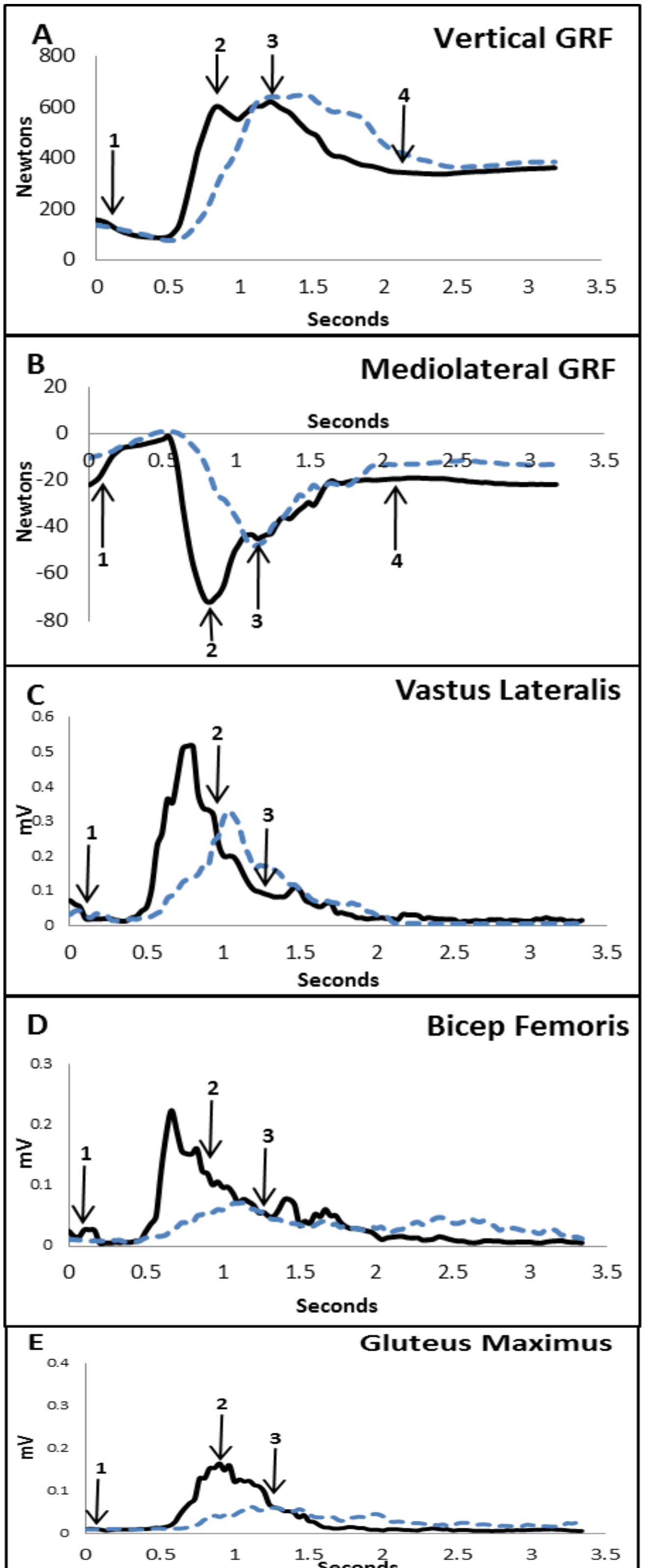

Figure 2: Comparison of 4 inch (dotted) and 8 inch (solid) step-up task phases:
1. Initiation, 2. Toe-off, 3. Contact, 4. Stability
A. Stability Leg (Z) GRF
B. Stability Leg (X) GRF
C. EMG Vastus Lateralis
D. EMG Biceps Femoris
E. EMG Gluteus Maximus

CONCLUSIONS

These results provide a baseline standard for understanding lower extremity muscle group patterns actively involved in performance of lateral side stepping tasks. These distinct phases in the step up task were found to be consistent for all subjects. The results illustrate coordination in the muscle activity patterns of different muscle groups during task modulation with prominent firing of the quadriceps, hamstrings and the hip abductor/extensor muscles for the side step up task. Future studies will examine OA subjects and determine if there is both a phase shift and amplitude change. This could be useful in defining kinematic and activation patterns for identifying early onset of the disease as well as rehabilitation protocols prior to surgery.

REFERENCES

1. Bhatia D., et al. "Coordination between lower limb muscles in different locomotion activities", *IJBET*, **6 (2)**, 23-30, 2011**.**
2. Childs J.D., et al. "Alterations in lower extremity movement and muscle activation patterns in individuals with knee osteoarthritis", *Clin. Biom.*, **19**, 44-49, 2004.
3. De Luca, C.J., "The use of surface electromyography in biomechanics", *Journal of App.Biom.*, **13 (2)**, 135–163, 1997.
4. Likivainio T., et al. "Physical function and properties of Quadriceps femoris muscle in men with knee Osteoarthritis", *A. Phys. Med.Rehabil*, **89**, 2185-2193, 2008.
5. Pai Y.C., et al. "Alteration in multijoint dynamics in patients with bilateral knee osteoarthritis", *Arthritis Rheum.*, **37 (9)**, 1297-304, 1994.
6. Rana S., et al. "Delayed onset of Quadriceps activity and altered knee joint kinematics during stair stepping in individuals with knee Osteoarthritis", *A.Phys Med. Rehab.*, **83**, 1080-1086, 2002.
7. Rana S. H., et al. "Hip Muscle Weakness in Individuals with Medial Knee Osteoarthritis", *Arthritis Care & Research*, **62 (8)**, 1190-1193, 2010.

THE EFFECTS OF UPPER EXTREMITY LYMPHEDEMA ON DOMINANT LIMB 3-DIMENSIONAL SCAPULAR KINEMATICS AND UPPER EXTREMITY FUNCTION IN SURVIVORS OF BREAST CANCER

Linda Biggers, Peter Rundquist

University of Indianapolis, Indianapolis, IN, USA
email: prundquist@uindy.edu

INTRODUCTION

Breast cancer is the most common form of cancer in women [1]. It is estimated that up to one third of breast cancer survivors will be diagnosed with lymphedema [2]. Lymphedema may lead to difficulty performing activities of daily living above 90° elevation, discomfort, and sensation of heaviness [1,3].

There is little research on the effects of lymphedema on scapular kinematics. Crosbie et al compared the shoulder and spinal kinematics of women post unilateral mastectomy for breast cancer to a control group. They found increased scapular upward rotation (UR) of the involved limb. Lymphedema was an exclusion criterion in their study [4].

Three research hypotheses were investigated: 1) Involved limb volume would be significantly greater than the noninvolved. 2) Affected scapular kinematics at peak humerus to trunk elevation in the plane of choice would be significantly less than the unaffected. 3) Both involved limb volume and scapular kinematics would be significantly correlated to the Penn Shoulder Score (PSS).

METHODS

This study included 12 participants with unilateral lymphedema in their dominant limb post-mastectomy. Eleven were right arm dominant. One was left arm dominant. Arm volume was measured with a volumeter. Scapular UR, internal rotation (IR), and posterior tipping (PT) during humerus to trunk elevation in the plane of choice (POC) were assessed using a 3-dimensional electromagnetic motion capture system. Humerus, scapula, and trunk segment locations and rotation sequences were performed as recommended by the International Society of Biomechanics [5]. Participants performed each motion three times. The peak value across the trials was utilized for data analysis. Shoulder function was assessed using the PSS.

Data analyses included paired tests comparing limb volume and scapular kinematics and correlations between the factors of interest and PSS. Significance level was $p \leq 0.05$.

RESULTS AND DISCUSSION

All of the variables were normally distributed except for limb volume. Participants' age, PSS, and affected limb volume are outlined in table 1.

Limb volume was found to be statistically significantly more in the involved than the noninvolved limb (z = -3.059, p = .002). The volume differences are outlined in Figure 1. Scapular UR at peak elevation in POC was statistically significantly less in the involved than the non-involved limb (t = -2.749, p = .019). The comparative scapula to trunk kinematics are outlined in Figure 2.

The PSS correlation and scapular PT was statistically significant. The Pearson correlation for involved scapular posterior tipping at peak humerus to trunk elevation in the POC and the PSS was (r = .871, p = .000). Correlation results are outlined in table 2.

The first hypothesis was supported. The involved limbs had significantly more volume than the noninvolved. The second hypothesis was partially supported as scapular UR was found to be significantly different between extremities. The third hypothesis was also partially supported as a significant correlation of kinematics of scapular PT was found to correlate with the PSS but girth was not found to be correlated.

Our results do not support Crosbie et al's overall results. However, they are similar to one of Crosbie et al's secondary findings. They found significantly less scapular UR in participants who had had a mastectomy on their dominant extremity than those that had had a mastectomy on their non-dominant extremity [4].

Ludwig et al studied the alterations of shoulder kinematics in participants with symptoms of shoulder impingement and found, in relation to the group without impingement, the group with impingement showed decreased scapular UR and decreased scapular PT during humerus to trunk elevation [6]. Our results showed decreased scapular UR which may predispose the participants to shoulder impingement. The increased scapular PT at may be a compensation to avoid this. Increased PT may lessen the likelihood of the developing shoulder impingement.

While the finding of a correlation of scapular PT to the PSS was significant, the other scapular motions were not. An alternative shoulder functional scale may be more appropriate. Since the time of the initial investigation, a lymphedema specific ICF tool has been identified and may be more appropriate for use in further studies.

CONCLUSIONS

Limb volume is greater and scapular UR is less in participants with lymphedema post-breast cancer surgery. Scapular PT is correlated to function. Further study is recommended to more fully determine the effect of lymphedema on the upper extremity in this population.

REFERENCES

1. Morrell RM, et al. *Mayo Clin Proc* **80**, 1480-1484, 2005.
2. Thomas-Maclean R, et al. *Oncol Nurs Forum* **35**, 65 -71, 2008.
3. Kwan W et al. *J Clin Oncol* **20**, 4242-4248, 2002.
4. Crosbie J, et al. *Phys Ther* **90**, 679-692, 2010.
5. Wu G, et al. *J Biomech*. **38**, 980-992, 2005.
6. Ludewig PM, et al. *Phys Ther* **80**, 276-291, 2000.

Table 1: Participant demographics

Volume (ml)	Median 2960	
	Mean	**S.D.**
Age (years)	56.3	12.3
PSS	72.6	17.0

Table 2: Correlations Between PSS and Factors of Interest

	Volume	UR	IR	PT
PSS r	-.263	.049	.571	.871
p	.419	.879	.053	.000

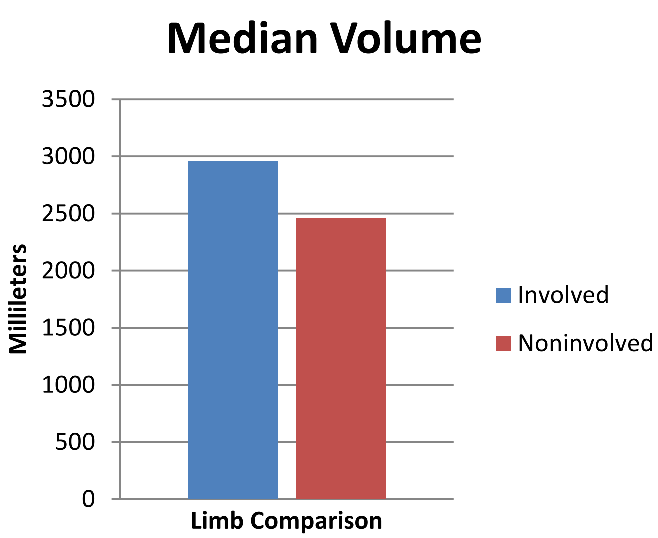

Figure 1: Comparative Limb Volume

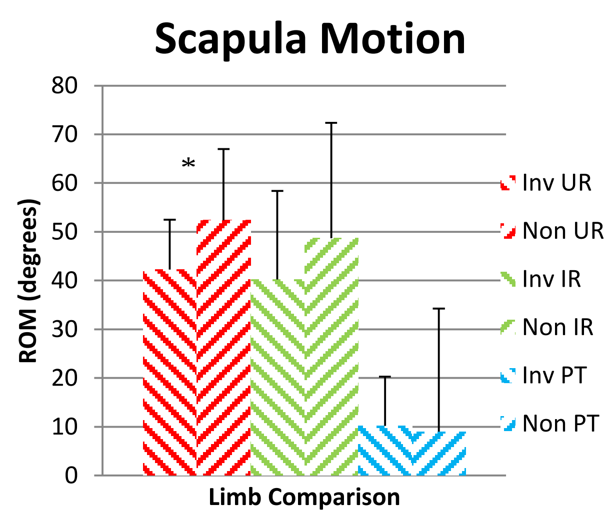

Figure 2: Comparative Scapula to Trunk Motion

STABILITY RADIUS AS A METHOD FOR COMPARING THE DYNAMICS OF NEUROMECHANICAL SYSTEMS

[1]Jeffrey T. Bingham and [1,2]Lena H. Ting

[1]Georgia Institute of Technology, Atlanta, GA, USA
[2]Emory University, Atlanta, GA, USA
email: bingjeff@gatech.edu, web: http://neuro.gatech.edu/groups/ting

INTRODUCTION

Robust motor behaviors emerge from neuromechanical interactions, however even with computational models these interactions are difficult to compare and analyze. One particular challenge is the characteristic of neuromechanical systems being capable of achieving similar motor performance for a multitude of neural and biomechanical configurations. For example, in frontal plane balance control, similar center-of-mass (CoM) kinematics is observed in response to support surface perturbations in subjects when standing at wide and narrow stances. Our models of frontal plane balance with delayed feedback control suggest that delayed neural feedback gains must necessarily change under these disparate biomechanical conditions [1]. However, previously we have lacked the computational tools to quantitatively compare dynamical behavior across different neuromechanical conditions.

Classical stability tools are generally not robust for analysis of neuromechanical systems, which may be non-linear, have multiple inputs and outputs, and include feedback delays. For example, gain/phase-margin, can only be used to compare the stability of single-input-single-output, linear-time-invariant feedback systems. More sophisticated stability techniques based on spectral, or eigen-value, analysis (alpha-stability, halving time, etc.) solve some of these issues, but do not offer robust metrics because sensitivity of model parameters to system stability is not accounted for.

Here we present the *stability radius*, a technique from robust control theory that provides a scalar measure of the smallest perturbation to any system parameter that would result in instability. The mathematical theory is derived from the field of pseudo-spectral analysis [2], which in turn is a generalization of spectral analysis. It is general and can be applied to multi-input-multi-output (MIMO) systems, which may be non-linear, of arbitrary size, and have feedback delays [3,4,5]. Furthermore, stability radius can be used to test the sensitivity of system stability to model parameters. Thus, the stability radius can be used to compare the stability of the same system with different parameters as well as between different systems with similar parameters.

We present the basic technique of using stability radius to compare the stability of neuromechanical systems with an example from postural control of frontal plane balance. We identify the stability radii of different stance widths in a frontal plane model of standing balance with delayed feedback and quantify the neural control parameters that produce a similar level of resistance to a physical disturbance across stance widths.

METHODS

We examined a delayed second order system that modeled human frontal-plane standing balance as a four-bar linkage (Fig 1A) with delayed position, k_p, and velocity, k_v, feedback using nominal anthropometric parameters, see [1] for more details:

$$\boldsymbol{I}(q)\ddot{q}(t) + \boldsymbol{V}(q,\dot{q})\dot{q}(t) + \boldsymbol{G}(q) = -C\left(k_p q(t-\tau) + k_v \dot{q}(t-\tau)\right)$$

Stability radius was computed for this system by reformulating the governing equations into a state space description, with states, x, and delay, τ. It was then linearized about the equilibrium state, $\tilde{x}$, to form the linearized system with non-delayed matrix, $\boldsymbol{A}$, and delayed matrix, $\boldsymbol{A_d}$:

$$\dot{\tilde{x}} = \boldsymbol{A}\tilde{x}(t) + \boldsymbol{A_d}\tilde{x}(t-\tau)$$

Next, the linearized system matrices were tested for stability by checking that all eigen-values of the following sum, $\boldsymbol{H}$, were strictly negative:

$$\boldsymbol{H} = \boldsymbol{A} + \boldsymbol{A_d}$$

Finally, the stability radius, r, was calculated for all stable delayed feedback parameters, k_p and k_v, for narrow (0.5) to wide (2.0) stance ratios (s = stance width / hip width), where $z \in \mathbb{C}$, $\Re(z) = 0$ implies $z = j\omega$ and σ_{min} was the smallest singular value:

$$r = \min_{\Re(z)=0} \sigma_{min}(\, z\boldsymbol{I} - \boldsymbol{A} - \boldsymbol{A_d} e^{-\tau z})$$

RESULTS AND DISCUSSION

The maximum stability radius (r=0.92) at preferred stance (s=1.0) was found when k_p=1540 N/rad and k_v=405 N/rad/s (Fig 1B). These stable feedback gain pairs were the least sensitive to changes in system parameters. This implied that these gain pairs produced the most stable behavior in the presence of modeling errors, state estimate error, and external disturbances. This illustrates how stability of different feedback parameters values (k_p, k_v) in the same biomechanical posture can be compared.

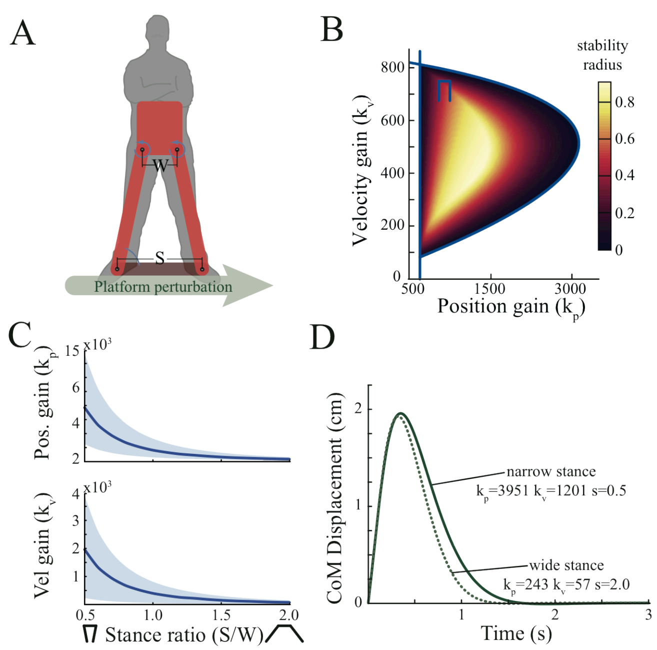

Figure 1: A) Four-bar linkage model B) Stability radii for s=1.0 C) k_p and k_v for constant stability radius (r=0.8) across stance ratios (–) and stable range (area) D) Model response with $q_o = [0\, rad, 10\, \frac{rad}{s}]$, r = 0.80 and s = 0.5 (–) & 2.0 (···)

To compare the stability of different biomechanical postures, k_p and k_v gains were found that resulted in same the stability radius across stance widths. Prior modeling results only identified a range of feasible feedback gains at each stance (shaded area) to reject a disturbance, such as motion of the floor, but did not allow direct comparison of specific conditions across stance widths. The feedback gains that maintained the same stability radius (r=0.8) across stance widths (Fig. 1C - line) required k_p and k_v to increase by 22.6 times from wide to narrow stance. Simulations of models with these gains subjected to external disturbances had similar responses across stances (Fig 1D).

CONCLUSIONS

The stability radius presented utilizes unstructured perturbations and is a measure of the smallest perturbation to *any* system parameter (i.e. any element in $\boldsymbol{A}$ or $\boldsymbol{A_d}$) that would result in instability. Perturbations that utilize known system structure can be used to identify less restrictive estimates of stability, see [3] for more.

Stability radius is a useful metric for comparing and analyzing the dynamics of inherently complex neuromechanical systems. This method provides a simple scalar descriptor of the stability of non-linear MIMO systems with time delays, and the sensitivity of system stability to model parameters. It is also predictive of responses to external disturbances and offers a way to compare different conditions of the same and different systems.

REFERENCES

1. Bingham JT, Choi JT & Ting LH. *J Neurophysiology*, **106**, 437-48, 2011.
2. Trefethen LN & Embree M. *Spectra and Pseudospectra*, Princeton Univ. Press, 2005.
3. Hinrichsen D & Pritchard AJ. (1986). *Systems & Control Letters* **7**, 1-10, 1986.
4. Qiu L, et al. *Automatica* **31**, 879-90, 1995.
5. Michiels W, et al. *Linear Algebra and its Applications*. **418**, 315-35, 2006.

ACKNOWLEDGEMENTS

Funding sources: NIH HD46922 & NS 53822

A COMPARISON OF KNEE MOMENTS DURING A LATERAL CUTTING MANEUVER: SHOD VS. BAREFOOT

Brianna Bisesti, Casey Cottle, Michael Lawrence, Lara Carlson

University of New England, Biddeford ME
email: bbisesti@une.edu

INTRODUCTION

Noncontact anterior cruciate ligament (ACL) injuries often occur during cutting and landing maneuvers [1]. Lateral cutting maneuvers are seen commonly in most sports, and create the mechanism of injury for a noncontact ACL injury [1,2,3]. Movements of almost full knee extension, combined with external or internal tibial rotation [4] occur during a lateral cutting maneuver that predisposes an athlete to a potential noncontact ACL injury. There has been much research on ACL injuries in the shod population; however, there is no evidence pertaining to barefoot sports, which are played in areas around the world, such as Brazil and Africa [5].

Running barefoot has been the focus of recent research; however, there has been minimal research involving other barefoot sports. In barefoot running, the athlete has more of a forefoot or midfoot strike, whereas shod runners have a rearfoot strike [6]. By varying foot strike, changes may transfer up the kinetic chain to the knees and hips.

Currently there is no research on lateral cutting maneuvers while barefoot. However lateral cutting maneuvers have been directly related to causing a noncontact ACL injury due to the increased extension, adduction and external rotation knee movements [7]. The combination of a high extension, adduction and external rotation knee moments create the highest load on the ACL, which can cause a rupture [1,7].

Beiser et al. determined the peak knee moments during the weight acceptance (WA) phase; (heel strike to the first trough after the peak vertical ground reaction force [7]) during lateral cutting. It is plausible that performing a lateral cutting maneuver barefoot could alter the kinetics of the lower limb, which may create a dangerous scenario in an already precarious maneuver.

Therefore, the purpose of this study was to determine if knee moments differ between shod (SD) and barefoot (BF) conditions during lateral cutting maneuvers. Peak knee extension, adduction, and external rotation moments during the WA phase were compared between conditions. We hypothesized that the BF condition would have a greater extension, adduction, and external rotation knee moments than the SD condition.

METHODS

Twelve NCAA Division III athletes (6 males; 6 females) without lower limb pathologies participated in this study (age, 20.2 $\pm$ 1.48 yr; mass, 71.17 $\pm$ 11.3 kg; height, 1.7 $\pm$ 0.06 m). All subjects gave their written informed consent to participate in this study, which was approved by the University's Institutional Review Board. The peak extension, adduction, and external rotation knee moments during a cutting maneuver were tracked during the WA phase using a cluster marker set [7].

The motion of each subject was analyzed during 5 trials of 45 degree lateral cutting maneuver for each limb in both barefoot and shod conditions. Speed for all trials was set at 4.3 m/s and was controlled using a Brower laser timing device [2]. Trials were collected bilaterally; however, for this investigation only the dominant side was analyzed. Dominance was determined as the foot used to kick a ball. The cutting maneuver was performed on an indoor rubber track (Super X, All Sports Enterprises, Conshohocken, PA).

Kinematic data were collected with 8 Oqus Series-3 cameras (Qualisys, Gothenburg, Sweden) was set at 240 Hz and kinetic data were collected by an AMTI BP400600 force plate (AMTI Watertown, MA) set at 2400Hz. Visual 3D (C-motion, Germantown, MD) was used to apply a Butterworth filter with a cutoff of 12 Hz [2] to kinematic data and a filter with a cutoff of 50Hz to analog data, as determined by retaining 95% of signal power through a fast Fourier transformation. Inverse dynamics were used to calculate internal joint moments at the during the WA phase. Peak knee extension, adduction, and external rotation moments in the WA phase were then found.

Independent t-tests were used to determine whether the knee moments were greater in the BF or SD condition for each direction (extension, adduction and external rotation). Statistical analyses were performed using SPSS Version 19 (IBM, Chicago, IL) and statistical significance was accepted at $p < .05$.

RESULTS AND DISCUSSION

This is one of the first studies to examine athletic tasks/maneuvers between BF and SD scenarios. This study focused on variables that have been linked to ACL stress. Our hypothesis was not supported, as no significant differences were found in the peak extension knee moments between conditions, and the SD condition produced greater peak adduction and peak external rotation moments about the knee (Table 1).

The results of this study suggest that lateral cutting while BF may place less stress on the ACL than when SD. Decreased knee moments in the BF condition may be due to; increased co-contraction of musculature about the knee [8], altering kinetic and kinematics diverting greater loads to the ankle joint, or decreasing ground reaction forces by the limb in the WA phase.

CONCLUSION

In summary BF lateral cutting provides no more stress on the ACL than when SD. Therefore, further investigations should study other phases of stance such as the peak push off phase and the final push off phase. In addition, other lower limb joints should also be considered. A limitation of this study is that none of the subjects regularly participated in field sports BF. Nonetheless, our results propose that BF lateral cutting produces no more risk as compared to SD in individuals unaccustomed to BF competition.

REFERENCES

1. O'Connor KM, et al. *J Appl Biomech* **25**(1); 9-21, 2009.
2. Griffin L, et al. *J Am Acad Orthop Surg* **34**(9); 141-50, 2000.
3. Cochrane JL, et al. *Med Sci Sports Exerc* **42**(8); 1535-44, 2010.
4. Bencke J, et al. *J Electromyogr Kinesiol* **21**(2); 371-5, 2011.
5. Boshoff GB. *J Sport Manag* **11**(1); 69-79, 1997.
6. Liberman D, et al. *Nature* **463**(7280); 531-5, 2010.
7. Beiser T, et al. *Med Sci Sports Exerc* **33**(7); 1168-75, 2001.
8. Beiser T, et al. *Med Sci Sports Exerc* **35**(1); 119-27, 2003.

Table 1: Knee Moments (Nm/kg), Mean ± SD

	Extension		Adduction		External Rotation	
	BF	SD	BF	SD	BF	SD
Knee Moment	1.88 ± 0.60	2.17 ± 0.88	0.71 ± 0.33*	1.50 ± 1.04	-0.27 ± 0.19*	-0.42 ± 0.41

Barefoot = BF; Shod = SD

*denotes difference ($p < .05$) from SD.

USING STATIONARY AND NON-STATIONARY MEASURES OF BALANCE TO ASSESS HANDSTAND PERFORMACE

Glen Blenkinsop, Matthew Pain and Michael Hiley

Loughborough University, Loughborough, UK
email: G.Blenkinsop@lboro.ac.uk; web: www.lboro.ac.uk

INTRODUCTION

The analysis of balance in quiet stance often employs techniques that assume the trajectory of the centre of pressure (COP) to be a stationary signal. However, research has shown otherwise [1], leading to the employment of more sophisticated non-stationary data analysis techniques, such as approximate entropy [2] and detrended fluctuation analysis [3].

Research examining balance in handstand has continued to employ traditional stationary methods to analyse the trajectory of COP. Similar to normal stance, this research has shown that sway in the anterior-posterior direction is larger than in the medio-lateral direction and increases during eyes closed conditions [4] and with restricted central or peripheral vision [5]. However, no research has shown these traditional measures of balance to be sensitive to differences in COP trajectories between hand balancers of different abilities. Furthermore, no study has attempted to analyse the trajectory of the COP during handstand using non-stationary signal processing techniques. The aim of the present study was to assess whether stationary and non-stationary signal processing methods are sensitive to differences in COP trajectories for hand balancers of different abilities.

METHODS

Beginner (n=6), intermediate (n=5) and expert (n=6) hand balancers were recruited and grouped based on maximum handstand time and gymnastic ability. COP was measured for a maximum of 20 seconds via two Bertec force platforms (100 Hz) during 10 handstand trials. Data were filtered using a Butterworth zero lag fourth order low pass filter with a cut-off frequency of 10 Hz. Sway path, standard deviation (SD), mean sway velocity (mean SV), approximate entropy (ApEn) and short and long range detrended fluctuation analysis (DFA) were calculated from filtered COP trajectories in the mediolateral (ML) and anterioposterior (AP) directions for each trial. All balance measures were averaged across all trials, and grouped data was compared using an independent sample ANOVA, with a Tukey post hoc test, at the 0.05 level of significance.

Furthermore, the relationship between the trial duration and each balance measure was determined via a Pearson's linear correlation for all trials that finished before the maximum allowed time of 20 seconds

RESULTS AND DISCUSSION

Statistical analysis showed there to be a significant difference between group means for SD ML, SD AP, ApEn ML, ApEn AP, short range DFA AP, long range DFA ML and long range DFA AP (see table 1). Even though these measures were sensitive to changes in COP trajectories between beginners and experts, only ApEn in the AP direction was also sensitive to changes between beginners and intermediates and between intermediates and experts. In addition, short range DFA in the AP direction was sensitive to changes between intermediate and expert hand balancers, but not between beginner and intermediate hand balancers. These results may support the supposition that, when compared to more traditional measures of balance, non-stationary processing techniques are more appropriate for assessing balance performance based on COP trajectories. Higher ApEn values for the elite group suggests that as individuals become more proficient in hand balance, the less regular their control of balance becomes.

Pearson's linear correlations found a reasonable relationship between the duration of each handstand trial and SD AP and SD ML; and a good relationship between the duration of each handstand trial and ApEn AP and ApEn ML (see Table 1). Although the duration of these trials used for further analysis were within a relatively small range, ApEn AP showed a good relationship to handstand performance based on time in the handstand position (see Figure 1). Future research may wish to assess this relationship further, either as a means of assessing learning progress in a hand balance activity, or as a way of predicting the duration of handstands based on performance in trials of shorter durations, which may be helpful for reducing the effect of fatigue during numerous handstand trials.

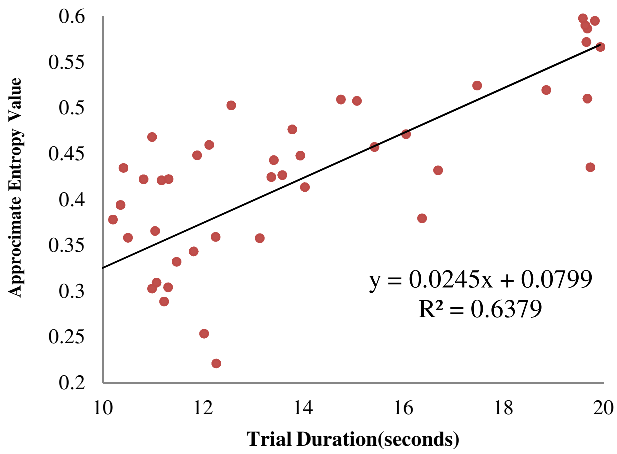

Figure 1: Scatter plot showing the relationship between ApEn AP and trial length for those handstands that ended before 20 seconds.

CONCLUSIONS

Traditional measures of balance based on COP trajectories are sensitive to large changes in balance performance, for instance between beginner and expert hand balancers. However, only non-stationary analysis methods in the AP direction, such as ApEn, are sensitive enough to distinguish between intermediate hand balancers and beginners and/or experts. There is a good relationship between the duration of handstand trials and ApEn values in both the AP and ML directions, but further study is required to explore this relationship further.

REFERENCES

1. Newell, K.M., et al. Gait & Posture, **6**, 56-62, 1997.
2. Pincus, S. Chaos, **5**, 110-117, 1995.
3. Peng, C-K., et al. Physical Review E, **49**, 1685-1689, 1994.
4. Asseman, F., et al. Int J Sports Med, **26**, 116-119, 2005.
5. Gautier, G., et al. J Sport Sciences, **25**, 1271-1278, 2007.

Table 1: Group means and standard deviation (SD) for traditional and non-stationary measures of balance; R^2 values from Pearson's correlations of trial duration against each balance measure.

	Beginner	Intermediate	Expert	R^2
	Mean ± SD	Mean ± SD	Mean ± SD	
Sway Path (mm)	1075.55 ± 186.76	904.58 ± 214.18	814.24 ± 72.55	0.10967
SD ML (mm) *[b]	8.96 ± 2.02	7.25 ± 1.46	5.24 ± 0.69	0.28168
SD AP (mm) *[b]	15.66 ± 1.95	12.37 ± 2.88	10.16 ± 1.35	0.28107
mean SV (mm/s)	107.56 ± 18.68	90.46 ± 21.42	81.42 ± 7.26	0.10967
ApEn ML*[b]	0.50 ± 0.05	0.54 ± 0.03	0.60 ± 0.03	0.56093
ApEn AP*[abc]	0.35 ± 0.02	0.45 ± 0.03	0.51 ± 0.02	0.63794
DFA ML (short range)	2.38 ± 0.01	2.37 ± 0.04	2.38 ± 0.01	0.00000
DFA ML (long range) *[b]	1.57 ± 0.06	1.51 ± 0.10	1.44 ± 0.05	0.03834
DFA AP (short range) *[bc]	2.40 ± 0.01	2.41 ± 0.01	2.38 ± 0.01	0.03109
DFA AP (long range) *[b]	1.59 ± 0.07	1.57 ± 0.11	1.44 ± 0.05	0.04970

(* significant difference at the 0.05 level; a=significant difference between beginner and intermediate groups; b=significant difference between beginner and expert groups; c=significant difference between intermediate and expert groups)

THE ISSUE OF TISSUE: A COMPARISON OF KINEMATIC MODELS IN OBESE ADULTS

Wayne J. Board, Derek J. Haight, and Raymond C. Browning

Colorado State University, Fort Collins, CO, USA
email: ray.browning@colostate.edu, web: http://pal.colostate.edu

INTRODUCTION

Collecting accurate kinematic data in obese individuals is challenging due to the excessive soft tissue that makes locating and tracking the motion of the skeletal system difficult. Studies of obese participants have typically used standard models developed for non-obese (e.g., modified Helen Hayes model) to characterize the movement of body segments, with no or only slight modifications to account for the increased soft tissue. This may lead to errors in joint angles, net muscle moments (NMM), and joint powers, particularly in hip and knee [1]. Prior attempts to account for excessive soft tissue include relocating markers (e.g. laterally at the pelvis), using a functional joint center method [2], and dual plane fluoroscopy [3]. However, these methods have limitations as they adjust for incorrect landmark location in only one axis/plane, are being debated regarding methodology and accuracy in an obese population with limited range of motion [3], or require expensive imaging technology, respectively.

The purpose of this study was to develop data collection methods and models that minimize the effects of excessive soft tissue and thus can more accurately quantify lower extremity kinematics and kinetics in obese adults. We hypothesized that the kinematics and kinetics would be different between models, especially between a standard model and models that accounted for more of the soft tissue in obese.

METHODS

Eleven obese, 94.7 (11.5) kg, 34.1 (4.0) kg/m^2, (mean (SD)) adult volunteers participated in this study. Body anthropometrics were obtained via DEXA. Each subject walked on level, dual-belt, force-measuring treadmill (Bertec) at 1.25 m/s. We measured ground reaction forces and moments at 1000 Hz via the treadmill and three-dimensional lower extremity kinematics via a 10-camera motion capture system (Vicon Nexus) at 100 Hz. Thirty-one single, passive, reflective markers were placed over the torso, pelvis, and lower limbs. Marker-clusters (four non-collinear markers attached to a contoured plate) were placed on the sacrum, thighs, and shanks. Digitized marker locations were placed at the ASIS and iliac crests via a digitizing pointer (C-Motion).

Five kinematic models were generated using different combinations of reflective markers, marker-clusters, virtual markers, and digitized landmarks. Hip joint centers were estimated (Bell, 1990) using various pelvic markers/landmarks. **1) Limited marker set (LM)**: A modified Helen Hayes (plug-in gait) model was created using 20 single, passive, reflective markers: five on the torso, the ASIS, sacrum, one marker from each thigh cluster, the lateral condyles of the knees, one marker from each shank cluster, the lateral malleoli, the heels, and second metatarsal heads. **2) Limited marker set with virtual markers (LV)**: same as LM with the exception of the ASIS markers which were adjusted posteriorly by a pelvic width/depth ratio and medially by the DEXA measured inter-ASIS distance. **3) LV built from ground up (LVG)**: same as model LMS-VM with the exception that the model was built from the foot segments up, rather than from the pelvis. **4) LVG with inverse kinematic joint constraints applied (LVGI). 5) Full marker set (FMS)**: All reflective markers were used in this model with the exception of the ASIS and iliac crests, which used the digitized ASIS and iliac crest landmarks.

We calculated the hip, knee, and ankle angles, and net muscle moments via standard inverse dynamics techniques (C-Motion/Visual 3D). A repeated-measures ANOVA (SigmaPlot) determined how the model affected kinematic and kinetic variables.

Necessary post-hoc comparisons were performed using Tukey's method. A criterion of $p<0.05$ defined significance.

RESULTS AND DISCUSSION

Peak flexion and extension angles during stance, were significantly different ($P<0.05$) between models for hip and knee (mean differences 11% and 14%, respectively). Peak ankle plantar-flexor angles, NMM, and powers were similar between models. Peak hip flexor moments differed ($P<0.001$) between LM and all other models (Figure 1). Early stance, peak, knee extensor NMM were different ($P<0.001$) between all models. Late stance, peak knee flexor NMM was significantly different between LM and all other models.

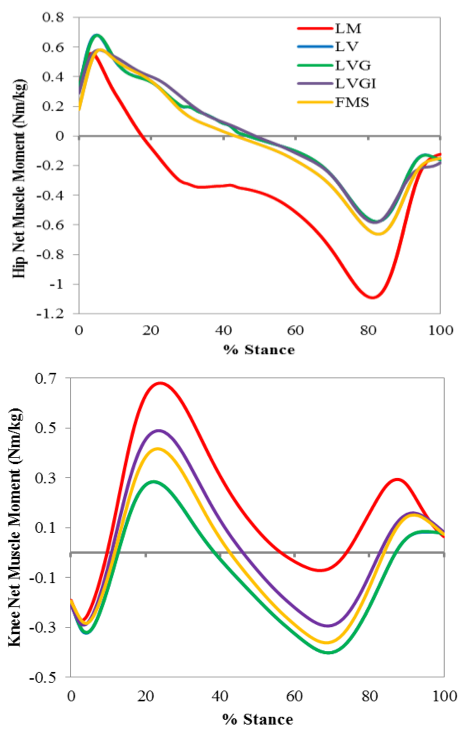

Figure 1: Mean sagittal plane NMM (Nm/kg) versus percent of stance for five kinematic models: LM, LV, LVG, LVGI, and FMS. Positive NMM are extensor/plantarflexor.

Peak hip positive power (energy generation) in early stance was significantly different (Figure 2) between LM and other models. Late stance, peak knee negative power (energy absorption) was different ($P<0.001$) between LM and the other models (Figure 2). The substantially different kinematics and kinetics (particularly at the hip) across the models highlights the need for methods and models to account for soft tissue in obese adults.

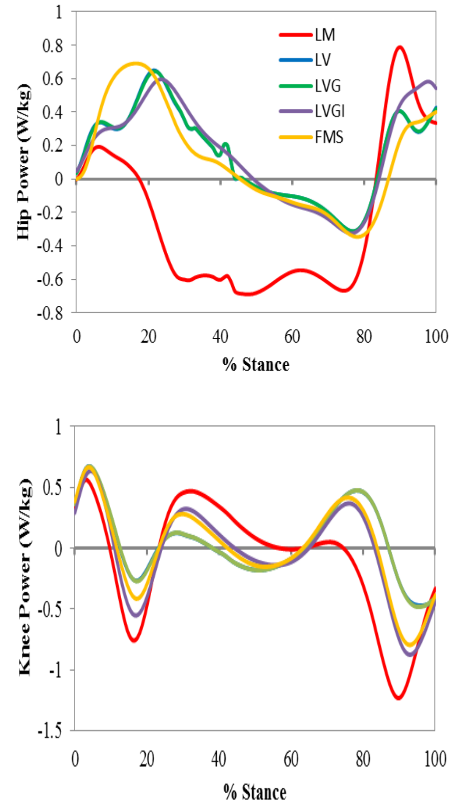

Figure 2: Mean joint powers (W/kg) versus percent of stance for the five models studied. Positive power is energy generation and negative is energy absorption.

CONCLUSIONS

The type of kinematic data collection method and model used to study gait in obese adults can have a substantial effect on biomechanical variables. Future biomechanics research using obese individuals should clearly describe the method and model development, so that results and interpretations can be evaluated on their likely accuracy.

REFERENCES

1. Stagni, R., et al. *J Biomech*, **33**(11), 1479-87, 2000.
2. Piazza, S.J., et al. *J Biomech*, **37**(3), 349-56, 2004.
3. Bingham J., et al., et al. *Trans ASME*, **128,** 588-95, 2006.

ACKNOWLEDGEMENTS

This research was supported by a grant from the CSU College of Applied Human Sciences and NIH grant R03AR059264.

POSTURAL CONTROL MODEL OF SPASTICITY IN PERSONS WITH MULTIPLE SCLEROSIS

[1]Morgan K. Boes, [2]Elizabeth T. Hsiao-Wecksler, [3]Robert W. Motl, and [3]Jacob J. Sosnoff
[1]Bioengineering, [2] Mechanical Science and Engineering, [3]Kinesiology and Community Health
University of Illinois, Urbana, IL, USA
email: mboes2@illinois.edu

INTRODUCTION

Multiple sclerosis (MS) is a neurological disease affecting the myelin sheaths of nerves in the central nervous system. One symptom caused by demyelination and its location is spasticity, a velocity-dependent tightness or resistance to stretch of the muscle. Previous research indicated that spasticity was associated with worse postural sway in persons with MS [1]. However, it is unknown why spasticity should result in greater postural sway. Mathematical models of the postural control system may help to clarify this apparent relationship between spasticity and sway.

Closed-loop inverted single link pendulum models with time delayed proportional-integral-derivative (PID) or proportional-derivative (PD) control in the anterioposterior (AP) direction are traditionally the models of choice for examining the upright standing postural control system (e.g., [2, 3]). Recent work has also used the inverted pendulum model to examine sway in the mediolateral (ML) direction [4]. Inverted pendulum models in the AP plane have shown that parameters, such as stiffness and damping in the neurological controller and physiological noise, increase as postural sway increases due to aging [2, 5].

METHODS

As per previous modeling work [2-4], the inverted pendulum represented the human body. The neural controller was represented by a PID controller with a neutral set point, and proportional, derivative, and integral gains (K_p, K_d, and K_i). Additional control components were included which account for the passive components of body at the ankle (stiffness K_{pass} and damping B_{pass}) (Figure 1a). The input noise characteristics, which simulate physiological noise such as breathing, were determined by two gains, K_N and τ_N. K_N was the gain of a low pass filter on the input noise, and τ_N was $1/f_c$, where f_c is the cutoff frequency of the low pass filter. The last parameter was the time delay in the feedback control concerning the transmission and processing time of neurological signals, τ_d. The body parameters were set to represent a 50th percentile Caucasian adult female who sways only at the ankle joint (mass 62 kg, height of center of mass 0.85 m, moment of inertia in AP (J_B= 61 kg·m^2), and ML directions (J_B = 60 kg·m^2)) (Figure 1b) [6].

The postural control data of 16 subjects with MS (9 high, 7 low spasticity) and sixteen age- and sex-matched controls (44±3 y, 14 females, 2 males) were used in the current study and were previously presented [1]. There was no significant difference in disability status (EDSS) between spasticity groups.

Five model parameters (K_p, K_D, K_N, K_{pass}, B_{pass}) were optimized to match participant COP data. Traditional COP measures such as 95% power frequency, sway range, and maximum distance were calculated from the output of the model simulation for each direction, and were then compared to similarly computed measures from the participant COP data [1]. The difference in these parameters was minimized to find the optimum model gains. As in the previous work, the model was divided into three test groups (healthy controls and persons with MS with low and high spasticity). Independent samples *t*-tests were used to compare the model-created traditional parameters to subject parameters. Univariate ANOVA tests with group as the between-subject factor were used to compare model gains. All statistical analyses were completed with SPSS version 17.0 (SPSS, Inc, Chicago, IL).

RESULTS/DISCUSSION

There were no significant differences between the experimental subject traditional COP parameters and corresponding model simulation parameters for any test group. Therefore the models recreated traditional sway parameters for the two MS and control group as noted previously [1].

The model gains used to achieve the simulated COP trajectories were analyzed (Table 1). In the AP direction, the low spasticity model had significantly higher K_p-AP (p=0.05) and lower K_{pass}-AP (p=0.02). In the ML direction, analysis revealed that the high spasticity model had a significantly higher K_N-ML than the controls model (p=0.04).

Table 1: Significant model gains (p < 0.05).

	Control	MS- low spasticity	MS- high spasticity
K_p-AP	10.3 ± 1.1	12.1 ± 2.9**	10.8 ± 1.0
K_{pass}-AP	10.7 ± 0.6	9.4 ± 1.6**	10.4 ± 0.6
K_N-ML	0.5 ± 0.3	2.2 ± 3.5	3.3 ± 3.6*

* Different from control
** Different from control and MS-high spasticity

Since differences were seen between the control and MS-high spasticity group, as well as between the control and MS-low spasticity group, it is likely that these differences are related to spasticity as well as to MS. Persons with MS and low spasticity potentially use different compensatory mechanisms, than those with high spasticity, in the AP direction to help control instability in their posture caused in part by the neurological signal degradation due to MS. It is possible that a difference in persons with MS and high spasticity and controls is not seen in the AP direction, as persons with high spasticity may be unable to modulate the sway in the AP direction due to higher levels of spasticity, and thus compensate by swaying in the ML direction. One could speculate that the increased K_N-ML physiologically represents the degradation of the neural signal transduction in persons with MS [2].

CONCLUSIONS

The goal of this study was to determine if the difference in experimental COP measures between controls and persons with MS could be recreated in inverted pendulum models of AP and ML postural sway and which model gains varied to cause the group differences in traditional COP parameters.

These significant differences in gains suggest that persons with MS use different control strategies depending on the level of spasticity than healthy persons to maintain postural control, such as increasing sway in the ML direction, where they have a larger base of support or modulating the stiffness of muscles to better control sway.

Results from this study can be used to inform future research on postural control and the role of spasticity in persons with MS, as well as rehabilitation to regain normal postural control.

ACKNOWLEDGMENTS

This projected was supported in part by Pilot Research Award from the National Multiple Sclerosis Society (# PP1099) and Steven Schwid Memorial Research Scholarship.

REFERENCES

1. Sosnoff, J.J.,et al. Arch Phys Med Rehabil, 2010. **91**(1): 93-9.
2. Maurer, C. and R.J. Peterka, J Neurophysiol, 2005. **93**(1): 189-200.
3. Masani, K., A.H. Vette, and M.R. Popovic, Gait Posture, 2006. **23**(2):164-72.
4. Valles, K.D., et al., Conf Proc IEEE Eng Med Biol Soc, 2006. **1**: 4576-9.
5. Cenciarini, M., et al.,Biomedical Engineering, IEEE Transactions on, 2010. **57**(2): 267-275.
6. Zatsiorsky, V.M., *Kinetics of human motion*, Champaign, IL: Human Kinetics, 2002.

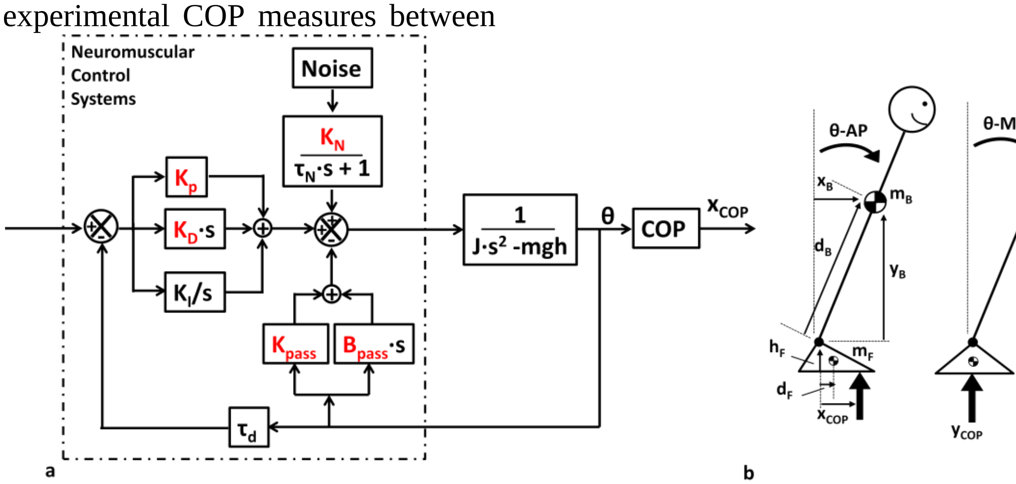

Figure 1: a. Time-delayed PID active controller with passive stiffness-damping and affected by physiological noise used for AP and ML simulations. **b.** AP and ML pendulum parameters for calculating COP.

THE INFLUENCE OF CONCENTRIC VS. ECCENTRIC MUSCLE CONTROL ON 3D AND DYNAMIC PATELLOFEMORAL CONTACT KINEMATICS

[1]Bhushan S. Borotikar, [1]Ali A. Siddiqui and [1]Frances T. Sheehan

[1]Rehabilitation Medicine Department, CC, NIH, Bethesda, MD, USA
email: borotikarbs@mail.nih.gov, web: http://www.cc.nih.gov/rmd/fab/

INTRODUCTION

Patellofemoral (PF) osteoarthritis and its potential precursor idiopathic PF pain are common, costly, and debilitating diseases [1]. As altered PF cartilage contact mechanics has been theorized as the main cause of cartilage wear, it is critical to understand and evaluate PF contact mechanics in order to develop evidence-based clinical treatments. Despite a long history and span of studies focusing on PF contact, to date there are no data available for *in vivo*, dynamic PF contact mechanics. Since cartilage contact is a dynamic phenomenon influenced by muscle force and other *in vivo* conditions, the research in this field is shifting focus from purely cadaver-based to *in vivo* studies. However, the current *in vivo* techniques remain static and their validity has not been demonstrated.

Thus, the objective of this study was threefold: 1) Demonstrate the feasibility of computationally determining 3D, *in vivo* PF cartilage contact kinematics (area and location) during a dynamic and volitional lower extremity muscle control activity, 2) report normative PF contact kinematics, and 3) compare PF contact kinematics during knee flexion with that during knee extension.

METHODS

Seven healthy volunteers (3 males, 4 females, age 24$\pm$6.1 years, height 172.3$\pm$11.3cms, and weight 70.1$\pm$15.2 kg.) with no prior history of PF pain participated in this IRB approved study.

MRI data acquisition: Subjects lay supine with their knee placed on a wedge and with flexible transmit-receive coils securely placed around the knee joint. Dynamic cine-PC (CPC) magnetic resonance images were acquired while subjects performed an open kinetic chain flexion-extension exercise inside the bore of 3T (Philips Medical Systems, Best, NL) Scanner [2]. A multi-plane cine (MPC) data was acquired in the same setting with subjects performing the same dynamic exercise as CPC [3]. All dynamic data were represented using 24 time frames with an actual temporal resolution equal to 62msec. Subsequently, the wedge was removed and the lower limb was placed in the anatomically neutral position and 3D static sagittal MR images (0.27mm^{2}x1mm, fat-saturated, gradient-recalled-echo sequence) were acquired using an 8-channel knee coil.

MRI data processing: Three-dimensional patellar and femoral bone kinematics were derived from the CPC data as previously reported [2]. Static 3D patellar and femoral bone models were created by segmenting high resolution static scans in MIPAV (Medical Image Processing and Visualization, NIH, Bethesda, MD). Similarly, sparse dynamic patellar and femoral bone models were created by segmenting MPC data at the full extension time frame. The sparse models were then shape matched to their respective static bone models (Geomagic Inc., Research Triangle Park, NC). This process transformed the static bone models to their respective full extension dynamic pose [3].

Cartilage Surface model: Point clouds representing the patellar and femoral cartilage surfaces were created by segmenting the sagittal static scans. These point clouds were then reconstructed using a thin-plate spline (TPS) mathematical surface [4]. Surface fitting errors were set to match the static MRI pixel resolution. The fitted TPS surfaces were re-sampled with a rectangular grid and subsequently trimmed to closely fit the cartilage morphology.

Cartilage contact kinematics: An in-house MATLAB (Mathworks inc., Natick, MA) algorithm was used to determine patellar kinematics with respect to femur. Cartilage surface models were then transformed to dynamic full-extension position using the dynamic (full extension MPC) to static bone transformations quantified earlier. CPC PF bone kinematics were used to define the cartilage surface location and orientation throughout the flexion-extension cycle. For each time-frame, the distance from each resampled grid point on femoral to patellar cartilage surface was determined using surface normal from that point and patellar TPS surface equation [4]. Consequently, surface overlap was defined using a threshold value of 0.3mm and area of contact was determined by summing the area of each resampled element on femoral surface that corresponded with the overlap. The contact area centroid was determined as the weighted sum of each rectangular patch (product of area and coordinate location) divided by total contact area.

Flexion-Extension contact analysis: For the purpose of this study, contact area was scaled by the ratio of the average epicondylar width to individual epicondylar width in order to eliminate size as a confounding variable. Absolute contact area was interpolated to single knee angle increments for averaging across subjects. The contact areas during the extension portion of the cycle were compared to the contact areas in the flexion portion using a paired Student's t-test at increments of 1° knee angle with Bonferroni-type false discovery rate (FDR) estimation for multiple comparisons for the range over which all the subjects were represented.

RESULTS AND DISCUSSION

To the authors' knowledge, this is the first study to report accurate, 3D, dynamic *in vivo* PF contact kinematics, acquired non-invasively and directly during an activity requiring active muscle control. Peak mean contact area reached 612.9 mm^2 at 34° of knee angle during flexion. There was a significant difference in the flexion and extension contact areas at all knee angles ($p<0.05$, Figure 1), which could be attributed to the active muscle control involved in the study. In their static, *in vivo* MRI data on healthy individuals (n=10), Salsich and associates [5] compared PF contact areas between quadriceps loaded and relaxed condition and found no significant differences. However, static nature of this study could have resulted in cartilage relaxation leading to no difference in contact areas.

Contact area location (centroid) also showed a consistent pattern moving from the lateral to medial side during flexion cycle. However, no such consistency could be recognized during extension cycle. This may give insights to pathology as loss of motor pattern flexibility may lead to extensive cartilage wear.

PF pain syndrome tends to be more prevalent in females as compared to males, but there is no data available that indicates differences in cartilage contact kinematics between genders. We did not compare genders in this study due to inadequate power, yet work is ongoing in this area. Although the accuracy of this technique is close to sub-millimeter mark and has been reported [3], a sensitivity analysis to check the reliability of the technique is warranted.

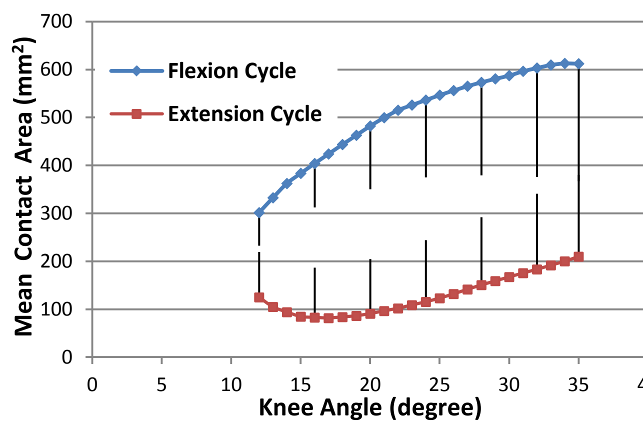

Figure 1: Mean (with 1 SD lines) contact areas at each knee angle during flexion and extension cycle.

CONCLUSIONS

Dynamic muscle control influences PF contact kinematics in healthy volunteers. Findings of this study will likely lead to improved understanding of the pathways leading to PF pain and osteoarthritis.

REFERENCES

1. Utting et. al. *Knee* **12**, 362-65, 2005
2. Seisler and Sheehan. *IEEE Trans Biomed Eng.* **54**, 1333-1341, 2007.
3. Borotikar et. al. *JOB*. **EPub**. Jan 2012
4. Boyd et. al. *J Biomech Eng.* **121**, 525-532, 1999
5. Salsich et. al. *CORR.* **417**, 277-284, 2003.

ACCURATE RECONSTRUCTION OF FORENSIC BIOMECHANICS CASES

Susan M. Bowley, Ph.D.
[1]Bowley Consulting, LLC, Sunnyvale, CA USA, bowleyconsulting@gmail.com, http://www.bowleyconsulting.org

INTRODUCTION
Injury causation biomechanics is used in forensic work to help determine the likely cause of an accident involving an injury. Normal human movements such as walking or running are very well understood and can be easily reconstructed. However, unique human movements, which are most typical for forensic cases, are not well understood nor easily reconstructed. Verbal description of these movements alone does not help a non-scientific audience understand and accurately visualize the unique biomechanics involved. In this paper we discuss a unique motion capture method we have adopted for use in our forensic work. This motion capture system allows us to not only capture the unique biomechanics of human movement for each case, but more importantly, it allows us to capture movements in the exact setting where the accident occurred, without constraints of a laboratory or use of reflective markers and video tracking. Several cases are presented wherein we have captured the unique biomechanics of human movement, and integrated these movements into high fidelity animations in order to accurately reconstruct the injury causation biomechanics. Animations allow us to visually illustrate opinions about how an injury occurred, and are most useful when actual reconstruction of an accident would be unsafe and costly.

METHODS
We use a reflector-less inertial-based wireless motion capture (mocap) system (Xsens MVN) to recreate and digitize the unique human movements of interest for each specific case. Typically this mocap is done on location at the actual accident site, or at a suitable alternative site. The forensic biomechanics expert serves as the "director" and instructs each mocap performer to recreate the movements of interest. Multiple data acquisition "takes" with the performer are acquired via proprietary data acquisition software (Xsens Studio). Each "take" is also filmed via video camera for reference. Afterwards, all mocap data are then exported to common motion capture file formats (BVH, and FBX). Further data manipulation or "clean up" is then completed in another software package (MotionBuilder, AutoDesk) in order to correct common acquisition errors, such as feet passing through the ground surface plane. Clean mocap data files are then exported for use in animation software (3DStudioMax, AutoDesk) for further manipulation.

RESULTS
The first forensic case example is shown in Figure 1. This case involves an adult woman carrying a child, walking across a street in the crosswalk. The pedestrians were struck by a vehicle moving at approximately 45mph and were both thrown approximately 50 feet. The adult had severe trauma and debilitating injuries and the child recovered completely. We used motion capture at the actual accident site to recreate the biomechanics of the adult carrying a child across the street. In the animation, we show the movement of the vehicle and pedestrians to the point of impact.

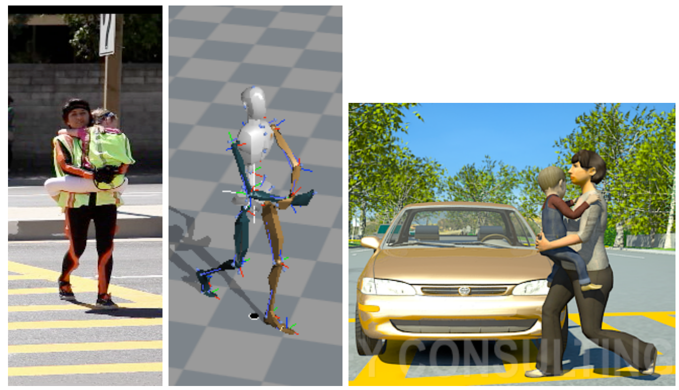

Figure 1: Case Example 1 – Pedestrians vs. Auto. Video reference (left), Motion capture (center), and Animation (right).

The second forensic case example is shown in Figure 2. This case involves an elderly man descending a stairway who fell near the bottom of the stairs. He suffered a hip fracture, requiring surgical intervention. We used motion capture at a similar stairway to capture the biomechanics of descending the stairs and the fall. The animation shows the complete movement during decent and fall to the ground.

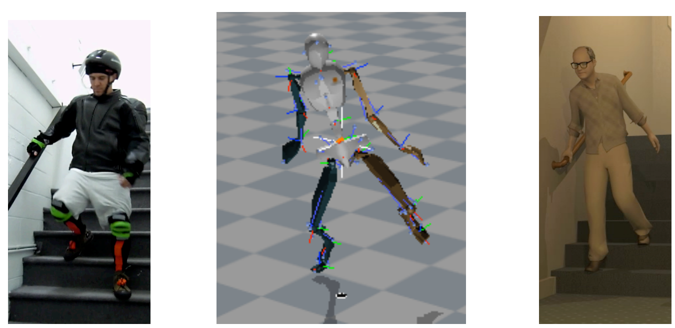

Figure 2: Case Example 2 – Fall Down Stairs. Video reference (left), Motion capture (center), Animation (right).

DISCUSSION & CONCLUSIONS
We have found that using our methods to recreate human biomechanics, which are captured at the actual accident site, greatly enhance the visual impact of our animations. Since the data is from real human movement, the results appear real and natural to the viewer. We hope others working in forensic biomechanics will find these same techniques useful to their specific cases under investigation.

SAGITTAL KINEMATICS & KINETICS OF MIDFOOT/FOREFOOT RUNNING AFTER 4 WEEKS OF TRAINING

[1]Elizabeth R. Boyer, and [1]Timothy R. Derrick

[1]Iowa State University, Ames, IA, USA
email: ehageman@iastate.edu , web: http:// www.kin.hs.iastate.edu/

INTRODUCTION

Transitioning from a heel strike running pattern to a midfoot/forefoot strike pattern undoubtedly results in different kinematics (by definition at foot contact) and kinetics [1]. To our knowledge, no one has compared sagittal plane angles, moments, and powers for the ankle, knee, and hip after training rearfoot strikers to run mid/forefoot. Therefore, the **purpose** of this study was to train heel strikers to run mid/forefoot over 4 weeks (8 sessions) and note how their lower extremity sagittal plane kinematics and kinetics change.

METHODS

Eleven recreational heel-striker runners volunteered for this study (mean±SD, age: 32±8 yrs; mass: 69.8±9.3 kg; height: 1.72±0.06 m) Participants visited the lab initially and performed 10 heel strike and 10 mid/forefoot overground running trials, both at preferred running velocity (3.25±0.31 m/s). For the next 4 weeks, participants came in twice a week (8 total training sessions) and ran on the treadmill with a mid/forefoot strike pattern for 15 minutes at their preferred velocity. For the first week, participants were instructed to use their normal heel strike pattern for their usual weekly running outside training sessions. For the remaining 3 weeks, they were instructed to increase their mid/forefoot running outside of training by 33% each week (up to 100% by week 4). Approximately 1-week after the 8 training sessions, participants again performed the 20 overground trials.

Kinematic data were collected with an 8-camera Vicon system (200 Hz; filtered at 20 Hz). Kinetic data were collected by two in ground AMTI force plates (1600 Hz, filtered at 20 Hz). Sagittal joint angles, moments, and powers were calculated for the ankle, knee, and hip, and ensemble curves were created. Moments were normalized to body weight.

Effect sizes greater than 1.0 were used to identify differences between pre-and post-training.

RESULTS AND DISCUSSION

As shown in Figure 1, there is very little difference in any of the sagittal plane angles, moments, or powers after 4 weeks of training. The only dependent variable that was outside 1 standard deviation of the pre-training mean was peak dorsiflexion angle. Greater dorsiflexion after training was likely a result of allowing the heel to lower closer to the ground instead of remaining high on their forefoot.

In a similar gait retraining study using audible feedback, three runners with patellofemoral knee pain were able to reduce pain and decrease peak vertical ground reaction forces and loading rates (Cheung & Davis, 2011). They did not report subsequent kinematics or moments and powers, so comparisons cannot be made. However, one may infer that there would be corresponding changes in kinematics that would account for these changes in reaction forces and loading rates. Regardless, there are several differences between their intervention/protocol and ours which may account for differences in results. First, their 8 training sessions extended over two weeks, opposed to our 4 weeks. Second, they incorporated additional warm-ups, including 15 minutes of light-resistance cycling. Their subjects were all females who suffered patellofemoral pain syndrome and ours currently had no lower extremity injury. Finally, Cheun & Davis collected their kinetic data during treadmill running, whereas we collected ours during overground running. Perhaps our participants showed greater sagittal plane kinematic and kinetic changes during treadmill running (which is how they were monitored) but were not able to transfer any adaptations to overground running. However, they were instructed to practice mid/forefoot striking outside the treadmill training sessions, and most people did run outside. Therefore, 4 weeks of training to transition from heel strike to mid/forefoot running may not be sufficient to see significant changes in biomechanics in the sagittal plane.

CONCLUSIONS

In conclusion, after 4 weeks of training to switch from a heel strike running pattern to mid/forefoot, sagittal plane lower extremity kinetics and kinematics did not change very much. The only difference was an increase in peak dorsiflexion angle post-training. Perhaps the investigated biomechanics do not change significantly with practice, they were not retained for 1 week between training and re-testing, or it takes longer than 4 weeks of training to see significant differences.

REFERENCES

1. Cheung RTH & Davis IS. *J Ortho & Sports Phys Ther* **41**(32), 914-9, 2011.

ACKNOWLEDGEMENTS
The authors would like to thank New Balance Athletic Shoe, Inc. for providing financial support for the study.

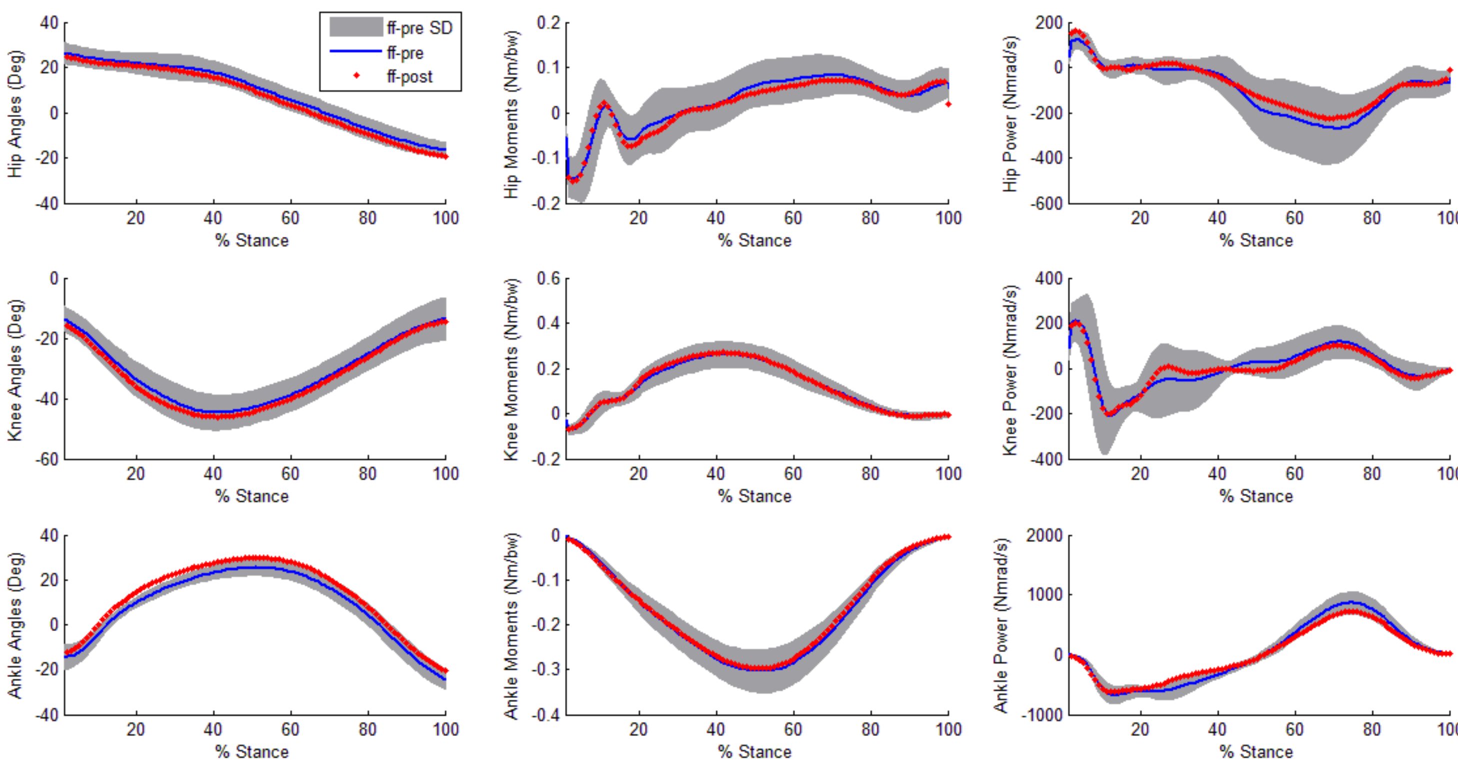

Figure 1. Ensemble curves for sagittal plane joint angles, moments, and powers for the hip, knee, and ankle. Pre-training forefoot running (ff-pre) is shown as a solid blue line plus or minus one standard deviation (gray shaded area). A red dotted line represents the mean after 4 weeks of training.

METABOLIC COST AND LOWER EXTREMITY MUSCLE ACTIVITY DURING CONSTANT SPEED WALKING AT DIFFERENT STRIDE FREQUENCIES

[1,2]Angela Boynton and [3]Todd Royer
[1]U. S. Army Research Laboratory, Aberdeen Proving Ground, MD, USA
[2]Program in Biomechanics and Movement Science, University of Delaware, Newark, DE, USA
[3]Department of Kinesiology & Applied Physiology, University of Delaware, Newark, DE, USA
email: angela.c.boynton.civ@mail.mil

INTRODUCTION

At a given speed, individuals tend to select a stride frequency that minimizes energy expenditure, and deviations from that preferred stride frequency (PSF) result in an increase in metabolic cost [1]. As stride frequency changes, so does the mechanical work done by the legs and the net mechanical efficiency associated with doing that work [1]. Changes in the mechanical requirements of gait progression may be reflected by modifications in muscle activation patterns as measured by surface EMG. Despite the fact that metabolic cost has been consistently shown to increase with decreased stride frequency, average EMG activity of several lower extremity muscles have been reported to decrease with decreases in cadence [2]. However, soleus and gastrocnemii integrated muscle activity (iEMG) has also been found to increase with decreased stride frequency at a fixed walking speed [3]. The effect of forced cadence walking on metabolic cost and muscle activity are of interest from a military standpoint. During foot marches, Soldiers walk at a constant speed with a stride frequency set by one individual in the group. The potential increase in systemic and/or local muscle fatigue associated with doing so could have a negative impact on Soldier performance. Therefore, the purpose of this study was to quantify changes in metabolic rate (MR) and lower extremity muscle activity associated with walking at normal, high and low cadences at a fixed speed. We hypothesized that MR would increase with deviations from PSF, and that changes in gait cycle iEMG would parallel changes in MR.

METHODS

Data were collected for five healthy males recruited from the Aberdeen Proving Ground, MD civilian and military population (age: 29.2±6.1 years, body mass: 85.9±24.7 kg). Subjects walked on a treadmill at 1.34 m/s for 5-minute periods. During each trial, they matched their footfalls to a metronome set at their PSF, PSF+10% or PSF-10%. A portable cardiopulmonary system (Cosmed USA, Chicago, IL) continuously sampled expired gases throughout each trial. The average rate of oxygen consumption was calculated from the final minute of data, converted to watts and normalized to the subject's body mass in kg to obtain metabolic rate. During the final minute of each trial, myoelectric activity in the right rectus femoris (RF), biceps femoris (BF), tibialis anterior (TA) and medial gastrocnemius (MGAS) were recorded for 20 sec at 1200 Hz using a portable EMG system (Delsys, Inc, Boston, MA). Heel strike was determined using a footswitch attached under the heel of the right foot and connected to the EMG system. Raw EMG signals were rectified and then smoothed using a 4^{th}-order, zero-lag, low pass Butterworth filter with a cut-off frequency of 5 Hz. The filtered EMG signals were then time normalized to individual strides and an ensemble average for each muscle was generated using a minimum of six strides. Next, iEMG was obtained by integrating the ensemble average curve of each muscle using a dt equal to the mean stride time for the given condition divided by 100. Finally, the iEMG value for each muscle was normalized to its PSF iEMG value. This is an ongoing study and data have been collected for only a small number of participants thus far. Therefore, only descriptive statistics were calculated for each of the variables.

RESULTS

Mean PSF normalized to leg length was 60.7±2.7 strides/min/m. For the PSF-10% and PSF+10% conditions normalized stride frequencies were

56.2±2.3 and 66.1±3.8 strides/min/m, respectively. As expected, MR increased approximately 5% from the PSF condition with a 10% increase or decrease in stride frequency. The magnitude and direction of changes in lower extremity iEMG appear to depend on the muscle in question, and whether stride frequency is higher or lower than PSF (Figure 1). Deviations from PSF appear to have relatively little effect on RF iEMG over a stride. Gait cycle iEMG of both BF and TA tended to increase with a 10% increase or decrease in stride frequency. However, increased cadence appears to more strongly affect BF activity than does decreased cadence, while the opposite seems to be true for TA activity. Contrary to our hypothesis, MGAS iEMG tended to increase with a decrease in stride frequency, but decreased when subjects walked at PSF+10%.

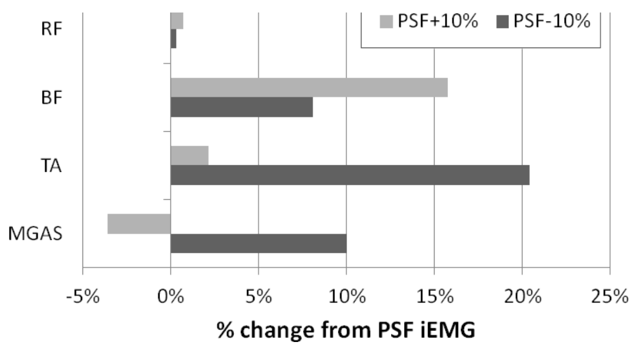

Figure 1: Changes in stride frequency during constant speed walking affect gait cycle iEMG of lower extremity muscles.

DISCUSSION

The purpose of this study was to quantify and compare changes in lower extremity muscle activity with those in metabolic cost during constant speed walking at stride frequencies higher and lower than preferred. The effect of stride frequency on MR is fairly well established and our results are consistent with other studies [1]. However, our results do not appear to support the hypothesis that changes in lower extremity iEMG would increase with MR. Of the four muscles evaluated, only the changes in BF iEMG appear to mirror those in MR. Therefore, changes in MR may not reflect levels of local muscle fatigue in Soldiers during extended periods of fixed-cadence marching.

Yang and Winter [2] reported decreases in average RF, BF and TA activity as stride frequency was reduced from 115 to 75 steps/min at an uncontrolled walking speed. While RF iEMG does not appear to change with stride frequency, average EMG tended to decrease with decreasing stride frequency. This decrease in RF activity may be related to a decrease in the acceleration required to initiate leg swing at lower cadences. In the same way, while BF iEMG increased with a 10% deviation from PSF, average EMG in the BF was greater at PSF+10% than either PSF or PSF-10%. In contrast, the average EMG for TA was approximately 10% higher for the increased and decreased stride frequency conditions than during the PSF walking. This suggests that the previously reported decrease in TA activity was more likely related to the concurrent reduction in walking speed than change is stride frequency. From the ensemble average TA curves, the observed increase in average EMG with decreased cadence appears to be primarily due to an increase in activity during mid-swing where gravity must be overcome to keep the foot parallel to the floor. The observed effect of stride frequency on MGAS iEMG is consistent with that of a previous study [3] and may be related to the positive ankle mechanical power associated with each stride frequency [1].

CONCLUSIONS

The gait cycle iEMG of selected lower extremity muscles appears to be sensitive to changes in stride frequency when walking at a constant speed. Changes in iEMG of individual leg muscles do not necessarily reflect the increases in MR associated with increasing and decreasing cadence from PSF. Further study is needed to determine the impact of increases in lower extremity muscle activity during fixed-cadence walking on Soldier performance.

REFERENCES

1. Umberger BR & Martin PE. *J Exp Biol* **210,** 3255-3265, 2007.
2. Yang JF & Winter DA. *Electroencephalogr Clin Neurophysiol* **60,** 485-491, 1985.
3. Cawsey RP et al. *Dynamic Walking Proc,* 2009.

BIOMECHANICAL ANALYSIS OF BASKETBALL FREE THROW SHOOTING

Steve Bradley and Joel R. Martin

The Pennsylvania State University, University Park, PA, USA
email: jrm496@psu.edu

INTRODUCTION

The free-throw shot is a motion that most players will perform tens or even hundreds of thousands times in their lives, and yet the league average for the highest level of basketball in the world, the National Basketball Association, was only 76.3 percent this past season. Previous research on basketball shooting has focused mainly on ball motion and kinetics. There has not been much exploration into free-throw biomechanics.

This study is intended to add to and elaborate on the very limited data available [1, 2, 3] on the movement patterns used by basketball players to shoot a free- throw. Specifically, we have three goals: 1) to identify the basic pattern of body joint motions during a free throw shot, 2) to determine the differences between the motions of made and missed shots, and 3) to identify differences in movement patterns between players that make a high percentage versus players that make a low percentage of their free throw shots.

METHODS

Nine test subjects were asked to shoot a set of free-throws using a NCAA regulation sized ball, basket, and free-throw line dimensions. Subjects were all male and reported playing recreationally on a regular basis. Subjects were filmed from the side with a digital video camera shooting twenty-five shots and the results of each shot were recorded (i.e. missed long, short, left, right, etc.). The video was recorded at thirty frames per second. Five makes and five misses from each shooter were chosen for further analysis. Analysis was limited to 2D.

Data for nine points (ball, fingertip, wrist, elbow, shoulder, hip, knee, ankle, toe) was digitized using MaxTRAQ motion analysis software. A total of twenty-six frames were digitized for each shot with the twentieth frame being regarded as the release point of the shot. The digitized points were then exported for filtering and post-processing.

The digitized points were post-processed in MATLAB. The joint angles were computed for the wrist, elbow, shoulder, hip, knee and ankle. The torso ankle was computed as the angle between a vertical vector projected from the hip and a vector connecting the hip and shoulder joints. The center of mass (COM) was assumed to be at the hip. The main data of interest was: 1) joint angles at release, 2) peak joint angular velocities prior to release (linear velocity in x- and y-direction for the COM), and 3) timing of the peak joint angular velocities relative to release. A qualitative analysis was performed on the joint angle vs. time data for the shooter that made the highest percentage of his shots and the shooter that made the lowest percentage of the shots. Repeated measure ANOVAs were performed to test for statistically significant differences between made and missed shots for all measures.

RESULTS AND DISCUSSION

All shooters displayed a stereotypical shooting pattern characterized by a proximal to distal pattern of joint motion in both the upper and lower body joints. The joint angles at release were amazingly similar across all shooters. The peak joint angular velocities and timing of peak joint angular velocities were much more variable across shooters suggesting that these measures may be the parameters differentiating “good” and “bad” shooters.

<u>Joint angles at release:</u> the mean joint angles at release are shown in Figure 1 for makes, misses, and all shots (overall). There were no significant differences in release angles for any single joint between makes and misses.

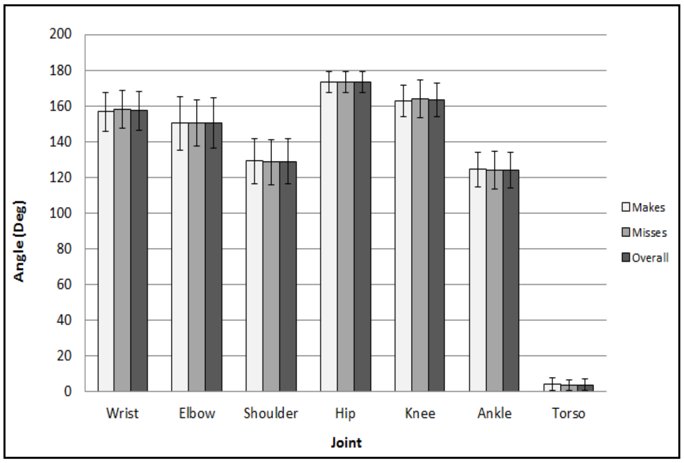

Figure 1: Mean values of joint angles at release. Error bars are standard deviation.

Peak joint angular velocities: the mean peak joint angular velocities are shown in Figure 2. The peak joint angular velocities increased in the proximal to distal direction with the wrist and elbow displaying the highest peak angular velocities. There were no statistically significant differences in peak joint angular velocity for any single joint between makes and misses.

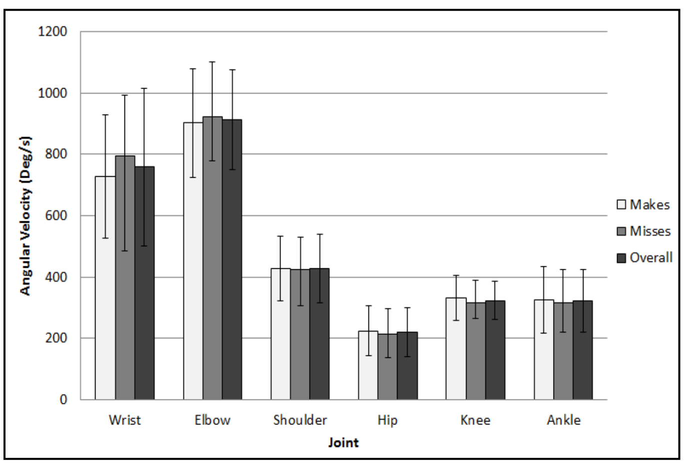

Figure 2: Mean joint peak angular velocities. Error bars are standard deviation.

Timing of peak joint angular velocities: the mean timing of peak joint angular velocity for each joint and COM (x- and y-directions) is shown in Figure 3. Generally, for both the upper and lower body joints the proximal joints reached their peak velocity first and the distal joints followed. The wrist and elbow reached peak joint angular velocity very close to release.

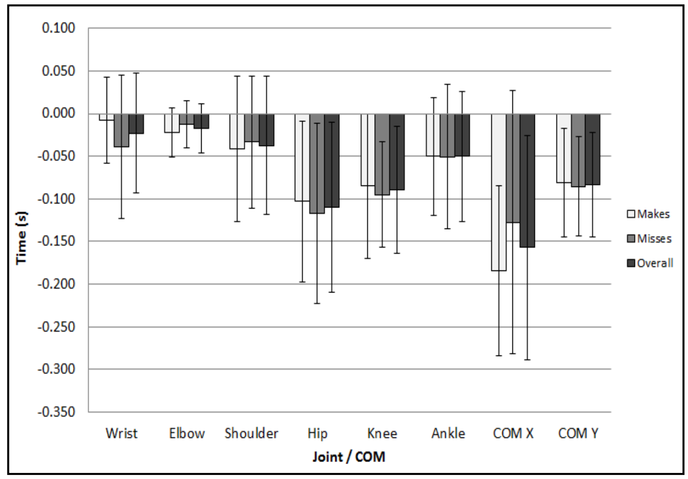

Figure 3: Mean timing of peak joint angular velocities and center of mass velocity relative to release. Error bars are standard deviation.

High vs. low percentage shooter comparison: the upper and lower body movement patterns between the players that made the highest percentage vs. the player that made the lowest percentage of shots revealed several differences. The shooting motion of the good shooter displayed stable joint posture prior to start of shooting motion and then a “smoother” extension of the joints through release. The shot to shot variability of joint motion of the good shooter was less than the poor shooter.

CONCLUSIONS

The results indicated that the free throw shot is characterized by a proximal to distal pattern of peak joint angular velocities prior to release. The coordination of peak joint angular velocities appears to be the most critical factor in determining the success of a shot. Stable joint postures and a smooth movement through release appear to be characteristics of more successful shooting motions.

REFERENCES

1. Brancazio PJ, *Am J Phys* **49(4)**, 356-365, 1979.
2. Hudson JL, *A biomechanical analysis by skill level of free throw shooting in basketball*, Academic Publishers, 1982.
3. Tan A & Miller G, *Am J Phys* 49(6), 542-544, 1981.

SPATIOTEMPORAL GAIT ASYMMETRY IS RELATED TO BALANCE/FALL RISK IN INDIVIDUALS WITH CHRONIC STROKE

Claire E. Bradley[1], Clinton J. Wutzke[2], Steve Zinder[1,2], Michael D. Lewek[1,2,3]

[1]Department of Sport and Exercise Science, [2]Interdisciplinary Program in Human Movement Science, [3]Division of Physical Therapy
The University of North Carolina at Chapel Hill
email: mlewek@med.unc.edu

INTRODUCTION

Approximately 800,000 strokes occur each year in the United States [1]. After a stroke, gait patterns are frequently slow and spatiotemporally asymmetric [2]. This is purported to lead to decreased balance, which is of particular concern as impaired balance can subsequently lead to falls and injury [3].

The purpose of this study was to determine if relationships exist between spatiotemporal gait asymmetry (measured at both comfortable and fast overground walking speeds) and measures of static and dynamic balance in individuals with chronic stroke. We hypothesized that individuals with greater spatiotemporal gait asymmetry would exhibit reduced measures of balance.

The presence of significant relationships between spatiotemporal gait asymmetry and measures of static and dynamic balance would suggest that rehabilitation programs that target asymmetric gait may also improve balance and reduce fall-risk.

METHODS

All subjects read, understood and signed an institution approved IRB consent form. Thirty-nine people $\geq$ 6 months post stroke (23 M, 16 F; age: 56.7±10.5 years; height: 172.3±10.2cm; weight: 87.5±10.2kg; 54±60 months post stroke) completed three passes across a 14 foot GaitRite mat, at both comfortable and fast gait speeds.

Measures of spatiotemporal asymmetry were calculated as ratios (non-paretic to paretic) using step length (SLA), stance time (STA), and swing time (SwTA) during both comfortable and fast walking speeds. All ratio values were inverted, if necessary, to ensure values $\geq$ 1.0, so that increased ratios indicated increased inter-limb asymmetry.

Static and dynamic balance measures were assessed using the Berg Balance Scale (BBS), step width (SW) during gait, and the percent of weight borne through the paretic limb (%P) during quiet standing. The weight borne through each limb was measured (~ 1 sec) as the subject stood unsupported with each foot on separate Bertec force plates.

Pearson and Spearman rank correlations were conducted to determine strength of relationships between ratios of spatiotemporal asymmetry and measures of static and dynamic balance. Significance was determined a priori at α=0.05.

RESULTS AND DISCUSSION

Mean comfortable gait speed was 0.65±0.27 m/s (range 0.16 to 1.15 m/s) whereas mean fast gait speed was 0.88±0.42 m/s (range 0.19 to 1.76 m/s). At the comfortable gait speed step length asymmetry was 1.26±0.37, stance time asymmetry was 1.16±0.12, and swing time asymmetry was 1.45±0.44. Asymmetry ratios at the fast walking speed were 1.22±0.36 (step length), 1.38±0.36 (swing time), and 1.15±0.12 (stance time).

The mean Berg Balance Scale score was 48±6 (maximum of 56). Mean step width was 16.89±5.63 cm at the comfortable speed and 16.85±6.15 cm at the fast walking speed. The mean percent of weight borne through the paretic limb was 44.99±8.46%.

At the comfortable gait speed, step length asymmetry (p=0.022), stance time asymmetry (p<0.001), and swing time asymmetry (p<0.001) were positively correlated with step width. Step length ($p<0.001$) and swing time ($p=0.025$) asymmetries were negatively correlated with Berg Balance Scale score. None of the measures of gait asymmetry were correlated with weight distribution between limbs (all $p>0.227$).

During fast walking, step length asymmetry ($p=0.044$), stance time asymmetry ($p<0.001$) and swing time asymmetry ($p<0.001$) were positively correlated with step width during gait. Step length asymmetry ($p<0.001$) and swing time asymmetry ($p=0.005$) were negatively correlated with Berg Balance Scale scores. Additionally, stance time asymmetry ($p=0.010$) was negatively correlated with weight distribution between limbs.

Our hypothesis that people post-stroke with increased spatiotemporal asymmetries would also have greater impairments in static and dynamic balance, was supported.

Spatiotemporal measures were more highly correlated with the dynamics measures of balance (step width) than static measures of balance (%P). This is not surprising given the walking is a dynamic task.

There was no difference in the number or magnitude of significant correlations between comfortable and fast walking speeds. This suggests that comparable relationships exist for walking at both comfortable and fast speed. Further work is needed to determine if spatiotemporal gait asymmetries at fast gait speed represents an increased risk of falls for individuals with chronic stroke.

CONCLUSIONS

These results indicate that spatiotemporal gait asymmetries are related to measures of dynamic balance in people with chronic stroke. This relationship may suggest that people post-stroke with increased spatiotemporal asymmetry are at greater risk of falling than those with more symmetrical gait. Therefore, rehabilitation programs that can improve spatiotemporal asymmetry, may subsequently improve balance and reduce fall risk.

REFERENCES

1. Roger, V.L., et al., *Circulation*, **123**(4): p. e18-e209, 2011.
2. Patterson, K.K., et al., *Neurorehabil Neural Repair*, **24**(9): p. 783-90, 2010.
3. Mackintosh, S.F., et al., *Arch Phys Med Rehabil*, **87**(12): p. 1583-9, 2006.

Table 1: Correlations between spatiotemporal asymmetries and measures of balance (SW=step width; BBS=Berg Balance Scale; %P=percent weight bearing through paretic limb in quiet stance) during comfortable and fast walking speeds.

Correlation between	Comfortable Gait Speed (CGS)	Fast Gait Speed (FGS)
BBS and STA	R = -0.280; p = 0.203	R = -0.281; p = 0.083
BBS and SwTA	R = -0.358; p = 0.025	R = -0.437; p = 0.005
BBS and SLA	R = -0.614; p < 0.001	R = -0.631; p < 0.001
%P and STA	R = -0.280; p = 0.084	R = -0.405; p = 0.010
%P and SwTA	R = -0.198; p = 0.227	R = -0.252; p = 0.122
%P and SLA	R = -0.218; p = 0.182	R = -0.195; p = 0.234
SW and STA	R = 0.552; p < 0.001	R = 0.562; p < 0.001
SW and SwTA	R = 0.599; p < 0.001	R = 0.664; p < 0.001
SW and SLA	R = 0.367; p = 0.022	R = 0.325; p = 0.044

OBESITY MODIFIES CANINE GAIT

[1]Robert Brady, [1]Alexis Sidiropoulos [1]Hunter Bennett, [1]Patrick Rider, [1]Zachary Domire, [1]Paul DeVita

[1]East Carolina University, Greenville NC, USA
Email: bradyr05@students.ecu.edu

INTRODUCTION

Canine obesity has been increasing in the US over the past several years(1). Increasing obesity in canines is positively correlated with diabetes, heart disease, and ultimately premature mortality(1). Obesity in canines also appears to result in degenerative joint diseases such as hip, and elbow osteoarthritis(1). Longitudinal studies have shown the prevalence of arthritis in obese canines is greater and occurs sooner than in their leaner, age and breed matched counterparts(2). An increase in fat mass in canines is thought to yield higher forces in the musculoskeletal system. These higher joint forces during gait could lead to the onset and progression of arthritic changes in obese canines. The purpose of the present study is to compare, for the first time, joint kinematic and ground reaction force variables between lean and obese pure breed or mixed breed canines during walking and trotting.

METHODS

Walking and trotting sagittal plane joint kinematics and ground reaction forces for front and rear limbs were obtained from lean (n = 8) and obese (n = 6) mixed breed canines with motion capture and force plate instruments. Obesity was measured using the Purina Obesity Scale ranging 1-9 with 4-5 being lean and 8-9 being obese (Fig 4). Walking was characterized as a speed of 1.8±0.2 m/s, and trotting as 2.5±0.2 m/s. Groups were compared utilizing independent samples t-test and alpha set at $p<0.05$. Written informed consent was obtained from the canine owners as well as proof of current Rabies vaccination status. All methods were approved by the ECU Animal Use Committee and IRB approval was granted before any testing occurred.

RESULTS AND DISCUSSION

Obese dogs had ~ 20% greater range of motion during stance phase at the shoulder, elbow, hip, and hock compared to the lean at both a walk and a trot (Figs 1 and 2). Obese canines also had ~25% greater vertical ground reaction forces compared to lean while walking and trotting (Fig 3).

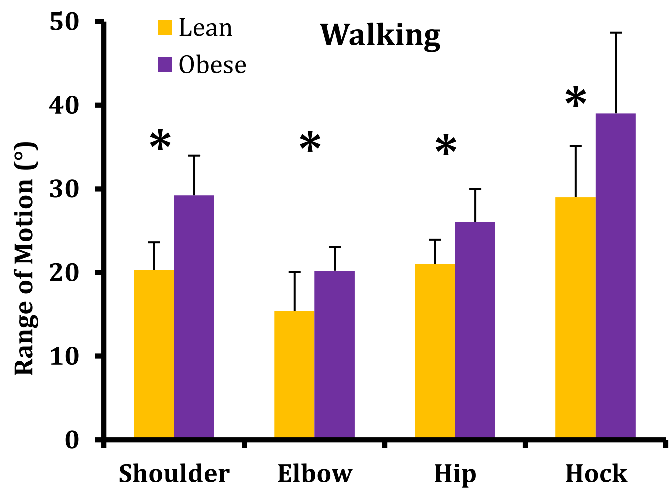

Figure 1: Sagittal plane range of motion during stance at a Walk: * indicates p<.05

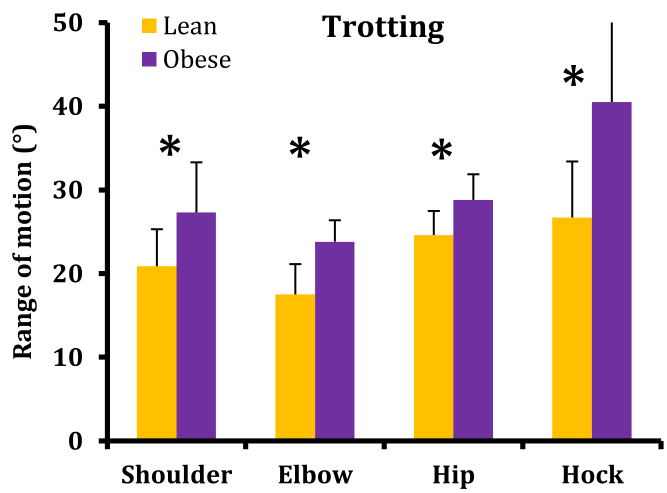

Figure 2: Sagittal plane range of motion during stance at a walk: * indicates p<.05

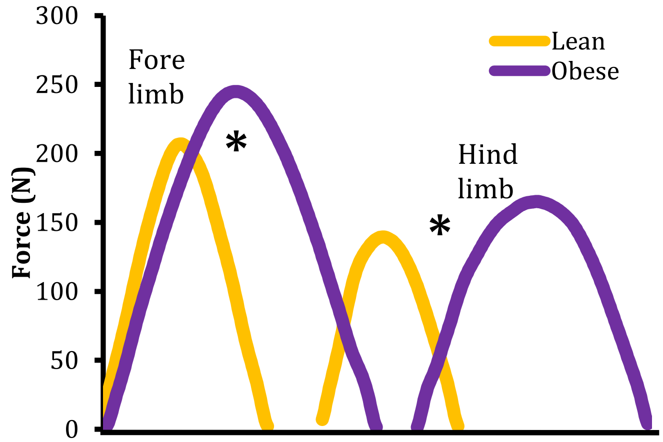

Figure 3: Vertical ground forces at a trot:
* indicates p<.05

Larger joint ROMs in obese vs lean canines were surprising and differ from human and comparative biology among species. Larger, heavier animals such as elephants typically have less ROM about a joint(3). The observed increase in ROM would presumably increase the lever arm of the ground reaction force to the joint center. This increased lever arm along with the larger ground reaction forces would cause an increase in the torques surrounding the joint increasing joint compressive and shear forces. The inability of canines to adapt to obesity by reducing their joint ROM to protect the joints may be one contributor of the increase in osteoarthritis seen with obesity in canines.

CONCLUSIONS

As the prevalence of obesity rises in the canine population, it is important to understand the ramifications of excess weight on their musculoskeletal system and other organ systems. Obese canines seem to not incorporate the same alterations in gait as obese humans, or even other larger animals such as elephants(3), in that obese compared to lean canines exhibit greater ranges of motion throughout the stance phase on both the front and hind limbs. This increased flexion and extension during stance may be one mechanism by which obese canines are promoting osteoarthritis development. Lean vs obese canine gait is not currently well documented in the literature and further studies are needed to continue learning how obesity affects other animals and different coping strategies that may arise.

REFERENCES

1: Courcier, E, et al. "An epidemiological study of environmental factors associated with canine obesity." *Journal of Small Animal Practice* **51** (2010): 362-367.
2: Marshall, W, et al. "A review of osteoarthritis and obesity: current understanding of the relationship and benefit of obesity treatment and prevention in the dog." *Vet Comp Orthop Traumatol* **22** (2009): 339-345
3: Langman, V, et al. "Moving cheaply: energetics of walking in the African elephant." *Journal of Experimental Biology* **198** (1995): 629-632.

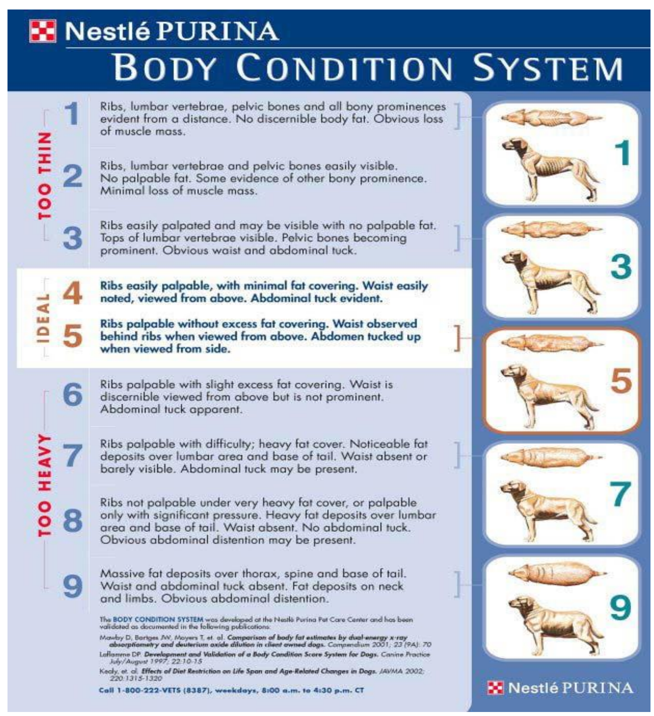

Figure 4: Purina Body Condition Scoring System.

Table 1: Subject Characteristics Data

	Age (Months)	Mass (kg)	Length (cm)	Height (cm)	Circumference (cm)	BCS
Lean	30.6±17.7	24±5.4	75.7±8.6	30.2±3.0	53.6±5.6	4.4±0.5
Obese	43.7±12.1	31.8±9.1	72.4±8.1	29.21±3.8	68±13.5	8.5±0.8

TIBIAL SLOPE AND KNEE FLEXION MODERATE MUSCLE INDUCED STRAIN IN THE ANTERIOR CRUCIATE LIGAMENT

[1]Ryan Breighner, [2]Zac Domire, [3]James R. Slauterbeck, and [4]Javad Hashemi

[1]Texas Tech University, Lubbock, TX, USA; [2]East Carolina University, Greenville, NC, USA;
[3]University of Vermont, Burlington, VT, USA; [4]Florida Atlantic University, Boca Raton, FL, USA
email: jhashemi@fau.edu

INTRODUCTION

Previous in-vitro studies have examined the role of quadriceps and hamstrings forces on the anterior cruciate ligament (ACL) of the knee [1]. The general effects of muscle activity and knee flexion angle on ACL loading have been well established [2]. However, these previous studies were not conducted in context of the geometry of the tibial plateau. Of particular interest are geometries that have been shown to relate to ACL injury status in-vivo [3].

To this end, the present study sought to quantify ACL loading under muscle activity at several flexion angles. The individual tibial geometry risk factors, lateral tibial slope (LTS), medial tibial slope (MTS), and the depth of the medial tibial plateau (MTD) were measured and used in statistical analyses to assess their potential role in moderating muscle induced ACL strain.

It was hypothesized that quadriceps and hamstrings applications would, increase and decrease ACL strain, respectively. Additionally, knee flexion was hypothesized to result in decreased ACL strain due to hamstrings application. Further, it was hypothesized that steeper posterior tibial slopes and shallow medial tibial depths would result in greater ACL strain under muscle loading. A custom-built in-vitro knee loading machine was used to apply fixed levels of quadriceps and hamstrings forces to previously MR imaged cadaver knees. ACL strain was monitored using a strain transducer as these muscle forces were applied.

METHODS

Ten unmatched cadaver knees were used in this study (6 M, 4 F, age: 48.9(8.1) years). Tri-planar T2-weighted MR image sequences were obtained using a 1.5T Siemens Magnetom clinical MRI machine. Prior to imaging, the knees were partially thawed (~ 2hrs at room temperature) to improve image quality. Measurements of medial tibial depth (MTD), medial tibial slope (MTS), and lateral tibial slope (LTS) were made using the method outlined by Hashemi, et al. [4].

The knees were then dissected to the capsule level and fitted with sections of nylon strapping to facilitate attachment of muscle-force actuation cables at physiologically appropriate locations. The magnitudes of muscle forces used were 200N and 80N for the quadriceps and hamstrings forces, respectively, after Li, et al. [1]. These forces were applied at four flexion angles (10°, 20°, 30°, and 40°). Across all flexion angles, muscle lines of actuation were kept parallel to the femur.

The testing procedure began with instrumenting the antero-medial bundle of the ACL with a differential variable reluctance transducer (DVRT) and then installing the knee in the simulator. After cycling the knee in flexion to precondition the remaining soft tissues, the knee was placed in one of the four flexion angles. ACL elongation was then measured at baseline, during quadriceps application, and again during hamstrings application. Strain was calculated from DVRT length, using the length at baseline as the gage length.

RESULTS

Tibial geometry values (table 1) all fell within the ranges of values reported previously in the literature [3, 4]. Averaged ACL strains under quadriceps (Q) and quadriceps/hamstrings (Q/H) loading are shown in figure 1. Tests for normality revealed that the strain data were non-normally distributed. Appropriate power transformations were applied to the strain values to normalize their distribution. Repeated measures models were fit to the transformed data for both Q and Q/H conditions.

Table 1. Tibial geometry measurements.

	MTS (°)	LTS (°)	MTD (mm)
Mean	6.7	6.9	2.75
SD	2.87	3.46	0.64
Max	11.0	14.0	3.8
Min	1.0	2.0	1.9

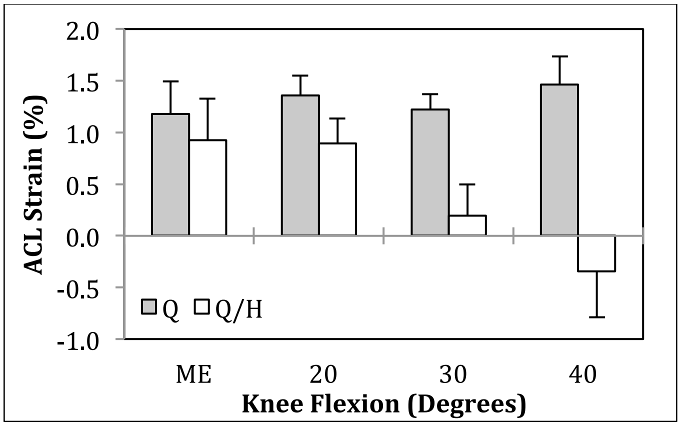

Figure 1. ACL strain due to quadriceps and quadriceps/hamstrings loading at various flexion angles (Mean ± SD).

Model parameters describing strain due to quadriceps and the decrease arising from hamstrings activity are shown in tables 2 and 3, respectively.

Table 2. Q-only model parameters

Factor	Estimate	t	p-value
Intercept	0.465	2.17	0.062
Flex	0.021	6.00	<0.001
LTS	0.102	3.65	<0.001
Flex*LTS	-0.003	-6.06	<0.001

Table 3. Q/H model parameters.

Factor	Estimate	t	p-value
Intercept	0.781	14.19	<0.001
Flex	0.011	7.86	<0.001
LTS	-0.013	-2.41	0.017
MTS	-0.017	-2.66	0.009

DISCUSSION

Under application of isolated quadriceps loading, flexion angle, lateral tibial slope (LTS), and their interaction are significant model parameters. The presence of interaction in this model makes direct interpretation of the main effects difficult, however the significant interaction between LTS and knee flexion indicates that they have opposing effects on ACL strain induced by application of the quadriceps. Applying the extrema of LTS values found in the knees and the range of flexion values to the model, it is apparent that greater flexion and lower LTS values result in lower ACL strain, in general. However this trend is not maintained beyond 30 degrees of flexion.

The analysis of ACL strain under the application of quadriceps/hamstrings loading indicates that steeper MTS and LTS significantly reduce the amount that hamstrings activation lowers ACL strain. Additionally, deeper knee flexion increased the reduction in strain (see figure 1). Medial tibial depth (MTD) was not found to significantly influence ACL strain under either loading condition despite its association with ACL injury status [3]. The reason for this may be the type of loading used in this study. ACL injury typically arises from dynamic events in which multiplanar loading of the knee occurs, however the current study examined only static loading in the sagittal plane.

CONCLUSIONS

This study indicates that knee flexion angle and tibial geometry moderate ACL loading due to muscle forces. These findings demonstrate that steep tibial slope is associated with increased ACL strain, supporting existing research that has found individuals with increased tibial slope to be at greater risk of ACL injury [3]. While the present study does not directly simulate injurious activities or loading conditions, the findings do indicate that individuals with steeper tibial slopes are biomechanically disadvantaged with regard to how their knees transmit forces and respond to loading. Lastly, the interaction between flexion and tibial geometry suggests that individuals at risk of injury due to steep tibial slopes may benefit from adopting movement strategies that maintain deeper knee flexion prior to weight acceptance.

REFERENCES

1. Li G, et al. *J Biomech* **32**, 395-400, 1998.
2. Markolf KL, et al. *Am J Sports Med* **32**, 1144-1149, 2004.
3. Hashemi J, et al. *Am J Sports Med* **38**, 54-62, 2010.
4. Hashemi J, et al. *J Bone Joint Surg Am* **90**, 2724-2734, 2008.

QUANTIFICATION OF MULTI-SEGMENTAL SPINE MOVEMENT DURING GAIT

Scott P. Breloff and Li-Shan Chou

Motion Analysis Lab, Department of Human Physiology, University of Oregon, Eugene, OR, USA
email: chou@uoregon.edu, web: http://biomechanics.uoregon.edu/MAL/index.html

INTRODUCTION

The area between the 7th cervical and 5th lumbar vertebrae is commonly classified as the 'trunk' segment. This segment has been commonly used to describe back/spine motion during gait using surface markers [1]. The detail in which this single segment approach is able to describe the motion of the spine is limited because the trunk segment contains eighteen bones with over thirty joints. Thus it becomes obvious that a more detailed method is needed to describe the motion of the back during gait.

Quantifying the motion between adjacent spinal segments will allow us to better examine the complexity of spine motion during gait. This information could be incorporated with more comprehensive spine dynamics models to enhance the understanding of injury mechanisms or injury prevention, such as low back pain (LBP). Thus, the purpose of this study is to develop a motion capture method which would demonstrate the importance of quantifying individual spinal movement during locomotion and assess its repeatability. To do this, spine kinematics of adjacent segments were examined and compared during level ground walking on two separate testing days.

METHODS

Ten (6M & 4F) young subjects (26.5 ± 4.3 yrs) participated in the study. All subjects read and signed informed consent approved by the Institutional Review Board.

Subjects came in for two testing sessions on non-consecutive days. On both days, a total of 65 (static trial) or 58 (dynamic trial) markers were placed on the subjects. The maker set used was a combination of a modified Helen Hayes along with an adaptation

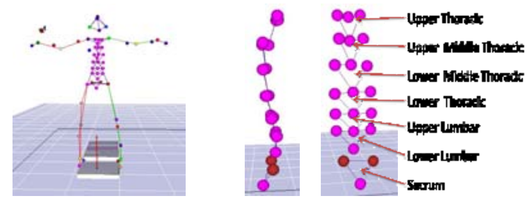

Figure 1: Anterior view of motion capture marker set with enhancements of the spine tracking markers. Sagittal view 2nd and posterior 3rd moving left to right.

from [2] (**Figure 1**). The subjects then preformed the level ground walking with barefoot at their self-selected paces.

A MATLAB® (Mathworks, Natick, MA) program was used to calculate three-dimensional angles between each adjoining spinal segments from heel strike (HS) to toe off (TO). Two more angles were calculated: (1) between the most distal segment (sacrum) and most proximal (upper thorax) segment and (2) between the sacrum and a segment defined by the most caudal back maker (S1) and the two shoulder markers. Both were considered different definitions of the "entire back" angle.

Ranges of motion were calculated for each for the eight angles as follows: (1)Sac-to-UpThx, (2)Sac-t-oC7, (3)Sacr-to-Low Lum, (4) Low Lum-to-Up Lum, (5) Up Lum-to-Low Thx, (6) Low Thx-to-Middle Low Thx, (7) Mid Low Thx-to-Mid Up Tx, and (8) Mid Up Thx-to-Up Thx (Table 1). The range of motion (RoM) for each joint angle was calculated to determine if the spine motion was repeatable between days. It has been shown that multiple spine motion patterns exist between healthy subjects [3]. Thereby increasing the difficulty when comparing motions between subjects, therefore it was decided the RoM was a viable measure to assess repeatability of spine motion [3]. T-tests, with equal variances not assumed (Welch's), compared RoM between the two testing days. Only the flexion-extension RoM will be discussed.

RESULTS AND DISCUSSION

Figure 2 shows the motion patterns during gait for the entire back (a) and three adjacent spine segments: (b) Sacrum to Lower Lumbar, (c) Lower Thorax to Middle Lower Thorax, and (d) Upper Lumbar to Lower Thorax. The figures show similar patterns between (a) & (b). This could be expected because the measured joint is the same. Both angles have the distal sacrum segment and both proximal segments are defined caudally by the S1 marker. Thus the defined joint becomes the relative motion between the sacrum segment and the S1 defined proximal segment. However, it is important to note that different motion patterns are displayed by angles derived from more superior paired segments (c & d). Table 1 displays the mean RoM for all eight angles. Five of the eight angles were shown to have similar RoMs between days. The three angles which were not (5-7) are located in the middle of the spine.

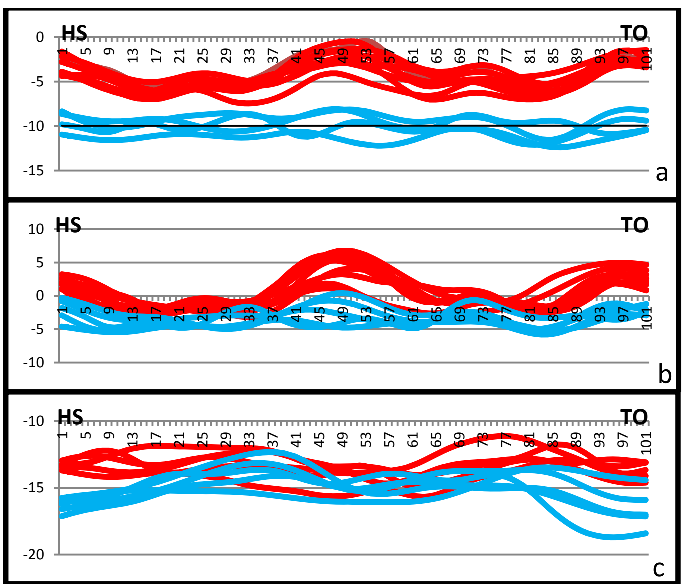

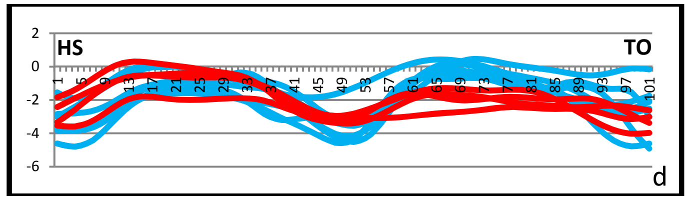

Figure 2: Sagittal plane angles (-ive; flexion) of adjacent segments: a)Sacrum to C7(1), b)Sacrum to LowerLumbar(2) c)LowerThorax to MiddleLowerThorax(6), d)Upper Lumbar to Lower Thorax(5) from HS to TO for one subject two different testing days. Red is first day and blue is second day.

CONCLUSIONS

The present study demonstrated promising results from the examination of detailed spine motions during gait. The results illustrated differences in joint angle patterns between those quantified with a single back segment and multiple spine segments. Such differentiation in movement patterns among individual spinal segments would be helpful in better understanding injury mechanism of LBP, and its prevention.

Most RoM values were found to be repeatable between testing days. Though uncertain, possible explanations for the non-repeatable RoMs could be a fatigue muscle response (specifically superior erector spine group) between the different days. Changes in RoM and patterns could be detected between healthy and pathologic population, similar to the lower extremity joint angles.

REFERENCES

1. Vogt L & Banzer W. *Gait & Posture*, **9**, 18-23, 1999
2. Preuss, RA. & Popovic MR. *J. of Electromyography and Kinesiology* **20**, 823-832, 2010
3. Gatton ML & Pearcy MJ. *Clinical Biomech* 14, 376-383, 1999.

Table 1: Means Standard Deviations of the Ranges of Motion for Adjoining Spine Segments.

Joint Angle (deg)	**Adjacent Spine Segment Angles**							
	1	**2**	**3**	**4**	**5**	**6**	**7**	**8**
Visit 1	6.1 ± 1.7	5.5 ± 1.7	7.14 ± 1.9	5.7 ± 3.1	4.4 ± 2.1	3.5 ± 1.6	4.6 ± 2.1	6.3 ± 5.9
Visit 2	6.4 ± 2.7	6.0 ± 2.9	6.58 ± 3.1	4.5 ± 4.9	3.3 ± 1.6	2.6 ± 1.2	2.6 ± 2.6	4.9 ± 2.1
p-Value	0.42	0.34	0.30	0.15	0.01	0.00	0.00	0.11

CHARACTERISATION OF AGAROSE GEL AS A TISSUE MIMICKING MATERIAL (TMM) FOR USE IN AN ANTHROPOMORPHIC TEST OBJECT INVESTIGATING THE ACOUSTIC LOCALISATION OF CORONARY STENOSIS

[1]MP Brewin, [1]SE Greenwald, [2]S Shaw, [2]C Kruse, [2]JR Whiteman and [3]MJ Birch

1. Blizard Institute, Barts and The London School of Medicine and Dentistry, Queen Mary, University of London, UK; 2. BICOM, Institute of Computational Mathematics, Brunel University, UK; 3. Clinical Physics, Barts & the London NHS Trust, UK

email: m.p.brewin@qmul.ac.uk

INTRODUCTION

As plaque builds up in a coronary artery, blood flow past the stenosed region becomes turbulent and thus creates chaotically varying wall shear stresses in the wake. These shears drive low amplitude acoustic shear waves through the soft tissue in the thorax which then appear at the chest wall and can be measured non-invasively by placing sensors on the skin. This acoustic surface signature has the potential to provide a cheap non-invasive means of diagnosing coronary heart disease [1].

In order to test this diagnostic tool, we have chosen to use agarose gel may be used as a tissue mimicking material in the construction of an anthropomorphic chest phantom. Numerical analysts (Brunel) are writing software that will describe wave motion in these gels with a view to simulating *in silico* the response of the chest wall to the shear waves generated by turbulence in a stenosed coronary artery. Simultaneously, mathematicians at North Carolina State University are developing inverse solver software to determine, from the chest wall signal, the location of the causal stenosis in the thorax. This mathematical loop creates an iterative means of characterizing the source and suggests a cheap non-invasive computational diagnosis tool.

METHODS

The acoustic properties of the gel were determined using established measurement methods [2]. The quasi static compressive elastic modulus and Poisson's ratio of the gel were determined by loading specimens with known masses and optically measuring the resulting axial and transverse strains. Cylindrical gel specimens were subjected to a static compressive load which was then rapidly released, allowing the specimen to undergo free, damped oscillations, see figure 1. These displacements, typically 200 μm, were measured by an inductive linear displacement transducer (Nano-DVRT, Microstrain, USA) and the time-amplitude data were captured. The data sets were used to obtain the time constant of the damping and the real part of the dynamic elastic modulus. The gels were also subjected to a quasi one dimensional shear stress, which was again rapidly released, thus generating damped shearing oscillations. The real and imaginary parts of the complex shear modulus were then derived.

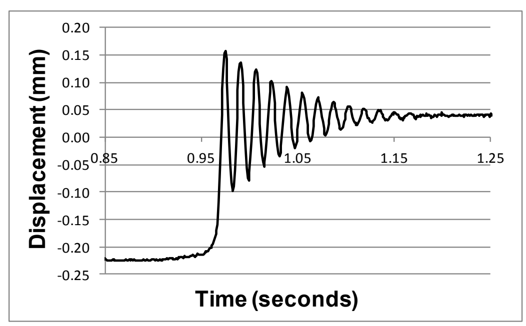

Figure 1: An example of a free damped oscillation.

RESULTS AND DISCUSSION

Initial results on 3% agar water-based gel show a Young's modulus of approximately 130 - 140 kPa and a Poisson's ratio of 0.43. The shear wave speed and attenuation were, respectively, of 3.2 - 7.4 ms^{-1} and 3 - 8 dB cm^{-1} in the frequency range 300 - 2000 Hz. Time-amplitude data for both the free and shear damped oscillations will be shown along with their derived elastic shear moduli components. Elasticity data derived from these data sets will be presented in another abstract from our group.

CONCLUSION

We conclude that, using the experimental set up described above, we are able to determine both the acoustic and elastic properties of tissue mimicking viscoelastic gels with sufficient accuracy, repeatability and precision to test the computational model.

REFERENCES

1. Semmlow J and Rahalkar K, *Annu. Rev. Biomed. Eng.,* **9**:449–69, 2007.
2. Brewin MP, et al, *J. Ultrasound Med. Biol.*, **34** (8):1292-1306, 2008

ACKNOWLEDGEMENTS

This work is supported by the Engineering and Physical Sciences Research Council (EPSRC) [EP/H011072/1 and EP/H011285/1].

THE RELATIONSHIP BETWEEN LEG DOMINANCE AND KNEE MECHANICS DURING THE CUTTING MANEUVER

[1]Scott Brown, [1]Clark Dickin, [1]Henry Wang

[1]Ball State University, Muncie, IN, USA
email: srbrown@bsu.edu web: http://bsu.edu/biomechanics

INTRODUCTION

Females have shown a 3-9 times greater risk for anterior cruciate ligament (ACL) disruption compared to their male counterpart while participating in sports that involve high risk jumping or cutting maneuvers [4]. These ACL injuries are non-contact (NC) in nature and are shown to occur more frequently in field and court sports such as soccer, rugby and basketball [1, 2]. Soccer is known as a predominantly lower extremity sport, where athletes are required to run, cut and kick over a 90 minute period. During this time, an estimated 60-80% of all injuries occur at the ACL [2, 3]. Female soccer players have also shown close to a 70% greater chance of sustaining an ACL disruption to their support leg or non-dominant limb (NDL) when compared to their kicking leg or dominant limb (DL) [2]. To date, few studies have looked into the role of limb dominance as a possible mechanism for NC ACL injuries in female soccer players.

Therefore, the purpose of this study was to examine the relationship between leg dominance and knee mechanics to provide further information about the etiology of ACL injury. We hypothesized that when compared to the DL, during the first-half of stance, the NDL will demonstrate altered knee joint mechanics.

METHODS

Fourteen healthy females who were NCAA Division I varsity soccer players volunteered as subjects for this study (age: 19.6 ± 1.3 yrs; body height: 168.0 ± 4.3 cm; body mass: 62.4 ± 6.1 kg). All subjects had a minimum of twelve years of soccer experience (14.1 ± 0.8 yrs) and at least one year of collegiate experience (1.9 ± 1.0 yrs). Prior to participation, each subject signed an informed consent document approved by the university IRB.

Subjects were fitted in standardized testing attire and asked to perform a five minute warm-up on a treadmill at a self-selected speed. Subjects were then instructed to perform a cutting maneuver; where they sprinted full speed a distance of 5m and then performed an evasive maneuver (planting on one leg and pushing off to the other leg in a new direction) at a 45° angle with their DL and NDL. Subjects were required to perform five successful cuts on each side given in a random order.

Three dimension kinematics and kinetics data were collected using a 12-camera motion capture system (240 Hz) (VICON Inc., Oxford Metric, London, England) and two AMTI force platforms (2400 Hz) (Advanced Mechanical Technologies Inc., Watertown, MA, USA). After the cutting trials, subjects performed bilateral isokinetic testing using a Cybex Norm dynamometer (Lumex, Ronkonkoma, NY, USA) at a speed of 60°/sec to evaluate knee muscle strength.

Power, moments, and angles in the knee were assessed during stance of the cutting maneuver. Paired Student t-tests were used to examine differences in knee mechanics between legs during the cutting maneuver. Significant level was set at 0.05.

RESULTS AND DISCUSSION

Knee joint mechanics in the DL and NDL were presented in Table 1. Subjects showed greater ($P=0.01$) power absorption in the NDL and greater ($P=0.04$) power production in the DL. The NDL also showed a greater ($P=0.02$) peak internal rotation angle. In addition, no differences ($P>0.05$)

in knee extensor and flexor isokinetic torques between the two limbs were shown.

The purpose of this study was to examine the relationship between leg dominance and knee mechanics during the cutting maneuver in healthy female soccer players. The results of this study were in agreement with our original hypothesis noting the NDL to demonstrate altered knee joint kinetics and kinematics. During the first half of stance, subjects exhibited significantly greater peak knee absorption power in their NDL. Although power absorption is expected in the knee during weight acceptance, it was interesting to discover that the magnitude of that power increased from the DL to the NDL. Increased power absorption reflects that increased energy is absorbed by the knee musculature and connective tissues such as ACL. Thus, it is possible that the NDL's ACL may experience increased strain at weight acceptance of cutting. In addition, there is increased internal knee rotation in the NDL during cutting; increased internal knee rotation could also place the ACL under high tension [5, 7]. Thus, the increased power absorption coupled with greater internal knee rotation may result in increased risk of NDL ACL injury. Conversely, the DL demonstrated a significant increase in power production during the second half of stance. Similar studies have found that skill level holds an inference on cutting mechanics [6]. If the DL should possess more skill than the NDL, than an increase in power production in the DL would be expected in the cutting maneuver.

In this study, both limbs demonstrated similar knee extensor and flexor isokinetic torques. The similar knee strength between the limbs may be a result of proper strength training procedures at the collegiate level. Indeed, we failed to find a significant difference in the knee extensor moment between the limbs during cutting. Having equivalent limb strength in the DL and NDL could potentially decrease the variability in knee moments by stabilizing and strengthening the rigidity of the joint complex.

CONCLUSIONS

The results of this study show that a difference in knee mechanics during cutting does exist between the dominant and non-dominant limb. The findings of this study will increase the knowledge base of ACL injury in females and aid in the design of more appropriate neuromuscular, plyometric and strength training protocols for injury prevention.

REFERENCES

1. Agel J, et al. *Am J Sports Med* **33**, 524-530, 2005.
2. Brophy RH, et al. *Br J Sports Med* **44**, 694-697, 2010.
3. Dick R, et al. *J Athl Train* **42**, 278-285, 2007.
4. Gwinn DE, et al. *Am J Sports Med* **28**, 98-102, 2000.
5. Olsen OE, et al. *Am J Sports Med* **32**, 1002-1012, 2004.
6. Sigward SM and Powers CM. *Clin Biomech* **21**, 740-747, 2006.
7. Wascher DC, et al. *J Bone Joint Surg Am* **75**, 377-386, 1993.

Table 1: Knee joint mechanics in the DL and NDL during the cutting maneuver [mean (standard deviation)].

Dependent variables	Conditions		
	DL	**NDL**	**P value**
Knee joint mechanics			
Power absorption (W/kg)	16.10 (3.79)	18.56 (5.76)	0.014*
Power production (W/kg)	13.00 (2.59)	11.33 (2.51)	0.038*
Peak internal rotation (°)	19.05 (5.76)	22.45 (5.25)	0.018*
Peak isokinetic extensor torque (Nm/kg)	160.91 (38.09)	162.05 (30.78)	0.817
Peak isokinetic flexor torque (Nm/kg)	83.83 (18.22)	84.81 (16.24)	0.643

* Denotes a significant difference between DL and NDL.

EXPERIMENTS & THEORY FOR CURVED PATH HUMAN LOCOMOTION

Geoffrey L. Brown and Manoj Srinivasan

The Ohio State University, Columbus, OH, USA
Web: http://movement.osu.edu

INTRODUCTION

Everyday life requires us to walk on paths much more complex than just straight lines. The purpose of this study is to understand the mechanics and energy expenditure during human walking when required to travel along curved paths, using a mixture of experiment and theory.

First, we test the hypothesis that, for a given linear speed, the energy expenditure per unit time will increase as the radius of curvature of the path of travel decreases. Second, we would like to explain the experimental observation that people walking in tighter circles walk at a slower speed when allowed to walk at their preferred comfortable speed [1]. We hypothesize that this trend may be explained by a shift in the energy optimum speed of walking as radius changes. We use both a computer model and energy optimization on the one hand and human subject energetics experiments on the other.

METHODS

This study is composed of two parts: experimental results from human subjects walking around circles and a computer simulation using a 3d model of a biped walker improving upon previous 2d models [2].

Simulation & Computer Optimization

Using a simple computer model of a biped, we compute the energy optimal gait for walking in a circle. The biped model has a point mass with two legs that can change length, using a single articulated joint (Figure 1), has no flight phase modeled and infinitesimal double stance phase. Analogous to [2], we used computer optimization to determine the initial conditions, the leg forces and the hip motion that satisfies the constraints and minimizes the energy cost function, subject to constraints for walking in a circle with periodic steps. The cost function we chose to minimize was cost per unit length – consisting of 3 cost pieces: a cost for work done and force exerted by stance leg, a swing cost [3,4] and resting cost. The optimized cost per unit length was found for a range of different speeds and radii in order to make inferences about overall energy cost trends.

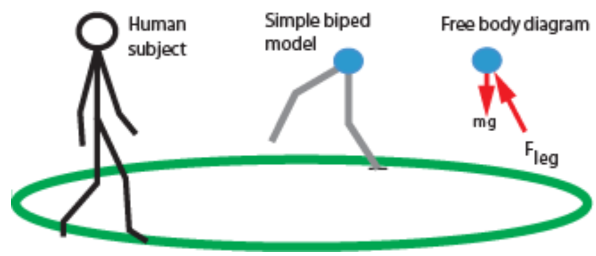

Figure 1: Cost per unit length versus speed and radius for simulated walking, obtained from computer optimization.

Experiment

We measured the metabolic rate of people walking in circles of different radii at different speeds, using the Oxycon™ Mobile metabolic testing system. This system measures the energy expenditure by sensing the change in oxygen content between inhaled and exhaled air to determine the rate at which the body is consuming oxygen. Subjects are asked to walk at a prescribed pace around specified circular paths of varying radii (1 to 5 m) for approximately 3-5 minutes, at speeds ranging from 0.75 m/s to 1.5 m/s (approximately). Pace is maintained using a timer to track subject lap times and provide audible feedback for speed corrections. Research approved by OSU's IRB.

RESULTS AND DISCUSSION

Simulation & Computer Optimization

The optimal motion obtained from this simulation produced a hip trajectory that followed close to a circular arc about the point of contact. Also, the forces obtained also show large spikes at the beginning and end of the stance phase representing push-off and heel-strike, as in [2]. The optimal energy cost per unit length is shown in Figure 2. The optimal walking speed at a range of radii is shown in Figure 3. We see a general trend of increasing optimal speed with increasing radius.

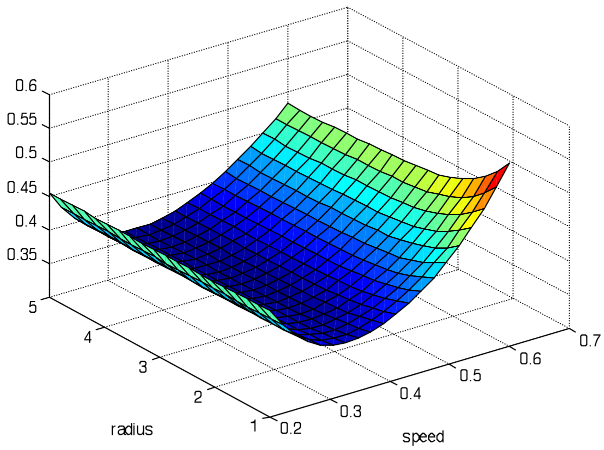

Figure 2: Cost per unit length versus speed and radius for simulated walking, obtained from computer optimization in non-dimensional units.

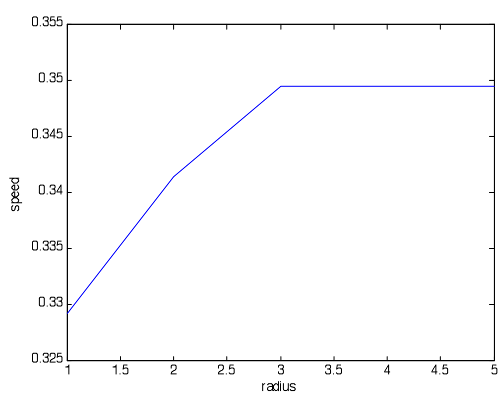

Figure 3: Optimum speed versus radius for simulated walking. All units are in non-dimensional quantities.

Experimental results

The experimental results are shown in Figures 3 and 4. The data shown in Figure 3 is obtained from a best fit surface of the experimental data, using a model of the form: $dE/dt = (A+B.v^2) + (1/R)(C_3+C_4 .v^2)$. where A, B, C, and D are found from the data using a weighted least squares approach. The surface shown in Figure 3 is this entire function divided by velocity to obtain cost per length.

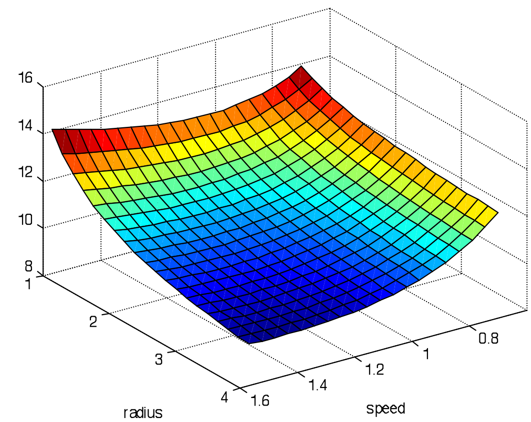

Figure 4: Fit of cost per unit length versus speed and radius from human subject experiments for one stubject.

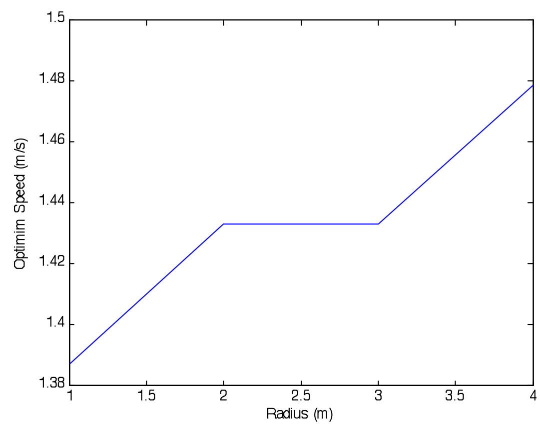

Figure 5: Optimum speed versus radius for actual walking.

We have established that our two hypothesis are consistent with energy optimally, and our data so far with a human subject. We hope to refine orur theory to

REFERENCES

1. S. Vieilledent, et al. *Neuroscience Letters,* **305**, 65-69.
2. M. Srinivasan and A. Ruina. *Nature,* **439**, 72-75, 2006.
3. J. Doke, J. M. Donelan, and A. D. Kuo. *The Journal of Experimental Biology*, **208**, 439-445.
4. M. Srinivasan, *Ph.D dissertation,* Cornell University, 2006.

THE EFFECT OF THORACIC KYPHOSIS AND SAGITTAL PLANE ALIGNMENT ON VERTEBRAL COMPRESSIVE LOADING

[1,2]Alexander G. Bruno, [2,3]Dennis E. Anderson, [2]John D'Agostino, and [2,3]Mary L. Bouxsein

[1]Harvard-MIT Health Sciences and Technology Program, Cambridge, MA, USA
[2]Center for Advanced Orthopaedic Studies, Beth Israel Deaconess Medical Center, Boston, MA, USA
[3]Department of Orthopedic Surgery, Harvard Medical School, Boston, MA, USA
email: agbruno@mit.edu, web: http://www.bouxseinlab.org/

INTRODUCTION

Hyperkyphosis of the thoracic spine is a strong and independent risk factor for vertebral fractures. One possible mechanism underlying this increased fracture risk is an increased moment arm between the spine and the superincumbent body weight that it must support, which has the net effect of increasing vertebral loading and thus fracture risk [1]. In an effort to maintain stability, upright posture, and horizontal eye gaze, there are multiple postural adjustments that an individual can employ in response to an age-related increase in thoracic kyphosis [2]. However, it is not known how these adjustments might interact with the thoracic kyphosis angle to influence forces applied to the vertebrae. The purpose of this study was to determine the effect of increased thoracic kyphosis on the magnitude of vertebral compressive loading during two different standing tasks, and to examine how three different posture conditions (an uncompensated increase in thoracic kyphosis, a compensated increase in thoracic kyphosis, and maintenance of congruency between the lumbar and thoracic spine) interact with the thoracic kyphosis angle to affect vertebral compressive loading.

METHODS

We used a static musculoskeletal model of the spine [3] to estimate vertebral compressive force at T8 and T12 for two different activities: 1) upright standing with arms hanging down and 2) upright standing with elbows flexed to 90° and 5 kg weights in each hand. Baseline spinal curvature and pelvic orientation for the model were created using average values from the literature [4]. For each activity, we examined three different posture conditions: 1) an uncompensated increase in thoracic kyphosis; 2) increasing thoracic kyphosis with a compensatory postural adjustment, in this case tilting the pelvis posteriorly; and 3) increasing thoracic kyphosis concomitantly with lumbar lordosis to maintain congruency, which means that the thoracic and lumbar curves are proportional and balance each other. For the uncompensated posture condition, the T1-T12 Cobb angle was varied from 50° to 75° while all other spino-pelvic parameters remained fixed at their baseline values. For the compensated posture condition, pelvic tilt was varied (10° to 15.31° in 0.23° increments) concomitantly with the T1-T12 Cobb angle (50° to 75° in 1° increments) to maintain the sagittal alignment of the head and neck directly above the hip joint. For the congruent posture condition, the L1-L5 Cobb angle was varied (43° to 52.1° in 0.36° increments) concomitantly with the T1-T12 Cobb angle (50° to 75° in 1° increments) to maintain the sagittal alignment of the head and neck directly above the hip joint.

RESULTS AND DISCUSSION

Compressive force was higher at T12 than T8 and compressive force was higher for standing with weight in the hands than standing with no weight. At both T8 and T12, compressive loading increased with increasing thoracic kyphosis for each of the three postures, with the increase in loading being greatest for the uncompensated posture, followed by the compensated posture, and finally the congruent posture (Fig. 1).

Increasing thoracic kyphosis increased vertebral compressive loading more in the uncompensated condition than in the compensated or congruent conditions because it shifted a greater amount of body mass forward. This generated higher flexion moments which required larger muscle forces to equilibrate. The congruent and compensated posture conditions countered the anterior shift in body mass associated with an increasing thoracic kyphosis, with the congruent posture condition being more effective. The clinical implication is that some older individuals who have a very high thoracic kyphosis angle may not be at an elevated risk for fracture because they have congruent posture. In comparison, those who have an age-related increase in thoracic kyphosis, and do not have a congruent spinal configuration, may have a greater risk for fracture than someone with the same thoracic kyphosis angle but who maintains a congruent posture.

CONCLUSIONS

We suggest that the current theory ascribing increased spinal loading to greater amounts of thoracic kyphosis is overly simplistic as it does not take into account other postural adjustments that accompany age-related increases in thoracic kyphosis, and which act to modulate any increases in loading. Our results indicate that in addition to measuring thoracic kyphosis angle, it is also necessary to evaluate overall posture and spino-pelvic alignment when assessing one's risk for degenerative spinal pathology due to altered spine biomechanics, such as vertebral fractures. When treating spinal deformities, clinicians should strive to restore congruent posture because of its positive effects on spinal loading, balance, and eye gaze.

REFERENCES

1. Briggs AM, et al. *Osteoporosis International* **18**, 575-584, 2007.
2. Knight R, et al. *White Paper on Sagittal Plane Alignment,* Scoliosis Research Society, 2003.
3. Iyer S, et al. *Clinical Biomechanics* **25**, 853-858, 2010.
4. Bernhardt M, et al. *Spine* **14**, 717-721, 1989.

ACKNOWLEDGEMENTS

This work was supported by grants R01AR053986, T32AG023480, and F31AG041629 from the NIH.

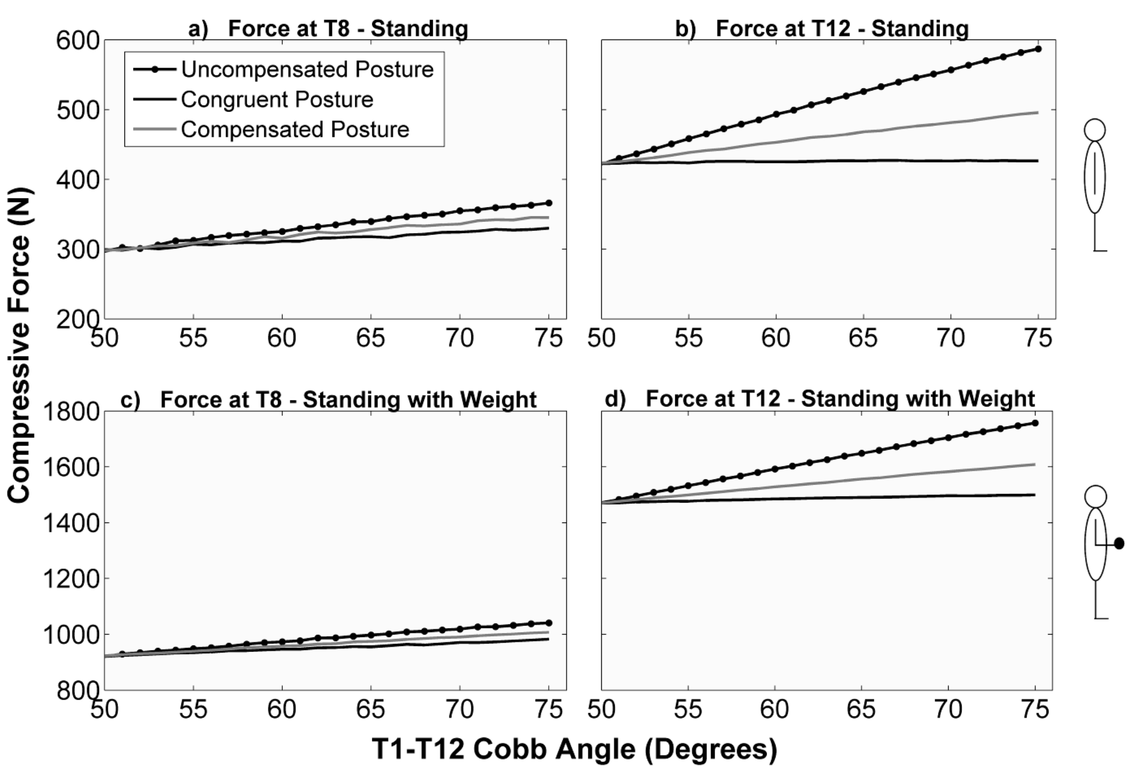

Figure 1: Compressive force (Newtons) on T8 and T12 as a function of T1-T12 Cobb angle (degrees) for two activities, as well as the three different postures.

LINGERING IMPAIRMENTS IN POSTURAL CONTROL, DESPITE SYMPTOM RESOLUTION, FOLLOWING A CONCUSSION

Thomas A. Buckley, Tiffen G. Tapia-Lovler, and Barry A. Munkasy

Georgia Southern University, Statesboro, GA, USA
email: TBuckley@Georgiasouthern.edu
web: http://www.georgiasouthern.edu/biomechanicslab

INTRODUCTION

Impaired postural control is a cardinal symptom of a concussions. Current guidelines recommend a multifaceted approach to acute and ongoing concussion management; however, many protocols allow return to participation or initiation of a graded exercise program once the individual self-reports they are symptom free. [1] Previous investigations have identified lingering impairments in postural control up to 30 days post-injury, but lacked specific comparison to clinical measures. Gait initiation, literally the act of beginning to walk, has successfully identified impairments in postural control in a wide range of patient populations. Therefore, the purpose of this study was to evaluate postural control on the day the individual self-reported being symptom free to their healthy baseline performance.

METHODS

The 22 participants (Age: 19.1 $\pm$ 1.0 years old, HT: 1.73 $\pm$ 0.16m, WT: 73.4 $\pm$ 27.4kg, MTBI history: 0.95 $\pm$ 1.51, 40.9%) were all NCAA Division I student-athletes. All participants underwent Gait Initiation (GI) assessment on three separate occasions: 1) during a baseline screening during the individuals pre-participation physical examination (PRE), 2) within 24 hours of suffering a MTBI (DAY 1), and 3) on the day the participant self-reported being symptom free (S/s FREE) following their concussion (4.3 $\pm$ 2.8 days post-injury)

All participants completed 5 trials of self-selected pace cued GI on each testing day. Participants began each trial with one foot each on adjacent forceplates, initiated movement in response to a verbal cue, and proceeded down a 7m walkway with the initial step on a forceplate. (Figure 1)

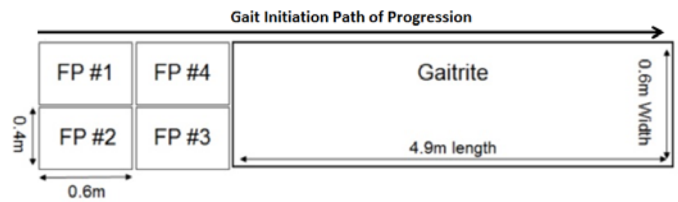

Figure 1. Lab Set-up. Participants begin the trials standing on forceplate 1 & 2 and walked from left to right with their initial step onto forceplate 3 or 4.

The kinetic data were sampled at 1,000 Hz from the 4 forceplates (AMTI, Watertown, MA, USA). The four dependent variables quantified were the center of pressure displacement during the anticipatory postural adjustment (APA) phases of GI in the posterior and lateral direction and the resulting step length and step velocity calculated from kinetic data. The dependent variables were compared between the three testing sessions with a one-way ANOVA and significant main effects were followed up with a Tukey post-hoc test (alpha = .05).

RESULTS AND DISCUSSION

The participant's concussions in this study were graded retrospectively based on the Cantu revised evidence based guidelines and were classified as grade II (symptoms lasting longer than 24 hours but less than 7 days). [2] The post-injury loss of consciousness rate was 22.7% and the post-traumatic amnesia rate was 31.8%.

There was a significant main effect for both the posterior (F: 21.537, p<0.001) and lateral (F: 5.641, p=0.006) displacement of the COP during the APA phase. Follow-up testing revealed significant differences for posterior displacement of the COP between PRE and Day 1 ($p<0.001$) and PRE and S/s FREE ($p<0.001$). Similarly, significant differences were noted for lateral COP displacement between PRE and Day 1 ($p=0.006$) and PRE and S/s FREE ($p=0.047$).

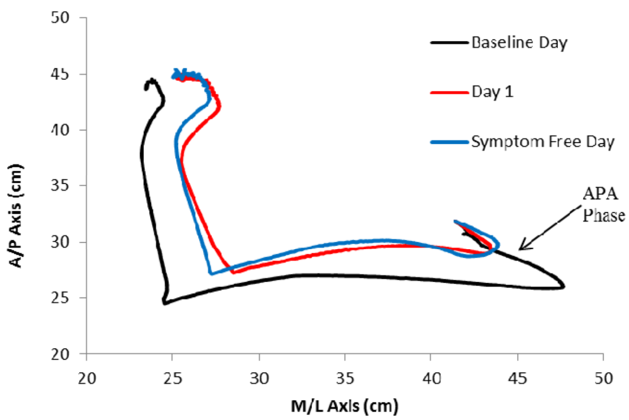

Figure 2. Exemplar COP displacements between the three testing dates.

There was a significant main effect for step length (F: 3.565, $p=0.035$) and step velocity (F: 3.346, $P=0.042$). However, post-hoc testing only identified a difference in step length between PRE and Day 1 ($p=0.027$). There were no differences between PRE and S/s FREE for either variable. (Table1).

Table 1. Mean and standard deviation for each variable on each testing day. * indicates significant difference from PRE.

	PRE	Day 1	S/s FREE
APA Posterior (cm)	5.17 + 1.87	2.25 + 1.37*	2.87 + 1.41*
APA Lateral (cm)	5.03 + 2.06	3.09 + 1.76*	3.57 + 2.14*
Step Length (m)	0.69 + 0.11	0.59 + 0.10*	0.65 + 0.11
Step Velocity (m/s)	0.72 + 0.13	0.62 + 0.18	0.72 + 0.15

The results of this study suggest that impairments in postural control persist despite the resolution of self-reported symptoms following a concussion. Specifically, these results suggest that APAs may be a more sensitive indicator of lingering impairments in postural control post–concussion than traditional stepping characteristics during locomotion activities.

These results further suggest the post–concussion subjects utilized a conservative strategy to initiate gait. Recently, stroke research has suggested that cued GI is under supraspinal control, specifically the supplementary motor area. [3] The results of this study may further the understanding of impairments in postural control post–concussion by potentially identifying a specific supraspinal structure contributing to the impairment.

Clinically, these results are meaningful as they indicate that impairments in postural control persist beyond the injured individuals self-report of symptoms. Simple reliance on patient self-report may allow premature return to participation which may predispose the individual to both short and long-term neuropathologies.

CONCLUSIONS

These findings further recent studies which have suggested that impairments in postural control following a MTBI may persist longer than previously suspected.[4] More sophisticated biomechanical analysis of postural control may be required to more sensitively identify recovery from MTBI.

REFERENCES

1. McCrory P, et al. Consensus statement on concussion in sport: the 3rd International Conference on Concussion in Sport held in Zurich, November 2008. *J Athl Train.* Jul-Aug 2009;**44**(4):434–448.
2. Cantu RC. Posttraumatic Retrograde and Anterograde Amnesia: Pathophysiology and Implications in Grading and Safe Return to Play. *J Athl Train.* 2001;**36**(3):244–248.
3. Wang J, et al. Functional MRI in the assessment of cortical activation during gait-related imaginary tasks. *J Neural Transm.* 2009;**116**(9): 1087–92.
4. Slobounov S, et al. Alterations of Postural Responses to Visual Field Motion in Mild Traumatic Brain Injury. *Neurosurgery.* 2006; **58**(7): 134–139.

ACKNOWLEDGEMENTS
Supported by: NINDS 1R15NS070744-01A1

ADAPTATION OF PLANTARFLEXOR MUSCLE ACTIVITY DURING GAIT

[1]Alison M. Bunchman, [1]Molly A. Wellinghoff and [1]Jesse C. Dean

[1]Medical University of South Carolina, Charleston, SC, USA
email: deaje@musc.edu

INTRODUCTION

Humans often appear to prefer movement patterns that minimize energetic cost, but it is not clear how these patterns are identified. Energetic cost is related to system mechanics, as shown for a simple bouncing task in which moving at the resonant frequency minimizes energetic cost and allows the plantarflexors to remain nearly isometric [1, 2]. Therefore, identification of the optimal movement pattern could be driven by either metabolic feedback or proprioceptive feedback of the body's mechanical state. We have recently shown that humans do not initially prefer to bounce at the resonant frequency, but gradually adapt toward it over time, indicating that feedback is necessary to choose the preferred movement pattern [3].

Activating muscles to remain near isometric may also have metabolic benefits in more complex tasks, including locomotion. During walking, the plantarflexors remain nearly isometric for much of the stance phase as elastic energy is stored in the Achilles tendon [4]. This near isometric behavior persists when slope is varied, requiring substantial changes in muscle activity [5]. However, it is not clear whether humans modify their muscle activation patterns through a feedback-dependent process as observed during bouncing. Alternatively, muscle activity changes could be driven by a switch to a new feed-forward motor plan, or could be an immediate reflexive response to the new slope [6].

The purpose of this study was to investigate the time course of changes in muscle activation during gait following alterations in slope. We hypothesized that in response to a slope change, humans would gradually adapt their plantarflexor activation patterns during the gait phase when elastic energy is stored in the Achilles tendon. Secondarily, we hypothesized that increasing cognitive load would disrupt the adaptation process.

METHODS

Seven young (23±1 yrs), healthy subjects participated in an experiment which they were told was investigating distracted walking. Subjects completed three 5-minute treadmill walking trials at 1.25 m/s. The first trial allowed subjects to accommodate to the treadmill. The order of the final two trials was randomized, and subjects wore glasses to block their lower visual field. In these trials, the treadmill slope was alternated between 0% and 1% uphill grades once each minute. The slope changes were quite slow (~5 s).

In a single-task walking trial, subjects were instructed to keep their eyes focused on a white dot projected onto a screen in front of them. In a dual-task walking trial, subjects performed a Stroop test, a common method of increasing cognitive load [7]. For all trials, we measured bilateral medial gastrocnemius (MG) and soleus (SO) EMG. Upon completion of the experiment, subjects were asked several questions, including whether the slope changed while they were walking.

For analysis, plantarflexor muscle activity was processed and normalized by the peak value during an average stride in the final minute of the initial trial. For each stride, EMG traces were divided into Storage and Return phases (Fig. 1), as previously defined [6], and averaged. This abstract focuses on gradual changes in Storage phase muscle activity. These muscle activity values were grouped into 5-second bins and averaged. Following each slope

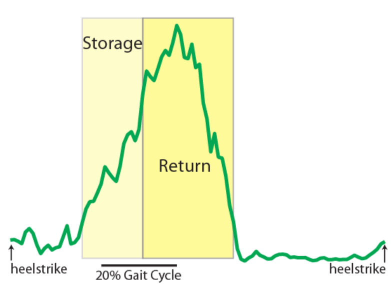

Figure 1. A typical pattern of MG activity during a stride is divided into a Storage phase, when energy is stored in the Achilles tendon, and a Return phase, when the tendon shortens [6].

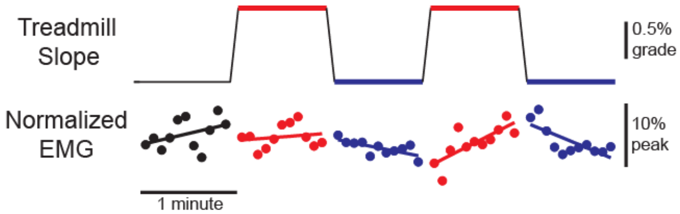

Figure 2. Treadmill slope and average Storage phase MG activity are plotted over the course of the single-task walking condition. Solid lines in the lower panel indicate the best-fit.

change (from 0→1% or from 1→0%) we calculated the change in Storage phase muscle activity over time, which was considered a sign of adaptation. We performed repeated measures ANOVAs to test for significant effects of the changes in slope.

RESULTS AND DISCUSSION

Subjects were not consciously aware of the small changes in treadmill slope, as none of the seven subjects reported that a slope change occurred.

During single-task walking, plantarflexor muscle activity varied in response to a slope change, as illustrated for MG (Fig. 2). Increases in treadmill slope tended to cause subsequent gradual increases in Storage phase EMG. Conversely, decreases in slope caused gradual decreases in Storage phase EMG. For both MG and SO, the direction of the slope change significantly ($p<0.05$) influenced the subsequent adaptation (Fig. 3A).

Dual-task walking, implemented in the form of a Stroop test, appeared to reduce the magnitude of adaptation (Fig. 3B). While changes in slope still significantly ($p<0.05$) affected subsequent MG adaptation, the magnitude of the average change was smaller than in single-task walking. Slope changes did not significantly affect SO adaptation.

Our results provide evidence that gradual adaptation of muscle activation patterns occurs during steady-state gait. Importantly, this adaptation was observed during the Storage phase of stance, when appropriate activation of the plantarflexors will allow elastic energy to be stored in the Achilles tendon. This adaptation process does not appear to require conscious control, as subjects did not report being aware that the treadmill slope had changed. However, adaptation may involve the cortex, as it was reduced when cognitive load was increased.

CONCLUSIONS

The gradual adaptation of plantarflexor activity over time supports our proposal that humans may optimize cyclical behavior by driving near-isometric muscle behavior [3]. Humans could potentially use proprioceptive feedback of the body's mechanical state to perform this optimization, with subsequent metabolic benefits [8]. Future work could integrate ultrasound measurements to quantify whether musculotendon length changes are predicted by the proposed optimization process.

REFERENCES

1. Takeshita D, et al. *J App Phys* **101**, 111-8, 2006.
2. Dean JC, Kuo AD. *J App Phys* **110**, 873-880, 2011.
3. Merritt KJ, et al. *J Neurophys* In Press, 2012.
4. Ishikawa M, et al. *J App Phys* **99**, 603-8, 2005.
5. Lichtwark GA, Wilson AM. *J Exp Biol* **209**, 4379-88, 2006.
6. af Klint R, et al. *J Phys* **586**, 4643-8, 2008.
7. Dingwell JB, et al. *J Neuroeng Rehabil* **21**, 5-12, 2008.
8. Raburn CE, et al. *J Exp Biol* **214**, 3768-74, 2011.

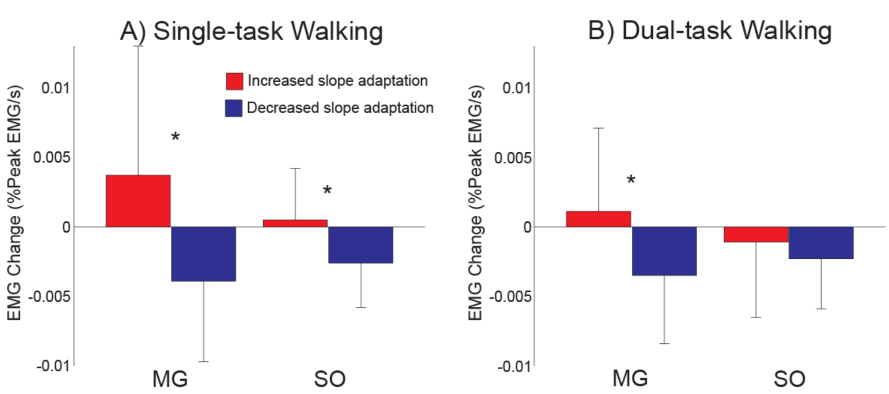

Figure 3. The average change in Storage phase muscle activity is plotted for single-task (A) and dual-task (B) walking. The direction of the slope change (from 0→1% or from 1→0%) had a significant effect on the subsequent adaptation for both muscles during single-task walking and for MG during dual-task walking. Asterisks indicate significant differences. It should be noted that there was substantial variability in this adaptation (see error bar size). This may be due to the relatively small slope changes imposed.

A QUADRUPEDAL POSTURAL CONTROLLER WITH PHYSIOLOGICAL DELAYS REVEALS THE NEED FOR MULTI-LEVEL STABILITY

Nathan Bunderson

Georgia Institute of Technology, Atlanta, GA, USA
email: nbunderson@gatech.edu, web: http://ap.gatech.edu

INTRODUCTION

Animals have a variety of tools with which to stabilize against postural perturbations. These include the intrinsic viscoelasticity of muscle, as well as short and long latency neural feedback mechanisms. To what extent each of these contributes to postural stability is a matter of intense debate. While control strategies have been inferred from measured physical quantities such as ground reaction forces, electromyograms, and joint kinematics [1], it is difficult to obtain sufficient data from experiments to form a clear picture of how the various elements are coordinated. On the other hand simplified biomechanical models do not accurately describe generic traits of musculoskeletal systems such as muscle and joint redundancy. We present a model for postural stability which includes redundant joints and muscles and analyze the response of the model to postural perturbations under two control strategies. In particular we demonstrate how intrinsic, short latency, and long latency components may work together to stabilize the entire biomechanical system and how this coordination is only apparent in the redundant system.

METHODS

The musculoskeletal model is comprised of a 6 degree of freedom trunk segment and four limbs which have been described previously [2]. Each limb has 6 kinematic degrees of freedom (3 at the hip, 2 at the knee, 1 at the ankle) and 31 muscles. The initial ground reaction forces at each limb are 1/4th the weight vector. The total force in each muscle is the sum of undelayed intrinsic forces (F_I), reflexive (20ms delay) forces (F_R), and control (120ms delay) forces (F_C). The total muscle force has a minimum (0) and maximum (*Fmax*, unique to each muscle) allowable value.

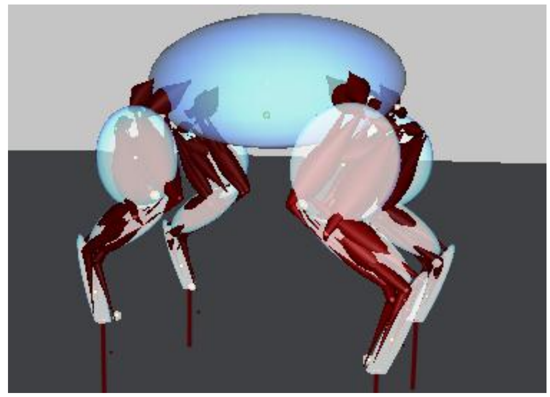

Figure 1: The musculoskeletal model with 30 kinematic degrees of freedom and 124 muscles.

The intrinsic forces are modeled with a parallel spring and damper acting on the instantaneous change in length from the initial muscle length and instantaneous velocity. Reflexive forces are modeled with a similar parallel spring and damper acting on the delayed (20ms) length and velocity values.

The control forces are the sum of constant background forces (minimum muscle effort solution to achieve equilibrium with the given initial ground reaction forces) and delayed control forces. The delayed muscle control forces are calculated to minimize the sum of squared ground reaction forces and squared generalized coordinate accelerations of an internal model. The internal model is constructed from delayed (120ms) state information. The delayed muscle control forces must also result in a net force and torque acting on the internal model center of mass which is equivalent to that which would be produced by a virtual parallel spring damper attached to the internal model center of mass. The controller has similarities to previous work by others [3].

Two sets of intrinsic, reflexive, and control viscoelastic parameters were chosen. The ***IRC*** condition had control viscoelasticity chosen such that the center of mass had optimal damping ratio and undamped natural frequency of 1/120Hz. The remaining four viscoelastic parameters were minimized with the constraint that the simulation be stable. The ***I*** condition had no reflexive or control forces and intrinsic viscoelasticity was chosen to achieve a stable response with maximum center of mass excursion.

A 3 N force was applied for 10 ms to the center of mass of the trunk segment in the "anterior" direction. The perturbation response of the model was simulated for the ***IRC*** and ***I*** conditions.

RESULTS AND DISCUSSION

The model was able to recover from the perturbation under both ***IRC*** and ***I*** conditions (Fig. 2a). However, under the ***IRC*** condition the model had 68% greater center of mass excursion than under the ***I*** condition demonstrating a more compliant response. In addition while the timing of maximum center of mass excursion was nearly the same for both models, the ***IRC*** recovered more quickly.

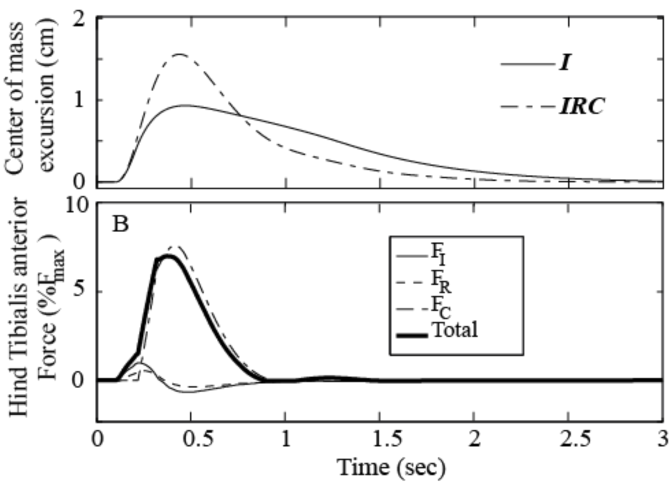

Figure 2: a) The deviation of center of mass for the quadruped under the two conditions. b) Muscle force components as a function of time in Tibialis anterior of the right hindlimb under ***IRC*** conditions.

When any of the individual viscoelastic parameters of the ***IRC*** model were decreased the model did not recover from the perturbation. The failure mode was dramatically different depending on which element was decreased. When reflexive or control parameters were decreased the model "gracefully" fell over. When intrinsic parameters were decreased the model failed more quickly. The joints of the limb began to deviate and/or oscillate dramatically before the center of mass of the model had deviated by even 1 cm. The different failure modes highlight the concept of multi-level stability. Intrinsic components stabilize the joints locally and delayed components stabilize the quadruped as a whole. By including sufficient intrinsic stability the delayed controller is free to ignore local variables and only stabilize the integrated "global" variables such as center of mass dynamics. This type of behavior cannot be observed in reduced models where global and local variables cannot be differentiated.

The relative contributions of each force component for each muscle were analyzed for the ***IRC*** condition. The Tibialis anterior of the right "hindlimb" has a peak total force and peak control force of about 7% *Fmax* and peak reflex and intrinsic forces are less than 1% *Fmax* (Fig. 2b). On average, the ratio of peak delayed control force to peak intrinsic force was found to be 5.2. It is sometimes argued that the magnitude of EMG associated with spinal reflex delays is insignificant compared with the longer latency EMG. We have demonstrated that our model in fact fails when the relatively small reflexive components are removed.

CONCLUSIONS

Stability must be achieved at multiple levels as part of the response to postural perturbations. The levels range from local (joint) to global (center of mass) and the various components of the neuromuscular system may be responsible for stability at the various levels.

REFERENCES

1. Winter DA, et al. *J Neurophysiol* **80**, 1211-1221, 1998.
2. Burkholder TJ, Nichols TR. *J Morphol* **261**, 118-129, 2004.
3. Ye Y, Liu KC. *ACM Transactions on Graphics* **29**, 2010.

KINEMATICS, KINETICS AND MUSCLE ACTIVATION PATTERNS OF THE UPPER EXTREMITY DURING SIMULATED FORWARD FALLS.

[1]Timothy A. Burkhart, [2]Don Clarke, [2]David M. Andrews

[1]Western University, London, Ontario, Canada
[2]University of Windsor, Windsor, Ontario, Canada

INTRODUCTION

The instinctive mechanism of extending the upper extremities in front of the body, while protecting the head and torso during a fall, can place large impulsive forces on the distal upper extremity. While past investigations have provided insight into the effects of muscle activation and joint kinematics on the impact forces [1], they have generally been limited by the fall simulation methods (*e.g.* anticipated falls limited to a single plane of motion). Therefore, the purpose of this study was to explore the effects of fall type and fall height on the kinematics, kinetics, and muscle activation of the upper extremity using a fall simulation method that can more accurately simulate forward fall motion.

METHODS

A Propelled Upper Limb fall ARrest Impact System (PULARIS) [2] was used to simulate the impact phase of a forward fall on twenty participants (10 male; 10 female; 23±3.0 years). Participants were suspended by torso and leg straps, attached to two solenoid controlled quick releases, subsequently attached to the bottom tracking of PULARIS (Figure 1). A drive chain that was connected to two PULARIS attached sprockets and a motor, controlled by an AC drive, allowed PULARIS to move in the forward and backward directions. A slotted optical switch with a light emitting diode, sandwiched one of the sprockets and was used to count the number of sprocket teeth that passed as PULARIS was moved backwards between the release point (rear edge of force platforms) and the start point (~ 1.9 m away from the force platforms), prior to each trial.

PULARIS propelled the participants forward towards the force platforms (Figure 1) at a velocity of approximately 1.0 m/s (velocity could be adjusted by changing the start position of PULARIS). The quick releases were activated (i.e. participant dropped) as the hands passed the release point and an impact occurred to the palm of each hand.

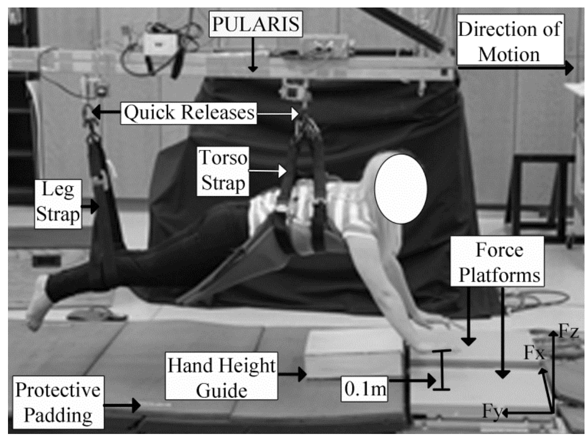

Figure 1: Experimental set-up for a straight arm 0.10 m fall.

Participants experienced all combinations of two fall heights (0.05 m and 0.10 m) and three fall types (straight-arm (worst case scenario); bent-arm (20^o flexion angle about the elbow); and self-selected (participants instructed to minimize impact)). "No-fall" trials were also included in an attempt to maintain the unpredictability associated with actual forward fall events.

Muscle activation levels were collected from six muscles of the upper extremity (Figure 2) and three marker sets were used to track the motion of the hand, forearm, and arm segments. Three-dimensional joint angles were calculated and a wrist marker was used to calculate wrist velocity.

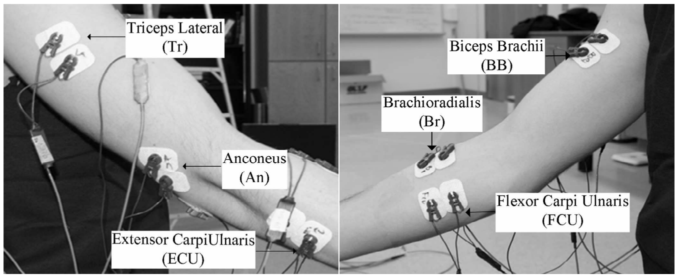

Figure 2: Placement of the EMG electrodes.

The average EMG and joint angles were calculated over four separate fall phases: i) start-release: PULARIS start to quick release; ii) release-impact: quick release to Fz impulse initiation; iii) impact-peak: Peak impulse initiation to peak Fz; and iv) peak-end: peak Fz to Fz cessation.

Three-way (2 fall height x 3 fall types x 2 sex) repeated measures ANOVAs, were performed on the force variables (peak, load rate, impulse) from the three force axes (Figure 1). Four-way (2 fall heights x 3 fall types x 2 sex x 4 fall phases) repeated measures ANOVAs were used to analyse the EMG and joint angle data. The reliability of PULARIS produced hip velocities and hand forces were assessed with Intra-class Correlation Coefficients (ICCs).

RESULTS AND DISCUSSION

Mean hip velocity and hand force ICCs of 0.72 and 0.70 were found respectively. The mean (SD) peak resultant wrist velocity was 1.5 (0.4) m/s, agreeing well with previously reported wrist velocities during catch trial falls [3]. A mean (SD) peak resultant impact force of 345 (18) N was recorded and peak Fx, as well as Fx and Fz load rate increased between 0.05 m and 0.10 m heights. With respect to fall type, the straight arm fall resulted in a significantly greater Fy impulse and Fy and Fz load rate.

Fall height, but not fall type, significantly affected wrist angle, resulting in a more extended posture during the 0.10 m (-22.9^{o}) compared to the 0.05 m falls (-19.5^{o}). Between release-impact and impact-peak, the change in elbow flexion angle was greater during the self-selected and bent-arm trials compared to the straight arm-falls; a pattern also seen in the wrist flexion/ extension angles. Therefore, it is likely that it was the change in joint angles over the duration of the impact that determined the magnitude and effect of the impact force variables.

Overall, Tr and ECU exhibited the highest mean (SD) peak muscle activation levels at 40.2 (21.9) % MVC, and 46.0 (18.8) % MVC, respectively. The majority of the muscles tested peaked before the peak force and the average EMG was significantly different between all fall phases for all muscles (Figure 3). This suggests that muscle activation begins to increase before the impulse onset; an indication of the muscle's preparation for impact.

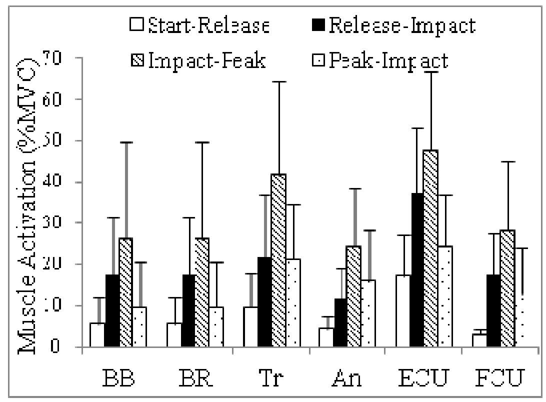

Figure 3: Muscle activity across the four impact phases for all muscles.

CONCLUSIONS

Overall, PULARIS is a reliable fall simulation method capable of producing accurate forward fall kinetics and kinematics. The results of this study suggest that, to some extent, individuals are capable of selecting an upper extremity posture that allows them to minimize the effects of an impact. This study has also confirmed the presence of a preparatory muscle activation response as a strategy in preparing for and reacting to a forward fall.

REFERENCES

1. DeGoede KM, et al. *J Biomech*, **35**, 843-848, 2002
2. Burkhart TA, et al. *J Biomech Eng*, in-press
3. Troy KL, et al. *Clin. Biomech*, **22**, 1088-1095

ACKNOWLEDGEMENTS

NSERC

PREDICTING DISTAL RADIUS BONE STRAINS AND INJURY IN RESPONSE TO IMPACTS TO FAILURE USING MULTI-AXIAL ACCELEROMETERS.

[1]Timothy A. Burkhart, [1]Cynthia E. Dunning, [2]David M. Andrews

[1]Western University, London, Ontario, Canada
[2]University of Windsor, Windsor, Ontario, Canada

INTRODUCTION

Measuring a bone's response to impact has traditionally been done using strain gauges that are attached directly to the bone. However, in addition to being invasive (*in vivo*), strain gauges are expensive, are generally used only once, and can be difficult to assemble and attach to the specimens being tested. While accelerometers are an attractive tool to overcome these limitations [1], little data are available relating measured accelerations to bone injury or surface strains. Therefore, the purpose of the current study was to determine the efficacy of multi-axial accelerometers for predicting injury to bone and assess the relationship between accelerations and bone surface strains.

METHODS

Eight (4 male; 5 left; mean (SD) age 61.0 (9.7) years) fresh-frozen human cadaveric radius specimens were potted to mimic the position of the radius during a forward fall and were loaded at incrementally increasing impact intensities using a custom built impact system [2,3]. The loading protocol consisted of an initial 20J impact followed by subsequent impacts of 10J increments until failure occurred; three specific impact events were noted: i) Pre-fracture (non-damaging impact 20J impact) ii) crack event (non-propagating damage) and; iii) fracture (propagating damage).

Compressive and tensile strain components were calculated from three strain gauge rosettes (two distal, one proximal). Two tri-axial accelerometers (one distal, one proximal) recorded the axial and off-axis accelerations (Figure 1).

Logistic generalized estimating equations (GEEs) were used to develop injury prediction models with strain and accelerations acting as the independent

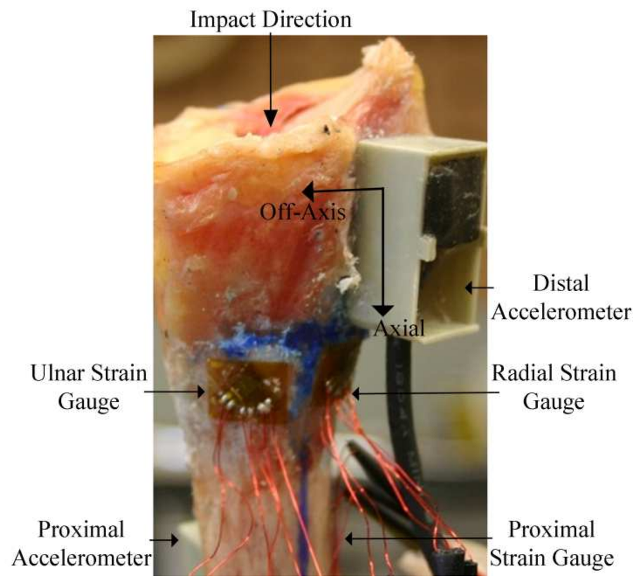

Figure 1: Locations of the strain gauges and accelerometers (including axes of interest).

variables, while linear GEEs were used to develop strain prediction models based on the axial and off-axis acceleration inputs (peak acceleration and acceleration rate). The logistic and linear models were assessed according to the R^2 and the Quasi-Likelihood under Independence model Criterion (QIC) value, such that smaller values represent better models, respectively.

Finally, shock propagation velocity was calculated based on the strain and acceleration data, separately. A 2x3 (2 velocity calculation methods x 3 impact events) repeated measures ANOVA was used to establish if significant mean differences existed between the propagation velocity calculation methods.

RESULTS AND DISCUSSION

A multi-variate acceleration model, specifically the combination of peak distal resultant acceleration and donor BMI was shown to provide the best prediction of bone fracture (Table 1). This is supportive of past work that has shown the risk of fracture to decrease with increasing BMI values [4].

Similar to the multi-variate acceleration models, the best injury prediction model, based on strain, was one that accounted for the combination of peak compressive strain and compressive strain rate at the ulnar gauge (Table 1). This model suggests that the gauge measurements are more equipped to predict the failure when it occurs in the vicinity of the gauge itself. The majority of the specimens failed at or near the ulnar side of the radius, coinciding with the site of the ulnar strain gauge; very little damage occurred at the radial gauge location.

Table 1: Summary of the acceleration- and strain-only injury prediction models.

Models	QIC	Intercept	β	p
Intercept-only	22.1			
Multi-variate Acceleration				
Distal Resultant	9.4	-9.4	-0.01	<0.01
BMI (kg/m^2)			-0.05	0.001
Multi-variate Strain				
Ulnar Gauge Compression	19.6	-2.4	-0.001	0.001
Ulnar Gauge Compression Rate			1.8E-7	0.04

Linear GEEs that contained peak axial and peak off-axis acceleration were found to provide the best estimate of the radial gauge compressive and tensile strains, respectively (Table 2). However, these accelerations were not good predictors of the strains measured from the ulnar gauge site. This suggests that the accelerations can only provide a reasonably good estimate of the strains at the site of the accelerometer, as the accelerometer was placed just distal to the radial gauge.

Table 2: Summary of the acceleration-based strain prediction models.

Model	Intercept	β	p	R^2
Radial Gauge Compression				
Peak Axial	-675.8	-9.6	<0.001	0.8
Radial Gauge Tension				
Peak Off-Axis	833.9	-3.9	0.01	0.7

The overall mean (SD) shock wave velocity decreased significantly from the pre-fracture (101.7 (62.3) m/s) to the fracture event (18.0 (9.2) m/s) (Figure 2) and this may indicate the presence of bone micro-fractures. However, no significant difference in the calculation of the shock propagation velocity between the two instrumentation methods was found (Figure 2).

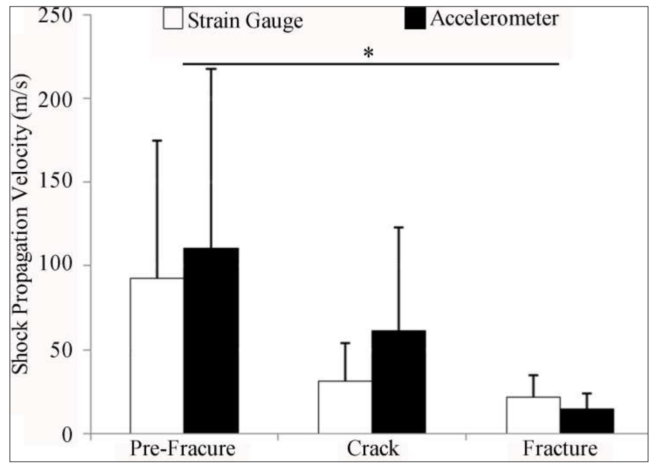

Figure 2: Comparison of shock propagation velocity calculated with the strain gauge and accelerometer data and across all impact events (*p<0.05).

CONCLUSIONS

This study suggests that accelerometers provide a reasonably good estimate of the bone surface strains traditionally measured with strain gauges. This is highlighted by the strong relationship between strains and accelerations and the similarity in the calculation of shock propagation velocity using both methods. However, accelerometers should only be used to infer the response of bone in the direct vicinity of the accelerometer.

REFERENCES

1. Burkhart TA, et al. *J Appl Biomech* **26**, 281-289.
2. Burkhart TA, et al. *J Biomech* **44**, 2725-2755.
3.Quenneville CE, et al. *J Biomech Eng* **132**, 1-4.
4. DeLaet C, et al. *Osteo Int* **16**, 1330-1338.

AKNOWLEDGEMENTS

NSERC, CSB travel award, University of Windsor, Western University.

A COMPARISON OF THE EFFECT OF FOAM-BOX CASTED AND PLASTER-CASTED ORTHOTICS ON THE NORMAL FOOT POPULATION USING BI-PLANAR X-RAY FLUOROSCOPY

[1,2]Kristen M. Bushey, [1,2]Megan E.R. Balsdon, [3]Colin Dombroski, [1,2]Thomas R. Jenkyn
[1]Wolf Orthopeadic Biomechanics Laboratory, Fowler Kennedy Sport Medicine Clinic, London, ON, Canada
[2]The University of Western Ontario, London, ON, Canada
[3]SoleScience, Fowler Kennedy Sport Medicine Clinic, London, ON, Canada
email: tjenkyn@uwo.ca web: http://www.eng.uwo.ca/people/tjenkyn/

INTRODUCTION

Orthotics are frequently prescribed for the conservative treatment of musculoskeletal disorders of the foot and ankle such as pes cavus or pes planus. Pes cavus is defined as having a high arch whereas pes planus is defined as having a low arch in the foot. The normal population is considered to have an arch in between pes cavus and pes planus. Orthotics are thought to alter the motion of the bones of the foot by applying constraint or support to various structures on the plantar surface.

Two commonly used techniques for casting the foot for an orthotic include: plaster wrap and foam box. The foam box technique has the practitioner guide the patient's foot into a foam tray that takes a negative impression of the foot while in the subtalar neutral position [1]. The plaster casting technique requires the patient lie prone in a figure four position during the process. A negative impression of the foot is taken while being locked in the subtalar neutral position [1]. While plaster casting has historically been the standard method, foam box has increased in popularity

Bi-planar x-ray fluoroscopy has been demonstrated to be a feasible method for measuring foot bone motions during in-vivo weight bearing gait [2]. To the authors' knowledge, a three-dimensional (3D) bi-planar x-ray fluoroscopy study of the foot during orthotic use in the normal population has not yet been done. Bi-planar x-ray fluoroscopy is used to compare the motion of the calcaneus in 3D to determine overall pronation of the foot during gait. Pronation is defined as the combination of external rotation, dorsi-flexion, and eversion. Five conditions were tested: barefoot, soft and rigid foam box orthotics, and soft and rigid plaster casted orthotic. It was hypothesized that the greatest pronation would occur during barefoot walking and the least during the rigid orthotic conditions. It was also hypothesized that there would be no statistical difference in the foam box and plaster casted orthotics ability in reducing foot pronation.

METHODS

Six (6) volunteers with normal arches were fitted with four pairs of custom-made orthotics by the same Canadian Certified Pedorthist using the foam box and the plaster casting technique. The orthotics were made with both a 4mm plastazote (soft) and 3mm RCH-500 (rigid) material as per usual clinical practice. Each volunteer walked along a custom-made wooden platform that raised their feet to the height of the two fluoroscopy units (SIREMOBIL; Compact-L; Siemens, Malvern, PA). On the platform each volunteer was able to walk normally and fully weight bearing past the fluoroscopes. The left foot was imaged during stance phase from an oblique, dorsal-medial to plantar-lateral view while simultaneously imaged from a sagittal plane view.

Each volunteer was instructed to walk along the platform at their preferred pace while the fluoroscopes recorded the images simultaneously at 30 frames per second. Each trial condition was repeated twice, ensuring that the entire hindfoot and tarsus were visible at all times. Five conditions were tested in a randomized order: 1) barefoot, 2) soft foam box orthotic, 3) rigid foam box orthotic, 4) soft plaster casted orthotic, 5) rigid plaster casted orthotic. The four custom-made orthotics were constructed with a deep heel cup intended to limit the pronation of the calcaneus during stance. Each volunteer had a computer tomography (CT) scan completed on their left foot.

The fluoroscope images were digitized on the control PC and stored as a tiff format. Each frame was post-processed using custom-written software

(MATLAB; Mathworks Inc., Natick, MA). A calibration algorithm allowed the experimental set-up to be recreated in the virtual environment (Rhinoceros; Robert McNeel & Associates, Seattle WA, USA). Using the CT image the calcaneus, tibia and fibula were segmented and bony landmarks were identified and marked (OsiriX; Advanced Open-Source PACS Workstation DICOM Viewer, Antoine Rosset, USA). The individual bone coordinate systems for the calcaneus and tibia/fibula (Fig. 1) were based on the International Society of Biomechanics standard. The change in pronation can then be determined during each condition using the barefoot (control) condition as the baseline value [3]. Using custom-written software internal rotation, plantar-flexion, and inversion angles were calculated. The bones involved in this calculation were the calcaneus, tibia, and fibula.

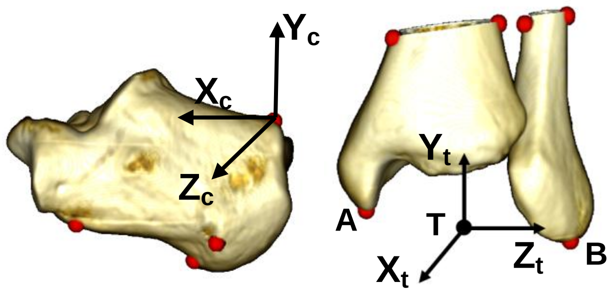

Figure 1: Calcaneus (left) and Tibia/Fibula (right) bone coordinate systems. The origin of the tibia/fibula is the midpoint of A and B.

Each data set was evaluated for statistical significance using an ANOVA repeated measures test using SPSS (SPSS; IBM Corp., Armonk, NY).

RESULTS AND DISCUSSION

The effect of the foam hard/soft orthotic as well as the plaster hard/soft orthotic is summarized in table 1. Both orthotic types show a significant change in alignment with $p<0.05$ in the ANOVA two repeated measures test. This means that these variables should follow a normal distribution pattern where 99.5% of all cases will fall within two standard deviations (SD) [4].

When the effect of the foam casted orthotics was analyzed it is evident that a reduction in pronation occurs. However, the internal rotation measurement for the foam hard orthotic is not statistically significant. A reduction in pronation was also evident in the plaster casted orthotics. However the change associated with the plantar-flexion angle does not have statistical significance in the plaster hard orthotic.

A comparison of the foam rigid and the plaster rigid showed there was no statistical difference with the change in pronation between the casting method. A comparison of the foam soft and plaster soft showed there was no statistical difference between the casting methods when measuring the change in pronation. The statistical analysis is to be revisited when all potential patients have been fully analyzed to ensure the model is as accurate as possible.

CONCLUSIONS

The results indicate orthotics reduce calcaneal pronation as the foot is in mid-stance during gait. The method of casting and material chosen does not change the amount of pronation by a statistically significant value.

REFERENCES

1. Laughton, C, et al., *J Am Pod Med As.* ***92****, 261-268.*
2. Kedgley, AE, et al. *J Biomech* **42**, 1350-1354, 2009.
3. Wu,G., et al., *J Biomech* **35**, 543-548.
4. Norman, G.R., et al., PDQ Statistics (3rd ed.) 5-52.

Table 1: Change in the internal/external rotation, plantar-flexion/dorsi-flexion, and inversion/eversion angle by comparison to the barefoot (control) condition. All entries in degrees.

Condition	Internal Rotation	Plantar-flexion	Inversion
Foam Hard	3.20±3.71	36.85±6.29	17.07±6.80
Foam Soft	7.56±2.31	23.54±5.80	17.57±7.34
Plaster Hard	4.54±1.48	7.45±11.6	8.74±6.06
Plaster Soft	1.70±1.51	14.17±6.65	5.76±4.07

Note: A negative value represents the opposite motion (i.e. negative inversion would mean the foot is actually experiencing eversion).

SENSORY REWEIGHTING DURING POSTURAL CONTROL IN ADULTS WITH DIFFERENT SPORT EXPERTISE: A PILOT STUDY

[1]Albert Busquets, [2]Silvia Aranda, [1]Michel Marina, and [1, 3]Rosa Angulo-Barroso

[1]INEFC, National Institute of Physical Education, University of Barcelona, Spain
[2]EUSES, School of Health and Sport, University of Girona, Spain
[3]Center for Human Growth and Development, University of Michigan, MI, USA
email: albert.busquets@inefc.net

INTRODUCTION

Individual control of posture requires an adequate fit between the information from sensory inputs (i.e. perception) and neuromuscular responses (i.e. action) [1,2,3]. The relative contribution of sensory information, originating from visual, proprioceptive, and vestibular system, is dynamically adjusted to changes in environmental, organismic or task conditions [4,5,6]. Regarding changes in environmental constraints, differences in the capability to reweight sensory information can be observed when individuals are exposed in the same trial to different sensory conditions (for example, an initial period of no-manipulation preceding a sensory manipulation period and finishing with a no-manipulation period). In relation to the organismic constraints, the accumulation of expertise capabilities [7,8] could also impact postural control. Expertise capabilities are usually defined by the amount of practice [9]. Gymnastics has been extensively studied in relation to postural control due to this sport's high balance requirement to perform complex acrobatics and to restore equilibrium after their completion. Authors [10,11,12] suggested that high-level gymnastics can improve the capability of reweighting sensory information. It would be interesting to know whether gymnastic practice could produce enhanced attributes relevant to postural control compared to ball-based sports such as soccer, softball and rugby. The main goal of this study was to investigate the reweighting processes to adjust standing posture when proprioception and vision were altered in adults with different sport expertise.

METHODS

All subjects participated in sports activities without any high competitive objective. Gymnastics skill level was used to divide participants in: low-level-gymnasts (LG, n=5, 22.2±6.3 years), they were enrolled in regional gymnastic competitions and non-gymnasts (NG, n=5, 17.9±4.1 years), who were engaged in different regional sport competitions such as rugby, soccer or softball. Participants were 14.5 years old or older given that several studies suggested an adult-like balance performance from age 12 [13]. Two identical vibrators were securely strapped to the lower legs just above the center of the ankle joint. Following Tjernström, Oredsson, and Magnusson [14], the center of each vibrator was placed over the Achilles tendon, 85Hz vibration frequency with 1mm of amplitude was applied. Participants were asked to stand with both feet on a force plate (Kistler 9286AA, Switzerland). The position of both feet was marked to maintain similar position and support area across trials. This support area was calculated for each participant and used to normalize postural control variables. The testing session consisted in two blocks (eyes open, EO, and eyes closed, EC) of three 45 s trials. The order of the 6 trials was randomized across subjects. During the trials participant were required to stay in quiet stance during 15 consecutive seconds without vibration (pre-vibration period, 1-15 s), 10 s with vibration (vibration period, 16-25 s), and 20 s without vibration (post-vibration period, 26-45 s) (Figure 1). Rest intervals of 3 minutes were given between the blocks and trials because vibration of tendons can have long after effects on postural stabilization [15]. The force plate signals of each trial were sampled at 500 Hz and filtered using a Butterworth Low-pass fourth order recursive filter [16] with a cut-off frequency set at 10Hz. Filtered data were used to assess displacement of the COP in anterior-posterior (AP) direction separately for each period of the trial (pre-vibration, vibration, and post-vibration). The AP sway of the COP was normalized by the support area. In order to characterize COP, we computed the following variables using custom software developed in Matlab version 7.01 (Mathworks R14): (1) trajectory (Traj); (2) mean velocity (Vel); (3) standard deviation (SD); (4) maximum distance (maxDis); and (5) peak velocity (pVel). To assess differences in reweighting processes when proprioception is altered in relation to gymnastics skill level, we used 2 (Group) x 2 (Condition) x 3 (Period) ANOVAs in which group (NG and LG) was between factor while condition (EO and EC) and period (pre-vibration, vibration, and post-vibration) were within participant factors. Tukey multiple comparison post hocs were used for establishing differences between groups. P values were adjusted using Bonferroni's method when appropriate and statistical significance was set at $p<.05$ level. All tests were performed with SPSS 13.

RESULTS AND DISCUSSION

Results of this study showed that balance and reweighting processes of both groups, the non-gymnasts (NG) and low-level-gymnasts (LG), were similar (Table 1). Amount of practice and skill level could modify organismic constraints [9,17]. High skill level produce enhanced physical, perceptual, and physiological attributes than lower skill level [18,19,20,21]. It was suggested that differences in postural control might be effected by the level at which the sport is trained [22]. In fact, other studies conducted with high-level-gymnasts [11,12] found a better ability to adapt postural control in gymnasts. However, in adults, the low-level performing gymnastics seemed not to produce enhanced in postural control than other ball-based sports practiced at similar level. Given the small sample, these results should be taken with caution. Future studies should increase the sample and include high-level performance gymnasts

ANOVAs yielded significant Condition x Period interactions for standard deviation and maximum distance of the sway (Table 1). Interestingly, eyes open and eyes closed sowed no differences in the pre-vibration period while differences existed during the vibration and post-vibration periods. To examine whether low level sport practice minimizes the contribution of vision during quiet standing tasks without vibration, future studies should include a control group without sport practice experience. Values of all balance sway variables (trajectory, mean velocity, standard deviation, maximum distance, and peak of velocity) during the vibration period increased compared to pre-vibration period. Similarly, participants could not decrease these values to initial level during the post-vibration period (Table 1). One may think that proprioceptive re-weighting to control balance may not be completed in 20 seconds. In addition, variables selected to characterize the COP displacement may be were gross to detect the reweighting process accurately. Trajectory, distance, velocities, and standard deviation were calculated over the entire post-vibration period. Future studies should partition this period to extract the sway response after termination of vibration effects.

REFERENCES

1. Hatzitaki V. et al. *Journal of Motor Behavior,* **34**, 161-170. 2002
2. Nourrit D. et al. *Journal of Sports Sciences,* **18**, 201-212. 2000
3. Walter C. et al. *Research Quarterly for Exercise and Sport,* **69**, 326-333.1998
4. Jeka J. et al. *Experimental Brain Research,* **134**, 107-125. 2000
5. King BR. et al. *Journal of Neurophysiology,* **101**, 315-322. 2009
6. Peterka RJ. et al. *Journal of Neurophysiology,* **91**, 410-423. 2004
7. Gautier G. et al. *Human Movement Science,* **28**, 129-140. 2009
8. Marin L. et al. *Journal of Sports Sciences,* **17**, 615-626. 1999
9. Paillard T. et al. *British Journal of Sports Medicine,* **36**, 304-305. 2002
10. Gautier G. et al. *Journal of Motor Behavior,* **40**, 400-408. 2008
11. Gautier G. et al. *Gait & Posture,* **28**, 46-51. 2008
12. Vuillerme N. et al. *Neuroscience Letters,* **311**, 73-76. 2001

13. Peterson ML. et al. *Gait & Posture, 23*(4), 455-463. 2006
14. Tjernstrom F. et al. *Journal of Vestibular Research,* **16**, 257-264. 2006
15. Wierzbicka MM. et al. *Journal of Neurophysiology,* **79**, 143-150. 1998
16. Winter DA. et al. *Biomechanics and motor control of human movement*. John Wiley and Sons. 1990
17. Lamoth CJ. et al. *Gait & Posture,* **29**, 546-551. 2009
18. Gabbett T. et al. *Journal of Strength and Conditioning Research*, **21**, 902-908. 2007
19. Milton J. et al. *Neuroimage,* **35**, 804-813. 2007
20. Sbriccoli P. et al. *European Journal of Applied Physiology*, **108**, 1269-1280. 2010
21. Williams AM. et al. *Journal of Motor Behavior,* **34**, 197-207. 2002
22. Asseman FB. et al. *Gait & Posture*, **27**, 76-81. 2008

ACKNOWLEDGEMENTS

We would thank to *Maxon Motor Iberica, S.A.* and *Sabater Grup* for their technological support.

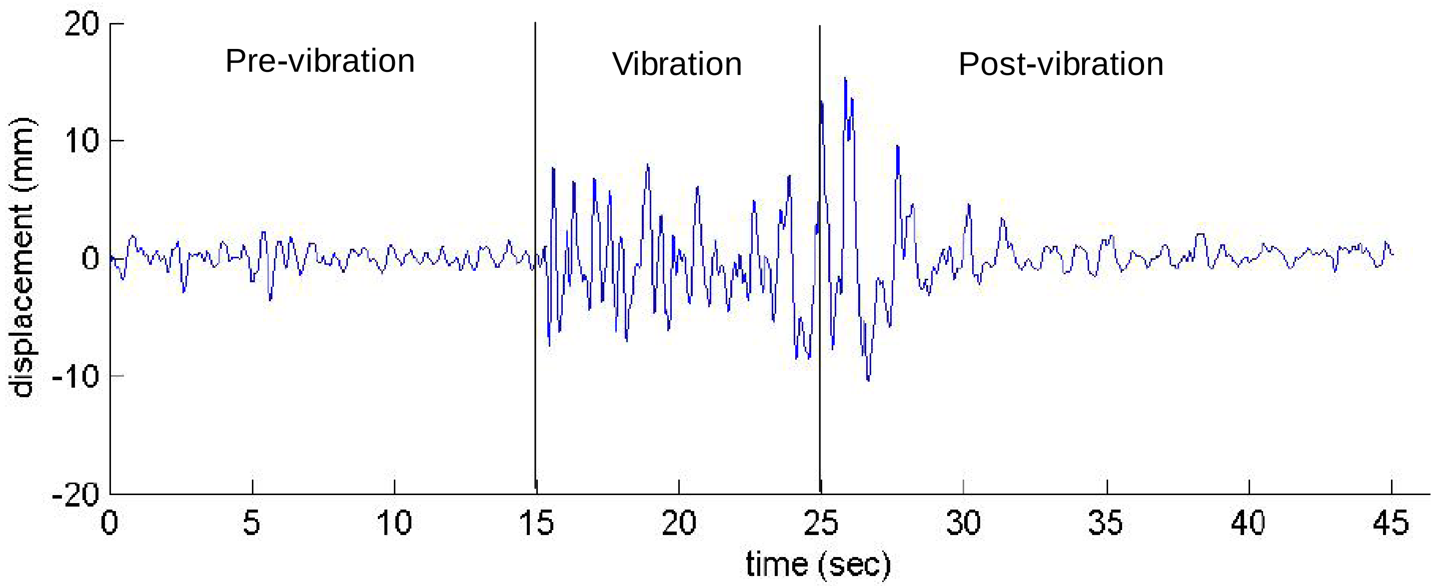

Figure 1: Example of the COP displacement in the anterior-posterior axis (AP) during one trial with eyes closed. In addition, pre-vibration, vibration, and post-vibration periods are drawn.

Table 1. Significant results of two (Group) x two (Condition) x three (Period) ANOVA with repeated measures.

Variable name	Main effects and interaction	F	Degrees of freedom	p	Partial η^2	Power	Post-hocs
Trajectory	Condition	20.78	1,8	.002	.722	.98	EO < EC
	Period	39.86	2,7	.000	.833	1.00	pre-vibr < post-vibr < vibration
Mean velocity	Condition	22.93	1,8	.001	.741	.99	EO < EC
	Period	38.94	2,7	.000	.830	1.00	pre-vibr < post-vibr < vibration
Standard deviation	ConditionxPeriod	6.86	2,7	.007	.461	.86	Vibration period: EO < EC Post-vibr: EO < EC EO: pre-vibr < vibration & post-vibr EC: pre-vibr < vibration & post-vibr
	Condition	63.32	1,8	.000	.888	1.00	EO < EC
	Period	52.85	2,7	.000	.938	1.00	pre-vibr < vibration & post-vibr
Maximum distance	ConditionxPeriod	4.59	2,7	.027	.365	.69	Vibration period: EO < EC Post-vibr: EO < EC EO: pre-vibr < vibration & post-vibr EC: pre-vibr < vibration & post-vibr
	Condition	40.32	1,8	.000	.834	1.00	EO < EC
	Period	22.46	2,7	.000	.737	1.00	pre-vibr < vibration & post-vibr
Peak velocity	Condition	7.03	1,8	.029	.468	.64	EO < EC
	Period	27.36	2,7	.000	.946	1.00	pre-vibr < vibration & post-vibr

Pre-vibr: pre-vibration period, post-vibr: post- vibration period; EO: eyes open; EC: eyes closed

QUANTIFYING INCREASED SKILL USING MEASURED BICYCLE KINEMATICS AS RIDERS LEARN TO RIDE BICYCLES

Stephen M. Cain, Dale A. Ulrich and Noel C. Perkins

University of Michigan, Ann Arbor, MI, USA
email: smcain@umich.edu

INTRODUCTION

Currently, it is difficult to determine when a novice bicycle rider is ready to ride without training wheels or external assistance. The basic strategy required to keep a bicycle upright, steering into the lean, has been utilized to stabilize bicycle models [1] and robot bicycles. Bicycles that are self-stable demonstrate the ability to steer into the lean automatically [2]. During successful riding, changes in the steer angle lag changes in the roll angle and are highly correlated; cross-correlation can be used to quantify this relationship [3]. We hypothesized that as a rider learned to ride a bicycle the peak cross-correlation between steer and roll angular velocities would increase, indicating that the rider is internalizing the critical relationship between steer and roll.

METHODS

We measured kinematics of the bicycles ridden by 10 participants as they progressed through a bicycle training camp provided by Lose the Training Wheels (www.losethetrainingwheels.org). The camp spans 5 consecutive days with individual instruction for 75 minutes per day. Children enter the camp without the ability to ride a bicycle and either learn to ride a bicycle or make significant progress towards riding a bicycle by the end of the camp. The subjects had a range of disabilities including Down syndrome (n = 3), autism spectrum disorder (n = 5), cerebral palsy (n = 1), and attention deficit hyperactivity disorder (n = 1). The training camp utilizes adapted bicycles with crowned rollers in place of the rear wheel (Fig. 1A). Unlike training wheels, the crowned rollers allow the bicycles to roll/lean similar to traditional bicycles. As a rider demonstrates improvement, the bicycle is altered by increasing the gearing or by changing to a more crowned roller that accentuates bicycle tipping (Fig. 1B). All riders, regardless of skill, are moved onto a traditional bicycle on the last day of the camp. Handles attached to the rear of the bicycle allow trainers to assist riders as needed. A detailed description of the camp training protocol can be found in [4]. Out of 10 subjects, 6 learned to ride a traditional bicycle without assistance.

Figure 1: (A) The adapted bicycles used by Lose the Training Wheels utilize crowned rollers in place of a rear wheel. (B) The most crowned roller (bottom) accentuates bicycle tipping.

We employed three synchronized wireless inertial measurement units (IMUs) to measure bicycle kinematics during each session for each rider. Each IMU includes a 3-axis accelerometer and a 3-axis angular rate gyro. A frame mounted IMU allows us to resolve the roll, yaw, and pitch rates of the bicycle frame, a stem mounted IMU allows us to resolve the steering rate, and a wheel mounted IMU allows us to calculate bicycle speed and the pedaling cadence of the rider. Our goal was to disrupt the training session as little as possible and therefore no special instruction or explanations were given to the riders.

For each trial, we calculated the average speed, standard deviations of steer and roll angular velocities and normalized cross-correlation [5] between steer and roll angular velocities. We assessed differences between groups using paired t-tests (α = 0.05). To evaluate the change of a variable with time, we calculated the slope of the linear least-squares fit to the variable versus time and performed a two-tailed t-test to detect slopes significantly different from zero (α = 0.05).

RESULTS AND DISCUSSION

The peak cross-correlation between steer and roll angular velocities (Fig. 2) increased significantly with time ($t = 5.944$, $p < 0.001$) and was significantly greater for riders who ultimately succeeded in riding a traditional bike without assistance ($t = 3.567$, $p = 0.009$). This finding suggests that rider learning is quantified by increased correlation between bicycle steer rate and roll rate. In essence, learning to steer in the direction of lean is an essential skill in learning to ride a bicycle.

The peak cross-correlations did not increase similarly for all riders, suggesting that the adapted bicycles are an effective balance training tool for some riders (e.g. subjects A and B) but are not effective for other riders (e.g. subjects C, D, and J). However, learning to balance a bicycle is only one part of learning to ride. Riders must also learn how to get on a bicycle, how to start pedaling/riding, how to avoid obstacles, and how to stop safely, among other skills. The benefit of adapted bicycles and other training aids are that they allow riders to become familiar with the controls of a bicycle and the attention and physical demands that riding a bicycle requires.

Average speed increased with time ($t = 4.591$, $p = 0.001$) and the standard deviation of the roll rate increased with time ($t = 3.864$, $p = 0.004$), likely due to the increased gearing and more crowned rollers used as a rider progresses through the camp. The standard deviation of the steer rate also increased with time ($t = 2.690$, $p = 0.025$), suggesting that initially fearful riders learn to relax their arms and use the handlebars to control and balance the bicycles.

CONCLUSIONS

By employing three synchronized wireless IMUs, we measured bicycle kinematics of riders during a bicycle training camp to quantify the changes that occur as riders learn to ride traditional bicycles. We found that riders learn to steer in the direction of the lean, an essential skill in learning to ride a bicycle. This acquired skill was quantified by computing the peak cross-correlation between steer and roll angular velocities. Our methodology could be used to evaluate the effectiveness of existing training techniques and to help evaluate or to develop new methods for teaching novice riders.

REFERENCES

1. Schwab AL, et al. *Proceedings of 4ECSC*, St. Petersburg, Russia, 2008.
2. Kooijman JDG, et al. *Science* **332**, 339-342, 2011.
3. Doyle AJR. PhD Thesis, University of Sheffield, 1987.
4. Ulrich DA, et al. *Physical Therapy* **91**, 1463-1477, 2011.
5. Sheridan TB and WR Ferrell, *Man-Machine Systems*, The MIT Press, 1974.

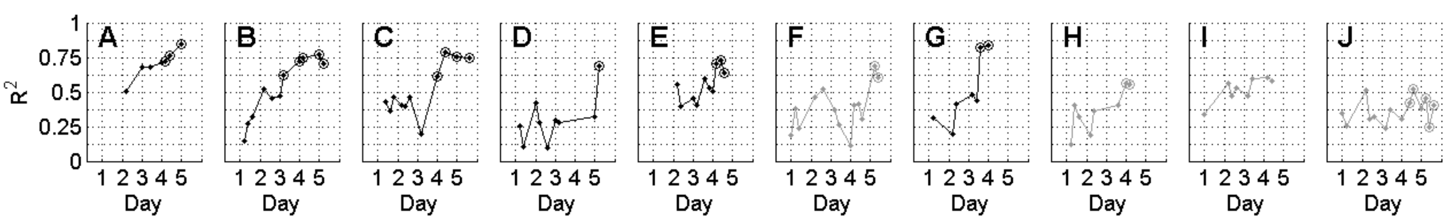

Figure 2: Peak cross-correlation between steer and roll angular velocities squared (R^2) for individual riders (labeled A-J) are plotted versus days in training. Data for riders that learned to ride a traditional bicycle unassisted are plotted in black (n = 6), whereas riders who did not are plotted in gray (n = 4). Trials on adapted bicycles are plotted as dots, whereas trials on traditional bicycles are plotted as circles. The peak cross-correlation increased time ($t = 5.944$, $p < 0.001$) and was greater for riders who ultimately succeeded in riding a traditional bicycle without assistance ($t = 3.567$, $p = 0.009$).

OPTICALLY BASED INDENTATION FOR BRAIN TISSUE: A NEW HISTOLOGICAL APPROACH

Saranya Canchi, Yu Hong, Sung Jin Lee, Malisa Sarntinoranont, Ghatu Subhash and Michael A. King

University of Florida, Gainesville, FL, USA
email: canchisaranya@ufl.edu

INTRODUCTION

Bulk mechanical properties of brain tissue are important to predict and understand reaction to injury or diseases. Change in local mechanical properties can also be an indicator of disease pathology. Indentation is a popular method for measuring the biomechanical properties of soft tissue. Indentation combined with the deep tissue imaging capability of optical coherence tomography (OCT) makes an efficient system to study mechanics of soft tissue [1]. This system offers unique advantages of real time imaging and high resolution. A schematic of the OCT – indentation system is shown in Figure 1.

Microglia activation within the brain leads to changes in morphology [2].This change in morphology can be an indicator of effects of mechanical stresses or strains on brain tissue. As the percentage of the microglia cells is small in the brain (20%) a new histological protocol is being developed to study changes in microglia morphology under varying mechanical influences. Along with microglia, astrocytes, which are most abundant type of glial cells in brain, will also be assayed to study their injury response. The staining procedure is combined with a clearing technique to obtain fluorescent optically clear samples for confocal imaging [3].

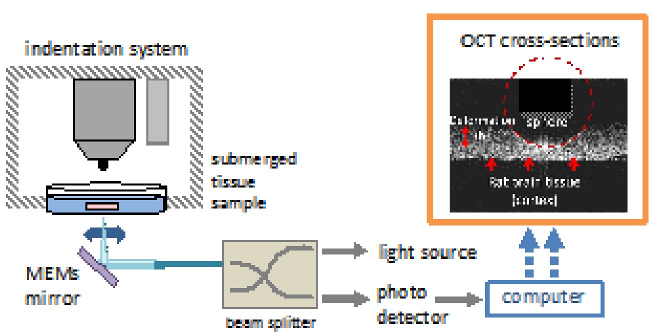

Figure 1: Schematic of indentation system with the optical coherence imaging system. Through thickness scans will be used to reconstruct indentation profiles and track deformation of internal structures (fibers & tissue interfaces).

METHODS

The brain tissue samples were obtained from adult Sprague Dawley rats. The rats were anesthetized by isoflurane and euthanized. The surgery was compliant with the NIH guidelines of animal use and regulations of the Animal Care and Use Committee of University of Florida. The excised brain was sliced using a Vibratome (Leica VT 1000A, Leica Microsystems Inc., Germany). The slices were divided into two groups (control and indented) and submerged in oxygenated aCSF. One solution with 2μM Texas red hydrazide and another with 1μM acetylated-low density lipoprotein (Ac-LDL) were prepared. After 30 minutes the slices are transferred to fresh aCSF. The slices were kept alive using a perfusion chamber for the duration of the experiment.

The tissue slices were mechanically tested using spherical indenter and visualized in real time using the OCT system [1]. Creep under constant loading of spherical beads was measured.Continuous OCT imaging provides cross-sectional images of slices with a fixed field of view during mechanical testing. Top and bottom surfaces of slices as well as internal boundaries and structures are observed.

The tissue slices were fixed after testing in 4% paraformaldehyde and DAPI stained. Optical clearing of the fixed tissue is carried out using a solution of 1:2 benzyl alcohol: benzyl benzoate (BABB). The tissue slices were dehydrated using graded methanol series of 50%, 70%, 95% and 100%. This procedure was followed by soaking in 1:1 methanol: BABB solution followed by soaking in pure BABB. All steps in clearing the tissue were carried out at room temperature. The optically cleared tissue samples are then imaged using confocal microscope to obtain a through thickness stack of the tissue slice images.

RESULTS AND DISCUSSION

Data from the OCT-indentation system provides displacement vs. time curves under constant loading. This information is used to compute the local viscoelastic material properties. The equilibrium shear modulus of the tissue is computed which is an indication of the bulk material stiffness. The time-dependent and spatially-varying mechanical properties provide insight into structural interactions with brain tissues.

Staining assays are being developed to study the effect of mechanical loading on individual glial cells in the brain. The symbiotic injury response of microglia and astrocytes will be studied with indentation. The staining protocol will also be tested for its sensitivity to detect change in morphology of the glial cells with loading. Figure 2 shows clusters of astrocytes in the dentate gyrus region of the hippocampus from an adult rat brain. Figure 3 shows inactive microglia from a control test slice(no indentation). In a previous study by our group, fluoroJade C and DAPI assays were used to quantify the percentage of degenerating neurons. Changes in percentage degeneration with time after slicing has been determined [4]. This method for quantifying degenerating neurons will be used in conjunction with microglia and astrocyte staining**.**

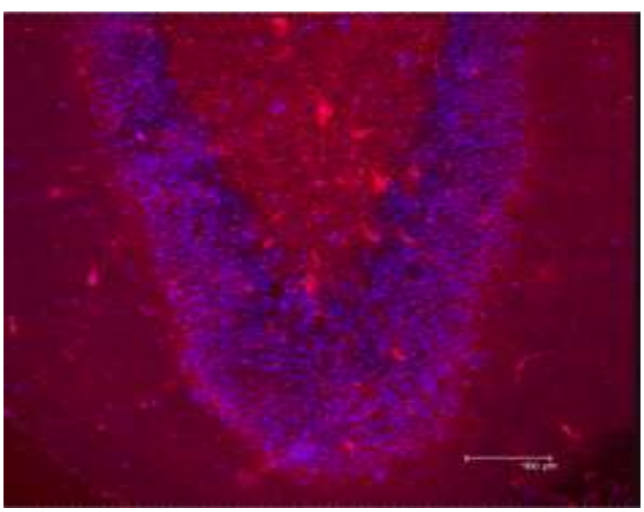

Figure 2: Confocal composite image of DAPI and Texas red hydrazide staining of dente gyrus in adult rat.

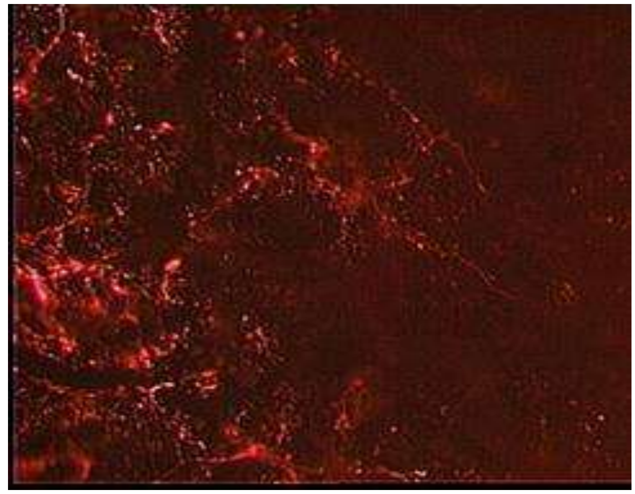

Figure 3: Ac-LDL stained brain tissue slice depicting features of an individual microglia cell.

CONCLUSIONS

An OCT based indentation system for measuring local and bulk mechanical properties of tissue has been established. A histological protocol to quantify the changes in cell morphology with mechanical force is being developed and will be calibrated against undeformed tissue slices subjected to the same environmental conditions. This system will also be used to measure properties of tissue slices subjected to high strain rate loading as part of ongoing mechanical testing.

REFERENCES

1. S J Lee et al., **“**Optically based-indentation technique for acute rat brain tissue slices and thin biomaterials”, J. Biomedical materials research, Part B, Applied biomaterials, 97(1), 84-95, 2011.
2. Perry HV et al, “Microglia in neurodegenerative disease”, *Nature Reviews Neurology 6,*193-201, 2010.
3. Sonia G. Parra et al., "Multiphoton microscopy of cleared mouse organs", J. Biomed. Opt. 15, 2010
4. Malisa Sarntinoranont et al., “ High-strain-rate brain injury model using submerged acute rat brain tissue slices”. Journal of neurotrauma 9(2), 418-29, 2012.

AN EXTERNALLY POWERED AND CONTROLLED ANKLE-FOOT PROSTHESIS FOR USE IN PUSH-OFF EXPERIMENTS

Joshua M. Caputo and Steven H. Collins
Carnegie Mellon University, Pittsburgh, PA, USA
email: jmcaputo@andrew.cmu.edu, web: http://biomechatronics.cit.cmu.edu

INTRODUCTION

Over 1/2 a million Americans are currently affected by major lower limb amputation [1]. Due to the lack of muscle tissue and the limitations of currently available prostheses [2], people suffering from unilateral transtibial amputation experience a 20% increase in metabolic energy expenditure during normal walking [3]. As a result of this and other mobility challenges, these amputees experience a decrease in quality of life [4]. A prosthesis which replaces the lost net positive work of the ankle joint can help reduce energy consumption [5]. Currently this mobility challenge is being addressed through the development of mobile prostheses. This design process faces many challenges as the objective to provide useful powered ankle push-off is at odds with the constraints of mobility. The limitations of current actuator and energy storage technologies are unavoidable, while packaging and weight further constrain designs. Thus, it is difficult to make maximally beneficial design decisions through methods other than trial and error. Thus, the development process is costly, time-consuming and results in devices that cannot guarantee optimal performance. In order to better understand the important design parameters, it is necessary to measure their effect on performance through controlled experiments. To this end, we propose the use of a tethered prosthesis, which avoids the mobility design challenges by offloading the actuator and controller to a workbench which run from wall power. This device is thus capable of implementing a variety of ankle control strategies which can be systematically studied in parameter sweeps. For instance, the device could be used to determine the relationship between push-off work and metabolic energy consumption during walking, providing useful information to the designers of future mobile devices.

METHODS

Testbed Design: We developed an experimental prosthesis testbed (Fig. 1) which provides powered ankle push-off work to subjects walking on a treadmill. The prosthesis (Fig. 2) is powered and controlled by a 1.61 kW servomotor (Baldor Electric Co.) and real-time controller (DS1103, dSPACE Inc.). The single degree of freedom prosthesis attaches to the amputee's residual limb and is actuated via a flexible Bowden-cable transmission by the motor using a series-elastic torque control scheme.

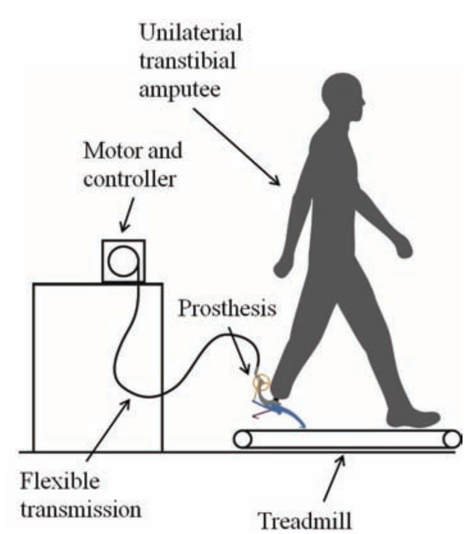

Figure 1: Schematic of the experimental testbed.

Testbed Evaluation: In order to measure the torque-control bandwidth of the system, benchtop tests were conducted. This was done by fixing the adapter and the toe segment and commanding a sinusoidally varying torque. In order to determine the system's torque tracking ability during experimental conditions, walking tests were conducted at 1.25 m/s with an able-bodied subject wearing the prosthesis via a simulator boot. Torque commands were generated by a desired torque relationship of the form: $\tau = k\theta + C_w W_n \text{sign}(\omega)$, where W_n is selected such that $C_w = 1$ corresponds to the push-off work seen during normal walking for an average able-bodied adult male. Tests were conducted using a variety of C_w values.

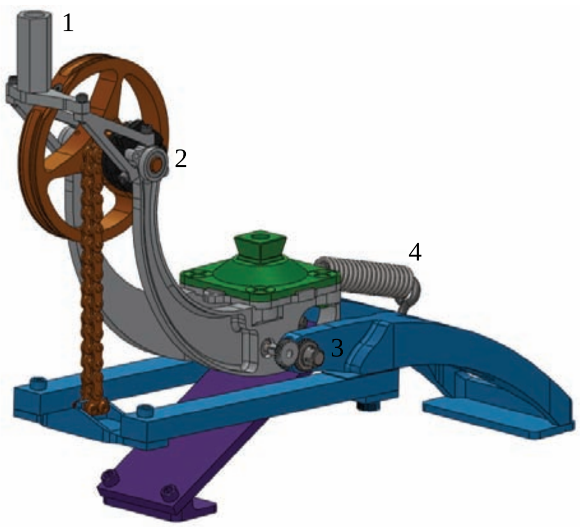

Figure 2: CAD model of the prosthesis. The transmission attaches at 1, where the inner cable continues to the pulley/sprocket and roller chain (orange). This pulls on series leaf springs (blue), thus rotating the toe segment about the ankle joint (3). Encoders at 2 and 3 measure spring deflection (in turn torque through a calibration procedure). A heel spring (purple) cushions impact at heel strike. An extension spring at 4 lifts toe during swing. A standard prosthesis attachment appears in green.

RESULTS AND DISCUSSION

The lightweight (1kg) prosthesis (Fig. 3) can provide up to 232 Nm of push-off torque and a range of motion of 14 degrees dorsiflexion to 29 degrees plantarflexion. These specifications were selected to be 150% of those exhibited by able-bodied subjects during normal walking and are limited only by motor, controller, and transmission selection and the structure of the prosthesis.

Benchtop tests revealed the -3dB gain bandwidth to be 11.6 Hz for a 75Nm sinusoidal torque input. Walking tests demonstrated the ability of the system to track the desired ankle torque-angle relationship and provide systematically varied quantities of push-off work (Fig. 4).

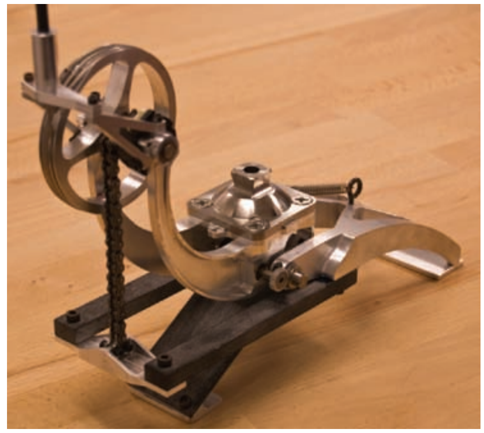

Figure 3: photograph of prosthesis prototype.

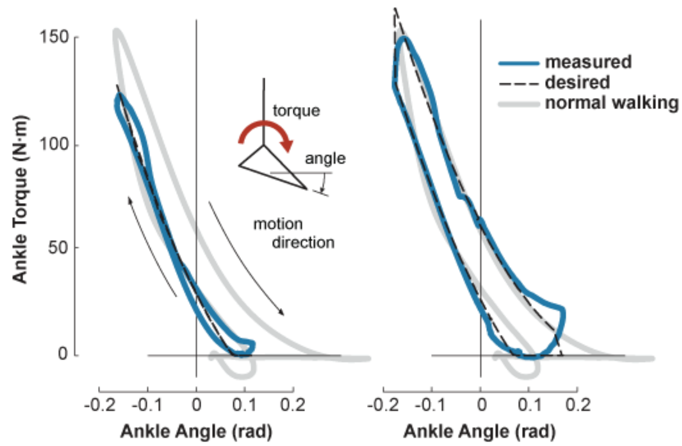

Figure 4: Results from walking tests. Data depicted is representative of an average step over the course of the trial. Two value of push-off work are shown, $C_w = 0$ on the left and $C_w = 1$ on the right.

We will conduct a full experiment with amputee subjects in order to determine the relationship between ankle push-off work and metabolic energy consumption. We will select a breadth of conditions which allow us to determine the limits of assistance for unilateral transtibial amputees.

REFERENCES

1. Ziegler-Graham K, et al. *Arch Phys Med Rehabil* **89**, 422-429, 2008
2. Waters R, et al. *Gait & Posture* **9**, 207-231, 1999
3. Molen, NH, et al. *Eur J Appl Physiol Occup Physiol* **31**, 173-185, 1973
4. Zidarov D, et al. *Arch Phys Med Rehabil* **90**, 1953-1959, 2009
5. Herr H, et al. *Proc R Soc B*, 2011

EFFECT OF AGE AND LEAN DIRECTION ON THE THRESHOLD OF BALANCE RECOVERY IN YOUNGER, MIDDLE-AGED AND OLDER ADULTS

Evelyne Carbonneau and Cécile Smeesters

Research Center on Aging, Sherbrooke QC, Canada
Human Performance and Safety Research Group (PERSEUS), Sherbrooke QC, Canada
Department of Mechanical Engineering, Université de Sherbrooke, Sherbrooke QC, Canada
e-mail: Cecile.Smeesters@USherbrooke.ca web: http://www.usherbrooke.ca/gmecanique

INTRODUCTION

The rate per 100 000 of fatal and nonfatal unintentional injuries due to falls increases exponentially with age above 50yrs [1]. However, the critical age at which balance recovery abilities decrease significantly has not been determined.

Furthermore, only 2 studies have explored balance recovery in response to large postural perturbations, at the threshold of balance recovery, in more than one direction. Both Hsiao and Robinovitch (support translation) [2] and Telonio and Smeesters (initial lean) [3] showed that balance recovery was more difficult for backward falls than sideways and forward falls.

Finally, to our knowledge, no studies at the threshold of balance recovery, where avoiding a fall is not always possible, have included middle-aged adults (35-60yrs).

Therefore, the purpose of this study was to determine the effect of age and lean direction on the threshold of balance recovery, not only in healthy younger and older adults, but also in healthy middle-aged adults.

METHODS

We determined the maximum forward, sideways and backward lean angles from which 20 younger adults (YA: mean±SD=32.4±7.7yrs, range=18-44yrs), 20 middle-aged adults (MA: 57.1±7.6yrs, 45-69yrs) and 12 older adults (OA: 77.2±4.9yrs, 70-86yrs) could be suddenly released and still recover balance. Balance recovery was successful if participants used no more than one step and less than 20% body weight was supported by the safety harness. Starting at 5deg, the initial lean angle was increased in 5.0-2.5deg increments at each successful trial, until participants failed to recover balance twice at a given initial lean angle.

Using 4 force platforms (OR6-7, AMTI, Newton MA), 2 load cells (FD-2 and MC3A, AMTI, Newton MA) and 4 optoelectronic position sensors (Optotrak, NDI, Waterloo ON) with 24 markers, the following kinematic variables were obtained: maximum lean angle as well as reaction time, weight transfer time, step time, step velocity and step length at the maximum lean angle.

For all kinematic variables, two-way analyses of variance with repeated measures were used to determine the overall effects of age, lean direction and their interaction. For each lean direction, the effect of age on all our kinematic variables was also more finely investigated using one-way analyses of variance and post-hoc paired t-tests with a Bonferroni correction. Finally, exponential regressions for each lean direction were used to determine the age at which the maximum lean angles decreased below one standard deviation of the theoretical mean value at age zero.

RESULTS AND DISCUSSION

Both age and lean direction had significant overall effects on all kinematic variables ($p<0.001$, Table 1), except for step time with age and reaction time with direction. Interactions between age and direction also existed for maximum lean angle, weight transfer time and step velocity ($p\leq0.047$).

In particular, the maximum lean angles decreased with age for all 3 lean directions ($p<0.001$, Table 1), with all post-hoc comparisons significant, except

Table 1: Effect of age and lean direction on kinematic variables at the maximum lean angles (mean±SD).

Lean Direction	Age	Maximum Lean Angle (deg)	Reaction Time (ms)	Weight Transfer Time (ms)	Step Time (ms)	Step Velocity (m/s)	Step Length (mm)
Forward (F)	**YA**	26.0±4.7	73±11	147±19	201±19	4.60±0.68	924±130
	MA	18.9±5.7	83±10	156±24	204±28	3.67±0.75	748±181
	OA	9.7±6.5	90±19	265±97	230±61	2.47±1.11	543±214
	$p_{Age F}$	**<0.001**	**0.002**	**<0.001**	0.080	**<0.001**	**<0.001**
Sideways (S)	**YA**	19.3±4.3	76±15	143±30	181±36	3.35±0.59	599±122
	MA	15.5±4.2	77±10	167±32	174±17	2.86±0.44	499±98
	OA	7.0±5.8	84±14	245±156	181±27	2.04±0.62	368±124
	$p_{Age S}$	**<0.001**	0.233	**<0.001**	0.679	**<0.001**	**<0.001**
Backward (B)	**YA**	18.3±3.1	72±10	114±21	209±28	3.44±0.39	722±136
	MA	15.8±3.8	76±10	134±47	196±24	2.92±0.59	579±160
	OA	8.9±6.5	90±12	164±39	215±68	1.84±0.85	394±177
	$p_{Age B}$	**<0.001**	**<0.001**	**0.003**	0.375	**<0.001**	**<0.001**
p_{Age}		**<0.001**	**<0.001**	**<0.001**	0.117	**<0.001**	**<0.001**
$p_{Age \times Lean\ direction}$		**0.004**	0.200	**0.047**	0.464	**<0.001**	0.060
$p_{Lean\ direction}$		**<0.001**	0.447	**<0.001**	**<0.001**	**<0.001**	**<0.001**

YA: Younger Adults (N=20), MA: Middle-aged Adults (N=20), OA: Older Adults (N=12).
Significant p-values ($p \leq 0.05$) are **bolded**. For maximum lean angle contrasts: * $p \leq 0.05$, ** $p \leq 0.01$, *** $p \leq 0.001$.

for OA vs MA for backward leans. At the maximum lean angles, age increased reaction time for forward and backward leans ($p \leq 0.002$) and weight transfer time for all 3 lean directions ($p \leq 0.003$). Age also decreased step velocity ($p<0.001$) and step length ($p<0.001$) for all 3 lean directions.

Finally, exponential regressions showed that the maximum forward, sideways and backward lean angles decreased below one standard deviation of the theoretical mean value at age zero over age 53, 58 and 66yrs, respectively (Figure 1).

CONCLUSIONS

We have determined, for the first time, the forward, sideways and backward thresholds of balance recovery in middle-aged adults. In particular, we showed both age and lean direction effects on the ability to recover balance and avoid a fall. Moreover, the critical ages at which balance recovery abilities decrease significantly found in this study could provide guidelines for when to start screening ageing adults to prevent future falls.

REFERENCES

1. *WISQARS*, Centers for Disease Control and Prevention, 2007.
2. Hsiao ET and Robinovitch SN. *J Biomech* **31**, 1-9, 1998.
3. Telonio A and Smeesters C. *31st Annu Meet Am Soc Biomech*, Stanford CA, 2007.

ACKNOWLEDGEMENTS

Hamel and Schoeb for technical assistance and NSERC grant 298229-2009 for financial support.

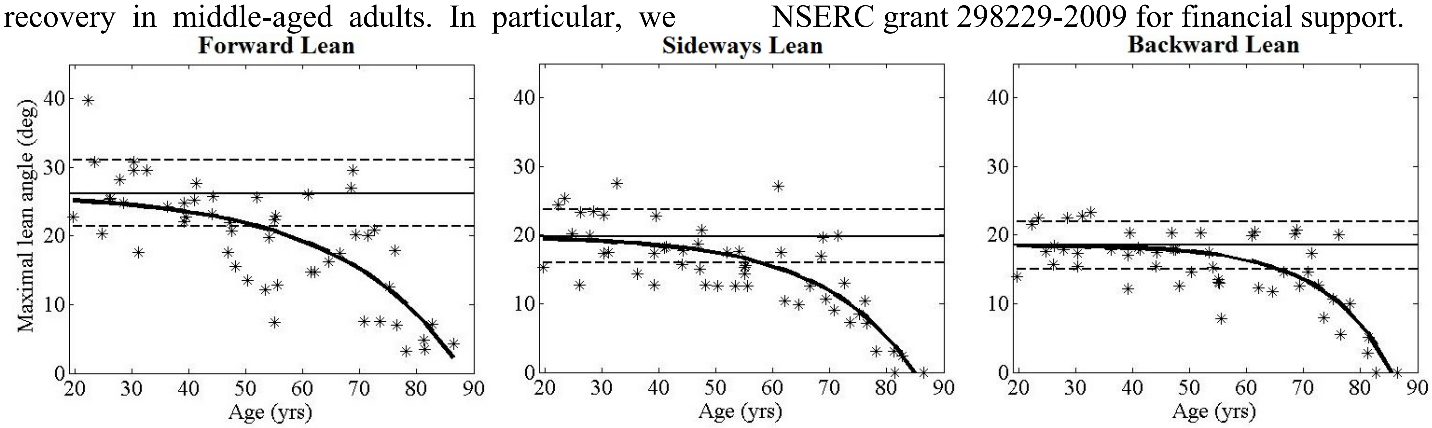

Figure 1: Exponential regressions of the maximum lean angles with respect to age (thick solid line). Theoretical mean ± standard deviation (thin solid and dashed lines) value at age zero.

A NOVEL ELASTIC LOADING-BASED EXERCISE PROGRAM IMPROVES BOTH STRENGTH AND POWER AT THE ANKLE JOINT

Jon D. Carey, Troy J. Rand and Sara A. Myers, PhD

Nebraska Biomechanics Core Facility, University of Nebraska at Omaha
email: jcarey@unomaha.edu, web: http://nbcf.unomaha.edu

INTRODUCTION

The ankle joint plays a key role in human movement. Walking, running, balance, jumping and athletic performance all rely to varying degrees on strength and power generated at the ankle. Thus, this joint is frequently targeted by exercise professionals for strength and power improvements. In recent years elastic bands have successfully been added to many college-level and adult strength training programs to increase athletic strength and power. The mechanisms behind these improvements are not fully understood, but may involve changes in lift kinetic and kinematic measures resulting changes in muscle recruitment patterns [1,2] This study is unique, however, in that it uses the bands alone, with no other exercise equipment. The authors are not aware of any other studies utilizing the bands as a resistance training tool exclusively. The goal of this study was to determine whether an elastic loading-based exercise program using elastic bands can improve strength and average power produced by the ankle. The elastic bands used are a large version of a rubber band, about one meter in length, with varying widths which provide different levels of resistance.

METHODS

Ten healthy young subjects (7 males, 3 females, age: 24.2 $\pm$ 3.7 years; height: 172.4 $\pm$ 9.95 cm; weight: 73.1 $\pm$ 13.08 kg) with no contraindications to exercise, and no previous history of ankle injury participated in this study. One subject's data was removed due to a collection error, resulting in nine subjets completing the study. Subjects underwent elastic band exercise training instruction with a fitness professional and then completed the elastic band exercise protocol (unsupervised) three days per week for eight weeks.

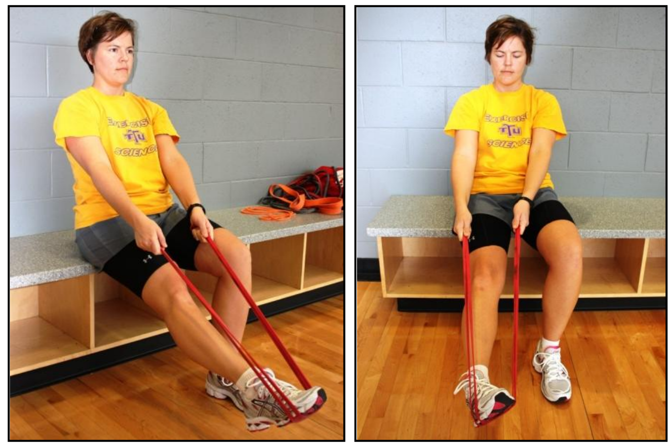

Figure 1: Ankle Specific Exercises (left, plantar/ dorsiflexion and right, inversion/eversion.

The exercise protocol included 10 lower-extremity exercises, with two (plantarflexion/ dorsiflexion and inversion/eversion against band tesion) exercises specifically targeting the ankle. Workouts were varied so different exercises were performed during each session. Pre- and post-exercise training strength testing was performed utilizing the Biodex 3 Isokinetic Dynamometer (Biodex Medical Systems, Shirley, NY) All subjects performing the Ankle Plantarflexion/Dorsiflexion tests for speed and average power. The strength test utilizes a fixed maximum movement speed of 60°/second for movement from full dorsiflexion to full plantarflexion and back, for five repetitions, while the average power test uses a fixed maximum movement speed of 180°/second. Subjects were instructed to give maximal effort throughout all five repetitions.

The Biodex Dynamomenter provides a score for strength (torque/BW) and average power for

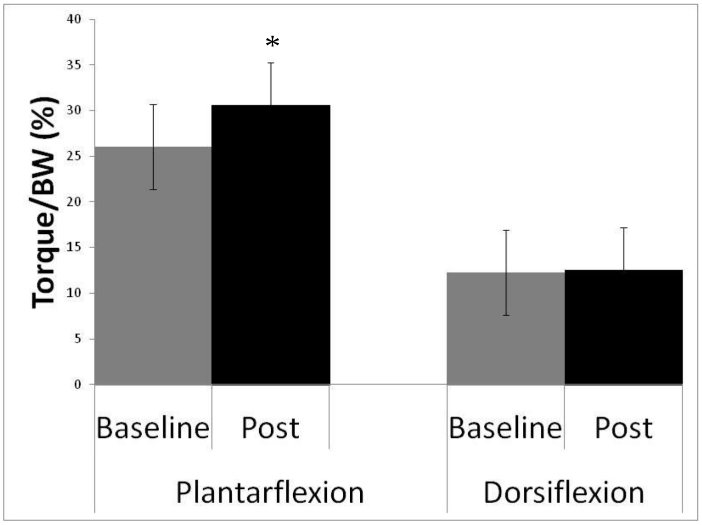

Figure 2: Ankle Strength Pre- and Post-Exercise Protocol Comparison

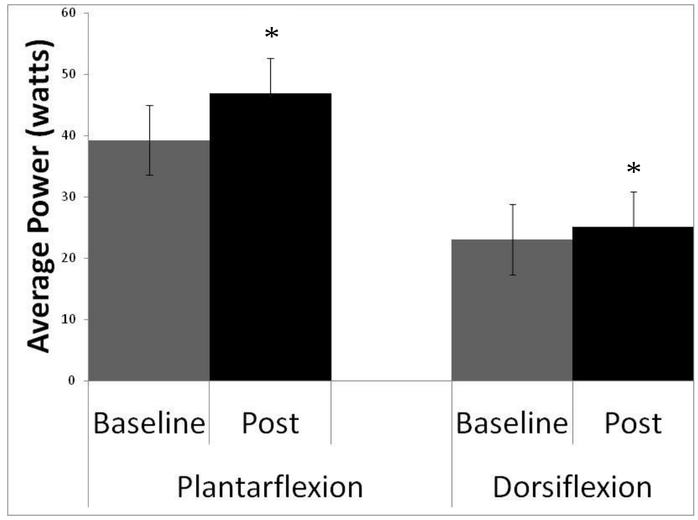

Figure 3: Ankle Power Pre- and Post-Exercise Protocol Comparison

dorsiflexion and plantarflexion for each leg. Strength and average power for right and left legs of each subject were included in the analysis. Baseline and post-exercise scores were compared using dependent t-tests. Significance was set at $p = 0.05$.

RESULTS AND DISCUSSION

Scores for both Strength and Average Power improved from Baseline to Post-Protocol testing, with statistical significance achieved in all but one category. Plantarflexion Strenth, as measured by torque/bodyweight, improved from 26.02% to 30.57% torque/BW ($p = 0.01$). Dorsiflexion Strength improved from 12.25% to 12.5%. of torque/BW ($p = 0.53$). With regard to power improvements, Plantarflexion Average Power improved from 39.24 watts to 46.83 watts ($p = 0.04$). Dorsiflexion Average Power increased from 23.02 watts to 25.05 watts ($p = 0.03$).

Broading the subjects' age, demographic, and activity range may be beneficial during future research in this area. Eldery and sedentary individuals were not included in the study. These individuals may have greater potential for strength and power gains than young healthy subjects who are already more active and may exhibit higher levels of postural control.

CONCLUSION

We conluded that exercise training using an elastic loading-based methodology such as elastic bands show promise for improving ankle strength and power. Further research in this area should involve larger sample sizes, and a variety of age ranges and activity levels. Protocol experimentation should also be considered.

REFERENCES

1. Stevenson GS, et al. *Journal of Strength and Conditioning Research* 2944-2954, 2010.

2. Anderson, C, et al. *Journal of Strength and Conditioning Research*, 567-574, 2008.

ACKNOWLEDGEMENTS

This work was supported by the NIH/NIA (F31AG032788), Nebraska Research Initiative, the NASA Nebraska Space Grant Fellowship Program and the University of Nebraska at Omaha's Committee for Research and Creative Activity.

VERTICAL TRAJECTORY OF CENTER OF MASS IS MAINTAINED WITH INCREASED VERTICAL STIFFNESS WHILE CARRYING LOAD

Robert R. Caron, Robert C. Wagenaar, Cara L. Lewis, Elliot Saltzman and Kenneth G. Holt

Boston University, College of Health and Rehabilitation Sciences: Sargent College, Boston, MA, USA
email: rcaron@bu.edu

INTRODUCTION

Despite the extensive literature on various kinematic adaptations in gait pattern while carrying load [5], little is known about the effects of load on the movement of the center of mass (COM) and the underlying mechanisms that help to control locomotion during load carriage. The amplitude and shape of the vertical COM trajectory during stance phase in unloaded gait ensures a maximal exchange of kinetic and potential energy and minimizes metabolic cost [9]. Increases in vertical stiffness have been shown to maintain vertical COM trajectory during stance with [4] and without [7] load; however, the literature does not adequately quantify how vertical stiffness changes across a wide range of incremental loads. The purpose of this study is to examine the underlying vertical stiffness dynamics that support the shape and amplitude of the vertical COM trajectory while load is manipulated at a constant walking velocity.

METHODS

Seventeen subjects (9 males, 8 females, age 25.4 ± 5.2 years; mass 70.6 ± 11.0 kg; height 1.7 ± 0.07 m) walked on a treadmill (Kistler Instrument Corporation, Amherst, MA) at a constant preferred walking velocity while load was systematically added and removed using a calibrated load manipulation apparatus. Loads began at 12.5% bodyweight (BW) and were increased in 2.5% BW increments up to 30% BW, using water in a rear torso carried backpack. A 40% BW load was then added to the pack before loads were decreased in the reverse order. Kinematic data were collected using an Optotrak 3020 System (Northern Digital Inc., Waterloo, Ontario, Canada) at 100 Hz.

The position of the total system COM (COM_{TSYS} of body plus loaded pack) was estimated using kinematic data with known body mass and anthropometric ratios found in de Leva [1]. The known volume and estimated spatial distribution of the water in the tank were used to estimate the contribution of the backpack to the COM_{TSYS}. Vertical COM_{TSYS} trajectory was time-normalized to stance duration and filtered using a zero-phase, 2nd order, Butterworth bandpass filter with a high (1/4 step frequency) and low (10Hz) passband to allow for comparisons of the shapes of the trajectories despite differences in the mean vertical trajectories across trials [6].

Mean vertical stiffness (k_v) was measured as the slope of the linear fit to the force vs. displacement curve during the descending phase of the COM_{TSYS} position trajectory during stance (see Fig. 1b) as in

$$-k_v = \frac{M\ddot{x}}{(x - x_0)}$$

where M is the total system mass, $\ddot{x}$ is the vertical acceleration of the COM_{TSYS}, x_0 is the equilibrium position of the COM_{TSYS} assumed to be located at the mean vertical position of the COM_{TSYS} and x is the current vertical position of the COM_{TSYS}.

The mean COM_{TSYS} trajectory for each condition was compared to the mean ascending 12.5% BW condition +/- 1 and 2 standard deviations (SD). Regions of deviation (ROD) measures [10] were used to assess deviations in the shape and amplitude of the mean vertical COM_{TSYS} trajectory for each condition within subjects.

Separate linear regression analyses were conducted for the vertical stiffness measure on the range of loads for the ascending (12.5%-A to 30%-A) and descending (30%-D to 12.5%-D) portions of the manipulation. Based on the linear regressions, actual mean values of vertical stiffness at 40% BW were compared to predicted mean values using 95% confidence intervals (CI) for ascending and descending analyses separately.

RESULTS

The mean of the COM_{TSYS} vertical trajectory curve increased proportionately to load during stance (Fig. 1a). Visual inspection of the ROD plots (Fig. 1b) for all conditions within each subject confirmed that the shape and amplitude of the COM_{TSYS} vertical trajectory was maintained across all loads within a narrow band (+/- 2 SD), relative to the mean trajectory of the ascending 12.5% BW condition. The mean COM_{TSYS} vertical trajectory curve remained within a +/- 1 SD band for most of stance. The average SD was 1.44mm +/- 0.25mm.

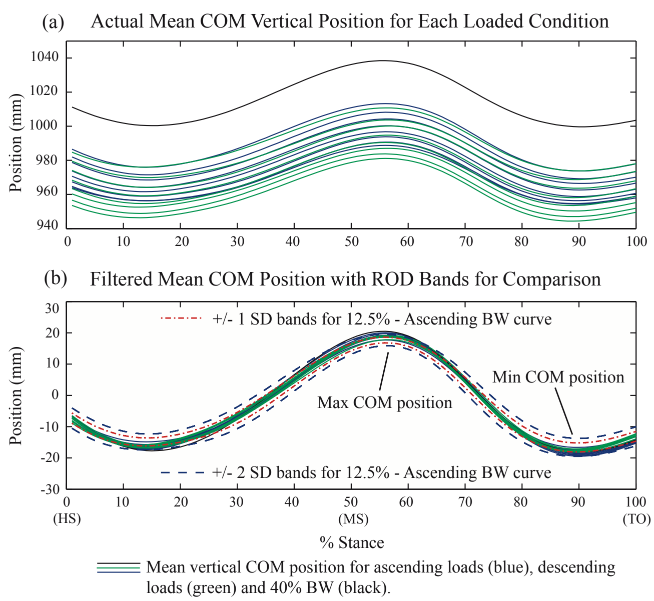

Figure 1: The mean height of the COM_{TSYS} position increased linearly with load (a), while the shape and amplitude of vertical COM_{TSYS} trajectory remained within a narrow band across all load conditions (b). Vertical stiffness was measured during the time of max to min COM vertical position during stance.

The linear regression results (Table 1) showed that vertical stiffness increased linearly with load.

Actual measures of vertical stiffness (Table 1) at 40% BW were within the 95% CI for both ascending and descending prediction equations.

DISCUSSION

Our findings suggest that linear increases in vertical stiffness help to maintain the shape and amplitude of vertical COM_{TSYS} trajectory during stance across a wide range of loads. While other kinematic adaptations may occur with increasing load [5], it appears that vertical COM_{TSYS} trajectory is an important kinematic invariant irrespective of load.

Prior research has attributed increased vertical stiffness to increased stiffness about lower-extremity joints [2]. A question that remains is whether increases in rotational stiffness in lower-extremity joints scale linearly with each other as loads increase. Such a finding would suggest that quasi-joint stiffness is controlled by a single outgoing neural signal rather than by control of individual segments – a significant advantage in managing load. Identification of the stiffness dynamics underlying vertical COM_{TSYS} trajectory may also have important implications for development of variable-stiffness exoskeletons based on either powered mechanical actuators [3], or passive tensegrity structures [8].

REFERENCES

1. de Leva. *J Biomech*, **32** (9), 1223-1230, 1996.
2. Farley CT, et al., *J Biomech*, **32**, 267-273, 1999.
3. Herr, HM. *J Neuroengin Rehab*, **6** (21), 1-9, 2009.
4. Holt KG, et al., *J Biomech*, **36**, 465-471, 2003.
5. Knapik JJ, et al., *Mil Med*, **169**, 45-56, 2004.
6. Kubo M, et al., *Gait Posture*, **23**, 512-518, 2006.
7. Lee CE, et al., *J Exper Bio*, **201**, 2935-2944, 1998.
8. Levin, SM. *Textbook Musculoskeletal Medicine*, Oxford University Press, 2006.
9. Ortega JD, et al., *J App Phys*, **99**, 2099-2107, 2005.
10. Shorter KA, et al., *Clin Biomech*, **23**, 459-467, 2008

Table 1: Regression coefficients for estimating vertical stiffness from ascending and descending loads. R^2 values are significant at the p >.001 level. SEE = Standard error of the estimate, β_0 = y-intercept, β_1 = slope. Mean vertical stiffness values are presented, with lower and upper 95% CI for predicted means, at 40% BW.

Regression for Ascending Load Conditions (12.5% - 30% BW)						
R^2	SEE	β_0	β_1	*Actual 40% BW*	*Lower CI 40% BW*	*Upper CI 40% BW*
0.969	63.65	9437.87	54.13	11857.83	11007.02	12199.17

Regression for Descending Load Conditions (30% - 12.5% BW)						
R^2	SEE	β_0	β_1	*Actual 40% BW*	*Lower CI 40% BW*	*Upper CI 40% BW*
0.992	38.15	9318.57	62.92	11857.83	11478.25	12192.82

WEIGHT BEARING ASYMMETRIES AND CHANGES IN COP TRAJECTORIES: UNILATERAL ERTL AMPUTEES VS NON-AMPUTEES

[1]Abigail L. Carpenter, [1]Jeremy D. Smith, [2]Cory L. Christiansen, and [1]Gary D. Heise
[1]Biomechanics Laboratory, University of Northern Colorado, Greeley, CO
[2]Interdisciplinary Movement Science Lab, University of Colorado, Anschutz Medical Campus, Denver, CO
email: abigail.carpenter@unco.edu, web: www.unco.edu/nhs/ses

INTRODUCTION

Lower extremity amputation often results in a weight bearing asymmetry between prosthetic and intact sides for unilateral amputees. This asymmetry is thought to contribute to greater fluctuations in center of pressure (COP) trajectories during quiet standing for unilateral amputees [1]. Specifically, medial-lateral (ML) and anterior-posterior (AP) COP excursions and velocities are greater for the prosthetic side compared to the intact leg or leg of a non-amputee [1-3].

Transtibial osteomyoplastic amputation, commonly referred to as the "Ertl technique", is designed to improve the healing process of the residual limb by improved surgical remodeling of the amputation site [4]. The Ertl technique involves sealing off the medullary cavity of the amputated bones via a bone bridge and/or by salvaging some of the periosteum during the amputation and using the periosteum to cover the exposed end of the medullary cavity. Although effects of the Ertl technique on wound healing and tissue recovery have been described in the research literature [e.g., 4], little is known about functional outcomes following an Ertl amputation.

The purpose of the study was to determine how bilateral postural control in unilateral, transtibial amputees who received an Ertl-type amputation compares with an age-matched non-amputee control group. Our expectation was that as demands on the postural control system increased the intact leg would be more relied on to control posture as evidenced by an increased weight bearing on the intact leg, whereas asymmetry in the control group would be unaltered across conditions.

METHODS

Five unilateral, transtibial amputees who received an Ertl amputation (age = 38 ± 7 yrs, height = 1.8 ± 0.1 m, mass = 79.8 ± 13.8 kg) and five age-matched controls (age = 38 ± 8 yrs, height = 1.8 ± 0.1 m, mass = 81.3 ± 17.1 kg; right limb dominant) participated in this study. Ground reaction force (GRF) data (1000 Hz) from two plates (one under each foot) were collected while participants stood on 1) a rigid surface with eyes open (RSEO), 2) a rigid surface with eyes closed (RSEC), 3) a compliant surface with eyes open (CSEO), and 4) a compliant surface with eyes closed (CSEC). Vertical GRFs (VGRF) and COP data were resampled at 100 Hz prior to analysis. Only the middle 20 s of each 30 s trial were analyzed. For VGRFs, the mean for each leg was determined over the entire 20 sec trial to assess weight bearing asymmetry. For COP data, four commonly used measures from the literature were identified; mean AP and ML COP velocities and mean AP and ML frequencies. A series of three-factor ANOVA's (Limb, Surface, and Vision) were used to determine the effects of each condition on COP and VGRF measures. Significant main effects were reported at $p \leq .05$ and interaction effects at $p \leq .10$.

RESULTS AND DISCUSSION

Weight bearing asymmetries in Ertl amputees were approximately 4% when standing on a rigid surface with their eyes open or closed (Figure 1). This weight bearing asymmetry was similar to the control group for the rigid surface. In addition, a 6% weight bearing asymmetry has been reported for skilled prosthetic users with a unilateral, transtibial amputation [1]. However, for both controls and amputees significant leg by surface ($p < .03$, $p < .05$, respectively) and leg by vision ($p < .09$, $p < .10$, respectively) interactions were observed. This suggested as demand on the postural system increased, amputees distributed more weight to the prosthetic side and controls distributed more weight to the left side. As Figure 1 illustrates, weight bearing asymmetry was exacerbated more in amputees than controls as demand increased, particularly on the compliant surface.

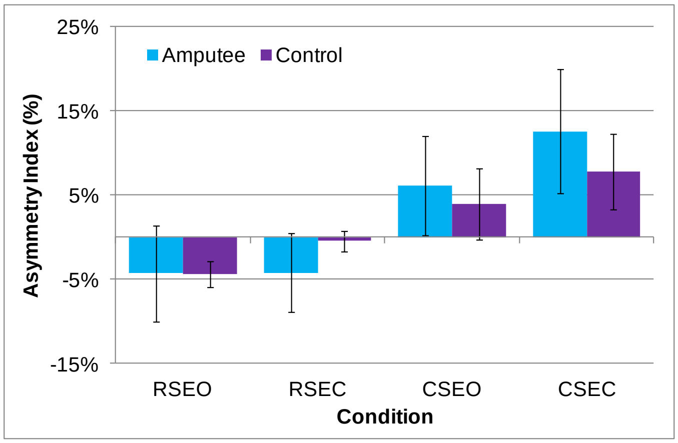

Figure 1: Weight bearing asymmetries across quiet standing conditions. Asymmetry was determined by dividing the difference between limbs by the average value for both legs. Positive percentages indicate the prosthetic side value was larger, and for controls the left leg value was larger.

For COP based measures in amputees, interaction effects between limb and surface ($p < .07$) and limb and vision ($p < .01$) occurred for mean AP COP velocity. However, mean ML COP velocity in amputees only exhibited an interaction between limb and visual input ($p < .06$). In general, as postural demands increased mean COP velocity for the prosthetic side increased to a greater extent than the intact side (Figure 2). Interestingly, our results are contrary to results from the literature where COP velocities are generally greater for the intact leg, rather than the prosthetic side. In the control group, no limb interaction effects were observed with AP or ML velocity measures, but main effects for surface ($p < .01$, $p < .01$, respectively) and vision ($p < .02$, $p < .02$, respectively) were detected. Thus, in the control group COP velocity was not dependent on the leg, but did increase with the eyes closed on the compliant surface.

For mean AP COP frequency, amputees revealed interaction effects for both limb by surface ($p < .02$) and limb by vision ($p < .03$), suggesting changes in AP frequency depend not only on prosthetic or intact leg, but also upon the surface or vision condition. Controls, however, only showed changes based on visual input ($p < .05$) with no dependence on leg. ML frequency in amputees was dependent on limb ($p < .01$), with a greater frequency for the intact limb. In controls, limb was only significant based on changes in surface ($p < .05$).

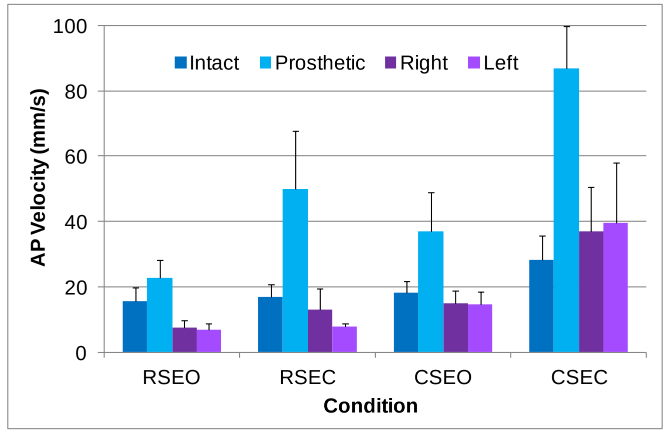

Figure 2: COP AP mean velocity across conditions.

CONCLUSIONS

Ertl amputees relied more on the prosthetic leg to control posture as demands increased, whereas control subjects relied more on the left limb. Surprisingly, it appears that Ertl amputees relied on the prosthetic side for stability, whereas controls relied on the non-dominant leg for stability. Further research is needed with comparisons between Ertl amputees and traditional amputees to determine whether this observation is unique to Ertl amputees.

REFERENCES

1. Mayer et al. (2011). *BMC Musculoskeletal Disorders*, 12, 118-124.
2. Buckley et al. (2002). *Am J Phys Med Rehabil*, 81, 13-20.
3. Hlavackova et al. (2011). *Plos One*, 6, e19661.
4. Dionne et al. (2009). *J Prosth Orthot*, 21, 64-70.

ACKNOWLEDGEMENTS

We would like to acknowledge Dr. David Hahn for assistance with recruitment and his medical expertise with this project.

A COMPUTATIONAL MODEL TO ESTIMATE PRE-STRESS BETWEEN BRAIN TISSUE AND A NEEDLE USED FOR CONVECTION ENHACED DELIVERY

Fernando Casanova, Paul R. Carney and Malisa Sarntinoranont
University of Florida, Gainesville, FL, USA
E-mail: fcasanova@ufl.edu

INTRODUCTION

Convection enhanced delivery (CED) is a drug delivery technique for treatment of neurological diseases such as epilepsy, Parkinson's diseases and brain tumors that respond poorly to systemic delivery due to the blood-brain barrier. Frequently, the infused fluid preferentially flows along the outer needle wall toward the surface instead of penetrating into and spreading out into surrounding tissue (backflow). Previous mathematical models have been developed to calculate the backflow distance and infusion pressure as a function of flow rate considering the tissue as a porous media with a linear elastic solid matrix [1,2]. However, these models do not consider the pre-stress existing between the needle and the tissue because of the strain caused during the needle insertion. In our previous study [3], we have developed a model to estimate the backflow distance during CED in agarose hydrogel which includes pre-stress. In this study, we developed a finite element model to simulate the needle insertion process and estimate the pre-stress existing between the cannula wall and the tissue.

METHODS

A finite element model was developed to model needle insertion. A 2D model with axial symmetry and a linear elastic material was assumed. Tissue was simulated as a cylinder of 5 mm radius and 10 mm height. At the beginning of the simulation a set of points were defined inside the tissue domain. These points were used to track the displacements of the tissue and to save the stresses during the simulation. Then a mesh of triangular elements over the tissue was created. Boundary conditions were used to simulate the tissue moving against the needle. The bottom surface of the tissue was displaced a distance (δ) towards the needle at constant speed and the displacement was restricted at the needle surface. Two geometries of needle were evaluated: a solid rod and a hollow cylinder. The solid needle (**Fig. 1a**), simulates the case when the needle is full of confined uncompressible fluid. The hollow cylinder simulates the case when fluid within the needle is not confined and fluids and tissues are free to move up into the core of the needle (**Fig. 1b**).

At every time step, stresses and displacements were calculated on the mesh from equilibrium equations using COMSOL Multiphysics (v. 3.5., Burlington, MA). Stresses and displacements were then interpolated to the predefined points in the tissue domain, and the coordinates of the points were updated. With each time step, a new mesh was defined in which bottom and the upper surfaces were displaced a distance (δ) and needle remained stationary, see Fig. 1. In the inner part of the needle a friction coefficient of 0.32 was applied based on pull-out tests in tissue [5].

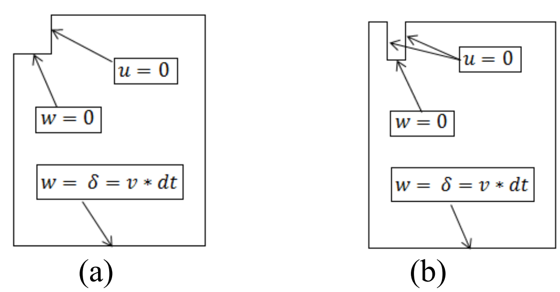

Fig. 1 Boundary conditions; u = displacement in radial direction, w = displacement in z direction, v = speed of the needle.

The model accounted for rupture of tissues at the needle tip. Once the von Mises stress reach a maximum value (S_{ut}), stresses at that point were set to zero if they were greater than zero. These points were not able to support tractions or shear stresses. Mechanical properties of brain tissues where obtained from data reported by Franceschini et al

[4] and were found to be 9.6 kPa and 10 kPa for the Young modulus and S_{ut} respectively. Simulations were performed for five needle diameters: 0.18, 0.23, 0.31, 0.36, and 0.46 mm with a depth of 15 times the needle radius. The pre-stress was calculated to be the average radial stress in the outer needle wall. Infusion pressure (P_0) was estimated as $P_0 = \frac{\sigma_r}{1-\phi}$ which was obtained assuming continuity in the fluid pressure at the boundary between the infusate and the porous media [3]. In the last equation σ_r is the pre-stress and ϕ is the porosity.

RESULTS AND DISCUSSION

The simulated force needed to insert a 0.2 mm diameter rod into the brain was compared with experimental values on rat brain at the same speed (0.8 mm/s) reported by Sharp et al. [5]. Relatively good agreement was obtained until ~1 mm of penetration. Beyond 1 mm, increased differences in forces may be because of the tissue heterogeneity and friction on the outer needle wall, factors which were not considered in the model. **Fig. 2a** and **2b** shows the simulated displacement of the points (tissue) near the solid and the hollow needle respectively due to the penetration of the needle in the tissue. In the hollow needle, part of the tissue moves inside the core. Along the outside needle wall, the tissue is more organized and uniformly displaced than that in the solid needle. In both needle cases, a zone of compressed material was formed immediately under the needle tip. This zone moved downwards together with the needle, and tissue below this compressed zone moved to the sides.

No significant difference in the predicted pre-stress was found for the needle diameters simulated (**Fig. 3**). Slightly smaller and more uniform values of pre-stress were obtained for the hollow needle.

For a tissue porosity of 0.26, the average infusion pressure was predicted to be 2.8 kPa for the solid needle and 2.6 kPa for the hollow needle. These values are inside the range of measured pressures reported by Chen et al. [6] during infusion at 0.5 µl/min into porcine brain.

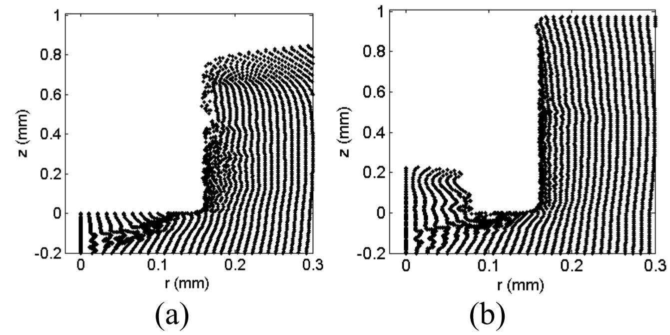

Fig. 2 Displacement field near the needle; (a) closed needle (b) hollow needle.

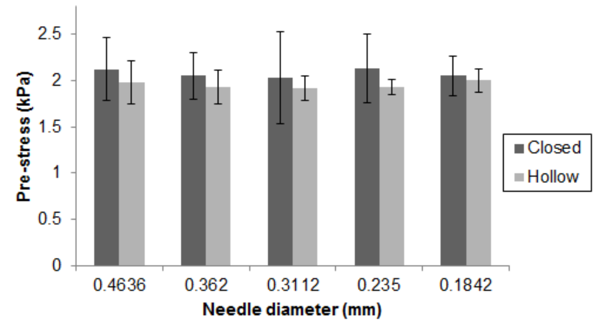

Fig. 3 Pre-stress as a function of needle diameter for closed and hollow needles.

CONCLUSIONS

Pre-stress in brain tissue was determined to be independent of the needle diameter. Also, no important difference between pre-stresses in closed and hollow needles were found. These results suggest that when backflow takes place, infusion pressure is independent of the needle diameter. However, this will not hold if tissue moves inside the core, since tissue clogging will affect infusion pressure.

REFERENCES

1. Morrison PF, et al. *Am. J. Physiology* **277**, 1218-1229, 1999.
2. Raghavan R, et al. *Phys Med Biol* **55**, 281-304, 2010.
3. Casanova F, et al. *J Biomechanical Engineering*, In press.
4. Franceschini G, et al. *J Mech and Phys of Solids*, **54**, 2592-2620.
5. Sharp AA, et al. *IEEE Trans Biomed Eng*, **55**, 45-53.
6. Chen ZJ, et al. *J Neurosurg*, 101, 314-322.

INSIGHTS INTO THE FOOTSTRIKE PATTERNS OF WOMEN DISTANCE RUNNERS

[1,2]Peter R. Cavanagh, [1]Molly D. Glauberman, [1]Karl T. Manner, [1]Kara Sawyer, [2]Santosh Devasia

Departments of [1]Orthopaedics and Sports Medicine and [2]Mechanical Engineering
University of Washington, Seattle, WA, USA
email: cavanagh@uw.edu

INTRODUCTION

Tibial stress fractures account for nearly 50% of all stress fractures experienced by athletes [1,2]. Women appear to sustain more tibial fractures than men, and distance runners are more likely to have stress fractures of the pelvis and long bones of the leg than the foot [3]. While some studies have found that ground reaction force (GRF) characteristics are unrelated to stress fracture history [4], recent reports have implicated the initial characteristics of the footstrike in stress responses [5,6]. This has led to efforts to modify the loading rate at footstrike [7].

The aim of this study was to establish the reliability of tibial accelerometry for characterizing the footstrike and to develop a new model of factors affecting the first peak of the ground reaction force.

METHODS

We used a treadmill with an embedded Kistler force platform together with a leg-mounted acceleration monitoring unit (AMU) to measure ground reaction forces and tibial accelerations/angular velocities respectively. The AMU consisted of a tri-axial accelerometer (±12 g) and a tri-axial rate gyro (±2000º/sec). AMU data were transmitted wirelessly to a local CPU via Bluetooth radio. The overall dimensions of the AMU were 40 mm x 22 mm x 12 mm with a packaged mass of 21 grams (including battery).

Thirty injury-free women distance runners were recruited to the study (18-40 years old, weekly mileage > 20). The sensor was positioned 5 cm above the medial malleolus along the medial tibial border. To eliminate slipping, it was placed over a self-adhesive bandage and then tightened to 5 pounds of tension with a Velcro strap.

Each subject was tested on two separate days. Before each data collection session, subjects completed a 5 minute warm-up on the treadmill. Data for five 90 second trials at a speed of 3.13 m/s were collected each day from the leg with the highest initial peak of axial tibial acceleration. The AMU was removed and remounted between each trial on a given day. Data for one trial from each limb on visit 1 was also compared for an analysis of asymmetry.

RESULTS AND DISCUSSION

The absolute magnitude of the mean peak axial tibial acceleration varied for all runners over a 2.6-fold range from 4.0 to 10.6 g. This peak acceleration was only moderately related to body weight (r^2=0.21 Fig. 1).

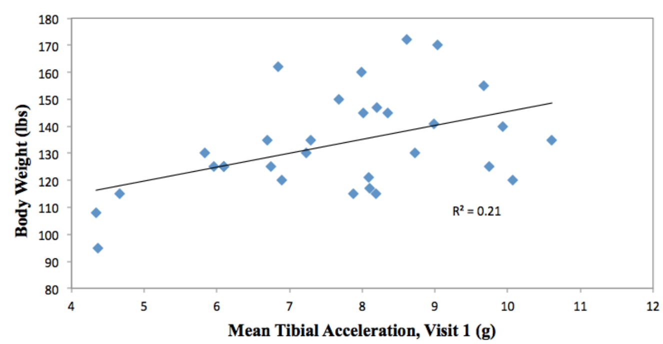

Figure 1: The relationship between the first peak of tibial axial acceleration and body weight (r^2=0.21)

A one-way repeated measures ANOVA using time as a fixed factor (5 trials in one visit) and subjects as a repeated measure was conducted. Using the Greenhouse-Geisser correction (with n=24 subjects), time was not significant (F(2.1,47.6) = 0.7406, p=0.4864) indicating that peak acceleration values at footstrike did not vary between applications of the AMU on the same day.

Similar high reliability was obtained when comparing results on the same subject over separate days. Between the first and second visit, mean peak accelerations showed low variability with an r^2 of 0.92 (Fig. 2).

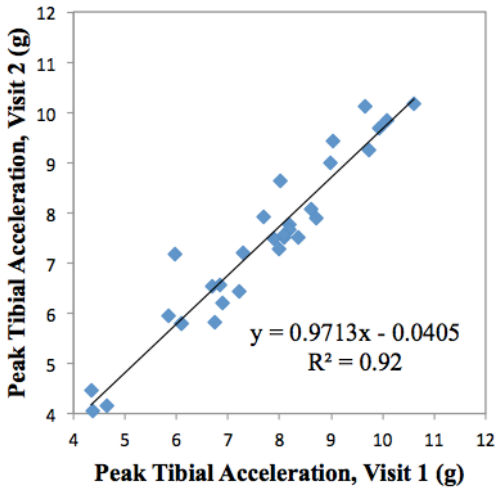

Figure 2: The comparison of mean peak axial tibial acceleration on the first and second visits for each subject.

Asymmetries were commonly observed between the tibial accelerations in the right and left legs. The mean absolute percentage difference between sides was 9.9%, with a range from 0.2% to 29.2%.

In order to explore reasons for the large differences in footstrike characteristics between subjects, a simple analytical model was developed (Fig. 3). The potential energy lost by the total body center of mass from initial contact to the first peak of the ground reaction force was equated with the energy stored in a linear spring representing the foot/shoe and a torsional spring representing the ankle.

This model predicts that the magnitude of the first peak in the ground reaction force is as follows:

$$Fz/mg = 2h/(h1 + h2)$$

where h is the change in height of the total body center of mass between footstrike and the first peak in the ground reaction force and $h1$ and $h2$ are the deflections of the ankle and the foot/shoe in the same time interval.

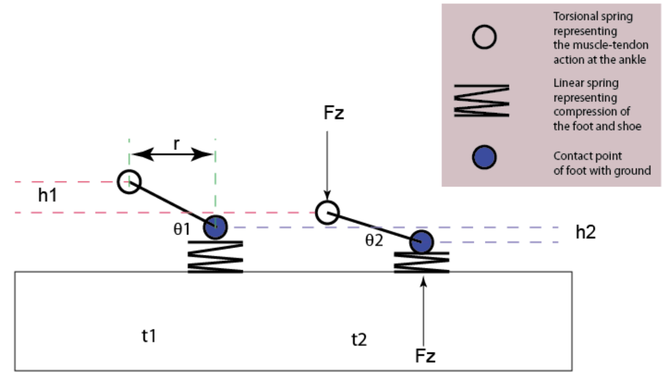

Figure 3: Simple model of the foot and ankle at footstrike. The ankle is represented as a torsional spring and the foot/shoe as a linear spring.

Future work will be directed towards an experimental examination of these predicted determinants of peak initial ground reaction force and to an exploration of the relationship between tibial acceleration and ground reaction force.

REFERENCES

1. Matheson G, et al. *American Journal of Sports Medicine,* **15**, 46-58, 1987.
2. Iwamoto J, et al. *Journal of Orthopaedic Science: Official Journal of the Japanese Orthopaedic Association,* **8**, 273-278, 2003.
3. Bennell K, et al. *American Journal of Sports Medicine,* **24**, 211-217, 1996.
4. Bennell K, et al. *Med Sci Sports Exerc.* 2004 Mar; **36**(3):397-404.
5. Davis IS, et al. *Medicine and Science in Sports and Exercise.* 2004; **35**,S58.
6. Zadpoor AA, et al. *Clin Biomech.* 2011 Jan **26**(1):23-8.
7. Crowell J et al. *Orthop Sports Phys Ther.* 2010 **40**(4):206-13.

ACKNOWLEDGEMENTS

This work was supported by the Women's Sports Medicine and Lifetime Fitness Endowment at the University of Washington. The assistance of Adrienne Nova, Tamre Cardozo, and Cristine Agresta is much appreciated.

CHANGES IN SPATIOTEMPORAL GAIT CHARACTERISTICS WHEN ANTICIPATING SLIPPERY FLOORS IN YOUNG AND OLDER ADULTS

April J. Chambers and Rakié Cham

University of Pittsburgh, Pittsburgh, PA, USA
email: ajcst49@pitt.edu, web: http://www.odar.pitt.edu/HMBL

INTRODUCTION

Slips and falls are a major cause of occupational injury in young and older adults [1,2]. Gait characteristics are important in fall research. Falling history and hazardous slips have been associated with decreased gait speed, increased step length, and decreased cadence [3,4]. Proactive strategies, balance control mechanisms that take place before encountering a potential disturbance, serve to counteract the destabilizing effect of a disturbance. They have been shown to reduce slip probability and reliance on reactive strategies in avoiding a fall [5,6]. Age-related differences in proactive strategies are reported across studies are not consistent with some research finding older adults adopting a more cautious gait consisting of reduced gait speed, shorten step length, and increased gait variability [6,7]. However, these cautious gait adaptations have also been noted as risk factors for falls and may increase fall risk, rather than protect against it [3,4,7,8].

A better understanding of the changes in spatiotemporal gait characteristics when anticipating a slippery floor is important for injury prevention and may further explain the high prevalence of slip-related falls in older adults. The goal of this study was to investigate the impact of anticipating slippery floors on spatiotemporal gait characteristics, including gait speed control, during walking on dry surfaces in young and older adults.

METHODS

Eighteen healthy young (20-33 years) and thirteen healthy older adults (55-67 years) participated in this study after written informed consent approved by the University of Pittsburgh Institutional Review Board was obtained. Whole body motion data were collected using a custom marker set as participants walked at a self-selected pace across an 8.5 meter walkway (Moyer et al., 2006). Participants were informed that the first few trials would be dry to ensure natural gait and three to five dry trials were collected, "baseline dry". Without the participant's knowledge, the diluted glycerol solution was applied to the left/leading foot-floor interface and an "unexpected slip" was recorded. Subjects were then alerted that all remaining trials might be slippery but no further specific information was provided and they walked on a dry surface, "anticipation dry".

General spatiotemporal gait characteristics, gait speed (m/s), cadence (steps/min), and step length (cm) were derived. The first two anticipation dry trials were used and compared to the baseline trials. Age- and baseline/anticipation-related differences in each spatiotemporal gait variable of interest were determined using a repeated measures ANOVA with age group (Y/O), anticipation condition (baseline/anticipation) and their interaction effects as independent fixed effects. Subject was included as a random effect. Statistical significance was set at 0.05.

RESULTS AND DISCUSSION

Anticipating slippery floors increased cadence ($p<0.001$) in both young and older adults (Figure 1). Specifically, cadence significantly increased by 6.04 steps/min in young adults and by 5.93 steps/min in older adults during anticipation compared to baseline. This gait adaptation is beneficial to reducing slip risk, as increased cadence has been shown to reduce the risk of experiencing a hazardous slip [3]. In general, younger adults took longer steps than older adults ($p=0.003$). Additionally, step length significantly increased in young adults by 1.06 cm while significantly decreasing 1.67 cm in older adults during anticipation trials (p=0.0095) (Figure 1). Increased step length as a component of a proactive strategy to reduce slip risk may be maladaptive. Increased step length has been linked to increased RCOF and thus increased slip risk [3-5]. The aforementioned effects on step length and cadence, in combination, cause the gait speed in young adults to significantly increase by 0.10 m/s during anticipation (p=0.003). Gait speed in older adults was not significantly different during anticipation trials compared to baseline walking (Figure 1). Increased, or at least maintaining baseline gait speed, is a beneficial component of a proactive strategy, as slower gait speeds have been related to increased fall risk [2].

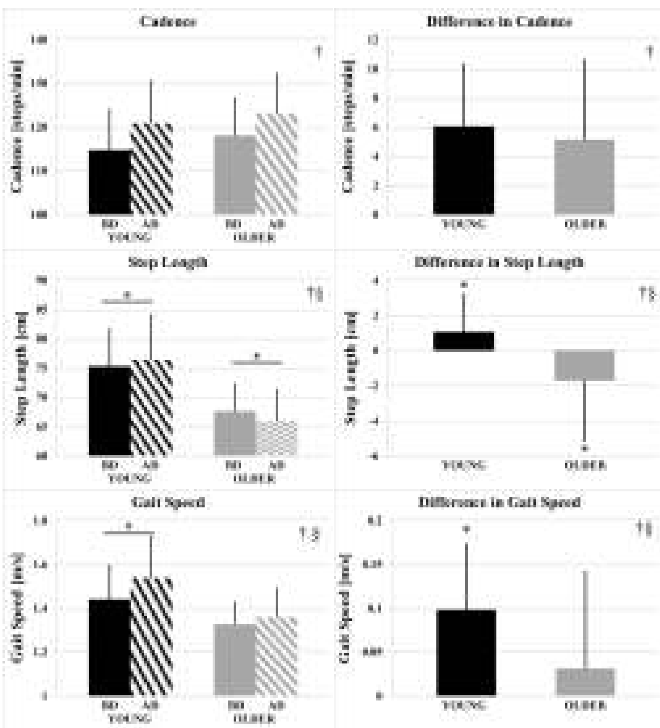

Figure 1: Effect of anticipation on gait speed, cadence and step length. Left column: baseline dry (BD) shown as solid bars and anticipation dry (AD) as hashed bars with young adults in black and older adults in gray. Right column: mean of within subject differences are provided with young adults in black and older adults in gray. Significant is provided in the top right corner with † denoting anticipation and § denoting age group. * represents a significant interaction effect. Standard deviations are provided.

Due to laboratory constraints, the gait parameters calculated were based on a limited number of steps. Additionally, the older subject group was arguably not sufficiently old enough to demonstrate significantly altered gait parameters compared to the young subject group. Different trends in proactive strategies might be seen in elderly adults.

CONCLUSIONS

Interestingly, older adults were able to implement a more conservative proactive strategy consisting of maintaining gait speed without increasing step length. Young adults implemented a potentially more risky proactive strategy consisting of increasing gait speed through a combination of increased step length and increased cadence. Additional research is necessary to determine the effect of these changes in gait speed control on slip risk during walking and if these age-related differences in proactive gait adaptations are associated with reducing future slip events.

REFERENCES

1. Liberty Mutual. 2010 Workplace Safety Index, 2010.
2. Hausdorff JM, et al. *Arch Phys Med Rehabil* **82**, 1050-1056, 2001.
3. Moyer BE, et al. *Ergonomics* **49**, 329-343, 2006.
4. Cham R & Redfern MS. *Gait Posture* **15**, 159-171, 2002.
5. Lockhart TE, et al. *Gait Posture*, **26**, 142-149, 2007.
6. Menz HB, et al. *Gait Posture*, **25**, 243-249, 2007.
7. Delbaere K, et al. *J Gerontol* **64**, 237-242, 2009.

ACKNOWLEDGEMENTS

Funding source: NIOSH R03 OH007533
Neurological screening: Dr. Joseph Furman

THE EFFECT OF EXTENDED DURATIONS OF WALKING IN OCCUPATIONAL FOOTWEAR ON BALANCE

Harish Chander[1], John C.Garner[1], Chip Wade[2], Jennica Roche[3], Nicole C.Dabbs[1], Rebecca L. MacNeill[1]

[1]Applied Biomechanics Laboratory, University of Mississippi, University, MS
[2]TigErgonomics Laboratory, Auburn University, Auburn, AL
[3]Human Movement & Balance Laboratory, University of Pittsburgh, Pittsburgh, PA
email: hchander@olemiss.edu

INTRODUCTION

Hazards and challenges present in the workplace pose a number of potential risks for injury and illness. Nearly 3.1 million nonfatal workplace injuries and illnesses were reported in 2010 [1]. A large portion of the injuries are attributed to slip and fall incidents, which have been positively correlated to balance decrements. Furthermore, 45% of all falls have been attributed to inappropriate footwear [2]. Previous studies have shown decrements in balance as a result of different footwear [2] and after an increased workload over a specific period of time [2,3]. Occupational footwear is often designed for safety and may fail to allow appropriate foot biomechanics during normal gait and standing. As such, the functionality of occupational footwear may impact balance characteristics over time. The purpose of the study is to examine the differences in balance while wearing different types of occupational footwear for extended durations.

METHODS

Fourteen healthy male adults (age: 23.6±1.2 yrs; ht: 181±5.3 cm; mass: 89.2±14.6 kg), with no history of orthopedic, musculoskeletal, cardiovascular, neurological and vestibular abnormalities completed the study. The experimental session included an extended duration of walking (4 hours) with balance measured at 30min intervals (Pre, 30, 60, 90, 120, 150, 180, 210 & 240 min). The standing balance protocol assessment was done using the six conditions of the Neurocom Equitest SOT with sway referencing capabilities of the platform and the visual surround (EO, EC, EOSRV, EOSRP, ECSRP and EOSRVP). The values of the dependent sway variables were derived from the center of pressure (CoP) movement. The average sway velocity (VEL) and the root-mean-square (RMS) sway of the CoP were used to characterize the postural sway in the anterior-posterior (APVEL & APRMS) and the medio-lateral (MLVEL & MLRMS) directions during the 60-second testing period. Participants were randomly assigned 3 different types of occupational footwear: Work Boots (WB) (mass 0.39±0.06 kg), Tactical Boots (TB) (mass 0.53±0.08 kg) and Low Top Shoes (LT) (mass 0.89±0.05 kg) with a minimum of 72 hours of rest between conditions.

RESULTS AND DISCUSSION

Balance dependent variables were evaluated using a 3 x 9 (Footwear [WB,TB, LT]) x (Extended duration of walking intervals [Pre, 30, 60, 90, 120, 150, 180, 210 & 240] RMANOVA and independently for the six SOT balance conditions (EO, EC, EOSRV, EOSRP, ECSRP and EOSRVP) to identify any existing differences within the exposure time as well as the footwear types. Significant differences were found over time in the EO, EC, EOSRV & EOSRP for MLRMS. Differences between footwear were seen in the APRMS and MLRMS for EC and the EOSRP for MLRMS, illustrated in Figures 1-3.

These results indicate a decrement in balance performance over time but the differences were limited to MLRMS. The decline in balance may be attributed to fatigue resulting from an extended duration of walking/standing, supporting previous literature. Significant differences were found among the WB, TB and LT, with the LT having higher RMS sway. The LT resulted in a relatively greater balance decrement, especially when vision was absent and with conflicting somatosensory input. The WB and TB, despite having a greater mass, had less balance decrement, which may be related to their elevated boot shaft height. Results from this data suggest that the high boot shaft supports the ankle, in turn attenuating fatigue, thus resisting balance decrements.

CONCLUSION

The current study accounts for balance decrements in a simulated occupational workload of standing and walking over an extended period of time with three commonly used occupational footwear. The findings from the study may help offer recommendations for efficient footwear design for the industrial populations to help resist fatigue and help prevent slip and fall-related injuries. Future research on the mechanical characteristics of the footwear are recommended to have a better understanding of the footwear functions and their importance in postural stability.

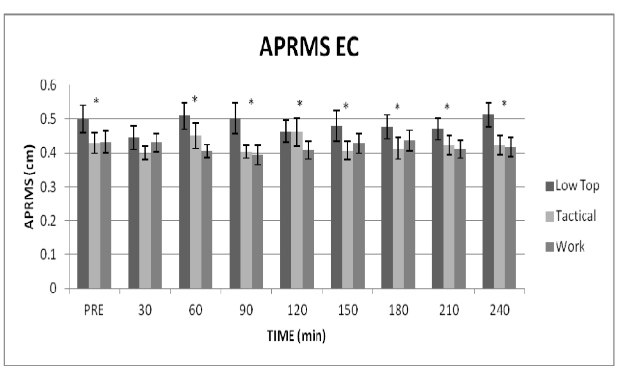

Figure 1: Eyes closed AP Sway RMS

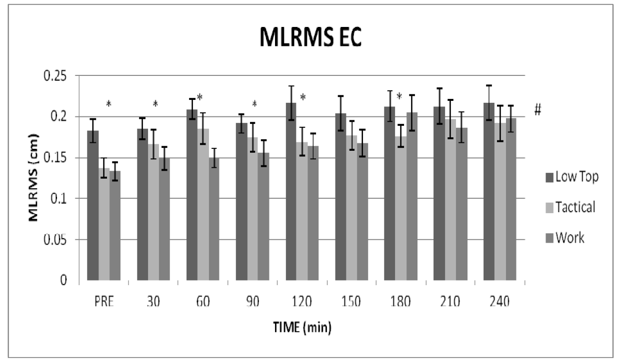

Figure 2: Eyes closed ML Sway RMS

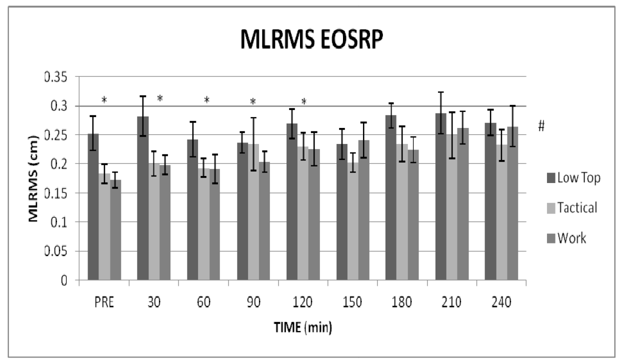

Figure 3: Eyes open sway referenced platform ML Sway RMS

REFERENCES

1. Bureau of Labor Statistics: 2010.
2. Menant et al. (2008). *Arch Phys Med Rehabil*; 89:1970-1976.
3. Yaggie & McGregor (2002). *Arch Phys Med Rehabil*;83:224-228.
4. Gribble & Hertel (2004).*Arch Phys Med Rehabil*; 85:589-592.

MAGNITUDE AND TIME COURSE OF ADAPTATION DURING WALKING WITH A PASSIVE ELASTIC EXOSKELETON

Charalambos C. Charalambous[1], Jesse C. Dean[1]
[1]Medical University of South Carolina, SC, USA
Email: charalam@musc.edu

INTRODUCTION

It is believed that various control systems in the CNS contribute to locomotion [1]. However, evidence from simulations and physical robots has shown that stable walking can be generated by the passive dynamics of the lower extremities without the need for active control and energy input (i.e. passive dynamic walking) [2].

After a neurological injury, either to the brain or spinal cord, maximal step frequency often limits gait speed [3, 4]. Previous simulations have revealed that biarticular springs crossing the hip and knee can increase step frequency, without the need for active control [5]. Human-like gait speeds and leg swing kinematic patterns may thus be generated via such an actuation strategy without additional energetic input.

These simulation results led us to develop a passive elastic exoskeleton with biarticular springs crossing the hip and knee. In pilot experiments, walking with the exoskeleton decreased hamstring activity during mid-swing yet increased metabolic cost. It is unknown if longer gait training with the exoskeleton can promote adaptation, as revealed by energetic cost and muscle activity. A recent study has demonstrated intra- and inter-day adaptation in muscle activities and kinematics during walking with a robotic ankle exoskeleton [6].

The aim of this study was to quantify the magnitude and time course of the adaptation of muscle activity during walking with a passive elastic exoskeleton. We hypothesized that subjects would gradually adapt to assistance provided by the passive elastic exoskeleton, reducing metabolic cost and muscle activity during swing.

METHODS

A lightweight (5 kg) exoskeleton consisting of a fiberglass pelvic brace and aluminum segments of adjustable length was attached lateral to the thigh and shank (Fig. 1). The exoskeleton's hip and knee joints were aligned with the participants' corresponding joints. Padded plastic cuffs around the shank and thigh mechanically linked the user to the device. Extension springs (k = 2000 N/m) were placed in series with wires running along grooved aluminum sheaves at the hip and knee. Based on simulations, a knee to hip moment arm ratio of 0.33 (i.e. 2.5cm/7.6 cm) was chosen [5].

A total of ten neurologically uninjured adults (6F, 27 ± 4 yrs), walked on a treadmill at 1.20 m/s under four conditions: normal walking with no exoskeleton (NoEXO; 6 minutes); walking with the exoskeleton but without springs (PRE; 6 minutes); walking with the exoskeleton and springs (EXO; 30 minutes), and walking with the exoskeleton but without springs (POST; 6 minutes).

Electromyographic (EMG) activity**,** spatiotemporal and metabolic cost data were collected for each condition. Spatiotemporal data were used to quantify stride timing. EMG data of five leg muscles (vastus medialis, VMd; rectus femoris, RF; semitendinosus, ST; biceps femoris, BF; and gluteus medius, GMd) were processed, divided into strides and gait phases, averaged, and normalized by the peak values during normal walking.

In order to quantify muscle activity adaptation, we calculated the time to steady state [6]. ANOVAs were used to test the effect of: 1) time on EMG during the EXO condition (N=8; 5F), and 2) walking condition on EMG and metabolic cost in the 6^{th} minute of walking (N=9; 5F). In cases where a significant effect was revealed, post hoc analyses were utilized.

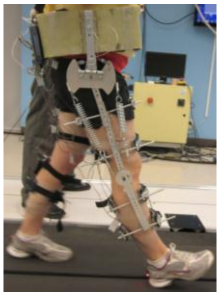

Figure 1. Participant walking on a treadmill wearing a passive elastic exoskeleton with two-joint springs crossing the hip and knee.

RESULTS AND DISCUSSION

In the EXO condition, a statistically significant effect of time was revealed for BF during mid-swing ($p<0.0001$) and late swing ($p=0.0004$), ST during mid-swing ($p=0.029$), and RF during initial swing ($p=0.011$). Since steady state was reached within 12 minutes for all muscles (e.g., Fig. 2), for the second analysis, we included both the 6th minute (EXO6) and 12th minute (EXO12) of walking.

Across conditions, a statistically significant effect was revealed for BF activity during mid-swing ($p<0.0001$) and late swing ($p=0.046$), ST activity during mid-swing ($p<0.0001$), and metabolic cost ($p<0.0001$). Surprisingly, no significant effect of walking condition was revealed for RF activity during initial swing ($p=0.26$). During mid-swing, BF EMG was significantly decreased in EXO6 and EXO12 compared to other conditions, while during late swing, BF EMG was significantly decreased in EXO12 only compared to NoEXO (Fig.3). ST EMG was the lowest in EXO12. Unexpectedly, the addition of springs to the exoskeleton significantly increased metabolic cost.

As hypothesized, muscle activity gradually decreased after springs were added to the exoskeleton. This implies that participants were able to adapt their muscle activation to take advantage of assistance provided by the exoskeleton.

Adding springs decreased hamstring activity during mid- and late swing phases. However, there was no

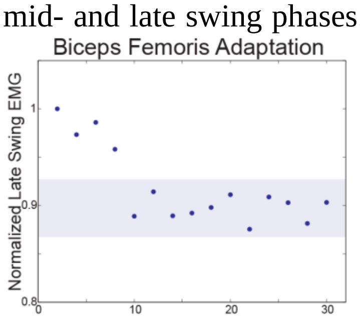

Figure 2. Group data is averaged across 15 time points during the EXO trial. Shaded area is the Mean ± 2SD of group mean of the final 10 minutes of walking.

significant effect of the exoskeleton on RF EMG during pre- or initial swing. It is possible that the anterior springs were not fully lengthened during these phases, or that subjects were less willing to reduce muscle activity during phases in which these muscles produce positive work. Lastly, increases in metabolic cost might be attributed to the fact that GMd activity increased during stance, as participants preferred to walk with wider steps after springs were attached.

CONCLUSIONS

A lightweight exoskeleton worn while walking on a treadmill allowed users to adapt their muscle activation during specific gait phases within a short time period. Though such a device can potentially be a useful gait assistance aid for people with neurological impairments, future work will test the optimal mechanical properties of the exoskeleton.

REFERENCES

1. Nielsen JB, *Neuroscientist* **9**, 195-204, 2003.
2. Kuo AD, et al. *Phys Ther* **90**, 157-74, 2010.
3. Bayat R, et al. *Neurorehabil Neural* Repair **19**, 115-24, 2005.
4. Pepin A, et al. *Spinal Cord* **41**, 271-9, 2003.
5. Dean JC, et al. *J R Soc Interface* **6**, 561-73, 2009.
6. Gordon KE, et al. *J Biomech* **40**, 2636-44, 2007.

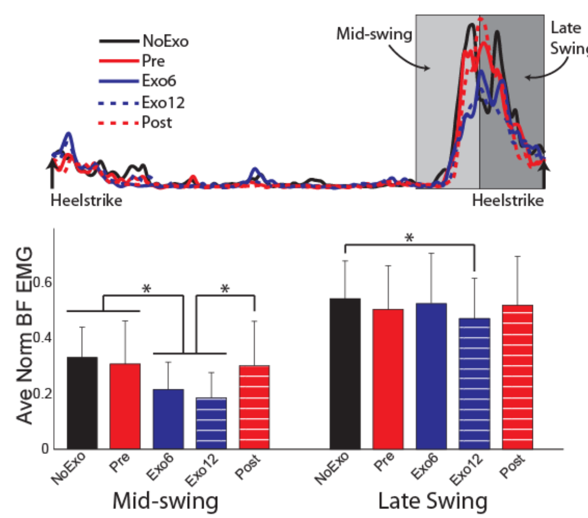

Figure 3. Changes in BF activity for a single subject (top) and averaged group data (bottom). Group data is averaged separately over Mid-swing (73-87%) and Late Swing (87-100%). Asterisks indicate post-hoc significance.

A METHOD FOR MEASURING 3D KINEMATICS OF THE MANDIBLE USING MODIFIED CONE-BEAM COMPUTERIZED TOMOGRAPHY

Chien-Chih Chen[1,2], Cheng-Chung Lin[3], Yunn-Jy Chen[2], Shih-Wun Hong[3] and Tung-Wu Lu[3*]

[1] Department of Dentistry, Cardinal Tien Hospital, Taiwan, R.O.C.
[2] School of Dentistry, National Taiwan University, Taiwan, R.O.C.
[3] Institute of Biomedical Engineering, National Taiwan University, Taiwan, R.O.C.
email: twlu@ntu.edu.tw

INTRODUCTION

Knowledge of the kinematics of the mandible relative to the maxilla is helpful for a better understanding of the normal function of the temporomandibular joint, and for the study of the etiology, diagnosis and subsequent treatment of temporomandibular disorders[1]. Accurate measurement of the three-dimensional (3D) motion of the mandible *in vivo* is essential. Existing techniques are either of limited accuracy or requiring the use of trans-oral devices that interfere with jaw movements. The current study aimed to develop further an existing 3D fluoroscopy method for measuring 3D, *in vivo* mandibular kinematics using cone-beam computerized tomography (CBCT) and its modified function of fluoroscopy imaging; and to determine the accuracy of the method on a healthy subject during opening/closing and chewing movements.

MATERIALS & METHODS

A female (age: 35 years; height: 157 cm; mass: 50 kg) participated in the current study with informed written consent as approved by the Institutional Research Board. Her maxilla and mandible were each fitted with four radiopaque crystal markers which were attached in the embrasures of the central incisors, canine and first premolar, and molars. The marker positions relative to the bones were determined using CBCT (i-CAT, Imaging Sciences International Inc., U.S.A.) with a voxel size of 0.4 mm. The segmentation and 3D reconstruction of the mandible, maxilla and radiopaque markers from the CBCT data were performed using a commercial software (Amira, Visage Imaging Inc., Berlin, Germany). The imaging for the *in vivo* measurement of the mandible kinematics was performed using the fluoroscopy function of the modified i-CAT system, giving images of sizes of 756 x 960 pixels with a pixel size of 0.254 mm x 0.254 mm at a sampling rate of 7.5 frame/s.

The subject, seated on a height-adjustable chair with her head fixed to the head-support by a belt, was first imaged by the fluoroscopy and CBCT with the mandible in the rest position. Fluoroscopy imaging was also performed at static positions with the mouth open at distances of 1 and 2 cm, as well as during opening-closing and chewing.

With the 3D fluoroscopy method, the mandibular kinematics was obtained by registering the 3D static bone models to the 2D dynamic fluoroscopic images. The formation of the fluoroscopic image of a bone was modeled as an ideal perspective projection of a point source X-ray through the bone onto the image plane. Each of the modeled X-rays went through a number of voxels of the CT volume of the bone in space. The Hounsfield numbers of these voxels were integrated along the ray and projected onto the imaging plane to obtain a digitally reconstructed radiograph (DRR). A bone model in space was defined as "registered" to the fluoroscopy image when its DRR best matched the fluoroscopic image according to a similarity measure called the weighted edge-matching score (WEMS)[2].

The measurement errors were calculated as the differences in translations and rotations between the registered bone poses using the WEMS method and the gold standard obtained using the roentgen single-plane photogrammetric analysis (RSPA) method[3]. The errors in the mandibular rotations and in the translations at both mandibular condyles were ensemble-averaged over all the image frames of all the static tests and over all the image frames of the movement cycle for each dynamic test, giving means and standard deviations. A general procedure of the study is illustrated in Fig. 1.

RESULTS

In static conditions, the means (SD) of the translation and rotation errors were all less than 0.1 (0.9) mm and 0.2° (0.6°), respectively. For dynamic tests, the means (SD) of the translation and rotation errors over the movement cycle were all less than 1.0 (1.4) mm and 0.2° (0.7°), respectively (Table 1).

DISCUSSION

The current study aimed to develop further a 3D fluoroscopy method for measuring 3D, *in vivo* kinematics of the mandible with CBCT and its modified fluoroscopy function; and to determine experimentally the accuracy and precision of the method on a healthy subject during opening/closing and chewing movements. The method was shown to have measurement errors less than 1.0 (1.4) mm for all translations, and 0.2° (0.7°) for all rotations, much smaller than previously published errors associated with skin marker movement artifacts using non-contact techniques[4].

In vivo measurement of the 3D mandibular motion without the use of interfering trans-oral devices is expected to have great potential in relevant dental clinical applications. The current method does not rely on markers or trans-oral devices so it would be useful for accurate measurement of the 3D, unlimited mandibular kinematics in the assessment of patients with missing or unstable teeth during more complicated movements.

The current method takes advantage of the CBCT system, enabling the measurement of the mandibular kinematics with a lower dose of radiation. With the modified CBCT system, both the CBCT and fluoroscopy imaging could be carried out without moving the subjects, largely reducing the time required for the measurement and any potential artifacts that might exist during the transfer between systems and affect the subsequent data analysis.

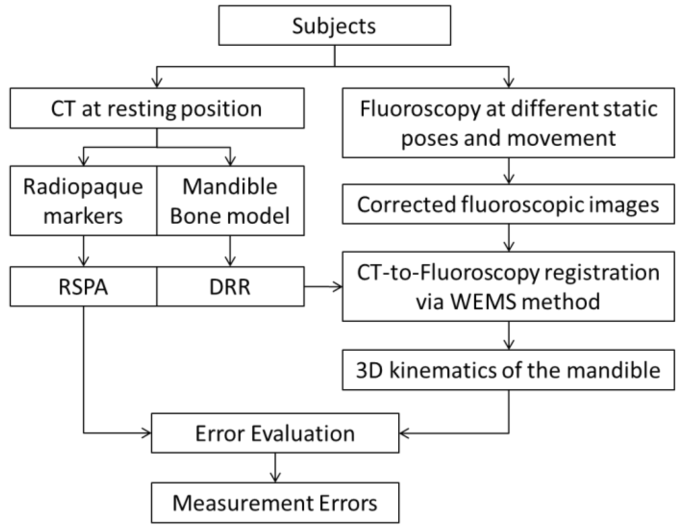

Figure 1: The general procedure of the experiments, image registration and error evaluation.

CONCLUSIONS

A 3D fluoroscopy method based on dental CBCT was proposed for measuring *in vivo* the kinematics of the mandible during static and dynamic movements. The method was shown experimentally to have measurement errors less than 1.0 (1.4) mm for all translations, and 0.2° (0.7°) for all rotations. These results suggest that the method can be used to measure the *in vivo* kinematics of the mandible during functional activities.

REFERENCES

1. Miyashita K et al. J Oral Rehabil. 1998;25:545-552
2. Tsai T-Y et al. Medical Physics. 2010;37:1273
3. Yuan X et al. J Bone Joint Surg Br. 2002;84:908-914
4. Chen C-C et al. Journal of Dental Sciences. 2011;6:95-101

Table 1: Means and standard deviations of the errors associated to the proposed method for measuring mandibular kinematics during static and dynamic tests

Joint Angle (deg)	**Error Components**					
	X	**Y**	**Z**	α	β	γ
Static	0.1 ± 0.2	0.0 ± 0.1	0.1 ± 0.9	0.1 ± 0.5	0.2 ± 0.6	0.2 ± 0.3
Open-Close	-0.1 ±0.2	0.1 ± 0.1	0.2 ± 1.2	0.2 ± 0.5	0.0 ± 0.7	0.0 ± 0.3
Chewing	-0.2 ±0.2	0.1 ± 0.1	1.0 ± 1.4	-0.2 ± 0.4	0.0 ± 0.6	-0.1 ± 0.3

Partnered human-robot stepping based on interactive forces at the hand

[1]Tiffany L. Chen, [1,2]J. Lucas McKay, [1]Tapomayukh Bhattacharjee,
[2,3]Madeleine E. Hackney, [1]Charles C. Kemp, and [1,2]Lena H. Ting

[1]Georgia Institute of Technology, Atlanta, GA, USA
[2]Emory University, Atlanta, GA, USA
[3]Atlanta VA Medical Center Rehabilitation R&D Center of Excellence, Atlanta, GA, USA
email: tiffany.chen@gatech.edu, web: http://healthcare-robotics.com/

INTRODUCTION

Cody is a humanoid robot that uses forces at its hands as cues for its movement. Using these force cues from human users, Cody has been successfully led by the hand to navigate through an obstacle course and to navigate close to a patient bedside [1]. We hypothesized that principles allowing Cody to be led by the hand could also be used for other cooperative human interactions.

Here we use partner dance as a model for cooperative physical interactions. In partner dance, motor goals (e.g., timing, direction, speed) are communicated through forces at the hands to maintain spatiotemporal synchrony between the motion of the leader and follower. Rehabilitative partner dance has been demonstrated to improve balance and gait skill for people with Parkinson's disease [2]. Thus, this work could aid our understanding of how instructors and therapists use physical interactions to aid in motor learning and rehabilitation.

We tested whether Cody could follow an experienced dancer in partnered stepping. We varied the stiffness of the robot's arms and control gain relating the measured force at the robot's hands to the commanded velocity of the robot's mobile base to see whether the robot could serve as a dance partner, and whether we could alter subjective and objective measures of dance synchrony.

METHODS

Cody is a human-scale statically stable robot weighing roughly 160 kg (Figure 1). The robot is comprised of Meka A1 arms, a Segway omni-directional base, and a Festo 1DoF vertical linear actuator. Force/torque sensors were mounted on each of the robot's wrists (ATI Mini45). The controller for the movement of Cody's base is:

$$\dot{x}_F = c \cdot f \tag{1}$$

where $\dot{x}_F$ is the commanded forward/backward velocity for the robot's mobile base, c is a constant velocity gain, and f is the sum of the forces measured at the end effectors in the forward/backward direction [1].

Figure 1: Experimental setup. Participant is shown on left wearing optical tracking markers. Robot Cody is shown on right.

We asked one participant (Female; Age: 45 years; 20 years dance experience) to lead the robot Cody in partnered stepping. The participant was instructed to hold onto the rubber balls that serve as Cody's hands and to walk backward three steps at 84 beats per minute, pause and tap her moving foot next to her stance foot, then walk forward three steps. This was repeated for four cycles. We measured the position of the human leader's sternum x_L, the position of the robot follower x_F, and the position of the participant's hands x_H using the NaturalPoint OptiTrak motion capture system.

We independently varied the velocity gain of the robot c (*high*: 0.02 m/sN vs. *low*: 0.01 m/sN) and the effective stiffness at the robot's hands when guided in the forward/backward direction (*high*: 822±269 N/m vs. *low*: 741±208 N/m). We ran three repetitions of each of these four treatments in random order. At the end of each trial, we administered a self-report questionnaire that assessed the participant's perception of how well Cody followed the participant on a 7-point Likert scale (1 = "Strongly Disagree," 4 = "Neutral," and 7 = "Strongly Agree"). We also performed a two-way ANOVA independently on each of the questionnaire responses and other measures.

RESULTS AND DISCUSSION

On average, the participant agreed with the statement that Cody was fun to dance with (Table 1) which supports the notion that Cody can successfully participate in partnered stepping. Furthermore, Cody followed closely behind the leader (Figure 2), lagging behind the human by 0.34±0.01 seconds across all treatments. The mean stepping speed was 0.13±0.01 m/s in both directions, and the mean distance between the human and robot was 0.52±0.01 m across trials.

Since the robot is very heavy and cannot be easily pushed, its motion was not based on power transfer by the human, but was due only to the controller's transformation of forces at the hand to commanded base velocity. Mean forces at the hand were 9.9±3.4 and -9.5±3.6 N for guiding the robot forward and backward, respectively, and were fairly constant across the forward and backward steps (Figure 2).

Table 1: Questionnaire ANOVA results (gain).

Question	High Gain	Low Gain	*p*
Cody was easy to move with.	5.8±0.3	4.7±0.3	0.01
Cody was too stiff.	3.0±0.4	4.8±0.4	0.02
Cody was fun to dance with.	5.5±0.2	4.8±0.2	0.05
Cody gave just enough space.	5.5±0.3	4.2 ±0.3	0.007

Table 2: Questionnaire ANOVA results (stiffness).

Question	High Stiff	Low Stiff	*p*
Cody gave just enough space.	4.3±0.3	5.3±0.3	0.03

The questionnaire results strongly suggest that the participant favored the high velocity gain setting over the low setting (Table 1) while there was a trend toward favoring the low stiffness over the high stiffness setting (Table 2). Low velocity gain resulted in larger CoM-CoM distances (*low:* 0.54±0.3 m vs. *high*: 0.52±0.3 m, p=0.005). Also, significantly higher forces between the human and robot were measured in the low versus high gain condition (*forward: high:* 6.9±0.6 N vs. *low*: 12.9±1.8 N, p<0.001; *backward: high:* -6.6±1.0 N vs. *low*: -12.4±2.8 N, p=0.002). These results are consistent with the low gain condition resembling a less proficient dance partner that lags further behind the leader and requires higher force cues.

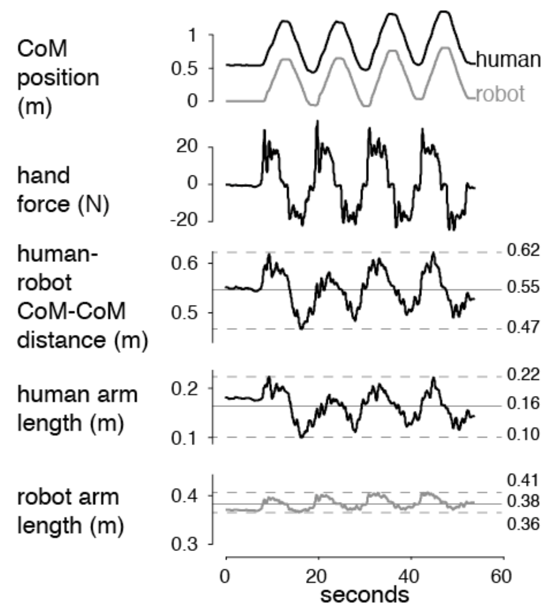

Figure 2: Forces and kinematics during partnered human-robot stepping.

CONCLUSIONS

Our results demonstrate that a humanoid robot can successfully follow the motor intentions of a human leader by interpreting the forces at the hand. The algorithm we used for leading the robot by the hand was minimally altered, suggesting common principles for cooperative physical interactions. The experienced dance leader partner preferred the condition in which the distance between the leader and follower and the forces at the hand were lower. In the future we will compare these results to those of human-human dancing and of dancers of different skill levels.

REFERENCES

1. Chen TL and Kemp CC. *Adv Robotics*, **25**, 605-627, 2011.
2. Hackney ME and Earhart GM. *Neurorehab Neural Re*, **24**, 384-392, 2010.

Altered Movement Strategy during Sit-to-Walk in Elderly Adults with History of Falling

Tzurei Chen and Li-Shan Chou

Motion Analysis Lab, Department of Human Physiology, University of Oregon, Eugene, Oregon, USA
E-mail: chou@uoregon.edu, Web: biomechanics.uoregon.edu/MAL/index.html

INTRODUCTION

Approximately one-third of older adults (65 years or older) are reported to have fallen annually. Most falls in elderly adults occur during daily activities [1,2]. Many of these activities require successful movement transitions, such as from sitting to walking. Sit-to-walk (STW) is not a sequential arrangement of two individual tasks but requires a smooth transition from sit-to-stand (STS) to gait initiation at seat-off instant [3]. However, such smooth transition is not observed in elderly adults [4,5]. Compared to young individuals, elderly adults generated a less horizontal center of mass (COM) momentum at seat-off in order to maintain a more stable upright posture before walking [4,5].

While the COM motion has been described for elderly adults during STW, investigating relation between movement strategy and joint kinetic during STW can aid in understanding potential mechanisms behind an altered STW in elderly. Therefore, the purpose of this study was to examine the differences in the movement strategy and joint kinetics during STW among three groups: healthy young adults (YA), healthy elderly adults (EA) and elderly fallers (EF).

METHODS

Ten healthy YAs (age = 25.0 ± 2.76 yrs), ten EAs (age = 77.0 ± 4.3 yrs) and ten EFs (age = 77.7 ± 9.3 yrs) have been recruited and tested in this study. EFs were those who had reported two or more falls in the prior year. Subjects were instructed to stand up from a bench, walk 3 meters, turn around, return to the chair and sit down at a self-selected speed (TUG). Subjects were told that they will be timed during the task. Whole body motion data were captured with an 8-camera motion analysis system (Motion Analysis Corp., Santa Rosa, CA). A total of 29 markers were placed on the subject's bony landmarks [6]. An adjustable height bench was placed on one force plate in order to detect the seat-off point of the STW period. The other force plate was placed under the foot that supports the subject's weight while he/she stands up.

Inclination angle of the line formed by the COM and lateral ankle marker of supporting limb was computed for each frame during STW. Sagittal plane trunk angle is also identified during STW. The hip, knee and ankle joint flexion/extension moment and the propulsion and braking impulse of the supporting limb (stance limb) during STW were investigated.

RESULTS AND DISCUSSION

The time required to complete TUG for YA, EA and EF were 7.94 ± 0.94 (STW: 1.32 ± 0.16), 9.90 ± 1.53 (STW: 1.48 ± 0.15) and 12.70 ± 3.84 (STW: 1.90 ± 0.57) seconds, respectively.

The magnitude of anterior-posterior COM-Ankle angle (AP COM-Ankle angle) was significantly greater in YA and EA than EF at seat-off (-4.06 ± 2.31, -3.03 ± 2.57, 0.51 ± 2.19, $p < 0.001$, $p = 0.007$ respectively). A negative value indicates that COM is located posterior to the ankle position. A small AP COM-ankle angle suggested that EF placed their COM within the base of support to achieve a stable posture before gait initiation. Sagittal plane trunk angles at seat-off did not differ significantly among groups (YA=36.5^{o}, EA=31.4 ^{o}, EF=32.9 ^{o}, $p = 0.333$). These results indicated that EF did not bend their trunk excessively to bring their COM closer to the supporting limb, instead they changed the ankle position.

While COM-ankle angle provide posture alignment information, ground reaction forces (GRF) and joint kinetics of the supporting limb can provide insight into the underlying mechanisms of muscular control. All groups demonstrated a braking impulse follow by a propulsive impulse at push off as shown by the AP GRF (Figure 1). When compared to YA and EA, EF demonstrated a significantly greater braking impulse and smaller propulsive impulse ($p < .001$). This greater braking impulse is used to reduce the forward COM momentum, and results in a longer STW time. The braking impulse in STS has been reported to be greater than the braking impulse during STW motion [3]. This could indicate that EF attempted to achieve an upright position before initiating gait.

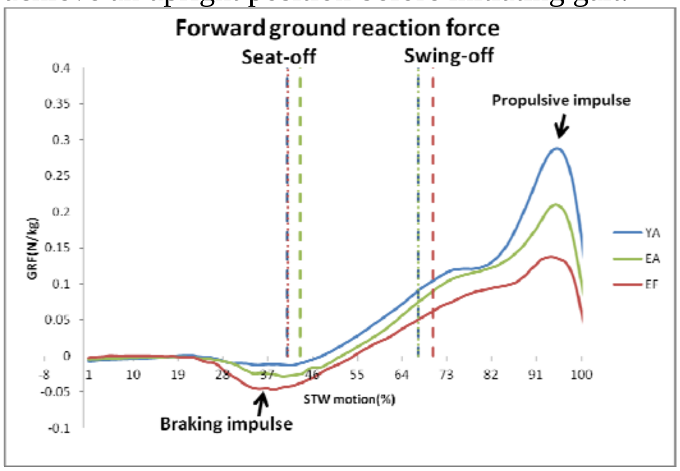

Figure 1: Mean forward GRF of the supporting limb during STW for YA, EA and EF.

YA demonstrated a trend of generating a larger hip extensor moment at seat-off than EA and EF (0.83 ± 0.16, 0.66 ± 0.31, 0.67 ± 0.14 respectively, $p = 0.179$). Smaller hip moment may suggest that EA and EF have relatively weaker hip extensor muscle. The knee extensor moment did not differ among groups (0.58 ± 0.19, 0.56 ± 0.24, 0.52 ± 0.17 respectively, $p = 0.770$). Significant differences in the sagittal plane ankle moment were found between groups at seat-off and swing-off (Figure 2, $p < .001$). Both YA and EA showed a dorsi-flexor moment while EF demonstrated a plantar-flexor moment at seat-off and swing-off. This could be related to the reduced ankle dorsi-flexor strength that has been reported in elderly adults with a history of multiple falls [7]. In addition, due to a reduced forward COM momentum and smaller hip/knee extensor movements, EF had to use their ankle plantar-flexor to push up to a standing position.

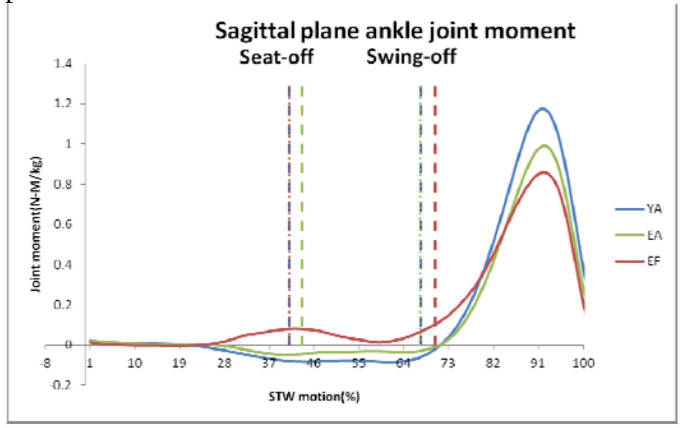

Figure 2: Mean sagittal plane angle joint moment of the supporting limb during STW for three groups. A negative value indicates a dorsi-flexor moment.

CONCLUSION

The results of this study suggest that EF tried to maintain a stable posture prior to walking during this dynamic STW task. They adjusted their foot (ankle) positions so that their COM could be located slightly anterior to ankle. In addition, EF increased the braking impulse to reduce their forward COM momentum. With small hip and knee extensor moments in EF, the above mentioned adjustments result in a greater ankle plantar-flexor moment at seat-off during STW.

REFERENCES

1. Berg, W.P., Alessio H.M. et al. (1997). *Age Ageing*, *26*, 261-8
2. Alexander, B.H., Rivara, F.P., and Wolf, M.E. (1992). *Am J Public Health*, *82*, 1020-3.
3. Magnan, A., B.J. McFadyen, and G. St-Vincent, (1996), Gait & Posture, 4, 232-41.
4. Buckley, T., et al. (2009). *J Biomech*, 42, 2318-22.
5. Kouta, M. and K. Shinkoda. (2008), *J physical therapy science*, 20, 185-9.
6. Chou, L. S., Kaufman, K. R., et al. (2003). *Gait & Posture*, 18: 125-33.
7. Wolfson et al. (1995), J Gerontology Series A, 50A, 64-7.

OLDER ADULTS EXHIBIT AN IMPAIRED ABILITY TO PREDICT MOVEMENT ACCURACY DUE TO GREATER MOTOR OUTPUT VARIABILITY

Yen-Ting Chen, Minhyuk Kwon, Jessica C Reid, Emily J Fox and Evangelos A Christou

University of Florida, Gainesville, FL, USA
email: eachristou@ufl.edu, web: http://hhp.ufl.edu/apk/ces/affil/npl/Home.htm

INTRODUCTION

The ability to predict movement accuracy is an important feature of the human motor system because it is necessary to make subsequent adjustments for the accurate execution of motor tasks [1]. The ability to predict is influenced by efference copy, sensory feedback and motor output variability [2]. During goal-directed movements, older adults are less accurate compared with young adults. The impaired accuracy in older adults may be associated with an impaired ability to predict their performance. It is unknown whether older adults can predict goal-directed movements equally well as young adults. The purpose of this study, therefore, was to compare the predictive ability of young and older adults during goal-directed movements with the elbow and ankle joints. We hypothesized that older adults will exhibit an impaired ability to predict endpoint accuracy due to greater motor output variability.

METHODS

Twenty young (25.1 ± 3.9 yrs, 10 men) and twenty older adults (71.5 ± 4.8 yrs, 10 men) participated in the study. Across two days, each subject performed 100 trials of ankle dorsiflexion and 100 trials of elbow flexion movements. The order of the limb movements was counterbalanced. During each trial, subjects attempted to match their peak position to a target. The movements were unloaded.

The target displacement was 9˚ for the ankle joint and 18˚ for the elbow joint, thus normalizing the movement to ~13% of the available range of motion for each joint. The time to target was 180 ms for both movements. After each trial, subjects predicted the endpoint of their performance by reporting the endpoint coordinates (position and time) of the peak displacement. After the prediction, visual feedback of the movement trajectory and target was provided.

Endpoint error was quantified as the absolute deviation of the endpoint displacement from the targeted position and time. Predicted endpoint error was quantified as the absolute deviation of the predicted endpoint displacement from the actual endpoint displacement. Endpoint variability was quantified independently for position and time. We used the coefficient of variation to quantify the endpoint position and time variability.

RESULTS AND DISCUSSION

Older adults exhibited greater overall error, positional variability, and time variability compared with young adults. The rate of practice-induced adaptation for the task was similar for young and older adults (young: -31.1 ± 2.5 %; older: -33.9% ± 3.0%).

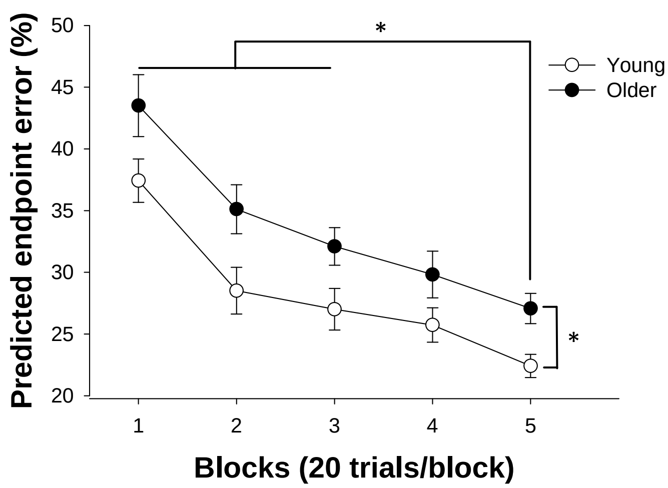

Figure 1: The ability of older adults to predict endpoint error was less accurate than young adults.

Older adults exhibited an impaired ability to predict the accuracy of goal-directed movements compared with young adults for both the upper and lower limb (Fig. 1). The ability of both young and older adults to predict endpoint accuracy improved with practice of the task (young: -34.8% ± 2.5%; older: -36.7% ± 2.5%). The predicted overall error was strongly associated with the actual endpoint error (Fig. 2; R^2=0.47).

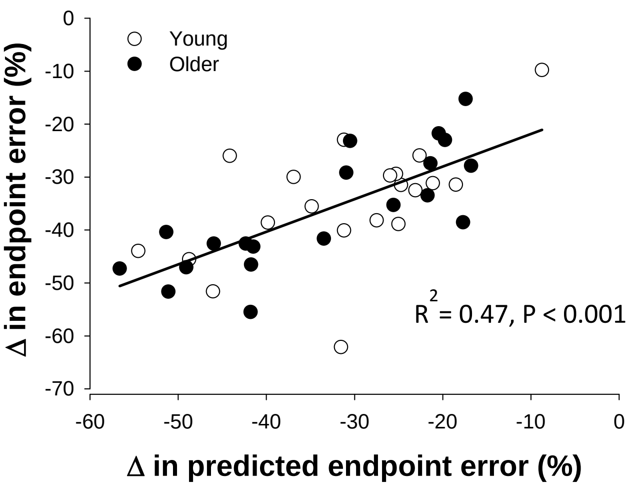

Figure 2: The predicted endpoint error was strongly associated with the actual endpoint error.

We examined the contribution of positional and time variability to the predicted endpoint error with a stepwise multiple linear regression model. We found that only time variability was associated with predicted endpoint accuracy (R^2=0.66; Fig. 3).

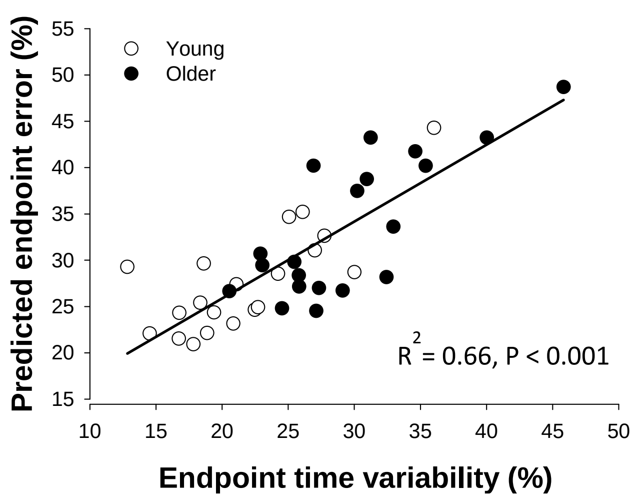

Figure 3: The time variability was strongly associated with predicted overall error.

The ability to accurately predict movements likely depends upon numerous factors including sensory feedback, efference copy, and motor output variability [2]. Our findings suggest that both young and older adults improve their prediction ability after 100 practice trials. Interestingly, this improvement in prediction ability explained about 50% of the improvement in endpoint accuracy for both groups.

We demonstrate for the first time that older adults exhibit an impaired ability to predict their own performance. This impairment is strongly associated with the amplified time variability in older adults. Therefore, motor output variability appears to be a strong contributing factor to the impaired prediction ability in older adults.

CONCLUSIONS

This experiment provides novel findings that aging impairs the ability to predict movement accuracy, likely due to motor output variability.

REFERENCES

1. Van Beer, et al. *Philos Trans R Soc Lond B Bio Sci* **357**, 1137-1145, 2004.
2. Wolpert, et al. *Nat Rev Neurosci* **12**, 739-751, 2011.

ACKNOWLEDGEMENTS

This work was supported by National Institute on Aging Grant R01 AG-031769 to E. A. Christou.

POSTURE AND ACTIVATION DEPENDENT VARIATIONS IN SHEAR WAVE SPEED IN THE GASTROCNEMIUS MUSCLE AND APONEUROSIS

Laura Chernak, Ryan DeWall and Darryl Thelen

University of Wisconsin-Madison, Madison, WI, USA
email: lchernak@wisc.edu web: http://engr.wisc.edu/groups/nmbl

INTRODUCTION

Musculotendon tissue interactions are strongly dependent on the morphological and mechanical characteristics of the aponeurosis [1]. Despite its mechanical significance, the material properties of the aponeurosis are not well understood. In fact, the literature reports conflicting results concerning the relative stiffness of tendon and aponeurosis tissue [2, 3], which may arise from the challenge of collecting repeatable measures from the *in vivo*, intact aponeurosis. The newly developed elastography technique of Supersonic Shear Imaging (SSI) may address this challenge. This novel ultrasonic method uses acoustic radiation force to induce transient shear waves within tissue, which are then tracked using high frame rate imaging [4]. In prior studies, SSI has shown promise in obtaining repeatable mechanical measures from the relaxed gastrocnemius [5], and has also demonstrated the ability to capture an increase in muscle stiffness with contraction [6].

In the current study, we investigated the capability of SSI to characterize load and posture dependent changes in aponeurosis tissue stiffness. It was hypothesized that shear wave speed, which is related to tissue stiffness [7], would be greater in the aponeurosis than the muscle, and would increase in both tissues with contraction. We also investigated the effect on shear wave speed of varying the knee angle, which modulates the length of the biarticular gastrocnemius.

METHODS

Data were collected from five healthy young adults. Subjects were asked to lie prone on an examination table while ultrasonic shear wave data were collected from the lateral gastrocnemius (AixPlorer Scanner, Supersonic Imagine, Aix en Provence, France). Five SSI images were collected during passive relaxation and active isometric contraction of the gastrocnemius at knee angles of 0°, 45° and 90°.

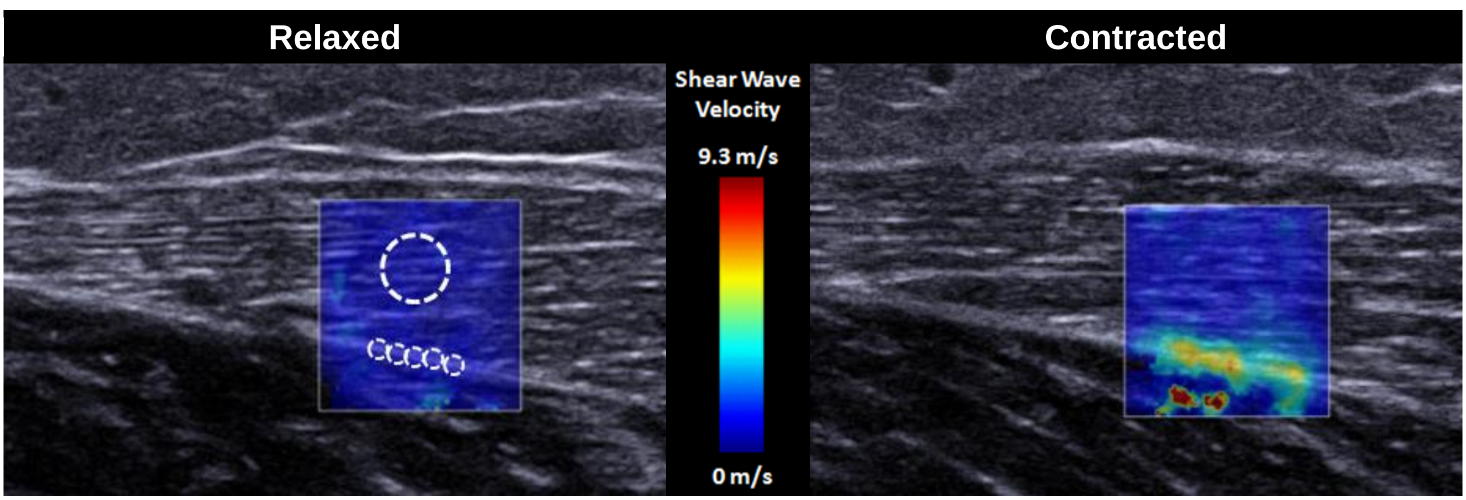

Figure 1: Representative B-mode images with shear wave speed information collected at a 45° knee angle. Average shear wave speeds were obtained from a 4 mm diameter ROI within the muscle belly and from five 1 mm diameter ROIs along the aponeurosis as shown in the image on the left. The increase in shear wave speed along the aponeurosis with active muscle contraction is clear from the bright yellow color noted along the anatomical structure.

Following data collection, shear wave speeds within the tissues were obtained from regions of interest (ROIs) manually placed within the muscle belly and along the aponeurosis (Fig. 1). Paired t-tests were used to evaluate the influence of contraction state and knee angle on shear wave speed.

RESULTS AND DISCUSSION

The muscle shear wave speeds ranged from 2.1-4.4 m/s, which is comparable to results reported previously for the gastrocnemius [5, 6]. As hypothesized, the aponeurosis demonstrated significantly higher shear wave speeds than the muscle for all knee angles. Also as hypothesized, shear wave speed increased significantly for both tissues when contracted at all knee angles, except the muscle at a 90° knee angle.

An increase in knee flexion led to a significant decrease in shear wave speed in the aponeurosis in the relaxed state, with a similar trend noted in the muscle (Fig. 2). This is consistent with the lower passive stiffness that is expected in the shortened gastrocnemius in a flexed knee posture (90°). Muscle shear wave speed was found to be highest when the muscle was active and lengthened (0°, extended knee). Aponeurosis stiffness also increased in the contracted state, but there was no significant effect of knee angle on stiffness, which may indicate the tissue is beyond the toe region of the stress-strain curve for all contracted states.

The results from this preliminary study suggest that SSI is capable of distinguishing posture and activation dependent changes in the mechanical properties of the gastrocnemius and aponeurosis tissues. Hence, this new, noninvasive, quantitative technology has substantial potential for both basic biomechanics and clinical applications. For example, it may be feasible to use the shear wave speed measures to characterize changes in tissue mechanical properties with injury, exercise and clinical treatment. We note that direct evaluation of the free tendon remains challenging due to the high stiffness of tendon which facilitates shear wave speeds that may exceed the current maximum measurable speed of the scanner (16.3 m/s). While elastic modulus can be ascertained from shear wave speed in homogeneous isotropic materials [4], further work is needed to better understand shear wave propagation in fibrous tissues with complex architectures.

REFERENCES

1. Rehorn MR, et al., *J Biomech* **43**, 2574-81, 2010.
2. Magnusson SP, et al., **177**, 185-95, 2003.
3. Lieber RL, et al., **261**, C86-92, 1991.
4. Bercoff J, et al., *IEEE Trans Ultrason Ferroelectr Freq Control* **51**, 396-409, 2004.
5. Arda K, et al., *AJR Am J Roentgenol* **197**, 532-6, 2011.
6. Shinohara M, et al., *Muscle Nerve* **42**, 438-41, 2010.
7. D'Onofrio M, et al., *AJR Am J Roentgenol* **195**, 132-6, 2010.

ACKNOWLEDGEMENTS

NIH AR056201, Kenneth Lee, MD.

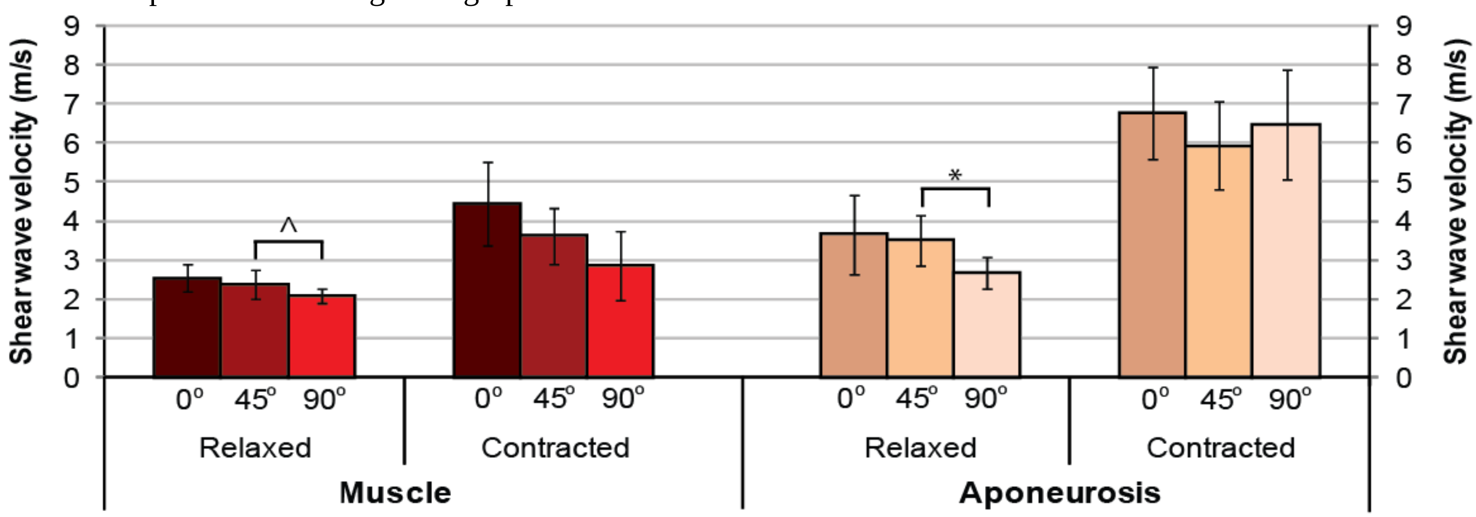

Figure 2: The effect of knee angle (0°, 45° and 90°) on average shear wave speeds (mean ± SD) in the muscle and aponeurosis tissues. *$p < 0.05$, ^$p < 0.10$

POSTURE AND ACTIVATION DEPENDENT VARIATIONS IN SHEAR WAVE SPEED IN THE GASTROCNEMIUS MUSCLE AND APONEUROSIS

Laura Chernak, Ryan DeWall and Darryl Thelen

University of Wisconsin-Madison, Madison, WI, USA
email: lchernak@wisc.edu web: http://engr.wisc.edu/groups/nmbl

INTRODUCTION

Musculotendon tissue interactions are strongly dependent on the morphological and mechanical characteristics of the aponeurosis [1]. Despite its mechanical significance, the material properties of the aponeurosis are not well understood. In fact, the literature reports conflicting results concerning the relative stiffness of tendon and aponeurosis tissue [2, 3], which may arise from the challenge of collecting repeatable measures from the *in vivo*, intact aponeurosis. The newly developed elastography technique of Supersonic Shear Imaging (SSI) may address this challenge. This novel ultrasonic method uses acoustic radiation force to induce transient shear waves within tissue, which are then tracked using high frame rate imaging [4]. In prior studies, SSI has shown promise in obtaining repeatable mechanical measures from the relaxed gastrocnemius [5], and has also demonstrated the ability to capture an increase in muscle stiffness with contraction [6].

In the current study, we investigated the capability of SSI to characterize load and posture dependent changes in aponeurosis tissue stiffness. It was hypothesized that shear wave speed, which is related to tissue stiffness [7], would be greater in the aponeurosis than the muscle, and would increase in both tissues with contraction. We also investigated the effect on shear wave speed of varying the knee angle, which modulates the length of the biarticular gastrocnemius.

METHODS

Data were collected from five healthy young adults. Subjects were asked to lie prone on an examination table while ultrasonic shear wave data were collected from the lateral gastrocnemius (AixPlorer Scanner, Supersonic Imagine, Aix en Provence, France). Five SSI images were collected during passive relaxation and active isometric contraction of the gastrocnemius at knee angles of 0°, 45° and 90°.

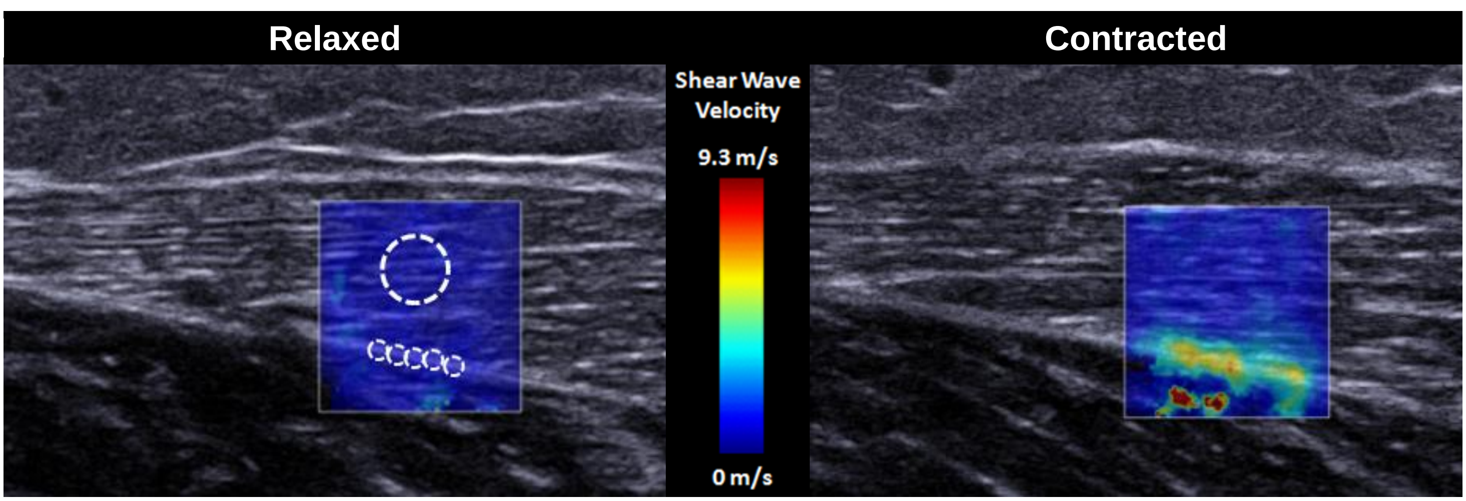

Figure 1: Representative B-mode images with shear wave speed information collected at a 45° knee angle. Average shear wave speeds were obtained from a 4 mm diameter ROI within the muscle belly and from five 1 mm diameter ROIs along the aponeurosis as shown in the image on the left. The increase in shear wave speed along the aponeurosis with active muscle contraction is clear from the bright yellow color noted along the anatomical structure.

Following data collection, shear wave speeds within the tissues were obtained from regions of interest (ROIs) manually placed within the muscle belly and along the aponeurosis (Fig. 1). Paired t-tests were used to evaluate the influence of contraction state and knee angle on shear wave speed.

RESULTS AND DISCUSSION

The muscle shear wave speeds ranged from 2.1-4.4 m/s, which is comparable to results reported previously for the gastrocnemius [5, 6]. As hypothesized, the aponeurosis demonstrated significantly higher shear wave speeds than the muscle for all knee angles. Also as hypothesized, shear wave speed increased significantly for both tissues when contracted at all knee angles, except the muscle at a 90° knee angle.

An increase in knee flexion led to a significant decrease in shear wave speed in the aponeurosis in the relaxed state, with a similar trend noted in the muscle (Fig. 2). This is consistent with the lower passive stiffness that is expected in the shortened gastrocnemius in a flexed knee posture (90°). Muscle shear wave speed was found to be highest when the muscle was active and lengthened (0°, extended knee). Aponeurosis stiffness also increased in the contracted state, but there was no significant effect of knee angle on stiffness, which may indicate the tissue is beyond the toe region of the stress-strain curve for all contracted states.

The results from this preliminary study suggest that SSI is capable of distinguishing posture and activation dependent changes in the mechanical properties of the gastrocnemius and aponeurosis tissues. Hence, this new, noninvasive, quantitative technology has substantial potential for both basic biomechanics and clinical applications. For example, it may be feasible to use the shear wave speed measures to characterize changes in tissue mechanical properties with injury, exercise and clinical treatment. We note that direct evaluation of the free tendon remains challenging due to the high stiffness of tendon which facilitates shear wave speeds that may exceed the current maximum measurable speed of the scanner (16.3 m/s). While elastic modulus can be ascertained from shear wave speed in homogeneous isotropic materials [4], further work is needed to better understand shear wave propagation in fibrous tissues with complex architectures.

REFERENCES

1. Rehorn MR, et al., *J Biomech* **43**, 2574-81, 2010.
2. Magnusson SP, et al., **177**, 185-95, 2003.
3. Lieber RL, et al., **261**, C86-92, 1991.
4. Bercoff J, et al., *IEEE Trans Ultrason Ferroelectr Freq Control* **51**, 396-409, 2004.
5. Arda K, et al., *AJR Am J Roentgenol* **197**, 532-6, 2011.
6. Shinohara M, et al., *Muscle Nerve* **42**, 438-41, 2010.
7. D'Onofrio M, et al., *AJR Am J Roentgenol* **195**, 132-6, 2010.

ACKNOWLEDGEMENTS

NIH AR056201, Kenneth Lee, MD.

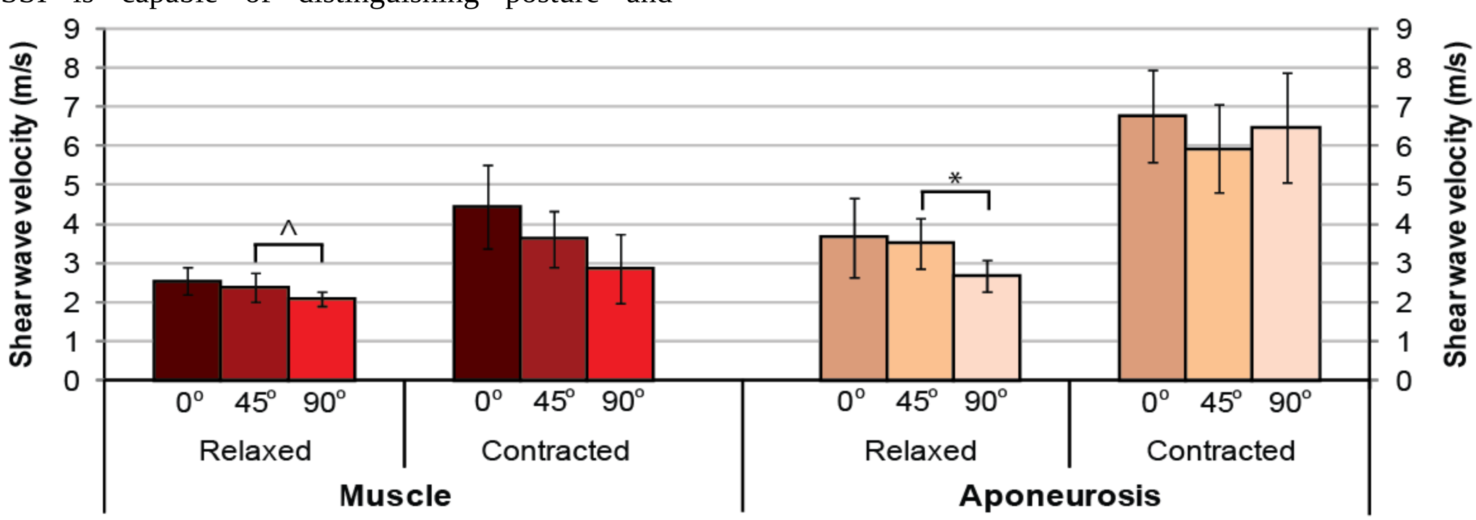

Figure 2: The effect of knee angle (0°, 45° and 90°) on average shear wave speeds (mean ± SD) in the muscle and aponeurosis tissues. *p < 0.05, ^p < 0.10

MODULATION OF STIFFNESS ON IMPACT LOADINGS DURING RUNNING

[1]Roy T.H. Cheung, [1]Michael J. Rainbow, [2]Allison Altman, [1]Irene S. Davis

[1]Harvard Medical School, Cambridge, MA, USA
[2]University of Delaware, Newark, DE, USA
email: isdavis@partners.org, web: http://www.runsnrc.org

INTRODUCTION

Tibial stress fractures are one of the most common injuries that runners sustain. Studies have demonstrated that tibial stress fractures are related to loading parameters, such as peak tibial shock (TS), average (VALR), and instantaneous loading rates (VILR) of the vertical ground reaction force (GRF) [1,2]. It has also been shown that these loading parameters can be reduced through a gait retraining program using real-time biomechanical feedback [3]. Through retraining, runners were able to reduce their tibial shock by approximately 50%, using a number of ankle and knee adaptive strategies [4]. However, there is likely some commonality among all of the strategies that resulted in reduced TS and loading rates.

The mass-spring model has been widely used to evaluate different running techniques. This model predicts the vertical ground reaction force given mass, initial vertical velocity, and stiffness. A modified model with dual stiffness values was established to more accurately predict the vertical GRF than a single, average stiffness value [5]. The transition from high (K_H) and low (K_L) stiffness follows the pattern of impact phase and propulsive phase, respectively, in a GRF curve in running. Additionally, vertical velocity at initial contact (VV) provides information about the flight phase and indirectly indicates the vertical displacement throughout the flight phase. Since the gait retraining focused on reducing loading during impact [3], it is plausible that the reduction of impact loading may be resulted from a lower K_H or VV, but not K_L. Therefore, the purpose of this study was to examine these variables before and after gait retraining. In addition, relationships between reduction in impact loading and changes in K_H, and VV were explored. It was hypothesized that vertical stiffness during impact phase (K_H) and vertical velocity at initial contact (VV) would be reduced following gait retraining and such reductions were correlated with the reduction of impact loading parameters.

METHODS

Sixteen recreational runners (9 females, 7 males; age= 24.9±6.8 years; height= 1.75±0.09 m; mass= 75.4±14.8 kg) with high tibial shock (≥8 g) were recruited in this study. All participants were regular runners (≥10 miles per week) with a heel-strike landing pattern and free from any active injuries.

All subjects underwent a baseline gait analysis. The leg with higher tibial shock prior to training was identified as the tested limb. A lightweight accelerometer (Model 356A32, PCB Piezotronics Inc., Depew, NY) was securely taped to the anteromedial aspect of the distal tibia of the tested limb, aligned with its long axis. All participants ran at 3.7 m/s (±5%) across a force plate (Bertec Corp., Worthington, OH) located in the center of a 23-m runway. The sampling rate of accelerometer and force plate was 1080 Hz. All underwent a 2-week gait retraining protocol that has previously been reported [3]. In brief, subjects were instructed to run 'softer and quieter' with the visual guidance from biofeedback of their real-time TS and a reference line representing 50% of their pre-training TS. Participants were again assessed after gait retraining

Accelerometer and GRF data were filtered with a dual pass Butterworth filter at 75 Hz and 50 Hz respectively. Data from five running trials were averaged for each subject. We calculated the COM acceleration by dividing the vertical GRF by body mass. Vertical velocity and displacement were obtained by a single- and a double-integration of COM acceleration. We found the integration constant by assuming that the net vertical velocity during stance phase was zero. The slopes of the most linear portion in the two transitions of the force-displacement hysteresis graph represented K_H and K_L [5] (**Figure 1**).

Paired-sample t tests were used to compare TS, VALR, VILR, K_H, K_L, and VV before and after gait retraining. Pearson's correlations were used to explore the association between impact loading reduction and changes in K_H, K_L, and VV.

RESULTS AND DISCUSSION

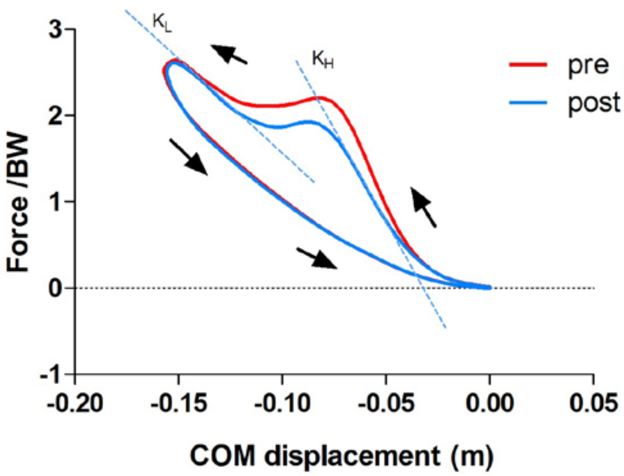

Figure 1: Hysteresis curve of a representative subject (Mean of five trials). K_H and K_L represent high- and low-stiffness of the COM during the stance phase of the running cycle.

As previously reported, there were significant reductions in TS and loading rates following the retraining [3]. K_H and VV were also reduced following gait retraining (**Table 1**). K_L remained unchanged. These findings indicate that runners lowered the TS and load rates by reducing K_H. K_H is associated with the impact phase of running, which was the focus of the retraining program. As the retraining did not influence the propulsive phase of the vertical ground reaction force, the lack of change in K_L was not surprising.

As expected, we also found a strong relationship between K_H reduction with reduction in TS (r_p=0.765, p=0.001), VALR (r_p=0.903, p<0.001), and VILR (r_p=0.890, p<0.001). This suggests that the greater the reduction in vertical stiffness at impact, the lower the impact loading. Conversely, reductions in VV were not related to reductions in any of the loading variables. However, a lower vertical velocity of the COM at impact does suggest less vertical displacement of the COM over the entire running cycle following gait retraining. Less vertical displacement reduces the total kinetic energy that needs to be dissipated.

As stiffness is modulated by muscular activity, future studies should explore the effect of gait retraining on electromyographic changes in selected hip, knee and ankle muscles. This information would be useful to those developing strengthening protocols to augment the retraining programs.

CONCLUSIONS

Despite differing adaptive strategies at the ankle and knee joints, individuals all appear to modulate their COM dynamics, in terms of reducing vertical stiffness, in order to reduce their tibial shock and load rates after gait retraining.

REFERENCES

1. Davis IS, et al. *Med Sci Sports Exerc* **35**, S58, 2004.
2. Milner CE, et al. *Med Sci Sports Exerc* **38**, 323-8, 2006.
3. Crowell HP, et al. *Clin Biomech* **26**, 78-83, 2011.
4. Bowser B, et al. *Med Sci Sports Exerc* **43**, 15, 2011.
5. Hunter I. *J Sports Sci Med* **2**, 139-43, 2003.

Table 1: Loading variables and dynamics of COM in runners before and after gait retraining. (Mean and SD)

	TS (g)	VALR (BW s^{-1})	VILR (BW s^{-1})	K_H (kNm^{-1})	K_L (kNm^{-1})	VV (ms^{-1})
Pre training	10.71 ± 2.6	117.0 ± 31.2	97.2 ± 26.0	39.0 ± 10.0	14.2 ± 4.2	1.94 ± 0.16
Post training	5.89 ± 2.7	77.9 ± 28.5	66.3 ± 25.3	27.2 ± 9.3	14.4 ± 4.2	1.84 ± 0.16
% change	-45.1%	-31.7%	-30.8%	-28.2%	+3.3%	-5.3%
P	<0.001	<0.001	<0.001	<0.001	0.860	<0.001

THE EFFECT OF VIBROTACTILE STIMULATION ON LONG RANGE CORRELATION OF STRIDE INTERVAL TIME SERIES AMONG DIFFERENT WALKING SPEEDS

[1,2]Jung Hung Chien, [1,2]Chun-Kai Huang, [1]Srikant Vallabhajosula, [1]Mukul Mukherjee
[1,2]Ka-Chun Siu, [1,2]Nicholas Stergiou

[1]Nebraska Biomechanics Core Facility, University of Nebraska at Omaha, Omaha, NE, USA
[2]College of Public Health, University of Nebraska Medical Center, Omaha, NE, USA
email: jchien@unomaha.edu web: http://nbcf.unomaha.edu/

INTRODUCTION

Successful postural control requires the integration of three major sensory systems: visual, somatosensory, and vestibular system[1]. A decline in postural control (e.g. increasing body sway) is common in patients with diabetic neuropathy, stroke and individuals with increasing age[2-4]. One way of addressing this problem is using vibrotactile stimulation (VS) [2-4]. VS has shown to increase the detectability of weak somatosensory signals and reduce postural sway during standing[2-4]. For locomotion, it has been shown that stride interval variability (an indicator of falls) decreased when VS was applied on the insole of elderly fallers as they walked at their Preferred Walking Speed (PWS)[5]. However, as we move at speeds higher/lower than PWS, stride interval variability is affected[6]. Specifically, when the speeds become higher/lower, the long range correlation of the stride interval time series was more persistent than the PWS[6]. This means that at speeds higher/lower than PWS, locomotion is more rigid as opposed to PWS where there is more variability. However, it is not known how VS will affect this relationship as we walk at speeds different from the PWS. It is crucial to answer this question because the presence of long range correlations in stride interval variability has been found to be related to the balance control during walking[7] and changes in walking speeds[6]. Therefore, our current study attempted to answer this question. We hypothesized that VS can influence the long range correlations of stride interval time series among different walking speeds.

METHODS

Ten healthy young individuals participated in this study. Participants were excluded if they had a history of cardiovascular, neurological, and/or musculoskeletal disorders. Three-dimensional motion of markers attached to anatomical locations was collected by the 3D Investigator motion capture system (Northern Digital Inc., Waterloo, Ontario, Canada). Participants then completed 10 five-minute trials at each of the following percentages of their PWS: 80%, 90%, 100%, 110% and 120% with and without the VS. The stride interval was defined as the time between two consecutive heel contacts of the same leg using the heel marker position data via custom software (MatLab, Mathworks, Inc., Natick, MA). Two hundred and fifty consecutive strides were used for data analysis in each trial based on the maximum number of strides available from the slowest walking participant. All trials were then cut to this length. Detrended Fluctuation Analysis (DFA) was performed on the stride interval time series of each trial. The DFA was used to determine the strength of long-range correlations over time and provide a measure of the *temporal structure* of variability (α-value). If the α-value is equal to 0.5, the motion is considered to be a random walk. If the α-value is greater than 0.5, the long-range correlation is a positively persistent long range correlation. This means that two stride intervals a certain distance apart (depends on window size) are positively related; when one increases, the other also increases. Whereas if the α-value is smaller than 0.5, the long-range correlation is anti-persistent. This means that two stride intervals a certain distance, are negatively related; when one increases, the other decreases. The range of window sizes of the DFA was selected from $n_1 = 4$ to $n_m = N/4$, where N is the number of stride intervals[6]. The vibrotactile

Figure 1. The vibrotactile stimulation system.

stimulation system contains: three vibrating elements, called tactors (C2, Engineering Acoustics, FL, USA.), which were embedded in a lab-designed custom insole to produce vibrations to the plantar foot surface. The vibrations were generated from a set of signals, whose frequency and magnitude were set independently for each foot, from a portable control unit (Fig. 1). The frequency of VS was set to 250Hz and magnitude was set to 17.5 db. To identify the relationship of the dependent variable (α-values) with percentage of PWS, trend analyses were utilized. A two-way (2 conditions x 5 speeds) repeated measure ANOVA was used to investigate the effect of VS on the α-values of the stride interval time series for the different speeds. Post hoc analysis was performed using the Tukey test when a significant main effect was found. Statistical analysis was completed in SPSS 16.0 (IBM Corporation, Armond, NY).

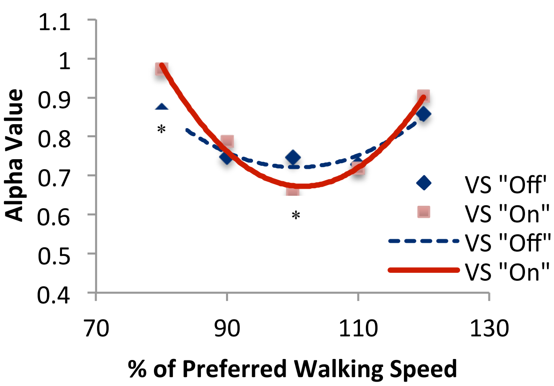

Figure 2: Group means of α values of the stride interval time series from five different walking conditions: (80%, 90%, 100%, 110% and 120% of preferred walking speeds). *: $p < 0.05$.

RESULTS AND DISCUSSION

Significant quadratic relationships were found between the α-values of the stride interval time series and the percentage of PWS when VS were "On" (F = 4.425, $p = 0.004$) and "Off" (F = 3.061, $p = 0.002$) (Fig. 2). A significant interaction was shown between conditions and walking speeds (F = 3.156, $p = 0.045$). The Post hoc test showed that the α-value was significantly smaller when VS was "On" than when VS was "Off" at 100% of PWS. In addition, the α-value was significantly larger when VS was "On" than when VS was "Off" at 80% of PWS.

In the present study, we investigated how VS affects the long range correlation of stride interval time series among different speeds. We found that a quadratic relationship exists in the α-values of DFA (a temporal structure variability measure) when VS was "On" and "Off". This result showed that regardless the status of VS ("On" or "Off"), the temporal structure of gait variability exhibited long-range correlations revealing a fractal-like scaling behavior. The smaller α-values at PWS indicate that gait variability at PWS exhibits more effective adaptability than at faster or slower speeds[6]. The significantly lower α-values when VS was "On" than when VS was "Off" indicates that VS increased this characteristic and made the system even more adaptable to environmental stresses. Within the dynamic system framework, lower α-values at PWS when VS was "On" represented a more stable system, which might enhance dynamic balance during walking[6]. However, higher α-values when VS was "On" than when VS was "Off" constrained this adaptability at slowest walking condition (80% of PWS). Therefore, VS affects locomotion at different speeds, differently than normal locomotion.

CONCLUSIONS

Noise-based devices, such as vibrating shoe insoles can affect the effective adaptability of a locomotor system. However, this effect depends on the walking speed.

REFERENCES

1. Patla AE, et al., *J Exp Psychol Hum Percept Perform* **17**, 603-634, 1991.
2. Priplata AA, et al., *Lancet* **362**, 1123-11234, 2003.
3. Priplata AA, et al., *Phys Rev Lett* **89**, 238101, 2002.
4. Priplata AA, et al., *Ann Neurol* **59**, 4-12, 2006.
5. Galica AM, et al., *Gait Posture* **30**, 383-387, 2009
6. Jordan K, et al., *Exerc. Sport Sci. Rev* **36,** 200-204, 2008
7. Hausdorff JM. *Chaos* **19,** 026113, 2009.

ACKNOWLEDGEMENTS

This work was funded by NASA EPSCoR NNX11AM06A.

CLINICAL BALANCE MEASURES ARE ASSOCIATED WITH VARIABILITY OF INTER-JOINT COORDINATION DURING WALKING IN ELDERLY ADULTS

Shiu-Ling Chiu and Li-Shan Chou
Department of Human Physiology, University of Oregon, Eugene, Oregon 97403, USA.
email: chou@uoregon.edu, web: http://biomechanics.uoregon.edu

INTRODUCTION

Fall is a serious problem in elderly adults. High variability of various gait parameters has been reported to be associated with high risks of fall [1]. However, such association remains to be investigated. Walking is a dynamic task that involves higher orders of neuromuscular controls integrating with sensory inputs to produce coordinated limb movements [2]. Examining the inter-joint coordination that directly reflects the neuromuscular control and comparing its variability between healthy and fall-prone elderly adults may provide insights into the underlying mechanisms of fall risks. Also, clinical implication for the variability of inter-joint coordination requires further exploration. The purpose of this study was to examine the characteristics of inter-joint coordination variability in healthy (non-fallers) and fall-prone (fallers) elderly adults and to determine its correlations to commonly used clinical balance measures.

METHODS

Thirty elderly adults were recruited and divided into two groups. Fifteen healthy elderly subjects (8 men, age = 75.7 ± 4.7 yrs, BMI = 26.7 ± 4.1 kg/m^2) and 15 elderly subjects who had experienced at least two unintentional falls to the ground in the year prior to the testing date (3 men, age = 72.9 ± 4.1 yrs, BMI = 29.6 ± 8.4 kg/m^2, # of falls = 3.2 ± 1.2). A 10-camera motion analysis system (Motion Analysis Corp., Santa Rosa, CA) was used to collect the whole body motion data during level walking. All subjects were asked to walk along a 10-m walkway with self-selected comfortable speed. A total of 29 reflective markers were placed on bony landmarks. Five successful walking trials were collected from each subject for data analysis. Sagittal plane joint kinematics of the bilateral lower extremities was calculated by using OrthoTrak kinematic analysis software (Motion Analysis Corp).

Continuous relative phase (CRP), derived from the phase portraits of two adjacent joints (hip-knee or knee-ankle), was used to investigate the variability of inter-joint coordination [3]. The variability of inter-joint coordination for each subject was calculated as the average standard deviation of all points on the ensemble CRP curve over a gait cycle, namely the deviation phase (DP). Clinical balance tests, including Burg Balance Scale (BBS), Dynamic Gait Index (DGI) and Time Up and GO (TUG), were performed. Independent *t*-test was used to detect group differences in walking speeds and measures from clinical balance tests. Group differences in DP values were examined using ANOVA with walking speeds as covariates [3]. Pearson correlation coefficient was used to determine the correlations between DP values of all subjects and clinical balance tests.

RESULTS AND DISCUSSION

The non-fallers walked significantly faster than the fallers (p=0.003, Table 1). The fallers showed poorer performances in clinical balance tests when compared to the non-fallers (p<0.003; Table 1).

For the variability of inter-joint coordination, no significant group differences were detected in hip-knee DP values (Fig. 1). The differences observed in the variability of hip-knee inter-joint coordination in the stance phase were due to different walking speeds. However, significant group differences were detected in knee-ankle DP values (Fig. 2). The fallers had significantly greater knee-ankle DP values in the stance phase but smaller knee-ankle DP values in the swing phase, as compared to the non-fallers (p=0.03 and p=0.04, respectively). During stance, higher variability of knee-ankle inter-joint coordination in fallers may indicate a lack of steady control for body weight supports. In contrast, during swing, lower variability of knee-ankle inter-joint coordination in fallers could suggest a poor adaptive control for swing foot trajectories.

The hip-knee DP values demonstrated a negative correlation with DGI (p=0.001), the knee-ankle DP values had a negative correlation with DGI (p=0.016) and a positive correlation with TUG (p=0.049). This indicated that high variability of hip-knee and knee-ankle inter-joint coordination in the stance phase are associated with poor balance controls in elderly adults.

CONCLUSIONS

Our results suggested that the clinical implication for the variability of inter-joint coordination during walking in elderly adults could be identified by DGI. The variability differences in knee-ankle inter-joint coordination between non-fallers and fallers may contribute to the fall risks in fallers during walking. While the proximal joints play important roles in maintaining dynamic balance and modulating walking speeds during walking [3,4], the fine tuning of distal joints seem to be critical for a secure control strategy against falling in elderly adults.

REFERENCES

1.Hausdorff, JM. *Hum Move Sci.* **26**, 555-589, 2007.

2.Winter, DA. *Phys Ther* **72**, 45-53, 1992.

3.Chiu, SL, et al. *J of Biom* **45**, 275-280, 2012.

4.Winter, DA. *Gait & Posture* **3**, 193-214, 1995.

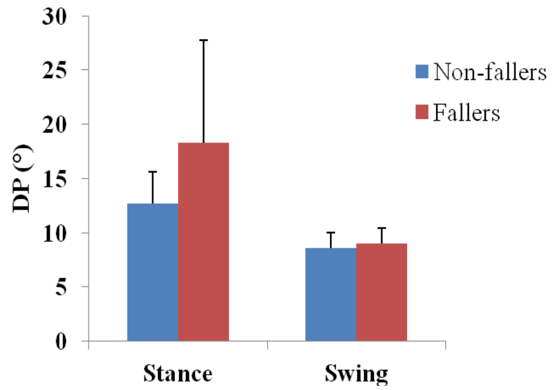

Figure 1: Variability of hip-knee inter-joint coordination in stance and swing phases.

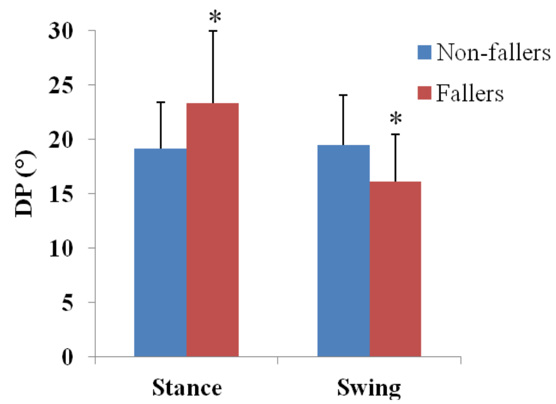

Figure 2: Variability of knee-ankle inter-joint coordination in stance and swing phases. (* group differences)

Table 1: Mean (SD) of walking speeds and clinical balance tests for non-fallers and fallers.

	Non-faller	Faller
Gait velocity (m/s)	1.22 (0.14)	1.07 (0.12) *
BBS	55.47 (0.74)	53.44 (1.15) *
DGI	23.60 (0.74)	22.56 (1.03) *
TUG (s)	7.49 (1.20)	9.06 (1.26) *

*Significant group differences, p<0.05.

Table 1: Pearson correlation coefficient (r) between overall DP values and clinical balance tests.

	Stance		Swing	
Clinical tests	Hip-Knee	Knee-Ankle	Hip-Knee	Knee-Ankle
BBS	-0.187	-0.284	-0.062	0.275
DGI	-0.559 *	-0.437 *	-0.100	-0.021
TUG (s)	0.236	0.362 *	0.313	-0.235

*Significant correlation, p<0.05.

ANALYSIS OF THE BIOMECHANICAL CHARACTERISTICS OF THE SPINAL INTERSPINOUS IMPLANTS

[1]Dae Kyung Choi, [1]Yoon Hyuk Kim and [2]Kyungsoo Kim

[1]University of Kyung Hee, Yongin, Gyeonggi, KOREA
[2]University of Kyonggi, Suwon, Gyeonggi, KOREA
email: yoonhkim@khu.ac.kr

INTRODUCTION

Spinal decompression surgery with spinal fusion is a widely used surgical procedure for the treatment of degenerative spine in the lumbar spine. However, it has been known that spinal decompression surgery causes the spinal instability. Some cadaveric and finite element (FE) studies have reported that adjacent segment degeneration may reduce adverse effects on the adjacent levels resulting from fusion by maintaining physiologic ROM as well as pressure. Therefore the interspinous implants have been recently used due to its advantages such as motion preserving and less subsidence of the implant to the osteoporotic bone.

Some of biomechanical studies have been performed to analyze biomechanical behaviors of the lumbar spine with interspinous implants [1-3]. Those studies have reported that interspinous implants affect increase of spinal stabilization and decrease of intradiscal pressure in extension [1]. However, the various influences by different types of interspinous implants on the lumbar spine are still unknown. In this study, the biomechanical effects of interspinous process implants was investigated for various implants under extension loading condition based on finite element analysis.

METHODS

A three dimensional FE model of a lumbar spinal motion segment from L3 to L4 was reconstructed from 1-mm thickness of computed tomography (CT) images. The CT images were taken from a healthy male volunteer whose height and age were 175 cm and 21 years old.

The FE model consists of two vertebrae, one intervertebral disc, and seven major ligaments (anterior longitude ligament (ALL), posterior longitude ligament (PLL), flaval ligament (FL), inter transverse ligament (ITL), inter spinal ligament (ISL), supra spinal ligament (SSL), and capsular ligament (CL)). The information of material properties and the attachment points of ligaments were taken from literatures [4,5].

In this study, biomechanical characteristics of Coflex (Paradigm Spine, Wurmlingen, Germany), Wallis (Abbott Laboratories, Bordeaux, France), Viking (Sintea Plustek, Assago, Italy) and Interspinous Spacer (Seohancare, Gyeonggi, Korea) were investigated.

Each three dimensional CAD model of the implants was made based on respective designs. Material properties of titanium (E=113GPa, v=0.3) was adapted for the FE model of Coflex, and polyehteretherketone (PEEK; E=4GPa, v=0.25) for the models of Wallis, Viking and Interspinous Spacer (Fig. 1a). The individual FE model of the lumbar spine, in which each interspinous implant was inserted by its surgical protocol, was generated (Coflex, Wallis, Viking and Interspinous Spacer) (Fig. 1b). Nonlinear surface to surface contact conditions with a frictional coefficient of 0.2 were assumed between the implant and the bone in all models.

Inferior plane of L4 vertebra was fixed in all directions and pure extension moment of 7.5 Nm was applied on the superior plane of L3 vertebra in each model. The intersegmental rotation angle of the motion segment and von-Mises stress on the interspinous process were analyzed using ABAQUS Standard™ (SIMULIA, Providence, RI, USA).

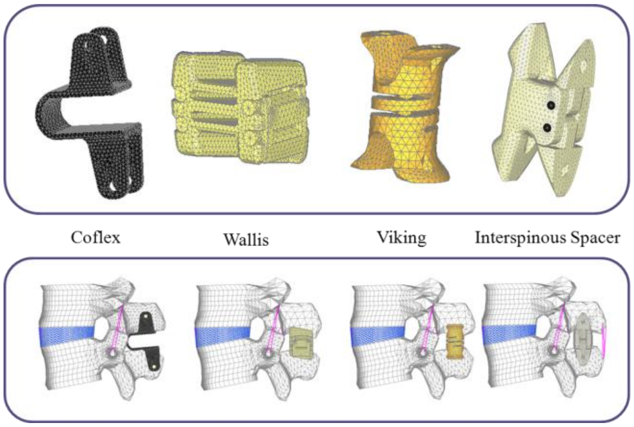

Figure 1: Integrated four kinds of interspinous implants into the validated FE model of the lumbar spine.

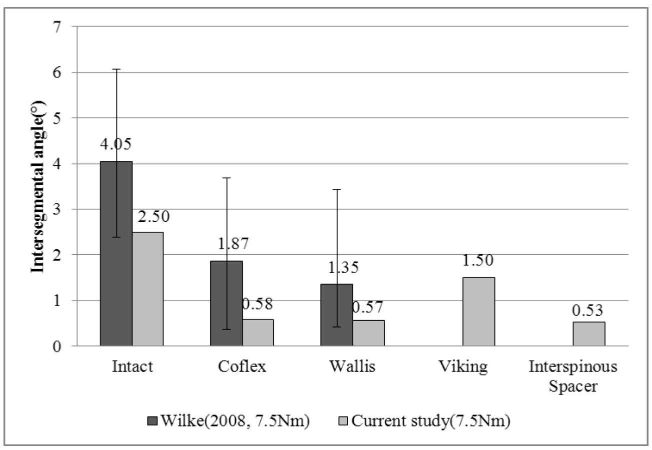

Figure 2: Comparison of intersegmental rotation angle in L3-L4 motion segment under extension.

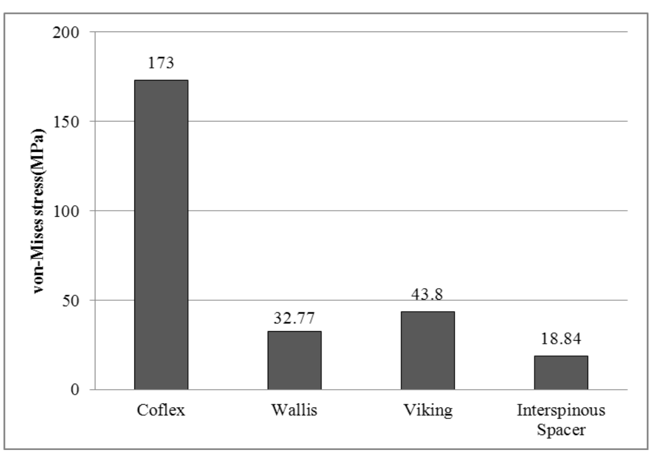

Figure 3: Comparison of von-Mises stress on interspinous process under extension.

RESULTS AND DISCUSSION

The intersegmental rotation angles were decreased by 88%, 89%, 70% and 90% compared with the intact motion segment with Wallis, Viking and Interspinous Spacer, respectively (Fig. 2). Thus, all implanted model showed higher stability than the intact lumbar spine in extension.

The maximum von-Mises stresses in the interspinous process were 173 MPa, 33.8 MPa, 43.8 MPa and 18.8 MPa for the Coflex, Wallis, Viking and Interspinous Spacer, respectively (Fig. 3). The Coflex showed higher maximum von-Mises stresses than any other implants.

Titanium was used for the Coflex interspinous implant. High young's modulus of titanium may cause subsidence of the implant to the osteoporotic bone. The results of this study showed similar trends with the results from previous studies [1,2].

CONCLUSIONS

We analyzed biomechanical characteristics of different types of interspinous implants. While all kinds of interspinous implants studied in this study increased stability of motions segment in extension, tremendously different values of maximum von-Mises stress was shown in each implant. Therefore, the influence of interspinous implants on subsidence of interspinous process should be considered in the interspinous implant surgery, as well as the increase of stability of motion segment. The results of this study could be useful for evaluating and selecting surgical options and implants in spinal surgeries.

REFERENCES

1. Wilke HJ, et al. *Eur Spine J* **17**, 1049-1056, 2008.
2. Kabir SM, et al. *Spine* **35**, 1499-1506, 2010.
3. Kettler A, et al. *Clin Biomech* **23**, 242-247, 2008.
4. Moore KL, et al. *Clinically Oriented Anatomy*, Lippincott Williams & Wilkins, Ltd., 2006.
5. White AA, et al. *Clinical Biomechanics of the Spine*, Lippincott Williams & Wilkins, Ltd., 1990.

ACKNOWLEDGEMENTS

This research was supported by 2009 National Agenda Project (NAP) funded by Korea Research Council of Fundamental Science & Technology (P-09-JC-LU63-C01).

AGE-RELATED CHANGES IN DYNAMIC COMPRESSIVE PROPERTIES OF SOFT TISSUES OVER THE HIP REGION MEASURED BY FORCED VIBRATION

[1]Woochol Joseph Choi, [1,2]Stephen N. Robinovitch

[1]Biomedical Physiology & Kinesiology, Simon Fraser University, Burnaby, BC, Canada
[2]School of Engineering Science, Simon Fraser University, Burnaby, BC, Canada
email: woocholc@sfu.ca

INTRODUCTION

Hip fractures are a major cause of death and disability in older adults, and over 90% of cases are caused by falls. Risk for hip fracture increases exponentially with age, and this may be due, in part, to age-related changes in the mechanical properties of soft tissues over the hip region, which act as a natural "shock absorber" for attenuating and distributing impact forces applied to the bone. In this study, we measured the stiffness and damping of soft tissues over the hip region during forced vibration, and examined how these parameters associate with age, contact sites over the hip region, baseline tissue compression, and soft tissue thickness as measured by ultrasound.

METHODS

Participants included 17 young women (aged 19-35, and ranging in body mass index (BMI) between 15 and 25) and 17 older women (over age 65, and ranging in BMI between 19 and 39).

In a first session, participants lay on a bed having a gap at the hip region (Figure 1a). A mechanical indenter, consisting of a 10 cm diameter circular plate, was centered over the hip region. The indenter was vibrated sinusoidally by a mechanical shaker (LDS shaker V408, Bruel & Kjaer), with an amplitude of 1 mm, and frequency sweeping from 5 to 30 Hz at a rate of 1 Hz/s. Trials were acquired over the greater trochanter (GT), 5 cm inferior to the GT, and 5 cm inferior & posterior to the GT (Figure 1b). Trials were acquired at baseline levels of tissue compression of 40 and 60 N for young participants, and (due to safety reason) only 40 N for older adults. During the trials, force and displacement were measured from a load cell (MLP100, Transducer Techniques) and linear position transducer (MLT 38000102, Honeywell) mounted on the indenter.

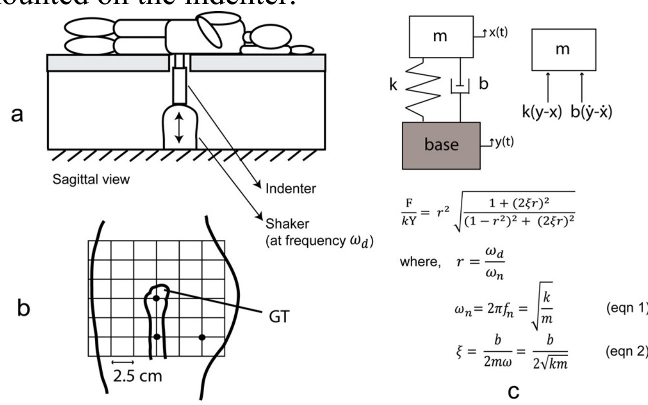

Figure 1: a. Experimental setup; b. Test sites (indicated as filled circles); c. Base excitation model.

We fit the shaker data with a single degree of freedom mass-spring-damper model with base excitation [1] (Figure 1c) to estimate soft tissue stiffness and damping (see equations 1-2 in Figure 1c). The effective mass of each subject was estimated as 50% of body mass [2]. The damping ratio (zeta) for each subject was determined by best-fitting the model force traces to experimental data using least squares.

In a second session, we used ultrasound (SonixRP, Ultrasonix) to measure the thickness of skin, fat, and muscle layers at the intender contact site, including total thickness. Care was taken to ensure consistent positioning and contact pressure between the ultrasound probe and skin.

We used ANOVA (with alpha=0.05) to test whether stiffness and damping constants associated with contact site, baseline tissue compression, soft tissue thickness (included as a covariate), and age (included as a grouping factor). We also used t-test to compare soft tissue thickness between young and older adults.

RESULTS AND DISCUSSION

Effect of age and contact site: Both stiffness and damping associated with age, but not with contact site, and there were no interactions. On average, stiffness was 48% greater and damping was 18% greater in older than young adults (87 versus 59 kN/m, 888 versus 756 N-s/m; $p<0.05$; Figure 2). Neither parameter associated with total tissue thickness, or the thickness of skin, fat, or muscle ($p>0.05$). Average values of muscle and total thickness were not different in young and older adults (Table 1), although skin and fat thickness in certain sites were different ($p<0.05$).

These results indicate that, older adults exhibit greater compressive stiffness and damping at the hip region, and will therefore experience more force at the proximal femur for the same fall conditions. We were surprised that stiffness and damping did not depend on soft tissue thickness, and that no differences were observed between young and older adults in tissue thickness.

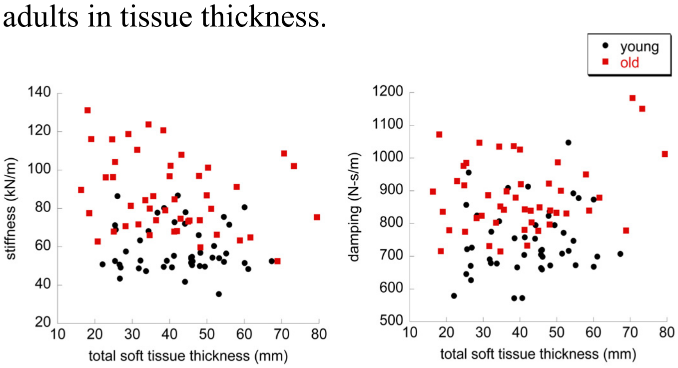

Figure 2: Age-related changes in stiffness and damping values, and observed lack of association with total soft tissue thickness.

Effect of baseline tissue compression: In young adults, baseline compression influenced the observed damping but not stiffness. Damping was 45.1% greater in trials involving 60 N than 40 N of baseline compression (1108 versus 764 N-s/m; $p<0.0005$; Figure 3). Stiffness was 62.4 kN/m in 60 N trials and 58.9 kN/m in 40 N trials ($p>0.14$). This indicates linear behaviour for stiffness, but not damping, over the operating range of our tests.

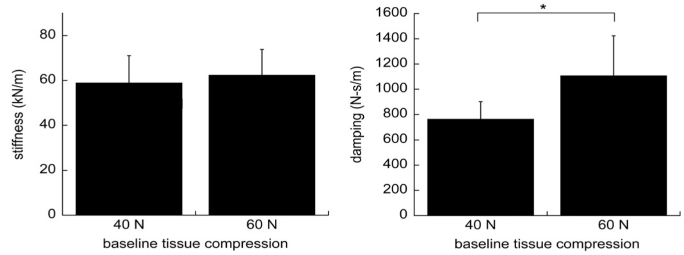

Figure 3: Soft tissue exhibited constant stiffness (left) but non-linear damping (right).

CONCLUSIONS

We used forced vibration to quantify the stiffness and damping of soft tissue over the hip region in young and older women. We found that older women have 48% greater stiffness, and will thus experience greater contact force during a fall on the hip. This may contribute to the exponential increase in rates of hip fracture with age. Soft tissue thickness did not influence tissue properties, and baseline compressive force influenced damping but not stiffness, over the range of conditions we examined. The lack of an observed effect of tissue thickness might relate to the dominant effect of in-series structures such as fat, which don't vary much between individuals, but are of relatively low stiffness compared to the underlying muscle.

Table 1: Average soft tissue thickness (mm) over the hip region (with SD shown in parentheses).

		young	old
Total	GT	32.1 (7.2)	30.4 (14.9)
	5 cm inf	44.9 (8.6)	40.8 (13.2)
	5 cm inf & post	49.9 (9.5)	48.0 (12.6)
Skin	GT	1.2 (0.3)	1.4 (0.5)
	5 cm inf	1.2 (0.3)	1.6 (0.4)*
	5 cm inf & post	1.2 (0.5)	1.2 (0.3)
Fat	GT	3.5 (2.1)	2.1 (2.1)
	5 cm inf	3.6 (1.4)	2.7 (2.0)
	5 cm inf & post	3.6 (1.7)	2.2 (1.1)*
Muscle	GT	27.2 (5.9)	26.7 (14.1)
	5 cm inf	40.6 (7.0)	36.5 (12.7)
	5 cm inf & post	45.0 (9.3)	44.5 (12.0)

* $p<0.05$

REFERENCES

1. Inman DJ, *Engineering Vibration*, Prentice-Hall, 1996.
2. Robinovitch SN, et al. *Ann Biomed Eng* **25**(3), 499-50, 1997.

COMPARISON BETWEEN SQUAT JUMP vs. WEIGHTED SQUAT JUMP: SIMULATION STUDY.

[1]Giuseppe Cimadoro, [2]Alberto Minetti, [3]Matt Pain, [4]Jacque Van Hoecke, [1]Giampiero Alberti, [5]Nicolas Babault, [3]Fred Yeadon.

[1]University of Milan, Department of Sport, Nutrition and Health Science, Milano, ITALY
[2]University of Milan, Physio-Mechanics Laboratory, Department of Human Physiology, Milano, ITALY
[3]Loughborough University, Gymnastic Research Centre, Loughborough, UNITED KINGDOM
[4]University of Burgundy, Cognition, Action et Plasticité Sensorimotrice Laboratory, Dijon, FRANCE
[5]University of Burgundy, Centre d'Expertise de la Performance, Dijon, FRANCE

email: giuseppe.cimadoro@unimi.it, web: http://www.unimi.it/

INTRODUCTION

Computer simulation has been used in sport science to better understand human motion, by optimizing sport techniques of common tasks such as walking, running, and vertical jumping [1]. Biomechanical models often use average muscle characteristics to provide general predictions. In this process the model is usually constructed from generic parameters and thus the model does not represent any of the subjects it is compared against and may not even represent an average of the subjects. An alternative is to use subject specific models where model parameters are equal to the same parameters measured on the subject, and compare a simulation to the single subject performance. Here one-subject's characteristics were incorporated into computer simulations that were used to address questions about his individual response to different jump conditions. From a mechanical point of view, vertical jumping can be compared to an inverted pendulum and, many authors have investigated neuromuscular function in a computational way using different kind of software packages to explore neuromechanical perspectives in the study of jumping. The aim of this study was to examine differences in technique between a squat jump and a squat jump with added weight by utilizing a subject specific model implemented in Working Model 2D.

METHODS

A subject specific four segment whole body model was constructed using Working Model 2D®. An individual male athlete performed body weight squat jumps (SJ_{bw}) and squat jumps with an added 40% of body weight ($SJ_{+40\%}$). Anthropometric characteristics were calculated from the subject according to Chandler (1975). Maximum torque (T, N.m) profiles of the hip and knee extensors, and ankle plantar flexors were determined via dynamometer measurements (Biodex,US) at different angles (ϕ, deg) and concentric angular velocities (ω, deg/s), coupled with force plate isometric corrections to the ankle torques. Positional data were also corrected to ensure real bone alignment. Torque data were fitted with a 4-parameter hyperbolic function and neuromuscular activations were represented using a quintic function [2]. Kinematic and force plate data from a subject were obtained for matching purposes (Fig.1). The optimal solutions that best matched a subject's actual SJ_{bw} and $SJ_{+40\%}$ were calculated with a brute-force optimization algorithm using a cost-function including hip, knee and ankle angles and the vertical velocity of the hip at toe-off for the SJ_{bw} and adding the vertical velocity of the barbell for the $SJ_{+40\%}$.

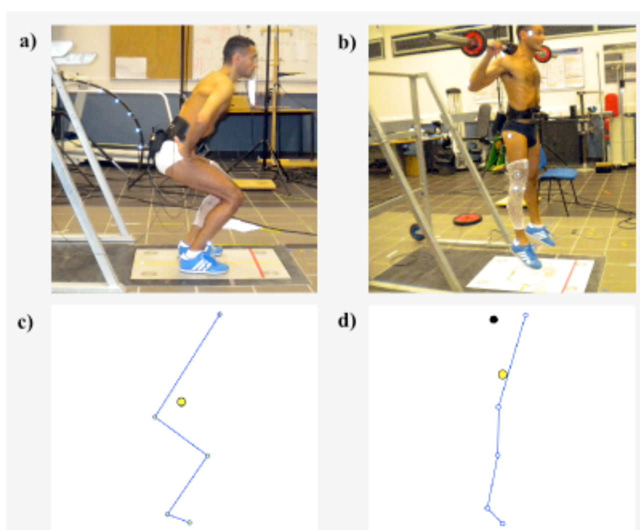

Figure 1: a) SJ_{bw} start position; b) Subject performing $SJ_{+40\%}$; c) and d) stick models, SJ_{bw}start position and $SJ_{+40\%}$ fly phase.

RESULTS AND DISCUSSION

SIM gave a set of activation patterns (Table 1.) that best matched actual performances. A proximal-to-distal sequence of muscle activation (from hip to knee to ankle) confirmed data from literature [3]. Height jump was 0.24m (SJ_{bw}), 0.21m (SJ_{bw}SIM), 0.16 ($SJ_{+40\%}$), 0.15 ($SJ_{+40\%}$SIM). The SJ_{bw} vertical GRF peak was 1450N vs. 1361N SJ_{bw}SIM, (SJ_{bw}>6.14%); $SJ_{+40\%}$ gave 1674N vs. 1482N $SJ_{+40\%}$SIM ($SJ_{+40\%}$>11.5%); (Fig.2). Net power was calculated [4] for SJ_{bw} 955W vs. SIM SJ_{bw} 798W (SJ_{bw}>16.4%) and, $SJ_{+40\%}$ 999W vs. SIM $SJ_{+40\%}$ 856W ($SJ_{+40\%}$>14%).

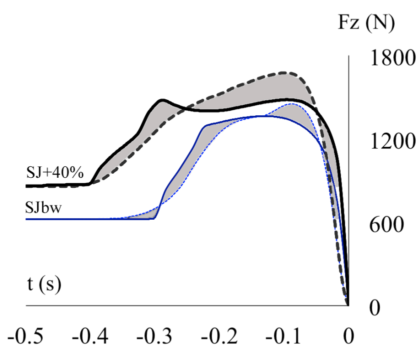

Figure 2: Vertical component of the ground reaction force: SJ_{bw} vs. SIM SJ_{bw}, RMS error=6.5%; $SJ_{+40\%}$ vs. SIM $SJ_{+40\%}$, RMS error=9.8%. Solid lines=actual jumps; dashed lines=SIM. Shaded area represents difference in relation to the net impulse.

Mechanical energy was greater for both actual jumps with regard to simulations, data are shown in table 2. Rectified sEMG (Fig.3), showed that the model should take into account activation decrease, in fact SIM GRF with full activation are both greater than actual jumps close to toe-off phase.

CONCLUSIONS

Further investigations to improve the accuracy of the current model are strongly recommended to make predictions more precise.

REFERENCES

1. Pandy, et al. *J Biomech* **23**, 1185-1198, 1990.
2. Yeadon, MR. et al. *J Biomech* **23**, 476-482, 2006.
3. Pandy, MG., Zajac, FE. *J Biomech* **24**, 1-10, 1991.
4. Hatze, H. *J of Appl Biomech* **14**, 127-140, 1990.

Table 1: Data set obtained from matching simulation at 60Hz for SJ_{bw} and $SJ_{+40\%}$

Data/Joints	Hip	Knee	Ankle
SJ_{bw} Opt_{ramp} (s)	0.099	0.171	0.160
SJ_{bw} Opt_{onset} (s)	-	0.008	0.014
$SJ_{+40\%}$ Opt_{ramp} (s)	0.075	0.164	0.136
$SJ_{+40\%}$ Opt_{onset} (s)	-	0.003	0.007

Fig. 3: Activation function compared with normalized rectified sEMG. A) SJ_{bw} chart; B) $SJ_{+40\%}$. 0=Toe-off.

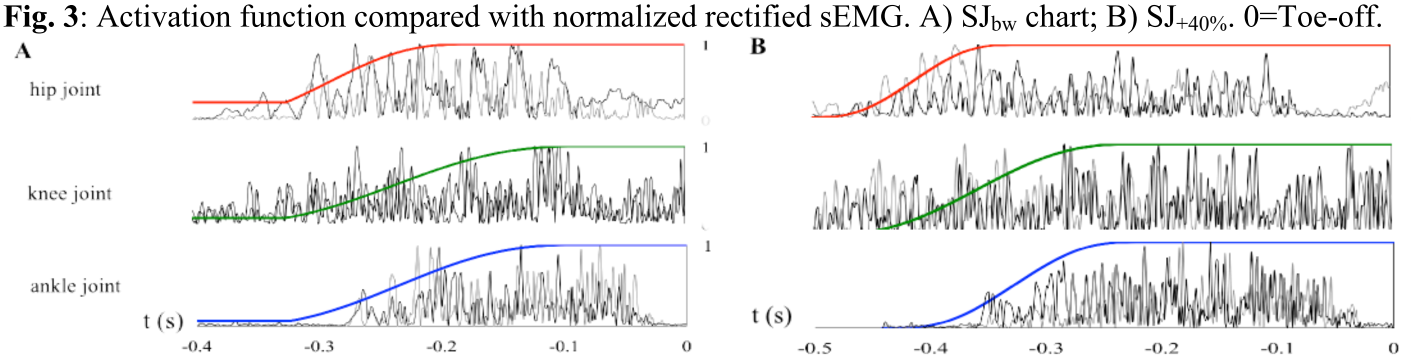

Table 2: Parameters at the instant of the toe-off for both SJ_{bw} and $SJ_{+40\%}$.

Parameters/Jumping	Actual SJ_{bw}	SIM SJ_{bw}	Actual $SJ_{+40\%}$	SIM $SJ_{+40\%}$
Hip (ϕ, deg)	169.3	166.2	167.9	145
Knee (ϕ, deg)	174.5	173.9	172.2	158.4
Ankle (ϕ, deg)	34.2	34.8	31.9	35.1
Hip (Y vel.,m/s)	2.38	2.285	2.067	1.910
Barbell (Y vel.,m/s)	-	-	2.216	1.999
E_k (J)	148	131	142	132
$E_{p,g}$ (J)	945	676	1100	1066
$E_k + E_{p,g}$ (J)	1093	807	1242	1198

TASK-SPECIFIC DIFFERENCES IN THE CORTICAL CONTRIBUTION TO WALKING ARE REVEALED BY 30-60 HZ OSCILLATORY ACTIVITY

[1,2]David J. Clark, [3,4]Steven A. Kautz, [1]Andrew R. Bauer, [5]Yen-Ting Chen and [5]Evangelos A. Christou

[1]Brain Rehabilitation Research Center, Malcom Randall VA Medical Center, Gainesville, FL, USA
[2]Department of Aging and Geriatric Research, University of Florida, Gainesville, FL, USA
[3]Ralph H. Johnson VA Medical Center, Charleston, SC, USA
[4]Department of Health Sciences and Research, Medical University of South Carolina, Charleston, SC, USA
[5]Department of Applied Physiology and Kinesiology, University of Florida, Gainesville, FL, USA
email: davidclark@ufl.edu

INTRODUCTION

Older adults exhibit heightened cortical activation to control coordinated motor tasks, including walking. A potential consequence is that cortical demand of motor control competes with cortical demand of other information-processing tasks, such as attending to environmental stimuli. Such a competition may threaten the safety of walking, particularly in a community setting with physical and/or cognitively challenging conditions. Investigations are needed to determine the extent to which altered cortical demand may affect the safety of walking. A promising approach is to indirectly gauge corticospinal drive by measuring the common oscillatory activity from pairs of muscles using surface electromyography (EMG). Oscillations in the Piper frequency band (30-60Hz) have previously been shown to be modulated by corticospinal input.

We hypothesized that Piper band oscillatory activity during normal walking would be: 1) greater than dual-task walking because of competition for cortical resources, 2) similar to fast walking because cortical facilitation of walking speed acts through an intermediate locomotor pathway, and 3) lower than step lengthening because voluntary gait pattern modifications are directed by the corticospinal tract.

METHODS

Participants walked on a motor driven treadmill in a motion analysis laboratory. Participants performed four different walking tasks: 1) Normal walking at each individual's perceived normal walking speed; 2) Fast walking at each individual's perceived fastest safe speed; 3) Dual-task walking (normal walking plus a cognitive working memory task (auditory 2-back test)); 4) Long step (every sixth gait cycle) during otherwise normal steady state walking.

EMG was recorded from plantarflexor muscles soleus and medial gastrocnemius because of their important role for forward propulsion and because common oscillatory EMG activity is most readily detected between synergistic muscles. EMG cross-wavelet analysis was conducted according to the description provided in an earlier publication [1].

Two-way repeated measures ANOVA (4 walking tasks x 2 legs) was used to examine cross-wavelet power within the 30-60 Hz band (i.e., Piper band oscillatory activity) for each leg and for each of the four walking tasks. Post-hoc analysis was performed by independently comparing typical walking to each other walking task using separate two-way repeated-measures ANOVA models (2 tasks x 2 legs).

RESULTS AND DISCUSSION

Seventeen older adults (70.1 ± 3.9, 9M/8F) participated in the study. There was a significant main effect for walking task ($p < 0.001$) and for leg ($p = 0.031$) for Piper band oscillatory EMG activity. Post hoc analysis of pairs of walking tasks (normal walking versus each other task) revealed reduced Piper band oscillatory activity during dual-task walking ($p=0.02$) with no leg x walking task interaction ($p=0.27$), unchanged Piper band oscillatory activity during fast walking ($p = 0.15$) with no leg x walking task interaction ($p=.726$), and heightened Piper band oscillatory activity when talking a left long step ($p < 0.001$) with the right side increasing significantly more than the left side (leg x walking task interaction $p = 0.02$). To illustrate the difference in Piper band oscillatory activity across tasks, we also calculated the percent change relative to typical walking for each subject, task and side. Group means and 95% confidence intervals are presented in Figure 1.

It is interesting that reduced oscillatory activity during dual-tasking was more consistent across participants for the right leg compared to the left leg (see Figure 1). This suggests that dual-task interference may have been more prominent in the left hemisphere (i.e., contralateral to the more affected leg). Indeed, the cognitive task that we used in this study involves verbal comprehension and working memory processes that have been shown to depend primarily on left frontal and parietal cortical regions.[2]

Figure 1.

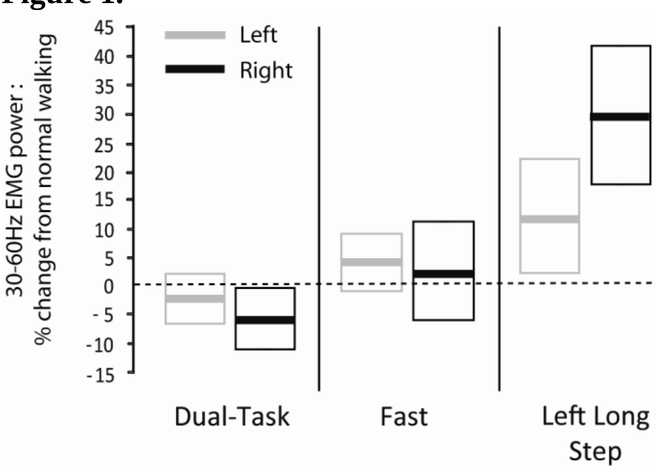

As hypothesized, we did not observe a significant difference in Piper band oscillatory activity between typical and fast walking. Although plantarflexor activation magnitude is known to increase substantially with faster walking speed, our findings indicate that the corticospinal pathway is not responsible for this increase. Rather, our findings support the notion that cortical control of walking speed is primarily limited to regulating the excitability of an intermediate locomotor pathway [3,4], that does not substantially affect Piper band oscillatory activity. In contrast, taking a longer step during otherwise steady state walking yielded a considerable increase in Piper band activity. This is consistent with the notion that gait pattern modifications are controlled by integrating a corticospinal command with the ongoing locomotor pattern.[5,6] Importantly, the Piper band activity in the left and right plantarflexors during the left long step differed in a way that is consistent with task demands. In an earlier study it was shown that increasing propulsive ground reaction force by the stance (i.e., right) leg is the primary mechanism by which step length is modulated, and that the plantarflexor muscle group is a major contributor.[6]

CONCLUSIONS

The findings of this study support the hypothesis that Piper band oscillatory EMG activity in the plantarflexor muscle group quantifies differences in corticospinal drive across walking tasks in healthy older adults. These finding have important implications for using EMG oscillatory activity to investigate locomotor control strategies used under different walking conditions, and how these strategies may change with aging, injury or disease.

REFERENCES

1. de Miranda Marzullo, A.C., et al., *Neural control of the lips differs for young and older adults following a perturbation.* Exp Brain Res, 2010. **206**(3): p. 319-27.
2. Glascher, J., et al., *Lesion mapping of cognitive abilities linked to intelligence.* Neuron, 2009. **61**(5): p. 681-91.
3. Matsuyama, K., et al., *Locomotor role of the corticoreticular-reticulospinal-spinal interneuronal system*. 2004, Elsevier: Amsterdam. p. 239-249.
4. Grillner, S., et al., *Neural bases of goal-directed locomotion in vertebrates--an overview.* Brain Res Rev, 2008. **57**(1): p. 2-12.
5. Drew, T., W. Jiang, and W. Widajewicz, *Contributions of the motor cortex to the control of the hindlimbs during locomotion in the cat.* Brain Res Brain Res Rev, 2002. **40**(1-3): p. 178-91.
6. Varraine, E., M. Bonnard, and J. Pailhous, *Intentional on-line adaptation of stride length in human walking.* Exp Brain Res, 2000. **130**(2): p. 248-57.

RATE OF LOADING AND LOWER EXTREMITY SAGITTAL PLANE BIOMECHANICS WHEN LANDING FROM A DROP-JUMP: SHOD AND BAREFOOT COMPARISIONS BETWEEN GENDERS

Robert Cochrane, Brian McNeaney, Michael Lawrence, Erin Hartigan
University of New England, Portland ME
E-mail: rcochrane@une.edu

INTRODUCTION

High rates of loading during running have been correlated to injury [1]. Barefoot running reduces the rate of loading by modifying lower extremity landing patterns, specifically a change at initial contact from a rearfoot strike pattern to a more midfoot or forefoot strike [1]. Females tend to land from a drop jump with decreased hip flexion and increased knee flexion compared to males; resulting in a more erect and upright posture [2]. This stiffer female landing pattern may predispose females to injury [3]. The typical female landing pattern of altered joint kinetics and kinematics compared to males may shorten the amount of time that vertical ground reaction forces (VGRF) are allowed to dissipate through the human body; therefore increasing the rate of loading. The purposes of this study were to investigate whether females: 1) land with higher rates of loading when barefoot and shod compared to males and 2) use less hip and knee flexion and ankle dorsiflexion angles, and greater hip and knee extension and ankle plantarflexion moments while barefoot compared to males.

METHODS

Twenty-three healthy, uninjured subjects (12 males and 11 females, mean age of 24.05 years ± 2.9 years, mean mass of 73.20 kg ± 9.45 kg, and mean height of 1.69 m ± 0.076 m) each performed 20 drop-jumps (10 barefoot and 10 shod) from a 0.71 meter box. The retro-reflective markers were placed on the anterior and posterior upper body and pelvis, medial/lateral leg, the anterior, lateral, and posterior ankle/foot and anterior, lateral, and posterior ankle/shoe. Eight Oqus Series-3 cameras (Qualisys, Gothenburg, Sweden) set at 240 Hz were used to capture 3-demenstional video of subjects performing drop jumps by tracking retro reflective markers placed on subjects. Force data were collected using 2 force plates (AMTI, Watertown, MA) set at a frequency of 2400 Hz. Visual 3D (C-motion, Germantown, MD) was used to apply a Butterworth filter with a cutoff of 12 Hz.

Of the 10 barefoot and shod trials, 5 trials of each condition that were not statistical outliers and did not have data gaps were selected for analysis. Sagittal plane hip, knee and ankle joint angles, internal joint moments and rate of loading were calculated using customized code written in MATLAB (MathWorks, Natick, MA). Internal joint moments and rate of loading data were normalized to subject mass. Joint moments were calculated at peak knee flexion using inverse dynamics. Rate of loading was defined as average of the slopes generated in the VGRF-time curve from initial contact to the maximum peak [4].

Statistical software was used to compare the conditions and genders for the dominant limb only. (SPSS, IBM- IBM Corporation, Somers, NY). A mixed model repeated measures ANOVA with a within factor of condition and a between factor of gender was used to compare shoe conditions and genders, respectively. If interaction effects existed, Post Hoc analyses were run to determine where the differences presented.

RESULTS and DISCUSSION

There were no main effects or interactions for rate of loading (Table 1). Biomechanical differences were found between genders and conditions. Subjects landed with significantly greater angles (hip flexion, knee flexion and ankle dorsiflexion) and moments (hip extension, knee extension and ankle plantarflexion) when barefoot (Table 1). Females landed with less knee and hip extension moments compared to males regardless of barefoot or shod conditions (Table 1). Researchers suggest that barefoot running may create a learning strategy and neuromuscular adaptations in order to reduce

the mechanical stress on the body that results in a reduced rate of loading [5,6]. Differences in rate of loading when landing
barefoot versus shod were not found likely due to a lack of neuromuscular adaptations and motor learning that must occur in subjects while barefoot landing in order to reduce mechanical stresses and rate of loading. Our subjects completed limited trials of landing, whereas barefoot running studies expose the subject to more landing opportunities while barefoot. Furthermore, the subject appears to contact the ground with their mid to forefoot when they land from a jump, regardless of shod or barefoot.

Conclusion

Lower extremity angles and moments increased when barefoot compared to shod, however altered mechanics did not result in rate of loading differences between conditions (Table 1). We did not find that females landed with less hip and knee angles while barefoot compared to males, yet our females did not land with different angles compared to males while shod either. However, females did land with less knee and hip moments across conditions suggesting that landing barefoot did not influence gender differences. Though we did not hypothesize that ankle differences would occur, shoe condition and gender differences existed at the ankle.

REFERENCES

1. Lieberman, D. E., Venkadesn, M., Werbel, W. A., Daoud, A. I., D'Andrea, S., Davis, I. S., Mang'Eni, R. O., Pitsiladis, *Nature*, **463**, 531-535. 2010
2. Decker, M. J., Torry, M. R., Wyland, D. J., Sterett, W. I., Steadman, J. R. *Clin Biomech*, ***18***, 662-669, 2003
3. Arendt, E., Dick, R., *Am. J. Sports Med*, **23**, 694-701. 1995
4. Decker, M. J., Torry, M. R., Noonan, T. J., Riviere, A., Sterett, W. I., *Med Sci Sport Exerc*, ***34***, 1408-1413, 2002
5. Divert, C., Mornieux, G., Baur, H., Mayer, F., Belli, A. *Int J Sports Me*, **26**, 593-598. 2005
6. Lieberman, D. E., Venkadesn, M., Werbel, W. A., Daoud, A. I., D'Andrea, S., Davis, I. S., Mang'Eni, R. O., Pitsiladis, Y. *Nature*, **463**, 531-535, 2010

ACKNOWLEDGEMENTS

Department of Physical Therapy, University of New England; Human Performance Lab, Saco, ME; Casey Cottle and Stacy Lee for their assistance during data collection

Table 1: Means and Standard Deviations Variables during Shod and Barefoot Conditions

	Male Shod	Female Shod	Male BF	Female BF
Rate of Loading (N/kg/s)	47.32 ± 27.02	67.27 ± 27.89	41.35 ± 33.16	60.93 ± 30.02
Hip Flexion Angle (Degrees)	98.93 ± 13.38 ǂ	100.05 ± 17.69 ǂ	116.28 ± 11.71	115.58 ± 16.72
Hip Extension Moment (Nm/kg)	-2.12 ± 0.58 ǂ	-1.67 ± 0.35 ǂ	2.61 ± 0.82	2.02 ± 0.37*
Knee Flexion Angle (Degrees)	-103.31 ± 17.69 ǂ	-90.55 ± 19.66 ǂ	-119.28 ± 14.8	-102.89 ± 17.38
Knee Extension Moment (Nm/kg)	1.87 ± 0.54 ǂ	1.29 ± 0.42 ǂ	2.06 ± 0.51	1.40 ± 0.52*
Ankle Dorsiflexion Angle (Degrees)	25.77 ± 3.97 ǂ	22.41 ± 4.48 ǂ	23.31 ± 6.90	19.05 ± 4.57*
Ankle Plantarflexion Moment (Nm/kg)	-1.29 ± 0.32 ǂ	-0.99 ± 0.2 ǂ	-1.46 ± 0.48	-1.26 ± 0.23

* Difference between Gender; ǂ Difference between Condition

WALKING SPEED OVERGROUND AND ON A FEEDBACK-CONTROLLED TREADMILL

John-David Collins, Pinata Sessoms, and Jamie Bartlett

Naval Health Research Center, San Diego, California
e-mail: john-david.collins@med.navy.mil

INTRODUCTION

Immersive virtual environments have been used to simulate walking overground with visual surround and treadmill components. This enables subjects to be exposed to complex physical and/or cognitive situations within a safe environment. The Naval Health Research Center in San Diego, CA, operates a Computer Assisted Rehabilitation Environment (CAREN) (Motek Medical BV, Amsterdam, The Netherlands). This device is one of only a few within the U.S. Department of Defense and includes a 10-foot-tall, 180-degree surround screen with dual-belt instrumented treadmill mounted on a six-degree-of-freedom platform. The CAREN system provides a way to modulate treadmill speed using hands-free, positional feedback control. Several researchers have used this method to control treadmill speed for physical therapy but have not compared it with traditional methods of treadmill control [1,2].

This study examined able-bodied adults walking in a synchronized immersive environment utilizing two different speed-control methods: a game controller and positional feedback. These variables were compared with each other and also with overground gait variables collected on a GAITRite gait assessment walkway (CIR Systems, Inc., Haverton, PA).

METHODS

Nine subjects (mean age 31 ± 5.07 years, weight 59.74 ± 9.26 kg, height 167.72 ± 7.47 cm) walked under three self-selected speed conditions (fast, normal, and slow) using two different speed-control methods. Subjects walked with a hand controller (HC) to incrementally increase the treadmill speed until a comfortable speed was reached for each condition. They passed the controller to an attending researcher prior to data acquisition. Under the feedback-controlled condition (i.e., self-paced [SP]) the fore/aft position of the subject's retroreflective pelvic markers on the treadmill-controlled belt speed. As the subject walked near the front, the treadmill speed increased and vice versa. Once up to speed, we recorded data for 30 seconds during each condition. All treadmill trials were randomized. An endless virtual hallway was displayed on the screen. Optic flow of the moving image was synchronized with the speed of the treadmill. A 12-camera Vicon motion capture system (OMG Plc, Oxford, U.K.) capturing a full-body marker set at 120 Hz was used for all motion data. Subjects walked overground (OG) at their preferred walking speed across the 24-foot-long GAITRite walkway. Three walking trials were averaged and recorded for comparison.

RESULTS AND DISCUSSION

Using a one-way repeated-measures analysis of variance with a Greenhouse-Geisser correction to evaluate the differences in speed-control methods (HC, SP, and OG) for normal self-selected walking, there was a significant effect for speed [Wilks' Lambda = 0.40, $F(2,7) = 5.25$, $p = 0.041$, multivariate partial eta squared = 0.60]. Post hoc tests using the Bonferroni correction revealed that OG was significantly faster than walking on the treadmill using either the HC ($P = 0.039$) or the SP method ($P = 0.031$) of speed control. Normal walking conditions on the treadmill (HC and SP) were not significantly different from each other ($p = 1.00$) (Figure 1).

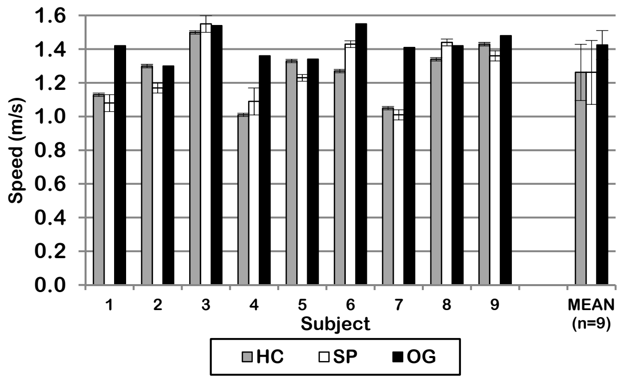

Figure 1. Individual and mean normal walking speeds by condition: hand controller (HC), feedback control (SP), and overground walking (OG). The chart shows values and standard deviation bars.

A paired-samples *t* test was conducted for each walking speed condition (self-selected slow, normal, and fast) to evaluate the differences in speed between the different treadmill control conditions (HC and SP) (Figure 2). There were no significant differences between HC and SP control methods for fast and normal walking ($p = 0.952$ and $p = 1.00$, respectively). Subjects walked significantly faster using the SP ($M = 0.90$, $SD = 0.22$) control versus HC [$M = 0.80$, $SD = 0.24$, $t(8) = -3.24$, $p = 0.01$] during the slow walking conditions. The eta squared statistic (0.57) indicated a large effect size.

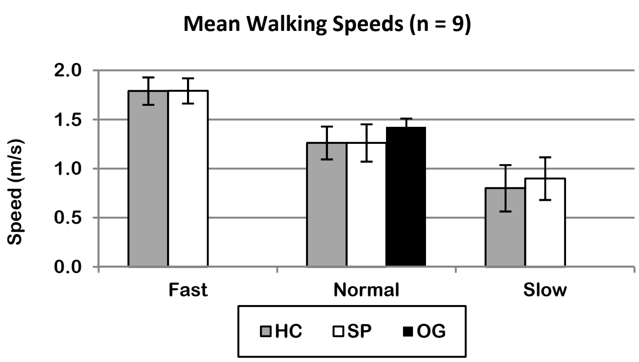

Figure 2. Mean walking speeds for each speed condition. The chart shows values and standard deviation bars.

When comparing normal speeds, OG walking was significantly faster than either treadmill control condition. This means that even with visual surround synchronized with the treadmill speeds, there is still a difference between treadmill walking on the CAREN and OG walking. Despite the differences between overground and treadmill walking speeds, the virtual environment is an effective laboratory tool to assess gait. User feedback from this study suggests that SP treadmill walking is relatively straightforward and easy to control.

Using SP treadmill control allows for more subject autonomy while walking in a virtual environment. The benefits of using the SP method of treadmill control are it allows a hands-free, more complete immersion in the virtual environment; and it provides the ability for subjects to walk in a scene, slow down, or stop to complete any number of tasks and under their own volition to begin walking again. This study demonstrates that subject's preferred walking speeds are similar between feedback-controlled walking and using a hand controller. Thus, the SP method of control should be used in future studies, particularly those in which dual tasking is important to measure cognitive and physical performance.

REFERENCES

1. Kizony R, Levin MF, Hughey L, Perez C, and Fung J. *Physical Therapy* **90,** 252-260, 2010.
2. Lamontagne A, Fung J, McFadyen BJ, and Faubert J, Journal of NeuroEngineering and Rehabilitation. **4**, 22, 2007.

ACKNOWLEDGMENTS

Many thanks to Kathrine Service and Jordan Sturdy and the entire PhyCore lab for assistance in data collection and processing.

This work was supported under Work Unit No. 60818. The views expressed are those of the authors and do not reflect the official policy or position of the Department of the Navy, Department of Defense, or the U.S. Government. Approved for public release; distribution is unlimited. This research was conducted in compliance with all applicable federal regulations governing the protection of human subjects (Protocol NHRC.2011.0002).

EXERCISE EFFICIENCY AND MITOCHONDRIAL COUPLING IN THE ELDERLY

Kevin E. Conley and Sharon Jubrias

University of Washington, Seattle, WA, USA
email: kconley@uw.edu, web: http://depts.washington.edu/tcmi/index.html

INTRODUCTION

Low locomotory efficiency has been found to have important impact on activities of daily living of the elderly [1]. A difference of 30% in the energetic cost of walking has been found between young and elderly subjects and suggests that muscle energetic changes are a major contributor to age-related inefficiency of locomotion [2,3]. A change in contractile efficiency is the conventional explanation for differences in exercise efficiency [4], but elderly muscle has a greater content of the more efficient type I fibers than younger muscle [5,6] and therefore would be expected to become more efficient – not less [4]. Thus a shift in muscle fiber type does not explain reduced exercise efficiency in elderly subjects.

A role of mitochondria in exercise efficiency comes from Whipp and Wasserman's [7] evaluation of the cascade of efficiencies that underly exercise. Their analysis revealed that contractile (0.5) and mitochondrial (0.6) efficiencies contributed equally to cycling efficiency (so-called delta efficiency, 0.3) in human quadriceps (i.e., 0.3 = 0.5 x 0.6). The lower mitochondrial coupling efficiency evident in elderly muscle of humans and animals [8,9] would therefore have the potential to reduce the power output per O_2 in exercising elderly. Thus, the mitochondrial uncoupling found with age in humans[8] is a likely contributor to the reduced exercise efficiency of elderly subjects.

To evaluate the contribution of contractile and mitochondrial coupling efficiency to exercise efficiency, we determined the underlying efficiencies in adult and elderly subjects. First, we determined **exercise efficiency** (i.e., delta efficiency) from oxygen uptake and power output measured on the cycle ergometer. Second, we used a simple method to estimate **contractile efficiency** of the quadriceps in vivo. Third, we determined **mitochondrial coupling efficiency** using a combination of in vivo and biopsy determinations [10].

Oxygen consumption on a cycle ergometer was evaluated in 9 adult (mean: 38.8 yrs) and 39 elderly subjects (mean: 68.8 yrs), revealing a decline in exercise efficiency (delta efficiency, ε_D) from 0.27$\pm$ 0.01 (mean$\pm$SEM) to 0.22$\pm$0.01 between age groups (Figure 1). Contractile-coupling efficiency (ε_C) determined from leg power output at VO_2max and ATP generation determined from magnetic resonance spectroscopy yielded values in adults (0.50$\pm$0.05) and elderly (0.58$\pm$0.04) in agreement with independent measures. Mitochondrial coupling efficiency (ε_M) was determined from $\varepsilon_D/\varepsilon_C$ to yield values reflective of well-coupled mitochondria (0.58$\pm$0.08) in adults, but indicative of significant uncoupling in the elderly (0.44$\pm$0.03). These e_M values were confirmed in measurements from muscle biopsy material from these subjects (adult: 0.57$\pm$0.08; elderly: 0.41$\pm$0.03) consistent with uncoupling as the basis of the mitochondrial dysfunction in these elderly. Thus, reduced mitochondrial efficiency (ε_M) is a key part of the exercise inefficiency found in the elderly subjects and may be an important part of the loss of exercise performance with age. The new insight from this analysis is the role of mitochondrial efficiency in the decline in exercise efficiency in the elderly.

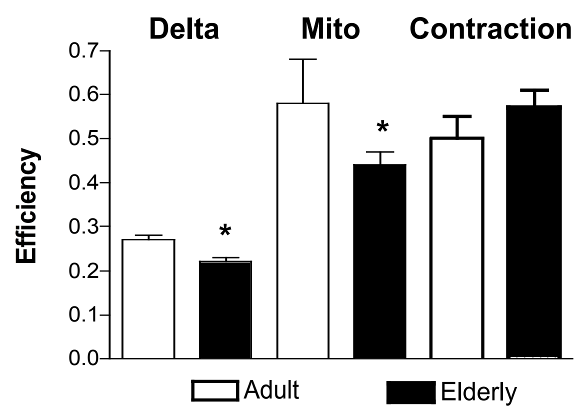

Figure 1. **Impact of age on the cascade of efficiencies underlying exercise.** The decline in mitochondrial efficiency (Mito) is a key factor in the decline in delta efficiency (Delta) with age. *P<0.05

REVERSAL OF MITO DYSFUNCTION IMPROVES EXERCISE PERFORMANCE IN ELDERLY.

Recent studies suggest that mitochondrial uncoupling may improve with an endurance training program based on the increase in coupling reported in isolated mitochondria in young subjects [11]. To evaluate the impact of exercise training, 39 male and female subjects (69.2 $\pm$ 0.6 yr) were divided into groups for a 6-month program of no training, endurance training (ET) or resistance training (RT). Only ET elevated the oxidative phosphorylation capacity in vivo (ATP_{max}). Improved mitochondrial function was evident from muscle biopsies based on the greater ATP_{max} per mitochondrial content ($ATP_{max}/V_V[mt,f]$). No change in muscle fiber type was found [12]. These results suggest that reduced mitochondrial functional capacity (low $ATP_{max}/V_V[mt,f]$, consistent with uncoupling of ATP from O_2 uptake) can be reversed.

Our second question was whether improved $ATP_{max}/V_V[mt,f]$ elevated exercise efficiency and the coupling of power output of the legs, P_{max}, to VO_2max to improve exercise performance. Again, ET alone significantly improved delta efficiency (ε_D, Δ2%) as well as P_{max} (17%) without a significant change in VO_2max. This rise in P_{max} per VO_2max paralleled the greater mitochondrial coupling ($ATP_{max}/V_V[mt,f]$) in the vastus lateralis in these subjects with ET (Figure 2). This association suggests that improved coupling of leg power output per VO_2 both during exercise (ε_D) and at the aerobic limit $\Delta(P_{max}/VO_2max)$ reflects an elevation in mitochondrial coupling, as evidenced by $\Delta(ATP_{max}/V_V[mt,f])$ in the vastus lateralis. Thus, a substantial increase in exercise performance as measured by greater leg power output per VO_2max in the elderly resulted from improvements in mitochondrial coupling efficiency after ET. These results demonstrate that mitochondrial uncoupling plays an important role in the reduced exercise efficiency with age and that the reversal of this uncoupling with ET can raise exercise performance that was lost with age in these elderly subjects.

ACKNOWLEDGEMENTS

Thanks go to M. Elaine Cress, Peter Esselman, Barbara Inglin and Chris Mogadam for their participation in these studies. Supported by NIH grants: AG10853, AR41928, RC2AG036606, RC2AG036594.

REFERENCES CITED

1 Martin, P. E., Rothstein, D. E. & Larish, D. D. Effects of age and physical activity status on the speed-aerobic demand relationship of walking. *J Appl Physiol* **73**, 200-206 (1992).

2 Malatesta, D. *et al.* Energy cost of walking and gait instability in healthy 65- and 80-yr-olds. *J Appl Physiol* **95**, 2248-2256 (2003).

3 Ortega, J. D. & Farley, C. T. Individual limb work does not explain the greater metabolic cost of walking in elderly adults. *J Appl Physiol* **102**, 2266-2273 (2007).

4 Coyle, E. F., Sidossis, L. S., Horowitz, J. F. & Beltz, J. D. Cycling efficiency is related to the percentage of type I muscle fibers. *Med Sci Sports Exerc* **24**, 782-788 (1992).

5 Deschenes, M. R. Effects of aging on muscle fibre type and size. *Sports Med* **34**, 809-824 (2004).

6 Lexell, J. Human aging, muscle mass, and fiber type composition. *J Gerontol* **50A**, 11-16 (1995).

7 Whipp, B. J. & Wasserman, K. Efficiency of muscular work. *J Appl Physiol* **26**, 644-648 (1969).

8 Amara, C. E. *et al.* Mild mitochondrial uncoupling impacts cellular aging in human muscles in vivo. *Proc Natl Acad Sci U S A* **104**, 1057-1062 (2007).

9 Marcinek, D. J., Schenkman, K. A., Ciesielski, W. A., Lee, D. & Conley, K. E. Reduced mitochondrial coupling in vivo alters cellular energetics in aged mouse skeletal muscle. *J Physiol* **569**, 467-473 (2005).

10 Conley, K. E., Jubrias, S. A. & Esselman, P. E. Oxidative capacity and aging in human muscle [published erratum appears in J Physiol 2001 Jun 15;533 Pt 3:921]. *J Physiol* **526.1**, 203-210 (2000).

11 Fernstrom, M., Tonkonogi, M. & Sahlin, K. Effects of acute and chronic endurance exercise on mitochondrial uncoupling in human skeletal muscle. *J Physiol* **554**, 755-763 (2004).

12 Jubrias, S. A., Esselman, P. C., Price, L. B., Cress, M. E. & Conley, K. E. Large energetic adaptations of elderly muscle to resistance and endurance training. *J Appl Physiol* **90**, 1663-1670. (2001).

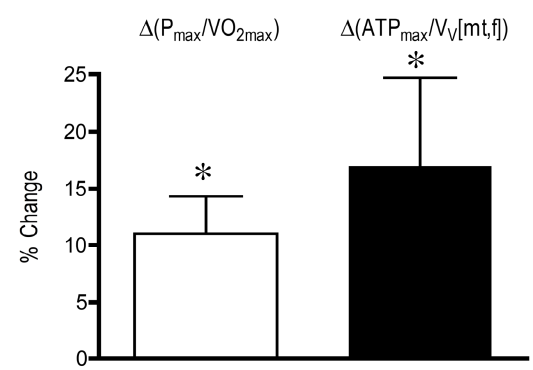

Figure 2. **Improved exercise ($\Delta(P_{max}/VO_2max)$) and mitochondrial coupling ($\Delta(ATP_{max}/V_V[mt,f])$) in the ET group** (Jubrias *et al.*, 2001). *P<0.05.

EFFECT OF ENHANCED ECCENTRIC RESISTANCE DURING THE SQUAT EXERCISE ON LOWER EXTREMITY STABILITY AND STRENGTH

+Conrad BP, Hankins DA, Barone T, Sonya Tang, MacMillan M

+University of Florida, Gainesville, FL, USA
Human Dynamics Labs
E-mail: bconrad@ufl.edu   Web: http://www.ortho.ufl.edu/motion-lab

Introduction

Females have a 4-6X higher risk of sustaining a non-contact anterior cruciate ligament (ACL) injury compared to males, when competing in the same cutting and jumping sports.[1,2] High knee abduction moments in female athletes during a jump landing task are associated with increased risk of sustaining an ACL injury.[3] Stability of the lower extremity is dependent on the intrinsic joint supportive structures and extrinsic musculotendinous stabilizers. Knee stability and joint moments can be quantified during the sudden deceleration of the body after a drop from a height. During the jump landing task, muscular force absorption and dissipation occurs exclusively eccentrically, during the forced lengthening of the involved musculature. Recent, compelling evidence suggests that eccentrically focused resistance exercise may induce superior increases in muscle mass and leg function at a lower cardiovascular and metabolic cost compared to concentrically focused resistance exercise. It therefore follows that training which strengthens the muscles that protect weight bearing joints from large dangerous external forces should include acclimatization to gradually increasing eccentric resistance exercises. The purpose of this project was to evaluate the effectiveness of a eccentric focused squat strengthening program on the reduction of knee abduction forces in females.

Methods

This study was designed as a prospective, randomized controlled trial. Physically active females age 18-24 years old with no prior history of knee injury were selected as participants for the study. Baseline and post-intervention analyses of jump landing mechanics were performed using the drop vertical jump test (DVJT).[3] Joint kinematics were measured using a 12 camera motion analysis system (Motion Analysis Corp, Santa Rosa, CA), sampled at 200Hz. Ground reaction force was measured with two AMTI force platforms (AMTI, Inc., Watertown, MA), sampled at 1200Hz. Data analysis was performed in Visual 3D to calculate joint angles, forces, and moments of the knee during the initial drop landing.

Participants were randomized to one of two 12 week training programs: either control training group (CON) or eccentric focused training group (ECC). The CON group performed a traditional squat exercise program where the concentric and eccentric resistance is equal. The ECC group performed a novel squat program where the eccentric resistance is initiated at the one repetition maximum and progressively increased during training, while the concentric resistance is maintained at traditional levels. The training portion of the study began one week after the testing session and post-intervention analyses were conducted one week after completion of training.

Results

For this analysis, data from 19 participants were available. Four subjects withdrew from the study due to reasons unrelated to the experimental protocol, and therefore had no post intervention analysis. Nine subjects in the CON group and six subjects in the ECC completed both baseline and post-intervention testing. The ECC group had a significant decrease in flexion moment following training compared to an increase in knee flexion moment in the CON group (effect size = 1.8, $p = 0.008$). No significant difference in abduction or torsion moments (p = 0.847, p = 0.645) were observed for the right side. There were no significant differences in pairwise comparisons of flexion, abduction, or torsional moments between CON and ECC control vs. treatment for the left knee (p = 0.422, p = 0.517, p = 0.295).

Discussion

Participants who utilized a standard squat exercise training program, experienced an increase in peak knee abduction moment during jump landing. Participants in the eccentric focused squat training group did not experience an increase in peak knee abduction moment. The eccentric squat training program may have a protective effect on knee stability, while accentuating increases in strength. The study provides promising data that eccentric strengthening of additional musculotendinous stabilizers such as the hamstrings, not just the quadriceps alone, may be required to significantly enhance knee stability.

The link between knee abduction loading and increased risk for ACL injury is well documented. Epidemiological studies have additionally suggested a gender based disparity in the rate of ACL injuries during sports related movements. While stability of the knee is primarily maintained by the intrinsic ligaments of the joint, enhanced extrinsic musculotendinous stabilizers of the knee may serve a protective effect in limiting future injury. Many studies posed that high mechanical loading and eccentric muscle action are essential in optimizing exercise induced hypertrophy. Eccentric training has the capability of overloading the muscle to a greater extent and to enhance muscle mass, strength and power when compared to training concentrically. This study demonstrated that, contrary to standard squat training, eccentric focused squat training did not have a negative effect on knee loading in healthy females. It remains to be determined if an eccentric focused squat training program can reduce the risk ACL injury in females.

Conclusion

This project addresses the important issue of reducing the risk of ACL injuries in females. The results of this study can be used to develop an eccentrically focused training program to reduce the knee joint moments, and subsequently, the risk of ACL injury in female athletes.

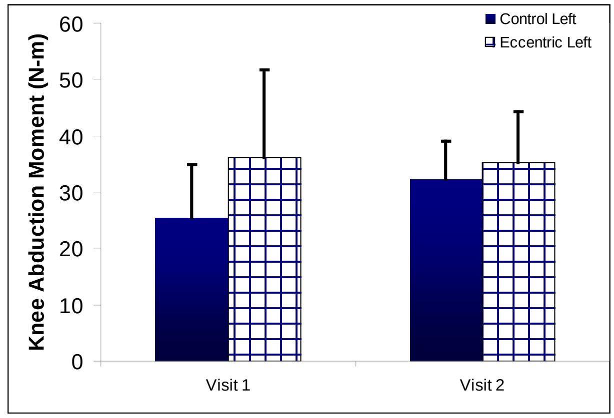

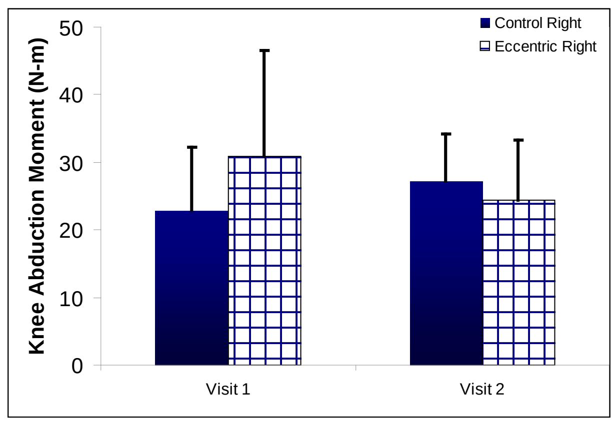

Figure 1. Left (top) and Right (bottom). Following the training program, subjects in the Concentric squat group had a higher knee abduction moment, while subjects in the Eccentric group maintained, or slightly decreased their abduction moment.

References

1. Arendt E, Dick R. AJSM 1995 Dec;23(6):694 -701.
2. Malone, etal. J South Orthop Assoc 1993;2(1):36–39.
3. Hewett TE, etal. AJSM 2005 Apr;33(4):492 -501.

COMPUTERIZED GAIT ANALYSIS AND LUMBAR RANGE OF MOTION ASSESSMENTS IN PEOPLE WITH LUMBAR SPINAL STENOSIS

Bryan P. Conrad, Abdullah Z. Abbasi, Heather K. Vincent, Amanda Seay, and David J. Kennedy[1]

[1] University of Florida, Gainesville, FL, USA
Spine and Sports Interventional Center at Shands Rehabilitation Hospital
E-mail: bconrad@ufl.edu Web: http://www.ortho.ufl.edu/motion-lab

INTRODUCTION

Age-related degeneration of the spine can reduce intervertebral disk height, ossify spinal ligaments and cause deterioration of the lumbar facet joints. These changes reduce the spinal canal lumen diameter and induce spinal stenosis. Spinal stenosis in the lumbar region causes pain or numbness in the low back and legs. As the disease progresses, ambulation and gait may be impaired. Self-report measures such as the Oswestry Disability Index (ODI), Medical Outcomes Short Form 12 (SF12), and Visual Analog Scales of pain (VAS) are routinely used in the clinical setting to capture data related to lumbar pain symptoms, function and perceived disability. The associations between self-report measures and objective measures of physical function in patients with lumbar spinal stenosis are not well characterized. The purpose of this study was to determine the correlation between ODI, SF12 and VAS scores and temporospatial measures of gait, three-dimensional lumbar range of motion (3D-ROM), and lumbar proprioception. The results of this study will provide evidence from which clinicians can make informed decisions as to which self-reporting measures are associated with lumbar functional status in patients with lumbar spinal stenosis.

METHODS

Patients with symptomatic lumbar spinal stenosis (N=25; age=62±14; 14 women) were enrolled in this study. Each subject completed the ODI, SF12, and VAS (during activity). Gait analysis was then performed using an instrumented walkway (GaitRite®; CIR Systems, Inc.; Havertown, PA). Three trials of each subject walking at a self-selected pace were collected and the temporospatial parameters were averaged together for analysis. Lumbar 3D-ROM was measured using an electromagnetic tracking system (Liberty, Polhemus Inc, Colchester, VT). Sensors were placed on L1 and L5 locations and joint angles were calculated for each of the three anatomical planes. In the 3D-ROM protocol, subjects were instructed to move as far as they could tolerate in flexion, extension, right and left lateral bending, and right and left axial rotation. The maximum envelope of motion in each plane was reported. Lumbar proprioception was measured by having the subject attempt to reproduce a position of lumbar spine angulation that had been previously set by the experimenter (target position). When the subject perceived that the target had been reached, the lumbar angulation was measured and compared to the actual target position. The difference between the target position and the subjects attempted repositioning is the repositioning error (RE). Linear regression was performed to determine the correlation between self report scores and gait analysis parameters (specifically stride length, cadence, and velocity).

RESULTS

The ODI was strongly correlated with stride length (r^2=0.58, $p<0.05$) and gait velocity (r^2=0.70, $p<0.05$) and weakly correlated with cadence (r^2=0.18, p=0.042). The SF12 was weakly correlated with stride length (r^2=0.182, p=0.042), but had no correlation with cadence or gait velocity. VAS was weakly correlated with velocity (r^2=0.189, p=0.038), and cadence (r^2=0.177, p=0.045), but had no correlation with stride length. There was no significant correlation between lumbar 3D-ROM or proprioception and any of the self-report measures.

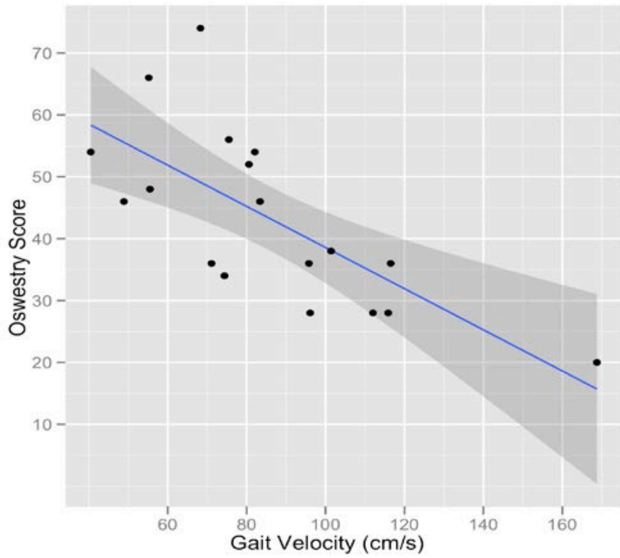

Figure 1. Oswestry Disability Index (ODI) and gait velocity were significantly correlated (r^2 = 0.5062, p= 0.000929), with faster velocity being associated with less disability (lower ODI score).

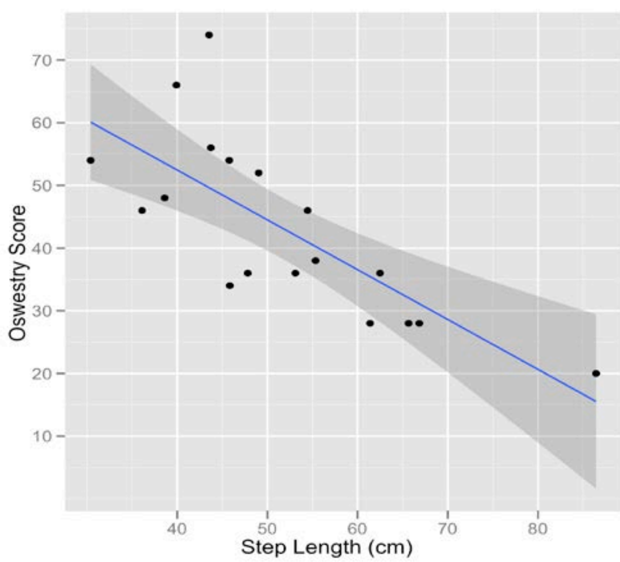

Figure 2. Oswestry Disability Index (ODI) and step length were significantly correlated (r^2 = 0.5788, p= 0.000246), with longer step lengths being associated with less disability (lower ODI score).

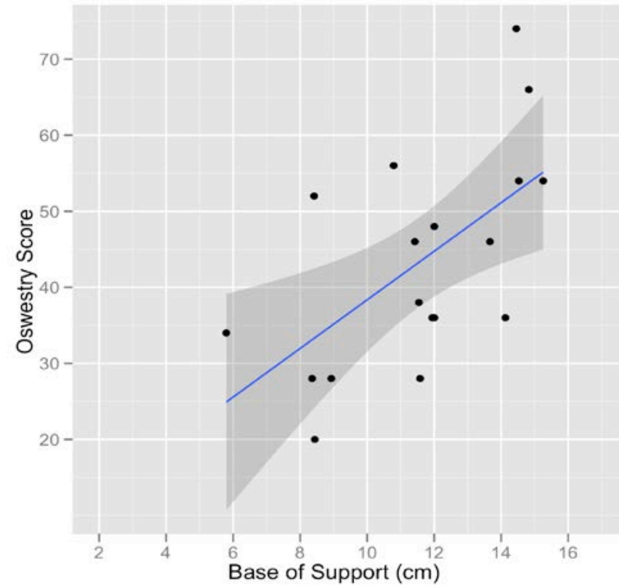

Figure 3. Oswestry Disability Index (ODI) and base of support were significantly correlated (r^2 = 0.3628, p=0.00817), with a narrower base of support being associated with less disability (lower ODI score).

DISCUSSION

Compared with SF12 and VAS, the ODI may be useful in the clinical setting to estimate the patient's walking ability. The lack of associations between the SF12 and VAS and walking ability was likely due to the non-specificity of these tools for back pain, The ODI content has some questions that relate directly to the functional tests, such as walking and pain during body motion and this may in part explain the higher correlations observed between gait and the ODI relative to the other tools.

ACKNOWLEDGMENTS

We appreciate the assistance of the Spine and Sports Intervention Center at Shands Rehab Hospital, in particular Patti O'Steen, Angie Korab, Lisa Herber, Sharon Presley, Shelly Hines.

DISCLOSURE STATEMENT

The authors have no conflicts of interest to report.

EFFECTIVENESS OF CERVICOTHORACIC ORTHOSES FOR IMMOBILIZING AN UNSTABLE CERVICOTHORACIC JUNCTION INJURY

Bryan P Conrad*; Glenn Rechtine**; Mark Prasarn§; Gianluca Del Rossi†; MaryBeth Horodyski*

* Department of Orthopaedics and Rehabilitation, University of Florida, Gainesville FL
** Bay Pines VA Health Care System, Bay Pines, FL
§Department of Orthopaedics, University of Texas Medical School, Houston TX
†Department of Orthopaedics, University of South Florida, Tampa FL

E-mail: bconrad@ufl.edu   Web: http://www.ortho.ufl.edu/motion-lab

INTRODUCTION

One of the primary goals of a cervicothoracic orthosis (CTO) is to provide stabilization and unloading to the spine in the presence of unstable fractures in both pre- and post-operative situations. In healthy volunteers with stable spines, CTO's have proven to be very effective in minimizing global and segmental motion in the cervical spine.[1] However, it is currently unknown whether CTO's will have the same effectiveness in immobilizing an unstable spine segment. The purpose of this study was to evaluate two modern CTO devices compared to a cervical collar to evaluate their ability to stabilize a complete segmental injury at the cervicothoracic junction.

METHODS

Four lightly embalmed whole body cadavers were utilized for this study. A global instability was created at the C7-T1 level by resecting the anterior and posterior ligaments, intervertebral disc, and facet joint. An electromagnetic motion analysis system (Liberty, Polhemus Inc. Colchester, VT) was used to capture segmental motion. Sensors affixed to the vertebral bodies of C7 and T1 using custom made mounting brackets. Four different conditions were evaluated: Aspen CTO, MiamiJ CTO, Aspen Vista cervical collar and no collar. The amount of motion allowed by each condition was then evaluated during a passive range of motion maneuver. A force sensor was utilized to standardize the amount of force applied during each range of motion maneuver. The motion generated during the application of each orthosis was also measured.

Figure 1. Images of the collar devices. From left to right: MiamiJ CTO, Aspen CTO, Aspen Vista Cervical Collar.

RESULTS

Each of the orthoses provided significant reduction of flexion/extension motion compared to wearing no collar, however there were no statistical differences between any of the orthoses. The Aspen CTO provided a restriction of flexion/extension motion of 82%, the MiamiJ CTO 85% and the Aspen cervical collar 58% compared to wearing no orthotic device. For axial rotation motion, the reduction was 66%, 71% and 57% for the Aspen CTO, MiamiJ CTO and Aspen cervical collar, respectively. For lateral bending motion, the reduction was 46%, 56% and 29% for the Aspen CTO, MiamiJ CTO and Aspen cervical collar, respectively. During orthoses application, the Aspen CTO has significantly less lateral bending motion than Aspen cervical collar, with no other significant differences.

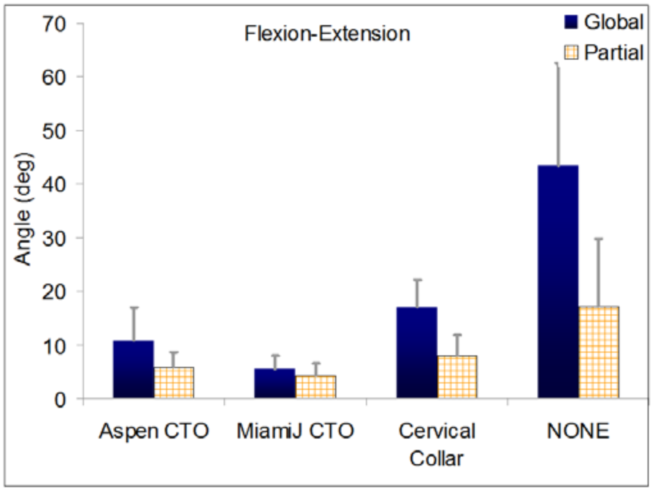

Figure 2. Flexion Extension motion.

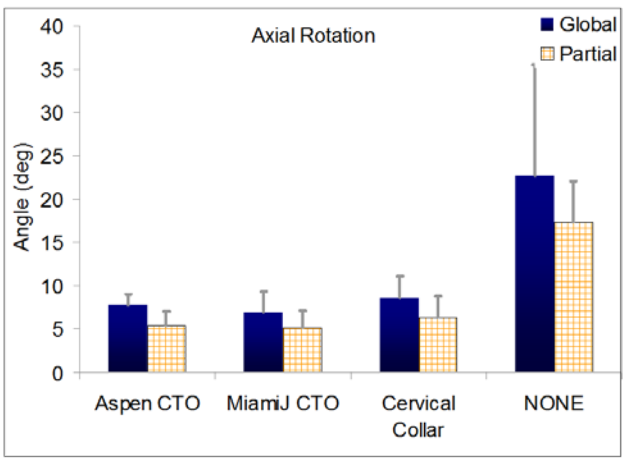

Figure 3. Axial Rotation motion.

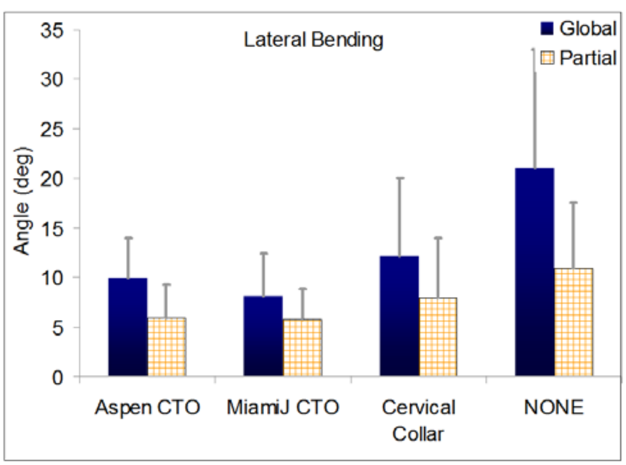

Figure 4. Lateral Bending motion.

CONCLUSION

Even in the presence of a catasrophic unstable cervicothoracic junction injury, CTO's can effectively reduce intervertebral motion. Although the motion is not eliminated, it is reduced to be approximately within the physiologic range. Although, there were no statistically significant differences between the CTO devices and the collar for the range of motion evaluation, in all cases the collar allowed more motion than either CTO.

REFERENCES

1. Gavin TM, Carandang G, Havey R, et al. Biomechanical analysis of cervical orthoses in flexion and extension: a comparison of cervical collars and cervical thoracic orthoses. *J Rehabil Res Dev*. 2003;40(6):527-537.

CREATING PHYSIOLOGICALLY REALISTIC VERTEBRAL FRACTURES

Nicole C. Corbiere, Kathleen A. Lewicki, Lisa M. Ferrucci, Kathleen A. Issen, and Laurel Kuxhaus

Clarkson University, Potsdam, NY, USA
email: lkuxhaus@clarkson.edu; website: http://www.people.clarkson.edu/~lkuxhaus/

INTRODUCTION

Approximately 50% of women and 25% of men will have an osteoporosis-related fracture after the age of 50, [1] yet the micro-mechanical origin of these fractures remains unclear. To understand compression fracture formation in cancellous bone, physiologically accurate loading conditions are necessary. Mechanical testing of vertebrae is relatively common, but the boundary conditions and specimen orientation with respect to the loading direction are frequently neglected or not considered. Cores of cancellous bone are often used [2] or the endplates are removed [3], creating unrealistic boundary conditions. For accurate results, motion segments must be physiologically loaded: the loading direction must pass through the center of the intervertebral disc [4]. The immediate research goal is to create physiologically realistic compression fractures in vertebrae. The proposed method is validated using Micro-Computed Tomography (µCT) and cervine vertebrae.

METHODS

Six 3-vertebrae segments from a fresh-frozen six month old male deer were loaded to create a vertebral fracture. MicroCT scans were taken before and after loading. A Potting Alignment Apparatus (PAA, Figure 1) ensures physiologically accurate boundary conditions and consistent loading of all specimens.

In preparation for mechanical loading, each 3-vertebrae segment was potted in Bondo™ (Auto Body Filler, 3M, St. Paul, MN) with half of the cranial and half of the caudal vertebrae of the segment submerged. The PAA ensures that the compressive load will be transferred through the center of the vertebral disc. An exploded view of these components is provided in Figure 2.

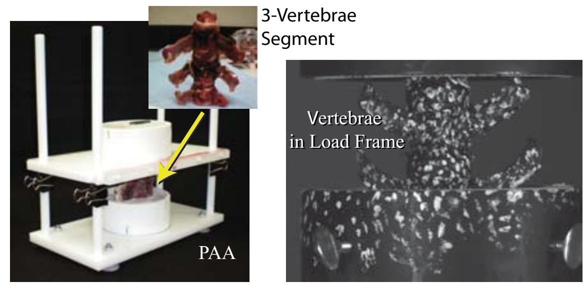

Figure 1: Potting Alignment Apparatus (left) and loading fixture with painted* vertebrae in load frame (right).
*Pattern for surface strain characterization, not mentioned here.

The PAA was leveled. A stopper was placed on the PAA to prevent rotation of the vertebrae during the curing and loading processes. A tube of machinable LE grade garolite was placed in the stopper to prevent adhesion of a rod to the Bondo™, which is poured in the PVC pipe slice. The rod was inserted in the garolite tube and the motion segment (cranial vertebra first) was slid down the rod to ensure vertical alignment of the spinal canal. A surface level was used on the rod to ensure vertebral bodies remained parallel to the loading direction and the vertebrae were secured during curing using a clamp. The vertebrae were then inverted and the process was repeated to pot the caudal vertebra.

After removing the metal alignment rod, each potted 3-vertebrae motion segment was then placed into a loading fixture (Figure 1), gripped in the load

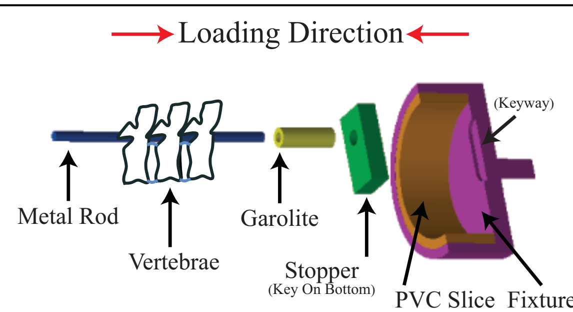

Figure 2: Components involved in alignment.

frame (Instron 1331, Norwood, MA), and compressed at a rate of 0.5mm/min until a noticeable load drop was observed (Figure 3). Each 3-vertebrae segment was scanned in a µCT scanner (GE Phoenix Nanotom, Wunstorf, Germany) prior to and after loading at a resolution of 20.07µm. These scans were visually inspected to determine fracture location.

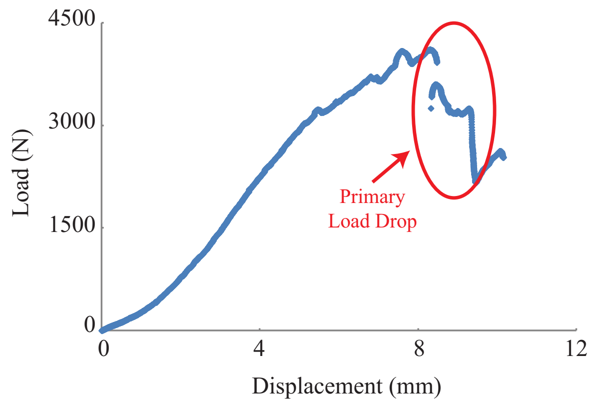

Figure 3: Representative example of a load-displacement curve (L1, L2, L3 segment).

RESULTS AND DISCUSSION

Burst fractures were created in all six motion segments. The primary load drop (Figure 3) indicates cancellous bone micro-structural collapse, whereas the smaller load drops may be disc rupture. A µCT scan (Figure 4) of a compressed motion segment shows a fracture propagating from the cranial vertebra at the caudal endplate. This endplate fracture is representative of a traumatic burst fracture [5]. The life span of deer is short and thus it is unlikely that a cervine specimen would have osteoporosis. Therefore, a burst fracture, rather than a compression fracture, is expected in these healthy, non-osteoporotic, cervine specimens.

Limitations of this work include the use of cervine vertebrae. If osteoporotic human vertebrae were used, the fracture may initiate in the vertebral body. A straight spinal cord canal is also assumed, which is reasonable for a 3-vertebrae motion segment.

CONCLUSIONS

This alignment and loading method for a 3-vertebrae motion segment produced a physiological

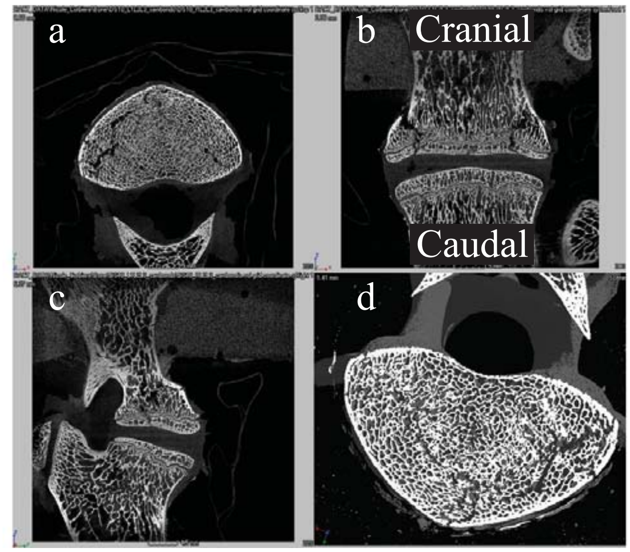

Figure 4: Example µCT scan of fracture site (L1, L2, L3 segment). (a) transverse plane view, (b) dorsal plane view, (c) sagittal plane view, and (d) 3D transverse view.

vertebral fracture in six 3-vertebrae motion segments. The PAA permits the physiologic specimen orientation to be reproduced in the load frame fixture. Thus, this method allows accurate load transfer boundary conditions through the discs and is appropriate for use in future studies of vertebral compression fracture initiation. Future studies may include quantifying the failure region(s) of vertebral micro-architecture in healthy and osteoporotic human vertebrae.

REFERENCES

1. *National Osteoporosis Foundation*, Fast Facts – Fractures, 2011.
2. Rapillard, L., et al. *J Biomech* **39**, 2133-2139, 2006.
3. Ebbesen, E. N., et al. *Bone* **25**, 713-724, 1999.
4. Brown, S. H. M., et al. *J Biomech* **41**, 122-127, 2008.
5. Jiang, G., et al. *Bone* **47**, 111-116, 2010.

ACKNOWLEDGEMENTS

We thank Mathew Ingraham for load frame expertise, Dr. David Morrison for load frame training, Jon Young for machining, and Dr. Richard Gonzalez for anatomy and dissection knowledge.

The Influence of Fatigue on Landing Mechanics in Youth Male Lacrosse Athletes

[1]Nelson Cortes, [2]Eric Greska, [2]Julie Bamberg, [2]Stacie Ringleb and [2]Bonnie Van Lunen

[1]George Mason University, Manassas, VA, USA
[2] Old Dominion University, Norfolk, VA, USA
email: ncortes@gmu.edu

INTRODUCTION

Over the past decade, youth lacrosse participation has substantially increased across the United States [1]. The inherent movements within lacrosse require cutting and pivoting tasks, which can potentially generate an increased risk for noncontact knee injuries similar to those seen in basketball and soccer athletes. As well, fatigue has been shown to have a detrimental effect on lower extremity biomechanics, potentially increasing the risk for injury [2, 3]. Yet, the effects of fatigue on lower extremity biomechanics in the young adolescent athletic population have not been addressed. Therefore, the purpose of this study was to assess the effects of a fatigue protocol [Slow Linear Oxidative Fatigue Protocol (SLO-FP)] on lower extremity biomechanics during side-step cutting task (SCT) in adolescent male lacrosse athletes

METHODS

Lower extremity biomechanics of twenty-four male recreational lacrosse players (11.6 ± 1.5 years; 153.9 ± 14.0 cm; 44.7 ± 2.2 kg) were obtained before and after completion of a fatigue protocol occurring in a single session. For the testing sessions, participants performed five trials of a side-step cutting task at pre and post-fatigue protocol with the dominant limb. The task was displayed in a randomly unanticipated order through custom-made software. A VO2peak test was performed prior to the SLO-FP. The SLO-FP consisted of four intervals; each interval included four-minutes of jogging (speed set at 70% max VO2peak speed) and one-minute of running (speed set at 90% max VO2peak speed) for a total of 20 minutes [4]. Eight high-speed VICON cameras (Vicon Motion Systems Ltd, Oxford, UK) sampling at 300Hz and two Bertec Force Plates (Model 4060-10, Bertec Corporation, Columbus, OH, USA) sampling at 1200Hz were used to track marker trajectory and ground reaction forces, respectively. From the standing (static) trial, a lower body kinematic model was created for each participant using Visual 3D (C-Motion, Rockville MD, USA). The kinematic model was used to quantify the motion at the hip, knee, and ankle joints. The standing trial with a circular motion of the pelvis was used to estimate a functional hip joint center [2]. Based on a power spectrum analysis, marker trajectory was filtered with a fourth-order Butterworth zero lag filter with a 7 Hz cutoff frequency, whereas ground reaction force data were filtered with a similar filter with a 25 Hz cutoff frequency. Dependent variables included knee flexion (KF) angle, hip flexion (HF) angle, knee abduction moment (KABM), hip abduction (HAB), hip abduction moment (HABM) and vertical ground reaction force (VGRF) at initial contact. Repeated measures ANOVA's were conducted to compare statistical differences between pre and post SLO-FP. Alpha level was set a priori at 0.05

RESULTS AND DISCUSSION

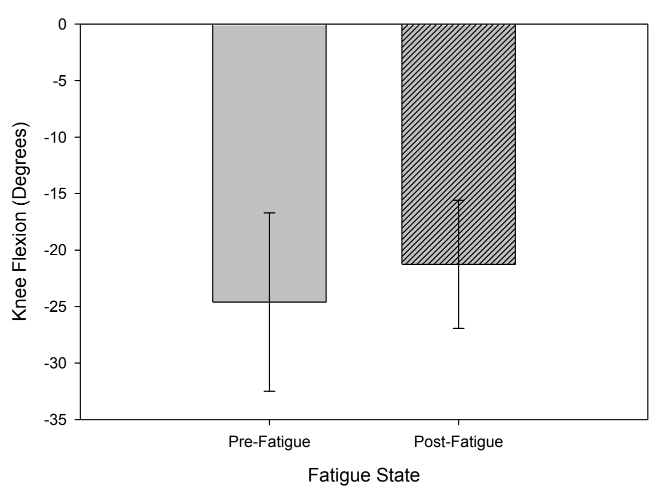

Figure 1: Knee flexion angle at initial contact presented a significant difference between pre and post-fatigue.

Fatigue significantly altered some kinetics and kinematics at the hip and knee. In particular, a decrease in VGRF was attained after the fatigue protocol (pre: 0.256 ± 0.123 N/mBW to post: 0.185 ± 0.15 N/mBW, p = 0.037) (Figure 1). Decreased knee flexion (pre: -24.51 ± 7.9˚ to post: -20.96 ± 5.39˚, p = 0.018) and knee adductor moment were also attained (pre: 0.851 ± 0.135 Nm/Kgm to post: 0.016 ± 0.096 Nm/Kgm, p = 0.016). Peak hip flexion also decreased after the fatigue protocol (pre: 56.31 ± 17.48˚ to post: 51.88 ± 16.25˚, p = 0.003), and the hip became less abducted post-fatigue when compared with pre-fatigue (pre:-14.85 ± 5.08˚ to post:-12.33 ± 5.98˚, p = 0.002) (Figure 2). A shift from a hip adductor moment to an abductor moment was observed (pre: 0.034 ± 0.22 Nm/Kgm to post: -1.52 ± 0.21 Nm/Kgm, p = 0.019).

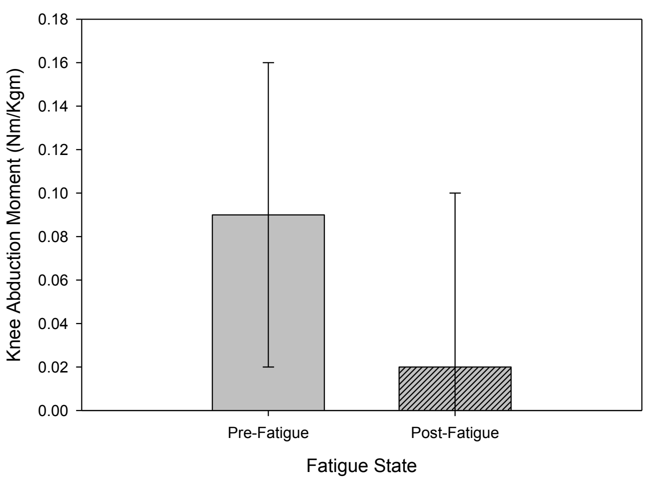

Figure 2: Knee abduction moment at initial contact attained a significant difference between pre and post-fatigue.

The extended posture through decreased knee and hip flexion angles causes greater quadriceps pull at the knee, which increases the anterior translational pull on the tibia, which prevents proper co-contraction of the hamstring muscle group [5]. This increase in anterior translation may contribute to the stress placed on the ACL, which can increase the risk for injury. Unexpectedly, we found a decrease in knee adduction moment but no difference was found for knee abduction angle. The lack of difference for knee abduction angle contradicts previous research [6]. It is important to note that this finding is inconsistent within the literature. There are studies that found an increase in knee abduction moment and angles with an inconsistency within gender. Few have reported significant increases for both men and women after a fatigue protocol, while others reported an increase just for women [7, 8]. Our study did not find an effect of fatigue on knee abduction angles. This supports the notion that our participants were not at increased risk for ACL injury after a fatigue protocol.

CONCLUSIONS

Post-fatigue, the adolescent athletes adopted a cutting position that has been shown to potentially increase the demands at the knee ligamentous structures. These demands are suggested to increase the likelihood of noncontact knee injuries. It is important that injury prevention programs start at early ages, and take into account the effects of fatigue.

REFERENCES

1. McCulloch PC, Bach BR. *Orthopedics* **30**, 29-34, 2007.
2. Mclean SG, Samorezov JE. *Med Sci Sports Exerc* **41**, 1662-1673, 2009.
3. Sanna G, O'Connor, KM. *Clin Biomech* **23**, 946-954, 2008.
4. Lucci S, et al. *J Sci Med Sport* **14**, 453-459, 2011
5. Padua DA, et al. *J Athl Train* **41**, 294-304, 2006.
6. Borotikar, et al. *Clin Biomech* **23**, 81-92, 2008.
7. Chappell JD, et al. *Am J Sports Med* **33**, 1022-1029, 2005.
8. McLean SG, et al. *Med Sci Sports Exerc* **39**, 502-514, 2007.

POWER TRAINING POST-STROKE ENGAGES NEURAL CIRCUITS AT SPINAL AND SUPRASPINAL LEVELS

[1]Manuela Corti, [1]Carolynn Patten

[1]University of Florida, Gainesville, FL, USA
[2]Brain Rehabilitation Research Center – Malcom Randall VAMC, Gainesville, FL, USA
email: m.corti@phhp.ufl.edu

INTRODUCTION

Upper-extremity rehabilitation post-stroke typically focuses on repetitive execution of functional movements (e.g., functional task practice (FTP)), ostensibly to facilitate neural plasticity. High intensity activities, especially strengthening, have traditionally been avoided in neurological disorders because they are assumed to increase spasticity and impair motor performance. Our combined work to date suggests that dynamic high-intensity resistance training (i.e., POWER) does not increase spasticity and is an effective treatment that can induce restoration of more normal movement parameters, including: isometric maximal voluntary force, isovelocity torques, neuromuscular activation, kinematics and stretch-reflex modulation. However, our previous studies have not measured the effect of therapeutic intervention involving POWER training on neural circuits at the supraspinal level.

Our overall objective is to improve our understanding of mechanisms underlying recovery post-stroke by using a multimodal investigative approach that provides insight into the dynamic relationship between neurophysiology and motor behavior. This study evaluated the effect of 2 weeks of HYBRID training (POWER + FTP) using clinical tests and three-dimensional motion-analysis of reaching, H-reflex measures to test spinal circuitry, and TMS to measure cortical circuits. Our central hypothesis is that intervention involving POWER increases central neural drive during functional voluntary movement. Here we sought to identify concurrent behavioral and neural adaptations at the spinal and supraspinal levels.

METHODS

The participant in this single-subject design was a 66-year-old, right hand dominant, white female, 5-months following a venous infarction associated with cortical vein thrombosis involving the arm-hand knob region and the subcortical posterior half of white matter. The lesion resulted in left hemiparesis affecting mainly the UE with absence of cognitive impairment. This single-subject design involved two weeks of HYBRID therapy. Prior to, immediately following and one-month follow-up, participant underwent to a blinded multimodal evaluation. Evaluation included the following measurements: 1) UE muscles strength tests; 2) kinematics analysis during a functional task to measure motor control; 3) H-reflex to test presynaptic inhibition (D1) and homosynaptic post-activation depression (PAD), TMS to measure cortical and interhemispheric networks.

HYBRID intervention consisted of combined POWER training followed by FTP for 3 hours daily, 5 days per week, for two weeks. POWER involved five reciprocal upper-limb movements: shoulder abduction/adduction, shoulder flexion/extension, shoulder external/internal rotation, transverse plane elbow flexion/extension and wrist flexion/extension. FTP involved practice of functional tasks using a progression of six therapeutic goals and nine activity categories.

RESULTS AND DISCUSSION

Kinematics revealed increased elbow and shoulder range of motion post-HYBRID training. These results suggest improved motor control during the functional reaching task. Behavioral improvements were partially maintained at follow-up. H-reflex indicated reduced H_{max}/M_{max} and H_{slope}/M_{slope} ratios, increased PAD and D1 inhibition progressively post-HYBRID and at follow-up. These results suggest reduced spinal excitability, and increased presynaptic and homosynaptic inhibition of the monosynptic reflex in the affected UE. TMS data at post-HYBRID evaluation indicated: 1) increased RC slopes in the affected hemisphere and reduced RC slopes in the unaffected hemisphere; 2) increased ipsilateral silent period (iSP) from the affected-to-unaffected hemisphere, and reduced iSP from the unaffected-to-affected hemisphere – indicating rebalancing of IHI; 3) reduced contralateral SP (cSP) duration and its RC slope in both affected and unaffected hemispheres – indicating improvement intracortical inhibition; 4) increased short intracortical inhibition (SICI) in the affected hemisphere and decreased SICI in the unaffected hemisphere – indicating improvement of another mechanism of intracortical inhibition. These improvements were partially maintained at follow-up evaluation.

The positive outcomes of HYBRID training can most likely be attributed to: a) the well-recognized and profound neural adaptations induced by POWER training, and b) therapeutic intensity, which promotes improvement by challenging the subject's capacity. Neural adaptations induced by resistance training occur: 1) at the level of the spinal cord, which is caused by changes in synaptic efficacy within the motoneuron pool, and 2) at the supraspinal level, including adaptations such as increased activation within the cortical circuitry. Our results suggest that HYBRID training induces improved modulation of the spinal mechanisms controlling homosynaptic (PAD) and presynaptic (D1) pathways of the arc reflex. Improvements in modulation of the homosynaptic arc reflex (PAD) may suggest improvement in the efficacy of the Ia fibre-motoneurone synapse. Improvements in the presynaptic (D1) mechanisms may suggest improvement of the impaired descending inhibitory control from higher cortical structures post-stroke (i.e. improved dis-inhibition).

TMS data confirm positive treatment effects on inhibitory and excitatory supraspinal pathways. Cortical excitability, and its interhemispheric influence (i.e. inhibition) on the unaffected hemisphere, improved in the affected hemisphere. These findings together suggest a more balanced cortical excitability and interhemispheric interaction. In addition, our results suggest improved modulation of the inhibitory pathways within the motor cortex mediated by GABAb (cSP) and GABAa (SICI). In accordance with previous studies, our study showed motor recovery associated with reduction of SP duration, usually prolonged post-stroke, and increased SICI, usually reduced post-stroke. As we hypothesized, the intensity of the HYBRID treatment may have indirectly improved the impaired modulation of the cortical inhibition pathways by engaging increased participation of the nervous system and eliciting greater voluntary cortical drive.

CONCLUSIONS

Our findings support our hypothesis that POWER promotes enhanced central neural drive in the ipsilesional hemisphere and may represent potential driver of cortical reorganization including modulation of intracortical and interhemipsheric inhibition. Further, our data reveal that it is possible to induce concurrent neurophysiological changes at spinal and supraspinal levels, associated with behavioral change that constitutes functional recovery. Our results compel us to investigate these mechanisms with future larger scale research studies, which may inform how individual characteristics interact with mechanisms of neural recovery.

REFERENCES

1. Aymard C, et al. Brain **123**, 1688-1702, 2000.
2. Perez MA, et al. Topics in Stroke Rehabilitation **16**(4), 254-269, 2009.
3. Kimiskidis VK, et al. Exp Brain Research **163**, 21-31, 2005.
4. Corti M, et al. Neurorehabil and Neural Repair [Epub, Feb 22, 2012] PMID:22357633
5. Patten C, et al. J Neurol Phys Ther **30**, 99-115, 2006.

ACKNOWLEDGEMENTS

This work was supported by a Brooks Foundation Endowment Pilot grant, VA RR&D Merit Review #B3964R, VA RR&D Research Career Scientist Award (CP), and a University of Florida Fellowship (MC).

EFFECTS OF SERRATUS ANTERIOR MUSCLE FATIGUE ON SCAPULAR KINIMATICS

Oren Costantini, Amitabh Dashottar, and John Borstad
The Ohio State University, Columbus, OH, USA

INTRODUCTION

Shoulder pain accounts for an average of 8.6 million physician visits each year in the United States. Data obtained from the U.S. Department of Health and Human Services show that more than 6% of these cases annual cases were attributed to rotator cuff problems. Neer proposed a mechanism of rotator cuff degradation, where the rotator cuff tendons were compressed in the subacromial space. This was coined as Subacromial Impingement Syndrome (SIS). SIS has become the most common diagnosis of shoulder pain, accounting for 44% to 65% of all complaints of shoulder pain during a physician's office visit. Scapular dyskinesis is a common clinical finding in patients with SIS and Rotator Cuff pathology. The pattern of scapular kinematics associated with SIS is decreased scapular posterior tilting, decreased upward rotation (UR), and increased scapular internal rotation (IR) from normal kinematics. Several studies have recorded scapular motion alterations due to fatigue. Though the results vary between these studies, due in part to the variety of fatigue tasks chosen, they consistently reflect changes in scapular kinematics. Ludewig & Cook reported increased upper and lower trapezius (UT & LT) activation and decreased serratus anterior (SA) activation in addition to decreased scapular posterior tilting during arm elevation in construction workers with SIS. Cools et al showed imbalances between the muscle activation ratios of UT and SA in athletes with SIS. SA is positioned to contribute to all three normal scapula rotations, upward and internal rotation, and posterior tilting. SA is the primary muscle which serves to anteriorly translate and internally rotate the scapula about the thorax. SA also is responsible for maintaining the contact of the scapula and the thoracic wall and serves to posteriorly tilt the scapula as the humerus is elevated. If fatigued, the SA can be expected to alter the motion of the scapula through its inability to perform on its unique line of action and through the compensation strategies of synergistic musculature. This study proposed to fatigue the SA, bilaterally and in multiple stages, using a task to isolate fatigue to the SA, and examine the effect this has on scapular kinematics. The purpose of this study was to examine the effects of SA fatigue on scapular kinematics.

METHODS

Seventeen healthy subjects, without existing shoulder pathology, were recruited for this study. Each subject was asked to participate in a single measurement session consisting of two types of tasks: Fatigue and Kinematic. Baseline measurements of maximum voluntary contractions (MVC) and pre-fatigue kinematics were taken at the start of testing. Subject then performed a fatigue task, for one minute, and repeated the kinematic tasks. This process was then repeated with the subject holding the fatigue task for as long as possible.

To determine the level of fatigue each subject experienced, EMG and subject reported Borg CR10 scores were be recorded for each fatigue task. EMG data was collected using a Delsys Bagnoli 8-EMG system with sensors placed on the UT, LT, Pectoralis Major (Pec), and SA muscles bilaterally. The EMG data from each task was normalized against the MVC for each of the four muscles, recorded at the beginning of the session. Kinematic data was collected in 3D using a Flock of Birds electromagnetic system in conjunction with Motion Monitor software. A total of five of these sensors were placed on the body: one on each upper arm, one on each acromion process, and one on the sternum. These sensors were digitized using the protocol recommended by the International Society of Biomechanics.

The fatigue task consisted of a resisted supine reaching task previously demonstrated to bias fatigue to SA. The resistance given to each subject was 20% body weight applied using a therapeutic resistance band. Subjects protracted their arms at a 30° angle, supported by an inclined table, and held this position. Normalized EMG data, collected in 10-second intervals, were used to quantify fatigue in each muscle. An 8% mean power frequency(MPF) decline has been described as the minimum threshold to indicate fatigue.

The kinematic tasks included raising and lowering the arms in the scapular plane and lifting a light weight in the frontal plane. Each task was performed five times. Euler angles for humeral elevation, scapular IR, UR, and scapular tipping were calculated. The motions of the scapula between 30° and 120° of humeral elevation were measured against baseline values and compared to reported scapular motions in shoulders with pathology.

RESULTS AND DISCUSSION

Kinematics: Arm dominance was shown to significantly affect all three rotations of the scapula in both kinematic tasks across all fatigue conditions ($P<.05$). To determine individual rotation changes between conditions, subjects were grouped based on direction of change. This was done due to variations in kinematic alteration within and across subjects. In scapular plane abduction most subjects gained IR and lost UR on both sides as fatigue progressed ($p<.05$), however the dominant shoulder showed significant kinematic alterations in the reverse directions as well ($p<.05$). Scapular posterior tilting of the dominant shoulder increased while that of the non-dominant decreased ($p<.05$). In frontal plane lifting the dominant arm showed significant kinematic alterations in both directions for all scapular rotations ($p<.05$) except loss of UR ($p=.056$). The non-dominant shoulder experienced a consistent gains in IR and losses in posterior tilt and UR ($p<.05$) as fatigue progressed. These statistically significant variations in kinematic patterns with the progression of fatigue of the dominant shoulder support the findings of McCully et al and suggest that compensation strategies are acquired and therefore vary from shoulder to shoulder. The findings on the non-dominant shoulder are similar to those reported by Ludwig & Cook on patients with SIS.

Fatigue: Results of EMG analysis were less clear than those of the kinematics. Due to the limited number of subjects, most results were derived qualitatively. In the first fatigue task SA was the only muscle to show significant changes in EMG MPF with time ($p<.05$). Overall this decline was only 5.5% and did not qualify as fatigue based on the accepted standard (8%). Separating the analysis by side shows an 8% decline in the non-dominant SA and a 3.2% decline in the dominant; though side to side differences were not found to be statistically significant. The second fatigue task had no significant MPF declines.

Qualitative inspection, specifically joint amplitude spectrum analysis (JASA), shows that for the first fatigue task SA and Pec show signs of increased fatigue and activation over time while UT and LT show minimal fatigue and activation. In the second fatigue task SA shows force decreases, UT and LT show primarily fatigue, and Pec shows a mixture of both. This suggests that in the first fatigue task fatigue has been biased to SA and that in the second task fatigue is more global and SA is experiencing a lower load.

CONCLUSIONS

Alterations in scapular kinematics of healthy subjects, as fatigue progresses, show similarities to reported scapular kinematics of patients with SIS, however, these motion patterns vary between subjects and suggest that compensation strategies are acquired. This means injury prevention may be trainable. SA fatigue was demonstrated qualitatively but further investigation is needed to clarify its role in these kinematic alterations.

REFERENCES

1. McClure, P. et al. *Physical Therapy*, **86**(8):1075–1090, 2006.
2. Neer C.S. *J Bone Joint Surg Am*, **54**(1):41–50, 1972.
3. Cools, A. et al. *British Journal of Sports Medicine*, **38**(1):64–68, 2004.
4. Ludewig, P. et al. *Physical Therapy*, **80**(3):276–291, 2000
5. McCully, S. et al. *Clinical Biomechanics* **21**:545-553, 2006

ULNA SIMULATION ASSESSES SENSITIVITY TO BONE ELASTIC MODULUS VARIATIONS IN A MRTA TEST

[1,2]John R. Cotton, [3]Lyn Bowman, and [1]Chad Stroud
[1]Mechanical Engineering, Ohio University, Athens, OH, USA
[2]Biomedical Engineering, Ohio University, Athens, OH, USA
[3]Biological Sciences, Ohio University, Athens, OH, USA
email: cotton@ohio.edu, web: http://www.ohio.edu/people/cotton/

INTRODUCTION

Unlike DXA and pQCT, Mechanical Response Tissue Analysis (MRTA) provides a direct, non-invasive, radiation-free, measurement of a long bone's mechanical integrity.[1] In MRTA, low amplitude oscillatory forces spanning frequencies from 50 to 1500 Hz are applied to skin overlying the bone and mechanical parameters are estimated from the resulting frequency response function. The bone's bending stiffness is then used to estimate an averaged *EI* value assuming a uniform cross-section beam.

We built a finite element (FE) model of a human ulna to compare the estimates of *EI* from two equations—one based on static deflection, one on modal frequency. Both assume a uniform cross-section beam. We validated the FE model by static and dynamic experiments, and then simulated static three-point bending and modal vibration of the ulna. We then examined the sensitivity of these two estimates to local differences in the elastic modulus, *E*.

METHODS

We scanned a fourth generation composite ulna (Sawbones, Pacific Research Laboratories, WA, USA) using a clinical CT scanner. Scans were segmented using Avizo (VSG, Merignac, France) into "cortical" (short fiber epoxy) and "cancellous" (polyurethane foam) material. A solid mesh was created with linear tetrahedra and over 47000 nodes. The mesh was exported into MSC.Marc (Santa Ana, CA). Cortical bone was assigned a density ρ of 1.64 g/cc, while cancellous bone had E = 155 MPa and ρ = 0.27 g/cc, as reported by the manufacturer. The cortical E value was calibrated to match our experimental static three-point bend test. Boundary conditions replicated a simply supported beam. The ulna was oriented with the load applied to the dorsal border and supports on the anterior aspect. The ulna span L was 243 mm between the supports.

Static three-point bend tests were simulated with a mid-span load F of 10 N. Results were calibrated to an actual static three-point bend test of the composite ulna. Both simulation and experiment calculated *EI* using the Euler beam solution

$$EI = \frac{L^3}{48}\frac{F}{d} \qquad (1)$$

where d is the deflection at the load. We then simulated a modal analysis of the ulna to find the frequency of the first mode of vibration, f_1, which was used to calculate *EI* by

$$EI = \mu\left[\frac{2 f_1 L^2}{\pi}\right]^2 \qquad (2)$$

where μ is the mass per unit length of the ulna. Experimental dynamic tests of the composite ulna applied a swept-sine mid-span load with frequencies from 50-400 Hz. We compared this to a harmonic simulation with the same conditions.

To examine sensitivity of *EI* measurements to local differences in E, we increased and decreased E by 10% in four 10 mm long sub-regions of cortical bone (C1-C4 in Figure 1) and compared *EI* calculations from equations (1) and (2) to a simulation with a constant cortical E.

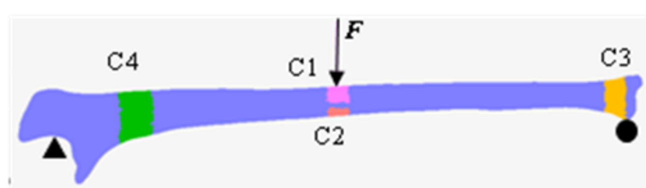

Figure 1: The ulna and four sub-regions (C1, C2, C3, C4) where cortical modulus values were varied. Supports and applied force F are shown.

RESULTS AND DISCUSSION

The physical three-point bend test of the composite ulna and equation (1) yielded an *EI* of 12.6 N·m^2. This was matched in our FE simulation by applying a constant cortical *E* of 11.3 GPa, a value between the 10 and 16 GPa moduli reported by the manufacturer for transverse and longitudinal directions, respectively. The frequency response of the FE model matched well with experiment (Figure 2) giving confidence in our FE model.

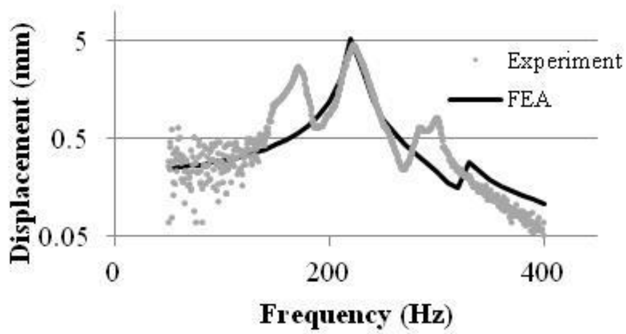

Figure 2. Harmonic response of simulation and experiment. Note: Data amplitude is normalized.

EI estimates from modal analysis and Equation (2) were ~2% larger than those from three-point bending and equation (1), perhaps due to the extra mass beyond the supports moving in vibration.

In the sensitivity analyses, when any sub-region modulus was increased and decreased the calculated *EI* values slightly increased and decreased, respectively. Further, Table 1 shows that *E* changes in center sub-regions (1 or 1&2 together) had much larger effects on *EI* than changes in sub-regions near the ends (3 or 4) despite the volume of sub-region 4 being > 2.5 times larger than C1&C2 combined. Figure 3 attempts to normalize the effects of altering local *E* by dividing the percent *EI* change by the percent sub-region volume.

CONCLUSIONS

This study used static and dynamic FE simulations of a realistic ulna and uniform beam equations to calculate an average *EI*. These mechanical methods are capable of detecting small local variations in the elastic modulus, but the sensitivity is greatest at mid span and least at the ends. Estimates of *EI* and sensitivities to local differences in elastic modulus are slightly different between methods and equations used for the interpretation. These findings show a role for modeling to guide further development of MRTA and interpretations of results based on its use, such as [2,3].

Table 1. Results of static and modal simulations with sub-region modulus variations. Also presented is the percent of model volume in the sub-regions.

Region	Percent model volume ΔVol (%)	% Change in calculated *EI*			
		Static		Modal	
		E ↑	*E* ↓	*E* ↑	*E* ↓
C1	0.90	0.56	-0.62	0.36	-0.45
C2&C2	1.83	0.97	-1.12	0.72	-0.90
C3	1.11	0.03	-0.01	0.00	-0.09
C4	4.64	0.05	-0.03	0.00	-0.09

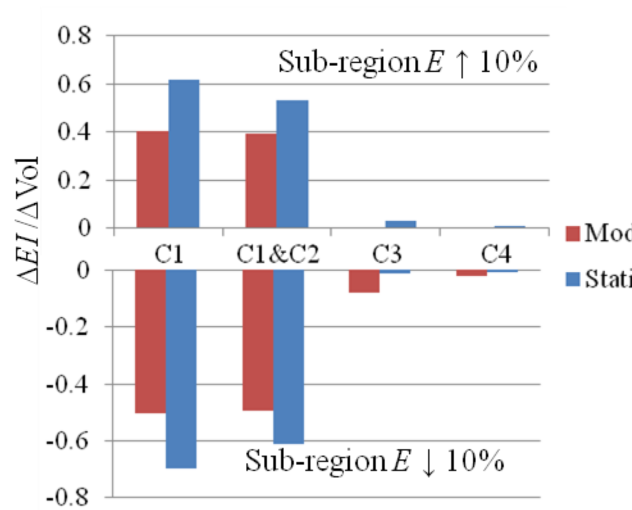

Figure 3. Volume adjusted effect of changing E in a subregion.

REFERENCES

1. Steele, CR, et al. *J Biomech Eng* **110**,87–96, 1988.
2. Miller, LE, et al. *Bone*, **41**, 685-689, 2007.
3. Wynnyckyj, C, et al., *Bone*, **44**, 840-848, 2009.

ACKNOWLEDGEMENTS

Thanks to Larry Witmer (OUCOM) and O'Bleness Memorial Hospital for performing the CT scans. Chad Stroud (B.S. student) was supported in this work by the Ohio University PACE program.

Knee Kinematics and Kinetics during Descent of a Navy Ship Ladder

[1]Jonathan D. Coulter, [1]Sebastian Y. Bawab, [2]Joshua T. Weinhandl and [1]Stacie I. Ringleb

[1] Department of Mechanical and Aerospace Engineering, [2] Department of Human Movement Sciences
Old Dominion University, VA, USA
email: sringleb@odu.edu, web: www.odu.edu/~sringleb

INTRODUCTION

Knee disorders have been associated with walking on hard surfaces and stair ambulation [1]. Patellofemoral pain syndrome (PFPS) has been diagnosed as pain arising in the anterior part of the knee [2]. PFPS has been linked to military populations [2,3], particularly in individuals who regularly use the unusual and constrained configuration of Navy ship ladders [3]. From 1994 to 1996, the chief cause for orthopaedic medical disability boards at the Naval Medical Center in San Diego, CA was patellofemoral pain [3].

The relationship between descent of Navy ship ladders and external knee flexion moments is not well established. To the knowledge of this study, only one study has compared traditional stair to Navy ship ladder external knee moments [3]. The study found that knee flexion moments were greater in descent than ascent of the ship ladder [3]. Thus, the purpose of this study was to compare external knee flexion moments during the descent of Navy ship ladders to external knee flexion moments during descent of traditional staircases from the literature.

METHODS

A replica of the most commonly used ship ladder from the USS Forrest Sherman (DD931) was constructed. The tread depth, rise and overlap were 12.7cm, 22.54cm, and 0.4763cm, respectively. The angle of the steps was approximately 61°. The replica ladder contained 4 steps and attached to a platform that allowed the subjects to take a full step before hitting the force plates. Two Bertec force (Bertec, Columbus, OH) plates were rigidly fixed to the second and third steps from the ground.

Data were collected from three active duty Navy sailors, (2 males and 1 female, age=21±1.15 yrs, BMI=79.62±10.3 kg, height=170.7±13.6 cm). They did not have any previous history of knee surgery and were knee injury free for the past 6 months. A total of 50 retro reflective markers were attached to the feet, shanks, thighs, pelvis, trunk, back and shoulders of the subjects. Kinematic data were collected at 300 Hz using 8 VICON (Vicon, Oxford, UK) cameras and kinetic data were collected at 1200 Hz. VICON Nexus was used to simultaneously collect kinematic and kinetic data. Three trials of data were collected during the subjects' descent of the ship ladder.

Kinematic and kinetic data were exported to Visual3D (C-Motion, Germantown, MD) for post processing. Knee moments and ground reaction forces were normalized to body mass.

RESULTS AND DISCUSSION

Peak knee flexion occurred at 99% of stance with an angle of 92.6 ± 7° (Figure 1A). The peak vertical ground reaction force occurred at 22% of stance with a magnitude of 10.8 ± 1 N/Kg and at 32 ± 6° of left knee flexion (Figure 1B). The peak external knee moment was 1.89 ± 0.15 Nm/Kg and it occurred at 76% of stance and at 67 ± 5.5° of knee flexion (Figure 1C).

Peak knee flexion and peak knee moment were 91.8±5.9° and 0.91±0.21 Nm/kg, respectively when collected on conventional stairs at an angle of 31.3° [4]. While the peak knee flexion on conventional stairs was similar to the peak knee flexion on the Navy ship ladder, the peak knee moment on conventional stairs was 48% of the magnitude of the knee moment measured on the Navy ship ladder. Similarly, data collected on three males using a replica of a ship ladder with a tread depth, rise, overlap and incline of 15.2 cm, 24.1 cm, 2.5 cm and 58°, respectively, found higher knee moments than reported on conventional stairs [3]. Specifically, the average peak external knee flexion moment was 252 ± 17 Nm, which was greater than the 147 Nm moment reported on conventional stairs [5].

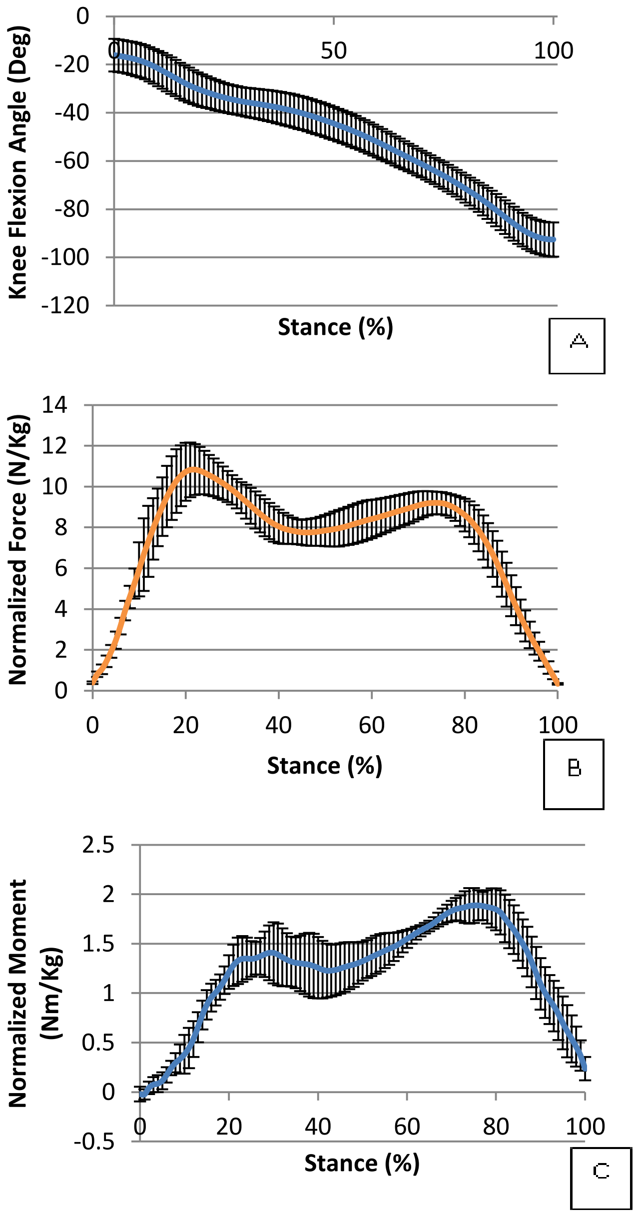

Figure 1: A –The stance leg exhibits flexion without extension. B –The vertical ground reaction force from 'heel strike' to 'heel off', maximum forces occur during the beginning half of stance. C – The sagittal plane knee moment, normalized to body mass, is greatest during the latter half of stance

The increased knee moments experienced on Navy ship ladders may contribute to anterior knee pain seen in active duty sailors. The narrow tread causes the feet to strike heel first, thus taking away the gastrosoleous lever arm and the complete rise of the ladder is felt due to the reaching with the heel instead of stretching out with the toes for the next step [3], thus resulting in the higher knee moments.

These increased moments lead to increased patellofemoral joint forces [6]. Strategies to minimize these patellofemoral joint force and knee joint moments, such as strength training and/or bracing should be investigated. Also, decreasing the rise in the step and thus adding more steps could be helpful in reducing the knee joint moments and patellofemoral joint forces; however this may not be possible due to the space constraints within a ship.

CONCLUSIONS

The results confirm higher knee moments on navy ship ladders compared to traditional stairs [3]. Thus, if traditional stairs have the potential to cause knee disorders [1], sailors who spend time on hard deck surfaces and Navy ship ladders also have the potential to be at greater risk for similar knee disorders. Thus, potential approaches to reducing the moments and forces in the knee such as strength training and/or bracing and modifications to the rise of the step should be investigated.

REFERENCES

1. Morken T, et al. *J Occup Med* **57**, 112-117, 2007
2. Crossley KM et al. *J Ortho Res* **22**, 267-274, 2004.
3. Crabb ID, et al. *Trans Annu Meet Ortho Res*. Atlanta, GA, 1996.
4. Reeves ND, et al. *J Electromyogr Kinesiol* **18**, 218-227, 2008.
5. Andriacchi TP, et al. *J Bone Joint Surg* **68**, 749-757, 1980.
6. Costigan, P. A. et al. *Gait & Post* **16**, 31-37, 2002.

ACKNOWLEDGEMENTS

NSF-STEM Marine Engineering Scholarship.
Thanks to CDR Luis Sanchez, Jr., CO USS Forrest Sherman, for allowing us to board and measure the ship's ladders.
Thanks to Eric Greska, Haroon Osmanzada, Mike Samaan, Julie Choisne and Dr. Matthew C. Hoch for assisting with data collection.

INVESTIGATING THE ETIOLOGY OF VIBRATION-INDUCED LOW BACK PAIN

Timothy D. Craig, Joseph S. Soltys, and Sara E. Wilson

University of Kansas, Lawrence, KS, USA
email: sewilson@ku.edu

INTRODUCTION

Numerous studies have examined occupational factors thought to contribute to back pain. Vibration, particularly whole body vibration (WBV) in seated vehicle operators, has been identified as a risk factor for LBP. This abstract will describe a series of experiments conducted in our laboratory to examine changes in neuromotor control with vibration exposure and factors such as frequency and transmissibility that can contribute to these effects.

METHODS

Transmissibility of vibration from seat to spine was examined using accelerometers at the seat and L3 vertebrae, a lumbar electrogoniometer centered between T12 and S1, and the muscular response of the erector spinae (ES) using integrated EMG. Transmissibility was determined by the ratios of the amplitudes between the three measures.

Vibration effects on neuromotor control were tested using several measures including: 1. Position sense error (measured as the error in a subject's ability to reproduce a lumbar angle), 2. sudden load response, 3. seated sway (mean sway speed), 4. pursuit task tracking, and 5. fMRI BOLD measurements. Protocols included measurements taken pre, during, and post vibration exposure using either whole body vertical vibration of the seat pan or a local vibration applied directly to the erector spinae musculature at the L3 level.

RESULTS AND DISCUSSION

Results of the vertically oriented WBV testing indicated two things: 1. mechanical transmission from the seat to the spine motion and rotation and 2. transmission of spine extension/flexion rotation to muscular response. The first peaked at 4-6 Hz and diminished at higher frequencies similar to other such studies in the literature [1]. The second was observed to remain relatively constant as a function of frequency and amplitude with peaks at 6 and 10-12 Hz. Muscle activation was seen to have a decreased time delay with frequency suggesting a transition between neuromuscular response pathways (polysynaptic vs. monosynaptic loops and voluntary vs. reflex response).

Changes in neuromotor response to vibration

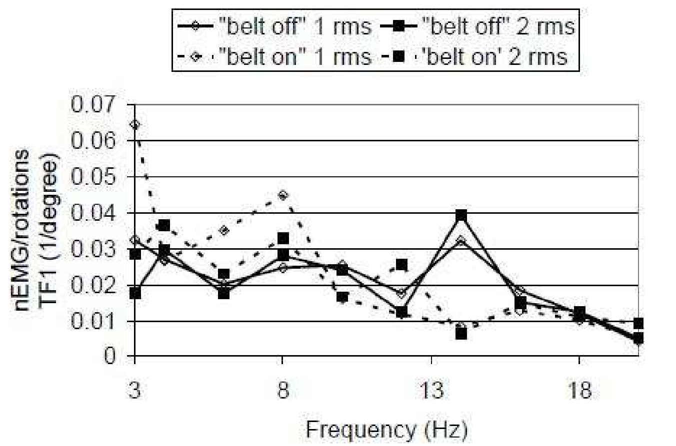

Figure 1: The transmission function ($TF1_{magnitude}$) between lumbar rotation and normalized erector spinae EMG (nEMG) was found to remain generally constant for frequencies less than 14Hz. Other than 14Hz, lumbar belt use had little effect on this magnitude ratio.

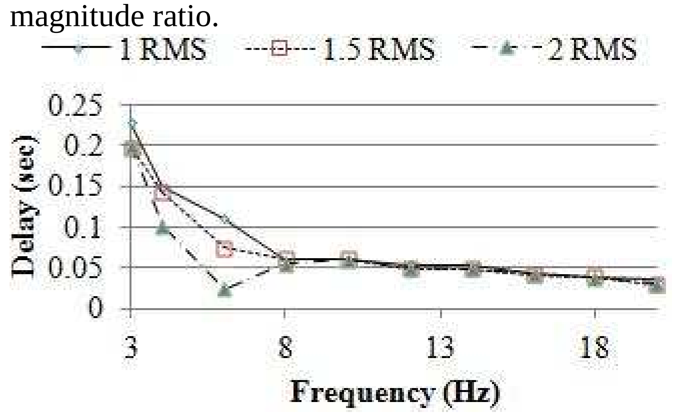

Figure 2: The time delay between lumbar extension and neuromuscular activation was measured as the time between peak rotation and the corresponding peak EMG from the ER musculature for a cycle within each frequency.

applied directly to the musculature (20 Hz vibration at the L3 erector spinae(ES)) included an increased position sense error of 24.6% and an increased sudden loading response time by 9.6% relative to pre-vibration. Post-vibration position sense error increased 11.3% in the reposition test and 12.7% for the sudden loading response time relative to pre-vibration [2].

Similar results were observed when examining the effects of 5 Hz vertical WBV through the seat. In the post-vibration position sense error increased 39.0% and the sudden loading response time increased 10% compared to the pre-vibration condition. These increases in position error and response time suggest that proprioceptive changes may be a mechanism for altered low back stability and increased risk for low back pain [3].

To examine the effects of these proprioceptive changes on lumbar dynamics, a seated sway protocol was used. Using center of pressure (COP) mean sway speed as the measurement, it was observed that the mean sway speed was doubled during a 44.5Hz localized vibration applied to the L3 level ES muscles [4].

To move closer to an occupationally relevant measure, the latest experiment examines the effects of 20 minutes of vertical WBV of random frequency (derived from dump truck seat vibration data) on a trunk pursuit task. The pursuit task consists of a constant velocity target moving about a circular path. By controlling posture of the spine, the subject can follow the target with their COP. RMS error in this tracking is currently being examined.

Finally, to examine the motor pathways contributing to these proprioceptive changes, functional magnetic resonance imaging (fMRI) has been used to examine changes in cortical activity with local muscle vibration in the arm, pre, during and post vibration exposure during a tracking task. Significant brain activations were found in premotor, supplemental motor, somatosensory association, prefrontal cortex, cingulate gyrus, and insula during and immediately post vibration relative to baseline [4].

The included neuromotor control studies have generally focused on single frequency and application mode (WBV or local) vibration exposure. However, occupational exposures can include a mixture of frequencies, amplitudes, orientations, application locations, and durations. As the transmissibility data suggests, the neuromotor effects of vibration may vary with frequency and amplitude in particular.

Future directions will include extending these experiments to examine the effects of vibration in an occupational setting. This would also allow for examination of extended duration well beyond those experienced thus far in the lab. In addition, it is desired to examine the effects of shocks along with the vibration as shocks may represent sudden loading events during vibration exposure.

REFERENCES

1. Pope MH, Wilder DG, Magnusson ML. A review of studies on seated whole body vibration and low back pain. Proc Inst Mech Eng H 1999;213(6):435-46.
2. Arashanapalli M, Wilson SE. Paraspinal muscle vibration alters dynamic motion of the trunk. J Biomech Eng 2008;130(2):021001.
3. Li L. The Effect of Whole Body Vibration on Position Sense and Dynamic Low Back Stability. Lawrence: University of Kansas; 2006.
4. Soltys JS. The Role of the Central Nervous System in the Integration of Proprioceptive Information. Lawrence: University of Kansas; 2011.

ACKNOWLEDGEMENTS

This research was possible with the contributions of Lu Li, Maneesha Arashanapalli, Raghu Channamallu, Farhana Lamis, Vinay Reddy, and Pradeep Abraham.

Table 1: Summary of results for studies examining Pre-During-Post vibration effects.

Vibration Frequency	Location Applied	Conditions Compared	Measurement	Result
44.5 Hz	Local (right ES)	Pre – During	Mean Sway Speed	+ 100%
20 Hz	Local (ES)	Pre – During	Sudden Load Response Time	+ 9.6%
20 Hz	Local (ES)	Pre – During	Reposition Error	+ 24.6%
20 Hz	Local (ES)	Pre – Post	Reposition Error	+ 11.3%
20 Hz	Local (ES)	Pre – Post	Sudden Load Response Time	+ 12.7%
5 Hz	Vertical WBV	Pre – Post	Sudden Load Response Time	+ 10%
5 Hz	Vertical WBV	Pre – Post	Reposition Error	+ 39.0%
5 Hz	Horizontal WBV	Pre – Post	Sudden Load Response Time	+ 10%
5 Hz	Horizontal WBV	Pre – Post	Reposition Error	+ 39.0%

EFFECT OF RUNNING CLASSES ON RUNNING KINEMATICS AND ECONOMY

Daniel Craighead[1], Nick Lehecka[2], Deborah L. King[1]

[1]Ithaca College, Ithaca, NY, USA
[2]Fast Splits, Boston, MA, USA
email: dking@ithaca.edu, web: http://www.ithaca.edu/hshp/ess

INTRODUCTION

The last decade has seen popularization of barefoot and minimalist footwear running along with promotion of running methods such as POSE and CHI running. Common amongst these running trends is a goal of increasing stride rate (SR) and decreasing stride length (SL). Increases in SR in barefoot (or minimalist) and POSE running are typically accompanied by changes in foot strike pattern, joint angles during impact as well as impact forces [1,2,3,4,5]. Barefoot running is associated with lower running economy [1,6], due primarily to mass. Reductions in running economy have not been reported in POSE running [2,3,4].

While running classes emphasizing decreasing stride rate, lowering impact forces, and a midfoot strike pattern are popular, their success is typically undocumented. The primary purpose of this study was to determine if 8 weeks of running practice offered by a local running store and focusing on one simple instruction along with occasional video feedback was effective in eliciting kinematic changes in recreational runners. A secondary purpose was to determine if the running classes had an effect on running economy.

METHODS

Eighteen recreational and fitness runners free from injury participated in the study after giving their informed consent. To be included, runners had to run 3 to 5 days a week, 3 to 5 miles per day at a self reported pace between 6 and 6.7 mph. All runners regularly competed in road, trail, or triathlon events.

Each subject completed three sessions on a treadmill at a 6.3 mph (2.8 m/s). Session 1 was a familiarization run of 30 minutes on the treadmill. During session 2, sagittal kinematics, VO_2, heart rate (HR), and rating of perceived exertion (RPE) were collected during a 15 minute run. Subjects were then matched into treatment and control groups. The treatment group completed 5 running classes over 8 weeks. The running classes focused on lifting the stance leg early from the ground and bringing the foot towards the butt. The subjects received one on one and group instruction during classes; individual video was taken and critiqued as a group. The control group received weekly educational materials on running training. All subjects were instructed to maintain their normal training program. After 8 weeks, subjects returned for session 3 which was identical to session 2.

Kinematic data were obtain with a high speed video camera (250 Hz) placed perpendicular to the sagittal plane and a 2D calibration was performed. Retro reflective markers were used to define thigh, leg, and foot segments. Five strides of running were recorded at minutes 5 at 10. Video data were subsequently analyzed with Vicon Motus. Variables of interest included lower extremity joint and segment angles and angular velocities, SR, SL, vertical displacement, and foot position at contact. HR, RPE, and VO_2 were measured during the last 5 minutes of the run. Kinematic data were analyzed using 2 x 2 x 2 ANOVA with repeated measures across session (pre and post) and time (minute 5 and 10) while physiological data were analyzed with a 2 x 2 ANOVA with repeated measures across session (pre and post). Alpha was set to 0.05.

RESULTS AND DISCUSSION

There were no differences in the kinematic data from minute 5 to 10. Data from the 10 total strides were averaged and subsequent analyzes were completed using 2 x 2 ANOVA with repeated measures across session (pre and post).

SR was significantly higher and SL significantly shorter for the treatment group following the 8 weeks of running classes (Figure 1). Effect sizes for both SR and SL were large, both over 1.0. The SR and SL of the treatment group changes were not accompanied by significant changes in joint or segment angles or in foot position at contact. There were no differences in VO_2, HR, or RPE for either group following the 8 week period.

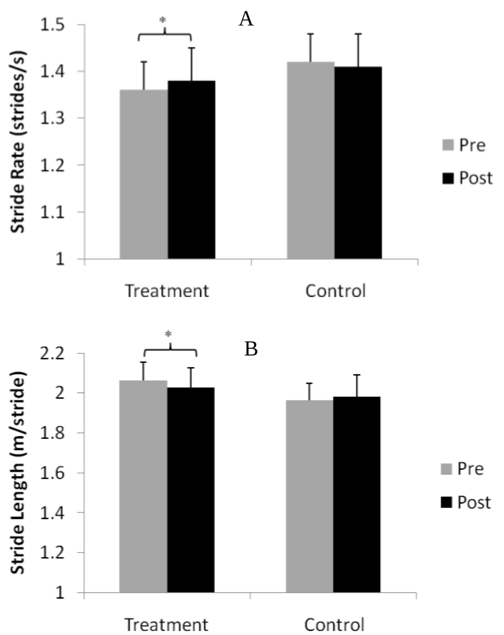

Figure 1. Average SR (A) and SL (B) for treatment and control groups pre and post 8 weeks. Error bars are SD. * $p < 0.05$.

Previous research has reported changes in knee and/or ankle angles just prior to or just after contact along with the foot landing closer, horizontally, to the hips following POSE training [2,3,4]. None of these studies saw an improvement in running economy; in fact one study had an increase in oxygen cost following 12 weeks of instruction [4]. However, Fletcher, et al. [2] reported a non significant 3 second drop in 2.4 km time trial.

The training protocol in these studies involved focusing on attaining and transitioning from the POSE position accompanied by an early lift of the heel from the ground. The intensive instruction involving specially designed drills to facilitate learning the POSE method [2,3,4] may have resulted in more uniform kinematic adaptations by the runners and may have accounted for the significant changes in knee and ankle angles before and after contact with the ground.

Conversely, the runners in our study, focused on lifting the leg early from the ground. It was theorized that bringing the back leg off the ground sooner would result in the front leg reversing motion earlier to maintain a symmetrical running pattern with the legs in opposition. Without focusing on the contact position, it appears that our runners used a variety of solutions to adjust their kinematics while achieving the sought after increases in SR. Previous studies that have demonstrated increases in SR have also found reductions in impact force, typically attributed to lower vertical displacements of the COM and changing foot strike patterns [3]. Our treatment group, however, did not have significant changes in foot strike position or vertical oscillation, and thus may not have realized reductions in impact forces.

CONCLUSIONS

Running classes focusing on one simple instruction with only basic video reinforcement are effective at increasing stride rate and decreasing stride length. However, the specific kinematic adaptations of the runners appear to be varied. Future studies may be warranted to determine if reductions in impact forces accompany the changes in SR and SL.

REFERENCES

1. Squadrone R & Gallozzi, C. *J Sports Med Phys Fitness*, **49**, 6-13, 2009.
2. Fletcher G, et al. *Int J Sports Sci & Coaching* **3**, 365-380, 2008.
3. Arendse, RE, et al. *Med Sci Sports Exerc*, **36**, 272-277, 2004.
4. Dallam, GM, et al., *J Sports Sci*, **23**, 757-764, 2005.
5. Lieberman, DE, et al. *Nature*, **463**, 531-536, 2010.
6. Hanson, NJ, et al. *Int J Sports Med*, **32**, 401-406, 2011.

ANTERIOR, BUT NOT POSTERIOR COMPENSATORY STEPPING THRESHOLDS, ARE REDUCED WITH AGE

[1]Jeremy R. Crenshaw and [1]Mark D. Grabiner

[1]University of Illinois at Chicago, Chicago, IL, USA
email: crenshaw.jeremy@mayo.edu

INTRODUCTION

The proportion of injuries due to unintentional falls increases with age [1]. This trend may be reduced by identifying factors that decline with age, are related to fall risk, and are modifiable through intervention.

The ability to recover from a disturbance without taking an anterior compensatory step is reduced with age [2-6] and is further degraded for older adults with a recent fall history [5]. Age-related reductions in anterior stepping thresholds, or disturbance displacements beyond which an anterior step is elicited, have been observed using a waist-pull disturbance method [4]. Compared to waist pulls, surface translations may reveal a more pronounced effect of age [7].

Unlike anterior steps, age-related declines in the ability to avoid posterior steps have not been apparent [2, 6]. However, the influence of age on posterior stepping thresholds has not been quantified.

The purpose of this study was to characterize the influence of age on anterior and posterior stepping thresholds—measures that potentially relate to fall risk—using a surface-translation method. It was hypothesized that anterior, but not posterior stepping thresholds would be reduced with age.

METHODS

Thirteen young adults (31.1 ± 0.8 years), 11 middle-aged adults (57.6 ± 2.5 years), and 11 older adults (73.8 ± 5.3) participated in this study. Anterior and posterior surface translations were delivered as subjects stood on a microprocessor-controlled treadmill (ActiveStep®, Simbex, Lebanon, NH). Subjects were instructed to "try not to step." Single-stepping thresholds ($d_{threshold}$) were defined as the largest displacement at a specified peak treadmill-belt velocity (v_{belt}) for which a subject could avoid stepping. Absolute v_{belt} ranged from 16 cm/s to 64 cm/s. Absolute treadmill belt displacements ranged from 4 cm to 30 cm. The margin of stability (*MOS*), a spatial measure that is proportional to the impulse needed to unbalance a subject [8], was used to estimate minimum dynamic stability at $d_{threshold}$. *MOS* was calculated as:

$$MOS = d + \left(\frac{v}{\sqrt{g/l}} \right)$$

Subjects were positioned facing the +x direction. For anterior disturbances, $d = x_{toe} - x_{COM}$ and $v = v_{toe} - v_{COM}$. x_{COM} and v_{COM} are the anteroposterior body COM position and velocity, respectively. x_{toe} and v_{toe} are the anteroposterior position and velocity of the toe marker, respectively. For posterior disturbances, $d = x_{COM} - x_{heel}$ and $v = v_{COM} - v_{heel}$. x_{heel} and v_{heel} are the anteroposterior position and velocity of the heel marker, respectively. $g = 9.81$ m/s^2. l is the sagittal plane distance between the ankle center and the COM.

Stepwise multiple regressions were conducted with *age*, $\log_{10} v_{belt}$ (expressed as a percentage of foot length), and an *age* x $\log_{10} v_{belt}$ interaction as independent variables. $d_{threshold}$ (% foot length) and minimum margin of stability (MOS_{min}, expressed in cm) were used as dependent variables. In the case of a significant *age* x $\log_{10} v_{belt}$ interaction, one-way ANOVA's were conducted at each v_{belt} between young, middle-aged, and older subjects.

RESULTS AND DISCUSSION

Anterior $d_{threshold}$ was reduced with age (Fig. 1). For every decade of increasing *age*, $d_{threshold}$ was reduced by about 5% foot length:

$d_{threshold} = 277.79 - 0.47(age) - 91.19(\log_{10} v_{belt})$
($R^2 = 0.450$, $p < 0.001$)

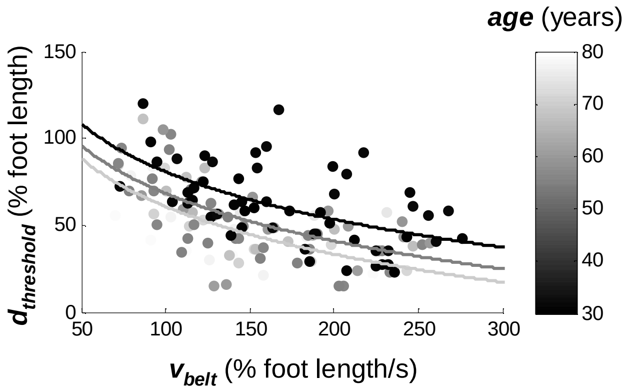

Figure 1: Anterior $d_{threshold}$ as a function of v_{belt}. Increasing *age* is represented by a gradient transition from black to grey. Regression functions are displayed for the average ages of young, middle-aged, and older adults.

Age did not appear to reduce the MOS_{min} that could be overcome without taking a step. The regression equation for anterior MOS_{min} contained an *age* x $\log_{10} v_{belt}$ interaction. Separate one-way ANOVA's at each v_{belt} revealed no significant ($p \geq 0.052$) main effects of age group on MOS_{min}. With age, smaller displacements were needed for subjects to become dynamically unstable to the point of requiring a step. Reduced thresholds may be due to an age-related decline in the ability to absorb kinetic energy and minimize the change in momentum of the COM [3, 9].

Age did not influence posterior $d_{threshold}$ (Fig. 2):

$d_{threshold} = 234.33 - 93.11(\log_{10} v_{belt})$
($R^2 = 0.358$, $p < 0.001$)

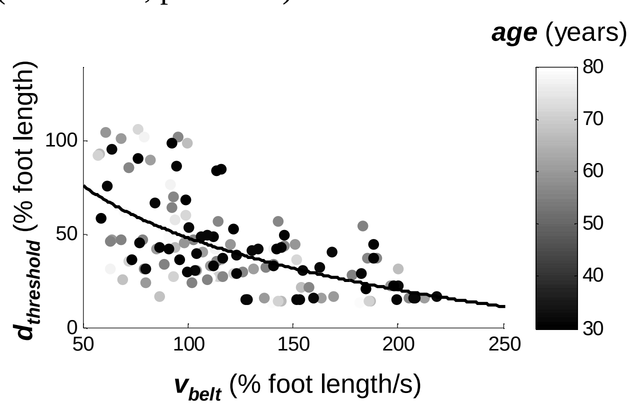

Figure 2: Posterior $d_{threshold}$ as a function of v_{belt}.

Previous literature has suggested that there are no age-related declines in kinetic energy absorption in response to posterior disturbances [9], which may explain why age did not affect posterior $d_{threshold}$.

The MOS_{min} associated with posterior thresholds became larger with age:

$MOS_{min} = 35.03 + 0.03(age) - 17.34(\log_{10} v_{belt})$
($R^2 = 0.587$, $p < 0.001$)

Younger subjects recovered from smaller MOS_{min} without stepping than older subjects. However, the influence of *age* on MOS_{min} did not have a substantial effect on posterior $d_{threshold}$.

CONCLUSIONS

This study is the first to demonstrate reduced anterior, but not posterior, stepping thresholds by adults as young as 55 years. Previous literature suggests that the ability to avoid anterior steps is retrospectively related to fall risk [5]. Additional study is needed to determine if declines in anterior stepping thresholds are prospectively related to fall risk and amenable to intervention.

REFERENCES

1. CDC WISQARS www.cdc.gov/injury/wisqars/index.html
2. Hall CD, et al. *J Gerontol A Biol Sci Med Sci* **54A**, M507-M513, 1999.
3. Jensen JL, et al. *Exp Aging Res* **27**, 361-376, 2001.
4. Mille M-L, et al. *J Neurophysiol* **90**, 666-674, 2003.
5. Pai YC, et al. *J Biomech* **31**, 1111-1118, 1998.
6. Schulz BW, et al. *Gait Posture*. **22**, 198-209, 2005.
7. Mansfield A, et al. *J Biomech* **42**, 1023-1031, 2009.
8. Hof AL, et al. *J Biomech*. **38**, 1-8, 2005.
9. Hall CD, et al. *J Am Geriatr Soc*. **50**, 1782-1788, 2002.

ACKNOWLEDGEMENTS

Funding by the CDC (RO1CE001430)

BATTING CAGE PERFORMANCE OF VARIOUS YOUTH BASEBALL BATS

J.J. Crisco, Michael J. Rainbow, Bethany Wilcox, and Joel B. Schwartz

Department of Orthopaedics, Warren Alpert Medical of Brown University and Rhode Island Hospital, USA
email: joseph_crisco@brown.edu, web: www.brownbiomechanics.org

INTRODUCTION

With the development of new materials and fabrication technologies, non-wood baseball bats can be constructed to provide a significant increase in performance over traditional wood bats. This increase in performance has motivated the sports governing bodies to more fully understand and regulate bat performance. Performance at most levels of play is standardized through compliance testing utilizing laboratory based methods. At some youth levels bat performance is not regulated. The aim of this study was to determine the batting cage performance of wood and non-wood baseball bats used at the youth level.

METHODS

Twenty two (n = 22) right-handed male players (mean age: 16, range 13-18) participated in a batting cage study after IRB approval and informed written consent and assent. Thirteen bat models, ten non-wood (A,C, D, G, H, I, J, K, L and M) and three wood (Wood), from six different manufacturers were used. Five bats of each model were prepared for testing by applying four evenly-spaced square markers of retro-reflective tape circumferentially at five locations along the length of the bat. Rawlings (St. Louis, MO) R100 baseballs (n = 300) were prepared with six uniformly arranged square markers and pitched (range 48-58 mph) from 40 ft with a pitching machine (Iron Mike MP5, Master Pitching Machine Kansas City MO). Players participated in multiple batting sessions consisting of twenty-five pitches with a single bat. The order of bats swung by players was selected randomly. Not all bats were swung by all players. The ball and bat were tracked at 300 Hz by eight Oqus 5-Series infrared sensing Qualisys cameras (Qualisys, Gothenburg, Sweden).

Pitched and batted ball velocities were determined by best-fit least-squares to the coordinates as a function of time. The location of ball impact on the bat was determined by intersecting the incoming pitch vector with the bat vector at the impact frame. Bat swing speed was defined as the speed of the bat at this location at the time of impact (Fig. 1).

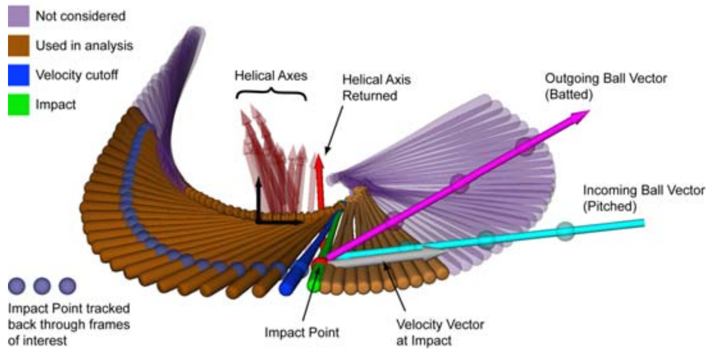

Figure 1: A typical hit in which the 3-D kinematics of the bat and ball are tracked and analyzed.

Batted ball speeds were compared using a one-way ANOVA with a post-hoc Bonferroni's multiple comparison test with Wood (wood models were grouped together) as the control. Bat impact and angular speeds were also analyzed as a function of bat moment of inertia about the knob (MOI_{knob}) by linear regressions first for each individual player, then by age group.

RESULTS AND DISCUSSION

Batted ball speed, bat impact speed and angular speed were significantly faster ($p < 0.001$) for bat models A and K than for Wood (Fig. 2). Mean differences were 4.0 and 3.6 m/s, 1.4 and 2.5 m/s, and 166 and 309 deg./s, respectively. Batted ball speeds were significantly faster for model J by a mean of 1.5 m/s, while significantly slower for model H by a mean of 2.0 m/s when compared with Wood. Bat impact speeds for models D and L were also significantly faster when compared with Wood by a mean of 1.1 and 1.7 m/s, respectively.

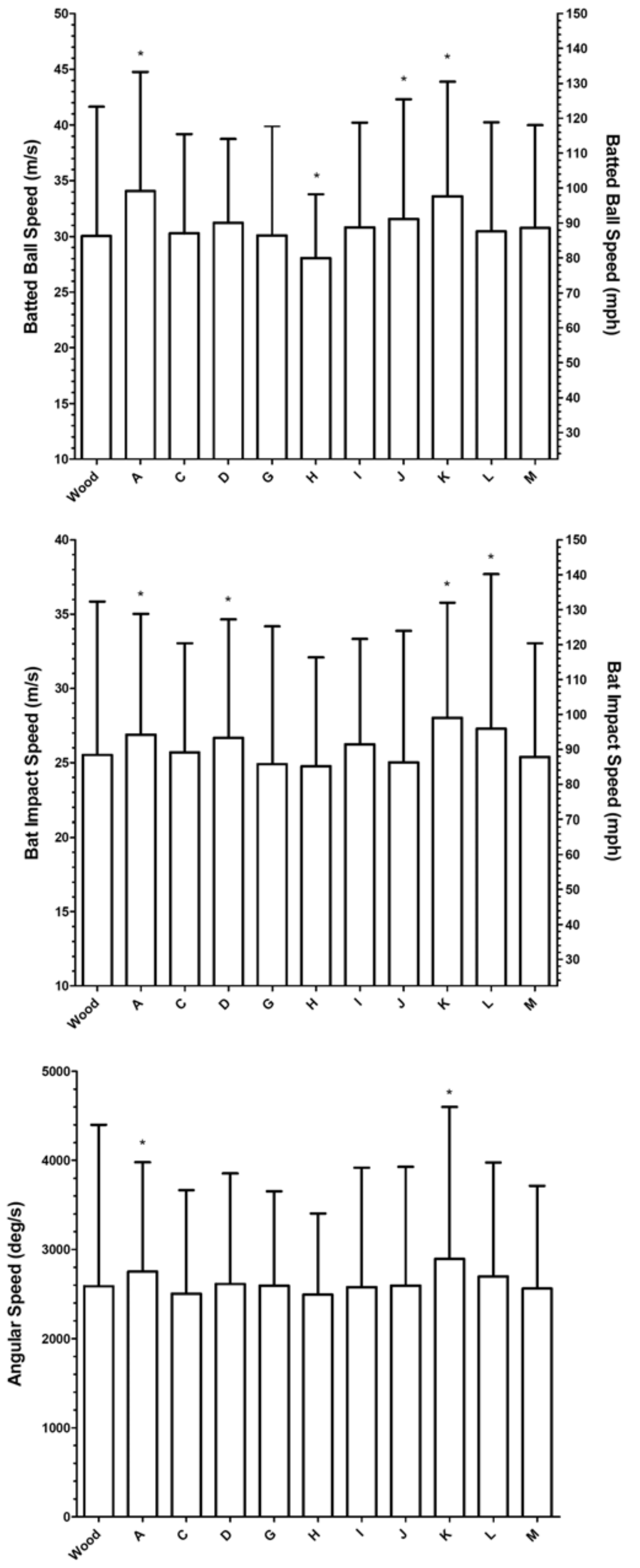

Figure 2: Three non-wood bat models (A, K, J) hit the ball significantly (*, p< 0.05) faster than Wood.

The bat impact speed significantly ($p < 0.05$) decreased with increasing MOI_{knob} of the bat model for the 13, 14 and 15 yr. age groups (Fig. 3). The slopes of the regression for each of these age groups was 24.4 ± 1.4, 28.3 ± 7.7, and 28.7 ± 4.3 m/s per kgm^2, respectively. There was no significant change in bat impact speed with bat MOI_{knob} for any of the other age groups, nor was there a significant change in angular swing rate with any age group.

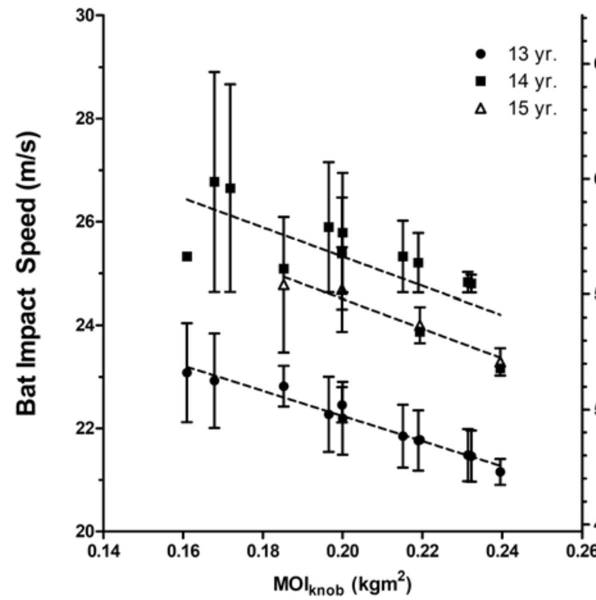

Figure 3: In the younger age groups, bats with lower moment of inertia (MOI) were swung faster.

CONCLUSIONS

This study found differences in batted ball speed and bat swing speeds between non-wood and Wood bats. Two non-wood bat models out-performed Wood bats and 8 of the 10 non-wood bats performed similar to or less than Wood. Younger players swung the lighter bats faster than the heavier bats, but swing speed alone was not a predictor of batted ball speed. This is most likely because of the complex relationship between MOI, swing speed, and the elastic performance of the barrel, often referred to as the trampoline effect.

ACKNOWLEDGEMENTS

Funding was provided by USA Baseball. The opinions expressed herein are those of the authors and do not necessarily reflect those of USA Baseball.

STRIDE LENGTH COMPENSATIONS AND THEIR IMPACTS ON BRACE-TRANSFER GROUND FORCES IN BASEBALL PITCHERS

[1]Ryan L. Crotin and [2]Dan K. Ramsey
[1,2]University at Buffalo, Buffalo, NY, USA
email: rlcrotin@buffalo.edu
Website: http://sphhp.buffalo.edu/ens/biomechanics/index.php

INTRODUCTION

Increased exertion in baseball pitchers can impair neuromuscular performance, alter biomechanical consistency, reduce competitive success, and increase risk of injury [1-3]. To manage exertion, pitch count monitoring has been enforced to maintain balance between applied orthopedic stress and the tissues' ability to tolerate high velocity loads [1,3].

Elevated pitch counts can decrease the throwing arm's rotator cuff strength, alter trunk and lead knee flexion, and affects shoulder kinematics at maximal external rotation [1-3]. The aforementioned changes in kinematics can be considered compensatory. The desired outcome associated to compensatory biomechanics is the maintenance of peak ball velocity while under a state of fatigue.

Pitching exertion can impact lower body power generation altering brace-transfer ground reaction forces [1-3]. The brace-transfer phase is a critical transition from linear to rotational momentum [1]. The onset of the phase is visualized by stride foot contact ending at maximal external rotation of the throwing shoulder [1]. To our knowledge, this study is the first to examine stride length compensations and their impacts on the brace-transfer phase in baseball pitchers. We hypothesize that stride length changes will impact brace-transfer ground reaction forces and impulses, while maintaining peak ball velocity.

METHODS

Nineteen collegiate and elite level high school pitchers (15 right-hand dominant, 4 left-hand dominant) were recruited for the study. Subject characteristics were the following: (height 1.84 ±0.054m; weight 82.14 ±0.054kg; age 18.63 ±1.67 years). An eight-camera, VICON MX20 motion analysis system (Oxford Metrics, UK), and Visual 3D software (C-Motion, MD) analyzed kinematics recorded at 240Hz. Peak knee height (PKH), stride foot contact (SFC), maximal external shoulder rotation (MER), and ball release (BR) provided hallmark events for time normalization of the data. Brace-transfer phase data was examined, which occurred from SFC to MER. The throwing hand and baseball were modeled and tracked to indicate peak throwing hand velocities at the point of ball release.

Pitchers participated in a randomized cross-over study approved by the University at Buffalo's Human Subjects Institutional Review Board. Pitchers threw two simulated games, where each subject pitched at 25% increased stride in meters (OS), and 25% reduced stride in meters (US) from desired stride length (DSL). For all trials, stride lengths were determined as the distance between the drive foot calcaneus at PKH to the calcaneus of the stride foot at the onset of SFC. SFC was identified when the landing foot registered a vertical ground reaction force exceeding 0.05 N/kg. Ground reaction force data was sampled at 960Hz and normalized to body weight for both drive and stride legs (Kistler Instrument Corp., Amherst, NY). Game simulations began with a standardized general warm-up, followed by 25-30 warm-up pitches. The last 5 warm-up pitches were thrown at 100% effort at DSL. Two warm-up pitches thrown at the highest velocities were visually inspected using software (Oxford Metrics, UK) and then averaged to determine each pitcher's DSL. Following the determination of DSL, force plates were marked to indicate drive foot and stride foot landing placement for OS and US simulated games. Ten pitches were thrown at either OS or US to acclimatize pitchers to each simulated game.

Twenty pitches were thrown per inning with a ratio of 3 fastballs to 1 change-up. Approximately 15 seconds rest was allocated between pitches with 9 minutes rest prescribed between innings. Mean vertical, anterior/posterior shear ground reaction forces, as well as normalized impulses were analyzed during the brace-transfer phase. Means were derived from the two highest velocity pitches observed in the first and last innings. Peak linear hand and ball velocities were recorded to accompany ground reaction force data. Independent t-tests (SPSS 20, Chicago, IL) assessed ground reaction force differences between OS and US pitching at $p \leq 0.05$. Ball velocities were recorded by a professional model radar gun for all pitches thrown (Jugs Sports, Tualatin, OR).

RESULTS

Mean DSL, OS, and US were calculated in meters and normalized to percent body height (DSL: 1.24 ±0.173m; 67.3 ±8.9%BHT); (OS: 1.39 ±0.15m, 75.9 ±7.2%BHT); (US: 0.95 ±0.15m, 51.9 ±7.8%BHT). Peak linear hand and ball velocities were not statistically different despite altered stride lengths (Table 1).

TABLE 1:
Peak Throwing Hand and Ball Velocities Associated to Stride Length Compensations

	Hand Velocity	Ball Velocity
OS	20.58 ±1.56m/s	126.29 ± 8.46 km/h
US	20.13 ±1.50m/s	126.32 ±7.66 km/h
	P=0.367	P=0.984

Table 1: OS (Overstride), US (Understride).

Reduced weighting of the drive leg and increased weighting of the stride leg appeared to be a trend for OS. Greater posterior shear forces were applied by both drive and stride legs for OS versus US. Greater normalized impulses were observed in OS for the drive leg. No changes in impulse occurred between groups for the stride leg (See Table 2 and Table 3).

TABLE 2:
Drive Leg Brace-Transfer Ground Reaction Forces and Normalized Impulses

Force	Overstride	Understride	P value
GRFZ	0.20 ±0.142 N/kg	0.31 ±0.198 N/kg	P=0.056
GRFY	-0.011 ±0.142 N/kg	0.050 ±0.627 N/kg	P<0.001
IMPZ	70.8 ±0.857 Ns	66.2 ±0.857 Ns	P<0.001
IMPY	25.0 ±0.857 Ns	20.0 ±0.255 Ns	P<0.001

Table 2: Ground reaction forces; GRFZ (vertical), GRFY (anterior+/posterior- shear), IMPZ (vertical impulse), IMPY (anterior+/posterior- impulse).

TABLE 3:
Stride Leg Brace-Transfer Ground Reaction Forces and Normalized Impulses

Force	Overstride	Understride	P value
GRFZ	0.95 ±0.384 N/kg	0.69 ±0.411 N/kg	P=0.056
GRFY	-0.57 ±0.245 N/kg	-0.34 ±0.198 N/kg	P=0.002
IMPZ	7.84 ±5.34 Ns	6.30 ±5.29 Ns	P=0.372
IMPY	-4.60 ±3.30 Ns	-3.11 ±0.267 Ns	P=0.123

Table 3: Ground reaction forces; GRFZ (vertical), GRFY (anterior+/posterior- shear), IMPZ (vertical impulse), IMPY (anterior+/posterior- impulse)

DISCUSSION

The results indicate that stride length compensations can maintain peak ball and hand velocities. If exertion causes stride length reduction, drive impulse and bracing forces decrease. If exertion causes an increase in stride, drive impulse and bracing forces increase about the brace-transfer phase. Orthopedic consequences associated to compensatory stride length adaptations are unknown in baseball pitchers. As such, adopted movement strategies can effect ground reaction force profiles and have the potential to be pathomechanic. Further investigation is required to identify how stride length changes exacerbate tensile and compression stress to the throwing shoulder and elbow. As a protective measure, ground reaction force monitoring may be efficacious in denoting changes in lower body power generation and bracing.

REFERENCES

1. Escamilla RF, Barrentine SW, Fleisig GS, Zheng N, Takada Y, Kingsley D, and Andrews JR. *Pitching biomechanics as a pitcher approaches muscular fatigue during a simulated baseball game*. Am J Sports Med **35**(1), p. 23, 2007.

2. Mullaney MJ, McHugh MP, Donofrio TM, and Nicholas SJ. *Upper and lower extremity muscle fatigue after a baseball pitching performance*. Am J Sports Med **33**(1), p. 108, 2005.

3. Murray TA, Cook TD, Werner SL, Schlegel TF, and Hawkins RJ. *The effects of extended play on professional baseball pitchers. Am J Sports Med* **29**(2), p. 137, 2001.

ANTERIOR AND MIDDLE DELTOID ARE FUNCTIONALLY CRITICAL TARGETS FOR NERVE TRANSFER FOLLOWING C5-C6 ROOT AVULSION INJURY

[1,2]Dustin L. Crouch, [3]Johannes Plate, [3]Zhongyu Li and [1,2]Katherine R. Saul

[1] Virginia Tech-Wake Forest School of Biomedical Engineering and Sciences, Winston-Salem, NC, USA
[2]Department of Biomedical Engineering, Wake Forest School of Medicine, Winston-Salem, NC, USA
[3]Department of Orthopaedic Surgery, Wake Forest School of Medicine, Winston-Salem, NC, USA
email: dcrouch@wakehealth.edu, web: http://www.sbes.vt.edu/kholzbau/MoBL/

INTRODUCTION

The deltoid and teres minor muscles, which are innervated by the axillary nerve, are paralyzed following brachial plexus avulsion injury of the C5 and C6 nerve roots. A nerve transfer to the axillary nerve is commonly performed to restore abduction strength. During this procedure, the radial nerve branch innervating the long head of the triceps is transferred to the anterior branch of the axillary nerve. Depending on the axillary nerve anatomy, either the entire deltoid or the anterior and middle compartments of the deltoid are restored, while teres minor remains paralyzed [1]. While this technique increases the likelihood that useful abduction strength is recovered, it is unclear whether overall function can be improved if teres minor and posterior deltoid are restored in addition to the anterior and middle deltoid compartments. Therefore, we used a musculoskeletal model to assess the biomechanical roles of teres minor and the three deltoid compartments in the context of isometric strength and shoulder movement.

METHODS

We used a computational musculoskeletal model of the upper limb [2] implemented for dynamic simulation [3] in OpenSim [4]. The model was simplified to represent 5 degrees of freedom at the shoulder, elbow, and forearm, and included 32 muscle compartments crossing the shoulder and elbow joints. Four scenarios were developed in which muscles were selectively paralyzed to investigate the biomechanical role of teres minor and the anterior, middle, and posterior deltoid muscle compartments (Table 1). Muscles were assumed to be unimpaired unless otherwise indicated. Paralyzed muscles were allowed to generate passive muscle forces only.

Table 1: Scenario descriptions

Scenario	Paralyzed muscles and muscle compartments*
unimpaired	none
1	teres minor
2	teres minor, posterior deltoid
3	teres minor, deltoid (all compartments)

*Muscles not listed were assumed to be unimpaired.

Maximum isometric abduction and external rotation strength were calculated for each scenario by summing the maximum isometric joint moment that each muscle could generate in a given posture. Abduction strength was calculated at 45° shoulder elevation in the frontal plane with the elbow fully extended. External shoulder rotation strength was calculated with the arm and forearm in neutral posture and the elbow flexed to 90°.

To understand how differences in shoulder strength among scenarios may affect movement performance, we conducted dynamic simulations of abduction from 0° to 90° in the frontal plane with the elbow extended and the forearm in a neutral posture. We used a computed muscle control (CMC) algorithm to compute the muscle activations required to track the movement as accurately as possible while minimizing a cost function related to muscle effort [5]. Shoulder elevation and flexion angles were evaluated to determine whether each scenario could abduct the shoulder to 90° and maintain neutral shoulder flexion.

RESULTS AND DISCUSSION

The largest differences in shoulder strength were observed for abduction (Fig.1). Compared to the unimpaired scenario, isometric abduction moment when both teres minor and posterior deltoid were paralyzed (scenario 2) was only 4.2% lower, while isometric abduction moment when teres minor and all deltoid compartments were paralyzed (scenario 3) was 62.0% lower. External rotation moment decreased only as much as 16.1% when teres minor and deltoid were paralyzed. These results suggest that teres minor and posterior deltoid contribute less to shoulder strength than do the anterior and middle deltoid compartments.

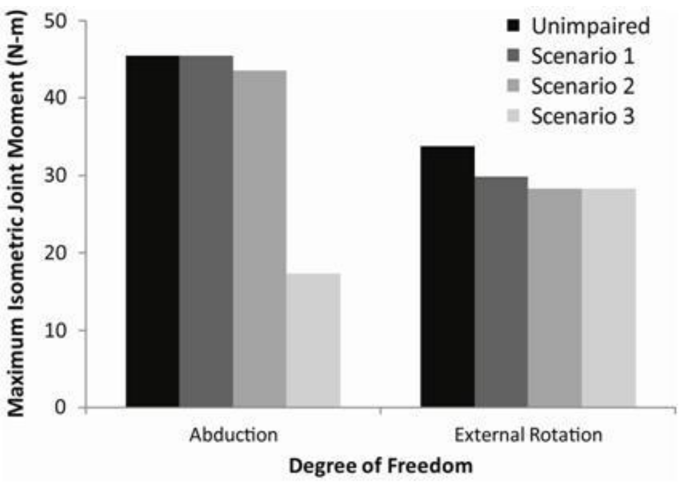

Figure 1: Maximum isometric shoulder joint moments were similar when the anterior and middle deltoid compartments were not paralyzed (unimpaired, scenario 1, and scenario 2).

Scenarios in which the anterior and middle deltoid compartments were not paralyzed (unimpaired, scenario 1, and scenario 2) could simulate the abduction movement to within 4° of the desired shoulder elevation angle with less than 4° of anterior flexion (Fig.2). However, when the entire deltoid muscle was paralyzed (scenario 3), the model was least capable among all scenarios of accurately simulating the abduction movement trajectory. Therefore, paralysis of the posterior deltoid and teres minor had relatively little effect on the ability of scenarios 1 and 2 to track the abduction movement.

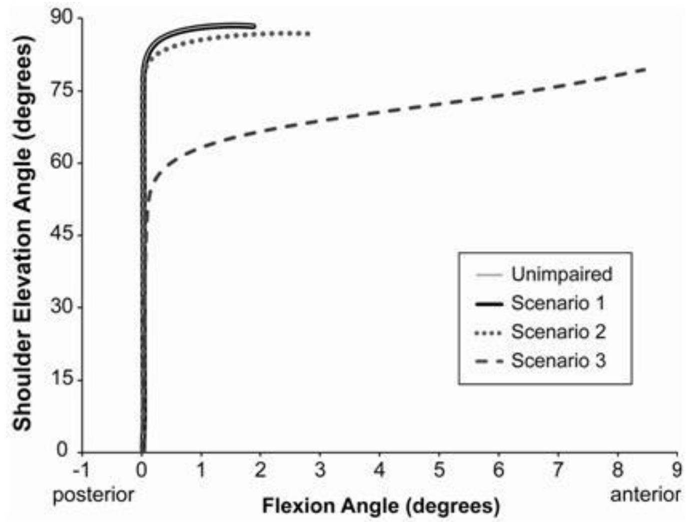

Figure 2: Scenario 3 exhibited the least accuracy when attempting to simulate the abduction movement. Joint angles of scenario 1 and the unimpaired scenario are coincident.

CONCLUSIONS

Based on the findings of this study, the anterior and middle deltoid compartments contribute most to shoulder strength and movement ability, compared to teres minor and posterior deltoid. Therefore, reinnervating teres minor and posterior deltoid may yield little additional functional benefit. Understanding the biomechanical consequences of axillary nerve transfers is important for surgical planning and predicting functional outcomes in clinical practice, particularly when multiple orthopaedic procedures are indicated.

REFERENCES

1. Leechavengvongs S, et al. *J Hand Surg*, **28A**(4), 633-638, 2003.
2. Holzbaur KRS, et al. *Ann Biomed Eng* **33**, 829-840.
3. Daly M, et al. *ASB Conf Proceedings*, State College, PA, 2009.
4. Delp SL, et al. *IEEE Trans Biomed Eng* **54**, 1940-1950.
5. Thelen DG, Anderson FC. *J Biomech* **39**, 1107-1115.

ACKNOWLEDGEMENTS

This work was supported by the National Institutes of Health (NIH 5R24HD050821-02) and the Wake Forest School of Medicine.

ANTICIPATORY ACTIVATION OF THE ERECTOR SPINAE AND MULTIFIDUS IN PATIENTS WITH AND WITHOUT LOW BACK PAIN

[1]Stuart J. Currie, [1]Casey A. Myers, [1]Bradley S. Davidson, and [2]Brian A. Enebo

[1]University of Denver, Denver, CO USA
[2]University of Colorado Hospital, Denver, CO USA
email: stuart.currie@du.edu

INTRODUCTION

Low back pain (LBP) is a disabling, pervasive, and costly medical condition that affects up to 80% of the US population [1]. Although previous investigations demonstrated a link between muscle activity and LBP, the relationship is dependent on variables such as the movement type, posture, and diagnostic group [2]. The cause of low back pain is often multifactorial, so the relationship between pain and the muscles that stabilize the spine is of interest to both clinicians and researchers alike.

Conflicting evidence exists regarding paraspinal muscle activity in patients with LBP. Hypertonicity is a generally accepted clinical correlate of low back pain; however, some studies have demonstrated decreased electromyographic (EMG) amplitude in participants with LBP when compared to healthy controls [2]. It is not clear how activation amplitude contributes to spine stability, and recent attention has been given to timing and coordination of paraspinal muscle activation. For instance, patients with chronic LPB have delayed response of various trunk muscles during activities such as task performance, spinal loading, and anticipation of limb movement [3].

The *multifidus* (MF) and *erector spinae* (ES) muscles are extensor muscles that contribute to lumbar spine stability. However, the principle action of the MF is posterior sagittal rotation on a segmental level [4] while the lever arm of ES may best contribute to broad motions. Rapid shoulder flexion produces moments on the spine that are counteracted by activity in the lumbar musculature. Recent investigations of paraspinal timing and coordination in preparation for self-generated arm movements indicate a movement dependent difference in timing between the ES and the MF in a healthy population [5]. However, it is not clear whether this pattern of timing in the paraspinal musculature is similar in the presence of LBP. The objective of this investigation was to assess the differences in MF and ES activation timing during rapid arm flexion in participants with and without LBP. We hypothesized that onset of MF activity would occur before ES in both groups.

METHODS

Two males and nine females participated in this investigation, seven without a history of LBP and four with LBP at the time of testing verbally rated between two and seven (out of ten). EMG activity was recorded from the MF and ES at the L2 spinal level during voluntary shoulder flexion with fine wire electrodes [6] and surface electrodes, respectively. A single motion capture marker was placed on the wrist and used to calculate the onset timing of arm flexion.

With feet shoulder width apart, participants performed rapid shoulder flexion movements from neutral to approximately 60 degrees from vertical. Initiation of the movement immediately followed verbal cues of “Ready?” followed 1-2 seconds later by “Go!”. Participants were instructed that speed was the primary goal of the movement.

EMG signals were sampled at 2000 Hz and bandpass filtered (4th order Butterworth , 15-350Hz) then transformed using the Teager-Kaiser Energy operator [7]. Data were full-wave rectified and filtered (4th order low pass Butterworth, 50Hz cutoff) to create a linear envelope. EMG onset was defined as exceeding a threshold of baseline plus 15 standard deviations 200ms before or after onset of arm movement (peak acceleration of wrist marker). All onset timings were verified by visual inspection.

Differences in muscle activation onsets between muscles (MF, ES) were tested using one-directional paired *t*-tests within each group (Healthy, LBP). Level of significance was set at $\alpha=0.05$. Effect sizes for each comparison were assessed using Cohen's *d*.

RESULTS AND DISCUSSION

Muscle activation onsets in both the MF and ES occurred before onset of the arm flexion (Figure 1) and the mean activation onset ranged between 64.8msec and 105.3msec before arm flexion (Table 1). In the healthy group, the MF onset occurred 30.2±21.6% earlier than ES onset ($p=0.025$, $d=1.19$). In the LBP group, there was no difference between MF and ES onset ($p=0.123$, $d=0.334$).

Table 1: Mean ± SD of EMG onset (msec) preceding peak arm acceleration.

Group	MF	ES
Pain	74.5 ± 33.0	64.8 ± 24.7
Healthy	105.3 ± 43.4	68.0 ± 12.7

Earlier onset of MF activity during rapid arm flexion occurred in the healthy group, but not in the pain group. While standing, rapid arm flexion creates a flexion moment on the spine that is stabilized by an extension moment produced by the paraspinal musculature. Previous findings in healthy participants demonstrated earlier activation of the deep fibers of the MF compared to the ES in an extension activity [5]. This investigation confirms this coordination in the healthy group with a flexion movement, but not the LBP group. Earlier onset of the MF indicates an anticipatory role of the MF and provides evidence for stabilizing function role of the MF that may take advantage of compressive action when activated.

Mean ES activity for both the pain and the healthy group were similar (64.8msec, 68.0msec), which indicates that earlier onset of MF activity in the healthy group was responsible for differences found in this investigation. It unclear what role MF/ES coordination plays in spinal stability or how MF dysfunction in patients with chronic LBP may affect this relationship. Underlying causes of MF dys-function may be related to several factors such as

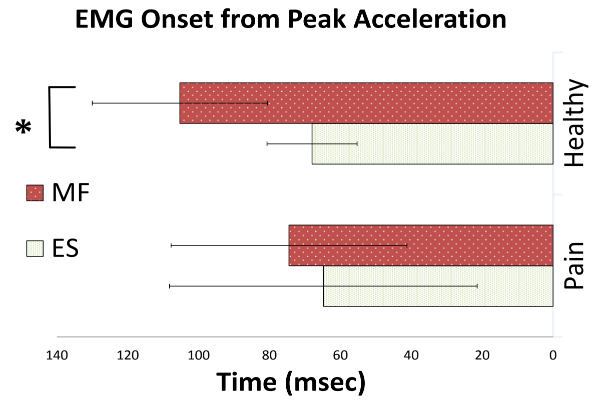

Figure 1: Mean onset of MF and ES activity from peak acceleration of the arm. All values occur earlier than arm acceleration. (* indicates $p<0.05$)

pain inhibition or fatty infiltration that accompanies LBP. [8] The timing difference found in this study is juxtaposed with the measures of EMG amplitude and clinical hypertonicity and suggests the importance of further examination of MF activation timing in various populations and tasks.

In summary, anticipatory onset of MF and ES activity measured during rapid arm flexion in healthy participants are different in healthy participants but not in LBP participants. It remains unclear what role activation timing plays in spine stability. Additional investigations of paraspinal muscle timing and coordination may provide insight into healthy and pathologic mechanisms of motor control in spine stability.

REFERENCES

1. Vallfors B. *Scand J Rehab Med* **11**, 1-98, 1985.
2. van Dieen J. *J Elect Kines* **13**, 333-351, 2003.
3. Panjabi MM. *Eur Spine J* **15**, 668-676, 2006.
4. Macintosh JE. *Clin Biomech* **1**, 205-213, 1986.
5. Moseley GL. *Spine* **27**, E29-E36, 2002.
6. Haig MD et al. *Muscle Nerve* **14**, 521-526, 1991.
7. Li X et al. *Ann Biomed Eng* **35**, 1532-1538, 2007.
8. Freeman. *Phys Med Rehab* **2**, 142-146, 2010.

AKNOWLEDGEMEN T

This work was supported in part by grant R00 AT004983-03 (to BSD) from NIH (NCCAM).

MARGIN OF STABILITY AS A METRIC FOR BALANCE IMPAIRMENT IN MULTIPLE SCLEROSIS

[1,2]Eric L. Cutler, [1,2]Shane R. Wurdeman, [1]Denise McGrath, [1]Sara A. Myers, [1,2]Nicholas Stergiou and [3]Jessie M. Huisinga

[1]Nebraska Biomechanics Core Facility, University of Nebraska at Omaha, Omaha, NE, USA
[2]University of Nebraska Medical Center, Omaha, NE, USA
[3]University of Kansas Medical Center, Kansas City, KS, USA
email: ecutler@unomaha.edu, web: nbcf.unomaha.edu

INTRODUCTION

Multiple sclerosis (MS) is a chronic disease of the nervous system. This potentially debilitating disorder often results in a general degradation of motor function. In particular, MS patients have been shown to exhibit altered balance dynamics while standing [1]. This altered balance is characterized by a large amount of postural sway [1]. Increased postural sway has also been observed in the medial-lateral direction during walking, even in patients with very mild MS [2].

Traditionally, static measurements taken during quiet standing have been utilized to assess balance impairment in MS patients [3]. Unfortunately, many of these approaches fail to account for aspects of balance during dynamic activities such as walking. It is particularly important to investigate balance during walking because this has been shown to correlate with fall risk in MS patients [4]. It would be pertinent to use a metric that accounts for not only the position of the center of mass or center of pressure but also its velocity. One such system that includes center of mass motion is the extrapolated center of mass motion and margin of stability [5].
This model utilizes the well established inverted pendulum analog of gait to characterize dynamic balance. The application of this unique metric could produce valuable new insights into the dynamic balance of gait in MS patients. Thus, the purpose of this study was to investigate the differences in dynamic balance between MS subjects and healthy controls in the medial-lateral direction utilizing the margin of stability [5].

METHODS

Ten healthy controls and ten MS subjects were used for this study. Lower extremity kinematics (12 camera Motion Analysis; 60Hz) were collected while each subject walked over ground at a self selected pace. Five trials were collected for each subject. A custom MATLAB code was used to calculate the margin of stability. The initial computational step was to calculate the eigenfrequency (ω_0) of the inverted pendulum using leg length (l) and the acceleration due to gravity (g).

$$\omega_0 = \sqrt{\frac{g}{l}}$$

Subsequently, the margin of stability was calculated for each trial using the position (x) and velocity (v) of the subject's center of mass and boundary of support of the right foot (u_{max}).

$$b = \left|u_{max} - \left(x + \frac{v}{\omega_0}\right)\right|$$

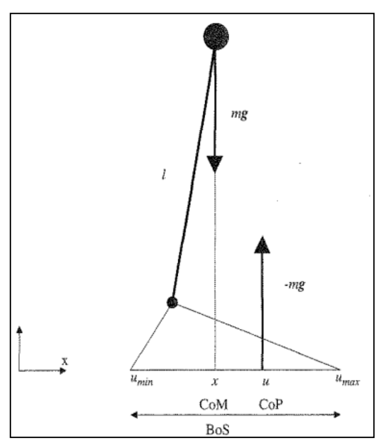

Figure 1: A schematic of the inverse pendulum model used to calculate margin of stability [5].

The mean, maximum, minimum, and range for the margin of stability were calculated and used as the outcome variables of this study. An independent t-test was used to test for significant differences with alpha at the 0.05 level.

RESULTS AND DISCUSSION

The mean and minimum values of the margin of stability exhibited very little difference between groups (<1 cm) (Figure 2). However, the maximum and range values displayed more substantial differences between groups. Notably, the maximum margin of stability experienced during gait was greater for MS subjects than for healthy controls and the minimum margin of stability experienced during gait was less for MS subjects than healthy controls. This resulted in a greater numerical range for margin of stability for MS subjects than for controls. Only the margin of stability range reached the statistically significant level.

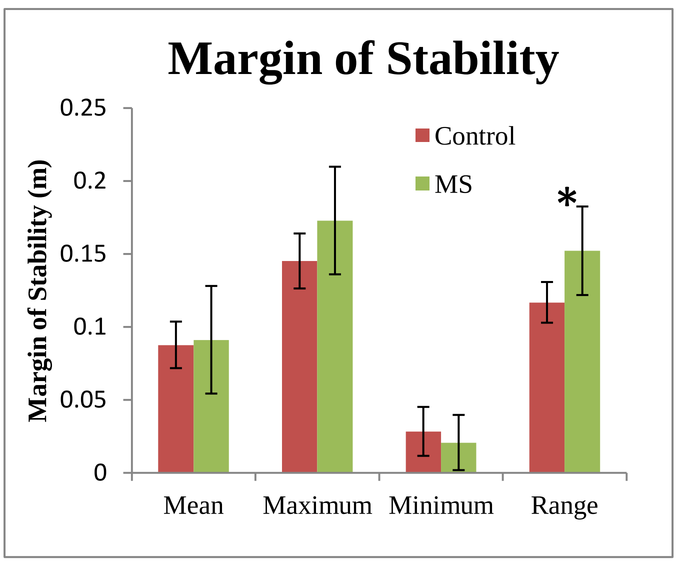

Figure 2: Margin of stability for MS vs. control subjects. *Sig. MS vs. control, $p<0.05$.

As the margin of stability decreases, the associated gait is considered to be more mechanically unstable. As the extrapolated center of mass nears the border of support a fall becomes more likely to occur [5]. The results indicate that neither the mean nor the minimum of the margin of stability are significantly affected by the presence of MS. This would indicate that MS does not move the medial-lateral path of the extrapolated center of mass toward the boundary of support. The presence of MS, however, does seem to increase the divergence of the trajectory of the extrapolated center of mass through the gait cycle. The increased range in margin of stability demonstrates greater medial-lateral travel of the extrapolated center of mass. This serves as confirmation of the greater side-to-side sway observed in the gait of subjects with MS [2].

CONCLUSIONS

The use of the margin of stability metric in this study confirms previous findings regarding increased medial-lateral sway in MS patients during gait. However, a more mechanically unstable gait as defined by a decreased margin of stability was not observed in this population.

REFERENCES

1. Karst GM, Venema DM, Roehrs TG, Tyler AE. *J Neurol Phys Ther* **29,** 170-80, 2005.
2. Spain RI, et al. *Gait Posture* **In Press**, 2012.
3. Cattaneo D, Regola A, Meotti M. *Disab Rehab* **28**, 789-795, 2006.
4. Cattaneo D, et al. *Arch Phys Med Rehab* **83**, 864-867, 2002.
5. Hof AL, Gazendam MGJ, Sinke WE. *J Biomech* **38**, 1-8, 2005.

ACKNOWLEDGEMENTS

This work was generously supported by a University of Nebraska Medical Center College of Public Health First Year Doctoral Fellowship.

GENDER EFFECTS ON LOWER EXTREMITY BIOMECHANICS IN ADOLESCENT PATIENTS FOLLOWING ACL RECONSTRUCTION

Boyi Dai, Robert J. Butler, William E. Garrett, Robin M. Queen

Duke University, Durham, NC, USA
email: bdai@email.unc.edu web: http://klab.surgery.duke.edu/

INTRODUCTION

Anterior cruciate ligament (ACL) injury is a common sports related knee injury. Females have a higher ACL injury rate in most sports when the injury rate is normalized to sports exposures [1]. Gender differences in neuromuscular control have been identified as a factor that contributes to the disparity in ACL injury rates. Females tend to have restricted sagittal plane motion and a rigid landing pattern during athletic tasks that are associated with a higher ACL loading [2].

ACL reconstruction (ACL-R) is usually performed for patients with the goal of restoring knee stability and increasing the chance to return to sports. However, ACL re-injury rates are more than 20% in adolescent and young athletes who have returned to sports following ACL-R [3,4]. Abnormal neuromuscular control has been observed in ACL injured patients and has been associated with an increased risk for ACL re-injury [4].

Post-operative rehabilitation plays an important role in modifying ACL re-injury risk factors before patients are returned to sports. However, it is unclear if gender differences in lower extremity biomechanics exist in adolescent patients following ACL-R. Understanding the gender differences would provide insight into whether we should consider gender as a factor during rehabilitation as well as during re-injury risk evaluation.

METHODS

Fourteen female (Age: 15.9 ± 1.3 yr; Height: 1.64 ± 0.03 m; Mass: 65.4 ± 11.9 kg; Time following ACL-R: 6.2 ± 0.6 mo) and 9 male (Age: 16.5 ± 1.1 yr; Height: 1.78 ± 0.1 m; Mass: 82.8 ± 15.2 kg; Time following ACL-R: 6.2 ± 0.7 mo) adolescent subjects participated in the study. Three-dimensional kinematic and ground reaction force (GRF) data were collected bilaterally during 5 trials of a vertical stop-jump task. Lower extremity kinematics and kinetics were processed bilaterally for the 2-footed landing phase during the stop-jump task. Cardan angles were calculated for sagittal plane ankle, knee, and hip joints. An inverse dynamic approach was used to calculate sagittal plane internal joint resultant moments. GRFs were normalized to subject's body weight. Joint moments were normalized to subject's body weight multiplied by body height. The dependant variables included ankle range of motion (ROM), knee ROM, hip ROM, peak impact vertical GRF, peak propulsion vertical GRF, peak posterior GRF, average ankle moment, average knee moment, and average hip moment. Each dependent variable was analyzed using a mixed-model ANOVA with side (surgical vs. non-surgical) as the within-subject factor and gender (female vs. male) as the between-subject factor. A Type I error rate was set at 0.05 for statistical significance.

RESULTS AND DISCUSSION

Males had a higher jump height (0.45 vs. 0.32 m, $p < 0.01$) and faster approaching speed (2.47 vs. 1.95 m/s, $p = 0.01$) during the stop-jump task than females. In regards to kinematic and kinetic variables (Table 1), no significant interaction was observed for all dependant variables ($p > 0.05$). No significant side or gender effects were found for ankle ROM, knee ROM, hip ROM, and average hip moment ($p > 0.05$). The non-surgical side had significantly higher peak impact vertical GRF, peak propulsion vertical GRF, peak posterior GRF, average ankle moment, and average knee moment than the surgical side for both males and females ($p < 0.05$). Males had significantly higher peak posterior GRF than females for both surgical and non-surgical sides ($p < 0.05$).

Adolescent patients 6-month following ACL reconstruction have demonstrated significant kinetic asymmetries between surgical and non-surgical sides during a stop-jump task. The asymmetries existed in both males and females and did not tend to change cross gender. Since the asymmetries are associated with increased risk of ACL re-injury [4], one goal of rehabilitation should be decreasing the asymmetries for both male and female patients.

Male and female adolescent patients 6-months following ACL-R exhibit similar lower extremity kinematics. These results are contradictory to previous studies which have observed decreased sagittal plane motion in healthy females compared to healthy males [2]. One potential explanation is that both male and female patients have possessed similar high risk neuromuscular control patterns that could have contributed to their primary ACL injury. It is also possible that the primary ACL injury has altered the patients' neuromuscular control, resulting in similar patterns between genders.

No gender differences were observed for kinetic variables except the peak posterior GRF. Males and females had similar strategies to absorb landing forces and generate take-off forces in the vertical direction. The contributions of joint moments for either surgical or non-surgical side to complete the stop-jump task were also similar between males and females. The higher peak posterior GRF in males was likely due to a faster approaching speed.

Contrary to primary ACL injury rates, which are higher in females than in males, ACL re-injury rates are similar between adolescent male and female adolescent patients [3]. Results from the current study potentially support the published findings of similar ACL re-injury rates between genders.

CONCLUSIONS

Kinetic asymmetries between the surgical and non-surgical side were observed in male and female adolescent patients 6-month following ACL-R. The asymmetries were not different between genders. Male and female patients demonstrated similar lower extremity biomechanics to complete a stop-jump task. The similar patterns could have existed before the injury or were the result of the primary ACL injury. The findings of the current study suggest that the gender difference in a healthy population might not be applicable to ACL-R patients and should be considered during rehabilitation and injury risk evaluations.

REFERENCES

1. Prodromos CC, et al. *Arthroscopy* **23**, 1320-1325, 2007.
2. Malinzak RA, et al. *Clinical Biomechanics* **16**, 438-445, 2001.
3. Shelbourne KD, et al. *Sports Health* **1**, 236-241, 2009.
4. Paterno MV, et al. *Am J Sports Med* **38**, 1968-1978, 2010.

ACKNOWLEDGEMENTS

This work was supported by a research grant from DonJoy Orthopaedic, LLC. We would like to thank Mary Russell for her assistance in data collection.

Table 1: Means, SD and p values for surgical and non-surgical sides in males and females

Dependant Variables	Female S side	Female NS side	Male S side	Male NS side	*p* value Gender	*p* value Side	*p* value Interaction
Ankle ROM (Degs)	21 ± 14	23 ± 15	16 ± 10	18 ± 10	0.33	0.41	0.90
Knee ROM	53 ± 10	56 ± 10	53 ± 11	53 ± 13	0.68	0.71	0.65
Hip ROM	17 ± 7	18 ± 7	18 ± 14	18 ± 15	1.00	0.95	0.87
Impact VGRF (BW)	1.5 ± 0.4	1.9 ± 0.5	1.7 ± 0.5	2.1 ± 0.6	0.34	**<0.01**	0.89
Propulsion VGRF	1.2 ± 0.2	1.4 ± 0.2	1.2 ± 0.2	1.4 ± 0.2	0.85	**<0.01**	0.64
Posterior GRF	0.6 ± 0.2	0.7 ± 0.2	0.9 ± 0.4	1.0 ± 0.2	**0.01**	**0.02**	0.61
Ankle moment (BW*BH)	0.05 ± 0.01	0.06± 0.02	0.05 ± 0.01	0.05 ± 0.01	0.35	**<0.01**	0.28
Knee moment	0.06 ± 0.02	0.08 ± 0.01	0.06 ± 0.02	0.09 ± 0.02	0.97	**<0.01**	0.49
Hip moment	0.06 ± 0.01	0.07 ± 0.02	0.07 ± 0.01	0.08 ± 0.01	0.25	0.06	0.18

*S: Surgical; NS: Non-surgical; ROM: Range of motion; VGRF: Vertical ground reaction forces.

ESTIMATING ACL FORCE FROM LOWER EXTREMITY KINEMATICS AND KINETICS

Boyi Dai, Bing Yu

The University of North Carolina at Chapel Hill, Chapel Hill, NC, USA
email: bdai@email.unc.edu web: http://www.med.unc.edu/ahs/physical/

INTRODUCTION

The majority of anterior cruciate ligament (ACL) injuries happened during the early phase of landing, cutting, or pivoting tasks with a non-contract mechanism [1]. An ACL injury occurs when the load applied on the ACL exceeds its maximum loading capacity. In *vitro* studies [2] have demonstrated that anterior shear force applied at the proximal tibia is the primary contributor to the ACL loading. The effects of anterior shear force on ACL loading is largely depended on knee flexion angle [2]. Knee valgus, varus, and internal rotation moments also contribute to ACL loading [2].

To assess ACL force during dynamic movements, previous studies have used in *vivo* measurement [3,4] and musculoskeletal modeling [5,6]. In *vivo* measurement is highly accurate but either invasive [3] or resource demanding [4]. Musculoskeletal modeling is non-invasive, but most models involve electromyography signal process [5] and complicated optimization which might limit its application [6]. The purpose of the current study was to evaluate the face validity of a musculoskeletal model that was developed to estimate ACL force directly from the time series data of lower extremity kinematics and kinetics.

METHODS

Fifteen recreational athletes (8 males, 7 females; age: 22.5 ± 3.4 yr; height: 1.7 ± 0.1 m; mass: 69.1 ± 8.3 kg) participated in the study. Three-dimensional kinematic and ground reaction force data were collected for the subject's dominant limb during two conditions of a vertical stop-jump task [7]. During the first condition, the subject was instructed to jump as high as possible following the 2-footed landing. During the second condition, the subject was instructed to land with increased knee flexion at the initial contact of the 2-footed landing and jump as high as possible. For the 2-footed landing phase, Cardan angle were used to calculated 3-D ankle, knee, and hip joint angles. Inverse dynamic was performed to calculate 3-D ankle, knee, and hip joint resultant moments and forces.

A musculoskeletal model was developed to estimate ACL force. The components that contributed to ACL loading included tibia anterior shear force, pure knee flexion-extension, tibia internal rotation moment, and tibia varus / valgus moment. To calculate tibia anterior shear force, gastrocnemius force, hamstring force, and patellar tendon force were estimated using a modified torque driven model [8]. In the model, muscle moment arms were modeled as a function of joint angles. Muscle peak forces, lines of action as well as joint geometries were obtained from the literature. To resolve muscle redundancy, it was assumed that there was no muscle co-contraction at the ankle and hip joints. It was also assumed that the force distributions for different muscles that crossed ankle and hip joints were depended on muscle peak forces and moment arms. The muscle forces and knee joint resultant moment and force were used to calculate tibiofemoral contact force and tibia anterior shear force [5,7].

The effects of tibia anterior shear force, pure knee flexion-extension, tibial internal rotation, and tibia varus / valgus moments on ACL force were based on a cadaver study which has documented the ACL force under different external loading conditions [2]. It was assumed that the relationship between ACL force and each external loading was linear. It was also assumed that the ACL loadings caused by each external loading were independent to each other and additive [5,7].

The face validity of the current model was evaluated from three aspects. First of all, if the peak ACL force estimated from the model was within the range of peak ACL forces measured in previous *vivo* studies [3,4], the face validity of the model would be supported. Secondly, a video analysis study [1] found that the timing of ACL injuries usually occurred within the first 40 milliseconds (ms) after the initial foot contact. If the timing of the peak ACL force estimated from the model was within the first 40 ms after initial contact, the face validity of the model would be supported. Thirdly, one in *vivo* study [9] has shown that landing with increased knee flexion decreased peak ACL length. If the peak ACL force estimated from the model was lower during the increased knee flexion landing condition than the preferred landing condition, the face validity of the model would be supported.

RESULTS AND DISCUSSION

The estimated peak ACL forces were **715.7 ± 299.3 N** (Mean ± SD) for the preferred landing condition and **349.6 ± 201.7 N** for the increased knee flexion condition. The estimated timings for peak ACL forces were **34.2 ± 9.7 ms** after initial foot contact for the preferred landing condition and **25.0 ± 10.1 ms** after initial foot contact for the increased knee flexion condition. Pair t-test showed that the peak ACL force during the increased knee flexion condition was significantly lower than the preferred landing condition ($\boldsymbol{p < 0.001}$).

Crulli et al. [3] used strain gauge to measure in *vivo* ACL strain during a hop landing tasks. The estimated peak ACL force was 505 N. Taylor et al. [4] employed a fluoroscope with MRI technique to measure in *vivo* ACL strain during a drop vertical jump task. The estimated peak ACL force was 1109 N during pre-landing and 647 N during landing. In the current study, the estimated peak ACL force during the preferred landing condition was 716 N which was consistent with previous in *vivo* studies.

The timing of ACL injuries usually occurred within the first 40 ms after the initial foot contact [1]. Therefore, it was expected that the timing of peak ACL force would occur during the early landing phase. The timing of the peak ACL force estimated from the model was generally less than 40 ms which was consistent with the video analysis study.

Brown et al. [9] have demonstrated that landing with increased knee flexion decreased peak ACL strain in *vivo*. In the current study, the peak ACL force during the increased landing condition was less than the preferred landing condition and the results supported the face validity of the model. The decrease in ACL force caused by increased knee flexion was mainly because of changes in patella tendon - tibia shaft angle, hamstring tendon - tibia shaft angle, and ACL elevation angle which were all considered in the model.

The major assumption of the model was that there was no muscle co-contraction at the ankle and hip joints. The muscle forces estimated from the current model should be compatible to previous optimization models which usually minimize a cost function to resolve muscle redundancy [6]. Different from most models, the current model estimated ACL force directly from the time series of lower extremity kinematics and kinetics data which were generally reported in motion analysis studies.

CONCLUSIONS

A musculoskeletal model has been developed to estimate ACL force from lower extremity kinematics and kinetics. The model has demonstrated good face validity in peak ACL force magnitude, peak ACL force timing, and sensitivity of ACL force to knee flexion angle. The model might be applied to evaluate intervention effects on ACL loading. Future studies are needed to evaluate the content validity of the model.

REFERENCES

1. Koga H, et al. *Am J Sports Med* **38**, 2218-2225, 2010.
2. Markolf KL, et al. *J Bone Joint Surg Am* **78**, 1728-1734, 1996.
3. Cerulli G, et al. *Knee Surg Sports Traumatol Arthrosc* **11**, 307-311, 2003.
4. Taylor KA, et al. *J Biomech* **44**, 365-371, 2011.
5. Kernozek TW, et al. *Clin Biomech* **23**, 1279-1286, 2008.
6. Laughlin WA, et al. *J Biomech* **44**, 1845-1851, 2011.
7. Lin CF, et al. *J Biomech* **42**, 418-423, 2009.
8. DeVita P, et al. *J Appl Biomech* **17**, 297-231, 2001.
9. Brown DW, et al. *Proceedings of ORS,* San Francisco, CA, USA, 2012.

IMPACT OF DUAL-TASKING ON LOWER JOINT DYNAMICS DURING STAIR ASCENSION

[1]Austin J. Davidson, [1]Srikant Vallabhajosula, [1]Chi Wei Tan, [1]Mukul Mukherjee, [1,2]Ka-Chun Siu, [1]Jennifer M. Yentes, [1]Denise McGrath, [1]Sara A. Myers

[1]University of Nebraska at Omaha, Omaha, NE, USA
[2] University of Nebraska Medical Center, Omaha, NE, USA
email: ajdavidson@unomaha.edu, web: http://nbcf.unomaha.edu/

INTRODUCTION

Stair-climbing is a daily activity, often done while simultaneously performing other tasks such as talking or carrying a laundry basket. Adults over the age of 60 indicated stair ascension as one of the most challenging daily tasks [1]. Moreover, there is a high risk of falls for the elderly during stair-climbing [1]. Reasons for such a high risk can be examined through gait characteristics. Lower-extremity joint moments have been found to be significantly higher during stair ascension compared to over-ground walking [1]. While previous studies have explored the biomechanics of stair-climbing, only one study has explored the effect of dual-tasking while climbing stairs. That study showed there is increased attentional demand for older adults as they ascend stairs while performing an additional cognitive task [2]. Thus, it has been suggested that dual-tasking could increase the risk of falls while climbing stairs [2]. Hence, the objective of the current study is to evaluate the joint dynamics (moments and powers) during stair-climbing while dual-tasking to identify any changes that take place which could potentially lead to falls. We hypothesized that a significant difference in joint moments and powers would occur as a result of dual-tasking during stair ascension and this difference would occur between consecutive ipsilateral steps.

METHODS

Ten healthy young adults (6 males; 23.9±2.8 years; 175.98±0.06 cm; 71.3±8.6 kg) were recruited to participate in the current study. Kinematics (Motion Analysis System; 60 Hz) and kinetics (AMTI; 600 Hz) data were collected as participants ascended a custom-built four-step staircase (angle of staircase rise = 32.73°). The first and third steps had built-in force platforms, which allowed us to collect force data from two consecutive ipsilateral steps. Ten trials of stair ascension were performed in four conditions, randomized among subjects. The first condition required subjects to walk up the stairs without performing any other task (control). The second condition required subjects to ascend the stairs while counting backwards by sevens starting from a random three-digit number that was given to them at the start of each trial (cognitive). For the third condition, subjects ascended the stairs while carrying an opaque light-weight box (motor). The fourth condition combined tasks from conditions 2 and 3 (combined). In all the conditions, the subjects were asked to take their first step with the dominant foot. A 2x4 (2 steps x 4 conditions) repeated measures ANOVA was applied to compare speed, joint moments and powers of the lower extremities. Bonferroni pairwise comparisons were used to determine the significant differences between the conditions. For measures that showed significant differences, a repeated measures ANCOVA was performed with speed as the covariate.

RESULTS AND DISCUSSION

Condition main effect results indicate that performing a cognitively challenging task has a greater influence than a motor task on how people climb stairs (Table 1). Specifically, this influence was seen immediately after foot-strike where the ankle experiences dorsiflexion (braking) and the knee and hip joints undergo extension (weight-acceptance). Lesser values of the corresponding powers were seen primarily during the conditions with additional cognitive task. Moreover, the peak ankle plantar flexor moment occurs during push-off indicating that during the cognitive conditions, participants produced a lesser moment to lift their foot. *Step main effect results* are outlined in Table 2. At the first step, participants seem to produce lesser moments at the ankle (during braking and push-off), while producing greater moments at the hip (during weight acceptance) and at knee (during push-off). This may be due to participants taking a more cautious first step to familiarize with the staircase, after which subjects took a less cautious second step. *Step-Condition interaction* indicates that while ascending the first step, the power absorption at the ankle was similar during braking phase in all the conditions (blue solid line in Figure 1).

But while ascending the second step, participants increased the power absorbed at the ankle only in the control and motor conditions (red solid line in Figure 1). Once the participants completed the first step, due to the familiarity of the task, they were able to absorb greater power during the control and motor conditions. However, in the cognitive and combined conditions, due to the additional cognitive demand, the participants may not have been able to alter their peak ankle power absorption. Overall, the control and motor conditions were similar to each other, but differed from the cognitive and combined conditions. Also, participants ascended the stairs slowly in the cognitive and combined conditions for all the steps and at the second step during all the conditions. With speed as a covariate, differences between conditions remained for peak ankle power absorption and peak ankle dorsiflexor moment suggesting that other variables (in Tables 1 and 2) were primarily influenced by speed. Participants exhibited similar greater ankle power absorption at both the steps during motor and control conditions compared with the two cognitive conditions (dotted lines, Figure 1). In both the cognitive conditions, less ankle power was absorbed at the second step compared to first step. Also, reduced peak ankle dorsiflexor moment was observed at the second step compared with the first step. These results could imply that the force generated during braking phase was less during cognitive conditions. This reduced force could be due to additional cognitive resources used by the central nervous system in these conditions or due to different foot positioning at foot-strike. Such observations could be important with respect to older adults ascending stairs while dual-tasking, as they ascend more slowly and operate closer to their maximal capabilities while ascending stairs [3].

CONCLUSION

Based on our hypothesis, dual tasking had a significant impact on joint dynamics and the impact was greater while performing a cognitive secondary task. This was true even after accounting for reduced speed during dual-task conditions.

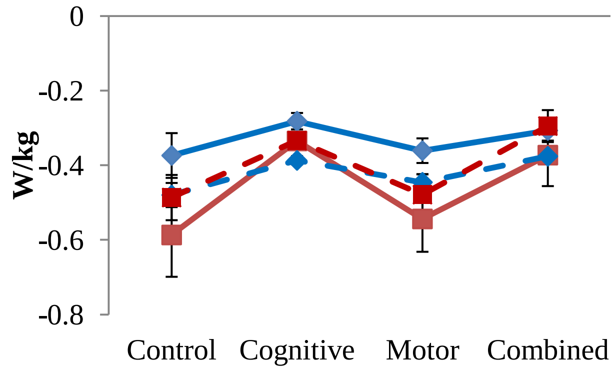

Figure 1: Mean (SE) of peak ankle power absorption, which showed a significant step x condition interaction (P=0.006); step 1 (blue diamond); step 2 (red square); before adjusting for speed (solid line); after adjusting for speed (dashed line).

REFERENCES

1.Novak, AC, et al. *Gait Posture* **33**, 54-60, 2011.
2.Ojha, HA, et al. *Phys Ther* **89**, 1080-1088, 2009.
3.Reeves, ND, et al. *J Electromyogr Kinesiol* **19**, e57-68, 2009.

ACKNOWLEDGEMENTS

Funding provided by the National Aeronautics and Space Administration (Grant No. NNX11AM06A) and National Institute of Health (Grant No. 1R011AG034995-01A1).

Table 2: Mean (SE) in Nm/kg of dependent variables that showed significant step main effect; * indicates significance vs. Step 2

Dependent Variable	Step 1	Step 2
Peak Ankle Dorsiflexor Moment	-0.04 (0.01) *	-0.06 (0.01)
Peak Ankle Plantar Flexor Moment	1.58 (0.06) *	1.77 (0.08)
Peak Knee Flexor Moment	-1.03 (0.07) *	-0.91 (0.07)
Peak Hip Extensor Moment	0.35 (0.04) *	0.26 (0.05)

Table 1: Mean (SE) of dependent variables that showed significant condition main effect; * indicates significance vs. Control; ^ indicates significance vs. Cognitive; # indicates significance vs. Motor.

Dependent Variables	Control	Cognitive	Motor	Combined
Peak Ankle Plantar Flexor Moment (Nm/kg)	1.75 (0.07)	1.61 (0.08)*	1.74 (0.06)^	1.61 (0.06)*#
Peak Ankle Power Absorption (W/kg)	-0.48 (0.08)	-0.31 (0.04)	-0.45 (0.05)^	-0.34 (0.05)
Peak Knee Power Generation (W/kg)	1.70 (0.17)	1.51 (0.11)	1.74 (0.15)	1.52 (0.13)
Peak Hip Power Generation (W/kg)	1.15 (0.07)	0.92 (0.08)*	1.16 (0.08)	0.93 (0.08)

EFFECT OF OBESITY AND OVERWEIGHT ON POSTURAL BALANCE IN CHILDREN FROM 7 TO 14-YEARS-OLD

[1]Ana de David [1]Marcella Barbacena

[1]University of Brasilia. Brasilia. DF. Brazil

email: acdavid@unb.br web: http://www.unb.br

INTRODUCTION

In addition to the metabolic and cardiac diseases, already well documented, the obesity affects the musculoskeletal development and may have long-term implications during adulthood. When compared to normal-weight children obese children have showed poor motor competence [1]. However, it is not clear how overweight and obesity affect the postural balance during childhood and early adolescence. Increased instability and major dependency on vision system have been reported [2,3]. On the other hand, some investigations have found no differences between normal-weight and obese children balance during the quiet standing posture [4,5]. Therefore, the purpose of this study was to verify the association between postural balance and age from 7 to 14 years-old in obese, overweight and normal weight children.

METHODS

The postural balance of 438 subjects from 7 to 14 years-old (201 normal weight, 136 overweight and 101 obese) was assessed. They were divided into four age groups (7-8, 9-10, 11-12 and 13-14) for each three weight status groups (normal weight, overweight and obese) using Cole et al [6]. An AMTI AccuSway Plus force plate at a frequency of 100Hz was used to measure the anterior-posterior amplitude (COPap), medio-lateral amplitude (COPml), mean velocity (COPvel) and 95% area of the ellipse (COParea). The subjects were tested for three trials (30 s) standing in comfortable feet apart and eyes open. The normal data distribution was verified by Kolgomorov-Smirnov test while Pearson correlation coefficient was used to verify association between age and COP parameters for each weight status group. Differences between weight status groups were verified using analysis of variance test. Pairwise comparisons were performed using Tukey post-hoc test ($p<0.05$).

RESULTS AND DISCUSSION

Figure 1 and Figure 2 provide descriptive statistics for COPvel and COParea. As to be expected, balance becomes better as age increases. Obese group had significant ($p<0.01$) greater sway for 13-14 years-old than normal weight and overweight groups only for COParea. There is no other significant difference between groups. For COParea the variability is higher than for COPvel mainly for 7-8 years-old group.

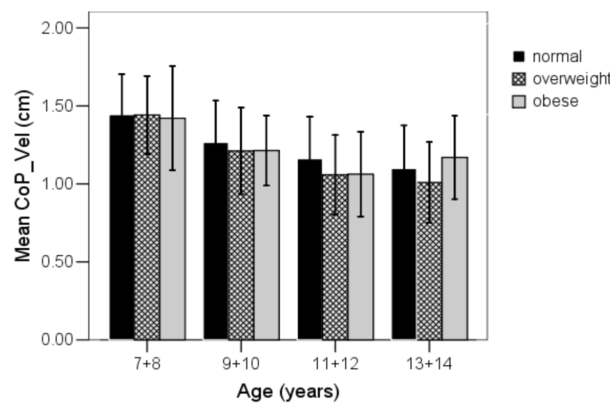

Figure 1: COPvel (mean ± sd) by age for weight status groups.

Moderate correlations are found between age and balance variables for normal weight and overweight groups as shown in Table 1 while obese group had poorest correlation with no-significant values for COParea, COPml and COPap. COPvel showed stronger correlation with age than the other measures for all groups. COPml is more associated with age than COPap for normal weight and overweight groups.

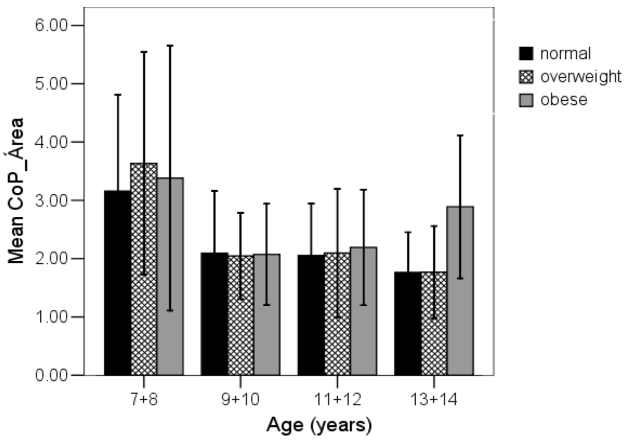

Figure 2: COParea (mean ± sd) by age for weight status groups.

An increase in body weight has been correlated to an decrease in balance stability [2,3,7]. However, our results did not indicate this same situation. Significant differences were found between obese and normal weight groups and obese and overweight groups only for 13-14 years-old group in COParea. On the same way has not been found any clear underlying sensory organization impairments that may affect standing balance performance in overweight children compared to normal weight peers [4].

Body weight was found to correlate with COPap parameters and not with COPml parameters in adults males and females [7]. However, our results showed better association of age 7 to 14-years with COPml than COPap parameters.

Similar with others studies about the effect of obesity on balance in children, postural balance was measured during quiet double leg stance using natural base of support. This less challenging foot position might explain the absence of BMI group differences. Significantly lower motor coordination in overweight and obese children when compared to normal-weight children on more dynamic situations support this idea [1].

CONCLUSIONS

According our results balance improves from 7 to 14-years-old in a similar way in normal weight, overweight and obese children for quiet standing double leg posture. It seems related more with age than with weight status. COPvel and COPml has stronger association with balance than COPap for normal-weight and overweight children on this age.

REFERENCES

1.Lopes VP. Et al. *J Sci Med Sport.* **15**. 38-43. 2012.
2.Hue O. et al. *Gait Posture.* **26**. 32-38. 2007.
3.D´Hont E. et al. *Gait Posture.* **33**. 179-184. 2011.
4.D´Hont E. et al. *Clin Biom.* **26**. 84-89. 2011.
5. Pau M. et al. *Gait Posture.* **35**. 378-382. 2012.
6. Cole TJ et al. *British Med J.* **320**. 1-6. 2000.
7.Menegoni F. et al. *Epidemiology*. **17**. 1951-1956.

Table 1: Pearson´s coefficient correlation values between age and COP variables.

		COP_Vel	COP_Area	COP_ML	COP_AP
Normal-weight	(n=201)	-.40*	-.39*	-.41*	-.26*
Overweight	(n=136)	-.51*	-.42*	-.47*	-.34*
Obese	(n=101)	-.37*	-.12	-.18	-.06

* Correlation is significant at the 0.01 level (2-tailed)

EVALUATION OF SHOULDER JOINT ARTHTOKINEMATICS IN PHYSICALLY DISABLED ATHLETES

[1]Aynur Demirel,[1] Nevin Ergun

[1]Hacettepe University, Ankara, TURKEY

email:aynurdemirel629@hotmail.com

INTRODUCTION

Repeated throwing motions causes hyper angulations between rotator cuff and superior part of labrum in some of overhead athletes and ıt effects shoulder kinematics negatively (1,2). The limitation of any part of the joints composes shoulder-arm complex could be limited shoulder movements in normal range and scapulahumeral rythm could be fail. On the other hand increased mobility of shoulder joint has a poor stability (3). Proprioception is a key component of joint stability. The role of proprioception in shoulder complex to produce synergistic control of the muscle groups, and to prevent a kind of potential instability of shoulder (4,5). The range of shoulder internal rotation values were smaller in the baseball athletes dominant shoulders than handball, volleyball and basketball athletes' dominant shoulders (2). In the literature a study found that there were limitations in external and internal rotation range of motion in wheelchair basketball athletes (8). There are limited study in the literature about shoulder kinematics in disabled athletes and also there was no study comparing overhead and underhead disabled athletes shoulder complex arthrokinematics. The aim of this study was to determine differences in physically disabled athletes shoulder artrokinematics who use shoulder joint at 90 degree, above and below of this degree in sports activity.

METHODS

Thirty-four athletes who have independent trunk control, don't have structural scoliosis and surgical operations during recent one year, playing sport with wheelchair at least two years were included in the study. (22 M, 12 F, age: 30.24±7.58 yrs. sport age: 5.6±3.48 yrs.) 15 wheelchair basketball and tennis player in the category of sport which use dynamic movement area above 90°(overhead), 19 para table tennis, para archery and shooting players in the category of sport which use dynamic and static movement area at 90° and below (underhead) were participated. Range of motion (ROM) of shoulder movements , shoulder joint position sense (JPS) were evaluated. ROM of shoulder joint were assessed in supine position with universal goniometer in flexion, extension, abduction, adduction, horizontal aduction , external and internal rotation movements in both shoulders. JPS were assessed with Baseline Bubble Inclinometer (Fabrication Enterprises Inc, White Plains, New York 10602) at two different degrees of external and internal rotation movements (for internal rotation 15°, 45° and for external rotation 45°, 75°) All measurements were repeated three times and mean values of measurements were calculated and differences between target and mean values were recorded as failure score. (Figure 1) the group difference were analysed with Mann- Whitney U test.

Figure1: JPS measurements in external and internal rotation movements.

RESULTS AND DISCUSSION

There were significant differences in horizontal adduction and external rotation ROM values in both shoulders. Underhead group showed higher values in horizontal adduction and external rotation motions than overhead groups ($p<0.05$). There were significant differences in internal rotation ROM values only in non-dominant shoulder between groups ($p<0.05$). There were no significant differences between groups in flexion, extension,abduction, adduction ROM values ($p>0.05$). (Table 1) There were differences in JPS at 45°of external rotation in both shoulder between groups. Underhead group showed closer values to the target value than overhead group ($p<0.05$). (Figure 2)

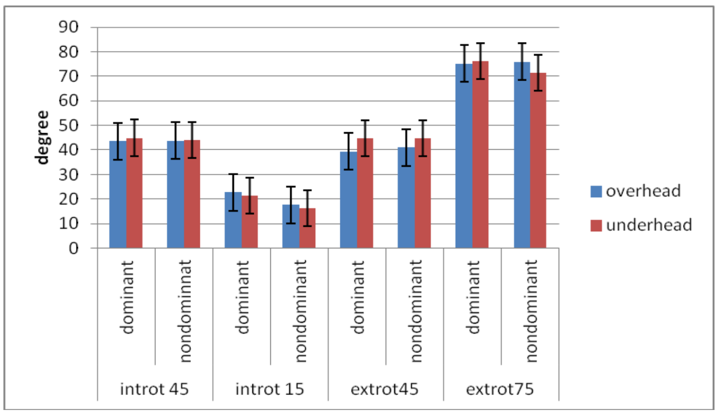

Figure 2: JPS results between groups.

Table 1: Descriptive statistics of ROM values.

		Hor.Add.(°)		Int .Rot(°)		Ext.Rot. (°)	
	G	Mean±SD	p	Mean±SD	p	Mean±SD	p
Dominant Shoulder	U O	45.6 ± 3.8 42.1 ±3.9	**.013***	62.9 ± 6.1 68.53 ± 10.8	.066	92.3± 3.6 84.07 ±7.7	**< 0.001***
Non-dominant Shoulder	U O	44.8 ± 3.4 41.2 ± 3.5	**.005***	60.3 ± 4.7 65.5 ± 11.1	**.048***	90.7 ± 2.7 87.9 ± 3.3	**.014***

*p<0.05 , U: underhead , O: overhead

CONCLUSIONS

In this study, we found differences in shoulder ROM and JPS between overhead and underhead disabled athletes. According to our result it could be depend on adaptive changes in arthrokinematics associated with sport. Further studies more athlete need to inclueded and computer aided motion analyses systems should be used to make detailed analyses for shoulder arthrokinematics in wheelchair athlete population.

REFERENCES

1. Rockwood CA. *The Shoulder*, Philedelphia, Saunders, 2004.
2. Krishan SG. *The Shoulder and Overhead Athlete*, Lippincott Williams & Wilkins, 2004.
3. Wilk KE, et al. *J Orthopaedic and Sports Physical Therapy* **18,** 365-378, 1993.
4. Boyar A. *J Isokinetics and Exercise Science* **15,** 111-116, 2007.
5. Myers JB. et al. *J Athletic Training* **35**, 351-363,2000.
6. Bezciler E. Master of Science Thesis, Abant İzzet Baysal University, Bolu, 2007.

MAPPING THE MECHANICAL TOPOGRAPHY OF HEALTHY TIBIAL CARTILAGE

Jessica M. Deneweth, Stephen M. Sylvia, Kelly E. Newman, Scott G. McLean, and Ellen M. Arruda

[1]University of Michigan, Ann Arbor, MI, USA
email: jmden@umich.edu

INTRODUCTION

Tibial plateau cartilage has been suggested to exhibit mechanical heterogeneity across its surface [1, 2]. This finding forms the fundamental basis for the tenet that altered joint biomechanics induce knee osteoarthritis (OA) [3]. The extent to which this heterogeneity consistently presents for healthy human knees subjected to physiological loading rates, however, remains unknown. This knowledge is critical to elucidating the role of biomechanics in knee OA. We hypothesized that healthy human tibial plateau cartilage would exhibit substantial physiologic mechanical variability across its surface, that this heterogeneity would form a distinct geographical pattern, and that this pattern would be consistent across individuals.

METHODS

Specimens. Eight fresh-frozen female cadaveric knees (age: 41-54; BMI: 14-20) without history of lower limb injury, surgery, or movement disorder; osteoarthritis; or osteoporosis were used in this study. Full-depth cylindrical cartilage samples were extracted from non-fibrillated cartilage, as identified by an India ink test[4], from 21 standardized sites across the tibial surface using a 4-mm diameter round hole hand punch and a scalpel (Figure 1).

Mechanical testing. Each sample was tested in unconfined compression using an innovative custom-built high-speed material testing apparatus. Samples remained immersed in standard phosphate-buffered saline solution throughout testing. After a pre-conditioning sequence, each sample underwent three compression trials at 100% strain/sec to 20% peak strain while simultaneous force and video were recorded at 1000 frames/sec. These loading parameters were selected to replicate cartilage deformation during normal gait [5].

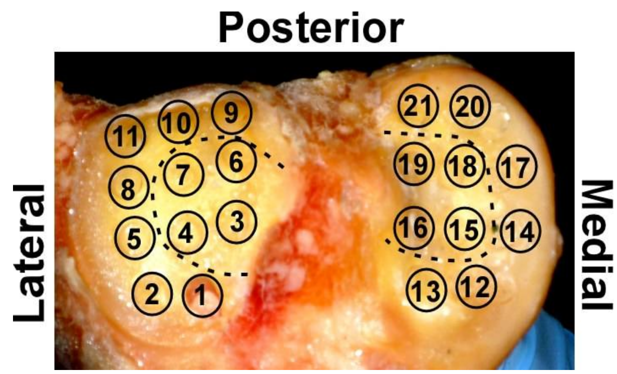

Figure 1. Cartilage sample sites. Dashed lines denote typical inner margins of the menisci.

Data Analysis. The average nominal strain along the thickness of the explant was calculated using commercial digital image correlation software (VIC-2D 2009, Correlated Solutions, Columbia, SC). Nominal stress was calculated by dividing the recorded force by the undeformed cross-sectional area of the explant. The elastic tangent modulus at 10% strain ($E_{10\%}$) was calculated, averaged across trials, and combined across knees to determine the mean and standard deviation of $E_{10\%}$ for four explicit tibial plateau regions: not covered by meniscus (I); covered by meniscus – anterior (II); covered by meniscus – exterior (III); and covered by meniscus – posterior (IV). The mean regional values of $E_{10\%}$ were submitted to a mixed model repeated measures analysis of variance to determine the effects of plateau (n=2, medial or lateral), region (n=4), and their interaction on $E_{10\%}$. Bonferroni-adjusted pairwise comparisons were made for all main effects. Pairwise effect sizes were calculated using Cohen's d. Significance was denoted by an alpha level of 0.05.

RESULTS AND DISCUSSION

When tested at a physiological compressive strain and strain rate, tibial plateau cartilage manifested substantial topographical heterogeneity. In general, the stiffest region in each knee displayed $E_{10\%}$ that was three or more times larger than the softest region. Furthermore, this non-uniformity followed a consistent pattern across individuals (Figure 2A).

There was not a significant effect due to plateau (p = 0.3613), indicating that the heterogeneity on each plateau could be approximated using the same pattern. Region I had a significantly lower value of $E_{10\%}$ compared to Region III (p = 0.0034, Figure 2B) and Region IV (p = 0.0085). Similarly, Region II was significantly less stiff than Regions III and IV (p = 0.0075 and p = 0.0188, respectively). No significant differences were present between Regions I and II (p = 1.00) and Regions III and IV (p = 1.00). Examining the effect sizes for these two pairs, the mean differences between III and IV on the medial plateau can be classified as weak (d = 0.09), between I and II and between III and IV on the lateral plateau as small (d = 0.34 and 0.27, respectively), and between I and II on the medial plateau as borderline moderate (d = 0.48).

These findings suggest that representing tibial plateau cartilage with a single elastic modulus is inaccurate. Moreover, the mechanical heterogeneity elicited by physiologically-relevant compression appears to be reasonably approximated by three regions, listed in order of increasing modulus: not covered by meniscus, covered by meniscus – anterior, and covered by meniscus – exterior/posterior. Biomechanical patterns posited to contribute to knee OA development (i.e., increased anterior tibial translation[6]), therefore appear to shift primary loading posteriorly, away from central compliant (i.e., mechanically viable) regions to those over three times as stiff. Further work must be done to determine how such a shift may directly compromise cartilage health.

CONCLUSION

This study is the first to our knowledge to map the physiologic elastic tangent modulus across the entire healthy human tibial plateau. We determined that non-osteoarthritic female proximal tibia cartilage exhibits a distinct topographic pattern in its physiologic elastic tangent modulus. This pattern is

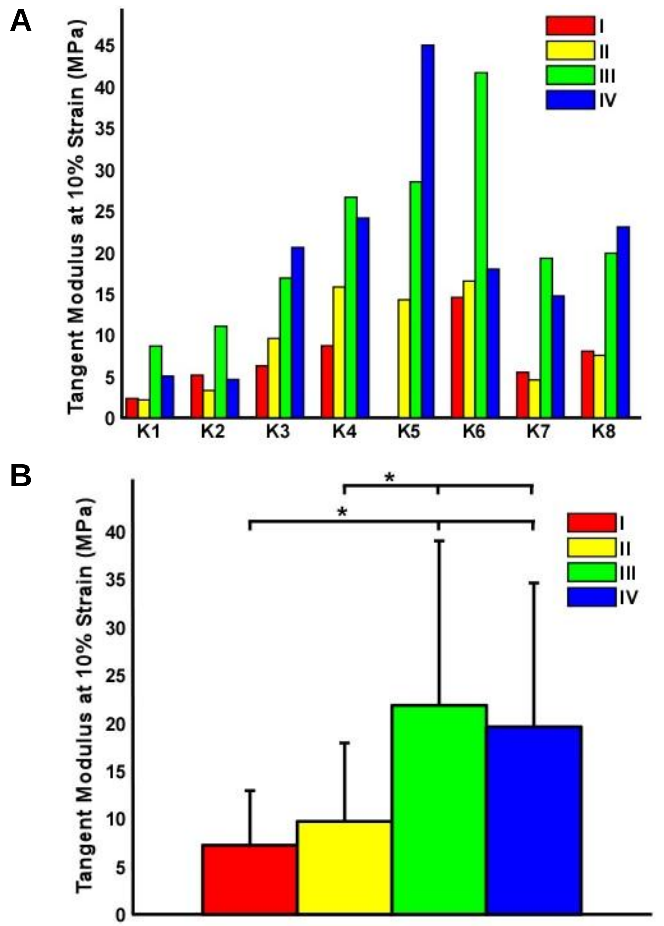

Figure 2. Regional $E_{10\%}$ for individual knees (A) and averaged across all knees (B). Vertical bars denote one standard deviation. * indicates $p < 0.05$.

consistent on both sides of the joint and across individuals, which suggests that it is a viable foundation for investigating the interaction between joint biomechanics and knee OA development. Computational knee models can benefit from these data, as well. Future work will expand this analysis to cartilage from distal femurs and male knees.

REFERENCES

1. Swann, A.C., et al. *Br J Rheumatol* **1**. 16-25, 1993.
2. Barker, M.K., et al. *Rheumatology (Oxford)* **3**. 274-84, 2001.
3. Andriacchi, T.P., et al. *Ann Biomed Eng* **3**. 447-57, 2004.
4. Meachim, G. *Ann Rheum Dis* **6**. 457-64, 1972.
5. Liu, F., et al. *J Biomech* **4**. 658-65, 2010.
6. Haughom, B., et al. *Knee* 2011.

A COMPARISON OF POSITION MEASUREMENT ACCURACY USING TWO DIFFERENT CAMERA ARRANGEMENTS

W. Matt Denning, Iain Hunter, and Matthew K. Seeley

Brigham Young University, Provo, UT, USA
Email: mdenning@byu.edu

INTRODUCTION

Motion analysis, using high-speed video and reflective markers placed on anatomical landmarks, is an important measurement method in biomechanical research. The accurate measurement of reflective marker position during motion is vital for various biomechanical analyses. Researchers have studied the influence of marker placement and size, and calibration technique on the accuracy of marker position measurement [1, 2]; however, it is unclear if/how the distance between the video cameras and reflective markers influence marker position measurement accuracy. We currently use two primary camera arrangements in our lab. One is an arrangement that uses cameras placed on the floor, relatively close to the subjects (~2 m). The other arrangement involves cameras that are mounted on the wall at a relatively far distance from the subjects (~4 m). The purpose of this study was to determine whether one of these two camera arrangements results in a more accurate measurement of reflective marker position. We hypothesized that an increased distance between cameras and reflective markers would result in decreased marker position measurement accuracy.

METHODS

Spatial position was measured for four 13-mm static reflective markers. These markers were placed in a known position and the distance between each marker was calculated using the measured (using high-speed video) and known positions. We also measured position for one dynamic reflective marker after it had been dropped into the motion capture volume from a height of 1.5-m. Position data for three trials were averaged for both the static and dynamic reflective markers. For the dynamic marker, vertical acceleration was derived using a central differences approach. All of these measurements were made using two camera arrangements: (1) a relatively close arrangement, with cameras positioned 2 m from a set global origin, and (2) a relatively far arrangement, with cameras positioned 4 m from a set global origin (Figure 1). Six MX13T cameras, two MXF20 cameras, and two MXT20 cameras, and VICON Nexus software (VICON, Santa Monica, CA, USA) were used to collect the position data (240 Hz). A wand calibration was completed using 2000 images spaced throughout a 1 × 1 × 1m volume. A calibration error of less than 0.2 was accepted as a successful calibration for each camera, as is recommended by the manufacturer.

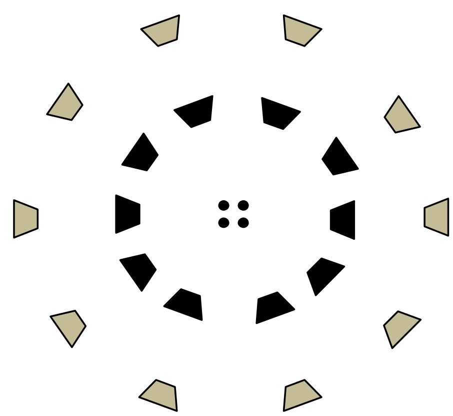

Figure 1: A representation of the two camera arrangements. Dark and light trapezoids represent the close and far camera arrangements, respectively. Small black spheres represent the static markers.

The independent variable was camera arrangement (close and far). Dependent variables were: (1) root mean square error (RMSE: the difference between the known and measured distances (between the static markers)), and (2) vertical acceleration of the dynamic marker within and without the calibrated motion capture volume. We used a one tailed *t*-test to test the effect of the independent variable on the dependent variables ($\alpha = 0.05$).

RESULTS AND DISCUSSION

The present results did not support our hypothesis. Mean RMSE for the relatively close position (0.28 mm) was not statistically different from mean RMSE for the relatively far position (0.49 mm; p = 0.12; Figure 2). Similarly, no significant difference in vertical acceleration was noted between the close and far camera arrangements (p = 0.44; Table 1). There is no statistical difference in position measurement accuracy between close and far camera arrangements.

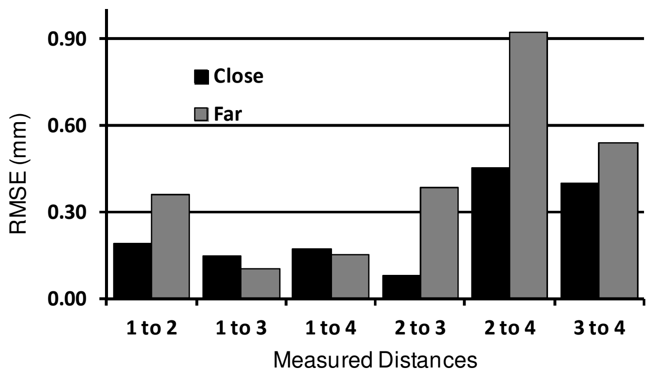

Figure 2: Difference in marker distance (relative to the known distance) for two camera arrangements.

Mean vertical acceleration for the dynamic marker, for the close and far camera arrangements, within and without the calibration volume, is shown in Figure 3. Although this was not the primary purpose of the present study and a statistical analysis was not performed, vertical acceleration for the relatively far camera arrangement appear to have been more variable (Figure 3 and Table 1). This implies that the position data were more variable for the far camera arrangement. Moreover, standard deviations outside the calibration volume are much higher for the far camera arrangement (Table 1), supporting the idea that it is important to measure position within the calibrated volume, especially when accelerations need to be calculated. Additionally, as noise increases when deriving acceleration from position data, perhaps a different smoothing technique should be used to eliminate noise from the true signal, when accelerations are calculated outside the calibration volume.

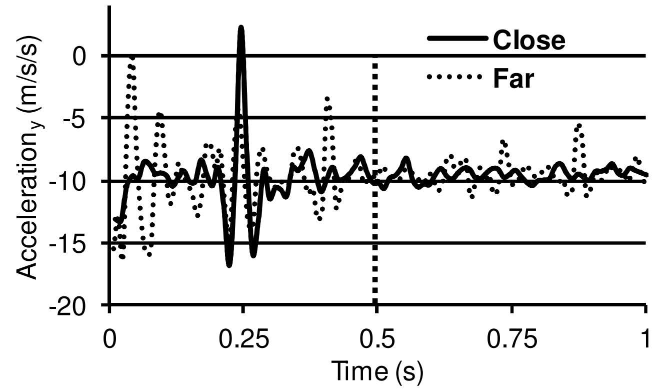

Figure 3: Vertical acceleration for the dynamic marker, plotted against time, for the two camera arrangements. Acceleration to the left of the vertical dotted line occurred without the calibration volume. It appears that vertical acceleration was more stable when measured in the volume.

In conclusion, the purpose of this project was to determine whether camera distance affects position measurement accuracy. Statistically, position measurement accuracy was similar for close and far camera arrangements. Additionally, accuracy is greatest when the measurement occurs inside the calibrated volume. Future research could strengthen these findings by using additional markers to further investigate the influence of camera placement on position and acceleration accuracy.

REFERENCES

1. Windolf M, et al. *J Biomech* **41**, 2776-2780, 2004.
2. Telfer S, et al. *Gait & Post* **32**, 536-539, 2010.

Table 1: Average accelerations (m/s/s) within and without the calibration volume.

	Without		Within	
	Close	**Far**	**Close**	**Far**
Mean	-9.86	-10.0	-9.48	-9.52
SD	4.42	6.29	0.92	1.92

Tibial Stresses in Habitual and Converted Forefoot and Rearfoot Strike Runners

[1]Timothy R. Derrick, [2]William Brent Edwards and [3]Brandon D. Rooney

[1]Iowa State University, Ames, IA, USA
[2]University of Illinois at Chicago, Chicago, IL, USA
[3]Brooks Sports Inc, Bothell, WA, USA
email: tderrick@iastate.edu web: http://www.kin.hs.iastate.edu/

INTRODUCTION

Biomechanics researchers often rely on surrogate measurements as estimates of the internal forces responsible for injury. For instance, vertical ground reaction forces are often measured to evaluate the potential for lower extremity stress fractures even though the vertical ground reaction force magnitudes are roughly 2.5 body weights (BW) while the forces that the tibia experiences are 10-15 BW [1]. In this paper we used a series of models to estimate the tibial stresses in a group of habitual forefoot runners (FF) running with a forefoot running style (ff) and a rearfoot running style (rf) and compared them to a group of habitual rearfoot runners (RF) running with both styles.

METHODS

Fifteen FF and 15 RF strike competitive long distance runners were recruited. Participants were provided the same brand and model of running shoes. Runners self selected a training pace to be used during the study and 21 retro-reflective markers were placed on the right leg, shoe, pelvis, and trunk. Runners completed 10 running trials while running with a ff running style and 10 trials running with a rf running style while position data (200 Hz, Vicon MX, Vicon, Centennial, CO, USA) and force data (2000 Hz, AMTI, Watertown, MA) were recorded.

All analyses were done using custom Matlab programs. Kinematic and kinetic data were low-pass filtered at 20 Hz [2]. A rigid body model was used with inverse dynamics to estimate 3D joint moments at the lower extremity joints. A musculo-skeletal model was used to estimate muscle insertions, origins, moment arms and maximal dynamic muscle forces of 43 lower extremity muscles [4]. Actual muscle forces were estimated using static optimization. Hip moments in all three planes, sagittal knee moment and sagittal/frontal ankle moments were used to constrain the solution. Muscle forces were also bounded by zero and the maximal dynamic force estimated by the musculo-skeletal model. The optimization criterion was minimization of the sum of the muscle stresses squared. Muscle forces and joint reaction forces were used to estimate the 3D moments and forces at a tibial cross-section approximately 75% of the length of the tibia from the proximal end. These loads were calculated at each 1% of stance and used as input to a finite element model. The model used a CT scan (VAKHUM data set; http://www.ulb.ac.be/project/vakhum/) to create a finite element mesh and then the forces and moments from each individual runner were applied to the model. The model was implemented using VA-Batts software [5] and resulted in normal stress estimates within each quadrant of the bone cross-section (AM=anterior-medial, AL=anterior-lateral, PM=posterior medial, PL=posterior lateral). Peak values in each quadrant were identified for statistical analysis.

Multivariate analysis of variance was used to detect differences between FF runners and RF runners and between ff and rf running styles. Alpha level was set to .05.

RESULTS

The FF and RF groups were both composed of 12 males and 3 females. The groups were not significantly different in age (21.3 ± 2.1 yr), body mass (64.70 ± 8.10 kg), height (1.78 ± 0.08 m), or mileage (61.8 ± 21.2 mi/wk) ($p>0.05$). The mean running velocities for the FF and RF groups were 4.39±0.24 and 4.26±0.27 m/s, respectively (p=.082). The stance time was not significantly different between groups (p=.125).

Multivariate tests indicated no differences between the FF and RF runners (p=.121) but a significant difference between the ff and rf running styles (p<.001). The interaction was not significant (p=.293). Univariate tests indicated greater ff running compressive stresses during the ff condition in the AM, PM and PL quadrants (Table 1).

Table 1. Means (sd) for group (RF and FF) and running style (rf and ff) compressive stresses (MPa) in each quadrant of a cross section 75% from the proximal end of the tibia.

Stress	RF		FF	
Quadrant	rf	ff	rf	ff
AM	-128 (34.1)	-136 (35.7)	-135 (34.6)	-141 (39.6)
AL	-109 (28.9)	-134 (31.6)	-108 (25.4)	-130 (44.9)
PM	-128 (41.5)	-121 (33.1)	-139 (43.2)	-132 (32.9)
PL	-30 (7.9)	-31 (7.7)	-66 (15.9)	-65 (12.3)

DISCUSSION

Although ff running reduces the vertical impact peak relative to rf running, it requires greater plantar flexor activity. Since the gastrocnemius muscle crosses the knee joint, it requires greater cocontraction at the knee to create a similar net moment. Even though the increased muscle forces work to reduce the total moment acting at the cross-section (Figure 1), it is not enough to reduce the stresses because of the increased compressive force caused by the muscles. This resulted in increased stress in 3 of the 4 quadrants.

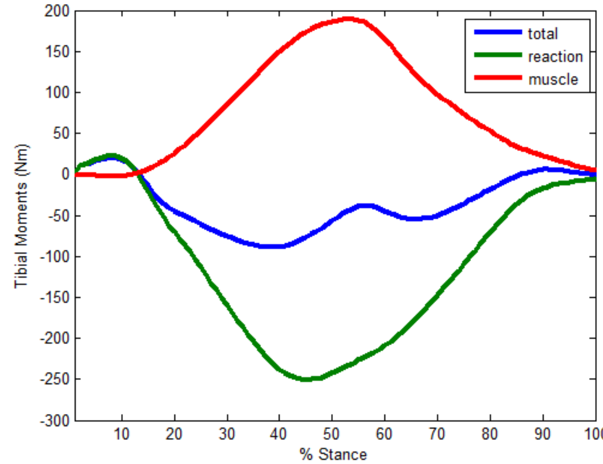

Figure 1. Ensemble average of RFrf **t**ibial moments about a mediolateral axis at 75% from the proximal end. The muscle moment (top curve) partially offsets the reaction moment (bottom curve) to reduce the total moment (middle curve).

The method described has the advantage that it accounts for the geometry of the bone and it uses the muscles that cross the selected site but no other muscles. It is also possible to analyze many more trials than a standard finite element model of the entire bone. The disadvantage is that a standardized, unscaled mesh was used in the application of forces and moments. Individual models would allow for differences in bone geometry and density. The model also suffers from a lack of a fibula – it was assumed that the tibia bore the entire load.

REFERENCES

1. Scott, SH and Winter DA. *MSSE* **22(3)**, 357-369, 1990.
2. Bisseling, RW, and Hof, AL. *JOB*, **39**, 2438-2444, 2006.
3. Vaughan CL, et al. *Dynamics of human gait*. Human Kinetics, Champaign, IL.1992.
4. Delp, SL and Loan, PJ. *Comp Biol Med*, **25(1)**, 21-24.
5. Kourtis, LC, et al. *Comp Meth Biomech and Biomed Eng*, **11(5)**, 463-476, 2008.

COMMON HEAD ACCELERATION EXPOSURES IN THE EARLY PEDIATRIC POPULATION

[1]Daniel M. Desautels and Elaine R. Serina, Ph.D.

[1]Talas Engineering, Inc., Hayward, CA, USA
email: ddesautels@talasinc.com, web: http://talasinc.com

INTRODUCTION

The potential for head injuries among children is of great concern, yet there is very little data on head loads experienced by the early pediatric population. In order to understand tolerance limits for head injury, it is useful to determine the levels of exposure during non-injurious events. Infants and toddlers experience sudden head accelerations as they learn to crawl and walk, and when interacting with parents or caregivers. These head accelerations occur in events with and without direct head contact. The purpose of this study was to investigate head acceleration exposures during commonly experienced, non-injurious events in infants and toddlers.

METHODS

Testing was performed using a Child Restraint/Air Bag Interaction (CRABI) 12-month old anthropomorphic test device (ATD) on various surfaces. The CRABI is a biofidelic crash test dummy, the specifications of which were included in the U.S. Code of Federal Regulations in 2000 [1].

A variety of tests representing common, non-injurious head acceleration events in the early pediatric population were performed. Tests involved direct head contact (fall sideways from sitting, fall backward from sitting, fall forward from crawling, and head butt) and no direct head contact (vigorous bounce on knee, fall onto buttocks from standing). The fall tests were performed on an innerspring crib mattress and on an outdoor grass (blend of rye, poa, and kakulia) area. A mother of an approximately one year old child performed the bounce on knee and head butt events as she normally would with her child. Each test was performed three times.

For the falling tests, the ATD was released from its initial position and dropped solely under the influence of gravity. In the tests which began from a seated position, a slight force was applied to the ATD in the direction of the intended fall until the ATD became unbalanced. In the tests which began from a standing position, the ATD was initially supported by hand. In the tests which began from a crawling position, the ATD was supported on its knees with its arms hanging down, hands brushing the ground, and with its face approximately 5 inches above the test surface. Figure 1 shows the initial position of the ATD in various test configurations.

Figure 1: CRABI ATD initial positions on the different test surfaces (head butt not shown).

The ATD was instrumented with three uni-axial accelerometers (Endevco 7264C-2000TZ-2-360-M17) mounted in the head. Data was sampled at 10 kHz and anti-alias filtered at 2 kHz (GMH Engineering DataBrick 3). Post-processing included low-pass filtering at 1.65 kHz to comply with the Society of Automotive Engineers (SAE) class 1000 requirements.

RESULTS AND DISCUSSION

Peak resultant accelerations and head injury criterion (HIC_{15}) values were calculated for each test and averaged for each event (Figure 2). HIC_{15} is often used to assess the likelihood of head injury. In the fall backward from sitting test on grass, a data system failure resulted in the analysis of only one of the three pulses.

The highest results from the direct head contact tests on both the crib mattress and grass were obtained in the fall backward from sitting test, followed by the fall sideways from sitting test, and then the fall forward from crawling test. Overall, average acceleration and HIC_{15} values recorded on grass were greater than those on the crib mattress. However, the results in the fall onto buttocks from standing test were similar on both surfaces. This suggests that the nature of the contact surface may not have a significant effect on head accelerations in events which do not involve a direct head contact.

Average accelerations and HIC_{15} values were not always higher in the direct head contact events when compared to those without a direct head contact. The bounce on knee test resulted in both acceleration and HIC_{15} values which were higher than the head butt test as well as all three direct head contact events on the crib mattress even though the bounce on knee test did not involve a direct head contact.

A limitation of this study is the lack of mobility of the extremity joints distal to the hip and shoulder. Particularly in the fall forward from crawling and fall onto buttocks from standing tests, this resulted in a large variability in the data and possible movement of the ATD that is different from a human.

This study serves to fill an important gap in the published literature. The results from this study are comparable to the acceleration levels reported among older children (aged 8-11) during non-injurious playground activities [2] and extend the knowledge of head acceleration exposures to a younger population.

CONCLUSIONS

Results of testing with a CRABI 12-month ATD indicate that common non-injurious events for infants and toddlers generate average peak resultant head accelerations of 4.9-22.0g, with associated HIC_{15} values of 0.7-17. These results are for a much younger age than previously documented, and are the first step in filling an important void in the published literature.

REFERENCES

1. 49 CFR Part 572, Subpart R.
2. Bussone, WR, et al. *SAE 2009-01-0383*, 2009.

ACKNOWLEDGEMENTS

Thanks to Kirsten White, Taylor Buckman, and Michael Caldarelli for assistance with this study.

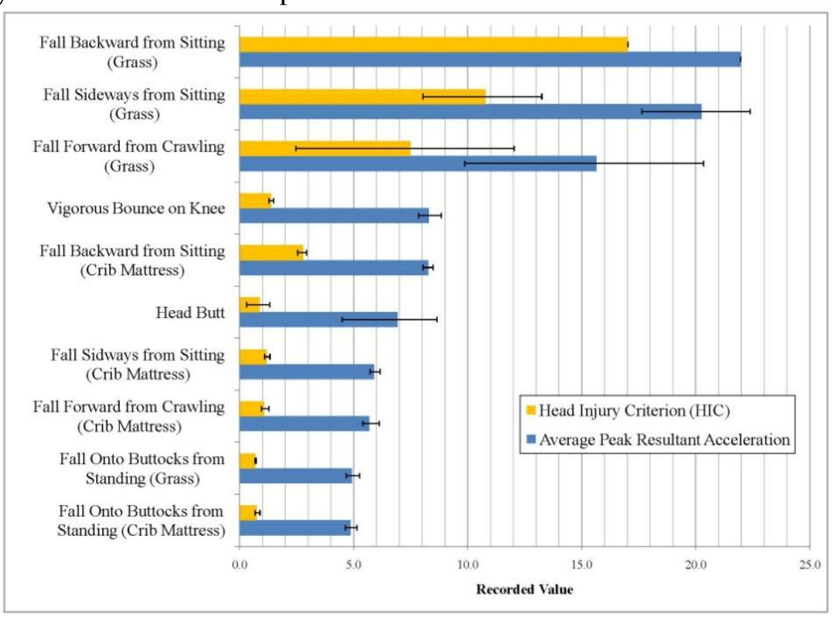

Figure 2: Average peak resultant acceleration and HIC_{15} values from each test event (error bars show ranges).

TIBIOFEMORAL JOINT ARTICULAR SURFACE MOTION GENDER DIFFERENCES IN SUBJECT SPECIFIC AND GENERIC KNEE MODELS

Robert H. Deusinger, Dequan Zou, Melanie Koleini, Kirk Smith, Gretchen Hensley, Timothy E. Machan

Washington University School of Medicine, St. Louis, MO, USA
Email: deusingerb@wustl.edu Web: http://pt.wustl.edu

INTRODUCTION

Excessive anterior cruciate ligament (ACL) force and distorted joint surface motion (kinematics) are components of tibiofemoral joint (TFJ) mechanics hypothesized as links to ACL injury and osteoarthritis (OA) [1]. We have investigated differences between ACL injured and healthy knees [2] and between genders [3] of in vivo anterior tibial translation and TFJ surface rolling and gliding using a 2-D computational TFJ model during weight bearing and non-weight bearing activities. The geometry of the tibiofemoral joint is complex, asymmetric within individuals, and may also differ between genders [4]. The current study is a progression from our 2D TFJ model [5] toward development of a skeletal geometry framework based subject specific 3D computational TFJ model to study knee osteoarthritis. Therefore, the current study examines relative motion of the TFJ articular surfaces by quantifying percent rolling and gliding of the femur condyles relative to the tibia condyles using both a subject specific 2D model (SSM) and a generic 2D model (GM). The characteristic rolling and gliding of the femur condyles relative to tibial condyles were compared between the SSM and GM models for both male and female subjects.

METHODS

Eighteen healthy adults, 9 men and 9 women, participated in this study (age 27.5±6.5; height 171±9 cm; body mass 78.7±19.3 kg). Before testing, all subjects signed informed-consent forms approved by the Washington University Human Studies Committee. Kinematic data for sit to stand was collected using a Vicon motion capture system (Vicon Motion Systems, Oxford, UK). Subjects were recorded during sit to stand from a chair without using their arms. A computed tomography (CT) scan of the right knee of each subject was obtained and analyzed according to an IRB approved research protocol.

Subjects' femur geometric dimensions were determined from 6 skeletal landmark (SL) locations identified on CT scans of the lateral femoral condyle (LFC) and medial femoral condyle (MFC) using methodology developed in earlier research [4]. The SLs were used to define 2 planes that bisect the LFC and MFC, respectively (Fig. 1). For the SSM, femoral curvature geometry was represented by two circular arcs connected with an elliptical curve [5] for the LFC and MFC respectively. The SLs of the surfaces of both the lateral and medial femoral condyles were used to derive the geometric measurements that individualized the 2D model for each subject. Percent rolling and gliding were the joint surface kinematics calculated in this study. Analysis was performed in the sagittal plane. A 2D knee model [2] which uses 2-cm radius and 4-cm radius circular arcs connected with an elliptical curve served as the GM for comparison to the SSM which consisted of a LFC and a MFC.

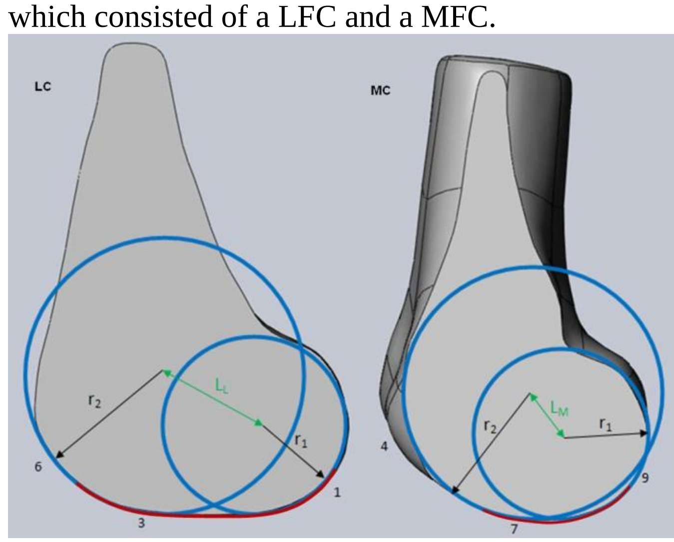

Figure 1. Cross sections of the femur LFC and MFC

Each trial was analyzed for knee joint excursion from sitting through full standing. Three trials were obtained for each subject using the geometric dimensions of the respective GM and the SSM. Although the SSM uses the same two circle concept to determine the joint surface geometry as the GM, the SSM is based on two individual condyles, and their individual SLs (Fig. 1). We hypothesized the SSM would be strongly correlated to the GM.

RESULTS AND DISCUSSION

All trials were processed individually and data were normalized as percent of activity. For both models, percent rolling reached peak values earlier for females than males (Tab. 1 and Fig. 2). Mean percent rolling tended to be higher for males than females for both models (Tab. 2). Peak percent rolling was higher for males in both models, higher in both genders for SSM MFC than LFC, and highest in males and females for the GM, and highest in females for the GM (Tab. 1). Mean percent rolling throughout TFJ excursion was higher in males than females for both models, highest for males and females in the SSM MFC, and lowest in the SSM LFC for both genders (Tab. 2). Although both models produced wide variations among subjects in both genders, strong Pearson r correlation coefficients were evident between the two models for % rolling (Tab. 3).

CONCLUSIONS

The SSM quantified rolling and gliding of both LFC and MFC relative to the tibia. Strong correlation of SSM to GM demonstrates high concurrent validity for the SSM. We believe results of this study merit continued development of a subject specific 3D computational TFJ model based on CT derived ISDs.

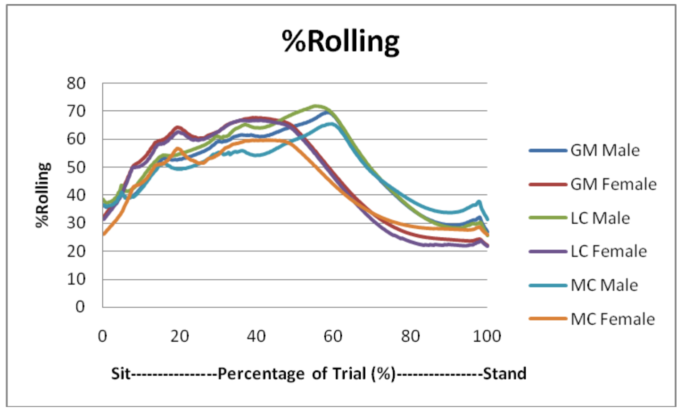

Figure 2. Comparison of percent rolling during sit to stand for the GM and for the SSM LFC and SSM MFC of female and male subjects

REFERENCES

1. Wilson DR, et al. *Rheumatic Disease Clinics of North America*, 34, 605-622, 2008.
2. Hollman JH, Deusinger RH, Van Dillen LR, et al. *Physical Therapy*, 82(10), 960-972, 2002.
3. Hollman JH, Deusinger RH, Van Dillen LR, et al. *Clin Orthop Rel Res*, 413, 208-221, 2003.
4. Zou D, Deusinger RH, Smith KE, Koleini M. *Proceedings of IEEE/ICME CME*, China, 2011.
5. Hollman JH, Deusinger RH, Van Dillen LR, et al. *Jrnl Sport Rehabil*, 12(2), 143-161, 2003.

ACKNOWLEDGEMENTS

This publication was made possible by Grant Number UL1RR024992 from the National Center for Research Resources (NCRR), National Institutes of Health (NIH), and NIH Roadmap for Medical Research. Its contents are solely the responsibility of the authors and do not necessarily represent the official view of NCRR or NIH.

Table 1: %Rolling and timing (% of trial) mean peaks during sit to stand of GM and SSM

Model	Generic Model		Subject Specific Model-LFC		Subject Specific Model-MFC	
	% of Trial	%Roll	% of Trial	%Roll	% of Trial	%Roll
Male	46.68 ± 10.45	83.63 ± 12.18	45.44 ± 10.52	67.01 ± 10.91	52.54 ± 9.81	80.54 ± 11.09
Female	37.02 ± 10.17	77.66 ± 16.67	39.79 ± 9.90	54.10 ± 17.69	40.69 ± 8.59	68.03 ± 17.33

Table 2: Mean %Rolling of sit to stand for male and female subjects from start to end of trial

%Rolling	Generic Model	Subject Specific Model	
		LFC	MFC
Male	48.19 ± 2.82	46.54 ± 3.62	55.18 ± 3.55
Female	43.68 ± 5.78	39.37 ± 7.26	49.28 ± 6.71

Table 3: Pearson r's for %Rolling

r	Generic Model	SSM	
		LFC	MFC
Generic	1		
LFC	0.808	1	
MFC	0.821	0.780	1

MODULATING STRIDE LENGTH & WALKING VELOCITY BY YOUNG & OLD ADULTS

[1]P DeVita, [1]P Rider, [1]A Sidiropoulos, [1]T Copple, [1]Z Domire & [2]T Hortobagyi,
[1]East Carolina University, Greenville, NC, [2]University of Groningen, Groningen, The Netherlands
email: devitap@ecu.edu website: http://www.ecu.edu/cs-hhp/exss/biomechlab.cfm

INTRODUCTION

Young and old adults walk with stereotypical yet distinctly different kinematics and joint power patterns. Old vs. young adults use shorter steps and slower velocities, greater power and work at the proximal hip and less power and work at the distal ankle (1,3,4). Despite these well-established adaptations with age however, we have yet to systematically explore the inter-relationships between power and work produced by lower extremity muscles and basic walking kinematics in old adults. This knowledge is important because reduced step length (SL) and velocity with age have been correlated with increased pathology and mortality risk (5). Although some evidence shows that old adults increase hip but not ankle power to walk faster (e.g. 2), the question how do old adults manipulate SL and walking velocity (i.e. change SL and velocity) is largely unexplored. We propose that understanding how old adults manipulate SL and velocity will provide a biomechanical basis for exercise programs aimed at increasing these basic walking characteristics in this population. We also propose the mechanical plasticity paradigm of distal-to-proximal shift in joint powers with age is a basis for the hypothesis that old adults modulate SL and velocity more so through hip muscle function and less so through ankle muscle function than young adults. The purposes of these studies were to compare the relationships between hip, knee, and ankle joint work and peak powers and SL and velocity between young and old adults.

METHODS

SL, walking velocity and joint powers were derived from 3D lower limb kinematics and ground forces in two separate experiments. SL: 16 young (22 yr, 75 kg) and 22 old (76 yr, 67 kg) adults each walked 20 trials at 1.50 ms^{-1} using various SLs per trial ranging from 0.52 to 1.22 m. Velocity: 22 young (20 yr, 69 kg) and 22 old (74 yr, 69 kg) adults each walked 20 trials using various velocities per trial ranging from 0.62 to 2.71 m s^{-1}. All participants provided written informed consent in accordance with University protocol. Relationships between positive sagittal plane joint work and SL and peak positive sagittal plane joint powers and velocity were derived through curvilinear regressions for the entire samples as population based assessments of SL (760 total trials) and velocity (880 total trials) modulation. The same relationships were identified for each individual participant in each experiment as single-subject based assessments and these were averaged within each age group through Fisher transformations. We assumed that since work from joint powers is the underlying cause of walking, correlations relating joint work and SL and velocity would reveal cause and effect outcomes.

RESULTS AND DISCUSSION

Joint power and work showed mechanical plasticity with age in both experiments. Averaged over all trials in each experiment, old adults had greater hip power and work and lower ankle power and work in both data sets (data not shown, t-test, $p<0.05$). The population analyses showed different modulation schemas for SL and walking velocity (fig 1). SL was modulated mainly through distal ankle joint function (highest explained variance) and minimal proximal hip joint function, especially in old adults. Alternately, velocity was modulated through a slight proximal to distal preference with the hip having stronger work & power relationships with velocity than the ankle. Overall, strengths of all joint relationships were surprisingly low with no population based measure exceeding 60% explained variance. The strongest relationships with SL and velocity however were seen in the summed work and power variables across all joints. ***We observed therefore that humans modulate SL and walking velocity by modulating the total work and power from the lower limb more so than by modulating individual joint mechanical output.***

The single-subject analyses provided greater insight into SL and velocity modulation (figs 1-3). These data had regression equations similar in form to the population equations (i.e. quadratic). More critically however, the single-subject analyses showed much stronger associations for each variable compared to the population data. ***We emphasize that nearly all individual participants in all variables showed stronger associations than the population results.*** Therefore, while the population analyses provided a general overview of SL and velocity modulation in walking, these data failed to describe precisely how humans modulate fundamental walking kinematics.

As in the population based analysis, single-subject analyses showed that total limb work and power better predicted SL and velocity than single joint predictions. The individual analyses also confirmed the proximal to distal gradient for SL and the distal to proximal gradient in velocity but only for old adults. Young adults in contrast had nearly identical contributions from each joint for both SL and velocity modulation. Thus, old adults appear to shift to a more dominant distal joint or proximal joint to modulate SL and velocity, respectively. The single-dominant joint strategy in old may be reflective of their reduced ability to control multiple joints as well as do young adults.

CONCLUSIONS

Population based analyses underestimated the strength of the relationships between SL and joint work and walking velocity and joint power. Single subject analyses showed uniformly strong relationships among each joint and SL and velocity in young adults (r^2~0.80). Old adults however had a weak relationship between hip work and SL but a strong relationship between hip power and walking velocity. Current data failed to support the hypothesis that old adults modulate SL and velocity more so through hip muscle function and less so through ankle muscle function than young adults.

REFERENCES

1. DeVita P, et al. *J App Phys*, **88**, 1804-1811, 2000.
2. Judge J, et al. *J Geront*, **51**, M303-312, 1996.
3. Karamanidis K, et al. *Annals Biomed Eng*, **37**, 467-476, 2009.
4. Silder A, et al. *J Biomech,* **41,** 1520–1527, 2008.
5. Studentski S, et al. *JAMA*, **305**, 20-58, 2011.

Figure 1. Explained variances (Coef. of Determination) between stride length & joint work and walking velocity & peak powers.

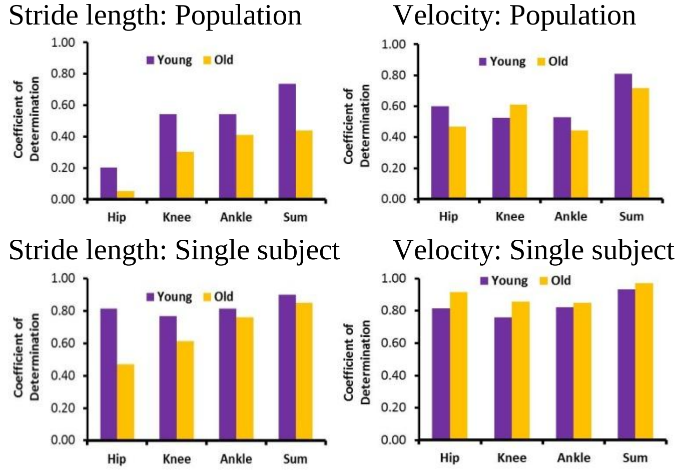

Figure 2: Stride Length vs joint work. Black: population; Red: representative individual

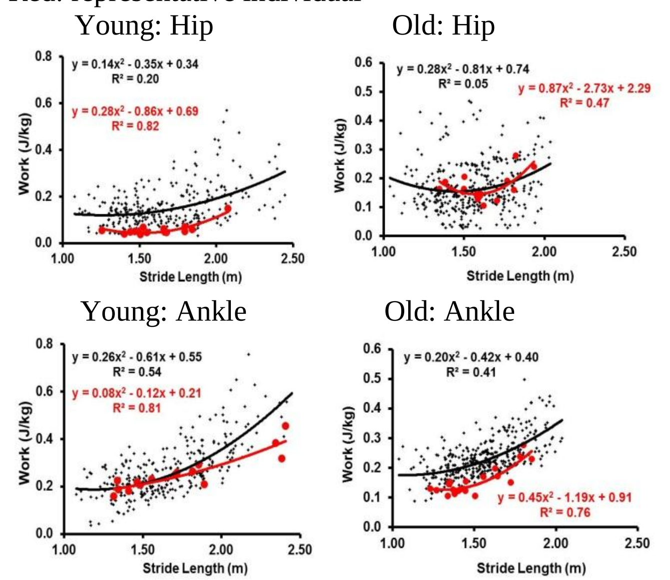

Figure 3: Walking velocity vs peak joint powers. Black: population; Red: representative individual

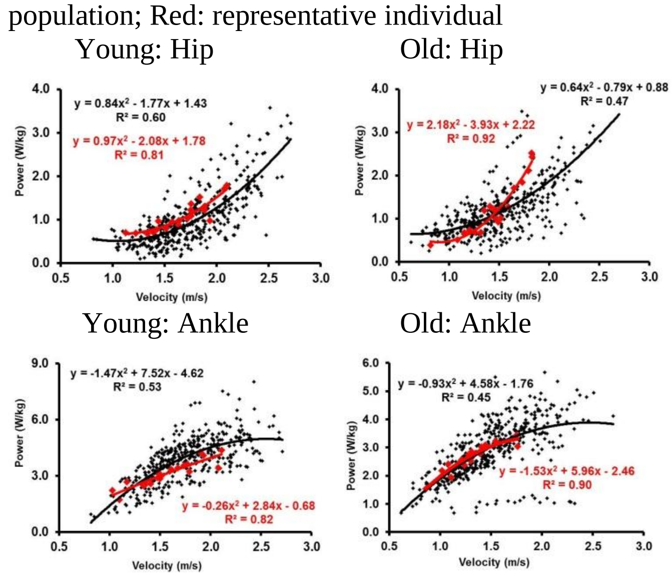

GROUND REACTION FORCES DURING TREADMILL EXERCISE ON THE INTERNATIONAL SPACE STATION

[1]John K. De Witt, [1]Renita S. Fincke, [1]Mark E. Guilliams, and [2]Lori L. Ploutz-Snyder
[1]Wyle Science, Technology and Engineering Group , Houston, TX, USA; [2]Universities Space Research Association, Houston, TX, USA. email: john.k.dewitt@nasa.gov

INTRODUCTION

Astronauts perform treadmill exercise during long duration spaceflight to maintain their physical health. There are limited data available that quantify the ground reaction forces (GRF) developed during exercise in microgravity [1,2,3]. The treadmill currently used on the International Space Station (ISS) is equipped with load sensors that measure GRF during normal exercise. The purpose of this investigation was to quantify the GRF during typical exercise on the ISS. The study is ongoing and the data presented are from a subset of subjects who have completed the evaluation.

METHODS

Six astronauts completed preflight ground testing and inflight testing throughout their ISS mission. The single preflight testing session occurred in the Exercise Physiology and Countermeasures Laboratory at NASA Johnson Space Center (1G). Each astronaut walked or ran at speeds ranging from 1.5 to 9.5 mph in 0.5 mph increments on a Kistler Gaitway Instrumented Treadmill (Kistler Instrument Corp., Amherst, NY). Vertical GRF were recorded at 1000 Hz for 30 s at each speed. Ground data were used as baseline for comparison with inflight data.

Once aboard ISS, each subject completed data collection sessions in microgravity (0G) as part of their normal exercise session for the day. The actual protocol performed varied from subject-to-subject and between sessions because it could not be standardized due to logistical reasons. However, sessions were designed to include multiple 30-s trials at varying speeds. The 3 to 6 data collection sessions were scheduled to span the entire mission of each crewmember and were separated by approximately 25 to 30 days.

Three-dimensional GRF data were collected at 250 Hz. Subjects maintained contact with the treadmill by using a harness attached to elastomer bungees. The ISS treadmill is a Force treadmill (Woodway USA Inc., Waukesha, WI) customized for onboard use. The treadmill is mounted on a dampening system to reduce the transmission of vibration to the ISS.

GRF data were downlinked and post-processed in the laboratory using custom MATLAB scripts (The MathWorks, Natick, MA). Algorithms were developed to identify the onset of heel strike and toe-off for each footfall. Peak force and impulse were computed for each footfall, as well as the respective means over each trial.

RESULTS AND DISCUSSION

Vertical GRF trajectories in 0G were very similar to those typically obtained in 1G (Fig. 1). Footfalls demonstrate clear impact and propulsive force peaks.

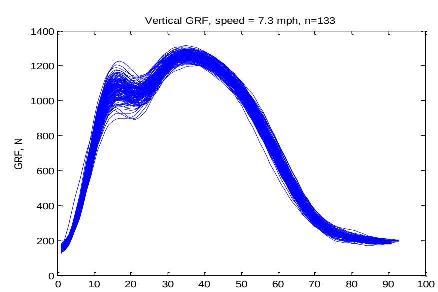

Figure 1: Typical GRF trajectories during running at 7.3 mph in 0G.

Peak GRFs were less at each speed in 0G than in 1G, which was expected given that subjects typically exercised in 0G with external loads (EL) that were less than their 1G body weight (BW). However, when GRFs for each subject were normalized (by BW for 1G and EL for each 0G session), subjects tended to generate similar peak forces between gravitational conditions at all running speeds (Fig 2).

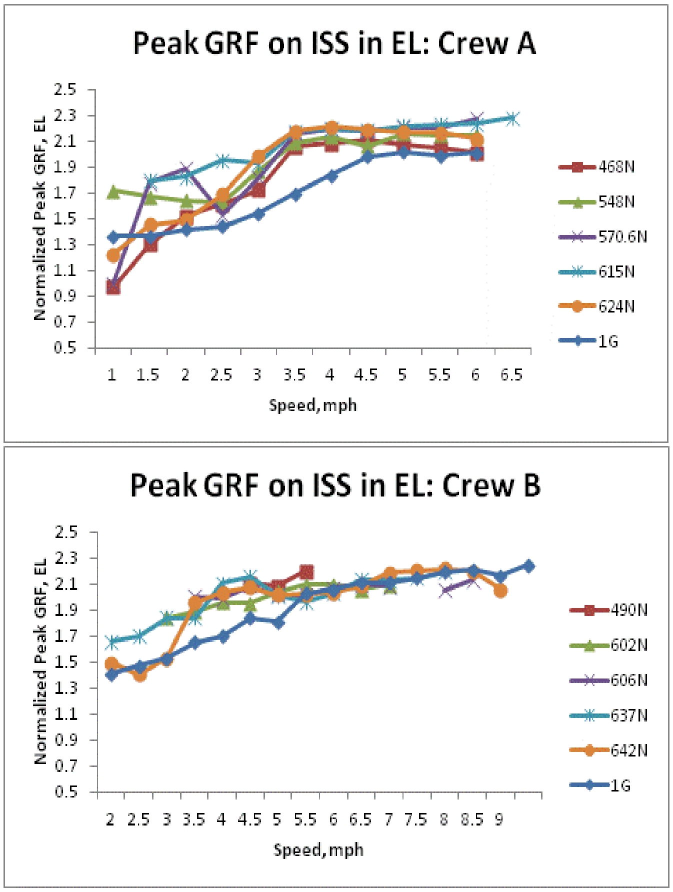

Figure 2: Mean peak GRF for two subjects in 1G and 0G normalized by EL across exercise speeds. Note that in 1G, bodyweight (BW) is the EL. Each plot represents a 0G session at the given EL in addition to the 1G plot.

The 'dose' of force has been hypothesized to be an important factor for bone health [4]. Impulses, which are analogous to the 'force dose' were similar across EL and did not decrease with increasing speed (Fig 3). However, in 1G impulse decreased as speed increased. This suggests that at higher speeds, impulse in 0G may be similar to that occurring in 1G.

CONCLUSIONS

GRF data from treadmill exercise on ISS suggest that subjects generate similar footfall patterns in 0G as in 1G. Peak forces are less in 0G, but data suggest that subjects adjust the propulsive force based on the EL. It is possible that subjects attempt to optimize flight time by reducing propulsive GRF proportionally to EL.

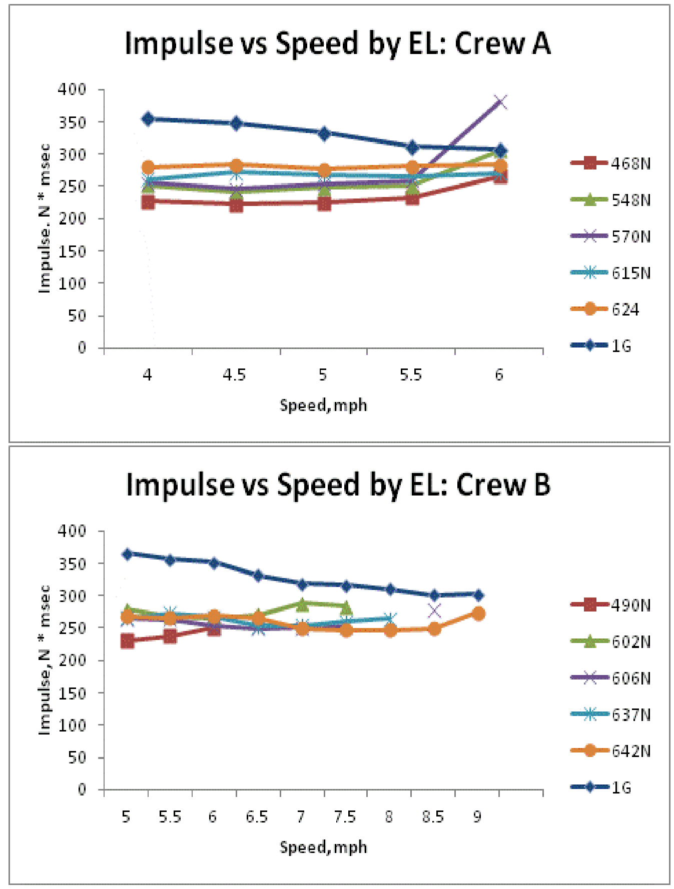

Figure 3. Mean impulse per footfall for two subjects in 1G and 0G.

In addition, while peak GRF are less in 0G than 1G, impulse generated at faster speeds between G-conditions may be similar, suggesting that exercising at higher speeds in 0G may be more similar to 1G than previously thought. The data from this investigation will provide greater insight regarding the quantification of exercise in 0G.

REFERENCES

1. Cavanagh PR, et al. *J Biomech* **43**, 2182-2188, 2010.
2. De Witt JK, et al., *Aviat Space Environ Med* **81**, 1092-1099, 2010.
3. Genc KO, et al. *J Biomech* **43**, 3020-3027, 2010.
4. Genc KO, et al. *Aviat Space Environ Med* **80**, 919-926, 2009.

CERVICAL AND MASTICATORY MUSCLES ACTIVITY DURING A 30 MINUTES LAPTOP TYPING TASK – A PRELIMINARY STUDY

[1]Barbara Diaz, [1]Edward Hernandez, and [1]Inae. C. Gadotti

[1]Florida International University, Miami, FL, USA
email: igadotti@fiu.edu, web: http://cnhs.fiu.edu/programs/pt/index.html

INTRODUCTION

Computer use continues to become more common in both work and home environments. Musculoskeletal disorders (MSDs) are considered to be an important negative effect of computer use. Lower displays, such as that in a laptop design, are associated with changes in head and neck posture and muscle activity of cervical muscles. Estimates of muscle activity have been used to assess musculoskeletal demands.[1] Overload of cervical muscles may also influence the masticatory muscles activity because of the neuroanatomical and biomechanical connections between cervical spine and masticatory regions.[2] No studies were found that investigate cervical and masticatory muscles during a laptop typing task. A better understanding of muscle activation patterns would help establish guidelines and recommendations for laptop usage in order to decrease the incidence of musculoskeletal disorders. The objective of this study was to evaluate the muscle activity of cervical and masticatory muscles during a 30 minutes typing task using a laptop.

METHODS

Fifteen healthy students (11 females and 4 males) participated in this study. Subjects had a mean age of 27±3 years with no history of surgery or trauma in the head and neck region, bone pathology, arthritic or other inflammatory disorders, neurological deficits, and temporomandibular disorders. The average of laptop usage by the participants was 5 hours and 15 minutes per day. The typing task was performed by each subject for 30 minutes using a 15” Laptop with a built-in palm rest. The chair used was adjustable with no armrest. The task included several standardized texts to type using the Rapid Typing program (version 4.0). Norotrode 20™ Bipolar Silver/Silver Chloride electrodes were used to capture surface electromyographic (EMG) activity from Motion Analysis System (MA 300- XII). EMG data was captured every 5 minutes for a period of 10 seconds throughout the entire 30 minutes of the typing task (total of 7 data captures) from upper trapezius, sternocleidomastoid, cervical erector spinae, masseter, and digastrics muscles from subjects’ dominant side. EMG data was processed and displayed using Visual3D (C-Motion Inc.; Germantown, MD) and normalized using the mean of each data set captured. A one-way ANOVA was used to assess if there were any differences among the data captures for each muscle. Statistical significance was set at $p<0.05$. The statistical analysis was performed using SPSS (version 18). This study was approved by Internal Review Board from the Committee Office of Research Integrity at Florida International University.

RESULTS AND DISCUSSION

No statistical significant change was found for EMG activity for the muscles tested. However, a trend towards increasing EMG activity was found for upper trapezius and sternocleidomastoid muscles ($p>0.6$), and a trend towards increasing EMG activity from the third to 7th data capture was found for cervical erector spinae muscle with a borderline significance of 0.05 for p-value. Masseter and digastric muscles did not show any trend in muscle activity changes.

More subjects need to be included and/or more time should be added for the typing task to determine if significant changes occur in muscle activity of the cervical and masticatory muscles. Based on the trend of activity observed, possible increase of cervical flexion with perhaps forward head posture may have happened during the typing task which explains the tendency of increasing activity of the cervical muscles. However, postural analysis during the typing task should be analyzed to further test this assumption.

REFERENCES

1. Straker, L., & Mekhora, K. An evaluation of visual display unit placement by electromyography, posture, discomfort and preference. *Int J of Ind Ergonomics*, ***26***, 389-398 2000.
2. Kraus S. Temporomandibular Disorders, Head and Orofacial Pain: Cervical Spine Considerations. *Dent Clin North Am* **51** 161-193 2007

ACKNOWLEDGEMENTS

We would like to thank Mario Novo, the laboratory technician for the help with the data collection.

STATIC FOOT STRUCTURE AND KNEE KINEMATICS DURING RUNNING

[1]Christopher A. DiCesare, [1]Jeffrey A. Taylor-Haas, [1]Kathryn C. Hickey,
[1,2]Gregory D. Myer, [3]Eric J. Hegedus, and [1,2]Kevin R. Ford

[1]Cincinnati Children's Hospital, Cincinnati, OH, USA
[2]University of Cincinnati, Cincinnati, OH, USA
[3]High Point University, High Point, NC, USA

INTRODUCTION

Structural properties of the foot affect lower extremity biomechanics during dynamic activities. As the structural components provide the initial shock absorption complex for the lower extremities, anatomical abnormalities in foot structure may disrupt the lower extremity arthrokinematics and the proximal kinetic chain. More specifically, evidence indicates that foot arch height may be associated with chronic injury mechanics in certain populations. Runners with high foot arch tend to acquire more bone and ankle injuries, while runners with low foot arch more commonly incur soft tissue and knee injuries, including patellar tendinitis and patellofemoral pain (PFP) [1]. Low foot arch can be associated with excessive pronation of the foot, which may result in tibial abduction, a contributing factor to knee valgus. Excessive foot pronation in early stance of dynamic tasks likely initiates increased lower extremity frontal plane alignment and may contribute to PFP incidence in young athletes. While increased knee abduction during prolonged running has been identified in subgroups of athletes with PFP [2], clarification of the association between structural foot properties and lower extremity mechanics may assist in delineation of risk factors that underlie knee injury in athletes, particularly runners. The purpose of this study was to examine the association between static arch measurements and knee kinematics during running.

METHODS

Twenty-four collegiate cross-country runners participated in this study. The Arch Height Index Measurement System was used to quantify arch height, foot length, and truncated foot length in each of the study participants. Standing foot arch height at 50% total foot length and truncated foot length, measured from the heel to the head of the first metatarsal, were used to calculate arch height index (AHI) for each participant as described by Williams et al. [3]. Relative arch deformation (RAD), a measure of arch mobility incorporating the height of the dorsum of the foot, was also calculated for each participant from standing and seated arch height measurements [3]. Reflective markers were placed on each participant with a minimum of three tracking markers used per segment. Motion data were collected at 240 Hz using a 10-camera motion capture system (Eagle, Motion Analysis Corp., Santa Rosa, CA). Each participant underwent a treadmill run at a self-selected speed. Kinematic data were calculated using Visual3D (C-Motion, Inc. Germantown, MD), and 25 steps were isolated and averaged using MATLAB (The Mathworks, Inc., Natick, MA) for analysis. Statistical analysis included tests for significant correlations between AHI, RAD, and knee flexion and abduction angle at the events of initial contact and peak abduction during the stance phase of running.

RESULTS AND DISCUSSION

Subjects exhibited a mean AHI of 0.326 (0.027) and RAD of 1.036 (0.352) N^{-1}. Significant correlations were observed between AHI and peak knee abduction ($r = 0.60$; $p = 0.002$) and RAD and peak knee abduction ($r = -0.48$; $p = 0.017$) (Figures 1 and 2). Significant correlations were observed between AHI and peak knee external rotation ($r = 0.7$; $p < 0.001$) but not RAD ($p = 0.13$). No significant associations were noted between either AHI or RAD with respect to knee flexion.

The exact relationship between anatomical structure, altered running kinematics, and running injuries is unclear. Among those previously described in the literature is the relationship between foot structure and injuries common among runners [1]. In the current study, runners with low arch exhibited higher external knee rotation at initial contact, likely as a consequence of greater foot pronation and eversion excursion. Accompanying this interaction is the potential for increased dynamic Q angle and misalignment of the patellofemoral joint, which in theory may lead to abnormal patellofemoral contact pressure, overuse and injury [4]. The results of the present study indicate that runners with low arch height and/or high relative arch deformation exhibit increased knee abduction during the stance phase of running. These findings are inconsistent with previous research [5], which found no significant correlation between AHI and knee valgus at the beginning or end of a prolonged run.

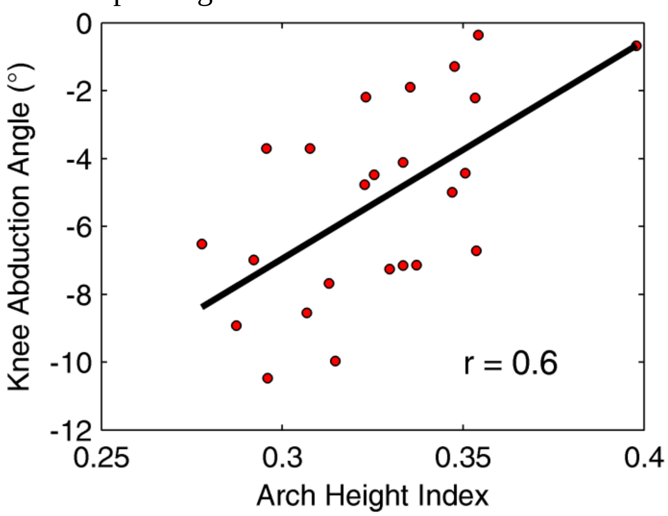

Figure 1. Relationship between AHI and peak abduction angle in collegiate runners.

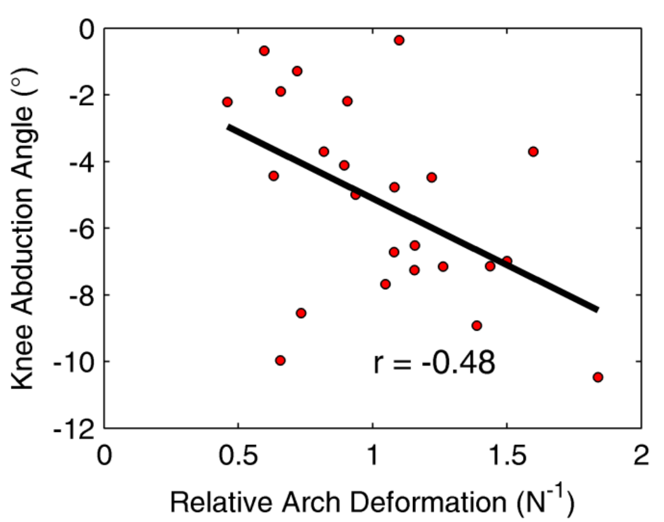

Figure 2. Relationship between RAD and peak knee abduction angle in collegiate runners.

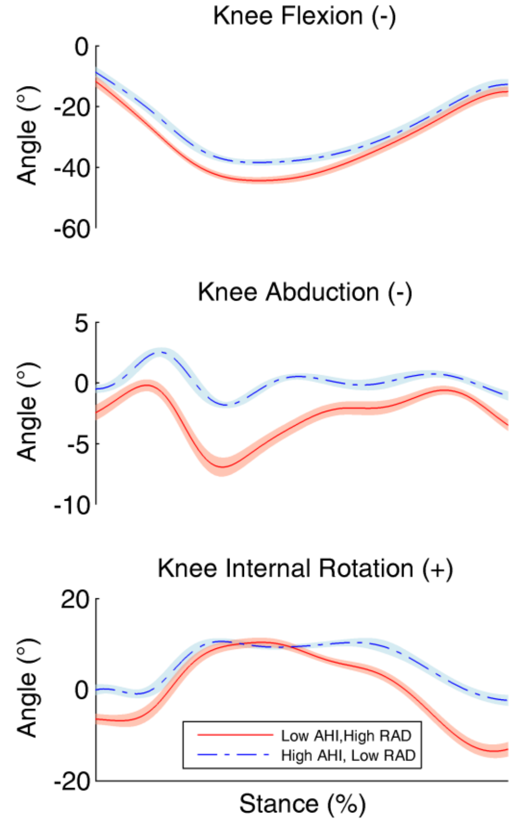

Figure 3. Representative subject with low AHI (0.29) and high RAD (1.5 N^{-1}) displayed solid red line. Representative subject with high AHI (0.34) and low RAD (0.7 N^{-1}) displayed dashed blue line.

CONCLUSIONS

The relationship between foot structure and knee abduction during dynamic activity indicates that foot structure likely contributes to altered arthrokinematics which, in turn, may contribute to certain overuse injuries in specialized athletic populations, particularly runners. This relationship warrants further examination in order to more accurately determine the direct linkage to injury in the proposed population.

REFERENCES

1. Williams DS, et al. *Cl Biom* **16**, 341-347, 2001.
2. Dierks TA, et al. *Med Sci Sp Ex* **43**, 693-700, 2011.
3. Williams DS, et al. *Phys Ther* **80**, 864-871, 2000.
4. Powers CM, *J Orth Sp Phys Ther* **33**, 639-646, 2003.
5. Dierks TA, et al. *J Orth Sp Phys Ther* **38**, 448-456, 2008.

POSTURAL SWAY CHANGES IN ALTERED SENSORY ENVIRONMENTS FOLLOWING INDIVIDUALIZED WHOLE BODY VIBRATION

D. Clark Dickin, Ryan Hubble, Jacqueline Heath, Eduardo Beltran and Mason Haggerty

Biomechanics Laboratory - Ball State University, Muncie, IN, USA
Email: dcdickin@bsu.edu web: http://www.bsu.edu/biomechanics

INTRODUCTION

Research has shown that whole body vibration (WBV) can produce positive effects on postural control. One explanation of the mechanism contributing to increased performance is an alteration or activation of the muscle spindle. In an attempt to elicit an increased level of activation from the stretch reflex, through heightened activation of the muscle spindle, frequencies ranging from 10Hz to 50Hz have been used [1]. If WBV can increase the activity level of the muscle spindle, the spindle could then become primed for easier activation in future muscular contractions [2]. For individuals with impairments in postural stability this increased level of activation may result in a quicker and more vigorous reflexive response to the postural challenge. Alternatively, the exposure to vibration may serve as a training stimulus much like strength training when the exposure is used longitudinally.

Despite these findings, no conclusive evidence exists indicating a frequency range that elicits optimal beneficial effects on postural control. Previous studies assessing WBV and postural control have used one frequency across subjects. However, recent finding suggests that each individual may have a particular frequency to which their muscles respond most vigorously [3]. This individualized frequency may help to alleviate the equivocality of past studies and more clearly define the vibration parameters that effect the greatest change on motor control. If each individual is vibrated at their specific individualized frequency the post-effects of WBV may become clearer and increase the utility of the training method. Also impacting the effectiveness of WBV is the overall duration of the exposure. As such it was the purpose of this investigation to determine the effect of using an individualized vibration protocol on postural sway in altered sensory environments and to determine the effect of vibration duration on measures of postural sway.

METHODS

Twenty healthy young adults were assessed in both altered and unaltered sensory environments across two days. During the first visit the individualized frequency was determined through the frequencies of 20-50 Hz (Pro-Vibe, Pneumex; Sandpoint, ID) while assessing EMG activity of the vastus lateralis muscle. During the second visit, each participant completed three 4-minute WBV exposures at their individualized frequency with balance assessments prior to the first exposure, after each vibration exposure and at 10 and 20 minutes post vibration. In total, the participants performed six assessments of balance and three periods of vibration. Each of the five sensory conditions was presented in a random order for each individual and for each testing session. Postural sway was assessed using the measures of mean sway velocity in the A/P and M/L directions as well as sway path length and sway area from data collected using a NeuroCom SMART Balance Master in five sensory environments: stable support surface and room (Baseline), eyes open with moving floor (EOF), eyes open with moving room (EOR), eyes open with moving room and floor (EOFR), and eyes closed with moving floor (ECF).

Design: To determine the effects of vibration on postural sway separate RM-MANOVA's were used for each of the five sensory conditions for the measures of COG ML & AP velocity, sway length and sway area. Follow-up univariate and pairwise contrasts were performed where appropriate. Significance was set at $p \leq 0.05$ for all tests.

RESULTS AND DISCUSSION

The exposure to an individualized frequency of WBV resulted in changes to postural sway both in unaltered and altered sensory environments in addition to differential changes in sway as a function of multiple exposures. When the individual was required to depend upon vestibular information (ECF and EOFR) there was an overall trend of decreased AP sway velocity and overall sway-path length across trials regardless of when balance was assessed (Figure 1). For these conditions it is possible that the individuals were continuing to adapt to the novel sensory environment across the testing trials despite research suggesting that the conditions are stable after two exposures during a single session [4]. Alternatively the exposure to WBV may have elicited improved sensory awareness and responsiveness on these conditions and resulted in improved control of postural sway [1].

When the environment was not altered (Baseline) or when the individual was required to depend more upon vision for postural control (EOF) the effects of WBV became more varied (Figure 1). Specifically, in the unaltered baseline condition the highest levels of AP sway velocity, sway-area and sway length were recorded during the first or third vibration period and resulted in significant differences between one or more of the vibration condition(s) and both the pre-vibration and 20-min post vibration periods. When somatosensory information was made inaccurate (EOF) similar results to the baseline condition were found. Again the highest levels of AP sway velocity, sway path length and sway area occurred during the vibration trials with the addition of peak levels of ML sway velocity. Taken together the findings from these two sensory conditions suggest an impaired ability to control postural sway immediately following exposure(s) to WBV.

Through using individualized vibration frequencies significant changes in postural sway across multiple sensory environments were elicited. Although the changes resulted in reduced postural control in less complex environments the effects were transient in nature and dissipated within 20 minutes of the vibration. What is unknown is how these effects will translate across multiple testing sessions when individualized frequency WBV is used as a training modality much like resistance training or in combination with a balance training program.

REFERENCES

[1] Dickin DC, et al. *Hum Movement Sci* (in press)

[2] Cardinale M, Bosco C. *Exerc Sport Sci Rev* **31** 3-7, 2003

[3] Di Giminiani R. et al. *J Sports Sci* 2009; 27(2):169-177.

[4] Dickin DC, Clark, S. *Clin.J.Sport.Med*; 17(2): 109-115.

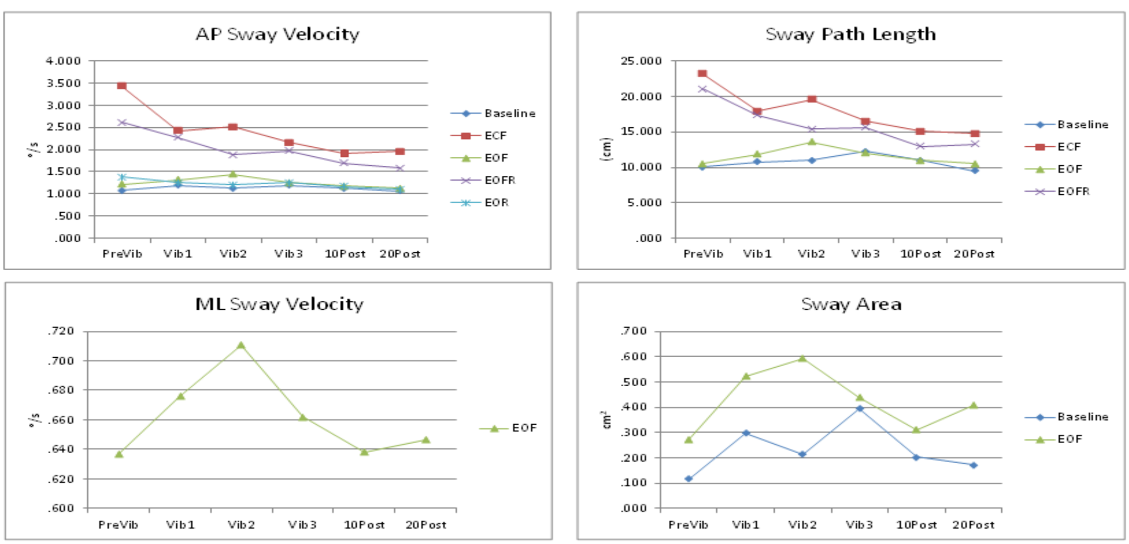

Figure 1: Illustrates sensory conditions with significant differences on each dependent measure

DETERMINING STABILIZATION TIME USING A NEGATIVE EXPONENTIAL MATHEMATICAL MODEL

Angela DiDomenico, Raymond W. McGorry and Jacob J. Banks

Liberty Mutual Research Institute for Safety, Hopkinton, MA, USA
email: angela.didomenico@libertymutual.com
web: http://libertymutualgroup.com/researchinstitute

INTRODUCTION

Volitional transitions to an erect posture require implementation of various motor control programs to achieve the desired posture but still maintain control of inertial components at the end of the movement [1]. The stabilization phase of such transitions is characterized by body oscillations reflected by fluctuations in the movement of the center of pressure (CoP), which regularly changes direction while decreasing to a steady state [2].

Various methods for determining *stabilization time* (i.e. initiation of steady state) have been presented in the literature, usually for very controlled movements. Many methods require comparisons with a baseline threshold or compare current values with an initial position. Generalizability of these methods to transitions in which the initial and final foot positions are not identical is limited. Comparisons of values (e.g. CoP velocity) within a trial do not have these limitations.

Rabuffetti, et al. [2] examined changes in center of mass (CoM) acceleration data to quantify aspects of postural stabilization performance after three transient movements related to activities of daily living. Analysis was limited to the anterior-posterior component of the CoM acceleration since the tasks occurred mainly in the sagittal plane. A negative exponential mathematical model was applied to the CoM acceleration data. Based on the parameters of the function, the time needed to stabilize was calculated. The purpose of the current research was to explore a modification of this methodology by examining the feasibility of applying a negative exponential mathematical model to CoP velocity data to determine stabilization times following multi-planar transitions.

METHODS

Participants
Forty-five healthy men, between 18 and 65 years of age, volunteered to participate in the study. Mean (sd) age, height and body mass of the participants were 40.5 (14.8) years, 1.77 (0.07) m and 83.6 (14.1) kg, respectively.

Experimental Protocol
As part of a larger study, participants were instructed to maintain a static forward kneeling posture for 60 s. An auditory signal prompted participants to transition to an erect posture at a self-selected pace ending with feet approximately shoulder width apart. Upon standing, participants were instructed to look straight ahead at a target and remain as still as possible for the duration of the trial. Total duration of the trial was 20 s. Minimal instruction regarding the transition was provided to elicit more natural movements. A minimum rest period of one minute was provided between each of three replications. Kinematic data were collected at 100 Hz using a 12-camera infrared motion capture system (Motion Analysis Corp., Santa Rosa CA). CoP position data was sampled from two 40 cm x 60 cm force plates (Kistler Instruments AG, Winterthur, Switzerland) at 100 Hz.

Data Processing
Motion and force data were filtered using zero-lag fourth-order low-pass Butterworth filters at 8 Hz and 6 Hz, respectively. The beginning of the stabilization phase (t_0) was identified as when the thoracic (T1) marker reached 99% of the mean vertical height achieved during the last 500 ms of the trial and at least 10% of the participant's body weight was supported by each leg. CoP data were collected for 20 s because this duration was

sufficient to allow individuals to reach a steady erect posture, since the transient component of the CoP signal was contained primarily in the first 5 s.

The task generally resulted in movement within the antero-posterior and medio-lateral planes, so the resultant CoP velocity was calculated by using finite differences applied to the resultant CoP. The CoP velocity time series was smoothed using a window of 0.5 s duration with a sliding step of 0.1 s. Mean CoP velocity was computed within each window to create a new time series.

Data Analysis

A negative exponential mathematical model was fit to the data (Fig. 1) using equation 1. Y_0 represented the CoP velocity at the beginning of the stabilization phase corresponding to t_0. The parameter τ was related to the decay rate of the function and Y_∞ was the asymptotic value. As indicated by Rabuffetti et al. [2], τ is proportional to the time needed to stabilize (i.e. reach a steady state posture) and Y_∞ represents the value of the steady state CoP velocity within the trial. Based on a negative exponential mathematical model, it is generally accepted that three times the value of τ approximates the time required for the initial CoP velocity, Y_0, to decrease to Y_∞. This value represents the stabilization time, T_s.

$$Y = k * e^{-t/\tau} + Y_\infty \qquad (1)$$

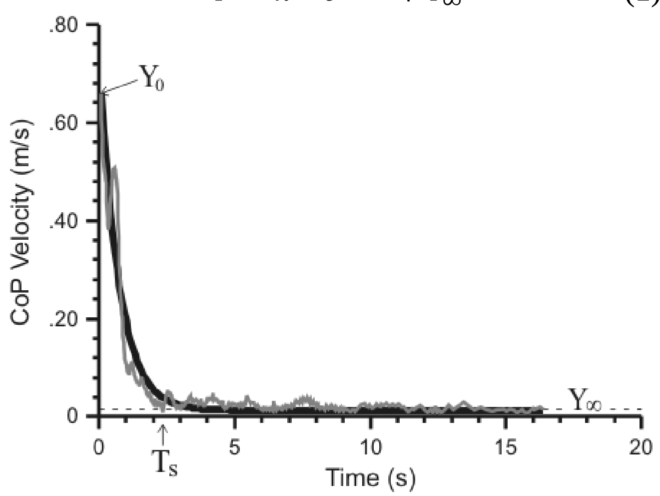

Figure 1: Example of a negative exponential mathematical model (black curve) fit to a CoP velocity time series (gray curve).

RESULTS AND DISCUSSION

CoP velocity data obtained from 135 trials (45 participants, three replications) was fit to a negative exponential mathematical model to determine T_s. This point in time indicated the beginning of the oscillatory nature of a typical steady state erect posture.

Mean (sd) values for R^2 were 0.92 (0.05). The data were well represented by the negative exponential mathematical model as indicated by large values of R^2. The parameter Y_∞ characterized the magnitude of the CoP velocity during the erect steady state portion of the transition. Mean (sd) values of 0.14 (0.05) m/s seemed reasonable as they were not substantially different from values obtained during quiet standing. Applicability of the method to the multi-planar transitions seemed reasonable with T_s mean (sd) values of 2.11 (0.096) s.

Transitional movements towards an erect posture are controlled and generally require further stabilization after the initial conclusion of the transition before a steady-state posture is reached [3]. A preponderance of the research regarding the calculation of stabilization times has emphasized movement only in the sagittal plane. However, volitional movements and other perturbations may cause movements in multiple planes. Many of the methods presented in the current literature would not generalize to such situations. Fitting a negative exponential mathematical model to CoP velocity data is a promising method for determining systematic stabilization times that may be extremely generalizable.

REFERENCES

1. Crenna P. et al. *J Physiology*, **573**, 1059-1072, 2001.
2. Rabuffetti, M., et al. *IEEE Trans. Neural Syst. Rehabil. Eng*. **19**, 420-426, 2011.
3. McKinley P. and Pedotti, A. *Exp. Brain Res.* **90**, 427-440, 1992.

A NOVEL IMPACTION SYSTEM TO MODEL CARTILAGE INJURY IN LIVING RABBIT KNEES

[1]Diestelmeier BW; [1]Tochigi, Y; [1]Rudert, MJ; [1]Fredericks, DC; [1]Arunakul, M; [1]Brown, TD; [1]McKinley, TO

[1]University of Iowa, Iowa City, IA, USA
email: yuki-tochigi@uiowa.edu, web: http://poppy.obrl.uiowa.edu

INTRODUCTION

In post-traumatic osteoarthritis (PTOA), death and dysfunction of chondrocytes associated with acute cartilage injury presumably play an important role in triggering the pathomechanical cascade that eventually leads to whole-joint degeneration. To study details of the disease mechanisms, or to pilot treatment(s) to amend the disease process, a survival animal model in which OA predictably develops after mechanically-introduced acute cartilage injury is crucial. The cartilage injury must be introduced in the primary weight-bearing region. To create such acute cartilage injury in living rabbit knees, a novel impaction system has been developed. In an earlier study, it had been confirmed that this system is capable of creating full-thickness cartilage injury on the medial femoral condyle, where cartilage is thickest (Figure 1). The level of injury severity was regarded as "critical" in the sense that the full-thickness cartilage damage persisted for more than 8 weeks, being accompanied by degenerative changes on the opposing medial tibial surface [3]. In the present study, this impaction system was utilized to create graded cartilage injury in living rabbit knees. It was hypothesized that the magnitude of impaction insult would be controllable by modulating energy delivery.

METHODS

Sixty-nine New Zealand White rabbits were subjected to blunt impaction insult to the left knee, with institutional approval. By approaching through a posterior arthrotomy, the posterior aspect of the medial femoral condyle could be bluntly impacted using the novel impaction system (Figure 2). In this system, the rabbit was positioned prone, in order to impact cartilage in the primary weight-bearing region of the medial femoral condyle at 135 degrees of knee flexion (representative of the habitual physiologic knee position for rabbits in cage confinement). The leg fixation platform (Figure 3) held the distal femur in the V-shaped groove, which was designed to conform to the anterior bone contour of the femoral condyles, with the bone compacted toward the groove via a cannulated bone pusher [3]. This bone pusher was placed with guidance of a 1.25 mm K-wire, providing additional stability in the proximal-distal direction, without locally damaging the cartilage [3].

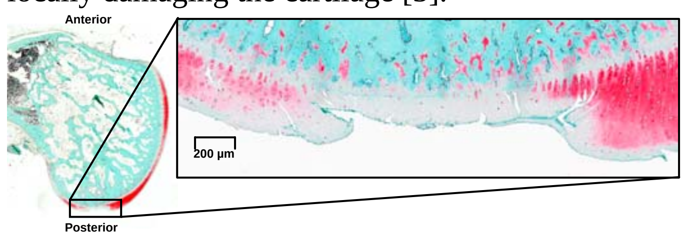

Figure 1: Cartilage histology of a rabbit knee (the medial femoral condyle) at 7 days after a 3.0 J impaction.

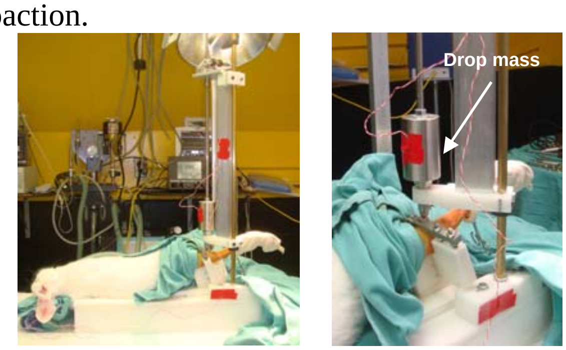

Figure 2: Drop-tower device for rabbit knee cartilage blunt impaction.

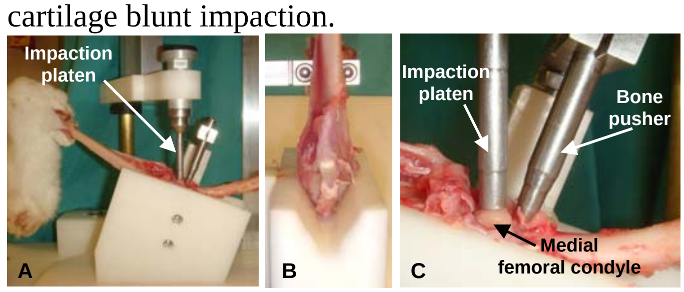

Figure 3: Custom leg-holding platform (A), V-shaped groove (B), and cannulated bone pusher (C) with denuded rabbit cadaver knee for visual clarity.

With the left thigh mounted on the leg fixation platform, a metal platen was placed on the medial femoral surface. This metal platen had a flat, oversized impaction face (diameter 7 mm) so that edge loading effects were alleviated, and that the distribution of impaction force across the contact area was relatively uniform. An impaction force pulse was delivered by a drop mass (1.55 kg). The magnitude of the energy delivery was 2.0 J (drop height 13.2 cm) for 45 animals, 3.0 J (19.7 cm) for 20 animals, and 4.0 J (26.2 cm) for 4 animals. The impaction magnitude was measured using an accelerometer mounted in the drop mass. Using the acceleration signal (sampled at 30 kHz), the history of compressive force during each impaction was determined. The impulse was verified by integrating the force curve. With pressure sensitive film (Fujifilm Co., Tokyo, Japan), the measured contact area between the metal platen and cartilage during impaction was used to estimate the peak contact stress, using rabbit cadaveric knees.

Data were statistically compared between impaction magnitudes using the single factor ANOVA test with a significance level set at $p < 0.05$.

RESULTS AND DISCUSSION

The data indicated that peak contact forces of 819 ± 98, 1037 ± 99, and 1313 ± 46 N, and impulses of 2.9 ± 0.1, 3.4 ± 0.1, and 3.9 ± 0.1 N-sec (Figure 4) were achieved, with energy delivery levels of 2.0, 3.0, and 4.0 J, respectively. The data also indicated a time-to-peak contact force of 2.2 ± 0.5 msec, across all energy delivery levels. None of the 69 animals tested exhibited a fracture complication. The cadaver validation experiment data indicated the peak contact stresses were approximately 70 or 100 MPa for 2.0 or 3.0 J impactions, respectively.

The peak contact force and impulse results demonstrate that the impaction magnitude was well discriminated between the 2.0, 3.0, and 4.0 J deliveries. Therefore, the novel impaction system can effectively control the severity of impaction by adjusting the level of energy delivery. The peak contact force developed was equivalent to or higher than that in previous studies [1,2], which had a peak contact force of approximately 800 N with a much higher energy delivery (23 J), using a pendulum-based system. Also, the time-to-peak force was especially short when compared to the 18 ± 2 msec in the previous studies [1,2]. A possible explanation for these differences is the rigidity of leg fixation achieved by the custom platform. Despite these differences, however, the peak contact stresses for both impaction systems were similar [1,2].

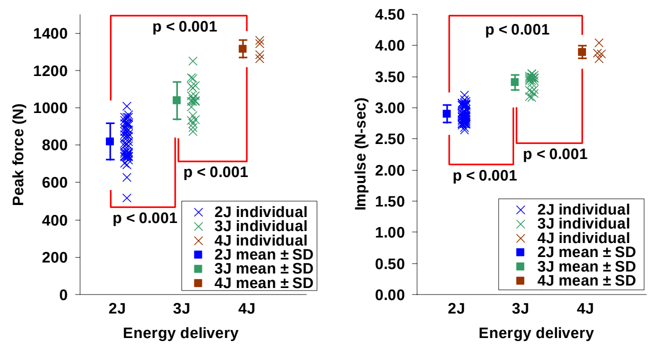

Figure 4: Peak force (left) and impulse (right) in survival animal impactions.

The peak contact stress values reported here are highly supra-physiologic, and so is the loading rate. Presumably, these have permitted creating full-thickness cartilage injury (Figure 1) that shares characteristics of cartilage pathology observed in human clinical intraarticular fractures. To our best knowledge, this impaction system for the first time has enabled such high magnitude of blunt impaction insult to cartilage in the primary weight-bearing region of the rabbit knee *in vivo*.

CONCLUSIONS

These data suggest that this impaction system is effective for modeling graded acute cartilage injury in living rabbit knees, facilitating translational research to improve orthopaedic treatment for PTOA.

REFERENCES

1. Borrelli J, Jr. et al. *JOR*, **27.3**, 347-352, 2009.
2. Borrelli J, Jr. et al. *JOR*, **28.10**, 1307-1314, 2010.
3. Tochigi Y, et al. *OARSI abstract*, #136, 2011.

ACKNOWLEDGEMENTS

NIH CORT Grant P50 AR055533
DOD Grant W81XWH-10-1-0864

QUANTIFICATION IMPACTION SYSTEM FOR A LARGE SURVIVAL MODEL OF INTRAARTICULAR FRACTURE

[1]Diestelmeier BW; [1]Rudert, MJ; [1]Tochigi, Y; [1]Baer, TE; [1]Fredericks, DC; [1]Brown, TD

[1]University of Iowa, Iowa City, IA, USA
email: yuki-tochigi@uiowa.edu, web: http://poppy.obrl.uiowa.edu

INTRODUCTION

Intraarticular fractures (IAFs) are a leading cause of post-traumatic osteoarthritis (PTOA). Despite the latest orthopaedic (typically surgical) treatment techniques, the risk of OA after IAFs has remained unacceptably high. This has led recent research to place an alternative emphasis on preserving viable metabolically-effective cells by means of biological adjunct therapy. In laboratory (*in vitro*) research, several types of agents have proven potentially effective for this new treatment strategy.

In order to facilitate the translation of these scientific developments to clinical practice, a new mechanical insult technique to create a large animal survival model of human IAF has been developed [1]. In this technique, the porcine hock (ankle) is subjected to an impaction insult that replicates the typical mechanism of human distal tibial (pilon) IAFs. To implement this new fracture insult technique in survival animal surgery, a pendulum-based impaction system, equipped with measurement devices to consistently quantify the impaction magnitude, has also been developed.

The objective of the present study was to validate the measurement devices through a series of experimentations. It was hypothesized that energy absorption could be quantified as the difference between the pre-impact and post-impact energies.

METHODS

The pendulum impaction device (Figure 1) was equipped with a rotary potentiometer to measure the pendulum's kinetic energy (pre-impact energy) and a "sled" system to measure the spring energy required to stop the sled's forward progress (post-impact energy).

To test the energy absorption measurement, a validation study was conducted using polyurethane foam surrogates as stand-ins for pig hocks. Twenty-one surrogates were penetrated at modulated impaction magnitudes using an indenter rigidly fixed to the sled. The penetration depth of the surrogates was measured and compared to the energy measurements. Concurrently, optical kinematic measurements and digital video were collected at 4 kHz using a Qualisys Motion Capture System (Qualisys AB, Gothenburg, Sweden) (Figure 2). The 3D position data was then used to determine the distance between the pendulum and indenter. As this distance decreased, the surrogate was absorbing energy and being penetrated.

Similarly, energy measurements, optical kinematic measurements, and digital video were collected for five porcine hock specimens that were impacted with a 35 J impaction magnitude (Figure 2).

This energy absorption measurement technique was also utilized to quantify the magnitude of impaction in a survival animal study, in which IAFs were created in four porcine hocks *in vivo* (in four different animals).

RESULTS AND DISCUSSION

The optical kinematic data for the surrogate and porcine hock impactions exhibited similar specimen deformation patterns, which increased sharply after initial impact then gradually leveled off (Figure 3, Figure 4). From the digital video, it was evident that the surrogate and porcine hock were damaged shortly after the time of initial contact. The energy absorption data exhibited a statistically significant correlation with the penetration depth ($r = 0.990$, $p < 0.001$, Figure 5). The culmination of data collected confirms that energy absorption can be quantified using this impaction system.

Energy absorption measured in the fracture insult *in vivo* ranged from 12 to 32 J (Figure 6). Except for Animal #1 (which needed four impactions for fracture, up to 45 J of energy delivery), the energy absorption magnitude was relatively consistent.

FIGURES

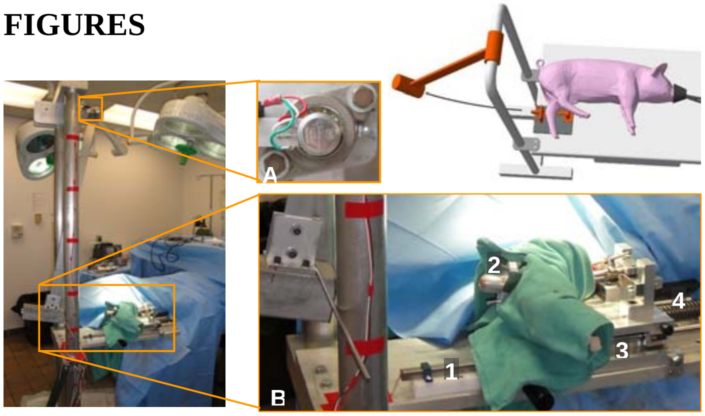

Figure 1: Pendulum impaction device, including a rotary potentiometer that measures the pendulum's linear velocity (A), linear potentiometer that measures the sled's linear displacement (B1), specimen anchorage system (B2), minimum-friction sled on linear bearings (B3), and a coil spring that resists the sled's forward motion (B4).

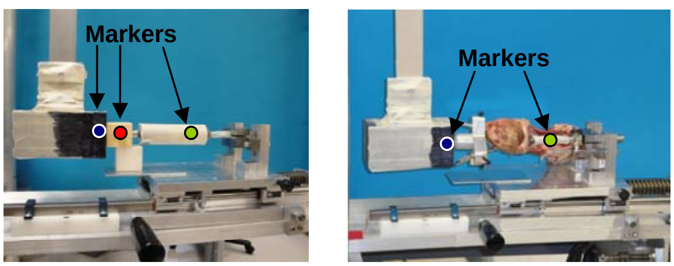

Figure 2: Qualisys Motion Capture System setup for the foam surrogate (left) and porcine hock specimen (right).

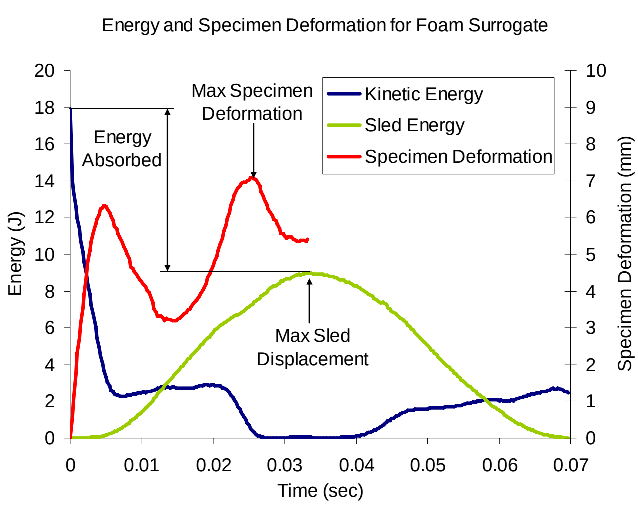

Figure 3: Energy and specimen deformation data for the surrogate impactions.

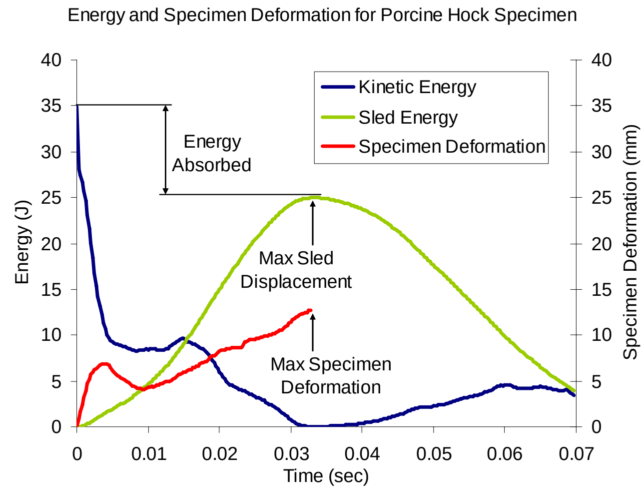

Figure 4: Energy and specimen deformation data for the porcine hock specimen impactions.

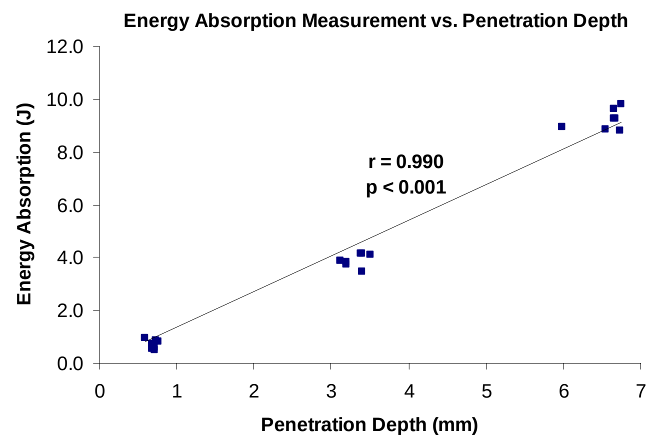

Figure 5: Relationship plotted for energy absorption and penetration depth measurements.

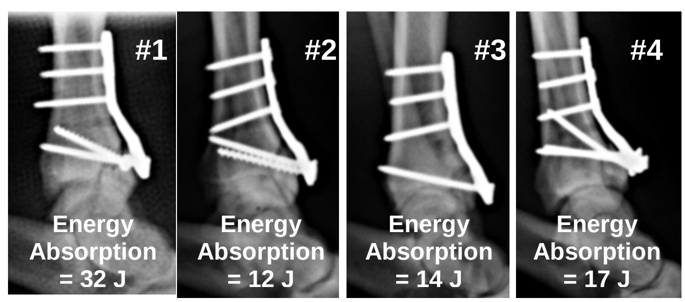

Figure 6: One day post-fracture radiographs and energy absorption measurements for Animals #1 - #4.

REFERENCES

1. Tochigi Y, et al. *ORS abstract*, #355, 2010.

ACKNOWLEDGEMENTS

NIH CORT Grant P50 AR055533
DOD Grant W81XWH-10-1-0864
DOD Grant W81XWH-11-1-0583

SIMPLE PREDICTIVE MODELS REVEAL STEP-TO-STEP CONTROL OF WALKING

[1] Jonathan B. Dingwell, [1] Nicole K. Bohnsack, [2] Joseph P. Cusumano
[1] University of Texas, Austin, TX, USA
[2] Pennsylvania State University, State College, PA, USA
E-Mail: jdingwell@austin.utexas.edu, Web: http://www.edb.utexas.edu/faculty/dingwell/

INTRODUCTION

"The purpose of models is not to fit the data but to sharpen the questions"
– Samuel Karlin, Mathematician

It is widely accepted that when people walk they try, on average, to minimize energy cost. Indeed, models that minimize energy cost do replicate average walking and running behavior [1]. However, neuronal noise [2] presents a significant challenge for walking control and predictions of *average* behavior do not explain the *variability* ubiquitously observed in human movements [3,4].

When subjects walk on a motorized treadmill, they could try (at each step) to stay in the same absolute *position*. Alternatively, they could try (at each step) to walk at the same *speed* as the treadmill [5]. *On average*, these 2 strategies appear identical: if you try to walk at the same *speed*, you will stay in the same average position; if you try to stay in the same *position*, you will walk at the same average speed. However, we demonstrate here that these two control strategies predict very *different* patterns of stride-to-stride *fluctuations*.

METHODS

Walking on a treadmill operating at belt speed v only *requires* that one stay on the treadmill [5]:

$$-L_{TM}/2 < \sum_{n=1}^{N}\left(L_n - v\cdot T_n\right) < +L_{TM}/2\,, \qquad (1)$$

where $L_n - v\cdot T_n$ is the net displacement for stride n and L_{TM} is the length of the treadmill belt. Any sequence $[T_n, L_n]$ that satisfies (1) will accomplish the task [5]. Because of equifinality [3,4], there are an infinite number of strategies people could use to do this. Specific strategies can be formulated as *goal functions* [4] that predict different "Goal Equivalent Manifolds" (GEM; e.g., Fig. 1) for walking. We tested two such strategies: maintaining constant *position* and maintaining constant *speed*.

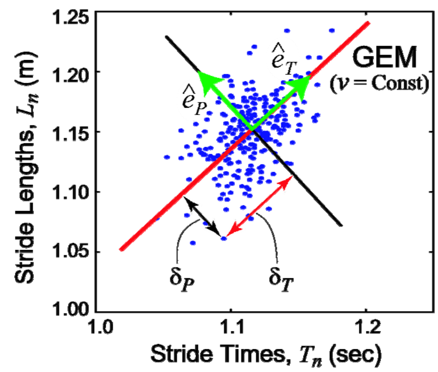

Fig. 1 – *Speed* Control: All combinations $[T_n, L_n]$ that satisfy $L_n/T_n = v$ define a "Goal Equivalent Manifold" (GEM) for the strategy to maintain constant speed. (Adapted from [3]).

Several stochastic control models [6] of the form

$$\mathbf{x}_{n+1} = \mathbf{x}_n + G(I+N)\mathbf{u}(\mathbf{x}_n) + \eta\,, \qquad (2)$$

were constructed, where $\mathbf{x}_n = [T_n, L_n]^T$, $\mathbf{u}(\mathbf{x}_n) = [u_1, u_2]^T$ was a vector of control inputs with gains G, N was multiplicative (motor) noise, and η was additive (sensory / perceptual) noise. Different controllers were found by minimizing the expected value of the cost function

$$C = \alpha e^2 + \beta p^2 + \gamma u_1^2 + \delta u_2^2\,, \qquad (3)$$

where αe^2 penalized the error, e, relative to each specified goal function, and βp^2 penalized the distance, p, of $\mathbf{x}_n$ from some preferred operating point, $\mathbf{x}^*$ [5,6]. The "Speed" controller was defined by $\mathbf{x}_n = [L_n, T_n]^T$ and $e_{Spd} = L_n - vT_n$ [5]. The "Position" controller was defined by $\mathbf{x}_n = [L_n, T_n, D_n]^T$ and $e_{Pos} = D_n + (L_n - vT_n)$. For each controller, we simulated both pure "Minimum Intervention Prinicpal" (MIP) type control [3] (i.e., $\beta = 0$; G = I) and an "over-correcting" controller [5] (i.e., $\beta \neq 0$; G $\neq I$). For each model, the controller's goal was to drive its $e \to 0$ in a probabilistic sense [3,5,6]. For each control model, we simulated 30 walking trials of 1000 strides each.

To test our model predictions, 17 healthy volunteers (age 18-28) walked on a level treadmill (Woodway USA) at their preferred speed [5]. 3D movements of their feet were recorded continuously for 2 trials of 5 min each and used to compute time series of T_n and L_n, as well as stride speeds ($S_n=L_n/T_n$), and absolute displacements (D_n) for each stride, *n*.

Detrended Fluctuation Analyses (DFA) [7] yielded scaling exponents, α, for all time series. Values of $\alpha < \frac{1}{2}$ indicate that stride-to-stride deviations are corrected rapidly [5]. Values of $\alpha > \frac{1}{2}$ indicate that deviations on average go *un*corrected (i.e., "persist") [5]. $\alpha = 1\frac{1}{2}$ indicates Brownian motion.

RESULTS AND DISCUSSION

All simulations for all 4 model formulations successfully achieved the walking task: i.e., they all satisfied Eq. (1). Thus, each model represented a perfectly viable strategy for walking on a treadmill. The task itself did *not* "constrain" subjects in any way to force them to adopt any one specific strategy [5]. Likewise, all 4 models maintained the same *average* position (centered on the treadmill belt) and walked at the same *average* speed as the treadmill.

Conversely, both MIP models ("PM" and "SM") exhibited *strongly* persistent dynamics ($\alpha \gg 1$) for both L_n and T_n that did *not* match humans ("HU"; Fig. 2). Both *position* control models ("PM" and "PO") yielded $\alpha(D_n) \leq \sim\frac{1}{2}$ and $\alpha(S_n) \ll \frac{1}{2}$, while the *speed* control models ("SM" and "SO") yielded $\alpha(S_n) \leq \sim\frac{1}{2}$ and $\alpha(D_n) \leq \sim 1\frac{1}{2}$. These findings were consistent with theoretical predictions [5,7].

Thus, all 4 stochastic models predicted very similar *average* behavior, but completely *different* stride-to-stride fluctuation dynamics. The *only* model that adequately captured the experimental fluctuation dynamics of all analyzed time series was the over-correcting speed controller ("SO") [5]. Thus, the hypothesis that humans control speed while walking on a treadmill was supported. The hypothesis that humans control absolute position was rejected.

Formulating hypotheses on specific movement strategies using goal functions, and then testing those hypotheses with relatively simple stochastic control models, allows one to successfully distinguish different movement regulation strategies that may otherwise be indistinguishable.

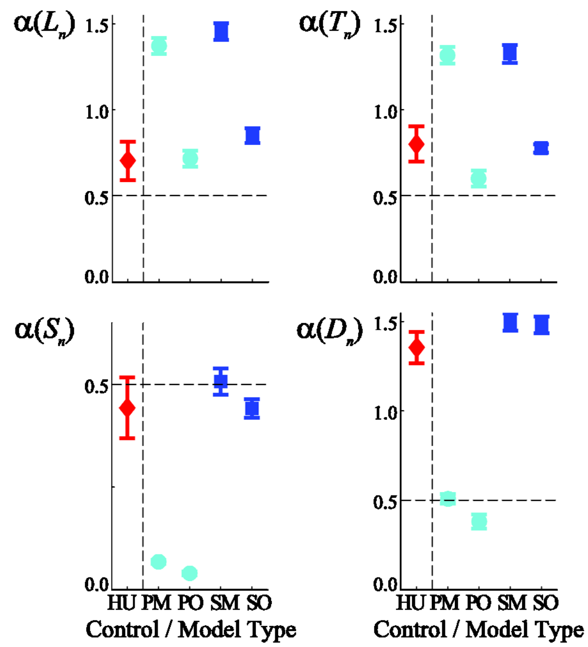

Fig. 2 – DFA (α) Results: Data for stride length (L_n), stride time (T_n), stride speed ($S_n=L_n/T_n$), and treadmill displacements (D_n). Each sub-plot shows data for humans (HU), the Position control models (P_), and the Speed control models (S_). For each model, results reflect pure MIP (_M) control and "over-correcting" (_O) control.

These results have important implications for rehabilitation. For example, allowing some intra-limb kinematic variability during training improves rehab outcomes [8]… But variability of *what* variables?... And *how much* is "optimal"? The approach outlined here can identify exactly which variability is important and which is irrelevant.

REFERENCES

1. Srinivasan M & Ruina A. *Nature*, **439**:72-75, 2006.
2. Faisal AA et al. *Nat. Rev. Neurosci.*, 9:292–303, 2008.
3. Todorov E. *Nature Neurosci.*, **7**: 907-915, 2004.
4. Cusumano JP & Cesari P. *Biol. Cybern.*, **94**: 367-379, 2006.
5. Dingwell JB, John J, & Cusumano JP. *PLoS Comput. Biol.*, 6(7):e1000856, 2010.
6. John J & Cusumano JP. *ASME IDETC Conf. Proc.*, **48027**: 707-716 (Paper no. DETC2007-35380)
7. Peng C.-K. et al. *Nature*, **356**:168-170, 1992.
8. Lewek MD, et al., *Phys. Ther.* **89**:829-39, 2009.

ACKNOWLEDGEMENTS

Funded by Whitaker #RG-02-0354 (to JBD), NIH # EB007638 (to JBD), and NSF #0625764 (to JPC).

NEUROMUSCULAR ASYMMETRIES AND DEFICIENCIES OF ACTIVE ADOLESCENT VOLLEYBALL PLAYERS WITH PATELLOFEMORAL PAIN

[1]Stephanie L Di Stasi, [2]Gregory D. Myer, [3]Jessica Wertz, [1]Kari Stammen, and [1,2,3]Timothy E. Hewett

[1]The Ohio State University, Sports Health and Performance Institute, Columbus, OH, USA
[2]Cincinnati Children's Hospital Medical Center, Cincinnati, OH, USA
[3]The Ohio State University, Division of Sports Medicine, Columbus, OH, USA
email: stephanie.distasi@osumc.edu

INTRODUCTION

Patellofemoral pain (PFP) is a common and potentially debilitating knee pathology experienced by active individuals. Interestingly, females are more than twice as likely to develop PFP compared to their male counterparts [1]. Sex-specific neuromuscular deficits are the hypothesized mechanism related to the differential risk for PFP.

Quadriceps weakness [2] and abnormal frontal plane mechanics [3] are characteristic of female athletes with PFP, and have been implicated in its pathogenesis. More specifically, high external knee abduction moments were identified in young female athletes who went on to develop PFP over the course of a sports season [3]. It is unknown whether these deficits persist in females with PFP and if they coincide with clinically important strength deficits.

Asymmetries in normal joint kinematics and kinetics may have detrimental effects not only on functional performance but also the onset and progression of osteoarthritis in the injured athlete. The presence of neuromuscular asymmetries in adolescent females with PFP; however, has not been well described. The purpose of this study was to compare asymmetries in thigh muscle torque and knee mechanics during a drop vertical jump task between females with and without complaints of PFP.

METHODS

Twenty-three high school female volleyball players (age: 14.9 ± 0.9 years, mass: 63.1 ± 8.1 kg, 168.8 ± 4.5 cm) underwent isokinetic quadriceps and hamstrings testing of both limbs and three-dimensional motion analysis of a drop vertical jump (DVJ). Athletes with PFP (N = 5) were identified by a score less than 100% on the Anterior Knee Pain Scale [4] and did not differ from the group without PFP with regard to age, mass, or height ($P \geq 0.4$). The Institutional Review Board approved all study methods, and all subjects and their parents provided informed consent prior to participation.

Isokinetic testing was performed with the patients seated and secured in a Biodex dynamometer. Peak knee flexor and extensor torque from 10 repetitions of 300 degree/second concentric trials was captured and used to calculate hamstrings-quadriceps (HQ), quadriceps symmetry and hamstrings symmetry ratios. Kinematic and kinetic data during a DVJ [3] were sampled at 240Hz and 1200Hz, respectively, and then low-pass filtered at 12Hz using a bi-directional Butterworth filter. Joint motion and external moments were calculated using rigid body analysis and inverse dynamics with custom Visual 3D (C-motion Inc., Germantown MD) and Matlab (Mathworks Inc. Natick, MA) coding. Biomechanical variables of interest (frontal plane knee excursions and peak external joint moments) were calculated during the landing phase (initial contact to minimum center of mass) of the DVJ.

Independent and paired t-tests were used to identify differences between-group (PFP and no PFP) and within-group limb asymmetries where moderate effect sizes were identified (ES ≥ 0.05). *A priori* statistical significance was set at $P < 0.05$.

RESULTS AND DISCUSSION

Females with PFP demonstrated lower HQ ratios than females without PFP ($P < 0.03$, ES > 1.26) (Figure 1). Only females with PFP presented with significant differences in HQ ratios between limbs

(P = 0.001, ES = 1.15). Quadriceps (P = 0.19, ES = 0.66) and hamstrings strength (ES = 0.23) symmetry were not different between groups.

Frontal plane knee joint excursion did not differ between groups or between the limbs of either group (ES ≤ 0.50) (Figure 2). Similarly, external knee abduction moments did not differ between groups (P > 0.18, ES ≤ 0.70) (Figure 3). However, frontal plane knee moments were significantly different between the limbs of females with PFP (P = 0.02, ES = 2.48).

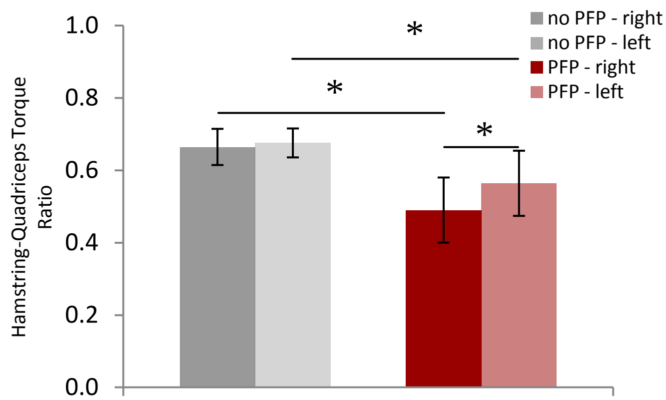

Figure 1: HQ torque ratio (Nm) during isokinetic testing at 300 deg/sec (Means ± 95% confidence intervals). * $P < 0.05$

Neuromuscular asymmetries in strength and frontal plane knee mechanics were identified only in females with PFP. Although the PFP cohort was small, these differences appear clinically meaningful and highlight neuromuscular impairments that may contribute or relate to the onset and persistence of PFP.

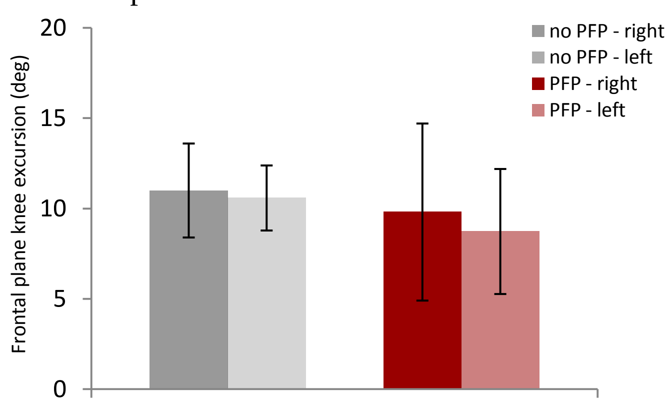

Figure 2: Frontal plane knee excursion during landing phase of drop vertical jump (Means ± 95% confidence intervals).

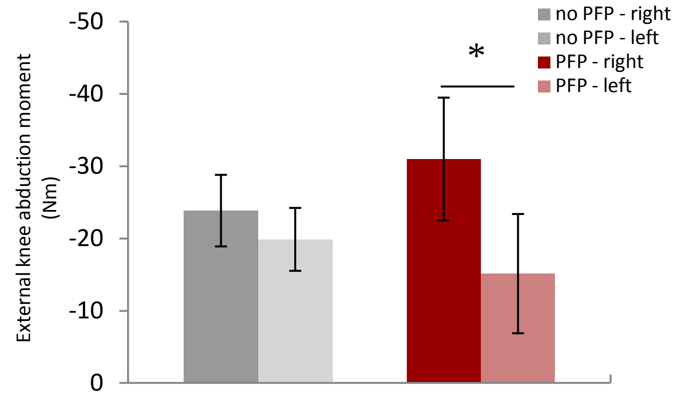

Figure 3: Peak external knee abduction moment during landing phase of drop vertical jump (Means ± 95% confidence intervals). * $P < 0.05$

CONCLUSIONS

Significant neuromuscular deficits and asymmetries were identified in the group of adolescent female athletes with a history of PFP. Persistence of these impairments without rehabilitation may not only have negative consequences on sports performance but may also increase risk for other knee pathology [3].

Future, larger cohort studies of athletic females with PFP will allow for analyses of relationships between strength and movement asymmetries and will provide data to inform effective clinical interventions for these individuals. Hereafter, studies should also evaluate the effectiveness of movement retraining, inclusive of targeted hamstrings and quadriceps strengthening, for resolution of clinically meaningful neuromuscular asymmetries and deficiencies in this population.

REFERENCES

1. Boling M, et al. *Scand J Med Sci Sports* **20**, 725-730, 2010.
2. Callaghan MJ and Oldham JA. *Br J Sports Med* **38**, 295-299, 2004.
3. Myer GD, et al. *Clin Biomech* **25**, 700-707, 2010.
4. Kujala UM, et al 2003. *Athrosc* **9**, 159-163, 1993.

ACKNOWLEDGEMENTS

This study was funded by National Institutes of Health Grants R01 AR055563 and AR056259.

A MARKOV CHAIN MODEL PREDICTS EARLY FAILURE OF ROTATOR CUFF TEAR REPAIRS

[1]Drew Michael S. Donnell, [1]James E. Carpenter, [1]Bruce S. Miller, and [1]Richard E. Hughes
[1]Department of Orthopaedic Surgery, University of Michigan, Ann Arbor, MI, USA
Email: rehughes@umich.edu

INTRODUCTION

Prior investigations have reported high rates of tendon re-tear following surgical repair of rotator cuffs. In a study performed at our institution, we reported a re-tear rate of 41% in large and massive tears within two years of surgery (B.S.M. & J.E.C.) [1]. We previously developed a model based on structural reliability to estimate the probability of re-tear, but it provided a single estimate over time [2]. Such an estimate fails to capture a critical aspect of the clinical picture, i.e. the majority of failures occur within the first six months. The purpose of this study was to develop a mathematical model to explain the nonlinear survival functions derived from long-term analyses of rotator cuff repairs. Additionally, we sought to demonstrate how the model could guide interventions to reduce re-tear rates.

METHODS

Two sources of clinical data were used to evaluate the model. In the dataset developed by our group, we had access to the primary data. Re-tear data were prospectively collected on twenty-two consecutive patients who presented for arthroscopic repair of a large (>3 cm) or massive rotator cuff tear. All subjects had magnetic resonance imaging (MRI) or ultrasound-confirmed full-thickness tears of the rotator cuff prior to surgery. Ultrasound evaluations were performed at seven time points post-operatively: 2 days, 2 weeks, 6 weeks, 3 months, 6 months, 12 months, and 24 months. The second source of data was a published prospective study 107 consecutive surgically treated rotator cuff tear patients [3]. A median follow-up time of 8 years was reported. Kaplan-Meier estimates of the respective survivor functions, *S(t)*, were then constructed from the data using SAS 9.1.3 Service pack 4 (SAS Institute, Cary, NC).

A time-inhomogeneous two-state Markov chain model was used to represent the survival of the surgical repair. A stochastic process was defined as $\{X_t \mid t=0,1,2,3,\ldots\}$, where t indexed the beginning of the day following surgery (t=0 represents the time of surgery). The two states in the model consist of (1) intact repair (X_t=1), and (2) re-tear of repair (X_t=2) at the beginning of post-op day. The transition probability matrix for this stochastic process was defined as

$$P^{(t,t+1)} = \begin{bmatrix} (1-p_t) & p_t \\ 0 & 1 \end{bmatrix}$$

We modeled the day of surgery as having a successfully repaired rotator cuff at the beginning of the day, i.e. the row vector of state probabilities at time t=0 was π=[1 0]. The probability of being in state 1 at time t, which corresponds to having an intact cuff at post-op day t, was

$$\text{Prob}\left[X_t = 1\right] = \pi P^{(0,t)} = \prod_{i=0}^{t-1}\left(1-p_i\right)$$

This is the model's estimate of the survivor function, *S(t)*.

The probability of failure on a single loading event was estimated using structural reliability theory, which models the capacity of a structure to withstand load and the applied load as random variables. Probability theory is used to derive the probability of the load exceeding the capacity, which gives an estimate of p_t. The parameters defining the load distribution were derived from published electromyographic data of the supraspinatus recorded during passive external rotation [4]. These data were combined with a simple model of muscle force production to estimate the mean and standard deviation of the load applied to the surgical repair. The muscle model was the product of the fraction of maximum activation, physiological cross-sectional area (6.65 cm^2), specific tension (22.5 N/cm^2), and the cosine of the pennation angle (5.1 degrees). The resulting mean and standard deviation of load at t=0 were 40.1 N and 78.7 N, respectively. We assumed that the mean load increased linearly for six months until it reached a level corresponding to maximal activation. The parameters for the capacity distribution were obtained from a cadaver and animal studies of repair strength. The initial mean and standard deviation of repair capacity were 320 N and 96.9 N, respectively. Tissue healing was incorporated in the model by assuming the mean capacity increased linearly during the first 6 months of biological healing to a value of 1890 N, which was the mean failure load measured at 6 months post-op in a sheep model of rotator cuff repair.

A quality improvement simulation was then employed to evaluate the effect of manipulating the means and standard deviations and capacity distributions on cuff repair survival at 2 years.

RESULTS

The model predicted a survival function that fell almost entirely within the 95% confidence intervals of the Kaplan-Meier estimates found in both sources of clinical data (Fig. 1). The two-year survival probability was predicted to be 76%, which was higher than the Kaplan-Meier estimates of Miller and Kluger (59% and 67%, respectively).

The quality improvement simulation predicted that decreasing the standard deviation of the load and increasing the standard deviation of the capacity by half increased the 2-year survival probability to 98% and 78%, respectively, all other factors unchanged. Meanwhile, increasing the mean of the load and decreasing the mean of the capacity by half increased the 2-year survival probability to 88% and 80%, respectively, all other factors unchanged.

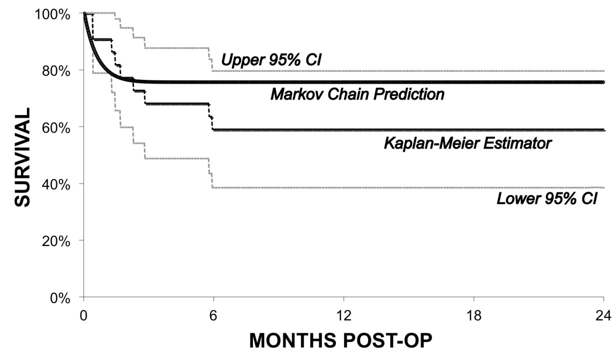

Figure 1: Kaplan-Meier estimate of $S(t)$ observed by Miller et al., 95% confidence interval for $S(t)$, and Markov chain model predictions.

DISCUSSION

The model predicted the nonlinear behavior of the survival function in the early post-operative period and suggested that lowering the variance of supraspinatus muscle loading may be the most effective method for decreasing the rate of re-tears. However, the model over-estimated the two-year survival probability. This may be caused by errors in the assumed load, capacity, and rate of change over the post-operative period. It may be possible to improve the biomechanical model by incorporating a more detailed representation of biological healing.

CONCLUSIONS

Structural reliability-based Markov chain modeling of soft-tissue repairs is a paradigm shift from deterministic modeling. While imperfect and assumption-dependent, the model can predict results of population-based clinical studies and may prove valuable by informing future quality improvement initiatives.

REFERENCES

1. Miller BS, et al. *Am J Sports Med* **39**(10), 2064-2070, 2011.
2. Donnell DM, et al. *Proceedings of the 57th ORS Meeting,* Long Beach, CA, USA, 2011.
3. Kluger R, et al. *Am J Sports Med* **39**(10), 2071-2081, 2011.

A TOOL FOR EVALUATING INDIVIDUAL CONTRIBUTION IN TEAMWORK

Patrik Doucet

Université de Sherbrooke, QC, CANADA

INTRODUCTION

In 1992, the Department of Mechanical Engineering at the Université de Sherbrooke launched a pilot experiment: the completion of major design projects in the last two years of its undergraduate program. The goal was to enable students to have an authentic design experience and hence to develop a skill that is important for engineers. The experiment was so successful that since 1996, all undergraduate students have been required to participate in the activity [1]. In 15 years, nearly 200 projects have been completed, from a bicycle adapted to handicapped children, through electric vehicles, to an acrobatic plane.

These types of projects generally require teams of eight or so students. However, when they have to work together, especially over such a long period, students often experience difficulties. The main irritating aspect is that contributions vary from one student to another. The question now arises: How can students' individual contributions be suitably evaluated in teamwork?

METHODS

The results of this work are mainly based on a heuristic approach, which was established in 1998. At the time, the activity was evaluated by means of an individual logbook (35%); a project report (40%); an oral presentation (10%); a weekly follow-up (5%); and a self-evaluation (10%).

This self-evaluation mechanism did not function well. Despite the setting out of specific criteria and teachers' efforts to raise awareness regarding appropriate self-evaluation, it became apparent over the years that this mechanism was becoming something of an object of ridicule among students, as shown by the last average calculated (μ (x) = 9.8/10).

To counter this trend, a decision was made to couple self-evaluation (5%) with evaluation by peers (5%). Despite this addition, however, the average remained high (μ (x) $\approx$ 9/10). In addition, students desired that more weight be given to the project report in their final grades.

After some reflection and discussion, the idea of using a weighting factor (β) was introduced. Rather than calculate individual contribution as a mark (10%), it was transformed into a factor by which to multiply marks for teamwork. The student's final grade thus broke down as follows: logbook (35%) + β x [report (50%) + oral presentation (10%) + weekly follow-up (5%)].

To avoid excessive penalties or rewards, an interval was fixed: $0.90 \leq \beta \leq 1.10$. The principle of coupling self-evaluation with peer evaluation was maintained. Although the average should have been situated around 1.00, it nevertheless remained high (μ (x) $\approx$ 1.05). Moreover, a new problem was observed: the more conscientious students evaluated themselves more strictly.

To address this problem, the idea of having several evaluations of individual contribution was tested. Since students had the opportunity to adjust their contribution from one evaluation to another, they were quick to accept the procedure. This approach also proved an excellent way to stimulate discussion on the participation of different members.

Hence, if three evaluations were required, the formula became $\beta_{Final} = \beta_1 \times \beta_2 \times \beta_3$. Since $0.90 \leq \beta_i \leq 1.10$, then $0.73 \leq \beta_{Final} \leq 1.33$. This interval consequently became a threat to any students who, in a spirit of laziness or strategy, scarcely contributed to the project; the difference in their final grade could be substantial.

However, this process was very time-intensive. Additionally, certain students continued to assign themselves excessively high grades.

RESULTS AND DISCUSSION

Following these observations and analyses, an interesting innovation was introduced: the MLE Matrix,[1] which replaced the self-evaluation mechanism coupled with evaluation by peers. The fundamental principle is based on a well-known mechanism: distributing points between members. For example, for a given criterion, a team with eight members will have eight points to distribute.

The innovation lies in the way the points are distributed [2]. Students do not evaluate themselves directly. Instead, for each criterion, a given student evaluates whether each of his teammates contributed MORE than he did ("M"), LESS than he did ("L") or to a degree EQUIVALENT to his own contribution ("E"). The evaluation he receives for a given criterion is thus a function of his evaluation of his teammates:

- If a student gives an "M" to all other teammates, he acknowledges that their contribution was greater and therefore, logically, he deserves an "L";
- Conversely, if the student gives an "L" to all other teammates, he receives an "M";
- Finally, if the student considers that some student contributions were equivalent to his own, the student automatically obtains an "E".

Based on this notation in terms of "M," "L," and "E," the point distribution is calculated [3]. After completing his evaluation grid, the evaluating student has produced a preliminary weighting factor (β_{prel}) for himself and each of his teammates. The operation must be completed by each member of the team. Once all the evaluations are completed, the weighting factor for a given student is obtained by averaging all the evaluations completed regarding this student, that is, his own and that of his teammates.

If more than one evaluation is done during a course, all these steps must be followed anew. This obviously requires a digital medium. At first, Excel files were used. However, in view of the growing popularity of the tool and the files' lack of user-friendliness, a decision was made to create a database and web interfaces.

Today, students access a web page, sign in, and choose an evaluation to complete and submit. After the period required for accessibility, the teacher can access the tool and extract the results, which are already compiled. Although it is fairly user-friendly, in the medium term there are plans to reprogram the tool with a view to integrating it into the Moodle platform. New features will then be possible, for example varying minimum and maximum values of weighting factors ($\beta_{min} \le \beta_i \le \beta_{max}$); giving more weight to a given criterion; or modifying the evaluation criteria to include, for example, specific criteria that a team may give itself to evaluate the expected contributions.

CONCLUSIONS

For almost 10 years, the MLE Matrix has been used to evaluate the individual contributions of students in most courses involving substantial teamwork projects. It is generally appreciated by students. The improvements being planned for Moodle are also promising.

Moreover, the tool reveals a team's internal dynamics, an element to which teachers often do not have access. The tool is now also used to identify conflicts and problems within teams, enabling subsequent intervention with a view to improving group performance.

REFERENCES

[1] Charron, F. et al. *Proceedings of the ASEE Annual Conference*, Montreal, Canada, 2002.
[2] Doucet, P. *RES Academica*, 22(2), 247-263, 2004.
[3] Gagnon L., Doucet P., *Recueil de considérations pédagogiques*. Unpublished paper, available on request.

[1] The original French designation is *Matrice PME,* with PME standing for "*PLUS que*," "*MOINS que*," "*ÉGAL à*."

INTERVENTION FOR IMPROVING PROJECT TEAMS

Patrik Doucet

Université de Sherbrooke, QC, CANADA

INTRODUCTION

Following a pilot experiment launched in 1992, all students in the mechanical engineering program at the Université de Sherbrooke must, as of 1996, complete a major design project. The projects are carried out in teams of eight students on average. Two mandatory courses (one credit each) are offered to prepare the students to work in teams.

The first one is offered in the second semester of the program. It addresses efficient time management, effective management of meetings [6], and Myers-Briggs personality types. The second one is offered in the final semester and addresses the dynamics of an effective team [5], leadership styles, conflict management, active listening, and feedback [6].

In approaching their design project, the students therefore have basic knowledge on teamwork. Even so, different difficulties have been noted over time, for instance the exclusion of a team member, and the restrictions placed on the actions of certain members. An analysis of the situation was required.

METHODS

To establish a strategy for improving guidance of project teams, a few explanations for such difficulties were needed. They hinged on three important characteristics of the design projects: workload, motivation, and project length [4].

First, the workload in these projects is substantial. Given the number of credits (12), each student should devote 560 hours to the project. In reality, however, few invest less than 700 hours and some devote more than 1,000. It is important to keep in mind that students also have other courses.

Second, motivation in the project varies. For some, it is an opportunity to turn a dream into a reality. For others, it is a mandatory pedagogical activity to be able to graduate. This does not generate the same excitement and thus, not the same amount of work.

Third, the project length is considerable. In a smaller project (spanning one semester, for example), the team is often dissolved before conflicts erupt. Over a two-year period, however, irritating factors accumulate and lead to conflicts.

These three characteristics interact and make teamwork critical:

- Motivation in the project affects the workload that students accept to take on;
- The workload (quantity and nature) varies over time and affects student motivation;
- The project length positively or negatively affects student motivation.

The experiment has shown that conflicts generally erupted in the last third of the project, when stress related to deadlines is at its peak. However, at this stage in the project, it is often too late to remedy the situation. Analysis of the conditions leading to conflicts has allowed the development of a general plan for prevention and intervention within teams.

RESULTS AND DISCUSSION

To improve the situation, three guidance measures were established: 1) a "charter" for teamwork; 2) evaluation by peers and the MLE Matrix [2]; and 3) coaching in interpersonal relationships. These measures do not replace good practices in teamwork, but rather complement them.

First, it is suggested that students develop a teamwork charter [1]. In this charter, they lay down a set of rules of conduct that they deem important. This activity is optional. Many teams do develop a charter and are encouraged to revise it in due course. Subjects typically addressed include:

- Meetings: their planning, duration, management, and follow-up in terms of actions to take;
- Decision-making modes: generally a consensus, sometimes a majority vote;
- Conflict management: approach, style, potential recourse to a mediator;
- Irritating factors to prohibit: lateness, failure to listen, rude comments;
- Signatures, attesting each student' commitment.

Then a tool enabling the evaluation of individual contributions is used: the MLE Matrix. Individual contribution is evaluated three times per semester, for two reasons. The first is to encourage ongoing participation among students, as the mark for each evaluation is multiplied between them and the final product weights the students' final grade [2].

The second reason is that this evaluation enables the teacher to monitor the team's well-being. Students sometimes hesitate to openly admit that their team is not doing well, that there is discord. In a matter of minutes, the MLE Matrix reveals the dynamics at play in a given team. For example, Figure 1 presents the results of a dysfunctional team's coevaluation. The issue is with student three: All his teammates assigned him $0.91 \leq \beta \leq 0.94$, suggesting that they consider his contribution low; he himself has given him a fairly high mark ($\beta = 0.98$), as he obviously does not want to be penalized.

β given / β received	Student 1	Student 2	Student 3	Student 4	Student 5	Student 6
Student 1	1.02	1.03	0.94	0.96	1.04	1.02
Student 2	1.01	1.01	0.91	0.99	1.05	1.01
Student 3	1.00	1.00	0.98	1.00	1.02	1.00
Student 4	1.03	1.00	0.92	0.99	1.05	1.01
Student 5	1.01	1.01	0.93	0.99	1.03	1.02
Student 6	1.03	1.01	0.91	0.98	1.07	1.01
$\boldsymbol{\beta_{final}}$	**1.02**	**1.01**	**0.93**	**0.99**	**1.04**	**1.01**

Figure 1: Example of a dysfunctional team

What is the cause of this dysfunction? It may be a "surfer," meaning a student who is taking advantage of the work of others without really contributing to the team project. It may also be a student who has trouble fitting into the team, or who is contributing adequately but who has been known in the past to be a somewhat poor worker. Regardless, the experiment and the literature indicate that intervention is required in such teams. In fact, the earlier an intervention takes place, the more the situation can be improved. In some cases it is even preferable to disturb a group that seems to be experiencing difficulties but does not dare to talk about it [3].

This is where the latest measure established—coaching in interpersonal relationships—proves useful [7]. This intervention technique aims to offer effective support to groups experiencing difficulties. The intervention takes place directly between the teacher and the team members. This type of coaching is underpinned by a relationship in which the coached subject holds the most important place; the coach only asks questions; and the coach does not need to be an expert, since the less he knows, the less he will be inclined to supply answers.

CONCLUSIONS

Having students work in teams to complete large-scale projects is extremely rich in terms of learning opportunities. However, considering the workload required, variable motivation in the project, and the project length, such teams may run into difficulties. It is possible to attempt to prevent some of these (with the help of teaching or a teamwork charter). However, there will always be tensions susceptible of degenerating into conflict. It is thus important to be able to detect them (MLE Matrix) and, where needed, intervene (coaching).

REFERENCES

[1] Aranda, E. K. et al. *Teams: Structure, Process, Culture, and Politics*, Prentice Hall, 1998.

[2] Doucet, P. *Proceedings of ASB 2012*, 2012.

[3] Doucet, P., *Doctoral thesis*, available on demand, 2008.

[4] Doucet, P. *RES Academica*, 22(2), 247-263, 2004.

[5] Katzenbach, J. R. et al. *The wisdom of teams*, Harper Buisness, 2003.

[6] Scholtes, P. R. et al. *The Team Handbook*, Oriel, 2003.

[7] Whitmore, J. *Coaching for performance*, Brealey, 2002.

Characterization of Coupled Wrist and Forearm Stiffness

[1]Will Drake and [1,2]Steven K. Charles

[1]Department of Mechanical Engineering and [2]Neuroscience Center
Brigham Young University, Provo, UT
email: will.b.drake@gmail.com, skcharles@byu.edu

INTRODUCTION

Wrist stiffness has been shown to have a greater effect on wrist dynamics than inertia and damping for all but the fastest wrist rotations [1]. Therefore, making coordinated wrist rotations requires that humans predict and compensate for the effects of wrist stiffness. Because wrist stiffness is anisotropic (with greater stiffness in radial-ulnar deviation than flexion-extension), some movement directions require more torque than others. We suspect that humans may use their forearm to allow their wrist to rotate along "paths of least resistance." Evaluating this hypothesis requires knowledge of the stiffness encountered during wrist *and* forearm movements. Previous research has only measured the passive stiffness of the wrist *or* forearm separately. While these measurements inform us of the stiffness encountered during wrist or forearm movements, humans rarely move in pure wrist or pure forearm movements—upper limb movements usually involve combinations of wrist and forearm movements. The present study characterizes the passive stiffness of the wrist and forearm throughout their combined three degrees of freedom in flexion/extension (FE), radial/ulnar deviation (RUD), and pronation/supination (PS).

METHODS

Subjects are seated at a rehabilitation robot (Interactive Motion Technologies, Watertown, MA) capable of actuating the forearm and wrist in PS, FE, and RUD. Because wrist range of motion (ROM) varies by as much as 30% due to finger constraint [2], the subject's right hand is constrained in a custom mounting fixture that allows unrestricted motion to the subject's fingers. The robot is calibrated to align the subject's wrist and forearm according to the ISB's definition of neutral joint position [3].

During data collection, the subject's wrist and forearm are simultaneously rotated through 81 combinations of FE, RUD, and PS spanning the range of motion ±15° around the joint's neutral position. To exclude the effects of short-range-stiffness, test movements are extended an additional 3° on each end, for a total movement of 21°. The 3° end-bands are not included in the data analysis.

Preliminary studies of wrist stiffness in one degree of freedom have shown a strong correlation to test-velocities over the range of 0.04 to 0.8 rad/s, with stiffness estimates leveling off below 0.1 rad/s. Therefore, we chose a nominal test velocity of 0.09 rad/s.

The subject is instructed to remain relaxed and not to interfere with the robot's movements. To ensure that muscles are passive, muscle activity is monitored by EMG sensors on the subject's major wrist muscles as well as pronator teres (forearm pronator) and biceps (a secondary supinator). Measurements with unintended muscle activity are excluded from the results.

Whitehead et al. [4] showed an increase in passive muscle stiffness of up to 40.8% ±13.0% following eccentric exercise. Leger and Milner showed a 15% reduction in wrist ROM after exercise but no significant increase in passive stiffness over the range ±3°. Because the range of the current study goes far beyond that used by Leger and Milner [5], subjects are instructed not to perform strenuous exercise 48 hours prior to the test session.

The data from the successful test runs form a three-dimensional torque-displacement vector field and are linearized via multiple linear regression to produce two 3x3 stiffness tensors for each subject (one for outbound movements and one for inbound movements). The anti-symmetric portion of the stiffness tensor is generally negligible and can be discarded [6]. The remaining (symmetric) portion of the stiffness tensor is conservative and can be plotted as a stiffness ellipsoid.

RESULTS AND DISCUSSION

The torque-displacement vector field was well approximated by a linear fit (r-squared values ranged between 0.7134 and 0.9884), resulting in 3x3 stiffness tensors for outbound and inbound movements (Table 1). The stiffness ellipsoid (Figure 1) is anisotropic (not the same in all directions), with the lowest stiffness in FE. The stiffness in RUD is comparable to the stiffness in PS. The stiffness ellipsoid is also tilted in certain directions (its principal axes do not coincide with the anatomical axes), coupling the degrees of freedom. For example, our data agree with previous studies which reported that the FE and RUD are coupled through stiffness [1], meaning that a movement in FE requires a torque in RUD as well as in FE. Our data also show coupling between FE and PS, but little coupling between RUD and PS.

CONCLUSIONS

A thorough characterization of the passive stiffness of the wrist and forearm is essential to understanding how the neuromuscular system accomplishes wrist and forearm movements. The present study expands upon previous work by characterizing the passive stiffness of the wrist and forearm throughout the entire three-dimensional space of PS, FE, and RUD. Our results show that passive stiffness in FE is much less than that in RUD or PS, with the "path of least resistance" following a line from flexion/radial deviation to extension/ulnar deviation. This result coincides with clinical observations of the "dart throwers" motion.

REFERENCES

1. Charles SK, and Hogan N, *J Biomech*, **44**(4), 614–621, 2011.
2. Gehrmann SV, et al., *J Hand Surgery*, **33**(8), 1287–1292, 2008.
3. Wu G, et al., *J Biomech*, **38**, 981–992, 2005.
4. Whitehead NP, et al., *J Phys,* **533**(2), 593–604, 2001.
5. Leger AB, and Milner TE, *Euro J App Phys*, **82**, 472–479, 2000.
6. Hogan N, *Bio Cyber,* **52**, 315–331, 1985.

Figure 1: Stiffness ellipsoid for outbound movements (left plot), with three orthogonal projections (three right plots). Negative extension is flexion, negative radial deviation is ulnar deviation, and negative pronation is supination.

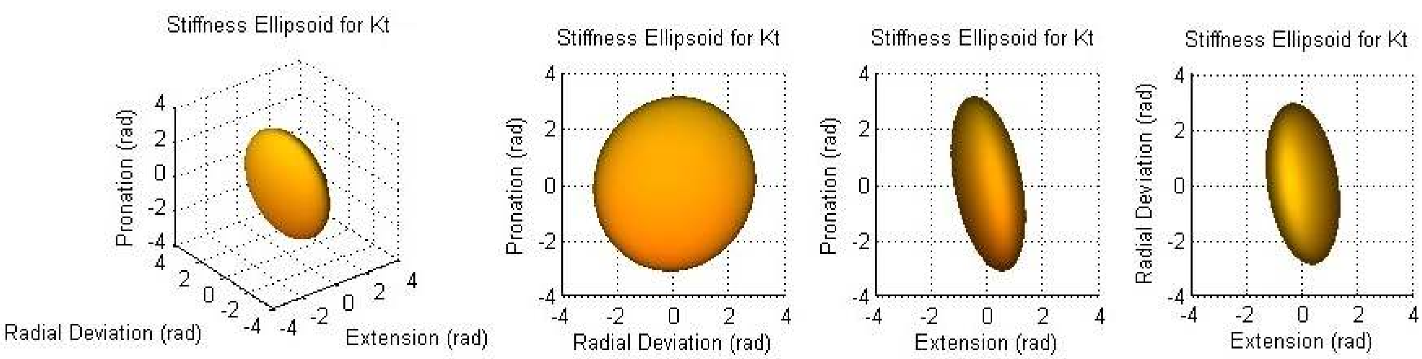

Table 1: Summary of passive wrist stiffness tensor for outbound and inbound movements.

	Stiffness (Nm/rad)					
	FE/FE	**FE/RUD**	**FE/PS**	**RUD/RUD**	**RUD/PS**	**PS/PS**
Outbound	1.3167	-0.2302	-0.3609	2.9457	0.0679	3.1116
Inbound	0.4633	-0.2861	-0.3017	2.1226	0.0933	2.7056

COMPUTER NAVIGATION AS AN INVESTIGATIONAL TOOL FOR ACL RECONSTRUCTION

[1, 2]Elizabeth Drewniak-Watts, [2]Robert Shalvoy, and [1,2]Susan D'Andrea

[1]Center for Restorative and Regenerative Medicine, Providence VA Medical Center, Providence, RI, USA
[2]Department of Orthopaedics, Alpert Medical School of Brown University, Providence, RI, USA
email: Susan.D'Andrea@va.gov

INTRODUCTION

Anterior cruciate ligament (ACL) rupture is one of the most common injuries among young, active individuals. It is estimated that nearly 250,000 ACLs ruptures annually in the US [1]. Individuals hoping to return to an active lifestyle generally opt for surgical treatment, which aims to restore knee joint kinematics. Computer-assisted navigation systems allow the surgeon to collect objective measures regarding graft placement and intra-operative knee kinematics while providing improved accuracy and consistency within the operating room. The information generated from these surgical techniques is a potentially valuable research tool [1]. The goal of this pilot study was to use computer navigation surgical data in combination with gait analysis to evaluate tibial rotation following ACL-reconstruction. It was hypothesized that tibial rotation measured via computer navigation would correlate with kinematic data captured one year post ACL reconstruction, and that ACL reconstruction would restore the range of knee joint rotation to levels similar to the subjects' contra-lateral limb.

METHODS

Ten subjects (5M, 5F; age: 31.1±10.3 years) with unilateral ACL ruptures underwent reconstructive surgery performed with a computer navigation system (OrthoPilot®, Tuttlingen, Germany) by the same primary surgeon. Internal and external tibial rotation measurements were recorded with the knee flexed to 30° prior to and following single-bundle ACL reconstruction.

Subjects who were at least 12 months post-reconstruction were recruited for testing in the Gait and Motion Analysis Laboratory at the Providence VA Medical Center. Retro-reflective skin markers were place on bony landmarks on the subjects' lower body and feet. An 8-camera 3D motion tracking system (Qualisys, Gothenburg, Sweden) was used to track a series of tasks at frequencies ranging from 100-300Hz. Tasks included: (1) walking at a self-selected pace, (2) descending from stairs and pivoting, and (3) landing from a 40cm platform and pivoting [2]. Tasks were completed in a randomized order and subjects perform ten trials per task.

Tibial rotation was calculated from marker data using Visual3D (C-Motion, Inc., Germantown, MD). Custom Matlab (Mathworks, Natick, MA) code was used to time-normalize tibial rotation data and determine peak values for external rotation (ER) and internal rotation (IR). Tibial range of motion (ROM) was calculated with the addition of the maximal internal and external rotation values. Walking task data was separated into stance and swing phases, stair descent and landing tasks were evaluated from initial foot contact to the subsequent step.

Mean (±SD) ER, IR, and ROM values were calculated for both intra-operative and gait data. Linear regression was used to assess correlations between data collected with these two methods. Differences in ACL-reconstructed and contra-lateral control tibial rotations were evaluated for significance using paired t-tests. A significant value of $p<0.05$ was set *a priori*.

RESULTS AND DISCUSSION

The goal of this pilot study was to investigate the use of a computer navigation system in combination with gait analysis to evaluate tibial rotation following ACL reconstruction. As expected, intra-operative ER, IR, and ROM values significantly decreased following ACL-reconstruction (Table 1).

Table 1: Intra-operative pre- and post-ACL reconstruction tibial rotation means±SD.

	Pre	Post	P-value
ER	15.5±3.4°	12.3±3.2°	0.005
IR	24.7±4.2°	17.9±4.2°	<0.001
ROM	40.2±5.8°	30.2±6.0°	<0.001

Tibial ROM of the ACL-reconstructed joint did not significantly differ from the contra-lateral intact limb during walking, stair decent, or landing. ACL-reconstructed knee kinematics, however, were not restored, as demonstrated by significant differences in the peak ER and IR values (Fig 1a and b). These findings contrast with those of Ristanis *et al* [2], who, using similar dynamic tasks, demonstrated that while tibial rotation significantly differed between ACL subjects and healthy control subjects, there were no differences between ACL-reconstructed knees and their contra-lateral controls.

Although the results presented here contradict those of Ristanis and colleagues [2], both studies support the theory that abnormal rotational kinematics are present in individuals with ACL rupture and subsequent reconstruction [3]. Abnormal tibial rotation will lead to altered loading at the knee and the degeneration of articular cartilage predisposing this patient population to osteoarthritis. Moving forward, this work will be strengthened by gait analysis prior to surgery. These additional time points will help strengthen the relationship between surgical outcome and functional performance post reconstruction.

This study was limited by the small sample size, the inability to measure intra-operative tibial rotation values of the contra-lateral intact knee, and a lack of an uninjured control group. Due to these limitations, we were not able to find a correlation between intra-operative data (ER, IR and ROM) and the same data collected during dynamic tasks performed in the gait lab one-year post-operatively.

a.)

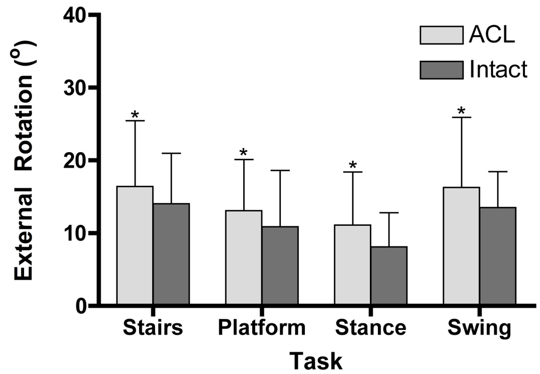

b.)

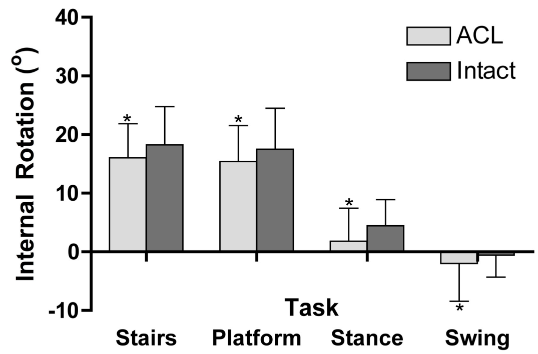

Figure 1: (a.) ER and (b.) IR means±SD for ACL-reconstructed and intact (contra-lateral control) knees. * denotes significant different between ACL and intact (p<0.05).

CONCLUSIONS

Future studies with larger sample sizes and additional time points prior to surgery could further demonstrate the relationship between surgical methods and functional outcomes in patients with ACL reconstruction using computer navigation. This work could be enhanced with imaging techniques, such as biplanar fluoroscopy.

REFERENCES

1. Cheng T, et al. *The Knee,* **19**, 73-7, 2012.
2. Ristanis S, et al. *Arthroscopy* **21**, 1323-9, 2005.
3. Scanlan SF, et al. JBiomech 43, 1817-22, 2010.

Kinematic Analysis of Volleyball Spiking Maneuver

[1]Nicholas Dunbar, B.Sc.; [1]Terese L. Chmielewski, Ph.D.; [1]Susan Tillman, P.T.; [2]Nigel Zheng, Ph.D.; [1]Bryan P. Conrad, Ph.D.

[1]University of Florida, Gainesville, FL, USA
[2]University of North Carolina at Charlotte, Charlotte, NC, USA
email: conradbp@ortho.ufl.edu, web: http://www.ortho.ufl.edu/motion-lab

INTRODUCTION

The purpose of this study is to evaluate the correlation between kinematic parameters and ball speed during a volleyball spiking maneuver. By accentuating the parameters that have the strongest correlation to ball speed, athletes can enhance their athletic performance. It is our hypothesis that higher rotational velocities of the pelvis and trunk and a greater range of shoulder external rotation will be correlated with faster ball speed after contact. A secondary aim of this study is to begin accumulating injury data over the playing careers of the athletes involved. This data can form a baseline to assess which kinematic parameters might be associated with injury.

METHODS

Cohort
Fourteen healthy collegiate Division I female volleyball athletes served as subjects. All participants played the position of either middle blocker or outside hitter. None of the subjects were injured or recovering from injury at the time of testing. The subjects had a mean mass and height of 75±6.2 kg and 1.85±0.03 m.

Data Collection
After obtaining informed consent, each athlete's spiking mechanics were evaluated in an indoor laboratory (Figure 1). A standard volleyball net was arranged in the lab at regulation height (2.24 m). An experienced volleyball coach set the ball for each trial. Subjects started from a self-selected position about 3-4 m from the net, and approached the net at approximately a 45^{o} angle. The set was timed such that it arrived in the hitting position when the athlete was at the peak of their jump. Subjects each took several warm-up trials to become acclimated to the lab environment and to become familiar with the timing and height of the set. For the recorded trials, the participants were instructed to spike the ball with full effort. Five spikes were recorded for each athlete and the trial with the highest ball velocity was used for this analysis.

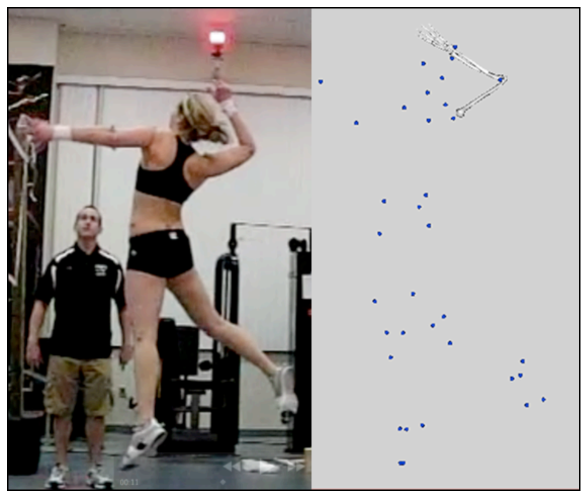

Figure 1. Indoor testing conditions and marker set used to evaluate volleyball kinematics.

Marker Set
A total of fifteen reflective markers (12mm diameter) were used to track landmarks used in the kinematics analysis (Figure 1). Markers were attached bilaterally at the lateral superior tip of the acromions, humeral epicondyles, greater femoral trochanters, lateral femoral epicondyles, lateral malleoli, and lateral to the fifth metatarsal. One marker was attached to the non-hitting wrist between radial and ulnar styloids and on the hitting wrist, two markers were placed, one each on the radial and ulnar styloids. One additional marker was attached to the ball to track the trajectory and velocity after contact.

Data Processing
A 14 camera high speed motion analysis system (Motion Analysis Corp, Santa Rosa, CA) was used to track the marker positions during each trial. Images were collected at a rate of 200 Hz and digitized using EvaRT software. A custom designed software package was used to calculate all kinematic parameters. This software has been previously used to analyze the kinematics of baseball pitchers[1].

Rotational speed was measured as the angular velocity of the pelvis, upper torso, shoulder internal rotation, and elbow extension. Timing was evaluated by defining the time of lead foot contact as 0% and the time of ball contact as 100%. The timing of peak velocity measures was calculated using this definition. A linear regression analysis was used to quantify the relationship between the kinematic parameters and ball speed.

RESULTS

Earlier peak pelvic angular velocity (Figure 2, p=0.039) and greater maximum shoulder external rotation (Figure 3, p=0.045) are both associated with higher ball speed. Other kinematic parameters were not significantly correlated to ball speed (Table 1).

DISCUSSION

From this study, we have observed two kinematic parameters that are significantly correlated with ball speed. The kinematic sequence of the spiking motion begins with pelvic rotation, then torso rotation followed by shoulder and elbow rotation. The initiation of this sequence has a greater impact on ball speed than the rotational velocities generated.

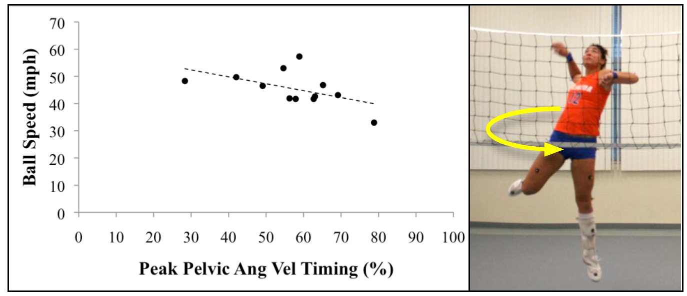

Figure 2: Earlier peak pelvic angular velocity was positively correlated with higher ball speed.

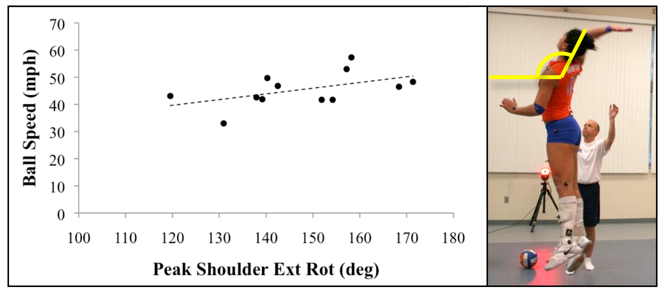

Figure 3: Peak shoulder external rotation was positively correlated with higher ball speed.

REFERENCES

1. Escamilla RF, et al. *Kinematic comparisons of 1996 Olympic baseball pitchers*. J Sports Sci. Sep 2001;**19**(9):665-676.

ACKNOWLEDGEMENTS

The authors would like to thank Miguel de Cardenas, Natalie Sanchez, Bill Vann, and David Velasquez for their collaborative efforts with this study.

Table 1: Averaged kinematic measures and timing recorded during volleyball spiking.

Parameter (Peak)	Average	STDEV	Range	Timing
Ball Speed (mph)	45	6.30	24.3	n/a
Shoulder Ext Rot (deg)	148	15.28	51.80	85.90 ± 3.79
Angular Velocity (deg/s)				
Pelvis	424	206.53	685.65	57.17 ± 13.07
Torso	277	102.72	322.79	86.49 ± 5.24
Shoulder (internal)	3637	1960.25	6945.62	103.81 ± 2.05
Elbow	1862	671.41	2293.80	96.26 ± 1.33

THE INFLUENCE OF UPPER BODY STABILITY ON PEAK KNEE LOADING DURING SIDESTEPPING: IMPLICATIONS FOR ATHLETE SCREENING AND ACL INJURY RISK

[1]David W. Edmonds, [2]David G. Lloyd, and [1]Cyril J. Donnelly

[1]The School of sport Science, Exercise and Health, The University of Western Australia, Perth, Western Australia, AUS; [2]Musculoskeletal Research Program, Griffith Health Institute, Griffith University, Australia.
email: D.Edmonds@westnet.com.au

INTRODUCTION

Anterior cruciate ligament (ACL) injuries are among the most severe knee injuries an athlete can sustain in sport[1], with over half of non-contact injuries occurring during sidestepping situations[2]. Biomechanical analysis of sidestepping shows that both external valgus and internal rotation are elevated relative to straight line running; the same loading patterns shown to elevate ACL strain in cadaveric knee models[3,4]. Clinically relevant measures of upper body stability in the medial/lateral (ML) plane have been shown to be a predictor of ACL injuries in college level athletes[5]. However, the causal mechanisms that link upper body stability to the biomechanical factors associated with ACL injury risk, such as peak joint loading, have yet to be identified. The purpose of this investigation is to determine whether clinically relevant measures of upper body stability are associated with peak knee joint loading and subsequent ACL injury risk during non-contact sidestepping sport tasks.

METHODS

The experimental design consisted of two phases, (1) a clinically relevant upper body stability assessment, and (2) the UWA sidestepping protocol [2, 3]. Participants (Table 1) were exposed to five release perturbations in four directions at 40% of their maximal voluntary contraction (MVC) in the trunk segment's flexion-extension (FE) and medial-lateral (ML) plane of motion. With the arms restrained to the trunk, the angular motion of the head, arms and trunk center of mass (HAT) following a release perturbation was measured by calculating the weighted average motion of the head, upper trunk and lower trunk/pelvis segments (fig. 1).

Table 1: Participant Information

Measurement	n	Mean	Standard Deviation
Height (m)	18	1.83	0.06
Weight (kg)	18	76.7	7.8
BMI (kg/m²)	18	22.8	1.8

Peak knee moments across the weight acceptance phase during unplanned (UnSS) non-contact sidestepping tasks were also recorded. A backward linear stepwise regression was used to determine if HAT CoM angular displacement following a release perturbation was correlated with mean peak knee moments during UnSS.

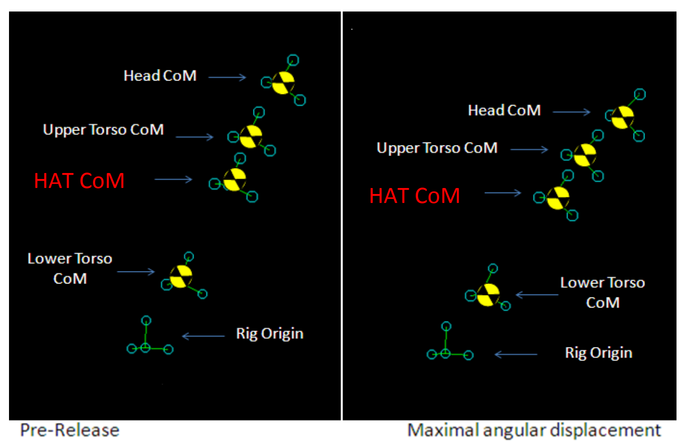

Figure 1: An example of a release perturbation showing the movement of the CoM of each trunk segment.

Table 2: Backward stepwise linear regression between peak mean knee loading ($Nm.m^{-1}.kg^{-1}$) recorded during UnSS and peak angular HAT CoM displacement following a release perturbation.

Perturbation Direction	n	Varus Knee Moment	R^2	β	p
Flexion	16	UnSS			0.164
Extension	16	Total Model	0.635	0.835	0.003*
Lateral	18	p = 0.002*	0.635	-0.993	0.001*
Medial	18	R^2=0.635			0.364
Perturbation Direction	**n**	**Flexion Knee Moment**	**R^2**	**β**	**p**
Flexion	16	UnSS			0.662
Extension	16	Total Model	0.373	0.611	0.016*
Lateral	18	p = 0.016*			0.481
Medial	18	R^2=0.373			0.563

RESULTS AND DISCUSSION

Significant correlations were shown between a combination of good lateral stability and poor extension stability with increased varus knee loading UnSS ($p = 0.002$, $R^2 = 0.635$) (Table 2). A positive correlation was observed between poor extension stability and increased flexion knee moments during UnSS ($p = 0.016$; $R^2 = 0.373$) (Table 2). These results suggest that an athlete with poor stability in the FE plane will display elevated valgus and flexion knee moments during non-contact UnSS tasks.

Adding to previous literature [5], these results show that upper body stability in the FE plane may be an important factor associated with ACL injury risk and a clinically relevant screening tool to identify "high-risk" athletes. It was apparent that the release forces (% MVC) used in this study were different to those used previously [5] (fig. 2), and may have been why the FE plane of motion was identified as a predictor of elevated peak knee loading and ACL injury risk in this investigation. It is then recommended that release perturbations are customised to each individual's MVC in each release direction if they are used in the future to identify "high-risk" athletes.

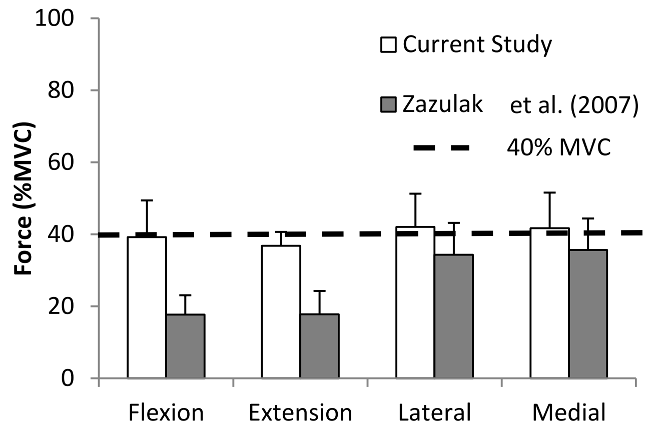

Figure 2: Mean trunk isometric force shown as a percentage of MVC. Values reported for current investigation and for Zazulak et al, (2007). Dotted line used to indicate 40% MVC

CONCLUSIONS

Clinically relevant estimates of an athlete's upper body stability can predict peak knee joint loading during non-contact sidestepping sport tasks. Stability in the FE plane of motion was identified as the best predictor of peak knee moments in both the FE and ML planes. This is an important finding as ACL injury risk is the greatest when flexion moments are combined with frontal plane knee moments. Finally, results suggest that clinically relevant measures of upper body stability may be used as a screening tool to identify athletes at increased risk of ACL injury.

REFERENCES

1. Boden B, et al. *Orthopedics* **23,** 573-578, 2000
2. Cochrane J, et al., *J. Sci. Med. Sport* **10,** 96-104, 2007
3. Besier T, et al., *Med. Sci. Sports Exerc.* **33,** 1176-1181, 2001
4. Markolf K, et al. *J. Orthop.* **13,** 930-935, 1995
5. Zazulak B, et al, *Am. J. Sports Med.* **35,** 1123-1130, 2007
6. Arendt E and Dick R. *Am J Sports Med* **23**, 694-701, 1995.

A LINEAR ACTUATED TORSIONAL DEVICE TO REPLICATE CLINICALLY RELEVANT SPIRAL FRACTURES IN LONG BONE

W. Brent Edwards and Karen L. Troy

University of Illinois at Chicago, Chicago, IL, USA
email: edwardsb@uic.edu, web: http://www.uic.edu/ahs/biomechanics

INTRODUCTION

In an effort to better understand the etiology of low-energy spiral fracture, we would like to carry out biomechanical tests of long bones loaded in torsion to ultimate failure. Although, our laboratory is equipped with a materials testing machine (858 Mini Bionix II, MTS, Inc., Minneapolis, MN), this machine has a single linear actuator, and due to budget constraints we are unable to purchase the company's Torsional Actuator Upgrade Kit. Here we develop, validate, and apply a linear actuated torsional device to replicate clinically relevant spiral fractures in long bones.

METHODS

Development:

The principal operation of the device is to transform vertical displacement of the material testing machine's linear actuator into rotational movement by way of a steel spur gear and rack system [1]. The spur gear is mounted to, and housed within, a cast aluminum frame using a steel tapered-roller bearing and roller assembly (Fig. 1). The cast aluminum frame is bolted to the material testing machine's working base, along with a chrome-moly rectangular bar directed orthogonal to the machine's linear actuator. The testing sample is attached to the system using two aluminum pots; the proximal pot is coupled to the spur gear and thus free to rotate, while the distal pot is attached to the rectangular bar and fixed in rotation. The position of the distal pot is adjustable along the length of the rectangular bar, thereby allowing testing samples of varying size. The rack is attached to the factory load cell placed in series with the linear actuator and guided with a lateral support containing two needle bearings.

Depending on the direction of linear actuation, the spur gear can rotate either clockwise or counterclockwise so that long bones from both left and right limbs can be loaded in internal or external rotation. Measured values of axial force F and linear displacement d from the factory load cell and LVDT, respectively, are used to directly calculate torque T and angular rotation α. The relationship between F (N) and T (Nm) is:

$$T = (F-f)r$$

where r is the moment arm, or pitch radius, of the spur gear (0.0635 m), and f is the friction required for the device's mechanical operation. For both clockwise and counterclockwise rotation we found f to be negligible (~0.1 Nm), thereby simplifying the equation to:

$$T = 0.0635F.$$

The relationship between d (m) and α (°) is:

$$\alpha = 180d/\pi r.$$

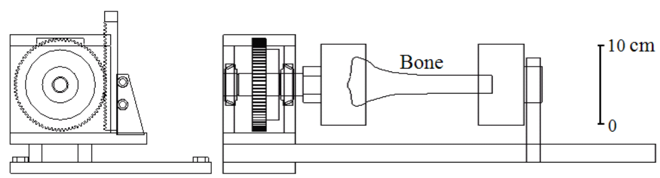

Figure 1. Front (left) and side (right) illustrations of the linear actuated torsional device.

Validation:

Accuracy and precision of the device was assessed using a cast acrylic rod (8528K33; McMaster-Carr, Chicago, IL) of known size (19.05 mm diameter) and material properties (E = 3.1 GPa, ν = 0.375). Acrylic has a linear torque-rotation curve that can be solved analytically using the following equation:

$$\theta = TL/GJ \qquad G = E/2(1+\nu) \qquad J = \pi D^4/32$$

where θ is the angle of rotation, L is the rod length, G is the shear modulus, and J is the polar moment of inertia. The rod was loaded experimentally at a fixed rotation rate of 9.023 °/s up to 30 Nm. The test was performed 5 times each in the clockwise and counterclockwise directions and experimental and analytical torque curves were compared using simple linear regression. The mean Pearson's r coefficient and standard error of the estimate (SEE) were used as measures of experimental accuracy; the coefficient of variation in regression slopes provided information about experimental precision.

Application:
The device was used to replicate a clinically relevant spiral fracture in the proximal tibia, such as that observed in subjects with spinal cord injury [2]. A proximal tibia (15 cm) was obtained from a 64 yr old male formalin-fixed cadaver. The proximal and distal most 2 cm of bone were potted in PMMA, leaving 11 cm of bone exposed. A strain gage rosette (WA-06-030WR-120; Micromeasurements Group Inc, Raleigh, NC) was mounted to the bone's anteriomedial surface. Following ten cycles of conditioning, the bone was loaded at a rotation rate of 9.023 °/s until fracture (Fig. 2). The fracture type and ultimate torque and rotation were noted. Strain gage data were analyzed to ensure mechanical conditions were in line with those expected from pure torsion.

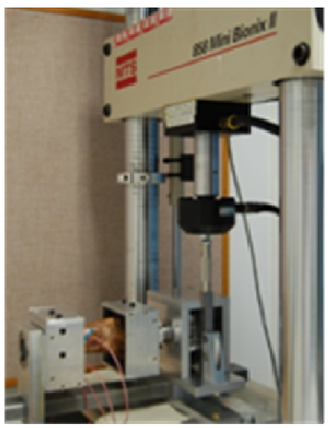

Figure 2. Linear actuated torsional device with potted cadaveric specimen.

RESULTS AND DISCUSSION
Accuracy of the device was excellent for both clockwise and counterclockwise rotation. Analytical and measured torque of the acrylic rod illustrated near perfect correlations, SEEs less than 0.2 Nm across the 30 Nm range, and slopes of unity (Table 1). Precision was also excellent with the CV of the regression slopes being less than 0.3%.

Table 1. Mean (SD) linear regression parameters comparing analytical and measured torque from five clockwise (CW) and counterclockwise (CCW) rotations of a cast acrylic rod.

	r	SEE (Nm)	slope	CV (%)
CW	1.00 (0.00)	0.16 (0.00)	1.02 (0.00)	0.09
CCW	1.00 (0.00)	0.20 (0.01)	1.01 (0.00)	0.27

The cadaveric tibia illustrated a spiral fracture pattern at ultimate torque and rotation values of 158.5 Nm and 8.8°, respectively (Fig. 3). In general, the strain environment mimicked that of a prismatic cylinder loaded in pure torsion. Principal strains were similar in magnitude and oriented near 45° relative to the bone's longitudinal axis. Likewise, the strain environment along the bone's longitudinal and transverse axes was predominately shear with some normal strain, which can be explained by constrained warping of the specimen as well as its complex geometry.

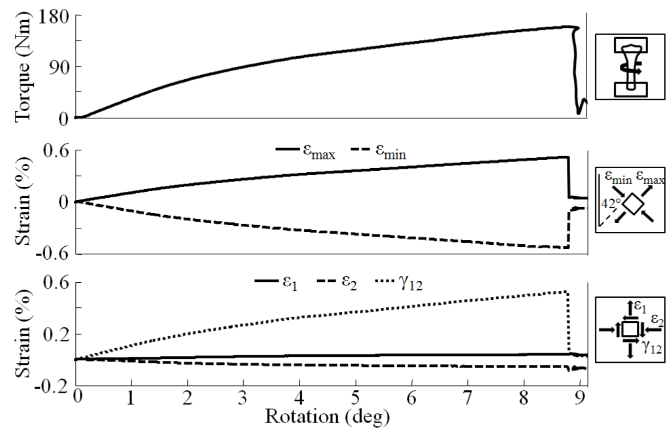

Figure 3. Torque and anteriomedial surface principal (ε_{max}, ε_{min}), normal (ε_1, ε_2) and shear (γ_{12}) strains versus rotation for cadaveric proximal tibia loaded to failure.

The device is currently limited to a maximum torque of ~318 Nm and an angular rotation of ~90° due to the 5 kN factory load cell and the 100 mm stroke of the linear actuator, respectively. Nonetheless, these limits are well above ultimate torque (mean 101, range 57-178 Nm) and rotation (mean 24, range 14-37°) values for human whole-tibiae at high rates of loading [3].

CONCLUSIONS
We developed, validated, and applied a linear actuated torsional device. The device is accurate, precise, and capable of replicating clinically relevant spiral fractures in long bones. Although the application of this paper dealt specifically with spiral fracture of the proximal tibia, the device presented is applicable to any torsional testing of long bone when only a linear actuator is available.

REFERENCES
1. Damián Z. *Instrum. & Dev.*, **3**, 34-37, 1997.
2. Keating J. *Disabil. Rehabil.*, **14**, 108-109 1992.
3. Martens M. *J. Biomech.*, **13**, 667-676, 1980.

ACKNOWLEDGEMENTS
NIH/NIAMS F32 AR061964

DXA DERIVED MEASURES OF BONE MINERAL CAN RELIABLY PREDICT MECHANICAL BEHAVIOR OF PROXIMAL TIBIAS LOADED IN TORSION

W. Brent Edwards and Karen L. Troy

University of Illinois at Chicago, Chicago, IL, USA
email: edwardsb@uic.edu, web: http://www.uic.edu/ahs/biomechanics

INTRODUCTION

Spinal cord injury (SCI) is characterized by marked bone loss at regions below the neurological lesion. The clinical consequence of this reduction in bone is an increased lifetime risk for low-energy fracture that is two times greater than the general population [1]. Regions of the knee, e.g., the proximal tibia, are among the locations most prone to fracture in the SCI population [2]. These fractures often occur during a fall or transfer from a wheelchair (i.e., twisting or catching of the lower-extremity) [2].

The current fracture risk assessment tools for the general public are inadequate for people with SCI. In part, this is because the locations of routine fracture do not correspond between these two groups. Therefore, the ability to predict mechanical behavior at the knee under a physiologically relevant mode of loading may serve as an important clinical tool to assess fracture risk in the SCI population. The purpose of this study was to statistically evaluate methods for predicting proximal tibia mechanical behavior in torsion from DXA derived measures of bone mineral.

METHODS

Twenty tibial specimens were excised from formalin-fixed cadavers (age 70.0 ± 15.6 yrs, 9 men/11 women, 15 right limbs/5 left limbs). Osteotomy was performed 15 cm below the intercondylar eminence and the proximal and distal most 2 cm of bone were potted in PMMA, leaving 11 cm of bone exposed. Bone mineral content (BMC) and density (BMD) of the entire proximal tibia – immersed in water – were acquired using a Hologic QDR-4500 (Hologic, Waltham, MA) with the lumbar spine acquisition software.

Tibiae were loaded in internal rotation using a materials testing machine (858 Mini Bionix II, MTS, Inc., Minneapolis, MN) with a custom linear actuated torsional device. The device has an experimental error less than 0.2 Nm and is repeatable to within 0.3% (companion abstract). Following 10 conditioning cycles, tibiae were loaded at a rotation rate of 9.023 °/s until fracture. Torque and rotation data were collected at 1000 Hz.

Six parameters were calculated from the torque-rotation curves including: rotational stiffness K, torque T_{yield} and rotation θ_{yield} at yield, torque $T_{ultimate}$ and rotation $\theta_{ultimate}$ at ultimate failure, and work to failure W. K was calculated from a 1st order polynomial fit of the initial linear portion of the curve, yield point was defined by a 5% offset of the torque to linear elastic projection, ultimate failure corresponded to the instant of maximum torque, and W was the area underneath the curve (Fig. 1).

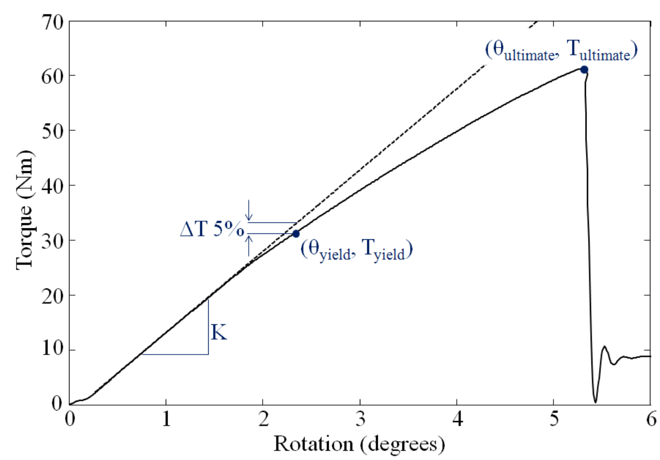

Figure 1. Representative torque-rotation curve (solid line) and corresponding linear elastic projection (dashed line) used to calculate mechanical behavior parameters.

Specimens were assigned to either a "training" set or a "test" set (10 specimens each). Set allocation was based on BMD ranks of the entire sample, in which every other ranked specimen was assigned to a specific set. Linear regressions were used to predict mechanical behavior from BMC and BMD using data from the training set. The reliability of these regressions were then tested by applying them to the test set (i.e., we tested how reliable regression equations were when applied to a new sample). Three statistics were used to examine reliability [3]: "cross-validation" r^2, "shrinkage on cross-validation", and "predicted" r^2. The cross-validation r^2 is obtained from the correlation between observed and predicted values in the test set. The shrinkage on cross validation is the difference between the training set r^2 and the cross-validation r^2. The predicted r^2 is a more conservative statistic which takes the form:

$$\text{predicted } r^2 = 1 - \sum\left(y_i - \hat{y}_i\right)^2 / \sum\left(y_i - \bar{y}\right)^2.$$

Predicted r^2 is not a least squares estimate because $\hat{y}_i$'s come from a model fit on different data (i.e., the training set). Predicted r^2 can also be a negative number for models with no predictive value.

RESULTS AND DISCUSSION

After dividing specimens into two groups based on BMD, the training and test sets consisted of 5 men/5 women and 4 men/6 women, respectively. Independent sampled t-tests confirmed the two groups did not differ in terms of age, BMC, or mechanical behavior ($p \geq 0.37$ for all comparisons).

The relationships between DXA derived measures of bone mineral and mechanical behavior of the proximal tibia are summarized in Tables 1 (BMC) and 2 (BMD). $T_{ultimate}$, K, and W illustrated relatively high correlations with bone mineral, while θ_{yield}, T_{yield} and $\theta_{ultimate}$ illustrated relatively low correlations with bone mineral. In general, BMC explained a larger amount of variance in mechanical behavior than BMD. The strongest and most reliable correlation was between BMC (g) and $T_{ultimate}$ (Nm), wherein, the regression equation was:

$$T_{ultimate} = 2.75 \times BMC + 2.47 \qquad (p<0.001).$$

This study was limited by the use of formalin-fixed specimens from a non-SCI population. Fixation can influence bone mechanical properties [4] and prolonged disuse may induce bone micro-structural changes. While these limitations may affect the coefficients of the regression equations developed herein, they would not be expected to influence the strength and reliability of the predictions and thus the interpretation of our findings.

CONCLUSIONS

Non-invasive measures of bone mechanical behavior at the knee may improve upon the current fracture risk assessment tools for the SCI population. Our data suggest that DXA derived measures of bone mineral can reliably predict mechanical behavior of proximal tibias loaded in torsion. BMC and BMD explained 60% to 90% of the variance in $T_{ultimate}$, K, and W. Future work will compare these findings to quantitative computed tomography and the finite element method.

REFERENCES

1. Vestergaard P. *Spinal Cord* **36**, 790-796, 1998.
2. Morse LR. *Osteoporosis Int* **20**, 385-392, 2009.
3. Cody DD. *J Biomech* **32**, 1013-1020, 1999.
4. Stefan U. *Bone* **47**, 1048-1053, 2010.

ACKNOWLEDGEMENTS

NIH/NIAMS F32 AR061964

Table 1. Relationships between DXA derived BMC and mechanical parameters of the proximal tibia.

	K	T_{yield}	θ_{yield}	$T_{ultimate}$	$\theta_{ultimate}$	W
Training set r^2	0.750	0.534	0.724	0.932	0.025	0.750
Cross-validation r^2	0.863	0.323	0.487	0.902	0.386	0.715
Shrinkage on cross-validation	-0.113	0.211	0.236	0.031	-0.361	0.035
Predicted r^2	0.853	0.278	0.461	0.851	-0.016	0.615

Table 2. Relationships between DXA derived BMD and mechanical parameters of the proximal tibia.

	K	T_{yield}	θ_{yield}	$T_{ultimate}$	$\theta_{ultimate}$	W
Training set r^2	0.461	0.338	0.625	0.755	0.143	0.778
Cross-validation r^2	0.675	0.332	0.394	0.788	0.489	0.666
Shrinkage on cross-validation	-0.215	0.006	0.231	-0.034	-0.346	0.112
Predicted r^2	0.604	0.233	0.389	0.718	0.157	0.599

TWO-DIMENSIONAL PARAMETER STUDY TO CHARACTERIZE PERFORMANCE OF ANKLE-FOOT ORTHOSIS JOINT IMPEDANCE CONTROL

Matthew R. Eicholtz and Steven H. Collins

Carnegie Mellon University, Pittsburgh, PA, USA
email: meicholt@andrew.cmu.edu, web: http://biomechatronics.cit.cmu.edu

INTRODUCTION

Active orthoses and exoskeletons show great potential for improving human locomotion in able-bodied and neurologically-impaired individuals [1]. Despite marked progress to that end, improvements in key performance measures are lacking. One such measure is metabolic cost, and to our knowledge, there is currently no powered lower-limb assistive device that provides an energetic benefit for walking when compared to normal conditions.

While there are many determinants contributing to user performance, two important factors are emphasized here. First, the device-user interface is affected by design parameters such as mass and geometric considerations. In particular, adding mass to the body has been shown to exact a proportional increase in metabolic energy during walking, with increasing energy change as the mass is moved distally from the body center of mass [2]. This result provides a clear directive for lightweight orthoses and exoskeletons, which necessitates highly efficient (or alternatively, external) actuators. Second, walking performance is directly related to the choice of control architecture and moreover, to the selection of parameter values *within* a given architecture. This suggests the need for systematic, experimental comparisons between and within different control schemes.

We propose a two-dimensional parameter study on joint impedance control using an ankle-foot orthosis (AFO) experimental testbed. We targeted the ankle joint because its muscle-tendons generate half of the power used in normal walking [3]. We selected joint impedance control because it enables systematic regulation of joint work, which seems to affect metabolic cost [4], and has led to promising results in a recent prosthesis experiment [5].

METHODS

Mechanical Design
The testbed includes a powerful motor and control hardware, a lightweight (~0.6 kg), minimally-restrictive ankle orthosis (Fig. 1), and a flexible tether between them. The AFO provides assistive plantarflexor torque in parallel to the leg during stance via fiberglass leaf springs (Gordon Composites). The details of the design can be found elsewhere [6].

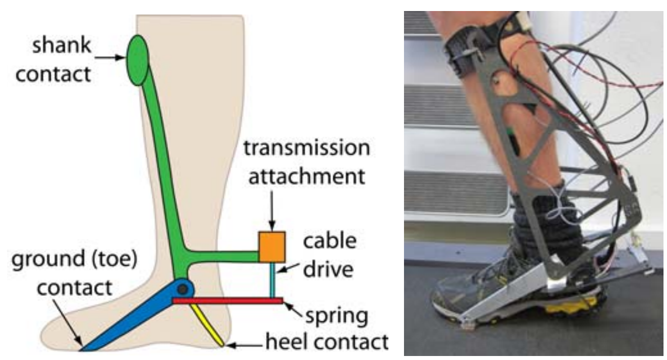

Figure 1: *(left)* Schematic of the ankle orthosis. A flexible transmission connects the device to an offboard motor and control hardware (not pictured). *(right)* Photograph of the pilot prototype.

Experimental Design
For joint impedance control, desired assistive ankle torque is a function of joint state. The control law used in this experiment is:

$$\tau_d = \left[k_i f_1(\theta_a) + c_w f_2(\dot{\theta}_a)\right]\gamma$$

where τ_d is desired ankle assistive torque, k_i is a stiffness parameter, $f_1(\theta_a)$ defines a virtual spring, c_w is a work loop parameter, $f_2(\dot{\theta}_a)$ is a (filtered) step function that switches at zero ankle velocity, and γ is gait phase (0 for swing, 1 for stance). The two parameters that will be systematically varied in this study are k_i and c_w, which together define a work loop in torque-angle space. The nominal values for these variables are 1, corresponding to the maximum expected net work done by the assistive device over a stride.

In the proposed experiment, neurologically-intact subjects will walk at normal speed (1.25 $m*s^{-1}$) on a treadmill while wearing the unilateral ankle-foot orthosis. For one set of trials, the stiffness will vary while the net work will remain constant. For a second set of trials, the stiffness will remain constant while the net work is varied. The intersection of these one-dimensional conditions will be determined *a priori* using the best parameter set from pilot tests.

Kinematic data is provided by an encoder mounted on the AFO ankle joint (US Digital, E8P Series). Assistive torque is estimated using strain gages fixed to the springs in a Wheatstone bridge configuration (Omega, SGD-13/350). Muscle activity of the soleus and medial gastrocnemius for the assisted leg is measured using surface electromyography (Delsys Inc.). The raw EMG data is (1) high-pass filtered (3^{rd} order Butterworth, cutoff frequency = 20Hz) to remove movement artifact, (2) full-wave rectified, and (3) low-pass filtered (3^{rd} order Butterworth, cutoff frequency = 6Hz) to smooth the signal. Metabolic rate is computed as the linear combination of carbon dioxide production and oxygen consumption, measured using portable indirect respirometry equipment (Jaeger).

Initial experimental hypotheses include: (1) increasing generalized stiffness will increase changes in ankle dynamics, (2) varying the net work constant will affect muscle activity and, therefore, metabolic cost, and (3) there exists a set of parameters that produces a local minimum for metabolic cost.

RESULTS AND DISCUSSION

Preliminary pilot data (Fig. 2) demonstrates the ability to accurately track desired assistive torques and vary the generalized stiffness. While some controller parameters still need tuning prior to the experiment, these results are encouraging and instantiate the feasibility of our control approach. In the future, we may use mathematical models to predict an optimal parameter set for a given user and test the predictions using the control architecture described here.

REFERENCES

1. Dollar AM and Herr H. *IEEE Trans Rob* **24**, 1-15, 2008.
2. Browning RC, et al. *Med Sci Sports Exerc* **39**, 515-525, 2007.
3. Farris DJ and Sawicki GS. *J R Soc Interface* **doi,** 10.1098/rsif.2011.0182, 2011.
4. Collins SH and Kuo AD. *PLoS ONE* **5**, e9307, 2010.
5. Sup F, et al. *Proc IEEE Int Conf Rehabil Robot*, 638-644, 2009.
6. Eicholtz MR and Collins SH. *Proc 6th Annual Conf Dynamic Walking*, Jena, Germany, 2011.

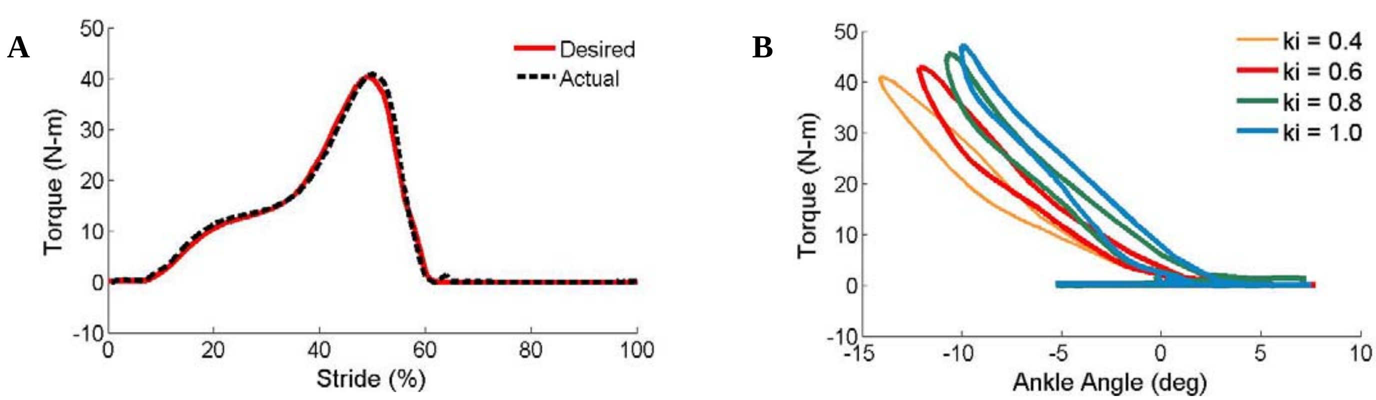

Figure 2: Averaged pilot results (~1 min, 50-60 steps) using AFO impedance control. **(A)** Sample of desired torque tracking as a function of stride (beginning at heel contact). **(B)** Net assistive work loops for trials where stiffness was varied but net work remained constant.

EXPEDITED COMPUTATIONAL ANALYSIS OF FRACTURE OF CERAMIC THA LINERS: OBESITY AND STRIPE WEAR CONSIDERATIONS

[1,2]Jacob M. Elkins; [1]Douglas R. Pedersen; [1,2]John J. Callaghan and [1,2]Thomas D. Brown

Departments of [1]Orthopaedics and [2]Biomedical Engineering, University of Iowa, Iowa City, IA;
email: jacob-elkins@uiowa.edu

INTRODUCTION

As of 2009, ceramic-on-ceramic bearings were estimated to represent 14% of the US market share for total hip arthroplasty (THA) [1]. However, fracture of ceramic liners remains a substantial concern, with incidence estimated at 1-2% [2]. Unfortunately, quantifying ceramic fracture risk is challenging. Surrogate physical models of liner fracture risk have been developed [3]. However, their associated cost and complexity preclude extensive parametric analysis. Computational (Finite Element, FE) linear elastic fracture mechanics (LEFM) models [4] are logistically challenging, and require extraordinary computational and analyst effort, since the location of crack nucleation must be known (or assumed) *a priori*, specialized elements must be used, and the model needs to be re-meshed at each increment of solution progression. However, a recent FE modeling advancement known as eXtended Finite Element Modeling (XFEM) has enabled a paradigm shift in this area. XFEM allows for modeling both the initiation and propagation of fractures without the requirement for specialized elements or meshes. To explore the use of XFEM as a modeling vehicle for ceramic liner fracture, and to investigate the relationships between stripe wear, obesity and cup orientation on liner fracture risk, an XFEM model of ceramic liner fracture is here reported.

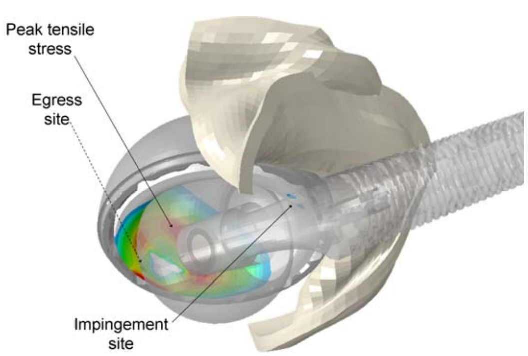

Fig 1: The (global) FE model consisted of THA hardware and the hip capsule. High tensile stress develop after impingement-associated head subluxation and subsequent edge loading

METHODS

Liner fracture risk for 36mm alumina bearings was studied by simulating two fracture-prone motions: stooping and squatting [5]. Twenty-five distinct cup orientations were considered, with variants of both acetabular inclination and anteversion. Four separate body mass indices (BMIs) were considered: normal (25 kg/m^2) and three levels of obesity (33, 42 and 50). Material properties were modified to simulate alumina with and without the presence of micro-flaws. A total of 600 FE simulations were performed: 200 (global) FE analyses of impingement and subluxation, with each global simulation followed by two (micro-flawed or non-flawed) XFEM analyses. The model was validated by corroboration with a previously published ceramic liner fracture study [3] (Fig. 2).

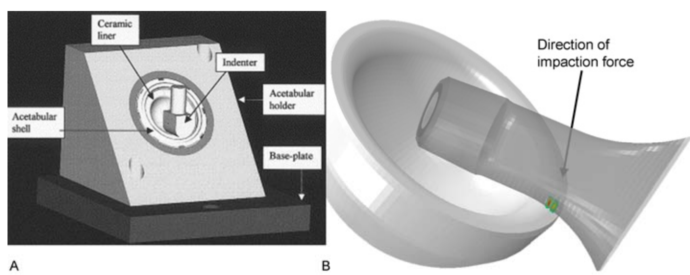

Figure 2: The XFEM corroboration series was conducted by computationally replicating the neck-on-liner impact fracture scenario of a previously reported physical investigation (A, reproduced from [3]). For the XFEM series (B), the femoral neck was displaced toward the liner under displacement control for several variations in total displacement.

RESULTS AND DISCUSSION

For the physical corroboration series, a threshold impaction force of 24.5 kN was computed to cause fracture of the liner (Fig. 3). The corresponding fracture threshold force measured experimentally [3] was 23 kN, lending strong credence to the credibility of the computational results.

Of the 400 distinct XFEM simulations run, fracture occurred in 108. The majority of fractures initiated in the posterior region of the cup and typically propagated toward the edge (Fig. 4). This site corresponded to the approximate location of maximum tensile stress (Fig. 1). Of 200 XFEM simulations with flaw-free alumina, fracture occurred in only eight instances, all of them involving obesity. Each of these occurred with cups in ≤ 37° inclination and in 0° anteversion. For 200 corresponding simulations with micro-flawed alumina, fracture propensity was greatest for cups with higher (edge-loading-associated) scraping wear, independent of BMI (Fig. 5). Both scraping wear (Fig. 6) and fracture (Fig. 5) increased with increased BMI. Fracture risk was greatest for cups with lower inclination (average 42° for fractured cases vs. 48° for non-fractured cases, $p<10^{-4}$) and lower anteversion (9° vs. 20°, $p<10^{-10}$) (Fig. 7).

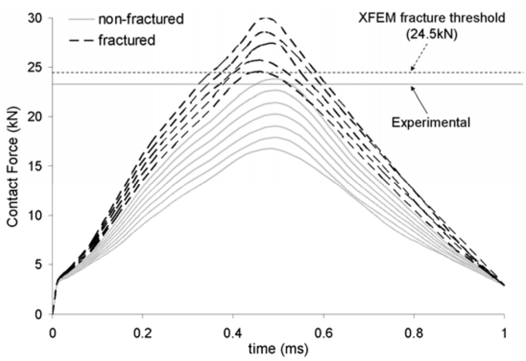

Fig. 3: Neck-on-liner fracture XFEM corroboration from physical experiment (3). A fracture threshold force of 24.5 kN was determined. These compare favorably to the experimental threshold of 23 kN.

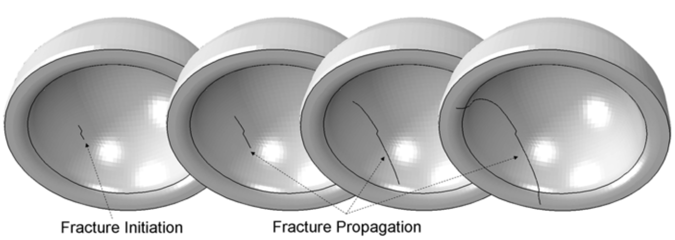

Fig. 4: Fractures typically initiated in the posterior region of the cup during head subluxation, and then propagated bidirectionally toward the edge.

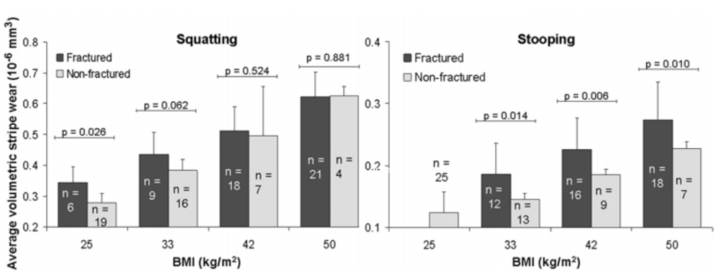

Fig. 5: For both squatting and stooping, fracture risk was greater for simulations with increased edge-loading-associated stripe wear.

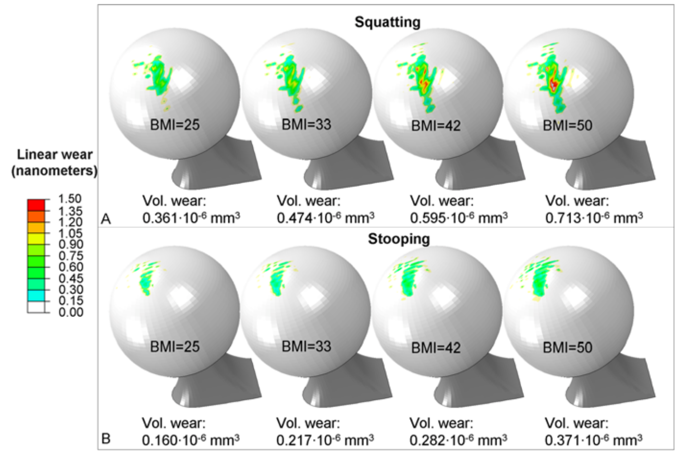

Fig 6: For squatting and stooping, linear and volumetric stripe wear increased for increased BMI.

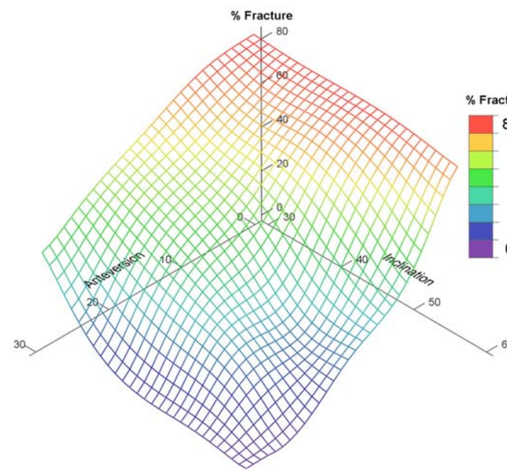

Fig 7: Cup-orientation-dependence of fracture percentages encountered for all 200 simulations of micro-flawed alumina liners.

CONCLUSIONS

In summary, an expedited computational formulation, XFEM, was utilized for novel systematic analysis of ceramic fracture in THA. To the authors' knowledge, this study represents the first application of XFEM to orthopaedic implants. The study corroborated recent clinical observations of increased risk of ceramic liner fracture for obese patients. A strong association was identified between stripe wear severity and fracture risk, for instances of both normal and elevated body weight.

REFERENCES

1. Bozic KJ, et al. *JBJS* **81**, 508-525, 2009
2. Capello WN et al. *J.Arthroplasty* **23**, 39-43, 2008
3. Maher SA et al. *J.Arthroplasty* **18**, 936-941, 2003
4. Elkins JM et al. *J.Arthroplasty* 2012 [accepted]
5. Nadzadi ME et al. *J.Biomech* **36**, 577-591, 2003

ACKNOWLEDGEMENTS

NIH (AR53553, AR46601, UL1 RR024979) and the Veterans Administration.

Mimetic Jar Device Capable of Measuring Dynamic Opening Forces: Development and Validation

[1]Arin M. Ellingson, [1]Michelle Ferkul, [1]Corey McGee, [1]Virgil G Mathiowetz, [1]David J. Nuckley

[1]University of Minnesota, Minneapolis, MN USA
email: dnuckley@umn.edu, web: http://www.mbrl.umn.edu

INTRODUCTION

On a daily basis, individuals open household jars without considering the biomechanical requirements involved, but for some people this task can be difficult to complete. Those with osteoarthritis, fibromyalgia or other neuromuscular conditions need to make accommodations to their hand kinetics to successfully open a jar with minimal pain. Unfortunately, there exists little data to help clinicians suggest proper hand kinetics for these individuals.

Many jar instruments have been developed to attempt to address these large populations; however, none of these jar instruments include a combination of : a six-axis load cell capable of measuring the total compensatory forces applied to the jar lid, multiple lid grip sensors, and a torque limiter to repeatedly simulate the experience of opening a sealed jar [1-8]. Similarly, those who have quantified the forces and moments acting upon a jar have created instruments that are not true to form and presumably alter the natural requirements of the task. Thus, we developed a life-like device to measure the full kinetics of the hand during jar opening, including both grip forces and resultant forces applied to the jar in six degrees of freedom. This instrument was validated by bench top and healthy human subject testing. Subsequent testing with this jar device may help clinicians advise suitable hand kinetics for individuals with neuromuscular conditions to maximize their effective forces on the jar and minimize pain during jar opening.

METHODS

A jar device was designed and constructed so as to measure the 6-axes of forces and moments applied to the jar between the two hands as well as the grip forces on the lid (Fig. 1). This jar device utilized a torque limiter set to 2.4 Nm and the jar lid would open freely for 45º to provide a similar experience to opening a real jar. The lid was equipped with 5 mm force sensing resistors (FSR) to measure the force magnitude and direction of force application while gripping the lid (Fig. 1B). The instrumentation of the jar was designed to work with two interchangeable lids: 83 mm (Fig. 1A) and 55 mm (Fig. 1C). Each of these jars utilizes the same load cell and torque limiter and a size appropriate instrumented lid with identical force sensing transducers. The large jar is outfitted with 6 sensors equally spaced radially around the lid, while the small jar has 4.

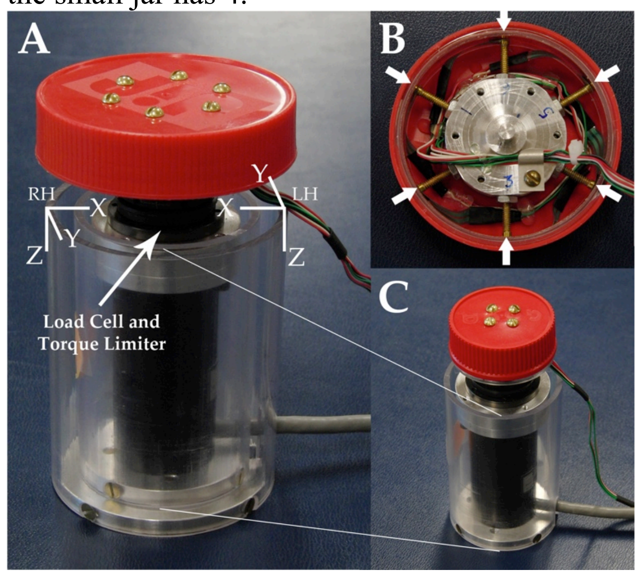

Figure 1- Force Sensing Jar with Opening Action. *A- Image of the large jar with size and textural finish similar to a typical peanut butter jar. Arrow indicates 6- degrees of freedom load cell equipped with torque limiter set to 2.4 Nm. RH is the coordinate system used for right handed subjects and LH is the coordinate system used for left handed subjects. B- Image of underside of jar lid. Arrows indicate positioning of force transducers to record grip forces on lid. C- Image of the smaller jar, which is contained within the large jar, utilizes the same load cell and torque limiter. The lid is interchangeable.*

In an effort to validate this force feedback jar, we enrolled 115 healthy subjects to perform the jar opening task and define the range of forces applied to the larger jar. This IRB approved study involved healthy volunteers (age: 24 ±6 yrs; sex: 44 males/71 females) without diagnosed osteoarthritis or hand pain. A repeated measures study was conducted on 36 healthy subjects (age: 31 yrs; sex: 6 males/30 females; hand dominance: 30R/6L) using the small jar set-up. The subjects repeated the experiment to evaluate the repeatability of individual's force application.

RESULTS AND DISCUSSION

The jar opening events measured a number of different kinematic approaches and similarly different kinetics on the jar.

Two representative trials were selected to show an efficient (A) and an inefficient (B) opening of a jar, respectively (Fig. 2). To open a jar, one must apply a torque and a downward axial force to the jar; any additional torques and forces are unnecessary and inefficient.

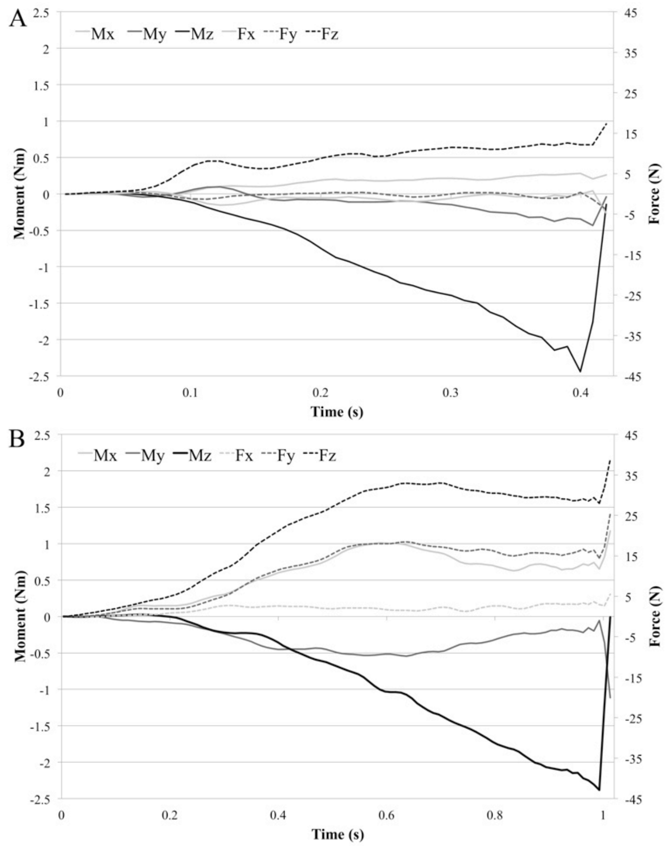

Figure 2- Force Time History. A- Efficient Jar Opening**. B-** Inefficient Jar Opening.

The orientation of the jar lid resultant grip forces can be seen in figure 3 which depicts the grip force vectors leading up to jar opening where the longest vector represents that force immediately prior to opening. This research effort involved the design and construction of a jar with simulated and reproducible opening action and the capability to measure both jar and lid forces and jar moments.

The jar instrument provided reproducible results between and within subjects and revealed interesting patterns of jar kinetics in healthy individuals. As we begin to study patients with difficulties opening jars, we expect the patterns and differences to become even greater.

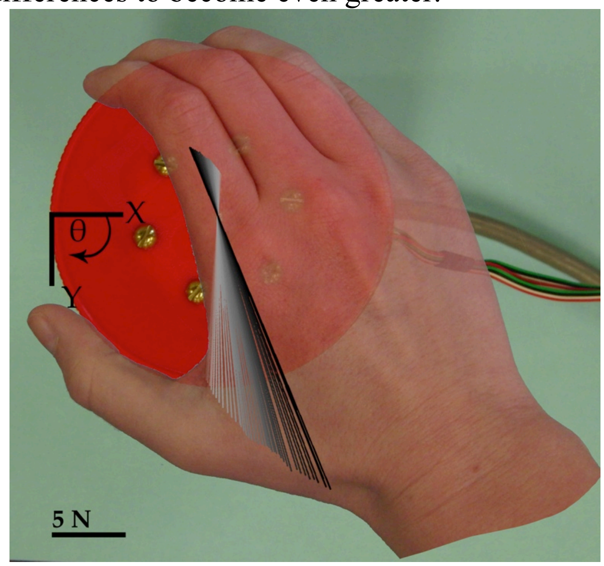

Figure 3- - ***Grip Force Overlay on the Hand / Jar.*** *Resultant grip force vectors are shown on the hand / jar up to opening (black line) for a representative data.*

CONCLUSIONS

This jar device for measuring the forces applied to a jar during opening has great promise in helping to quantify the hand force requirements of those diagnose and treat patients with osteoarthritis, fibromyalgia or other neuromuscular conditions as well as recommend hand kinetics tom maximize effective forces and minimize pain during jar opening without alternating the natural experiences of the test subjects.

REFERENCES

[1]Carse B et al. *Med Eng Phys.* 2011; [2]Chang JH et al. *Ergonomics.* 2008; [3]Fowler NK et al. *Clin Biomech.* 1999; [4]Fowler NK et al. *J Biomech.* 1999; [5]Kuo et al. *Proc Inst Mech Eng H.* 2009; [6]Pataky T et al. *Ergonomics.* 2004; [7]Voorbiji et al. *Appl Ergon.* 2002; [8]Shim JK et al. *J Apply Physiol.* 2004

Table 1- Summary Statistics and Interclass Correlations of Forces and Moments on Jar at the Instant before Opening

	Fx (N)	Fy (N)	Fz (N)	Mx (Nm)	My (Nm)	Mz (Nm)
Average	-10.6	17.72	29.61	1.17	0.96	-2.38
STD	4.7	7.1	12.22	0.43	0.4	0.24
r(p)	0.55(0.001)	0.78(<0.001)	0.61(<0.001)	0.54(0.001)	0.58(<0.001)	0.75(<0.001)
ICC	0.715	0.852	0.766	0.687	0.733	0.857

HELICAL AXIS PATTERNS OF MOTION FOR THE HEALTHY TO SEVERELY DEGENERATED LUMBAR INTERVERTEBRAL DISC

[1]Arin M. Ellingson and [1]David J. Nuckley

[1]University of Minnesota, Minneapolis, MN, USA
email: ellin224@umn.edu web: http://mbrl.umn.edu

INTRODUCTION

Chronic low back pain is one of the most prevalent health complaints in the US, with an estimated 70-85% of the population developing back pain at some point in their life [1]. Unfortunately, while the intervertebral disc has been the most implicated tissue in low back pain, correlations between changes in the intervertebral disc and clinically measurable parameters, which may enable diagnostic staging of degeneration, have not been well established.

It has been shown that patients with low back pain exhibit more out of plane motion during bending, suggesting that a functional kinematics outcome may be a sensitive predictor of lumbar disc degeneration [2, 3]. Early degenerative changes may enable someone to produce the same range of motion despite tissue morphologic changes taking place. However, it is unlikely that the precise three-dimensional pathway of each vertebrae during that motion is preserved and traditional range of motion measurements do not capture this. Using a three-dimensional helical axis (HA) approach to understand the pathway of intersegmental vertebral motion we can now understand the natural coupling behavior of the lumbar spine throughout the degenerative process. *The purpose of this study was to establish helical axis patterns for lumbar spine motion in healthy and degenerative intervertebral disc samples.*

METHODS

Eighteen osteoligamentous cadaveric lumbar spines (L3-S1) were acquired from the UofM Bequest Program (ave age: 53.2±15.5 yrs; range: 21-71 yrs). Each specimen was examined using conventional MR imaging and biomechanically exercised in the cardinal planes. MR imaging was performed on a Siemens 3T scanner (Magnetom Trio; Siemens Healthcare). Conventional T2-weighted sagittal anatomic images were acquired for Pfirrmann disc grading [4].

After imaging, the specimens were embedded in polymethylmethacrylate and tested in a six-axis Spine Kinetic Simulator (8821 Biopuls, Instron, Norwood, MA). Pure moments of up to 7 Nm were applied sinusoidally (0.015 Hz). Three cycles were performed and the final cycle was analyzed. Load and moment data was collected at 100 Hz. Segmental displacements were recorded using a 3D visual motion analysis 5-camera system (Vicon MX-F40NIR, Vicon Motion Systems, Centennial, CO) capturing a four ball infrared reflecting marker set attached to each vertebral body. A custom digitizer was used to locate three anatomical points (mid-sagittal anterior, left and right lateral) to establish a local coordinate system. This coordinate system was used to display each HA as it relates to its own anatomy, captured by MRI.

Three representative lumbar spines were selected, based on their Pfirrmann grade, for helical axis analysis. This included one specimen from grades 1, 3, and 5. Helical axes for the L4-L5 functional spinal unit (FSU) were computed at 0.1 Nm increments from 0N through neutral zone to 6 Nm in flexion, extension, and lateral bending [5, 6]. There were 60 total vectors for each direction of bending. The following HA parameters were measured: unit vector of HA, rotation about the HA, translation along the HA and the anatomical location of the HA. The location of where the helical axis crosses the mid-sagittal plane, for flexion/extension, and the coronal plane, for lateral bending, was normalized by the disc's height, width and anterior-posterior dimensions.

RESULTS AND DISCUSSION

Figure 1 displays the computed helical axes during all bending directions over-laid on a representative

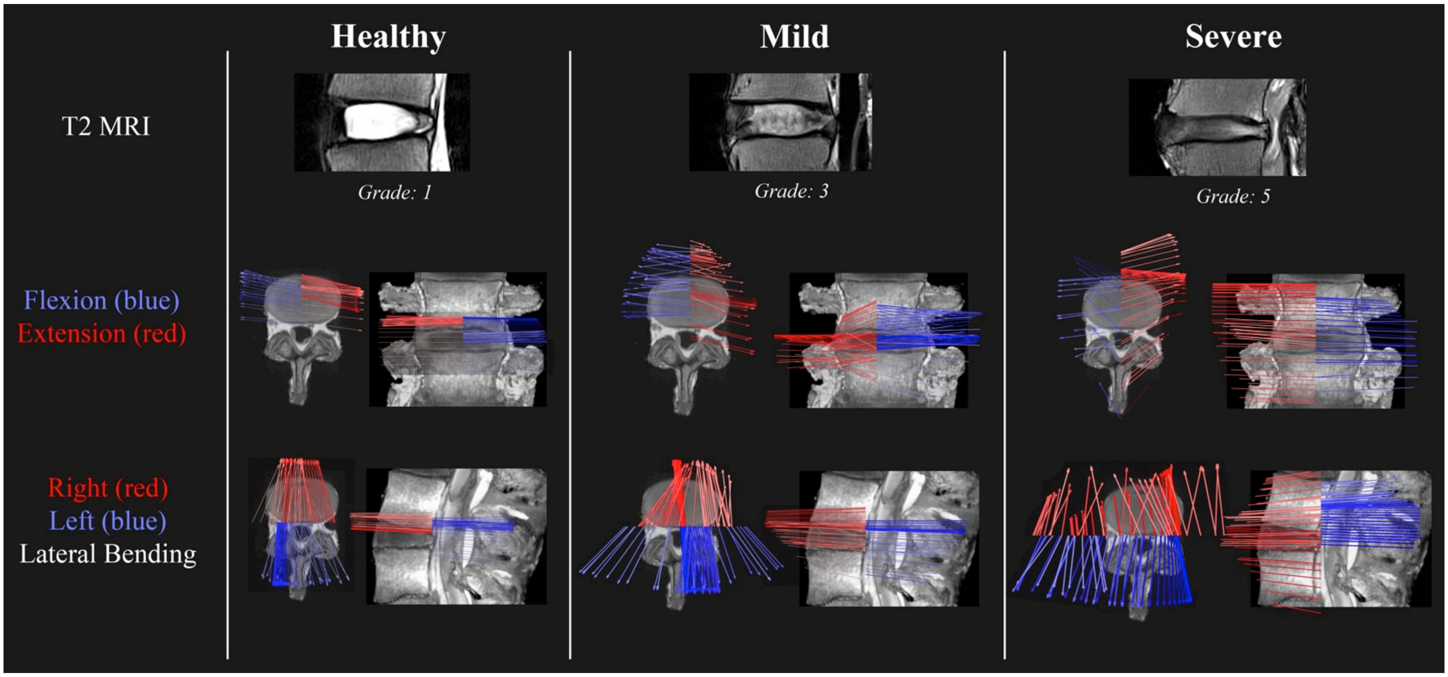

Figure 1- Helical Axis Patterns of the Healthy, Mild, and Severely Degenerated Lumbar Spine (L4-L5). T2 weighted MRI images show the healthy of the intervertebral disc and the corresponding Pfirrmann grade. Flexion (blue), extension (red), right (red) and left (blue) lateral bending helical axes are laid over top a representative lumbar spine. All HA locations are normalized to each respective FSU's disc dimensions. The healthy HA generally reside in the disc space, where as degeneration worsens, the location of the HA spreads and the orientation is less congruent. HA are computed from 0-6 Nm at 0.1 Nm steps. The colors of the vectors start at red/blue at the neutral zone (0Nm) and fade as they approach the end range of motion (6Nm)

MR image of a lumbar spine. All HA locations are normalized to each respective FSU's disc dimensions. The T2 weighted MR image shows the health of the disc and Pfirrmann grade associated. Vectors appear dark red/blue at the neutral zone (0 Nm) and lighten towards the end range of motion (6 Nm).

This preliminary work demonstrates there is a relationship between disc health and the patterns of helical axes throughout motion. The healthy specimen exhibited very tight HA, especially at the beginning of bending. Generally all the vectors reside within the disc space. As degeneration worsens the normalized location of the vectors spread drastically and the orientation of the vectors are less congruent. This indicates that the smoothness and condensed motion of the healthy disc is disrupted by degeneration in such a way so as to produce motions, which are less conserved.

CONCLUSION

The current presentation of the data do not allow for greater generalizations across the degenerative spectrum. Statistical comparison of the multiple HA parameters collected will represent a significant contribution towards the functional definition of disc degeneration. This ongoing work aims to link imaging and functional helical axis parameters in a factorial model describing the progression of disc degeneration. This may become the foundation for a potential clinical tool for assessing spinal health.

REFERENCES

[1] G.B. Andersson, Lancet, 354 (1999) 581-585.
[2] T. Lund, T. Nydegger, D. Schlenzka, T.R. Oxland, Spine (Phila Pa 1976), 27 (2002) 1865-1874.
[3] I.A. Stokes, D.G. Wilder, J.W. Frymoyer, M.H. Pope, Spine (Phila Pa 1976), 6 (1981) 233-240.
[4] C.W. Pfirrmann, A. Metzdorf, M. Zanetti, J. Hodler, N. Boos, Spine (Phila Pa 1976), 26 (2001) 1873-1878.
[5] C.W. Spoor, F.E. Veldpaus, J Biomech, 13 (1980) 391-393.
[6] H.J. Woltring, R. Huiskes, A. de Lange, F.E. Veldpaus, J Biomech, 18 (1985) 379-389.

The Metabolic and Mechanical Costs of Step-Time Asymmetry in Walking

[1]Richard Ellis, [1]Kevin Howard, and [1]Rodger Kram

[1]Departement of Integrative Physiology, University of Colorado, Boulder, CO, USA
email: richgellis@gmail.com

INTRODUCTION

Asymmetry is a major feature of numerous gait pathologies. Restoring gait symmetry has therefore been used as a clinical outcome variable for individuals recovering from stroke, amputation, joint replacement and physical trauma [e.g. 1]. Despite this, this is yet no evidence that gait symmetry is optimal even in healthy adults. Indeed, recent modeling studies suggest that the costs of small asymmetries may be minimal [2]. It has already been shown that step times both slower- and faster-than-preferred are mechanically and metabolically more expensive then preferred steps [3]. Here we ask: is there an inherent cost to gait asymmetry beyond that imposed by slow or fast steps? We also explore the mechanical power generated during asymmetric walking.

Hypothesis 1: The metabolic cost of walking with asymmetric steps will be greater than for walking with symmetric steps.

Hypothesis 2: This increased metabolic cost can be explained by greater mechanical power production.

METHODS

10 healthy subjects (5M/5F, 174±20cm, 68±10kg, 26±6yrs) each completed 9 walking trials at 1.25 m/s on a dual-belt force treadmill. Each trial involved walking at different symmetric and asymmetric step time combinations. Throughout the protocol, subjects received both auditory cues and visual feedback of their step time symmetry ratio, calculated as:

We define a step as from heel strike of the contralateral foot to the heel strike of the ipsilateral foot (e.g. right step time is left heel strike to right heel strike). Because of how we calculated SR, the right leg was always the 'slow' leg, with a step time greater than the left leg and slower than preferred (Fig 1). Correspondingly, the left leg was the 'fast' leg for all subjects. Our symmetric conditions had steps times +25, +12.5, 0, -12.5, -25% faster or slower than preferred (SR 1.0). Of our 4 asymmetric conditions, 3 had similar, less asymmetric SR's (1.25, 1.29 and 1.33) with right and left step times +25/-0, +12.5/-12.5, and +0/-25% different from preferred. One condition had a higher SR (1.66), with steps +25/-25% from preferred.

We used expired gas analysis to calculate subject's metabolic power. We calculated the mechanical power from measured ground reaction forces using the individual limbs method [4].

RESULTS AND DISCUSSION

Our symmetric results confirmed that faster and slower symmetric steps are more expensive than preferred steps. Our +25% condition resulted in a ~0.97 W kg^{-1} (+30%) increase in the net metabolic power while our -25% condition resulted in a 1.35 W kg^{-1} (+42%) increase in metabolic power (Fig 2A).

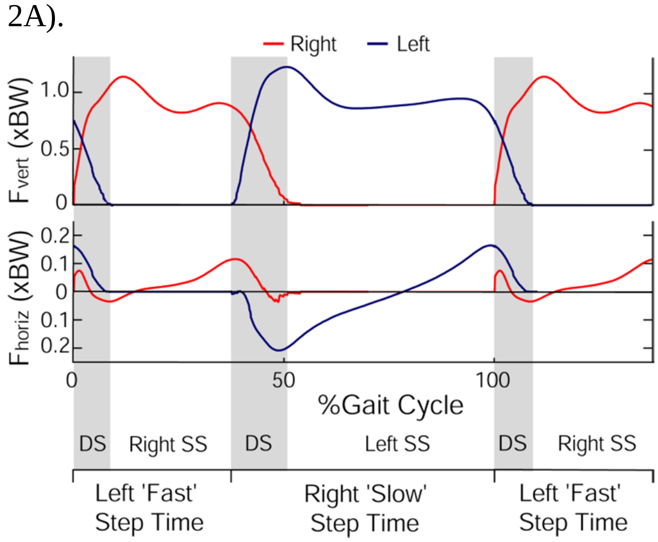

Fig 1: Average ground reaction forces for the +25/-25 condition. DS= double support. SS=single support. Right step time was longer then left step time, resulting in a symmetry ratio, resulting in a SR > 1.00.

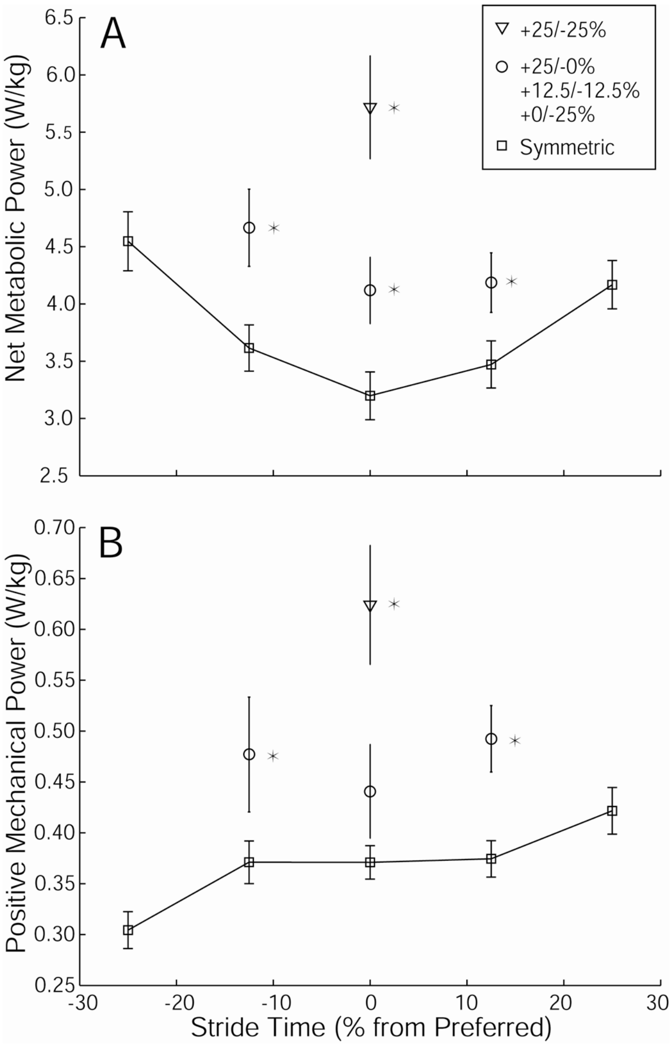

Fig 2: A) Metabolic power increased with step times further from preferred and with increasing asymmetry. B) Positive mechanical power performed on the center of mass increased with increasing stride time and with increasing asymmetry. =SR 1.66, ○ =SR ~1.3, □ =SR 1.0. * Significantly different from average of comparable fast and slow symmetric steps (paired t-test, α=.05).

Positive mechanical power increased with increasing symmetric step time i.e. long steps (Fig 2B). Each 12.5% increase in step time required ~0.024 W kg^{-1} (+6%) greater mechanical power output.

Subjects were able to reach the target stride times but did not walk quite as asymmetrically as the target symmetry ratio for the +0/-25 and +12.5/-12.5 conditions. Each of the asymmetric conditions was metabolically more expensive than the average of the corresponding fast/fast and slow/slow symmetric steps, supporting hypothesis 1 (All comparisons p<0.001, paired t-test).

We also observed a modest (~0.10 W/kg) increase in the mechanical power required for our three less asymmetric conditions, which was significant for all but the +12.5/-12.5 condition. We observed a large amount of variability in the strategies employed by our subjects to complete the task. Interestingly, some subjects performed less positive and negative mechanical work for an asymmetric stride than for a symmetric stride under each of the +12.5/-12.5, +25/-0 and +0/-25% conditions.

We also observed a substantial shift in when during the stride this work was performed, as well as a shift in the function of each leg. On average, the 'fast' leg performed more than half of the positive work per stride. Further, both legs had redistributed when they were producing power relative to normal walking. For example, the 'fast' leg produced net power during single support while also absorbing more power as the leading leg during each step-to-step transition.

CONCLUSIONS

Step-time asymmetry resulted in a clear metabolic penalty, which increased with increasing asymmetry. In our specific paradigm, we observed a reorganization of how when during the stride each leg was producing and absorbing power. The 'slow' leg produced net positive power while the 'fast' leg primarily absorbed power, which was distributed differently across the stride than we observed for symmetric walking. We suggest that the greater metabolic cost of walking asymmetrically is caused both by an increase in positive work performed on the center of mass and by an unequal distribution of this work between the legs and across a stride. Overall, we find that symmetry is optimal for healthy, generally symmetric individuals, as it requires less metabolic power, although this does not endorse the idea of imposing symmetry on individuals with pathological gait asymmetry.

REFERENCES

1. Maria et al. 2003. *Gait & Post.* **18** 23-28.
2. Srinivasan. 2009. *Interface*. **8** 74-98.
3. Umberger et al. 2007. *J. Exp. Bio.* **210** 3255-3265.
4. Donelan et al. 2002. *J. Biomech **35** 117-124.*

INDUCED ALTERATIONS OF INTERLIMB COORDINATION CAUSED BY THE USE OF A SPLIT-BELT TREADMILL

Jonathan M. Elrod, Brian M. Hoover, Ryan T. Roemmich, and Chris J. Hass

University of Florida, Gainesville, Florida, USA
Email: jonrod88@ufl.edu

INTRODUCTION

Human bipedal gait requires the production of a continuous rhythmic cycle of arm and leg swings. However, in a select number of clinical populations the rhythmic nature of this process may be impaired and gait asymmetries can develop. In order to maintain dynamic stability during ambulation a certain degree of coordination between the upper and lower extremities must be maintained. Investigations into stroke rehabilitation techniques have shown that training utilizing a split-belt treadmill can be beneficial in reducing gait asymmetries. Following acute training sessions on a split-belt treadmill the reductions in asymmetry carry over to overground walking [1]. Split-belt treadmills differ from traditional treadmills in that there is a belt beneath each foot which can be independently controlled. Typical training protocols have the more affected limb walk at a rate that is twice as fast as the least affected limb. Currently, little is known about how the gait adaptations produced acutely by a split-belt treadmill modulates human interlimb coordination. Therefore, the purpose of this study was to examine the effects of split-belt treadmill walking (SBTW) on the interlimb coordination of the upper and lower extremities. Additionally changes in coordination states based upon the degree of split between the lower limbs were investigated.

METHODS

A group of twelve healthy young adults between the ages of 18-25 were recruited. All participants signed an informed consent form approved by the Institutional Review Board. A series of passive retroreflective markers were attached to bony landmarks that were identified by manual palpation according to the Vicon Plug-in-Gait marker set (Vicon Nexus, Oxford, UK). All participants were acclimated to walking on the instrumented split-belt treadmill while at a self-selected gait velocity for several minutes. Following acclimation to the treadmill the participants were asked to identify the fastest velocity they felt comfortable walking for a period of ten minutes.

The participants walked at this velocity for one minute. Following that one minute period, the belt corresponding to the participant's dominant side was slowed four times in intervals of 90 seconds. Dominance was determined by asking the participants, "If you had to kick a soccer ball which leg would you use?" The belt speed was decreased in a descending stepwise manner to speeds set at percentages (90%, 70%, 50%, & 30%) of their fast-selected velocity.

Kinematic data were captured during the last 60 seconds of the 90 second interval using an 8-camera motion capture system collecting at a frequency of 120 Hz. Upper and lower extremity coordination was quantified by determining point estimate of relative phase (PERP) and cross-covariance (COV) measures using a customized MATLAB code (Math Works, Natick, MA). PERP was defined as the contralateral phase difference in time of maximum shoulder flexion and maximum hip flexion normalized to the duration of the stride cycle [2]. Analysis was performed on only the final 60 seconds of each condition to allow for adaptation to each split condition [3]. A 2x5 (belt condition x belt velocity) repeated measures ANOVA was performed in SPSS, with an a priori α level of $p \leq 0.05$. Post hoc comparisons were made using Bonferroni's method.

RESULTS

Coordination between the non-dominant shoulder and dominant hip exhibited a significant belt velocity main effect. Differences in coordination patterns were observed in both PERP and COV measures (p= 0.03; p= 0.01, respectively). COV values were also shown to exhibit a significant belt velocity effect for the dominant shoulder and non-dominant hip (p= 0.007).

Post hoc comparisons of the non-dominant shoulder and dominant hip measures revealed differences in the fast-selected gait velocity condition compared to the split condition at 30% of the fast-selected gait velocity for COV measures (p= 0.004). Similar results were found when comparing the 30% and 90% of the fast speed conditions (p= 0.018). Additional comparisons of the non-dominant shoulder and dominant hip relative phase values showed distinct differences between the fast-selected gait condition and the split condition at 30% of the fast-selected gait velocity (p= 0.029).

Furthermore, significant differences were detected for the COV measures of the dominant shoulder and non-dominant hip between the split condition at 30% of the fast-selected gait velocity and the split conditions of 50% and 70% of the fast-selected gait velocity (p= 0.034; p= 0.044, respectively). Comparisons between the 30% and 90% of the fast speed conditions, as well as the 30% and fast-selected showed statistical trends (p= 0.063; p= 0.061) (Table 1).

CONCLUSIONS

SBTW induced well-defined changes in the interlimb coordination patterns of the upper and lower limbs. Coordination was greatly diminished when the velocity of the dominant limb was at 30% of the fast-selected velocity. The results of this study would suggest that therapeutic interventions using a split-belt treadmill would not want to exceed a speed ratio of 3:1 between belts to minimize the risk of disruption to the interlimb coordination patterns.

REFERENCES

1. Reisman DS, Wityk R, Silver K, and Bastian AJ. Split-belt treadmill adaptation transfers to overground walking in persons poststroke. *Neurorehabil Neural Repair* **23**, 735-744, 2009.
2. Ford MP, Wagenaar RC, and Newell KM. Arm constraint and walking in healthy adults. *Gait Posture* **26**, 135-141, 2007.
3. Dietz V, Zijlstra W, Duysens J. Human neuronal interlimb coordination during split-belt locomotion. *Exp Brain Res* **101**, 513-520, 1994.

Table 1: Observed means (±SD) of dependent variables for each testing condition. Each symbol (β, γ, δ, ε, and θ) represents significant differences between the designated gait speed compared to 30% of the fast selected gait speed for the specified dependent variable based upon post hoc comparisons with p≤ 0.05.

		Fast-Selected	**Split-90%**	**Split- 70%**	**Split-50%**	**Split-30%**
Dominant Shoulder/ Non-dominant Hip	**COV**	0.90 ± 0.07	0.90 ± 0.06	0.89 ± 0.09 β	0.87 ± .11 γ	0.78 ± 0.22βγ
	PERP (º)	21.2 ± 9.83	25.34 ± 10.25	23.77 ± 9.57	26.34 ± 18.49	35.17 ± 32.65
Non-dominant Shoulder/ Dominant Hip	**COV**	0.92 ± 0.05 δ	0.92 ± 0.03 ε	0.90 ± 0.04	0.89 ± 0.06	0.86 ± 0.07δε
	PERP (º)	23.25 ± 10.56θ	25.75 ± 10.16	25.38 ± 9.86	25.9 ± 10.92	31.23 ± 10.04θ

.

KINEMATICAL AND LOAD SHARING EFFECT OF A NOVEL POSTERIOR DYNAMIC STABIIZATION SYSTEM IMPLNATED IN LUMBAR SPINE

[1]D. U. Erbulut, [2]A. Kiapour, [3]T. Oktenoglu, [1,3]A.F.Ozer and [2]V. Goel

[1]Koc University, Istanbul, Turkey
[2]University of Toledo, Oh, USA
[3]VehbiKoc Foundation American Hospital, Istanbul, Turkey
email: derbulut@ku.edu.tr

INTRODUCTION

Posterior dynamic stabilization systems (PDS) has been proposed as an alternative solution for treatment of degenerative disc disease. PDS systems are designed to restore the kinematics of destabilized segment to its intact state.

The objective of this study was to investigate the biomechanical effect of a novel PDS system on lumbar spine. A cadaveric experiment followed by a Finite Element (FE) modeling approach were used for this purpose.

MATERIALS AND METHODS

The dynamic stabilization system included a set of dynamic rod and dynamic screws. The diameters of each coil was so that there was no gap between each layer. To perform the cadaver testing, six fresh-frozen human lumbar spine specimens were used. The specimens were screened and the CT images were obtained to ensure that the specimens are healthy and free of any abnormality.

Each specimen was cleaned and was potted an either ends prior to mounting on the testing machine, Figure 1. A set of LEDs, attached to a rigid plate, was affixed to each vertebrae to track the spatial motion at each level. Rods and screws were attached to the upper rigid block at the cranial end of the specimen for applying the physiological bending moment. Each specimen was tested as intact and instrumented state. The instrumentation was performed at L4-L5 level and included two surgical cases: Dynamic Screw and Dynamic Rod (DSDR) and Rigid Screw and Rigid Rod (RSRD). The screws and rods were made of stainless steel. For the surgical cases, a diskectomy was performed at the index level prior to instrumentation.

Both intact and instrumented cases were subjected to a pure bending moment which was applied in increments of 1.5, 3.0, 4.5, 7.0 and 10 Nm (maximum) to simulate physiological flexion (Flex), extension (Ext), lateral bending (LB), and axial rotation (AR). The OptoTrak camera system was used to capture the instantaneous spatial coordinate of each LED and use these coordinates to compute the relative kinematics of each motion segment. A statistical analysis was performed on the obtained kinematic data using two-tailed paired Student's t-tests to determine whether significant changes in motion occurred after implantation. Repeated measures analysis of variance (ANOVA) followed by the Neuman-Keul's test was used to detect statistically differences between treatment intervention. A 95% confidence interval was assessed. P-values less than 0.05 were considered a significantly different.

A finite element (FE) evaluation was followed by cadaver experiment using a nonlinear and 3D model of L1-S1 segment, Figure 1. This model consists all main physiological features of the actual spine including bone, intervertebral disc and ligament group [1]. The FE model was validated with cadaveric data through simulation of same surgical scenarios the discectomy followed by instrumentation at L4-L5 same as *in vitro*. A 3D model of each instrumented construct was obtained, meshed and placed at L4-L5 of the FE model to simulate each surgical intervention. The rod ends were fixed into screw heads in each construct and screw shafts were affixed to pedicle hole at each level. A frictionless contact formulation was defined between coils of the left and right dynamic rods in the dynamic stabilized model. The kinematic results obtained from the FE cases were compared with those of *in vitro* experiment for validation of the model, then the FE model was used to predict the important biomechanical feature i.e. peak stresses in the screws.

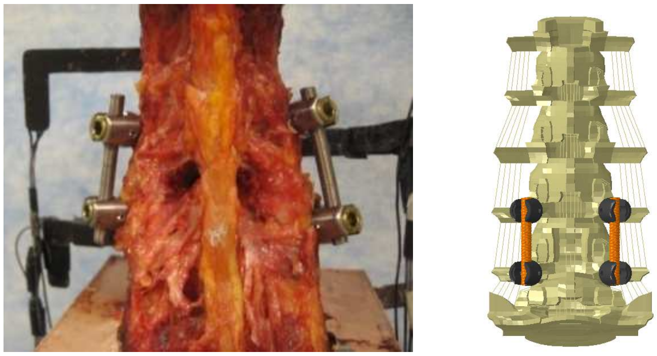

Figure 1: Lumbar spine instrumented at L4-L5: Cadaver spine (left), FE spine (right).

RESULTS

Post dynamic stabilization, the ROM was observed for all motion directions, Flex, Ext, LB and AR (Figure 2). At the treated segment, L4-L5, a statistically significant reduction in motion was observed for RSRR fixation in flexion ($p<0.024$), extension ($P<0.020$) and bending ($P<0.024$) (33%Flex, 56%Ext, 44%LB and 55%AR). After implantation, DSDR restored motion close to intact in all loading directions ($P>0.05$) (7,4º Flex, 5,4º Ext, 4,4ºLB, 4,9ºAR).

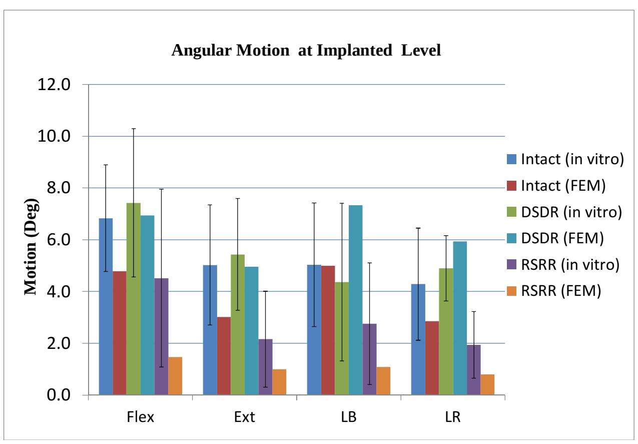

Figure 2: The FE data of range of motion compared with experimental data for intact vs. instrumented cases.

The FE model has ROM predictions for DSDR and RSRR within the range of experiment. In the FE model, the DSDR had motions with values of 6.9^0, 5^0, 7.3 and 5.9^0 in flexion, extension, left bending and rotation respectively. FE analysis predicted that the peak stress at the screw tail in DSDR case was 35, 26, 49 and 21MPa in Flex, Ext, LB and LR in respectively (Figure 3). In DSDR model these values were 108, 89, 110 and 128MPa respectively (Figure 3).

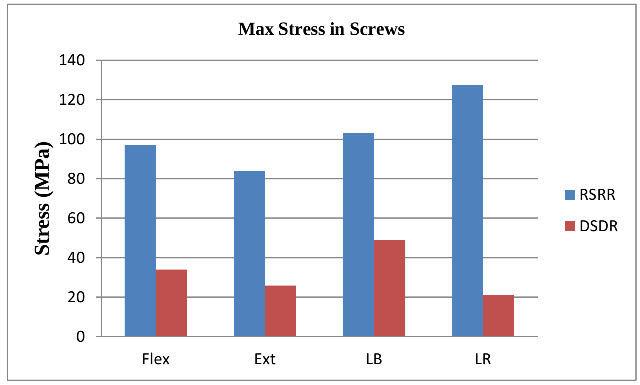

Figure 3: Peak stress in the pedicle screw in rigid and dynamic systems.

DISCUSSION

Both *in vitroo* and FE simulations showed that all systems were able to stabilize the treated segment where DSDR restored the kinematics to intact. The data showed that the rigid system provides more constrained on the treated level. Dynamic system allowed near normal kinematic at the treated level which is resulted with less load distribution on the screw than rigid systems. The novel dynamic instrumentation avoids adjacent disc hypermobility.
Rigid systems might cause screw failure due to high stress on the screw tails. However novel dynamic rod prevented high stress on the pedicle screws by preserving the normal spinal motion. These results may suggest that the novel dynamic instrumentation may be used for back pain treatment. Clinical investigation still remains for DSDR system in order to verify the system functionality.

REFERENCES

[1] Goel VK, et al. SAS Journal, **1**, 55-62, 2007.

INFLUENCE OF VARIOUS HEIGHTS AND SURFACES ON NEUROMUSCULAR STRATEGIES DURING DROP LANDINGS.

Emily M. Esselman, Abigail L. Carpenter, Jeremy D. Smith, Gary D. Heise
University of Northern Colorado
email: esse0585@bears.unco.edu

INTRODUCTION

Drop landings are a common component of sport and exercise training programs and often play an important role in successful sport performance [1]. In order to absorb and distribute ground reaction forces, controlling one's body during the landing offers substantial challenges. In drop landings, the goal is to decrease the body's momentum, absorb impact forces, stabilize the body, and prevent harmful joint rotations [2]. Previous research on drop landing strategies in gymnasts from various heights onto surfaces simulating gymnastics landing mats [3, 4] focused on lower body kinematics and loading rates. Additionally, some attention has been given to identifying changes in landing techniques using joint angles and muscle activation comparisons from different heights [5], but this approach did not examine muscle co-activation. The aim of the current study was to examine muscle activity during landing, including co-activation, across various drop heights and landing surfaces. In addition, joint angles were evaluated to examine the relationships between joint kinematics of the lower extremity during variations of drop landings. Therefore, the goal of this study was to better understand how drop height and landing surface influence muscle co-activation and limb position at contact during a drop landing.

METHODS

Simultaneous capture of motion, force, and electromyographic (EMG) data of 14 adults (mass = 72.2 ± 13.7 kg, height = 1.8 ± .1 m, age = 22 ± 2 yrs) were collected. Participants were excluded if they currently had a musculoskeletal injury of the lower extremity had an injury within the previous three months. Surface electrodes were placed on the following muscles of the non-dominant side: rectus femoris (RF); vastus lateralis (VL); medial hamstrings (MH); gastrocnemius (GAS); tibialis anterior (TA). Following electrode placement volunteers were asked to perform a maximum voluntary contraction (MVC) using isometric settings on an isokinetic dynamometer (Biodex Medical Systems, Shirley, NY). The trial with the greatest EMG amplitude for the muscle of focus was used later to normalize EMG amplitude during landing. Participants dropped from two plyometric boxes; a tall box (61.5 cm) and a short box (30.5 cm) onto the force plate. In addition to landing on the rigid force platform, they landed on a compliant surface, which was a viscoelastic foam pad commonly used to disrupt proprioceptive feedback (Airex AG Specialty Foams, Sins, Switzerland). For each condition, participants completed three trials for a total of 12 drops. The trial sequence was randomized.

The landing phase was defined as beginning 150 ms prior to initial contact, and ending when the velocity of the center of mass returned to zero. DC-bias was removed from the EMG signals. Then EMG signals were full-wave rectified low-pass filtered (cut-off 15 Hz), and normalized to the appropriate MVC. Kinematic data were computed using VICON's plug-in-gait model (VICON, Denver, CO). Muscle co-activation groups were chosen based on primary muscle functions at the joints of interest. GAS and TA were examined because of their actions at the ankle joint. RF, VL, and MH were examined because of hip and knee actions, and all muscles that cross the knee joint were included in the third co-activation measure (RF, VL, MH, and GAS). Muscle onset and cessation were identified manually by a single experimenter and durations of co-activation were calculated using custom software (MATLAB r2010a, MathWorks, Lowell, MA). Two-way repeated measures ANOVAs were used to determine differences in joint angles at landing and muscle co-activation between surface conditions and drop height. Significant ($p< .05$) results are reported.

RESULTS AND DISCUSSION

Regarding lower extremity joint angles at contact, significant differences in hip ($F_{1,13} = 6.84$, $p = .021$) and knee angles ($F_{1,13} = 8.09$, $p = .014$) were found for surface conditions, suggesting participants' hip and knee joints were more flexed when landing on a rigid surface (Figure 1). This is consistent with previous findings [4] and Lee et al. [5] suggest this strategy may be used to aid in reducing the force experienced by increasing the duration of landing. At the ankle, a significant main effect was identified for drop height and an interaction was found. Thus, the increase in ankle plantarflexion from rigid to compliant surface was greater when dropping from the tall box as compared with the small box ($F_{1,13} = 4.72$, $p = .049$).

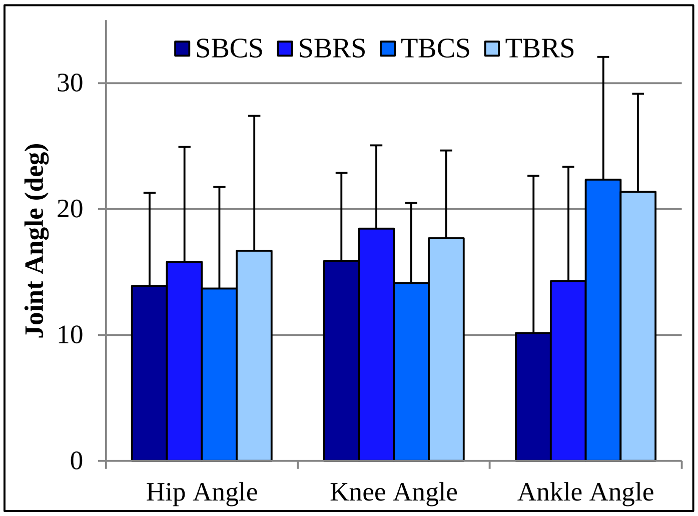

Figure 1: Hip flexion, knee flexion, and ankle plantarflexion at contact.

Co-activation between GAS and TA and among RF, VL, and MH were not affected by changes in surface or drop height. The combined co-activation among all muscles considered that cross the knee (RF, VL, MH, and GAS) revealed a significant main effect for surface condition ($F_{1,13} = 5.68$, $p = .033$).

When landing on the compliant surface the decreased joint flexion, coupled with greater co-activation of muscles crossing the knee joint suggest participants adopted a strategy with greater leg stiffness. However, when landing on a rigid surface, increased hip and knee joint flexion coupled with decreased muscle co-activation suggests a less stiff leg at landing.

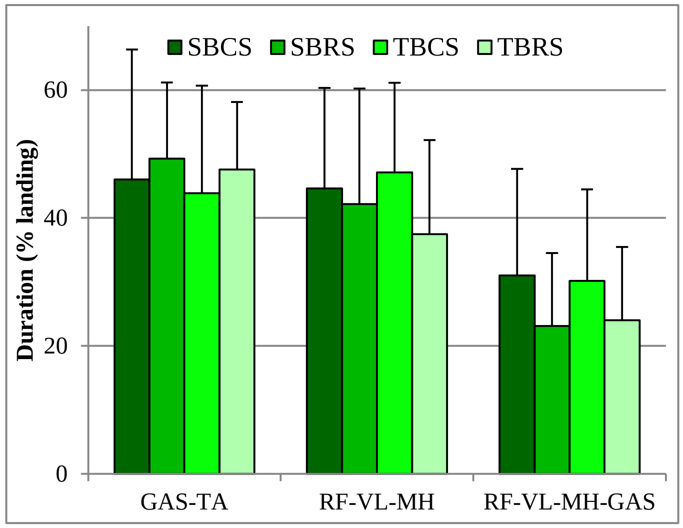

Figure 2: Muscle co-activation durations, expressed as a % of the landing phase. GAS-TA were co-active an average of 45-50% for the four conditions, RF, VL and MH were co-activated approximately 37-47%. However, when adding GAS to the RF, VL and MH combination, co-activation for all muscles at the knee decreased to between 23-30%.

CONCLUSIONS

Findings from this study suggest that drop height had minimal influence on preferred landing strategies as evidenced by the lack of significant effects on all variables except the ankle angle. Landing on different surfaces, however, did indicate a change in preferred landing strategies, specifically participants adopted a strategy that was more consistent with a stiffer leg when landing on a compliant surface.

REFERENCES

1. Yeow CH, et al. *J Biomech* **42**, 1967-1973, 2009.
2. Ambegaonkar JP, et al. *J Str Cond Res* **25**, 2781-2788, 2011.
3. McNitt-Gray JL, et al. *J Biomech* **9**, 173-190, 1993.
4. McNitt-Gray JL, et al. *J Biomech* **10**, 237-252, 1994.
5. Lee S, et al. *J Phys Ther Sci* **23**, 303-305, 2011

REMOVAL OF PAIN FROM PATIENTS WITH SHOULDER IMPINGEMENT RESULTS IN ALTERATIONS IN SHOULDER MUSCLE ACTIVITY & SCAPULAR KINEMATICS

[1] Luke R. Ettinger M.S, [2] Mathew M. Shapiro M.D, [1] Andrew R. Karduna Ph.D

[1] University of Oregon, Eugene, OR, USA
[2] Slocum Orthopaedics, Eugene, OR, USA
email: lettinge@gmail.com

INTRODUCTION

Pain has often been recognized as playing an important role in the neuromotor control of scapular posture and shoulder stability [1]. Understanding the relationship between pain and neuromuscular control is vital to the treatment and rehabilitation of patients with painful shoulder disorders. Lund et al. suggested that pain increases the activity in the antagonist muscle and decreases the activity in the agonist muscle during voluntary movement [2]. Experimentally induced pain to the subacromial bursa has been shown to increase antagonist muscle activation during arm elevation (latissamus dorsi); however, for agonist muscles variable results have been reported [3]. Additionally, it is likely that muscles respond differently when pain is acute (experimental) versus chronic (patient population). We hypothesize that patients with subacromial impingement syndrome will have reductions in antagonist muscle activity and increased agonist muscle activity when pain is reduced via a subacromial anesthetic injection. In addition, we hypothesize that pain inhibition will induce changes in scapular kinematics that reflect the compensatory changes seen in muscle activation.

METHODS

Seven patients with a mean age of 58.3 (±7.34) years diagnosed with stage 2 subacromial impingement syndrome were included in this study. Patients having had shoulder surgery on the symptomatic side, a positive Spurling test, traumatic shoulder dislocation or instability in the past 3 months, reproduction of shoulder pain with active or passive cervical range of motion, or signs of a rotator cuff tear (drop-arm test, lag signs, gross external rotation weakness assessed by a manual muscle test, or positive image findings) were not included in this study. Surface EMG activity was measured from seven shoulder muscles (anterior, middle and posterior deltoid, latissamus dorsi, upper and lower trapezius and serratus anterior) on the affected arm during three arm elevation trials in the scapular plane. Each arm elevation trial was performed isokinetically at approximately 30 degrees per second. Three dimensional scapular kinematic data were measured using an electromagnetic tracking device (Polhemus Fastrak). Digitization of anatomic landmarks followed the proposed ISB standards [4]. All EMG electrodes were positioned using recommendations by Cram et al. [5]. Subjects completed a visual analog scale (VAS) questionnaire depicting their worst pain immediately following the arm elevation task. All data were collected before and after a subacromial injection of 3cc 2% Lidocaine followed by an additional injection of 6cc 0.5% Marcaine with Epinephrine and 1 cc Depo-Medrol. Normalization of EMG was calculated by percent maximal voluntary contraction (MVC) of each muscle during a 5 second contraction, where the amplitude of the contraction was determined by the root mean squared (rms) over the middle two seconds of the muscle contraction. Each muscle's MVC was determined in a unique testing position after a subacromial injection, with approximately 20 seconds of rest between testing different muscles. No sensors were removed between the pre and post injection tests. All EMG data were sampled at 1200 Hz. All motion data were sampled at 40 Hz.

RESULTS

Following an anesthetic subacromial injection, there was a reduction in pain of approximately 62%; pre injection VAS 6.3/10 ± 2.4, post injection VAS

2.8/10 ± 1.4. After patients received subacromial injections, antagonist muscle activity decreased (latissamus dorsi). Additionally, it appears that most agonist muscles had a decrease in activity post injection as well (anterior deltoid, lower trapezius and serratus anterior), with the exception of upper trapezius, which increased in activity post injection (Figure 1). No trends for scapular upward or external rotation were noticed following an anesthetic injection. However, patients tended toward a more anteriorly tilted scapular position at all levels of humeral elevation following a subacromial injection (Figure 2).

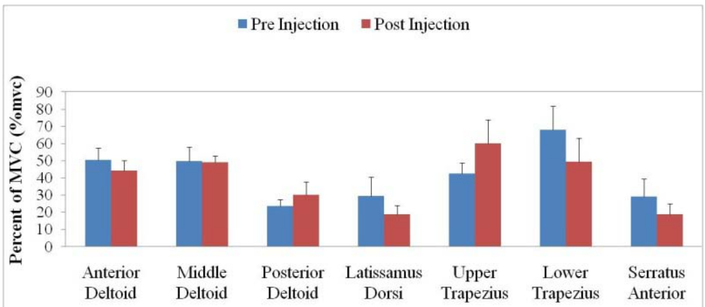

Figure 1: Muscle activity during isokinetic arm elevation at 90 degrees of humeral elevation.

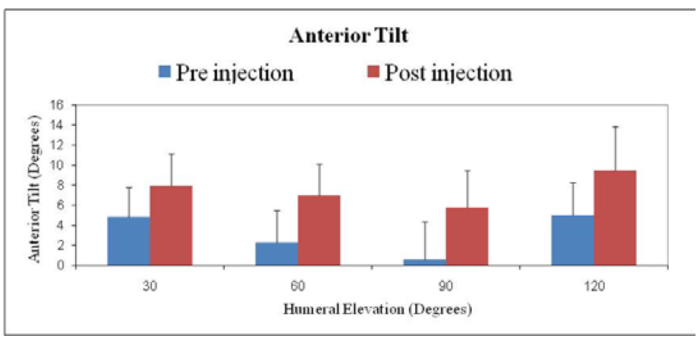

Figure 2: Scapular tilt during isokinetic arm elevation pre (blue) and post (red) injection.

DISCUSSION

Scapular posterior tilt and upward rotation have been reported to increase the subacromial distance and may bring relief to patients with subacromial impingement [1]. In general our patients had a slight increase in scapular anterior tilting post injection. This finding may be explained by the 10% reduction in MVC of serratus anterior activation after pain was reduced. For scapular upward rotation, no changes were observed following injection. Interestingly, both agonists (lower trapezius and serratus anterior) and antagonists (latissamus dorsi) had decreased activation post injection. This finding may explain why no kinematic changes were observed for scapular upward or external rotation. We predicted a decrease in muscle pain may be related to a reduction in antagonist muscle activation and an increase in agonist activation. For antagoinist muscle activity our hypothesis was supported; however, we found mixed resluts for agonist activity. It is possible that agonist muscles such as serratus anterior and lower trapezius have greater activation during pain and may help to compensate by decreasing scapular anterior tilt and increase scapular upward rotation. Additionally, it is possible that when pain is reduced, the neurologic mechanisms that recruit these scapular stabilizers are altered.

CONCLUSIONS

These findings suggest that pain may naturally induce compensatory scapular mechanics by reducing scapular anterior tilting. The effects of a local anesthetic injection influenced pain reduction in all patients tested. Pain dis-inhibition seems to have an effect on scapular muscle activity and scapular anterior tilting. The lack in changes for scapular rotation may indicate that kinematic and muscle adaptations occur over time. Kinematic adjustments to a pain free shoulder may not occur immediately. Agonist muscle activation did not behave uniformly following the injection, therefore generalized pain adaptation models as described by Lund et al. may not explain scapular adaptive patterns to chronic joint pain.

REFERENCES

1. Ludewig P. *Physical Therap*, **80**, 276–291, 2000.
2. Lund JP. *Can J Physiol Pharm*, **69**, 683–669, 1991.
3. Diederichsen LP. *Exp Brain Res*, **194**, 329–337, 2009.
4. Wu G. *Journal of Biomechanics*, **38,** 981–992, 2005.
5. Cram JR. *Aspen Publishers*, 400–410, 1998.

EMG NORMALIZATION TECHNIQUES FOR PATIENTS WITH PAIN

Luke R. Ettinger M.S, Jason Weiss, Andrew R. Karduna Ph.D.

[1]University of Oregon, Eugene, OR, USA
email: lettinge@gmail.com

INTRODUCTION

Electromyography (EMG) is a technique used for measuring electrical activity of skeletal muscles. EMG has been used clinically to help diagnose pathologies consisting of muscle weakness, fatigue and neurologic disorders, to name a few. From a recent review of studies using EMG to compare differences between patients with subacromial impingement syndrome versus healthy controls, differences between groups were attributed to neurologic and/or musclular compensation [1]. There are several limitations to these studies, including differences in the sensor placement (motor neurons being sampled) as well as variability between patients. Therefore, in order to compare individuals, EMG is often normalized to a maximal voluntary contraction (MVC). Khan et al., reported that experimentally induced muscle pain caused significant reductions in muscle activation during MVC; however, submaximally no changes in muscle activity were observed [2]. Therefore, it is the goal of the study to measure the effect of pain on commonly used MVC normalization techniques. It is hypothesised that MVC will be increased once pain is reduced in patients with subacromial impingement recieving a subacromial injection of anesthetic. Additionally, it is hypothesised that pain will cause an over-estimation of muscle activity during submaximal tasks due to errors in normalization technique.

METHODS

Seven patients with a mean age of 58.3 (±7.34) diagnosed with stage 2 subacromial impingement syndrome were included in this study. Patients suspected on having full thickness rotator cuff tears, cervical or neurologic disorders were not included in this study. Surface EMG activity was measured from seven shoulder muscles on the affected arm during an arm elevation task, where patients were asked to complete three arm elevation trials in the scapular plane before a subacromial injection. Arm elevation was approximately 30 degrees per second. Humeral elevation data were measured using an electromagnetic tracking device (Polhemus Fastrak), data were sampled at 40 Hz. All EMG electrodes were positioned using recommendations by Cram et al. [3] (Figure 1). Normalization of EMG was calculated by percent maximal voluntary contraction (MVC) of each muscle during a 5 second contraction, where the amplitude of the contraction was determined by the root mean squared (rms) data over the middle 2 seconds of the muscle contraction. Each muscle's MVC was determined in a unique testing position, with approximately 20 seconds of rest between testing different muscles, MVC tests were performed before and after the subacromial injection. EMG from the arm elevation task before the subacromial injection were analyzed two ways, first by normalizing EMG to an MVC pre injection. Second, EMG data were normalized to an MVC post injection. MVC data were collected before and after a subacromial injection of 3cc 2% Lidocaine followed by an additional injection of 6cc 0.5% Marcaine and 1 cc Depo-Medrol. No sensors were removed between the pre and post injection tests. All EMG data were collected at 1200 Hz. Subjects completed a visual analog scale (VAS) questionnaire during the arm elevation trial depicting their worst pain during the task. A two-way repeated measures ANOVA were run to test for differences in MVC (mV) pre and post injection for each of the 7 muscles tested. A separate 2-way ANOVA was run to test for differences in percent MVC pre and post injection during an arm elevation trial (pre injection) at four levels of humeral elevation (30, 60, 90 and 120 degrees). For simplicity purposes, in the second analysis, only Anterior Deltoid data are presented here.

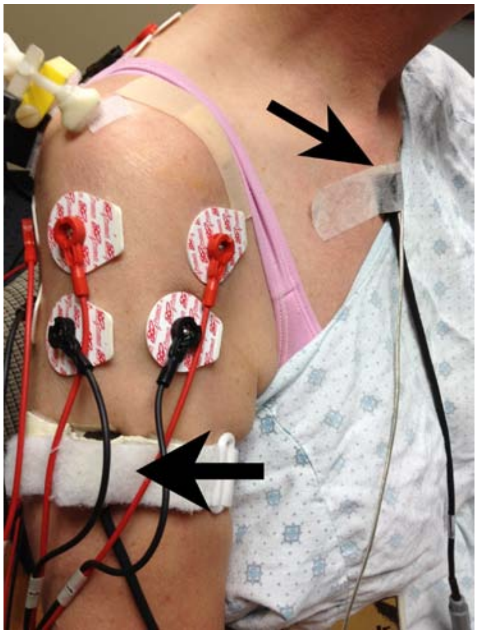

Figure 1: Experimental setup. Arrows indicate humeral and thoracic sensors. Emg setup for anterior, middle and posterior deltoid muscles.

RESULTS

Anesthetic subacromial injection resulted in a reduction in pain of approximately 62%; pre injection VAS 6.3/10 ± 2.4, post injection VAS 2.8/10 ± 1.4.

Results of the ANOVA test indicate that post injection MVC's (0.333 ± 0.066 mV) were greater than pre injection (0.251 ± 0.049 mV) MVC's, p = 0.02. Additionally, there was a significant main effect of muscle on EMG activity $p < 0.001$.

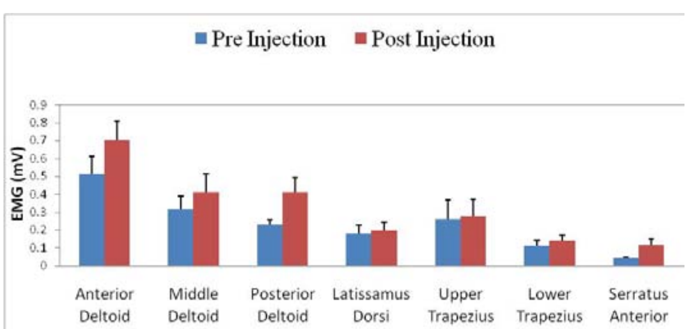

Figure 2: Pre and post injection MVC values for each shoulder muscle tested. Post MVC values are on average 0.082 mV higher than pre MVC values.

Results of the ANOVA test for the percent MVC contribution to arm elevation for anterior deltoid by normalization technique (pre and post injection) at four levels of humeral elevation angle indicate that pre injection normalization overestimates the percent MVC by 20% on average, p = 0.001.

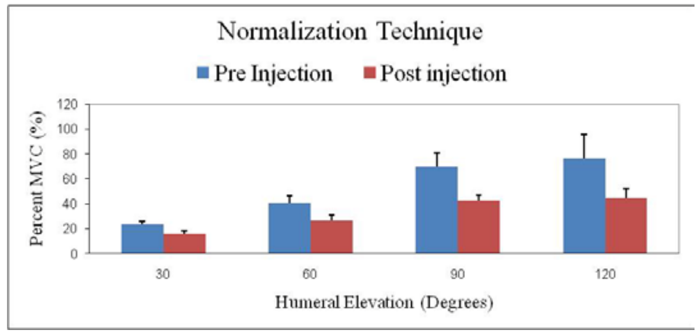

Figure 3: Percent MVC contribution of Anterior Deltoid for each level of humeral elevation angle using pre and post injection normalization values.

DISCUSSION

Normalization techniques are useful when trying to compare the EMG of individuals. However, our results indicate that normalization to a MVC in the patient population is confounded by pain and can cause an over estimation of submaximal muscle activity. This finding is due to the fact that maximal voluntary contractions appear to have weaker electrical activity in the presence of pain. Normalizaiton to a pain free MVC, such as after anesthetic injection, may reduce this error. However, anesthetic injections may also reduce the contractability of the muscle if the anesthetic drug comes into contact with efferent nerve fibers. Our patients all recieved an anesthetic injection to the subacromial bursa. It is believed that an anesthetic injection to this area causes little, to no disruption in the contractability of the surrounding musculature. Therefore, the technique of MVC described in this study may be useful in future studies examining differences between patients with subacromial impingement and healthy controls.

REFERENCES

1. Phadke V. *Rev Bras Fisoter*. **13**: 1-9, 2009.
2. Kahn S. I, *J Appl Physiol*. **111**: 743–750, 2011.
3. Cram JR. *Aspen Publishers*, 400 – 410, 1998.

THE EFFECTS OF WEARING A SPRING-LOADED ANKLE EXOSKELETON ON SOLEUS MUSCLE MECHANICS DURING TWO-LEGGED HOPPING IN HUMANS

Dominic Farris & Gregory S. Sawicki
North Carolina State University and University of North Carolina-Chapel Hill, Raleigh, NC, USA
Email: djfarris@ncsu.edu

Introduction

Assistive exoskeletons have the potential to aid locomotor recovery and restore walking function in neuro-muscularly and musculo-skeletally impaired individuals (e.g. post-stroke or spinal cord injury). They also may be used to augment locomotor performance in healthy individuals by reducing the metabolic cost of locomotion or reducing skeletal loading. Whilst these devices have been shown to be effective in replacing joint moments and powers, little is known about how they influence the underlying muscle function.

Neuro-muscularly intact humans rely on ankle plantar-flexor muscles to provide a considerable proportion of the mechanical work required for locomotion (40-50%)[1]. The main plantar-flexors (Gastrocnemius and Soleus) insert on the calcaneous via the compliant Achilles tendon. The series compliance provided by the Achilles allows these muscles to contract relatively isometrically during most of stance in walking and running, whilst the tendon stores and returns elastic energy [2]. This is an efficient way for the muscle-tendon units to produce force and provide work at the ankle joint. Thus, these mechanisms help to reduce the metabolic energy required for locomotion.

The use of spring-loaded ankle exoskeletons could reduce the required contribution of the plantar-flexors to ankle joint kinetics during cyclic motions but, they might also perturb the 'tuned' interaction of muscle and tendon. The purpose of this study was to investigate the effects of using spring-loaded ankle exoskeletons on soleus muscle mechanics during a cyclic motion (two-legged hopping).

Methods

Seven healthy male participants hopped at a range of frequencies (2.2, 2.5, 2.8 & 3.2 Hz) in 3 conditions: with bilateral spring-loaded ankle exoskeletons (SE); without exoskeletons (NE); & with bilateral spring-less exoskeletons (NS). The exoskeletons consisted of a carbon fiber cuff around the upper calf connected to a carbon fiber foot segment and training shoe by aluminium struts and a freely rotating joint on the medial and lateral sides. When the spring was attached, it connected the heel of the foot segment to the dorsal aspect of the cuff with the resting length set at an ankle angle of 127°. The linear stiffness of the springs was 5 kN/m.

A stationary instrumented treadmill was used to record ground reaction forces (Bertec, 980 Hz). Motion capture (Vicon, 120 Hz) was used to determine kinematics for a four segment (Pelvis, thigh, shank & foot) inertial model of the right leg. These were combined in a typical inverse dynamics analysis to compute ankle, knee and hip joint moments and powers using Visual 3D software (C-motion Inc.). EMG data were also recorded for soleus, gastrocnemius and tibialis anterior.

B-mode ultrasound images of Soleus muscle fascicles were recorded synchronously with the kinematics & kinetics using a linear array 128 element transducer (Telemed, 50 Hz). Manual digitization of these images provided a measurement of soleus fascicle length and pennation angle. Soleus muscle-tendon unit (MTU) lengths were calculated from regression equations using the ankle angle as input. A simple geometric model was then used to calculate series elastic element (SEE, the elastic tendon & aponeurosis in series with soleus) lengths. Forces in the SEE were modeled as the flexion-extension ankle joint moment divided by the Achilles tendon moment arm, multiplied by the relative physiological cross sectional area of soleus within the plantar-flexors. An adjustment of this force for pennation angle yielded the fascicle forces. Fascicle and SEE velocities were multiplied by their respective forces to give fascicle and SEE powers. Powers were integrated to calculate the positive and negative work done by each and this was divided by time to obtain average positive power of the fascicle (P^+_{FAS}) and SEE (P^+_{SEE}).

Results & Discussion

The results presented are for hopping at 2.5 Hz only. The use of spring-loaded ankle exoskeletons resulted in reduced force production by soleus and reduced average length of the SEE and MTU (Table 1). This was associated with lesser soleus EMG magnitude just after landing and a reduced positive power contribution from the SEE (Table 1, Fig 1d).

When hopping in assistive spring-loaded ankle exoskeletons, participants reduced the contribution of the soleus MTU to overall power production by reducing muscle activation in the early part of ground contact and thus reducing muscle force production. This limited the absolute lengths to which the SEE could be stretched (less force equates to less stretch) and thus limited the storage and return of elastic energy in the SEE and the overall length of the MTU. With less energy stored and returned by the SEE, the fascicles were able to maintain a similar power output across conditions by balancing their length change and force production. It should be noted that the relative length change of the SEE was similar between conditions, indicating that the shortening of the SEE with assistance may have taken it to a non-linear region of its length-tension relationship.

Conclusions

The use of spring-loaded ankle exoskeletons may reduce the overall work required of the soleus MTU but it does so by reducing SEE energy storage rather than fascicle work.

[1] Farris DJ & Sawicki GS. (2012). J. R. Soc. Interface. 9: 110-118.
[2] Lichtwark et al. (2007). J. Biomech. 40: 157-164

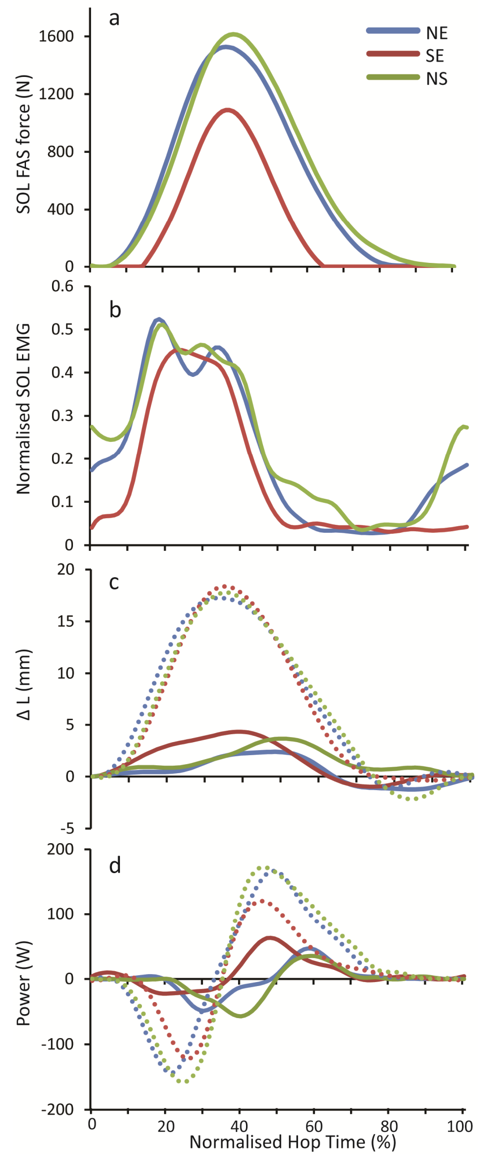

Fig 1. Soleus fascicle force (a); soleus root mean squared EMG (b); fascicle (solid) & SEE (dotted) length change (c) and power (d) over a hop. Data are group means.

Table 1. Group mean (sd) maximum soleus force; total excursion of soleus (ΔL); average length of soleus ($\bar{L}$) and average positive power output of soleus (P^+). The latter three are broken down into fascicle (FAS), SEE and MTU.

	Max SOL Force (N)	ΔL (mm) FAS	ΔL (mm) SEE	ΔL (mm) MTU	$\bar{L}$ (mm) FAS	$\bar{L}$ (mm) SEE	$\bar{L}$ (mm) MTU	$\bar{P}^+$ (W) FAS	$\bar{P}^+$ (W) SEE	$\bar{P}^+$ (W) MTU
NE	1623 (187)*	10 (2)	38 (11)	42 (1)	39 (3)	253 (9)*	291 (8)*	14 (2)	40 (5)*	40 (4)*
SE	1166 (194)	15 (2)	39 (6)	48 (1)	38 (4)	237 (7)	272 (6)	15 (3)	25 (3)	30 (4)
NS	1667 (119)*	9 (2)*	39 (8)	42 (2)	41 (4)	246 (8)*	285 (8)*	13 (2)	45 (4)*	40 (4)*

*Indicates significant difference from the SE condition (P<0.05, paired t-test)

DYNAMIC STABILITY OF INDIVIDUALS WITH AND WITHOUT UNILATERAL TRANS-TIBIAL AMPUTATIONS WALKING IN DESTABILIZING ENVIRONMENTS

[1]Kathryn A. Faust, [1,2]Kevin Terry, [2]Jonathan B. Dingwell, and [1]Jason M. Wilken

[1] Department of Orthopedics and Rehabilitation, Center for the Intrepid,
Brooke Army Medical Center, Ft. Sam Houston, TX, USA
[2] Department of Kinesiology, University of Texas at Austin, Austin, TX, USA
email: kathryn.a.faust.ctr@us.army.mil

INTRODUCTION

The purpose of this study was to determine how trans-tibial amputation alters the ability to respond to small-amplitude continuous visual or mechanical perturbations during walking. Vision is crucial for maintaining balance during walking. So is somatosensory feedback, which is severely disrupted in patients with amputation [1]. However, to date there are no data defining how these patients use visual and/or somatosensory information to walk. Here, healthy individuals' responses were compared to unilateral trans-tibial amputee patients' responses during continuous mediolateral perturbations of the walking surface or visual field. This is the first study to determine how amputation affects global and local dynamic stability during exposure to external perturbations while walking.

METHODS

Thirteen healthy individuals (24.8±6.9yrs) and nine patients (30.7±6.8yrs) with a unilateral trans-tibial amputation provided written informed consent prior to participation. All subjects walked on a 2m x 3m treadmill embedded in a 4m dia. moveable platform in a Computer Assisted Rehabilitation Environment (CAREN) virtual reality system (Motek, Amsterdam, Netherlands). Subjects' movements were tracked using 24 Vicon motion analysis cameras (Vicon, Oxford, UK).

Participants completed a 6-min warm-up followed by five 3-min trials under each of the following test conditions: no perturbation (NP), platform (PLAT) or visual field (VIS) perturbations. The order of the perturbation trials was randomized. All perturbations were applied as pseudo-random translations in the mediolateral direction [2,3]. The perturbation amplitudes used here were based on those used previously [3].

Orbital stability (maxFM) quantifies how purely periodic systems respond to perturbations discretely from one cycle to the next [2,4]. Local stability (λ^*_S) quantifies how the system responds to very small perturbations continuously in real time [2,5]. $\lambda^*_S > 0$ indicate instability. MaxFM > 1 indicate instability. For both λ^*_S and maxFM, larger values indicate greater sensitivity to perturbations. We calculated these exponents using previously published methods [2,4,5] using velocity trajectories of mediolateral C7 marker movements [2,4]. Both variables were calculated using a 5-dimensional delay-embedded state space [5] of C7 velocity with a time delay of τ=30 samples. For both maxFM and λ^*_S, a 2-way mixed repeated measures MANOVA with condition as the within factor and group as the between factor was used to determine the main effects for NP, PLAT and VIS perturbation trials.

RESULTS AND DISCUSSION

Consistent with previous work [2], orbital and short-term local instability both increased for platform and visual perturbed walking compared to unperturbed walking. In the mediolateral direction, patients exhibited slightly decreased maxFM during PLAT ($p<0.001$) and slightly increased λ^*_S during NP ($p<0.025$) compared to controls (Fig. 1). During VIS, patients exhibited slightly lesser λ^*_S than controls ($p<0.014$) (Fig. 1). While these differences were statistically significant, they were relatively small in magnitude.

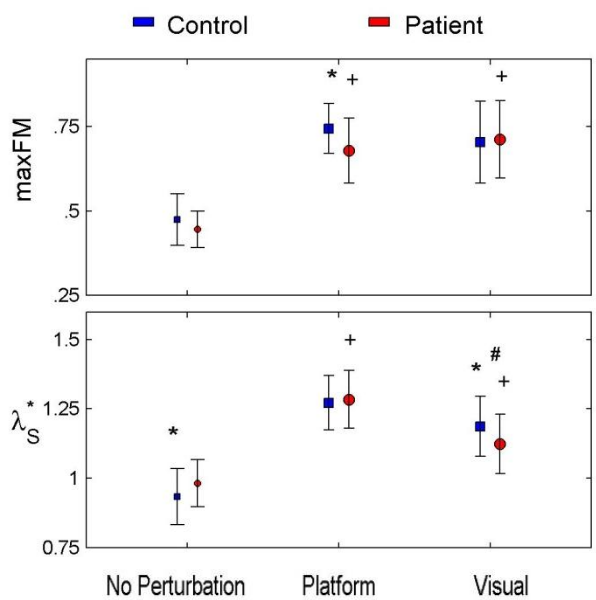

Figure 1: Dynamic walking stability (mean±SD) for NP, PLAT and VIS conditions. The * indicates a significant difference between control and patient. The + indicates that the perturbed condition is significantly different from the unperturbed condition for both groups. The # indicates a significant difference between PLAT and VIS for patients.

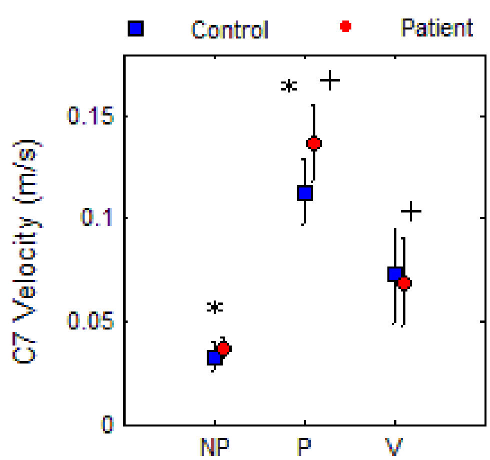

Figure 2: C7 velocity variability (mean±SD) for NP, PLAT and VIS conditions. The * indicates significantly different from control to patient. The + indicates that each condition was significantly different from each other condition.

For comparison, kinematic variability measured using the mediolateral C7 marker velocity (Fig. 2) was greater for patients during both the NP ($p<0.008$) and PLAT ($p<0.000$). The C7 velocity variability was also significantly different between conditions for both patients and controls ($p<0.000$).

Due to the lack of distal somatosensory feedback, we anticipated that the patients would rely more heavily on the visual feedback and therefore be more variable and less stable during VIS. Patients were, however, more stable during VIS (λ^*_S), and PLAT (maxFM) than controls and more stable (λ^*_S) during the VIS than PLAT ($p < 0.00$). Variability results were not consistent with stability analyses with patients being more variable during the PLAT.

Although significant, the between-group differences for all measures were quite small and not likely of functional relevance. The inconsistent results may be the product of a young, highly active and otherwise healthy population. This may be one reason we did not see larger differences in their dynamic stability during walking. The differing results for stability and variability measures further suggest that these measures do not quantify the same physiologic phenomenon.

CONCLUSIONS

Young, active patients with unilateral trans-tibial amputation were no less stable, locally or orbitally, than the controls when being mechanically or visually perturbed.

REFERENCES

1. Warren, W. H. , et al. (1996) *J EXP PSYCHOL* **22**(4): 818-838.
2. McAndrew, P.M., Wilken, J.M., & Dingwell, J.B., (2011) *J Biomech* **44** (4): 644-649.
3. McAndrew PM, et al., *J Biomech* **43(8)**:1470-75, 2010.
4. Dingwell, J.B. & Kang, H.G., (2007) *J Biomech Eng* **129** (4): 586-593.
5. Dingwell, J.B. & Cusumano, J.P, (2000) *Chaos* **10** (4): 848-863.

ACKNOWLEDGEMENTS

Supported by grant 5R01HD059844-02 from NIH (NICHD).

The view(s) expressed herein are those of the author(s) and do not reflect the official policy or position of Brooke Army Medical Center, U.S. Army Medical Department, U.S. Army Office of the Surgeon General, Department of the Army, Department of Defense or the U.S. Government.

SPATIOTEMPORAL PARAMETERS OF UPHILL, LEVEL AND DOWNHILL WALKING ARE SIMILAR BETWEEN TREADMILL AND OVERGROUND SURFACES

[1]Rebecca E. Fellin, [1]Joseph F. Seay, [2]Karen N. Gregorczyk and [2]Leif Hasselquist

[1]US Army Research Institute of Environmental Medicine, Natick, MA, USA
[2]US Army Natick Soldier Research, Development & Engineering Center, Natick, MA, USA
email: rebecca.e.fellin.ctr@us.army.mil

INTRODUCTION

Treadmill walking gait analyses are frequently conducted due to their ease of collecting multiple strides of data, minimal space required and ability to finely control speed. The question of whether treadmill (TM) walking gait replicates overground (OG) walking gait on a level surface, has been extensively studied. From a spatiotemporal perspective, TM walking on a level surface generally simulates OG walking [2,5].

Additionally, treadmills are advantageous to compactly simulate common outdoor terrain changes, such as uphill and downhill locomotion. Results of spatiotemporal parameters during uphill and downhill walking are mixed. In one OG study, stride length increased during both uphill and downhill walking when compared to level walking [4]. However, cadence decreased with uphill walking and increased with downhill walking, which may be due to subject's selecting a separate self-selected walking speed for each grade. In an OG study where speed was controlled, no differences in stride length in uphill walking were observed [1]. In contrast, during TM walking at consistent speed across grades, stride length increased during downhill walking and decreased during uphill walking compared to level walking [3]. No study to date has comprehensively assessed TM and OG walking at multiple grades. Therefore, the purpose of this study was to compare uphill, level and downhill walking gait between treadmill and overground modes at a constant speed.

METHODS

11 subjects aged 20.7 ± 2.9 years, height 1.71 ± 0.06 m and weight 73.0 ± 6.4 kg volunteered to participate in this study. Subjects completed four separate sessions, an orientation and then 3 sessions of OG and TM walking for 1 grade (downhill, -6% grade; level, 0% grade or uphill, +6% grade) per session. Session order and OG and TM order within a session were counterbalanced across subjects. Subject self-selected speed was determined during a 3 minute bout of OG walking on a level surface, which was then utilized for all data collections. The OG range of speeds was self-selected speed ± 5%. Subject instrumentation included a sagittal plane marker set with reflective markers placed on the torso, pelvis and lower extremity. OG data were collected on a 12 m grade-adjustable walkway. Subjects had several warm-up trials to acclimate to the OG capture volume, following which three trials comprising several strides of marker data were collected at 120 Hz (QTM, Qualisys Medical AB, Gothenburg, Sweden). A minimum of 6 strides total were used for the OG data analysis. The TM walking trials were conducted on a split-belt treadmill (AMTI, Watertown, MA, USA) with two belts (107 x 56 cm) in a fore/aft configuration. Kinematic data were collected after a 5 minute warm-up within the same capture volume as the OG data. Six consecutive strides of TM data from both lower extremities were selected for analysis.

Kinematic data were filtered at 6 Hz in Visual 3D (C-motion, Germantown, MD, USA). Heelstrike and toe-off were determined as the maximum anterior heel position and maximum posterior toe position relative to the pelvis, respectively [6]. This method was used for consistency between OG and TM trials. Cycle time, stride length, cadence and double support time were calculated in Visual 3D, with the first 3 variables averaged across limbs. 2x3 repeated measures ANOVAs were used to evaluate differences in mode (TM, OG) and grade (uphill, level or downhill) (SPSS version 19, IBM, Armonk, NY, USA). When indicated, a post-hoc t-test was conducted using a Sidak adjustment for repeated measures. Effect sizes (ES) were calculated to aid in interpretation of results.

RESULTS AND DISCUSSION

Grade influenced spatiotemporal parameters during both TM and OG walking (Table 1). Post-hoc testing indicated that compared to level walking, subjects walking downhill had decreased double support and cycle times and a faster cadence. Compared to downhill walking, subjects walking uphill had increased double support and cycle times, slower cadence and longer strides. There were no significant difference between level and uphill walking. There were no differences between TM and OG walking nor was there an interaction between grade and mode.

This research was the first report the authors are aware of that compared graded walking in both TM and OG modes. Regardless of grade, TM and OG walking were consistent from a spatiotemporal perspective. Speed was tightly controlled in this study, which may explain the lack of differences between TM and OG walking. In addition to the OG speed limited to ± 5% of the subject's self-selected OG walking speed, actual speed was calculated from stride length and cycle time in Visual 3D. Statistically, there were no differences in actual speed across mode and grade, which indicated that speed was consistent across the strides analyzed.

Increases in stride length and cycle time during uphill compared to downhill walking were similar to those reported by Leroux and colleagues during TM walking at constant speed [3]. However, they found no change in gait-cycle proportions while this study found changes in double support. In this study cadence was faster downhill than uphill, similar to McIntosh and colleagues, who studied subjects OG at self-selected speeds [4]. The stride length results of this study were opposite possibly because this study controlled speed across grades.

The changes with grade were small in magnitude. The average within-subject differences between uphill and downhill walking were <0.1 s for timing variables, 3.6 steps/min and 0.05 m in stride length. Despite these small differences, double support time had a moderate ES (≥.5) between downhill and uphill walking. ES for other variables between uphill and downhill walking were 0.28-0.47. Between downhill and level walking ES were small (< 0.46). It remains unclear what the clinical implications were of these small, but consistent, changes in double support with different grades.

One potential limitation of this study was collecting between grade data in multiple sessions. However, this limitation was mitigated with tight speed control and utilizing subject's self-selected speed.

CONCLUSIONS

Spatiotemporal parameters were similar between overground and treadmill walking. Regardless of whether subjects were walking overground or on a treadmill, spatiotemporal parameters responded in similar fashion to changes in grade.

REFERENCES

1. Lay et al. *J Biomech* **39**, 1621-1628, 2006.
2. Lee and Hilder. *J Appl Physiol* **104**, 747-755, 2008.
3. Leroux et al. *Gait Posture* **15**, 64-74, 2002.
4. McIntosh AS, et al. *J Biomech* **39**, 2491-2502, 2006.
5. Riley PO, et al. *Gait Posture* **26**, 17-24, 2007.
6. Zeni JA, et al. *Gait Posture* **27**, 710-714, 2007.

ACKNOWLEDGEMENTS

Shane Sauer for data processing assistance. Carolyn K. Bensel and Jeffrey M. Schiffman for study design and implementation assistance.

Table 1: Spatiotemporal parameters (mean (SD)) for downhill (D), level (L) and uphill (U) grades during treadmill (TM) and overground (OG) walking. P values (analysis collapsed across modes) include Sidak adjustment, significance in **bold**.

Variable	**Downhill (-6%)**		**Level (0%)**		**Uphill (+6%)**		**P values**		
	OG	**TM**	**OG**	**TM**	**OG**	**TM**	**D/L**	**D/U**	**L/U**
Double Support (s)	0.30(0.03)	0.29(0.03)	0.32(0.03)	0.31(0.03)	0.34(0.04)	0.32(0.03)	**p< .001**	**p< .001**	p= .056
Cycle Time (s)	1.09(0.06)	1.10(0.06)	1.11(0.07)	1.12(0.07)	1.14(0.08)	1.12(0.06)	**p= .015**	**p= .002**	p= .215
Cadence (steps/min)	110.0(6.3)	109.8(6.1)	108.3(6.5)	107.7(6.8)	105.6(7.1)	107.2(6.3)	**p= .011**	**p= .001**	p= .241
Stride Length (m)	1.49(0.08)	1.48(0.10)	1.52(0.10)	1.53(0.13)	1.54(0.11)	1.53(0.13)	p= .058	**p= .023**	p= .661

DEVELOPMENT OF AN EFFICIENT FLUID-STRUCTURE INTERACTION SOLVER FOR APPLICATIONS TO THE VASCULAR SYSTEM

[1]Chessy Fernandez, [1]Scott Berceli, [2]Marc Garbey, [1]Nam H. Kim, and [1]Roger Tran-Son-Tay

[1]University of Florida, Gainesville, FL, USA
[2]University of Houston, Houston, TX, USA
email: chessy@ufl.edu

INTRODUCTION

Physical forces stand among the primary factors that regulate blood vessel response. While increased wall shear promotes luminal expansion, elevated circumferential wall stress supports wall thickening and stabilization of the lumen size [1-3]. The interaction of these two divergent responses can lead to significant patient to patient variability in observed clinical outcomes. Coupled solutions of these competitive processes can be modeled with the use of finite element (FE) packages. Hindering these commercially available finite element packages from real time clinical analysis is the fact that they require a complex modeling process for patient-specific arterial geometry and exhaust computational power and time for evaluating the fluid dynamics of the aneurysm. The proposed fluid-structure interaction (FSI) solver tackles the problems faced with current FE packages by creating a simpler modeling process by sharing a grid scheme and speeding up the computational time.

METHODS

Using an Eulerian staggered grid scheme and an immersed boundary method, the fluid and structure are coupled through the pressure and the vessel wall. The Navier-Stokes equations (Equation 1) assume an incompressible flow and are solved using a central finite difference scheme. The structural analysis (Equation 2) utilizes a novel topographical approach with a level set method to track the vessel wall within a fixed grid scheme. The structural analysis assumes a linear elastic model with an axisymmetric geometry.

In Equation (1), U is the fluid velocity, p is the pressure, ν is the kinematic viscosity, and f is the forcing term for the immersed boundary method [3].

$$\begin{aligned}
&\partial_t U + (U.\nabla)U + \nabla p - \nu\nabla.(\nabla U) = f \text{ in } \Omega \\
&\mathrm{div}(\mathrm{U}) = 0 \text{ in } \Omega \\
&U = g \text{ on } \partial\Omega
\end{aligned} \tag{1}$$

$$[\mathbf{K}]\{\mathbf{Q}\} = \{\mathbf{P}\} \tag{2}$$

In Equation (2) **[K]** represents the stiffness matrix, **{Q}** the displacements, and **{P}** the nodal forces caused by the boundary pressure [4]. Equation (2) is used to calculate a new boundary geometry using the level set method for a given boundary pressure while Equation (1) is used to calculate the velocity and pressure for a given boundary geometry.

Verification and validation tests were performed using simplistic geometries. Assuming a Poiseuille flow, a straight axisymmetric cylindrical vessel was used to test the fluid and solid modules separately as well as the FSI solver. The ends of the tube were unfixed in order for the wall to expand and uniform material properties were used along the entire length of the vessel. The average human blood pressure was used to provide an intraluminal pressure.

RESULTS AND DISCUSSION

A stability and convergence analysis was performed separately for the fluid model and the solid model to verify the solution has converged. Three grid sizes were used and the solution converged as expected showing that the solution is independent of the grid size and the solution stabilized. Fluid and solid models were decoupled and verified by comparison to analytical solutions and found to be in good agreement. Results obtained with a commercially available computational software (ADINA, Boston, MA) and our FSI model are shown in Table 2 and Figure 1. Comparison showed that the solutions matched within reasonable error. Figure 1 shows the velocity and wall displacement for both FSI simulations. The analytical solutions for both the fluid and solid domains were calculated and found to be in good agreement with the results. Stability and convergence analyses were performed on the FSI solver and found the solution has converged and was independent of the grid size.

Table 1: Physical Parameters for Model Geometry

Parameter	**Values**
Straight Wall Geometry	
Artery Diameter	20 mm
Total Length	150 mm
Wall Thickness	2 mm
Fluid/Material Properties	
Elastic Modulus	3 x 10^6 dynes/cm^2
Internal Pressure	100 mmHg
Kinematic Viscosity	0.04 poise
Poisson's Ratio	0.45
Centerline Velocity	27 cm/s

Table 2: Comparison between FSI model and ADINA

FSI straight axisymmetric model	
Parameter	**Percent Difference**
Outlet Centerline Velocity	1.43 %
Wall Displacement	<1%
Inlet Fluid Pressure	-2.9%

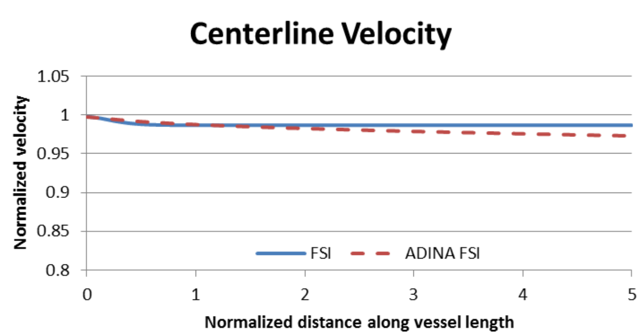

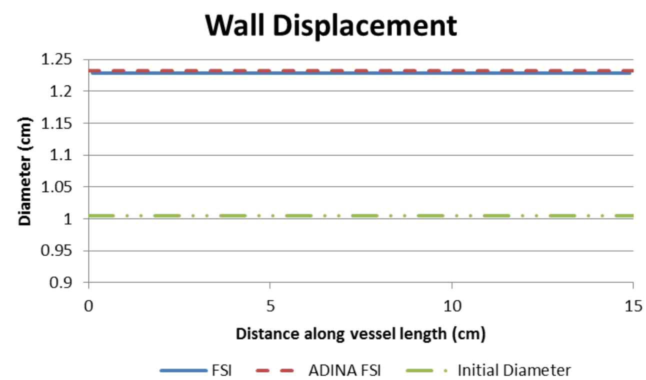

Figure 1: Velocity and wall comparisons of ADINA and FSI model for straight axisymmetric geometry.

Preliminary results show that the FSI analysis has the potential to provide valuable information and have been comparable to ADINA. However, more complex geometries need to be tested. Simulations on aneurysmal geometries are currently being performed in both ADINA and FSI models. Stability and convergence analyses are being performed to ensure the solution has converged. Comparison to other FSI simulations in literature will also be performed to check the accuracy of the FSI solver. The FSI analysis provides a novel numerical scheme that could potentially cut computational time while sacrificing some accuracy with more complex geometries. Making this scheme novel is the elimination of extra modeling found in most software packages. Future versions of this solver should include a 3-D analysis and incorporation of a pulsatile simulation to better represent blood vessels. While sacrificing minimal accuracy, the solution should be enough to determine the stresses that regulate blood vessel response to provide better diagnosis and treatment in a clinical setting.

REFERENCES

1. Jiang, Z, et al. *Am J Physiol Heart Circ Physiol*, **286**, H240-H245, 2004.
2. Glasgov S. *Circulation*, **89**, 2888-2891, 1994.
3. Vorp, DA. *J Biomech*, **40**, 1887-1902, 2007.
4. Garbey, M and F Pacull. *Int J Numer Meth Fluids*, **57**, 473-496, 2007.
5. Kim N and Y Chang. *Comput Methods Appl Mech Engrg*, **194**, 3291-3314, 2005.

GAIT INITIATION IMPAIRMENTS IN ESSENTIAL TREMOR AND PARKINSON'S DISEASE

Kristina Fernandez, Ryan Roemmich, Elizabeth Stegemöller, Joe Nocera, and Chris Hass

University of Florida, Gainesville, FL, USA

Email: stina11@ufl.edu

INTRODUCTION

Gait initiation (GI) involves a shift from a static, stable state to a destabilizing, dynamic state of locomotion. It is a challenging task that demands balance and postural control due to a decreasing base of support, from a two leg stance to an alternating single leg stance. GI is a complex transition phase consisting of anticipatory postural adjustments (APAs) that provide the momentum needed for efficient forward motion. Indeed, failure to generate sufficient forward momentum during GI has been shown to lead to overall poorer GI performance as evidenced by decreased step length and decreased step velocity. Because GI requires a separation of the center of mass (COM) from the center of pressure (COP), it has been used as an investigative tool to observe balance dysfunction and postural instability [1].

Parkinson's disease (PD) is characterized by a degenerative loss of dopaminergic neurons in the substantia nigra of the basal ganglia. The main symptoms of PD are tremor, rigidity, and bradykinesia, and it is common for PD patients to exhibit stooped posture, shuffling, and freezing of gait. The basal ganglia are commonly understood as essential in planning and initiating movement, and thus APAs have been shown to be diminished in persons with PD leading to shorter, slower steps during GI. Furthermore, it has been shown that persons with PD have shorter COP-COM distances compared to healthy older adults, indicating a decline in postural control and momentum generation.

Essential Tremor (ET) is a neurodegenerative movement disorder that is characterized by an involuntary shaking predominantly in the hands, arms, neck, and head that worsens with movement. Recent research indicates that ET is caused by brainstem and cerebellar dysfunction. In addition to the basal ganglia, both the brainstem and the cerebellum also play an important role in GI. Although ET is the most prevalent movement disorder, little is known about how ET deficits affect dynamic control and postural stability, particularly during GI.

Because there are no quantifiable diagnostic measures for PD or ET, PD and ET are discernible only by clinical criteria. Since these two neurological disorders share common characteristics of tremor and gait disturbances, there is a greater possibility for misdiagnoses, as approximately 30-50 % of persons with ET are misdiagnosed with PD or other tremor disorders [2]. Due to differences in neuropathology between PD and ET, we expect that GI in persons with ET will resemble healthy older adults more closely than persons with PD. This study aims to utilize GI as a quantifiable measure to aid in the clinical diagnostic process of PD and ET.

METHODS

Ninety-three participants, 23 persons with ET (67.5 ± 6.0 y, 172.4 ± 8.4 cm, 99.0 ± 19.8 kg), 32 with PD (67.5 ± 7.4 y, 170.3 ± 6.1 cm, 82.6 ± 14.4 kg), and 38 healthy older adults (68.1 ± 5.8 y, 169.1 ± 5.8 cm, 79.3 ± 16.1 kg) participated. All PD participants were tested at their self-reported best medicated state. None of the PD subjects displayed signs of dyskinesia or non-purposeful movements. Similarly, persons with ET were optimally treated during testing.

GI trials began with the participant standing quietly on force platform (Bertec, Columbus Ohio) mounted flush with the laboratory floor. Initial positioning of the feet was self-selected. In response to an auditory signal, the participants initiated walking and continued to walk for several steps. Each participant performed three to five trials.

Kinematic data were collected using an 3D Optical Capture system (Vicon Peak, Oxford, UK) collecting at 120Hz. Thirty-five passive reflective markers were attached to the body in accordance with the Vicon Plug-in-Gait marker system. We manually distinguished two events during GI that separated the COP trace into three distinct phases as defined by previous research on APAs [3].

The following outcome measures were collected for the three phases of gait initiation: (1) S1 anteroposterior (AP) displacement, (2) S1 mediolateral (ML) displacement, (3) S2 ML displacement, (4) S3 AP displacement, (5) S1 AP velocity, (6) S1 ML velocity, (7) S3 AP velocity, and (8) S2 ML velocity.

We analyzed mean differences among the HOA, ET, and PD groups using Mann-Whitney U-tests with Bonferroni corrections for multiple comparisons for all COP variables. Level of significance was set at .05 for the Mann-Whitney U-tests (prior to Bonferroni correction).

RESULTS AND DISCUSSION

Persons with PD had a significantly diminished S1 AP displacement (17.8 ± 9.5 vs. 27.2 ± 19.3 mm, p=.003), S1 ML displacement (17.9 ± 11.1 vs. 24.4 ± 15.6 mm, p=.017), S1 AP velocity (52.0 ± 26.9 vs. 101.6 ± 62.4 mm/s, p<.001) and S1 ML velocity (52.8 ± 26.3 vs. 88.3 ± 55.4 mm/s, p=.002) in comparison to healthy older controls. Persons with ET had a significantly diminished S3 AP displacement (70.9 ± 27.6 vs. 87.7 ± 42.4 mm, p=.013) in comparison to healthy older controls. When comparing persons with ET to those with PD, persons with PD had significantly decreased S1 AP (52.0 ± 26.9 vs. 94.9 ± 71.7 mm/s, p=.004) and S1 ML (52.8 ± 26.3 vs. 86.1 ± 54.6 mm/s. p=.005) velocities than persons with ET.

Persons with PD exhibit disturbances during GI, and advanced cases display freezing of gait. This disturbance in GI is due to dopaminergic dysfunction of the basal ganglia, and potentially

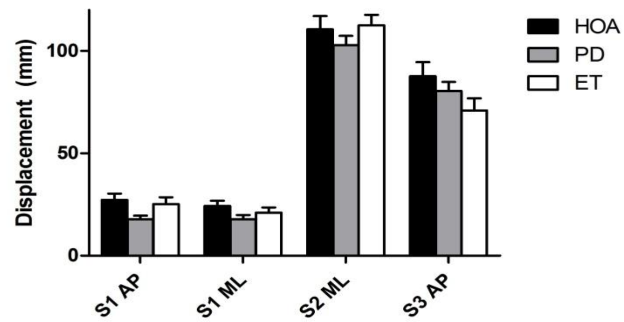

Figure 1. APA displacements during GI in healthy older adults and in persons with PD and ET.

dysfunction of the pedunculopontine nucleus. However, our results suggest that persons with ET also exhibit GI disturbances despite experiencing lesser dopaminergic deficits. Furthermore, previous research has shown that the brainstem and cerebellum are affected in ET. As the cerebellum and basal ganglia both send descending signals to the brainstem to regulate locomotion, we postulate that dysfunction of brainstem structures may be the cause of GI deficits in persons with ET. Thus, GI impairment may be more severe in PD due to the compounding nature of basal ganglia and brainstem deficits whereas GI impairments in ET likely are localized to brainstem control.

REFERENCES

1. Hass C.J., Waddell D.E, Fleming R.P., Juncos J.L., Gregor R.J. Gait Initiation and Dynamic Balance Control in Parkinson’s Disease. Archives of Physical Medicine and Rehabilitation, Volume 86, 2172-2176, 2005.

2. Jain, S., Lo, S.E., Louis E.D. Common Misdiagnosis of a Common Neurological Disorder: How Are We Misdiagnosing Essential Tremor. Archives of Neurology, Volume 63, 1100-1104, 2006.

3. Hass, C.J., Gregor, R.J., Waddell, D.E., Oliver, A., Smith, D.W., Fleming, R.P., Wolf, S.L. Influence of Tai Chi Training on COP trajectory during Gait Initiation in Healthy Older Adults. Archives of Physical Medicine and Rehabilitation, Volume 85, 1593-1598, 2004.

SIMULATION PREDICTIONS OF PROSTHETIC FOOT AND MUSCLE FUNCTION IN RESPONSE TO ALTERED FOOT STIFFNESS DURING BELOW-KNEE AMPUTEE GAIT

[1]Nicholas P. Fey, [2]Glenn K. Klute and [1]Richard R. Neptune

[1]Department of Mechanical Engineering, The University of Texas at Austin, Austin, TX, USA
[2]Department of Veterans Affairs, Puget Sound Health Care System, Seattle, WA, USA
email: nicholas.fey@gmail.com web: http://www.me.utexas.edu/~neptune

INTRODUCTION

Elastic energy storage and return (ESAR) prosthetic feet have been developed to improve the walking performance of lower-limb amputees. Unilateral below-knee amputees often have asymmetrical gait patterns that lead to elevated metabolic cost and increased prevalence of joint disorders compared to non-amputees [for review, see 1]. These abnormalities are due to the loss of the ankle muscles, which provide needed body support, forward propulsion and leg swing initiation during non-amputee walking [2], and the use of prosthetic devices that insufficiently restore these functions.

Foot stiffness is an important design variable that governs the ESAR qualities of prosthetic feet. Previously, we used selective laser sintering (SLS) to systematically vary prosthetic foot stiffness and assess its influence on the walking mechanics of unilateral below-knee amputees [3]. These results suggested that as stiffness decreases, adaptations of the intact leg are required to provide increased body support. However, decreasing stiffness also increased the late-stance energy return of the prosthetic feet and decreased residual leg hamstring activity, suggesting that more compliant feet may provide increased forward propulsion [e.g., 4, 5].

Identifying the causal relationships between foot stiffness and the function of the foot and limb muscles is needed to improve foot design and provide prescription rationale in an effort to improve amputee mobility. The purpose of this study was to develop forward dynamics simulations of unilateral below-knee amputee walking using a range of foot stiffness levels to identify how altering stiffness influences prosthetic foot and muscle function.

METHODS

Forward dynamics simulations of amputee walking with three levels of foot stiffness were generated using a musculoskeletal model developed in SIMM/Dynamics Pipeline (Musculographics, Inc.). Hill-type musculotendon actuators drove the simulations using bimodal excitation patterns. A simulated annealing optimization algorithm was used to identify the excitation patterns necessary to emulate group-averaged kinematic and ground reaction force (GRF) experimental tracking data of 12 below-knee amputees walking overground at 1.2 m/s with three SLS ESAR prosthetic feet of varying stiffness [3]. The prosthetic feet used included nominal, compliant and stiff SLS ESAR feet manufactured from Rilsan™ D80 (Nylon 11, Arkema, Inc.). The nominal foot matched the stiffness of a widely prescribed commercial carbon fiber ESAR foot (Highlander™, Freedom Innovations, LLC), while the compliant and stiff feet were 50% less and 50% more stiff, respectively.

A distributed stiffness prosthetic foot model of the three feet was developed and consisted of 18 rotational degrees-of-freedom, which connected the segments of the keel and heel (Fig. 1). A viscoelastic element applied a passive torque at each degree-of-freedom with a stiffness based on material properties of Nylon 11 and the measured geometry of the three prosthetic feet, and linear damping based on previous work [3].

Prosthetic foot and muscle contributions to body forward propulsion (anterior-posterior GRF) and vertical support (vertical GRF) were quantified using a GRF decomposition technique [5]. In addition, their contributions to trunk forward propulsion (horizontal trunk power) and support (vertical trunk power) as well as residual leg swing (total mechanical power of the leg) were quantified using a segment power analysis [5].

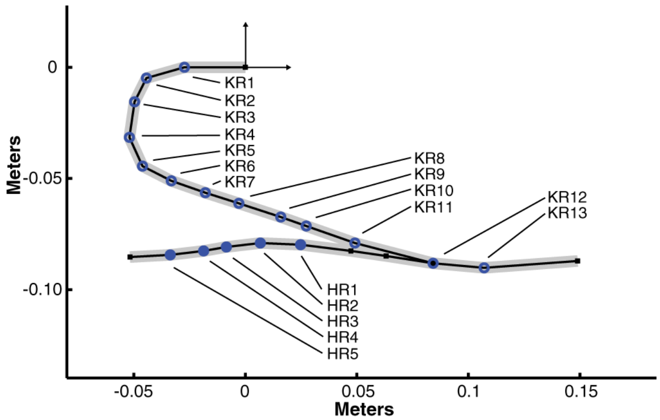

Figure 1: Prosthetic foot model including 13 keel (KR1-KR13) and 5 heel (HR1-HR5) rotational degrees-of-freedom.

RESULTS AND DISCUSSION

As prosthetic foot stiffness decreased, substantial differences in prosthetic keel function were observed, while heel function was similar across simulations. During the first half of residual leg stance, the keel provided increased body support and braking (i.e., negative A/P GRF; Fig. 2). During the second half of stance, the keel contributions to propulsion decreased while contributions to body support increased. In addition, the keel had a decreased negative contribution to residual leg swing (i.e., it absorbed less leg energy). Overall, the biomechanical functions of the keel during stance were consistent with the functional roles of the soleus during non-amputee walking [2]. The increased keel contributions to braking and residual leg swing as foot stiffness decreased were consistent with experimentally-observed increases in the residual leg braking GRF and prosthetic foot late-stance energy return, respectively [3].

As a result of these altered keel functions as stiffness decreased, muscle compensations were observed such as the residual hamstrings providing decreased body support and increased forward propulsion during the first half of stance (Fig. 2). In addition, throughout stance the residual leg rectus femoris generated increased braking (Fig. 2) as it redistributed increased energy from the leg to the trunk for propulsion. These altered muscle functions are consistent with the residual leg hamstrings needing to provide less propulsion during the second half of stance and experimentally-observed decreased hamstring muscle activity [3].

Also during the second half of residual leg stance, the intact leg vasti had increased contributions to body support and braking, consistent with experimentally-observed increased intact leg braking GRF, vasti muscle activity and knee extensor moments [3].

CONCLUSIONS

Prosthetic foot stiffness influences keel and residual and intact leg muscle function. While the identified muscle functions were consistent with non-amputee walking [e.g., 4, 6], the magnitude of the contributions were modulated in response to the changes in foot stiffness. Future work should seek to optimize foot stiffness to minimize important biomechanical quantities such as joint loading and/or metabolic cost.

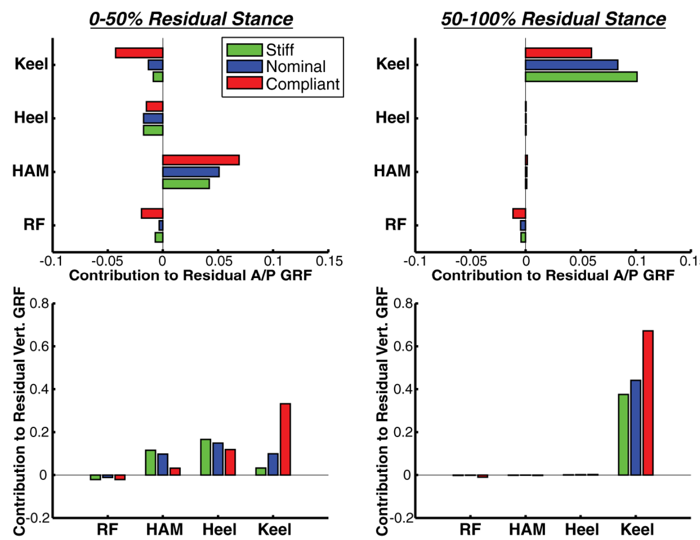

Figure 2: Mean prosthetic keel and heel and residual leg rectus femoris (RF) and hamstring (HAM) contributions to body support and forward propulsion (GRFs/body weight).

REFERENCES

1. Gailey R, et al. *J Rehabil Res Dev* **45** (1), 15-29, 2008.
2. Neptune RR, et al. *J Biomech* **34**(11), 1387-98, 2001.
3. Fey NP, et al. *Clin Biomech* **26**(10), 1025-32, 2011.
4. Liu MQ, et al. *J Biomech* **39**(14), 2623-30, 2006.
5. Neptune RR, et al. *Gait Posture* **19**(2), 194-205, 2004.

ACKNOWLEDGEMENTS

This work was funded by the NSF grant 0346514 and VA grant 1 I01 RX000311.

A COMPARISON OF VOLLEYBALL BLOCKING TECHNIQUES: JUMPING VELOCITIES AND EFFECTIVE BLOCKING AREAS

Travis Ficklin, Megan Schipper, and Robin Lund
Biomechanics Laboratory, University of Northern Iowa, Cedar Falls, IA, USA
email: travis.ficklin@uni.edu

INTRODUCTION

Effective blocking in volleyball is dependent upon forceful jumping and hand position both above and penetrating over the net. A recent study has shown these variables to vary with the choice of a traditional blocking technique (TR) versus a swing blocking technique (SW) [1]. The full effect of technique choice on lateral jumping velocity and effective blocking area (A_B) remains unclear. The purpose of this study was to compare TR technique to SW technique in terms of body center of mass (c.m.) projectile motion and effective A_B.

METHODS

Nine intercollegiate volleyball players executed maximum effort TR and SW blocking techniques in a counterbalanced order. Each subject started in a "ready" position with both feet in a rectangle marked on a volleyball court. This rectangle was 82.5 cm by 45 cm and was placed 30 cm from the court's centerline such that its long axis was parallel to the plane of the net and exactly centered at the midpoint of the centerline. A blue square "target" was affixed to the top of the net at a distance of 150 cm from the antenna denoting out of bounds. Therefore, each subject started from the middle of the court and moved rightward a distance of 3.0 m to execute each block as though the opponent's attack was coming from above the blue target.

Two high-definition video cameras shooting at 60 Hz were used to record each block. One camera was placed with its optical axis perpendicular to the plane of the net and 30 m behind the subject. Video from this camera was used to digitize body landmark data to obtain c.m. locations and A_B in a plane parallel to the net. The second camera was positioned with its optical axis in the plane of the net and directed along the top of the net. Video from this camera was used to digitize hand position with respect to the top of the net to measure height and penetration of the hands during the block. Calibration points allowed converting from digitized measurements to standard units.

To calculate projectile takeoff velocities of the c.m., its position in the plane of the net was calculated at takeoff (X_0,Y_0) and touchdown (X,Y). Horizontal and vertical takeoff velocities (V_X and V_Y respectively) were calculated using the formulas: $V_X = (X - X_0) / t$ and $V_Y = (Y - Y_0 + 1/2gt^2) / t$; where t was the time of flight based on the number of frames between liftoff and touchdown, and g was the acceleration due to gravity (9.81 m/s^2). It was then possible to predict the vertical displacement of the c.m. in flight (H) by the formula: $H = V_Y^2 / 2g$.

To calculate A_B, six defining points were digitized (see Fig. 1) on the extended arms and hands in each frame during flight in which the wrist joints were both at a level higher than the top of the net, and the area of the resulting polygon in the plane of the net was calculated.

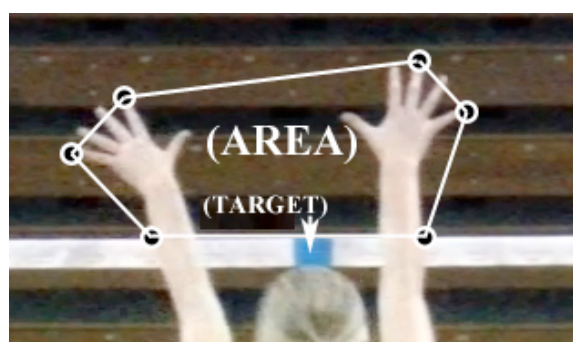

Figure 1. Method to determine planar blocking area and "target" tape.

Because blocking performance depends not only on the blocking area presented by the blocker, but also upon the duration of the block, area was plotted versus blocking time (t_{BLOCK}), defined as the time period in which the hands were above the net, and then integrated to yield A_B.

The approach time taken by each subject to move from starting position to the initiation of takeoff (t_{APP}) was also calculated as the time between the instant the right foot left the ground to start the lateral approach and the instant that a second foot touched the ground to begin the two-footed takeoff.

To measure hand penetration across the plane of the net, the centroid of the locations of the most distal fingers of each hand were measured in the vertical (Y_{PEN}) and horizontal (X_{PEN}) direction.

Variable means were compared between the SW and TR conditions using paired t-tests ($\alpha = .05$) and the results are presented in Table 1.

RESULTS AND DISCUSSION

V_X, V_Y, and H were all greater for SW, resulting in a markedly different c.m. path during flight (see Fig 2). For the hands, t_{BLOCK}, A_B, X_{PEN}, and Y_{PEN} were all greater for SW. Only t_{APP} was less for SW.

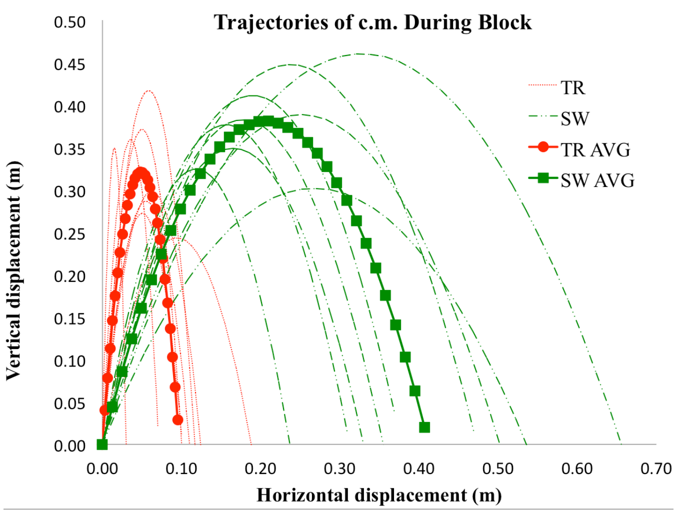

Figure 2. Trajectories of c.m. for TR and SW airborne phases (with respect to location of c.m. at takeoff). Average TR trajectory is marked by red circles. Average SW trajectory is marked by green squares.

The increased V_Y and H for SW found in the present study are consistent with previous findings made using other techniques [1], but are presented here with analysis of A_B. Taken together with increased t_{BLOCK}, X_{PEN}, and Y_{PEN}, the greater A_B and H for SW could allow for a very effective block compared by these criteria with the TR technique.

However, given that adjusting to the attack could be vital to the success of the block, it is important for coaches and athletes to consider the implications of the greater V_X and lesser t_{APP} associated with SW.

Taken together, they mean that the player commits to an airborne trajectory earlier than in TR, and once committed, the c.m. travels further laterally while airborne. In blocking a target, this means that more of the lateral distance covered in reaching the target would be made while airborne, wherein no adjustment to the c.m. path can be made.

Considering the advantages of the SW technique found here, it is interesting that many volleyball programs are able to exclusively use the TR technique successfully. It may be possible that beyond a certain point, increased H may not continue to increase blocking advantage. Given the overall goal of the block, increasing jump height in itself does not necessarily equate to increased blocking success.

It may be that one advantage of the TR technique lies in being able to make later adjustments in response to opponent deception or a misreading of the attack. These later adjustments before committing to an airborne path could allow for leaving options open slightly longer.

Table 1.	**TR**	**SW**	**p val**
$\mathbf{V_X}$ (m/s)	0.19 ± 0.13	0.74 ± 0.24	p < .01
$\mathbf{V_Y}$ (m/s)	2.51 ± 0.21	2.73 ± 0.19	p < .01
H (m)	0.32 ± 0.05	0.38 ± 0.05	p < .01
$\mathbf{t_{APP}}$ (s)	1.21 ± 0.11	1.08 ± 0.08	p < .01
$\mathbf{t_{BLOCK}}$ (s)	0.40 ± 0.04	0.46 ± 0.04	p < .01
$\mathbf{A_B}$ ($cm^2 \cdot s$)	618 ± 112	729 ± 107	p < .01
$\mathbf{X_{PEN}}$ (cm)	14.2 ± 5.7	17.0 ± 2.9	p < .05
$\mathbf{Y_{PEN}}$ (cm)	33.2 ± 5.0	36.5 ± 4.2	p < .01

REFERENCES

1. Neves, TJ, et al. *J Sports Sci and Med* **10**: 452-457, 2011.

SCAPULOHUMERAL KINEMATICS IN INDIVIDUALS WITH UPPER EXTREMITY IMPAIRMENT FROM STROKE

Margaret A Finley and Stephanie Combs
Krannert School of Physical Therapy, University of Indianapolis
email: finleym@uindy.edu, web: http://pt.uindy.edu/

INTRODUCTION

The mobility of the shoulder girdle is a complex interaction of arthrology and neuromotor control[1]. Over 780,000 persons in the United States have a new or recurrent stroke each year. Residual, motor impairments such as weakness and incoordination can lead to changes in shoulder function and mobility. Alterations in shoulder elevation and scapular upward rotation are related to shoulder pain in persons with hemiparesis from subacute stroke[2,3]. Despite therapeutic efforts, as many as 80% of persons with stroke continue to have residual deficits, particularly within the paretic, affected limb. Additionally, it has been suggested that in individuals with stroke the upper extremity ipsilateral (“less affected”) to the lesion may also exhibit deficits. However, there is little literature that examines the scapulohumeral kinematics of the paretic and less affected limbs in persons with chronic stroke and that compares the less affected limb kinematics to individuals without upper extremity impairment.

METHODS

Fifteen individuals (63.8±17.5 yrs) with impairment from chronic stroke and 15 healthy, aged matched individuals (62.1±8.4yrs.) were evaluated. Motor impairment in those with stroke was measured with the Fugl-Myer Upper Extremity Motor Assessment (FM_UE). The FM_UE is a valid and reliable tool with a maximal score of 66. Three-dimensional kinematic data of the upper extremities was collected as participants performed three repetitions of arm elevation at a self-selected velocity and in their plane of choice. Participants were instructed to “lift your arm overhead in the most comfortable manner.” Kinematics were collected with the Motion Monitor™ short range transmitter system (Innsport, Chicago, IL) with use of “mini-bird” sensors (Ascension Technology, Burlington, VT). This system has a reported position accuracy of 0.07 inches/0.5 degrees at a 36 inch range with a resolution of .03 inch/0.1 degrees (Ascension Technology, Burlington, VT). The standardized shoulder protocol for the description of shoulder motions and global coordinate system (GCS) asrecommended by the International Shoulder Group (ISG) of the International Society of Biomechanics was followed[4]. The scapula was defined in respect to the thorax (scapulothoracic) and the humerus with to respect to the thorax (humerothoracic). Three repetitions from each extremity were collected with order of extremity randomized. Humeorthoracic (HT), scapulothoracic (ST) and glenohumeral (GH) kinematics were determined from the final repetition. Scapulohumeral rhythm (SHR) was calculated as the ratio of the change in glenohumeral elevation to change in scapulaothoraic upward rotation. Independent t-tests ($p \leq 0.05$) compared the between group differences of the control and the less affected limb while paired t-tests assessed differences with participants less affected limb vs. paretic limb. Three participants with stroke were unable to elevate about 70°, therefore, were not included in the paretic limb analysis. Given the small sample, Cohen's *d* was calculated to determine the strength of the comparative relationships with effect size defined as small ($d \geq 0.2$), medium ($d \geq 0.5$) or large ($d \geq 0.8$).

RESULTS AND DISCUSSION

The scapulohumeral kinematics of participants with stroke were highly variable across all motions. Plane of elevation was significantly different between the control group and the less affected limb of the stroke group throughout the elevation motion, with the less affected limb elevation occurring more in the scapular plane and the control limb in the frontal plane (Figure 1). No difference was found between the less affected and paretic limb plane of elevation.

Figure 1: Plane of humerothoracic elevation

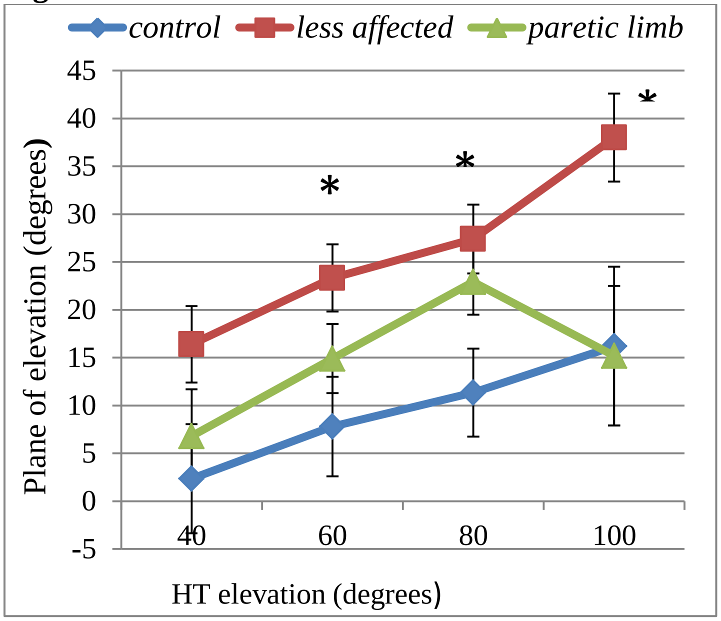

*= p≤ 0.05 control vs. less affected limb

Although not statistically different (p=0.07), a medium effect size (δ = 0.70) was found in mean peak HT elevation with reduced elevation in the less affected limb, compared to the control. As with previous research, greater mean peak HT elevation (p=0.03) was achieved by the less affected limb (118°) than the paretic limb (104°) within the stroke group.[2] At peak elevation, compared to the control group, the less affected limb demonstrated increased scapular internal rotation (IR) as indicated by a large effect size (δ = 0.93). Medium effect sizes were also found for reduced posterior scapular tipping (PT) of the less affected limb compared to control at HT elevation of 60° (δ=0 .70), 80° (δ = 0.72) and 100° (δ = 0.73). Compared with the control group and the paretic limb, SHR was increased (p=0.01) in the less affected limb. (Figure 2) Given the large variability in impairment and movement patterns no other statistically significant differences between limbs were revealed among the kinematics within the group with stroke.

CONCLUSIONS

The majority of shoulder complaints involve frequent use of the arm at, or above shoulder level. There is growing evidence associating abnormal scapulothoracic kinematics with a variety of shoulder pathologies. During HT elevation the scapula should upwardly rotate and posteriorly tilt with external rotation occurring at end range of elevation. [5] Given anatomical relationships, it is believed that reductions in scapular upward rotation and posterior tilt during arm elevation could reduce the available subacromial space, potentially contributing to development of impingement as well as providing a poorer environment for tissue healing. The lack of scapular ER with decreased posterior scapular tipping found in this pilot study may be a precursor to the development of shoulder pathology in the less affected limb of persons with stroke. Given the limited elevation range of the paretic limb, the less affected limb in persons with stroke often must accomplish the majority of overhead activities. Therefore, assessment of scapulothoracic kinematics is important in understanding potential mechanisms of injury.

Figure 2: Scapulohumeral Rhythm

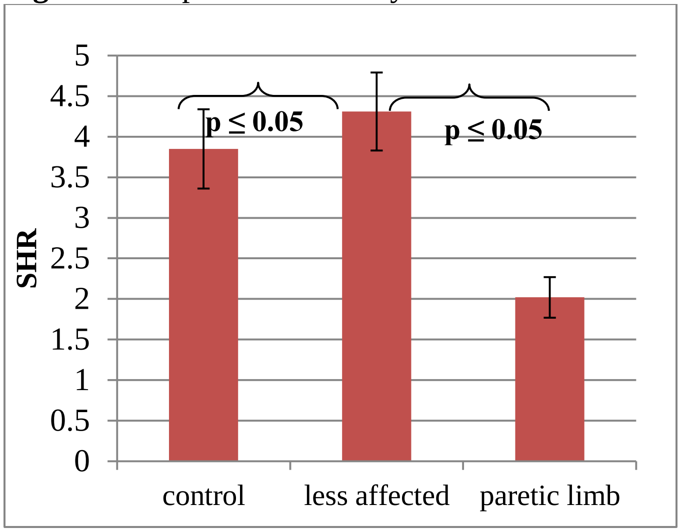

REFERENCES

1.Halder AM, et al *Orthop Clin North Am*; 31(2):159-76, 2000.
2.Niessen M et al *J Rehabil Med;* **40**(6):482-486, 2008
3.Hardwick DD, Lang C. *Proceedings of the CSM of the APTA*; 2008.
4.Wu G, et al. *J Biomech* 38(5): 981-992, 2005
5. Ludwig, P. & Reynolds, J. , *J Orthop Sports Phys Ther*;39(2),20.

PEAK AND NONUNIFORM FIBER STRETCH INCREASE IN THE BICEPS FEMORIS LONG HEAD MUSCLE AT FASTER SPRINTING SPEEDS

[1]Niccolo Fiorentino, [2]Elizabeth Chumanov, [2,3]Darryl Thelen, [1,4]Silvia Blemker

Departments of [1]Mechanical & Aerospace Engineering and [4]Biomedical Engineering, University of Virginia, Charlottesville, VA
Departments of [2]Mechanical & Aerospace Engineering and [3]Biomedical Engineering, University of Wisconsin-Madison, Madison, WI
e-mail: niccolo@virginia.edu, web: http://www.mae.virginia.edu/muscle

INTRODUCTION

Acute muscle strain injury remains a prevalent problem for athletes participating in high-speed sports, such as soccer, rugby and track and field [1]. The hamstrings commonly suffer injury, with the biceps femoris long head (BFlh) injured most often. Recent whole-body simulations of sprinting gait showed that musculotendon stretch at the end of the swing phase is independent of speed [2]. We hypothesize that speed-dependent increases in *localized* stretch may still occur and contribute to increased injury risk at high speed. The goal of this work was to use finite element (FE) modeling to determine internal tissue kinematics throughout the BFlh and to find peak fiber stretch as sprinting speed increases. We hypothesized that peak localized fiber stretch increases as running speed increases.

METHODS

Mesh generation

Twelve (N = 12) University of Virginia Track and Field athletes (five male) participating in short distance events provided informed consent and were imaged in accordance with Institutional Review Board guidelines. Athletes had no history of hamstring strain injury and were positioned in the head-first prone position inside a 3T Siemens Trio Magnetic Resonance (MR) Scanner. High-resolution (0.7 x 0.7 mm^2) axial plane images were acquired with a T1-weighted Dixon sequence [3]. Musculotendon measurements, including axial plane muscle widths, muscle length, aponeuroses width and length, and tendon length, were made on MR images and averaged across all athletes (Fig. 1). Average musculotendon measurements were used as the dimensions for the FE mesh [4]. The FE mesh was generated with TrueGrid software (XYZ Scientific Applications) and included 692 hexahedral elements and 1077 nodes.

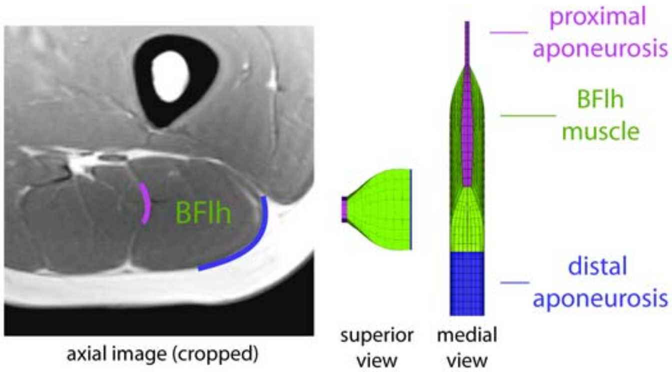

Figure 1. FE model generation. High-resolution axial plane MR images were used to measure the dimensions of the BFlh musculotendon unit. The FE mesh was based on average dimensions of all athletes.

FE simulations

Muscle and connective tissue were modeled as a transversely isotropic, hyperelastic, quasi-incompressible material [5]. Simulations were run on the implicit FE solver Nike3D (Lawrence Livermore National Lab). Muscle activation and muscle length change were based on forward dynamic simulations of sprinting gait at 70%, 85% and 100% of maximum speed (7.8 m/s) (Fig. 2) [2]. The BFlh musculotendon unit was fixed at the superior end of the proximal external tendon (i.e., at the hip) and change in length was applied to the inferior end of the distal aponeurosis (i.e., at the knee). Muscle activation was applied uniformly to the BFlh, and the level of activation modulated muscle's known active force-length curve [6].

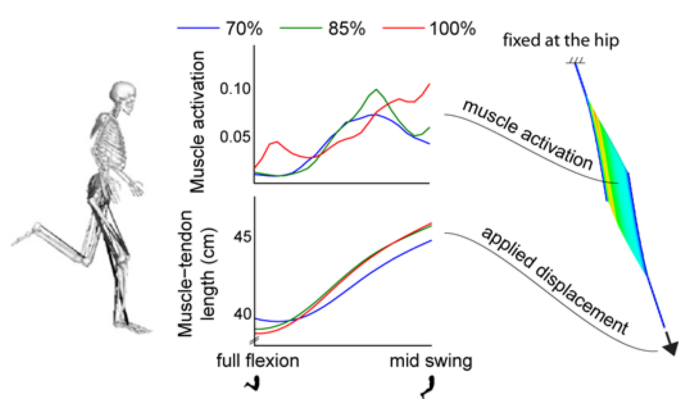

Figure 2. FE simulation. Muscle activation and musculotendon unit lengthening boundary conditions were based on whole-body forward dynamic simulations of sprinting gait [2].

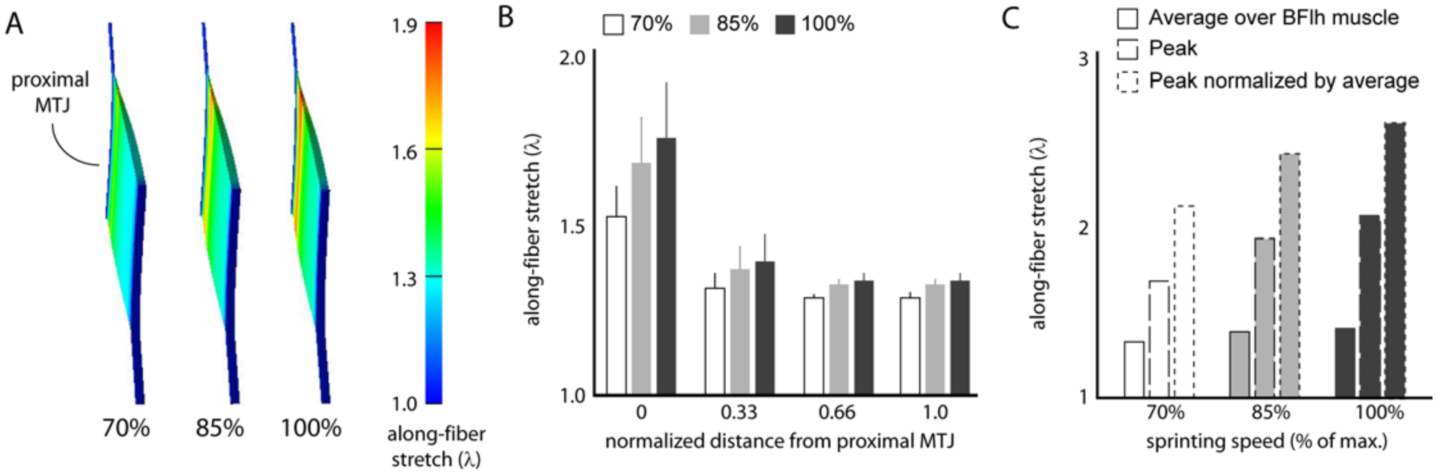

Figure 3. Simulation results. Sprinting simulations of the BFlh musculotendon unit demonstrate higher along-fiber stretch (λ) with faster running speed (shown in longitudinal cross section), particularly near the proximal myotendinous junction (MTJ) (A). Average fiber stretch (+ standard deviation) increased with sprinting speed in all regions of the muscle, with the largest increase in the tissue near the proximal MTJ (B). Average fiber stretch, peak fiber stretch and peak fiber stretch normalized by average fiber stretch increased with sprinting speed (C).

Simulation analysis

We calculated along-fiber stretch values at the midpoint of the swing phase of sprinting gait, where full knee flexion represented the reference configuration. Average fiber stretch values were calculated over the entire BFlh and at multiple evenly spaced regions from the proximal myotendinous junction (MTJ), and peak fiber stretch was found over the entire BFlh.

RESULTS & DISCUSSION

Fiber stretch was found to be non-uniform throughout the BFlh muscle; the non-uniformity of the fiber stretches increased with increasing sprinting speed (Fig. 3A). Regionally, fiber stretch was highest near the proximal myotendinous junction (MTJ), which is where injuries occur most commonly [7], and decreased as a function of distance from the MTJ (Fig. 3B). Peak fiber stretch values near the proximal MTJ increased with increasing running speed (1.69, 1.94 and 2.07 for sprinting at 70%, 85% and 100% of maximum speed, respectively) (Fig. 3C).

The average fiber stretch across the entire muscle was 1.33 (SD 0.09), 1.39 (SD 0.13) and 1.41 (SD 0.15) for sprinting at 70%, 85% and 100% of maximum speed. The relative increase in the average whole-muscle fiber stretch from 70% to 85% speed (18%) and from 85% to 100% (5%) agreed well with fiber stretch values from whole-body simulations (26% and 9%, respectively) at the midpoint of the swing phase of sprinting [2]. However, the peak localized fiber stretch values increased with sprinting speed more than the average fiber stretch (Fig. 3C). In other words, peak fiber stretch, normalized by average fiber stretch, increased with sprinting speed (2.13, 2.44 and 2.62 at 70%, 85% and 100% of max. (Fig. 3C).

Elevated localized fiber stretch with increasing sprinting speed provides a possible explanation for why acute strain injuries are more prevalent in high-speed sports, such as track and field. At faster running speeds, increased muscle activation is required to slow down the lower limb in preparation for foot contact; thus, higher localized fiber stretch is likely the result of increased muscle activation. The results reported here also support the hypothesis that large localized tissue strain is the injury mechanism in lengthening contractions, given that the highest muscle fiber stretch was found where injury is observed most often (the proximal myotendinous junction) [7].

REFERENCES

1. Bennell and Crossley. *Aust J Sci Med Sport* **28**, 69-75, 1996.
2. Chumanov, et al. *Med Sci Sports Exerc* **43**, 525-532, 2011.
3. Dixon. *Radiology* **153**, 189-194, 1984.
4. Rehorn and Blemker. *J Biomech* **43**, 2574-2581, 2010.
5. Blemker, et al. *J Biomech* **38**, 657-665, 2005.
6. Zajac. *Crit Rev Biomed Eng* **17**, 359-411, 1989.
7. Askling, et al. *Am J Sports Med* **35**, 197-206, 2007.

ACKNOWLEDGEMENTS

NIH RO1 AR056201 and the Achievement Rewards for College Scientists Program provided funding sources for this work.

COMPARISON OF STRESS DISTRIBUTION PATTERNS WITHIN TRIGONAL, QUADRADLE, AND HEXAGONAL SCREW DRIVE DESIGNS OF AN ACL INTERFERENCE SCREW USING FINITE ELEMENT ANALYSIS

[1]Jonquil R. Flowers B.S., [1]Matthew B. McCullough, Ph.D.

[1]North Carolina A&T State University, Greensboro, NC, USA
email: jrflowe1@ncat.edu

INTRODUCTION

The anterior cruciate ligament (ACL) is the most often injured ligament of the knee with well over 100,000 ACL injuries in the U.S. annually [1]. Surgical reconstruction is a widely accepted treatment option and can succeed in restoring joint stability [2]. It is an arthroscopic surgery that involves replacing the damaged ACL with a soft tissue autograft or allograft. Interference screws are used to ensure secure fixation of the graft by compressing it against the wall of the bone tunnel, consequently keeping graft slippage minimal and the graft sufficiently taut.

There are two classes of materials commonly used for ACL interference screws, metallic (i.e. titanium) and bioabsorbable polymers. The ideal interference screw can be described as "best of both worlds" having high mechanical strength, creating a secure initial fixation, being biodegradable, biocompatible, and allowing for osseointegration, and causing no MRI interference. In spite of numerous advances in material development, questions remain about the impact of design on screw performance. This is particularly important with regard to design of the screw head. Stripping/breakage of the screw head or drive was observed in the head of the screw in previous studies [3]. Once a screw is stripped, it cannot be fully inserted, reducing contact area between the screw and the walls of the bone tunnel. Consequently, reducing the ultimate pullout load and increasing graft slippage. The objective of this study was to use finite element analysis to compare three different drive designs (trigonal, quadrangle, and hexagonal) to evaluate stress in the screw head. This can provide critical insight into the causes of the stripping mechanism within the screw drive.

METHODS

Three 3-D computer models of an ACL interference screw were designed in SolidWorks 2010 (SolidWorks Corp., Waltham, MA). These models were 15 mm in length and had a 5 mm outer diameter and a 1.7 3mm inner diameter (cannulated). They each had a different drive design in the screw head, a trigonal drive, a quadrangle drive, and a hexagonal drive (Figure 1). The screw geometry was imported into the ANSYS 11.0 (ANYS, Inc., Canonsburg, PA) finite element software. Within ANSYS Workbench, the model was meshed and a static analysis was run to simulate a torque within the drive of the screw. In all the simulations the model was constrained by eliminating all degrees of freedom of the nodes on the outer surface of the screw. In addition, all simulations used Titanium material properties ($E = 9.6E10$ Pa, $\upsilon = 0.36$) with a 2.5 Nm torque applied within the screw's drive. The model with the trigonal drive design had 6008 nodes and 2957 elements, the model with the quadrangle drive design had 5771 nodes and 2800 elements, and the model with the hexagonal drive design had 5493 nodes and 2586 elements. The monitored outputs were shear and von Mises' stress distribution within the drive design of the screw head.

RESULTS AND DISCUSSION

The maximum shear stress and maximum von Mises' stress were observed in the corners of the drive design, an example of the von Mises stress is seen in (Figure 1). The trigonal drive design had a maximum shear stress of 122.48 MPa and a maximum von Mises' of 212.16 MPa. The quadrangle drive design had a maximum shear stress of 81.627 MPa and a maximum von Mises' of

141.38 MPa. The hexagonal drive design had a maximum shear stress of 79.47 MPa and a maximum von Mises' of 137.65 MPa.

From these results, the maximum stress values of the quadrangle and hexagonal drive designs were similar, while the trigonal drive designs stress values were greater. It also appears like the stress has a greater distribution for the hexagonal drive design which has the greatest surface area.

CONCLUSIONS

In order to eliminate insertion failure of ACL interference screws due to stripping and breaking, it is necessary to decrease the maximum stress values and increase the stress distribution. This can be done with drive designs that have greater contact area with the screw driver. Future studies could investigate other screw drive designs such as the torx, turbine, and trilobe drive designs.

REFERENCES

1. Woo, S. L.-Y., et. al. *Appl Mech Rev.* **43**(5), S143-S149, 1990
2. Beynnon BD, et. al. *Am J Sports Med* November **33**, 1751-1767, 2005
3. Weiler A, et. al., *Am J Sports Med* January **26**, 119-128, 1998

ACKNOWLEDGEMENTS

Thank you to Dr. McCullough your support and encouragement.

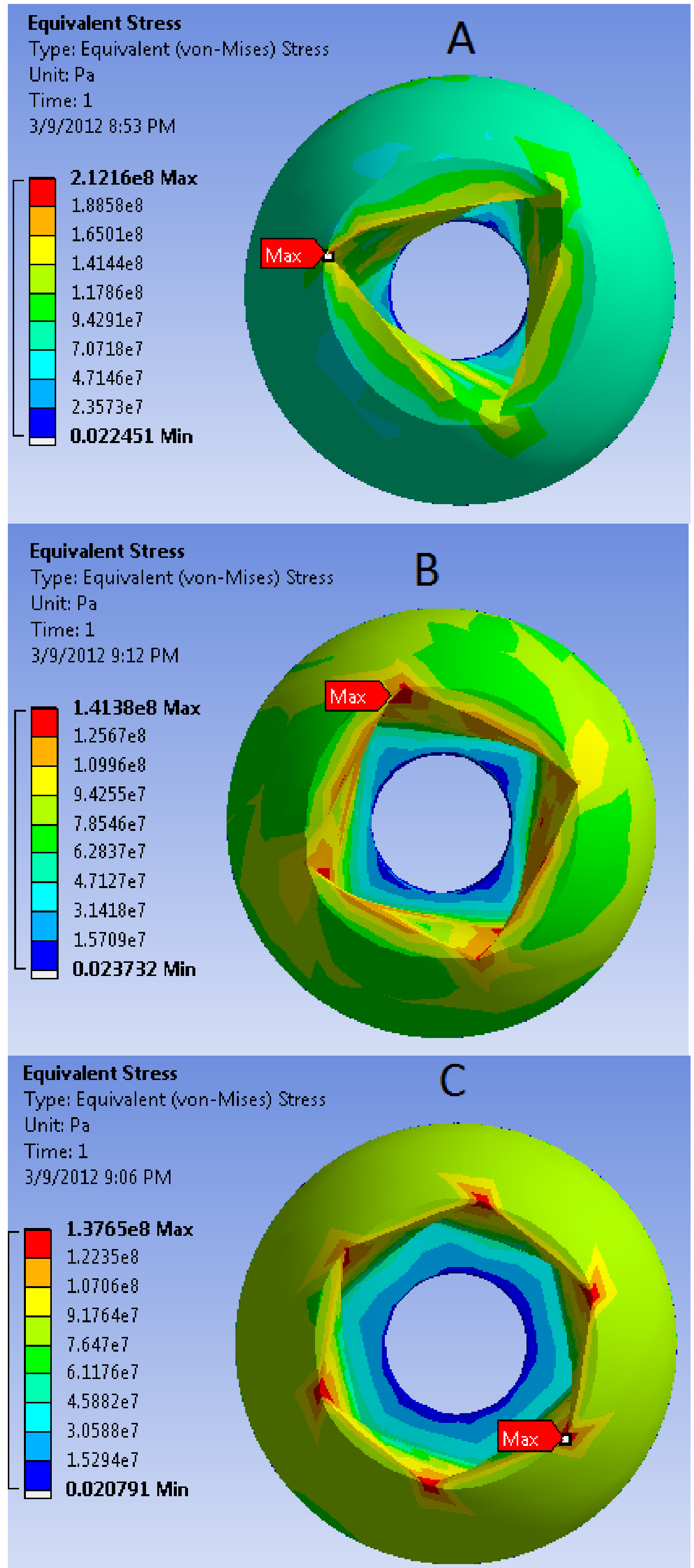

Figure 1: Von Mises Stress Results
A. Trigonal Drive Design B. Quadrangle Drive Design C. Hexagonal Drive Design

TRUNK ENDURANCE STRENGTH AND RUNNING BIOMECHANICS AFTER ILIOTIBIAL BAND SYNDROME

Eric Foch, Julie Pfeiffer, and Clare E. Milner
University of Tennessee, Knoxville, TN, USA
email: efoch@utk.edu

INTRODUCTION

Iliotibial band syndrome (ITBS) is the second most commonly reported overuse running injury [1]. Proximal factors such as hip kinematics may play a role in the development of ITBS [2]. Additionally, excessive trunk motion may also be associated with ITBS. A stable lumbo-pelvic-hip complex, or "core," provides a solid foundation for lower extremity motion during running. A reduced ability to limit excess frontal plane trunk and pelvis motion could medially shift the whole body center of mass away from the stance limb. This shift would result in a larger moment arm between the knee joint center and resultant ground reaction force. Therefore, a greater internal knee abduction moment may result [3]. An increased joint moment could increase the tensile strain experienced by the iliotibial band [3]. In the sagittal plane, increased anterior pelvic tilt may be due to core muscle weakness, in particular rectus abdominis. This imbalance may be compensated for by positioning the trunk more vertical [3]. Core endurance strength can be tested in the clinic via a series of tests that focus on different aspects of the lumbo-pelvic-hip complex. Frontal and sagittal plane trunk muscular endurance imbalances may exist in runners who develop ITBS. Therefore, the purpose of this investigation was to determine if differences in trunk endurance strength exist between female runners with and without a history of ITBS. We also sought to determine if trunk, pelvis, and hip kinematic and knee kinetic differences exist between groups during running. It was hypothesized that trunk endurance strength would be less in runners with a history of ITBS than controls. Second, we hypothesized that the ITBS group would exhibit greater peak frontal and sagittal plane trunk and pelvis angles, frontal plane hip angles and knee moment than controls.

METHODS

As part of an ongoing investigation examining knee overuse injuries, fourteen currently healthy female runners aged between 18 and 35 years old were recruited. All procedures were approved by the Institutional Review Board prior to the commencement of the study. All participants provided written informed consent to participate. Runners with a history of ITBS (n = 7; age: 25.9 ± 3.5 years; height: 1.67 ± 0.06 m; mass: 57.0 ± 4.3 kg; weekly mileage: 29.0 ± 19.6 $mi \cdot wk^{-1}$) were matched for age and mileage with a control group (n = 7; age: 23.6 ± 9.3 years; height: 1.66 ± 0.06 m; mass: 57.6 ± 3.5 kg; weekly mileage: 23.6 ± 9.3 $mi \cdot wk^{-1}$). Running data were collected using standard three-dimensional motion capture techniques. Participants' lower extremities and trunk were instrumented with passive reflective markers. Standard laboratory footwear was worn by participants. Marker trajectories were collected using a 9 camera optoelectric motion capture system sampling at 120 Hz. Participants ran at a velocity of 3.5 $m \cdot s^{-1}$ (± 5%) over a 17 m runway for 5 acceptable trials. A force plate sampling at 1200 Hz was used to determine the stance phase. After completing the running trials, trunk endurance strength was tested. Specifically, trunk and pelvis core endurance were measured using three clinical tests extensor dynamic endurance, side-bridge, and partial curl-up. For the extensor dynamic endurance and partial curl-up tests, participants performed as many repetitions as possible while maintaining a cadence of 25 beats per minute set by a metronome. The side-bridge test was measured as the total time participants were able to keep their right hip off the table. A test was terminated if the participant was given more than one correction of technique or speed. Alternatively, the participant ended the test if she felt unable to continue. Kinematic data were processed using a joint coordinate systems method. Peak values of the dependent variables from five running trials were extracted from the first 60% of stance phase: lateral trunk flexion, forward trunk lean, contralateral pelvic drop, anterior pelvic tilt, hip adduction angle, and internal knee abduction moment. Dependent variables from the running trials were averaged for each participant and group. Data were analyzed using descriptive statistics and effect size. Moderate effects were considered clinically relevant (≥ 0.5).

RESULTS AND DISCUSSION

Large effect sizes were associated with fewer repetitions performed in the partial curl-up test, greater time maintaining a side-bridge position, and greater lateral trunk flexion towards the stance limb in the ITBS group compared to controls (Table 1). A moderate effect was associated with smaller forward trunk lean angle, greater contralateral pelvic drop, and increased internal knee abduction moment in the ITBS group than controls. All other dependent variables had small effect sizes or no effect.

The purpose of this investigation was to determine if frontal and sagittal plane trunk muscular endurance and kinematics and knee kinetic differences exist between female runners with and without a history of ITBS. Our findings partially support the hypotheses. In the sagittal plane, runners with previous ITBS have less trunk flexor endurance and a more vertical trunk, but similar pelvic tilt. It is unclear whether these sagittal plane differences are related to ITBS. In the frontal plane, contralateral pelvic drop tends to shift the mass of the trunk away from the stance limb [3]. It has been suggested that displacement of the large of mass of the trunk away from the stance limb may increase the internal knee abduction moment [3]. The ITBS group had contralateral pelvic drop and lateral trunk lean away from the stance limb, whereas controls remained more upright. Therefore, the increased internal knee abduction moment exhibited in the ITBS group may be due to positioning the trunk farther away from the stance limb in the frontal plane.

CONCLUSIONS

Our preliminary data indicates that female runners with a history of ITBS exhibit decreased trunk flexor endurance strength compared to controls, coupled with a more vertical trunk placement. Frontal plane kinematic differences indicate that the previous ITBS group shifts upper body mass away from the stance limb. This shift increases knee moment and contributes to increasing the tensile strain on the iliotibial band.

REFERENCES

1. Lun V, et al. *Br J Sports Med*, **38**, 576-580, 2004.
2. Noehren B, et al. *Clin Biomech*, **22**, 951-960, 2007.
3. Powers CM. *J Orthop Sports Phys Ther*, **40**, 42-51, 2010.

Table 1: Variables of interest during running and strength tests (mean ± standard deviation)

	ITBS	Control	Effect Size
Peak Hip Adduction Angle	13.6 ± 3.5º	14.4 ± 3.3º	0.25
Peak Anterior Pelvic Tilt*	-1.9 ± 5.5º	-3.1 ± 2.3º	0.29
Peak Contralateral Pelvic Drop	4.4 ± 2.0º	3.4 ± 1.7º	0.51
Peak Forward Trunk Lean	5.4 ± 5.1º	8.8 ± 3.6º	0.74
Peak Lateral Trunk Flexion	3.1 ± 3.4º	0.2 ± 1.6º	1.07
Knee Abduction Moment	1.1 ± 0.2 Nm/kg	0.9 ± 0.4 Nm/kg	0.60
Partial Curl-Up Test	23 ± 12 reps	44 ± 10 reps	1.3
Trunk Extension Test	31 ± 9 reps	30 ± 5 reps	0.2
Side-Bridge Test	118 ± 27 seconds	90 ± 28 seconds	0.9

*The negative sign indicates that the pelvis was tilted posteriorly in both groups.

REAL-TIME BIOFEEDBACK FOR ACL INJURY PREVENTION

[1,2]Kevin R. Ford, [1]Christopher DiCesare, [1,2]Gregory D. Myer, [1,2,3]Timothy E. Hewett

[1]Cincinnati Children's Hospital, Cincinnati, OH, USA
[2]University of Cincinnati, Cincinnati, OH, USA
[3]Ohio State University, Columbus, OH, USA

INTRODUCTION

Traumatic and debilitating anterior cruciate ligament (ACL) injuries occur at a 2 to 10-fold greater rate in female compared to male athletes. Prospectively measured knee abduction load is a modifiable risk factor that predicts future ACL injury in young female athletes. Neuromuscular training that targets the underlying mechanics that influence increased knee abduction load effectively reduces ACL injury. However, low athlete compliance and implementation have resulted in a lack of widespread reduction in ACL incidence. Innovative biofeedback modalities that focus on proper movement technique are viable options to improve both compliance and implementation issues. Biofeedback training is a method that enables an athlete to learn how to alter biomechanical and physiological function by receiving biomechanical and physiological data during real-time or immediately after a task. The goal of this form of training is to facilitate motor learning of improved and safe movement patterns without the need for continued use of biofeedback. The purpose of this study was to compare the effects of two different modes of real-time biofeedback during a squat on drop vertical jump landing mechanics.

METHODS

A crossover study design was used to test the effects of two methods of real-time biofeedback during repetitive double leg squats. Baseline and post training drop vertical jumps (DVJ) were collected to determine if either training method transferred to another activity. Female high school soccer players (n=4) participated in this pilot study. Kinetic biofeedback (KNbf) and kinematic biofeedback (KMbf) order were randomly allocated to each subject. Each subject was instrumented with 43 markers attached with double sided tape with a minimum of three tracking markers placed on each right and left lower extremity segment (foot, shank, thigh) and trunk (pelvis, thorax). Motion and force data were collected at 240 Hz and 1200 Hz, respectively, using a 10 camera motion capture system (RaptorE, Motion Analysis Corp., Santa Rosa, CA) and multiple force platforms (AMTI, Watertown, MA). A standing static trial for each subject was collected to define the neutral kinematic posture. Kinematic analysis and real-time biofeedback was performed in Visual 3D (C-Motion, Inc. Germantown, MD).

Figure 1: Example of initial setup and double leg squat with real-time biofeedback.

Three DVJ trials were collected prior to and following each feedback condition (Figure 1). During the feedback conditions, a monitor displaying a real-time animation of the subject and a data curve with a highlighted goal region was positioned in front of the subject. Subjects were instructed to keep the curve within the highlighted region. Three trials of 10 double leg squat repetitions were collected and displayed in real-time. Knee abduction/adduction angle was displayed for the KMbf condition. Knee abduction/adduction moment was displayed for the KNbf condition. Paired t-tests were used to determine differences in knee abduction moment and angle in DVJ from baseline to post feedback.

RESULTS AND DISCUSSION

Maximum knee abduction moment during DVJ landing was significantly decreased following KNbf ($p=0.038$). Subjects exhibited a 32.8% improvement in knee abduction moment from baseline to post KNbf. The reduced knee abduction moment during the DVJ following KMbf (5.7%) was not statistically different. Maximum knee abduction angle was significantly decreased following KNbf ($p=0.003$) but not following KMbf ($p=0.08$). Subjects exhibited a 31.5% improvement in knee abduction angle from baseline to post KNbf compared to a 16.3% change post KMbf.

Knee adduction moment averaged over all subjects during squat biofeedback is presented in Figure 2. During the eccentric and concentric phases of the squat, subjects were able maintain feedback torque within the goal region for 80.8% of the trials during KNbf compared to only 29.3% of the trials during KMbf (Figure 2).

Intervention studies that have successfully reduced ACL injuries utilized analysis of movement biomechanics and feedback regarding proper body position and technique [1]. Education and enforced awareness of dangerous positions and mechanisms of ACL injury decreases ACL injuries. The results from this pilot study indicate that KNbf technique modications during squat biofeedback may rapidly transfer to dynamic drop landings.

Recent studies with real-time gait retraining have reinforced the concept of providing critical feedback with detailed real-time motion analysis data [2,3,4]. Both Barrios et al. [2] and Noehren et al. [4] utilized a similar motion analysis system to provide real-time feedback to modify a risk factor related to different knee pathologies. Both immediate and longer term improvement were identified.

CONCLUSIONS

The innovative biofeedback employed in the current study reduced knee abduction load and posture from baseline to post training during a DVJ. While the immediate improvements are important, long term retention of adapted motor performance is critical for overall success of an intervention. Retention should be further investigated to determine both the change in mechanics and injury reduction effects.

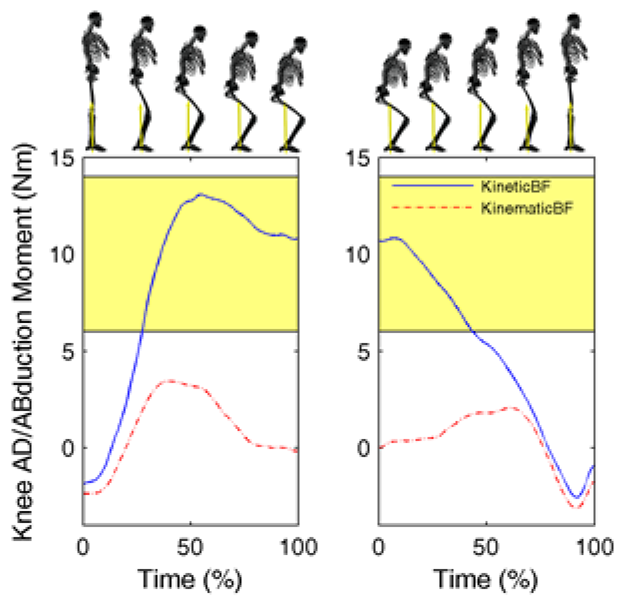

Figure 2: Average knee adduction (positive) curve during eccentric (left) and concentric (right) phases of the squat. Yellow shaded region was the target goal during each kinetic feedback squat.

REFERENCES

1. Hewett TE et al. *Am J Sports Med*, **28**, 490-498, 2006.
2. Barrios JA et al. *J Biomech*, **43**, 2208-2213, 2010.
3. Crowell HP et al. *J Orthop Sports Phys Ther*, **40**, 206-213, 2010.
4. Noehren B et al. *Br J Sports Med*, 2010.

MEDIAL LONGITUDINAL ARCH CHARACTERISTICS DURING RUNNING

Steph Forrester

Sports Technology Research Group, Loughborough University, Loughborough, UK
email: s.forrester@lboro.ac.uk, web: http://sti.lboro.ac.uk

INTRODUCTION

Foot type, and in particular medial longitudinal arch (MLA) height, is considered to be a key factor in running injuries [1]. Commonly, clinicians assess foot function based on static measurements, such as arch height index. However, these measures largely neglect the contribution of lower limb muscles which can influence foot function during dynamic movement. Indeed, static MLA measures are typically found to correlate poorly with MLA movement during dynamic activities [2]. Previous studies characterizing MLA behavior under dynamic movement conditions have mainly been limited to walking [2]. This study aimed to characterize and compare MLA deformation and loading between heelstrike and forefoot running.

METHODS

Eight male recreational athletes with normal arches [3] gave written informed consent (age 21 ± 2; height 1.75 ± 0.09 m; body mass 68.8 ± 11.5 kg; all mean ± SD). Each performed standing trials for their right foot with 10% and 90% body weight loading conditions. Digital scales were used to control the loading and digital photographs (Panasonic Lumix DMC-TZ7, 10.1 MP) of the medial foot were taken to allow static arch properties to be determined [4].

All subjects completed barefoot trials for heelstrike and forefoot running across a force platform at a comfortable speed. The order of run techniques was randomized and in each case five good trials for right foot contact with the force platform were performed. Ground reaction forces (1200 Hz, Kistler 9281CA) were measured together with 3D lower body kinematics using a 12 camera motion analysis system (200 Hz, Vicon Nexus). Twenty six retro-reflective markers were positioned using the lower body plug in gait model (16 markers), with additional markers on the greater trochanter, first metatarsal head, navicular tuberosity, medial calcaneus and distal hallux.

Arch height index (AHI) and static arch stiffness (AS-S) were obtained from the digital photographs (ImageJ, NIH, Bethesda, USA). The AHI followed [1] while AS-S was defined as the change in loading divided by the change in dorsum height at 50% of foot length between the 10% and 90% body weight (bw) conditions. For the gait trials, arch length (AL) was calculated as the 3D distance from the medial calcaneus to the first metatarsal head and navicular height (NH) as the 3D perpendicular distance from the arch length line to the navicular tuberosity. Arch stiffness (AS-D) values were obtained for the early (ES) and late (LS) stance phases of ground contact as the slope of the best fit line through the ground reaction force (GRF) component acting in the NH direction versus NH. Early stance was defined as starting at the end of the GRF_{NH} impact peak (heelstrike) or 10% of ground contact time (forefoot) to the GRF_{NH} active peak. Late stance was defined as from minimum NH to 90% of ground contact time.

The effect of running technique (heelstrike versus forefoot) on MLA deformation and loading characteristics was assessed using paired samples t-tests ($p \leq 0.05$).

RESULTS AND DISCUSSION

The static arch measurements gave group mean AHI values of 0.355 ± 0.007 (10% bw) and 0.332 ± 0.008 (90% bw), similar to those reported in [4], and confirmed the normal arch classification for each subject. Group mean static arch stiffness was 155 ± 26 N mm^{-1}.

There were no significant differences in dynamic arch stiffness between heelstrike and forefoot running (Table 1) or between early and late stance. This was somewhat surprising given the differences in technique during early stance; for heelstrike running the arch is not directly loaded until after the impact peak and thereafter from heel-to-toe, while for forefoot running the arch is loaded from touchdown and from toe-to-heel. The large standard deviation in AS-D_{ES} for heelstrike running may have prevented any systematic differences from being identified. The stiffness was higher during late stance for both running techniques, in agreement with previous studies [5].

Table 1. Summary of the dynamic MLA deformation and loading results.

	HEELSTRIKE		**FOREFOOT**	
Velocity (m s^{-1})	3.49 ± 0.46		3.43 ± 0.46	
Stance time (s)	0.209 ± 0.019		0.218 ± 0.036	
Arch stiffness				
AS-D_{ES} (N mm^{-1})	175 ± 54		157 ± 25	
AS-D_{LS} (N mm^{-1})	220 ± 29		200 ± 30	
Navicular height				
$NH_{RESTING}$ (mm)	28.9 ± 5.4			
NH_{MIN} (%resting)	67.0 ± 10.7		64.6 ± 9.3	
$t_{NH,MIN}$ (%stance)	48.5 ± 5.2		46.3 ± 2.3	
NH_{RANGE} (%resting)	*29.1 ± 4.5		35.2 ± 7.6	
Arch length				
$AL_{RESTING}$ (mm)	148 ± 9			
AL_{MAX} (%resting)	106.8 ± 2.1		106.8 ± 2.3	
$t_{AL,MAX}$ (%stance)	47.3 ± 10.7		50.9 ± 6.3	
AL_{RANGE} (%resting)	6.51 ± 2.01		7.44 ± 1.8	
Peak Active Force	(bw)	(%stance)	(bw)	(%stance)
GRF_Z (bw)	2.47 ± 0.11	*39.7 ± 5.5	2.51 ± 0.09	47.8 ± 1.3
GRF_{NH} (bw)	2.34 ± 0.16	*38.2 ± 4.4	2.30 ± 0.19	47.0 ± 1.7
GRF_{AL} (bw)	*0.56 ± 0.11	*77.0 ± 1.9	0.85 ± 0.09	72.0 ± 1.1

* indicates significant difference between heelstrike and forefoot running ($p<0.05$)

Although NH and AL demonstrated similar trends for both running techniques (Figure 1) the movement range (deformation) for NH was significantly greater in forefoot running ($p=0.008$; Table 1). This resulted from a higher value of NH at touchdown, presumably due to the differences in lower limb kinematics and pre-activation between running techniques at this point, combined with a (non-significant) lower minimum NH during mid-stance (Figure 1a).

The GRF_{NH} were of similar shape, but lower magnitude, to the vertical GRF. Beyond the impact peak they were very similar between running techniques (Figure 2a). The GRF_{AL} were lower for heelstrike running throughout stance (Table 1 and Figure 2b). The timings of the peak active force for both NH and AL showed significant differences between running techniques. Notably, NH_{MIN} and peak GRF_{NH} almost coincided for forefoot running (46% and 47% of stance respectively), but were > 10% of stance apart for heelstrike running (49% and 38% respectively).

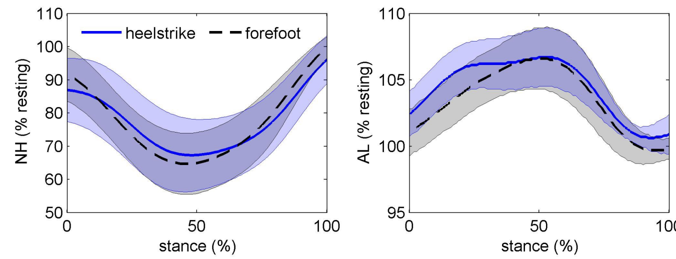

(a) navicular height (b) arch length

Figure 1: Group mean (±SD) NH and AL for heelstrike and forefoot running.

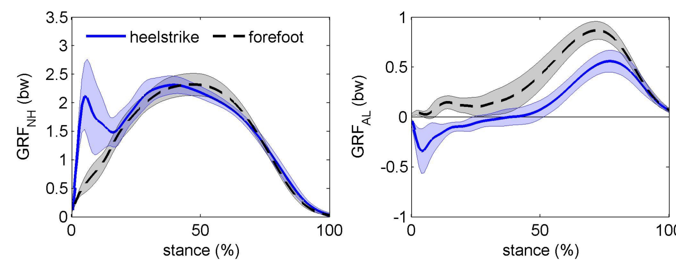

(a) navicular height (b) arch length

Figure 2: Group mean (±SD) GRF components in NH and AL directions for heelstrike and forefoot running.

CONCLUSIONS

Clear differences in MLA deformation and loading characteristics between heelstrike and forefoot running were observed. Characterizing MLA function during running may be beneficial to improving our understanding of many running injuries.

REFERENCES

1. Williams DS & McClay IS. *Phys Ther*, **80**, 864-871, 2000.
2. Cashmere T, et al. *Foot Ankle Int*, **20**, 112-118, 2010.
3. Williams DS, et al. *Gait Posture*, **19**, 263-269, 2004.
4. Pohl MB & Farr L. *J Foot Ankle Res,* **3**, 14.
5. Hageman ER, et al., *Proceedings 34th ASB*, Providence, RI, 2010.

DO SKELETAL MUSCLE PROPERTIES RECOVER FOLLOWING REPEAT BOTULINUM TOXIN TYPE-A INJECTIONS?

[1]Rafael Fortuna, [1]Monika Horisberger, [2]Marco Aurelio Vaz, [1]Walter Herzog
[1]Human Performance Laboratory, University of Calgary, Canada
[2]School of Physical Education, Federal University of Rio Grande do Sul, Brazil
email: rfortuna@kin.ucalgary.ca

INTRODUCTION

Botulinum toxin type-A (BTX-A) is a frequently used treatment modality for a variety of neuromuscular disorders with the primary aim to relax spastic muscles. When injected into spastic muscles, it prevents the release of acetylcholine at the motor nerve endings, thus inducing a dose-dependent muscle paralysis [1].

Although considered safe, previous studies have suggested that BTX-A injections cause muscle atrophy and contractile material loss in injected and contralateral non-injected muscles [2,3]. BTX-A treatments often comprise repeat injections separated by 3-4 month intervals due to the reversible and time limited action of the toxin [4]. Depending on the BTX-A injection/recovery protocol, muscle function may be compromised following repeat BTX-A treatments and this could severely impair muscle function once BTX-A treatment has been finished. However, muscle recovery following BTX-A treatments, and its long term effects, are anecdotal with no systematic research backing the clinical claims.

Therefore, the purpose of this study was to investigate if muscle properties can fully recover within six months following monthly BTX-A injections given over a half year period.

METHODS

Twenty-seven skeletally mature one year old female NZW rabbits were divided into 5 groups as follow: Control (*n*=5), BTX-A+0M (*n*=5), BTX-A+1M (*n*=5), BTX-A+3M (*n*=5), BTX-A+6M (*n*=7). Control group rabbits received equal volume saline injections as experimental rabbits. Experimental rabbits received intramuscular monthly BTX-A injections (3.5U/kg) unilaterally into the quadriceps femoris musculature for six months, and were evaluated after 0, 1, 3, and 6 months of recovery (BTX-A+0M/+1M/+3M/+6M; respectively).

Outcome measures included isometric knee extensor strength, muscle mass, and contractile material percentage in quadriceps femoris injected and contralateral non-injected muscles. Muscle mass and strength were assessed by weighing the muscles and measuring the maximal isometric strength via femoral nerve stimulation throughout the entire knee range of motion. The contractile material percentage was determined histologically by the area fraction of contractile material to total muscle cross-sectional area.

A two way mixed model ANOVA with the main factors leg (injected and contralateral non-injected) and groups (Control, BTX-A+0M/+1M/+3M/+6M) was performed ($\alpha=0.05$).

RESULTS

Isometric knee extensor strength was partially and completely recovered in the injected and contralateral non-injected hindlimbs, respectively for BTX-A+6M group rabbits. Peak knee extensor strength in the BTX-A injected hindlimbs was reached after 1 month of recovery (BTX-A+1M), with no further recover for BTX-A+3M and BTX-A+6M group rabbits (Fig 1). Muscle mass recovered in a similar manner to strength (results not shown).

The contractile material for Control group rabbits was around 96%. BTX-A+0M group rabbits had a significant reduction in the contractile material for the injected (63%) and contralateral non-injected (79%) hindlimbs. The contractile material was partially recovered in the injected hindlimbs for the BTX-A+6M but not for the BTX-A+1M and BTX-A+3M group rabbits when compared to BTX-A+0M group rabbits. The contractile material in the contralateral non-injected hindlimbs showed no recovery in the BTX-A+1M/3M/6M compared to the BTX-A+0M rabbits (Fig 2).

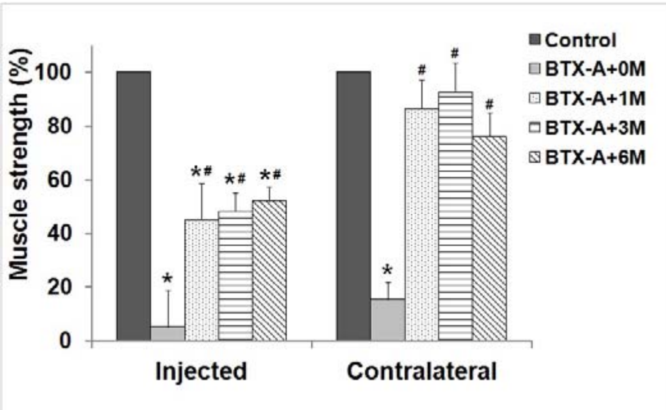

Figure 1 Mean (±1SE) knee extensor strength normalized to control group rabbits (dark bars). *****compared to Control; #compared to BTX-A+0M group (p<0.05).

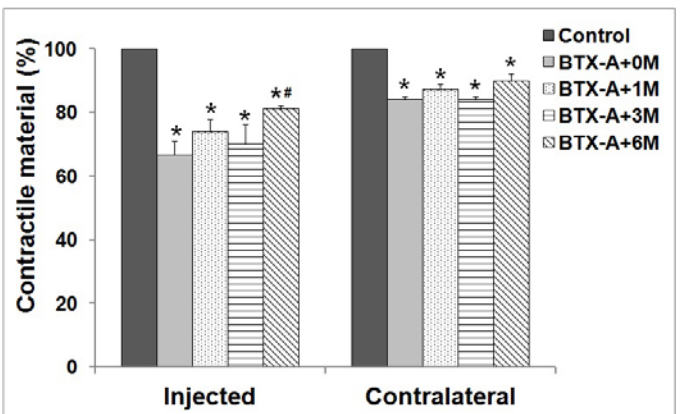

Figure 2 Mean (±1SE) contractile material normalized to control group rabbits (dark bars). *compared to control; #compared to BTX-A+0M group (p<0.05).

DISCUSSION AND CONCLUSIONS

Isometric knee extensor strength, muscle mass and the area fraction of contractile material was not fully recovered in injected and contralateral non-injected quadriceps femoris muscles after six months of recovery. While knee extensor strength and muscle mass recovered to a certain degree, there was no apparent improvement in the area fraction of contractile material, suggesting that muscle mass and strength recovery occur at a different rate than the recovery of the contractile material. Since contractile material is typically not evaluated in patients suffering from spasticity following repeat BTX-A treatments, measurements of muscle strength, volume and mass may not appropriately reflect the long-term structural changes in skeletal muscles following repeat BTX-A treatments.

The dramatic recovery of strength in the BTX-A injected muscles of the 1 month recovery group compared to the 0 month recovery group suggests that the effects of BTX-A on acetylcholine release inhibition wore off primarily between the 0 and 1 month recovery period. Considering that the injections were given at the beginning of each month, the 0 month recovery rabbits were 1 month post the last injection, while the 1 month recovery rabbits were 2 months post injection. Our results, therefore, are consistent with previous findings that BTX-A effects rapidly decrease after approximately four weeks following the last BTX-A injection [5]. They also suggest that BTX-A affected not only the target muscles, but also the quadriceps muscles of the contralateral hindlimbs that were not injected and were not targeted in this investigation. Future studies will need to address the fact that long-term recovery following BTX-A treatment may affects no-target muscles and may lead to non-reversible damage of the injected musculature.

REFERENCES

1. Brin MF, *Muscle & Nerve* **6**, 148-168, 1997.
2. Fortuna R, et al. *J. of Biomechanics* **44**, 39-44, 2011.
3. Graham HK, et al. *Gait and Posture* **11**, 67-79, 2000.
4. Schroeder AS, et al. *Movement disorders* **24**, 1494-1503, 2009.
5. De Paiva A, et al. *PNAS* **96**:3200-3205, 1999

ACKNOWLEDGEMENTS

Capes–Brazil; NSERC-CIHR Collaborative Health Research Projects, the Canada Research Chair Program; Cerebral Palsy International Research Foundation and the Killam Foundation.

STEP COUNTS USING A TRI-AXIAL ACCELEROMETER DURING ACTIVITY

Emma Fortune, Vipul Lugade, Melissa Morrow and Kenton R. Kaufman

[1]Mayo Clinic, Rochester, MN, USA
email: kenton.kaufman@mayo.edu, web: http://mayoresearch.mayo.edu/mayo/research/biomechanics

INTRODUCTION

Physical activity has been associated with health improvements in a number of populations. Step counting is one of the most commonly used measures of physical activity [1]. Due to their small size and light weight, the use of wearable sensors for step counts has been investigated in many studies [2, 3] as they are suitable for home deployment. One of the main issues with step counts as a physical activity measure is that a high level of accuracy is needed. The aim of this study was to validate step detection using a tri-axial accelerometer in healthy adults.

METHODS

Accelerometer and video data were acquired from 10 (2 M, 8 F) healthy adults using custom built activity monitors strapped bilaterally on the ankles, waist and thigh as they performed a 5 minute protocol in the laboratory. The protocol consisted of static and dynamic activities involving standing, sitting, shuffling feet while standing and sitting, lying, walking, stair climbing and jogging. At the time of evaluation, the mean age and BMI of the subjects were 33.4±10.49 yrs, and 23.6±2.7 kg/m^2, respectively. The study protocol was approved by the Mayo Clinic IRB and written informed consent was obtained before participation. Each activity monitor incorporated a tri-axial accelerometer (±16g) and sampled each axis at 100 Hz. Video data were simultaneously acquired at 60 Hz using a handheld camera and were synchronized to the accelerometer data by three vertical jumps performed by the subjects prior to the protocol.

Steps were manually counted in the video data using Windows Movie Maker. Accelerometer data were analyzed offline using MATLAB. The calibrated acceleration signals were filtered using a median filter (with n=3) and separated into its gravitational component by using a third-order zero phase lag elliptical low pass filter, with a cutoff frequency of 0.25 Hz, 0.01 dB passband ripple and -100 dB stopband ripple. Subtracting the gravitational component from the original signal provided the bodily motion component [4].

Waist and thigh angles were used to identify upright standing postures. Activity was characterized as jogging when the signal magnitude area of the bodily motion component of the waist exceeded 0.8 g and as walking (including stair climbing) when it was between 0.135 g and 0.8 g for epochs of 1 s. During identified walking and jogging segments, the anteroposterior accelerations of the right and left ankles were analyzed using a peak detection method with adaptive thresholds to calculate the number of steps taken [5]. Step counts were validated against the steps counted manually from the video data (gold standard). The sensitivity, positive predictive value (PPV) and agreement were calculated for the group.

RESULTS AND DISCUSSION

The average sensitivity (Fig. 1), positive predictive value (Fig. 2) and agreement (Fig. 3) of step counts in this study were 96, 97 and 98%. The 2% average difference in agreement from the manual step count was due mostly to segments of activity with shuffling of the feet while standing and segments with less than 5 steps. The results of this study suggest that this method would be suitable for counting steps using tri-axial accelerometers placed bilaterally on the ankles and waist in a free living environment.

With some subjects, step counts were less accurate, mostly due to small inaccuracies of the detection of the walking and jogging segments at the beginnings and ends (walking activity detection had a sensitivity of 98.0% (1.3%) and a PPV of 95.5% (3.5%), while jogging activity detection had a sensitivity of 94.5% (6.8%) and a PPV of 98.8% (2%)), resulting in one or more missing steps at the beginning and end of the activity.

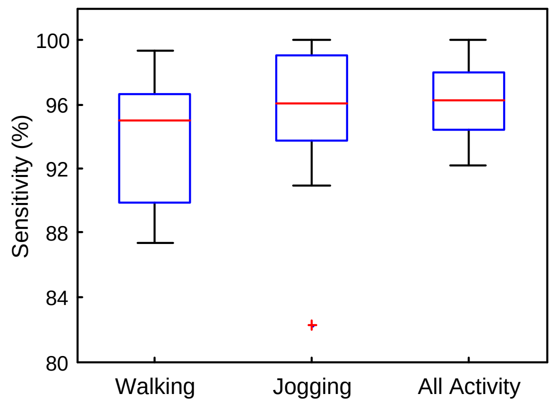

Figure 1: Step detection sensitivity. The red line represents the median, the bottom and top lines of the box are 25th and 75th percentiles, and the whiskers extend to ± 2.7SD. Crosses are outliers.

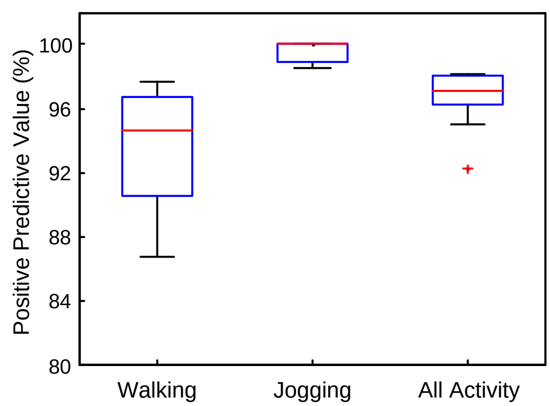

Figure 2: Step detection positive predictive values.

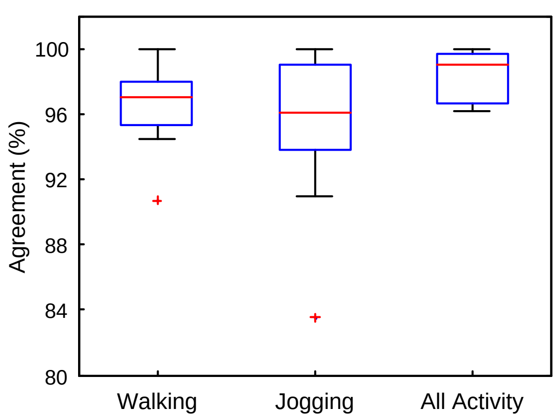

Figure 3: Agreement between steps detected and manual step counts.

The number of steps taken for each segment ranged from 2 to 115. The accuracy of the step detection would be expected to increase for longer segments of walking and jogging activity as the inaccuracies occur at the beginning and end of the segments. Previous studies have shown that the most accurate pedometers can give step counts within ±3% of the manual step count, with step counts being classed as 'acceptable' when within ±10% [3].

The higher average sensitivity (Fig. 1) and positive predictive values (Fig. 2) obtained with step detection during jogging (95 and 100%) in comparison to walking (94 and 94%) were due to the consistent and higher accelerations. An even higher level of accuracy of step detection would be expected in free living as the confined space of a laboratory sometimes resulted in the subjects moving unnaturally by turning often and taking smaller steps. The advantage of using an accelerometer for step counting is that it can also provide data such as gait event timings, amplitudes, and other temporal parameters derived from these.

CONCLUSIONS

The results suggest that the analysis methods are suitable for step counting in free living using tri-axial accelerometers on the ankles, waist and thigh, which remains to be tested in future work.

ACKNOWLEDGEMENTS

Funding provided by DOD DM090896, NIH T32 HD07447 and NIH K12 HD065987.

REFERENCES

1. Thomas J, et al. *Research methods in physical activity*: Human Kinetics Publishers, 2005.
2. Dijkstra B, et al. *Age & Aging* **37**, 436-441, 2008.
3. Schneider PL, et al. *Medicine and Science in Sports and Exercise* **36**, 331-5, 2004.
4. Karantonis DM, et al. *Information Technology in Biomedicine, IEEE Trans* **10**, 156-67, 2006.
5. Greene BR, et al. *Medical and Biological Engineering and Computing* **48**, 1251-1260, 2010.

THE EFFECTS OF VISUAL FEEDBACK AND AGING ON FORCE OSCILLATIONS WITHIN 0-1 Hz

Emily J. Fox, Harsimran S. Baweja, Changki Kim, David E. Vaillancourt, and Evangelos A. Christou
University of Florida, Gainesville, FL, USA
email: eachristou@ufl.edu; web: http://hhp.ufl.edu/apk/ces/affil/npl/Home.htm

INTRODUCTION

Oscillations in motor output change in specific frequency bins and have important implications for understanding healthy aging and pathological motor control. Force output primarily comprises of oscillations from 0-4 Hz; however, most of the modulation comes from 0-1 Hz and the power within this bin is associated with force control [1,2]. Despite this, prior studies have assumed that the oscillations from 0-1 Hz respond uniformly rather than considering the presence of sub-frequencies *within* 0-1 Hz.

It is important to examine the modulation of sub-frequencies within 0-1 Hz because these sub-frequencies may originate from physiological processes, such as those associated with visuomotor integration and aging. For example, manipulation of visual feedback, either by removing it or changing the magnification, alters force oscillations from 0-1 Hz [1]. Additionally, age-associated differences in force control may be due to modulation of force from 0-1 Hz [2]. Furthermore, the age-associated differences in force control are exacerbated when visual feedback is magnified [3].

Our purpose was to determine whether modulation of specific sub-frequencies *within* 0-1Hz contribute to changes in force control associated with manipulation of visual feedback and aging.

METHODS

Ten young adults (25± 4 yrs, 5 men) and ten older adults (71± 5 yrs, 4 men) participated and performed the following: 1) MVC with abduction of the index finger; 2) Constant force task with abduction of the index finger; 3) repetition of the MVC task. During the constant force task, we manipulated visual feedback by changing the visual angle or removing it. Changing the visual angle altered the amplitude of the force fluctuations viewed by the subject [3].

Each subject performed three trials at each visual angle (0.05°, 0.5°, 1.5°) at 2% MVC. We counter balanced the order for the visual feedback conditions (vision and no vision) and the order of the three visual angles was random. The 2% MVC force was chosen because age-associated differences in force control are consistently evident at low-force levels [4].

Subjects were instructed to increase their force (blue line) to match the target force (red line) within 5 s, and then to maintain their force on the target as accurately as possible for 30 s. During the no visual feedback condition, visual feedback was removed after 15 s.

The middle 6 s of force data were used to calculate the mean force and the coefficient of variation. The frequency data were divided into seven bins: 0, 0.16, 0.33, 0.50, 0.66, 0.83, and 1.00 Hz and the percent of power was calculated for each bin, relative to the total power from 0-1.0 Hz.

RESULTS AND DISCUSSION

To determine whether modulation of force output within 0-1 Hz is different with and without visual feedback we compared the no visual feedback condition with the visual feedback condition at the highest visual angle (1.5^{o}). During the no visual feedback condition, both groups exhibited greater force oscillations from 0 to 0.33 Hz and lesser oscillations from 0.66 to 1.0 Hz. In contrast, magnification of visual feedback (visual angles of 0.50^{o} and 1.5^{o}) decreased force oscillations from 0-0.16 Hz and increased force oscillations from 0.86-1.0 Hz (Figure 1).

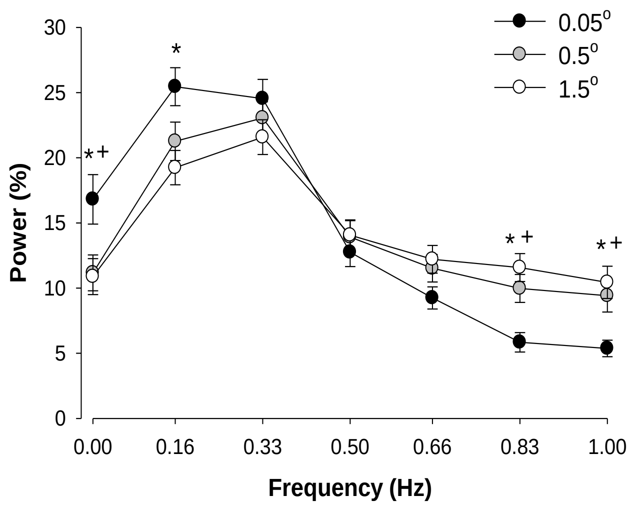

Figure 1: The interaction of visual angle and frequency bins within 0-1 Hz.

Older adults demonstrated a greater increase in the variability of force with magnification of visual feedback compared with young adults (P=0.05). Furthermore, older adults exhibited differential force modulation within 0-1 Hz compared with young adults (P<0.05). Specifically, older adults exhibited greater power from 0-0.16 Hz and lesser power from 0.66-0.83 Hz (Figure 2).

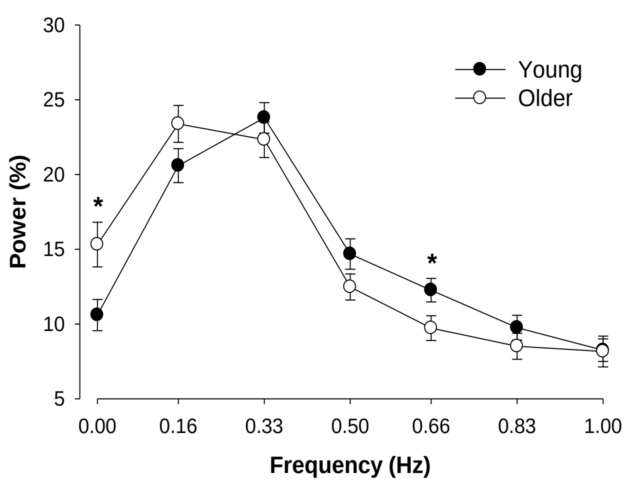

Figure 2: The interaction of age and frequency bins within 0-1 Hz.

We used multiple linear regression models to predict the change in CV of force at the highest visual angle (relative to the no visual feedback condition) from the change in power of the seven frequency bins within 0-1 Hz. The change in CV of force was predicted by a multiple-regression model that included the modulation at 0.16 Hz, 0.33 Hz, 0.5 Hz, 0.66 Hz, and 0.83 Hz (R^2 = 0.8, P = 0.01).

Our findings suggest that sub-frequencies in force output within 0-1 Hz are modulated with changes in visual feedback and aging. Modulation of these low-frequency oscillations may be associated with underlying processes such as central drive to the motor unit pool or breathing. The age-associated changes in low-frequency oscillations may be related to increases in motor unit discharge rate variability [5]. Additionally, our results suggest that alterations in visuomotor integration may underlie the age-associated differences in force modulation with magnification of visual feedback. This finding may be related to age-related changes in neuroanatomic structures [6] as well as the increased attentional demands associated with magnification of visual feedback.

CONCLUSIONS

Overall, examination of force oscillations within 0-1 Hz is critical for understanding the effects of visual feedback and aging on force control. Our findings have important implications for identifying underlying mechanisms associated with force control and may potentially influence the development of training strategies for individuals with motor impairments.

REFERENCES

1. Baweja HS, et al. *Europ J Appl Physiol* **108**, 935-943, 2010.
2. Vaillancourt DE and Newell KM. *J Appl Physiol* **94**, 903-912, 2003.
3. Kennedy DM and Christou EA. *Exp Brain Res* **213**, 351-361, 2011.
4. Christou EA and Tracy BL. *Movement System Variability*, 199-215, 2005.
5. Kornatz KW, et al. *J Appl Physiol* 98, 2072-2080, 2005.
6. Coombes SA, et al. *J Neurophsiol* **103**, 2114-2123, 2010.

ACKNOWLEDGEMENTS

This work was supported by National Institute on Aging Grant R01 AG-031769 to E. A. Christou.

INFLUENCE OF SHOD & BAREFOOT GAIT ON SINGLE SUPPORT & DOUBLE SUPPORT

John Fox, Braden Romer, Jay Patel, Jared Rehm, and Wendi Weimar

Auburn University, Auburn, AL, USA
email: jwf0007@auburn.edu, web: http://education.auburn.edu/kine/

INTRODUCTION

For many, everyday life involves gait, whether walking across the parking lot into the grocery store, strolling into the kitchen for an afternoon snack, or exercise. Hence, the role gait plays in human life demands a better understanding of the biomechanical implications involved. However, one does not have to search long to see that a great deal of biomechanical research is oriented toward this goal. Amongst these studies on gait, research into effects of shod versus barefoot gait has emerged. One such study suggests that barefoot gait is advantageous due to better foot strike patterns [1]. Other research has demonstrated decreased stride length and increased cadence when walking without shoes [2]. This indicates that a potential difference in the timing of gait phases occurs when shod versus barefoot, particularly double support time and single support time.

The purpose of this study was to measure the effects of shod and barefoot gait and two different self-selected paces on the single support and double support phases.

METHODS

Twenty (10 female, 10 male) participants volunteered for the study. Participants were healthy and without lower extremity injury for at least one year prior to participation in the study. The average age of the participating group was 23.7±2.4 years (m±SD) and the average body mass was 73.6±12.2kg. Participants walked on an instrumented walkway (GAITRite, CIR Systems, Inc., Havertown, PA, USA) under four separate conditions. Each condition required six trials. For each of the six trials single support and double support time was measured as a percentage of the entire gait cycle. Trials began with a 3.5m lead-in, followed by walking over the 4.25m GAITRite mat, then a 3.5m walkout for a total of 11.25m per trial.

Conditions included in the study were: participants walking shod at a self-selected pace (SHFW), barefoot at a self-selected pace (BFFW), shod while walking faster than self-selected pace (SHF), and barefoot while walking faster than self-selected pace (BFF). During the SHF and BFF conditions, participants were provided the verbal instructions that they were to imagine they were late to a meeting. All participants were provided the same verbal cue, by the same investigator, at identical points during the data collection process. Participants were dressed in identical polyester clothing and utilized commercially available non-running athletic shoes for all shod trials.

A 2 (Gender) x 4 (Condition) MANOVA was conducted using SPSS (IBM SPSS Campus Edition, IBM Corporation, Somers, NY). Dependent variables were single support time and double support time. Bonferroni post-hoc analyses were conducted to determine where significant differences ($p<0.05$) existed among conditions.

RESULTS AND DISCUSSION

Results showed no main effect for gender ($F_{(2,71)}$ = 2.437, p = 0.095, $\eta^2 = 0.064$)on the dependent variables, but for condition there was a main effect ($F_{(6,144)}$ = 12.129, p < 0.001, $\eta^2 = 0.336$). There was no significant interaction effect. Follow-up analyses indicated a significant difference between all conditions except BFFW and SHF (p = .171) for single support time. In addition, for double support time significant differences were found between all conditions except BFFW and SHF (p = .071).

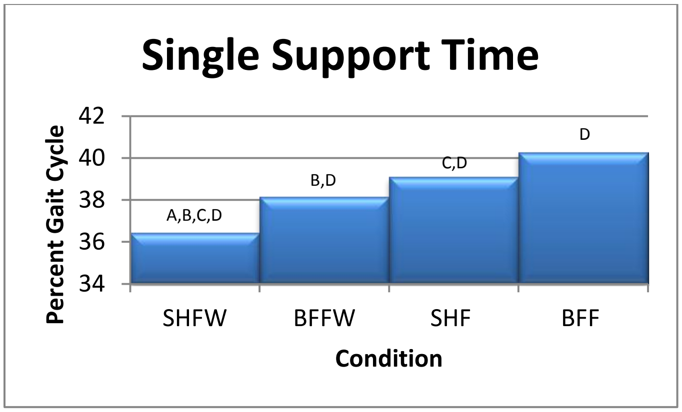

Figure 1: All conditions were significantly different, with the exception of BFFW and SHF.

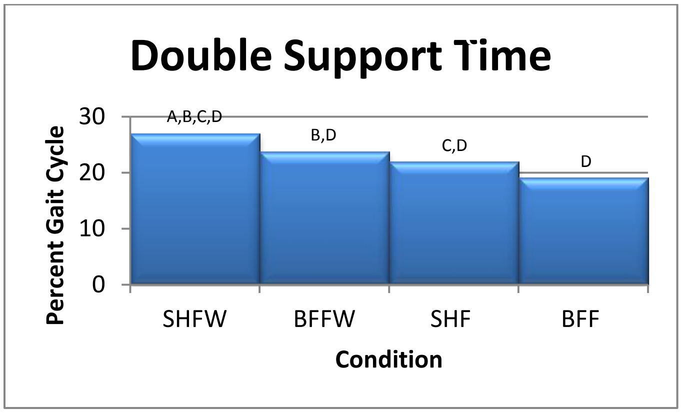

Figure 2: All conditions were significantly different, with the exception of BFFW and SHF.

CONCLUSIONS

The research conducted here demonstrates differences in gait characteristics when walking shod versus barefoot and at different speeds. It is not surprising that gender differences in single and double support were not found, since these variables were represented as a percentage of the gait cycle. However, similar to recent publications on running [1] and walking [2, 3], variations were found between shod and barefoot conditions. As shown in Figure 1, the amount of time spent in the single support phase increases when going from the shod to barefoot condition and when walking at a fast self-selected pace. Conversely, Figure 2 shows that the amount of time spent in double support decreases when changing from the shod to barefoot condition and when velocity increases. This is consistent with research showing that as speed increases single support time increases and double support time decreases [4] These results also support research indicating that wearing shoes decreases single support time and increases double support time [3]. Further research should be conducted to determine whether increases single support time during barefoot gait and higher velocity conditions aids in the attenuation of peak ground reaction forces.

REFERENCES

1. Leiberman DE, et al. *Nature* **463**, 531 – 353, 2010.
2. Shakoor N, Block JA. *Arthritis Rheum* **54(9)**, 2923 – 2927, 2006.
3. Lythgo N, Wilson C, Galea M. *Gait Posture* **30**, 502 – 506, 2009.
4. van Hedel HJA, Tomatis L, Müller, R. *Gait Posture* **24**, 35 – 45, 2006.

HOW DOES AGE AFFECT INDIVIDUAL LEG MECHANICS DURING UPHILL AND DOWNHILL WALKING?

Jason R. Franz, Alyse Kehler, Lauren E. MacDonald, and Rodger Kram

University of Colorado, Boulder, CO, USA
Email: jason.franz@colorado.edu web: http://www.colorado.edu/intphys/research/locomotion.html

INTRODUCTION

Unlike most gait laboratories, the world is not flat. Uphill and downhill walking present biomechanical challenges to old adults seeking to maintain their independence. We know that in young adults walking over level ground, the collision of the leading leg during double support dissipates mechanical energy. The trailing leg replaces this dissipated energy by generating mechanical power to restore and redirect the center of mass (CoM) velocity upward and forward. Thus, during level walking, the leading and trailing legs simultaneously perform negative and positive mechanical work, respectively [1]. However, old adults generate significantly less trailing leg mechanical power during level walking. To compensate, they perform greater positive work during the single support phase of the subsequent step [3,4].

Unlike level walking, we recently discovered that both the leading and trailing legs of healthy young adults contribute progressively more to power generation with steeper uphill grade and to power absorption with steeper downhill grade [2]. Advanced age may bring changes in the biomechanics of individual leg function that uniquely impair uphill or downhill walking ability in old adults.

We quantified individual leg mechanical power during level, uphill, and downhill walking in old adults and compared with young adult data reported previously [2]. We hypothesized that, compared to young adults, old adults would 1) generate less mechanical power with the trailing leg during uphill walking and 2) absorb greater mechanical power with the trailing leg during downhill walking.

METHODS

10 old (4M/6F, 72 ± 5 yrs, 65.0 ± 13.3 kg) and 11 young (6M/5F, 26 ± 5 yrs, 71.0 ± 12.3 kg) subjects walked at 1.25 m/s on a dual-belt, force-measuring treadmill [2] at seven grades (0, ±3°, ±6°, ±9°). All subjects were healthy and exercised regularly. We recorded ground reaction force (GRF) components parallel, perpendicular, and lateral to the treadmill surface for the right leg (Fig. 1). Assuming symmetry, we phase shifted the right leg GRFs by 50% of a stride and reversed the polarity of the lateral forces to emulate the forces exerted by the left leg.

We used the individual limbs method (ILM) [1] to

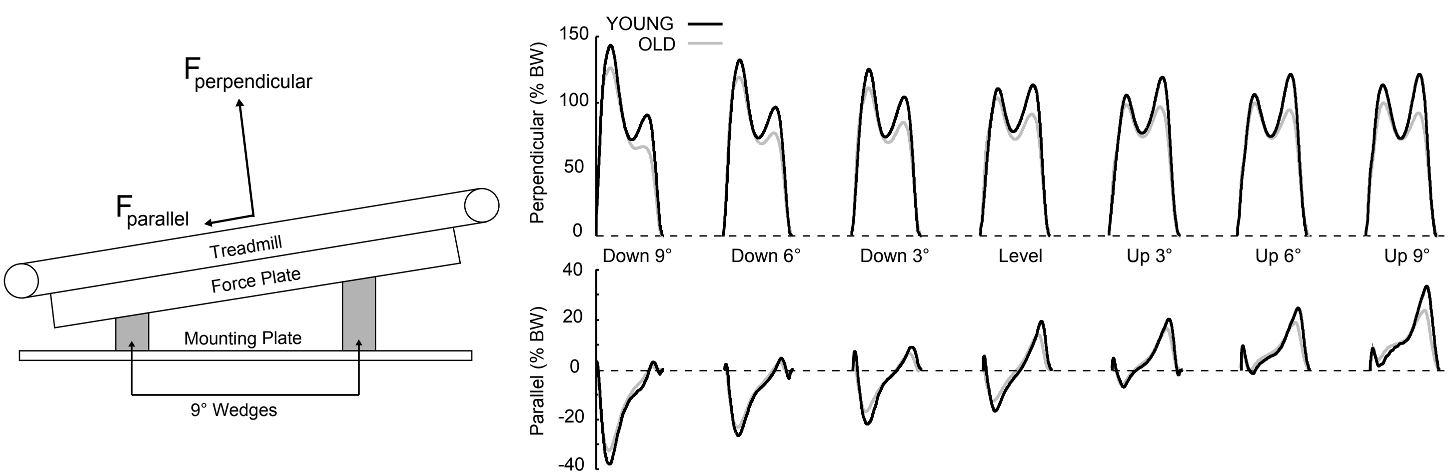

Figure 1. Average ground reaction force (GRF) components perpendicular and parallel to the treadmill surface. Note the reduced propulsive GRF peaks in old vs. young adults.

calculate the mechanical power generated/absorbed by each leg over 15 consecutive strides per condition. In short, the ILM involves computing instantaneous mechanical power as the dot product of individual leg GRF and CoM velocity. An analysis of variance (ANOVA) for repeated measures tested for significant effects of age and grade with a p<0.05 criterion.

RESULTS AND DISCUSSION

Old adults exhibited smaller propulsive GRF peaks than young adults, and this was exacerbated with steeper uphill grade (Fig. 1). As hypothesized, compared to young adults walking at the same speed, old adults generated significantly less trailing leg mechanical power during the double support phase of level (-41%) and uphill (-25% at 9°) walking (Fig. 2A). Old adults compensated by generating greater mechanical power during the single support phase of the subsequent step (e.g., +111% at 0° and +16% at 9°) (Fig 2B). The total mechanical power generated/absorbed over a step remained the same as young adults. The reduced trailing leg mechanical power generated by old adults during level and uphill walking is consistent with the distal (ankle extensor muscles) to proximal (hip extensor muscles) shift in leg muscle recruitment that occurs with advanced age [5]. We plan to test this idea by quantifying the net mechanical work performed by muscles crossing the hip, knee, and ankle. In contrast with our second hypothesis, we found no differences in mechanical power absorption between young and old adults during downhill walking. However, old adults did so with smaller peak perpendicular GRFs (Fig. 1), perhaps indicating an eccentric muscle impairment.

CONCLUSIONS

Old adults exhibit reduced trailing leg propulsive function during level and uphill walking. They compensate during single support, presumably through a greater reliance on hip extensor muscles. However, the distinct functions of the individual legs during uphill and downhill walking are preserved with advanced age. During double support, the leading and trailing legs of young and old adults both contribute progressively more to power generation with steeper uphill grade and to power absorption with steeper downhill grade. We plan to investigate therapeutic strategies that might improve the propulsive mechanics of old adults to maintain their uphill walking ability and thus their independence.

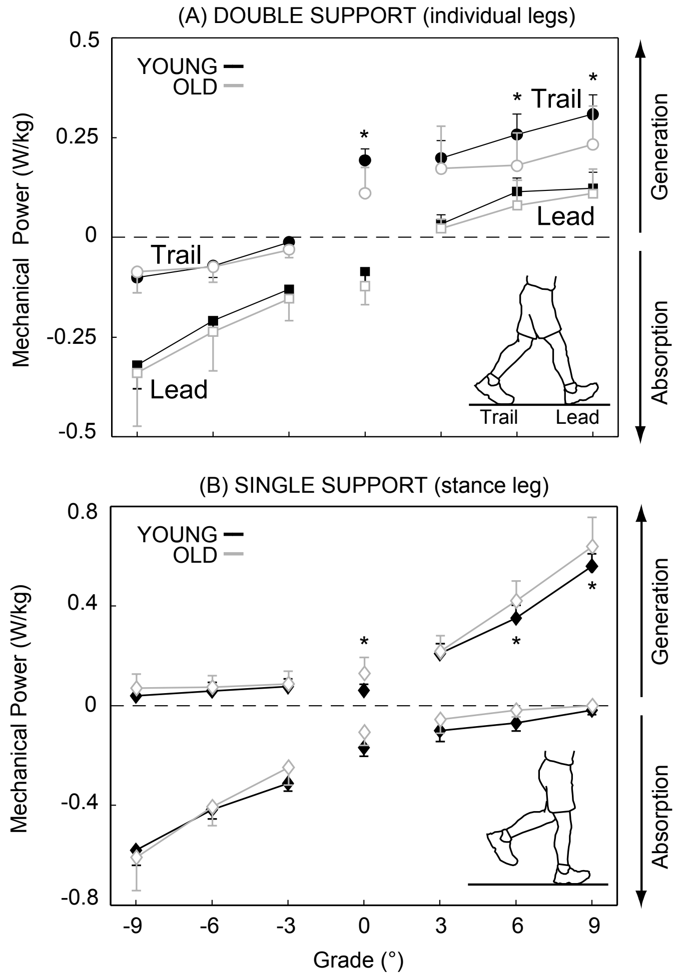

Figure 2. Average (SD) mechanical power during (A) double and (B) single support. Asterisks (*) indicate significant differences between young and old adults (p<0.05).

REFERENCES

1. Donelan JM, Kram R, Kuo AD, *J Biomech* 35, 117-24. 2002.
2. Franz JR, Lyddon NE, Kram R, *J Biomech* 45(2), 257-62, 2012.
3. Hernandez A, et al., *Gait & Posture* 30, 217-22, 2009.
4. Ortega JD, Farley CT, *J Appl Physiol* 102, 2266-73, 2007.
5. DeVita P, Hortobagyi T, *J Appl Physiol* 88: 1804-11, 2000.

ACKNOWLEDGEMENTS

Supported by NIH (5T32AG000279) and by a student Grant-in-Aid Award from the American Society of Biomechanics.

COMPARISON OF UNICOMPARTMENTAL KNEE ARTHROPLASTY AND HEALTHY LIMB FOR KNEE MOMENTS GENERATED DURING STAIR ASCENT

[1]Yang-Chieh Fu, [2,3]Tracy L. Kinsey, [2]Ormonde M. Mahoney, [1]Cathleen N. Brown, [1]Kathy J. Simpson

[1]Department of Kinesiology, University of Georgia, Athens, GA, USA
[2]Athens Orthopedic Clinic, Athens, GA, USA
[3]Department of Epidemiology, University of North Carolina, Chapel Hill, NC, USA

E-mail: ycfu@uga.edu web: http://www.coe.uga.edu/kinesiology/research-service/biomechanics/

INTRODUCTION

With improvement of implant design and surgical techniques, use of unicompartmental knee arthroplasty (UKA) has increased recently [1]. This surgery replaces the most damaged knee compartment, either the medial (MED) or lateral (LAT). However, biomechanical evidence to support the efficacy of UKA is still lacking, especially LAT-UKA. Stair ascent is a high-demanding functional activity. Interlimb asymmetry is a common clinical indicator to evaluate performance after joint reconstruction and to identify abnormal mechanics. Atypical joint mechanics are associated with osteoarthritis (OA) progression and implant wear [2]. Therefore, the purpose of the study was to compare the interlimb symmetry of the knee joint moments displayed during stair ascent of MED-UKA and LAT-UKA individuals.

METHODS

17 MED-UKA (14 iBalance Unicondylar Knee®, Arthrex; 3 Zimmer® Unicompartmental High Flex Knee System, Zimmer), and 9 LAT-UKA (6 iBalance; 3 Zimmer) healthy participants were recruited (Table 1) [3]. Leg dominance was defined as the limb used to kick a ball. All participants had a UKA performed by the author (OMM) at least 6 mo. prior to testing (range: 6 mo to 3 yr). All participants provided informed consent. Reflective markers (30) were placed on the lower body segments. Marker trajectories were captured using high-speed cameras (120 fps). Ground reaction forces were collected at 1200 Hz via a force platform mounted in the floor and another flush with the 1st step. Participants walked up 4 stairs barefoot at a self-selected speed starting with 1 limb for 5 trials and then the other limb for another 5 trials. The order of starting limb was counterbalanced among participants.

Knee moments were generated for each limb of the support phase of the 1st step. Different knee moment patterns among participants existed [3]. Therefore, variables common to all patterns were analyzed: peak knee extensor, abductor, and external rotator moment magnitudes and times to those peak moments. Paired t-tests were applied to determine interlimb differences within each UKA group (α = 0.05). A difference score for each variable was determined: value of UKA minus nonUKA limb. 95% confidence intervals (CIs) of difference scores also were reported.

RESULTS AND DISCUSSION

No interlimb difference was detected for ascent stride velocity (Table 1). The average ascent velocities of both groups were slower than a reported value (0.44 ± 0.06 m/s) for stair ascent of healthy older adults [3]. No time to peak moments were significantly different (p = 0.263 - 0.937), likely due to interparticipant variability.

For moment magnitudes, the MED-UKA group displayed greater peak extensor moment for the nonUKA limb than the UKA limb (Table 2). The extensor moment is generated to raise the body during the support phase. One possible reason for this outcome may be related to differences in leg strength, although this is not known from our data. Weaker leg strength of total knee replacement limbs has been reported [4]. Another explanation is that UKA individuals might also protect their surgical limb by leaning the body to the non-diseased limb. Habituation of limb protection has been shown for other populations [5]. However, this suggestion also cannot be proven at present. Limb dominance is not a likely reason (Table 1). Peak extensor moments of the UKA limb of both groups (MED: 1.21 ± 0.19; LAT: 1.02 ± 0.17 N·m·(body mass · leg length)$^{-1}$) were similar to values (1.30 ± 0.23) in the literature [3], suggesting that the moments generated by LAT- and MED-UKA groups are not abnormal.

In both groups, UKA limbs demonstrated greater peak abductor moments than nonUKA limbs. A possible reason may be the preference to shift the center of mass toward the nonUKA limb, thereby requiring greater abductor moment during late stance phase. A similar strategy has been noted during level walking for OA population [5], and it is reasonable that UKA population uses same strategy during stair ascent. Therefore, OA progression and implant wear may be of concern for the MED-UKA and LAT-UKA groups, respectively [2, 5, 6].

Sample size was a study limitation, especially on LAT-UKA group. *Posthoc* power analysis showed that desired group sample size was 20.

CONCLUSIONS

In conclusion, both MED- and LAT-UKA individuals demonstrate adequate knee extensor moments during stair ascent for both limbs compared to the literature. Greater UKA limb abductor moments were displayed by both groups. However, whether these differences are clinically significant and related to abnormal wear on the affected articular surfaces needs further examination.

REFERENCES

1. Geller, J. A., et al., J. *Knee Surg*, **21**, 7-14, 2008.
2. Milner C. E., *Gait & Posture* **28**, 69-73, 2008.
3. Fu, Y.-C., et al., *Annual meeting of ASB*, Long Beach, CA, USA, 2011.
4. Rossi, M. D. et al,. *Strength & Conditioning Journal*, **33**, 88-99, 2011.
5. Huang S.-C. et al., *Med Eng & Phy*, **30**, 997-1003, 2008.
6. Hopkins A. R. et al., *Med Eng & Phy*, **32**, 14-21, 2010.

Table 1: Participant characteristics (mean ± SD). Also presented: Average stride velocity (m·s^{-1}) and frequency of participants (% participants) whose UKA limb was their dominant limb.

Group	Gender (n)	Age (yrs)	Height (cm)	Mass (kg)	Stride Velocity (m·s^{-1})	Leg Dominance Freq (%)
MED-UKA	M: 6; F: 11	68.0 ± 7.4	162.7 ± 7.1	74.1 ± 12.3	0.38 ± 0.08	58.8
LAT-UKA	M: 3; F: 6	63.1 ± 7.8	167.2 ± 6.4	71.1 ± 13.3	0.37 ± 0.05	77.8

Table 2: Means ($\bar{X}$) and 95% confidence interval (lower (LB) and upper (UB) bound) of difference scores for peak knee joint moment magnitudes (N·m·(body mass · leg length)$^{-1}$).

	MED-UKA				LAT-UKA			
	$\bar{X}$	LB	UB	*p*	X	LB	UB	*p*
Extensor Moment	-0.08	-0.16	-0.01	*0.030	-0.36	-0.79	0.07	0.087
Abductor Moment	0.22	0.08	0.36	*0.005	0.15	0.04	0.26	*0.013
External Rotator Moment	-0.02	-0.06	0.02	0.298	-0.01	-0.04	0.02	0.471

Note. A positive or negative value indicates the UKA limb was greater or lesser, respectively, than the nonUKA limb. * = significant difference ($p < 0.05$).

In vivo three-dimensional analysis of the thoracic spine in trunk rotation

[1]Takahito Fujimori, [1]Motoki Iwasaki, [1]Yukitaka Nagamoto, [2]Takahiro Ishii, [1]Masafumi Kashii, [1]Tsuyoshi Murase, [3]Kazuomi Sugamoto, and [1]Hideki Yoshikawa.

[1]Department of Orthopedic Surgery and [3]Orthopedic Biomaterial Science, Osaka University Graduate School of Medicine, Osaka, Japan
[2] Department of Orthopedic Surgery, Kaizuka City Hospital, Osaka, Japan
email: takahito-f@hotmail.co.jp

INTRODUCTION

Spinal biomechanics is essential for understanding of the pathogenesis of spinal disorders and therapies. Compared with other regions of the spine, the thoracic spine is unique in both anatomy and potential disorders. Coupled motions of cervical and lumbar spine have been well described. However, there is less information about kinematics of the thoracic spine because of difficulty in analyzing its subtle motions. The purpose of our study was to demonstrate in vivo each intervertebral motion and coupled motion of the thoracic spine in trunk rotation by using three-dimensional imaging technique.

METHODS

Our subjects were 13 healthy male volunteers. Low-dose functional computed tomography (CT) scans were obtained for 3 positions for each subjects. Subjects were placed in neutral position that was defined as being supine on the flat CT table. Subjects were instructed to rotate actively their shoulder girdles along with the axis of the body trunk. Rotational positions were defined as twisting the trunk at a maximum to the right and left side within the range that subjects did not feel pain or discomfort. Motion analysis was performed on an original VTK viewer that was previously reported [1, 2]. Contour of each vertebra was semiautomatically extracted from 3D CT at a specific threshold. The segmented vertebra in the neutral position was superimposed on other positions automatically by voxel-based registration. The translation was converted into the relative motion with respect to the inferior adjacent vertebra on the local coordinate axis (Fig1) [3]. We also computed relative motion of T1 vertebra to L1 vertebra for better understanding.

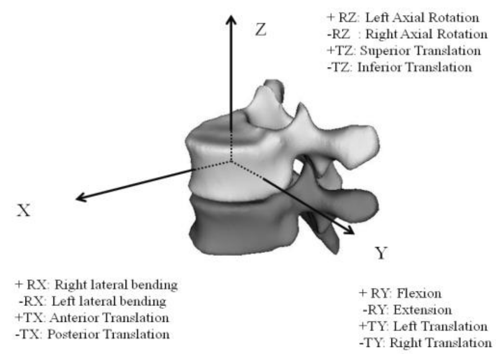

Figure 1: Local orthogonal coordinate system. The origin locates middle point between two centers of endplates.

The accuracy of this analysis system was: 0.19° in flexion–extension, 0.13° in axial rotation, 0.21° in lateral bending, 0.13 mm in lateral translation, 0.15 mm in superoinferior translation, and 0.31 mm in anteroposterior translation, as described in detail previously [4].

RESULTS AND DISCUSSION

At maximum rotation, mean ROM (± standard deviation) of T1 with respect to L1 at one side were 24.9°±4.9° for axial rotation, 7.6°±6.0° for coupled lateral bending in the same direction as axial rotation and 1.8°±12.4° for coupled flexion.

Segmental rotations and coupled motions were summarized in Table1. Axial rotation was significantly larger at middle segments (T6-T11) than at upper segments (T1-T6) and at lower segments (T11-L1) (Fig. 2).

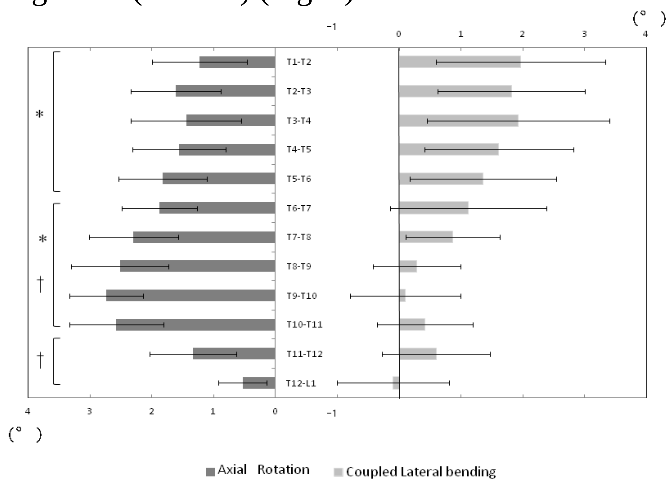

Figure2: Mean range of motions (*bar*) and standard deviation (*line*) of axial rotations (*left*) and coupled lateral bending (*right*) of one side in trunk rotations.
*, † P<0.01

We speculated that intact rib cage stabilized rotational motions at T1-T6 segments. Coupled lateral bending with axial rotation was observed predominantly in the same direction as axial rotation except T12-L1. Our results showed that coupled lateral bending with main rotation occurred in the same direction in the upper thoracic spine in common with the cervical spine, however, possibly occurred in the opposite directions at middle and lower thoracic spine in a similar pattern of the lumbar spine. Coupled flexion-extension was slight flexion. Coupled translations were hardly observed.

CONCLUSIONS

We firstly conducted a study to measure in vivo three-dimensional kinematics of each consecutive segment of the thoracic spine by using three-dimensional imaging technique.

REFERENCES

1. Ishii T, et al. *Spine* **29**, 2826-31, 2004.
2. Nagamoto Y, et al. *Spine* **36**, 778-83, 2011.
3. Stokes IA, et al. *Spine* **19**, 236-48, 1994.
4. Fujimori T, et al. *J Neurosurg Spine* [2011 in press.

Table 1: Mean (±SD) range of motion of the thoracic spine during axial rotation in normal subjects on one side.

Levels	Main axial rotation (°)	Coupled lateral bending (°)*	Coupled flexion extension (°)†	Coupled lateral translation (mm)§	Coupled SI translation (mm)‡	Coupled AP translation (mm)**
T1-T2	1.2 (0.8)	2.0 (1.4)	0.0 (2.1)	-0.1 (0.5)	0.1 (0.7)	0.1 (0.5)
T2-T3	1.6 (0.7)	1.8 (1.2)	-0.1 (1.5)	0.0 (0.6)	0.0 (0.6)	0.0 (0.4)
T3-T4	1.4 (0.9)	1.9 (1.5)	0.3 (1.4)	0.0 (0.5)	0.0 (0.4)	0.1 (0.4)
T4-T5	1.6 (0.8)	1.6 (1.2)	0.7 (1.0)	-0.1 (0.4)	-0.1 (0.4)	0.2 (0.3)
T5-T6	1.8 (0.7)	1.4 (1.2)	0.1 (1.0)	-0.1 (0.4)	0.0 (0.3)	0.0 (0.3)
T6-T7	1.9 (0.6)	1.1 (1.3)	0.2 (1.0)	0.0 (0.3)	-0.1 (0.3)	0.0 (0.3)
T7-T8	2.3 (0.7)	0.9 (0.8)	0.1 (0.7)	0.0 (0.3)	0.0 (0.2)	0.0 (0.2)
T8-T9	2.5 (0.8)	0.3 (0.7)	0.4 (0.5)	0.0 (0.4)	-0.1 (0.1)	0.1 (0.1)
T9-T10	2.7 (0.6)	0.1 (0.9)	0.4 (0.6)	0.0 (0.5)	0.0 (0.1)	0.1 (0.2)
T10-T11	2.6 (0.8)	0.4 (0.8)	0.5 (0.8)	0.0 (0.5)	0.0 (0.1)	0.1 (0.2)
T11-T12	1.3 (0.7)	0.6 (0.9)	1.0 (1.1)	0.0 (0.3)	0.0 (0.1)	0.3 (0.4)
T12-L1	0.5 (0.4)	-0.1 (0.9)	0.9 (0.9)	0.1 (0.4)	-0.1 (0.2)	0.3 (0.4)

SI: superoinferior; AP: anteroposterior
*: positive means lateral bending to the same direction as axial rotation; †: positive means flexion; §: positive means lateral translation to the same direction as axial rotation; ‡: positive means superior translation; **: positive means anterior translation

MOMENTUM CONTROL STRATEGIES DURING WALKING IN ELDERLY FALLERS

Masahiro Fujimoto and Li-Shan Chou

Motion Analysis Lab, Department of Human Physiology, University of Oregon, Eugene, OR, USA
email: chou@uoregon.edu, web: http://biomechanics.uoregon.edu/MAL/

INTRODUCTION

Dynamic balance control during walking has been assessed in terms of the interaction between position and velocity of the whole body center of mass (COM) and the base of support [1], where insufficient COM momentum could be a cause for gait imbalance. Given that acceleration induces changes in velocity, investigating how the COM momentum is regulated during walking would allow us to better differentiate individuals with different balance control abilities. The objective of this study was to establish a region of stability (ROS) using COM acceleration and to characterize differences in COM control. Strategies for COM control during walking among healthy young, elderly, and elderly fallers were compared using regions of stability derived by COM velocity and acceleration (ROSv and ROSa, respectively).

METHODS

A single-link-plus-foot inverted pendulum model was used to define ROSv and ROSa at the instant of toe-off (TO) (Fig.1). The boundaries of the ROSv in the anteroposterior (AP) direction were derived using the following equation [2]:

$$-\tilde{X}_{TO} \le \dot{\tilde{X}}_{TO} \le 1-\tilde{X}_{TO} \qquad (1)$$

where $\tilde{X}_{TO}$ and $\dot{\tilde{X}}_{TO}$ are normalized COM position and velocity at TO in AP direction, defined as $\tilde{X}_{TO} = (X_{TO} - X_h)/L_f$, $\dot{\tilde{X}}_{TO} = \dot{X}_{TO}/(L_f\omega_0)$ ($\omega_0 = \sqrt{g/l}$, $L_f = X_t - X_h$: foot length, Xh and Xt: the heel and toe positions, l: pendulum length). Similarly, the ROSv in the mediolateral (ML) direction was obtained:

$$-\tilde{Y}_{TO} \le \dot{\tilde{Y}}_{TO} \le 1-\tilde{Y}_{TO} \qquad (2)$$

where $\tilde{Y}_{TO}$ and $\dot{\tilde{Y}}_{TO}$ are normalized COM position and velocity at TO in the ML direction, defined as $\tilde{Y}_{TO} = (Y_{TO} - Y_{ma})/Lw$, $\dot{\tilde{Y}}_{TO} = \dot{Y}_{TO}/(L_w\omega_0)$ ($\omega_0 = \sqrt{g/l}$, $Lw = Y_{la} - Y_{ma}$: ankle width, Y_{ma} and Y_{la}: the medial and lateral ankles).

The ROSa was defined as the region confined by peak COM acceleration needed to be generated prior to TO. COM position and velocity when the COM velocity becomes its minimum prior to TO were used as initial COM position and velocity. The boundaries of the ROSa in the AP direction were derived using the following equation:

$$\frac{(\tilde{X}_{TO}+A)B}{\tilde{X}_{TO}-\tilde{X}_i}\dot{X}_i < \ddot{\tilde{X}}_p < \frac{(1-\tilde{X}_{TO}+A)(1-B)}{\tilde{X}_{TO}-\tilde{X}_i}\dot{X}_i \qquad (3)$$

where $A = \dot{X}_i/(\omega_0 L_f)$, $B = \tilde{X}_{TO} + (\dot{X}_i - 2)/(\omega_0 L_f)$, $\tilde{X}_i$ is the initial COM position defined as $\tilde{X}_i = X_i/L_f$. $\ddot{\tilde{X}}_p$ is the normalized peak COM acceleration prior to TO defined as $\ddot{\tilde{X}}_p = \ddot{X}_p/\omega_0{}^2 L_f$. Similarly, COM position when the COM velocity becomes zero prior to TO was used as initial COM position (Yi) in the ML direction. The boundaries of the ROSa in the ML direction were derived using the following equation:

$$-\frac{Y_{ma}-Y_{TO}}{Y_{TO}-Y_i}\tilde{Y}_{TO} \le \ddot{\tilde{Y}}_p \le \frac{Y_{la}-Y_{TO}}{Y_{TO}-Y_i}(1-\tilde{Y}_{TO}) \qquad (4)$$

where $\ddot{\tilde{Y}}_p$ is the normalized peak COM acceleration defined as $\ddot{\tilde{Y}}_p = \ddot{Y}_p/\omega_0{}^2 L_w$.

Fifteen healthy young adults [Young], 15 healthy elderly adults [Elderly], and 15 elderly adults with a history of falls [Fallers] participated in this study. The inclusion criterion for Fallers was a self-report of two or more falls within the year prior to the study [3]. Subjects were asked to walk barefoot at a self-selected pace. Motion data were captured with

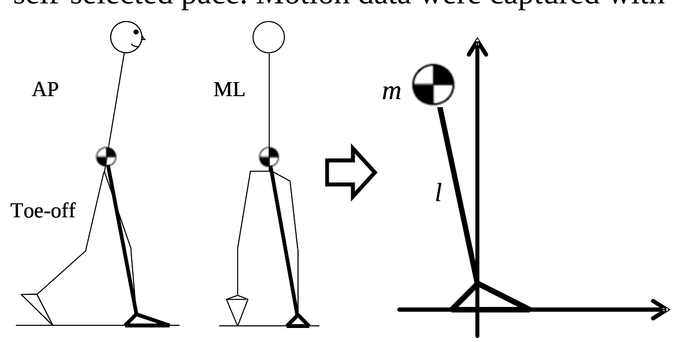

Figure 1: An inverted pendulum model

a motion analysis system (MotionAnalysis, Santa Rosa, CA) at 60 Hz. A total of 29 reflective markers were placed on each subject's bony landmarks. One-way ANOVA was used to detect group differences. Significance level was set at α=0.05.

RESULTS AND DISCUSSION

The COM of Fallers was located significantly anterior to those for Young and Elderly groups, with significantly smaller COM velocity at TO, which placed their mean data point inside the boundaries of the ROSv (Fig.2). Similar results were obtained in the ROSa in the AP direction, where the data for Fallers were significantly closer to the forward boundary of the ROSa for Fallers group (Fig.3).

Normalized peak COM acceleration prior to TO differed significantly between Young and Elderly groups (Fig.3), although no significant difference was detected in normalized COM velocity at TO between them (Fig.2). Both groups also showed similar peak COM velocity. The momentum was controlled differently even though similar momentum was observed during walking. COM acceleration could be a more sensitive measure to differentiate individuals with different balance control abilities.

No significant differences were detected in COM position, normalized COM velocity at TO, and normalized peak COM acceleration prior to TO in the ML direction (Fig.4 and 5). Fallers appeared to use a more conservative strategy in momentum control in the AP direction, as indicated by their data located significantly closer to the boundaries of the ROSv and ROSa, but not in the ML direction.

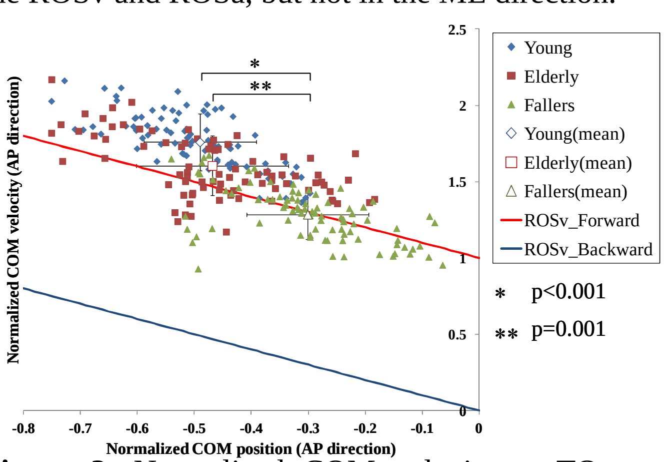

Figure 2: Normalized COM velocity at TO vs. normalized COM position in AP direction.

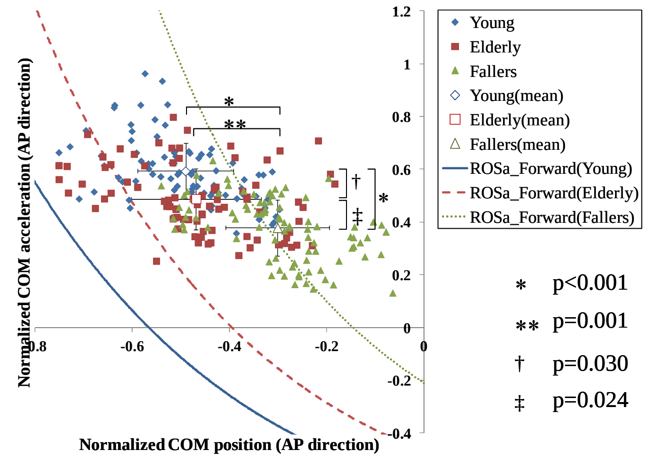

Figure 3: Normalized peak COM acceleration prior to TO vs. normalized COM position at TO in AP direction.

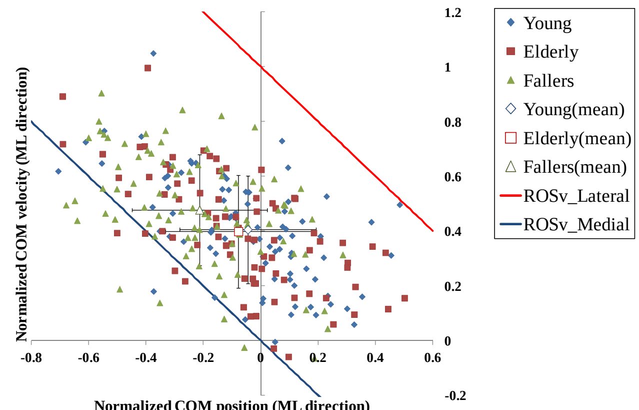

Figure 4: Normalized COM velocity at TO vs. normalized COM position in ML direction

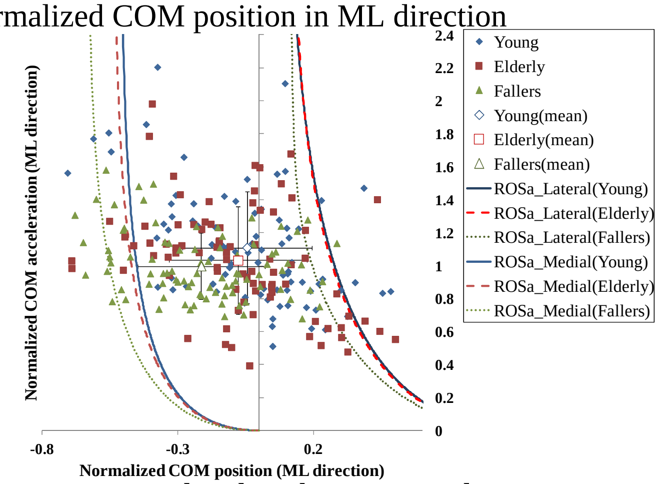

Figure 5: Normalized peak COM acceleration prior to TO vs. normalized COM position at TO in ML direction.

REFERENCES

1. Yang F, et al. *Ann Biomed Eng.* **37**(12), 2606-2614, 2009.
2. Hof AL, et al. *J Biomech* **38**(1), 1-8, 2005.
3. Shumway-Cook A, et al. *Phys Ther* **77**(8), 812-819, 1997.

DESIGNING TRAINING SAMPLE SIZE FOR SUPPORT VECTOR MACHINES BASED ON KINEMATIC GAIT DATA

[1]Reginaldo K Fukuchi, [2]Lisa Stirling and [1]Reed Ferber

[1]Running Injury Clinic, [2] Faculty of Kinesiology, University of Calgary
email: r.fukuchi@ucalgary.ca, web: http://www.runninginjuryclinic.com

INTRODUCTION

Traditionally, biomechanical gait data are analyzed using discrete variables and a univariate statistical approach. In contrast, the multivariate and complex pathoaetiology of a running-related musculoskeletal injury often demands a more robust analysis [1]. Support Vector Machines (SVMs) have recently been applied to analyze biomechanical data due to its ability to identify complex associations amongst many discrete gait variables [2]. However, the number of observations required to train the SVM classifier to solve biomechanics classification problems is still unknown. For this reason, generic rule-of-thumb approaches have been used suggesting that a very large sample size is required to provide appropriate training for optimal classification. Unfortunately in clinical studies, large samples are usually not readily available. In addition, large sample sizes may be wasteful when fewer samples may result in optimal classification. Furthermore, a large sample size does not guarantee that one will obtain optimal classification since the groups may considerably overlap in their distribution, even in high-dimensional space. Therefore, it is paramount to a priori approximate the sample size in biomechanical studies. Hence, the aim of this study is to provide guidance to plan the appropriate sample size for SVM training classification based on discrete kinematic gait variables.

METHODS

Some of the parameters used in the present study were obtained from a previously published data [2]. The current study assessed the performance of the SVM algorithm in classifying young and elderly runners based on discrete gait kinematic variables obtained from a three-dimensional motion capture system. In addition to the overall classification, the variables carrying the most combined discriminative information were selected using a feature selection algorithm combined with the SVM. It was found that six variables, out of the 31 originally input into the algorithm, were required to achieve 100% classification accuracy [2]. The sample size estimation was obtained using the approach similar to Guo et al. [3]. To do so, the discriminant features were first obtained and consisted of the six-discriminant variables selected from the previous study [2]. In addition, their effects sizes were obtained after the data were transformed in the natural logarithm scale. The effect size to be used in the algorithm was calculated as the ratio of the absolute mean difference between groups ($\mu=|s_1-s_2|$) across discriminant variables and the common standard deviation across groups (σ) [3]. Thus, a vector containing the effect sizes was obtained and the smallest fold difference was employed. In addition, a matrix with the same dimension as the original data set (34 observations and 31 variables) was then generated and the effect size was introduced using the first six variables, thus representing the discriminant variables. Moreover, the remaining 25 variables were created assuming they exhibited the same distribution among groups ($\mu=0$; $\sigma=1$). Therefore, the number of observations and the effect sizes could be altered while the nature of the original data was preserved. One hundred simulations were carried out using the generated data as an input to the classifier where the number of observations and the effect size varied. The chosen metric to assess the ability of the classifier in predicting class membership was the classification accuracy rate (CAR): the average proportion of correctly classified observations across testing subsets [2]. Hence, a distribution of CARs across 100 simulated data sets was obtained and used in the final calculation. Finally, to assess the statistical power of the SVM algorithm, a null distribution of CARs had to be generated. This distribution consisted of CARs obtained when only non-discriminant variables were used in the SVM classifier and the algorithm would likely perform no better than a 50% accuracy rate for binary classification. The statistical power was determined by computing the percentage of observed CARs that was greater than the 0.95th percentile of the null distribution [2]. The power calculations were performed over a range of effect sizes (0-1 with increments of 0.25) and sample sizes (15-150 observations per group with increments of 15).

RESULTS AND DISCUSSION

The smallest fold difference across discriminant features of the original data set was 0.26 (effect size). Although this effect size underestimates the true fold difference, it was identical to the largest standardized fold change proposed by a previous study [3]. Therefore, the effect size used in the present study will likely produce conservative sample size.

The Figure illustrates the dependence of the statistical power on the effect size across a range of sample sizes. As expected, the statistical power increases along with the effect size. In addition, steeper curves arise when larger sample data were used for training. Furthermore, the power did not considerably change when the effect size was 0.5 and the sample size was equal to or larger than 60 observations. Therefore, it may be suggested that 17 subjects per group used in previous study [2] may not sufficiently train the SVM algorithm to classify young and elderly runners based on kinematics data.

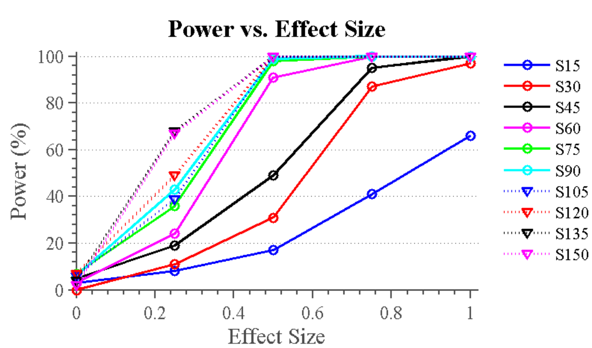

Figure: Relationship between statistical power (y-axis) and Effect size (x-axis) across a range of sample sizes (S15-S150).

The null distribution presented average CAR of 49.5% (±8.7%) across sample sizes when the effect size was set to 0.5, suggesting that the classifier could not predict the group membership more accurately than random chance. The ratio of informative and non-informative features (signal to noise ratio) in the present study was 0.19 (6/25). Although, the removal of non-informative features would possibly have enhanced the performance of the SVM classifier, we decided to include both types of features in the simulations as a more realistic approach due to the typical nature of biomechanics data.

The application of the present findings is limited to the use of the SVM classifier to solve binary classification problems considering discrete gait kinematic variables in young and elderly runners. Additional studies are necessary to estimate the training size and should consider the effects of imbalance in class distribution and dependence among features and varying signal to noise ratio.

CONCLUSIONS

The application of a method to determine a priori sample size for SVM classifier-based approaches using biomechanics gait data was described. Based on the effect size associated with the proportion of discriminant and non-discriminant features, one may obtain a reasonable estimation of the sample size required to build the classifier.

REFERENCES

1.Chau T. *Gait & Posture* 13, 49-66, 2001.
2.Fukuchi RK, et al. *J Biomech* **44**, 540-542, 2011.
3.Guo Y, et al. *BMC Bioinformatics* 11:447, 2010.
4.Dobbin KK, et al. *Clinic Cancer Res* 14, 108-114, 2008.

ACKNOWLEDGEMENTS

RKF wishes to thank CAPES Foundation (Ministry of Education of Brazil) for his scholarship. Reed Ferber is primarily funded through Alberta Innovates: Health Solutions.

THE INFLUENCE OF WEDGED INSOLES ON KNEE AND ANKLE MOMENTS AND ANGULAR IMPULSES DURING WALKING

Claudiane A. Fukuchi, Ryan T. Lewinson, Jay T. Worobets, Darren J. Stefanyshyn

Human Performance Laboratory, Faculty of Kinesiology, University of Calgary.
email: c.fukuchi@ucalgary.ca

INTRODUCTION

High frontal plane knee joint angular impulse has been associated with patellofemoral pain syndrome (PFPS) and knee osteoarthritis (OA) [1,2]. Interventions that reduce frontal plane knee joint loading may provide clinical benefits. Wedged insoles have widely been proposed as one form of such an intervention. It has been shown that a laterally wedged insole can effectively decrease the peak frontal plane knee moments and reduce knee OA progression [3]. Medially wedged insoles have been associated with a reduced ankle inversion moment during stance [4]. Nevertheless, it is still unknown whether wedged insoles can reduce the knee joint frontal plane moments without increasing the loading in the ankle joint. Therefore, the purpose of this study was to investigate the effects of lateral and medial wedged insoles on knee and ankle joint moments and angular impulses during walking.

METHODS

Ten healthy males (height: 178.6 ± 7.8 cm, mass: 78.1 ± 7.6 kg, age: 25.7 ± 3.1 years) participated in this study. Informed written consent in accordance with the University of Calgary's Ethics Committee was obtained from all subjects prior to testing.

Each subject performed five walking trials in each of the following conditions: a neutral condition, a 6º lateral wedge (LW6), a 9º lateral wedge (LW9), a 6º medial wedge (MW6), and a 9º medial wedge (MW9). The neutral condition was performed with a neutral running shoe (adidas adiZero Aegis 2.0). Each wedge was made out of ethylene vinyl acetate (EVA) and was inserted into the neutral shoe condition.

Retro-reflective markers were attached to the right shank and shoe and the position of each marker was recorded with an eight camera high-speed motion analysis system at 240 Hz (Motion Analysis Corp., Santa Rosa, CA), while the subjects walked on a 10m walkway at 1.4 m/s. Ground reaction forces were collected at 2400Hz using a force platform (Kistler AG, Winterhur, Switzerland). A walking trial was considered valid if the subject planted their right foot near the middle of the force platform and their walking speed was within 5% of the target speed.

Internal knee and ankle moments were calculated using an inverse dynamics approach with Kintrak 7.0 (Motion Analysis Corp.). The angular impulses were calculated by integrating the joint moments over stance time. A repeated measure ANOVA (α=0.05) was performed in SPSS (SPSS inc., USA) to determine whether there was a wedge effect on the frontal plane knee and ankle joint moments and angular impulses.

RESULTS AND DISCUSSION

The laterally wedged condition decreased knee abduction moment and knee abduction impulse whereas the opposite was found for the medially wedged condition. Statistical differences ($p < 0.05$) were found between lateral and medial conditions (Table 1). Larger differences were noticed when higher amounts of lateral (LW9) and medial (MW9) wedge were compared. Figure 1 highlights a descending knee abduction moment pattern from the higher medial wedge (MW9) to the opposite higher lateral wedge (LW9), particularly in the first peak. Smaller knee frontal plane loadings have been associated with prevention of the progression of knee OA [3]. Previous prospective studies showed an association between higher knee angular impulse in the frontal plane and PFPS and the severity of knee OA [1,2]. Therefore, the reduced knee frontal plane loadings obtained with the lateral wedge would possibly prevent PFPS and slow the progression of knee OA. Nonetheless, further studies investigating these particular populations need to be conducted to provide additional insights.

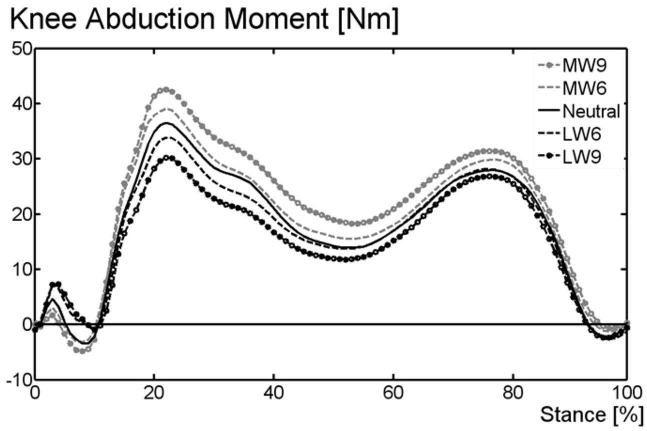

Figure 1: Mean time-series knee abduction joint moment across shoe conditions.

On the other hand, the ankle inversion moment and the ankle inversion impulse showed a tendency to increase with the lateral wedges while the medial wedges showed opposite effects (Fig 2). Table 1 details the mean and standard deviation of the ankle joint moments which were statistically different ($p < 0.05$) between conditions. Similarly to the knee, the effects of the wedges were more evident when higher amounts of lateral (LW9) and medial (MW9) wedge were compared.

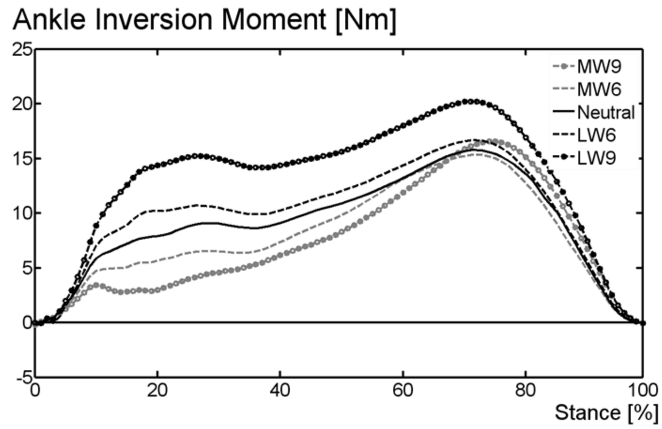

Figure 2: Mean time-series ankle inversion joint moment across shoe conditions.

CONCLUSIONS

These findings suggest that the decrease of the knee joint moment was associated with an increase at the ankle joint. The lateral wedge was effective in reducing knee frontal plane loadings during walking. In particular, the magnitude of the knee abduction moment was inversely proportional to the wedge amount. Therefore, a lateral wedge could be a method to avoid progressive degeneration of the knee joint that leads to knee OA.

REFERENCES

1. Stefanyshyn et al., *Am J Sports Med* **34**, 1844-1851, 2006.
2. Thorp et al., *Arthritis Rheum* **54**, 3842-3849, 2006.
3. Radzimski et al., *Knee*, 2011 [Epub ahead of print].
4. Novick et al., *Phys Ther***,** 72:S78, 1992.

Table 1: Means and standard deviations in each shoe condition.

	MW9	MW6	NEUTRAL	LW6	LW9
Peak Knee Abduction Moment [Nm]	42.5 (13.9)$_{a,b}$	39.3 (12.8)$_{a}$	37.3 (12.4)	33.7 (12.4)$_{e}$	30.3 (10.8)$_{d,e}$
Knee Abduction Impulse [Nm]	15.5 (5.9)$_{a,b}$	14.1 (4.9)$_{a}$	13.7 (5.6)	12.3 (5.2)$_{e}$	11.1 (4.3)$_{d,e}$
Peak Ankle Inversion Moment [Nm]	17.8 (3.4)	16.1 (2.9)$_{a}$	16.9 (2.8)	18.6 (4.8)	21.9 (4.5)$_{d}$
Ankle Inversion Impulse [Nm]	5.7 (1.3)$_{a}$	5.9 (1.3)$_{a}$	6.5 (1.4)$_{a}$	7.8 (1.6)	9.9 (2.1)$_{c,d,e}$

Subscript letters indicates sample group for which there are significant mean differences ($p < 0.05$): $_{a\,=}$ LW9, $_{b\,=}$ LW6, $_{c\,=}$ Neutral, $_{d\,=}$ MW6, $_{e\,=}$ MW9.

JOINT ANGLES AND JOINT MOMENTS FOLLOWING NEUROMUSCULAR FATIGUE IN FUTSAL PLAYERS

[1]Reginaldo K Fukuchi, [1]Claudiane Fukuchi, [2]Mauro Dinato, [2]Luiz Riani and [3]Marcos Duarte

[1]Faculty of Kinesiology, University of Calgary
[2]Instituto Vita, São Paulo, Brazil
[3]Biomedical Engineering Program, Federal University of ABC, Brazil
email: r.fukuchi@ucalgary.ca

INTRODUCTION

Futsal has recently been increasing its popularity worldwide. However, futsal has also exhibited approximately 2.5 higher injury rates as opposed to soccer with a greater proportion of non-contact injuries [1]. Since futsal involves multiple-sprints and more high-intensity phases than in soccer, neuromuscular fatigue is likely a concern due its potential to influence biomechanical risk factors for injuries. In addition, futsal players usually need to perform sprints with frequent changes in direction which expose them to high mechanical demands. Although the influence of neuromuscular fatigue on lower extremity biomechanics during sport-related tasks has widely been investigated in the literature [2], to date there is no study involving futsal. Therefore, the aim of this study was to describe the biomechanics alterations of the lower extremity joints when performing an anticipated cutting maneuver at maximum exertion. We hypothesized that there would be an overall decrease in joint angles, joint moments and ground reaction forces (GRF) parameters following neuromuscular fatigue.

METHODS

Eight healthy elite male futsal players (height: 174±5 cm, mass: 75±8 kg, age: 24±3 years) volunteered in this study. This study was approved by the ethics committee of Instituto Vita. The subjects were evaluated while performing cutting maneuvers before and after they underwent in a fatigue protocol. The protocol consisted of running on a treadmill at a speed that corresponded to the one above the second anaerobic threshold (previously determined by a VO_2max test) until maximally fatigued. To collect kinematic data, clusters of retro-reflective markers were attached on the pelvis, thigh, shank and foot of the left leg. Individual markers were also placed on anatomical landmarks to define the segmental co-ordinate systems during the standing calibration trial. Six high-speed cameras (Vicon Inc.) collected 3D marker coordinates at 250 Hz and a force platform (AMTI Inc.) acquire the GRF data at 500 Hz, during the cutting task. To perform the task, the subjects had to run at their maximum speed, hit the force platform with their left foot and cut 45º to the right. They were allowed to practice as many trials as they need. The kinematic and kinetic data were filtered at 10 Hz with a sixth order Butterworth filter. The joint angles and internal joint moments were calculated using standard inverse dynamics approach.

The resultant velocity of the pelvic centroid markers, in the anterior-posterior and medio-lateral directions, was computed to verify whether the subjects' speed was similar between conditions. The stance phase (initial contact (IC) to toe-off) was time normalized from 0% to 100%. Five valid trials were included and the following discrete variables were extracted for the hip, knee and ankle joints in all anatomical planes: IC angle, IC moment, peak angle, peak moment, and peak GRF. Peak angles and peak moments at the peak GRF vertical were also quantified. Furthermore, the knee and ankle frontal plane angular impulses (integral of the joint moment-time curve) were calculated. Paired t-tests were used to compare conditions ($\alpha=0.05$). The computations were performed in Matlab 7.0 (Mathworks Inc).

RESULTS AND DISCUSSION

The resultant velocity of the centroid of the pelvic markers was not different ($p=0.36$) between conditions (4.1±0.4 m/s vs. 4.2±0.2 m/s). Hence, as requested, the subjects maintained the same performance before and after fatigue. The average subjects' speed was higher to the one reported previously [3], thus the results may not be comparable across studies. We decided to instruct the participants to run at their maximum speed since the mechanical demands would likely be similar to the one experienced in real situations.

The decreased ankle abduction at IC resulted in lower peak ankle abduction after fatigue (Figure 1b). In fact, Lucci et al. [3] found that subjects tended to land in more overall erect posture following a fatigue protocol. A smaller IC hip abduction moment and a decreased peak hip flexion moment were also found after fatigue. Indeed, the overall lower extremity joint moments were previously reported smaller following neuromuscular fatigue [2].

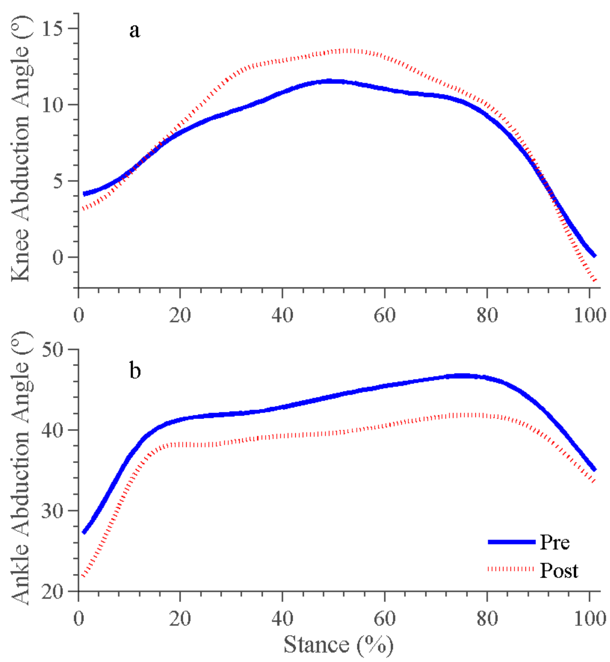

Figure 1: Mean time-series of knee (a) and ankle (b) transverse plane angles across participants.

The fatigued players exhibited an increased knee internal rotation (IR) angle (Figure 1a). Lucci et al. [3] reported similar findings in female collegiate soccer players. The increased IR of the tibia over the femur may result in a greater strain in the ACL.

In contrast, knee frontal plane angle and moment did not differ. Certainly, the effects of fatigue in this particular movement are not well understood [2]. GRF peaks were also not altered by neuromuscular fatigue. It is possible that participants could have adapted better to fatigue than recreational players, since they were used to perform similar tasks. Therefore, this may partly explain the lack of differences, in particular in the frontal plane of the knee.

CONCLUSIONS

This preliminary study was the first to highlight the possible detrimental effects of neuromuscular fatigue on lower extremity biomechanics in elite futsal players. In particular, the increased peak knee IR angle after fatigue may result in higher strain on the ACL and thus result in an increased risk of ACL injury. Further studies with a large sample size are needed to determine the association between the biomechanics response and injury risk.

REFERENCES

1. Junge, A, et al. Br J Sports Med **44**, 1089-1092, 2010.
2. Santamaria, LJ, et al. J Orthop Sports Phys Ther 40, 464-473, 2010.
3. Lucci, S, et al. J Sci Med Sport, **14,** 453-459, 2011.

ACKNOWLEDGEMENTS

RKF wish to thank CAPES Foundation for his scholarship.

Table 1: Mean (±1SD) values of the analyzed biomechanical variables, and the P-values of the t-tests comparisons between conditions.

Variable	Pre-Fatigue	Post-Fatigue	p-value
IC Ankle Angle Z (^{o})	27.18±9.64	21.92±8.76	0.001
Peak Ankle Angle Z (^{o})	49.04±7.07	44.62±5.40	0.03
IC Hip Moment Y (N·m)	-115.01±47.03	-93.87±39.04	0.03
Peak Hip Moment X (N·m)	87.39±36.41	70.98±28.64	0.02
Hip Angle X @ peak GRFa-p (^{o})	51.82±10.94	46.96±11.58	0.04
Knee Angle Z @ peak KFLX (^{o})	10.68±7.74	13.07±6.65	0.04

Loading history of the mechanical properties of human heel pads

Daniel J. Gales[1,2] and John H. Challis[1]

[1] Biomechanics Laboratory, Department of Kinesiology, The Pennsylvania State University, University Park, PA, USA
[2] Lock Haven University of Pennsylvania, Lock Haven, PA, USA
E-mail: djg153@psu.edu

INTRODUCTION

Typically during both walking and running the first part of the body to make contact with the ground is the heel pad. During running Cavanagh and LaFortune (1980) reported mean impact peak vertical ground reaction forces of two times body weight for shod rear-foot heel strikers. The role of the heel pad has been identified as providing both shock reduction and absorption, affording some protection for the body to injuries of the skeletal or muscular system (Rome, 1998).

Each foot has a period during gait when it is not in contact with the ground, presumably during which the heel pad has the potential to recover from the previous loading. Research examining the temporal characteristics of gait have reported that the stride time intervals during walking (Hausdorff et al., 1995) and running (Jordan et al., 2007) demonstrate long term correlations. Therefore, the stride interval times are not normally distributed but have fractal like properties.

During gait the heel pad strikes the ground multiple times, the heel pads mechanical properties on each footfall could be influenced by the previous footfall or footfalls. For example, if the heel pad has not recovered before the heel hits the ground again then presumably the heel pad will have different mechanical properties. The time interval between footfalls varies in a fractal style for both walking and running (Hausdorff et al., 1995; Jordan et al., 2007), but does this time series influence heel pad mechanical properties during the repeated footfalls? Therefore the purpose of this study was to examine if the heel pad mechanical properties differ during multiple simulated footfalls under varying time series. This is achieved by examining the mechanical properties of cadaver heel pads during selected footfalls during different time series producing 800 heel pad impacts.

METHODS

Eleven injury free runners were recruited for this study; each ran on an instrumented treadmill at their preferred running speed for eight minutes. The treadmill had two force plates under the belt; these plates permitted determination of the vertical ground reaction forces. From the force profiles the intervals between footfalls was computed. Examination of the time interval between footfalls using the Detrended Fluctuation Analysis (Peng et al., 1994) showed the presence of long-term correlations. The time intervals between strides for one representative subject were used as the time intervals between loadings when the cadaver heel pads were tested.

Eight fresh-frozen cadaver feet were thawed to room temperature before completing all procedures. All tissues superior to a 45 mm horizontal line marked on the foot above the uncompressed heel were removed using blunt dissection. Heel pads remained fixed to the calcaneus and the foot and toes and overlying skin remained intact throughout the testing procedures.

Dynamic mechanical testing of the heel pads was completed using a servo-hydraulic material test system (MTS model 858) operating in force control and programmed to compress these specimens 808 times to a maximum impact peak based on subject data scaled to body weight. Each heel pad was subjected to three stride time interval conditions: minimum in the experimental time series, the maximum, and actual (physiological) time series. For all conditions applied force and pad displacement were collected at 500 Hz, from which the heel pad deformation, hysteresis, and stiffness were computed.

RESULTS AND DISCUSSION

In the Physiological time series there were seven stride intervals which were equal in duration to the minimum stride interval, therefore the heel pad mechanical properties were compared for the seven subsequent loading for the Physiological and Minimum time series (Table 1). These comparisons indicated a statistically significant difference between heel pad stiffness at 50% body weight between the conditions ($p < 0.05$). In a similar fashion seven stride intervals were identified in the Physiological time series which were equal in duration to the maximum stride interval (Table 2). These comparisons indicated a statistically significant difference between heel pad hysteresis and maximum deformation between the conditions ($p < 0.05$).

These results indicate that the physiological time series associated with the loadings on the human heel pad during gait change the mechanical response of the heel pad to loadings. These results warrant further investigation, to find their cause and their influence on in vivo loadings.

REFERENCES

Cavanagh, PR and Lafortune, MA (1995). *J Biomech*, 13:397-406.

Hausdorff, JM et al. (1995). *J Appl Physiol*, 78:349-58.

Jordan, K et al. (2007). *Hum Mov Sci*, 26:87-102.

Peng, CK et al. (1994). *Phys Rev E*, 49:1685-1689

Rome, K. (1998). *The Foot*, 8:179-85.

Table 1. Means (±standard deviation) of heel pad mechanical properties for 7 selected footfalls with minimum rest time.

Condition	Maximum Deformation (mm)	Hysteresis (%)	Maximum Stiffness ($N.mm^{-1}$)	Stiffness at 50% BW ($N.mm^{-1}$)
Minimum	2.2 ± 0.5	54.8 ± 4.8	316.6 ± 107.5	268.3± 83.5
Physiological	2.2 ± 0.4	54.7 ± 5.7	322.5 ± 95.8	285.3± 83.6

Table 2. Means (±standard deviation) of heel pad mechanical properties for 7 selected footfalls with maximum rest time.

Condition	Maximum Deformation (mm)	Hysteresis (%)	Maximum Stiffness ($N.mm^{-1}$)	Stiffness at 50% BW ($N.mm^{-1}$)
Maximum	2.3 ± 0.5	55.6 ± 4.5	308.6 ± 100.9	269.5± 92.2
Physiological	2.2 ± 0.5	54.0 ± 5.0	314.7 ± 92.2	278.5± 77.1

INVESTIGATION OF PROSTHETIC SOCKET INTERFACE PRESSURE AND GAIT IN TRANSTIBIAL AMPUTEES: EFFECTS OF SUSPENSION TYPES AND SOCKET ALIGNMENT

Fan Gao and Susan Kapp

UT Southwestern Medical Center at Dallas, TX, USA
email: fan.gao@utsouthwestern.edu, web: http://www.utsouthwestern.edu/findfac/

INTRODUCTION

Socket interface is essential in prosthetics and plays an important role in the control of function and delivery of comfort. Studies have shown that socket interface pressure is closely related to the comfort level [1-3]. Socket alignment and fit are closely related. However, most of the studies only focused on one aspect instead of both. Comfort and function are tightly related to the socket design and alignment and poor design and alignment is usually accompanied with discomfort and skin breakdown and/or ulceration and could eventually result in rejection. In practice, practitioners always try their best to achieve optimal socket design and alignment if possible. The object of this study is therefore to quantify the pressure distribution of gel liner socket interface with and without locking-pin in transtibial amputees with systematic adjustment of socket alignment. The outcome of the proposed study will help us better understand the effects of suspension types and socket alignment and provide clinical recommendation.

METHODS

Subjects: Ten unilateral transtibial amputees participated in the study. The subjects were patients of the UT Southwestern prosthetics & orthotics clinic and the devices were fabricated by certified prosthetist. The subjects were recruited if they use gel liner with locking pin and they have received the definitive device.

Equipment: Two F-socket pressure sensors were used to register the pressure distribution around the anterior and lateral sides of the residual limb (Tekscan Inc., USA). GAITRite (CIR Systems, Inc. PA, USA) was used to obtain spatiotemporal characteristics of gait. In addition, a digital video camera was used and an LED was used to synchronize the signals captured by GAITRite and Tekscan.

Figure 1. Residual limb with F-socket sensor.

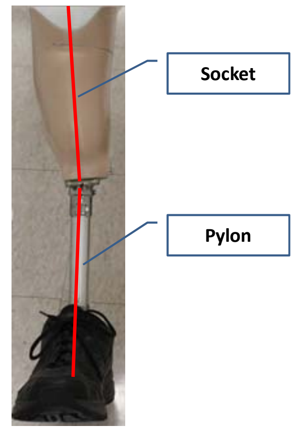

Figure 2. Socket alignment adjustment in frontal plane.

Test protocol: F-socket sensors were carefully calibrated before the test. At the beginning of the test, the individual fingers of the F-socket pressure sensor (Tekscan Inc., USA) were separated to better accommodate the residual limb. The sensors were placed on the residual limb covering the lateral and anterior of the limb (Fig. 1) using double-sided tape. The socket alignment which was approved and carefully adjusted by a certified prosthetist was assumed to be the 'neutral' position and served as the reference for socket alignment adjustment. The socket alignment was systematically adjusted in both sagittal and frontal planes with a deviation of 5 degrees (Figure 2). In total, five socket alignments were tested including neutral, flexion, extension, adduction and abduction of 5 degrees. After each socket alignment adjustment, subjects were instructed to walk cross the GAITRite mat at self-paced speed. Each condition was repeated three times. The order of socket alignment adjustment was randomized. After the subjects finished all conditions the locking pin was taken out and a sleeve was used to provide socket suspension. Then similar to the test with locking pin, socket alignment was systematically changed. In addition, a visual analogue scale (0 – 10 where 0 represents the most uncomfortable and 10 represents the most comfortable) was used to evaluate the socket fit and comfort for each condition.

Data analysis: Three trials were pooled together and spatiotemporal characteristics including step length, step time, velocity, cadence (steps/min), heel-to-heel base support, single support (percentage of gait cycle), double support (percentage of gait cycle), swing phase, stance phase and toe in/out angle were obtained directly from GAITRite. Peak pressure was identified during stance phase and was averaged across steps and trials. The visual analogue scale was digitized to obtain the score in the range of 0 to 10.

RESULTS AND DISCUSSION

Here results of one subject are presented. The subject tended to walk faster with locking pin and socket set in neutral position. For example, the walking speeds with locking pin are .69 m/s and .64 m/s for socket set in neutral and flexion respectively. Without locking pin, the speed is slightly lower, .67 m/s. In addition, stride length peaks when the socket is set at neutral position (108±10.9 cm) and is shortest when the socket is set at abduction (100±10.8 cm) on the amputated side. The socket alignment also influenced the stance phase on the amputated side. For example, with locking pin the stance phase as a percentage of the gait cycle is 61.9%, 62.4%, 63.9%, 64.4% and 61.6% for neutral, flexion, extension, adduction and abduction respectively. Without locking pin, the stance phase as a percentage of the gait cycle is slightly increased across the socket alignments except extension. For instance, with socket set at abduction, the stance phase (%) increased from 61.6% to 63.5%. Support base is also closely related to the socket alignment and suspension types. Specifically, with socket set neutral and locking pin, the base support is the narrowest (13.5±3.6 cm) while the base support jumped to 21.1±4.2 cm when the socket was set at abduction without locking pin. Socket alignment affects the socket interface pressure distribution systematically which agrees with previous studies. In addition, the peak pressure under sensitive zones, such as fibula head is significantly higher (e.g. 180 Kpa) with locking pin than that without locking pin (e.g. 40 Kpa). The subject, in general was more satisfied with locking pin which was reflected by favorable rating. For example, the subject gave a score of 9 for neutral socket alignment with locking pin and a score of 2 for abduction socket alignment without locking pin. It appears that for this subject, socket abduction and flexion was among the least satisfied and locking pin appears important without which the score dropped to 1 under neutral socket alignment.

Conclusions/summary

The pilot results did indicate that there is a strong interaction between the socket alignment and suspension type. In addition, it should note that though systematic socket alignment adjustment did impact the interface pressure and gait, the influence is multiple-faceted. Though the visual analogue scale indicates that neutral alignment provides the most satisfied fit, this is not always strongly supported by the outcome measures including the socket pressure and gait. It is believed that very few key parameters (e.g. peak pressure on sensitive areas, gait speed etc.) might not be sufficient to capture the whole picture and a comprehensive evaluation is always needed especially during the clinical practice when the quantitative tools are not available. The outcome of this study might help us better understand the effects of suspension types and socket alignment and provide useful clinical recommendation.

REFERENCES

1. E. S. Neumann, P. D. Pe, J Prosthet Orthot 13, 99 (2001).
2. E. S. Neumann, J. S. Wong, R. L. Drollinger, J Prosthet Orthot 17, 12 (2005).
3. J. Sanders, Pressure Ulcer Research: Current And Future Perspectives, (2005).

ACKNOWLEDGEMENTS

This study was supported by American Orthotic and Prosthetic Association (EBP- 043010).

COMPARISON OF FIRST AND SECOND GENERATION ROCKER BOTTOM SHOES

Jacob Gardner, Songning Zhang, Max Paquette, Clare Milner, and Eric Foch
University of Tennessee, Knoxville, TN, USA
email: jgardn25@utk.edu, web: http://web.utk.edu/~sals/resources/biomechanics_laboratory.html

INTRODUCTION

The use of rocker bottom shoes has become very popular in recent years. It is thought that these types of shoes may be beneficial in enhancing lower extremity muscle tone, reducing pressure on the feet, and providing an added exercise benefit during walking [1,2]. Our lab has conducted comprehensive gait analyses on two generations of rocker bottom shoes (Dockers Active Balance) designed as dress shoes for men [3].

The results of the first study (generation 1 compared with its respective control shoe) revealed that the unstable shoe had increased mediolateral (ML) center of pressure (COP) displacement, decreased anteroposterior (AP) COP displacement, increased 1st peak vertical ground reaction force (vGRF) loading rate, decreased second peak vGRF, and increased braking peak GRF. Additionally, the unstable shoe resulted in decreased ankle plantarflexion ROM, and increased the ankle eversion ROM. For kinetics, the unstable shoe had a decreased peak dorsiflexion moment and an increased peak inversion moment. The results from the second generation shoe compared to its respective control shoe revealed nearly identical results as the first generation shoe compared to its respective control shoe, although the second generation shoe had a lower profile design. The purpose of this abstract was to compare GRF, COP, and ankle kinematic and kinetic variables between the two versions of the unstable shoes and examine related changes in shoe characteristics.

METHODS

Fifteen males in the first study (age: 41.1 ± 4.6 yrs; height: 1.77 ± 0.7 m; mass: 83.2 ± 11.5 kg; BMI: 26.5 ± 2.8) and 14 males in the second study (age: 45.6 ± 8.4 yrs; height: 1.81 ± 0.07 m; mass: 80.6 ± 9.4 kg; BMI: 24.7 ± 2.2) participated. Each subject performed 5 walking trials in a control shoe and an unstable shoe at 1.3 m/s.

Figure 1: 1st generation (A) and 2nd generation (B) test shoes.

A nine-camera motion analysis system (240 Hz, Vicon Motion Analysis Inc., UK) was used to track reflective markers placed on the trunk, pelvis, and bilateral thighs, shanks, and feet. Two force platforms (1200 Hz, Advanced Mechanical Technology Inc.) were synchronized with the motion analysis system to measure the ground reaction forces. Visual3D software suite (C-Motion, Inc.) was used to compute the 3D kinematic and kinetic variables of the ankle joint. Joint moments were computed as internal moments.

Variables in the test shoes that were statistically different from their respective control shoes for each study were extracted for comparison. The differences between the two shoe generations were compared using an independent samples t-test for each variable of interest (18.0, SPSS). To quantify shoe characteristics, the slope of the heel and forefoot regions of the test shoes were calculated using the following equations.

$$S_{FT} = \frac{L_{ft}}{f} \times 100 \qquad S_{HL} = \frac{L_{hl}}{r} \times 100 \qquad (1)$$

$$\alpha_{FT} = \frac{t}{f} \qquad \alpha_{FT} = \frac{t}{f} \qquad (2)$$

Where S_{FT}: forefoot slope percentage, L_{ft}: forefoot slope length, f: forefoot length, S_{HL}: heel slope percentage, L_{hl}: heel slope length, r: heel length, α_{FT}: forefoot slope angle, α_{HL}: heel slope angle, t: toe height, and h: heel height. It is important to note, that while the two studies were similar in methodology, the subjects were not the same for both studies (although there was some overlap).

RESULTS AND DISCUSSION

The results of independent samples t-tests comparing means of the subject age, height, mass, and BMI from the two studies showed that BMI was the only variable that was different ($p = 0.036$). Quantitative shoe characteristics can be found in Table 1. The largest difference noted between the two shoe designs was the angle of the heel slope which was decreased by almost 10 degrees in the second generation shoe.

Table 1. Quantitative shoe measurements.

	S_{HL}	S_{FT}	α_{HL}	α_{FT}
Gen 1	108.8%	105.5%	23.4°	17.1°
Gen 2	104.4%	102.8%	13.7°	18.9°

Independent t-tests revealed that only two gait variables were significantly different between the two shoe generations, AP COP ($p = 0.001$), and peak vertical GRF ($p = 0.042$, Table 2). In the 2nd generation shoe, AP COP range of motion was 9 cm longer compared to the 1st generation shoe. Since the average shoe size between the groups was similar (approximately size 10), the larger AP COP in the 2nd generation shoe was likely a result of a smaller curved profile, especially the heel region. This reduced heel slope may likely introduce a more posterior heel contact. This may also indicate that the subjects using the 1st generation shoe may not have utilized the full length of the shoe sole. The 2nd generation shoe also decreased the 1st peak vertical ground reaction force by about 0.05 BW. Since the second peak vGRF was not different between the shoes, the decreased 1st peak is also likely a result of the 2nd generation shoe's smaller heel slope.

CONCLUSIONS

One of the reasons for changing the shoe design was to decrease the profile to make the transition between heel strike and toe off more seamless during stance. Based on the key variables selected, the findings from the lower profile construction of the 2nd generation shoe did not greatly differ from that of its first generation counterpart. This suggests that a lower profile rocker bottom shoe may be just as effective at achieving the desired "unstable" effects while promoting a smoother transition from heel contact through mid-stance. While this study did not evaluate other brands of unstable shoes, it provided evidence to suggest that large bulky soles may not be necessary, and that a lower profile sole design may accomplish similar desired outcomes.

REFERENCES

1. Nigg B, et al. *Clin Biomech* **21**, 82-88, 2006a
2. Romkes J, et al. *Clin Biomech* **21**, 75-81, 2006.
3. Zhang S, et al. *ASB abstract*, 2011.

ACKNOWLEDGEMENTS

The projects were supported in part by funding from Genesco Inc.

Table 2. Mean ± SD of selected gait variables between the two shoe generations.

	ML COP (m)	*AP COP (m)	*1st Peak vGRF (BW)	vGRF load rate (BW/s)	Peak braking GRF (BW)	2nd Peak vGRF (BW)	Eversion ROM (°)	Peak INV Moment (Nm/kg)
1st Gen	-0.06 ± 0.02	0.18 ± 0.04	1.16 ± 0.08	8.27 ± 2.10	-0.23 ± 0.02	1.11 ± 0.05	-6.87 ± 3.45	0.14 ± 0.04
2nd Gen	-0.07 ± 0.02	0.26 ± 0.02	1.11 ± 0.05	7.69 ± 1.97	-0.21 ± 0.02	1.08 ± 0.03	-8.81 ± 2.34	0.14 ± 0.05
p-value	0.651	**0.000**	**0.042**	0.447	0.093	0.057	0.091	0.729

[*] Significant difference between shoe generations.

COMPARISON OF POWERED AND UNPOWERED PROSTHESES IN PATIENTS WITH TRANSTIBIAL AMPUTATION WALKING ON A ROCK SURFACE *

Deanna H. Gates, Jennifer M. Aldridge and Jason M. Wilken

Department of Orthopaedics and Rehabilitation, Center for the Intrepid, Brooke Army Medical Center, Ft. Sam Houston, TX, USA
email: Deanna.H.Gates@gmail.com

INTRODUCTION

Recent research has focused on the design of intelligent prosthetic ankle devices with the goal of adapting the behavior of the device to accommodate all walking surfaces that an individual encounters in daily life. One surface that is particularly difficult for persons with transtibial amputation (TTA) is uneven ground. Patients with TTA have an increased frequency of falling on uneven ground [1], possibly because of limited ankle joint mobility on the prosthetic side, and lack of distal muscles and sensory feedback from the lower limb [2].

The BiOM (iWalk, Cambridge, MA) is an ankle/foot prosthesis that claims to provide active power during the stance phase while accommodating for real time terrain changes [3]. Unlike a passive device, it may not always provide exactly the same response to loading, which may lead users to adopt a more cautious strategy. As such, a passive device may be preferable when encountering novel surfaces. The purpose of this study was to determine if individuals with transtibial amputation altered their gait kinematics when wearing the BiOM ankle prosthesis compared to a passive energy storage and return (ESR) prosthesis when walking on a loose rock surface.

METHODS

11 young adults (10 male, 1 female) with traumatic unilateral transtibial amputation participated. Subjects came to the lab for two separate data collections. During the first session, they wore their clinically prescribed ESR prosthesis. After this session, they were given the powered BiOM prosthesis and provided a three week acclimation period. They then returned for a second session while wearing the BiOM.

During each session, subjects walked over a loose rock surface, previously described in [4,5]. Kinematic data from 57 reflective markers were used to track full body kinematics at 120 Hz using a 26-camera motion capture system (Motion Analysis, Santa Rosa, CA). Walking speeds were normalized to each subject's leg length, l, according to the Froude number, Fn. Subjects walked at three controlled speeds (Fn = 0.10, 0.16, 0.23) and their self-selected walking velocity (SSWV). A total of five left and five right strides were collected at each speed. All subjects wore their own athletic shoes during data collection.

Comparisons of SSWV were made using paired t-test. Comparison of all other dependent measures were made using repeated measures ANOVAs with prosthetic type (BiOM, ESR), walking speed (1-3, SSWV), and limb (prosthetic, intact) as fixed factors.

RESULTS AND DISCUSSION

Patients had a 10% higher SSWV wearing the powered BiOM than an energy-storage and return (ESR) prosthesis (ESR: 1.05± 0.17, BiOM: 1.16 ± 0.018 m/s, $p = 0.031$; Fig. 1A). There were no differences in step width ($p = 0.686$) or step length ($p = 0.058$) between prostheses. A significant Limb × Prosthesis interaction indicated that the difference between the limbs was slightly greater when patients used the ESR compared to the BiOM ($p = 0.039$; Fig. 1B).

There were several significant differences in the patient's kinematics when wearing the different devices (Fig. 2). Patients exhibited increased ankle plantarflexion throughout the gait cycle when wearing the BiOM compared to the ESR prosthesis. Specifically, patients increased ankle plantarflexion during early stance, and push-off, and decreased ankle dorsiflexion during late stance and swing ($p < 0.025$). The increased plantarflexion at push-off occurred only on the prosthetic limb ($p_{\text{Limb × Prosthesis}} = 0.002$). Patients also exhibited a small, but significant, decrease in knee flexion during early stance with the BiOM ($p = 0.047$; Fig. 2).

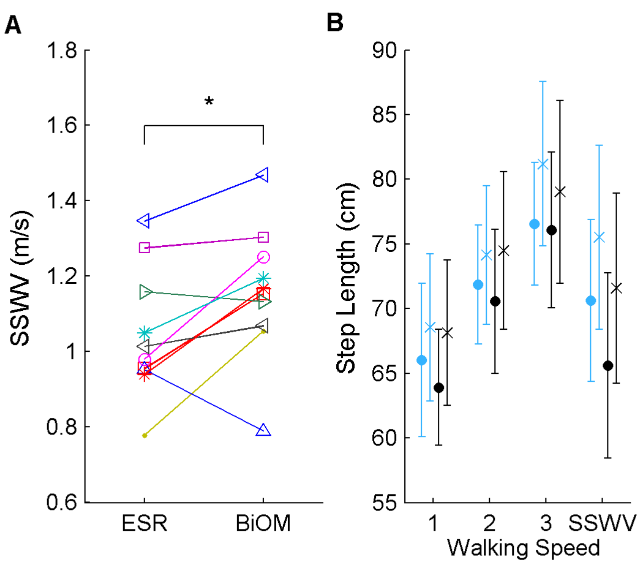

Figure 1: *A) SSWV is shown for each subject with each prostheses. B) Step length is shown for patients using the BiOM (blue) and ESR (black). 'x' is intact limb and 'o' is prosthetic limb.*

Changes with walking speed were similar to those reported previously in patients with transtibial amputation walking with ESR prostheses [5]. There were no Prosthesis × Speed interaction effects, indicating that the patients responded similarly to changes in speed when walking in either prosthesis.

CONCLUSIONS

The patients with transtibial amputations in this study were able to successfully traverse the rock surface in both prostheses tested. Patients walked with similar step width in both devices. They also increased their SSWV while using the BiOM. Together, these results suggest that patients did not adopt a more cautious strategy while using the BiOM. When wearing the BiOM, patients exhibited ankle plantarflexion during push-off, similar to that of healthy controls (Fig. 2). The change in ankle kinematics did not result in any changes in hip or knee kinematics between devices, however.

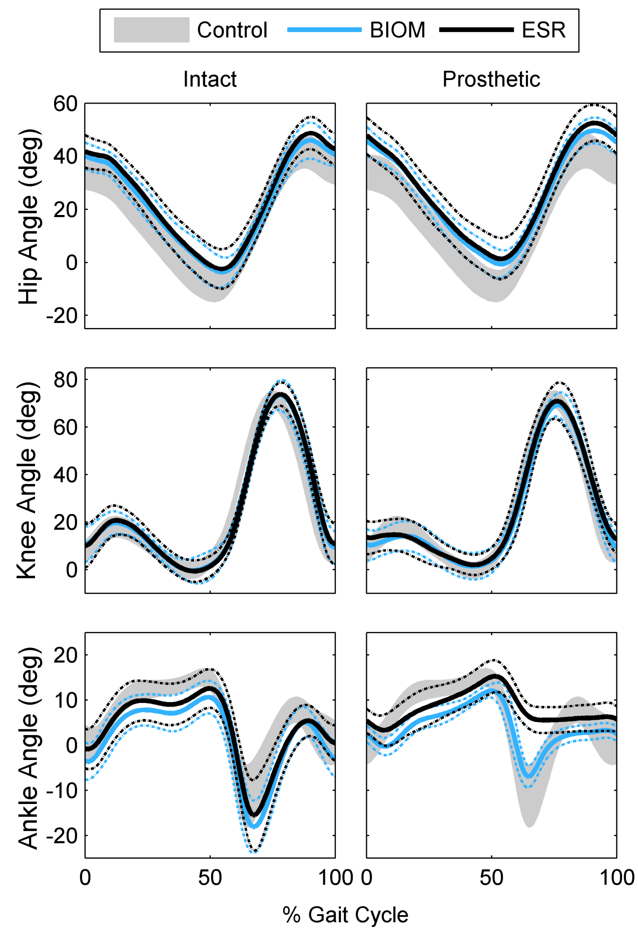

Figure 2: *The average (solid line) and standard deviation (dotted line) of the lower extremity kinematics are shown across subjects for their intact side (left) and prosthetic side (right) at controlled speed 2. The gray band represents normative data on this surface from [3].*

REFERENCES

1.Ülger Ö, et al. *Top Ger Rehabil* **26**, 2010.
2.Viton JM, et al. *Prosthet Orthot Int* **24**: 108-116, 2000.
3. "The BiOM by iWalk." from http://iwalk.com/.
4.Gates DH, et al. *Gait Posture* **35**: 36-42, 2012.
5.Gates DH, et al. *Gait Posture*, In Press.

ACKNOWLEDGEMENTS

Support provided by the U.S. Army Telemedicine & Advanced Technology Research Center.

* The view(s) expressed herein are those of the author(s) and do not reflect the official policy or position of Brooke Army Medical Center, the U.S. Army Medical Department, the U.S. Army Office of the Surgeon General, the Department of the Army, Department of Defense or the U.S. Government.

A MODELING FRAMEWORK FOR EXAMINING CHANGES IN FEMORAL STRENGTH DUE TO LONG DURATION BEDREST

[1]Kerim O. Genc and [2]Peter R. Cavanagh

[1]Simpleware Ltd. Exeter UK
[2]University of Washington, Seattle, WA, USA
email: k.genc@simpleware.com, www.simpleware.com

INTRODUCTION

Despite the use of exercise countermeasures, computed tomography-based (CT) bone mineral density (BMD) changes in astronauts continue to be a serious medical consequence of long duration spaceflight [1]. BMD losses of up to 1.5% per month have been observed in the hips of crewmembers on 4-6 month missions on board the International Space Station (ISS) [1].

We conducted a bedrest study to examine the effect of individualized loading profiles on bone homeostasis by calculating bone mineral density (BMD) changes from CT scans [2]. The goal of the bedrest study was to expand this BMD analysis and examine the use of CT and voxel-based subject-specific finite element (FE) models to quantify the changes in femoral strength. The purpose of the current study was to develop a modeling framework and workflow to go from CT images to FE model, based on the methods used by Joyce Keyak [3], but using readily available commercial software. A sensitivity analysis of the model parameters was also explored.

METHODS

Eleven subjects (6 male, 5 female), were randomized to control (n=6) or treatment (exercise; n=5) groups and confined for 12 weeks to 6-degree head-down bedrest in the General Clinical Research Center at the Cleveland Clinic. The treatment group underwent individualized daily exercise programs in the Zero Gravity Locomotion Simulator (ZLS) designed to replace their daily mechanical load stimulus experienced during free-living [4]. QCT scans of the proximal femur were obtained pre-and post-bedrest (Sensation 64 – Siemens Medical USA Inc. Malvern, PA) at the following settings: 3mm slice thickness, 0.7325 ± 0.05 mm^2 pixels, 120 kVp, 180 mA and the standard soft tissue reconstruction kernel.

A five-sample calibration phantom (Figure 1) with known equivalent K_2PO_4 and H_2O densities (Mindways Software Inc. – Austin, TX) was placed below the hips during each scan.

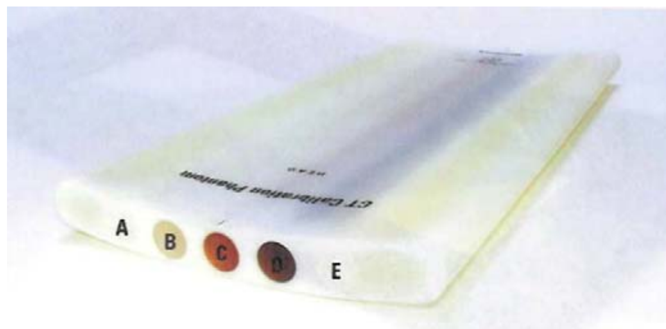

Figure 1: Mindways 5-sample K_2HPO_4 and H_2O equivalent density calibration phantom placed under each subject during CT data collection. Each sample with known densities is labeled A through E.

Coefficients for the linear calibration equations used to convert Hounsfield Units (HU) to BMD (ash density - ρ_{ash} - g/cm^3) for all pixels in each CT slice were calculated in terms of known phantom equivalent densities using custom software provided by Mindways. The linear calibration coefficients for each slice were averaged across all slices to define a linear HU to ρ_{ash} calibration equation for each scan.

The CT dataset was imported into the ScanIP+FE software environment (Simpleware Ltd, Exeter, UK), window where leveling procedures were carried out and the right proximal femur was segmented from the top of the femoral head to just below the lesser trochanter via the use of semi-automated algorithms.

The calculated HU to ρ_{ash} calibration coefficients and ρ_{ash} to Elastic Modulus (E - MPa) coefficients from the literature [5,6] were then used to calculate E for each voxel. A Poisons ratio of 0.4 was used [3]. A three-dimensional voxel-based FE model using heterogeneous linear isotropic material properties was generated from the segmented mask.

Due to variability in subject positioning during the CT scans, the FE models were aligned using the Iterative Closest Point (ICP) algorithm [7]. These models were then exported to ABAQUS (Dassault Systemes, Providence, RI) for FE analysis. A loading condition representing a fall onto the posterolateral aspect of the greater trochanter was modeled (Figure 2).

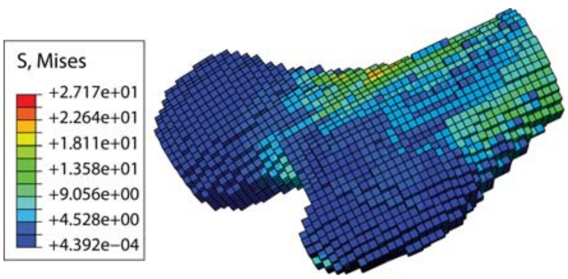

Figure 2: Stress distribution within an exemplar FE model of the right proximal femur of one subject under loading representing a fall onto the posterolateral aspect of the greater trochanter.

MATLAB (Mathworks, Natick, MA) was then used to assign strength values to each voxel and to predict fracture load of a femur by calculating a factor of safety (FOS) for each element [3]. A sensitivity analysis was performed on an FE model built from a pre-and post-bedrest CT data set from a control subject to examine the effect of variations in the following parameters on the calculated failure load: (1) element edge length, which directly affects voxel size and mesh density, (2) the size of the area of load application on the femoral head and (3) the number of nodes constrained at the greater trochanter. We varied the element edge length from 3 to 2 to 1mm. We varied the radius of the circular area of load application from 2 to 20mm in 1mm increments. Finally, we varied the number of nodes constrained at the greater trochanter from 10 to 150 in 10 node increments in the 3mm edge length model, 20 to 300 in 20 node increments in the 2mm edge length model and 30 to 450 in 30 node increments in the 1mm edge length model.

RESULTS AND DISCUSSION

The results indicate that a model with element edge lengths of 2mm, a 15mm radius for an applied load area and 160 constrained nodes at the greater trochanter balanced the sensitivity of the model with the computational time. Using these parameters, the failure loads and locations in the proximal femur showed a pattern consistent with previous models from the literature.

CONCLUSION

The modeling framework shown has allowed an efficient method of using readily available commercial software and phantoms to build and analyze calibrated FE models from medical CT scans.

REFERENCES

1. Lang TF, et al. *J Bone Miner Res* **19**, 1006-12 2004.
2. Genc KO, et al. *American Society of Biomechanics*, University Park, PA, USA, 2009.
3. Keyak JH, et al. *J Biomech* **31**, 125-33, 1998.
4. Genc KO et al. *Aviat Space Environ Med*, **80**, 919-26, 2009.
5. Keyak JH et al. *J Biomed Mater Res* **28**, 1329-36 1994.
6. Keller TS. *J Biomech* **27**, 1159-68, 1994.
7. Besl PJ and McKay ND. *IEEE PAMI* **14**, 239-56, 1992

ACKNOWLEDGEMENTS

This work was supported by NASA grants NNX08BA58G and NNJ05HE72G, by the National Space Biomedical Research Institute through NASA NCC 9-58 and in part by the National Institutes of Health, National Center for Research Resources, CTSA 1UL1RR024989. The advice of Dr. Joyce Keyak and Dr. Ross Cotton and Keenan Brown during this study has been much appreciated.

AUTOMATED ANALYSIS OF 3D GLENOID VERSION

[1]Soheil Ghafurian, [2]Balazs Galdi, [2]Virak Tan, and [1]Kang Li

[1]Department of Industrial & Systems Engineering, Rutgers University, Piscataway, NJ, USA
[2]Department of Orthopaedics, University of Medicine and Dentistry in New Jersey, New Jersey Medical School, Newark, NJ, USA
Email: kl419@rci.rutgers.edu

INTRODUCTION

Optimal glenoid orientation and placement are essential for shoulder function. Abnormal glenoid orientation has been associated with many shoulder pathologies such as glenohumeral instability[1], osteoarthritis [2], and rotator cut tears [3]. Improper placement of the glenoid component could result in glenoid loosening [4] and has been considered as a leading cause of total shoulder arthroplasty failures [5]. Therefore, it is important to characterize the natural glenoid orientation.

The most common measure for characterizing the glenoid orientation and placement is the angle of the glenoid surface in relation to the body of the scapula, which is generally referred to as "glenoid version." [6] A few studies have been conducted to estimate the glenoid version [1-6]. What limited these previous studies, however, was that visual inspections and subjective judgments were required in determining the bony landmarks and glenoid surface from the image data and therefore intra- and inter- observer variability were inevitable.

The primary goal of this study was to establish an automated method for determining glenoid version. The second goal of this study was to examine the inter-subject variability of the version.

METHODS

We reviewed the orthopedic trauma database of our institution from 2003 to 2008. Patients with isolated minimally displaced greater tuberosity fractures (<2mm) who had undergone CT scan of the shoulder were selected. Those patients with fractures of the glenoid or scapular body, prior deformity, or evidence of gleno-humeral arthritis were excluded. Three-dimensional models of the scapulae were reconstructed from the CT scans of patients using the itk-SNAP software. The models which missed the scapular inferior tips were also excluded. In total 12 scapulae were included in this study.

These selected models were then loaded into a custom-made program, which can automatically detect the anatomical features including the scapula inferior tip, the confluence of the spine of the scapula and the medial border of the body, coracoid, acromion, and glenoid face (Figure 1). The glenoid face was determined based on the normal orientation of the points in the glenoid. The glenoid center was defined as the centroid of the glenoid face. The scapular plane was determined by three points, the scapula inferior tip, the confluence of the spine of the scapula and the medial border of the body, and the glenoid center. The acromion and coracoid were defined as the most lateral points with regard to the scapula plane.

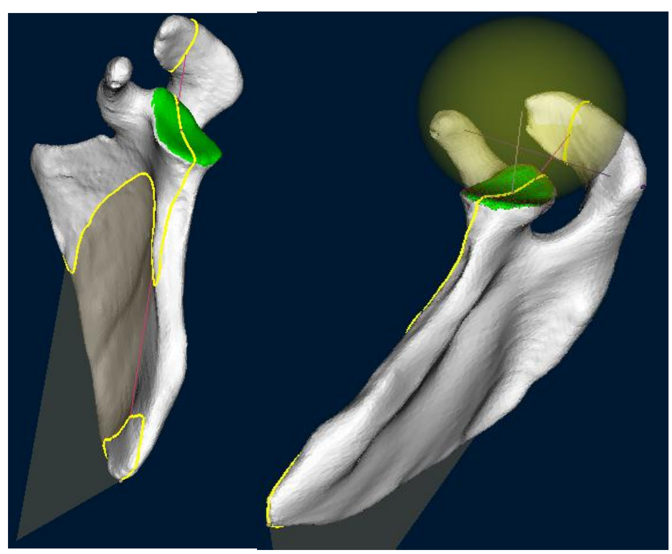

Figure 1: The anatomical features (the pink spheres and the green surface) identified using the

automated method. The yellow line illustrates the scapular plane.

The three-dimensional fulcrum axis was defined as the line connecting the coracoid and acromion. The three-dimensional glenoid version was measured by the angle between the fulcrum axis and the glenoid plane. This was done by fitting a sphere into the glenoid face and the defining the line between the center of the glenoid and the center of the sphere as the normal of the glenoid plane (Figure 2).

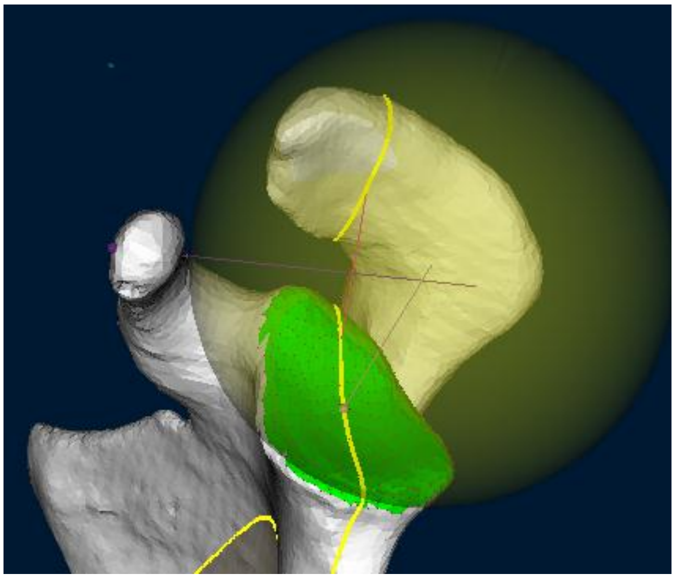

Figure 2: The fitting sphere and 3D glenoid version. The fulcrum axis is seen as the purple line and the green region is the glenoid face. The line connecting the glenoid center and the center of the sphere is the normal of the glenoid plane.

RESULTS AND DISCUSSION

The proposed method automatically processed the CT-acquired 3D scapula models and was able to measure 3D glenoid version within 30 seconds. The mean (±standard deviation) of the 3D glenoid version was -3.1° (±6.08°). Compared with previous 3D glenoid version studies [7, 8], the result from this study was free of the intra- and inter-observer variability, thus more reliable.

Establishment of true glenoid version in the setting of shoulder arthoplasty is of vital importance as improper version of components may lead to abnormal loading of the glenoid component and poor clinical results. Our reliable result established the relationship between extra-articular landmarks and glenoid surface. Such a result may allow a more accurate estimation of glenoid bone loss and normal version for reconstructive purposes, especially in the presence of arthritic and post-traumatic changes.

REFERENCES

1. Brewer, B.J., et al., J Bone Joint Surg Am, 1986. **68**(5): p. 724-31.
2. Mullaji, A.B., et al., J Bone Joint Surg Br, 1994. **76**(3): p. 384-8.
3. Bishop, J.L., et al., J Shoulder Elbow Surg, 2009. **18**(2): p. 231-6.
4. Iannotti, J.P., et al., J Shoulder Elbow Surg, 2005. **14**(1 Suppl S): p. 111S-121S.
5. Strauss, E.J., et al., J Shoulder Elbow Surg, 2009. **18**(5): p. 819-33.
6. Nyffeler, R.W., et al.,. J Shoulder Elbow Surg, 2003. **12**(5): p. 493-6.
7. Ganapathi, A., et al., J Shoulder Elbow Surg, 2011. **20**(2): p. 234-44.
8. Budge, M.D., et al., J Shoulder Elbow Surg, 2011. **20**(4): p. 577-83.

ACKNOWLEDGEMENTS

This work was supported in part by the Charles and Johanna Busch Memorial Fund.

MOVEMENT STRATEGY AND ARM USE REDISTRIBUTE SIT-TO-STAND JOINT MOMENTS

[1]Jason C. Gillette, [2]Catherine A. Stevermer and [3]Michelle Hall

[1]Iowa State University, Ames, IA, USA
[2]Des Moines University, Des Moines, IA, USA
[3]University of Melbourne, Victoria, Australia
email: gillette@iastate.edu

INTRODUCTION

The capability to move from a sitting to a standing position is essential for mobility and is associated with independent living. For those who struggle with sit-so-stand, potential compensations include utilizing different movement strategies [1-3] and using armrest support. Three common sit-to-stand movement strategies are momentum, stabilization, and vertical. The momentum strategy involves trunk/hip flexion to generate momentum and then trunk/hip/knee extension to complete the sit-to-stand movement. This is the most common strategy utilized by young, healthy adults. The stabilization strategy involves trunk/hip flexion to achieve a stable 'nose over toes' posture, then knee extension, and then trunk/hip extension. Such a strategy may be preferred by someone with balance deficits and/or fear of falling. The vertical strategy involves knee/hip extension without trunk/hip flexion to rise straight up from a sitting position during sit-to-stand. Although difficult even for some young healthy adults, this movement strategy may be required for those with low back pain, during pregnancy, or after total hip replacement. The use of armrest support should be beneficial to those with strength deficits such as hip extensor weakness and may be particularly helpful for those who utilize the vertical strategy.

The purpose of this study was to determine lower extremity joint moments during sit-to-stand as a function of movement strategy and arm use. It was hypothesized that the stabilization strategy would result in increased hip extension moments and the vertical strategy would result in increased knee extension moments. It was also hypothesized that the use of arm support would result in reduced hip extension moments.

METHODS

Twenty-two individuals (gender 10 M/12 F, age 23±2 yr, height 1.71±0.08 m, mass 78±20 kg) participated in this study. Verbal cues were 'normal' and 'regular' for the momentum strategy; 'forward bending' and 'nose over toes' for the stabilization strategy; and 'keep back straight' and 'do not bend forward' for the vertical strategy. The seated surface was a 46 cm wooden bench with no back support. When using arm support, hands were placed on 9 cm armrests attached to the bench. After demonstration and practice, each participant completed 3 repetitions of 6 conditions (3 movement strategies x 2 arm support options). Twenty-four reflective markers were tracked during the sit-to-stand movements by an 8-camera motion analysis system (Vicon). Participants placed each foot on a separate in-ground force platform (AMTI).

Sit-to-stand movements were analyzed from elevation onset to vertical stabilization as determined from the combined right and left vertical ground reaction forces [4]. Using inverse dynamics, right and left maximum ankle plantarflexion, knee extension, external knee valgus, hip extension, and hip abduction moments were calculated, transformed to the distal segment coordinate system, and normalized by body mass. All calculations were determined using Matlab, averaged across 3 trials, and averaged for right and left legs. Multivariate ANOVA was used to test for main effects of movement strategy, arm support, and their interactions with a significance level of $p<0.05$ (SPSS). When significant main effects were found, post hoc Scheffe comparisons were utilized for movement strategy effects and univariate ANOVA for arm support effects with a Bonferroni adjustment of 5 ($p<0.01$).

RESULTS AND DISCUSSION

Significant differences in peak joint moments as a function of movement strategy and arm support are shown in Table 1. Ankle plantarflexion moments were decreased with the vertical strategy and increased with the stabilization strategy. Knee extension moments were decreased with the stabilization strategy and increased with the vertical strategy. Knee extension moments were also decreased with armrest support. Hip extension moments were decreased with the vertical strategy and with armrest support. Hip extension moments approached a significant increase when using the stabilization strategy (p=0.013). Knee extension and hip extension moments were dependent upon both movement strategy and arm support, thus meriting further examination. Knee extension moments ranged from 0.435±0.127 Nm/kg when using the stabilization strategy with armrest support to 0.804±0.122 Nm/kg when using the vertical strategy with no arm support. Hip extension moments ranged from 0.475±0.148 Nm/kg when using the vertical strategy with armrest support to 0.909±0.161 Nm/kg when using the stabilization strategy with no arm support. Knee valgus and hip abduction moments were not significantly changed by movement strategy or arm support.

The hypothesis that hip extension moments would increase with the stabilization strategy was not supported, although this comparison approached significance. The hypothesis that knee extension moments would increase with the vertical strategy was supported by a 20% increase. The hypothesis that hip extension moments would decrease with armrest support was supported by a 24% reduction. In terms of percent differences, the most dramatic changes were a 36% increase in ankle plantarflexion moments with the stabilization strategy and a 44% reduction in ankle plantarflexion moments with the vertical strategy. These distinct changes were likely due to differences in peak ankle dorsiflexion angle between the movement strategies.

Results of this study can be used to make basic observations regarding sit-to-stand movements. The stabilization strategy was described as an option for those with balance deficits and also may also benefit those with knee extensor weakness. However, the stabilization strategy relies more heavily on ankle plantarflexors and strengthening exercises may be in order. The vertical strategy was listed as an alternative for individuals with back/hip pain or reduced range of motion and succeeded in reducing hip extensor and even ankle plantarflexor requirements. However, the vertical strategy has higher knee extensor requirements, potentially exceeding strength capacity, but which may be offset by the use of armrests.

REFERENCES

1. Schenkman ML, et al. *Clin Biomech* **11**, 153-158, 1996.
2. Mazza C, et al. *J Am Geriatr Soc* **52**, 1750-1754, 2004.
3. Scarborough DM, et al. *J Rehabil Res Dev* **44**, 33-42, 2007.
4. Gillette JC, Stevermer CA. *Gait Posture* **35**, 78-82, 2012.

Table 1: The effects of movement strategy and arm support on sit-to-stand joint moments.

	Peak Joint Moments (Nm/kg)				
	Ankle Plantarflexion	**Knee Extension**	**Knee Valgus**	**Hip Extension**	**Hip Abduction**
Momentum	0.281 ± 0.110	0.651 ± 0.127	0.092 ± 0.063	0.732 ± 0.193	0.266 ± 0.102
Stabilization	**0.381 ± 0.148↑**	**0.504 ± 0.145↓**	0.090 ± 0.061	0.834 ± 0.164	0.272 ± 0.125
Vertical	**0.158 ± 0.091↓**	**0.781 ± 0.115↑**	0.112 ± 0.079	**0.591 ± 0.201↓**	0.284 ± 0.151
No Support	0.255 ± 0.149	0.691 ± 0.155	0.104 ± 0.071	0.816 ± 0.196	0.287 ± 0.141
Armrests	0.292 ± 0.148	**0.600 ± 0.177↓**	0.093 ± 0.065	**0.622 ± 0.179↓**	0.261 ± 0.110

↑ indicates significant increases with respect to momentum strategy ($p<0.01$), ↓ indicates significant decreases with respect to momentum strategy or no arm support ($p<0.01$)

ACCURACY OF SELF-REPORTED FOOTSTRIKE PATERNS AND LOADING RATES ASSOCIATED WITH TRADITIONAL AND MINIMALIST RUNNING SHOES

[1]Donald L. Goss, [1]Michael D. Lewek, [1]Bing Yu, and [1]Michael T. Gross

[1]The University of North Carolina at Chapel Hill
email: dgoss@email.unc.edu

INTRODUCTION

Since the advent of the modern running shoe in the 1970's, approximately 75-80% of runners have adopted a rearfoot strike pattern.[1,2] Using this strike pattern increases horizontal braking forces and vertical loading rates.[3] Some experts in the industry have recommended a departure from traditional running shoes with cushioned heels in favor of adopting "minimalist" running shoes. The assertion is that wearing minimalist shoes simulates barefoot running and will force runners to adopt a more anterior footstrike pattern than traditional shoes, thus reducing loading rates and internal knee moments in an effort to reduce injuries.

The purposes of this study were to evaluate the accuracy of self-reported footstrike patterns in traditional shoe wearers (TS) and minimalist shoe wearers (MS) and to report the average vertical loading rates among these runners.

METHODS

Fifty-seven male and female runners (22 TS- and 35 MS) who reported wearing the same type of footwear for at least 6 months during running were asked to report their footstrike tendencies on flat, level surfaces. Runners were then evaluated in the final minute of a five minute run at a self-selected speed on a Bertec instrumented treadmill. Center of pressure data and slow motion videos from a Sony Handycam were used to classify footstrike pattern dichotomously: either rearfoot or anterior (non-rearfoot).

Chi-squared analysis was used to compare self-reported to actual footstrike pattern. A one-way analysis of variance (ANOVA) was used to compare average vertical loading rates (determined from 20-80% of impact peak or 3-12% stance phase in the absence of an impact peak) and peak vertical ground reaction forces among the following groups: TS with rearfoot strike pattern (TSR), MS with anterior foot strike pattern (MSA), and MS with rearfoot strike pattern (MSR). Post- hoc testing was conducted using Tukey's HSD.

RESULTS

Prior to running, 20 of the 22 (90.9%) TS runners reported utilizing a rearfoot strike pattern. All 22 TS runners, however, exhibited a rearfoot striking pattern. Prior to running, all 35 MS runners reported utilizing an anterior footstrike pattern. Out of the 35 MS runners, 23 demonstrated an anterior footstrike pattern and 12 demonstrated a rearfoot strike pattern. Accuracy of self-reported footstrike pattern in MS runners was 23/35 (65.7%) and overall accuracy of self-reported footstrike pattern was 43/57 (75.4%).

Actual footstrike differed statistically from self-reported footstrike ($X^2 = 6.90$, 1df, $p = .01$, $n = 57$). (Table) Loading rates differed among groups ($F = 15.24$, $p < 0.001$). Average vertical loading rates differed among groups (Figure 1, $F = 15.26$, $p < 0.001$, TSR-MSR $p < .001$, TSR-MSA $p=0.18$, MSA-MSR $p < 0.001$). Peak vertical ground reaction force did not differ among groups (Figure 2, $F = 0.74$, $p = 0.48$).

Table: Self-reported vs. actual footstrike pattern.

Footstrike pattern	Reported	Actual
Rear footstrike	20	34
Anterior footstrike	37	23

$X^2 = 6.90$, 1df, $p = .01$, $n = 57$

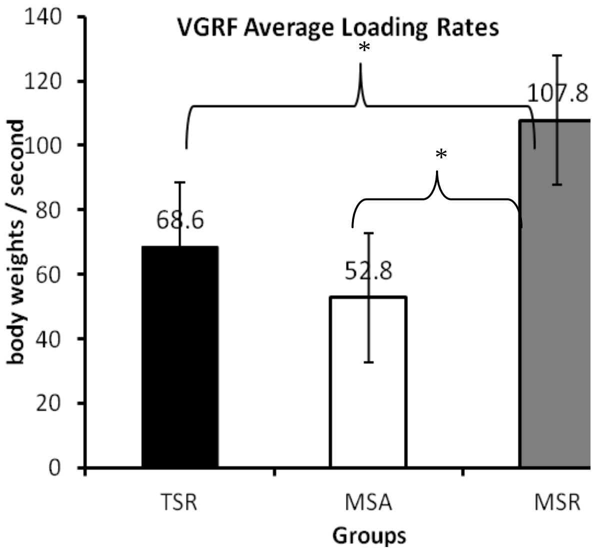

Figure 1: Average vertical loading rates for rearfoot striking runners in traditional shoes (TSR), anterior footstriking runners in minimalist shoes (MSA), and rearfoot striking runners in minimalist shoes (MSR).

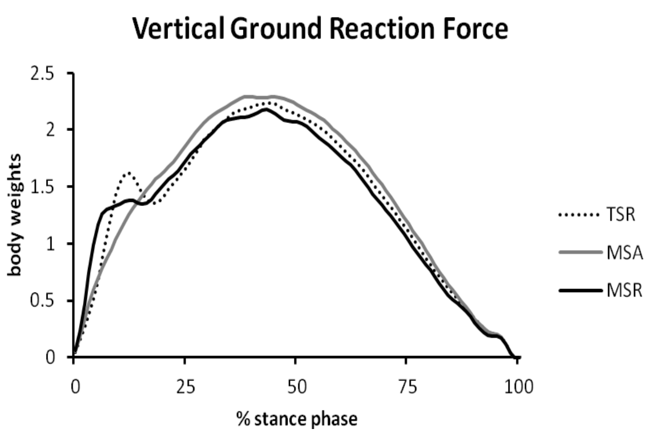

Figure 2: Vertical ground reaction force curves for rearfoot striking runners in traditional shoes (TSR), anterior footstriking runners in minimalist shoes (MSA), and rearfoot striking runners in minimalist shoes (MSR).

DISCUSSION

McCarthy et al. observed 50% of females still demonstrating a rearfoot strike pattern two weeks after transitioning to minimalist footwear.[4] Despite at least six months of accommodation and 24.6 ± 25.7 months in minimalist running shoes, approximately 1/3 of the MS runners in our sample demonstrated a rearfoot strike pattern and potentially injurious ground reaction force loading rates.

Greater loading rates have been associated with stress fractures[5], patellofemoral pain syndrome[6], and plantar fasciitis.[7] Clinicians and runners should understand that running in minimalist shoes with a rearfoot strike pattern may increase the risk of incurring lower extremity musculoskeletal injury.

CONCLUSIONS

Approximately 1/3 of experienced MS runners in this sample misclassified their footstrike pattern, and demonstrated a rearfoot strike pattern with potentially injurious loading rates.

REFERENCES

1. Hasegawa H, Yamauchi T, Kraemer WJ. Foot strike patterns of runners at the 15-km point during an elite-level half marathon. *J Strength Cond Res.* 2007;21(3):888-893.
2. Lieberman DE, Venkadesan M, Werbel WA, et al. Foot strike patterns and collision forces in habitually barefoot versus shod runners. *Nature.* 2010;463(7280):531-535.
3. Arendse RE, Noakes TD, Azevedo LB, Romanov N, Schwellnus MP, Fletcher G. Reduced eccentric loading of the knee with the pose running method. *Med Sci Sports Exerc.* 2004;36(2):272-277.
4. McCarthy CPJK, T; et al. Like Barefoot, Only Better. *ACE Certified News.* 2011;September 2011:8-12.
5. Zadpoor AA, Nikooyan AA. The relationship between lower-extremity stress fractures and the ground reaction force: a systematic review. *Clin Biomech (Bristol, Avon).* 2011;26(1):23-28.
6. Davis I. Vertical Impact Loading in Runners with a History of Patellofemoral Pain Syndrome. Baltimore, MD: American College of Sports Medicine; 2010.
7. Pohl MB, Hamill J, Davis IS. Biomechanical and anatomic factors associated with a history of plantar fasciitis in female runners. *Clin J Sport Med.*2009;19(5):372-376.

BIOMECHANICAL AND METABOLIC IMPLICATIONS OF WEARING A POWERED EXOSKELETON TO CARRY A BACKPACK LOAD

[1]Karen N. Gregorczyk, [1]Albert A. Adams, [2]Meghan P. O'Donovan, [1]Jeffrey M. Schiffman, [1]Carolyn K. Bensel, and [1]Michael L. Brown

[1]U.S. Army Natick Soldier Research, Development and Engineering Center, Natick, MA, USA
[2] Oakridge Institute for Science and Engineering, Post Graduate Research Participation Program, Belcamp, MD
email: karen.gregorczyk@us.army.mil

INTRODUCTION

Carrying heavy backpack loads in mountainous terrains can negatively impact soldiers' overall mission effectiveness. A wearable, assistive device for bearing loads that reduces soldiers' energy consumption or preserves their fitness to fight after prolonged marches could have widespread application in military environments. We previously evaluated a prototype of a quasi-passive exoskeleton designed to assist in bearing a backpack load and found that using the device on a level grade altered gait mechanics and increased oxygen consumption by approximately 60%, as compared to standard load carriage [1]. Recently, a prototype of a powered exoskeleton (PEXO) was developed to off-load the vertical component of backpack loads and assist the user against gravity throughout the gait cycle via powered hip and knee joints. The physiological effects of carrying loads with the PEXO, which weighed 39.54 kg, have not been reported. This study was conducted to quantify the physiological and gait effects of the PEXO on users carrying a military load at various grades.

METHODS

Eight healthy U.S. Army infantry soldiers (mean: age = 23.8 yrs, stature = 1.77 m, weight = 76.5 kg) participated in the study. Testing consisted of 9-min trials of walking at 1.34 m/s on a treadmill while carrying a 39.5-kg military load (Fig. 1). All subjects were tested at -6%, 0%, and 6% grades carrying the load with the PEXO and without the PEXO (Control). The orders of testing of the device and the grade conditions were balanced. Breath-by-breath oxygen consumption (VO_2) data were collected using the COSMED K4b^2 between minutes 5 and 7 of each trial and then averaged over the 2-min period. The VO_2 data (ml/min) were normalized to body mass, VO_2BM (ml/kg/min). Heart rate, HR (bpm), was recorded every 15 s between minutes 5 and 7 of each trial with the Polar RS400 monitor and averaged over the 2 min. Kinematic data were collected using 12 Oqus cameras (Qualisys) operating at 120 Hz. Prior to data collection, each subject completed, on average, 3.25 h of familiarization with the PEXO, including treadmill walking at the specified speed and grades with and without the load. A 2-way repeated measures ANOVA was performed for device (Control, PEXO) x grade (-6%, 0%, and 6%) with alpha set at .05 and *t*-tests done as appropriate.

RESULTS AND DISCUSSION

There were significant main effects of device and of grade on VO_2, VO_2BM, and HR (Table 1), but the interaction was not significant (p>.05). VO_2 (p=.001) and VO_2BM (p=.001) were higher by 39% and HR (p=.000) was higher by 26% with the PEXO compared to the Control. For the main effect of grade, VO_2, VO_2BM, and HR increased significantly with each increase in grade (p=.000).

Analyses of the kinematic data revealed significant main effects of device on trunk angle (p=.000), trunk range of motion (ROM; p=.017), maximum hip angle (p=.000), minimum hip angle (p=.000), and maximum knee angle (p=.001). Significant main effects of grade were found for trunk angle (p=.000), trunk ROM (p=.010), maximum hip angle (p=.000), minimum hip angle (p=.000), hip ROM (p=.000), maximum knee angle (p=.000), and maximum ankle angle (p=.014). Overall, wearing the PEXO altered normal gait patterns of load carriage (Fig. 2). Subjects adopted a specific gait pattern with the PEXO where they straightened the knees at heel strike, locking out the device knee joint, to transfer the load to the ground. Subjects found this gait difficult at the 6% grade where the knee is typically in a flexed position at heel strike.

Figure 1: Soldier wearing the PEXO with the military load attached while walking on the treadmill at 1.34 m/s.

CONCLUSIONS

Like the quasi-passive exoskeleton we evaluated previously [1], the PEXO resulted in higher metabolic costs and heart rates and altered gait mechanics during treadmill walking at various grades compared to standard load carriage. The physiological burden was somewhat lower with the PEXO than with the earlier version, probably due to the powered knee and hip joints. However, adding power was not sufficient to produce a device that augments human load-carriage performance. Other researchers have suggested that mistiming of the power applied to the joints may cause a destabilization of the users' gait, increasing metabolic cost [2]. Additional factors contributing to the increase in VO_2 may include the weight of the PEXO and controlling the MOI of the load and device. The findings here highlight the importance of continuing research to extend understanding of fundamental engineering and biomechanical mechanisms that must function in a complementary manner if efforts to develop exoskeletons for load-carriage assistance are to succeed.

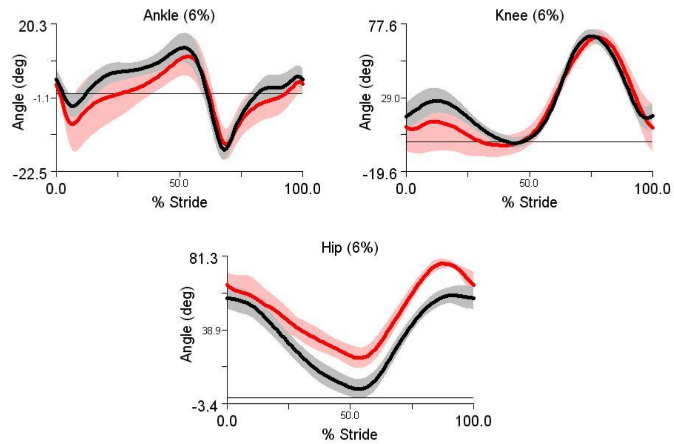

Figure 2: Means (solid line: red = PEXO; black = Control) and standard deviations (shaded region) for ankle, knee and hip angles as a percentage of stride for subjects walking at 1.34 m/s at the 6% grade (*n* = 8).

REFERENCES

1. Gregorczyk KN, et al. *Ergonomics* **53**, 1263-1275, 2010.
2. Walsh CJ, et al. *Int J Hum Robot* **4**, 487-506, 2007.

Table 1: Means (SD) of physiological variables for the device and for the grade conditions (*n* = 8).

	Device		Grade		
	Control	**PEXO**	**-6%**	**0%**	**6%**
VO_2 (ml/min)	1470.08^{A} (541.63)	2047.90^{B} (546.40)	1263.59^{X} (339.24)	1604.03^{Y} (389.08)	2409.34^{Z} (411.94)
VO_2BM (ml/min/kg)	19.27^{A} (7.07)	26.82^{B} (7.09)	16.51^{X} (4.08)	20.99^{Y} (4.83)	31.63^{Z} (5.53)
HR (bpm)	124.95^{A} (25.59)	157.31^{B} (23.90)	120.47^{X} (21.88)	137.13^{Y} (25.23)	165.81^{Z} (21.92)

Note: Within device and within grade, means that do not share the same letter were found to be significantly different (p<.05) in ANOVA or post-hoc tests.

EFFECTS OF A BIOMECHANICAL ENERGY HARVESTING ANKLE DEVICE ON GAIT KINETICS

Robert Gregory, Rebecca Zifchock, Stephane Manuel and William Brechue

U.S. Military Academy, West Point, NY, USA
email: robert.gregory@usma.edu web: http://www.usma.edu/dpe

INTRODUCTION

The average U.S. Army infantry soldier in present theaters of operation carries a typical load of approximately 95 lbs on multiple day missions [1]. Due to the proliferation of electronic devices in the field, the need for batteries to power these devices has increased. Because batteries are a large percentage of pack weight during load carriage, the U.S. Army is exploring alternative methods of power generation.

One possible solution is to enable the soldier to harvest biomechanical energy that is generated during walking. The Soldier Power Regeneration Kit (SPaRK; SpringActive, Inc.; Tempe, AZ) is a device designed to generate power from the eccentric muscular actions at the ankle joint during walking by using a spring to slow rotation of the shank with respect to the foot during mid-stance. It is worn on the outside of standard military footwear and current prototypes produce 3-6 W of continuous power output [2].

In theory, power production from eccentric muscle activity should assist the braking motion of the body during walking and therefore have no associated metabolic cost. However, the SPaRK device has a mass of 1.9 kg. Previous research has found that the addition of weight to the ankle joint during gait resulted in increased joint moments; these joint moments were linked with increased metabolic energy expenditure [3]. In addition, deviations from normal gait patterns have been shown to be indicative of an individual's susceptibility to injury [4, 5]. Therefore, the purpose of this study was to assess the effects of wearing a biomechanical energy harvesting device on gait kinetics. It was hypothesized that the use of the SPaRK device will result in increased vertical ground reaction forces, weight acceptance and push off rates, and impulse.

METHODS

Six individuals (4 M, 2 F; age: 34.0 ± 5.0 yr, height: 1.68 ± 0.05 m, mass: 69.6 ± 8.9 kg) volunteered to participate in this study. All participants provided written informed consent in accordance with the procedures established by the Institutional Review Board of the U.S. Military Academy.

The participants walked on an instrumented treadmill (Kistler Gaitway II; Winterthur, SUI) for 7-10 min at 4.83 km/h (3.0 mph) for each of four conditions: 1) No rucksack/boots only, 2) No rucksack/boots with SPaRK, 3) Rucksack (30% BW load)/boots only, and 4) Rucksack (30% BW load)/boots with SPaRK. Ground reaction force (GRF) data were collected during the final minute of walking at a sampling rate of 250 Hz.

The following kinetic variables were analyzed:

1) first peak force – the maximum vertical GRF during the first half of the stance phase;
2) mid-support force – the minimum vertical GRF between the first and second peak forces;
3) second peak force – the maximum vertical GRF during the second half of the stance phase;
4) weight acceptance rate – the slope of the vertical GRF time curve during the loading phase, taken from heel contact to the first peak force;
5) push off rate – the slope of the vertical GRF time curve during the unloading phase, taken from the second peak force to toe off; and
6) impulse – the area under the vertical GRF time curve from heel contact to toe off.

The kinetic variables were averaged across both right and left legs for 30 strides per condition for each participant. A paired *t* test was used to assess the effects of the SPaRK device on gait kinetics while walking both with and without a rucksack. Statistical significance was set at the $P \leq 0.05$ level.

RESULTS AND DISCUSSION

There was only one significant difference in gait kinetics as a result of wearing a biomechanical energy harvesting device at the ankle: the second peak force (associated with the propulsive phase of gait) increased when using the SPaRK device during walking both with (+9.3%; $P < 0.05$) and without (+11.9%; $P < 0.05$) a rucksack (see Table 1). Due to the increase in the second peak force when using the SPaRK device, there was also a strong trend for an increased push off rate during walking both with (+10.0%; $P = 0.09$) and without (+6.2%; $P = 0.12$) a rucksack (see Table 1). There were no differences between the first peak force (which is associated with the braking phase of gait), the mid-support force, the weight acceptance rate, and impulse when using the SPaRK device during walking both with and without a rucksack.

The lack of differences in gait kinetics (with the exception of the second peak force during the propulsive phase of gait) suggests that utilizing the SPaRK device during walking both with and without a rucksack does not significantly alter lower extremity loading as compared to wearing boots only. Therefore, it appears that wearing a biomechanical energy harvesting ankle device may not predispose individuals to injuries that could possibly occur as a result of long-term alterations in gait mechanics.

Future studies will utilize a larger sample size in order to more accurately assess the effects of the SPaRK device on gait mechanics, since the small sample size ($N = 6$) used in this study may have allowed the overall effects to be disproportionately influenced by individuals who had a particularly strong response to the device. In addition, follow-on research will incorporate trials longer than 10 min that should be more representative of the long-term gait adaptations and alterations that may occur when using the SPaRK device.

CONCLUSIONS

The SPaRK device allowed the study participants to maintain normal gait kinematics (not reported here) and kinetics with negligible increases in metabolic cost while achieving 2.5-3.5 W of power output per leg during walking at 4.83 km/h (3.0 mph). This prototype demonstrates the feasibility of a soldier-ready biomechanical energy harvesting ankle device for field use.

REFERENCES

1. Tunnel HD. *Red Devils: Tactical Perspectives from Iraq*, Combat Studies Institute Press, 2010.
2. SpringActive, Inc. http://www.springactive.com/spark.php.
3. Browning RC, et al. *Med Sci Sports Exerc* **39**, 515-525, 2007.
4. Crossley K, et al. *Med Sci Sports Exerc* **31**, 1088-1093, 1999.
5. Pohl MB, et al. *J Biomech* **41**, 1160-1165, 2008.

ACKNOWLEDGEMENTS

The authors would like to acknowledge the support of the U.S. Army Natick Soldier Research, Development and Engineering Center in conducting this preliminary study.

Table 1: Gait kinetics (mean ± SD) during walking with and without the SPaRK device.

	Walk w/o Rucksack		Walk w/Rucksack	
	Boots Only	w/SPaRK	Boots Only	w/SPaRK
First Peak Force (BW)	1.20 ± 0.08	1.33 ± 0.16	1.55 ± 0.15	1.65 ± 0.17
Mid-Support Force (BW)	0.74 ± 0.04	0.75 ± 0.07	0.89 ± 0.10	0.87 ± 0.08
Second Peak Force (BW)	1.20 ± 0.04	1.35 ± 0.14	1.53 ± 0.04	1.67 ± 0.12
Weight Acceptance Rate (BW/s)	8.18 ± 1.05	10.64 ± 5.73	10.60 ± 1.45	13.14 ± 5.25
Push Off Rate (BW/s)	9.40 ± 0.94	9.98 ± 1.26	12.05 ± 1.03	13.25 ± 1.93
Impulse (BW·s)	0.58 ± 0.02	0.61 ± 0.05	0.74 ± 0.03	0.76 ± 0.04

The Effects of Leg Dominance, Neuromuscular Training, and Fatigue on Bilateral Lower Extremity Kinematics

[1]Eric Greska, [2]Nelson Cortes, [1]Stacie Ringleb, [1]Michael Samaan, and [1]Bonnie Van Lunen

[1]Old Dominion University, Norfolk, VA, USA
[2]George Mason University, Fairfax, VA, USA
email: egreska@odu.edu

INTRODUCTION

Neuromuscular training programs aimed at reducing anterior cruciate ligament (ACL) injuries have demonstrated positive effects in reducing the occurrence of such injuries. Strength, flexibility, agility, and plyometric training have been included in such training programs, aimed at trying to alter landing mechanics. When influenced by fatigue, neuromuscular control strategies and biomechanical parameters demonstrate alterations [1]. There is a lack of information regarding how training programs impact neuromechanical control with regards to leg dominance and fatigue status. Therefore, the purpose of this study was to determine the effects of a neuromuscular training program on bilateral lower extremity kinematics during a fatigued status while performing a sidestep cutting task.

METHODS

At pre- and post-training, bilateral lower extremity kinematics of 14 female collegiate soccer athletes (19.6 ± 1.0 years, 1.68 ± 0.06 m, 64.8 ± 5.7 Kg) were obtained while undergoing a dynamic fatigue protocol. For the testing sessions, participants alternated between performing an unanticipated sidestep cutting task, with the dominant and non-dominant legs, and performing a dynamic fatigue battery. Participants were required to complete six valid trials (3 for each leg) of the sidestep cutting task prior to beginning the dynamic fatigue battery. To control the unanticipation factor, the task was visually displayed in a random order through custom-made software [2]. The dynamic fatigue battery consisted of four functional tasks that included: 5 vertical jumps (80% of their maximum), 5 parallel squats, 5-10-5 agility drill and step-ups onto a 20-cm box. Participants rotated between the sidestep cutting tasks and the dynamic fatigue battery until they were deemed physiologically fatigued. Eight high-speed Vicon cameras (Vicon Motion Systems Ltd, Oxford, UK) sampling at 250Hz and two Bertec Force Plates (Model 4060-NC, Bertec Corporation, Columbus, OH, USA) sampling at 2000Hz were used to track marker trajectory and ground reaction forces, respectively. A lower body kinematic model was created from each participants' static trial using Visual 3D (C-Motion, Rockville MD, USA), and was used to quantify hip, knee, and ankle joint angles. Functional hip joint centers were estimated from a standing trial performing a circular motion of the pelvis [3]. Based on a power spectrum analysis, marker trajectory was filtered using a fourth-order Butterworth zero lag filter with a 6 Hz cutoff frequency, whereas ground reaction force data were filtered using a similar filter with a 12 Hz cutoff frequency. The training program spanned 10 weeks and consisted of a single session each week. Sessions were performed under fatigue at the end of practice and consisted of plyometric and agility drills. Separate 2 (Training) x 2(Leg dominance) x 2(Fatigue status) repeated measures ANOVA's were performed for each dependent variable at initial contact and peak knee abduction moment. A Bonferroni adjusted alpha level was set *a priori* at 0.004.

RESULTS AND DISCUSSION

Multiple significant differences were found for hip, knee, and ankle joint angles (Table 1). For the main effect of training, significant differences were found for hip flexion at initial contact (IC) ($p < 0.001$) and peak knee abduction moment (PKABM) ($p = 0.004$), demonstrating a more extended position post-training. Ankle flexion at PKABM also displayed a significant difference ($p = 0.002$) for the main effect of training. For the main effect of fatigue, significant differences were exhibited for hip flexion (p = 0.001) and rotation (p = 0.004) at IC, and knee flexion (p < 0.001) and hip rotation (p < 0.001) at PKABM. No significant differences were exhibited for the main effect of leg dominance or for any interaction effects at IC and PKABM (p > 0.004).

With regards to the training program, the kinematic differences noted for hip flexion may have a potential negative impact on ACL injury risk, as the participants were landing in a more extended position about the hip post-training. As well, the decrease in ankle dorsiflexion at PKABM demonstrates a further extended position at post-training. It has been reported that decreased hip flexion and a heel-to-toe foot strike are possible factors that can influence the risk of incurring a non-contact ACL injury [4]. Fatigue further effected the extended position of hip flexion at IC, and placed the knee in a more extended position at PKABM. As hip internal rotation has been implicated as a mechanism involved in non-contact ACL injury occurrence, the decrease seen at both IC and PKABM post-fatigue may be a protective alteration for controlling motion about the knee when landing in a more extended position. As no significant differences were noted between the dominant and non-dominant legs, leg dominance does not appear to influence non-contact ACL injury risk factors in this population. Kinetic analyses of the lower extremities were not included with the kinematics analysis, therefore is not possible assess the extent to which the kinematic changes influence non-contact ACL injury risk.

CONCLUSIONS

Lower extremity kinematics were effected by neuromuscular training and fatigue during a sidestep cutting task. At post-training and post-fatigue, the participants demonstrated positions of less flexion about the hip and knee bilaterally, which may demonstrate that the training program did not decrease non-contact ACL injury risk factors.

REFERENCES

1. Mclean SG, Samorezov JE. *Med Sci Sports Exerc* **41**, 1662-1673, 2009.
2. Cortes N, et al. *Sports Biomech* **10**, 22-34, 2011.
3. Schwartz MH, Rozumalski A. *J Biomech* **38**, 107-116, 2005.
4. Cortes N, et al. *J Appl Biomech*. **23**, 289-299, 2007

Table 1. Descriptive statistics for hip, knee, and ankle kinematics at initial contact and peak knee abduction moment.

	Pre-Training				Post-Training			
	Dominant		Non-Dominant		Dominant		Non-Dominant	
Rotation (°)	Pre-Fatigue	Post-Fatigue	Pre-Fatigue	Post-Fatigue	Pre-Fatigue	Post-Fatigue	Pre-Fatigue	Post-Fatigue
Initial Contact								
Knee Flexion	-27.0±7.3	-21.9±9.0	-28.0±8.0	-23.4±8.9	-19.6±8.4	-18.5±7.3	-26.6±7.2	-22.5±11.0
Knee Abduction	0.5±4.0	0.6±3.7	-1.7±3.9	-1.5±3.8	0.1±3.0	-0.7±3.4	-2.2±3.1	-2.0±3.7
Knee Rotation	9.0±6.9	6.4±5.5	8.2±7.3	8.0±6.8	8.4±7.3	9.1±6.5	10.3±4.9	8.2±5.1
Hip Flexion[a,b]	50.1±11.2	44.3±10.1	49.5±10.2	45.7±12.0	41.8±6.4	37.1±7.9	43.3±8.1	39.3±9.1
Hip Abduction	-12.0±5.7	-8.1±7.5	-9.5±7.5	-7.5±7.2	-11.3±8.2	-9.0±7.8	-11.0±7.0	-8.2±6.6
Hip Rotation[b]	17.4±4.8	15.9±4.6	17.9±6.1	15.7±5.4	12.2±7.8	9.8±6.9	15.1±5.9	13.0±8.4
Ankle Flexion	2.7±5.5	2.2±6.3	1.2±7.8	0.1±8.0	-1.4±10.8	-0.2±9.0	-3.4±9.1	-0.7±9.2
Peak Knee Abduction Moment								
Knee Flexion[b]	-44.8±6.8	-41.6±8.4	-42.5±4.6	-40.9±6.3	-38.8±7.2	-34.9±6.6	-42.6±5.7	-39.7±6.3
Knee Abduction	1.6±4.6	1.9±3.8	-1.7±3.8	-2.0±3.9	0.0±4.2	-0.4±4.6	-2.2±4.5	-1.4±4.6
Knee Rotation	14.7±5.6	14.4±5.6	14.6±5.9	16.8±5.8	14.8±5.7	15.1±4.8	15.4±3.5	15.7±3.0
Hip Flexion[a]	49.4±11.0	42.5±11.1	47.2±10.0	42.4±12.9	42.0±6.0	37.2±7.7	41.3±7.8	37.6±10.3
Hip Abduction	-14.2±6.0	-10.3±8.3	-12.7±7.8	-10.1±6.4	-12.9±8.6	-9.5±8.3	-13.8±6.7	-10.7±7.0
Hip Rotation[b]	15.9±4.7	11.8±5.7	14.3±4.9	10.7±6.7	9.4±6.4	8.3±5.6	11.8±6.1	8.4±6.5
Ankle Flexion[a]	12.3±6.0	13.0±9.9	12.9±6.0	15.3±5.8	6.6±9.4	5.0±7.4	11.2±7.7	9.8±5.2

Knee flexion, abduction, and external rotation, and hip extension, abduction, and external rotation denoted by negative (-) joint rotations

[a] - significant effect of training

[b] - significant effect of fatigue

HANDGRIP FORCE AND UPPER-LIMB KINETICS DURING HANDCYCLING

Jason Griswold and Kotaro Sasaki

Boise State University, Boise, ID, USA
email: kosasaki@boisestate.edu

INTRODUCTION

Chronic wheelchair users often suffer from poor physical fitness and conditions such as obesity and diabetes, partially due to their sedentary lifestyles [1]. Manual wheelchair users are also frequently inflicted with shoulder injuries and pain [2], which may limit their active involvement in exercise activities using wheelchairs. Handcycling is one of the few well-tolerated exercises [3], and therefore, could become a life-time exercise mode for those individuals. In order to improve handcycling performance (e.g., prolong the exercise duration and increase power), the forces generated in the upper limbs need to be effectively applied to the handgrips to generate crank power. However, only a few studies have measured handgrip forces during handcycling [4]. The lack of handgrip force information also impedes upper-limb kinetic analyses during the exercise. Therefore, the purpose of this study was to investigate how the upper limbs generate joint moments and handgrip forces during handcycling.

METHODS

Six healthy right-handed male subjects (age 23.0 ± 3.3 years old, height 1.81 ± 0.09 m, body mass 75.3 ± 6.8 kg) volunteered to participate in the study. The experimental protocol was approved by the Boise State University institutional review board, and written informed consent was obtained from each subject. The subjects were instructed to perform synchronous handcycling on a racing handcycle (Top End Force, Invacare, Elyria, OH) at a constant cadence of 60 rpm, and at three different crank resistances (50, 70, and 90 watts). The crank resistance was controlled by a bicycle trainer (CompuTrainer, RacerMate, Inc., Seattle, WA) that was attached to the front wheel of the handcycle. The seat position was adjusted such that the subject's elbows were slightly flexed when the handgrips were in the farthest position from the shoulder, and the subject's eye level was slightly above the crank axis. After being accustomed to handcycling and warming up for ten minutes, the subjects performed handcycling for 45 seconds at randomly assigned crank resistance. A three-minute resting period was assigned between trials to minimize fatigue. Because bilateral symmetry was assumed in the synchronous handcycling, all data were collected only from the right upper limb. Kinematic data were collected at 100 Hz for 15 seconds in the middle of the 45-second trial, using a motion capture system (Vicon 460 series with eight cameras, Oxford, UK) and 28 reflective markers attached to the trunk and the right upper limb. Handgrip forces and couples were collected simultaneously at 2000 Hz using a six-axis load cell (MC1, Advanced Mechanical Technology, Inc., Watertown, MA) installed in the right handgrip. Crank angles were computed from the trajectories of six markers attached to the handgrip. Zero-degree crank angle was defined at maximum elbow extension.

The kinematic and force data were low-pass filtered at 6 and 15 Hz, respectively, using second-order zero-lag Butterworth filters. All data were time-normalized to the crank angle, and averaged within and then across subjects. The handgrip forces were decomposed into two components: the force component that contributes to crank power generation (i.e., tangential component to the circular path of the handgrip center), and the component that does not contribute to crank power. Upper-limb joint moments were computed using an upper-limb model [5] that was scaled to each subject in OpenSim [6]. Statistical significance in peak handgrip forces and joint moments was tested using repeated measures ANOVA ($p = 0.05$) with post-hoc Tukey-Kramer multiple comparisons.

RESULTS AND DISCUSSION

The handgrip force that contributed to crank power showed two peaks (Fig. 1a). The first peak was generally greater than the second peak. This indicates that greater crank power is generated during the pulling phase (0-180° crank angles) compared to the pushing phase (180-360° crank angles). These peak forces increased as the resistance increased. In contrast, the peak magnitude of non-contributing handgrip force was statistically unchanged at three crank resistances (Fig. 1b at 0° crank angle).

Joint moments increased in general as crank resistance increased. Elbow flexion moment and elevation plane moment had the largest increase during the pulling and pushing phases, respectively (Fig 2a, b). The peak moments at 90 watts were significantly greater than the corresponding peak moments at 70 and 50 watts. This indicates that the elbow flexors and shoulder flexors (e.g., the anterior deltoid) may contribute to generating crank power during the pulling and pushing phases, respectively.

This pilot study investigated the handgrip forces and upper-limb joint moments during handcycling at different crank resistance. To our knowledge, three-dimensional handcycling grip forces have been analyzed in only one study [4]. The present study showed that the non-contributing handgrip forces were relatively insensitive to the increase in crank resistance. This may indicate that the effectiveness of handgrip forces (e.g., the ratio of contributing- and total handgrip forces) might be greater at higher crank resistance. Further investigation with a larger number of subjects is required to confirm this result. Previous studies of cycling and wheelchair locomotion have suggested that attempting to reduce non-contributing force components does not necessarily increase the efficiency of the motor activities [7, 8]. Therefore, solely focusing on reducing non-contributing handgrip forces might not increase the effectiveness of handcycling. Future studies are planned to investigate the mechanical efficiency in handcycling at a muscular level.

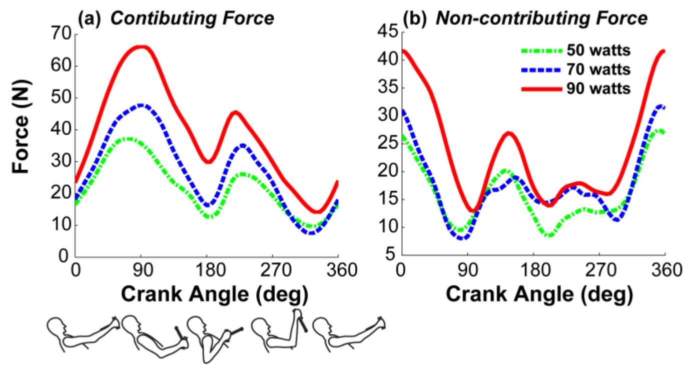

Figure 1: Group-averaged handgrip forces during handcycling at three crank resistances: (a) force component contributing to crank power, (b) non-contributing force component.

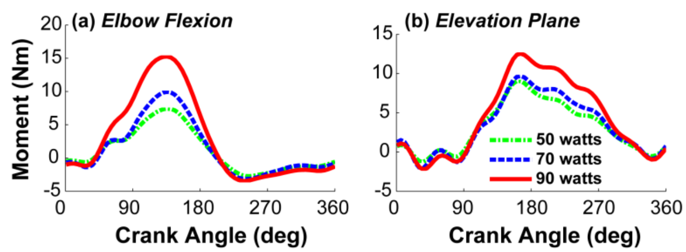

Figure 2: Group-averaged joint moments during handcycling at three crank resistances: (a) elbow flexion, (b) shoulder elevation plane angle.

REFERENCES

1. Bauman WA and Spungen AM. *Metabolism* **43**, 749-756, 1994.
2. Boninger ML, et al. *Arch Phys Med Rehabil* **84**, 1615-1620, 2003.
3. Dyson-Hudson TA, et al. *Arch Phys Med Rehabil* **88**, 1727-1729, 2007.
4. Arnet U, et al. *Med Eng Phys* **34**, 78-84, 2012.
5. Holzbaur KR, et al. *Ann Biomed Eng* **33**, 829-840, 2005.
6. Delp SL, et al. *IEEE Trans Biomed Eng* **54**, 1940-1950, 2007.
7. Kautz SA and Neptune RR. *Exerc Sport Sci Rev* **30**, 159-165, 2002.
8. Bregman DJ, et al. *Clin Biomech* **24**, 13-19, 2009.

ACKNOWLEDGEMENTS
The authors are grateful to Dr. Eric Dugan for lending the bicycle trainer used in this study.

PRIMING THE MOTOR SYSTEM
PASSIVE AND ACTIVE MOVEMENTS INDUCE DISTINCT GABAergic EFFECTS

[1]Albina Guri, [1,2]Manuela Corti and [1,2]Carolynn Patten

[1]University of Florida, Gainesville, FL, USA
[2]Malcom Randall VA Medical Center, Gainesville, FL, USA
email: aguri@ufl.edu

INTRODUCTION

Following stroke, the brain undergoes plastic changes including: diminished neural connectivity within the ipsilesional hemisphere contributing to imbalanced inter-hemispheric inhibition and over-excitability of the contralesional hemisphere. Therapeutic interventions that reduce inter-hemispheric competition may improve motor function and contribute to rehabilitative treatments [3]. Priming by a method knows as Active-Passive Bilateral Activity (APBA) can improve the overall balance of inter-hemisperic inhibition, increasing TCI from AH-to-UH as well as intracortical inhibition (SICI) in the UH [1].

Here we use the Davey technique [2] to investigate activity in cortical inhibitory circuits following passive and voluntary motor activity. According to [2], EMG suppression in response to sub-threshold TMS corresponds to activation of cortical inhibitory interneurons mediated by GABA involved in motor activity.

METHODS

In this UF IRB-01 approved study we used sub-threshold transcranial magnetic stimulation (TMS) [2] to elicit EMG suppression and investigate the effects of passive and resisted movements on corticomotor drive. Four healthy females, aged 18 to 22 years, participated. Sub-threshold TMS (~0.7x MT) was delivered to the contralateral hemisphere during sustained isometric contraction of the first dorsal interosseus (FDI): at rest, following passive, and following active-resisted wrist flexion/extension movements. To determine the persistence of exercise effects on the cortical circuitry, two participants were re-tested following a 10-15 minute rest period

RESULTS AND DISCUSSION

Our data reveal that both passive and active exercises modulate neural inhibition and in many cases produced a marked facilitation. Following passive movement, the magnitude and duration of EMG suppression was markedly increased. Following active-resisted movement, increased EMG suppression was followed by facilitation. This facilitation may be a key phenomenon to improving the efficacy of neurorehabilitation interventions.

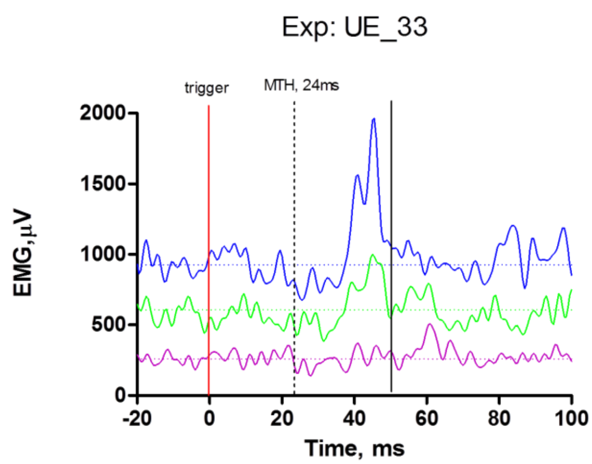

Figure 1: Dotted line corresponds with MEP latency. Subject 33 reveals EMG suppression in the baseline condition (purple line). Following PASSIVE movements (green line), EMG suppression is deeper and followed by a notable facilitation observed at ~50 ms (black cursor). These effects are augmented following ACTIVE, resisted exercise (blue line).

While it is expected that the facilitation induced by active and passive movements diminishes with time, our data in two participants suggest the facilitation persisted 10-15 minutes post-exercise. We intend to conduct more experiments to fully understand the time course of this phenomenon.

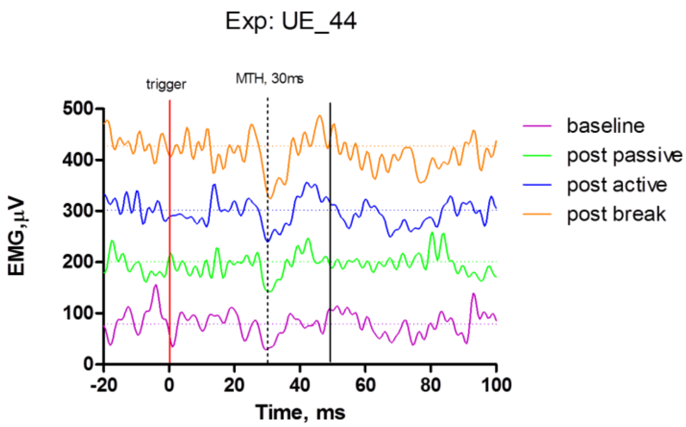

Figures 2: Subject 40 was re-tested 10-15 minutes following post-exercise. Persistent post-exercise facilitation is observed.

There is great interest in identifying adjuvant treatments to partner with traditional rehabilitation. Candidates argued to produce priming effects include: pharmacologic agents (e.g., amphetamine, L-dopa, D-cycloserine), repetitive TMS (rTMS), mental practice, and passive movement (in the form of APBA). It is recognized that exercise produces significant neuromodulatory effects without significant negative side effects. However, the specific mechanisms have not been fully explored.

These data illustrate neural mechanisms involved in activities used for priming and suggest that priming prior to traditional rehabilitation treatment could enhance neural excitation and therefore increase the effectiveness of treatment. Before this method can be applied in stroke rehabilitation more research needs to be done on healthy individuals to determine the magnitude, consistency and persistence of these effects. Further, effects will likely differ in persons post-stroke because the functioning of inhibitory cortical circuits is impaired. Our ongoing work seeks to develop our understanding of this phenomenon.

CONCLUSIONS

EMG suppression, as first described by [2], reflects activation of GABA-mediated cortico-cortico inhibitory interneurons. Because these interneurons are activated by cortical neurons, EMG suppression is used to confirm cortical involvement in the motor task (e.g., corticomotor drive). Consistent with the motor priming hypothesis proposed by [1] enhanced EMG suppression observed following passive movement is consistent with enhanced corticomotor drive. Our data suggest a neural mechanism by movement-related activation and feedback influence the cortical circuitry. These effects will likely differ in persons post-stroke because cortical circuits are impaired. Regardless, both passive and active-resisted movements offer a non-invasive approach to increase cortical excitability, induce 'priming' and potentially enhance treatment efficacy.

REFERENCES

1.Stinear CM, et al. *Brain*, **131**, 1381-1890, 2008
2.Davey NJ, et al. *Journa*l, 1994
3.Dimyan,M.A.,&Cohen, L. G. *Neurorehabilitation and Neural Repair*, **24**(2), 125-135, 2010

ACKNOWLEDGEMENTS

VA RR&D Research Career Scientist (F7823S) (Patten, PI)

MESOZOIC SPEED DEMONS: FLIGHT PERFORMANCE OF ANUROGNATHID PTEROSAURS

Michael Habib, Justin Hall

University of Southern California, Los Angeles, CA, USA
email: biologyinmotion@gmail.com web: http://www.pterosaur.net

INTRODUCTION

High performance flying animals, such as those that rapidly chase flying insects at high levels of maneuverability, are useful models for the biologically inspired design of micro-air vehicles. They also present intriguing test cases for understanding the limits of musculoskeletal system performance. Modern examples of such animals include small, fast-flying birds like swifts, as well as many insectivorous bats. It has been previously suggested that a specific group of pterosaurs, the anurognathids, might also have been high performance insectivores [1]. If this hypothesis can be supported in a quantitative context, then anurognathid anatomy could provide an additional, unique morphological solution to the problem of highly maneuvered, pursuit flight.

Here, we utilize metrics known to predict general mechanical load capacity in living flyers to test the hypothesis that anurognathids were high performance pursuit insectivores. We find strong support for this hypothesis, and further provide a methodology that should be generally applicable to reconstructing performance in many extinct flying animals. In this manner, we utilize anurognathids as a case study for the application of biomechanical principles to extinct flyers.

METHODS

The avian comparative dataset comprises a total of 239 individuals representing 36 species. The bat dataset comprises 50 individuals representing 23 species. All specimens were received on loan from the Smithsonian Museum of Natural History in Washington, DC. The humerus and femur were taken from one side of each specimen (left and right sides were chosen randomly). Specimens were chosen based on completeness and condition of long bone elements. Both females and males were used for each species, though the specimens were chosen at random with respect to sex. We utilized peripheral quantitative computed tomography (pQCT) scans at the midshaft of each humerus and femur to obtain cross-sectional images and geometric data for cross sections. Our methodology for estimating geometric resistance to bending in the limb bones of the avian comparisons and *Anurognathus* has been used with success for comparing fossil and living species previously [2,3].

Measurements of external breadths and cortical thickness were taken using CT imaging of birds from the Smithsonian's National Museum of Natural History (NMNH) in Washington, DC. Measurements of external breadths and cortical thickness were taken manually for *Anurognathus* at the Bavarian State Palaeontological Collection (BSPG) in Munich, Germany (cortical breadth was measured from broken elements). Two specimens of *Anurognathus* were made available for study at BSPG in 2007. Other pterosaurs, used for comparison, were measured at the Smithsonian's National Museum of Natural History (NMNH) in Washington, DC, the Texas Memorial Museum (TMM) in Austin, TX, and the Bavarian State Palaeontological Collection (BSPG) in Munich, Germany. To calculate the polar section modulus for a hollow section that closely approaches a true ellipse, the polar second moment of area (J) was calculated for both the outer and inner diameters using:

$$J=0.25\pi(b^4a/b+a^4b/a)$$

The inner diameter value (medullary cavity J) is then subtracted from the total, solid section value of J. We then calculated the final value of Zp as cortical J/average radius of section (in the x and y planes).

RESULTS AND DISCUSSION

Compared to most birds and other pterosaurs, the section modulus of the humeri in *Anurognathus* are greatly elevated (Figure 1).

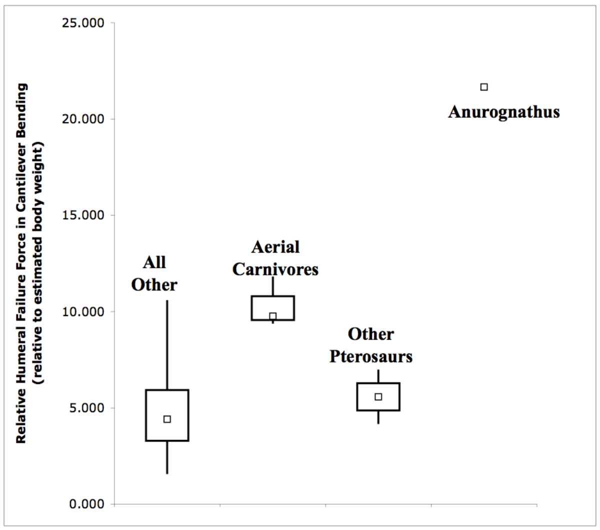

Figure 1: Humeral section modulus of *Anurognathus* compared to other pterosaurs, as well as a sample of modern birds. "All other" represents birds that are not aerial carnivores.

A strong pattern was also found when humeral diameters were compared across birds, bats, and anurognathid pterosaurs: known pursuit insectivores and anurognathids all have similar, and comparatively large, humeral diameters when compared by use of a General Linear Model with post-hoc Tukey tests.

The extreme strength in bending of the *Anurognathus* humerus implies that hunting on the wing was important. The proportions of humeral diameter in *Anurognathus*, relative to total body size, are particularly indicative of a high-performance aerial hawker, being especially similar to those of swiftlets and vespertilionid bats (e.g. *Lasiurus*). However, we also found that the hindlimb was relatively robust. This 'balanced' geometric strength (i.e. both forelimb and hindlimb elements are robust relative to body size) might be indicative of an ecology that included powerful ground movement

There are no extant flyers known to be adapted to both powerful ground motion and extensive aerial hawking, but we see no reason to expect that pterosaur ecologies would necessarily conform exactly to living ecotypes. The limb length proportions in anurognathids are somewhat similar to those of *Desmodus*, which launches at a relatively steep angle. Combined with the observation that *Anurognathus* possessed robust forelimb and hindlimb elements, along with expanded space for proximal limb musculature we suggest that climb out would have been particularly rapid and steep.

CONCLUSIONS

Fossil species present unique challenges in comparative biomechanics because they are unavoidably poorly known relative to living animals. However, because the vast majority of all species that have lived on Earth are extinct, the fossil record may be able to provide a wealth of information on previously unrecognized evolutionary solutions to biomechanical problems. Anurognathid pterosaurs are a strong example of an extinct group whose morphology appears to carry useful information for understanding the limits of performance in animal locomotion.

REFERENCES

1. Bennett SC. *Paläontologische Zeitschrift,* 81: 376-398, 2007.
2. Habib M. *Zitteliana*. B28: 161-168, 2008
3. Witton M, Habib M. *PLoS ONE*. 5(11): e13982

ACKNOWLEDGEMENTS

We wish to thank the Jurassic Foundation for graciously funding this research project. Our thanks also go to Mark Witton for ongoing collaboration and assistance with anurognathid biology.

Effects of Volitional Preemptive Abdominal Contraction on Trunk and Lower Extremity Biomechanics and Neuromuscular Control During a Drop Vertical Jump

R. Haddas, T. Hooper, P. Sizer, C.R. James

Texas Tech University Health Sciences Center, Lubbock, TX, USA
email: r.haddas@ttuhsc.edu

INTRODUCTION

Anterior cruciate ligament (ACL) injuries continue to be a significant concern relative to short- and long-term effects on quality of life and participation in physical activity [1]. Recognizing individuals who have an increased risk for ACL injury and discovering interventions that may reduce their risk are important to patients, clinicians, and researchers. Altered neuromuscular control plays a prominent role in most ACL injury models. Previous research has focused primarily on examining the neuromuscular control of the lower extremity (LE) [2]. However, LE control also may be influenced by activation of the abdominal muscles [3]. The effects of abdominal muscle contraction may be transmitted to the LE via the pelvis, which provides a mechanical link between the trunk and the LE thus influencing the entire chain [4]. Although, volitional preemptive abdominal contraction (VPAC) has been shown to improve spine stability [5], very little is known about the effects of VPAC on trunk and LE biomechanics and neuromuscular control in healthy individuals, with implications for ACL injury risk. Therefore, the purpose of our study was to determine the effects of VPAC on trunk and LE biomechanics and neuromuscular control during a drop vertical jump (DVJ). We hypothesized that VPAC, would improve trunk and LE stabilization and neuromuscular control during the landing phase of the DVJ.

METHODS

A repeated measures design was used to examine the effects of VPAC using an abdominal bracing strategy [5] on biomechanical and neuromuscular control variables measured during a DVJ from two heights. Thirty two healthy and active subjects (17 men and 15 women; M±SD age 24.6±2.4 yr, height 1.76±0.12 m, and mass 77.6±19.0 kg) participated after providing informed consent. Volunteers were excluded if they had LE pain, history of LE or lumbar spine surgery, active abdominal or gastrointestinal condition, or if pregnant. Subjects were taught and allowed to practice VPAC. The presence of VPAC during the DVJ was verified by a review of the recorded electromyographic (EMG) data immediately after each trial. Eighteen reflective markers were placed on the LE and trunk. Surface EMG electrodes were placed over eight muscles on the right side LE and trunk. Each subject performed three successful DVJs from a raised platform from each of two heights (30 and 50 cm) with and without VPAC, presented in a random order. 3D kinematic data were recorded using an 8 camera Vicon-Peak system (120 Hz), while ground reaction force (GRF; Bertec Corp.) and EMG (Noraxon, Inc.) were recorded simultaneously (1200 Hz). Data were pre-processed using Motus (Vicon-Peak), exported and reduced using custom laboratory algorithms developed in Matlab (Mathworks). Dependent variables included trunk, hip, knee and ankle joint angles, and internal joint moments in 3D, sagittal plane LE joint powers, EMG root mean square (RMS) amplitudes pre- and post-initial ground contact. A total of 96 independent variables were incorporated in an exploratory analysis. Kinematic maxima, minima, range of motion and values at initial contact, kinetic maxima, minima and impulse, and the pre- and post-contact EMG RMS values were analyzed statistically (SPSS; $\alpha=0.05$).

RESULTS AND DISCUSSION

At the 30 cm landing height, VPAC resulted in statistically significant ($P \leq 0.05$) greater knee internal rotation angle, greater knee flexion range of motion, greater knee internal abduction moment, greater knee energy absorption, greater medial hamstring post contact activity, greater trunk left rotation, and greater external oblique activity pre- and post-contact (Table 1).

At the 50 cm landing height, VPAC resulted in statistically significant ($P \leq 0.05$) less ankle inversion angle, greater knee flexion angle at contact, greater medial hamstring activity pre- and post-contact, greater hip flexion angle at contact, less hip energy absorption, greater trunk left rotation angle post contact, greater trunk left rotation angle at contact, greater external oblique muscle activity pre-contact, and less external oblique muscle activity post-contact (Table 2).

CONCLUSIONS

VPAC altered LE and trunk biomechanics and neuromuscular control when performing DVJ from 30 and 50 cm heights, although not all changes were consistent with greater knee protection. More potential clinical advantages were observed at the lower height, where increased medial hamstring activity, knee flexion and knee energy absorption during VPAC suggest an enhanced protective LE response. Similarly, VPAC triggered increased external oblique activity that may indicate enhanced trunk stability under lower loading conditions, when more neuromuscular control options are available. The demands of the 50 cm DVJ may have superseded the effectiveness of VPAC. Similarly, competing neuromuscular control requirements (trunk vs. LE) may have resulted in less attention to the abdominal contraction, and greater attention to the task at the higher height. Further study is needed to determine whether VPAC is effective for reducing ACL injury risk. The effects of VPAC on pelvis motion and relative motion among spinal segments should be examined as well.

REFERENCES

1. Arendt E, et al. Am J Sports Med **23**, 694-701, 1995.
2. Hewett TE, et al. Instr Course Lect **56**, 397-406, 2007.
3. Hodges PW, et el. Ergonomics **40**, 1220-1230, 1997.
4. Duval K, et al. Gait Posture **32**, 637-640, 2010.
5. Stanton T, et al. Spine **33**, 694-701, 2008.

ACKNOWLEDGMENTS

Graduate students Lee Atkins, Natalie Burg, Nathan Jarman, Vittal Nagar.

Table 1: Mean (SD) values for 30 cm drop vertical jump with and without VPAC (statistically significant variables only).

	Knee					**Trunk**		
Condition	Internal rotation (deg)	Flexion (deg)	Internal abduction moment (Nm)	Energy absorption (W)	Medial hamstring post contact (mV)	Left rotation (deg)	External oblique pre contact (mV)	External oblique post contact (mV)
VPAC	33.7 (13.6)	44.9 (13.7)	15.4 (6.4)	37.3 (69.0)	0.000392 (0.000273)	0.34 (0. 15)	0.000201 (0.000123)	0.000199 (0.000117)
Without VPAC	31.0 (10.9)	40.9 (12.5)	15.0 (6.6)	29.7 (64.1)	0.000343 (0.000239)	0. 28 (0.16)	0.000165 (0.000133)	0.000169 (0.0000968)

Table 2: Mean (SD) values for 50 cm drop vertical jump with and without VPAC (statistically significant variables only).

	Ankle	**Knee**			**Hip**		**Trunk**			
Condition	Inversion (deg)	Flexion at contact (deg)	Medial hamstring pre contact (mV)	Medial hamstring post Contact (mV)	Flexion at contact (deg)	Energy absorption (W)	Left rotation at contact (deg)	Left rotation post contact (deg)	External oblique pre contact (mV)	External oblique post contact (mV)
VPAC	9.9 (8.9)	19.1 (7.9)	0.000219 (0.000163)	0.000334 (0.000274)	27.2 (6.8)	277.6 (253.6)	1.29 (0.08)	1.29 (0.08)	0.000231 (0.000138)	0.000177 (0.000101)
Without VPAC	14.2 (8.1)	16.5 (8.0)	0.000164 (0.000112)	0.000311 (0.000301)	25.4 (7.2)	301.6 (254.3)	1.25 (0.13)	1.26 (0.11)	0.000197 (0.000119)	0.000209 (0.000113)

CORRELATIONS BETWEEN RUNNING CADENCE AND KINEMATICS

[1]Jocelyn F. Hafer, [2]Allison M. Brown, [1]Howard J. Hillstrom

[1]Hospital for Special Surgery, New York, NY, USA
[2]University of Medicine and Dentistry of New Jersey, Newark, NJ, USA
email: haferj@hss.edu

INTRODUCTION

Certain lower extremity kinematics have been shown to be related to injury in runners. An extended knee and increased angle of the tibia with respect to vertical at initial contact have been associated with running injury, especially tibial stress fractures [1, 2]. Additionally, "overstriding" has been shown to increase loads during running [1, 3]. Cadence retraining has become a popular intervention for the reduction of potentially injurious kinematics (such as those mentioned above) and treatment or prevention of running injury. It has been shown that increasing cadence in runners with patellofemoral pain decreases both pain and the horizontal distance of heel strike in front of the body (an estimate of overstriding) [4]. While a cadence of 90 strides/minute is often anecdotally deemed optimal, it is not known if this value should be applied to all runners or if runners respond differently to cadence alterations. One cadence may not produce the same kinematic pattern across all runners. The purpose of this study was to determine if kinematics that have been tied to overuse injuries are correlated with cadence in healthy runners. The authors hypothesize that cadence will be positively correlated with knee flexion (KF) at initial contact and negatively correlated with heel strike distance (HSD) and tibial angle with respect to vertical (TA) at initial contact. Additionally, increased KF should correlate with decreased TA (and vice versa) and increased HSD should correlate with decreased KF and increased TA.

METHODS

This study included 20 healthy female runners. All were rearfoot strikers who had been injury free for at least 6 months prior to data collection.

Participants ran on a treadmill at their self-selected speed. 30 seconds of 3D motion capture data were collected after a 3 minute warm-up period. Cadence was calculated as twice the number of right heel strikes in the 30-second period. Right-sided KF, TA, and HSD were calculated at initial contact. HSD was defined as the horizontal sagittal-plane distance between a virtual mid-malleolar point and the center of the pelvis. Bivariate Pearson correlations were calculated between all variables with significance set at $p<0.05$.

RESULTS AND DISCUSSION

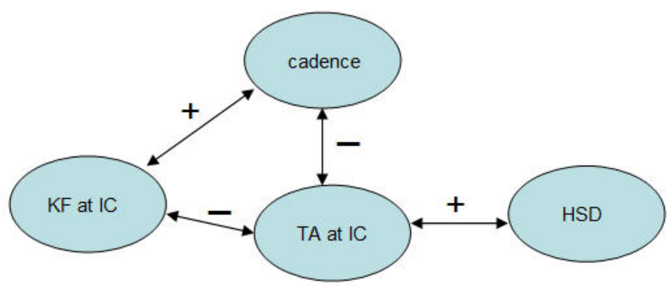

Figure 1: Correlation directions between variables. Only significant correlations are displayed.

KF was positively correlated with cadence (r=0.64, p=0.002). HSD (r=0.08, p=0.73) and TA (r=-0.16, p=0.5) showed no correlation with cadence.

TA was correlated with both KF (r=-0.59, p=0.006) and HSD (r=0.76, p=0.000). See Table 1 below for correlation table.

While there is a positive correlation between cadence and KF, there is no correlation between cadence and TA or HSD. TA correlations with KF and HSD are in expected directions from previous literature.

CONCLUSIONS

Despite the lack of correlation between cadence and TA or KF, the TA correlations with KF and HSD suggest there may be another parameter that would more clearly describe the relationship between cadence and risky kinematic variables. Future research should examine more proximal kinematics such as pelvic tilt and rotation, trunk lean, and hip flexion in relation to cadence. These variables may influence the relationship between pelvis and foot positioning and may more closely represent variations in running styles.

Additionally, the range of kinematic values in these runners may not have reached potentially injurious levels. Injured runners may display different correlations in these parameters.

When looking at healthy runners at a single time point, the relationship between cadence and potentially injurious kinematics is unclear. A "less than optimal" cadence may not directly cause potentially injurious kinematics.

REFERENCES

1. Hamill J, et al. *Hum Movement Sci*, **14**, 45-60, 1995.
2. Heiderscheit BC, et al. *Med Sci Sport Exer*, **43**(2) 296-302, 2011.
3. Derrick TR, *Med Sci Sport Exer*, **36**(5) 832-837, 2004.
4. Heiderscheit BC, *CSM Proceedings*, San Diego, CA, 2010.

Table 1: Pearson correlation coefficients. * indicates $p<0.05$.

	Cadence	KF	TA	HSD
Cadence	1			
KF	0.64*	1		
TA	-0.16	-0.59*	1	
HSD	0.082	-0.11	0.76*	1

SLOW UPHILL WALKING: BETTER FOR THE KNEES OF OBESE ADULTS?

Derek J. Haight, Michelle M. Reynolds, Wayne J. Board, Trevor Connor, Raymond C. Browning

Colorado State University, Fort Collins, CO, USA
Email: Derek.Haight@Colostate.edu, Web: http://pal.colostate.edu

INTRODUCTION

Obese individuals need physical activity options that expend energy while reducing the risk of acute or chronic musculoskeletal injuries. While walking is a common physical activity recommendation for obese adults, net muscle moments (NMMs), a proxy measure for joint loading, increase with walking speed [1]. Walking at a relatively slow speed up a moderate grade may be an alternative form of exercise that maintains exercise intensity while reducing joint loads [2]. NMMs may give inaccurate indications of load during movements where significant muscle co-activation occurs (e.g. uphill walking), but musculoskeletal models (OpenSim) can be used to estimate these loads [3]. The purpose of this study was to quantify knee joint contact forces (JCFs) in obese (OB) and non-obese (NO) adults during fast, level and slow, uphill walking. We hypothesized that absolute JCFs would be greater in obese and would decrease during uphill vs. level walking.

METHODS

We collected kinematic and kinetic data as 10 OB subjects (mass=94.9(11.7)kg, BMI=34(4.3)kg·m^{-2}) and 10 NO subjects (mass=67.2(12.0) kg,BMI= 21.2(2.1) kg·m^{-2}) walked on a dual-belt force-measuring treadmill (Bertec) at speed/grade combinations of 1.50 m·s^{-1}/0 deg and 0.75 m·s^{-1}/6 deg. We used a modified Helen Hayes marker set to identify anatomical landmarks and define lower extremity segments for the NO subjects. For OB subjects, we used a more extensive marker set, including digitized ASIS and iliac crest markers, to help account for excess adipose tissue. Kinematic data was collecting using a 10-camera motion capture system (Vicon) recording at 100 Hz. Force data was collected at 1000 Hz.

We scaled a three-dimensional OpenSim musculoskeletal model with 23 degrees of freedom (DOF) and 92 individual muscle actuators to each subject. The knee joint was modeled as a single DOF hinge joint with anterior–posterior (AP) translation as a function of flexion and extension. We used OpenSim [3] to calculate sagittal NMMs and individual muscle forces using inverse dynamics and static optimization, respectively, for five gait cycles per subject at each speed/grade combination. We determined each JCF in the tibial reference frame from the vector sum of the joint reaction force and the individual muscle forces crossing the knee joint.

We used two-factor ANOVAs with repeated measures to determine how obesity and speed/grade affected peak knee NMMs and JCFs. We performed necessary post-hoc comparisons using the Holm-Sidak method.

RESULTS AND DISCUSSION

As hypothesized, knee JCFs were much greater in OB compared to NO individuals (Fig 1). When participants walked uphill at the slower speed, JCFs were reduced during weight acceptance but not late stance. When normalized to BW, peak axial knee JCFs were not significantly different between level and uphill walking in both OB and NO groups (Fig. 2). Peak AP knee JCFs during early stance were similar across groups and speed/grade combinations (Fig 2).

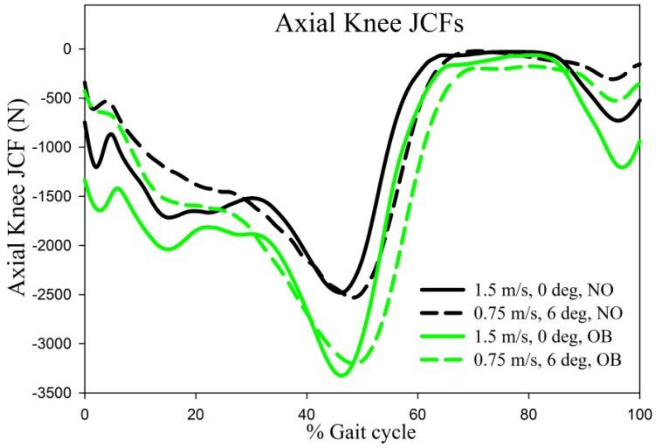

Figure 2: Absolute Axial Knee JCFs

Our results suggest that while the absolute knee joint loads are certainly greater in obese adults, these individuals walk in a way that reduces the loads, particularly during early stance. One possible explanation is that obese walk with a straighter leg, but we did not find this in our data. Another possibility is that these individuals are using their hip to provide support during this phase of the gait cycle. It must be noted however, that it is likely that the magnitude of the load, combined with the medial distribution of this load, is the mechanical contributor to knee joint pathology in obese adults.

The finding that early stance knee joint loads were reduced when individuals walked uphill at a slower speed suggests that this walking speed/grade may be an effective physical activity prescription for obese individuals. While the axial knee joint loading was reduced, the rate at which this load is applied is also significantly reduced compared to level walking because of longer stance times due to the slow speed.

An important secondary finding from our study is the relatively poor relationship between the peak NMM at the knee and the JCF. While peak extensor NMM decreased by 69% during uphill vs. level walking, JCF decreased by a more modest 30%. This suggests caution should be used when estimating joint loading via NMMs.

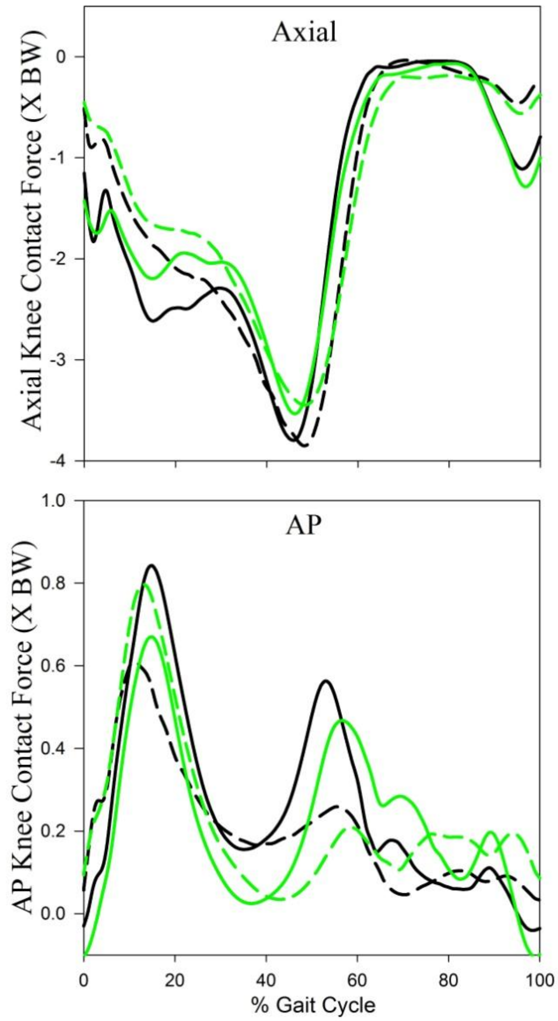

Figure 3: Normalized Axial and AP Knee JCFs

CONCLUSIONS

Obese individuals appear to adopt a gait that reduces knee joint loads during early-mid stance. Slow uphill walking may be an effective way to reduce early-stance knee joint loading in an obese population while maintaining aerobic intensity

ACKNOWLEDGEMENTS

This research was supported by a grant from the CSU College of Applied Human Sciences and NIH Grant R03AR059264.

REFERENCES

1. Browning, R.C. et al. MSSE **33**, 1632-1641, 2007.
2. Ehlen, K.A. et al. MSSE **43,** 1251-1259, 2011.
3. Delp, S.L. et al. *IEEE Trans Biom Eng.* **54,** 1940-1950, 2007

MOTIONS OF THE THUMB CARPOMETACARPAL (CMC) JOINT ARE COUPLED DURING THE INITIATION OF THREE FUNCTIONAL TASKS

[1]Eni Halilaj, [1]Michael J. Rainbow, [1]Christopher Got, [1]Joel B. Schwartz, [2]Amy Ladd, [1]Arnold-Peter C. Weiss, [1]Douglas C. Moore, [1]J.J. Crisco

[1]Department of Orthopaedics, Warren Alpert Medical School of Brown University, Providence, RI
[2]Stanford School of Medicine, Palo Alto, CA
email: Joseph_Crisco@brown.edu

INTRODUCTION

Evolution of the thumb carpometacarpal (CMC) joint has highly enhanced human dexterity, as much of the thumb's mobility and wide range of motion are due to the saddle geometry of the trapezio-metacarpal articulation. Functionality of the thumb CMC joint is commonly hindered by osteoarthritis – a critical condition that necessitates the study of normal and pathological CMC biomechanics. Currently there is little data on *in vivo* thumb CMC motion. Therefore, the purpose of this study was to evaluate *in vivo* motion of the first metacarpal (MC1) with respect to the trapezium (TPM), in a healthy population, as the hand is moved from neutral to three functional tasks: jar grasp, key pinch, and jar twist.

METHODS

24 volunteers, 12 males (age 38.7±11.7 yrs.) and 12 females (age 43.2±15.8 yrs.) were CT scanned with their dominant wrist in neutral, jar grasp, key pinch, and jar twist positions. To standardize wrist positioning across subjects, an adjustable wrist and thumb splint was used for the neutral scan and custom-designed polycarbonate mechanical jigs were used for the functional tasks (Fig. 1).

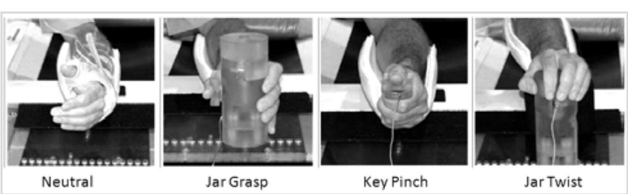

Figure 1: Experimental set-up for the neutral pose and the three functional tasks during CT image volume acquisition.

CT volume images were generated with a 16-slice clinical CT scanner (General Electric, Milwaukee, WI) at tube settings of 80kVp and 80mA, slice thickness of 0.625mm, and in-plane resolution of ~0.3mm x 0.3mm. Wrist bones were manually segmented from the neutral position CT volumes using Mimics software (Materialise, Leuven, Belgium) and 3-D bone models were exported as meshed surfaces. Bone kinematics for the three functional positions were obtained with an established markerless bone registration algorithm. Anatomical coordinate systems were constructed for the trapezium (TPM) and first metacarpal (MC1) by using the principal curvature directions of the saddle shaped articulating surfaces as guiding features. MC1 posture with respect to the TPM was expressed in terms of a joint coordinate system (JCS; Fig. 2), after Grood and Suntay. Motion from the neutral position to the functional positions was defined as the difference in MC1 posture. CMC flexion/extension was defined as rotation about the anatomically-defined radial-ulnar axis (X), while abduction/adduction was defined as rotation about the dorsal-volar axis (Z) and internal-external rotation was defined as rotation about an axis that is perpendicular to the other two axes (Y).

Linear regression analysis was used to evaluate the relationships between flexion/extension, abduction/adduction, and internal/external rotation of the MC1 with respect to the TPM for each of the three tasks (SigmaPlot, Systat Software, Inc., CA).

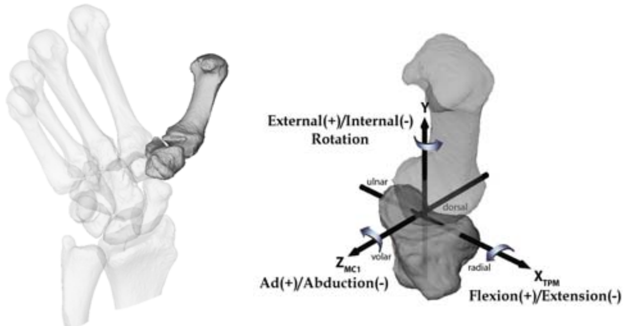

Figure 2: Volar view of the right wrist and the thumb CMC joint (*left*) and the joint coordinate system (JCS, *right*), where flexion/extension occurs around the X-axis, ab/adduction occurs around the Z-axis, and internal/external rotation around the Y-axis.

RESULTS

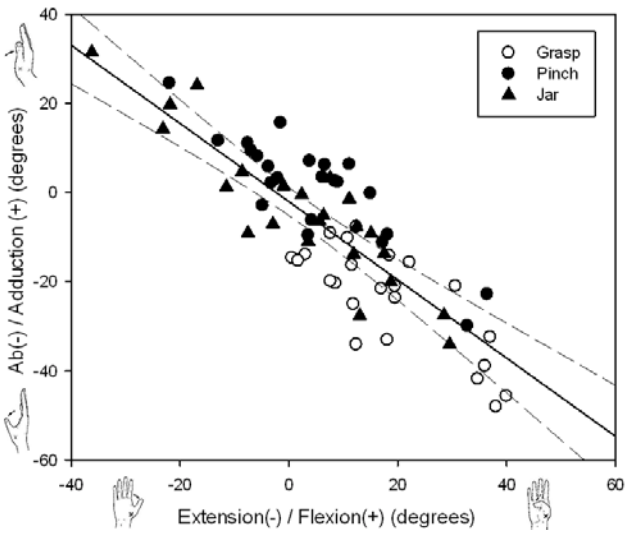

Figure 3: Flexion was significantly coupled with abduction, and extension was significantly coupled with adduction, for CMC motion from the neutral position to all three tasks ([0,0] represents posture of the thumb in neutral position).

Motion of the thumb from neutral to key pinch and jar twist was accomplished with MC1 extension, adduction, and external rotation or with MC1 flexion, abduction, and internal rotation, while grasp was accomplished with MC1 flexion, abduction and internal rotation only (Fig. 3). The three rotational components of MC1 motion were significantly coupled. The strongest coupling occurred between flexion/extension and abduction/adduction, where, for all three tasks, 10 degrees of flexion/extension were accompanied by nearly 10 degrees of ab/adduction ($p<0.0001$, $R^2 = 0.74$; Fig. 3). Internal/external rotation correlated with both flexion/extension and ab/adduction ($p<0.0001$, $R^2 = 0.46$).

DISCUSSION

The study sought to determine whether there were specific patterns of rotational motion of the CMC joint that occurred with positioning of the thumb for three functional tasks. We found that when the hand was moved from the neutral position to a key pinch, jar grasp, or jar twist position, the three rotational components of MC1 motion were significantly correlated, even though the final positions were substantially different. Given the anatomy of the thumb CMC joint, this coupling is less likely to reflect bony constraints and more likely to reflect a “functional coupling” at the level of the neuromuscular system. While our results must be viewed in the context of our experimental design, which might have constrained CMC motion, they generally agree with findings from a previous marker based motion tracking study that measured the operational workspace of the thumb, reporting coupled flexion/extension and ab/adduction at the CMC joint[3].

CONCLUSIONS

This study provides insights into the *in vivo* biomechanics of the thumb CMC joint that should increase our fundamental understanding of this complex joint and lead to improved diagnosis and treatment of OA, which is highly prevalent at this joint.

ACKNOWLEDGEMENT

Funded by American Foundation for Surgery of the Hand (AFSH) and NIH AR059185.

CHANGES IN *IN VIVO* KNEE CONTACT FORCE THROUGH GAIT MODIFICATION

[1]Allison L. Hall, [2]Thor F. Besier, [3]Amy Silder, [3]Scott L. Delp,
[4]Darryl D. D'Lima, [1]Benjamin J. Fregly

[1]Department of Mechanical & Aerospace Engineering, University of Florida, Gainesville, FL, USA
[2]Auckland Bioengineering Institute, University of Auckland, Auckland, New Zealand
[3]Departments of Bioengineering, Mechanical Engineering and Orthopaedic Surgery, Stanford University, Stanford, CA, USA
[4]Shiley Center for Orthopaedic Research & Education, Scripps Clinic, La Jolla, CA, USA
email: allisonlhall@ufl.edu, web: http://www.mae.ufl.edu/~fregly/

INTRODUCTION

Gait modification represents a non-invasive method for reducing knee joint loading in patients with knee osteoarthritis. Previous studies have shown that a variety of gait modifications are effective in reducing the external knee adduction moment [e.g., 1-3]. The external knee adduction moment is often used as a surrogate measure of medial compartment force. However, a recent study showed that reductions in the external knee adduction moment do not guarantee reductions in medial compartment loads [4]. Therefore, direct measurement of changes in knee contact force is important for determining the effectiveness of gait modifications. A previous study found that medial thrust gait and walking with hiking poles reduced contact force in a patient with a force-measuring knee replacement [5]. The purpose of this study was to investigate the effects of additional gait modifications (mild crouch, moderate crouch, forefoot strike and bouncy gait) and four configurations of hiking poles on medial and lateral contact forces measured by a force-measuring knee replacement.

METHODS

Experimental data were collected from one patient implanted with a force-measuring knee replacement (male, right knee, age: 88 years, mass: 64.8 kg) [6]. Institutional review board approval and informed consent were obtained prior to testing. Internal knee contact force data were recorded from a custom force-measuring implant [7] and external ground reaction force data were recorded from three force plates (Bertec Corp., Columbus, OH). Data were simultaneously collected while the patient performed five trials of ten different overground gait patterns: normal, mild crouch, moderate crouch, medial thrust, forefoot strike, bouncy, and four hiking pole configurations (combinations of short and long poles with normal and wide pole placement). The patient was given verbal instruction and allowed time to learn each gait modification.

Medial and lateral contact force data were calculated from the implant's force transducer data using a previously validated regression equation developed for the patient's implant [8]. Medial and lateral contact force at 25%, 50%, and 75% of stance phase, and the average value over all of stance phase (0-100%) were averaged across 10 stance phases for each gait modification. Changes in contact force for the modified gaits relative to normal gait were determined by a Kruskal-Wallis test. When significant ($p < 0.05$) differences were found in the Kruskal-Wallis test, pairwise comparisons using a Tukey's Honestly Significant Difference correction were performed.

RESULTS AND DISCUSSION

Walking with hiking poles was the most effective gait modification for reducing *in vivo* contact force, consistent with a previous study [5]. Medial and lateral contact forces were significantly reduced at 50% and 75% of stance phase and over all of stance phase (0-100%) for walking with hiking poles (Table 1). Walking with long hiking poles and wide pole placement was the most effective configuration for reducing contact forces (Table 1). Walking with hiking poles has been suggested to reduce knee contact force by transferring some of the vertical ground reaction force through the hiking pole [5] and by reducing the external knee adduction moment [4]. Post-hoc statistical testing showed that the vertical ground reaction force was significantly reduced compared to normal gait at 75% of stance phase for walking with long hiking poles and normal and wide pole placement and short hiking poles with wide pole placement. Thus, these results suggest that walking with hiking poles is effective in offloading the knee joint by reducing medial and lateral contact force during stance phase.

Both mild and moderate crouch gait modifications significantly reduced lateral contact force at times during stance phase (Table 1). However, the knee contact force was transferred from the lateral to the medial compartment, as medial contact force was increased during the crouch gait modifications (Table 1). These results suggest that patients who exhibit crouch gait may transfer knee joint loads from the lateral to the medial compartment and may be at increased risk for developing medial compartment knee osteoarthritis.

No other gait modifications were found to significantly reduce *in vivo* contact forces during stance phase (Table 1). In particular, no gait modification was effective at reducing contact force at 25% of stance. In a previous study, medial contact force was reduced in early stance when walking with hiking poles [5]. However, in this study, none of the hiking pole gaits were effective in reducing contact force in early stance. A post-hoc analysis revealed that hiking pole contact with the ground was delayed after heel strike for all hiking pole configurations, reducing the effectiveness of the hiking poles in early stance. With additional practice, patients may be able to reduce the delay in hiking pole contact and may be able to reduce contact force in early stance.

CONCLUSIONS

Walking with hiking poles was found to be the most effective gait modification for reducing medial and lateral contact force during stance. An optimal configuration of hiking pole gait (long hiking poles and wide pole placement) reduced medial and lateral contact force over the stance phase by 18% and 14%, respectively. Patients with knee osteoarthritis may consider walking with hiking poles to reduce knee joint loading and minimize further damage to the articular surfaces of the knee.

REFERENCES

1. Guo M, et al. *Gait Posture* **26**, 436-41, 2007.
2. Mundermann A, et al. *J Biomech* **41**, 165-70, 2008.
3. Fregly BJ, et al. *IEEE Trans Biomed Eng* **54**, 1687-95, 2007.
4. Walter JP, et al. *J Orthop Res* **28**, 1348-54, 2010.
5. Fregly BJ, et al. *J Orthop Res* **27**, 1016-21, 2009.
6. Fregly BJ, et al. *J Orthop Res* **30**, 503-13, 2012.
7. D'Lima DD, et al. *J Biomech* **38**, 299-304, 2005.
8. Zhao D, et al. *J Orthop Res* **25**, 789-97, 2007.

ACKNOWLEDGMENTS

This study was funded by NIH grants R01EB009351 and R21HD053490.

Table 1: Percent difference values calculated for each gait modification relative to normal gait. Bold values indicate statistically significant differences from normal gait.

	Medial Contact Force				**Lateral Contact Force**			
Gait Modification	25%	50%	75%	0-100%	25%	50%	75%	0-100%
Mild Crouch	14	-2	-6	4	**-23**	-15	-16	**-12**
Moderate Crouch	-1	18	5	13	-11	-11	**-29**	-9
Medial Thrust	-14	-4	-1	-4	-11	-8	-12	-10
Forefoot Strike	-9	-1	-4	1	-1	9	-17	-8
Bouncy	4	7	-9	3	4	14	**-36**	-11
Poles – Short, Normal	-3	-14	-14	-8	-7	-14	-13	-7
Poles – Long, Normal	-6	-17	-18	-13	-14	-13	-6	-6
Poles – Short, Wide	2	-15	**-21**	-8	-3	-17	**-19**	-9
Poles – Long, Wide	-5	**-28**	**-34**	**-18**	-13	**-26**	**-23**	**-14**

HINDWING FUNCTION IN FOUR-WINGED FEATHERED DINOSAURS

[1,2] Justin T. Hall, [1,2] Michael B. Habib, [4] David W. E. Hone and [2] Luis M. Chiappe

[1] University of Southern California, Los Angeles, CA, USA
[2] Natural History Museum of Los Angeles County, Los Angeles, CA, USA
[3] Chatham University, Pittsburgh, PA, USA
[4] University College Dublin, Dublin, Ireland

email: halljt@usc.edu

INTRODUCTION

The evolution of powered flight in birds remains a contentious issue in vertebrate paleontology. The diminutive predatory dinosaur *Microraptor gui* preserves evidence of extensive, lift-generating feathers on each manus and forearm, but also preserves evidence of lift-generating feathers associated with the hindlimbs, effectively forming a pair of “hindwings”.

Phylogenetic analyses consistently place *M. gui* among Dromaeosauridae and thus close to the origin of birds. Combined with anatomical and functional studies, this indicates that flight evolved at least once within the lineage originating with the common ancestor of birds and dromaeosaurids. Thus, flight performance in *M. gui* may represent an ancestral four-winged stage in avian flight evolution. Alternatively, the evolution of flight may not have represented a single monophyletic event and there could be multiple abandoned body plans attempting to solve flight performance issues. Under such a case, *M. gui* may represent an alternative solution to aerodynamic issues experienced by early flying theropods.

Prior authors modeled the hindlimb of *M. gui* in a strongly abducted four-winged gliding position [1-3] that may require an anatomically implausible orientation of the hip socket [4]. We suggest an alternative model in which the hindwings were generally held below the body during steady flight, but deployed unilaterally, or bilaterally, to produce additional roll and yaw during unsteady flight maneuvers, such as turning. In this way, the hindwings could serve as control surfaces, enhancing maneuverability. This model is supported aerodynamically and is consistent with described anatomy for this animal, requiring no unusual positioning of the hindlimb.

METHODS

Our proposed model for hindwing use in *Microraptor gui* is based upon proportionalities between wing loading and turning ability in flying systems. Three factors are of interest: minimum speed, turning radius, and turning rate.

All three proportionalities arise from the basic equation for lift production: $L= C_L(\rho V2S)/2$, where L is the force of lift, C_L is the coefficient of lift, ρ is the density of the fluid medium, U is the velocity relative to the fluid, and S is the lifting area.

The minimum steady-state speed of a gliding animal can be determined by setting the lift (L) equal to body weight (W). This yields: $W=C_L(\rho V2S)/2$, which can be rearranged to yield: $(2W/S \rho C_L)0.5=Vmin$.

A flyer that can maintain level flight at speed V in a circle of radius R accelerates towards the center at V^2/R. That acceleration is caused by the component of the lift oriented towards the center of the rotation, and generated by initiating a roll. $L\sin\theta$ gives the inward component of lift, where θ is the banking angle. The force towards the center of the circle must be equal to the product of body mass (M) and acceleration towards the center of the circle, yielding: $MV^2/R=L\sin\theta$. Substitution from previous equations then gives: $MV^2/R=C_L(\rho V^2S)/2\sin\theta$, which can be solved for turning radius: $R=2M/\rho SC_L\sin\theta$. The rate of aerial turning relies on multiple factors including rate of roll, which is proportional to the difference in lift produced from the left and right sides. Initiating roll begins to produce vertical lift, which further increases the rate of roll, producing an exponential impact on roll rate. There is an additional influence of the yawing moment developed from the horizontal component of the lift from a unilaterally deployed hindwing (given by $L\sin\theta$). The yawing moment would push the cranial end of the animal into the turn (opposite to sign of the yaw). This produces the proportionality equation: $\Delta A_{roll} = K\int[(\cos(\theta)]^2 - \sin(\theta)\, d\theta$, which can be solved to yield: $\Delta A_{roll} = \frac{1}{2} K[(\theta+\sin(\theta)+2)(\cos(\theta))]$

RESULTS AND DISCUSSION

Deployment of the hindwings in *Microraptor* would have had a relatively modest effect on minimum speed, because wing loading is equal to W/S. Thus, Vmin is proportional to the square root of the wing loading and only decreases slightly during hindwing deployment.

However, the turning radius is proportional to mass unit wing loading (M/S). This direct linear proportionality indicates that deploying a single hindwing during a bank would reduce turning radius by the added proportional wing area. For *M. gui*, we estimate that deploying a single hindwing through moderate abduction of the limb would reduce turning radius by approximately 30-40%.

We calculate that the area of the hindwing in *M. gui* is equal to that of the forewing. Turn rate can thus be solved for any bank angle of interest. For example, at a 45 ^{o} bank there is an estimated 85% increase in turning rate.

The extent to which *Microraptor gui* possessed the flight control capabilities of modern birds is uncertain. Regardless, by utilizing the 'hindwings' according to our model, this animal would have been highly maneuverable in flight. Our new model suggests a potential function for the hindwings in *M. gui* and a plausible explanation for the origins of these conspicuous structures. Control function would be sensitive to small expansions of the hindlimb feathers, but critically would not require a simultaneous modification towards a sprawling hip. Our model is also advantageous in that it makes testable predictions about future observations of hindwing morphology in dinosaurs. If hindlimb lifting surfaces were principally associated with control function, then we should expect hindwings to reach their largest size in volant dinosaurs from cluttered environments, with comparatively primitive flight ability, and relatively long, narrow forewings. Broader forewings and/or more open environments would both reduce the relative importance of additional control surfaces beyond the forewings and tail. An advanced flight apparatus also allows the forewings to be utilized as the primary (or even sole) control surfaces.

While prior models have focused almost exclusively on sustained gliding, we suggest that control may have been more critical in *Microraptor gui*. *M. gui* was an active predator that occupied a forested environment with many obstacles to avoid during flight, clearly control and maneuverability would have been critical to successfully navigating such an environment. Control, both to avoid collisions with objects and land where the animal desired, would be a strong selective pressure, where a missed landing or an accident could mean wasted energy in recovering a desired position or even death. While efficiency of travel is a hallmark of gliding animals where the maximum amount of lateral distance can be acquired for the minimum investment in vertical gain, control may also be of great significance.

Our control-based model should therefore be considered when constructing potential modes of transport in *Microraptor gui*, and other four-winged dinosaurs. Furthermore, we assert that any hypotheses regarding the origin of flight in dinosaurs should bear in mind the importance of flight control and associated selective pressures.

REFERENCES

1. Xu X, Zhou Z, Wang X, Kuang X, Zhang F, Du X. *Nature*, 421(6921): 335-340. 2003.
2. Chatterjee S, Templin RJ. *Geological Society of America Special Paper* 376. 2004.
3. Alexander DE, Gong E, Martin LD, Burnham DA, Falk AR. *PNAS* 107: 2972–2976. 2010
4. J Brougham, SL Brusatte. *PNAS* 107: 155. 2010

IDENTIFYING FALLERS AND NON-FALLERS USING GAIT VARIABILITY INDICATORS BASED ON METHODS PROPOSED FOR HEART RATE ASSESSMENT

Camilla Zamfolini Hallal[1]; Nise Ribeiro Marques[1]; Dain LaRoche[2]; Edgar Ramos Vieira[3]; Deborah Hebling Spinoso[1]; Luciano Fernandes Crozara[1]; Mary Hellen Morcelli[1]; Mauro Gonçalves[1,4]

[1]Biomechanics Laboratory. São Paulo State University. Biosciences Institute IB/UNESP. Rio Claro. SP. Brazil.
[2] Department of Kinesiology, University of New Hampshire, Durham, USA.
[3] Departament of Physiotherapy, Florida International University, Miami, USA.
[4] Departament of Physical Education. São Paulo State University. Biosciences Institute IB/UNESP. Rio Claro. São Paulo. Brazil.

.

INTRODUCTION

Falls are the major cause of injury and injury-related death in older adults [1]. The risk of falls is multifactorial, 50% or more occur during walking [2]. The prevention of falls in older adults includes early detection of gait biomechanical abnormalities [3]. Hence, kinematic gait analysis is one of the most used methods to identify changes in this motor task [4].

Variability of kinematic parameters is sensitive to assess the effect of aging on motor control during walking, and may help assess the risk of falls in older adults [5]. Heart rate variability has been widely studied in cardiology to determine heart health, and, several statistical methods have been used to analyze heart rate variability that could be applied to gait variability. Despite heart rate and kinematic gait measures resulting from different physiological phenomena, they exhibit similar properties, such as a cyclical occurrence over time [6]. Thus, it is plausible to use similar procedures to analyze heart rate variability in the time domain to calculate step time variability during walking.

The aim of this study was to assess what method of variability evaluation previously used in heart rate evaluations would best distinguish between fallers and non-fallers based on temporal kinematic variability.

METHODS

Subjects

Thirty-five physically active volunteers participated in this study, including 16 older female fallers (67.4 ±7.34 yr) and 19 older female non-fallers (66.5±6.2 yr). The volunteers were classified as fallers if they reported falling in the 12 months before the study [7].

Procedures

First, the subjects' preferred treadmill walking speed was determined, and then a 10-minute familiarization session walking on the treadmill at this speed was completed. After familiarization, the volunteers walked for an additional three minutes on the treadmill to record the temporal kinematic gait parameters of stance time, swing time and step time. These parameters were recorded by four footswitches (Noraxon®, Arizona, USA) placed under the feet of the volunteers in the region of the heel, toe, base of the halux and the fifth metatarsal to determine the phases of gait. The signal of the footswitches was recorded at a sample frequency of 2000 Hz. We studied step time, stance time and swing time temporal kinematic parameters because they can be recorded using low-cost equipment (footswitch) applicable for use in physical rehabilitation centers.

Data Analysis

Data from 40 consecutive gait cycles were analyzed and the signals of the footswitches were processed in Matlab (Mathworks®, Natick, USA) using custom algorithms. Six statistical methods used to calculate heart rate variability were applied to determine the variability of stance time, swing time and step time of both groups [8]. 1) SDNN represents the standard deviation of all the interstride intervals, expressed in ms. 2) SDANN is the standard deviation of the means of the interstride intervals taken every 5 strides, expressed in ms. 3) SDNNi represents the mean of the standard deviations of the interstride intervals determined every 5 strides, expressed in ms. 4) The rMSSD is the root-mean square of the differences between interstride intervals, expressed in ms. 5) CV is the coefficient of variation calculated as the standard deviation of the interstride intervals divided by the mean of the interstride intervals, expressed as a percentage. 6) The triangular index is a geometric method calculated based on the construction of a density histogram of the interstride intervals, which has on the horizontal axis, the length of intervals and on the vertical axis, the frequency at which each interval occurred. The junction of the points of the histogram columns forms a triangle that expresses the variability of intervals. The triangular index corresponds to the width of the base of the triangle [9].

Pearson correlations were used to evaluate the relationship between the different methods. Multivariate analysis of variance was used to compare the variability scores of each method between fallers and non-fallers. Stepwise discriminant analysis was used to identify which method best predicted group participation, and determine the specificity and sensitivity of each method. The six gait variability measures were entered into separate stepwise discriminant analyses for each gait phase (three analyses were performed). The significance level was set at $p<0.05$ for all tests.

RESULTS AND DISCUSSION

Most methods were moderately associated. The correlation between SDNNi and rMSSD was the strongest in stance time, swing time and stride time variability estimation ($r= 0.948$, $p<0.01$ for stance time; $r=0.947$, $p<0.01$ for swing time; $r=0.948$, $p<0.01$ for step time). The predictor model that used the SDNN for stance time resulted in the best identification of group participation ($p<0.001$, sensitivity=100%, specificity=100%, table 1).

The identification of older people at risk for falling is critical to the adoption of prevention strategies. This study investigated the possibility of identifying older female fallers by temporal kinematic variability using a low-cost method [10]. The results showed that older female fallers are best identified using SDNN of stance time to calculate kinematic gait variability. The SDANN and triangular index methods can also be used, respectively for the swing time and step time variability analyses, however they have lower sensitivity and specificity.

CONCLUSIONS

A low-cost gait assessment system, such as a footswitch, may be used to distinguish older female fallers and non-fallers using stance time variability calculated by SDNN method.

REFERENCES

1. Schulz BW, Lloyd JD, William E. Gait & Posture **32**(1),18-22, 2010.

2.Talbot LA, et al. *BCM Pub Health* ; **5**,86-90,2005.

3. Kuptniratsaikul V, et al. *Clin Interv Aging* **11**(6), 111-117, 2011.

4. Kirkwood RN, et al. *Gait & Posture* **34**(1), 60-64, 2011.

5. Callisaya ML, et al. *Gait & Posture* **34**, 443–450, 2011.

6. Hausdorff JM. *J Neuro Eng Rehab* **2**(19), 2005.

7. Tucker MG, et al. *Arch Phys Med Rehabil* **91**, 2010.

8. Vanderlei LCM, et al. *Rev Bras Cir Cardiovasc* **24**(2), 205-217, 2009.

9. Rajendra et al. *Med Bio Eng Comput* **44**, 1031-1051, 2006)

10. Pijnappels M, et al. *Eur J Appl Physiol* **102**, 585–592, 2008.

ACKNOWLEDGEMENTS

The authors wish to thanks the funding providing by FAPESP, CNPq and Fundunesp.

Table 1: Significant predictor variables from stepwise discriminant analyses for each phase of gait.

Gait phase	Predictive variable	*p*	Discriminant analysis (sensitivity/specificity %)
Stance Time	SDNN	<0.001	100/100
Swing Time	SDANN	0.047	56/78
Stride Time	Triangle index	0.004	50/91

LOWER LIMB MUSCLE COACTIVATION IN YOUNGER AND OLDER ADULTS DURING DUAL-TASK GAIT

[1]Camilla Z. Hallal, [1]Nise Ribeiro Marques, [1]Deborah Hebling Spinoso, [2]Denis Brunt, [2]Edgar Ramos Vieira,[1]Mauro Gonçalves

[1] São Paulo State University, Rio Claro, SP, Brazil
[2] Florida International University, Miami, FL, USA

INTRODUCTION

Aging is related with changes in sensory and motor functions. These progressive declines can impair the ability to perform complex motor tasks and are associated with the high rate of falls among older adults. The risk of falls is multifactorial and more than 50% of cases of older adult falls occur during gait [1,2]. Gait planning, regulation and performance require high levels of dedicated attention and cognition. Thus, when gait is held in conjunction with other cognitively demanding task, performance of both tasks can be impaired. Concomitantly performance of cognitive and motor tasks can change the postural control and muscle coactivation patterns increasing the risk of falls [3,4]. Further understanding of these potential changes is needed. The objective of this study was to evaluate lower limb muscle coactivation levels in healthy younger and older adults during normal and dual-task gait conditions.

METHODS

Subjects
Thirty-five physically active volunteers participated in this study, including 17 younger (22±2) and 18 older women (65±3). All participating older women had low risk of falls based on the Berg Balance Scale (55±1).

Procedures
The gait tests were performed on a treadmill. Surface electromyographic activity (sEMG) of the tibialis anterior (TA), gastrocnemius lateralis (GL), and soleus (SO) muscles was measured. Subjects walked on the treadmill to determine their preferred speed. Data were then collected in two different gait conditions: normal gait and functional dual-task gait. During the latter, the volunteers were told to walk on the treadmill at their preferred speed and at the same time pay attention to a mock traffic light which changed to one of three colors randomly. When the lights changed color the volunteers had to say which color was lit.

Data Analysis
sEMG during the 10 initial gait cycles of both conditions was analyzed. The linear envelope sEMG data from each muscle of each participant was normalized by the mean sEMG during the normal gait condition. The percentage of agonist/antagonist coactivation (*%COACT*) for the muscles TA/GL and TA/SO was calculated using the equation [5]:

$$\%COACT = 2 * \frac{\text{common area A \& B}}{\text{area A + area B}} * 100$$

Where:

- *%COACT* is the percentage of coactivation between the agonist/antagonist muscles;
- area A is the area below the processed EMG curve of muscle A;
- area B is the area below the processed EMG curve of muscle B, and
- common area A & B is the common area of activity of muscles A and B.

To compare muscle coactivation during the gait conditions, the Student T test (within group) and the Student T test for independent samples (between groups) were used at the significance level of $p<0.05$.

RESULTS AND DISCUSSION

The older group had higher levels of coactivation than the younger group during both gait conditions ($p < 0.005$) (Figure 1). Increased coactivation might be used to optimize power generation and compensate for aging-related neuromotor functioning decline (e.g. reduced strength, power and proportion of fast twitch fibers, and increased response time). Coactivation-induced joint stiffness can be a strategy to increase joint rigidity during stance to compensate for aging-related strength decreases and/or ligament laxity [6,7]. Older women may coactivate ankle muscles to maintain the dynamic equilibrium. However, increase in stiffness is not always a good response because it might contribute to increased risk of falls [8]. Increase in stiffness can be an indicator of inefficiency and increased energy expenditure due to the coactivation of agonist and antagonist muscles [5]. Thus, high percentages of coactivation can result in mechanical disadvantages, favoring the onset of fatigue, limiting the duration of activities, and increasing the risk of falls [9].

There were no significant differences between normal and dual task gait conditions. However, there was a small trend showing a tendency to increased levels of coactivation during the dual task condition in the older group but not in the younger group. Larger sample studies with less intra-group variability are required to evaluate this trend.

The older women who participated in this study were physically active and were classified as having low risk of falls. So these factors may interfere with the performance the tasks evaluated.

CONCLUSIONS

The older women group had higher levels of lower limb muscle coactivation. There were no significant differences on the muscle coactivation levels between normal and dual task gait, but larger studies are encouraged because the older women seem to tend to have higher levels of coactivation during dual task gait.

REFERENCES

1.Talbot LA, et al. *BCM Pub Health* ; **5**,86-90,2005.

2. Bassey EJ. *Rev Clin Geront* **7**,289-297, 1997.

3. Schulz BW, et al. *Gait&Post* **32,**18-22.2010.

4. Abbud GAC, et al. *Gait&Post* **30**,227-232,2009.

5. Candotti CT, et al. *JEK* **19**,915-921,2009.

6. Ishida et al. *Med & Biol Eng & Comp* **46**,213-221,2008.

7. Schmitz et al. *JEK* **19,**1085–1091,2008.

8. Cenciarini et al. *IEEE* **57,**267-275,2010.

9. Ortega et al. *J App Phys* **102**,2266-2273,2007.

ACKNOWLEDGEMENTS

This project was funded by grants from the following Brazilian agencies Conselho Nacional de Desenvolvimento Científico e Tecnológico (CNPq), Fundação de Amparo à Pesquisa do Estado de São Paulo (FAPESP), Coordenadoria de Aperfeiçoamento de Pessoal de Nível Superior (CAPES) and Fundação para o Desenvolvimento da UNESP (FUNDUNESP).

Figure 1: Percent of coactivation between tibialis anterior (TA) and gastrocnemius lateralis (GL), and between TA and soleus (SO) muscles during normal and dual task gait conditions.

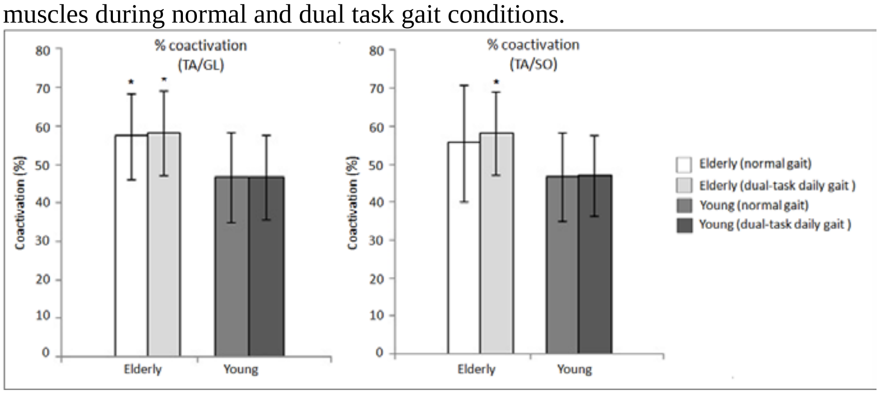

*p<0,05 between older and younger women.

STRENGTH, POWER AND ELECTROMYOGRAPHIC PERFORMANCE OF HIP MUSCULATURE IN OLDER FEMALE FALLERS AND NON-FALLERS

[1]Camilla Z. Hallal, [1]Mary H. Morcelli, [1]Luciano F. Crozara, [1]Nise R. Marques, [1]Denise Martineli Rossi, [2]Dain P. LaRoche, [1]Mauro Gonçalves and [3]Marcelo T. Navega

[1]Sao Paulo State University, Rio Claro, SP, Brazil
[2]University of New Hampshire, Durham, NH, USA
[3]Sao Paulo State University, Marilia, SP, Brazil

email: camillazhallal@yahoo.com.br, web: http://www.rc.unesp.br/ib/efisica/biomecanica2011/contato.php

INTRODUCTION

Falling is a serious problem in the elderly, mainly due to its negative impact on the quality of life of this population and increased public health costs (Bento et al. 2010). The etiology of falls is multifactorial, so developing a broad understanding of the biomechanical and physiological factors associated with increased risk of falling in the elderly is extremely important (LaRoche et al. 2010).

It is known that the weakness of hip muscles can challenge balance during gait and impair rapid torque production (Mendis et al. 2009). The neuromuscular performance of the ankle and knee musculature has been well studied in fallers and non-fallers but a comprehensive comparison of hip function is lacking, despite some authors considering it crucial in the prevention of falls (Wert et al. 2010). Thus, this study aimed to compare the neuromuscular capacity of older female fallers and non-fallers during hip flexion, extension, abduction and adduction.

METHODS

Subjects

The participants of this study were forty-four older women (60-85 years), divided in two groups: fallers (n=20) and non-fallers (n=24), based on their report of having fallen or not fallen during a period of one year before the study. There were no significant differences in body mass, age and stature between groups. All subjects were classified as physically active.

Procedures

Maximal strength and power were obtained using an isokinetic protocol that consisted of five concentric contractions at velocities of 30 and 120°/sec for hip flexion and extension, and 30 and 180°/sec for hip abduction and adduction.

Surface EMG signals were recorded at a sample frequency of 2000 Hz from the internal oblique (IO), multifidus (MU), gluteus maximus (GM), biceps femoris (BF) and rectus femoris (RF) muscles.

Data Analysis

The torque obtained from the dynamometer was smoothed with a low pass filter (4th order, 6 Hz), and peak torque and power (torque x velocity) were determined for each joint action. Peak torque was measured from lower speeds (30°/sec) whereas peak power was measured from the higher speeds (120 and 180°/sec). Peak torque and power were then normalized to the body mass of each volunteer.

The EMG signals of the OI, RF, MU, GM and BF muscles were processed in the time domain using full-wave rectification and a low pass filter (4^{th} order and cut-off of 6 Hz) 50 ms before and after peak torque. Then, the linear envelop values were normalized by the group mean of each muscle activation. The EMG of the RF was obtained during hip flexion, GM and BF during hip extension, and the ratio of the OI/Mu EMG during hip flexion, extension, abduction and adduction.

The normality of data were tested using the Shapiro Wilk test and Independent samples t-tests and Mann-Whitney tests were used as appropriate to test for group differences. The significance level was set at $P<0.05$. Data are reported as mean (SD) for normally distributed data and median (range) for data that were not normally distributed.

RESULTS AND DISCUSSION

EMG, strength, and power data are shown in Table 1. Older female non-fallers were stronger than fallers for hip extension, abduction and adduction (17,11%, 21,73% and 24,16% stronger respectively). It was also found that non-fallers had higher muscle power than fallers during hip abduction, flexion and extension (20,1%, 16,31% and 23,94% more power respectively).

EMG data showed that during hip flexion fallers had higher RF activation than non-fallers. However, during hip extension non-fallers had higher GM activation than fallers, while for BF, fallers had higher activation. With respect to OI/MU EMG ratio, fallers had lower values than non-fallers in all the movements analyzed.

The findings of this study suggest that the ability to produce torque during dynamic contractions is associated with a history of falling in older women. Furthermore, it is suggested that elderly fallers may have impaired excitation-contraction coupling during flexion and extension of the hip, since a higher activation of the RF and BF muscles, respectively, was not sufficient to produce a torque equal to or greater than that of elderly non-fallers (LaRoche et al. 2010). Additionally, the impairment of the adduction and abduction torque by the elderly fallers suggests the potential for lateral instability and justifies the increased risk of falls in this group.

The IO/MU EMG ratio observed in this study suggest that elderly fallers have a reduced ability to stabilize the trunk during movements of the hip joint, which may contribute to an increased risk of falls.

CONCLUSIONS

Older female fallers had a lower capacity to produce torque and muscle power at the hip joint. In addition, fallers required greater muscle activation to achieve the same or less torque than non-fallers, which may increase the incidence of fatigue and, consequently, lead to an increased risk of falls in this population.

REFERENCES

1. Bento PCB, et al. *Clinical Biomechanics* **25**, 450-454, 2010.
2. LaRoche DP, et al. *J Electromyogr Kinesiology* **20**, 482-488, 2010.
3. Mendis MD, et al. *Gait Posture* **30**, 533-537, 2009.
4. Wert DM, et al. *Phys Ther* **90**, 977-985, 2010.

ACKNOWLEDGEMENTS

This project was funded by grants from Conselho Nacional de Desenvolvimento Científico e Tecnológico (CNPq), Fundação de Amparo à Pesquisa do Estado de São Paulo (FAPESP), Coordenadoria de Aperfeiçoamento de Pessoal de Nível Superior (CAPES) and Fundação para o Desenvolvimento da UNESP (FUNDUNESP).

Table 1: Comparisons between older female fallers and non-fallers for EMG, strength, and power. Data are reported as median (range).

Variable	**Fallers (n=20)**	**Non-Fallers (n=22)**	***P***
Hip adduction torque ($N \cdot m \cdot kg^{-1}$)	47.33 (10.55)	62.40 (18.58)	0.003*
Hip abduction torque ($N \cdot m \cdot kg^{-1}$)	67.74 (16.31)	86.54 (20.64)	0.02*
Hip flexion torque ($N \cdot m \cdot kg^{-1}$)	51.17 (16.05)	58.77 (19.16)	0.17
Hip extension torque ($N \cdot m \cdot kg^{-1}$)	134.57 (41.43)	162.33(42.81)	0.037*
Hip flexion power ($W.\ kg^{-1}$)	84.35 (38.21)	100.87 (24.01)	0.02*
Hip extension power ($W.\ kg^{-1}$)	186.28 (69.77)	244.88 (72.71)	0.01*
Hip abduction power ($W.\ kg^{-1}$)	189.87 (78.25)	237.63 (81.48)	0.04*
Hip adduction power ($W.\ kg^{-1}$)	126.79 (38.98)	154.04 (52.53)	0.13
Rectus femoris activation (%)	99.5 (99.3 - 102.4)	96.7 (94.5 - 118.3)	0.0001*
Biceps femoris activation (%)	100.9 (95.5 - 101.4)	81.1 (80.4 - 86.6)	0.0001*
Gluteus maximus activation (%)	101.1 (93.7 - 102.2)	102.8 (85.9 - 104.9)	0.0001*
Internal oblique/Multifidus EMG ratio (flexion)	2.95 (2.91 - 4.95)	4.56 (4.55 - 5.97)	0.0001*
Internal oblique/Multifidus EMG ratio (extension)	0.59 (0.52 - 0.87)	0.9 (0.85 - 1.15)	0.0001*
Internal oblique/Multifidus EMG ratio (adduction)	1.12 (0.85 - 1.16)	2.88 (2.72 - 9.4)	0.0001*
Internal oblique/Multifidus EMG ratio (abduction)	1.23 (1.22 - 2.47)	2.25 (2.24 - 3.17)	0.0001*

* Significant difference between fallers and non-fallers groups.

THE INFLUENCE OF REPETITIVE LOADS ON FOOT SENSITIVITY AND DYNAMIC BALANCE

Stephanie Hamilton, Louisa Raisbeck and Karen Roemer

Michigan Technological University, Houghton, MI, USA
email: shamilto@mtu.edu

INTRODUCTION

Loss of balance and falls are a health cost factor because of temporal or long term loss of functional independence and injuries in various age groups [1]. Cutaneous foot sensation (FS) provides important information to the brain about the foot's contact with the ground. FS has been artificially reduced in several studies in order to establish its role in balance, and decreased FS has been demonstrated to be limiting factor for balance [2,3]. Influencing factors on FS are known to be age, neuropathies, injuries, and temperature [5,7,8]. There is currently limited research with respect to the influence of increased load on FS. It is known that overload decreases balance [6], therefore, this research will emphasize the influence of repetitive external load on FS and postural stability. It is hypothesized that repetitive additional load will negatively affect FS, sway area (SA) and time to failure (TTF) of the balance task.

METHODS

Ten healthy subjects (age: 19.5±1.5, 5 female, 5 male, BMI: 20.9kg/m^2±2.9) attended three sessions, each with a randomly assigned intervention. The interventions were comprised of resting (RST), unloaded walking (UW), or loaded walking (LW). The RST intervention required subjects to remain seated in a chair for the duration. During both walking interventions, the participants walked wearing only socks on wood floor. The loaded walking required participants to wear a weighted vest that increased their BMI by 9. Pre and post intervention, FS was tested using Semmes-Weinstein monofilaments at five locations on the foot and balance was assessed by measuring SA and TTF during 4 unipedal reaching stances combining alternating vision (eyes open (EO), and eyes closed (EC)) and surface (stable surface (SS), and unstable surface (US)). These balance tasks were performed on the subject's dominant leg as determined by the Balance Recovery Test. Data was standardized according to pretest data to calculate change.

RESULTS AND DISCUSSION

SA measured during the ECUS trial increased significantly greater following RST compared with UW (p=.03). TTF increased for RST while decreasing for UW (p=.01).

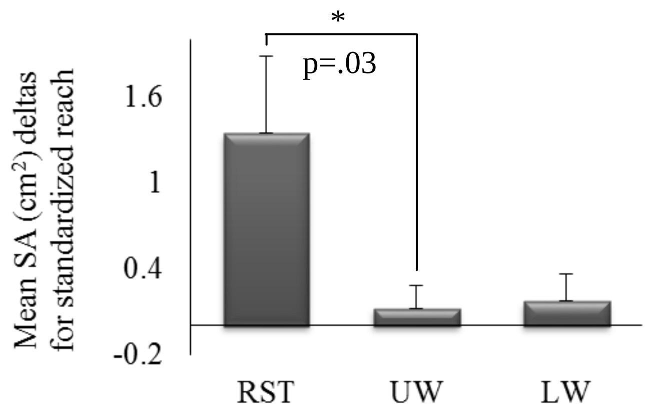

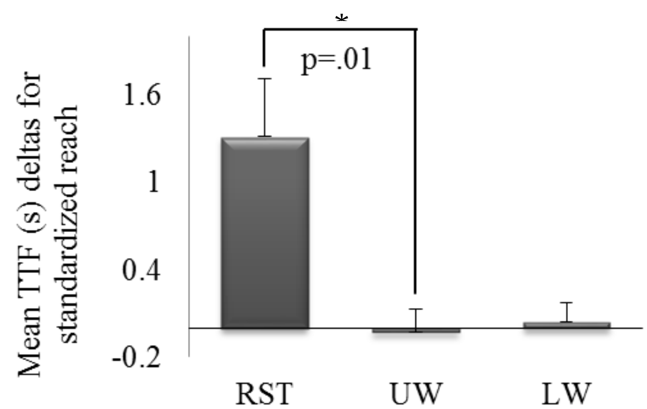

Figures: 1a) Mean SA deltas shown for each ECUS trial following intervention. 1b) Mean TTF deltas shown for ECUS trial following intervention.

It appears that the RST intervention has a significant impact on TTF and SA, indicating improvement on balance.

TTF increased following RST, while SA increased as well to a greater extent following RST compared with UW and LW. While SA is typically used as an indication of balance performance with smaller area indicating improved balance [5], when combined with the increase in TTF, this seems to indicate that RST may cause balance to improve compared to the other interventions. Subjects may have benefitted from RST condition, decreasing any potential fatigue or loading of the feet, allowing them to maintain the balance stance longer, increasing TTF, but also increasing SA concurrently.

A complementary effect of vision and fatigue may have caused participants to step off the pressure sensing mat sooner following the UW and LW interventions, resulting in a shorter TTF and less SA compared with RST intervention.

SA and TTF were unchanged following the EOSS, ECSS, and EOUS conditions. This lack of difference can be explained according to the surface and the vision conditions. Surface plays an important role with regards to balance. Yi & Park [10] examined the effect of using a spongy surface for balance tasks, and found that the spongy surface provided similar results to other artificial sensation reducing methods, increasing cutaneous FS threshold. SS may lessen the degree of difficulty in the stance due to the provision of cues from the cutaneous mechanoreceptors providing pressure information for the body to respond to compared with US. This can be seen by the interventions affecting the ECUS task instead of the ECSS task. Though vision is removed from the ECSS task, the stable surface appears to provide enough afferent information for the body to maintain postural stability. Vision also has a great effect on balance. Strang et al [9] found that vision seemed to provide enough information for the body to overcome any fatigue or reduction in FS. This is shown by the EOUS task specifically, as even with the challenging surface, SA remained unchanged following the interventions.

Against expectations, FS remained unchanged following all interventions. The interventions may not have exceeded the impacts imposed on the foot prior to the appointment. This information is unknown, as it was not regulated for this study. Additionally, foot sole temperature has been demonstrated to have an effect on FS [7]. The subjects' feet may have experienced an increase in temperature during the walking interventions due to increased circulation of the foot. This temperature increase may have been enough compared with the cooler environment where the baseline testing took place to affect testing results.

CONCLUSIONS

The RST intervention resulted in improved balance for the ECUS condition. This indicates that periods of rest could reduce daily fatigue effects that may decrease the ability to balance. Though it was hypothesized that the repetitive impacts with and without the load would negatively affect balance, the reverse was shown as the RST intervention seemed to improve balance. Further research should be performed to differentiate whether this increase in TTF and consequently SA is related to the recovery from fatigue accumulated during previous activities.

REFERENCES

1. Costs of Falls Among Older Adults. http://www.cdc.gov/HomeandRecreationalSafety/Falls/fallcost.html, 2011.
2. Hong, S.L., et al. *Neurosci Lett*, **423**, 104-108, 2007.
3. Meyer, P.F., et al. *Exp Brain Res*, **156**, 505-512, 2004.
4. Nashner, LM & McCollum,G. *Behav Brain Sci*, **8**, 135-150, 1985.
5. Perry, S.D. *Neurosci Lett*, **392**, 62-67, 2006.
6. Qu, X.D., & Nussbaum, M.A. *Gait Posture*, **29**, 23-30, 2009.
7. Schlee, G., et al. *Clin Neurophysiol*, **120**, 1548-1551, 2009.
8. Simmons, R. W., et al. *Diabetes Res Clin Pr*, **36**, 153-160, 1997.
9. Strang, A.J, et al. *Eur J Appl Physiol*, **111**, 1485, 2011.
10. Yi, Y. W., & Park, S. *Exp Brain Res*, **195**, 361-369, 2009.

Characterization of Interlamellar Shear Properties of the Annulus Fibrosus

Sang Kuy Han, Chao-Wei Chen, Yu Chen, Adam. H. Hsieh

University of Maryland, College Park, MD, USA
email: sangkuy.han@hotmail.com, web: http://www.bioe.umd.edu/orthomechlab

INTRODUCTION

The intervertebral disc (IVD) is a highly heterogeneous structure and has a functional role of load bearing and stress distribution between adjacent vertebrae in the spine [1]. Complex interplay among the cartilaginous endplate, annulus fibrosus (AF), and nucleus pulposus determines the mechanical function of the IVD. Failure of structural integrity is associated with the onset of IVD degeneration. For instance, delamination between lamellae of the AF is a crucial stage of IVD herniation. Excessive shear stress between lamellae mainly causes delamination [2]. Therefore, the quantification of structural integrity of IVD has been widely studied to elucidate relationships between IVD mechanics and degeneration. However, significant gaps remain in our understanding of interlamellar mechanical behavior during IVD loading. In order to circumvent potentially confounding tissue deformations and identify local variations in strain, this study sought to develop and implement a mechanical shear testing system that incorporates a three dimensional meso-structural optical image technique to measure interfacial behavior between lamellae. Additionally, we introduce more physiological loading regimes by applying combinatorial normal and shear loads to tissue specimens.

METHODS

Fresh-frozen porcine thoracic motion segments (two adjacent vertebrae with IVD) were obtained from common source. AF specimens consisting of two or multiple adjacent lamellar layers were cut to approximatly 7 mm axial × 7 mm circumferential dimensions. Specimen thicknesses were approximately 1 mm for two layer specimens and 7-8 mm for multiple layers in the radial direction. Specimens were hydrated via phosphate buffer solution prior to and during shear tests. A custom-designed shear testing fixture was designed, and a commercial material testing system was used (Testbench, Bose ElectroForce, Fig 1). Two load cells were attached to the bottom fixture plate for detecting axial and lateral force, respectively. In order to secure the specimen between the moving and fixed plates, a small amount of Vetbond tissue glue was applied to the two plates before placing the specimen. A 0.3 N of pre-compressive load was applied to ensure contact. A 12% of shear load was applied with two different strain rates, 0.3 and 0.86 %/s.

Swept-source Optical Coherent Tomography (SSOCT) was incorporated to the material testing system (Testbench, Bose ElectroForce) for visualizing tissue deformation and detecting any slide of tissue from the fixture plate following shear load (Fig. 1a). SSOCT is centered at 1300 nm with 100nm bandwidth (8 µm axial and 11.7 µm transverse resolutions under a 4 x objective, NA=0.1). 2.8mW was delivered on IVD. OCT acquired $6 \times 6 \times 1.8$ mm^3 volume in $512 \times 512 \times 512$ pixel.

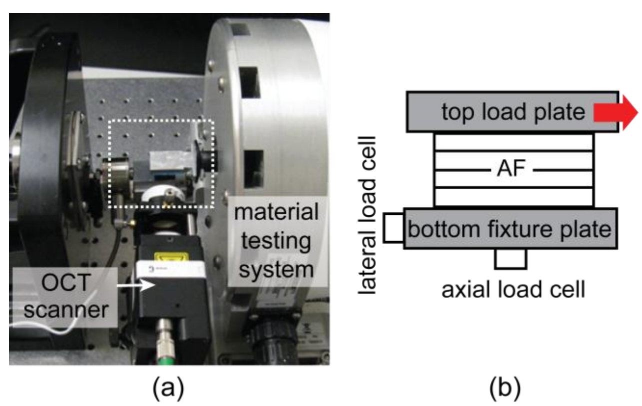

Figure 1: Custom-designed shear testing system for AF experiments; a: shear testing system with OCT scanner, b: schematic illustration for the area marked with the dashed line in a.

RESULTS AND DISCUSSION

OCT images visualize AF structures before and after shear load. OCT images provide overall tissue deformation (Fig. 2).

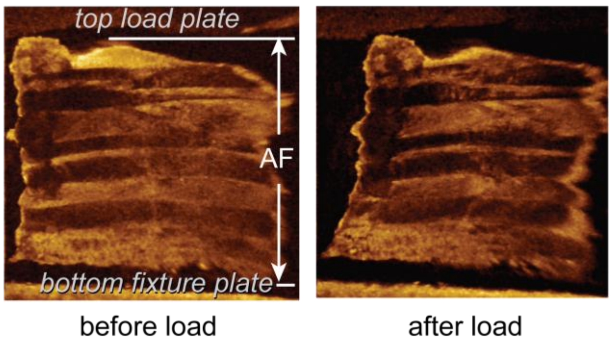

Figure 2: Typical example of multiple lamellae of annulus fibrosus before and after shear load taken by OCT image. OCT images visualize the tissue structure and deformations.

As expected, a 14 % shear strain with higher strain rate, 0.86 %/s, resulted in larger reaction force (46.45g = 0.16 N) compared to slower strain rate, 0.3 %/s (28g) (Fig. 3a). Shear stiffness, 3.3 N/mm, following 14 % of mechanical shear was larger in 0.86 %/s strain rate compared to 2.0 N/mm for 3 %/s specimens (Fig. 3b).

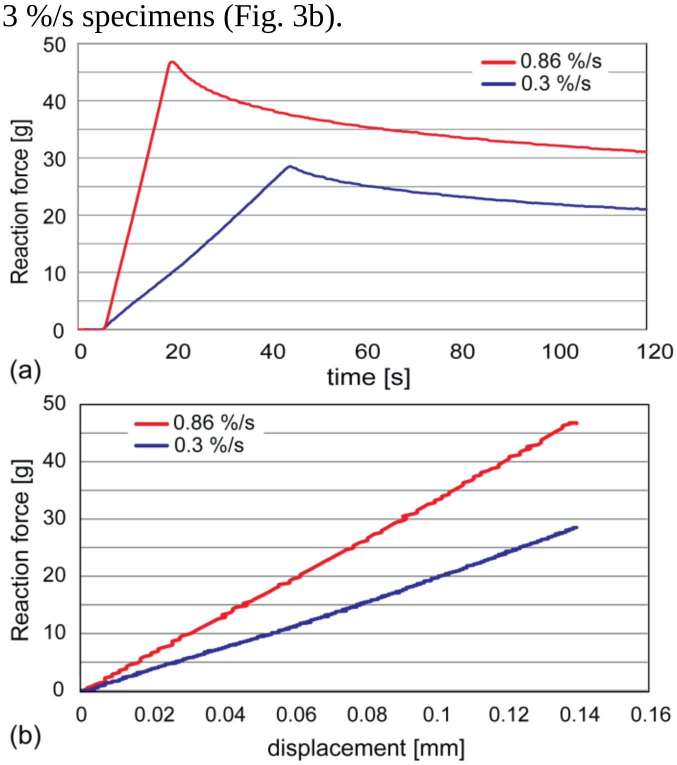

Figure 3: Typical example of the material behavior of inter-lamellae from two lamellae layers test following shear load. (a) reaction force shown as function of time, (b) reaction force *vs* displacement.

In the previous study using a lamellar lap test [3], the tensile and in-plane shear strains in the adjacent annular layers introduce additional complexity to the analysis of material properties between lamellae following shear load. For example, the highly non-linear behavior of reaction force in a small displacement region of shear load could potentially be largely associated with fibril reorientation within each of the adjacent annular layers, in addition to deformations between lamellae. In contrast with this lap test study, shear load was applied to the whole area of lamella plane in our testing setup (Fig. 1b). Therefore, it can be suggested that the testing system in this study measured the material properties of inter-lamellae with less compound effect from the extensibility of the adjacent lamellae.

Using OCT imaging to visualize tissue deformations provides several advantages to verify mechanical test procedure. For instance, we were able to verify the Vetbond-mediated tissue-shear fixture interfacial integrity, which we found deficient in sandpaper-coated fixtures (data not shown). This ensured that the mechanical response during loading and stress relaxation is due completely to the tissue, itself. Furthermore, we plan to utilize such OCT images for mapping strain fields within localized regions of tissue following shear load using image registration analysis.

CONCLUSIONS

This study provides a novel method to characterize the material properties of inter-lamellae in physiological load conditions. Based on the results from this study, it can be concluded that the material properties of inter-lamellae is viscoelastic, i.e., stress relaxation, strain-rate dependent material property.

REFERENCES

1. White AA and Panjabi MM. Clinical Biomechanics of the Spine. Lippincott, 1978.
2. Goel VK, et al. Spine. **20**, 689-698, 1995.
3. Gregory DE, et al., *J Biomech* **44**, 97-102, 2012.

ACKNOWLEDGEMENTS

NIH R21 AR059325

HOW DO LOWER LIMB MUSCLES SCALE ACROSS INDIVIDUALS?

[1]Geoffrey Handsfield, [2]Lindsay Sauer, [2]Joseph Hart, [2]Mark Abel, [1,3]Craig Meyer, and [1,2,4]Silvia S. Blemker
Depts. of [1]Biomedical Engineering, [2]Orthopaedic Surgery, [3]Radiology, [4]Mechanical and Aerospace Engineering
University of Virginia, Charlottesville, VA
Email: gh8hq@virginia.edu; Web: http://www.mae.virginia.edu/muscle/

INTRODUCTION

Determination of scaling relationships for musculoskeletal architecture is important for understanding fundamental shape and size principles in biology, estimating clinical subject parameters, and generating realistic musculoskeletal models. Currently, only limited knowledge exists on how muscle sizes may scale across individuals. Moreover, most currently used architecture data are based on cadaveric studies, which typically represent elderly populations and may not represent the muscle architecture for active, healthy individuals. In this study, we collected magnetic resonance (MR) images of the lower limb of a cohort of young healthy adults and adolescent boys in order to answer the following questions: *(i)* how do muscle volumes scale with height and mass?, *(ii)* how do individual muscle volumes scale relative to each other?, and *(iii)* how do muscle volumes scale with bone volume?

METHODS

Ten healthy adults (five women) with the following parameters (mean±S.D.): age: 25.2±4 *years*, height: 175±9 *cm*, weight: 69.8±12.1 *kg* and five healthy adolescent boys: 13.8±0.8 *years*, 167.8±6.5 *cm*, 65.0±11.2 *kg*, all with no prior history of lower limb injury were scanned on a 3T Siemens Trio MRI scanner. Axial images were acquired from the twelfth thoracic vertebra to the ankle joint using a non-Cartesian gradient echo sequence. Scanning parameters were as follows: TE/TR/α: 3.8 *ms*/ 800 *ms*/ 90°, field of view: 400 *mm* × 400 *mm*, slice thickness: 5 *mm*, in plane spatial resolution: 1.1 *mm* × 1.1 *mm*. Additionally, a Chebyshev approximation was applied for semi-automatic off-resonance correction [1]. Thirty-five muscles in the hip, knee, and ankle were segmented using an in-house segmentation program written in Matlab. The volumes of each muscle and bone in the lower limb were calculated. The volumes of all of the muscles and all of the bones were summed for each subject to obtain the total muscle volume and total bone volume, respectively, of the limb.

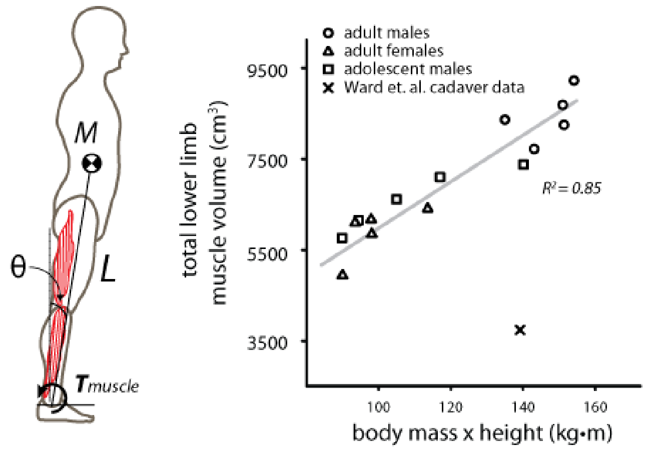

Figure 1: Left: schematic of the mechanical principle of muscle volume scaling. The quantity of lower limb muscle needed to support and move a subject will be a function of both the mass of the subject and the length over which the muscle(s) are acting on the center of mass. Right: plot of lower limb muscle volume as a function of body mass x height. Literature value [3] for cadaver muscle volume vs. height and mass is shown (X).

RESULTS AND DISCUSSION

These data allowed us to probe the relationship between total muscle volume of the lower limb and subject parameters such as mass and height. We used an analytical mechanical model of the lower limb (Fig. 1, left) to predict this relationship. Briefly, muscle volume has been previously related to muscle torque [2]:

$$T_{muscle} \propto V_{muscle}$$

The torque needed to support a human standing is given by the product of mass, length, gravitational acceleration, and the cosine of the leg angle from vertical:

$$T_{supp} = M \cdot L \cdot g \cdot \cos\theta$$

Under the assumption that length, L, and subject height scale together, it follows that muscle volume scales linearly with body mass and height. Both the analytical model and the MRI-based volume results (Fig. 1, right) support a mass-height scaling for lower limb muscle volume. This relationship was statistically more correlative than a scaling by mass or height alone.

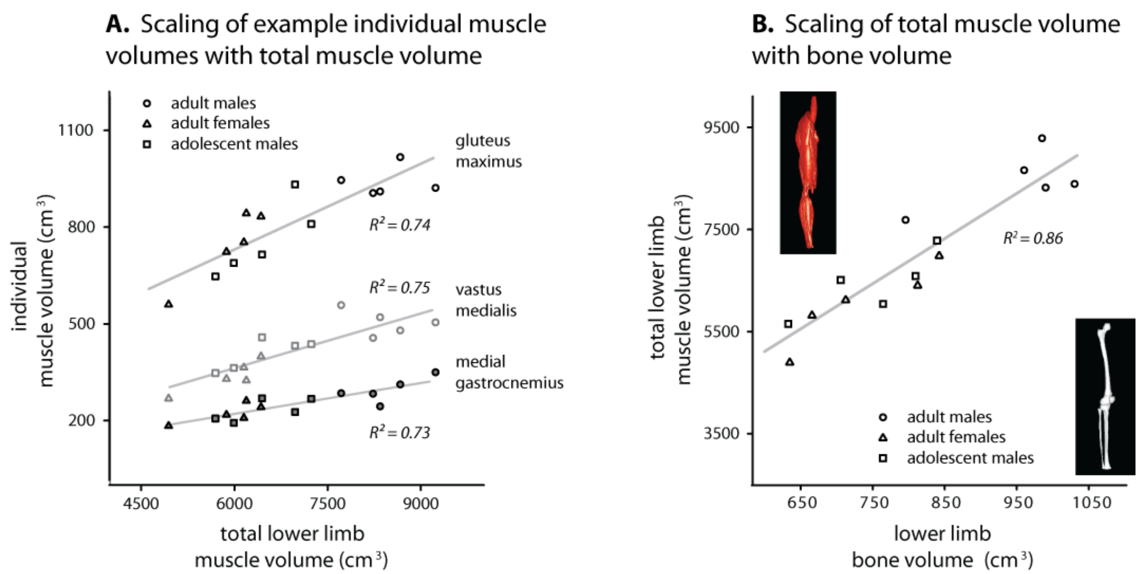

Figure 2: Scaling relationships for muscles in the lower limb. A. linear scalings for muscles crossing the three joints in the lower limb; the volume of each muscle can be well-approximated as a constant proportion of the total lower limb musculature. B. linear relationship between muscle volume and bone volume for subjects ranging in age and body size.

Interestingly, when our results for healthy active subjects were compared to literature values for cadaver muscle architecture [3], the cadavers' lower limb muscle volume was less than half of what would be expected from a healthy subject of the same mass and height (Fig. 1). This result explains why previous musculoskeletal models based on cadaver lower limb architecture have had to scale peak isometric tension by 200% in order to produce *in vivo* isometric joint moments [4].

For individual muscles of the lower limb there is a statistical correlation between total lower limb muscle volume and the volume of the individual muscle. Three examples are given (Fig. 2A). The linear regressions shown here can be thought of as muscle fraction averages for our population. On average, each of our subjects' muscles represents a constant proportion of their total lower limb musculature.

For the entire population included in this study, a statistical correlation between total muscle volume and total bone volume of the lower limb was observed (Fig. 2B). The muscles and bones of a limb are inextricably mechanically linked in movement and locomotion. It is compelling that a linear scaling exists between these parameters for a subject population that ranges in age, size, and sex.

CONCLUSIONS

This work demonstrates scaling relationships for muscle volumes across healthy adult and adolescent populations. Lower limb muscle and bone volumes scale together, as do individual muscles contained in the limb. Furthermore, these results suggest that muscle volumes scale linearly with height and mass across individuals. This height-mass scaling relationship can be used to approximate healthy subject muscle volume from height and mass or compare patients' muscle volumes against those observed in a healthy population.

REFERENCES

1. W Chen, C Sica, and CH Meyer. *Magn. Res. in Med.* **60,** 5: 1104-1111, 2008.
2. KRS Holzbaur et. al. *J Biomech* **40**, 742-749, 2007.
3. SR Ward et. al. *Clin Ortop Relat Res*. **467**: 1074-1082, 2009.
4. EM Arnold et. al. *Annals of Biomed. Eng.* **38**, 2: 269-279, 2010.

ACKNOWLEDGEMENTS

We wish to acknowledge members of the Multi-scale Muscle Mechanics Lab at the University of Virginia for assistance with this project. Special thanks are owed to Drew Gilliam, Nic Fiorentino, Kelly Anderson, Mary Boyles, Colin Maloney, and Clara Tran. Funding for this work was provided by the Wallace H. Coulter Foundation.

COMPARISON BETWEEN NINTENDO WII FIT AND CONVENTIONAL REHABILITATION ON FUNCTIONAL PERFORMANCE OUTCOMES AFTER HAMSTRING ANTERIOR CRUCIATE LIGAMENT RECONSTRUCTION

[1]Gulcan Harput, [1]Bunyamin Haksever, [1]Burak Ulusoy, [1]Gul Baltaci, [2]Hamza Ozer

[1] Hacettepe University, Ankara, TURKEY
[2] Gazi University, Ankara, TURKEY
email: aktasgulcan@yahoo.com

INTRODUCTION

Rehabilitation after Anterior Cruciate Ligament (ACL) reconstruction is essential for knee functional outcomes [1]. Since clinical practices in the management of ACL injury are varied, there is no standard agreement on the ideal treatment algorithm for individuals with ACL reconstruction. All protocols aim to enhance the neuromuscular control of the knee following ACL injury, or reconstruction may result in better outcomes in terms of returning back to functional activities and a reduced rate of re-injury [2]. The Wii Balance Board (WBB) (Nintendo, Kyoto, Japan), the part of the popular video game Wii Fit, designed as a video game controller, is predominantly used in combination with a video game console and its associated software. Given the capacity for providing instant feedback and the potential for enhanced motivation levels, this system has already been integrated into the neurological rehabilitation programs of subjects with balance defects [3]. Although increasing interest in Wii rehabilitation, there is no study about Wii rehabilitation in ACL reconstruction. The aim of this study was to determine the acceptability of the Nintendo Wii Fit compared to the conventional rehabilitation as a therapy tool for patients with ACL reconstruction.

METHODS

Thirty males who underwent unilateral arthroscopic ACL reconstruction with hamstring tendon graft by the same surgeon participated in this study. The subjects were divided into two groups by using randomized sampling which was computer generated with a basic random number generator. One of the groups was trained with Nintendo Wii Fit system (Figure 1) and the other group enrolled into conventional ACL rehabilitation program [4] during three months after reconstruction.

The bowling and skiing games in Wii Sports, Boxing, Football and Balance Board within Sports Pro Series were chosen for their potential to influence physical and functional movement, cognitive functioning, and driving. Each game was tried for 15 minutes. Each subject participated in one-hour rehabilitation sessions and accomplished 3 sessions per week (Figure 1).

Functional examinations included the measurements of the balance using modified star excursion balance test (SEBT), coordination, and proprioception and response time using functional squat system (Figure 2).

Figure 1: Balance exercises on the Nintendo Wii Fit Balance board.

The data were analyzed by using Friedman Test with time as the repeated-measures factor for outcome measures, and Mann Whitney U Test was used to determine the group differences at the first, 8th and 12th weeks of the rehab. Wilcoxon Test was used for time of test differences in each group. The level of significance was set at $p<0.05$

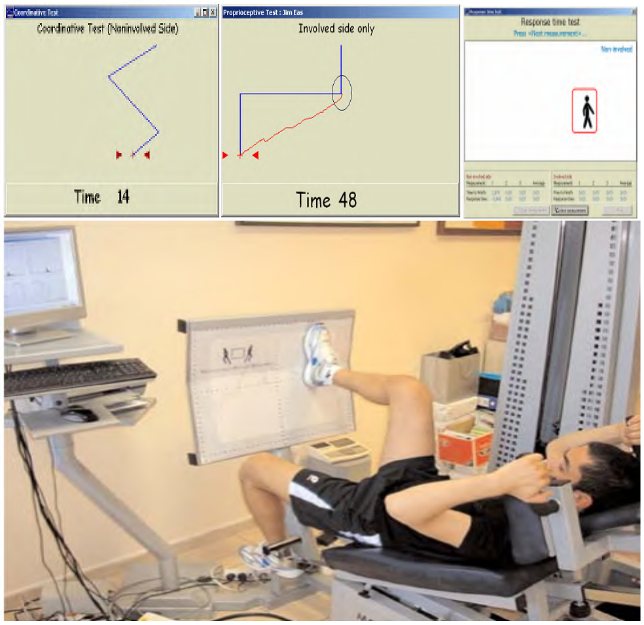

Figure 2: Functional squat system and the coordinative, proprioception and response time test, respectively.

RESULTS and DISCUSSION

There was no significant difference between Wii Fit and conventional groups with respect to dynamic balance, and functional squat tests including coordination, proprioception and response time at the first, 8th and 12th weeks of the rehabilitation ($p>0.05$).As a consequence of the repeated measures for each group, SEBT (Figure 3), coordination and proprioception test (Figure 4) results significantly differed depending on time ($p<0.05$).

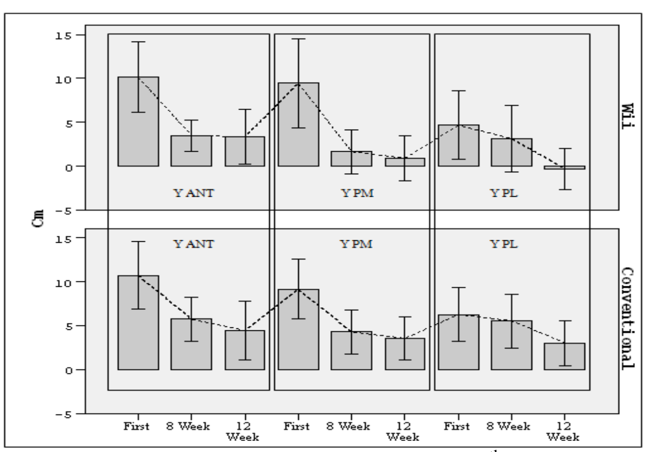

Figure 3: SEBT test results at 1, 8 and 12th weeks in both groups (ANT: anterior division, PM: Posteromedial division, PL: Posterolateral division).

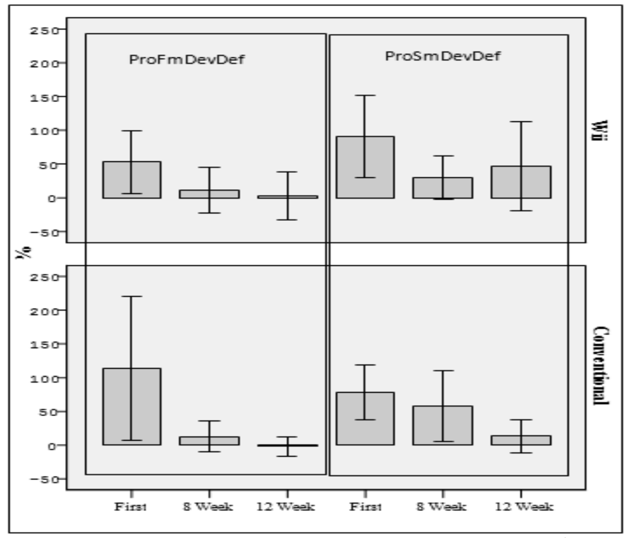

Figure 4: Proprioception test results at 1, 8 and 12th weeks in both groups.

There was a significant difference in coordination test between first and 8th weeks of the rehab in Wii group ($p=0.017$). The proprioception test including deviation first movement deficit was recognized as significantly different in both groups between the first and 12th weeks of the rehab (Wii: $p=0.032$, Con: $p=0.012$).

CONCLUSIONS

It is obvious that Wii Fit and conventional training programs which were conducted within a mean time frame of 12 weeks are important in ACL rehabilitation. However, it is not clear whether one is significantly more effective in restoring neuromuscular control and increasing the functional performance. Instead of conventional rehabilitation, Wii Fit Balance program might be recommended since it is safe, feasible, cheap and fun.

REFERENCES

1. Yosmaoglu HB et al. *J Sport Rehabil* **20**(2), 207-18, 2011.
2. Aune A et al. *Am J Sports Med* **29**(6), 722–728, 2001.
3. Deutsch JE et al. *Phys Ther* **88**(10), 1196–207, 2008.
4. Grinsven SV, et al. *Knee Surg Sports Traumatol Arthros* **18**, 1128–1144, 2010.

EVALUATION OF ANKLE MUSCULAR ACTIVATION DURING SELECTED BALANCE EXERCISES ON DIFFERENT BALANCE PLATFORMS

[1]Gulcan Harput, [1]Nevin Ergun, [2]Hayri Ertan and [1]A. Ruhi Soylu

[1] Hacettepe University, Ankara, TURKEY
[2] Anadolu University, Eskisehir, TURKEY
email: aktasgulcan@yahoo.com

INTRODUCTION

The ankle injuries are the most common type of injuries with an incidence of about 25% of all injuries across all sports. 95% of ankle injuries involve lateral ankle sprain that causes a rupture of the anterior talofibular ligament [1]. Ankle muscles, especially peroneus longus, gastrocnemius, tibialis anterior, tibialis posterior have a great role in stabilizing the ankle during daily activities and sports maneuvers such as cutting and jumping [2, 4]. If there is any functional or anatomical deficiency in ankle muscles, the stresses are formed during activities countered by ligaments or joint structures [5]. A proprioceptive impairment in the ankle resulting from injuries has been well documented [1, 2, 3, 5]. Therefore, balance trainings are used to improve balance ability so as to protect injuries, or to diminish the rate of injury risk after the injuries [4]. Balance training supports the neuromuscular mechanisms responsible for the co-contraction of agonist and antagonist muscles that enhance joint stability [3, 5, 6]. It has been showed that unstable surfaces provide sudden alterations and make training more dynamic, and possibly more applicable to a sporting context [3]. However, there are limited studies which show the activation of the ankle muscles during balance exercises on balance surfaces, and thus it is hard to decide which exercises on which platforms are proper to our exercise protocol. The aim of this study was to investigate whether the activation of peroneus longus (PL), tibialis anterior (TA) and gastrocnemius medialis (GKm) muscles differ during four different closed kinetic chain exercises on wobble board and BOSU platforms.

METHODS

23 healthy subjects (12 F, 11 M) (age: 23.2±1.5 yrs; height: 170.1±9.3 cm; weight: 66.4±12.2 kg; BMI: 22.8±2.5 kg/m^2) were included in this study. Four different balance exercises (forward lunge, side lunge, single limb stance, single limb squat) were performed on wobble board and BOSU during 15 seconds **(Figure 1).** The activation of PL, TA and GKm muscles during exercises were recorded by using surface electromyography (Delsys, Boston, MA). Pass band of EMG amplifier, sampling rate, maximum intra-electrode impedance and common mode rejection ratio (CMMR) were 8–500 Hz, 1000 Hz, 6 kOhm and 95 dB respectively [7]. Butterworth filter (8Hz) was applied to clear up movement artifacts. Integrated EMG (iEMG) was calculated and used for statistical analyses. Non-parametric tests were performed for statistical analysis.

Figure 1: forward lunge (FL), side lunge (SL), single limb squat (SLSQ) and single limb stance (SLST) respectively.

RESULTS AND DISCUSSION

The activations of the other muscles except for GKm were found to be the same in terms of both platforms ($p>0.05$). The activation of GKm muscle was recorded to be higher in SLSQ exercise on

BOSU (p=0.021) (**Figure 4**). PL and GKm muscles revealed maximum activation in SLST exercise, while the maximum activation of TA muscle was in SL exercise.

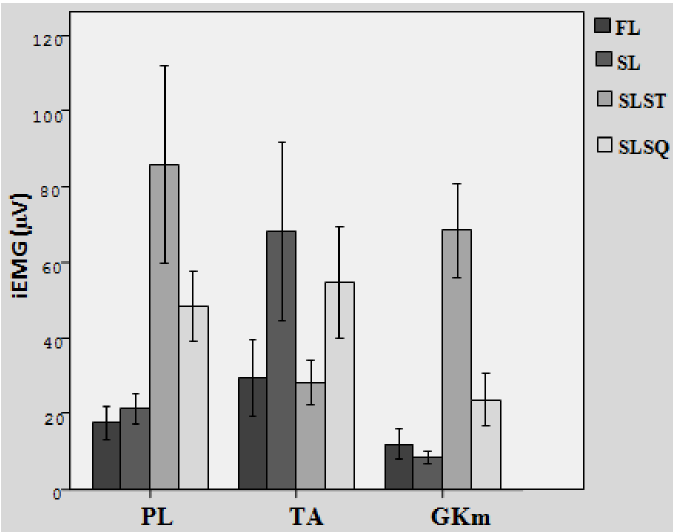

Figure 2: EMG activation of PL, TA and GKm muscles on wobble board in FL, SL, SLST and SLSQ exercises.

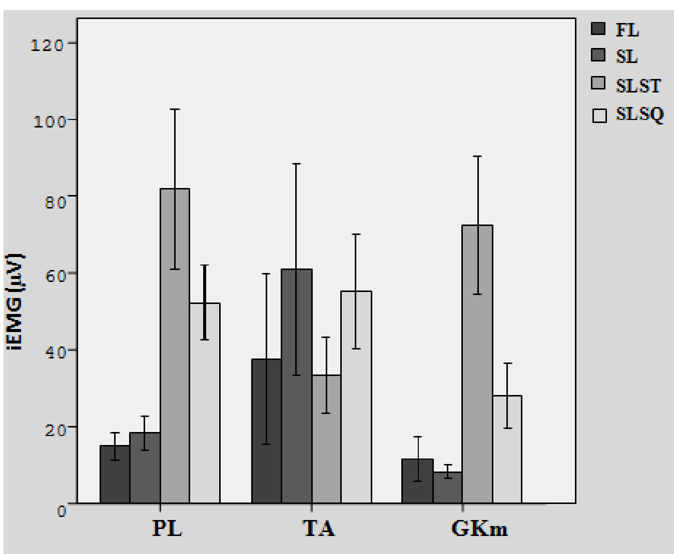

Figure 3: EMG activation of PL, TA and GKm muscles on BOSU in FL, SL, SLST and SLSQ exercises.

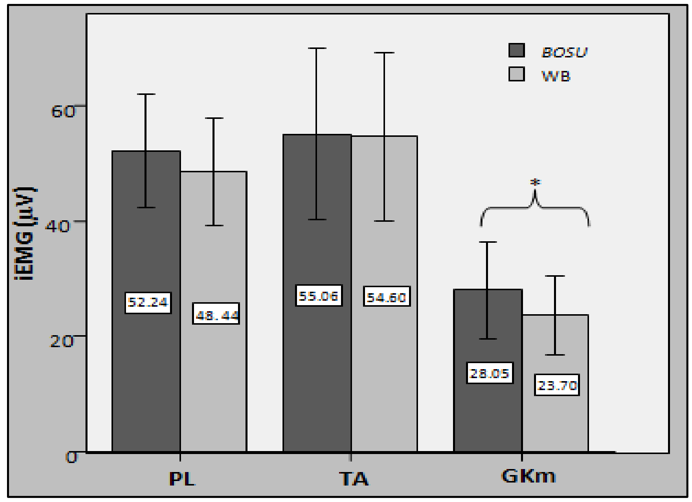

Figure 4: The difference between BOSU and Wobble board in terms of PL, TA and GKm muscles EMG activation in SLSQ exercise.

CONCLUSIONS

SLST was regarded to be the most effective exercise for training both PL and GKm muscles, and to display the most co-contraction of all muscles, which were tested. On the other hand, SL exercise could be more effective to train TA. As PL and TA muscle activations were similar in four exercises on wobble board and BOSU, only one platform could be said to be adequate for training these muscles. Further investigations are needed to create evaluation and exercise protocols following injuries.

REFERENCES

1. Hupperets, MDW. et al. *Sports Med* **39**,591-605, 2009.
2. Eisen, TC. et al. *J Strength Cond Res* **24(7)**, 1740-1745, 2010.
3. Zech, A. et al. *J Athl Train* **45(4)**, 392-403, 2010.
4. Page, P. *Journal of Bodywork and Movement Therapies* **(10)**, 77-84, 2006.
5. Wikstrom, E. et al. *Sports Med* **36(5)**, 393-410, 2006.
6. Lee, AJY. et al.*Clin Biomech* **23**, 1065-1072, 2008.
7. Soylu, AR. et al. *Human Mov Sci* **25(6)**, 767-74, 2006.

THE RELATIONSHIP BETWEEN AMBULATORY ACTIVITY PATTERNS AND KINEMATIC VARIABILITY

[1]Ryan M. Hasenkamp, [1]Shane Wurdeman and [1]Sara Myers

[1]University of Nebraska at Omaha, Omaha, NE, USA
email: rhasenkamp@unomaha.edu, web: biomech.unomaha.edu

INTRODUCTION

Analysis of the variability present in movement patterns provides insight and understanding of the underlying motor control in a given movement. Natural fluctuations occur in movement and this inherent variability can be quantified through linear and nonlinear mathematical algorithms. A temporally ordered gait pattern is thought to be "healthy" and allows individuals the freedom to adjust to their environment[1]. Healthy young adults are thought to demonstrate optimal amount and temporal structure of variability and deviations from this status of variability have been associated with aging, disease and delayed development[1,3]. However, current scientific methods for assessing gait kinematic variability are limited to laboratory-based environments, which may not accurately reflect what occurs throughout daily ambulation. An alternative device, which can capture movements throughout the day, is an accelerometer. These portable, easy to use, and inexpensive devices measure ambulatory activity patterns and may provide similar information about motor control of movements as gait kinematic variability. The purpose of this pilot study was to investigate the relationship between ambulatory activity as measured through an accelerometer and gait kinematic variability. We hypothesized that variability of ambulatory activity and gait kinematic measures are strongly related.

METHODS

Seven healthy young adults (age: 25.3 ± 4.2 years, weight: 80.6 ± 19.7 kg, height: 175.4 ± 13.2 cm) were recruited to participate in this pilot study. Subjects were asked to walk on a treadmill while simultaneously wearing an accelerometer at the hip. First subjects walked at a slow self-selected speed (2.2 ± 0.6 mph) for five minutes. Then in order to determine if the relationship was consistent with different speeds, subjects walked at a fast self-selected speed (3.1 ± 0.6 mph) for five minutes. Subjects walked on a treadmill while 3D marker trajectories (60 Hz; Motion Analysis Corp., Santa Rosa, CA) were recorded. Simultaneously, an accelerometer (30 Hz; ActiGraph GT3X, Pensacola, FL) worn at the hip recorded raw acceleration (milli-Gs). Continuous joint angle time series were calculated for the ankle, knee, and hip (Figure 1). Measures of temporal structure of gait kinematic variability calculated were the Lyapunov Exponent using procedures according to Wolf's algorithm and approximate entropy (4,5). For the ambulatory activity, the raw acceleration time series was analyzed. Measures of temporal structure of ambulatory variability were the Lyapunov Exponent and approximate entropy (4,5). Pearson's correlations were used to calculate the relationship between gait kinematics and the acceleration.

RESULTS AND DISCUSSION

Results from this pilot study are presented in Table 1. There was a significant, positive relationship between the Lyapunov exponent of ambulatory activity and gait kinematic variability at the hip during the slow condition ($r = 0.77$). Additionally, there were several moderate, but non-significant correlations. Specifically, there was a moderate, positive relationship between gait kinematic and ambulatory activity variability for Lyapunov exponent at the ankle during the slow self-selected speed, and moderate, negative correlations for approximate entropy at the knee during the slow self-selected speed, and for the approximate entropy at the ankle and the knee during the fast speed. It is very interesting that the only significant, strong relationship occurred at the hip. This result provides evidence that there is a relationship between variability of ambulatory activity and gait kinematic variability. The hip likely shows the strongest correlation due to the fact that the accelerometer was placed at the hip.

As seen in Figure 1, the accelerometer time series shows similar oscillations as seen in the hip kinematic time series. Lyapunov exponent and approximate entropy are good statistical measures because these time series show periodic oscillations.

Figure 1. Sample of ankle, knee, and hip kinematic time series (solid line) with accelerometer time series (dashed line).

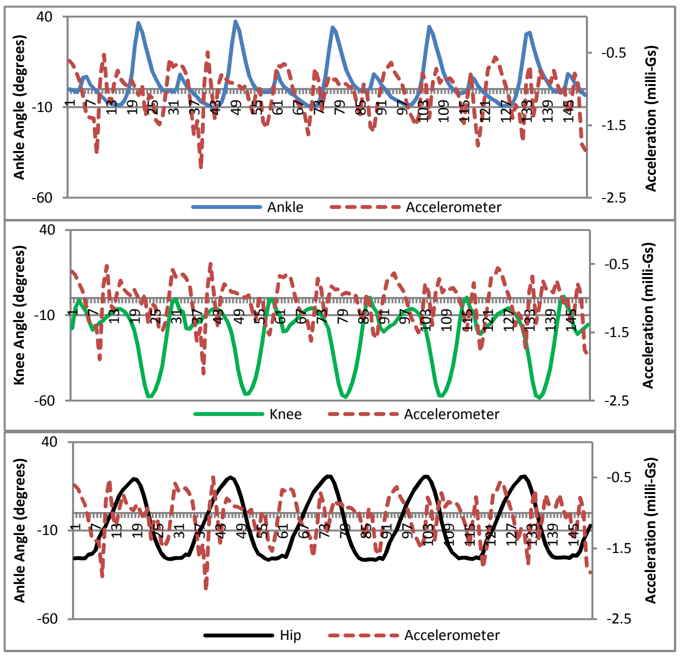

A limitation of this pilot study is the small sample size, which can be particularly limiting in a correlation analysis. This likely explains the large differences in the relationship between the variability of ambulatory activity and gait kinematic variability for different measures.

CONCLUSION

There was a strong, significant relationship between the Lyapunov exponent of the hip joint angle and ambulatory activity while walking at a slow self-selected speed. Further work may investigate the relationship between kinematics and an accelerometer located at various lower extremity positions. Furthermore increasing the size of the sample may lead to improved ability to reveal a relationship between these two measures.

REFERENCES

1. Stergiou N et al. *J Neurol Phys Ther*. 2006 Sep;**30**(3):120-9
2. Cavanaugh JT et al. J Am Geriatr Soc. 2007 Jan;**55**(1):120-4.
3. Myers S et al. J Vasc Surg. 2009 Apr;**49**(4):924-931.
4. Wolf A et al. Phsica D. 1985 July;**16**(3):285-317
5. Pincus S. Proc Natl Acad Sci USA. 1991 Mar;**88**:2297-2301

Table 1. Group means ± standard deviation for Lyapunov Exponent and Approximate Entropy of acceleration and kinematics of the ankle, knee, and hip.

Dependent Variable	Kinematics	Accelerometer	*r* value	Coefficient of Determination
Condition 1 – Slow Speed				
Lyapunov Exponent Ankle	1.302 ± 0.38	1.799 ± 0.71	0.59	0.349
Lyapunov Exponent Knee	0.871 ± 0.31	1.799 ± 0.71	0.17	0.028
Lyapunov Exponent Hip	0.672 ± 0.25	1.799 ± 0.71	0.77*	0.593
Approximate Entropy Ankle	0.415 ± 0.09	1.618 ± 0.12	-0.04	0.002
Approximate Entropy Knee	0.261 ± 0.06	1.618 ± 0.12	-0.69	0.472
Approximate Entropy Hip	0.232 ± 0.04	1.618 ± 0.12	0.31	0.098
Condition 2 – Fast Speed				
Lyapunov Exponent Ankle	1.260 ± 0.40	1.347 ± 0.21	0.16	0.024
Lyapunov Exponent Knee	0.878 ± 0.35	1.347 ± 0.21	-0.43	0.189
Lyapunov Exponent Hip	0.614 ± 0.18	1.347 ± 0.21	-0.34	0.113
Approximate Entropy Ankle	0.453 ± 0.11	1.415 ± 0.14	-0.54	0.287
Approximate Entropy Knee	0.295 ± 0.06	1.415 ± 0.14	-0.54	0.287
Approximate Entropy Hip	0.224 ± 0.03	1.415 ± 0.14	0.01	0.0001

Note: * $p < 0.05$, significant correlation

MECHANICAL DEMAND DISTRIBUTION DURING SHOD AND NOVICE BAREFOOT RUNNING

Rami Hashish, Sachithra Samarawickrame, Kush Gaur and George Salem
University of Southern California, Los Angeles, CA, USA
email: rhashish@usc.edu web: http://pt2.usc.edu/labs/mbrl/

INTRODUCTION

Research regarding barefoot (BF) running has demonstrated that habitual BF runners present with a more anterior foot strike compared to their habitually shod (SH) counterparts [1]. A forefoot strike is associated with a decrease in peak impact collision forces [1], and thus a reduced potential for knee overuse injuries. This is of particular clinical importance considering that the knee is the most commonly injured site from running participation, accounting for approximately 42% of all injuries [2]. However, these same loading characteristics may lead to an increase in eccentric demand about the ankle, which could potentially result in soft tissue injuries of the foot and ankle. Therefore, the purpose of this preliminary investigation was to examine the change in footfall pattern, and mechanical demand at the knee and ankle during SH and novice BF running.

METHODS

Three habitually SH distance runners performed 4-8 trials of SH and BF over-ground running at the Jaquelin Perry Musculoskeletal Biomechanics Research Laboratory. All subjects performed SH running at a self-selected velocity, which was between 3.7-5.5 meters/second. The BF running trials were also performed at a self-selected velocity, which was within 5% of the SH running speed. All subjects included in the study ran a minimum of 12 kilometers per week, and reported no significant injuries over the preceding 12 months.

Kinematics were recorded using a Qualisys motion capture system (Gothenburg, Sweden) at 250 Hz. Three-dimensional kinetics were recorded from AMTI force platforms (Watertown, MA) at 1500 Hz. Initial contact (IC) was defined as a minimum of 20 Newtons vertical ground reaction force (vGRF). The absorption (ABS) phase was defined from IC to peak knee flexion during the stance phase [3]. The support impulse was calculated as the sum of the sagittal plane extensor impulses during ABS [4]. Joint power was calculated as the product of the moment and angular velocity. Mechanical work was then computed utilizing a custom written program in Matlab (MathWorks Inc., Natick, MA) that integrates the negative portion (energy ABS) of the respective joint power curves [3]. Mean absolute differences, or relative contributions and the associated effect sizes (ES; Cohen's *d*) between the conditions are reported.

RESULTS AND DISCUSSION

Ankle Angle
Relative to SH running, novice BF runners demonstrated a mean increase of 23.45^{o} in ankle plantar flexion at IC (ES = 3.53).

Support Impulse
Compared to SH running, BF running resulted in a 4.2% mean reduction to the support impulse by the knee (ES = 1.89) and a 7.5% mean increase in contribution by the ankle (ES = 6.07).

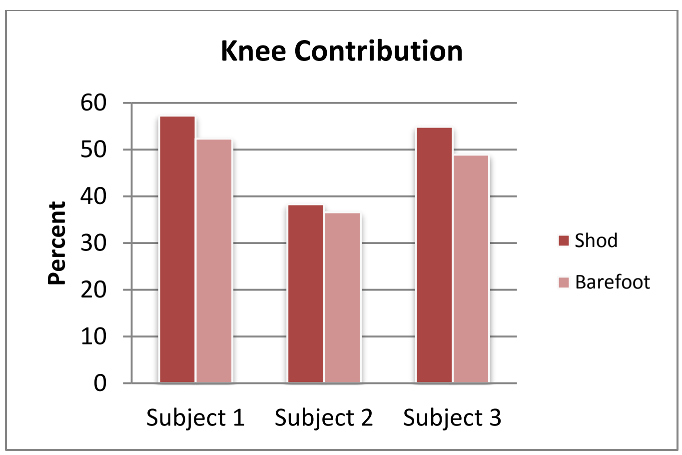

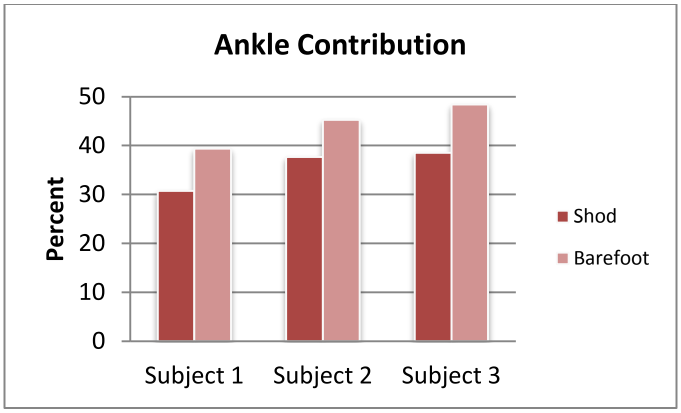

Figure 1: Knee (top) and ankle (bottom) contribution to the support impulse during SH and novice BF running for the three subjects.

Relative to SH running, Subject 2 demonstrated a negligible change in knee contribution, yet an increase in demand at the ankle during novice BF running (7.6%). The findings suggest that this participant potentially shifted demand away from the hip, rather than the knee, to the ankle.

Energy Absorption

Relative to SH running, novice BF runners demonstrated a negligible change in mean energy ABS by the knee (-6.1 J/Kg; ES = 0.30), but an increase at the ankle (18.1 J/Kg; ES = 1.60).

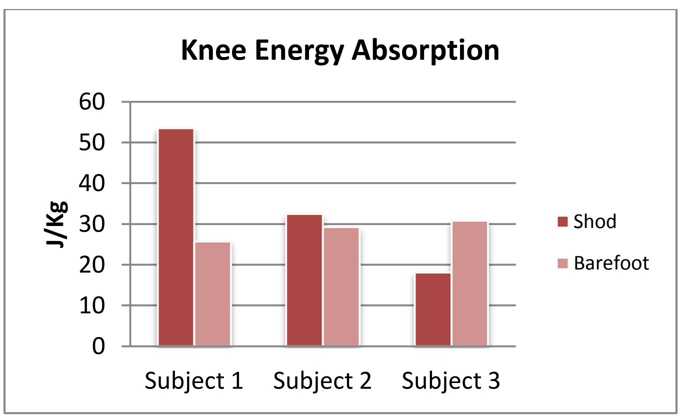

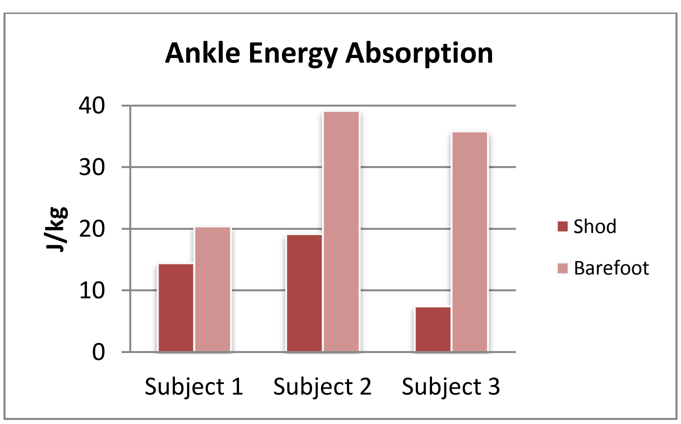

Figure 2: Knee (top) and ankle (bottom) energy absorption during SH and novice BF running for the three subjects.

Relative to SH running, Subject 3 demonstrated increases in knee (12.7 J/Kg) and ankle (28.4 J/Kg) energy ABS during novice BF running. The findings suggest that this running pattern may have been less energy efficient for this particular participant.

CONCLUSIONS

The cumulative findings from this preliminary investigation suggest that relative to SH running, novice BF runners shift mechanical demand away from the knee and to the ankle. Although the benefit of BF running is associated with a forefoot strike, this footfall pattern results in a more anteriorly located vGRF vector, thereby increasing eccentric demand to the ankle. If this demand is too great, it could result in myotendinous strains, potentially including tears to the Triceps Surae, as well as Achilles and/or Tibialis Posterior tendinopathy. It is plausible, however, that an appropriate transition to BF running may help to negate these deleterious effects [5]. These findings will inform the design of expanded, controlled prospective studies, which are needed to better understand the effects of a BF transitional period on lower extremity dynamics in habitually SH runners.

REFERENCES

1. Lieberman DE, et al. *Nature* **463**, 531-535, 2010.
2. Taunton JE, et al. *Br J Sports Med* **36**, 95-101, 2002.
3. Heiderscheit BC, et al. *Med Sci Sports Exerc* **43**, 296-302, 2011.
4. Flanagan SP, et al. *J Strength Cond Res* **18**, 599-605, 2004.
5. Hashish R, et al. Proceedings from *American College of Sports Medicine*, 2012.

IMMEDIATE APPLICATION OF CYCLIC COMPRESSIVE LOADING ATTENUATES SECONDARY HYPOXIC INJURY FOLOWING DAMAGING ECCENTRIC EXERCISE

[2*]Caroline Haas, [1*]Sarah M. Abshire, [1]Timothy A. Butterfield, and [2]Thomas M. Best
[1]University of Kentucky, Lexington, KY, USA
[2]The Ohio State University, Columbus, OH, USA
*contributed equally to this work
email: caroline.haas@osumc.edu
Website: http://www.mc.uky.edu/athletic_training/butterfield

INTRODUCTION

The loss of function following eccentric exercise (EEX) is associated with immediate subcellular damage [1] that is further exacerbated by secondary hypoxic injury [2] that can delay the recovery of force production for several weeks [3]. Recently, we have shown that cyclic compressive loading (CCL) accelerates the recovery of muscle form and function when immediately applied to muscle following intense, damaging EEX [4]. We hypothesize CCL attenuates secondary hypoxic injury in skeletal muscle by modulating the immune response to EEX, thereby indicating a time-dependency for CCL efficacy. In this study we assess the temporal effects of delayed vs immediate CCL application following EEX, to further understand the influence of CCL on cellular (immune) and mechanical (function) responses in exercised muscle.

METHODS

Eighteen skeletally mature NZW rabbits were instrumented with bilateral peroneal nerve cuffs to allow stimulation of the tibialis anterior (TA) muscles [4]. Following a single bout of damaging EEX (7 sets of 10 reps [4], rabbits were randomly assigned to 15 minute immediate CCL (0.5Hz, 10N) (n=6), 48 hour delayed CCL (0.5Hz, 10N) (n=6), or exercised, non-massaged control (n=6). A torque-angle relationship was obtained for 21 tibiotarsal joint angles (55° to 155° in 5° increments) pre and post EEX and following four consecutive days of CCL or non-CCL (control). CCL was performed via a customized device that allowed quantifiable, repeatable loading [5]. 24 hours after the final CCL day, animals were euthanized and the TA muscles were weighed and flash frozen in liquid nitrogen and stored at -80ºC for analyses.

To assess the time-dependent influence of CCL on function, a recovery index (RI) was defined as a contrast of peak torque at the three fixed time points (pre-exercise, post-exercise, and post four days of CCL).

$$RI = \left(1 - \left(\frac{(pre\_EEX - post\_CCL)}{pre\_EEX} \middle/ \frac{(pre\_EEX - post\_EEX)}{pre\_EEX} \right) \right)$$

The denominator quantified the immediate loss of peak torque (day one, post EEX), and the numerator measured delayed loss of torque (post CCL) with respect to pre EEX values. An RI of 1 denotes full recovery of peak torque to pre EEX value.

TA muscles were sectioned at 8um thickness for immunohistochemistry staining. Sectioned tissues were fixed for 10 minutes in ice cold acetone, washed in 0.1M PBS then quenched for 10 minutes in 3% H_2O_2 and washed again in 0.1M PBS. Sections were then blocked for 1h at room temperature (RT) with 2% bovine serum albumin (BSA). Primary antibody (Mouse anti-Rabbit Macrophage Clone RAM11 (1:50) Dako, Carpinteria, CA or Mouse anti-Rabbit cd11b (1:50) or Mouse anti-Rabbit T-Cells and Neutrophils RPN3/57 (1:50) AbD Serotec, Raleigh, NC) for 90 minutes at RT. Sections were then washed with 0.1M PBS with 0.1% Tween-20 before incubation in Immpress anti-mouse Ig Detection Kit (Vector Labs, Burlingame, CA) for 30 minutes at RT. Sections were then washed in 0.1M PBS with 0.1% Tween-20 before incubation in TSA amplification kit for 20 min at RT. After a final wash in 0.1M PBS with 0.1% Tween-20, sections were stained with Dapi and coverslipped with Vectashield (Vector Labs, Burlingame, CA).

Muscle sections were viewed with a Zeiss Axio Imager M.1 microscope (Carl Zeiss, Thornwood, NY) at 20x and five random fields for each limb with each of the three antibodies were photographed for cell quantification. Positively labeled cells were then counted for each of the five photos and the numbers were averaged for each animal limb. Only stained areas that co-localized with Dapi stained nuclei were counted as positively stained cells.

RESULTS AND DISCUSSION

EEX produced an average 49% (± 13%) decrease in peak isometric torque output (n=18 hindlimbs; 6 immediate, 6 delay, and 6 exercised, non-massaged). Both immediate and delayed application of massage showed significant improvement of recovery of peak torque as compared to the exercised, non-massaged control (p=0.0005 and p=0.0135, respectively). Immediate application of massage produced a significant 79% increase in peak torque recovery as compared to the exercised, non-massaged control (p=0.0005). However, 48 hour delay of massage onset produced a significant 47% reduction of peak torque recovery compared to recovery produced by immediate application (p=0.0115) (Figure 1).

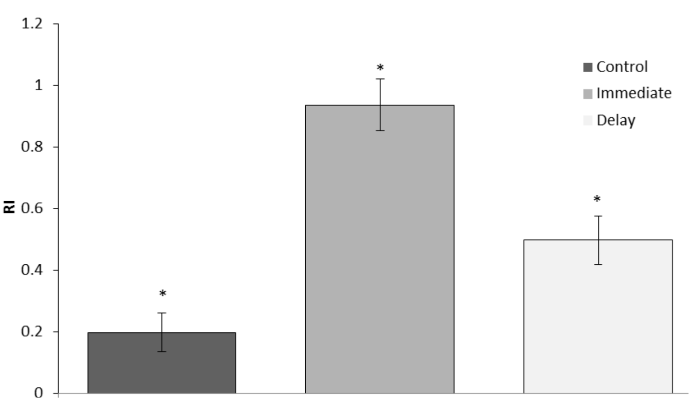

Figure 1: Immediate application of CCL produced greatest recovery as compared to delayed CCL (RI=0.94 ±.08 vs. 0.49 ± .07, respectively). However both application times of CCL produced a significantly greater recovery than control (RI=0.19 ± .06)

Muscle wet weight for the exercised, non-CCL group (4.01 ± 0.10g) was significantly higher than both the immediate (2.75 ± 0.09g) and delayed (3.34 ± 0.15g) CCL groups (p= 0.0003 and 0.0005, respectively. There was also a significant difference in wet weight between the immediate and delay CCL groups (p=.0005).

The exercised non-CCL control animals had significantly higher number of RPN3/57 positive neutrophils (42.87 ± 48.23) compared to the immediate CCL group (12.83 ± 11.58) and the delayed CCL group (27.20 ± 28.76), $p < 0.05$. The exercised non-CCL control animals also had a significantly higher number of RAM11 positive macrophages (16.96 ± 20.17) compared to the immediate (7.16 ± 10.31) and delayed (24.57 ± 41.42), $p < 0.05$) CCL groups.

CONCLUSIONS

Application of CCL immediately following damaging EEX attenuated the infiltration of neutrophils and macrophages in skeletal muscle, and facilitated recovery of function to near pre-exercise levels. Delayed application of CCL following EEX was less effective in restoring function, and was associated with more edema and greater infiltration of immune cells. These data provide support for the immunomodulating effects of CCL and its effect on associated secondary hypoxic injury and recovery of function following muscle injury.

REFERENCES

1. Butterfield TA. *ESSR* **38**, 51-60, 2010
2. Toumi H, F'Guyer S, Best TM. *J. Anat* **4**, 459-470, 2006
3. Sayers SP, Clarkson PM. *Eur J Appl Physiol* **84**,122-126, 2001
4. Butterfield TA, et al. *Med. Sci. Sports Exerc* **40**, 1289–1296, 2008.
5. Zeng, H, et al. *J. Med. Devices* **2**, 027530, 2008.

ACKNOWLEDGEMENTS

Supported by award R01AT004922 from the NIH (NCCAM) to TMB

DECELERATION: RELATIONSHIP BETWEEN BODY POSITION AND VELOCITY

Kathryn L. Havens, Susan M. Sigward
Human Performance Laboratory
Division of Biokinesiology and Physical Therapy
University of Southern California, Los Angeles, CA, USA
email: khavens@usc.edu, web: www.usc.edu/go/mbrl

INTRODUCTION

The distance between the body's center of mass (COM) and center of pressure (COP) has been shown to be related to the anterior velocity of the COM at initial contact of the terminating step during gait. Specifically, the COM must be positioned posterior to the COP in order to come to a complete stop without falling. A faster horizontal velocity requires a more posterior position.[1]

It is not clear if the anterior velocity of the COM or its required change in velocity during the task is more important for this relationship. Considering that velocity is zero at the end of gait termination, velocity at initial contact is equivalent to the change in anterior velocity. This relationship would need to be assessed during tasks that require ongoing motion. In order to determine the effect of velocity requirements on COM position, we examined tasks with deceleration demands such that the change in velocity should differ from that of initial contact: running, cutting at two angles, and running termination.

The purpose of this study was to determine whether relationships exist between the anterior-posterior COM position relative to the COP and the anterior COM velocity at initial contact and the change in anterior velocity during tasks with varying deceleration demands.

METHODS

Seven healthy, recreationally active individuals (4 females; 19-25 yrs) with no history of previous knee injury participated. Average height and weight was 1.75 ± 0.1 m and 69.2 ± 8.2 kg, respectively.

Subjects performed a straight running task, two sidestep cutting tasks (to 45˚ and 90˚) and a stopping task. For the running task, subjects ran for 15 meters. For the cutting tasks, subjects ran 7.5 meters, planted their dominant foot on the force plate and changed direction away from the plant leg at a 45° or 90˚ and continued running for 7.5 meters. For the stop task, subjects ran 7.5 meters and came to a complete stop (Fig. 1). All tasks were performed as fast as possible.

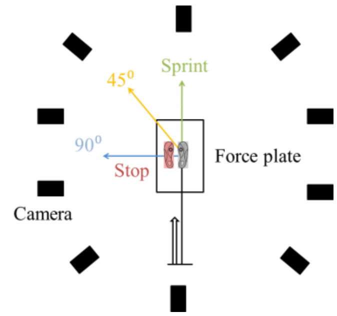

Figure 1: Experimental set-up for right dominant subject. Open arrow indicates original line of progression.

Three-dimensional kinematics were collected using a 10-camera motion capture system (Qualisys, Inc. Sweden), 250 Hz. Ground reaction forces (GRF) were quantified using AMTI force platforms (Newton, MA, USA), 1500 Hz. Whole body COM was calculated as the weighted sum of the COM of all 15 modeled segments (Visual3D™, C-Motion, Inc., Rockville, MD, USA). COP location, the application point of the resultant GRF vector, was determined from force plate recordings.

The distance between the COM and COP was calculated in the anterior-posterior (AP) direction and normalized by height at initial contact. COM anterior velocity was also calculated at initial contact. Change in velocity was represented by the AP ground reaction force impulse (GRI), which was calculated as the integration of the GRF-time curve and normalized by body weight impulse (BWI).[3] GRI was considered during the braking phase of stance, defined as the time during which the AP GRF vector was directed posteriorly. During stopping, braking was defined as time during which COM velocity remained greater than 5% of peak running trial velocity (~0.3m/s).[4] Data were averaged across four trials. Pearson's correlations were used to assess whether relationships exist between COM position and COM velocity and change velocity. Multiple stepwise regression was used to determine the best predictor of COM position. Differences in velocity requirements were assessed using a one-way ANOVA; paired t-tests were used for post hoc analysis ($p \leq 0.05$).

RESULTS AND DISCUSSION

These tasks represented a range of velocity and change in velocity (impulse) demands. A statistically significant difference was found between tasks in anterior velocity at initial contact ($p<0.001$) and GRI ($p<0.001$). All pairwise comparisons were significant ($p<0.05$), with the only exception being the GRI between the 45˚ cut and stop tasks ($p=1.0$). (Table 1)

	Run	45˚ Cut	90˚ Cut	Stop
Velocity (m/s)	6.42 ± 0.48	5.57 ± 0.58	4.18 ± 0.35	2.72 ± 0.67
Impulse/ BWI (ratio)	0.06 ± 0.01	0.35 ± 0.09	0.61 ± 0.06	0.35 ± 0.10

Table 1: COM anterior velocity and GRI

Braking ground reaction force impulse was the only predictor of AP COM-COP separation. ($r=0.806$, $R^2=0.649$ $p<0.001$). (Fig. 1) Greater AP separation was associated with greater impulse. While a statistically significant relationship was found between peak AP COM-COP separation and anterior COM velocity ($r=-0.519$, $R^2=0.270$, $p=0.005$), it did not enter into the regression equation. (Fig. 2)

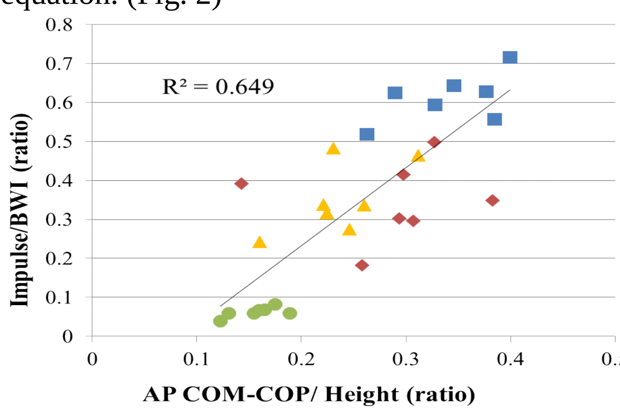

Figure 1: Posterior COM position relative to COP versus braking ground reaction force impulse; *Green circles*: Run, *Yellow triangles*: 45˚ cut, *Blue squares:* 90˚ cut, *Red diamonds*: Stop

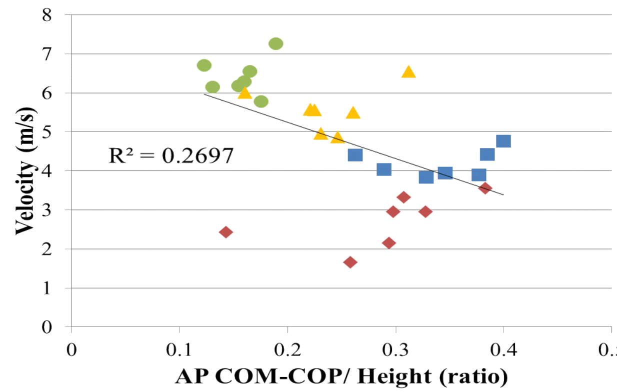

Figure 2: Posterior COM position relative to COP versus COM velocity

These experimental tasks had different velocity requirements. Speeds at initial contact and deceleration requirements were different, (Table 1) which allowed for comparisons between the two velocity variables.

Change in velocity requirements appear to be a more important determinant of COM position than velocity at a single time point. (Fig. 1) When more deceleration was required, subjects positioned their COM more posterior to their COP. The relationship between COM posterior position and velocity at initial contact was opposite of that seen during gait termination (Fig. 2). This suggests the relationship observed during walking gait termination is related to the change in velocity demand (coming to a complete stop) and not the anterior velocity itself.

CONCLUSIONS

Together, these data suggest that during ongoing tasks, the change in anterior velocity is a more important determinant of COM position than anterior velocity at initial contact. However, these data only represent seven subjects. A larger sample size would be needed to determine whether the differences reported here represent real differences in strategies.

REFERENCES

1. Pai YC, et al. *J Biomech* **30**, 347-353, 1997.
2. Sheppard JM, et al. *J Sports Sci* **24**, 919-932, 2006.
3. Munro CF, et al. *J Biomech* **20,** 147-155, 1987.
4. Cao C, et al. *Gait Posture* **8,** 103-109, 1998.

STABILOGRAM DIFFUSION ANALYSIS APPLIED TO DYNAMIC STABILITY: ONE-LEGGED LANDING FROM A SHORT HOP

[1]Gary D. Heise, [1]Jeremy D. Smith and [2]Kathy Liu

[1]University of Northern Colorado, Greeley, CO, USA
[2]University of Delaware, Newark, DE, USA
email: gary.heise@unco.edu, web: http://www.unco.edu/nhs/ses/

INTRODUCTION

Dynamic stability describes the process of transitioning from movement to a quiet, standing posture. Time-to-stability (TTS), based on the diminishing fluctuations in ground reaction forces and center-of-pressure (COP) trajectories, is often used to assess this transition [1]. Static postural stability is often assessed by analyzing the displacement of the COP while a person stands quietly on a force platform [2]. These approaches result in gross indicators of overall stability, but are criticized because of the limited physiological meaning that can be derived from the dependent variables. Typically, protocols that examine responses to perturbations, changes to sensory systems (e.g., vision), and differences in injury status are used in conjunction with the aforementioned approaches.

Collins and DeLuca [3] introduced a method of assessing stabilograms based on techniques from statistical mechanics. Their intent was to introduce a method that resulted in more physiologically meaningful results. Their stabilogram-diffusion analysis (SDA) modeled quiet standing as a system of coupled, correlated random walks [3]. The mean squared displacement between COP coordinates and their respective time interval are plotted (see Figure 1) and a critical point is identified where the slope changes from very steep to much shallower. The resulting two regions of the stabilogram-diffusion plot (short-term and long-term) have been suggested to be associated with postural control changes from a primarily open-loop process to a closed-loop process. The purpose of the present investigation was to apply this SDA to a dynamic stability protocol, where a person hops, lands on one foot, and gains stability (as in TTS studies). It is intended that further insights will be gained into how individuals become stable at the end of a dynamic task.

METHODS

Twenty healthy, recreationally active men (n=9) and women (n=11) volunteered for this study (age = 28 ± 4 yrs, body mass = 73.3 ± 21.5 kg, body height = 173.4 cm ± 10.5 cm). Participants were asked to complete a hopping task onto an AMTI force platform (barefoot, landing with dominant leg). After taking two steps, individuals took a forward hop from 100% of their leg length. Three trials were collected and analyzed for each person.

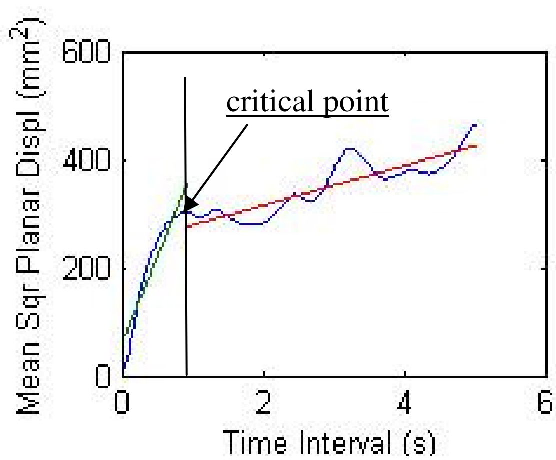

Figure 1: A representative resultant, planar stabilogram-diffusion plot. The vertical line goes through the critical point, which splits the plot into short-term and long-term regions. Least squares linear fits are shown in each region.

Ground reaction force data were collected at 100 Hz for 10 s after landing. COP coordinates were calculated and a SDA was applied to the COP-time series following the procedures of Collins and DeLuca [3]. From the mean square displacement-time interval plots, a critical value was determined that identified the short-term and long-term regions.

Diffusion coefficients (D_S, D_L) were calculated as one-half the slope of each least-squares linear fit to each region of the plot (see Figure 1). Similarly, scaling coefficients (H_S, H_L) were calculated from log-log plots of these curves [3]. These coefficients, values of the critical points, and R^2 values for line fits were compared to static stability results.

RESULTS AND DISCUSSION

Coefficients from the SDA assessment for dynamic stability in the present study were greater than values reported for static tests (see Table 1). Data from two sources [3, 4] are also shown in Table 1 for comparison. Collins and DeLuca [3] reported data for two separate groups, which differed in how many trials each participant attempted.

Table 1: Mean diffusion coefficients (D, $mm^2 \cdot s^{-1}$) and scaling exponents (H) for the short- (S) and long-term (L) regions of the SDA.

	D_S	D_L	H_S	H_L
Means	450.59	36.86	0.49	0.13
SDs	(181.66)	(23.64)	(0.04)	(0.08)
Means [3a]	6.74	1.76	0.76	0.28
Means [3b]	11.21	3.05	0.76	0.34
Means [4]	11.00	2.10	0.80	0.24

Note: Mean values from [3] are from two different groups (a, b) and mean values from [4] are from 30-s trials (they also analyzed data after 60 and 90 s).

The diffusion coefficients and scaling exponents from the linear fitted lines resulted in mean R^2 values greater than 0.95, except for D_L, which had a large range of values and a mean of 0.54.

In the present study, the mean critical point coordinates were (0.72 s, 587 mm^2) as compared to (1.04 s, 13 mm^2) from Collins and DeLuca [3] and (1.02 s, 16 mm^2) from Doyle et al. [4]. For all trials in the present study, this critical point was clearly identified, which was not the case in a previous study [3]. The critical time interval has been suggested to be indicative of a switch from open loop to closed loop control. Based on the previous suggestions, the critical time interval identified in the present study suggests that a switch between control processes took place at shorter time intervals in our dynamic task. This may be due to the less stable condition (one-legged standing after landing) compared to static, two-legged conditions or possibly the difference between the dynamic and static tasks themselves.

In addition, the values of the mean square displacement for the critical point and the diffusion coefficients are greater than values for static stability [3, 4]. Because one-legged standing after a short hop results in much greater movement of the COP during stabilization, it is not surprising that mean square displacements calculated across longer and longer time intervals would be greater.

In the present study, the mean short-term scaling exponent (H_S), resulted in a value of 0.49, with values from all 20 participants ranging from 0.40 to 0.54. This is a fundamental departure from the two-legged static SDA, where H_S was greater than 0.5 in all subjects [3]. Classical Brownian motion exists when H = 0.5, thus in the present study, COP movements over short-term intervals are purely random. The extremely high values of D_S support this interpretation. After the critical point, the mean long-term scaling exponent (H_L) decreased to 0.13, which describes nonrandom COP movements over longer time intervals. Taken together, these results suggest control for this stabilization task changes from a non-regulated process to a more tightly controlled one (e.g., closed loop) [3].

CONCLUSIONS

Compared to two-legged static stability, SDA for one-legged landings from a hop resulted in random COP motion over short-term intervals and a much clearer transition to tighter postural control.

REFERENCES

1. Wikstrom, EA, et al. *J Athletic Training* **39**, 247-253, 2004.
2. Prieto TE, et al. *IEEE Trans Biomed Eng* **43**, 956-966, 1996.
3. Collins JJ, DeLuca CJ. *Exp Brain Res* **95**, 308-318, 1993.
4. Doyle RJ, et al. *Gait & Posture* **27**, 223-230, 2008.

REDUCED AND ASYMMETRIC TRUNK STIFFNESS AMONG UNILATERAL LOWER-LIMB AMPUTEES DURING MULTI-DIRECTIONAL TRUNK PERTURBATIONS

Brad D. Hendershot and Maury A. Nussbaum

Virginia Tech, Blacksburg, VA, USA
email: nussbaum@vt.edu

INTRODUCTION

Low back pain (LBP) represents a significant secondary disability among persons with lower-limb amputation [1]. Substantial biomechanical evidence suggests altered and asymmetric movements and muscular control strategies that could alter the mechanics of the spine during amputee gait and locomotion [2]. Spine biomechanics (e.g., loading and stability) are largely influenced by passive mechanical properties of the spine and surrounding trunk musculature. Viscoelastic tissues of the passive spine can develop altered mechanical properties in response to changing loading patterns, rates, and magnitudes [3]. Alterations in amputee gait and locomotion could therefore lead to musculoskeletal imbalances, contributing to further reductions in mobility and causing pain. The goal of the present study was to quantify alterations and/or asymmetries in passive trunk stiffness among unilateral lower-limb amputees (LLAs), using multi-directional trunk perturbations.

METHODS

Six male unilateral LLAs and six male, non-amputee matched controls participated (Table 1), after completing an informed consent procedure approved by the Virginia Tech IRB.

Table 1: Mean (SD) anthropometric characteristics.

	LLAs *(n=6)*	Controls *(n=6)*
Age (yr)	36.5 (19.8)	34.3 (14.5)
Stature (cm)	176.0 (3.2)	174.0 (3.2)
Body mass (kg)	76.7 (11.9)	81.7 (12.1)

Participants were randomly exposed to trunk perturbations in the following directions: anterior, right- and left-oriented lateral bending. During each sequence, participants stood upright and relaxed in a structure that restrained the pelvis and lower limbs. A pseudorandomly-timed sequence of 12 rapid (~40ms) horizontal position perturbations (±5mm) were applied to the trunk at ~T8 via a servomotor (Kollmorgen AKM53K, Radford, VA, USA), rigid rod, and chest harness. The harness was designed such that the rigid connecting rod can be attached with a quick-release pin for connection in both the anterior and mediolateral directions (participants were rotated 90˚ depending on perturbation direction; Fig. 1).

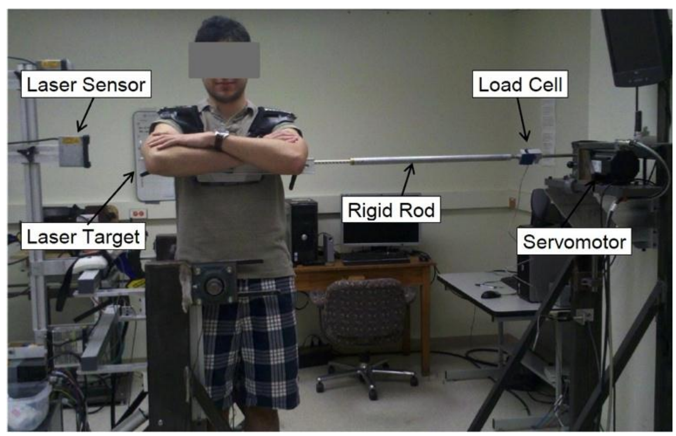

Figure 1: Experimental set-up demonstrating a participant in the left-oriented position. Participants' arms were similarly folded across the chest for all three perturbation directions.

During position perturbations, trunk displacements were measured with a CCD laser displacement sensor (Keyence LKG150, Osaka, Japan) and motor encoder. Applied forces were measured using a load cell in-line with the rigid rod (Interface SM2000, Scottsdale, AZ, USA). All data were sampled at 1000 Hz, and filtered with a 10Hz, bi-directional, low-pass filter [4]. Mechanical properties were estimated by relating measured trunk kinematics to trunk kinetics during each perturbation pulse, and by modeling the trunk/harness-rod connecting device as a 2DOF system [4]. Each degree of freedom has parameters of stiffness, damping, and mass, determined using a least squares curvefit algorithm in MATLAB™. Trunk damping was assumed to be negligible [5], and was forced to zero for these analyses to better represent changes in stiffness. Curve fits were restricted to the period of movement (~40ms) to ensure that there were no contributions from involuntary muscle reflexes.

Mixed-factor analyses of variance (ANOVA) were used to compare trunk stiffnesses between perturbation directions among LLAs and controls. Statistical analyses were conducted using JMP 9 (SAS Software, Cary, NC, USA), with a significance level of $p < 0.05$. Among LLAs, lateral bending perturbations were identified as ipsilateral or contralateral to the side of amputation, and results were pooled for both right- (n=4) and left-leg (n=2) amputees.

RESULTS AND DISCUSSION

Trunk stiffness was higher among controls than LLAs in all perturbation directions (Fig. 2), a difference that approached significance (p=0.063). There was also a significant group x perturbation direction interaction (p=0.001) on trunk stiffness. Among controls, trunk stiffness was higher (p<0.0001) in right- and left-oriented lateral bending perturbations [15.3 (3.1) kN/m] than anteriorly-directed [13.3 (2.9) kN/m], but bilaterally similar (p = 0.57; i.e., no asymmetries). Larger lateral bending stiffness of the trunk is consistent with previous research [6,7], and is likely caused by additional passive stiffness resulting from the geometry of the trunk musculature in the frontal plane [8]. Among LLAs, however, trunk stiffness was significantly lower (p<0.0001) during ipsilateral perturbations than contralateral perturbations (Fig. 2). Bilateral asymmetries in trunk stiffness may be a result of muscle atrophy ipsilateral to the side of amputation, and hypertrophy of trunk musculature contralateral to the side of amputation.

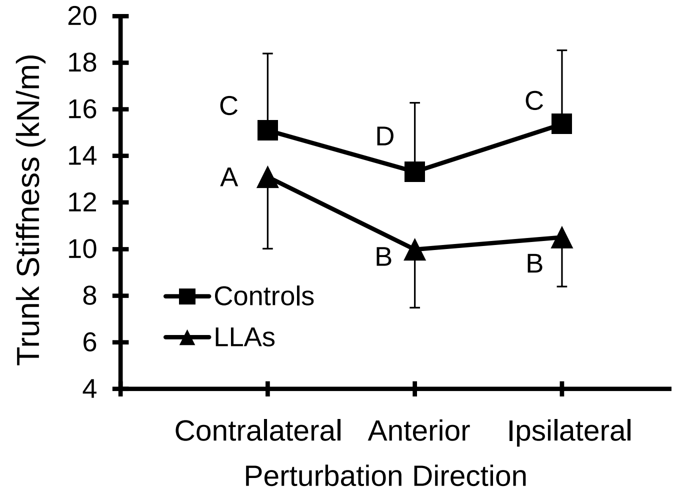

Figure 2: Trunk stiffness among LLAs and matched controls. Letters represent significant within group differences between perturbation directions. Error bars indicate standard deviations.

CONCLUSIONS

Reduced and asymmetric trunk stiffness among LLAs suggests substantial alterations in passive mechanical properties of the spine and surrounding trunk musculature. Further, muscle disuse atrophy could lead to reduced trunk stiffness among LLAs, specifically ipsilateral to the side of amputation, due to preferential use of the intact side of the body. Such reductions and asymmetries in trunk stiffness could represent an increased susceptibility for spinal instability, abnormal spinal loads, and thus an increased risk of LBP among persons with lower-limb amputation.

REFERENCES

1.Smith D et al. *Clin Orthop Relat Res* **361**, 29-38, 1999
2.Gailey R et al. *JRRD* **45**, 15-30, 2008.
3.Adams MA et al. *Clin Biomech* **11**, 194-200, 1996.
4.Bazrgari B et al. *CMBBE* (In Press)
5.Gardner-Morse MG et al. *J Biomech* **34**, 457-63, 2001.
6.McGill S et al. *Spine* **19**, 696-704, 1994.
7.Brown SHM et al. *J Electromyogr Kinesiol* **19**, 727-36, 2009.
8.Brown SHM et al. *Hum Movement Sci* **26**, 113-23, 2007.

THE EFFECT OF AGE AND MOVEMENT DIRECTION ON RAPID AND TARGETED CENTER OF PRESSURE SUBMOVEMENTS WHILE CROUCHING

Manuel E. Hernandez MS[1], James Ashton-Miller PhD[1,2], and Neil B. Alexander MD[3]

[1]Department of Biomedical Engineering, [2]Department of Mechanical Engineering,[3]Department of Internal Medicine, The University of Michigan, Ann Arbor, Michigan.
Email: manueleh@umich.edu   Web: www.med.umich.edu/geriatrics/moblab/

INTRODUCTION

Difficulty bending down to the floor is associated with an increased fall-risk among older adults [1]. Rapid center of pressure (COP) movements are often needed to avoid falls, yet older women are slower than young women, particularly when moving posteriorly [2]. Limitations in the use of balance recovery responses while crouching provide a mechanism for increased fall risk among older adults.

The overall goal of this study was to determine the effect of age, movement direction, and body configuration on COP submovements. We hypothesized that in comparison to young women, older women would display smaller but more numerous submovements with longer interpeak intervals, particularly during posterior movements.

METHODS

Subjects. Healthy young (mean±SD, age 23±3 years, N=13) and healthy older females (age 76±6 years, N=12) were recruited from the local community. Young women were taller (164±6 cm vs. 159±5 cm), but did not differ in weight, body mass index, or foot length.

Protocol. Subjects performed rapid targeted COP movements, while standing or crouching on top of a force plate and using hand support for stabilization. Trials corresponded to varying movement directions (anterior vs. posterior), varying target sizes (2, 3 and 4-cm), and body configuration (crouching vs. upright stance). A time-varying (1-3 sec) auditory tone was used to cue the start of the COP movement. Data collection was performed in a single experimental session in a laboratory setting.

Data Analysis. Submovements were extracted using a scattershot algorithm first proposed by Rohrer and Hogan (2006). Discrete COP movements were used to calculate the overall number of submovements, amplitude, and interpeak intervals. Repeated measures mixed-model analyses of variance were used to examine the effects of age while controlling for movement direction, target size, and body configuration. $P < 0.05$ was considered statistically significant.

RESULTS AND DISCUSSION

Overall, older women used more submovements, decreased COP peak magnitudes, and longer interpeak intervals ($P < .05$, Fig. 1) than young women. In comparison to an upright stance, COP submovements during a crouched stance were more numerous and smaller in magnitude ($P < .005$). Posterior movements used smaller peak magnitudes than anterior movements ($P < .001$). Furthermore, when moving posteriorly rather than anteriorly, older women used disproportionately smaller peak magnitudes than young women ($P < .05$, i.e., significant age x movement direction effect).

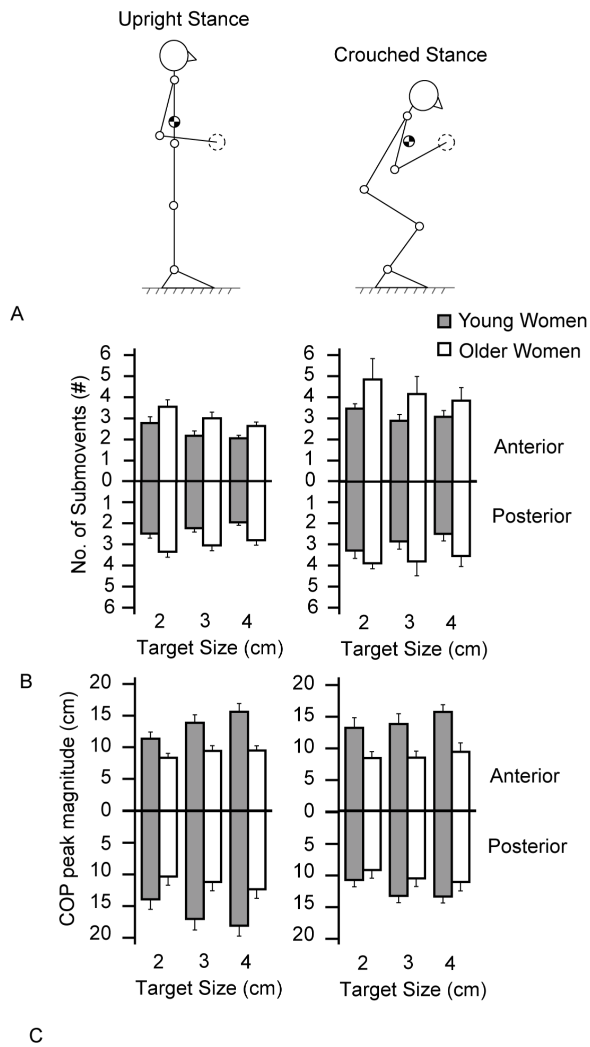

Figure 1: (A) Body configuration in typical upright and crouched stance. (B) Mean (SE) number of COP submovements and (C) COP peak magnitudes of anterior and posterior movements during 2-cm, 3-cm, and 4-cm trials.

Age-related changes observed in the number of submovements as well as the peak magnitude and interpeak interval of individual submovements are consistent with prior studies [2,4]. The submovement structure identified in this study provides a mechanism for the slower speeds seen in the movements of older adults. Crouching was found to lead to the use of more conservative postural control strategies in both young and older women, in comparison to an upright stance. However, as hand support was provided throughout this experiment, greater age-related changes between the upright and crouching stance may be observed through unsupported trials in a future study.

CONCLUSIONS

We conclude that COP submovement extraction via a scattershot algorithm can be used to identify age-related changes while standing and crouching. The use of smaller COP submovements by older women, particularly when moving posteriorly, may provide further evidence of a compensatory strategy for preventing backward falls.

REFERENCES

1. O'Loughlin, JL et al. (1993). *Am J Epidemiol ,* **137**, 342-354.
2. Hernandez, ME et al. (2012). *Hum Mov Sci,* **doi: 10.1016/j.humov.2011.11.002**.
3. Rohrer, B and Hogan, N (2006). *Biol Cybern,* **94**, 409-414.
4. Ketcham, CJ et al. (2002). *J Gerontol ,* **57B**, P54-P64.

ACKNOWLEDGEMENTS

We would like to thank collaborators in the Mobility Research Center for their assistance with data collection and the National Institutes of Health for NRSA Grant AG24689, which helped support this project.

ESTIMATING PEAK ACHILLES TENDON FORCES IN YOUTH DURING LOCOMOTION USING HIP ACCELERATION

[1]Jennifer Neugebauer and [1,2]David Hawkins
[1] Biomedical Engineering Graduate Group
[2] Department of Neurobiology, Physiology & Behavior
University of California, Davis, Davis, CA, USA
email: jmneugebauer@ucdavis.edu

INTRODUCTION

Estimating forces sustained by a musculoskeletal structure such as the Achilles tendon (AT) during locomotion is of interest for many applications. Quantifying peak AT forces (F_{AT}) is commonly limited to laboratory settings that are equipped with sophisticated motion capture systems. Recent developments using activity monitors (AMs) [1,2,3] provide novel methodology to estimate peak vertical ground reaction forces (pVGRFs) during gait using regression equations and hip acceleration as measured by an AM. The purpose of this investigation was to explore expanding this approach to estimate peak F_{AT} during locomotion by developing a preliminary regression equation for peak F_{AT} using hip acceleration, measured by an AM, and subject specific characteristics.

METHODS

3 girls (11.8 ± 1.0 years) and 3 boys (13.6 ± 0.6 years), a subset of subjects from another study in our laboratory, had their height and mass determined to the nearest 0.5 cm and 0.1 kg, respectively (Table 1). The AT moment arm was measured (in triplicate) as the perpendicular distance between the mid-substance of the AT and the medial malleolus while subjects stood with weight evenly distributed across both feet.

Subjects wore a randomly assigned Biotrainer AM (IM Systems, Baltimore, MD; 15 second epochs, 40 Hz sampling rate, 40 gain) secured on their waistband over the lateral most aspect of their right iliac crest. Kinematic (240 Hz) and ground reaction force (960 Hz) data were collected simultaneously using a four camera video system (Motion Analysis, Santa Rosa, CA) and a force plate (FP) (Kistler Corporation, Model 9281B, Amherst, NY), respectively.

Subjects completed a minimum of 3 walking (speeds 0.8-2.2 m/s) and 3 running (2.3-3.8 m/s) trials along a 90 m path that included the FP about 6 m from the starting point and four turns along two hallways. Locomotion speed was determined using electronic timing gates located 2 m on either side of the FP and synchronized with FP data acquisition. Inter-segmental forces and moments were determined via inverse dynamics (ID) methods using the video and FP data (Kintrak, Motion Analysis, Santa Rosa, CA). For all trials, peak F_{AT} was calculated by dividing the peak plantar flexion moment during the stance phase of gait by the AT moment arm (termed ID peak F_{AT}).

R (R Foundation for Statistical Computing, Vienna, Austria) was used to develop a preliminary mixed effects regression model to predict peak F_{AT}. This regression model was not designed to be statistically powered. The regression model initially included fixed effects (hip AM acceleration (g), subject mass (kg), subject height (cm), sex, type of locomotion, and AM acceleration-type of locomotion interaction) and random effects (subject, AM acceleration by subject, and an error term). A cutoff of $p < 0.05$ was used to determine if effects were included in the model. Based on the final regression model, ID and predicted peak F_{AT} were compared for each subject and all trials.

RESULTS AND DISCUSSION

In general, for each subject, as peak F_{AT} increased, AM acceleration increased. The final regression model used to predict the natural log of peak F_{AT} included the fixed effects of hip AM acceleration (g), subject height (cm), and type of locomotion (walk = 0, run = 1) (Equation 1).

$$Y_{ij} = 3.29 + X_{ij1}0.29 + X_{i2}0.02 + X_{ij3}0.26 + e_{ij} \quad [1]$$

where:

Y_{ij} = log transformed peak F_{AT} (ln(N)) for subject i, trial j
X_{ij1} = hip AM acceleration (g)
X_{i2} = subject height (cm)
X_{ij3} = type of locomotion (walk = 0, run = 1)
e_{ij} = error in trial j for subject i

Sex, subject mass, and AM acceleration-type of locomotion interaction ($p > 0.19$) as well as subject specific random effects ($p > 0.78$) were not included in the regression model.

The natural log of peak F_{AT} was predicted using Equation 1 for all trials, converted to peak F_{AT}, and compared with the ID peak F_{AT} (Figure 1).

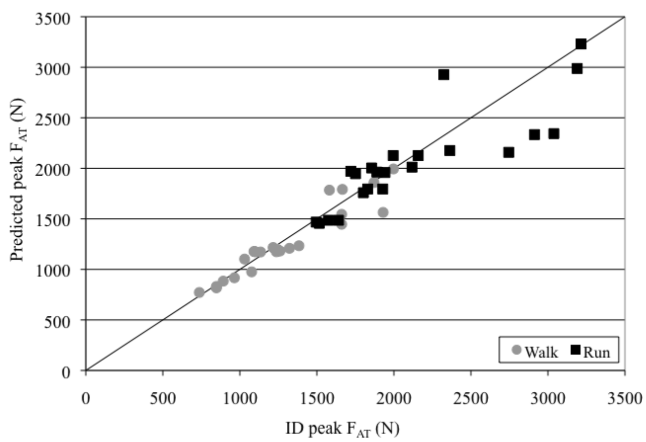

Figure 1. Predicted and ID peak F_{AT} for all subjects and all trials (r^2 =0.878, $p < 0.001$).

For all subjects, the average absolute and the average absolute percent difference between ID and predicted peak F_{AT} were 138.9 N (± 131.6 N) and 7.7 % (± 6.3 %), respectively (Table 1).

A preliminary regression model was developed to estimate peak F_{AT} during walking and running. To date, similar methods to estimate peak F_{AT} using hip AM acceleration have not been reported. The low average percent difference between ID and predicted peak F_{AT} for all subjects (7.7%) suggests that regression models of this type may provide reasonable estimates of peak F_{AT} for most subjects tested. However, as illustrated by the large absolute percent difference for Subject 3 (20.2%), the regression equation has room for improving.

The lack of significance of the random effects in predicting peak F_{AT} is likely a reflection of the unequal trial numbers as well as the small number of subjects. Before applying the regression model to predict peak F_{AT} in future applications, more subjects are needed to further develop the equation. Although not statistically powered, the accuracy of the prediction suggests that further exploration of this approach is warranted to fully develop a statistically powered equation to estimate peak F_{AT} using hip accelerations quantified using an AM.

REFERENCES

1. Collins, et al. *Proceedings of ASB 2011*, Long Beach, CA, USA, 2011.
2. Janz, et al. *Pediatr Exerc Sci* **15**, 34-43, 2003.
3. Neugebauer, et al. *MSSE* **42**, 270-271, 2010.

Table 1. Subject demographics, number of trials, and the average (avg) absolute (abs) difference (diff) and avg abs % diff between ID and predicted peak F_{AT}.

Subject	Sex	# of Trials	Age (years)	Height (cm)	Mass (kg)	Avg Abs Diff (N)	Avg Abs % Diff (%)
1	M	7	13.5	176.3	72.0	166.3	7.0
2	F	6	10.9	156.6	57.3	102.7	6.3
3	M	7	13.8	168.0	48.3	392.1	20.2
4	F	6	12.9	146.7	42.7	66.5	4.7
5	M	8	12.6	140.0	31.9	47.4	4.1
6	F	11	11.7	157.4	41.1	56.4	3.7
All Subjects: Avg ± Std Dev			12.6 ± 1.1	157.5 ± 13.3	48.9 ± 14.1	138.9 ± 131.6	7.7 ± 6.3
Males: Avg ± Std Dev			13.3 ± 0.6	161.4 ± 19.0	50.7 ± 20.2	201.9 ± 175.1	10.4 ± 8.6
Females: Avg ± Std Dev			11.8 ± 1.0	153.6 ± 6.0	47.0 ± 8.9	75.2 ± 24.3	4.9 ± 1.3

LATENT PROFILE ANALYSIS: GROUPING SUBJECTS BY BIOMECHANICAL PREDICTORS OF INCREASED KAM & POTENTIAL RISK FOR ACL INJURY

[1, 2] Hewett, T E; [2] Ford, KR; [2] Xu, YY; [2] Khoury J; [1,2]Myer, GD
[1]The Ohio State University, Columbus, OH,
[2] Cincinnati Children's Hospital Research Foundation, Cincinnati, OH,
Email: tim.hewett@osumc.edu or tim.hewett@cchmc.org.

INTRODUCTION

Over 120,000 anterior cruciate ligament (ACL) injuries occur each year in the United States. External loads on the knee in the coronal plane, specifically knee abduction moment (KAM), predict ACL injury risk with high sensitivity and specificity. Neuromuscular deficits associated with increased KAM appear to increase with age and proliferate with the onset of maturation. Profile analysis is a potentially important tool for characterization of the biomechanical and neuromuscular risk factor mechanisms that underlie ACL injury risk. This study utilized a novel cluster analytic technique, Latent Profile Analysis (LPA), to study the effects of multiple biomechanical and neuromuscular risk factors associated with KAM during a Drop Vertical Jump (DVJ), and a Single Leg Cross-Over Drop (SCD). The purpose of this work was to understand coupling between biomechanical and neuromuscular risk factors and their effects on KAM. We hypothesized that these variables would place subjects into distinct groups related to KAM.

METHODS

A total of 624 athletes from 52 basketball, soccer and volleyball teams were screened prior to their competitive season. During the screening, the athletes were asked to perform two different types of tasks for which biomechanical measures were taken: DVJ and SCD. For each task, 3 trials were performed. We used LPA to examine whether subjects could be grouped into distinct profiles based on biomechanical characteristics (task measured) determined *a priori*: GRF (DVJ), HAdT (SCD), hip moment (HIPADD maximum, from SCD), hip moment (HIPM_SCD minimum, SCD), hip moments (DVJ), and pelvis angle (SCD). For each of these six variables, we used values from the trial with the peak KAM within the specified task.

LPA created distinct neuromuscular profiles so that the heterogeneity of response pattern of the biomechanical characteristics was minimized within each profile and maximized across profiles. Initially, two profiles were specified for the LPA model, then, in a stepwise fashion, the number of profiles specified was increased by one. At each step, changes in Bayesian information criteria (BIC), adjusted for sample size, was used to assess model fit and identify the number of profiles needed. The number of profiles was deemed adequate when no significant drop in BIC was seen when the profile number was increased. In addition, the Lo-Mendell-Rubin adjusted likelihood ratio test was used to determine the optimal number of profiles.[5] It was necessary to account for the correlation between some of these variables; in particular maximum hip moment and GRFv and HAdT. The LPA was implemented using Mplus 5.[6] Validation of profile group involved examination as an independent predictor of KAM. Statistical analyses were conducted using Analysis of Variance (ANOVA). Differences were considered statistically significant at $p<0.05$.

RESULTS AND DISCUSSION

LPA resulted in three profiles. The three profiles are significantly different in most of the pair-wise comparisons of the means for these six variables. Figure 1 depicts the means and standard errors of the standardized score of each variable. For presentation purposes it is necessary to show the standardized values as the variables are on different scales, with large variance in mean values. The profiles also showed significant differences in characteristics;

athletes' age, pubertal stage, body mass, height and BMI. Profile I was smallest for these anthropological measures and mostly not post-pubertal, while profile III was largest with respect to the anthropological measures and mostly post-pubertal.

The validation analysis showed that profile group was significantly associated with KAM from the DVJ task. Profile II and III had a significant greater KAM value than Profile I, both with and without adjustment for age and pubertal stage. We also examined KAM during the SCD task as most of the six biomechanical variables used values from the SCD trial with peak KAM, with the exceptions of GRF and hip moment DVJ, which used the DVJ trial with peak KAM. Peak KAM during the SCD was significantly different across the profiles.

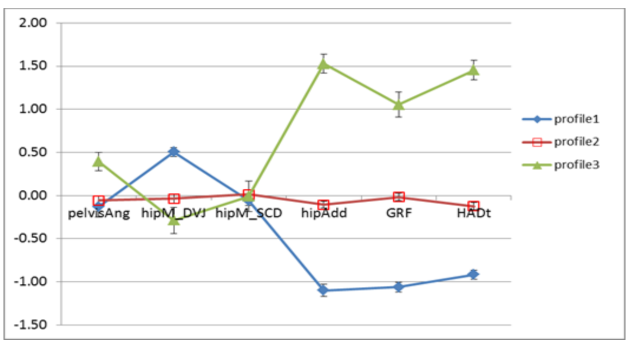

Figure 1 Profile mean and SE values of standardized biomechanical variables

To the investigators' knowledge, this is the first study to use LPA analysis of biomechanical landing data to create KAM and potentially ACL injury risk profiles. LPA provided greater group separation using multiple combined movement analyses and three distinct profiles were observed using peak measures. Group differences in peak KAM across the profiles were significant (II > I and III>I), whether unadjusted or adjusted for age and pubertal stage. Profile I is more likely to consist of younger and pre-pubertal athletes, while Profile III is more likely to consist of older and post-pubertal athletes.
Earlier studies by Hewett et al. [3] and Ford et al. [1,2] demonstrated that KAM increases with maturation and high KAM was consistently observed in those subjects that went on to ACL injury.[4] These findings begin to explain the clinical incidence of LPA groups; yet, further study is needed to investigate this phenomenon. We continue to examine LPA models and will validate them post intervention to determine potential emergent profiles that result from neuromuscular training. Large cohort Multi-Center studies of prediction of KAM and ACL injury risk with measured and demonstrably high validity and reliability will be the focus of future analyses.

CONCLUSIONS

Understanding the interaction between biomechanical and neuromuscular risk factors can help explain underlying mechanics to ACL injury factors and may help to predict relative risk.

REFERENCES:

[1] Ford KR, et al. *J App Bio.* **27**, 215-222. 2010.
[2] Ford KR, et al. *Med Sci Sport Ex.* **42**, 1923-1931. 2010.
[3] Hewett TE et al. *J. Bone Joint Surg*, 2004 Aug; 86-A(8): 1601-8. *2004*
[4] Hewett TE, et al. *Am J Sport Med.* **33**, 492-501. 2005.
[5] Lo Y, et al., *Biometrika*. **88**, 767-778. 2001.
[6] Muthen L.K., Muthen B.O. (2007) – Mplus User's Guide, Version 5

ACKNOWLEDGEMENTS

This study was funded by National Institutes of Health Grants R01 AR055563, AR049735 and AR056259.

GLOSSARY

GRF *–Ground Reaction Force during the DVJ*
HADT *- Hip Abduction Moment during the SCD*
HIPADD *–Hip Adduction Moment Max during SCD*
HIPM_SCD *- Hip Adduction Moment Min during SCD*
HIPM_DVJ *–Hip Adduction Moment Min during DVJ*
Pelvis Ang: *Peak Frontal Plane Pelvis angle during* SC

A BIOMECHANICAL COMPARISON OF THREE BACKPACK FRAMES DURING TREADMILL WALKING

[1]Brian K. Higginson, [1]Kaya L. Mills, [2]Kimberly A. Pribanic, [3]Jana E. Hollins and [3]Daniel P. Heil

[1]Gonzaga University, Spokane, WA, USA
[2]Mystery Ranch LTD, Bozeman, MT, USA
[3]Montana State University, Bozeman, MT, USA
email: higginson@gonzaga.edu

INTRODUCTION

It is well established in the load carriage research that the magnitude of the external load, as well as positioning of the load within a backpack, can influence select cardiorespiratory and metabolic measures. It has also been suggested that these measures may not be sensitive enough to detect differences in load carriage conditions and that measures such as muscle activation and gait and postural kinematics should be used [1]. Few studies have focused on how backpack frame design may impact these same parameters. Therefore, the purpose of this study was to compare muscle activation and kinematic variables for three backpack frames (MOLLE, FILBE, and NICE) during treadmill walking, all of which are commonly used in branches of the U.S. Armed Forces.

METHODS

Backpack-experienced subjects (18 men, 4 women; Mean ± SD: 32±8 yrs, 79.7±7.7 kg) completed 4 successive 15-min walking trials at a fixed treadmill speed (1.34 m/s) and grade (2%). The Control trial (walking without a backpack) was always tested first, while the order of the three backpack frames tested were counterbalanced. Trials 2-4 corresponded to wearing one of 3 military backpack frames (MOLLE, FILBE, NICE), each of which was loaded with a 26.6 kg bag load. In addition to the backpack load, each subject walked on the treadmill while carrying a Rubber Ducky rifle (M-16A2) in front (i.e., simulating carrying a rifle on patrol), which weighed another 4.1 kg (30.7 kg total load). During each trial, subjects were filmed in the frontal and sagittal planes to characterize upper body posture and lower-limb gait kinematics at heel strike and heel-off, which were then averaged over five strides. Finally, electromyography (EMG) measures were recorded using a telemetry-based surface EMG electrode system for select lower extremity muscles (biceps femoris, BF; rectus femoris, RF; lateral head of the gastrocnemius, LG), and normalized to the Control (unloaded) condition. All kinematic and muscle activation measures were summarized at two time points (minute 6 and 12) for each trial. Each variable was then summarized by Trial (Control, MOLLE, FILBE, NICE) and time point (mins 6 and 12) and then evaluated using a multivariate 2-factor repeated measures analysis of variance (RM ANOVA) and Sheffe's test for post-hoc evaluations (α=0.05).

RESULTS AND DISCUSSION

Postural and lower limb kinematics were significantly altered during the load carriage trials when compared to the Control condition. At heel strike, wearing a heavily loaded pack resulted in a 17-19 degree increase in trunk angle when compared to the Control condition. Statistically, this forward lean was significantly less (P=0.045) for the MOLLE (17-17.8 degrees) than the FILBE (18.4-19.1 degrees), but neither of these were statistically different from the NICE frame. Lower limb kinematics were also significantly different than the Control condition with an increase in thigh flexion angle and decrease in both knee and leg flexion angles (P<0.01). These lower limb kinematic adaptations are commonly seen throughout the load carriage literature [2]. Greater knee flexion while carrying heavy loads facilitates absorption of the impact forces experienced at heel strike and is accomplished through a concomitant increase in both thigh and leg flexion angles.

At heel-off, the load carriage conditions resulted in an increase in trunk flexion angle ($P<0.001$), thigh extension angle ($P<0.001$), leg flexion angle ($P<0.01$) and knee angle ($P<0.05$) when compared to the unloaded condition. Comparison between frame types at heel-off indicated that the FILBE frame resulted in the greatest thigh angles ($P<0.05$) when compared to the other two frames tested, greater knee angles ($P<0.05$) than the MOLLE frame, and significantly greater trunk flexion angle than the NICE frame ($P<0.05$). Unlike the heel strike phase of gait, there was an effect of load carriage duration during the heel-off phase, with a significant increase in trunk flexion ($P=0.025$) and thigh extension angles ($P=0.016$) from minute 6 to minute 12.

Previous studies have shown that stride length tends to increase, with a subsequent decrease in stride frequency, during load carriage [2, 5]. These gait adaptations were not seen in the present study when comparing the loaded and unloaded conditions. Although there were no differences observed in stride length, stride frequency, or stride width between the four testing conditions, stride width tended (non-significantly) to be widest for the FILBE and most narrow for the NICE frame. Stride parameters were, however, sensitive to load carriage duration, with stride frequency decreasing and stride length increasing from minute 6 to minute 12 ($P<0.001$).

During load carriage, a two-fold increase (1.79-2.46) in muscle activation was seen for both the LG ($P<0.001$) and RF ($P<0.01$) muscles when compared to the Control condition. The BF muscle was relatively unaffected by the additional load of the packs (0.96-1.08). These findings are consistent with those found by others investigating the change in muscle activation of lower extremity muscles during prolonged load carriage while carrying loads of 20-40% of body weight [3], and those looking at the effect of external load magnitude on muscle activation changes while walking [4]. Interestingly, RF muscle activation in the current study tended to be about 40-50% lower when using the FILBE frame when compared to the two other frames (although this difference was not statistically significant). This may be explained by the differences seen in trunk, thigh, and knee angles while wearing this frame when compared to the MOLLE and NICE frames.

CONCLUSIONS

Although most of the kinematic and muscle activation differences seen between frame types were relatively small, all were associated with the FILBE frame. While any one of these trends in itself may not be overly important, the collection of trends and significances points toward use of the FILBE frame having a greater biomechanical influence on the body than either the MOLLE or NICE frames.

Kinematic and stride parameter changes observed between minute 6 and minute 12 indicate that load carriage duration may influence the physiological and biomechanical responses to load carriage. In the current study, load carriage duration was limited to 15 minutes per frame tested. It is reasonable to assume that larger differences in these measures may emerge between frame types when load carriage duration is increased (i.e., fatigue is induced), and may warrant further investigation.

REFERENCES

1. Bobet J, and Norman RW. *Eur J App Phy Occup Phys* 53(1), 71-75.
2. Majumdar D, Sudan Pal M, and Majumdar D. *Ergonomics* 53(6), 782-791.
3. Simpson KM, Munro BJ, and Steele JR. *J Electromyogr Kinesiol* 21(5), 782-788.
4. Knapik J, Harman E, and Reynolds K. *Appl Ergon* 27(3), 207-216.
5. Birrell SA and Haslam RA. *Ergonomics* 52(10), 1298-1304.

COMPARISION OF PATELLA BONE STRESS BETWEEN INDIVIDUALS WITH AND WITHOUT PATELLOFEMORAL PAIN

[1]Kai-Yu Ho, [1]Christopher M. Powers

[1]University of Southern California, Los Angeles, CA, USA
email: kaiyuho@usc.edu, web: http://pt.usc.edu/labs/mbrl

INTRODUCTION

Patellofemoral pain (PFP) is the most common overuse injury of the lower extremity. It has been hypothesized that PFP is the result of increased pressure on highly innervated subchondral bone.[1] A recent finite element (FE) modeling study has suggested that persons with PFP demonstrate elevated hydrostatic pressure and octahedral shear stress in patella articular cartilage.[2] It is unclear however how cartilage stress influence stress within the pain-sensitive subchondral bone layer. The purpose of the current study was to test the hypothesis that females with PFP exhibit elevated patella bone stress compared to pain-free controls.

METHODS

To date, seven females with PFP, and 7 pain-free females have participated in this on-going study. Subjects were matched based on age, weight, height, and physical activity level.

Input parameters for the FE model included: 1) PFJ geometry, 2) elastic modulus of patella, 3) weight-bearing PFJ kinematics, and 4) quadriceps muscle forces (Fig. 1). PFJ geometry was obtained from sagittal plane, water-fat IDEAL magnetic resonance imaging (MRI) acquired with a 3.0T MRI scanner (General Electric Healthcare; Fig. 1A). Voxel-wise bone density of patella was estimated from IDEAL in-phase MRI with the assistance of a calcium hydroxyapatite phantom[3] and the voxel-wise elastic modulus was consequently computed.[4] The elastic modulus of each element was calculated by retrieving the elasticity of the closest voxel to the element's centroid. The patella was then divided into 200 linear material regions based on the elastic modulus distribution of the patella (Fig.1B). The FE mesh of cartilage and bone was then registered to the position of each structure on the weight-bearing MRI (Fig.1C). Quadriceps muscle forces were estimated using a previously described EMG driven model (Fig.1D).[5]

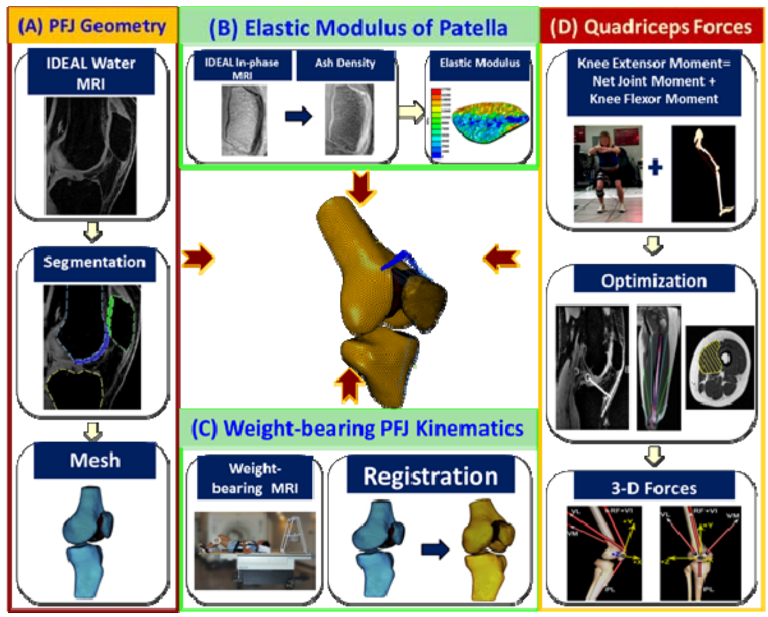

Figure 1: Pipeline of patellofemoral joint FE model.

For each model, the femur and tibia were modeled as rigid structures and the cartilage of the patella and femur was modeled as homogeneous isotropic tetrahedral continuum elements (elastic modulus of 4 MPa and Poisson ratio of 0.47). The patella was modeled as heterogeneous isotropic tetrahedral continuum elements with Poisson ratio of 0.3. Quadriceps muscles were divided into 3 functional groups (rectus femoris/vastus intermedius, vastus medialis, and vastus lateralis) made up of 6 equivalent uniaxial connector elements.[2] The patellar tendon was modeled as 6 uniaxial, tension-only elements with stiffness of 4334 N/mm.

The peak and average stresses at the cartilage-bone interface were quantified in terms of 2 invariants: 1) von Mises stress, and 2) compressive stress. To establish a clinically meaningful measure of average stress, only elements with a stress higher than the 90^{th} percentile were considered while computing the average stress.[6] This threshold was used to identify the highest risk for bone initial failure.[6] As an indirect assessment of the validity of each FE simulation, the estimated contact area and final patella position predicted by the models were compared to the actual contact area and patella position measured from the weight-bearing MRI using previously published procedures.[7]

Independent t tests were used to compare 1) peak and average von Mises stresses, and 2) peak and average compressive stresses between the PFP and control subjects. The significance level was set as 0.05.

RESULTS AND DISCUSSION

In general, more concentrated stress was observed on the lateral facet of the patella in the PFP subjects while a more evenly distributed stress pattern was observed in the control subjects (Fig. 2). When compared to the pain-free controls, individuals with PFP exhibited significantly greater peak and average von Mises stress as well as peak and average compressive stress (Table 1).

Contact areas estimated by the model were within 19.3 mm^2 (5.0 %) of contact areas measured from the weight-bearing MRI. In addition, the average lateral patella displacement predicted by the FE models were within 0.02 (3.0 %) of those measured from the weight-bearing images.

Previous literature has reported that elevated bone stress is associated with bone tissue damage.[8] We propose that the elevated bone stress observed in the current study may contribute to bone tissue injury (e.g., MRI-detected bone marrow lesions) and patellofemoral symptoms in persons with PFP.

Future efforts will focus on increasing the sample size and relating stress values to pain, function, and location of BML's to better understand the underlying pathomechanics of this poorly understood clinical condition.

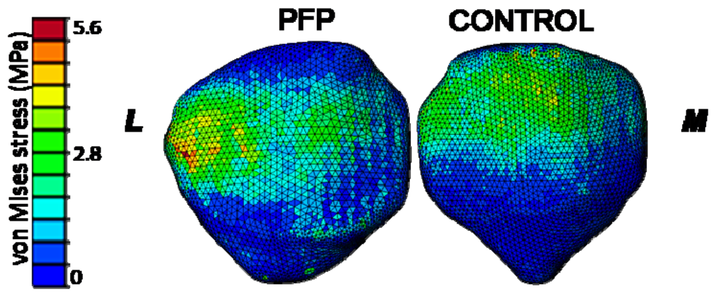

Figure 2: von Mises stress distribution of PFP and control subjects is demonstrated in a posterior view of patella. L and M indicate lateral and medial.

REFERENCES

1. Dye SF. *Clin Orthop Relat Res* 100-110, 2005.
2. Farrokhi S, et al. *Osteoarthritis Cartilage* **19**, 287-294, 2011.
3. Ho KY, et al. *J Magn Reson Imaging* (In review).
4. Keyak JH, et al. *Clin Orthop Relat Res* 219-228, 2005.
5. Chen YJ, et al. *J Appl Biomech* **26**, 415-423, 2010.
6. Eswara SK, et al. *Bone* **41**, 733-739, 2007.
7. Powers CM, et al. *Med Sci Sports Exerc* **36**, 1226-1232, 2004.
8. Nagaraja S, et al. *J Biomech* **38**, 707-716, 2005.

ACKNOWLEDGEMENTS

This study is supported by the International Society of Biomechanics Student Dissertation Award and the 3.0T MRI Pilot Research Grant from Radiology Department at the University of Southern California.

Table 1: Peak and average von Mises stress and compressive stress at the cartilage-bone interface of patella

	PFP	CONTROL	P value
Peak von Mises Stress (MPa)	5.58±1.22*	3.52±0.81	0.003
Average von Mises Stress (MPa)	3.75±0.98*	2.16±0.69	0.004
Peak Compressive Stress (MPa)	5.64±2.25*	3.06±1.07	0.018
Average Compressive Stress (MPa)	2.13±0.57*	1.12±0.30	0.001

Values are presented as mean±SD. * indicates a significant difference from the control group.

SPRING-MASS CHARACTERISTICS DURING OVERGROUND RUNNING IN AMPUTEES USING RUNNING SPECIFIC PROSTHESES

[1,2]Hiroaki Hobara, [2]Brian S Baum and [2]Jae Kun Shim

[1]Japan Society for the Promotions of Science, Tokyo, JPN
[2]University of Maryland, College Park, MD, USA
email: h.hobara@gmail.com

INTRODUCTION

Spring-like behavior is a general feature of a "bouncing gait" such as running, hopping or jumping. To describe this type of gait, the whole body is often modeled with a "spring-mass model" which consists of a body mass supported by a spring [1]. In this model, stiffness of the leg spring (leg stiffness; K_{leg}) is defined as the ratio of the total leg spring compression (ΔL) to peak vertical ground reaction force at the middle of the stance phase. Previous study demonstrated that running humans adjust the apparent spring-like behavior for different speeds by increasing the angle swept (θ) by the stance limb while keeping the K_{leg} nearly constant [2].

Carbon fiber running-specific prostheses (RSP) can allow individuals with lower extremity amputation to run by partly providing spring-like leg function in their amputated leg [3]. However, a very limited number of studies offer insights into spring-mass characteristics during running in amputees. The aim of this study was to investigate the effect of running speed on spring-mass characteristics during amputee running using RSP.

METHODS

Eight male subjects with unilateral transtibial amputation (mean age = 32.0 ± 10.2 years, height = 1.80 ± 0.07 m, mass = 82.3 ± 13.0 kg) volunteered to participate in the experiment. Each subject used his own RSP. Subjects ran overground around a 100-m long track at 2.5, 3.0 and 3.5 m/s, respectively. Ten six-degree-of-freedom force platforms (Kistler, Amherst, NY) embedded in the track in series collected ground reaction forces sampled at 1000 Hz. Subjects completed at least five successful trials for each leg at each of three running velocities. The order for prescribed running velocities was randomized.

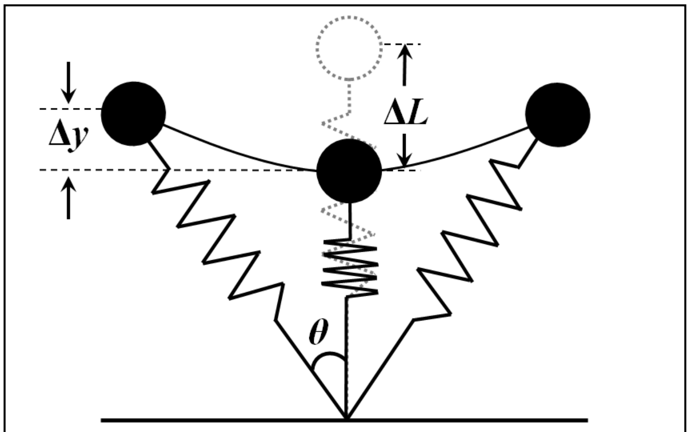

Figure 1: Spring-mass model for running. The leg spring is compressed during the first half of the stance phase and rebounds during the second half. Maximal vertical displacement of the center of mass and leg spring compression during ground contact is represented by Δy and ΔL, respectively. Half of the angle swept by the leg spring during the ground contact is denoted by θ.

From ground reaction force data, we determined step frequency (f) and stance time (t_c) in both intact and prosthetic limb (INT and PST, respectively). The K_{leg} was calculated utilizing the spring–mass model (Figure 1). During running, the peaks of ground reaction force and leg compression coincide in the middle of the ground contact phase. At this point, K_{leg} can be calculated as the ratio of peak vertical ground reaction force (F_{peak}) to peak leg compression in the spring (ΔL) when the leg spring was maximally compressed:

$$K_{leg} = F_{peak} / \Delta L \qquad (1).$$

The ΔL was calculated from the maximum vertical displacement of the center of mass (Δy), the initial length of the leg spring L_0, and half of the angle swept by the leg spring while it was in contact with the ground (θ):

$$\Delta L = \Delta y + L_0 (1- \cos\theta) \quad (2)$$

with

$$\theta = \sin^{-1} (ut_c /2L_0) \quad (3)$$

where u is the forward velocity of the body (in m/s) and t_c is the ground contact time at each step [2, 4].

A two-way repeated measure ANOVA and Bonferoni post hoc multiple comparison test were performed to compare the INT and PST limb at three velocities.

RESULTS AND DISCUSSION

K_{leg} remained constant in both legs for three velocities (Figure 2-A). However, there were significant differences in the K_{leg} between INT and PST at 3.5 m/s ($p<0.05$). Further, while it did not reach statistical significance, K_{leg} in the INT was greater than the PST at 3.0 m/s ($p = 0.052$). These results contrast with previous study which stated that there were no distinct differences in the K_{leg} between the legs in amputee running at slow speed (less than 5 m/s) [5]. The cause of this discrepancy could involve methodological differences, such as treadmill running in the previous study [5] and overground running in the current study.

The differences in K_{leg} between the INT and PST was mainly due to the differences in F_{peak}, but not to ΔL (Figure 2-B and C). One potential explanation for the invariant ΔL across speed may be that amputee runners using RSP would strive for similar center of mass movement in both legs at the expense of ground reaction force. Indeed, as previous study suggested, human subjects would use a simple control strategy (i.e., apparent stiffness regulation) that results in smooth center of mass movements during bouncing gait [6]. Further, there were no significant differences in θ between the legs at all running speed (Figure 2-D). In other

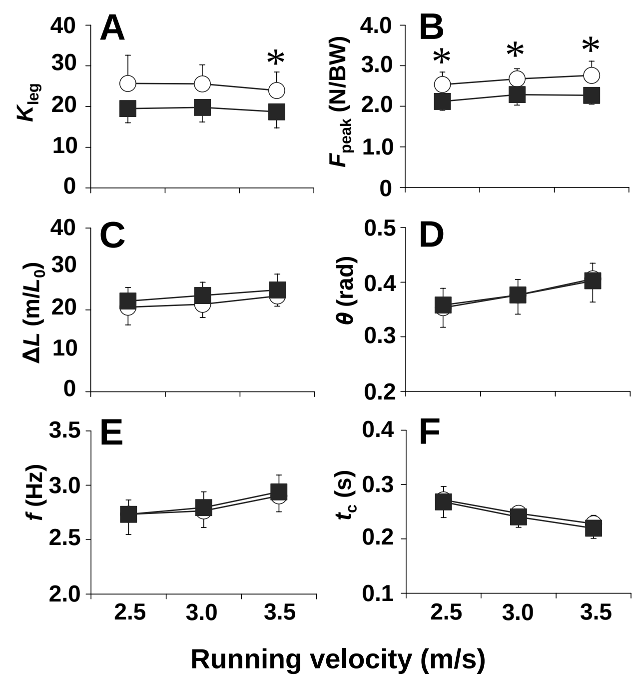

Figure 2: Comparison of K_{leg} (A), F_{peak} (B), ΔL (C), f (D), t_c (E) and θ (F) between INT (○) PST (■) for three velocities. An asterisk indicate significant differences between the legs; p <0.05.

words, both angle of attack and angle swept by the leg during ground contact is similar between the legs. The results also indicate that maintaining the natural center of mass movement in both legs may be an invariant characteristic of running in amputees.

According to previous studies, K_{leg} is influenced by not only f, but also t_c [4, 7]. In the present study, there were no significant differences in f and t_c between the legs at all velocities (Figure 2-E and F). These results indicated that current results definitely eliminate potential effects of f and t_c on K_{leg} and that RSP have a lower stiffness than intact limb.

REFERENCES

1. Blickhan R. *J Biomech* **22**, 1217-1227, 1989.
2. He J, et al. *J Appl Physiol* **71**, 863-870, 1991.
3. Nolan L. *Foot Ankle Sug* **14**, 125-129, 2008.
4. Farley& Gonzalez. *J Biomech* **29**, 181-186, 1996.
5. McGowan et al. *J Roy Soc Int*, in press.
6. Bobbert & Casius. *Roy Soc B* 366, 1516-29, 2011.
7. Morin et al. *J Biomech* **40**, 3341-3348, 2007.

A NOVEL METHODOLOGY USING PRINCIPAL COMPONENT ANALYSIS TO QUANTIFY GLOBAL BILATERAL ASYMMETRY OF HUMAN GAIT

[1]Stefan Hoerzer, [1]Christian Maurer, [1,2]Peter Federolf, [1]Vincent von Tscharner, [1]Jennifer Baltich and [1]Benno M. Nigg

[1]Human Performance Laboratory, Faculty of Kinesiology, University of Calgary, Calgary, Canada
[2]Norwegian School of Sport Sciences, Oslo, Norway
email: shoerzer@kin.ucalgary.ca, web: www.kin.ucalgary.ca/hpl/

INTRODUCTION

Gait asymmetry in the able-bodied population is an important consideration for clinicians and may also be important for physical activities, gait evaluation, clinical decisions for patients requiring rehabilitation for one or both of the lower extremities, and in artificial limb design [1]. Asymmetry of human gait has been investigated for many years using a variety of analysis approaches [2-4]. Although these analysis approaches provide suitable values to assess gait asymmetry on a local level (e.g. at specific joints), conclusive statements about the global aspect of gait asymmetry, the influence of specific interventions (e.g. shoes and orthotics), and the importance of specific biomechanical variables are difficult to make due to a multitude of asymmetry values per subject.

Therefore, the purpose of this study is: (a) to use principal component analysis (PCA) to develop a global asymmetry index (GASI), (b) to quantify global gait asymmetry of able-bodied subjects running with and without shoes, and (c) to determine which biomechanical variables are important for the GASI.

METHODS

Kinematic and kinetic data of 15 able-bodied subjects (25.4 years ± 4.4 SD) performing 5 barefoot and 5 shod over-ground running trials (4.0 ± 0.6 ms^{-1}) for each leg were collected. Based on the 5 running trials, 30 different biomechanical variables of the hip, knee, and ankle were computed, normalized over the stance phase (0-100 %) and averaged. In order to compare variables with different physical units, the biomechanical variables were normalized. The biomechanical variables of both leg and shoe conditions were normalized with respect to the peak value of the corresponding variable (e.g. knee moments were normalized to the peak knee moment). Subsequently, a vector ($\boldsymbol{q}$) was created for each leg that included all the normalized biomechanical variables in series. Gait asymmetry was isolated by calculating a difference vector ($\Delta\boldsymbol{q}$) between the vectors of the right and the left leg. PCA was applied to a matrix containing the difference vector of each subject (s). Finally, the difference vector of each subject was projected onto the first 10 (i = 1…10) principal components (PCs). Equation 1 calculates the projections (P) of the difference vector onto the 10 PCs:

$$\mathbf{P_{si}} = \langle \Delta\boldsymbol{q}_\mathbf{s} \mid \mathbf{PC_i} \rangle \qquad (1)$$

The GASI of a subject was determined using equation 2 which calculates the Euclidean distance of the projections within the 10 PCs:

$$\mathbf{GASI_s} = \sqrt{\sum_{\mathbf{i=1}}^{\mathbf{10}} (\mathbf{P_{si}})^2} \qquad (2)$$

In order to reveal which biomechanical variables were important for the GASI, the variables with a high contribution to the 10 individual PCs were identified. The degree of contribution was determined by analyzing the factor loadings of the PCs. The calculation of the GASI and the determination of the important variables were carried out separately for the barefoot and shod conditions.

RESULTS AND DISCUSSION

The GASI provided a single representative value for global bilateral asymmetry of human gait (Fig. 1).

The GASI of the able-bodied subjects running barefoot ranged between 3.1 and 9.3 (mean: 5.2 ± 1.7 SD). The range of the GASI in the shod condition was 3.3 to 7.7 (mean: 5.0 ± 1.3 SD). Although a conclusive statement is difficult to make based on the small sample size and the use of an able-bodied cohort, it may be speculated that a GASI under 10 is still in a non-pathological range. However, the changes of the GASI between barefoot and shod condition were inconsistent and subject-specific. These inconsistencies might be due to subject-specific sources of gait asymmetry. More precisely, the subject-specific sources of gait asymmetry, such as different combinations of structural and/or neuromuscular factors [5], might have caused subjects to react differently to the shoe condition and resulted in different GASI changes.

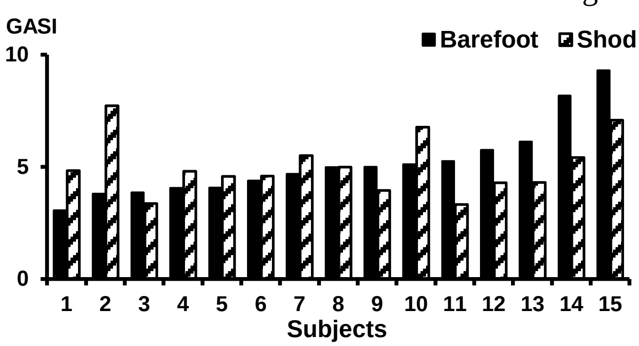

Figure 1: Global gait asymmetry index (GASI) of barefoot and shod running for 15 subjects, arranged by increasing GASI of barefoot running.

Figure 2 presents the biomechanical variables that were important for the GASI by showing how often a variable had a high contribution to the 10 individual PCs. In total, 18 variables for barefoot running and 23 variables for shod running had a high contribution to at least one PC. These important variables described approximately 90 % and 97 % of the mean GASI in the barefoot and shod conditions, respectively. Lastly, the hip joint had the highest number of important biomechanical variables for the 10 PCs and therefore for the GASI. It is speculated that this could be due to two functional reasons: (1) less anatomical restrictions at the hip joint compared to the knee and ankle joints and (2) asymmetries of the ankle and/or knee joints which propagate to the hip joint based on the anatomical connection between these lower extremity joints.

CONCLUSIONS

The GASI developed in this study provided for the first time a measure of the global aspect of gait asymmetry. Additionally, the examples of the influence of an intervention (shoe) and the importance of specific biomechanical variables with respect to global gait asymmetry were presented. The GASI developed in this study will allow for a better definition of physiological and pathological ranges of gait asymmetry. This knowledge can help researchers and clinicians to improve the evaluation and rehabilitation of gait.

REFERENCES

1. Sadeghi H, et al. *Gait & Posture* **12**, 34-45, 2000.
2. Robinson RO, et al. *J. Manipulative Physiol. Ther.* **10,** 172-176, 1987.
3. Sadeghi H. *Gait & Posture* **17**, 197-204, 2003.
4. Zifchock RA, et al. *Gait & Posture* **27**, 622-627, 2008.
5. Vagenas G. & Hoshizaki B. *Int. J. of Sport Biomechanics* **4,** 220-230, 1988.

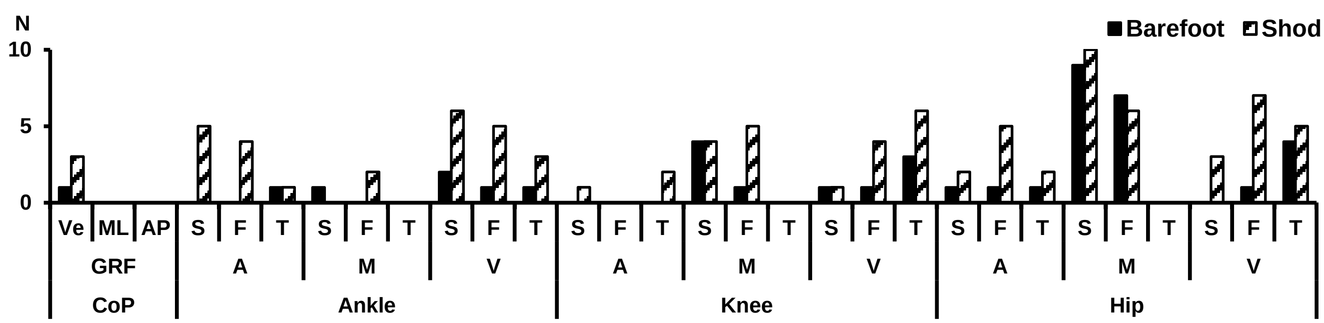

Figure 2: Number of high contribution occurrences of a biomechanical variable to the 10 principal components (Ve-Vertical; ML-Medial Lateral; AP-Anterior Posterior; GRF-Ground Reaction Force; CoP-Centre of Pressure; S-Sagittal Plane; F-Frontal Plane; T-Transverse Plane; A-Angle; M-Moment; V-Velocity).

VIBRATION IMPAIRS PROPRIOCEPTION DURING ACTIVE CYCLICAL ANKLE MOVEMENTS

[1]Taylor C. Holmes, [1]Lisa M. Floyd and [1]Jesse C. Dean

[1]Medical University of South Carolina, Charleston, SC, USA
email: deaje@musc.edu

INTRODUCTION

Accurate information about the mechanical state of the body is a vital element of functional motor control. The role of proprioception in human motor control has commonly been investigated using vibration. Essentially, tendon vibration causes many small stretches of the musculotendon complex, evoking a sense of larger length changes than are actually occurring [1]. However, recent findings in the upper extremity have demonstrated that vibration does not influence position sense when muscles are actively supporting or moving a load, as the body's mechanical state may instead be derived from sense of effort [2].

In the lower extremity, functional tasks such as locomotion require active, cyclical movements. However, the effects of vibration at the ankle have primarily been investigated either when the joint is moved passively [3], or undergoes a simple, ballistic-like motion [4]. It is unclear whether vibration would influence motor control during more functional tasks, when sense of effort may also play a role.

The purpose of this study was to test whether altering proprioception with vibration would influence active, cyclical ankle movements. We hypothesized that vibration would cause subjects to overestimate the amplitude of ankle movements. We also hypothesized that vibration would be more effective during slower movements in which subjects had more time to respond to feedback. Finally, we hypothesized that the frequency of vibration would influence its effectiveness.

METHODS

Twelve young (24±1 yrs), healthy subjects performed a series of 30s ankle oscillation trials while lying prone. Ankle angle (plantar/dorsi-flexion) was quantified using LED markers placed on the medial and lateral sides of the knee, ankle, and foot of each leg. Custom-built vibrators were strapped over the distal tendons of the right plantarflexors and dorsiflexors.

For all trials, subjects were instructed to match the motion of their left and right ankles, and given real-time visual feedback of their left ankle angle on a computer screen. Movement amplitude (5, 7.5, or 10^{o}) was prescribed with a visual target, while movement period (1 or 3 s) was prescribed using a metronome. Each subject performed trials with no vibration and with 80-Hz vibration, the optimal frequency to activate muscle spindles [1]. Additionally, subgroups of subjects (n=4 per subgroup) performed trials with 40-Hz, 120-Hz, and 160-Hz vibration. Each trial condition was repeated 3 times in randomized order, for a total of 54 trials.

To quantify the ability of subjects to match bilateral ankle motion, we calculated the Amplitude Ratio for each movement condition. Amplitude Ratio was defined as the average amplitude of right ankle motion divided by the average amplitude of left ankle motion (Fig. 1). An Amplitude Ratio of 1.0 would indicate that both ankles moved through the same range of motion. We performed repeated measures ANOVAs to determine if movement condition significantly influenced Amplitude Ratio.

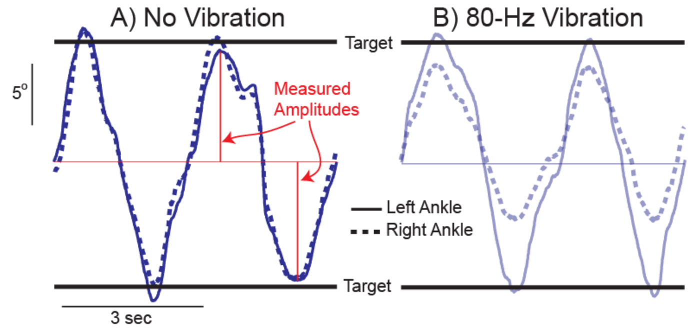

Figure 1. Typical ankle movement patterns (and measured amplitudes) are shown for a single subject for trials with no vibration (A) and 80-Hz vibration applied to the right ankle (B).

RESULTS AND DISCUSSION

Application of 80-Hz vibration clearly influenced motion of the vibrated ankle (Fig. 1). 80-Hz vibration had a significant main effect ($p<0.0001$) on the Amplitude Ratio (Fig. 2), as the right ankle moved through a smaller range of motion when vibration was applied. The Amplitude Ratio for each vibrated movement condition was significantly smaller than the Amplitude Ratio for all non-vibrated movement conditions. These results demonstrate that humans use proprioceptive feedback to scale their movements, even during active rhythmic tasks.

Characteristics of the movement pattern (prescribed amplitude and period) modulated the effect of 80-Hz vibration (Fig. 2). Across all non-vibrated movement conditions, the Amplitude Ratios were not significantly different, indicating that subjects were equally able to match their bilateral movements independent of amplitude and period. However, 80-Hz vibration had a larger effect during small amplitude movements (interaction $p=0.0003$). 80-Hz vibration also had a larger effect during long period movements (interaction $p<0.0001$). In both cases, disturbing proprioception had a larger effect for movement conditions in which velocities were lower, potentially allowing more time for feedback to play a role in controlling movement.

Vibration frequency influenced its effectiveness. In all subgroups, 80-Hz vibration significantly decreased the Amplitude Ratio ($p<0.0001$). 40-Hz vibration did not significantly affect Amplitude Ratio (Fig. 3A). In contrast, higher frequency vibration (120- and 160-Hz) decreased Amplitude Ratio significantly more than 80-Hz vibration (Fig. 3B-C). These results contradict our expectation that 80-Hz vibration would most effectively disturb proprioception, possibly because vibration amplitude scaled with vibration frequency.

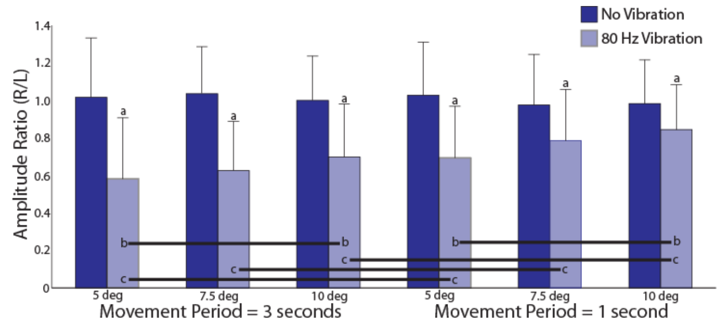

Figure 2. The effects of 80-Hz vibration on Amplitude Ratio were modulated by movement pattern characteristics. Post-hoc significance is indicated symbolically (a=smaller than all non-vibrated conditions; b=difference between 5^{o} and 10^{o} amplitudes; c=difference between 1s and 3s periods).

CONCLUSIONS

Vibration influenced Amplitude Ratio, indicating that peripheral feedback contributes to motor control during active, cyclical ankle movements. However, this effect was weakened during faster motions, in which feed-forward commands may play a larger role. Additionally, controlling the vibration frequency influenced the magnitude of its effect. These results suggest that we may be able to use vibration to investigate the proposed role of proprioceptive feedback in the optimization of cyclical movements [5] or to improve lower extremity function in clinical populations [6].

REFERENCES

1. Roll JP, Vedel JP. *Exp Brain Res* **47**, 177-90, 1982.
2. Ansems GE, et al. *J Physiol* **576**, 445-55, 2006.
3. van Deursen RWM, et al. *Exp Brain Res* **120**, 1-8, 1998.
4. Khudados E, et al. *J Neurol Neurosurg Psych* **67**, 504-10, 1999.
5. Raburn CE, et al. *J Exp Biol* **214**, 3768-74, 2011.
6. Conrad MO, et al. *J Neurophysiol* **106**, 1480-8, 2011.

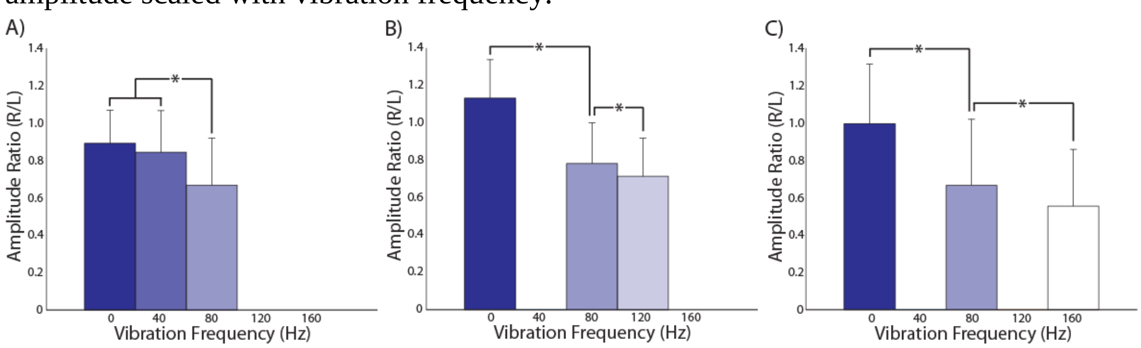

Figure 3. Vibration frequency significantly influenced its effect on Amplitude Ratio, as shown for all three subgroups in panels A, B, and C.

DESIGN OF SUSPENDED LOAD BACKPACKS FOR YOUNG URBAN PROFESSIONALS

[1]Melissa Holtz and [2]Dustyn Roberts

[1]New York University, New York, NY, USA
[2]Polytechnic Institute of New York University, Brooklyn, NY, USA
email: mah482@nyu.edu

INTRODUCTION

According to the United Nations [1], as of 2008, a majority of the population lives in cities for the first time in history.[1] Mobility is an increasing problem for these city dwellers especially as they use public transportation and carry belongings with them on their backs throughout their day. Additionally, many urban professionals, particularly those under age 40, rely on electronics such as smartphones (0.028 kg), tablet PCs (0.45 kg), and laptops (1.36 kg and up). As young, urban professionals travel for work and school, they bring these electronics with them every day. An ergonomic bag aims to protect a human's back from injury and fatigue. As technology develops enabling reduction of the vertical force of loads on the carrier, bags can enable higher loads to be carried with less injury [2].

This population's load carrying behavior has not been well studied. Most load carrying studies tend to focus on military loads of approximately 27 kg [2], schoolchildren's loads of approximately 9 kg, or other profession-specific loads such as apple pickers. Studies of traditional "locked" backpacks test compression, distribution of pressure and padding, and strap placement. These locked backpacks, as Larry Rome explained [2], impose large peak forces on the wearer as the loaded backpack is accelerated with vertical motion of the pelvis during each step. Larry Rome proved that suspending the load could reduce vertical movement of the system's center of mass, force on the carrier, and the metabolic cost of carrying loads. However, this suspended-load energy harvesting backpack was developed for heavy, military loads, and with six pounds for the frame alone, would not be appropriate for daily urban use.

This study intended to test loads of a different magnitude. The goal of this initial feasibility study was to determine if a spring mounted suspended load carrying system was a viable option for reducing fatigue experienced by young urban professionals during every day load carrying scenarios.

METHODS

The bags of 80 subjects (48 women, 32 men) were weighed with a Pelouze heavy duty temperature compensated scale. Most subjects were young professionals and computer science graduate students, age 25-35, who carry laptops and smart phones with them on a daily basis, in a single bag, either backpack (both shoulders), tote (one shoulder), or messenger (diagonal across body) shape.

Previous studies determined that vertical center of mass (COM) excursion ranges from 0.027 to 0.048 m during walking for this age group [3]. [3] The mean of that range, was used for initial testing.

The spring constant necessary to suspend the load was calculated through Hooke's Law ($F = kx$) from the average bag weight and COM excursion.

One subject (1.6256 m, 511.5 newtons, female) was recruited for initial prototype testing. Extension springs with the proper spring constant were used in a spring-loaded mass prototype, including a Dyneema lightweight and strong bag with an appropriate load inside. The spring-loaded mass was attached to a frame and its movement was observed relative to a subject's hips while a subject walked at a self selected pace. To trace the COM of the subject versus the COM of the spring loaded mass, lights were attached to both COMs. A long exposure photograph was taken to show the motion via a light path coming from separate light marker on the subject's hip and on the bouncing mass.

RESULTS

The lightweight frame constructed for testing is shown in Figure 1.

Figure 1: Initial prototype of lightweight frame system.

The average daily load of young urban professionals in New York City was calculated to be approximately 5 kg. The average weight of subjects' bags was 50 N. The mean COM excursion was determined from literature to be 0.035 m. The spring constant k was determined to be 1442 N/m**.**

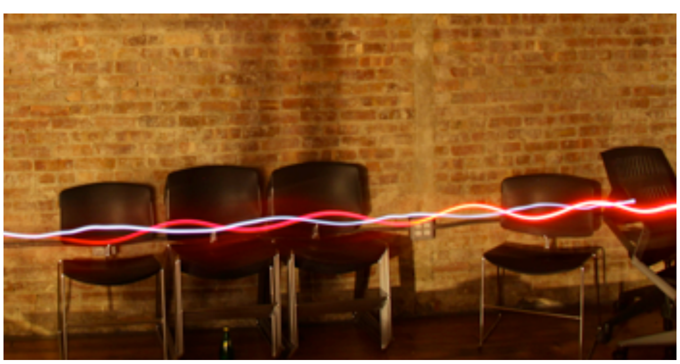

Figure 2: Long exposure photograph indicating out of phase movement of the COMs of the load and the subject. The white light is on the subject, red light is on the bag.

In this feasibility test, the lights showed the mass was moving out of phase with the carrier's gait as expected (Figure 2).

DISCUSSION

The preliminary results indicate that this spring and frame system can in fact uncouple the vertical excursion of the load from the COM excursion of the subject at a load commonly carried by a young, urban professional. This study is part of a larger ongoing study examining the relationship between walking biomechanics, load carrying, and bag design. To date, several early bag prototypes have been developed. Future work will include optimizing the spring constants to improve the loads' ability to move out of phase with the subject. Additionally, a more ergonomic physical prototype will be created, featuring an improved minimal frame as pictured in Figure 1.

This next version of the prototype will involve attaching the spring setup to a frame to allow it to be used for longer periods of time comfortably. The frame will be updated to make it as minimal and lightweight as possible. Though initially this study has characterized the kinematics of how the suspended load travels in relation to the body, future studies will also measure kinetics. This research represents a first step in developing a daily use urban load suspension system.

REFERENCES

1. "Latest Publications." *Urbanization: A Majority in Cities: Population & Development : UNFPA*. United Nations Population Fund. Web. <http://www.unfpa.org/pds/urbanization.htm>.
2. L. C. Rome, L. Flynn, and T. D. Yoo, "Biomechanics: Rubber Bands Reduce the Cost of Carrying Loads," *Nature*, vol. 444, no. 7122, pp. 1023–1024, Dec. 2006.
3. Orendurff, Michael S., Ava Segal, Glenn Klute, Jocelyn Berge, Eric Rohr, and Nancy Kadel. "The Effect of Walking Speed on Center of Mass Displacement."*Journal of Rehabilitation Research & Development,* **41**, 6A, 829-834, 2004.

Development of a test system to study brain tissue damage due to cavitation

Yu Hong, Saranya Canchi, Michael King, Sung Jin Lee, Malisa Sarntinoranont and Ghatu Subhash

University of Florida, Gainesville, FL, USA
email: yuhong@ufl.edu

INTRODUCTION

Blast-induced traumatic brain injury (bTBI) has received increasing attention in recent years. Numerous theories are currently being evaluated by various research groups to indentify the causes of TBI. One issue that has remained controversial is the initiation of cavitation in the brain due to the incident shock waves and the resulting negative pressure. In this study we focus on regions of tension that may, particularly in cerebrospinal fluid (CSF), cause cavitation. Cavitation from negative pressure at the contrecoup site in the brain has been hypothesized as early as 1948 [1]. However whether or not cavitation occurs, few studies have studied brain tissue damage caused by cavitation especially for mild bTBI. The objective of this research is to develop a system to introduce and control cavitation around a live brain tissue slice to detect damage due to the shock waves caused by the collapse of bubbles.

METHODS

To introduce cavitation, the slices were submerged in a fluid-filled (water or artificial CSF, *aCSF*) plastic chamber with a 2 mm height with a sealed piston at one end. The chamber was placed in a polymeric split Hopkinson pressure bar system, see Figure 1, which was designed to pull the fluid chamber away from the fixed piston. The striker bar was launched at 15 psi from the gas gun, and upon impact with the incident bar. The wave velocity in the bar was 2230 m/s, and the duration of stress wave was ~565 μs. This stress wave loading was imparted to aluminum U-shape feet which impacted the back holder of the test chamber. The piston was held in place using a clamp which was fixed to the test platform. In this way, fluid in the chamber was placed under a tensile load which caused negative pressure and cavitation.

Cavitation was captured using a high-speed imaging system (Vision Research, Wayne, NJ) that was triggered from the acoustic signal generated by the gas gun. The camera was set at approximately 100,000 frames per second. Total test duration was relatively short (~5 min). A high frequency pressure transducer (ICP 113B24, 2000 Hz sampling rate over 5 μs, PCB Piezotronics Inc., Depew, NY) embedded at the top of the test specimen holder was used to measure fluid pressure.

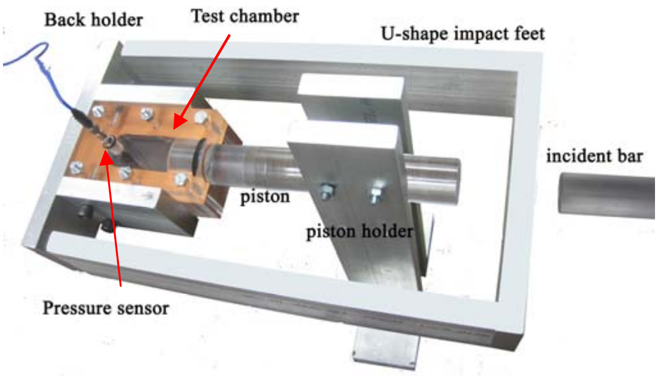

Figure 1. Polymeric split Hopkinson bar system introducing cavitation into a fluid chamber.

In addition to these tests, live rat brain tissue slices will be used to test this system. Protocols and procedures for this study have been approved by the University of Florida Institutional Animal Care and Use Committee. Fluoro-Jade C and DAPI staining will also be used to detect neuronal tissue damage. Brain tissue slices stained with FJC (green fluorescence) and DAPI (blue) will be imaged with a fluorescent microscope within dentate gyrus (DG), CA1, and CA3 regions of the hippocampus which have a high density of neurons. Degenerating neurons (with FJC images) and total cells (with DAPI images) within select fields of view will be counted via a custom MATLAB subroutine. Histological methodologies have been completed for the case of no cavitation see Figure 2.

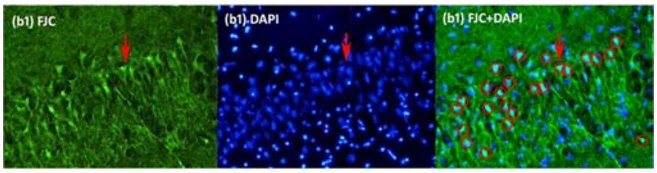

Figure 2. FJC and DAPI images of the hippocampus. Bright green regions show degenerating neurons and bright blue regions indicate cell neurons. The percentage of neural degeneration was determined by overlaying these images.

RESULTS AND DISCUSSION

Within the developed tension system, gas bubbles formed at different locations. Bubbles suddenly appeared, grew and underwent collapse within a time span of approximately 1.8 ms, see Figure 3.
Negative pressure was recorded by the pressure sensor. With a 15 psi air gun setting, the pressure in the test chamber reached approximately -12 psi. Negative pressure may be controlled by varying air gun pressure. Since pressure directly affects bubble size, further control of bubble size may also be achieved. Control of bubble location may also be achieved by seeding bubbles at specific sites.

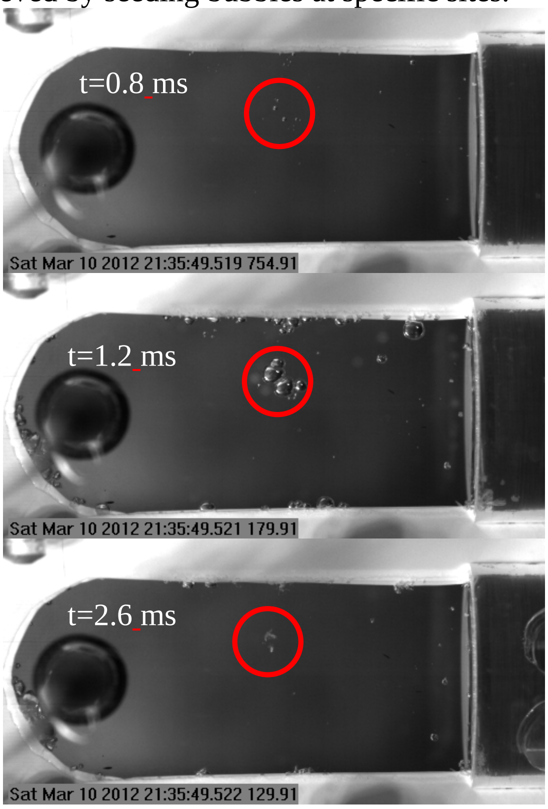

Figure 3. Cavitation introduced by negative pressure. The red circle shows bubble appearance, growth and collapse. Cavitation appeared during testing at 0.8 ms, grew to the maximum size ~1.2 ms, and collapsed at 2.6 ms.

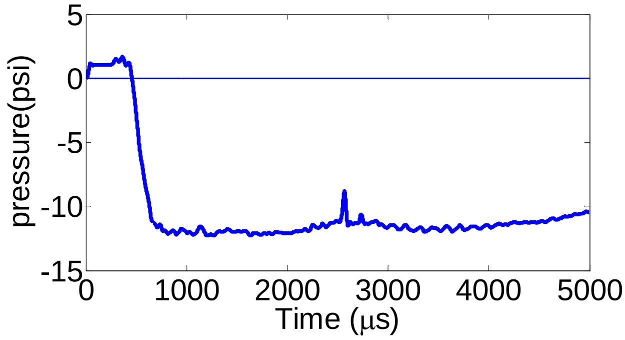

Figure 4. Negative pressure measured in the fluid chamber during cavitation. Pressure went down to approximately -12 psi; cavitation was observed at these negative pressures.

CONCLUSION

This new PSHPB tension test system has the ability to introduce cavitation in a fluid-filled chamber by providing a negative pressure. Controlled pressure testing will provide more control over bubble size and position. In ongoing studies, neural injury due to cavitation will be studied by introducing rat brain tissue slices to this system. Histological methodologies have been completed for the case of no cavitation within hippocampal regions.

REFERENCES

1. Ward, J.W., et al., “A mechanism of concussion: A Theory.” Science, 1948. 107:349-353
2. Miller, D.L., "Overview of experimental studies of biological effects of medical ultrasound caused by gas body activation and inertial cavitation." *Progress in Biophysics & MolecularBiology*, **93**(1-3), 2007. p. 314-330.
3. Brennen, C., *Cavitation and Bubble Dynamics*. 1995, New York: Oxford University Press.

ACKNOWLEDGEMENTS

The authors would like to thank Dr. Stephen Blackband for kindly allowing us to use his laboratory facilities during animal surgery. This research was funded in part by the Army Research Office (Award Number W911NF-10-1-0276).

KNEE JOINT LOADING DURING A COMPENSATORY STEP: PRELIMINARY DATA FOR OBSERVING REOVERY RESPONSES IN KNEE OSTEOARTHRITIC PATIENTS

[1]Mackenzie L. Hoops, [1]Noah Rosenblatt, [1]Andrew Skoirchet, [1]Mark D. Grabiner

[1]University of Illinois at Chicago, Chicago, IL, USA
email: mhoops2@uic.edu, web: http://www.uic.edu/ahs/biomechanics/

INTRODUCTION

Patients with lower extremity osteoarthritis (OA) have a 25% greater incidence of falls compared to disease-free controls [1]. However, the underlying causes and mechanisms are unknown. In older adults, tripping is the most commonly reported cause for a fall [2]. Following a trip, a compensatory step is required to restore dynamic stability and avoid a fall. A compensatory step can elicit high loads at the knee joint [3], which in the presence of OA can elicit knee pain. Pain, or anticipation of pain may impair the ability to successfully perform the compensatory step.

Knee joint moments can be used as surrogate measures for knee joint loading considering larger moments contribute to larger joint forces. In patients with painful knee OA, compensatory strategies to reduce the knee extension and abduction moments during walking are common [4,5]. Similar compensatory strategies, implemented to reduce pain by decreasing the compressive force at the knee joint, may influence success of a compensatory stepping response.

Differences in foot placement during a compensatory step alter the knee joint moments due to changes in moment arms and/or ground reaction forces. A wider step may increase the knee abduction moment while a longer step may lead to greater knee extensor moment. However, the extent to which knee loading is concomitantly influenced by step width and step length during a compensatory step have not been examined. Such information may inform the design of fall-prevention interventions for people with lower extremity OA that focus on compensatory stepping. Thus, the purpose of this preliminary study was to examine relationships of foot placement and internal knee moments (as surrogate measures of knee joint loading) on the stance and stepping limbs in healthy young subjects.

METHODS

Nine healthy young adults (7 females, age 22.7$\pm$2.5 years, 165.0$\pm$5.6 mm, 61.0$\pm$8.4 kg) participated in this study. Subjects performed a maximum of 25 compensatory steps with the right leg after a self initiated loss of dynamic stability. Subjects were instructed to "lean forward slowly until you feel that you are about to fall, and at the last moment possible, step forward with your right foot".

Frontal and sagittal plane kinetics of the stepping and stance limbs during the compensatory step were collected using motion capture (120 Hz, Motion Analysis, Santa Rosa, CA) and two force platforms (1200 Hz, AMTI, Waterton, MA). The center of mass (COM) for each subject was estimated using a ten segment model and anthropometric estimations [6]. OrthoTrak (Santa Rosa, CA) and custom software (MATLAB, Natick, MA) were used to compute:

- Peak internal knee abduction and knee extension moments for the stepping limb during the 500 ms after recovery step touchdown.
- Peak internal knee abduction and knee extension moments for the stance limb prior to recovery step touchdown.
- Frontal and sagittal plane distance of the COM from the centroid of the stepping foot at recovery step touchdown (reflecting step width and step length, respectively).

Paired t-tests were used to compare moment data between the stepping and stance limb. Pearson product correlations quantified the strength of the relationships between knee moments and step length and step width. Significance was set at 0.05. Statistics were performed with SPSS 17.0 (Chicago, IL).

RESULTS AND DISCUSSION

Both the stance and stepping limbs were subjected to high loading conditions during the compensatory step. Peak knee extension moment were significantly greater on the stepping limb compared to the stance limb (Table 1, $p<0.01$), and were four to five times that during normal walking [7]. The knee abduction moments on the stance limb were significantly greater than that on the stepping limb (Table 1, $p<0.01$) and were nearly three times that during normal walking [7]. It is unknown if patients with knee OA favor one limb or another during compensatory stepping responses such as that used in the present study. Regardless, the results suggest that the most-affected limb of patients with knee OA, whether it is the stance or stepping limb, will likely experience high loading conditions unless a different strategy is used to avoid falling.

For the stepping limb, longer compensatory steps were associated with larger knee extension moments (r^2=0.52, p=0.01). Longer compensatory steps have been associated with an increased ability to recover from a trip [8]. However, to the extent that a longer step may increase joint loading, and potentially be painful for a person with knee OA, the ability to successfully perform the compensatory step and avoid a fall following a trip may be compromised. Further, patients with knee OA often have decreased quadriceps strength [9]. Some patients with knee OA display “quadriceps avoidance” during walking that is thought to reduce the contact forces at the knee [10]. Both decreased strength and quadriceps avoidance may influence the ability to perform a compensatory step independent of the influence of pain.

Knee moments on the stance limb were also related to recovery foot placement during the compensatory step. Longer steps were associated with larger knee extension moments (r^2=0.50, p=0.02) and wider steps tended to be associated with larger abduction moments (r^2=0.30, p=0.06). This suggests that for those with knee OA who choose to step with the least-affected limb, loading on the stance (most-affected) limb could be reduced by changes in foot placement.

While the data suggest that individuals with longer and wider steps tend to have larger knee joint moments on the stance and stepping limb, subjects were not instructed to step to specific positions. An important question related to a fall prevention intervention is whether these step kinematics are modifiable. Further, it is unknown if patients with knee OA will demonstrate similar trends and if knee loads can be reduced with changes in step position.

CONCLUSIONS

During a task used as a surrogate for a recovery from a trip, healthy young subjects performing the compensatory step with wider and longer steps had larger knee extension and abduction moments on the stepping and stance limbs. For patients with knee OA, larger moments associated with wider and longer compensatory steps may cause pain or be perceived by the subject to have the potential to cause pain. This may negatively affect the ability to perform the task. A possible approach to an intervention intended to reduce trip-related falls in patients with knee OA may involve focusing on recovery steps that are shorter. Although a performance trade-off would require more rapid, potentially additional, recovery steps, this may be both a suitable and achievable strategy for persons with knee OA.

REFERENCES

1. Prieto-Alhambra D, et al. *2011 American College of Rheumatology Annual Meeting*, Chicago IL.
2. Berg WP, et al. *Age and Ageing* **26**, 261-268, 1997.
3. Cyr M, Smeesters C. *J Biomech* **40**, 2857-2864, 2007.
4. Hurwitz DE, et al. *J Ortho Res* **18**, 572-579, 2000.
5. Kaufman KR, et al. *J Biomech* **34**, 907-915, 2001.
6. Winter DA. *Biomechanics and Motor Control of Human Movement*, John Wiley & Sons, Ltd., 2005.
7. Messier SP, et al. *Osteoarth Cartilage* **19**, 272-280, 2011.
8. Owings TM, et al. *Clin Biomch* **16**, 813-819, 2001.
9. Slemenda C, et al. *Ann Intern Med* **127**, 97-104, 1997.
10. Messier SP. *MSSE* **26**, 1446-1452, 1994.

Table 1: Knee joint moments for the stance and stepping limbs during the 500 ms after touchdown of a compensatory step

	Stepping Limb	Stance Limb
Mean Peak Abduction Moment (Nm/kg)	0.41 ± 0.30	0.98 ± 0.15
Mean Peak Extension Moment (Nm/kg)	2.01 ±0.43	0.14 ± 0.13

Pain During Ergonomic Hand Drive Wheelchair Propulsion

[1]Patty Hovis, [1]Lisa A. Zukowski, [1]Jaimie A. Roper, [1]Dana Otzel, [1]Orit Shechtman, [1]Mark Bishop, and [1]Mark. D. Tillman

[1]University of Florida, Gainesville, FL, USA
email: phovis@ufl.edu

INTRODUCTION

Approximately 3.3 million individuals use a wheelchair or similar device for mobility [1]. Pain and dysfunction with wheelchair use has prevalence as high as 70% [2]. Pain with manual wheeling leads to loss of mobility and independence and subsequent reductions in quality of life. The occurrence and/or severity of pain and dysfunction may be minimized though ergonomic optimization of manual wheelchair propulsion systems.

Ergonomic optimization has been addressed through different wheelchair designs. De Woulde et al. [3] reported that a lever wheelchair produced more power when compared to a manual wheelchair and a crank wheelchair. Further Requejo et al. [4] found that the lever wheelchair design had the advantage of eliminating the extraneous forces (medial/lateral forces) with propulsion. Such a lever design is in production in our lab that utilizes a lever with an adjustable grip Ergonomic Hand Drive (EHD). Our EHD propels the wheelchair through a ratchet lever system and accommodates user anthropometrics.

Accordingly, the purpose of this study is to evaluate and compare pain intensity, push frequency, and maximal volume of oxygen consumption (VO2) in a group of participants who are habitual wheelchair users propelling an EHD wheelchair and a conventional manual wheelchair (CMW). Since increased age of the individual increases the risk of degenerative changes of the shoulder, an age range of 18 to 30 years will delineate our younger age group with over 30 years being the older age group. The younger age range was chosen to avoid degenerative changes seen with older adults with spinal cord injury [5}. We hypothesize using an EHD would result in decreased pain intensity, decreased VO2, and no change in push frequency compared to the CMW for both age groups.

METHODS

Fourteen full-time manual wheelchair users [younger group (N = 5) means 25.2±4.5 yrs, 66.0±10.8 kg, 169.2±12.4 cm; older group (N=9) means 47.1±4.4 yrs, 79.5±17.9 kg, 175.7±13.2 cm) participated in the study. All participants were medically and functionally stable and at least six months post injury. All participants provided written informed consent in conjunction with the universities institutional review board.

The same chair was used for EHD and CMW wheeling (the levers rotated back and out of the way during CMW propulsion) and the order of the testing on each device was randomized. Participants wheeled for three and a half minutes around a 99.3 m semi-circular course in the gymnasium while push frequency was manually measured and VO2 recorded from a portable device (Cosmed K4b2 Portable Metabolic System). Push frequency and VO2 were obtained for the last 30 seconds of each trial (during physiological steady state). Pain visual analogue scale (VAS) ratings were acquired via ratings on a 10 cm visual analog scale after using each chair. Higher pain VAS ratings indicate higher pain intensity.

The push count obtained during the last 30 seconds of three and a half minutes of wheeling was converted to push frequency by dividing by time. Relative VO2 (mL/kg/min) was calculated from the absolute VO2 obtained from the metabolic unit. A mixed model ANOVA (within – type of propulsion unit; between – age) was used to measure how the dependent measures of pain, VO2, and push frequency are affected by chair design and age. Alpha was set at $p \leq 0.05$.

RESULTS AND DISCUSSION

No significant interaction was found for chair type or age with pain [$F(1,12) = 3.273$, $p = 0.096$, $\eta^2 = 0.214$] in the two way ANOVA. In addition, no significant main effects were found in this analysis for chair type or age with pain [$F(1,12) = 1.592$, $p = 0.231$, $\eta^2 = 0.117$]. Also, no significant interaction for chair type or age with VO2 were found [$F(1,12) = 0.445$, $p = 0.517$, $\eta^2 = 0.036$], as well as, no significant main effects [$F(1,12) = 1.435$, $p = 0.254$, $\eta^2 = 0.107$]. Furthermore, no significant interaction or main effect was found for chair type or age with push frequency [$F(1,12) = 4.688$, $p = 0.052$, $\eta^2 = 0.280$; $F(1,12) = 0.124$, $p = 0.731$, $\eta^2 = 0.010$ respectively].

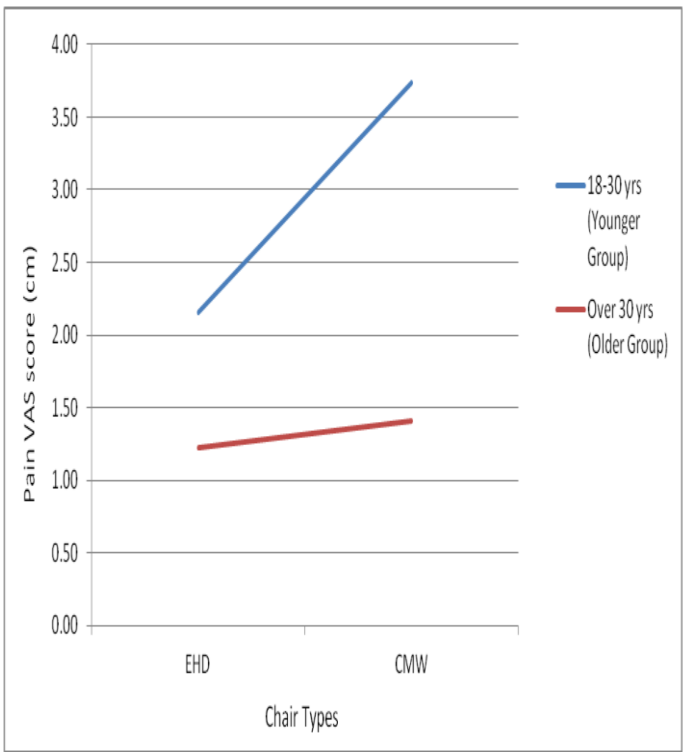

Figure 1: The interaction of age pain intensity mean scores between the EHD and CMW.

Preliminary results showed no significant difference in pain intensity while wheeling in an EHD wheelchair versus a CMW for age. Additionally, neither VO2 nor push frequency significantly differed with chair type or age at the 0.05 threshold that we had set for this experiment. However, there was weak evidence of an interaction observed for pain ($p = 0.096$) and push frequency ($p = 0.052$). We had moderate effect sizes (0.21, and 0.28) but were only powered 50% to find true effects

CONCLUSIONS

Our findings suggests that the age of the individuals and which chair design they use may affect pain intensity and push frequency - younger individuals may have less pain using the lever, whereas the older individual's pain intensity is not affected by chair type (Fig. 1). Future work should include pre and post pain data that includes quality of pain. Also, identify the mechanical efficiency of the EHD during propulsion and how it may relate to risk of pain with shoulder impingement. Last, a larger group of participants should be followed.

REFERENCES

1. U.S. Census Bureau. Americans with Disabilities: 2005 Current Population Reports, http://www.census.gov/prod/2008pubs/p70-117.pdf., 2008.
2. Salisbury, SK, et al. *Spinal cord*, **44**, 723–728, 2006.
3. van der Woude, LH, et al. *Am J Phys Med Rehabil*, **80**, 765-777, 2001.
4. Requejo, PS, et al. *J Spinal Cord Med*, **31**, 568-577, 2008.
5. Lal, S. *Spinal Cord* **36**, 186 – 189, 1998.

ACKNOWLEDGEMENTS

Supported by the Clinical and Translational Science Institute Pilot & Collaborative Research Projects (NIH). The hand drive mechanism used in this study is the intellectual property of Shands Healthcare.

DUAL-TASK WALKING AND COMPUTERIZED COGNITIVE TESTS IN ASSESSING CONCUSSED HIGH SCHOOL ATHLETES

David Howell, Louis Osternig and Li-Shan Chou

Department of Human Physiology, University of Oregon, Eugene, OR, USA
email: chou@uoregon.edu, web: http://biomechanics.uoregon.edu/MAL

INTRODUCTION

An estimated 1.6 – 3.8 million sport related concussions occur each year [1], yet proper care and treatment is still poorly understood. Many methods of assessment such as computerized neuropsychological testing (NP) have been advocated in the management of concussion [2]. Although this type of measurement gives an indication of cognitive ability, it provides little data regarding motor function. Little investigation has been conducted about motor performance deficits seen longitudinally after mTBI in adolescent populations. Therefore, the purposes of this study are to identify gait performance characteristics and the relationships between computerized cognitive testing modules and gait under different conditions over a period of two months post-concussion. We hypothesized that divided-attention walking and executive function would reveal deficits post-concussion that are longer lasting than those found with commonly used cognitive tests.

METHODS

High school athletes who suffered a concussion were identified by a certified Athletic Trainer. Each concussion subject (n=20) underwent examination in the following five time increments: within 72 hours of injury, one week, two weeks, one month, and two months post injury. Matched, healthy controls (n=20) completed the same testing protocol at the same time increments. Each subject completed NP tests which assessed cognitive disturbances post-concussion. The tests used and analyzed were the ImPACT [3] (ImPACT Applications, Pittsburgh, PA) and Task Switching Test [4] (TS). Dependent variables examined for the ImPACT were the visual memory composite score and self-report symptom score and for the TS was the switch cost calculation. To assess whole body motion, a set of 29 reflective markers were placed on bony landmarks of the participant. A ten-camera motion analysis system (Motion Analysis Corp., Santa Rosa, CA, USA) was used to capture and reconstruct the three-dimensional trajectory of surface markers. Gait velocity was then calculated using Orthotrack analysis software (Motion Analysis Corp.) and normalized by height. The dependent variable examined was the difference in gait velocity between a single-task (level walking) and a dual-task condition involving level walking while simultaneously performing specific cognitive tasks (spelling backwards, counting serial 6s or 7s backwards, or months in reverse order).

A two way, mixed effects analysis of variance was used to examine between group (concussion and control) and within-group (testing time) effects for the dependent variables. To determine the relationship between gait and cognitive performance, Pearson's correlation coefficients were computed for combined groups on all combinations of cognitive tests and the dual task variable (SPSS Inc., Chicago, IL, USA).

RESULTS AND DISCUSSION

There was a significant effect of group (p = .01) and testing day (p < .001; Figure 1) for the switch cost (TS), and a significant interaction for the visual memory (p = .007; Figure 1) and symptom score (p = .001) components of ImPACT. Upon analysis of group effects, differences for visual memory were seen at the 72 hour ($p < .001$) and 1 week assessment ($p < .001$). There was a main effect of group ($p = .025$) and day ($p = .002$) for gait velocity between dual and single-task conditions (Figure 2).

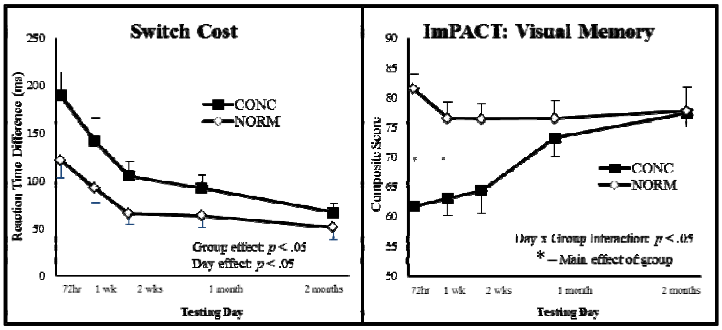

Figure 1: Comparison between two types of cognitive tests: The task switch (left) and ImPACT (right)

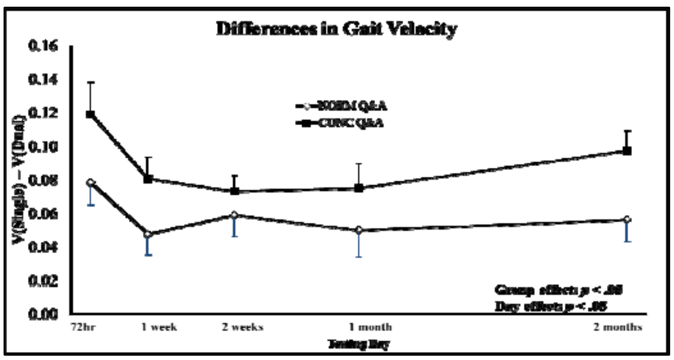

Figure 2: The difference in gait velocity between a single task (level walking) and simultaneous dual task in concussed and healthy high school athletes.

Moderate, but significant, correlations were found between the switch cost measure and the dual task effect at the two week assessment ($r = 0.347$, $p = 0.026$; Figure 3) and between the visual memory composite score and dual task effect ($r = -0.361$, $p = 0.021$) at one week post-concussion.

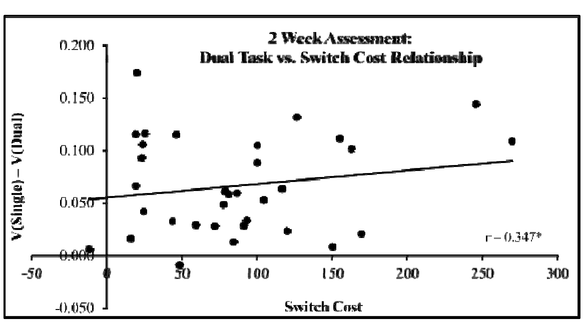

Figure 3: Grouped comparison between the switch cost (TS) and gait velocity dual task difference revealed a moderate correlation at the two week testing period. This is one of two correlations found between all NP test and gait variables.

No other significant correlations were found between motor performance and NP test performance across the two month testing period.

These data revealed deficits which were present throughout the two months of testing for concussion subjects for TS and gait velocity difference between dual and single task conditions. The visual memory component of the ImPACT resolved within two weeks of injury while the switch cost (TS), an executive function probe, and divided-undivided attention gait velocity difference showed group differences throughout the two month testing period. This could be an indication of a prolonged deficit in a region of the brain which is employed in complex motor tasks and could be susceptible to concussion, particularly in high school aged athletes.

The moderate correlation between NP tests and gait velocity condition difference is similar to previous findings [5] for college athletes. NP tests are used as one form in return to physical activity decisions. However, it must be noted that the ability to move and effectively protect oneself against concussion may still be compromised even though cognitive testing shows an individual has returned to normal. Further examination of dynamic motor function following concussion may be warranted in the assessment, diagnosis, and treatment of this injury.

CONCLUSIONS

Within high school athletes, complex motor tasks may better represent the cognitive demands instigated once they have returned to physical activity and daily life rather than traditional cognitive testing.

REFERENCES

1. Langlois et al. *J Head Trauma Rehab*, **21**, 375, 2006.
2. Van Kampen et al. *Am J Sport Med*, **34**, 1630-1635, 2006.
3. Iverson et al. *Arch Clin Neuropsychol*, **19**, 961-962, 2004.
4. Mayr and Bell. *Psychol Sci*, **17**, 774-780, 2006.
5. Parker et al. *Brit J Sport Med*, **41**, 868-873, 2007.

SINGLE LEG HOP LANDING BIOMECHANICS AND ASSOCIATION WITH SYMMETRY INDEX FOLLOWING MENISCECTOMY

[1]Chao-Jung Hsieh, [2] Terese Chmielewski

[1, 2]University of Florida, Gainesville, FL, USA
email: chaojung@phhp.ufl.edu

INTRODUCTION

The single-leg hop for distance is a commonly used functional test in rehabilitation for knee injury or surgery. Results on the test have been used to guide clinical decision-making following anterior cruciate ligament (ACL) injury or reconstruction. For example, symmetry between limbs of 85% or greater has been suggested as satisfactory for safely returning to sports activity[2]. Few studies have reported symmetry on the single leg hop test following meniscectomy has been studied less because the surgery is less invasive than ligament reconstruction. In addition, few studies have examined landing kinematics and kinetics on the single leg hop test following meniscectomy. However, landing from a hop places high demands on the lower limb to absorb ground reaction force, and poor force absorption may be a factor in the high incidence of knee osteoarthritis following meniscectomy.

The purpose of this study was to investigate in subjects with meniscectomy: (1) differences in single leg hop landing biomechanics between limbs, and (2) the relationship between the single leg hop test symmetry index and landing biomechanics on the surgical limb.

METHODS

Subjects with meniscectomy were selected to participate if they met the following criteria: (1) age 15-35 years, (2) traumatic-onset meniscal tears, (3) surgery performed within 1 year of injury, (4) meniscal tears confirmed at the time of surgery, (5) unilateral injury, (6) no concomitant other ligamentous injury > Grade II, and (7) no previous knee injury and surgery. At the time of testing, all subjects had undergone a supervised physical therapy program for 6 weeks.

Single leg hop test

Subjects first stood on the non-surgical limb and hopped forward as far as possible, landing on the same limb and holding for 3 seconds. The test was repeated on the surgical limb. Practice trials were performed for each limb until hop distance was stable. Three trials were then collected and the distances were averaged. The symmetry index was calculated using the following formula: [(average distance on surgical limb/ average distance on non-surgical limb) *100].

Landing biomechanics

Retro-reflective markers placed on anatomical landmarks and tracking shells were used to monitor lower limb motion. Marker positions were recorded with a six-camera, three-dimensional motion capture system (Motion Analysis Corporation, Santa Rosa, CA) collecting at 120 Hz. Synchronized force data were sampled at 1200 Hz with a six-component force plate (Advanced Mechanical Technology Inc.; Watertown, MA). Subjects performed a single leg hop test onto the force plate at 80% of the average hop distance and held their landing position for 3 seconds. Subjects performed at least 3 practice trials, and 3 successful trials were recorded.

Kinematic and kinetic variables were analyzed during the landing phase, including sagittal plane knee excursion (initial contact to peak knee flexion), peak vertical ground reaction force (PVGRF), time from initial contact to PVGRF and rate of loading. Rate of loading was calculated using the following formula: PVGRF/time from initial contact to PVGRF. PVGRF and rate of loading were both normalized for body weight.

Paired-sample t-tests analyzed the difference in single leg hop landing biomechanics between limbs. Pearson product-moment correlation was used to determine the association between the single leg hop symmetry index and biomechanical variables on the surgical limb.

RESULTS AND DISCUSSION

Twelve male subjects (age = 20.9 ± 1.4 years) participated in the study. The mean height and weight were 181.7 ±1.7 cm and 102.6 ± 8.8 kg, respectively. The mean time from injury to testing was 4.2 ± 3.2 months. The side of meniscectomy was lateral for 7 subjects and medial for 5 subjects.

The single leg hop symmetry index was 87.8± 1.2 %. The surgical limb demonstrated decreased sagittal plane knee excursion compared to the non-surgical side (Surgical = 32.5 ± 7.2°, Non-surgical = 40.8 ± 9.1°; p=0.008). The PVGRF was not significantly different between limbs (Surgical = 2.5 ± 0.6 BW, Non-surgical = 2.5 ± 0.6 BW; p=0.661). Compared to the non-surgical limb, the surgical limb demonstrated a trend toward increased time from initial contact to PVGRF (Surgical = 0.056 ± 0.015 s, Non-surgical = 0.049 ± 0.012 s; p=0.083) and decreased rate of loading (Surgical = 50.1 ± 18.5 BW/s, Non-surgical = 55.5 ± 18.5 BW/s; p=0.087).

A significant negative correlation (r=-0.595, p=0.041) was found between the single leg hop symmetry index and the time from initial contact to PVGRF on the surgical limb. No correlation was found between single leg hop symmetry index and sagittal plane knee excursion (r=0.050, p=0.878) or PVGRF (r=0.454, p=0.138) or rate of loading (r=0.468, p=0.125) on the surgical limb.

The mean single leg hop symmetry index met the current standard for returning to sport activation in ACL reconstruction is 85%. However, 4 of 12 subjects in this study were below this criterion. Asymmetry was seen in the landing biomechanics of a single leg hop. The surgical limb demonstrated a significant decrease in knee motion and the rate of force application to the body. This reduced loading strategy may lead to a reduced force absorption capacity, which indicates greater impact force at the knee. However, additional investigation is needed to examine whether the decreased knee motion is compensated by greater hip and/or ankle motion.

An interesting finding of this study was the negative correlation between the single leg hop symmetry index and time from initial contact to PVGRF on the surgical limb. This finding may indicate that subjects with meniscectomy who need more time to absorb force on the surgical limb may not be able to hop as far on the surgical limb. This finding may provide insight for clinicians to develop rehabilitation interventions to improve surgical limb hopping distance following meniscectomy.

CONCLUSIONS

Our findings indicate that following meniscectomy, the surgical limb displayed decreased sagittal plane knee excursion, increased time from initial contact to PVGRF and decreased rate of loading. The single leg hop symmetry index was negatively correlated with the time from initial contact to PVGRF on the surgical limb. Our findings provide insight for developing rehabilitation interventions to correct limb asymmetry in landing of a single leg hop and improve surgical limb hopping distance following meniscectomy. Future studies should examine the hip and ankle motion during landing of a single leg hop.

REFERENCES

1. DeVita P, Skelly WA. *Med Sci Sports Exerc* **32**, 812-819, 2000.
2. Fitzgerald GK, Lephart SM, Hwang JH, et al. *J Orthop Sports Phys Ther* **31**, 588-597, 2001
3. Decker MJ, Torry MR, Noonan TJ, et al. *Med Sci Sports Exerc* **34**,1408–1413, 2002.

RELATIONSHIPS BETWEEN ELECTROMYOGRAPHY AND OXYGEN CONSUMPTION IN DIFFERENT WORK LOADS – ROWING EXERCISE

[1]Hsiang Yi Hsu, [2]Wei Hsien Hong, [2*]Hui Ju Wang

Department of Sports Medicine, China Medical University, Taichung, Taiwan
*: Corresponding Author
email: shaq19850310@gmail.com

INTRODUCTION

The evaluation of sport performance is imperative to athletes, especially in accordance with several identifying elements, such as oxygen uptake (VO_2), and muscle activity[1]. It is incontestable that physical fatigue is fully considered as the perplexing period during training and thus the relationship between $\dot{V}O_2$ and muscle activity can be referred to as the major determinants to predict the athlete's performance[2]. Rowing exercise has been viewed as an endurance training activity. However, the mechanism of fatigue during rowing is not fully investigated. This study aimed at differentiating the contribution of prime movers in rowing exercise at different intensities. Also, the physical fatigue time point was investigated along with changes in $\dot{V}O_2$.

METHODS

Four college students were recruited and performed rowing exercise on a rowing ergometer (Concept II, Concept Inc., Morrisville, VT). Oxygen consumption was measured by a computerized system (MetaMax 3B, Cortex, Germany). Furthermore, subjects' muscle activities were recorded by electromyography (EMG) (SX230, BioMetrics Ltd., UK) which is supported by a portable data logger. The muscles involved in rowing exercise, namely biceps brachii, triceps, flexor/extensor carpi muscle, latissimus dorsi, erector spinae, rectus femoris and hamstring were included for EMG evaluation. Subjects were first requested to row at the maximal power output (Watt) to exhaustion within 3 min. Then, they underwent rowing tests at 60%, 70% and 80% of maximal power output respectively in different days. On the day of test, work load was gradually increased to desired level and EMG signals and $\dot{V}O_2$ were recorded simultaneously. EMG variables (median frequency and mean value), was sampled at 1000Hz and analyzed by a self-developed MATLAB program.

RESULTS AND DISCUSSION

Our results showed that the activation of leg and back muscles increased in proportion to the work load increase (Fig 1).

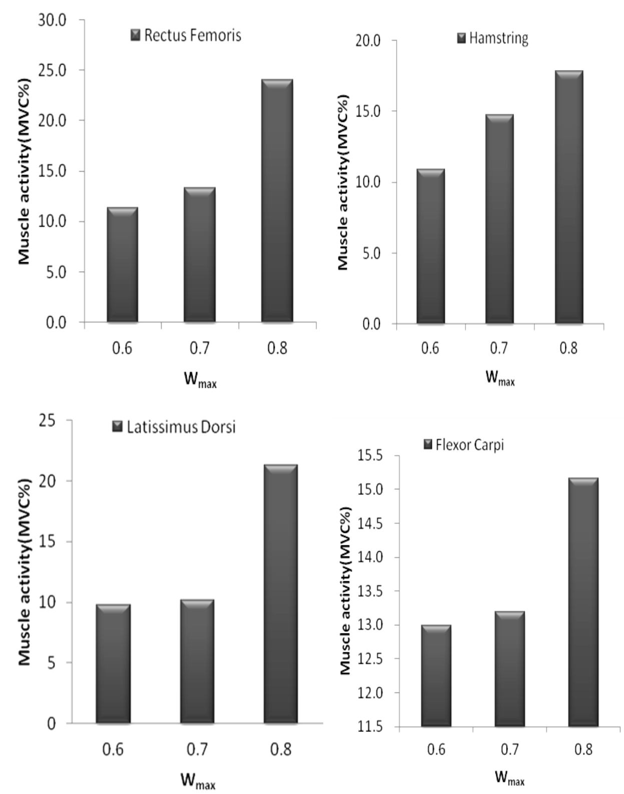

Figure 1: Electromyography (EMG) mean value at different work loads – Rectus femoris, Hamstring, Latissimus dorsi and Flexor Carpi muscle.

However, biceps brachii activity remained relative stable regardless of exercise intensities (Fig 2), suggesting that the standard rowing movement focuses mainly on the coordination of back and thigh muscles.

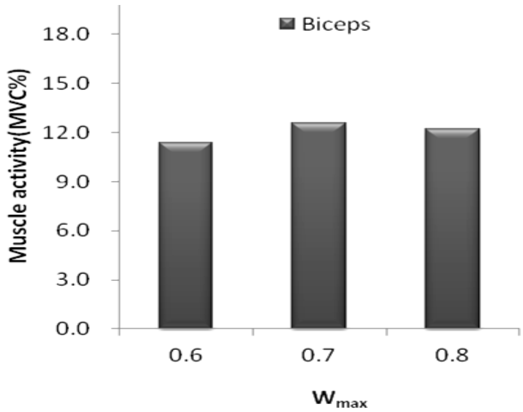

Figure 2: Electromyography (EMG) mean value at different work loads – biceps brachii.

Besides, the physical fatigue time point was found within 24.8 second according to the median frequency of muscle activity (Fig 3). Meanwhile, a concomitant change in O_2 consumption also occurred at the same time frame (Fig 4). These results indicated that oxygen consumption can reflect changes in muscle activities in rowing exercise.

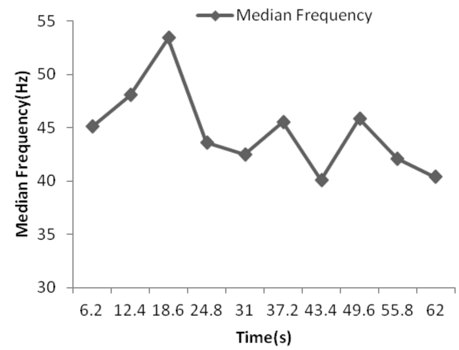

Figure 3: EMG variable, median frequency, within 80% maximal power output.

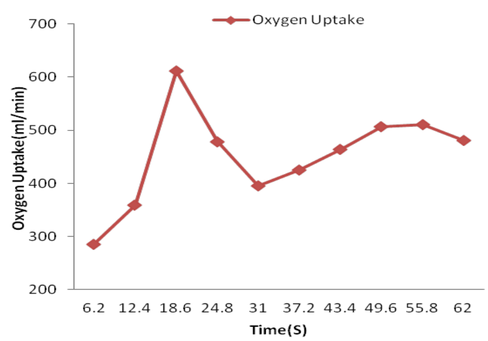

Figure 4: The oxygen uptake volume within 80% maximal power output

REFERENCES

1. Maestu, J., et al., *J Strength Cond Res*, **20**(4): p. 824-8, 2006.
2. Hug, F., et al., *Clin Physiol Funct Imaging*, **24**(1): p. 25-32, 2004.

.

REDUCED LIGHT INTENSITY ALTERS SPATIOTEMPORAL GAIT PATTERNS DURING TREADMILL WALKING

[1,2]Chun-Kai Huang, [1,2]Jung Hung Chien, [1]Mukul Mukherjee and [1,2]Ka-Chun Siu

[1]Nebraska Biomechanics Core Facility, University of Nebraska at Omaha, Omaha, NE, USA
[2]College of Public Health, University of Nebraska Medical Center, Omaha, NE, USA
email: chuang@unomaha.edu web: http://nbcf.unomaha.edu/

INTRODUCTION

Conditions which reduce light intensity (dim lighting, restricted vision) impairs the ability to identify hazards, and is one of the in-home risk factors of fall [1, 2]. Humans rely on visual information perceived from the surroundings to react [3], and use the perceived information to maintain balance by adjusting foot-placement during walking [4]. However, the effect of reduced light intensity on spatiotemporal gait patterns is not clear, especially during treadmill walking.

The aim of this study was to investigate the effect of reduced light intensity on gait patterns during treadmill walking. We hypothesized that walking with reduced light intensity would decrease step length, increase double support time, and increase step length and double support time variability.

METHODS

Twelve healthy adults (mean age= 24.4 ± 2.8 years; leg length = 84.67 ± 4.46 cm) walked on a treadmill (Bertec Corp. Columbus, OH) with a virtual corridor projected in front of the subjects (Fig. 1).

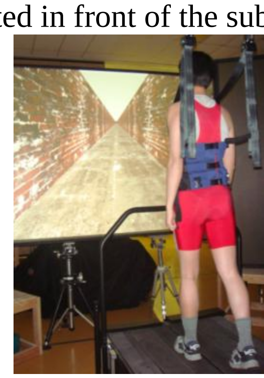

Figure 1: A subject walking on a treadmill with a safety harness while a virtual environment was presenting in front of him.

Each subject walked five minutes at their self-selected pace for familiarization followed by three two-minute treadmill walking trials in the following conditions by wearing: 1. A pair of clear goggles (Fig. 2: left); 2. Goggles attached with one layer of window film which reduced the amount of light intensity from 7.9 lx to 3.7 lx; 3. Goggles attached with two layers of window film which reduced the amount of light intensity from 7.9 lx to 2.2 lx (Fig. 2: right).

Figure 2: The clear goggles used as control condition (left) and goggles attached with 2-layered window films to reduce light intensity (right).

Three-dimensional spatiotemporal data were collected using NDI motion capture system at 100 Hz (Northern Digital Inc, Waterloo, Canada). Gait parameters (step length and double support time) were calculated. Step length was defined as the distance between two consecutive heel strikes of the same leg. Double support time was the time duration in each gait cycle when two feet were in contact with the treadmill belt. Group means and variability (coefficient of variance, CV) of both step length, and double support time were evaluated.

To eliminate between-subject anthropometric disparities, we normalized each subject's step length to his/her leg length (distance between greater trochantor and lateral malleolus).

One-way ANOVA with repeated measure was applied to compare all the spatiotemporal gait parameters collected in the three conditions. Pairwise comparison tests with Bonferroni adjustment were performed when significant effects were found. The significance level was set at 0.05.

RESULTS AND DISCUSSION

Light intensity showed the main effect on spatiotemporal gait parameters in terms of step length ($p < 0.01$), double support time ($p = 0.02$), and the corresponding CVs ($p < 0.05$). The follow-up comparisons indicated step length and double support time were significantly decreased ($p < 0.03$; Fig. 3) whereas the CV of double support time was significantly increased when light intensity was reduced in the two-layer Goggles condition compared to other conditions.

In addition, significant linear trends were revealed in step length ($p < 0.01$), double support time ($p < 0.01$) as well as the corresponding CVs ($p < 0.05$). These results indicate that gait patterns differ with the changes of light intensities.

The reduced light intensity led to a short step length, which may have led to increased cadence and decreased double support time to maintain the constant treadmill speed.

CONCLUSIONS

Overall, the present study provides evidence that vision plays an essential role during treadmill walking. The results support our hypothesis that subjects used a conservative gait pattern during walking in conditions with reduced light intensity in terms of decreased their step length.

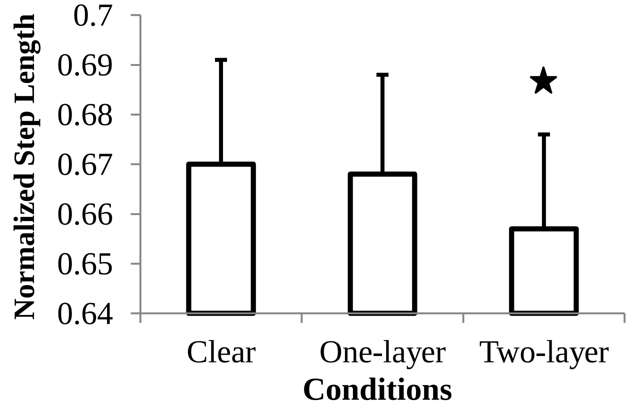

Figure 3: Compared to other conditions, normalized Step length was decreased significantly (asterisk) when subjects wore the two-layered window films goggles and walked on the treadmill.

REFERENCES

1. Bell J, et al. *DHHS (NIOSH) Publication* **2011-123**, 2010.
2. Helbostad JL, et al. *Gait Posture* **30**, 233-238, 2009.
3. Gibson JJ. *The Ecological Approach to Visual Perception*, Houghton Mifflin, 1979.
4. Patla AE, et al. *Exp Brain Res* **128**, 441-450, 1999.

ACKNOWLEGEMENTS

This project was supported by NSAS Nebraska Space Grant & EPSCoR and NASA Nebraska Space Grant Fellowships.

Table 1: Descriptive statistics of gait patterns in different conditions

	Clear	**One-Layer**	**Two-Layer**
Normalized Step Length	0.67	0.67	0.66 *
CV of Step Length	0.02	0.02	0.03
Double Support Time	28.24	28.16	27.65 *
CV of Double Support Time	0.06	0.06	0.07 *

Note: CV: coefficient of variance;

*Significant difference when compared the condition of two-layered window films goggles with the other conditions ($p < 0.05$).

EXPERIMENTAL DESIGN USING PARTICLE SWARM OPTIMIZATION

[1]Richard E. Hughes and [2]Mark L. Palmer
[1]Department of Orthopaedic Surgery, University of Michigan, Ann Arbor, MI, USA
[2]School of Kinesiology, University of Michigan, Ann Arbor, MI, USA
email: rehughes@umich.edu web: http://www-personal.umich.edu/~rehughes/index.html

INTRODUCTION

Computational models are important tools for understanding biomechanical systems. The scientific process is most powerful when experiments are designed to differentiate between competing models. The experimenter must explore the entire space of experimental conditions to select ones that will produce the largest difference in model behavior. It would be helpful to have an automated method for searching the space of experimental parameters to assist the investigator in selecting experimental conditions. Therefore, the goal of this project was to develop a computational method for designing experiments to differentiate between competing biomechanical models. While the ultimate goal is to develop a method for computationally intensive models (FEA, etc.), we started by developing a method for a small-scale muscle force prediction model. Two variants of a ten-muscle low back muscle force prediction model were used as a proof-of-concept for the method.

METHODS

The approach was to use a nonlinear optimization model to select two experimental conditions that maximally differentiate between competing model predictions. We assume that two distinct mathematical models (1 and 2) of the biomechanical system exist that map independent variables to dependent variable values (denote the mapping for the ith model as $y = f_i(\mathbf{x})$). We assume that EMG measurements are made on one muscle. If loading of the torso is conducted under isometric conditions in the experiment, it is reasonable to assume a monotonically increasing relationship between muscle force and EMG. Thus, the goals of our model is to find two loading conditions, $\mathbf{x}^A$ and $\mathbf{x}^B$, that create model predictions such that an increase or decrease in EMG measurements from experimental condition A to experimental condition B will imply that either Model 1 or Model 2 is inconsistent with experimental results (or both). Such an experimental design would allow the investigator to pursue the Popperian paradigm of falsifying one or both of the models.[1] To achieve this design, we propose solving two nonlinear optimization problems. The first model seeks sagittal and frontal plane moments that maximize the difference in muscle force magnitudes predicted by Models 1 and 2 over a prescribed set of possible experimental loadings, $\mathbf{\Omega}$:

$$\underset{\mathbf{x}^A \in \mathbf{\Omega}}{Max}\ \Theta\left(\mathbf{x}^A\right) = f_1\left(\mathbf{x}^A\right) - f_2\left(\mathbf{x}^A\right) \qquad (1)$$

The second optimization model seeks to maximize the difference in muscle force magnitudes predicted by Model 1 and Model 2:

$$\underset{\mathbf{x}^B \in \mathbf{\Omega}}{Max}\ \Psi\left(\mathbf{x}^B\right) = f_2\left(\mathbf{x}^B\right) - f_1\left(\mathbf{x}^B\right) \qquad (2)$$

Note $\Psi(\mathbf{x}) = -\Theta(\mathbf{x})$. Ideally, equation (1) will produce a moment loading (“condition A”) that make the muscle force predicted by Model 1 much greater than the force predicted by Model 2. Conversely, (2) will find a loading condition (“condition B”) that make the Model 2 prediction much greater than the Model 1 prediction. If such experimental conditions can be identified then changes in EMG between condition A and condition B can be used to refute Model 1 or Model 2. If EMG is greater in condition B than condition A then Model 1 is inconsistent with the data. If EMG is greater in condition A than in condition B then Model 2 is not supported by the data. If EMG is the same in both conditions then neither model is consistent with the data (although the experiment must have sufficient statistical power to confidently make such a claim).

The approach was applied to two variants of a published model used for predicting muscle forces in the lumbar region of the torso.[2] One version of the model (Model 1) used the double linear programming scheme to select muscle forces that minimize the spinal compression force subject to the strictest possible muscle stress limits in the first step.[3] The alternate version (Model 2) minimized the sum of cubed muscle stresses and without imposing upper bounds on muscle force.[4,5]

The optimization problems (1) and (2) were solved using particle swarm optimization (PSO).[6] The dependent variable of interest was the left erector spinae (LES), so $y = f_i(\mathbf{x}) = LES\ force$. The independent variables were X (sagittal), Y (frontal), and Z (transverse) moments. The region of allowable values for experimental conditions was a hypercube having sides of length 20 N.m and centered at the origin. PSO simulations were run with 10 particles and 20 time steps. Initial particle locations were randomly selected using uniform distributions over the hypercube. Particle velocities were also randomly distributed chosen using uniform distributions [0,0.5] for each dimension. All simulation code was written in MATLAB (v.R2011b). Simulations were performed on a single core of a quad core computers running Windows Vista.

RESULTS

PSO found loading conditions that produced substantially different left erector spinae force predictions. Figure 1 shows LES predictions for Model 1 and Model 2 for two loading conditions, A and B. Loading condition A was 2.1 and -10.0 N.m for the X and Y axes respectively; loading condition B was 10.0 and -9.1 N.m for the corresponding axes. The model produced predictions that could easily be interpreted if an experiment were conducted to collect EMG under static conditions.

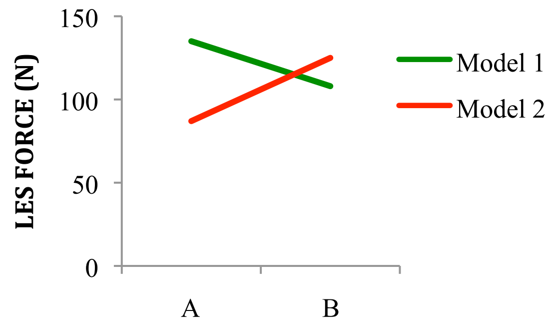

Figure 1: Predicted left erector spinae (LES) force by Model 1 and Model 2 for two experimental conditions (A and B).

DISCUSSION

These results demonstrate the feasibility of using particle swarm optimization to select experimental conditions that would produce distinctly different and testable predictions. If the experiment were conducted under static conditions, an increase in LES EMG from condition A to B would imply that Model 1 is inconsistent with the data; if it decreased from A to B then Model 2 would be inconsistent. Equal EMG values would be inconsistent with both.

REFERENCES

1. Miller, D (Ed.) *Popper Selections*. Princeton: Princeton University Press, 1985.
2. Schultz AB, et al. *J. Ortho. Res*. **1**, 77-91, 1983.
3. Bean JC, et al. *J. Biomech*. **21**, 59-66, 1988.
4. Crowninshield RD and Brand RA, *J. Biomech*. **14**, 793-801, 1981.
5. Hughes RE, et al. *J. Ortho. Res*. **12**, 689-698.
6. Kennedy J and Eberhart RC, Proc. IEEE int'l conf. on neural networks Vol. IV, pp. 1942-1948, 1995.

COHERENCE ANALYSIS REVEALS ALTERED POSTURAL CONTROL DURING STANDING IN PERSONS WITH MULTIPLE SCLEROSIS

[1]Jessie M. Huisinga, [2]Martina Mancini, [2]Chris Veys, and [2]Fay B. Horak
[1]University of Kansas Medical Center, Kansas City, KS, USA
[2]Oregon Health and Science University, Portland, OR, USA
email: jhuisinga@kumc.edu

INTRODUCTION

Postural control may be measured in persons with Multiple Sclerosis (PwMS) using both clinical and laboratory methods. Because balance problems are highly prevalent in this population, it is important to understand the adaptations that PwMS make to maintain postural control during standing and walking given their slowed somatosensory and motor pathways. Most studies investigating postural control assume the body moves as an inverted pendulum when, in fact, the upper body must be precisely balanced upon the legs to control position of the body center of mass motion during standing. Healthy adults move the trunk and legs together in an ankle strategy at frequencies below 1 Hz and then add a hip strategy at higher frequencies of sway [1] but it is not known how MS affects multi-segmental postural control strategies. PwMS exhibit a larger center of pressure sway area compared to healthy controls even when standing with eyes open [2]. Additionally, PwMS display a late, exaggerated response to perturbations, which is related to delayed somatosensory evoked potentials [3]. It is likely that delayed somatosensory-triggered postural responses require movement adaptations to maintain body equilibrium. The present study uses inertial sensors to measure acceleration of multiple body segments during quiet standing. The purpose of this study was to investigate how PwMS and age-matched healthy control subjects coordinate their trunk and leg segments at different frequencies during quiet standing. Coherence analysis allows for examination of the relationship between two segments across oscillating frequencies. We hypothesized that PwMS would have impaired multi-segmental coordination during stance posture displayed by reduced trunk-leg sway coherence.

METHODS

Eighteen PwMS (age 41.8 ± 9.3 yrs, self-reported EDSS 3.85 ± 1.34) and 12 healthy, age-matched healthy controls (age 38.8 ± 10.0 yrs) participated. Subjects were outfitted with 6 MTX Xsens sensors (49A33G15, Xsens, Enschede, NL, USA) sampling at 50 Hz. The sensors contained 3D accelerometers (± 1.7 g) and 3D gyroscopes (± 300º/s range) mounted on: (i) sternum, (ii) sacrum (L5 level), (iii) right and left wrist, (iv) right and left lower leg. Subjects stood quietly for 30 seconds with eyes open (EO) and closed (EC) for three trials in each condition. Acceleration data in the antero-posterior direction from the sacrum (trunk segment) and right ankle (leg segment) sensors were used for the analysis. Coherence was calculated for each trial as the absolute value of the cross spectral density of the trunk and leg acceleration, squared and divided by the product of trunk and leg power spectral density [1]. The mean of coherence was then examined at 5 frequencies (0, 0.5, 1.0, 1.5, 2.0 Hz). A linear mixed model (Group x Frequency) analysis was performed for both EO and EC conditions.

RESULTS

A significant effect of Group was found for coherence in the EO ($F=27.58$, $p<0.001$) and the EC ($F=45.23$, $p<0.001$) conditions where coherence was lower in PwMS compared to controls in both conditions. There was a significant effect of Frequency for both EO ($F=71.44$, $p<0.001$) and EC ($F=74.67$, $p<0.001$) conditions where coherence decreased as frequency increased in both groups. There was a significant interaction between Group and Frequency during EO ($F=9.53$, $p<0.001$) and EC ($F=3.34$, $p=0.012$). In the EO condition, coherence was lower in PwMS at 0 and 0.5 Hz but was the same in both groups at 1.0, 1.5, and 2.0 Hz

(Figure 1, top). In the EC condition, coherence was the same at 0.5 Hz but was decreased in PwMS at all other frequencies (Figure 1, bottom).

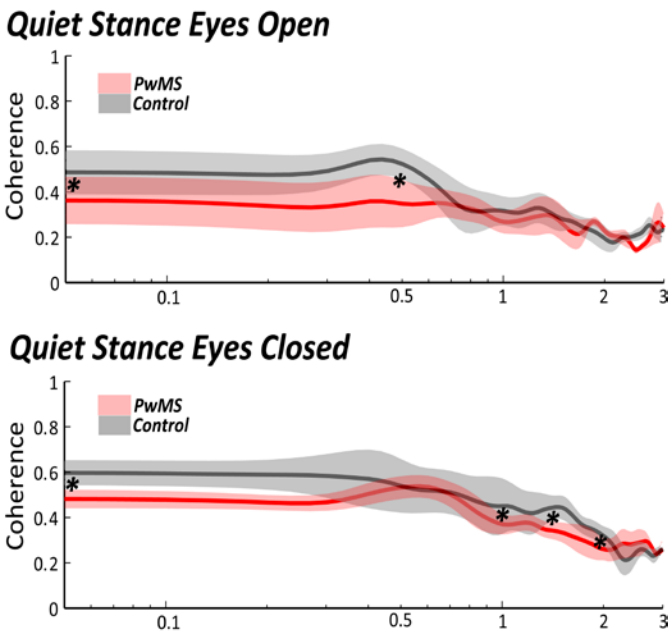

Figure 1: Coherence values across frequencies for both groups with eyes open (top) and eyes closed (bottom). *indicates a significant difference between groups.

DISCUSSION

Results indicate that PwMS use different strategies than controls to maintain balance during quiet standing. In healthy controls, coherence is expected to decrease as the frequency of oscillation increases [1]. This study also observed this finding, but also found that in PwMS, coherence is at a lower level than controls even at low oscillation frequencies. Thus, in the EO condition, it appears that at low frequencies, PwMS are using a mixed, strategy (moving at both the ankle and hip) whereas controls are using more of an ankle strategy. As frequency increases, both groups gradually increase use of a mixed strategy.

In contrast to EO, the EC condition resulted in differences in coherence between groups primarily at the higher frequencies. As frequency increases, coherence in PwMS stays lower than in controls. Thus, visual feedback appears to be able to substitute for delayed and reduced somatosensory feedback at higher frequencies of postural sway.

We will next determine how changes in coordination of upper and lower body segments during stance relates to delays in somatosensory feedback loops for postural control among PwMS.

REFERENCES

1. Creath et al. *Neurosci Lett* **377**, 75-80, 2005.
2. Van Emmerik, et al. *Gait Posture* **32**, 608-14, 2010.
3. Cameron, et al. *Somatosens Mot Res* **25**, 113-22, 2008.

ACKNOWLEDGEMENTS

This work was supported by the National Multiple Sclerosis Society, the Medical Research Foundation of Oregon, and the NIA.

MANIPULATION OF THE STRUCTURE OF GAIT VARIABILITY WITH RHYTHMIC AUDITORY STIMULUS

[1]Nathaniel Hunt, [1,2]Joshua L. Haworth, [1]Denise McGrath, [1]Sara Myers, [1,2]Nicholas Stergiou
[1]University of Nebraska at Omaha, Omaha, NE, USA
[2]University of Nebraska Medical Center, Omaha, NE, USA
email: nhunt@unomaha.edu, web: http://biomech.unomaha.edu/

INTRODUCTION

Gait is a rhythmic behavior that may be analyzed via discrete measures that are taken once per cycle, such as inter-stride interval. Nonlinear analyses of a series of discrete measures such as fractal scaling (an inverse power law relationship between two measures) and entropy (a measure of disorder and unpredictability) are important complements to the more traditional linear analyses [1]. Nonlinear measures provide the investigator additional information on the temporal structure of a time series. Previous quantification of gait variability using nonlinear analyses in young healthy walkers has identified a particular structure of gait variability within this population. This natural gait variability has been associated with the capacity to adapt to a dynamic environment. In contrast, aging and pathological conditions have been associated with altered entropy (more disordered gait) and fractal scaling properties (loss of long-range correlations) that suggest reduced capacity for adaptive gait [2, 3]. While gait therapies often focus on restoration of linear measures like mean step length or mean cadence, few, if any studies investigate the restoration of nonlinear measures of gait. We approach the restoration of nonlinear measures by *driving gait with a rhythmic auditory stimulus*.

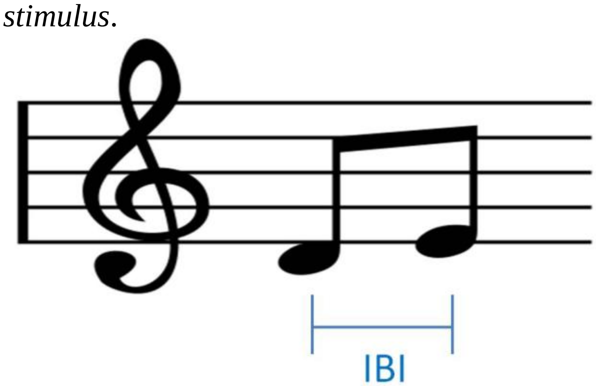

Figure 1. The inter-beat interval (IBI) is the amount of time between the onset of two successive notes.

When people walk in synchrony with music, the inter-stride interval of gait is roughly equivalent to an integer multiple of the inter-beat interval of the music (Figure 1). A strong, natural auditory motor coupling in humans promotes this synchrony; people will very easily and often unconsciously move to the beat of music. We propose that it is possible to restore the fractal scaling properties of gait that degenerate with aging and disease by taking advantage of this natural tendency to synchronize to auditory rhythms. This may be achieved by designing an individualized rhythmic auditory stimulus in which the series of inter-beat intervals exhibits the target nonlinear properties of gait. Therefore, the purpose of this study was firstly to test whether we can successfully manipulate fractal scaling of inter-stride interval gait variability in young healthy adults.

METHODS

Eleven healthy adults (age: 23.5$\pm$3.2 years; preferred walking speed: 1.01$\pm$0.11 meters/second; average cadence: 1.65$\pm$0.10 Hz; 7 male) participated in the study. We designed the rhythmic auditory stimulus to the music of Für Elise. The mean and standard deviation of the inter-beat interval was designed to match that of each subject as they walked on the treadmill at their preferred walking speed, with no stimulus. The music was manipulated so that the time series of the inter-beat intervals matched the temporal structure of either a metronome, fractional Gaussian white noise, or the Lorenz system. We selected parameters for the Lorenz equations that are known to generate entropy values between periodic and random dynamics via mathematical chaos, which is similar to the dynamics that have been observed in healthy human walking. These stimuli were specifically chosen for their entropic properties which increase monotonically from the metronome to the Lorenz to the random white noise conditions. In the no music condition, the entropy of the subject's natural gait variability is driven by endogenous dynamics. Natural gait variability exhibits entropy values between completely periodic (metronome) and completely random (white noise) dynamics, with somewhat greater entropy values than the Lorenz system [1]. Subjects walked on a Bertec Instrumented Treadmill. Each subject first walked at their preferred walking speed for five minutes with no stimulus. Each subject then completed five minutes of treadmill walking while listening to an auditory stimulus, followed by five minutes of seated rest for each of the four conditions in a randomized order. The stimulus was delivered through an Olympus digital voice recorder WS-600S and AKG K55 over the ear stereo headphones. Three-dimensional kinematics was collected at 100 Hz (Optotrak Certus system; First Principles software; Northern Digital Inc., Waterloo, Canada). Inter-stride intervals were calculated as the time difference between successive maximums of the anterior displacement of the toe marker of the same foot. Analysis of fractal scaling of the inter-stride interval series was performed with the Detrended Fluctuation Analysis algorithm, resulting in the scaling exponent α [3]. Trend analysis was performed to investigate the relationship between the entropy of the driving signal and the fractal scaling of the stride interval variability. A repeated measures ANOVA was performed to compare group means between the tested conditions.

RESULTS AND DISCUSSION

Trend analysis across conditions (ordered in terms of increasing entropy) found no significant linear trends. A significant quadratic trend was found for the α values across conditions ($F_{1,36} = 5.281$; Figure 2). This indicates that as the entropy of the driving signal increases monotonically from periodic to chaotic to random dynamics, the structure of stride time variability goes from uncorrelated to persistent fractal scaling and then back towards uncorrelated, in line with the theoretical model presented in [1]. Repeated measures ANOVA found no significant differences in α value between conditions. A lack of significant differences between the means may be due to the stationarity constraint imposed by walking on a treadmill of finite length, as well as the altered relationship between velocity and visual information.

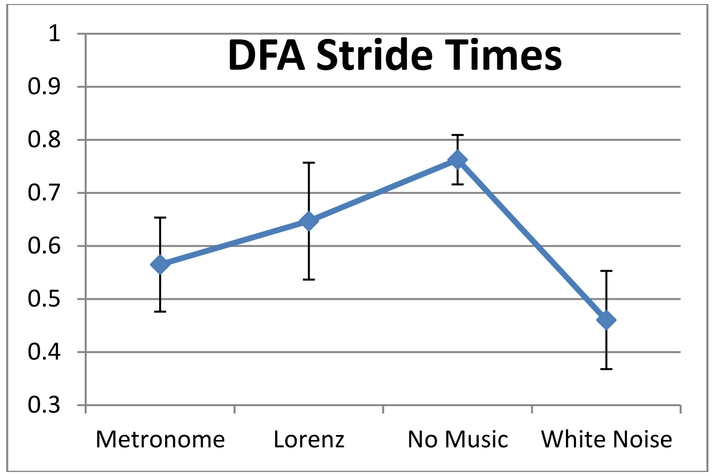

Figure 2. Mean α values with error bars representing the standard error of the mean. Values are from the dominant leg of 11 subjects walking on a treadmill.

CONCLUSIONS

The presence of a quadratic trend with an inverted U shape suggests that our technique may be able to manipulate the temporal structure of inter-stride interval. Our present work is exploring rhythmic auditory stimulus during overground walking with additional temporal structures, tested in pathological gaits.

REFERENCES

1. Stergiou N, Decker L. *Human Movement Science* **30**, 869-88, 2011.
2. Buzzi U, Stergiou N, Kurz M, Hageman P, Heidel J. *Clinical Biomechanics* **18(5)**, 435-43, 2003.
3. Hausdorff J, Mitchell S, Firtion R, Peng C, Cudkowicz M, Wei J, et al. *Journal of Applied Physiology*, **82(1)**, 262-9, 1997.

ACKNOWLEDGEMENTS

Funding was provided by the National Aeronautics and Space Administration (Grant No. NNX11AM06A), Autism Speaks (Grant #7070), and the Nebraska Research Initiative.

EMG Activity while Alter-g Treadmill Running

Iain Hunter, Matthew K Seeley, J Ty Hopkins, Michael Collins, and Jared Franson
Brigham Young University, Provo, UT, USA
Email: iain_hunter@byu.edu

INTRODUCTION

The Alter-g treadmill is a popular cross-training method for runners. The treadmill reduces impact forces to allow injured runners to recover from injuries while still performing their preferred mode of training [1]. Some lower-body muscles involved in running utilize lower activations due to the smaller ground reaction forces [2]. The Alter-g treadmill creates an upwards force due to the pressure difference between the lower and upper body. While this will relieve the stress on the bones and decrease muscles activation for certain muscles during stance, this may not assist in swinging the legs horizontally. Thus some injuries may not be effectively treated using the Alter-g treadmill when the injury is related to repositioning the limbs during the swing phase of running. For example, the hip adductor muscles are very active during the swing phase to keep the leg moving forwards in the correct directions. So, the Alter-g may not have a positive impact on injuries like hip adductor tendonitis.

Figure 1: Alter-g treadmill running.

This study investigated muscle activation of 12 muscles of the lower body throughout the gait cycle at 40, 60,80, and 100% of body weight.

METHODS

Eleven NCAA Division I male cross-country runners participated in the study after signing an informed consent. Delsys Trigno Wireless electrodes were placed over the following muscles of the right leg: Gluteus maximus, gluteus medius, medial hamstring, lateral hamstring, vastus medialis, vastus lateralis, rectus femoris, hip adductors, gasctrocnemius, soleus, peroneus longus, and tibialis anterior. Electrodes were placed at an estimated point midway between the muscle insertion and the innervation zone. Placement was confirmed using manual muscle testing.

After electrodes were placed (sampling at 4000 Hz), subjects ran for two minutes at 100% body weight at 4.47 m/s (6:00 min/mi). After the first two minutes of running, subjects continued at the same pace at 40%, 60%, 80% and 100% of body weight in random order for two more minutes at each body weight.

Mean root mean square amplitudes were calculated during the first half of stance, second half of stance, full stance, and swing phases. The specific phase of interest for each muscle was determined by when the largest EMG amplitudes occurred. If the amplitude remained relatively high throughout stance, then the entire stance phase was included in the analysis.

A simple linear regression was completed for each muscle at certain phases of interest for that specific muscle with an alpha of 0.05.

RESULTS AND DISCUSSION

Most muscles utilized a lower activation as more body weight was supported (Table 1). Generally, it appears that the muscles involved in support of the body used less activation as body weight was supported. However, for the hip adductors during the swing phase and the hamstrings during stance, a significant trend was not observed.

Interpretation of these results should be considered with care. A significant slope is encouraging, but some slopes were fairly small (Figure 2). For example the peroneus longus had a significant slope, but did not decrease in activity nearly as much as many other muscles.

Table 1: Linear regression p-values for each muscle during the primary time of interest (the phase of the gait cycle when activation was highest).

Muscle and Phase	*p*-value
Hip Adductors Swing	*P*=0.63
Vastus Lateralis Stance	*p*<0.01
Rectus Femoris Stance	*p*<0.01
Vastus Medialis Stance	*p*<0.01
Gluteus Medialis Stance	*p*=0.02
Gluteus Maximus Stance	*p*=0.07
Medial Hamstring First Half of Stance	*p*=0.22
Lateral Hamstring First Half of Stance	*p*=0.44
Peroneus Longus Stance	*p*<0.01
Soleus Stance	*p*<0.01
Tibialis Anterior First Half of Stance	*p*<0.01
Gascrocnemius Stance	*p*<0.01

So, someone with an ankle inversion injury or tendonitis of the peroneus longus should run with a relatively low body weight. However, someone with patella tendonitis may be safe running with only a small amount of body weight supported since the vastus medialis, vastus lateralis, and rectus femoris activities decrease dramatically as more body weight is supported.

Another purpose of Alter-g treadmill running is known as over-distance training. Some elite marathoners use the Alter-g treadmill to add to their weekly mileage without adding as much stress to their bodies. The results of this study show the decreases in stress, if any, each muscle and tendon will receive as some of their body weight is supported. Thus, if there are concerns about the stress on a specific muscle or tendon, this study can be used to aid in selecting an appropriate amount of body weight that should be supported.

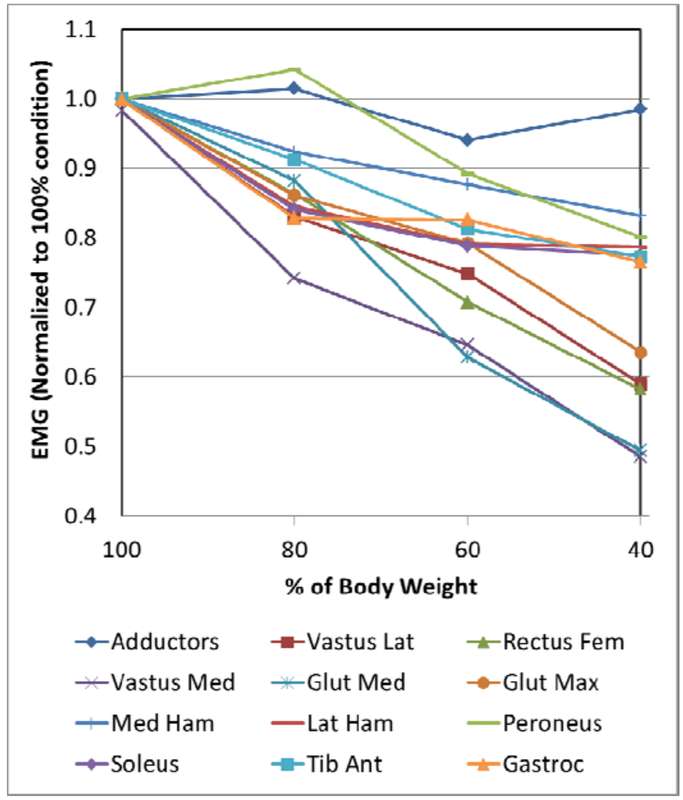

Figure 2: Muscle activity versus % of body weight supported for each muscle tested.

CONCLUSIONS

The Alter-g treadmill is a useful intervention for certain running related injuries. This is accomplished due to lower ground forces and lower activation of the muscles connected with certain injuries.

However, other injuries, such as hip adductor and hamstring tendonitis or strains may require alternative cross-training to relieve the stress on those areas as healing progresses. Runners should also take care in determining which amount of body weight should be supported according to how much the muscle activation decreases for the muscle related to the injury of concern.

REFERENCES

1. Cutuk A, et al. *J Appl Physiol* **101**, 771-777, 2006.
2. Liebenberg J, et al. *J Sports Sci* **29**, 207-2149, 2011.

INVESTIGATING THE LINK BETWEEN KINEMATIC DEVIATIONS AND RECOVERY RESPONSE TO UNEXPECTED SLIPS

Pilwon Hur and Kurt Beschorner

Industrial and Manufacturing Engineering, University of Wisconsin-Milwaukee, Milwaukee, WI
E-mail: hur@uwm.edu, beschorn@uwm.edu
Web: www4.uwm.edu/ceas/faculty_profiles/KEBeschorner.html

INTRODUCTION

Falls are one of the main contributors to occupational injuries. Falls account for approximately 24% of non-fatal injuries and 13% of fatal injuries in the workplace [1]. Slipping is the leading cause of falling accidents that occur on the same level ground. In response to a slip, a complex recovery response is initiated to prevent the fall. While this recovery response is critical for regaining balance, the sensory modalities that trigger the response are not well understood.

Previous research has indicated that degradation in the sensory system due to aging may increase slip risk [3]. As a first step towards identifying the systems responsible for detecting a slip, the order of deviations to the lower-body joint angles (relevant to proprioception) and vertical foot forces (relevant to somatosensation) has been identified. Vertical forces and slipping-leg knee angles are known to deviate before the onset of the recovery response or other joint angles indicating that foot somatosensation and knee angle may be responsible for detecting the slip [4]. This study aims to continue to examine the relationship between kinematic deviations and motor response by correlating the onsets of deviations with the onset of muscle response.

METHODS

Nine healthy young adults (4 male and 5 female, age=22-33 yrs) participated in this study. Subjects were fitted with a set of 56 reflective markers, 4 surface electromyography (EMG) electrodes. Subjects were donned with a harness to prevent falling due to slipping throughout the trials. All subjects were provided tight-fitting clothing and standard shoes to minimize marker error and ensure constant shoe-floor friction conditions, respectively.

Subjects were informed that the floor would be dry. The five known dry conditions were followed by an unexpected slip trial. The unexpected slip was induced by applying a thin layer of a diluted glycerol contamination (90% glycerol and 10% water) to the floor surface above the force platform [4]. Motion capture system (Motion Analysis Co, Santa Rosa, CA) collected marker data to compute ankle, knee, and hip joint angles. Subjects walked across four force plates that measured ground reaction forces (GRF). During slipping trial, slipping contaminant was applied on the third force plate. All subjects gave informed consent prior to their participation and this research was approved by the University Institutional Review Board

Several variables were measured that are believed to be relevant to sensory afferents. Joint angles of the ankle, knee and hip for ipsilateral to the slip were measured for proprioception. Vertical and shear GRFs for the slipping leg were collected via forceplate for somatosensation at foot. Four surface EMG signals (Delsys, Boston, MA) were collected to determine the motor response to unexpected slip at the following muscles:(1) rectus femoris (RF), (2) tibialis anterior (TA), (3) medial gastrocnemius (MG), and (4) medial hamstring (MH).

The time that variables deviated during a slip from the baseline walking conditions was denoted deviation time (*TimeDev*). *TimeDev* was defined as the minimum time when the normalized deviation of each variable from the baseline exceeded 1.96 similar to [4], which is equivalent to 95% confidence interval of the baseline walking (Fig 1).

$$Deviation = \frac{Variable_{perturbed} - \text{mean}\left(Variable_{baseline}\right)}{\text{stdev}\left(Variable_{baseline}\right)}$$

A repeated measures ANOVA was used to investigate *TimeDev*'s for each variable were significantly different. Pearson's correlation analysis was performed to determine how sensory responses (joint angles and ground reaction forces) were related to motor response (muscle activation). Significance level was set to 0.05 (SPSS v17, Chicago, IL).

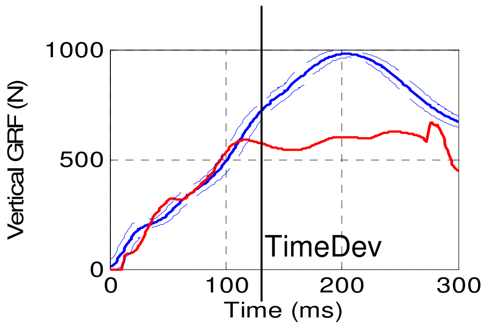

Fig 1 Representative vertical GRF for the mean baseline (solid blue) +/- standard deviations (dashed blue) and the slip (red). The vertical line represents the time of deviation.

RESULTS AND DISCUSSION

A repeated measures ANOVA found that *TimeDev*'s were significantly different ($p<0.01$). The order of deviations were similar to [4] with ground reaction forces deviating first followed by knee angle, ankle angle and hip angle. Anterior/posterior ground reaction forces deviated around the same time as the vertical force, while medial-lateral force deviation occurred later in stance. Note that all motor responses to unexpected slip occurred after the kinematic deviations to the ipsilateral leg. The order of muscle onsets were medial hamstring, tibialis anterior, medial gastroc and then rectus femoris similar to published research on unexpected slips [5].

Pearson's correlation analysis found that *TimeDev*'s for ankle ($r=0.73$, $p=0.027$) and hip ($r=0.68$, $p=0.043$) joint angles were significantly correlated with *TimeDev* for MH. *TimeDev* for hip ($r=0.70$, $p=0.037$) joint angle was significantly correlated with *TimeDev* for TA. None of the kinematic deviations were correlated with MG or RF.

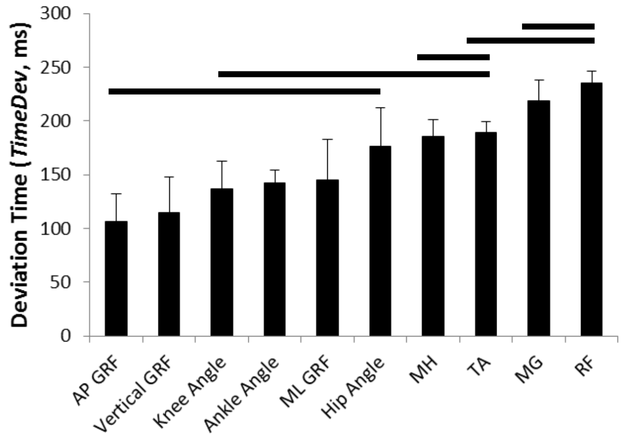

Fig 2 Average deviation times (*TimeDev*) for each variable. Error bar is ± SE. Thick lines represent groups of variables that have no statistical significance.

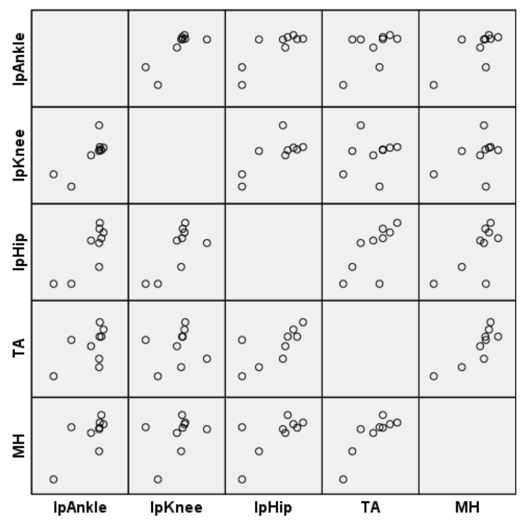

Fig 3 Scatter plot showing correlation between *TimeDev*'s for ankle, knee, hip joint angles, TA and MH.

CONCLUSION

While ground reaction forces and knee joint angles deviated first, they were not correlated with the timing of muscle onset in response to slipping. Several kinematic measures deviate prior to muscle onset and muscle onsets were best correlated with ankle and hip angles (which deviate later in stance). This may indicate that the central nervous system waits for multiple afferents to deviate before initiating the recovery response. Therefore, sensory deficits to any of the lower-body systems may inhibit the body's ability to respond to a slip.

REFERENCES

1. U.S. Department of Labor-Bureau of Labor Statistcs, 2009
2. Courtney et al, *Ergonomics*, V44(13) 1118-1137, 2001
3. Lockhart et al., *Safety Science*. 40(7-8) 689-703, 2002
4. Beschorner et al., *IIE Occ Ergo and Hum Fact*, DOI:10.1080/21577323.2012.660904, 2012.
5. Chambers and Cham, *Gait Posture* 25, 565-72, 2007.

Age-related differences in the stepping response to laterally-directed disturbances

[1]Christopher P. Hurt, [1]Mark D. Grabiner
[1]Department of Kinesiology and Nutrition, University of Illinois at Chicago, Chicago, IL, USA
churt2@uic.edu, URL:http://www.uic.edu/ahs/biomechanics

INTRODUCTION

The maintenance of frontal plane dynamic stability requires that the motion of the center of mass (COM) is arrested before it extends beyond the lateral edge of the base of support (BOS). If the COM extends beyond the BOS the risk of a laterally-directed fall increases. This is particularly problematic for older adults considering that falls to the side increase the risk of hip fracture 600% compared to forward or backward-directed falls [1]. A key means by which dynamic stability can be restored is a compensatory stepping response (CSR).

Age-related differences have been reported in the compensatory stepping response (CSR) following laterally-directed postural disturbances. Most notably, older adults more often utilize multiple recovery steps compared to younger adults [2, 3]. The extent to which multiple-step CSRs are used is associated with an increase in prospective fall-risk [4].

The utilization of multiple steps could reflect the lack of instructions requiring a single step response. However, mechanistically, the use of multiple steps may also result from the failure of the initial CSR to restore dynamic stability. This may be a function of the CSR utilized. Following laterally-directed postural disturbances three forms of the CSR have been identified [2, 3].

A sidestep sequence (SSS) and a crossover step (COS) are the most common strategies used to recover from platform-based postural disturbances. Observationally, older adults appear to prefer a sidestep sequence (SSS) [2] whereas younger adults utilize both SSS and COS [2,5]. It has been reported that young subjects performing a COS are less stable than those performing a SSS [5] however, the dynamic stability of older adults recovering from laterally-directed platform-based postural disturbances has not been described.

The purpose of this study was to investigate the laterally-directed stepping responses of older and younger adults following similar laterally-directed postural disturbances that required a step in every trial. We hypothesized that compared to younger adults, older adults would utilize a SSS to a greater extent than a COS. We also hypothesized that older adults would be less dynamically stable than younger adults upon completion of the initial recovery step.

METHODS

Ten healthy young adults (6 women and 4 men, 172.5±9.3cm, 67.9±12.4 kg) with an average age of 24± 2.0 years and eighteen older adults (9 women and 9 men, height: 174.9± 8.6 cm, mass 82.6± 15.8 kg), with an average age of 72.8± 5.2 years, volunteered to participate in this institutionally reviewed and approved study. All subjects were healthy, free from any musculoskeletal or neurological disorder that may have limited functional mobility.

Subjects were exposed to 20 lateral disturbances (10 to the left and right) for which the direction was randomized. The postural disturbances were delivered via a microprocessor controlled stepper motor-driven treadmill (Simbex, Lebanon NH). The disturbance waveform was triangular in shape and had a peak velocity and total displacement of 1.0 ms^{-1} and 0.24 m, respectively. The disturbances were sufficient to elicit a stepping response in all trials. Initial stance width was standardized. Subjects were instructed to "do whatever it takes to recover your balance".

Recovery strategies were documented for each subject. Step efficiency was defined as the number of extra steps utilized to laterally extend the BOS beyond the initial CSR. Kinematics of the CSR were collected using a motion capture system (Motion Analysis, Santa Rosa, CA). The COM for each subject was estimated based on a ten segment model and anthropometric estimations [7]. COM velocity was calculated using a first-central difference algorithm. Dynamic stability was quantified as the margin of stability (MOS) [8].

$MOS = BOS_{lat} - xCOM$

- BOS_{lat}=Most lateral position of the BOS
- $xCOM = COM + v_{COM} / \sqrt{9.8/(1.34 * \text{leg length})}$.

The minimum MOS (MOSmin) that occurs coincidently with or shortly after footstrike was quantified. The between group difference in the relative frequency of the CSR utilized was compared using a Mann-Whitney U test. The between group difference in MOSmin was compared using a two factor ANOVA (age X step). Lastly, the between group difference in step efficiency compared using a Mann-Whitney U test. Significance was set at 0.05.

RESULTS AND DISCUSSION

Older and younger adults utilized a SSS in 73% and 68% of trials, respectively (p=0.271, Table 1). The recovery response of older and younger adults included extra recovery steps in 25% and 15% of all stepping trials, respectively (p=0.294). COS resulted in the use of extra steps with greater frequency than the SSS (p<0.001). Older adults utilized extra steps in 87% of the COS trials, compared to 38% of younger adults executing a COS (p=0.028, Table 1). For older adults, the extra COS step responses resulted from a recovery step that was insufficient to re-establish stability (i.e. a negative MOS) in 40 of 82 stepping trials.

Significant differences in the MOSmin of the recovery responses were detected within the statistical model. The step X age interaction was not significant (p=0.068 Figure 1, top). Significant main effects of step and age were detected (p<0.001, p=0.031 respectively). Older adults established a MOSmin that, on average, was 40% smaller than that of younger adults. Further, subjects performing a SSS established a MOSmin that was three times larger in magnitude than COS.

With respect to older adults, on average, a the MOSmin of those utilizing a SSS and a COS were 117 ± 43mm and 14 ± 30 mm, respectively. Given the similarities between SSS and COS in lateral velocity of the COM during the initial CSR (Figure1, bottom), the extra steps utilized for the COS response likely relate to the differences in the established distance between the COM and BOS afforded by the recovery step (201±48 mm for SSS, 82±51 mm for COS p<0.001).

Table 1. Frequency data of recovery responses and step efficiency across group and step

	Older Adults		Younger Adults	
	Single Step	Extra Step	Single Step	Extra Step
Crossover step	12	82	35	22
Sidestep Sequence	244	10	124	4

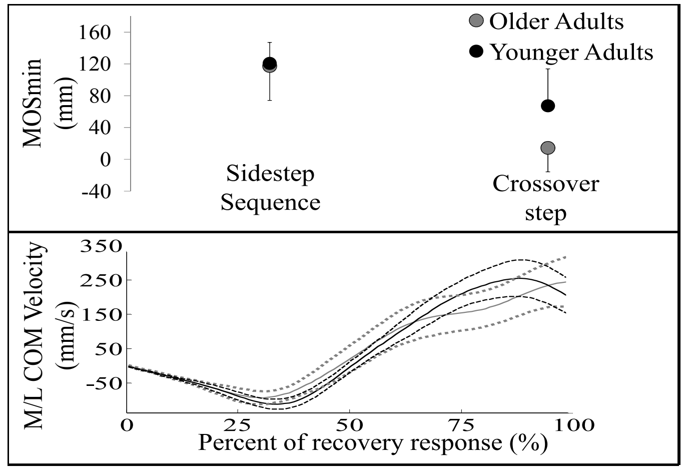

Figure 1. (TOP) MOSmin as a function of group and recovery step. (BOTTOM) Lateral COM velocity and 95% C.I. of first step for a single step SSS (black) and extra step COS (grey) of older adults

The current results suggest that a SSS is more effective than a COS at re-establishing dynamic stability. Previously it has been shown that the use of a COS also increases the risk of a limb collision which may increase fall-risk [2,3], This has been used as a rationale to train older adults to avoid performing a COS [9]. However, in the present study, only one between-limb collision occurred. Thus, it may be more useful to train older adults to more effectively execute a COS considering that this type of step may be situationally necessary to recovery stability.

CONCLUSIONS

Subjects responded to laterally-directed platform disturbances by primarily utilizing a SSS with no differences in re-establishing dynamic stability or step efficiency. However, when considering a COS response, older adults were more likely to utilize a dynamically unstable step response that required extra steps compared to younger adults. Biomechanically this related to the established difference between COM and BOS and not necessarily to reduced control of the COM while stepping. These results provide a target to improve the COS recovery response of older adults.

References

1. Greespan SL et al. *JAMA*. 12:128-33, 1994
2. Maki BE. *J Gerontol* **55**, M27—M277, 2000.
3. Mille et al. *Clin Biomech*. 20:707-616. 2000
4. Hilliard .MJ. Arch.of Phy sMed Rehab **89**, 1708-1713, 2008
5. Hurt et al. *Exp Brain* 214:557-566.2011
6. Johnson et al. *Arch Phys Med Rehab* 85:593-7,2004
7. Winter DA. *Biomechanics and Motor Control of Human Movement,* John Wiley & Sons, Ltd., 2005.
8. Hoff A. et al. *J Biomech* **38**, 1-8, 2005.
9. Mansfield et al. *BMC Geriatric* 7, 12, 2007.

Age-related differences in the maintenance of frontal plane dynamic stability while stepping to targets

[1]Christopher P. Hurt, [1]Mark D. Grabiner
[1]Department of Kinesiology and Nutrition, University of Illinois at Chicago, Chicago, IL, USA
churt2@uic.edu, URL:http://www.uic.edu/ahs/biomechanics

Introduction

Laterally-directed steps are commonly utilized to circumvent an obstacle or to avoid an undesirable step location during gait. The increased lateral COM motion required to execute the step must then be arrested and reversed if the previous direction of travel (i.e. forward), as well as stability, is to be maintained. Previous research has suggested that older adults may be especially vulnerable to lateral instability [1, 2, 3]. Thus, relative to normal walking, maintaining control of the position and velocity of the COM with respect to the base of support (BOS) while performing a laterally-directed step could be particularly difficult for older adults. This may relate to the marked reductions in force generating capacity of the hip abductors-adductors [4], which are primarily responsible for controlling frontal plane COM motion during stance [5, 6].

The purpose of the present study was to investigate the age-related differences of subjects performing crossover (COS) and sidesteps (SS) to three different targeted step widths while walking. We hypothesized that older adults would generate a significantly smaller hip abductor moment compared to younger adults particularly at the longer step targets. Similarly, given the importance of the hip abductors in regulating dynamic stability, we hypothesized that older adults would be less dynamically stable while performing COS and SS than younger adults, particularly at the longer step targets for which the largest abduction moments would be expected.

Methods

Nineteen young adults (9 males, age: 22.9±3.1 years, height: 174.3±10.2 cm, mass: 71.7±13.0 kg) and eighteen older adults (9 males, age: 72.8± 5.2 years, height: 174.9± 8.6 cm, mass 78.0± 16.3 kg) volunteered to participate in this institutionally reviewed and approved study. All subjects were healthy and free from any musculoskeletal or neurological disorder that may have limited functional mobility.

Subjects walked along an eight meter carpeted walkway with demarcated lanes on the walkway surface (Figure 1). All laterally-directed step trials were executed with subjects' dominant limb as the stepping limb to targets placed at three locations on a force plate. Subjects performed five SS trials at each distance followed by five COS trials at each distance. Subjects were instructed to walk at a speed that was comfortable to them.

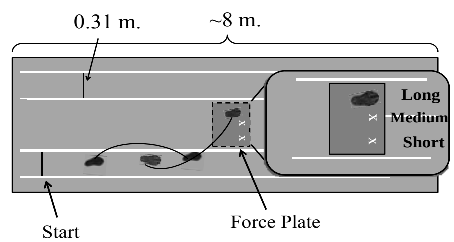

Figure 1. Schematic diagram of the experimental setup. The step sequence for a crossover step is presented for a right-limb-dominant subject. Also illustrated are the targets to which subjects stepped during the data collection (inset). Subjects performed the same protocol for sidesteps.

Kinematics of the laterally-directed step were collected using a motion capture system (Motion Analysis, Santa Rosa, CA). The COM location for each subject was determined based on a ten segment model and regression equations [5].

Margin of stability (MOS) was utilized to quantify the instantaneous dynamic stability.
The equation for MOS was as follows [6]:
MOS= BOS_{lat} - xCOM

- BOS_{lat}=Most lateral position of the BOS
- xCOM = COM + v_{COM}/ $\sqrt{(9.8/(1.34*\text{leg length}))}$.

The average value for MOS was computed from heelstrike to contralateral toe-off of the laterally-directed step. Internal hip abduction moments were computed from the synchronized motion capture and force plate data using commercial software package (Orthotrak, Motion Analysis Corporation, Santa Rosa, CA). For all trials the initial peak of the bi-modal abduction moment was extracted from the continuous bi-modal curve.

We tested the hypothesis that the peak abduction hip moment of older adults would be significantly smaller than that of younger adults particularly at the longer step targets with a three-factor (step X target X age) ANOVA with repeated measures on the step and target terms.

To test the hypothesis that older adults would be less dynamically stable than younger adults, particularly at the longer step targets, we utilized a mixed three-factor (step X target X age) ANOVA with repeated measures on the target and step terms. *Post hoc* tests on the simple effects of significant interactions were performed if significant interactions were detected in the model. Significance was set at 0.05.

Results and Discussion

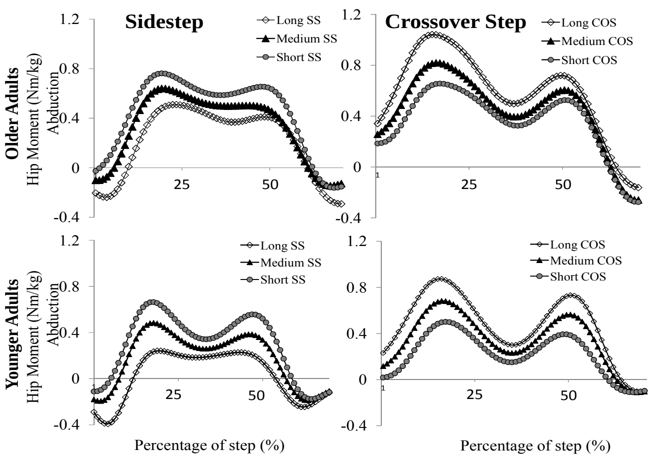

Figure 2. Hip moment curves of subjects stepping to targets. Older adults (Top panels) and younger adults (Bottom panels) performing sidesteps (left panel) and crossover steps (right panel) across three targeted conditions.

The general pattern of internal abduction hip moment generation between the stepping targets was similar across subjects for COS and SS (Figure 2). COS to the long targets resulted in the largest peak abduction moment while long SS resulted in the smallest peak abduction moment. A main effect of age was detected for the peak abduction moment ($p<0.001$). On average older adults generated a peak hip abduction moment that was 30% larger than younger adults across targeted COS and SS (Figure 3). COS resulted in greater abduction moment than a SS particularly at the long and medium step targets ($p<0.001$). Older adults were

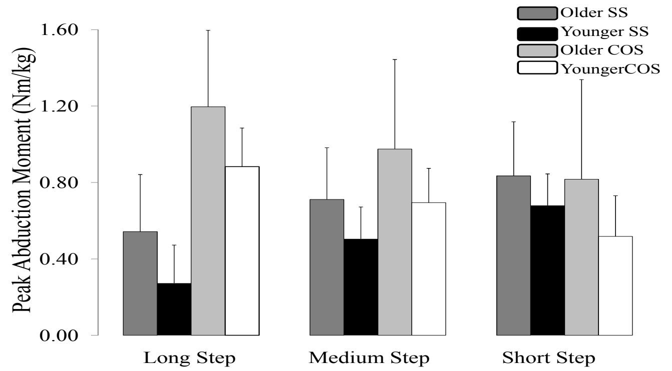

Figure 3. Peak abduction moments of laterally-directed step across group and step type (i.e. COS and SS).

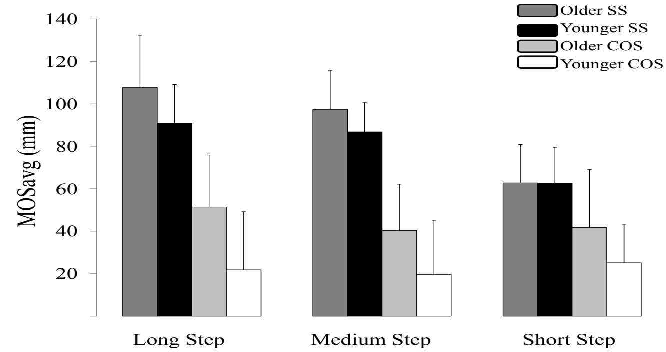

Figure 4. MOSavg of laterally-directed steps across group and step type (i.e. COS and SS).

as stable or more-stable than younger adults (Figure 4) specifically for the long and medium steps ($p<0.003$). For both groups, the execution of a SS resulted in a larger MOS than the execution of a COS at all targeted distances ($p<0.001$).

Conclusion

Age-related differences existed in the performance of targeted laterally-directed steps. Surprisingly, peak hip abduction moments were larger in older adults. This may reflect greater muscular effort by older adults as an attempt to reduce the likelihood of becoming unstable. Contrary to findings related to platform-based disturbances [1,2,3], older adults were as stable or more -stable than younger adults It is possible that the reactive nature of platform-based disturbances, compared to the proactive nature of voluntary stepping may explain the differences in these results.

References

1. Maki. J Gerontol **55**, M27:M277, 2000.
2. Mille et al. Clin Biomech. 20:707-616. 2005
3. Hilliard .MJ. *Arch.of Phy sMed Rehab* **89**, 1708-1713, 2008
4. MacKinnon & Winter J Biomech 26: 633-644, 1993
5. Pandy, Lin,Kim J Biomech 43:2055-2064,2011
6. Johnson et al. Arch Phys Med Rehab 85:593-7,2004

BIOMECHANICAL RELATIONSHIP BETWEEN THE PROPERTIES OF COLLAGEN FIBERS IN DIFFERENT REGIONS OF ANNULUS MATRIX AND THE DECOMPRESSION OF DISC TISSUES

[1]Mozammil Hussain

[1]Logan University, Division of Research, Chesterfield, MO, USA
email: mozammil.hussain@logan.edu

INTRODUCTION

Degeneration related neck and low back pain involving abnormal disc pressures/herniations has been shown to be relieved by spinal decompression therapy that widens intervertebral disc space, spinal canal, and neural foramen [1]. The underlying physiological mechanism that has been theorized behind this discogenic pain relief is the decrease in disc stresses [2,3] and dead cells [4], leading to an overall increase in the disc tissue metabolism [5] and the endplate vascular channels necessary for disc nutrient transport [6]. How the traction forces used in decompression therapy benefit disc health through stress re-distribution in discs is still not fully understood. Do the surrounding fibers in disc extracellular tissue matrix have any major role in the stress re-distribution?

Degeneration in discs begins in inner nucleus pulposus (NP). As degeneration advances, the load is shifted from inner NP to outer annulus fibrosus (AF). Degenerative signs are noted not only in the AF tissue matrix in the form of tears and delamination, but they also involve changes related to the annular fibers [7,8]. By resisting tensile loads, these fibers affect the mechanics of the discs through re-orientation and bulging. Despite past research have reported the annular stresses in degenerative discs, the relative contributions of degenerative properties in annular fibers, such as incompleteness and slackness, to the overall degenerative disc response are not completely known.

The aim of the present study is to understand the re-distribution of stresses in the discs consisting of degenerative fibers when the traction forces are applied on the compressed discs.

METHODS

The current study used an intact finite element (FE) model of a normal C5-C6 disc segment that was validated under axial forces [3]. Cortical bone, cancellous bone, endplates, AF, NP, and 6 layers of collagen fibers were included in the model. The collagen fibers were embedded into AF tissue matrix between the superior and inferior disc-endplate interfaces, arranged in a zigzag (X) fashion, and oriented at an angle of ±70° with respect to the horizontal plane. AF tissue matrix was divided into 3 regions – outer, middle, and inner – with 2 fiber layers in each of the AF regions. Tissue material properties of the spinal structures were referenced from the literature.

5 FE models (Model O, Model M, Model I, Model OM, and Model MI) were developed from the intact model with degenerative fiber modifications in different AF regions, respectively (outer AF, middle AF, inner AF, outer-middle AF, and middle-inner AF). First, incompleteness in fibers was modeled as a morphological modification by reducing the fiber length by 50% (in a wedge (>) fashion) originating from superior or inferior disc-endplate interface up to mid disc-height, compared to the complete length of fibers running between the superior and inferior disc-endplate interfaces in the intact model. Second, slackness in fibers as a tissue material modification was modeled by decreasing the fiber elasticity, by 30%, compared to the fiber elasticity in the intact model.

To simulate the *in vivo* disc pressure under upper body weight (50 N); the FE models were subjected to compression (C), by applying a pressure load on the superior C5 surface. Next, the models were decompressed (17 N), by applying a traction force (T). The inferior C6 surface was constrained in 3 perpendicular planes. Meshing and analysis were performed using the FE software ABAQUS (Dassault Systemes Simulia Corp, Providence, Richmond, USA). At the end of compression and decompression, stress profiles in AF and NP tissues were investigated and normalized with respect to the normal intact FE model. Normalized stress changes were used to formulate a NP/AF ratio – a parameter representing greater changes in NP than in AF, for the ratio greater than 1 and vice versa.

RESULTS AND DISCUSSION

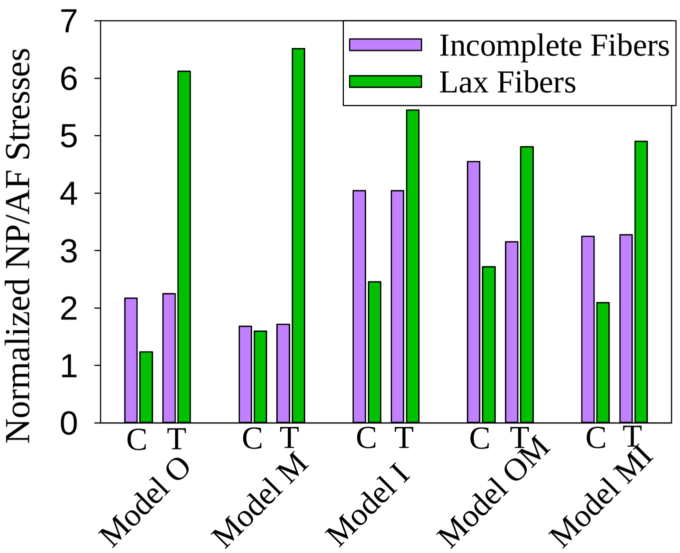

Figure 1: Ratio of normalized NP stress changes to AF stress changes, under compression and traction forces, for different modifications of fibers in various AF regions

For both incompleteness and laxity in annular fibers, a ratio (NP/AF) value of greater than unity was found (Figure 1) that indicated the NP stress changes are higher than the AF stress changes. With fiber modifications (incompleteness, laxity), ratio of NP/AF compressive stress changes were: Model O (2.17, 1.24), Model M (1.68, 1.60), Model I (4.04, 2.46), Model OM (4.55, 2.72), and Model MI (3.25, 2.09); and that of decompressive stress changes were: Model O (2.25, 6.12), Model M (1.72, 6.52), Model I (4.04, 5.45), Model OM (3.15, 4.80), and Model MI (3.27, 4.90).

NP tissues appeared to be more responsive than AF tissues. The load sharing between NP and AF was more affected by incomplete fibers than lax ones in compression; whereas, it was more affected by lax fibers than incomplete ones in decompression.

At the end of compression and decompression, no significant changes in NP/AF ratio were observed with incomplete fibers; however, an increase in the NP/AF ratio was noted with lax fibers. Therefore, elasticity of fibers played an important role in tissue decompression than that in tissue compression.

One of the limitations in the present study includes the development of the FE model from the anthropometric spinal dimensions, rather than from the computed tomographic image scans. Also, only 6 concentric rings of fibers were modeled, compared to the 15-20 rings of fibers. It is recommended the findings of this computational analysis be verified with other comparable biomechanical studies.

CONCLUSIONS

Spinal decompression technique used as a non-surgical interventional procedure for the discogenic pain relief may be more beneficial in the disc regions that have complete length of collagen fibers, although the fiber elasticity should also be taken into subsequent consideration when this intervention is applied to the degenerated discs.

REFERENCES

1. Sari H, et al. *Physiotherapy Theory and Practice* **21**, 3-11, 2005.
2. Gay RE, et al. *The Spine Journal* **8**, 982-990, 2008.
3. Hussain M, et al. *J Manipulative & Physiological Therapeutics* **33**, 252-260, 2010.
4. Kroeber M, et al. *Spine* **30**, 181-187, 2005.
5. Guehring T, et al. *Spine* **31**, 1658-1665, 2006.
6. Hee HT, et al. *Spine* **36**, 505-511, 2011.
7. Tsuji H, et al. *Spine* **18**, 204-210, 1993.
8. Schmidt H, et al. *Medical Engineering & Physics*, **31**, 642-649, 2009.

IS THERE A GOLD STANDARD FOR ROTATIONAL ALIGNMENT OF THE TIBIAL COMPONENT DURING TKA?

[1]Erin E. Hutter; [1]Jeffrey F. Granger; [1]Matthew D. Beal; [1]Robert A. Siston
[1]The Ohio State University, Columbus, OH
siston.1@osu.edu

INTRODUCTION

A successful total knee arthroplasty (TKA) is dependent on many factors, but component alignment is particularly critical. Aligning the femoral component parallel to the transepicondylar axis is generally regarded as the optimal rotational position, since it has been shown to produce a balanced joint, optimize patellar tracking, and minimize patellofemoral shear forces [1,2]. Unlike the femur, a gold standard for rotational alignment of the tibial component has not been established. A wide variety of landmarks can be used during surgery including the medial border of tibial tubercle, the medial third of the tibial tubercle, the projected femoral transepicondylar axis, the PCL attachment, and the transverse axis of the tibia [3,4]. It is not currently understood how the choice of one of these alignments over the others impacts the stability or kinematics of the TKA knee. The purpose of this study was to examine the relationship of tibial component rotational alignment to passive knee kinematics and stability.

METHODS

We have performed a series of experiments using a custom, image-based surgical navigation system on 9 cadaveric knee specimens containing all structures distal to the pelvis. Prior to testing, all specimens were CT scanned (2 mm slices) in order to precisely locate the transepicodylar axis on the femur and several landmarks on the tibia. We used these data to define 4 tibial axes. The TEA was the projection of the femoral transepicondylar axis onto the tibial plateau with the knee in full extension. The transverse axis (TA) was defined as the line between the most medial and the most lateral points on the tibial plateau. The medial border axis (MBA) and the medial third axis (MTA) were defined as the lines between the PCL attachment and the medial border or the medial one third of the tibial tubercle, respectively.

A TKA was performed on each specimen using a Zimmer Natural Knee PCL-retaining model. After the knee was exposed, optical reference frames were attached to the femur and the tibia and anatomic reference frames were established [5]. The specimen was then registered to the CT data using an iterative closest point method [6] to ensure that the femoral component was rotationally aligned to the transepicondylar axis, while the tibial component was aligned within 1° to the 4 different tibial axes of interest using a customized tibial component.

Passive kinematics and varus-valgus stability data for the knee in full extension were recorded before and after prosthesis implantation. Passive kinematics were recorded as we have done previously [5]. To characterize joint stability, the force-displacement relationship of the knee was measured using the surgical navigation system and a custom stability device (Figure 1) that enabled us to accurately apply known loads and record resultant displacements [7].

Figure 1: Custom stability device used to obtain force-displacement data

Knee stability was evaluated by analyzing the force-displacement curves for varus-valgus laxity (the amount of motion in degrees) under ±10 and ±20 N·m loads and stiffness (slope of the curve) at ±20 N·m [8, 9]. Passive kinematics were analyzed by determining the amount of varus-valgus motion, screw-home rotation, and anterior-posterior translation while the knee was passively flexed and extended [5]. Repeated measures analysis of variance (ANOVA) was used to determine if tibial rotational alignment has a statistically significant effect on these factors. When a significant effect was present ($p \leq 0.05$), Tukey's test was used to as a post-hoc test.

RESULTS and DISCUSSION

Our study showed that significant differences ($p \leq 0.02$) in stability exist between the native knees and the 4 different tibial rotational alignment axes, but there was little change ($p \geq 0.28$) based on the rotational alignment of the tibial component (Figure 2). For a given knee, TKA results in a "softer" knee with a 4.6±2.7° average increase in laxity and a 4.0±2.7 N·m/° average decrease in stiffness when a ±20 N·m load is applied.

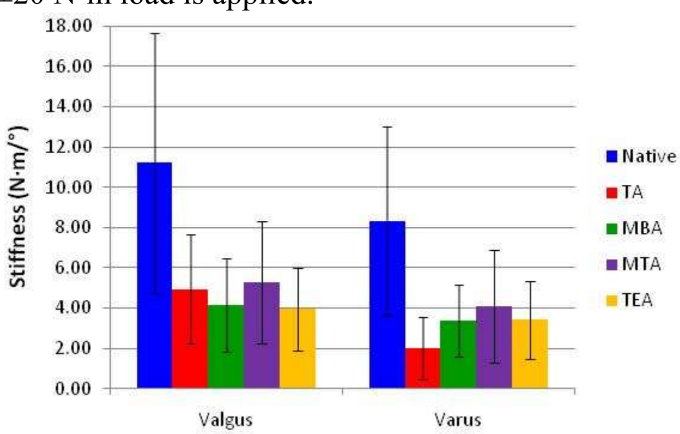

Figure 2: Stiffness under 20 N·m load for a representative specimen

Anterior translation of the femur and screw-home motion during passive flexion also showed an increase ($p \leq 0.05$) after TKA, but once again, tibial rotational alignment did not appear to affect these parameters ($p \geq 0.28$). When comparing native to TKA knees, anterior translation increased by an average of 5.6±4.0 mm and screw-home (5°-105° flexion) increased by 6.7±2.8° on average.

However, varus-valgus motion was affected ($p \leq 0.001$) by the rotational alignment of the tibial component in early flexion (Figure 3). Aligning to the MBA or the TA was shown to minimize the valgus deviation between the normal and the TKA knee, but it is debatable whether this small difference (4.2±1.1°) is clinically relevant.

We did note large variability in our measurements between specimens for all 5 conditions. We believe the variability seen across different knees maybe the result of high variability in the tibial anatomy. We discovered that the angle between the most internal and the most external axis across knees ranged from 8.9° to 27.1°, which is similar to other researchers [3]. Additionally, the most internal and external axes were not consistent across specimens.

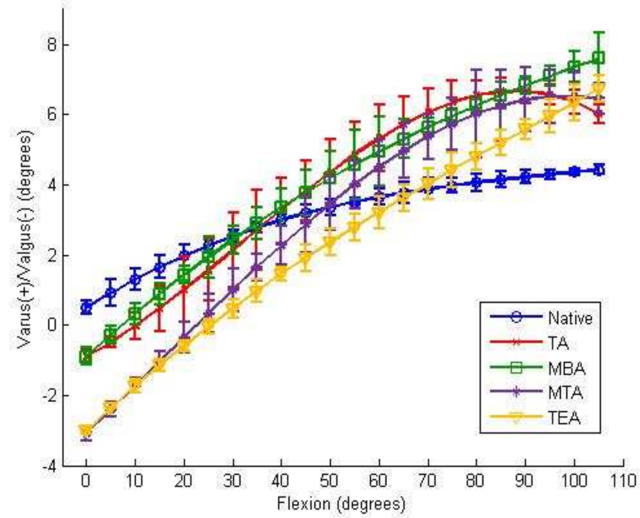

Figure 3: Passive kinematics for a representative specimen

CONCLUSIONS

Considering the importance of surgical technique in TKA, our results suggest that surgeons who align the tibial component to any of the axes in this study may be expected to have stability results consistent with their peers who may be using a different axis. Given the large variability between specimens, this study further suggests that there is not a gold standard for the rotational alignment of the tibial component that can be recommended for use on all patients at this time.

REFERENCES

1. Miller, MC, et al. *CORR* **392** 38-45, 2001.
2. Olcott, CW, et al. *CORR* **367** 39-42, 1999.
3. Akagi, M, et al. *CORR* **436** 172-176, 2005.
4. Siston, RA, et al. *CORR* **452** 65-69, 2006.
5. Siston, RA, et al. *JOR* **24** 1607-1614, 2006.
6. Besl, PJ, et al. *IEEE Patt Anal Mach Intel* **14** 239-256, 1992.
7. Siston, RA, et al. *ASME SBC* 373-374, 2009.
8. Markolf, KL, et al. *JBJS* **58** 583-594, 1976.
9. Siston, RA, et al. *CORR* **463** 43-49, 2007.

ENDPOINT INSTRUCTIONS RESULT IN HIGHER PROPRIOCEPTIVE ACUITY THAN JOINT ANGLE INSTRUCTIONS

Jacqlyn S. Hyler and Andrew R. Karduna
University of Oregon, Eugene, OR, USA
email: jhyler@uoregon.edu, web: http://biomechanics.uoregon.edu/obl

INTRODUCTION

Proprioception – the ability to sense both limb position and movement in the absence of vision – is crucial for accurate and coordinated motor strategies. Numerous sensory modalities give rise to proprioception, making it difficult to determine which strategies the CNS employs to make sensory-motor transformations. One strategy would be for the CNS to determine joint angles from sensory information and combine this information with known segment lengths, to indirectly determine endpoint position [1]. An alternate strategy would be for the CNS to directly determine endpoint position from sensory information. Under this strategy, the CNS could skip the intermediate step of calculating joint angles [2]. Most proprioceptive investigations evaluate perception of joint angles. However if the CNS employs an endpoint strategy, more reliable estimates of proprioception would be obtained by evaluating perception of endpoint (hand/foot) position. Therefore the aim of this study was to investigate these alternate control strategies by comparing two types of instruction on the accuracy, precision, and interjoint coordination during an active positioning - active repositioning reaching task.

METHODS

A total of 12 subjects, with a mean age of 20.3 ± 2.7 years have participated in the ongoing study. All subjects were right hand dominant and had no history of elbow or shoulder pathology. Subjects were seated on a kneeling chair to avoid tactile cues and then fitted with a head-mounted display to inhibit visual cues. Target positions were presented via custom-made Labview® software and required equal angular excursion at the shoulder and elbow in the sagittal plane (Fig. 1). The three targets were: 45˚/45˚, 60˚/60˚, and 75˚/75˚ corresponding to shoulder flexion and elbow flexion, respectively. Once the target position was reached, subjects remained positioned in the target for three seconds before returning their arm to their side. Subjects then actively repositioned themselves into the target. During the positioning period, subjects were given one of two instructions: (1) memorize hand location or (2) memorize shoulder and elbow angles. Instructions were blocked and randomized. Targets were also randomized and six trials were presented for each target.

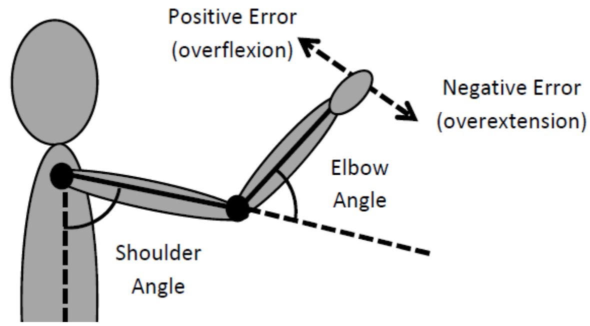

Figure 1. Experimental Setup

Data were collected via a Polhemus Fastrak® (Colchester, VT) with receivers placed on the thorax, scapula and dorsum of the wrist. Bony landmarks were digitized in accordance with ISB recommended anatomical coordinate systems [3]. A total of six separate two-way repeated measures ANOVAs (2 instructions x 3 targets) were run with the following dependent variables: endpoint accuracy and precision, shoulder accuracy and precision, and elbow accuracy and precision. Where significant main effects and interactions were found, post hoc analysis was performed. Accuracy was defined as constant error while precision was defined as variable error [4].

RESULTS

Data collection is ongoing. Thus the following results only represent preliminary findings.

Accuracy Across Instructions. Endpoint, shoulder, and elbow accuracy were unaffected by instruction (P = 0.27, P = 0.96, P = 0.35, respectively).

Accuracy Across Targets. Endpoint accuracy was influenced by target location (P = 0.04) with smaller errors occurring at greater excursions. The shoulder consistently overshoot the target by approximately 4˚ and was not sensitive to target location (P = 0.85). However the elbow was affected by target location (P < 0.01), overshooting lower excursions and undershooting higher excursions (Fig. 2).

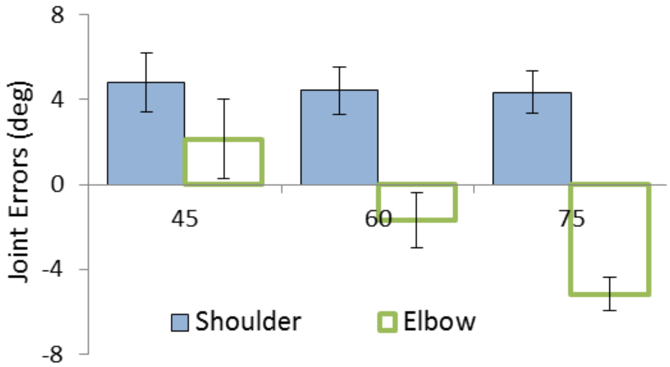

Figure 2. Joint Accuracy Across Targets

Precision Across Instructions. Endpoint precision improved when endpoint instructions were given (P = 0.07; Fig. 3). Smaller variable errors were present at the shoulder under endpoint instructions (P = 0.09) while variable errors at the elbow were unaffected (P = 0.63).

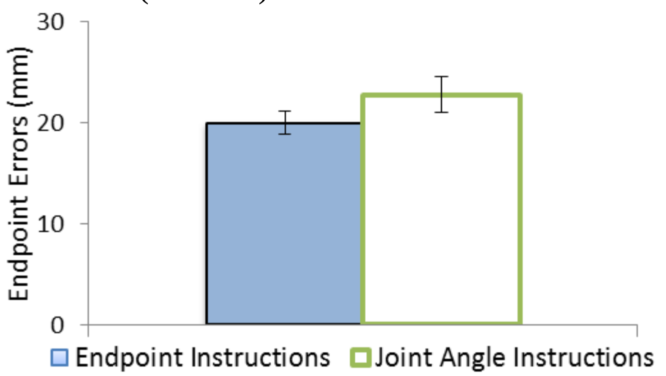

Figure 3. Endpoint Precision Across Instructions

Precision Across Targets. Endpoint precision was influenced by target location (P = 0.01) with smaller errors occurring at greater excursions. Neither the shoulder nor elbow were influenced by target location (P = 0.23, P = 0.81, respectively).

DISCUSSION

Instructions. We found that endpoint precision improved if subjects focused their attention to hand position instead of joint angles. This outcome can be explained by improved precision at the shoulder under these same instructions. Although the elbow was not influenced by instructions, the lever arm controlled by the elbow is shorter than the lever arm controlled by the shoulder. Therefore improvements at the shoulder are desired for greater endpoint accuracy in comparison to the elbow. Precision reflects the degree of noise in sensory signals and in the processing of those signals. Since sensory signals were kept constant by repeating target locations, our results show there was less noise in central processing when hand position was estimated versus joint angles. Consequently, our results provide evidence that the CNS directly determines endpoint position from sensory signals. This finding may be important in assisting populations with sensory deficits. Furthermore, experiments in which subjects estimate hand position are likely to give a better indication of the actual precision of proprioception than would joint angle estimates.

Targets. We found that endpoint accuracy improved at targets requiring greater angular excursion. This outcome is the result of superior coordination between the shoulder and elbow at higher excursions. Muscle spindles are sensitive to changes in muscle length and are recognized as the primary peripheral contributor to proprioception. It follows that proprioception should vary based on limb configuration. However an explanation for improved endpoint accuracy and interjoint coordination at greater excursions is not straightforward. It is possible that the increasing torque demands on the shoulder associated with greater excursions may lead to improved endpoint resolution. Additionally, greater excursion at the shoulder and elbow brings the hand closer to the head and shoulder joint. It has been suggested by other authors that targets located closer to the origin of movement are more acutely resolved [5].

REFERENCES

1. Soechting JF. *Brain Res* **248**, 392-395, 1982.
2. Cho S, et al. *Int J Neural* Syst, **5**, 87-101, 1994.
3. Wu G, et al. *J Biomech* **38**, 981-992, 2005.
4. Schmidt RA, et al. *Motor Control & Learning: A Behavioral Emphasis*, Human Kinetics, 1982.
5. Van Beers RJ. Et al. *Exp Brain Res* **122**, 367-377, 1998.

PENNATION ANGLE VARIABILITY IN HUMAN WHOLE MUSCLE

[1]Benjamin W. Infantolino and [2]John H. Challis

[1]Penn State University – Berks, Reading, PA, USA
[2]Penn State University, University Park, PA, USA
email: bwi100@psu.edu

INTRODUCTION

Traditionally muscle pennation angles are either measured on the surface of a dissected muscle using a goniometer [1], or measured in vivo using an imaging technique such as ultrasound [2] which displays a single cross-section of muscle. Magnetic Resonance Imaging (MRI) produces images throughout the muscle in the three planes and in two of the planes (frontal and sagittal), pennation angles can be measured. By measuring the pennation angle in both planes for all images, the variability of pennation angle can be quantified. The purpose of this study was to describe the variability of pennation angle observed throughout the First Dorsal Interosseous (FDI) muscle. Pennation angles were measured using MRI of the FDI muscle.

METHODS

One FDI muscle was removed from each of two embalmed cadavers for a total of two FDI muscles. Each muscle was removed using the methods described in Infantolino and Challis [1] to ensure complete removal of the muscle and the tendon. The cadaver characteristics were: Cadaver 1: female, 76 years old, 152 cm in height, 67.37 kg in mass, cause of death – end stage congestive heart failure; Cadaver 2: male, 72 years old, 160 cm in height, 72.60 kg in mass, cause of death – esophageal carcinoma.

To reduce the MRI scanning time the tissue was immersed in a 1.5% Magnevist (Bayer Health Care, Wayne, NJ) phosphor-buffered saline solution for 7 days. The achieved short T1 (33 ms) and T2 (7 ms) times allowed for fast imaging with a high contrast-to-noise ratio. To prevent the tissue from drying out and to minimize magnetic susceptibility artifacts during scanning the specimens were surrounded by a flourinert liquid FC-43 (3M, St. Paul, MN). All experiments were conducted using a vertical wide bore 14.1 tesla Varian MRI system (Varian Inc., Palo Alto, CA) with direct drive technology. A commercially available millipede resonator (Varian) with an inner diameter of 40 mm was used to acquire three-dimensional spin echo images of the muscle tissue. A standard imaging experiment with an isotropic resolution of 75 μm comprised a field of view of 45 x 20 x 20 mm^3 and a matrix size of 600 x 268 (75% partial Fourier: 201) x 268. With 12 averages and a repetition time of 75 ms (echo time 11.7 ms) the total scan time was 13.5 hours. MATLAB (The MathWorks, Inc., Natick, MA) was used for post-processing. By zero-filling each direction by a factor of two the pixel resolution of the standard imaging experiment was 37.5 μm isotropically.

The software Mimics (Materialise, Leuven, Belgium) was used to measure the pennation in each image for the medial-lateral and anterior posterior image planes (37.5 μm thick slices). One angle measurement was taken along the medial-lateral axis (Figure 1) while two measurements were taken along the anterior-posterior axis for each slice (Figure 2) because of the two headed nature of the muscle. Measures of pennation were made with an attempt to use the same location in the muscle throughout the different slices. In addition, for one image in each imaging plane the pennation angles of all fibers were measured. This was to demonstrate the variability in pennation angles that could be measured within the same image. In this case the measures were made in a plane which approximates the superficial surface used when making measures on cadavers using a goniometer.

RESULTS AND DISCUSSION

Along the medial-lateral axis the first cadaver muscle was 16.8 mm long (448 slices), while in the second it was 10.8 mm long (287 slices). In the anterior-posterior axis the first muscle was 11.4 mm long (305 slices) and the second cadaver muscle was 8.9 mm long (237 slices).

Nearly all the pennation angles throughout the muscle demonstrated non-normal distributions assessed using an Anderson-Darling statistic ($p < 0.05$ for all measures but one). The multiple pennation angle measures in one image demonstrated a coefficient of variation of 57% for the medial-lateral axis, 33% for the first metacarpal head of the FDI, and 19% for the second metacarpal head of the FDI for the first cadaver. All of these measures demonstrated normal distributions. This variability in pennation angle has functional significance as pennation angles were measured above 15^{o} which is the angle at which Zajac [3] stated that pennation angle makes a contribution to muscle force production.

CONCLUSIONS

The non-normal distribution of pennation angles in an anatomical plane hints at a more complex distribution of fascicles than assumed when a single pennation angle is used to represent an entire muscle. Therefore, this distribution indicates that a single pennation angle may not be an appropriately measure to describe the arrangement of muscle fascicles in a whole muscle. The multiple measures of the pennation angles within one image demonstrate that many pennation angles can be observed and these pennation angles can vary by an amount that can have functional significance.

REFERENCES

1. Infantolino BW, and Challis JH. *J Anat* **216**, 463-469, 2010.
2. Narici M. *J Electromyography Kinesiol* **9**, 97-103, 1999.
3. Zajac FE. *Crit Rev Biomed Eng* **17**, 359-411, 1989

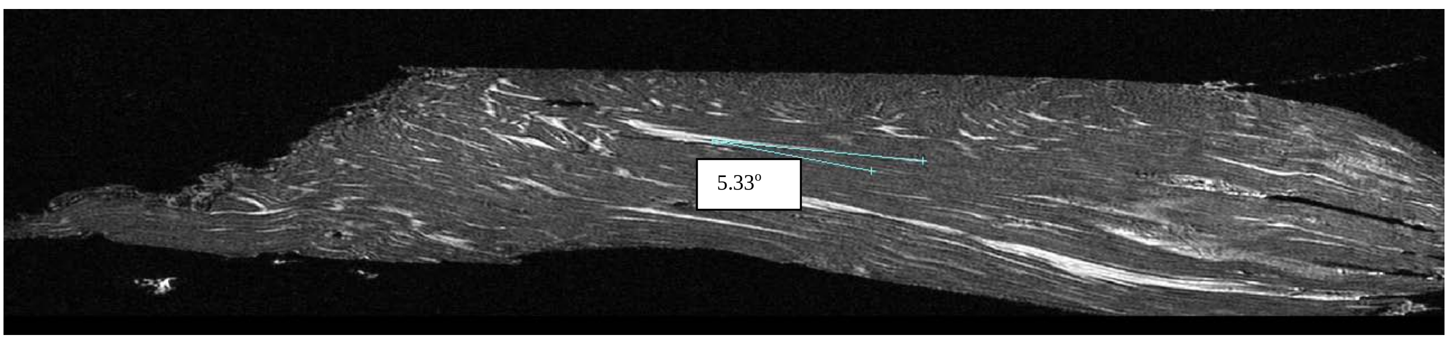

Figure 1. Pennation angle measured in an image along the medial-lateral plane of cadaver one, where the dashed line represents the aponeurosis while the solid line represents the line of action of the fiber.

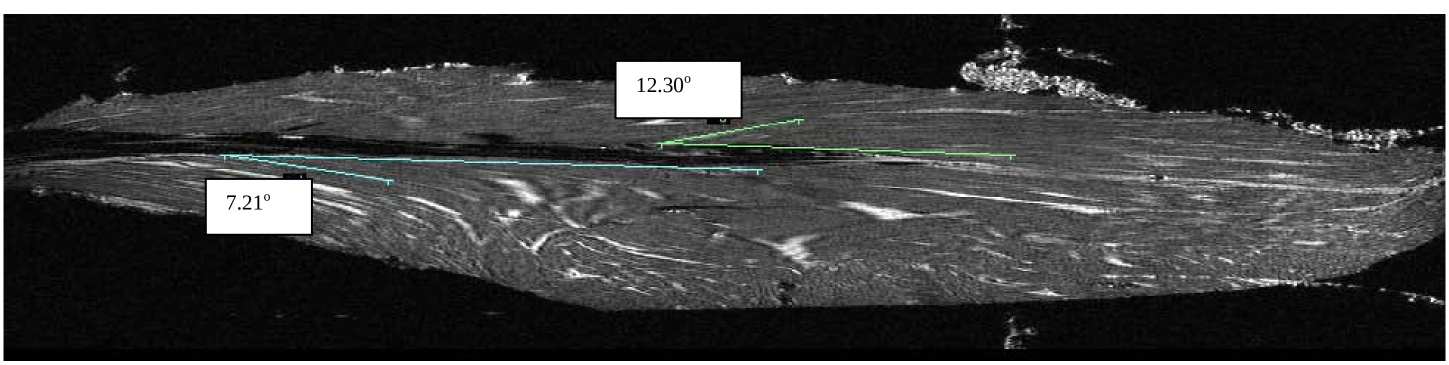

Figure 2. Pennation angles measured in an image along the anterior-posterior plane of cadaver one, where the dashed line represents the aponeurosis while the solid line represents the line of action of the fiber.

COMPUTER METHODS FOR DESIGNING ARTIFICIAL TALUS BONE IN THE ANKLE JOINT

[1]Kamrul Islam, [1]Ashlee Dobbe, [1]Samer M. Adeeb, [1]Marwan El-Rich, [1]Kajsa Duke, and [1]Nadr M. Jomha

[1]University of Alberta, Edmonton, AB, Canada
email: adeeb@ualberta.ca, web: http:// www.ualberta.ca/~adeeb/index.htm

INTRODUCTION

The talus bone is one of the most important bones in the ankle joint. With the majority of its surface covered with a thin layer of articular cartilage, it transmits the entire load of the lower portion of the musculo-skeletal system [1]. Fracturing of the talus bone is a common occurrence in younger members of the population that can result in death of the bone with subsequent collapse and development of severe osteoarthritis. Given these realities, talus bone replacement through use of an implant has become a possible option in orthopaedic surgery in order to promote proper functioning of the ankle joint [2]. The restoration of proper ankle joint function through surgery is an unresolved challenge due to the lack of refinement of implant design for whole talar replacements. Proper joint kinematics not only depends on the load-carrying capacities of implants, but also on restoring the proper three dimensional shape (i.e., complex articulating surfaces). Therefore, better understandings of ankle anatomy and morphology are integral to successful talus bone replacement using an implant. The primary objective of this study is to develop a robust computer-based methodology by which to design an implant of the ankle joint for talus bone replacement using high resolution CT imaging.

METHODS

Computed Tomographic (CT) images of the ankles of four subjects (3 males, 1 female) were used for this pilot study to take into account the inter-patient variation. In each of the four subjects, the talus bone was intact. The CT scan machine software produced DICOM images which were then imported into the 3D image modelling software, MIMICS. MIMICS is an image processing software which generates a 3D model using the segmented images of each CT slice. Pixel threshold values of 242 HU to 2080 HU were used for each of the four subjects during the segmentation. Finally, 3D reconstructed geometry of the talus was created using MIMICS. Two independent observers created the geometry of the talus bone, in order to capture inter-observer variability. Following the digitization; the 3D geometries of the talus bone were imported into the Geomagic Studio/Qualify 12. The 3D geometries for the talus bone of the same given subject created by two observers were aligned using a built-in algorithm of Geomagic for best fit. Following the alignment, the two geometries were compared using a custom tool 3D comparison in order to measure the 3D deviation, and then quantify inter-observer variability for a given subject. The volumes (V) of the talus were also compared. Quantification of the respective volumes of each of the talus bones shows that the talus bone of the human ankle joint varies from subject to subject (male/female). A scaling technique has been attempted in this study in order to identify any relationship between different subjects and thus come up with a few custom-made talus bone implants which will fit all subjects. Since the talus bone is very irregular in shape, in order to make custom implants we need to create the implant that will best fit a given patient's ankle joint. We are thus, in the interest of better design optimization, focusing in this preliminary study on the three articulating surfaces i.e., talar dome (articulates with the tibial plafond), sub-talar surface (articulates with the calcaneus), and the talar head (articulates with the navicular) of the talus bone. In this pilot study, in order to establish the applicability of the scaling approach, subject 1 was set as the reference model, and the other three subjects were used as testing models. After quantifying the volume of all four subjects, the ratios of volume of the reference model (subject 1) to test models (subject 2, subject 3, and subject 4) were calculated, and finally the cubic roots of all three ratios (x_1, x_2, x_3) were estimated. Finally, the test models were scaled up by this number (x_1, x_2, x_3) using the custom uniform scaling tool bar of Geomagic Qualify. (The new test models were, accordingly, subject $2x_1$, subject $3x_2$, and subject $4x_3$). Afterwards, the reference model and test models (one at a time) were aligned using the previously described procedure (using the best fit alignment algorithm) for 3D comparison. Table 2 shows the output parameter generated from the 3D comparison.

RESULTS AND DISCUSSION

Fig. 1 depicts the 3D prototype models of the talus bone of four different subjects, printed in a 3D printer using the VRML (virtual reality modeling language) file of Geomagic. Fig. 2 shows the 3D comparison between the reference model and the new test models (subject $2x_1$, subject $3x_2$, and subject $4x_3$).

Figure 1: 3D prototype models of 4 different talus bones.

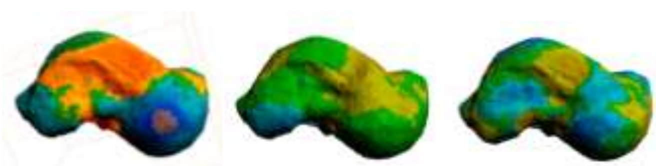

Figure 2: 3D comparison between reference and test models.

Table 1 shows the interobserver variation in digitizing the 3D geometries of the talus bones of the four subjects. Volume measurement was set as a base criterion in this study. It is also notable that the average inter-observer 3D deviation is in the range of 0.03-0.26 mm.

Table 1: Inter-observer measurement (mm)

Subjects	Observer 1 (volume)	Observer 2 (volume)	% difference
Subject 1	49139	50293	2.3
Subject 2	32994	32805	0.6
Subject 3	43729	43324	0.9
Subject 4	27509	27926	1.5

Table 2 shows the detailed measurements found using the scaling approach. In this study we focused on the average deviation following the 3D comparison in order to mimic the global behavior of this scaling approach. Articular surface is a prime concern in any biomechanical analyses. Therfore, in order to mimic the local behavior, the maximum deviations between the reference model and the new test models in the three articular surfaces were estimated, and were found to be less than 2.5 mm (in all cases).

CONCLUSIONS

The robust and simple technique developed based on the scaling approach in order to design a custom implant for the talus bone was shown to be very promising. The cubic root of the difference in volume was shown to be the best factor in choosing the proper implant size for a person with a damaged talus. The volume can be obtained from the contralateral talus. To the author's best knowledge this stands as the first attempt to develop a process to design a talar body implant which might be applicable for all patients. Future work will focus on the deviation between the left and right talus. Future studies will also implement this technique on more subjects to confirm these findings.

REFERENCES

1. Manter J.T. *Anat. Rec. 96*, 313-321, 1946.
2. Leardini A. *Clin Biomech* **16**, 706-709, 200

Table 2: Output of 3D model comparisons after incorporating scaling approach (mm)

New Test Model	Reference Model Volume (V_1)	Test Model Volume (V_2)	Scale Factor, $x = \sqrt[3]{(V_1/V_2)}$	Average Deviation Between Reference and New Test Model (+/-)
subject $2x_1$	49139	32998	1.14	+0.734/-0.76
subject $3x_2$	49139	43729	1.04	+0.784/-0.706
subject $4x_3$	49139	27509	1.21	+0.996/-0.863

DEVELOPMENT OF A SUBJECT-SPECIFIC VERTICAL GROUND CONTACT FORCE MODEL

Jennifer N. Jackson, Chris J. Hass and Benjamin J. Fregly

University of Florida, Gainesville, FL, USA
email: jnjrun18@ufl.edu, web: http://www.mae.ufl.edu/~fregly/

INTRODUCTION

In computational modeling of gait, it is easier to apply ground reaction forces and moments to the foot to prevent the model from falling through the floor than it is to model deformable foot-ground interactions. While applying ground reactions is satisfactory for many purposes, an unconstrained foot path simplifies prediction of new gait motions. Previous musculoskeletal models used independent viscoelastic elements to model contact between the foot and ground [1,2], but these models used pre-determined parameter values (i.e., not subject-specific) to replicate running [1] or part of a gait cycle [2].

This study seeks to develop a deformable subject-specific vertical ground contact force (vGRF) model that matches a full cycle of experimental gait data for one foot. The model uses viscoelastic elements whose parameter values are calibrated to the subject's ground reaction and foot motion data. Matching of the experimental data is performed in two stages: 1) calibration using one gait trial to determine spring and foot parameters, and 2) testing of the calibrated parameters using additional gait trials not used in the calibration process.

METHODS

The foot-ground contact model was developed using five trials of motion capture and ground reaction force and moment data collected from a healthy subject. The study was IRB approved and the subject gave informed consent. A two-segment (hindfoot and toes) dynamic foot model was constructed possessing seven degrees of freedom. The equations of motion were derived using Autolev symbolic manipulation software (OnLine Dynamics, Sunnyvale, CA). The foot model was incorporated into a Matlab (The Mathworks, Natick, MA) program to define each viscoelastic element's location in its respective segment (hindfoot or toes). An inverse kinematics analysis was then used to determine translations and rotations of the foot in the lab frame and toe flexion with respect to the hindfoot during locomotion. Foot model parameter values were determined from static trial data.

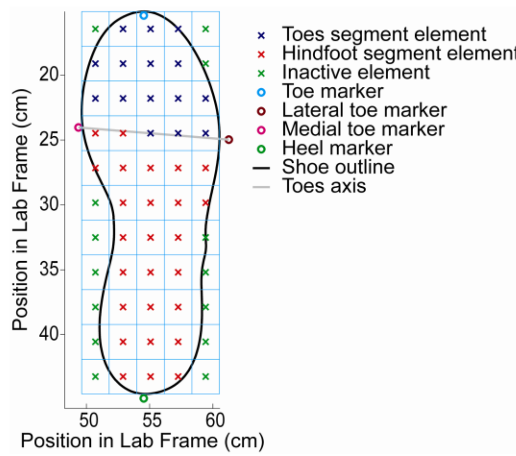

Figure 1: Spring placement for the right foot.

During the static trial, each foot was outlined using a marker wand to determine foot shape and size (Fig. 1). Addidas Samba sneakers were specifically used for this study because the bottom is flat and possesses minimal cushioning. The heel, toe, and medial and lateral toe markers were used to define a uniform rectangular grid (5 x 11 elements) whose long axis was aligned with the heel-to-toe marker direction. A linear spring-damper element was placed at the center of each grid element. The location of each spring-damper element was defined relative to its respective foot segment (i.e., hindfoot or toes). The initial vertical locations of the spring-damper elements in the toes segment varied along a parabolic surface between the toe tip and the toes axis. The motion of the hindfoot and toes segments was used to determine the vertical deformation and deformation rate of each viscoelastic element throughout the gait cycle.

Vertical contact force generated by each viscoelastic element, F_{N_j}, was modeled using nonlinear damping:

$$F_{N_j} = \sum_{i,j} k_i (y_{i,j} - y_{0_i})(1 + c_i \dot{y}_{i,j}) \qquad (1)$$

In this equation, k is the spring stiffness, y and $\dot{y}$ are the spring deformation and deformation rate, respectively, c is the damping coefficient, y_0 is the change in vertical position within the foot segment, i is the spring number, and j is the time frame. The nonlinear damping term produces physically realistic hysteresis during spring compression [5], as opposed to linear damping terms that exhibit force discontinuities at the transitions into and out of contact. The contact forces from each element were added together to get the total vGRF at each time frame.

A constrained non-linear optimization algorithm modified the kinematics, vertical position of the spring-damper elements in the hindfoot and toes segments, and springs parameter values to best match the experimental vertical ground reaction force curve. The cost function minimized $\sum 1/k_i + c_i$ (i.e., maximize spring stiffness values and minimize damping value) subject to constraints on marker position errors and vGRF errors. k and c values were bounded to be greater than zero. Optimized parameters were then applied to four additional gait trials excluded from calibration.

RESULTS AND DISCUSSION

The foot-ground contact model was able to generate vGRF curves that closely matched experimental data. The RMS errors for the vGRF curves were 4.2 N for the calibration trial and 4.9, 6.3, 5.6, and 11.9 N for the four testing trials. The marker errors were within 1 mm of the best fit to the experimental marker data determined from [4]. The spring constants were all positive and the optimizer drove all of the damping coefficients to zero. However, damping may be needed for accurate anterior-posterior or medial-lateral ground contact force calculation, as well as other motions. The magnitude of spring stiffness values, k, mirrored the wear pattern on the bottom of the subject's shoe (Fig. 2), indicating the areas of high force: the heel and across the ball of the foot. While the modifications to the kinematic curves were small, the model was sensitive to the flexion/extension of the toes and hindfoot rotations about the anterior-posterior and superior-inferior axes.

The goal of this study was to develop a subject-specific vertical foot-ground contact model that reproduces experimental vGRF curves. The model successfully reproduced experimental data for four gait trials that were excluded from model calibration. Future work will focus on improving the current model and exploring the grid density of the springs, modeling of the toes surface, and parameterization of the kinematics. This study provides a valuable first step toward developing subject-specific foot-ground contact models. This work could help simplify prediction of new walking motions by allowing free alteration of the foot path.

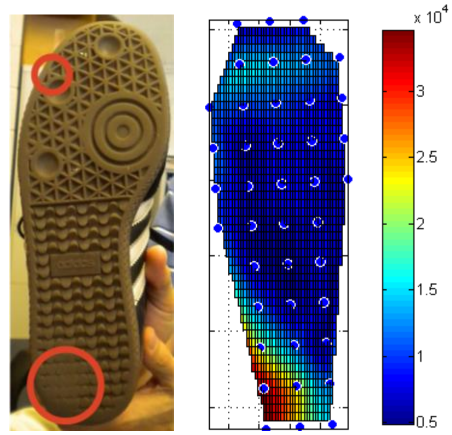

Figure 2: Comparison of wear on the bottom of subject's shoe vs. spring stiffness surface plot. Red circles indicate higher wear areas.

REFERENCES

1. Neptune R, et al. *Comp Methods Biomech Biomed Eng* **3**, 321-334, 2000.
2. Maboobin A, et al. *J Biomech* **43**, 1532-39, 2010.
3. Fregly, et al. *IEEE Trans on Biomed Eng* **54**, 1687-95, 2007.
4. Soderkvist, I and Wedin, P. *J Biomech* **26**, 1473-77, 1993.
5. Hunt, K and Crossley, F. *J Appl Mech* **42**, 440-45, 1975.

ACKNOWLEDGMENTS

This work was funded by NSF Grant CBET 1052754.

RESIDUAL ELIMINATION ALGORITHM IMPROVEMENTS FOR FORWARD DYNAMIC SIMULATION OF GAIT

Jennifer N. Jackson, Chris J. Hass and Benjamin J. Fregly

University of Florida, Gainesville, FL, USA
email: jnjrun18@ufl.edu, web: www.mae.ufl.edu/~fregly

INTRODUCTION

During inverse dynamic simulations of human movement, residual forces and torques acting on the pelvis arise from noise and inaccuracies in experimental data [1]. These physically unrealistic quantities are necessary to balance the equations of motion. To address this problem, Remy and Thelen developed a residual elimination algorithm (REA) that uses forward dynamic simulation to yield dynamically consistent accelerations that satisfy the whole-body equations of motion and track experimental marker motion data [2]. However, the original REA approach is unable to reproduce foot marker motion accurately. This limitation is problematic for applications requiring precise positioning of the feet (e.g., foot-ground contact models).

This study seeks to achieve better matching of foot marker motion with the REA method by investigating modifications to: 1) marker weights, 2) tracked acceleration curves, 3) feedback gains, and 4) model parameter values. In addition, greater back flexibility may also help the model achieve better matching of all marker motion. Thus, the potential benefit of using a two-joint back model is investigated.

METHODS

To evaluate our enhanced REA method, motion capture and ground reaction data were collected from a single healthy subject performing overground gait. The study was IRB approved and the subject gave informed consent. The experimental gait data were analyzed using an existing dynamic full-body gait model [3] that was later modified to include a second back joint. The three-dimensional model consists of 27 degrees of freedom and 14 (single-joint back) or 15 (two-joint back) segments. For the two-joint back model, back flexibility was increased without increasing the number of generalized coordinates in the model by defining the rotations of both back joints using the same three generalized coordinates. The equations of motion were derived using Autolev symbolic manipulation software (OnLine Dynamics, Sunnyvale, CA).

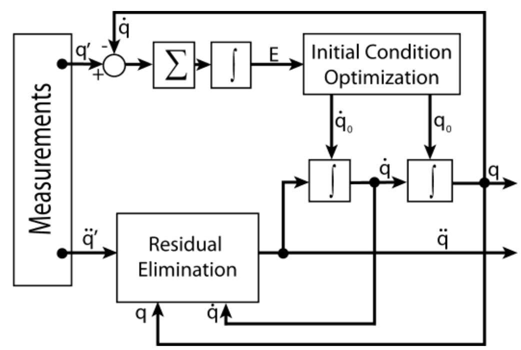

Figure 1: Schematic of the original residual elimination algorithm [2].

The original REA method [2] (Fig. 1) finds new initial conditions and generalized accelerations that eliminate pelvis residual loads while tracking measured marker motions. At the initial time frame, the method uses the pseudoinverse to calculate the minimum changes in generalized accelerations required to balance an underdetermined system of whole-body dynamics equations. Acceleration changes are calculated relative to desired values defined by an optimal feedback strategy:

$$\ddot{q}^* = \ddot{q}' + k_v(\dot{q}' - \dot{q}) + k_p(q' - q) \qquad (1)$$

In this equation, $\ddot{q}^*$ is the desired generalized acceleration, k_p is a feedback gain on joint position error, k_v is a feedback gain on joint velocity error, q is a model generalized coordinate value (along with one time derivative), and q' is an experimental generalized coordinate value derived from inverse kinematics (along with two time derivatives). The updated generalized accelerations are numerically integrated and the process is repeated for each subsequent time frame. An optimization repeats the entire numerical integration process by updating the initial conditions until errors between experimental and model marker positions are minimized.

To improve the ability of the original REA method to match foot marker motion accurately, four modifications to the method were investigated. First, the marker weights were adjusted to 100 for the feet (to closely track the feet), 10 for the shoulder (to prevent the trunk from falling over), and 0.2 to 1 for all other markers weights. Second, the experimental curves being tracked in Eq. (1) were varied by allowing the optimizer to adjust poly-Fourier coefficients that parameterized the *q'* curves. This change accounts for inaccurate generalized speed and acceleration curves derived from differentiating noisy generalized coordinate trajectories. Third, we used nine different k_p values (instead of one) with associated k_v values defined by

$$k_v = 2\sqrt{k_p} \tag{2}$$

to drive the feedback error terms to zero in a critically damped manner [4]. Fourth, select joint and inertial parameter values in the model were also included as design variables to facilitate correct foot positioning while maintaining zero pelvis residual loads.

RESULTS AND DISCUSSION

Use of the four modifications together resulted in significantly better foot marker tracking as well as improved leg marker tracking (Table 1), especially when the two-joint back model was used. Pelvis residual forces and torques remained below 1e-8 N and Nm, respectively, for all cases.

These modifications generally resulted in a reduction in marker error with minimal alteration in kinematics compared to the original REA formulation. Allowing the tracked accelerations to vary resulted in small but reasonable changes in the marker trajectories [2]. The optimized kinematics showed slightly more rotation of the pelvis and torso to reduce overall marker errors. The model does not account for shoulder internal/external rotation, which may contribute to higher marker errors for the arm. Splitting the trunk into two segments reduced almost all marker errors compared to a single-segment trunk while still eliminating pelvis residuals, highlighting the benefit of greater trunk flexibility.

We also performed a sensitivity study to determine the impact of each modification separately and in pairs. When tested separately, tracked acceleration curve adjustments had the most impact on foot marker error reduction. Testing combinations of modifications showed that the use of all four modifications simultaneously resulted in the best overall results, not only for the foot markers but also for most of the other markers.

With these improvements, REA-generated simulations can be used for applications that utilize foot-ground contact models, where foot location is important for modeling foot-floor interaction. These findings also demonstrate the need for greater back flexibility to improve marker tracking in computational walking models.

Table 1: RMS marker distance errors for all time frames. Units are in mm. BJM = Back Joint Model.

Segment	Original REA	New REA (1 BJM)	New REA (2 BJM)
Pelvis	19.25	21.08	14.63
Thigh	21.55	24.89	18.64
Shank	20.02	16.13	13.23
Foot	20.75	2.59	2.98
Arm	34.79	47.82	44.66
Leg	20.56	15.47	12.05
All	24.06	22.13	19.08

REFERENCES

1. Cahouet V, et al. *J Biomech* **35**, 1507-13, 2002.
2. Remy C, et al. *J Biomech Eng* **131**, 031005, 2009.
3. Fregly BJ, et al. *IEEE Trans Biomed Eng* **54**, 1687-95, 2007.
4. Anderson F, et al. *OpenSim User's Guide*, 230, 2001.

ACKNOWLEDGEMENTS

This work was funded by NSF Grant CBET 1052754.

OBJECTIVE EVALUATION OF CHRONIC ANKLE INSTABILITY AND BALANCE EXERCISE TREATMENT

[1]Tarang K. Jain, [2]Clayton N. Wauneka and [1]Wen Liu

[1]University of Kansas Medical Center, Kansas City, KS, USA
[2]University of Kansas, Lawrence, KS, USA
email: tjain@kumc.edu, web: http://www.ptrs.kumc.edu/research/neuromuscular-research-lab/index.html

INTRODUCTION

Lateral ankle inversion sprains occur frequently in sports and recreational activities. Although the majority of patients recover completely after their first moderate/severe ankle sprain, disabling symptoms of pain and swelling, feelings of instability, and recurrent sprains continue to affect 15% - 60% of people despite treatments [1]. There are conflicting results in literature regarding the role of suggested etiological factors of Chronic Ankle Instability (CAI) including ankle joint laxity, proprioceptive deficiencies, peroneal muscle weakness, and the elongated muscle response time. In spite of the disagreement regarding CAI etiological factors, balance training is widely used in rehabilitation clinics for patients with CAI [2]. Past studies have reported the effect of balance training on CAI, but strong evidence with a definitive result is still missing. Furthermore, the mechanism that explains the effect of balance training on CAI is still unclear [2]. Therefore, the objective of this research was to determine the effect of balance training intervention on the ankle joint laxity, peroneal muscle weakness, and ankle proprioception in patients with CAI using quantitative biomechanical and neuromuscular measurements.

METHODS

We tested two groups of patients with unilateral CAI before and after a 4-week balance training program in the Neuromuscular Research Laboratory at The University of Kansas Medical Center. Subjects were randomly assigned to either experimental or control group with 4 subjects (2 males, 2 females; age, 35.2±6.3 years, height, 175.2±6.5 cm; weight, 87.88±21.1 kg) in the experimental group and 6 subjects (2 males, 4 females; age, 36.3±8.6 years, height, 168.9±11.8 cm; weight, 80.43±18.6 kg) in the control group. Subjects in the experimental group participated in a balance training program prescribed over a 4-week time period (3 times per week) whereas subjects in the control group didn't receive balance training. The balance training program consisted of single limb standing, using both static and dynamic balance components. Ankle joint laxity, peroneal muscle strength, and ankle proprioception were measured using the Biodex dynamometer in the seated position for both the affected and unaffected legs pre- and post- training in both groups.

Ankle laxity testing was done at 20^{o} of ankle plantar flexion. The Biodex machine performed full inversion/eversion ranges of motions while the movement angle and joint resistance were recorded (torque-angle curve). The ankle peroneal muscle isometric strength was determined at 15^{0} of ankle inversion (peak torque). Additionally, isokinetic testing of the ankle peroneal muscles was also performed at a rotational velocity of 120^{0}/s for concentric contractions to determine peroneal muscle strength (peak torque). The ankle proprioception positioning-repositioning test was done passively at 15^{0} and 30^{0} of ankle inversion with the subjects blinded. The error in degrees between the reference angle and the repositioned angle was recorded.

The recorded data was processed using lab-made Matlab programs (Mathworks Inc.). The outcome measures for the affected and unaffected leg at the baseline, and pre-post intervention in both the groups were examined using a one-sided independent t-test and one-sided t-test within the groups, respectively.

RESULTS

The affected leg showed increased laxity, decreased peroneal muscle strength, and decreased ankle proprioception as compared to the unaffected leg at the baseline. The ankle joint laxity, peroneal muscle strength, and ankle proprioception in the affected leg were found to be improved by balance training intervention as compared to the control group.

The ankle stiffness improved for both eversion and inversion motions following balance training in the experimental group (pre-test: eversion slope, -0.072±0.05 and inversion slope, -0.050±0.05; post-training: eversion slope, -0.115±0.11 and inversion slope, -0.063±0.02), but it did not reach significance (eversion, p=0.166; inversion, p=0.461). In the control group, the ankle stiffness decreased for both eversion and inversion motions (pre-test: eversion slope, -0.104±.05 and inversion slope, -.067±0.02; post-test: eversion slope, -0.097±0.06 and inversion slope, -0.044±0.01), but were not found to be significant.

The isometric peroneal muscle strength following balance training improved significantly as compared to isokinetic peroneal muscle strength for patients in the experimental group. The peak torque produced during isometric strength test increased significantly following balance training (pre-test: 11.69±3.05 Nm; post-training: 16.18±.4.57 Nm; p=.05). However, the control group showed a decrease in peak torque produced during isometric strength test, but it was not found to be significant. The isokinetic strength test showed the similar trend as isometric strength test for both experimental and control group but the peak torques observed pre-and post-testing showed no significant difference.

The ankle joint proprioception for the experimental group patients improved significantly in 30^0 of ankle inversion (p=.002) but not for 15^0 ankle inversion (p=0.07). In contrast, the control group patients were less accurate in matching the target position post-testing in both 15^0 and 30^0 ankle inversion tests and error magnitudes were found to be significant in 30^0 ankle inversion (p=0.007).

DISCUSSION

The findings of the present study confirm that a proprioceptive and strength deficit exists in patients with CAI: specifically, the perception of ankle inversion movement and isometric peroneal strength is impaired. CAI has long been thought to occur in part because the initial sprain causes deficit in proprioception. The articular de-afferentation may lead to high risk of re-injury at the ankle joint in challenging positions which may further lead to chronic ankle instability. Similarly, lesion to either the afferent or efferent nerves during repeated injuries may also lead to impaired neuromuscular control of the ankle joint, in turn affecting the peroneal muscle strength. Balance training—long known to help some patients decrease the level of pain—may help retrain the nervous system to re-establish more normal neural connections and help re-establish the neuromuscular control around the ankle joint. There was no significant difference in the ankle stiffness, isokinetic peroneal muscle strength, or proprioception at 15^0 ankle inversion in the study, but that may be due to the small subject sample size. A similar argument can be made for positive findings in our study but we hope to establish a clear pattern as we enroll more subjects into our ongoing study. Classification of individuals with CAI based on impairments or treatment response may lead to more efficient conservative management. The results of the proposed study will help researchers and clinicians to develop more focused and effective diagnostic tools and treatment approaches for CAI in the future.

REFERENCES

1. Gutierrez, G.M., T.W. Kaminski, and A.T. Douex, *Neuromuscular control and ankle instability*. PM R, 2009. **1**(4): p. 359-65.
2. Hale, S.A., J. Hertel, and L.C. Olmsted-Kramer, *The effect of a 4-week comprehensive rehabilitation program on postural control and lower extremity function in individuals with chronic ankle instability*. J Orthop Sports Phys Ther, 2007. **37**(6): p. 303-11.

MODELING THE DEMANDS OF A DANCE JUMP: A MISMATCH BETWEEN MECHANICAL DEMANDS AND AESTHETIC CONSTRAINTS

Danielle N. Jarvis, MS, ATC and Francisco J. Valero-Cuevas, PhD
University of Southern California, Los Angeles, CA, USA
Email: dnjarvis@usc.edu   Web: http://pt.usc.edu/labs/mbrl

INTRODUCTION

Many athletic activities require jumping maneuvers, and strategies for maximizing height in a vertical jump have been studied previously [1,2]. However, most athletic activities incorporate a variety of jumping techniques, including jumps in many different directions. The demands of these jumps and the ways that they differ from a standard vertical jump have not been determined.

Dancers perform jumps in many different directions, with very specific aesthetic constraints regarding how the body should look while in the air. For example, in a saut de chat, the dancer takes off from one leg and extends both legs into the air before landing on the front foot. This jump requires propulsion forward as well as vertical height to allow the dancer to achieve the required position.

The purpose of this study was to determine the feasible force output of the takeoff leg during postures used in takeoff for a vertical jump and a saut de chat as well as to compare the force production capabilities during maximal vertical jumps and during traveling jumps leaving the ground at a 45° angle.

METHODS

A three-link model of the lower limb with seven muscles (gluteus maximus, rectus femoris, hamstrings, vasti group, gastrocnemius, soleus, and tibialis anterior) was used (Figure 1). A coordinate system was established such that hip flexion, knee extension, and ankle dorsiflexion were positive torques, and the Jacobian was calculated by taking the partial derivative of the Geometric Model.

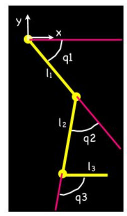

Geometric Model

$x = l_1c_1 + l_2c_{12} + l_3c_{123}$

$y = l_1s_1 + l_2s_2 + l_3c_{123}$

$\alpha = q_1 + q_2 + q_3$

Jacobian

$$J = \begin{bmatrix} -l_1s_1 - l_2s_2 - l_3s_{123} & -l_2s_{12} - l_3s_{123} & -l_3s_{123} \\ l_1c_1 + l_2c_{12} + l_3c_{123} & l_2c_{12} + l_3c_{123} & l_3c_{123} \\ 1 & 1 & 1 \end{bmatrix}$$

Figure 1: Coordinate system and Geometric Model used for Jacobian calculation (J).

Takeoff postures and limb lengths were derived from kinematic data of a dancer performing a saut de chat and an athlete performing a maximal vertical jump (Vicon 612 motion capture system, Oxford, UK). Moment arm, muscle length, and maximal force production from each muscle were taken from previously published data [3,4]. Force production for each muscle was determined using the muscle length and an estimated curve representing the length-tension relationship of muscle.

Coordination patterns and endpoint force production were determined using the inverse Jacobian transpose, moment arm matrix, and force matrix ($F=J^{-T}RF_0a$) [5]. Optimization functions were used to determine maximal force production in a vertical direction with as well as to maximize force production in a traveling jump (at a 45° angle posterior), with no torque production in either case. The model allows for the prediction of the force vector produced by maximal activation of each muscle. Feasible force sets representative of the force production capabilities of the limb were determined by finding the convex hull of all the possible outputs resulting from different activation patterns of each muscle [6].

RESULTS

Optimization functions showed that less endpoint force could be produced during the traveling jump (~200N) than during a vertical jump (~500N).

The posture used by athletes for a maximal vertical jump has a larger feasible force set than the posture used by dancers for a saut de chat (Figure 2).

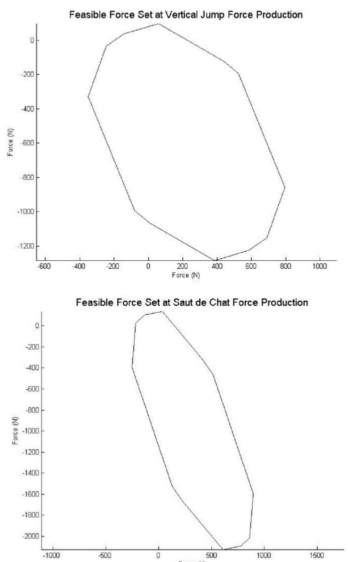

Figure 2. Feasible force set during saut de chat takeoff (top) and vertical jump takeoff (bottom).

DISCUSSION

The posture used for a saut de chat did not allow for as much endpoint force production as the posture used for a maximal vertical jump, which indicates that dancers may need to train for jumping differently from other athletes.

The feasible force sets show that force production in the posture used for vertical jumps (more flexion at all 3 joints) looks more appropriate for producing greater force at a 45° angle than the posture that is used by dancers in a saut de chat jump. The vertical jump force set is larger overall, and extends further in a posterior direction. While using more flexion may be beneficial for producing more force, the aesthetic demands of dance require the movement to look graceful and effortless, and this posture may take away from that appearance. Also, the saut de chat jump requires full extension of the legs in the air, which is likely more difficult when coming from a position of more flexion. However, it is possible that using slightly more flexion during the preparation for the jump may allow for more successful jump performance overall.

CONCLUSIONS

Modeling of vertical jump and saut de chat takeoffs demonstrated that the posture used for maximal vertical jumps appears more appropriate for producing force than the posture used by dancers in a saut de chat. There appears to be a mismatch between the optimal mechanics of the jump and the required aesthetics of the movement. While the position in the air at the height of the jump is the most important aspect of the saut de chat, it is possible that using slightly more flexion during the preparation phase of the jump may be beneficial for dancers.

REFERENCES

1. Pandy MG et al. *J Biomech* **23**, 1185-1198, 1990.
2. Bobbert MF, Van Soest AJ. *Med Sci Sports Exerc* **26**, 1012-1020, 1994.
3. Arnold EM et al. *Ann Biomed Eng* **38**, 269-279, 2010.
4. Ward SR et al. *Clin Orthop Rel Res* **467**, 1074-1082, 2009.
5. Valero-Cuevas FJ. *Progress in Motor Control*. Springer, 2009.
6. Kutch JJ, Valero-Cuevas FJ. *J Biomech* **44**, 1264-1270, 2011.

CORRELATION ANALYSIS OF UPPER EXTREMITY KINEMATICS FOR MANUAL WHEELCHAIR PROPULSION

Chandrasekaran Jayaraman, Iris M. K. Hsu, Yae-Jin Moon, Elizabeth T. Hsiao-Wecksler, Ian M. Rice, Carolyn Beck, Jacob J. Sosnoff
University of Illinois at Urbana-Champaign, Urbana, IL.
jsosnoff@illinois.edu

INTRODUCTION

Manual wheelchair users are at high risk of developing shoulder pain. Consequently, mechanisms and factors that contribute to shoulder pain in manual wheelchair users have been a topic of scientific inquiry. Researchers to date have studied the effect of various parameters of wheelchair design, kinematic and kinetic propulsion mechanics related to shoulder pain [1]. However, there has been less focus on the coupling between arm segments during wheelchair propulsion. There are numerous ways to examine coupling in a biomechanical system. A traditional approach is the Pearson product moment correlation (PPMC). The reliability of PPMC to study walking behavior is well known [2,3]. Importantly, this technique provides complementary information to traditional kinematic analysis. To our knowledge, there has been no application of the PPMC method to study wheelchair propulsion. The purpose of this cross sectional preliminary study was to examine coupling of the upper extremity during wheelchair propulsion in experienced manual wheelchair users. Additionally, we examined whether correlational analyses are sensitive to shoulder pain in wheelchair users.

METHOD

Kinematic data of wheelchair propulsion from eight participants (age=26±12 yrs) with spinal cord injury (five without shoulder pain and three with shoulder pain) from the local community were collected for this study. All were manual wheelchair users, who used a wheelchair for more than a year as their primary means of mobility. Injury diagnosis included six participants with SCI at level T1-T12, one participant with SCI at level C7, and one participant with spina bifida.

Each participant's wheelchair was fitted bilaterally with force and moment sensing wheels (SmartWheel; Three Rivers Holdings LLC; Mesa, AZ, USA) and placed on a stationary roller with a tie-down system. The participants were asked to propel at steady state speeds of 1.1 m/s (fast), 0.7 m/s (slow) and a self-selected speed for three minutes each. These speeds were chosen based on pilot testing using the setup. The sequence of speeds was randomized across participants. A speedometer was used to provide real-time velocity feedback to the participant. Twenty-two reflective markers were placed on bony landmarks and the SmartWheel axles, to define the trunk, upper arm, forearm, hand, as well as the position of the wheelchair and wheels. Kinematic data of wheelchair propulsion were collected using motion capture equipment (Cortex 2.5, Motion Analysis Co.; Santa Rosa, CA, USA) at 100Hz.

Only sagittal plane data from arm segment markers, namely radial styloid (RS), ulnar styloid (US), acromion process (AC) and lateral epicondyle (EL) were correlated and are discussed henceforth. A Pearson Product Moment Correlation (PPMC) at zero lag was computed for the kinematic data between the arm segment joints (Figure 1).

RESULTS and DISCUSSION

Table 1 shows a comparison of the PPMC values obtained between joints on the same side (intra-arm) of the arm (left AC with left EL, and right AC with right EL) between the WSP and NSP groups. Table 2 shows this comparison for the joints (AC with EL) across the right and left arm (inter-arm) joints between the NSP and WSP group. Similar trends were observed in the slow and self-selected speed conditions. The PPMC values for the no pain group were consistently negative (~ -0.8) for both the inter-arm and intra-arm segment joints.

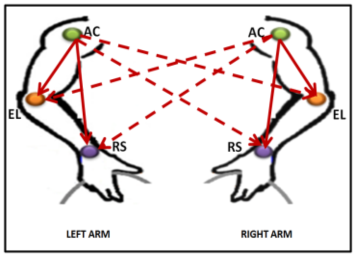

Figure 1: Different inter-arm and intra-arm joints between which PPMC was computed. AC (Acromion), EL (Lateral epicondyle) and RS (Radial Styloid). Dotted line shows inter-arm joint pairings and solid line shows intra-arm joint pairings for which PPMC were computed.

Table 1:Average PPMC values for fast (1.1 m/s) speed. (Intra-arm segments)

Avg PPMC values	**No Shoulder Pain Group NSP**	**Shoulder Pain Group WSP**
Between left AC-left EL joint	-0.76	0.28
Between right AC-right EL joint	-0.88	0.27

Table 2: Average PPMC values for fast (1.1 m/s) speed. (Inter-arm segments)

Avg PPMC values	**No Shoulder Pain Group(NSP)**	**Shoulder Pain Group WSP**
Between left AC-right AC joint	-0.85	0.30
Between left EL-right EL joint	-0.82	0.73

The group with shoulder pain had consistent positive PPMC values (ranging from 0.3 to 0.7) between the intra-arm and inter-arm segment joints. The magnitude of the PPMC values signifies the strength of in-phase motion (positive PPMC) or out-of-phase motion (negative PPMC) between the arm segment joints (both inter-arm and intra-arm) during the cycle. The group with shoulder pain show positive PPMC values, which could mean that the motion executed by these participant's between their AC and EL joints were in-phase, demonstrating a more constrained range of motion movement pattern. Whereas the group without pain, tend to have negative PPMC values, indicating a comparatively more unconstrained range of motion.

CONCLUSIONS

This investigation hypothesized that a propulsion pattern difference exists between manual wheelchair users with and without shoulder pain. This study is one of the first to identify pattern differences between arm joint motion for MW users with and without shoulder pain. The PPMC values on the upper extremity motion data for the "with pain (WSP)" and "without pain (NSP)" groups showed opposite trends. The PPMC values for the no pain group were consistently negative while for the group with shoulder pain the PPMC values were positive. These results suggest that shoulder pain influences the propulsion mechanics in MW users. The PPMC values calculated quantifies this. It is maintained that PPMC values indicates a constraint on the range of motion due to prevalence of pain. A limitation of the current set of data is its small sample size. This study, however, is still in progress; we anticipate that additional test participants will follow the current results and improve statistical power.

ACKNOWLEDGEMENTS

The study is supported by the National Institute of Health grant #1R21HD066129-01A1. The authors would also like to thank Mike Socie, Katie White, and Amy DeFilippo for their assistance in experimental preparation and data collection.

REFERENCES

1. Boninger, ML.,, et al. *Arch Phys Med Rehabil May;83(5):718-23.*
2. Derrick, TR., et al. *Medicine and science in sports and exercise,* 26(7): 919-928,*1994.*
3. Stergiou, N., et al. *Medicine and science in sports and exercise,* 31(11):1645-1655, 1999.

FORCE ENHANCEMENT: AN EVOLUTIONARY STRATEGY TO REDUCE THE METABOLIC COST OF MUSCLE CONTRACTION?

Venus Joumaa and Walter Herzog

University of Calgary, Calgary, AB, Canada
email: walter@kin.ucalgary.ca, web: http://herzogdspace.kin.ucalgary

INTRODUCTION

When a skeletal muscle is actively stretched, its force is substantially greater than the force obtained for a muscle contracting purely isometrically [1]. This phenomenon has been observed for more than fifty years, is an accpeted property of skeletal muscle contraction, and has been termed (residual) force enhancement [2]. When performing experiments on force enhancement in human skeletal muscles, we observed that the additional force produced in the enhanced state was not associated with an increase in muscle activation. In fact, in the force enhanced state, a given submaximal force could be maintained with substantially lower activation than the same force in an isometric reference contraction [3]. This observation led to the idea that maybe force in the enhanced state was produced at a metaboliccaly lower cost than force in the isometric reference state. However, there is no study in the literature on metabolic cost of muscle contraction in the force enhanced state. Therefore, the purpose of this study was to test the hypothesis that force in the enhanced state was metabolically cheaper compared to force in the isometric reference state. If this hypothesis was supported, it could point to new mechanisms of force enhancement and might reveal an evolutionary purpose for this property of skeletal muscle.

METHODS

We used skinned fibers from the rabbit psoas muscle (n=37) that were isolated and set up in a standard mechanical testing apparatus as described previously [4]. One set of fibers (n=15) was stretched passively to an average sarcomere length of 2.4µm and an isometric reference contraction was performed. These fibers were then stretched passively to an average sarcomere length of 2.8µm for another isometric reference contraction. Then, the fibers were actively stretched from 2.4-2.8µm to induce force enhancement. For each isometric reference and each stretch test contraction, fibers were transferred into a fresh activation solution bath for measurement of the metabolic cost of contraction and were held there for exactly 40s. The same testing was performed for a second set of fibers (n=22), however these fibers were tested isometrically at average sarcomere lengths of 2.4 and 3.2µm, and the corresponding stretch test contraction (to induce force enhancement) was performed using an active stretch from 2.4-3.2µm. Forces were measured continuously using a commercial load cell and displacements were imposed using a computer controlled motor as, described previously [4].
Metabolic cost measurements were made over a 40s period by measuring the ATP activity using an enzyme coupled assay as described previously [5]. A non-parametric Wilcoxon test (α=0.05) was used to compare the metabolic cost per unit force for fibers in the isometric reference state and fibers in the force enhanced state following active stretching.

RESULTS

Force enhancement: Stretching of fibers from an average sarcomere length of 2.4 to 2.8µm resulted in a force enhancement of 7.7% (±3.7%) and stretching of fibers from 2.4 to 3.2µm resulted in a force enhancement of 14.2% (±4.2%). Force enhancement occurred in all fibers and was statistically significant ($p<0.01$; Table 1).
Metabolic cost: The metabolic cost per unit of force was reduced by 12.4% (±3.2%) and by 20.7% (±4.4%) for the fibers that were stretched actively to average sarcomere lengths of 2.8 and 3.2µm, respectively compared to the corresponding

isometric reference contractions. This reduction in metabolic cost was observed for each fiber and was statistically significant ($p<0.01$; Table 1).

DISCUSSION AND CONCLUSIONS

Force enhancement in skinned fibers from rabbit psoas muscles, induced by active stretching, was associated with a substantial decrease in the metabolic cost per unit force. The reduction in metabolic cost was greater, on average, than the observed force enhancement because the increased force in the enhanced state was associated with a lower metabolic cost than that measured during the isometric reference contractions. This result strongly suggests that force enhancement is associated with the "engagement" of a passive structural component rather than an increase in cross-bridge based forces.

We have previously shown that the structural protein titin is a calcium activatable spring, and have speculated that titin-associated force enhancement could be achieved by titin binding to actin in an activation/force dependent manner [6]. If this was indeed the case, then one would expect a relationship between the savings of metabolic cost in the force enhanced state with the passive force enhancement. Passive force enhancement increased with stretch magnitude (Table 1) and, as expected, was linearly related to the reduction in metabolic cost in the force enhanced compared to the isometric reference state ($r=0.78$; $p<0.01$). Furthermore, the reduction in metabolic cost was greater when the stretch magnitude was increased (Table1). Together, these results support the idea that the reduced metabolic cost in the force enhanced state is likely associated with the recruitment of a passive structural element, such as titin .

The results of this study also question the common notion that force enhancement evolved as a mechanism to increase force of muscles during everyday movements. Evolution might have favored the "force enhancement" mechanism not primarily for the purpose of increasing force, but for decreasing the metabolic cost of human movement.

REFERENCES

1. Abbott BC, et al. *J Physiol* **117**:77-86, 1952
2. Herzog W, et al. *J Physiol* **574** :635-642, 2006
3. Oskouei A, et al. *Eur J Appl Physiol* **98**:22-29, 2006
4. Joumaa V, et al. *Am J Physiol (Cell)* **294**:74-78, 2008
5. Glyn H, et al. *J Physiol* **365**:259-276, 1985
6. Leonard TR et al. *Am J Physiol (Cell)* **299:**14-20, 2010

ACKNOWLEDGEMENTS

The Natural Sciences and Engineering Research Council (NSERC) of Canada, The Killam Foundation, and the CIHR Canada Research Chair for Molecular and Cellular Biomechanics.

Sarcomere Length (μm)	Reduction in ATP/unit of force (%)	Passive force enhancement (%)	Residual force enhancement (%)
2.8 (n=15)	12.4±3.2*	18.4±1.9*	7.7±3.7*
3.2 (n=22)	20.7±4.4*#	38.6±3.7*#	14.2±4.2*#
2.8 and 3.2 (n=37)	17.2±4.1*	29.5±4.2*	11.3±3.6*

Table 1: Percentage change in ATPase activity and residual and passive force enhancement. Values are Means±SEM. Percentage reduction in ATP cost per unit of force, passive force enhancement, and residual force enhancement observed after active stretches from an average sarcomere length (SL) of 2.4 μm to average sarcomere lengths of 2.8 and 3.2 μm compared to purely isometric contractions performed at sarcomere lengths of 2.8 and 3.2 μm. * indicates a significant change compared to the corresponding purely isometric contraction at the corresponding final length, # indicates a significant increase compared to an average sarcomere length of 2.8 μm (Wilcoxon test, $p<0.01$).

CORRELATIONS BETWEEN TEMPOROMANDIBULAR DISC DAMAGE AND BULK SHEAR MECHANICS

[1]Cassandra Juran and [1]Peter S. McFetridge

[1]University of Florida, Gainesville, FL, USA
email: pmcfetridge@bme.ufl.edu, web: http://www.ufl.edu

INTRODUCTION

The Temporomandibular Joint (TMJ) is a complex hinge and gliding joint that induces significant shear loads onto the fibrocartilage TMJ disc during jaw motion. The majority of published biomechanical analysis has focused on the TMJ discs compressive properties [1, 2, 3] and have found that the disc possesses significant regional variation [4]. While compressive properties are important during joint loading, the TMJ has primarily a sliding joint function that induces compressive as well as significant shear forces. The purpose of this study was to assess regional variation in the discs collective compressive and shear loading characteristics under physiologically relevant loads and to correlate those mechanical findings to common clinical observations of disc perforation and damage.

METHODS

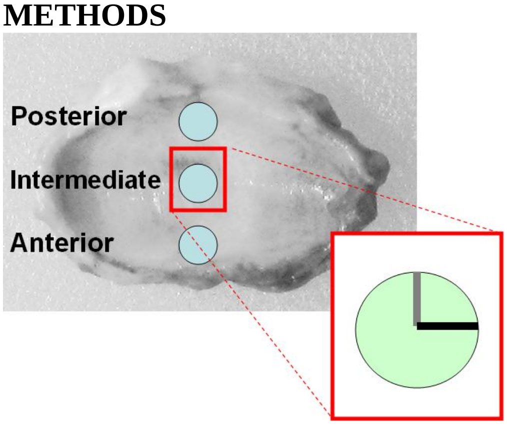

Figure 1: Illustration of regional sampling and directional notation for proper orientation during shear testing (grey line – anterior to posterior direction, black line – medial to lateral direction).

In these investigations the regional shear and compressive characteristics of the porcine TMJ disc and the interconnectivity and dependency of these characteristics on one another and variables relevant to physiologic function: frequency, shear and compressive strain, have been evaluated. Porcine TMJ disc regional punches (Fig 1) were compressed between an axially translating bottom platen and a 2.5cm diameter indenter within a hydrated testing chamber, and oriented either to axially load in the anterior to posterior direction or the medial to lateral direction. Discs were cyclically sheared at 0.5, 1, or 5 Hz to 1, 3, or 5% shear strain. Results of the cyclic loading tests were analyzed by calculating the hysteresis, peak stresses, and the instantaneous and steady-state compressive (E_{int}, E_{ss}) and shear moduli (G_{int}, G_{ss}). Standard Deviation and one-way analysis of variance (ANOVA) were used to determine statistical significance, established using the Tukey-Kramer's Test (p = 0.05, n = 9).

RESULTS AND DISCUSSION

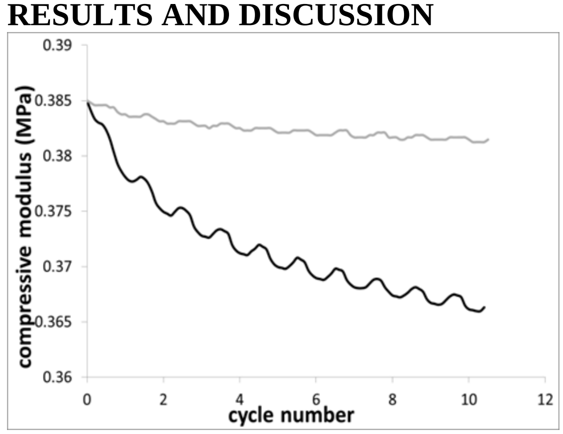

Figure 2: Change in posterior region's compressive modulus when cyclic shear strain is applied in the anterior to posterior or medial to lateral direction (black line – anterior to posterior direction, grey line – medial to lateral direction).

Within the anterior and intermediate regions of the disc when sheared in the anterior to posterior direction both shear and compressive modulus experienced a significant decrease from the instantaneous to steady-state values; while the posterior region's compressive modulus decreased approximately 5% (Fig 2 anterior to posterior) from E_{int} to E_{ss}, no significant loss of shear modulus was noted (Fig 3, posterior A-P). All regions retained their shear modulus within 0.5% of initial values when shear was applied in the medial to lateral direction (Fig 3 all regions M-L).

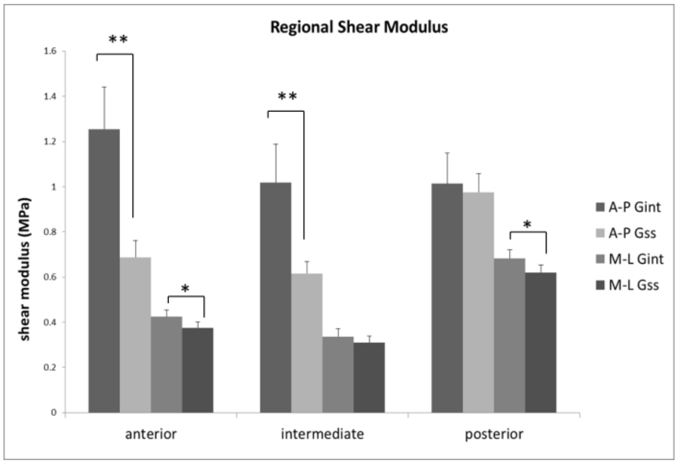

Figure 3: **Mean regional values of the instantaneous and steady state shear modulus of each disc region.** The anterior and central regions experience a significant decrease in shear modulus when strained in the Anterior-Posterior (A-P) direction. This increased elasticity is not seen in the posterior region or in any of the regions under Medial-Lateral (M-L) strain (*, $P < 0.05$; **, $P < 0.01$).

The lack of significant shear softening, decrease from G_{int} to G_{ss} values, in the posterior region is hypothesized to be a function of the extracellular environment make-up. The posterior band of the disc contains lower glycosaminoglycan (GAG) content and higher elastin protein content than the anterior or intermediate zones. GAGs are highly hydrophilic sugar chains that act to maintain the disc's resistance to pressure by trapping water within the matrix. While collagen Type I is the predominant structural protein of the disc, an increased density of elastin fibers in the posterior region [5] may impart more resilience to tensile and shear forces; as observed in our biomechanical results.

These investigations show the steady state shear modulus is stiffest in the discs posterior region, indicating this region is different structurally and in composition. These mechanical results are in agreement with clinical observations of regional disc damage. It is clinically accepted that TMJ disc perforations occur most frequently in the discs lateral-posterior region. We hypothesize that this retained stiffness with repeated shear strain applications limits the disc's ability to distribute (disseminate) loads away from the impact point, leading to greater residual localized stress summation. It is further hypothesized that these localized stress' result in material fatigue and eventual failure, seen clinically as disc perforations.

CONCLUSIONS

The ability of the TMJ disc to act as a bumper between the articulating skeletal structures of the TMJ is fundamental to jaw movement, thus it is paramount to understand the mechanical response of an undamaged TMJ disc when exposed to loading similar to that experienced in vivo. These results suggest a strong correlation between the disc's regional shear mechanics and clinical observation that the posterior region is almost exclusively the zone in which the disc perforates.

REFERENCES

1. Allen K, Athanasiou K. *Annals of Biomedical Engineering* 951-962, 2005.
2. Lumpkins S, McFetridge P. *Journal of Biomedical Materials Research Part a*, 784-791, 2009.
3. Tanaka E, del Pozo R, Tanaka M, Aoyama J, Hanaoka K, Nakajima A *et al*. *Journal of Biomedical Materials Research Part a*, 761-765, 2003.
4. Allen K, Athanasiou K. *Tissue Engineering*, 1183-1196, 2006.

WHICH MUSCLES LIMIT THE ABILITY OF OLDER ADULTS TO RECOVER BALANCE?

[1]Norio Kadono and [2]Michael J. Pavol

[1]University of Ottawa, Ottawa, ON, Canada
[2]Oregon State University, Corvallis, OR, USA
email: mike.pavol@oregonstate.edu

INTRODUCTION

Backward falls are a major concern for older adults. One factor thought to contribute to falls by older adults is aging-related losses in muscle strength [1]. In particular, muscle weakness may limit the ability of older adults to support the weight of the body and stop its motion following a recovery step [2]. Consistent with this, a modeling study found that typical aging-related changes in muscle strength increased the minimum step length needed to restore static balance following a backward balance loss [3]. The purpose of the study was to determine which muscle groups were the greatest contributors to this decreased ability of older adults to recover from a backward balance loss by stepping.

METHODS

A six-link, sagittal-plane musculoskeletal model was used to simulate balance recovery by older adults after touchdown of a backward recovery step [3]. The model included front and rear feet, rear leg, rear thigh, head-arms-torso, and front thigh-and-leg segments. The rear foot, representing the foot that took the step, was fixed to the ground. The front foot was constrained to slide along the ground. Ten Hill-type musculotendon actuators controlled the rear limb. These included uniarticular flexor and extensor actuators across the ankle, knee, and hip and biarticular ankle extensor/knee flexor, knee extensor/hip flexor, and hip extensor/knee flexor actuators. The front limb moved passively. Passive moments enforced anatomical ranges of motion.

Each musculotendon actuator consisted of three elements: contractile (*CE*), passive elastic (*PE*), and series elastic (*SE*). Active force generation by the *CE* was determined by a neural excitation signal (n_i), excitation-activation dynamics, and length-tension and force-velocity relationships. The *PE* and *SE* elements were nonlinear springs. The properties of each actuator were specified by a set of parameter values. These were found by adjusting a set of values that were derived from the literature to model the strength of young adults. Adjustments made to simulate the effects of aging were to decrease the *CE* maximum isometric force (-25%) and the ratio of Type II to Type I fibers (-30%) and to increase the *CE* deactivation time constant (+20%) and the *PE* and *SE* stiffness (+8%).

Using the model, the rear boundary of the feasible region for balance recovery was determined for initial backward and downward velocities of 30% body height/s by the body center of mass (*COM*) and hips, respectively. These velocities are associated with a high risk of falling [3]. To locate the boundary, either the initial hip height (Z_{HIP}, in % body height) or the initial *COM* horizontal position (X_{COM}, in % foot length from the rear heel) was chosen. Then, using repeated numerical simulations and a simulated annealing optimization algorithm, the minimum value of the other variable was found from which static balance could be restored within 1 s. The initial joint angles and velocities, initial *CE* activation levels (a_i), and n_i were the "control" variables. Antagonist uniarticular actuators were controlled by a single n_i such that only one of each pair was excited at a time. Biarticular actuators were controlled individually. The n_i were parameterized by the start time, magnitude, and stop time of five periods of constant excitation, connected by linear changes in excitation. The cost function minimized was:

$$I_{COST} = f_0 + \sum g_m + \sum h_n$$

where f_0 was the initial X_{COM} or Z_{HIP}, the g_m were penalties for violating continuous constraints on the ground reaction forces during movement, and the h_n were penalties for violating the constraints on the final state. The penalty functions required the model to bring itself to a statically stable, near-stationary state in a manner feasible in real life.

For each final optimization solution, the peak n_i to each actuator and the peak a_i of each actuator, as a proportion of maximum, were determined from the corresponding balance recovery simulation. Simulation results were sampled at 20 Hz.

RESULTS AND DISCUSSION

Three initial (X_{COM}, Z_{HIP}) from which recovery of static balance was possible were identified along the rear boundary of the feasible region. In each of these solutions, the peak n_i of the ankle flexors and of the uniarticular knee and hip extensors were at least .87, .91, and .97, respectively (Table 1), with large n_i seen in these actuators for sustained periods (>100 ms) during the early part of balance recovery. Similar results were found for the peak a_i (Table 2). The knee extensor/hip flexor and hip extensor/knee flexor actuators also had large peak n_i, the former at the two highest Z_{HIP} and the latter at the lowest Z_{HIP}. These peaks occurred late in balance recovery. The knee extensor/hip flexor also always had an initial a_i of .93 or greater; however, this high a_i was short-lived (<50 ms). No other actuator exhibited a peak n_i greater than .71 or a peak a_i greater than .85.

The rear boundary of the feasible region in this study is an indicator of the smallest backward step that would allow the recovery of static balance if the *COM* and hips were moving backward and downward, respectively, at 30% body height/s at step touchdown. The sustained, near-maximal n_i and a_i seen in multiple muscle groups during balance recovery from initial (X_{COM}, Z_{HIP}) along the rear boundary suggest that the muscle strength of older adults is a limiting factor that determines the smallest step length that can be successfully used to recover from a backward balance loss. The results further suggest that the ankle flexors and the knee and hip extensors are the muscle groups whose strength most limits the ability of older adults to arrest the body's backward and downward motion following too short of a recovery step. This finding is consistent with the role of these muscle groups in balance and/or weight support.

CONCLUSIONS

Muscle strength of the ankle flexors and knee and hip extensors appears to be a limiting factor for the ability of older adults to restore static balance if they take too short of a recovery step following a backward balance loss. Training to improve the strength of these muscle groups may therefore help older adults to prevent backward falls.

REFERENCES

1. Moreland JD, et al. *J Am Geriatr Soc* **52**, 1121-1129, 2004.
2. Madigan ML, Lloyd EM. *J Gerontol Med Sci* **60A**, 910-914, 2005.
3. Kadono N, Pavol M. *ASB 33rd Annual Meeting*, State College, PA, USA, 2009.

ACKNOWLEDGEMENTS

Funded by the Ringe Faculty Excellence Fund for Life Quality and Longevity and the OSU Center for Healthy Aging Research.

Table 1: Peak neural excitation signals (n_i) during balance recovery as a function of the initial state of the body.

(X_{COM}, Z_{HIP})	AE	AE/KF	AF	KE	KE/HF	KF	HE	HE/KF	HF
(62.4, 48.5)	0	.69	.99*	.91*	.86	0	.98*	.76	.09
(63.7, 47.5)	0	.37	.91*	.99*	.91*	.71	.97*	.70	0
(67.0, 46.6)	0	.31	.87	.99*	.49	0	.99*	.95*	0

A=Ankle, K=Knee, H=Hip; E=Extensors, F=Flexors; X/Y=Biarticular muscle; *=peak excitation ≥.9

Table 2: Peak muscle activation levels (a_i) during balance recovery as a function of the initial state of the body.

(X_{COM}, Z_{HIP})	AE	AE/KF	AF	KE	KE/HF	KF	HE	HE/KF	HF
(62.4, 48.5)	.85	.69	.99*	.91*	.99*	.54	.98*	.73	.42
(63.7, 47.5)	.14	.83	.91*	.99*	.93*	.71	.97*	.73	.19
(67.0, 46.6)	.79	.60	.87	.99*	.99*	.54	.99*	.95*	.73

A=Ankle, K=Knee, H=Hip; E=Extensors, F=Flexors; X/Y=Biarticular muscle; *=peak activation ≥.9

MEASURING 3D TIBIOFEMORAL KINEMATICS AND CONTACT USING DYNAMIC VOLUMETRIC MAGNETIC RESONANCE IMAGING

Jarred Kaiser, Robert Bradford, Kevin Johnson, Oliver Wieben, Darryl G. Thelen

University of Wisconsin, Madison, WI
email: jmkaiser2@wisc.edu **web:** http://www.engr.wisc.edu/groups/nmbl/index.html

INTRODUCTION

Dynamic magnetic resonance imaging (MRI) can characterize musculoskeletal mechanics during movement. Previously, both real-time [1] and cine phase contrast (PC) [2] sequences have been used to measure *in vivo* skeletal kinematics. However, both sequences are only able to image a single plane within reasonable scan times. While cine-PC provides 3D velocity information which can be integrated to estimate out-of-plane motion, it remains challenging to register 3D skeletal positions in space. This limits the capacity of using MRI-based measures to characterize inter-articular contact patterns. The purpose of this study was to investigate the use of dynamic volumetric MRI to measure 3D tibiofemoral kinematics. Volumetric imaging is achieved using radially under-sampled trajectories, termed vastly under-sampled isotropic projections (VIPR), to obtain isotropic resolution within a reasonable scan time. We show that this imaging technique can be coupled with a functional loading device and simultaneous knee angle measures to characterize both 3D joint motion and cartilage contact patterns.

METHODS

Ten healthy subjects (5 F; 24.6 ± 3.2 y; 65.1 ± 5.0 kg) who had no history of past knee injuries, pathologies, surgeries, or chronic pain were imaged bilaterally. High resolution static images (0.37 mm cubic voxels) of each knee were first obtained in a 3.0T MR scanner. Subject-specific bone and cartilage models of the tibia and femur were segmented from these images, and local anatomical coordinate systems were defined [3].

Subjects were then asked to perform a cyclic knee flexion-extension task at 0.5 Hz for 5 min while lying supine in the scanner, with their lower limb attached to a MR-compatible knee loading device. The device applies an inertial load to the lower leg in response to cyclic motion, resulting in peak quadriceps loading with knee flexion as seen in the load acceptance phase of gait. Knee angle was monitored in real-time using a MR-compatible rotary encoder attached to the device's rotation axis. Volumetric images (1.5 mm cubic voxels, 160x160x160 resolution) were continuously collected using a spoiled gradient (SPGR) sequence in conjunction with VIPR. The encoder data was then used to retrospectively sort the MR data into 60 equally sized bins over the 2 s knee motion cycle, from which 60 volumetric images were generated. The high resolution bone models were then co-registered to the volumetric dynamic images at each frame of the motion (Fig. 1). Co-registration was achieved using numerical optimization to determine the bone positions and orientations that minimized the sum-squared intensities of the dynamic images at the locations of the bone model vertices. Tibiofemoral joint angles (flexion-adduction-rotation order) were then determined based on the orientation of the tibia relative to the femur.

For a subset of subjects (n=3), the reconstructed knee kinematics were used to characterize cartilage contact. This was done using a proximity functions between articulating cartilage [4]. Center of contact was defined as the weighted average location of overlapping vertices.

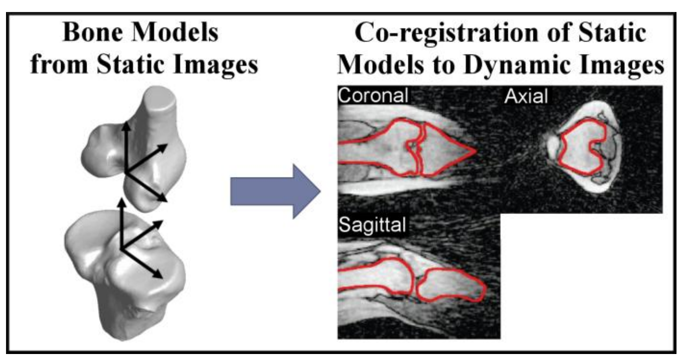

Figure 1. High resolution bone/cartilage models are co-registered with dynamic images.

RESULTS

All subjects exhibited internal tibia rotation (7.8 ± 3.5°) with knee flexion (35.8 ± 3.8°), characteristic of the screw-home mechanism. The internal tibia rotation angles were greater than those previously measured during unloaded knee motion with cine-PC [2]. This difference may be due to the quadriceps loading induced by the loading device, as the average tibia rotation trajectory agreed extremely well with kinematic measures during the load acceptance phase of gait (Fig. 2) [5]. Estimated cartilage contact patterns exhibited greater contact excursion on the lateral condyle (Fig. 3), consistent with contact measures obtained during weight-bearing knee flexion using biplane fluoroscopy [6].

DISCUSSION

We believe this study represents the first fully dynamic volumetric MRI of skeletal motion. A key to our approach is use of radially under-sampled acquisitions which allow for isotropic images to be obtained in reasonable scan times. Subjects had to perform cyclic knee flexion-extension within a scanner for 5 min. In a separate study, we showed that the device induces repeatable loading [7] with peak knee extension moments of ~0.5 Nm/kg in flexion. This loading is at the low end of knee extension moments seen in walking, making the task no more fatiguing than a slow walk. The dynamic images we obtained are relatively low-resolution, but have sufficient contrast at the edges of the bone to resolve the position and orientation of rigid bone segments. We are now in the process of building a motion phantom to assess the absolute accuracy of kinematics measured using this imaging

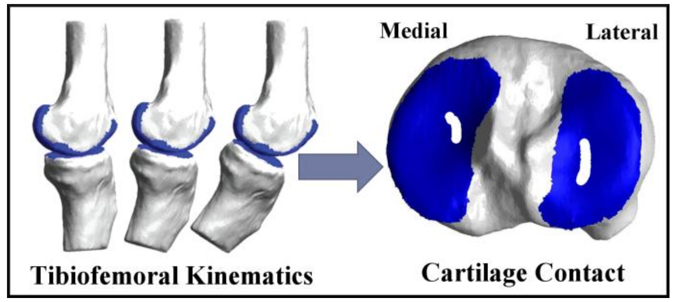

Figure 3. Cartilage models can be combined with tibiofemoral kinematics to calculate cartilage contact through the cyclic task.

technique. Yet, when cartilage models were added to the bone models, realistic contact patterns were estimated based on simple proximity measures. Hence, we believe the new dynamic imaging approach could prove useful for investigating how cartilage contact changes with ligament injury and reconstructive surgery, which is important given the potential for small changes in contact to give rise to the onset of osteoarthritis.

REFERENCES

1. Draper CE, et al. *J Orthop Res* **27**, 571, 2009.
2. Seisler AR, et al. *IEEE Trans BME* **54**, 9, 2007.
3. Miranda DL, et al. *J Biomech* **43**, 4, 2010.
4. Larsen E, et al.. Tech Rep TR99-018, Dept of Comp Sci, Uni N Carolina, Chapel Hill, 1999.
5. Lafortune M, et al. *J Biomech* **25**, 11, 1992.
6. DeFrate, LE, et al. *J Biomech* **37**, 1499, 2004.
7. Silder, A, et al. *J Med Devices* **3**, 53, 2009.

ACKNOWLEDGEMENTS

NIH AR056201, NSF 0966535, Robert W. Bolz Distinguished Graduate Fellowship Program

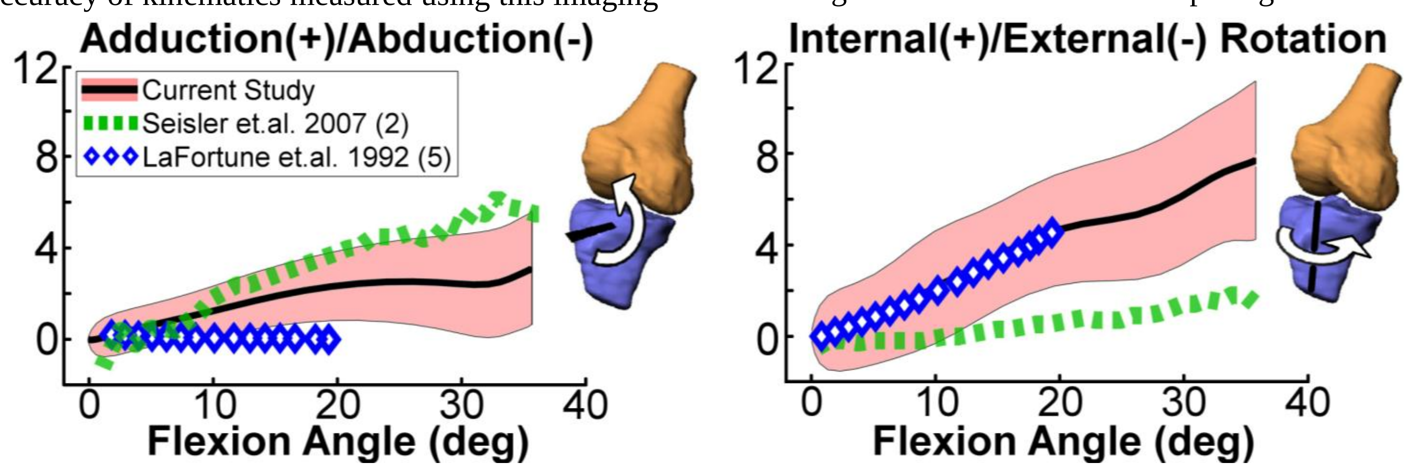

Figure 2. Tibiofemoral rotations (deg) of gait measured with intra-cortical pins (5), unloaded knee flexion measured with cine PC MRI (2) and loaded knee flexion measured with SPGR-VIPR MRI.

DESIGNING BIOMECHANICS COURSES FOR SIGNIFICANT LEARNING: FINK MODEL APPLIED AT CAL POLY POMONA

Hyun Gu Kang

Kinesiology and Health Promotion, California State Polytechnic University, Pomona CA, USA
email: hgkang@csupomona.edu, web: http://www.csupomona.edu/~hgkang

INTRODUCTION

How do I get students to really learn biomechanics? How do I make the students care about biomechanics? There are many specific tools address issues related to student difficulty in particular topics and concepts. However, all of these tools individually or together many not be very effective unless they fit into a greater cohesive structure that promotes student learning.

Presented here is a comprehensive framework to design a course for significant learning [1]. These methods were developed by L. Dee Fink, a course design consultant and author. The application of these concepts at Cal Poly Pomona are presented.

METHODS

To achieve learning, the instructor must first consider the **Situational Factors**: student composition, instructor's capabilities, and institutional requirements. Then, the course need to be **Learner-Centered** rather than content-centered. That is, a course need to be designed around skills the students need to demonstrate at the end of the course, rather than the content that need to be covered. The instructor needs to structure the course so that students do achieve the goals necessary. That is, the learning goals, the teaching /learning activities, and the feedback/assessments need to be aligned with each other. For example, a 100% lecture class will not help students develop creative problem solving skills, since they don't have the opportunity to get the necessary practice and feedback.

Fink found that students find course contents memorable when they not only contain high-level cognitive requirements, but also affective, personal content. He organizes the paradigm of learning into six categories:

1. **Content/ Foundational Knowledge**: understanding and remembering facts, terms, formulas, concepts, principles, etc.
2. **Application**: Thinking skills, such as critical thinking, creative activities, problem solving, as well as communication and managing projects
3. **Integration/Synthesis**: Making connections with other ideas, subjects, people.
4. **Human Dimensions**: Learning about and changing one's self, and interacting with others
5. **Caring**: Identifying or changing one's feelings, interests, or values.
6. **Learning how to learn**: Becoming a better student, learning how to find answers to a question, and becoming self-directed.

Notice that the first three are analogous to Bloom's Taxonomy of Learning. However, for significant learning to occur, the course also needs to emphasize personal and affective aspects. Each aspect of learning necessary involves others, and targeting one will support the others. This paradigm can be applied to any course, from arts to engineering. Particularly in biomechanics, it is easier to relate any of the concepts directly to how students encounter the world.

To formulate significant learning goals, the instructor must complete the statement: "A year (or two) after this course if over, I want and hope that students will ...." Once the learning goals are defined, then the course now can be designed "backwards." Assessments need to be designed to test whether students in fact can do .... Now, rest of the course prepares the students for the assessments. This does involves "teaching to the test" which is the desired outcome as long as the "test" effectively assesses the necessary learning. Once the assessments (tests, projects, papers, etc.) are defined, the instructor needs to consider instructional activities. **Active Learning** activities effectively involve student participation in and outside of the classroom. **Rich Learning Experiences** (projects, etc.) can attain several kinds of learning simultaneously. **Reflection activities** give students time to think about what and how they are learning. Finally, these activities and the assessments need to fit into a comprehensive whole.

RESULTS AND DISCUSSION

This design method was applied to the Introductory Biomechanics class at California State Polytechnic University, Pomona (hereafter Cal Poly Pomona). The course is required for all 600+ Kinesiology majors options, including about 25% whose curriculum does not require physics. Course objectives are also approved by the California Commission on Teacher Credentialing to meet teacher education needs. We expect students to be able to:

1. Apply anatomical position and movement terminology when describing specific activities
2. Identify major muscles for specific activities
3. Describe movement using appropriate kinematic terminology and mathematical methods
4. Use Newtonian mechanics to derive determinants of movement
5. Critically analyze movement using basic anatomical and biomechanical knowledge

To that end, the following assessments were created using the Fink model:
Dance Analysis: Take a dance, and describe it using proper anatomical terminology to a blind person who wants to learn. Achieves Content, Application, Human Dimension learning
Biomechanics Article Reviews: Discuss author views, and test their claims on students themselves. Achieves content, application, integration, and caring learning
Muscular Analysis: Describe the phases of movement and muscles used in an activity that you perform on video and analyze. Achieves Content, Application, human dimension learning
Sand Pit Safety Design (group work): Using world-record data, determine the amount of sand necessary to maintain safety. Achieves all six learning types.
Activity Modification (group work): Modify an activity to be more accessible to those with disabilities. Achieves all six learning types.
Equipment Design (group work): Create the next big fitness product! Achieves all six learning types.
Teaching Project: (group work): Teach a new biomechanics topic to the class. Achieves all six learning types.

To prepare for these assessments, in-class time is spent on Immediate Feedback quizzes of content or application, creating a lesson, and describing movements and kinematics in videos and in person. Kinesthetic activities are used, such as trying different activity variations to determine what modifications work, jumping on the force plate to see how landing styles affect ground reaction forces, etc. Students need to report what impact the course content is having on their personal life outside of kinesiology, and need to write a reflection on the group work and teaching experience as to how they like to learn.

Data is not available to compare how effective this course is vs. my previous teaching, as this course design was implemented very early in my teaching career. There are still many aspects of the course that do not integrate well, and improving the course will be an on-going effort.

CONCLUSIONS

For more information, Fink's book [1] is an helpful resource. The website www.designlearning.org also gives examples from many contributors. L. Dee Fink runs workshops at universities (see www.deefinkandassociates.com).

REFERENCES

1. Fink LD. *Creating Significant Learning Experiences*, Jossey-Bass, 2003.

ACKNOWLEDGEMENTS
Cal Poly Pomona Provost's Office

NATURAL GAIT MAY NOT BE NEUTRAL: IT ALL DEPENDS ON HOW YOU FEEL

Gu Eon Kang and Melissa Gross

University of Michigan, Ann Arbor, MI, USA
email: guekang@umich.edu, web: http://www.umich.edu/~mgross

INTRODUCTION

Emotion is observable in body movement, even during walking [1]. When observers detect an emotion during walking, gait kinematics have been shown to differ between those walkers who felt the emotion and those who just displayed the emotion without feeling it [2], suggesting that the kinematic cues used for emotion decoding may not always be the same as those produced during emotion encoding. In this study, we examined gait kinematics in trials in which a target emotion was felt compared with neutral trials in which no target emotions were felt, regardless of whether or not the emotions were recognized. Gait studies are based on "natural" walking trials, without consideration of how the walker feels. If gait data are collected when a participant is feeling an emotion, gait data may not actually represent natural walking with neutral feeling, and gait studies with a repeated measures design over time may be affected by differences in a participant's mood as well as the experimental variable of interest. The purpose of this study was to assess the differences in gait kinematics between trials in which an emotion was felt compared to neutral trials in which no emotions were felt.

METHODS

This study was based on a secondary analysis of data collected previously in our lab [3,4]. Motion data were collected from 62 young healthy individuals while they walked with five target emotions (anger, sadness, joy, contentment and neutral). After each trial, participants rated the intensity that they felt target and non-target emotions (awe, fear, surprise and disgust) during walking using a 5-item Likert scale. Emotions were considered *felt* if Likert scale score for the target emotion was $\geq$ 2 (0=not at all; 1=a little bit 2=moderately; 3=a great deal; 4=extremely); if < 2, the emotion was *not felt*.

Motion data were acquired with a 6 camera (60/120 Hz) motion analysis system (Motion Analysis Co.). Marker coordinate data were filtered at 6 Hz with Butterworth filter. Gait kinematics were analyzed using Visual 3D (C-Motion Inc.). Outcome variables were gait parameters (velocity, stride length, cadence), postural angles (neck extension, shoulder girdle protraction and depression, trunk and thoracic spine extension), and joint range of motion (ROM) (shoulder, elbow, wrist and hip flexion, knee extension, ankle plantarflexion, trunk lateral tilt and trunk rotation).

Trials were selected in which only one emotion was *felt*. For example, trials were categorized as angry if anger was *felt* and the other target emotions were *not felt*. Trials were categorized as sad, joyful or content in the same way. Trials were categorized as neutral if none of the target emotions were *felt*. A mixed model with random walker effects and fixed effects of emotional trials and neutral trials was used to test significant difference (p<.05).

RESULTS AND DISCUSSION

Mean mood intensities were *felt* at levels > 3 for angry, sad, and joy trials, and > 2 for content trials; all other target emotions were < 1 (*not felt*) (Table 1). For neutral trials, mean mood intensities were < 1 (*not felt*) for all target emotions.

Gait parameters were significantly different in angry and joyful trials compared to neutral trials. Gait velocity, stride length and cadence in angry trials (1.43 m/s; 1.44 m; 118 steps/min) were 22, 12 and 8% greater (all p<.001), respectively, than neutral trials (1.17 m/s; 1.29 m; 109 steps/min). In joyful trials, gait velocity and cadence (1.29 m/s; 113 steps/min) were 10 and 4% greater (all p<.01), respectively, and stride length was 4% greater (p<.05) than neutral trials. Gait velocity, stride length and cadence did not change significantly in sad (1.15 m/s; 1.3 m; 106 steps/min) and content trials (1.26 m/s; 1.33 m; 112 steps/min).

Differences in postural angles were significant in angry and sad trials. In angry trials, the trunk and thoracic spine were more flexed (1.9° and 1.5°; $p<.01$ and $p<.05$, respectively) and the shoulders were more protracted and elevated (2.3° and 5.3°; $p<.05$ and $p<.001$, respectively) than in neutral trials. Mean neck angles decreased 2° in angry trials but the difference was not significant. In sad trials, neck and trunk were more flexed (8.3° and 2°; $p<.001$ and $p<.05$, respectively) and the shoulders were more elevated (4°; $p<.05$) compared to neutral trials. Shoulder protraction and thoracic spine extension were similar between sad and neutral trials. In joyful and content trials, neck extension and trunk flexion were greater (1.2° and 1° for joy; 2.4° and 1.5° for contentment, respectively) compared to neutral trials, but the difference was not significant. Shoulder protraction and elevation and the thoracic spine extension were similar between joyful and neutral trials and content and neutral trials.

Joint ROM increased in angry trials compared to neutral. ROM increased for the elbow (24%; 7°; $p<.05$), hip and ankle (all 13%; 5° and 3°; $p<.001$ and $p<.01$, respectively), and knee (4%; 2°; $p<.05$). Trunk lateral tilt and rotation increased (all 15%; 1° and 3°; $p<.01$ and $p<.05$, respectively). In sad trials, trunk rotation decreased (7%; 1°; $p<.05$) compared to neutral trials. In joyful trials, ROM increased for the wrist, hip and ankle (30, 7 and 12%; 2°, 3° and 3°; all $p<.01$, respectively). Trunk lateral tilt increased slightly (5%; $p<.01$) but the difference was likely too small to be meaningful. In content trials, ROM increased for the knee and ankle (5 and 16%; 3° and 4°; all $p<.05$, respectively).

The data reported here differ from other studies because only trials in which the target emotions were *felt* were included in the analysis, regardless of whether or not the target emotions were recognized. In these *felt* trials, the postural gait variables (neck, thoracic spine, trunk and shoulder girdle mean angles) were affected more for the negative emotions (anger and sadness) than for the positive emotions (joy and contentment), compared to neutral. In contrast, the velocity-dependent gait parameters were affected more for the high arousal emotions (anger and joy) than for the low arousal emotions (sadness and contentment), compared to neutral. Gait kinematics seemed to be most sensitive to the feeling of anger, since both postural and velocity-dependent kinematics were affected.

CONCLUSIONS

The results of this study show that gait kinematics and posture are affected when emotions are felt compared to neutral trials in which no particular emotion is felt. Some of the emotion-related differences occurred even when gait speeds were similar. These results suggest that it may be important to include assessment of participant feelings in experimental protocols particularly if differences in outcome variables are expected to be small, or if postural variables are included.

REFERENCES

1. Gross MM et al. *Human Movement Science* 31, 202 – 221, 2012.
2. Kang G and Gross MM. Proc Amer Soc Biomechanics, Long Beach, CA, USA, 2011.
3. Crane EA et al. In: England D (Ed.), *Whole Body Interaction*, Springer, 2011.
4. Edgeworth R et al. Proc Amer Soc Biomechanics, Ann Arbor, MI, USA, 2008.

Table 1: Mean mood intensity, number of *felt* trials and percent of female walkers analyzed for each emotion.

Emotion	**Mood Intensity**				**Trials**	**Female**
	Anger	**Sadness**	**Joy**	**Contentment**	**(n)**	**(%)**
Neutral	0.1	0.1	0.1	0.4	31	45
Anger	**3.5**	0.5	0.0	0.0	33	45
Sadness	0.4	**3.5**	0.0	0.1	33	54
Joy	0.0	0.0	**3.3**	0.8	20	50
Contentment	0.0	0.9	0.7	**2.7**	23	47

FLEXIBLE FRAMEWORK FOR TESTING POSTURAL CONTROL MODELS: EVIDENCE FOR INTERMITTENT CONTROL?

[1]Hyun Gu Kang and [2]Gregory J. Murdock

[1] Kinesiology and Health Promotion and [2]Computer Science,
California State Polytechnic University, Pomona, California

email: hgkang@csupomona.edu   www.csupomona.edu/~hgkang

INTRODUCTION

A wide variety of models have been proposed to describe postural sway during quiet standing. One approach in the engineering context is the PID-feedback approach. Postural control parameters are determined from transfer functions based on inputs and outputs. This approach assumes linearity of controller and the system dynamics. Another model that has been proposed is the intermittent control [1], where the controller is active for short bursts only as necessary. This is in contrast to the usual PD/PID model where controller gains are fixed and the controller is active continuously. Testing this model is more difficult, as typical linear system identification and control theory methods do not work well with such non-linear control strategies.

Our goal is to describe a flexible modeling approach that does not require linearity of the controller, and does not require perturbations to be applied to the standing person. Here we will apply this approach to two different models: the continuous feedback PD control, and intermittent control.

METHODS

Data was used from the MOBILIZE Boston Study, a prospective study examining risk factors for falls, including pain, cerebral hypoperfusion, and foot disorders in the older population [2]. The study includes a representative population sample of 765 elderly volunteers age 70 or above from the Boston area. COP data were available in 725 participants, who were 77.9±5.3 years old, with height of 1.63±0.10 m and weight of 74.1±19.7 kg. 64% were female.

Subjects stood barefoot with eyes open on a force platform (Kistler 9286AA). The center of pressure (COP) data were sampled at 240 Hz in anteroposterior (AP) direction. Subjects five quiet standing trials, 30 seconds each. After accounting for various technical or data collection issues, 3308 trials were analyzed.

The postural system was modeled as an inverted pendulum with passive and active stabilization. From the COP data, the center of mass (COM) excursions were determined using zero-point to zero-point double integration technique [3] and from there, postural angle $\theta(t)$, angular velocity $\dot{\theta}(t)$, and acceleration $\ddot{\theta}(t)$ were calculated. The basic candidate model structure was [4]:

$$I\ddot{\theta} = mgh\,\theta - K\theta - B\dot{\theta} - f_p(\theta(t-\tau)) - f_d(\dot{\theta}(t-\tau)) + \xi(t) \qquad \text{[Equation 1]}$$

where I = moment of inertia about the ankle,
K = passive stiffness of the body (at the ankle); B = passive damping; τ = time delay in the response of the neuromuscular system; $f_p(\ )$ and $f_d(\ )$ = function of the position feedback for each model; $\theta(t-\tau)$ and $\dot{\theta}(t-\tau)$ = time delayed information of angular position and velocity of the body; $\xi(t)$ = noise.

Two models were considered. 1. Continuous control model: Here, $f_p(\theta(t-\tau)) = P\,\theta(t-\tau)$ and $f_d(\dot{\theta}(t-\tau))$=$D\,\dot{\theta}(t-\tau)$, so that feedback is a linear function of the angular position and velocity with delays.

2. Intermittent control model: Here, feedback control only occurs when the pendulum has moved away from the vertical (|θ|>0), yet it keeps moving away (|$\dot{\theta}$|>0). In this model,

$$f_p(\theta(t-\tau)) = P\,\theta(t-\tau) \text{ and } f_d(\dot{\theta}(t-\tau)) = D\dot{\theta}(t-\tau) \quad \text{for } \theta(t-\tau)\dot{\theta}(t-\tau)>0 \qquad \text{[Equation 2]}$$

$$f_p(\theta(t-\tau)) = 0 \text{ and } f_d(\dot{\theta}(t-\tau)) = 0 \quad \text{otherwise}$$

The model parameters (K, B, P, D) were solved as a multiple linear regression over a range of physiologically plausible time delay, τ (tau) of 40-400 ms, and τ with the best fit was selected. For each τ, model fit was determined as R^2.

RESULTS AND DISCUSSION

Model 1: Continuous Control. Despite high R^2, this model produced valid results for <1% of the trials, as most of D were negative. Also, the model defaulted to τ=42 ms. Our method did not identify a meaningful parameter set or time delay in the nervous system. This was due to lower τ making the time delayed kinematics variables more correlated with original kinematics.

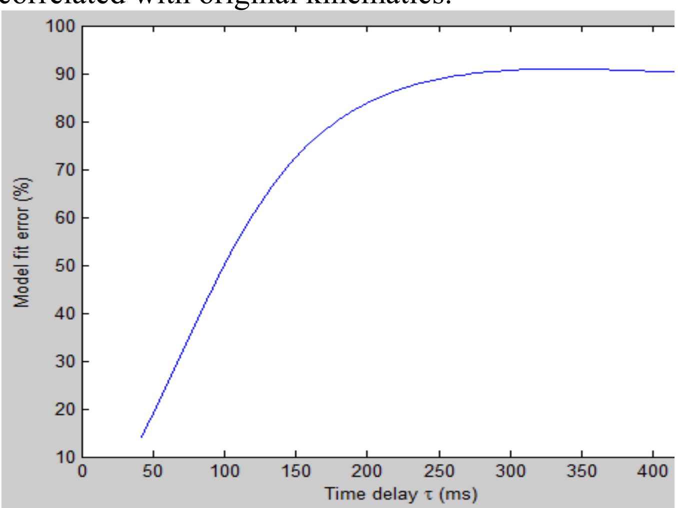

Figure 1: Sample model fit error vs. τ in continuous control. Model fit becomes worse with increasing time delay.

Model 2: Intermittent Control. This model produced valid results for 93.1% of the trials. The method does find a reasonable time delay of 214±72 ms in the population (Table 1). Fit improved even at these time delays because the intermittent control feedback variables were no longer correlated with the original kinematic variables. Overall, this model fit the data better (Table 1) and yielded parsimonious time delays.

CONCLUSIONS

Our preliminary work does not provide a strong or definitive evidence for a particular postural control theory. However, this flexible modeling approach allows the testing on non-linear models of postural control that have been proposed yet have been difficult to test experimentally. Future work will include refinement of methods that would provide a stronger evidence for any particular postural control theory or model.

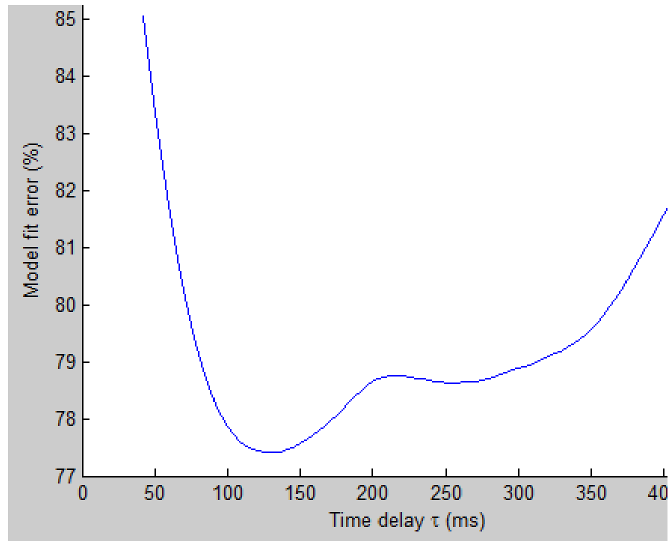

Figure 2: Sample model fit error vs. τ in intermittent control. Here, τ of ~130ms provides the best fit.

REFERENCES

1.Loram ID et al. *J Physiol* 589:307-24 2011.
2. Leveille SG et al. *BMC Geriatr.* 8:16, 2008.
3.Zatsiorsky VM et al. *J Biomech* **31**, 161-4, 1998.
4.Asai Y et al. *PLoS One*. 4:e6169, 2009.

ACKNOWLEDGEMENTS

NIA P01AG 004390 and T32AG023480

Table 1: Postural model parameter estimates

	Continuous control	Intermittent control	
K	945.3±297.9	515.1±174.4	Nm-rad
B	1677.6±560.4	93.5±58.5	Nm-rad/s
P	288.2±145.4	110.3±79.4	Nm-rad
D	-1691±77.6	151.5±89.1	Nm-rad/s
τ	42±0	214±72	ms
R^2	94.5±3.9	21.7±8.5	%
% valid	<1%	93.1	%

DEVELOPMENT OF A DEMENTIA-SPECIFIC GAIT PROFILE: APPLICATION OF SIGNAL DETECTION THEORY

[1,2]Tasos Karakostas, [3]Hsiang Simon, and [2,4]Davis Boyd

[1]Rehabilitation Institute of Chicago, Chicago, IL, USA
[2]Medical University of South Carolina, Charleston, SC, USA
[3]Texas Tech University, Lubbock, TX, USA
[4]University of North Carolina, Charlotte, NC, USA
email: tkarakosta@ric.org

INTRODUCTION

The rate at which elderly are being diagnosed with dementia has accelerated over the recent years and it is alarming [1]. They are three times more likely to fall and over three times more likely to have severe injury compared to cognitively unimpaired elderly [2]. Consequently, recently there is an interest in the identification of biomarkers that can contribute towards, or establish, early detection and diagnosis of dementia.

One of the characteristics of dementia is the inability of the patient to allocate attentional resources to concurrent tasks [1]. Consequently, towards the identification of biomarkers for the early detection of dementia, recent studies have used walking gait in conjunction with another cognitive or motor task and contrast performance to walking gait as a stand-alone task [3-5]. Typically, the temporal-spatial parameters of gait are being evaluated to identify individuals with the disease, the type of dementia and its progression.

However, in every study all temporal-spatial gait descriptors are being evaluated and, typically, the non-specific velocity, double limb support and stride variability are reported as significant. It was the purpose, therefore, of this study to identify the minimum number of temporal-spatial gait characteristics that discriminate individuals with dementia irrespective of task.

METHODS

We used gait as a stand-alone task and in conjunction with a cognitive task, i.e., walking while talking about a subject's topic of interest. Thirteen elderly, seven with moderate to severe dementia, living in a secured dementia facility and six of normal cognition, aging normally, living independently in long-term care (control group) participated in our investigation. This was a sample of convenience which will form the foundation for a larger clinical study. Subjects had no orthopaedic defects. They could ambulate without assistive devices for 10 meters or more and none was taking medications that could affect stability and gait.

The gait parameters of interest were obtained using the GAITRite® Gold, a 6.10m instrumented with sensors walkway (CIR Systems Inc., Clifton, NJ) sampling at 120 Hz. Talking data while walking was obtained using Olympus DS 330 digital recorders and a clip-on Sony microphone ECM 717, which were less alarming to the residents with dementia. For the purposes of this report we will focus on the gait performance of the subjects.

To collect the temporal-spatial gait parameters, the instrumentation was brought to the subjects' residence. Each participant was asked to walked at a self-selected pace. Three sets of trials were collected. During the first set subjects walked normally. During the second set, each participant walked while talking to one of the investigators that the participant was familiar with. The investigator facilitated the conversation. Talking involved anything the participant desired to talk about.

To identify the minimum set of temporal-spatial descriptors that can distinguish the walking patterns of normal aging individuals from those with dementia, i.e., to identify the dementia-specific walking profile, signal detection theory (SDT) was used [6]. SDT was also used for discriminating across walking conditions, i.e., walking while talking and just walking. SDT was complemented by constructing the receiver operator characteristic curves [7].

RESULTS AND DISCUSSION

The results (See Figure 1 and Figure 2) suggest that only six of the thirteen temporal-spatial variables: Stride Time, Stride Width, Single Support Time, Toe In/Out, Swing Time, and Stride Length were needed to discriminate individuals with dementia from the normally ageing cohort irrespective of whether individuals were tested using gait as a stand-alone task or under a dual task paradigm. Consideration of additional variables made no noticeable difference in the ability to differentiate between the two cohorts. The variable that had the most discriminating power across walking tasks, irrespective of cognitive status, was the double support time.

Our study is the first to provide a gait-specific profile for individuals with dementia irrespective of the walking task. It is also the first to report on the effect of task on gait performance irrespective of pathology. The descriptors can be considered true predictors of dementia, because they are specific to condition whereas velocity and stride variability identified by previous studies are non-specific.

We believe that this study, strengthened by a future validation, can provide a strategy for clinicians to assess dementia based on a gait-specific profile of patients with dementia focusing on less than half of the traditional time-distance gait descriptors; furthermore, it can potentially provide a new tool for assessing the effectiveness of related interventions by monitoring changes in the performance of the dementia-specific gait descriptors.

REFERENCES

1.Morgan D, et al. *Can J Ag*, **26**, 19-32, 2007.

2.Hauer K, et al. *Am J Phys Med Rehab*, **85**, 847-857, 2006.

3.Snijders A, et al. *J Neur Transm*, **114**, 1315-1321, 2007.

4.Verghese J, et al. *J Am Ger Soc*, **56**, 1244-1251, 2008.

5.Verghese J, e al. *J Neur Neuros Psych*, **78**, 929-935, 2007.

6.Nabeshima A, et al., *Ger Geront Intern*, **7**, 160-166, 2007.

7.Tanner WP, et al., *Psych Rev*, **61**, 401-409, 1954.

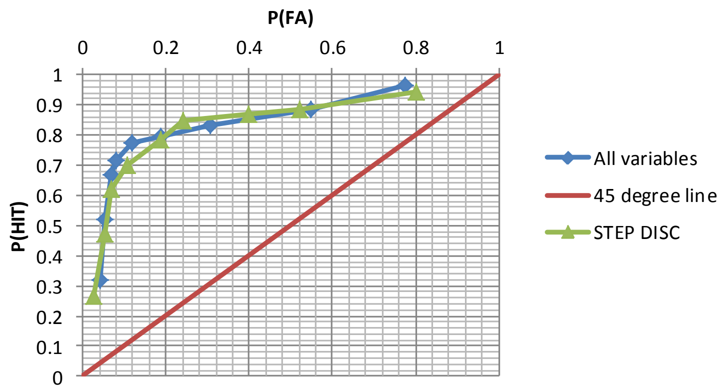

Figure 1. ROC curve when all gait variables (All variables) are used to discriminate the individuals with dementia from those of normal aging plotted against the respective ROC curve for the minimum six gait descriptors (STEP DISC). The plot represents the probability of false positives (P(FA)) against the probability of true positives (P(HIT)).

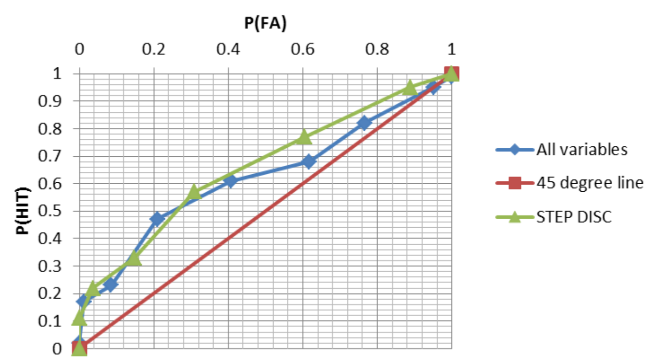

Figure 1. ROC curve when all gait variables (All variables) are used to discriminate the walking task, plotted against the respective ROC curve for the double support time (STEP DISC). The plot represents the probability of false positives (P(FA)) against the probability of true positives (P(HIT)).

MAXIMUM VOLUNTARY FORCE PRODUCTION CHANGES WITH VISUAL FEEDBACK MODULATION DURING MULTI-FINGER PRESSING

[1]Sohit Karol, [1]Kyung Koh, [1]Hyun Joon Kwon and [1,2]Jae Kun Shim
[1]University of Maryland, College Park, Maryland, USA
[2] Department of Mechanical Engineering, Kyung Hee University, Global Campus, Korea
Email:skarol@umd.edu, web: www.sph.umd.edu/KNES/faculty/jkshim/neuromechanics

INTRODUCTION

The human hand is an excellent example of an effector capable of producing wide range of forces to conduct day to day manipulation tasks like pressing, grasping and rotating objects (Johansson and Flanagan 2009). Studies on sedentary subjects measuring isokinetic torque production at the knee joints, as well as the quadriceps and hamstrings have shown a significant increase in the torque production capacity with the presence of online visual feedback (Larivière, Gagnon et al. 2009). Despite a number of studies investigating the role of visual feedback in sub maximal finger force production tasks and reports on increased isokinetic torque production in the presence of visual feedback, it is not known how the real time visual feedback affects the isometric MVF production by the fingers during isometric pressing. The purpose of the present study is to investigate the effect of visual feedback and its modulation on MVF during a multi-finger pressing task in four conditions: baseline condition (BC), hard condition (HC), neutral condition (NC) and easy condition (EC).

METHODS

Ten healthy male volunteers (age: 21.3±2.3 years, body mass: 72.3±3.9 kg, height: 1.7±0.4 m), without any history of neurological disorders participated in the study. For measuring the MVF, a customized device that has been used in previous experiments on multi-finger pressing by our group was used (Karol, Kim et al. 2011). For the BC, subjects performed five conditions of the MVF task in flexion with individual fingers as well as all the four fingers pressing together. During each trial, all fingers were inserted in the thimbles, and subjects were asked to produce maximum isometric force with a task finger(s) in flexion over a 7s interval.

Following the determination of MVF in BC, subjects were presented with different visual feedback conditions in a randomized order. Three levels of visual feedback were presented to the subjects. In the NC, the baseline force, shown as a yellow horizontal bar on the screen represented the true value of the corresponding task-finger MVF produced in the BC. The real-time task-finger force produced by the subjects was shown with a red horizontal bar, which moved in the downward direction towards the yellow bar when the subjects applied force on the sensors. In the HC, the visual scale was modulated such that subjects had to produce 140% of the MVF recorded in the BC, in order to reach the yellow bar representing the baseline force. In the EC, the subjects had to produce 60% of the MVF in the BC in order to reach the yellow bar. In all the experimental conditions, an auditory cue was given to the subjects, marking the beginning and ending of the trial. The changes in MVF under different visual feedback conditions were statistically analyzed using repeated measures ANOVA. The within subject factor was the feedback condition (4 levels: BC, NC, HC and EC). The level of significance was set at 0.05 for all the comparisons.

RESULTS AND DISCUSSION

The MVF for individual fingers as well as all the four fingers pressing together, during BC, NC, HC and EC have been presented in Table 1. Amongst the individual finger pressing tasks, the MVF values increased significantly for the middle and little fingers with the presence of visual feedback. The results were supported by ANOVA ($F_{1,9}$ = 56.5, P<.05; $F_{1,9}$ = 6.3; p<.05). MVF values were also significantly greater with the presence of visual feedback for all the four fingers pressing together. The results were supported by ANOVA

($F_{3,9} = 15.3$; $p<.05$). Within the three visual feedback conditions, the HC produced significantly higher forces in the four fingers pressing task compared to NC and EC (Fig. 2). The results were supported by ANOVA ($F_{2,9} = 5.5$; $p<.05$; $F_{3,9} = 20.26$; $p<.01$).

Since it is safe to assume that the experimental design of the present study did not alter the biomechanical factors, increase in MVF with the presence of visual feedback could be attributed to the changes in motor commands emanating from the CNS. Studies on sub-maximal isometric force production have shown that in the absence of tactile feedback, visual feedback plays an important role in producing accurate forces (Hong, Brown et al. 2008). However, it is not yet clear if the compensatory mechanism involving visual feedback during sub-maximal tasks and maximal force production tasks is the same. Previous studies on maximum torque production in isokinetic tasks have reported a significantly improved performance when subjects are verbally motivated or psychologically aroused (Coombes, Tandonnet et al. 2009). Since MVF production is primarily thought to be controlled in a feed forward manner, it is possible that the increase in MVF with visual feedback and by scaling the visual feedback are mediated by such psychological factors. As an example, presenting the visual target of the baseline MVF could have motivated subjects to reach, or potentially surpass that target. Regardless of the mechanism, results from this study suggest that the CNS has the capacity to significantly increase the magnitude of motor commands. In addition, making the task easier as well as harder could further increase the magnitude of motor commands as long as the subjects are not aware of those changes. Changes in MVF could also be attributed to the changes in perceived finger force production, although factor was not evaluated in this study and needs to be investigated further (Jones 1986; Li 2006).

REFERENCES

1. Johansson R, et al. *Nat Rev Neurosci* **10**:345-359, 2009.
2. Larivière C, et al. *J Biomech* **42**:1498-1505.
3. Karol S, et al. *Exp Br Res* **208**: 359-367.
4. Hong S, et al. *Percept Psychophys* **70**: 306-313.
5. Coombes S, et al. *Neurosci Lett* **396**: 192-196.
6. Jones LA, Psychol Bull **100**:29-42.

Table 1. Maximum Voluntary Force (MVF) production by index, middle, ring, little and all the fingers in different experimental conditions.

	Maximum Voluntary Force (N)			
	BC	HC	NC	EC
Index	45±4	55±5	51±5	52±5
Middle	43±5	52±5	51±5	53±4
Ring	34±7	36±3	34±4	33±5
Little	29±3	37±6	33±3	30±3
All	101±11	123±14	119±12	116±10

THE EFFECT OF ANESTHETIC HIP JOINT INJECTIONS ON GAIT

David J. Kennedy, Deepa Sun, Abdullah Z. Abbasi, Heather Vincent, Amanda Seay, and Bryan P. Conrad [1]

[1] University of Florida, Gainesville, FL, USA
Spine and Sports Interventional Center at Shands Rehabilitation Hospital
E-mail: bconrad@ufl.edu   Web: http://www.ortho.ufl.edu/motion-lab

INTRODUCTION

Fluoroscopically guided hip joint injections with a local anesthetic have been utilized for both diagnostic purposes in patients with suspected hip joint pain. From a diagnostic standpoint the injection of a local anesthetic should result in a profound rapid onset (although short term) decrease in pain if the injection site is indeed the primary pain generator. However diagnostic injections have been shown to have a significant placebo response when measuring pain scores only. We therefore proposed to study the immediate effects of fluoroscopically guided local anesthetic injections of suspected painful hip joints on gait kinematics. Our hypothesis is that immediately following an injection of local anesthetic, gait function will be improved, with patients walking faster, with longer steps, and larger base of support in those patients that have a positive decrease in self-reported pain scores.

METHODS

The study consisted of eighteen patients who received a hip joint injection with a local anesthetic for suspected intra-articular hip pathology. Before receiving the injection, each subject completed gait analysis using an instrumented walkway (GaitRite®; CIR Systems, Inc.; Havertown, PA). Immediately after the injection, gait analysis testing was repeated. Three trials of each subject walking at a self-selected pace were collected and averaged together for analysis. A paired t-test was used to evaluate whether differences in gait (specifically stride length, cadence, base of support and velocity) were present after the injection.

RESULTS

The average age of the patients receiving a hip joint injection was 50±13 years. Immediately following injection, patients reported a significant decrease in VAS pain scores (from 6.0 to 2.3, $p = 0.001$). Following the injection, patients walked faster ($p=0.017$) and took longer steps ($p = 0.044$), Table 1 and Figure 1. There was no change in the patients' base of support or cadence.

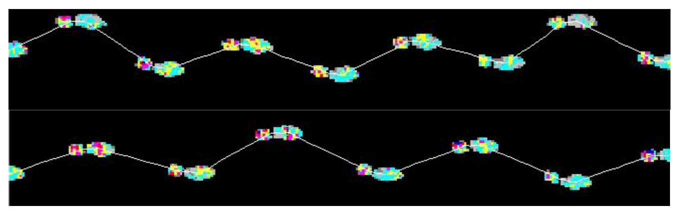

Figure 1. Gait recordings before (above) and after (below) Hip Joint injection. Velocity and stride length were significantly increased after injection

DISCUSSION

Our hypothesis, that gait would be positively affected immediately following hip joint injection was partially supported by the data. Following a hip joint injection patients immediately increased their gait velocity by 6% and increased their stride length by 3%. These results mirror the reported response for patient pain level, but at a much smaller magnitude (62% decrease in pain score). This study provides a quantitative evaluation of the diagnostic effect of anesthetic injections. This has a potential impact on improved functional movement by increasing gait speed. These results have several implications on clinical practice, such as discharged instructions and post-injection care. Questions remain regarding the durability of this effect and the short term effects of hip corticosteroid injections. The results of this study will allow clinicians to better understand the mechanism of hip joint pain. This study also provides novel information regarding the functional abilities of patients immediately after they receive an anesthetic injection.

ACKNOWLEDGMENTS

We appreciate the assistance of the Spine and Sports Intervention Center at Shands Rehab Hospital, in particular Patti O'Steen, Angie Korab, Lisa DeVault, Sharon Presley, Shelli Hines.

DISCLOSURE STATEMENT

The authors have no conflicts of interest to report.

Table 1. Summary of gait parameters before and after hip joint injection. Significant Pre/Post differences are denoted with *.

Cohort	Time	Pain	Velocity (cm/s)	Stride Length (cm)	Base of Support (cm)	Cadence (steps/min)
Hip Joint	Pre-Injection	6.0	98 ± 21	115 ± 20	12 ± 3	102 ± 10
	Post-Injection	2.3*	104 ± 25*	119 ± 20*	12 ± 3	104 ± 15

HIGHLY AUTOMATED METHODS FOR SUBJECT-SPECIFIC, POPULATION-WIDE INVESTIGATIONS OF HABITUAL CONTACT STRESS EXPOSURE IN THE KNEE

[1]Andrew M. Kern, [1]Neil A. Segal, [2]John A. Lynch, [3]Leena Sharma, and [1]Donald D. Anderson
– and the Multicenter Osteoarthritis Study Group –

[1]University of Iowa, Iowa City, IA, USA; [2]University of California–San Francisco, San Francisco, CA, USA; [3]Northwestern University, Chicago, IL, USA
e-mail: andrew-kern@uiowa.edu; web: http://poppy.obrl.uiowa.edu

INTRODUCTION

The contact stress in a joint is a critical factor in its health and maintenance. Computational methods have been developed to estimate joint contact stress,[1,2] but analyses using these methods have been limited to tens of subjects, due to inherent complexities in subject-specific modeling. Much larger numbers of subjects will need to be analyzed to achieve the statistical power necessary to clarify the role of contact stress in joint pathology.

The Multicenter Osteoarthritis Study (MOST) is a prospective observational study of older adults with frequent knee symptoms or at risk for developing symptomatic knee OA.[3] Large-scale studies such as MOST present a unique opportunity to use longitudinal imaging data to assess the relationship between contact stress and pathology. This paper describes highly automated methods developed to use data from 150 knees from the MOST cohort to predict articular contact stress (Figure 1).

METHODS

Subjects had a 1.5T knee MRI obtained at baseline using a FLASH VIBE sequence, with a 0.3x0.3x1.5 mm resolution. Bone surfaces were segmented manually on an interactive pen display using OsiriX software (OsiriX Foundation, Geneva, Switzerland), and the 3D point clouds were wrapped using Geomagic Studio software (Geomagic, Inc., Research Triangle Park, NC). The Geomagic software was scripted to automate this process.

MR images were acquired with the subject in a relaxed supine position. Accurate mechanical modeling requires that bone surfaces be aligned to a functional loaded apposition. Posterior-anterior fixed-flexion standing radiographs acquired using a standardized protocol were used in a 3D-to-2D registration of bone surfaces to a loaded apposition.

A feature-based 3D-to-2D alignment algorithm was written in MATLAB (The MathWorks, Natick, MA). The algorithm requires a 3D triangulated surface for each bone, as well as a 2D binary tracing of the relevant bony edges obtained from a standing radiograph. The radiographic imaging protocol was reproduced in a 3D virtual scene with the bone model initialized at the center of the film. Ray casting was used to project a bone edge silhouette of the model onto the virtual radiographic film. This silhouette was then compared to the bone edge tracing to drive an alignment optimization.

Covariance matrix adaptation evolution strategy (CMA-ES) [4], a meta-heuristic global optimizer that requires few parameters to be selected *a priori*, was utilized to iteratively manipulate bone models through the 3D space to achieve this alignment.

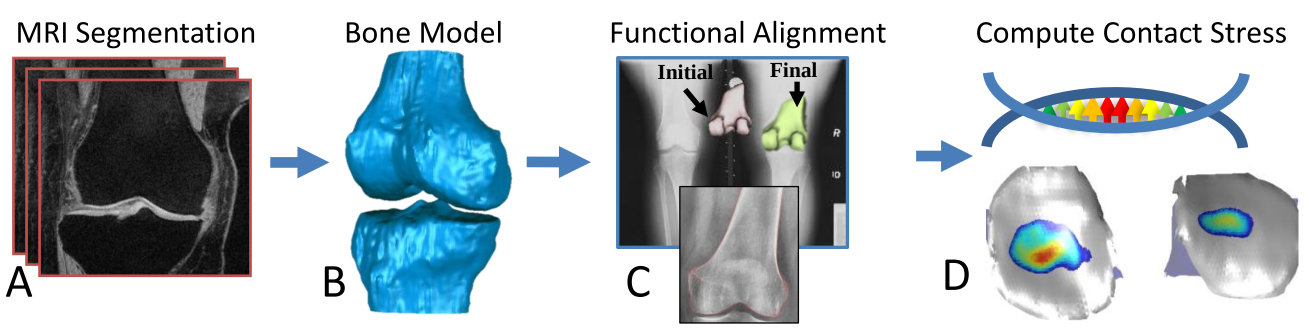

Figure 1. Methodology for subject-specific, population-wide investigations of habitual contact stress exposure in the knee. MR images are segmented to produce bone model (a-b), which are aligned to a standing radiograph using a ray casting algorithm (c). Contact stress is computed using discrete element analysis (d).

Cartilage and subchondral bone surfaces obtained previously using validated manual segmentation methods [5] were also available in the MOST data. Segmentations of the cartilage surface and of the bone/cartilage interface were wrapped as 3D triangulated models using Geomagic Studio, and registered to the functional loaded apposition.

Cartilage thickness maps were generated and stored for use in the contact stress analysis. Contact stress was evaluated using a discrete element analysis (DEA) algorithm written in MATLAB.[1] Femoral and tibial cartilage layers were treated as beds of independent elastic springs anchored to an underlying rigid bone surface. Contact stress was computed from the apparent penetration of the articular surfaces.

RESULTS AND DISCUSSION

The methods described proved a highly efficient means for obtaining contact stress estimates in the knees studied. Manual tracing of the bone surfaces accounted for the majority of time expenditure, at ~2 hours of user time per knee. Automated knee segmentation methods (e.g., [6]) are fast becoming available, and they will allow for large reductions in the user time required to complete this task.

Alignments were completed in approximately 4 minutes per bone, involving over 8,000 cost function evaluations. Initial alignment optimization failed approximately 20% of the time, resulting in a poor alignment. This was easily identified by either examination of objective function cost or visual examination. All alignments with errant solutions were re-run. Solutions which would not optimize acceptably (appropriate cost function value) with repeated trials were flagged for re-tracing of the 2D radiograph. As expected, alignment had the highest variability orthogonal to the film direction. This variability can be mitigated by using an average of multiple trials, or using *a priori* knowledge of joint anatomy to control alignment along this direction. Future studies using simultaneous bi-planar imaging techniques would greatly reduce this issue.

Contact stress computations were completed in ~3 minutes per knee and produced reasonable contact stress distributions (Figure 2). Peak computed contact stress across all 150 knees was 4.8±3.1 MPa and mean contact stress was 1.8±0.87 MPa.

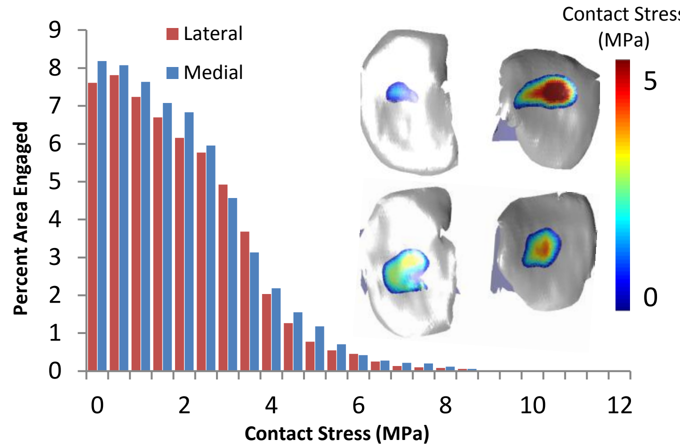

Figure 2. An area engagement histogram is shown, averaged across all 150 knees analyzed. The distribution is further broken down by compartment (medial vs. lateral). Two representative contact stress distributions are also shown.

Due to the extensive use of automation in model creation, alignment, and contact stress computation, procedures for verifying the quality of individual results need to be established. For the purposes of this study, results for each step were examined visually in the case of model creation and contact stress, or by a more objective measure (objective function cost) for alignment. Future methods need to be developed to specifically flag poor solutions and return them to the investigator.

CONCLUSIONS

The described methods provide a practical framework for utilizing information from large epidemiological studies to compute contact stress exposures. The methods were demonstrated using 150 subjects from the MOST study. Future addition of automated segmentation and quality control methods will significantly decrease investigator time investment and further improve results.

ACKNOWLEDGEMENTS

Funded by grants from NIH/NIAMS (AR48939 and AR55533) and NIH/NIA (AG18832, AG18820, AG18947, and AG19069).

REFERENCES

1. Anderson DD et al. *J Appl Biomech* **26**:215-23, 2010.
2. Bei Y, Fregly BJ. *Med Eng Phys*. **26**:777-89, 2004.
3. http://most.ucsf.edu/
4. Hansen et al. *IEEE Int'l. Conf. on Genetic Algorithms*, 1996
5. Eckstein F, Wirth W. *Arthritis* 2011, Article ID 475684.
6. Yin Y et al. *IEEE Trans Med Imaging* **29**:2023-37, 2010

3D-TO-2D REGISTRATION FOR THE EOS BIPLANAR RADIOGRAPHIC IMAGING SYSTEM

Andrew M. Kern, Lu Kang, Thomas E. Baer, Neil A. Segal, Donald D. Anderson
University of Iowa, Iowa City, IA, USA
e-mail: andrew-kern@uiowa.edu; web: http://poppy.obrl.uiowa.edu

INTRODUCTION

Accurate alignment of 3D bone models to a functional weight-bearing apposition is a critical step in studying in vivo joint alignment, kinematics, and contact stress.[1] This is because conventional MRI and CT imaging techniques require a subject to be imaged in a relaxed, unloaded pose. A secondary fluoroscopic or radiographic image of the subject has typically been used to conduct the alignment of a segmented 3D bone model to a 2D-imaged pose of the functionally loaded joint. Single-view registration approaches have reduced accuracy in the plane normal to the image detector, and bi-planar techniques often rely upon purpose-built devices limited to the research realm.

The EOS clinical imaging system (EOS Imaging, Paris, France) uses two orthogonal vertically scanning fan beam sources capable of providing simultaneous bi-planar imaging of a subject's entire body in a standing position. The EOS presents a unique opportunity to obtain a weight-bearing skeletal snapshot in clinical settings. A 3D-to-2D alignment methodology has been developed for use on the EOS, taking into account its unique layout and features. The performance of these methods is here reported using a phantom radio-opaque device imaged at a known position. And, several knees have been studied.

METHODS

A 3D-to-2D alignment algorithm was written in MATLAB (The MathWorks, Natick, MA) using a feature-based alignment approach. The algorithm requires a bone model segmented from a 3D imaging modality (CT or MRI), and a binary segmentation of internal and external bone edge features for each EOS view. A semi-automated segmentation algorithm was used to generate a binary tracing of internal and external edge features of the desired bone on the EOS images.

A 3D virtual scene replicating the EOS system was created, with the bone model placed at the center of

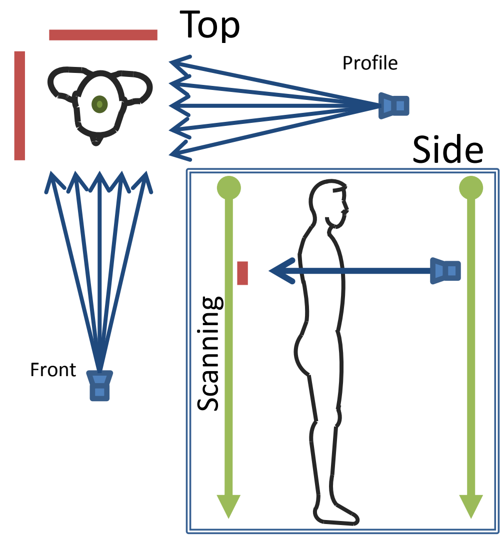

Figure 1. Top and side views of EOS imaging scene. X-rays are collimated to a fan beam when viewed from the top and to a flat beam when viewed from the side. The detector is a single row of pixels arranged horizontally, which scans in the vertical direction. Output images are from two detectors (red) located at the isocenter (green circle) of the system

the virtual scene. (Fig. 1) A ray casting algorithm was used to detect silhouette edges of the bone model and project them onto the virtual EOS detector. This edge projection is compared to the binary edge tracing obtained from the EOS image and provides a basis for comparison between the virtual alignment of the 3D model and the alignment of the subject during scan acquisition.[2] For each iterated pose of the bone, the ray casting operation reports a goodness-of-fit value for the coronal and sagittal views, which are combined to form a single objective function for optimization.

Covariance matrix adaptation evolution strategy (CMA-ES) [3], a meta-heuristic global optimizer that requires few parameters to be selected *a priori*, was utilized to iteratively manipulate bone models through the 3D space to achieve this alignment.

Evaluation of the registration system performance was done first using a phantom device constructed of five steel cylinders positioned diagonally across a square acrylic mounting board, at 2 inch offsets. The device was centered in the EOS workspace and scanned. Alignments were performed using this

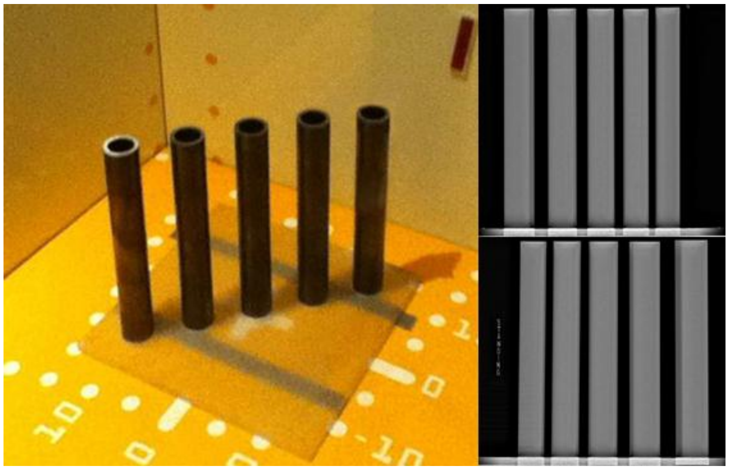

Figure 2: Placement of "phantom" device within EOS system. Resulting EOS images can be viewed in the front (top right) and profile (bottom right) views.

scan and 3D CAD models of the phantom device. The alignment values served as a basis for comparison between the known position of the device in the scanner and the aligned position of the virtual device.

A secondary evaluation was performed on two human knees in which an MRI scan was completed and segmented manually to generate a 3D bone model. Each knee was placed roughly over the isocenter (point in space in which the central beam of the sources intersect) of the EOS system and imaged. The 3D bone models were then aligned to these scans repeatedly to obtain baseline variability information between multiple alignments.

RESULTS AND DISCUSSION

The alignment performed on the metal calibration cylinders took ~10 minutes per cylinder and was performed in an entirely automated fashion. There was a slight offset (-1.2 and 0.93mm) in the initial placement of the validation device when compared

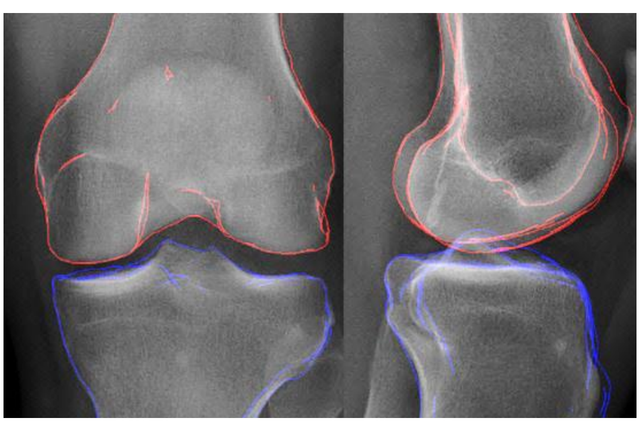

Figure 3: Optimized alignment of femur model to EOS scan. Edge silhouette of femur (red) and tibia (blue) model can be seen to match the image well.

to the isocenter of the EOS workspace. This was computed by measuring the distance of the central tube from isocenter of the image following alignment. The offset was then uniformly applied to all other cylinders. Comparing the experimentally aligned axis to the theoretical axis of each cylinder showed an unsigned error of 0.09±0.06 mm (mean±SD), indicating excellent performance of the alignment algorithm in translation. This result is comparable to other bi-plane 3D-to-2D registration methods which typically report accuracy on the order of ±0.1 mm/degree.[1]

Alignment for the two knees required ~10 minutes each, and operated in a fully automated manner. Due to the heuristic nature of CMA-ES optimization, it was necessary to verify that it consistently converges to a global minimum. Standard deviations were computed across 10 trials for each tibia and femur. The most variable translational component was ±0.05 mm for the femur and ±0.06 mm for the tibia. Rotational variability was found to be ±0.1 degrees for the femur and ±0.12 degrees for the tibia. These results demonstrate that the optimization algorithm consistently converged upon a minimum. Visually, the alignments appeared to match the contour of the radiograph accurately in both coronal and sagittal views. (Fig 3)

CONCLUSIONS

The EOS imaging system presents an opportunity to obtain standardized simultaneous weight bearing bi-planar radiographic images of subjects in a scanner meant for clinical purposes. The alignment algorithm introduced in this paper comprises an adaptation of similar prior algorithms to the unique source and detector layout of the EOS system [2,4]. It was demonstrated that alignments comparable in accuracy to those of custom-built devices can be achieved using these methods.

ACKNOWLEDGEMENTS

Funded by grants from NIH/NIAMS (AR48939, AR55533), NIH/NIA (AG18832, AG18820, AG18947, AG19069, and AG030945) and the American Geriatrics Society.

REFERENCES

1. Fregly et al. *J. Orthop Res*. 26(9) 1173-9, 2008.
2. Mahfouz et al. *IEEE Trans Med Imaging*. 22(12) 2003.
3. Hansen et al. *IEEE Int'l. Conf. on Genetic Algorithms*, 1996
4. Markelj et al. *Med Image Anal*, 2010.

EFFECTS OF KINESIO-TAPE ON PAIN AND 3-D SCAPULAR KINEMATICS INPATIENTS WITH SHOULDER IMPINGEMENET SYNDROME DURING SCAPTION: A Randomized, Double blinded, Placebo-controlled Study

Roshanak Keshavarz[1], Amir Massoud Arab[1], Hassan Shakeri[1], Farhad Tabatabai Ghomshe[2], Ahmad Raeissadat[3]

1. Department of Physiotherapy, University of Social Welfare and Rehabilitation Sciences, Tehran, Iran
2. Department of Ergonomy, University of Social Welfare and Rehabilitation Sciences, Tehran, Iran
3. Department of Rehabilitation Sciences, Medical University of Beheshti, Tehram, Iran

Introduction and aims of the study: To determine the effects of kinesio tape (KT) application on the improvement of the pain intensity and 3-D scapular kinematics immediately after taping and 1 week in patients with shoulder impingement syndrome during arm elevation and lowering in the scapular plane.

Method: 30 patients with shoulder impingement syndrome participated in this study which is randomized controlled trial and were assigned randomly to a control (N = 15, mean age = 46.53 ± 13.31) and an experimental group (N = 15, mean age = 46.6 ± 14.24(.The patients in the experimental group received a standardized therapeutic KT application. The standardized, placebo neutral taping was applied for control group. Visual analogue scale (VAS) for pain intensity and scapular movements were measured (30°, 60°, 90°, 110°) by motion analyzer at baseline and 1 week after KT application.

Results: The result of repeated measures analysis of variance (ANOVA) showed a significant change in pain intensity at movement (P = 0.009) and at night (P = 0.04) immediately after taping was significantly greater in the experimental group than in the control group. Also, a (2 x 2 x 4 x 2) ANOVA with repeated measures was used to analyze scapular kinematics changes and scapular lateral tilt had meaning effect (p=0.000) between experimental group.

Conclusions: This study provides a clinically relevant description of the KT just has main effective factor in Scapular Lateral Tilt, also an immediate improvement in the pain intensity among experimental group.

CORRELATION BETWEEN KT ARTHROMETER DATA AND ACL STRAIN SUGGESTS DIAGNOSTIC IMPORTANCE

[1]Ata M. Kiapour, [2]Carmen E. Quatman, [2]Samuel C. Wordeman, [1]Jason W. Levine, [1]Richard C. Ditto, [2,3]Mark V. Paterno, [1]Vijay K. Goel, [1]Constantine K. Demetropoulos, [2,3]Timothy E. Hewett

[1]University of Toledo, Engineering Center for Orthopaedic Excellence (ECORE) Toledo, OH
[2]The Ohio State University, Sports Health and Performance Institute, Columbus, OH,
[3]Cincinnati Children's Hospital Medical Center, Sports Medicine Biodynamics Center, Cincinnati, OH

INTRODUCTION

The CompuKT knee arthrometer is used to quantify AP tibial translation relative to the femur and demonstrates good to excellent intra-rater reliability [1,2,3]. The CompuKT is used diagnostically to generate load-displacement data to evaluate ACL integrity [2,3], and as a research tool to evaluate ACL stiffness in healthy and pathologic subjects [4]. Little data has been generated to correlate these measurements with ACL strain. The purpose of this study was to evaluate the relationships between ACL strain and CompuKT force-displacement curves.

METHODS

20 cadaveric lower limbs (46±6 yrs) were tested using a CompuKT to evaluate ACL integrity and generate load-displacement curves. In all tests, AP loads were cycled (±30 lbs) using standard protocol by a single tester. This test is conducted at 20-35° of knee flexion. As the ACL provides approximately 87% of the restraint to anterior tibial translation (ATT) at this flexion angle range [5,6,7], it is likely that the load-displacement curve is a good representation of ACL integrity. Subsequently, two parapatellar incisions were used to arthroscopically place a DVRT displacement transducer on the ACL (AM bundle), and specimens were retested. The relationship between peak ACL strain and CompuKT force-displacement data at 30 lb were evaluated using a general regression model and an ANOVA with post hoc Bonferroni correction.

Figure 1: ACL Strain versus ATT (KT Displacement)

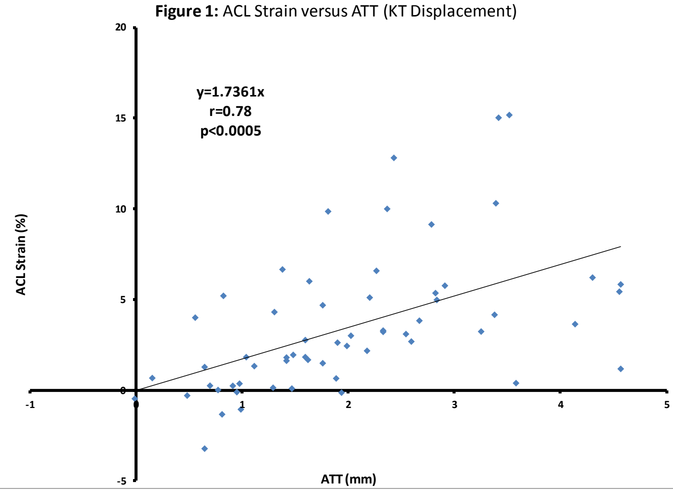

RESULTS

No significant difference in ATT was observed between testing sessions (2.8±1.4 mm prior and 3.0±1.1 mm after DVRT insertion). Peak ACL strain during knee arthrometry was 4.9±4.3%. Both ACL strain ($p=0.02$) and ATT ($p<0.0005$) were significantly related to anterior shear load. Linear regression analysis (Figure 1) with the assumption that 0 mm ATT corresponds with 0% ACL strain (y-intercept = 0) demonstrated a Pearson's correlation coefficient (r) of 0.78 ($P<0.0005$).

DISCUSSION

Anterior shear load (30 lb) during knee arthrometry is significantly related to both ACL strain and ATT. Arthroscopic DVRT insertion did not affect ATT. A significant linear relationship was demonstrated between ATT and ACL strain. This relationship indicates that the knee arthrometry is a good indicator of ACL strain at 20-35° of flexion, and therefore, has intrinsic value in the evaluation of ACL loading characteristics and the diagnosis of a functionally compromised ACL. Development of more quantifiable methods to utilize knee arthrometry data may help improve prevention strategies and ACL injury mechanism studies.

ACKNOWLEDGEMENTS

The authors would like to thank Laura Buckenmeyer for assistance with data analysis. The authors also acknowledge funding support from the National Institutes of Health Grants RO1-AR049735 and R01-AR056259.

REFERENCES:

1-Myer et al, AJSM, 2008
2-Daniel et al, JBJS, 1985
3-Myrer et al, AJSM, 1996
4-Romani et al, *J Womens Health, 2003*
5-Markolf et al, JBJS, 1976
6-Fukubayashi et al, JBJS, 1982
7-Markolf et al, JBJS, 1978

KNEE ARTICULAR CARTILAGE PRESSURE DISTRIBUTION UNDER SINGLE- AND MULTI-AXIS LOADING CONDITIONS: IMPLICATIONS FOR ACL INJURY MECHANISM

[1]Ata M. Kiapour, [2] Carmen E. Quatman, [1]Vijay K. Goel, [1]Richard C. Ditto, [2]Samuel C. Wordeman, [1]Jason W. Levine, [2,3]Timothy E. Hewett, [1]Constantine K. Demetropoulos

[1] Engineering Center for Orthopaedic Research Excellence (ECORE), Departments of Bioengineering and Orthopaedic Surgery, University of Toledo, Toledo, OH, USA
[2] Sports Health and Performance Institute, Departments of Biomedical Engineering and Orthpaedic Surgery, The Ohio State University, Columbus, OH, USA
[3] Sports Medicine Biodynamics Center, Cincinnati Children's Hospital, OH, USA
Email: Constantine.Demetropoulos@utoledo.edu Web: www.bioe.eng.utoledo.edu

INTRODUCTION

Acute anterior cruciate ligament (ACL) injury is one of the most common and devastating knee injuries, which is often associated with bony contusions of the lateral tibial plateau [1]. Previous studies have shown that abduction and internal rotation moments are critical factors in the mechanism of ACL injury [2]. The purpose of this study was to determine the effects of abduction and internal rotation moments on the pressure distribution of the tibiofemoral lateral compartment under single- and multi-axis loading conditions. We hypothesized that there is a relationship between intra-articular pressure distribution patterns and the mechanism of loading the ACL under injurious conditions. This relationship may enhance our knowledge of ACL injury mechanisms. Such insight could improve current prevention strategies designed to reduce the risk of ACL injury and damage to secondary structures acting to decrease associated posttraumatic knee osteoarthritis.

METHODS

16 fresh frozen cadaveric lower limbs (45±7 years, 8 females and 8 males) were sectioned at the mid-shaft of the femur and potted in polyester resin. The quadriceps (rectus femoris) and hamstrings (semitendinosus, biceps femoris and semimembranosus) tendons were isolated and sutured inside metal tendon grips for the application of simulated muscle forces. Specimens were tested using a custom designed passive six-degree of freedom Force Couple Testing System (FCTS). This system utilizes servo-electric actuators to drive a cable–pulley system that generates an unconstrained pure moment from full extension through 90˚ of flexion. A K-Scan sensor (Tekscan Inc, Boston, MA) was used to map tibiofemoral articular pressure distribution. This system allows for the bicondylar tracking of pressure distribution with high resolution (0.1 MPa and 0.1 mm).

Prior to use, each sensor was laminated, then equilibrated and calibrated based on manufacturer recommendations. With the anterior horn of the medial and lateral meniscus dissected from the tibial plateau, the sensor was arthroscopically placed into the medial and lateral compartments below the menisci. Care was taken to avoid crinkling of the sensors, while sensors were sutured to the knee capsule to avoid relative translations.

An external fixation frame was attached to the tibia such that the centers of the pulleys were located about the knee center of rotation. External loads were applied to specimens using a combination of static weights and cable-pulley systems through the external fixation frame.

Simulated muscle forces (400 N quadriceps and 200 N hamstrings) were used as a baseline. The following loading conditions were applied to each specimen in addition to the baseline, while the specimens were cycled from 0˚ to 90˚ of flexion:

5, 10 and 15 Nm of pure abduction, 5, 10 and 15 Nm of pure internal rotation, 15 Nm abduction + 5 Nm internal rotation and 15 Nm abduction + 10 Nm internal rotation.

Data were analyzed using Analysis of Variance (ANOVA) with a post-hoc Bonferroni Correction for multiple comparisons and general linear model (GLM) to investigate the effects of each loading parameters on articular pressure distribution. Differences were considered statistically significant for $p<0.05$.

RESULTS AND DISCUSSION

Increased abduction and internal rotation produced higher intra-articular peak pressure (Figure 1). While higher internal rotation moved the location of the center of pressure (COP) in the anterior-posterior (A-P) direction (Figure 2), no significant medial-lateral (M-L) translation of the COP was observed under simulated loading conditions (Figure 3). At 25˚ of flexion, 15 Nm of Abduction significantly increased intra-articular peak pressure in the lateral compartment from 6.0±3.5 MPa to 9.1±2.6 MPa (P<0.0005), while the COP was not affected. 15 Nm of internal rotation increased intra-articular peak pressure in the lateral compartment to 6.5±3.2 MPa and moved the COP by 1.6±0.7 mm posteriorly. Combined 15 Nm abduction and 10 Nm internal rotation generated the highest intra-articular peak pressure (9.7±1.8 MPa, P=0.002).

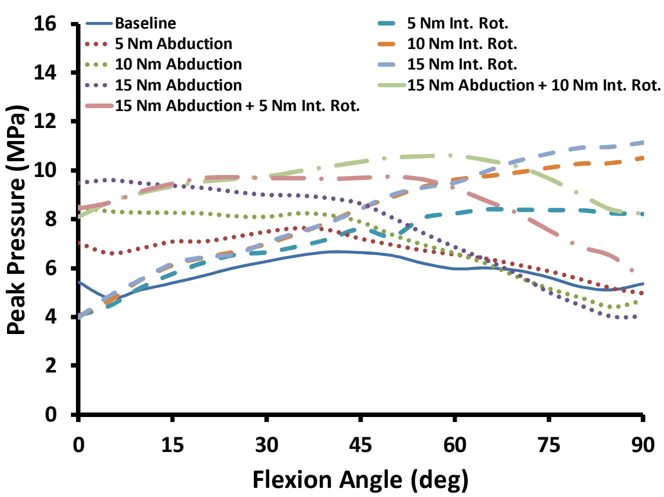

Figure 1: Average lateral peak pressure (MPa).

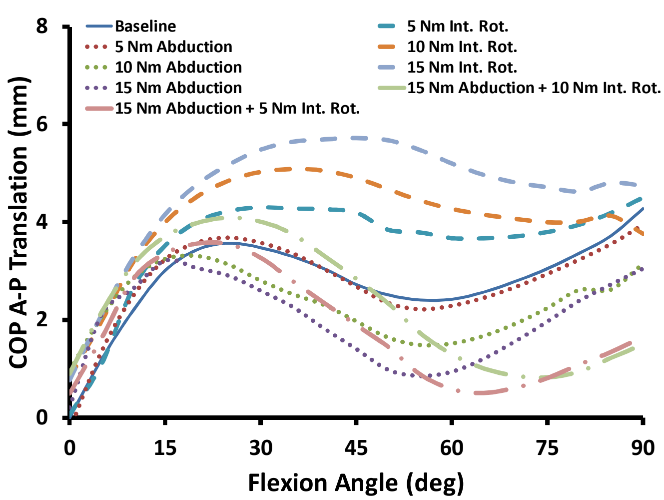

Figure 2: Average lateral COP A-P translation (mm) Posterior (+), Anterior (-).

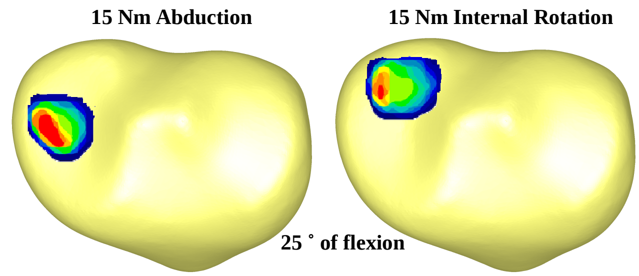

Figure 3: Lateral tibial plateau pressure distribution.

The GLM demonstrated that internal rotation significantly affects A-P translation of COP in the lateral compartment (p=0.03). Further, abduction moment significantly increase intra-articular peak pressure across the knee lateral compartment (p<0.0005). The combination of abduction and internal rotation moments increased the intra-articular peak pressure, while translating the COP posteriorly. However this amount of COP translation was not substantial, which could be due to low magnitudes of applied axial rotation moments. Further, data suggested that the lateral COP will move to its most posterior location between 15-30˚ of knee flexion and coming back toward the initial position an again translating posteriorly in deep flexion under all modes of loading except pure internal rotation. No substantial A-P translation of the COP was observed after the first peak posterior translation under pure internal rotation. This peak posterior translation of the COP at low knee flexion angles can be an indication of the 'screw-home' mechanism.

CONCLUSIONS

To the author's knowledge, this is the first time that knee intra-articular pressure distribution has been investigated under single- and multi-axis loading conditions over a range of flexion. Relatively low magnitudes of external loads were used in this study to avoid structural damage to both soft and boney tissues. Our findings support our hypothesis that there is a relationship between intra-articular pressure distribution patterns and knee loading mechanisms in a way that abduction will cause high pressure concentration in the mid-lateral tibial plateau while internal rotation will cause high pressure across the postereolateral tibial plateau.

REFERENCES

1.Spindler KP, et al. *AJSM* **21**,551-557, 1993.
2.Kiapour AM, et al. *ORS Annual Meeting*, 2012.

ACKNOWLEDGEMENTS

This study was funded by National Institutes of Health (R01 AR056259 and R01 AR049375).

CONTACT STRESS ANALYSIS OF THE RADIAL HEAD AND RADIAL HEAD IMPLANTS

[1]Sunghwan Kim, and [1,2]Mark Carl Miller

[1]University of Pittsburgh, Pittsburgh, PA, USA
[2]Allegheny General Hospital, Pittsburgh, PA USA
email: mcmiller@wpahs.org

INTRODUCTION

Radial head fractures are the most common fractures occurring in about 30% of the fractures involving the elbow joints [1, 2]. While fractures of the radial head and neck are usually the result of a fall on the outstretched arm [3], the radial head can also be fractured by the direct impact or high energy trauma. Radial head replacement is conducted when the radial head is comminuted associated with a joint dislocation or instability and ORIF (Open Reduction and Internal Fixation) is not advisable [4]. There are basically two choices for radial head implants: monoblock and bipolar. The purpose of this study is to compare these two different types of implants with the native radial head by investigating contact stresses and areas using Finite Element (FE) Analysis.

METHODS

A 3-D FE model was constructed from computed tomography of a cadaveric elbow using Mimics medical imaging software (Materialise, Leuven, Belgium) and Geomagic studio (Geomagic inc., Triangle Park, NC). The elbow was modeled in neutral supination/pronation and flexed at 90°. Two FE implant models were created by replacing the native radial head with radial head implants: one with monoblock implant (Avanta) and the other with bipolar implant (KMI). The geometry of each implant was obtained using an optical comparator and a coordinate measuring machine, and then drawn in SolidWorks (SolidWorks Corp, Concord, MA). The FE models included cartilage, the annular ligament and the radial collateral ligament. Cartilage was assumed to have a uniform thickness of 0.8 mm. Three stiff spring elements were used to model the ligaments. Cartilage, ligament and implants were modeled as isotropic materials whereas bone was modeled as transversely isotropic. The native elbow FE mesh is shown in Figure 1. Material properties of bone, cartilage, ligament, and implant are listed in Table 1. The proximal end of the humerus and distal end of ulna were constrained in all directions. All the nodes on the distal surface for the native radius and monoblock implant were coupled in the loading direction so that the surface did not rotate and remained perpendicular to the loading direction at all times. For the bipolar implant, only the center node on the distal surface was fixed in medial-lateral and anterior-posterior directions so that the implant was free to rotate medial-laterally and anterior-posteriorly. Axial loads of 100, 200, and 300N were applied on the distal surface of the radial head or implant. The finite element package, ANSYS (ANSYS Inc., Canosburg, PA), was used for the calculations of contact stresses in the contact region. Contact areas were calculated from the ANSYS results using MATLAB.

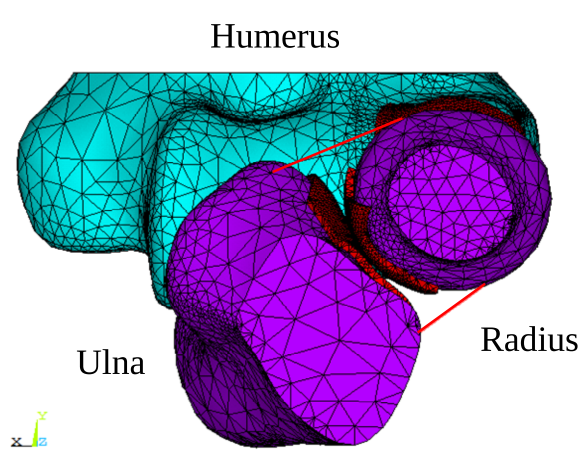

Figure 1: FE mesh of the native elbow joint.

RESULTS AND DISCUSSION

The maximum contact stresses and contact areas are shown in Figures 2 and 3 respectively. A linear relationship was found in both the maximum contact stress and contact area with the applied load. Compared to the native radial head, the maximum contact stresses for both implants were at least twice as large. The maximum contact stresses for both implants reached 20MPa under the applied load of 300N. Between monoblock and bipolar implants, the maximum contact stresses and the computed contact areas were very similar. There was approximately 50% reduction of the contact areas for implants compared to the native radial head, which concurs with the findings with Vitor et al. [5]. Vitor measured contact areas of the native radial head and implant using dental impression material under 100N of applied load and found there was an average of 68% reduction in contact joint area with implant relative to the native radial head.

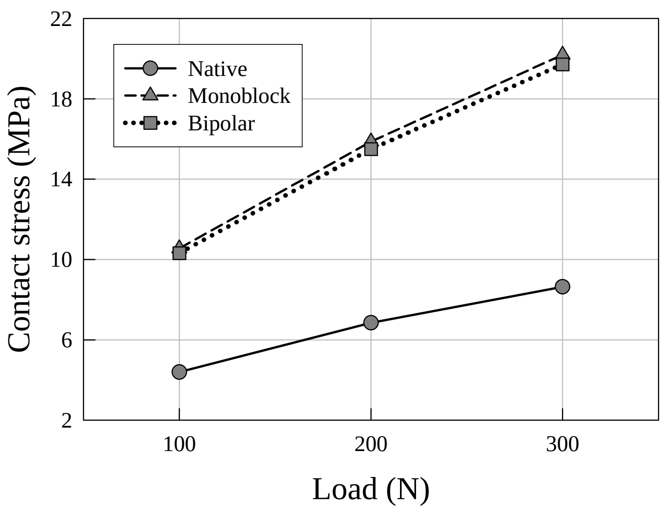

Figure 2: Maximum contact stress comparison.

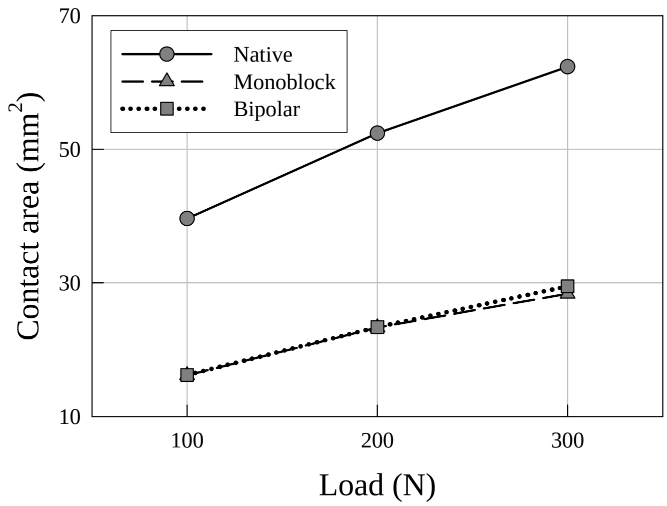

Figure 3: Contact area comparison.

CONCLUSIONS

In this study, finite element models for the native elbow and radial head replaced elbows with two different types of implants were created. The maximum contact stresses and contact areas were compared. A significant reduction in contact areas and increase in contact stresses with both implants were found. There was no difference between monoblock and bipolar implants in both the maximum contact stresses and contact areas.

REFERENCES

1. Morrey BF. *The elbow and its disorders*, Philadelphia, PA, USA, 2000.
2. Taylor TK, et al. *J Bone Joint Surg Br* **46**, 83-88, 1964.
3. Odelberg-Johnsson G. *Acta Radiologica* **3**, 45-53, 1924.
4. Ring D, et al. *J Bone Joint Surg Am* **84-A**, 1811-1815, 2002.
5. Victor SL, et al. *Clinical Biomechanics* **18**, 115-118, 2003.

Table 1: Material properties.

Part	Elastic modulus (GPa)	Poisson's ratio
Humerus	E_x=E_z=7, E_y=11.5, G_{xy}=G_{yz}=3.5, G_{zx}=2.6	0.3
Ulna, Radius	E_x=E_y=7, E_z=11.5, G_{xy}=2.6, G_{yz}=G_{zx}=3.5	0.3
Implant	220	0.3
Cartilage	0.012	0.45

TASK DIFFICULTY EXACERBATES THE AGE ASSOCIATED DIFFERENCES IN FORCE CONTROL

Changki Kim, Tanya Onushko and Evangelos Christou

University of Florida, Gainesville, FL, USA
Email: eachristou@ufl.edu, web: http://hhp.ufl.edu/npl

INTRODUCTION

Aging impairs the ability of older adults to control their motor output. This is evident during various single joint tasks (1) and during movements that require the coordination of joints within a limb (intralimb) and across limbs (interlimb). Because older adults exhibit greater brain activity than young adults during such tasks (2) it is proposed that they use greater attentional resources to accomplish the task. This is supported by literature that increases attentional demands by adding a secondary task, either a cognitive (3) or a motor task (4). Although these findings suggest that there should be an interaction between age and task difficulty, there is little direct evidence of how task difficulty can influence the age-associated differences in the control of motor output. In this study we vary task difficulty during a two-finger force coordination task by changing the relative timing between the two fingers. The purpose of this study, therefore, was to determine if the age-associated differences in motor performance exacerbate with task difficulty.

METHODS

Six young (23.8 ± 3.8 yrs) and five older adults (73 ± 11.1 yrs) were instructed to track a moving target on a monitor by controlling isometric abduction forces of the index and little fingers. A 'Lissajous Plot' which shows two finger forces as a dot in coordinates was used for visual feedback. X axis indicated index finger force and Y axis indicated little finger force. Each finger's target force range was 5-15% of its maximal voluntary contraction (MVC). Subjects performed five different tracking tasks. The level of difficulty of the finger coordination pattern was dependent on the relative timing (phase) of force generation between the index and little fingers (0°, 45°, 90°, 135°, 180° relative phase). The 0° task was expected to be the easiest task, whereas the 90° task was expected to be the hardest task (5).

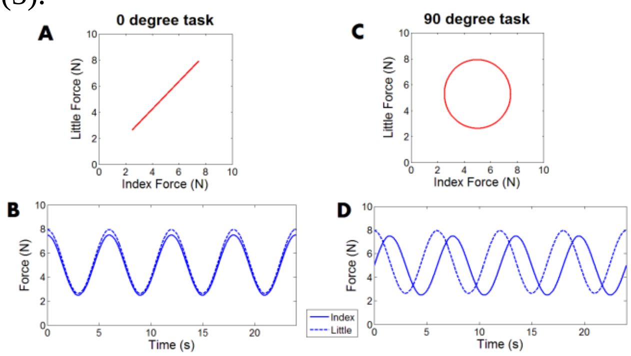

Figure 1: Example of an easy (0° relative phase) and a hard task (90° relative phase). Panels A and C show the Lissajous visual feedback for 0° and 90° respectively. Panels B and D demonstrate the required force and time for each finger.

The order of the five tasks was randomly assigned and subjects performed five trials for each task. We quantified temporal error (sum of the timing delay between the force trace and target for each finger (s)), overall error (sum of the normalized root mean square error (RMSE) of two fingers (%)), and force variability (sum of the force variance from each finger (N)).

RESULTS AND DISCUSSION

For the temporal error, there was a significant age x task interaction ($P < 0.05$), which indicated that the age-associated differences exacerbated at (90°) the most difficult task (Figure 2).

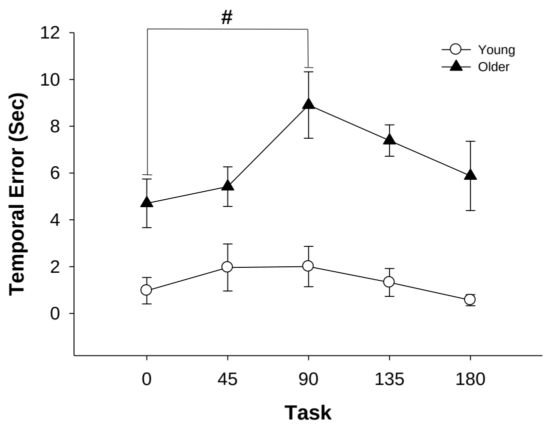

Figure 2: Older adults exhibited greater temporal error than young adults, especially at 90° task.

Older adults exhibited greater overall error compared with young adults across all tasks ($P=0.01$; 70.35 ± 3.46 vs. 144.93 ± 12.26 %). The age x task interaction was not significant. Finally, older adults exhibited greater force variability than young adults across all tasks ($P=0.009$; 0.05 ± 0.007 vs. 0.28 ± 0.04 N). There was a significant age x task interaction, which indicated that the age-associated differences were greater at the 45^{o} task compared with the other tasks.

In this study we examined age-associated differences by varying the task difficulty of a novel coordination model that incorporates forces from two fingers. Similar to previous work we demonstrate that the most difficult task to perform for our coordination model was at 90° phase and the easiest was at 0°. We provide novel evidence that the age-associated differences, at least for temporal errors, are exacerbated with task difficulty. In addition, older adults exhibit greater overall error and variability compared with young adults.

CONCLUSIONS

Aging impairs the ability to coordinate finger forces, especially during more difficult tasks. This impaired finger coordination with aging may lead to deficiencies in manual dexterity and activities of daily living.

REFERENCES

1. Carlton LG, et al. *J Appl Physiol*, Illinois, US, 2002.
2. Ward N.S. *Ageing Res. Rev.*, 5, 239–254, 2006.
3. Falkenstein M, et al. *Brain Res*, 2011 Sep 26; 1414: 66-76.
4. Shinohara M, et al. *J Appl Physiol*, In press.
5. Haken H, Kelso JA, Bunz H. *Biol Cybern*, 51(5):347-56, 1985.

ACKNOWLEDGEMENTS

This work was supported by National Institute on Aging Grant R01 AG-031769 to E.A. Christou.

Comparison of Kinematic, Kinetic, and Mechanical Work Data between Traditional and Bone Bridge Amputation Techniques During Fast Walking One Year Post Ambulation Without an Assistive Device

Trevor Kingsbury[1], Nancy Thesing[1], John David Collins[2], Joseph Carney[1], Marilynn Wyatt[1]
[1]Naval Medical Center, San Diego, CA; [2] Naval Health Research Center, San Diego, CA
E-mail: trevor.kingsbury@med.navy.mil

Introduction:
The Global War on Terrorism has produced a large number of severely injured active duty service members who at the time of injury were active and fit. Due to improvements in personal body armor and other technology, soldiers are surviving blasts, mostly from improvised explosive devices (IED's), but incurring grave extremity injuries. Many of these injuries result in limb amputation, with transtibial amputations accounting for approximately 27% of total traumatic amputations[1]. There are two principle techniques for performing a trans-tibial amputation: the Traditional technique championed by Burgess creates a long posterior myocutaneous flap and does not create a bone bridge between the distal tibia and fibula;[2] while the bone bridging osteomyoplasty championed by Ertl and modified by others, creates an osseous bridge between the tibia and fibula[3-5]. Current research fails to provide conclusive data supporting either the bone bridging amputation technique or the traditional transtibial amputation technique as functionally superior for below knee amputation[6]. We have evaluated and reported functional outcomes of patients walking at a self-selected speed, finding that subjects with a bone bridge have greater ground reaction forces in late stance, but that the length of the residual limb could play a greater role than the surgical condition[7]. The purpose of this study is to further examine the differences in functional outcomes between these two patient groups walking at fast speeds utilizing kinematic, kinetic, and mechanical work parameters during ambulation with secondary interest on the effect of residual limb length on functional outcomes.

Methods:
Following IRB approval, a retrospective review of 14 active duty military members, age 18-45, who had undergone a unilateral, transtibial amputation, was conducted. All subjects were male with an average age of 24.8 (range 20-28), height 178.2 cm (range 168-187.2), and weight 87.7 kg (range 60-113). Subjects wore their everyday walking prosthesis that was customized to their liking and walking skill. All subjects wore a carbon fiber ankle, but no effort was made to control the specific brand. All subjects were studied at least one year post ambulation without an assistive device.

Three dimensional gait analysis data were collected with a 12-camera Motion Analysis Corporation (MAC) system (Motion Analysis Corp., Santa Rosa, CA), and four AMTI (AMTI, Watertown, MA) force plates embedded in the floor. Data were collected and processed with Cortex (MAC) software at 120 Hz and low pass filtered using a fourth order Butterworth filter with a frequency of 6 Hz. Kinematic and kinetic data analyses were done using a combination of Visual3D (C-Motion Inc., Germantown, MD) and OrthoTrak (MAC) software programs, with patients walking at a fast walking pace, where the subject was instructed to walk as fast as they felt they could safely move without breaking into a jog or run. At least six full strides with three force plate strikes were processed and averaged for each leg. Parameters evaluated included velocity, cadence, step and stride length, symmetry variables, mechanical work normalized to body weight and stride length (J/kg*m), and vertical ground reaction force data: F1, the peak vertical force during initial contact, and F3, the peak vertical force in terminal stance. Due to the nonparametric nature of the data, the Wilcox W rank test was used to compare the two surgical groups.

Results:
Functional outcomes are presented in Tables 1-3, with significant differences in bold. The primary significant differences were in residual limb length, with bone bridge patients having significantly longer residual limb lengths, and increased F3 vertical ground reaction forces. A linear regression of residual limb length and F3 force showed no significant correlation.

Discussion:
This is the first study to use instrumented motion analysis techniques to evaluate for differences in functional outcomes between bone bridge and traditional trans-tibial amputation procedures. Our results indicate that there may be a clinically significant functional difference between the two surgical techniques. Originally, during self-selected walking, we found that bone bridge patients had higher F3 roll off forces, but this finding was seemingly mitigated by the fact that as residual limb length increased, irregardless of surgical condition, F3 roll off force increased. During the fast condition, no such link was found between residual limb length and roll off force. Rather, the only significant difference was seen between surgical conditions. One often proposed benefit with a bone bridge amputation is the concept that it facilitates distal socket loading. This is the first functional data that provides support to this idea. It would seem that the bridge may allow for greater

force transmittal during “push” off in terminal stance. It would be useful to explore this finding during other high level functional activities such as running and cycling. We are also enrolling additional subjects in order to increase the overall power of the study.

Disclaimer:
"The views expressed in this article are those of the authors and do not necessarily reflect the official policy or position of the Department of the Navy, Department of Defense, or the United States Government."

References:

1. Mayfield JA, Reiber GE, Maynard C, Czerniecki JM, Caps MT, Sangeorzan BJ. Trends in lower limb amputation in the Veterans Health Administration, 1989-1998. *Journal of Rehabilitation Research & Development* 2000 Jan-Feb;37(1):23-30.
2. Burgess EM, Romano RL, Zettl JH, Schrock RD,Jr. Amputations of the leg for peripheral vascular insufficiency. *Journal of Bone & Joint Surgery - American Volume* 1971 Jul;53(5):874-890.
3. Ertl J. Uber amputationsstumpfe. *Chirurg* 1949;20:218-24.
4. Deffer PA, Moll JK, LaNoue AM. The Ertl osteoplastic below-knee amputation [abstract]. *Journal of Bone & Joint Surgery - American Volume* 1971;53(1028).
5. Loon HE. Below-knee amputation surgery. *Artif Limbs* 1963;8:86-99.
6. Pinzur MS, Beck J, Himes R, Callaci J. Distal tibiofibular bone-bridging in transtibial amputation. *Journal of Bone & Joint Surgery - American Volume* 2008 Dec;90(12):2682-2687.
7. Kingsbury T, Spies A, Wyatt M. Comparison of Mechanical Work between Traditional and Ertl Amputation Techniques. *GCMAS Conference*, Bethesda, MD; April 2011.

Figure 1: Descriptive Statistics: Mean ± Standard Deviation (Minimum, Maximum)

	Traditional Group	Bone Bridge Group	Wilcoxon W	Exact Sig (2-tailed)
Height (cm)	179.77 ± 6.08 (170.20, 187.20)	176.57 ± 5.78 (168.00, 184.50)	45	0.383
Weight (kg)	90.33 ± 17.35 (60.00, 113.00)	85.07 ± 11.83 (67.00, 101.00)	48	0.62
Age (years)	24.14 ± 2.79 (20.0, 27.0)	25.43 ± 1.81 (23.0, 28.0)	47	0.535
Residual Limb Length [Radiograph] (cm)	13.70 ± 2.78 (8.00, 16.50)	17.74 ± 1.15 (16.30, 19.00)	29	**0.001**

Figure 2: Kinetic and Mechanical Work Data

		Traditional	Bone Bridge		
		Mean ± SD	**Mean ± SD**	**Wilcoxon W**	**Exact Sig (2-tailed)**
F1 (Normalized to Body Weight)	PL	1.40 ± 0.27 (0.98, 1.85)	1.34 ± 0.17 (1.09, 1.50)	49	0.645
	NPL	1.48 ± 0.14 (1.27, 1.66)	1.42 ± 0.16 (1.28, 1.67)	47	0.482
F3 (Normalized to Body Weight)	PL	0.87 ± 0.16 (.63, 1.02)	1.01 ± 0.07 (.88, 1.09)	37	**0.048**
	NPL	1.07 ± 0.15 (.77, 1.22)	1.17 ± 0.08 (1.06, 1.32)	42	0.182
Mechanical Work (J/kg*m)	PL	6.04 ± 0.43 (5.64, 6,72)	6.02 ± 0.61 (5.38, 7.29)	48	0.565
	NPL	6.03 ± 0.33 (5.71, 6.44)	5.95 ± 0.69 (5.38, 7.33)	45	0.338

Figure 3: Temporal Spatial/Kinematic Data (PL = prosthetic leg, NPL = non prosthetic leg)

	Traditional	Bone Bridge		
	Mean ± SD (Min, Max)	**Mean ± SD (Min, Max)**	**Wilcoxon W**	**Exact Sig (2-tailed)**
Velocity (cm/s)	191.03 ± 16.39 (169.00, 215.00)	190.74 ± 21.42 (154.00, 213.00)	52	1
Cadence (steps/min)	131.57 ± 12.24 (115.85, 152.00)	131.28 ± 12.86 (111.00, 147.97)	52	1
Stride Length (cm)	174.85 ± 16.12 (153.00, 195.40)	174.03 ± 8.05 (166.00, 185.00)	52	1
Step Width (cm)	13.84 ± 2.47 (10.57, 18.50)	14.24 ± 3.08 (10.90, 20.50)	50	0.805
Step Length [PL] (cm)	89.07 ± 10.63 (75.00, 103.10)	90.50 ± 5.41 (84.00, 98.00)	50	0.805
Step Length [NPL] (cm)	85.34 ± 7.84 (71.00, 92.49)	83.75 ± 3.55 (80.28, 91.00)	47	0.535
Single Support [PL] (% Gait Cycle)	37.45 ± 1.77 (35.00, 39.93)	37.21 ± 0.80 (36.00, 38.45)	50.5	0.805
Single Support [NPL] (% Gait Cycle)	39.55 ± 1.62 (37.00, 42.00)	39.37 ± 1.42 (37.00, 41.00)	50.5	0.805
Stance [PL] (% Gait Cycle)	60.45 ± 1.62 (58.00, 63.00)	60.63 ± 1.42 (59.00, 63.00)	50.5	0.805
Stance [NPL] (% Gait Cycle)	62.70 ± 1.76 (60.07, 65.00)	62.79 ± 0.80 (61.55, 64.00)	52	1

CONTROL OF THE CAT PAW TRAJECTORY DURING WALKING ON A FLAT SURFACE AND HORIZONTAL LADDER

[1]Alexander N. Klishko, [1]Bradley J. Farrell, [2]Irina N. Beloozerova, [3]Mark L. Latash, [1]Boris I. Prilutsky

[1]School of Applied Physiology, Georgia Institute of Technology, Atlanta, GA, USA
[2] Barrow Neurological Institute, Phoenix, AZ, USA
[3]Department of Kinesiology, Penn State University, State College, PA, USA
email: aklishko3@gatech.edu, web: http://www.ap.gatech.edu/Prilutsky/BiomechanicsMotorControl.php

INTRODUCTION

In a recent study of simple walking and skilled precise stepping in the cat [1] it has been shown that during swing the fore- and hind-paws have highly stereotyped, bell shaped horizontal velocity profile. This finding suggests that paw trajectory may be actively regulated and stabilized by the motor control system. The extent to which a specific movement variable is controlled in a redundant musculoskeletal system can be determined using analysis within the uncontrolled manifold (UCM) hypothesis [2, 3]. We tested the following hypotheses: (1) Paw trajectory during the swing phase of walking is stabilized by co-varied changes in joint angles, (2a) the quantitative index of paw trajectory stabilization depends on the type of locomotor behavior (simple walking vs. precise stepping) and (2b) the paw trajectory stabilization is different for fore- and hindlimbs.

METHODS

The UCM hypothesis suggests that the motor control system, acting in a space of generalized coordinates of the musculo-skeletal system (elemental variables, e.g. limb joint angles and Cartesian coordinates of the most proximal limb joint), limits most variance of elemental variables across repeated cycles to a sub-space (UCM) corresponding to desired values of a performance variable (e.g., paw trajectory) [2,3]. This is achieved by co-varying elemental variables such that variance of the performance variable is minimal. By comparing the relative amounts of variance within the UCM and within the sub-space orthogonal to UCM (ORT, variance that affects performance), one can estimate the extent to which the paw trajectory is stabilized: $IMA = (\sigma^2_{\parallel} - \sigma^2_{\perp}) / \sigma^2$, where *IMA* is an index of motor abundance [3], $\sigma^2_{\parallel}$ is UCM variance, $\sigma^2_{\perp}$ is ORT variance, and σ^2 is total variance, each normalized to the number of degrees of freedom in the corresponding space. *IMA* above zero indicates that the paw trajectory is stabilized by co-varying the limb elemental variables.

Three adult cats were trained to walk along a horizontal walkway on the flat surface (simple walking) and on a horizontal ladder (with 5-cm wide rungs) using food reward. High-speed motion capture system (Vicon, UK) was used to record 3D positions of reflective markers on the fore- and hindlimbs. Low-pass filtered marker coordinates were used to compute elemental variables of limb movements for multiple walking cycles of each cat. In selected trials, a high speed step motor moved a rung (MR) by 5 cm either away or toward the walking cat 1 or 2 strides before the animal stepped on the MR. The UCM variance $\sigma^2_{\parallel}$ at each normalized time slice was computed as the total variance projection to the null-space of the Jacobian matrix, which related performance variables to elemental variables. The ORT variance was calculated as $\sigma^2_{\perp} = \sigma^2 - \sigma^2_{\parallel}$. Examples of patterns of the UCM and ORT variances and *IMA* for the forelimb of one cat walking on the ladder are shown in Fig. 1.

RESULTS AND DISCUSSION

We found the following (Figs. 2-3): (1) The *IMA* during both locomotor tasks was above zero during initial and late swing. (2) In mid-swing of both tasks the *IMA* typically had low positive values, or was

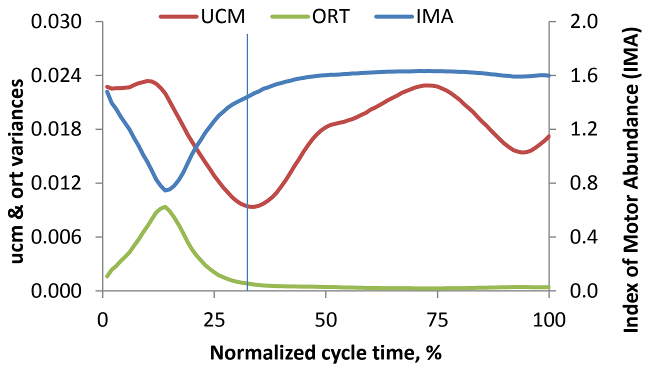

Figure 1: Representative patterns of normalized UCM and ORT variance, and *IMA*. Vertical line separates swing from stance.

close to zero or negative. (3) The IMA for the hindlimbs during mid-swing of ladder walking had negative values of larger absolute magnitude than during level walking. (4) The IMA for the forelimbs was higher, i.e., the forelimb paw trajectory was more stabilized than that of the hindlimbs during the swing phase.

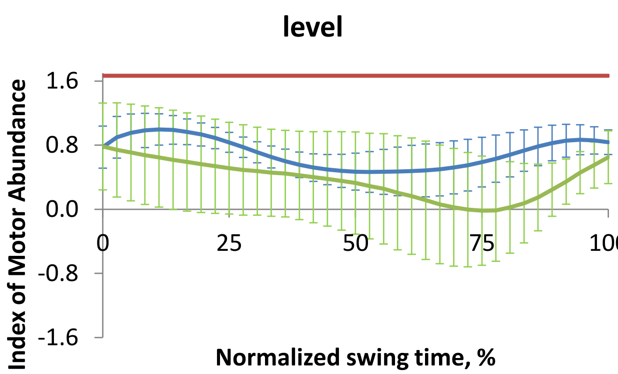

Figure 2: IMA during swing for the forelimb (blue) and hindlimb (green) during simple walking. Red horizontal line is the maximum value of *IMA*.

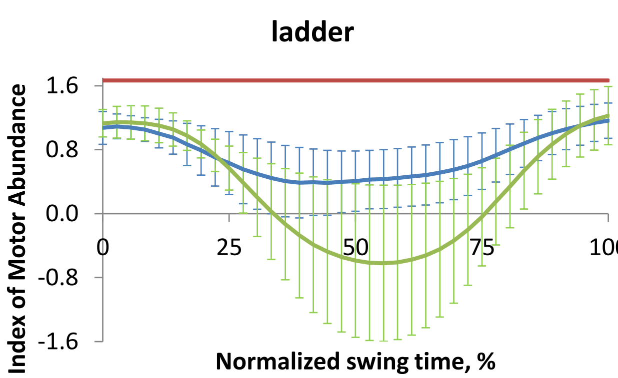

Figure 3: IMA during swing for the forelimb (blue) and hindlimb (green) during ladder walking.

Walking on a ladder (Fig. 4, green) was associated with more paw stabilization than simple walking (Fig. 4, black), and paw stabilization increased further when the cat could see the MR moving while it was preparing to step on the MR (Fig. 4, orange).

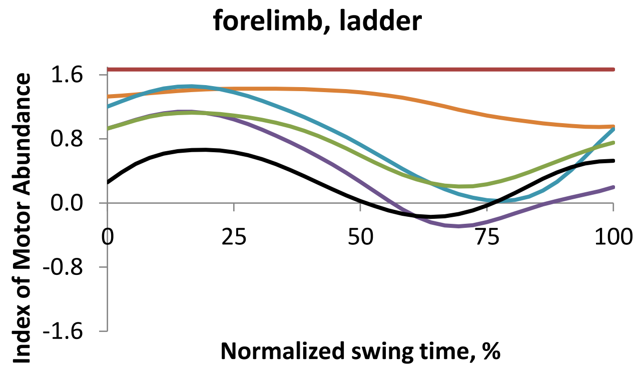

Figure 4: IMA during swing for the forelimb during simple (black) and ladder walking (green); blue line indicates step on the rung moved away from the cat; purple line, step on the rung moved toward the cat; and orange line, step preceding the step on the moved rung when cat was preparing to step on it. Red horizontal line is the *IMA* maximum.

CONCLUSIONS

We found high indices of stabilization of the paw trajectory at the beginning and end of the swing phase. This stabilization was higher for forelimbs than hindlimbs and was progressively higher during walking on a stationary ladder and ladder with a moving rung. Low or absent paw stabilization was found in mid-swing of all studied locomotor behaviors. The UCM analysis allows for insights into the organization of stepping at the kinematic level.

REFERENCES

1. Beloozerova et al., *J Neurophysiol* **103**, 2285-3000, 2010.
2. Scholz JP, Schoner G, *Exp Brain Res* **126**, 289-306, 1999.
3. Latash ML, *Motor Control* **11,** 276-308, 2007.

ACKNOWLEDGEMENTS

Supported by NIH grants EB012855 to BIP and NS-058659 to INB and by the Center for Human Movement Studies at Georgia Tech.

The Relationship Between Lower Extremity Joint Power during Sit to Stand and Clinical Measures of Function Among Subjects Post Hip Fracture

[1]Janet A. Kneiss, [2]Jeffrey Houck and [2]Tiffany Hilton
[1]MGH Institute of Health Professions, Boston, MA, USA
[2]Ithaca College, Rochester, NY, USA
email: jkneiss@mghihp.edu

INTRODUCTION

Individuals post hip fracture experience a loss of physical function (>50% loss of lower extremity function) and increased risks of falls despite return of functional independence[1]. Decreased lower extremity power at the hip and knee may contribute to decreased function and falls risk[2]. However, it is unknown if lower extremity power at the hip or knee is associated with clinical measures of function [3]. Decreases in whole limb kinetics (both knee and hip may occur) or joint specific decreases may be associated with functional deficits. Understanding the association between lower extremity power and measures of functional performance may facilitate targeted rehabilitation interventions that improve physical function post hip fracture. Therefore the purpose of this study was to determine the association of hip and knee kinetics during a sit to stand task with clinical measures of function.

METHODS

Twenty Nine subjects (7 male, 22 female; age=80 ± 7.3) post hip fracture and participated in this study. All subjects were community dwelling and recently discharged from home care physical therapy. Average time from their hip fracture was approximately 2.5 ± .86 months. An Optotrak Motion Analysis System (Northern Digital Inc, CAN) and Motion Monitor Software (Innsport Training Inc, USA) collected kinetic and kinematic data at a sample rate of 60 Hz and a low pass filter rate of 6 Hz. Angles were then produced and calculated from a Cardan angle Z-X-Y sequence of rotations. Hip and knee moments and powers calculated from the appropriate angles and ground reaction force (collected at 1000 Hz using Kistler force plates under each foot). Subjects were asked to perform sit to stand "as fast as possible" three times. Time to rise was calculated from seat off to upright posture. Data were averaged over the three trials and pearson product moments were used to determine the relationship between clinical measures of function (Gait Speed (GS), BBS (Berg Balance Scale), Lower Extremity Measure (LEM)) and hip/ knee power.

RESULTS AND DISCUSSION

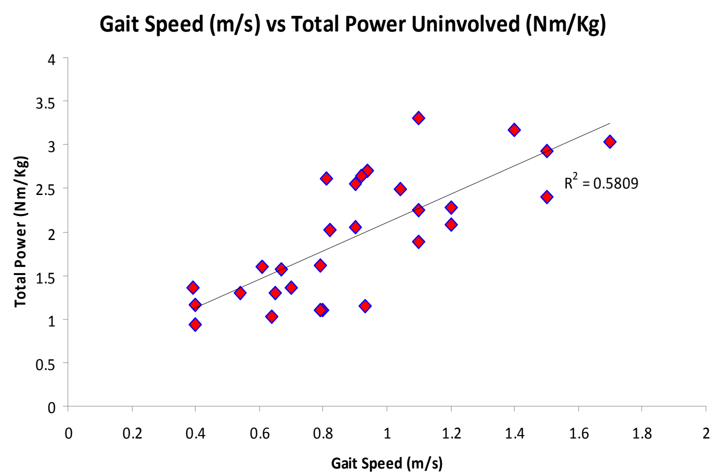

Figure 1: Correlation between Total Power (hip + knee) of the involved limb and Gait Speed.

Subjects' post hip fracture (HF), who were recently discharged from homecare physical therapy, had moderate functional deficits. Average scores for the BBS, GS and LEM (43.7±6.03, .9±.3, 81±11) were

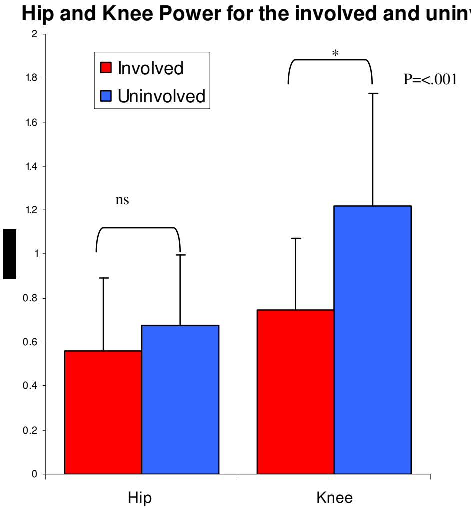

Figure 2: Hip and knee powers for the involved and uninvolved limb.

below clinical cut-points for minimal functional loss. Hip and knee power on the uninvolved limb (p=<.001; HFuninvolved 1.96±0.72 Nm/Kg HFinvolved, 1.23±0.57 Nm/Kg) was significantly higher than hip and knee power on the involved limb. Physical function is moderately correlated with higher levels of hip and knee power on the uninvolved side (table 1, figure 1). The new findings of our study show that individuals post HF achieve higher levels of physical function with higher knee power on the uninvolved limb (figure 2) rather than higher levels of hip power on the uninvolved side. Further, lower extremity power is moderately correlated with Gait Speed and Functional Performance (BBS) but not self-report function (Table 1). Together these findings suggest that improving knee power on the uninvolved side may improve physical function post hip fracture.

CONCLUSIONS

Subjects post hip fracture who have been recently discharged from home care physical therapy achieve higher levels of physical function with higher knee power of the uninvolved limb. Interventions targeted at improving knee power on the uninvolved limb may improve physical function post hip fracture.

REFERENCES

1. Magaziner, J., W. Hawkes, and J.R. Hebel, Recovery from hip fracture in eight areas of function. *J.Gerontol.A Biol.Sci.Med.Sci.*, 2000. 55: p. M498.
2. Portegijs, E., et al., Asymmetrical lower extremity power deficit as a risk factor for injurious falls in healthy older women. *Journal of the American Geriatrics Society*, 2006. 54(3): p. 551-3.
3. Puthoff ML, Nielsen DH. Relationships among impairments in lower-extremity strength and power, functional limitations and disability in older adults. *Physical Therapy*. 2007;87: p. 1334-1337.

ACKNOWLEDGEMENTS

The authors are grateful for support from NIH: NIAMS; Center for Research Translation,Grant#:1P50AR054041-02).

TABLE 1. Pearson Product Moment correlations for hip and knee power and clinical variables

	Gait Speed	Berg Balance Scale	Lower Extremity Measure
Hip Power Involved Nm/Kg	.562**	.398*	ns
Hip Power Uninvolved Nm/Kg	.468*	.421*	ns
Knee Power Involved Nm/Kg	.683**	.448*	ns
Knee Power Uninvolved Nm/Kg	.659**	.660**	ns
Total Power Involved Nm/Kg	.586**	.464*	ns
Total Power Uninvolved Nm/Kg	.774**	.671*	ns

P-values represent results of a two-tailed Pearson Product Moment. * denotes significance at a set alpha level of p<.05 ** denotes significance at a set alpha level of p<.001 Abbreviation: ns, not significant

STUDY ON ANTHROPOMETRIC MEASUREMENT ON KOREAN SKELETAL SYSTEMS BASED ON CADAVERIC CT IMAGES

[1]Cheolwoong Ko, [1]Deokyeon Cho and [1]Keyoungjin Chun

[1]Gerontechnology R&D Group, Korea Institute of Industrial Technology (KITECH), Cheonan, Korea
email: cheko@kitech.re.kr web: http://www.kitech.re.kr/

INTRODUCTION

Recently, human models developed based on measurement data of human bodies have been effectively used to study human-related biomechanical characteristics in various research fields. Several research bodies in the USA, Europe, and Japan have expressed significant interest in developing human models for their own people. Basically, as the human models developed in foreign countries show remarkable differences in physique, it is not desirable to directly utilize their model information for the construction and evaluation of Korean human models. In Korea, recently, the Digital Korean project has been initiated; however, anthropometric studies on Korean skeletal systems remain insufficient. This study developed 3D morphological skeletal models of Korean adults and the elderly close to standard Korean body sizes, and also performed anthropometrical comparison/analysis to provide basic data for the development of Korean human models.

METHODS

In this study, the CT data of 4 adult and 4 elderly cadavers were obtained (Table 1), which are close to the standard physique of Koreans (5th Measurement, 2004). The CT images (Pixel size: 0.832mm, Gap: 1 mm) were provided by KISTI (Korea Institute of Science and Technology Information, South Korea). ROI (Range of Interest) was extracted based on the CT images. 3D skeletal models were reconstructed using Mimics 13.0 (Materialise Inc., Belgium) and Hypermesh 7.0 (Altair Engineering Inc., USA) (Figure 1).

This study performed morphological analysis on Korean adults and the elderly based on reconstructed 3D models for the selected 8 major

Table 1: Information of Korean cadavers

Cadaver	Gender	Number	Age (Year)	Weight (kg)	Height (cm)
Adult	Male	4	25~34	(70~72)	172~174
Elderly	Male	4	60~69	(65~67)	164~165

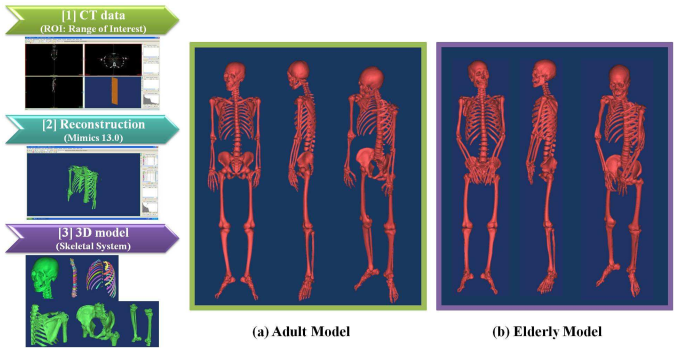

Figure 1: 3D reconstruction models of Korean adults and the elderly based on cadaveric CT images

bones (skull, humerus, radius, ulna, ilium, femur, tibia and fibula). The measurement references were cited from published literature. For the skull, the skull breadth (SkB) and height (SkH) were measured. For the humerus, the humeral length (HuL), lower width (HuLW), body minimum diameter (HuMD) and bone-marrow cavity diameter (HuCD) were measured. For the radius, the radial length (RaL), maximum head diameter (RaMHD) and body minimum diameter (RaMD) were measured. For the ulna, the ulna length (UlL), minimum circumference (UlMC) and body minimum diameter (UlMD) were measured. In the case of the ilium, this study defined the anatomical reference points (A~E) from the origin (O) of the 3D coordinate system perpendicular to the reference axis of the anterior superior iliac spine and pubic symphysis. For the femur, femoral length (FeL), proximal breadth (FePB) and midshaft transverse diameter (FeMTD) were measured. For the tibia, the tibial length (TiL), maximum head diameter

(TiMHD) and body minimum diameter (TiMD) were measured. Finally, for the fibula, the fibula length (FiL) and body minimum diameter (FiMD) were measured (Figure 2).

RESULTS and DISCUSSION

Based on the measurement data of each skeleton, dimensional differences between Korean adults and the elderly were analyzed through anthropometric study of the 8 skeletons (Table 2). It was found that the measurement values of the FeL, TiL, FiL and OA of adults were higher than those of the elderly by 6.1%, 9.7%, 10.7% and 12.6%, respectively. From this result, it can be determined that the lower bodies of Korean adults are obviously more developed than those of the elderly (Table 2).

CONCLUSIONS

This study performed anthropometric measurement and comparison on the skeletal systems of Korean adults and the elderly. It was found that the length of each bone in the elderly was remarkably shorter than that in the adults. The limitation of this work was that only 4 cadavers were available for anthropometric measurement. However, it is expected that the data accumulated by this process can be effectively used to develop Korean skeletal models and various orthopedic implants (spine, hip, knee, etc.) suitable for Koreans.

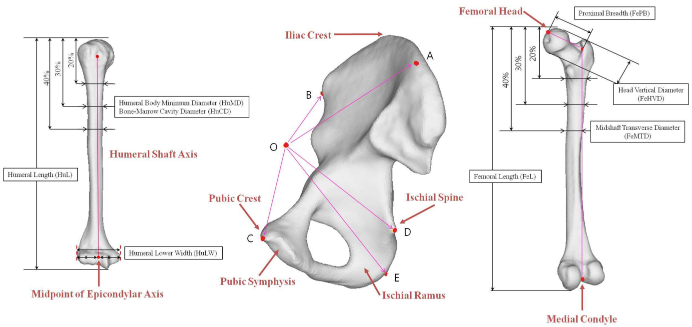

Figure 2: Reference of anthropometric measurements in case of humerus, ilium and femur

ACKNOWLEDGEMENTS

This study was financially supported by Korea Institute of Industrial Technology (KITECH).

Table 2: Summary of anthropometric measurements for Korean skeletons
(+: adult > the elderly, -: adult < the elderly)

Skeleton	Measurement	Average Dimension (mm)		Dimension difference (%)
		Adult	Elderly	
Skull	**SkB**	146.0	140.1	4.2 (+)
	SkH	224.4	210.4	6.6 (+)
Humerus [1]	**HuL**	318.3	301.1	5.7 (+)
	HuLW	62.1	60.7	2.2 (+)
	20% HuMD-CD	23.6	25.2	6.5 (-)
	30% HuMD-CD	21.9	23.1	5.1 (-)
	40% HuMD-CD	20.5	21.1	2.8 (-)
Radius	**RaL**	242.4	224.7	7.9 (+)
	RaMHD	21.1	21.4	1.8 (-)
	10% RaMD	15.4	16.2	5.3 (-)
	20% RaMD	14.0	15.0	6.7 (-)
Ulna	**UlL**	259.2	246.0	5.3 (+)
	UlMC	11.0	11.6	5.1 (-)
	10% UlMD	17.9	17.9	0.3 (-)
	20% UlMD	18.1	18.6	2.7 (-)
Ilium [2]	**OA**	145.9	129.5	12.6 (+)
	OB	120.9	124.1	2.6 (-)
	OC	72.5	76.2	4.9 (-)
	OD	121.9	121.4	0.4 (-)
	OE	157.4	149.6	5.2 (+)
Femur [3]	**FeL**	452.1	425.9	6.1 (+)
	FePB	70.6	66.9	5.5 (+)
	20% FeMTD	36.7	36.3	1.0 (+)
	30% FeMTD	30.7	31.6	2.8 (-)
	40% FeMTD	29.9	31.1	4.1 (-)
Tibia	**TiL**	373.2	340.1	9.7 (+)
	TiMHD	84.8	77.3	9.8 (+)
	10% TiMD	43.1	42.3	1.8 (+)
	20% TiMD	33.4	34.4	2.7 (-)
	50% TiMD	25.1	25.5	1.6 (-)
Fibula	**FiL**	371.3	335.4	10.7 (+)
	10% FiMD	16.8	15.7	6.6 (+)
	20% FiMD	15.7	14.0	12.1 (+)
	50% FiMD	15.8	13.6	16.5 (+)

REFERENCES

1. W. D. Murray, et al., Scaling of peak moment arms of elbow muscles with upper extremity bone dimensions, Journal of Biomechanics, Vol. 35, No. 1, pp. 19-26, 2002.
2. P. N. Gonzalez, et al., Geometric Morphometric Approach to Sex Extimation of Human Pelvis″, Forensic Science International, Vol. 189, No. 3, pp. 68-74, 2009.
3. Taner Ziylan, et al., An Analysis of Anatolian Human Femur Anthropometry, Turkish Journal of Medical Science, Vol.32, No.3, pp.231-235, 2002.

STUDY ON WHEELBASE DESIGN PARAMETERS OF A SHOWER CARRIER THROUGH DRIVABILITY TESTS

[1]Cheolwoong Ko, [1]Deokyeon Cho and [1]Keyoungjin Chun

[1]Gerontechnology R&D Group, Korea Institute of Industrial Technology (KITECH), Cheonan, Korea
email: cheko@kitech.re.kr web: http://www.kitech.re.kr/

INTRODUCTION

Korea already became an aging society in 2000 (population over 65: 7%), and elderly care is also becoming a major social problem in Korea. Recently, the number of the elderly in care facilities has increased. Generally, the 4 major elements of the activity of daily life (ADL) in elderly care facilities are eating, defecating, transferring/moving, and bathing/showering. Basically, bathing/showering activities are very important for the improvement of the quality of life (QoL) of the elderly. However, more than one caregiver are needed for showering/bathing-care activities, imposing a great deal of muscle burden on caregivers. As a result of this, it is imperative to introduce bathing/showering-assisting equipment into elderly care facilities.

The shower carrier is a representative piece of showering-assisting equipment, and various R&Ds on lightweight, compactness, lifting stroke, wheelbase, etc. are being performed for its optimal development. Especially, the wheelbase is considered a key design factor which directly affects the muscle burden of the caregivers. However, studies on the shower carrier wheelbase remain insufficient in Korea. In this study, muscle activities of subjects were measured through drivability tests using a shower carrier prototype, and the optimal design parameters of the wheelbase were proposed.

METHODS

A shower carrier prototype was newly developed for the drivability tests (Figure 1). Also, to investigate the driving characteristics according to wheelbase design parameters, a wheelbase plate with holes (Material: Al alloy, Size: 1,900x700x10mm) was newly fabricated to adjust the wheel position. The wheelbase was adjustable

Bed Length(mm)	1,900
Bed Width(mm)	650
Bed Height(mm)	600~1,100
Stroke(mm)	500
Wheel Size	Ø125
Weight	65kg

Figure 1: Newly developed shower carrier prototype

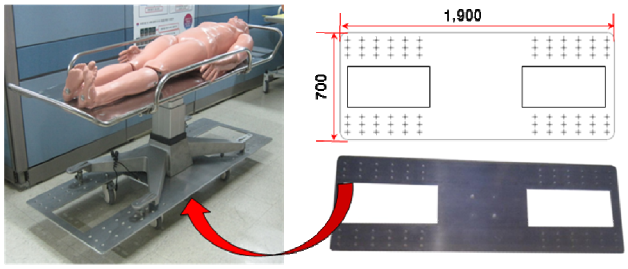

Figure 2: Shower carrier prototype equipped with a wheelbase plate for drivability tests

in the length direction of 800mm~1,800mm (6 types, gap 200mm) and in the width direction of 400~600mm (3 types, gap 100mm), fixing the wheelbase plate under the base frame of the shower carrier prototype (Figure 2).

This study selected 5 Korean females in their 40s (Age: 45±2.5, Height: 152.5±4.5cm, Height of elbow: 104.5±4.5cm, Shoulder width: 38.3±2.3cm, and Body weight: 52.5±3.5kg) as subjects. Also, 7 muscles in the upper body of the subjects (DM/Deltoid Muscle, BBM/Biceps Brachii Muscle, FCUM/Flexor Carpi Ulnaris Muscle, TM/Trapezius Muscle, TBM/Triceps Brachii Muscle, ECRLM/Extensor Carpi Radialis Longus, and ESM/Erector Spinae Muscle) were selected, which are expected to be activated during the drivability tests. EMG sensors were attached on the selected muscles to measure muscle activities (Figure 3), and Telemyo 2400T-G2 (Noraxon Inc., USA) was used.

For the tests, 3 types of driving patterns were selected; straight, 90°-clockwise (CW) and 90°-

counterclockwise (CCW) rotations (Figure 4). The tests were repeated 8 times per driving pattern (3 types) and wheelbase combination (6*3=18 types), resulting in a total of 432 times per subject, and the measurement results of the 6 tests, excluding maximum/minimum values, were analyzed.

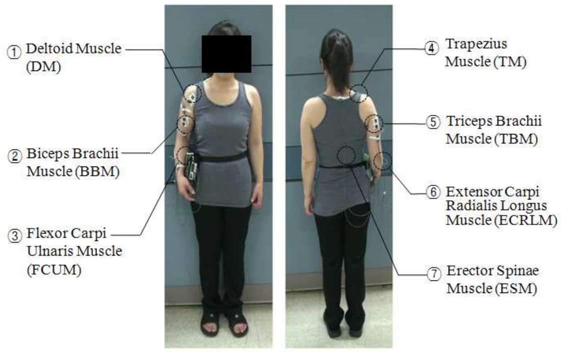

Figure 3: EMG sensors attached to female subjects

Figure 4: Three types of driving patterns

RESULTS and DISCUSSION

The muscle activities measured in the upper limbs (UL: BBM, FCUM, TBM, ECRLM) and the TM of the subjects did not show significant differences according to the design parameters of the length/width direction of the wheelbase. However, the DM (Ave. 27.2%) and ESM (Ave. 23.7%) in the straight track showed relatively noticeable muscle activities. On the other hand, in the rotation tracks, relatively high muscle activities were measured in the ESM (Ave. 25.1% from CW and Ave. 23.8% from CCW).

From the analysis on the wheelbase parameters corresponding to the first three low values from the minimum muscle activity for the DM and/or ESM in each test track (Figure 5, Figure 6), it was found that most of the wheelbase parameters showed approximately 1,400mm in length direction and 400mm in width direction. Based on these results, this study selected the optimal design of a wheelbase as 1400 x 400mm for a shower carrier capable of reducing the muscle burden of female caregivers (Figure 7).

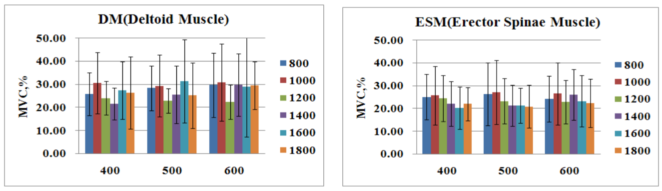

Figure 5: Comparison of muscle activities in the straight

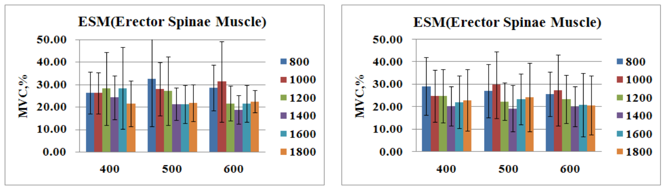

Figure 6: Comparison of muscle activities in CW (Left) and CCW (Right) rotation tracks

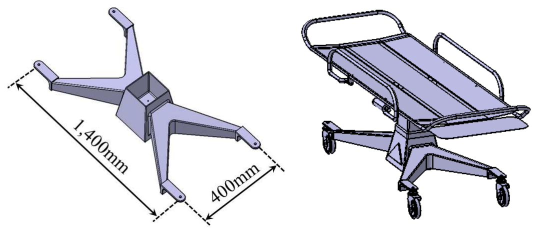

Figure 7: 3D model of shower carrier with newly designed wheelbase parameters

CONCLUSIONS

In this study, the muscle activities of 5 Korean female subjects in their 40s were measured and analyzed through drivability tests. For the tests, a shower carrier prototype equipped with a wheelbase plate was newly developed. In the case of the straight driving pattern, significantly high muscle activities were observed from the DM and ESM, while significantly noticeable muscle activities were measured from the ESM in the case of the CW/CCW rotation tracks. By analyzing the wheelbase parameters corresponding to the first three low values from the minimum for each test track, the wheelbase of 1,400 x 400mm was selected as being optimal for the purpose of reducing the muscle burden of female caregivers.

ACKNOWLEDGEMENTS

This study was performed with assistance from the research fund of the Ministry of Health and Welfare of Korea (A101945).

ALTERED KINEMATICS BETWEEN FLAT AND CURVED TREADMILLS DO NOT CAUSE INCREASED ENERGY EXPENDITURE

[1]Whitney Korgan, [1]Shane R. Wurdeman, [1]Jennifer M. Yentes, [1]Sara A. Myers, [1,2]Nicholas Stergiou

[1]University of Nebraska at Omaha, NE, USA
[2]University of Nebraska Medical Center, Omaha, NE, USA
e-mail: swurdeman@unomaha.edu, web: http://nbcf.unomaha.edu

INTRODUCTION

Our previous study [1] challenged the notion that a minimized vertical displacement of the body's center of mass (COM) coincides with reduced energy expenditure. In that study, subjects walked on a flat treadmill and a curved treadmill. The curved treadmill has an arc shaped walking platform similar to the path of motion of the COM when walking overground but inverted. Thus, this design counters the arc motion of the COM, reducing the vertical displacement of the COM. We believed this experimental design allowed a more natural walking motion as opposed to requiring subjects to alter their gait by either taking shorter steps or walking with increased knee flexion [2]. By either reducing step length or utilizing increased knee flexion, an increase in energetics may have occurred as a secondary effect of the altered gait. Our previous study did not examine the gait beyond an anecdotal report of similar walking patterns. Therefore, the purpose of this study was a retrospective analysis of the kinematics of our previous study to determine if individuals walked with similar gaits between the two conditions. We hypothesized that joint angles would be similar between the two treadmills due to the more natural gait utilized.

METHODS

Five subjects (age: 23.00 ± 2.61 years, ht: 183.39 ± 4.23 cm, mass: 84.63 ± 9.72 kg) walked (random order: 0.67, 1.12, and 1.56 m/s) on both a standard flat treadmill and a curved treadmill (Woodway®, Waukesha, WI, shown in Figure 1). Three different speeds were chosen based upon previous work[3]. Subjects walked for three minutes with breaks between trials as necessary to prevent fatigue. Twenty-seven retroreflective markers affixed to the lower limbs were used to record three-dimensional kinematics (60Hz; Motion Analysis Corp., Santa Rosa, CA). Ankle, knee, and hip joint range of motion for each gait cycle were calculated and averaged over the entire trial through custom Matlab software. Significant differences for joint angle ranges of motion for the right leg were tested for each joint through 2x3 (treadmill x speed) fully repeated measures ANOVA (α=0.05).

Figure 1: Subject walking on the Woodway®.

RESULTS AND DISCUSSION

The knee flexion range of motion for the curved treadmill was significantly less than the flat treadmill (p=0.032). The hip flexion range of motion for the curved treadmill was significantly greater than the flat treadmill (p=0.047). The ankle joint range of motion was not significantly different between treadmills (p=0.479). Differences between speeds did not reach significance nor were there any interactions (Figure 2).

In our previous study [1], we found that the difference in energy expenditure between the two treadmills was greatest at 1.56 m/s, which was also the greatest difference in terms of displacement for the COM. We hypothesized that the curved treadmill and the flat treadmill permitted similar natural gaits for the subjects. Our hypotheses were not supported. Subjects ambulated with different ranges of motion at the hip and knee joints. However, to the contrary of what we found with energy expenditure [1], there was not a significant effect of speed. Previously as speed increased, subjects had a greater increase in energy expenditure on the curved treadmill than the flat treadmill [1]. Thus, if altered gait mechanics between the treadmills had been the cause of the increased energy expenditure measured with the curved treadmill, then we would have expected a similar effect of speed on the gait kinematics. Furthermore, our previous study examining energy expenditure found the differences between the curved and flat treadmill were not significant at the slowest speed (0.67 m/s) [1]. This further highlights the lack of impact from the changes in joint ranges of motion at the hip and knee since these were different at 0.67 m/s. A closer examination of the group means (Figure 2), would suggest that while the effect of speed was not significant, the slowest speed had ranges of motion that were least similar.

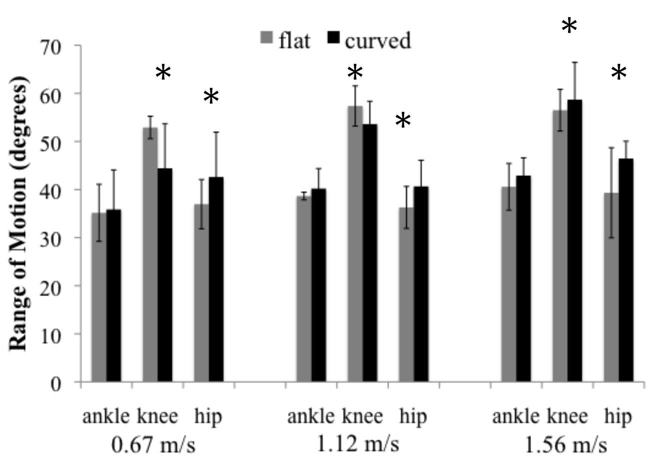

Figure 2: Comparison of each joint angle's range of motion while walking on the flat vs. curved treadmill. *Sig. at $p<0.05$.

We previously demonstrated that reducing displacement of the COM in a more natural fashion by using a curved treadmill results in increased energy expenditure [1]. The results presented here have provided evidence that our previous results do not appear to be a secondary effect of an altered gait strategy. Our findings would seem to indicate that the most energy efficient gait has an "optimal" amount of vertical displacement, permitting a healthy exchange between potential and kinetic energy but also not requiring excessive movement.

CONCLUSIONS

The consequences of a completely reduced displacement of the COM need to be better understood to improve rehabilitation protocols. Specifically, outlining a potential "optimal" amount of displacement during gait that results in minimal energy expenditure is important. By using the unique curved treadmill, we were able to minimize vertical displacement of the body's COM and measure a coinciding increase in energy expenditure [1]. Our results in this study indicate that the curved treadmill does cause changes in joint ranges of motion. Importantly, these changes were not the result of speed manipulation. This contrasts our findings with energy expenditure and vertical displacement of the COM which showed a significant effect for speed (i.e. differences in energy expenditure and vertical displacement of the COM between the flat and curved treadmills increased with faster speed). Thus, while we found significant differences at the hip and knee joint between the treadmills, our results support the notion that overly minimized vertical displacement of the COM can cause increased energy expenditure.

REFERENCES

1. Korgan et al. *Proceedings of GCMAS'12*, Grand Rapids, MI, USA, 2012.
2. Gordon et al. *Arch Phys Med Rehabil* **90**, 136-144, 2009.
3. Snyder et al. *J Strength Cond Res* **25**: S109, 2011.

ACKNOWLEDGEMENTS

Support was provided through a NASA Nebraska Space Grant & EPSCoR fellowship.

AGE DIFFERENCES IN THE STABILIZATION OF SWING FOOT TRAJECTORY IN THE FRONTAL PLANE

Vennila Krishnan[1], Noah J. Rosenblatt[1], Mark L. Latash[2], and Mark D. Grabiner[1]
[1]Department of Kinesiology and Nutrition, University of Illinois at Chicago, IL 60612
[2]Department of Kinesiology, Pennsylvania State University, University Park, PA 16802
e-mail: vennila@uic.edu, URL:http://www.uic.edu/ahs/biomechanics

INTRODUCTION

Increased gait variability can accompany increased age and has been associated with gait impairment and disability [1, 2]. Of particular importance is step width variability (SWV) [3, 4]. Stabilizing the foot in frontal plane during the swing phase of gait contributes to step width and SWV. In this study, we explored stabilization of the frontal plane swing foot trajectory using the framework of the uncontrolled manifold hypothesis (UCM)[5, 6]. With respect to swing foot trajectory the UCM hypothesis assumes that variance in the joint configuration space is organized in such a way that it is mostly confined to a sub-space that does not affect swing foot trajectory (V_{UCM}). Relatively little variance is expected orthogonal to the UCM (V_{ORT}). If $V_{UCM} > V_{ORT}$, it may be concluded that a multi-joint synergy stabilizes swing foot trajectory. We used a synergy index reflecting the relative amount of V_{UCM} in total joint configuration variance to quantify synergies stabilizing swing foot trajectory. Earlier studies have reported significantly reduced synergy indices in the elderly[7, 8]. In the present study, we tested three hypotheses: (1) there will be a kinematic synergy stabilizing the swing foot trajectory; (2) the synergy indices will be smaller in older adults; and (3) SWV will correlate with the index of stabilization of frontal plane swing foot trajectory.

METHODS

Eight healthy young adults (24.4±4.5 years) and 9 older adults (70.8±6.9 years) walked across an 8 m laboratory walkway at their preferred speed. Full-body, three dimensional kinematics were acquired using motion capture and from which a four segment (stance limb, pelvis, swing-limb thigh and swing-limb shank) geometric model with seven degrees of freedom was used to derive the frontal plane ankle joint center trajectory. Ankle joint trajectory was used as a proxy for the swing foot trajectory. Each swing phase of the gait cycle was time normalized to 100%. At one percent increments during the swing phase, UCM was approximated as the null-space of the Jacobian (a matrix of the partial derivatives that corresponded to changes in the ankle joint trajectory with respect to the mean segment angles). For each increment, deviations from these means were resolved into projections onto the V_{UCM} and orthogonal to the V_{ORT}, where V_{ORT} and V_{UCM} are the variance per degree of freedom and V_{TOT} is the total variance. We then computed a synergy index:

$$\Delta V = \frac{V_{UCM} - V_{ORT}}{V_{TOT}}$$

A higher synergy index signifies a greater stabilization of the swing foot trajectory. For statistical analysis, ΔV values were z-transformed (ΔV_Z). Step width was determined as the frontal plane distance between the foot centroids of consecutive stance phases. SWV was operationalized as the standard deviation [3, 4]. A mixed design ANOVA (group * variance) was used to determine if V_{UCM} was higher than V_{ORT} in both the groups. A higher V_{UCM} would confirm that the swing foot trajectory is stabilized. Independent sample t-tests were used to compare the younger and the older subjects for the following parameters: SWV, the average ΔV_Z and the slope of the ΔV after the peak value till the end of the swing phase. Pearson's correlation determined the strength of the relationship between SWV and average ΔV_Z.

RESULTS AND DISCUSSION

A main effect of variance in the UCM analysis confirmed that the swing foot trajectory was stabilized in both the groups ($V_{UCM} > V_{ORT}$), ($F_{(1,15)}=76.6$, $p<0.01$). On average, older subjects had larger SWV than the younger subjects ($p<0.01$).

The average ΔV_Z revealed that younger participants had higher synergy indices (Table 1) than the older subjects ($p<0.05$).

Table 1: Results with mean ± SE.

	Young	Old
SWV(mm)	24.28±1.87	40.19±3.16
Average ΔV_Z	0.66±0.03	0.49±0.03
Slope ΔV	-0.02±.002	-.04 ± .003

Both groups showed a consistent pattern of ΔV with a peak value in the middle of the swing phase and a decrease towards the moment of touch-down (negative slope - Figure 1). However, the older subjects had a steeper negative slope of ΔV than the younger subjects ($p<0.01$), possibly reflecting a greater rate of loss of synergy towards the end of the swing phase in the older when compared to the young adults.

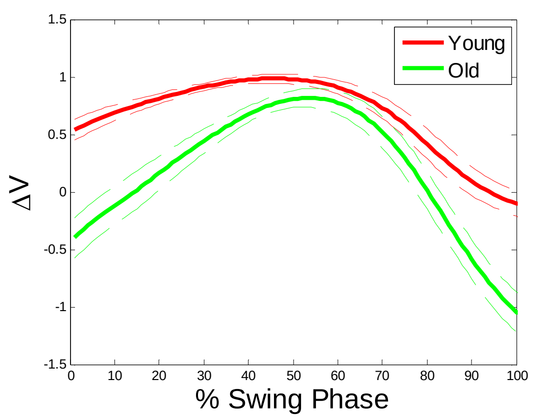

Figure 1: Index of variance (ΔV) of the younger and older subjects with standard errors (dotted lines).

Figure 2 shows the significant negative relationship between the overall SWV and the average ΔV_Z, r=-0.56, $p<0.05$.

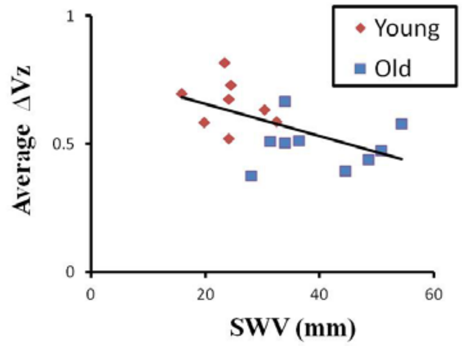

Figure 2: SWV and the average ΔVz for the young and the older adults.

CONCLUSION

The results suggest that a multi-joint kinematic synergy stabilizes the swing foot trajectory in both groups. The decline in the synergy index towards the end of the swing phase in both the groups may be associated with preparing a soft touch-down/heel strike[9]. The synergy index was significantly smaller in older as compared to the young adults. In addition, the stabilization of the swing foot was negatively correlated with the SWV. As the SWV increased, the stabilization of the swing foot (as computed by the average ΔV_Z) decreased. This lower synergy indices and increased step width variability in the older group could reflect the age-related deterioration of sensorimotor function. Thus, we conclude that normal aging affects the stabilization of the swing foot trajectory which is associated with decreased precision of frontal plane foot placement.

REFERENCES

1. Brach et al., Journal of Engineering and Rehabilitation, 2005;2(21):0003-2.
2. Maki BE et al., The Journals of Gerontology Series 2000;55(5):M270.
3. Owings TM, Grabiner MD. J Biomech 2004;37(6):935-8.
4. Owings TM, Grabiner MD Gait Posture 2004;20(1):26-9.
5. Scholz JP, Schoner G. Experimental Brain Research 1999;126(3):289-306.
6. Latash ML et al., Exerc Sport Sci Rev 2002;30(1):26.
7. Park J et al., Experimental Brain Research 2011;212(1):1-18.
8. Kapur S et al., J Appl Physiol 2010;109(6):1827-41.
9. Winter DA. Physical Therapy 1992;72(1):45-53.

SCRATCH-BASED DAMAGE QUANTIFICATION AND WEAR PREDICTION IN TOTAL HIP ARTHROPLASTY

[1]Karen Kruger, [2]Nishant Tikekar, [1]Anneliese Heiner, [1]Thomas Baer, [2]John Lannutti, and [1]Thomas Brown
[1]University of Iowa, Iowa City, IA, USA
[2]Ohio State University, Columbus, OH, USA
email: karen-kruger@uiowa.edu, web: http://poppy.obrl.uiowa.edu

INTRODUCTION

Aseptic loosening due to polyethylene wear remains a leading cause of failure in total hip arthroplasty (THA), particularly in the late term. Retrieval studies have shown that third body damage, especially scratching of the femoral head, can involve dramatic wear acceleration. A direct link between femoral head scratch damage and wear acceleration however, is unknown.

To date, mapping of femoral head damage on a global implant level has been limited to representation by standard surface roughness parameters, usually the average roughness, R_a. Attempts to relate average regional roughness parameters to clinical wear rates however, have proven difficult [1]. Average surface roughness alone fails to suitably describe scratch damage as observed in retrievals, because that measure is unable to distinguish between large groups of fine scratches versus one or a few severe scratches.

This study presents a novel technique that allows for localization and quantification of regions of femoral head damage on a scratch-wise basis, using a combination of masked photography and optical profilometry. A finite element (FE) model for THA wear was then used to predict wear acceleration due to the actual spatial scratch damage pattern. The model utilizes a purpose-developed algorithm to allow local wear acceleration to be dependent on the properties and orientations of individual scratches overpassing a given site on the polyethylene liner.

METHODS

Scratch Detection and Quantification

Illustratively, two retrieval femoral heads were used to demonstrate this technique. Sample 1 was revised 5.1 years post-op for septic loosening. Sample 2 was revised 6.2 years post-op due to dislocation. Photographs were taken of each femoral head using a novel masking technique (Figure 1). Canny edge detection [2] was performed on the photographs in order to detect regions of damage. A Hough transform [2] was then utilized to discretize damage regions into straight-line scratch segments.

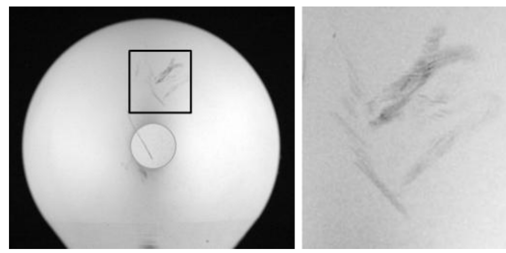

Figure 1: Photograph of femoral head damage (Sample #1)

Damaged regions were scanned using a Bruker Contour GT optical profilometer. Scans over an area of 45 mm^2 in sample 1 and 49 mm^2 in sample 2 were taken to analyze all damaged areas detected in the image analysis. These scans were used to determine the scratch lip heights for each individual scratch segment detected in the photographs. These data were then used to simulate femoral head damage in the FE model.

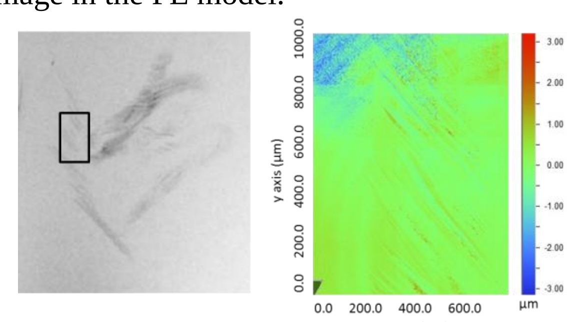

Figure 2: Optical profilometry of a selected region

A convergence study was conducted to determine the number of sampling points needed to accurately assign a lip height to each scratch segment. Based on these results, the peak profile height needed to be measured every 10 µm along individual scratch segments, the average of which was assigned to be the scratch lip height for that scratch segment.

Finite Element Analysis

An experimentally validated finite element model for THA wear was implemented in ABAQUS v6.9.1, using the adaptive meshing capabilities of the UMESHMOTION subroutine. Wear was determined using the Archard wear formula, which calculates the spatial distribution of wear depth as a function of contact pressure, sliding distance, and a wear coefficient based on the tribological properties of the surfaces in contact. This approach has been validated (10% error) by replication of physically measured wear for femoral head specimens on which specific scratch patterns had been stylus-ruled [3, 4].

Femoral head scratches, along with their corresponding lip heights, were modeled for the detected scratch locations. When an area of the acetabular cup was overpassed by a femoral head scratch, the wear coefficient was elevated based on the lip height of that specific scratch, using a bench-study-based relationship [5]. At each time increment, the angle between the orientation of the scratch and its direction of motion was calculated. When this angle was highly acute, the wear was correspondingly elevated, as was reported in physical wear tests [6]. Simulations of this model were run to one million standard gait cycles, with linear and volumetric wear calculated.

RESULTS AND DISCUSSION

The image analysis detected 101 individual scratch segments with scratch lip heights ranging from 0.1 µm to 4 µm in sample 1, and 62 segments with scratch lip heights ranging from 0.6 µm to 5.3 µm in sample 2 (Figure 3). The R_a values of scanned areas ranged from 0.153 µm to 0.638 µm, an increase from R_a values typically observed on undamaged femoral heads, which are usually approximately 0.007 µm.

Compared to the baseline simulation for a non-roughened femoral head, the FE models of the damaged retrieval heads showed a 37.5% increase in volumetric wear for sample 1 and a 15.6% increase for sample 2 (Figure 4).

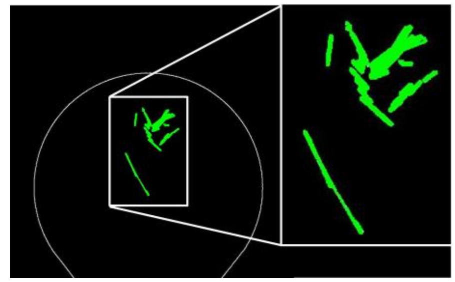

Figure 3: Image analysis result of damage detection

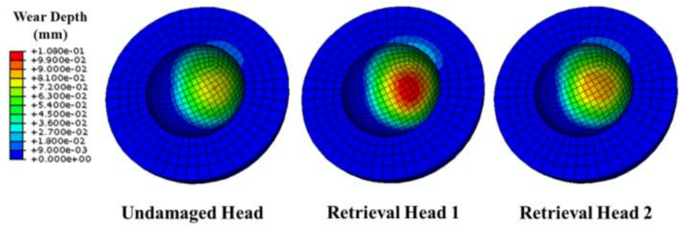

Figure 4: Wear depth of undamaged and retrieval models

CONCLUSIONS

This technique represents the first demonstration of mapping whole head retrieval damage on a scratch-specific basis. Representation of damage using this technique allows simulation of damage observed on specific retrieval femoral heads. The FE model affords physiologically significant predictions of wear acceleration due to actual 3rd body damage patterns observed *in vivo*. In its current embodiment, this approach is capable of modeling up to 12,000 discrete scratch increments, thus allowing even severely damaged heads to be modeled.

REFERENCES

1. Hall, R.M., et al, Med Eng Phys, 1997. 19(8): p.711-719.
2. Sonka, et al, Image Processing, 2007.
3. Barbour, et al. Proc Inst Mech Eng H, 2000. 214(6): p. 569-76.
4. Kruger, K.M., Brown, T.D., 20th Annual pre-ORS, Berkeley, CA, 2012.
5. Dowson, D., et al. Wear, 1987. 119(3): p. 277-293.
6. Glennon, L.P., et al. J Biomech Eng, 2008. 130(5): p. 051006.

ACKNOWLEDGEMENTS

This research was funded by NIH AR05778.

ON THE POTENTIAL OF COMPUTATIONAL MATHEMATICS IN THE DIAGNOSIS OF CORONARY HEART DISEASE

[1]Carola Kruse, [1]Simon Shaw and [1]JR Whiteman,
[2]MP Brewin, [2]SE Greenwald, [3]MJ Birch,
[4]HT Banks, [4]ZR Kenz, [4]S Hu

[1]BICOM, Institute of Computational Mathematics, Brunel University, England;
[2]Blizard Institute, Barts and The London School of Medicine and Dentistry, Queen Mary, University of London, England;
[3]Clinical Physics, Barts & The London NHS Trust, England;
[4]Center for Research in Scientific Computation, North Carolina State University, Raleigh, USA

INTRODUCTION

This talk is concerned with a project exploring the use of computational modelling for the diagnosis of coronary heart disease (CHD). As plaque builds up in a coronary artery blood flow past the stenosed region becomes turbulent and creates abnormal variations in wall shear stresses. These shears drive low amplitude acoustic shear waves through the soft tissue in the thorax which appear at the chest wall and can be measured non-invasively by placing sensors on the skin. This acoustic surface signature has the potential to provide a cheap non-invasive means of diagnosing CHD [1]. The development of such a test has been described as 'one of the holy grails of diagnostic cardiology' [2].

METHODS

The first part of this talk will outline a multi-disciplinary international collaboration on a proof-of-concept investigation which connects computational applied mathematics to experimental biomechanical technology. In the initial stage of this project biomedical physicists (Brewin, Greenwald and Birch) are building cylindrical chest phantoms from tissue mimicking (viscoelastic) agarose gel which will simulate the process described above in a wet lab environment. Numerical analysts (Kruse, Shaw and Whiteman) are writing dry lab computer software that will predict wave motion in these gels with a view to simulating *in silico* the response of the chest wall to the shear waves generated by an atherosclerotic coronary artery. Simultaneously, another group of mathematicians (North Carolina State University) are developing inverse solver software which attempts to determine the source of a given chest wall signal. The loop: source to signal (Brunel) and signal back to source (NC State), creates an iterative means of characterising the source given only the signal and suggests a cheap non-invasive computational diagnosis tool based on the numerical solution of partial differential equations. The wet lab results will be used to provide input parameters to the software as well as, at a later stage, to validate it.

RESULTS AND DISCUSSION

Axial symmetry is being exploited for this first stage of the project. The second part of this talk will describe the construction of the forward solver in the resulting 2D axial cross section. For this we consider a two-dimensional space-time 'viscodynamic' problem using a wave equation incorporating Zener (also known as a 'standard linear solid' or 'Maxwell solid') and Kelvin-Voigt models for viscoelasticity. We use a spectral finite element method in space and a high order discontinuous Galerkin finite element discretization in time using normalized Legendre polynomials. This choice allows the decoupling of the linear system following the technique of [3].

The overall potential of the scheme will be addressed in terms of computational accuracy and load, and the need and scope for both coarse and fine grained parallelism will be discussed.

CONCLUSIONS

By reference to our experimental data we will see that our computational scheme is both accurate and efficient enough for this simulation. Moreover we will illustrate the interplay between the number of time steps and the polynomial degree of the temporal approximation in terms of computational load and solution accuracy.

REFERENCES

1. Banks HT and Pinter G, *Multiscale Model. Simul.* **3**, 395–412, 2005.
2. Semmlow J and Rahalkar K, *Annu. Rev. Biomed. Eng.* **9**, 449–69, 2007.
3. Werder T *et al., Comput. Methods Appl. Mech. Engrg.* **190**, 6685 – 6708, 2001.

ACKNOWLEDGEMENTS

This work is supported by the Engineering and Physical Sciences Research Council [EP/H011072/1 and EP/H011285/1].

MEASUREMENT OF MTPJ CARTILAGE THICKNESS DISTRIBUTION USING 14T MRI

[1]Atul Kumar, [2]Donghoon Lee, [3]Peter R. Cavanagh

[1] Asian Institute of Tele-surgery, Chang Bing Show Chwan Memorial Hospital, Changhua, Taiwan R.O.C.
Departments of [2]Radiology and [3]Orthopaedics and Sports Medicine
University of Washington, Seattle, WA, USA
email: sharmaatul11@gmail.com

INTRODUCTION

The first metatarsophalangeal joint (MTPJ1) plays a crucial role in human locomotor movements [1,2,3] but little is known about the articular cartilage of this joint. Previous studies to determine the MTPJ1 cartilage thickness have used the creep indentation [4] or histomorphometric techniques [5]. To the best of our knowledge, imaging has not yet been used for this purpose although it has the potential to provide a profile of the three-dimensional distribution of the cartilage. The objective of the current work is to determine the distribution of cartilage thickness in the region of the first metatarsal head (MTH1) which articulates with proximal phalanx using 14T MRI.

METHODS

MRI images of MTPJ1 specimens, harvested from two cadaver feet, were acquired with a 14T scanner. A turbo spin echo pulse sequence was used with voxel size of 0.05 x 0.05 x 0.10 mm^3 (for a specimen from a 75 year old female) and 0.04 x 0.04 x 0.04 mm^3 (for a specimen from a 77 year old male).

Edge pixels in the grayscale transverse images (Figure 1a) of the MTH1 were identified with the Canny edge detector. In the image, the articular surface of the cartilage was called the 'outer border' while the interface between the cartilage region and the subchondral bone was called the 'inner border'. The outer border was identified semi-automatically. A best-fit circle was calculated for the outer border and a vector to the center of the circle from each outer-border pixel was calculated. Each pixel on the outer border was grown along its respective vector until it crossed a pixel with intensity above a given threshold. The last pixel along each vector defined the 'inner border' of the cartilage region. The total number of pixels along the individual vector defined the 'depth' of the cartilage at this point. A moving average was used to smooth the inner border leading to the result shown in Figure 1b.

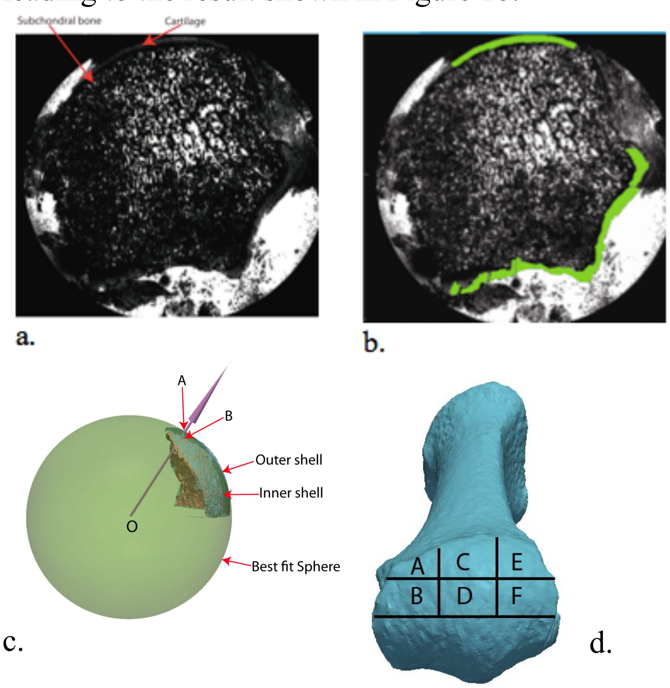

Figure 1: a. Transverse image of MTH1; b. Result of cartilage segmentation (green region); c. Cartilage thickness calculation from the cartilage shell; d. Regional division of MTH1 for the calculation of median cartilage thickness.

A three-dimensional reconstruction of the cartilage shell was assembled by stacking the outer and the inner borders of the cartilage in 3-D space. The surfaces were represented as a point cluster. A best fit sphere was calculated for the outer surface (Figure 1c). Vectors joining the center (O) of the sphere and each point (A) on the outer shell of the cartilage were calculated. The distance between the point (A) on the outer surface and the corresponding point (B) on the inner surface nearest to the vector OA was calculated as the thickness of the cartilage at the point A.

RESULTS AND DISCUSSION

The cartilage shell was divided into six regions (Figure 1d) and the median thickness in each region was calculated (Table 1). The average of these median thicknesses was 0.73±0.07mm. The thickest cartilage was observed in region D (0.79 mm) and thinnest was observed in region E (0.59 mm). These results lie within the range of thicknesses measured in previous studies using other methods [4,5].

A resolution up to 0.04 x 0.04 x 0.04 mm per voxel was achieved with 14T MRI which enabled the study of the thin (< 1mm) highly curved cartilage. Information regarding cartilage thickness distribution supplements current estimates of MTH1 geometry made from osteological specimens or CT scans and this can be helpful in the design of MTH1 implants. The incorporation of cartilage thickness distribution in finite element models may provide more precise estimations of stress distributions for computational analysis of the foot. The thickness distribution can also be used for the calculation of cartilage volume which correlates well with the radiographic grade of osteoarthritis.

The current study has a number of limitations: 1) the study used only two specimens; 2) The surface data of the cartilage shell required substantial smoothing; 3) The current cartilage segmentation method is based on a gray scale intensity threshold which may vary between specimens due to technical issues.

CONCLUSIONS

An approach towards cartilage thickness measurement using 14T MRI imaging of MTH1 has been presented. The results obtained were similar to those obtained from histomorphometric analysis. The proposed approach can also be useful for other bones that have cartilage thickness in the sub-millimeter range.

REFERENCES

1. Cavanagh PR, et al. *Foot & Ankle*, **7**(5) 5, 262-76, Apr. 1987.
2. Stokes IA, et al. *Clinical Orthopaedics and Related Research,* **142**, 64-72, 2012.
3. Hutton WC, et al. *Clinical Orthopaedics and Related Research,* **157**, 7-13, 1981.
4. Athanasiou KA, et al. *Clinical Orthopaedics and Related Research,* **348**, 269-81, 1998.
5. Muehleman C, et al. *Journal of Anatomy*, **197** Pt 4, pp. 687-91, 2000.

ACKNOWLEDGEMENTS

This work was supported in part by the National Institutes of Health (5R01 HD037433).

Table 1: Mean (± standard deviation) thickness of the cartilage in six regions of the MTH1 articular surface.

Region	A	B	C	D	E	F
Thickness (in mm)	0.74±0.13	0.77±0.24	0.76±0.32	0.79±0.17	0.59±0.04	0.75±0.21

THE GAIT PATTERN OF CHILDREN WITH CEREBRAL PALSY HAS GREATER STOCHASTIC FEATURES

Max J. Kurz and Regina Harbourne

Munroe-Meyer Institute, University of Nebraska Medical Center, Omaha, Nebraska
email: mkurz@unmc.edu, web: http://www.unmc.edu/mmi/

INTRODUCTION

Children with cerebral palsy (CP) demonstrate a more variable stepping pattern than their typically developing peers [1]. Gait variations have been noted to arise from subtle corrections in the motor command to overcome perceived errors in the stepping pattern and mechanical perturbations. Alternative evidence suggests that these variations may stem from stochastic features that at contaminate the motor command at the sensor and neuronal processing level [2,3]. However, separation of these deterministic and stochastic sources that promote variability in the motor output has historically been a challenge, and has rarely been evaluated in children with CP [3]. Since CP is associated with damage along the thalamocortical and corticospinal tracts [4], it is possible that the accentuated variability seen in these children may be a result of an increased presence of stochastic features in motor output. However, it is alternatively plausible that the gait variations seen in these children are a result of inconsistencies in properly selecting and formulating a successful stepping pattern. To begin to address this knowledge gap, we used a Langevin approach to evaluate differences in the deterministic and stochastic features that may be contributing to the variability present in the stepping pattern of children with CP [5].

METHODS

Ten children with spastic diplegic CP (Age = 7.8 $\pm$ 2.8 yrs.) and nine typically developing (TD) children (Age = 8.0 $\pm$ 2.4 yrs.) participated in this investigation. The children walked on a treadmill for two minutes at 0.8 m/s, which is a speed that has been previously reported for children with CP while walking in the community. The position of reflective markers placed on the heel, toe, ankle and the sacrum were recorded with a three-dimensional motion capture system (120 Hz). The marker positions were filtered with a low-pass zero lag digital filter at 6 Hz. Since the position of the children on the treadmill may drift, the difference in the horizontal position of the sacrum and the right ankle marker at foot-contact was used to quantify the stepping kinematics. The stepping kinematic data was differenced to ensure that the data was stationary and that the mean of the stepping pattern was zero. The standard deviation of the differenced stepping kinematics was calculated to determine the amount of gait variability present in the respective groups.

We evaluated the change in the stepping kinematics as a Langevin process

$$\dot{x}(t) = D^{(1)}(x) + \sqrt{2D^{(2)}(x)}\Gamma(t)$$

where $D^{(1)}(x)$ was the drift coefficient, $D^{(2)}(x)$ was the diffusion coefficient and $\Gamma(t)$ was the Langevin force [5]. The drift coefficient represented the deterministic changes in the gait pattern from one step to the next, while the diffusion coefficient represented the stochastic features present in the stepping kinematics. Reconstruction of the amount of drift and diffusion present in the stepping kinematics was based on a conditional probability distribution that represented the probability of the system to be in state x' at time t+τ. The amount of drift and diffusion from the respective states was calculated as follows

$$D^{(n)}(x) = \lim_{\tau \to 0} \frac{1}{\tau} \int \frac{[x' - x]^n}{n!} P(x', t+\tau \mid x, t)dx'$$

where t represents time, τ represent a change in time from the initial state, and P(x',t+t | x,t) is the conditional probability distribution established from the stepping kinematics [5]. The coefficients were evaluated by fitting a first and second order polynomial to the reconstructed drift and diffusion processes present in the collected data (Figure 1).

RESULTS AND DISCUSSION

Concurrent with what has been previously reported [1], our results also show that children with CP have a greater amount of variability in the stepping kinematics compared to TD children (CP= 29.6 ± 3 mm; TD = 22.3 ± 2 mm; p=0.03). However, the slope and intercept of the line fitted to the reconstructed drift of the stepping kinematics (Figure 1A) was not significantly different between the children with CP and the TD children (p>0.05). This indicated that both groups were capable of adapting the stepping kinematics to perturbations in a similar fashion. In addition, this suggests that subtle adjustments in the stepping motor command were most likely not the reason that the children with CP had a greater amount of variability in their stepping kinematics. This notion was further confirmed by a lack of correlation between the amount of variability in the stepping kinematics and the drift coefficient (p>0.05).

For both groups, the reconstruction of the amount of diffusion present in stepping kinematics had an inverted parabolic shape with the mean of the differenced stepping kinematics located where the stochastic features were at a minimum (Figure 1B). Although divergence away from this preferred state resulted in an increased amount of stochastic features, the coefficient of the second order polynomial was not significantly different (p>0.05). However, the amount of diffusion evaluated at the local minimum of the polynomial was significantly higher for the children with CP (CP= 0.16 ± 0.03 mm; TD= 0.08 ± .01 mm; p=0.01). This indicated that children with CP had a greater amount of stochastic features in their stepping kinematics. Moreover, we found that the amount of diffusion at the local minimum had a strong positive correlation (r=0.89; p<0.0001) with the standard deviation of the stepping kinematics. Indicating that greater variability in the stepping pattern was associated with the presence of more stochastic features.

Together, these results imply that the differences in the variability present in the stepping kinematics of children with CP and TD children are most likely related to stochastic features. We suspect that these stochastic features partly arise from the damage present in the thalamocortical and cortical spinal tracts [4]. Alternatively, it is possible that the stochastic features may arise from muscular spasticity. To address this knowledge gap, our current investigations are directed at identifying the stochastic features in the gait are amplified in children with greater sensorimotor impairments.

REFERENCES

1. Katz-Leurer M, et al. *Dev Neurorehab* **12**:100-105, 2009.
2. Faisal AA, et al. *Nature Neurosci* **9**:292-303, 2008.
3. Chu WTV & Sanger TD *Mov Disorder* **24**:1299-1305, 2009.
4. Hoon AH, et al. *Dev Med Child Neurol* **51**:697-704,2009.
5. van Mourik AM, et al. *Physics Let A* **351**:13-17, 2006.

A.

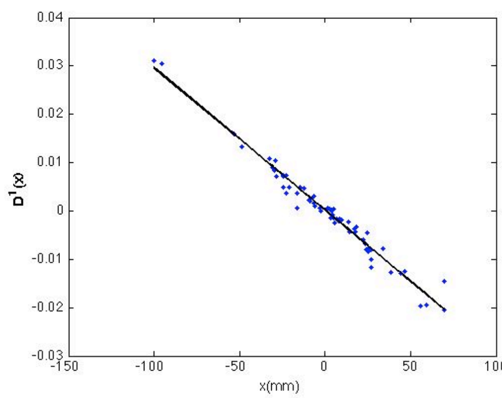

B.

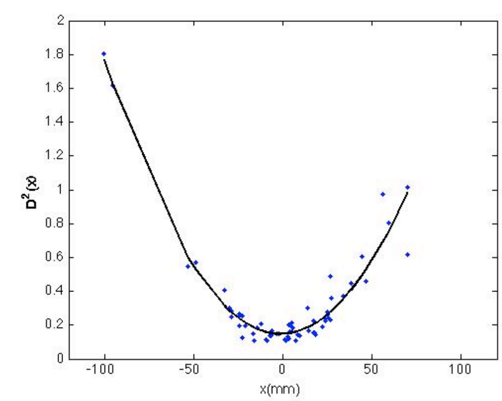

Figure 1. Exemplary reconstructed drift (A) and diffusion of the stepping kinematics (B) for a child with cerebral palsy. Zero represents the mean of the differenced data. This point coincides with where the stochastic features of the gait are minimized.

CHILDREN WITH CEREBRAL PALSY DO MORE POSITIVE MECHANICAL WORK AFTER GAIT REHABILITATION

Max J. Kurz, Wayne Stuberg, David J. Arpin and Megan Gosselin

Munroe-Meyer Institute, University of Nebraska Medical Center, Omaha, NE, USA
email: mkurz@unmc.edu web: http://www.unmc.edu/mmi/

INTRODUCTION

Cerebral palsy (CP) results from a perinatal brain insult that often impacts the integrity of the coordination between the brain and the muscles. The poor brain-muscle coordination has been previously noted to hinder the child's ability to properly perform mechanical work on the center of mass during gait [1,2]. However, no investigations have explored the ability of the current therapeutic trends to improve the ability of children with CP to perform mechanical work during gait. Our recent clinical trails have shown that body weight supported gait rehabilitation can improve the walking speed and gross motor function of children with CP [3,4]. We suspect that these changes are a result of an improved ability of the muscles to perform mechanical work. To address this knowledge gap, we examined the changes in the mechanical work performed by the legs after body weight supported gait rehabilitation.

METHODS

Nine children (Age = 12 $\pm$ 1 yrs.) with CP who had a Gross Motor Function Classification Score (GMFCS) of II participated in this investigation. A GMFCS of II indicates that the child has a notable walking impairment, but does not require an assistive mobility device (i.e., forearm crutches, wheeled walker) for community ambulation. All of the children had spastic diplegia. The children participated in a body weight supported gait rehabilitation program that was performed three days a week for 6-weeks. The therapeutic protocol started with no more than 40% of the child's body weight supported by an overhead suspension system, and was reduced each week until no more than 10% of the body weight was supported during the final week of therapy. The speed of the treadmill was increased each week to encourage a faster walking pace. However, this pace did not exceed 75% of the child's aged determined maximum heart rate. The gait rehabilitation and assessments described below were performed with the child wearing their prescribed ankle-foot orthoses.

Each child underwent a three-dimensional gait analysis before and after the gait rehabilitation. The three-dimensional lower extremity joint kinematics were captured with an 8-camera motion capture system, and a series of four force plates were used to measure the ground reaction forces for each leg. Inverse dynamics were used to calculate the respective joint moments during the stance phase, and the joint powers were calculated from the product of the joint moments and joint angular velocities. The positive and negative work performed by the ankle, knee and hip joints were calculated by integrating the respective power curves. The positive and negative work performed across the lower extremity joints was summed to quantify the net mechanical work. The average net mechanical work was determined from three trials, and was normalized to the child's body mass. Lastly, the average net mechanical work performed during the stance phase was separated and evaluated for the double and single support phases.

The individual leg ground reaction force components were summed and integrated to determine the instantaneous forward velocity, and vertical displacement of the center of mass. Subsequently, these variables were used to quantify the changes in the potential energy and forward kinetic energy profiles. The amount of positive external work performed on the center of mass in the respective directions was calculated by summing the incremental changes in the energy profiles. The average external mechanical work values were also calculated from the same three trials, and normalized by the child's body mass.

The child's gait adaptability and endurance were additionally assessed. Adaptability was evaluated by having the child walk as fast as possible for 10 meters, while the distance walked in 6-minutes was used to evaluate changes in the child's endurance.

RESULTS AND DISCUSSION

There was no difference in the pre-post walking speeds during the biomechanical data collections (Pre= 1.1$\pm$0.05 m/s; Post = 1.1$\pm$0.06 m/s; $p>0.05$). Although the children were walking at a similar speed, the net mechanical work performed by the joints during the single support phase was different after gait rehabilitation (Figure 1A; p=0.02). Prior to the gait rehabilitation, the net mechanical work had a negative bias, which indicated that the children were performing more eccentric work on the center of mass during single support. This result is similar to what has been previously reported in the literature [2]. However, after gait rehabilitation, the net work performed by the joints was positive indicating that the children improved their ability to lift and accelerate the center of mass during single support. This finding was supported by an increase in the amount of external positive work that was performed in the vertical direction after gait training (Figure 1B; p=0.03). Recent muscle-driven stimulations have suggested that children with CP use abnormal muscular activation patterns to vertically lift and accelerate the center of mass during single support [5]. Potentially, our results may indicate that gait training can help to resolve these aberrant muscular control strategies.

Further inspection of the data reveled that there was no change in the net mechanical work performed by the joints during the double support phase (Pre = 0.02 $\pm$ 0.06 J Kg^{-1}; Post = -0.02 $\pm$ 0.05 J Kg^{-1}; $p>0.05$). Additionally, gait training did not influence the external mechanical work performed on the center of mass in the forward direction (Pre = 0.42 $\pm$ 0.06 J Kg^{-1}; Post =0.49 $\pm$ 0.07 J Kg^{-1}; $p>0.05$).

After the gait training the children were able to walk faster for 10-meters (Pre = 6.9 $\pm$ 0.4 sec; Post = 6.1 $\pm$ 0.4 sec; p=0.002), and for a longer distance during

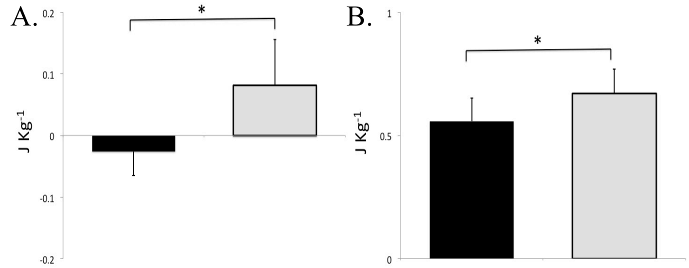

Figure 1. A) Net mechanical work performed by the joints during single support, B) External mechanical work performed on the center of mass in the vertical direction. Black bars are baseline, grey bars are after gait rehabilitation. *p<0.05

the 6-minutes (Pre = 383 $\pm$ 27 m; Post = 437 $\pm$ 29 m; p=0.01). These clinical outcomes indicate that the gait patterns of the children were more adaptable, and they had better muscular endurance after the gait training. These functional changes support the notion that the positive mechanical work performed during single support after gait training represents a clinically relevant improvement in the walking biomechanics of the children.

CONCLUSIONS

Our results are the first to show that gait training can improve the mechanical work performed by children with CP during single support. More importantly, these biomechanical changes appear to be coupled with an improved gait adaptability and endurance. Altogether these results provide evidence that body weight supported gait training is an advantageous therapy for children with CP. Further investigations of the therapeutic parameters that best augment these beneficial biomechanical changes are warranted.

REFERENCES

1. Kurz MJ et al. *Gait & Posture* **31**, 347-350, 2010.
2. Onley SJ et al. *Phys Ther* 70:431-438, 1990.
3. Kurz MJ et al. *Dev Neurorehabil* **14**:87-93, 2011.
4. Kurz MJ et al. *Ped Phys Ther* **23**:232-239, 2011.
5. Steele et al. *J Biomech* **43**:2099-2105, 2010.

ACKNOWLEDGEMENTS

Partial funding for this investigation was provided by the Pediatrics Section of the American Physical Therapy Association.

IMPAIRED ENDPOINT ACCURACY IN OLDER ADULTS IS ASSOCIATED WITH GREATER TIME VARIABILITY

Minhyuk Kwon, Yen-Ting Chen, Jessica C Reid, Emily J Fox, Evangelos A Christou

University of Florida, Gainesville, FL, USA
Email: eachristou@hhp.ufl.edu, web: http://hhp.ufl.edu/npl

INTRODUCTION

The accuracy of goal-directed movements is a critical component of numerous functional activities. Older adults, however, are less accurate than young adults during goal-directed movements [2, 4]. These age-associated differences in accuracy may be due to slower adaptation to the task by older adults. For example, when young and older adults repeated 100 goal-directed isometric contractions with the index finger, the age-associated differences in accuracy were evident only during the initial 40 practice trials [3]. Following that initial adaptation, endpoint accuracy was similar for the two age groups. This raises the following research question: "*Are there age-associated differences in endpoint accuracy during goal-directed movements and do these differences persist after the initial adaptation to the task?*"

Furthermore, endpoint accuracy during goal-directed movements may depend on the limb that is used to perform the task. Young adults, for instance, exhibit greater endpoint accuracy with the upper compared with the lower limb during goal-directed isometric tasks [1]. However, recent evidence indicates that aging exacerbates differences in positional variability, particularly for the lower limb [5]. The purpose of this study, therefore, was to compare the endpoint accuracy and variability of young and older adults during goal-directed movements with the upper and lower limb.

METHODS

Twenty young (25.1 ± 3.9 years, 10 females) and twenty older adults (71.5 ± 4.8 years, 10 females) participated in two sessions across two days. On each day, the subject performed 100 trials of a goal-directed movement either with the upper limb or with the lower limb. The goal-directed movements involved accurately matching the peak displacement of the limb to a target by performing ankle dorsiflexion or elbow flexion. The movements were unloaded and the order of the upper and lower limb movements was counterbalanced. The target displacement was 9º for the elbow and 18º for the ankle. Therefore the target displacement for the each limb was ~ 13% of the available range of motion for each joint. The time to target was 180 ms for both movements. After each trial, visual feedback of the subjects' movement trajectory was provided for 5 s. To compare the motor output, independent of the initial practice-induced adaptations, we analyzed the last 40 trials from each subject. Endpoint accuracy was quantified by calculating the overall error, which was based on the orthogonal relationship of the endpoint time and position errors, relative to the target goal. Endpoint position error and time error were calculated as the absolute deviation from the targeted range of motion (position) and time. Endpoint position variability and endpoint time variability were quantified by calculating the coefficient of variation of the peak displacement and time to peak displacement.

RESULTS AND DISCUSSION

Older adults exhibited impaired endpoint accuracy with both limbs as evidenced by greater overall endpoint error ($P < 0.05$; Fig. 1).

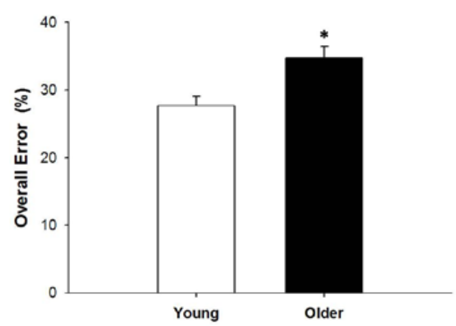

Figure 1: Older adults exhibit greater overall endpoint error than young adults.

Furthermore, older adults exhibited significantly greater positional and time endpoint variability compared with young adults ($P < 0.05$; Fig. 2).

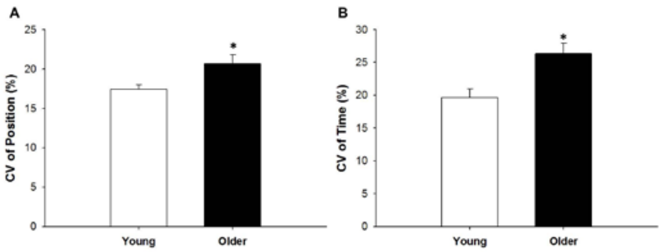

Figure 2: Older adults exhibited greater positional variability (A) and time variability (B)

To examine the association between the age-associated differences in the endpoint accuracy and endpoint variability during goal-directed movements with the upper and lower limb, we performed a multiple stepwise linear regression analysis. Our results indicated that time variability, but not positional variability predicted the impaired endpoint accuracy in older adults ($R^2 = 0.7$, $P < 0.001$; Fig. 3).

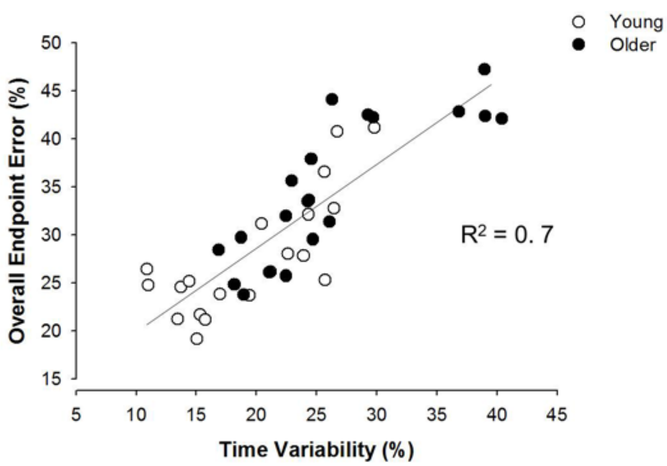

Figure 3: Overall endpoint error is strongly associated with time variability.

Independent of age, subjects exhibited greater overall endpoint error and time variability with the lower limb compared with the upper limb ($P < 0.05$).

Our results demonstrate for the first time that aging impairs the endpoint accuracy of goal-directed movements, independent of the initial practice-induced adaptations. We also provide evidence that this impairment is associated with greater time variability in older adults. In addition, our results suggest that movement control and accuracy is better for the upper limb compared with the lower limb. This result extends previous findings on isometric goal-directed contractions and positional holding task [1, 5].

CONCLUSION

Aging impairs movement end-point accuracy due to greater time variability. This impairment is consistent for both limbs.

REFERENCES

1. Christou, EA. et al. *J Mot Behav* **35**, 322-324, 2003.
2. Christou, EA. et al. *Movement System Variability*.199-215, Human Kinetics, 2005
3. Christou, EA. et al. *J Neurophysiol* **97**, 3340-3350, 2007.
4. Christou, EA. *Exerc Sport Sci Rev* **39**, 77-84. 2010.
5. Kwon, M. et al. *J Mot Behav* **43**, 357-360, 2011.

ACKNOWLEDGEMENTS

This study was supported by R01 AG031769 to Evangelos A. Christou.

ARE INTERNAL-EXTERNAL ROTATIONAL MOMENTS IN ACL DEFICIENT SUBJECTS DIFFERENT THAN THOSE IN HEALTHY SUBJECTS?

[1]Amelia S. Lanier, [2]Toran D. Macleod, [1]Kurt Manal, and [1]Thomas S. Buchanan

[1]Delaware Rehabilitation Institute, University of Delaware, Newark, DE, USA
[2]Department of Radiology &Biomedical Imaging University of California, San Francisco, CA, USA
email: alanier@udel.edu, web: http://www.udel.edu/dri

INTRODUCTION

Impairment of the anterior cruciate ligament (ACL) is a common injury causing rotational instability of the knee joint. Evaluating how patients respond in the absence of an ACL can help identify compensation strategies and potential patient response to rehabilitation efforts. However, it is difficult to directly evaluate ACL-deficient patients in internal and external rotations due to the risk of further injury. We developed a technique using standing target matching that is able to actively test subjects in internal and external rotations [1]. The aim of this study was to evaluate the standing target matching taskôs ability to challenge ACL-deficient patients in internal and external rotational moments and we hypothesized ACL injured subjects would exhibit larger external rotation moments during knee extension when compared to healthy subjects.

METHODS

Ten subjects participated in this study; four (2 males, 2 females) had no history of knee injury and six (3 males, 3 females) sustained complete isolated ACL rupture within 6 months prior to testing. All subjects were regular participants (> 50 hrs/year) in level I and II sports requiring running and cutting.

Subjects stood barefoot approximately hip-width apart on two force plates, a separate force plate for each foot (OR-6, AMTI, Watertown, MA, USA). One foot was selected at random to control a cursor and was coined the *mobilizer*. The limb not controlling the cursor but still maintaining stability for the subject was coined the *stabilizer*. Anterior/Posterior and Medial/Lateral shear forces controlled the cursorôs movement in the anterior-posterior-medial-lateral plane respectively. Internal/External rotation moments controlled a needle on the cursor which rotated counterclockwise for internal rotation and clockwise for external rotation. A projector was used to display the cursor on a screen in front of the subject to provide visual feedback of the subjectsô shear and rotational forces/moments. The standing target matching task required subjects to position the cursor, described earlier, on a target consisting of two concentric circles (Figure 1) using the mobilizing limb while kinematic and force plate measurements were taken from the stabilizing limb (the limb of interest in this study). Targets appeared one at a time on the screen at one of eighteen positions around a circle (located at 20° increments in the anterior-posterior-medial-lateral plane). Subjects were required to hold the cursor within the narrow target for 500 ms before the trial was considered successful. 72 targets were matched bilaterally (both feet performed the mobilizer task). A force of 30% of maximum anterior or posterior shear of the mobilizing limb, whichever was greater (collected prior to trials) was required to move the

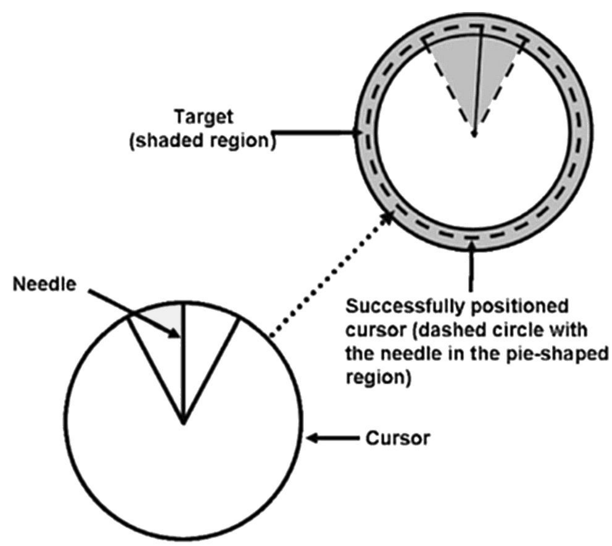

Figure 1: Depiction of the cursor used in standing target matching and successfully positioned cursor within target.

cursor to each target. Additionally, the mobilizing limb was required to minimize internal/external rotations loads by maintaining the needle in a narrow region of the cursor corresponding to 30% of maximum internal/external rotation. Lastly, subjects received no visual feedback of stabilizing limb.

Ground reaction force (GRF) data was collected via two force plates at 1000 Hz. Motion capture data was collected at 50 Hz via an 8 camera system (Qualysis Motion Capture System, Gothenburg, Sweden). Retro-reflective markers were placed on the subjectsô anatomical landmarks. Additionally markers adhered to rigid shells were placed on the thighs and shanks of subjects to aid in tracking motion of the lower limbs. Transverse knee moment for both limbs was calculated in Visual 3D using both GRF and kinematic data collected during the 500 ms period the cursor was located in the target.

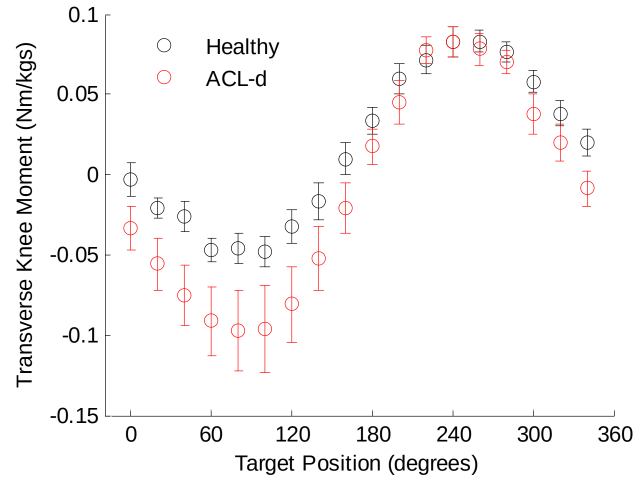

Figure 2: Average and standard error of the transverse knee moment normalized to body weight for each target position for healthy and ACL-d subjects while the limb is acting as the stabilizer. The ACL deficient limb is reported for ACL-d subjects. Here, 0°=abduction, 90°=extension, 180°=adduction and 270°=flexion

RESULTS AND DISCUSSION

External rotation, denoted as the negative transverse knee moment, of the stabilizing limb during knee extension was observed to be higher in ACL-d subjects when compared to healthy subjects (Figure 2), supporting our hypothesis. There were no differences in rotation moments during knee flexion between healthy and ACL-deficient subjects.

Being that the ACL restricts anterior tibial translation and internal rotation [2], measuring changes in external rotation for the stabilizing limb can provide insight to the effectiveness of this task to challenge the ACL-d subjects. For the targets 0° to 180°, the subjects are moving in the forward direction corresponding to knee extension. Near full extension (i.e., target position = 90°) the ACL acts as a major restraint to internal rotation [3]. In the absence of this restraint muscles surrounding the knee joint must produce a larger external rotation moment. Specifically, the ACL deficient subjects are acting to limit internal rotation of the tibia. At target positions corresponding to knee extension the ACL-d subjects maintain an internally rotated tibia confirming the external rotation moment is acting to limit internal rotation of the tibia. In this manner the standing target matching task is requiring subjects to maintain rotational stability in the absence of the ACL.

CONCLUSIONS

We believe that the standing target matching protocol is effectively challenging ACL deficient subjects in internal and external rotations in a safe and controlled manner. The ACL deficient limb is exhibiting higher external rotation moments during knee extension as a preventative measure in the absence of the passive restraint provided by the ACL. Future studies using this task can be used to understand stabilization strategies in both ACL deficient and ACL reconstructed populations.

REFERENCES

1. MacLeod, TD, et al. *Proceedings of ASB '11*, Long Beach, CA, USA, 2011.
2. Duthon, VB, et al. *Knee Surg Sports Trauamtol Arthrosc*, **14**, 204-213,2006.
3. Logerstedt DS, et al. *J Orthop Sports Phys Ther,* **40**, A1-A37, 2010.

ACKNOWLEDGEMENTS

The authors wish to thank NIH R01-AR046386.

NEAR-INFRARED LIGHT THERAPY DELAYS THE ONSET OF SKELETAL MUSCLE FATIGUE

Kelly A. Larkin, Evangelos A. Christou, Harsimran S. Baweja, Molly A Moore, Mark D. Tillman, Steven Z. George, Paul A. Borsa

University of Florida, Gainesville, FL, USA
Email: klarkin@hhp.ufl.edu

INTRODUCTION

Near-infrared light therapy has been implicated as an effective ergogenic aid to delay the onset of fatigue (1; 2). The most common manifestation of fatigue is impairment in muscle function and an inability to perform work. Fatigue is typically quantified with decreased force capacity within a target muscle (3). However, no studies have directly examined the ergogenic properties of near-infrared light therapy and its ability to enhance muscle activity, delay the onset of fatigue and prevent losses in muscular strength. The purpose of this work was to determine a therapeutic dose-response to near-infrared light therapy that will increase time to task failure (TTF) and muscle activation when performing a submaximal sustained contraction.

METHODS

The design of the study was a cross-over repeated measures, where each subject serves as their own control and receives all three treatments. A commercially available FDA approved Class IV phototherapeutic device (Lite Cure, LLC., Newark, DE) was used covering the muscle belly of the first dorsal interosseous (FDI). The electromyographic (EMG) activity from the FDI was recorded throughout the fatigue task. Neural activation of the FDI was quantified as the RMS amplitude of the EMG signal. Each subject received a 4 minute treatment. Each subject received 3 different doses of Phototherapy treatment (sham, 240 Joules, 480 Joules) during three separate testing sessions. Nine right hand dominant healthy collegiate aged participants (24.3 ± 4.9 yrs, 171.7 ± 7.8 cm, 71.2 ± 11.6 kg) with no current history of injury to the upper extremity, or previous history/pathology that would compromise hand function. The dependent variables were time to task failure when performing a submaximal isometric contraction following treatment with near-infrared light therapy. In addition we examined changes in muscular strength quantified as changes in 1 repetition maximum (1 RM).

RESULTS AND DISCUSSION

Time to task failure increased significantly following the 240J treatment compared with the sham treatment (391.56 ± 57.21 vs. 302.33 ± 55.93s; $P<0.032$; Figure 1). Although, the 480J treatment elicited a greater time to task failure it was not significantly different from sham (363.11 ± 60.61 vs. 302.33 ± 55.93s; $P=0.202$; Figure 1).

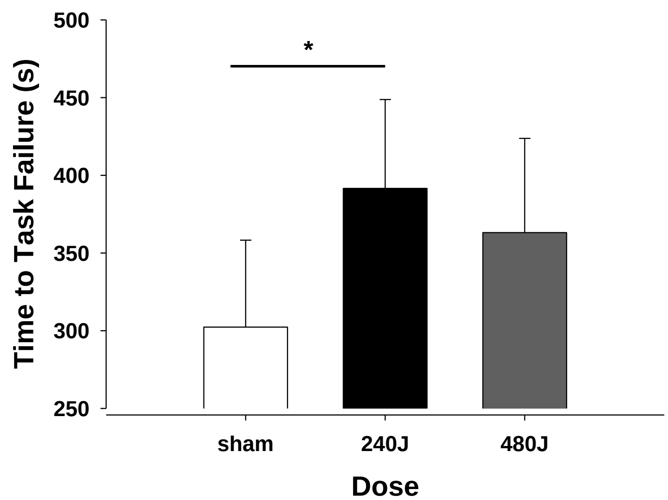

Figure 1. Time to task failure for a submaximal sustained contraction with the FDI. TTF was significantly (*) prolonged following a 240J treatment of near-infrared light therapy.

In addition, the treatment changed muscle activity. The EMG amplitude of the FDI was greater with the

240J and 480J treatments compared with the sham (Figure 2). This difference, however, did not reach statistically significant levels.

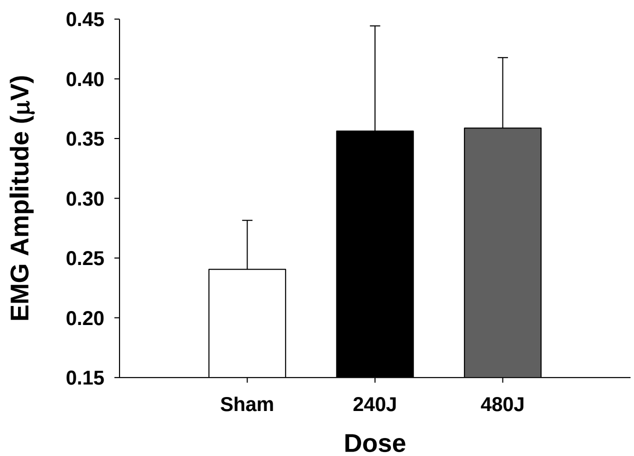

Figure 2. Change in EMG amplitude following 3 different treatments (sham, 240J, 480J) of near-infrared light therapy.

The decrease in 1RM following the sustained isometric contraction task was similar for all treatments, sham (21.2%), 240J (22.8%) and 480J (21.2%).

Our results, therefore, suggest that the 240J treatment was the most beneficial treatment to prolong time to task failure. On average, subjects sustained the submaximal isometric task 26% longer than when they received the sham. Because the 240J treatment also increased the muscle activity of the FDI, it is possible that the longer time to task failure was related to changes in the activation of the agonist muscle.

CONCLUSIONS

Our findings implicate a 240J dose of near infrared light therapy as an effective non-invasive ergogenic modality for health care providers to enhance time to task failure and potentially delay the onset of musculoskeletal fatigue. Future research studies are necessary to identify the mechanisms responsible for the prolonged time to task failure observed.

REFERENCES

1. Leal Junior ECP, Lopes-Martins RAB, de Almeida P, Ramos L, Iversen VV, Bjordal JM. Effect of low-level laser therapy (GaAs 904 nm) in skeletal muscle fatigue and biochemical markers of muscle damage in rats. Eur. J. Appl. Physiol 2010 Apr;**108**(6):1083–1088.[cited 2010 Oct 25]

2. Baroni BM, Leal Junior ECP, Geremia JM, Diefenthaeler F, Vaz MA. Effect of light-emitting diodes therapy (LEDT) on knee extensor muscle fatigue. Photomed Laser Surg 2010 Oct;**28**(5):653–658.[cited 2011 May 26]

3. Enoka RM, Duchateau J. Muscle fatigue: what, why and how it influences muscle function. J. Physiol. (Lond.) 2008 Jan;**586**(1):11–23.[cited 2011 May 26]

AGING IS ALL RELATIVE: MODELING THE RELATIONSHIP BETWEEN STRENGTH AND FATIGUE ON ENDURANCE TIME IN OLDER ADULTS

[1]Laura Frey Law, [1]Keith Avin, [1]Aruna Tumuluri

[1]University of Iowa, Iowa City, IA, USA
email: laura-freylaw@uiowa.edu

INTRODUCTION

Older adults fatigue less than younger adults for controlled relative-intensity tasks, particularly sustained and intermittent isometric contractions [1]. However this seems in opposition to anecdotal evidence that people fatigue more readily with advancing age.

To compare fatigue development between individuals, it is common to standardize the test contraction intensity to a percentage of the individual's maximum voluntary contraction (% max). Thus, the actual torque produced varies for each person, but the relative intensity is constant across individuals. Conversely, functional tasks require some level of joint torque, which may be proportional to total body mass, such as walking, stair climbing, or the sit-to-stand transfer, but not necessarily to peak strength. Thus, the relative intensity of the task (% max) will increase as strength decreases. The purpose of this study was to model the degree to which age-related advantages in fatigue resistance for relative-intensity tasks can be lost (or reversed) when considering functional tasks with varied levels of strength loss.

METHODS

To investigate this question, we modeled time to task failure (endurance time, ET), a widely utilized and accepted measure of fatigability, for various knee extension task intensities. Functional tasks can require a wide range of relative intensities, for example, sit-to-stand has been reported to require torques from 34% to 80% of maximum knee extension strength [2-5]. Thus, we chose to consider a range of reference task intensities (i.e. for young adults) in our analyses: 20, 30, 40, 50, and 60% of max. Assuming matching body mass and anthropometry, the relative intensity required to perform a functional task will depend on the peak strength (i.e., the denominator), as the numerator is assumed constant. With aging, strength declines can range from losses of 34 – 38% [6, 7] to 63% [3, 4] compared to young adults. Correspondingly, the increases in task intensity with strength decline (e.g.., aging) to perform a given task can be estimated by multiplying the reference task intensity (for young adults) by: 1/(1 – strength decline). For example, a 15% decrease in strength translates to an increase in relative intensity of (1/0.85)*reference task %max = 1.11*ref% or 11% increase. For our analyses, we analyzed a range of possible strength declines with aging: 0%, 15%, 35%, and 55%.

The second step of the process involved estimating the young vs. old adult intensity-ET curves. Starting with intensity- ET models developed for young adults [8], we applied observed age differences in fatigue (i.e., moderate effect sizes for constant relative intensity contractions = 0.53) [1] to develop fatigue curves for old adults. Using these intensity-ET curves, we modeled time to failure for each reference task intensity (i.e., young adult) and the corresponding ETs for old adults for each of the 4 strength decline levels (i.e., altered task intensities due to changed denominators). Thus for each task intensity (20, 30, 40, 50, and 60), 5 ETs were modeled.

RESULTS AND DISCUSSION

The young and old adult intensity – ET curves for knee extension are shown in Figure 1. The old adult curve is shifted up and to the right, reflecting the moderate increase in fatigue resistance observed in previous studies [1]. For each reference task intensity, the resulting increase in relative task intensity with increasing declines in strength are provided in Table 1. The corresponding ETs for each relative intensity and age group are also provided in Table 1. One reference task intensity (i.e., 30% max) and the corresponding higher intensities due to strength declines are shown in Figure 1 as one example. Note that for a constant relative task intensity, i.e., 30% max, the old adult can sustain the task 18% longer than the young adult. However, with even a small decline in strength (i.e., 15% loss, 18% increase in relative intensity), the ET is 12% less than the young (see Figure 1, Table 1).

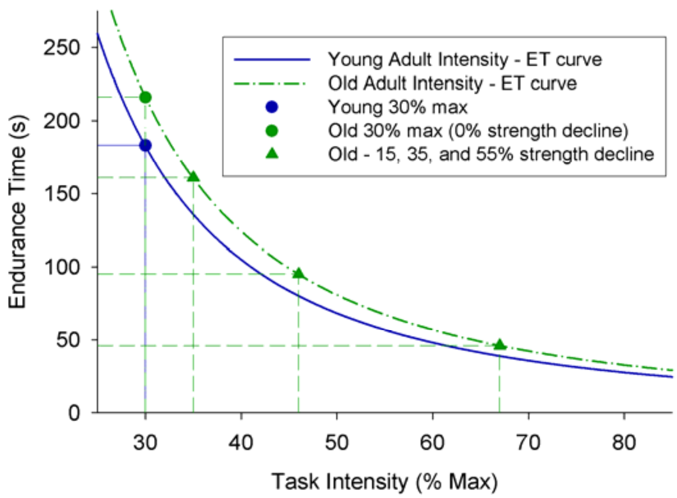

Figure 1: Young (solid blue line) [8] versus old (dashed green line) adult intensity-ET curves for the knee joint, with estimated ETs for a task intensity of 30% for the young adult, and the corresponding intensities for a range of strength declines in the older adult (0% – 55% decline in strength).

The differences in modeled task intensities we investigated for the older vs younger adults are consistent with previous studies. For example. the relative intensities required to complete the sit-to-stand task ranges from no difference between age groups [2] to nearly double the relative intensity (i.e., 78 -99% vs 34 – 42% max) for old vs young cohorts [3, 4].

CONCLUSIONS

We conclude that while fatigue resistance can improve with age, even small decrements in strength more than offset this advantage when considering the relative task intensities required to complete a functional task. This explains the apparent discrepancy between standardized fatigue studies and anecdotal observations with aging.

REFERENCES

1. Avin, KG et al., 2011. *Phys Ther* **91**, 1153-1165.
2. Bieryla, KA, et al., 2009. *J Electromyogr Kinesiol* **19**, 139-144.
3. Hortobagyi, T, et al., 2003. *J Gerontol A Biol Sci Med Sci* **58**, M453-460.
4. Hughes, MA, et al., 1996. *J Biomech* **29**, 1509-1513.
5. Kotake, T, et al., 1993. *Arch Phys Med Rehabil* **74**, 1095-1099.
6. Alexander, NB, et al., 1997. *Muscle Nerve* **Suppl 5**, S56-59.
7. Stoll, T, et al., 2000. *Clin Rheumatol* **19**, 105-113.
8. Frey Law, LA et al., 2010. *Ergonomics* **53**, 109-129.

ACKNOWLEDGEMENTS

The authors were funded in part by National Institutes for Health, K01AR056134 (LFL), NRSA F31 AR056175 (KA), the Foundation for Physical Therapy (KA), and the Virtual Soldier Research Group at The University of Iowa (LFL, AT).

Table 1: Results for 5 reference task intensities demonstrating the increase in intensity due to strength declines and their expected endurance times (ET) for young (reference) and old adults.

	Young Adult (Reference)		Old Adult (0% loss in strength)		Old Adult (15% loss in strength)		Old Adult (35% loss in strength)		Old Adult (55% loss in strength)	
Task	Intensity	ET (s)	Intensity	ET (s)	Intensity	ET (s)	Intensity	ET (s)	Intensity	ET (s)
1	20%	398	20%	471	24%	332	31%	203	44%	103
2	30%	183	30%	216	35%	161	46%	95	67%	46
3	40%	105	40%	124	47%	91	62%	53	89%	27
4	50%	68	50%	80	59%	59	77%	35	-	-
5	60%	48	60%	57	71%	41	92%	25	-	-

THE EFFECT OF LOAD ON MOVEMENT COORDINATION DURING SLED TOWING

[1]Michael Lawrence, [2]Daniel Leib, [2]Cara Masterson and [1]Erin Hartigan

[1]University of New England, Portland, ME, USA
[2]Boise State University, Boise, ID, USA
email: mlawrence3@une.edu

INTRODUCTION

Towing sleds while walking is a popular resistance exercise for the healthy athlete. One reason for the popularity of sled towing is that it is widely believed to be a 'functional' exercise. Preliminary research suggests towing while walking can increases lower extremity moment impulses; however whether towing a sled utilizes the same coordination patterns as un-resisted walking is unknown. While altered patterns may not be as relevant to a healthy athlete, sled towing is also sometimes used in the rehabilitation of athletes who sustained a lower extremity injury (anterior cruciate ligament rupture) with the goal of regaining movement symmetry. The addition of resistance to walking may induce a shift to a coordination patterns not consistent with normal gait and may not aid in the retraining of normal gait movement patterns.

Dynamic systems theory (DST) provides a framework for analyzing optimal coordination patterns and how patterns of functional movement are produced [1]. Segmental relations may be analyzed as a measurement of coordination and can be measured utilizing continuous relative phase angles (CRP). CRP uses a segment's angular position and angular velocity compressed into lower-order variables to assess coordination patterns and variability. Too much variation deteriorates the stability of the system and may lead to injury or undesired adaptations while too little does not allow for adaptation to perturbations [2]. Determining differences in attractor states can be done by assessing mean absolute continuous relative phase (MARP) while variability of movement can be measured by calculating deviation phase (DP), which is the mean standard deviation of the relative phase angle [3].

The goal of this study is to determine if towing sleds at two different loads (20 and 50% body weight (BW)) produce different lower extremity coordinative movement patterns and if those patterns are more or less variable than normal walking.

METHODS

13 healthy, uninjured subjects (9 males; 4 females), aged 21.0±1.9 years, were recruited for this study. Lower extremity motion during stance phase of gait was tracked using a cluster marker set.

Subjects completed 5 conditions: normal walking and sled towing with two loads (20 and 50% BW) with attachment at the waist and the shoulder. After walking, the order of towing conditions was randomized. For the purposes of this study only the attachment site at the waist was analyzed. Walking speed was set at 1.3 m/s for all conditions and was controlled using a Brower laser timing device [4]. Trials were collected bilaterally, but for this investigation only the dominant side was analyzed. Dominance was determined as the foot used to kick a ball; every subject was right limb dominant. Five stance phases of each condition were analyzed. Sleds were towed over an indoor rubber track (Super X, All Sports Enterprises). Kinematic data were collected with 8 Oqus Series-3 cameras (Qualisys AB, Gothenburg, Sweden) set at 60Hz. Visual 3D (C-motion, Germantown, MD) was used to apply a Butterworth filter with a cutoff of 6Hz to kinematic data.

Global sagittal segmental angles for the right foot, thigh, and shank were calculated in Visual3D, differentiated to obtain velocities, and both measures were normalized to stance. Phase plots were developed by plotting angular velocity verses angular position and phase angles were calculated according to the method of Stergiou et al [5]. Relative phase angles were then calculated between adjacent segments and MARP and DP were then calculated as described by Stergiou [3].

Two one-way ANOVAs with multiple comparisons (one for each segment pairing) were then performed using MATLAB 2011b (MathWorks, Natick, MA).

RESULTS AND DISCUSSION

MARP between the shank and thigh was significantly different ($p = 0.002$), with the 50% BW load being different than either normal walking or the 20% BW load. The difference in MARP indicates the movement pattern between the shank and thigh was altered when towing with the 50% BW load. MARP during normal walking and the 20% BW load were not significantly different. The DP was not significantly different for any comparisons, meaning there was not an increase or decrease in variability between loads, even when a new coordination pattern emerged. This study suggests that a large load (50% of BW) is required to alter inter-limb coordination patterns when the load is attached near the center of mass, such as attachment at the waist.

These results also suggest that the movement pattern between the shank and thigh is the first to be altered by the addition of resistance. Further investigations on the CRP of other movements is needed to determine if this pattern holds true for most movements or if movement pattern alteration is more specific upon load placement.

CONCLUSIONS

Towing sleds with a 20% BW load did not produce movement patterns that were different than normal walking. Therefore using a 20% BW load with a waist attachment may be an appropriate scenario to provide resistance to the lower limbs and still utilize a movement pattern consistent with normal walking.

Future studies should investigate differences seen using a finer load gradient to determine a more precise load threshold as well as between limbs comparisons. Future research should also investigate more dynamic resisted moments such as sprinting while towing sleds, towing a parachute, or wearing a weight vest to determine if a more dynamic movement is more easily changed to a different coordinative movement pattern. Although such movements have been previously investigated, conclusions were generally drawn using more traditional gait parameters, such as lower limb angles at specific gait events [6]. It may be that a high order analysis such as the comparison of continuous relative phase angles could provide more informative results.

REFERENCES

1. Scholz, J.P., *Dynamic pattern theory--some implications for therapeutics.* Phys Ther, 1990. **70**(12): p. 827-43.
2. Davids, K., S. Bennett, and K.M. Newell, *Movement system variability*. 2006, Champaign, IL: Human Kinetics. xii, 363 p.
3. Stergiou, N., *Innovative analyses of human movement*. 2004, Champaign, IL: Human Kinetics. xi, 331 p.
4. Bastien, G.J., et al., *Effect of load and speed on the energetic cost of human walking.* Eur J Appl Physiol, 2005. **94**(1-2): p. 76-83.
5. Stergiou, N., et al., *Intralimb coordination following obstacle clearance during running: the effect of obstacle height.* Gait Posture, 2001. **13**(3): p. 210-20.
6. Cronin, J., et al., *Effects of weighted vests and sled towing on sprint kinematics.* Sports Biomechanics, 2008. **7**(2): p. 160-72.

The Effect of Kinesio Taping on Kinematics and Muscle activity for Subjects with Neck Pain

Su-Ya Lee, Guan-Bo Chen, Mei-Ling Chou, Fong-Chin Su

Department of Biomedical Engineering, National Cheng Kung University, Tainan, TAIWAN
Email: panda740324@yahoo.com.tw

INTRODUCTION

Neck pain is widely prevalent in the working-age population and 5% of neck pain patients suffer from neck disability. Neck pain, obviously, resulted from highly repetitive work with arms' raise, neck forward posture and cervical muscle contraction. Previous studies showed neck pain patients decreased the range of motion (ROM) of flexion, extension, axial rotation and lateral bending; furthermore, neck pain patients increased movement variability at the same time.

Circumduction movement, definitely, is made up of lateral flexion and rotation in cervical joint, able to make subjects to do maximal joint movement with effort. According to previous studies, neck pain patients were prone to decrease deep muscle activity and increased superficial muscle activity. To determine the effects of kinesio taping on kinematics and electromyography (EMG) between normal and mild neck pain individuals during cervical circumduction should allow for better therapy prescription.

METHODS

Twelve men and women, age range from 20 to 35 years old, volunteered to participate in this study. Subjects were divided into two groups which based on the score of neck disability index (NDI), which is linked to the level of neck disorder. The score of NDI which is less than 8 was fully considered as normal subject and the score of NDI that is between 8 and 16 was defined as mild neck pain subject. The subjects who have severe neck disorders, trauma, cervical joint instability spasmodic torticollis, frequent migraine, peripheral nerve entrapment, shoulder diseases, inflammatory rheumatic diseases, severe psychiatric illness were excluded.

This study used three-dimensional motion-testing device (Electromagnetic Motion Tracking System, Polhemus, USA) to measure cervical ROM (Figure 1) and AMT-8 EMG system (Bortec, Inc. Calgary, AB, CA) to measure muscle activity on sternocleidomastoid (SCM) and upper trapezius. The kinesio taping was tapped on the upper trapezius muscle (Figure 2). Both of groups, without using kinesio taping, were initially asked to perform circumduction movement. Then subjects, with using kinesio taping, perform the circumduction movement again. The results for angle of joint movements and muscle activity were compared using paired t test. The significance was set at p<0.05.

Figure 1. The placement of motion-testing device

Figure 2. The placement of kinesio taping

RESULTS AND DISCUSSION

During counterclockwise circumduction, the neck pain group, without using kinesio taping on upper trapezius muscle, had significantly decreased extension ROM(p<0.05), which was compared to subjects without neck pain (Figure 3). The motion of left rotation and left side bending tended to decrease the ROM in neck pain subjects. Although there were no significant differences in ROM of clockwise circumduction, showing that the ROM in extension and left rotation was declined in neck pain subjects as well. Otherwise, neck pain subjects had less muscle activity during counterclockwise and clockwise movement (Figure 4).

Results show that there was no significant difference in the motion of counterclockwise and clockwise circumduction for subjects with or without neck pain after using kinesio taping (Figure 5); however, it was found that neck pain patients tended to decrease muscle activity in left sternocleidomastoid, right sternocleidomastoid, left upper trapezius and right upper trapezius after using kinesio taping (Figure 6). Besides, there were no consistence results in muscle activity for subjects without neck pain after kinesio taping intervention.

CONCLUSIONS

Kinesio taping could change muscle activity for subjects with neck pain. However, kinesio taping wasn't able to alter the joint movements of cervical circumduction either counterclockwise or clockwise circumduction for subjects with or without neck pain.

REFERENCES

[1] Szeto G.P. et al., 2009. *Man Ther* 14, 338-45.
[2] Sjolander P. et al.,2008.*Man Ther* 13, 122-131.

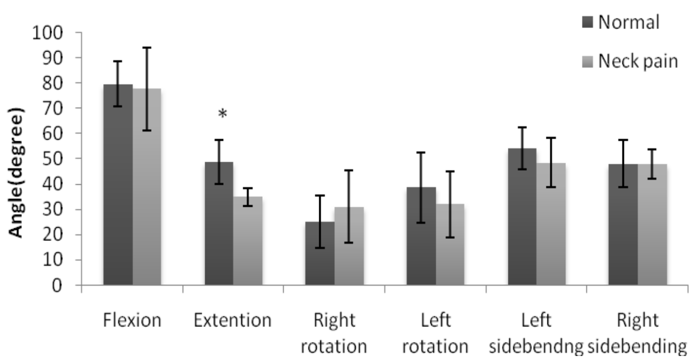

Figure 3. Joint movements in counterclockwise circumductionfor both groups without kinesio taping*p<0.05

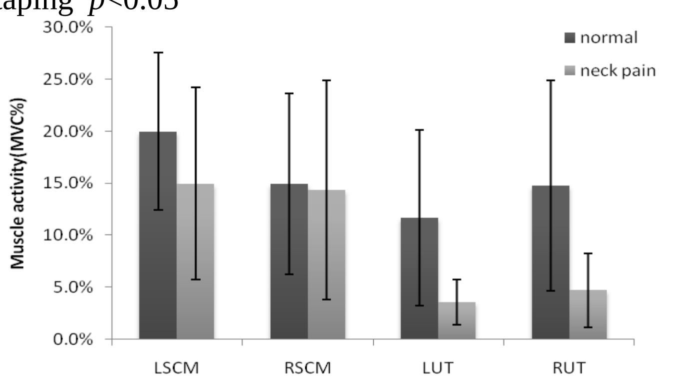

Figure 4. Muscle activity in clockwise circumduction for both groups without kinesio taping

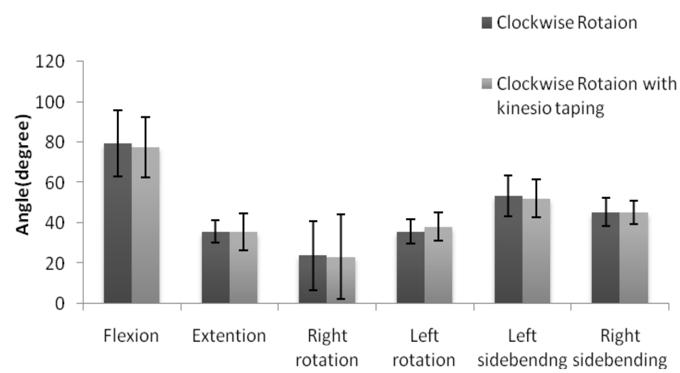

Figure 5. Joint movements in clockwise circumduction for neck pain subjects with kinesio taping

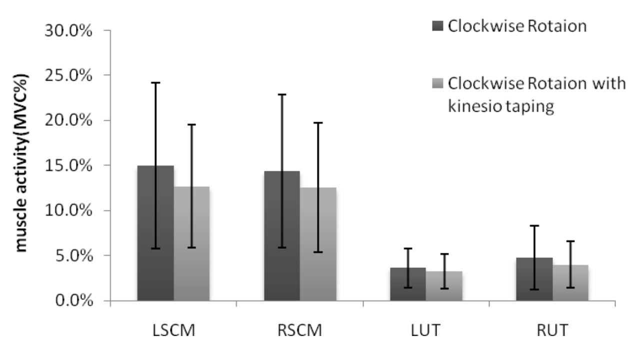

Figure6. Muscle activity in clockwise circumduction for neck pain subjects with kinesio taping

A NEW APPROACH TO UNDERSTAND POSTURAL INSTABILITY IN YOUNG CHILDREN WITH AUTISM SPECTRUM DISORDERS

[1]Hyokeun. Lee, [1]Shinichi Amano, [2]Kim Fournier, [1]Krestin Radonovich, [1]Chris J. Hass

[1]University of Florida, Gainesville, FL, USA
[2]University of Texas Pan American, Edinburg, TX, USA
email: leehk82@ufl.edu

INTRODUCTION

Self-stimulatory behavior is one of the characteristics in children with autism spectrum disorders (ASD). Self-stimulation causes repetitive and stereotypic behavior such as unusual ritualistic hand and body movement. Previous research suggests that these unusual movements in children with ASD may stem from one of the motor control deficits. Furthermore, this abnormal motor control ability manifests in impaired postural stability in children with ASD [1].

Numerous studies support a deficit in the postural control ability of children with ASD during quiet stance. Unfortunately, most studies solely focused on standing posture and the comparison of postural control ability between children with ASD and typically developing (TD) children, not emphasizing the underlying mechanism through which such differences occur. Thus, to further understand to the breadth of postural control abilities, we calculated and evaluated the 'Approximate Entropy' (ApEn) during quiet sitting [2]. Approximate Entropy is regarded one of the reliable and predictable parameters to assess postural control, or more importantly, is believed to provide insight into the structural nature of how the movement is controlled [3]. It is generally believed that a decrease in value of nonlinear measures such as ApEn are indicative of a less complex system.

For our present study, we hypothesized that children with ASD would have a difficulty with postural control in quiet sitting as a result of motor control deficits and these deficits would be highlighted by lower ApEn values in the COP time series data.

METHODS

For quite sitting performance, 16 children diagnosed with ASD (5.3±1.2 yrs, 114.8±11.5 cm, 23.7±6.5 kg) and 16 TD children (6.1±1.3 yrs, 114.5±7.4 cm, 20.3±3.0 kg) participated. All children and their legal guardians provided written informed consent as approved by the University of Florida institutional review board.

During quiet sitting trials, children were asked to sit quietly while watching a video segment with engaging images and sounds (Baby Einstein Mozart, The Baby Einstein Company, LLC).

Ground reaction forces and moments were recorded from a force plate embedded level with the laboratory floor (Type 4060–10, Bertec Corp., Columbus, OH) 360 Hz) while the children sat as still as possible on a child size stool with their feet firmly on the floor. Four, 120 s experimental trials were collected. The location of the center of pressure (COP) was calculated from the force plate data and each trial was divided into 20 s time intervals for the determination of ApEn data. ApEn values for the anteroposterior (ApEnx) and mediolateral (ApEny) components were calculated using customized Matlab software (Mathworks, Natick, MA). Independent T-test were used to compare performance between ASD and TD children with an aprior level of significance of $p \leq 0.05$. All statistical tests were performed using SPSS 16.0 for Windows (Chicago, Illinois).

RESULTS

First of all, there was a significant difference in COP sway area between children with ASD and TD ($p < 0.05$). Children with ASD showed 238% greater sway area values than children with TD. In addition, children with ASD showed significantly smaller ApEn values in both the anteroposterior (AP) and mediolateral (ML) direction compared to TD children. The ApEn values were 28% smaller in AP direction and 31% smaller in the ML direction.

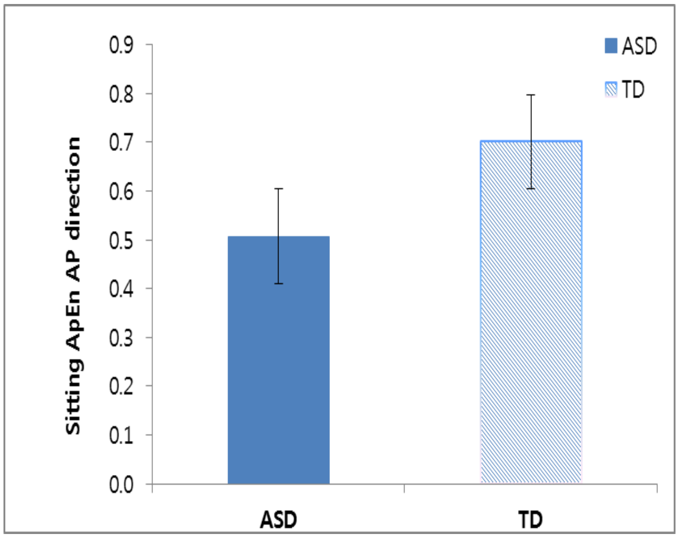

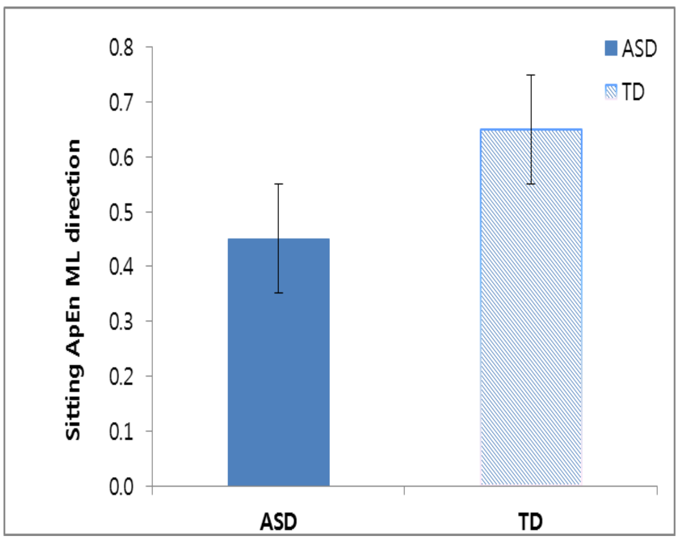

Figure 1: Box plot for ApEn on AP and ML direction.

DISCUSSION

Our results showed that children with ASD had smaller ApEn in the both AP and ML direction compared to TD children. Smaller ApEn values indicate a reduced complexity of the COP time series data. This suggests that children with ASD possess more regularity in shifting their body weight while sitting quietly. The findings of the current study are aligned to previous findings reporting that clinical population with motor control deficits show relatively lower COP variability with a regular pattern when compared to age matched controls.

CONCLUSIONS

The ApEn results from present study suggest that postural control during quiet sitting is influenced by nonstrategic repetitive behavior and is believed to be indicative of more widespread motor control deficit associated with the disorder. To further elucidate disruptions in postural control system of individuals with ASD, dynamic and functional movements such as gait initiation and sit-to walk should be examined in future.

REFERENCES

1. Fournier K, et al. J *Autism and Developmental Disorders* 2010 Oct;40(10):1227-40.
2. Bodifish, J. et al. J *Autism and Developmental Disorders*, 30, 237-43, 2000
3. James T Cavanaugh, et al. *J NeuroEng and Rehab*, 4:42, 2007.
4. Pincus, SM. Proc Natl Acad Sci USA, 88(6): 2297-301, 1991

ACKNOWLEDGEMENTS

Autism Speaks #CH/1964/01-201007-065-00-00

Associations between motor unit recruitment and the rates of strain, force rise and relaxation

Sabrina S.M. Lee[1], Maria de Boef-Miara[2], Allison S. Arnold[2], Andrew A. Biewener[2], James M. Wakeling[1]
[1]Department of Biomedical Physiology and Kinesiology, Simon Fraser University, Burnaby, Canada,
[2]Department of Organismic and Evolutionary Biology, Harvard University, Cambridge, USA
sabrina_lee_4@sfu.ca

INTRODUCTION

Muscles are able to produce the forces required for a wide range of locomotor tasks — tasks requiring different fascicle strains and strain rates. Different motor unit types have specific physiological and mechanical properties (i.e. strain rates and activation-deactivation rates), and there is evidence that during rapid locomotor tasks, preferential recruitment of faster motor unit types occurs [1,2]. However, the mechanical factors that influence motor unit recruitment remain unclear. Myoelectric signals with higher frequency content have been associated with greater fascicle strain rates [1,2], suggesting that there may be a mechanical basis for preferentially recruiting faster motor units. However, whether preferential recruitment of faster motor units is also associated with faster force rise and relaxation rates is not known. The focus of this study is to determine if different motor units are recruited in task-specific patterns during locomotion and to assess whether recruitment is influenced by mechanical factors such as strain, strain rate, force, and force rise-relaxation rates.

METHODS

Six African pygmy goats (*Capra hircus;* 3 males, 3 females, age 21 ± 15.5 months, mass 25.85 ± 6.20 kg) were tested at Harvard University's Concord Field Station. Electromyography (EMG), fascicle strain, and tendon force of the lateral and medial gastrocnemius muscles were recorded using surgically implanted offset twist-hook bipolar silver-wire electrodes (0.1mm, California Fine Wire Inc.), sonomicrometry crystals (2mm, Sonometrics Inc.), and a tendon buckle on the Achilles tendon, respectively. Recordings were made during different gaits (walk, trot, and gallop) on a level and incline surface on a treadmill (Fig. 1).

We used wavelet analysis, a time-frequency decomposition technique [3], and principal component analysis (PCA) to identify the major features of the myoelectric intensity spectra. The angle, θ, formed between the vector of the first and second principal component, PCI-PCII, loading scores and the PCII loading score axis was used to quantify the contribution of high and low frequency content in the myoelectric signal (Fig. 2). A signal with a small angle θ has a positive contribution from the PCII loading score and is interpreted as having relatively high frequency content associated with faster motor unit recruitment. Analysis of variance was conducted to compare myoelectric intensity, angle θ, and mechanical factors (muscle force, force rise-relaxation rates, fascicle strain, and strain rates) between muscles, gaits, and grades. A general linear model analysis of covariance was conducted to identify significant associations between angle θ and myoelectric intensity and the mechanical factors.

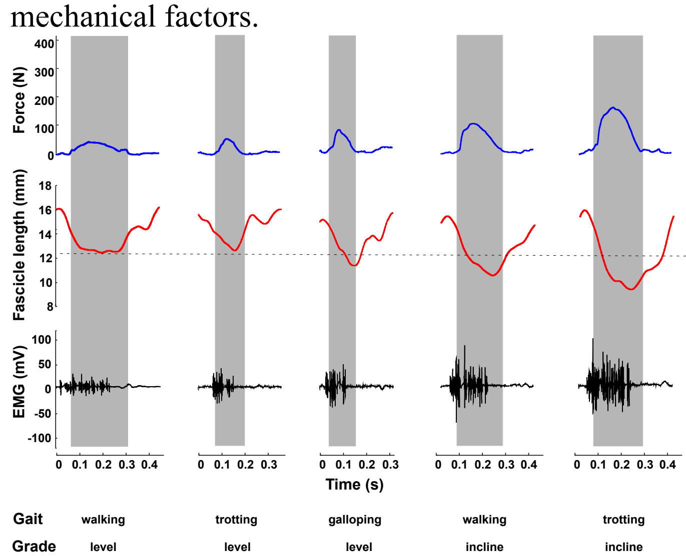

Figure 1: Representative lateral gastronecmius force (blue), fascicle length (red), and myoelectric signals from fine-wire EMG (black) of a goat during different locomotor tasks. Shaded grey area indicates stance phase.

RESULTS AND DISCUSSION

Myoelectric intensity, fascicle strain, strain rate, force, and force rise-relaxation rates all increased as gait velocity increased from walking to trotting to galloping ($p<0.05$). These measures were greater during locomotion on an incline surface compared to the same level speed ($p<0.001$).

Angle θ decreased as gait velocity increased from level walking to trotting to galloping (Figure 2), suggesting that different motor units were recruited depending on the task. At faster speeds, the myoelectric signal contained higher frequency components. This shift to higher frequencies was due to a decrease in the low frequency components and an increase in the high frequency components of the spectra, indicating that a greater number of fast motor units were recruited while fewer slow motor units were recruited. These results support previous observations in other animals and man that faster motor units may be preferentially recruited for tasks that require rapid shortening-lengthening cycles [2,3]. EMG recordings from the LG had smaller values of angle θ (higher frequency content) than recordings from the MG. This finding is consistent with previous work on *in situ* motor unit recruitment in goats [4] and is mostly likely caused by the higher proportion of fast fibres within the goat LG (unpublished immunohistochemistry results).

Although we found no evidence that faster motor units were recruited for tasks that required rapid force rise-relaxation rates, we did find that preferential recruitment of faster motor units was associated with faster shortening fascicle strain rates in some cases (Table 1, $p<0.001$). Thus, the increased shortening velocities of faster motor units may provide benefits at faster locomotor speeds.

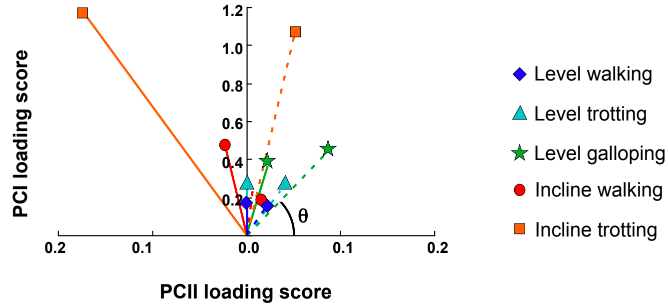

Figure 2: PCA of the myoelectric signals. PC I and II loading scores for MG (solid) and LG (dotted) during different locomotor tasks reveal differences in myoelectric frequency content and motor unit recruitment

CONCLUSIONS

We observed that motor units in the goat LG and MG muscles are recruited in patterns that are task-specific during locomotion. We also observed cases where preferential recruitment of faster fibres was related to faster fascicle shortening strain rates. These findings offer crucial insight into the basic neuromechanical mechanisms of producing movement.

REFERENCES

1. Wakeling JM, et al. *J R Soc Interface* **3**, 533-544, 2006.
2. Hodson-Tole E, et al. *J Exp Biol* **211**, 1893-1902, 2008.
3. Von Tscharner V. *J Electromyogr Kinesiol* **10**, 433-445, 2000.
4. Lee SSM et al. *J Electromyogr Kinesiol* **21**, 557-565.

ACKNOWLEDGEMENTS

We thank Drs. Jennifer Carr and Carlos Moreno for assistance during data collection. This work was supported by the NIH (R01AR055648).

Table 1: Summary of the effect of mechanical and excitation variables on angle θ. The arrows denote the direction of association: ↑ positive and ↓ negative when the covariates are significant ($p<0.05$).

Variables	Total intensity	Strain	Strain rate	Force	Force rate
Force rise	↓		↑	↓	
Force relaxation	↓	↓	↑	↓	

Changes in Muscle Co-activation in Spinal Cord Injured Individuals After Body-Weight Supported Treadmill Training

[1]Sabrina S.M. Lee, [2]Katherine Pauhl, [1]Erika Harder, [2]Tania Lam, [1]James M. Wakeling[1]
[1]Simon Fraser University, Burnaby, BC, Canada
[2]University of British Columbia, BC, Canada
E-mail: sabrina_lee_4@sfu.ca

INTRODUCTION

Locomotor training with body weight supported treadmill training (BWSTT) is a commonly used rehabilitation tool for retraining individuals with incomplete spinal cord injury (SCI) [1]. It is often augmented with robotic devices to assist leg movements [2], however, there is recent evidence that resistance to leg movements, instead of assistive forces, results in increased flexor muscle activity through enhanced afferent feedback [3]. As sufficient foot clearance can be problematic for SCI individuals, the timing of muscle activation is crucial for normal gait. Electromyography (EMG) is often used to measure muscle activity, in addition to kinematics and kinetic measurements to evaluate gait function. Recent methods of using wavelet analysis to resolve EMG signals into frequency components provide information beyond the standard timing and amplitude measures [4,5]. The purpose of this study is to investigate the influence of BWSTT on co-activation between antagonistic muscles using wavelet analysis.

METHODS

We tested individuals (n=7, 42.0±14.3 yrs, 1.75±0.12 m, 79.7±22.6 kg) who had incurred an incomplete spinal cord injury due to a non-progressive lesion above the thoracic level of T10, at least 12 months prior to recruiting to the study. Subjects were tested pre- and post- training where they walked on a treadmill while in body weight supported harness (the minimum support necessary) at their self-selected comfortable and maximum speeds. EMG data were collected bilaterally from the tibialis anterior (TA), medial gastrocnemius (MG), rectus femoris (RF), and biceps femoris (BF) (Delsys, Boston, MA). Force sensitive resistors were used to detect foot contact and toe-off. After the initial visit, subjects participated in a BWSTT program where they walked on a treadmill with a harness that supported a percentage of their body weight, while the Lokomat device applied velocity-dependent moment against the hip and knee joints in the sagittal plane that was scaled to their maximum hip and knee flexor voluntary contraction (Lokomat: Hocoma, AG, Volketswil, Switzerland). All subjects underwent 45 minutes walking session, three days a week, for a total of 36 sessions. Age-, gender-, and height-matched healthy individuals (n=10, 40.0±12.8yrs, 1.75±0.09m, 74.5±13.6kg) were also tested at the same % body weight support and velocities as their matched SCI. Data for approximately 50 strides per subject from the pre- and post-training tests were analysed. EMG signals were resolved into time-frequency components using wavelet analysis [4,5]. The mean intensity at each wavelet domain (10 wavelets ranging from 19.29 Hz to 395.4 Hz) was calculated to generate an intensity spectrum. The correlation coefficient, r, was calculated for the EMG intensities between pairs of antagonistic muscles at each frequency band to generate a correlation spectrum. The intensity spectra and correlation spectra were analysed using principal component analysis [5]. We calculated an *EMG-normalcy score* as the resultant distance between the principal component loading scores for each antagonistic muscle pair and the mean principal component loading scores for the control subjects. ANOVA was performed to determine the effect of training, antagonistic muscle pair, speed, gait phase, and subject (random) on the mean correlation coefficient with Tukey post-hoc tests when appropriate.

RESULTS AND DISCUSSION

For the TA-MG muscles, the correlation coefficient of pre-training SCI was significantly greater than that of healthy controls ($p = 0.02$) and tended to be greater than that of post-training SCI (Fig. 1). BWSTT decreased the correlation between the MG-TA muscles especially at the mid-range frequencies (Fig. 1). Correlation and coordination of the RF and BF also improved after BWSTT (Fig. 1), although not as substantially as the more proximal muscles. The EMG normalcy-score, calculated from the PCI and PCII loading scores (Fig. 2) were significantly less after training for MG-TA ($p = 0.03$), indicating that muscle function improved during training.

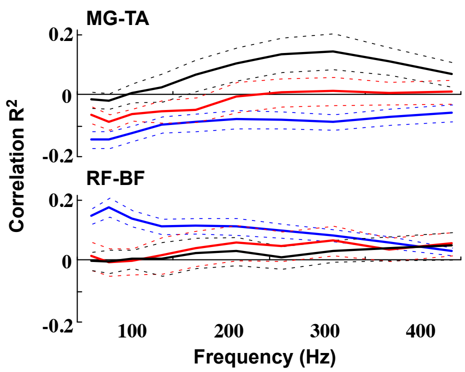

Figure 1: Correlation spectra of EMG intensities between muscles of healthy controls (blue), pre-training SCI (black), and post-training SCI (red) of the antagonistic pairs of muscles: 1) medial gastrocnemius (MG) and tibialis anterior (TA) and 2) rectus femoris (RF) and biceps femoris (BF).

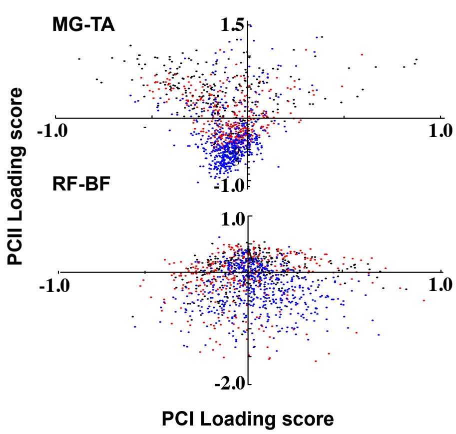

Figure 2: First and second principal component (PCI and PCII) loading scores of intensity and correlation spectra of healthy controls (blue), pre-training SCI (black), and post-training SCI (red) of the antagonistic pairs of muscles: 1) medial gastrocnemius (MG) and tibialis anterior (TA) and 2) rectus femoris (RF) and biceps femoris (BF).

Body weight supported treadmill training with resistance at the hip and knee joints appears to decrease the co-activation of the MG-TA muscles during gait. We are currently analyzing a set of similar data for a group of SCI individuals that underwent BWSTT with assistive forces applied to the hip and knee joints for comparison. Using wavelet analysis, we can calculate the intensity and correlation between antagonistic muscles over a range of frequencies. This EMG method considers the variation in frequency components in the EMG signal and is therefore more informative of muscle activity than traditional methods. This is useful in developing and assessing training interventions as specific frequencies can be targeted. Application of this EMG analysis to quantify and evaluate muscle dysfunction and coordination in SCI offers new insights into the fundamental mechanisms behind SCI impaired gait and into the effectiveness of rehabilitation treatments.

CONCLUSIONS

Body weight supported treadmill training with resistance at the hip and knee joints is an effective rehabilitation training that improves co-activation of antagonistic muscles. By employing advanced EMG processing techniques such as wavelet analysis and principal component analysis, information about the frequency content of the EMG signal can be obtained which is more informative that traditional methods and provides insight into muscle dysfunction and coordination in SCI individuals.

REFERENCES

1. Barbeu H, et al. *Curr Opin Neurolo* **14**, 735-740, 2001.
2. Behrman AL, et al. *Phys Ther* **85**, 1356-1371, 2005.
3. Lam T, et al. *Neurorehabil Neural Repair* **22,** 438-446, 2008.
4. Von Tscharner V. *J. Electromyo Kines* **10**, 433-445, 2000.
5. Wakeling JM. *Gait and Posture* **25**, 580-589, 2007.

Individuals with Diminished Hip Abductor Muscle Strength Exhibit Higher Moments & Neuromuscular Activation at the Ankle during Unipedal Balance Tasks

Szu-Ping Lee and Christopher Powers

University of Southern California, Los Angeles, CA, USA
email:szupingl@usc.edu web:http://pt2.usc.edu/labs/mbrl/index.html

INTRODUCTION

Coordinated control of the hip and ankle is important for maintaining postural stability.[1] The hip provides a greater degree of modulation of the body center of mass (COM), while the ankle fine-tunes the COM location and maintains effective foot contact to the supporting surface.[2,3] Existing literature suggests that diminished hip muscle strength is associated with loss of postural stability,[4,5] however the associated compensatory adaptations in lower extremity control have not been elucidated. It is plausible that persons with diminished hip muscle strength may exhibit increased reliance on the ankle to reposition the body COM (ie ankle strategy).[6] If true, this could explain the findings of several clinical studies that have reported hip muscle weakness is often associated with recurrent ankle sprain and soft tissue injuries.[7,8]

The purpose of the current study was to compare postural stability, as well as frontal plane moments and neuromuscular activation at the ankle during unipedal balance tasks in females with contrasting levels of hip abductor muscle strength. When compared to persons with stronger hip abductors, we hypothesized that individuals with diminished hip abductor strength would exhibit: 1) increased medial-lateral center of pressure (COP) displacement, 2) increased ankle inverter and everter moments, and 3) increased activation of the peroneus longus and tibialis anterior.

METHODS

Forty-five females between the ages of 23 to 34 participated in this study. All subjects were recreationally active and free of any existing injuries, pain or history of surgery to the lower extremity and the lower back.

Hip abductor muscle strength was assessed using a previously described weightbearing method.[9] More specifically, subjects' hip abductor force generation capacity was assessed in a squat position (50° knee flexion and 30° hip flexion) using a force tranducer connected to a non-stretchable fabric belt wrapping around the distal ends of both femurs (Figure 1)

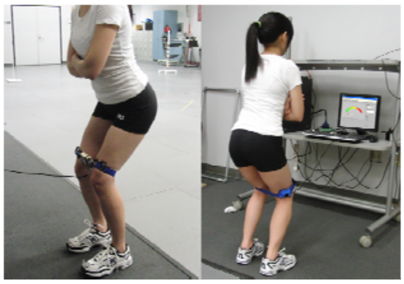

Fig 1: Weightbearing Assessment of Hip Abductor Strength

COP, ankle kinematic and kinetic data were collected using a force platform (AMTI, MA, USA, sampling frequency = 1500Hz), and a 11-camera motion capture system (Qualisys, Gothenburg, Sweden, sampling frequency = 250Hz). EMG signals from the peroneus longus (PL) and tibialis anterior (TA) were recorded using a EMG system (MA-300, Motion Lab Systems, LA, USA, sampling frequency = 1500Hz).

Static Standing Balance Task

Participants were instructed to stand on the preferred leg with the hip and knee of the stance leg extended, and the arms folded across the front of the chest. Subjects were informed that the goal of the task was to stand as steady as possible for a duration of 20 seconds. A total of 3 static balance trials were collected.

Dynamic Step-down Balance Task

Participants were instructed to lower themselves from an elevated force platform, touch their heel on the lower step, then return to the starting position over a 2-second period (Figure 2). The height of the step was normalized to the each subjects' height (10% of body height).[10] A metronome (set at 30 beats per minute) was used to guide the rate of the step-down task. One trial consisted of 5 consecutive up-and-down repetitions (10 seconds). A total of 3 dynamic balance trials were obtained.

Figure 2: Dynamic Step-down Balance Task

The biomechanical variables of interest included the mean medial-lateral COP displacement, peak ankle inverter and everter moments, and PL and TA activation amplitude during each of the balance tasks. The mean values from 3 trials for each condition were used for statistical analysis.

Participants were ranked based on their hip abductor muscle strength. The top 33% of the participants were categorized as the strong group (n=15) and the lower 33% as the weak group (n=15). To determine if postural stability, ankle biomechanics, and neuromuscular activation of the ankle muscles varied between groups across the two balance tasks, 2 x 2 (group x task) mixed analyses of variance (ANOVAs) tests with task as a repeated factor were performed. Significance level for all statistical procedures was set at 0.05. Effect size of the group difference in each dependent variable was presented by a Cohen's D value.

RESULTS AND DISCUSSION

Significant group effect was observed for mean medial-lateral COP displacement, and peak ankle inverter and everter moments. When averaged across tasks, individuals with low hip abductor muscle strength exhibited greater medial-lateral COP displacement, and greater peak inverter and everter moments (Table 1). With respect to neuromuscular activation, a significant group effect (no interaction) was observed for PL muscle EMG amplitude when averaged across tasks. On average, subjects in the weak group exhibited significantly higher PL activation when compared to the strong group (Table 1) No significant main effect or interaction was observed for TA activation.

CONCLUSION

Persons with relatively weak hip abductors exhibited decreased medial-lateral postural stability and increased utilization of an ankle strategy to maintain balance. This was reflected by the findings fo decreased medial-lateral postural stability as well as increased frontal plane ankle moments and increased peroneus longus activation. We propose that hip abductor weakness may, in part, explain clinical observations of increased risk of ankle injury in this population. Therefore, hip abductor muscle performance should be considered as part of the evaluation of persons with diminished balance and/or recurrent ankle injury.

REFERENCES

1. Runge et al. *Gait Posture*. 1999;10(2):161-70.
2. Hoogvliet et al. *Arch Phys Med Rehabil.* 1997;78(3):284-9.
3. Riemann et al. *Arch Phys Med Rehabil.* 2003;84(1):90-5.
4. Gribble & Hertel *J Electromyogr Kinesiol*. 2004;14(6):641-6.
5. Bisson et al. *Gait Posture*. 2011;33(1):83-7.
6. Nashner & Mccollum *Behavioral and Brain Sciences.* 1985;8(1):135-150.
7. Kulig et al. *J Orthop Sports Phys Ther*.41(9):687-94.
8. Friel et al. *J Athl Train.* 2006;41(1):74-8.
9. Lee & Powers *Proceedings of American Society of Biomechanics Annual Meeting*; Long Beach, CA 2011.
10. Willson & Davis *Clin Biomech* . 2008;23(2):203-11.

ACKNOWLEDGEMENTS

This study is partially supported by the International Society of Biomechanics Student Dissertation Award

Table 2: Group differences for each variable of interest (averaged across both tasks)

	Weak	Strong	p-value	Cohen's D
Mean medial-lateral COP displacement (mm)	13.6 ± 11.7	9.8 ± 6.0	0.046	0.41
Ankle kinetic variable (Nm/kg)				
Peak inverter moment	0.31 ± 0.10	0.25 ± 0.11	0.03	0.57
Peak everter moment	0.04 ± 0.06	-0.02 ± 0.07	0.01	0.92
EMG activation amplitude (% MVIC)				
PL	0.46 ± 0.12	0.36 ± 0.15	0.003	0.78
TA	0.21 ± 0.10	0.18 ± 0.09	0.17	0.39

STUDY ON LUMBAR MORPHOLOGICAL MEASUREMENTS OF KOREAN ADULTS AND THE ELDERLY

[1]Euiseok Lee, [1]Ilgyu Kang, [1]Sunghyuk Park, [1]Jaehyuk Yang,
[2]Deokyeon Cho, [2]Cheolwoong Ko and [2]Keyoungjin Chun

[1]Korea University Guro Hospital, Seoul, Korea
[2]Korea Institute of Industrial Technology (KITECH), Cheonan, Korea
email: cheko@kitech.re.kr web: http://www.kitech.re.kr

INTRODUCTION

The chair system is a common piece of equipment utilized for various purposes in daily life. Due to the rapidly aging society of Korea, the need for a chair system appropriate for the elderly has mounted. The current chair systems, however, do not fully conform to a structure that is ergonomically suitable and convenient for the elderly. This seems to be mainly due to the lack of biomechanical information in relation to changes in the posture of skeletal systems, such as the spine, that occur with age. Recently in Korea, a chair system was designed in consideration of human body shapes, however, there have been few systematic studies based on the analysis of skeletal morphology.

To acquire anthropometric information of the human lumbar useful for the optimal development of an ergonomic chair system, this study compared Korean lumbar shapes in various postures. With Korean males in their 20's and elderly males in their 60's, X-ray examination on the lumbar was conducted in defined postures, and the lordotic angles and the end plate angles between the vertebral bodies were measured and analyzed based on these X-ray images.

METHODS

This study newly fabricated a simplified chair device with 3 segmental rigid plates that can be adjusted to various angles (0°, 30°, 60°, 90°) (Figure 1) to obtain lumbar shape information (L1～L5) for each posture. The subjects included 7 Korean males in their 20's (Height: 171.7±5.3cm, Weight: 71.3±9.9kg) and 7 Korean elderly males in their 60's (Height: 163.6±5.6cm, Weight: 63.9±9.0kg), close to the Korean standard sizes according to a Korean body measurement survey (Sizekorea, 2004). Those who had been diagnosed with mental disorders, lumbar problems during the last 6 months or had a suspicious medical history were excluded from being subjects. This study was approved by the Institutional Review Board (IRB NO. MD10024). A total of 5 conditions (Supine, Angle 30°, 60°, 90° and Standing) were defined, and the subjects maintained neutral postures while the X-rays were being taken (Figure 2). For the X-ray images, Mimics 13.1 (Materialise, Belgium) was utilized to analyze the lordotic angles and end plate angles between the vertebral bodies (Figure 3, Figure 4).

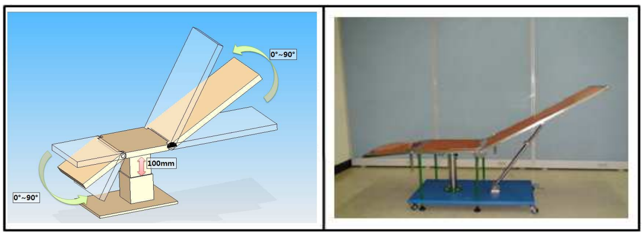

Figure 1: Simplified chair device with 3 segmental rigid plates for X-ray examination

Figure 2: X-ray examination conditions (Supine, Angle 30°, 60°, 90° and Standing)

RESULTS AND DISCUSSION

According to the measured results of the adults in their 20's (Figure 5, Table 1), the largest lordotic angle (φ) was observed in the standing condition (56.28°) while the angle declined in general from the supine to the 30°, 60° and 90°-seating conditions. As for the end plate angles (φ1~φ5) between the vertebral bodies (L1~L5), φ5 was largely measured in comparison to φ1~φ4. In case of the elderly in their 60's (Figure 5, Table 1), the largest lordotic angle (φ) was found in the standing condition (58.88°) while the angle declined in general from the supine to the 30°, 60° and 90°-seating conditions. However, the changes in lordotic angles at the standing, supine and 30°-seating conditions were remarkably small compared to those of the adults in their 20's, which indicated the lumbar characteristics of the elderly. As for the end plate angles (φ1~φ5) between the vertebral bodies (L1~L5), φ5 was larger than φ1~φ4.

CONCLUSIONS

This study comparatively analyzed the lordotic angles and plate angles between the vertebral bodies through X-ray examination on Korean adults and the elderly. It is expected that the data accumulated by this process will be useful for the development of ergonomically suitable chair systems.

ACKNOWLEDGEMENTS
This study was funded by the Ministry of Health and Welfare of Korea (A101945).

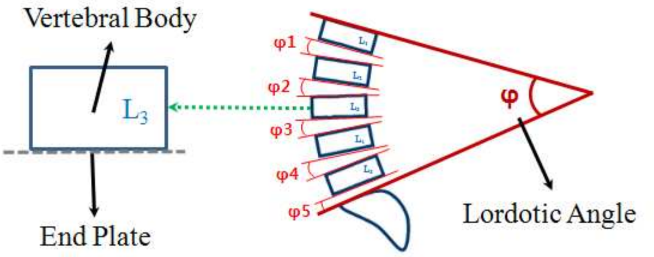

Figure 3: Measurement location of angles in lumbar

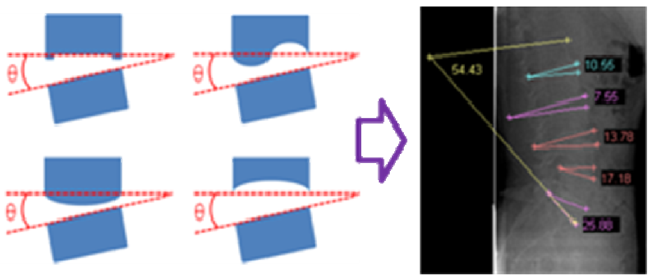

Figure 4: Measurement references of angles in lumbar based on the X-ray images

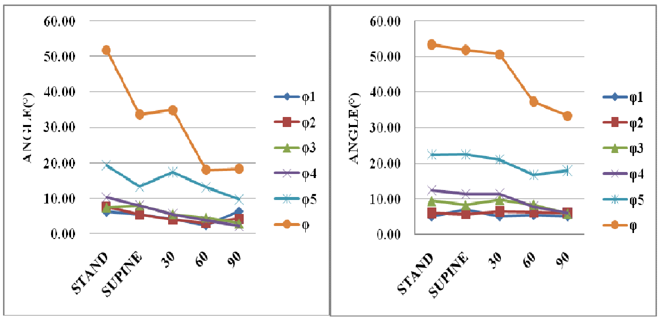

Figure 5: Measurement results of angles in lumbar (Left: adults / Right: the elderly)

Table1: Summary of lumbar angles based on X-ray images of Korean adults and the elderly

Positions		STAND		SUPINE		30°		60°		90°	
		Angle(°)	S.D.	Angle(°)	S.D.	Angle(°)	S.D.	Angle(°)	S.D.	Angle(°)	S.D.
Adults in their 20s	φ1	6.22	2.91	5.57	3.44	4.16	3.30	2.35	2.05	6.39	2.48
	φ2	7.68	2.72	5.50	1.31	4.03	1.50	3.07	1.30	4.28	1.79
	φ3	7.47	3.12	7.97	3.53	5.57	3.18	4.58	1.73	2.96	3.92
	φ4	10.21	3.83	8.05	2.13	5.50	3.74	3.71	1.12	2.16	3.64
	φ5	19.39	7.77	13.28	7.40	17.33	7.83	13.20	9.82	9.68	2.58
	φ	**51.79**	**5.00**	**33.68**	**15.35**	**34.94**	**13.07**	**18.01**	**12.39**	**18.31**	**17.91**
The Elderly in their 60s	φ1	5.04	1.51	7.07	1.84	5.07	2.30	5.44	1.75	5.04	1.24
	φ2	6.07	2.27	5.75	1.68	6.43	2.57	6.32	3.44	6.08	3.78
	φ3	9.44	2.07	8.29	3.12	9.81	4.16	8.43	2.75	5.85	2.87
	φ4	12.46	4.16	11.38	4.45	11.39	4.98	7.78	3.66	6.11	4.99
	φ5	22.42	7.13	22.49	4.11	21.11	6.22	16.71	11.39	18.00	11.20
	φ	**53.44**	**16.77**	**51.92**	**10.08**	**50.63**	**12.63**	**37.28**	**18.56**	**33.41**	**15.88**

JOINT KINEMATICS IN CHIMPANZEE AND HUMAN BIPEDAL WALKING

[1]Leng-Feng Lee, [2]Matthew C. O'Neill, [2]Brigitte Demes, [1]Michelle D. LaBoda,
[2]Nathan E. Thompson, [2]Susan G. Larson, [2]Jack T. Stern Jr. and [1]Brian. R. Umberger

[1]University of Massachusetts Amherst, Amherst, MA, USA
[2]Stony Brook University School of Medicine, Stony Brook, NY, USA
email: umberger@kin.umass.edu, web: http://www.umass.edu/locomotion

INTRODUCTION

As a facultative biped and our closest living relative, the chimpanzee (*Pan troglodytes*) has long provided important context for understanding the evolution of bipedalism in humans. While there has long been an interest in chimpanzee bipedalism [e.g., 2], there have been few detailed reports of gait kinematics in chimpanzees walking bipedally [e.g., 3]. In particular, there have been no direct comparisons of three-dimensional (3D) joint kinematics between chimpanzees and humans.

The similarities and differences between the bent-hip, bent-knee form of locomotion employed by great apes and the upright, straight-legged locomotion of modern humans, particularly for motions outside of the sagittal plane, are not well understood. Such data will be necessary to fully appreciate how differences in morphology influence locomotor performance. As a first step in that direction, we present here preliminary data on 3D hind limb joint kinematics in chimpanzees walking bipedally, and compare the results with lower limb joint kinematics from humans.

METHODS

Data were collected on two chimpanzees (age: 5.2 ± 0.2 yr, mass: 21.9 ± 1.7 kg, hip height: 0.34 ± 0.01 m) and six humans (age: 29.2 ± 4.9 yr, mass: 66.3 ± 15.1 kg, standing height: 1.67 ± 0.07 m) walking overground, with data for both species collected in a laboratory setting. All experimental procedures were approved by the relevant ethics boards, and the human subjects provided informed consent. The chimpanzees walked at a self-selected speed (1.3 ± 0.2 m/s) as they followed an animal trainer offering a juice reward. The human subjects all walked at a standardized speed of 1.2 m/s. Anatomical landmarks on the pelvis and hind/lower limbs were marked using non-toxic paint for the chimpanzees and reflective, spherical markers for the humans. 3D coordinates of the markers were recorded using high-speed motion capture systems.

Joint angles over the full gait cycle (ipsilateral foot contact to ipsilateral foot contact) were computed using OpenSim software. Generic chimpanzee [5] and human [1] musculoskeletal models were scaled to match the sizes of the subjects, and an inverse kinematics procedure was used to compute joint angles. All joint angles had values of zero degrees in a reference, upright standing posture (e.g., full knee extension), and the directions of positive angular displacements are indicated in the vertical axis labels in Fig. 1. Joint angle data for three trials were first averaged within each subject; then data were averaged across subjects within a species. Joint angle minimum (Min), maximum (Max), and range of motion (ROM=Max-Min) values were determined from the average curves for both species. Given the small and uneven sample sizes, no statistical comparisons were performed.

Table 1: Joint angle Min, Max, and ROM values in degrees. H - hip; K - knee; A - ankle.

		H Flex	H Add	H Rot	K Flex	A Flex
Chimp	Min	30.7	-22.7	-31.6	17.6	-24.0
	Max	54.8	-10.1	7.0	94.4	14.9
	ROM	24.1	12.6	38.6	76.8	38.9
Human	Min	-7.1	-7.5	-3.5	2.9	-12.5
	Max	35.4	8.4	3.9	75.0	11.3
	ROM	42.5	15.9	7.4	72.1	23.8

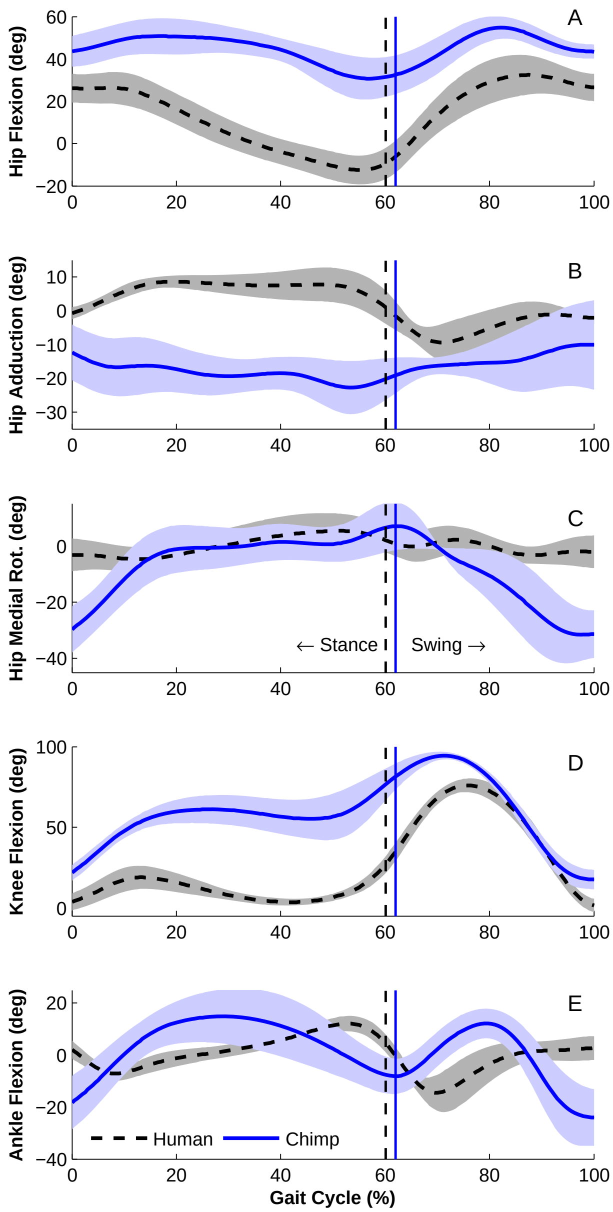

Figure 1: Joint angles for chimpanzee and human walking (shaded area is one standard deviation).

RESULTS AND DISCUSSION

The patterns for hip and knee joint flexion were similar in chimpanzees and humans; however, chimpanzees walked with their hip (Fig. 1A, Table 1) and knee (Fig. 1D, Table 1) maintained in a more flexed posture, reflecting a bent-hip, bent-knee gait. The pattern of ankle joint motion (Fig. 1E) differed between species, which was associated with a less prominent heel-strike in the chimpanzees. The greatest difference in sagittal plane ROM was a smaller excursion of the hip joint in chimpanzees (Table 1), which will act to reduce stride length.

There were also striking differences in hip kinematics outside of the sagittal plane. Unlike humans, whose hips are adducted in stance and abducted in swing, chimpanzees maintained the hip joint in 10-20° of abduction over the whole gait cycle (Fig. 1B). Chimpanzees also used ~30° more medial/lateral rotation ROM over the gait cycle than humans (Table 1). The chimpanzee hip was maximally laterally rotated at initial foot contact, and rapidly rotated medially during the early part of the stance phase (Fig. 1C). The combination of abduction and lateral rotation observed in the chimpanzees at initial foot contact will serve to increase stride length, compensating for the limited sagittal plane hip joint ROM.

In contrast to the differences between our human and chimpanzee subjects, the chimpanzee results were similar to 3D joint kinematics reported for bipedal walking in macaques [4], except for the ankle joint angle being offset more in the direction of flexion in the macaques.

CONCLUSIONS

While the observation that bipedal chimpanzees display more hip and knee flexion than humans is not novel, this 3D analysis reveals that chimpanzees also utilize a greater degree of hip abduction and rotation than humans, as well as a distinctive pattern of ankle motion. This host of adaptations reflects a unique solution to biomechanical challenges faced by a facultative biped.

REFERENCES

1. Delp S, et al. *Trans BME* **37**, 757-767, 1990.
2. Elftman H. *J Mammal* **25**, 67-71, 1944.
3. Kimura T, et al. *Folia Primat* **80**, 45-62, 2009.
4. Ogihara N, et al. *J Hum Evol* **58**, 252-261, 2010.
5. Umberger B, et al. *Proceedings of ASB*, Long Beach, CA, USA, 2011.

ACKNOWLEDGEMENTS

Supported by NSF BCS-0935321 & BCS-0935327.

KINEMATIC EFFECTS OF BIOMECHANICAL ENERGY HARVEST AT THE ANKLE: IMPLICATIONS FOR INJURY SUSCEPTIBILITY

Adam Leemans, Rebecca Zifchock, Robert Gregory, William Brechue

United States Military Academy, West Point, NY, USA
email: rebecca.zifchock@usma.edu

INTRODUCTION

One of the largest contributors to the heavy loads borne by soldiers during combat is battery weight, which typically accounts for 20% of a combat load in theatre [1]. One possible method, currently being pursued by the US Army as a way to reduce battery weight, is to enable soldiers to harvest biomechanical energy that they generate during walking. The Soldier Power Regeneration Kit (SPaRK, Spring Active; Tempe AZ) is a device that has been designed to generate power from the eccentric muscle actions at the ankle during walking by using a spring to slow rotation at the ankle during mid-stance. It is worn on the outside of standard military footwear, and current prototypes produce 5-7 W of continuous output (Spring Active).

In theory, power production from eccentric muscle activity should assist the braking motions of the body, and therefore have no metabolic cost. However, the SPaRK has a mass of 1.9 kg on each ankle, and previous studies have found increased metabolic costs and joint moments when weight is attached at the ankle [2]. Surprisingly, there is little research that examines the effects of ankle weight on joint kinematics. Deviations from typical, healthy gait patterns have been shown to be indicative of an individual's susceptibility to injury [3, 4]. Therefore, it is important to assess the effect of wearing a device such as this on gait kinematics. The purpose of this study was to examine the effects of an ankle-mounted energy harvester device on five joint angles where deviant gait patterns have been linked to overuse injuries: hip adduction, hip flexion, knee adduction, knee flexion, and ankle dorsiflexion. Altered kinematics were anticipated while wearing the active SPaRK device, as well as while wearing a disengaged SPaRK device, used to simulate ankle weight only (without power generation).

METHODS

Six subjects volunteered to participate in this institutionally-approved protocol. Three-dimensional instrumented gait analysis was conducted as each participant walked under three conditions: combat boots (BOOTS), combat boots with the SPaRK device attached but not generating power (WEIGHT), and combat boots with the SPaRK device attached and generating power (SPARK). They walked for approximately 10 minutes until they reached a metabolic steady state and data were collected in the final minute of walking. The markers were tracked using a nine-camera system operating at 250 Hz (Motion Analysis Corp.; Santa Rosa, CA). The raw data were then tracked and trimmed to six strides. Tracked data were then analyzed using custom code written in Visual 3D (C-Motion; Germantown, MD), and the peak value of each joint actions of interest was identified during stance-phase. Repeated measures ANOVAs were used to compare averaged peak values among the BOOTS, WEIGHT, and SPARK conditions. Statistical significance was set at $p \leq 0.05$.

RESULTS AND DISCUSSION

There were no significant differences among the three conditions for any of the variables of interest (Table 1). Hip adduction was reduced in the

WEIGHT and SPARK conditions by 14% and 21%, respectively, as compared to the BOOTS condition. Ankle dorsiflexion was increased in the SPARK condition by 29% as compared to the BOOTS condition. However, due to the small sample size, many of those apparent differences were driven by individuals who reacted particularly strongly to the WEIGHT or SPARK conditions.

The lack of significant differences between conditions suggests that additional weight, whether it is a power-generating or not, may not affect lower extremity kinematics in a consistent manner. Therefore, it is possible that wearing an ankle-mounted energy harvesting device may not influence injury susceptibility as it relates to altered gait kinematics.

It is important to acknowledge several limitations of this preliminary study. First, a larger sample size is important for identifying potential trends in the individuals who reacted more strongly to the WEIGHT and/or SPARK conditions. Additionally, although the participants walked for approximately 10 minutes prior to data collection, these results may not be indicative of the long-term effects of this ankle-mounted device on gait kinematics.

CONCLUSIONS

These preliminary results suggest that the ankle may be a feasible location for mounting an energy harvester device, and that weight at the ankle may not consistently alter an individual's kinematics.

REFERENCES

[1] Shaffer E. Unburdening the Soldier through innovations in battery, power component technology, US Army Research Laboratory. 15 Mar 2011.
[2] Browning R, et al. *Med Sci Sports Exerc,* **39** (3), 515-525, 2007.
[3] Noehren B, et al. *Clin Biomech*. **22**, 951-956, 2007.
[4] Zifchock R, et al. Hum Mov Sci, **27**, 888-902, 2008.

ACKNOWLEDGEMENTS

The authors would like to acknowledge support from U.S. Army Natick Soldier, RDEC in conducting this preliminary study.

Table 1: Means, Standard Deviations, and Statistical Results

	Hip Flexion, deg	Hip Adduction, deg	Knee Flexion, deg	Knee Adduction, deg	Ankle Dorsiflexion, deg
BOOTS	30.7 ±8.0	7.4 ±4.5	48.2 ±3.6	3.5 ±4.2	6.0 ±2.6
WEIGHT	31.3 ±5.5	6.4 ±3.5	51.5 ±2.1	3.8 ±2.9	6.3 ±2.6
SPARK	34.8 ±5.5	6.7 ±5.4	49.7 ±7.3	3.7 ±3.9	6.9 ±4.1
p-value	0.28	0.29	0.50	0.95	0.74
BOOTS-WEIGHT	-0.6 ±2.6	1.0 ±1.4	-3.3 ±3.7	-0.3 ±2.5	-0.3 ±4.5
% Diff	-1.9%	13.9%	-6.6%	-7.5%	4.1%
BOOTS-SPARK	-2.3 ±3.5	1.5 ±1.7	-1.5 ±6.7	-0.2 ±1.2	-1.9 ±6.5
% Diff	-7.2%	20.1%	-3.1%	-4.5%	29.4%

Biomechanical Effects of Component Alignment Variability in Total Knee Arthroplasty: A Computer Simulation Study of an Oxford Rig

[1]Sean Lemke, [1]Matthew D. Beal, [2]Stephen J. Piazza, and [1]Robert A. Siston

[1]The Ohio State University, Columbus, OH, USA
[2]Pennsylvania State University, University Park, PA, USA
email: siston.1@osu.edu

INTRODUCTION

While total knee arthroplasty (TKA) is an effective method for alleviating pain due to joint diseases such as osteoarthritis (OA), many patients have sub-optimal functional outcomes such as an inability to climb stairs and perform other tasks that are important in their daily lives [1]. Surgical technique is a key factor in the outcomes of a TKA [2], but a high degree of variability exists in the alignment of the femoral and tibial components. Due to difficulty in identifying proper anatomic landmarks during surgery, internal/external malalignment of the femoral component can be as high as 13° internal and 16° external, and the alignment of tibial component can range from 44° internal to 46° external [3,4]. In the frontal plane, the components have been historically aligned to create a neutral mechanical axis [5], but more recent research shows potential functional advantages to a “natural” or “kinematic” alignment [6]. Clinical studies have shown the posterior slope of the tibial component vary from -1° to 10°, and flexion of the femoral component varies from 0° to 7° [7].

We believe that variability in component alignment may contribute to the variability in post-operative functional outcomes, but a definitive link between alignment and outcomes has not yet been established. We have previously shown that variability in component alignment in the transverse plane affects ligament forces, knee kinematics, and quadriceps force [8], but the effects of malalignment in the sagittal and frontal planes remains unknown. The purpose of this study was to characterize the relationship between femoral and tibial component orientation in all three planes during a TKA on ligament forces, knee kinematics, and quadriceps force for a cruciate retaining knee implant during a simple squat motion using a forward dynamic simulation of the Oxford Rig device.

METHODS

Using methods similar to those of Thompson et.al. [8], we used a forward dynamic model of the ‘Oxford Rig’, which is commonly used for testing cadaveric samples in the flexed knee stance [9]. The forward dynamic model simulates controlled knee flexion from 20°-120°. To simulate 50% body weight, a 30 kg mass was placed at the pelvis. Resistance to lowering of the pelvis was provided by a lumped quadriceps muscle whose force was determined using a proportional derivative controller. Articular contact forces were determined using a rigid body spring model [10]. Knee angles were found using the convention determined using Grood and Suntay [11].

A cruciate retaining implant design (Scorpio CR; Stryker, Inc.) was used in all simulations. Tibial and femoral component alignments were varied individually and in combination over ranges of 6° varus to 6° valgus, 15° internal to 15° external, and 5° anterior to 10° posterior. The relationship between component alignment and the outcome variables was examined using a regression analysis, where linear, quadratic, and interaction effects were explored. Component alignments with a significant effect ($p \leq 0.05$) and with coefficients greater than 1 in the resultant regression equation are summarized in Table 1, and those alignments with the largest coefficients are bolded. Results from 133 simulations with an alignment change in only one plane are presented here; our study of component malalignment in multiple planes is still in process.

RESULTS AND DISCUSSION

Ligament Forces

Internally rotating the femoral component increases the MCL force in late flexion. Placing either component in valgus generates a MCL force in early flexion that is reduced in late flexion. The combination of both components in valgus generates a greater force than the variation of one component (Figure 1). LCL force is increased only when there are changes in the alignment of both tibial and femoral components. The PCL is most affected by changes in femoral component alignment in the transverse and sagittal planes in deep flexion.

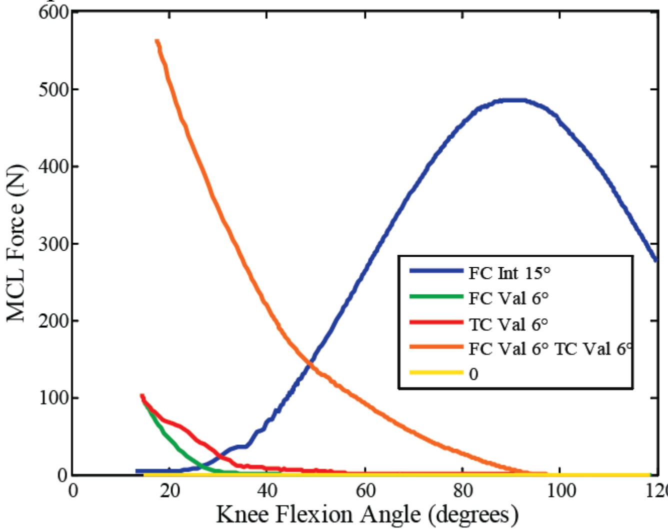

Figure 1: Effect of Femoral (FC) and Tibial (TC) component alignment on MCL Force.

Knee Kinematics

Changing femoral component alignment in the frontal and transverse planes has different effects on knee kinematics (Figure 2), but variation in the frontal plane has a slightly larger effect.

Quadriceps Force

Quadriceps force is affected by alignment of both components in the frontal and sagittal planes with the greatest increase in force caused by femoral component alignment in the sagittal plane

CONCLUSIONS

Understanding the relationship between component malalignment and functional outcomes will facilitate the design of new prosthetic components and surgical techniques. The current study suggests that femoral alignment in the frontal and transverse planes and tibial alignment in the frontal plane require the most attention at the time of surgery.

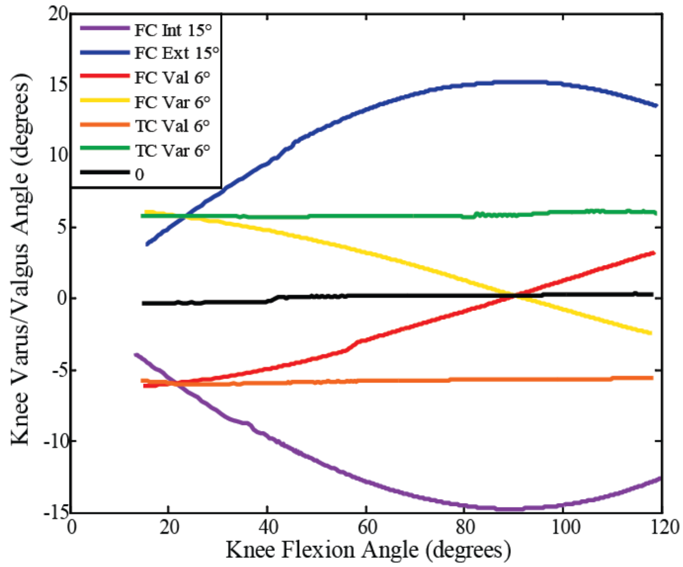

Figure 2: Effects of FC and TC alignment on knee varus/valgus angle.

REFERENCES

1. Weiss, J.M., et al. *CORR*, 172-188, 2002.
2. Stulberg, S.D., et al. *JBJS Am* **84-A Suppl 2**, 90-98, 2002.
3. Siston, R.A., et al. *CORR* **452**, 65-69, 2006.
4. Siston, R.A.,et al. *JBJS Am* **87**,2276-2280, 2005.
5. Jeffery, R.S., et. al. *JBJS Br* **73**, 709-714, 1991.
6. Howell, S.M., et. al. *Orthopedics* **31,** 857-863, 2008.
7. Chauhan, S.K., et al. *JBJS Br* **86**, 372-377, 2004.
8. Thompson, J.A., et. al. *JOR* **29**, 969-975, 2011
9. Zavatsky, A.B. *J Biomech* **30**, 277-280, 1997.
10. Landon, R.L., et al. *Comput Method Appl M* **198,** 2339-2346, 2009.
11. Grood, E.S., Suntay, W.J. *J Biomech Eng* **105**, 136-144, 1983

Table 1: Alignment Factors Contributing to Biomechanical Parameters (Principal Alignment in Bold)

Biomechanical Parameters	Component Alignment Plane		
	Transverse	Frontal	Sagittal
Knee Varus/Valgus Angle	Femoral	**Femoral**	
PCL Force at 120° of Knee Flexion	Femoral, Tibial	Femoral, Tibial,	Femoral, **Tibial**
LCL Force at 20° of Knee Flexion	Femoral	**Femoral, Tibial**	
MCL Force at 20° & 90° of Knee Flexion	**Femoral**, Tibial **(90°)**	**Femoral, Tibial (20°)**	
Quad Force at 120° of Knee Flexion	Femoral	Femoral, Tibial	**Femoral**, Tibial

INCREASING RUNNING STEP RATE REDUCES PATELLOFEMORAL JOINT FORCES

Rachel L. Lenhart, Christa M. Wille, Elizabeth S. Chumanov, Bryan C. Heiderscheit and Darryl G. Thelen

University of Wisconsin-Madison, Madison, WI, USA
email: rlenhart@wisc.edu, web: http://www.engr.wisc.edu/groups/nmbl/

INTRODUCTION

Anterior knee pain is a common ailment among runners, thought to be triggered in part by the repetitive compressive stress between the patella and femur. The patellofemoral (PF) compressive joint force has been estimated to reach 5.6-7.6 times body weight during running [1,2]. Since PF joint force is influenced by both quadriceps loading and knee flexion angle [3,4], strategies to modulate these parameters may decrease PF compressive forces and ameliorate pain. A recent study showed that a subtle increase in step rate can reduce peak knee flexion and the internal knee extension moment during the loading response phase of running [5]. The purpose of this study was to use computational musculoskeletal models to investigate how step rate modulation affects PF joint loading. We hypothesized that an increase in step rate would reduce PF joint forces, arising from the coupled effect of a reduced knee extension moment and knee flexion angle during stance.

METHODS

We measured whole body kinematics and foot-floor reactions during treadmill running in 23 healthy, experienced runners (14 males, mean ± SD: age = 37.0 ± 14.7 yr, mass = 69.8 ± 9.2 kg, height = 177.6 ± 9.9 cm, 5+ months experience, run 44.6 ± 23.2 km/wk). Each subject ran at his/her preferred running speed under three cadence conditions: 90%, 100% and 110% of preferred step rate. Step rate was maintained via an auditory metronome and confirmed by ground reaction forces.

Joint forces were analyzed using a lower extremity model with 44 muscles acting about the hip, knee and ankle joints [6]. The model was adapted to include a 1-degree of freedom PF joint, in which the patella could translate along a constrained path relative to the femur. Quadriceps muscle and patellar tendon forces were applied to the proximal and distal ends of the patella, respectively. For each subject, the model was first scaled to subject-specific segment lengths. Inverse kinematics was then used to compute the joint angles at each frame of the running motions. Patella position along the constrained path was set assuming the patellar tendon remained a constant length [6]. We then used numerical optimization ($min \sum V_i \bar{F}_i^2$, V=volume) to compute the lower extremity patellar tendon and muscle forces (F_i) necessary to generate the measured joint angle accelerations at each frame of the motion. The magnitude of the PF joint reaction force vector was then computed, with peak PF force averaged over five strides for each step rate. The effect of step rate on peak PF joint force was investigated using paired t-tests with $p<0.05$ establishing significance.

RESULTS AND DISCUSSION

Peak PF joint force occurred during the loading response of stance, with a second smaller peak seen during swing limb initiation (Figure 1). Step rate and PF joint force were inversely related for all subjects, with the lowest PF joint forces observed at the highest step rates (Figure 1).

PF joint forces reached a magnitude of 5.1 (±0.9) times body weight at a preferred step rate (Figure 2). Decreasing step rate increased PF joint force by an average (±SD) of 17.3% (±9.4), while increasing step rate decreased PF joint force by 15.4% (±7.4) ($p<0.05$). These percent changes exceed the previously observed change in knee extension moment seen with the same step rate manipulation [5]. The additional benefit is likely derived from running with a more extended limb at a higher step rate. These runners exhibited a 3.5 deg decrease in knee flexion at the higher step rate [5].

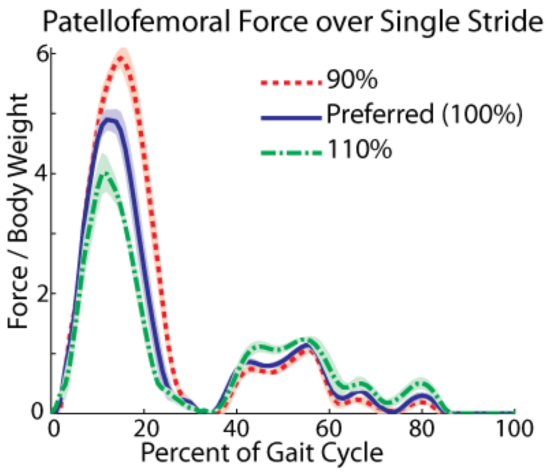

Figure 1: Average (± 1 SD) patellofemoral joint force for a subject running at a decreased (90%), preferred (100%), and increased (110%) step rate.

CONCLUSIONS

Running places high compressive forces on the PF joint, which is likely a contributor to anterior knee pain syndrome commonly observed in distance runners. This study demonstrates that a simple running form modification (i.e. increasing step rate 10% above one's preferred) can be used to substantially diminish peak PF joint force. This biomechanical benefit appears to be due to two factors: a) the ground reaction force passing closer to the knee and reducing the loading on the quadriceps, and b) a more extended knee posture at midstance resulting in a less obtuse angle between the quadriceps and patellar tendons (Figure 3). Therefore, increasing step rate is an effective way to decrease patellofemoral joint forces, and may prove to be a useful, simple strategy for addressing anterior knee pain issues in distance runners.

ACKNOWLEDGEMENTS

NIH 1UL1RR025011, UW Medical Scientist Training Program, UW Sports Medicine Classic

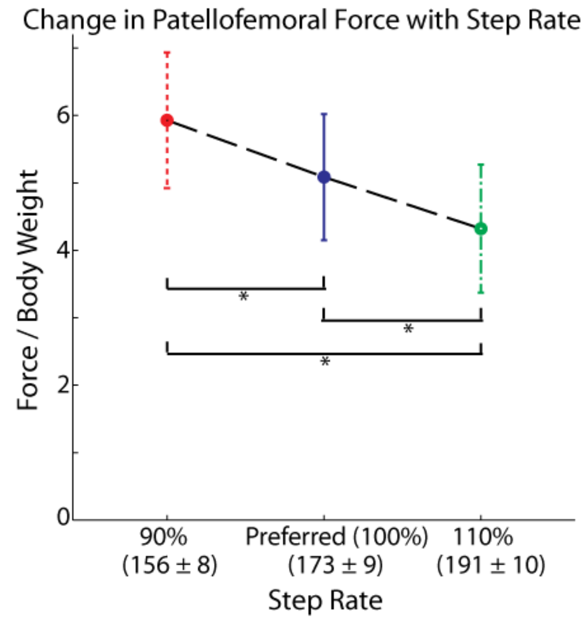

Figure 2: Patellofemoral joint force is inversely related to step rate (mean ± 1SD step rate is shown, *$p<0.05$)

REFERENCES

1. Scott SH and DA Winter. *Med Sci Sports Exerc*, **22**, 357-369, 1990.
2. Flynn TW et al. *JOSPT*, **21**, 277-282, 1995.
3. Reilly DT et al. *Acta orthop Scandinav*, **43**, 126-137, 1972.
4. Ward SR et al. *Clin Biomech*, **19**, 1040-1047, 2004.
5. Heiderscheit BC, et al. *Med Sci Sports Exerc*, **43**, 296-302, 2011.
6. Arnold EM et al. *Ann Biomed Eng*, **38**, 269-279.

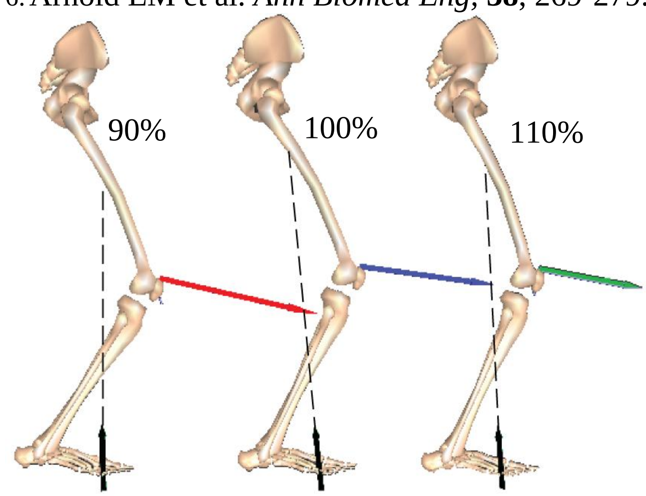

Figure 3: Representative depiction of limb position, ground reactions and peak PF joint force at the 90%, preferred, and 110% step rate conditions.

ALTERED HIP MOVEMENT IN FEMALES WITH HIP PAIN DURING SINGLE LEG STEP DOWN

[1]Cara L. Lewis

[1]Boston University, Boston, MA, USA
email: lewisc@bu.edu, web: people.bu.edu/lewisc

INTRODUCTION

Over the past 15 years, increased attention has been paid to hip pain in young adults. Acetabular labral tears have been recognized as a source of pain, while femoroacetabular impingement (FAI) has been implicated as a cause of labral tears, hip pain, and osteoarthritis (OA). In FAI, hip pain occurs in the presence of structural anomalies of the acetabulum or femur. These structural anomalies are thought to cause abnormal impingement during hip motion. Current treatment for FAI is primarily surgical to correct the structural anomaly. While a connection between structural anomalies and hip pain certainly exists, some evidence suggests that structure is not the only factor contributing to hip pain. Recent studies demonstrate that the structural features of FAI are present in over 50% of people who do not have hip pain [1, 2] and are often present bilaterally despite unilateral pain [3]. Also, in a case report of a female patient with FAI, Austin and colleagues [4] demonstrated that reduction in hip adduction and internal rotation using a simple elastic brace during functional movements resulted in decreased pain, indicating that surgery is not the only treatment option. The concurrent reduction in pain with modification of hip motion suggests that movement patterns may contribute to hip pain in people with FAI.

To date, however, these movement patterns have not been fully studied. Therefore, the purpose of this ongoing study is to compare the movement patterns of adults with hip pain to adults without hip pain, and to test for limb-specific differences in these patterns that may be contributing to the hip pain. We hypothesize that subjects with hip pain will have less hip flexion and more hip adduction when standing on the painful side than control subjects. We also hypothesize that subjects with hip pain will have more hip adduction when standing on the painful side than when standing on the uninvolved side. This project may redirect treatment for people with hip pain and FAI by identifying specific movement patterns which could be targeted by inexpensive and non-invasive therapeutic interventions such as neuromuscular retraining.

METHODS

As part of an ongoing study, data were collected from six female subjects with hip pain (age: 30.5 year (range: 21-40); mass: 63.0 ± 10.3 kg; height: 1.68 ± 0.05 m). All six subjects with hip pain had right sided pain in the groin / anterior hip that increased with activity. Each subject's pain was reproduced with passive hip flexion, adduction and medial rotation (anterior impingement test), a test that may indicate an anterior labral tear or FAI. Data from six painfree matched females (age: 25.0 year (range: 18-46); mass: 58.2 ± 7.6 kg; height: 1.63 ± 0.08 m) were also collected. All control subjects had no pain with the impingement test nor with a resisted straight leg raise.

Kinematic data were collected using a motion capture system while the subject performed a single-leg step down and return task. With one foot on the step, the subject slowly lowered herself until the contralateral heel touched the ground, and then returned to the starting position, completing the entire motion in approximately 2 seconds. The task was repeated 5 times with each leg. Visual 3D (C-Motion, Inc, Germantown, MD) was used to calculate hip joint peak angles and excursions.

Pain data were collected during the step down task. After each trial, subjects were asked to rate their hip pain on a scale from 0 to 10 with 10 being the greatest pain.

RESULTS AND DISCUSSION

During the step down task, females with anterior hip pain flexed the hip less than females without hip pain. Females with pain had a higher peak hip adduction angle when standing on the right (painful) leg than when standing on the left leg. The adduction angle on the painful limb with similar to the peak right hip adduction in females without pain; however, females without pain were more symmetric.

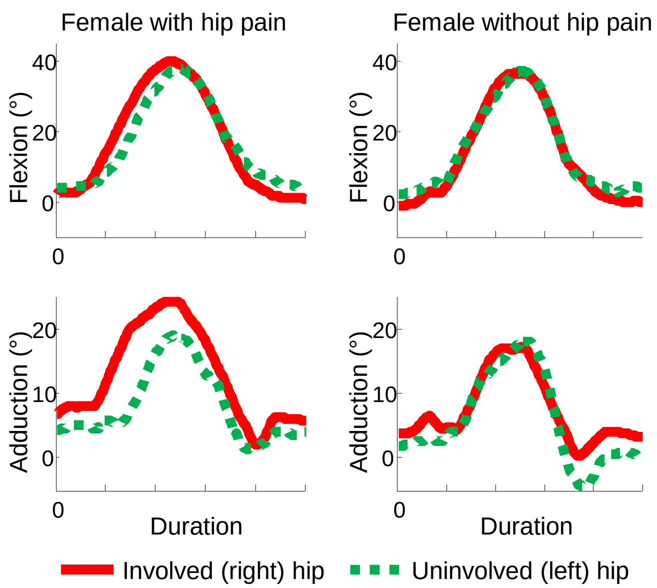

Figure 1: Single subject data performing the step down and return task. The female with hip pain has less symmetric adduction than the female without hip pain, and has greater adduction on the involved side than the uninvolved.

The females with hip pain reported pain in the involved hip of 1-4/10. All control subjects reported 0/10 pain. For one hip pain subject, the increased hip adduction on the involved side was visually noted during testing. Therefore, additional trials were collected while giving verbal cues to contract the gluteal muscles and keep the pelvis level. During these cued trials, the subject reported no hip pain and demonstrated 4 degrees less peak hip adduction than during the trials without cues.

These preliminary results indicate that increased hip adduction during single-leg step down may contribute to anterior hip pain in women, and that this altered movement pattern may be corrected with verbal cues.

CONCLUSIONS

Anterior hip pain is an increasingly common complaint of young active adults; however there is a limited understanding of appropriate interventions. Based on the preliminary results of this study, movement patterns should be evaluated in individuals with anterior hip pain in order to direct non-operative treatment. Changing how someone moves, particularly decreasing hip adduction, may help reduce hip pain.

REFERENCES

1. Kang A, et al. *Amer J Sports Med*, **38**, 1160-1165, 2010.
2. Pollard T, et al. *J Bone Joint Surg Br*, **92**, 209-216, 2010.
3. Allen D, et al. *J Bone Joint Surg Br*, **91**, 589-594, 2009.
4. Austin A, et al. *J Orthop Sports Phys Ther*, **38**, 558-565, 2008.

ACKNOWLEDGEMENTS

These data were collected and analyzed with the assistance of Kaitlyn Chin, Erin Garibay, Anne Khuu, Adam Linsalata, and Ashley Rex.

Table 1: Peak stance hip angles in degrees during single-leg step down (mean ± SD).

	Females with Hip Pain		**Females without Hip Pain**	
	Hip Flexion	**Hip Adduction**	**Hip Flexion**	**Hip Adduction**
Involved (Right)	33.3 ± 5.0	18.6 ± 3.9	38.1 ± 4.6	17.7 ± 4.2
Uninvolved (Left)	31.3 ± 1.8	13.4 ± 4.5	38.9 ± 5.0	18.2 ± 5.0

INFLUENCE OF ECCENTRIC BODY WEIGHT ON THE KNEE BALANCE OF OBESE PATIENTS

Jihui Li, Edward MacMahon and Mark Theiss
Inova Fairfax Hospital, Falls Church, VA, USA
email: jihui.li@inova.org

INTRODUCTION

Leg alignment and ligaments release are critical to the success of a total knee replacement (TKR) surgery. Proper surgery needs to achieve a stable knee with balanced pressures between the medial and lateral condyles [1]. During single leg standing and walking, the center of body mass is normally medial to the femoral head. This eccentric loading will produce a lateral thrust force to the knee joint and may increase the pressure under the medical condyle if the lateral thrust force can not be compensated by muscle and ligament forces [2]. Obesity can increase this lateral thrust force beyond the normal compensation limits. As a result, continuous overloading on the medical condyle will lead to complications such as unstable knee, lateral lift-off and excessive valgus knee [3].

Mechanical axis of the leg has been the basis for TKR alignment in the last thirty years. 5° of valgus cut on distal femur was recommended to address the high body weight in obese patients [4]. High complication rates indicated that the 5° valgus is insufficient to compensate for the lateral thrust force generated by a high BMI. However, no guideline has been established to adjust the cut angle based on body weight, pelvis width, and lateral thrust force. One the first step, the relationship among lateral thrust force, body weight and loading distance needs to be investigated.

In this study we used cadaver legs to develop a biomechanical model and illustrate the pathway from the center of body mass to the pressure distribution of the knee condyles. We hypothesized that the lateral thrust force has a linear relationship with eccentric body weight, loading distance and pressures under both condyles.

METHODS

Two right cadaveric legs (one male donor and one female donor) were harvested and soft tissues were removed. All knee ligaments were untouched. The legs were laid on a plywood board with the ankle fixed with a hinge (Fig. 1). The pelvis was represented by an alumina beam (length *D*), which was attached to the femoral head on one side and to a wheel on the other side. The wheel was in contact with a steel block fixed onto the plywood board and its freedom in horizontal direction was restricted. Two pressure sensors (Tekscan Inc., South Boston, MA) were inserted into the knee joint to measure the pressure distributions under the medical and lateral condyles (*P1* and *P2*). A series of dead weights (*W*, 15, 22.5, 25, 30 and 40 lbs) were added on the beam to simulate the body weight of different patients. The loads were also moved along the beam (*r*, loading distance from the femoral head) to simulate the horizontal motion of body during gait. Due to the loading procedure, the pressure under the medical condyle would be higher than that under the lateral condyle. A load cell (100 lbs range) was attached on the lateral side of the knee joint and advanced through a screw to push the knee joint toward its original position until the medical pressure equals to lateral pressure. The recorded force at this balance condition was called lateral thrust compensation force (F_t), which should equal to the lateral thrust force but at opposite direction. We expected F_t has a linear relationship with body weight, loading distance and the pressures under the two condyles:

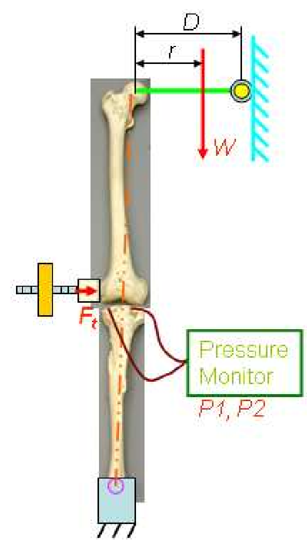

Figure 1. Setup of the test

$$F_t = aW + br + cP1 + dP2 + e \qquad (1)$$

where *a* to *d* are coefficients and *e* is intercept. Regression analysis was conducted to determine the value of the coefficients and statistical significance was defined as P<0.05.

RESULTS

The application of the lateral thrust compensation force significantly reduced the pressure difference between medical and lateral condyles (Fig. 2). Higher body weight generated higher condyle pressures (Fig. 3), and larger lateral thrust compensation force was needed to keep the balance of knee joint (Fig. 4). This rule also existed when studying the relationship between loading distance and body weight (Fig. 5). Regression analysis showed the linear model (Equation 1) is:

$$F_t = 0.16W + 0.67r - 0.03P1 + 0.06P2 - 4.48 \quad (2)$$

And the P-values were all smaller than 0.01.

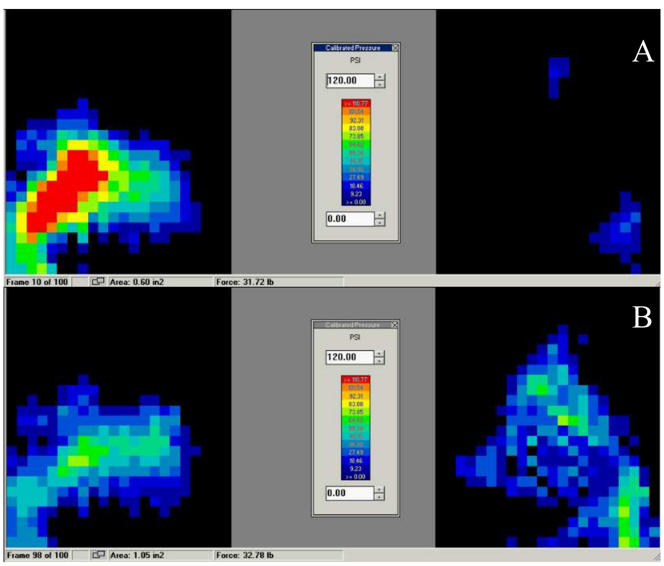

Figure 2: Pressure distribution under medial (left) and lateral (right) condyles before (A) and after (B) the lateral thrust compensation force was added.

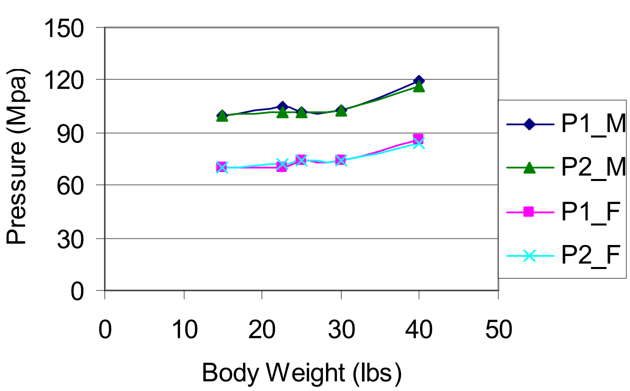

Figure 3: Body weights vs. condyle pressures in both male and female specimens.

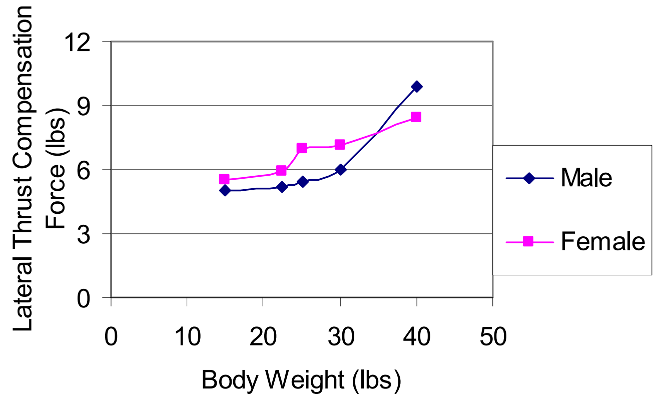

Figure 4: Lateral thrust compensation force vs. body weights in both male and female specimens.

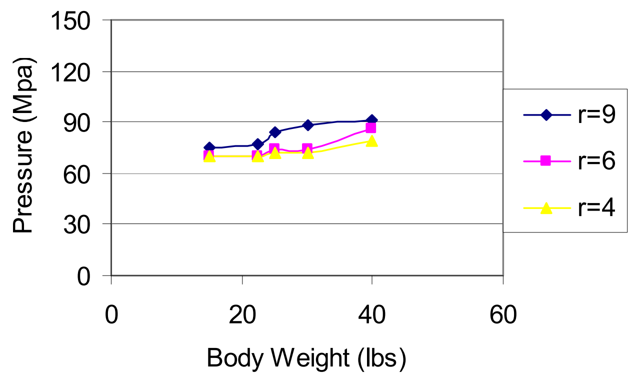

Figure 5: Body weights vs. medial condyle pressures in male specimens when *r* was adjusted.

DISCUSSION

This study demonstrated that both eccentric body weight and loading distance linearly relate to the lateral thrust compensation force. It indicated that the difficulty of balancing the knee joint will increase progressively with the rise of patients' BMI and pelvis width. Future study is planned to include the cut angles of the femur and tibia in the biomechanical model, and the goal is to set up a guideline for surgeons to properly conduct TKR alignment for obese patients. The major limitations of this study were the utilization of cadaveric specimens.

REFERENCES

1. Hsu et al., Clin Orthop Relat Res, 1990.
2. Shelburn et al., J Orthop Res, 1990.
3. Niu et al., Arthritis Rheum, 2010.
4. Insall et al., Instr Course Lect, 1981.

GAIT MODE RECOGNITION USING AN INERTIA MEASUREMENT UNIT ON A POWERED ANKLE-FOOT-ORTHOSIS

Yifan David Li, Elizabeth T. Hsiao-Wecksler
University of Illinois, Urbana, IL, USA
email: yifanli4@illinois.edu

INTRODUCTION

Ankle-foot orthoses have significant potential as both assistance and rehabilitation devices for individuals with below-the-knee muscle weakness. Recently, we have developed a portable powered ankle-foot orthosis (PPAFO), which can provide modest dorsiflexor or plantarflexor torque [1]. The untethered design can allow walking outside of the laboratory or clinic.

One of the challenges that any powered lower limb orthotic or prosthetic device must address for activities in the real world is its ability to recognize gait modes (level ground walking, stairs, ramps, etc.) and adapt to mode changes promptly. There are two critical aspects of this problem. First, the gait mode has to be recognized at the earliest possible time to prevent potential misfiring (e.g., plantarflexor assistance during stair descent). Failing to do so can increase the fall risk of the wearer dramatically. Second, the device must have enough sensors to reliably detect gait mode. In the PPAFO, the original sensor array had only three sensors (heel and toe contact force and ankle joint angle). This construction limited sensing ability.

In commercially available prosthetic legs, manual switches have been broadly used to toggle actuation control between gait modes, i.e., the user has to manually change the mode by either flexing the knee [2] or tapping the device multiple times [3].

In this study, an inertial measurement unit (IMU) based scheme was proposed to enhance the sensor array and allow for tracking of real-time 3D position and orientation of the AFO for gait mode recognition. IMU use for foot position tracking is not a trivial problem. Therefore, the goal of this pilot study was to precisely identify foot position and gait mode at the very beginning of a mode change.

METHODS

An inertial measurement unit (VectorNav, VN-100) was attached to the foot section of the PPAFO (Fig. 1). This IMU contains an accelerometer, gyroscope and magnetometer to compute real-time position and orientation. The magnetometer was not used in this study due to poor reliability issues with indoor activities.

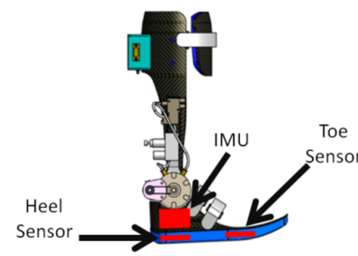

Figure 1: The experimental setup of the PPAFO. The shank and foot piece are connected by a pneumatic rotary actuator, which can provide dorsi- or plantarflexor torque. The IMU is attached to the foot plate close to the heel sensor.

The acceleration and gyro data were sent to the PPAFO onboard controller (Texas Instruments, TMS320F28335), and combined with force measurement at the heel (Fig. 1), to track 3D position of the PPAFO in real time.

First, we need to find the accelerations of the IMU in a fixed global coordinate system (a_x, a_y, a_z) from the accelerometer and gyroscope data,

$$\begin{bmatrix} a_x \\ a_y \\ a_z \end{bmatrix} = R(q_0, q_1, q_2, q_3) \begin{bmatrix} r_1 \\ r_2 \\ r_3 \end{bmatrix} - \begin{bmatrix} 0 \\ 0 \\ g \end{bmatrix} \quad (1)$$

where, r_1, r_2, and r_3 are the local accelerations from the accelerometer, g is gravitational acceleration, and q_0, q_1, q_2, and q_3 are for the quaternion vector that describe IMU orientation. The quaternion coordinate system was used to avoid the gimbal lock problem. R is the rotation matrix from IMU coordinates to the fixed global coordinates.

Second, given the acceleration vector $\boldsymbol{a}(t)$ and initial conditions ($\boldsymbol{v}(0)$, $\boldsymbol{p}(0)$), continuous position of the foot $\boldsymbol{p}(t)$ can be computed as a function of time,

$$\boldsymbol{v}(t) = \boldsymbol{v}(0) + \int_0^t \boldsymbol{a}(t)dt \quad (2)$$

$$\boldsymbol{p}(t) = \boldsymbol{p}(0) + \int_0^t \boldsymbol{v}(t)dt \quad (3)$$

Next, to compensate for sensor drift, which is a problem with IMUs, the velocities estimated from Eqn. 2 were corrected at each heel strike (Fig.2). The velocity was set to be zero within 0.2 seconds of the heel strike to avoid the error introduced by heel strike shock.

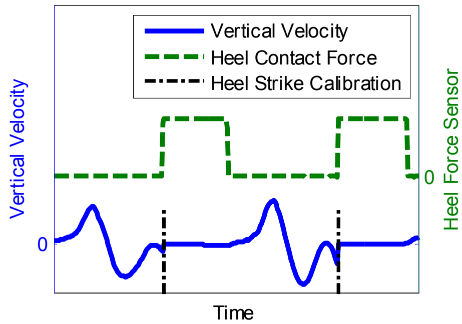

Figure 2: Velocity correction of IMU tracking based on heel contact. At each heel contact, the velocity of the heel and IMU are assumed to be zero; IMU velocity is then re-zeroed.

With the real-time position, the gait mode can be recognized by comparing the vertical position Z at each heel strike to the previous value of Z (Fig.3)

$$Mode(n) = \begin{cases} Ascent & Z(n) - Z(n-1) > T \\ Descent & Z(n) - Z(n-1) < -T \\ Level & |Z(n) - Z(n-1)| < T \end{cases} \quad (4)$$

where T is a manually tuned threshold parameter, and $Z(n)$ is the vertical position at n^{th} heel strike.

As a preliminary test, we had one subject (age: 25yr, body mass: 85kg, height: 180cm) wear the PPAFO and walked on one indoor and one outdoor set of stairs (with 12 and 6 stairs, respectively), for three times in each direction (12 trials in total). The subject took multiple steps on level ground before and after the stairs at both locations. The PPAFO was passive, without actuation.

RESULTS AND DISCUSSION

Among the 12 trials, 4 trials had significant gyro drift and lost track of elevation before the trial ended. Further investigation is needed to resolve this IMU reliability problem.

For the trials that correctly maintained orientation tracking, the estimated vertical positions were recorded and compared to their true values (Table 1). It was also demonstrated that the algorithm successfully identified all the level and stair modes with no error.

A representative trial is demonstrated in Fig.3. Starting from level mode, ascent mode was detected after the fourth heel strike (the first time the right foot hit the stairs). Similarly, at the seventh heel strike, the level mode was detected.

Table 1: Average (± standard deviation) change in vertical position per step for all trials. True values for stair height are indicated in parentheses.

Height (cm)	Indoor (16)	Outdoor (13)
Level	1.2 ± 1.3	1.6 ± 1.2
Ascent	16.1 ± 1.7	14.6 ± 1.3
Descent	-16.8 ± 2.1	-12.1 ± 1.7

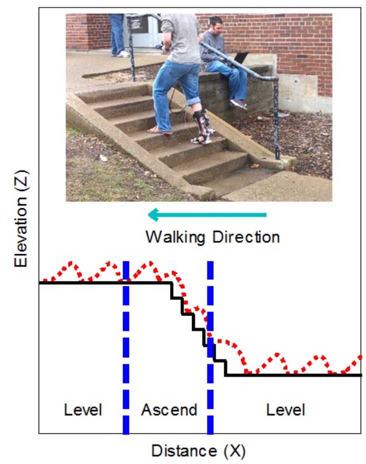

Figure 3: Stair-ascent gait mode recognition. Blue dashed lines indicate when gait mode changes were recognized.

CONCLUSIONS

An IMU-based AFO position tracking and gait mode recognition algorithm was proposed to detect stair ascent/descent events at the earliest possible times. Future work includes increasing the reliability of the orientation tracking, finding the optimal threshold value T for consistently recognizing stairs and not uneven terrain, and providing ankle actuation based on gait mode information.

ACKNOWLEDGEMENTS

Support by the NSF ERC for Compact and Efficient Fluid Power (#0540834). The authors thank Dr. Dan Block, Matt Petrucci., Morgan Boes, Louis Diberardino, and Richard Kesler for experimental help, and VectorNav, Inc. for donating the IMU.

REFERENCES

[1] K. A. Shorter, *et al.*, *JRRD,* vol. 48, Nov 4 2011.
[2] S. Au, *et al.*, *Neural Networks,* vol. 21, pp. 654-666, 2008.
[3] OttoBock. (2002). *The Electronic C-Leg® Knee Joint System: Instructions for Use*. Available: http://www.ottobockus.com

USE OF MARKER-LESS MOTION CAPTURE APPROACH FOR CONSTRUCTION FIELD WORKERS' BIOMECHANICAL ANALYSIS

Chunxia Li, SangHyun Lee, and Thomas J. Armstrong

University of Michigan, Ann Arbor, MI, USA
email: shdpm@umich.edu

INTRODUCTION

We propose computer vision-based biomechanical analysis for construction field workers. Taking into account the fact that the number of fatalities in construction is the highest among all industries [1], and that the unsafe acts and behavior of workers cause 80% to 90% of accidents in construction [3,5,7], the systematic understanding of field construction workers' unsafe behavior has great potential to contribute to the reduction of injuries and fatalities in construction. Though techniques do exist to study unsafe acts (e.g., surveys, focus groups, video analysis, and laboratory experiments), these techniques may not be suitable for measuring the physical demands exerted on workers under real conditions (i.e., biomechanical analysis). To address this issue, we aim to develop a computer vision-based marker-less biomechanical analysis system, which will extract workers' skeletons (without any marker attached to the workers) captured from ordinary network surveillance video cameras; the skeletons will be used for biomechanical analysis with estimated force information. The paper first compares the accuracy of the proposed marker-less motion tracking system with that of a commercial system with ladder climbing in the lab. Second, it demonstrates how postures determined using marker-less motion tracking can be used to evaluate biomechanical loads for a quasi-static case.

METHODS

We use two ordinary network surveillance cameras to record a subject climbing a ladder. 2D skeletons are extracted from each video set using an articulated pose estimation algorithm with flexible mixtures-of-parts [2]. In this algorithm, the human body is decomposed into local body parts such as the upper arm, lower arm, torso, upper leg, and lower leg. The local body parts are represented by a non-oriented pictorial structure that illustrates the relationships among them. Then, the 2D skeleton is inferred based on the detected body parts. Once we have 2D skeletons from each video set, 3D skeletons are reconstructed using a Euclidean reconstruction algorithm [4]. Figure 1 illustrates the reconstructed 3D skeleton from a ladder climbing.

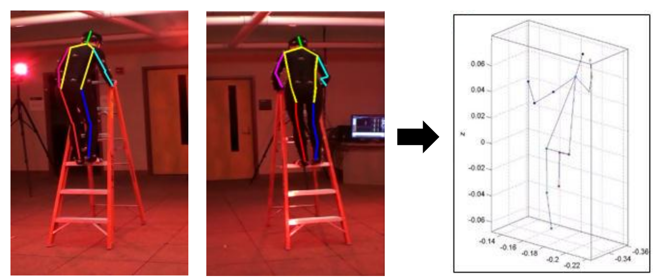

Figure 1: 3D reconstruction of 2D skeletons from ordinary network cameras.

With the 3D skeletons, biomechanical analysis can be performed using estimated (or assumed) force information. First, the body segment angles, which can be obtained from each pose in a frame, are calculated using 3D skeleton joint coordinates. The force data are assumed based on the climbing pattern. For example, if the hand or foot is in the air, the external load of this hand or foot can be assumed to be zero. In addition, one hand force can be assumed to be 11.5% of body weight [6], and foot force can be range between 48% and 60% [8] (based on the data close to the subject). With such force and pose information in each frame, the quasi-static biomechanical analysis was implemented using the University of Michigan 3D SSPP [9].

RESULTS AND DISCUSSION

We compared the accuracy of 3D skeletons developed with our marker-less approach to those developed with the commercial marker-based motion capture system (i.e., VICON). One possible way for accuracy measurement is comparing each body segment's length between the two systems. To do this, we measure one female subject's the mean length of the head, trunk, upper left and right arms, lower left and right arms, upper left and right legs, and lower left and right legs (1,000 frames). The average of the Normalized Root Mean Square Error (NRMSE: RMS divided by max-min value) of these segments between anthropometry data of the subject and VICON's output is 0.163 (0 is perfect agreement), while the average of the NRMSE between the anthropometry data and the proposed approach is 0.317. The head, trunk, and lower left and right legs showed high accuracy (less than 0.1 in NRMSE), but the lower left and right arms and upper left and right legs showed low accuracy (0.26-0.46 in NRMSE). This is because the lower left and right legs and upper left and right legs are susceptible to occlusions in ladder climbing. We performed quasi-static biomechanical analysis using the first 50 frames in 3D SSPP (see Figure 2). Based on this analysis, the elbow and shoulder are the parts that regularly endure forceful exertion during this climbing process (10% and 17% capable respectively - see Figure 2). In addition to their important role in climbing, the shoulder and elbows are common sites of work-related injuries.

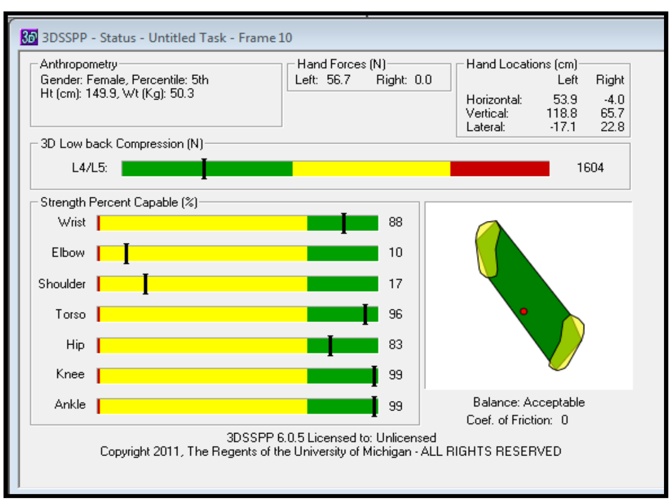

Figure 2: Biomechanical analysis using 3D SSPP

CONCLUSIONS

A computer vision-based marker-less motion capture approach is proposed. Based on the preliminary study, its feasibility is demonstrated, illustrating how biomechanical analysis can be achieved using ladder climbing. This analysis was based on a static analysis. We are currently working on improving the accuracy of 3D skeletons and the use of OpenSim for dynamic analysis [10].

REFERENCES

1. U.S. Bureau of Labor Statistics. (2011). National Census of Fatal Occupational Injuries in 2010. <http://www.bls.gov/news.release/pdf/cfoi.pdf> (Mar. 9, 2012).
2. Yang, Y., Ramanan, D. (2009). Articulated pose estimation with flexible mixtures of parts. CVPR
3. Helen, L. and Rowlinson, S. (2005). Occupational health and safety in construction project management. new York, 157-158.
4. Hartley, R., Zisserman, A. (2004). 3D reconstruction of cameras and structure. Multiple View Geometry in Computer Vision, Cambridge University Press, 2nd, West Nyack, NY: 262-278.
5. Salminen, S. and Tallberg, T., (1996). Human errors in fatal and serious occupational accidents in Finland." Ergonomics, 39 (7), 980–988.
6. Bloswick, D.S. and Chaffin, D.B. (1990). An ergonomic analysis of the ladder climbing activity. Int. J. Ind. Ergon. 6: 17-27.
7. Heinrich, H. W., Petersen, D. and Roos, N. (1980). Industrial Accident Prevention. McGraw-Hill, Inc., New York.
8. McIntyre, D.R., (1979). The effects of rung spacing on the mechanics of ladder ascent. PhD dissertation, Department of Physical Education, University of Oregon.
9. Center of Ergonomics. (2011). <http://www.engin.umich.edu/dept/ioe/3DSSPP/ > (Mar. 9, 2012).
10. OpenSim. <https://simtk.org/home/opensim> (Mar. 7, 2012).

ACKNOWLEDGEMENTS

We appreciate Mr. SangUk Han (University of Illinois at Urbana-Champaign) for his contribution to validation. We also acknowledge the financial support from the National Science Foundation (CMMI 1161123).

PREDICTING IN VITRO ARTICULAR CARTILAGE WEAR IN THE PATELLOFEMORAL JOINT USING FINITE ELEMENT MODELING

[1]Lingmin Li, [2]Shantanu Patil, [2]Nick Steklov, [3]Won Bae,
[2]Darryl D. D'Lima, [3]Robert L. Sah, [1]Benjamin J. Fregly

[1]Department of Mechanical and Aerospace Engineering, University of Florida, Gainesville, FL
[2]Shiley Center for Orthopaedic Research & Education, Scripps Clinic, La Jolla, CA
[3]Department of Bioengineering, University of California-San Diego, La Jolla, CA
email: lingminl@ufl.edu web: http://www.mae.ufl.edu/~fregly

INTRODUCTION

The mechanism by which altered knee joint motions and loads (e.g., following anterior cruciate ligament injury) contribute to the development of knee osteoarthritis (OA) is not well understood. One hypothesis is that articular cartilage degradation is initiated when altered knee kinematics increase loading on certain regions of the articular surfaces and decrease loading on other regions [1]. As a step toward computational simulation of the *in vivo* mechanobiological process of knee OA development, this study uses a finite element model to simulate *in vitro* patellofemoral (PF) articular cartilage wear observed for a cadaver specimen tested in a knee simulator machine. The goal was to evaluate a specimen-specific model of the experimentally worn PF joint.

METHODS

A single cadaveric PF joint specimen was wear tested in an AMTI multi-axial knee simulator machine (Figure 1, left). Experimental cartilage damage was visualized using India ink and measured using pre- and post-test laser scans. Experimental details have been previously reported in Li et al. [2].

A computational model of the specimen in the knee simulator machine was constructed using customized FEBio finite element code [3]. Geometry for the model was provided by CAD models of the machine components and laser scan data of the femur and patella before and after testing. Elements were generated using TrueGrid and a mesh density converging study was performed. Articular cartilage on the femur and patella was modeled as deformable. The femur bone was modeled as a rigid body with prescribed motion. The patella bone and most machine components were modeled as rigid. Interacting machine components were modeled as deformable with contact between them. A Young's modulus 15 MPa and Poisson's ratio of 0.46 for the cartilage layers was chosen by reproducing Tekscan static pressure mesurements with the model. Resulting errors in predicted contact force and area on the medial and lateral sides were less than 5%.

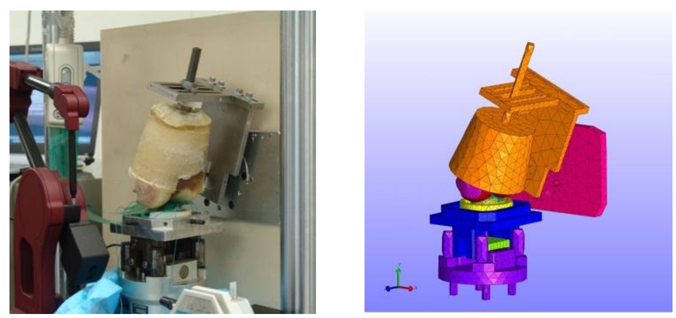

Figure 1: Experimental set-up for *in vitro* PF wear testing on an AMTI Force 5 machine (left), and computational model of the specimen and knee simulator machine (right).

The finite element model was used to predict the articular cartilage wear observed on the femur and patella over the 375,000 cycles of simulated gait. The wear predictions were based on Archard's wear law and were implemented using two approaches. The first approach (i.e., "non-progressive") involved a single one-cycle dynamic simulation. Wear depth at each surface location due to one loading cycle was calculated and extrapolated to 375,000 cycles. The second approach (i.e., “progressive”) involved a sequence of 10 dynamic simulations. Wear depth at each surface location due to one loading cycle was calculated and extrapolated to 37,500 cycles. The nodes of each surface element on the femur and patella were offset by these wear depths, and the process was repeated for 9 additoinal simulations. For both approaches, a constant wear factor was chosen that provided the best match of the progressive results to the experimentally measured maximum wear depths on both bones.

RESULTS AND DISCUSSION

Predicted wear areas and locations of maximum of wear showed good qualitative agreement with the experimental wear areas visualized by removal of India ink (Figure 2). In both the non-progressive and the progressive simulation, a hen-shaped wear band was observed on the central region of patella, and a butterfly-shaped wear region was observed on the trochlear groove of the femur.

Predicted wear depths also showed good quantitative agreement with experimental wear depths measured using the pre- and post-test laser scans. For the experiment and both wear simulation approaches, the patella exhibited more wear than the femur did, and the ratio of patellar to femoral maximum wear depth was similar in all cases (Figure 2). The progressive approach reproduced the experimental wear depths the best, though the less costly non-progressive approach predicted wear areas almost as well. Each dynamic simulation required only 20 minutes of CPU time.

Compared to the elastic foundation contact model [2], the finite element modeling approach can simulate more complex contact situations such as the tibiofemoral joint with menisci, and it provides additional information beyond normal surface pressure (e.g., subsurface normal and shear stress/strain) that may be useful for developing an appropriate *in vivo* cartilage adaptation law [4].

Compared to elastic material properties, biphasic cartilage properties can introduce beneficial damping behavior. However, biphasic materials significantly increase computation time for dynamic simulations. Furthermore, studies have reported that for dynamic loading at physiological frequencies, articular cartilage responds roughly as an elastic material [5].

CONCLUSIONS

Finite element simulation of *in vitro* articular cartilage wear of the PF joint provides a good foundation for extending the work to simulations of other joints, both *in vitro* and *in vivo*. This step will involve additional challenges such as *in vivo* measurement of knee kinematics, estimation of *in vivo* contact loads, modeling of the menisci, and identification of an appropriate *in vivo* cartilage adaptation law.

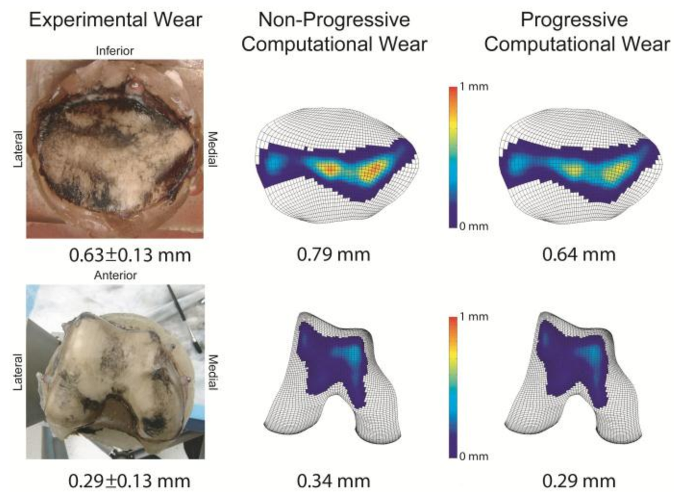

Figure 2: Wear results for the patella (top row) and femur (bottom row). Left column is experimental wear areas (white areas are worn regions) and depths. Middle column is predicted wear areas and depths from the non-progressive approach. Right column is predicted wear areas and depths from the progressive approach.

REFERENCES

1. Andriacchi TP, et al., 2009, *J Bone Joint Surg Am*, **91** Suppl 1, pp. 95-101.
2. Li L, et al., 2011, *J Biomech*, **44**(8), pp. 1507-1513.
3. Maas SA, et al., 2012, "FEBio: Finite element for biomechanics", *J Biomech Eng, (in press)*.
4. Wilson W, et al., 2006, *J Orthop Res*, **24**(2), pp. 220-228.
5. Garcia JJ, et al., 1998, *J Biomech Eng*, **120**(5), pp. 608-613.

COMPUTER PLANNING OF ARTHROSCOPIC FEMOROACETABULAR IMPINGEMENT SURGERY

Jihui Li and Mark Theiss

Inova Fairfax Hospital, Falls Church, VA, USA
email: jihui.li@inova.org

INTRODUCTION

Femoroacetabular impingement (FAI) syndrome is a hip disorder due to abnormal contact between the anterior acetabular rim and the femoral neck. It was recognized as an etiology of pain and early osteoarthritis of the hip, especially in young and active patients [1]. Surgical intervention for FAI consists of debridement of soft tissue and bony deformities to restore normal range of motion (ROM) of hip joint. Surgical hip dislocation and open osteochondroplasty have been considered the standard of treatment and the early and midterm clinical outcomes are promising [2].

Arthroscopic management of FAI is a less invasive approach emerged in recent years. Early reports suggested favorable clinical outcomes, and major complications included incomplete reshaping and over resection of the impingement deformities [3, 4]. Imaging techniques such as three-dimensional CT and MRI can help surgeons to understand the shape of the deformity. However, no available technique can lay out a surgical plan that can determine a proper amount of bone needs to be removed and achieve optimal ROM of the hip joint. The purpose of this research was to develop a computer technique that can plan arthroscopic FAI surgeries and predict the improvement in hip ROM.

METHODS

Three cam FAI patients (P1: male, 18 yo; P2: female, 48 yo; P3: male, 18 yo) were enrolled in this study. CT images were used to reconstruct 3D geometric models of the hip and pelvis in Mimics (Materialise Inc., Leuven, Belgium). The 3D models were then forwarded to computer aided design software UG/NX6 (Siemens PLM, Plano, TX) to observe the deformity of the proximal femur. Arthroscopic FAI surgeries were planned by removing the bone deformity virtually (Fig. 1).

The geometric models of the preoperative and postoperative hip joint were forwarded to finite element analysis (FEA) software ABAQUS (SIMULIA Inc., Providence, RI). Corresponding FEA models were created. Bone's Young's modulus was 20 GPa, Poisson ratio was 0.3. The friction coefficient between femoral head and acetabular socket was 0.01. The neutral position of the hip was defined when the pelvic coordinate system was parallel with the femoral coordinate system, and the hip center was the rotation center. Physiological loads were added to each hip joint to rotate the femur around the anatomical axes starting from the neutral position. An impingement was detected when the femoral neck contacted with acetabular rim or the femoral head detached from acetabular socket (Fig. 2 and 3). The flexion and abduction ROM were monitored during the motion simulation.

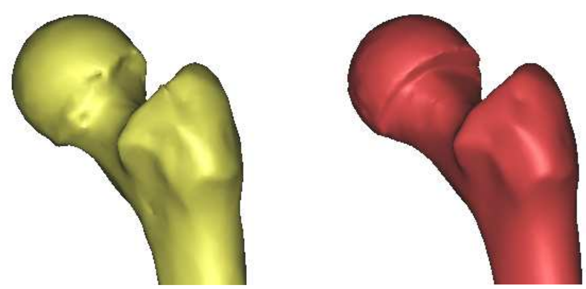

Figure 1. P2: before (left) and after (right) the virtual arthroscopic FAI surgery.

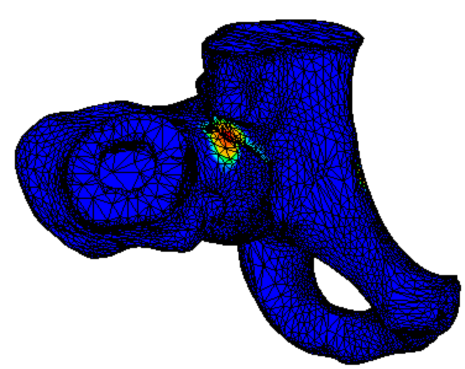

Figure 2. Impingement detection during flexion.

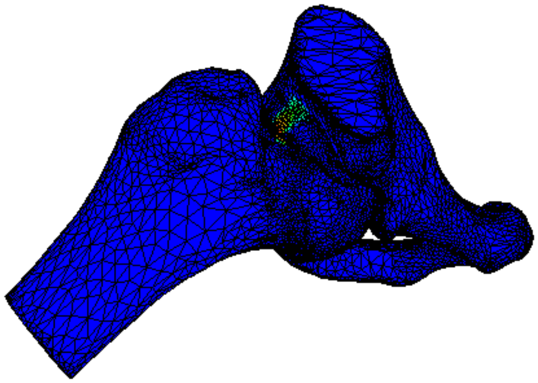

Figure 3. Impingement detection during abduction.

RESULTS

The comparison between the preoperative and postoperative ROM showed improved ROM in all patients (Table 1). P1's preoperative ROM was much lower than those of P2 and P3. P1's ROM improvements were relatively higher, but the flexion ROM was still lower than the other two specimens.

Table 1: Preoperative and postoperative ROM of the specimens.

Speci-men	Flexion		Abduction	
	Preop	Postop	Preop	Postop
P1	45.6	75.0	49.4	67.9
P2	105.5	112.4	57.2	60.2
P3	102.5	109.8	58.8	63.0

DISCUSSION AND CONCLUSIONS

The results demonstrated that the computer technique developed in this study was able to plan arthroscopic FAI surgeries and predict the improvement in hip ROM. In the future, this technique can be incorporated into surgical navigation systems so that the execution of the surgery is accurate and the clinical outcomes are predictable.

P1 had a notable bony prominence at the anterolateral head-neck junction. Although a large amount of bone was removed from the area, result of motion simulation indicated the debridement was not sufficient. This again validated the importance of the preoperational planning and outcome prediction in arthroscopic FAI surgery. The ROM of P2 and P3 were in agreement with Tannast et al. [5].

The major limitation of this study was that no cartilage and labrum were included in the computer model. With those tissues the actual ROM of the specimens might be lower than current results. Another limitation was that the application of FEA in this study might significantly slow the motion simulation and outcome estimation. However, the contact pressure provided extra information for surgeons to evaluate the surgical plan. In future study extension, adduction, internal and external rotation will be simulated as well to better understand the hip's ROM and plan the arthroscopic FAI surgery.

REFERENCES

1. Ganz R, et al. Clin Orthop Relat Res. 2003; 417:112-20.
2. Beaulé, P E, et al. J Bone Jt Surg. 2007; 89-A:773-779
3. Larson CM, et al. Arthroscopy. 2009; 25(10):1183-92.
4. Philippon, MJ, et al. Clin J Sport Med. 2006; 25: 299-308.
5. Tannast M, et al. J Orthop Res. 2007; 25(1):122-31.

SENSORY REWEIGHTING FOR VISUALLY INDUCED ROLL TILT PERCEPTION UNDER SENSORY CONFLICT CONDITIONS

[1]Hyerim Lim, [1]Heewon Park and [1]Sukyung Park

[1] Mechanical Engineering dept. KAIST, Daejon, Korea
email: sukyungp@kaist.ac.kr , web: http://biomt.kaist.ac.kr/

INTRODUCTION

Human perceives the body motion by integrating redundant sensory information [1]. When multiple sensory motion cues contribute to motion perception, the different relative sensory weights were applied for different sensory conditions. One prevalent assumption for the integration of multi-sensory information is the weighted sum of each sensory cue based on its relative reliability which was often quantitatively modeled using optimal estimator framework [2]. The optimal estimator such as Kalman filter generates the best estimation of body movement from multiple sensory motion cues with most weight for the least variable and uncertain sensory cue. Although the direct output of Kalman filter is the estimated body movement, it is noteworthy that the most of the previous studies indirectly measured the consequence of sensory reweighting using sensorimotor performance, such as body sway or joint kinematics. Therefore, the measure of perceived motion in response to various sensory conditions could provide more direct measurement of sensory reweighting. In this study, we quantified a sensory reweighting for the perception of visually induced roll tilt perception under sensory conflict condition using a Kalman filter.

METHODS

Empirical perception data from four healthy young subjects were obtained from roll tilt vection protocols and the change in sensory weight for various sensory conditions was obtained by fitting empirical data of subjective horizontal.

Four young subjects who don't have sensory disorder participated in this research. Subjects signed written informed consent obtained according to KAIST IRB protocols. A sinusoidal roll tilt visual cues at 0.08 Hz was provided to the subject using three 19 inch LCD monitor. This visual stimulus induced a vection cues so that the subjects felt like the room is rotating. Subjects were instructed to maintain upright posture, so subjects sway their body not to fall down in the imaginary rotating room. Also, subjects were instructed to make the somatosensory bar horizontal. If subjects feel the room is rotating, they will rotate the somatosensory bar. Two sensory conditions were applied to the subjects: consistent and sensory conflict conditions. During consistent sensory condition, subject were free to generated visually induced body sway, whereas the subjects' movement were restricted by the side-contact guide, so that only the visual cues were provided for roll tilt but not for vestibular nor proprioception.

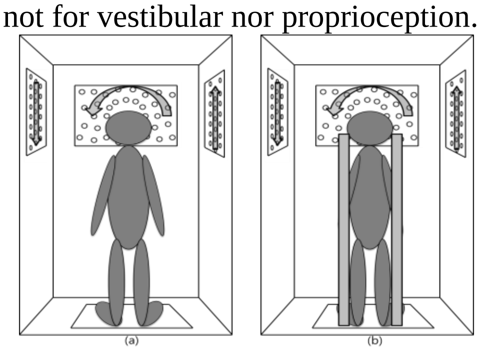

Figure 1: Experimental protocol of roll tilt perception of consistent (left) and conflict (right) sensory condition.

Kalman filter was used as an internal model that estimates body movement based on the multi-sensory information in a way best use the reliable sensory data (Fig. 2). Due to the low frequency of the visual stimulus, subjects sway their body like one segment. Thus, we can model the human as single pendulum system, and we can get plant dynamics. In this experiment vision and vestibular are main sensory organs. Thus, we examined contribution of vision and vestibular to the motion perception and we used vision and vestibular dynamics as sensor dynamic. To maintaining the upright posture (ref=0), sinusoidal visual stimulus acts as disturbance. Thus, we set visual stimulus as disturbance.

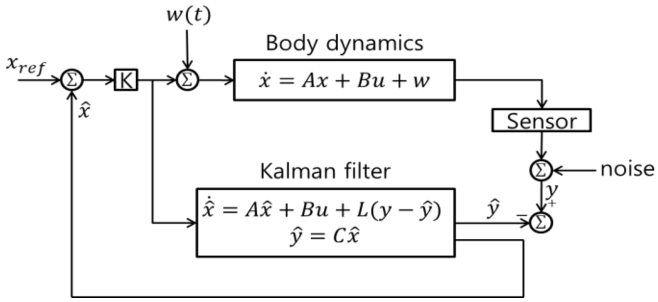

Figure 2: Block diagram of sensory reweighting model using Kalman filter.

To quantify sensory reweighting, Kalman gain L, was tuned to best match the empirical perception data. To fit the perception data, we measured the degree of somatosensory bar and the change of COP. Data were divided by cycle by cycle. To get magnitude of each cycle, data were fit with a sinusoidal function of 0.08 Hz. We compared mean magnitudes of each tests. Also, to analyze the weights of sensory information, we adjust kalman gain L and determined the weight of sensory information.

RESULTS AND DISCUSSION

The magnitude of somatosensory bar rotation reduced in conflict sensory condition. Also, vection-on-time was increased in conflict sensory condition. It means that in sensory consistent condition, roll tilt perception was increased.

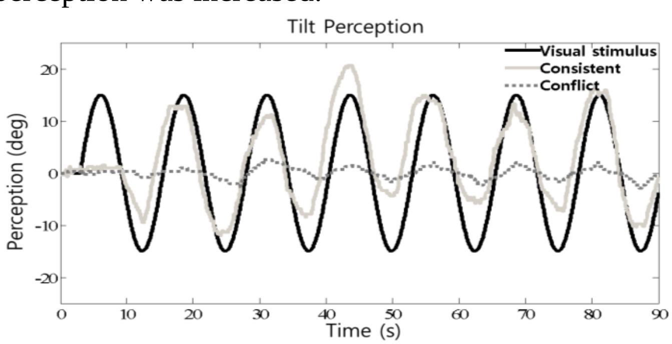

Figure 3: Tilt perception in consistent sensory condition and conflict sensory condition.

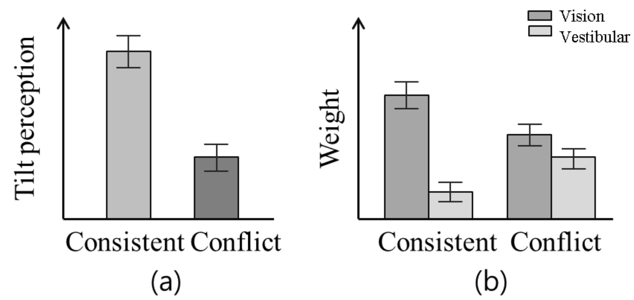

Figure 4: (a) Magnitude of tilt perception and (b) weights of vision and vestibular.

When subjects were free to sway, weight of vision was larger than that of vestibular. It means that visual information is dominant compared to other sensory information. Thus, even the room is not rotating, subjects feel the room is rotating. However, when subjects were in conflict sensory condition, weight of sensory information changed. Weight of visual information reduced and weight of vestibular increased. We can interpret this change in this way. If human are certain that the room is not rotating, human trust vestibular information more compared to the first case. Thus, weight of visual information reduces and weight of vestibular information increases.

CONCLUSIONS

Human integrate redundant sensory information in different weight to estimate motion perception. Results imply that the nervous system increases the dependency on the reliable visual cue when unexpected sensory conflict exists and the sensory reweighting is performed.

REFERENCES

1. Horak FB, Macpherson JM (1996) Postural orientation and equilibrium. In: Rowell L, Sheppard J (eds) Exercise: regulation and integration of multiple systems. Oxford University Press, New York, pp 255-292.
2. Kuo AD (2005) An Optimal state estimation model of sensory integration in human postural balance *J. Neural Eng.* **2** 235-49

ACKNOWLEDGEMENTS

This research was supported by SOT Program funded by the Ministry of Education, Science and Technology (#2010-0013306)

VARYING FOAM SURFACE THICKNESS DOES NOT AFFECT LANDING EMG PRE-ACTIVATION IN ACTIVE FEMALES

Nadine M. Lippa, David E. Krzeminski, James T. Goetz, Scott G. Piland, James W. Rawlins, Trenton E. Gould

The University of Southern Mississippi, Hattiesburg, MS, USA
e-mail: nadine.lippa@eagles.usm.edu, web: www.usm.edu/shpm

INTRODUCTION

Dissonance exists regarding the efficacy of foam to improve performance or reduce injury. The effects of foam in reducing proprioception [1], decreasing peak force [2], and increasing eversion pre-activation in peroneous longus [3] have been studied. Excessive pre-activation in running may be correlated with fatigue and reduced performance [4]. Varying loading rate by using softer foams was shown to alter pre-activation [5]. Optimum foam thickness for walking and running has not been well-defined by researchers. With increased interest in minimalist running, midsole thickness is being reduced with little peer-reviewed investigation. The purpose of this study was to determine how varying foam thickness affects the degree of pre-activation required during a single-leg landing task.

METHODS

Ten females (age 24±2.3 years, height 164±6.3 cm, weight 65±10.4 kg) that reported running activity of at least 30 min, 3x/week gave informed consent to participate in the study. Participants were excluded for illnesses affecting balance, recent lower extremity injury, or pregnancy. The University's Institutional Review Board approved the study. All analyses were completed on the right limb.

After skin preparation with abrasive pads and alcohol swipe, circular pre-gelled 10 mm bipolar Ag–AgCl surface electrodes (EL503; Biopac Systems, Inc., Goleta, CA) were placed in parallel (inter-electrode distance 35 mm) between the distal motor point and the distal tendon of the tibialis anterior (TA), lateral gastrocnemius (LG), and vastus medialis (VM) muscles in accordance with SENIAM recommendations. The sEMG data (1000 Hz) were acquired (44.6 N foot contact switch plate threshold for trigger onset) via a 3 channel data acquisition system (MP100, Biopac Systems, Goleta, CA; amplification 20 V/mV, low pass 500 Hz, high pass 10 Hz, common mode rejection ratio 110 dB min at 60 Hz, input resistance 2 MΩ).

Impact-resistant polyurethane foam with measured properties (Table 1) similar to shoe midsoles was varied in thickness (¼", ½", 1", 2").

Table 1: Foam properties summary. Second row data (*) approximate traditional running shoes [6].

Material Class	Shore A Hardness	Density (g/cm^3)	Cell Type	Cell size
Polyurethane (PU)	30A	0.05	Open-cell	500 µm
EVA or PU*	>25A	0.17- 0.25	Closed-cell	200 µm

Participants were randomly presented with each surface and allowed to habituate to each thickness by stepping down 7.5 in (standard step) for several unmeasured trials before testing began. The stepping platform was adjusted between foam conditions to maintain the vertical and horizontal distance from platform to foam/ground. Each of the four foam conditions was repeated 10 times. A no-foam control condition also received 10 steps, totaling 50 trials per participant.

The sEMG signals were rectified using a root mean square (RMS) algorithm (AcqKnowledge v.3.9.1, Biopac Systems, Goleta, CA) with a 15 ms time constant. The RMS waveforms were ensemble averaged across the ten trials for each condition. Pre-activation onset was determined by the intersection of two regression lines (OriginPro8, OriginLab, Northampton, MA) fitted to the RMS wave's incline and pre-contraction baseline. Using the calculated onset and triggered landing time, mean RMS amplitude (V), integrated RMS energy (V·s), and pre-activation duration period (ms) variables were determined. Nine separate multivariate one-way repeated measure ANOVAs examined differences in mean RMS amplitude, integrated RMS energy and pre-activation duration across the three muscle conditions. Alpha level was set at p=.05. All analyses were performed using SPSS Statistics (V. 16.0; IBM Corp., New York).

RESULTS AND DISCUSSION

No significant main within effects were observed (Figure 1). If varying foam thickness does not affect pre-activation, a transition to thinner shoes may be acceptable for foams that have a sufficiently high modulus and thickness to avoid "bottoming out" under the increased load of running. However, there was a within subjects contrast effect (Figure 1, bottom; p=.017) for LG mean amplitude, indicating a linear trend of decreasing amplitude with increasing thickness. The lack of within subjects main effect differences was observed potentially due to the high inter-subject variability in landing strategy. Since participants were stepping off a platform rather than running, the differences in necessary muscle tuning between foams may have been immeasurable. Additionally, the foam was chosen based on a hardness property, which is similar to other literature methods. For example, a previous study measured pre-activation as a function of frequency of the input energy, which was altered under the assumption that loading rate changes with shoe hardness [7]. However, surface properties such as hardness may prove to be poor predictors of loading rate. A more accurate correlate may be compressive modulus, the ratio of applied stress to strain. Foams dissipate energy via bulk mechanisms such as compression, cell face bending, and molecular-level interactions between polymer chains [8]. Furthermore, input signal frequency and pre-activation may be affected by inherent material properties and not simply loading rate. Although thickness did not elicit a within subjects main effect, the results warrant further research into the midsole foam properties and any subsequent effects on muscle tuning.

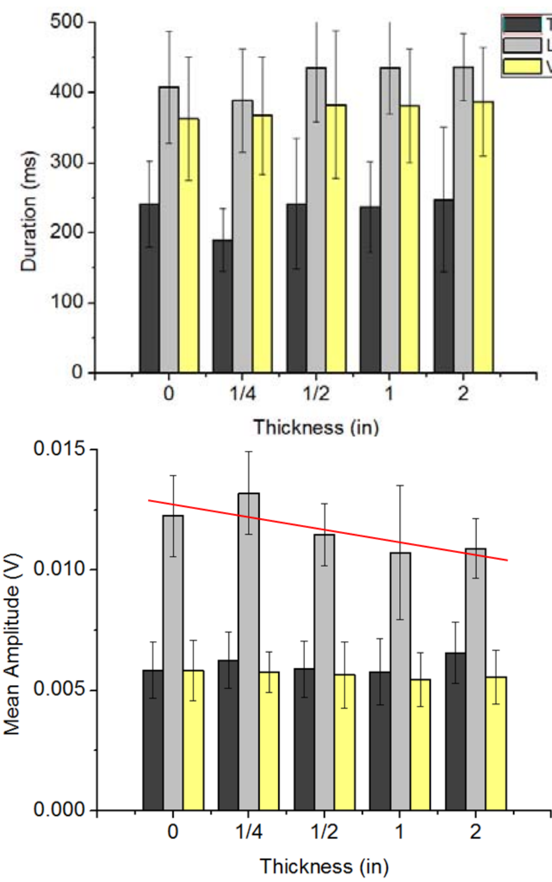

Figure 1: LG Duration (top) and Mean Amplitude (bottom) with 95% confidence intervals. The red fit line highlights contrast test; p=.017.

REFERENCES

1.Robbins S, et al. *Age Ageing* **24**, 67-72, 1995.
2.Shorten M, et al. *6th Symposium on Footwear Biomechanics*; Univ Otago, New Zealand 2003.
3.Ramanathan A, et al. *Foot and Ankle Surgery* **17**, 218-23, 2011.
4.Even-Tzur N, et al. *Bio-Med Mat's & Eng* **16**, 289-99, 2006.
5.Nigg B. *Clin J Sport Med* **11**, 2-9, 2001
6.Mills N. *Poly Foams Handbook*, Elsevier, 2007.
7.Nigg BM, et al. *J Appl Phys* **91**, 1307-17, 2001.
8.Ashby MF. *Metal Trans A* **14A**, 1755-69, 1983.

ON THE FATIGUE LIFE OF THE ANTERIOR CRUCIATE LIGAMENT DURING SIMULATED PIVOT LANDINGS

David B. Lipps, Edward M. Wojtys and James A. Ashton-Miller

University of Michigan, Ann Arbor, MI, USA
email: dlipps@umich.edu, web: http://me-engin.umich.edu/brl

INTRODUCTION

Passive collagenous structures such as rabbit medial collateral ligament exhibit fatigue behavior under cyclic loading: the larger the magnitude of repetitive loading, the fewer the number of loading cycles until failure [1]. A knowledge gap exists as to whether the human ACL might also exhibit fatigue behavior under cyclic loading. If so, this would help explain why an ACL rupture can occur during a common athletic maneuver that has been performed hundreds, if not thousands, of times before without injury. In addition, since smaller ACL cross-sectional area (CSA) and greater lateral tibial slope (LTS) increase peak ACL strain during simulated jump landings [2], might these morphological factors affect ACL fatigue life by increasing peak ACL strain? To find out, we tested the null hypotheses that landing force, gender, CSA, or LTS will not affect the number of cycles to ACL failure during repeated simulated pivot landings.

METHODS

Ten pairs of human lower extremities (5 females) from donors of similar age, height and weight (53(7) years, 174(9) cm and 69(9) Kg) with no visual scars or deformities were harvested and dissected, leaving the ligamentous knee structures intact along with the muscle tendons of the quadriceps, medial and lateral hamstrings, and medial and lateral gastrocnemius. Prior to testing, all knees underwent 3-Tesla T2-weighted MR imaging (Phillips scanner, 3D-PE sequence, field of view: 330 mm, slice thickness: 0.7 mm); the ACL CSA and LTS were measured using established methods in OsiriX (v3.9, open source) [2].

Using a published testing apparatus [2], the matched pairs of knees were tested under repetitive simulated pivot landings until ACL failure was achieved, with one knee having been randomized to a three-times body-weight (3*BW) pivot landing and the paired knee to a 4*BW pivot landing. The simulated quadriceps, hamstrings, and gastrocnemius muscles were pre-tensioned to place the knee in 20 degrees flexion prior to each trial. The knees underwent 5 non-pivot trials (compression + knee flexion) to adjust the height and mass of the drop weight on the apparatus in order to achieve the impulsive 3*BW or 4*BW simulated landing force. After the fifth trial, an impulsive 32(7) Nm internal tibial torque was added to place the ACL under large peak strain [2]. Cumulative peak relative strain of the anteromedial bundle (‘AM’) of the ACL was monitored (@ distal 1/3 location) with a DVRT (Microstrain Inc, Burlington, VT) from the first rotation trial. Tibiofemoral kinematics were measured at 400 Hz using optoelectronic marker triads on the proximal tibia and distal femur (Optotrak Certus, NDI, Waterloo, ON) to measure relative and absolute changes in tibiofemoral 3-D translations and rotations. The 3-D forces and moments applied to the knee joint were monitored at 2 kHz with paired 6-axis AMTI load cells on the distal femur and proximal tibia.

The testing protocol concluded when (a) the ligament had clearly failed, (b) a 3-mm increase in the absolute anterior tibial translation had occurred, or (c) a minimum of 60 trials were performed. The ACL was visually inspected for signs of tearing on the AM as well as the posterolateral (PL) bundles. A Cox regression model with shared frailty was performed in Stata (v12) to predict the number of cycles to ACL failure, with gender, simulated landing force, ACL cross-sectional area, and lateral tibial slope as covariates, and $p < 0.05$ being significant. For the purposes of the analysis, the ACL was considered to have failed if a complete or partial tear or an avulsion occurred, or absolute anterior tibial translation increased by 3 mm.

RESULTS AND DISCUSSION

The null hypotheses were rejected: a greater landing force and a smaller ACL cross-sectional area are significantly associated with a reduced number of cycles to ACL failure (Table 1). Thirteen of 20 knees failed during testing. There was one complete tear, six tears of the PL bundle (one combined with AM tear), two tibial avulsions, and four greater than 3 mm increases in anterior tibial translation with visible elongation of the PL bundle (Fig. 1). No knees showed visual signs of MCL damage. Relative to the first rotation trial, there was a mean (SD) increase of 4.0(2.2) mm anterior tibial translation and $3.3(1.1)^{o}$ internal tibial rotation in the 13 failed knees. Peak AM-ACL cumulative relative strain averaged 16% by the failure cycle.

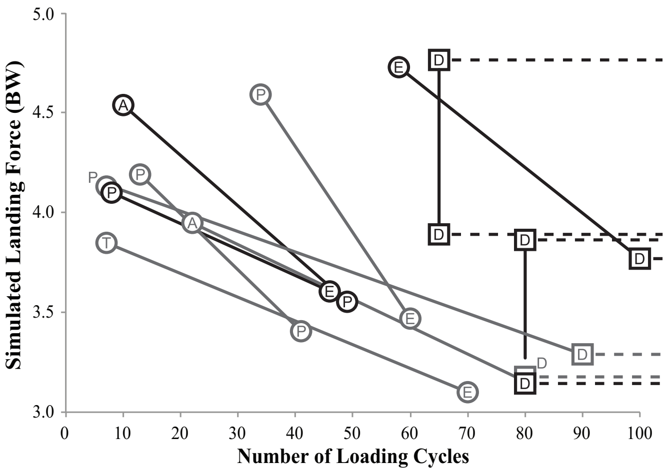

Figure 1: Scatterplot of simulated landing force vs. number of loading cycles. Legend: circle – failed, square – intact; black – male, grey – female; T – complete tear; P – partial tear; A – avulsion; E – >3mm anterior tibial translation; D – did not fail.

Table 1: Cox regression results for 20 knees with shared frailty term (theta) to control for matched-pairs. Abbreviations: CSA – cross-sectional area; LTS: lateral tibial slope.

	Hazard Ratio	95% CI	P
Landing Force	6.77	1.03-44.4	**0.04**
Gender	2.29	0.25-21.1	0.46
ACL CSA	0.89	0.79-0.99	**0.03**
LTS	0.88	0.64-1.21	0.43
Theta	1.22		0.06

Wald $X^2 = 9.64$; $p = 0.047$

Partial tears of the PL bundle, as well as tibial avulsions, have previously been reported in quasi-static torsional failures without muscle forces [3]. A 3-mm increase in anterior tibial translation was used because it has been found arthroscopically in 85% of complete ACL tears [4]. Four knees reached a 3-mm increase with no macroscopic tearing despite visible elongation of the PL bundle; it is likely that these knees underwent intra-substance damage and histology will be used to examine this. The tears and elongation of the PL bundle shown in this study supports the PL bundle's role in providing torsional stability of the knee. While only 10% of symptomatic ACL tears are reported as 'partial' tears [5], our results suggest that many PL tears may go undetected because an intact AM bundle continues to provide resistance to anterior tibial translation [6].

Limitations include the possibility that one or both DVRT barbs might have initiated failure in the AM bundle. But, since only one knee had a partial AM tear occurring distal to the DVRT, and because the majority of ACLs sustained a PL tear, this is unlikely to have significantly influenced the results.

CONCLUSIONS

This is the first evidence that the human ACL demonstrates fatigue failure. Greater landing force and smaller ACL CSA significantly reduced the number of cycles to ACL failure under repetitive 3 - 4*BW simulated pivot landings.

REFERENCES

1. Thornton G et al. *Clin Biomech*, **22**:932-40, 2007.
2. Lipps DB et al. *Am J Sports Med*, **40**:32-40, 2012.
3. Meyer EG et al. *Am J Sports Med*, **36**:1966-77, 2008.
4. Daniel D et al. *Am J Sports Med*, **13**:401-7, 1985.
5. Siebold R & Fu F. *Arthroscopy*, **24**:1289-98, 2008.
6. Hole RL et al. *Am J Sports Med*, **24**:556-60, 1996.

ACKNOWLEDGEMENTS

Funding: PHS grant R01 AR054821. Assistance: Dr. Catherine Brandon, Suzan Lowe, Dr. Youkeun Oh, Mélanie Beaulieu, and Jessica Deneweth.

PELVIC EXCURSION DURING WALKING POST-STROKE

[1,2]Virginia L. Little, [2]Theresa E. McGuirk, [2]Lindsay A. Perry and [1,2]Carolynn Patten

[1]University of Florida, Gainesville, FL, USA
[2] Brain Rehabilitation Research Center - Malcom Randall VAMC, Gainesville, FL, USA
email: ginnylittle@phhp.ufl.edu

INTRODUCTION

Dyscoordination and atypical muscle activation patterns are hallmarks of stroke-related walking dysfunction. While these impairments can readily be attributed to disruptions of neural control, skeletal malalignment, specifically at the pelvis, is also a prominent, and underappreciated, sequela post-stroke. Biomechanical malalignment places muscles at disadvantageous length-tension relationships impairing muscle activation and movement efficiency [1,2]. The direct consequences of biomechanical malalignment on walking function remain poorly understood. The magnitude of altered pelvic excursion and how these alterations affect the coordination and control of walking have not been studied in persons post-stroke. Of note, activation and coordination deficits are revealed in both the paretic and nonparetic limbs post-stroke [3-6].

We hypothesized that excessive pelvic excursion during gait would correspond with: 1) impaired ankle plantarflexor and hip flexor power in late stance/early swing, and 2) disrupted muscle activation patterns.

METHODS

Here we studied 19 participants (59.4±13.9yrs; 15 male) with chronic (40.7±34.4mo) post-stroke hemiparesis compared to 19 non-disabled controls (54.32±8.21yrs; 10 male). Participants walked on an instrumented split-belt treadmill at self-selected walking speed while biomechanical variables were assessed including: pelvic excursion, magnitude of hip (H1, H3) and ankle (A2) powers, peak hip extension range of motion, and activation patterns (EMG) of the tibialis anterior (TA), medial gastrocnemius (MG), and soleus (SO). Clinical data including gait speed and Fugl-Myer scores were also obtained.

Pelvic excursion was defined as pelvic motion with respect to the lab reference frame; quantified in three planes. Hemiparetic participants were allocated to pelvic excursion deviation categories based on the magnitude of deviation in pelvic excursion relative to controls.

ANOVA was used to determine if pelvic excursion deviation categories identified differences in clinical data, biomechanical gait parameters, and temporal muscle activation patterns (EMG).

RESULTS AND DISCUSSION

Classification based on pelvic excursion identified three distinct groups: Types I, II, and III, representing progressively increased magnitudes of deviation relative to controls.

Clinical Data
All participant groups presented with slower gait speed (Type I: 0.54 m/s, Type II: 0.41 m/s, Type III: 0.43 m/s; p <0.001) than the control group (0.96 m/s). However, no differences in gait speed, age (p = 0.70) or Fugl-Meyer synergy score (p = 0.32) were detected between Types I, II and III.

Biomechanical parameters
Differences in peak hip extension were revealed by classification on pelvic excursion deviation. The magnitude of peak hip extension was significantly lower for the paretic than the nonparetic leg for the Type III group (p = 0.03).

Joint powers responsible for the stance-to-swing transition also demonstrated disrupted patterns across groups (Fig. 1). Nonparetic and paretic differences were detected between the Type I and Type III groups in A2 magnitude ($p = 0.001$), and between the Type II and Type III groups in H1 magnitude ($p = 0.02$). The control and Type I groups produced higher magnitudes of H3 than the Type II and Type III groups ($p < 0.0001$).

EMG

All three participant groups revealed differences in MG EMG across the gait cycle. The Type I group maintained a normal MG modulation pattern through late stance, while the Type II group demonstrated a stepwise pattern through late stance, and the Type III group presented with no modulation through late stance. Additionally, during loading response, all participant categories revealed a significantly greater proportion of MG EMG activity than the control group ($p < 0.0001$).

Discussion

Static pelvic position did not correlate with pelvic excursion during gait. Additionally, clinical data failed to distinguish between variables of interest. However, the classification scheme based on pelvic excursion deviation differentiated group-specific walking patterns in stroke survivors.

The Type III group, with the greatest pelvic excursion, demonstrated the most pronounced reduction in H3 in late stance/early swing and reduced A2, with the greatest asymmetry between legs. Taken together, these findings provide initial evidence in support of our first hypothesis.

All groups also showed evidence of altered EMG patterns in the medial gastrocnemius, demonstrating a significant redistribution of muscle activity across the gait cycle providing support for our second hypothesis. Many treatment approaches for so-called "foot-drop" focus on augmenting TA activity to produce foot clearance. Our data suggest more effective treatment options might target EMG timing of multiple muscles, including the deficient activity of the plantarflexors during late stance in preparation for transition to swing.

CONCLUSIONS

As hypothesized, excessive pelvic excursion is related to walking impairment post-stroke. Here we present first evidence of detrimental effects on joint power production and EMG patterns.

Lack of correlation between static pelvic position and pelvic excursion during walking underscores the importance of this novel assessment scheme to understanding the role of dynamic pelvic control post-stroke. Additional work is needed to further understand specific neuromechanical contributions to walking impairment post-stroke and identify appropriate, targeted interventions to engage these mechanisms and promote neuromotor recovery.

REFERENCES

1. Lieber RL. *Acta Anat.* 1997;**159**(2-3):84-89.
2. Marks R, et al. *JTheor Biol.* 1994; **170**(3):283-9.
3. Kautz, S.A. and C. Patten. *J Neurophysiol*, 2005. **93**(5):2460-73.
4. Horstman, A.M., et al. *Clin Physiol Funct Imaging*, 2008. **28**(4):251-61.
5. Simon, A.M., et al. Conf Proc IEEE Eng Med Biol Soc, 2009. **1**:5294-9.
6. Garry, M.I., et al. *Hum Mov Sci*, 2005. **24**(5-6): 849-64.

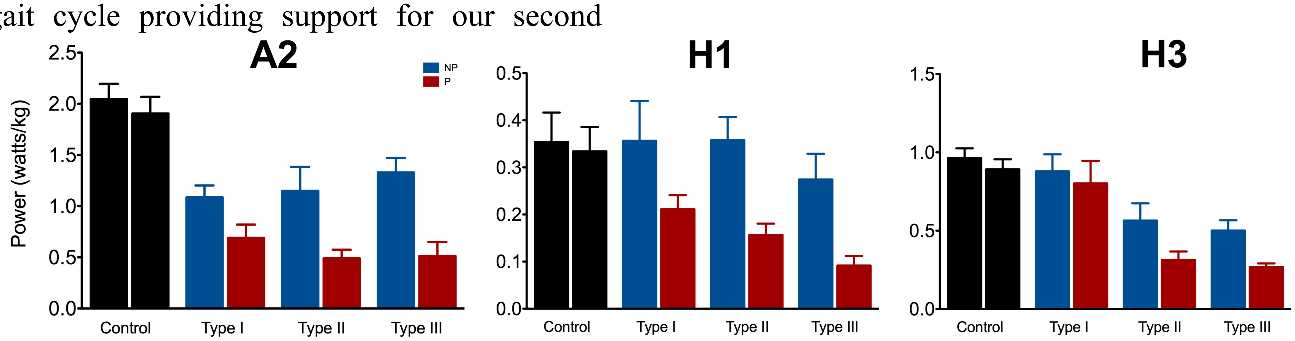

Figure 1: Joint powers during the stance-to-swing transition. Black bars represent symmetric joint powers between the right and left legs of controls. Blue and red bars represent nonparetic and paretic legs of participants post-stroke, respectively. *Abbreviations:* A2 – concentric ankle plantarflexor power during pre-swing, H1 – concentric hip extensor power in early stance, H3 – concentric hip flexor power during late stance and early swing.

IS THE PROBLEM REALLY FOOT-DROP?

[1,2]Virginia L. Little, [1,2]Theresa E. McGuirk and [1,2]Carolynn Patten

[1]University of Florida, Gainesville, FL, USA
[2]Brain Rehabilitation Research Center - Malcom Randall VAMC, Gainesville, FL, USA
email: ginnylittle@phhp.ufl.edu

INTRODUCTION

Impaired paretic swing limb advancement (SLA) is a hallmark of gait following stroke. The common school of thought posits 'foot drop' (impaired dorsiflexor function) as the primary cause of decreased paretic limb clearance during swing. SLA involves vertical shortening of the swing, relative to the stance, limb with simultaneous contributions from all three joints: hip, knee and ankle. Kinematic analyses illustrate reduced joint excursions throughout the paretic limb following stroke [1]. However, the influence of individual joint angular excursions during swing on toe clearance remains unknown. Sensitivity analysis enables determination of the influence of respective joint angles on toe clearance [2]. Here we investigated toe clearance sensitivity ($TC_{sensitivity}$) at: i) minimal toe clearance and ii) maximal limb shortening, during paretic limb swing, to the: hip, knee, and ankle joints. We hypothesized: 1) minimal toe clearance would be lower in participants post-stroke, but 2) toe clearance sensitivity to ankle dorsiflexion at either gait milestone would not differ between controls and participants post-stroke.

METHODS

We studied 16 participants (age: 57±14.37yrs; 13 male) with chronic (4.21±1.93yrs) post-stroke hemiparesis during overground walking at self-selected speed (SSWS) and 10 healthy controls who walked at matched speeds. Lower extremity kinematics were collected with 3D motion analysis. All participants post-stroke presented with lower extremity (LE) motor dysfunction (LE Fugl Meyer synergy: 15/22 ±2.78) and gait impairment (SSWS: 0.54m/s ±0.26).

Toe clearance sensitivity was defined as the partial derivative of toe clearance with respect to the paretic hip, knee, and ankle joints. We calculated $TC_{sensitivity}$ to sagittal plane changes in the lower extremity joint angles throughout swing, thus a planar model was used (*Fig. 1*).

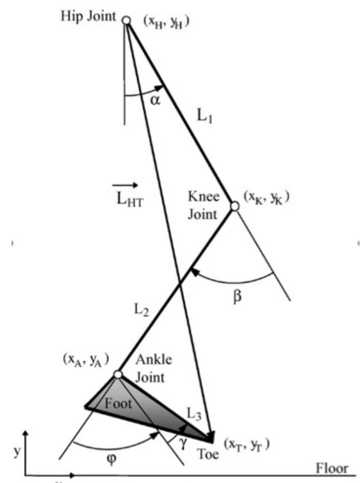

Figure 1: Free-body diagram used for sensitivity analysis [2].

Student's *t*-test was used to test for group differences in minimum toe clearance during swing. ANOVA was used to test for group x joint interactions for joint angle and $TC_{sensitivity}$ at two points: 1) minimum toe clearance and 2) maximum paretic leg shortening, in swing. After correction for multiple tests, statistical significance was established at $p<0.008$.

RESULTS AND DISCUSSION

Surprisingly, participants post-stroke revealed greater minimal toe clearance in swing ($p=0.001$; *Fig* 2). Maximum hip flexion and ankle dorsiflexion during swing did not differ between groups ($p>0.05$). However, as expected, maximum knee flexion during swing was reduced post-stroke ($p<0.0001$).

Minimum toe clearance in swing

Minimum toe clearance (TC_{min}) during swing occurred at approximately 73% and 74% of the gait cycle for controls and participants post-stroke, respectively. At TC_{min}, the joint angles of the hip and ankle did not differ between groups; however, the knee angle was reduced in participants post-stroke (26±15 degrees), relative to controls (48±12 degrees; $p<0.0001$). $TC_{sensitivity}$ to ankle dorsiflexion at TC_{min} did not differ between groups ($p>0.05$; Fig.3)). Interestingly, the pattern of $TC_{sensitivity}$ was reversed in the hip and knee between groups. $TC_{ensitivity}$ to 1) hip flexion and 2) knee flexion was exaggerated and reduced, respectively post-stroke ($p<0.0001$).

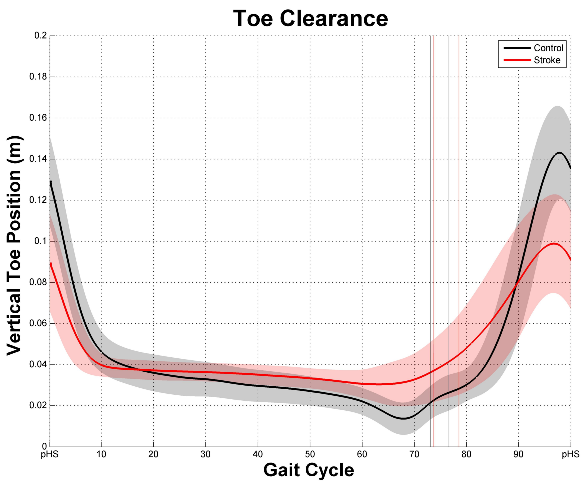

Figure 2: Vertical trajectory of the toe marker across the gait cycle. Black and red vertical lines denote the instance of: 1) minimal toe clearance in swing and 2) maximum leg shortening for controls and participants post-stroke, respectively.

Maximum paretic leg shortening in swing

Maximum paretic leg shortening (PL_{short}) occurred at approximately 77% and 79% of the gait cycle for controls and participants post-stroke, respectively. At PL_{short}, the joint angles for the hip and ankle did not differ between groups; however, the knee angle was reduced in participants post-stroke (24±14 degrees), relative to controls (49±11 degrees; $p<0.0001$). $TC_{sensitivity}$ to ankle dorsiflexion at PL_{short} did not differ between groups ($p>0.05$; Fig.3). In contrast, $TC_{sensitivity}$ to hip flexion was higher in participants post-stroke whereas the opposite was true for knee flexion ($p<0.0001$).

CONCLUSIONS

Given that minimal toe clearance during swing was higher post-stroke than controls, two conclusions can be made. First, limited toe clearance (i.e., dorsiflexion function) during SLA may not be as problematic as usually considered. Second, exaggerated toe clearance likely results from: 1) impaired inter-joint coordination at the stance-to-swing transition, or 2) a compensatory mechanism.

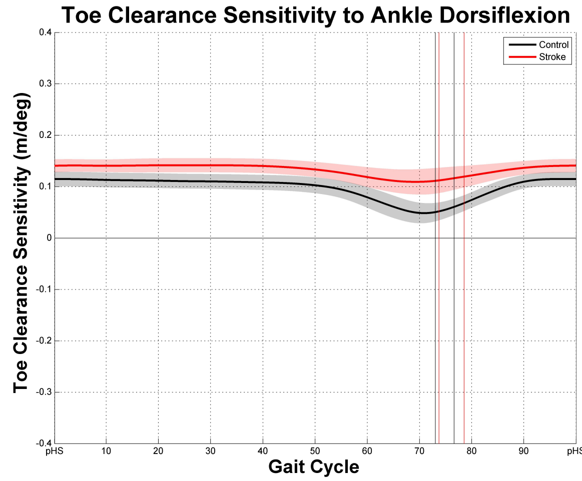

Figure 3: Toe clearance sensitivity relative to ankle dorsiflexion. Black and red vertical lines denote the instance of: 1) minimal toe clearance in swing and 2) maximum leg shortening for controls and participants post-stroke, respectively.

The lack of difference between groups in ankle angle and $TC_{sensitivity}$ to ankle dorsiflexion at both TC_{min} and PL_{short} argue against dorsiflexor dysfunction as the primary impairment of SLA in persons post-stroke. Further, reversal of $TC_{sensitivity}$, to hip and knee flexion between groups, at both gait cycle milestones suggests impairment of the dynamic coordination between these joints. The reduced ankle angle at both points suggests the causal mechanism may be impairment of the dynamic contribution to knee flexion by the gastrocnemius muscle in preparation for swing.

REFERENCES

1. Olney SJ & Richards C. *Gait & Posture* **4**,136-48, 1996.
2. Mossabhoy MA & Gard SA. *Gait & Posture* **24**, 493-501, 2006.

ACKNOWLEDGEMENTS

We thank Eric Topp for assistance with the sensitivity analysis. This work was supported by: VA RR&D Project B540231, Research Career Scientist Award (F7823S) to Dr. Carolynn Patten and the Foundation for Physical Therapy (VLL). Virginia Little, PT, NCS is supported by the NIH T32 Neuromuscular Plasticity Training Grant (No. 5 T32 HD043730-08, K Vandenborne, PI).

RELIABILITY AND PRECISION OF THE RESISTANCE ZONE AND LAXITY ZONE FOR SHOULDER INTERNAL AND EXTERNAL ROTATION

[1]Beven P. Livingston, [1]Jeff T. Wight, [2]Erik A. Wikstrom, [3]Mark D. Tillman

[1]University of North Florida, Jacksonville, FL, USA
email: j.wight@unf.edu, web: http://www.unf.edu/brooks/movement_science/
[2]University of North Carolina at Charlotte, Charlotte, NC, USA
[3]University of Florida, Gainesville, FL, USA

INTRODUCTION

Shoulder flexibility studies have traditionally focused on end range of motion only. Recent studies, however, have expanded shoulder flexibility analysis by assessing the passive torque that is generated by the shoulder as it is rotated to the end range of motion [1,2]. The torque may have great clinical relevance, especially for internal rotation (IR) and external rotation (ER). Therefore, it is critical to establishing reliable torque measures. In this study we assess the torque-angle relationship for the entire shoulder IR/ER motion. The purpose is to determine the intrasession, intersession, and intertester reliability and precision of the shoulder's laxity zone (LZ) and resistance zone (RZ). Studying the LZ and RZ is important because it helps to determine when soft tissues begin stretching and the joint motion allowed after stretching begins.

METHODS

Fifteen healthy male controls (age = 20.7 ± 1.1 years) participated. Participants had no history of shoulder surgery, injuries, or pain. Informed consent was obtained.

A custom device was constructed to assess the torque-angle relationship for shoulder ER and IR. The device consisted of a chair (reclined 30° from vertical) and a wheel. The participant's forearm was secured to the wheel. The investigator internally and externally rotated the shoulder by slowly pulling on a cable that caused the wheel to rotate. A potentiometer was mounted to the wheel (to assess shoulder displacement). The free end of the cable passed through a pulley that was attached to a load cell (to assess the torque). Data was sampled at 100 Hz.

Custom programs were written in LabVIEW software to collect and process the data. The torque-angle data was averaged into ½ degree increments. A least-squares best-fit line was used to model the torque-angle data (Figure 1). From the best-fit line, we identified the shoulder angle where 1N·m of torque was first generated. For both ER and IR, the laxity zone began at the neutral shoulder position (0°) and ended at the angle where 1N·m of torque was first generated. The resistance zone began at the angle where 1N·m of torque was first generated and ended at the end ROM.

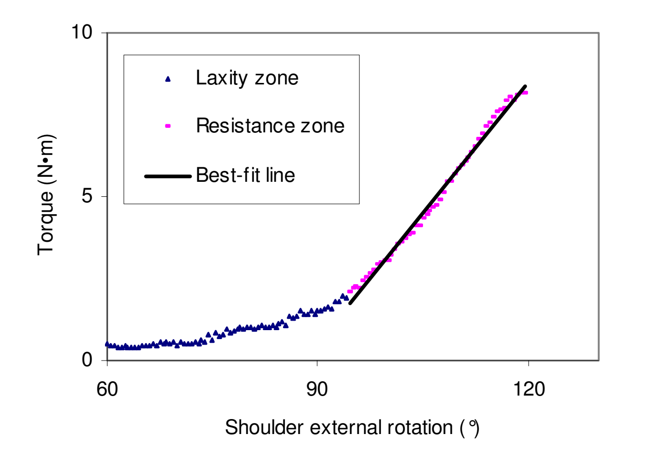

Figure 1: A least-squares best-fit line was used to model the resistance zone.

Participants had their flexibility analyzed twice within 7-10 days. On day 1, a single investigator analyzed both shoulders twice (for intrasession testing). On day 2, the first assessment was completed by the original investigator (for intersession testing) and the second assessment was completed by a second investigator (for intertester testing).

Intraclass correlation coefficients ($ICC_{2,1}$) were used to test reliability. For the LZ and RZ, intrasession, intersession, intertester reliability were calculated for each shoulder (dominant and non-dominant) and direction (IR and ER). This resulted in 24 total ICC scores (12 for each zone). The precision of measurement was estimated by calculating the standard error of measurement (SEM). Dependent t-tests were used to determine if the ICC and SEM scores were significantly different between the LZ and RZ. A standard alpha level ($p = 0.05$) was used.

RESULTS AND DISCUSSION

For ER, the LZ (83.0° ± 11.1°) was much greater than the RZ (25.0° ± 5.2°). For IR, the LZ (73.1° ± 8.4°) was also much greater than the RZ (21.3° ± 5.7°).

Reliability and precision results are presented in Table 1. The overall ICC score for the laxity zone was good (0.81). Only 1 of the 12 ICC scores was poor/moderate. The ICC scores for the resistance zone were not as strong. The RZ ICC score (0.63) was significantly lower ($p<0.05$). Four of the 12 RZ ICC scores were poor/moderate (< 0.6).

Interestingly, there was no difference in the standard error of measure between the LZ (3.5 ± 0.9°) and RZ (3.1 ± 0.7°). For both, the overall precision appeared to be quite good.

CONCLUSIONS

The RZ and LZ appear to have a similarly small standard error of measure. Interestingly, the resistance zone appears to be more sensitive to these errors as evidenced by its reduced ICC scores. The laxity zone is much greater in size than the resistance zone; the laxity zone comprises the majority of the motion for shoulder ER and IR. It is important to determine if the smaller RZ is therefore more susceptible to errors.

There were no dramatic differences between intrasession, intersession, and intertester ICC and SEM scores. All three analyses contained multiple ICC scores over 0.8 and SEM scores that were primarily less than 3.5°. Similarly, there were no obvious differences between the two shoulders (dominant and non-dominant) and two motions (ER and IR). This suggests that there is great potential to assess the measures bilaterally, for both motions, on different days, using different investigators.

It is recommended that LZ and RZ assessment be incorporated for clinical exams and research. LZ and RZ assessment may help to 1) better quantify shoulder flexibility and 2) improve the ability to diagnose, treat, and prevent injuries.

REFERENCES

1. Beardsley CL et al. *Clin Biomech.* 2010;25(8):759-64.

2. Novotny JE et al. *J Orthop Res.* 2000;18(2):190-4

Table 1: Reliability (ICC) and precision (SEM) of the laxity zone and resistance zone.

		DER	NDER	DIR	NDIR
Intrasession	**LZ**	0.82 (4.9°)	0.94 (2.0°)	0.88 (2.5°)	0.84 (2.5°)
	RZ	0.57 (3.6°)	0.72 (2.1°)	0.79 (3.0°)	0.63 (2.9°)
Intersession	**LZ**	0.86 (3.6°)	0.80 (4.7°)	0.77 (3.5°)	0.55 (4.7°)
	RZ	0.83 (2.0°)	0.28 (4.9°)	0.75 (2.8°)	0.47 (3.7°)
Intertester	**LZ**	0.89 (3.2°)	0.76 (4.2°)	0.84 (3.1°)	0.72 (3.4°)
	RZ	0.68 (3.0°)	0.55 (2.8°)	0.64 (3.5°)	0.62 (3.1°)

DER = dominant shoulder external rotation; NDER = non-dominant shoulder external rotation; DIR = dominant shoulder internal rotation; NDIR = non-dominant shoulder internal rotation

INTERHEMISPHERIC INHIBITION AND MOTOR LATERALIZATION: RELATIONSHIP TO AGE

[1,2]Neha Lodha, [1,2]Manuela Corti, [1,2]William J. Triggs and [1,2]Carolynn Patten

[1]University of Florida, Gainesville, FL, USA
[2]Brain Rehabilitation Research Center – Malcom Randall VAMC, Gainesville, FL, USA
email: lodhaneha@hhp.ufl.edu

INTRODUCTION

Asymmetries in inter-hemispheric function are hypothesized to relate to behavioral changes in motor lateralization. However, it remains unknown, how interhemispheric inhibition is altered as a function of age. Further, whether age related hemispheric asymmetries relate to motor lateralization has not been examined before. We hypothesized that interhemispheric inhibition from the non-dominant hemisphere to dominant hemisphere would reduce with advancing age. Further, motor lateralization will correlate positively with age.

METHODS

Twenty-five healthy individuals (10 male and 15 female) with age range 20-76 (m = 39.16 ± 16.605) participated. Motor laterality was determined using the Edinburgh Handedness Inventory and finger-tapping speed. Finger Tapping Difference (dominant-non-dominant hand) = 5.760 ± 0.82 confirmed all individuals were right handed. Interhemispheric inhibition was determined by ipsilateral silent periods obtained during transcranial magnetic stimulation (TMS). Motor Laterality is computed as finger tapping ratio difference [(Dom)/(Dom+NDom) – 0.5] . A positive ratio difference value indicates greater dominant hand lateralization.

RESULTS

The interhemispheric inhibition from non-dominant to dominant hemisphere (iSP duration) is negatively correlated with age ($r = -.41$, $p < 0.05$). Motor laterality revealed a significant positive correlation to age ($r = 0.48$, $p < 0.05$). Further, independent sample t-test revealed the younger group (age <40, N= 14) had significantly greater ipsilateral silent period duration (m=53.86 ± 17.01 ms) than older group (m=38.62 ± 12.80 ms) Further, the younger group demonstrate reduced finger tapping ratio difference (m=0.24 ± .02) than the older group (m=0.48 ± .02). The correlation between iSP duration from non-dominant to dominant hemisphere and finger tapping is not significant.

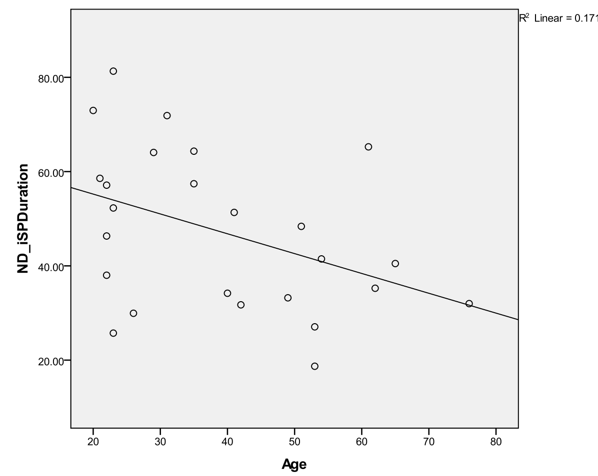

Figure 1: Correlation between iSP duration (ms) and age

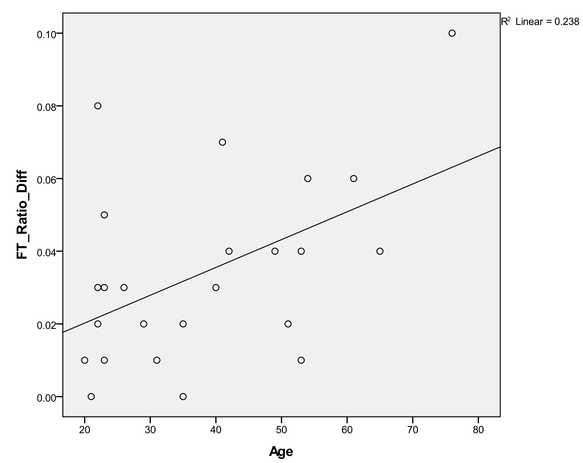

Figure 2: Correlation between finger tapping speed and age

DISCUSSION

Ipsilateral silent period duration revealed that inter-hemispheric inhibition from non-dominant to dominant hemisphere decreases with advancing age. Further, motor lateralization towards dominant hand increases with aging. Collectively, these findings show that aging leads to reduced inhibition of the dominant hemispheric contributing to increased motor lateralization. Moreover, the present findings have significant implications on how neurological deficits such as stroke may interfere with imbalances in inter-hemispheric function resulting in asymmetric motor function.

KINEMATIC VARIABILITY AT THE SHOULDER IS NOT RELATED TO SHOULDER PAIN DURING MANUAL WHEELCHAIR PROPULSION

Jessica Longworth and Karen Troy
Department of Kinesiology and Nutrition, University of Illinois at Chicago, IL, USA
email: jlongw3@uic.edu web: http://www.uic.edu/ahs/biomechanics

INTRODUCTION

The population of manual wheelchair users is increasing at a faster rate than that of the general population, contributing to a disproportionately high prevalence of shoulder pain and injury [1]. Most therapeutic interventions do not provide adequate alleviation for shoulder pain [2]. Unlike recreational activities such as running and cycling, wheelchair propulsion is an unavoidable activity and rest is not a viable alternative.

The upper extremities did not evolve as and are not conditioned to be the primary movers for mobility. It is theorized that the repetitive nature of wheelchair propulsion and the relatively large forces imposed are risk factors for pain and injury [2]. Consequences include a limited range of motion (ROM) and altered movement patterns [3]; however, quantifying these adaptations remains inconsistent.

It is reasonable to assume that these adaptations occur over time and that early detection is possible with indices that are more sensitive than those historically used. The purpose of this study is to quantify temporal and spatial characteristics of wheelchair propulsion in individuals with and without self-reported shoulder pain. In support of the loss of complexity theory [4] that biological systems lose their ability to adapt to varying conditions due to age or disease, we hypothesize that individuals with shoulder pain will have less ROM and thus, less cycle-to-cycle propulsion variability in the shoulder.

METHODS

22 subjects who use a manual wheelchair as a primary means of mobility were recruited for this institutionally approved study. All subjects gave written informed consent and completed the Wheelchair Users Shoulder Pain Index (WUSPI) and Shoulder Pain and Disability Index (SPADI). Both questionnaires were coded 0-10 with 0 meaning no pain.

A 3D motion capture system operating at 120 Hz (Motion Analysis, Santa Rosa, CA) was used to collect kinematic data. 18 reflective markers were placed on the trunk and upper extremities to create a 7-segment rigid body model [5]. Subjects propelled their wheelchair at a constant velocity on rollers (McClain, USA) for 2 min. A trial completed by each subject at a fixed speed between 2.0 and 3.0 km/h was analyzed.

Segment angles of the right upper extremity were calculated using custom software [5]. Kinematics were calculated relative to the global reference frame and were described using: plane of elevation (rotation about global vertical, with 0° being oriented forward), elevation angle (with vertical being 0° and horizontal being 90°), and axial rotation (with 0° in anatomic position) [6]. The data from each subject were divided into propulsion cycles that started and ended at the beginning of the push phase. ROM for each variable was calculated by subtracting the mean minimum angle from the maximum achieved during propulsion. Phase planes were plotted for each variable (Fig. 1) and centroid locations of phase planes were calculated for each propulsion cycle [7].

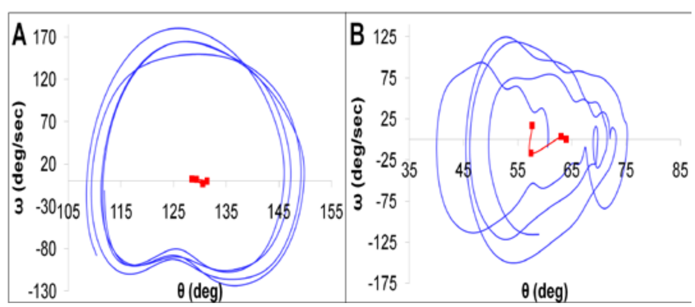

Figure 1 Phase planes for shoulder elevation angle and angular velocity during 4 propulsion cycles. Square symbols indicate centroid locations for each cycle. **A** low variability subject. **B** high variability subject.

The total path length the centroid traveled during consecutive propulsion cycles, divided by the total number of analyzed cycles, was calculated. The resulting quantity was the mean distance the centroid traveled between consecutive cycles, which we will consider variability. Pearson's correlations were used to determine the relationship between shoulder ROM and centroid path length.

Subjects were retrospectively classified as having shoulder pain if they reported pain on both questionnaires. Student's t-tests were used to compare shoulder ROM and variability between the pain and no pain groups.

RESULTS and DISCUSSION

Descriptive statistics by pain classification are presented in Table 1. The pain group had more females (p=0.040) and was older (p=0.045).

Table 1 Descriptive statistics by pain classification.

	Pain	No pain
Male/female	10/4	8/0
Age	38±11 yr	28±8 yr
Height	1.8±0.10	1.8±0.10 m
Mass	85.8±18.9 kg	80.3±25.6 kg
Wheelchair use	11±7 yr	8±7 yr
WUSPI	1.3±1.0	0.1±0.1
SPADI	3.2±2.1	0.2±0.6

Four of 9 possible combinations of upper arm ROM and centroid path length were significantly correlated (Table 2). Elevation angle was not correlated with any other angle. There were no differences between pain groups for internal rotation, elevation angle and plane of elevation ROM or centroid path length (Table 3).

Table 2 Correlations between centroid path length and humeral ROM (* p≤0.05).

	Int Rot path	Elev Ang path	Pl Elev path
Int Rot ROM	r=0.607*	r=0.032	r=0.510*
Elev Ang ROM	r=-0.232	r=-0.155	r=-0.120*
Pl Elev ROM	r=0.463*	r=0.047	r=0.522*

Table 3 ROM and path length by pain classification (mean±SD).

	Pain	No pain
Int Rot ROM	67±23	91±31
Elev Ang ROM	68±8	64±9
Pl Elev ROM	73±27	88±21
Int Rot path	5.9±3.3	7.2±9.0
Elev Ang path	2.9±1.5	2.8±1.0
Pl Elev path	5.8±3.7	5.9±4.6

It is possible that shoulder pain does not influence upper arm propulsion kinematics. It can be argued that wheelchair pushrims provide constraints to the upper extremity that minimizes the available movement coordination patterns. However, we have previously demonstrated that shoulder variability during propulsion is larger in individuals with a low level of control over their trunk [ASB abstract].

Alternately, it is possible that pain does influence upper arm variability during propulsion, but that our method of quantification is not sensitive to this condition. However, gait and running literature provide evidence in support of the hypothesis that kinematic variability decreases in the presence of injury, including the study used to develop our methods [7]. This suggests that our findings are not a result of metric insensitivity.

Lastly, the absence of a difference may be due to our subject sample. These subjects are part of an ongoing study in which they were not recruited based on the presence of shoulder pain. In fact, a post-hoc analysis revealed no difference between groups in active ROM at rest suggesting their pain is not severe enough to compromise ROM. Additionally, the questionnaires used provide information about shoulder pain experienced during the "previous week." This implies the pain group did not necessarily have pain at the time of testing. A similar study should be completed to ensure a type II error was not committed.

CONCLUSIONS

Although there were correlations between some ROM and centroid path length variables, our hypothesis that shoulder pain will be associated with less ROM and less cycle-to-cycle variability was not supported. Our results are in opposition to the theory that pain and injury compromise a system's ability to adapt to changing environments.

REFERENCES

1.US Census Bureau, 2000.
2.Subbarao, et al. *J Sp Cord Med* **18(1)**, 9-13, 1995.
3.Ballinger, et al. *Arch Phys Med Rehab* **81(12)**, 1575-81, 2000.
4.Pool. *Science* **243(4891)**, 604-7, 1989.
5.Troy KL. *Disabil Rehabil AT* **6(1)**, 22-28, 2011.
6. Wu G, et al. *J Biomech* **38**, 981-992, 2005.
7.DiBerardino LA, et al. *Clin Biomech* **25**, 552-556, 2010.

PARAMETERIZING AND VALIDATING A THREE COMPARTMENT MUSCLE FATIGUE MODEL FOR ISOMETRIC TASKS

[1]John M. Looft, [1]Laura Frey Law

[1]University of Iowa, Iowa City, IA, USA
email: laura-freylaw@uiowa.edu

INTRODUCTION

Muscle fatigue is a risk for musculoskeletal injuries [1]; however, there are very few predictive analytical tools available to model this complex process. Classically, muscle fatigue has been classified by the intensity-endurance time (ET) curve in the ergonomic literature [2], referred to as "Rohmert Curves". Several authors have provided updated versions of Rhomert Curves [3, 4]. Recently, a large meta-analysis of 194 publications involving experimental fatigue data confirmed joint-specific intensity-ET relationships [5].

We developed a three-compartment predictive fatigue model, modified from Liu et al (2002) [6] composed of three muscle states: active (M_A), fatigued (M_F), and resting (M_R). Our primary modification was the addition of a controller, C(t), defining the activation and deactivation between the resting and active states [7]. The rate of muscle fatigue and recovery, i.e., the "flow" between states is defined by two parameters (F & R). This model qualitatively reproduced expected intensity-ET relationships [7], but the purpose of this study was to determine optimal parameter values and validate the model against joint-specific intensity-ET relationships for isometric contractions reported by Frey Law and Avin (2010) [5].

METHODS

A two-stage global optimization search strategy was employed to determine the optimal F and R parameter values for each joint. The first stage involved a course grid of potential F and R parameter ranging from 0.0001 to 0.1 in increments of 0.0001 for nine task intensities ranging from 10-90% of maximum effort in 10% increments. This resulted in a total of 9,000,000 simulations (1,000,000 F and R combinations for each of the nine intensities). The second stage involved a refined grid search around the best values found from the first grid search in increments of 0.00001. This produced 8572 additional simulations for each of the 9 relative intensities for a total of 77,148 simulations in the second stage. Thus a total of 9.08 million simulations were performed to determine the optimal F and R parameters for each joint.

Error was calculated as the root mean square (RMS) between the predicted and expected ETs across the 9 task intensities using the joint-specific intensity-ET power equations [5] as the expected values. The optimal F and R combinations for each joint were chosen as those with the lowest mean RMS error. We defined a minimum criterion for "adequate" model accuracy as having a majority of the optimized ETs fall within the 95% prediction intervals (PI) for each joint region (i.e. minimum of 5 of the 9 intensities).

To validate these values, the model was also evaluated across a new set of 9 task intensities (15-95 % max, in increments of 10%) that were not part of the optimization process.

RESULTS AND DISCUSSION

The optimal, joint-specific, F and R values found as a result of the global optimization search strategy are located in Table 1. The resulting ET errors using the original optimization intensities and the test intensities are also provided in Table 1. The model well surpassed our minimum criterion for each joint, with a minimum of 7 of 9 ET predictions falling within the expected 95% PI, using the "optimized intensities" (Table 1). Across each joint, the highest intensities (>80% max) were the most difficult to maintain inside the 95% prediction intervals (see Figure 1 as an example).

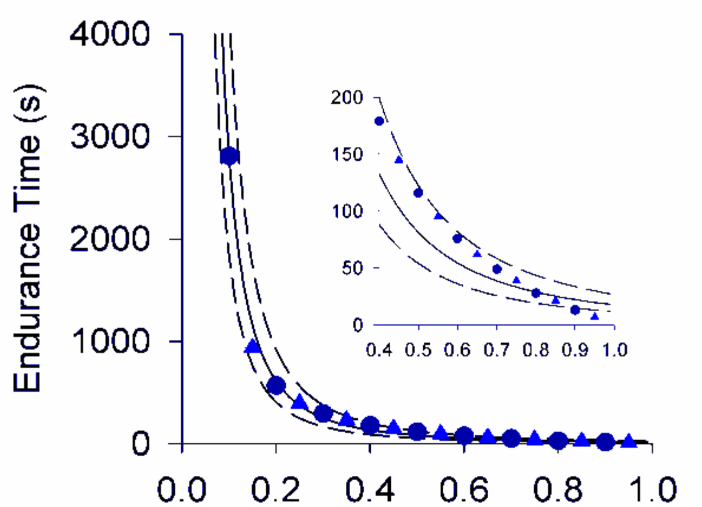

Figure 1: Model predictions using optimal F and R parameter values (optimized intensities = circles, test intensities = triangles) for the elbow.

The model predicted the expected intensity-ET curves well for the test intensities as well. A previous meta-analysis of the fatigue literature [5] determined that variations in ET range from 29-47% (by joint regions). Whereas the model's mean relative errors did not exceed 20%. Thus the mean model errors where well below normal variation.

CONCLUSIONS

The main finding of this study is that the three compartment muscle fatigue model can accurately predict ET for isometric contractions across a wide range of intensities for multiple joint regions. This suggests this relatively simple biophysical model of fatigue may provide a valid means of predicting fatigue for sustained isometric contractions.

REFERENCES

1. Sejersted, O.M. and G. Sjogaard, Physiol Rev, 2000. **80**(4): p. 1411-81.
2. Rohmert, W., Internationale Zeitschrift Fur Angewandte Physiologie, Einschliesslich Arbeitsphysiologie, 1960. **18**: p. 123-164.
3. Hagberg, M., Ergonomics, 1981. **24**(7): p. 543-555.
4. Monod, H. and J. Scherrer, Ergonomics, 1965. **8**(1-4): p. 329-338.
5. Frey Law, L.A. and K.G. Avin, Ergonomics, 2010. **53**(1): p. 109-129.
6. Liu, J., R. Brown, and G. Yue, Biophysical Journal, 2002. **82**(5): p. 2344-2359.
7. Xia, T. and L.A. Frey Law, Journal of Biomechanics, 2008. **41**(14): p. 3046-3052.

ACKNOWLEDGEMENTS

The authors were funded in part by National Institutes for Health, K01AR056134, United Council for Automotive Research (USCAR, Dearborn, MI), and the University of Iowa Heartland Center Graduate Student Fellowship.

Table 1: Optimal fatigue, F, and recovery, R, parameters by joint region.

Joint Region	F	R	Within 95% PI*	Optimization Intensities† RMS Error (s)	Optimization Intensities† Relative Error (%)	Test Intensities‡ RMS Error (s)	Test Intensities‡ Relative Error (%)
Ankle	0.00589	0.00058	8/9	11.2	0.6	28.2	-4.0
Knee	0.01500	0.00149	8/9	6.7	14.0	15.4	-17.0
Trunk	0.00755	0.00075	8/9	9.3	2.2	23.1	-1.9
Shoulder	0.01820	0.00168	8/9	2.7	-6.9	6.1	-10.0
Elbow	0.00912	0.00094	8/9	9.9	12.0	25.5	7.9
Hand/Grip	0.00980	0.00064	7/9	5.6	16.2	6.0	-20.0
General	0.00970	0.00091	8/9	7.3	2.4	11.8	-2.0

† Optimization task intensities: 10% - 90% of maximum, in 10% increments (total of 9 simulations).
‡ Test task intensities: 15% - 95% of maximum, in 10% increments (total of 9 simulations).
* Based on Prediction Intervals determined by Frey Law and Avin (2010), assessed using the 9 optimization intensities.

INTER-JOINT COORDINATION IN PATIENTS WITH CERVICAL SPONDYLOSIS DURING OBSTACLE-CROSSING

[1]Tung-Wu Lu, [1]Zhi-You Chen, [2]Dar-Ming Lai, [1]Wei-Ching Lo

[1] Institute of Biomedical Engineering, National Taiwan University, Taipei, Taiwan
[2] Division of Neurosurgery, Department of Surgery, National Taiwan University Hospital, Taipei, Taiwan
email: twlu@ntu.edu.tw

INTRODUCTION

Cervical spondylosis (CS) is a frequent clinical problem characterized by symptoms and signs consistent with cervical spine and spinal cord structural abnormalities [1]. Previous studies have shown that the level of disc prolapse among CS patients in the surgical group mostly occurred around C5 and C6 [2]. Cervical spondylosis with myelopathy (CSM) can affect several motor and sensory pathways travelling along the cord [3]. Balance dysfunction due to CS or CSM can result in falls during walking and obstacle-crossing, leading to physical injuries. Obstacle-crossing during walking is essentially a multi-joint movement, requiring precise swing foot control and a high level of inter-joint coordination of the stance and swing limbs [4-5]. The stability of the coordination patterns, a fundamental feature of functional action, is also essential. Failure to meet these requirements will lead to falls. The purpose of this study was to compare patterns and variability of the inter-joint coordination between the CS group and healthy control group when crossing obstacles of different heights.

METHODS

Eleven patients with CS at the C4-C5 or C5-C6 level (age: 61.88±12.03 years, height: 160.05±7.42 cm, weight: 64.12±12.36 kg, leg length (LL): 80.81±5.23 cm) and 11 normal controls (age: 53.45±8.71 yrs, height: 158.38±5.85 cm, weight: 60.74±15.21 kg, leg length (LL): 78.83±2.11 cm) participated in the current study with written informed consent.

In a gait laboratory, each subject walked and crossed a height-adjustable obstacle at a self-selected speed across an 8-meter walkway. Forty-one infrared-retroreflective markers were used to track the motion of the body segments. Three-dimensional trajectories of the markers were measured using a 7-camera motion capture system (Vicon 512, Oxford Metrics Group, UK). Test conditions included obstacle-crossing of three different heights (10%, 20% and 30% LL). For each subject, a total of six successful trials, three for each limb leading, were obtained.

Joint angles and angular velocities were calculated and used to obtain the phase angles for each joint [4-5]. Continuous relative phase (CRP) between two adjacent joints was then calculated by subtracting the phase angle of the distal joint from that of the proximal. A parameter called deviation phase (DP) was calculated by averaging the standard deviations of the ensemble-averaged CRP curve points for the stance and swing phase for each obstacle height [4-5]. The group and height effects on all the calculated variables were tested using two-factor repeated measures ANOVA using SPSS (Version 17, Chicago, IL). A significance level of 0.05 was set for all statistical tests.

RESULTS AND DISCUSSION

In general, the CRP curves of the leading limb in the CS group were significantly different from those of the control group (Fig. 1) while no significant differences were found for the trailing limb. The CS group showed significantly smaller CRP values for the leading joints when the leading and trailing toes were above the obstacle, except for the hip-knee at trailing toe crossing (Fig. 1). These results suggest that the inter-joint coordination of the leading limb but not the trailing limb was altered with CS.

Significantly increased variability of the inter-joint coordination was observed in the leading limb of the CS group, as indicated by the increased DP values, except for the knee-ankle (Fig. 2). As for the trailing limb, the variability of the inter-joint coordination was not significantly different between groups except also for the knee-ankle coordination. During trailing limb crossing, the CS group showed increased variability in the trailing swing knee-ankle coordination but decreased variability in the leading stance knee-ankle coordination. No significant height effects were found for all the variables.

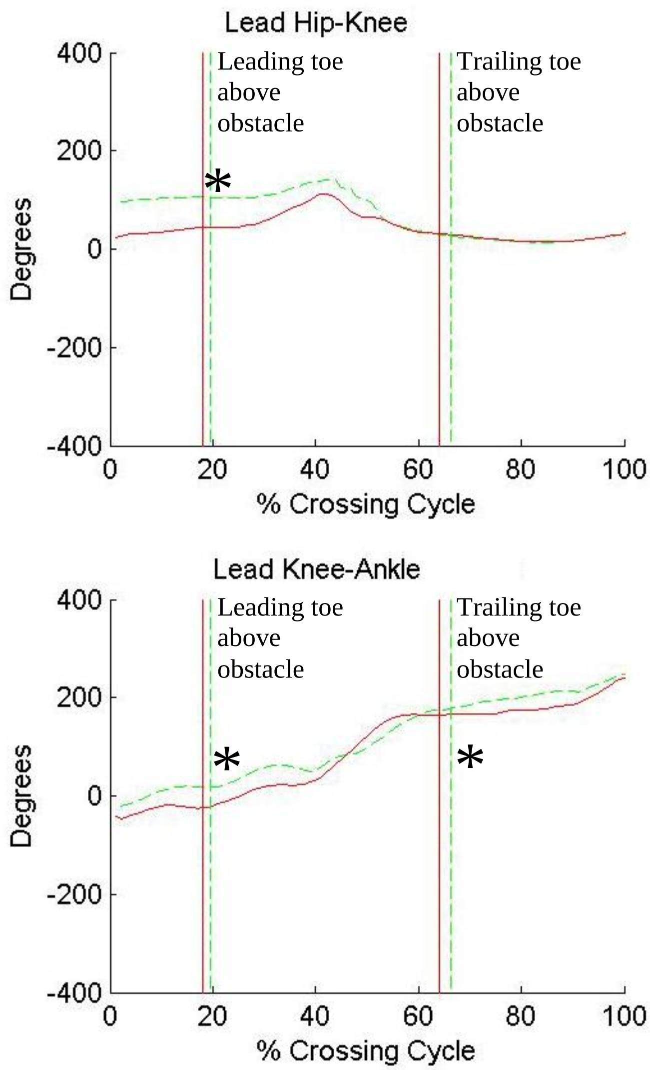

Figure 1: Ensemble-averaged CRP of hip-knee and knee-ankle of the leading limb for the CS (red) and control (green) groups when crossing obstacles of 20% LL. '*' significant group difference ($p<0.05$)

The current results showed that during leading limb crossing, the stability of the control of this motor task in the CS group was compromised mainly owing to the altered patterns and increased variability of the hip-knee coordination in the leading limb. This may lead to increased variability of the end-point control, increasing the risk of tripping. During trailing limb crossing, the increased variability of the trailing swing knee-ankle appeared to be a major determinant of the stability of the task while the reduced variability of the leading stance knee-ankle may be a strategy to compensate for it. The observed changes of the patterns and increased variability in the inter-joint coordination in patients with CS may be a result of impaired sensory function and reduced muscle strength in the lower limbs which often occur in this patient group.

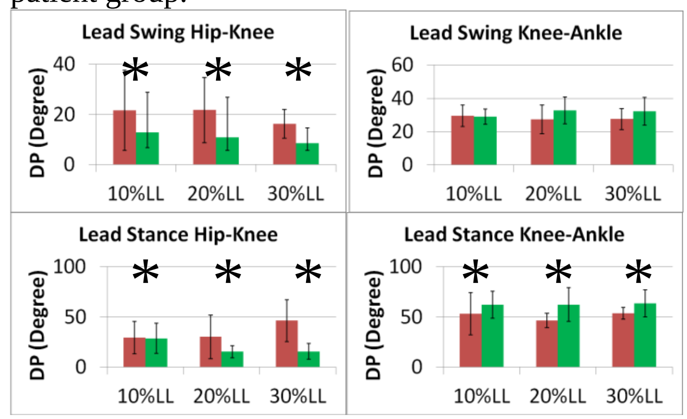

Figure 2: Comparisons of the DP values for the leading limb between CS (red) and control (green) groups during stance and swing phases. An asterisk indicates significant group difference ($p<0.05$).

CONCLUSION

During obstacle-crossing, patients with CS showed different and less stable inter-joint coordination in both the leading limb and distal part of the trailing limb when compared to controls. This suggests that clinical rehabilitation programs should include strategies to restore not only the primary motion of individual joints but also the coordination of movements between joints.

REFERENCES

1. Nardone A, et al. *J Rehabil Med* **40**, 539-547, 2008.
2. Kelsey JL, et al. *J Bone Joint Surg Am* **66**, 907-914, 1984.
3. Takayama H, et al. *Spine* **30**, 83-86, 2005.
4. Yen HC, et al. *J Biomech* **42**, 2501-2506, 2009.
5. Wang TM, et al. *J Biomech* **42**, 2349-2356, 2009.

POSTURE AND ACTIVITY DETECTION USING A TRI-AXIAL ACCELEROMETER

Vipul Lugade, Emma Fortune, Melissa Morrow, Kenton Kaufman

Mayo Clinic, Rochester, MN, USA
email: kaufman.kenton@mayo.edu, web: http://mayoresearch.mayo.edu/mayo/research/biomechanics/

INTRODUCTION

Quantifying activity levels among healthy older adults and patients can provide objective information on sedentary behavior and physical function [1]. In order to accurately quantify activity in the free-living environment, a robust method for classifying posture and activity needs to be established. Therefore, the purpose of this study was to validate the identification of static postures and dynamic activity from acceleration data against a gold standard of visual inspection from video recordings.

METHODS

Video and acceleration data were collected from 12 healthy adults (9 females; age (SD) of 34.0 (9.7) years; BMI (SD) of 24.7 (5.5) kg/m^2). Subjects were asked to perform an approximately 5 minute series of static and dynamic activities, consisting of sitting, standing, lying, walking, jogging and stair climbing in the laboratory. Additionally, subjects were asked to 'shuffle' their body to simulate activity during selected sitting and standing tasks. A hand held camera collected video data at 60Hz. Custom built activity monitors (±16g) collected tri-axial accelerations at 100 Hz. The study protocol was approved by the Mayo Clinic IRB, with written informed consent obtained prior to data collection.

Event durations were determined by two investigators for each static and dynamic activity using Windows Movie Maker. Timings for accelerometer classification were determined from two activity monitors attached with straps to the waist and right thigh. Accelerometers were synchronized with video data from three vertical jumps performed prior to the prescribed protocol.

Acceleration signals from the waist were used to differentiate dynamic versus static activity [2]. Data were separated into its gravitational component by using a third-order zero phase lag elliptical low pass filter, with a cutoff frequency of 0.25 Hz, 0.01 dB passband ripple and -100 dB stopband ripple. Subtracting the gravitational component from the original signal provided the bodily motion. The bodily motion component determined static versus dynamic activity, with a threshold greater than 0.135 *g* for the signal magnitude area identified as activity [3]. The gravity component provided the tilt angle (θ) of the device using $\theta = arccos(a/g)$ [4].

Lying down was determined when the waist angle was between 50 and 130 degrees and upright postures between 0 and 50 degrees, in relation to gravity. For upright postures, standing and sitting were differentiated based on a thigh angle threshold of 45 degrees [4]. Among active tasks, walking and jogging were differentiated based on a threshold of 0.80 *g* for the signal magnitude area. Transition periods between lying, sitting and standing were also identified. Classified data were organized into one second windows for video and accelerometer data. Sensitivity and positive predictive value (PPV) were used to assess accelerometer identification of posture at each second. Bland-Altman plots assessed differences in total time of activity for video and accelerometer identification. Inter-rater reliability was assessed using intra-class correlations (ICC).

RESULTS AND DISCUSSION

ICC values were greater than 0.95 for all activity, except transitions (ICC = 0.69). The acceleration at the waist during the protocol discriminated static and dynamic activities at 95% sensitivity (Figure 1). Further discrimination of the static postures demonstrated average sensitivities above 85% for sitting, standing and lying down. Total time in activity demonstrated up to 7 second discrepancy with video identification across the entire protocol (Figure 2). Among dynamic activities, walking and jogging sensitivity were greater than 90%. Standing and transitions had the greatest variability in classification. Average PPV were greater than 85%

for all static and dynamic orientations. These results suggest that a tri-axial accelerometer could be utilized to accurately track individuals in their free-living environment and are similar to those previously reported [2,4].

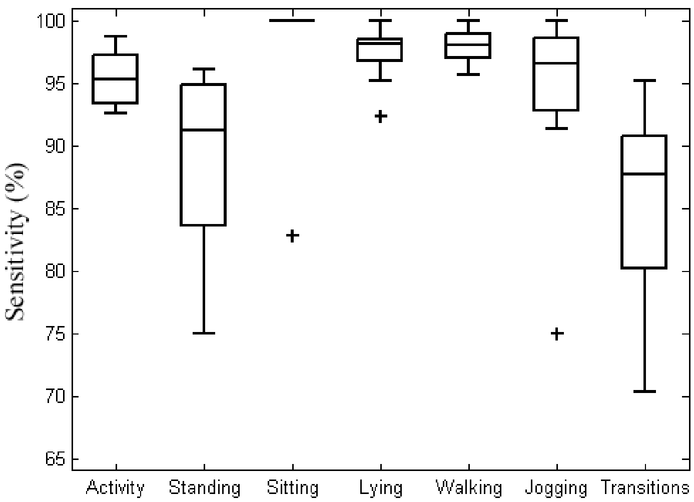

Figure 1. Sensitivity of the activity classification algorithm. The central line represents the median, the edges of the box are 25th and 75th percentiles, and the whiskers extend to ± 2.7SD. Crosses are outliers.

While average sensitivities across subjects for the activity monitor were strong, four subjects demonstrated reduced sensitivity and PPV in static posture. Among these subjects, differences were observed in body morphology and monitor placement. Subjects were asked to don the waist marker at the level of the navel, and slight offsets in monitor orientation during static upright posture produced tilt angles of greater than 0 degrees.

Additionally, during the protocol, all subjects were asked to perform 15 second sitting and standing tasks while ‘shuffling,’ to recreate daily activity. While some subjects voluntarily moved slightly, greater shuffling resulted in an increased number of false negatives. When assessing ‘non-shuffling’ sitting and standing tasks, all subjects classifications approached sensitivity and PPV values of 95%.

Not including ‘shuffling’ tasks, classification errors occurred at the beginning or end of a given posture or transition. These differences can be attributed to rounding of both the accelerometer and video data to one second windows. Greater resolution in window size would provide even greater accuracy.

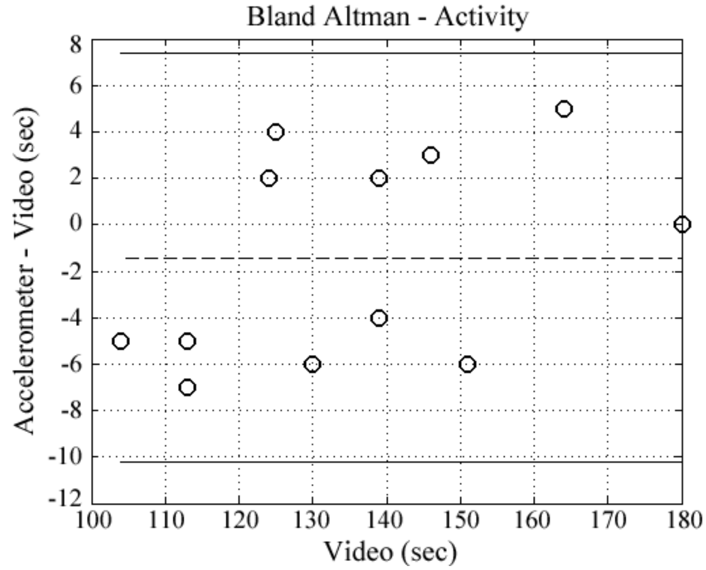

Figure 2. Differences in total time spent in dynamic activity versus static postures for the accelerometer and video recordings among the 12 subjects. Horizontal lines indicate ± 1.96 SD from the mean.

A limitation of this study is the current inability to differentiate level walking from stair climbing. While further analysis will investigate the differences in these two tasks, it is noted that subjects in this study were ambulating at similar speeds when walking and stair climbing, with upright activity properly identified during these tasks. The strength of this study is in the inclusion of a range of body types (BMI range: 19.9 to 40.1 kg/m^2) with a less constrained testing procedure that includes more natural movements. In conclusion, the use of activity monitors with tri-axial accelerometers can predict activity and static postures among the general population during activities of daily living.

ACKNOWLEDGEMENTS

Funding provided by NIH T32 HD07447, NIH K12 HD065987, and DOD DM090896.

REFERENCES

1. Oliver M., et al. *Prevent Med.* **51,** 357-360, 2010.
2. Karantonis D., et al. *Inform\ Tech Biomedicine, IEEE Transactions.* **10**, 156-167, 2006.
3. Mathie M., et al. *Med & Biol Engr & Comp.* **41**, 296-301, 2003.
4. Lyons G., et al. *Med Engr & Physics*. **27**, 497-504, 2005.

A COMPUTATIONAL MODEL FOR CONVECTION-ENHANCED DELIVERY IN A HIND LIMB TUMOR

[1]K.N. Magdoom-Mohamed, [1]Gregory. L. Pishko and [1]Malisa Sarntinoranont

[1]Dept of Mechanical and Aerospace Engineering, University of Florida, Gainesville, FL, USA

email: msarnt@ufl.edu

INTRODUCTION

Systemic drug delivery to malignant tumors involving macromolecular therapeutic agents is challenging for many reasons. Amongst them is their chaotic microvasculature and higher interstitial fluid pressure (IFP) which often leads to inadequate and uneven uptake in solid tumors [1,2]. Localized drug delivery can circumvent such obstacles and convection-enhanced delivery (CED) has emerged as a promising local drug delivery technique. CED is controlled infusion of the drug directly into the tissue, thereby utilizing both convection and diffusion for distributing macromolecules. In this study, a three dimensional computational porous media transport model based on voxelized modeling methodology was developed for predicting the interstitial fluid flow and distribution of albumin tracer following CED at the hind-limb tumor in mice. The model accounted for the actual tumor microvasculature obtained through dynamic contrast enhanced-magnetic resonance imaging (DCE-MRI). A sensitivity analysis was also performed to study the effects of varying hydraulic conductivity maps on fluid flow and tracer transport.

METHODS

The study was divided into two parts. First the spatially-varying transport properties (rate transfer constant between plasma and extracellular space, K^{trans} and porosity, φ) of the KHT murine sarcoma were found using DCE-MRI data following bolus tail vein injection of MR visible tracer gadolinium-diethylene-triamine penta-acetic acid (Gd-DTPA, MW ~ 590 Da) in the mice. This portion of the study was performed earlier by our group [3] and its data (K^{trans} and φ maps) was used for this study. The focus of the current work is on the second part which involves incorporating the above calculated variable transport properties into a computational porous media model for predicting fluid flow and albumin transport by CED.

Mathematical Model

The tissue continuum was modeled as a porous media. The continuity equation with an additional point source (infusion site) was combined with Darcy's law to solve for interstitial fluid pressure and velocity. Spatially varying hydraulic conductivity given by the following relation [4] was used,

$$K = K_0 \, e^{m\phi}$$

Here K and K_0 are the actual and baseline tissue hydraulic conductivity and m is an empirical exponent.

Albumin tracer (MW ~ 66 kDa) transport was modeled using a convection-diffusion equation without any sources or sinks. The concentration in the transport equation was normalized ($\hat{C}$) using the concentration at the infusion site.

Spatially varying transport properties were implemented into the model as follows. The transvascular diffusive flux term in the transport equation was spatially varied by scaling it with K^{trans}. Assuming similar patterns of leakiness for tracer and plasma, normalized values of K^{trans} (obtained by dividing it with its average value) were used to scale the fluid filtration rate per unit volume in the continuity equation. Model parameter values were identical to those in [3].

Computational Method

The governing equations were solved at each voxel using commercial computational fluid dynamics

(CFD) solver (FLUENT v12.0.16, ANSYS Inc) over a rectangular mesh with element size equal to that of the MRI voxel size (0.104 x 0.104 x 1 mm^3). User-defined functions were used to specify K, K^{trans}, φ and variable source terms in the continuity equation, in each voxel. Infusion simulations were carried out for 2 hrs. A zero fluid pressure condition was applied along the cut ends and the remaining outer boundaries of the geometry were assigned as wall with a normal mass flux approximately equal to zero. Initial conditions for tracer transport assumed no tracer in the tissue, $\hat{C} = 0$ except at the infusion site (center of the tumor) which is one voxel, where it was set to a normalized value of 1 at all the times during the transport simulation. Baseline simulations were carried out at $m = 0$ and sensitivity analysis was performed for $m = 4$ and 8.

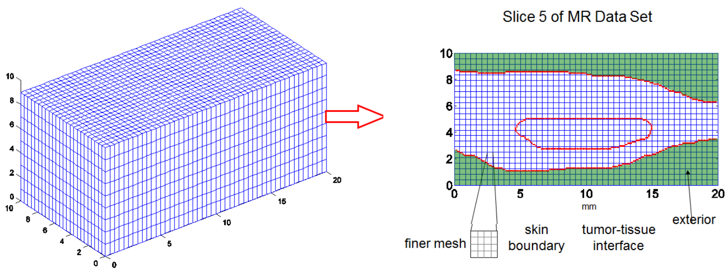

Figure 1: Schematic of voxelized mesh and detailed view of slice 5 of MR data set showing the hind limb with tumor.

RESULTS AND DISCUSSION

The model was able to capture asymmetric albumin distribution shown experimentally in previous sarcoma CED studies [5]. Also captured was the linear relation between distribution volume (tissue volume covered by at least 1% infused albumin) and infusion volume typically observed with CED. Albumin distribution was found to be sensitive to changes in hydraulic conductivity maps. Increasing hydraulic conductivity (via higher values of m) lowered the tumor IFP and raised the distribution volume within the whole leg. However within the tumor, the distribution volume decreased with increasing values of m, at later time points.

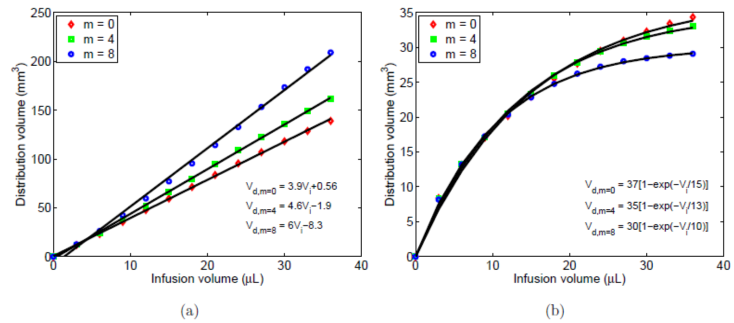

Figure 2 : Variation of distribution volume with infusion volume for whole leg (left) and tumor (right)

CONCLUSIONS

These results demonstrate the importance of non-linear tissue swelling behavior in targeted infusion drug delivery to tumors. To our knowledge, this is the first image-based tumor model that incorporates the actual tumor microvasculature, and predicts heterogeneous drug distribution following CED. With further development, such models could potentially optimize patient-specific cancer treatments and explore the effects of heterogeneity on tracer transport in tumors.

REFERENCES

1. Fukumura D, et al. *Microcirculation* **17(3)**, 206-25, 2010.
2. Heldin CH, et al. *Nat Rev Cancer* **4(10),** 806-813, 2004.
3. Pishko GL, et al. *Ann Biomed Eng* **39(9)**, 2360-2373, 2011.
4. Lai WM and Mow VC. *Biorheology* **17 (1-2)**, 111-123, 1980.
5. Boucher Y et al. *Br J Cancer* **78(11)**, 1442-1448, 1998.

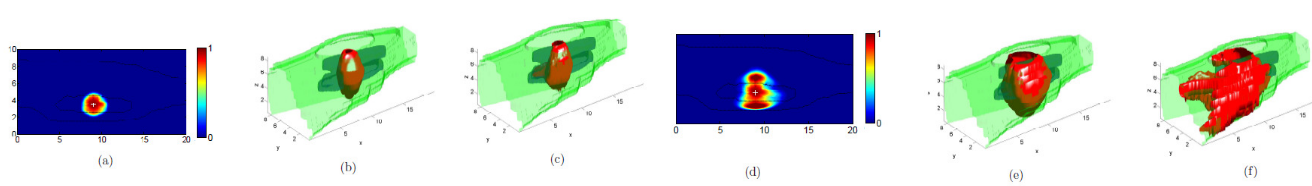

Figure 3 : Distribution of predicted albumin concentration at t = 30 and 120 mins. First column shows the contours at the infused slice, second and third column shows the whole leg iso-surfaces at *m* = 0 and 8 at t = 30 mins. Similarly, the contours and iso-surfaces of albumin concentration at t = 120 mins are shown in the last three columns. (Green – skin boundary, red – drug distribution and blue – tumor)

UPPER BODY KINEMATICS OF BILATERAL TRANSTIBIAL PROSTHESIS USERS DURING GAIT

[1]Matthew J. Major, [2]Rebecca Stine, [3]Megan Hodgson and [1,2]Steven A. Gard

[1]Northwestern University Prosthetics-Orthotics Center,
Dept. of PM&R, Feinberg School of Medicine, Chicago, IL, USA
[2]Jesse Brown VA Medical Center, Chicago, IL, USA
[3]Johns Hopkins University, Baltimore, MD, USA
email: matthew-major@northwestern.edu, web: www.nupoc.northwestern.edu/

INTRODUCTION

Compared to the gait characteristics of persons with unilateral transtibial amputations, bilateral transtibial amputee gait has received relatively less attention. Recent investigations on this topic have demonstrated that, due to the nature of their disability, bilateral transtibial amputees walk with significantly reduced self-selected speeds and increased step width compared to able-bodied controls [1]. Furthermore, despite close to normal knee and hip joint kinematics, these individuals display considerable hip-hiking during swing phase [1]. These compensatory gait mechanisms may contribute to their increased metabolic cost of 33 to 107 percent relative to able-bodied controls [2]. However, the clinically observed unique upper body motions of these individuals, which are substantially different from able-bodied ambulators, have not yet been quantitatively described. Therefore, the purpose of this study was to quantify upper body kinematics of bilateral transtibial amputees during steady-state walking. Further understanding of these dynamics may help inform prosthetic prescription to satisfy the unique ambulatory and rehabilitation needs of these individuals.

METHODS

A retrospective analysis was performed on a subset of ten subjects (51±18 yrs, 1.73±0.08 m, 82±16 kg) from a previous investigation on the gait characteristics of bilateral transtibial amputees [1]. Participants were fit with a Seattle Lightfoot II prosthetic foot and rigid pylon to standardize prosthesis configuration between subjects, then permitted two weeks for acclimation prior to data collection. During testing, subjects performed overground walking trials at three self-selected speeds: “normal,” “fastest comfortable” (fast), and “slowest comfortable” (slow). Kinematic data were collected with an eight camera motion capture system (Motion Analysis Corporation (MAC), Santa Rosa, CA) at 120 Hz, and kinetic data were collected with six embedded force plates (AMTI, Watertown, MA) at 960 Hz. Upper body kinematics, joint range-of-motion (ROM), step width and walking speed were estimated using a modified Helen Hayes marker set and post-processed with OrthoTrak software (MAC). Dominant arm swing frequency was estimated from the power spectral density profile of a single wrist marker. As upper body dynamics affect the vertical ground reaction, or free vertical, moment [3,4], this kinetic parameter was also calculated [4]. Amputee kinematic data were averaged over all ten subjects, whilst kinetic data were averaged over only nine subjects due to a hardware malfunction. Data for thirteen age- and speed-matched able-bodied controls (51±6 yrs, 1.72±0.09 m, 74±15 kg) walking at self-selected speeds were used for baseline comparison. A repeated-measures ANOVA was used to statistically analyze between-speed differences of amputee parameters (α=0.05).

RESULTS AND DISCUSSION

Data for controls were matched to the fastest walking speed of the amputee subjects (Table 1). At similar walking speeds, amputee elbow flexion/extension ROM was comparable to controls, but amputee shoulder flexion/extension ROM and shoulder abduction were greater at all walking speeds. Similar to able-bodied individuals [2], flexion/extension ROM of the elbow (p=0.001) and shoulder (p=0.002) joints increased with walking speed. Most noticeably, amputee subjects displayed a sinusoidal profile of lateral trunk flexion with a

ROM that was substantially greater than controls (Figure 1), coupled with a wide step width (Table 1). Both lateral trunk flexion ROM (p=0.601) and step width (p=0.145) remained similar irrespective of walking speed. A previous study has suggested that bilateral transtibial amputees walk with a wide step width to maintain a larger medial-lateral (ML) base of support due to a perception of instability [1]. Given this abducted gait, such exaggerated shoulder ROM and lateral trunk flexion may be expected, in which bilateral amputees must shift their center of mass from one foot to the other across this wide base of support [2]. These subjects may abduct their shoulders to facilitate this transfer and promote ML stability, with increased necessity at higher walking speeds (peak shoulder abduction increased with increasing speed (p=0.002)). Furthermore, lateral trunk flexion slightly preceded pelvic obliquity, which may indicate that the pelvis is following trunk movement rather than directly facilitating hip-hiking for foot ground clearance.

Dominant arm swing frequency remained more closely matched to stride than step frequency when walking at slower speeds (<0.75 m/s) for the majority (4 of 7) of subjects. This behavior has also been observed in unilateral transfemoral amputees, which is counter to the motion of able-bodied individuals [5]. This pattern may be an artifact of the near in-phase temporal relationship between lateral trunk flexion and hip flexion displayed by these subjects for maintaining forward ambulation.

Bilateral amputee subjects displayed greater ML ground reaction force magnitudes throughout stance compared to controls across all walking speeds (Table 1), with moderate increases in peak forces as speed increased (p=0.006). These excessive ML forces may be reflective of a greater lateral 'push' required to transition from one leg to the other during double support stance. As walking speed increased, the free vertical moment shifted into purely external rotation (applied to the foot), but peak moments during stance were not significantly different between walking speeds (p=0.079).

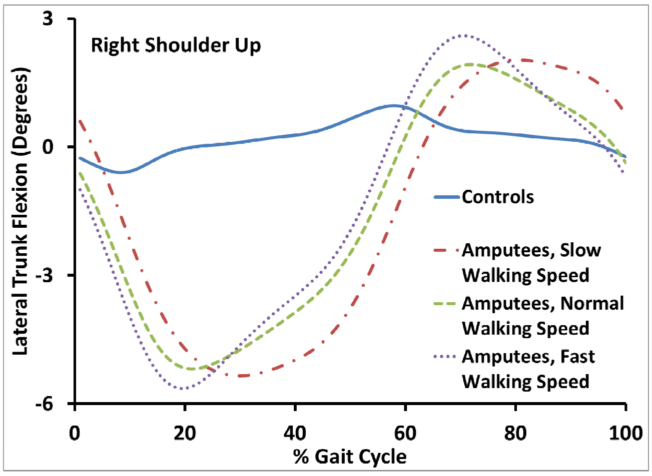

Figure 1: Lateral trunk flexion.

CONCLUSIONS

At similar walking speeds, bilateral transtibial amputees walked with wider step widths than age-matched controls. Importantly, amputees walked with exaggerated lateral trunk flexion coupled with large ML ground reaction forces. Lateral trunk flexion toward the stance limb preceded contralateral pelvic rise and hip flexion slightly at slow, normal, and fast self-selected walking speeds. Further studies are needed to determine if prosthetic components can be designed to reduce both stance width and excessive lateral trunk flexion during the gait of bilateral transtibial amputees.

REFERENCES

1. Su PF, et al. *J Rehabil Res Dev* **44**, 491-502, 2007.
2. Perry J and Burnfield JM. *Gait Analysis: Normal and Pathological Function* 2nd *Ed.*, Slack, 2010.
3. Collins SH, et al. *Proc Biol Sci* **276**, 3679-88, 2009.
4. Li Y, et al. *J Exp Biol* **204**, 47-58, 2001.
5. Donker SF, et al. *Acta Psychol* **110**, 265-88, 2002.

Table 1: Gait parameters for amputee subjects walking at three speeds (slow, normal, and fast) and controls.

	Slow	Normal	Fast	Controls
Walking Speed (m/s)	0.7±0.1	1.0±0.2	1.3±0.3	1.3±0.1
Step Width (cm)	19.7±4.2	19.4±4.0	18.6±3.5	12.2±2.7
Peak ML Force (%Body Weight)	8.0±1.9	8.8±1.9	9.3±1.5	6.6±1.7

Knee Joint Loading after ACL Reconstruction: Influence of Graft Type

Kurt Manal, Emily Gardinier, Lynn Snyder-Mackler and Thomas Buchanan

University of Delaware, Newark, DE, USA
email: manal@udel.edu

INTRODUCTION

There is a high incidence of knee osteoarthritis (OA) following ACL reconstruction [1]. Many factors likely contribute to the onset and progression of knee OA including altered muscle and joint contact forces. Signs and symptoms can take 5 or more years to develop [2], and may be related to small differences in knee loading associated with subtle changes in gait mechanics repeated of over many gait cycles. Muscle forces contribute significantly to joint compressive load and thus surgical procedures which alter a muscle's force generating potential can have a direct influence on knee joint loading.

The autologous semitendinosous-gracilis (STG) graft procedure is commonly used in ACL reconstruction. The STG procedure involves harvesting the patients' semitendinosous and gracilis tendons and bundling them together to form a surrogate ACL. This causes an immediate change in the way forces are transmitted across the knee. Further, morphological changes occur with time including hypertrophy of the semimembranosous and biceps femoris muscles. Such changes are not seen in patients reconstructed using a transplanted cadaveric ACL (ie., allograft). The flexor musculature in patients undergoing STG autograft reconstruction is altered in ways not experienced by those reconstructed using a cadaveric allograft.

The purpose of this study was to evaluate if hamstrings muscle force and medial compartment loading differ between patients reconstructed using an STG autograft compared to the allograft procedure. We hypothesized that changes to the flexor mechanism subsequent to reconstruction would result in different muscle forces and peak loading between groups.

METHODS

Ten subjects approximately 6 months post-op participated in this study. Five had the STG autograft procedure and 5 had an allograft reconstruction (Table 1). All subjects demonstrated full knee range of motion, minimal effusion, ≥70% quadriceps index and ability to hop on the injured limb without pain. The study was Institutional Review Board approved and all subjects provided informed consent prior to testing.

Table 1. Subject demographics

	Autograft (n=5)	Allograft (n=5)
Age (yrs)	27.4.±1.67	32.8±11.0
Height (m)	1.73±0.09	1.76±0.06
Mass (kg)	75.7±16.6	93.8±13.5
Walking Speed (m/s)	1.59±0.10	1.49±0.09

Stance phase kinematics and kinetics were collected using standard video-based motion capture and analyzed with Visual3D (C-motion, Inc). An EMG-driven model was used to estimate muscle forces for 10 muscles crossing the knee [3]. Electromyography (EMG) was collected for the following muscles: biceps femoris long head (BFL), semimembranosus (SM), rectus femoris (RF), vastus medialis and lateralis (VM & VL), and the medial and lateral Gastrocnemii (MG & LG). EMG for the Vastus intermedius (VI) was equal to the average of the VM & VL, with Semitendinous (ST) and Biceps Femoris Short head (BFS) equal to the SM and BFL. The ST was set to 0 for subjects in the STG autograft group representing a complete loss of the ST due to harvesting the tendon. Subjects performed isolated maximum voluntary isometric contractions for EMG normalization. Medial compartment force was calculated using a frontal plane moment-balancing algorithm [4]. Contact forces were time-normalized to 101 samples and reported as bodyweights (BWs). Three trials per subject were averaged in this manner.

RESULTS AND DISCUSSION

Subjects in both groups walked at a similar speed and thus speed was not a confounding factor (Table 1). Both groups exhibited similar patterns and relative distribution of hamstrings force. Peak force for the BFL and SM was approximately 5% BW greater for the STG autograft subjects. Additional subjects are being added to our data set to better evaluate the clinical significance of this finding.

In contrast, quadriceps force for the STG autograft group was larger compared to the allograft subjects (Figure 1). This finding was unexpected as both surgeries did not directly involve the quadriceps. Further, the large increase in quadriceps force was disproportional to the relatively small increase in hamstrings force. This is clinically relevant as the quadriceps contribute to knee loading during weight acceptance with peak muscle and contact forces occurring at approximately 20% stance (Figures 1 & 2). Sharma and colleagues reported an association between quadriceps strength and increased likelihood of developing knee OA [5]. Whether subjects with stronger quadriceps actually generated larger forces during gait could not be determined from their study however it is consistent with the idea that greater loading is associated with onset and progression. The STG autograft reconstructed subjects in our study used greater quadriceps force and this may place them at greater risk of developing knee OA.

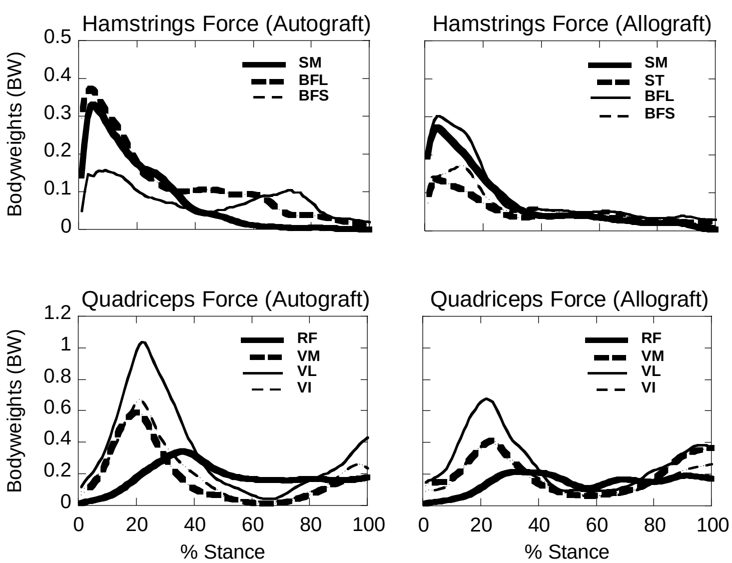

Figure 1. Ensemble averaged muscle forces (n=5 per group). Note that peak quadriceps force was larger for the Autograft group and occurred at 20% of stance.

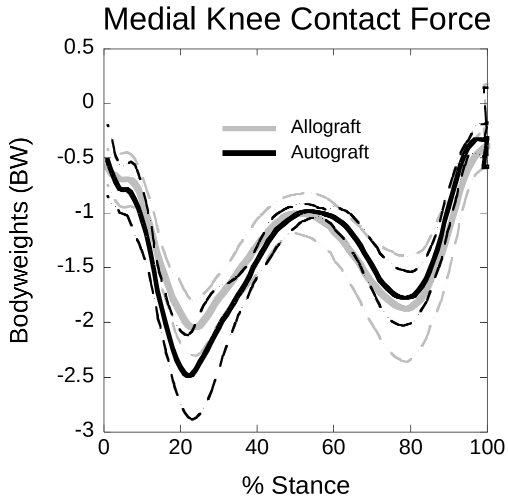

Figure 2. Ensemble averaged medial compartment contact force (n=5 per group; dashed line = SD). Note that peak contact occurs at same time as peak Vasti force (Figure 1).

CONCLUSIONS

Subjects with the STG autograft had slightly greater peak hamstrings force (~ 5% BW) compared to the allograft patients. Quadriceps force for the STG subjects was much larger, and this was directly related to greater medial compartment loading compared to the allograft reconstructed. This finding may have clinical implications related to the high incidence of knee OA seen after ACL reconstruction. It is premature to conclude the autograft group may be at greater risk of developing OA. Additional subjects and longitudinal follow-up are needed to critically evaluate the influence of graft type on joint loading. This work is underway.

REFERENCES

1. Fleming BC, et al. *Curr Opin Orthop*. 2005 October ; 16(5): 354–362.
2. Daniel DM, et al. Am J Sports Med 1994;22:632–644.
3. Buchanan TS, et al. *J Appl Biomech* **20**, 367-95, 2004.
4. Winby CR, et al. Journal of Biomechanics 42 (2009) 2294–2300
5. Sharma L, et al. *Ann Intern Med.* 2003;138:613-619.

ACKNOWLEDGEMENTS

Supported by NIH R01-AR046386

FACTORS ASSOCIATED WITH PRESSURE ULCERS: THE EFFECTS OF SHEAR LOADS ON BLOOD FLOW

Abinand Manorama and Tamara Reid Bush

Michigan State University, East Lansing, MI, USA

email: reidtama@msu.edu, web: http://www.egr.msu.edu/bdrl

INTRODUCTION

Pressure ulcers are localized areas of breakdown in the skin and underlying tissues that can extend down to the bone. These wounds are major health concerns and affect approximately 3 million people in the United States. Individuals who have limited mobility and spend a significant time in the seated posture, such as spinal cord injured and elderly, are highly susceptible to pressure ulcers.

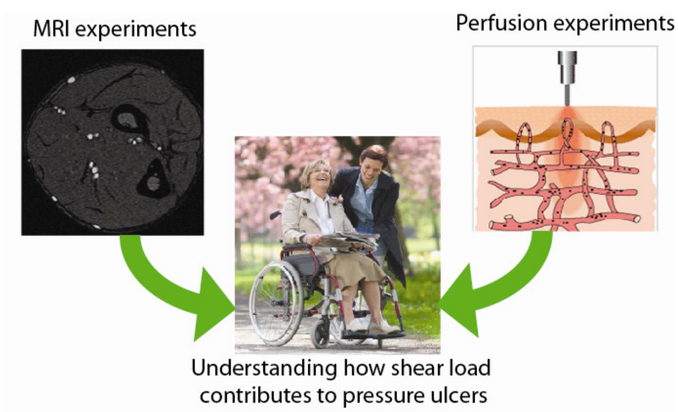

Figure 1: General workflow of the study

Current ulcer prevention methods focus on minimizing the normal loads (pressure) by shifting the individual's posture at regular intervals. However, these preventive measures have not been highly successful. When in a seated position, the body is consistently exposed not only to normal but also shear loads [1, 2] though, few studies have investigated the effects of shear loading on the skin. Additionally, there have been two theories which describe the mechanism of pressure ulcer propagation. One suggests that ulcers propagate at the skin level and proceed inwards to the muscle [3]. The other theory suggests that the tissue breakdown initiates at the muscular level and later propagates to the dermal and epidermal regions [4].

Because the health of the skin heavily relies on blood flow and perfusion, the goal of this work was to investigate the effects of shear loads on blood flow in vessels as well as perfusion of the skin (Figure 1). By studying these responses, insights can be garnered as to which theory of ulcer propagation is most likely.

METHODS

<u>MRI experiment:</u> This experiment investigated blood flow in the larger vessels of the forearm and was conducted in a MRI setting. The forearm was selected as the test site because it was easily accessible for measurements. Magnetic Resonance Angiography (MRA) was used to obtain blood flow measures in the vessels of ten healthy male participants, with an average age of 28 (SD 9) years.

Each participant lay prone on the scanner bed with his right forearm inside a cylindrical magnetic coil beneath a pressure cuff (Figure 2). Next, the scanner bed along with the participant was translated into the MRI scanner, and loads were applied to the participant's forearm.

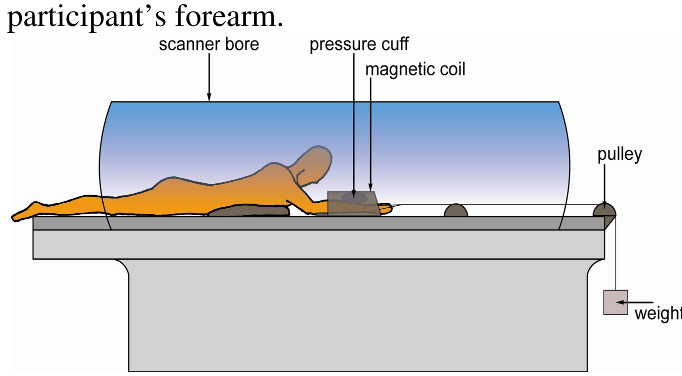

Figure 2: MRI experimental setup

There were three loading conditions: baseline (no load), normal load, and normal plus shear load. The normal load was applied by inflating a pressure cuff placed between the magnetic coil and the top of the forearm. The cuff was inflated to a pressure of 20 mm Hg which resulted in an average force of 17 N. A pulley-weight system was used to apply shear loads on the forearm. A wrist band was secured around the participant's wrist so that when the weight (20N) was attached to the rope, shear loading was applied to the skin. This load was large enough to apply shear, without measurably displacing the arm.

During each of these loading conditions, the blood flow in the anterior interosseous artery (AIOA) and basilic vein (BV) were measured.

Perfusion experiment: While the MRI experiment measured the blood flow in larger vessels, the perfusion experiment measured the blood perfusion in the capillaries of the skin in the forearm. Laser Doppler Perfusion Monitoring (LDPM) was used to measure the perfusion and transcutaneous oxygen (tcpO2) in the skin.

A total of 15 participants (seven male and eight female) with an average age of 23 (SD 2.4) years were tested. The participants were seated in an office chair, with their right forearm placed on a load cell assembly located on a table in front of the individual. Two probes, one to measure the blood perfusion and the other to measure tcpO2, were attached non-invasively to the subject's forearm while a load cell measured the normal and shear forces. Three conditions were evaluated: baseline (no load), the normal load of the forearm, and the normal load of the forearm plus a subject-induced shear load.

RESULTS AND DISCUSSION

The blood flow rates in the AIOA and the BV were obtained from the angiography data for the three conditions from the MRI experiment. A decreasing trend of blood flow in both the vessels was observed (Figure 3), with the largest flow rate in the baseline condition and the lowest flow rate in the combined loading condition.

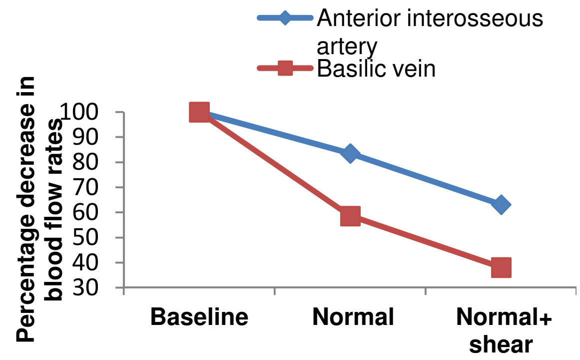

Figure 3: Decreasing blood flow with applied loads

Although the differences in mean blood flow were not statistically significant, medium to high effect sizes were obtained. Specifically, for the comparisons of blood flow between normal load condition and combined load condition, an effect size of 0.65 was obtained for the AIOA, and 0.43 for the BV. These effect sizes suggested statistical significance would be likely with a larger sample size.

Analysis conducted with the perfusion data showed a significant decrease in blood perfusion ($p=0.023$) and tcpO2 levels ($p<0.001$) with the application of shear load in addition to the normal load.

CONCLUSIONS

From the results of the two experiments, it is evident that the blood flow decreases in the AIOA and BV vessels and at the superficial level, with the addition of shear loads. Furthermore, the decrease in tcpO2 indicates a decrease in nutrients to the skin and other surrounding tissues, thus increasing the potential for tissue necrosis.

The results of our experiments indicate that both theories of ulcer propagation are possible, because the deeper vessel flow as well as the superficial flow were affected.

REFERENCES

1. R.H.M. Goossens et al. (1997) *Scand J. Rehabil Med,* 29, 131–136.
2. T.R. Bush & R.P. Hubbard. (2007) *J Biomech Eng-T ASME*, 129, 58–65.
3. C. Bansal et al. (2005) *Int J Dermatol*, 44, 805-
4. R.K. Daniel et al. (1981) *Arch Phys Med Rehab*, 62, 492-8

The Use of a Platform for Dynamic Simulation of Movement: Application to Balance Recovery

Misagh Mansouri, Ashley E. Clark and Jeffrey A. Reinbolt

University of Tennessee, Knoxville, TN, USA
email: misagh@utk.edu, web: http://rrg.utk.edu

INTRODUCTION

Numerical simulations play an important role in solving complex engineering problems and have the potential to revolutionize medical decision making and treatment strategies. Whereas experimental data from clinical studies aids in the evaluation and treatment of movement abnormalities as seen in children with cerebral palsy, it remains difficult to elucidate mechanisms responsible for these abnormal movements. Simulation offers a means of integrating experimental data, anatomical models, and dynamic principles to thoroughly understand human movement and perform "what if" studies for optimal treatment planning.

Stiff-knee gait is a prevalent movement disorder among children with cerebral palsy that could benefit from simulations. Rectus femoris transfer surgery, a common treatment for stiff-knee gait, reattaches the distal tendon of this two-joint muscle to a new site such as the sartorius insertion on the tibia. Biarticular muscles, such as the rectus femoris, play a unique role in motor control. As a biarticular muscle, rectus femoris may offer unrecognized benefits to maintain balance.

In this study, we used a simulation platform including an OpenSim and MATLAB interface [1] to perform forward dynamic simulations and applied the closed-loop control capability of this interface to investigate the influence of biarticular muscles on balance recovery. Our goal was to use the rapid model-based design and control of the interface by implementing the previously developed stretch-reflex controller [2] in MATLAB. We then employed the controller to maintain the whole-body center of mass (CoM) displacements in response to support-surface translations for simulations of preoperative, unilateral, and bilateral rectus femoris transferred models.

METHODS

Musculoskeletal Models and Platform Dynamics

A three-dimensional musculoskeletal model with 92 muscle-tendon actuators and 23 degrees of freedom was created in OpenSim (Fig. 1). The model was scaled to represent the size of the patient using previously collected gait analysis data [3, 4]. A pre-surgical simulation (Fig. 1a) was altered to represent surgical transfer of the rectus femoris to the sartorius for both a unilateral (Fig. 1b) and bilateral case [4]. The foot-ground interface was modeled using elastic foundation contact and the feet were based on cadaver foot geometry [5].

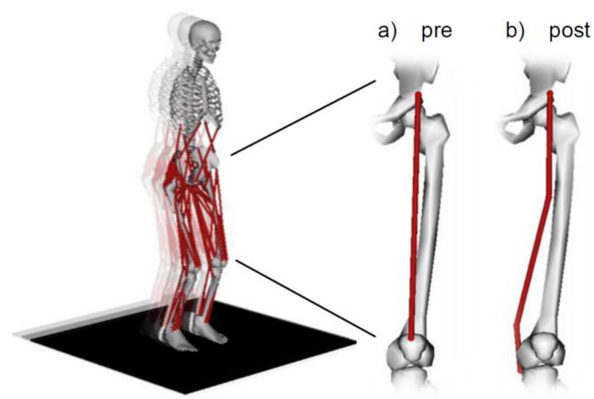

Figure 1: Musculoskeletal model of a patient with cerebral palsy on an anteriorly translating support surface, and biarticular attachments for the rectus femoris muscle (a) pre- and (b) post-surgical transfer to the sartorius.

Stretch-Reflex Controller

The mechanism used to maintain balance was based on a muscle stretch-reflex control model [6]. The closed-loop stretch–reflex controller was implemented in Simulink as an "Embedded MATLAB Function" (Fig. 2). Simulink used the interface to integrate state derivatives of the musculoskeletal model and generates new states based on the feedback controls. Each simulation included 0.25 seconds of quiet standing, 0.35 seconds of support-surface translation (6 cm in the anterior and posterior directions, with a peak velocity of 23 cm/s [2]). Controller gains for the stretch-reflex were found using MATLAB's Optimization Toolbox to keep the CoM position above the base of support. This controller is analogous (but not identical) to monosynaptic reflexes and afferent mechanisms (e.g., muscle spindles and Golgi tendon organs) responsible for lower-level motor control, and should not be affected following surgical transfer; thus, the same stretch-reflex controller was used for all model simulations.

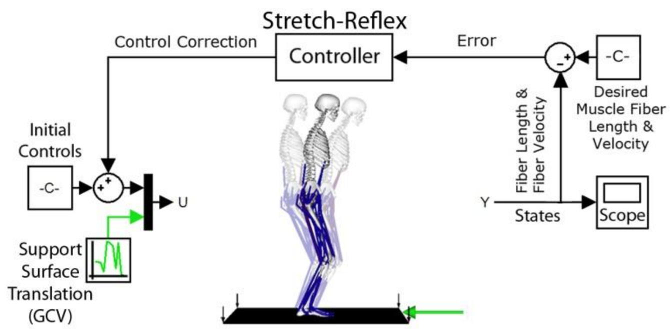

Figure 2: Closed-loop Simulink model of balance recovery using a muscle stretch-reflex controller. The controller uses the muscle's fiber length and velocity to generate a control correction to maintain the CoM position above the base of support.

RESULTS AND DISCUSSION

The closed-loop stretch-reflex controller was developed in Simulink using MATLAB's rapid design and control capabilities to demonstrate the application of a platform for dynamic simulation to investigate the influence of biarticular muscles on balance recovery. The platform not only made the procedure of implementing the previously written C++ code [3] easier but also provided access to all MATLAB toolboxes and numerical solvers.

The CoM had various displacements in the anterior-posterior directions relative to support-surface translations for preoperative, unilateral, and bilateral tendon transfers (Fig. 3). For the anterior translation, all three cases recovered balance; however, the preoperative model recovered faster than the post-surgical ones. For the posterior translation, the post-surgical models maintained balance while the pre-surgical one did not.

Patient-specific simulation is a powerful tool to investigate the role of rectus femoris tendon transfer in control tasks. Our results suggest that rectus femoris tendon transfer will change the balance recovery, illustrating the biomechanical uniqueness that biarticular muscles have in motor control. Future study is necessary to include higher-level motor control and investigate other treatments (e.g., hamstrings lengthening) for other movement abnormalities (e.g., crouch gait).

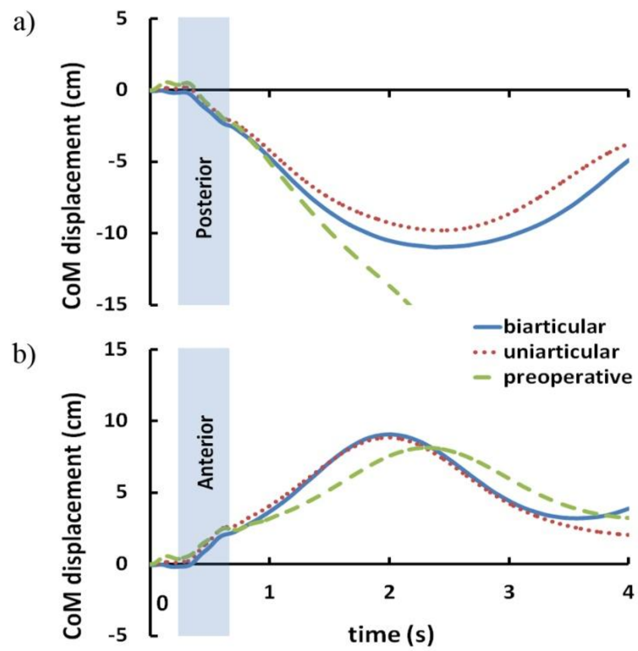

Figure 3: Center of mass (CoM) displacements relative to the support-surface translating (a) posterior and (b) anterior for simulations of preoperative, unilateral, and bilateral tendon transfer. The shaded regions highlight the duration of support-surface translations.

REFERENCES

1. Mansouri M, et al. *Proc. of ASB10*, Providence, RI, 2010.
2. Clark AE, et al. *Proc. of BMES11*, Hartford,CT, 2011.
3. Goldberg SR, et al. *J Biomech* **39**, 689-698, 2006.
4. Fox MD, et al. *J Biomech* **42**, 614-619, 2009.
5. Erdemir A, et al. *J Biomech. Eng.* **131(9),** 094502, 2009.
6. Feng CJ, et al. *IEEE Proc.* **20-5**:2317-20. 1998.

ASSOCIATION BETWEEN STRENGTH, KINEMATICS, AND THE ENERGY COST OF WALKING IN OLDER, FEMALE FALLERS AND NON-FALLERS

[1]Nise R. Marques, [1]Camilla Z. Hallal, [2]Dain P. LaRoche, [1]Luciano F. Crozara, [1]Mary H. Morcelli, [1]Aline Harumi Karuka, Marcelo Tavella Navega[3] and [1]Mauro Gonçalves
[1]São Paulo State University, Rio Claro, SP, Brazil
[2]University of New Hampshire, Durham, NH, USA
[3]Sao Paulo State University, Marilia, SP, Brazil
email: nisermarques@yahoo.com.br, web: http://www.rc.unesp.br/ib/efisica/biomecanica2011/contato.php

INTRODUCTION

Walking is the most executed movement during daily activities and is essential to functional independence in older adults. However, aging causes changes in the neuromuscular system that result in abnormal gait during walking. Despite the documented changes in the biomechanical parameters of gait, the causes for an increased oxygen cost of walking (Cw) in older adults remain unclear [1].

Most falls occur during walking, and poor gait performance has been indicated as a major contributing factor to falling. In addition, higher energy expenditure during walking in older adults could cause clinically significant increases in task difficulty and fatigue rate [2]. Consequently, our study aimed to determine the contributions of gait biomechanics, muscle activation, and hip, knee and ankle strength to Cw in older women with and without a history of falls.

METHODS

Subjects

Data of thirty-seven older women were considered for this study. Volunteers were separated into two groups according to their report of having fallen or not fallen over the one year period before the study. This resulted in 15 volunteers in the faller group and 22 volunteers in the non-faller group. The subjects had an average age of 67.5 ± 7.1 yr, body mass of 65.9 ± 11.9 kg, body mass index of 28 ± 4.4 kg m^{-2}, and preferred treadmill walking speed of 0.9 ± 0.2 m s^{-1}, which were not different between groups (all $p > 0.1$).

Procedures

Data collection was performed on two separate days. On the first day, hip, knee and ankle maximal, voluntary, joint torques were recorded isokinetically at 120 deg s^{-1} for both flexion and extension movements. On the second day, volunteers were familiarized with treadmill walking at their preferred speed. Then, indirect calorimetry was used to measure oxygen uptake (VO_2) first in a sitting, resting posture and second, during an 8-minute treadmill walk. Lower-extremity gait kinematic parameters were also recorded during a 1-minute period of the walk using a three-dimensional, optical motion system.

EMG signals were recorded at a sample frequency of 2000 Hz for the following muscles: internal oblique (IO), multifidus (MU), gluteus maximus (GM), biceps femoris (BF), rectus femoris (RF), tibiallis anterior (TA) and gastrocnemius lateralis (GL).

Data Analysis

The average VO_2 recorded between minutes 3-6 of the walking trial was used to calculate Cw. The resting, body mass-normalized VO_2 was subtracted from the walking, body mass-normalized VO_2 and this difference was divided by the gait speed chosen by each volunteer.

For strength measures, the peak torque was normalized by the mass of each volunteer. The EMG signal was processed using full-wave rectification and a low pass filter (4^{th} order and cut-off of 10 Hz) at 100 ms before and after heel contact and toe-off of ten consecutive strides. Then, the linear envelope values were normalized by the mean of each muscle activation.

Stride length, stride time, ankle angle at heel contact and hip angle at toe-off were analyzed using motion data and were averaged over ten consecutive strides These measures were chosen as they have been previously shown to be related to Cw.

The statistical analysis compared strength, gait kinematic variables, and Cw between groups using the student's t-test for independent samples. Also, Spearman correlation coefficients were computed to quantify the association between the Cw and each gait, muscle activation, and torque measure. The significance level was set at $p < 0.05$ for all tests.

RESULTS AND DISCUSSION

When comparing female fallers and non-fallers, we found that knee extensor maximal voluntary torque was 28% higher in non-fallers than in fallers ($p = 0.01$) and the hip angle at toe-off was four degrees higher in non-fallers than in fallers ($p = 0.01$; Table 1).

For non-fallers, only age was associated with Cw ($r = 0.6$, $p = 0.01$). However, for fallers, we found that a higher activation of GM during initial stance was associated with a higher Cw. For example, Cw was correlated to GM activation before heel contact ($r = 0.5$, $p = 0.03$) and GM activation after heel contact ($r = 0.7$, $p = 0.01$).

The most novel finding of this study is that in female, older fallers, impaired knee extensor strength may cause a greater reliance on the hip extensors during walking. This compensation was demonstrated by a high hip angle at toe-off and high levels of hip extensor activation at initial stance.

During initial stance, hip stabilizer muscles such as GM and gluteus medius are recruited to reduce the displacement of the center of mass in the sagittal plane [3]. We could therefore suggest that in older, female fallers the decreased knee extensor strength may reduce the capacity of quadriceps to perform negative work and stabilize the knee. In turn, a reduced capacity to absorb work at the knee may result in diminished return of energy, more positive work, and an increased Cw.

Reduced knee extensor strength could shift the burden of body support to the hip extensors, challenge hip joint stability, and increase hip stabilizer muscle activation. According to Hortobágyi et al. (2011) high levels of muscle coactivation, which is a compensatory adaptation to maintain stability, is also related to an increased Cw.

CONCLUSIONS

In older, female non-fallers age was the only factor that related to the Cw, while in older fallers, kinematic and muscle activation parameters were related to the Cw. We speculate that in the fallers observed in this study that poor knee extensor strength could cause compensatory adaptations at the hip, such as high levels of GM activation at initial stance. Thus, abnormal gait patterns could increase the Cw which could contribute to the onset of fatigue and increased fall risk in older people.

REFERENCES

[1] Wert DM, et al. *Phys Ther* **90**, 977-985, 2010.
[2] Hortobágyi T, et al. *J Gerontol A Biol Sci Med Sci* **69**, 541-547, 2011.
[3] Liu MQ, et al. *J Biomech* **39**, 2623-2630, 2006.

ACKNOWLEDGEMENTS

This project was funded by grants from Conselho Nacional de Desenvolvimento Científico e Tecnológico (CNPq), Fundação de Amparo à Pesquisa do Estado de São Paulo (FAPESP), Coordenadoria de Aperfeiçoamento de Pessoal de Nível Superior (CAPES) and Fundação para o Desenvolvimento da UNESP (FUNDUNESP).

Table 1: Comparisons between fallers and non-fallers for Cw, strength and kinematic measurements.

Variable	Faller Group (n=15)	Non-Faller Group (n=22)	P
Cost of walking ($ml \cdot kg^{-1} \cdot min^{-1} \cdot m^{-1} \cdot s^{-1}$)	9.3 (4.3)	8.7 (2.9)	0.6
Knee flexor torque ($N \cdot m \cdot kg^{-1}$)	0.54 (0.26)	0.55 (0.14)	0.8
Knee extensor torque ($N \cdot m \cdot kg^{-1}$)	0.69 (0.2)	0.96 (0.24)	0.02*
Hip flexor torque ($N \cdot m \cdot kg^{-1}$)	0.68 (0.26)	0.74 (0.19)	0.4
Hip extensor torque ($N \cdot m \cdot kg^{-1}$)	0.78 (0.23)	0.89 (0.36)	0.2
Ankle plantarflexor torque ($N \cdot m \cdot kg^{-1}$)	0.31 (0.19)	0.33 (0.13)	0.7
Ankle dorsiflexor torque ($N \cdot m \cdot kg^{-1}$)	0.28 (0.11)	0.31 (0.13)	0.3
Stride time (s)	2.3 (0.89)	2.6 (0.9)	0.3
Stride length (mm)	509.3 (61.9)	497.2 (70.7)	0.6
Ankle angle at heel contact (deg)	6.4 (4.3)	5.9 (4.4)	0.2
Hip angle at toe-off (deg)	9.5 (4.8)	5.4 (4.7)	0.01*

* Significant difference ($p < 0.05$) between faller and non-faller groups. Values are mean (SD).

USING ANKLE BRACING INFLUENCES THE TORQUE RATIO AMONG ANKLE STABILIZERS MUSCLES AFTER SIMULATION BASKETBALL MATCH-PLAY?

[1]Nise R. Marques, [1]Alex Castro, [1]Fernanda C. Milanezi, [1]Almeida Neto AF, [1]Luciano F. Crozara, [1]Mauro Gonçalves

[1]Sao Paulo State University, Rio Claro, SP, Brazil
email: ax.castro@yahoo.com.br, web: http://www.rc.unesp.br/ib/efisica/biomecanica2011/contato.php

INTRODUCTION

Ankle inversion sprains are the most common injuries during sports activities, particularly in sports that involve jump, run and change of direction, such as basketball, which 41.1% these injuries are occurred(Waterman et al, 2010). Aiming to minimize the severity and incidence of ankle sprain some preventive features are used, such as the use of ankle brace (Cordova et al, 2009). However, due to difficulty in to analyze the muscular demands in real game, the possible effects of the use of braces during basketball practice are still in the clear. Therefore, this study aimed to analyze the evertor eccentric/concentric invertor (EVE_{EXC}/INV_{CON}) functional torque ratio, obtained in different ranges of motion during inversion, before and after an exercise protocol at the same intensity of basketball match-play, with and without ankle brace.

METHODS

Subjects
The participants of this study were ten healthy college basketball players (mass=80.57 ± 9.73 kg kg; age=19.82 ± 1.94 years; height=181.5 ± 9.47 cm; body fat=13.93 ± 5.34 %).

Procedures
The participants performed an exercise at the intensity of basketball match-play into two conditions: with and without ankle brace (BR and NB, respectively). The test was composed by a succession of intermittent physical effort distributed in four periods of 10 min each. This protocol was designed, considering the mechanical and physiological demands of a basketball match-play. Previously to the start of the trial (Evaluation 1) and after 2° (Evaluation 2) and 4° (Evaluation 3) periods, the subjects performed five maximal isokinetic concentric and eccentric contractions of ankle invertors and evertors muscles at 60º/s and 120°/s, separated by 2 min rest.

Data Analysis
EVE_{EXC}/INV_{CON} functional torque ratios were calculated separately based on angle-specific torque obtained at 0°, 5°, 10°, 15° and 20° ankle joint angles. The EVE_{EXC}/INV_{CON} functional torque ratio representative for ankle inversion was determined as the maximal eccentric evertor torque divided by maximal concentric invertor torque calculated at each specific joint angles.
After using Shapiro-Wilk's test to verify the normality of the data a repeated measures analysis of variance (ANOVA) was used to compare torque ratio values between the condition (with and without ankle brace), assessment (Evaluation 1, 2 and 3) and joint angle (0º, 5º, 10º, 15º e 20º). The significant level was set at p < 0.05. Data are reported using mean and standard deviation.

RESULTS AND DISCUSSION

There were founded changes only in the torque ratio values versus joint angle: For the torque ratio values at 60º/s (NB), was verified increase of 5-10º (10%, p=0.002) and 10-15º (12%, p=0.003) (Evaluation 1), 5-10º (9%, p=0.006) and 10-15º (15%, p=0.045) (Evaluation 3), decrease 0-5º (9%, p=0.013). Whereas to BR was verified increase of 5-10º (10%, p=0.008) and 10-15º (13%, p=0.019) (Evaluation 1), 5-10º (10%, p=0.043) (Evaluation 2), 5-10º (13%, p=0.017) (Evaluation 3).
For the torque ratio values at 120º/s (NB), was verified increase of 0-5º (13%, p=0.039) (Evaluation 1) and 5-10º (9%, p=0.007) (Evaluation 3). Whereas to BR the torque ratio increase of 5-10º (10%, p=0.011) (Evaluation 1) and 0-5º (15%, p<0.001) (Evaluation 2).

Studies have found, that an increase in this ratio toward end range (from 0 ° neutral position to 30° inversion angle) is pointed as a preventive neuromuscular strategy to ankle inversion sprain (Yildiz et al, 2003), once the inversion ankle sprains usually occur toward the range of motion of 0°-30° (Wright et al., 2000). The present study, verified an increase of torque ratio values with increase of joint angles, predominantly at 60 °/s and during the Evaluation 1. These results suggest that the increases of the torque ratio, toward the end range of motion, can be compromised after exercise protocol in intensity of basketball match-play, especially, during high speed movements, increasing the risk of injury.

On the other hand, considering that the use of ankle brace reduces approximately 70% of ankle sprains during sports practice, as well as the occurrence and severity of this injury in basketball, we can supposed that the ankle brace should reduce injuries without to compromise the functional reason of the ankle stabilizing muscles. According to Cordova et al. (2010) and Waterman et al. (2010) the mechanical limitations caused by the use of ankle brace on range and speed of ankle motion did not cause impairments to the athletic performance.

CONCLUSIONS

The use of ankle bracing does not change the functional torque ratio in different ranges of inversion motion, after an exercise at the intensity of basketball match-play. However, this exercise seems to alter the functional behavior of the ankle muscular balance throughout the range ankle inversion, especially at higher isokinetic speeds.

REFERENCES

1. Cordova ML, et al. *Journal of Electromyography and Kinesiology* **20**,348-353, 2010.
2. Waterman BR, et al. *Journal of Bone and Joint Surgery* **92**,2279-2284, 2010.
3. Yildiz Y, et al. *Journal of Sports Science and Medicine*. **2**,70-76,2003.
4. Wright IC, et al. *Journal of Biomechanics* **33,**513-519, 2000.

ACKNOWLEDGEMENTS

This project was funded by grants from Conselho Nacional de Desenvolvimento Científico e Tecnológico (CNPq) and Fundação de Amparo à Pesquisa do Estado de São Paulo (FAPESP.

Table 1: Comparisons of torque ratio between joint angle, condition and evaluation.

Joint Angle	No Brace			Brace		
	Evaluation 1	**Evaluation 2**	**Evaluation 3**	**Evaluation 1**	**Evaluation 2**	**Evaluation 3**
60º/s						
0º	0.94 (0.25)	1.05 (0.31)	0.92 (0.27)	1.10 (0.44)	1.00 (0.46)	1.01 (0.44)
5º	0.97 (0.24)	0.96 (0.25)*	0.92 (0.16)	1.07 (0.42)	0.87 (0.25)	0.95 (0.39)
10º	1.08 (0.30)*	1.05 (0.31)	1.13 (0.25)*	1.18 (0.48)*	0.96 (0.26)*	1.09 (0.52)*
15º	1.22 (0.36)*	1.23 (0.37)	1.28 (0.39)*	1.35 (0.63)*	1.06 (0.38)	1.10 (0.57)
20º	1.43 (0.60)	1.34 (0.53)	1.43 (0.64)	1.13 (0.52)	1.43 (1.45)	1.22 (0.70)
120º/s						
0º	0.91 (0.23)	0.96 (9.3)	0.95 (0.32)	0.99 (0.31)	0.89 (0.34)	1.00 (0.33)
5º	1.04 (0.25)*	1.03 (79.9)	1.07 (0.24)	1.10 (0.23)*	1.04 (0.38)*	0.97 (0.24)
10º	1.10 (0.35)	1.13 (9.9)	1.17 (0.30)*	1.21 (0.30)	1.06 (0.31)	1.06 (0.39)
15º	1.14 (0.38)	1.09 (0.26)	1.16 (0.33)	1.11 (0.26)	1.07 (0.35)	1.08 (0.37)
20º	1.23 (0.61)	1.37 (0.30)	1.30 (0.46)	0.99 (0.35)	1.17 (0.44)	1.09 (0.60)

*Significant difference (p<0.05) when compared to prior joint angle.

Performance Optimality and Variability Studied at the Level of Hypothetical Commands

[1]Joel R. Martin, [2]Alexander V. Terekhov, [1]Mark L. Latash, and [1]Vladimir M. Zatsiorsky

[1]The Pennsylvania State University, University Park, PA, USA
[2]Universite Pierre et Marie Curie, Paris, France
email: *jrm496@psu.edu*

INTRODUCTION

It is generally assumed that motor actions are performed in an optimal manner based on minimization of some cost function. At the same time movements display a certain amount of variability across repetitions. Recently, two experimental approaches of been developed to analyze these features of motor performance. *Analytical inverse optimization* [ANIO; 1] allows for reconstructing the cost function from experimental recordings. The cost function is additive with linear constraints. The *uncontrolled manifold* hypothesis [UCM, reviewed in 2] allows for partitioning of variance into "good" (V_{GOOD}) and "bad" variance (V_{BAD}). V_{GOOD} does not affect task performance while V_{BAD} harms performance.

These methods have been applied to analyzing finger forces in a multi-finger pressing task previously [3]. It was shown that these methods are complementary, as they allow analyzing different aspects of motor performance.

During multi-finger pressing finger forces are not independent of each other. The *enslaving* [4] and *force deficit* [5] behaviors result in: a) some finger(s) involuntarily producing force when other finger(s) are instructed to voluntarily produce force (enslaving) and b) decreasing in force produced by a single finger in a multi-finger maximum voluntary contraction (MVC) task compared to the same finger in a single finger MVC task (force deficit).

A hypothesis has been suggested [4,5,6] that the central nervous system (CNS) sends out neural commands (NC's) to fingers that account for enslaving and force deficit. The NC's are related to finger forces by the following relationship:

$$[F] = [IFC][NC] \tag{1}$$

where $[F]$ is a (4×1) vector of finger forces, $[IFC]$ is a (4×4) inter-finger connection matrix accounting for enslaving and force deficit, and $[NC]$ is a (4×1) vector of NC's.

The purpose of the current study was to examine if the cost function could be reconstructed from the NC's. Failure to reconstruct the cost function would imply that it is not additive in regards to the NC's. Successfully reconstructing the cost function would allow for the comparison of the ANIO and UCM results between force and NC data.

METHODS

Eleven healthy right-handed male subjects volunteered to be in the study. The experimental protocol consisted of three sessions:

1) During the first session MVC contractions were recorded for each of the 15 finger pressing combinations. These data were used to estimate the $[IFC]$ of equation 1 using a neural network (NN) model. The NN was previously validated to accurately model finger interaction during MVC contractions [4,5].

2) During the second session subjects were required to press with all four fingers to match a total force (y-axis) and a total moment (x-axis) target that appeared as a point on a grid that was generated on the computer screen. There were five total force targets and five total moment targets. Targets were scaled based on MVC values. Each of the twenty five force-moment combinations were repeated five times (125 total trials). Force data of each finger were averaged during a 2 s window of each trial. The force data from a single trial were then converted to NC data by the following relationship:

$$[NC] = [IFC]^{-1}[F] \tag{2}$$

The force and NC data were averaged across trials of the same force-moment target combinations. The cost-functions with respect to each data type were reconstructed. Using principal component analysis

(PCA) it was checked whether the data were confined to a two-dimensional hyperplane. Since the data were distributed on a plane, the cost function was assumed to be a quadratic function of the form:

$$J = \frac{1}{2}\sum_{j=1}^{4} k_j^x(x_j)^2 + \sum_{j=1}^{4} w_j^x(x_j) \quad (3)$$

where x_j is the force or NC of the *j*th finger, k_j^x is the second order coefficient of data type *x* and w_j^x is the first order coefficient of data type *x*. The linear constraints were of the form:

$$[C][EV] = [B] \quad (4)$$

where [*C*] is a (2×4) matrix of constraints, [*EV*] is the (4×1) vector of elemental variables and [*B*] is a (2×1) vector of target force and target moment. The dihedral angle [D-angle; 1,3] between the planes of the experimental and optimal solutions was used as a measure of the ability of the cost function to approximate the experimental data over the range of target forces and moments used.

3) The third session consisted of an additional 75 trials of five different force-moment conditions (15 trials each condition). These trials were used to perform the UCM analysis. UCM analysis requires elemental and performance variables to be selected. The elemental variables were either the force or the NC data. The performance variables tested were: a) total force, b) total moment, and c) both total force and total moment. A Jacobian (constraint matrix from ANIO) related changes in elemental variables to changes in the performance variable. The variance within the null-space of the Jacobian was defined as V_{GOOD}. Variance orthogonal to this subspace is V_{BAD}. An index, ΔV, was computed that measured the relative variance in the UCM:

$$\Delta V = \frac{V_{GOOD} - V_{BAD}}{V_{TOT}} \quad (5)$$

where V_{TOT} is the total variance and was used to normalize the ΔV index.

Repeated measure ANOVAs were used to test whether the elemental variable type (force or NC data) had a significant effect on the outcome data of each analysis method.

RESULTS AND DISCUSSION

Neural network modeling: the *IFC*'s computed from the models resulted in computation of NC values that were, in most instances, between 0 and 1.

PCA: the first two PC's explained 96.2±0.6% and 94.1±0.7% of the variance of force and NC data, respectively. This satisfied the assumption that both data types were confined to a two-dimensional hyperplane.

ANIO: the D-angle was 4.46±1.21° and 4.39±0.89° for the force and NC data, respectively. The effect of elemental variable type on D-angle was insignificant ($F_{1,10} = 0.158$, $p > 0.700$).

UCM: In regards to all tested performance variables ΔV and normalized V_{GOOD} were higher for NC data than for the force data. This difference was statistically significant in all cases ($p < 0.005$ for all).

In regards to the ANIO results it was not clear which data type outperformed the other. The UCM results indicate that the variance of the NC data is structured more favorably than that of the force data.

CONCLUSIONS

Overall, the major findings are: (1) it is plausible that the CNS controls NC's instead of more easily measured mechanical variables and (2) the ANIO and UCM methods are complementary data analysis approaches.

REFERENCES

1. Terekhov AV, et al. *J Math Biol* **61**, 423-453, 2010.
2. Latash ML, et al. *Exerc Sport Sci Rev* **30**, 26-31, 2002.
3. Park J, et al. *Exp Brain Res* **207**, 119-132, 2010.
4. Zatsiorsky VM, et al. *Biol Cybern* **79**, 139-150, 1998.
5. Li ZM, et al. *Neurocomputing* **47**, 259-275, 2002.
6. Danion F, et al. *Biol Cybern* **88**, 91-98, 2003.

ACKNOWLEDGEMENTS

We would like to thank Dr. Jaebum Park and Dr. Zong-Ming Li for their assistance with this study. This research was supported by NIH grants AR-048563, AG-018751, and NS-035032.

COMPARISON OF FINGER INTERACTION MATRIX COMPUTATION TECHNIQUES

[1]Joel Martin, [2]Alexander V. Terekhov, [1]Mark L. Latash, and [1]Vladimir M. Zatsiorsky

[1]The Pennsylvania State University, University Park, PA, USA
[2]Universite Pierre et Marie Curie, Paris, France
email: *jrm496@psu.edu*

INTRODUCTION

During multi-finger pressing and prehension tasks fingers are not independent of one another. The behaviors of *enslaving* [1] and *force deficit* [2,3] limit finger independence. Enslaving is the name that has been given to the behavior of fingers producing force unintentionally when other fingers are instructed by the performer to intentionally produce force. Force deficit is the behavior of individual fingers producing less force in a multi-finger maximal voluntary contraction (MVC) task than in a single-finger MVC task. The force deficit increases as more fingers as added to the task.

The mode control hypothesis was proposed as the manner in which neural commands (NC's) from the central nervous system (CNS) are delivered to muscles and result in a pattern of movement or force production by the periphery [1,4,5]. The hypothesis states that the NCs are scaled from 0 to 1; with 0 being no intentional force production and 1 being maximal force production. The hypothesis, which was developed with finger interaction in mind, accounts for behaviors such as enslaving and force deficit. The basic assumption of the hypothesis is the CNS manipulates muscle modes according to the task and that sending a NC to a single finger results in force production of other fingers as well, which the CNS accounts for when it sends the mode commands. A general relation between finger forces and NC's depends on finger connections (mechanical and neural) as well as number of fingers involved. The mathematical relation proposed by Danion et al. [5] was:

$$[F] = \mathrm{G}[IFC][NC] \qquad (1)$$

where $[F]$ is a (4×1) vector of finger forces, G is gain factor that is inversely proportional to the number of fingers explicitly involved, $[IFC]$ is an inter-finger connection matrix that accounts for enslaving and does not depend on the number of explicitly involved fingers, and $[NC]$ is a (4×1) vector of mode commands. This simple model was found to predict finger forces well in the MVC tasks involving different numbers of intentionally active fingers.

Neural network (NN) models have also been used to transform NC's to forces produced by fingers [1, 4]. Previous NN models have been comprised of three layers: 1) the input layer that models a central neural drive; 2) the hidden layer that models extrinsic muscles; and 3) the output layer that models the force output of fingers. As it was shown by Zatsiorsky et al. [1] the whole action of the neural network can be described by a simple equation:

$$[F] = (1/N)[w][NC] + [v][NC] \qquad (2)$$

where $[w]$ is a (4×4) matrix of connection weights between the fingers, $[v]$ is a (4×4) diagonal matrix and N is the number of explicitly involved fingers.

The purpose of this paper is to compare the techniques purposed by Danion et al. [5] and the NN modeling approach of estimating finger forces from NCs.

METHODS

Eleven healthy right-handed male subjects volunteered to be in the study. Subjects were asked to press with all fifteen combinations of one-, two-, three-, and four-finger combinations to produce a MVC. Normal forces were recorded with piezoelectric force sensors. The forces of each finger at the instant of peak MVC for the instructed combination were extracted.

The $[IFC]$ was computed for the Danion et al. [5] method and the NN method [1,4]. The Danion et al. method only required forces from the single-finger trials while the NN method requires forces from all fifteen finger combinations.

The [*IFC*] of each method were used to predict finger forces in each of the fifteen MVC finger combination conditions using relationship in equation 1. The finger(s) that were instructed to press had the NC set to 1, the NC of non-instructed fingers was set to 0. The predicted force was compared to the experimental force for all four fingers. The error was computed as the absolute difference between the experimental and modeled force.

Various mathematical properties of the matrices were computed. Matlab commands were used to compute the determinant, inverse of determinant, trace and singular values of the matrices. The sum of the non-diagonal elements was computed and then the ratio of this value to the trace (sum of diagonal elements) was calculated. Repeated measure ANOVAs were used to test for differences between the methods.

RESULTS AND DISCUSSION

The total MVC forces predicted by the two methods were very close to the experimental MVC forces. Due to the mathematics of the Danion et al. method the single-finger MVC trials predicted all the finger forces with zero error. The NN method better predicted MVC values for the multi-finger MVC trials. For all multi-finger pressing combinations the individual finger errors between experimental and modeled values were less for the NN method (Figure 1).

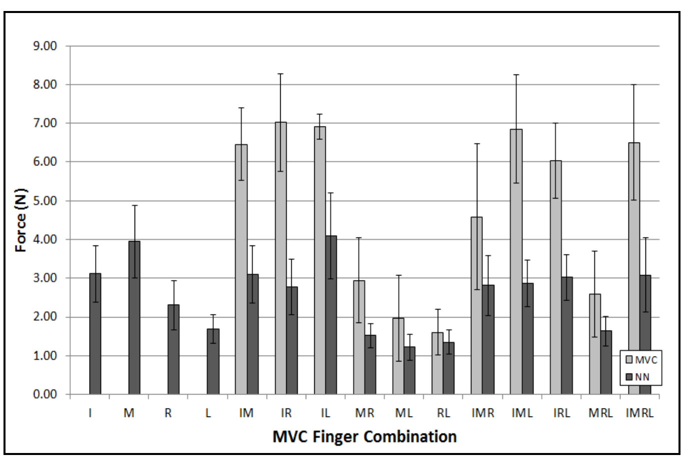

Figure 1: Comparison of force error between experimental finger forces and forces predicted by the Danion et al. and neural network based methods for the index finger.

The diagonal elements of the [*IFC*] for the Danion et al. method were less than those of the NN method ($F_{1,10} = 9.759$, $p < 0.05$). The off-diagonal elements were smaller for the NN method than the Danion et al. method ($F_{1,10} = 33.971$, $p < 0.001$). The ratio of the sum of off-diagonal elements to sum of diagonal elements was higher for the NN method ($F_{1,10} = 36.716$, $p < 0.001$).

There was no significant difference for the determinant or the inverse of the determinant between the methods ($p > 0.05$). The singular values of the [*IFC*] were significantly affected by the main effect of computation METHOD ($F_{1,10} = 9.425$, $p < 0.05$). The maximum singular value ($F_{1,10} = 2.196$, $p > 0.16$) was not significantly affected by METHOD; however, the minimum singular value was ($F_{1,10} = 28.302$, $p < 0.001$) . In general the singular values were larger for the NN method. The ratio of maximum to minimum singular values was almost significantly ($F_{1,10} = 4.219$, $p > 0.06$) larger for the NN method.

CONCLUSIONS

The results suggest that the NN method is preferable when dealing with multi-finger pressing tasks. Subtle differences in the [*IFC*] mathematical properties appear to explain why the transformation from NC's to forces is more accurate for the NN method. The fact that levels of enslaving and force deficit vary from person to person due to things such as practice make it advisable to use a model that takes more finger combinations into account so that these behaviors are more precisely modeled on an individual basis.

REFERENCES

1. Zatsiorsky, et al. *Biol Cybern* **79**, 139-150, 1998.
2. Ohtsuki T, *Ergonomics* **24**, 21-36, 1981.
3. Li ZM, *Exp Brain Res* **119**, 276-286, 1998.
4. Li ZM et al., *Neurocomputing* **47**, 259-275, 2002.
5. Danion F, et al., *Biol Cybern* **88**, 91-98, 2003.

BIOMECHANICAL ANALYSIS OF DISCRETE VERSUS CYCLIC REACHING IN SURVIVORS OF STROKE

Crystal L. Massie, Matthew P. Malcolm, David Greene, and Raymond C. Browning

Colorado State University, Fort Collins, CO, USA
email: crystal.massie@colostate.edu website: pal.colostate.edu

INTRODUCTION

Stroke rehabilitation interventions incorporate discrete and/or cyclic reaching tasks, yet no biomechanical comparison exists between these two movements in survivors of stroke. Some of our previous research has demonstrated that survivors of stroke respond differently to interventions that incorporate discrete versus cyclic reaching [1, 2], suggesting that the task structure may be an important aspect for rehabilitation scientists and clinicians to consider.

We hypothesized that survivors of stroke would use more compensatory patterns (e.g., trunk flexion) and slower movements when reaching with the stroke-affected side compared to the less-affected side. We also wanted to explore which aspects of reaching were different between discrete and cyclic reaching in survivors of stroke as these may be important considerations for stroke interventions.

METHODS

Seventeen survivors of stroke (10 male; 9 left CVA; mean age of 65.6 ± 11.9 years) in the chronic stage of recovery (mean 3.7 ± 3.1 years post-stroke) participated. Subjects met gross and fine-motor criteria for intensive interventions (e.g., ability to extend wrist). Subjects sat comfortably in a chair and were asked to reach between two targets 0.35 m apart (anterior-posterior direction) at a height of 0.71 m (approximate height of a computer desk). The close target was at an initial starting position with the shoulder at neutral and the elbow at 90 degrees of flexion. Subjects were instructed to reach as quickly and as accurately as possible. The pressure sensitive targets were used to quantify beginning/end of reaching cycles. Five discrete trials and one trial of cyclic reaching (5 cycles) were performed with both the affected and less-affected upper-extremity; order of trials was randomized. Motion of reflective markers on the torso and arms were recorded (100Hz) via a 7-camera Vicon system. Electromyography (EMG) data of selected upper extremity muscles were recorded (2000Hz) with a Noraxon system and synchronized with the motion capture data. Kinematic and EMG data were processed in Visual 3D™ for outcome measures of interest including:

- Range of motion (ROM, degrees) between the two targets for shoulder, elbow, anterior trunk flexion, and trunk rotation during forward reach
- Muscle activation patterns for anterior deltoid, biceps, and triceps
- Time to reach between each target (sec)
- Variable error at target contact (accuracy)

Averaged data for the 5 reaching cycles and were analyzed with RMANOVA (significance $p<0.05$).

RESULTS AND DISCUSSION

The ROM for the shoulder, elbow and trunk are shown in Figure 1. Participants used significantly less shoulder flexion ROM when reaching with the stroke-affected side compared to the less-affected side ($F=25.8$, $p<0.001$). A main effect for type of reach was observed ($F=8.0$, $p=0.01$) with greater shoulder flexion ROM associated with discrete reach. Similar to shoulder flexion, participants had significantly less elbow extension ROM when reaching with stroke-affected side compared to the less-affected side ($F=70.6$, $p<0.001$). There was a significant main effect for type of task ($F=11.1$, $p=0.004$); the post-hoc test for the stroke-affected was not significant ($t=-1.2$, $p=0.23$), but there was a significant difference when using the less-affected side ($t=-3.7$, $p=0.002$). Participants used significantly greater trunk flexion ROM when using the stroke-affected side compared to the less-affected side, but the trunk flexion ROM did not differ between the cyclic and discrete reaches ($F=58.9$, $p < 0.001$, $F=0.8$, $p = 0.4$, respectively). A significant interaction was observed in the degree of trunk rotation ROM ($F=8.2$, $p = 0.01$). Post-hoc analyses determined significantly more trunk rotation when reaching cyclically with the stroke-affected side (t=2.9, p=0.011), but no differences in task when using the less-affected side (t=0.2, p=0.8).

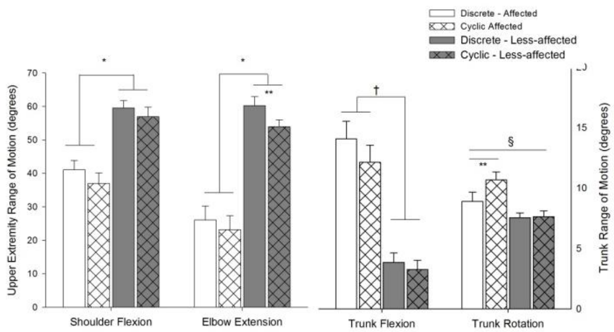

Figure 1: Range of motion for shoulder flexion, elbow extension, trunk flexion, and trunk rotation as participants reached from the proximal target to the distal target. * denotes a main effect for sides (stroke-affected and less-affected) and a main effect for tasks (discrete and cyclic), † denotes a main effect for side, § denotes a significant side by task interaction, and ** denotes a significant difference for type of reaching.

As demonstrated in Figure 1, stroke survivors used significantly more trunk rotation when reaching cyclically compared to discrete reaching. One potential factor that may influence the degree of trunk rotation is the difference in generating muscle activity of the anterior deltoid. As depicted in Figure 2, survivors of stroke had significantly lower levels of anterior deltoid activation compared to reaching with the less-affected side. Although the causal relationship between EMG activation and kinematics remains difficult to determine, the current results suggest that the proximal musculature may be an important consideration when designing clinical interventions.

Motor performance was generally slower when using the stroke-affected side, yet variability at target contacts was not different between sides. Participants reached significantly slower using the stroke-affected side compared to the less-affected side (F=25.4, p < 0.001), but no differences in the type of reach. The average time to complete a reach was 1.1 ± 0.5 seconds for the stroke-affected side (both discrete and cyclic), and 0.69 ± 0.3 seconds for discrete and 0.66 ± 0.3 seconds for cyclic with the less-affected side. The error at target contact was not significantly different (p>0.05) between the stroke-affected and less-affected side and the type of reach performed (0.5cm cyclic and 0.4cm discrete for stroke-affected and 0.3cm cyclic and 0.4cm discrete for less-affected).

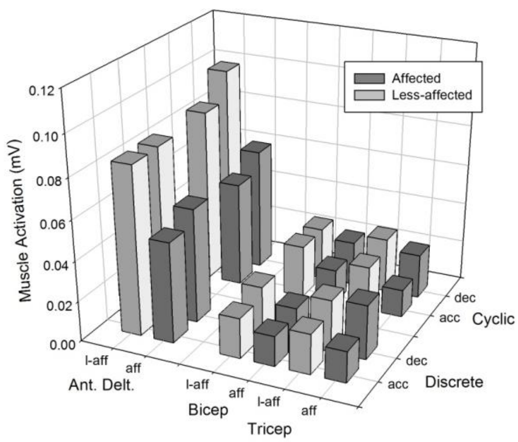

Figure 2. Muscle activation patterns of the anterior deltoid, biceps, and triceps muscles for both the affected and less-affected side during discrete and cyclic reaching. There was significantly less activation of the anterior deltoid muscle when using the stroke-affected side.

CONCLUSIONS

Survivors of stroke used a distinct trunk rotation compensatory strategy for cyclic reaching compared to discrete reaching. This represents a novel strategy that may contribute to overcoming decreased proximal muscle activation. These findings suggest that cyclic reaching provides a unique motor learning opportunity that can be used during interventions without decreases in motor performance, i.e., accuracy at target contact.

REFERENCES

1. Massie C, et al. *Archives of Physical Medicine and Rehabilitation*, 90, 571-579, 2009.
2. Malcolm MP, et al. *Topics in Stroke Rehabilitation*,16, 69-79, 2009.

ACKNOWLEDGEMENTS

C. Massie was awarded a student grant-in-aid by the American Society of Biomechanics in 2011. This project was partially supported by the American Heart Association (10PRE3750001 and 10GRNT4580008).

THE EFFECTS OF FATIGUE ON THE RECOVERY FROM A POSTURAL PERTURBATION

[1]Matthew McClain, Jennifer Popp, Henry Wang, D. Clark Dickin

[1]Ball State University, Muncie, Indiana USA
email: mamcclain@bsu.edu, web: http://www.bsu.edu/biomechanics

INTRODUCTION

Currently, fall related injuries are a major problem among older adults and children ages 14 and younger[1]. These injuries include, but are not limited to, severe-fractures, internal injuries, and concussions. A common method for understanding postural stability is to perturb the support surface on which an individual stands[2]. During normal stance, an individual maintains their center of mass within their base-of-support. However, during a postural perturbation the body is displaced, leading to disequilibrium.

This instability is further exacerbated when an individual is fatigued. Recently, literature has shown that muscle fatigue of the lower extremity leg musculature is a major contributor to postural instability. Muscle fatigue has been shown to affect various biomechanical gait factors that have been associated with a higher risk of falling in young and older adults. By understanding what internal or external factors are crucial in the recovery of a fall, we can improve the standard of care prescribed by health care professionals.

With that being said, the purpose of this study was to assess the effects of fatigue on the recovery from a postural perturbation. More specifically, how does fatigue affect an individual's trunk lean and response time? It was hypothesized that muscle fatigue would result in greater trunk lean and a slower response time in healthy adults.

METHODS

Seven healthy young adults, male and female, participated in the study. Upon arrival, the study was fully explained and participants were asked to complete a health questionnaire as well as sign an informed consent. Reflective markers were placed on various landmarks on the body. Prior to assessing the postural perturbation, the participants walked for five minutes on a force instrumented treadmill at 1.0 m/s (2.24 mph). Following the five minute walk, 10 postural perturbation trials were collected. During the postural perturbation, the treadmill accelerated to 1.0 m/s in approximately 150 ms and continued for 5 seconds thereafter[3]. Subjects were instructed to maintain balance and continue walking for 5 seconds. Immediately following the pre-fatigue perturbations, participants began the fatigue protocol consisting of a 5 minute bout of the Queen's College Step Test and body weight squats. A maximum vertical jump (MVJ) test was used to assess fatigue level. Fatigue was assessed after each 5 minute bout. When the subject failed to reach 80% of the MVJ he/she was considered fatigued and began post-fatigue perturbations. Post-fatigue perturbations consisted of five initial post-fatigue attempts, with five additional perturbations at 10-minutes post and again at 20-minute post fatigue.

Design: To determine the effects of fatigue on the recovery from a postural perturbation separate RM-ANOVA's were used for the measures of trunk lean (toe-off and at heel strike) and for response time (toe off and heel strike) at four separate times (PrePert, PostPost, 10Pert, and 20Pert). Follow-up pairwise contrasts were performed where appropriate. Significance was set at $p \leq 0.05$ for all tests.

RESULTS AND DISCUSSION

Significant changes in trunk lean at heel strike where found between the Pre-Fatigue Perturbation trials and 20-minutes Post Fatigue Perturbation trials. However, no other significant effects were found between the other conditions.

Table 1: Trunk Lean (degrees)

Trial	Heel Strike	Toe Off
PrePert	11.70 (3.79)	6.54 (4.57)
PostPert	11.20 (3.55)	6.53 (3.21)
10Pert	10.39 (3.13)	6.46 (3.60)
20Pert	*9.70 (4.52)	5.83 (4.56)

(* indicates significant difference from PrePert)

Table 1: Time to HS and TO (milliseconds)

Trial	Heel Strike	Toe Off
PrePert	0.43 (0.03)	0.24 (0.02)
PostPert	0.43 (0.05)	0.25 (0.04)
10Pert	0.42 (0.03)	0.24 (0.02)
20Pert	0.42 (0.03)	0.25 (0.02)

(* indicates significant difference from PrePert)

Trunk lean was reduced at 20-minutes post fatigue ($9.70 \pm 4.52°$) when compared to pre fatigue trunk lean ($11.70 \pm 3.79°$). The first 5 trials were removed from analysis to take out any learning affect from the results. However, it is possible that a learning affect still could have altered the results in the pre-perturbation trials. Prior to the 20-minute post fatigue trials, the subjects had 20 trials of experience. Thus, they likely developed strategies to best react to the perturbation.

This data suggests that fatigue does not affect recovery from a perturbation. These results are contradictory to the results from Owings et al. who found a reduction in trunk lean and reaction time[3]. However, there are many differences between Owings et al. study and this study. First, Owings et al. used an older population. An older population is already at risk for falling and differences between fatigue and not-fatigue would be expected Additionally, Owings et al. compared falling trials to non-falling trials. In this study we used young, healthy adults and compared successful trials to one another.

By analyzing successful trials in response to fatigue we are trying to better understand the factors and potential changes that could impact a successful perturbation trial. If using an older population we could further highlight how an individual controls posture in light of external challenges.

It is believed that differences in this healthy, young population would be expected on a kinetic and physiologic level. This study is part of a larger study that looked at various electromyography and kinetic variables.

CONCLUSIONS

In conclusion, the results of this study suggest that fatigue does not play a major role in altering the degree of upper body lean or temporal aspects of stepping during a postural perturbation in a young adult population. Future studies could look at the impact of a higher degree of fatigue or different populations to better understand the factors that contribute to successful and unsuccessful recoveries from postural challenge.

REFERENCES

1. Tinsworth DK, et al. *Special Study: Injuries and deaths associated with children's playground equipment,* Washington, DC, USA, 2001.
2. Horak FB, et al. *Physical Therapy* **77**, 517-533, 1997.
3. Owings TM, et al. *Clinical Biomechanics*, **16**, 813-819, 2001.

ACKNOWLEDGEMENTS

The author would like to thank Dr. Clark Dickin, Dr. Henry Wang, and Dr. Jennifer Popp for their help and guidance in this study.

TORSO KINEMATICS DURING GAIT DIFFER BETWEEN PREGNANT FALLERS AND NON-FALLERS

[1,2]Jean L. McCrory, [2]April J. Chambers, [2,3]Ashi Daftary, and [2]Mark S. Redfern

[1]West Virginia University, Morgantown, WV, USA, [2]University of Pittsburgh, Pittsburgh, PA, USA, [3]West Penn Allegheny Health System, Pittsburgh, PA, USA
email: jmccrory@hsc.wvu.edu

INTRODUCTION

More than 27% of women fall while pregnant [1, 2]. Falls are a leading cause of trauma-related hospital admissions during pregnancy [3]. Changes in gait during pregnancy have been hypothesized to be a reason for increased falls. Several authors have examined pregnancy-related alterations to gait mechanics, such as increased anterior pelvic tilt, hip flexion, and stance phase hip adduction, as well as a wider base of support [4]. We previously reported increased thoracic extension and greater frontal plane movement of C7 during gait and increased movement of the center of mass in the third trimester [5, 6]. Also, Wu et al. reported a reduction in thoracic and pelvic rotational ROMs in late-stage pregnancy [7].

Little research has examined biomechanical differences between pregnant women who fall and those who do not. Pregnant fallers exhibit an attenuated response to a perturbation to standing balance, while pregnant non-fallers respond similarly to non-pregnant women [8]. However, torso kinematics between pregnant fallers and non-fallers have not been examined.

The purpose of this study was to determine if pregnant fallers exhibit different torso kinematics and step width during gait than pregnant non-fallers and non-pregnant control women. Given that we have previously found increased movement of C7 with advanced pregnancy [5], we hypothesized that pregnant fallers would demonstrate increased mediolateral motion of the C7 and L3L4 spinal segments, greater angular ranges of motion of the thorax and pelvis and a smaller step width.

METHODS

Forty one pregnant women (age: 29.5±4.9 yrs, hgt: 1.7±0.7 m, 2nd tri. mass: 74.7±12.1 kg, 3rd tri. mass: 81.6±11.0 kg) and 40 non-pregnant controls (age: 26.5±6.4 yrs, hgt: 1.7±0.6 m, mass: 66.0±8.9 kg) participated. Data were collected on the pregnant women in the middle of their 2nd and 3rd trimesters and on the control women in the week following menses.

Informed consent was obtained during the subjects' first visit. At each visit, pregnant subjects were surveyed about their history of falls while pregnant. A fall was defined as a loss of balance such that another part of the body other than a foot touched the ground. Fifteen pregnant subjects were classified as 'fallers' by having at least one fall and14 as 'non-fallers'. Twelve pregnant subjects withdrew from the study prior to their 3rd trimester visit. Their data are not included in this analysis.

Kinematic data were recorded with an 8 camera movement analysis system (120 Hz). A modified Helen Hayes marker set was used. Specifically, to examine torso kinematics, markers were placed on the posterior aspects of C7 and the L3L4 spinal segments. Additionally, markers were placed on the acromion processes, manubrium, xiphoid process, T10, and bilateral ASIS and PSIS landmarks. Markers placed on the most posterior aspect of the heel were used to assess step width.

Right foot heel contact (RHC) and left foot toe off (LTO) were determined from force plate data (1080 Hz). The 3D angles of the thorax (i.e. upper torso) and pelvis were determined at RHC. The frontal plane movement of the C7 and L3L4 markers and the ranges of motion of the thorax and pelvis during gait were determined between RHC and LTO. Step width was calculated as the distance between the heel markers in the lab-referenced frontal plane. Average walking velocity was calculated from the L3L4 marker.

Variables were organized into three categories for statistical analysis: linear ROM variables, angular position at heel-contact variables, and angular ROM variables. The linear ROM variables consisted of the frontal plane movement of C7 and L3L4 and step width. The angular position at heel contact variables included the angle of the thorax and pelvis about the local X-axis (flexion/extension), Y-axis (lateral lean), and Z-axis (rotation). Similarly, the angular ROM variables included the 3D ROMs of the thorax and pelvis from RHC to LTO.

A multivariate analysis of covariance (MANCOVA) was performed on each category of data ($\alpha=0.05$). The independent variables were trimester and fall group (i.e. pregnant faller, pregnant non-faller, and non-pregnant control). Walking velocity was the covariate in each analysis. If significant differences were found among fall groups, a Tukey post-hoc analysis was performed ($\alpha=0.05$). The effect of "trimester" has been reported elsewhere [5].

RESULTS AND DISCUSSION

Pregnant fallers exhibited less thoracic lateral lean at RHC when compared to the pregnant non-fallers and controls (pregnant fallers: 0.1±2.3º, pregnant non-fallers: 1.6±2.7º, controls: 1.1±2.6º, p=0.001). Pregnant fallers also demonstrated less thoracic rotational ROM (p=0.036) during the gait cycle when compared to the pregnant non-fallers (pregnant fallers: 7.0± 2.4º; pregnant non-fallers: 7.8±2.9º), although neither group was significantly different from the controls (7.5±2.4º).

Pregnant non-fallers demonstrated greater values on several variables than pregnant fallers and controls. Step width was greatest in the pregnant non-fallers (9.9±4.0 cm) compared to the pregnant fallers (8.1±2.9 cm) and controls (8.7±3.5 cm) (p=0.001). Pregnant non-fallers demonstrated greater thoracic rotation at RHC (2.8±3.7º) than the pregnant fallers (0.6±3.9º) and controls (0.9±3.4º) (p=0.001). Compared to pregnant fallers and controls, pregnant non-fallers exhibited greater frontal plane ROM of the thorax during the gait cycle (pregnant non-fallers: 4.8±2.8º, pregnant fallers: 4.2±2.6º, controls: 4.1±1.9º, p=0.03).

In every variable that differed between pregnant fallers and non-fallers, the magnitude of that variable was greater in the pregnant non-fallers, implying that pregnant non-fallers demonstrate greater torso movement than do the pregnant fallers. This may be indicative of greater torso flexibility or less rigidity that would allow the pregnant non-fallers to be more likely to successfully overcome a trip or a slip. Also, the greater step width of the pregnant non-fallers would increase the base of support, thus increasing stability. Increased step width was also noted by Foti et al. [4].

It is unlikely that this greater frontal and transverse plane movement in pregnant non-fallers is related to abdominal size (i.e. circumference) or weight gain because pregnant fallers and non-fallers did not differ on either of these factors [8]. Wu et al. reported truncated torso rotations during gait in advanced pregnancy [7], but did not compare between fallers and non-fallers.

CONCLUSION

Pregnancy-associated alterations to gait biomechanics differed between in pregnant fallers and non-fallers. These differences may be indicative of a more rigid trunk and greater instability in the pregnant fallers.

REFERENCES

1. Dunning K et al. *Am J Indus Med* **44**; 664-72, 2003.
2. Dunning K et al. *Matern Child Health J.* **14**; 720-5, 2010.
3. Gardner JG et al. *J Biomch* **38**; 1861-8, 2004.
4. Foti T et al. *J Bone Joint Surg* **82-A**; 625-32, 2000.
5. McCrory et al. *ACSM* San Francisco, CA. 2012.
6. Enders L et al. *BMES* Pittsburgh, PA. 2009.
7. Wu W et al. *Clin Biom* **19**; 480-8, 2004.
8. McCrory J et al. *Brit J Obs Gyn* **117**; 954-62, 2010.

ACKNOWLEDGEMENTS

This research was supported by NIOSH K01 OH8548

METABOLIC COST OF MAINTAINING BALANCE DURING A PERTURBED GAIT TASK IS RELATED TO GAIT VARIABILITY

[1]Denise McGrath, [1]Shane R. Wurdeman, [1]Jennifer M. Yentes, [1]Nathaniel Hunt, [1]Sara A. Myers, [1]Nicholas Stergiou

[1]University of Nebraska at Omaha, Omaha, NE, USA
e-mail: dmcgrath@unomaha.edu web: http://nbcf.unomaha.edu

INTRODUCTION

We have previously shown increased VO_2 when subjects were asked to walk on a curved treadmill, compared to a standard flat treadmill, despite a reduction in the vertical displacement of the center of mass (COM) when walking on the curved treadmill [1]. Using a model derived from Workman and Armstrong [2] and proposed by Hoffman et al. [3], we sought to determine the metabolic cost related to balance maintenance while walking, as distinct from the energy required to perform the mechanical work of walking. Walking on a curved treadmill enables us to address this question as the natural movement characteristics of gait are preserved, yet the curve presents a subtle postural control challenge. Thus, we hypothesized that the metabolic cost associated with maintenance of balance during walking is increased when walking on the curved treadmill, whereas the metabolic cost of locomotion is unchanged. Additionally, we investigated the variability of the COM during walking. We hypothesized that walking on the curved treadmill would lead to changes in the amount and temporal structure of variability of the COM, and that these alterations in motor control would be related to the increased metabolic cost associated with maintenance of balance during walking.

METHODS

Five subjects (age: 23.00 ± 2.61 years, height: 183.39 ± 4.23 cm, mass: 84.63 ± 9.72 kg) walked at three speeds (random order: 0.67, 1.12, and 1.56 m/s) on a standard treadmill and a curved treadmill (Woodway®, Waukesha, WI). The curved treadmill consists of a concave, non-motorized belt that is mobilized by the person walking on the treadmill. The walker places their foot on the concave sloping belt, and the foot moves down and backwards, assisted by the slope. Each trial was three minutes long with breaks between trials as necessary to prevent fatigue. Steady state oxygen consumption relative to body mass (VO_2) (K4b2, Cosmed, Chicago, IL) was recorded at rest and during all walking trials. The VO_2 data at three different speeds were used to calculate the characteristics of Hoffman's three-compartment model [2] by plotting the VO_2 against squared walking speed. Linear regression was performed to obtain the slopes and intercepts from these equations. The model defines the three compartments as follows: compartment 1 is the basal metabolic rate, compartment 2 (C2) is the metabolic cost associated with maintaining balance and compartment 3 (C3) is the metabolic cost associated with walking. C2 is calculated by subtracting basal metabolic rate (in our case we used the resting VO_2) from the intercept, which theoretically defines the metabolic demand associated with zero walking speed. C3 is described by the slope of the regression line. This is illustrated in Figure 1 below. We performed dependent t-tests to compare C2 and C3 between conditions. We then analyzed the relationships between C2, C3, and the variability of COM. Displacement of COM was approximated using a retroreflective marker placed on the sacrum (60Hz; Motion Analysis Corp., Santa Rosa, CA). Displacement of the COM in the medial-lateral and anterior-posterior direction was quantified using the dispersion about the individual's mean COM displacement (i.e. standard deviation) and maximum range of displacement across all steps within each trial. The largest Lyapunov exponent was calculated from the sacral marker time series in units of bits/s[4]. The Lyapunov exponent quantifies the exponential rate of divergence of adjacent trajectories in phase space. The proximity of adjacent trajectories is indicative of a stable attractor. Smaller Lyapunov exponent values reflect a more stable attractor while larger values reflect the opposite. Differences in the Lyapunov exponent, dispersion and range of COM displacement in the medial-lateral and anterior-posterior directions were examined using dependent t-tests.

RESULTS AND DISCUSSION

Subjects demonstrated increased C2 values on the curved treadmill ($p=0.006$) compared to the flat treadmill and no differences in C3 between conditions ($p=0.44$). Our results showed reduced range and standard deviation and increased Lyapunov exponent of the COM displacement in both anterior-posterior and medial-lateral directions on the curved treadmill, compared to the standard treadmill (Table 1). These findings are consistent with previous research that has reported an inverse relationship between the amount and temporal structure of gait variability. The results suggest that walking on the curved treadmill requires careful body positioning to optimize the return from the slope. While this requires the subjects to constrain the amount of variability of their movement (i.e. range and standard deviation), it led to a more unpredictable temporal organization of variability, as evidenced by an increased Lyapunov exponent.

Table 1: Mean and standard deviation values of the Lyapunov Exponent (LyE), Range and Standard Deviation (SD) of the sacral marker in the anterior-posterior (AP) and medial-lateral (ML) directions, on the standard and curved treadmill.

	Standard	Curved	p-value
LyE AP (bits/s)	0.97(0.44)	1.38 (0.6)	0.070
LyE ML (bits/s)	0.99 (0.23)	1.29 (0.17)	0.000
Range AP (cm)	250.12 (46.7)	126.38 (22.9)	0.000
Range ML (cm)	162.9 (21.2)	144.5 (22.4)	0.010
SD AP (cm)	48.1 (11.4)	19.7 (3.0)	0.000
SD ML (cm)	28.7 (4.8)	25.7 (4.5)	0.002

Correlation analysis revealed the Lyapunov Exponent in the medial-lateral direction to be the most highly correlated with C2, with a significant and positive correlations observed at all speeds (0.67m/s ($r=0.63$), 1.12m/s ($r=0.80$) and 1.56m/s ($r=0.83$)). Medial-lateral standard deviation of COM displacement also showed a significant negative correlation with C2 at 0.67m/s ($r=-0.85$) and 1.12m/s ($r=-0.65$). Range AP showed a significant negative correlation with C2 at the fastest speed ($r=-0.7$). This study showed that walking on a curved treadmill (where walking is actively controlled compared to unconstrained walking on a flat treadmill) causes a more unpredictable gait in terms of nonlinear stride-to-stride fluctuations in the medial-lateral direction that is strongly related to increased metabolic cost. We surmise that while the subject is attempting to control his/her position on the curved treadmill in order to hit the right spot on the slope, the attractor becomes unstable as constant correction and readjustment is required.

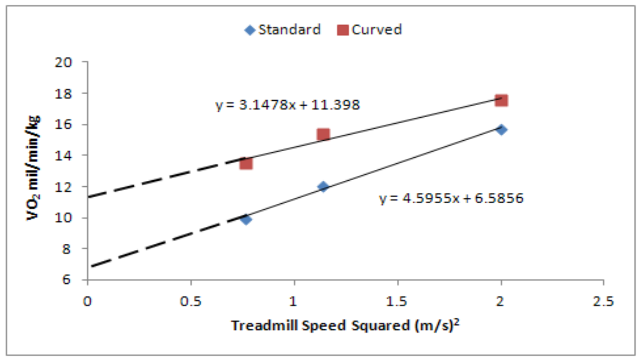

Figure 1: VO_2 regression equations for Subject 2 when walking on the curved and flat treadmill. Note that for this subject, the intercept, which relates to C2, is higher in the curved treadmill condition, but the slope, which relates to C3 is lower.

CONCLUSIONS

The study participants optimized walking in terms of motor control strategies, and not energy consumption. This strategy was adopted in response to altered task constraints, and came at a metabolic cost. These findings further elucidate the relationship between unstable gait behaviors and increased energy cost.

REFERENCES

1. Korgan W, et al. *Proceedings of GCMAS*, Grand Rapids, MI, USA, 2012
2. Workman JM and Armstrong BW, *J Appl Physiol* **61**(4):1369-74, 1986
3. Hoffman MD, et al. *Arch Phys Med Rehabil* **78**(4):385-92, 1997
4. Wolf, A. et al, *Physica* D **16**, 285-317, 1985

EFFECTS OF LONG-TERM USE OF ANKLE TAPING ON BALANCE

Stephanie F. McGregor, Samuel T. Johnson and Michael J. Pavol

Oregon State University, Corvallis, OR, USA
email: mike.pavol@oregonstate.edu

INTRODUCTION

Ankle ligament sprains are the most common injury in collegiate athletes [1] and ankle taping is often used by athletes during rehabilitation after a sprain. Many athletes also continue to tape their ankles as a preventative measure. Taping has been shown to enhance ankle proprioception [2] which, in theory, should improve balance, thereby potentially aiding in injury prevention. Yet most studies have found ankle taping to either have no effect on or to worsen balance [3]. A factor that has not been studied, however, is whether the effects of ankle taping on balance change with regular, long-term use. It has been suggested that ankle taping is most effective at preventing ankle sprains in previously injured athletes [4]. Thus, it may be that, with long-term use of taping, the body better adapts to the associated changes in sensory input and ankle stiffness. This study therefore compared the effects of ankle taping on balance between athletes who regularly tape their ankles and those who do not tape their ankles.

METHODS

Fourteen NCAA Division 1 gymnasts were tested after they provided informed consent. Gymnasts were studied because balance plays a large role in the sport and because long-term, regular use of ankle taping is common. Six participants always taped one or both ankles for gymnastics over the preceding three months ("tapers" group) and eight never did ("non-tapers" group). No participant had sprained an ankle in the six weeks preceding testing.

The participants' ability to balance on one foot was measured using a force platform (Bertec, Columbus, OH). Participants who tape only one ankle were tested on that foot. Non-tapers, as well as tapers who tape both ankles, were tested on the foot with the more "normal" ankle. If both ankles were similar with regards to these criteria, the foot tested was selected randomly.

Each participant was tested with and without ankle taping under each of four conditions: with eyes open and eyes closed, both with and without a 5 cm-thick block of foam between the foot and force platform. Participants performed three trials for each condition. They were to try to remain still, with the other foot raised slightly by flexing the hip and knee, legs apart, and hands on the hips, as best they could. A trial continued until the participant touched the other foot to the ground or 30 s elapsed, whichever occurred first. Trials of less than 15 s were repeated. Whether participants were tested with or without taping first and the order in which the conditions were tested were counterbalanced. An athletic trainer performed the taping.

Ground reaction force data were collected at 100 Hz during each trial and low-pass filtered at 12 Hz. Balance measures analyzed were the extent of center of pressure (COP) motion, quantified by the standard deviation of COP position, and the mean speed of the COP in the anteroposterior (AP) and mediolateral (ML) directions, with the 2 s before ground contact by the other foot excluded. Values were averaged across the three like trials. Mixed four-factor analyses of variance (ANOVA) were performed to assess the effects of ankle taping as a function of group, vision condition, and surface. Effects were considered significant at $p<.05$ in the ANOVA and at $p<.025$ in the post hoc testing.

RESULTS AND DISCUSSION

For all four balance measures investigated, the effects of ankle taping differed between eyes-open and eyes-closed conditions. When the eyes were open, ankle taping had no effect on the extent or speed of COP motion ($p>.025$). However, ankle taping had a generally negative effect on balancing with the eyes closed. Under eyes-closed conditions, taping was associated with greater COP AP motion, regardless of surface, and greater COP ML motion when on solid ground (Figure 1). These effects did not differ between tapers and non-tapers.

In contrast, effects of ankle taping on the speed of COP motion differed between groups. Under eyes-closed conditions, tapers exhibited faster COP AP motion and non-tapers exhibited slower COP ML motion with the ankle taped versus without tape, regardless of surface (Figure 2). No corresponding effects were seen in the other group. Otherwise, the two groups differed only in that tapers exhibited lesser COP AP motion than non-tapers, regardless of taping, vision, or surface (Figure 1).

The present results are consistent with those of other studies in finding that ankle taping did not improve balance [3]. That negative effects of taping were observed only with the eyes closed suggests that participants had difficulty integrating into their control of balance changes in somatosensory input that resulted from the presence of the taping. Furthermore, as is seen in the results for the speed of COP motion, the effects of taping on balance differed between tapers and non-tapers in a manner suggestive of greater negative effects of ankle taping with long-term, regular use. Of interest, however, is that the extent and speed of COP motion in the tapers when taped appear to have been similar to those of non-tapers without taping. It may thus be that the tapers had adapted their control of balance over time in such a way as to compensate for the negative effects of the ankle taping.

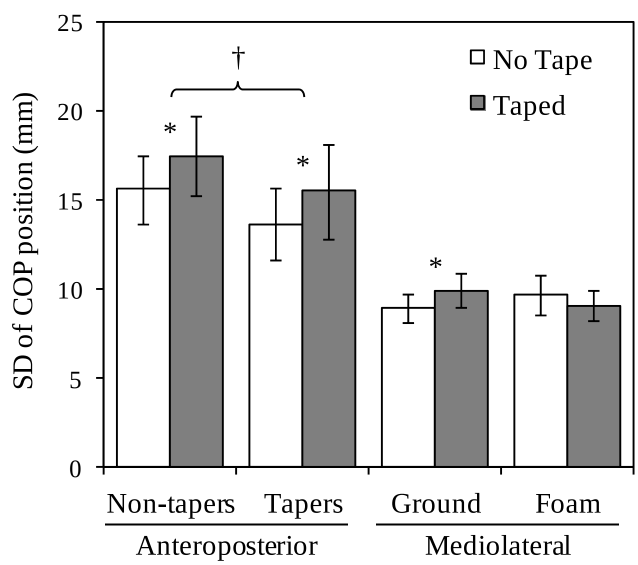

Figure 1: Standard deviation (SD) of COP position while balancing with eyes closed. * = p<.025 for effect of taping; † = p<.05 for main effect of group.

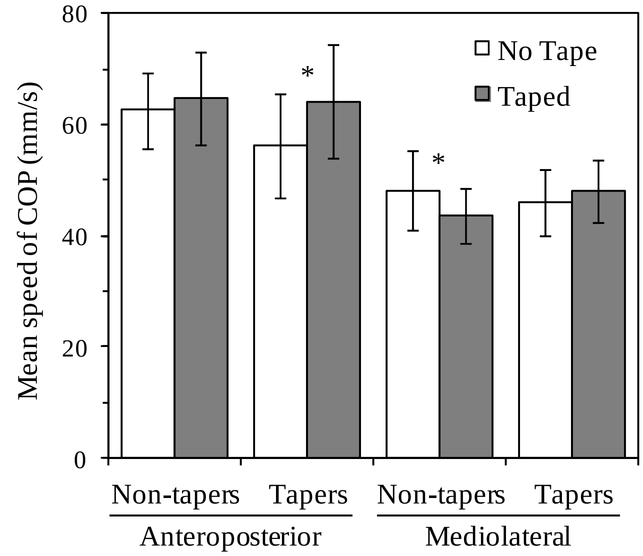

Figure 2: Mean speed of the COP while balancing with eyes closed. * = p<.025 for effect of taping.

CONCLUSIONS

In general, the results support the conclusion that ankle taping is detrimental to balancing ability. The results also support the conclusion that the negative effects of ankle taping on balance increase with long-term, regular use. However, long-term ankle tapers may adjust their balancing technique to account for the negative effects of taping.

REFERENCES

1. Hootman J, et al. *J Athl Train* **42**, 311-319, 2007.
2. Robbins S, et al. *Br J Sports Med* **29**, 242-247, 1995.
3. Cordova M, et al. *J Athl Train* **37**, 446-457, 2002.
4. Verhagen E & Bay K. *Br J Sports Med* **44**, 1082-1088, 2010.

ACKNOWLEDGEMENTS

Funded through the HHMI Summer Undergraduate Research Program and the URISC program at OSU.

STATISTICALLY-SIGNIFICANT CONTRASTS BETWEEN EMG WAVEFORMS REVEALED USING WAVELET-BASED FUNCTIONAL ANOVA

J. Lucas McKay,[1] Torrence D.J. Welch,[1,2] Brani Vidakovic,[1] and Lena H. Ting[1]

[1]Emory University and Georgia Institute of Technology, Atlanta, GA, USA
[2]Exponent, Inc., Phoenix AZ
email: j.lucas.mckay@emory.edu

INTRODUCTION

We often want to compare the shapes of temporal waveforms, but traditional statistical methods cannot reveal differences between curves without sacrificing temporal resolution or power. Waveform features that are clearly identifiable through visual inspection may not be revealed in statistical tests like ANOVA applied across time points due to the large number of comparisons (Figure 1A). Instead, a common approach to overcome this problem is to apply statistical tests to mean values over a time bin of interest, sacrificing temporal resolution of interesting features.

Here, we developed wavelet-based functional ANOVA (wfANOVA), a technique that retains temporal resolution and power by performing statistical inference in the wavelet domain (Figure 1B). When expressed in the wavelet domain, temporally-localized waveform features tend to be well represented by a few wavelets, which are temporally-localized, orthogonal functions, rather than by many time samples. Applying statistical tests to individual wavelet coefficients yields fewer significant differences across experimental conditions, reducing the number of required tests and retaining power [1]. wfANOVA differs from previous applications of the wavelet transform to EMG because differences across experimental conditions identified in the wavelet domain are transformed back to the time domain for visualization as contrast curves, rather than being reported in the wavelet domain.

Supported by NIH R01 NS058322.

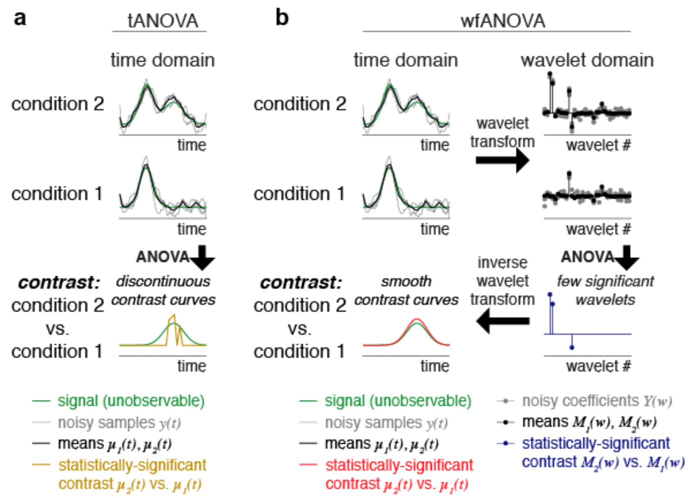

Figure 1: Schematic comparison of ANOVA performed on timepoints (tANOVA) to wfANOVA performed on wavelet coefficients.

METHODS

We compared the ability of wfANOVA and time point ANOVA (tANOVA) to identify contrast curves in previously published EMG waveforms from a balance task [2]. Subjects withstood anterior translation perturbations of the support surface. When perturbation characteristics were varied, muscle activation during the initial burst (IB; 100-250 ms after perturbation onset) scaled with peak acceleration (varied among 0.2, 0.3, and 0.4 g), and muscle activation during the plateau region (PR; 250-400 ms) scaled with peak velocity (25, 30, 35, and 40 cm/s) (Figure 2).

Wavelet transform: EMG waveforms were transformed to the wavelet domain (third-order coiflet) in Matlab software.

ANOVA: Each wavelet coefficient (wfANOVA) or time point (tANOVA) was subjected to three-factor fixed-effects ANOVA (velocity × acceleration × subject; α=0.05). In the wavelet domain, we assumed the following ANOVA model for each wavelet coefficient:

$$Y_{ijkn}(\mathbf{w}) = M(\mathbf{w}) + A_i(\mathbf{w}) + B_j(\mathbf{w}) + C_k(\mathbf{w}) + E_{ijkn}(\mathbf{w})$$

where $M(\mathbf{w})$ designates the wavelet coefficients of the grand mean, $A_i(\mathbf{w})$ designates the effects of velocity level i, $B_j(\mathbf{w})$ designates the effects of acceleration level j, $C_k(\mathbf{w})$ designates the effects of subject k, and $E_{ijkn}(\mathbf{w})$ designates Gaussian noise. Similarly, in the time domain, we assumed the following ANOVA model for each time point:

$$y_{ijkn}(t) = \mu(t) + \alpha_i(t) + \beta_j(t) + \gamma_k(t) + \varepsilon_{ijkn}(t).$$

Post-hoc tests: Wavelet coefficients or time points corresponding to significant initial F-tests were then evaluated for significant contrast across velocity or acceleration levels with post-hoc Scheffe tests. Post-hoc tests were conducted at significance levels Bonferroni-corrected by the number of significant initial F-tests.

Contrast curves: Statistically significant contrasts in coefficient magnitude were assembled into wavelet domain contrast curves and transformed back to the time domain for visualization.

RESULTS and DISCUSSION

wfANOVA contrast curves reveal the magnitude as well as the shape of significant differences over time, whereas tANOVA revealed differences between conditions only at discontinuous timepoints (Figure 2, red vs. yellow). wfANOVA velocity contrast curves (Figure 2, V1-V3, red) were nonzero during PR, while acceleration contrast curves were nonzero during IB (Figure 2, A1-A2, red), confirming previously described scaling relationships [2] without assuming analysis time bins *a priori*. In contrast, mean difference curves contained large features that rejected as insignificant by wfANOVA (Figure 2, V3: black vs. red during IB).

Due to the compression properties of the wavelet transform, wfANOVA identified 1/3 fewer significant F-tests than tANOVA, increasing the statistical power of subsequent post-hoc tests (40±5 significant F-tests, wfANOVA; vs. 160±39, tANOVA; $p < 0.015$; t-test). The number of significant tests could be further decreased by initial thresholding of small wavelet coefficients [3]. When applied to simulated EMG data in which the underlying contrast curves were known, wfANOVA revealed underlying contrasts with high precision (R^2=0.89±0.19), superior to tANOVA (R^2=0.69±0.40).

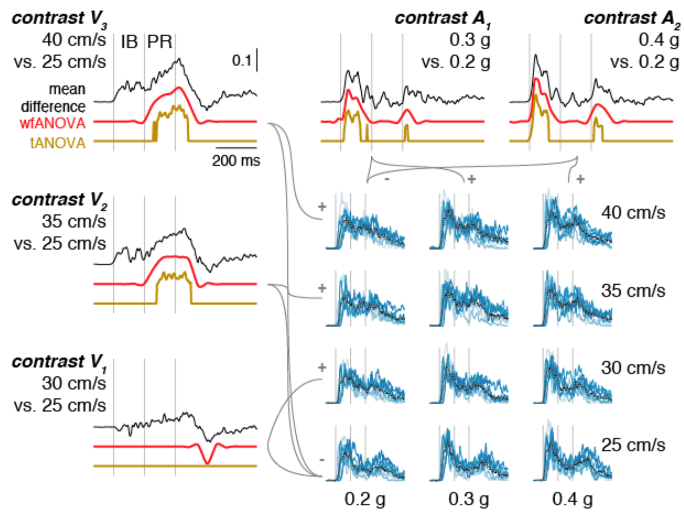

Figure 2: Comparison of contrast curves identified in recorded EMG data (blue, subject means) with wfANOVA (red) and tANOVA (yellow).

CONCLUSIONS

wfANOVA is a general tool for identifying contrasts in waveforms that is superior to current time-domain methods. wfANOVA could be applied to any spatio-temporal waveforms, including H-reflex timecourses, and kinematic data such as joint angle timecourses. Future extensions of wfANOVA could be used to compare model predictions to data with better fidelity than metrics like R^2, which may penalize high-frequency components while ignoring differences in overall waveform shape.

REFERENCES

1. Angelini, C and Vidakovic, B. in: *Wavelets and Their Applications*, M. Krishna, R. Radha, and S. Thangvelu, eds. Allied Publishers Private Limited, 2003, pp. 31-45.
2. Welch, TDJ and Ting, LH. *J Neurophysiol* **101**, 3294-3309, 2009.
3. Unser M, and Aldroubi A. *Proc IEEE* **84**, 626-638, 1996.

LOWER EXTREMITY WORK IS ASSOCIATED WITH CLUB HEAD VELOCITY DURING THE GOLF SWING IN EXPERIENCED GOLFERS

[1]Michael P. McNally, [2]Nicholas A. Yontz, [1]Ajit M.W. Chaudhari, PhD

[1]Ohio State University Wexner Medical Center, Columbus, OH, USA
[2]Nike Inc., Beaverton, OR, USA
Email: Michael.mcnally@osumc.edu

INTRODUCTION

The golf swing is a complex whole body movement, requiring the coordination of multiple joints to achieve the maximum power while still producing an accurate shot. Despite the strong interest by players and coaches in improving the golf swing, most of the scientific literature has focused on either the role of the pelvis and trunk interaction, or the ground reaction forces which occur during the swing to generate club head energy. A significant lack of scientific evidence exists to explain how lower extremity biomechanics relate to club head velocity during the golf swing. Only one known study has investigated lower extremity biomechanics during the golf swing, using computer modeling to estimate the amount of work performed by the total body, including the lower extremities [1]. However, this study did not investigate what relationship may exist between lower extremity biomechanics and club head velocity or collect data from enough subjects to permit any generalizations in their results beyond the four individuals they measured.

For this study, we tested the hypothesis that greater lower body net work would be associated with greater club head velocity. In addition, we hypothesized that individual joints of the lower extremity would have different joint work contributions to club head velocity, and that golfers of different skill levels would show different influences of overall, side to side, and individual joint work from the lower extremities during the golf swing.

METHODS

Forty-one subjects were recruited from local country clubs and golf teams and divided into four groups (Elite, Low, Mid, High) based on their self-reported handicap or team status. A passive optical three-dimensional motion capture system (Vicon Inc., Oxford UK) was used to collect kinematics of the body while subjects used their own driver to hit golf balls into a net placed approximately 3 m down the target line. Force plates were used to capture ground reaction forces from lead and trail legs throughout the swing. A single representative trial with the most complete trajectory data from each subject was chosen for data analysis.

Standard inverse dynamics equations were used to calculate joint kinetics of the lower extremities, including the intersegmental power flow from the distal segment to proximal segment across the joint using Vicon Bodybuilder software. Total work ($Work_{Total}$) was estimated by summing the integrated powers of all six primary lower extremity joints (hips, knees, ankles) throughout the downswing. Lead leg work ($Work_{Lead}$) and trail leg work ($Work_{Trail}$) were similarly estimated by summing the integrated powers of the hip, knee, and ankle joints on their respective sides.

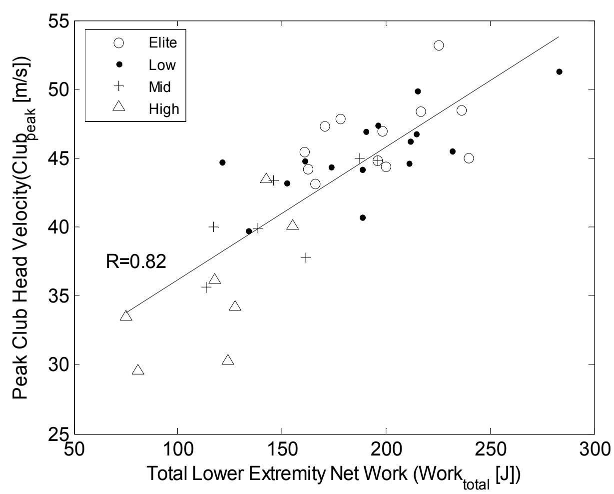

Figure 1. Peak club head velocity vs. total lower extremity work for all subjects.

Correlations were calculated between peak club head velocity ($Club_{Peak}$) and $Work_{Total}$, $Work_{Lead}$, $Work_{Trail}$, and individual joint work. Comparisons of $Work_{Total}$, $Work_{Lead}$, $Work_{Trail}$, and individual joint work between the four groups were performed using a MANOVA analysis with Tukey's post hoc test for analysis of significant variables.

RESULTS AND DISCUSSION

There was a strong correlation ($R = 0.82$) observed between $Work_{Total}$ and peak club head velocity ($Club_{Peak}$; Figure 1), which suggests the lower extremities may play a significant role in the development of club head velocity during the golf swing. A strong correlation also was observed between $Work_{Lead}$ and $Club_{Peak}$ ($R = 0.72$). Only a moderate correlation was seen between $Work_{Trail}$ and $Club_{Peak}$ ($R = 0.54$), suggesting that the lead leg might play a greater role in the development of club head velocity than the trail leg.

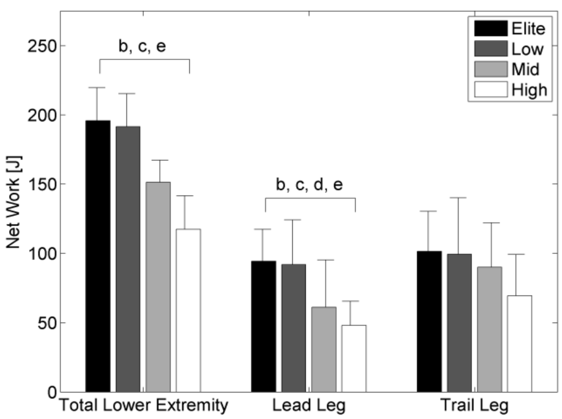

Figure 2 – Comparison between groups for $Work_{Total}$, $Work_{Lead}$, and $Work_{Trail}$.
b = Elite > Mid, c = Elite > High
d = Low > Mid, e = Low > High

Comparison between groups showed that the Elite group performed significantly greater $Work_{total}$ than Mid and High groups (195±28 J vs. 151±32 J and 117±30 J; $p=0.05$ and $p<0.01$), and the Low group performed significantly greater work than the High group (191±41 J vs. 117±30 J; $p<0.01$; Figure 2). When divided into lead and trail legs, differences were only seen in $Work_{lead}$, where both Elite and Low groups were significantly greater than both Mid and High groups (94±24 J and 92±24 J vs. 61±16 J and 48±24 J; $p<0.05$). Individual joint work was also different between groups at the lead knee (Elite > High; $p = 0.02$) and lead ankle (Elite > Mid; $p = 0.05$). These results provide further evidence that players of a higher skill level use their lower extremities to a greater extent during the downswing than golfers of a lesser skill level, especially the lead leg. More skilled golfers may also be utilizing more distal joints of their lead leg to generate energy in addition to the hips.

While this study provides evidence that the lower extremities play a role in the production of club head velocity during the golf swing, the exact mechanism of how they generate that energy to accelerate the club head is still unknown. The increased work by the lower extremities may be related to an upward pull generated by the body as suggested by Chu et al [2]. Increased lower extremity work may also be related to an increased magnitude of weight transfer from the trail leg to the lead leg, which has been shown by multiple studies to relate to club head velocity.

CONCLUSIONS

This study is one of the first to explore the role of the lower extremities in the development of club head velocity. In this study we show strong relationships between the work performed by the lead leg and club head velocity, though this may not be as important as the total amount of work performed by the lower extremity to generate club head velocity. Future work needs to be done to validate these results, as well as to further investigate the lower extremity mechanisms which aid in developing club head velocity.

REFERENCES

1. Nesbit SM and Serrano M. *Journal of Sports Science and Medicine.* **4**, 520-533, 2005.
2. Chu Y et al. *Journal of Sports Sciences* **28(11)**, 1251-1259, 2010.

FMVSS 218 Compliance Testing: Evaluation of Lateral Acceleration and Brain Injury

Nicholas Merrier, BS[1], Sean D. Shimada, Ph.D.[1]

[1]Biomechanical Consultants of California, Davis, CA, USA
email: sean@motionsandforces.com

INTRODUCTION

The side of the head is one of the most vulnerable impact locations for riders in real motorcycle accidents [1]. The sides of the head, where skull bone is relatively thin, have a lower tolerance to impact [1,2]. Side impacts produced the highest HIC values, linear accelerations, rotational accelerations, and durations of unconsciousness [3]. For impacts of the same severity but of different configurations, lateral impacts have been shown to result in higher levels of accelerations of the head than frontal or occipital impacts. The level of force and acceleration imposed on the rider's head can be decreased by wearing a Department of Transportation (DOT) approved motorcycle helmet. Yet, alleviation of all potential brain injuries is limited with respect to a helmet's dampening characteristics. Translational acceleration causes focal brain injuries whereas rotational acceleration causes both focal and diffuse injuries [4]. Focal injuries, such as contusions or hematomas, are lesions where the damage is locally defined [4]. Diffuse injuries are those injuries with axonal, neural, and microvascular effects and brain swelling [4]. It is known that rotational acceleration can produce more severe focal and diffuse brain injuries than translational acceleration; however, current helmet design emphasizes the evaluation of translational acceleration [5]. In this study, DOT helmet verification tests were examined to determine the effectiveness of a motorcycle helmet in preventing rotational brain injuries from lateral impacts. Implementing the measure of rotational acceleration could result in higher standards for helmet design and provide the rider better protection against both rotational and translational acceleration brain injuries.

METHODS

An accumulation of side impact headform translational acceleration data points for the subject study were obtained through Federal Motor Vehicle Safety Standards (FMVSS) 218 compliance testing reports from 2003 to 2011 [6]. In order to determine whether a difference exists in the acceleration data based upon the type of helmet configuration, the translational acceleration data were separated into three helmet configurations: complete facial, full, and partial. This study additionally examined the difference in the translational data compiled between DOT approved helmets and novelty (non-DOT approved) helmets. Furthermore, incorporating matching helmet configurations with similar foam liner material, data were separated based upon differences in the shell material (Acrylonitrile Butadiene Styrene (ABS), Polycarbonate (PC) and fiberglass) to characterize shell attenuation properties. Finally, to observe the influence of foam properties, data were separated by differences in foam type (Expanded Polystyrene (EPS) and Polystyrene (PS)). The Head Injury Criteria (HIC) and Abbreviated Injury Scale (AIS) were used to determine the efficacy of the various motorcycle helmet characteristics.

RESULTS AND DISCUSSION

From a total of 143 DOT motorcycle helmets tested, the average experienced side impact headform translational acceleration was 183 g. The complete facial, full, and partial helmet's average translational headform accelerations were 173 g, 180 g, and 195 g, respectively. ABS shell material achieved the lowest headform acceleration at 165 g while the highest headform acceleration was fiberglass shell material (184 g). EPS foam average headform acceleration was 173 g. In comparison, PS foam had an average headform acceleration of 178 g. Our data of partial style novelty helmets indicated that headform accelerations were approximately five times the partial headform accelerations of the DOT approved helmets. Rotational accelerations are derived from the translational accelerations following the same correlation.

The average helmet translational acceleration of 183 g corresponds to an HIC score of 1,303 [7], which falls well above the National Highway Traffic Safety Administration (NHTSA) HIC_{15} maximum allowable value of 700 [8] and is associated with AIS 4 representing mild Diffuse Axonal Injury (DAI) [9]. The average calculated rotational acceleration was 16,219 rad/s^2 resulting in an HIC score greater than 1860 [10] and corresponds with the AIS measure of 6 indicating severe DAI where death may occur [9].

In this study, motorcycle helmets demonstrated less protection for the prevention of brain injuries during lateral impacts when compared to frontal or crown impacts. Demarco observed tapering of the force attenuating liner foam on the sides of helmets, suggesting weaker force absorbing ability [11]. On the side of the helmet where the radius of curvature is larger, it is more prone to experiencing excessive displacements, which lead to the full compaction of the foam with a steep increase in the transmitted forces [12]. The different radiuses of curvature on the sides of helmets yield to different deformation properties than frontal or crown sites. Essentially, the shells are relatively flexible for side impacts due to the edge flexibility compared with crown impacts where they are stiff [13]. This flexibility results from lower stiffness associated with larger shell curvature [1]. Thermoplastic shells absorb energy by both buckling and by permanent plastic deformation, whereas fiberglass shells dissipate energy by matrix and fiber cracking and delamination [12]. At more flexible sites, such as the side of the helmet, shell impact force attenuation may be lower. Sides of the helmet with higher shell curvature or near the edges need denser foam [12]. Motorcyclists could benefit from designing motorcycle helmets to alternate degree of foam density depending on the specific impact locations of the helmet in order to maximize protective properties.

CONCLUSIONS

Motorcycle helmets have limitations with respect to mitigating all injuries but can reduce the severity of head and brain injuries. Rotational accelerations are known to cause more severe injuries; nonetheless current helmet verification test standards only measure translational accelerations [5]. Our study revealed that a helmet may not prevent significant rotational acceleration brain injuries even when a helmet meets the FMVSS 218 standard. More examination should be given to the side of the head because of the weakness from head tolerance and helmet performance at these locations. Reducing the overall severity of rider brain injuries may be achieved by considering the measure of rotational acceleration into the FMVSS 218 compliance testing. Employing the measurement of rotational acceleration would result in higher standards for helmet design and may provide better protection for motorcyclist.

REFERENCES

1. Schuaeib, FM, et al. *Journal of Materials Processing Technology* **123**, 046-421, 2002.
2. Crandall, JR, *SAE* 960094, 1996.
3. Hodgson VR, *SAE* 831618, 1983.
4. Schmitt K. *Trauma Biomechanics.* Springer, 2007.
5. Nahum A. *The Biomechanics of Trauma*. Prentice Hall, 1985.
6. Compliance Database. Office of Vehicle Safety Compliance. [Online] NHTSA, 2003-2011
7. Zellmer, H, *SAE* 933113, 1993.
8. Eppinger R, *NHTSA* Department of Transportation, 2000.
9. Tyrell, DC, et al. *Crashworthiness and Occupant Protection in Transportation Systems*, **30**, 539-557, 1995.
10. Dalmases, C. *Head Injury Protection For Pedestrians*. VDM, 2010.
11. Demarco AL, et al. *Accident Analysis and Prevention* **42**, 1778-1784, 2010.
12. Cernicchi A, et al. *International Journal of Crashworthiness* **13**, 451-467, 2008.
13. Gilchrist A, et al. *Accident Analysis and Prevention* **28**, 525-535, 1996.

IMPACT OF THE LOADING TYPE ON THE BIOMECHANICS OF THE CERVICAL SPINE

Wissal Mesfar, Ph.D and Kodjo Moglo, Ph.D

Royal Military College of Canada, Kingston, Ontario, Canada
email: wissal.mesfar@rmc.ca

INTRODUCTION

The determination of the cervical spine response under different major movement continues to be the objective of many studies, either experimental or numerical. In fact, understanding of the biomechanics of the cervical spine provides further insights into the underlying mechanisms of injuries and physical conditions. This can of great added value by improving prevention, diagnosis and rehabilitation. The FE models are recognized as a reliable tool to obtain information which would otherwise be very difficult to obtain through the experimental studies [1]. Internal stresses, contact forces between the facets and spinal motion segments are from data provided by FE simulations when the model is subjected to complex boundary and loading conditions. The principal movements of the cervical spine are the flexion-extension, Left and Right lateral bending and Left and Right axial rotation. In this study and based on our developed FE model, we aim to determine the impact of applied moment at the different planes on the contact force at the facets joint of the cephalic cervical vertebrae.

METHODS

A 3D nonlinear head and neck (HN) complex finite element (FE) model was developed and constructed based on CT scans and MRI images. The reconstruction of the bone structures (C1-T1 and the head) was based on CT scan images; however the reconstruction of the intervertebral discs was based on MRI images. The FE model consists of bony structures and their cartilage facet joints, intervertebral discs and all the ligaments. The non-linear material properties for the ligaments were considered based on the study of Shim et al. [2]. The transverse ligament is modeled as a bundle and all the other ligaments are each modeled by a number of uniaxial elements with non-linear material properties. However, linear and homogenous properties for the annulus and nucleus and the cartilage were considered. The bony structures were considered as rigid due to their greater stiffness to the adjacent soft tissue structures. For stable unconstrained boundary conditions, T1 is fixed while the cervical vertebrae are left free. In order to quantify the effect of the moment applied at different planes to the centre of mass of the head (CMH), a moment of 2.0N.m was applied to simulate the left and right lateral bending, the left and right axial Rotation and the Flexion movement.

For the extension movement, only 1.2N.m was applied. Only the contact force (CF) in the right cephalic vertebrae facets joint will be presented in this abstract. The CF in the left side can be determined by deduction. In fact the response is almost symmetric with a very minor difference due to the absence of perfect symmetry of the head and neck joint complex.

RESULTS & DISCUSSION

Under 2.0 N.m applied to simulate the Right lateral bending, the contact force was found only in the right facets joint. It reaches the maximum of 58N at the level C1-C2 and ~35N at C0-C1 level and ~31N at C2-C3 level (Fig. 1). The contact force does not exist in the left facets joints due to widening of the left facets under the right lateral bending movement. Under the left lateral bending moment, a very similar response is

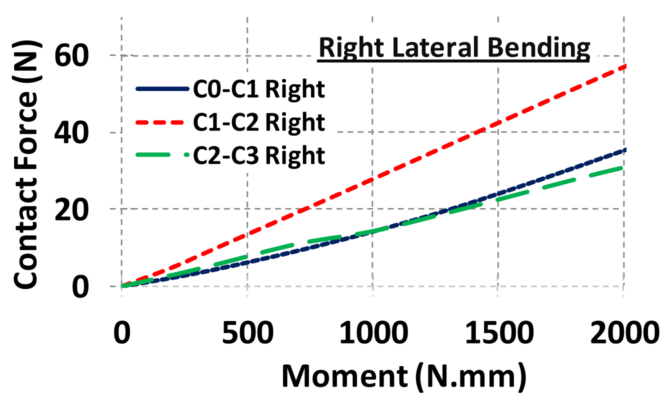

Figure 1: Contact force at the cephalic right facets joint under the right lateral bending moment.

Under the right axial rotation moment, the CF at the right C1-C2 level increases with the applied moment and reaches a maximum of 40N at 2N.m moment. However, the CF at the right level C0-C1 increases with the applied moment only after applying 0.6N.m and reaches a maximum of 40N at 2.0N.m. The CF at the level C2-C3 is nil which can indicate that no contact exists at this level (Fig.2). On the other hand, the application of left axial rotation moment increases the CF at the whole cephalic cervical vertebrae facets joints for 0N.m and also the maximum contact force is computed at the level C0-C1 then at C2-C3 and after at C1-C2 level under 2N.m loading (Fig.3). The joint response at the left facets under the right axial moment is similar to results shown in Fig.3 and under the left axial moment is similar to the results shown in Fig.2.

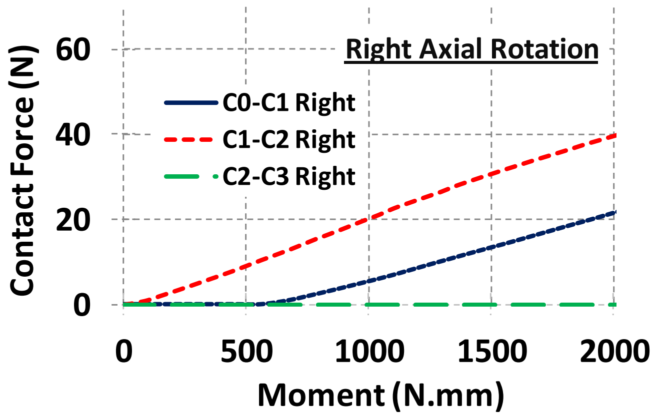

Figure 2: Contact force at the cephalic right facets joint under the right axial rotation moment.

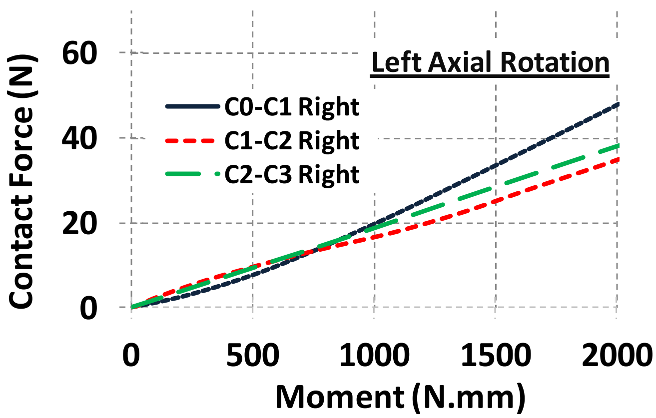

Figure 3: Contact force at the cephalic right facets joint under the left axial rotation moment.

The last moment simulated in this study is the one applied at the sagittal plane. The application of flexion moment induces an increase of the contact force at the right facets C0-C1 and C1-C2 to reach a maximum at C1-C2 level of 42N under 2N.m. At the level C0-C1 the maximum CF computed at 2N.m is 25N. The CF at the level C2-C3, however, is zero. In fact the widening of the C2-C3 facet joint is induced by the flexion moment (Fig. 4). The response of the left facets joints is completely similar to the right side due to the symmetric nature of the loading and the boundary conditions.

Finally, the response of the joint under a 1.2N.m extension is shown in Fig.5. The contact force at the right facet joints C1-C2 and C2-C3 increase with the moment and they are very close in magnitude to reach a maximum of 30N at 1.2N.m. However, the CF at the level C0-C1 is zero until ~0.7N.m and after it starts to increase with the applied moment to reach 15.5N at 1.2N.m (Fig.5). The response of the left facets joints are similar due to the same reasons of the flexion loading case.

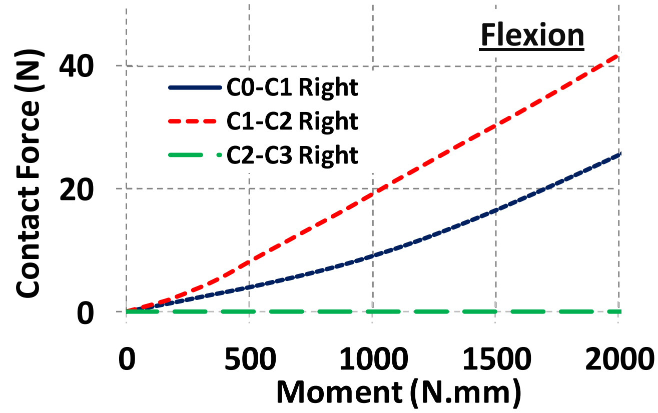

Figure 4: Contact force at the cephalic right facets joint under the flexion moment.

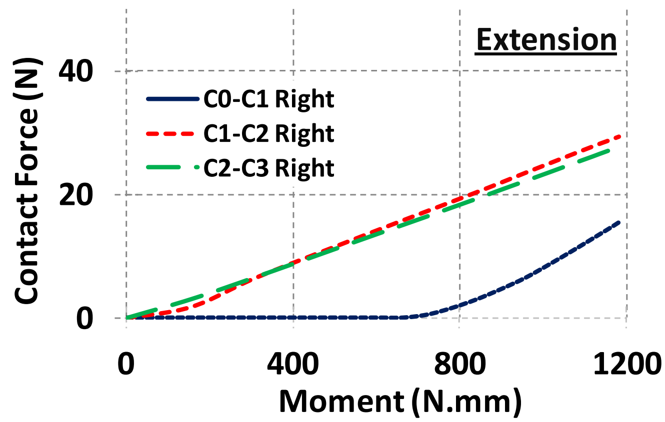

Figure 5: Contact force at the cephalic right facets joint under the extension moment.

CONCLUSION

This study evaluated the effect of the applied moment to the CMH at different planes on the contact force at the cephalic facets joints. The CF computed at the facets joints vary widely with the loading. Except of the left axial rotation movement, the CF at the right facet joint is greater at C1-C2 than the other levels. The results can identify clearly which facet joint is in contact under such specific loading moments and can also quantify the magnitude of the CF. These results may be of great interest to the clinicians and surgeons to prevent certain injuries for a specific cervical joint problems and also improve our understanding of the biomechanics and the response of the joint.

REFERENCES

1. Panjabi, M.M., *Spine* **23**(24), 2684–2700, 1998.
2. Shim VPW et al. *Exp. Mechanics*, 46, 77–89, 2006.

ACKNOWLEDGEMENTS

The financial support from the Canadian Dept. of National Defence (DTAES 6 SGHRP) is gratefully acknowledged.

A NOVEL STATISTICAL METHOD FOR EMG-TO-MOMENT ESTIMATION DURING GAIT

Andrew J. Meyer[1], Carolynn Patten[2,3] and Benjamin J. Fregly[1]

[1] Department of Mechanical & Aerospace Engineering, University of Florida, Gainesville, FL, USA
[2] Department of Physical Therapy, University of Florida, Gainesville, FL, USA
[3] VA Brain Rehabilitation Research Center, Gainesville, FL, USA
email: ixradgst@ufl.edu, web: http://www.mae.ufl.edu/~fregly

INTRODUCTION

Application of neuromusculoskeletal models to clinical problems will likely require model customization to the unique anatomical and neurological conditions of each patient. Unfortunately, current modeling methods make model customization to patient data difficult, especially for model parameter values related to muscle-tendon actuators and musculoskeletal geometry [1]. Improved methods are needed so that patient-specific neural control capabilities and limitations can be easily incorporated into predictive gait optimizations to be used for intervention planning purposes.

This study presents a novel statistical method for predicting net joint moments directly from electromyographic (EMG) and kinematic data. The method could allow measured or simulated muscle EMG signals to control dynamic skeletal models directly without the need for explicit Hill-type muscle-tendon models or complex musculoskeletal geometry. In this study, we describe the approach for generating an over-determined system of equations for statistical EMG-to-moment estimation, and we present an initial evaluation of the approach using the knee flexion-extension moment during gait.

METHODS

Video motion (Vicon Corp., Oxford, UK), EMG (Motion Lab Systems, Baton Rouge, LA), and ground reaction data were recorded simultaneously from a single healthy subject walking on an instrumented split-belt treadmill (Bertec Corp., Columbus, OH). Institutional review board approval and subject informed consent were obtained. The subject walked at a speed of 1.2 m/s while performing his normal gait pattern (125 cycles) and a toe-out gait pattern (50 cycles). Surface EMG data were collected from eight muscles: gastrocnemius medialis and lateralis, rectus femoris, vastus medialis and lateralis, biceps femoris, semimembranosis, and semitendonosis.

EMG data were processed in a manner similar to previously published methods [2]. Raw EMG signals were high-pass filtered at 30 Hz, demeaned, rectified, and finally low-pass filtered at 6 Hz. After these steps, each EMG signal was normalized to maximum value over all gait cycles.

Knee flexion moment, angle, and angular speed were calculated using a customizable 27 degree-of-freedom (DOF) full-body dynamic walking model. Model Properties were calibrated to the subject's video motion and ground reaction data using previously published optimization methods [3]. For each of the 150 gait cycles, an inverse dynamics analysis was performed with the calibrated subject-specific model to calculate the knee flexion-extension moment at 51 normalized time points across the gait cycle. Joint motions required for inverse dynamics were obtained via inverse kinematics performed with the calibrated model.

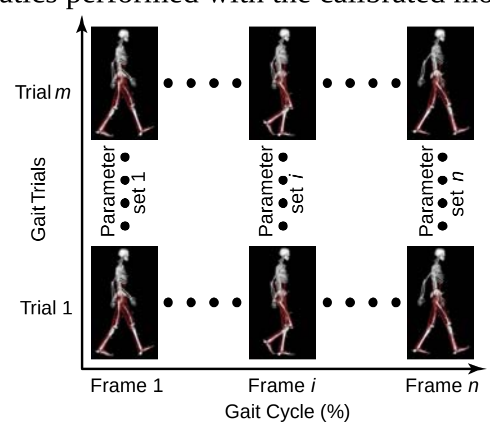

Figure 1: Graphical portrayal of the statistical moment estimation method.

To turn processed muscle EMG signals and knee kinematics into a knee flexion-extension moments, we developed a novel computational method called "statistical moment estimation" (SME). SME is different from existing EMG-to-moment estimation methods (e.g., [4]) in that model parameter values are constant only at normalized time points in a motion cycle rather than across the motion cycle (Fig. 1). To obtain unique model parameter values at each normalized time point, we collect at least twice as many motion cycles as unknown model parameter values. Since gait is a periodic motion, we assume that kinematic and kinetic conditions at each joint vary within a small range at each normalized time point. We then employ the Taylor series concept from mathematics to define how the joint moment to be estimated varies away from its operating point as a function of local changes in EMG patterns and kinematics.

For this initial evaluation of SME, we linearized the mathematical form of a Hill-type muscle model to derive the following approximate EMG-to-moment relationship:

$$M(\theta,\dot{\theta},t)=\left(\sum_{i=1}^{8}\frac{e^{A_i\varepsilon_i(t-\tau)}-1}{e^{A}-1}\left[c_{i1}+c_{i2}\theta+c_{i3}\theta^2+c_{i4}\dot{\theta}\right]\right)+\left[c_5+c_6\theta\right] \qquad (1)$$

In this equation, ε_i represents the processed EMG signal for muscle *i*, *t* represents time, τ represents a constant EMG-to-activation time delay (50 ms based on [2]), A_i is a nonlinear EMG-to-activation exponent for muscle *i* that ranges between -3 and 0 [2], θ is the knee flexion angle, $\dot{\theta}$ is the knee flexion angular speed, c_{i1} through c_{i4} are constants accounting for force-length, and force-velocity properties for muscle *i*, and c_5 and c_6 are passive force-length terms for all muscles lumped together. The *c* coefficients are mathematically constrained to vary smoothly between time frames.

We performed two evaluations of our proposed SME method using the 150 knee flexion-extension moment curves calculated from the treadmill gait data. Each evaluation followed a "calibrate-test" approach, where 100 gait cycles were used to solve Eq. (1) at the 51 normalized time points in the gait cycle, and then the resulting model parameter values were used to test the estimated knee flexion moments using 25 additional gait cycles. The first evaluation used 100 normal gait cycles for calibration and the remaining 25 normal gait cycles for testing, while the second evaluation used 75 normal and 25 toe-out gait cycles for calibration and 25 toe-out gait cycles for testing. We used Matlab's fmincon optimizer to make repeated guesses for A_i (i = 1,…,8) while the cost function used the current guesses and linear regression to solve for the best-fit coefficients c_{ij} (i = 1,…,8, j=1,2,3), c_5, and c_6.

RESULTS AND DISCUSSION

Overall, the knee flexion moment curves predicted by SME were reasonably accurate for normal and toe-out gait (Fig. 2). RMS prediction errors were 3.1 Nm for normal gait and 3.9 Nm for toe-out gait.

The knee flexion-extension moment estimates generated in this study suggest that the statistical moment estimation idea has merit. Moment estimates were reasonable for toe-out gait, even though the calibration was performed primarily using normal gait data. This fact shows that the method may be able to predict the knee flexion moment for subjects with erratic or asymmetric gait patterns, such as subjects who have had a stroke.

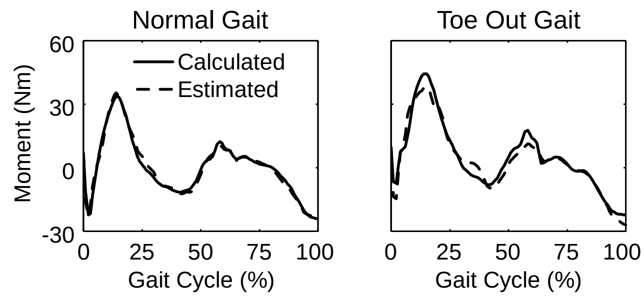

Figure 2: Inverse dynamic and SME knee flexion moment curves during treadmill gait.

Our proposed statistical EMG-to-moment estimation method possesses several advantages as well as disadvantages. On the positive side, the model to be fitted in Eq. (1) is very simple with a low number of parameters, allowing for unique determination of model parameter values at any normalized time frame given enough gait cycles. SME also eliminates the need for explicit muscle-tendon models and complex musculoskeletal geometry. Thus, SME could permit measured or simulated EMG signals to control dynamic skeletal models directly, simplifying incorporation of patient-specific neural control capabilities and limitations directly into predictive gait optimizations. On the negative side, each fitted SME model will only be accurate for a specific normalized time point in the gait cycle. Also, the method will only work for periodic motions, and it requires a large number of motion cycles to formulate an over-determined system of equations at each normalized time point in the motion cycle.

REFERENCES

1. Fregly BJ, et al. *J Orthop Res*, **30**, 503-513, 2012,
2. Lloyd DG, Besier TF. *J Biomech* **36**, 765-776, 2003.
3. Reinbolt JA, et al. *Med Eng Phys* **30**, 434-443, 2008.
4. Olney SJ, Winter DM. *J Biomech* **18**, 9-20, 1985.

ACKNOWLEDGMENTS

Thus study was funded by NIH grant R01EB009351.

ARE EXTERNAL KNEE LOAD AND EMG MEASURES STRONG INDICATORS OF INTERNAL KNEE CONTACT FORCES DURING GAIT?

Andrew J. Meyer[1], Darryl D. D'Lima[2], Scott A. Banks[1], David G. Lloyd[3], Thor F. Besier[4], Clifford W. Colwell[2], and Benjamin J. Fregly[1]

[1]Department of Mechanical & Aerospace Engineering, University of Florida, Gainesville, FL, USA
[2] Shiley Center for Orthopaedic Research & Education, Scripps Clinic, La Jolla, CA
[3] Griffith Health Institute, Griffith University, Queensland, Australia
[4] Auckland Bioengineering Institute, University of Auckland, Auckland, New Zealand
email: AMeyer1987@gmail.com, web: http://www.mae.ufl.edu/~fregly

INTRODUCTION

Researchers have sought to explain the development and progression of knee osteoarthritis using *in vivo* estimates of knee contact forces. Unfortunately, it is not possible to measure knee contact forces in a clinical environment. Studies often estimate knee contact forces using a variety of external measures. The recent development of instrumented knee implants, such as the eTibia design [1], has provided access to *in vivo* knee contact force data during gait and other activities. This study explores the correlations between relevant external measures (i.e., inverse dynamics knee loads and EMG signals) and internal knee contact forces measured by an instrumented implant.

METHODS

We collected video motion, ground reaction, and surface EMG data from a single subject with valgus alignment implanted with an eTibia instrumented tibial tray [1]. The subject performed five trials of four overground gait patterns: normal, medial thrust, walking pole, and trunk sway gait. Surface EMG signals were collected from seven muscles: biceps femoris long head, vastus medialis and lateralis, rectus femoris, gastrocnemius medialis and lateralis, and tensor fascia latae. Institutional review board and patient informed consent were obtained. The data used in the study have been made available as part of the second Grand Challenge Competition to Predict *In Vivo* Knee Loads [2].

EMG data were processed in a manner similar to previously published methods [3]. Raw EMG signals were high-pass filtered at 30 Hz, demeaned, rectified, and finally low-pass filtered at 6 Hz. Each EMG signal was normalized to its maximum value over all gait cycles.

Inverse dynamics knee loads were calculated using a previously published 27 degree-of-freedom (DOF) full-body dynamic walking model [4]. For this study, knee superior-inferior force, adduction-abduction moment, and flexion-extension moment were of particular interest. Joint positions and orientations in the model, along with segment inertial properties, were calibrated to isolated joint motion and gait trials using previously published optimization methods [4].

Medial and lateral contact forces were calculated from the six eTibia loads using regression equations generated for this subject [5]. A regression equation was generated and tested for contact force in each compartment using static analyses performed with an elastic foundation contact model. The final regression equations were highly accurate for calculating medial and lateral contact force from eTibia measurements [5].

Correlations between peak values of external inverse dynamic and EMG measures and corresponding peak values of internal contact forces were quantified using a series of linear regression analyses. The regression models fitted first peak, second peak, and both peaks together of medial, lateral, and total contact force as a function of closest peak values of superior force, adduction moment, absolute value of flexion moment, and/or EMG signals. Inverse dynamics peaks closest to each contact force peak were selected for analysis. Only the superior force (F_y) and flexion moment (T_z) were included in the total contact force regressions since the adduction moment (T_x) should only affect medial-lateral load split. In a separate set of step-wise regressions, EMG values taken 50 ms before each contact force peak were used in place of the flexion moment peaks. The step-wise regression started with all EMG signals included and iteratively removed the EMG signal with the highest

p value until either all remaining EMG signals had p values less than 0.05. Only statistically significant EMG signals are reported in this abstract.

Table 1: Regression equations and associated fitting errors. RMS errors are in units of bodyweight.

Peak	Force	Regression Equation	R^2	RMS
First	Total	$c_1F_y+c_2$	0.35	0.381
		$c_1F_y+c_2T_z+c_3$	0.52	0.337
	Medial	$c_1F_y+c_2$	0.38	0.163
		$c_1F_y+c_2T_x+c_3$	0.48	0.154
		$c_1F_y+c_2T_x+c_3T_z+c_4$	0.49	0.157
	Lateral	$c_1F_y+c_2$	0.17	0.280
		$c_1F_y+c_2T_x+c_3$	0.76	0.156
		$c_1F_y+c_2T_x+c_3T_z+c_4$	0.77	0.157
Second	Total	$c_1F_y+c_2$	0.06	0.267
		$c_1F_y+c_2T_z+c_3$	0.07	0.274
	Medial	$c_1F_y+c_2$	0.15	0.184
		$c_1F_y+c_2T_x+c_3$	0.48	0.149
		$c_1F_y+c_2T_x+c_3T_z+c_4$	0.48	0.153
	Lateral	$c_1F_y+c_2$	0.00	0.175
		$c_1F_y+c_2T_x+c_3$	0.00	0.180
		$c_1F_y+c_2T_x+c_3T_z+c_4$	0.01	0.185
Both	Total	$c_1F_y+c_2$	0.49	0.339
		$c_1F_y+c_2T_z+c_3$	0.53	0.332
		$c_1F_y+c_2E_{MVastii}+c_3E_{BicFem}+c_4$	0.60	0.309
	Medial	$c_1F_y+c_2$	0.78	0.171
		$c_1F_y+c_2T_x+c_3$	0.78	0.173
		$c_1F_y+c_2T_x+c_3T_z+c_4$	0.79	0.170
		$c_1F_y+c_2T_x+c_3E_{MVastii}+c_4E_{TFL}+c_5$	0.84	0.152
	Lateral	$c_1F_y+c_2$	0.01	0.243
		$c_1F_y+c_2T_x+c_3$	0.39	0.192
		$c_1F_y+c_2T_x+c_3T_z+c_4$	0.39	0.195

RESULTS AND DISCUSSION

While some contact force peaks exhibited strong correlations with external measures, these measures did not generally account for a significant amount of variability in the internal contact forces. The first peak of lateral contact force correlated strongly with adduction moment and superior force with an R^2 value of 0.76. However, in spite of this high R^2 value, the associated RMS errors were of the same order of magnitude as those of medial contact force, which had a much lower R^2 value of 0.48. For this valgus patient, medial and lateral contact force peaks were almost equivalent in magnitude, making comparison of error magnitudes between the two sides reasonable. EMG signals were found to be significantly correlated only with total and medial contact force, and only when both contact force peaks were included in the regression analyses. Even so, addition of EMG signals yielded only small improvements in R^2 values and RMS errors.

The results of this study suggest that caution should be exercised when using inverse dynamics loads and EMG signals as indicators of knee contact forces. In this subject, changes in external measures were generally not indicative of changes in medial, lateral, or total contact force. It is unknown whether this finding applies to other subjects as well.

The knee adduction moment did not correlate strongly with medial contact force as is generally believed. A likely explanation is that the adduction moment only alters the distribution of force between the two compartments. Changes in total contact force may skew the medial contact force correlations. For example, two significantly different adduction moment values may result in the same medial contact force if the total contact force increases. For this reason, changes in total contact force should be accounted for before using the adduction moment to estimate the load split between the medial and lateral compartments.

Even though muscle EMG signals did not correlate well with contact force peaks, muscle forces may still correlate well. The superior force from inverse dynamics was only half of the total contact force recorded by the implant. This finding suggests that as much as half of the variation in knee contact force occurs as a result of muscles and/or ligaments, the most significant factor likely being muscles. With the use of advanced EMG-to-force modeling methods, a strong correlation between contact force and muscle force may exist.

REFERENCES

1. Kirking B, et al. *J Biomech* **39**, 1744-51, 2006.
2. Fregly BJ, et al. *J Orthop Res* **30**, 503-13, 2012.
3. Lloyd DG, et al. *J Biomech* **36,** 765-6, 2003.
4. Fregly BJ, et al. *IEEE Trans. Biomed Eng* **54,** 1687-95, 2007.
5. Meyer, A. et al. *Proc. of ASME Summer Bioengineering Conference*, Farmington, PA, 2011.

ACKNOWLEDGMENTS

Thus study was funded by NIH grant R01EB009351.

WHY DO HUMANS WALK THE WAY WE DO? EVIDENCE FROM DYNAMIC SIMULATIONS

Ross H. Miller

Queen's University, Kingston, ON, Canada
email: ross.miller@queensu.ca, web: http://me.queensu.ca/HMRC

INTRODUCTION

Walking is likely the most widely studied motion in human movement science, but despite this volume of research, we know surprisingly little about why humans walk the way they do. The relationships between the speed, stride length, and metabolic cost of human walking, along with the associated limb motions and joint kinetics, suggest that walking has characteristics of an optimal control problem, where the stereotypical muscle activation sequences of walking minimize some optimality criterion that quantifies the objective of the motion. Previous studies have suggested this criterion may be the metabolic cost, i.e. the energy expended per unit distance traveled [1,2], but this argument is not universally accepted [3,4].

The purpose of this study was to contribute evidence on the existence of a unique optimality criterion for human walking, from the perspective of musculoskeletal modeling and computer simulation of locomotor behavior. The approach taken was to generate forward dynamics simulations that minimized various candidate criteria, which were then compared to experimental data from walking humans. The underlying assumption is that the humans are presumably minimizing the true, unknown criterion while they walk.

METHODS

Thirteen simulations of one stride of walking were generated using a 2D forward dynamics model and dynamic optimization procedure (Fig. 1; [5]). The model consisted of a trunk and two legs, and each leg was actuated by nine Hill muscle models. Muscle energy expenditure rates and the metabolic cost of walking were calculated using equations that predicted the Hill model's rates of thermal and mechanical energy liberation [6].

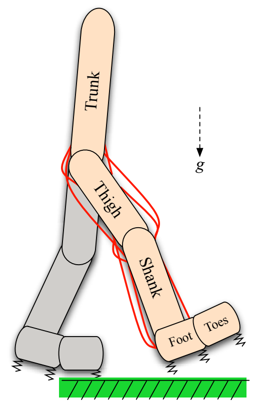

Figure 1: Diagram of the musculoskeletal model used to simulate human walking. The left leg's muscles are not shown. See reference [5] for more details.

The model's muscle excitation patterns, initial generalized speeds, and stride duration were optimized over the time for one stride to minimize (or in some cases maximize) a specified optimality criterion. The criteria evaluated included the metabolic cost of transport, various functions of muscle stress and muscle activation, and the vertical excursion of the center of mass, among others. Simulations were restricted via soft constraints to be periodic, steady-speed, and bilaterally symmetric.

The simulation results were compared to experimental motion capture, ground reaction force (GRF), electromyographic (EMG), and metabolic data measured from 21 human who walked at a self-selected "normal" walking speed and had heights and body masses similar to the model. The model's ability to produce realistic walking motions was validated in a data tracking simulation, where the results matched the mean experimental joint angles and GRF to within 1.42 between-subjects standard deviations (SD) on average.

RESULTS AND DISCUSSION

The simulation that minimized the metabolic cost deviated from the mean experimental joint angles and GRF by 1.86 SD on average. Some other simulations had mechanics with similar accuracy

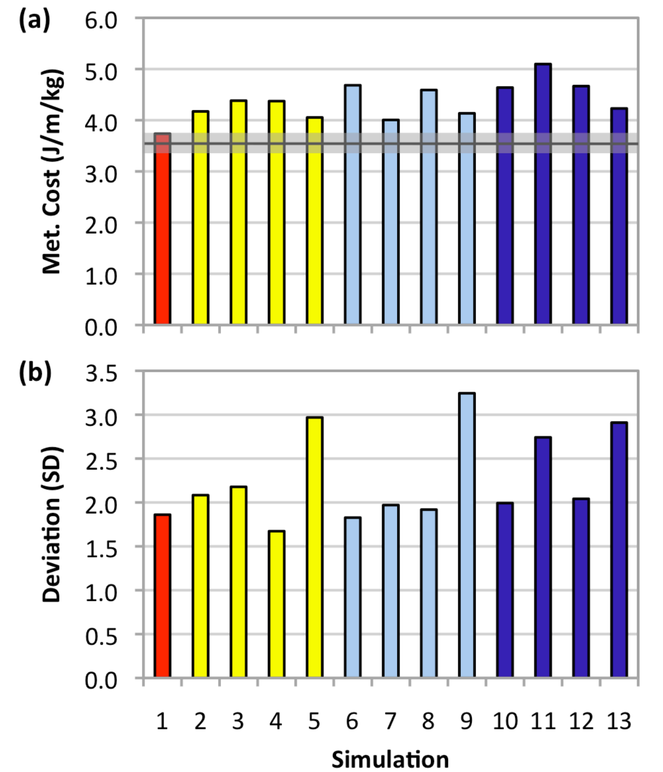

Figure 2: (a) Simulated metabolic costs and (b) average deviations from the experimental joint angles and GRF. Red bar is the minimum metabolic cost simulation. Yellow bars minimized stress-based criteria. Light blue bars minimized activation-based criteria. Dark blue bars minimized other criteria of interest. The shaded grey area in (a) is one standard deviation above and below the average human metabolic cost (3.52 J/m/kg).

(Fig. 2a). For example, minimizing the sum of cubed muscle stress integrals produced an average deviation of 1.67 SD. However, the "minimum metabolic cost" simulation was the only simulation with a realistic metabolic cost (3.74 J/m/kg, 0.98 SD above the human mean). The metabolic costs for all others simulations were at least 2.21 SD above the human mean (Fig. 2b). The "minimum metabolic cost" simulation also had the most realistic muscle excitation timing, with an average deviation from the EMG on/off timing of 10.4%.

The "min/max" criterion suggested by Rasmussen et al. [7] and Ackermann and van den Bogert [3] was not supported in these simulations. Minimizing the maximum muscle activation or stress integrals predicted less realistic simulations than minimizing the sum of integrals raised to a small integer power. Minimizing the vertical center-of-mass excursion produced the gait a very high metabolic cost (4.64 J/m/kg, over five SD above the human mean). This result supports previous arguments against an extreme interpretation of the "six determinants of gait" theory [8]. Maximizing the pendular energy exchange of the center of mass (the "inverted pendulum" paradigm) produced some of the least realistic results (5.10 J/m/kg, 2.74 SD).

CONCLUSION

While several optimality criteria predicted realistic mechanics, a realistic metabolic cost resulted only from minimizing the metabolic cost itself. Previous simulation studies assessing optimality criteria for walking either assumed that a single criterion is adequate [2] or made no quantitative comparisons with human experimental data [3]. Within the limitations of a 2D simulation model, the results suggest that the metabolic cost is prioritized for minimization by the neuromuscular system, more so than other variables associated with the cost or effort level of walking. A goal-oriented explanation for the gross mechanics and muscle activity of walking, where muscle actions are coordinated to produce a gait that maximizes the potential distance traveled for a given energy budget, is consistent with evolutionary theories on bipedalism offering an energetic benefit for long-distance migration [9]. It remains to be explained how or if the nervous system estimates and modulates the metabolic cost.

REFERENCES

1. Ralston HJ. *Int Z Angew Physiol* **17**, 277-283, 1958.
2. Anderson FC & Pandy MG. *J Biomech Engr* **123**, 381-390, 2001.
3. Ackermann M & van den Bogert AJ. *J Biomech* **43**, 1055-1060, 2010.
4. Carrier DR, et al. *PNAS* **108**, 18631-18636, 2011.
5. Miller RH, et al. *Proc R Soc B*, in press.
6. Umberger BR, et al. *Comp Meth Biomech Biomed Engr* **6**, 99-111, 2003.
7. Rasmussen J, et al. *J Biomech* **34**, 409-415, 2001.
8. Kuo AD. *Hum Mov Sci* **26**, 617-656, 2007.
9. Sockol MD, et al. *PNAS* **104**, 12265-12269, 2007.

DISCRIMINATING BETWEEN KNEE OSTEOARTHRITIS SEVERITY LEVELS IN WALKING USING ONLY FORCE PLATFORM DATA

Ross H. Miller, Scott C.E. Brandon, and Kevin J. Deluzio

Queen's University, Kingston, ON, Canada
email: ross.miller@queensu.ca, web: http://me.queensu.ca/HMRC

INTRODUCTION

Features of the knee adduction moment (KAM) during walking have previously distinguished between the presence and severity level of knee osteoarthritis (OA) [1-3]. Calculating the KAM requires the collection and processing of both motion capture and force platform data, followed by application of biomechanical modeling techniques. Consequently, calculating and interpreting the KAM can be difficult in clinical settings that may not have a fully equipped gait lab or may lack personnel with extensive training in biomechanical data collection, analysis, and modeling. A simpler surrogate measure for joint loading would be useful under these circumstances.

The internal KAM arises primarily from the need to balance the external adduction moment generated about the knee by the ground reaction force (GRF). The GRF provides no explicit information on knee or shank kinematics, but during stance, the shank is approximately vertical, and the frontal plane axes of the knee and force platform are approximately aligned. Therefore, the waveform resulting from the product of the GRF magnitude and its angle in the force platform's frontal plane (termed the *frontal load approximation*, FLA) should in theory approximate the KAM waveform.

In this study, we compared common waveform features of the KAM and FLA and assessed whether the FLA can distinguish between OA severity levels in a similar fashion to the KAM.

METHODS

Motion capture and GRF gait analysis data were collected from 198 participants who walked at self-selected normal speeds. Seventy-one participants had healthy knees with no evidence of OA, 66 had moderate knee OA, and 61 had severe knee OA [4]. Linked segment models were defined from each participant's calibration trials, and 3D internal joint moments were calculated by inverse dynamics [5].

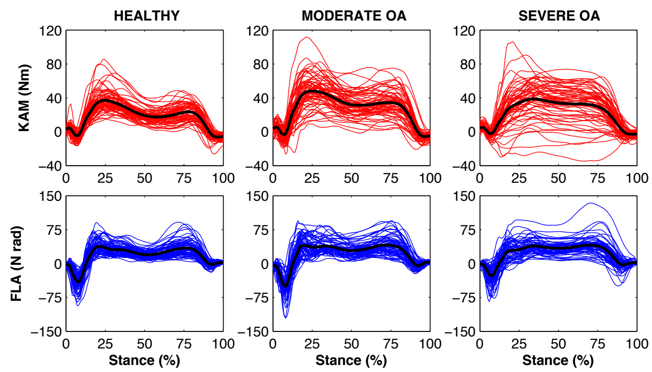

Figure 1: KAM (top) and FLA (bottom) waveforms for healthy, moderate OA, and severe OA groups. Colored waves are individual subjects. Black waves are group means.

Principal component analysis (PCA) was used to transform the KAM and FLA waveforms into sets of statistically uncorrelated principal components (PCs; [6]). Features described by the PCs were identified by reconstructing waveforms from high and low PC scores. The PC scores were compared between groups using analysis of variance (α = 0.05, β = 0.80). Group membership was predicted from PC scores using linear discriminant analysis.

RESULTS AND DISCUSSION

For both the KAM and the FLA (Fig. 1), the first PC described the overall waveform magnitude, and the second PC described the amplitude of the first peak in early stance. The first two PCs accounted for 89% of the variance in the KAM and 72% of the variance in the FLA. The peak KAM in absolute

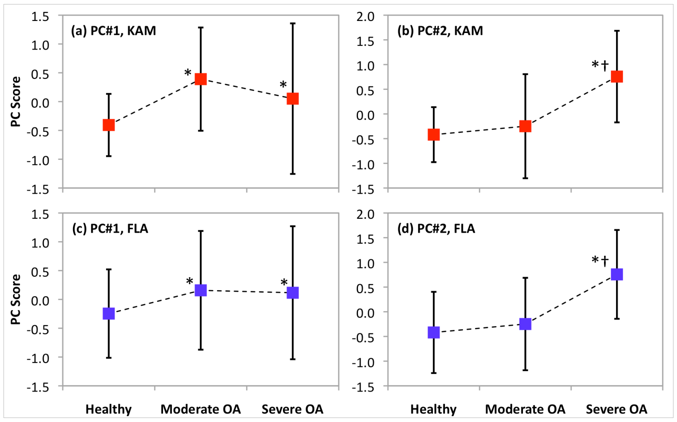

Figure 2: Mean PC scores of each group for (a) the first PC of the KAM, (b) the second PC of the KAM, (c) the first PC of the FLA, and (d) the second PC of the FLA. Error bars are +/- one standard deviation. * = significantly different from healthy group. † = significantly different from healthy group and moderate OA group.

units (Nm) distinguished (p < 0.05) healthy from moderate OA and moderate OA from severe OA, but these distinctions vanished when the data were scaled by body mass. The peak FLA distinguished moderate OA from healthy in raw units (N rad) and distinguished both moderate OA and severe OA from healthy when scaled by body mass.

For both the KAM and the FLA, the first PC score for both the moderate and severe OA groups was significantly greater than the normal group. The second PC score for the severe OA group was significantly greater than the healthy and moderate OA groups (Fig. 2).

Linear discriminant analysis of the KAM PCs correctly distinguished healthy from moderate OA at a 75% rate, healthy from severe OA at 89%, and severe from moderate OA at 76%. For the FLA PCs, rates were 74%, 86%, and 81%, respectively.

CONCLUSIONS

In summary, peak stance phase values of both the KAM and the FLA could distinguish between samples of healthy, moderate OA, and severe OA individuals, but the two variables distinguished different groups from one another in some cases, and responded differently to body mass scaling. However, when the principal components of the KAM and the FLA were assessed, the same waveform features accounted for the most variance in both variables, and the PC scores for these features distinguished between the same groups for both variables. In addition, the PC scores correctly predicted group memberships at similar rates for both variables.

These results suggest that principal components of the FLA can distinguish between knee OA severity levels as well as the KAM. The FLA may thus be a useful surrogate measure of the KAM. The FLA is attractive for clinical use because it requires no motion capture data and no modeling.

It is worth noting that the KAM is not actually a "load" from a structural mechanics perspective. Walter et al. [7] reported that changes in the actual knee joint load induced by a gait intervention are not necessarily reflected by changes in the KAM. It remains to be seen if alternative surrogate loading measures such as the FLA are reflective of changes in joint loading.

Although the peak magnitude of the KAM is often described as an important factor in knee OA onset and progression, most studies have not found a difference in KAM peaks between healthy and OA samples [8]. Alternative analyses of knee joint mechanics, such as PCA, may be needed to consistently identify the presence and severity of knee OA from biomechanical data.

REFERENCES

1. Sharma L, et al. *Arthritis Rheum* **41**, 1233-1240, 1998.
2. Baliunas AJ, et al. *Osteoarthritis Cartilage* **10**, 573-579, 2002.
3. Deluzio KJ & Astephen JL. *Gait Posture* **25**, 86-93, 2007.
4. Kellgren LH & Lawrence JS. *Ann Rheum Dis* **16**, 494-502, 1957.
5. Landry SC, et al. *J Biomech* **40**, 1754-1761, 2007.
6. Deluzio KJ, et al. *Hum Mov Sci* **16**, 201-217, 1997.
7. Walter JP, et al. *J Orthop Res* **28**, 1348-1354, 2010.
8. Foroughi N, et al. *Knee* **16**, 303-309, 2009.

MUSCLE ACTIVATION CHANGES ACROSS THREE DIFFERENT SKATE SKIING TECHNIQUES

[1]Kaya L. Mills, [2]Daniel P. Heil, and [1]Brian K. Higginson

[1]Gonzaga University, Spokane, WA, USA
[2]Montana State University, Bozeman, MT, USA
email: higginson@gonzaga.edu

INTRODUCTION

Previous research on skate skiing has traditionally focused on physiological measures, with less focus on biomechanical factors [1,2]. Of the biomechanics research, there is very little information concerning muscle activation patterns and changes observed during the different skate ski techniques. Of the muscle research, most appear to be devoted to the diagonal stride or double poling [2]. In addition, there currently exists no reliable method to determine skate skiing strategy (e.g., transition from V1 to V2, amount of time spent using V1 to the left vs. right, etc) utilized by a skier during on-snow training or during actual race conditions. It has been suggested that appropriate ski technique selection may affect ski performance [2]. This information could potentially benefit coaches and athletes alike. Therefore, the purpose of this study was twofold: 1) to characterize the changes in unilateral muscle activation of upper and lower extremity muscles while skate skiing utilizing three different skate techniques and 2) determine if muscle activation information can be used to reliably detect changes in ski technique while skiing.

METHODS

Eleven members (5 male, 6 female) of the Montana State University Nordic Ski Team (Mean±SD: 169.5±8.2 cm, 63.5±7.6 kg, 2.90±0.22 m/s) skate skied for two minutes at a self selected speed on an oversized treadmill utilizing three skate ski techniques: V1 to the right (V1RT), V1 to the left (V1LT) and V2 (V2). Muscle activation measures were recorded using a telemetry-based surface electromyography (EMG) system for select upper extremity (biceps brachii, BB; lateral head of the triceps, LT; and posterior deltoid, PD) and lower extremity (tibialis anterior, TA; biceps femoris, BF; and lateral gastrocnemius, LG) muscles. An inertial sensor was mounted to the right ski pole tip and used to determine pole contact with the treadmill surface. Unilateral muscle activation of the right side upper and lower extremity muscles were sampled at 1500 Hz and averaged over five strides (defined by six subsequent pole contacts). Total and average muscle activation was evaluated using a Multivariate Repeated Measures Analysis of Variance (RM ANOVA) and Sheffe's test for post-hoc evaluations (α=0.05) to determine if there was a systemic change in muscle activation across the three skate ski techniques. Discriminant Function Analysis was used to predict group membership (skate ski technique) using these muscle activation measures.

RESULTS AND DISCUSSION

Total muscle activation was shown to be a more sensitive measure of muscle activation changes across ski techniques with significant differences found in five of the six muscles tested, whereas differences were only found in two of the six muscles tested using average muscle activation. Average muscle activation was significantly less in both BB and LT for V1RT than both V1LT (P = 0.001 and P = 0.003, respectively) and V2 (P = 0.002 and P = 0.001, respectively). There were no other noticeable differences in average muscle activation measures found across ski techniques.

Significant changes in total muscle activation was seen across ski techniques in all muscles instrumented except BF (P = 0.310). Like average muscle activation, total muscle activation for BB was significantly less during V1RT than for both V1LT (P = 0.001) and V2 (P = 0.003). For LT, total muscle activation was significantly greater for

V1LT than both V1RT ($P = 0.001$) and V2 ($P = 0.012$). For the remaining muscles (PD, TA, and LG), total muscle activation was greater during V1RT and V1LT than V2 ($P < 0.001$).

These results indicate that no single muscle can be used to differentiate between the three skate ski techniques used in the current study, yet all muscles found to significantly differ between techniques can differentiate one technique from the other two. It was found that average muscle activation for the BB and LT, and total muscle activation of the BB could effectively differentiate V1RT from both V1LT and V2. Total muscle activation of the PD, TA, and LG muscles were found to result in greater muscle activation during V2 than both of the V1 techniques. Finally, LT was the only muscle that resulted in greater total activation during V1LT than both V1RT and V2.

Discriminant Function Analysis was performed to predict group membership (skate skiing technique) using the total muscle activation measures that were found to be significant in the RM ANOVA (BB, LT, PD, TA, and LG). Two discriminant functions were identified (Wilke's Lambda = 0.144, $P < 0.001$; Wilke's Lambda = 0.550, $P = 0.002$, for functions 1 and 2, respectively), with function 1 accounting for 77.4% of the total solution variance and function 2 accounting for the remaining 22.6%. Total LG activation was most highly correlated to function 1 ($r = -0.334$), with LT ($r = 0.771$), TA ($r = 0.680$), BB ($r = 0.529$), and PD ($r = 0.471$) most highly correlated to function 2. Classification results indicate that 93.9% of the cases were correctly classified, with only one case for V1RT and one case for V2 being misclassified as V1LT. There was no classification error associated with V1LT.

In a similar study it was found that the preferred poling side of the skier affected the classification error associated with each ski technique [4]. In the current study, eight of the 11 skiers indicated that the right side was their preferred poling side. The same analysis performed on this subgroup of eight subjects resulted in 100% of all cases being correctly identified (Wilke's Lambda = 0.091, $P < 0.001$; Wilke's Lambda = 0.437, $P = 0.002$, for functions 1 and 2, respectively).

CONCLUSIONS

The current study indicates that muscles activation of the upper and lower extremities change across skate ski techniques and that these changes can be used to determine selected skate technique at a fixed skiing speed. It is reasonable to believe that the predictive ability of muscle activation data on group membership may also be influenced by speed and grade and should be considered in future studies.

REFERENCES

1. Millet GP, Boissiere D, and Candau R. *J Sports Sci* 21(1); 3-11.
2. Kvamme B, Jakobsen V, Hetland S, and Smith G. *Eur J Appl Physiol* 95(2-3); 205-212.
3. Lindinger SJ, Holmberg HC, Muller E, and Rapp W *Eur J App Physiol* 106(3); 353-363.
4. Higginson BH, Mills KL, and Heil DP. *Proceedings of ICSNS'12,* Vuokatti, Finland, 2012.

CHANGING STEP WIDTH ALTERS LOWER EXTREMITY KINEMATICS DURING RUNNING

Clare E. Milner, Richard A. Brindle, Songning Zhang, Eugene C. Fitzhugh

University of Tennessee, Knoxville, TN, USA
Email: milner@utk.edu

INTRODUCTION

Frontal and transverse plane lower extremity kinematics are associated with overuse knee injuries in runners [1, 2]. Step width is a frontal plane variable which may influence lower extremity kinematics while running. Previous research has reported that rearfoot angle changes with step width alterations during running [3]. The effects of changes in step width during running on the knee and hip have not been reported. Furthermore, differences in hip and knee kinematics are also apparent between male and female runners [4]. The purpose of this study was to determine the effect of changing step width during running on lower extremity kinematics in healthy male and female runners. We hypothesized that peak hip, knee and rearfoot angles during running will differ among the step width conditions and between genders.

METHODS

Twenty six healthy runners participated in this study, half of them male. Participants were between the ages of 18 and 35 years old, and have been running at least 15 miles a week for at least a year (age: 24.7 ±3.9; height: 1.7 ±0.1; weight: 66.0 ±9.3; miles/week: 31.3 ±18.0). Each participant provided written informed consent and completed a Physical Activity Readiness Questionnaire before participating. Participants' leg length was measured. A nine camera motion capture system collected marker position data at 120 Hz. Ground reaction force data were collected at 1200 Hz using a force plate synchronized with the motion capture system. Running velocity (3.5 m/s +/-5%) was monitored via two photocells and a timer. Participants ran with their preferred step width for the control condition. The order of the subsequent experimental conditions was randomized. During the wide condition, participants ran with a step width of 20% leg length. During the narrow condition, participants ran with a step width of 0% leg length. Target step width was indicated by tape placed along the runway. Participants took several practice trials for each condition. Five right side trials were collected per condition. Data were processed using joint coordinate systems and rigid body assumptions. The dependent variables were peak hip adduction angle, peak hip internal rotation angle, peak knee internal rotation angle, and peak rearfoot eversion angle. The dependent variables and step width were each analyzed statistically using a 2 x 3 (gender x step width) mixed model ANOVA. Least significant difference post hoc tests determined where any significant differences lay for step width or interaction effects. Differences were considered significant if $p < 0.05$.

RESULTS AND DISCUSSION

The step width during running was altered from preferred width in both narrow and wide conditions ($p < 0.001$), and was similar in men and women ($p = 0.454$) with no interaction effect (Table 1). In general, there was a continuous increase in peak values for the dependent variables as step width changed from wide, to preferred, to narrow. Greater peak angles for the hip and knee dependent variables have been associated with overuse knee injuries in runners. There were no interactions between step width condition and gender for any dependent variable ($p > 0.05$), indicating that men and women responded similarly to changes in step width during running. However, several variables differed between men and women, with women tending to have larger peak angles. Specifically, peak hip adduction angle was larger with narrower steps ($p = <0.001$) and in women ($p = 0.012$). Peak hip internal rotation angle was similar across step widths ($p = 0.071$) and gender ($p = 0.438$). Peak knee internal rotation decreased slightly as step width decreased ($p = 0.004$), and was larger in women ($p = 0.044$). Peak rearfoot eversion angle increased as step width decreased ($p = <0.001$) and was similar in men and women ($p = 0.100$).

There was an inverse relationship between step width and peak hip adduction angle. Thus, running with narrow steps causes hip adduction more like that of runners with overuse knee injury [1, 2]. The opposite was also found: running with wide steps reduces peak hip adduction angle. This may be beneficial in runners with excessive hip adduction.

The inverse relationship between step width and peak rearfoot eversion angle has been reported previously [3]. Peak hip adduction angle and peak knee internal rotation angle during running were larger in women than men. Greater peak hip adduction angle in female compared to male runners has been reported previously [4].

CONCLUSION

Changing step width influences hip and rearfoot kinematics during running. Running with wider steps reduced peak hip adduction and rearfoot eversion angles in healthy runners.

REFERENCES

[1] Willson JD, et al. *Clin Biomech* **23**, 203-211, 2008.
[2] Ferber R, et al. *J Orthop Sports Phys Ther* **40**, 52-58, 2010.
[3] Pohl MB, et al. *Clin Biomech* **21**, 175-183, 2006.
[4] Ferber R, et al. *Clin Biomech* **18**, 350-357, 2003.

Table 1: Dependent variables among step width conditions, mean (standard deviations)

	Gender	Narrow	Preferred	Wide
Step Width (cm)*	Male	1.2 (3.8)	6.0 (4.8)	15.7 (2.5)
	Female	0.4 (2.8)	5.0 (3.5)	15.0 (2.5)
Peak Hip Adduction Angle (˚)*	Male	12.9 (3.2)	12.4 (3.4)	8.0 (3.3)
	Female	17.1 (3.6)	15.0 (3.9)	12.0 (4.0)
Peak Hip Internal Rotation Angle (˚)	Male	10.6 (5.1)	11.0 (5.4)	9.9 (5.5)
	Female	8.7 (4.8)	9.4 (4.5)	8.9 (4.4)
Peak Knee Internal Rotation Angle (˚)	Male	1.3 (5.4)^{W}	1.5 (5.7) ^{W}	2.2 (5.7)^{NP}
	Female	5.2 (4.2)^{W}	5.7 (4.4) ^{W}	6.3 (3.7)^{NP}
Peak Rearfoot Eversion Angle (˚)*	Male	6.0 (3.7)	5.2 (3.4)	3.6 (3.8)
	Female	8.7 (4.0)	7.4 (3.9)	6.3 (4.5)

Post-hoc tests indicate significant differences among step width conditions: *all different; different to ^{N}narrow, ^{P}preferred, ^{W}wide.

A NOVEL HIGH-ORDER ELEMENT FOR THE ANALYSIS OF HEART VALVE LEAFLET TISSUE MECHANICS

Hadi Mohammadi, Walter Herzog

The Human Performance Lab, Faculty of Kinesiology, University of Calgary, Calgary, Canada

email: hadim74@gmail.com

INTRODUCTION

Modeling heart valve leaflet tissue is challenging because the degree of anisotropy changes from one layer to the next due to changes in collagen fiber density and orientation. Also, constitutive models describing the mechanical properties of the leaflet structure are not available. Here, we develop a high-order, single element to approximate the material properties of the heart valve leaflet tissue. This element accounts for the nonlinearity in leaflet properties using a bilinear material model, it is composed of a two-dimensional FE in the principal directions, and a p-type FE in the direction of thickness. The element is easy to implement, and is efficient and quick compared to commercially available elements.

METHODS

The heart valve leaflet was modeled using 183 high-order elements (Fig. 1A). The schematic 3D structure of the element is shown in Fig. 1B.

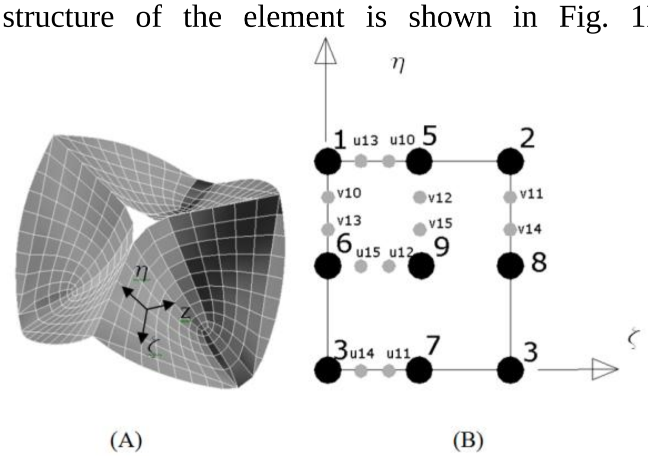

Figure 1: Geometry of the heart valve leaflet modeled using 183 high-order elements (A), and a single high-order element with its major and minor nodes (B).

It consists of 21 nodes with nonlinear boundaries. Each element has 55 degrees of freedom: 15,15, and 25 in each of the principal displacement directions (ζ, η and z, respectively) at each node, as shown in Fig.1 .

The 3D displacement field of an element is based on a 2D element in the ζη-plane that is extended in the z-direction using a 1D linear, parabolic, or cubic Lagrange interpolation function. The in-plane displacement field is a combination of trigonometric and polynomial functions which is obtained by a tensor product of a 2D high order element shape function in the ζη- plane and a 1D Lagrange interpolation function in the z-direction such that:

$$u\,(\zeta,\eta,z) = \sum_{i=1}^{t}\Big(\sum_{k=1}^{p} N_i^u(\zeta,\eta)\,.\,u_{ik}\Big).\,N_k(z)$$

$$v\,(\zeta,\eta,z) = \sum_{i=1}^{r}\Big(\sum_{k=1}^{p} N_i^v(\zeta,\eta)\,.\,v_{ik}\Big).\,N_k(z)$$

$$w\,(\zeta,\eta,z) = \sum_{i=1}^{s}\Big(\sum_{k=1}^{p} N_i^w(\zeta,\eta)\,.\,w_{ik}\Big).\,N_k(z)$$

where t, r and s are DOFs of the components of displacement vectors, i.e., u, v and w on each element, respectively. P is the order of the polynomial used for the Lagrange interpolation function in the direction of z, where P=2, 3 and 4 for a linear, parabolic and cubic function, respectively, and u_{ik}, v_{ik} and w_{ik} are the components of the displacement vector at node ik.

RESULTS AND DISCUSSION

Fig. 2 shows the maximum principal stresses over two layers applied on a single leaflet tissue. The principal stresses differ between the top and bottom layer. The maxima of the first principal stress in the top and bottom layer are 580 kPa and 602 kPa, respectively. The maximum principal stress is located below the corners where the leaflet attaches to the stent (Fig. 2A) [1].

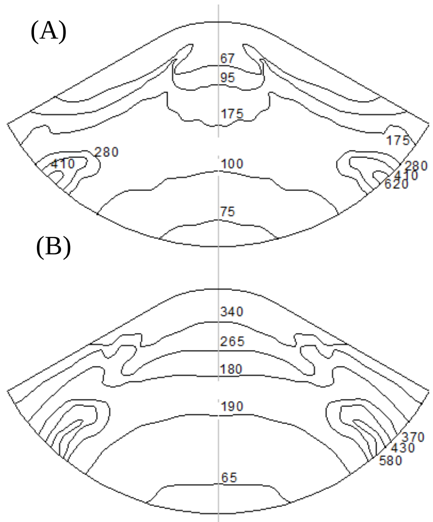

Figure 2: Maximum principal stress distribution on the top (A) and bottom layer of the leaflet (B). Contact between the leaflets was ignored. Values are in kPa.

Fig. 3 shows values of stress including in-plane stress (Max. shear stress) and out-of-plane stresses (longitudinal and transversal normal stresses) with respect to the labelled locations. The direction shown in Fig. 3A is the midline of the leaflet, or the axis of symmetry, and in Fig. 3B, it is the path where maximum values of stresses occur. As shown in Fig. 3, the critical values of stress do not occur along the midline where the maximum deformation occurs. However, longitudinal normal stress, transversal normal stress, and maximum shear stress are maximum in the area close to the corners on the attachment of the leaflet to the stent.

CONCLUSIONS

A new high-order element which is anisotropic and bilinear (material nonlinearity) has been developed to mechanically analyze a trileaflet natural aortic heart valve tissue. Stress patterns, maximum principal stresses, Cauchy stress tensor and distribution of bending moments and the values of longitudinal stresses, the contact area between to adjacent leaflets and in-plane and out-of plane stresses in closing phase have been calculated. The proposed element is less complex, and thus much faster, than an equivalent nonlinear finite element. The technique has similar accuracy as the equivalent nonlinear FEM solution, but solutions are obtained in a fraction of the CPU time. Also, given that defining a strain energy density function for soft tissues generally is so difficult, if not impossible, this element can be easily developed to possess any degree of anisotropy using a bilinear material model.

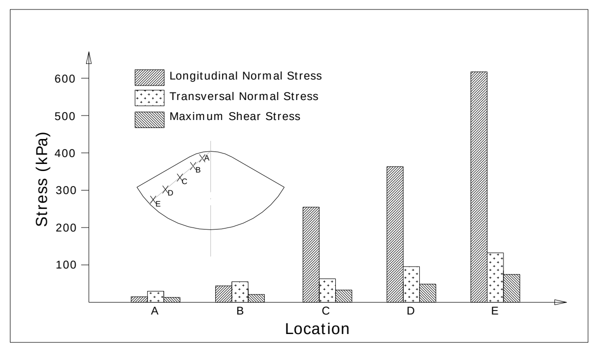

Figure 3: Longitudinal normal stress, transversal normal stress and the maximum shear stress with respect to labeled locations, (A) on the midline of the leaflet, (B) on the line passing over the maximum values.

REFERENCE

Mohammadi H et al. *IMECH, part H, J Eng. in Med.*, **223**(6); 697–711, 2009.

ACKNOWLEDGEMENTS

Alberta Innovates-Health Solutions, The Canada Research Chair Programme and the Killam Foundation.

FOREFOOT ORIENTATION ANGLE DETERMINES DURATION AND AMPLITUDE OF PRONATION DURING WALKING

[1]Gail Monaghan, [1]Cara L Lewis, [1]Wen-Hao Hsu, [1]Elliot Saltzman, [2]Joseph Hamill, [1]Kenneth G. Holt

[1]Boston University, MA, USA
[2]University of Massachusetts, Amherst, MA, USA
email:gmm9@bu.edu

INTRODUCTION

Prior research has shown that an individual with a large forefoot varus has a greater risk of having hip pain from osteoarthritis and is five times as likely to have a total hip replacement[1]. However, the biomechanical mechanisms that link foot structure to injury are not well understood. It is proposed that this may be because of two factors. First, the traditional clinical measure of foot structure has poor reliability and questionable validity[2]. Second, few studies include forefoot kinematics when investigating the relationship between foot structure and injury. The purposes of this study were twofold: 1) to determine the relationship between a newly developed non-weight bearing clinical measure of forefoot and rearfoot orientation, and measures of forefoot and rearfoot orientation at ground contact during gait; and 2) to determine the difference in duration and amplitude of pronation between two groups divided on degree of varus foot orientation.

METHODS

Fourteen subjects participated (23.6 ± 4.9 years of age). All subjects had a right forefoot varus greater than or equal to 15° using a new clinical orientation measure. For this measure, clinical rearfoot and forefoot orientations were obtained from digital photographs using Canvas X (ACD Systems). The photographs were taken with the participant in prone position. The newly developed measure assessed orientation relative to an external (vs. internal) reference frame. Specifically, the new rearfoot orientation was assessed as the angle formed by a line bisecting the calcaneus and the horizontal edge of the table (Fig 1, A). The new forefoot orientation was determined by the angle formed by the line connecting the first and fifth metatarsal heads and the table (Fig 1, B).

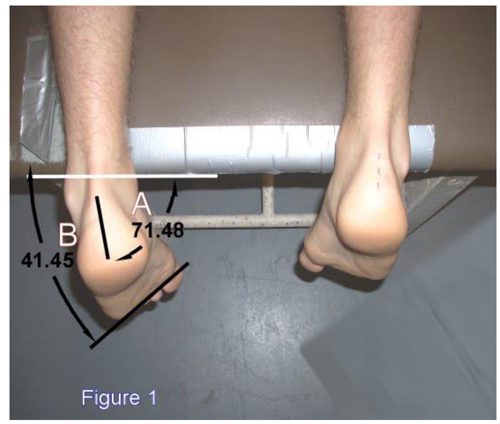

Figure 1: New clinical measure: Rearfoot (90° - A) and Forefoot (B) orientation to the ground with the ankle joint held in neutral

Three dimensional (3D) kinematics of the right foot were obtained using a motion capture system, during over ground walking. Data were collected using eight cameras arranged around a force plate. Participants wore sandals (Bite LLC). Thirteen ankle and foot markers were used based on the model of Leardini et al (1997)[3].

Participants walked at three speeds: slow, preferred and fast. 3D segment angles were calculated using Visual 3D software with an x (flexion/extension), y (abduction/adduction), and z (axial rotation) Cardan rotation sequence. Stance interval was identified using ground reaction force data. Angles were referenced to those measured during standing and time normalized from 0-100 percent. Forefoot orientation and rearfoot orientation were measured at forefoot and rearfoot contact respectively as determined from marker data. Duration of forefoot pronation was defined as the percent of stance between contact and forefoot re-supination. Likewise, duration of rearfoot pronation was the percent of stance between contact and rearfoot re-supination. A General Estimating Equation Analysis (GEE, Linear) was used to test if the new clinical forefoot and rearfoot orientation measures could predict forefoot and rearfoot orientation at contact. Participants in this study were grouped twice into equal groups of Large or Moderate orientation angles: once based on forefoot varus orientation and once based on rearfoot orientation at contact (Table 1). Two separate two factor ANOVAs were performed for forefoot and rearfoot. The two factors were group (Large and Moderate) and speed (preferred, slow, fast).

Table 1: Means and S.E of Group Orientation Angles at contact

Groups	Forefoot Grouping	Rearfoot Grouping
Moderate	2.6° ± 1.1	0.7° ± 0.5
Large	5.4° ± 1.4	3.1° ± 1.3

RESULTS AND DISCUSSION

The new clinical measure of forefoot orientation predicted the forefoot orientation at ground contact ($p<.01$, W=18.7). This indicates that an individual with a greater clinical forefoot varus will have a larger forefoot varus orientation when the forefoot contacts the ground. Clinical rearfoot orientation did not predict rearfoot orientation at contact ($p =1.0$, W=.00). Speed did not influence either rearfoot or forefoot contact orientations.

The group of individuals with large forefoot varus orientation at forefoot contact had greater amplitude (4.1° ± .7 versus 7.8° ± .7, $p < .01$) and duration (64.1% ± 1.1 versus 67.7% ± 1.1, $p = .05$) of forefoot pronation than the group with a moderate forefoot varus orientation at forefoot contact (Fig 2). The Large and Moderate groups based on rearfoot varus orientation at contact were not significantly different in amplitude (3.5° ± .80 versus 5.6° ± .80, $p =.1$) or duration (71.0% ± 2.2 versus 72.1% ± 2.2, $p=.75$) of rearfoot pronation.

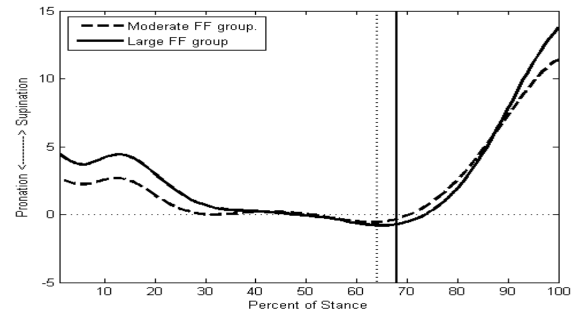

Figure 2: Mean trajectories of groups indicating amplitude and duration of forefoot pronation. Vertical lines indicate where pronation ended for the Moderate (dotted) and Large (solid) groups.

The relation between increased hip injury risk and increased pronation amplitude and duration can be explained by the functional relationship between the foot and the hip[4]. The relative timing of forefoot, rearfoot, tibia and femur motion may be disrupted in an individual when forefoot pronation is prolonged. Consistent with Gross et al’s (2007) finding that a large forefoot, not rearfoot, varus is associated with injury, this study suggests that it is a large forefoot varus which predicts greater and prolonged forefoot pronation associated with injury. In contrast, most studies investigating mechanisms of injury report only rearfoot kinematics and most orthoses prescribed for foot related injuries only address rearfoot structure and movement.

CONCLUSION

This study suggests that a new clinical measure of forefoot structure using an extrinsic reference frame can predict forefoot behavior during gait and that forefoot structure may significantly contribute to musculoskeletal injuries associated with foot function.

REFERENCES

1. Gross KD, et al. *Arthritis &Rheumatism* 2007; **6**: 2933-2938
2. Van Gheluwe B, et al. *J.Am.Podiatr.Med.Assoc.* 2002; **92**: 317-326
3. Leardini A, et al. *Gait Posture* 2007; **25**: 453-462
4. Souza TR, et al. *Clin.Biomech.* (Bristol, Avon) 2010; **25**: 745-748.

BOUNDARY CONDITIONS AFFECT MECHANICAL BEHAVIOR OF *IN-SITU* CHONDROCYTES.

[1]E.K. Moo, [2]S.K. Han, [2]A. Jinha, [2]Z. Abusara, [1]N.A. Abu Osman, [1]B Pingguan-Murphy, [2]W. Herzog

[1]Department of Biomedical Engineering, University of Malaya, Kuala Lumpur, Malaysia
[2]Human Performance Laboratory, University of Calgary, Canada

INTRODUCTION

Osteoarthritis is a joint disease associated, among many other things, with lesions of the articular cartilage. These lesions are thought to accelerate the progression of articular cartilage tissue degradation, and are known to change the structural environment of cells. The mechanical behavior of chondrocytes also depends significantly on the structural integrity of its environment [1]. For example, a hypotonic-challenge affects cells with an intact extracellular matrix (ECM) differently than a cell near the border of a cartilage lesion [1].

Therefore, we suspect that the boundary conditions affect the mechanical behavior of *in-situ* chondrocytes substantially. The objective of this study was to investigate the mechanical behavior of *in-situ* chondrocytes exposed to different boundary conditions: (i) chondrocytes surrounded by an intact ECM; and (ii) chondrocytes close to the edge of an articular cartilage lesion. We hypothesized that the chondrocytes near the lesion would deform more than cells in the intact ECM.

METHODS

Osteochondral blocks (10 x 10 x 5 mm) were harvested from the medial side of metacarpo-phalangeal joints of skeletally mature cows on the day of slaughtering. These blocks were washed three times with phosphate buffered saline (PBS) before being cultured in serum-free DMEM (Dulbecco's Modified Eagle's Medium, Sigma Aldrich) until the day of the experiment, which was always within a week of harvest.

On the day of the experiment, a cylindrical punch was used to obtain a 6 mm diameter full-thickness cartilage/bone sample at the centre of the osteochondral block. The surrounding cartilage tissue was cut away using a scalpel. The osteochondral block was incubated in 8.33 µM Calcein AM (excitation 488 nm; emission 515 nm, Molecular Probes, Invitrogen) and 220 µM Vybrant CFDA SE Cell Tracer (excitation 490nm; emission 520 nm, Molecular Probes, Invitrogen, USA) for 30 minutes each. After incubation, samples were rinsed in dye-free PBS for 15 minutes following staining. Osteochondral samples were then rigidly fixed in a specimen holder using dental cement. Care was taken to ensure that the articular surface was horizontal. During testing, samples were fully immersed in the serum-free DMEM solution to prevent dehydration of the cartilage surface. Prior to the mechanical testing, cartilage thickness was measured using the needle indentation technique at positions near the circumference of the cylindrical cartilage tissue layer [2].

All mechanical tests and imaging were conducted using a custom-designed piezo-electrically driven indentation system that allows for imaging of cells in the intact cartilage attached to its native bone [3]. An average pre-load of 0.15 N was applied to define the contact point between the glass indentor (diameter = 1.64 mm) and the articular surface. A nominal tissue strain of 15% was applied to the articular surface at loading rate of 3µm/s. The target strain was then maintained for 20 minutes until near steady state conditions were achieved. After strain application, the load was released and the cartilage was allowed to recover for another 20 minutes.

Two photon laser scanning microscopy was used to minimize photobleaching of the tissue and photodamage to the cells. A 40x/0.8 N.A., 0.17 mm coverglass corrected water immersion objective (Zeiss Inc., Germany) coupled with a Charmeleon XR infrared laser (Coherent Inc., USA) was used to capture cell images at a resolution of 0.41 x 0.41 µm with optical slice thickness of 1 µm. Images from superficial zone chondrocytes (up to 30 µm from the articular surface) were captured at three time points: before loading, at steady-state during the 15% strain loading, and during recovery when steady state had been reached.

Three-dimensional reconstruction of chondrocytes was then performed using custom-written software (VTK, the Visualized toolkit: Kitware Inc.) for the calculation of cell shape change. Local ECM strain was determined from the change in spacing of paired cells (used as local markers) at different tissue thickness.

RESULTS AND DISCUSSION

No tissue swelling was observed prior to the experiment. At 15% nominal tissue strain, the local ECM strain in the superficial zone showed a compressive strain of 26% in the intact tissue while the ECM strain close to the cutting edge was merely 20%. Cell height (in the loading direction) decreased by 6.8% for cells located near lesions and 14.1% for cells in the intact tissue (Figure 1).

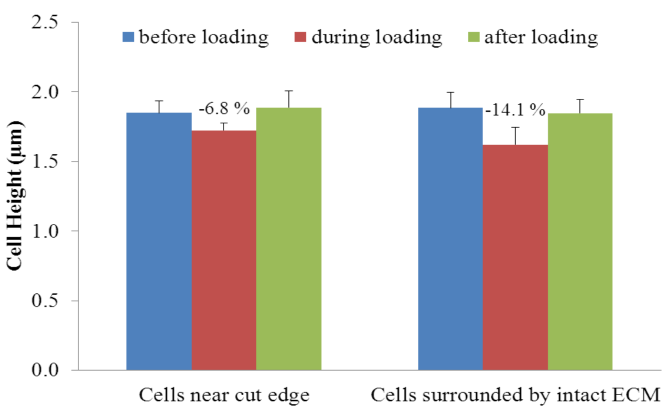

Figure 1. Cell height change before, during, and after application of a 15% nominal tissue strain.

Our preliminary results indicate that chondrocytes near a lesion deform less than chondrocytes surrounded by the intact ECM. This result was unexpected, as we hypothesized that chondrocytes near lesions would be less protected from mechanical perturbations and thus deform more. However, during mechanical compression of the tissue, chondrocytes surrounded by an intact ECM are compressed in the loading direction (green cells in Figure 2), while the tissue near lesions expands sideways, in addition to the axial compressive strain. Therefore, cells near lesions are avoiding the full brunt of the compressive mechanical load, by being displaced laterally, and thus deforming less in the loading (axial) direction (orange cells in Figure 2). Further measurements and finite element loading of this scenario will need to be made to confirm these preliminary findings.

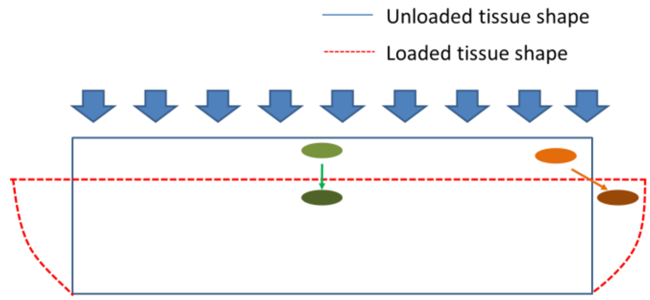

Figure 2. Shape of the cartilage tissue layer before and after compression. The blue arrows indicate the direction of compression. The green cells are surrounded by intact ECM while the orange cells are near the edge of a lesion.

Our preliminary results suggest that cells near lesions deform differently than cells in the intact ECM. Chondrocyte deformation is thought to be a crucial factor in the biosynthetic response of cells and thus the maintenance and health of articular cartilage. Therefore, we suggest that cells in the intact ECM and near lesions will produce different biological responses that may affect the repair capacity of cells near lesions.

REFERENCES

1. Turunen et al. *Biomech Model Mechanobiol*, In Press, 2011
2. Herzog et al. *J Biomech* **31**, 1137-1145, 1998.
3. Han et al. *Med Eng Phys* **31**, 1038-1042, 2009.
4. Guilak et al. *Osteoarthritis Cartilage* **2**, 91-101, 1994

ACKNOWLEDGEMENTS

Alberta Innovates Health Solutions Team Grant on Osteoarthritis, International Society of Biomechanics, Killam Foundation, Canada Research Chair Programme for Cellular and Molecular Biomechanics, Malaysia UM/MOHE HIR grant.

MUSCLE FORCE ESTIMATES DURING THE WEIGHT-ACCEPTANCE PHASE OF SINGLE-LEG JUMP LANDING

[1]Kristin D. Morgan, [2]Cyril J. Donnelly, and [1]Jeffrey A. Reinbolt

[1]University of Tennessee, Knoxville, TN, USA
[2]The University of Western Australia, Perth, Western Australia, AUS
email: kmorga12@utk.edu web: http://rrg.utk.edu

INTRODUCTION

Over 200,000 anterior cruciate ligament (ACL) injuries occur in the United States every year [1, 2], with the majority of non-contact injuries occurring during jump landing sport tasks [3, 4]. Low knee flexion angles, elevated knee valgus moments, and anterior tibia translation contribute to elevated ACL strain and injury during landing tasks [5-7]. Muscle forces during landing may determine injury risk.

Muscles support the knee and could potentially reduce ACL injury risk during jump landing tasks. Presently, several methods are available for estimating muscle contributions during sport tasks associated with elevated ACL injury. Surface electromyography (sEMG) [7] and co-contraction indices estimate muscle activity during landing. However, these methods do not account for muscle architecture or changes in muscle moment arms during dynamic sport tasks, preventing these methods from estimating muscle forces. Computed muscle control (CMC) has recently been used to provide valuable insights into the roles individual muscles play during dynamic movements [8, 9].

The purpose of this study was to use CMC to estimate the forces crossing the knee during a single-leg landing tasks. The ability to identify how individual muscles function to support the knee and affect ACL injury risk during a single-leg jump landing may provide researchers with a better understanding of landing biomechanics and the ability to improve methods to reduce injury risk.

METHODS

Experimental kinematic, kinetic and sEMG data for six muscles (vastus medialis, vastus lateralis, medial and lateral gastrocnemius and medial and lateral hamstrings) were recorded from two male Australian football players conducting a single-leg jump landing task. Subject-specific simulations were created in OpenSim for each participant (Fig. 1) [10]. Inverse kinematics was used to derive the joint angles from the experimental kinematic data. Then OpenSim's residual reduction algorithm was used to create dynamically consistent simulations with the experimentally recorded ground reaction forces (peak residual forces less than 4N, peak residual moments less than 8Nm). CMC was used to estimate muscle excitations and subsequently muscle forces during the weight-acceptance phase of single-leg jump landing. During the simulation, minimum excitation levels for six muscles were bounded to excitations observed experimentally from their sEMG measurements. Muscle excitations estimated from CMC were compared to experimentally recorded sEMG data for the six muscles (Fig. 2). Muscle force estimates for nine muscles were normalized with respect to their individual maximum isometric force values used during the simulation (Fig. 3).

(a) (b)

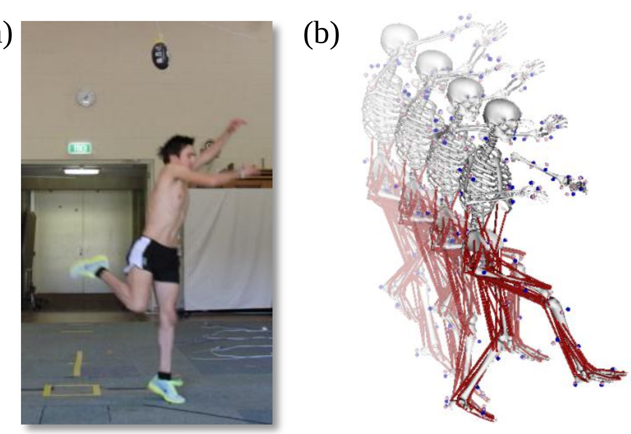

Figure 1: (a) Subject performing single-leg jump landing. (b) Simulation of single-leg jump landing task (model with 23 degrees of freedom and 92 muscle-tendon actuators).

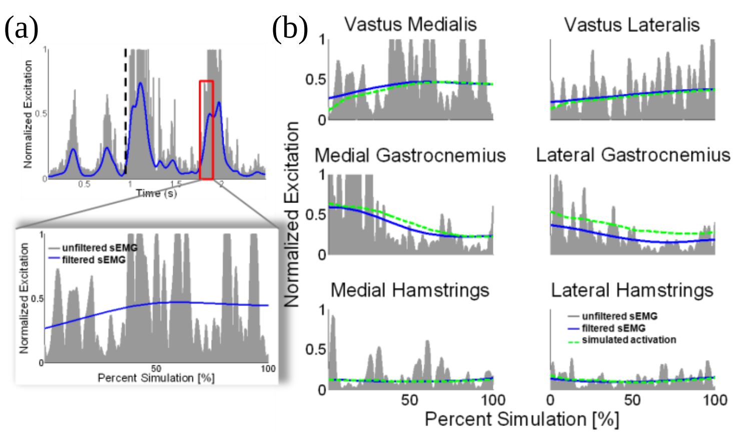

Figure 2: Comparison of sEMG and simulated muscle excitations. (a) Unfiltered and filtered sEMG for the vastus medialis where vertical dashed line indicates start of jump and simulation is during weight-acceptance. (b) Experimental sEMG and simulated muscle excitations estimated during the weight-acceptance phase of single-leg jump landing for subject 1.

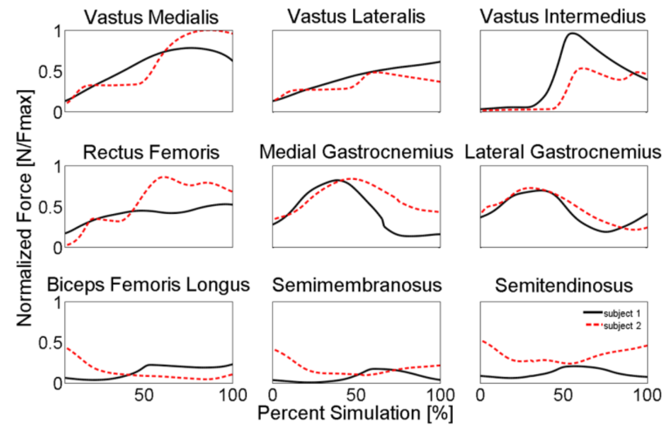

Figure 3: Muscle force estimates solved for via CMC during the weight acceptance phase of single-leg jump landing. Muscle forces are normalized to their respective maximum isometric force values used during the simulation for both subjects.

RESULTS AND DISCUSSION

The largest muscle force estimates during the weight-acceptance phase of single-leg jump landing in decreasing order were the quadriceps and gastrocnemius followed by the hamstrings (Fig. 3). This result agrees with the primary motor control task during landing of producing a support moment [11] capable of maintaining the center of mass in an upright position. The gastrocnemius plays a much larger role than the hamstrings muscles in dynamic knee movements during single-leg landing. Further analysis is necessary to determine whether muscles may be selectively recruited [12] based on moment arms to support the knee from externally valgus knee loading during single-leg jump landing.

CONCLUSIONS

Simulations can be used to estimate individual muscle force contributions during the weight-acceptance phase of single-leg jump landing. Currently, these results suggest that the quadriceps and gastrocnemius muscles are the primary muscles utilized to support the knee and may potentially affect ACL injury risk from external knee loading during single-leg jump landing. Additional subjects are being analyzed to determine if these muscle strategies are simulation specific or if they can be generalized to the single-leg jump landing sport task.

ACKNOWLEDGEMENTS

We thank Caroline Finch, David Lloyd and Bruce Elliott for providing experimental data (NHMRC grant: 400937).

REFERENCES

1. Arendt E and Dick R. *Am J Sports Med* **23**, 694-701, 1995.
2. DeMorat G, et al. *Am J Sports Med* **32**, 477-83, 2004.
3. Ekegren CL, et al. *J Orthop Sports Phys Ther* **39**, 665-74, 2009.
4. Hewett TE, et al. *Am J Sports Med* **24**, 765-73, 1996.
5. Hagood S, et al. *Am J Sports Med* **18**, 182-7, 1990.
6. Walla DJ, et al. *Am J Sports Med* **9**, 13-34, 1985.
7. Podraza JT and SC White. *The Knee* **17**, 291-5, 2010.
8. Anderson FC, et al. *Diagnosis and Management of Movement Abnormalities in Cerebral Palsy*, Cambridge Press, 2005.
9. Thelen DG, et al. *J Biomech* **36**, 321-8, 2003.
10. Hamner SR, et al. *J Biomech* **43**, 2709-16, 2010.
11. Winter DA *J Biomech* **13**, 923-27, 1980.
12. Besier TF, et al. *Med Sci Sports Exerc.* **35 (1)**, 119-27, 2003.

COUPLING OF OSCILLATORY MOTION: THE IMPACT OF VOLUNTARY AND PHSYIOLOGICAL TREMOR ON POSTURE

S.Morrison[1], N., Cortes[2], G.Kerr[3,4], K.M.Newell[5],
[1]School of Physical Therapy, Old Dominion University, [2]School of Recreation, Health, and Tourism, George Mason University, [3]School of Human Movement Studies, QUT, [4]Institute of Health and Biomedical Innovation, QUT, [5]Department of Kinesiology, Pennsylvania State University. Email: smorriso@odu.edu

INTRODUCTION

For optimal control and stability of motion, the ability to minimize any impact intrinsic oscillations generated in one part of the body has on different parts of the body would appear to be desirable. Postural motion and physiological tremor have both been described as periodic, involuntary, approximately rhythmical motions that reflect healthy functioning of a dynamical neuromuscular system. For healthy adults, there is no evidence of coupling between the oscillations – the tremor in one arm is uncoupled to that in the contralateral limb or to postural motion [1, 2]. However, there is a tendency for increased coupling between tremor and postural motion when tremor is amplified as for Parkinson's disease [2]. One issue that has not been resolved is whether the pattern inter-limb tremor coupling and tremor-sway coupling relations are preserved or altered when tremulous oscillations are amplified in healthy adults. This study was designed to 1) assess the relation between voluntary and involuntary tremor responses and postural motion and, 2) to examine the differences in regards to the time-and frequency dependent structure of tremor under voluntary and involuntary conditions.

METHODS

Twelve right-handed individuals (age 20-30 years) participated in this study. Subjects performed two conditions where bilateral limb acceleration (tremor), surface EMG activity and postural motion were collected. The conditions were; postural tremor (involuntary) and simulated (voluntary). For the postural tremor tasks, participants performed a pointing task with their arms held parallel to the ground [3]. For the simulated movements, rapid alternating wrist flexion-extension movements (at 5 Hz) were performed with both arms. All conditions were performed while standing on a Bertec balance plate. Hand and finger tremor were measured using uniaxial accelerometers which were attached to the hand (middle of third metacarpal) and index finger (dorsal distal aspect) of each arm. Bilateral EMG activity was collected from the wrist flexors (flexor digitorum) and extensors (extensor digitorum). Six 30 s trials were collected for each condition. All data were sampled at 1000 Hz.

Time and frequency analyses were performed on the tremor, EMG and COP data. Estimation of the degree of coupling between selected signals (e.g. COP-tremor, tremor-tremor) was determined using cross-correlation and coherence analyses.

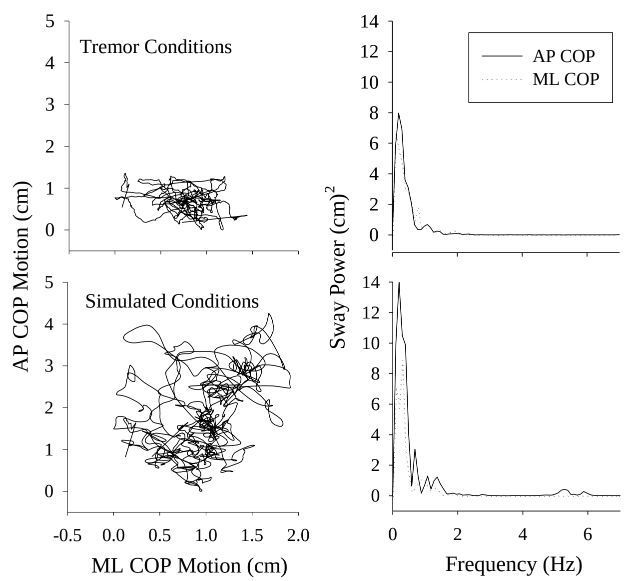

Fig 1. Example of the differences in AP/ML COP motion and the respective frequency plots between the postural tremor and simulated conditions.

RESULTS AND DISCUSSION

The results of the time and frequency analysis revealed a significant difference between conditions in terms of the both amplitude and frequency for all signals. As shown in figure 1, the COP profile during the tremor tasks was of lower amplitude and characterized by a single, peak (0.28-0.30 Hz). In contrasts, under simulated conditions, there were two notable frequency peaks in the COP signal; one between 0.41-0.86 Hz and a second between 4-6 Hz. A similar result was found for the tremor (accelerometer) signals where differences in both amplitude and peak frequency were observed between conditions. For the tremor condition, low amplitude peaks were seen in each arm between 2-4 Hz (2.98-3.11 Hz) and 7-14 Hz (7.75-8.86 Hz). For the simulated conditions, a single, higher amplitude peak was present between 4-6 Hz (4.98-5.16 Hz).

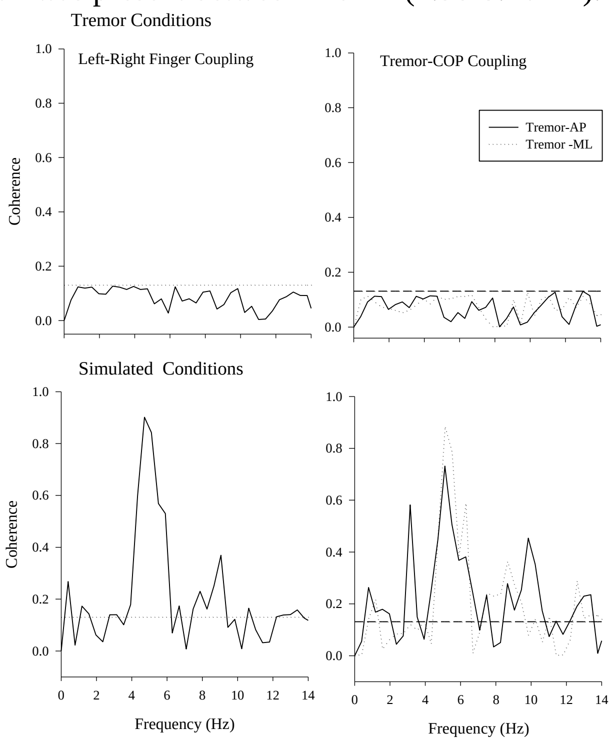

Fig 2. Representative coherence plots for the left-right tremor and the tremor-COP relations. All data was obtained from the same subject during a single trial within each condition.

Coupling analyses revealed significant differences between conditions. For the tremor tasks, there was no evidence of any coupling between arms (r's <0.12), between the tremor and COP motion (r's <0.07) or between the AP and ML postural motion (r's< 0.14). However, under simulated conditions, tremor-tremor and tremor-COP coupling increased significantly (r's=0.62-0.72). As shown in figure 2, the coherence results provided a similar pattern with no evidence of coupling under tremor conditions (coherence<0.14) while coupling increased during the simulated tasks (coherence=0.76-0.93). For this analysis, these significant peaks were observed between 4-6 Hz.

Together, a strong pattern of differences in amplitude, frequency and coupling were found between the simulated and tremor tasks. For tremor conditions, the lack of any inter-limb or tremor-COP relations is consistent with previous reports [2] and indicates that participants were effectively able to dissociate oscillations from sway or tremor from impacting on each other. The increased coupling reported for simulated conditions may result from voluntarily increasing the neural drive to selected muscle groups to perform this task. This increased motion within the upper limb could then have a destabilizing effect on balance, resulting in increased COP motion. Another consequence of increasing the neural drive to the muscles of the upper limb could be an overflow effect to the lower limb muscles. Irrespective of whether the increase in sway was produced in response to the destabilizing effect of the upper limb motion and/or as a result of any potential neural overflow effect, it is obvious that the effects of performing voluntary oscillating actions are wide-spread, impacting on inter-limb coupling and postural motion.

CONCLUSIONS

Overall, there was no evidence of any coupling between physiological tremor in any limb or postural sway. In contrast, when required to simulate a 5 Hz tremor in the upper limbs, there was strong coupling between these oscillations and postural motion and a significant increase in the amount of postural motion. Together, the results support the view that, for involuntary tremor tasks, the control of postural stability is performed in an independent manner to that of the control (minimization) of upper limb tremor. However, voluntarily generating tremulous oscillations not only constrains the limbs to act coherently but this task also has a negative impact on postural stability.

REFERENCES

1. Marsden C, et al. (1969) *Electroencephalogr Clin Neurophys* **27**: 179-185.
2. Kerr G, Morrison S, Silburn P (2008) *Movement Disorders* **23**: 386-394.
3. Morrison S, Sosnoff J (2009) *Journal of Motor Behavior* **41**: 274-283.

INFLUENCE OF SEX AND SEVERITY ON THE EXTERNAL ADDUCTION MOMENT IN MEDIAL COMPARTMENT KNEE OSTEOARTHRITIS

Melissa M. B. Morrow and Kenton R. Kaufman

Mayo Clinic, Rochester, MN, USA
email: kaufman.kenton@mayo.edu
web: http://mayoresearch.mayo.edu/mayo/research/biomechanics/

INTRODUCTION

The interplay of biomechanics and the pathophysiology of knee osteoarthritis (OA) has been investigated for insight into the progression of the disease and the increased incidence and prevalence in women. The relationship between the knee external adduction moment and loading of the medial tibiofemoral compartment has garnered a lot of scientific attention as a key contributor to medial compartment knee OA development [1]. While the basic association between medial knee OA and adduction moment is not disputed, conflicting results remain for the presence of differences in adduction moment between sexes and across Kellgren and Lawrence grades of OA severity in adults with medial knee OA. The lack of consensus across studies with regards to sex and severity may be attributed to small sample sizes. Therefore, the purpose of this study was to investigate the effects of sex and severity on the knee adduction moment in adults with medial compartment knee OA in a sufficiently large sample.

METHODS

The study sample consisted of 306 subjects with knee OA who were consented for participation. While the majority of subjects had bilateral, multi-compartment OA involvement, this analysis excluded those with no medial compartment OA and reduced the sample size to 294 subjects (221 women and 73 men, Table 1).

Bilateral x-ray examinations were performed using standard techniques to obtain weight-bearing knee x-rays. Radiographic OA grade was determined by a single musculoskeletal radiologist according to the Kellgren and Lawrence system [2]. OA severity was stratified into early (grades 1,2) and advanced (grades 3,4). Knee moments were determined from a standard lower extremity gait analysis during level walking [3]. The peak knee external adduction moment was identified for each subject and normalized to height and body weight.

A Chi-square test was used to test disease severity proportions across sexes. A two-way ANOVA was used to test the main effects of sex and severity (fixed effects) and their interaction on the dependent variable, peak knee adduction moment. Additionally, an ANCOVA was used to adjust the effects of sex and severity on the peak knee adduction moment to age and velocity during level walking. For all analyses, only data from the most severe knee for each subject was included based on OA grade. In the case of equivalent severity, the average of the left and right peak knee moment was used. Statistical significance was set at $p < .05$.

Table 1. Subject demographics and variables of interest

	Women mean (95% CI)	**Men** mean (95% CI)
n	221	73
Age (yrs)	56.5 (55.1-57.9)	59.2 (56.6-61.6)
BMI (kg/m2)	32.3 (31.4-33.2)	30.4 (29.0-3l.6)
Velocity (cm/s)	114.6 (112.8-116.5)	118.1 (114.8-121.5)
Adduction moment: Early OA (% Ht-Wt)	1.6 (1.5-1.7)	1.9 (1.8-2.1)
Adduction moment: Advanced OA (%Ht-Wt)	2.1 (1.9-2.2)	2.5 (2.2-2.8)
Early OA^ (n)	124	42
Advanced OA^ (n)	97	31

^Chi-square test, p=0.8312

RESULTS AND DISCUSSION

There was no difference in disease severity between men and women (Table 1). There were significant effects of sex and OA severity on peak knee adduction moment (Table 2). Women had significantly lower adduction moments than men and the adduction moment significantly increased with OA severity (Figure 1). There was no significant effect of the interaction of sex and severity; therefore, while women had consistently lower knee adduction moments than men, the adduction moment slope between early and advanced OA was similar between sexes. Sex and severity remained significant after adjusting for age and velocity (Table 2).

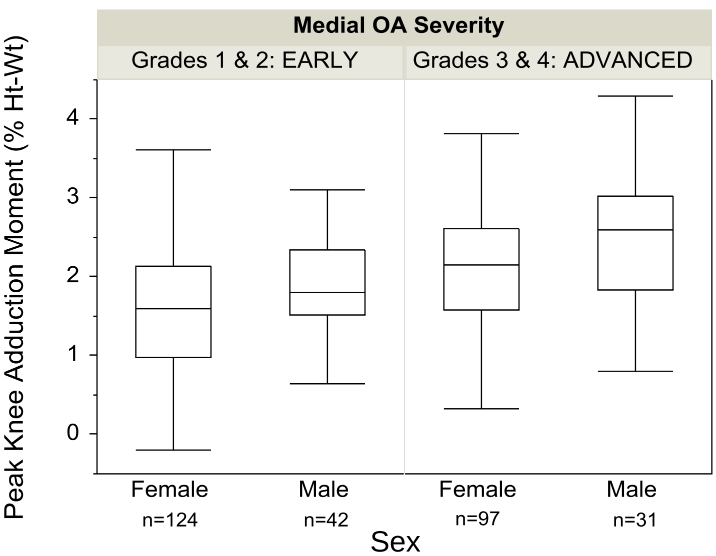

Figure 1. Peak knee adduction moment stratified by sex and OA grade.

The sex differences reported here contrast with the conclusions found by McKean et al. [4] wherein no differences in peak knee adduction moment were detected between sexes which was most likely due to the under powered analysis from a small sample size (24 men, 15 women). However, our results do concur with other previous studies [5]. The increase in peak adduction moment between early and advanced disease severity found here was similar to results reported by Sharma et al. [1], but refute many of the previous reports [5-6].

Lower peak adduction moments in adults with knee OA have been hypothesized as compensatory techniques used to limit loading and/or pain associated with knee OA [4]. The present study did not compare against a disease free cohort and previous comparisons between OA and normal gait are inconclusive, so it remains to be seen as to whether both sexes reduce their medial loading patterns in early OA to compensate for pain. Additionally, the cross-sectional nature of this study does not allow for conclusions on whether the increased adduction moments during advanced OA are causative or responsive to the disease. This study only considered the peak adduction moment while further investigations are warranted into the midstance and second peak adduction moments [6].

CONCLUSIONS

The peak knee adduction moment during medial compartment knee OA is larger in men as compared to women and larger in advanced OA as compared to early OA. Further investigations into longitudinal sex differences in knee biomechanics during progressive knee OA are recommended.

Table 2. Sex and severity effects on peak knee adduction moment adjusting for age and velocity.

	ANOVA		ANCOVA	
	F Ratio	p	β	p
Sex	6.51	0.0112*	0.17	0.0011*
OA Severity	25.21	<.0001*	0.52	<.0001*
Sex * OA Severity	0.07	0.7954	-	-
Age	-	-	0.00	0.2524
Velocity	-	-	0.00	0.2096

*Statistical significance

REFERENCES

1. Sharma L, et al. *Arth Rheum* **41**, 1233-1240, 1998.
2. Kellgren J, and Lawrence J. *Ann Rheum Dis* **16**, 494-501, 1957.
3. Kaufman KR, et al. *J Biomech* **34**, 907-915, 2001.
4. McKean KA, et al. *Clin Biomech* **22**, 400-409, 2007.
5. Sims EL, et al. *J Wom Aging* **21**, 159-170, 2009.
6. Astephen JL, et al. *J Ortho Res* **26**, 332-41, 2008.

ACKNOWLEDGEMENTS

This study was funded in part by NIH K12HD065987 and NIH R01AR048768.

FF GRAPHS AND GROUND REACTION FORCE

[1]Juan C. Muñoz, [2]Gustavo Represas, [3]María Vales Flores and [4]Roberto Cassibba

[1,2,3,4] Instituto de Ciencias de la Rehabilitación y el Movimiento
Universidad Nacional de San Martín, BS AS, Argentina
[1,4]Universidad Nacional de Tres de Febrero, BS AS, Argentina
[1,3]Universidad Favaloro, BS AS, Argentina
[2]Centro Nacional de Alto Rendimiento Deportivo, BS AS, Argentina
email: profjcm@hotmail.com

INTRODUCTION

The pattern of ground reaction force (GRF) during stance phase was presented originally by Elftman [1]. When a person walks, the vertical, antero-posterior and medial-lateral components of the GRF are continuously changing in direction and magnitude, progressing towards the ball and the toe.

At normal gait, the simultaneous representation of the vector formed by vertical and horizontal components of the GRF –in function of position of center of pressure during the support- usually displayed in the so called "butterfly diagram". This diagram was proposed by the Italians Silvano Boccardi, Gigliola Chiesa and Antonio Pedotti in 1977 (Fig. 1) [2]. If we now combine antero-posterior and vertical components of the GRF, we obtain a two dimensional vector in sagittal plane. It is, possibly, the most popular representation of this type of diagrams.

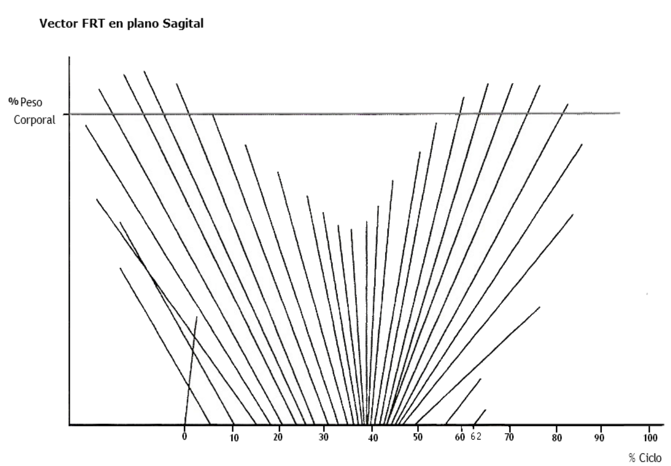

Figure 1: Butterfly Diagram in sagittal plane [3].

As can be seen, that diagram presents a shape of a butterfly wing. The envelope of all vectors presents a pattern characterized by two maxima and one minimum. Initially, when foot contacts the ground, the first few vectors are pointing forwards while absorbing the shock due to the heel strike. Immediately, at the beginning of stance, GRF vectors are inclined backwards, contrary to the direction of movement, producing body deceleration. In the later stages, the leg pushes the ground down and backwards, and the GRF pushes the entire body up and forward and the vector inclination faces the movement, according to Newton´s third Law of motion. The velocity with which the center of pressure moves on the ground is immediately readable as the density of the vectors. The center of pressure is moving monotonously in the direction of progression and is showing an evident plateau in the later stages of the stance which results in correspondent closeness of the vector [4].

The GRF components can be used to derive joint forces and moments acting at the ankle, knee and hip, but the laborious nature of that process has intimidated to most clinicians. For that reason, it was required a visual presentation of the GRF acting in a particular plane combined with a visual image of the patient's ambulation. The visual GRF vector would enable a clinician to see immediately the implication of those forces to the joints in question [5].

However, there are many other implications and applications derived from the relationships between the components of the GRF, not requiring be seen immediately, but they can bring relevant information.

In this article we present the force-force graphs (FF graphs), some applications to normal and prosthetic gait, and propose the use of these type of graphs to extend the knowledge of the ground reaction force.

METHODS

The first GRF data correspond for an adult subject in normal gait. After that, was performed a study on amputee person, who used knee prosthesis with uniaxial joint and a SACH foot.

The tests were performed at the gait laboratory of CeNARD, National Center for High Performance Sports, in our country.

The FF graphics were constructed by taking all possible combinations: GRFz vs. GRFx; GRFz vs. GRFy and GRFy vs. GRFz. In this paper, GRFx represents the antero-posterior ground reaction force exerted by the soil onto the foot, and GRFz the vertical component of the ground reaction force.

Studies were replicated in similar cases, obtaining results without significant differences for each of the two types of selected categories. We understand that force-force curves obtained have characteristic patterns, depending on the situation to which they relate.

RESULTS AND DISCUSSION

The results corresponding to the normal gait, in sagittal plane, can be observed in figure 2. The force shows an anterior direction to the right of ordinate axis (vertical axis), while in the left region it presents posterior direction.

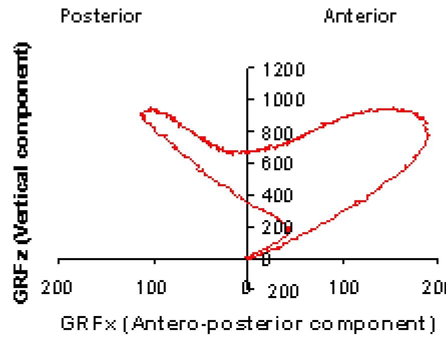

Figure 2: Vertical GRF (Fz) against antero-posterior GRF (Fx), for a subject with normal free gait speed.

In the first moments of initial support, a gradual increase of the force in anterior direction is observed. When it reaches a value close to 50 N -and the vertical force is slightly higher than the 100N -, the curve changes its direction. While the vertical component continues to grow, the component with anterior direction decreases to become zero at the intersection of the curve with the vertical axis. Then, the chart is continued in the left region, reaching a peak corresponding to the maximum body deceleration (braking). From there, the vertical force decreases its numeric value and its direction gets progressively more vertical, reaching its lowest value during the mid stance phase. Subsequently, there is a new intersection of the graph with the vertical axis where, for an instant, the GRF vector exerts no action antero-posterior. From there, the curve moves to the right and reaches a new maximum, corresponding to the impulsion, to finally decrease until becoming zero in the complete foot takeoff.

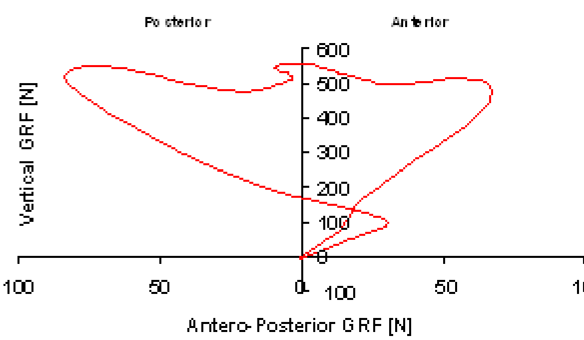

Figure 3: GRFz vs. GRFx for a person with a knee prosthesis (Amputee leg)

For the prosthetic gait, important differences are clearly visualized (Fig. 3). This FF curve represents

GRF on the prostethic foot for a person with transfemoral amputation. In this situation, there are three peaks at the upper zone, and it is notorious how the curve changes its direction, oscillating back and front when the force is almost vertical.

There is also an important difference between the force-time curves and force-force curves. Should be noted that, while the first ones are functions, in general, the second ones are not. Each element of the FF domain graphs can map to more than one element in the codomain. In the examples analyzed, is clearly observed that the curves intersect the ordinate axis more than once, and therefore, this mathematical relationship is not a function.

CONCLUSIONS

Certainly, butterflies diagrams are a special type of FF graphs, where the regions under the curves show graphically the vectors. To our knowledge, the representation given by the Italian researcher undoubtedly has many virtues as we have seen, but also some limitations.

advantages:
• It shows the direction and sense of GRF vector at all times of the stance phase of walking, running, etc.
• Displays if the GRF passes behind, ahead or just on the joint at a specific time.
• Sets quickly, and by direct observation, if the torque produced by the GRF (at each joint in particular) is flexor or extensor, adductor or abductor, etc.

disadvantages:
• Many times, overlapping lines does not allow to see the envelope curve, which is a FF curve in many cases.
• It is difficult to follow the course of the curve from its beginning to its end point. By contrast, a diagram FF facilitates this monitoring, especially when it is accompanied by small arrows indicating the direction of path.
• To clarify the picture, vector of the butterfly diagrams are presented spaced. This is achieved by taking times much greater than those required to draw the FF curve.

Basically, both representations differ in their origin, in its intention. The butterfly diagrams are intended principally to show the GRF vectors. By contrast, FF graphs are interested primarily in the plotted curve, which often manifests itself as the envelope of those. Furthermore, although in both cases it is possible to identify and analyze characteristic points, its detection is easier if the vectors are not present. These reasons make us think that, in some cases, the analysis of graphs FF may prove more productive than the analysis of Pedotti diagrams, though in many others the last ones follow presenting advantages

As others analysis, FF diagrams could be applied to many situations, sports, health, ergonomics, etc.

Other charts that we believe would be extremely interesting and useful, which we are currently working and analyzing them, are the force-angle diagrams. These graphs will enable us to know the GRF's values in terms of joint angles. We can thus obtain curves of GRF vs. ankle angle, GRF vs. knee angle, GRF vs. hip angle, etc.

Finally, we propose the use of FF and FA graphs to study and its application to new phenomena.

REFERENCES

1. Elf Elftman, H. *Am J of Physiol*; 125: 339-356, 1939.
2. Silvano B, Chiesa G and Pedotti A. *Amer J. Phys. Med*, 56(4) .163-182, 1977.
3. Perry, J. *Gait analysis. Normal and pathological function*. Slack Incorporated. Second edition. Thorofare, 2010.
4. Marasović T, Cecić M, Zanchi V. *Proceedings of the 9th WSEAS.* International Conference on Simulation, Modelling and Optimization. Budapest, 2009.

Tait JH. and Rose GK, FRCS. *Journal of Medical Engineering & Technology*. Vol.3 N°5, 1979, with correction.

THE MEDIAL ULNAR COLLATERAL LIGAMENT CARRIES NO LOAD DURING PASSIVE FLEXION AND EXTENSION

[1]Muturi G Muriuki; [1,2]Patrick J Schimoler; [1,2]Bradley C Campbell; [1]Michael A Vaccariello; [1]Edward Snell; [1]Sam Akhavan; [1]Patrick J DeMeo; [1,2,]Mark Carl Miller

[1]Allegheny General Hospital, West Penn Allegheny Health System, Pittsburgh, PA,
[2]University of Pittsburgh, Pittsburgh, PA
mcmiller@wpahs.org

INTRODUCTION

Injuries to the medial ulnar collateral ligament (mUCL) are common in athletes participating in sports that involve an overhead throwing motion. Surgical repair usually involves reconstruction of the anterior bundle of the mUCL using a graft connecting the humerus and ulna. Whether this graft is looped through tunnels on one side and anchored on the other or is anchored on both sides, graft placement and tensioning may have substantial effects on successful outcome. The flexion angle at which the graft is tensioned may also contribute to the success of the repair.[1]

Our aim in this study was solely to determine a desirable graft tension for medial ulnar collateral ligament surgery. Under the working assumption that the desirable tension would equal the force in the native anterior bundle of the mUCL, this force was measured during passive flexion-extension of the elbow.

METHODS

The humerus, ulna, and mUCL of eleven male cadaveric elbows (avg. age 61 ± 7; range 52-75) were exposed while the joint capsule and interosseous membrane were left intact. The humerus and ulna were placed in PVC cylinders aligned with the longitudinal axis of each segment and held in place within each cylinder by two-part polyester resin (3M, St Paul, MN). The humerus of each specimen was fixed to a rigid base and the ulna of each was clamped to the end effector of a 6 DOF robot (Stäubli AG, Horgen, Switzerland). (Figure 1) At full extension, the forearm was directed straight upwards.

Figure 1: Elbow specimen mounted in robot manipulator

A 6 DOF load cell on the robot end effector was used to find the passive flexion path of the elbow (JR-3 Inc., Woodland, CA). The passive path minimized all forces as well as pronation-supination and varus-valgus moments during a flexion movement of 90°. The kinematic steps in the passive path were recorded for subsequent replay.

The rigid attachments of the ulna and humerus were unbolted and an oscillating saw was used to resect the distal humerus, the proximal radius and the proximal ulna, leaving the origin and insertion of the ligament intact. The resection removed all tissue at the elbow except for the anterior bundle of the medial ulnar collateral ligament. The rigid attachments of the humerus and ulna were then rebolted to the robot.

The robot then moved to the positions of 0°, 30°, 45°, 60°, and 90° of flexion. At each of the five flexion angles, the robot performed small proximally- and larger distally-directed distractions along the direction of the long axis of the ulna. Two trials were performed at each of the five flexion angles and force and displacement data were collected for all distractions.

RESULTS AND DISCUSSION

At the neutral position, i.e. prior to distraction, the average mUCL forces measured by the 6 DOF load cell at the five flexion angles were all less than 10 N. Distally directed distractions of 0.5mm along the long axis of the ulna produced small increases in force, with the average force remaining under 11N. (Figure 2) For distally directed distractions, the force along the ulnar axis always dominated the resultant forces shown in the figure. Only slight reductions in load were observed for proximally directed distractions of 0.5mm (Figure 2),

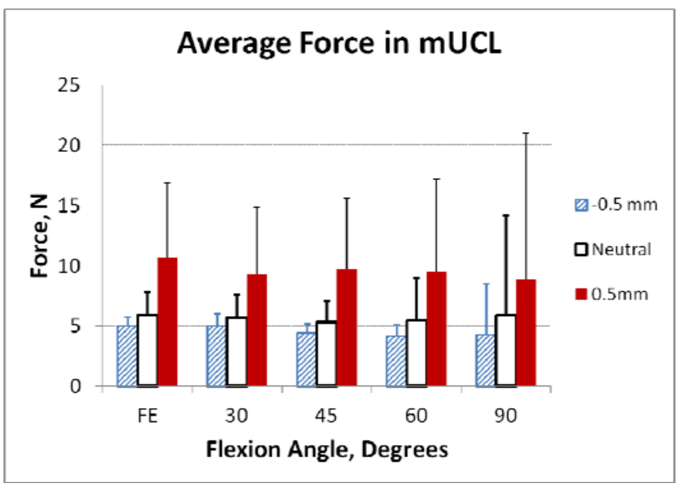

Figure 2: Average resultant force in the medial ulnar collateral ligament at both the original (neutral) position and 0.5 mm distractions in the proximal (-0.5mm) and distal (0.5mm) directions. FE represents Full Extension. (n = 11)

These results show that the medial ulnar collateral ligament carries negligible load at five points on the passive flexion-extension path of the elbow. This result, coupled with the observed changes in load for proximally and distally directed distraction of 0.5mm, suggests that the ligament is close to its slack length during the passive flexion and extension arc from full extension to 90 degrees.

The increase in load observed for distally directed distractions indicates how deviations from the passive flexion path, such as those caused by a valgus moment, could cause the medial ulnar collateral ligament to experience injurious levels of force. Small deviations would be unlikely to lead to damage even if the small deviations were repetitive.

The loading mechanism of the current work is strictly limited to distraction. Valgus loading of the elbow during overhand throwing also has the potential to cause the mUCL to contact the medial side of the condyle at the joint line, which was not considered in this study.

The average force measured in the mUCL declined slightly with flexion angle. This was observed for forces at the neutral and distracted positions. This decline, however, was small and its effect on ligament strains would probably be negligible. Investigation of the strain state in the ligament is currently underway.

CONCLUSIONS

We found that the medial ulnar collateral ligament carries essentially no load during passive flexion and extension. This result indicates that minimal tension should be placed on grafts during ulnar collateral ligament replacement surgery and that this tension should not increase during unloaded flexion/extension.

REFERENCES

Bowers, A.L., et al., J Shoulder Elbow Surg, 2010. **19**(2 Suppl): p. 110-7.

DISTURBANCES TO INTRINSIC STIFFNESS AND REFLEXIVE MUSCLE RESPONSES FOLLOWING REPEATED STATIC TRUNK FLEXION

Khoirul Muslim, B. Hendershot, N. Toosizadeh, M.A. Nussbaum, B. Bazrgari, and M.L. Madigan

Virginia Tech, Blacksburg, VA, USA
email: nussbaum@vt.edu

INTRODUCTION

Occupations involving frequent flexed trunk postures are associated with a higher incidence of low back pain (LBP) [1]. A single exposure to static trunk flexion leads to creep deformation of trunk viscoelastic tissues, reducing passive trunk stiffness [2]. Such reductions in passive trunk stiffness require neuromuscular compensation to maintain mechanical equilibrium and stability of the spine [2], and may require a longer time for recovery than the initial exposure duration [3]. Repeated static flexion may thus result in an accumulation of disturbances to trunk mechanical and neuromuscular behaviors. In this study, the effects of flexion duration and duty cycle on trunk intrinsic stiffness and reflex response were investigated.

METHODS

Healthy young adults with no self-reported history of LBP participated, after completing an informed consent procedure approved by the Virginia Tech IRB. Participants included six males with mean (SD) age = 23(2) yr, stature = 177.9 (3.7) cm, and body mass = 71.6 (8.4) kg. Respective values for six females were 25.7 (1.7) yr, 163.6 (4.5) cm, and 58.3 (2.9) kg. Trunk posture was monitored using electromagnetic sensors (Xsens, Los Angeles, CA, USA) over the T12 spinous processes, and muscle activity (EMG) was recorded using bipolar surface electrodes over the bilateral erector spinae, external obliques, and rectus abdominis muscles. Participants completed six counterbalanced experimental sessions involving exposure to all combinations of three durations (1, 2, and 4 min) of static flexion, and two flexion duty cycles (33% and 50% exposure relative to exposure + rest durations).

During the experiment, participants stood in a rigid metal frame designed to restrain the pelvis and lower limbs in a fixed, but comfortable posture. Static trunk flexion was achieved by bending forward in a controlled manner until minimal trunk extensor muscle activity was observed, indicating a relaxed flexed posture. This procedure was expected to induce creep deformation of passive posterior tissues. Participants repeated a sequence of static flexion-rest-flexion according to the assigned duration and duty cycle; this was done continuously, for 48-minute periods.

A pseudorandomly-timed sequence of 12 anterior-posterior position perturbations of ±5mm were applied to the trunk at ~T8 via a servomotor (Kollmorgen, Radford, VA), rigid rod, and chest harness (Fig. 1), prior to and immediately following exposure periods. During these perturbations, participants maintained a constant sub-maximal extensor effort of 10% MVC using real-time visual feedback of EMG. Trunk displacements were measured with both the servomotor encoder and a laser displacement sensor (Keyence, Osaka, Japan), while reaction forces were measured using an in-line load cell (Interface SM2000, Scottsdale, AZ, USA).

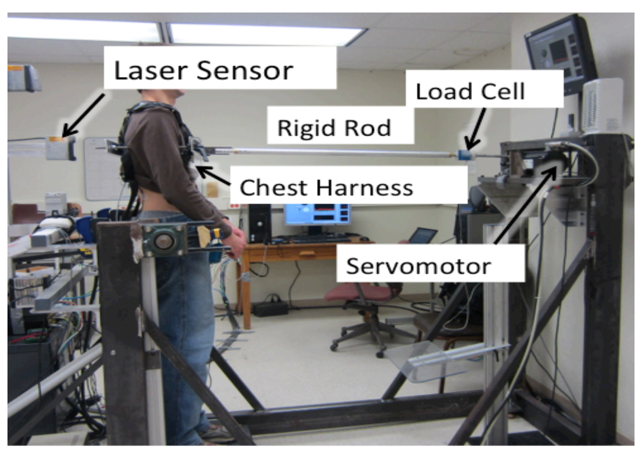

Figure 1: Experimental set-up demonstrating a participant during neuromuscular measurement.

Neuromuscular behaviors were characterized by several measures. Reflex delay was determined as the time between perturbation onset and reflexive muscle response for each anteriorly directed perturbation (via EMG) [4]. Intrinsic trunk stiffness was quantified by relating measured trunk kinematics to trunk kinetics during the reflex delay [5]. Reflex response was estimated by subtracting the intrinsic response from measured trunk kinetics and was correlated to delayed trunk velocity to estimate reflex gain [5]. The overall effects (i.e., differences between neuromuscular measures at t=0 and t=48 min) of flexion duration, duty cycle, and gender were assessed using mixed-factor analyses of variance (ANOVA). Statistical significance was determined when $p < 0.05$.

RESULTS AND DISCUSSION

Mean (SD) pre-exposure trunk stiffness was higher (p<0.0001) among males than females, at 8300 (1262) and 6252 (922) N/m, respectively. Intrinsic trunk stiffness decreased significantly with increasing flexion duration (p=0.01) and in the higher duty cycle (p=0.04). Muscle reflex delays were comparable (p=0.19) between males [62(5) ms] and females [65(3) ms], and were unaffected by trunk flexion duration (p=0.37) or duty cycle (p=0.27). These results indicate that a longer duration of static flexion and insufficient rest periods between these increase the severity of changes to intrinsic stiffness. Since background muscle activity during perturbations was maintained at the same level, the decrement in intrinsic stiffness was most likely caused by alterations in passive mechanical trunk properties, indicating accumulated creep deformation following repeated static flexion [6].

Pre-exposure reflex gain did not differ (p=0.73) between genders. Though not significant (p=0.09), reflex gains decreased with increasing duty cycle. Another measure of reflex response (i.e., maximum reflex force) decreased (p=0.03) with increasing duty cycle, but was similar across flexion durations. There was a gender effect (p=0.005) on reflex gain, with females having substantially larger decreases after exposure. These decreased reflex responses are consistent with evidence from feline models, in which a decreased reflex response was found following prolonged cyclic lumbar flexion-extension [6]. Repetitive or cyclic tasks are presumably responsible for developing laxity in the viscoelastic tissues that may diminish the intensity of muscular activation.

CONCLUSIONS

Increased reflexive responses have been suggested as compensatory adaptations to decreases in passive trunk stiffness following prolonged static flexion [2,5]. The present results (Fig. 2), however, suggest that repeated static flexion decreases both passive trunk stiffness and reflexive responses. Specifically, longer flexion durations or shorter rest periods between flexion induce more severe changes. Hence, simultaneous decreases in both passive trunk stiffness and reflexive responses may increase the risk for spinal instability and low-back injury following repeated static flexion tasks.

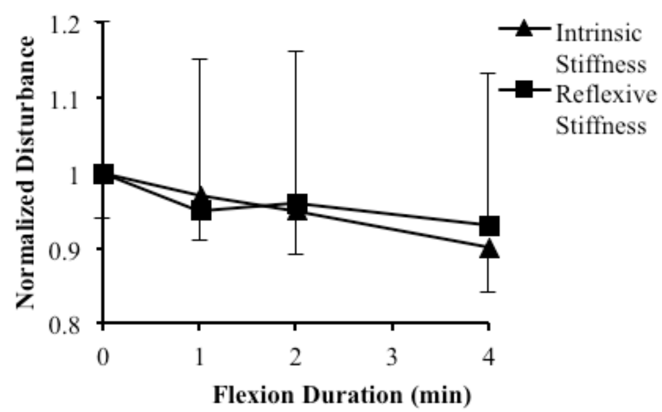

Figure 2: Effects of flexion duration on trunk intrinsic stiffness and reflexive gain following repeated static flexion. Values are normalized to pre-exposure measures

REFERENCES

1. BLS. *Nonfatal Occupational Injuries And Illnesses Requiring Days Away From Work*, 2009
2. Bazrgari B, *et al. Ergonomics* **54**: 1043-1052, 2011
3. Ekström L, *et al. J Eng in Med*, **210**: 249-258, 1996
4. Granata KP, *et al. J Biomech* **37**: 241-247, 2004
5. Hendershot B, *et al. Clin Biomech* **26**: 250-256, 2011
6. Solomonow M. *J Electromyogr Kinesiol* **22**: 155–175, 2012

ACKNOWLEDGEMENTS

This work was supported by Award Number R01 OH004089 from the CDC. Its contents are solely the responsibility of the authors and do not necessarily represent the official views of the CDC.

CALCULATING THUMB AND INDEX FINGER POSTURES DURING PINCH WITH A MINIMAL MARKER SET

[1]Raviraj Nataraj, [1,2,3]Zong-Ming Li

Department of [1]Biomedical Engineering, [2]Orthopaedic Surgery, and [3]Physical Medicine and Rehabilitation, Cleveland Clinic, Cleveland, OH, USA
email: liz4@ccf.org, web: http://www.facebook.com/handlab

INTRODUCTION

Motion capture methods employing infrared cameras to track three-dimensional (3-D) movements of retroreflective markers placed on the hand and digits have been regularly employed [1]. However, marker-based sources of error include inaccurate marker placement, marker occlusion from camera view, and passive skin movement. To mitigate these errors, this study presents methods for anatomical coordinate system alignment and subsequent calculation of 3-D changes in finger posture using a minimal number of markers. A protocol employing nail marker clusters and a digit alignment device (DAD) has been previously established for tracking orientation of the distal thumb and index finger segments [2]. In this study, the aforementioned protocol is extended to calculate the orientation of the middle and proximal segments of both digits. Techniques for coordinate system transformations, inverse kinematics, and constrained optimization were applied.

METHODS

Three participating subjects signed informed consent forms approved by the local institutional review board. All were able-bodied and neither showed nor reported orthopedic problems or functional deficits. All 3-D marker position data were tracked using a VICON® motion capture system sampling at 100Hz. A static trial using the DAD was performed to determine transformations to identify anatomically-aligned coordinate systems during a dynamic trial with ten repetitions of precision pinch. This eliminated the requirement of the experimenter to accurately align marker clusters upon placement. Given anatomical constraints of the thumb and fingers [3], it was hypothesized that only one additional marker cluster (placed dorsally on hand, along third metacarpal) was needed as a global reference frame for the digits.

Transformations between dorsal-surface segment endpoints and adjacent marker clusters were established from another static trial to track these endpoints dynamically (Figure 1). The *index finger cluster* determined the index finger tip and DIP (distal interphalangeal) positions, and the *thumb cluster* determined the thumb tip and IP (interphalangeal) positions. The *hand cluster* determined the thumb CMC (carpometacarpal) and index finger MCP (metacarpophalangeal) positions. The index finger PIP (proximal interphalangeal) and thumb MCP positions were measured statically relative to other endpoints only to calculate lengths (L_1, L_2) of adjacent digit segments.

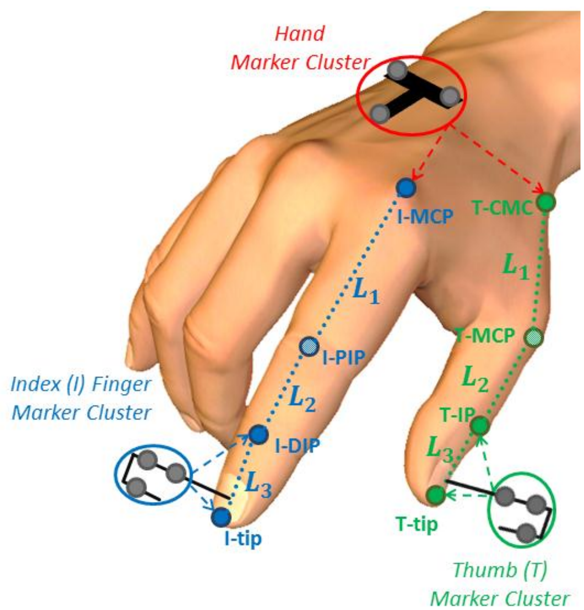

Figure 1: Minimal marker set and location of dorsal-surface segment endpoints to be tracked dynamically or used to calculate digit segment lengths.

Kinematic models were developed to solve the posture for each digit from all available marker-based data. All segments were assumed to be rigid bodies and all connecting joints to be purely rotational. Additional constraints were based on the number of degrees of freedom (DOFs) at each joint. Deterministic inverse kinematics solutions were analytically derived for sufficiently constrained model cases. Solutions for the remaining underdetermined cases were derived by constrained optimization. The cost function minimized MCP and IP axial rotations [3].

To assess the solution results, additional marker clusters were placed on the proximal and middle segments of both digits for comparison. Aligned coordinate systems were determined for these comparison clusters using the DAD. Euler rotations of flexion-extension, abduction-adduction, and internal-external rotation were then computed between adjacent segments for both the solution and comparison data.

RESULTS AND DISCUSSION

Figure 2 shows sample rotation results at the index MCP location for both model-based solution and comparison data. The flexion-extension and abduction-adduction DOFs underwent larger excursions (>10°) and had correspondingly larger mean differentials of 12.7°, 7.5°, respectively, between the comparison and solution data. Solution and comparison results were highly correlated ($R^2 > 0.98$) for both DOFs. Internal-external rotation underwent notably smaller excursions, which suggests this DOF was comparatively negligible. Correspondingly, this DOF had a relatively lower differential (1.9°) and lower correlation ($R^2 = 0.29$).

The average solution-comparison differential for all rotational DOFs across the index finger and thumb were 6.0±7.7° and 15.3±13.7°, respectively. The larger differential at the thumb was attributed to more complex joint function. The thumb CMC joint may have non-perpendicular axes of rotation [4], which was not considered for the inter-segment kinematics in this study. Furthermore, conventional anatomical notions suggest the thumb be modeled by up to 6 DOFs [3]. Thumb postures were best estimated by solution model cases of only 3 DOFs since only precision pinch was investigated. For pinching, changes in thumb posture were notably less compared to the index finger.

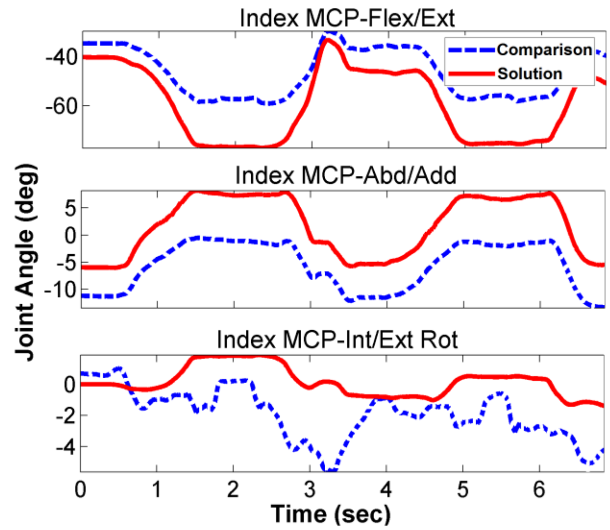

Figure 2: Sample Euler rotation angle results from model-based solution and comparison data at index MCP location over two precision pinches. Extension, abduction, and external rotation are denoted as positive values.

The methods presented in this study provide robust means to solve segment orientations of hand digits. Requirements to accurately place additional markers are reduced. This improves reliability of rotation angle computations by mitigating sources of error directly due to skin-surface placement of markers. In the future, we seek to validate our models with additional subjects. Furthermore, similar kinematic models could be developed and verified for hand function tasks beyond precision pinch and involving additional finger digits (e.g., whole hand grasp).

REFERENCES

1. Cerveri P, et al. *Ann Biomed Eng* **27**, 173-180, 2007.
2. Mondello T, et al. *ASB*, Long Beach, CA, 2011
3. Gonzalez MH, et al. *J Am Soc Surg Hand*, **5**, 48-60, 2005.
4. A. Hollister, et al. *J Orthop Res*, **10**, 454-60, 1992.

ACKNOWLEDGEMENTS

NIH R01 AR056964

DISTINCT FEATURES OF GRIP FORCE CHARACTERIZE PARKINSON'S DISEASE AND ATYPICAL PARKISONIAN DISORDERS

KA Neely, PhD[1], PJ Planetta, PhD[1], J Prodoehl, PhD[2], DM Corcos, PhD[2, 3, 4, 5], CL Comella, MD[6], CG Goetz, MD[6], KL Shannon, MD[6], DE Vaillancourt, PhD[1,7,8]

[1]Department of Applied Physiology and Kinesiology, University of Florida, Gainesville, FL, USA
[2]Department of Kinesiology, University of Illinois at Chicago, Chicago, IL, USA
[3]Department of Bioengineering, University of Illinois at Chicago, Chicago, IL, USA
[4]Department of Physical Therapy, University of Illinois at Chicago, Chicago, IL, USA
[5]Department of Neurological Sciences, University of Illinois at Chicago, Chicago, IL, USA
[6]Department of Neurological Sciences, Rush University Medical Center, Chicago, IL, USA
[7]Department of Neurology, University of Florida, Gainesville, FL, USA
[8]Department of Biomedical Engineering, University of Florida, Gainesville, FL, USA

Email: kaneely@ufl.edu, web: lrnlab.org

INTRODUCTION

The goal of this study was to determine how measures of precision grip force differ among healthy individuals and patients with Parkinson's disease (PD), the parkinsonian variant of multiple system atrophy (MSAp), and progressive supranuclear palsy (PSP). Patients with PD are characterized by a slower rate of force increase[1-4], a slower rate of force decrease[3, 5, 6], and the production of abnormally large grip forces when lifting[2] and holding[1] an object. Further, patients with early stage PD have difficulty with the rapid contraction and relaxation of hand muscles required for precision gripping [7].

METHODS

We studied 52 participants: 14 PD, 15 MSAp, 8 PSP, and 15 healthy individuals. All patients were diagnosed by a movement disorders trained neurologist and were tested off anti-parkinsonian medication. The severity of parkinsonism was measured by the UPDRS part III and ranged from 12 to 65 with a mean (SD) of 33.16 (11.69).

Participants completed two force tasks ("same" and "different") wherein force pulses were produced for 2 s, followed by 1 s of rest. Ten pulses plus rest were completed to achieve 30 s of force. Force intervals were interleaved with 30 s of rest. A visual display provided online feedback and cued the onset/offset of force. In the "same" task, target amplitude was always 15% of the participant's maximum voluntary contraction (MVC). In the "different" task, target amplitude varied unpredictably.

Eight dependent measures were calculated: MVC, the mean force produced between the beginning and end of force production, the standard deviation of mean force, the duration of the force interval, the mean rate of change during the ramp up to the target, and the mean rate of change during the decrease to baseline (i.e., rest), and the number of pulses produced per force interval.

RESULTS AND DISCUSSION

MSAp and PSP were weaker than PD and healthy individuals. In addition, MSAp and PSP were more variable than PD and healthy individuals.

As shown in Figures 1A and 1B, patients with PD, MSAp, and PSP were characterized by slower rates of change (contracting and relaxing) relative to healthy individuals. Figure 1C shows that patients with PD, MSAp, and PSP produced longer pulse durations than healthy individuals. Last, Figure 1D shows that PSP patients had a specific difficulty stopping the rhythmic production of pulses: PSP produced more force pulses, within and beyond the force interval, than all other groups.

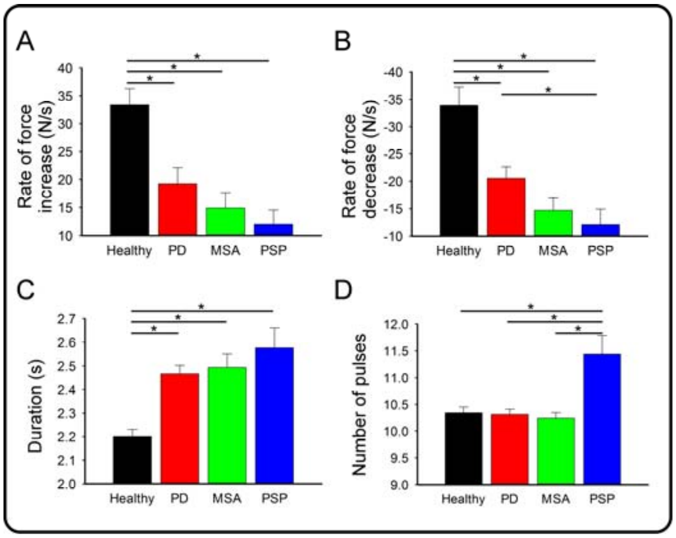

Figure 1: Mean rate of force increase (N/s) for each group. B: Mean rate of force decrease (N/s) for each group. C: Mean duration of force pulse (s) for each group. D: Mean number of pulses for each group. Asterisks (*) identify a significant mean difference at an alpha level of .05.

Table 1 reports the significant findings from the ROC analysis. In particular, the analysis revealed that pulse duration differentiated Parkinsonism from health with a high degree of sensitivity and specificity. The number of pulses produced distinguished PSP from PD and MSAp with a high degree of sensitivity specificity.

CONCLUSIONS

Although patients with Parkinsonism were slow to increase decrease force, weakness and greater variability of force control were specific features of atypical forms of Parkinsonism (PSP and MSAp). Patients with PSP had difficulty stopping the production of grip force, a finding that distinguished them from MSAp. This feature may represent a motor control deficit specific to PSP.

REFERENCES

1. Fellows, S.J. and Noth, J. *Movement disorders: official journal of the Movement Disorder Society*, 2004.
2. Fellows, S.J., et al. *Brain: a journal of neurology*, 1998.
3. Jordan, N., et al. *Journal of neurology, neurosurgery, and psychiatry*, 1992.
4. Stelmach, G.E. and Worringham, C.J. *Neuropsychologia*, 1988.
5. Corcos, D.M., et al. *Annals of Neurology*, 1996.
6. Robichaud, J.A., et al. *Movement Disorders*, 2005.
7. Spraker, M.B., et al. *Human brain mapping*, 2010.

ACKNOWLEDGEMENTS

Supported by NIH R01 NS52318 and R01 NS48587.

Table 1: Receiver Operating Characteristic Curves

Classification State	Variable	AUC	Cutoff	Specificity	Sensitivity
Health v. Disease	Duration of pulse	0.9532	2.295	89.19%	86.67%
PD v. PSP	Number of pulses	0.9509	10.56	87.50%	85.71%
MSAp v. PSP	Number of pulses	0.9542	10.56	87.50%	86.67%

INFLUENCE OF LECTURE SLIDE COMPLETENESS ON STUDENT LEARNING IN A BIOMECHANICS COURSE WITHIN A PHYSICAL THERAPY CURRICULUM

Erika Nelson-Wong, Heidi Eigsti, Amy Hammerich and Nicole Marcisz

Regis University, Denver, CO, USA
email: enelsonw@regis.edu

INTRODUCTION

There are consistent discrepancies between student and faculty attitudes and beliefs regarding the completeness of lecture presentation material provided to students [1,2]. Anecdotal evidence gathered through informal surveys of students enrolled in the Doctor of Physical Therapy (DPT) school at Regis University suggest that students have a preference for access to complete lecture slides/notes prior to and during lectures. A common rationale for this preference is that note-taking during lecture interferes with the ability to listen, and students are afraid of missing critical information. Faculty commonly express the opinion that providing incomplete lecture slides/notes facilitates student engagement through note-taking and encourages class participation, a belief that has been supported in the literature [3]. The purpose of this study was to investigate the influence of differences in lecture slide completeness on student recall and retention in a foundation level biomechanics course taught to DPT students. The hypothesis was that less complete lecture slide formats would result in better recall and retention performance than complete lecture slide formats.

METHODS

A cohort of 66 entry-level DPT students beginning the first term in the School of Physical Therapy at Regis University was included in this study. This was a repeated measures design, where three different levels of lecture slide completeness were used on different days. Slide formats included: Complete (100% of content included on slides), Fill-in-the-blank (75% of content included, with selected words missing requiring students to fill them in) and Incomplete (50% of content included in a bulleted/outline format). All lecture slides were posted on a web-based learning management system 24 hours prior to the lecture, in accordance with school policies. Immediate recall was assessed through a quiz given at the end of the lecture, and retention was assessed with re-administration of the same quiz 1 week later. Quiz format was multiple choice and included 7 questions. Quiz scores (percent correct) were entered into a 3 x 2 within factor ANOVA, with 3 levels of slide format and repeated measure of quiz timing. Students who were absent from class and missed a quiz had their data excluded from the analysis. Significance criterion was set *a priori* at .05, and pairwise comparisons (paired t-tests with Bonferroni adjusted alpha) were used for *post hoc* analysis where necessary.

RESULTS

Of the 66 students, 8 were excluded due to class absences, leaving a sample of 58 students. The student cohort was 45% male, and 70% were in the 20-25 year age bracket. For immediate recall, quiz scores were 75.0 (20.1)% for Complete, 88.2 (13.6)% for Fill-in-the-blank, and 87.6 (15.5)% for Incomplete. For 1-week retention, quiz scores were 74.4 (22.1)% for Complete, 85.9 (15.2)% for Fill-in-the-blank, and 86.5 (14.1)% for Incomplete. There was a significant main effect of slide format ($F_{2,57}$=18.2, p<.001). *Post hoc* pairwise comparisons revealed significant differences between Complete and Fill-in-the-blank (t=4.3, p<.001), Complete and Incomplete (t=4.8, p<.001), and no significant differences between Fill-in-the-blank and Incomplete (t=0.23, p=.82) formats. There were no significant differences seen between recall and retention performance and no interactions between quiz timing and slide format. Recall and retention quiz performance for each slide format are shown in Figure 1.

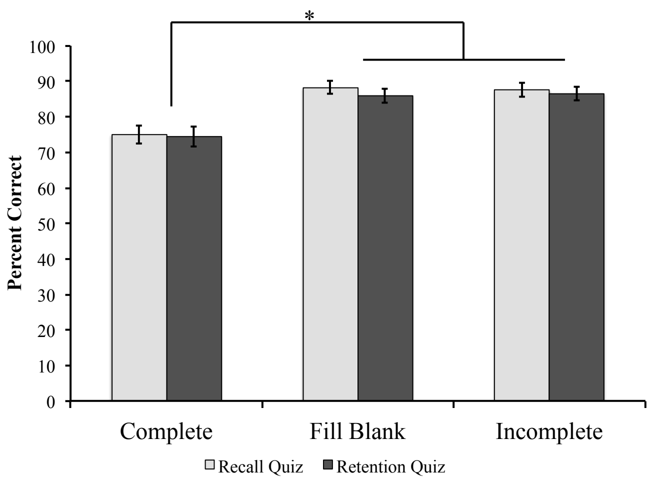

Figure 1: Students had higher recall and retention quiz performance with both Fill-in-the-blank and Incomplete compared to Complete slide formats. (*p< .001)

DISCUSSION

The hypothesis that student performance in a Biomechanics course would be better with less complete lecture slide formats was supported. This is consistent with findings from other studies that have shown student learning is enhanced when note-taking is required [4]. Using fill-in-the-blank or outline slide formats is a commonly used method for encouraging note-taking [3,4]. These findings are consistent with Larsen, who found that the highest student recall occurred with incomplete and the lowest with complete slide formats in a cohort of undergraduate business school students being taught negotiation skills [3].

This study was a part of a larger research project that is investigating student performance in other content areas (Physiology and Research Methods/Statistics) in the same student cohort, as well as interactions between students' stated preferences for slide format and actual performance. Preliminary findings including different content areas have shown that the influence of slide completeness on learning, as assessed by recall and retention quizzes, is not consistent across courses.

This leads to the question of whether a standard approach can be adopted as a 'best practice' for enhancement of student learning, or if it should be viewed as course or instructor-specific. While the findings from this study are consistent with the published literature, it may be that the content area in biomechanics (taught at the DPT curriculum level) involved concrete problem solving similar to other research, and concepts in the other two courses were more abstract.

Additionally, potential interactions with individual instructor lecture delivery style and slide format on student performance cannot be ruled out. For future studies the influence of instructor style could be mitigated in two ways: different instructors should assess slide formats within the same course, and a single instructor should assess slide formats across different courses.

CONCLUSION

In conclusion, less complete slides enhanced both recall and retention performance in a biomechanics course taught to physical therapy students. There were inconsistencies between courses in the optimal level of slide completeness, further exploration of interactions between instructor and course content is warranted. Individual instructors may wish to assess the influence of slide completeness within their own courses to determine which format promotes the best student learning outcomes in their academic setting.

REFERENCES

1. McClennon M & Isaacs G. *Austr Vet J,* **80**, 626-629, 2008.
2. Marsh EJ & Sink HE. *Appl Cognit Psychol,* **24**, 691-706, 2010.
3. Larsen RB. *Computers & Education,* **53**, 1278-1284, 2009.
4. Stefanou C et al. *Learning Environ Res,* **11**, 1-17, 2008

ACKNOWLEDGEMENTS

The authors would like to thank the Regis University PT Class of 2014 for engaging in this study and enduring an exceptionally high number of pop quizzes during their Fall 2011 term.

COMPARISON OF TIBIAL TORSION MEASUREMENTS USING MOTION CAPTURE, PHYSICAL THERAPY EVALUATION, AND COMPUTED TOMOGRAPHY

Cassie Nguyen[1], Nicole M. Mueske[2], Tishya A. L. Wren[1,2]

[1]University of Southern California, Los Angeles, CA, USA
[2]Children's Hospital Los Angeles, CA, USA
email: cassieng@usc.edu

INTRODUCTION

Abnormal tibial torsion is a common problem that may significantly impact muscle lever arms and force production in children with conditions such as cerebral palsy and spina bifida. While there are many existing methods to measure tibial torsion, computed tomography (CT) has become the accepted standard; however, it is costly and requires a CT scan [1]. More practical methods using various clinical techniques have also been used, but accuracy of these clinical measures has been questioned. The purpose of this study was to compare three methods of measuring tibial torsion: an imaging method using CT (gold standard), a clinical method, and a computational method using motion capture technology.

METHODS

10 healthy children (5 males, 5 females, age 11.6 ± 3.3 yrs) underwent three different measures of tibial torsion bilaterally, using CT, physical therapy evaluation (PT), and motion capture. To measure tibial torsion from axial CT images, the angle was measured between a posterior femoral axis at the proximal end of the tibia and a bimalleolar axis at the distal tibia. The posterior femoral axis was drawn tangent to the posterior condyles, just above the knee. The bimalleolar axis was drawn bisecting the medial and lateral malleoli, just above the ankle (Figure 1).

For the motion capture measurements, markers were placed on 4 anatomical landmarks: the medial and lateral knee corresponding to the knee flexion axis, and the medial and lateral malleoli at points corresponding to the transmalleolar axis. Marker positions were recorded during standing using a 3-D motion capture system (Vicon Motion Systems, Oxford, UK), and Vicon Workstation software was used to calculate the angular offset between the two axes defined by the knee and ankle markers.

Measurements were compared using correlation coefficients and Bland-Altman plots of the difference between measurements [2].

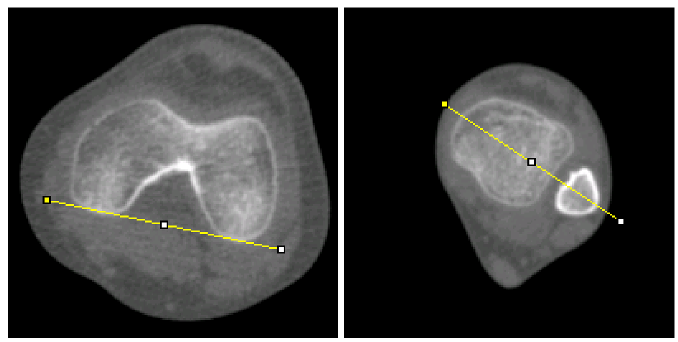

Figure 1. CT images of the posterior femoral axis (left) and bimalleolar axis (right) used to measure tibial torsion.

RESULTS AND DISCUSSION

The coefficient of variation (CV) was used to evaluate the repeatability of the CT measures. Average CV was 6.4±1.6%. To reduce variability, 2 individuals made 3 measurements each and the results were averaged for the subsequent analyses.

All three measurements were moderately correlated (Table 1). The Vicon measurements had a higher correlation with CT than the PT measurements.

	PT	Vicon	CT
PT	1	0.44	0.47
Vicon		1	0.57
CT			1

Table 1. Correlation coefficients comparing the 3 methods of measurement.

To evaluate agreement between measurements, the difference was plotted against the mean. Threshold lines indicate the mean difference and two standard deviations above and below the mean. By plotting the difference against the mean, offsets between measurements become evident. The PT and Vicon measurements had little offset between them (mean difference 2.0º) whereas they both had an offset of approximately 20º with the CT measurements (mean difference 22.4º for PT and 20.4º for Vicon) (Figure 2).

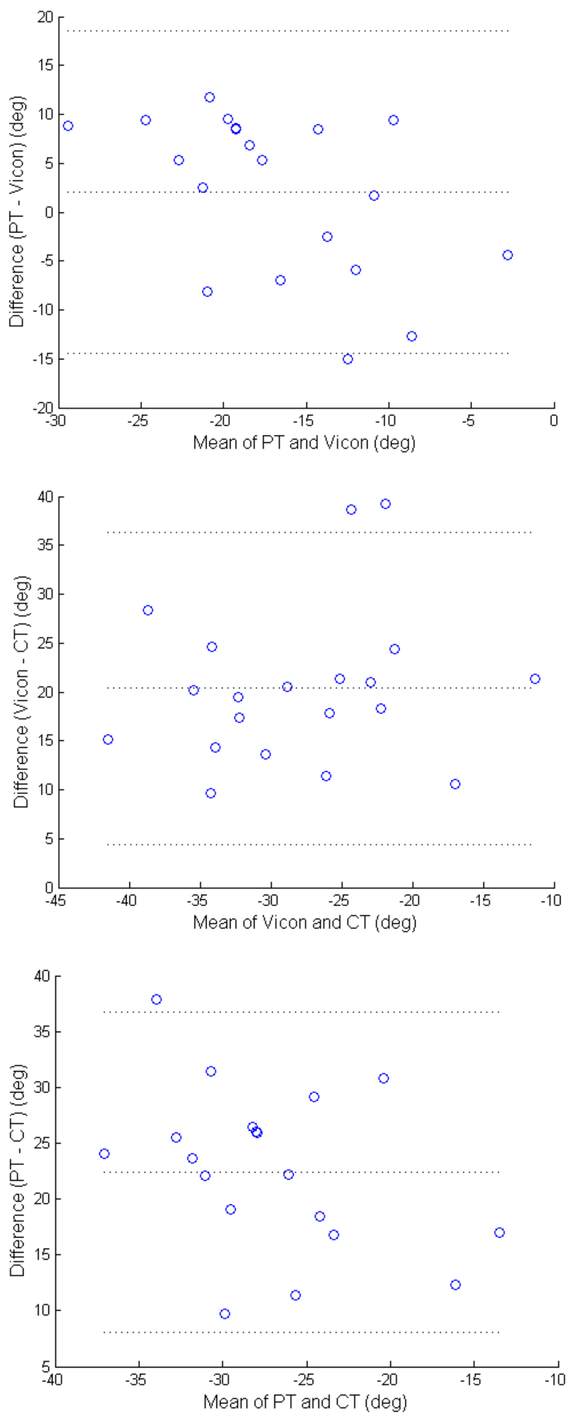

Figure 2. Bland-Altman plots comparing PT, Vicon, and CT measurements of tibial torsion.

CONCLUSIONS

The three methods of measuring tibial torsion were moderately correlated; however, there was a 20° offset between the clinical and CT measurements. This discrepancy is consistent with past research [3]. Both the PT and Vicon measures used the same landmark identification and were intended to locate the same axes identified on the CT images. However, the 20° offset suggests that clinical evaluation identifies different axes than those defined based on anatomy. When using clinical methods to measure tibial torsion, this 20° offset may need to be considered in the final outcome.

Compared with CT measures, Vicon had a slightly higher correlation and lower offset than PT measures, suggesting that Vicon may be a better method than PT. The Vicon system calculates the angle between the knee and ankle axes, while the PT method requires the extra step of visually assessing this angle. Also, both the CT and Vicon measures were done with the knee extended, while the PT measurement was done with the knee flexed. The differences between PT and Vicon in this study were small, and repeatability of the measures was not investigated. More research is needed to determine if one of the clinical methods should be recommended over the other.

REFERENCES

1. Tamari K, et al. *Clinical Anatomy* **18**, 46-55, 2005.
2. Bland JM, et al. *Lancet*. **i**, 307-310, 1986.
3. Milner CE, et al. *J Anat.* **193**, 139-144, 1998.

ACKNOWLEDGEMENTS

Support provided by NIH-NICHD Grant# 5R01HD059826

MODELING INTRA-TRIAL VARIABILITY OF A REDUDANT PLANAR REACHING TASK

[1]Hung P. Nguyen, [2]Joseph P. Cusumano and [1]Jonathan B. Dingwell

[1]University of Texas, Austin, TX, USA
[2]Pennsylvania State University, State College, PA, USA
email: hpnguyen@utexas.edu

INTRODUCTION

Humans can perform highly redundant tasks with high accuracy and repeatability because of the large number of articulating joints and the even larger number of muscles that coordinate the movement of these joints. The nervous system possesses a robust control mechanism that regulates its performance from one movement to the next. This control framework not only resolves redundancy but also creates a system that is highly adaptable to noise. However, the control mechanisms that regulate these processes are still largely unknown. There is currently no unified control framework that adequately addresses the issues of optimality of redundancy and stochastic noise during motor performance. These issues have been examined experimentally using geometry-based uncontrolled manifold approach [1] and related data analysis methods [2]. However, these methods generally use the structure of the between-trial variation to predict motor control while ignoring the between-trial dynamics. Here we will apply a more rigorous analytical approach to understand these control mechanisms [3-4].

METHODS

If the goal is to reach at a constant average speed, S, then the strategy is mathematically defined by a relationship between movement distance, *D*, and movement time, *T*. For each trial, there is an infinite combination of $[D, T]$ that yields the exact same speed. Any solution that satisfies the goal (i.e., constant S) lies on the solution manifold of distance and time (Fig. 1A). This is defined as a Goal Equivalent Manifold (GEM) [5]. Experimentally, subjects performed a planar reaching task while exploring the redundancy in distance and time from trial-to-trial for two different GEMs (Fig. 1).

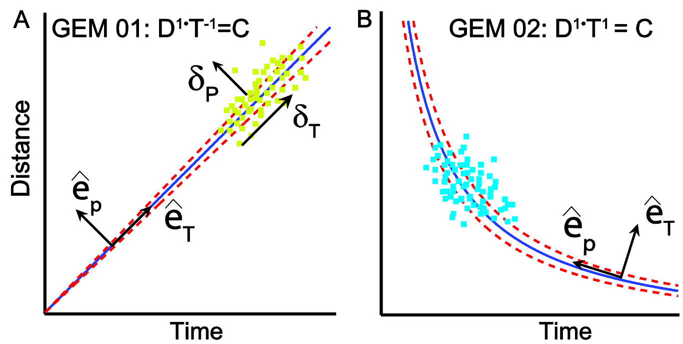

Figure 1: Two different GEMs generated by manipulating the coefficient of $[m, n]$ that define the relationship between distance and time. .

The between-trial controller can be expressed by a general form [3]

$$\mathbf{x}_{k+1} = \mathbf{x}_k + \mathbf{G}[\mathbf{I} + \mathbf{N}]\mathbf{u}(\mathbf{x}_k) + \boldsymbol{\eta} \qquad (1)$$

Where $\mathbf{x} = [D_k, T_k]$ is the current distance and time and $\mathbf{x}_{k+1}$ is the distance and time of the next reaching movement. $\mathbf{u}(\mathbf{x}_k)$ is the control effort and $\mathbf{G}(2x2)$ is a diagonal gain matrix. $\mathbf{N}(2x2)$ is the diagonal multiplicative (sensory/perceptual) noise matrix and $\boldsymbol{\eta}(2x1)$ denotes the *additive noise* (motor output noise). These noise terms represent the stochasticities that are inherent in human motor system.

The "next trial" is calculated by solving (1). The control input $\mathbf{u}(\mathbf{x}_k)$ is calculated by solving an optimization problem with the following cost function.

$$Min\left\{ C = \alpha e^2 + \beta p^2 + \gamma u_1^2 + \delta u_2^2 \right. \qquad (2)$$

Each of these terms represents a critical feature of stochastic optimal control. The first term, αe^2, is the error penalty which measures the absolute deviation from the goal of the task and is dependent on the definition of the GEM. The second term, βp^2, represents the deviation away from preferred operating point, $[D^*, T^*]$, along the GEM and $[\gamma u_1^2,\ \delta u_2^2]$ represent the control inputs.

To quantify the between-trial dynamics, we used discrete stability analysis:

$$\mathbf{x}_{n+1} = \lambda \cdot \mathbf{x}_n + \xi_n, \tag{3}$$

where $\mathbf{x}$ was modeled as a one-dimensional mapping from $\mathbf{x}_n$ to $\mathbf{x}_{n+1}$ with ξ_n denoting the stochastic process in the system. Values of $0 < |\lambda| < 1$ correspond to stable movements, with smaller values of λ indicating more rapid corrections of between-trial deviations. The between-trial variability was calculated for direction that is tangential, δ_T, and perpendicular, δ_P, to the task goal.

Three different control architectures were examined by manipulating the cost function to test their robustness in replicating experimental results. When $\beta = 0$, this represents a pure Minimum Intervention Principle (MIP) controller. When $\beta \neq 0$, a preferred operating point (POP) was added to penalize deviation from this point. Lastly, a sub-optimal controller (SOP) where $\mathbf{G} \neq \mathbf{I}$ (eqn 1).

We simulated data for 400 consecutive trials of steady state behavior (i.e. after transient responses had died down). The model was used to predict experimental data obtained for three subjects performing two different GEMs (Fig. 1).

RESULTS AND DISCUSSION

All three controllers performed adequately to generate the average reaching distance and reaching time of each subject (Fig. 2A-B). However, the optimal controllers (MIP & POP) failed to capture the dynamic stability from trial-to-trial of each subject in the tangential, δ_T (Fig. 2C), and perpendicular direction, δ_P (Fig. 2D). The MIP model rapidly corrected deviations along the task-relevant direction, ($\lambda_{\delta_P} \approx 0$), and slowly corrected deviations along the task-irrelevant direction ($\lambda_{\delta_T} \approx 1$). The POP controller performed significantly better than MIP by more rapidly correcting for δ_T deviations; however, it still failed to capture the intra-trial dynamic in the δ_P (Fig. 2D) as exhibited by humans.

Conversely, the sub-optimal model (SOP) captured the between-trial dynamics exhibited by humans. The SOP controller allowed the system to under correct or over correct for deviations along δ_P and δ_T. These results from our model show that a rigorous analytical approach to understanding human behavior is essential in enhancing our abilities to *generalize* and *predict* the underlying dynamics rather than relying solely on descriptive experimental approach.

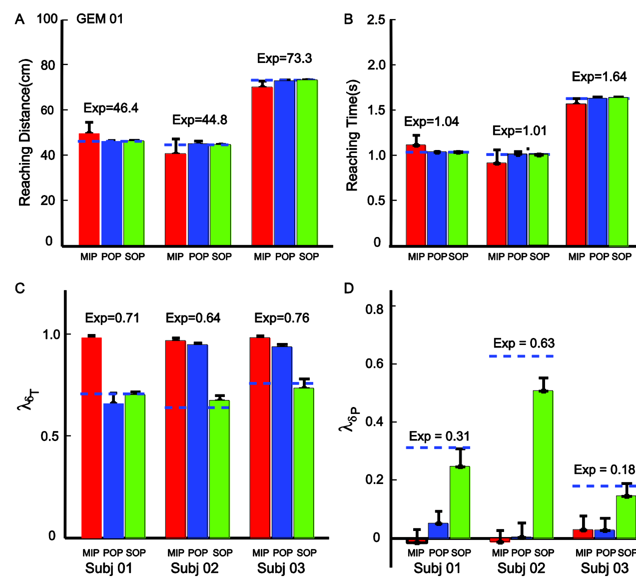

Figure 2: Experimental and simulation data for three different control architectures for three subjects for GEM 01 (Fig. 1). Qualitatively similar results were obtained for GEM 02.

REFERENCES

1. Scholz JP, et al. *Exp Brain Res,* **126,** 289-306, 1999.
2. Cohen RG, et al. *Exp Brain Res* **1,** 45-48, 2003.
3. John J, et al. *ASME Int Design Eng, Las Vegas,* NV, USA 2007
4. Dingwell JB, et al. *PLOS Comp Bio* **6,** e1000856, 2010.
5. Cusumano JP, et al. *Biol Cybern* **94,** 367-379, 2006.

THE GAIT VARIABILITY PROFILE OF PATIENTS WITH PARKINSON'S DISEASE WHEN COMPARED TO OLDER ADULTS WITH MOBILITY DISABILITY AND A HISTORY OF FALLS.

[1,2] Joe R. Nocera, [2]Michael Okun, [2]Jared Skinner, [2]Chris J. Hass

[1]Department of Veterans Affairs, Gainesville, FL, USA
[2]University of Florida, Gainesville, FL, USA
University of Florida Email: jnocera@ufl.edu

INTRODUCTION

Fluctuations in gait characteristics from one step to the next, or gait variability, have gained recent attention in the older adult (OA) literature. For example, research has demonstrated that an increase of 1% of stance time variability is associated with a 13% higher incidence of mobility disability (1). Further, research has demonstrated that greater variability in step length is associated with an increased risk of falls in OA (2). Despite the growing knowledge concerning the gait profile in OA, limited information has been presented on the gait variability characteristics of patients with Parkinson's disease (PD), particularly in a large sample. Therefore, the purpose of this abstract is to present gait variability profile of patients with PD and to compare this variability profile to previously published profiles of non-PD OA with mobility disability and a history of multiple falls.

METHODS

Data were collected on 368 ambulatory patients with a diagnosis of idiopathic PD by a Movement Disorders neurologist. These data were collected in the medicated state as part of their routine clinical exam at the Center for Movement Disorders and Neurorestoration.

Gait performance was measured with GaitRite instrumentation (CIR Systems Inc., Havertown, PA) consisting of an electronic walkway 5.8 m in length and 0.9 m in width. Subjects completed four, self-selected pace walks across the GaitRite walkway, initiating and terminating their walks 1 m fore and aft of the walkway to minimize acceleration/deceleration effects. Data from all four walks were combined and considered as a single test. The coefficient of variation (COV), (SD/mean), was used to qualify the variably of step length and stance time. On the same day as the gait evaluation, a movement disorders neurologist performed the modified Hoehn and Yahr (H&Y).

RESULTS AND DISCUSSION

The data indicates that those with highest PD severity (H&Y ≥ 3) were statically more variable in both step length and step width ($p<.05$) when compared to those less severe (H &Y ≤ 2) (Table 1). Further, the PD patients with the highest mobility function, as measured by a gait speed of $\geq$ 1m/s, demonstrated less variability in both step length and stance time ($p<.05$) (Table 1). Interesting, when comparing the PD group to previously published data on OA with mobility disability as well as history of multiple falls (1,2) the PD group demonstrated slower gait speed and more variability (Table 2).

Because stance time and step length variability are independent predictors of mobility disability and falls in OA understanding these characteristics in PD is critical. Our results suggest that the gait variability profile of PD patients, even early on in the disease process, places them at increased risk for disability and falls.

CONCLUSIONS

Understanding the predictors of falls and disability in persons with PD is vital for understanding disease outcomes and evaluating the effectiveness of targeted interventions. Our results suggest that those with PD have increased variability in key areas of gait that have been demonstrated to increase risks in older adults. Future research is needed to identify how these variables may predict disability and/or fall risk specific to PD.

REFERENCES

1. Brach JS, Studenski SA, Perera S, VanSwearing JM, Newman AB. Gait Variability and the Risk of Incident Mobility Disability in Community-Dwelling Older Adults. *J Gerontol A Bio Sci Med Sci*, 2007;62: 983-988.

2. Michele L. Callisaya ML, Blizzard L, Schmidt MD, Martin KL, McGinley JL, Sanders LM, Srikanth V Gait, gait variability and the risk of multiple incident falls in older people: a population-based study. *Age and Ageing* 2011; 40: 481-487.

Table 1. Demographics and gait profile of patients with PD divided by disease severity and gait speed (SD).

Characteristics	Complete Sample	H&Y ≤ 2	H&Y ≥ 3	Gait Speed <1.0m/s	Gait Speed ≥1m/s
n	368	183	51	174	194
Mean age	68.68 (10.41)	66.63 (10.01)	75.25 (9.09)	71.80 (10.08)	65.54 (10.97)
H&Y	2.19 (0.60)	1.92 (0.28)	3.16 (0.41)	2.43 (0.69)	2.02 (0.46)
Disease Duration, yrs	8.82 (5.17)	9.11 (5.42)	9.48 (5.02)	8.39 (4.80)	9.22 (5.47)
Gait Speed, m/s	0.98 (0.26)	1.06 (0.21)	0.80 (0.28)	0.76 (0.17)	1.18 (0.14)
COV- Step Length	0.06 (0.06)	0.05 (0.02)	0.09 (0.11)	0.08 (0.05)	0.05 (0.06)
COV- Stance Time	0.05 (0.03)	0.04 (0.01)	0.06 (0.03)	0.06 (0.04)	0.03 (0.02)

Table 2. Gait profile of patients with PD compare to OA with mobility disability and history of falls (SD).

Characteristics	PD	OA with history of falls	OA with mobility disability
n	368	66	222
Mean age	68.68 (10.41)	73.92 (8.4)	79.4 (4.3)
H&Y	2.19 (0.60)	na	na
Disease Duration, yrs	8.82 (5.17)	na	na
Gait Speed, m/s	0.98 (0.26)	1.08 (0.24)	1.04 (0.19)
COV- Step Length	0.06 (0.06)	0.03 (0.01)	0.03 (0.02)
COV- Stance Time	0.05 (0.03)	Data not available	0.04 (0.02)

PREDICTORS OF INITIAL IMPACT LOAD AND LOADING RATES IN RUNNERS

[1]Brian Noehren, [1]Michael B Pohl

[1]University of Kentucky, Lexington, KY,USA
email: bwn51@yahoo.com

INTRODUCTION

Over 35 million Americans engage in running for recreation and sport. Running, however, is associated with a high risk of developing a musculoskeletal overuse injury (1). While the risk of developing an injury is multimodal, running mechanics are believed to be an important contributing factor. Growing evidence suggests that common injuries such as tibial stress fractures and plantar fasciitis are associated with excessive initial impact peaks and loading rates of the vertical ground reaction force (GRF) (2,3). While strategies such as gait retraining and footwear modifications have been proposed to reduce the incidence of such overuse injuries, little is known about which kinematic and kinetic variables are most closely associated with high impact loading and loading rates (4). Clarification of this relationship would facilitate the development of subsequent treatment strategies to reduce the deleterious effects of high impact loading in injured runners.

The control of the stance limb in the sagittal plane at the instant of initial impact loading during running may provide important information regarding the type of gait pattern associated with high impacts. For instance, decreased joint angular excursions, smaller internal joint moments and powers, and faster joint velocities at the hip, knee and ankle may reflect decreased utilization of the muscles to absorb impact. Therefore, the purpose of this study was to determine which sagittal plane kinematics and kinetics at the hip, knee and ankle were most closely associated with initial impact loading and loading rates.

METHODS

Active males and females between the ages of 18-45 were recruited for this study. Upon entry into the study they underwent an instrumented gait analysis. Retro-reflective markers were placed on the extremities (5). Participants then ran between 2.8-3.3 m\s on an instrumented treadmill (Bertec OH, USA) capturing kinetic data at 1200 Hz. The marker trajectories were captured using a 15 motion capture system (Motion Analysis Corporation) at 200 Hz. Five consecutive stance phases were collected for each participant. Analog and kinematic data were low pass filtered at 35 Hz and 8 Hz respectively. Joint angles, moments, and velocities were subsequently calculated at the instant of the initial vertical GRF impact peak. In addition, joint excursions were calculated from initial contact to initial impact peak. The average loading rate was determined as the slope of the vertical GRF between 20-80% of the period between initial contact (20N) and impact peak.

A linear regression was used to assess which sagittal plane kinematic and kinetic variables were predictive of loading rates and initial impact peak. We had apriori determined that there was a poor correlation (R^2=0.14) between average loading rate and the initial impact peak. Thus we ran each as a separate dependent variable using a step wise regression.

RESULTS

One hundred and five individuals participated in this study. There were 16 males and 89 females in the study. The mean (stdev) of initial vertical impact peak was 1.6 (0.33) BW and average vertical loading rate was 78.3 (26) BW/s. We found a significant association between initial vertical GRF impact peak to knee flexion velocity, as well as hip extension power ($r= 0.610$, $R^2 =0.37$, $p< 0.01$) (figure 1). The average loading rate was significantly associated with knee flexion excursion and hip extension power ($r=0.467$, $R^2= 0.22$, and $p=0.02$) (Figure 2).

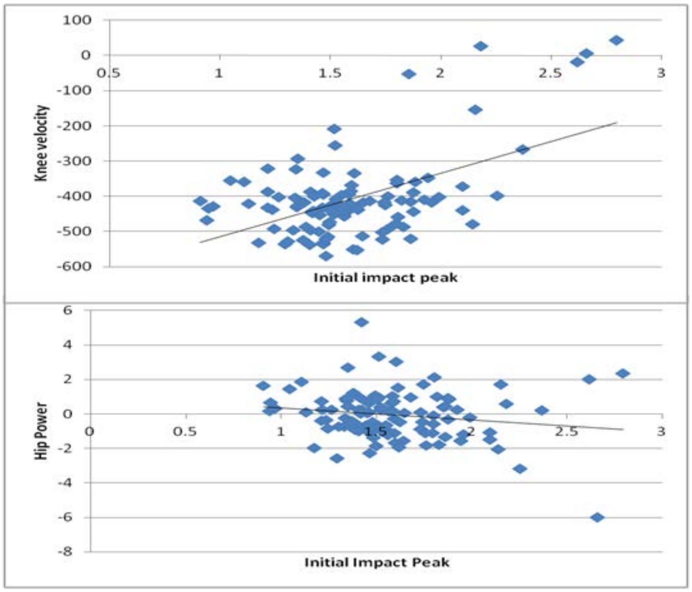

Figure 1: Scatter plots of the association between Initial impact peak with knee flexion velocity and Hip joint power.

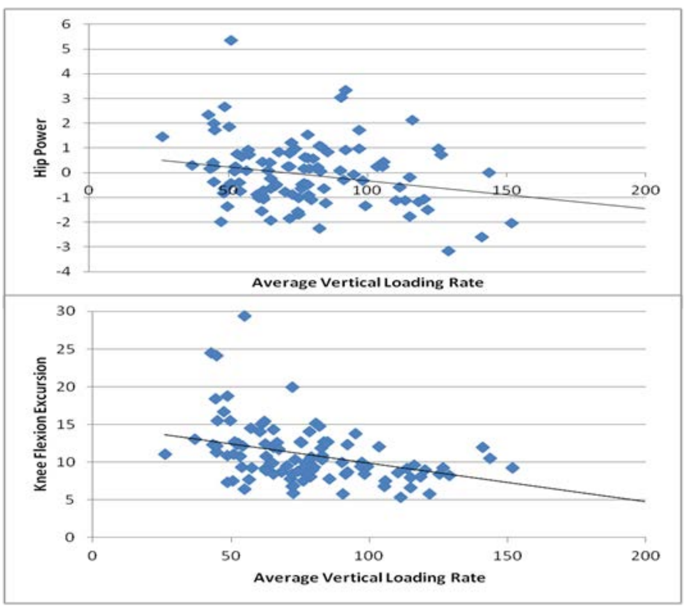

Figure 2: Scatter plots of the association between Average loading rate, hip joint power and knee flexion excursion.

DISCUSSION

Several variables that were significantly related to initial impact peak and average loading rate were identified. Contrary to our expectations, smaller values of knee flexion velocity were more closely associated with initial impact peak. Perhaps, smaller values may be indicative of a stiffening of the tibiofemoral joint in early stance. Additionally, when combined with a reduction in the use of the hip extensors in early stance this may lessen the ability of the lower extremity to attenuate impact loading.

Average loading rate was most associated with a reduction in knee flexion excursion and hip extensor power (figure 2). Less knee flexion excursion suggests that a smaller arc of motion over which to decelerate the limb is linked with greater loading rates. Also a reduction in the hip extensor power suggests less use of the hip extensor muscles to slow down the centre of mass early in stance.

Interestingly, no ankle variables were predictive of either average loading rate or initial impact peak. Perhaps the larger capacity of the hip and knee during early stance to decelerate and control the limb is more critical than foot control. Moreover, we did not find that any sagittal angles at the time of initial impact were predictive of impact peak or average loading rate. The initial angle may not be as critical as the joint velocities and power developed by the muscle in early stance. These data suggest that one potential strategy to lessen impact peaks and loading rates would be to use greater knee flexion excursion and to more fully utilize the hip extensors to help decelerate the limb at initial contact. Future studies are needed to confirm whether these gait patterns are also evident in injured populations that characteristically demonstrate greater impact peak and loading rates.

REFERENCES

1. Taunton JE, et al. *Br J Sports Med*, **36**, 95-101, 2002.
2. Milner CE, et al. *Med Sci Sports Exerc* **38**, 322-328, 2006.
3. Pohl MB, et al. *Clin J Sport Med*, **19**, 372-376 2009.
4. Crowell HP, et al. *Clin Biomech* **26**, 78-83 2011.
5. Noehren, B et al. *Clin Biomech* ***in press*** 2012.

DECREASED GAIT TRANSITION SPEEDS IN UNILATERAL, TRANSTIBIAL AMPUTEE GAIT

Tracy Norman and Young-Hui Chang
Comparative Neuromechanics Laboratory, School of Applied Physiology, Georgia Institute of Technology, Atlanta, GA
email: tnorman8@gatech.edu

INTRODUCTION

Unilateral, transtibial amputation causes a greatly diminished capacity to generate propulsive forces on the affected side. Collisional energy loss on the intact side is significantly higher than on the prosthetic side [1]. Modeling and experimental studies in control subjects has shown that ankle plantarflexor force production decreases near the gait transition speed (GTS) [2] as a result of high muscle fascicle shortening velocities [3]. Transitioning to a running gait at the same speed greatly reduces fascicle shortening velocity and increases force production of the plantarfelxor muscles [3].

We hypothesized that unilateral, transtibial amputees (AMP) will transition between gaits at a lower absolute speed than able bodied controls (AB) due to their decreased ability to generate propulsive forces on their amputated leg.

METHODS

Preliminary data were collected from two healthy, AB subjects (male = 1) and two healthy, AMP subjects (male = 2). All subjects were competitively fit. AMP were at least one year post traumatic amputation and regularly used their personal walking and running specific prostheses. Testing was completed over two days no more than one week apart.

Day 1: Determine Gait Transition Speed

GTS was determined for subjects by an incremental protocol similar to the one described by Prilutsky and Gregor [4]. Subjects habituated to walking and running on a single belt of a split-belt treadmill at self-selected speeds for 3 minutes with 2-minute rest periods. The incremental protocol to determine gait transition speed consists of two parts (A. increasing speed and B. decreasing treadmill speed), repeated three times.

Part A: Increasing Speed

Subjects stood on the non-moving treadmill belt while the second belt was running. Once the second belt reached the starting speed (1.3m/s for AB and 1.0m/s for AMP), subjects were instructed to step onto the moving belt. Once on the belt, subjects were given up to 30 seconds to both walk and run before indicating which gait was preferred. Subjects rested while the moving belt's speed was increased by 0.1 m/s. The task was then repeated. This continued until the subject passed a speed in which running was always the preferred gait. The subject's lowest preferred running speed was recorded as the transition speed. Subjects then rested for 2 minutes.

Part B: Decreasing Speed

Starting speeds were 2.6 and 2.3m/s for AB and AMP respectively. Once again the treadmill speed was adjusted by 0.1 m/s. The highest preferred walking speed was recorded as the transition speed.

AB subjects completed the entire incremental protocol (Part A and Part B) three times. The first time was used as practice. In total four transition speeds were collected and averaged to determine the subject's gait transition speed (GTS) AMP subjects completed the entire incremental protocol for both their walking prosthesis (W-AMP) and running prosthesis (R-AMP). Both the order of Part A and B and the order of W-AMP and R-AMP conditions were counterbalanced.

Day 2: Instrumented Split-Belt Collection

Three out of the four subjects completed 30 second walking trials at speeds of 50, 60, 70, 80, 90, 100, 110, 120, and 130% of their previously determined GTS as part of a larger protocol. One earlier collected control subject's 30 second walking trials were at speeds of 55, 70, 85, 100, 115, and 130% of his previously determined GTS (Subject BS). Subjects rested for 2 minutes between each trial. AMP subjects completed the protocol twice. W-AMP and R-AMP at appropriate scaled speeds in accordance with the walking prosthesis GTS and running prosthesis GTS respectively.

For all subjects, speeds were randomized and the order of prosthetic leg donning was counterbalanced in AMP subjects. Ground reaction force data was measured using a custom built, instrumented, split-belt treadmill (1,080 Hz, Advanced Mechanical Technology Incorporated, Water- town, MA, USA).

RESULTS & DISCUSSION

As we hypothesized the GTS of AMP subjects were lower than that of AB subjects (Fig. 1 and Table 1).

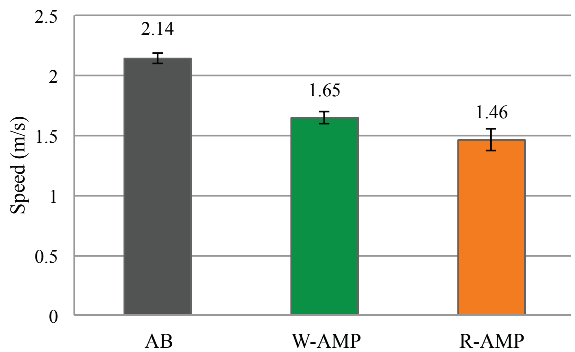

Figure 1: Average Gait Transition Speeds
All transition speeds recorded were averaged within each subject group (AB: 2.14 ± 0.05, W-AMP: 1.65 ± 0.05, R-AMP 1.46 ± 0.09).

Groups	GTS
AB	2.13 ± 0.05
	2.15 ± 0.04
W-AMP	1.66 ± 0.05
	1.63 ± 0.04
R-AMP	1.49 ± 0.09
	1.43 ± 0.08

Table 1: Individual Gait Transition Speeds

Anterior-posterior propulsive force impulses and force peaks of the AB subjects were consistent with previous observations, decreasing after 100% of the GTS (Fig. 2) [2]. Surprisingly, anterior-posterior propulsive force impulses and peaks continued to rise after the 100% GTS for both W-AMP subjects and R-AMP subjects. This may be explained by the lower absolute speed of the AMP subjects' trials allowing for slower muscle fascicle shortening velocities than in the controls.

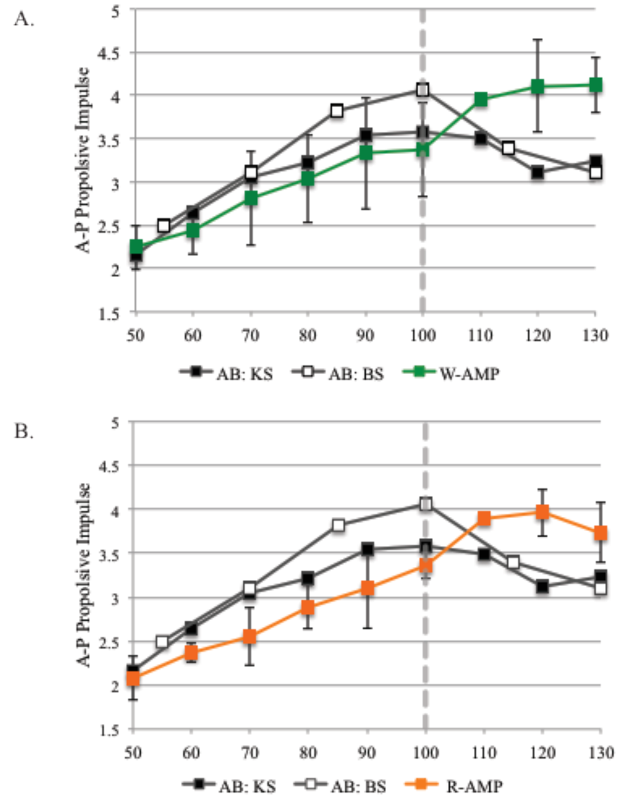

Figure 2: Anterior-Posterior Propulsive Impulse
Two representative AB control subjects are plotted in comparison to the (A) mean propulsive impulse for W-AMP subjects, and (B) mean propulsive impulse for R-AMP subjects. Preferred transition speeds for each group are denoted by the dashed grey line at 100%. (Note: Impulse for W-AMP at 110% of GTS only represents one AMP subject)

CONCLUSION

Unilateral, transtibial amputees transition between gaits at lower absolute speeds than able bodied controls. The gait transition in transtibial amputees appears to be triggered by something other than propulsive force or plantarflexor muscle force-velocity characteristics. Increased sample size and further investigation is planned to further pinpoint the cause of the decreased GTS.

ACKNOWLEDGEMENTS

Work supported in part by NIH grant R01NS069655 to YHC and NIH training fellowship NICHD 5T32HD055180 to TN.

REFERENCES

1. Adamczyk, PG and Kuo AD, *ASB Abstract,* 2011.
2. Neptune RR and Sasaki K, *J. Exp. Biology.* 208, 799-808, 2004.
3. Farris DJ and Sawicki GS, *PNAS.* 109(3), 977-982, 2012.
4. Prilutsky BI and Gregor RJ, *J. Exp. Biology.* 204, 2277-2287, 2001.

IS PUSH-OFF PROPULSION ENERGETICALLY OPTIMAL FOR ACCELERATED GAIT?

[1]Keonyoung Oh, [2]Joohyun Baek, [2]Jae-Kwan Ryu and [1]Sukyung Park

[1]Mechanical Engineering dept. KAIST, Daejon, Korea
[2] LIG Nex1, Mechanical Engineeering R&D Lab, Korea
email: sukyungp@kaist.ac.kr, web: http://biomt.kaist.ac.kr

INTRODUCTION

To maintain steady state level walking, a positive work is required to compensate energy loss through heel strike collisions during the gait cycle. When the amount of push-off propulsion is smaller than the concurrent collision loss by heel strike, additional center of mass (CoM) propulsion should be provided during the following single support phase. Experimental data showed that the compensatory push-off work during the double support phase almost matched with the collision loss, thereby almost negligible additional work was done to propel the CoM during the single support phase [1, 2]. The observed energy balance between the push-off and heel strike during the step-to-step transition appeared, from a simple biomechanical analysis, to be the energetically least costly gait [1-3]. However, the observed dominance of the push-off propulsion was mostly observed for steady gait trials, which brings into question whether the mechanical dominance and the energetic optimality of push-off propulsion would still hold for a transient gait response such as gait acceleration.

METHODS

In this study, we examined whether the push-off propulsion during the double support phase would serve as a major energy source for gait acceleration, and we examined the energetic optimality of accelerated gait using the simplest bipedal walking model [1, 2]. Seven healthy, young subjects participated in the over the ground walking experiments. The subjects either walked at four different constant gait speeds ranging from a self-selected to a maximum gait speed, or they accelerated their gait from zero to the maximum gait speed using a self-selected acceleration ratio. We measured the ground reaction force (GRF) of three consecutive steps and the corresponding leg configuration using force platforms and an optical marker system, respectively, and compared the mechanical work performed by the GRF during each single and double support phase. To examine the energetic optimality of the gait acceleration propelled by the measured push-off impulse, we compared the experimental data with the theoretical optimal push-off which was predicted from the gravitational impulse model [2]. Specific details are as follows..

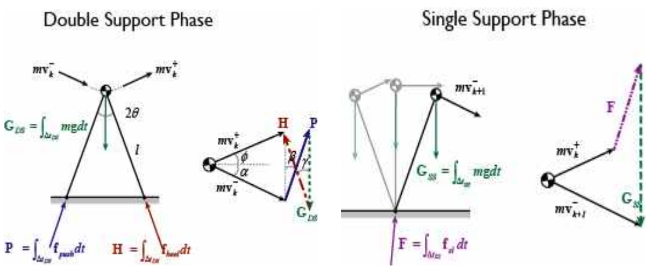

Figure 1: Momentum-impulse relationship.

The gravitational impulse model was used to predict the collision impulse and corresponding mechanical work. Consider the momentum change of a mass m during a double and single support phases by gravitational impulse (G), push-off (P) and heel strike (H) impulses as follows,

$$m\mathbf{v}_k^+ = m\mathbf{v}_k^- + (\mathbf{P} + \mathbf{H} + \mathbf{G}_{DS}),\quad m\mathbf{v}_{k+1}^- = m\mathbf{v}_k^+ + (\mathbf{F} + \mathbf{G}_{SS}) \quad (1)$$

where $\mathbf{v}_k^-$ and $\mathbf{v}_k^+$ are the pre- and post-collision velocities of the CoM during the double support phase of kth step, and is the pre-collision velocity of k+1 step's double support phase. The mechanical work performed by each impulse during the double support phase can be obtained from the expansion of the equations for the collisional energy change from previously published studies [3] as follows:

$$\begin{cases} WP_{DS} = \dfrac{P}{2m}\sin^2 2\theta \cdot \left(P + \dfrac{mv_k^-}{\tan 2\theta} - \dfrac{G_{DS}}{2\cos\theta} \right) \\ WH_{DS} = -\dfrac{1}{2} \cdot v_k^- \sin 2\theta \cdot \left\{ mv_k^- \sin 2\theta - P\cos 2\theta + G_{DS}\cos\theta \right\} \\ W_{SS} = -(WP_{DS} + WH_{DS}) + \dfrac{1}{2} \cdot mv_k^{-2} \rho(\rho + 2) \\ = \dfrac{-\sin^2 2\theta}{2m} \left\{ P - \left(mv_k^- \tan\theta + \dfrac{G_{DS}}{2\cos\theta} \right) \right\} \left(P + \dfrac{mv_k^-}{\tan\theta} \right) + \dfrac{1}{2} \cdot mv_k^{-2} \rho(\rho + 2) \end{cases} \quad (2)$$

Then, the push-off P^* that minimizes the CoM work throughout the gait cycle is computed as follows:

$$\begin{aligned} P^* &= \arg\min_{P^*} \left| WP_{DS} + W_{SS} \right| \\ &= \arg\min_{P^*} \left(\left| WH_{DS} \right| - \frac{1}{2} \cdot mv_k^{-2} \rho(\rho + 2) \right), \textit{ subject to } W_{SS} \geq 0 \end{aligned} \quad (3)$$

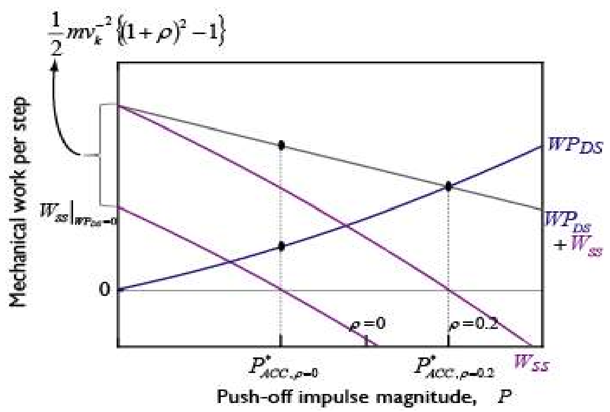

Figure 2: Model prediction of optimal push-offs.

By solving Eqn. (3) subject to the positive work constraint during the single support phase, i.e., $W_{SS} \geq 0$ [1], the model predicts the optimal push-off that minimizes the mechanical work done for the gait acceleration as a quadratic form of the acceleration ratio ρ.

RESULTS AND DISCUSSION

Although the gravitational impulse model predicted the optimal push-off that minimizes the total work input as a quadratic form of acceleration ratio, the push-off propulsion was slightly increased, and a significant increase in the mechanical work during the single support phase was observed. The results suggest that gait acceleration occurs while accommodating a feasible push-off propulsion constraint such as the finite magnitude of plantar flexor torques. Because the push-off force is known to be generated mostly by the plantar flexors and the elastic recoil of the tendon, the limited push-off forces are attributed to muscle mechanics. Studies have shown greatly reduced plantar flexion and isokinetic plantar flexion torques with angular velocity, which implies that generating greater push-off propulsion is more challenging to achieve at a high gait speed. Therefore, we suggest that the intrinsic muscle properties limit the increase in the push-off propulsion during an accelerated gait; thus, the subjects employed a more expensive acceleration strategy to increase their gait speed during the single support phase to accommodate the biomechanical constraint.

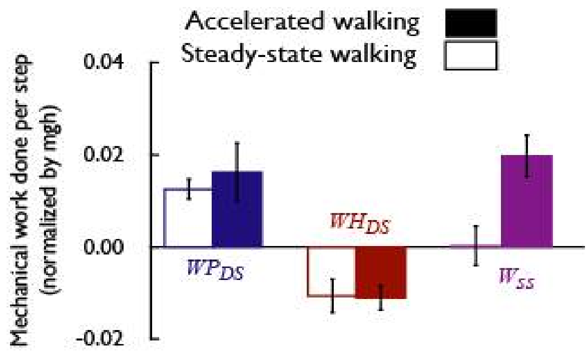

Figure 3: Mechanical work done during each gait phase for steady and accelerated walking.

CONCLUSIONS

Contradictory to the optimal push-off model prediction of an increase in the push-off proportional to the acceleration that minimizes mechanical energy cost, the empirical push-off propulsion was slightly increased, and a significant increase in the mechanical work during the single support phase was observed. The results suggest that gait acceleration occurs while accommodating a feasible push-off propulsion constraint.

REFERENCES

1. Kuo AD, *J Biomech Eng*, **124**, 113-120, 2002.
2. Yeom J and Park S, *J Biomech* **44**, 59-67, 2011
3. Ruina A et. al., *J Theor Biol* **237**, 170-192, 2005
4. Orendurff et.al., *Gait & posture* **27**, 603-61, 2008

ACKNOWLEDGEMENTS

This research was supported by LIG nex1 (G01110120)

SURGICAL SIMULATION: VALIDATING METHODS TO IMPROVE ORTHOPAEDIC RESIDENT SKILLS COMPETENCY

Gary T. Ohrt, Matthew D. Karam, Geb W. Thomas, Jenniefer Y. Kho, Tameem M. Yehyawi, J. Lawrence Marsh, Donald D. Anderson

The University of Iowa, Iowa City, IA
email: gary-ohrt@uiowa.edu web: http://poppy.obrl.uiowa.edu/

INTRODUCTION

Surgical reconstruction of fractured extremities is a complex procedure that orthopaedic residents must master during training. Currently, training is based on an apprenticeship model, which while beneficial, is not uniform and does not provide any means to assess skills competency. Surgical simulation can help address shortcomings in the training model by providing residents opportunities to (1) practice procedures that they may not otherwise perform and (2) practice said procedures efficiently until competency is achieved, (3) while limiting exposure of patients to undue risk.

However, before a surgical simulator construct can be used to assess competency, its scientific validity must be established.[1] A well-designed and rigorously validated simulator can provide quantitative, repeatable assessment of specific surgical skills and can predict performance in the operating room. Our long-term goal is to provide a beneficial surgical simulator module for fracture reconstruction that can be modified for different fracture models and anatomic locations.

METHODS

A simulation training and assessment program focused on improving articular fracture reduction skills in a tibial plafond model has been developed (Figure 1). The simulation uses various multi-segment, radio-dense polyurethane foam (bone surrogate) fracture patterns inside a synthetic soft tissue housing (Sawbones Inc.). The task is to reduce fragment displacement and fixate a three-segment fracture with Kirschner wires, operating through a limited anterior window in the soft tissue housing while using fluoroscopy for visualization.

Participant hand motions are tracked using a four-camera Qualisys motion capture system. The

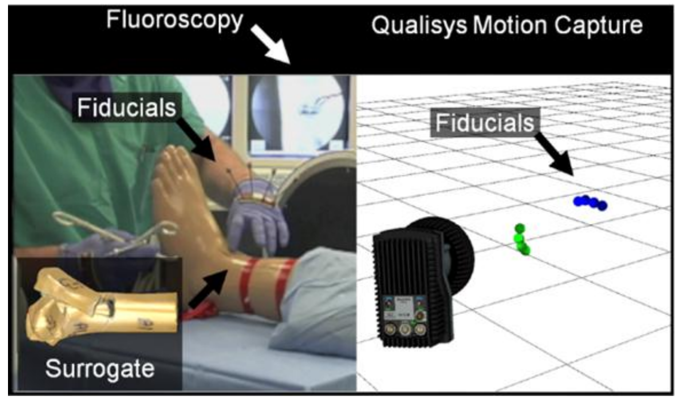

Figure 1. Left: In-progress simulation showing fiducials and soft-tissue housing. Bottom Left: Fracture surrogate pattern. Right: Fiducials shown in motion capture software.

simulation is synchronously recorded from multiple video sources, including from a head-mounted camera that enables determination of when and where attention is focused. The video streams are consolidated into a single composite split-screen video (Figure 2), for later one-on-one feedback from a surgeon/educator.

Residents were assessed on time-to-completion and objective error in reducing the fracture. The

Figure 2. Video of Simulation, Clockwise from Top Left: Head Mount, Top View, Fluoroscopy, Wide Angle.

reduction inaccuracy was assessed by comparing post hoc 3D laser scans to an ideal reconstruction of the fracture using Geomagic Qualify software (Geomagic Inc.). Motion capture data were processed to provide the number of discrete hand actions and cumulative hand motion distance. Radiation dose and fluoroscopy time were also recorded. The OSATS global surgical skills metric [3] was used to rate the residents on their performance in nine areas, and an overall score was calculated. The rating was done by a senior orthopaedic traumatologist.

In a prior study, we found that senior orthopaedic residents had more deliberate hand motions (less cumulative hand distance, a surrogate for less iatrogenic wound bed trauma) and scored better on task performance than more junior residents.[2]

Building upon that earlier work, a training program consisting of cognitive and motor skills modules was developed. The cognitive module was implemented through an online course that included a pretest, general knowledge about plafond fractures and fluoroscopy, and online video performance reviews. The motor skills module focused on acquiring motor skills by direct instruction and dedicated practice on a simulated model (different fracture pattern from test model), with real-time feedback from an orthopaedic traumatologist.

To evaluate the new training program, six first-year and six second-year orthopaedic residents were randomly assigned to either an intervention or control group. Simulations were run with both groups before and after training in the intervention group. Training occurred 24 to 48 hours prior to the second surgical simulation.

RESULTS AND DISCUSSION

There were no significant differences in the metric of articular surface step off (Table 1) attributable to training. However, both the control and intervention groups showed improvement of nearly 1 mm. Current analysis methodology does not yet account for the rotation of fragments, which may play a large role in quality of reduction, and may show a difference with the training.

Table 1: Fracture reconstruction inaccuracy

	Average Articular Displacement (mm)		
	Control	Intervention	P Value
Pre-Training	4.73	4.93	0.827
Post-Training	3.63	4.00	0.603
P Value	0.34	0.21	
Improvement	1.10	0.93	0.886

Judged by OSATS scores (higher score is better) from the pre and post training simulations (Table 2), there was a significant improvement associated with the intervention, while the control group did not experience significant improvement or worsening. This indicates that the training was effective in improving the aspects of fracture reduction that a senior orthopaedic surgeon would find important.

Table 2: OSATS Rating Scores

	OSATS Overall Score		
	Control	Intervention	P Value
Pre-Training	28.8	20.5	0.000
Post-Training	28.5	32.7	0.029
P Value	0.79	0.001	
Improvement	-0.3	12.2	0.003

CONCLUSIONS

The articular surface comparison results did not show significant differences between the control and intervention groups. However, the OSATS scoring showed a post intervention difference between the two groups.

REFERENCES

1. McDougall EM, et al. *J Endourol*. 2007**. 21(3)**:244-7**.**
2. Marsh JL, et al. *AOA Council of Residency Directors Conference*. 2011.
3. Martin JA et al. *Br J Surg*. 1997. **84(2)**:273-8.

ACKNOWLEDGEMENTS

This research was funded in part by grants from the Orthopaedic Research & Education Foundation, the OMeGA Medical Grants Association, the Orthopaedic Trauma Association, and NIH/NIAMS (AR055533 and AR054015).

MOTOR LEARNING IS ENHANCED IN OLDER ADULTS FOLLOWING TRAINING WITH A LESS DIFFICULT TASK

Tanya Onushko, Changki Kim, and Evangelos A. Christou

University of Florida, Gainesville, FL, USA
email: eachristou@ufl.edu web: http://hhp.ufl.edu/apk/ces/affil/npl/Home.htm

INTRODUCTION

Motor learning is impaired in older adults likely due to their inability to process information when practicing a novel motor task [1,2]. This motor learning impairment has been associated with degenerative as well as compensatory changes in the aging central and peripheral nervous systems [3,4]. Recent studies suggest that motor learning in older adults can be improved with training interventions that use a light load and focus on muscle coordination to improve movement control [5,6,7]. There is some evidence, however, that the age-associated differences in movement control are exacerbated during more difficult tasks. For example, force variability and error increases with dual motor tasking or the addition of a cognitive task compared with a unilateral motor task, especially for older adults [8]. It is not clear, however, whether these aging differences remain when the task difficulty increases with greater coordination demands. Furthermore, it is not clear whether there are any age-associated differences in motor learning when young and older adults train with an easy and a hard motor task. The purpose of this study, therefore, was to determine whether the difficulty of the training task affects motor learning in young and older adults.

METHODS

Eighteen young (Y) (23.3±3.3 years) and seventeen older (O) adults (72.9±8.2 years) participated in this study. Subjects were instructed to track a moving target (dot) on a computer monitor by controlling isometric abduction forces of the index and little fingers. The isometric force produced by the abduction of the index finger and the little finger were measured with single-axis force transducers (one per finger) (Futek LRF400 Futek Advanced Sensor Technology Inc. CA, USA) (Fig. 1A). Visual feedback of the finger abduction forces and the moving target's path were provided to subjects using a custom-written Matlab (Math Works Inc., Natick, Massachusetts, USA) program. A two-dimensional (X-Y) coordinate plane was displayed on the computer monitor. The X-axis represented the index finger force and the Y-axis represented the little finger force. The target force for both fingers varied from 5-15% of maximal voluntary contraction (MVC). The subjects' force feedback from the index and little fingers was displayed as a single cursor on the monitor using a force-force plot (also referred to as a Lissajous plot).

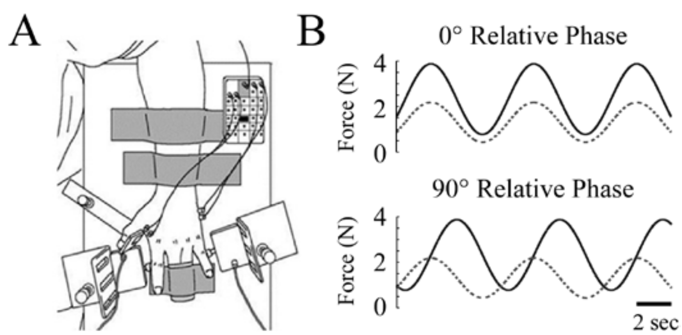

Figure 1: (A) Experimental setup. The proximal inter-phalangeal (PIP) joint of each finger was aligned perpendicular to the force transducer's axis. (B) Example of the 0º and 90º relative phases for the index (solid) and little (dotted) abduction finger forces. Force amplitude was dependent on individual finger abduction MVC.

Subjects were assigned to one of three groups (6 Y and 6 O per group) to determine whether training with a more or less difficult task would influence motor learning. The level of training difficulty was dependent on the relative timing (i.e. phase) of abduction force generation between the index and little fingers (Fig. 1B) [9]. The three groups were:

Easy (0º relative phase), Hard (90º relative phase) and Control (no training). Subjects practiced their assigned task for 80 trials (5 blocks x 16 trials per block) one day prior to the testing session. During the testing session, Easy, Hard and Control groups performed three transfer tracking tasks (45°, 135° and 180° relative phases) to test motor learning. The three tasks were presented in random order and subjects performed five trials for each task. We quantified force variability (sum of the variance of the force from each finger), overall error (sum of the root mean square error (RMSE) of each finger), and the timing error (sum of the timing delay between the target's trajectory and the force production for each finger).

RESULTS AND DISCUSSION

Overall, older adults compared with young adults exhibited greater force variability, greater RMSE values and greater timing errors during the training trials ($P < 0.05$). As expected, older adults in the Easy group had lower force variability, lower RMSE values, and lower timing errors compared to the Hard group ($P < 0.05$). The rate of improvement with training, however, was similar for the two tasks.

Motor learning was enhanced for both the young and older subjects who trained with the easy task compared with the hard task and the control group (Fig. 2). This was evident by lower RMSE and temporal errors and lower force variability during the transfer tasks (45°, 135° and 180° relative phases). The effect of training with the easy task on motor learning was greater for older adults (Fig. 2).

In this project we aimed to determine whether the difficulty of the training task affects motor learning in young and older adults. We demonstrate that task difficulty is important for motor learning. Surprisingly, we show that subjects who practiced with an easy task transferred to difficult tasks much better than subjects who trained with a difficult task. This is surprising because all of our transfer tasks were difficult and required alternating phase between the two fingers, similar to the hard training task. We also demonstrate that this effect is greater in older adults. Overall, this finding suggests that practicing a simple task can enhance motor learning and reduce errors and variability in force control in older adults to a level near young adults.

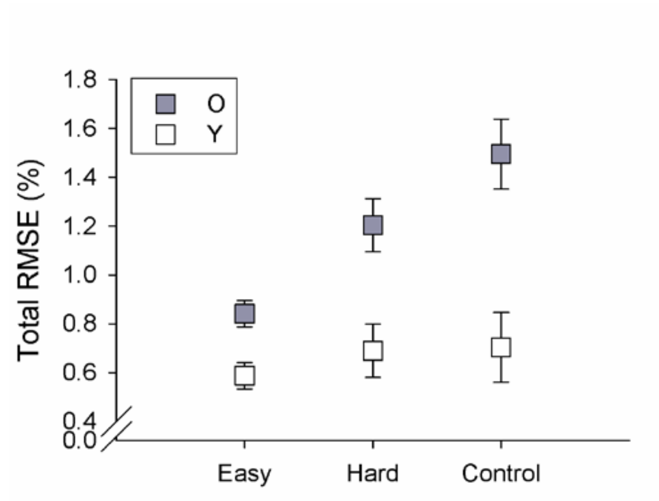

Figure 2: Average RMSE of the 45°, 135° and 180° relative phases for young (Y) and older (O) adults. Motor learning was enhanced in subjects who performed the Easy training.

CONCLUSIONS

Task difficulty is an important parameter for a training intervention to enhance motor learning. We provide evidence that motor learning is enhanced when training with an easy task compared with a hard task. These findings clearly suggest that training with a less difficult task can enhance motor learning in young and, especially, older adults when learning a novel fine motor task.

REFERENCES

1. Seidler RD. *Brain Res Bull* **70**: 337-346, 2006.
2. Seidler-Dobrin RD. *Exp Brain Res* **119**: 467-474, 1998
3. Christou EA. *Exerc Sport Sci Rev* **39**: 77-84, 2011.
4. Seidler RD. *Neurosci Biobehav Rev* **34**: 721-733, 2010.
5. Christou EA et al. *J Gerontol A Biol Sci Med Sci* **58**: 763-766, 2003.
6. Kornazt KW et al. *J Appl Physiol* **98**: 2072-2080, 2005.
7. Ranganathan et al. *J Gerontol A Biol Sci Med Sci* **56**: M518-M522, 2001.
8. Johnson et al. *J Appl Physiol* In press, 2012.
9. Haken H et al. *Biol Cybern* **51**, 347-356, 1985.

LOWER-LIMB ACCELERATION DURING SPRINT-START AND SELECTED POWER EXERCISES

[1]Thomas A. Ordelt and [2]Ashish Deshpande

[1]University of Maine, Orono, ME, USA
[2]University of Texas, Austin, TX, USA
email: thomas.ordelt@umit.maine.edu

INTRODUCTION

Many kinetic, kinematic and neuromuscular (EMG) aspects of sprint running and of strength and power exercises have been researched [1-4]. Little has been done, however, to directly compare the kinetics and kinematics of strength and power exercises to that of sprinting [5].
The purpose of this study was to determine the effect of load changes on angular accelerations of the ankle, knee and hip joints. Accelerations were measured in the squat (S), power clean (PC) and power hang clean (PHC), and compared to the accelerations in the push-off phase of the sprint start (SS). It was hypothesized that increases in load would cause significant changes in the acceleration patterns, and thus significant differences from the sprint start.

METHODS

Nine female NCAA Div. 1 track athletes (age 18.7 ± 0.9 yrs) performed 3 trials each of sprint-starts, single-leg squat jump (1S0) with 0% of 1RM, squat (jump) with 0, 25, 40% of 1RM, and power clean and power hang clean with 30, 50, 75, 100% of 1RM. An optical motion capture system (Vicon, 8 infrared-cameras, 250Hz) was used to track and calculate the trajectories of full-body and bar markers (Plug-in-Gait). The fastest trial of each exercise was determined and the minimum and maximum ankle, knee and hip joint angular accelerations (flexion-extension) under the different load conditions were calculated for the same side leg used in the front block of the SS (front leg) (Matlab 7.9.0). Data were smoothed with zero-lag Butterworth filter, 2nd order, 250 Hz sampling frequency, 12 Hz cut-off frequency. Within subjects, repeated measures ANOVAs with minimum and maximum angular acceleration as dependent variable, and load and joint as independent variables were followed by Least Square Difference post-hoc comparison (SPSS 19.0). Level of significance was set at $p<.05$.

RESULTS AND DISCUSSION

Figure 1 shows exemplary angular joint accelerations in one subject during the sprint start between start and front leg toe-off.

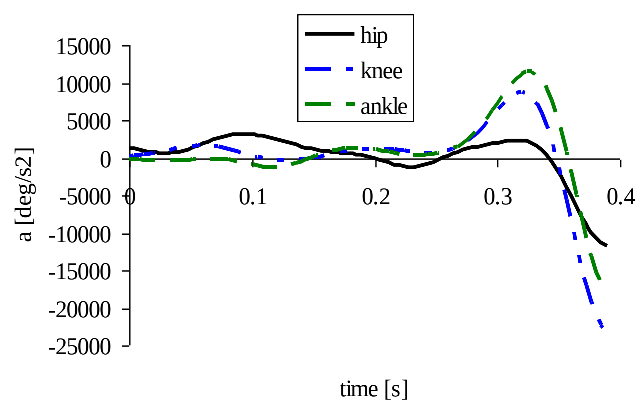

Figure 1: Angular acceleration of ankle, knee and hip joints during sprint start in subject 2.

F(11,44) for ankle amin was 13.4 ($p<.001$), for ankle amax was 13.6 ($p<.001$), for knee amin was 27.5 ($p<.001$), for knee amax was 5.1 ($p<.001$), for hip amin was 14.1 ($p<.001$), and for hip amax was 3.5 ($p=0.002$).
In pairwise comparisons, only for minimum ankle (S0-S25 $p=.01$, S0-S40 $p=.047$) and minimum hip acceleration (S0-S25 $p=.02$, S0-S40 $p=.003$, S25-S40 $p=.02$) in S (Fig. 2) (S0-S25 $p=.01$, S0-S40 $p=.047$) and for minimum knee acceleration in PHC (PHC30-PHC75 $p=.01$, PHC50-PHC75 $p=.02$) (Fig. 3) was a change in load significantly related to change in angular acceleration. PHC (knee amin)

and S (hip amin) behaved opposite in their respective load- acceleration patterns: Increase in load led to acceleration increase in the PHC, whereas increase in load resulted in acceleration decrease in the S. In PC, no clear tendencies were apparent.

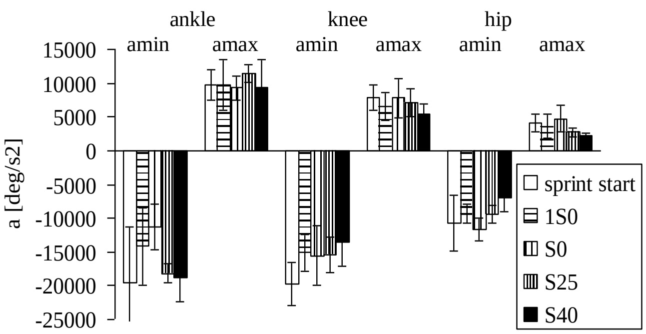

Figure 2: Angular acceleration of ankle, knee and hip joints in sprint start vs. squat at different loads (mean ± SD).

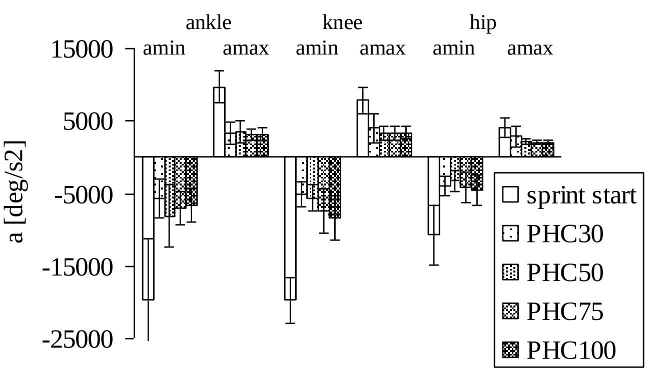

Figure 3: Angular acceleration of ankle, knee and hip joints in sprint start vs. power hang clean at different loads (mean ± SD).

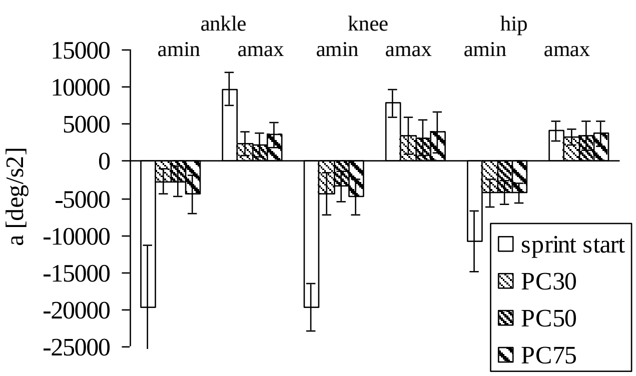

Figure 4: Angular acceleration of ankle, knee and hip joints in sprint start vs. power clean at different loads (mean ± SD).

Possibly, in order to successfully lift heavier loads, the reversal of direction from extension to flexion at the transition to the drop-under phase had to occur faster, resulting in an increase in minimum angular knee acceleration. The minimum angular hip acceleration showed a similar, statistically non-significant, tendency (Fig. 3). In S, however, there is no drop-under phase, so increasing load should more directly lead to decreasing acceleration (force-velocity curve). Maximum knee and hip angular accelerations in S behaved similarly, albeit not statistically significant (Fig. 2).
The angular accelerations in most exercises were significantly different from the accelerations in SS. Only 1S0, S0, and S25 were not significantly different, except for knee amin (SS-1S0 p=.01, SS-S0 p=.03, SS-S25 p=.02).

CONCLUSIONS

Load-induced changes in angular acceleration patterns during the concentric phase appear to be opposite in S and PHC. Higher load tended to decrease acceleration in S (except for the ankle), whereas in PHC higher load caused an increase in (minimum) acceleration (except for the ankle).
SS and no- or low-load squat jumps usually reported the highest positive and negative angular accelerations in ankle, knee, and hip. Their mean values were 2 - 4 times higher than the means from PC and PHC. The results of this study seem to indicate that the squat exercises 1S0, S0 and S25 are more specific to lower-limb acceleration patterns of the SS than are heavier squats and any of the PC or PHC loads. Thus, they should be more effective in achieving performance improvements and more efficient when practice time is limited.

REFERENCES

1. Harland MJ, et al. *Sports Medicine* **23**, 11-20, 1997.
2. Čoh M, et al. *Biology of Sport* **26**, 137-147, 2009.
3. McBride JM, et al. *J Strength Cond Res* **16**, 75-82, 2002.
4. Souza AL, et al. *J Strength Cond Res* **16**, 423–427, 2002.
5. Mero A, et al. *J Appl Biomech* **10**, 1-13, 1994.

THE DETERMINANTS OF WALKING ENEGETICS IN ELDERLY ADULTS

Justus D. Ortega

Humboldt State University, Arcata, CA, USA
email: jdo1@humboldt.edu, web: www.humboldt.edu/~jdo1

INTRODUCTION

Elderly adults consume more metabolic energy for walking than young adults across a range of speeds [1], yet the reason for the greater metabolic cost is unclear. During walking, the muscles of the body consume metabolic energy to generate force for such mechanical tasks as performing external mechanical work, stabilizing the body, supporting body weight, and swinging the limbs. However, other factors such as the efficiency of performing mechanical work and the co-activation of antagonist muscles may also contribute to the cost of performing these tasks of walking. Here, I review a series of studies that investigate some of the key determinants of walking energetics in elderly adults.

EFFICIENCY AND CO-ACTIVATION

During walking, stance limb muscles perform mechanical work to lift and accelerate the body's center of mass [2]. Although prior research shows that elderly adults do not perform more mechanical work than young adults [3, 4], it is possible that they perform mechanical work less efficiently as a result of increased co-activation of antagonist muscles.

Some evidence suggests that elderly adults use a greater level of antagonist muscle co-activation in walking [5]. Based on this evidence, we conducted a study that quantified delta mechanical efficiency and its relation to leg muscle co-activation during walking across a range of incline slopes. We hypothesized that elderly adults perform mechanical work less efficiently as a result of increased leg muscle co-activation.

To test this hypothesis, 13 healthy young (22±4 yrs) and 12 healthy elderly adults (75±3 yrs; mean±SD) walked at 1.3 m s^{-1} on a level treadmill and at five different uphill slopes (1.5, 3.0, 4.5, 6.0 and 7.5% grade). For each trial, we quantified metabolic power and Co-activation Index (CI) using indirect calorimetry and EMG during the last 2 minutes of each 7 minute trial. Delta efficiency was calculated as Δ mechanical power output/ Δ metabolic power consumption. We determined CI of two antagonist muscle pairs of the thigh segment (vastus medialis-biceps femoris and vastus lateralis-biceps femoris) and two of the shank segment (gastrocnemius-tibialis anterior and soleus-tibialis anterior). We calculated the CI of each muscle pair as the area of overlap between the agonist and antagonistic EMG signals [6]. CI about the thigh and shank (CITH, CISH) were then determined by averaging the pairs of co-activation indices about each segment.

Elderly adults consumed 12% more metabolic energy on average during walking than young adults and performed mechanical work less efficiently (29%, SEM 1) than young adults (33%, SEM 1) across the range of uphill slopes (p=0.006; Figure 1).

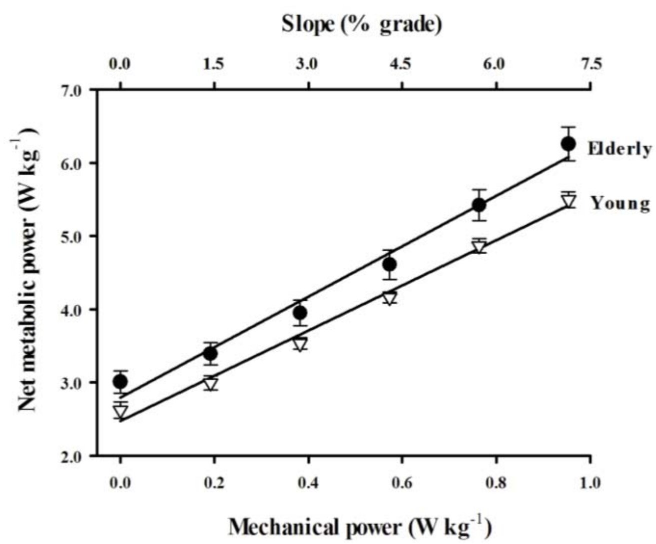

Figure 1: Net metabolic power consumption vs. uphill slope (top x-axis) and mechanical power output

While co-activation across the shank was similar between groups (~28%, p=0.927), elderly adults used more co-activation across the thigh (55%, SEM 3) than young adults (44%, SEM 3) (p=0.001). However, leg co-activation did not increase in either group across the range of uphill slopes (p=0.701) and was only weakly correlated to the metabolic cost of walking (r=0.233).

Although these results suggest elderly adults perform mechanical work less efficiently and use more leg muscle co-activation during steady-state uphill walking, other factors such as a greater cost of muscle force generation for supporting body weight may also contribute to the increased cost of walking in elderly adults.

COST OF SUPPORTING BODY WEIGHT

During walking, the muscles of the body consume metabolic energy to generate force necessary to support body weight. Previous walking studies have shown that the metabolic cost of supporting body weight accounts for as much as 28-33% of the total metabolic cost of walking in young adults [7]. In this study, we examined how force generation to support body weight contributes to the cost of walking in young and elderly adults. We hypothesized that body weight support incurs a substantially greater metabolic cost in elderly adults than young adults.

To test this hypothesis, 12 healthy young (26±4 yrs) and 12 healthy elderly (75±4 yrs) adults walked on a motorized treadmill at an intermediate speed of 1.3 m s^{-1} at four levels of body weight support (0%, 25%, 50%, and 75% of body weight). For each trial, we determined net metabolic cost and lower limb kinematics. We provided weight support by applying a nearly constant upward force to the pelvis and torso near the center of mass using a custom built harness and elastic pulley system as described by Griffin et al. [8].

Weight support reduced the rate of metabolic energy consumption to a greater extent in elderly subjects compared to young subjects ($p<0.0001$; Fig. 2). Across the range of weight support, metabolic cost decreased an average 50% (SD 7) in elderly adults, whereas metabolic cost only decreased by an average 31% (SD 8) in young adults.

Although elderly subjects used a faster step frequency and spent a shorter portion of the gait cycle in single limb support compared to young subjects, our kinematic analysis revealed that elderly subjects did not use a more flexed lower limb posture during the stance phase of walking compared to young adults.

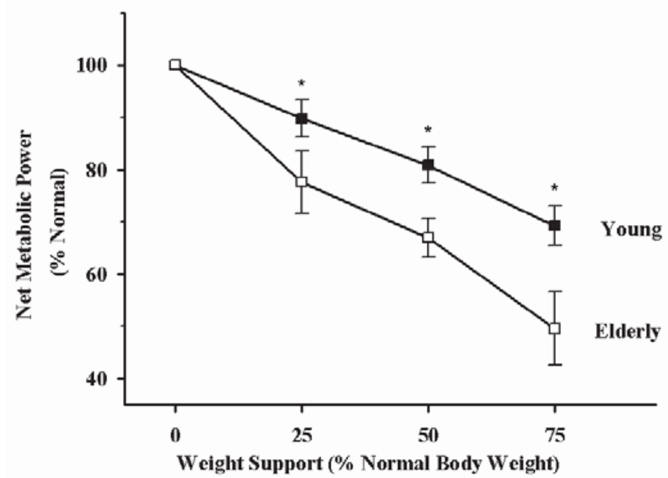

Figure 2: Net Metabolic Power as a function of Weight Support. Asterisk indicates significant differences from normal walking ($p<0.05$).

CONCLUSION

The results of these studies suggest that the increase cost of walking in elderly adults is due in part to an increased cost of supporting body weight and an increased co-activation of thigh muscles. While our results suggest body weight support comprises as much as 50% of the net metabolic cost of walking in elderly adults, it is likely that the increase cost of weight support is related to an increase in leg muscle co-activation. Although reduced mechanical efficiency appears to contribute to the cost of walking in elderly adults, the small difference between age groups suggests that reduced mechanical efficiency is not a primary determinant of the increased cost of walking in elderly adults.

REFERENCES

1. Martin, PE, et al. *J Appl Physiol*, **73,** 200-206, 1992.
2. Cavagna, GA, et al. *J Physiol*, **268**, 647-681, 1977.
3. Ortega, JD et al. *J Appl Physiol*, **102**, 2266-2273, 2007.
4. Mian, OS, et al. *Acta Physiol Scand*, **186**, 127-139, 2006.
5. Hortobágyi, T., et al. *Gait Post*, **29**, 558-564, 2009.
6. Falconer, K, et al. *Electromyogr Clin Neurophysiol*, **25**, 135-149, 1985.
7. Grabowski, A, et al. *J Appl Physiol*, **98**, 579-583, 2005.
8. Griffin, TM, et al. *J Appl Physiol*, **86**, 383-390, 1999.

KINEMATIC ANALYSIS OF GESTURE IN APHASIA

[1]Haroon Osmanzada, [1]Stacie I. Ringleb, [1]Michael A. Samaan, [2]Anastasia M. Raymer,
[1]Sebastian Y. Bawab
[1]Department of Mechanical and Aerospace Engineering and
[2]Department of Communication Disorders and Special Education, Old Dominion University, VA, USA
Email: SRingleb@odu.edu, web: www.odu.edu/~sringleb

INTRODUCTION

Gestural facilitation of naming (GES) is a method to treat word retrieval impairments in stroke-induced aphasia. This method involves asking a patient to use a gesture to activate the impaired language system [1]. A secondary outcome to this treatment may be improvement in motor patterns. Before changes in kinematics can be quantified during the GES treatment process, a kinematic of commonly used gestures within GES should be developed with healthy individuals and individuals with aphasia. The purpose of this study was to compare the upper extremity kinematics in a patient with aphasia with an age matched healthy individual during a slicing motion.

METHODS

Data were collected on three males diagnosed with aphasia following a left hemisphere stroke (age: 56.7±8.5 years) and three age matched (±8 years) healthy asymptomatic males (age58.3±12.3 years). All subjects were right hand dominant and data were collected on the left side. Electromagnetic sensors were placed on the spine, scapula, upper arm, forearm, and hand. The scapula sensor was attached to a scapula tracker with plastic screws [2]. Anatomic landmarks were digitized to define anatomic coordinate systems according to the standards from the international society of biomechanics (ISB) for upper extremity kinematics. The ISB standards were used to report the motions of the glenorohumeral joint, elbow and wrist [3]. Kinematic data were collected and analyzed using Polhemus LIBERTY™ (Polhemus, Inc., Colchester, VT) and The MotionMonitor™ (Innovative Sports Training, Chicago, IL).

Each participant was asked to perform a slicing gesture after being instructed to imagine slicing a loaf of bread. Participants made five slicing motions and the middle three cycles were used for analysis. Euler angles, following the ISB convention were exported from The MotionMonitor for the glenorohumeral joint, elbow and wrist. A custom MATLAB program was used to normalize each cycle of data to 100 points (i.e. from initiation to completion of each slice). Mean curves were generated from the three trials and ensemble averages were calculated for each group. The entire mean curve as well as the range of motion and location of the maximum and minimum motions were examined. Additionally, a custom MATLAB (R2010a, The MathWorks, Natick, MA) program was written for post processing kinematic variables including movement amplitude, trajectory duration and average velocity,. Movement amplitude is the distance the wrist travelled along the path of each cycle [4]. Trajectory duration is defined as the time taken to complete 1 cycle of slicing. Data from each group were compared to identify differences between the impaired and unimpaired individuals.

RESULTS AND DISCUSSION

Kinematics showed that the patients with aphasia had a greater range of motion when compared with their age matched controls in elbow flexion/extension (84±50° vs. 34±18°), elbow pronation/supination (11.5±7.4° vs. 2.6±1.3°), wrist flexion/extension (14.5±9.2° vs. 2.6±0.8°), wrist ab/adduction (14.5±9.2° vs. 3.8±0.7°), wrist pronation/supination (11.4±2.6° vs. 3.2±1.4°) and glenerohumaral elevation (23.0±7.4° vs. 7.6±4.6°). The standard deviations of these motions were also greater in the participants with aphasia and their cycle-to-cycle variability tended to be greater than that of their age matched counterpart (Figure 1), suggesting that the patients with aphasia may have less control over their motions compared to their healthy counterparts. Additionally, the end of the forward slicing motion appeared to occur earlier in the cycle of motion in participants with aphasia than their age matched controls (49±2% vs. 56±4%, Figure 1).

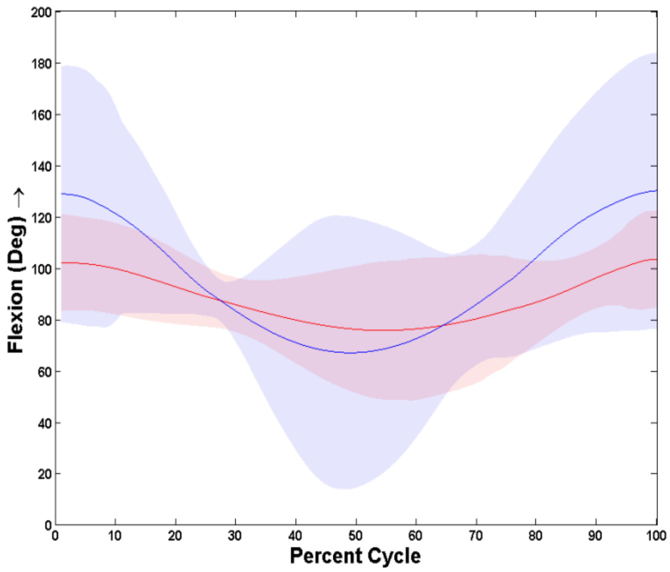

Figure 1. Mean and standard deviations of elbow flexion/extension in aphasia patients (blue) and age matched healthy volunteers (red). The data show differences in the movement pattern as well as a larger standard deviation in the patients with aphasia.

The movement amplitude showed that the patients with aphasia had a greater trajectory of motion than the healthy controls (74.3±38.5 cm vs. 35.5±21.9 cm), which makes sense, as the aphasia patients had a greater range of motion when the kinemtic data were examined. It took the aphasia patients longer to complete each cycle (1.3±0.2 seconds vs. 1.1±0.8 seconds); however, their mean velocity was faster than the age matched controls (0.6±0.3 m/s vs. 0.34±.07 m/s). Even though the aphasia patients were faster, it took them longer to complete a cycle because their slicing trajectory was larger than their age matched controls.

CONCLUSIONS

This preliminary study demonstrates that there is a difference between the kinematics of a slicing gesture between patients diagnosed with aphasia after a left hemispheric stroke and age matched controls. It is important to develop a database of these motions in both healthy individuals as well as in individuals diagnosed with aphasia. These data will be helpful in future studies that will quantify the effects of gestural facilitation of naming speech therapy on movement patterns.

REFERENCES

[1] Raymer et al., *Neuropsychological Rehabilitation*, *in press*, 2012.

[2] Karduna, A.R., et al., *J Biomech Eng* **123**(2), p. 184-90, 2001.

[3] Wu, G., et al., *J Biomech*, **38**(5): p. 981-992, 2005.

[4]. Clark, M.A., et al., *Brain*, **117 (Pt 5)**: p. 1093-106, 1994.

EFFECTS OF CORTICAL STIMULATION ON SENSORIMOTOR FUNCTIONS OF THE HAND IN HEALTHY OLD ADULTS

Pranav J. Parikh and Kelly J. Cole

Motor Control Laboratories
Department of Health and Human Physiology
University of Iowa, Iowa City, USA
email: pranav-parikh@uiowa.edu

INTRODUCTION

Transcranial anodal stimulation (tDCS) has shown promise to improve dexterous manipulation in healthy old adults [1]. However, underlying changes in the finger force control during object manipulation and specific neural mechanisms are not clear. In this study, we intend to understand the effects of tDCS to the contralateral M1 combined with motor training (MT) on moment-to-moment changes in the forces applied to the object during grasp and manipulation. We also measure performances on functional tasks in healthy elderly individuals.

METHODS

Right-handed able-bodied individuals aged between 60 and 85 years participated in a sham-controlled, cross-over, single-blinded study. The intervention comprised of tDCS in combination with repeated practice on the Grooved pegboard test (tDCS+MT) for 20 minutes. Each participant received anodal tDCS+MT and sham tDCS+MT in two separate sessions at least 5 days apart. Before and after the intervention, they performed a ‘key-slot’ task, which required inserting the slot on the object over the bar; an isometric force production task using a pinch grip with and without visual feedback; and the Grooved pegboard test.

RESULTS

Our preliminary results (n=6) showed that the reduction in time to complete the Grooved pegboard test and the key-slot task was similar following sham and anodal tDCS+MT. However relative to sham tDCS+MT, anodal tDCS+MT allowed participants to better retain the improved performance on the Grooved pegboard test 35 minutes later (Intervention×Time interaction; $p=0.042$).

For the isometric pinch grip task performed with vision, anodal tDCS+MT significantly increased the coefficient-of-variability (COV) of grip force than sham tDCS+MT (Intervention×Time interaction; $p=0.02$). In contrast, while inserting the slot on object over the stationary bar (key-slot task), moment-to-moment variability (standard deviation) in the horizontal force angles showed a strong trend towards reduction following anodal tDCS+MT, as compared to sham tDCS+MT (Intervention×Time interaction; $p=0.058$).

Taken together anodal tDCS+MT, but not sham tDCS+MT showed task-dependent effects on the force variability (Intervention×Task interaction; $p=0.004$).

Furthermore, the change in time to complete the pegboard test performed 35 mins after the tDCS+MT correlated with the change in horizontal force angle variability on the key-slot task ($r=0.626$; $p=0.03$), but not with the change in COV of grip force during the isometric pinch grip test ($p>0.1$).

DISCUSSION

Our results indicate that anodal tDCS+MT facilitates retention of learning on a skillful manual task in healthy old adults, which is consistent with other reports demonstrating the role of motor cortex in consolidation versus acquisition of learning on a skilled task. Furthermore, improved retention on the pegboard test was associated with reduced force variability on the key-slot task that demanded similar precise control over the forces applied to the object. These findings suggest that improvement in force steadiness is one of the potential mechanisms through which short-term anodal tDCS during motor training improved performance on a functional task that outlasted the intervention period.

Similar approaches with peripheral transcutaneous electrical nerve stimulation yield no effects in a small group of subjects, which prompted the change to direct cortical stimulation.

REFERENCES

1. Hummel FC, Heise K, Celnik P, Floel A, Gerloff C, Cohen LG. *Neurobiol Aging. 2010 Dec; 31(12): 2160-8.*

ACKNOWLEDGEMENTS

This study is supported by the American Society of Biomechanics Graduate Student Grant-in-Aid (2011-2012).

THE IMPACT OF OBESITY ON THE ACCURACY OF PREDICTING BODY FAT PERCENTAGE IN OLDER MEN

[1]Erica Parise, [1]April J. Chambers, [1,2]Jean L. McCrory, and [1]Rakié Cham

[1]University of Pittsburgh, Pittsburgh, PA, USA, [2]West Virginia University, Morgantown, WV, USA
email: ajcst49@pitt.edu, web: http://www.odar.pitt.edu/hmbl/index.html

INTRODUCTION

It is well-known that body composition is strongly correlated with health in older adults. Specifically, total body fat percentage (BF%) has been associated with risk for morbidity and mortality [1]. Several advanced methods for determining BF% have been established, such as underwater weighing and Dual-Energy X-ray Absorptiometry (DXA), which provide the greatest accuracy in prediction of BF% [2]. However, due to cost and other study limitations, these methods are not always a practical method for determining BF%.

BF% regression equations have been developed from several different anthropometric measurements, but equations using skinfold thickness (ST) from various locations on the body are the most popular in clinical use. The American College of Sports Medicine currently recommends the use of Jackson and Pollock body density (BD) equations combined with either Siri or Brozek BF% equations to estimate BF% [3,4,5]. Previous research has shown that BF% is affected by age and obesity [1]. The Jackson and Pollock equations were developed from a middle aged American population of non-obese men and women [2]. Because of this, these equations may not be well suited for prediction of BF% in elderly or obese populations.

In order to understand the effects of age and obesity on the accuracy of BF% predictive equations, the aim of this study was to compare BF% predicted by Jackson and Pollock equations to BF% determined by DXA in obese and non-obese men over the age of 65 years.

METHODS

Forty-one healthy men aged 65 or older, were divided into non-obese and obese subgroups based on body mass index (BMI) (BMI≤30, non-obese; BMI>30, obese) (Table 1). After obtaining written informed consent approved by the University of Pittsburgh Institutional Review Board, each participant underwent a whole body DXA scan (Hologic QDR 1000/W, Bedford, MA, USA) lying supine. Assumed densities for bone (2.5–3.0 g/cc), fat (0.9 g/cc), and lean (1.08 g/cc) tissue were used. Body fat % (BF%) was determined as total body fat mass/total body mass.

Table 1: Subject sample characteristics

Mean (SD) [Range]	Non-obese (n=21)	Obese (n=20)
Age (yrs)	76.00 (5.35) [65.68- 85.02]	74.54 (4.58) [66.46-82.24]
BMI	26.29 (2.59) [19.75-29.71]	33.86 (3.18) [30.14-41.26]
Mass (kg)	79.02 (10.48) [56.00-97.10]	102.05 (14.53) [83.30-133.81]
Height (m)	1.73 (0.06) [1.62-1.82]	1.73 (0.06) [1.62-1.85]

ST measurements were carried out with a Lange skinfold calliper (Beta Technology Inc, Cambridge, MD, USA) at chest, midaxillary, tricep, bicep, subscapular, abdomen, suprailiac, and thigh sites. Measurements were taken three times at each site and averaged across the three measurements. Body density (BD) was calculated using Jackson and Pollock 7 skinfold equation for men: $BD=1.112 - 0.00043499*(\text{sum of 7 SF}) + 0.00000055*(\text{sum of 7 SF})^2 - 0.00028826*(\text{age})$ [3]. BD was then converted to BF% using both Siri (JPS) and Brozek (JPB) equations [4,5].

Analysis of variance was performed on BF% using method type (DXA/JPS/JPB) and obesity (main effects and first order interactions) as fixed factors. Subject was a random factor in the model. Post hoc analyses included comparisons using a Tukey test. Statistical significance was set at 0.05. In addition to the statistical analysis, percent difference was calculated to aid in assessing the differences between DXA and the regression equations with DXA values of BF% being the gold standard.

RESULTS AND DISCUSSION

As expected, mean BF% from DXA was significantly greater in obese compared to non-obese groups ($p<0.0001$). Method type was also significantly different ($p<0.0001$). Post-hoc analysis revealed that DXA BF% was significantly different than JPB and JPS BF% in non-obese males. Specifically, both regressions (JPS and JPB) underestimated BF% in non-obese older males (Figure 1). This is consistent with previous literature which found that Jackson and Pollock equations significantly underestimated BF% in non-obese older men when using a 4-compartment model of body composition as the standard [6].

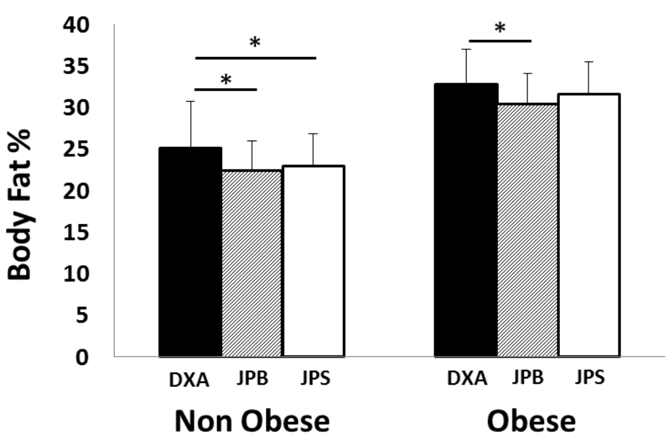

Figure 1: Mean BF% from DXA in black, Jackson & Pollock-Brozek (JPB) in gray, and Jackson & Pollock-Siri (JPS) in white in non-obese and obese men. * denotes significant differences between DXA and JPB, and DXA and JPS in non-obese, as well as between DXA and JPB in obese. Standard deviations are provided.

In obese males, JPB equations significantly underestimated BF%, but there was no significant different between JPS BF% and DXA BF% (Figure 1). This suggests that Jackson and Pollock equations may be better at predicting BF% in obese older men than non-obese. Previous literature found that another predictive equation was better able to estimate BF% in obese older men than in non-obese older men, but the population size for obese older men was small [2].

CONCLUSIONS

These results suggest that Jackson and Pollock equations may not be best suited for use in older male populations, for both obese and non-obese individuals. This is likely due to the use of a middle-aged healthy population to develop the Jackson and Pollock equations. Other predictive equations have been developed for older populations. Further evaluation of these and other predictive equations in older obese and non-obese populations, including females, is needed. This will allow for improved BF% estimations in older adults and in turn improve assessment of risk for morbidity and mortality.

REFERENCES

1. Kuczmarski RJ. *A J Clin Nutr* **50**, 1150-1157, 1989.
2. Guerra RS, et al. *J Nutr Health Aging.* **14**, 744-8, 2010.
3. Jackson AS, Pollock ML. *Br J Nutr* **40**, 497–504, 1978.
4. Siri WE. *Techniques for measuring body composition* 223-244, 1961.
5. Brozek J, et al. *Ann N Y Acad Sci* **26**, 113-40,1963.
6. Clasey JL, et al. *J Appl Physiol* **86**, 1728-1738, 1999.

ACKNOWLEDGEMENTS

Funding and support was provided by The Pittsburgh Claude D. Pepper Older Americans Independence Center (NIH P30 AG024827) & The University of Pittsburgh CTRC (NIH/NCRR/CTRC Grant 1 UL1 RR024153-01). Special thanks to Dr. S. Greenspan, Donna Medich & Adrienne Belasco.

Effect of L-dopa on multi-finger synergies and anticipatory synergy adjustments in Parkinson's disease

[1]Jaebum Park, [1]Vladimir Zatsiorsky, [2]Mechelle Lewis, [2]Xuemei Huang, and [1]Mark Latash
[1]Pennsylvania State University, University Park, PA, USA
[2]Pennsylvania State University, Hershey, PA, USA
email: jzp12@psu.edu

INTRODUCTION

Parkinson's disease (PD) is a progressive neurologic disorder caused by degeneration of dopamine neurons, leading to impaired motor coordination [1]. The gold standard of current therapy the dopamine replacement with L-dopa [2]. L-dopa has marked symptomatic effects on many clinical sings of PD. However, the effect of L-dopa on motor coordination has not been understood clearly, and it limits prospects for application and studying L-dopa treatment. We examined multi-finger coordination in patients with early-stage PD because problems in multi-finger coordination are frequently the first clinical signs in PD. Results of our previous study (in review, [5]) have suggested that PD is associated with significant impairment of multi-finger coordination. In particular, we observed decreased synergy indices in multi-finger accurate force production tasks and reduced anticipatory synergy adjustments (ASAs) in preparation for a quick force pulse production [3]. The aim of the current study was to investigate how L-dopa treatment affects the synergic action of fingers during multi-finger pressing tasks.

METHODS

<u>*Subject:*</u> Six patients with idiopathic Parkinson's disease (age: 58.4 ± 11.6 yrs, mean ± SD), Hoehn-Yahr stage less thant II (while "off" PD medications) were recruited. All patients were right-hand dominant. Each subject was tested twice on the same day, on- and off- L-dopa.

<u>*Equipment:*</u> Four piezoelectric force sensors were used to measure vertical forces produced by the fingers. The sensors were attached to a customized flat wooden panel (size: 140 × 90 × 5 mm).

<u>*Experimental Procedure:*</u> The experiment consisted of three blocks including (1) maximal voluntary contraction (MVC_{TOT}) tasks with the four fingers, (2) single-finger ramp tasks, and (3) quick force pulse production tasks. The subjects performed three sessions with the left and right hands in a balanced order, and each subject was tested twice, early in the morning (off) and 40 min after taking the first dosage (on) of L-dopa. The entire experiment for each visit lasted approximately one hour. During the single-finger ramp tasks, subjects were required to press with one of the fingers (the task finger) and match with the force template shown on the screen. The subjects were instructed to keep all fingers on the sensors, and both task and non-task finger forces were measured. During the quick force pulse production tasks, the subjects were asked to produce a steady-state level of force (set at 5% of MVC_{TOT}) for 3-4 s, and to produce quick force pulses to a target force level (set at 25%±5% of MVC_{TOT}) in a self-paced manner by pressing with all four fingers. Each subject performed 25-35 trials using each hand.

<u>*Data analysis:*</u> The enslaving matrix (E) was computed using the data from the single-finger ramp tasks, which reflects the involuntary force productions by non-task fingers. The time (t_0) of initiation of F_{TOT} change was defined as the time when the first derivative of force (dF/dt) reached 5% of its peak value in that particular trial. The time to reach F_{PEAK} (t_{PEAK}) was defined as the time of F_{PEAK} with respect to t_0. Further analysis used an index of multi-finger force stabilizing synergy computed within the framework of the uncontrolled manifold (UCM, [4]) hypothesis. First, variables reflecting intended finger involvement in force production (finger mode) were computed using the finger forces and the enslaving matrix, E. Second, the trials by each subject and in each condition were aligned with respect to t_0. After the trial alignment, finger mode variance across trials was quantified separately in two sub-spaces for each time sample. The first sub-space corresponded to a fixed value of F_{TOT} (V_{UCM}). The second sub-space was the orthogonal complement to the first one (V_{ORT}). Further, presence of synergy ($\Delta V > 0$) and its

strength were quantified by the relative amounts of V_{UCM} and V_{ORT} with respect to the total variance (V_{TOT}), which was computed for each time sample and formed a time function:

$$\Delta V(t) = \frac{V_{UCM}(t)/3 - V_{ORT}(t)/1}{V_{TOT}(t)/4} \qquad (1)$$

where each variance index is normalized by the number of degrees-of-freedom in the corresponding spaces. For further statistical analysis, ΔV was log-transformed (Fischer transformation) resulting in an index ΔV_Z. The average value of ΔV_Z was computed for the steady-state (between –600 and –400 ms before t_0). The time of initiation of changes in ΔV_Z (time of anticipatory synergy adjustment, t_{ASA}) was defined as the time when ΔV_Z dropped below its average steady-state value by more than two SDs. Negative values of t_{ASA} mean that ΔV_Z started to drop before the initiation of F_{TOT} changes.

RESULTS AND DISCUSSION

Timing index: The subjects were relatively faster in the time to F_{PEAK} on- L-dopa for both right and left hands (off: 0.29 ± 0.04 sec; on: 0.25 ± 0.02 sec, mean ± SD, $p < .05$). This finding confirms the well-documented effects of L-dopa on movement speed.

Synergy analysis of the quick pulse trials: During steady-state force production, positive ΔV indices were observed both off- and on-L-dopa. This means that the finger forces co-varied across trials to stabilize F_{TOT}. The magnitude of the synergy index, ΔV, was larger on the drug as compared to the off state for both hands ($p < .05$) (Fig. 1). The synergy index showed a trend to be higher in the left hand ($p = 0.06$). This result suggests that L-dopa has beneficial effects not only on such global indices of motor performance as speed but also on indices reflecting more subtle aspects of motor control such as multi-digit coordination.

Prior to the initiation of the force pulse, there was a drop in the synergy index (ASA), which was of a larger magnitude on-L-dopa: ΔV_z dropped earlier on the drug (off: –0.066 ± 0.04 sec; on: –0.194 ± 0.07 sec, mean ± SD, $p < .05$) (Fig. 1), and there was no difference in t_{ASA} between the two hands. ASAs reflect a particular aspect of feed-forward control [3]. The effects of L-dopa suggest that this drug can alleviate the effects of PD on feed-forward control.

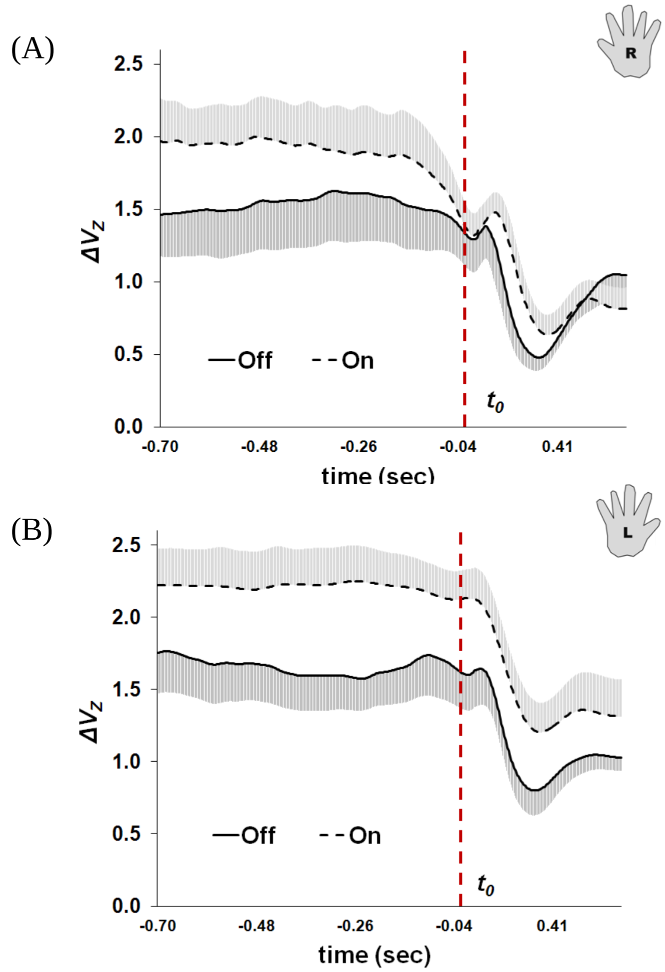

Figure 1: Variance of the total force (z-transformed ΔV, ΔV_Z) of the right **(A)** and left **(B)** hands for off- (dotted line) and on-drug (dashed line) during the discrete quick force production tasks. Average and standard error across subjects are presented. t_0 represents the time of initiation of F_{TOT} change.

CONCLUSIONS

1. L-dopa alleviates the detrimental effects of PD on multi-digit synergies.
2. An aspect of feed-forward control (ASAs) that is impaired in PD shows beneficial effects of L-dopa.

REFERENCES

1. Aruin AS, et al. *Neuroreport* **7**: 1794-1796, 1996
2. Bowen FB, and Brady E, Yahr MD, *Neurology* **23**: 1101-1106, 1973
3.Olafsdottir H, et al. *Neurosci Lett* **381**: 92-96, 2005
4. Scholz JP, and Schöner G, *Exp Brain Res* **126**: 289-306, 1999
5. Park J, et al. *J Neurophysiol* [In review]

BICYCLE RIDING, ARTERIAL COMPRESSION AND ERECTILE DYSFUNCTION

Sujeeth Parthiban[1], Christopher Yang[2], Loren Jones[2],Amit Baftiri[3],Craig Niederberger[2]

[1]Department of Bioengineering, University of Illinois at Chicago, Chicago, IL, USA - 60612.
[2]Department of Urology, University of Illinois at Chicago, Chicago, IL, USA-60612.
[3]Department of Radiology, University of Illinois at Chicago, Chicago, IL, USA -60612.

INTRODUCTION

A National survey approximately estimates 57 million people rode a bicycle in 2002. Males were more likely to ride bicycle than were females[1]. Another survey estimates US bicycles and accessories sales in 2010 to be 6 billion dollars. Several research studies implicated bicycle riding as risk factor for erectile dysfunction[2]. One possible reason is ischemic injury due to compression of perennial arteries between the bony pelvis and the bicycle seat. Previous studies attempted to measure this damage employed several indirect methods including computational models[3], pressure mats on a stationary bike[4], measuring transcutaneous oxygen pressure in the penis[5], MR imaging of the pelvic region[6], doppler flowmetry. None of these studies measured forces exerted directly on the perennial arteries and correlated to each riders occlusion force. Most of these studies are done on a stationary bike set up inside the lab. The objective of our study is to build a device to measure the forces exerted on the perennial arteries and develop a method to correlate the forces with each riders occlusion force. Another goal is to conduct the rides on the road where actual bike riding takes place. Recent publications[4] suggested that cutting off the nose from the saddles may help to prevent the damage to the arteries. Based on these findings several noseless seats came to market. We also wanted to test some of them in our study.

MATERIALS AND METHODS

In order to conduct our studies on road we decided to develop our own device which is portable and which does not alter the natural positioning or comfort of the rider. 1 lb Flexiforce® sensors were chosen to measure the forces on the artery because they are thin, flexible and virtually unnoticeable by the riders. Rabbit core module 4000 based device was developed which can record and store force from 8 different sensors. The device was powered by 4 AA batteries making it portable. The device was calibrated using Instron 8500 high rate system to convert the output from mV to force in newtons. A geometric template of sensor position was developed based on the anatomy of the perennial arteries so that sensors are placed on fixed locations along the artery. The four locations are marked as right proximal, right distal,left proximal and left distal according to their position on the artery. Using doppler ultrasound subject's perennial artery was identified. Then we slowly applied force on the artery using our force probe attached to our device until blood flow in the artery completely stops. The recorded force is the force required to completely close the artery and we call it as occlusion force. The procedure was repeated four times on each side so that we obtain the mean occlusion force for the right and left side. Four sensors were attached to the subject's skin over the perennial arteries as per the geometrical template using Tegaderm™. Subjects are asked to ride on a standard road course for 0.5 mile each seat. Six different test seats of varying shapes, sizes and padding are used. The seats were called by their commercial names and three of them had nose and three of them are noseless type. The subjects are asked to fill a short questionnaire about the comfort of the seats at the end. The recorded force values for each seat were downloaded and compared to the subject's mean occlusion force.

ANALYSIS

We identified the amount of time a rider spends above the occlusion force. This was done by adding up the points that had force value equal to or greater than the mean occlusion force. As time spent by the riders on each test seat varies we decided to express this value as percentage of total ride time. For example, a rider takes 300 seconds to complete the 0.5 lap for a particular seat. 50% occlusion time for that seat denotes the rider spends 150 seconds on or above his mean occlusion force. This means his artery is completely closed for 150 seconds.

RESULTS

The study so far had 15 volunteers (mean age: 34±12years, BMI: 24.20±2.8 metric units). The mean occlusion force required to occlude the artery for each subject varied from 7.7N to 12.12N. We observed slight difference in the right and left arterial mean occlusion force with maximum observed difference is within 1N.The average occlusion force for all the 15 subjects is 10.16±1.12N. Out of the 15 subjects 12 were significantly (more than 50%) occluding their artery during the road rides. Among them 4 subjects were only occluding in the seats with nose and were occluding less with noseless seats. The mean seat occlusion times are shown in the figure and ranged from 26% to 45%.

DISCUSSION

The mean occlusion force varied among subjects. This variation is independent of age and BMI. It more depends on the anatomy of the perenium. As expected most of the subjects showed significant occlusion on the three seats with nose. This is because the nose of the bike seat directly compresses the artery. To our surprise we observed significant occlusion times when subjects used the three noseless seats. So contrary to the popular belief the noseless seats still puts force on the arteries closing them. So they are still capable of causing erectile dysfunction. One possible reason why these noseless seats still occludes is because of the small sitting area. The subjects tend to push back further on those seats making them to sit right on their arteries instead of their pelvic bones. These noseless seats are rated poorly by the subjects for their comfort. Another interesting trend we observed is one seat which is good for a person is worse for another person in terms of occlusion time. In other words there is no single seat which we tested so far proved effective in minimizing the impact on the arteries.

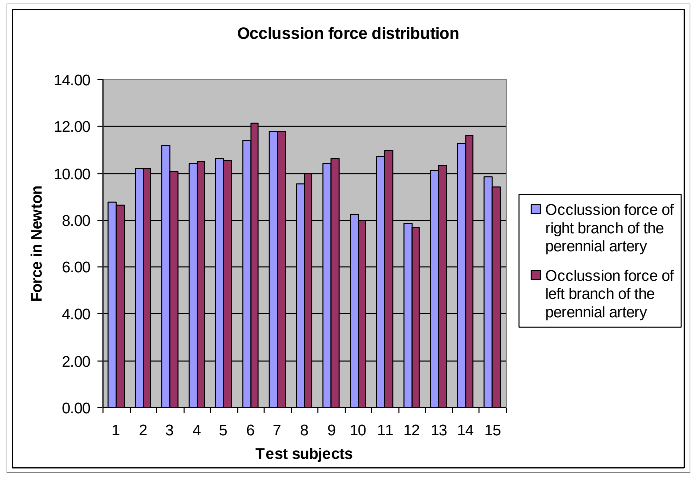

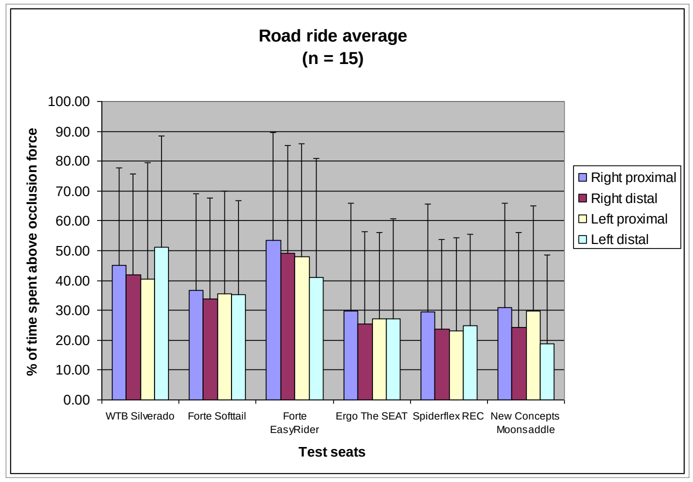

REFERENCES

(1) National Survey of pedestrian and bicyclist attitudes and behaviors.

(2) Sommer F et al,"Bicycle riding and erectile dysfunction: a review"J Sex Med. 2010 Jul;7(7):2346-58. Epub 2010 Jan 19

(3) Spears I. R., et al. “The Effect of Saddle Design on Stresses in the Perineum during Cycling”. Medicine and Science in Sports and Exercise, 2003.

(4) Lowe, Brian D, et. al.“Effect of Bicycle Saddle Designs on the Pressure to the Perineum of the Bicyclist”. Journal of the American College of Sports Medicine. 1055-1062. January 2004.

(5) Schwarzer U, et al.:”Genital numbness and erectile dysfunction in long distance cyclists”. J Urol Suppl 1999; 161:179.

(6) Bressel E., et al. “Influence of bicycle seat pressure on compression of the perineum: A MRI analysis”. Journal of Biomechanics, Nov. 2005.

Biomechanical loading of the sacrum in pre- and post operative adolescents idiopathic scoliosis

[1,2]Saba Pasha, [1,2,3] Carl-Eric Aubin, [2,3] Stefan Parent, [2,3] Hubert Labelle, [2,3] Jean-Marc Mac-Thiong

[1] Department of Mechanical Engineering, Ecole polytechnique de Montreal, Montreal, QC, CANADA
[2] Research Center, Sainte-Justine University Hospital Center, QC, CANADA
[3]Department of Surgery, Université de Montréal, QC, CANADA
email: saba.pasha@polymtl.ca

INTRODUCTION

Posterior spinal instrumentation and fusion techniques are used over decades to correct spinal deformities higher than 40 degrees in scoliotic subjects [1]. Although these methods are successfully decreased the spinal curvature in scoliosis, the biomechanical loading of the distal unfused vertebrae is not well studied after operation. Among unfused vertebrae sacrum, the connective vertebra between the spine and pelvis, is of special interest; the biomechanical loading of the sacrum contributes to the transferred load between the spine and lower extremities and hence impacts the postural equilibrium of the subject [2]. This study tries to present the biomechanical loading of the sacrum in scoliotic patients with different curve types before and after spinal fusion via a comprehensive finite element model (FEM).

METHODS

5 right thoracic and 5 left thoracolumbar/lumbar AIS female subjects who had undergone a posterior spinal instrumentation and fusion with an average of 16 months [12-18] follow-up were selected from the database in our institution. Exclusion criteria of receiving a previous spinal fusion surgery and a spinal deformity (Cobb angle) less than 20 degrees were applied. The medical dossier and pre- and post-operative bi-planar radiographs of the patients were consulted. A gender- age match group of 12 asymptomatic controls with no history of spinal disease were added to the protocol.

3-dimensional reconstruction of the spine, pelvis, ribcage, and the position of the femoral heads were created from digitized landmarks on the postero-anterior and lateral x-rays by a freeform deformation technique along with a detailed atlas of the spine, ribcage, and pelvis [3].

A patient specific osseo-ligamenteous FEM of the spine, ribcage, and pelvis was generated and personalized by means of the landmarks coordinates from the 3D reconstruction [4]. Mechanical properties of the FEM were derived from literature [4]. Beam elements were used to present the different components of the spine, ribcage and pelvis. Intercostal and intervertebral ligaments were modeled with tension-only spring elements while zygapophyseal joints were modeled using non-linear contact and spring elements. The nodes of the ribcage, pelvis, and vertebrae were interpolated to create the abdominal cavity wall. Later the internal and external structures of the trunk were connected by hedrahexal solid elements [4]. The position of the center of mass of trunk slices at the level of each vertebra was derived from literature and optimized in such a way that the geometry of the spine after application of the gravitational forces resembles the original geometry of the spine [4].

Biomechanical loading of the sacrum endplate due to the gravitational load was computed for the cohort of subjects. The compressive stress magnitude was normalized to the patient weight and scaled between the minimum and maximum values of the compressive stress measured on the sacrum endplate in individuals. The barycenter of the compressive stress on the sacrum endplate (COP_{S1}) was calculated by means of the sacrum radius and the magnitude of the compressive stress on the sacrum. The 2D position of the COP_{S1} in the transverse plane with respect to the center of the hip vertical axis (CHVA) was determined.

A cluster technique (K-means cluster, PAWS statistics 18.0) was used to divide the distributions of compressive stress on the sacrum endplate in two areas *i.e.* low stress and high stress areas. The position of the low and high stress areas was compared between pre- and post-operative scoliotic groups and controls. The projection of the position of the COP_{S1} on the transverse plane with respect to the CHVA was calculated and compared to the position of the center of mass (COM) in the three studied groups.

RESULTS AND DISCUSSION

Table 1 shows of the spine and pelvis parameters in the control and pre- and post-operative scoliotic groups *i.e.* RTs and TL/Ls.

The radiographs and high and low stress areas on the sacrum endplate are shown for one typical RT patient before and 10 months after surgery (Figure1).

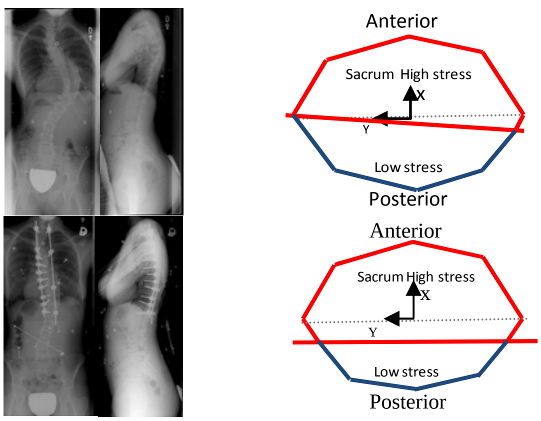

Figure 1. Radiographs and stress distribution on the sacrum endplate before and after surgery in a typical RT subject

Compressive stress on the sacrum was higher at the side of the spinal concavity before operation while the biomechanical loading of the sacrum appears symmetric after operation. No significant different was observed in the position of the COM and COP_{S1} between post-operative and control subjects $p>0.05$ while these parameters were significantly different between pre-operative and controls and pre-operative and post-operative subjects $p<0.05$. The differences between the position of the COM and the COP_{S1} were decreased in post-operative subjects when compared to same parameters before operation.

CONCLUSIONS

A patient-specific model of the spine and pelvis used to show the biomechanical impact of the spinal fusion on the sacral loading. Although sacrum remains unfused after spinal operation the results show the possible effect of the spinal fusion on equilibrating the sacral loading in scoliotic subgroups. This effect can be explained by the fact that the position of the center of mass after operation was more similar to the COM position in controls. The results suggest that the position of the COP_{S1} with respect to the position of CHVA and COM can be used as biomechanical parameters to evaluate scoliosis postural parameters pre- and post-operatively.

REFERENCES

1. Kim YJ, et al. *Spine* **31**, 291-298, 2006.
2. Jiang Y, et al. *Asian J Control* **8,** 297-306, 2006.
3. Kadoury S, et al. *J Spinal Disord Tech* **20**, 160-167. 2007.
4. Clin J, et al. *Med Biol Eng Comput* **49**, 967-977. 2011.

ACKNOWLEDGEMENTS

Funded by FQRNT and NSERC (Industrial Research Chair Program with Medtronic).

Table 1: Spine and pelvis average parameters in the three groups.

		Thoracic Cobb (°)	Lumbar Cobb (°)	Kyphosis (°)	Lordosis (°)	COP_{S1} (mm) With respect to CHVA		COM (mm) With respect to CHVA	
						Medio-lateral	Postero-anterior	Medio-lateral	Postero-anterior
Pre- op	**RT**	54	35	32	44	-7	-6	-14	3
	TL/L	40	55	32	43	10	-15	28	-6
Post-op	**RT**	25	15	29	53	5	-13	5	-10
	TL/L	22	24	26	50	4	-21	10	-17
Controls		-	-	47	50	3	-18	8	-23

THE ROLE OF THE LATISSIMUS DORSI MUSCLE IN PELVIC GIRDLE AND TRUNK ROTATIONS

Jaynesh Patel[1], Ande Sumner[1], John Fox[1], Braden Romer[1], Jared Rehm[1], Brian Campbell[2] and Wendi Weimar[1]

[1]Auburn University, Auburn, AL, USA
[2]University of Louisiana, Lafayette, Lafayette, LA, USA
email: pateljh@tigermail.auburn.edu, web: http://education.auburn.edu/kine/

INTRODUCTION

The role of the Latissimus Dorsi as a shoulder extensor, internal rotator, trunk extensor and trunk rotator has been well documented. Further, the Latissimus Dorsi is a large muscle with multiple attachment sites including the "posterior crest of the illium, back of the sacrum, and the spinous processes of the lumbar and lower six thoracic vertebrae (T6-T12) and slips from the lower three ribs, to the medial side of the intertubercular groove of the humerus" [1]. However, too often we consider the motions of a muscle at only one of the attachment sites and ignore the role of the muscle at the other attachment sites. It is usually thought that the primary role of the Latissimus Dorsi muscle is at the shoulder and as such the attachment sites on the spine and pelvis acts as anchors from which the muscles can pull in order to transmit force across the shoulder. But, what if the attachment site roles were reversed and the shoulder attachment served as the anchor and the joint motion happened at a different attachment site. This relationship has been demonstrated with axial trunk rotation and even trunk extension, however, the contribution of the Latissimus Dorsi to pelvic girdle and other trunk motions has gone largely overlooked.

This study examined the EMG activity of the Latissimus Dorsi muscle during six different pelvic girdle motions and trunk rotations including the following: Anterior pelvic girdle rotation (APGR), posterior pelvic girdle rotation (PPGR), left transverse pelvic girdle rotation (LTVPGR), right transverse pelvic girdle rotation (RTVPGR), left lateral pelvic girdle rotation (LLPGR), right lateral pelvic girdle rotation (RLPGR), trunk flexion (TF), trunk extension (TE), left lateral trunk flexion (LLTF) and right lateral trunk flexion (RLTF). Specifically, the aim of this study was to examine the role of the Latissimus Dorsi muscle during pelvic girdle and trunk rotations in relation to internal rotation of the shoulder (SIR).

METHODS

Fifteen (N=15) current resistance training men volunteered for participation in the study. No participant had a previous upper-extremity injury within the year prior to participation in the study. The age of the participants was 25.1±3.2 years (m±SD); height 1.81±.06 m and body mass 84.1±9 kg. The activity of the Latissimus Dorsi was recorded with a multichannel electromyography (EMG) amplifier/processor unit (MyoClinical, Noraxon USA INC; Scottsdale, AZ) using wet gelled bipolar Ag-AgCl disc surface electrode pairs (Blue Sensor SE, Ambu Inc. Denmark). The raw EMG signal was amplified with an input impedance of 10 MΩ, the gain set at 1000x, and a common mode rejection ratio of >115 dB. Further data processing included band passed filtered (6^{th} order Butterworth, with cut off frequencies of 8 and 535 Hz), and full wave rectified.

Surface EMG electrodes were placed over the muscle belly of the Latissimus Dorsi with a 2 cm inter-electrode distance. Electrode placement sites were shaved, abraded, and cleaned according to standard electromyographic procedures. The electrode placement was similar to that used by Lehman et al. (2004). Proper placement was verified by manual muscle testing.

The participant performed a maximum volitional isometric contraction (MVIC) of shoulder internal rotation, six different pelvic girdle rotations and then six different trunk rotations. The MVIC was taken as peak EMG values, collected in µv at approximately 90 degrees of internal rotation. It was hypothesized that there would be no statistically significant differences between the EMG recorded from the Latissimus Dorsi during the twelve pelvic girdle and trunk motions when compared to the EMG recorded from the Latissimus Dorsi during internal rotation at the shoulder.

A Paired Samples t-test was completed with samples including internal rotation of the shoulder paired with the six pelvic girdle rotations and six trunk rotations. Significance was set a priori at 0.05.

RESULTS AND DISCUSSION

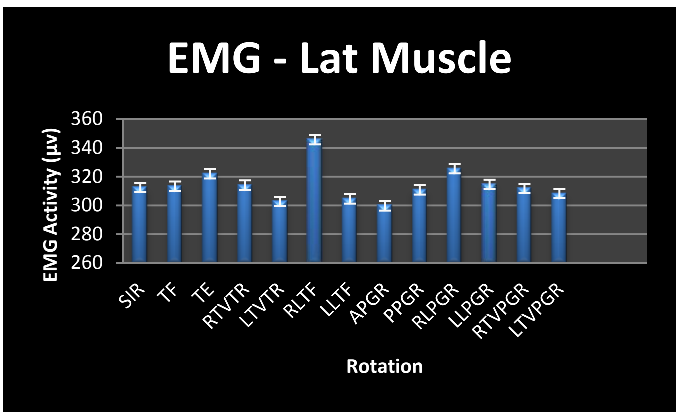

Figure 1: Isometric muscle actions of the twelve movements indicate that the Latissimus Dorsi muscle is active in all of these motions. There was a significant difference only between SIR* and RLTF* p=.002) only. However, this difference occurred due to greater EMG activity in RLTF than in SIR.

Figure 1 presents the EMG activity of the Latissimus Dorsi during the twelve pelvic and trunk motions. The following pelvic girdle and trunk motions produced EMG activity values greater than that of SIR but not significantly: SIR-TF (p=.916), SIR-TE (p=.168), SIR-RTVTR (p=.718), SIR-RLPGR (p=.323), and SIR-LLPGR (p=.863). Furthermore, EMG activity for the following motions had activity values lower, but not significantly different than the values for SIR: SIR-LTVPGR (p=.088), SIR-LLTF (p=.287), SIR-APGR (p=.072), SIR-PPGR (p=.829), SIR-RTVPGR (p=.918), and SIR-LTVPGR (p=.518).

CONCLUSIONS

These findings indicate that the Latissimus Dorsi contributes to six motions of the pelvic girdle and six motions of the trunk with the same (if not more) muscle activity than the matched motion of internal rotation at the shoulder. Further research is needed to determine how these combined motions affect the influence of the Latissimus Dorsi to specific joint motions.

REFERENCES

1. Thompson and Floyd. *Manual of Structural Kinesiology*. McGraw Hill, New York, NY. 1998.

2. Gregory J Lehman et al. *Variations in muscle activation levels during traditional latissimus dorsi weight training exercises: An experimental study.* Dyn Med. 2004; 3: 4. 2004 June 30.

DISTINCT PATTERNS OF RECOVERY FOLLOWING THERAPEUTIC INTERVENTION POST-STROKE: RESPONDERS VS. NON-RESPONDERS

[1]Shilpa Patil and [1,2]Carolynn Patten

[1]University of Florida, Gainesville, FL, USA
[2]Brain Rehabilitation Research Center - Malcom Randall VA Medical Center, Gainesville, FL, USA
email: patilsh@phhp.ufl.edu

INTRODUCTION

Walking recovery is one of the highest rehabilitation priorities for persons post-stroke. Hemiparetic gait is characterized with both kinematic and kinetic impairments in walking. [1] Decreased push-off (i.e., forward propulsion during the terminal phase of gait) contributes to slow walking speeds which characterize walking dysfunction post-stroke. However, detection of clinically meaningful effects is challenging, due in part to heterogeneity of population characteristics and interacting clinical factors including severity and chronicity. Here our goal was to differentiate kinematic and kinetic patterns of response to intervention in an effort to identify characteristics of therapeutic responders and non-responders.

METHODS

36 persons post-stroke (13.9 (S.D. 4.85) months post-stroke, 10 females) participated in a staged intervention including 15 sessions of unilateral lower-extremity power training followed by 9 sessions of clinic-based gait training. Walking function was studied at baseline and following each treatment phase using instrumented 3D-motion analysis. Participants were classified as "Responders" (RES) or "Non-responders" (NRES) on the basis of gait speed improvements exceeding a minimal important difference (MID) of 0.123 m/s, derived from baseline data. We studied kinematics and spatiotemporal parameters including: cadence, stride length, non-paretic (NP) step-length and paretic (P) double-limb support (DLS) phase 1 and 2, and kinetics including: the anterior-posterior (AP) ground reaction forces. The anterior-posterior (AP) impulse generated by the paretic (P) leg, relative to the non-paretic (NP) leg, provides a quantitative measure of the P leg's contribution to forward propulsion termed 'paretic propulsion' (Pp).

Walking speed is positively correlated with both AP impulse and Pp. Forward propulsion during walking was measured by dividing the AP ground reaction forces into 4 bins, defined by key features extracted from speed matched control data. Positive and negative impulses were calculated for each bin with Bins1 and 2 corresponding to early and late braking and Bins3 and 4 to early and late push-off, respectively. Paretic propulsion (Pp), calculated as paretic propulsive impulse/total propulsive impulse generated by both legs, was used here as a measure of the P leg's contribution to forward propulsion.[2]

RESULTS

Kinematics

Overall, significant improvements in gait speed were revealed post-intervention (p=0.0). However, by identifying RES vs. NRES, two distinct patterns of response emerged. RES improved gait speed (0.21 m/s, 31%, p=0.0) and NRES improved (0.06 m/s, 14%, p=0.0). (Fig. 1)

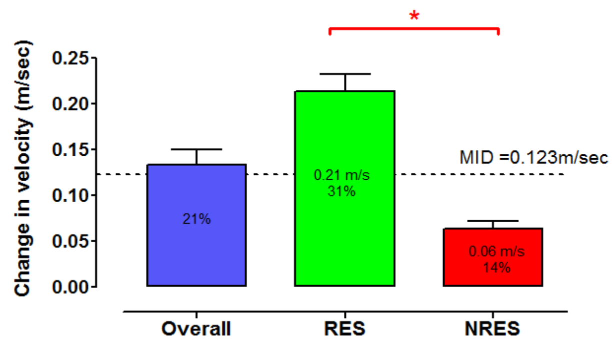

Figure 1: Change in gait velocity for the overall cohort, RES and NRES.

Although, both RES and NRES revealed statistically significant improvements in walking pattern, as reflected by changes in spatiotemporal parameters, these improvements were significantly greater in RES. Moreover, the percentage of individuals who responded by improving greater than 1 MID change were significantly higher in RES than NRES for cadence (**63.6% vs. 6.2%, p= .001**), stridelength (**90.9 vs. 18.8%, p<.001**), non-paretic step-length (**90.9% vs. 6.2%, p<.001**) and 1st paretic double-limb support (PDLS1) (**54.5% vs. 12.5%, p=.019**) respectively. Interestingly, at baseline the RES and NRES groups revealed equivalent gait speed (0.452±0.24 vs. 0.39±0.23 m/sec) and comparable scores on most clinical indicators (p >.05). Only PDLS1 differed between RES and NRES at baseline **(22.06 vs. 16.71% gait cycle, p=.021)** as shown in Fig. 2.

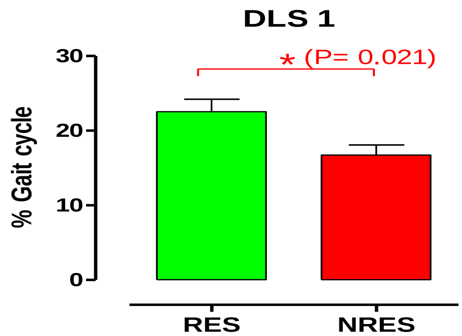

Figure 2: DLS phase 1 represented as percentage of gait cycle at baseline.

Kinetics

Significant overall improvements in Pp were revealed post-intervention **(p=0.002, 16.6 to 25.1%).** However, distinct patterns of response emerged between RES vs. NRES. Although, both RES (.21 m/s) and NRES (.06 m/s) demonstrated statistically significant improvements in walking speed, RES increased Pp, towards normal**, (from 14.7 to 29.2%, p=0.004)** and P propulsive impulses in Bins 3 and 4 by **107.21% and 139.57%**, respectively. Conversely, NRES reduced NP negative impulse in Bin2 by 34.18% with no change in Pp **(from 18.9 to 20.1%, p >.05)** as shown in Fig. 3. Interestingly, baseline gait speed and Pp (14.73±14.57 vs. 17.59±18.66%) were similar between RES and NRES, respectively.

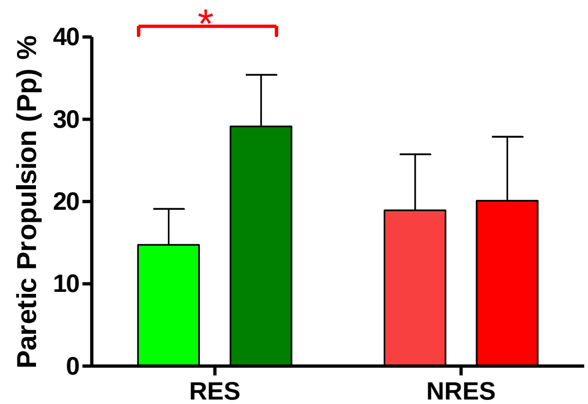

Figure 3: Pp (%) for both RES and NRES. The light green and red bars represent the value at baseline and the darker bars representing the value after the complete staged intervention.

DISCUSSION

These distinct patterns of behavioral response suggest important difference(s) in the capacity for motor recovery post-stroke between RES and NRES. Notably, baseline clinical equivalence in this sample reveals a significant limitation of existing clinical assessments for predicting treatment response. However, difference between the PDLS1 at baseline suggest that parameters reflecting inter-limb coupling are likely important to differentiation of these individuals.

Moreover, despite similarities at baseline, significant effects on AP-impulse and Pp contributing to increased gait speed were revealed post-intervention only in RES. In contrast, compensatory walking patterns appear to be exaggerated in NRES post-intervention.

REFERENCES

1. Olney SJ, et al. *Gait & Posture* **4,** 136-148, 1996.

2. Bowden MG, et al. *Stroke* **37,** 872-876, 2006

MUSCLE STIFFNESS AND RESPONSE TO EXERCISE IN CALORIC RESTRICTED AND AD LIBITUM-FED ELDERLY RATS

[1]Laura L. Pauwels, [1]Brittany Dowling, [1]Nkeonye Okafor, [2]Ryan E. Breighner and [3]Zachary J. Domire

[1]Texas Tech University, Lubbock, TX, USA
[2]Mayo Clinic, Rochester, MN, USA
[3]East Carolina University, Greenville, NC, USA
email: domirez@ecu.edu

INTRODUCTION

It is well known that the strength and size of skeletal muscle decrease significantly with age. This may be partly a result of elderly muscle having an impaired response to exercise, indicated by reduced activation of biochemical pathways responsible for muscle growth after resistance training compared to younger muscle [1,2]. Furthermore, it is known that advanced glycation end products accumulate in the muscle extracellular matrix of aged skeletal muscle [3] increasing tissue stiffness. It has been hypothesized that mechanotransduction mechanisms required for myocytes to sense mechanical stimuli may be compromised by this increased stiffness and this impairment may explain the reduced response to exercise in elderly muscle. Calorie restriction has been shown to lower levels of glycation compared to *ad libitum*-fed rats [4]. The purpose of this study was to compare caloric restricted rats to *ad libitum*-fed rats in order to test whether the activation of pathways responsible for muscle growth in response to exercise is increased in caloric restricted rats compared to age-matched controls and to determine if this response is related to muscle stiffness.

METHODS

This study was a pilot study involving five elderly male F344 rats age-matched to a 40% survival rate. Three rats were fed a lifelong caloric restricted diet, and two rats were fed *ad libitum* diets. All procedures were approved by the Texas Tech Institutional Animal Care and Use Committee. To perform resistance exercise, rats were first anesthetized and their left foot placed in the footplate of a rat dynamometer (Figure 1). Electrodes were placed subcutaneously to span the peroneal nerve to stimulate contraction of the dorsiflexor muscles. Rats performed three sets of ten maximum eccentric contractions of the plantar flexors and were immediately euthanized for muscle harvesting.

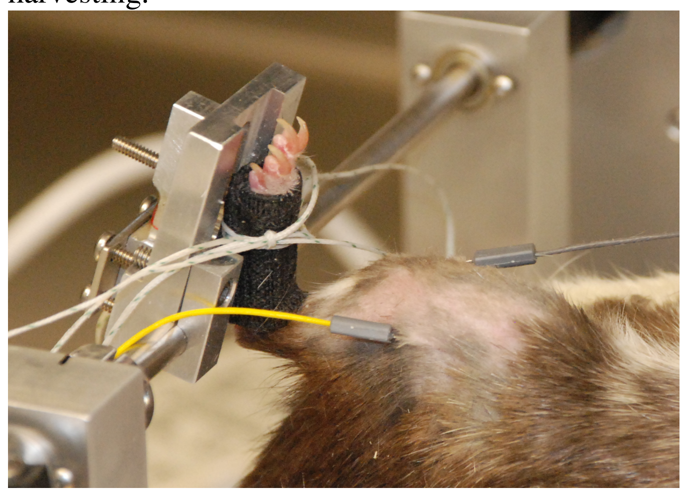

Figure 1. Resistance exercise set-up.

Material stiffness measurements of the right extensor digitorum longus (EDL) muscle were taken within one hour of sacrifice using a custom-built tensile tester. Muscle samples were positioned with approximately 25% of the muscle belly length in each clamp. The specimen was lengthened until a resistive force was developed, and the gauge length in this position was used as l_0. Force measurements were recorded as the specimen was lengthened until midbelly failure. CSA of the muscle was estimated as an ellipse using width and thickness measurements of the muscle midbelly when laid flat. Force was normalized to CSA, and length was normalized to l_0 to create a stress-strain curve. The Young's Modulus was calculated as the slope of a linear trend line fit to the roughly linear region of this curve (Figure 2).

The right and left tibialis anterior (TA) muscles were isolated immediately after sacrifice and frozen in liquid nitrogen. A measure of response to exercise was obtained by quantifying the activation of focal adhesion kinase (FAK), a membrane protein critical in mediating cellular responses to mechanical loading, including cell growth [5]. Activation of FAK was quantified by measuring the percentage of FAK that was phosphorylated using immunoprecipitation, western blotting, and immunodetection analysis.

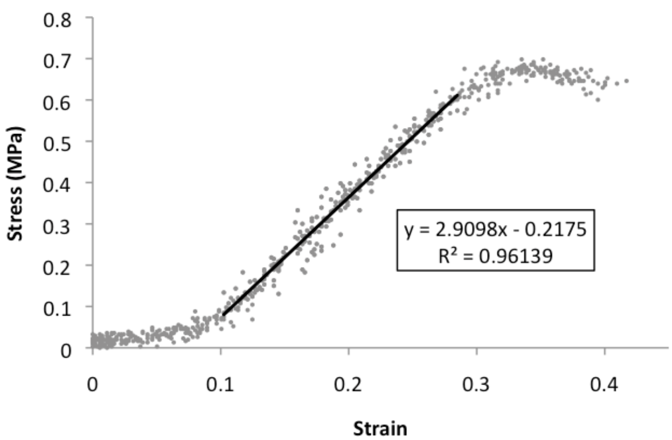

Figure 2. Sample stress-strain curve.

RESULTS AND DISCUSSION

The EDLs of the caloric restricted rats appear to be less stiff than those of the *ad libitum*-fed rats (Table 1). Because caloric restriction is known to lower levels of glycation compared to an *ad libitum* diet, the reduced muscle stiffness in the caloric restricted rats may be due to less glycation and crosslinking of the extracellular matrix.

Analysis of FAK phosphorylation in the tibialis anterior shows that *ad libitum*-fed rats displayed little far less FAK activation directly following resistance exercise compared to caloric restricted rats. Additionally, the phosphorylation percentage seems to decrease as stiffness increases.

CONCLUSIONS

Caloric restricted rats displayed decreased skeletal muscle stiffness as well as substantially increased activation of FAK following resistance exercise compared to *ad libitum*-fed rats. The reduced muscle stiffness in caloric restricted rats may be a result of decreased extracellular matrix glycation, and this decreased stiffness may explain their increased sensitivity to mechanical loading of the muscle. Although this pilot study cannot offer any firm conclusions, it provides support for further investigation into the effects that muscle stiffness may have on mechanotransduction and elderly muscle's decreased ability to respond to exercise as well as support for caloric restriction as a means to modulate muscle stiffness.

REFERENCES

1. Dennis et al. *Physiol Genomics* **32**, 393-400, 2008.
2. Owino et al. *FEBS* **505**, 259-263, 2001.
3. Snow LM et al. *J Gerontol* **64A**, 1204-10, 2007.
4. Cefalu WT et al. *J Gerontol* **50A**, B337-42, 1995.
5. Carson JA & Wei L. *J Appl Physiol* **88**, 337-43, 2000.

ACKNOWLEDGEMENTS

Funding for this project was provided by the ASB Graduate Student Grant-in-Aid. Special thanks to Dr. Boyd Butler for his assistance in our analysis of the FAK protein.

Table 1: Muscle stiffness and FAK activation in *ad libitum*-fed and caloric restricted rats.

	Ad Libitum Rats		Caloric Restricted Rats		
Young's Modulus of EDL (MPa)	3.8	3.1	2.0	2.1	2.9
FAK %Phosphorylation Exercise	1.95	2.83	9.2	9.42	8.73
FAK %Phosphorylation Control	1.62	1.76	1.81	1.73	0.99

THE EFFECT OF DIFFERENT FOAMS ON POSTUROGRAPHY MEASURES IN HEALTHY AND IMPAIRED POPULATIONS

Daniel J. Petit and Kimberly Edginton Bigelow

University of Dayton, Dayton, OH, USA
email: petitd1@udayton.edu

INTRODUCTION

The manipulation of available sensory inputs is an important component in static posturography testing to examine one's multisensory reweighting ability and to identify potential balance problems that would otherwise be masked by compensation [1,2]. Traditionally, to reduce the availability of proprioceptive input, subjects are asked to stand barefoot on a foam pad placed on top of the force platform [1]. However, the choice of what kind of foam block to use often falls on the shoulders of the investigator or clinician as it is rarely well defined in testing procedures. As such, a review of the relevant research reveals a wide range of the type and description of foam used.

Not surprisingly, previous research looking at the effect of surface has determined that the type of surface stood on, as measured by density, elasticity or even thickness, has a dramatic influence on balance [1,3,4]. While these studies have investigated the effect of varying foam types on outcome measures, it has not been well investigated whether choice of foam influences the ability to differentiate between healthy and impaired populations using posturography. This is especially important as standardization of posturography testing methods move forward.

Therefore, the purpose of this study was to investigate the effect of two types of foam (open-cell and closed-cell) on typical balance measurements and their impact on the ability to differentiate healthy and impaired populations.

METHODS

This study was part of a larger experiment and involved 15 individuals with multiple sclerosis (MS) and 15 age and gender matched individuals who served as healthy controls. The average age of MS participants was 48.5yrs ± 9.6yrs (4 Males, 11 Females) and average age for the control group was 47.7yrs ± 8.7yrs (4 Males, 11 Females). Potential subjects were excluded if they had known balance, joint, or sensory problems other than MS. All MS subjects were community ambulatory, not requiring the use of an assistive device to walk. All participants gave informed consent and all procedures were approved by the university's Institutional Review Board.

Anterior-posterior (A/P) and medial-lateral (M/L) center of pressure displacement data was collected using a 3-component force plate (Bertec Corp., Worthington, Ohio). Each trial lasted 30 seconds with a sampling rate of 1000 Hz. For this protocol, a form of the modified clinical test for sensory integration of balance (mCTSIB) was used where a total of six trials were completed in randomized order. The six trials included: (A) standing on balance plate surface with eyes open, (B) standing on balance plate surface with eyes closed, (C) standing on open-cell foam with eyes open, (D) standing on open-cell foam with eyes closed, (E) standing on closed-cell foam with eyes open, and (F) standing on closed-cell foam with eyes closed. Table 1 details the properties of the two foam blocks, as described in data sheets provided by the manufacturers.

Table 1. Foam properties

Type	Dimensions (LxWxH) (cm)	Density (kg/m^3)	UTS (kPa)
Open-cell	50.8x50.8x7.9	32.0	170.3
Closed-cell	47.3x38.4x6.7	55.0	260

A/P Sway Range, M/L Sway Range, and Mean Sway Velocity were calculated for each trial. The main effects of surface, eyes, and disease state, as well as all potential interactions, were analyzed through three-way repeated measure ANOVAs ($p < 0.05$) using SPSS software. Post-hoc analysis was also done to look at each foam type separately using two-way, repeated measures ANOVAs ($p < 0.05$).

RESULTS AND DISCUSSION

Table 2 summarizes the statistical findings as related to the effect of surface.

Table 2. P-values for Main Effects and Interactions related to Surface Type

	A/P Sway Range	M/L Sway Range	Mean Velocity
Surface	**>0.001***	**>0.001***	**>0.001***
Surface*Disease	0.055	0.132	**0.037***
Surface*Eyes	**>0.001***	**>0.001***	**>0.001***
Surface*Eyes* Disease	0.388	0.517	0.380

As expected, the surface did make a difference for all outcome measures (p = >0.001 for all), further supporting the importance of standardizing, or minimally reporting, foam properties if postural sway measures are to be compared across different research or clinical environments. For all three balance parameters, a post-hoc pairwise comparison revealed that all three surfaces (hard flat surface, open-cell foam, and closed-cell foam) resulted in statistically different sway outcomes with indications of poorest balance performance observed in the closed cell foam conditions. From this alone it is unclear, however, whether this surface is simply more challenging or whether the difficulty level may provide better discrimination between those who are able to perform well due to healthy function and those with impaired balance due to disease.

Therefore, of greater interest for this study was whether an interaction existed between surface and disease that would indicate that certain surfaces were better/worse at differentiating individuals with disease from those who were healthy. This could be especially important in improving the clinical utility of posturography which has been hindered by the fact that it is difficult to differentiate individual patients through static balance testing [5]. It was found that for Mean Velocity there was a statistically significant interaction (0.037), and in the A/P Sway Range the p-value also approached significance (0.055). In both cases observed power was < 0.80 suggesting that more subjects are needed to confirm and perhaps strengthen these findings. Post-hoc analysis for Mean Velocity revealed that the between-subject factor of disease was significant for the hard flat surface (p=0.018, effect size=0.184), open-cell foam (p=0.007, effect size=0.229), and closed-cell foam (p=0.007, effect size=0.238). Though further work is necessary with a larger subject population, this suggests that while the values may be drastically different there is not currently compelling findings that the choice of foam better improves the ability to discriminate between disease states.

CONCLUSIONS

While the surface used in posturography was shown to significantly affect measures of postural sway, findings did not strongly support that there is a single superior type of foam which would best differentiate between healthy and impaired balance. As such, until standardization can be reached it does not appear to matter whether open-cell or closed-cell foam is used, but characteristics of the foam are important to report to allow study comparison.

REFERENCES

1. Patel M, et al. *Gait Posture* **28**, 649-656, 2008.
2. Carver S, et al. *Biol Cybern* **95**, 123-134, 2006.
3. Federica D, et al. *Gait Posture* **29**, 158-160, 2009.
4. Wright A, et al. *Accid Anal Prev* **43**, 1480-1487, 2011.
5. Visser JE, et al. *Clin Neurophysiol* **119**, 2424-2436, 2008.

ACKNOWLEDGEMENTS

Funding for this work provided by the LEADER Consortium (NSF ADVANCE), University of Dayton Research Council, and the University of Dayton Graduate School. Statistical analysis was provided by DeAnne French of WSU SCC.

What Causes Slips, Trips, and Falls on the Fireground? A Survey

[1]Matthew N. Petrucci, [1]Brett Harton, [2]Karl S. Rosengren, [1]Gavin P. Horn, [1]Elizabeth T. Hsiao-Wecksler

[1]University of Illinois, Urbana, IL, USA [2]Northwestern University, Evanston, IL, USA
email: mpetrucc@illinois.edu

INTRODUCTION

Slips, trips, and falls are a prevalent cause of injury for firefighters on the fireground. In 2003, the National Fire Protection Agency (NFPA) reported 105 deaths and estimated that there were over 78,000 injuries among firefighters [1]. Of these injuries, 48% occurred on the fireground, resulting in an average of 24 injuries per 1000 fires. More than 27% percent of fireground injuries were attributed to falls, slips, or missed jumps, ranking second to injuries caused by overexertion and strain.

Despite the large quantity of data indicating that falls and loss of balance result in high injury rates and high rates of lost work time [2], efforts to understand the underlying mechanisms and develop possible interventions to reduce these events have been practically nonexistent. The failure to understand the causes of fall and slip injuries has serious consequences: since 1990, the annual number of injuries due to falls, slips, or missed jumps has remained relatively constant, even though the total number of firefighting injuries has substantially decreased over the same time period.

Many conditions within a firefighter's environment could contribute to the prevalence of falls and injuries while on call. However, there has been a lack of systematic investigation of the factors that might put firefighters at risks for falls. To address this issue, we generated a survey to assess potential factors related to slips, trips, and falls in order to potentially develop enhanced training programs and help guide the equipment redesign. Thus, the goal of this project was to identify factors that contribute to a firefighter's risk for a slip, trip, or fall (STF).

METHODS

An anonymous survey was conducted in conjunction with the Illinois Fire Safety Institute (IFSI) at the University of Illinois. Surveys were distributed by mail to all firefighters who had previously participated in a balance and gait study at IFSI [3]. In addition, the survey was made available on the IFSI website to any firefighter who wished to participate. All participants from the balance and gait study ($n = 148$) were male. Gender from the online participants ($n = 94$) is unknown. Demographic factors such as type of firefighter (volunteer, career, or a combination of the two), years of experience, and responses per month requiring bunker gear were asked. A total of 232 responses were received from 87 volunteer, 117 career, and 36 combination firefighters. The average experience was 11.6 ± 8.5 years across all participants, and the average number of fire calls per month requiring gear was 22.2 ± 26.1 per month.

Subjects were asked (1) if they had ever (a) personally experienced or (b) witnessed a slip, trip, or fall and to provide examples if they had, (2) if they had received any previous training to reduce STF when wearing their bunker gear, (3) how their ensemble affects their balance (strongly, slightly, or not at all), and (4) to rate how extensively personal protective equipment (PPE), footwear, self contained breathing apparatus (SCBA) mask, SCBA assembly, and training affect their ability to recover from slip and falls while firefighting on a scale of 1-5, with 1=negatively, 3=no effect, and 5=positively.

RESULTS AND DISCUSSION

Regarding the amount of falls witnessed or personally experienced, 73% of participants had experienced a STF while on call, whereas 84% had witnessed one. The leading cause of an STF both personally or witnessed was ice (Figure 1). This is consistent with previous findings from the NFPA, which identified some of the most common causes of STF's as being due to crossing or moving over objects, icy surfaces, steps or stairs, and wet surfaces [4].

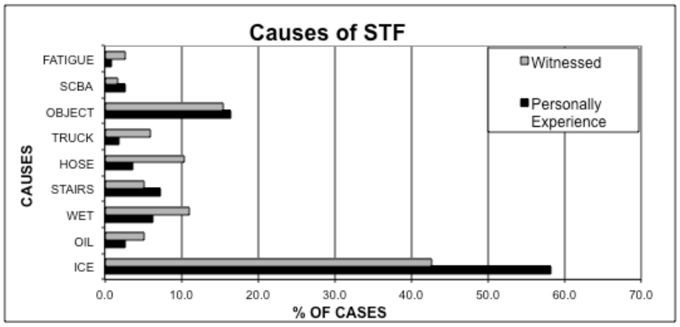

Figure 1: Self-reported causes of slips, trips or falls (STF) as percent of total cases either witnessed or personally experienced.

Eighty-six percent of the participants had not received training to reduce STF while wearing bunker gear, indicating the lack of attention given to prevention. Of the 14% who had received slip training, the majority of them found it to be effective, with only one participant saying it had a negative effect. These results suggest that firefighters find this type of training to be valuable and more programs similar to these could be beneficial for all types of firefighters.

When asked if they felt that the PPE ensemble affected their balance, 32% of the participants responded that it severely affected it, 61% responded that is only slightly affected them, and only 6% responded that it had no effect. Thus, the vast majority of respondents felt that their gear impacts mobility and balance.

Considering the items rated based on their effect on STF recovery (Table 1), the responses were varied with only training being given a positive rating. Footwear had an average rating of 3.0 (out of 5), suggesting that the participants did not feel like footwear had an effect on their ability to recover from a STF. This rating is interesting because multiple write-in comments given by the respondents specifically addressed how different types of footwear (e.g., rubber, leather) affected traction and may put the wearer at risk for falls. Future studies should include additional questions about specific footwear types. PPE, SCBA mask, and SCBA were all given negative ratings, with the SCBA apparatus having the lowest rating (1.9). These results suggest that firefighters perceive that these gear can inhibit their ability to recovery from a STF. These responses correspond with previous findings that SCBA pack weight can have a significant effect on gait parameters and ability to cross obstacles of challenging heights [3]. Thus, continued research is needed regarding PPE and SCBA apparatus design to further reduce their hindrance on slip, trip, and fall recovery.

Table 1: Total number of responses for how each item affects ability to recover from an STF. The average rating based on 5 point scale (5 to 1) is displayed in far right column.

Extent of Hindrance	*Positively, "Helps me recover" (5)*	*(4)*	*No Effect (3)*	*(2)*	*Negatively, "Hinders my ability" (1)*	**AVERAGE RATING**
Protective Clothing ensemble	10	27	79	80	46	**2.5**
Footwear	41	58	37	62	44	**3.0**
SCBA mask only	5	3	130	60	44	**2.4**
SCBA apparatus (complete)	5	11	25	108	93	**1.9**
Training	45	83	94	9	7	**3.6**

CONCLUSIONS

A survey was performed to gain a better understanding of which factors influence slip, trip and fall events on the fireground. Results suggest that firefighters should undergo STF-prevention training regardless of career path. More in-depth questions should be generated in follow-up surveys to further our understanding of different footwear materials and their effects on of slips, trips, and falls. Additionally, continued research should be done looking into how SCBA equipment and PPE can be redesigned to reduce slips, trips, and falls.

REFERENCES

1. Karter, M. J. *NFPA Journal*(Nov/Dec): p. 58, 2004
2. Ault, R. *Advantage* 3(36): 1-8, 2002
3. Park, K. *Ergonomics* 53(7): 882-891, 2010
4. Karter, M. J. *NFPA Journal*(Nov), 2003

ACKNOWLEDGEMENTS

This work was supported by grants from the Department of Homeland Security (#EMW-2006-FP-02459, and # EMW-2010-FP-01606).

Mechanical Cueing Using A Portable Powered Ankle-Foot Orthosis

[1]Matthew N. Petrucci, [2]Colum D. MacKinnon, [1]Elizabeth T. Hsiao-Wecksler

[1]University of Illinois, Urbana, IL, USA [2]Northwestern University, Evanston, IL, USA
email: mpetrucc@illinois.edu

INTRODUCTION

Approximately one third of individuals with late stage Parkinson's disease (PD) experience severe gait impairments, such as the inability to initiate gait (start hesitation) and episodic termination of forward movement (freezing of gait (FOG)). Start hesitation is associated with an impaired ability to generate the anticipatory postural adjustments (APAs) that are required to control posture and balance during gait initiation.

External cues (audio, visual, somatosensory) have been shown to facilitate gait initiation by improving the magnitude and timing of APAs, but the efficacy of cueing strategies is reduced by poor reliability in the home environment [1] and the reduced capacity of patients with PD to produce the forces required to generate an appropriate APA [2]. Thus, considerable need exists for intervention strategies that reliably assist with APA generation via force amplification.

Recent studies have shown that imposed perturbations that provide a small postural assist can significantly improve gait initiation in people with PD, but to date, no wearable device has been tested. Using healthy normal subjects, we investigated the use of a portable powered ankle-foot orthosis (PPAFO) [3] to provide a modest torque at the ankle as a mechanical cue to initiate gait.

METHODS

Five healthy normal subjects (4 male, 1 female, age 21±2 yrs, height 183.6±6.1 cm, weight 78.8±11.5 kg) participated in this study. Five test conditions were evaluated: (1) self-initiated in personal running shoes to provide normal baseline [baseline-shoe], (2) self-initiated trial in unpowered passive PPAFO to provide baseline while wearing PPAFO [baseline-passive], (3) acoustic go-cue in passive PPAFO to assess effect of acoustic cue [acoustic-passive], (4) acoustic go-cue with simultaneous mechanical assist from powered PPAFO to assess effect of acoustic and mechanical assist cue [acoustic-assist], and (5) mechanical assist cue only [assist]. Blocks of 5 trials were performed for each test condition (total of 25 trials per participant). For conditions 2-4, the PPAFO was fit to the test participant and worn on the right limb. The participant's personal running shoe was worn on the left limb.

Trials began with participants standing with their feet on two separate force plates (Bertec). During self-initiated trials, participants were instructed to initiate gait on their own within 5-10 seconds after hearing a warning signal. For all cued trials, an instructed-delay task was used [4]. This instructed-delay consisted of an acoustic warning cue presented 2.5 s before the imperative go-cue [4]. Instructed-delay warnings have been shown to significantly improve gait initiation in people with PD. Participants were instructed to initiate the first step with the right foot "as quickly as possible" and take a minimum of two steps forward.

Both the acoustic warning and go-cue were audible tones for 500 ms at 80 dB from a speaker. The mechanical assist cue began with a dorsiflexor torque for 330 ms followed by a subsequent plantarflexor torque for 83 ms. The actuation timings were based on average time to peak APA from onset to toe-off time in healthy control subjects [2]. The dorsiflexor torque magnitude was heuristically tuned before the gait trials to a magnitude that held the subject's foot at neutral while the plantarflexor torque was set at 9 Nm.

Ground reaction force (GRF) data were recorded from the two force plates. Bipolar surface EMG signals (Delsys) were recorded from an electrode placed over the right tibialis anterior (TA). GRF and EMG data were sampled at 1000 Hz. Force data were filtered using a low-pass Butterworth filter with a cut-off frequency of 15 Hz.

To quantify APA response to the different test conditions, vertical GRF and TA EMG data were analyzed. Specific parameters were time from go-cue to onset, time to peak GRF from onset, time to toe off from onset, and peak GRF amplitude. GRF values were normalized by subject body mass. GRF onset time was calculated based on change of more than three standard deviations from the mean signal recorded 2500 ms prior to the go-cue. EMG data were visually analyzed based on overall activation and behavior.

Repeated-measures ANOVA was used to examine the main effects of test condition on GRF parameters. Post hoc evaluation of interaction effects was examined using Tukey's Honestly Significant Test (HSD). Differences between conditions were considered to be significant at 0.05.

RESULTS AND DISCUSSION

Significant main effects were found between test conditions for peak amplitude ($p = .01$, $\beta = 0.88$), time from go-cue to onset ($p = 0.005$, $\beta = 0.91$), and time to peak from onset ($p = 0.02$, $\beta = .08$). There was no significant difference found for time to toe off from onset ($p = 0.31$, $\beta = 0.32$). Post hoc analysis suggested that the two conditions which included mechanical cueing were significantly different from baseline and auditory conditions for average peak amplitude and time to onset from go-cue (Table 1). For time to peak from onset, significant differences were found between acoustic-assist and baseline-passive only. Overall, data suggest that the mechanical assist cue conditions (with or without acoustic cue) resulted in highly consistent onset of APA behaviors, i.e., increased peak vertical GRF amplitude, shorter time to peak amplitude, and quickening of toe-off time to suggest faster step initiation. These findings could have potential implications for people with PD because these results are consistent with previous external purturbations studies where significantly shortened APA duration and earlier step onset for people with PD were observed [5,6].

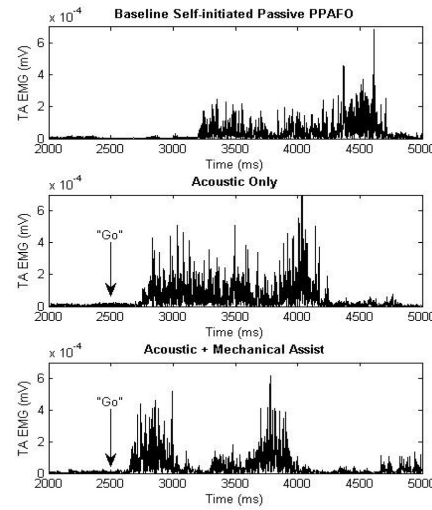

Figure 1: EMG recording from the right TA, during gait initiation trials

Mechanical cueing conditions demonstrated consistent EMG behaviors across all subjects. A consistent onset time of muscle activity was always observed. A bimodal pattern was consistently observed (i.e., TA activation during APA onset, suppression during plantarflexion, and activation during late toe-off (Figure 1). This implies that the PPAFO could aid in consistently inducing necessary muscle activation patterns required for APA production.

CONCLUSIONS

These preliminary data suggest that the mechanical assist from the PPAFO can signifcantly improve APA timing parameters and increase APA force production in healthy normal young adults. Further studies should include people with PD to test the feasibility of using the PPAFO for cueing of Parkinsonian gait.

REFERENCES

1. Nieuwboer, A *Mov Disord* **23 Suppl 2:** S475-481, 2008
2. Rogers, MW *J. of Neurophys* **208**(4): 557-567, 2011
3. Shorter, KA *JRRD* **48**(4): 459-472, 2011
4. MacKinnon, CD *J of Neurophys* **97**(6): 4368-4379, 2007
5. Rogers, MW *Exp. Brain Research* **208**(4): 557-567, 2010
6. Mille, ML *J Neurol Phys Ther* **33**(2): 88-95, 2009

Table 1: Vertical ground reaction force data. Superscripts indicate that the data are statistically the same as the condition shown.

Conditions (A-E)	(A) Baseline Shoe	(B) Baseline Passive	(C) Acoustic Only	(D) Acoustic + Mech Assist	(E) Mech Assist Only
Average Peak Amplitude (N/Kg)	1.3 ± 0.6^{B}	$1.4 \pm 0.5^{A,C}$	1.9 ± 0.6^{B}	2.5 ± 0.9^{E}	2.7 ± 0.7^{D}
Time to Onset from "Go" Cue (ms)	-	-	391 ± 194	215 ± 59^{E}	239 ± 83^{D}
Time to Peak from Onset (ms)	$318 \pm 125^{B,C,D,E}$	$356 \pm 144^{A,C,E}$	$317 \pm 120^{A,B,D,E}$	$263 \pm 73^{A,C,E}$	$284 \pm 97^{A,B,C,D}$
Time to Toe Off from Onset (ms)	$606 \pm 152^{B,C,D,E}$	$584 \pm 195^{A,C,D,E}$	$582 \pm 139^{A,B,D,E}$	$503 \pm 134^{A,B,C,E}$	$530 \pm 135^{A,B,C,D}$

GEOMETRIC ACCURACY OF PHYSICAL AND SURFACE MODELS CREATED FROM COMPUTED TOMOGRAPHY DATA

Geoffrey Piller, Sarah McCoy, Caitlin Collins, Scott Sokn, and Heidi-Lynn Ploeg

University of Wisconsin-Madison USA
email: smmccoy@wisc.edu

INTRODUCTION

When accurate physical models are fabricated from patient specific computed tomography (CT) data, the physical models can be used as a source of pre-operative planning, surgical template, or as replacement implants [1,2]. The creation of the physical models generally follows a three step process: 1. CT imaging; 2. three-dimensional (3D) surface model generation; 3. physical model fabrication. Quantifying the errors within each step can help reduce the overall error of the physical model. Therefore, the objective of the current study was to determine the accuracy of surface models and physical models created from CT data. The errors within the process that were quantified include the CT slice thickness and spacing, the algorithms used to create the 3D surface models from the thresholded CT data, and the creation of initial graphics exchange specification (IGES) computer aided design (CAD) models from the stereolithographic (STL) surface models. In addition this study looks at the accuracy of 3D bone models generated from magnetic resonance imaging (MRI) compared to CT data. The results of this study support the definition of application appropriate protocols to fabricate physical parts from CT data.

METHODS

Two cadaveric lower limb bones (one embalmed, one fresh) and three surrogate bones (femur, tibia, and hemi pelvis) were used in this study. The surrogate bones were CT scanned using five different CT scanners, (GE LightSpeed 16-slice and GE LightSpeed VCT 64-slice, Siemens SOMATOM Sensation 64-slice, Toshiba Aquilion 64-slice, Philips Brilliance 64-slice). The cadaveric bones were scanned using both the GE LightSpeed 16-slice and GE LightSpeed VCT 64-slice), in addition the fresh cadaveric femur and tibia were MRI scanned using the GE discovery. The effects of slice thickness and spacing were investigated at two levels referred to as “clinical” and “high.” The scan settings at these two levels were set according to the standards of the clinic and the maximum of the CT scanner brand.
The thresholded MRI and CT data were converted to STL files in the program MIMICS. To minimize the variance of the thresholding error in the current study, a standard protocol was defined and followed, between three users the difference in surface models was less than 0.07 mm. Therefore, the current study investigated the effect of the algorithms used to create the 3D surface models. Two algorithms were investigated: “High” and “Optimal.” The “High” algorithm did not smooth the surface and had a low tolerance causing it to follow the outer most edge of the outer most pixels. The “Optimal” algorithm smoothed the surface and reduced the number of triangles used to create the 3D surface model. The stl file was then converted into an IGES 3D CAD model. Titanium alloy (Ti) physical models of the fresh cadaveric pelvis and tibia were fabricated using electron beam melting (EBM). The bones and titanium physical models were laser scanned and the laser scan data were used to determine the error of the surface and physical models for all the bones (**Figure 1**).

Figure 1: (Top Left) Fresh cadaveric pelvis. (Bottom Left) Laser scan model derived from the fresh cadaveric pelvis. (Top Right) 3D STL model derived from CT data. (Bottom Right) Ti-6AL-4V ELI physical model.

RESULTS AND DISCUSSION

The largest source of error of those tested was the CT scan slice thickness and spacing. The errors, defined as the perpendicular distance from the laser scan data, in the surface models for cadaveric bone decreased from 0.84±0.87 mm to 0.57±0.66 mm by using CT data with a smaller slice thickness and spacing (Figure 2).

The next largest source of error determined in this study was the algorithm used to create the 3D surface models, which defined the amount of smoothing and triangle reduction of the 3D surface models. Surface models created without smoothing or triangle reduction were larger than the models created with smoothing and triangle reduction. The errors decreased from 0.71±0.60 mm to 0.57±0.66 mm by incorporating smoothing and triangle reduction in the algorithm to create STL surfaces from the thresholded CT data (Figure 2).

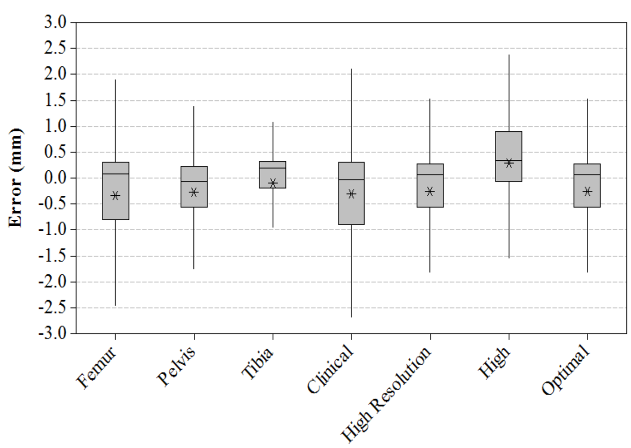

Figure 2: Summary of the STL surface model comparisons for the fresh cadaveric bones with the GE LightSpeed 16-Slice CT Scanner

The third largest source of error, the conversion from an STL file to an IGES file was minimal. There was no difference in the accuracy of surface models generated from CT data from 16-slice versus 64-slice CT scanners. A significant difference was found between the different brands of CT scanners however this was not investigated further due to the large number of parameters that could be varied between brands.

The error between the Ti physical model pelvis and the original cadaveric pelvis was 0.73±0.80 mm, which was higher than values obtained in the literature through the use of bony markers [2,3]. However the error between the Ti physical model tibia and the original cadaveric tibia was 0.42±0.63 mm, which was lower than that found in the literature [2,3]. The error from the MRI generated surface models were much higher than those from the CT surface models of the fresh cadaveric femur and tibia, with an overall error of 1.4±2.09 as compared to 0.67±1.056 mm for the CT surface models (figure 3).

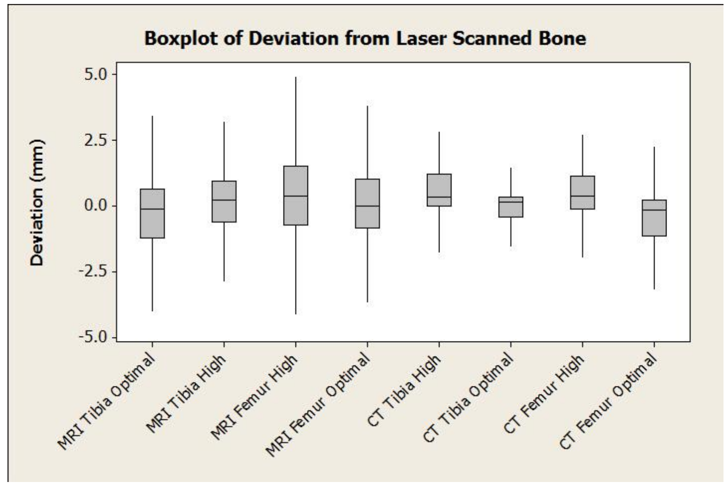

Figure 3: Comparison of CT and MRI surface models of the fresh cadaveric tibia and femur.

The errors in the EBM process were outside of the scope of this study and were not evaluated.

The results of this study provide a framework for capturing patient specific bone geometry for use in patient specific implants, pre-surgical planning, biomechanical models, and as surgical templates.

REFERENCES

1. Fisherman EK, et al. Three-dimensional imaging. Radiology, 1991
2. White D, Chelule KL, Seedhom BB. Accuracy of MRI vs CT imaging with particular reference to patient specific templates for total knee replacement surgery. Int J Med Robotics Comput Assist Surg, 2008; 4: 224-231.
3. Choi JY, et al. Analysis of errors in medical rapid prototyping models. *International Journal of Oral and Maxillofacial Surgery*, 2002; 31: 23-32. Viceconti M, et al. A new method for the automatic mesh generation of bone segments from CT data. *Journal of Medical Engineering and Technology*, 1999; 23: 77-81.

THALAMIC PROJECTION FIBER INTEGRITY IN DE NOVO PARKINSON'S DISEASE

P.J. Planetta[1], E.T. Schulze[2], E.K. Geary[2], J.G. Goldman[3], D.M. Corcos[3-6], D.M. Little[7,8], D.E. Vaillancourt[1,9,10]

[1]Department of Applied Physiology and Kinesiology, University of Florida, Gainesville, FL, USA
[2]Department of Neurology and Rehabilitation, University of Illinois at Chicago, Chicago, IL, USA
[3]Department of Neurological Sciences, Rush University Medical Center, Chicago, IL, USA
[4]Department of Kinesiology and Nutrition, University of Illinois at Chicago, Chicago, IL, USA
[5]Department of Physical Therapy, University of Illinois at Chicago, Chicago, IL, USA
[6]Department of Bioengineering, University of Illinois at Chicago, IL, USA
[7]VISN 17 Center of Excellence for Research on Returning War Veterans, Waco, TX, USA
[8]Department of Psychiatry, Texas A&M Health Sciences and Scott & White Healthcare, Temple, TX, USA
[9]Department of Neurology, University of Florida, Gainesville, FL, USA
[10]Department of Biomedical Engineering, University of Florida, Gainesville, FL, USA

email: planetta@ufl.edu, web: lrnlab.org

INTRODUCTION

The goal of this study was to examine the microstructural integrity of six thalamic regions in *de novo* Parkinson's disease (PD) patients relative to healthy controls using diffusion tensor imaging (DTI). Post-mortem studies of advanced PD have revealed disease-related inclusion pathology in specific thalamic nuclei [1,2]. However, most studies utilizing DTI to investigate the thalamus *in vivo* have focused on the thalamus as a single entity, and have not evaluated the integrity of specific nuclei or the critical cortical-subcortical fibers that project from the thalamus [3-5]. Further, these studies examined relatively advanced PD patients who had been taking antiparkinsonian medication, thus making it unclear whether differences between the patients and controls were caused by the disease, medication, or a combination of both.

METHODS

Forty subjects (20 with early-stage, untreated PD and 20 age- and sex-matched controls) were studied with a high-resolution DTI protocol at 3 Tesla to investigate the integrity of thalamic nuclei projection fibers. Two blinded, independent raters placed seed voxels in six thalamic regions: anterior nucleus (AN), ventral anterior nucleus (VA), ventral lateral nucleus (VL), dorsomedial nucleus (DM), ventral posterior lateral nucleus (VPL)/ventral posterior medial nucleus (VPM), and pulvinar (PU). Fractional anisotropy (FA) values were then calculated from the fibers projecting from the seed voxels in each thalamic region.

RESULTS AND DISCUSSION

As shown in Figure 1, FA values were reduced significantly in PD patients compared to controls in the fibers projecting from the thalamic regions AN, VA, and DM, but not the VPL/VPM and PU. There was also a marginally significant reduction in FA values from the VL projections of the PD patients. These findings were consistent across both raters.

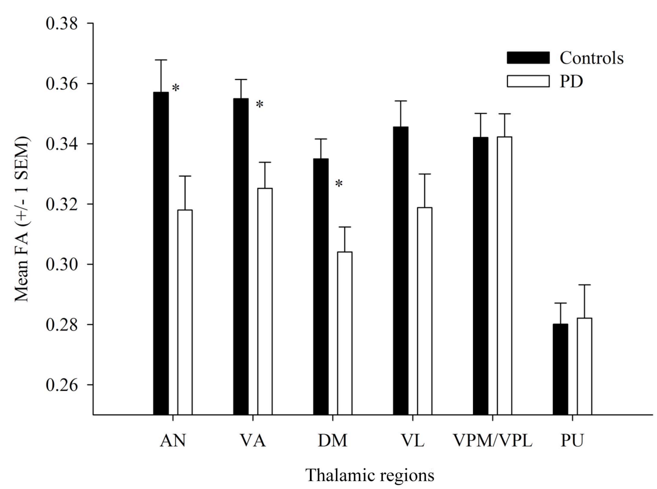

Figure 1: Mean (± SEM) FA values from each of the six thalamic regions for the control and PD groups. Asterisks (*) identify a significant mean difference at an alpha level of .05.

CONCLUSIONS

The present study provides preliminary *in vivo* evidence of thalamic projection fiber degeneration in *de novo* PD and sheds light on the extent of disrupted thalamic circuitry as a result of the disease itself. Specifically, we showed that nuclei involved in motor (VA and VL) and cognitive and affective (AN and DM) processes were disrupted, whereas those involved in sensory processes (VPL/VPM and PU) were relatively spared.

REFERENCES

1. Rüb U, et al. *Neurobiol Aging* **23**, 245-254, 2002.
2. Halliday GM. *Parkinsonism Relat Disord* **15**, S152-S155, 2009.
3. Zhan W, et al. *Mov Disord* **27**, 90-97, 2011.
4. Li W, et al. *Am J Neuroradiol* **31**, 1861-1866, 2010.
5. Péran P, et al. *Brain* **133**, 3423-3433, 2010.

ACKNOWLEDGEMENTS

This work was supported in part by grants from the Department of Defense/Congressionally Directed Medical Research Program (PT 075675), Michael J. Fox Foundation, and National Institutes of Health (R01-NS-52318, R01-NS-58487).

SOFTBALL WINDMILL PITCH: NECESSITY OF A PITCH COUNT

Cara Postlmayr, Tom Wu and Jennifer Ashley

Bridgewater State University, Bridgewater MA, USA
email: cara.postlmayr@gmail.com

INTRODUCTION

Softball has become a quickly growing sport all across the world. The growing number of girls participating in softball has lead to an increase in the amount of sports-related injuries. Softball windmill pitchers account for a high amount of injury incidents within the sport. Previous literatures have reported that the problem seems to be associated with a lack of regulations, proper strength and conditioning programs and the high repetitive stress placed on the shoulder joint [1,3]. According to Sauers et al. the most common reported site of injury in softball pitchers is the anterior aspect of the shoulder joint, accounting for 81% of injuries [4]. Marshall et al. found that out of all the positions on the team, the pitcher has the highest prevalence of injury accounting for 10.8% of the injuries [5]. This data is alarming, over half of active softball pitchers are reporting to have anterior shoulder pain. Therefore, the purpose of this study was to examine the fatigability of the upper limb mechanics in windmill pitching to determine if it was necessary to implement a pitch count to reduce shoulder injuries.

METHODS

Five female Division III college softball windmill pitchers participated in the study. These softball pitchers had no previous history of shoulder pain or injury. Each pitcher went through their normal warm up routine. Reflective markers were placed on their right hip, shoulder, elbow, and wrist joints. The five pitchers threw 70 fastball pitches, to prevent potential influence on joint mechanics from other pitching styles. Pitching trials of #1-10, #31-40 and #61-70 were recorded and analyzed with Ariel Performance Analysis System software. These ten pitch increments were chosen so that researchers were able to analyze the development of fatigue over time. After every 10 pitches, the pitcher took a 2-minute break. Softballs were provided to the pitchers and the team catcher participated in the study. A Sports Radar gun (Model: SRA3000) was placed behind the catcher to record the speed of the ball.

A two-dimensional kinematic analysis was conducted with a Casio Camera (Model: EX-FH25) operated at 120 Hz with the use of 500W artificial light. The digital filter function was applied to filter data at 8Hz. A one-way repeated measure ANOVA statistical analysis was conducted at $\alpha = 0.05$ and followed by a t-test with Bonferroni adjustment if a significant difference was found. Also, Pearson product moment correlation analyses were conducted to determine the relationship between the linear ball velocity and joint angular velocity. All statistical analyses were conducted with SPSS software.

RESULTS AND DISCUSSION

The results of this study showed that changes in joint angles of the shoulder, elbow and wrist at ball release were not statistically significant in the three pitching trial intervals (Table 1). In the beginning, middle and end intervals, the participants showed the shoulder joint angular velocity of 419 ± 245°, 396 ± 277°, and 391 ± 292°, respectively; the elbow joint angular velocities were -1206 ± 283°, -1006 ± 415°, and -970 ± 539°, respectively, and the wrist joint angular velocities were -549 ± 399°, -313 ± 244°, and -437 ± 370°, respectively. A positive joint angular velocity indicates an increase in joint angle at ball release while a negative joint angular velocity represents a decrease in joint angle at release. No statistically significant difference was found in the joint angular velocities of the shoulder, elbow and wrist in the three pitching trial intervals. The resultant linear ball velocity was found to be statistical significant with the one-way repeated measures ANOVA test (Table 1), but with the post hoc pairwise comparison analysis of t-test with Bonferroni adjustment no statistical significant difference was found.

From the Pearson product moment correlation analyses, the results showed that the shoulder joint angular velocity had a significant strong correlation with the linear ball velocity in the middle and end intervals (Table 2). A moderate correlation was observed in the elbow's angular velocity and a small correlation was noted in the wrist's angular velocity.

The findings from this study showed that the pitchers did not change their pitching mechanics from fatigability of pitching 70 fastballs. However, a trend of decreased in the ball velocity from the start of the trial to the end was observed. Hence, this study suggests that future studies should examine the rate of fatigue over a larger span of pitches. Also, due to a limited amount of pitches collected in this study, it was difficult to generalize the findings from this study to a softball pitcher whom normally pitches multiple games in a weekend tournament. A separate future study will be needed to examine the changes in pitching mechanics from pitching multiple games.

The pitchers in the present study demonstrated similar ball velocity as to the previous studies conducted by Barrentine et al. and Werner et al. whom found pitchers to throw at a ball velocity of 25 ± 2 m/s and 27 ± 2 m/s, respectively [1,3].

CONCLUSION

This study examined the mechanics of pitching fatigue in regards to necessity of implementing a pitch count. The results showed that there was no significant difference in joint angles and joint angular velocities from the beginning to the end of the trial. The preliminary findings suggest that it may not be necessary to implement a pitch count for pitchers who will throw 70 pitches and fewer in a game. However, a decrease in the ball velocity over time was observed in the study. Therefore, the findings may become significant with a larger pitching range supporting the need for future research to be performed on the kinematics of the windmill softball pitch. More specifically, future research studies should be focused on the shoulder joint since a strong correlation was observed in the middle and end intervals between the shoulder joint and ball velocity. This implies the importance of strengthening shoulder joint to reduce anterior shoulder injuries within the sport of softball.

REFERENCES

1. Barrentine SW, et al. *J Orthopedic Sports and Physical Therapy.* **28(**6), 405-415, 1998.
2. Richardson AB, et al. *J Sports Medicine* **8**, 159-163, 1980.
3. Werner SL, et al. *J Sports Medicine* **7**, 597-603, 2006.
4. Sauers EL, et al. *J Sport Rehabilitation* **20**, 100-114, 2011.
5. Marshall SW, et al. *J Athletic Training* **42**, 286-294, 2007.

Table 1: Comparisons of the dependant variables in the beginning, middle and end pitching trial intervals

Variables	**Beginning**	**Middle**	**End**	***p***
Shoulder (°)	6.4 ± 4.9	6.7 ± 4.4	6.2 ± 3.6	0.60
Elbow (°)	165 ± 5.7	168 ± 5.5	168 ± 6.9	0.15
Wrist (°)	174 ± 2.1	174 ± 2.2	174 ± 1.1	0.83
Ball (m/s)	25.5 ± 2.6	25.3 ± 2.4	24.9 ± 2.2	0.03*

*Statistical significant at $p < 0.05$

Table 2: Pearson product correlations between each joint angular velocity and linear ball velocity

Variables	**Beginning**	**Middle**	**End**
Shoulder	0.81	0.91*	0.96*
Elbow	0.73	0.30	0.70
Wrist	0.14	0.57	0.42

*Statistical significant

LOADING PATTERNS DURING A STEP-UP-AND-OVER TASK IN INDIVIDUALS FOLLOWING TOTAL KNEE ARTHROPLASTY

[1]Federico Pozzi, [1,2]Ali Alnhadi, [1]Joseph Zeni Jr., and [1]Lynn Snyder-Mackler.

[1]University of Delaware, Newark, DE, USA
[2]King Saud University, Riyadh, Saudi Arabia
email: fpozzi@udel.edu

INTRODUCTION

More than 500,000 Total Knee Arthroplasties (TKAs) are performed annually in the United States [1]. TKA successfully reduces pain and increases self-report of function, but patients continue to exhibit functional deficits and movement asymmetries after surgery [2]. Asymmetrical movement patterns have been found during walking and sit-to-stand tasks [3], and are partially related to the quadriceps strength of the operated limb [4]. The aim of this study was (1) to compare loading parameters between operated and non-operated limbs in subjects following unilateral TKA during a step-up-and-over task; and (2) investigate the relationship between quadriceps strength and limb loading during the same task.

METHODS

13 Individuals with unilateral TKA were evaluated for this study (Table 1). Subjects were excluded if they presented with any pathology (other than TKA) that could affect movement patterns.

Table 1. Subject demographic, mean (SD)

Gender	4M/9F
Age, years	68 (5)
Height, m	1.65 (0.07)
Weight, kg	88.04 (15.53)
BMI, kg/m^2	32.12 (5.80)
Time from surgery, months	14.30 (8.32)

A wooden step (height ~20cm) was fastened to a force platform. Participants were examined during a step-up-and-over task. Participants were instructed to step onto the step with one limb (stepping limb), transverse across the step, land with the contralateral limb (landing limb), and keep walking for ~5m. Both operated and non-operated limb were tested as the stepping and landing limb. 5 trials for each limb were collected.

Kinematic and kinetic data were collected during the step task using an 8 camera motion capture system (Vicon, Lake Forest, CA) and 2 force plates (Bertec Corp, Worthington, OH) (freq., 120Hz and 1080Hz respectively). Quadriceps strength was measured with an electromechanical dynamometer (Kin-kom, Chattex Corp., Harrison, TN). Subjects were positioned with the knee in 75° of flexion and asked to perform 3 sets of maximal voluntary isometric contractions (MVIC). The maximal value was then used for further analysis.

Visual3D software (C-Motion Inc., Germantown, MD) was used for the kinematic and inverse dynamic analysis. The peak knee flexion moment was calculated for the stepping limb (the limb on the step) limb. Sagittal ankle and knee angles at touchdown for the landing limb were calculated. Peak ground reaction force (GRF) and average loading rate (peak GRF/time-to-peak) were calculated as loading measures of the landing limb. Sagittal knee excursion during weight acceptance and average rate of power absorption (peak negative power/time-to-peak) at the knee of the landing limb were also calculated. All kinetic data were normalized according to body weight.

A paired-sample t-test was used to compare measures between operated and non-operated limb. Pearson correlation was used to investigate whether quadriceps strength of the operated limb was related to biomechanical parameters in both limbs.

RESULTS AND DISCUSSION

The operated limb was significantly weaker and was significantly more impaired than the non-operated limb (Table 2). There was no difference between limbs in sagittal plane angles at the knee or ankle at touchdown; however, the knee of the operated limb had less flexion excursion during the weight acceptance phase (p = .021). This suggested that individuals with unilateral TKA tended to land with a stiffer knee, when the operated knee was used as the landing limb. This stiff-knee movement pattern may be related to the tendency of the operated limb to have lower rate of energy absorption at touchdown (p = .083).

When assessing differences between limbs for the stepping limb, the operated limb presented with less knee flexion moment during the descent from the step (p = .018), suggesting that the ability of the operated limb to sustain the weight of the upper body was diminished. In the operated limb, sagittal knee moment was correlated to muscle strength, with weaker muscles demonstrating less knee flexion moment during the step-down portion of the task (r = 0.566, p = .035).

Poor control of the descent phase by the stepping limb appeared to increase loads on the landing limb. The operated knee quadriceps strength was inversely related to average loading rate of the non-operated limb at landing (r = -0.548, p = .05), indicating that individuals with weak operated quadriceps muscle presented with higher average loading rate at the non-operated knee during weight acceptance.

CONCLUSION

Significant asymmetries were found between the operated and non-operated limbs during the landing and stepping portions of the step-up-and-over task. Quadriceps weakness in the operated limb appeared to be related to asymmetrical movement pattern that may play a role in overloading the non-operated limb. Persistent excessive loading during functional activities might facilitate the degenerative process in the contralateral limb and increase risk of contralateral TKA.

Our future studies will include a larger sample size and we will compare these variables at different time points after TKA.

REFERENCES

1. Kurtz S, et al. *J Bone Joint Surg Am*. **89**, 780-785, 2007.
2. Walsh M, et al. *Phys Ther*. **78**, 248-258, 1998.
3. Mizner RL, et al. *J Orthop Res* **23**, 1083-1090, 2005.
4. Yoshida Y, et al. *Clin Biomech*. **23**, 2008.

ACKNOWLEDGMENTS

This study was funded by NIH- P20RR016458.

Table 2. Functional, strength, kinematic and kinetic data.

	Operated limb mean (SD)	**Non-operated limb** mean (SD)	*t-value*	*p-value*	Effect Size
Knee outcome survey, %	84.09 (13.70)	90.35 (12.03)	2.798	.016	0.77
Maximal voluntary isometric contraction, N	5.22 (2.12)	6.82 (2.51)	4.210	.001	1.16
Flexion moment (stepping leg), N*m/BW	1.01 (0.22)	1.16 (0.24)	2.642	.210	0.77
Ankle plantarflexion angle at touchdown, °	28.51 (4.47)	27.86 (5.26)	0.548	.594	0.15
Knee flexion angle at touchdown, °	11.95 (4.87)	10.69 (3.71)	0.866	.404	0.24
Knee excursion, °	15.07 (4.23)	18.78 (5.45)	2.304	.040	0.63
Peak GRF, N/BW	1.73 (0.22)	1.81 (0.24)	1.037	.320	0.28
Average loading rate, N/BW*s	17.40 (4.58)	19.41 (5.88)	1.530	.152	0.42
Average rate of power absorption, W/BW*s	1.36 (0.95)	2.07 (1.44)	1.893	.083	0.52

Abbreviation: GRF, ground reaction force.

DESIGN STUDY ON STABILITY AND SAFETY OF MEDIAN STERNOTOMY FIXATION

[1]Nathaniel Price, [1]Nam H. Kim, [2]Bryan Wilcox, and [2]Brian Hatcher

[1]University of Florida, Gainesville, FL
[2]Biomet, Jacksonville, FL
email: nkim@ufl.edu

INTRODUCTION

In mid-line sternotomies, many different sternal closure techniques have been proposed including wires, cables, bands, rigid fixation, and combinations of these techniques. Wire closure often yields poor bone union and sternal movement or instability. However, wire closure techniques are still the most prevalent technique in use today. A number of biomechanical studies have compared the stability of various closure techniques.

Biomechanical studies of sternal closure techniques are currently limited by the wide variability in sternum size, strength, and density. Synthesized bone models provide a greater degree of reproducibility, but currently lack the ability to represent the bi-material, cortical and cancellous, composition of natural bone. Finite element analysis (FEA) modeling allows for the consistent and reproducible study of a variety of interrelated material and geometric variables.

The objective of this study was to develop a model for evaluating the mechanical performance of 2 sternal closure techniques, rigid plate fixation and wire cerclage. A design study using FEA was performed to determine the effects of screw length, cortical thickness, and bone quality on the mechanical performance of a rigid sternal fixation system. The study analyzed the sternal separation and stresses that developed in the anterior cortical, intermediate cancellous, and posterior cortical regions. Lateral distraction and Rostral-Caudal shear (longitudinal shear) load cases were analyzed. The fixation systems analyzed were peri-sternal wires and the Biomet Microfixation SternaLock® Blu System.

METHODS

A two-level modeling approach was utilized in the design study. A global model consisting of two sternal halves was constructed to determine forces surrounding the plates or wires and to calculate sternal separation (Fig. 1). A local model consisting of a detailed bone model was constructed to determine stresses that developed in the plate, screws, and sternum (Fig. 2).

The mechanical properties and thickness of the cortical and cancellous bone layers were adjusted for the 2 models to simulate patients with variable bone quality. Medium strength cortical bone properties were applied to the global sternum model (Table 1). The plate was modeled as CP Ti Grade IV with an elastic modulus of 104.1 GPa [3]. The screws were modeled as Ti-6Al-4V with an elastic modulus of 112 GPa [3]. A lateral distraction load of 350 N was applied to simulate coughing [2]. A Rostral-Caudal shear load of 175 N was applied to simulate the average force on the sternum from lifting 25 lbs [2]. Average forces surrounding the plates and the sternal opening were recorded for each loading case.

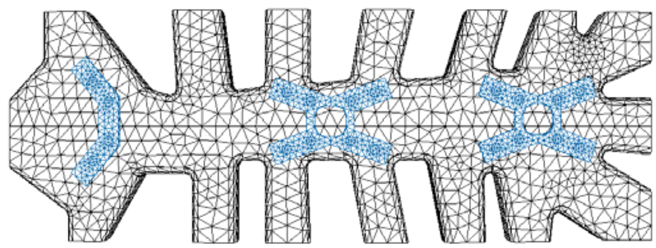

Figure 1: Global sternum model with Biomet Microfixation SternaLock® Blu System

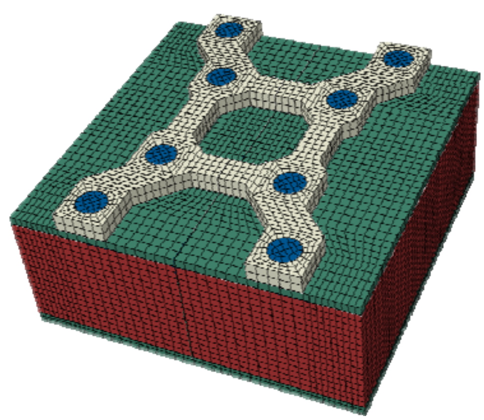

Figure 2: The local model was divided into cortical and cancellous layers with distinct material properties

In the local model, the screw lengths, bone properties, and cortical thickness were parameterized such that they could be easily changed in the design study. Lateral distraction and Rostral-Caudal shear loading cases were analyzed using the loads determined from the global model. Fixed displacements were applied until reaction forces matched the desired applied load. Screws were modeled as cylinders with rigid normal fixation to the plate (modeling the screw locking mechanism). The screw length was adjusted to correspond to 50% purchase in the bottom cortical or 80% purchase in the cancellous region. The cortical thickness was adjusted to 0.50, 0.75, and 1.00 mm while the bone thickness was held constant at 12 mm. The strength of the bone was adjusted to low, medium, and high strength as shown in Table 1.

Table 1 – Elastic Moduli of Bone (GPa) [1]

	Cortical	Cancellous
Low	6	0.04
Medium	12	1.1
High	25	2.2

RESULTS AND DISCUSSIONS

In the global model, sternal separation seen with wire fixation was 48-75 times more than with rigid plate fixation (0.317mm vs. 0.0066mm). Due to the low contact area between the wires and sternum, the stresses from the applied load were concentrated to the wires, with low distribution of load into the bone (Table 2).

In the local models, screw length and bone quality were seen to impact sternal separation and the distribution of load. Longer screws that engaged the posterior cortex resulted in less sternal separation than shorter screws. Additionally, more load was transferred from the plate into the surrounding bone with longer screws (Table 2).

The lateral distraction model resulted in a relatively high stress at the screw neck and stress concentration at the top cortical bone. The FEA results showed most loads are carried by the top cortical bone. In addition, it was shown that approximately 80% of the load was carried by the inner screws of the X-plate. Due to the low stiffness of the cancellous bone there were low stress levels in the cancellous region. Due to the high stiffness of the plate and screws there were low stress levels at the bottom cortical. The L-shaped plate exhibited similar behavior to the X-shaped plate.

The lateral distraction parameter study at 50% cortical purchase showed that increasing bone strength reduced the sternum gap and plate stress but increased the stress in the top cortical. When the screw length was decreased the cortical stress decreased but the sternum gap and plate stress increased. It was noted that the stress in the plate increased by approximately 80% when the screw length was decreased. The shorter screw length resulted in higher stresses in the cancellous region.

The shear loading analysis resulted in much lower stresses and sternum gaps. The results of the parameter study revealed trends similar to those in the lateral distraction loading.

Table 2 – Comparison of Separation and Stress Values for Different Closure Techniques in the Global Model

	Wire	Rigid Plate Fixation
Max. Gap (mm)	0.317	0.0066
Max. Bone Stress (MPa)	55	--
Max. Stress in Metal (MPa)	200	--

Table 3: Comparison of Separation and Stress Values for Different Screw Lengths in the Local Model

	Plate with Long Screws	Plate with Short Screws
Max. Bone Stress (MPa)	79	67
Max. Stress in Metal (MPa)	100	184

CONCLUSIONS

In general, FEA analysis demonstrated that stresses and sternum gap resulting from lateral distraction was significantly greater than for Rostral-Caudal shear. A comparison of wire closure to rigid fixation showed the stresses in plates was about half of the wire stress when proper screw sizes were used. The stress concentration at the top cortical bone was about 30% higher than the wire model.

The screw length and bone strength are the major factors for stress concentration and gap opening. The evaluation of the stress concentration in wire model needs to be evaluated in a different way because the wire diameter is too small compared to element size used in the bone for the local model.

Selection of the proper screw length to achieve purchase in the bottom cortical is very important in order to reduce the sternum gap, which can be achieved by measuring the sternal thickness. In addition, this model allows for an evaluation of screw location and plate design to be performed in order to design rigid fixation systems with optimal distribution of load. Future work to compare these results with bench testing is warranted.

REFERENCES

1. Jutley, R. S., et al. *Proceedings of the Institution of Mechanical Engineers, Part H: Journal of Engineering in Medicine* 216.5 (2002): 315-21.
2. Parker, R., et al. *The Thoracic and cardiovascular surgeon* 56.4 (2008): 190-4.
3. Niinomi, Mitsuo. *Materials Science and Engineering A* 243.1-2 (1998): 231-6.

EFFECTS OF EXERCISES FOR PREVENTION OF FEMORAL NECK FRACTURE BASED ON DYNAMICS AND FINITE-ELEMENT MOEL SIMULATION

Jing-Guang Qian[1], Hong Zhang[2], Zhaoxia Li[2], Rong Bian[1], Songning Zhang[3]

[1]Nanjing Institute of Physical Education, Nanjing, China, [2]Southeast University, Nanjing, China
[3]The University of Tennessee, Knoxville, TN, USA

INTRODUCTION

Femoral neck fracture has become common among elderly. World Health Organization (WHO) has designated the decade of 2000 as the "Decade of Bone and Joint Disease" [1]. Many clinical research studies argue that the prevention is particularly important for various fractures [2].

In order to study the impact of the fitness methods on femoral neck health, one method is using dynamics simulation to estimate and analyze the stress across the femoral neck during the process of fitness activities. The LifeMOD software package provides a suitable platform for conducting such evaluations using existing human body models, muscles and joints [3].

Our previous work on mechanisms of femoral neck fracture demonstrated that the bone mineral density of femoral neck and Ward's triangle in patients with femoral neck fracture is less than those in the normal population [4]. Under similar loading condition, the stress can easily reach the ultimate strength level of bone and lead to fractures. The results indicated that osteoporotic patients with a small femoral neck angle have a high risk of femoral neck fracture. For the high risk group, intervention should be implemented to prevent the fracture and targeted strengthening is recommended [4].

To study force distributions at several different sites of the femoral neck during human movements, CT image data of hip joint region were obtained. We established the finite element model of the hip joint with four material properties in Mimics (12.1). We then examined strains and strains at 12 different points of the femur in a standing posture under loading of body weight in ANSYS finite element software platform and the relationship of stress with bone mineral density [5].

In this study, the main objective was to examine how to improve bone strength through strengthening exercises governed by the Wolff's law and prevent femoral neck fractures. Specifically, a dynamics model and a three-dimensional finite element model were established to study kinematics and dynamics natures during the dynamic movements such as walking, squat, one leg standing, and two different lunges, investigate stress in the femoral neck region during these exercises, and identify optimal exercise(s) for this high risk patient group.

METHODS

A healthy participant volunteered to participate in the study and performed three trials in each of five movements: walking, squat, one-leg standing, forward lunge, lateral (left and right) lunge while three-dimensional (3D) kinematics was captured by a motion capture system (60 Hz, Motion Analysis system, CA). One of the trials was selected for further analysis. A skeletomuscular model was created in LifeMod, which was used to perform inverse and forward dynamics simulations on the five different movements in the LifeMod. Joint reaction forces and muscle forces related to the femoral neck fracture were obtained. Under the assumption of symmetry, only the joint reaction forces and muscle forces related to the left femur were estimated. According to analytical geometry, the loading data obtained through the LifeMod were transformed into the finite-element model of the left hip joint with four different material properties. The stress of the femoral neck regions were then computed and examined in order to obtain stress patterns associated with the different movements. In the five fitness activities, three movement phases, early, middle, and terminal phases were analyzed. Six hip region muscles, Iliacus, Gluteus maximus 1 (GlutMed1), Gluteus maximus 2 (GlutMax2), Psoas major (PsoasMaj) and Adductor magnus (AddMag), were included in the model. The origin and insertion of those muscles were implemented, and the muscle forces were computed in in the LifeMod.

RESULTS AND DISCUSSION

A customized MATLAB program was used to transform the joint reaction forces and muscle forces during the stance phase of the movements into the finite element model (FEM) in ANSYS. The FEM results of the stress distribution of the femoral neck showed that the stress was localized at the position 8 along the compression arc and the position 9 along the tension arc within the femoral neck (Table 1). In addition, the trabecular bone and tension lines of the Ward's triangle also demonstrated high stress.

The analysis of the five movement patterns found that the order of the maximum Von Mises stress of the stress arc observed within the compact and spongy bones in the movements were different. The compact bone received the greatest peak Von Mises stress in the forward lunge and the least stress in squat (Table 2). However, the spongy bone in the femoral neck region had the greatest stress in walking the least stress in squat.

CONCLUSIONS

This study demonstrated that it is effective to combine 3D human dynamics model with a 3D finite element model with muscle force inputs in studying influences of the movements on stress placed on femur. The forward lunge seems to be an effective method to prevent femoral neck fractures. High risk subjects of femoral neck fracture should avoid the side-step movements and using support. Finally, walking is an effective and simple method in improving bone mass of the Ward's triangle and preventing osteoporosis and femoral neck fracture.

REFERENCE

1. Zhang, X., et al. *Clin Rehab*，65-68, 2003.
2. Chen, W., et al. *Strait J Prevent Med*，15-17, 2001.
3. Ahn HS. *Dissertation*. The University of Tennessee Health Science Center，2005.
4. Qian, J. et al. *Clin Biom*, **24**, 47-52, 2009.
5. Qian, J. et al. *Proceedings of 2nd Int Conf Modeling and Simulation*, 2009.

Table 1. The maximum stress of the points in the five activities (MPa).

Stance	Walking		Squat		1-leg standing		Forward lunge		Lateral lunge	
	comp	tension	comp	tension	comp	tension	comp	tension	comp	tension
Early	18.1	13.81	3.09	1.83	13.88	10.1	64.73	49.37	3.98	3.47
Middle	10.51	7.53	4.82	3.59	14.81	10.59	57.41	42.73	5.22	9.02
Terminal	12.1	8.77	9.25	6.55	11.9	8.58	74.42	59.85	79.16	56.74
Node 19949	59.79		4.74		17.11		27.79		25.18	

Table 2. The order of the maximum stress on compact and spongy bones of performing the five activities.

	The order of Von Mises stress (maximum → minimum)
Compact bone	forward lunge > lateral lunge > walking > one-leg standing > squat
Spongy bone	Walking > forward lunge > lateral lunge> one-leg standing > squat

RESPONSE TO MEDIO-LATERAL PERTURBATIONS OF HUMAN WALKING AND RUNNING

[1]Mu Qiao, [2]Mark Hughes, and [3]Devin L. Jindrich
[1]Kinesiology Program, School of Nutrition & Health Promotion
[2]School of Engineering, Arizona State University
[3]Department of Kinesiology, California State University, San Marcos
email: mqiao1@asu.edu, website: http://www.limblab.org

INTRODUCTION

Walking and running can be described by simple templates (inverted pendulum and spring-mass) that can describe important aspects of Center of Mass (COM) movement. However, neither template can fully describe important requirements such as stability. During walking humans respond to medio-lateral (ML) perturbations by adjusting lateral foot placement [1]. Intrinsic spring-mass and muscle physiological properties can contribute to stabilizing running [2]. However, the active mechanisms used to maintain stability during running remain unknown. Moreover, whether different gaits employ different strategies to maintain stability is unclear. For example, longer stance time and higher duty factors during walking could allow for stabilizing responses to occur in fewer steps than during running, potentially using different mechanisms. We tested the response of humans to randomized ML perturbations in both walking and running on an instrumental split-belt treadmill. We hypothesized that 1) ML perturbations during walking are rejected faster than during running, and 2) during the double support phase of walking and stance in running ML perturbations are rejected faster than during single support in walking or flight in running.

We found that 1) recovery in walking after ML perturbations occurred earlier than during running, and fewer steps were required to return to the original movement pattern, 2) double support in walking/single support in running rejected ML perturbations faster than single support in walking/flight phase in running in terms of recovery instant and step number, 3) humans altered ML foot placement during single support in walking/flight phase in running after ML perturbations.

Key words: Medio-Lateral perturbation, stabilization, foot placement, walking, running

METHODS

A 3-D motion capture system (VICON®) recorded whole body kinematics while participants walked and ran on a custom-built instrumental split-belt treadmill that recorded GRF. We applied randomized ML impulse perturbation to 3 participants (age = 24.6 ± 7.9yrs; body weight (bw) = 71.2 ± 8.1kg; body height (bh) = 1.74 ± 0.02m, mean ± std, 2 male) in both walking (1.15 m/s) and running (1.57 m/s; Fig. 1). Impulsive 250ms, 5m/s^2 COM perturbations were generated using a linear stage motor (MPAS-A9060M-ALMC2C, Parker). Instantaneous COM was calculated using segmental locations and foot placement was determined using foot markers. The beginning of recovery was estimated as the instant when COM ML speed changed from lateral to medial. The recovery ended when COM fell within the range of normal ML variation.

Figure 1. Experiment setup with participant standing on a split-belt treadmill, attached to the linear motor, and secured to a gantry for safety. The linear motor was mounted to the left on the scissor table.

RESULTS AND DISCUSSION

Perturbation in single support in walking and flight phase in running involved changes in foot placement ipsilateral to COM (Fig. 2A, 3A). When perturbed in double support in walking or stance phase in running, there was little change in COM trajectory and foot placement (Fig. 2B, 3B).

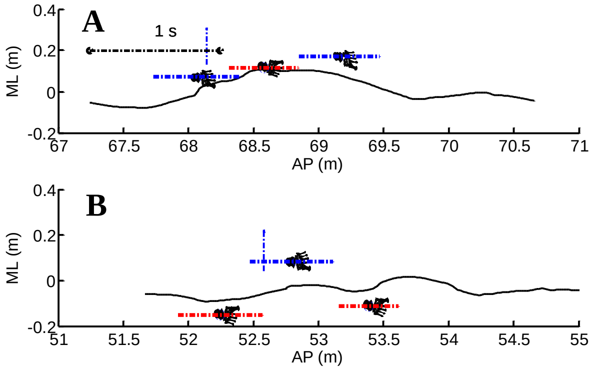

Figure 2: ML COM trajectory with foot placement in walking when perturbed in single (A) and double (B) support phase (+/- left/right). Perturbation to the left is indicated by vertical blue line. The duration of each foot contact was also shown with scale (left, blue; right red).

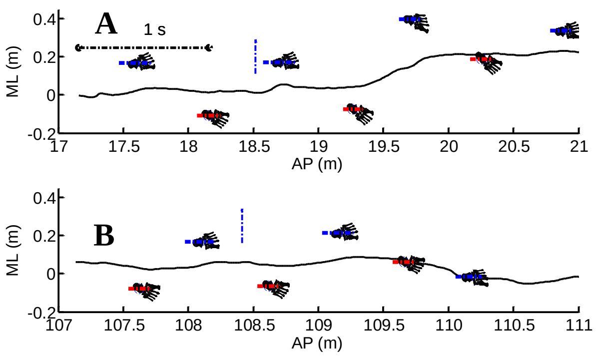

Figure 3: ML COM trajectory with foot placement in running when perturbed in flight (A) and single support (B). Symbols design follows Fig. 2.

Initiation of recovery for walking was faster than running (p_A < 0.001) and faster during double ("More") relative to single ("Less") support (p_B < 0.001). In walking, recovery initiation occurred at 0.96 ± 0.14/0.68 ± 0.20s for single/double support, respectively. For running recovery initiation occurred at 2.41 ± 0.83/1.17 ± 0.47s for flight/stance phase perturbations (Fig. 4).

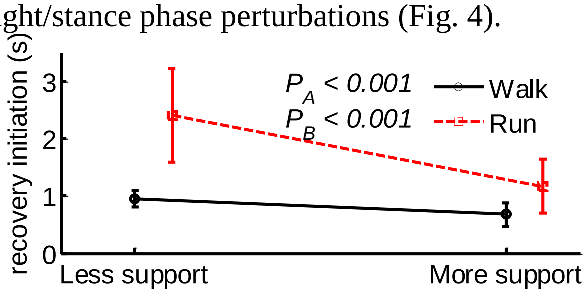

Figure 4: Factorial ANOVA on recovery beginning instant as influenced by gait and support phase. Factor A: gait (walk vs. run); Factor B: support phase ("less" vs. "more"). Less support in walking/running is single/flight phase, respectively. More support in walking/running is double support/stance phase, respectively. Mean ± m.s.e.

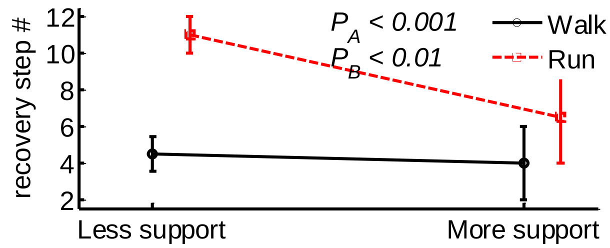

Figure 5: Factorial ANOVA on recovery step number as influenced by gait and support.

Significant main effects also showed that running required more steps for recovery than walking (p_A < 0.001). In walking 6.0 ± 2.5 steps were required to compensate for perturbations while 9.5 ± 3.4 steps in running were needed. The main effect also indicated that in single support of walking/flight phase of running more steps were required to recover than in double support in walking/stance in running (p_B < 0.01).

CONCLUSIONS

ML Perturbations in walking were rejected faster than running. Double support in walking/stance phase in running also provided faster recovery initiation, and fewer steps to recovery than single support in walking/flight phase in running.

These finding showed that 1) gait and 2) phase in each gait have different affordances for stabilizing ML perturbations. The contact of foot with ground provided the interface where, when necessary, humans redirected foot placement to the direction of ML perturbation and adjust GRF to maintain movement. The strategy was similar to spring-mass templates that stabilize running by redirecting foot placement [3]. Further, the joints in lower extremities, as well as the inherent limb and muscle properties may also contribute to rapid stabilization during ground contact [2].

REFERENCES

1. Hof, A.L., S.M. Vermerris, and W.A. Gjaltema, *Balance responses to lateral perturbations in human treadmill walking.* Journal of Experimental Biology, 2010. **213**(15): p. 2655-2664.
2. Jindrich, D.L. and R.J. Full, *Dynamic stabilization of rapid hexapedal locomotion.* Journal of Experimental Biology, 2002. **205**(Pt 18): p. 2803-2823.
3. Blickhan, R., et al., *Intelligence by mechanics.* Philosophical transactions.Series A, Mathematical, physical, and engineering sciences, 2007. **365**(1850): p. 199-220.

TRACKING HIGH-SPEED PATELLA MOTION USING BIPLANAR VIDEORADIOGRAPHY: AN ACCURACY STUDY

[1]Michael J. Rainbow, [1]Roy T.H. Cheung, [2]Daniel L Miranda, [2]Joel B Schwartz, [2]Joseph J Crisco, [1]Irene S Davis, [2]Braden C Fleming

[1]Harvard Medical School, Cambridge, MA, USA
[2]Brown University, Providence, RI, USA
email: braden_fleming@brown.edu

INTRODUCTION

Patellofemoral pain (PFP) is one of the most common disorders of the knee. However, the pathomechanics of PFP have not been fully elucidated. Our lack of understanding of PFP is partially due to difficulties with tracking the 3-D kinematics of the patellofemoral joint during important dynamic activities, such as running. Biplanar videoradiography can track dynamic 3-D bone motion with high accuracy, and is a promising modality for elucidating the pathomechanics of PFP. Recently, accuracies of 0.1 mm and 0.15º were reported when tracking motion of the distal femur, radius, and ulna [1]. However, the accuracy of markerless tracking algorithms inherently depends on bone morphology. Therefore, the purpose of this study was to evaluate the systematic error of a biplanar videoradiography system while tracking dynamic motion of the patella using a markerless bone registration algorithm. Secondarily, we introduce and evaluate a filtering step that directly operates on the 3-D transforms computed from biplanar videoradiography data.

METHODS

The biplanar videoradiography system was evaluated against an optical motion capture system (OMC) (Qualysis, Gothenburg Sweden). Three cadaveric patellae were used in this experiment. Each patella was embedded in urethane resin (Smooth-Cast, Easton, PA), and then CT scanned (Lightspeed, GE, Piscataway, NJ. 0.217x0.217x0.625mm^3). Three dynamic trials were captured for each patella according to the following procedure.

The patella along with six retroreflective markers (1 cm diam.) were attached to a custom designed impact pendulum. The pendulum rotated about axial bearings that confined it to planar rotation. The pendulum rotated until it impacted a cement block, where it underwent damped oscillations until it came to a resting position [1]. The biplanar videoradiography system and the OMC system were time synchronized and both recorded at 250 Hz.

The OMC marker data was filtered at 10 Hz with a lowpass Butterworth filter. The kinematic transforms of the OMC markers were computed from the resting position to each frame using least-squares methods. The kinematic transforms of the patellae were computed using custom markerless tracking software. Briefly, the software computed a transformation from CT-space to each frame by rotating and translating the CT volume such that digitally reconstructed radiographs (DRRs) were optimally matched to the biplanar videoradiography data [1]. These kinematic transforms were registered to the resting position of the pendulum and then converted into quaternions. A quaternion is represented by four parameters that can be directly filtered [2]. A dual pass Butterworth filter with a 10Hz cutoff was applied to the quaternion parameters before they were converted back to rotation matrices.

Helical axes of motion parameters were computed to facilitate the comparison between the OMC and biplanar videoradiography data. Because the motion was mechanically confined to planar rotational motion, only rotation about the helical axis and angular speed were considered in the analysis.

The error distribution and absolute error between OMC and biplanar videoradiography were computed for each patella and each trial. The error distribution was calculated as the mean of the difference between the OMC and biplanar videoradiography data. The absolute error was calculated as the root mean squared difference between the OMC and biplanar videoradiography data. Unfiltered (UF) rotation and angular speed errors were quantified using the filtered OMC data and unfiltered biplanar videoradiography data. Filtered (F) errors were quantified with filtered OMC data and filtered biplanar videoradiography data. Unpaired Student's t-tests with a Bonferoni adjusted alpha of 0.017 (0.05 / 3) were used to determine differences in error between patellae for filtered rotation and angular speed.

RESULTS AND DISCUSSION

There were no statistically significant differences in tracking errors between any patellae. Errors in rotation between OMC and biplanar videoradiography were low for both unfiltered and filtered conditions (**Table 1**). Absolute errors in rotation were also small (0.17º ± 0.07º). These errors were similar to reported errors of approximately 0.14º for the distal femur, radius, and ulna [1]. After filtering, an increase in the error distributions for angular speed was observed; however, the absolute error was reduced by 91% on average (**Figure 1**). These results confirm that filtered biplanar videoradiography can track the motion of the patella during dynamic activities with previously unattainable accuracy.

CONCLUSIONS

Angular errors in tracking the patella using biplanar videoradiography were low and did not depend on individual patellae. However, angular errors, likely due to small tracking errors, were amplified in the calculation of angular speed for both biplanar videoradiography and OMC. The applied quaternion filter adequately attenuated these errors without compromising the underlying signal. These data support the use of biplanar videoradiography for studying the pathomechanics of PFP.

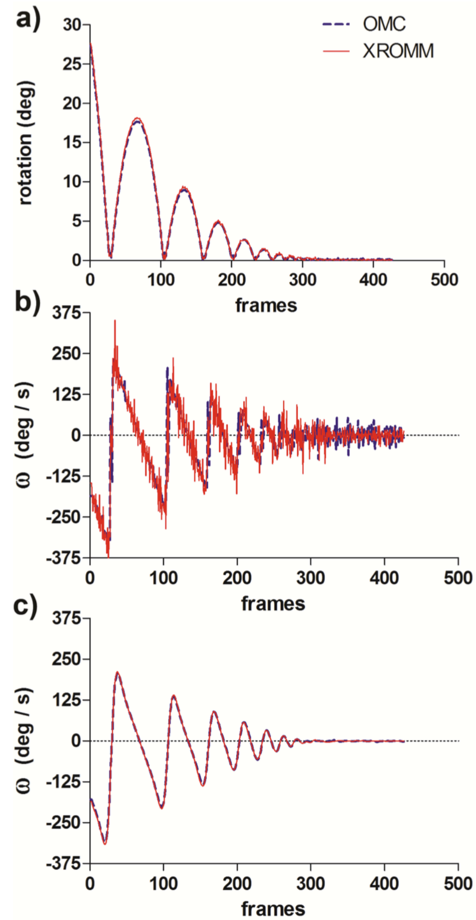

Figure 1: Errors in **a)** unfiltered rotations were amplified in the **b)** angular speed calculations. Filtering the biplanar videoradiography rotation matrices prior to calculating **c)** angular speed attenuated these errors by 91%.

REFERENCES

1. Miranda DL, *et al*, *J Biomech Eng.* 133, no. 12, 2011.
2. Coburn J and Crisco JJ, *J Biomech Eng* 127, 311-7, 2005.

Table 1: Errors in rotation and angular speed with (F) and without (UF) filtering (10Hz cutoff). (Mean and SD)

Patella	Rotational Error (deg)				Angular Speed Error (deg/s)			
	Error Distribution		Absolute Error		Error Distribution		Absolute Error	
	UF	F	UF	F	UF	F	UF	F
#1	-0.03 (0.06)	0.06 (0.08)	0.22 (0.01)	0.12 (0.08)	0.03 (0.03)	0.04 (0.19)	48.55 (4.72)	2.61 (0.40)
#2	-0.09 (0.03)	-0.02 (0.04)	0.25 (0.01)	0.15 (0.01)	-0.09 (0.06)	-0.15 (0.12)	39.09 (3.38)	3.87 (1.14)
#3	-0.17 (0.02)	-0.12 (0.02)	0.34 (0.02)	0.23 (0.04)	0.14 (0.16)	-0.31 (0.19)	42.44 (1.04)	5.20 (2.37)
Average	-0.10 (0.07)	-0.03 (0.09)	0.27 (0.05)	0.17 (0.07)	0.02 (0.13)	-0.14 (0.21)	43.36 (5.10)	3.89 (1.74)

COMMON CONTROL STRATEGIES FOR GENERATING ANGULAR IMPULSE IN FORWARD AND BACKWARD TRANSLATING TASKS

[1]Christopher R. Ramos, [2,3]Witaya Mathiyakom, [1,2]Jill L. McNitt-Gray
[1]Department of Biomedical Engineering, [2]Biological Sciences, USC, Los Angeles, CA
[3]Department of Physical Therapy, California State University, Northridge, CA
Email: mcnitt@usc.edu

INTRODUCTION

In complex whole-body movements that involve coordination of multiple joints, the nervous system appears to organize the human body into a number of operational subsystems using some type of hierarchical control [1]. By determining strategies that are invariant or variant across tasks performed by the same individual under various conditions, we can advance our understanding of the control structure [2,3,4] and facilitate learning.

Linear and angular impulse generation during well-practiced tasks relies on the interaction between the nervous system and the musculoskeletal system at the whole-body and subsystem levels. By studying two tasks requiring backward angular impulse generation, we have discovered that multijoint control at the joint torque and muscle level can transfer between tasks [2-4]. The distribution of these lower extremity net joint moments are known to be influenced by the orientation of reaction force relative to the lower extremity segments and the adjacent net joint moment [2-5]. Generation of lower extremity net joint moments also involves synergistic activation of the uniarticular and biarticular muscles crossing the knee and hip [2-4]. Based on this previous research, we hypothesized that satisfying the linear and angular impulse requirements of forward and backward somersaults involving either forward or backward translation would require between-task modifications in lower extremity control. We expected that differences in muscle activation patterns within subject across tasks would provide insight as to how the nervous system modifies multijoint control to satisfy task-specific objectives (linear and angular impulse generation requirements) at the total-body and subsystem levels.

METHODS

Seven (5 males, 2 females) skilled performers (national level divers) participated in this study. Each participant performed a series of backward (BS), inward (IS), forward (FS), and reverse (RS) somersault from a force plate onto a landing mat as part of a dry land training session. During the BS and IS tasks, the participant translated backwards and rotated either backward (BS) or forward (IS). During the FS and RS tasks, the participant translated forward and rotated either forward (FS) or backwards (RS).

Prior to data collection, the participants warmed up and acclimated to the experimental set up. Sagittal plane kinematics were recorded during each task (200 Hz, C^2S NAC Visual Systems, Burbank, CA, USA). Simultaneously, reaction forces were measured using a force plate (AMTI, 1200 Hz) and muscle activation patterns were monitored using surface electrodes (Konigsberg). EMG of the Gluteus Maximus (GMax), Semimembranosus (SM), Biceps Femoris (BF), Rectus Femoris (RF), and Vastus Lateralis (VL), were filtered (4^{th} order recursive Butterworth filter, 10–350 Hz). The magnitude of muscle activation was quantified using root-mean-squared (RMS) values (20 ms binned) [6]. The RMS values were normalized to maximum values obtained during isometric manual muscle tests [7] and averaged for each bin.

RESULTS AND DISCUSSION

Satisfying task-specific linear and angular impulse generation requirements, as observed during the dive take-off phase, requires coordination between multiple subsystems. Activation patterns of lower extremity muscles differed between backward and forward rotating tasks (BS, RS vs. IS, FS). Backward-rotating dives (BS, RS) used higher activation of the knee flexors (SM, BF) while forward-rotating dives (IS, FS) used higher activation of the knee extensors (RF, VL; Fig. 1). Activation of knee flexors (SM and BF) is consistent with generating a resultant reaction force acting anterior to the center of mass (CM) to create backward angular impulse. In contrast, activation of knee extensors (RF and VL) is consistent with generating a resultant reaction force acting posterior to the CM to create forward angular impulse.

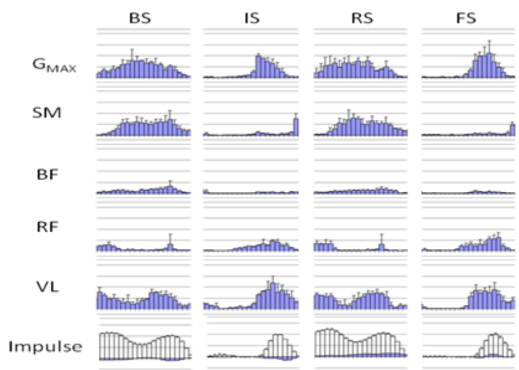

Figure 1. Average muscle activation and generated for all four tasks for an exemplary subject

Two different joint extension patterns were observed between subjects (Fig. 2). Just over half of the participants (4 of 7) simultaneously extended the knee and hip. The remaining participants (3 of 7) initiated lower extremity extension at the hip while the knee was stabilized. All participants using simultaneous knee-hip extension demonstrated early onset and prolonged activation of the SM and BF compared to the participants using hip extension with knee stabilization strategy.

During forward rotating tasks, redirection of the reaction force posterior to the CM involved activation of the RF regardless of translation direction. In contrast, during backward rotating tasks, redirect the reaction force anterior to the CM involved activation of the SM and BF regardless of translation direction. In addition, different participants satisfied the same mechanical objective using two different multijoint control strategies: simultaneous knee-hip extension; hip extension with knee stabilization.

Selective activation of the biarticular muscles may also serve as a means for coordinating joint kinetics at the knee and hip. Simultaneous knee-hip extension may serve as a mechanism to maintain the muscle-tendon-unit length of the biarticular muscles crossing the knee and hip. For example, extending the hip and knee together shortens the SM and BF at the hip, but lengthens them at the knee. These mechanisms may allow power transfer between the hip and knee joints [8].

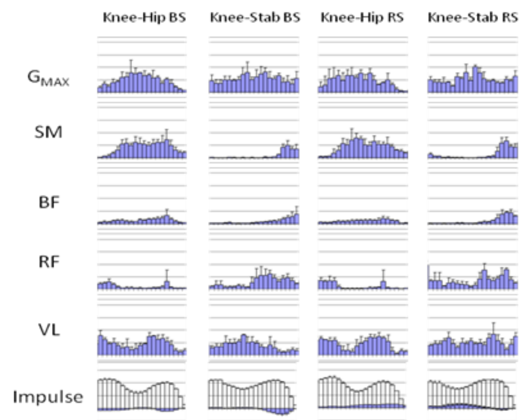

Figure 2. Average muscle activation patterns and impulse generated for knee-hip coordinated versus knee-stabilizing subject for back and reverse somersaults

How the lower extremity muscles were activated did not change the magnitude or direction of the net impulse generated during the task. Should greater reaction force be needed to increase the angular impulse, involving the SM and BF earlier in the take-off phase by using a knee-hip coordination strategy may prove advantageous. This hypothesis will be tested in future work using musculoskeletal modeling.

REFERENCES

1. Bernstein N. The co-ordination and regulations of movements. Pergamon Press, Oxford, 1967
2. Mathiyakom W, et al. *J Biomech* **39**, 990-1000. 2006.
3. Mathiyakom W, et al. *ExpBrain Res* **169**, 377-388, 2006.
4. McNitt-Gray JL, et al. *J Biomech* **34**, 1471-1482, 2001
5. McNitt-Gray JL et al. *Bio Cyb* **94**, 501-510, 2006
6. de Luca C. *J Appl Biomech* **13**, 135-163, 1997
7. Kendall FP et al. *Muscles testing and Function*, Williams & Walkins, 1993
8. van Ingen Schenau G. et al. *J Ana **155***, 1-5, 1987.

ACKNOWLEDGEMENTS

USA Diving Performance Enhancement Team and USC Biomechanics Research Team.

PATIENTS WITH PERIPHERAL ARTERIAL DISEASE EXHIBIT GREATER TOE CLEARANCE THAN HEALTHY CONTROLS

[1]Troy J. Rand, [1]Shane Wurdeman, [2]Jason M. Johanning, [2]Iraklis I. Pipinos, [1]Sara A. Myers

[1]Nebraska Biomechanics Core Facility, Omaha, NE, USA
[2]Department of Surgery, University of Nebraska Medical Center, Omaha, NE, USA
E-mail: trand@unomaha.edu Web: nbcf.unomaha.edu

INTRODUCTION

Peripheral arterial disease (PAD) affects over 8 million individuals in the United States, including 12-20% of all individuals 60 years of age and older [1]. PAD patients commonly suffer from intermittent claudication in the lower extremities, making walking difficult even for short distances. In addition, recent findings have shown that PAD patients experience 73% more falls than healthy controls, and have a significantly greater incidence of ambulatory stumbling and unsteadiness [2]. The minimum toe clearance (MTC) during the swing phase is considered a critical gait event when assessing fall risk. Since the majority of falls happens from contact between the swing leg and the ground or another object a smaller MTC is associated with an increased risk for falls [3]. It is possible that PAD patients have abnormal toe clearance prior to the onset of claudication pain, after the onset of claudication pain, or during both conditions, which could contribute to an increased risk of falls. The purpose of this study was to investigate the difference in MTC between healthy individuals and PAD patients both in pain-free and pain conditions. It has been shown that PAD patients exhibit a lower center of mass during the stance phase when compared to controls [4]. This result along with the increased number of falls observed in these patients, led us to hypothesize that PAD patients would exhibit a reduced MTC due to lower limb impairment.

METHODS

Ten PAD patients (age: 62.7 ±12.6 years; ht: 174.4 ±5.9 cm; wt: 80.4 ±20.2 kg) and ten healthy controls (age: 56.2 ±6.9 years; ht: 175.3 ±7.8 cm; wt: 89.6 ±19.7 kg) were screened and consented for participation in this study. All subjects walked on a treadmill at their self-selected pace while kinematic data was recorded (12-camera Motion Analysis Corp., Santa Ana, CA; 60Hz). We chose treadmill walking so we could collect the greatest amount of strides possible. PAD patients performed one walking trial in a pain-free state followed by one trial experiencing claudication pain. A virtual toe marker was created using the motion analysis post processing software to prevent interference with walking from a physical marker at the hallux. Independent t-tests were utilized to test for difference between controls vs. PAD pain-free and also controls vs. PAD pain conditions. A dependent t-test was utilized for the PAD pain-free vs. PAD pain conditions. Mean MTC and standard deviations were both analyzed. Significance was set at 0.05.

RESULTS AND DISCUSSION

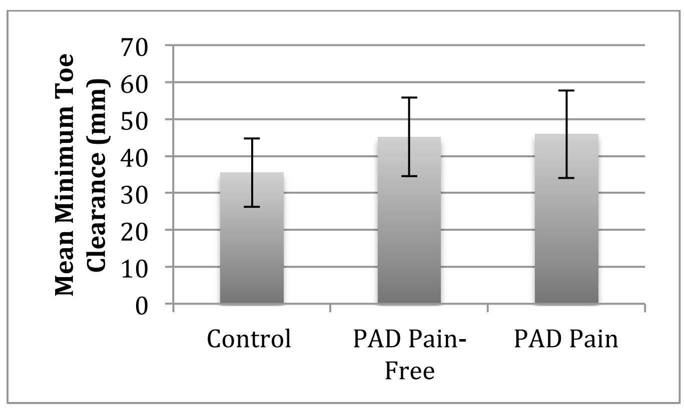

Figure 1: Group means for minimum toe clearance. Mean values are larger in PAD patients compared with controls. PAD Pain-Free vs. Control (p=0.044), PAD Pain vs. Control (p=0.042).

Contrary to our hypothesis, PAD patients had a significantly greater MTC on average in both the pain-free and pain conditions when compared to the healthy controls (Figure 1). No significant difference was found when comparing the pain-free and pain conditions. One explanation is other strategies may be used by PAD patients to overcome their ambulatory limitations. Previous research has shown decreased hip and ankle power during stance phase [5]. It is possible that patients may compensate for this by increasing the power at the hip during the swing phase causing a greater MTC. It is also possible that gait limitations such as reduced power during stance [5] or shortened stride length [6] cause the individual to lift their foot higher than someone who is comfortable walking and performs the task automatically.

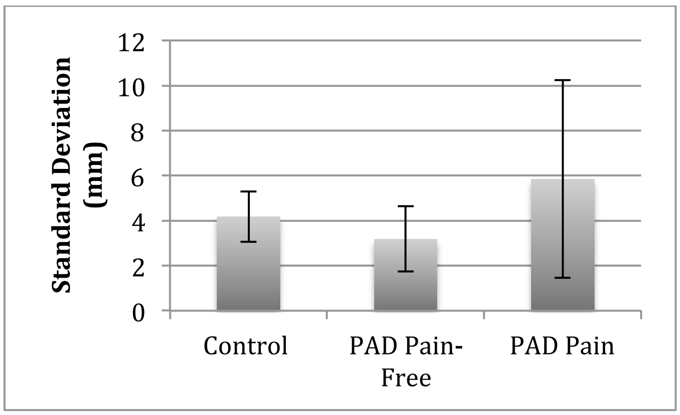

Figure 2: Group standard deviations for the PAD patients while experiencing pain was larger than the Pain-Free and Control conditions, although not found to be significant ($p=0.082$ and $p=0.0529$ respectively).

Regarding the average standard deviations, there were no significant differences between PAD patients and controls or between PAD pain-free and pain conditions (Figure 2). This was the result of the large variance in the heights of MTC throughout the trials, as evident through the large standard deviations of the average values. Thus, PAD patients on average exhibit a greater MTC, but certain strides throughout the gait cycle could possibly be lower and more unpredictable than healthy individuals, particularly when the patient is experiencing pain. One limitation with this study is in calculating the absolute values of the minimum toe clearance. The point of the toe was measured by calculating a virtual marker. Previous studies have utilized both virtual markers and physical markers to measure MTC [3]. Our calculation was based on the position of physical markers, which were placed on the metatarsal-phalangeal joint and the heel. This calculation made the assumption that the toe was even with the ground at the end of the foot, which did not account for the curved shape of shoes at the toe region. However, the same technique was implemented for all subjects, thus our technique is expected to be consistent for all subjects and thus we expect differences to be due to true gait alterations. Further investigation needs to be done to determine how the MTC changes over time and how MTC is related with falls in PAD patients. While the average toe clearance is greater, this study does not address changes in toe clearance as the duration of walking increases.

CONCLUSIONS

PAD patients have increased average MTC compared with healthy individuals. Current literature suggests that a smaller MTC results in increased falling [3]. Accordingly, these results could indicate that average MTC in the swing phase may not be a major cause of falling in PAD patients. However further research needs to be performed to make this determination, including examining the variability of MTC over time. There are many additional factors that could be contributing to increased falls in PAD patients. Future research should also consider these other factors, as well as the relationship between falls in PAD patients and MTC.

REFERENCES

1. Nehler, MP, et al. *Vasc Med,* **8**(2), 115-126, 2003.
2. Gardner, AW, Montgomery, PS. *J Gerontol A Biol Sci Med Sci,* **56**(7), M454-M458, 2001.
3. Lai, DT, et al. *Hum Mov Sci,* 2010.
4. Scott-Pandorf, MM, et al. *J Vasc Surg,* **46**(3), 491-499, 2007.
5. Koutakis, P, et al. *J Vasc Surg* **51**(1), 80-88, 2010.
6. Scherer, S, et al. *Arch Phys Med Rehabil* **79**, 529-531, 1998.

ACKNOWLEDGEMENTS

This work was supported by NIH/NIA (F31AG032788), NIH/NIA (1R01AG034995), NIDRR (H133G080023) and the Nebraska Research Initiative.

AVERAGE ANKLE DYNAMIC JOINT STIFFNESS DURING HEEL STRIKE RUNNING

[1]Alexander Razzook, [1]Charlie Gleason, [2]Richard Willy, [3]Rebecca Fellin, [4]Irene Davis and [1]Steven Stanhope
[1]University of Delaware, Newark, DE, USA
[2]Ohio University, Athens, OH, USA
[3]US Army Research Institute of Environmental Medicine, Natick, MA, USA
[4]Harvard Medical School, Cambridge, MA, USA
email: arazzook@udel.edu, web: http://www.udel.edu/kaap/research/biomechanicslab.html

INTRODUCTION

A passive dynamic ankle-foot orthosis (PD-AFO) is a type of ankle brace that acts like a torsional spring [1]. PD-AFOs are prescribed to patients with weakened plantar flexors. PD-AFOs are designed to be effective by supporting the natural forward progression of the shank over the stance foot [2]. Dynamic joint stiffness (DJS) has been defined as the instantaneous slope of the ankle moment plotted as a function of ankle angle [3].

Recently, PD-AFOs have been prescribed to limb salvage patients and utilized to restore both walking and running function [4]. Thus the need for PD-AFOs to provide optimal stiffness for both walking and running has been established. Therefore, the purpose of this study was to characterize average ankle DJS during the dorsiflexion interval of stance in heel toe running for both males and females.

METHODS

Twenty healthy males (ages 18-50 yr, body height 1.80 ± 0.06 m, and body weight 763.90 ± 97.51 N) and ten healthy females (ages 18-50 yr, body height 1.68 ± 0.08, and body weight 615.48 ± 9.12 N) rearfoot striker runners underwent unilateral lower extremity instrumented movement analysis. All subjects ran at an absolute speed of 3.35 m/s (1.77 – 2.20 body heights/s scaled). Speed was monitored by photocells and only trials ± 5% were accepted. Kinematic data were collected at 120 Hz using an eight-camera based motion capture system (Vicon Peak, Centennial, CO) and kinetic data were collected at 1080 Hz from a strain gauge force platform (AMTI, Watertown, MA). Kinematic target data and kinetic force data were both filtered using lowpass butterworth filters with a cutoff of 12 Hz and 50 Hz respectively.

Stance phase net plantar/dorsiflexion ankle moments and corresponding ankle angles for at least three trials were calculated using Visual3D (C-Motion, Germantown, MD). The average ankle DJS was calculated as the slope over the interval from the first occurrence of a plantar flexion moment (ZM) to maximum ankle dorsiflexion (MD) (See Figure 3). Ankle moment data were scaled by subject bodyweight (BW) and body height (BH). Student's t-tests were used to assess gender differences between ankle angles at heel strike (HS), the first occurrence of a plantar flexion moment (ZM), maximum dorsiflexion (MD) and terminal stance (TO); and the ankle moments at maximum dorsiflexion. Bivariate correlations were used to assess the effect of speed on average ankle DJS.

RESULTS AND DISCUSSION

There were no significant differences between female and male ankle angles at HS, ZM or MD ($p > 0.05$). However, female ankle angles (-21.9º) at TO were significantly different than males (-12.5º) ($p < 0.05$) (See Figure 1).

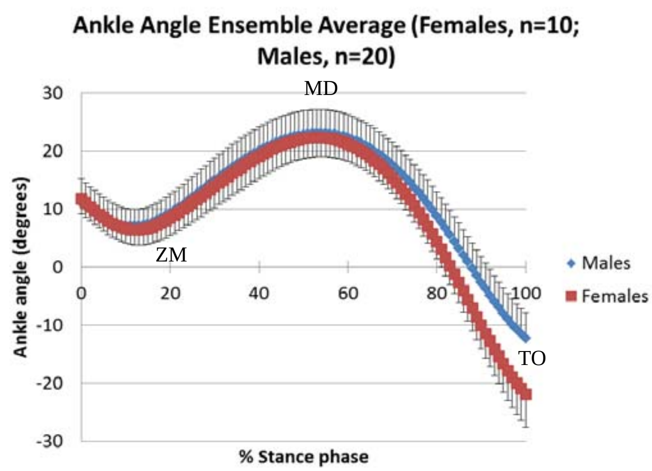

Figure 1: Ankle angle ensemble averages for 10 females and 20 males. Dorsiflexion is (+). Error bars denote 1 SD.

Females tended to have higher peak dorsiflexion moments in early stance and appeared to have lower peak plantar flexion moments during midstance but no statistically significant differences were found when looking at scaled data (See Figure 2).

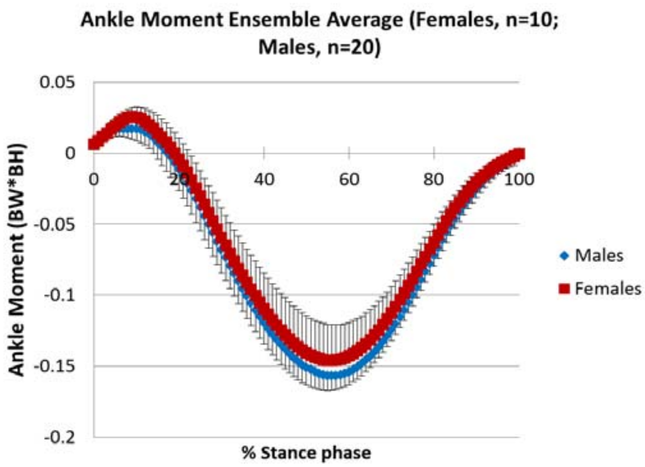

Figure 2: Ankle moment ensemble averages for 10 females and 20 males. A dorsiflexion moment is (+). Error bars denote 1 SD.

Female un-scaled average ankle DJS was 10.56 Nm/deg and was significantly different than the male ankle stiffness at 14.76 Nm/deg ($p < 0.05$). However, scaling moment values by BW and BH did not yield statistically significant differences ($p > 0.05$).

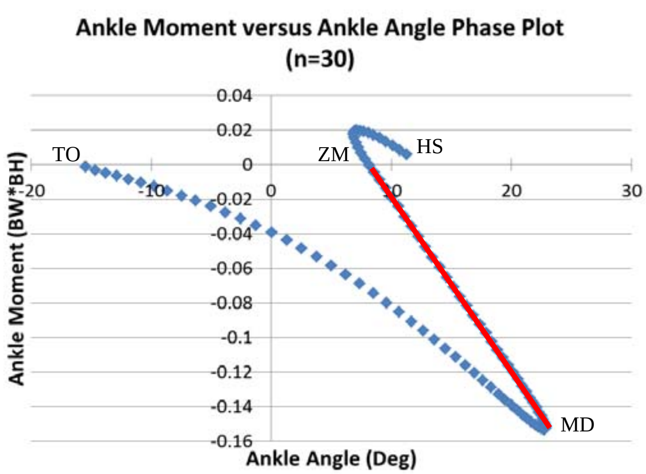

Figure 3: Group ensemble average (n=30) of ankle moment versus ankle angle. Dorsiflexion angle and moment are both (+). The red line denotes the interval that DJS is calculated from.

Figure 3 shows the ensemble average for all 30 subjects in a phase plot of ankle moment versus ankle angle. Subjects contacted the ground at HS, plantar flex slightly to achieve foot flat and then dorsiflexed as the shank rotated over the stance foot. ZM denoted the point at which the ankle moment transitioned from a dorsiflexion moment to a plantar flexion moment. Subjects continued to dorsiflex until MD and then plantar flexed concentrically until TO (See Figure 3). Average DJS appeared to have opposite relationships to speed for females and males but neither correlation was statistically significant (See Figure 4).

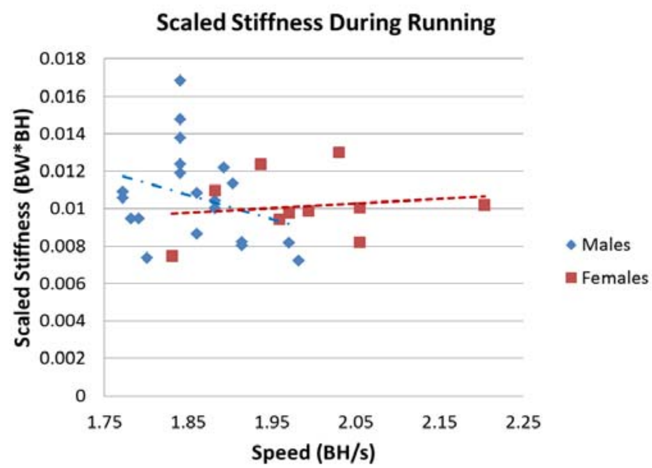

Figure 4: Average dynamic ankle joint stiffness for both males (r = .30; p = .19) and females (r = .15; p = .67).

CONCLUSIONS

These scaled data suggest that there are no gender differences for average ankle DJS once bodyweight and body height are accounted for and that speed does not appear to have a significant effect. Furthermore, it appears that a scaled relational database may be used to predict an individual's ankle DJS for running based on their bodyweight and body height which may be useful in tuning PD-AFOs for running.

REFERENCES

1. Nelson, KM et al. *Proc. of ASB*. Abstract 2003.
2. Yammoto et al. Arch Phys Med Rehabil, **86**, 162-166, 2005.
3. Davis, RB et al. *Gait and Posture.* **3**, 173, 1995
4. Patzkowski, J. et al. *J of Surg. Ortho. Adv.* **20(1)**, 8-11, 2011.

THE EFFECT OF LEG DOMINANCE ON STEP LENGTH IN SHOD AND BAREFOOT WALKING

Jared Rehm, Braden Romer, John Fox, Jay Patel, and Wendi Weimar

Auburn University, Auburn, AL, USA
email: jmr0020bhr0002@auburn.edu, web: http://education.auburn.edu/kine/

INTRODUCTION

It is sometimes assumed that a healthy individual will demonstrate symmetrical step lengths during walking gait and that dominance does not significantly affect step length. Previous research has supported this belief [1]. Previous research has also shown an increase in step length from barefoot to shod walking [2]. What is uncertain is if dominance and footwear affect walking gait when investigated together. Therefore, the purpose of this project was to determine the effects of leg dominance on step length in shod and barefoot walking.

METHODS

Nineteen (10 female, 9 male) healthy participants volunteered for participation in the study. No participant had a lower-extremity injury within the year prior to participation in the study. Age of the participants was 23.8±2.4 years (m±SD) and body mass was 73.7±12.5kg. Participants walked on an instrumented walkway (GAITRite, CIR Systems, Inc., Havertown, PA, USA) during four separate conditions, with each condition consisting of six trials. Kinematic data was averaged across the six trials. Each trial included a 3.5m lead-in, followed by walking over the 4.25m GAITRite mat, then a 3.5m walkout for a total of 11.25m per trial.

The four included conditions were: participants walking at a self-selected pace while shod (SHFW), self-selected pace while barefoot (BFFW), shod while walking faster than self-selected (SHF), barefoot while walking faster than self-selected (BFF). During the SHF and BFF conditions, participants were provided the verbal instructions that they were to imagine they were late to a meeting. All participants were provided the same verbal cue, by the same investigator, at identical points during the data collection process. Participants were dressed in identical polyester clothing and utilized commercially available non-running athletic shoes for all shod trials.

Dominance for each participant was determined by the having the participant kick a ball. The participant was instructed to kick the ball, without mention of dominance for the task. The foot chosen by the participant to strike the ball was determined to be the dominant foot. In this study, all participants were right-foot dominant.

A 4 (condition) × 2 (dominance) within-subjects ANOVA was conducted with dependence on step length. Post hoc analyses were conducted using least squares differences to determine significant differences ($p \leq .05$) between condition and dominance.

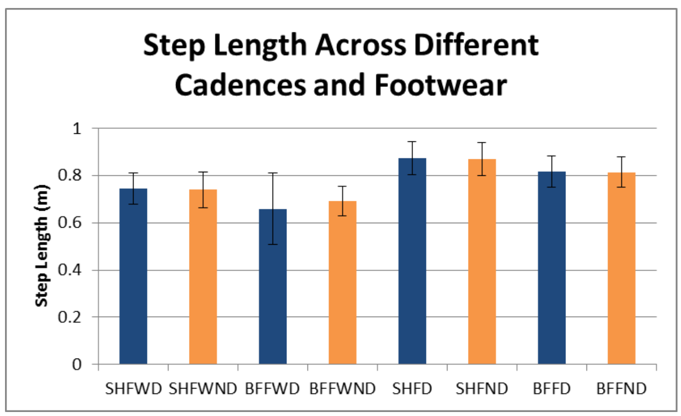

Figure 1: Blue bars indicate dominant and orange indicates non-dominant. All blue lines are significantly different from each other, and all orange lines are significantly different from each other. But the blue and orange bars are not significantly different from each other.

RESULTS AND DISCUSSION

As shown in Figure 1, when comparing step length between dominant and non-dominant legs, no significant effect was found ($F_{(1,18)}$=.272, p=.609,

η^2=.015). A significant main effect in step length was found between all conditions ($F_{(3,16)}$=58.41, $p \leq .007$, η^2=.764). No significant interaction effect was found between condition and dominance.

While the step length difference between the shod and barefoot conditions is not surprising, the persistence of this finding across different cadences is of some interest. Of particular note is the barefoot step length during the faster condition. This step length, while less than the shod condition for faster walking is longer than the step length during the shod self selected pace. This suggests that the barefoot step length can exceed the shod step length.

CONCLUSIONS

In support of previous literature, barefoot walking leads to a decrease in step length compared to shod walking [2]. In this study, this was found to be true across conditions of differing pace. No significant differences being found between step lengths for dominant versus non-dominant leg supports the practice of measuring one side of a person's gait in research using healthy gait patterns. However, further bilateral research is needed that would also include left-foot dominant participants to ensure that holds true for the left-foot dominant population. Future research should also investigate the kinematics of dominance under different conditions such as controlling velocity and cadence.

REFERENCES

1. Majumdar, D, et al. *Indian J Physiol Pharmacol*, **50 (1)**, 33-40, 2006
2. Zverev, Y. *Ann Hum Bio*, **33 (2)**, 161-176, 2006

DIFFERENCES IN STRIDE INTERVAL VARIABILITY DURING STAIR-CLIMBING AND TREADMILL WALKING

[1]Jessica J. Renz, [1]Srikant Vallabhajosula, [1]Nathaniel Hunt, [1]Jung Hung Chien, and [1,2]Nicholas Stergiou

[1]Nebraska Biomechanics Core Facility, University of Nebraska at Omaha, Omaha, NE, USA
[2] College of Public Health, University of Nebraska Medical Center, Omaha, NE, USA
email: jrenz@unomaha.edu, web: http://nbcf.unomaha.edu

INTRODUCTION

Stair climbing is an activity of daily living that is common yet challenging and exhausting. Many times multiple steps have to be covered and previous studies have investigated the kinematics and kinetics at various joints during stair-climbing [1,2]. Previous research has also shown that long-range correlations of stride intervals exist during overground walking, treadmill walking and running [3,4]. Particularly, the fluctuations that occur during the stride intervals of human walking have been shown to be persistent and self-similar. Thus, it has been suggested that human locomotion is fractal-like during overground walking, treadmill walking, and running [3,4]. However, it is unknown if this is also true for other types of locomotion like a stair-climbing task. Hence, the objective of the current study was to compare variability of stride time intervals during treadmill walking and stair-climbing and to determine if long-range correlations exist during stair-climbing.

METHODS

Nine healthy participants (5 females; 25.2±4.9years; 1.71±0.10m; 69.1±13.8kg) were recruited to participate in the study. Spatial-temporal data were collected using 12 high-speed cameras (Motion Analysis, Santa Rosa, CA) at 60Hz as the subjects performed continuous stair-climbing on the SC916 stairmill (StairMaster, Fitness Direct, San Diego, CA) without using the handrails. Subjects were asked to find the stepping rate that they were most comfortable at, and this was used as their preferred stepping rate. We confirmed the subject's preferred stepping rate by increasing the stepping rate until the subject reported discomfort with further increase in stepping rate. Once the preferred stepping rate was determined, spatial-temporal data was collected for three minutes at that rate.

As all the subjects demonstrated right leg dominance, right leg stride time was calculated using Matlab (Mathworks, Inc., Natick, MA). Right stride time was defined as the time between two consecutive toe-off events with the right leg and was calculated using the position of the marker placed on the head of the second meta-tarsal.

After walking on the stairmill, each subject rested for three minutes. Then the subjects were asked to walk on a treadmill (BodyGuard Fitness, Georges, QC, Canada) for five minutes at their preferred walking speed. Their preferred walking speed was determined similar to the procedure used to find the preferred stepping rate on the stairmill.

The mean, standard deviation (SD), and coefficient of variation (CV) of the right stride time were computed for each subject from the entire stairmill and treadmill walking trials. The SD and CV indicate the amount of variability in the stride time series. Additionally, long-range correlations of the right stride time were calculated using the Detrended Fluctuation Analysis (DFA) technique [5]. The DFA forms a sum of the time series from the minimum and maximum values of N provided, where N is the total number of data points in a time series. In the present study, N = 65 was used as that was the minimum number of strides across all the subjects. The range of the window size used was from n_1=4 to n_m=16 [4]. The DFA was used to determine the strength of the long-range correlations and provide a measure of temporal structure of the variability (α-value). If the outcome value of α is greater than 0.5 then the correlations are said to be positive persistent, meaning a long stride interval is followed by a long stride interval whereas a short stride interval is followed by another short stride interval. If the value of α is less than 0.5 the correlations are said to be anti-persistent, meaning long stride intervals are followed by short stride intervals whereas short stride intervals are followed by long stride intervals. If the α-value is equal to 0.5 then long-range correlations are said to be absent. A paired sample t-test comparing stairmill and treadmill walking was performed on all the dependent measures. The statistical significance was set at 0.05.

RESULTS AND DISCUSSION

Results are shown in Table 1. The preferred stepping rate for stairmill walking was 52.44 (11.58) steps/min and the preferred walking speed for treadmill walking was 2.67 (0.53) m/s. From DFA, the mean α-value for right stride time was obtained as 0.50 for stairmill walking and 0.64 for treadmill walking. An α-value of 0.50 for the stairmill walking indicates the presence of white noise and an absence of scaling and fractal behavior and that long-range correlations are absent [3]. This was confirmed by surrogation analysis where most subjects exhibited alpha-values that were not significantly different than the randomly shuffled surrogates of the same stride interval time series [6]. On the treadmill, an α-value of 0.64 shows that there are long-range correlations present and that these correlations are positively persistent, similar to results of previous studies [3,4]. The mean stride time, SD and CV for treadmill walking were significantly less than stairmill walking (all $P <$ 0.001). However, the mean alpha values were not significantly different ($P = 0.208$).

These significant differences could have been due to the difficulty associated with stairmill walking. Participants were more comfortable to walk on the treadmill at a greater stepping rate (lesser stride interval). Stairmill walking is a more strenuous and difficult task than treadmill walking and probably requires more involvement from central nervous system resources. It is possible that during stairmill walking, the brain considers each step as a new problem to solve and depends minimally on the feedback from the previous step(s). Mechanically, stairmill walking places constraints on the individual to produce sufficient vertical and forward motion of the foot to successfully accomplish the task. Perhaps, the individual must solve this problem at each step there by producing greater amount of variability and absence of long-range correlations during stairmill walking. We also speculate that the results could have been affected by the small length of stride interval data series (N = 65). Presently, we explore this issue by collecting longer time series during stairmill walking.

CONCLUSION

The results show that continuous stair-climbing differs from treadmill walking primarily in terms of the amount of variability.

REFERENCES

1. Hamel K. & Cavanagh P, *J Am Geriatr Soc* **52**, 563-567, 2004.
2. McFadyen B, et al. *J Biomech* **21,** 733-744, 1988.
3. Hausdorff J, et al. *J Appl Physiol* **78**, 349-58, 1995.
4. Jordan K, et al. *Gait Posture* **24**, 120-125, 2006.
5. Peng C-K, et al., *Phys Rev E* **49**, 1685-1689**,** 1994
6. Theiler J et al. *Physica D* **85**, 77, 1992.

ACKNOWLEDGEMENTS

Funding provided by the National Institute on Disability and Rehabilitation research (Grant No. H133G080023), National Institute of Health (Grant No. 1R011AG034995-01A1), the NASA Nebraska Space Grant & EPSCoR (Grant No. NNX11AM06A) and the Nebraska Research Initiative.

Table 1: Mean (SD) of dependent variables of right stride time of stairmill and treadmill walking; * indicates a significant difference between stairmill and treadmill walking; DFA – Detrended Fluctuation Analysis

Dependent Variable	**Stairmill**	**Treadmill**	**t-statistic**	**p-value**
Mean*	2.29 (0.42)	1.07 (0.10)	8.24	0.000035
Standard Deviation *	0.08 (0.03)	0.02 (0.01)	6.77	0.00014
Coefficient of Variation (%) *	3.47 (0.96)	1.34 (0.64)	9.54	0.000012
Alpha value from DFA	0.50 (0.26)	0.64 (0.29)	-1.37	0.21

EFFECT OF SEAT POSITION MODIFICATIONS ON UPPER EXTREMITY MECHANICAL LOADING DURING MANUAL WHEELCHAIR PROPULSION

[1, 4]Philip S. Requejo, [4]Sara J. Mulroy, [1]Joseph M. Munaretto,
[2]Marco A. Mendoza Blanco, [3]Edward Wagner, [1, 2]Jill L. McNitt-Gray,

[1]Department of Biomedical Engineering, [2]Biological Sciences, [3]Aerospace and Mechanical Engineering
[4]Rehabilitation Engineering, Rancho Los Amigos National Rehabilitation Center, Downey, CA
[1]University of Southern California, Los Angeles, CA, USA
mcnitt@usc.edu

INTRODUCTION

Repetitive mechanical loading of the shoulder during manual wheelchair (WC) propulsion has been associated with disabling shoulder pain that can significantly affect health and active community participation [1,2]. Because individuals with spinal cord injury (SCI) are dependent on the upper extremity during most of their activities of daily living, shoulder pain developed as a result of an acute incident or overuse is difficult to resolve.

Past efforts to reduce the mechanical demand on the upper extremity of manual WC users have focused on WC design and the interface with the WC user. For example, introducing modifications in materials and WC construction can significantly reduce the mass of the WC (e.g. >35% reduction between standard and ultralight chair), thereby reducing the magnitude of the tangential component of the reaction force (RF) needed to maintain WC speed. Incorporating WC components that are adjustable provides multiple solutions for achieving a desired elbow extension angle between 100-120 degrees when the wrist is at top-dead-center of the handrim [2]. Load exposure is affected by pushing frequency and the mechanical load experience during each propulsive cycle. Increasing the duration of hand contact may increase the duration of hand contact and reduce the average force, but not necessarily peak reaction forces during the impact or propulsive phases [5].

Identification of prospective preventative strategies for preserving shoulder function is imperative for manual WC users with SCI. Previous research indicates modifications in WC fitting can affect joint kinetics as well as muscle activation patterns during manual WC propulsion [2-4]. Our working hypothesis is that custom fitting of the WC to the individual WC user can create a functional workspace conducive for maintaining mobility and mitigating detrimental mechanical loading of the shoulder. Our purpose here is to show how modifications in seat position can alter upper extremity mechanical loading during manual WC propulsion. Modifications in axle position relative to the shoulder, arising from adjustments to seat position, orientation, and cushioning (Figure 1) are expected to affect segment kinematics and as a result upper extremity joint kinetics during manual WC propulsion [5,6].

METHODS

An experimental-based modeling approach was used to assess the sensitivity of shoulder net joint moments (NJM) and net joint forces (NJF) to changes in shoulder horizontal and vertical position relative to the rear wheel axle (Figure 2). Individuals with paraplegia volunteered to participate in accordance with the Institutional Review Board at the Rancho Los Amigos National Rehabilitation Center, Downey, CA. Kinematics, reaction forces at the hand-rim interface, and muscle activation patterns were quantified as participants propelled the WC using their self-selected free, fast and graded conditions[3,4,7]. Reflective markers were used to monitor the 3D motion of the hand, forearm, upper arm, trunk, and wheel segments (VICON, 50 Hz) and pushrim force was collected (SmartWheel 2500 Hz. The markers and upper extremity model to estimate wrist, elbow, and shoulder joint centers followed methods described in [7]. Foot-rest height was adjusted to each subject's preferences and anthropometry.

An experimentally validated 2D inverse dynamic model, incorporating subject-specific experimental tangential force, body segment parameters, and kinematic data, was used to determine the sensitivity of UE loading to modifications in shoulder/axis distance for an individual WC user [6]. Configuration of the forearm and upper arm body segments at an instant was determined using the law of Cosines and shoulder-axle distance and wrist angle under each seating condition (Figure 3). Mechanical loading during WC propulsion at the time of peak push was characterized by determining the elbow net joint moment (NJM) and shoulder NJM over a range of RF directions. Experimentally WC speed was maintained by preserving the tangential component of the RF and varying the magnitude of the radial component of the RF.

RESULTS AND DISCUSSION

Modifications in shoulder-axle distance and wrist location relative to the rim was found to influence how RF redirection distributes mechanical loading across the shoulder and elbow (Figure 4. Our simulation studies indicate that the effect of force redirection on elbow and shoulder NJMs depends on the seat configurations at specific times within the push phase. Simulated solution spaces at the time of peak RF during propulsion illustrate how redirection of the reaction force relative to the upper extremity segments is an effective means for shifting mechanical load (NJM, NJF) away from regions commonly experiencing pain during WCP (shoulder). If RF direction is constrained (due to friction, grip strength, etc.) solutions for redistributing the load will shift within the solution space.

CONCLUSIONS

By using an experimental-based subject-specific dynamic model, we can prospectively determine how multiple factors interact and affect mechanical loading under different seating conditions. Prospective determination of feasible solutions for an individual WC user will assist in preserving shoulder function by avoiding seat modifications that inadvertently contribute to detrimental mechanical loading of the shoulder.

REFERENCES

1. Finley, MA et al. (2004). *J RehabResDev*, 41(3), 395-402.
2. Consortium for SCI Medicine (2005), *J SCI Med.* 28(5).
3. Mulroy, SJ et al. (2005). *J Spinal Coard Med*. 28:214-221.
4. Mulroy, SJ et al. (2005). *J Spinal Coard Med*. 28:222-229.
5. Raina, S. et al. (2011). *Human Movement Science*.
6. Munaretto, JM et al. (2011).*Clinical Biomech*.27(3):255-62.
7. Rao, SS et al. (1996). *IEEE Trans Rehabil Eng*, 4:152-60.

Support: Spinal Cord Injury Model Systems (H133G110018)

ACKNOWLEDGEMENTS

Rancho Los Amigos National Rehabilitation Center and the USC Biomechanics Research Lab.

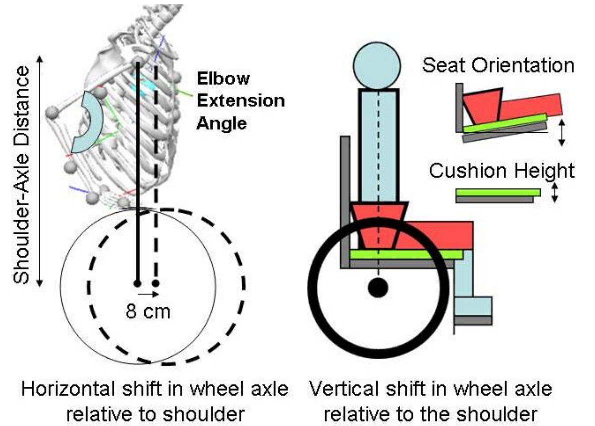

Figure 1. Effects of wheelchair (WC) modifications on shoulder-axle distance. Cushion height increases and seat orientation adjustments decrease shoulder-axle distance.

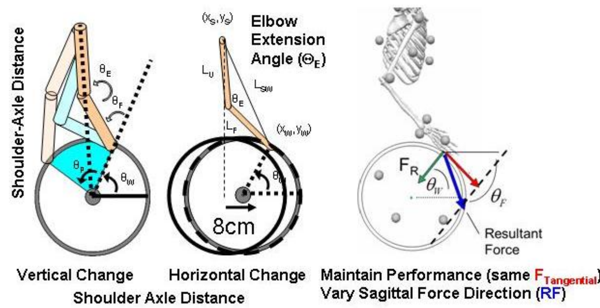

Figure 2. Kinematic and reaction force variables used to characterize the effect of changes in vertical and horizontal position of shoulder relative to rear wheel axle on mechanical loading of the upper extremity during manual wheelchair propulsion at comparable speeds.

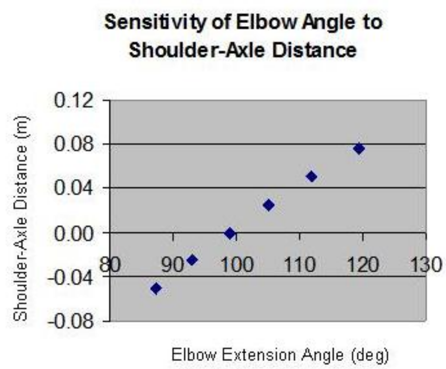

Figure 3. Elbow extension angle changes in relation to changes in shoulder-axle distance originating from combined effect of fitting modifications (e.g. seat cushioning (+) and orientation(-)).

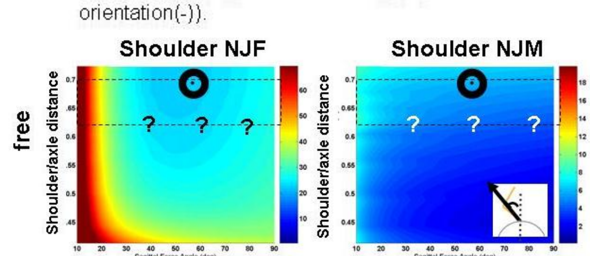

Figure 4. Model simulated shoulder net joint force (NJF) and net joint moment (NJM) during self-selected free propulsion when modifying shoulder axle distance (vertical axis). Experimental results are represented by black circle. Question marks reflect how the shoulder NJF and NJM magnitudes may change with changes in seat orientation (-) or seat cushioning (dotted lines) depending on the direction of the reaction force (horizontal axis).

VALIDATION OF A COMMERCIAL WEARABLE SENSOR SYSTEM FOR ACCURATELY MEASURING GAIT ON UNEVEN TERRAIN

Mark Tyler Rigsby and Kimberly Edginton Bigelow

University of Dayton, Dayton, OH, USA
email: Kimberly.Bigelow@udayton.edu

INTRODUCTION

Wearable sensor systems comprised of accelerometers and/or gyroscopes have gained popularity in recent years as a means of collecting physical activity and gait data in real-world environments [1,2]. Such systems open up a whole realm of possibilities for better understanding and determining true patient abilities and habits without the constraints associated with traditional motion analysis evaluations [1,2]. Though these systems have great promise, there is believed to be some trade-off in accuracy for the benefits of real-world monitoring [1,2]. Validation of such systems is paramount to ensure that the data collected appropriately reflects the subject's true gait.

Of particular interest is the validation of turn-key systems developed with clinical user-friendliness in mind. Unlike basic sensors, where raw accelerometer or gyroscope data can be manipulated and processed according to the user's expertise, many of these turn-key systems automate the post-processing of the data, showing only the ultimate outcome measures. If such systems produce highly accurate results, this has the potential to change practice as clinicians of all backgrounds would be able to utilize motion capture-type data. Unfortunately research to validate such systems has shown mixed results as related to their accuracy [e.g. 3,4]. The purpose of this study was therefore to validate one such commercially available wearable sensor system (MiniSun IDEEA) in outdoor environments over a span of age ranges.

METHODS

A total of 32 subjects participated in this study: 16 comprising the younger adult group (ages 18 – 38, mean age: 21.6 ± 2.3) and 16 comprising the middle-aged adult group (ages 45 – 65, mean age: 53.6 ± 5.0). All subjects were free of any injury, disease, or disorder that would affect their ability to walk. Subjects gave written informed consent and all procedures were approved by the university's IRB.

Each subject performed six 50 meter walking trials in an outdoor park: 3 on a paved, well maintained path and 3 across an area of mown grass to replicate uneven terrain that might be encountered during daily ambulation. Subjects were encouraged to walk at their natural pace and to wear their normal, comfortable walking or tennis shoes.

Data for each trial was collected with two systems: the commercially available wearable sensor system of interest (Intelligent Device for Energy Expenditure and Physical Activity (IDEEA), MiniSun LLC) and an inertial measurement system (Opal IMU, APDM Inc.) used for comparison. The IDEEA system consists of five bi-axial accelerometers placed on the feet, thighs, and sternum wired together to a data logger worn on the subject's waistband. The Opal IMU was placed on the L3 spinal process with an elastic belt and the tri-axial accelerometer feature was utilized for data collection.

The data from the IDEEA system was processed using the system's proprietary software. The data from the Opal IMU accelerometer was processed according to a published algorithm proposed by Moe-Nilssen [5], which has been used successfully to study gait, including in outdoor environments. Paired t-tests were performed to investigate the differences between the mean values of gait speed, cadence, step length, and gait duration obtained from the tri-axial accelerometer and the MiniSun

IDEEA for each age group, walking upon each surface ($p<0.05$).

RESULTS AND DISCUSSION

Statistically significant differences ($p<0.05$) were found between the systems for gait speed, cadence, and step length in both age groups and for both the even, paved path and the uneven terrain. In all cases the commercially available system underestimated the gait parameters as compared to standard raw accelerometer method. Table 1 provides the results for the trials occurring on the uneven terrain.

These results suggest that there is an accuracy trade-off using this system and its' automated proprietary post-processing software. Others who have investigated the validity of the IDEEA have reported similar underestimations, even when other gold standard comparisons are used [e.g. 3, 6]. However, these studies have been done over shorter distances, and it was hoped that better validity would be found when the distances better matched typical ambulation tasks. This was not the case, and as such researchers and clinicians should be cautious in extracting gait parameters from this particular system.

In contrast, however, gait cycle duration showed no statistically significant differences in any condition, suggesting good accuracy of this particular measure. If the IDEEA uses this information to calculate gait speed and cadence, similar to the estimation of gait parameters done using the raw acceleration data from the Opal, it would make sense for the IDEEA to be more accurate in calculating these parameters than it was. Though the proprietary nature of the IDEEA post-processing software prevents identification of why these values may be underestimated, this finding does suggest that there may be a refinement that can be done to the IDEEA algorithm to improve the device's accuracy.

There is a need to similarly examine other commercially available systems, particularly those like the IDEEA whose turn-key nature prevent comprehensive understanding of how the system functions. This will provide insight into which systems might be most ideal for clinical real-world monitoring of gait.

CONCLUSIONS

It was found that though easy to use, the commercially available MiniSun IDEEA wearable sensor system consistently underestimated measures of gait, other than cycle duration. This suggests it may not have the accuracy needed for motion analysis studies.

REFERENCES

1. Aminian K, et al. *Comput Animat Virtual Worlds* **15**, 79-94, 2004.
2. Yang C and Hsu Y. *Sensors* **10,** 7772-7788, 2010.
3. Maffiuletti NE, et al. *Gait Posture* **27,** 160-163, 2008.
4. Gardner MJ, et al. *Arch Orthop Traum Su* **127,** 223-227, 2007.
5. Moe-Nilssen R. *Clin Biomech* **13,** 328-335, 1998.
6. Gorelick ML, et al. *J Clin Physiol Funct Imaging* **29,** 271-276, 2009.

ACKNOWLEDGEMENTS

This work was supported by funds from the University of Dayton Graduate School (MTR) and the University of Dayton Research Council (KEB).

Table 1: Summary of Mean ± Standard Deviation Gait Parameters for Uneven Terrain, $^{**}p<0.01$, $^{***}p<0.001$

Age Group	18-38		45-65	
Parameter	Tri-axial Accelerometer	IDEEA	Tri-axial Accelerometer	IDEEA
Gait Speed (m/s)	1.32 ± 0.15	1.17 ± 0.12***	1.52 ± 0.21	1.36 ± 0.20***
Cadence (step/min)	104.93 ± 6.09	104.38 ± 6.24**	117.10 ± 9.98	115.71 ± 9.85***
Step Length (m)	0.76 ± 0.07	0.69 ± 0.05***	0.76 ± 0.06	0.72 ± 0.06**
Gait Cycle Duration (s)	1.14 ± 0.07	1.15 ± 0.07	1.03 ± 0.09	1.03 ± 0.09

EFFECTS OF REGIONAL FOOT PAIN ON PLANTAR PRESSURE AND LOADING

Jody L. Riskowski[1,2], Alyssa B. Dufour[1,3], Thomas J. Hagedorn[1], Virginia A. Casey[1], Marian T. Hannan[1,2]

[1]Institute of Aging Research, Hebrew SeniorLife, Boston, MA, 02131; [2]Harvard Medical School, Boston, MA, 02115; [3]Boston University School of Public Health, Boston, MA, 02118

INTRODUCTION

Foot pain affects one in four adults [1], but location of pain within the foot varies [2]. Given that the etiology of foot pain varies by region (e.g., heel pain can be a result of plantar fasciitis or forefoot pain can result from hallux valgus), the effects of foot pain on gait and movement may differ accordingly. Therefore, the purpose of this study was to evaluate the peak pressure and maximum force differences during gait by region of foot pain.

METHODS

This study included participants in the Framingham Foot Study [2] with data on regional foot pain, foot biomechanical measures, and foot disorders.

Foot scans were collected using a Tekscan Matscan pressure mat (Tekscan Inc, Boston, MA) at 40 Hz. For data collection, participants walked barefoot at a self-selected pace using the two-step method [3]. The Novel Automask software (Novel GmbH, Munich, Germany) masked scans into four regions: toes, forefoot, midfoot, and rearfoot.

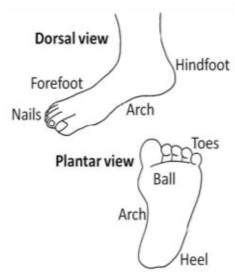

Figure 1: Regional foot pain picture [2].

Participants selected location(s) of foot pain from a graphic (Figure 1). To align with the four masked regions, the eight locations of pain were collapsed into four pain regions: toes, which included toe and nail pain; forefoot, which included forefoot and ball pain; midfoot, which included plantar or dorsal arch pain; and rearfoot, which included heel and hindfoot pain.

Each foot was classified into one of seven mutually exclusive groups based on region(s) of foot pain. These foot groups were: 1) toe pain only, 2) forefoot pain only, 3) midfoot pain only, 4) rearfoot pain only, 5) pain in two regions, 6) pain in three or more regions, and 7) no regional pain (referent).

A podiatric-trained examiner conducted a standardized, validated foot exam to determine the presence or absence of structural foot disorders. The foot disorders were: hallux valgus, hallux rigidus, claw toes, overlapping toes, and hammer toes.

Means and standard deviations of the participant demographic variables were calculated for each group. A per-foot analysis using linear regression was used to determine the association between the regional peak pressures and maximum forces and foot group, adjusting for age, gender, weight, and number of structural foot disorders. General Estimating Equations (GEE) were used to account for the correlation between right and left foot of the same person. All statistical analyses were conducted using the SAS statistical analysis package, version 9.2 (SAS Institute, Cary, NC), with alpha set to $p \leq 0.05$.

RESULTS

There were 3197 participants (6385 feet; seven feet were missing foot biomechanics data and two were missing foot disorder data) included in this analysis. Women were more likely to have toe pain only, forefoot pain only, and pain in multiple regions. Participants with rearfoot pain were younger than those without regional foot pain.

After adjustment (Figure 2), individuals with toe pain typically had lower rearfoot pressure and loading compared to those without regional foot pain. However, people with only forefoot or midfoot pain displayed higher rearfoot pressure and loading relative to the referent. Individuals with rearfoot pain typically showed lower toe pressure,

Table 1: Participant demographics. Data reported as mean (standard deviation), unless otherwise noted.

	Total Population	No Regional Foot Pain (Referent)	Toe Pain Only	Forefoot Pain Only	Midfoot Pain Only	Rearfoot Pain Only	Pain in Two Regions	Pain in Three or More Regions
Number of Feet (N)	6385	4886	262	228	78	267	481	183
Age (years)	66.2 (10.5)	66.3 (10.4)	68.0 (11.9)	65.8 (9.6)	64.1 (10.1)	64.3 (9.7)*	66.3 (11.3)	66.0 (11.1)
Women (%)	1795 (56)	2599 (53)	171 (65)*	170 (75)*	40 (51)	156 (58)	320 (67)*	131 (72)*
BMI (kg/m^2)	28.4 (5.5)	28.1 (5.2)*	28.1 (5.8)	29.8 (5.7)	29.2 (5.6)	29.9 (5.9)*	29.9 (6.3)*	30.0 (6.2)*
Foot Disorders (present)								
Hallux Valgus (%)	1763 (28)	1269 (26)	100 (38)*	80 (35)*	17 (22)	62 (23)	174 (36)*	61 (33)*
Claw Toes (%)	107 (2)	67 (1)	12 (5)	6 (3)	0	9 (3)	9 (2)	4 (2)
Hammer Toes (%)	1119 (18)	799 (16)	59 (23)*	43 (19)	20 (26)*	38 (14)	110 (23)*	50 (27)*
Overlapping Toes (%)	386 (6)	275 (6)	26 (10)*	12 (5)	5 (6)	20 (7)	34 (7)	14 (8)
Hallux Rigidus (%)	238 (4)	158 (3)	12 (5)	11 (5)	0	3 (1)	39 (8)	15 (8)

* represents significantly different from referent (no regional pain group)

with the rest of the foot regions showing similar forces and pressures to the referent group (i.e., no regional foot pain).

DISCUSSION & CONCLUSIONS

A common trait among feet with specific regional foot pain (e.g., pain only in the toes or only in the forefoot) was that plantar pressure and loading forces were not changed in the area of pain. The only group that did not show this trend was the midfoot pain group, who showed increased pressures and forces at the midfoot. Further, similar to prior work that suggested forefoot pain was associated with rearfoot dysfunction [4], our results showed higher plantar loading and pressure in the midfoot and rearfoot with forefoot pain. Future studies should evaluate how changing pressure profiles and loading patterns affect regional foot pain.

REFERENCES

1. Thomas MJ, et al. *Pain*, **152**, 2870-80, 2011.
2. Dufour AB, et al. *Arthritis Rheum*, **61,** 1352-58, 2009.
3. McPoil TG, et al. *J Am Podiatr Med Assoc*, **89,** 495-501, 1999.
4. Coughlin MJ. *J Bone Joint Surg Br*, **82**,781–90, 2000.

ACKNOWLEDGEMENTS

NIAMS RO1-AR047853, NIA T32 -AG023480.

Figure 2: Regional peak pressures and maximum forces relative to the referent (no regional pain). Blue indicates the region is significantly (p≤0.05) lower, red indicates the region is significantly (p≤0.05) higher, and white indicates the region is not significantly (p>0.05) different relative to the referent after adjustment.

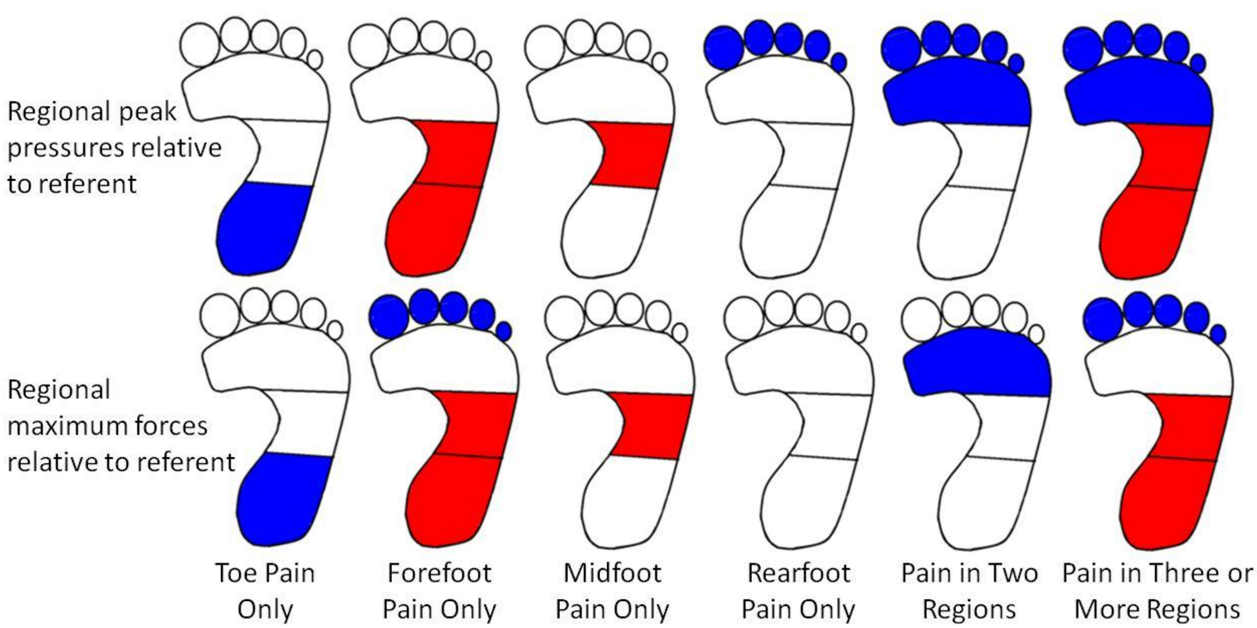

Balance Control During Tai Chi Movements

[1]Beverly L. Roberts, [2]Hongtao Li, [2]Roy Geib, [2]Gabi Waite, [3]Paul Lam, [4]Guido Pagnacco and [4]Elena Oggero

[1]University of Florida, Gainesville, FL, USA
[2]Indiana University School of Medicine Terre Haute, IN, USA
[3]Tai Chi for Health Institute, Sydney, Australia
[4]University of Wyoming, Laramie, WY, USA
email: robertsb@ufl.edu

INTRODUCTION

The slow continuous and controlled movements of tai chi require good motor control and balance. [1, 2] The more accomplished the practitioner the greater the quality of movements. The quality of tai chi would be expected to increase with practice and also those with certifications would be expected to meet certain minimal standards of quality. The purpose of this study was to compare balance while performing tai chi between tai chi experts and non-experts.

METHODS

Participants were recruited from a 10-day workshop on tai chi sponsored by the Tai Chi for Health Institute (TCHI). They had selected from one of several beginning and in depth level options for the workshop. People with prior knowledge of Sun style or Tai Chi for Arthritis that is based on this style were included in the study.

Balance was characterized by the movement of the center of pressure (COP) that was assessed by the CAPS™ Professional portable computerized force platform (Vestibular Technologies, LLC.). For the four experimental conditions, participants completed one of the Sun style movements (commence, open/close, single whip and wave hands). For the fifth experimental condition, they performed the four movements without stopping. They performed the experimental conditions while standing on the force platform. Participants were centered on the platform. On a start command, they began the tai chi movement, and repeated the movement for one minute.

Self-report was used to measure experience with tai chi (certifications and years engaged in the different types of tai chi; and master or senior trainer in TCHI). Master and senior trainers were classified as experts because they had good quality tai chi movements to be designated as such. The quality of the tai chi movements (understanding of the tai chi movements, quality of movement, application of tai chi principles, and physical relaxation) were rated on a 4-point Likert scale (0 “low” to 3 “high”) and ratings summed for maximum score of 12. Inter-rater reliability was 92%.

RESULTS

The 4 men and 17 women had an average age of 61 years (range 50 to 79, SD = 7.32). One master trainer had over 10 years of Sun style tai chi experience while two had 5 to 10 years. Two senior trainers had practiced a Sun style tai chi for 5 to 10 years while another for less than 5 years. All participants in the study were certified in Tai Chi for Arthritis that uses the Sun style movements used in the present study. They most frequently rated their health as excellent and very good (47.6% for each level) and only 1 rated it as fair.

For open/close and single whip, no significant differences in distance and velocity measures of the COP were found between the experts and non-experts. For commence and wave hands, the COP displayed statistically greater displacement to the limits of stability and velocity. (See Figure on next page for significant results). No significant differences were found for observed overall quality of movements, but master and senior trainers had greater observed relaxation with movements.

CONCLUSIONS

Greater motor control and balance are hallmarks of tai chi, and balance analysis revealed differences between experts and non-experts. The greater distance the COP moved in the experts in the present study may be associated with their ability to move closer to their limits of stability. Velocity then may have been higher because the COP had to cover a greater distance in the same amount of time than the non-experts. Alternately, the movements of the experts may have been more continuous while that of the non-expert may have been shaky with hesitations in the COP. Experts' greater confidence in the movements may also have reduced hesitations. Exploration of last two hypothesized explanations requires further research.

REFERENCES

1. Wu G, Millon D. Joint kinetics during Tai Chi gait and normal walking gait in young and elderly Tai Chi Chuan practitioners. *Clin Biomech (Bristol , Avon)* **23**,*787-95, 2008.*

2. Hong Y, Li JX. Biomechanics of Tai Chi: a review. *Sports Biomech, 6, 453-64,* 2007.

ACKNOWLEDGEMENTS

Funding from Indiana University School of Medicine-Terre Haute and the Alvin S. Levine Professorship to Roy W. Geib. Authors appreciate the space for data collection provided by St. Mary-of-the-Woods College. Authors thank Pratik Kalsaria, Josephine Riley and Safa Alakhdhair for assistance with the project.

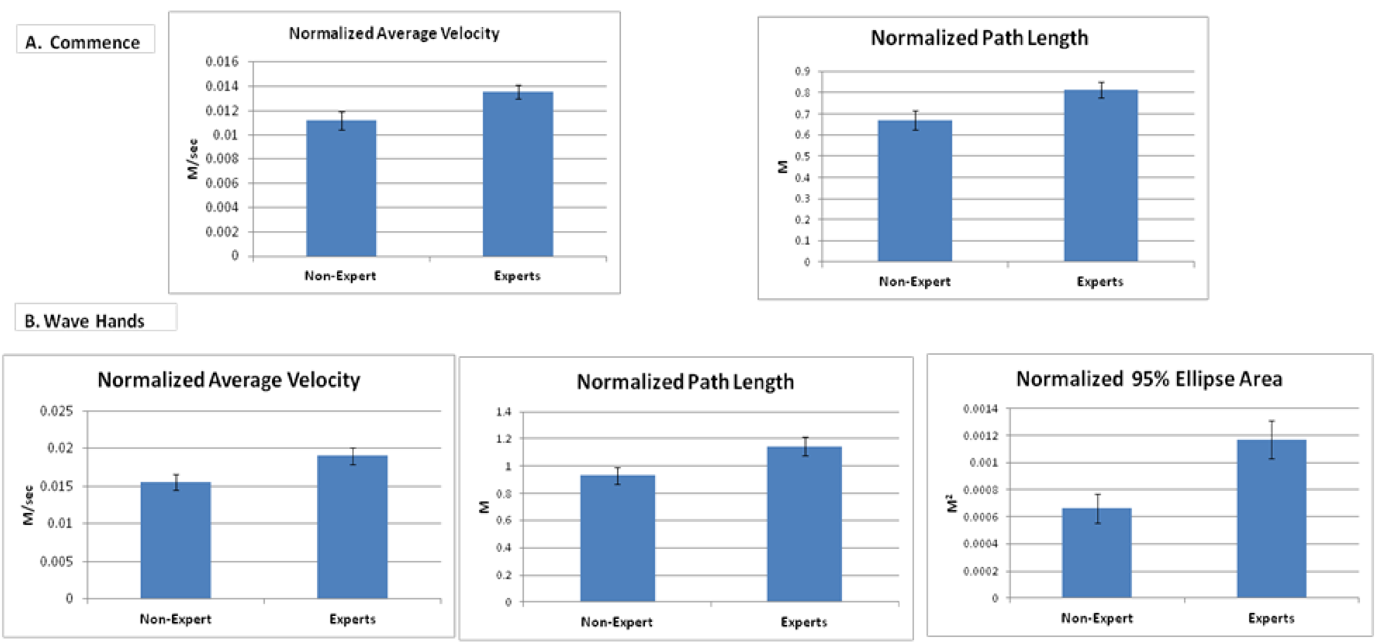

Figure 1: All COP indices were normalized by height in meters. Errors are standard errors. All differences were significant at P < .05

A PHENOMENOLOGICAL HUMAN ENERGY EXPENDITURE MODEL IN JOINT SPACE

Dustyn P. Roberts and Joo H. Kim

Polytechnic Institute of New York University, Brooklyn, NY, USA
email: jhkim@poly.edu

INTRODUCTION

In humans, metabolic energy is converted to mechanical work at the junction of tendon and bone [1]. However, there are several losses and inefficiencies that prevent direct transformation of metabolic energy to mechanical work. Metabolic energy consumed can be experimentally measured from indirect spirometry. This input energy is transformed into the mechanical work of motion and the balance is either stored or dissipated as thermal energy. The mechanical work at joints can be determined from standard gait analysis and inverse dynamics procedures that take input from a motion capture system and force plates and output kinematic and kinetic data. Since humans are subject to the first law of thermodynamics, when data is available on metabolic energy expenditure (EE) and joint mechanical work, the losses that occur in the transition of the former to the latter can be inferred.

Several phenomenological models have been developed that calculate metabolic EE based on output from Hill-type muscle models [2]. However, these require intricate dynamic muscle models that rely on geometric parameters that are often taken from static cadaver studies [3]. Recent work by Kim et al. [4] demonstrated the possibility of calculating metabolic EE in joint space when joint torques and angular velocities are known, which facilitates simulations. This work will take advantage of both methods to illustrate the implementation of a new phenomenological formulation of human EE.

MODEL DESCRIPTION

Anthropometric, kinematic, and kinetic data from [1] were used as inputs to the model. Most of the thermal energy dissipation for a healthy adult over the course of a day is attributable to the basal metabolic rate (BMR). Although there are several formulas for calculating BMR, the Mifflin-St Jeor equation is considered to be most likely to predict BMR within 10% of actual:

$$\dot{B} = 0.0485\left(9.99M + 6.25H - 4.92A + s\right)\ W$$

where M is body mass in kg, H is height in cm, A is age in years, s is +5 for males and -161 for females, and a conversion factor is used to get BMR in terms of SI units.

Physical activity increases BMR by 60% for light labor up to over 100% for heavy exertion. Kinematic and kinetic data from [1] were used characterize this physical activity in order to develop the remaining terms in the EE formula. The resultant actuator torque at each joint represents the sum of the moments created by each musculotendon unit (flexors and extensors) that acts on that joint. The joint mechanical power is the product of the torque and angular velocity for each degree of freedom (DOF):

$$P_i(t) = \dot{W}_i(t) = \tau_i(t)\dot{q}_i(\mathrm{t}) \quad \left(i = 1, \ldots, n\right)$$

where P is power, W is work, τ is torque, $\dot{q}$ is joint angular velocity, and n is the total number of DOFs. The torque and angular velocity can and do have different signs depending on the activity, and there is a metabolic cost associated with both positive and negative work. The work-related metabolic cost in muscle was estimated using an equation from [1]:

$$\frac{\textit{positive work}}{\eta_+} + \frac{\textit{negative work}}{\eta_-} = \textit{metabolic cost}$$

where the positive work efficiency η_+ is 0.25 and the negative work efficiency η_- is 1.2. To determine the whole body metabolic cost of gait based on the limited lower body dataset used, the average subject-specific metabolic EE rate above BMR during walking was estimated using an experimentally derived equation [5] to determine an acceptable multiplication factor.

From Hill's muscle models we know that the equation for the heat released from an active muscle has one term dependent on the muscle force independent of length changes (activation and maintenance heat h_{am}), one term dependent on the change in muscle length (shortening and lengthening heat h_{sl}), and one term that represents the mechanical work. If rates of EE are used instead of totals, and the equations are transformed into joint space since torque is related to force through the muscle moment arms, we can establish a phenomenological formulation of total metabolic EE:

$$\dot{E}(t) = \sum_{i=1}^{n} \left|\tau_i(t)\dot{q}_i(t)\right| + \sum_{i=1}^{n} h_{am}\left|\tau_i(t)\right| + \sum_{i=1}^{n} h_{sl}\left|\tau_i(t)\dot{q}_i(t)\right| + \dot{B}$$

where $\dot{E}$ is total EE rate and

$$h_{sl} = \begin{cases} h_{sl}+ & \text{if } \tau_i(t)\dot{q}_i(t) \geq 0 \\ h_{sl}- & \text{if } \tau_i(t)\dot{q}_i(t) < 0 \end{cases} \quad (i = 1, \ldots, n)$$

RESULTS

The mass of the subject was given in [1], the height was estimated based on accepted ratios of tibia length to total height, and the age of the subject was estimated to be 20 based on anthropometric reference data relating weight, height, and age. The BMR of the subject was 74.3 W, the average subject-specific metabolic EE above BMR was 185.2 W, so the total average EE rate for walking was 259.5 W. This target was used to develop the constants in the new equation for EE. Both the results from Winter's equation and the new formulation are shown in Figure 1.

DISCUSSION

The phenomenological model developed here shows a slightly different EE profile than that derived from [1] although the average metabolic rate is the same. This model is expected to more closely resemble the EE profile of an actual subject based on physiologically derived terms. It has been said that all models are wrong, but some are useful. This research represents the first step in developing a joint-space-based human EE equation for general tasks. Improvements in coefficient estimation and validation will be pursued in future work.

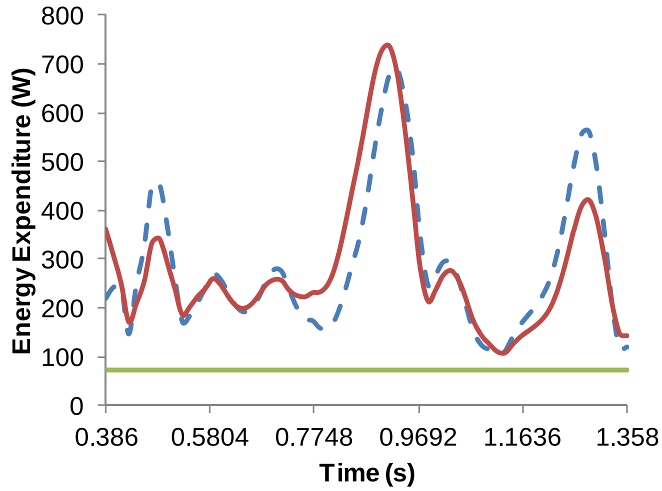

Figure 1: Total metabolic rate over one stride. The dashed blue line shows the formulation from [1], the solid red line shows the results of the current study, and the green line indicates BMR.

REFERENCES

1. D. A. Winter, *Biomechanics and Motor Control of Human Movement*, Wiley, 2009.
2. L. J. Bhargava, et al., "A Phenomenological Model for Estimating Metabolic Energy Consumption in Muscle Contraction," *J Biomech*, **37**, n. 1, 81–88, Jan. 2004.
3. K. Manal, D. P. Roberts, and T. S. Buchanan, "Can Pennation Angles Be Predicted from EMGs for the Primary Ankle Plantar and Dorsiflexors During Isometric Contractions?," *J Biomech*, **41**, n. 11, 2492–2497, Aug. 2008.
4. J. H. Kim, J. Yang, and K. Abdel-Malek, "Planning Load-Effective Dynamic Motions of Highly Articulated Human Model for Generic Tasks," *Robotica*, **27**, n. 5, 739–747, Sep. 2009.
5. P. G. Weyand, B. R. Smith, M. R. Puyau, and N. F. Butte, "The Mass-Specific Energy Cost of Human Walking Is Set by Stature," *J Exp Biol*, **213**, n. 23, 3972–3979, Dec. 2010.

ACKNOWLEDGEMENTS

This work was supported in part by a National Science Foundation Graduate Research Fellowship to D. Roberts under Grant No. DGE-1104522.

EVALUATING KNEE STABILITY AFTER TOTAL KNEE ARTHROPLASTY USING INERTIAL MEASUREMENT UNITS

[1]Dustyn P. Roberts, [2]Humera Khan, [1]Joo H. Kim, [2]James Slover, and [1,2]Peter S. Walker

[1]Polytechnic Institute of New York University, Brooklyn, NY, USA
[2]New York University Hospital for Joint Diseases, New York, NY, USA
email: jhkim@poly.edu

INTRODUCTION

Hundreds of thousands of total knee arthroplasties (TKA) and 22,000 TKA revisions are performed annually in the US alone. While most patients can perform activities of daily living (ADL) following successful recovery from TKA surgery, many experience instability under more stressful conditions [1], and instability is one of the major causes for revision surgery. Clinically, instability in TKA patients is attributed to misalignment or inadequate ligament balancing at surgery, as well as to joint laxity. A common symptom of knee instability is a patient report of the knee “giving way” [2]. Anterior/posterior (A/P) laxity varies considerably between TKA patients. However, research on anterior cruciate ligament (ACL) deficient knees has shown that passive knee laxity is *not* related to dynamic knee stability [2]. Existing methods of characterizing stability that include only spatial (vs. temporal) aspects are inadequate. Existing temporal methods rely on the periodicity of activities such as gait that are not applicable to non-periodic ADL. In order to explain the lay concept of joint stability with engineering rigor in such activities, new methods of characterization are needed that include temporal parameters that address the transient episodes of “giving way” reported by patients.

A sudden change in muscle forces that causes elevated acceleration and/or jerk can be an indicator of lack of stable control or instability in the underlying structure [3]. The aim of this study was to investigate the use of an inertial measurement unit (IMU) attached at the level of the tibial tuberosity as a tool to evaluate knee stability of TKA patients during ADL.

METHODS

There were 27 patients with unilateral or bilateral TKAs (66±8 years old, 11 males, 38 total TKA knees), and 18 healthy age-matched control subjects (60±6 years old, 7 males, 36 total control knees). An IMU (GLI Interactive LLC, Seattle, WA) set to 100 Hz was used for all testing. It was fixed with a strap over the tibial tuberosity of the subjects. Questionnaires on pain and instability were administered for each subject immediately following the experimental sessions. Both instability and pain were reported as none, mild, or severe in each test activity. All subjects gave informed consent, and experiments were approved by the Institutional Review Board.

Each subject completed five ADLs with the IMU on each leg: (1) walking 3 steps, (2) pivoting towards the test leg, (3) sit to stand, (4) step up/step down, and (5) pivoting opposite the test leg. For each of the five activities, the x (medial/lateral (M/L)), y (A/P), and z (superior/inferior (S/I)) components of linear acceleration were recorded. Ten parameters of interest were identified using a custom MATLAB program - five based on acceleration, and five based on jerk: the maximum, minimum, difference between these (delta), mean, and infinity norm (maximum absolute acceleration) of each trial. The resulting 150 parameters were analyzed statistically to determine which parameters were significantly different between patients and controls [4]

RESULTS

Out of the five activities, the patients reported more instability during Activity 4 – step up and step down – than in any other activity (Figure 1). Additionally, this was the only activity in which any patient reported severe instability. The patients also reported more pain during Activity 4 than in any other activity. This was also the only activity in which any patient reported severe pain.

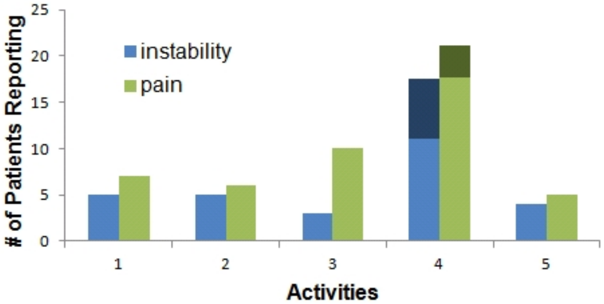

Figure 1: Instability and Pain by activity. All reports were mild except for darker blocks in activity four that indicate severe complaints

There was a statistically significant difference ($p < 0.05$) between groups on 23 parameters as determined by one-way ANOVAs. Of these parameters, 18 depended on components of acceleration in the A/P direction and 5 depended on components in the S/I direction. Six of these parameters were determined in Activity 4 – the activity during which the most pain and instability was reported. Of these 6 metrics, 3 were identifiable from acceleration data alone: the delta, the mean, and the infinity norm. Since Activity 4 involved a step up and a step down procedure, the delta and infinity norm were determined to better characterize the activity than the mean.

DISCUSSION

We have demonstrated that IMUs have potential in evaluating instability in patients following TKA surgery. The tests could be readily carried out in a clinical setting, were applicable to several ADL, and results provided a quantifiable indication of instability that correlated with patient-reported instability. The majority of the parameters of interest that showed significant differences between patients and controls were in the A/P direction, which was expected since the main plane of motion in all activities was the sagittal plane. Higher accelerations in patients vs. controls in the activities studied may be due to reduced control of the position of the knee joint. This is consistent with reports of reduced quadriceps muscle strength after TKA which can persist for 1-2 years. This is also seen in ACL deficient patients [5], where instability has been linked to quadriceps weakness.

A limitation of the study is that relative sliding motions between the tibia and the femur could not be characterized by one IMU mounted on the tibia. The study design could not distinguish whether the higher accelerations in TKA patients were due to relative motion of the tibia and femur or resultant motion at the joint. Future work will explore the use of two IMUs (one mounted on the tibia, one mounted on the femur) for better characterization of the relative motion.

REFERENCES

1. S. Parratte and M. W. Pagnano, “Instability After Total Knee Arthroplasty,” *Instr Course Lect*, **57**, 295–304, 2008.
2. L. Snyder-Mackler, G. K. Fitzgerald, A. R. Bartolozzi, and M. G. Ciccotti, “The Relationship Between Passive Joint Laxity and Functional Outcome After Anterior Cruciate Ligament Injury,” *Am. J. Sports Med.*, **25**, n. 2, 191 –195, Mar. 1997.
3. J. H. Kim, J. Yang, and K. Abdel-Malek, “Planning Load-Effective Dynamic Motions of Highly Articulated Human Model for Generic Tasks,” *Robotica*, **27**, n. 5, 739–747, Sep. 2009.
4. L. Palmerini, L. Rocchi, S. Mellone, F. Valzania, and L. Chiari, “Feature Selection for Accelerometer-Based Posture Analysis in Parkinsons disease,” *IEEE Trans. Inf. Technol. Biomed.*, **15**, n. 3, 481–490, 2011.
5. M. Lewek, K. Rudolph, M. Axe, and L. Snyder-Mackler, “The Effect of Insufficient Quadriceps Strength on Gait After Anterior Cruciate Ligament Reconstruction,” *Clin. Biomech.*, **17**, n. 1, 56–63, Jan. 2002.

ACKNOWLEDGEMENTS

This work was supported by the New York University and Polytechnic Institute of NYU Seed Grant for Collaborative Research and a National Science Foundation Graduate Research Fellowship to D. Roberts under Grant No. DGE-1104522.

More Is Not Always Better:
Consequences of Exoskeleton Assistance in a Compliant Muscle-Tendon System

[1]Benjamin Robertson [1]Gregory Sawicki
[1]UNC Chapel Hill/NC State University
Department of Biomedical Engineering
email: bdrober3@ncsu.edu

Introduction

Years of research on the mechanics and energetics of locomotion have established that compliant tissues (i.e. tendon and aponeurosis) are crucial in shaping efficient and stable locomotion [1]. Achieving a 'tuned' state in a compliant muscle-tendon unit (MTU) depends on optimal interaction between the frequency and amplitude of muscle activation, material properties of series elastic tissues, and actuation properties of the biological muscle (e.g. activation dynamics, force-length, and force-velocity). Maximizing elastic energy storage and return in complaint tissues allows series muscles to remain nearly isometric, reducing metabolic demand with little effect on MTU power output [2, 3]. It is not surprising, then, that humans prefer to use neuromuscular control strategies during cyclic movements that allow their muscles to operate with near-isometry when coupled with a series elastic tendon [3-5].

In recent years, there has been rapid progress in the development of wearable robotics designed to assist/enhance human movement [6, 7]. Despite technological advances, few studies have examined the effects of parallel mechanical assistance on underlying MTU interaction dynamics. Because it is difficult to make direct measurements of in-vivo MTU behavior, we developed a model of assisted human hopping to address key questions regarding human physiological response to wearable robotic assistance provided via a spring loaded exoskeleton (Exo). We hypothesize that 1) the coupled Exo-MTU system can produce periodic mechanical power output by trading off increased Exo stiffness with decreased muscle activation and that 2) the MTU will continue contracting with near-isometry under these conditions resulting in reduced CE power and force production.

Methods

The biological MTU in this model is comprised of a single Hill-type muscle, or contractile element (CE) in series with a Hookean tendon-spring, or series elastic element (SEE) operating with a fixed mechanical advantage on a mass under constant gravitational load. We based our muscle-tendon properties (F_{max} = 6000 N, v_{max} = .45 m/s, l_0 = .055 m, k_{CE} = 90,000 N/m, k_{SEE} = 180,000 N/m, l_{slack} = .237 m) and activation dynamics (*duty* = 10%, τ_{act} = .011 s, τ_{deact} = .068 s) on data documented for the human triceps surae-Achilles tendon complex [8]. We chose parameters for the load (M = 35 kg, in/out lever arm length ratio ~.33) to reflect realistic body weight and mechanical advantage seen at the ankle joint of a single limb during two-legged hopping.

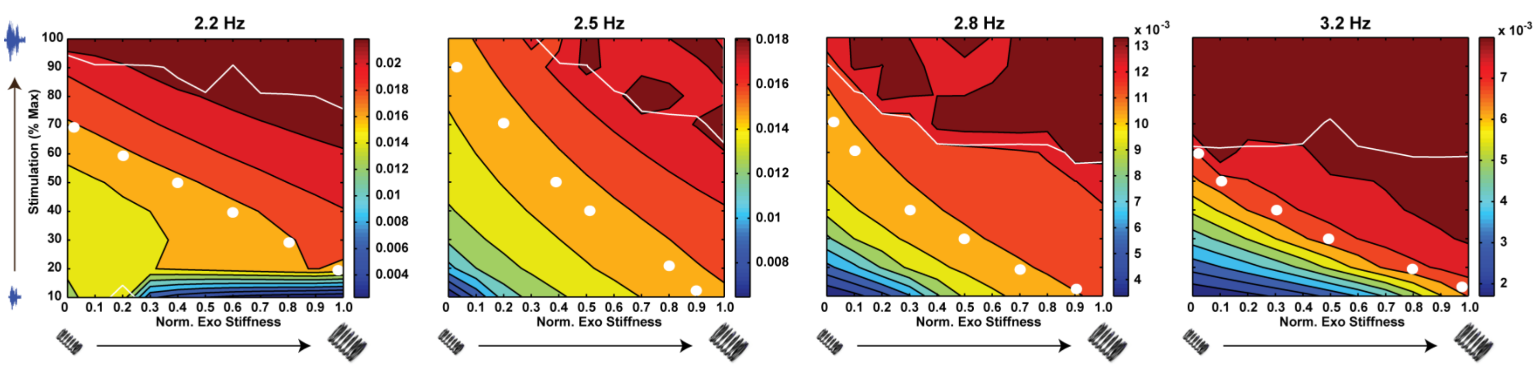

Figure 1: Plots of average positive power produced in the Exo-MTU system for each of the four operating frequencies over the full range of stimulation amplitude and exoskeleton stiffness. Exoskeleton stiffness is normalized to k_{MTU} and Power production to F_{max}*v_{max} for the CE. Contour scaling for each operating frequency is indicated by the colorbar to the right of each graph. Regions exhibiting non-periodic behavior are bordered in white, and points selected for further analysis are indicated by white dots. MTU and Exo component data for each dot can be seen in **Figure 2**.

To drive muscle force generation, we used a purely feed-forward neural control signal. The modeled muscle-tendon system was stimulated over a range of muscle activations (10-100% of maximum) and frequencies (2.2, 2.5, 2.8, and 3.2 Hz). We chose these operating frequencies because they reflect observed human behavior, and exhibit near-isometry for in-vivo and modeled conditions in the absence of assistance [4]. To model the effects of a wearable passive Exo at the ankle, we provide parallel assistance with a linear spring that has a slack length equal to the combined optimal muscle fascicle length (l_0) and series tendon slack length (l_{slack}). Modeled exoskeleton stiffness ranged from 0-100% of the stiffness of the purely passive MTU (k_{MTU} = 60,000 N/m). By varying activation amplitude, frequency, and coupled Exo-MTU stiffness we were able to explore how the addition of a passive linear spring in parallel with the human triceps surae-Achilles tendon complex affected the naturally efficient mechanics of the MTU.

Results/Discussion

At all frequencies, a majority of stimulation amplitude/Exo stiffness combinations resulted in mechanics that were periodic with stimulation. Non-periodic behavior was observed at every frequency for high Exo stiffness and high stimulation amplitude (**Figure 1**). The Exo was able to make significant contributions to MTU-Exo power and force production, particularly for low stimulation amplitude and high stiffness conditions (**Figure 2**). We observed contours of equal power production for the Exo-MTU system that spanned stiffness-stimulation parameter space at all frequencies by trading increasing exoskeleton stiffness for decreased muscle activation, in support of hypothesis 1. Power output from the CE was frequency dependent, increasing dramatically at the lowest frequency and decreasing only slightly at the highest with system power output held constant (**Figure 2**). Despite reductions in CE peak force and rate of force along these contours, there were consistent increases in CE average operating length/velocity and passive force. This indicates a loss of isometry and previously efficient MTU mechanics, contradicting hypothesis 2. All of these variations in mechanics will affect both metabolic cost and injury risk; what that effect will be, however, cannot be determined based on model results. Future experiments in humans will test model predicted variations in MTU mechanics when assistance is applied, and attempt to determine what, if any, mechanical aspects of assisted hopping drive metabolic cost and human preference.

References

[1] Alexander, R M, *Comp Biochem Physiol A Mol Integr Physiol,* vol. 133, pp. 1001-11, Dec 2002.

[2] Roberts, T J, et al., *J Exp Biol,* vol. 214, pp. 353-61, Feb 1 2011.

[3] Dean, J C, et al., *J Appl Physiol,* vol. 110, pp. 873-80, Apr 2011.

[4] Takeshita, D, et al., *J Appl Physiol,* vol. 101, pp. 111-8, Jul 2006.

[5] Ishikawa, M, et al., *J Appl Physiol,* vol. 99, pp. 603-8, Aug 2005.

[6] Ferris, D P, et al., *J Appl Physiol,* vol. 100, pp. 163-70, Jan 2006.

[7] Herr, H, *J Neuroeng Rehabil,* vol. 6, p. 21, 2009.

[8] Lichtwark, G A, et al., *J Theor Biol,* vol. 252, pp. 662-73, Jun 21 2008.

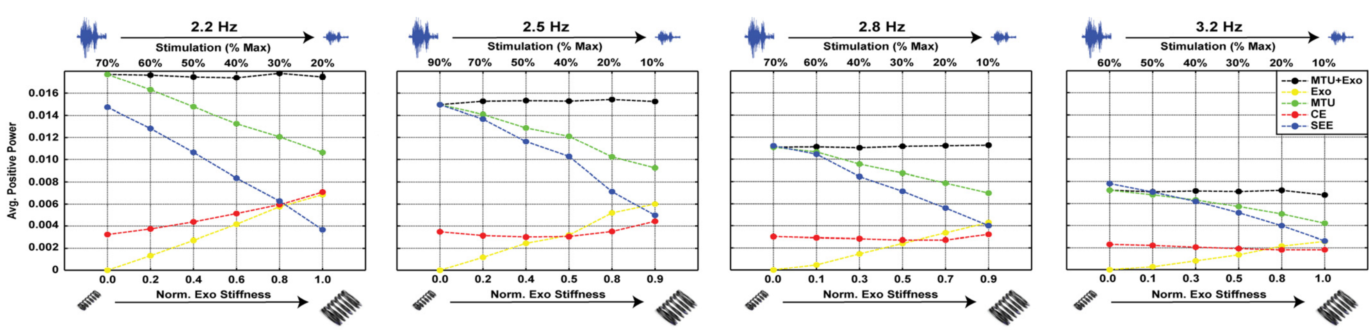

Figure 2: Plots of average positive power over a cycle of stimulation for each component of the MTU system. Each point corresponds to a white dot in the MTU-Exo average positive powers plotted in **Figure 1**, horizontal axes are not to scale. Moving from left to right decreases stiffness and increases activation.

LOCOMOTOR ADAPTIVE LEARNING IS IMPAIRED IN PERSONS WITH PARKINSON'S DISEASE

[1]Ryan T. Roemmich, [1]Joe R. Nocera, [1]Chris J. Hass

[1]University of Florida, Gainesville, FL, USA
Email: rroemmich@ufl.edu

INTRODUCTION

Locomotor adaptation is essential to maintain safe and efficient ambulation. Whether in response to changing external or internal environments, the ability to adapt gait patterns is essential to sustaining steady gait amidst changing walking conditions. The central nervous system facilitates adaptation by utilizing online feedback (reactive) and feedforward (predictive) control. While initial reactive responses to adaptation are likely spinally-mediated, feedforward predictive motor adaptation appears to be controlled by the cerebellum [1].

Locomotor adaptation has recently been studied in various populations by using split-belt treadmills (SBT). SBT differ from conventional treadmills in that there are two belts (one under each leg), each with a separate motor which allows the limbs to walk at different speeds simultaneously. During adaptation, gait parameters are initially asymmetric as stride length increases in the fast leg while stance time and step length increase in the slow leg. As the walker continues to adapt, stride length and stance time remain asymmetric while step length gradually returns to symmetry under cerebellar control [1].

Persons with Parkinson's disease (PD) are characterized by motor deficits resulting from degeneration of dopaminergic neurons within the basal ganglia. Recent research has suggested that the cerebellum becomes hyperactive in persons with PD as a compensatory response to basal ganglia dysfunction [2]. While this may be an appropriate response in order to preserve some motor function typically controlled by the basal ganglia, Jayaram and colleagues have demonstrated that depression of cerebellar inhibitory activity over the motor cortex is essential in facilitating locomotor adaptive learning [3]. Thus, we postulate that locomotor adaptation and adaptive learning may be impaired in persons with PD.

METHODS

Fifteen healthy young adults (HYA; age 22.3 ± 3.3 yr, 169.0 ± 8.6 cm, 65.8 ± 11.3 kg, 8 males, 7 females), fifteen persons with PD (age 60.5 ± 12.3 yr, 172.8 ± 4.3 cm, 82.4 ± 11.5 kg, 12 males, 3 females), and fourteen healthy older adults (HOA; age 61.1 ± 13.2 yr, 167.7 ± 7.2 cm, 71.2 ± 12.1 kg, 7 males, 7 females) participated. Sixteen passive reflective markers were attached to the lower body in accordance with the Vicon Plug-in-Gait lower body marker system. Kinematic data were collected using a 7-camera motion capture system (120 Hz; Vicon Nexus, Oxford, UK) as the participants walked on an instrumented SBT (Bertec Corporation, Columbus, OH).

All participants held onto the handrails for the duration of all treadmill sessions. The speed of both belts was gradually increased until the participants reported being at the "fastest speed they felt comfortable walking for 15 minutes". This speed was set as the "fast" walking speed while 50% of this speed was designated as the "slow" walking speed. During the SBT tasks, the belt under the nondominant leg in the control groups and the belt under the more-affected leg in the PD group was sped up to the fast speed while the belt under the contralateral leg remained at the slow speed. Participants walked under these conditions for 10 minutes (SPLIT). During the SPLIT condition, kinematic data were collected during intervals from 0:00-0:30 (EARLY adaptation), 4:30-5:00 (MID adaptation), and 9:30-10:00 (LATE adaptation). Immediately following the split-belt condition, the participants walked overground for 10 trials to wash out the split-belt adaptation. Then the participants walked under the same split-belt conditions again for three minutes (READAPT). Following the READAPT condition, the "fast" belt was slowed to the "slow" speed (POST-TIED). Participants walked under the POST-TIED conditions for five minutes. Data were also collected from 0:00-0:30 of the READAPT and EARLY POST conditions.

Heel strikes and toe offs were manually labeled in Vicon software based on marker velocity profiles. Stride length, stance time, and step length asymmetry were defined based on previous literature [1]. Repeated measures ANOVAs with Bonferroni post-hoc analyses were performed to analyze differences in asymmetry in stride length, stance time, and step length among groups and conditions. Level of significance for the ANOVAs were set at $\alpha = .05$.

RESULTS AND DISCUSSION

We observed main effects of group and condition as well as a significant group x condition interaction. There were no significant differences in the mean asymmetry measures among the groups during the EARLY, MID, and LATE adaptation conditions.

During the READAPT condition, there were no significant differences among the groups in stride length or stance time asymmetry. Step length asymmetry was significantly higher in the PD group than in the HYA group ($p<.05$).

During the EARLY POST condition, stride length asymmetry was significantly higher in the HYA group than in the PD group ($p<.05$). Stance time asymmetry was significantly higher in the HYA and HOA groups than the PD group ($p<.05$). Step length asymmetry was significantly higher in the HYA group than the PD group ($p<.05$).

HYA facilitated the greatest locomotor adaptive learning in that they were able to quickly reduce asymmetry during READAPT. This indicates that the HYA were able to store the gait pattern learned during the initial SPLIT condition and apply this learned pattern to the READAPT condition efficiently. Further, HYA retained the split-belt walking pattern into conventional treadmill walking, as demonstrated by the relatively high

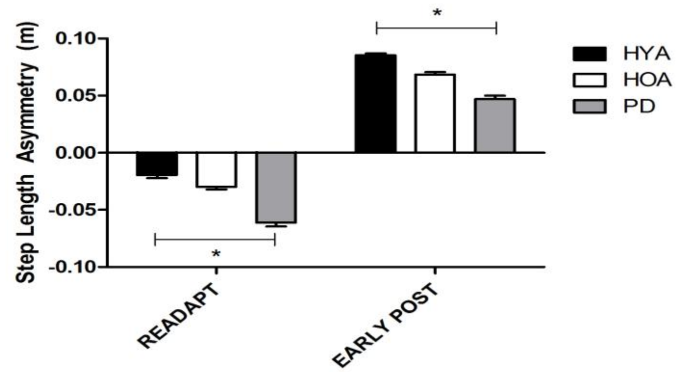

Figure 1. Step length asymmetry during READAPT and EARLY POST (* indicates $p<.05$).

asymmetry observed in EARLY POST. This provides further evidence to suggest that locomotor adaptive learning has occurred in HYA.

Our results also suggest that locomotor adaptive learning was impaired in persons with PD. PD demonstrated reduced retention of the split-belt gait pattern as evidenced by increases in asymmetry during READAPT when compared to HYA and decreases in asymmetry during EARLY POST when compared to HYA and HOA.

CONCLUSIONS

Though persons with PD retain the ability to adapt locomotor patterns, they do not appear to retain the ability to store new gait patterns to the same degree as neurologically-healthy controls. We postulate that restricted locomotor adaptive learning may be caused by hyperactivity in the cerebellum frequently observed in persons with PD.

REFERENCES

1. Morton SM, Bastian AJ. Cerebellar contributions to locomotor adaptations during splitbelt treadmill walking. *J Neurosci.* Sep 2006;26(36):9107-9116.
2. Yu H, Sternad D, Corcos DM, Vaillancourt DE. Role of hyperactive cerebellum and motor cortex in Parkinson's disease. *Neuroimage.* Mar 2007;35(1):222-233.
3. Jayaram G, Galea JM, Bastian AJ, Celnik P. Human locomotor adaptive learning is proportional to depression of cerebellar excitability. *Cereb Cortex.* Aug 2011;21(8):1901-1909.

THE INFLUENCE OF FILTERING CUTOFF FREQUENCY ON LANDING BIOMECHANICS MEASURED DURING A DROP VERTICAL JUMP

[1] Ben D. Roewer, [3,4] Kevin R. Ford Ph.D., [1,2,3,4] Gregory D. Myer Ph.D., [1,2,3,4] Timothy E. Hewett, Ph.D.

[1]Sports Health & Performance Institute, The Ohio State University, Columbus, OH 43221, USA
[2]Departments of Physiology and Cell Biology, Orthopaedic Surgery, Family Medicine and Biomedical Engineering, The Ohio State University, Columbus, OH 43221, USA
[3]Division of Sports Medicine, Cincinnati Children's Hospital Medical Center, 3333 Burnet Avenue, Cincinnati, OH 45229, USA
[4]Department of Pediatrics and Orthopaedic Surgery, College of Medicine, University of Cincinnati, Cincinnati, OH 45221, USA
Email: ben.roewer@osumc.edu, web: http://sportsmedicine.osu.edu/

INTRODUCTION

The drop vertical jump (DVJ) is a useful movement task for determining knee injury risk. Hewett et al. used the DVJ to prospectively screen young female athletes for future anterior cruciate ligament injuries [1]. Peak knee abduction moment (KAM) measured during a DVJ predicted future ACL injury risk with 78% sensitivity and 73% specificity. Prior investigators have purported that it is necessary to filter marker and force data at the same frequency in order to calculate accurate joint moment data [2]. Joint moments derived from inverse dynamic techniques may be large when kinematic and force plate data are not filtered at the same frequency; however, the potential for erroneous calculation of joint torques is largely dependent on the maneuver, the joint of interest and the axis of rotation and [3]. The purpose of the present study was to determine the effects of kinematic and kinetic filtering cutoff frequencies on the peak KAM calculated during a DVJ. We hypothesized that the choice of filtering cutoff frequency would not significantly affect the peak KAM nor would it significantly alter the order of subjects ranked based on their peak KAM.

METHODS

Twenty-two female high school volleyball players were tested prior to the onset of their sport seasons. Subject height, body mass and the average of three maximum vertical jump attempts were recorded. Forty-three 9 mm retroreflective markers were placed on anatomical landmarks. Each subject performed three DVJ trials from a 31cm tall box. Trials were accepted if the subject's feet made simultaneous and isolated contact with two force places embedded into the laboratory floor (Bertec corp. Worthington, OH). Three-dimensional marker position data were sampled at 240Hz using eight infrared cameras (Vicon, Oxford Metric Ltd. London, UK). Ground reaction force data were sampled at 1200Hz. Marker and force data were low-pass filtered at the same frequency (10Hz, 12Hz, and 15Hz) and also at mismatched frequencies (10-50Hz, 12-50Hz, 15-50Hz respectively) using a bi-directional Butterworth filter. Data were processed using custom Visual 3D (C-motion Inc. Germantown, MD) and Matlab (Mathworks Inc. Natick, MA) coding. Peak external KAM during 100% of stance was compared across all filtering conditions using an ANOVA with two repeated measures (limb x filtering cutoff frequency). Spearman rank correlation was used to test the effect of filtering condition on the rank order of athletes based on their peak KAMs. Significance for all tests was set at $\alpha < 0.05$. Statistical significance for the post hoc paired t-tests was adjusted using a Bonferonni correction ($\alpha < 0.003$).

RESULTS AND DISCUSSION

No effect of limb was detected ($p = 0.206$) so data for both limbs were collapsed and analyzed. A main effect of filtering condition was detected for peak KAM ($p < 0.001$). Significant differences in peak KAM were detected among all of the matched filtering conditions ($p < 0.003$), but no differences were detected among all of the mismatched filtering conditions ($p \geq 0.003$). The average mismatch-filtered peak KAM values were greater than the match-filtered peak KAM values ($p < 0.001$) (Fig. 1).

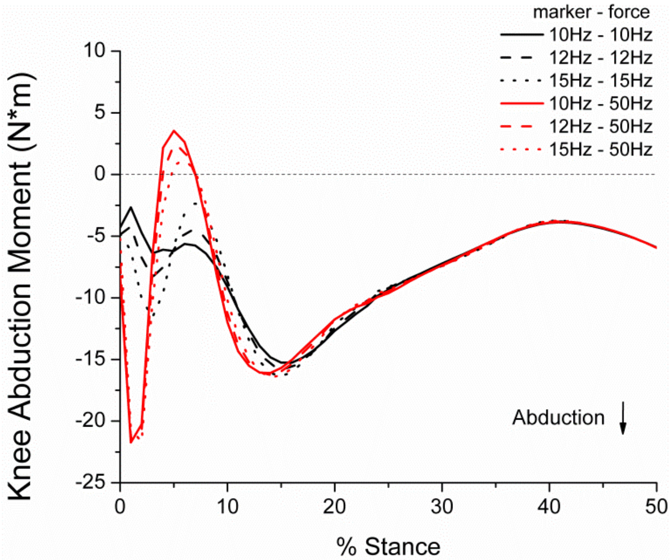

Figure 1: The average external knee abduction moment during the drop vertical jump for each filtering condition. Time-normalized data for the first 50% of stance are presented to clarify the effect of filtering condition on KAM near initial contact.

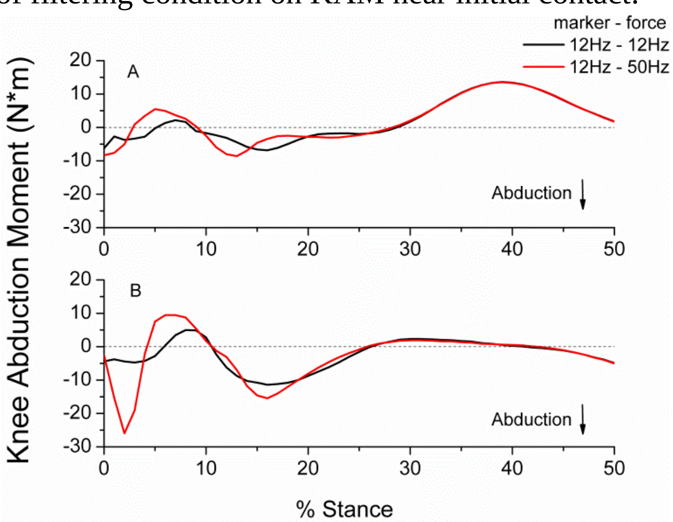

Figure 2: The average external knee abduction moment for two representative subjects produced under matched and mismatched filtering conditions.

The effect of mismatched filtering was not consistent across all subjects. Large KAMs were not observed at initial contact when matched filtering was applied. However, when mismatched filtering was applied, some subjects showed large KAMS at initial contact (Fig. 2B) while others did not (Fig. 2A).

The rank order of mismatch-filtered peak KAM values significantly covaried with the order of match-filtered peak KAM values ($p < 0.001$). In other words, athletes who had the largest peak KAMs when matched filtering was applied also had the largest peak KAMs when mismatched filtering was applied.

CONCLUSIONS

While filtering cutoff frequency affected the magnitude of the peak KAM calculated during a DVJ it did not affect the rank order of individual athletes. An important question remains unanswered: "Are the high knee moments reported by prior investigators [1] artifacts as postulated [2] or are they authentically large knee moments that may hold high predictive value for assessing future knee injury risk?"

REFERENCES

1. Hewett, et al. *American Journal of Sports Medicine*, **33**, 492-501, 2005.
2. Kristianslund, et al. *Journal of Biomechanics*, **45** 666-671, 2012.
3. Hewett, et al. *Journal of Biomechanics*, **In Press** 2012.

ACKNOWLEDGEMENTS

Funding was provided by the National Institutes of Health grants (RO1-AR049735, R01-AR055563, R01-AR056259).

Table 1: Peak knee abduction moment calculated for each filtering condition during 100% of stance for the drop vertical jump. (n=22). Means ± standard deviations are presented.

Cutoff frequency (marker – force)	**(10-10) Hz**	**(12-12) Hz**	**(15-15) Hz**	**(10-50) Hz**	**(12-50) Hz**	**(15-50) Hz**
Peak KAM (Nm)	-24.0 ± 11.7	-24.5 ± 11.3	-25.5 ± 11.0	-31.1 ± 10.7	-31.0 ± 10.2	-31.0 ± 10.1

RELIABILITY OF A NOVEL PROPRIOCEPTION TESTING DEVICE

[1]Juan D. Rojas, [2,3]J. Troy Blackburn, [3]Laurence E. Dahners, [3]Chris W. Olcott, [1,3]Paul S. Weinhold

University of North Carolina, Departments of [1]Biomedical Engineering, [2]Exercise & Sports Science, & [3]Orthopaedics
email: jrojas@live.unc.edu

INTRODUCTION

Impaired knee proprioception is believed to have a role in the risk of acute knee injury and the progression of knee osteoarthritis. New methods for evaluating knee proprioception are needed due to limitations of existing methods that include fair reliability, nonfunctional nature, and an inability to assess the effect of braces.

The purpose of this study was to develop a new three-dimensional target matching (3DTM) device for measuring knee proprioception and compare it to two existing methods: vibration perception threshold (VPT) and joint position sense (JPS) testing. It was hypothesized that the 3DTM task would show higher reliability than the JPS testing and limited correlation to the alternative methods due to its functional nature.

METHODS

20 healthy subjects (age: 20-65yrs; 11M, 9F) were tested across two sessions separated by one week using three evaluation methods; 3DTM, VPT, and JPS. The order of the presentation of the evaluation methods was counterbalanced.

For the 3DTM task, subjects were asked to locate eight radially located target switches with their dominant foot without vision of the target board (Figure 1). A LabVIEW program was used to generate a computer display indicating which target switch to press. Targets were randomly presented in one of four predetermined sequences. Subjects were allowed to run practice trials with a random sequence of targets with vision of the target board. Three different radii(10.1, 14, 17.8cm) for targets were presented in a counterbalanced manner with one trial per radius. Target misses and hits were detected with a foot switch and the target switch (one attempt) & recorded for each trial. The outcome measure calculated was the average # of misses/trial.

Figure 1: 3DTM task.

VPT was evaluated at the medial femoral condyle (MFC) and at the first metatarsophalangeal (MTP) joint. The vibration amplitude of a biothesiometer was steadily increased at a rate of approximately 1V/sec. Subjects were asked when they first felt the vibration, and then the vibration was increased a set amount and steadily decreased until not felt. This process was repeated 5 times in each location and ascending/descending detection voltages were recorded. The measurements of the ascending detection voltage were averaged.

In the JPS method, the subjects were asked to lie on a sliding reclined platform (15° relative to the horizontal) while bearing weight on one leg with the knee extended. The task was to reproduce knee flexion angles between 20-40° over 5 trials. Knee flexion angle was measured by electrolytic tilt sensors. The subjects were asked to slowly flex their knee until the investigator tapped them on the shoulder and hold that position for 5 seconds. Then, the subject was asked to return to full extension and reproduce the angle of flexion which was marked with an electronic trigger. The absolute error (degrees) of each trial was calculated.

Reliability across the two testing sessions was assessed by the intraclass correlation coefficient (2,1) and by the standard error of measurement(SEM). SEM's between methods were compared by F-test of the error variance normalized by the square of the mean. Associations between measures were calculated by Pearson correlation coefficients.

RESULTS AND DISCUSSION

Descriptive statistics and reliability assessments for the measures are shown (Table1). No correlation was found between the measures except between the VPT-MTP measurement and the average misses in radius 1 of the 3DTM method ($R=0.535$, $P<0.05$) (Figure 2).

The VPT methods showed excellent reliability, but are more nonfunctional in nature, prevent assessment of the effects of other devices such as braces, and are likely dominated by cutaneous receptor input. The JPS task was more functional in nature, but only showed fair reliability. The 3DTM showed good reliability, was more functional in nature and included motions in the frontal plane which may have clinical relevance to knee injury and disease mechanisms. In addition, the 3DTM task likely receives proprioceptive input from receptors of different types and locations.

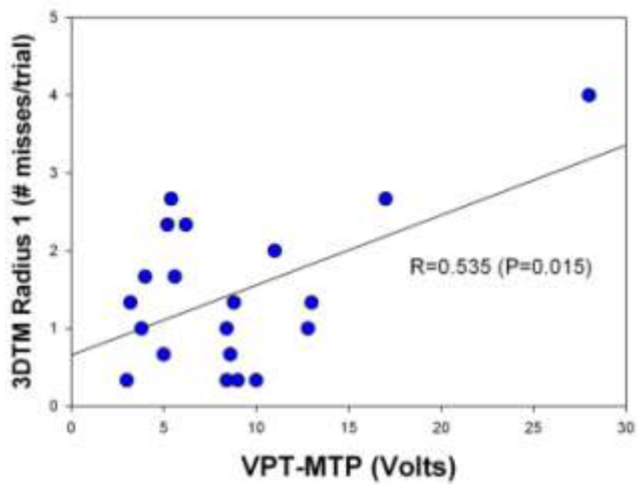

Figure 2: Correlation of 3DTM-radius1 vs. VPT-MTF measures.

CONCLUSIONS

The new 3DTM method shows promise due to its functional nature, good reliability, and its possible use with braces. The 3DTM was only associated with the VPT-MTP at the small radius target position and was not associated with the JPS measure. The 3DTM method might be improved with further refinement of the location of the radial target positions used in the evaluation.

ACKNOWLEDGEMENTS

Support provided by the Aileen Stock Research Fund.

Table 1: Proprioception measures across the two testing sessions (Mean± SD)

Method	Session 1	Session 2	ICC(2,1)	SEM(% of mean)
3DTM (miss/trial)	2.37 ± 1.33	2.11 ± 1.27	0.65 (good)	0.77(34%[A])
JPS (deg)	4.45 ± 2.76	3.68± 1.69	0.46 (fair)	1.68(41%[A])
VPT-MFC (V)	16.27 ± 8.76	15.94 ± 6.87	0.88(excellent)	2.70(17%[B])
VPT-MTP (V)	9.43 ± 6.42	8.82 ± 5.83	0.94(excellent)	1.35(15%[B])

A, B: SEM% values with a common letter did not differ ($F_{(20,20)}$, $P<0.05$)

THE EFFECT OF VARYING CADENCES ON SHOD & BAREFOOT GAIT KINEMATICS

Braden Romer, John Fox, Jay Patel, Jared Rehm, and Wendi Weimar

Auburn University, Auburn, AL, USA
email: bhr0002@auburn.edu, web: http://education.auburn.edu/kine/

INTRODUCTION

The significant increase in barefoot or minimalist footwear interest has forced its way into the retail markets, with numerous footwear manufacturers recognizing the commercial opportunities for this emerging market. While there is a definitive "pop-culture" influence for many individuals, as highlighted by Christopher McDougall's book *Born to Run*, recent research has also focused on the important differences in barefoot and shod gait [1]. One of the most immediate and significant adaptations to barefoot gait is the reduction in stride length and a corresponding rise in cadence. A point of debate among researchers is whether this increase in stride length is due to neural, mechanical, or a combination of factors. Previous research has found increased stride length when wearing athletic shoes as compared to flip-flops, which the authors hypothesized may be attributable to the increased mass of the athletic shoe [2]. However, more recent research has found that this relationship may not hold for all types of footwear as participants exhibited a longer stride length when wearing a heavier flip-flop as compared to a lighter version.

Therefore, the purpose of this study was to examine the relationship between barefoot and shod gait kinematics as a result of changes in walking speed.

METHODS

Twenty (10 female, 10 male) healthy participants volunteered for participation in the study. No participant had a lower-extremity injury within the year prior to participation in the study. Age of the participants was 23.7±2.4 years (m±SD) and body mass was 73.6±12.2kg. Participants walked on an instrumented walkway (GAITRite, CIR Systems, Inc., Havertown, PA, USA) during four separate conditions, with each condition consisting of six trials. Kinematic data was averaged across the six trials. Each trial included a 3.5m lead-in, followed by walking over the 4.25m GAITRite mat, then a 3.5m walkout for a total of 11.25m per trial.

The four included conditions were: participants walking at a self-selected pace while shod (SHFW), self-selected pace while barefoot (BFFW), shod while walking faster than self-selected (SHF), barefoot while walking faster than self-selected (BFF). During the SHF and BFF conditions, participants were provided the verbal instructions that they were to imagine they were late to a meeting. All participants were provided the same verbal cue, by the same investigator, at identical points during the data collection process. Participants were dressed in identical polyester clothing and utilized commercially available non-running athletic shoes for all shod trials.

A 2 (Gender) x 4 (Condition) MANOVA was completed with dependence on walking velocity, stride length, and cadence. Post-hoc analyses were completed utilizing a least squares difference test to determine if significant differences (p<0.05) existed between gender or footwear conditions.

RESULTS AND DISCUSSION

There was a significant main effect for gender ($F_{(3,70)} = 21.85$, $p < 0.001$, $\eta^2 = 0.48$) and condition ($F_{(9,170.51)} = 21.41$, $p < 0.001$, $\eta^2 = 0.46$) while the interaction effect was not significant. As indicated in Table 1, follow-up pairwise analyses indicated that men exhibited a significantly lower stride frequency (steps*min^{-1}) (p<0.001), walked significantly faster (p<0.036), and had significantly longer strides (p<0.001). Furthermore, significant differences were found between the cadences of all conditions, except SHFW-BFFW while significant differences were found for all velocities except

SHFW-BFFW and SHF-BFF. In addition to the aforementioned results, there were significant differences found in the stride length for all conditions (Figure 1). Participants walked slower in the free-walking (SHFW, BFFW) than the faster (SHF, BFF) conditions, indicating the investigator's instructions were successful. When shod was compared to barefoot, participants walked faster, had a lower cadence, and exhibited longer stride lengths.

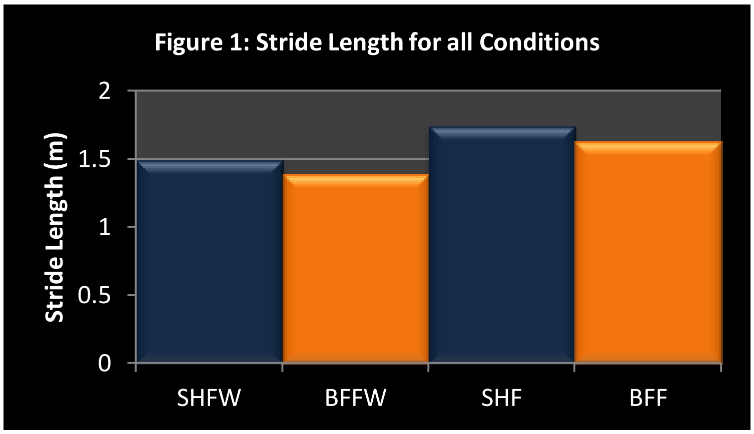

Significant differences in stride length were found ($p \leq 0.005$) between all conditions.

CONCLUSIONS

Similar to recent publications on running gait [1], considerable variations were found between shod and barefoot conditions. While the gender differences are not necessarily surprising, the fact that these differences held across all conditions was interesting. Even with the lack of significant differences in cadence between SHFW-BFFW, there were significant differences in the stride lengths. Despite increases in velocity, the relationships between shod and barefoot walking are maintained (i.e. decreases in stride length, increases in cadence). Similarly, the magnitude of the difference between shod and barefoot stride length and cadence appears to increase as velocity increases. Further research is needed to better understand the interaction between cadence and stride length during walking gait and understanding the mechanical and neurological factors involved in gait alterations.

REFERENCES

1. Leiberman, DE, et al. *Nature*, **463**, 531 – 353, 2010
2. Majundar, D, et al. *Indian J Physiol Pharmacol*, **50 (1)**, 33-40, 2006

Table 1: Kinematic variables across the four conditions.

		Male (n = 10)	**Female** (n = 10)	**Total** (n = 20)
SHFW	**Cadence** (steps*min^{-1})	110. 24 (±6.99)[1]	115.00 (±5.40)[1]	112.62 (±6.55)
	Velocity (ms^{-1})	1.45 (±0.16)[2]	1.34 (±0.09)[2]	1.39 (±0.14)
	Stride Length (m)	1.58 (±0.13)[3]	1.39 (±0.07)[3]	1.49 (±0.14)
BFFW	**Cadence** (steps*min^{-1})	114.21 (±5.40)[1]	119.37 (±6.68)[1]	116.79 (±7.54)
	Velocity (ms^{-1})	1.39 (±0.15)[2]	1.31 (±0.11)[2]	1.35 (±0.13)
	Stride Length (m)	1.46 (±0.13)[3]	1.32 (±0.07)[3]	1.39 (±0.12)
SHF	**Cadence** (steps*min^{-1})	125.71 (±7.93)[1]	135.21 (±6.73)[1]	130.46 (±8.66)
	Velocity (ms^{-1})	1.91 (±0.18)[2]	1.87 (±0.12)[2]	1.89 (±0.15)
	Stride Length (m)	1.83 (±0.11)[3]	1.66 (±0.11)[3]	1.74 (±0.14)
BFF	**Cadence** (steps*min^{-1})	131.73 (±8.43)[1]	141.15 (±8.24)[1]	136.44 (±9.44)
	Velocity (ms^{-1})	1.88 (±0.19)[2]	1.83 (±0.14)[2]	1.85 (±0.16)
	Stride Length (m)	1.71 (±0.18)[3]	1.56 (±0.10)[3]	1.63 (±0.12)

[1] Significant main effects for gender were found for Cadence ($p<0.001$)
[2] Significant main effects for gender were found for Velocity ($p<0.036$)
[3] Significant main effects for gender were found for Stride Length ($p<0.001$).

Variability of Strain and Strain Rate in the Human Tibial Diaphysis During Walking

[1]Tyler Rooks, [2]Daniel Leib, [2]Kotaro Sasaki, [2]Eric Dugan

[1]US Army Aeromedical Research Laboratory, Fort Rucker, AL, USA
[2]Boise State University, Boise, ID, USA
email: rooks.t@gmail.com

INTRODUCTION

With the prevalence of stress fractures in the military and athletes of all levels, reasearch into the pathology of this injury has taken flight in recent years. One area of research has focused on the role bone strain, which is known to be a factor in bone remodeling, has on stress fracture development. It has been difficult to perform studies in this area of research due to the invasiveness of *in vivo* measurements of the bone strain. Instrumentation for *in vivo* measurements is very difficult, introducing many uncertainties due to the quality of the contact between the bone and strain gauge. In addition to these uncertainties, *in vivo* measurements only provide strain information for a limited area in the locality of the strain gauge.

Recent work combining a subject specific musculoskeletal model with a flexible body (finite element model) has been shown to be a valid, time efficient method for calculating strain and strain rate[1,2,3]. Since this method does not involve *in vivo* measurements, it solves the problem of invasiveness, lessens the issues associated with instrumentation quality, and allows researchers to measure strain at multiple locations.

The goal of this study was to calculate a range of bone strain and strain rates at various potentially significant locations on the tibia.

METHODS

Experimental and imaging data was obtained from 13 healthy male subjects who were part of a larger study on tibial stress fractures. The subjects were asked to walk on an instrumented treadmill while collecting motion capture data to be used in creating a subject specific musculoskeletal model. This musculoskeletal model provided the framework for a flexible tibia to be used to calculate the strain and strain rate. The use of a flexible body, generated from the deformation modes of the bone, sufficiently decreases the degrees of freedom of the finite element model so that it can be used in a fully dynamic simulation.

The flexible tibia was generated by first segmenting the CT scanned tibia to regenerate a 3D solid model of the tibia geometry which was then meshed using a 3mm hexahedral mesh. Then, 600 material properties (300 for cortical bone and 300 for trabecular bone) calculated from the CT scan Hounsfield Units (HU) values for each element in the finite element model were applied to the mesh elements. Finally, a Craig-Bampton modal analysis was performed on the completed model to generate the deformation modes for the flexible tibia model.

The flexible tibia was then imported into the subject specific musculoskeletal model and aligned using motion capture markers and the corresponding nodes on the tibia model. After importing the flexible model into the subject-specific musculoskeletal model, the strain data from several reference locations around the tibial mid-shaft were obtained using subject-specific forward dynamics simulations. The strains and strain rates for several strides were averaged to obtain representative values for each subject. These representative values were then used to generate corridors for a homogenous population.

RESULTS AND DISCUSSION

The results showed a large variability in strain magnitude for a homogenous population. The mean peak and standard deviation for the maximum principal strain, minimum principal strain, and maximum shear strain can be seen for three locations in Table 1. Traditionally *in vivo* strain measurements only record the strain from a location on the anterior medial portion of the tibia near midshaft. Previous research has shown that this method of calculating strain results in realistic values of strain at that location[1,2,3]. The results for the anterior medial location shown in Table 1 below are similar to previous *in vivo* work and previous computational work[1,2,4]. A representative plot of the maximum shear strain, the maximum principal strain, and the minimum principal strain for the anterior medial location is shown in Figure 1 below.

This methodology provides a reasonable approach to calculating strain and strain rate in a dynamic simulation. As a computational simulation, this technique allows researchers to investivage the strain and strain rate at multiple locations that may be unaccessible for strain gauge staples. Future work in this area should focus on parametric studies of subjects whose tibia is instrumented in addition to collecting imaging, motion capture, and force plate data for calculating the strain and strain rate.

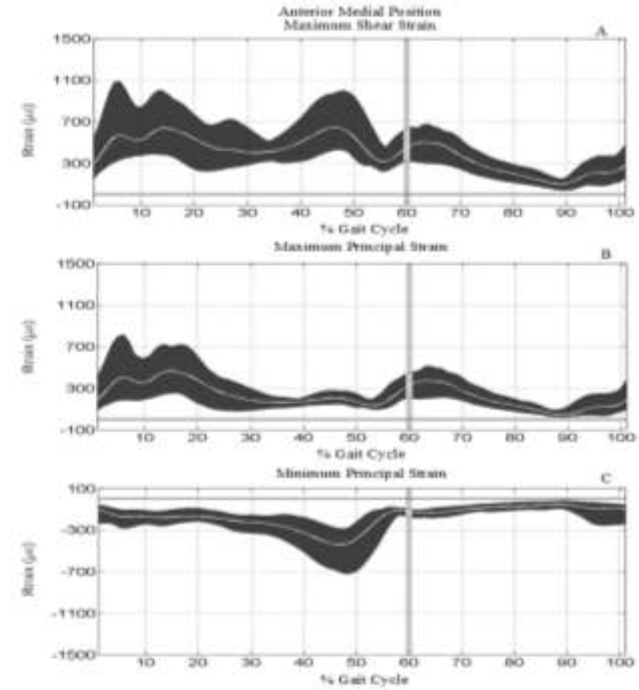

Figure 1: Expected Ranges of (A) Maximum Shear, (B) Maximum Principal, and (C) Minimum Principal Strains. The vertical bands indicate the typical timing of toe-off.

REFERENCES

1. Leib *et al*. ASB Regional Conference, 2011
2. Al Nazer *et al*. *J Biomech* 41, 1036-1043, 2008
3. Klodowski *et al*. ASME IDETCCIEC, 2009
4. Milgrom *et al*. *J Biomech* 37, 947-952, 2004

ACKNOWLEDGEMENTS

Funding source: US ARMY #W81XWH-08-1-0587

All experimental data was collected at Ball State University. All experimental procedures were approved by the University's Institutional Review Board and the subjects signed an informed consent form.

Table 1: Principal and Shear Strains and Strain Rates for Three Locations on the Tibia

		Simulated Staple (ST)			Anterior Medial			Posterior Medial		
		max	min	shear	max	min	shear	max	min	shear
strain	mean	543	-453	838	488	-473	814	533	-489	857
	std deviation	165	135	211	175	93	177	137	161	210
strain rate	mean	7921	-3494	10390	6946	-3588	8612	7531	-3657	9909
	std deviation	3249	1206	4494	2510	1221	3050	2758	1303	3788

HOP PERFORMANCE IN INDIVIDUALS WITH ANTERIOR CRUCIATE LIGAMENT INJURIES

[1,2]Paulien Roos, [1,2,3]Kate Button and [1,2]Robert van Deursen

[1]School of Healthcare Studies, Cardiff University, Cardiff, UK
[2]Arthritis Research UK Biomechanics and Bioengineering Centre, Cardiff, UK
[3]Cardiff and Vale University Health Board, Cardiff, UK
email: vandeursenr@cardiff.ac.uk web: http://www.cardiff.ac.uk/arcbbc

INTRODUCTION

ACL injury can have two major impacts; failure to return to pre-injury activity levels and future predisposition to osteoarthritis [1,2]. Rehabilitation is recommended to help individuals maximize their recovery and performance. Single leg hop is an exercise used in late stage rehabilitation and a tool to evaluate recovery and inform treatment selection [1] but there is insufficient biomechanical understanding of this activity.

The aims of this study were to investigate 1) if hop performance is altered in individuals with Anterior Cruciate Ligament (ACL) injury and 2) identify how kinematics and kinetics determine hop performance.

METHODS

19 individuals with ACL rupture (ACLD; height: 1.77±0.08 m, mass: 83.2±14.0 kg, age: 32±9 years, gender: 2 female, 17 male) and 19 individuals with ACL reconstruction (ACLR; height: 1.75±0.06 m, mass: 80.3±9.9 kg, age: 28±9 years, gender: 4 female, 16 male) were compared to 20 healthy controls (CONT; height: 1.74±0.11 m, mass: 74.8±16.5 kg, age: 29±8 years, gender: 8 female, 12 male). Individuals were asked to hop their maximum single leg hop distance and regain balance after landing. All ACL subjects hopped using their injured leg and the controls their dominant leg. Analysis focused on the landing phase. Ethical approval was obtained from South East Wales Local Research Ethics Committee.

Kinematic data were collected using a VICON motion analysis system (Oxford Metrics Group Ltd., UK) at 250 Hz. Reflective markers were placed using the 'Plug-in-Gait' full body marker set. Ground reaction force data were collected using a Kistler force plate (Kistler Instruments Ltd., Switzerland) at 1,000 Hz. Inverse dynamics calculations were performed within VICON Nexus software and data were processed and analyzed in Matlab R2010b (The Mathworks Inc., USA).

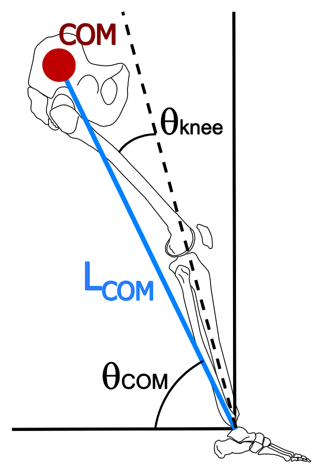

Figure 1: Schematic overview TIP model, with the COM angle (θ_{COM}), knee angle (θ_{knee}), and distance ankle to COM (L_{COM}).

To investigate the kinematics and kinetics a telescopic inverted pendulum (TIP) model approach was used (Fig. 1). Hopping can be simulated by an inverted pendulum model where the stance limb is modeled as a rigid segment that rotates around the ankle. The TIP model approach will show whether ACL injured individuals use a predominantly telescopic motion (large change in stance leg length) or predominately pendular motion (large change of the approach angle of the stance leg). Statistical differences for the output variables between the ACL and control groups were analyzed using a general linear model univariate analysis. Centre of mass (COM) velocity prior to landing was used as a co-variant.

RESULTS AND DISCUSSION

ACLR had a similar hop distance (D_{hop}) to CONT but ACLD hopped significantly shorter. Recovered hop distance for ACLR was achieved by a different kinematic/kinetic strategy compared to CONT. Both ACL groups had reduced range of knee motion (ROM_{knee}), reduced peak extensor moments ($M_{knee(max)}$), reduced knee angle at peak knee extensor moment and increased peak hip flexor moments (M_{hip}) during the landing phase compared to CONT. ACLD also had increased plantar flexion moments (M_{ankle}). The angle of the COM (θ_{COM}) and trunk lean (θ_{trunk}) at peak knee moment were not significantly different from CONT (Table 1).

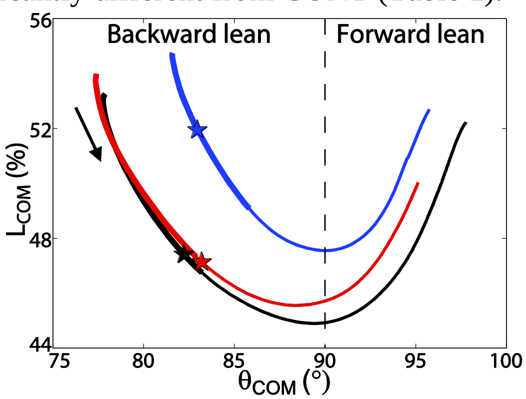

Figure 2: TIP model analysis with distance ankle to COM as percentage of body height (L_{COM}) against angle of the COM (θ_{COM}); black line is average data for CONT; red line for ACLR; blue line for ACLD. Stars indicate peak knee extensor moments. The arrow is the direction of movement.

TIP model analysis (Fig. 2) indicates that the ACL groups used a reduced range of flexion/extension at the knee throughout landing. The peak knee moment also occurred with the knee in a more extended position. This suggests that the ACL groups were in a more upright position throughout the landing phase and therefore used more of a pendular deceleration strategy. Whereas CONT flexed their knee through a greater range, had larger knee extensor moments and therefore used a more telescopic strategy. The ACL pendular strategy was further confirmed by their decreased knee extensor moments and increased M_{hip}. ACLD also had increased M_{ankle}. Pendular deceleration requires higher hip flexor and plantar flexor moments to decelerate and regain single leg balance.

CONCLUSIONS

Hop performance was reduced in ACLD but not in ACLR. However kinematics and kinetics of ACLR were very similar to ACLD. We suggest that the ACL groups used a more pendular deceleration strategy during landing. Therefore this shows that both ACL groups had not fully rehabilitated. Consequently hop distance may not be a good criterion for full recovery. Translation of these biomechanical results to clinical practice would indicate that training of soft landing techniques should be used to optimize control of knee joint loading. The challenge is to do this in an understandable and user-friendly manner.

REFERENCES

1. Arden CL, et al. *Br J Sports Med* **45**, 596-606, 2011.
2. Blagojevic M, et al. *Osteoarthr Cartil* **18**, 24-33, 2010.

ACKNOWLEDGEMENTS

Paul Rimmer and Abigail Bird for their help in data collection and processing. Dr. Roos is funded by Arthritis Research UK (Grant No 18461) and Dr Button is funded by Research Capacity Building Collaboration Wales.

Table 1: Mean hop output variables with standard errors. *: significant difference from CONT (p<0.025).

	D_{HOP} (m)	$M_{knee(max)}$ (N.m/body weight.m)	ROM_{knee}	θ_{knee} at $M_{knee(max)}$	θ_{COM} at $M_{knee(max)}$	$M_{hip(max)}$ (N.m/body weight.m)	$M_{ankle(max)}$ (N.m/body weight.m)	θ_{trunk} at $M_{knee(max)}$
CONT	1.34±0.04	0.41±0.02	70°±2	39°±1	82°±0.4	0.46±0.02	0.29±0.01	18°±1
ACLD	1.05±0.04*	0.33±0.02 *	58°±2 *	35°±1 *	83°±0.5	0.61±0.03 *	0.38±0.02 *	17°±1
ACLR	1.33±0.04	0.29±0.02 *	61°±2 *	35°±1 *	83°±0.4	0.60±0.02 *	0.31±0.01	18°±1

CONTROL OF CORONAL PLANE KINEMATICS AND KINETICS DURING A SINGLE LEG HOP FOR DISTANCE IN INDIVIDUALS WITH ANTERIOR CRUCIATE LIGAMENT INJURY

[1,2]Paulien Roos, [1,2,3]Kate Button, [1,2]Paul Rimmer and [1,2]Robert van Deursen

[1]School of Healthcare Studies, Cardiff University, Cardiff, UK
[2]Arthritis Research UK Biomechanics and Bioengineering Centre, Cardiff, UK
[3]Cardiff and Vale University Health Board, Cardiff, UK
email: RoosPE@cardiff.ac.uk, web: http://www.cardiff.ac.uk/arcbbc

INTRODUCTION

Anterior Cruciate Ligament (ACL) injury can result in failure to return to pre-injury activity levels and increase future predisposition to osteoarthritis [1]. Single leg hop for distance is an exercise used in late stage rehabilitation and a tool used to evaluate recovery and inform treatment selection [2]. Besides hop distance, coronal plane kinematics such as dynamic valgus/varus motion and fluency of movement are often used in rehabilitation to assess and modify movement of ACL injured individuals [3]. There is limited understanding of the biomechanical implications of movement adaptations used by ACL injured individuals and which adaptations may be advantageous.

The aims of this study were to: 1) investigate coronal plane adaptations during single leg hop for distance between individuals with ACL injury and healthy controls, and 2) identify the biomechanical implications of these adaptations.

METHODS

19 individuals with ACL rupture (ACLD; height: 1.77±0.08 m, mass: 83.2±14.0 kg, age: 32±9 years, gender: 2 female, 17 male), 19 with ACL reconstruction (ACLR; height: 1.75±0.06 m, mass: 80.3±9.9 kg, age: 28±9 years, gender: 4 female, 16 male) and 20 healthy controls (CONT; height: 1.74±0.11 m, mass: 74.8±16.5 kg, age: 29±8 years, gender: 8 female, 12 male) were asked to perform a single leg hop for distance and regain balance after landing. All ACL subjects hopped using their injured leg and CONT subjects used their dominant leg. Ethical approval was obtained from South East Wales Local Research Ethics Committee.

Kinematic data were collected using VICON (Oxford Metrics Group Ltd., UK) at 250 Hz. Markers were placed using the 'Plug-in-Gait' full-body marker-set. Ground reaction force (GRF) data of landing were collected using a Kistler force platform (Kistler Instruments Ltd., Switzerland) at 1,000 Hz. Inverse dynamics calculations were performed within VICON Nexus software and data were further analyzed in Matlab R2010b (The Mathworks Inc., USA). Analysis focused on the landing phase until the subject regained balance.

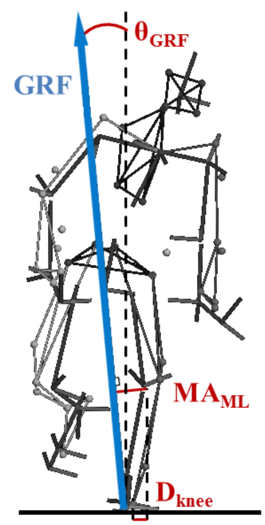

Figure 1) Graphical representation of the calculation of D_{knee}, MA_{ML} and θ_{GRF}.

Hop distance (D_{hop}) was calculated as the distance of the ankle between lift off and touch down. Other output variables were the peak adduction moment (M_{add}), which was normalized using body weight (BW) and height, the varus/valgus range of motion (ROM_{vv}), the orientation of the GRF force vector relative to the vertical at the peak adduction moment ($\theta_{GRF(pkadd)}$), the medio-lateral moment arm of the GRF vector with the knee at the peak knee extensor moment ($MA_{ML(pkm)}$, Fig. 1) and the maximum medio-lateral distance between the projection of the ankle and knee on the ground (D_{knee}, Fig. 1). Fluency of the knee movement in the coronal plane was calculated by a method adapted from [4]. It was defined as the number of times the velocity of the knee position in the coronal plane crossed zero, averaged per second.

Statistical differences between the ACL and CONT groups were analyzed using a general linear model univariate analysis. COM velocity prior to landing was used as co-variant.

RESULTS AND DISCUSSION

Five ACLD subjects could not perform a hop. Hop distance was significantly reduced in ACLD, while ACLR achieved similar hop distance compared to CONT (Table 2). Medio-lateral displacement of the knee (D_{knee}) was not altered in the ACL groups. ROM_{vv} was increased in both ACL groups and movement of the knee was significantly less fluent in ACLR and showed a trend to be less fluent in ACLD compared to CONT (Table 2). While the ACLD and ACLR used the same strategy with reduced medio-lateral control of the knee, ACLR attained a normal hop distance. It therefore appears that both ACL groups have not fully recovered.

Despite the larger ROM_{vv} in ACLD and ACLR, their peak M_{add} was not significantly different from those in CONT, when taking COM velocity prior to landing in consideration. The lower M_{add} in ACLD was related to their shorter hopping distance. The medio-lateral moment arms of the GRF vector with the knee ($MA_{ML(pkm)}$**)** were not different in ACLD, ACLR and CONT. The altered kinematics (ROM_{vv}, Fluency) were not correlated to joint loading (M_{add}, $\theta_{GRF(pkv)}$ or $MA_{ML(pkm)}$).

Assessment of knee control using varus/valgus ROM and fluency of movement therefore seems important to evaluate hop performance in knee patients. This could be used in addition to hop distance which is used as a clinical outcome measure.

CONCLUSIONS

Hop distance was fully recovered in ACLR with similar adduction moments to CONT. They were however unable to control the dynamic knee varus/valgus movement like CONT. End-stage rehabilitation tends to focus on medio-lateral control and fluency of knee movement [5]. This study highlights the importance of addressing this control, as it was not regained in both ACL groups even though hop distance was restored in ACLR.

REFERENCES

1. Blagojevic M, et al. *Osteoarthr Cartil* **18**, 24-33, 2010.
2. Arden CL, et al. *Br J Sports Med* **45**, 596-606, 2011.
3. Padua DA, et al. *Am J Sports Med* **37**, 1996-2003, 2009.
4. Smeulders MJC, et al. *Clin Rehab* **15**, 133-141, 2001.
5. Myer GD, et al. *Br J Sports Med* **45**, 245-252, 2010.

ACKNOWLEDGEMENTS

Abigail Bird for her help in data processing. Dr. Roos and Mr. Rimmer are funded by Arthritis Research UK (Grant No 18461). Dr. Button is funded by Research Capacity Building Collaboration Wales.

Table 2: Mean D_{hop}, D_{knee}, fluency, M_{add}, ROM_{vv}, $\theta_{GRF(pkv)}$, and $MA_{ML(pkm)}$, with standard deviations. A * indicates a significant difference at $p<0.025$ and a † a trend to significant difference from CONT at $p<0.05$.

	D_{hop} (m)	D_{knee} (m)	ROM_{vv} (°)	Fluency	M_{add} (N.m/BW.m)	$\theta_{GRF(pkv)}$ (°)	$MA_{ML(pkm)}$ (m)
CONT	1.34±0.04	0.07±0.02	19±1	5.7±0.3	0.18±0.02	1.2±0.1	0.10±0.01
ACLD	1.05±0.04*	0.07±0.02	27±1*	6.7±0.4†	0.14±0.02	1.6±0.2	0.09±0.01
ACLR	1.33±0.04	0.07±0.02	23±1*	7.2±0.3*	0.18±0.02	1.6±0.1†	0.10±0.01

THE INFLUENCE OF INCREASED DOF IN THE KNEE JOINT ON MUSCLE ACTIVATION TIMINGS AND FORCES IN A MUSCULOSKELETAL MODEL

[1,2]Paulien Roos, [3]Ilse Jonkers, Kate Button[1,2] and [1,2]Robert van Deursen

[1]School of Healthcare Studies, Cardiff University, Cardiff, UK
[2]Arthritis Research UK Biomechanics and Bioengineering Centre, Cardiff, UK
[3]Katholieke Universiteit Leuven, Leuven, Belgium
email: RoosPE@cardiff.ac.uk, web: http://www.cardiff.ac.uk/arcbbc

INTRODUCTION

Altered kinematics following a knee injury can lead to increased knee joint loading [1], which may lead to early onset osteoarthritis [2]. Muscle activation patterns influence contact forces in the knee [3]; muscle forces also play an important role in stabilizing the knee joint [3]. Knee injuries often result in altered muscle activation patterns but it is not known how exactly this influences knee loading. Musculoskeletal models allow investigation of the influence of altered muscle activation patterns on forces acting on the knee. Simulations with a full body model with a simplified knee joint can estimate muscle forces, which can be used as input in complex knee models to investigate detailed loading of the condyles [3]. This pilot study investigated the influence of increased knee joint degrees of freedom (DOF) on the accuracy of muscle onset and kinematic estimations. This will provide insight into the role of active control in frontal plane knee stability and will allow future investigation of the effect of altered muscle activations due to injury.

METHODS

One healthy subject (female, age 31 years, height 1.74 m, mass 59 kg) stood with feet shoulder width apart and body weight distributed over both legs (DS), body weight was slowly transferred to the left leg lifting the right leg slightly off the ground (TR1), this was held (ST) and then shifted back to both legs (TR2). This movement involved minimum knee flexion and allowed focus on the frontal plane. Kinematic data were collected at 250 Hz using a VICON system (Oxford Metrics Group Ltd., UK), and the 'Plug-in-Gait' marker set. Ground reaction force data were measured for each foot at 1,000 Hz using two force plates (Kistler Instruments Ltd., Switzerland). EMG data were collected at 1,000 Hz using a Noraxon Telemyo system. Electrodes were placed on the left leg on rectus femoris (RF), vastus lateralis (VL), vastus medialis (VM), tensor fascia latae (TFL), biceps femoris (BF), semimembranosus (SM), lateral (LG), and medial gastrocnemius (MG). Raw EMG was band-pass filtered (20-450 Hz) with a 4th order Butterworth, then full wave rectified, low-pass filtered (10 Hz) with a 4th order Butterworth, and normalized to maximum muscle activation of the simulations. Medio-lateral coactivation ($COACT_{Med\text{-}Lat}$) was calculated using the summed activation of the lateral muscles (VL, TFL, BF, LG) and of the medial muscles (VM, SM, MG) and applying the algorithm proposed by Winter [5]. Simulations were performed in OpenSim (v2.4.0, SimTK, USA). Marker positions and ground reaction force data were transformed and imported. The gait2392 Simbody model [4] was scaled using a calibration trial. Inverse kinematics calculations were performed, followed by Residual Reduction Analysis. Muscle activations and forces were computed using Computed Muscle Control. Muscle activations were low-pass filtered (10 Hz). The gait2392 model has a 1-DOF (sliding hinge joint) knee. A 2nd varus/valgus DOF was added and a simulation was performed using the same experimental data as with the 1-DOF knee model.

RESULTS AND DISCUSSION

Accuracy of the inverse kinematics was the same in the 1-DOF and 2-DOF knee model (squared error: 0.002 m; marker error RMS: 0.009 m). Kinematics differed minimally with maximum RMS differences in joint angles between the models of 0.6°. Adding a varus/valgus DOF influenced muscle activation patterns and forces, and how well muscle activation patterns agreed with EMG (Fig. 1, Table 1).

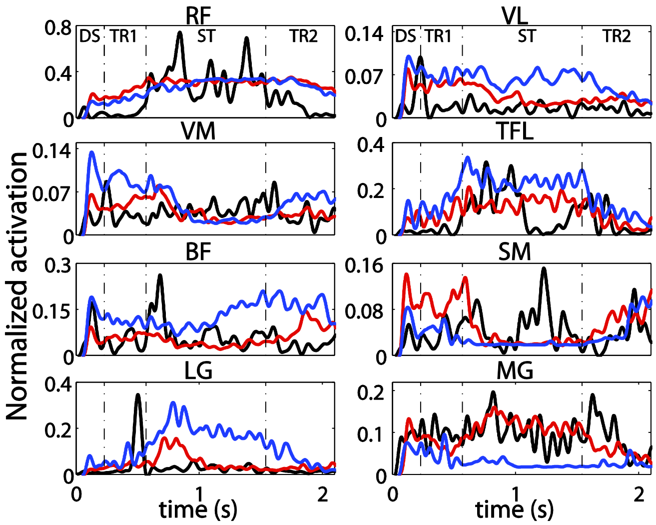

Figure 1: Normalized muscle activation with black lines: EMG data, red lines: simulations with 1-DOF knee, and blue lines: simulations with 2-DOF knee.

Peak differences in muscle force changed up to 236 N (table 1). In the DS and TR1 phases VM and BF activity and forces increased while SM activity and forces decreased in the 2-DOF compared to the 1-DOF knee simulation. This asymmetrical activation pattern in the upper leg at the anterior medial and posterior lateral side relates to control of varus/valgus movement of the knee. In the ST phase VL, TFL, BF and LG activity and forces increased, while MG decreased in the 2-DOF compared to the 1-DOF knee simulation. This increased lateral activation in the stance leg would be required to control the center of mass (which is medial of the center of pressure) and keep the right leg lifted off the ground. TR2 showed a similar pattern to DS and TR1 with increased VM, LG and BF activation and forces and decreased SM and MG in the 2-DOF compared to the 1-DOF knee simulation. This asymmetric activation pattern also relates to control of varus/valgus movement. Adding the varus/valgus DOF resulted in decreased $COACT_{Med\text{-}Lat}$ due to the increased activation of lateral muscles (Fig. 2). In the simulations muscle activations were optimized to minimize control and stability was not taken into account. Knee injured patients may have altered activation. Alternative optimization algorithms are needed to account for stability and altered control in patients. The model also did not account for medio-lateral stability provided by tibio-femoral contact and ligaments.

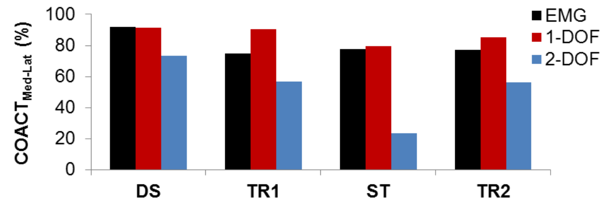

Figure 2: $COACT_{Med\text{-}Lat}$ for the differenct phases.

CONCLUSIONS

This study showed that adding varus/valgus DOF to the knee influenced muscle activation patterns and forces in simulations with a musculoskeletal model. Including a varus/valgus DOF resulted in decreased medio-lateral coactivation. This may indicate a need for alternative optimization algorithms that account for stability, or a need for a more comprehensive knee model. Further development of these methods is required before active control of the knee in the frontal plane and patient's muscle activity can be effectively explored through simulation.

REFERENCES

1. Walter J, et al. *Journal of Orthopaedic Research*, 1348-1354, 2010.
2. Blagojevic M, et al. *Osteoarthritis Cartilage*, **18**(1), 24-33, 2010.
3. Shelbourne KB, et al. *Journal of Orthopaedic Research*, **24**, 1983-1990, 2006
4. Delp SL, et al., *IEEE Trans Biomed Eng* **37**, 757-767, 1990.
5. Winter DA, *Biomechanics and Motor Control of Human* Movement, John Wiley & Sons, 2004.

ACKNOWLEDGEMENTS

Rebecca Hemming for her help with data collection. Dr. Roos is an Academic Fellow funded by Arthritis Research UK (Grant No 18461).

Table 1: Peak difference in muscle force between the simulations with the 1-DOF and 2-DOF knee as absolute value in N and normalized as percentage of the peak muscle force.

		RF	**VL**	**VM**	**TFL**	**BF**	**SM**	**LG**	**MG**
Difference	**N**	123	-96	-118	-40	-126	107	-145	236
	%	27%	46%	49%	44%	50%	43%	58%	56%

FRONTAL PLANE MECHANICS ARE ALTERED DURING SPLIT BELT TREADMILL WALKING IN YOUNG HEALTHY ADULTS

Jaimie A Roper, Ryan T. Roemmich, Mark T. Tillman, Chris J. Hass
University of Florida, Gainesville, FL, USA
email: jaimier@hhp.ufl.edu

INTRODUCTION

Split belt treadmills (SBT) consist of two independently-controlled belts (one under each leg) and have recently been used to induce locomotor adaptation in various populations. During SBT studies, gait speed is independently manipulated for each limb with one limb typically walking 2 times faster than the other. While spatiotemporal adaptation during SBT walking has been frequently analyzed in the sagittal plane,[1, 2] little is known about the changes in frontal plane mechanics that occur during SBT walking. However, because SBT walking requires one leg to walk twice as fast as the contralateral leg, we may be able to gather insight from previous work related to slow and fast walking. Indeed, prior research has indicated that gait speed may also alter frontal plane kinetics in healthy adults, particularly the knee adduction moment (KAM).[3] KAM reflects the loading in the medial compartment of the knee joint and is also related to progression of OA.[3]

The aim of this study was to examine the frontal plane mechanics during SBT walking in the propulsive and braking phases of stance for the ankle, knee, and hip joints bilaterally.

METHODS

Thirteen healthy participants walked on an instrumented SBT (Bertec Corporation, Columbus, OH) during three conditions: slow, fast and split. Participants initially selected his/her fastest comfortable walking speed (“fast” speed), then walked for two minutes with both belts moving at 50% of the fast speed (“slow” speed/slow condition) and two minutes with both belts moving at the fast speed (fast condition). The participants then walked for ten minutes with the self-reported nondominant leg moving at the fast speed and the dominant leg moving at the slow speed (split condition). Kinematic and kinetic data were recorded during the last 30 seconds of the slow, fast, and split conditions. Sixteen passive reflective markers were attached to the lower body in accordance with the Vicon Plug-in-Gait lower body marker system. Kinematic data were collected using a 7-camera motion capture system (120 Hz; Vicon Nexus, Oxford, UK).

Force recordings, marker position data and the individuals anthropometrics were used to calculate the frontal plane moments for the ankle, knee, and hip during the propulsive and braking phases of gait via inverse dynamics.

Joint moments and GRFs were normalized to body mass (kg) and temporally to 100% of the gait cycle. Braking phase was defined as the period from heel-strike to the first 50% of single-limb stance period. Propulsive phase was defined as the period from second 50% of the single-limb stance to toe off.[4] Frontal joint moment impulses for the ankle, knee and hip were calculated as the time integrals of the AP GRFs over the braking and propulsive phases, respectively.

Several 2x3 (limb x condition) repeated measures ANOVA with Bonferroni correction for pairwise comparisons was used to analyze mean differences among conditions and between limbs ($\alpha = .05$).

RESULTS AND DISCUSSION

Table 1 displays the means and standard deviations of frontal joint moment impulses for the ankle, knee, and hip for the non-dominant and dominant limbs during slow, fast, and SBT walking. There were no bilateral differences in the braking or propulsive GRF impulses during the slow, fast, and SBT conditions ($p > .05$).

Bilateral differences during slow and fast conditions

During the slow condition, hip adduction moment impulses were significantly higher for the “slow” versus the “fast” limb during the braking phase ($p = .027$).

Slow condition versus fast condition

During the slow condition, the non-dominant limb ankle adduction moment and KAM impulses, along with the dominant limb KAM impulses were significantly smaller compared to the fast condition during the braking phase ($p = .032$, p

= .002, p < .001). During slow walking, the dominant limb ankle adduction moment impulses were significantly higher compared to non-dominant limb walking during the propulsive phase (p = .006).

Fast limb vs. slow limb during SBT walking

During the split condition, KAM impulses along with hip adduction moment impulses were significantly larger for "slow limb" compared to the "fast" limb during braking phase (p = .006, p < .001, respectively). KAM impulses were significantly larger for the "fast limb" versus the "slow limb" during the propulsive phase (p = .011).

Fast limb during SBT walking vs. fast limb during fast walking

The "fast limb" ankle adduction moment, KAM and hip adduction moment impulses during SBT walking were smaller compared to the same limb during the fast condition for the braking phase (p = .035, p = .002, p = .007, respectively).

Slow limb during SBT walking vs. slow limb during slow walking

During the split condition the "slow limb" KAM and hip adduction moment impulses were larger compared to the same limb during the slow condition for the braking phase (p = .011, p = .001, respectively). The "slow limb" ankle adduction impulses were smaller compared to "slow limb" during the slow condition for the propulsive phase (p = .018).

The "fast limb" ankle, knee, and hip adduction moment impulses were all smaller during the split condition versus the same limb for the fast condition during the braking phase (116%, 34%, and 23% lower for slow, respectively). While the "slow limb" knee and hip adduction moment impulses were larger during the split condition compared to the same limb during the slow condition for the braking phase (30% and 23% smaller during the slow condition, respectively). "Slow limb" ankle adduction moment impulses were 96% smaller compared to the same limb during the slow condition for the propulsive phase.

Joint adduction moment impulses represent the amount of time exposed to a load in a specific joint.[3] A smaller moment impulse would represent a shorter exposure time to a load, and a larger moment impulse would imply a longer exposure time. The results of this study indicate that while walking on a SBT, adduction moment impulses may be smaller for the "fast limb" compared to fast conventional treadmill walking, and larger for the "slow limb" compared to slow conventional treadmill walking. The findings of this study demonstrate that participants can walk (with one limb) at a fast speed with lowered joint adduction moment impulses. Lowering frontal plane joint moment impulses particularly at the knee is important in patients with knee OA to prevent further progression or development of the disease. In addition, simultaneously maintaining and/or restoring a fast walking speed while reducing or preserving healthy joint adduction moment impulses is clinically important to perhaps reduce the incidence or progression of knee OA. However, further longitudinal research that addresses the disease process of OA specifically is needed to verify this statement.

REFERENCES

1. Stoquart G, et al. Neurophysiol Clin 2008.
2. Reisman DS et al. Neurorehabil Neural Repair 2009.
3. Robbins SM, et al. Gait Posture 2009.
4. Turns LJ et al.Arch Phys Med Rehabil 2007.

Table 1. Ankle, Knee, and Hip Adduction Moment Impulses during Braking and Propulsive phases for Slow, Fast, and Split walking.

	Ankle		*Knee*		*Hip*	
Braking	Slow limb	Fast Limb	Slow limb	Fast Limb	Slow limb	Fast Limb
Slow	1.50 (1.82)	-0.07 (1.96)	10.9 (4.71)	8.23 (3.51)	16.9 (4.16)	14.5 (3.43)
Fast	1.79 (1.60)	0.61 (2.31)	13.4 (4.97)	11.6 (3.99)	19.8 (3.69)	18.1 (3.74)
Split	1.24 (1.98)	-0.10 (1.91)	14.2 (6.24)	7.63 (3.01)	20.8 (4.13)	14.0 (3.70)
Propulsive	*Ankle*		*Knee*		*Hip*	
	Slow limb	Fast Limb	Slow limb	Fast Limb	Slow limb	Fast Limb
Slow	1.43 (1.88)	1.10 (1.85)	7.87 (3.80)	5.80 (3.25)	13.6 (6.45)	12.6 (5.78)
Fast	1.62 (1.92)	2.64 (2.39)	6.37 (2.99)	5.50 (3.74)	10.13 (8.98)	10.5 (8.57)
Split	0.05 (1.87)	2.59 (2.45)	7.20) (3.85)	4.88 (3.11)	14.4 (8.03)	8.34 (6.91)

MAINTAINING A CONSTANT MARGIN OF STABILITY ACROSS DYAMIC CONDITIONS MAY RELY ON DIFFERENT CONTROL STRATEGIES

[1]Noah J. Rosenblatt, [1]Christopher P. Hurt, [1]Mark D. Grabiner
[1]University of Illinois at Chicago, Chicago, IL, USA, email: nrosenbl@uic.edu, URL: http://www.uic.edu/ahs/biomechanics

INTRODUCTION

A simple rule sufficient for stable gait states that at ground contact, the swing foot should be placed a certain distance lateral to the extrapolated center of mass (XCOM), which is the sum of the center of mass (COM) position and normalized velocity [1]. This distance between the foot and XCOM, termed margin of stability (MOS), is a measure of dynamic stability and remains constant while walking. Indeed, across multiple walking conditions, step width (SW), a measure of foot placement traditionally related to dynamic stability, changes while the minimum MOS (MOS_{min}) does not vary [2,3]. During these conditions, variations in SW are associated with variations in frontal plane COM states [4], i.e. XCOM, such that a constant MOS_{min} results. If the allowable positions for frontal plane foot placement are limited, e.g walking in a crowd, then step width variability (SWV) would also be expected to decrease. This would in turn reduce ones' capacity to correct for XCOM variations. To maintain dynamic stability (MOS>0) the unimpaired motor system might be expected to decrease XCOM variability (XCOMV).

Decreased XCOMV however cannot describe how, or if, differential control over XCOM and dynamic stability is employed when frontal plane foot placement is limited. The XCOM trajectory reflects the net movement of all body segments. Consequently, multiple segmental configurations can result in the same XCOM motion, a concept referred to as motor redundancy [5]. To explain how the variability of redundant degrees of freedom is organized with respect to maintaining similar step-to-step XCOM motion, i.e. stabilization of XCOM, the uncontrolled manifold (UCM) analysis may be used [5]. The UCM analysis partitions the variance of segmental configurations into a component that keeps XCOM constant across steps ($UCM_{\parallel}$) and a component that destabilizes XCOM across steps ($UCM_{\perp}$) [5,6]. Greater variance within $UCM_{\parallel}$ ($UCM_{\parallel}/UCM_{\perp}>1.0$) suggests stabilization of XCOM. As $UCM_{\parallel}$ increases more movement patterns are used to achieve a particular XCOM. Greater variance within $UCM_{\perp}$ implies errors in segmental configurations lead to deviations from the mean XCOM although such destabilization need not imply dynamic instability (MOS<0). When foot placement is limited, increasing $UCM_{\parallel}$ and/or decreasing $UCM_{\perp}$ may be thought of as increasing control to stabilize XCOM and dynamic stability.

Figure 1. Four segment model (stance limb, pelvis, torso and swing limb) to derive mediolateral XCOM motion relative to the stance limb (left limb):

$$\begin{aligned}\mathrm{COM} = {} & m_1(a_1L_1\sin\theta_1)+ \\ & m_2(L_1+0.5L_2\cos\theta_2)+ \\ & m_3(L_1+0.5L_2\cos\theta_2+a_3L_3\sin\theta_3)+ \\ & m_4(L_1+L_2\cos\theta_2+b_4L_4\sin\theta_4)\end{aligned}$$

m=mass and L=length of segment *n* (m_n, L_n, respectively), θ_n=segment angle, a_n and b_n=distance from proximal and distal end of segment to its' COM. COM velocity taken as the derivative of COM.

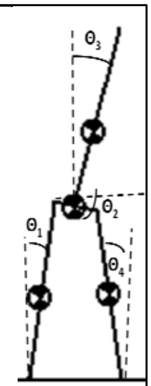

The purpose of this study was to quantify how dynamic stability is controlled when the demand for precision in frontal plane foot placement increases. We hypothesized that SWV and XCOMV would decrease, MOS would not vary and $UCM_{\parallel}/UCM_{\perp}$ would increase with increasing demand.

METHODS

Ten healthy, young adults (21.5±2.6 years) participated. Subjects completed 10 trials for each of three conditions in the following order: unconstrained walking (UW), constrained walking (CW) and beam walking (BW).

During UW, subjects walked across an 8 m laboratory walkway. Photoelectric timers measured speed and kinematics were collected using motion capture. For CW and BW walking speed was maintained to ±10% of UW speed. In the CW condition, two pairs of lines, with lines in each pair separated by 7.5 cm, were marked on the laboratory floor with the center of each pair separated by the mean SW during UW. Subjects were instructed to keep the left and right foot within the left- and right-most line pairs, respectively. For BW, two beams, 8 m x 7.5 cm (L x W), were raised 11.5 cm from a mounting platform and spaced an on-center distance equal to SW during UW. Subjects were instructed to keep the left and right foot within the left- and right-most beams, respectively. Anthropometric and kinematic data were used to calculate SW, SWV, XCOMV and MOS according to:

$$\textbf{MOS} = \textbf{COM} + [\textbf{COM}_{vel}/\sqrt{(9.8\ m/s^2/\ 1.34*\text{leg length})}\,] - \textbf{BOS}$$

where the first two terms are XCOM and the final, BOS (base of support), is the lateral- most position of the stance foot [2]. SW and minimum MOS during double support, MOS_{min}, were averaged across all steps.

Given that SW was expected to be similar across conditions, BOS was also expected to remain relatively constant. Thus to determine if MOS was differentially controlled across conditions UCM analysis was employed on XCOM. Briefly, mediolateral COM position and velocity was modeled using experimental data normalized to the gait cycle (Figure 1). At each percent of the cycle, the UCM was computed as the null space of the Jacobian (matrix of partial derivatives) evaluated at the mean segmental angles. For each step, deviations from these means were resolved into projections onto the UCM and orthogonal to the UCM. The square root of the mean squared length of these vectors, per degree of freedom, represents $UCM_{\parallel}$ and $UCM_{\perp}$ respectively [5,6]. Values for each component and for $UCM_{\parallel}/UCM_{\perp}$ were averaged over the first 10% of gait (just before MOS_{min}). Individual repeated measure ANOVAs were used to compare SW, SWV, XCOMV, MOS_{min}, and the ratio $UCM_{\parallel}/UCM_{\perp}$. In the event of a significant ratio a two way ANOVA (condition x component) was used to test for an interaction.

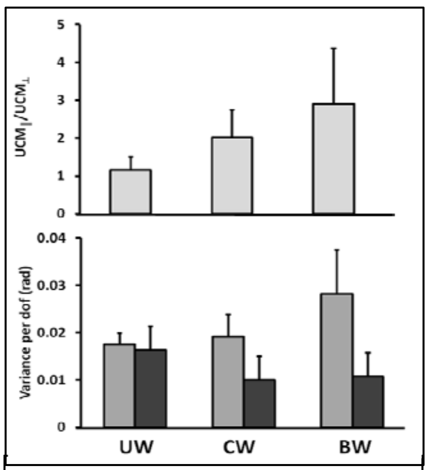

Figure 2. (Top) For the first 20% of gait $UCM_{\parallel}/UCM_{\perp}$ was >1.0 and significantly increased across conditions. (Bottom) The increased ratio resulted from an increasing $UCM_{\parallel}$ (light) and decreasing $UCM_{\perp}$ (dark)

Table 1. Kinematic data. * significantly different from BW (p<0.05); + significantly different from CW (p<.05).

	SW (mm)	MOS_{min} (mm)	SWV (mm)	XCOMV (mm)
UW	123.1±42.5	59.4±14.0	29.7±2.1	24.6±1.3
CW	119.9±39.9	60.0±12.9	18.6±0.8*	16.9±1.4*
BW	122.7±46.1	61.9±12.3	18.8±1.3*	10.4±0.8*,+

RESULTS AND DISCUSSION

Neither SW nor MOS_{min} differed between conditions (p=0.83 and p=0.37, respectively; Table 1). SWV for UW was larger than during either CW or BW (p=0.003) but was similar for CW and BW (p=0.88). XCOMV decreased significantly across all conditios (p=.003 for UW vs. CW; p=.01 for CW vs. BW). Similarly, UCM analysis revealed increasing control over XCOM across conditions (Figure 2). The ratio $UCM_{\parallel}/UCM_{\perp}$ increased from UW to CW (p=0.01), and again from CW to BW (p=0.048). The increased ratio was due to increasing $UCM_{\parallel}$ and concurrent decreasing $UCM_{\perp}$ (a significant interaction was observed; p<0.001).

Results suggest that changes in SWV reflect changes in precision of foot placement. As expected SWV during the CW condition was less than during the UW condition. It was expected that SWV would further decrease from CW to BW. Similar SWV for these conditions suggests that a lower limit for SWV may exist, potentially reflecting system noise under maximum precision. While SWV is thought to reflect “dynamic stability” (e.g. SWV changes with age and these changes are associated with fall-risk [7,8]), SWV may not relate to direct measures of dynamic stability, such as MOS_{min}. Across conditions, MOS_{min} was not significantly different.

Separately, reduced XCOMV and an invariant MOS_{min} may not imply increased control over dynamic stability. However, the increasing $UCM_{\parallel} > UCM_{\perp}$ ratio across conditions, resulting from both an increasing proportion of variance in joint configuration aligned with $UCM_{\parallel}$ *and* decreasing proportion within $UCM_{\perp}$, does suggest increased control. As variations in swing foot placement are limited, resulting in decreased SWV, the unimpaired motor system may exploit motor redundancy to achieve a constant MOS_{min}.

CONCLUSION

Across three conditions in which increasing constraint was placed on foot placement, only XCOMV and UCM analysis showed a systematic change. XCOMV and UCM analysis may be more sensitive measures of control of frontal plane dynamic stability and provide information not captured by SW, SWV or an invariant MOS_{min}.

REFERENCES

1. Hof AL, Hum Mov Sci. 2008;27(1):112-25
2. Rosenblatt NJ, Grabiner MD. Gait Posture. 2010;31(3):380-4.
3. Curtze C, Hof AL, Postema K, Otten B. Gait Posture. 2011; 33(2):292-
4. Hurt CP, et al. Gait Posture. 2010; 31(4):461-4
5. Scholz JP, Schoner G. Exp Brain Res. 1999;126:289-306.
6. Black DP, Smoth BA, Wu Jm Ulrich B. Exp Brain Res. 2007;183:511-21.
7. Brach JS, et al. Gait Posture. 2010;31(2):175-9.
8. Brach JS, et al. J Neuroeng Rehabil. 2005 Jul 26;2:21.

COMPARISON OF MODULE QUALITY AND WALKING PERFORMANCE OF HEMIPARETIC SUBJECTS PRE AND POST LOCOMOTOR REHABILITATION THERAPY

Rebecca L. Routson[1], David J. Clark[2], Mark G. Bowden[3,4], Steven A. Kautz[3,4] and Richard R. Neptune[1]

[1] Department of Mechanical Engineering, The University of Texas at Austin, Austin, TX
[2] Department of Aging and Geriatric Research, University of Florida, Gainesville FL
[3] Ralph H. Johnson VA Medical Center, Charleston, SC
[4] Department of Health Sciences and Research, Medical University of South Carolina, Charleston, SC
email: rebecca.routson@gmail.com, web: http://me.utexas.edu/~neptune

INTRODUCTION

In healthy subjects, electromyography (EMG) reveals that well-coordinated walking can be produced by exciting four co-activation modules: Module 1 (hip and knee extensors) in early stance, Module 2 (ankle plantarflexors) in late stance, Module 3 (tibialis anterior and rectus femoris) during swing, and Module 4 (hamstrings) in late swing and early stance [1]. These modules, comprised of timing and composition matrices that define muscle activity (Fig. 1), may reflect a neural strategy of co-activation through a reduced set of patterns.

Persons with post-stroke hemiparesis typically have fewer modules that are less well organized than healthy subjects [2]. Even in those subjects who had four modules post-stroke, the modules differed in composition and timing from those of healthy subjects. Since recent simulation analyses found modules have specific biomechanical functions during unimpaired walking [1], altering their timing or composition could adversely affect walking ability. Thus, interventions that restore normal module organization could significantly improve locomotor performance.

Studies investigating EMG throughout the post-stroke recovery process have proposed that improved walking performance can be accomplished by relying on an individual's own compensatory muscle activation patterns, rather than trying to improve muscle timing towards healthy patterns [3, 4]. However, the effect of rehabilitation on muscle activation timing, reflected by module organization, and hemiparetic walking performance has not been assessed. We propose that such an assessment would provide justification for selecting specific rehabilitation approaches that target improving module quality. Therefore, the goal of this study was to examine the influence of a locomotor rehabilitation therapy on module organization and post-stroke hemiparetic walking performance. Specifically, we assessed whether those subjects who had four modules pre-therapy improved their module quality post-therapy.

METHODS

Twenty-eight individuals with chronic post-stroke hemiparesis participated in a 12-week, 36 session locomotor training program including stepping on a treadmill with body weight support and manual assistance. Kinematics, ground reaction forces and EMG were collected pre- and post-therapy for each subject. Data were also collected from 19 aged-matched healthy subjects walking at self-selected speeds. Using a non-negative matrix factorization algorithm (NNMF) [2], the number of modules required to account for the variability of EMG recorded from eight muscles bilaterally were assessed.

Module quality was determined by comparing both module composition and timing in the hemiparetic subjects to average respective values in healthy subjects. Composition was assessed by comparing weighting factors for individual muscles using Pearson's correlation coefficient. Timing quality was calculated as the difference in timing peaks of the hemiparetic subjects as compared to the control group average. Biomechanical measures including self-selected speed (SS), paretic step length, paretic pre-swing leg angle and propulsion asymmetry as well as module quality measures were compared pre- and post-therapy using paired t-tests.

RESULTS AND DISCUSSION

Nine of the 28 hemiparetic subjects had four modules pre- and post-therapy. When comparing the magnitude and timing of the four modules of these nine subjects pre- and post-therapy, the only statistically significant change was that timing improved for the ankle plantarflexor module (Module 2; p=0.005). The post-therapy timing peak of this module was more defined and occurred later in stance, which more closely resembled the control group (compare Figs. 1b and 1c to 1a). Of the four biomechanical measures compared in these subjects, three were statistically (α=0.05) or marginally (α=0.10) significantly improved post-therapy. Those measures were SS speed (p=0.004), propulsion asymmetry (p=0.072), and pre-swing leg angle (p=0.022). Improvements in these measures (i.e., a faster speed, greater propulsion symmetry, and more extended leg angle) were likely directly related to the improved Module 2 timing since the plantar flexors have been shown to be important contributors to these biomechanical functions [1].

CONCLUSION

In subjects with four modules pre- and post-therapy, locomotor training resulted in improved timing of the ankle plantar flexor module (Module 2) and more extended paretic leg angles that allowed the hemiparetic subjects to walk faster and with more symmetrical (i.e., greater paretic leg) propulsion. Future work will investigate module quality post-therapy in those subjects who started with less than four modules pre-therapy to assess whether they are more or less likely to achieve a normal module organization.

REFERENCES

1. Neptune RR, et al., *J Biomech.* **42**, 1282-7, 2009.
2. Clark DJ, et al., *J Neurophysiol*, **103**, 884-57, 2010.
3. Den Otter AR, et al., *Clin Neurophysiol,* **117**, 4-15, 2006.
4. Buurke JH, et al., *Neurorehabil Neural Repair,* **22**, 676-83, 2008.

ACKNOWLEDGEMENTS

This work was supported by NIH Grant R01 HD46820, Department of Veterans Affairs RR&D Merit Review B3983-R, and the NSF GRFP. The contents are solely the responsibility of the authors and do not necessarily represent the official views of the NIH, NICHD, NSF, the Department of Veterans Affairs or the United States Government.

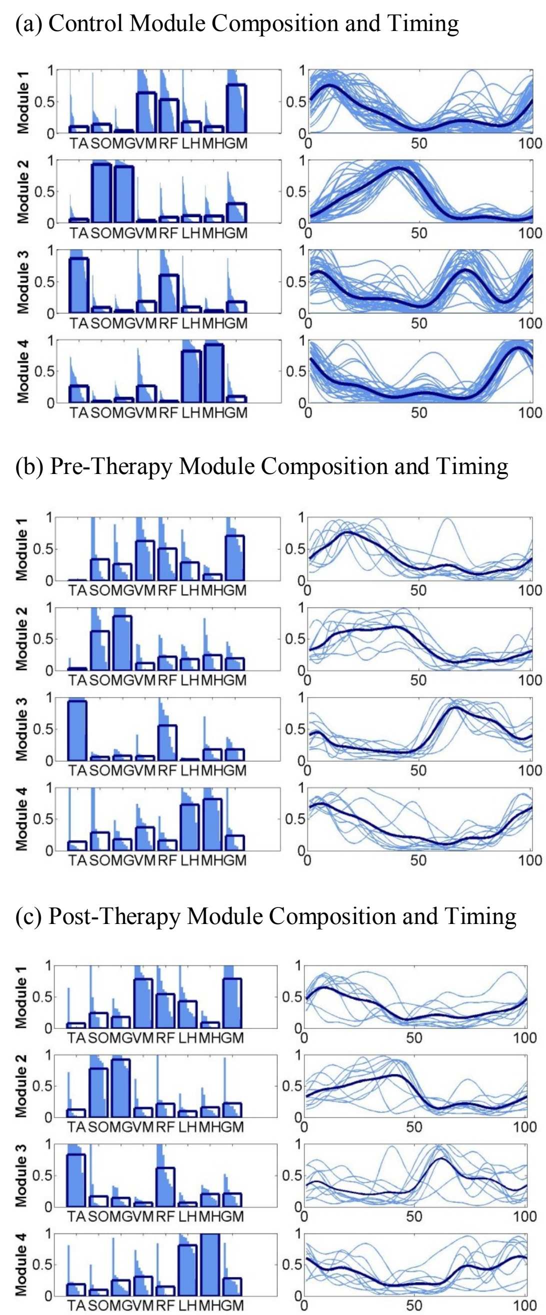

Figure 1: Module Composition (left) and Timing (right) with individual subject (light blue) and group average (dark blue) data: (a) Control Subjects, (b) Pre-Therapy (c) Post-Therapy.

ON THE ASCENT: THE SOLEUS OPERATING LENGTH IS CONSERVED TO THE ASCENDING LIMB OF THE FORCE-LENGTH CURVE ACROSS GAIT MECHANICS IN HUMANS

[1]Jonas Rubenson, [1]Neville, J. Pires, [1]Heok O. Loi, [2]Gavin J. Pinniger, [1]Damian G. Shannon

[1]School of Sport Science, Exercise and Health, University of Western Australia, Perth, Australia
[2]School of Anatomy, Physiology and Human Biology, University of Western Australia, Perth, Australia
email: jonas.rubenson@uwa.edu.au web: http:// www.uwa.edu.au/people/jonas.rubenson

INTRODUCTION

Where muscles operate on their force-length (F-L) curve and how their length operating ranges are modulated is important for understanding the control, mechanics and energetics of locomotion. Muscle function at the plateau region of the F-L relationship may be regarded as favorable since maximal force output is achieved for a given level of muscle activation. In contrast to this view, it has been hypothesized that muscles function on the part of the F-L curve that matches the *in vivo* functional demand of the muscle [1] (e.g. ascending limb for stretch-shorten cycles). Furthermore, it has been proposed that muscles operating along the ascending limb of the F-L relationship are better able to withstand lengthening perturbations and are thus inherently more stable [2].

The primary objective of this study was to establish the region of the F-L curve occupied by the soleus muscle (SOL) during walking and running in young adults using a novel experimental framework combining experimental subject-specific muscle length changes during gait with an experimental subject-specific muscle F-L relationship.

METHODS

Eight healthy, recreationally fit male subjects were recruited for this study (26 ± 3.51 years of age and 70.31 ± 9.18 kg; mean ± SD). Initially, a passive F-L relationships was determined for the SOL by recording simultaneous passive ankle joint torque (Biodex, M3, USA) and fascicle lengths (B-mode ultrasound; Telemed, Lithuania) across the ankle range of motion with the knee positioned at 130° to remove the torque contribution from the gastrocnemius muscles (Fig. 1). Joint torque was converted to muscle force based on a subject-specific Achilles moment arm and muscle pennation angle. An active F-L relationship was determined for the SOL from maximal isometric voluntary plantarflexion contractions with twitch interpolation, taking into account co-contraction (EMG-based estimates), synergist muscle contributions and changes in passive force.

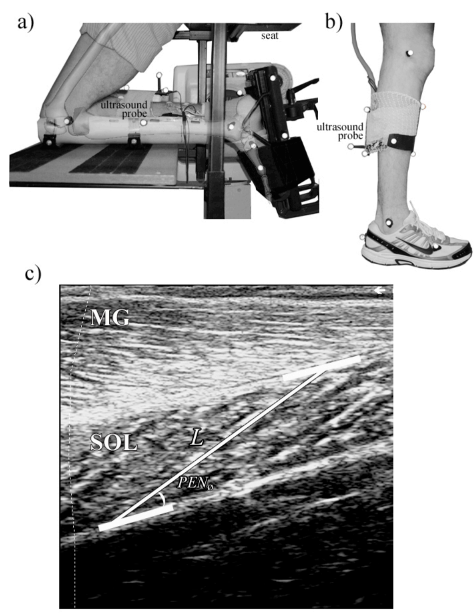

Figure 1: The experimental set-up for measuring subject-specific F-L properties **(a)** Dynamometer positioning **(b)** position of the ultrasound probe for walking and running trials; **(c)** representative ultrasound image of the soleus fascicles.

The experimental optimal fascicle length (L_0) was determined using a non-linear least square optimization routine implemented in MATLAB (The Mathworks, Natick, MA, USA) that minimized the sum of the squared differences between the experimental normalized peak active fascicle forces and those calculated from a theoretical whole-muscle F-L curve at the same normalized lengths [3].

The F-L operating range of the SOL during walking (preferred speed) and running (3 m s^{-1}) on a treadmill was examined by integrating motion analysis, B-mode ultrasound, EMG, and the subject's previously established F-L relationship within 2-3 days after the F-L assessments.

RESULTS AND DISCUSSION

All participants exhibited a plateau in the maximum voluntary SOL isometric force production. The estimated L_0 and the peak isometric force were 0.0377 ± 0.0069 m, and 3469.4 ± 720.0 N, respectively. The experimental data matched closely to the theoretical whole muscle F-L curve [3] (Fig. 2).

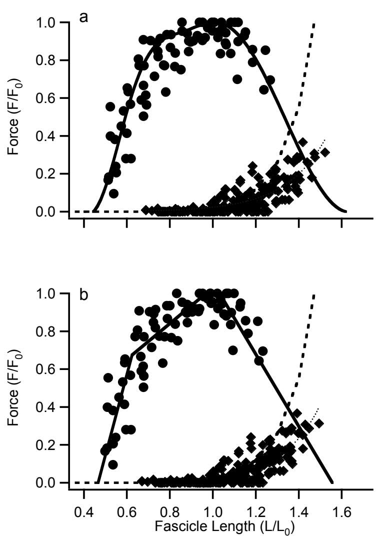

Figure 2: Normalized active and passive F-L relationship. **(a)** data fitted using a whole-muscle F-L relationship [3]; r^2 = 0.748 , and **(b)** using a theoretical sarcomere F-L relationship based on human filament lengths; r^2 = 0.763).

We found that the mean active muscle lengths reside predominantly on the shallow ascending limb of the F-L relationship in both gaits (0.70 – 0.94 L_0, walk; 0.65 – 0.99 L_0, run) (Fig. 3). The active operating lengths were conserved, despite a fundamentally different fascicle strain pattern between walking (stretch-shorten cycle) and running (near continuous shortening). Interestingly, individuals with shorter L_0 undergo smaller absolute muscle excursions (p<0.05) so that the normalized length changes during walking and running remain independent of L_0.

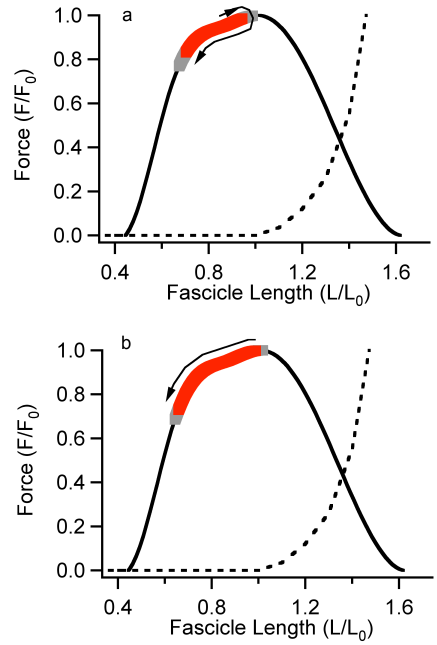

Figure 3: The thick red and grey lines represent active and inactive normalized muscle lengths across the stride, respectively. The arrow represents the direction of muscle strain from the start to end of muscle activation. **(a)** walking at the subjects' preferred treadmill speed **(b)** running at 3 m s^{-1}.

CONCLUSIONS

These findings indicate that the SOL operating length is highly conserved despite gait-dependant differences in muscle-tendon dynamics, and appear to be preferentially selected for stable force production compared to optimal force output.

REFERENCES

1. Herzog W et al. *J Biomech* **25**, 1329-1335, 1992.
2. Julian FJ & Morgan DL *J Physiol* **293,** 365-378, 1979
3. Zajac FE *Critical Reviews in Biomedical Engineering* **17**, 359-411, 1989.

ACKNOWLEDGEMENTS

Supported by a National Heart Foundation Grant (Australia) (G 09P 4469) to J.R.

FORWARD BENDING WITH INCREASED ERECTOR SPINAE FORCE HELPS REDUCE DISK HERNIATION RISK

[1]Steven A. Rundell, [1,2]Brian T. Weaver

[1]Armstrong Forensic Engineers, Milford, MI, USA
[2]Michigan State University, MI, USA
email: s.rundell@armstrongforensic.com, web: http://www.armstrongforensic.com

INTRODUCTION

Forward bending causes compression, anterior shear, and a flexion moment at the lumbar spine. A combination of posterior muscle and ligament forces must be generated in order to prevent excessive motion and restore upright posture.

It is generally believed that forward bending to 90 degrees while maintaining a straight or extended lumbar spine is biomechanically favorable compared to lifting with a rounded back[1]. However, simple static biomechanical models predict the same spinal loading regardless of lifting technique. Posterior muscle activation with concomitant facet engagement may reduce the compression experienced by the disc.

Therefore, the objective of the current study was to simulate forward bending with a previously validated finite element model of L4-L5 and determine if increasing posterior muscle force results in a reduction in disc pressure. We hypothesized that posterior muscle activation during forward bending would increase facet contact and reduce intradiscal pressure and nucleus extrusion forces thereby minimizing the contribution to progressive disc herniation.

METHODS

A finite element model of a ligamentous L4-L5 motion segment was generated from QCT data of a cadaveric spine. The model was validated using disc pressures, cortical and endplate strains, and kinematic data from peer reviewed literature[2, 3]. Development and validation of the model has been previously described[4, 5].

An additional validation was undertaken for the current study whereby the forces exerted from the nucleus to the surrounding annulus during combined compression and flexion were evaluated. A previously published cadaveric study demonstrated posterolateral disc protrusions when cadaveric specimens were stripped of their posterior elements, hyperflexed, and exposed to compression[6]. Therefore, the current L4-L5 model was stripped of its posterior elements and subjected to progressive increases in flexion of 2 degree increments (0 to 8 degrees) under a 2 kN compressive load.

For the intact model, an anterior shear force of 400 N and a flexion bending moment of 10 N*m was applied to the superior endplate of L4 to simulate forward bending. The inferior endplate of L5 was fixed rigidly in space. The posterior muscles, or erector spinae (ES), were simulated by attaching a force element between the spinous processes approximately 5.5 cm posterior of the joint center and perpendicular to the shear plane of the disc. ES forces of 0, 100, 200, 300, 400, 500, and 600 N were evaluated. Vector plots of nucleus extrusion forces and nucleus pressure was recorded.

RESULTS

Results from the validation study indicated increased posterolateral nucleus extrusion forces during combined compression and hyperflexion (Figure 1). This result is consistent with previously published experimental results[6].

Progressive increase of the ES force resulted in a general decrease in nucleus extrusion forces (Figure 2). Simulated bending with no ES force indicated force maxima in the posterolateral region. The nucleus pressure tended to decrease with increasing ES force for the “intact” model (Figure 3).

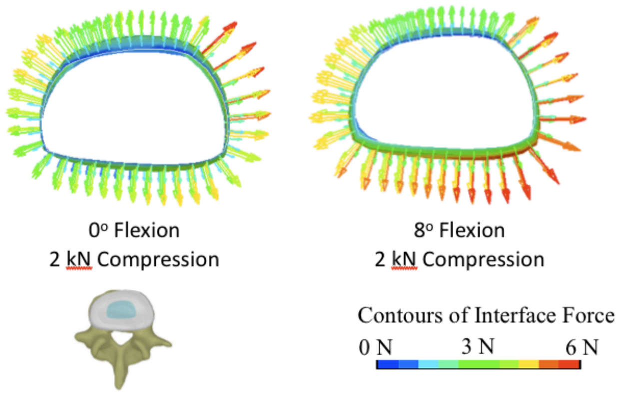

Figure 1. Vector plots indicating the force vectors generated by the nucleus (bottom left image indicates spine orientation). Results from the disc protrusion validation study indicated that combined hyperflexion and compression resulted in increased posteroloateral nucleus extrusion forces consistent with a previously published study (Adams, 1984)

A

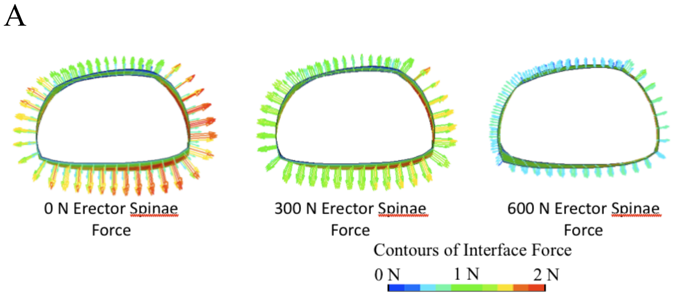

Figure 2. . Vector plots of nucleus extrusion forces during simulated bending. Results indicated a general decrease in nucleus extrusion forces as the erector spinae muscle force was increased (from left to right)

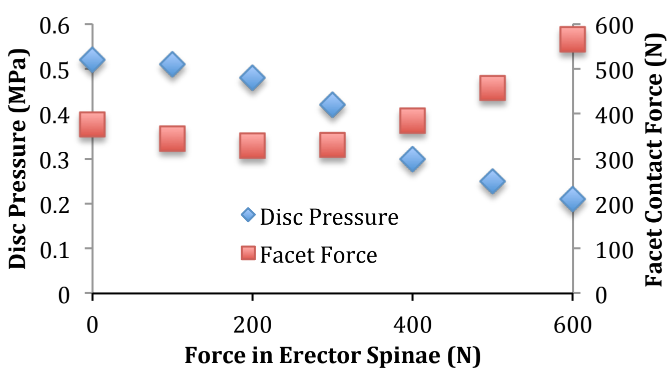

Figure 3. Graph depicting the disc pressure and facet contact force as a function of the force in the erector spinae.

DISCUSSION

Results from the current study are consistent with the hypothesis that posterior muscle activation can reduce disc pressure and nucleus extrusion forces. Exercises that promote strengthening of the erector spinae muscle may help in preventing the occurrence or progression of disc herniation.

Results from the current study indicate potential benefits for the disc by maintaining a strong core or keeping a straight back while performing bending lifts. A study on professional weightlifters documented a reduction in lumbar flexion just prior to lifting heavy weights while bent over (dead lift) [7]. The authors suggested several reasons for this including muscle control and geometric advantages, but do not indicate the potential for increased facet engagement. The authors calculated that during these heavy lifts the disc would be exposed to load levels on the order of 17 kN, which is substantially larger than known compressive failure loads [6]. A possible explanation for this discrepancy is the contribution of the facets. Results from the current study suggest that weightlifters are activating their ES in order to engage the facets prior to heavy lifting to offload the discs. Based on the current study, keeping a straight back or increasing the lumbar lordosis while lifting, or rather engaging your erector spinae to promote facet contact, will result in lower disc pressures and nucleus extrusion forces.

REFERENCES

1. Wilke, H.J., et al., *New in vivo measurements of pressures in the intervertebral disc in daily life.* Spine (Phila Pa 1976), 1999. **24**(8): p. 755-62.
2. Frei, H., et al., *The effect of nucleotomy on lumbar spine mechanics in compression and shear loading.* Spine, 2001. **26**(19): p. 2080-9.
3. Niosi, C.A., et al., *Biomechanical characterization of the three-dimensional kinematic behaviour of the Dynesys dynamic stabilization system: an in vitro study.* Eur Spine J, 2006. **15**(6): p. 913-22.
4. Rundell, S.A., et al., *Total disc replacement positioning affects facet contact forces and vertebral body strains.* Spine, 2008. **33**(23): p. 2510-7.
5. Rundell, S.A., et al., *Effect of nucleus replacement device properties on lumbar spine mechanics.* Spine (Phila Pa 1976), 2009. **34**(19): p. 2022-32.
6. Adams, M.A. and W.C. Hutton, *Gradual disc prolapse.* Spine, 1985. **10**(6): p. 524-31.
7. Cholewicki, J. and S.M. McGill, *Lumbar posterior ligament involvement during extremely heavy lifts estimated from fluoroscopic measurements.* J Biomech, 1992. **25**(1): p. 17-28.

Stretching with applied vibration increases triceps surae flexibility in patients with plantar fasciitis

[1]Elizabeth Russell, PhD,[1] Benjamin Thompson, MD[1,2]

[1]The Andrews Research and Education Institute, Gulf Breeze, FL, USA
[2]Milton Hospital Orthopaedic Department, Milton, MA, USA
email: elizabeth.russell@gmail.com

INTRODUCTION

Stretching the triceps surae complex is the most common conservative treatment for patients dealing with plantar fasciitis pain (1). Lengthening the triceps surae increases the ankle dorsiflexion range of motion and previous research has supported stretching to relieve plantar fasciitis pain. However, sometimes the muscle cannot be stretched enough to provide this relief (2). Stretching with locally-applied vibration induces acute increases in flexibility more than static stretching alone (3). It is possible that adding vibration to the stretching routines in plantar fasciitis patients may increase ankle dorsiflexion range of motion more than stretching alone in patients with plantar fasciitis.

The purpose of this study was to determine how stretching with vibration applied under the foot affected ankle dorsiflexion flexibility. It was hypothesized that stretching with vibration would improve flexibility more than static stretching alone.

METHODS

Fifty-three (N=53) male and female patients with current diagnosis of plantar fasciitis were recruited for this study. All patients used conservative therapies to treat their plantar fasciitis pain, such as stretching, ice, and rolling the arch of the foot.

Subjects were randomly assigned to either a control (N=27, mean age: 45.3 ± 13.3 yrs, height: 1.77 ± 0.1 m, BMI: 29.1 ± 7.5 kg/m^2) or experimental group (N=26, mean age: 49.5 ± 10.8 yrs, height: 1.67 ± 0.09 m, BMI: 27.4 ± 4.8 kg/m^2). The control group stretched on the platform with no vibration and the experimental group stretched with vibration. A vibrating platform (PowerPlate Pro5, 30 Hz, 2mm amplitude) was used to deliver the vibration under the foot. Subjects stretched by lunging forward, keeping the affected foot on the plate and the unaffected foot on a platform of equal height.

Prior to data collection, subjects were prone on an exam table while ankle dorsiflexion range of motion was recorded at 90 and 180 degrees of knee flexion. The center of a goniometer was aligned with the mark on the lateral malleolus and the arms were aligned with marks along the line of the fibula and on the head of the fifth metatarsal. Care was taken by the investigator to ensure that the subject's foot did not rotate out of plane when taking these measurements. In a subset of patients (N=15 in the control group and N=12 in the experimental group), weight-bearing measurements were also recorded with the knee of the effected limb fully extended, the foot flat on the ground and the feet oriented parallel along a line beneath the feet.

All subjects then stretched with their affected foot on the plate. The distance between the feet was not controlled and subjects were able to adjust this distance to gain the greatest stretch. Subjects were instructed to extend the knee of the affected foot and keep the heel flat on the platform while lunging forward to stretch the triceps surae complex only to the point of initial discomfort. Range of motion measures were repeated after the stretching bout.

Student's unpaired t-tests and effect sizes (4) were used to determine differences between the two groups for change in ankle dorsiflexion range of motion from baseline measures.

RESULTS

Stretching the triceps surae complex with vibration under the foot resulted in a greater increase in ankle dorsiflexion flexibility than stretching with no vibration at both 90 degrees (p=0.024, d=0.914) and at 180 degrees (p=0.014, d=0.707). This related to an absolute change of 0.7 ± 3.4 degrees in the control group and 2.7 ± 3.3 degrees in the experimental group. Percent change in flexibility from baseline measures are displayed in Figure 1.

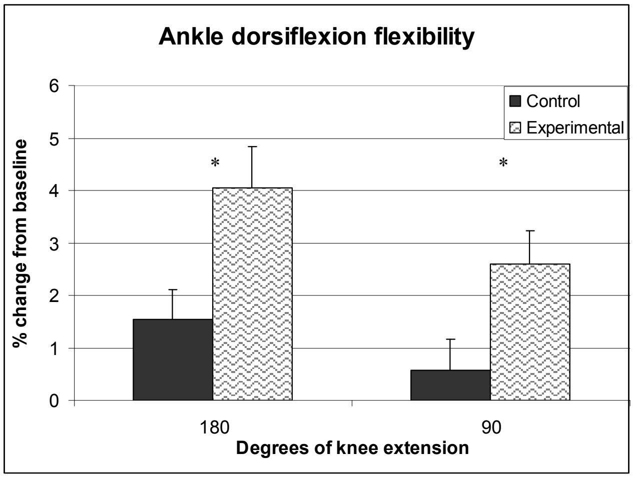

Figure 1: Mean percent change in ankle dorsiflexion flexibility during non-weight bearing and standard error bars. * indicates $p<0.05$.

For the subset of subjects who also performed weight-bearing measures, ankle dorsiflexion flexibility was not significantly different between the groups (p=0.071, d=0.759). There were no differences between groups for any of the subject characteristics of age (p=0.214), height, or body mass index.

CONCLUSIONS

In support of the hypothesis, stretching with vibration applied under the foot was a more effective way to increase flexibility in patients with plantar fasciitis than static stretching alone. The moderate-to-high effect sizes indicate that this effect was present when measured both weight-bearing and non-weight-bearing. Although conservative treatment for plantar fasciitis is stretching, previous research indicates that stretching cannot adequately lengthen the triceps surae complex (2). The use of vibration during stretching may augment flexibility. Feland et al. (5) reported that whole body vibration during stretching had long-term effects on flexibility retention in healthy populations. Therefore, it is possible that the positive effects of vibration during stretching may last longer than just the acute effect however this has not been studied in patient populations or with a population with plantar fasciitis.

Three mechanisms have been proposed that may play a role in flexibility enhancement with vibratory stimulation (6): increased blood flow, increased pain threshold, or induced relaxation of the muscle. Vibration increases blood flow to the targeted area, which then increases temperature and has been linked to muscle extensibility. It may also be the result of decreased pain sensation leading to the ability to stretch beyond initial discomfort. Lastly, vibration-induced flexibility may result from pre-synaptic inhibition of the Ia sensory fibers and the alpha motor neuron.

Patients often need to stretch the triceps surae complex in the morning or throughout the day to relieve some of the tension on the plantar fasciia during walking. Utilizing a form of vibration applied under the foot during their morning stretching routines may substantially improve mobility in this population. Future research will determine long-term successes of stretching with vibration on pain, function, and walking mechanics in plantar fasciitis patients.

REFERENCES

1. Digiovanni BF. *J Bone Joint Surg Am*, 88, 1775-1781, 2006.
2. Sands WA. *Med Sci Sports Exerc*, 38, 720-725, 2006
3. Grady JF. *J Foot Surg*, 30, 465-469, 1991.
4. Cohen J. *Statistical Power Analysis of the Behavioral Sciences (2nd Ed.)*, Erlbaum, 1990.
5. Feland JB. *Int J Sports Med*. 31, 584-589, 2010.
6. Issurin VB. *J Sports Sci*. 12, 561-566, 1994.

ACKNOWLEDGEMENTS

The authors thank Drs. Erik Nilssen and Joshua Hackel for assistance with subject recruitment and Athletes' Performance for use of their PowerPlate.

MAXIMAL DYNAMIC STABILITY OF WALKING COINCIDES WITH THE FREELY ADOPTED SPEED AND STRIDE FREQUENCY

[1]Daniel M. Russell, [2]Joshua L. Haworth and [3]Cesar Martinez-Garza

[1]Old Dominion University, Norfolk, VA, USA
[2]University of Nebraska - Omaha, NE, USA
[3]Pennsylvania State University - Berks, Reading, PA, USA

email: dmrussel@odu.edu, web: http:// hs.odu.edu/physther

INTRODUCTION

It has commonly been assumed that the movement patterns readily adopted by healthy individuals are most dynamically stable [1]. In walking, humans display a preference for a cadence predicted as the resonant frequency of a hybrid spring-pendulum [2]. This leads to the expectation that walking at resonance provides optimal dynamic stability. However, tests of this hypothesis have given mixed results [3-6]. A major criticism of all of these studies is that the measures used (e.g., standard deviation, harmonic ratio of power spectrum and approximate entropy) do not directly quantify local dynamic stability [7]. Instead, this can be estimated via the maximum Lyapunov Exponent (LyE), which quantifies the divergence of nearby trajectories in state space.

Another factor that may have influenced previous results is studying walking on a treadmill. Treadmills provide control and consistency of walking speed, but they have been shown to mask dynamic stability effects [7]. Therefore, studying overground walking offers the greater likelihood of finding stability effects due to walking cadence.

In order to provide a strong test of the hypothesis that walking is most dynamically stable at the preferred stride frequency, we computed maximum LyE for participants walking overground at 7 different individualized frequencies.

Walking at different stride frequencies overground leads to associated changes in speed, which have been shown to impact local dynamic stability [8]. In order to distinguish between the influence of speed and frequency on local dynamic stability, two different conditions were performed. The Free Speed condition (FS) required entraining to the target frequencies while freely adopting any speed. The Controlled Speed condition (CS) required the same stride frequencies to be performed at the preferred speed of walking.

METHODS

Ten (6 men) healthy, college aged students volunteered for this study. Participants walked overground along a 45.3 m walkway. Motion of the knees in the sagittal plane was recorded at 100 Hz using two electrogoniometers, from which the maximum LyE was computed. Average speed was determined via timing gates. To determine each participant's preferred gait, they walk down the walkway five times at their "most comfortable speed and stride rate." The last three trials were recorded, from which the average preferred speed (PS) and stride frequency (PSF) were computed.

The experimental trials required matching seven different cadences specified by an auditory metronome: PSF, ± 5, ± 10, ± 15 strides per minute). Participants performed all seven target frequencies in random order under their own freely elected walking speed (FS), before completing the same frequencies under a controlled walking speed (CS) condition. In CS participants were required to complete the walkway within ± 10% of the mean time from their preferred walking trials. Trials not completed within this time window were repeated, with the appropriate instruction to speed up or slow down. To avoid the influence of fatigue, one correct trial was needed for each condition.

RESULTS AND DISCUSSION

Participants readily matched the target metronome frequencies in both speed conditions. In the FS condition, walking speed increased linearly with cadence ($p<.05$, Fig. 1). This finding is consistent with previous research, which shows humans freely adopt higher stride frequencies when walking at faster speeds.

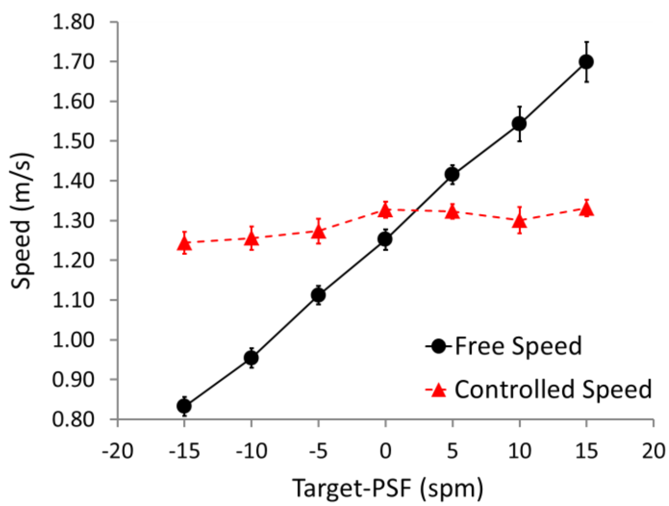

Figure 1: Mean walking speed at each target-preferred stride frequency (strides per minute) under Free Speed and Controlled Speed conditions. Error bars indicate the standard error.

The CS condition required participants to walk at the PS. Participants were able to match the different metronome frequencies and walk within the target speed window, however this required repeating some conditions for all but one participant.

The findings for the maximum LyE supported our main prediction (Fig. 1). Local dynamic stability was greatest (LyE was minimal) at the PFS ($p<.05$). This occurred when the participants were able to freely adopt any speed (FS condition) and when the walking speed was constrained to the PS (CS condition). The significant interaction ($p<.05$) indicates that constraining the speed further reduced the local dynamic stability of gait. At cadences less than the PSF, the CS condition required a speed faster than freely adopted which further decreased local dynamic stability. At cadences greater than PSF, the CS condition required speeds slower than freely adopted, also reducing local dynamic stability.

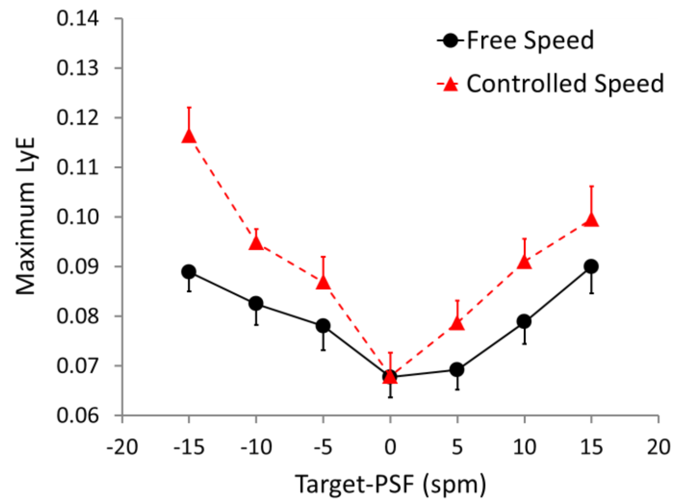

Figure 2: Mean maximum Lyapunov exponent for right knee motion at each target-preferred stride frequency (strides per minute) under Free Speed and Controlled Speed conditions. Error bars indicate the standard error.

CONCLUSIONS

In agreement with the hypothesis, local dynamic stability is maximal at the PSF of walking for healthy individuals. Requiring a speed different from that freely adopted further decreases local dynamic stability. In agreement with the hybrid spring-pendulum model of walking, humans appear to tune into the dynamic stability of their movement patterns [1,2].

REFERENCES

1. Kelso JAS. *Dynamic Patterns: The Self-organization of Brain and Behavior*, MIT Press, 1995.
2. Holt KG, et al. *Hum Movement Sci* **9**, 55-68, 1990.
3. Arif M, et al. *Meas Sci Rev* **4**, 29-40, 2004.
4. Danion F, et al. *Gait Posture* **18**, 69-77, 2003.
5. Holt KG, et al. *J Motor Behav* **27**, 164-178, 1995.
6. Latt MD, et al. *Exp Brain Res* **184**, 201-209, 2008.
7. Dingwell JB, et al. *J Biomech Eng* **123**, 27-32, 2001.
8. England SA, et al. *Gait Posture* **25**, 172-178, 2007.

USING MRI-BASED MUSCLE VOLUMES AND GAIT ANALYSIS TO QUANTIFY RELATIVE MUSCLE EFFORT IN CHILDREN WITH CEREBRAL PALSY

Shawn Russell, Geoffrey Handsfield, Mary Boyle, Lindsay Sauer,
Craig Meyer, Mark Abel, and Silvia S. Blemker

University of Virginia, Charlottesville, VA, USA
email: sdr2n@virginia.edu, web: http://www.mae.virginia.edu/muscle/

INTRODUCTION

Children with spastic cerebral palsy (CP) develop a wide variety of atypical movement patterns, which often lead to musculoskeletal impairments. Therefore, treatments for CP (e.g., muscle-tendon surgeries, botulin toxin injections, muscle strengthening exercises) are often targeted at correcting individual muscle impairments; however, treatment decisions are currently based only on global measurements of movement and function, which include a physical exam, visual observation of the patient's gait, motion capture data, and electromyographic measurements. The overall hypothesis of this research is that inclusion of direct measurements of individual muscle volumes in the treatment decision process will improve treatment outcomes.

The goal of this specific project was to *(i)* measure muscle volumes of six children with cerebral palsy along with age-matched controls, and *(ii)* explore a new method of interpreting gait measurements that takes into account, muscle volume measurements, the distribution of that volume within the leg, and provides an estimate of relative muscle effort for a given movement pattern.

METHODS

Six ambulatory (no assistive devices) children with spastic CP (2 female) 14.0±1.9 *years*, 159±13 *cm*, 58.8±12.1 *kg* were scanned on a 3T Siemens Trio MRI scanner. Thirty-five muscles in the hip, thigh, and shank were segmented using an in-house segmentation program written in Matlab. It has been previously shown that leg muscle volumes scale linearly with subject height and mass [1], so all muscle volumes were normalized by subject height and mass.

For each degree of freedom, we summed the normalized volumes of all the corresponding muscles to determine the total acting muscle volume. We define the volumetric moment for a particular joint's degree of freedom as the moment (normalized by height and mass) divided by the corresponding total acting muscle volume.

To determine the effects changes in muscle volume and distribution due to CP would have on the volumetric moment for normal gait, we analyzed the average normalized joint moments (Nm/kg) of typically developed (TD) children based on a database of 84 aged matched children.

In addition two CP subjects underwent a clinical gait evaluation where gait kinematics and kinetics of their self selected non assisted gait patterns were measured (Vicon PIG model). For these two subjects the volumetric moments were calculated based on their own gait patterns.

RESULTS AND DISCUSSION

In general the total leg muscle volume for the subjects with CP was lower (**Table 1**) than the average reported for typically developed children [1]. Differences in muscle distribution were also found between TD children and those with CP. TD children had larger percentage of their muscle

Table 1: Normalized muscle volumes and volume distributions

	Muscle Volume	Hip						Knee		Ankle			
	ml/kg*m	Ext	Flex	Abd	Add	Inter	Exter	Ext	Flex	Plant	Dorso	Inver	Ever
TD	58.4	16.6	14.0	5.7	8.2	5.2	11.3	15.0	12.0	9.8	3.1	2.1	1.1
CP01	37.0	10.9	8.3	4.7	5.2	4.0	8.1	9.8	6.8	5.5	1.7	1.2	0.6
CP02	40.5	12.0	8.7	5.2	5.2	4.4	9.1	10.2	8.3	6.3	2.1	1.4	0.8
CP03	50.4	13.9	12.3	6.4	7.1	5.1	10.6	14.8	7.9	6.6	2.4	1.8	0.9
CP04	46.0	10.8	9.8	5.2	6.0	4.8	9.7	14.3	8.4	7.0	1.6	1.7	0.7
CP05	56.0	17.3	14.3	6.4	8.7	5.6	12.2	14.2	10.9	8.2	2.4	1.2	1.2
CP06	37.3	11.1	8.4	5.0	4.8	4.2	9.2	9.6	6.4	5.3	1.8	1.4	0.9

volume in ankle dorsi and plantar flexors, and knee flexors, while children with CP had larger percentage of their muscle volume in the hip abductors, and internal and external rotators.

Analysis demonstrated that in order to achieve the gait pattern of a typically developed child, children with CP require a higher volumetric moment, for all motion other than hip abduction, than a typically developed child (**Figure 1**). This is particularly important at the ankle where energy is added most efficiently into the gait cycle.

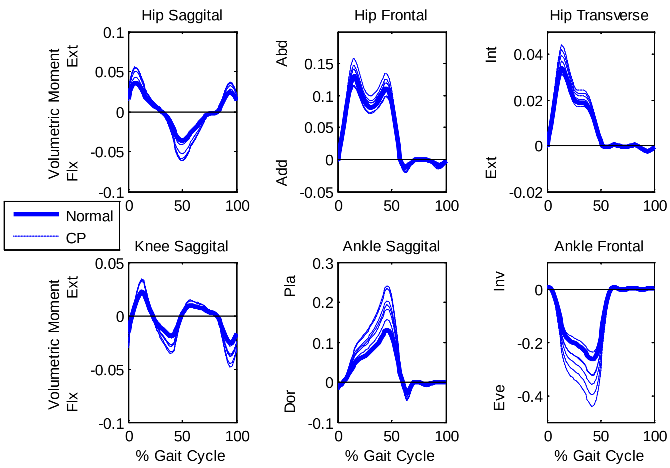

Figure 1: Moments of TD gait pattern normalized by the muscle volume distributions of a TD child and the volume distributions of children with CP.

When the gait moments generated by children with CP are normalized by corresponding muscle volumes and compared to the normal volumetric

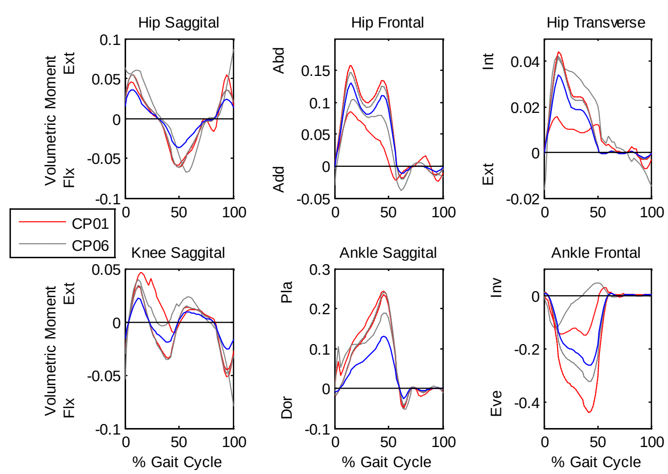

Figure 2: Moments of CP (dotted) and TD (dashed) gait normalized by the corresponding CP muscle volumes, TD reference (solid).

moments (**Figure 2**) we see similar patterns in the hip joint and ankle plantar flexion. However there are noticeable differences in knee flexion and ankle eversion. During stance phase, children with CP have their knees in hyperextension reducing the required moment in knee flexion where they have noticeably less muscle volume. Similarly ankle inversion moments are reduced to accommodate decreased eversion muscle volume.

It has been demonstrated that the moment generating capacity of a muscle is directly related to the volume of the muscle [2]. In optimization routines joint torque generation as a % of max torque generation is often used to predict muscle fatigue. The volumetric moment presented in this study can be used to quantify the ability and efficiency of individuals to produce desired motions with and without pathology on a joint action basis. The ability to decompose motions into their bases i.e. knee flexion, hip abduction, and understand each components contribution to the gross motor pattern will facilitate acute treatment or training of specific muscles in order to optimize the motion.

CONCLUSIONS

Understanding the effect of muscle volume and the distribution of that volume within the leg enables one to better identify the cause of individual gait pathologies, which will allow therapists and clinicians to develop rehab programs specifically targeted at developing muscles or muscle groups in order to facilitate efficient gait patterns.

REFERENCES

1. Handsfield. et al. *2012 ASB Annual Meeting*, Gainesville, FL, USA, (submitted).
2. Holzbaur. et al. *J Biomech*. **40**, 2442-2449, 2007.

ACKNOWLEDGEMENTS

Funding for this work was provided by the Wallace R. Coulter Foundation

ROBUST OPTICAL SENSOR FOR NONINVASIVE CARDIAC MONITORING

Michelle Sabick and Jami Johnson
Department of Mechanical & Biomedical Engineering, Boise State University, Boise, ID, USA
email: msabick@boisestate.edu, web: http://cobr.boisestate.edu

INTRODUCTION

Photoplethysmography (PPG) is a noninvasive method for studying skin blood volume pulsations. Blood-pressure waves that are generated by the heart propagate along the arteries of the skin, locally increasing and decreasing the tissue blood volume with the periodicity of heartbeats [1]. Photoplethysmography detects the blood volume changes through the use of narrow-band light-emitting diodes (LEDs) in the infrared or near-infrared region. Scattering of the optical radiation is generally detected in either transmission or reflection configuration by photodetectors.

Heart rate, respiratory rate, and tissue blood perfusion, as well as indicators of cardiac disorders and peripheral vascular diseases, can be extracted from the analysis of a single PPG trace [2]. Factors such as skin color, volume of adipose tissue, ambient light, sensor location, and movement artifacts have been known to affect the robustness and consistency of PPG signals [2]. A method of obtaining a reliable photoplethysmograph signal at various locations on the body, therefore, has the potential to be useful in clinical applications, as well as self-monitoring. Here, the development of a novel PPG sensor is described.

METHODS

Initially, an alpha prototype PPG sensor was developed using a single infrared emitter and detector. Reflection configuration was chosen for versatility and ease of sensor placement. Electronic filtering and signal processing techniques were designed to optimize the PPG signal and minimize the signal due to ambient light detection in the alpha prototype.

To quantify sensitivity of the sensor to body location, PPG signal intensity was obtained from four subjects at five different locations: the anterior and posterior surfaces of the wrist, posterior calf, posterior upper arm (trapezius), and center of the forehead to determine optimal sensor placement. Analysis was based on the intensity of the signal obtained with respect to baseline ambient light detection. Distinguishability of characteristic PPG contours was also considered.

The reflected radiation of the LED is generally directed toward the incident skin surface in a circular pattern. Therefore, a sensor with a ring of photodetectors was developed as a beta prototype. The ring diameter was optimized based on consistency of acquired signals and signal amplitude. Subsequently, the optimal ring was incorporated into a housing with an adjustable strap for convenient wearability. A conformable gel surrounds the optical components and makes contact with the skin. This reduces ambient light interference, motion of the sensor with respect to the skin, and vibration. This beta prototype is shown in Figure 1.

Figure 1: Photograph of beta prototype, which includes a ring of sensors, conformable gel, and housing with adjustable strap.

Filtering for the beta prototype is accomplished using LabVIEW software. This helps to reduce the power consumption and allows for a more versatile user interface. An algorithm was also developed to detect motion artifact, and noticeable changes in the PPG signal. Further development of the algorithm has the potential to detect when cardiac failure has occurred.

RESULTS AND DISCUSSION

Data obtained using the alpha prototype are displayed in Table 1. The average peak-to-peak signal at each body location is measured in decibels. The average amplitude of the PPG signal was comparable at each location, however the standard deviation varied. The most consistent signal amplitudes were obtained from the posterior wrist and upper arm.

Table 1: Peak amplitude data from alpha prototype.

Sensor Location	Amplitude (dB)	Std. Deviation
Anterior Wrist	4.53	1.79
Posterior Wrist	3.11	0.77
Calf	4.03	1.37
Upper Arm	4.86	0.44
Forehead	4.89	3.52

Features of PPG signals are influenced by factors such as health and age. The contours of a PPG signal, therefore, are distinct for each individual. A common feature, however, is the dicrotic notch. This feature can provide important diagnostic information regarding an individual's cardiac health. The dicrotic notch, in addition to other identifying characteristics, was visible in virtually all trials with the alpha prototype (Fig. 2)

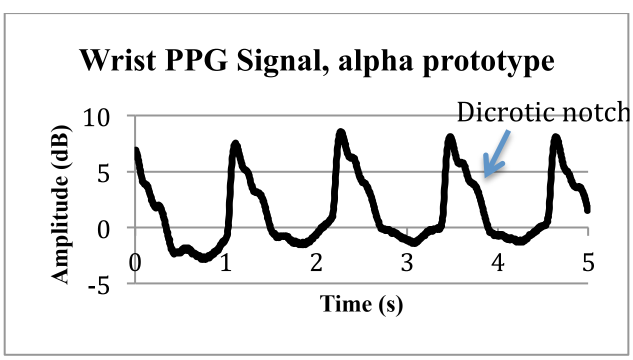

Figure 2: Data obtained from anterior wrist using alpha prototype, dicrotic notch denoted by blue arrow.

With the beta prototype, signals were easily obtained with distinct contours and scalable amplitude using the LabVIEW program. Data obtained using this configuration is displayed in Figure 3.

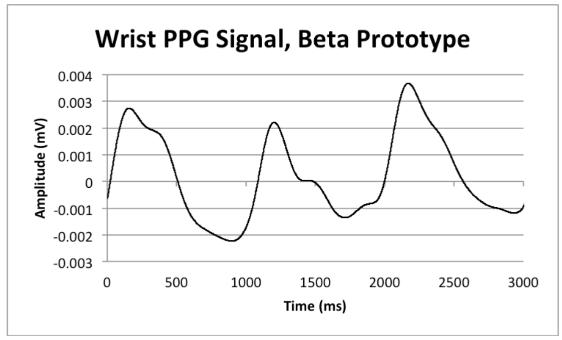

Figure 3: Data obtained from anterior wrist using beta prototype sensor and LabVIEW filtering.

Ambient light interference and motion artifact were reduced with the beta prototype. Further testing and development will work toward additional motion reduction through optimization of components.

CONCLUSIONS

The novel heart monitor sensor developed in this study increased reliability, versatility, robustness, and ease of use over traditionally configured sensors that use a single emitter-detector in reflection configuration.

While PPG has found clinical applications, its use is limited primarily to professional health care use, due in large part to the sensitivity of PPG signals to motion. Our technique shows promise for adaptable use of a PPG monitoring system in a variety of settings. Noninvasive self-monitoring of cardiovascular functions has the potential to provide useful information for health care providers, and overall improve patient care. Additional applications may include self-monitoring of basic cardiac parameters such as heart rate and oxygenation status for the average individual.

REFERENCES

1. Spigulis, J. *Applied Optics* **44**, 1850-1857, 2005.
2. Gailite, L, et al. *Lasers Med Sci* **23**, 189-193, 2008.

THE EFFECT OF UNILATERAL AND TOTAL MENISECTOMY ON POSTERIOR CRUCIATE LIGAMENT FORCES UNDER FEMORAL ANTERIOR DRAWER IN PASSIVE HUMAN KNEE AT FULL EXTENSION.

Sohaila El Sagheir, Kodjo Moglo

Department of Mechanical and Aerospace Engineering
Royal Military college of Canada, Kingston, Canada,
email: sohaila.el-sagheir@rmc.ca

INTRODUCTION

Unilateral and total menisectomy are common clinical procedures when the menisci are injured or torn. However, menisci excision severely impacts and disrupts the knee function. Previous studies focused on either unilateral or total menisectomy mostly at fixing axial rotation of femur or tibia but lacked a full comparison of both cases while including intact knee in both conditions of fixed and free femoral axial rotation. The objective of this study is to investigate which unilateral menisectomy (medial or lateral) has the highest impact on the posterior cruciate ligament (PCL) forces and comparing the results with total meniscectomy and normal intact knee. In addition to investigate if the behaviour will change by fixing or freeing the femoral axial rotation. Four sets of finite element analysis were processed on the same passive knee joint model (Figure 1): (1) Unilateral Lateral menisectomy, (2) Unilateral Medial menisectomy, (3) Total menisectomy, (4) Menisci Intact (control). All cases were analyzed under femoral anterior displacement of 3 mm in two boundary conditions (free and fixed femoral axial rotation). Only the tibio-femoral joint was considered in this study.

METHODS

A Finite Element knee joint model was used to conduct this study. The model was created based on MRI scans of the right knee (Male:45 yr-70 kg) which were used to extract the 3D geometry of the knee joint model. The 3D geometry of the skeletal knee skeletal was built using Mimics and Abaqus software. Articular cartilages and menisci were considered to behave as linear elastic isotropic as reported in the literature [1]. Ligaments were modeled as springs which have an elastic nonlinear behaviour [2]. Since bone stiffness is much higher than the soft tissues, bones are modeled as rigid bodies represented by a reference node and meshed with tetrahedral elements. Menisci and cartilages were meshed with 8 node hexahedron elements. Frictionless non-linear contact with finite sliding was assumed in all articulations. Tibia and Fibula were fixed in all D.O.F. An anterior displacement of 3 mm [3] was applied to the Femur with fixed and free axial rotation.

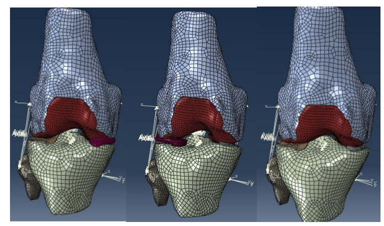

Figure 1: Knee joint model cases: Lateral menisectomy (left), Medial menisectomy (middle) and Total menisectomy (right)-Intact not shown

RESULTS AND DISCUSSION

In case of fixed femoral axial rotation, higher PCL forces were noticed in case of medial menisectomy than the corresponding lateral menisecotmy at displacements greater than 1 mm (Figure 2). PCL forces were (70N) and (88N) at 2 mm displacement, (127N) and (155N) at 3 mm displacement for lateral and medial menisectomy respectively. It was noticed that PCL forces resulting from medial menisectomy were the next highest value to those resulted from total menisectomy which agrees with [4,5] that medial compartment is the main resistance to femoral anterior displacement. Total menisectomy resulted in the highest PCL forces in all conditions. Results of intact case were within range with previous experimental studies [6]. In case of free femoral axial rotation, the model became looser and more flexible as the femur was free to rotate axially, lower PCL forces resulted due to the extra degree of freedom applied (free rotation) as less resistance to femoral drawer was noticed. Predicted results of PCL forces for the medial menisectomy were relatively higher than lateral menisectomy. Both maintained higher PCL forces than the intact case. However, a substantial increase of PCL forces resulted in total menisectomy (Figure 3). Predicted PCL forces were (13.5N) and (18N) at 2 mm anterior displacement, (20N) and (24N) at 3 mm anterior displacement for lateral and medial menisectomy respectively. Contact pressure on tibial cartilages were twice as high in case of medial menisectomy (0.9MPa) and (1.02MPa) than lateral menisectomy (0.5MPa) and (0.52MPa) in free and fixed axial rotation respectively. It is noticed that contact pressure resulted from medial menisectomy was close in value to that resulted from total menisectomy in both conditions (Table 1).

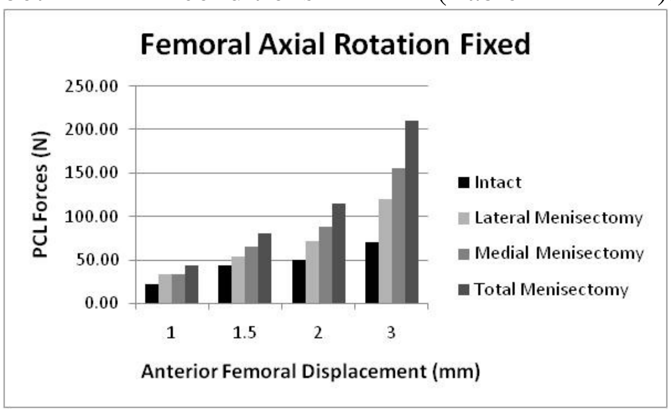

Figure 2: PCL forces vs anterior femoral displacement at full extension, for unilateral and total menisectomy-fixed axial rotation.

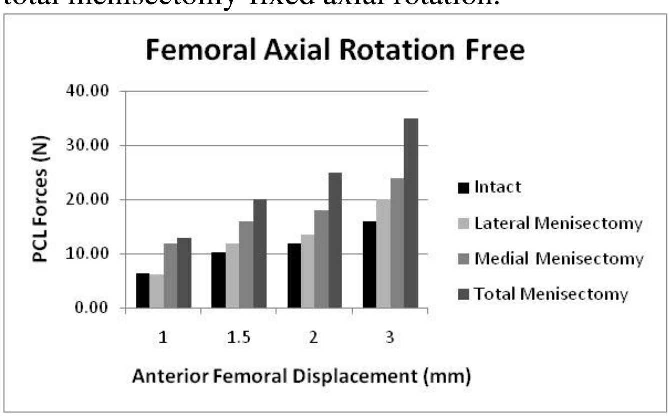

Figure 3: PCL forces versus anterior femoral displacement at full extension, for unilateral and total menisectomy-free axial rotation.

CONCLUSIONS

Total menisectomy resulted in the highest PCL forces in all conditions tested (most damaging condition), the next highest impacting condition was the unilateral medial menisectomy. Un-constraining femoral axial rotation, resulted in more looseness in the tibiofemoral joint, less resistance to the drawer and noticeably less PCL forces than that resulted in fixed rotation. However the same behavior was maintained in both conditions. This highlights that the medial compartment contributes more to load sharing (agrees with [4]) Contact pressure values on tibial cartilages due to medial menisectomy was very close to that due to total menisectomy (Table 1) in both conditions which indicates higher probability of cartilage degeneration. Clinically, this study's results show that unilateral medial menisectomy has a higher impact on knee joint function than lateral menisectomy in both conditions. Clinically, medial meniscus should have a higher priority for preservation either by grafting or transplantation [5]. Total menisectomy remains the most disrupting condition and should be avoided as a treatment. However, if absolutely necessary, total knee replacement should be utilized.

REFERENCES

1. Pena B, et al. 3D FE. Analysis of the combined behaviour of ligaments & menisci in healthy human knee joint. *Journal of Biomechanics* 39, 1686-1701 (2006).
2. Mesfar W, et al. Biomechanics of the knee joint in flexion under various quadriceps forces. *The Knee* 12 424-434 (2005).
3. Benjamin MA, et al. Measurement of Posterior Tibial Translation in the Posterior Cruciate Ligament-Reconstructed Knee. *The American Journal of sport medicine*, vol 31 (2003).
4. Shirazi A, et al. Biomechanical response of the passive knee joint under AP forces, *Clinical Biomechanics*, vol 13, 625-633 (1998).
5. Brain J, et al. Allograft Meniscal Transplantation. *Journal of bone and joint surgery,* vol 84-A, 1236-1249 (2002).
6. Lenschow S, et al. Joint Kinematics and in situ forces after single bundle PCL reconstruction. *Arch Orthop Trauma Surg* 126:253-259 (2006)

ACKNOWLEDGMENTS

This work is supported by Academic Research Program (ARP) and Aerospace Research Advisory Committee (AERAC)

Table 1: Contact Pressure (MPa) on tibial cartilages at 3 mm

	Intact	Lateral Menisectomy	Medial Menisectomy	Total Menisectomy
Free Axial Rotation	**0.56 MPa**	**0.5 MPa**	**0.9 MPa**	**1.15 MPa**
Fixed Axial Rotation	**0.5 MPa**	**0.52 MPa**	**1.02 MPa**	**1.18 MPa**

WRIST ROTATIONS ARE CONSIDERABLY LESS SMOOTH THAN REACHING MOVEMENTS

[1]Layne H. Salmond and [1,2]Steven K. Charles

[1]Department of Mechanical Engineering and [2]Neuroscience Center
Brigham Young University, Provo, UT, USA
email: lhsalmond@gmail.com and skcharles@byu.edu

INTRODUCTION

Early studies found that reaching movements are remarkably smooth, as demonstrated by the stereotypical bell-shaped velocity profile [1,2]. Later studies showed that the reaching movements of patients with certain disorders (such as stroke) are less smooth, but that movement smoothness improves with recovery [3]. Consequently, the smoothness of reaching movements may potentially be a way to diagnose and monitor recovery from disorders that affect reaching movements. This approach is especially appealing in rehabilitation robotics since the robot measures movement kinematics and could monitor changes in movement smoothness during therapy.

In contrast, despite the development and implementation of robotic rehabilitation for the wrist [4], little is known about the smoothness of wrist rotations. Consequently, wrist rotation smoothness cannot currently be used to diagnose or monitor recovery from disorders affecting wrist rotations.

The purpose of this study is to characterize the smoothness of unimpaired wrist rotations in order to establish a foundation for future diagnosis and monitoring of disorders affecting wrist rotations. More specifically, we characterized the smoothness of wrist rotations under different speed and movement direction conditions. Finally, to establish a point of reference to the well-known smoothness of reaching movements, we compared the smoothness of subjects' wrist rotations to the smoothness of their reaching movements.

METHODS

Five male and five female right-handed subjects (ages 18 to 26) with no neurological impairment were recruited to participate in this study. Each subject participated in six sessions, each session requiring either wrist or reaching movements at fast, comfortable, or slow speed. Fast, comfortable, and slow movements all required the same movement amplitude but were required to have durations of 300 ± 75ms, 550 ± 100ms, and 900 ± 150ms, respectively. For wrist rotation experiments, subjects had to rotate their wrist 15° in 8 directions involving flexion-extension (FE), radial-ulnar deviation (RUD), or a combination of FE and RUD. Pronation-supination of the forearm was constrained during the experiment. For reaching movement experiments, subjects had to reach 14cm in 8 directions in the horizontal plane. Their forearm rested in a sling to constrain vertical movement during the experiment. Subjects received visual feedback of their movements in the form of a cursor moving (in proportion to their wrist or reaching movements, whichever applied) on a screen in front of them. Subjects also received feedback of their movement duration to help them make movements within the required duration window.

We recorded subjects' wrist or reaching movements using electromagnetic motion sensors. From the kinematic data, we calculated three measures of smoothness: the number of maxima in speed per move, the symmetry of the speed profile (relative location of "center of mass" of speed profile), and the amount of integrated square jerk (relative to a minimum jerk movement). For each measure of smoothness, we tested (by ANOVA) for differences in wrist smoothness between speeds, movement directions, direction of travel, and subjects, and whether there were differences in smoothness between wrist and reaching movements. In this abstract, we present results for one of the measures of smoothness (the number of maxima in speed).

RESULTS

Wrist rotations were significantly less smooth than reaching movements ($p < 0.0001$, Fig. 1). Whether wrist or reaching movements, slower movements were less smooth than fast movements ($p < 0.0001$), but the effect of movement speed on smoothness was greater for wrist rotations (Fig. 1). Although the differences in the smoothness of wrist rotations with direction were not quite significant ($p = 0.0518$), they showed an interesting sinusoidal pattern in which movements involving radial deviation were more smooth than movements involving ulnar deviation (Fig. 2). Outbound movements were significantly smoother than inbound movements ($p < 0.0001$), though the difference in smoothness was small. The variability within a single subject was significantly smaller than the variability between subjects ($p < 0.0001$, Fig. 3).

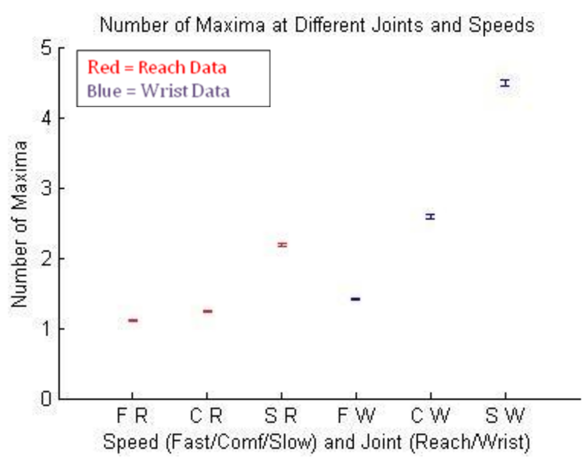

Figure 1: Reach and wrist moves at varying speeds. The error bars represent mean ± 1 standard error.

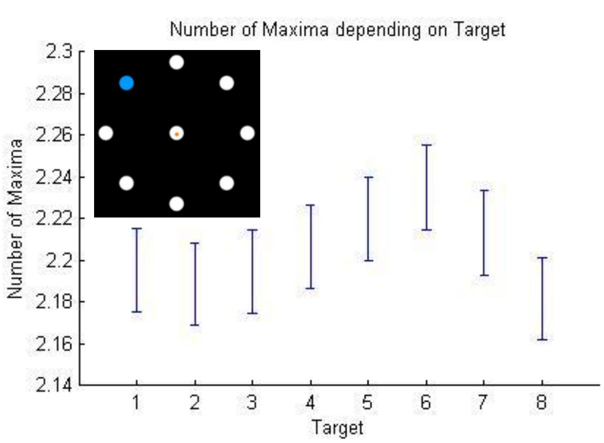

Figure 2: Wrist moves according to target, with #1 at 12 o'clock continuing clockwise to #8 (blue). The error bars represent mean ± 1 standard error.

DISCUSSION

Why are wrist rotations less smooth than reaching movements? One hypothesis is that the low-pass filtering properties of the wrist may not filter out neuromuscular noise as well as those of the arm. Variations between subjects are likely due to differences in the low-pass filtering properties of subjects' limbs (because of differences in limb inertia and joint stiffness and damping). Differences in smoothness between inbound and outbound wrist rotations may be due to differing effects of joint stiffness, the dominant effect in wrist dynamics [5].

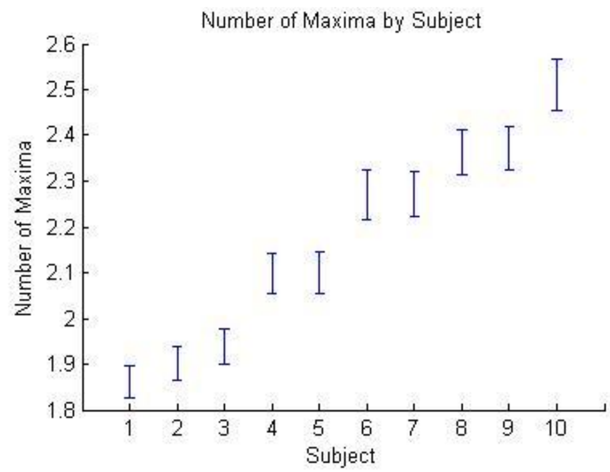

Figure 3: Number of maxima in wrist speed by subject. Subjects are ordered from least to most number of maxima. The error bars represent mean ± 1 standard error.

REFERENCES

1. Morasso P. *Experimental Brain Research* **42** (2), 223—227, 1981.
2. Atkeson CG, Hollerbach JM. *The Journal of Neuroscience* **5** (9), 2318—2330, 1985.
3. Rohrer B, et al. *The Journal of Neuroscience* **22** (18), 8297—8304, 2002.
4. Krebs HI, et al. *IEEE Transactions on Neural Systems and Rehabilitation Engineering* **15** (3), 327—335, 2007.
5. Charles SK, Hogan N. *Journal of Biomechanics* **44** (4), 614—621, 2011.

THE EFFECTS OF NEUROMUSCULAR FATIGUE ON COORDINATION VARIATION

[1]Michael Samaan, [2]Nelson Cortes, [1]Matthew Hoch, [1]Stacie I Ringleb, [1]Joshua T. Weinhandl, [1]Eric Greska, [1]Shawn Lucci, [1]David Quammen, [1]Sebastian Bawab, [3]James Onate

[1] Old Dominion University, Norfolk, VA, USA, [2]George Mason University, Manassas, VA, USA
[3]The Ohio State University, Columbus, Ohio, USA
email: SRingleb@odu.edu, web: www.odu.edu/~sringleb

INTRODUCTION

Various techniques have been developed and used to understand the effects of perturbations and injuries on lower extremity joint couplings through the calculation coordination variability within a particular task [1, 2]. Previous investigators used continuous relative phase [1], a modification of relative motion plots analysis, to examine joint couplings. However, this technique is designed for sinusoidal movement patterns and often requires normalization of data which often hinders the ability to interpret the findings as they relate to injury. To overcome these limitations, a vector coding (VC) method [2] was developed to allow for the simultaneous comparison of multiple trials through the use of angle-angle plots created between two segments.

Females exhibit a reduced variability in couplings that involved either the transverse or frontal planes [3, 4]. Specifically, the knee flexion-extension/knee rotation and knee flexion-extension/hip rotation couplings were reduced compared to males during the first 40% of stance in an unanticipated side step cut. From these data, it was hypothesized that a decrease in coordination pattern variability in particular joint couplings may help explain the increased risk of lower extremity injury in females [3].

Neuromuscular fatigue was shown to alter lower extremity kinematics, which may increase the risk of injury in female collegiate athletes [5]. Specifically, these athletes landed in a more extended position when fatigued, showing that fatigue had a detrimental effect on lower limb biomechanics at discrete time points. The purpose of this study was to improve our understanding of the effects of fatigue on the coordination variability of lower extremity joint couplings.

METHODS

Fifteen NCAA Division I female soccer players (mean age = 19.2 ± 0.8yrs; height = 1.67 ± 0.05m; mass = 61.7 ±8.1kg) were selected to participate in this study. In a previously published study, kinematic and kinetic data were collected for each participant as they performed four trials of an unanticipated side step cut using their dominant leg for both pre- and post-fatigue conditions [5]. The fatigue protocol consisted of dynamic movements such as sprinting, cutting, jumping and squatting at varying intensities within a short period of time.

A modified VC technique [2] was used to analyze variation between the pre- and post-fatigue trials, where zero and one represents no variability and high variability [6].. A custom MATLAB program (Mathworks, Inc., Natick, MA, USA) imported the kinematic data and performed the VC calculations. Four trials of the side step cut were analyzed for each subject for both the pre- and post-fatigue conditions. The stance phase of each trial, consisted of heel strike to toe-off and was normalized to 101 points.

Inter- and intra-limb couplings of the entire group between the hip and knee joints were analyzed using curve analysis during the deceleration phase (i.e., first 50% of stance). The pre- and post-fatigue variation curves along with their respective standard error bands were plotted simultaneously and areas of non-overlap were considered to be areas to investigate further. An area of non-overlap exists when the standard error bands of both curves do not intersect.

RESULTS AND DISCUSSION

An area of non-overlap was found in the hip flexion/hip rotation coupling during the first 5% of stance, where pre-fatigue presented higher variation values than post-fatigue (Fig. 1). This suggests that the athletes in this study are able to employ multiple movement strategies to accomplish the preliminary stage of the cutting task in an un-fatigued state. Many of the other couplings involving knee motion exhibited an opposite trend between 20-30% of stance. This suggests that the motion of the hip joint during the first 5% of the task may affect the motion of the knee joint at a later time period of the stance phase.

From the previously published study, significant differences were found for hip flexion-extension and rotation at initial contact after fatigue [5]. A direct comparison between the kinematics and joint coupling variation values cannot be made yet. However, the changes in planar kinematics along with the coupled motions with fatigue suggest that the deceleration around initial contact during cutting should be further investigated.

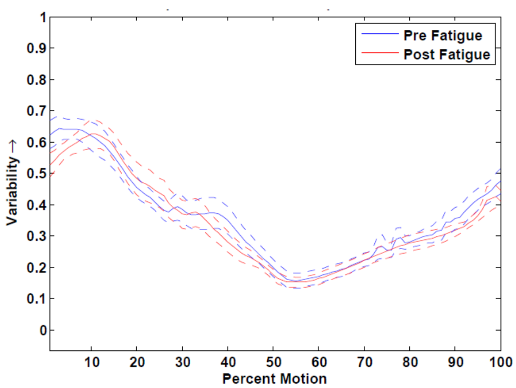

Figure 1 Hip Flexion-Extension/Knee Rotation

Hip and knee flexion-extension are coupled motions and this becomes evident from 20 to 30% of the cutting stance (Table 1). Many couplings (both inter- and intra-limb) involving knee flexion-extension present greater post fatigue variation during 20-30% of stance, including: knee flexion-extension/knee abduction-adduction, knee flexion-extension/knee rotation, hip flexion-extension/knee flexion-extension and hip abduction-adduction/knee flexion-extension. A similar trend was observed in variability patterns during running in individuals with patellofemoral pain syndrome [1].

A decrease in variation in a fatigued state in the hip flexion-extension/hip rotation coupling may be responsible for the increase in post-fatigue variation in many couplings involving knee flexion-extension. This may be a compensatory mechanism that the athletes are employing to accomplish the deceleration phase of the cutting task, however, the interpretation of these findings require further investigation.

CONCLUSIONS

Vector coding may be a useful technique that can be used to determine coordination variation during a particular task. Future studies should combine vector coding along with kinetic and neural assessments to help provide further insight into the non-contact ACL injury mechanism.

REFERENCES

1. Hamill, J et al. *Clin Biomech.* **14**, 297-308, 1999.
2. Tepavac D., et al. *J of App Biomech*. **17**, 259-270, 2001.
3. Pollard, C.D., et al. *Clin Biomech.* **19**, 1022-1031, 2004.
4. Heiderscheit, B.C., et al. *J of App Biomech*. **18**, 110-121, 2002.
5. Lucci, S., et al. *J of Sci & Med in Sp.* **14**(5), 453-459, 2011.
6. Mullineaux, D.R., et al. *J of Sp Sci*. **19**, 739-760, 2001.

Table 1: Chart indicating areas of non-overlap, where blue and red represent greater variability in pre- and post-fatigue, respectively. There were no areas of overlap beyond 50% of the stance phase of cutting.

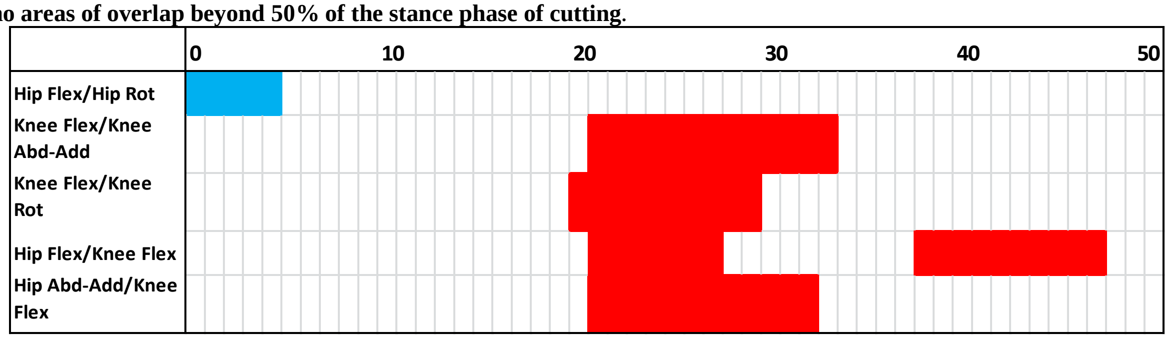

EXERTION MODULATES ANKLE JOINT CO-ACTIVATION DURING NOVEL BAREFOOT AND POST-TRANSITION BAREFOOT RUNNING CONDITIONS

Sachithra Samarawickrame, Rami Hashish, Kush Gaur and George Salem

University of Southern California, Los Angeles, CA, USA
email: ssamaraw@usc.edu web: www.pt2.usc.edu/labs/mbrl

INTRODUCTION

Transitioning from shod (SH) to barefoot (BF) running is becoming increasingly popular among recreational and competitive distance runners. During this transition, multi-segmental kinematics, kinetics, and neuromotor recruitment patterns will adapt to the lack of footwear. Barefoot running induces a fore-foot strike in a plantar-flexed position [1], thus causing an increase in the eccentric demand on the plantar-flexors during weight acceptance. These changes are likely to result in adaptations in muscle performance dynamics, including Agonist :antagonist co-activation, and resistance to the effects of exertion/fatigue. Muscle imbalances and fatigue are known to be contributory factors to running injuries, especially in less experienced runners [2]. The kinematic changes in a fatigued runner result from impairments of muscle performance, contributing to a change in running technique and speed. Muscle electromyographic (EMG) activation prior to foot strike (Preactivation- PR) has been suggested to be a requirement to prepare muscles for activation during the braking phase [3], and the co-activation of the Gastrocnemius (GAS) and Tibialis anterior (TA) are known to be altered during exertional running (4) . While the biomechanics of fatigued running has been reported for SH runners [5], there is no evidence to date of the effects of exertion/fatigue during BF running. Thus, the purpose of this preliminary study was to examine the effect of exertion on the GAS:TA EMG co-activation ratio under novice barefoot and post-transition barefoot conditions in habitually shod runners who undertook an 8-week transition to barefoot running.

METHODS

One female and one male habitually shod runner (Ages 26 and 34 years respectively) performed over-ground running at their self-selected speeds; as a novice BF runner and then as a post-transition BF runner after 8-weeks. Each runner ran under two conditions: pre-exertion and post exertion. A bout of exertion was defined as 20% of their running distance. Both subjects had a history of running a minimum of 12 km per week and reported no significant injuries over the preceding 12 months. The 8-week transition protocol used in this study was modified from that of Lieberman et al. [1]. EMG data was recorded through a Motion Lab SystemMA-420® (Baton Rouge, LA) system with surface electrodes on the TA, medial gastrocnemius and lateral gastrocnemius. Data was digitized via a 16-bit A/D converter (Qualysis®, Gothenburg, Sweden) and stored in the motion analysis system (Qualysis® QTM 2.4, Gothenburg, Sweden). The sampling rate was 1500 Hz. Data was processed using a Matlab® software program and is reported according to the methods described by Kellis et al.[6]. PR EMG was defined as the period of 100ms prior to foot contact (IC). EMG signals were normalized to the peak signal using the peak dynamic method. Each subject completed 6-8 trials in each condition and the normalized signal averaged. The activations of the two heads of the gastrocnemii were averaged to derive the GAS normalized activity. Simultaneous kinematic data were recorded using an 8- camera Qualisys motion capture system (Gothenburg, Sweden) at 250 Hz. The foot was modeled as a rigid segment and tracked using a dorsal marker cluster plate. Kinematic data were low pass filtered at 6 Hz and averaged over the available number of trials. Three-dimensional kinetics were recorded from AMTI force platforms (Watertown, MA) at 1500 Hz. Data is reported for the dominant lower limb of each subject. Foot contact was defined at a minimum of 20 N vertical ground reaction force.

RESULTS AND DISCUSSION

In the novel barefoot condition, the GAS: TA ratio increased after exertion by 21% and 31% (0.29 & 0.42) for the female and male subject respectively. Post–transition, the GAS: TA increased only by 14% and 13% (0.17 & 0.15). (Figure 1). The co-activation increased less due to exertion in the post-transition condition, demonstrating an overall change of 52.8% **(Cohen's D Effect Size (ES): 1.84).** These data should be reviewed together with the functional parameters.(Table 1). The ankle angle at IC is determined by the PR level.

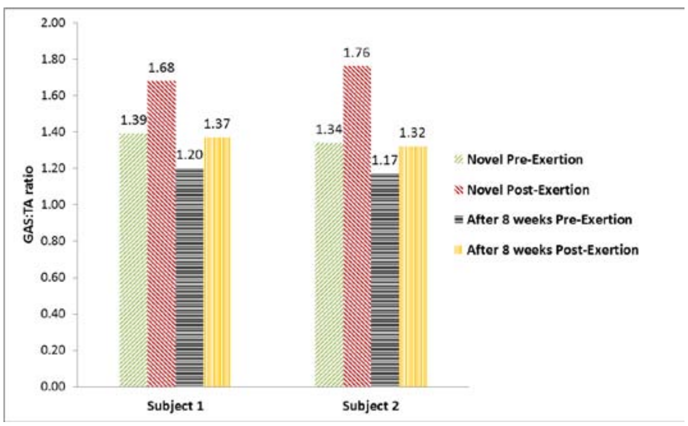

Figure 1: Mean GAS:TA ratio values for each subject, for each running condition.

CONCLUSIONS

These results demonstrate the effects of exertion on habitually SH runners running barefoot. It was seen that exertion increases the GAS:TA ratio. However, after 8 weeks of barefoot running, this effect is reduced. The changes that occur when switching from shod to barefoot running will dictate the new demands that are placed on the foot and ankle musculoskeletal and tendinous structures. These new demands may lead to beneficial effects such as strengthening of muscles and/or detrimental effects through repetitive overloading of muscles. These preliminary data will inform the design of expanded longitudinal studies and help prescription of safe and effective training protocols for persons transitioning from shod to barefoot running.

REFERENCES

1. Lieberman DE, et al. *Nature* **463**, 531-535, 2010.
2. Gerlach KE, et al. *Med Sci Sports Exercise* **37**, 657-663, 2005.
3. Kyrolainen H, *J Sport Sci* **10**, 1101-1109, 2005.
4. Mizrahi J, *Hum Mov Sci* **19**, 139-151, 2000.
5. Christina KA, *Hum Mov Sci* **20**, 257-276, 2001.
6. Kellis E, *J Ath Training* **46**, 11-19, 2011.

ACKNOWLEDGEMENTS

We gratefully acknowledge Dr. Sean Yu for his guidance during data processing.

Table 1: Summary of running speed and ankle angle data for the two subjects. IC= initial contact, BF= barefoot, BMI= body mass index, Negative ankle angle is plantarflexion.

Subject	BMI ($kg*m^{-2}$)	Running Condition	Mean speed ($m*s^{-1}$)		Mean Sagittal ankle angle at IC (°)	
			Pre-exertion	Post-exertion	Pre-exertion	Post-exertion
Subject 1	24.1	Novel BF	5.30	3.62	-03.3	+10.3
		Post-transition BF	4.33	3.90	-07.8	+03.1
Subject 2	22.8	Novel BF	3.73	2.59	-13.5	-04.3
		Post-transition BF	3.81	2.93	-07.8	-04.6

COMPARISON OF SARCOMERE HETEROGENEITY MEASURED IN PASSIVE LIVE AND FIXED MUSCLE

[1]Thomas G. Sandercock, [1]Alex R. Cash, and [1]Matthew C. Tresch

[1]Northwestern University, Chicago, IL, USA
email: t-sandercock@northwestern.edu

INTRODUCTION

Sarcomere length is a key parameter underlying muscle function. Within a muscle, the heterogeneity of sarcomere lengths affects global measures such as the muscle length-tension relationship and may provide insight into muscle stability and function. However, measuring sarcomere lengths in muscle is difficult and often requires with some surgical dissection of fibers and/or chemical fixation of muscle fibers. Here, we take advantage of new 2 photon imaging techniques to image sarcomere lengths in live muscles to examine the heterogeneity of sarcomere lengths. We then compare this in situ measurement of heterogeneity to measurements made using classical methods of fixing muscle, asking whether fixation alters sarcomere length measurements and increases sarcomere length heterogeneity.

METHODS

In anaesthetized adult mice the extensor digitorum muscle (EDL) was carefully freed from surrounding tissue and the tendons tied with silk suture (Fig. 1).

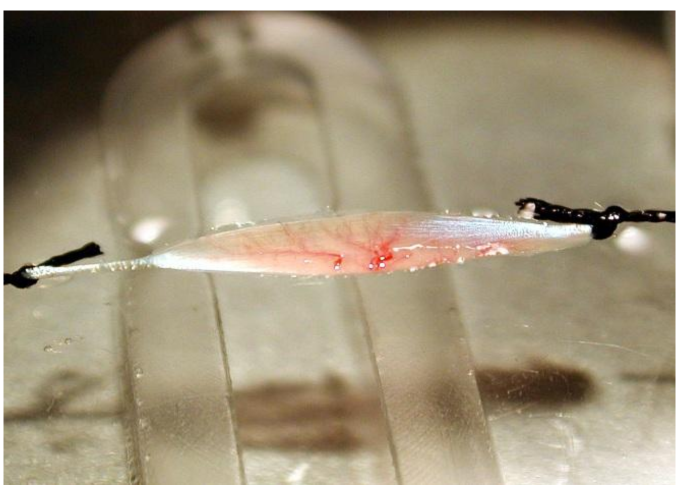

Fig. 1) Isolated mouse EDL.

Four muscles were imaged using 2P microscopy. The muscle was placed in ringers and stretched to slack length. The imaging technique is similar to that described by Llewellyn et al.[1] except the muscle was viewed from the surface and not penetrated with a microendoscope. Surface fibers were imaged up to a depth of 200µ using second harmonic generation (SHG) imaging (Bio-Rad 2100 MPD, tunable titanium-sapphire laser wavelength of 800 nm, Olympus 40x/NA0.8 water-dipping objective, filter and photo multiplier tube at λ 370-450 nm).

Four muscles (not the same as those imaged with 2P) were fixed and then imaged using a light microscope. The methods used are similar to those described by Loeb and Gans[2]. Briefly, the muscle was pinned at slack length, covered in paraformaldehyde for 24 hours, placed in dilute nitric acid for 24 hours, fiber bundles teased out using a glass probe, mounted on a microscope slide with DPX, and photographed using a light microscope with 60X objective.

RESULTS AND DISCUSSION

After establishing standard procedures in preliminary experiments, we consistently obtained good 2P images with clearly visible sarcomere striations. We were able measure sarcomere lengths to a depth of approximately 200 µ in all regions except under the collagen at the aponeurosis. Figure 2 shows a typical image of 5 muscle fibers obtained with 2P SHG imaging. Similar images were obtained from all 4 muscles. Sarcomere lengths were measured using a semi-automated computer program to count pixels. The mean sarcomere length across all muscles was 2.42µ. In-series sarcomere lengths showed considerable variability ranging ±0.14% from the mean sarcomere length (S.Dev. 0.08). This is consistent with the variability reported by Llewellyn et al.[1] Average sarcomere length measured in regions was uniform between and along the muscle fibers.

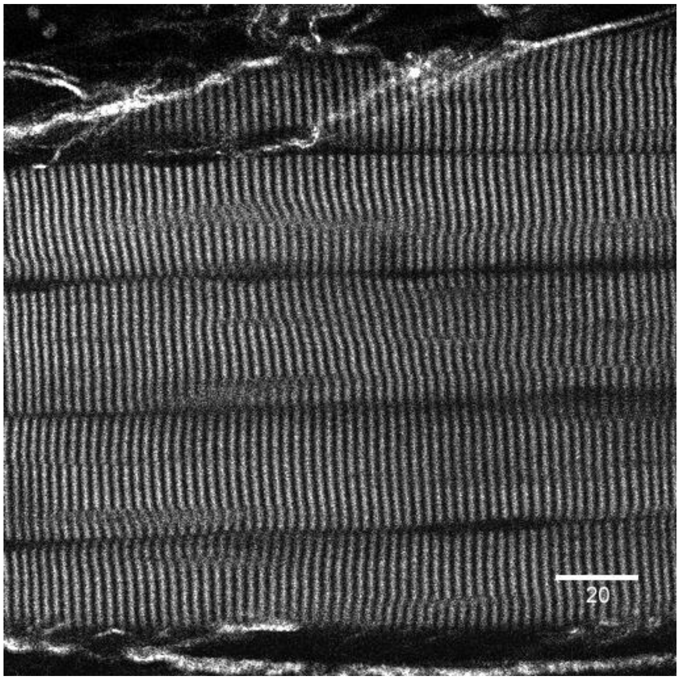

Fig. 2) Muscle fibers imaged with 2P microscopy. Fibers are near the surface of the muscle. Sarcomere spacing is clearly visable. Five muscle fibers can be seen. The white strands are collagen.

In contrast, many of the fibers in the fixed muscle showed irregularities when compared to the 2P SHG images. Figure 3 shows one of the best images obtained using fixed tissue. Sarcomeres are clearly visible but the fibers show considerable cross fiber shear. Such shear was never observed in the in situ measurements made using 2P. In other cases, sarcomeres were not visible at all or showed an even higher degree of disorder. In one of the muscles none of the 4 slides gave a good measurement of sarcomere spacing. In the remaining 3 muscles the mean sarcomere length was 2.05μ, considerably shorter than in the 2P measurements. Analysis of in-series sarcomere variability, taken from the best sections, showed variability ranged ±0.10% of the mean sarcomere length (S.Dev. 0.06). This is comparable to the variability seen in the 2P images.

The short sarcomere lengths measured in the fixed muscle suggests muscle shortening during the fixation. This may have occurred through slippage or stretch of silk threads holding the muscle. Ward et al.[3] showed when a metal clamp was used to hold a fiber segment during fixation mean sarcomere length matched laser measurements. Future experiments will try fixing the muscle in situ to eliminate this possibility.

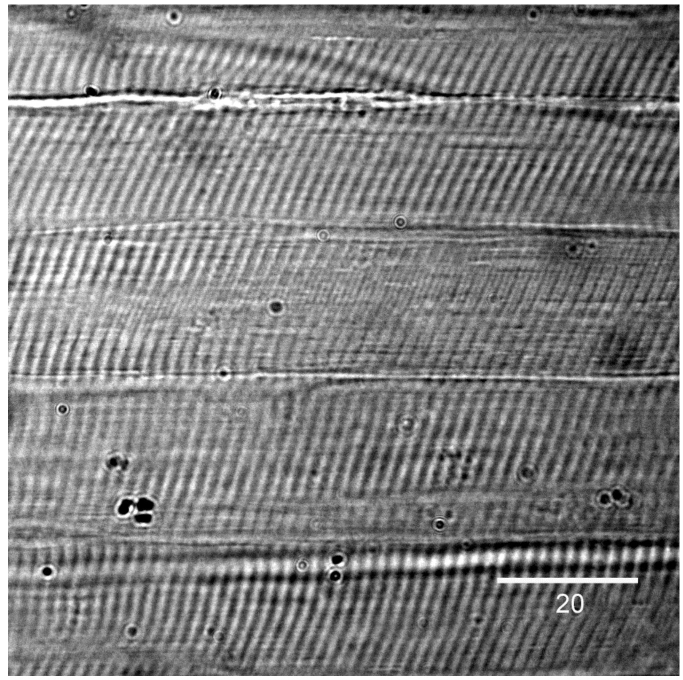

Fig. 3) Fixed muscle fibers imaged with light microscopy.

CONCLUSIONS

Two photon imaging was used to measure sarcomere heterogeneity in passive muscle held at rest length. In-series sarcomere variability was detected but mean sarcomere length along and between fibers was low. In fixed tissue, considerable distortion was observed, rendering measures of heterogeneity questionable. However, the best sections showed similar in-series variability to 2P measurements.

REFERENCES

1. Llewellyn ME, et.al. Nature 454(7205): 784-788, 2008.
2. Loeb GE, and Gans C. Electromyography for experimentalists. Univ. of Chicago Press, 1986.
3. Ward SR, et al. J Biomech 42: 193-196, 2009.

PROTOCOL TO ASSESS HYOID BONE DENSITY FOR PREDICTION OF FRACTURE

[1]Ozell P. Sanders, [2]L.D. Timmie Topoleski

[1]University of Maryland, Baltimore County Baltimore, MD, USA

email: oz1@umbc.edu

INTRODUCTION

In recent literature fracture of the hyoid bone is more common in manual strangulation as opposed to ligature strangulation but the results are not consistent enough to determine whether this outcome is typical of all manual strangulations [1]. There are several variables of the hyoid bone which must be considered to determine the cause of fracture. There is a need to minimize the number of variables and focus on the relationship between hyoid bone fracture and bone density at the site of fracture.

Previous studies have demonstrated multiple imaging techniques capable of determining the density of bone [2]. Bone imaging has the potential to determine the location a greatest risk of fracture which could lead to the development of a bone fracture risk factor. This study aims to contribute to the research on the cause of fracture in human hyoid bones in strangulation victims. In addition, this study will develop a novel protocol for the preparation and imaging procedure needed to assess cause of fracture in the human hyoid bone. Development of a protocol for determining bone density will involve the use of a microCT imaging.

METHODS

Hyoid complexes (n=2) were obtained from cadavers courtesy of the Chief Medical Examiner's Office of Maryland. The hyoid complexes were cleaned of adherent tissues and fat and rinsed in cold sterile. The specimens were dissected across the mid-sagittal plane yielding paired halves. Each half were vacuum-sealed in a food storage wrap using Seal-a-Meal vacuum food sealer and refrigerated at 4 °C until testing.

A Skyscan 1172 microCT was used for imaging. Prior to scanning, the CCD camera within the MicroCT machine must be aligned due to the rotation of the platform containing the specimen. After alignment is completed the hyoid bone specimen can be placed within the MicroCT scanner. In order to secure the hyoid bone during scanning, the specimens are secured onto a disc shaped platform using a pliable adhesive. The platform is then secured into the high precision stage. Once the specimen is fully fixated the flat field references can be completed. After a flat-field correction is preformed the pixel size is set to 17.2 μm, and "acquisition mode" is selected from the options menu. To initiate scanning the height is readjusted so that the specimens are within the camera's field of view. Each pixel size is 2000 x 1048 pixels. An oversized scan is used to segment the image through multiple scans. [3]

3-D reconstructed images are required to perform bone density images. Following the completion of the scans, the NRecon® software package is used in conjunction with six primary computer servers to reconstruct each specimen. A tiff image for each hyoid bone is opened in NRecon®.

After all artifacts are eliminated, reconstruction takes place using the CTan® analysis software package. An adaptive rendering algorithm is used with a tolerance of 1 μm and setting set to default. Each of the three-dimensional models were saved as a finite-element three-dimensional physical model in *.stl file format.

Bone mineral density (BMD) is a measure of the volumetric density of calcium hydroxyapatite (CaHA) in units of g/cm^3 The CTAn® software utilizes Hounsfield units of water and air was used to for BMD calibration.

RESULTS AND DISCUSSION

The results of the present study have shown that using the appropriate scanning parameters (Table 1) will generate a 3-D reconstructed image of a human hyoid bone (Fig. 1). Reconstructed images provided an overview of the human hyoid bone and cross-sectional images of the bone were achieved. These cross-sectional images are used to model the geometry of the hyoid bone. Using the 3-D reconstructed images as well as the Hounsfield units, the Skyscan 1172 can be calibrated in order to give bone mineral density measurements at a given cross-section.

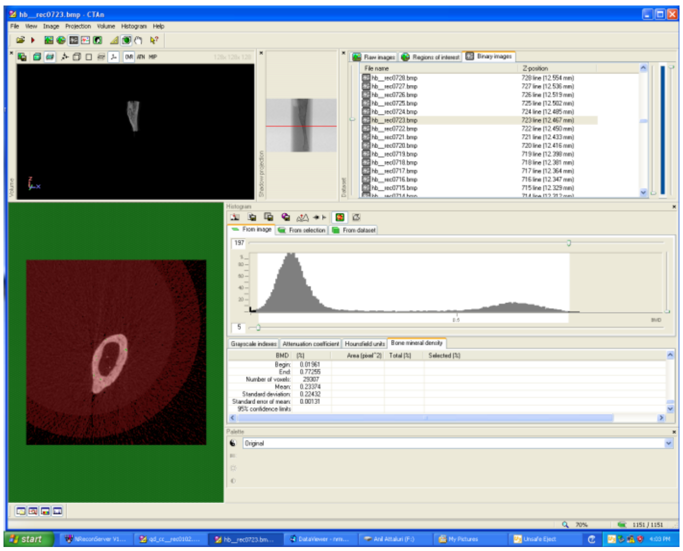

Figure 1: CTan® screen with bone mineral density determined

CONCLUSIONS

Several limitations were determined during the completion of this study. The most important fact is the limited sample size used for evaluating the protocol developed. A total of two samples were successful ran using the protocol developed. A larger sample size is necessary to validate the outlined protocol. Once the protocol established during this study has been validated testing should be carried out and data can be collected. The data collected can be used to determine the effects of bone density on the occurrence of fracture.

Future work in this ongoing investigation could study the effects of the associated soft tissue around the hyoid structure. Superficial structures, such as tracheal cartilage, subcutaneous fat, and even the skin could dampen the effects strangulation. A test could be developed to test these effects using a fully intact cadaver. However retrieval of the mentioned specimen could be difficult to obtain. Use of finite element modeling of the neck region could simplify the process.

REFERENCES

1. Griffith J, *Annals of NYAS, 45-56, 2010*
2. Pollanen M, Journal of Forensic Science (41), 1996

ACKNOWLEDGEMENTS

This work was funded in part by the LSAMP Bridge to the doctorate fellowship as part of the NSF AGEP program

Table 1: Scanning Parameters and Reconstruction Settings

X-Ray Voltage	Filter	Image Pixel Size	Rotation Step	Exposure Rate	Misalignment Compensation	Ring Artifact Reduction	Beam Hardening
60 kV	0.5 mm Aluminum	17.2 µm	0.4^{o}	1475	-1	15	60%

Graft Material Properties Affect Supraspinatus Force-Generating Capacity in a Simulated Rotator Cuff Repair

[1,2]Anthony C. Santago II; [1]Robert C.Weinschenk; [1]Sandeep Mannava; [1,2]Katherine R. Saul

[1]Wake Forest School of Medicine, Winston-Salem, NC
[2]Virginia Tech – Wake Forest School for Biomedical Engineering and Sciences, Winston-Salem, NC
email: asantag@wakehealth.edu website: http://www.sbes.vt.edu/kholzbau/MoBL/

INTRODUCTION

Surgical repair of chronically torn rotator cuff tendons are associated with a high rate (20-70%) of retear [1], which decreases shoulder strength and function compared to patients who do not retear. Operative repair of a torn rotator cuff, in which a retracted muscle-tendon unit is stretched to the humeral head insertion site, results in high passive forces that may contribute to recurrent tearing. Recently, graft materials have been used in an attempt to reduce these passive forces by bridging the tendon defects [2]. However, the influence of a bridging graft on active muscle force has not been evaluated. Further, the graft material properties vary widely, which may contribute to the mixed clinical repair results. We evaluated the effect of graft material selection in this recently developed bridging repair approach on the force-generating capacity of a surgically repaired supraspinatus using a computational shoulder model.

METHODS

To simulate a bridging repair of a chronic full-thickness supraspinatus tendon tear, a Hill-type mathematical representation of the supraspinatus muscle-tendon unit was implemented in Matlab (The Mathworks, Natick, MA). Optimal fiber length, pennation, peak force, resting tendon length, and the muscle-tendon path were obtained from a previously developed upper extremity model [3]. To represent the chronically retracted supraspinatus, resting tendon length was shortened from its uninjured length of 39.5mm to 9.5mm [4]. The path of the supraspinatus remained unchanged, representing the clinical goal of restoring the supraspinatus to the original insertion site. Each of the 5 simulated materials (AlloPatch [Musculoskeletal Transplant Foundation], Restore [DePuy Orthopedics], CuffPatch [Organogenesis], GraftJacket [LifeCell Corporation], TissueMend [TEI Biosciences]), was modeled in series with the muscle-tendon unit, with biomechanical properties based on their response to uniaxial tension tests [1]. Graft cross-sectional area was defined as manufactured graft thickness and the average width of the supraspinatus (25mm) [5]. Resting graft length was 30mm, corresponding to the tendon defect length. For each muscle-tendon-graft construct, an interative solver was used to determine maximal isometric force-generating capacity from 0 to 90° of abduction, dependent on muscle activation and fiber length. Peak activation of the muscle in each construct was determined such that the peak reported strain in the graft material was not exceeded for any muscle-tendon-graft length [1]. Force in the graft, muscle, and tendon were assumed to be equivalent and the total length of the muscle-tendon-graft unit in a given posture was determined from the muscle path in the kinematic model [4].

RESULTS AND DISCUSSION

Stiffer graft materials resulted in a higher total force-generating capacity of repaired supraspinatus constructs than compliant materials, but in all cases the capacity was reduced compared to uninjured supraspinatus. Allopatch, the stiffest and strongest material, resulted in the highest force-generating capacity for any repair. However, the peak force-generating capacity in the Allopatch repair was reduced on average 207N from the uninjured muscle-tendon for all abduction angles. Using GraftJacket, the most compliant graft material, resulted in the largest force reduction (401N) relative to an uninjured muscle-tendon unit. In all constructs, passive forces in the muscle were reduced throughout the range of motion to levels seen in an uninjured supraspinatus.

Reduced total force-generating capacity stemmed from two sources: reduced muscle activation and shortened muscle length due to graft stretch. To avoid exceeding the peak strain of these materials, and thus retearing the construct, muscle activation was reduced for all materials (Figure 1). None of the muscle-tendon-graft units could reach full activation during the first 14° of abduction, and only GraftJacket and Tissuemend repairs permitted full activation in any posture. As abduction angle increased, peak activation level increased for all graft materials.

More compliant graft materials were associated with increased stretch of the graft, resulting in an overall shortening of the supraspinatus muscle fibers to maintain total construct length (Figure 2).

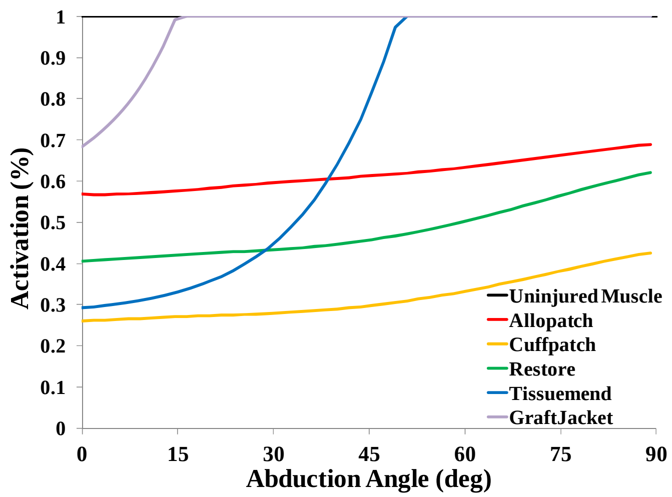

Figure 1: Peak activation vs. abduction angle for each graft material. Peak activation was not reached until 14° for any graft material.

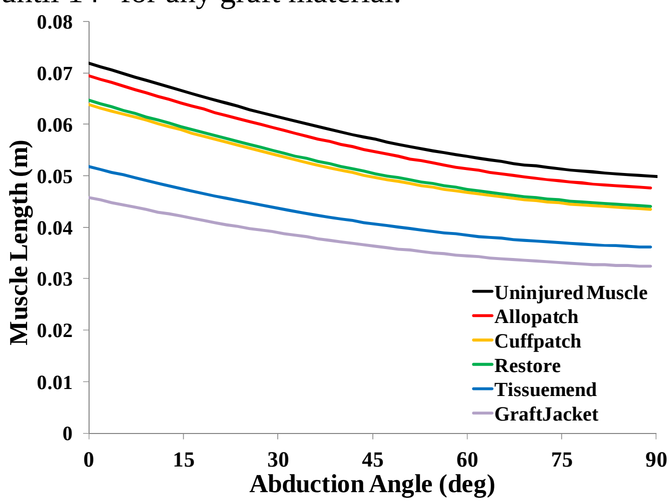

Figure 2: Muscle length vs. abduction angle for each graft material. GraftJacket, the most compliant material, resulted in the shortest muscle fibers throughout the range of motion.

This muscle shortening reduced the force-generating capacity of the muscle. As abduction angle increased, muscle-fiber length decreased even further, as a consequence of the shortening of the muscle path (Figure 2).

Our results suggest that existing graft materials have mechanical behavior unlike native tendon, which reduces the force-generating capacity of muscle as a consequence. Muscle activation was reduced for all materials to avoid graft mechanical failure and retear, further limiting the force-generating capacity of the repaired muscle. Thus, repaired supraspinatus force would be limited not only due to overall fiber shortening but reduced activation also.

These predictions are dependent on peak strain and stiffness relationships reported in the literature. Recent work [6] has reported peak stresses and linear modulus that exceed those used in this study for some materials. If those properties are increased, force-generating capacity of the repaired supraspinatus may increase as well. Further we do not model in-growth and biological remodeling of the graft material following implantation which may alter mechanical behavior.

CONCLUSIONS

Our simulations suggest that the active response of the repaired supraspinatus, and not soley the reduced passive force of the repair, should be considered when choosing a bridging repair. Stiffer materials more closely mimic native tendon in an uninjured supraspinatus; and thus may improve post-surgical rotator cuff function. However, even the stiffest of the currently available graft materials do not mimic native tendon. Future work will incorporate other factors, including muscle atrophy and fiber shortening, that are often associated with rotator cuff tear and which would further reduce the active production of muscle force.

REFERENCES

1. Aurora A, et al. *J Should Elb Surg*, **16**, S171-178, 2007.
2. Wong I, et al. *J Biomech*, **38**, 1861-1868, 2004.
3. Holzbaur K, et al. *Ann Biomed Eng*, **33**, 829-840, 2005.
4. Saul K, et al. *Clinical Biomech*, **26**, 804-810, 2011.
5. Rutolo C, et al. *Arthoscopy*, **20**, 246-249, 2004.
6. Chaudhury S, et al. *J Should Elb Surg*, in press, 2011.

ACTIVE CONTROL OF LATERAL BALANCE VARIES THROUGHOUT A STEP DURING TREADMILL WALKING

[1,2]Andrew Sawers and [1,3]Michael E. Hahn

[1]RR&D Center of Excellence, Department of Veterans Affairs, Departments of [2]Rehabilitation Medicine and [3]Mechanical Engineering, University of Washington, Seattle, WA, USA
email: sawera@u.washington.edu

INTRODUCTION

Step width variability is frequently used to assess the control of step-to-step lateral balance during locomotion [1-3]. An increase in step width variability has been interpreted as a sign of greater active control over lateral balance, while a decrease has been interpreted as a reduction in active control of lateral balance. However, since step width does not change within a step, the assessment of active control of lateral balance using step width variability is limited to step-to-step behavior, potentially missing important differences within a step. The consistency with which lateral balance is actively controlled throughout a step remains unknown. The objective of this study was to determine whether the need to actively control lateral balance is consistent throughout a step.

METHODS

Adults without impairment between 18 and 50 years of age with the ability to walk continuously for 20 minutes on a treadmill were recruited. All protocols were approved by Institutional Review Boards and written informed consent was obtained prior to enrollment. Following 15 minutes of acclimation to walking at 0.7 m/s on a split-belt instrumented treadmill (Bertec, Columbus, OH), 50 consecutive strides of whole-body marker coordinate data (57 markers) were collected (120 Hz) using a 12 camera motion-capture system (Vicon, Oxford, UK). These data were synchronized with ground reaction force data collected from the treadmill force platforms (1200 Hz). Filtered marker coordinates (6 Hz low-pass butterworth) and anthropometric data were combined to build a 15 segment whole-body model in Visual 3D (C-Motion, Germantown, MD). Whole-body COM position was calculated with a weighted sum approach. Using custom Matlab (The MathWorks, Natick, MA) code, the frontal plane COM-ankle angle [4] was calculated for all frames of data as the angle between a line connecting the whole-body COM and lateral malleolus and a vertical line projecting from the whole-body COM. Discrete values of the frontal plane COM-ankle angle for the dominant limb were then extracted across all 50 strides for each of the following gait events; ipsilateral heel-strike (iHS), peak medial-lateral COM velocity (pCOMV), contralateral toe-off (cTO) and ipsilateral mid-stance (iMSt). The standard deviation (SD) of the frontal plane COM-ankle angle was calculated for each gait event, across all 50 strides, for each participant. This variability (SD) was used to infer the extent to which lateral balance was actively controlled [1-3] during each gait event.

A repeated measures ANOVA (SPSS Inc., Chicago, IL) (two-tailed α-level = 0.025) was used to assess differences in frontal plane COM-ankle angle variability between each gait event. A Bonferroni correction was used for multiple comparisons (α = 0.0042).

RESULTS AND DISCUSSION

Twenty-one adults without impairment (age: 31 ± 7 years; height: 1.73 ± 0.11 m; mass: 70 ± 14 kg; gender: 11 male, 10 female) participated in the study. The frontal plane COM-ankle angle variability (SD) differed significantly between all gait events ($p<0.001$), decreasing progressively over a step (Fig. 1).

Based upon previous studies' interpretation of increased metric variability as a sign of greater active control over lateral balance, [1-3] our findings suggest that active control of lateral balance varies significantly within a step, and that the greatest degree of active control occurs at heel-strike, decreasing progressively thereafter. These results support previous work [5,6] which suggested that medial-lateral foot placement with respect to the COM at heel-strike was a critical determinant of lateral balance control.

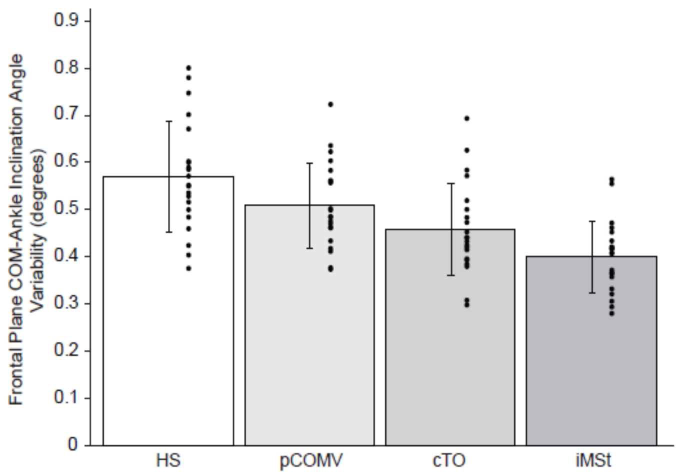

Figure 1: Level of active control of lateral balance within a step. Bars are the average variability (SD) of the frontal plane COM-ankle angle at each gait event. Dots represent individual subject variability (SD) of the frontal plane COM-ankle angle.

Our results expand upon previous work by suggesting that greater active control of medial-lateral balance at heel-strike may occur as a means to ensure adequate lateral stability in preparation for subsequent gait events, such as single limb stance, which pose greater challenge to lateral balance. This would reduce the need to exert a high level of active control across the remainder of stance phase when the available lateral balance control strategies are notably less efficient [5,6].

These results may directly impact the assessment and treatment of locomotor balance control impairments for a variety of patient populations. By assessing lateral balance control within a step, we may be able to detect phase-specific balance control impairments that would be overlooked using a step-to-step assessment of lateral balance control. For example, increased active control of lateral balance beyond heel-strike may be indicative of ineffective foot placement strategies, increasing the role of corrective stance phase joint moments. Excessive active control of lateral balance at heel-strike may signify difficulty or an inability to generate corrective frontal plane moments during stance, thus increasing the importance of foot placement strategies. The increased resolution offered by a within-step assessment may lead to the creation and prescription of more focused, patient-specific interventions that target phase-specific impairments.

Future work will need to validate these results using self-selected walking speeds, and examine how phase specific gait impairments such as ineffective foot placement strategies and an inability to generate corrective frontal plane moments affect active control of lateral balance within a step. The slow walking speed and lack of visual flow while walking on a treadmill may have affected the results of this study. However, the 15 minute acclimation period was intended to minimize these limitations.

CONCLUSIONS

Our results indicate the active control of lateral balance varies significantly within a step. These results could be used to improve the assessment and treatment of locomotor balance control impairments across a range of patient populations.

REFERENCES

1. Bauby CE, et al. *J Biomech* **33,** 1433-40, 2000.
2. Donelan JM, et al. *J Biomech* **37**, 1861-68, 2004.
3. Owings TM, et al. *Gait Posture* **20**, 26-9, 2004.
4. Chen CJ, et al. *Gait Posture* **31**, 391-3, 2010.
5. MacKinnon C, et al. *J Biomech* **26**, 633-44, 1993.
6. Kuo AD. *Int J Robot Res* **33**, 917-30, 1999.

ACKNOWLEDGEMENTS

This study was supported by the Department of Veterans Affairs, RR&D Service (grant A4843C).

COMPARING METABOLIC COSTS OF HARVESTING BIOMECHANICAL ENERGY FROM HUMAN MOTION VERSUS CARRYING BATTERIES FOR THE SAME ENERGY SUPPLY

Eliran Scherzter and Raziel Riemer

Ben-Gurion University of the Negev, Beer-Sheva, Israel
Email: rriemer@bgu.ac.il

INTRODUCTION

Biomechanical energy harvesting from human motion presents a promising and clean alternative to supplying electrical power by batteries to portable electronic devices. The harvesting idea relies on the fact that the human average energy expenditure (i.e., energy used by the body), $1.07*10^7$ Joule per day [1], is equivalent to carrying roughly 20kg of batteries. This fact has led to the development of several technological devices that convert human motion to electrical power [2, 3] and can thus supply electrical energy for users without electricity, such as hikers or residents of third-world countries.

When considering the use of biomechanical energy harvester versus carrying extra batteries, the metabolic cost of each of the options is a major decision criterion that users would wish to minimize. This paper presents research on development of a theoretical framework for comparing the costs of carrying batteries and using a biomechanical harvester device given the same energy provision. The developed framework takes into consideration the device's mass and location on the human body, whether ankle, knee or back, the person's walking speed and body mass, the electrical power production and the duration of use.

METHODS

One key component in the proposed framework concerns how the cost of carrying the extra mass depends on different body locations at different walking speeds. Pandolof [4] developed equations for mass carried on the back. Yet, equations for mass carried on the ankle or knee have not been reported in the literature. In this study we develop, based on experimental work, equations for all three locations for use within the framework.

The decision of whether to use a biomechanical harvester or to carry batteries for delivery of the same supply of needed electrical energy (e.g., during a 6-hour walk) depends on which of the two options requires less user effort in terms of metabolic cost. The metabolic cost difference in Watts can be formulated as follows:

1) $Metabolic\ difference = MH - MB$

Where MH is the metabolic cost using the harvester (Equation 2) and MB is the metabolic cost for carrying the batteries (Equation 3):

2) $MH = f_1(M, S, L)*BM + P*COH,$

Where f_1 calculates the metabolic cost of carrying a mass (normalized to user body mass), as a function of the mass carried M, the walking speed S, and the location of the mass on the body L. The mass location can be at the ankle, knee, or back. The user body mass is BM, the total electrical power harvested at a given walking speed is P, and the cost of harvesting is COH (dimensionless). This is defined as the additional metabolic power in watts required for generating 1 Watt of electric power [2].

The metabolic cost of using batteries is a function of the batteries' mass, carrying location and walking speed. In this study we assume that batteries are always carried on the back, and therefore the metabolic cost of batteries is:

3) $MB = f_1\ (BTM, S, L|L=\text{back})*BM$

Where BTM is the battery mass that provides the required amount of energy and can be calculated as follows (Equation 4):

4) $BTM = \frac{T*3600*P}{BD}$

Where T is the usage duration time in hours, meaning the actual time that the extra battery load is carried, P is the electric power output of the harvester device in Watts, and BD is the battery energy density in Joule per kg. Note that since food energy density is high, we ignore the weight of food required to support the extra metabolic cost of harvesting.

In order to calculate the cost of carrying a mass at given location, while walking at a given speed (f_1 at Equation 2), we conducted an experiment with 8 male subjects (Age: 24-30 years, Weight: 61-90 kg, Height: 173-190 cm). Each walked on a treadmill at slope zero while carrying a different mass at different body locations. At the ankle and the knee the loads on each side were 0, 0.5, 1.5, and 2 kg, and at the back the load was 0, 2, 7.2, 10.2, 16.2, and 22.2 kg. Each of the above weight conditions was performed at three walking speeds of 4, 5, 6 km/h. The Linear Mixed Model (LMM) with a Box-Cox power transformation method [5] was used to determine the equations for predicting the cost of carrying a mass as a function f_1 of its location and walking speed. For ankle or knee the mass refers to the total on both legs.

Once these equations are obtained, the metabolic costs for using a biomechanical harvester and for carrying extra batteries can be calculated for the different cases. For example, for a *case study* of relevance to hikers, a knee device with COH = 0.5, user mass = 75 kg, walking speed = 6 km/h, battery density (lithium) = $4.1*10^5$J/kg, knee harvester device power output = 6W (3W per each knee). To investigate in the next section at what device mass and trek duration would it be beneficial to use the harvester, we will vary the mass from 0.1 kg to 1 kg and the net walking time from 20 to 60 hours.

RESULTS AND DISCUSSION

Using experiment-obtained metabolic values, we fitted equations to predict the metabolic cost as a function of the added mass weight and the walking speed, at each of the three locations (Table 1), and then used these equations for f_1 in Equation 2.

Table 1: Metabolic cost as a function of walking speed and added weight at three body locations:

Location	**Equation** [W/kg]	**R^2**
Ankle	$e^{(0.67913+0.190769*speed+0.075217*weight)}$	0.78
Knee	$e^{(0.59+0.206*speed+0.059*weight)}$	0.83
Back	$e^{(0.51+0.22*speed+0.011*weight)}$	0.85

With the help of Equation 1, we calculated for the same energy supply the difference in metabolic cost between using an energy harvester and carrying batteries. The results for the above case study are presented in Table 2, with negative values in the highlighted cells showing the combinations of device mass and walking time under which harvesting energy is better metabolically than carrying batteries. As expected, the harvester is the preferred option for longer hikes and lower device masses.

Table 2: Metabolic difference for a knee device as a function of device mass and walking time, for case-study parameters: speed=6 km/h, COH=0.5, user mass=75 kg, battery=lithium, and electrical power 6W. Negative values indicate the conditions under which the harvesting option is better.

		Knee Device Mass [kg]								
		0.1	0.2	0.3	0.4	0.5	0.6	0.7	0.8	0.9
Walking Time [Hours]	20	1	4	7	10	13	15	18	21	24
	24	0	3	6	9	12	14	17	20	23
	28	-1	2	5	8	10	13	16	19	22
	32	-2	1	4	7	9	12	15	18	21
	36	-3	0	3	5	8	11	14	17	20
	40	-4	-1	1	4	7	10	13	16	19
	44	-5	-2	0	3	6	9	12	15	17
	48	-6	-4	-1	2	5	8	11	13	16
	52	-7	-5	-2	1	4	7	9	12	15
	56	-9	-6	-3	0	3	5	8	11	14
	60	-9	-7	-4	-1	2	4	7	10	13

We also applied this framework to Donalen's knee harvester [2], with the following parameters: 0.75 kg per knee, 12 W total power output (2 devices), 0.7COH, and 5 km/h walking speed. Our analysis shows that using the harvester device is better than carrying batteries for walking time longer than 50 hours. Future work should include slope walking. Furthermore, modification of this work could be applied to evaluate orthotists and exoskeletons.

REFERENCES

1. McArdle, W. D., F. I. Katch, et al. Exercise Physiology: Energy, Nutrition, and Human Performance**,** Lippincott Williams & Wilkins, 2001.
2. Donelan J. et al *J Science* **319**, 807, 2008.
3. Rome L. et al. *J Science* **309**, 1725-1728, 2005.
4. Pandlof B. et al. Predicting metabolic cost of running with and without backpack loads. Eur.J. Appl. Physiol. Occup. Physiol. 56:495-500, 1987.
5. Schertzer E & Riemer R. Meta-analysis to predict metabolic cost as a function of walking speed and added mass on different body parts. ASB 35th Annual Meeting, 2011.

AN ITERATIVE LEARNING CONTROLLER FOR AN ELBOW SIMULATOR TO MAINTAIN FLEXION ANGLE DURING SUPINATION

[1,2]Patrick J. Schimoler, [1]Jeffrey S. Vipperman, and [1,2]Mark Carl Miller

[1]University of Pittsburgh, Pittsburgh, PA, USA
[2]Allegheny General Hospital, Pittsburgh, PA, USA
email: pjs50@pitt.edu

INTRODUCTION

A clear picture of strength loss from conservative treatment of distal biceps rupture is necessary to weigh the risks of surgery [1]. An elbow joint motion simulator (JMS) provides one means to quantify strength loss by measuring the supination torque produced from various combinations of biceps and supinator tensions at different elbow orientations. Supination strength with the ulna rigidly constrained has already been measured with a JMS [2]. Performing the test with the ulna unconstrained would be significant because the triceps and brachialis are limited in their ability to manage the FE disturbance generated by the biceps acting as a supinator.

A multiple-input multiple-output controller is necessary to perform these unconstrained tests on a JMS. The trials are expected to be temporally short with identical initial conditions and a repetitive biceps disturbance, making iterative learning control (ILC) an appropriate solution [3]. The following describes the design of an ILC for maintaining the FE angle of an elbow JMS using the brachialis and triceps in the presence of a repetitive disturbance.

METHODS

An elbow JMS has been designed and validated [4] at Allegheny General Hospital. This system can actuate an elbow in PS and FE by means of cables attached to the muscle insertions along the muscles' physiologic lines of action. Equation 1 is a nonlinear model of the FE motion of the elbow shown in Figure 1.

$$I\ddot{\theta} + b\dot{\theta} = f_{br}(\theta, x_{br}) + f_{tr}(\theta, x_{tr}) + f_g(\theta) + M_b \quad (1)$$

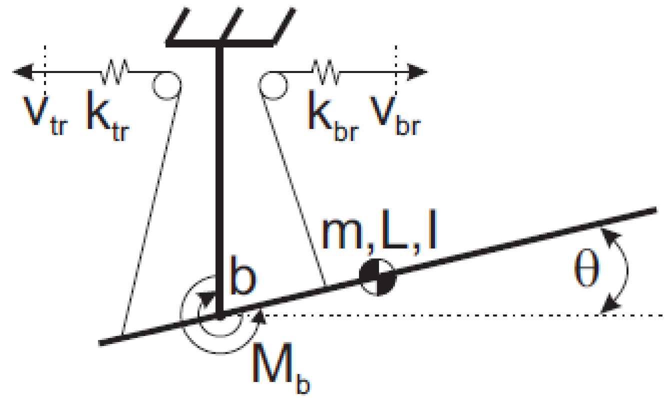

Figure 1: Diagram of the FE motion of the elbow JMS. The triceps and brachialis tendons connect to linear actuators whose velocities are inputs to the system, v_{tr} and v_{br}. The disturbance to the system is a moment resulting from biceps actuation, M_b.

For the study of supination strength, the major muscles involved are the biceps, brachialis, triceps, and supinator. In a given trial, the supinator and biceps will apply specified load profiles to an arm that is connected distally to a torque measuring load cell. The purpose of the ILC is to maintain a fixed FE angle and a specified brachialis tension through the generation of velocity input commands for the brachialis and triceps actuators during application of the biceps and supinator load profiles. The biceps actuation creates a concurrent FE moment, seen as a disturbance. The FE moment of the biceps is taken from the literature [5, 6].

The first step in the controller design is the linearization of equation (1) with a Taylor series expansion about the operating point. This linearization should be valid because the system will operate in the close vicinity of pre-chosen configurations. This linear model is used to populate a matrix, *H*, with Markov parameters, creating a linear map from a given input, u, to a given output, y. Matrix A, the inverse of H, maps the desired trajectory to a first attempt at the satisfactory velocity input signals.

$$y = Hu \tag{2}$$
$$u = H^{-1}y = Ay \tag{3}$$

The input signals and the biceps disturbance are applied to (1). The response of (1) can be used to calculate an error signal. The error signal and A can then be used iteratively to modify the previous input.

$$u_{i+1} = u_i + Ae_i \tag{4}$$

Iterations are performed until the error is within acceptable bounds.

The maximum error bounds have been chosen to be 0.5° in FE displacement and 0.25 N in brachialis tension. The design of this ILC follows Moore [3]. The nonlinear system was simulated with Matlab using a built-in Runge-Kutta method.

RESULTS AND DISCUSSION

Two iterations with the ILC on (1) were necessary to find inputs that kept the error within the chosen bounds. Figure 2 shows FE profiles over time for different iterations. Figure 3 shows the maximum error as a function of iteration number for both the FE angle and brachialis tension.

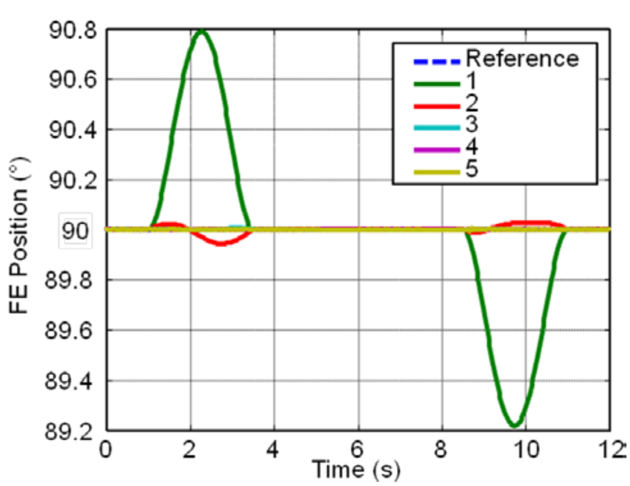

Figure 2: FE position as a function of time and iteration number for the nonlinear model simulation.

In this simulation, the first inputs to the nonlinear model were produced from two iterations on the linear model. These two iterations on the linear model ensured that all iterations performed on the nonlinear model were stable. This will also be done on the physical system to save time and protect equipment from unplanned large motions.

H does not always have an inverse as assumed above. Methods exist to deal with this situation [3].

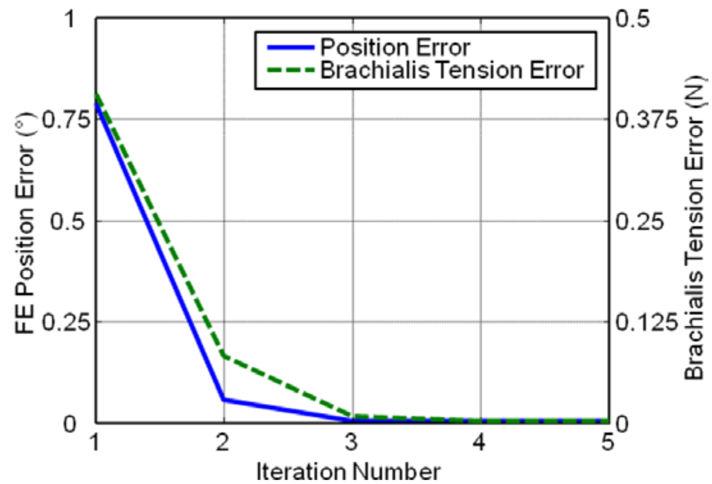

Figure 3: Position and brachialis tension error as a function of iteration number for the nonlinear model.

CONCLUSIONS

It has been demonstrated through simulation that an ILC can be used to control the FE position and stiffness of an elbow in a JMS through control of the brachialis and triceps in the presence of a disturbance.

REFERENCES

1. Freeman CR, et al. *J. Bone and Joint Surgery* **91**, 2329-2334, 2009.
2. Haugstvedt JR et al. *Acta. Orthop. Scand.* **72**, 629-634, 2001.
3. Moore KL, *ILC for Deterministic Systems*, Springer-Verlag, 1993.
4. Kuxhaus L, et al. *J. Med. Devices* **3,** 031002/1-7, 2009.
5. Ramsay JW, et al. *J. Biomech.* **42**, 463-473, 2009.
6. Hale R, et al. *J. Biomech.* **44**, 650-656, 2011.

THE IMPORTANCE OF ACCOUNTING FOR KNEE LAXITY WHEN SIMULATING GAIT

[1]Anne Schmitz and [1]Darryl G. Thelen

[1]University of Wisconsin, Madison, WI, USA
email: ambaus@wisc.edu, web: http://www.engr.wisc.edu/groups/nmbl/

INTRODUCTION

Musculoskeletal simulations of gait are commonly used to estimate muscle and joint forces. Such models typically represent the knee as a kinematic constraint that is independent of load [1]. However, the tibiofemoral joint bas been shown to exhibit load-dependent behavior during functional tasks [2,3]. For example, at the same extended knee posture, internal tibia rotation varies markedly between early stance, late stance, and terminal swing [2]. These variations in kinematics may be important to consider in gait simulations, since they alter muscle moment arms and the instantaneous joint axes [4]. Therefore, the goal of this study was to determine if a musculoskeletal simulation model that included a knee with laxity could predict secondary knee kinematics seen in walking.

METHODS

We started with a lower limb musculoskeletal model that included 44 musculotendons acting about the hip, knee and ankle joints [1]. The one degree of freedom (dof) knee in the model was replaced by a six dof tibiofemoral joint [5,6] and a one dof patellofemoral joint. Nineteen ligament bundles were represented including the MCL (5 bundles), LCL, popliteofibular ligament, ACL (2 bundles), PCL (2 bundles), posterior capsule (4 bundles), iliotibial band (ITB), and patellar ligament (3 bundles). Each ligament was represented as a nonlinear spring with origins and insertions based on [5] and wrapping about the femoral condyles accounted for. The geometry of the distal femur and cartilage was segmented from high resolution MRI images of a young male knee with average femoral geometry. The medial and lateral tibia plateaus were modeled as planes with posterior slopes of 2 and 7 deg, respectively [5]. Tibiofemoral contact forces were computed via an elastic foundation model [5]. The one dof patellofemoral joint allowed for the patella to translate within a constrained path relative to the femur, subject to quadriceps and patellar ligament forces acting on either end. The reference strains and stiffness values of the ligaments were adapted from the literature [5,6], with a minimal amount of tuning to ensure the model replicated literature measures of passive motion, anterior-posterior stiffness, and axial rotational tibiofemoral stiffness.

The model was used to simulate knee motion and loading during gait. To do this, computed muscle control (CMC) [7] was used to determine muscle excitations that drive the model to track normal knee flexion throughout a gait cycle. Muscle redundancy was resolved by minimizing the sum of muscle volume-weighted squared activations. During the simulation, measured ground reaction forces were directly applied to the foot and 3D pelvis, hip, and ankle motion were prescribed to track measured trajectories. Note that CMC was only used to track knee flexion, such that the other five dof at the tibiofemoral joint and the patella translation were predicted (Fig. 1). These predictions were compared to a gait simulation conducted with a one dof kinematic knee [1], in which all secondary tibiofemoral kinematics and patellofemoral motion were constrained functions of knee flexion. The kinematic constraint functions were obtained by passively flexing the knee model.

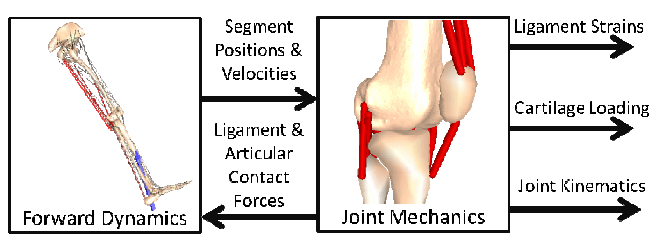

Figure 1. Forward dynamics and joint mechanics models were integrated simultaneously when simulating gait, providing predictions of muscle forces, ligament loads, cartilage contact, and secondary knee kinematics.

RESULTS

Predicted tibiofemoral kinematics differed from that assumed in a kinematic knee model but were generally consistent with direct bone pin measures during gait [2] (Fig. 2). Notably, internal tibia rotation occurs throughout much of stance and peaks near toe-off. Anterior tibia translation was greater during stance than assumed in the kinematic model, with the difference attributable to quadriceps activity during the load acceptance phase of gait. The patella also translated more superiorly in the co-simulation model due to compliance of the patellar ligament. A major advantage of the co-simulation model formulation is that it provides direct estimates of muscle, ligament, and joint contact forces. The shape of the simulated knee contact loading was consistent with measures obtained via instrumented implants [8]. ACL tension peaked during the load acceptance phase of gait, as suggested in [5].

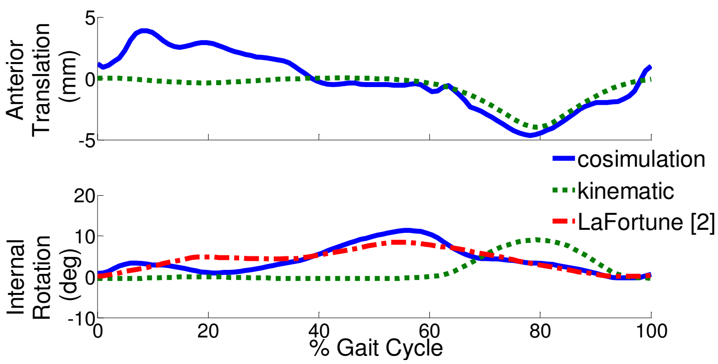

Figure 2: Predictions of secondary tibiofemoral kinematics during gait using cosimulation. Internal tibia rotation differs markedly from a kinematic model but is consistent with [2].

DISCUSSION

This study represents the first use of CMC to simulate movement using a joint that exhibits laxity. Previous formulations of CMC were only applicable for kinematics joints in which the multi-joint acceleration capacity of a muscle can be directly computed [7]. With a deformable joint, numerical integration is required to determine how individual muscles will induce motion as ligament and contact forces change over time. To overcome this challenge, we used short forward integrations (30ms) within CMC to assess muscle acceleration capacities, which were in turn used to determine excitations needed to track desired trajectories. We note that the full complement of musculoskeletal dynamics and joint mechanic equations are integrated together during the actual simulation.

It is noteworthy that the goal of tracking normal knee flexion directly predicts the secondary knee kinematics seen experimentally. Hence, secondary motions seem to arise naturally from the interaction of muscle, ligament, articular contact, and external forces acting on the systems. Such interactions likely become very important to consider when soft tissue restraints are compromised (e.g. ACL deficiency), resulting in the joint exhibiting even larger deviations from passive behavior. We note that this gait simulation only considered actuation at the knee. Future studies will include multi-joint muscle actuation to better understand the effect of inter-segmental dynamics and coordination on movement at the knee.

CONCLUSIONS

We conclude that a co-simulation model is important to account for load-dependent changes in knee kinematics during gait. This more rigorous formulation could be particularly important when investigating the effects of soft tissue injury, surgical reconstruction, and rehabilitation protocols on internal joint mechanics during movement.

REFERENCES

1.Arnold, E. M., et al. *Ann Biomed Eng* **38**, 269-279, 2010.
2.Lafortune, M. A., et al. *J Biomech* **25**, 347-357, 1992.
3.Andriacchi, T. P., et al. *Knee Mech: Update of Theor and Exp Anal* **38**, 293-298, 2005.
4.Schmitz, A., et al. *Proceedings of ASB,* Providence, RI, 2010.
5.Shelburne, K. B., et al. *J Orthop Research* **24**, 1983-1990, 2006.
6.Shin, C. S., et al. *J Biomech* **40**, 1145-1152, 2007.
7.Thelen, D. G., et al. *J Biomech* **39**, 1107-1115, 2006.
8.Fregly, B. J., et al. *J Orthop Research* 2011.

ACKNOWLEDGEMENTS

NSF Grant 0966535
NIH T32 AG000213 (P.I. Sanjay Asthana)

Age-related redistribution of hip and knee kinetics during out-and-back stepping

Brian W. Schulz

VA HSR&D/RR&D Center of Excellence, Maximizing Rehabilitation Outcomes, Tampa, FL, USA
email: Brian.Schulz@va.gov

INTRODUCTION

Maximum step length (MSL) is a quick clinical test that has been shown to predict fall risk [1], but the kinetics of this test are not yet fully understood. Previous work demonstrated that MSL is primarily correlated with knee and hip velocity, moment, and power, but older subjects reached their peak knee extensor moment at a different time than the young. However, the younger subjects also had greater MSL values, so this effect could have been due to changes in kinetics required to reach the longer step lengths attained by the young. To resolve this confound, younger and older subjects stepped out-and-back to target distances of 20-80% of their own height (ht) while kinematic and kinetic data were recorded. We hypothesized that knee extensor moment peaks would occur during knee extension (i.e. concentric phase) for step lengths <70%ht and during knee flexion (i.e. eccentric phase) for step lengths >70%ht in both younger and older adults.

METHODS

Unimpaired younger (N=14) and older (N=14) men and women (½ of each age group) stepped out-and-back 6 times (3 with each leg) to lines on the ground placed at 20-80%ht away from the starting position in increments of 10%. If the subject could step on or past the target line at least once with each leg, they progressed to the next step length. Full-body kinematic data were recorded as per previously validated methods [2]. Force plates under the stance foot and at all target locations were used to calculate stance and stepping hip and knee kinetics for the time interval between step out landing and return step liftoff (dual contact with feet apart) using Visual3D.

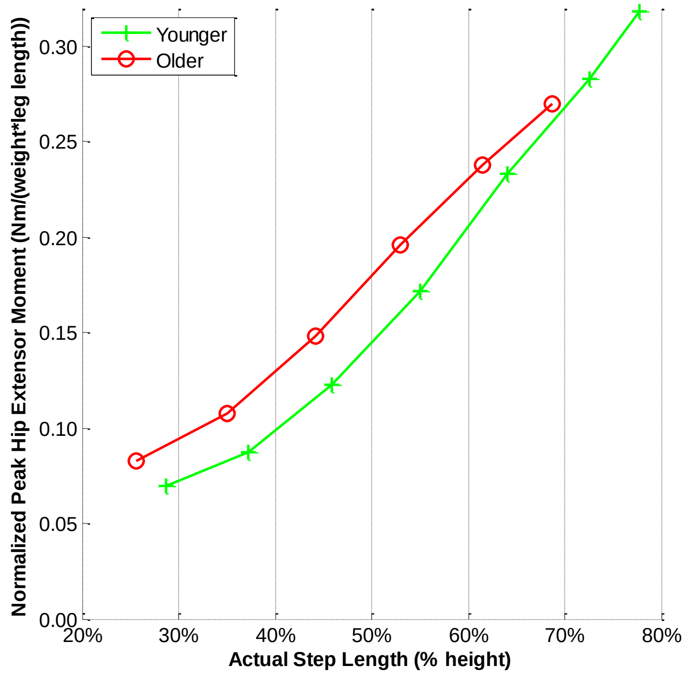

Figure 1: Peak stepping hip extensor moment by step length and age group.

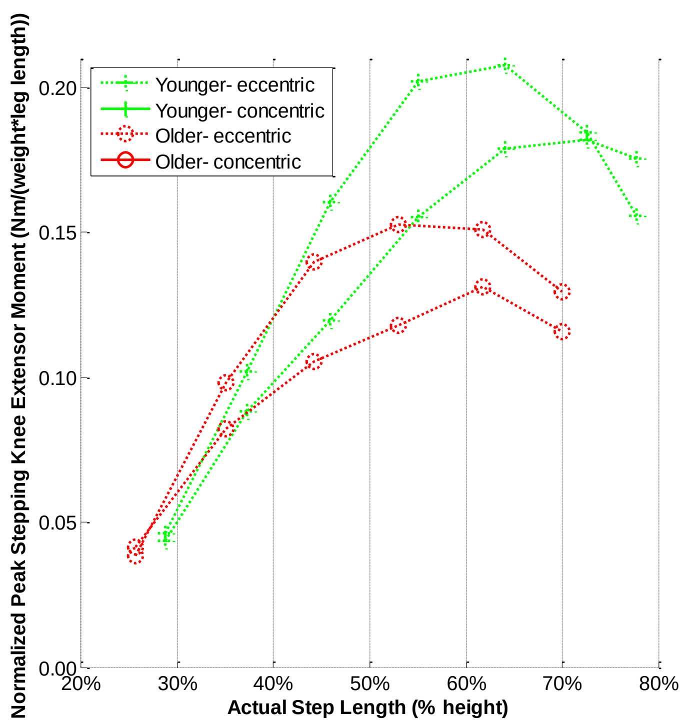

Figure 2: Peak stepping knee extensor moment by step length, age group, and knee rotation direction.

RESULTS AND DISCUSSION

All younger men and all but one younger woman stepped to 80%ht. Five older men stepped to 70%ht, one to 60%ht, and another to 50%ht. All older women successfully stepped only to 60%ht. Nearly every kinematic and kinetic variable increased significantly with step length. Men and Women were generally similar, with the few exceptions. Men used greater stepping hip extensor moments ($p=0.014$) and power generation ($p=0.027$) at all step lengths. Women kept their stepping hip more flexed during the stepping task, which was indicated by greater peak hip flexion and smaller peak extension angles.

Older subjects utilized greater stepping and stance hip extensor moments and powers ($p<0.006$), but less knee extensor moment and power ($p<0.0006$) than younger subjects to reach the same target step lengths (**Figs. 1-3**).

Peaks in knee extensor moments reached maximum values for steps of 50-60%ht, then decreased as step lengths increased further (**Fig. 2**). The rate of this decrease in peak knee extensor moment was greater during knee flexion (i.e. eccentric moment) than during extension (i.e. concentric moment). This tendency resulted in eccentric knee extensor moments exceeding concentric knee extensor moments for steps greater than 70%ht, which only the younger subjects were capable of attaining. This proximal redistribution of joint moments to improve performance at a given task is similar to what has been observed during gait, where older adults use hip extensors more and knee extensors and ankle plantarflexors less to walk at the same speed [3].

CONCLUSIONS

Unimpaired younger and older adults employ different kinetics to step out-and-back to similar lengths, with older subjects utilizing less extensor moment and power at the stepping knee and greater extensor moment and power at the stepping hip.

The hypothesis was partially supported in that peak eccentric knee moments did exceed peak concentric knee moments for steps beyond 70%ht, but we could not verify that this finding also applies to the older subjects because none were capable of stepping beyond 70%ht.

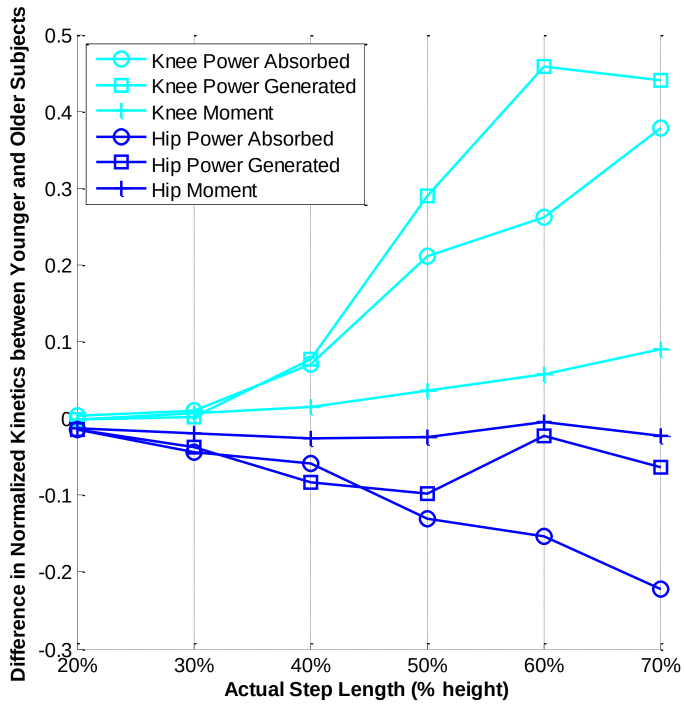

Figure 3: Difference in peak normalized hip and knee extensor kinetics between younger and older subjects (young value – old value) by target step length. Units for moments are Nm/(height*weight) and units for powers are W/(height*weight).

REFERENCES

1. Lindemann U, et al. *Aging Clin Exp Res **20**(5) 394-399, 2008*
2. Schulz BW, Kimmel W. *Clin Biomech* **25**(7) 687-692, 2010.
3. DeVita P, Hortobagyi T. *J Appl Physiol*, **88**(5) 1804-1811, 2000.

ACKNOWLEDGEMENTS

This work was supported by a VA RR&D Career Development Award (E4941W). I thank Wendy Kimmel and Pradeep Ambati for their assistance with data collection and Scott Barnett for statistical support. The contents of this manuscript are those of the authors alone and do not represent the views of the Department of Veterans Affairs or the United States Government.

A Framework for Visualizing Biomechanical Movement for Designers within 3D Modeling Programs

[1]Mathew Schwartz and [1]Janani Viswanathan

[1]University of Michigan, Ann Arbor, MI, USA

INTRODUCTION

In the past twenty years the power of the computer has drastically changed the ability to visualize information. Architects and designers have adopted this technology for many aspects of their workflow, however, there is still much to be done. The only diagrams architects are legally bound to are those of the ADA Standards [1]. These diagrams are outdated sectional drawings of how people move within space. Current research similar to this give simplified iso-surface representations of reach envelopes that may be useful for the engineering profession [2], but are of little use towards a user understanding the movement. The purpose of this research is to project a methodology for advanced visualization and integration of biomechanical movements within computer aided design tools (Figure 1).

METHODS

The method for integrating biomechanical visualizations is split into two sections. One avenue of the methodology is with motion capture technology and the other is with a forward kinematic algorithm. A motion capture session recorded two actions, one of an arm envelope and another of a person sitting in a chair. The reach envelope was recorded in order to compare the forward kinematic model as well as the difference in computational costs associated with mesh visualizations. The recording of a person sitting in a chair was used as a more complex movement for visualization. For the motion captured movements a 'snapshot' of the human form was recorded in different resolutions in order to represent time in a single frame. A forward kinematic algorithm was applied to a premade skeleton in the software Autodesk MAYA. The algorithm created a point cloud of a reach envelope that was visually compared by an overlay with the motion capture data. The forward kinematic algorithm used a cylindrical reference to prevent plotting of a point within a persons body. The algorithm used a user given variable to adjust for the maximum joint angles.

RESULTS AND DISCUSSION

The two methods of creating the human movement are presented as point clouds and mesh surfaces. These methods represent a movement occurring over time in a single form. The findings show the two types of visualizations aid in design differently depending on the resolution of the movement. If a high resolution is used, the movement becomes a single envelope describing the domain of the movement whereas a low resolution gives a visual understanding as to how the human interacted with the chair. The kinematic algorithm was adjusted to the motion capture subjects' joint extents. The resulting point cloud accurately described the reach envelope (Figure 2). The efficacy of the visualization is checked against the computational load within the program. For this study the program Autodesk 3D Studio Max was used to compare the frames per second (FPS) of the viewing window of each type of visualization. The goal was to maintain a FPS above 15 (half the rate of video). While the mesh surface did extremely well, with an FPS of 155, the point cloud ranged from 4 FPS to 90FPS, depending on the way in which the points were represented (Figure 3).

CONCLUSIONS

These findings indicate the most feasible method for visualizing biomechanical movements in an understandable way is through mesh surfaces. The mesh surfaces described are unique to reach envelope visualization in that instead of a single iso-surface [3], the entire human form is represented. This method of visualization allows for a more thorough understanding of the biomechanics behind a reach envelope. The use of a kinematic model instead of motion capture data would still require a human manikin to create these visualizations. This combination proves extremely useful, as the user is able to clearly compare the result of the kinematic model to what they know about biomechanics. This can also further enhance the benefit of a kinematic model with its ability to reconfigure.

REFERENCES

1. 2010 *ADA Standards for Accessible Design*, Title II (28 CFR part 35) and Title III (28 CFR part 36). Department of Justice
2. Blanchonette P, 2010. *Jack Human Modelling Tool: A Review*. Air Operations Division, DSTO Defence Science and Technology Organisation, Australian Government Department of Defence, Australia.
3. Yang, J. (J. & Abdel-Malek, K. *Human reach envelope and zone differentiation for ergonomic design Hum. Factors Man*., Wiley Subscription Services, Inc., A Wiley Company, 2009, Vol. **19**(1), pp. 15-34

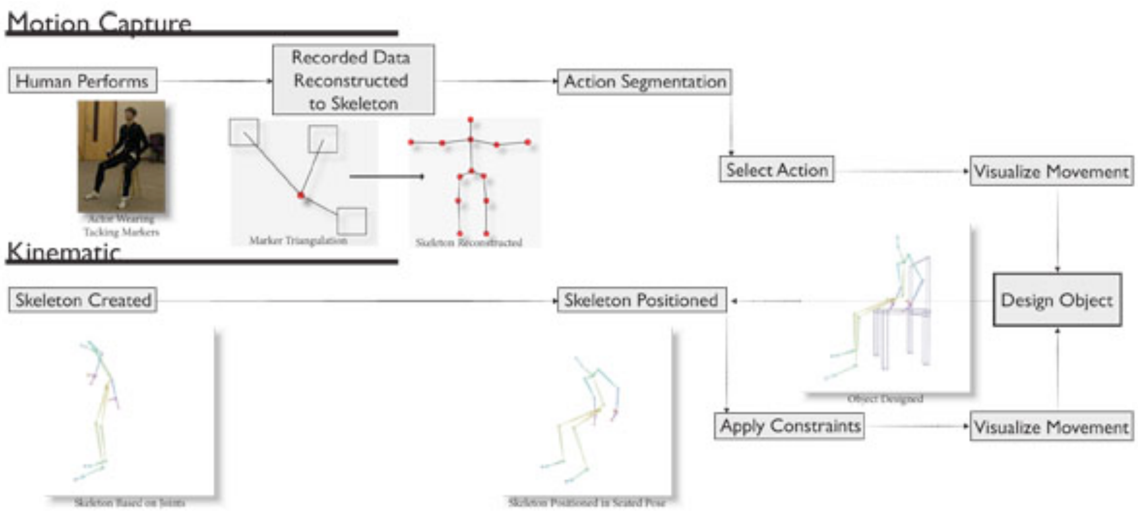

Figure 1: Motion Capture VS Kinematic Workflow for Designers

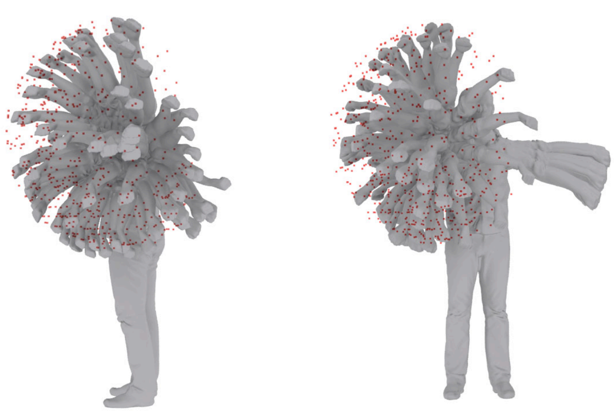

Figure 2: Overlay Comparison of motion capture mesh and kinematic point cloud

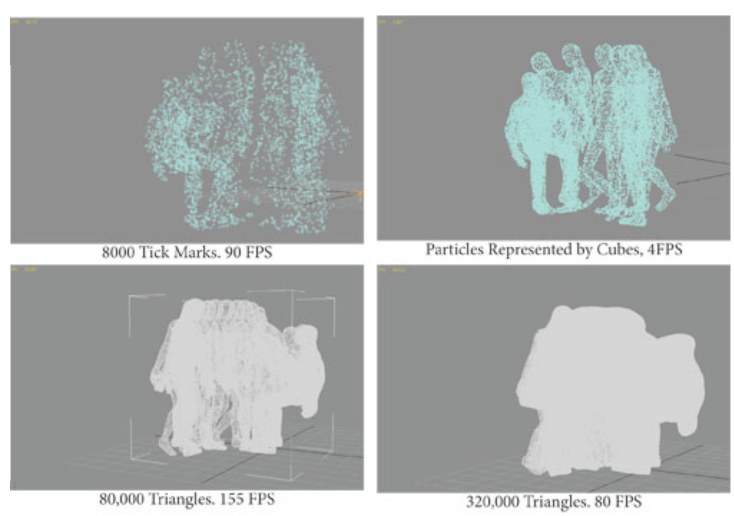

Figure 3: Frames Per Second (FPS) For varying resolutions of mesh and point clouds

THE EFFECT OF KNEE PAIN AND EFFUSION ON VERTICAL GROUND REACTION FORCE DURING WALKING

Matthew K. Seeley, Jihong Park, Iain Hunter, Devin Francom, Ben R. Black, and J. Ty Hopkins

Brigham Young University, Provo, UT, USA
email: matt_seeley@byu.edu; web: biomech.byu.edu

INTRODUCTION

Knee injuries are common and often result in quadriceps weakness [1]. This weakness likely alters movement mechanics, including ground reaction force and knee joint loading patterns. If allowed to persist, these mechanical alterations may contribute to knee joint degeneration. Researchers have reported that knee pain [2] and knee joint effusion [3] are related to knee injury and contribute to quadriceps weakness; however, the additive effect of knee pain and effusion on arthrogenic muscle inhibition and corresponding mechanical alterations is unclear. Independent effects of knee pain and effusion on movement mechanics have been studied, yet, pain or effusion rarely occur alone in knee injury. The purpose of this study was to evaluate the influence of anterior knee pain, knee joint effusion, and a combination of both of these stimuli on walking vertical ground reaction force (VGRF). Because the quadriceps contribute to VGRF during walking, we hypothesized that: (1) knee pain and effusion would independently decrease walking VGRF, and (2) knee pain and effusion, in combination, would further decrease walking VGRF, relative to pain and effusion alone.

METHODS

The independent variables were session (pain, effusion, pain and effusion, and control) and time (Times 1-3). The dependent variables were perceived pain, walking VGRF, and walking speed. Nineteen healthy subjects (10 males and 9 females; age = 22 ± 2 yrs; height: 1.73 ± 0.10 m; mass: 73 ± 16 kg) provided informed consent form and then participated.

Subjects completed four data collection sessions one week apart: (1) pain, (2) effusion, (3) pain and effusion, and (4) control. For each session, subjects performed nine walking trials at a preferred speed: three trials at Time 1, Time 2, and Time 3. Subjects performed landing trials after the walking trials; those results are not reported here. For each walking trial, subjects contacted a separate force platform with each foot. For the pain session, subjects first completed the Time 1 trials. Next, we injected 1 ml of hypertonic (5.0% NaCl) saline into the infrapatellar fat pad. Subjects then completed the Time 2 walking trials, rested for 20 minutes, and completed the Time 3 trials. The effusion session was identical, except that prior to the Time 2 trials, we injected sterile lidocaine for anesthetic purposes and 50 ml of isotonic (0.9% NaCl) saline into the superolateral knee joint. For the pain and effusion session, prior to the Time 2 trials, three injections were performed in the following order: lidocaine, 0.9% isotonic saline, and 5% hypertonic saline. All injections were performed in the right leg. No injections were performed for the control session. Two ANOVAs were used to compare (1) perceived pain, measured every two minutes using a 10-cm visual analog scale, and (2) walking speed between sessions and times ($\alpha = 0.05$). A functional analysis was used to compare VGRF between sessions and times ($\alpha = 0.05$); we used this analysis to compare VGRF as cubic functions rather than discrete values.

RESULTS AND DISCUSSION

Significant session × time interactions existed for each dependent variable. Mean perceived pain was greater for Time 2 than for Times 1 and 3, for each session except the control session (Figure 1). For Time 2, pain was greater than zero pain for 10, 6, and 16 min for the pain, effusion, and pain and effusion session, respectively. These pain levels were expected, although we were somewhat surprised by the elevated pain levels for the effusion session; we speculate that slight nociceptor

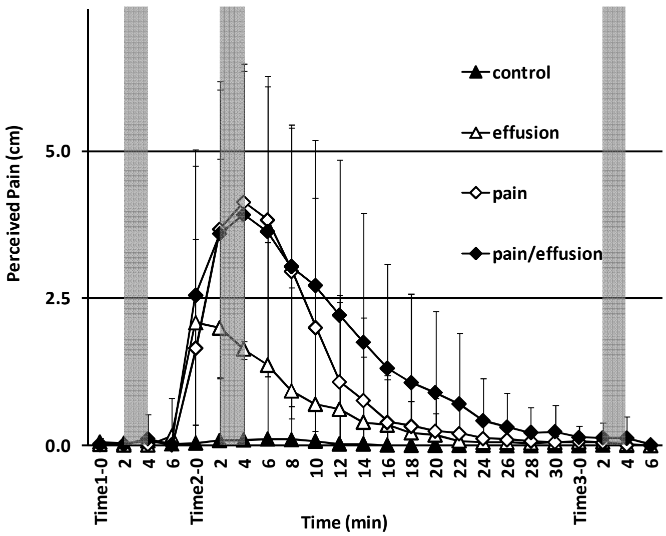

Figure 1: Perceived pain for all sessions. Time of walking trials is indicated by the shaded bars.

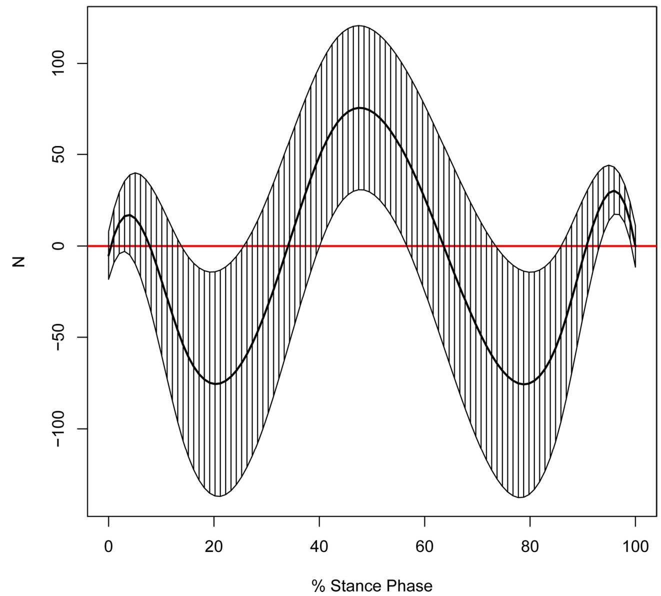

Figure 2: Functional analysis of VGRF (y axis) for the pain and effusion session. Time 2 VGRF was less than Time 1 VGRF at 20% and 80% of stance, but greater than Time 1 VGRF at 50% of stance. 95% confidence intervals are indicated by the shaded band.

stimulation occurred during this session and that this may have partially confounded the VGRF results. Contrary to our hypotheses, the only session that exhibited between-time differences for walking VGRF was the pain and effusion session. For this session only, walking VGRF for the involved leg was affected by time. For Time 2, VGRF was less at 20% and 80% of stance (impact and push-off peaks) relative to Times 1 and 3; however, VGRF was greater at midstance (Figure 2). We observed the opposite for the uninvolved leg for the same session: Time 2 VGRF was greater at 20 and 80% of stance than for Times 1 and 3, but were less at midstance. We are unsure why the pain and effusion sessions did not also significantly affect VGRF. Finally, although walking speed exhibited session × time interactions (Table 1), the observed VGRF differences probably should not be completely attributed to different walking speeds.

This is the first attempt to evaluate the independent effects of anterior knee pain, knee joint effusion, and the combined effects of these stimuli on walking mechanics. These findings show that simultaneous anterior knee pain and knee joint effusion alter walking VGRF. This is consistent with the idea that injury factors, such as pain and edema, can result in additive mechanical alterations to movement. We speculate that the VGRF alterations reported in this study cause abnormal knee joint loading patterns throughout stance and, under chronic circumstances, could lead to knee joint degeneration. Additional research should be conducted to evaluate this idea.

REFERENCES

1. Suter E, et al. *J App Biomech* **14**, 360-373, 1998.
2. Hodges P, et al. *Arthritis Rheum* **61**, 70-71, 2009.
3. Young A, et al. *Clin Orthop Relat Res* **219**, 21-27, 1998.

Table 1: Mean walking speeds for each session and time. Time 2 speed was significantly decreased, relative to Times 1 and 3, for all sessions except the control session.

Time	control	effusion	pain	pain and effusion
Time 1	1.32 (0.08)	1.35 (0.10)	1.33 (0.12)	1.34 (0.10)
Time 2	1.34 (0.09)	1.29 (0.10)	1.33 (0.16)	1.22 (0.13)
Time 3	1.34 (0.07)	1.31 (0.08)	1.30 (0.08)	1.29 (0.09)

A SCAPULOTHORACIC JOINT MODEL FOR FAST AND ACCURATE SIMULATIONS OF UPPER-EXTREMITY MOTION

[1]Ajay Seth, [2,3]Ricardo Matias, [3]António Veloso, [1]Scott Delp
[1]Stanford University, Stanford, CA, USA
[2]Polytechnic Institute of Setubal, Setúbal, Portugal
[3]Technical University of Lisbon, CIPER-FCT. Lisbon, Portugal
email: aseth@stanford.edu, web: http://www.stanford.edu/group/nmbl

INTRODUCTION

The human shoulder is a complex mechanism that provides maneuverability and support for performing a wide range of activities [1]. When observing the behavior of the shoulder, abnormal motion of the scapula is often indicative of pathology [2]. Unfortunately, the kinematics of the scapula are difficult to measure. Computer models of the shoulder may be combined with experimental measurements of shoulder motions to better understand scapular kinematics. Because irregularities in scapular movement often arise from abnormal forces in muscles and surrounding tissues [3] a model of the shoulder will be more useful if it predicts changes in scapula kinematics in response to muscle forces. Here, we present a biomechanical model of the scapulothoracic joint based on a novel multibody formulation [4] to enable fast and accurate kinematic analyses and dynamic simulations of the shoulder. The purpose of this study was to: 1) test the accuracy of scapula kinematics computed with the model and 2) verify that the model reduces the effects of measurement errors when evaluating scapula kinematics from motion capture data.

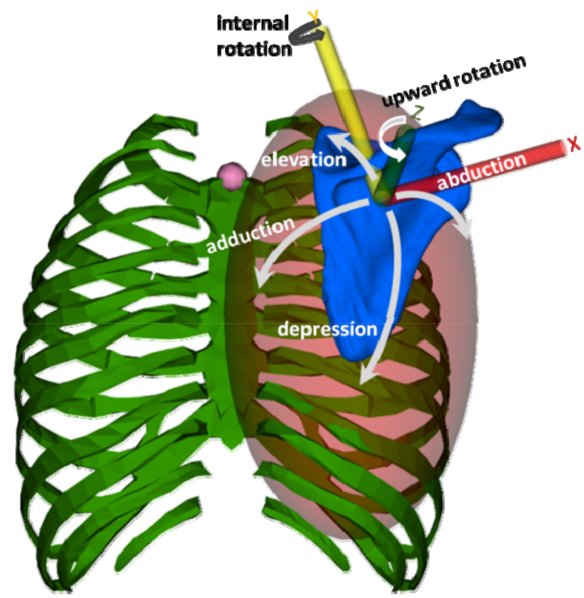

Figure 1: Four coordinates of the scapulothoracic joint. *Depression-elevation* and *adduction-abduction*, specify the location of the scapula (blue) on the thoracic surface (red ellipsoid) fixed to the thorax body (green); *upward-downward rotation*, about the scapula axis (Z) normal to the surface, and *internal rotation*, about the scapula's vertical (Y) axis, specify the orientation of the scapula with respect to the thorax at the point of contact. Joint frame (X,Y,Z) affixed to the scapula.

METHODS

The scapulothoracic joint model includes coupled translation and rotation of the scapula on the surface of the thorax [5] and is parameterized by four coordinates (Fig. 1). A mobilizer formulation [4] captures the biomechanically permissible kinematics of the scapula. The scapulothoracic joint model provides the reaction loads experienced by the scapula when acted upon by forces including inertial, gravity, muscle, and external forces. The scapulothoracic joint is composed of two mobilizers: an ellipsoid mobilizer and a pin mobilizer. The ellipsoid mobilizer enables the translation and rotation of the scapula on the thoracic surface and the pin mobilizer permits internal rotation about the scapula's Y-axis (Fig. 1). The ellipsoid surface reaction forces are not computed in order to solve the equations of motion; therefore, the low mass of the scapula does not require numerical methods for constraint stabilization during dynamical simulations. Instead the forces required to keep the scapula on the thorax (ellipsoid) surface can be obtained as joint reaction forces from a joint reactions analysis. The scapulothoracic joint was implemented and included as part of a multibody (thorax, scapula, humerus) model of the upper-extremity in OpenSim [6, 4].

We tested the ability of the model to reconstruct the kinematics of the scapula measured via bone-pins during flexion, abduction and rotation shoulder tasks [7]. We also assessed the effects of soft-tissue errors and marker noise as measured by deviation of markers on the skin from associated landmarks on the scapula [8]. From the mean of the measured peak skin marker errors and their standard deviation, we added Gaussian noise with means and standard deviations corresponding to the average and standard deviation of the measured peak errors. We added noise with 25, 50, 75, and 100% of the mean and standard deviation of the measured errors [8] to represent a range of noise levels. Noise was added as offsets in marker locations with the direction of the offset selected at random. 50 trials of synthetic marker data were generated for each noise level. Euler sequences were computed directly from the noisy marker data and from model markers affixed to the scapula after performing an inverse kinematics analysis. We analyzed each task with added noise (50 trials) and for each of the four noise levels.

RESULTS AND DISCUSSION

Bone-pin markers and model markers had a root-mean-squared error (RMSE) on average below 2mm (Table 1), which is small considering that the spatial resolution of the motion-capture system is approximately 1mm [7]. Inverse kinematics analyses for 600 trials were performed in OpenSim [6] and had an average run-time faster than 120 frames/s. The Euler angles describing the spatial orientation of the scapula computed using the scapulothoracic joint showed half to a third of the variability of those angles calculated directly from noisy markers (e.g. see Fig. 2) across all trials with greater relative improvement (i.e. 1/3 the variability) at higher noise levels. The mechanics imposed by the scapulothoracic joint reduce the effects of measurement errors and noise in marker locations compared to Euler angles evaluated directly from noisy markers (Fig. 2).

Table 1: Marker errors between model kinematics and bone-pin experiments (RMSE in mm). Marker definitions are according to ISB recommendations [9].

Activity	**Scapula**			**Thorax**			**Humerus**			**Mean**
(Markers)	**AA**	**AI**	**TS**	**IJ**	**C7**	**T8**	**EL**	**GH**	**EM**	(all)
Flexion	2.2	3.8	3.9	0.9	0.6	0.6	1.1	1.1	1.2	1.7
Abduction	3.0	2.6	3.3	0.9	0.6	0.8	1.7	1.7	1.7	1.8
Int./Ext. rot	1.8	1.7	3.2	1.6	0.9	0.7	0.6	1.4	0.4	1.4

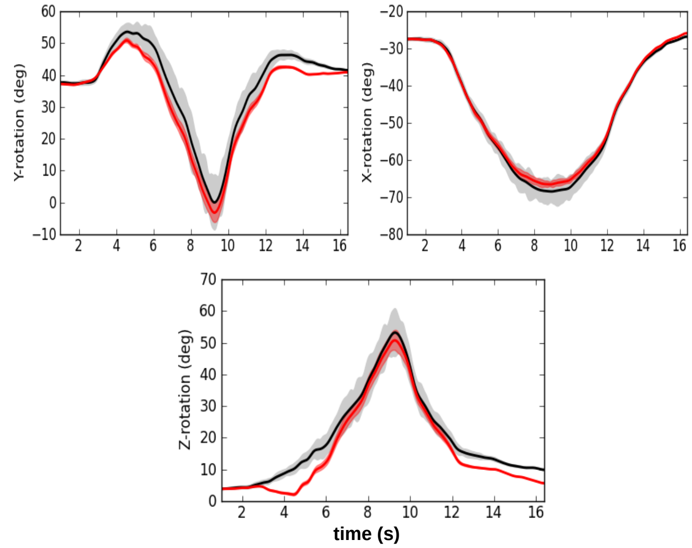

Figure 2: Body-fixed Euler-angles for scapula spatial orientation during flexion from model-based (red) and direct marker-based evaluations (black) for the 100% noise level. Mean in bold lines and ±1SD as shaded.

The scapulothoracic joint coordinates are intuitive to interpret and fully describe the kinematics of the scapula including the elevation and abduction translations of the scapula on the thorax surface. This is critical for describing pathological movements of the scapula. The application of the scapulothoracic joint also produces more reliable scapula kinematics in the presence of measurement errors and enables real-time inverse-kinematics analyses. This novel formulation of the scapulothoracic joint provides the foundation for developing fast and accurate dynamical simulations of the upper-extremity.

REFERENCES

1. Veeger et al. *J Biomech* **40**, 2119-29, 2007.
2. Struyf et al. *Scand J Med Sci Sports* **21**, 352–8, 2011.
3. Ludewig et al. *J Orthop Sports Phys Ther* **39**, 90-104, 2009a.
4. Seth et al. *Nonlinear Dynamics* **62**, 291–303, 2010.
5. van der Helm. *J Biomech* **27**, 551-69, 1994
6. Delp et al. *IEEE Trans Biomed Eng* **37**, 757-67, 2007.
7. Ludewig et al. *J Bone Joint Surg* **91**, 378-89, 2009b.
8. Matsui et al. *J Orthop Sci* **11**,180-4, 2006.
9. Wu et al. *J Biomech* **38**, 981-92, 2005.

ACKNOWLEDGEMENTS

We thank Paula Ludewig for the bone-pin data. Work supported by NIH grants U54 GM072970; R24 HD065690 and Portuguese STF grants FCT-PTDC/DES/103178/2008; PhD SFRH/BD/41846/2007.

A LABORATORY METHOD FOR EVALUATING DYNAMIC PROPERTIES OF EQUINE RACETRACK SURFACES

[1]Jacob J. Setterbo, [1]Thuy-Anh Chau, [1]Patricia B. Fyhrie, Mont Hubbard, Shrini K. Upadhyaya and [1]Susan M. Stover

[1]J D Wheat Veterinary Orthopedic Research Laboratory, University of California, Davis, CA, USA
[2]Department of Mechanical and Aerospace Engineering, University of California, Davis, CA, USA
[3]Department of Biological and Agricultural Engineering, University of California, Davis, CA, USA
email: smstover@ucdavis.edu, web: http://www.vetmed.ucdavis.edu/vorl

INTRODUCTION

Racetrack surface is a risk factor for racehorse injuries and fatalities. Dynamic surface properties are useful for understanding the relationships between surfaces and injury. A laboratory method would allow evaluation of surface materials in a controlled environment. The objective was to validate reconstruction of race surfaces in the laboratory by comparing in situ and laboratory measurements of dynamic surface properties.

METHODS

Using a track-testing device (TTD) designed to simulate equine hoof impact [1], impact tests were conducted on a dirt racetrack and a synthetic racetrack, and after reconstruction of the harvested surface materials in the laboratory. In situ compaction measurements were used to guide surface reconstruction in the laboratory. Dynamic surface properties were compared between in situ and laboratory settings using analysis of variance. Additionally, the relationships between racetrack TTD and compaction measurements were analyzed using stepwise multiple linear regression.

RESULTS AND DISCUSSION

Most racetrack-laboratory dynamic surface property differences were ≤10% of the respective racetrack averages, and these differences were often small relative to differences between dirt and synthetic surfaces. Compaction measurements correlated more strongly with TTD measurements on the synthetic surface than on the dirt surface, and compaction decelerations negatively correlated with TTD forces on the dirt surface.

Reconstruction of equine racetrack surfaces, guided by in situ compaction measurements, in the laboratory yielded impact data similar to that acquired in situ. The negative correlation between TTD and compaction measurements suggests lighter impact devices may not be appropriate for assessing dynamic surface properties relevant to the racehorse. The dynamic impact properties of race surfaces, and thus the effects of factors affecting surface behavior, can be evaluated on a small scale in the laboratory under controlled conditions.

CONCLUSIONS

The dynamic impact properties of equine race surfaces, and thus the effects of factors affecting surface behavior, can be evaluated on a small scale in the laboratory under controlled conditions.

REFERENCES

1. Setterbo JJ, et al. *Sports Engineering*, In Press 2011

ACKNOWLEDGEMENTS

The authors would like to thank Neil Willits, PhD for statistical assistance, and Golden Gate Fields and Pleasanton Racetrack for their cooperation.

DIFFERENCES IN RUNNING AND WALKING GAIT KINEMATICS DURING EARTH AND SIMULATED MARS AND LUNAR GRAVITATIONAL ENVIRONMENTS: PRELIMINARY INVESTIGATION

Robert Shapiro, Tommy Cunningham, Brian Wallace, Jaclyn Norberg, Megan Phillips, Megan Miller

University of Kentucky, Lexington, KY 40506
email: rshap01@uky.edu, web: http://www.coe.uky.edu/biodynamics/

INTRODUCTION

As part of a larger study (Kostas et al., 2011) to examine human responses to reduced gravity we examined alterations in walking and running gait kinematics. To simulate effects of Mars (40% g) and Moon (20% g) gravities we used a specialized treadmill that simulated hypogravity with lower body positive pressure (Alter-G treadmill, P200, Alter-G, Freemont, CA). Gait kinematics were compared to performance under 1g on a Bertec split belt treadmill (TM-09-P, Bertec, Columbus, OH). The purpose of the study was to compare basic gait parameters across gravity conditions and also compare the effect of running and walking in the Alter-G at 1 g with a traditional treadmill.

METHODS

Methods
Ten healthy subjects volunteered and provided informed consent prior to participation in this IRB approved investigation (height=1.74±0.12m, mass=76±15kg, age=25.8±4.4yrs). Subjects were provided running shoes, wore tight fitting clothing and were fitted with a pair of neoprene shorts which enabled them to be zipped into the Alter-G treadmill A modified Cleveland Clinic marker set using 3 and 4 marker rigid clusters for upper and lower extremities, with a total of 70 markers was applied strategically on each subject using double sided toupee tape. The markers were applied after the subject placed the neoprene shorts on to avoid moving any of the reflective markers.

For the purposes of this study two calibrated filming volumes were established using standard mocap procedures. A Bertec split belt treadmill with a force platform under each belt and the Alter-G treadmill were surrounded by 8 and 10 Eagle cameras (Motion Analysis, Santa Rosa, CA) respectively. Subjects initially stood on the Bertec and assumed a “t-pose” while the static anatomical calibration was collected for 3 seconds. Subjects then were allowed a warm-up on the Bertec treadmill. Following warm-up the subjects walked for approximately 1 minute at their self-selected walking pace (range 1.14-1.57m/s) and then ran at 3m/s for approximately another minute. A minimum of three ten second trials were collected for each condition. Subjects then entered the Alter-G treadmill and the neoprene shorts were zipped to the Alter-G canopy to create the seal needed to enable production of lower body positive pressure. Subjects walked at their selected pace and then ran at 3m/s at 100, 40 and 20% of body weight. The body weight condition was randomly assigned within the walk and run. Three ten second motion capture trials were collected for each condition. Video data were collected at 120 hz. The Bertec force platforms were synchronously sampled at 1200 Hz.

Data were tracked using Cortex software (v6.7, Motion Analysis Corp, Santa Rosa, Ca). Three-dimensional coordinate data were processed in Visual 3D (C-Motion Corp, Germantown, Md). Joint angles for the ankles and knees were determined using a standard Cardan angle rotation. Foot strike was determined by calculating the peak acceleration of the heel marker (5^{th} metatarsal head marker for midfoot strikers) in the direction opposite of foot progression. Take-off was determined by the vertical motion of the toe marker. The ability to determine these time points was verified by checking the predicited events against the force data from the Bertec treadmill. The determination of events was done prior to smoothing the data with a fourth order Butterworth low pass filter. The cut-off for motion data was 6

Hz. Time series data were normalized to single strides and reported as 101 data points per stride. Multiple strides were averaged for each condition for each subject. Events were used to determine stride time. Stride length was calculated as the product of stride time and treadmill velocity. Timing variables were calculated with a custom Matlab program (Mathworks, Natick, MA). Repeated measures ANOVA (EXCEL, Microsoft Corp, Redmond, WA) was used to compare differences across conditions for the following sagittal plane angle variables: ankle angle at impact, peak dorsiflexion, and peak plantar flexion at take-off; knee angle at foot strike, peak knee flexion during stance, knee angle at take-off and maximum flexion during swing. The Scheffé test used for post hoc analyses.(p=0.05). Only right leg joint kinematics are reported in this abstract.

RESULTS AND DISCUSSION

Stride length and rates (Table 1) were not significantly different when comparing the 1g conditions on both treadmills. For the 0.2g condition stride length was significantly longer that either 1g condition and stride rate was significantly lower than the 1g conditions. No differences were observed for single leg stance times during running which indicates that flight time for the 0.2g should be greater than the 1g conditions.
The sagittal plane ankle angle (Table 2) demonstrated significantly less dorsiflexion during stance in both hypogravity conditions during walking and running. At foot strike the only difference that was observed was for the 0.2g running condition indicating the foot landed at a much greater plantar flexion angle. Maximum plantar flexion tended to be greater in the hypogravity conditions for running and walking.

Knee angle data during walking was in significantly greater flexion at foot strike and in swing, just prior to foot strike. In running, an opposite pattern prior to foot strike was observed with the leg in significantly greater extension just prior foot strike. Since no difference in the knee angle at foot strike during running were observed this would indicate a rapid flexion motion to get the foot back to the ground during the 0.2g run. During swing the knee was observed to be in decreased flexion during walking and running but only the walking data were significantly different from the 1g conditions.

These preliminary findings of different lower leg kinematics particularly for the lunar gravity simulation may impact a variety of biomechanical and physiological parameters are need further investigation

REFERENCES

1. Kostas V, et al. *MSSE*, **43**, 823, 2011.

Table 1: Comparison of Stride Rates and Stride Lengths among all conditions.(AG=Alter-G treadmill)

	Walking (self-selected speed)				**Running (3m/s)**			
	1g AG	**0.4g AG**	**0.2g AG**	**1g Bertec**	**1g AG**	**0.4g AG**	**0.2g AG**	**1g Bertec**
Stride length (m)	1.39	1.46	1.55*	1.43	2.20	2.60	2.79*	2.16
Stride rate (st/s)	1.00	0.96	0.90*	0.99	1.39	1.17*	1.11*	1.39

*significantly different from both 1g conditions, p<0.05

Table 2: Sagittal plane ankle angle (degrees, positive direction is dorsiflexion, AG=Alter-G, Ber=Bertec).

	Angle at foot strike				**Max dorsiflexion in stance**				**Max plantar flexion**			
Motion	**1g AG**	**0.4AG**	**0.2AG**	**1g Ber**	**1g AG**	**0.4AG**	**0.2AG**	**1g Ber**	**1g AG**	**0.4AG**	**0.2AG**	**1g Ber**
Walk	-9.8	-10.9	-10.0	-9.8	2.0	-5.1*	-4.6*	0.2	-27.3	-34.9*	-36.4*	-26.3
Run	-5.6	-10.2	-15.5*	-5.8	10.9	2.7*	-2.6**	12.7	-36.4	-38.0	39.4[a]	-34.1

*significantly different from both 1g conditions, p<0.05
**significantly different from both 1g conditions and 0.4g condition, p<0.05
[a]significantly different from the 1g Bertec, p<0.05

Muscle activation strategy in the sand-swimming sandfish lizard (*Scincus scincus*)

[1]Sarah S. Sharpe*, and [1]Daniel I. Goldman

[1]Georgia Institute of Technology, Atlanta, GA, USA
*email: ssteinmetz3@gatech.edu, web: http://www.crablab.gatech.edu/

INTRODUCTION

Animal locomotion results from the complex interactions among the nervous system, internal biomechanics, and the surrounding physical environment. For desert dwelling animals that live on and within granular media (GM) [1], the neuromechanics of locomotion is relatively unexplored. Recent work on the sandfish (Fig. 1), a lizard native to the Sahara desert, reveals that it moves above surface using a diagonal gait with little body bending, but swims subsurface through sand using large amplitude traveling waves of body undulation [2]. Models of sand-swimming predict that a particular combination of wave amplitude and wavelength will maximize speed and minimize cost of transport [3], and experiments suggest that the sandfish targets these kinematics [2]. In GM, external resistance dominates while effects of body inertia are small. Thus, we hypothesize that the sandfish modulates neural strategy in response to the resistance force of the surrounding media to maintain the desired waveform.

Based on the observed kinematics, we predict little axial muscle activation during above-surface walking and a traveling wave of muscle activation during subsurface sand-swimming. Resistance force in GM is independent of speed (when speed approx. < 50 cm/s) due to the dominance of frictional forces between particles. However, external resistive force increases with depth beneath the surface and GM compaction. Therefore, during subsurface movement, we expect the muscle activity will scale with the depth of the animal and GM compaction, but not with speed.

To determine the neural strategy used by the sandfish during locomotion, we utilize high speed video and x-ray imaging with synchronized electromyogram (EMG) recordings of axial musculature. We investigate the effect of external forces and speed by examining EMG intensity at varying compaction, depths and swimming speeds.

Figure 1: Sandfish lizard on 0.3 mm glass beads.

METHODS

The granular substrate was prepared into repeatable compaction states using an air fluidized bed [2]. Compaction was characterized by the volume fraction, ϕ, defined as the ratio between the volume of the GM to the volume of its occupied space. We prepared the media into either a loosely (LP, $\phi \approx 0.58$) or closely (CP, $\phi \approx 0.63$) packed state. The granular substrate consisted of spherical glass particles that were similar in size (diameter = 0.27 ± 0.04 mm) and density (ρ = 2.5 g/cm^3) to particles found in sand dunes.

Sandfish were implanted with five bipolar hook electrodes in the epaxial musculature located approximately 4 mm away from the midline on one side of the body. These electrodes were implanted at the longitudinal position of 0.3, 0.5, 0.7, 0.9, and 1.1 of the snout-to-vent length (SVL), where 0 indicates snout position and 1 indicates vent. EMG recordings were amplified and filtered before data acquisition. For each detected EMG burst we quantified the EMG intensity I, defined as the ratio of the rectified integrated area of the EMG burst to the EMG duration. We calculated a best fit line between I and depth for each electrode. To compare across animals and electrodes we determined I_{rel} by normalizing I by the linear fit intensity at a consistent depth.

The sandfish were initially placed in a holding area separated from the GM by a gate. After the gate was lifted, sandfish ran onto and buried within the substrate. Above surface visible light video and subsurface x-ray video were recorded at 250 frames s^{-1} to capture dorsal kinematics. A separate side-view analysis with x-ray only was used to characterize angle of descent, θ_d.

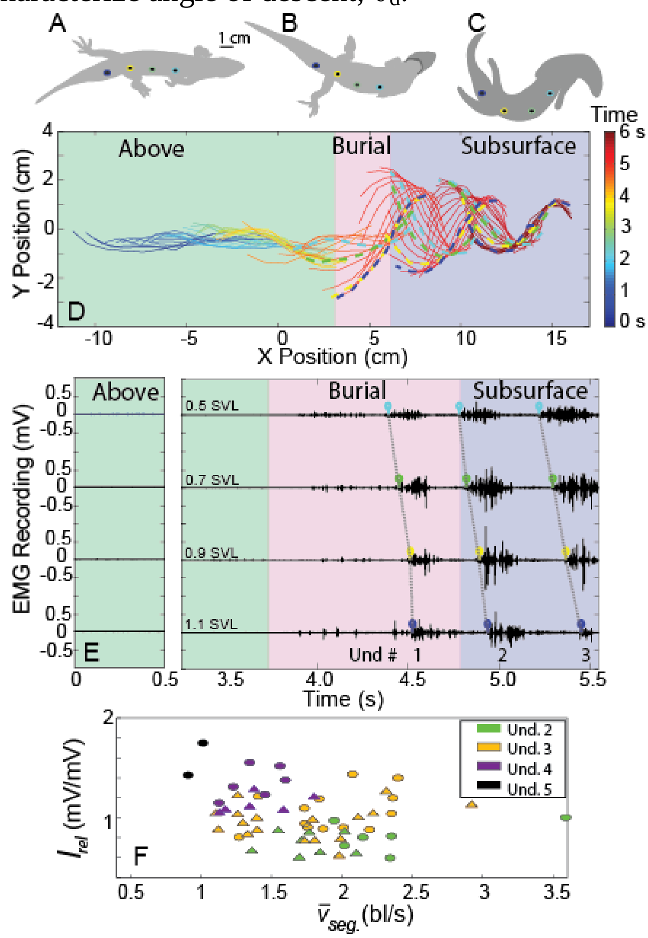

Figure 2: Sandfish kinematics and muscle activation. A sketch of the animal during (A) above surface walking, (B) burial and, (C) subsurface swimming. (D) The midline trajectories during the run and (E) the corresponding EMG. (F) The relative EMG intensity vs. average speeds. Greater undulation correspond to increased depth. Triangles are LP runs and circles are CP runs.

RESULTS AND DISCUSSION

On hard ground the sandfish utilized its limbs in a diagonal gait and little body bending (Fig 2A, D) was observed. During this movement no muscle activity was detected (Fig. 2E, green region). During subsurface sand-swimming, sandfish propagated an anterior-to-posterior traveling wave of axial bending down its body to move forward (Fig 2C, D), which corresponded to a wave of muscle activation (Fig.2 E). Sandfish descended into the media along a nearly linear trajectory with $\theta_d = 18.9 \pm 4.3°$ (N = 18) in LP and $\theta_d = 26.1 \pm 5°$ (N = 18) in CP states.

I_{rel} increased with depth (binned by undulation number) in both CP and LP preparations (Fig. 2F). As resistive force increased by 75% for CP and 67% for LP due to depth changes, I_{rel} increased by 63% for CP and 54% for LP for similar changes in depth demonstrating a positive correlation between muscle activation intensity and resistance force measurements [2].

Also in agreement with resistance force measurements, I_{rel} was independent of the velocity of the sandfish for a given depth ($P > 0.05$) for both CP and LP runs (Fig. 2F). Surprisingly, although resistance force increased by 50% from a LP to CP media, differences in I_{rel} were small in combined data (≈13%) and were only significant for one individual tested. We hypothesize that this difference could be attributed to the body interacting with disturbed material as the animal proceeds through the GM. LP media will tend to consolidate and CP media will dilate in response to shear force. Therefore, the ϕ immediately surrounding the animal could be similar in both preparations.

CONCLUSIONS

The muscle activation strategy in sand-swimming sandfish can be attributed to the unique physics of the granular medium. The discovery that muscle activation intensity increases with depth while the wavelength and wave amplitude do not suggests that the animal is targeting these kinematics and may be using sensory feedback to maintain this waveform to bury most rapidly [3].

REFERENCES

1. Arnold, EN *J Zool., Lond.* **235**, 351-388, 1995.
2. Maladen RD, et al. *Science* **325**, 314-318, 2009.
3. Maladen RD, et al. *J R Soc Interface* **8**, 1332-1345, 2011

A ROBUST KINEMATIC BASED EVENT DETECTION ALGORITHM THAT WORKS FOR WALKING AND RUNNING ON BOTH UPHILL AND DOWNHILL SURFACES

Riley C. Sheehan and Jinger S. Gottschall

The Department of Kinesiology, The Pennsylvania State University
University Park, PA, USA
email: rcs241@psu.edu web: http://biomechanics.psu.edu/nml/

INTRODUCTION

Gait analysis is a typical protocol utilized by medical practitioners, athletic coaches and basic scientists for the purpose of rehabilitation, performance, and research, respectively. A critical component of the process is the accurate detection of kinematic events such as foot-strike (FS) and foot-off (FO) in order to evaluate individual strides and phases. The ideal method of event detection is a force plate, which will register when the foot is in contact with the ground. However, the availability and practicality of force plates is low due to the high expense and complex logistics of mounting on a pathway or below a treadmill. Visual inspection of video data is an alternative, but this method is time consuming and prone to operator biases. Thus, it is beneficial to have an automated system for detecting FS and FO from kinematic data. To date, there are numerous algorithms with sufficient detection capabilities[1-4]. However, they are limited in that they have only been validated for level walking, and occasionally require user input to determine threshold values, which often differ between individuals and conditions. Therefore, our goal was to develop a robust algorithm that accurately detects gait events for both walking and running on level as well as uphill and downhill surfaces, and requires no threshold values or user input.

METHODS

Four healthy, college students (2 men, 2 women) walked at 1.25 m/s and ran at 3.0 m/s on an instrumented treadmill inclined at -6°, 0°, and +6°. We collected simultaneous vertical force data at 1000 Hz and kinematic marker position data at 100 Hz from the heel (calcaneus) and toe (1st metatarsal) of each foot. The timings for FS and FO of the left limb were determined using 4 methods:

1. force plates (FP)
2. walk/run up/down condition algorithm (WRUD)
3. vertical velocity (VVEL)[1]
4. modified vertical velocity (MVEL)

For the FP method of event detection, we initially down sampled the data to match the sampling frequency of the marker data. FS was considered as the frame when the vertical force first rose above 5% bodyweight and FO was defined as the first frame the vertical force dropped below. For the up and downhill conditions the threshold was adjusted to only include the percentage of body weight perpendicular to the belt surface.

For our WRUD method, we utilized the vertical marker positions to determine the gait events. FS was defined as the minimum vertical position of the heel marker. FO was defined as the minimum vertical position of a virtual marker placed in front of the toe marker 1/3 the distance between heel and toe markers. This virtual marker allowed us to estimate the position of the end of the participant's toe. For the uphill and downhill conditions, we calculated the marker coordinates with respect to the belt angle as:

$$y' = x \sin(\text{belt angle}) + y \cos(\text{belt angle})$$

The VVEL method by O'Connor et al.[1] combined the heel and toe markers to create a foot marker. The vertical velocity of the foot marker was calculated and FS was defined as a local minimum whereas FO was a local maxima. To ensure that the proper minima was located for the FS, the algorithm only detects minima when the heel marker is in the bottom 35% of its vertical range.

We modified the VVEL method, MVEL, with the same coordinate calculation as the WRUD method.

Finally, we compared the WRUD, VVEL, and MVEL algorithms to the force plate data by calculating the relative differences in terms of kinematic frames as algorithm frame – FP frame. Negative values indicate the predicted event occurred before the actual event while positive values indicate the predicted event occurred after the actual event.

RESULTS AND DISCUSSION

The WRUD algorithm detected FS and FO with similar errors across all conditions, while in its current form, the VVEL algorithm failed to detect events in the uphill condition. This was because the threshold imposed to detect the proper minima when the heel was close to the belt fails when the FS occurs above the FO as it does in uphill locomotion. For the level and downhill conditions, both algorithms detected FS with similar accuracy with the WRUD approximately 1-2 frames early and the VVEL approximately 0-1 frame early (Table 1). However, the VVEL algorithm incorrectly detected a FS up to 13 times for trials only containing 9 strides, whereas the WRUD algorithm had no false detections. We removed these inaccurate detections prior to comparison with FP values. The MVEL method worked for all conditions but similar to VVEL the original results contained false detections.

Table 1: Differences between FS event detection timings between force plate and kinematic methods. Negative values indicate predicted event occurred before actual event.

Condition\Method	WRUD	VVEL	MVEL
Level Walk	-1.6	0.0	0.0
Level Run	-1.5	-0.2	-0.2
Up Walk	-1.3	NA	-0.5
Up Run	0.4	NA	-1.4
Down Walk	-0.6	-0.3	0.1
Down Run	-1.5	-0.4	0.3

All three algorithms detected FO early, but the WRUD algorithm was closer to the FP values and more consistent across all conditions than VVEL and MVEL (Table 2). WRUD predicted FO 5-8 frames early for each condition. The VVEL predicted FO 10-11 frames early for level and downhill walking and only 1-5 frames early for running. The MVEL performed similar to the VVEL method but was one frame closer to the FP values for the downhill conditions. None of the methods falsely identified FO.

While each method had differences with the timings of FS and FO, they were consistent offsets rather than random errors. On average, there was only a 2 frame difference between the maximum and minimum error for each trial.

Table 2: Differences between FS event detection timings between force plate and kinematic methods. Negative values indicate predicted event occurred before actual event.

Condition\Method	WRUD	VVEL	MVEL
Level Walk	-7.3	-10.6	-10.6
Level Run	-6.4	-1.4	-1.4
Up Walk	-7.6	NA	-10.4
Up Run	-6.0	NA	-0.4
Down Walk	-7.9	-11.1	-10.3
Down Run	-5.3	-4.3	-3.0

CONCLUSIONS

Though each method identified FS and FO timings with similar accuracy, the WRUD algorithm offset was similar for all gait and hill conditions. The versatility of the WRUD algorithm is preferred because it utilizes surface angle and it does not rely on threshold values. However, the WRUD algorithm still has large errors in FO timings. This method could potentially be improved with an adjusted virtual toe definition. Also, the flexibility of the VVEL algorithm was easily improved by incorporating the coordinate system of the belt. Overall, the WRUD algorithm provides a starting point for a robust kinematic gait detection method that is easy to implement in a variety of conditions. Additionally, applying a simple coordinate transformation can improve the adaptability of any detection method. Perhaps clinicians and trainers could utilize this method for gait analysis with inexpensive reflective markers and free software.

REFERENCES

1. O'Connor, et al. *Gait Posture* **25**, 469-474, 2007.
2. Zeni, et al., *Gait Posture* **27**(4), 710-714, 2008.
3. Hreljac & Marshall, *J Biomech* **33**(6), 783-786, 2000.
4. Hsue, et al., *J Biomech* **40**(S2), S529, 2007.

THE INFLUENCE OF STEP FREQUENCY ON MUSCLE ACTIVITY DURING DOWNHILL RUNNING

Riley C. Sheehan, Ryan W. Lutz and Jinger S. Gottschall

The Department of Kinesiology, The Pennsylvania State University
University Park, PA, USA
email: rcs241@psu.edu web: http://biomechanics.psu.edu/nml/

INTRODUCTION

Sixty years ago Hogberg[1] asked, how does stride length and stride frequency influence energy expenditure during level running? The topic of how running mechanics dictate the metabolic cost of running continues to be a topic of interest. For instance, Snyder and Farley[2] recently addressed the question of whether stride frequency is less important during hill running due to the reduced capacity for elastic energy storage and return? Overall, they concluded that stride frequency affected metabolic cost similarly regardless of the slope. Our current aim was to evaluate the influence of frequency on muscle activity during downhill running and compare the differences in muscle activity to metabolic cost.

Minetti[3] demonstrated that the metabolic cost of running is minimized at an angle of -10% (6°) and is highly influenced by the ratio of positive to negative external work as well as the relative efficiencies of the muscle. The reduced expenditure during downhill running can be attributed to the small cost of eccentric contractions. However, the higher amount of negative work done by the muscles during downhill running has been related to an increase in the likelihood of injury[4]. Thus, it is important to understand the factors influencing downhill running mechanics for the minimization of both metabolic cost and injury.

Compared to level running, both metabolic cost and muscle activity are less during downhill running[3]. More specifically, ankle extensor concentric activity is less compared to level running, since the need for propulsion is reduced due to the aiding force of gravity. However, during stance, knee extensor muscle eccentric activity is greater to help dissipate energy and control the magnitude of knee flexion. During swing, knee flexor eccentric muscle activity is also greater to decelerate the leg and prepare for ground contact[5]. The purpose of this study was to determine how step frequency affects metabolic cost and muscle activity at the metabolically optimal grade of 6°. We hypothesized that during downhill running at a preferred step frequency, leg muscle activity and metabolic cost would be less than running downhill with step frequencies 15% slower and 15% faster.

METHODS

Seven healthy, college students (4 male, 3 female) ran at 3.0 m/s on a treadmill at 0° level and 6° downhill. First, the participants completed a warm-up of level running for 5 minutes and downhill running for 3 minutes. We determined their preferred downhill step frequency during the final minute of the downhill running bout. Next, the participants completed 4 randomized conditions where they matched stride frequency to a metronome: 0° with downhill preferred frequency (L), -6° with downhill preferred frequency (P), -6° with frequency 15% slower than preferred (S), and -6° with frequency 15% faster than preferred (F). For each condition we measured oxygen consumption during a 5-minute bout and averaged the values for the final 3 minutes.

Additionally, we collected simultaneous kinematic marker position data at 100 Hz from the heel (calcaneus) of each foot for step length measurements and electromyography (EMG) data at 1000 Hz from 4 muscles of the left leg, lateral gastrocnemius (LG), soleus (SL), biceps femoris (BF), and rectus femoris (RF). We took the mean value of the filtered and rectified EMG signal for each stride during mid-stance (20-57% of stance, mST), terminal stance (81-100% of stance, tST), initial swing (0-34% of swing, iSW), and mid-swing (34-60% of swing, mSW). The values for each stride were averaged for each participant, and normalized by dividing by the maximum value obtained during L, thus all values are reported as a percentage of level walking values.

The conditions were compared using a repeated-measures ANOVA and if appropriate, followed by a Newman Keuls post hoc test with a significance of $p < 0.05$.

RESULTS AND DISCUSSION

Based on the stride time calculations, the participants matched the metronome to obtain the required step frequencies. As expected, the metabolic cost was significantly less than L for all downhill conditions. Additionally, there was a trend ($p = 0.06$) for S to be greater than P at 78% of level compared to 72% of level, respectively.

The lower metabolic rate for the downhill conditions is likely due to the reduced need for propulsion during stance by both the LG and SL (Table 1). Yet during S, aerial and swing phases were longer resulting in greater iSW BF activity.

Table 1: Mean values of the variables for running downhill at preferred step frequency (P), 15% slower (S), and 15% fast (F). All values are presented as a percent of level walking values. Bold indicates significantly different from level. Underlined indicates significantly different from preferred. Significance at $p < 0.05$.

Variable\Condition	S	P	F
Metabolic Cost	**78**	**72**	**76**
LG mST	**84**	**71**	**68**
LG mSW	99	97	**139**
SL mST	88	**77**	**70**
BF iSW	**137**	100	104
BF mSW	109	107	<u>**146**</u>
RF tST	71	92	<u>**172**</u>

In contrast to S, F required muscle activity modulation for shorter stance times and step lengths. During tST, the RF was greater for F than all the other conditions helping to accelerate the leg forward to achieve a faster swing phase (Table 1). However, this also led to greater BF activity in mSW for F compared to all other conditions to slow the fast swinging leg to prepare it for stance. While these greater muscle activities for F compared to P would likely lead to a higher metabolic cost, it is possible that the F strategy also takes advantage of other energy saving mechanisms that counteract the cost of the extra muscle activity. The F condition also showed greater LG activity during mSW, for ankle extension. This finding demonstrates that participants likely ran on their toes during the F condition. Perhaps this strategy would maximize the storage and return of elastic energy[2,6].

CONCLUSIONS

Regardless of step frequency, metabolic cost was significantly lower during downhill running compared to level running, with the greatest difference at the preferred frequency. The small number of participants lowers the predictive power, but the trends in metabolic cost and muscle activation patterns suggest that the preferred frequency is a balance of metabolic and muscle influences. Slower frequencies require prolonged stance and swing times, which leads to greater muscle activity to provide added propulsion and delay the swing leg. In contrast, faster frequencies require shorter stance times and step lengths which cause muscles to have greater activity to accelerate the leg in early swing and decelerate it in mid-swing.

It is possible that the slow and fast step frequencies provide other energy saving mechanisms such as a longer aerial phases and greater elastic energy storage and return, respectively[2,6-7]. This compromise of factors on metabolic cost can hopefully be elucidated through investigation of a larger participant population and a greater number of variables including ankle and knee kinematics in addition to kinetics. It is also important to note that though these strategies may decrease metabolic cost, it is possible that they increase force measurements such as impact peaks and joint reaction forces and moments, which may also lead to the preferred frequency[4]. In the end, these findings may influence how individuals run downhill in order to minimize both cost and injury.

REFERENCES

1. Hogberg, P. Eur *J Appl Physiol* 14, 437-441, 1952.
2. Snyder & Farley *J Exp Biol* **214**, 2089-2095, 2011.
3. Minetti, et al. *J Exp Biol* **195**, 211-225, 1994.
4. Buczek & Cavanagh, *Med Sci Sports Exerc* **22**(5), 669-677, 1990.
5. Cai, et al. *Isokinet Exerc Sci* **18**(3), 163-168, 2010.
6. Cavagna, et al., *Am J Physiol* **2**(3), R243–R261, 1977.
7. Alexander, *J Exp Biol* **160**, 55-69, 1991.

INTERSEGMENTAL ADAPTATION OF LUMBAR SPINE ON DIFFERENT LOAD-CARRYING TYPES

[1] Jun Ho Shin, [1] Yong Hyun Park, [2]Young-Kwan Kim and [1]*Yoon Hyuk Kim

[1]University of Kyung Hee, Yongin, Gyeonggi, Korea
[2]University of Chonnam National, Gwangju, Korea
email: yoonhkim@khu.ac.kr

INTRODUCTION

Carrying bags including backpacks and shoulder bags are common applied loads in our daily lives to carry items without using hands. Previous studies have shown that a heavy bag could be a potential cause associated with neuromuscular disorders, especially chronic low-back pains [1,2]. This was because increased carrying loads [1] or locations of load relative to the trunk [2] significantly changed forward inclination of the trunk and induced more core muscle activations [3].

Previous studies, however, have not focused on in-depth investigation of the lumbar spine (LS; from L1 to S1) kinematics, which would be better address the causes of chronic problems associated with the lower back.

The purpose of this study was to investigate the kinematics of the LS in the level of intersegmental joint in response to increased carrying loads for two different load-carrying types during upright standing posture.

METHODS

Eight male college students (height 178.0±4.18 cm, weight 70.6±3.97 kg, age 22.6±1.41 years; mean±*SD*) having no neuromuscular disease participated in this study.

The dumbbell discs tied with ropes were used for a load-carrying item. Two different types, such as both shoulders' carrying and right shoulder's carrying, were tested. Four different loading conditions (0 kg, 5 kg, 10 kg and 15 kg corresponding to 0%, 7.5%, 15.0% and 22.5% body weight, respectively) were randomly assigned during the experiment. The reflected markers along the LS were attached on the lower back acromion processes and anterior/posterior superior iliac spines (Fig. 1a) after careful palpation were used for calculating trunk forward lean (TFL) angle.

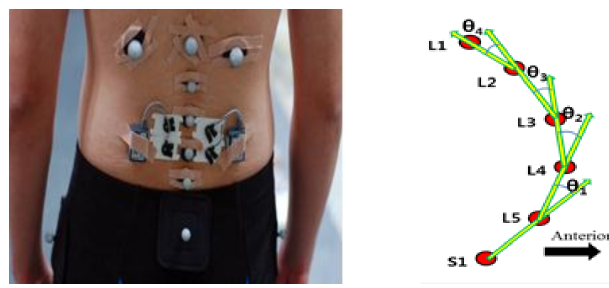

(a) (b)

Figure 1: (a) Locations of reflective markers around the LS (backside view), and (b) definition of intersegmental angles in the sagittal plane (θ_i = proximal segmental angle – distal segmental angle).

Locations of markers were captured by eight motion analysis cameras (Hawks®, Motion Analysis Co., USA) with a sampling frequency of 100Hz. TFL angle was defined as the relative angle of the trunk segment (mid-shoulder to mid-pelvis) with the vertical in the sagittal plane. Intersegmental angles of the LS were projected joint angles in the sagittal plane created by adjacent markers on the LS (Fig. 1). Axial rotation angle of the LS was the relative angle of the horizontal line of L1 created by two lateral markers with respect to the horizontal line created by two anterior superior iliac spines.

A two-way repeated measures analysis of variance (ANOVA) was used to see the interaction of load-carrying type and load amount. The statistical analysis was conducted in SPSS 12.0(SPSS Inc., USA). A family-wise significance was set at 0.05.

RESULTS AND DISCUSSION

There were only a main effect of type (P<0.05) and a main effect of loading (P<0.05). With increasing of loads, increased loads, both carrying types showed increased TFL, but the bilateral carrying (BC) demonstrated more TFL than the unilateral carrying (UC) (Table 1) [4, 5].

Table 1: Changes in TFL angle according to increased loads for different load-carrying types (mean±*SD*, Unit:°)

	5kg	10kg	15kg
BC	4.16±3.04 *	5.99±3.50*	8.15±7.40*
UC	1.02±2.43	2.75±2.34	7.23±7.75

* represent a significant different from 0 kg condition (P<0.05).

Intersegmental angles of the LS generally decreased in response to increased loads (Fig. 2), which consequently contributed to increased TFL. Differences between BC and UC became clear in the intersegmental angles of proximal motion segment (θ_3 and θ_4), so that a significant interaction was detected on θ_4 result (P<0.05).

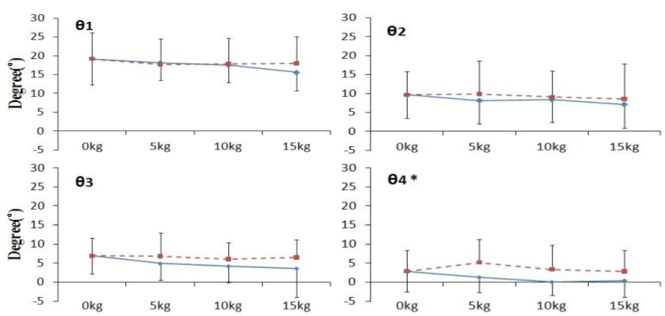

Figure 2: Changes in intersegment angles of the LS. * indicates that a significant interaction was detected at θ_4 (P<0.05).

A significant interaction of load magnitude and load-carrying type was detected (P<0.01). In UC, the counter-clockwise axial rotation of the LS (medial direction) was found in order to adapt the increased loads. Theses results mean that the LS would try to handle asymmetric loads with transverse motion medially, which relieves the dependency on TFL. However, this kinematic adaptation inevitably induced combined mechanical loadings on the LS (i.e., compression and torsion together), which could be a potential risk factor to neuromuscular disorders associated with the lower back.

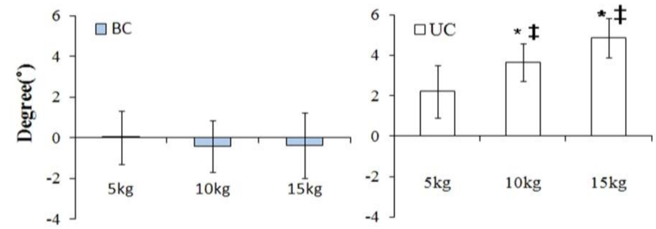

Figure 3: Changes in axial rotation angle of the LS responding to load-carrying types and load magnitudes. * represents a significant different from 0 kg condition (P<0.05) and ‡ a significant different from 5 kg condition (P<0.05).

CONCLUSIONS

As a carried load increases, trunk forward lean by the bilateral carrying was attributed to larger changes in intersegmental angles of proximal LS joints in the sagittal plane. For the unilateral carrying, the axial rotation of the LS in medial direction was the main adaptive strategy in response to increased asymmetric loads with small TFL. This adaptation as a result of UC tends to cause combined mechanical loadings on the LS, which could result in neuromuscular disorders associated with low-back pains.

REFERENCES

1.Grimmer K, et al. *BMC Musculoskeletal Disord*, 2002.
2. Chow DH, et al. Ergonomics, **48**, 642-656, 2005.
3. Negrini S, et al. *Spine*, **27**, 187-195, 2002.
4.Lindstrom HD, *Work: A Journal of Prevention*, **32**, 329-338, 2009.
5. Hong Y, et al. *Gait&Posture*, **17**, 28-33, 2003.

ACKNOWLEDGEMENTS

This research project was supported by the Sports Promotion Fund of Seoul Olympic Sports Promotion Foundation from Korean Ministry of Culture, Sports and Tourism, and National Agenda Project (NAP) funded by Korea Research Council of Fundamental Science and Technology (P-09-JC-LU63-C01).

TRIP RECOVERY STRATEGIES IN A UNILATERAL TRANSFEMORAL AMPUTEE

[1,2]Camila Shirota, [1]Ann M. Simon and [1,2]Todd A. Kuiken

[1]Northwestern University, Chicago, IL, USA
[2]Rehabilitation Institute of Chicago, Chicago, IL, USA
email: camila.shirota@u.northwestern.edu, web: www.ric.org/cbm

INTRODUCTION

Recovery from a trip requires coordination to maintain balance and continue walking. The choice of recovery strategy is strongly related to when the trip occurs in swing phase [1,2]. Elevating strategies (where the tripped foot is lifted in order to cross the obstacle) are used in response to trips in early and mid swing; lowering strategies (where the tripped foot is quickly lowered to the ground behind the obstacle, and the contralateral foot is the first to cross the obstacle) are employed in mid and late swing. A delayed lowering strategy (where the tripped foot is elevated but can not overcome the obstacle and is lowered to the ground, and the contralateral foot is the first to cross the obstacle) is used when the foot is caught behind the obstacle during an elevating strategy.

Recovering from a trip can be difficult for individuals with a lower limb amputation. Previous research shows that transfemoral amputees cannot always recover from trips on the side of their prosthesis [3]. Not much is known about the recovery strategies they use if they are able to maintain balance, if these strategies are consistent with those of non-amputees, or how they respond to trips on their sound side.

We investigated the trip-recovery strategies of a transfemoral amputee compared to non-amputee subjects. We also compared recovery strategies used following trips on the sound side with those following trips on the side with the prosthesis.

METHODS

One unilateral transfemoral amputee (21 years old) and 8 non-amputee (23.9 ± 2.4 years old) subjects participated in this study. The amputee subject wore her own socket and prosthesis (C-Leg, Otto Bock, Duderstadt, Germany) during the experiment.

Subjects walked at 1.4 m/s (non-amputee) or 0.92 m/s (amputee, self-selected) on a split-belt force treadmill. A custom device induced trip-like perturbations using retractable cords attached to each foot [4]. Custom software arrested the cord during swing phase of walking. Perturbations occurred in a random order on either leg from 10% to 70% of swing phase. Trials were separated by at least 1 min and 5 undisturbed walking trials were randomly distributed among the trip trials in order to obtain average walking kinematics.

Motion capture data, ground reaction forces, and tension on the tripping cables were recorded. Force plate data were used to determine heel strike and toe off. Trip onset was defined as the time between toe off and the onset of tension on the retractable cords, normalized by swing phase duration. Recovery strategies were identified from the trajectories of each foot following the perturbation and defined as:

- *elevating*: the tripped foot was lifted and placed ahead of a virtual obstacle (i.e., where the foot was perturbed);
- *delayed lowering*: the tripped foot was lifted and placed at or behind the virtual obstacle;
- *lowering*: the tripped foot was quickly lowered, and the contralateral foot was the first to cross the virtual obstacle;
- *additional*: the tripped foot was lowered, the contralateral foot was placed behind it, and the tripped foot was the first to cross the virtual obstacle on the following step.

RESULTS AND DISCUSSION

When tripped on the prosthesis side, the amputee subject employed recovery strategies similar to non-amputee subjects (Fig. 1) [2]. Elevating strategies occurred in early swing and lowering strategies in late swing. During mid-swing, elevating, delayed lowering, or lowering strategies were employed.

When tripped on the sound side during mid to late swing, the amputee subject used lowering strategies. During early swing, no elevating strategies were observed. Instead, the foot was lowered as it moved forward, as if the subject kicked the virtual obstacle.

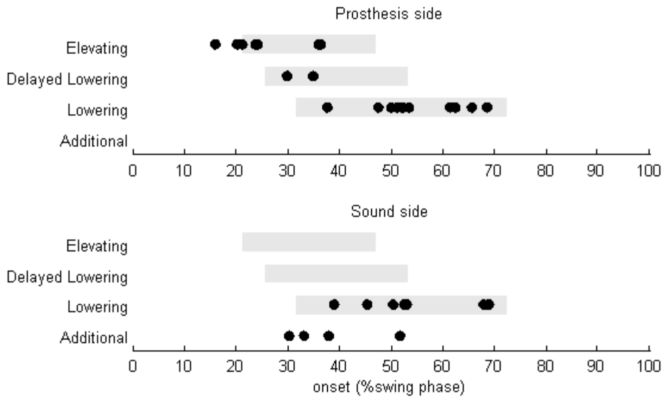

Figure 1: Strategy selection as a function of perturbation onset for trips on the prosthesis (top) and sound (bottom) sides for a transfemoral amputee. Shaded regions indicate range of non-amputee data.

This was more an indication of a failure of the custom tripping device to completely arrest the foot rather than an outcome of not using elevating recovery strategies on the sound side.

An additional recovery strategy, separate from the lowering strategy, was observed following trips during mid swing. In the lowering strategy, the sound side was lowered to the ground behind the obstacle and the prosthetic foot was the first to cross. In the additional strategy, after the sound side was lowered, the prosthetic foot was also lowered behind the obstacle, which was first crossed in the next stride by the sound side (i.e., tripped foot). These similarities and differences can be seen in the kinematic data (Fig.2), where we note that the prosthetic knee remained extended throughout the second stride. The subject consistently employed this additional strategy during mid swing.

Our study was limited to only one amputee subject, and more data is needed to determine if this additional strategy is used by other transfemoral amputees. Further investigation should also be done to determine if this population also employs elevating strategies following trips to the sound side in early swing.

CONCLUSIONS

The amputee subject consistently used similar recovery strategies to control subjects in response to trips on her prosthesis side. An additional recovery strategy was observed following trips on the sound side in mid swing. Further understanding the strategies individuals with a transfemoral amputation use to recover from trips may allow a powered lower limb prosthesis to be programmed with specific recovery mechanisms in order to prevent falls resulting from trips.

REFERENCES

1. Eng JJ, et al. *Exp Brain Res* **160**, 339-349, 1994.
2. Schillings AM, et al. *J Neurophysiol* **83**, 2093-2102, 2000.
3. Bellmann M, et al. *Arch Phys Med Rehabil* **91**, 644-652, 2010.
4. Shirota C, et al. *Conf Proc IEEE Eng Med Biol Soc*, Boston, MA, USA, 7833-7836, 2011.

ACKNOWLEDGEMENTS

This work was supported in part by the Brazilian Ministry of Education through the CAPES Foundation and the US Department of State under the CAPES/Fulbright scholarship BEX1691/07-4, and the Rice Foundation. The authors would like to thank Dr.Ann Barlow for revising and editing the manuscript.

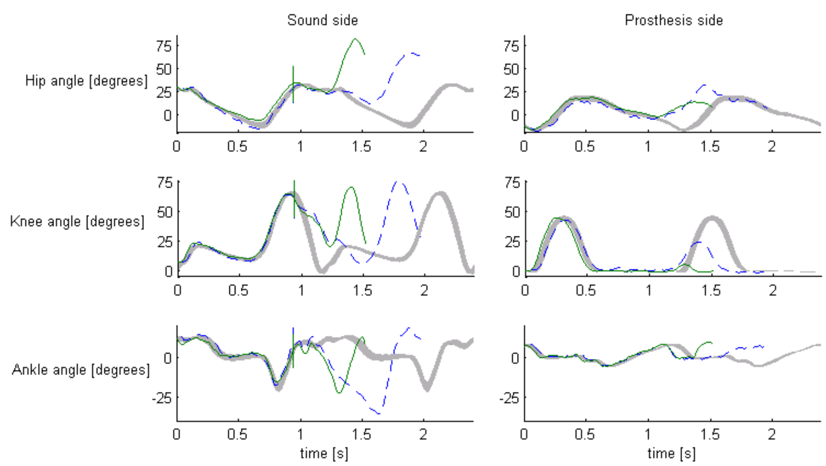

Figure 2: Kinematics of the sound and prosthesis sides following trips occurring at 40% of swing phase on the sound side. The subject employed two different strategies (lowering: dashed line, and additional: solid line). Data from two consecutive strides are shown. Trip onset is indicated by the vertical lines. The shaded area represents average walking kinematics plus or minus one standard deviation.

Suction and skin: the effect of vacuum loading on the skin of a common dolphin

[1]K. Alex Shorter, [2]Tom Hurst, [3]Mark Johnson, [2]Scott Cramer, [2]Darlene Ketten and [2]Michael Moore

[1]University of Michigan, Ann Arbor, MI, USA
[2]Woods Hole Oceanographic Institution, Woods Hole, MA, USA
[3]University of St. Andrews, St Andrews, Fife KY16 8LB, UK

INTRODUCTION

Many marine mammals spend most of their life below the water surface, necessitating specialised observational tools to track their behaviour. To address this need, archival tags have been developed to collect and store high-resolution sound, image and motion data for intervals of hours or days [1]. Given the short recording duration of these devices, non-invasive attachment methods, such as suction cups, are frequently used to minimize animal impact [2].

Suction cups generate attachment force by balancing two forces acting perpendicular to the substrate: the shape restoring force of the distorted cup and the vacuum force created by the pressure difference between the ambient environment and the cup interior. During attachment, the lip is flattened and a majority of the air within the cup is expelled. When the attachment force is relaxed, the cup attempts to return to its original shape with the lip acting as a check valve preventing ingress of the surrounding fluid. Because the lip is sealed, the increase in internal volume resulting from the cup relaxation creates a reduced internal pressure and corresponding increase in vacuum force. The internal volume of the cup continues to expand until a balance is reached between the pressure force and the restoring force of the cup. As such, the vacuum force is dependent on the material/shape stiffness of the cup (i.e., the force with which it opposes shape distortion) and the properties of the substrate material (e.g. the animal's skin).

If the skin surface is less stiff than the cup, the skin may deform more than the cup in balancing the vacuum force. The performance of the attachment is then critically dependent on the surface and stress-strain properties of the skin and its ability to maintain stiffness against a static force. This work presents the design and experimental demonstration of a custom measurement tool, termed the smart static suction cup (SSSCup), to facilitate the investigation of vacuum loading on cetacean skin.

METHODS

The SSSCup consists of a rigid acrylic half-dome, a molded silicone lip, a linear variable differential transformer (LVDT) to measure displacement of the skin (LT0617, Active Sensors, USA), a pressure sensor (US300, Measurement Specialties, USA) and two thermistors (192-102DEW-A01, Honeywell, USA). The thermistors are located in the tip of the displacement sensor and in the lip of the cup to make differential measurements of the skin temperature during loading. A peristaltic pump (200 series, Williamson Manufacturing, UK) creates a controllable vacuum force in the cup and is attached via flexible tubing and a pressure port on the top of the SSSCup. Sensor data are logged using a netbook and USB analog to digital converter (U6, LabJack U6). The whole system is battery powered and located in a splash proof case for portability.

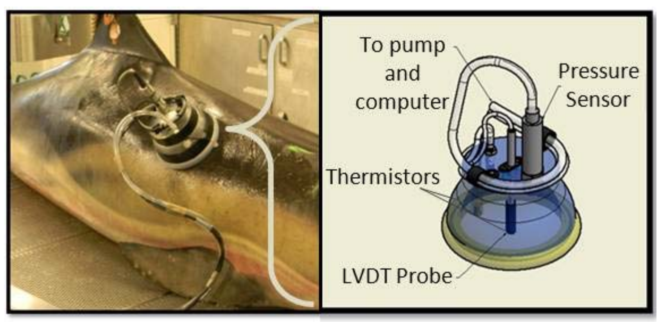

Figure 1: A mechanical drawing of the SSSCup assembly (right) and the SSSCup shown attached to the freshly stranded common dolphin (left).

Initial testing of the SSSCup was conducted on a common dolphin (*Delphinus delphis)* cadaver that had been frozen shortly after death. The cadaver was thawed just prior to testing, Figure 1. The setup pressure of a conventional suction cup when applied to an animal (-0.07 bar gage) was used for the initial trials of the SSSCup. The SSSCup was placed on an untested location on the body, and evacuated to the test vacuum. Pressure was held constant for 5 min and the test was replicated twice at different locations. To examine repetitive loading, the vacuum was increased to -0.1 bar, held for 2 min and released. This pressure profile was repeated three times in succession at two positions. To examine the long-term response of the skin, the SSSCup was brought to -0.1 bar and held for 1 hr.

Finally, to explore how the skin, blubber, fat and muscle of the animal cooperate with the suction cup in creating a vacuum force, a non-metallic version of the SSSCup was applied with a -0.1 bar load on the animal during a computed tomography (CT) scan of the cup/animal system. Scanning was conducted in the Computerized Scanning and Imaging (CSI) facility at the Woods Hole Oceanographic Institution

RESULTS AND DISCUSSION

The instrumented SSSCup recorded a mean skin displacement of 1.0 cm into the SSSCup in the static and dynamic loading trials, Table 1. This confirms that the substrate plays an important role in suction generation and implies that the substrate properties will influence vacuum formation and maintenance. Figure 2 illustrates the nonlinear response of the skin to the applied pressure during one cycle of dynamic loading. A nonlinear stiffness was observed as the skin deformed rapidly at the onset of the loading (0 to 3 sec) and then at a reduced rate until the maximum pressure was reached at ~19 sec. Following the release of the pressure, the skin rapidly returned to its original state. Creep was not observed during the constant loading portions of the dynamic trials, as illustrated by Figure 2 or during the 1 hr extended loading test.

Table 1: SSSCup displacement and pressure values.

Measurement	Static Trial 1	Static Trial 2	Dynamic Trial 1	Dynamic Trial 2	Long - Term
Mean Pressure (bar)	-0.07	-0.07	-0.1	-0.1	-0.1
Mean Displacement (cm)	1.0	1.0	1.0	1.0	1.0

The CT images provide a snap shot of the response of the animal skin during vacuum loading, Figure 3. The -0.1 bar loading creates a visible deformation compared to the unloaded side of the animal. Measurements taken from the images show a change in thickness of the subcutaneous fat and a small change to the blubber thickness, but not to the skin itself, Table 2.

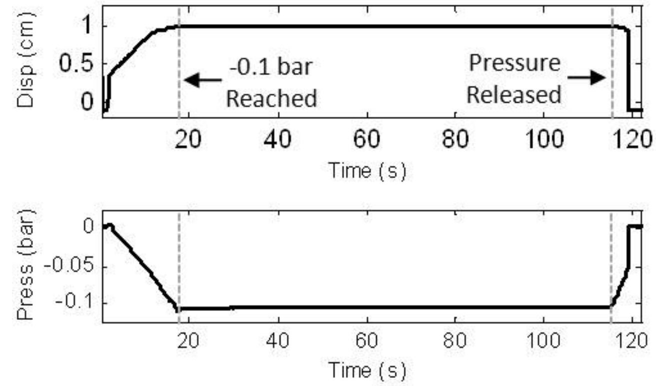

Figure 2: Response of the skin to pressure loading.

The measured displacement from the CT scan is comparable to the SSSCup measurement. The 0.3 cm difference observed in the measurements could be due to deformation created by the spring backed LVDT plunger tip and will be investigated in the future.

Table2: Displacement measurements from CT scan.

Condition	Pressure (bar)	Displacement (cm)	Fat (cm)	Blubber (cm)	Skin (cm)
CT Cup	-0.1	1.3	1.3	1.1	0.1
CT Control	0	NA	1.0	1.2	0.1

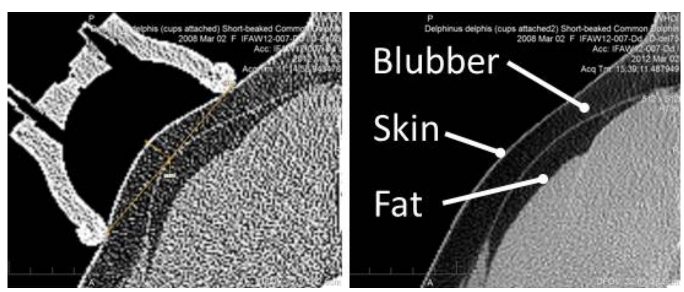

Figure 3: CT image of the non-metallic SSSCup (left) at -0.1 bar and the unloaded animal (right).

CONCLUSIONS

Direct measurement of the material properties of intact marine mammal skin will lead to improved performance of suction cups on marine mammals.

REFERENCES

1. Johnson M, Aguilar de Soto N, Madsen PT, (2009) Studying the behaviour and sensory ecology of marine mammals using acoustic recording tags. Marine Ecology Progress Series, 395:55-73.
2. Hooker SK, Baird RW (2001) Diving and ranging behaviour of odontocetes: a methodological review and critique. Mamm Rev 31:81-105.

TOE-IN GAIT REDUCES THE FIRST PEAK IN THE KNEE ADDUCTION MOMENT DURING WALKING IN KNEE OSTEOARTHRITIS PATIENTS

[1]Pete B. Shull, [1]Rebecca Shultz, [1]Amy Silder, [2]Thor F. Besier, [1]Mark R. Cutkosky and [1]Scott L. Delp

[1]Stanford University, Stanford, CA, USA
[2]The University of Auckland, Auckland, New Zealand

INTRODUCTION

The external knee adduction moment (KAM) typically shows two peaks during the stance phase of gait. The first, and larger, peak occurs during early stance and has been linked to the severity [1] and progression [2] of medial compartment knee osteoarthritis (OA), while the second, smaller peak occurs during late stance. Gait modification is a conservative method of reducing the KAM. Toe-out gait has been proposed as one type of gait modification, but this only lowers the second peak of the KAM [3]. Medial thrust gait has been shown to reduce both peaks of the KAM [4], but it also increases the external knee flexion moment, which can cancel out the medial compartment force reduction from a lower KAM [5]. Our aim was to use haptic (touch) feedback to train OA patients to reduce the first peak KAM without increasing the external knee flexion moment. We hypothesized that toe-in gait would move the knee medially, which would shorten the lever arm of the resultant ground reaction force (GRF) and reduce the KAM without increasing the knee flexion moment.

METHODS

Twelve subjects (5F/7M; age 60±12y; BMI 27±4) with medial compartment knee OA participated in this study. Subjects were required to have radiographic evidence of medial compartment knee OA, symptoms of medial compartment pain during the previous six weeks, and the ability to walk without assistance for at least 25 minutes. Gait retraining was focused on the leg with self-reported greatest knee pain. Three-dimensional lower extremity motion (60Hz) and forces (960Hz) were recorded using a Vicon motion capture system and a Bertec instrumented treadmill, respectively. Subjects walked at a self-selected pace with a previously-described marker set [6]. Subjects performed two trials: a baseline ‘normal’ gait followed by a toe-in gait in which they were encouraged to decrease foot progression angle by moving their toes inward. Gait kinematics and haptic feedback actuations were both conducted in real-time to help subjects learn to toe-in. A vibration motor was placed on the lateral shank and vibrated each time the frontal plane tibia angle was not decreased 0.75 deg from the baseline walking trial. Because foot progression angle and tibia angle are correlated [7], and because it is easier for subjects to sense vibrations from a motor placed on the shank than from one placed on the shoes [8], giving feedback on tibia angle is an effective method of training foot progression angle. Baseline and toe-in trials lasted two minutes each and the last 10 steps were recorded and averaged for analysis. Paired t-tests were used to detect differences between gait parameters at the $p \leq 0.05$ significance level.

RESULTS AND DISCUSSION

Toe-in gait reduced the first peak of the KAM but did not increase the knee flexion moment (Table 1, Fig. 1). In early stance, the knee shifted medially toward the GRF (Fig. 2). This shortened the lever arm of the GRF and reduced the KAM. In late stance, the knee remained medially shifted but this shift was offset by a medial shift in the center of pressure. This moved the GRF medially, away from the knee (Fig. 2). Thus, there was no net difference in KAM or lever arm at the time of the second peak of the KAM (Table 1).

Toe-in gait moved the knee position medially, reducing the lever arm of the GRF in a similar way as medial thrust gait [4]. However, medial thrust gait requires the foot progression angle to remain constant which may be unnatural since tibia angle and foot progression angle movements are naturally correlated [7]. Achieving a medial thrust gait may also require an increased knee flexion angle and a corresponding elevated knee flexion moment [5]. Toe-in gait allows the foot and shank to move together and does not increase the knee flexion

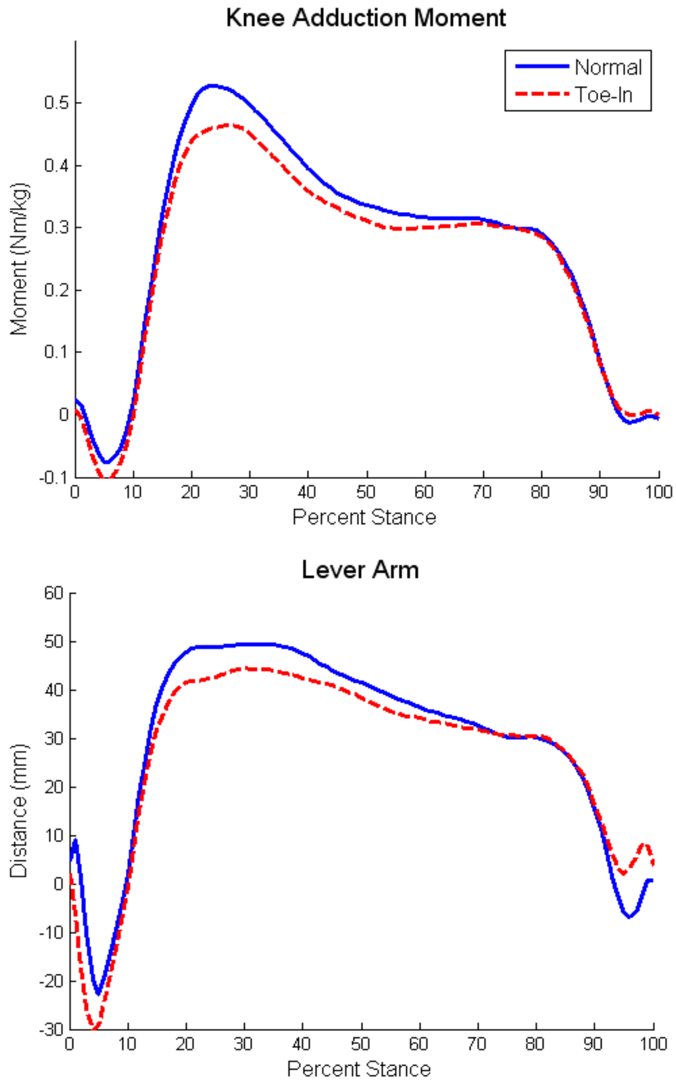

Figure 1: Ensemble curves (n=12). Positive lever arm distance occurs when knee center is lateral of GRF. Toe-in gait reduced the KAM in early stance.

moment typically observed during medial thrust gait.

CONCLUSIONS

Toe-in gait reduces the first peak knee adduction moment, which has been linked to the progression and severity of knee OA. Teaching OA patients to

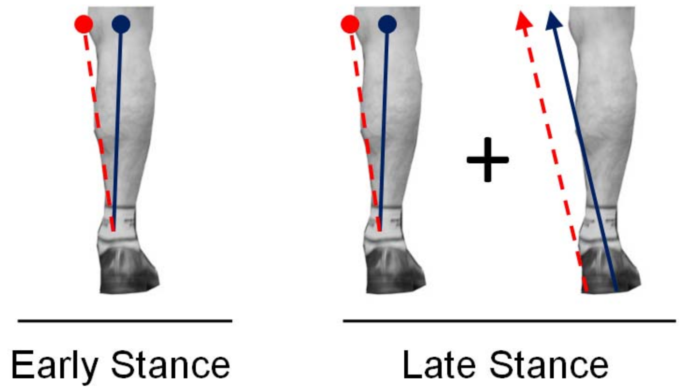

Figure 2: Components affecting the lever arm (solid line is normal gait, dashed line is toe-in gait, circles represent knee center position, arrows represent GRF line of action). In early stance, the tibia angle with toe-in gait causes a shift of the knee center medially which shortens the GRF lever arm. In late stance this is offset by the medial shift in center of pressure, which shifts the GRF medially.

toe-in is a promising alternative to invasive surgical procedures.

REFERENCES

1. Sharma L, et al. *Arth & Rheu* **41**, 1233-40, 1998.
2. Miyazaki T, et al. *Ann Rheu Dis* **61**, 617-622, 2002.
3. Guo M, et al. *Gait Posture* **26**, 436-441, 2007.
4. Fregly BJ, et al. *IEEE Trans Bio Eng*, **54**, 1687-95, 2007.
5. Walter J, et al. *J Ortho Res* **10**, 1348-54, 2010.
6. Shull PB, et al. *J Biomech* **44**, 1605-1609, 2011.
7. Shull PB, et al. *IEEE Hap. Symp.* 409-416, 2010.
8. Jirattigalachote W, et al. *IEEE Ro-Man Symp*, 401-406, 2011.

ACKNOWLEDGEMENTS

NSF HCC #1017826, Jason Dragoo, Stuart Goodman, Wisit Jirattigalachote, Stanford Human Performance Lab.

Table 1: Kinematic and kinetic variables at the first and second peak knee adduction moment (KAM)

	At First Peak KAM			At Second Peak KAM		
	Normal	*Toe-In*	*p-val*	*Normal*	*Toe-In*	*p-val*
Knee Add. Moment (Nm/kg)	0.54 ± 0.24	0.48 ± 0.23	< **0.01**	0.31 ± 0.21	0.30 ± 0.20	0.71
Lever Arm (mm)	51.9 ± 20.7	44.7 ± 18.4	< **0.01**	31.1 ± 21.4	31.4 ± 21.2	0.56
Knee Flex. Moment (Nm/kg)	0.25 ± 0.25	0.23 ± 0.23	0.60	-0.30 ± 0.14	-0.28 ± 0.13	0.58
Foot Progression Angle (deg)	3.3 ± 4.6	-2.1 ± 6.3	< **0.01**	3.3 ± 5.2	-2.5 ± 6.8	< **0.01**

SIX-WEEK GAIT RETRAINING PROGRAM FOR KNEE OSTEOARTHRITIS PATIENTS: LEARNING RETENTION AND SYMPTOM CHANGES

[1]Pete B. Shull, [1]Amy Silder, [1]Rebecca Shultz, [2]Thor F. Besier, [1]Scott L. Delp and [1]Mark R. Cutkosky

[1]Stanford University, Stanford, CA, USA
[2]The University of Auckland, Auckland, New Zealand

INTRODUCTION

Gait modification has been proposed as a conservative intervention to slow the progression of medial compartment knee osteoarthritis (OA) by lowering the external knee adduction moment (KAM) [1]. Previous gait modification studies for knee OA patients have involved only a single gait retraining session [2,3]. It is not known if OA patients can learn and retain an altered gait pattern over time, and whether reducing the KAM will improve knee pain and function after prolonged training. The purpose of this study was to train medial compartment knee OA patients to adopt new gait patterns with a reduced KAM using real-time sensing and haptic (touch) feedback over a six-week period. We hypothesized that it would take patients four weeks to learn to retain an altered gait pattern and that the overall learning rate would follow an exponential trajectory. We also hypothesized that patients would show improvements in knee pain and function after six weeks of gait retraining.

METHODS

Seven subjects (2F/5M; age 64±12y; BMI 27±4) with medial compartment OA participated in this study. Subjects had radiographic evidence of medial compartment knee OA, symptoms of medial compartment pain during the previous six weeks, and could walk without assistance for at least 25 minutes. Gait retraining was focused on the leg with self-reported greatest knee pain. Three-dimensional lower extremity motion (60Hz) and forces (960Hz) were recorded as subjects walked at a self selected pace on an instrumented treadmill [4]. Subjects completed seven testing sessions spaced one week apart. During the initial visit, real-time sensing and haptic feedback were used to train tibia and trunk angle changes, and data-driven models linking empirical changes in tibia and trunk to changes in the KAM were used to predict new gait patterns [4]. Subjects then verbally reported whether gait patterns predicted by the model were comfortable and sustainable; this input was used to aid in determining the final new gait pattern. The gait retraining protocol during the next six visits involved a one minute retention trial followed by three training trials of three minutes each. During the training trials, subjects received real-time haptic feedback on the tibia and trunk [4] to aid in achieving the new gait pattern established during the initial visit. Subjects could disregard haptic feedback if the new gait pattern began to feel uncomfortable or unsustainable. During the final training session (week 6), no feedback training was given, and only a retention trial was performed.

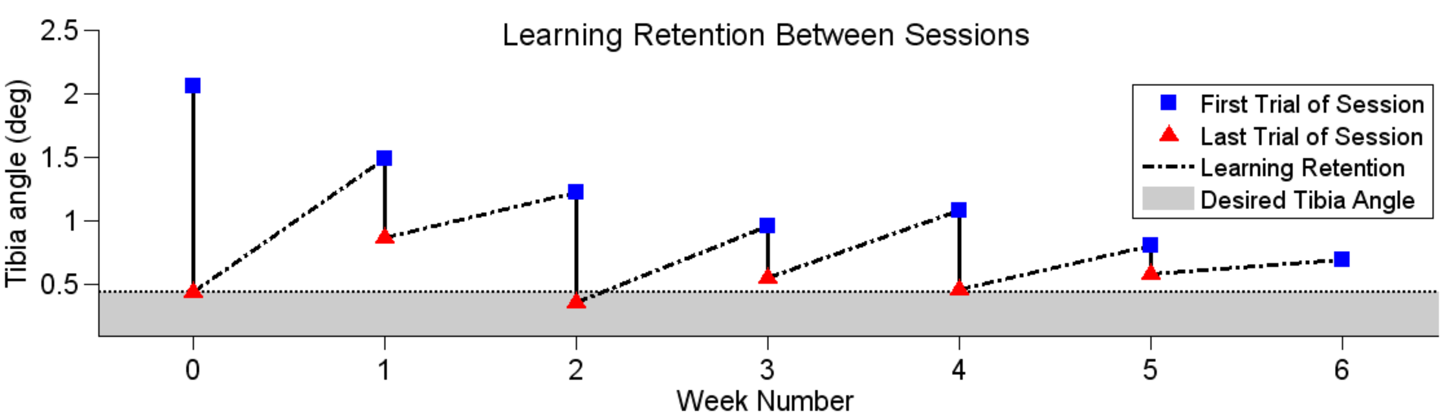

Figure 1: Mean tibia angle at the beginning and end of each training session. The first trial of week 0 is the baseline trial, and the first trial of weeks 1-6 are retention trials. Dotted lines show the degree of learning retention between sessions.

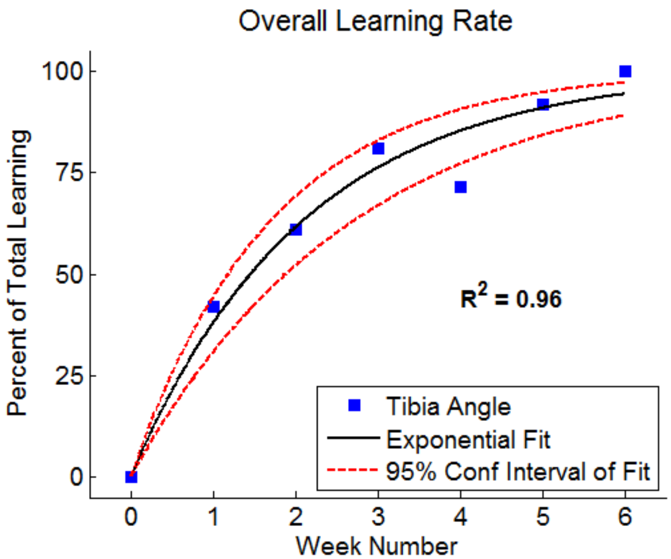

Figure 2: Mean tibia angle (first trial each session) as a percent of tibia angle on week 6. This followed an exponential trajectory, $y = 100*(1 - e^{(-0.48*x)})$.

Subjects filled out a WOMAC questionnaire at baseline and the beginning of the final training session to assess changes in pain and function. Paired t-tests were used to compare differences between gait parameters. The effect size of WOMAC pain and function for pre- and post-training was compared with the effect size expected from the placebo effect for OA treatments [5].

RESULTS AND DISCUSSION

Learning was not completely retained between sessions during the first four weeks ($p < 0.05$) as seen by an increase in tibia angle away from desired during each retention trial (Fig. 1). However, during the final two weeks, learning retention trials were not statistically different from the previous session's final trial ($p \geq 0.19$). Subject learning followed an exponential trajectory (Fig. 2). Approximately 90% of learning occurred during the first four weeks of training (evidenced in the retention trial on week 5, Fig. 2). Subjectively, patients began to internalize the new gaits by week 3 or 4 as evidenced by their more natural walking patterns and comments that walking in the new way now required, "less concentration." Gait patterns on the final session showed an average 22% KAM reduction as compared to baseline gaits ($p < 0.01$). Subjects reported improved knee pain and function. These improvements were statistically higher than expected improvements from the placebo effect ($p < 0.05$) (Fig. 3).

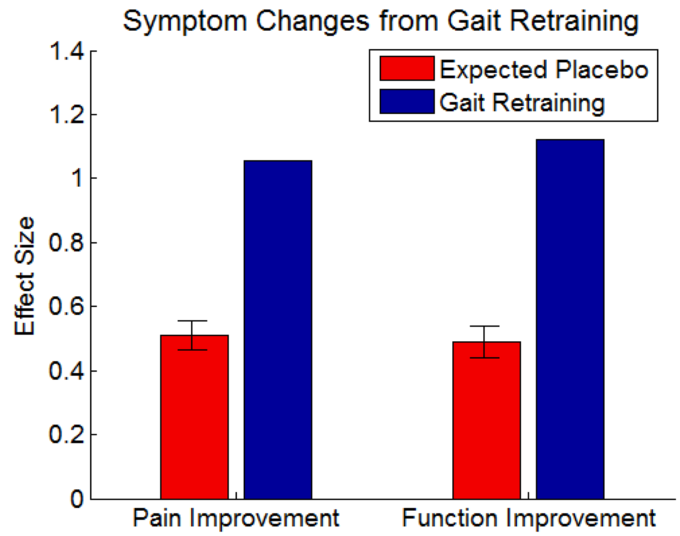

Figure 3: WOMAC knee pain and function effect size (mean difference between baseline and final divided by the standard deviation of the mean difference) of gait retraining compared to the expected placebo effect (compiled from 180 pain and 80 function OA placebo studies [5]). 95% conf interval for effect size of all placebo studies shown on expected placebo bar. Improvements for gait retraining are roughly twice as large as expected solely from the placebo effect.

CONCLUSIONS

Subjects experienced exponential learning patterns over time that resulted in a reduced KAM, reduced knee pain and improved knee function. Future gait retraining interventions should train knee OA patients for at least four consecutive weeks to ensure learning retention.

REFERENCES

1. Simic M, et al. *Arth Care & Res* **63**, 405-26, 2011.
2. Fregly BJ, et al. *J Ortho Res* **27**, 1016-21, 2009.
3. Guo M, et al. *Gait Posture* **26**, 436-441, 2007.
4. Shull PB, et al. *J Biomech* **44**, 1605-1609, 2011.
5. Zhang W, et al. *Ann Rheu Dis* **67**, 1716-23, 2008.

ACKNOWLEDGEMENTS

NSF HCC #1017826, Jason Dragoo, Stuart Goodman, Wisit Jirattigalachote, Stanford Human Performance Lab.

WHOLE-BODY ANGULAR MOMENTUM DURING STAIR ASCENT AND DESCENT

[1]Anne K. Silverman, [2]Richard R. Neptune, [3]Emily H. Sinitski and [3]Jason M. Wilken

[1]Department of Mechanical Engineering, Colorado School of Mines, Golden, CO, USA
[2]Department of Mechanical Engineering, The University of Texas at Austin, Austin, TX, USA
[3]Center for the Intrepid, Department of Orthopedics and Rehabilitation, Brooke Army Medical Center, Ft. Sam Houston, TX, USA
email: asilverm@mines.edu

INTRODUCTION

Whole-body angular momentum has been studied during level walking and is thought to be highly regulated over the gait cycle [1, 2]. In addition, this quantity is important in maintaining dynamic stability and recovering from trips [3]. The time rate of change of whole-body angular momentum equals the net external moment about the body center-of-mass (COM). Thus, angular momentum is largely affected by changes in foot placement and ground reaction forces (GRFs) [e.g., 2]. In addition, previous studies have shown that GRFs and joint kinetics vary while ascending and descending stairs [4, 5]. Therefore, the angular momentum trajectory during stair ascent and descent will likely be different from level walking.

Muscles are the primary contributors to whole-body angular momentum [6] and net joint moments. Previous studies have shown that greater net joint moments occur during stair walking [4, 5], suggesting that the magnitude of angular momentum may also be greater. Greater deviation of angular momentum from zero may lead to greater instability when walking on stairs. The purpose of this study was to analyze 3D angular momentum during stair ascent and descent. We tested the hypothesis that the range of angular momentum would be larger for stair walking relative to level walking. We analyzed joint moments to interpret the angular momentum results and gain insight into how whole-body angular momentum is controlled during stair walking.

METHODS

Thirty subjects walked at a fixed cadence (80 steps per minute) up and down 16 stairs as well as on a level walkway. Full-body kinematic and GRF data were collected at 120 and 1200 Hz, respectively. An inverse dynamics model was used to determine the COM location and velocity of each body segment including the head, torso, pelvis, upper arms, lower arms, thighs, shanks and feet. Whole-body angular momentum (H) about the COM was calculated as:

$$\vec{H} = \sum_{i=1}^{n}\left[\left(\vec{r}_i^{COM} - \vec{r}_{body}^{COM}\right) \times m_i\left(\vec{v}_i^{COM} - \vec{v}_{body}^{COM}\right) + I_i\vec{\omega}_i\right]$$

where $\vec{r}_i^{COM}$, $\vec{v}_i^{COM}$ and $\vec{\omega}_i$ are the position, velocity and angular velocity vectors of the i-th body segment's COM, $\vec{r}_{body}^{COM}$ and $\vec{v}_{body}^{COM}$ are the position and velocity vectors of the whole-body COM, m_i and I_i are the mass and moment of inertia of each segment, and n is the number of body segments. H was normalized by mass (kg), walking speed (m/s) and height (m) and analyzed over the left leg gait cycle. The range of each 3D angular momentum component, defined as the peak-to-peak value, was compared across the three conditions using a one-factor ANOVA for normally distributed data and Friedman's test for non-normally distributed data. When a significant main effect was found, pairwise comparisons were performed between each stair condition and level walking (α=0.05). Correlation analyses were performed between the range of angular momentum and peak joint moments.

RESULTS AND DISCUSSION

There were significant main effects in the range of H in the frontal, transverse and sagittal planes ($p<0.001$, Fig. 1). The ranges for stair descent and ascent were significantly larger than level walking in all three planes ($p<0.001$).

In the frontal plane, the range was strongly correlated with the peak hip abduction moment in late stance ($r=0.51$, $p<0.001$, $n=90$). This peak moment was reduced for stair ascent relative to level walking, which is in agreement with previous studies [5]. A reduced hip abduction moment suggests reduced contributions from the gluteus medius, which is a major contributor to this joint moment and frontal-plane H [7].

In the transverse plane, the range of H was much smaller than the other two planes, consistent with previous analyses of level walking [1, 2]. The range was correlated with peaks of the knee rotational moment in both early ($r=0.33$, $p<0.001$, $n=90$) and late stance ($r=0.33$, $p<0.001$, $n=90$).

In the sagittal plane, the range of H was significantly correlated with the peak knee extension/flexion moments in both early ($r=0.63$, $p<0.001$, $n=90$) and late stance ($r=0.29$, $p<0.001$, $n=90$). In early stance, the peak knee extension moment was significantly greater for stair ascent relative to level walking, consistent with previous studies [4, 5]. The vasti muscles contribute to the positive (backward) external moment in early stance during level walking [6]. Thus, greater output from the vasti is consistent with the greater increase (positive slope) in sagittal H seen during stair ascent in early stance (Fig. 1), and a greater range of H.

In late stance, the peak knee moment was extensor during stair descent and flexor during level walking and stair ascent, which is in agreement with previous studies [4]. Also in late stance, the vasti contribute negatively to the sagittal external moment during level walking [6]. Thus, greater negative contributions in late stance from the vasti may result in a greater decrease (negative slope) of H at this time during stair descent. A greater negative slope of the H trajectory would also result in a greater overall range of H.

CONCLUSIONS

These results suggest that there are differences in how angular momentum is controlled in stair ascent and descent relative to level walking. While differences were shown in all three planes, the differences in the frontal and sagittal planes were much larger than the transverse plane. The range was greater while ascending and descending stairs relative to level walking. Differences in the joint moments suggest differences in mechanisms used to control angular momentum during stair walking. These results provide a baseline for comparison to impaired populations who may have altered angular momentum trajectories [e.g., 2] and a greater risk of falling during stair walking.

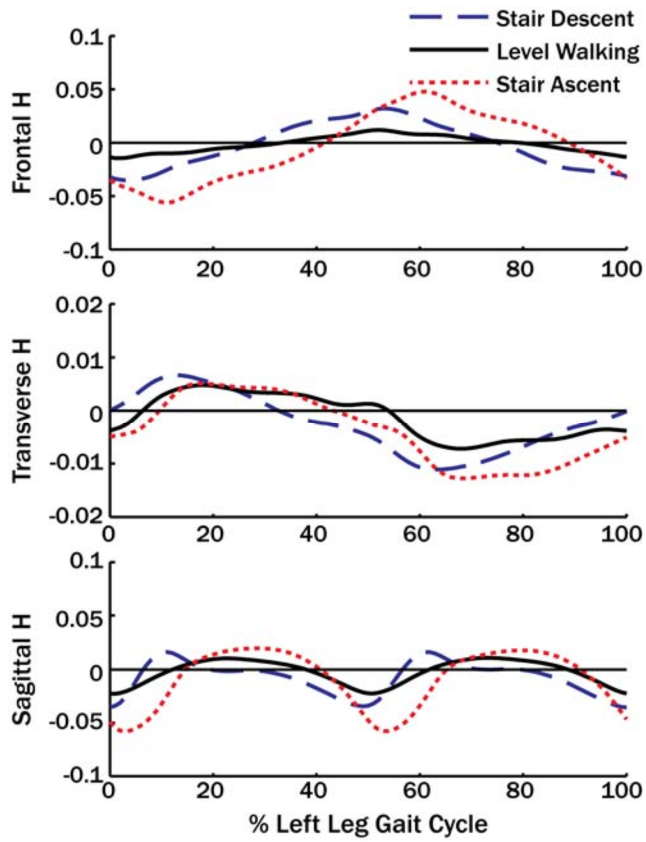

Figure 1: Normalized 3D angular momentum (H) for stair ascent, level walking and stair descent.

REFERENCES

1. Herr H et al. *J Exp Biol* **211**, 467-481, 2008.
2. Silverman A, et al. *J Biomech* **44**, 379-385, 2011.
3. Pijnappels M, et al. *J Biomech* **37**, 1811-1818, 2004.
4. McFadyen B, et al. *J Biomech* **21**, 733-744, 1988.
5. Nadeau S, et al. *Clin Biomech* **18**, 950-959, 2003.
6. Neptune, RR, et al. *J Biomech* **41**, 6-12, 2011.
7. Neptune, RR, et al. *Proceedings of ISB 2011 Conference*, **129**, Brussels, Belgium, 2011.

MUSCLE CONTRIBUTIONS TO WHOLE-BODY ANGULAR MOMENTUM DURING UNILATERAL BELOW-KNEE AMPUTEE WALKING

[1]Anne K. Silverman and [2]Richard R. Neptune

[1]Department of Mechanical Engineering, Colorado School of Mines, Golden, CO, USA
[2]Department of Mechanical Engineering, The University of Texas at Austin, Austin, TX, USA
email: asilverm@mines.edu

INTRODUCTION

Unilateral, below-knee amputees have altered angular momentum trajectories over the gait cycle relative to non-amputees [1]. However, it is unclear how individual muscles contribute to these altered patterns. The time rate of change of whole-body angular momentum equals the external moment about the body center-of-mass (COM). Muscles are the primary contributors to this moment due to their contributions to ground reaction forces (GRFs) [2]. Thus, muscles have a critical role in regulating whole-body angular momentum during human movement. Previous work has shown that the ankle muscles have large contributions to the external moment in the sagittal plane during non-amputee walking [2]. Thus, amputees must compensate to regulate their angular momentum and maintain dynamic stability during walking. In this study, we investigated individual muscle and prosthesis contributions to the external moment, and therefore the regulation of whole-body angular momentum, during amputee walking relative to non-amputee walking.

METHODS

A 3D musculoskeletal model with 14 body segments, 23 degrees of freedom, and 38 Hill-type musculotendon actuators per leg was developed in SIMM to represent a 70-kg non-amputee. The model was then altered to represent an amputee by removing the ankle muscles and adjusting the mass and inertial properties of the residual leg [3]. The ankle-foot prosthesis was modeled using a second-order passive spring at the ankle joint as:

$$\tau = a_0 + a_1\theta + a_2\omega + a_3\theta^2 + a_4\omega^2$$

where θ is the ankle angle, ω is the ankle velocity, and τ is the ankle torque. Constants a_0-a_4 were determined from a multiple regression analysis of experimentally-collected data. Muscle excitations were modeled using bimodal excitation patterns. Representative simulations of amputee and non-amputee walking were generated using a simulated annealing algorithm that optimized the muscle excitations such that the differences between experimental and simulated kinematics and GRFs were minimized. The experimental data consisted of group-averaged kinematic and GRF data from 14 amputees and 10 non-amputees walking at 1.2 ± 0.06 m/s [1].

Similar to our previous work [2], we quantified muscle and prosthesis contributions to the regulation of whole-body angular momentum by their contributions to the external moment, defined as:

$$\vec{M}_{EXT} = \dot{\vec{H}} = \vec{r} \times \vec{F}_{GRF}$$

where $\vec{r}$ is the position vector from the body COM to the foot center-of-pressure and $\vec{F}_{GRF}$ is the corresponding GRF. In this study, we focused on the sagittal plane, where the anterior/posterior (A/P) and vertical GRFs from each leg contribute to the external moment. Specifically, we determined muscle and prosthesis contributions to the external moment from the residual, intact and non-amputee legs over each respective stance phase.

RESULTS AND DISCUSSION

Overall, the muscle contributions in the intact and non-amputee legs were similar. The residual leg in the amputee simulation had a greater positive M_{EXT} in early stance and a greater negative M_{EXT} in mid-stance relative to the non-amputee simulation (Fig. 1). A larger magnitude of M_{EXT} will result in a greater change in the angular momentum trajectory, which is consistent with the greater range of sagittal-plane angular momentum observed experimentally in early residual-leg stance [1]. Also, individual muscle contributions to M_{EXT} were consistent with previous studies of non-amputee walking [2].

The vasti muscles contributed to a positive (backward) M_{EXT} from early to mid-stance in both the amputee and non-amputee simulations (Fig. 1). However, the residual leg had a larger positive contribution from the vasti muscles (Fig. 1). The greater net positive contribution from the vasti in the amputee simulation was the result of a reduced negative contribution to M_{EXT} due to a decreased contribution from the vasti to the A/P GRF.

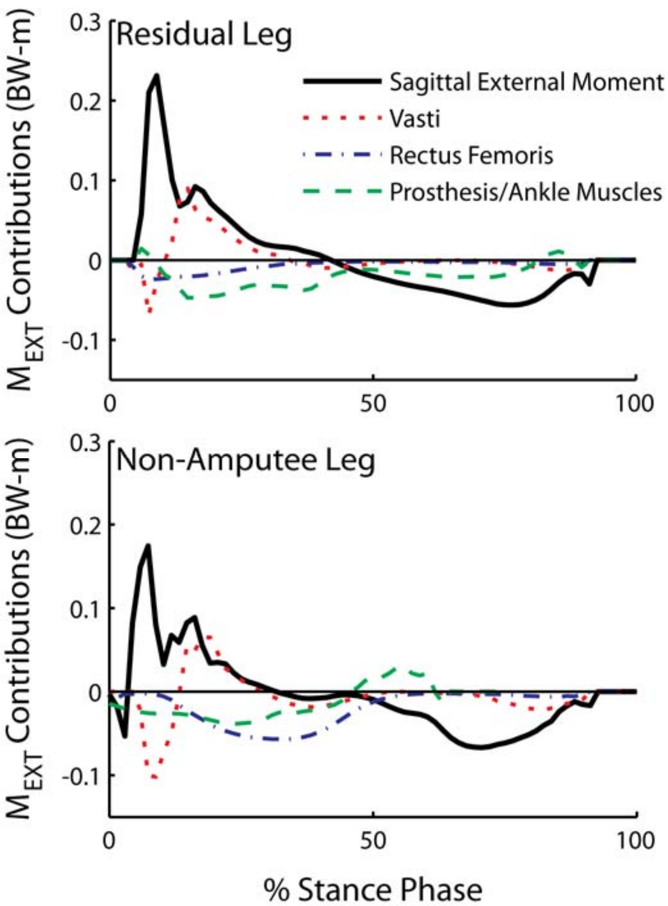

Figure 1: Muscle and prosthesis contributions to the sagittal-plane external moment during amputee and non-amputee walking (normalized by body weight (BW)). The prosthesis contributions are compared to the net contributions from all the muscles crossing the ankle joint in the non-amputee simulation.

Both the amputee and non-amputee simulations had negative (forward) contributions from the rectus femoris. The rectus femoris contribution in the amputee simulation was less negative than in the non-amputee simulation. Again, this was due to the reduced contribution to the negative A/P GRF in early stance.

The prosthesis functioned similarly to the non-amputee soleus muscle in that it contributed to a negative M_{EXT} for the majority of the stance phase. However, the contribution was more negative for the prosthesis relative to the soleus from early to mid-stance. In addition, the non-amputee simulation had a positive contribution from the tibialis anterior in early stance and the gastrocnemius in late stance, which was not present for the amputee simulation. Previous work has shown the prosthesis contributes substantially to body support, but provides less body propulsion in late stance relative to the ankle plantar flexors [4]. Thus, the prosthesis provided a negative (forward) M_{EXT} in late stance through its contributions to the vertical GRF, but had reduced positive contributions in late stance because it did not provide as large a propulsive A/P GRF compared to the ankle plantar flexors.

CONCLUSIONS

These results provide insight into how amputees regulate sagittal-plane angular momentum over the gait cycle. Amputees have lost the functional use of the residual-leg ankle muscles, which are important regulators of angular momentum in non-amputee walking. Altered contributions from the vasti and rectus femoris muscles contributed to a more positive M_{EXT} in early residual-leg stance, resulting in a greater range of angular momentum. Negative contributions from the prosthesis in late stance also contributed to the altered angular momentum trajectory.

REFERENCES

1. Silverman AK, et al. *J Biomech* **44**, 379-385, 2011.
2. Neptune, RR, et al. *J Biomech* **41**, 6-12, 2011.
3. Mattes SJ, et al. *Arch Phys Med Rehabil* **81**, 561-568, 2000.
4. Silverman, AK, et al. *Proceedings 2010 Annual ASB Meeting*, **34**, Providence, RI, 2010.

AGE RELATED CHANGES IN RUNNING

Julia Freedman Silvernail[1], Eric Rohr[2], Gert-Peter Brueggemann[3], Joseph Hamill[1]

[1] Biomechanics Laboratory, University of Massachusetts, Amherst, MA, USA
[2] Human Performance Laboratory, Brooks Sports Inc. Bothell, WA, USA
[3] Institute of Biomechanics and Orthopaedics, German Sports University, Cologne, Germany
Email: jfreedman@umass.kin.edu

INTRODUCTION

Running is a popular form of exercise and recreation and an activity that has been the subject of research for many years. In spite of this ongoing research, runners are frequently injured [1]. Participation in competitions, such as the New York City marathon, decreases rapidly after the age of 54 [2]. In addition, research has shown that runners over the age of 50 are at increased risk of being injured compared to younger runners [3]. What remains unknown is why some older runners have the ability to remain healthy and continue running.

In spite of the increased risk of injury, there is a paucity of research investigating older runners. Therefore, the purpose of this study was to compare gait in younger and older runners. We hypothesized that older runners would run with lower vertical loading rate, and greater knee flexion, and lower joint moments than younger runners.

METHODS

Thirty participants were recruited from the University community and consented to participate in the study. All participants were healthy runners who ran at least ten miles per week and were free of lower extremity injury. Participants were placed into two groups according to their age: Younger adults between the ages of 18 and 30; and Older adults between the ages of 45 and 65. Groups were matched by gender, age, height, mass and miles run each week (Table 1).

Participants were fitted with retro-reflective markers attached to the right lower extremity and were allowed to practice running trials. The laboratory consists of a 25 meter runway surrounded by an eight camera 3D motion capture system (Oqus, Qualysis, Inc., Gothenburg, Sweden) with a force platform (AMTI, Watertown, MA, USA) mounted flush with the floor in the center of the runway. Running trials consisted of participants running within 5% of 3.5 m/s while contacting the force platform with their right foot with a natural stride. Running velocity was monitored by two photo-electric sensors (Lafayette Instrument Company, Lafayette, IN, USA) placed six meters apart on either side of the force platform. Participants completed running trials while running in a standard running shoe provided by the lab. Kinematic and kinetic data were collected during trials at 240Hz and 1200Hz respectively.

Data were filtered with a low-pass Butterworth filter with a 12 Hz cut-off for the kinematic data and 50Hz cut-off for the kinetic data. Joint angles and moments were calculated for the ankle, knee and hip and stance time was determined. Values of joint angles and moments at footstrike and at their maximum points were determined. Joint angle range of motion (ROM) was calculated from the difference between the joint angle at footstrike to its maximum value during stance. Force variables of impact peak (F1) and vertical loading rate were calculated for all trials with an impact peak.

RESULTS

No differences were observed between younger and older runners for the investigated force variables or the stance time. Ankle and knee joint maximum angles, angle at footstrike and joint range of motion were similar between groups. Hip rotation and frontal plane maximum angles, angle at footstrike and range of motion were similar between groups. Knee and hip joint moments were similar between groups, as were transverse and frontal plane moments at the ankle.

Older adults ran with a more extended hip throughout stance (Figure 1). They had significantly greater amount of hip range of motion than younger adults ($p<0.05$). Maximum hip flexion, occurring near footstrike, was greater in younger adults than older adults ($p<0.05$), yet older adults reached a more extended hip position at the end of stance than the younger adults ($p<0.05$).

Younger adults ran with a significantly larger maximum plantar-flexion moment than older adults ($p<0.05$).

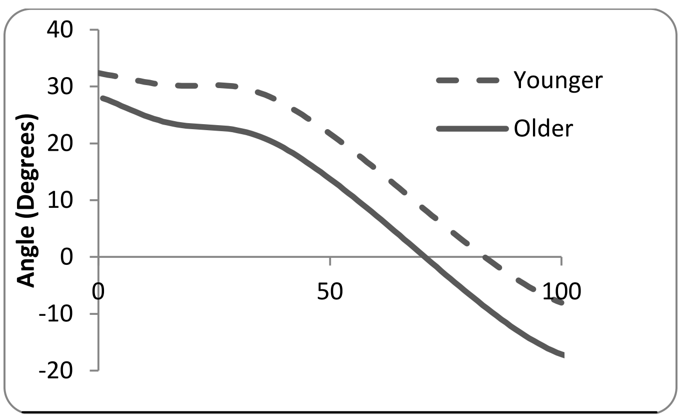

Figure 1: Mean sagittal plane hip angle during stance in younger and older adults.

DISCUSSION

Contrary to our hypotheses, younger and older runners ran with similar knee and ankle kinematics and similar ground reaction force characteristics. Despite a greater range of motion at the hip, older adults selected to run with a more extended hip. It is not known if this was a postural change or if it was a change made to avoid injury.

As hypothesized, older adults had a smaller maximum ankle plantar-flexion moment than younger adults. Yet this was the only joint that a decreased moment was observed.

In order to compare gait characteristics, all participants were asked to run at the same velocity. All participants provided a self-reported pace for their typical run. The preferred pace of the older runners was slower than that of the younger runners. Therefore, had participants run at their preferred running velocity differences may have been observed in a greater number of variables.

CONCLUSION

The observed differences between younger and older runners provide initial evidence of changes that are made with aging in running style. With further investigation, other differences in gait may be identified, and the changes that older runners may select to protect from injury can be determined.

REFERENCES

1. James SL, et al. *Am J Sports Med* 6(2), 1978.
2. Finisher Demographics, www.nycmarathon.org, 2011.
3. Taunton JE, et al. *British J Sports Med* 37, 2003.

ACKNOWLEDGEMENTS

This project was supported by Brooks Sports Inc.

Table 1: Group demographics: Mean (Standard Deviation)

	Gender	Age (years)	Height (m)	Mass (kg)	Miles Run/Week
Younger	4 Female; 11 Male	21.2 (3.1)	1.73 (0.07)	68.6 (7.9)	25.3 (15.8)
Older	4 Female; 11 Male	54.6 (6.4)	1.71 (0.07)	68.3 (7.8)	26.7 (13.1)

RELIABILITY OF LUMBAR VERTEBRA POSITION AND ORIENTATION MEASUREMENT USING WEIGHT-BEARING MRI

[1]Craig J. Simons, [1]Bradley S. Davidson, and [2]Loren Cobb

[1]University of Denver, Denver, CO, USA
[2]University of Colorado Denver, Denver, CO, USA
email: craig.simons@du.edu

INTRODUCTION

Low back pain and spinal instability are frequently linked to abnormal motion in the lumbar spine [1,2]. However, complex and inaccessible anatomy combined with small coupled intervertebral motions provide a challenging environment in which to accurately and reliably measure spine kinematics. Past investigations of *in vivo* spine kinematics have used computed tomography and conventional magnetic resonance (MR) imaging, which requires that the participant be supine [3] and restricts available range of motion at the joint of interest, particularly in sagittal plane.

Weight-bearing MRI, a relatively new technology, enables imaging while standing, sitting, or lying, and accommodates the full functional range of most joints. This versatility potentially provides a powerful tool to characterize healthy and pathologic structural kinematics, and to develop subject-specific rigid-body and finite element models.

Reconstructing the 3D position and orientation of a structure from MR images can be labor intensive. Weight-bearing MR images are produced using 0.5-0.6 Tesla magnets (1.5 Tesla in conventional MR), at short scan times to accommodate multiple images. Because of the reduced detail, time-saving automated segmentation and registration methods used in conventional MR are not reliable in weight-bearing MR. A previous investigation of the lumbar spine using weight-bearing MR relied upon the mean of five reconstructions performed by an individual to ensure reliable kinematics [4]. This substantial time investment currently limits the usefulness of weight-bearing MR in quantitative research and modeling applications.

The objective of this investigation was to assess the reliability of a novel semi-automated process to determine vertebral position and orientation from sagittal weight-bearing MR images across a full range of flexion/extension motions while standing. We hypothesized that the interrater reliability would be good (ICC>0.75) for vertebral position and orientation in the primary plane and moderate (ICC>0.5) for out-of-plane measurements.

METHODS

Participants attended a single data collection in which sagittal plane T1-weighted MR images were collected during one neutral posture while sitting and five flexion/extension postures (postural scans) while standing. The Fonar 0.6-Tesla Upright MRI was configured to maximize detail during the sitting scan and minimize imaging time during the five postural scans (Table 1). During the postural scans, the pelvis was restrained to isolate lumbar motion and a padded bar was placed under the torso to reduce movement artifact in the image.

We developed a unique registration method that superimposes high-detail vertebra with body-fixed coordinate systems (from seated scan) onto the

Table 1: MRI Scan Settings Sagittal Plane

	Slice Thickness	Slice Interval (mm)	# of Slices	Repetition Time (ms)	Echo Time (ms)	Scan Time (min)
High-Detail Scan	4	4	20	610	17.0	~5.0
Postural Scans	5	8	10	350	17.0	~2.75

same low-detail vertebra (from postural scans). Body-fixed coordinate systems were assigned to each high-detail vertebra similar to ISB recommendations (*x*-axis in right dir., *y*-axis in anterior dir., and *z*-axis in vertical dir.). Individual high-detail vertebral reconstructions were superimposed onto the low-detail reconstructions of the postural images using a K-D tree iterative closest point (ICP) algorithm that minimized the mean square error between points in the two reconstructions. The ICP algorithm generated translational and rotational transformation matrices to map between the individual vertebra from the sitting and the postural trials. Final position and orientation for each vertebra were referenced to a body-fixed coordinate system on the sacrum. Dependent variables included rectangular positions (x,y,z) and Cardan angles (α,β,γ) with respect to the sacral coordinate system.

Images of five flexion/extension postures taken from one participant were segmented and registered by three researchers (raters), each with a different level of experience. This resulted in 25 vertebral reconstructions available from each rater for analysis. The effect of rater on each dependent variable was assessed with a mixed-model ANOVA: fixed effect of rater and random effect of vertebra. Intraclass Correlation Coefficients (ICC model 2,1) were calculated for each dependent variable.

RESULTS AND DISCUSSION

ICCs indicated good interrater reliability for sagittal plane positions, y (ICC=0.966) and z (0.752), but poor reliability for the x (-0.098) position. ICCs indicated good interrater reliability for sagittal plane rotation, α (0.839), but poor reliability for second and third rotations, β (0.294) and γ (0.163). The effect of rater was statistically significant for each variable ($p<0.05$), and Tukey HSD demonstrated differences between the most experienced and least experienced in all variables.

Several factors may contribute to the low reliability of the *x*-position. First, ICC calculations are sensitive to error when lacking a large range of values relative to the sample variance. Because the mediolateral positions during flexion/extension are small, they are most prone to low ICCs. In addition, scan detail is reduced at the lateral edges of the images because the vertebra may not occupy the full thickness of the slice, and could lead to high rater error in the *x*-direction. Adding simultaneous coronal scans could improve the lateral results, but this would come at the expense of increased imaging time and participant fatigue.

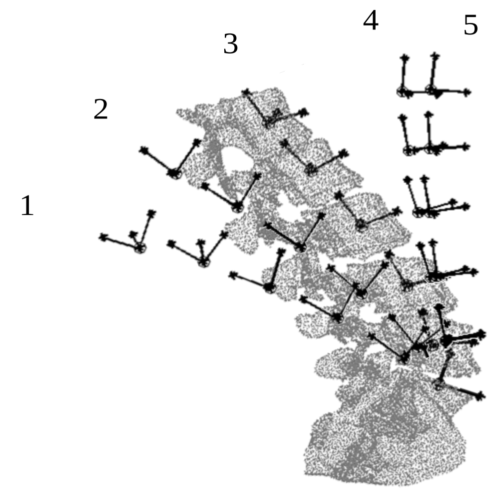

Figure 1: Coordinate systems for five postures with complete reconstruction shown in neutral posture (1 = full extension, 5 = full flexion)

In summary, this method of registration provides a fast and reliable technique to assess sagittal plane vertebral positions and orientations. Future refinements will improve reliability and these data will be used to develop predictive position and orientation estimates through machine learning applications.

REFERENCES

1. Panjabi MM. *J Electromyogr Kines* **13**, 371-379, 2003
2. Cholewicki J. *Clin. Biomech.* **11**, 1-15, 1996
3. Fujii R, et al. *Eur Spine J* **16**, 1867-1874, 2007
4. Cargill SC, et al. *Spine* **32**, 1242-1248, 2007

ACKNOWLEDGEMENTS

Thanks to MRI of America for providing access to the Fonar MR. This work was supported in part by grant R00 AT004983-03 (to BSD) from NIH (NCCAM).

DOES INTERLIMB KINEMATIC SYMMETRY EXIST DURING STAIR ASCENT AFTER UNICOMPARTMENTAL KNEE ARTHROPLASTY?

[1]Kathy J. Simpson, [1]Yang-Chieh Fu, [2,3]Tracy L. Kinsey, [1]Cathleen N. Brown, [2]Ormonde M. Mahoney

[1]University of Georgia, Athens, GA, USA
[2]Athens Orthopedic Clinic, Athens, GA, USA
[3]Department of Epidemiology, University of North Carolina, Chapel Hill, NC, USA
email: ksimpson@uga.edu web: http://www.coe.uga.edu/kinesiology/research-service/biomechanics/

INTRODUCTION

Unicompartmental knee arthroplasty (UKA) is a treatment option for people that have osteoarthritic disease primarily in the medial (MED) or lateral (LAT) tibio-femoral compartment. There are insufficient data to assess the biomechanics of UKA limbs for functional activities, especially for LAT-UKA [1], although the clinical outcomes and survival rates have been improving in recent years [2,3]. However, some surgeons are reluctant to use UKA [1]. Therefore, the purpose of the study was to determine the interlimb symmetry for gait and knee kinematics of individuals with MED and LAT UKA during a functional stair ascent task.

METHODS

Healthy unilateral UKA individuals, 17 MED-UKA and 9 LAT-UKA (respectively, age: 68.0 ± 7.4 yrs, 63.1 ± 7.8 yrs; ht: 162.7 ± 7.1 cm, 167.2 ± 6.4 cm; mass: 74.1 ± 12.3 kg, 71.1 ± 13.3 kg) with 14 and 9 iBalance Unicondylar Knee®, respectively, and 3 and 3 Zimmer® Unicompartmental High Flex Knee Systems, participated. All surgeries were performed by author OMM at least 6 mo. prior to testing. All participants provided informed consent. Reflective markers affixed to the lower extremities and locations of markers were collected using high-speed digital cameras (120 Hz) [4]. Participants walked up 4 stairs barefoot at a self-selected speed for 5 trials starting on each limb. The order of starting limb was counterbalanced.

For each trial, spatiotemporal variables were calculated for one stride starting at touchdown onto the 1st step. Angular knee joint displacements for the 1st step support phase were computed. For each UKA group, paired t-tests were applied to determine interlimb differences ($p < 0.05$). 95% CI were also generated for interlimb differences of each variable. Interlimb symmetry was classified qualitatively using the 'symmetry angle' method: *symmetry*: 0% - 5%; *low asymmetry*: 6% - 10%, and *asymmetry*: ≥ 11% [2]. The frequencies of individuals in each UKA group displaying these symmetry classifications were generated.

RESULTS AND DISCUSSION

Neither group demonstrated significant interlimb differences for any temporal ($p > .321$) variable. No knee displacement variables were significant (Table 1), either. This was due to the interparticipant variability of limb differences, as shown by the 95% CI and by the frequency distributions in Table 2 for symmetry/asymmetry of knee displacement variables.

Qualitatively, for both groups, knee flex/extension variables demonstrated interlimb symmetry by nearly all participants. However, few participants displayed adduction displacement symmetry, and ˜66% of participants in each UKA group displayed asymmetry. However, it is apparent for the adduction and internal/external directions, that the classification of symmetry/asymmetry, as well as the limb that demonstrated the greater knee joint asymmetry, varied among participants. Potential reasons for these variations include participant-dependent kinematic or kinetic stair-ascent strategies; factors related to the surgery, e.g., soft tissue release, pre-surgery knee varus/valgus malalignment; age and/or asymptomatic OA in the nonUKA limb [2]. However, the effects of these factors cannot be determined with this small sample size. Limb dominance was not strongly correlated with interlimb differences (r: ˉ.23 to .23).

Patil et al. [5] tested int/external rotation for 6 cadaver knees during machine testing under simulated stair ascent loading conditions. Rotations were similar during UKA and the nonoperated condition. They concluded that UKA had the potential to produce normal kinematic function. Some of our participants displayed rotation kinematics congruent with this finding.

CONCLUSIONS

For adduction and int/external rotation displacements during stair ascent, symmetries and asymmetries were likely affected by participant-related factors than the UKA components. Qualitatively, symmetries/asymmetries were similar for MED- and LAT-UKA groups. Therefore, understanding of the factors that affect ab/adduction and int/external roatation asymmetries of UKA individuals is needed. UKA participants do display symmetry for knee flex/extension motions.

REFERENCES

1. Verdonk, R., et al., *Knee Surg Sport Tra A*, **13**, 163-166, 2005.
2. Saccomanni, B., *Clin Rheumatol* **29**, 339-346, 2010.
3. Schiavone, E., et al., *Knee Surg Sport Tra A*, **20**, 579-585, 2012.
4. Fu, Y.-C., et al., *Annual meeting of ASB*, Long Beach, CA, USA, 2011.
5. Patil, S., et al., *J Bone Jt Surg*, **87-A**, 332-338, 2005.

Table 1: UKA and nonUKA (NUKA) limb means ± SD and *p* value of paired t-tests for knee angular displacement variables (deg.) of medial (MED) and lateral (LAT) UKA groups. Also shown: Lower (LB) and upper bounds (UB) of 95% CI of interlimb differences.

	MED-UKA Group					LAT-UKA Group				
	Limb Means			95% CI		Limb Means			95% CI	
Variable	UKA	NUKA	*p*	LB	UB	UKA	NonUKA	*p*	LB	UB
Extension	52.9 ± 5.1	54.3 ± 5.4	.198	-3.9	0.9	58.4 ± 6.1	55.9 ± 5.8	.215	-1.7	6.5
Flexion	84.8 ± 5.8	86.6 ± 5.7	.215	-4.9	1.2	88.0 ± 8.3	86.4 ± 8.9	.333	-2.0	5.2
Adduction	11.0 ± 5.1	9.3 ± 5.9	.349	-2.0	5.4	8.8 ± 6.9	11.2 ± 7.0	.230	-6.8	1.9
Int. Rot.	14.7 ± 4.9	15.1 ± 4.1	.693	-2.6	1.8	14.1 ± 7.3	15.6 ± 4.8	.439	-5.7	2.7
Ext. Rot.	22.9 ± 7.4	24.0 ± 9.4	.471	-4.3	2.1	22.1 ± 10.1	25.8 ± 8.0	.272	-10.9	3.5

Table 2. Frequencies of participants (% of participants of each UKA group) that exhibit each category of symmetry (Sym.) and asymmetry for knee joint displacement variables. For asymmetries, the limb demonstrating the greater magnitude is listed as UKA (arthroplasty) and NUKA (nonUKA) limb.

	MED-UKA					LAT-UKA				
		Low Asymmetry		High Asymmetry			Low Asymmetry		High Asymmetry	
Variable	Sym.	UKA	NUKA	UKA	NUKA	Sym.	UKA	NUKA	UKA	NUKA
Ext.	88.2	0.0	11.8	0.0	0.0	77.8	22.2	0.0	0.0	0.0
Flex.	94.1	0.0	5.9	0.0	0.0	100.0	0.0	0.0	0.0	0.0
Adduction	5.9	17.6	11.8	41.2	23.5	22.2	11.1	0.0	22.2	44.4
Int. Rot.	52.9	5.9	17.6	11.8	11.8	44.4	22.2	0.0	0.0	33.3
Ext. Rot.	35.3	23.5	23.5	5.9	11.8	33.3	22.2	11.1	0.0	33.3

ADAPTIVE CHANGES IN FINGER FORCE VARIANCE IN RESPONSE TO INDEX FINGER FATIGUE IN UNIMANUAL AND BIMANUAL TASKS

Tarkeshwar Singh, Vladimir. M. Zatsiorsky, and M. L. Latash
The Pennsylvania State University, University Park, PA, USA
email: tarkesh@psu.edu

INTRODUCTION

On the one hand, muscle fatigue causes a drop in the maximal voluntary contraction (MVC) force and also in the accuracy (measured as an increase in intra-trial variability) of force production by the fatigued elements. On the other hand, accuracy of tasks performed by redundant sets of elements may be relatively preserved. Previously, we have shown that this is achieved by the less affected elements showing an increased variance of their outputs accompanied by a strong negative co-variation among the outputs of all the elements [1]. To quantify the change in performance due to fatigue, we used the framework of the uncontrolled manifold (UCM) hypothesis [2]. The hypothesis assumes that the controller organizes covariation among elemental variables (finger modes (*m*) in our study) to stabilize a certain value of a performance variable (total force). We quantified variance in two sub-spaces within the *m* space, one corresponding to a fixed value of total force (V_{UCM}) and the other leading to changes in the total force (V_{ORT}, orthogonal to the UCM). Several fatigue studies have documented fatigue-induced decline in the maximal voluntary contraction force (MVC) and increased motor-unit synchronization [3] not only within the exercised limb but also in the non-exercised limb. Thus, our hypothesis was that the non-exercised hand would show effects on the two variance components (V_{UCM} and V_{ORT}) similar to those in the exercised hand, but possibly of smaller magnitude.

METHODS

Thirteen right-hand dominant participants (seven males) participated in the experiment. This study involved force production with the index and middle fingers of the left and right hands. Four six-component force sensors (Nano-17, ATI Industrial Automation, Garner, NC) were used to measure the normal forces generated by individual digits. Two force sensors (for the index and middle fingers) were attached to two customized flat panels for each of the hands (see Figure 1). Only the normal force data were collected from the sensors.

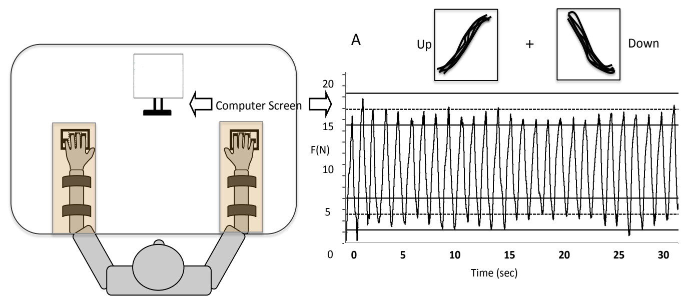

Figure 1: A schematic of the experimental setup; the bottom right part shows the feedback shown to the participants on the computer screen. The cycles were separated into force up and down half-cycles.

The participants performed unimanual and bimanual rhythmic accurate force production tasks (see Figure 1). Each participant made three visits to the Laboratory. The first visit was a practice session without a fatiguing exercise. The second and third sessions were separated exactly by one week. Within the second and third sessions, participants exercised the left index finger ($Left_{Fatigue}$) or the right index finger ($Right_{Fatigue}$). Three factors were manipulated: *fatigue* (two levels – before-fatigue and during-fatigue), *exercised-hand* (two levels – $Left_{Fatigue}$ and $Right_{Fatigue}$), and *Tested-hand* (exercised and non-exercised hand as levels).

RESULTS AND DISCUSSION

Before-fatigue, the right hand was stronger than the left hand by ~15%. A one-way MANOVA with MVC of I and IM as dependent variables and *Hand* (left and right hand as levels) as a factor revealed a significant main effect of *Hand* ($p<0.05$). Fatigue led to a significant reduction in the MVC produced by the I and IM finger combinations. The MVC of the exercised hand (ipsilateral fatigue) dropped more than the MVC of the non-exercised hand (contralateral fatigue). Fatigue led to a ~20% drop in MVC in the bimanual task. There were no differences between the hands in the root mean square error (RMSE) index prior to the fatiguing exercise. The ipsilateral effects of exercise were strong in the up direction; the RMSE of the left hand increased by ~27% and that of the right hand by ~22% (both $p<0.01$). There were no changes in the RMSE of the non-exercised hand. Fatigue did not have a significant effect on RMSE in the force-down direction. For the bimanual task, fatigue increased the RMSE by about ~14% in the up direction. The effect of *exercised-hand* was not significant.

Both exercises ($Left_{Fatigue}$ and $Right_{Fatigue}$) had strong ipsilateral effects on V_{UCM}. Ipsilateral fatigue also increased V_{ORT} but the increase in V_{ORT} was not as large as that of V_{UCM}. There were no contralateral effects of fatigue on V_{ORT}. Fatigue led to an increase in V_{UCM} in both exercised and non-exercised hands for both *force-up* and *force-down* segments (the black and gray columns in panels A and C of Figure 2) although only the increase in the exercised hand reached significance. For the bimanual task, fatigue increased V_{UCM} by about 80% on average. $Left_{Fatigue}$ increased V_{UCM} more than $Right_{Fatigue}$ by about 35%.

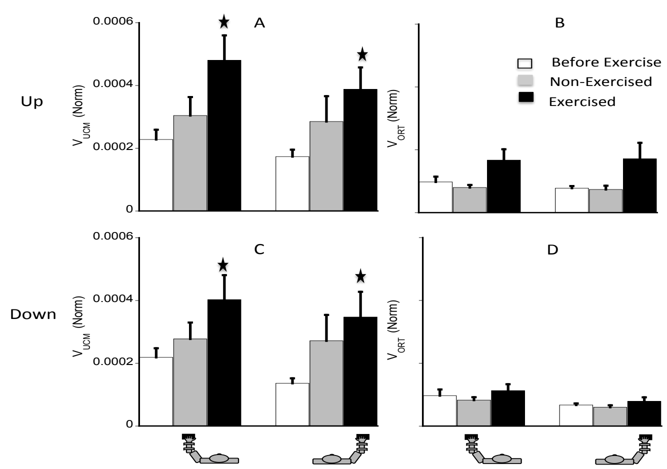

Figure 2: Average V_{UCM} (panel A) and V_{ORT} (panel B) for the up half-cycle. The left three bars show the means for the before-fatigue (white), non-fatigued (grey, contralateral fatigue), and fatigued (black, ipsilateral fatigue) condition. The right three bars show the means for the right hand.

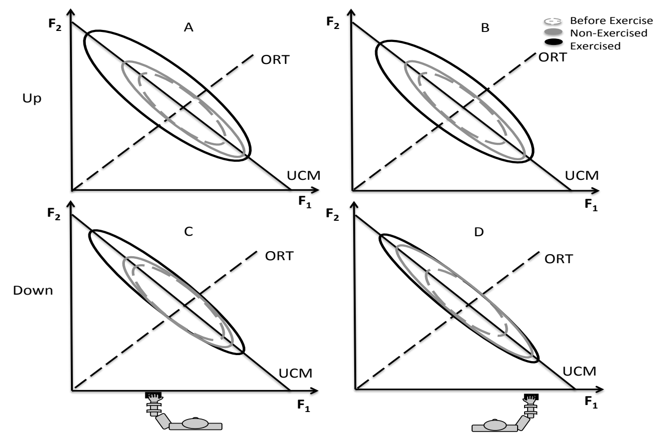

Figure 3: An illustration of hypothetical data point distributions for the task of accurate total force production with 2 fingers. A and B: In the force-up direction, for both the left (panel A) and the right hand (panel B), notice a larger increase in V_{UCM} than V_{ORT} during fatigue for the exercised hand. For the non-exercised hand, there is no change in V_{ORT} but V_{UCM} increases. C and D: In the force-down direction, for both the left (panel C) and the right hand (panel D), notice that there is no change in V_{ORT} for both the exercised hand as well as the non-exercised hand. V_{UCM} increases for the exercised as well as the non-exercised hand.

During one-hand tasks, both hands showed high indices of force-stabilizing synergies. These indices were larger in the left hand. Fatigue led to a general increase in synergy indices. Exercise by the left hand had stronger effects on synergy indices seen in both hands. Exercise by the right hand showed ipsilateral effects only. Smaller effects of fatigue were observed on accuracy of performance of the *force-down* segments of the force cycle as compared to the *force-up* segments (see Figure 3). The results confirmed the changes in multi-finger synergies stabilizing total force under fatigue and extended these observations to performance of the non-exercised hand. Some of the most unexpected results are the strong changes at the one-hand level, which was seen in two-hand tasks; the asymmetry of the effects seen in the right and left hands; and also of the effects seen during *force-up* and *force-down* segments.

REFERENCES

1.Singh et al. *J Neurophysiol,* **103:**2990-3000, 2010
2.Scholz et al. *Exp Brain Res,***126**, 289-306, 1999
3.Boonstra et al. *J Electromyogr Kines.18,717-731*, 2008

CHANGES IN GAIT OVER A 30 MINUTE WALKING SESSION IN OBESE INDIVIDUALS DO BIOMECHANICAL LOADS INCREASE IN PURSUIT OF WEIGHT LOSS?

[1]Bhupinder Singh, [2]Kathleen F. Janz, and [1]H.John Yack
[1]Program in Physical Therapy & Rehabilitation Sciences
[2]Department of Health and Sport Studies
University of Iowa, IA, USA
Email: bhupindersingh@uiowa.edu

INTRODUCTION

Walking, in combination with changes in diet, is commonly recommended for the treatment of obesity because it is a convenient physical activity that can be used to expend a significant amount of metabolic energy [1]. Exercise programs typically recommend walking for at least 30 minutes per session to comply with the current American College of Sports Medicine recommendations. It could be argued that 30 minute walking programs are too ambitious or too much for obese individuals [2]; however, there is no concrete evidence that documents the time dependent effects of these walking programs on gait mechanics in obese individuals. The purpose of this study is to assess the biomechanical gait changes in obese subjects over a 30 minute walking session. It is hypothesized that the hip and knee adduction and extensor moments, which are the primary modulators of frontal and sagittal plane load distribution, will increase in obese individuals, as they start to fatigue, resulting in more stress across the hip and the knee joint.

METHODS

Eight subjects mean age 37.4 ± 3.7 years; with BMI 39.2 ± 3.7 kg/m^2 participated in the study. Height, weight, waist circumference, hip circumference, resting BP, resting HR and SpO_2 were recorded. Infrared emitting diodes were applied to the lower limbs, pelvis, and trunk segments. Anatomical landmarks were digitized, relative to segment local coordinate systems, to create a link-based model. The gait evaluation was conducted along an 8 meter walkway using three-dimensional motion analysis system (Optotrak, NDI Inc., Ontario) and force plates (Kistler Instruments, Inc., NY). Tape marks were placed on the floor (based on their step length); so that the subject's natural approach to the force plates increased the probability of appropriate foot contact while they continuously walked back and forth at their predetermined self-selected speed. Treadmill session included total walking for 30 minutes out of which: Ebelling protocol (4 minutes at 0% incline and 4 minutes at 5% incline), was followed for the first 8 minutes [3]. On the treadmill, target heart rate was set between 65-85% of estimated maximum (208 - 0.7*age), SpO_2 was maintained above 93 and perceived exertion below 17 on the Borg scale. A post-treadmill gait analysis was conducted immediately following the treadmill protocol, with subjects sustaining the same speed as the initial pre-treadmill during a continuous overground test.

DATA ANALYSIS

Visual 3D software (C-Motion) was used for processing and the moments were normalized to body mass. A symmetry index was calculated to investigate differences in moments on the right and left side and the side with greater increase in the moments was used for further analysis. Paired t-tests ($p<0.05$) were performed to determine differences in mean peak hip and knee moments.

RESULTS AND DISCUSSION

The subjects walked at an average self-selected speed 3.06 miles/hr. All subjects reported similar fitness levels; $V0_2$ max calculated from the Ebelling protocol using speed on the treadmill, heart rate, age and gender was estimated to be 31.65 ± 3.48 ml/min/kg.

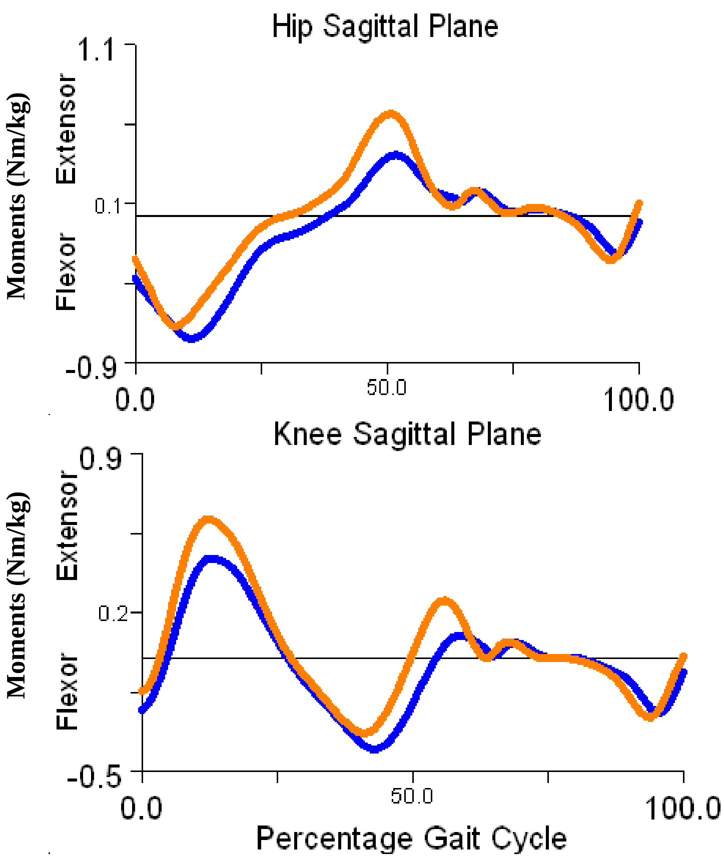

Figure 1: Representative data showing an increase in the knee and hip extensor moments (Nm/kg) post 30 minute treadmill walking (orange) as compared to pre treadmill (blue) during a complete gait cycle (toe-off to toe-off).

Analyzing the side with greater change, the peak hip adduction moment increased from 0.84 ± 0.26 Nm/kg at pre treadmill to 0.94 ± 0.19 Nm/kg (p= 0.06). Similarly, the knee adduction moments increased (p=0.21), however not significantly.
Hip moments during post treadmill were higher than the pre-treadmill session (p=0.009). The second knee peak extensor moment, associated with controlling the knee during the swing phase of gait cycle, also increased (p= 0.01). (Table 1)

The results showed an increase in the extensor moments at hip and knee after a 30 minute treadmill walking session. Hip extensor moments increased on both right and left side for all subjects except one. As the muscles fatigue, the increased hip extensor moments could be attributed to altered kinematics, e.g., increased flexion at the hip.
In the current study, some subjects showed an increase in knee adduction moments on one side whereas moments decreased on the other side suggesting compensations at other joints [4].

CONCLUSIONS

Our results show increases in extensor moments at both the hip and knee joints which points to greater muscle work and the possibility of increased joint stress. Increased muscle and joint stress can cause discomfort and can lead to non-compliance and attrition from the walking programs.

Taking into consideration time dependent changes in hip and knee joint kinetics may improve compliance to walking programs. Further analysis is being carried out to explore the compensations and the strategies adopted by the obese individuals as they fatigue during the 30 minute walking protocol.

REFERENCES:

1. Davis JN, (2006). Obesity, 14, 2259- 2266.
2. Browning RC, (2009). Journal of Biomechanics, 2, 2273–2278.
3. Waddoups L,(2008). Journal of Sports Sciences, 5,491-497.
4. Segal NA, (2009). Am J Phys Med Rehabilitation 88,180-188.

PEAK MOMENTS: PRE vs POST TREADMILL				
Moments(Nm/kg)	**Knee Adduction**	**Knee Extensor ***	**Hip Adduction**	**Hip Extensor ***
Pre treadmill	0.34 (0.14)	0.45 (0.27)	0.84 (0.26)	1.27 (0.42)
Post treadmill	0.44 (0.24)	0.89 (0.47)	0.94 (0.19)	0.68 (0.17)

Table 1: Represents the mean (standard deviation) of peak hip and knee adduction and extensor moments at pre and 30 minutes post treadmill for all subjects. * indicates significant difference between pre and post treadmill sessions.

EMPIRICAL PLANTAR PRESSURE INSOLE POSE ESTIMATION

Erik W. Sinsel, Maria K. Lebiedowska, Frank L. Buczek

National Institute for Occupational Safety and Health, Morgantown, WV, USA
email: Erik.Sinsel@cdc.hhs.gov

INTRODUCTION

Plantar pressure shoe insole center of pressure (COP) data have been used in whole body inverse dynamics analyses [1]. Errors in locating insole pose, or position and orientation, relative to the foot can introduce errors by altering the point of application of forces at the foot, and consequently the moment arm used to calculate joint moments. During the stance phase of gait, an anteroposterior (AP) shift in COP location of ±5 mm was found to produce errors in peak hip, knee, and ankle extensor and flexor joint moments of approximately 7%, on average [2].

Previous attempts to quantify the insole pose relative to the foot include mathematically aligning insole and force platform COP data using upright stance calibrations [1]. However, this method lacked independent verification of the insole pose. COP RMS error varied across the gait cycle, and was 8.6 mm AP during mid-stance. Plantar pressure insoles typically have lower spatial and data resolution than force platforms and may not measure all data relevant for calculating COP, such as tangential force components. The spatial location of the force platform COP would also contain some measurement error. These errors may propagate to the estimated insole pose.

We present a method for empirically quantifying the insole pose in the shoe, directly relating sensor cell location to the foot. It addresses the need for an independently-derived insole pose for use with inverse dynamics analyses. We demonstrate the method's use in assessing the impact of insole migration on plantar pressure insole COP data.

METHODS

Five subjects, three male and two female, were enrolled in a study approved by the agency Human Subjects Review Board, and gave informed consent. Subject age, height and body mass: mean 27 years SD (6), 173 cm (9.5), 65.9 kg (15.7), respectively. Subjects wore leather low-rise, soft-toe, work shoes instrumented with plantar pressure insoles (Pedar-X, Novel GmbH), and performed a series of lifting and self-paced walking trials. Marker trajectories were obtained at 100 Hz using a 14-camera Vicon Nexus system and insole data at 50 Hz. Kinematic modeling was performed in Visual3D (C-Motion, Inc.) and analysis in MATLAB (The Mathworks, Inc.).

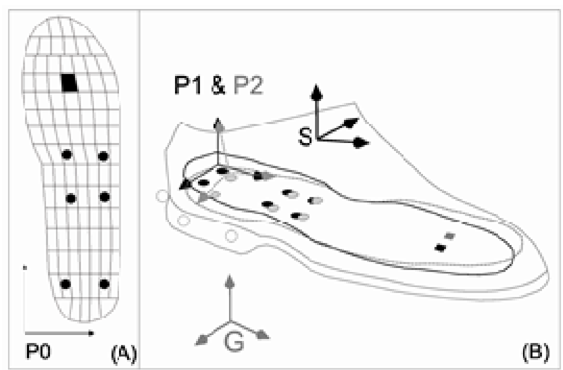

Figure 1: Global and local reference frames [3].

As described previously [3], manufacturer documentation was used to attach several 8-mm diameter disk markers to the insole (Fig. 1A). Prior to use, a flat insole calibration trial was collected, providing an undeformed insole reference frame (P0). The shoe was instrumented with motion capture markers used to create a local shoe reference frame (S), aligned with anteroposterior and mediolateral (ML) axes which defined the transverse plane (Fig. 1B). Pre- and post-use trials of the insole in the shoe provided the local insole reference frames in S as P1 and P2, respectively.

The axes of P0 were aligned with the manufacturer's coordinate system. The correspondence between the empirical insole markers' centroid in S and the centroid of nominal local sensor locations was used to locally translate P0's origin to be consistent with the insole specification [4]. Using the global reference frame (G) coordinates of the shoe and inserted insole markers, Visual3D software was used to perform a least squares fit of P0 onto the inserted insole marker locations, providing insole poses P1 and P2 in S. The root-mean-square (RMS) error between the insole marker locations in P1 and their nominal sensor locations in P0 was calculated (Table 1).

To demonstrate the method, for each subject a gait cycle from a walking trial was selected. A contiguous range of COP data for each foot was selected from initial to terminal contact, as reflected by insole data and verified by motion data. The insole COP was transformed into the shoe using P1, and compared to the similarly transformed COP using the potentially migrated P2 (Fig. 2). The migration-induced COP RMS error was calculated in the transverse plane of S (Table 1). Only overall observed migration was assessed, which may have occurred at any time.

RESULTS AND DISCUSSION

We found mean transverse RMS errors between the insole markers of P1, the inserted insole frame prior to use, and the corresponding sensors' nominal locations in the undeformed planar model to be 1.25 mm or less. Mean transverse COP RMS errors due to observed insole migration between P1 and P2 were found to be less than 1 mm.

Due to methodological differences, a direct comparison with the previous method is not possible. However, in the AP direction, the maximum insole frame RMS error of our method was 1.63 mm, compared to the mean 8.6 mm COP RMS error during mid-stance reported with the previous method.

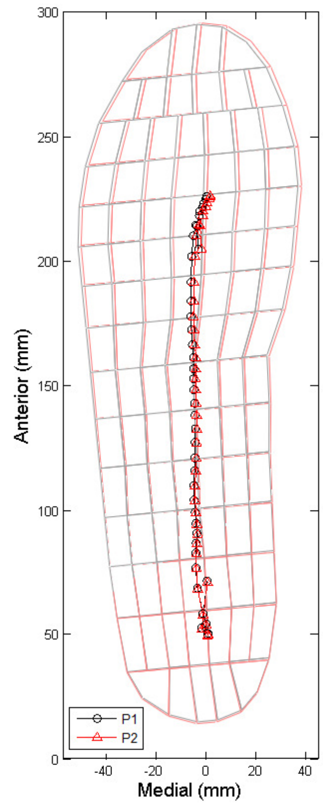

Figure 2: Example of COP in P1 and P2 in the transverse plane of S.

REFERENCES

1. Chumanov ES, et al. *Computational Methods Biomech. Biomed. Eng.* **13**: 505-514, 2010.
2. McCaw ST, et al. *J Biomech* **28**: 985-988, 1995.
3. Sinsel EW et al. *Proceedings of GCMAS'12*, Grand Rapids, MI, USA, 2012.
4. Horn, BKP, et al. *Journal of the Optical Society of America* **5**: 1127-1135, 1998.

DISCLAIMER

The findings and conclusions in this abstract have not been formally disseminated by the National Institute for Occupational Safety and Health and should not be construed to represent any agency determination or policy.

Table 1: RMS values for COP in P1 and P2 for consecutive left and right foot contacts during a single gait cycle per subject, and for the fit of the undeformed insole P0 in P1. Table combines left and right data (n=10).

	COP RMS (mm)			P1 Insole Frame RMS (mm)		
	AP	**ML**	**SI**	**AP**	**ML**	**SI**
Mean (SD)	0.97 (0.68)	0.89 (0.56)	4.12 (1.33)	0.88 (0.53)	1.25 (0.57)	2.48 (0.95)
Maximum	2.14	1.86	5.51	1.63	2.40	3.62

FREQUENCY DOMAIN ANALYSIS OF GROUND REACTION FORCE DOES NOT DIFFERENTIATE BETWEEN HYPERKINETIC AND HYPOKINETIC MOVEMENT DISORDERS.

Jared W. Skinner, Ryan Roemmich, Shinichi Amano, Elizabeth Stegemoller, Lori Altmann and Chris J. Hass

University of Florida, Gainesville, FL, USA
Email: jskinner1@ufl.edu

INTRODUCTION

Movement disorders can be clinically defined as neurologic conditions in which there is either an excess of movement (hyperkinetic) or a reduction of voluntary or automatic movements (hypokinetic). Essential tremor (ET) is a hyperkinetic disorder and is one of the most common movement disorders of older adults. ET is clinically characterized by an involuntary 4-10 Hz tremor that is most prevalent in the hands, arms, neck, and head that worsens with movement. Recent research indicates that ET is associated with brainstem and cerebellar dysfunction. Parkinson's disease (PD) on the other hand is the most recognized form of hypokinetic disorders. The cardinal symptoms of PD are 3-6Hz resting tremor, rigidity, postural instability and bradykinesia. PD is characterized by a degenerative loss of dopaminergic neurons in the substantia nigra of the basal ganglia.

The pathophysiologic changes occurring in the cerebellum and brain stem in ET and the basal ganglia in PD coupled with differences associated with resting and active tremor could elicit changes in functional performance such as gait and decrease the quality of life in the patients with these disorders. These two neurological disorders share similar characteristics of tremor and gait disturbance; thus there is the possibility for misdiagnoses. Indeed, approximately 30-50 % of patients with ET are misdiagnosed with PD or other tremor disorders [5].

During normal locomotion, each limb contributes forces to vertical support of the body in addition to providing braking and propulsive forces to maintain balance and forward velocity. The impairments in these movement disorders can have detrimental effects on the spatial-temporal characteristics of gait, such as reduced velocity, stride length, cadence, cycle length symmetry and disturbances in the support phase during gait [4].

The support phase can be evaluated via inspection of the ground reaction forces (GRF). In patients with PD and ET the GRF are reduced, which lead to increased gait and balance impairment [4]. The study of GRF during gait has been important in the identification and evaluation of gait in other patient populations [1-3]. One method that has gained attention is the use of frequency domain analysis. Assessing the frequency domain of patients' GRF may provide insight in early detection and distinguish characteristics of GRF in hypokinetic and hyperkinetic movement disorders. The purpose of this investigation was to compare the 99.5% frequency, median frequency and frequency bandwidth of the anterior-posterior and vertical GRF's in patients with PD and ET during over ground walking.

METHODS

Twenty six patients with PD (66.7±8.6.yr, 170.7±7.1cm, 80.16±12.6kg) and 15 patients with ET (67.8±7.9yr, 173.3±7.6cm, 88.4±10.6kg) participated in this investigation. Patients walked across an eight-meter long walkway containing three Bertec force plates (Bertec Corporation, Columbus, OH, USA) mounted flush to the laboratory floor. Subjects walked at a comfortable, self-selected pace while GRF were collected at a sampling rate of 360Hz. Starting positions were manipulated to ensure a complete and isolated foot-strike on the force plates. Ten isolated foot strikes were collected per participant. Frequency analysis was then performed by converting the GRF signal into its component frequencies in the anterior-posterior and vertical direction using fast fourier transformation by MATLAB (Matlab 7.6, Mathworks, Inc., Concord, MA, USA) software. Independent sample t-test was used to assess the frequency domain variables between the two groups.

RESULTS AND DISCUSSION

The self-selected walking speed was similar for both group: PD (1.03m/s) and ET (1.05m/s) (*P*=.69). In the anterior-posterior direction, no statistical difference between PD and ET was detected for the 99.5% frequency (*P* = .359), median frequency (*P* = .428) or frequency bandwidth (*P* = .422) (Table 1). Similarly, in the vertical direction, there was no statistical difference between PD and ET for the 99.5% frequency (*P* = .303), median frequency (*P* = .235) or frequency bandwidth (*P* = .147) (Table 1).

This purpose of the current investigation was to compare the frequency domain components of the GRF's during self-selected walking in patients with PD and ET. The results of the investigation suggest that the frequency components of the GRF in patients with ET and PD are not significantly different from each other, in the anterior-posterior and vertical direction. However, this investigation did not examine differences in the medial-lateral direction that may exist, and perhaps this direction of movement should be examined in future studies. Previous literature has shown that frequency analysis has the ability to determine differences in the frequency content in GRF with patients with specific movement disorders when compared to healthy older adults [1-3]. Given that PD and ET are both progressive disorders; it is possible that detection of GRF at differing stages of the disease may provide alternative results, which could lead to an earlier diagnosis and provide some insight on the results of this investigation. Progress is being made in the scientific knowledge and symptomatic treatment of movement disorders, but literature is still lacking in the pathophysiology of these disorders and its effect on motor control, muscle tone, gait and posture between hypokinetic and hyperkinetic movement disorders.

REFERENCES

1. Giakas G, Baltzopoulos V, Dangerfield PH, et al. Comparison of gait patterns between healthy and scoliotic patients using time and frequency domain analysis of ground reaction forces. Spine 1996;21:2235– 42.
2. White, R., I. Agouris, and E. Fletcher, Harmonic analysis of force platform data in normal and cerebral palsy gait. Clinical Biomechanics, 2005. 20(5): p. 508-516.
3. Wurdeman, S.R., et al., Multiple sclerosis affects the frequency content in the vertical ground reaction forces during walking. Clin Biomech (Bristol, Avon). 26(2): p. 207-12.
4. Pedersen, S.W., et al., Gait analysis, isokinetic muscle strength measurement in patients with Parkinson's disease. Scand J Rehabil Med, 1997. **29**(2): p. 67-74
5. Jain, S., Lo, S.E., Louis E.D. Common Misdiagnosis of a Common Neurological Disorder: How Are We Misdiagnosing Essential Tremor. Archives of Neurology, Volume 63, 1100-1104, 2006.

Table 1: GRF frequency values (Hz) for anterior-posterior and vertical directions for MS patients and PD patients

		PD Subjects Mean (SD) n=26	ET Subjects Mean (SD) n=15	P-Value
99.5%	A-P	17.43 (5.60)	15.64 (5.12)	.359
	Vertical	6.39 (2.31)	5.62 (1.71)	.303
Median	A-P	1.29 (0.20)	1.25 (0.14)	.428
	Vertical	0.45 (0.09)	0.42 (0.08)	.235
Bandwidth	A-P	1.20 (0.25)	1.14 (0.16)	.422
	Vertical	1.23 (0.29)	1.11 (0.27)	.147

BIOMECHANICAL DESIGN OF ROLLING CONTACT KNEE JOINT PROSTHESES

[1,2]Alexander H. Slocum, Jr., [3]Just L. Herder, PhD, [1]Kripa K. Varanasi, PhD

[1]Massachusetts Institute of Technology, Cambridge, MA
[2]Marshall University School of Medicine, Huntington, WV
[3]TU Delft, Delft, The Netherlands

INTRODUCTION

A four-bar linkage model of knee flexion/extension can be used to design prosthetic joints with improved load transfer characteristics. Rolling contact joints have improved lifetimes and could lead to reduced incidence of failure due to wear of the joint surfaces. It will be shown that by using knee anatomy to drive the design of the prosthesis, it can be designed to accurately mimic knee biomechanics in the primary degree of freedom of flexion/extension. Figure 1a shows a prototype rolling contact knee prosthesis. Additional degrees of freedom will be added in a deterministic manner to allow for mimicry of healthy tibio-femoral joint motion in 6 DOFs.

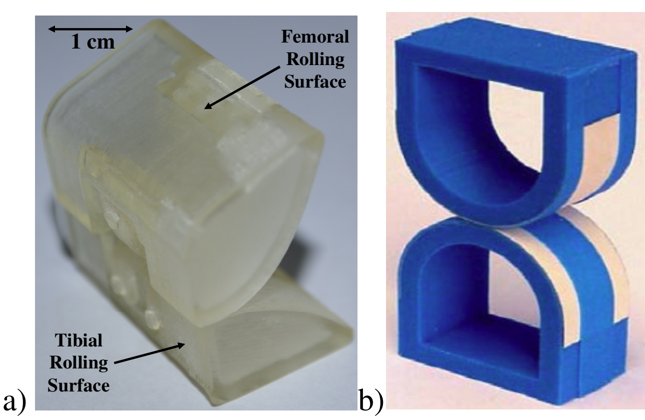

Figure 1: a) 3-D printed rolling contact prototype; b) sketch model of a flexure coupling.

METHODS

The concept of a rolling-contact joint is based on a flexure coupling, a sketch model of which can be seen in Figure 1b [1]. This joint morphology couples rotation with translation, similar to the way in which the femoral condyles articulate with the tibia and meniscus. The advantage of the flexure coupling is that it utilizes rolling contact to achieve a large range of motion. It can be shown that rolling contact joints have improved load transfer characteristics as a result of decreased parasitic forces at the joint interface.

The design process begins with a four-bar linkage model of the knee [2, which allows knee anatomy to deterministically drive the shape of the prosthesis. Figure 2 shows a schematic of the four-bar linkage model. The base link (in the tibia) is drawn between the ACL origin and the PCL insertion in the anterior and posterior proximal tibia, respectively. The links are lines of constraint drawn between the origin and insertion of the cruciate ligaments, and the follower is drawn between the origin of the PCL and the insertion of the ACL.

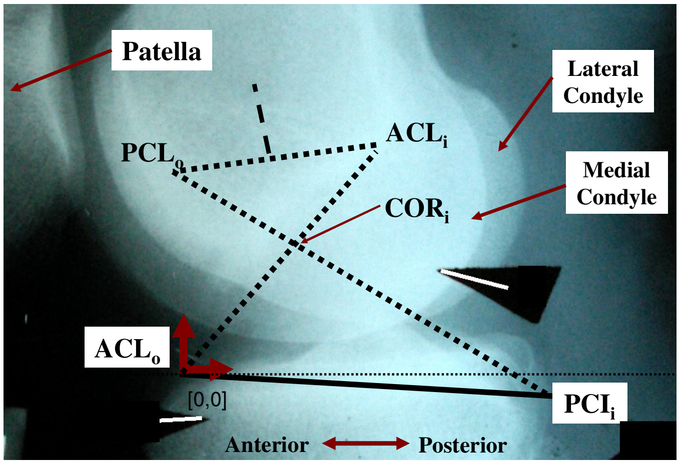

Figure 2: Four-bar linkage model of knee ligament lines of constraint sketched onto radiograph.

A solution to the forward kinematics problem for the four-bar linkage was found, and used to describe the motion of it's instantaneous center of rotation. Using this mathematical description of knee joint kinetics enabled synthesis of two rolling surfaces: a tibial and femoral component. The motion generated by the femoral component rolling over the tibial component accurately mimics to the flexion/extension motion of a healthy knee joint. Flexure straps are used to provide constraint for undesired motions and to prevent subluxation of the rolling surfaces [3, 4]. In the present embodiment, these constraints help to reproduce the primary flexion/extension motion of the knee.

RESULTS

A SolidWorks™ solid model of a rolling contact joint for use in a knee brace can be seen in Figure 3a. Contact stress analysis suggests that three common orthopaedic materials could be used to manufacture this joint: Ti6Al4V, CoCrMo, or SS316. Stainless steel was used to fabricate the prototype joint seen in Figure 3b, as it is more iteratively cost-effective.

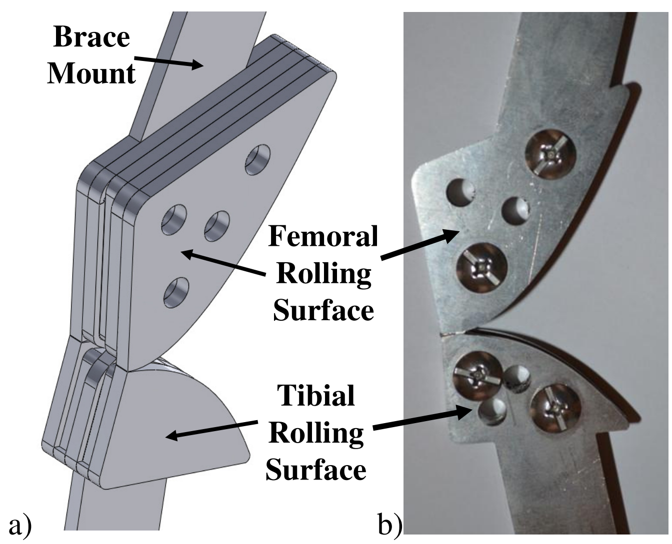

Figure 3: a) SolidWorks™ model of a rolling contact knee brace; b) 316SS laser-cut prototype.

DISCUSSION

It is known that knee motion is actually quite complex, as a result of changes in the orientation of the epicondylar axis, as well as internal rotation of the femur when the joint nears full extension [5]. The performance of the simple joint in Figure 3b must be evaluated, however, before additional degrees of freedom can be reliably added. Based on their required lifetimes, knee braces and prosthetic joints must withstand huge numbers of cycles. As such, the current prototype will be subjected to high-cycle tests to assess wear of the rolling surfaces and to evaluate fatigue and fracture modes of failure in the flexure straps.

CONCLUSIONS

A method of synthesizing rolling surfaces for prosthetic joints driven by the biomechanics of the healthy biological joint has been used to design a rolling contact knee brace.

REFERENCES

[1] Jeanneau, A., Herder, J., Laliberte, T., Gosselin, C., "A compliant Rolling Contact Joint and its Application in a 3-DOF Planar Parallel Mechanism with Kinematic Analysis", Proc. ASME Design Eng. Tech. Conf., Sept 28 - Oct 2, 2004, Salt Lake City, Utah, DETC2004-57264.

[2] Zavatsky, A. B., O'Connor, J. J., "A model of human knee ligaments in the sagittal plane Part 1: response to passive flexion". Proc Instn Mech Engrs 1992, Vol 206, pp. 125-134.

[3] Montierth, J. R., Todd, R. H., Howell, L. L., "Analysis of Elliptical Rolling Contact Joints in Compression". ASME Journal of Mechanical Design, March 2011, **133**:3, pp. 1-10.

[4] Cannon, J. R., Lusk, C. P., and Howell, L. L. "Compliant rolling-contact element mechanisms," Proceedings of the ASME International Design Engineering Technical Conferences and Computers and Information in Engineering Conference, DETC2005-84073.

[5] Williams, A., Logan, M., "Understanding Tibio-Femoral Motion". The Knee, **11**:2, pp. 81-88, 2004.

ACKNOWLEDGEMENTS

This work was funded by a CIMIT/MIT Medical Engineering Fellowship; Tom Dolan at Dolan's Welding & Steel Fabricating, Inc. (Johnstown, PA) cut the stainless steel components for the rolling contact joint.

TRIAL-TO-TRIAL CONTROL DYNAMICS IN REDUNDANT REACHING TASKS

[1,2] Rachel F. Smallwood, [3] Joseph P. Cusumano, [1] Jonathan B. Dingwell

[1] University of Texas, Austin, TX, USA
[2] University of Texas, San Antonio, TX, USA
[3] Pennsylvania State University, State College, PA, USA
E-Mail: jdingwell@austin.utexas.edu, Web: http://www.edb.utexas.edu/faculty/dingwell/

INTRODUCTION

A central question in neuroscience is how humans make accurate and repeatable movements in the face of biological noise [1] and redundancy [2,3]. For many tasks, one can precisely define the task goal *independent* of the performance or performer. When throwing darts, the goal is to hit the bull's-eye. This goal exists regardless of who throws the dart, how they throw it, or if any dart is thrown at all. For such tasks, one can define a precise map from the *performance* variables to the *goal* variables [3]. Task redundancies can create a manifold in the space of performance variables, referred to as a "Goal Equivalent Manifold" (GEM) [3-5]. For such tasks, all variations in performance *along* the GEM equally achieve the task goal. Any deviations in performance *perpendicular* to the GEM cause errors with respect to the task goal [3-5].

However, it is not known how generalizable these motor control processes are or if learning to exploit task redundancies requires having a physical task to perform. This study determined if subjects learned to adopt GEM-based control when presented with a generalized reaching task and given feedback based only on their performance relative to a GEM.

METHODS

We defined an infinite *family* of goal functions [3]:

$$G(D_i, T_i) = D_i^m \cdot T_i^n - c = 0 \quad \Rightarrow \quad D_i^m \cdot T_i^n = c \qquad (1)$$

where D_i was total reaching distance and T_i was total reaching time for trial i, and m, n and c were constants. The *task* was then to drive $G(D_i, T_i)$ to zero. We then tested two specific goal functions from this class. The first was defined by $n = -m$, which defined the task of trying to maintain constant average speed $(D/T = c)$ from trial to trial. The second GEM was defined by $n = +m$, which defined the task of trying to maintain constant $D \cdot T = c$ from trial to trial (Fig. 1).

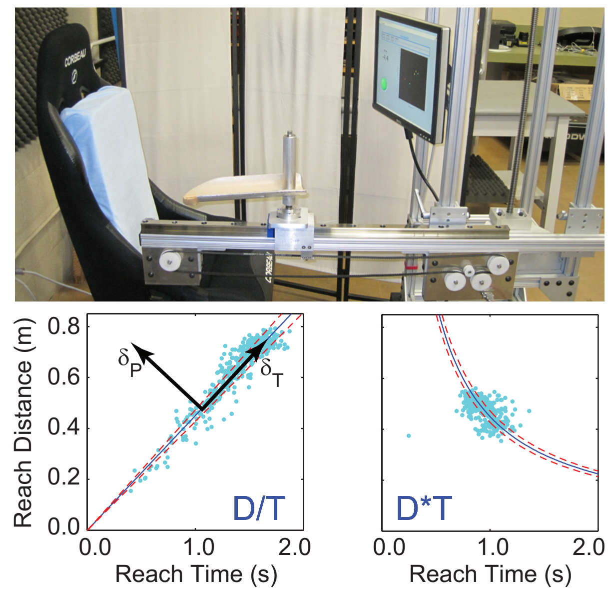

Figure 1: *Top*: Test apparatus with handle on linear bearing and video monitor for visual feedback. *Bottom*: Schematic of the GEMs for the 2 tasks tested. Subjects were *not* explicitly shown either GEM.

Ten healthy right-handed subjects participated. Subjects sat in a chair (Fig. 1) and made straight line reaching movements. They were not told what the specific goal for the movements was, only that there was a goal. After each reach, they were given feedback based on their performance in the form of an error (percent over or under the goal) and a graph that displayed their movement distance and time with color-coded points. Subjects were instructed to make their errors as close to zero as possible.

All subjects were given the exact same instructions and the same type of visual feedback for both reaching tasks. For each task, subjects performed 1800 total movements, divided over 2 consecutive days. Each subject performed both tasks at least 5 days apart. Five subjects did the $D{\cdot}T$ task first, while the other five subjects did the D/T task first.

Initial error magnitudes from each day were tested for learning, consolidation of learning, and generalization of learning across tasks. From the last 400 trials of each day, time series of D_i and T_i were extracted and then deviations tangent to (δ_T) and perpendicular to (δ_P) each GEM (Fig. 1) were computed [3,4]. We then calculated the normalized standard deviations of δ_P and δ_T [4] and linear stability multiplier, λ, for each time series using:

$$X_{i+1} = \lambda X_i + \xi_i \qquad (2)$$

where X corresponded to either δ_P or δ_T and ξ was a noise term. Values of $0 \le |\lambda| < 1$ correspond to stable movements, with smaller values of λ indicating more rapid corrections of cycle-to-cycle deviations. Data were analyzed using a combination of 2-factor and 3-factor, mixed effects balanced ANOVA's.

RESULTS AND DISCUSSION

Subjects showed significant evidence of learning and of consolidation of learning across consecutive days (not shown). Interestingly, each task elicited very *different* generalization effects when subjects switched to the other task (Fig. 2).

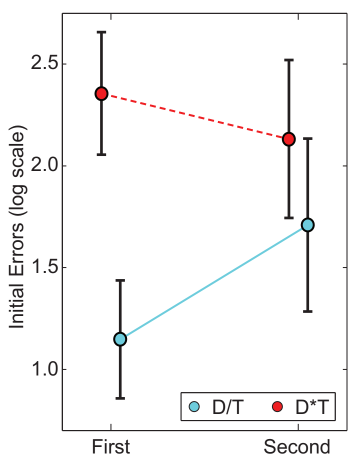

Figure 2: Initial errors exhibited different generalization effects: Learning the D/T task first *facilitated* learning of the $D{\cdot}T$ task. Conversely, learning the $D{\cdot}T$ task first *interfered with* learning the D/T task second. The Task × Order interaction effect was highly significant ($p = 0.007$).

For both tasks, subjects exhibited greater variability (Fig. 3, left) along the GEM (δ_T) than perpendicular to it (δ_P), although this effect was much stronger for the $D{\cdot}T$ task ($p < 0.0005$) than for the D/T task ($p = 0.019$). Subjects also corrected deviations (Fig. 3, right) in δ_P more rapidly (i.e., lower λ) than deviations in δ_P, and this effect was ~equally strong for both the $D{\cdot}T$ and D/T tasks ($p < 0.0005$).

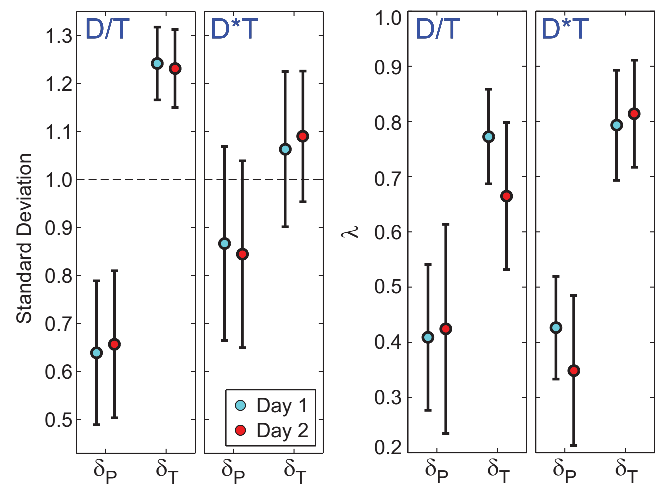

Figure 3: Normalized standard deviations and stability multipliers (λ) for both GEM's tested for both directions (δ_P and δ_T). Error bars indicate ±95% CI. All δ_P vs. δ_T comparisons were highly significant: all $p < 0.020$.

Thus, subjects were more variable in the task-irrelevant direction than in the direction where variability would lead to task errors [2,3]. Subjects corrected task-relevant deviations more rapidly than task-irrelevant deviations away from each GEM. Subjects exploited the $D{\cdot}T$ GEM redundancy to the same degree as the D/T GEM, despite exhibiting greater variance ratios for the D/T task. Variance measures [2] failed to capture the trial-to-trial *dynamics* of task performance [4]. Humans actively exploited task redundancies, even for these abstractly defined tasks where they did not have to.

REFERENCES

1. Faisal AA et al. *Nat Rev Neurosci*, 9:292–303, 2008.
2. Todorov E. *Nature Neurosci*, **7**: 907-915, 2004.
3. Cusumano JP & Cesari P. *Biol Cybern,* **94**(5): 367-379, 2006.
4. Dingwell JB, John J, & Cusumano JP. *PLoS Comput Biol*, 6(7):e1000856, 2010.
5. Gates DH & Dingwell JB. *Exp Brain Res*, **187**(4): 573-585, 2008.

ACKNOWLEDGEMENTS

Funded by NIH Grant #1-R03-HD058942-01.

PROBLEM- AND PROJECT-BASED LEARNING IN BIOENGINEERING: A CASE STUDY

[1]Cécile Smeesters, [2]Yves Bérubé-Lauzière, [1]Denis Rancourt,
[1]Ève Langelier, [3]Frédéric Balg and [2]Réjean Fontaine

[1]Department of Mechanical Engineering, Université de Sherbrooke, Sherbrooke QC, Canada
[2]Department of Electrical and Computer Engineering, Université de Sherbrooke, Sherbrooke QC, Canada
[3]Faculty of Medicine and Health Sciences, Université de Sherbrooke, Sherbrooke QC, Canada
e-mail: Cecile.Smeesters@USherbrooke.ca web: http://www.usherbrooke.ca/bioingenierie

CONTEXT

Problem- and project-based learning (PBL) is a student-centered teaching method in which students learn about a subject in the context of complex, multifaceted and realistic problems or projects.

Since 1996, the Department of Mechanical Engineering (ME) at the Université de Sherbrooke (UdeS) has used PBL within its undergraduate curriculum [1]. During each of the first 4 terms, the various courses are integrated together through a common term project. During the last 4 terms, students undertake a major design project (12 credits). Since 2001, the Department of Electrical and Computer Engineering (ECE) at the UdeS has also used PBL within its undergraduate curriculum [2]. During each of the first 6 terms, the entire course load is distributed and integrated into 2 to 3 week PBL units. During the last 2 terms, students also undertake a major design project (12 credits).

In 2001, Smeesters and Fontaine initiated a successful collaboration between these two departments and created the building blocks of a bioengineering concentration (12 course credits + 12 design project credits in a 120 credit Mechanical B.Eng.) and specialisation (6 course credits in a 120 credit Electrical and Computer B.Eng.). With the addition of 4 new bioengineering professors, this joint program took its current PBL form in 2006. Its purpose is to enable students to solve complex problems and to design projects in bioengineering.

A PBL BIOENGINEERING PROGRAM

Each of the 8 bioengineering units (Table 1) lasts 3 weeks and is composed of 3 core competences (Bloom's Taxonomy of Learning Domains):

- Human *anatomy* and physiology (knowledge)
- Bioengineering *modeling* (skill)
- Bioengineering *instrumentation* (skill)

These are integrated together through a 4th "design (skill), integration (skill) and communication (attitude)" competence by means of a common clinical, research or development problem.

The units span the various systems of the human body from cells and tissues to humans as a whole. Integration problems have included:

- Could you beat Usain Bolt at the 100 m dash?
- Design a wheelchair racing ergometer.
- Does leg stiffness vary with running speed?
- Do antibiotics affect rat tendon biomechanics?
- Can dialysis help a renal transplant patient?
- Design a chronotropic insufficiency pacemaker.
- Design a custom osteosynthesis fracture plate.
- Help diagnose and treat a patient with vertigo.

Each unit is taught by a team of 3 professors, one for each of the 3 core competences. All units have demonstrations, laboratories and/or hospital visits, and use selected readings from textbooks and/or journal articles. Evaluation is based on a scientific report [3] in which teams of 2 or 3 students present their solution to the integration problem (40%), as well as an individual student exam focussing on concepts (60%). Both the report and exam must always equally evaluate all 4 competences.

BENEFITS AND CHALLENGES

Some of the benefits of this PBL format have been:

- Dropout rates have decreased 20% (p=0.048).
- *Anatomy* grades improved by 5% (p=0.051).
- Integration problems and exam questions are now possible, given that the 3 core competences

are taught simultaneously (not sequentially).

- ME (63%) tend to do best in *Modeling*. ECE (31%) tend to do best in *Instrumentation*. Non-engineering students (6%) do just as well if not better than ME and ECE students (p=0.080).
- Mixed ME, ECE and non-engineering teams teach each other to produce better reports.
- Although stability in teaching tasks is endeavoured, integration problems and the core competence emphasised in each unit can change with the expertise of the professors.

This PBL format is not without its challenges:

- Staff resources being limited, this PBL format is far from traditional. The group size has been 11 students on average but as high as 26 (5-8 are traditional for PBL). A hybrid Lecture (passive) / PBL (active) format has thus been used.
- Working in teams of 3 professors is tricky. One team leader per unit is thus chosen to take on additional coordination tasks.
- To accommodate both under/graduate students who wanted only selected pairs of units (35%), an “à la carte” option was created. This required a savvy distribution of credits per unit (1.5), course (3) and department (1). It also required independence and equality (time, difficulty and competence proportions) between units.
- As a substantial portion of the grade can be based on PBL team reports, a way to evaluate individual contributions had to be developed.
- Finally, professors must be ready for the unexpected (ex: rain during field tests).

CONCLUSIONS

The multidisciplinary nature of bioengineering lends itself very well to PBL and has worked successfully at the UdeS for the past 6 years. However, it does have its challenges and must also adapt with time to changing needs.

REFERENCES

1. Charron F, et al. *Proc ASEE Annu Conf*, Montreal QC, 2002.
2. Lachiver G, et al. *IEEE Can Rev* **41**, 21-24, 2002.
3. Brand RA and Huiskes R. *J Biomech* **34**(11), 1371-1374, 2001.

ACKNOWLEDGEMENTS

To all the *Anatomy* professors and bioengineering teaching assistants for their PBL contributions.

Table 1: Bioengineering concentration and specialisation at the Université de Sherbrooke (1.5 credit per unit).

Weeks 1-3	**Unit 1 Biomedical Signals**	A Nervous A Tactile	M Axons M Proprioception	I Data acquisition	
	Unit 5 Classical Biofluids	A Digestive A Urinary	M Reynolds M Dialysis	I Echocardiographic imaging	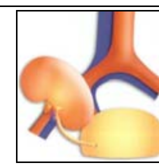
Weeks 4-6	**Unit 2 Musculoskeletal Statics**	A Muscle UL A Bones UL	M Contraction M Fracture	I Electromyograms	
	Unit 6 Hydraulic Biofluids	A Cardiovascular A Respiratory	M Circulation M Surfactant	I Electrocardiograms	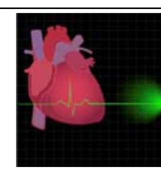
Weeks 7-9	**Unit 3 Musculoskeletal Dynamics**	A Mouvement A Locomotion	M Walking M Running	I Motion analysis	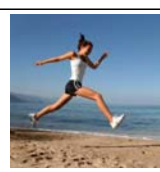
	Unit 7 Biomaterials	A Muscles LL A Bones LL	M Biomechanics M Design	I Tomographic imaging	
Weeks 10-12	**Unit 4 Tissue Biomechanics**	A Cells A Tissues	M Biomechanics M Mecanobiology	I Microscopy	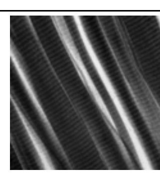
	Unit 8 Sensorimotor Control	A Visual A Vestibular	M Pupil M SC canals	I Magnetic resonance imaging	

A: *Anatomy*, M: *Modeling*, I: *Instrumentation*. UL: Upper Limbs, LL: Lower Limbs, SC: Semicircular.

INTER-SEGMENTAL COORDINATION VARIABILITY DURING LOCOMOTION – DO DIFFERENT ANALYTICAL APPROACHES TELL THE SAME STORY?

[1]Jo Armour Smith, [1]James Gordon and [1]Kornelia Kulig
Division of Biokinesiology and Physical Therapy, University of Southern California, Los Angeles, CA
email: joannesm@usc.edu, http://pt2.usc.edu/labs/mbrl

INTRODUCTION

Recent studies have utilized vector coding (VC), continuous relative phase (CRP) and principal components analysis (PCA) to quantify within-subject inter-segmental coordination variability in healthy subjects and in persons with neuromusculoskeletal disorders such as low back pain (LBP) [1,2,3]. These methods make somewhat different conceptual and mathematical assumptions, and initial evidence suggests that the choice of analytical method affects the magnitude and distribution of estimated variability [4]. The purpose of this study was to directly compare the results obtained from VC, CRP and PCA when quantifying the variability of inter-segmental coordination of the trunk during locomotion in a sample of persons with recurrent LBP and healthy controls.

METHODS

Four female subjects were recruited for this study. Two subjects (RLBP1 & 2) had a history of recurrent LBP but were in symptom remission at the time of the data collection. They were individually matched to two healthy controls by age, height, weight and activity level (CTRL1 & CTRL2). Motion capture markers were placed on the greater trochanters, sacrum, iliac crests and anterior superior iliac spines, and on the sternum, acromioclavicular joints and C7 spinous process to define a kinematic model for the pelvis and thorax respectively. Kinematics were collected at 250Hz (Qualisys AB, Gothenburg, Sweden).

Subjects walked at a controlled average speed of 1.5m/s. 11 stride cycles were analyzed for each subject. Stride cycle were time-normalized and angular displacement of the thorax and the pelvis in the axial plane was calculated (Visual3D software, C-Motion Inc, MD, USA). For VC, inter-segmental coordination was quantified as the coupling angle between the thorax and pelvis [4,5]. Coordination variability was defined as the variability of the coupling angle for each time point across repeated trials and was quantified as the angular deviation of the coupling angle using circular statistics [5]. For the CRP analysis, a normalized phase plane of angular displacement and velocity were constructed for each segment and a phase angle was calculated. Coordination was defined as the relative phase between the two segments [4,5]. Coordination variability was quantified as the angular deviation of the relative phase using circular statistics. For the PCA, the data were normalized to zero mean and unit variance. Inter-segmental coordination variability was quantified as the amount of data variance contained in the residual principal components after the dominant components had been removed from the data, and was expressed as a percentage of the total variance [2]

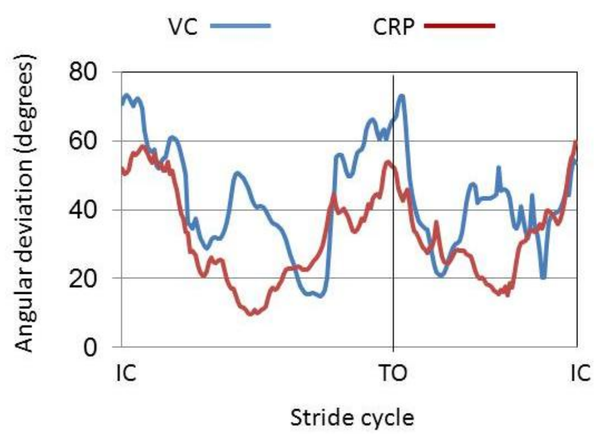

Figure 1. Time series of magnitude of variability over the stride cycle (CTRL1; IC = initial contact, TO = toe-off)

RESULTS AND DISCUSSION

The same inter-individual trends in mean angular deviation across the stride cycle were evident in the VC and CRP analyses. In this small sample there was no systematic difference in mean inter-segmental coordination variability between subjects with RLBP and healthy controls during locomotion. On average, mean variability calculated using VC was greater than that calculated using CRP, but this was not true for all subjects (average difference 3.3º, SD 6.6º). Coefficients for the cross correlation of the time series of angular deviation obtained using the VC and CRP approaches ($R[\tau = 0]$) were high, ranging from 0.89 (CTRL2) to 0.95 (CTRL1). However, the time-series patterns of variability obtained from VC and CRP over sub-phases of the stride cycle were not always in agreement (Fig. 1)

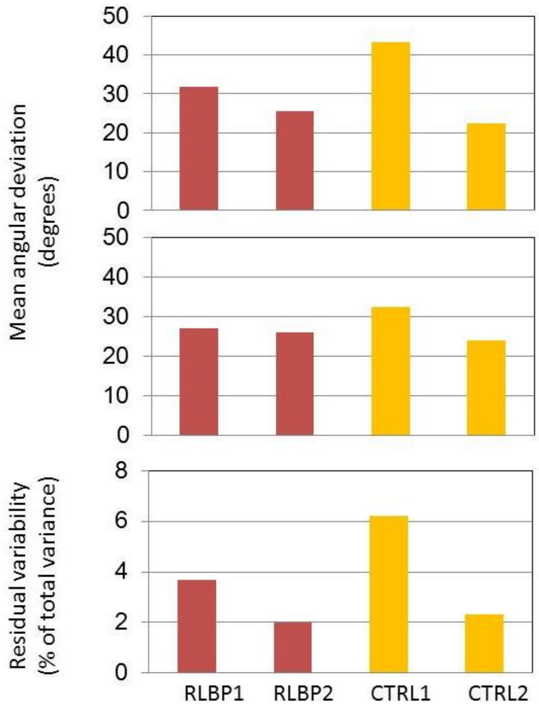

Figure 2: Comparison of individual results: VC: mean angular deviation of the coupling angle, (top); CRP: mean angular deviation of the relative phase, (center); PCA: residual variability, (bottom).

The first three principal modes obtained from the PCA analysis contained greater than 93% of the variance in the data for all subjects. The first two principal modes represented stride cycle oscillations of the pelvis and the thorax, whereas the higher order modes represented superimposed oscillations at higher frequencies. Based on the eigenvalue spectra and data projections onto the principal components, the first three components were selected as the global pattern, with the subsequent eight modes therefore comprising the residual variability. Coordination variability quantified using PCA had similar inter-individual trends as the VC and CRP analysis, but the relationship between the magnitude of variability in subjects RLBP2 and CTRL2 using this analysis was reversed (Fig. 2).

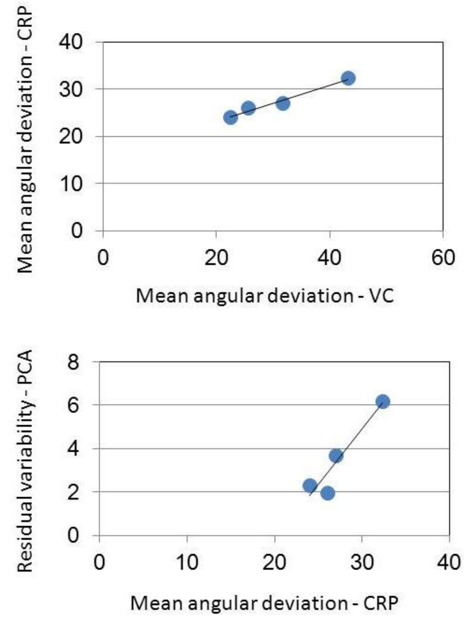

Figure 3: Relationship between mean variability calculated using VC and CRP (top) and mean variability and residual variability calculated using CRP and PCA (bottom).

Despite the differences both in data normalization and mathematical formulation of the three methods, there was a strong linear relationship between mean variability calculated using the VC and CRP methods and residual variability calculated using PCA (Fig.3).

CONCLUSIONS

Inter-individual trends in the magnitude of coordination variability were similar for all three analytical methods. This confirms that inter-segmental coordination variability is a robust locomotor characteristic, and that previously observed differences between subject groups are independent of the chosen analytical approaches.

REFERENCES

1. Pollard, CD et al. *J Appl Biomech,*, **21**, 143-152, 2005
2. Lamoth JC, et al. *Gait & Posture,* **23**, 230-239, 2006
3. Seay JF, et al. *Clin Biomech,* **26,** 572-578, 2011
4. Miller RH, et al. *J Biomech,* **43,** 2554-2560, 2010
5. Hamill J, et al. *J Appl Biomech*, **16**, 407-418, 2000

METABOLIC COSTS OF LOCOMOTION WHEN WALKING WITH AND WITHOUT ANKLE AND KNEE BRACES

Jeremy D. Smith, Caitlin Kievenaar, Victoria Falgien and Jennifer Wilmes

University of Northern Colorado, School of Sport and Exercise Science, Biomechanics Lab
email: jeremy.smith@unco.edu, web: www.unco.edu/nhs/ses

INTRODUCTION

Effective walking requires the ability to rotate the lower extremity joints in a coordinated manner to produce forward progression of the body. However, when joint function is impaired energetic penalties are often observed. There appears to be a relationship between joint impairment and energetic costs during walking. For example, in amputees, the higher the level of amputation, typically the higher the metabolic cost during walking; a transfemoral amputee expends ~0.24 $ml\cdot kg^{-1}\cdot m^{-1}$, a through-knee amputee expends ~0.20 $ml\cdot kg^{-1}\cdot m^{-1}$, and a transtibial amputee expends ~0.18 $ml\cdot kg^{-1}\cdot m^{-1}$ walking at their preferred speeds [1,2]. To better understand the influence of joint function on metabolic costs, previous researchers [2] have systematically casted each lower extremity joint and measured the effects on metabolic costs during walking. In general, greater metabolic costs occurred when more joints were restricted, which is consistent with results seen in higher levels of amputations. However, casting a joint requires the addition of a significant amount of mass that can also increase the metabolic cost of walking. The use of other lighter weight orthotics to restrict joint motion would minimize effects due to increased mass. A further limitation of the previous work [2] was that walking speed was not controlled and decreased with increased joint restriction. Therefore, the purpose of this study was to investigate the effects of restricted lower extremity motion on the metabolic costs of walking, and address limitations of previous work in this area.

METHODS

Four males and six females participated in this study (age = 22.67 ± 1.58yrs, weight = 70.4± 10.08kg, height = 171.33 ± 6.93 cm). Inclusion criteria for this study included: a) no lower extremity injury within the previous three months and b) participation on a competitive sports team. The University's IRB approved the study and all participants provided informed written consent prior to participation.

Participants were asked to complete a single laboratory session, in which they were asked to complete a series of 8-minute treadmill walking bouts under 4 different conditions. Participants walked at a fixed walking speed of 1.5 m/s velocity for all treadmill walking bouts. Participants were instructed on the operation of the treadmill they would be using during data collections and then practiced walking on the treadmill for a minimum of 10 minutes. During this treadmill practice, participants also practiced walking with the headgear and mouthpiece they were to wear during the actual data collection. Participants completed a series of 8-minute treadmill walking bouts under 4 different conditions while metabolic data were recorded. A minimum of at least 5 minutes was provided to participants to rest between conditions and give researchers time to change the bracing condition. The four conditions were: a) baseline (no bracing), b) knee brace only, c) ankle and knee brace and d) ankle brace only.

The rate of oxygen consumed and carbon dioxide produced (expressed in $ml\cdot kg^{-1}\cdot min^{-1}$) and heart rate (HR) were measured during the 8-minute trial. For each trial metabolic and heart rate data were averaged over the last two minutes and used in statistical analyses. Weir's equation [4] and a conversion to Joules was used to express the metabolic data as an energetic cost (Ecost) of walking (expressed in $J\cdot kg^{-1}\cdot s^{-1}$). Single factor ANOVAs with repeated measures were used to determine the effects of restricting lower extremity ($p<.05$ determined significance).

RESULTS AND DISCUSSION

Systematic increases in net metabolic cost (i.e., Net Ecost) and heart rate (HR) were observed during walking as the level of joint restriction increased (Figure 1). The bracing condition had a significant effect on Ecost ($F = 16.174$, $p < .001$) and HR ($F = 9.469$, $p = .002$). Follow-up pairwise comparisons showed that with the knee braced with or without the ankle also being braced, Ecost and HR were greater than baseline walking ($p<.005$ for all comparisons). When only the ankle was braced the observed increases in Ecost and HR over baseline walking was not significant. However, ankle bracing with knee bracing together significantly increased Ecost and HR compared to walking only with the knee braced ($p<.05$ for all comparisons).

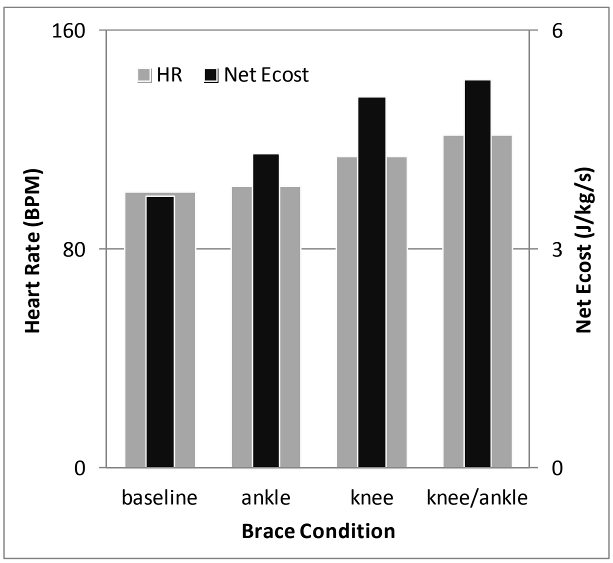

Figure 1: Effects of bracing on heart rate (fat bars) and net metabolic cost (skinny bars).

These results are consistent with trends that have been reported in the amputee literature. For example, Waters & Mulroy [1] found that when comparing across amputations levels in traumatic amputees Ecost was 14% and 43% higher in transtibial and transfemoral amputees compared to a non-amputee group walking at the same speed. Considering our results as relative increases compared to baseline walking we observed similar trends as reported by Waters and Mulroy [1] for higher amputation levels (Figure 2). Specifically, if you consider the ankle condition as a traumatic transtibial amputee our observed 16% increase is similar to the 14% increase reported for transtibial amputees. In addition, our observed 43% increase with the knee and ankle both braced is similar to that reported for transfemoral amputees compared to non-amputees. Comparing our results with those of Waters et al. [2] illustrates that the use of the lighter weight orthotic for restricting joint motion was more consistent with actual energetic costs seen in amputees. For example, for the cast condition which restricted knee and ankle motion, Waters et al. observed a 60% in Ecost compared to our 43% for the same condition. For the ankle cast only condition Waters et al. reported a 27-33% increase compared to our observed 16% increase. In conclusion, our results suggest that the higher costs of locomotion often reported for higher levels of amputation is likely due in large part to the loss of joint function resulting from the amputation.

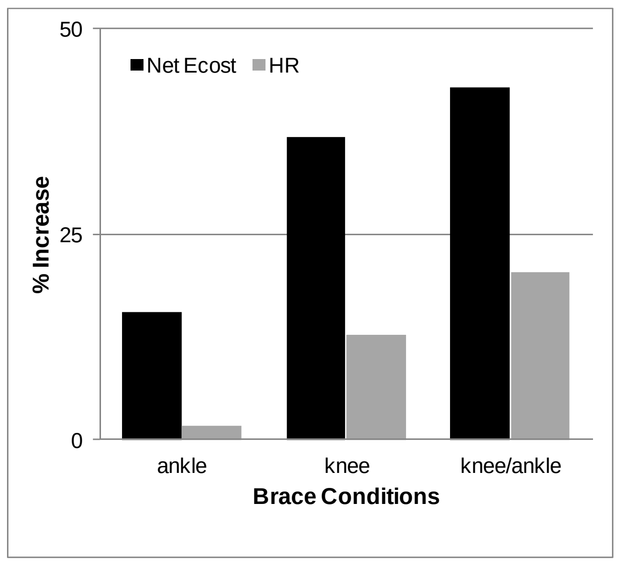

Figure 2: Relative percent increases in heart rate and net metabolic costs with bracing.

REFERENCES

1. Waters, RL & Mulroy, S (1999). *Gait and Posture* ***9****, 207-231*.
2. Waters RL et al. (1982). *J Bone Joint Surg Am*. ***64*****,** 896-899
3. Weir, J. B. (1949). *J Physiol*, ***109*****(1-2),** 1-9.

A Micromechanical Analysis on Diffuse Axonal Injury for Heterogeneous Brain Tissue

[1]M. Soheilypour, [1]M. Khorshidi, [1]M. Peyro, [2]A. Abolfathi, [1]M.H. Naei

[1]School of Mechanical Engineering, University of Tehran, Tehran, Iran
[2]School of Biomedical Engineering, Amirkabir University of Technology, Tehran, Iran
email: m.soheilypour@ut.ac.ir

INTRODUCTION

Due to the devastating nature of Diffuse Axonal Injury, numerous experimental (on animals) and analytical researches have devoted to study the mechanisms and consequences of this phenomenon. The limitations in experimental approaches and the need for microscopic investigation of DAI [1], lead the researchers to analytical and computational microscale models. However, many parameters make this subject sophisticated to study [2].
Geometrical intricacy is one of the exclusive characteristics of white matter and always has been simplified in some way in the previous models. This study intends to propose a micromechanical approach which could model and analyze parts of white matter with the most heterogeneous distribution of axons inside ECM. A finite element (FE) based method is implemented on dissociated culture of neurons to reach this goal.

METHODS

An image of rat's dissociated culture of hippocampal neurons is used (Figure 1-Left). Although the structure of dissociated culture of neurons is somehow different from that of brain, the image is a good representative of the geometry of the tissue and since there is almost no appropriate human brain image for this approach, it is just used to implement the method. However, the algorithm is applicable to any other image that would be at hand in near future.
Variational Asymptotic Method for Unit Cell Homogenization[3], *VAMUCH*, is used to analyze the model. This method is much more convenient and efficient than classical FE methods and gives the authors the opportunity to analyze the heterogeneous geometry of brain tissue. As a basic in homogenization methods, a unit cell is assumed

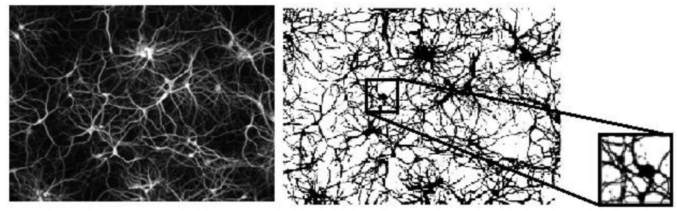

Figure 1: (Left) Dissociated culture of rat hippocampal neurons (Scale: approximately 700 microns), Paul De Koninck, Laval University, www.greenspine.ca
(Right) The digitized image and a selected RUC for the analysis

to be repeated to model the material (Figure 1-Right). VAMUCH uses a variational statement of Repeated Unit Cells, *RUCs*, through an asymptotic expansion of the energy function.
Since DAI is commonly induced by impact loadings which occur in less than 50 milliseconds [4], assuming axons and ECM to be elastic is a good approximation. Considering plane stress conditions, the model is meshed with 2D 9-node quadrilateral elements.
The influence of axon volume fraction and axon distribution on the overall and local properties of the brain tissue is studied. The response of the model to different external loadings is investigated to analyze the brain response in different situations. The results are verified by existing studies on different parts of the tissue [2], [5].

RESULTS AND DISCUSSION

The results of this study indicate that the axon volume fraction has a significant effect on the overall properties of the tissue (Figure 2). The noticeable increase of 1.8-5.9% in the properties with respect to 5% of increase in axon volume fraction shows the importance of this parameter on the tissue overall behavior. However, in a specific loading exerted to RUCs with different axon volume fractions, the maximum local stress exerted to axons, varies inconspicuously which shows the effect of axon distribution on the local stresses.

In different loading scenarios, axons which are parallel to the direction of loading bear more stress than others, i.e. axons with 0, 45, and 90 degrees to

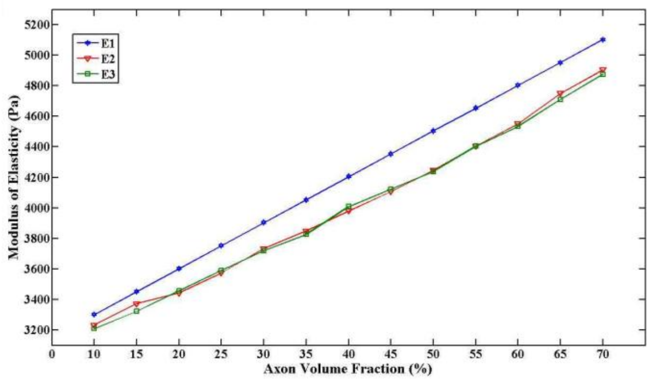

Figure 2: Change in Moduli of Elasticity of the tissue with respect to increase in Axon Volume Fraction (%)

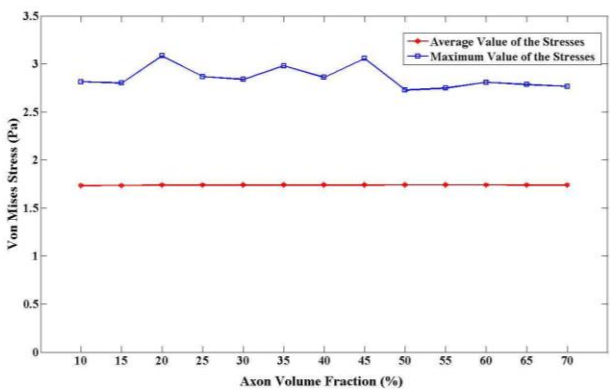

Figure 3: Maximum and average stresses for different volume fractions (shear loading)

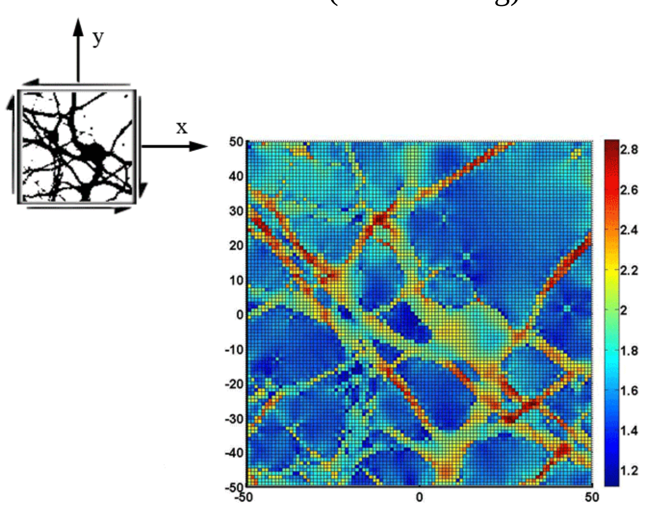

Figure 4: Local stress analysis (Von Mises stress). Subjected to shear loading

the x axis, in compression in x-direction, shear, and compression in y-direction loadings, respectively. The maximum stress in shear loaded model is about 1.54 times the maximum stress in compressed model. It can be concluded that the tissue is more vulnerable when subjected to shear loadings. The maximum local strain of axons, which are in the direction of the compression, is 1.43-1.51 times the applied strain which has close compatibility with Ref. 5.

CONCLUSIONS

A finite element based micromechanical model is proposed to model and analyze the heterogeneous white matter. The model is able to take into account even the most heterogeneous distributions of axons. The study reveals that the overall properties of the tissue are intensely dependent on the axon volume fraction. In addition, it is concluded that despite axon volume fraction, axon distribution affects the maximum local stress exerted to axons which shows the great significance of the micromechanical structure of the tissue and the importance of including the heterogeneous distribution of axons in the model.

Although each external impact on the brain tissue is a combination of shear and compressive loads, in some cases one of these types of loadings is the dominant one, e.g. shear in the sudden movement of head in a car accident. In this way, the mentioned conclusion that the tissue is more vulnerable when subjected to shear loading in comparison to compressive loadings, is in good consistency with the fact that TBI is commonly induced by shear loads [4].

REFERENCES

1. Smith DH, Meaney DF. *Neuroscientist* **6**, 483-495, 2000.
2. Abolfathi N, et al. *Comput Method Biomech* **12**, 249-262, 2009.
3. Yu W, Tang T. *Int J Solids Struct* **44**, 3738–3755, 2007.
4. Smith DH, et al. *J Head Trauma Rehabil* **18**, 307-316, 2003.
5. Cloots RJH, et al. *Biomech Model Mechanobiol* **10**, 413-422, 2011.

BIOMECHANICS CONSTRAINS VARIABILITY IN SPATIAL STRUCTURE OF MUSCLE COORDINATION FOR ENDPOINT FORCE GENERATION

[1]M. Hongchul Sohn, [1,2]J. Lucas McKay and [1,2]Lena H. Ting

[1]Georgia Institute of Technology, Atlanta, GA, USA
[2]Emory University, Atlanta, GA, USA
email: lting@emory.edu

INTRODUCTION

Due to biomechanical redundancy, multiple muscle coordination patterns can be used to generate the same endpoint force. Accordingly, muscle synergy patterns used to produce similar force vectors during balance control varies across individuals in both cats [1] and humans [2]. For example, in a synergy to produce a limb loading force vector (F_{W1}, down-backward), *vastus* (VAST) was recruited consistently at a high level across different animals, whereas the activation level of *gracilis* (GRAC) varied considerably across animals. On the other hand, in producing an unloading force vector (F_{W2}, up-forward), *sartorius* (SART) was always used, but *vastus* (VAST) was recruited at varying levels across animals.

We hypothesized that the constraints of limb biomechanics would predict the observed variability identified experimentally. Our approach was to identify the upper and lower bounds of individual muscle activation levels for generating endpoint force vectors in different directions and magnitudes. A similar approach has been used to demonstrate how muscle dysfunction affects the robustness of force generation [3].

Here we were particularly interested in the relation between the observed variability in measured EMG signals during a behavioral task, and the spatial structure of redundant muscle space defined by the biomechanics, with implication to neural strategies for selecting muscle coordination in muscle synergies. For example, muscles with consistently high activation would be "necessary", and muscles with more variability would be "optional" for a given task. We further compared the bounds to muscle coordination patterns predicted with alternate neural strategies defined by scaling [4] or minimum effort control.

METHODS

Using a detailed model of the cat hindlimb [5], we examined how the range of permissible activation levels of each muscle changes for the generation of endpoint force vectors when magnitude increases from 0 to maximal force. The posture of the static model was matched to the kinematics of 3 cats and used to map a 31D muscle activation vector $\vec{e}$ ($0 \leq e_m \leq 1$) to a 7D joint torque vector, determined by pre-multiplying the Jacobian transpose to a 6D combined endpoint force and moment vector $\vec{F}_{End} = [f_x, f_y, f_z, M_x, M_y, M_z]^{\mathrm{T}}$, with $\mathbf{J}^{\mathrm{T}}\vec{F}_{End} = \mathbf{R}\mathbf{F}_{AFL}\vec{e}$ ($\mathbf{J}^{\mathrm{T}}$: 7×6 Jacobian transpose, $\mathbf{R}$: 7×31 moment arm matrix, $\mathbf{F}_{AFL}$: 31×31 diagonal muscle scaling factors for active force generation).

Five experimental synergy force vectors in each cat [1] were used as the target endpoint force vector directions, where the maximum force magnitude in each direction ($\vec{F}_{W_i}^{\mathbf{MAX}}$, i=1~5) was found with linear programming. We identified the maximum (upper bound: $e_m^{\mathbf{UB}}$) and minimum (lower bound: $e_m^{\mathbf{LB}}$) possible activations of each muscle m, in producing an endpoint force of $\alpha \cdot \vec{F}_{W_i}^{\mathbf{MAX}}$ (α=0~1) with linear programming at each incremental step ($\Delta\alpha$=0.1) for the five force directions in each cat. For each force, we also found the muscle activation patterns predicted by 1) scaling the pattern for the maximal task [4], and 2) minimizing muscular effort (i.e., sum-squared activation).

RESULTS and DISCUSSION

The range of each muscle, which is the difference between $e_m^{\mathbf{UB}}$ and $e_m^{\mathbf{LB}}$ at a given α, changed anisotropically as the force magnitude increased (Fig. 1A and B, shaded). When the lower bound, $e_m^{\mathbf{LB}}$ becomes nonzero, it corresponds to the force magnitude (α) at which the muscle becomes necessary (Fig. 1A and B, bottom trace), whereas the upper bound $e_m^{\mathbf{UB}}$s defines the maximum allowable activity of the muscle (Fig. 1A and B, top trace). In many cases, these bounds converged at α=1. However, cases existed where these bounds did not converge (results not shown), reflecting the redundancy within joints.

Non-negativity of muscle activation profoundly affected the structure of the null-space associated with zero force production at α=0. The $e_m^{\mathbf{UB}}$s were limited by the relative torque-generating capability of each muscle. For example, GRAC had $e_m^{\mathbf{UB}}$ of 0.3 in one cat (Fig.1B) meaning that torque generated by activating this muscle higher than 0.3 cannot be counterbalanced by activation of other muscles. In contrast, when negative activation was allowed, the range spanned the full possible levels ($-1\leq e_m \leq 1$) for all muscles, showing its weak biological relevance.

In agreement with the prediction, muscles that were consistently activated across animals were necessary, whereas muscles that highly varied in its recruitment level were optional. For example, $e_m^{\mathbf{LB}}$ of VAST became immediately nonzero for F_{W1} and SART became necessary at $\boldsymbol{\alpha}$=0.6 for F_{W2} in one animal (Fig. 1A). Similarly, GRAC and VAST activity for F_{W1} and F_{W2}, respectively, had zero $e_m^{\mathbf{LB}}$ at all force levels (Fig. 1B). Although the observed variability was consistent with the model predictions, the magnitudes of experimental force vectors (Fig. 1A and B, vertical line) were actually small such that the $e_m^{\mathbf{LB}}$ s were zero for all muscles in one cat for F_{W1}, and in all cats for F_{W2}.

The consistent activation of muscle at before they are necessitated by biomechanical constraints may conform to a neural strategy where the pattern for the maximal task is scaled in sub-maximal tasks [4] (Fig. 1A and B, dashed line). Accordingly, both the scaling strategy and the minimum effort strategy (Fig. 1A and B, dots) predicted the activation of "necessary" muscles (VAST for F_{W1} and SART for F_{W2}) at the earliest nonzero $\boldsymbol{\alpha}$. However, "optional" muscles (GRAC for F_{W1} and VAST for F_{W2}) were never selected in either strategy.

Our results show that biomechanics places bounds on the variability of muscle activation patterns for endpoint force generation. Recruitment of optional muscles may reflect other goals such as stabilizing posture.

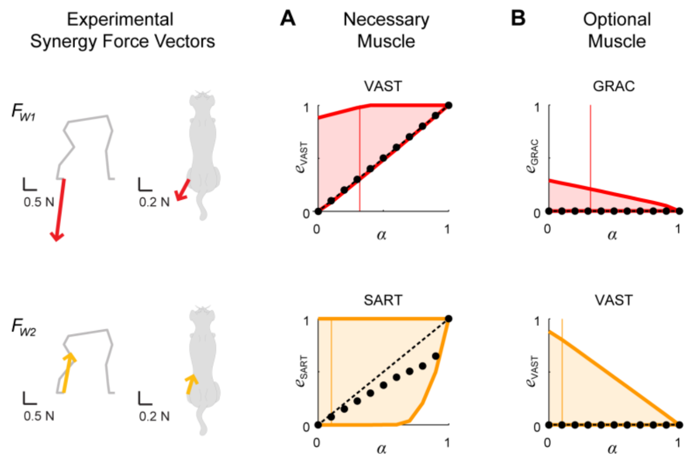

Figure 1: Upper (top trace) and lower (bottom trace) bounds for necessary (**A**) and optional (**B**) muscles show the range (shaded) of allowable variability in muscle activation for generating force in direction of the experimental synergy force vectors F_{W1} (red) and F_{W2} (yellow). Solutions for scaling (dashed line) and minimum effort (dots) strategy lie within the range, or on the lower bound.

REFERENCES

1. Torres-Oviedo *G, et al. J Neurophysiol*, 96, 1530-1546, 2006.
2. Chvatal SA, et al. *J Neurophysiol*, 106, 999-1015, 2011.
3. Kutch JJ, Valero-Cuevas FJ. *J Biomech*, 44, 1264-1270, 2011.
4. Valero-Cuevas FJ. *J Neurophysiol*, 83, 1469-1479, 2000.
5. Burkholder TJ, Nichols TR. *J Morph*, 261, 118-129, 2004.

ACKNOWLEDGEMENTS

NIH HD 46922

LANDING TECHNIQUE, NOT BODY MASS OR QUADRICEPS STRENGTH, IS ASSOCIATED WITH FORCE DURING JUMP-LANDING TASK IN MALE ATHLETES

Fredy M. Solis, Jon Van Den Boogaard, Jose Dominguez, Terese L. Chmielewski

University of Florida, Gainesville, FL, USA
email: freddy@ufl.edu

INTRODUCTION

Increased peak vertical ground reaction forces (PvGRF) during functional tasks may predispose athletes to lower extremity injury and be harmful to articular cartilage in the knee. Body weight, knee flexion angle and quadriceps strength have been associated with vertical ground reaction forces (GRF) during different functional tasks. The PvGRF during a single-leg landing task has not been widely reported and the association with body mass, knee flexion angle and quadriceps strength is unknown. The purpose of this study was to quantify PvGRF on each leg and investigate the association with body mass, knee flexion angle, and quadriceps strength during a forward drop-land task.

METHODS

Subjects: 56 males, Division I collegiate football athletes (BMI = 30 ± 4.6) were tested as part of preseason musculoskeletal screens. Subjects stood on the left leg, jumped off a 12 inch step and landed on a force plate. The procedure was repeated on the right leg. A single trial was used for analysis. Landing with entire foot on the force plate, hands on hips, eyes forward and balancing on single leg for three seconds constituted a good trial. An 11-camera motion capture system (Motion Analysis, Santa Rosa, CA) was used to collect kinematic data at 200 Hz. A force plate (AMTI, Watertown, MA) embedded in the floor was used to collect kinetic data at 1200Hz. Data were analyzed using Visual3D movement analysis software (C-Motion, Inc., Germantown, MD). Trajectories of the reflective markers were filtered with a low-pass, Butterworth digital filter using a cut-off frequency of 6 Hz. Kinetic force plate data were filtered with a low-pass, Butterworth digital filter using a cut-off frequency of 15 Hz. PvGRF and peak knee flexion angle were analyzed during the first 500 ms after initial contact with the force plate. An isokinetic dynamometer (60°/s) assessed peak knee extensor torque (PKET). Both PvGRF and PKET were normalized to body weight (BW). Pearson's correlation coefficients determined the associations between variables.

RESULTS AND DISCUSSION

The results of this study showed that normalized VGRF on the right was 3.4 ± 0.4 BW and on the left was 3.3 ± 0.3 BW. Only peak knee flexion angle was significantly associated with normalized PvGRF (right: $r = -.557$, $p < .001$; left: $r = -.526$, $p < .001$). Normalized PvGRF during the forward-land task exceeded 3 x BW. Despite the mean BMI for this sample being in the obese category, body mass was not associated with PvGRF.

CONCLUSIONS

Knee joint flexion showed an inverse relationship with normalized PvGRF, which means conditioning programs for these athletes should emphasize landing with greater knee flexion to reduce vertical forces on the lower extremity. Future research will determine if comparable PvGRF values and a similar association with peak knee flexion angle are found in a sedentary population.

POSTURAL SWAY CORRELATES OF PERCEIVED COMFORT IN POINTING TASKS

Stanislaw Solnik, Chase J. Coelho, Nemanja Pazin, Mark L. Latash,
David A. Rosenbaum, Vladimir M. Zatsiorsky

Pennsylvania State University, State College, PA, USA
email: szs13@psu.edu, web: http://www.mcl.psu.edu/

INTRODUCTION

People grasp objects differently depending on what they plan to do with the objects. One hypothesis concerning this tendency is based on the *end-state comfort effect*, which has been described as a tendency to grasp an object in an uncomfortable way that allows for a more comfortable final posture [1]. Following up on this hypothesis, we sought to introduce quantitative indices of "comfort" based on biomechanical variables. We hypothesized that *uncomfortable* positions would be associated with decreased stability. Toward that aim, we explored biomechanical measures of postural sway as possible correlates of subjective comfort ratings for a range of arm postures.

METHODS

Twelve right-handed, young adults (28 ± 3 years of age, 66.1 ± 13.0 kg of mass, 1.69 ± 0.11 m of height) volunteered for the study. During the experiment, subjects stood on a force plate (AMTI), with eyes open and with their feet at a comfortable width. The positions of the feet were recorded in all trials. To elicit specific arm positions, we placed a plastic hoop (diameter = 0.65 m) in front of the participant at two distances parallel to the frontal plane – at 40% and 80% of the participants' arm length. The center of the hoop was aligned with the subject's vertical midline at shoulder height. A reflective marker (target) was placed on the hoop either at 12, 3, 6, or 9 o'clock positions on a quasi-random basis (ensuring that all targets were used) over trials. Participants held a pointer (length = 0.29 m) using a power grip and were asked to point to the target with the tip of the pointer while keeping the hand close to the center of the hoop in the hoop's plane (Fig. 1). Subjects maintained each final grasp posture for 60 s while force plate data were collected (sampling rate = 100 Hz). Two minutes of rest were given after each trial. After data collection for each posture, subjects rated the perceived comfort (COMFORT) on a scale from 1 (least comfortable) to 5 (most comfortable). In total, each subject completed 8 arm postures (4 target positions × 2 distances).

Force plate data were low pass filtered at 10 Hz before center of pressures (COPs) were calculated. The COPs were then decomposed into rambling (Rm) and trembling (Tr) components, using a procedure described in [2]. In this analysis, Rm and Tr represent two different aspects of postural sway processes. Rm characterizes movement of the reference point with respect to which equilibrium is maintained. Tr is oscillation around the Rm trajectory. For each postural sway component (COP, Rm, Tr), we computed the area of the 95% confidence ellipse (AREA) and the root-mean-square error in the anterior-posterior direction (RMS).

To check for an interaction between postural sway components, we conducted two one-way MANOVAs for AREA and for RMS, with COMFORT as the independent factor and COP, Rm, and Tr as dependent variables. In addition, we used polyserial correlation [3] to estimate the strength of the relation between COMFORT and the postural sway components. All data analyses were performed in Matlab (Mathworks, Inc.) and SPSS (IBM Corp.).

RESULTS

The results are summarized in Table 1. Of all postural sway components, only Tr showed a significant correlation with COMFORT, both for AREA ($r = -0.45$, $p < 0.001$) and for RMS (r = -

0.41, p <0.001). One-way MANOVAs yielded a multivariate COMFORT main effect on postural sway components, both for AREA ($p < 0.001$) and for RMS ($p < 0.001$). Each of three separate univariate ANOVAs revealed a main effect of COMFORT on each AREA-based postural sway component (COP: $p = 0.025$; Rm: $p = 0.025$, and Tr: $p = 0.001$). Likewise three separate ANOVAs for each RMS-based component revealed a main effect of COMFORT (COP: $p = 0.016$; Rm: $p = 0.017$; and Tr: $p = 0.001$). A series of post-hoc (Tukey HSD) analyses showed that Tr values differed significantly between COMFORT ratings 1 vs. 4 and 5, both for AREA ($p < 0.001$) and RMS parameters ($p < 0.005$).

DISCUSSION

The present results suggest that during quiet standing, maintenance of arm postures with different comfort ratings has differential effects on the rambling (Rm) and trembling (Tr) components of postural sway. The data are consistent with the suggestion [2] that Rm and Tr represent different processes associated with postural stability. Rm has been associated with reference point migration with respect to which postural stability is maintained. Accordingly, Rm may have here represented spontaneous sway, which was larger for more comfortable arm postures, and postural correction, which was larger for less comfortable arm postures. Tr, meanwhile, has been assumed to represent restoring forces [4]. Accordingly, Tr may have increased here for less comfortable arm postures owing to the need for more muscle co-activation in the service of restoring forces when the arm postures were uncomfortable.

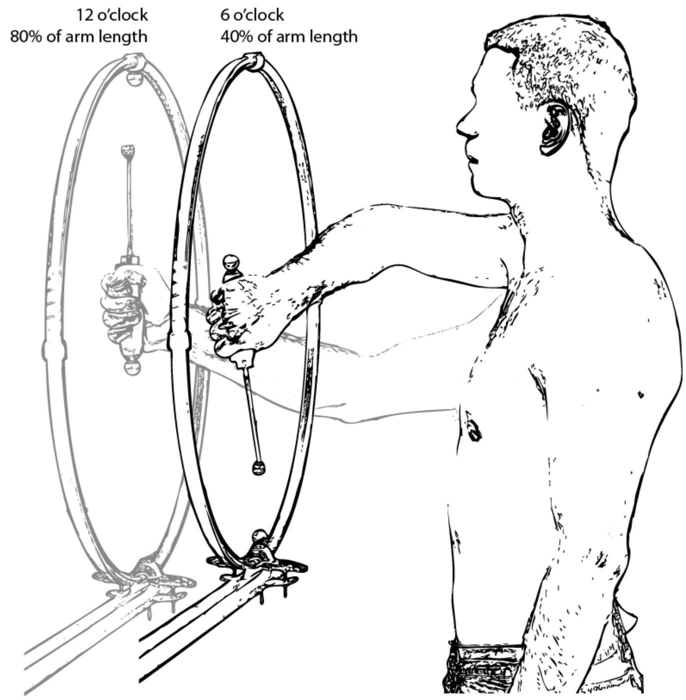

Figure 1. Example of two final grasp postures.

REFERENCES

1. Rosenbaum DA, et al. *Attention and performance XIII,* Hillsdale, NJ: Erlbaum, 1990.
2. Zatsiorsky VM, et al. *Motor Control* **3**, 28-38, 1999.
3. Jaspen N, *Psychomotorika* **11**, No. 1, 1946.
4. Zatsiorsky VM, et al. *Motor Control* **4**, 185-200, 2000.

Table 1. Left part of the table: Mean ±1 SE for each posture sway component grouped by comfort ratings. Right part of the table: Comfort ratings for each position. T denotes target position (o'clock). MdC denotes median comfort rating, where 1=least comfortable and 5=most comfortable.

		Comfort Rating				
		1	2	3	4	5
AREA (cm^2)	COP	1.49 ±0.24	1.45 ±0.18	1.59 ±0.36	0.81 ±0.11	1.39 ±0.22
	Rm	1.09 ±0.19	1.11 ±0.14	1.34 ±0.35	0.59 ±0.09	1.09 ±0.19
	Tr	0.103 ±0.012	0.069 ±0.009	0.062 ±0.008	0.040 ±0.005	0.056 ±0.007
RMS (cm)	COP	0.73 ±0.10	0.83 ±0.13	0.66 ±0.13	0.47 ±0.06	0.83 ±0.11
	Rm	0.71 ±0.10	0.82 ±0.14	0.64 ±0.13	0.46 ±0.06	0.82 ±0.11
	Tr	0.088 ±0.006	0.078 ±0.006	0.069 ±0.007	0.057 ±0.004	0.062 ±0.006

	T	MdC
40% arm length	12	4.5
	3	4.0
	6	2.0
	9	3.0
80% arm length	12	4.0
	3	3.5
	6	1.5
	9	2.0

Cortical Activations During a Joystick Pursuit Task with Modulated Spindle Afferents

[1]Joseph Soltys and [2]Sara E. Wilson

[1]University of Missouri Kansas City, Kansas City, MO, USA
[2]University of Kansas, Lawrence, KS, USA
email: jsoltys@ku.edu,

INTRODUCTION

Proprioceptive feedback derived from muscle spindle afferents is important to proper control of everyday tasks. The proprioceptive feedback loop (PFL) originates at the muscle spindle organ and the outgoing spindle afferents, continues with the integration of the afferent in the central nervous system (CNS) into an appropriate response, and returns as the efferent signal exciting the motor neurons that generate the final response. It is well documented that applied vibration results in increased task errors that may persist beyond exposure and/or a perceived movement when none exists (kinesthetic illusion) [1].

Spindle afferents entrained to an applied external vibration can explain performance changes during exposure[2]. Persistent performance errors are not as straight forward. Changes along each aspect of the PFL (afferent, CNS, efferent) may be responsible. However, both the muscle spindle afferent and the efferent motor excitability have been observed to recover relatively quickly (on the order of seconds)[3,4]. This leaves the CNS as the likely location for persistent errors after prolonged vibration exposure.

The objective of the current work was to identify locations in the CNS where proprioceptive errors arise due to vibration during a constant velocity joystick pursuit task. We hypothesized that subject pursuit velocity would deviate from baseline both during and post vibration and that cortical activations in sensorimotor locations including primary motor (M1), primary somatosensory (S1), and cingulate motor area (CMA) would be observed to change with vibration exposure.

METHODS

Ten young and healthy subjects (5F, 5M, 25.8 +/- 4.1 years old), all self reported as right-handed (tested arm) consented for the University of Kansas approved study. Assessment trials were conducted in a 3-Tesla fMRI (Siemans; Integra) (echo time 30 ms, repetition time 2000 ms, and slice thickness of 4 mm). A cross over design was used to present the following vibration conditions: pre-vibration (BL), during vibration (DV), immediately post-vibration (PV), and post-washout (PW). Subjects were randomly assigned to one of two groups determining the order of exposure. Vibration exposure and the washout period were each set at 15 minutes duration.

Subjects lay supine on the scanner table with legs bent and supported. Custom pneumatically driven vibrators were placed over supinating muscles of the forearm (biceps and supinator) while the subject gripped an MR compatible joystick (HHSC-JOY-1, Current Designs) secured on the subject's thigh. The pursuit task was then projected into the fMRI bore and presented in ABC block format the following pursuit task levels: 1) active pursuit with visual feedback, 2) active pursuit with no visual feedback, and 3) visual pursuit only.

The pursuit task was generated and joystick cursor locations were recorded using a LabVIEW (National Instruments) virtual instrument running at 40 Hz. The target cursor swept through 18° pronation to 18° supination (total of 36° per movement) at a frequency of 0.2 Hz. Average pursuit task velocities were calculated within each task block for each pronation/supination movement. A repeated measures ANOVA was performed in SPSS testing for significant differences in pursuit velocity with a simple contrast for post hoc analysis.

A general linear model, multi-subject, random effects (RFX) analysis using BrainVoyager (v.2.2) software was used to examine the functional data. Imaging data were transformed into standard Talairach space and significant BOLD activation was defined for activations with an uncorrected p-value ≤ 0.001 and a minimum cluster size of 3. BOLD imaging contrasts were set to be similar to those in the ANOVA. These contrasts included comparisons between: BL and DV, BL and PV, and DV and PV.

RESULTS AND DISCUSSION

Subject pursuit velocities without feedback were found to decrease from baseline DV ($p=0.000$) followed by a significant increase PV ($p=0.006$). This is the same pattern we had reported previously in a non-MR environment. Both of the current velocity deviations were similar, approximately ±0.5 °/s (we had previously observed a magnitude of ±1.2 °/s). No differences were observed between PW and BL.

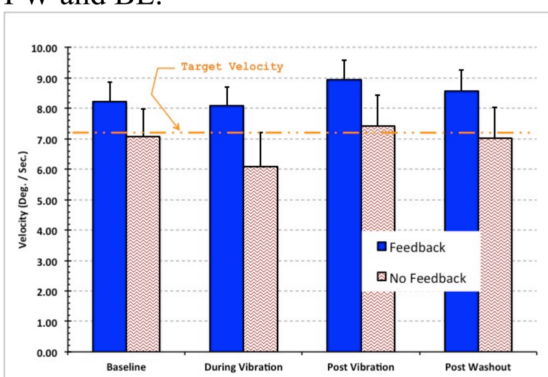

Figure 1: Average joystick pursuit velocity per task level and vibration condition.

Significant brain activations over baseline were observed in premotor (PMA), supplemental motor (SMA), somatosensory association (SSA), prefrontal cortex (PreF), cingulate gyrus, and insula during and immediately post vibration. Examination of the interactions indicated that in many previously mentioned active clusters; the applied vibration decreased the %BOLD signal change between task feedback levels, suggesting some form of habituation may be taking place. Post vibration activations suggested sensory locations increased over DV contributing supporting a recovery in sensory processing.

Additionally, clusters that would be expected to receive signaling from the anterior cingulate gyrus were consistently more active along with activations in the premotor cortex. In the BL and PV conditions activity shifted posteriorly in the cingulate gyrus and coincided with greater activity in the prefrontal cortex and parietal lobule, possibly indicating distinct pathways dependent on level of proprioceptive feedback.

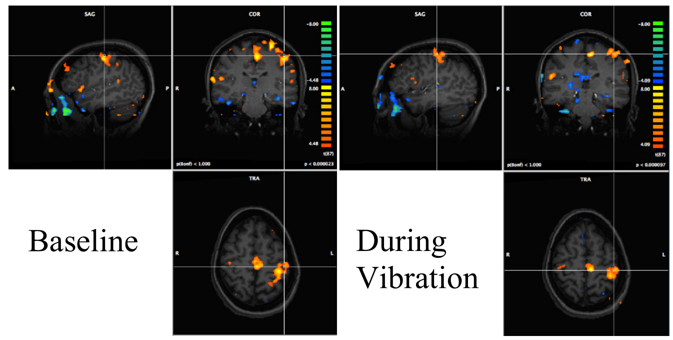

Figure 2: Example baseline and during vibration raw BOLD activations during pursuit task.

CONCLUSIONS

Pursuit task performance was consistent with vibration-induced errors found in literature. Early fMRI results suggest proprioceptive performance may be the result of more complex pathways than previously thought, involving co-activations in memory and association areas alongside sensory and motor locations. This potentially indicates multiple control strategies dependent upon the intensity of proprioceptive feedback.

REFERENCES

1. Li, L., et al., *Int. Journal of Ind. Ergo.* **38**, 792-800, 2008.
2. Cordo GS. *Proceedings of NACOB'08,* Ann Arbor, MI, USA, 2008.
3. Forner-Cordero A, et al., *Behavioral. Brain Research.* **190***:41-49, 2008*
4. Ribot-Ciscar E., et al. *Neurosci Letters*, **258**: 147-50, 1998.

ACKNOWLEDGEMENTS

The authors would like to thank Dr. Cary Savage and the staff at Hoglund Brain Imaging Center for their help. This study was also funded in part by an ASB student Grant-In-Aid award.

TISSUE DEFORMATION IN THE SEATED BUTTOCKS MODEL

[1]Sharon Eve Sonenblum, [2]John Cathcart, [2]John Winder and [1]Stephen H. Sprigle

[1]Georgia Institute of Technology, Atlanta, GA, USA

[2]University of Ulster, Belfast, UK

email: sharon.sonenblum@coa.gatech.edu web: rearlab.gatech.edu

INTRODUCTION

Pressure ulcer development remains a costly secondary complication for certain wheelchair users, impacting activities of daily living, employment and overall quality of life [1,2]. Wheelchair users are prescribed cushions in an attempt to prevent the formation of pressure ulcers. Currently, clinicians select cushions based largely upon their clinical experience; limited evidence is available to support their decisions.

Biomechanical and physiological characteristics of individuals may diminish the buttock's ability to resist damaging deformation and lead to a greater risk of pressure ulcer development. Deformation Resistance (DR) is defined as the intrinsic characteristic of an individual's soft tissues to withstand extrinsic applied forces. Persons with poor DR require greater attention in finding a cushion that accommodates the buttocks with minimal buttocks deformation. These cushions can be described as having high Shape Compliance (SC). SC is defined as the ability of a cushion to support the buttocks with minimal buttocks deformation. SC can be considered a metric of cushion performance, so is characteristic of the design and material construction of the cushion.

This study sought to study SC and DR in a phantom buttocks model. Specifically, the study evaluated the effects of different wheelchair cushions and buttocks geometry on tissue deformation.

METHODS

Two phantom buttocks models were created based on geometric shapes that reflect the anthropometry of ischial tuberosity (IT) spacing and bitrochanteric breadth (Figure 1). The elastomeric shell was made using Dragon Skin FX-Pro® (Smooth-On, Inc., Easton, PA) mixed with silicone thinner to a stiffness of 30kPa. The models had different tissue thicknesses and sphere diameters (Table 1), representing body types with different DR.

Figure 1. Foreground: Elastomeric gel buttocks model. Background: rigid substructure.

Table 1. Design features of two buttocks models.

Model	Elastomer thickness under sphere	Sphere diameter (IT Model)
A	35 mm	10 cm
B	20 mm	20 cm

Deformation data were collected using a Siemens Trio 3T MRI scanner. Coronal, T1 images were collected with a 2mm slice thickness. To document a reference, unloaded condition, the model was scanned upside down. Afterwards, the buttocks was flipped over and placed on top of a wheelchair cushion. Loading was applied to simulate a 70kg and 84kg person. Cushions tested included Roho Hi Profile, Jay2, 3" HR45 foam, Varilite Evolution, Motion Concepts Matrx, Vicair Vector, and a rigid surface.

MRI scans were imported into Analyze AVW v9.0 and converted to isotropic volumetric data (each voxel dimension was 1.68 mm). The model "soft tissue" was segmented using a simple threshold. We computed two different measurements on both the left and right sides: tissue thickness under the sphere (or IT model) and tissue volume under the sphere. Both measures were made through the middle slice of the buttock model. The volumetric measurement was made by projecting a 25 mm diameter cylinder through the model from top to bottom, and centered in the sphere. This region was selected to include the elastomer beneath the peak of the sphere. The volume of buttocks model material within this cylinder was calculated by counting voxels in the thresholded region and multiplying by the voxel volume. Two observers performed the analysis, and both were blinded to the model, cushion, and loading conditions. An analysis of repeatability and agreement showed good results.

Data analysis addressed three questions. First, loading conditions were compared in a paired t-test to see if increased load increased deformation. Second, we analysed the benefit of the presence of a wheelchair cushion by comparing the amount of deformation under load on a rigid surface with deformation on wheelchair cushions. This comparison was made across both models using a one-way ANOVA. Finally, we looked at the impact wheelchair cushion and buttocks model design on deformation using a 2-way ANOVA.

RESULTS AND DISCUSSION

A paired t-test across loading conditions revealed no significant differences in linear or volumetric deformation. Therefore, data across loading conditions were combined.

When loaded on a rigid surface (no cushion), Model A had a 65% change in thickness and a 62% change in volume. Model B experienced a 41% change in thickness and 35% change in volume. Not surprisingly, the use of a wheelchair cushion reduced the deformation significantly ($p<0.001$) (Figure 2). While the model deformation seen on a rigid surface was comparable with thickness changes measured in able-bodied humans, the model deformation when loaded on a cushion was much smaller than published human data [3]. Differences in cushions, loading parameters and/or representativeness of the models may factor into the explanation of differences.

The 2-way ANOVA revealed that both model and cushion design played a significant role in the amount of deformation experienced by the buttocks model, although the interaction effect was not significant (Table 2). Model B, which had thinner tissue but a less peaked sphere, experienced less deformation than Model A on all surfaces

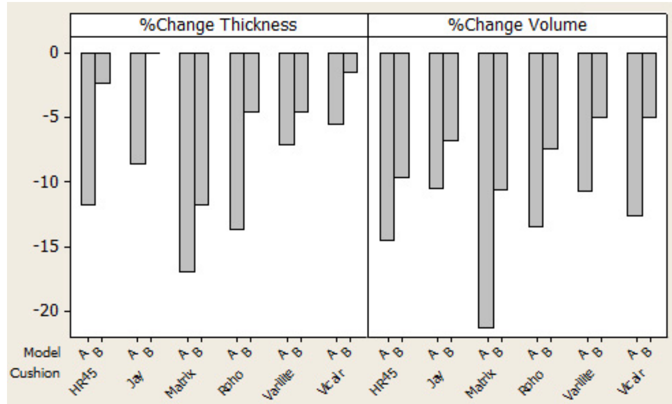

Figure 2. % Change in thickness (left) and volume (right) in a 25mm diameter region under the sphere (IT model). Figure shows the mean of left and right.

Table 2. P-values from the 2-way ANOVA of percent change in thickness and volume.

	Thickness		Volume	
	Left	Right	Left	Right
Model	0.005	0.084	<0.001	<0.001
Cushion	0.060	0.050	<0.001	0.001

CONCLUSIONS

This study represents the first analysis of Shape Compliance of wheelchair cushions. While these methods successfully demonstrate differences in DR and SC, it is difficult to define cushion performance using the models and measurements presented. More complex measures of deformation such as the gradient might be necessary to better stratify cushions. Validation of the approach using human data is planned.

REFERENCES

1. Raghavan P, et al. *Clin Rehab*. **17**(8):879-84, 2003.
2. Langemo DK, et al. *Adv skin wound care*. **13**(5):225-35, 2000.
3. Shabshin, N., G., et al. *J Rehabil Res Dev* **47**(1): 31-42, 2010

ACKNOWLEDGEMENTS

The project was supported by the Center for Advanced Brain Imaging and the mobilityRERC at Georgia Tech. Software and hardware for analysis were contributed by Roho, Inc.

THE EFFECTS OF A 6 WEEK INTERVENTION PROGRAM ON LOWER LIMB JOINT MOMENT ASYMMETRY IN HEALTHY FEMALE COLLEGIATE ATHLETES

Lee Spencer, Ali St Jeanos, Mike Wynot, Michael Lawrence, and Erin Hartigan

University of New England, Portland, ME, USA
Email: rspencer1@une.edu

INTRODUCTION

Of all sport-like tasks, cutting and drop jumping tasks are associated with having the highest injury rates [1,2]. Lower limb asymmetry, the difference in a kinematic or kinetic parameter between limbs, is a risk factor for musculoskeletal injuries in athletes, especially female athletes [1,3,4]. Asymmetrical joint moments can increase risk of injury in musculoskeletal structures forced to compensate to maintain limb support [5,6]. The total support moment (TSM) of a limb is the sum of each individual joints (hip, knee, ankle) [7]. It describes the synergistic role of these joints in each limb to maintain the body upright at any instance [7]. Asymmetrical quadriceps and hamstring isokinetic strength values may also increase injury risk [7,8,9]. Lower extremity asymmetry in joint moments and isokinetic strength may be caused by limb dominance [7], which may be influenced by intervention programs composed of plyometric, balance, and resistance training [3,4,10,11]. However, whether neuromuscular training that includes plyometrics, resistance, and speed training alters limb differences is unknown. Therefore, the purpose of this study was to assess the effects of a neuromuscular training on isokinetic knee strength and joint moments during cutting and drop jump landing tasks between dominant and non-dominant limbs in healthy female collegiate athletes. We hypothesized that 1) at pre-intervention, the dominant limb's isokinetic strength values and joint moments during both tasks will be greater than the non-dominant limb, and 2) at post-intervention, isokinetic strength values and joint moments will increase compared to pre-intervention and limb differences will resolve .

METHODS

Twelve healthy, female, collegiate softball and lacrosse players participated in a bi-weekly, 6-week neuromuscular training program with speed, agility, and landing progressions. Limb dominance was determined by which foot they kicked a ball with. Data were collected pre and post training including: peak torque throughout range of motion isokinetic knee flexion and extension strength bilaterally at 180^0/s using a S4 Biodex dynamometer (Biodex Medical Systems Inc, Shirley, NY); lower extremity motion using an 8 camera 3-dimensional motion analysis system (Qualisys, Gothenburg, Sweden); and ground reaction forces using 3 6-channel force plates (AMTI, Watertown, MA). Each participant performed each task until 5 usable trials were collected. Inverse dynamics were used to calculate sagittal plane hip, knee, and ankle joint moments at peak knee flexion during stance. This instant during the weight acceptance phase of gait is when the limb is most vulnerable to injury [12]. Total support moments were calculated by using the formula by Winter et al. $M_s = M_k - M_a - M_h$ [8]. Repeated measures analysis of variance was used to assess differences between limbs and over time for isokinetic strength and joint moments during both tasks. Post hoc tests were run when differences were found.

RESULTS AND DISCUSSION

Cutting: Limb differences existed for the knee (non-dominant [ND] > dominant [D], p<.001) and total support moments (TSMs) (D > ND, p=.001). Joint moments increased over time for the knee (p=.002). No interaction effects (limb x time) were found at the hip, knee, or total support moment (TSM). **Jumping:** Limb differences were found for the hip, knee, and TSMs (Table 1). There was an interaction effect, indicating that joint moments at peak knee flexion (PKF) responded differently between limbs over time for the jumping task. **Strength Data:** There were no main effects or interaction effect in knee flexion or extension strength data.

Our hypothesis that strength and moments would be greater in the dominant limb was supported only for knee moments during the drop jump landing tasks. Unexpectedly, the moments in the ND limb were greater than the D limb for TSMs during both tasks, hip moments during jumping, and knee moments during cutting. Furthermore, no limb differences occurred in strength values or hip moments during cutting. After the intervention, our athletes increased their knee moments while cutting despite no differences in knee extension and flexion strength. During the jumping task, only the D knee's extension moments increased. These results suggest that neuromuscular changes may explain increases in joint moments without concurrent strength changes. Laterality and the nature of the task (unilateral cuts vs. bilateral drop jump landing) may influence the different D and ND moment profiles.

CONCLUSIONS

Our intervention successfully increased moments in at least one joint for each task; however limb differences in lower extremity joint moment and isokinetic knee strength were not altered in our female softball and lacrosse athletes. Joint moment increases without concurrent increases in strength at 180^0/second suggest the specific training may have improved neuromuscular control.

REFERENCES

1. Pollard CD et al. *Clin J Sport Med* **17**, 38-42**,** 2007.
2. Cochrane JL et al. *Med Sci Sports Exerc* **42**, 1535-1544, 2010.
3. Chappell JD and Limpisvasti O. *Am J Sport Med* 36, 1081-1086, 2008.
4. Sadeghi H et al. *Gait Posture* **12,** 34–45, 2000.
5. Myer GD et al. *J Strength Cond Res* **20**, 345-353, 2006.
6. Herman DC et al. *Am J Sports Med* **36**, 733-740, 2008.
7. Winter DA and Eng J. *Behav Brain Res* **67**, 111-120, 1995.
8. Winter DA. *J Biomech* **13**, 923-927, 1980.
9. Winter DA. *Biomechanics and motor control of human movement*, John Wiley and Sons, Ltd., 1990.
10. Hadzica V et al. *Isokinet Exerc Sci* **18**, 31–37, 2010.
11. Devan MR et al. *J Athl Train* **39**, 263–267, 2004.
12. Trowbridge C et al. *J Athl Train* **40**, S-90, 2005.
13. Myer GD et al. *J Strength Cond Res* **19**, 51-60, 2005.
14. Slocker de Arce A, et al. *Isokinet Exerc Sci* **9**, 151-154, 2001.

Table 1: Joint Moments at Peak Knee Flexion (Nm/kg) in the Non-Dominant Limb and Dominant Limb while Drop Jump Landing

	Non-Dominant Limb	Dominant Limb	P value
Pre Hip Extension	-1.630 (0.425)	-1.292 (0.345)	< 0.001*
Post Hip Extension	-2.144 (0.395)	-1.575 (0.296)	< 0.001*
Pre Knee Extension	1.001 (0.247)	1.380 (0.317)	< 0.001*
Post Knee Extension	1.143 (0.285)	1.656 (0.389)	< 0.001*
Pre TSM	3.913 (0.713)	3.518 (0.678)	0.002*
Post TSM	4.763 (0.654)	4.150 (0.614)	0.008*

*Statistical significance ($p < 0.05$)

ALTERED SCAPULOHUMERAL COORDINATION IN INDIVIDUALS WITH SCAPULAR DYSKINESIS

[1]Bryan A Spinelli, PT, MS, OCS, CLT and David Ebaugh, PT PhD
[1]Department of Physical Therapy and Rehabilitation Sciences, Drexel University, Philadelphia, PA, USA
email: bas62@drexel.edu

INTRODUCTION

Clinicians commonly perform visual assessment of scapulohumeral motion when they evaluate an individual with shoulder pain. The reason for this is that alteration of the coordinated motion between the scapula and humerus is believed to be a contributing factor for development of shoulder pain and dysfunction [1]. However, evidence supporting this belief is limited and a recent study failed to find an association between altered scapulohumeral motion (scapular dyskinesis) and shoulder pain [2]. This may be secondary to the possibility that only certain patterns of altered scapulohumeral coordination are harmful. Garofalo et al [3] proposed a method for assessing patterns of continuous 3-dimensional scapulohumeral motion by deriving averaged motion patterns and minimal detectable change bands (MDCB) from individuals without shoulder pain, and then individually comparing subjects with shoulder pathology to these graphs. In this study we used this method to assess the coordination of scapulohumeral motion in individuals who were identified as having visible scapular dyskinesis on a physical exam.

METHODS

Nineteen subjects (mean age 24.5±3.9 years; 13 females; 9 dominant side tested) without current shoulder pain were consented to participate in the study. All subjects underwent a visual assessment of scapulohumeral motion by three examiners. Motion was assessed by viewing subjects from behind during 5 repetitions of bilateral sagittal plane arm elevation. Motion was rated as ideal (normal) or dyskinetic (subtle or obvious) according to the operational definitions described by McClure et al [2]. Final rating of each subject's motion was based on the majority rating amongst the examiners.

Following visual assessment, an electromagnetic device (Polhemus Liberty) was used to collect 3-D kinematic data from the scapula, humerus, and trunk at 240Hz as the subjects repeated 5 repetitions of bilateral sagittal plane arm elevation. Digitized anatomical landmarks and joint coordinate systems generally followed the standards of the International Society of Biomechanics [4]. Scapular motion was described by the following rotations: upward/downward rotation (UR/DR), internal/external rotation (IR/ER), anterior/posterior tilt (AT/PT), as well as clavicular elevation/depression (CE/CD) and clavicular protraction/retraction (CP/CR). Humeral motion was described as elevation of the humerus with respect to the scapula (glenohumeral elevation), and elevation of the humerus with respect to the thorax (humerothoracic elevation). Kinematic data were filtered with a zero lag 4^{th} order Butterworth filter (8Hz), and resampled to 101 data points using linear interpolation for a common range of humerothoracic elevation amongst all subjects (30° - 130°).

Relative motion graphs were used to describe the coordinated motion between the scapula and humerus and clavicle and humerus. In a relative motion graph the coupling angle for each scapular or clavicular rotation is plotted on the Y-axis and percent of glenohumeral elevation on the X-axis [5]. A coupling angle of 45 degrees indicates 1:1 motion between the scapula or clavicle and humerus. Coupling angles greater than 45 degrees indicate more scapular or clavicular motion, while coupling angle less than 45 degrees indicate more humeral motion. Averaged relative motion graphs with 95% MDCB were created from data of subjects who were determined to have ideal scapulohumeral motion based on the visual examination. MDCB was calculated as follows: MDCB = mean +/- 1.96 x standard error of the measure (SEM) x $\sqrt{2}$; SEM =

SD x (1-ICC); ICC (3,3) (Intraclass correlation coefficients based on data collected from two separate days). Subjects rated as having either subtle or obvious scapular dyskinesis were individually compared to the averaged relative motion graphs and MDCB derived from subjects with normal scapulohumeral motion. Subjects with scapular dyskinesis were classified as having altered scapulohumeral coordination if their relation motion pattern fell outside the MDCB.

RESULTS AND DISCUSSION

Ten subjects (52.6%) were visually rated as having scapular dyskinesis (2 obvious, 8 subtle). All subjects with scapular dyskinesis demonstrated altered coordination patterns in at least one of the scapular or clavicular relative motion graphs. However, a consistent pattern of altered coordination across subjects did not exist. An example of a subject rated as having scapular dyskinesis and their scapulohumeral and claviculohumeral coordination patterns compared to subjects with ideal visual scapular motion are illustrated in Figure 1.

These findings demonstrate the feasibility of using relative motion graphs to identify altered patterns of scapulohumeral and claviculohumeral coordination. This approach expands upon traditional measures of assessing scapular and clavicular angular positions at select angles of humeral elevation by assessing the relationships between scapulohumeral and claviculohumeral motion over the movement cycle.

It is important to note that none of the subjects in this study had shoulder pain, which raises the question of whether or not all patterns of altered coordination are harmful. We plan to use the method described in this study in a larger group of subjects with and without shoulder pain in an attempt to determine if certain patterns of altered coordination are associated with shoulder pain.

REFERENCES

1. Ludewig P, et al. *JOSPT* 39, 90-104, 2009.
2. McClure P, et al. *J Athl Train* **44**, 160-164, 2009.
3. Garofalo P, et al. *Medical & biological engineering & computing* **47,** 475-486, 2009.
4. Wu G, et al. *J Biomech* **38,** 981-992, 2005.
5. Sparrow W., et al. *J of Motor Behavior* **19,** 115-129, 1987.

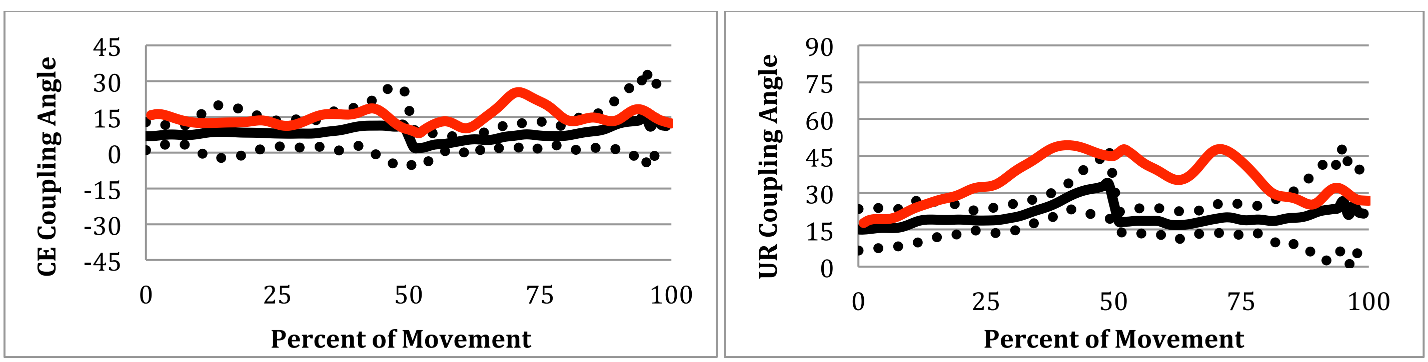

Figure 1: Relative Motion graphs. Mean of normal subjects (solid black) & +/- MDCBs (dashed black). Single subject with aberrant visual scapular motion (red).

SIMPLE FE MODELS OF THE FOREFOOT FOR USE IN THE DESIGN OF THERAPEUTIC FOOTWEAR FOR DIABETIC PATIENTS

[1]Thomas A. Spirka, [2]Ahmet Erdemir and [1]Peter Cavanagh

[1]University of Washington, Seattle, WA, USA
[2]Cleveland Clinic, Cleveland, OH, USA
email: cavanagh@uw.edu

INTRODUCTION

Therapeutic footwear is frequently recommended for neuropathic diabetic patients to reduce their risk of the developing ulcers. Due to the high pressures that often occur under the bony prominences of the metatarsal heads (MTHs), therapeutic footwear is often designed to reduce the plantar pressure (PP) in this region. Subject-specific finite element (FE) models have been proposed to assist in footwear design[1], but in order to be clinically useful, such models need to be simple to generate and must have fast solution times. Here, we propose a simplified FE model of the metatarsal head region of the foot based on patient specific measurements to test the effect of potential footwear interventions on PP distribution.

METHODS

CT images of the left foot of a 46 year old male with Type I diabetes were acquired. To characterize the location and size of the MTHs the measurements listed in Table 1 were made. Briefly, the model assumed that the metatarsal heads were spheres having diameters equal to widest portion of the MTH. The spacing between MTHs was determined by locating the approximate center of each head relative to the center of its neighbor from the CT. Lastly, the tissue thickness under each MTH was determined from the CT by identifying the lowest point on the each MTH and measuring the thickness of the unloaded tissue from this point to the plantar surface.

The MTHs were modeled as rigid bodies and were embedded in a block representing soft tissue so that the thickness of tissue under the MTH corresponded to the measured tissue thickness. The tissue was modeled as a hyperelastic Ogden material that was in contact with a rigid body representing the floor (coefficient of friction = 0.5). The model was loaded by distributing a 300N load over the 5 MTHs in an effort to reproduce the barefoot pressure distributions observed using an Emed® pedography platform (Novel GMBH Munich, Germany). This generated input conditions for the modeling of two types of insole footwear interventions designed to reduce plantar pressure: a flat ¼” thick foam insole and a ¼” thick foam insole with cylindrical cutouts under the MTHs. Different materials including firm plastozote, poron and microcell puff were examined in the modeling of the flat insole[2,3]. The cutout insole was modeled as being constructed from firm plastozote.

RESULTS AND DISCUSSION

Figure 2 presents the pressure distributions predicted by the finite element model. As can be seen in the pressure distribution measured from the subject using the Emed platform, the regions of the greatest pressure are under the 1st and 5th MTH. This result was duplicated in the original model constructed with no footwear interventions. Adding insoles did alleviate the high pressure present under the 1st MTH but was not as successful at reducing the high pressures under the 5th MTH. The models predicted that insoles constructed of firmer materials would be more successful at reducing plantar pressure than softer materials. The models also indicated that removing material from the insole by way of cylindrical cutouts under the regions of highest plantar pressure would reduce the plantar pressure in these regions. However, high pressure regions were initially noted in the regions where the foot would come into contact with the edges of the cutout. These stress concentrations were alleviated by beveling the edges of the cutout.

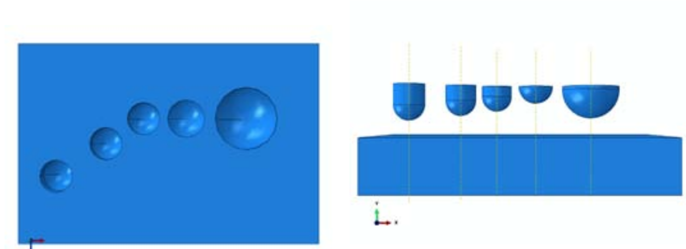

(A) (B)

Figure 1: Finite element model (A) shows an overhead view of the relative location of the MTHs relative to one another. (B) Shows the relative positions of the MTHs relative to the rigid floor surface

Table 1: Measurements made from the subject's CT scan used to construct FE models of MTH region

Maximum Diameter of MTHs	
1st MTH	25 mm
2nd MTH	15 mm
3rd MTH	13 mm
4th MTH	13 mm
5th MTH	13 mm
Spacing between MTHs	
MTH1 to MTH 2	Med-Lat Distance 24 mm Ant-Post Distance 0 mm
MTH 2 to MTH 3	Med-Lat Distance 17 mm Ant-Post Distance 0 mm
MTH 3 to MTH 4	Med-Lat Distance 15 mm Ant-Post Distance 10 mm
MTH 4 to MTH 5	Med-Lat Distance 20 mm Ant-Post Distance 13 mm
Thickness of Unloaded Tissue Under Metatarsal Heads	
1st MTH	8 mm
2nd MTH	14 mm
3rd MTH	10.5 mm
4th MTH	8.5 mm
5th MTH	6.5 mm

CONCLUSIONS

The main benefit of this model is that it would allow an orthotist to gain insight into how potential foot interventions would impact the pressure distributions and determine if those interventions would have the desired effect or if modifications are needed to achieve the desired pressure relief. Construction of the models and all FEM runs were completed rapidly (run time of 3 hours per model) in contrast to our previous experience with full-scale anatomically accurate foot models for which a single simulation required several weeks to converge.

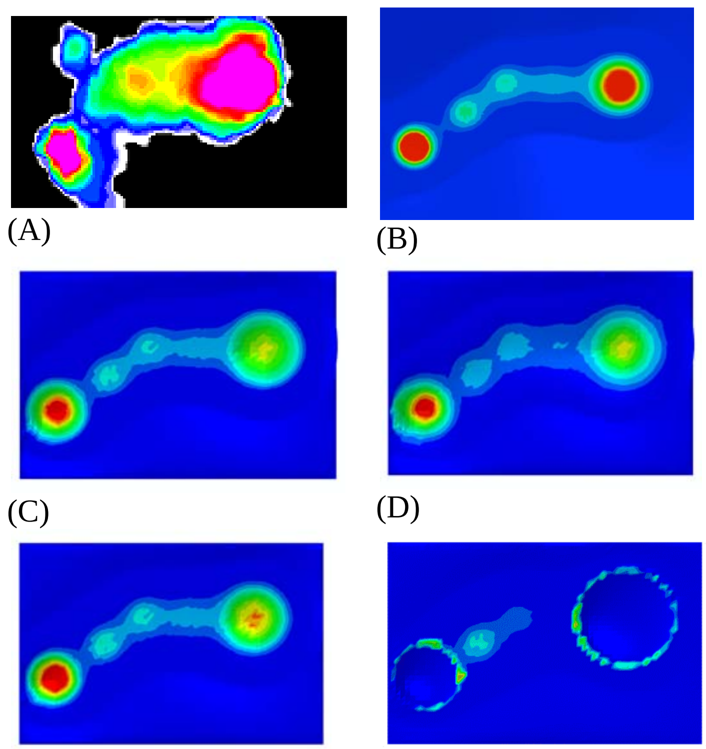

(A) (B) (C) (D) (E) (F)

Figure 2: (A) Barefoot pressure distribution measured by Pedar. (B) FEM prediction of barefoot plantar pressure distribution (C) FEM prediction of adding a firm plastazote insole (D) FEM prediction of effect of incorporating a Poron insole (E) FEM prediction of effect of incorporating a Puff insole (F) Effect of incorporating beveled cylindrical cutouts under the 1st and 5th MTH in the firm platazote insole.

REFERENCES

1. Cheung JT et al. *Arch.Phys.Med.Rehabil* **86**, 353-358, 2005.
2. Goske S, et al. *J Biomech* **39** 2363-2370 2006
3. Budhabhatti SP, et al. *J Biomech Eng* **129**, 750 756, 2007

LOWER EXTREMITY JOINT MOMENTS DURING THE ACTIVE PEAK VERTICAL GROUND REACTION FORCE IN THREE DIFFERENT RUNNING CONDITIONS

[1]Tyler Standifird, [1]Wayne Johnson, [1]Iain Hunter and [1]Sarah Ridge

[1]Brigham Young University, Provo, UT, USA
email: tstandifird@gmail.com

INTRODUCTION

The benefits of exercise are numerous and as such many people participate in exercise programs. Running has become one of the primary forms of exercise with over 36 million Americans running at least once and over 10.5 million at least 100 days in 2003 [1]. Many runners sustain lower extremity running injuries, with some rates as high as 79% in recreational runners [2]. Current research is replete with explorations as to causes and cures of common running related injuries.

Barefoot and other minimalist running has gathered increasing interest in recent years. During running, a runner will have to withstand forces up to three times their body weight and these forces can lead to a variety of lower extremity injury [3,2]. Barefoot running has been found to lower these forces during the stance phase of running as a result of altered mechanics [3]. Additionally, elevated lower extremity joint moments may contribute to the development of overuse injury [4] and barefoot running has been shown to reduce joint moments of the lower extremity [5].

Many companies are now designing shoes aimed at capturing the benefits of barefoot running while still allowing some protection for the foot on potentially harmful running surfaces. The Vibram FiveFingers (VF®) running shoe has been designed specifically for this purpose. Previous research has shown that the VF® is effective at mimicking kinematic variables during running [6] though no study has compared joint moments between VF®, barefoot and shod running.

METHODS

Twenty-five healthy recreational runners (sixteen male and nine female) participated in this study. Following a warm-up of running the length of the lab, subjects ran in VF®, barefoot and shoes (Nike Air Pegasus) in a randomized order at a speed of 3.84 m/s, controlled with timing lights. Force and position data was collected for the stance phase of gait until the subject achieved complete foot contact on the force platform without altering gait (determined by two researchers). This was done until the subject completed three successful trials in each running condition. Joint moments in the sagittal plane at the ankle, knee and hip were calculated during the peak vertical ground reaction force (PVGRF) in Visual 3d and averaged for the three successful running trials.

RESULTS AND DISCUSSION

At the ankle, the shod condition led to lower plantarflexion moments when compared with VF® and barefoot running (Table 1). At the knee, the shod condition led to elevated extension moments when compared with VF® and barefoot running. The only significant differences between hip extension moments were seen when comparing shod and barefoot running. When comparing VF® and barefoot running there were no significant differences found when comparing joint moments at the ankle, knee and hip in the sagittal plane.

No difference was found between the PVGRF values between the three conditions. As a result, it is apparent that the differences in joint moments are not a result of differences in the forces experienced by our subjects, but rather altered running mechanics. Reductions in joint moments can potentially lead to a smaller number of running related injuries. The knee is the most common location of lower extremity joint injury [2] and should be one of the primary areas of focus when considering a reduction in injury. Our subjects experienced reduced joint moments at the knee during VF® and barefoot running when compared with shoes and may offer a means for reducing injury at that joint.

When considering incidence of injury it is also important to consider the aspects of Wolff's law and how these reduce forces could potentially impact the strength of the bone and soft tissue of the lower extremity. Elevated forces could cause alterations in the structures of the lower extremity that would allow the subject to withstand higher forces. A reduction in forces, over time, could possibly lead to similar rates of injury if the bones and surrounding tissues become weaker as a result of decrease joint moments.

Athletes and coaches looking to improve upon performance while reducing injury prevalence need to keep in mind the aspects of Wolff's law relating to forces and the associated adaptations. When taking this law into consideration, they could add variety to a program in order to strengthen the associated bones, joints and muscles. This could be done through cross training, running in a variety of shoes and exercises specifically aimed at strengthening the associated structures through elevated stresses. Individual differences should be taken into consideration when planning any type of training program aimed to increase performance and decrease injury.

CONCLUSIONS

The VF® was developed to mimic barefoot running while offering some protection to the runner's foot. Our study compared barefoot running and running in VF® to running in standard running shoes. Results from this study found that the VF® does closely mimic barefoot running in regards to joint moments during the PVGRF in the sagittal plane. There were no differences when considering the joint moments during VF® and barefoot running. Though the VF® did not reduce joint moments in the sagittal plane at the ankle and hip, the shoe did reduce impact forces at the knee, the site of the highest incidence of running related injuries. Prospective studies aimed at combining a reduction in joint moments with strengthening of associated structures should be carried out to truly understand how the alterations associated with VF® and other minimalist running changes long term incidence of injury.

REFERENCES

1. Paluska SA, *Sports Med* **35**, 991-1014, 2005
2. van Gent RN, et al. *Br J Sports Med* **41**, 469-480, 2007
3. Lieberman DE, et al. *Nature* **463**, 531-535, 2010
4. Scott SH, et al *Med Sci Sports Exerc* **22**, 357-369, 1990
5. Kerrigan DC, et al. *PM R,* **1**, 1058-1063, 2009
6. Squadrone R, et al. *Journal of Sports Medicine and Physical Fitness* **49**, 6-13, 2009

Table 1: Joint moments at the active peak vertical ground reaction force
B=Significant difference from barefoot
V=Significant difference from Vibram®

Joint	Barefoot	Vibram	Shoe
Ankle Plantarflexion Moment (Nm/kgm)	1.49	1.43	1.21[BV]
Knee Extension Moment (Nm/kgm)	1.86	1.96	2.26[BV]
Hip Extension (Nm/kgm)	1.49	1.43	1.35[B]

A GENERAL APPROACH TO MUSCLE WRAPPING OVER MULTIPLE SURFACES

Ian Stavness, Michael Sherman and Scott Delp

Stanford University, Stanford, CA, USA
email: stavness@stanford.edu

INTRODUCTION

In musculoskeletal simulations muscle forces are transmitted along curves intended to represent the centroid of each muscle's path. The curves are assumed to take the shortest path wrapping around geometric surfaces that represent bones and other structures. The length and rate of length change of a muscle's path affect computed muscle force and the geometry of a muscle's path determines how muscle force is delivered to bones. Errors in representing how muscles wrap may degrade simulation accuracy and performance.

A common approach to represent muscle wrapping uses approximate discretized wrapping curves [1]. In dynamics simulations, discontinuous changes in wrapping paths due to discretization can degrade simulation performance. Another approach to model muscle wrapping uses analytical equations for simple shapes such as spheres and cylinders [2, 3]. This approach does not generalize to muscle paths that wrap around more than two surfaces or complex wrapping surfaces.

Here we introduce a novel formulation to compute smooth wrapping curves for arbitrary numbers of wrap surfaces. The formulation permits the use of general smooth geometric surfaces with implicit or parametric representations and incorporates fast analytical equations for the special cases of simple shapes. This method generates smooth wrapping paths suitable for high-order time integration, and allows biomechanical models of the spine, finger, shoulder, and other systems to incorporate wrapping paths over multiple anatomical structures with complex shapes.

METHODS

Our formulation computes the minimum length wrapping path over multiple surfaces by finding the location of two wrapping points per surface such that joining paths are straight lines, wrapping paths are geodesic curves, and joining paths connect smoothly with wrapping paths (Figure 1).

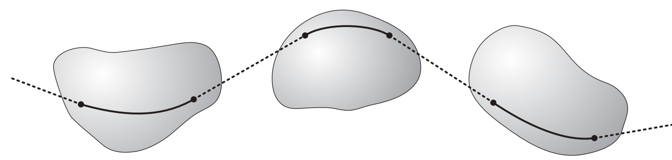

Figure 1: The shortest path wrapping n surfaces is represented with two wrapping points on each surface, straight joining paths (dotted lines), and geodesic wrapping paths (solid lines).

A geodesic curve is nominally the shortest path along a smooth surface and is uniquely defined for a point and direction on that surface. Our formulation ensures that the path remains smooth as wrapping paths lift off wrapping surfaces during dynamic simulations. In the case of an implicit surface representation, $\phi(\boldsymbol{r}) = 0$, with gradient, $\boldsymbol{n} \equiv \nabla\phi$, we aim to find the location of wrapping points, $\boldsymbol{p}$ and $\boldsymbol{q}$, that satisfy the conditions illustrated in Figure 2.

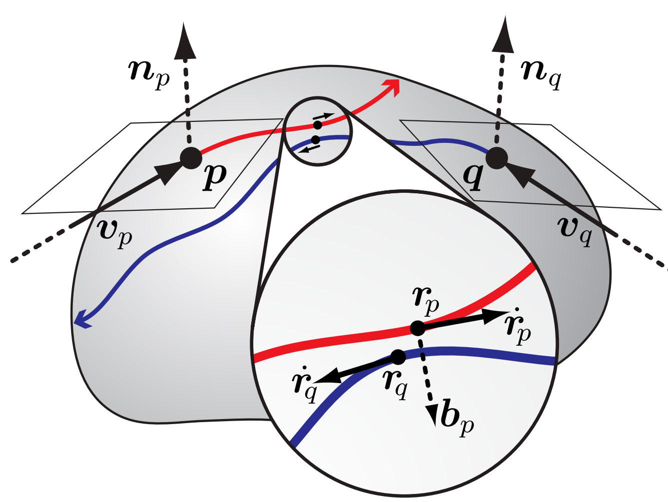

Figure 2: The local conditions that must be satisfied to find the shortest wrapping path. Wrapping points $\boldsymbol{p}$ and $\boldsymbol{q}$ must lie on the wrapping surface and straight-line joining paths $\boldsymbol{v}_p$ and $\boldsymbol{v}_q$ must be tangent to the surface. The geodesic curve originating from point $\boldsymbol{p}$ in the direction of $\boldsymbol{v}_p$ (red line) and the geodesic curve originating from point $\boldsymbol{q}$ in the direction $\boldsymbol{v}_q$ (blue line) must connect smoothly.

The wrapping conditions can be stated as follows:

1. Wrapping points lie on the wrapping surface:

$$\begin{aligned}\phi(\boldsymbol{p}) &= 0\\ \phi(\boldsymbol{q}) &= 0\end{aligned} \tag{1}$$

2. Joining paths are tangent to the wrapping surface:

$$\begin{aligned}\boldsymbol{n}_p \cdot \boldsymbol{v}_p &= 0\\ \boldsymbol{n}_q \cdot \boldsymbol{v}_q &= 0\end{aligned} \tag{2}$$

where $\boldsymbol{n}$ is the surface normal ($\boldsymbol{n} \equiv \nabla\phi$ for implicit surface representations).

3. The geodesic curves originating from the two wrapping points must connect smoothly:

$$\begin{aligned}\boldsymbol{b}_p \cdot (\boldsymbol{r}_q - \boldsymbol{r}_p) &= 0\\ \boldsymbol{b}_p \cdot \dot{\boldsymbol{r}}_q &= 0\end{aligned} \tag{3}$$

where $\boldsymbol{b}_p \equiv \dot{\boldsymbol{r}}_p \times \boldsymbol{n}_p$, and $\boldsymbol{r}_p$ and $\boldsymbol{r}_q$ are the closest points on the geodesic curves from $\boldsymbol{p}$ and $\boldsymbol{q}$.

We compose a system of equations using conditions (1), (2), and (3) for all n wrapping surfaces as:

$$\boldsymbol{F}(\boldsymbol{x}) = 0, \quad \boldsymbol{x} \equiv \left(\boldsymbol{p}_1^T\ \boldsymbol{q}_1^T\ \ldots\ \boldsymbol{p}_n^T\ \boldsymbol{q}_n^T\right)^T \tag{4}$$

The size of the system is $6\,n_{\text{implicit}} + 4\,n_{\text{parametric}}$, since condition (1) is automatically satisfied for parametric surface representations. We solve (4) as a root-finding problem using Newton's method with a banded Jacobian to find wrapping point locations across all n surfaces. Fast convergence requires good initial conditions; to achieve this we take advantage of temporal coherence for wrapping in dynamic simulations.

For general smooth surfaces, we find geodesic curves using numerical integration. For this purpose, we use the mechanical analogy that a particle moving along a surface with acceleration normal to the surface will trace a geodesic path [4]. For a particle $\boldsymbol{r}$, we solve the differential equation $\boldsymbol{M}\ddot{\boldsymbol{r}} = -\boldsymbol{G}^T\lambda$ subject to $\phi(\boldsymbol{r}) = 0$, which leads to:

$$\begin{pmatrix}\boldsymbol{M} & \boldsymbol{G}^T\\ \boldsymbol{G} & 0\end{pmatrix}\begin{pmatrix}\ddot{\boldsymbol{r}}\\ \lambda\end{pmatrix} = \begin{pmatrix}0\\ -\dot{\boldsymbol{G}}\dot{\boldsymbol{r}}\end{pmatrix}$$

where $\boldsymbol{G}^T \equiv \boldsymbol{n}$ and λ is the Lagrange multiplier that satisfies the implicit surface constraint.

For spheres, cylinders and other surfaces of revolution, it is straightforward to replace the general geodesic condition (3) with analytical equations to improve speed.

RESULTS AND DISCUSSION

We evaluated the accuracy of our approach using a combined sphere-cylinder test case reported in [3]. We chose initial wrapping points on the straight-line path between the fixed end points (Figure 3, dotted line). Our computed wrapping path (Figure 3, solid line) has a length of 22.437 cm, which matches the exact solution reported in [3]. We also simulated test cases for wrapping multiple bicubic spline surfaces, ellipsoids, spheres, and cylinders as shown in Figure 4. Videos and source code are available at http://simtk.org/home/wrap. This method provides high performance muscle wrapping for simulation of musculoskeletal dynamics.

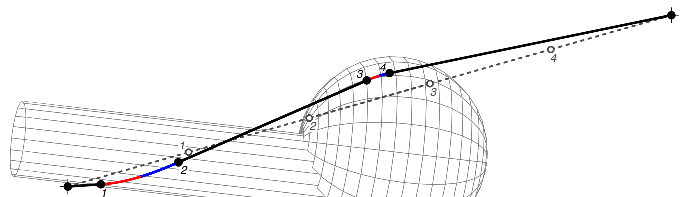

Figure 3: Result for wrapping over the sphere-cylinder test case from [3]. The initial path is denoted by the dotted line.

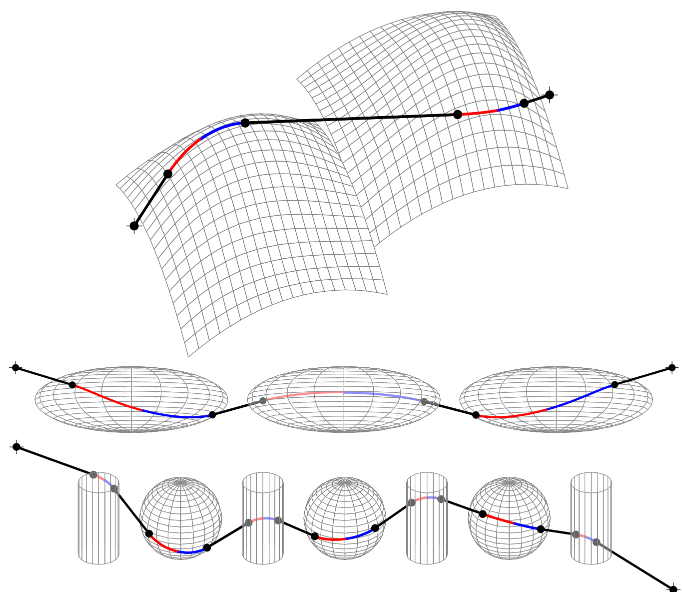

Figure 4: Results for wrapping over multiple surfaces: two bicubic spline surface patches (top), three ellipsoids (middle), and seven spheres and cylinders (bottom).

REFERENCES

1. Delp and Loan, *Comput Biol Med*, **25**(1), 21–34, 1995.
2. Garner and Pandy. *CMBBE*, **3**(1), 1–30, 2000.
3. Marsden et al., *IMechE PartH*, **222**(7), 1081–95, 2008.
4. DeSapio et al., *Multiby Syst Dyn*, **19**(3), 303–22, 2008.

AN MRI-COMPATIBLE DEVICE FOR OBTAINING PATIENT-SPECIFIC PLANTAR SOFT TISSUE MATERIAL PROPERTIES

[1,2] Michael J. Stebbins, [1] Michael J. Fassbind, [2,3] Peter R. Cavanagh, [4] David R. Haynor, [4] Baocheng Chu and [1,2,3] William R. Ledoux

[1]RR&D Center of Excellence for Limb Loss Prevention and Prosthetic Engineering, Department of Veterans Affairs; Departments of [2]Mechanical Engineering, [3]Orthopaedics and Sports Medicine, and [4]Radiology, University of Washington
email: wrledoux@u.washington.edu, web: www.amputation.research.va.gov

INTRODUCTION

More than 60% of all nontraumatic lower-limb amputations occur in people with diabetes [1]. Diabetes has been shown to increase the stiffness of the plantar soft tissue in cadaveric samples [2], which could cause a shift in the location and/or magnitude of peak stresses inside of the foot. A previous MRI study measured internal deformation of the foot *in vivo* under quasi-static loading [3]. The purpose of this study is to develop an MRI-compatible device for obtaining patient-specific plantar soft tissue material properties using dynamic *in vivo* loading.

METHODS

A cyclic, displacement-controlled, compressive load was applied to the foot while gated magnetic resonance imaging (MRI) obtained internal deformation data at multiple points on the loading /unloading curve. A water-based hydraulic loading device (Fig. 1) was designed to produce a sine wave displacement curve with maximum peak amplitude of 20mm at a 0.1 Hz rate. Inside the MR control

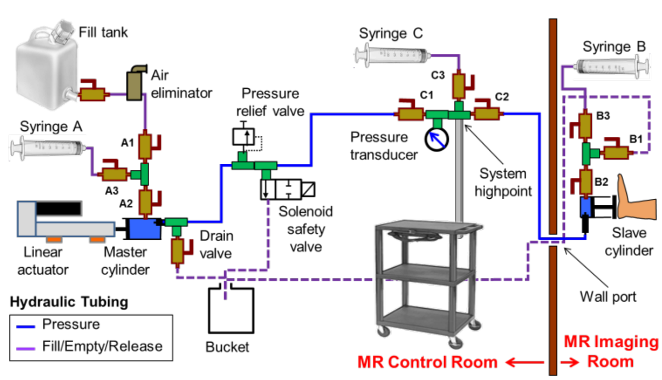

Figure 1: Schematic of hydraulic loading device.

room, the master piston was driven by a stepper motor-powered linear actuator. High-pressure tubing connecting the master and slave cylinders passed through ports in the dividing wall between the MR imaging room and the control room.

To ensure MRI compatibility, all equipment inside the imaging room (save for several small hardware items) was non-metallic. The plantar surface of the foot contacted a platen attached to the slave piston, which could be adjusted to facilitate forefoot or hindfoot testing (Fig. 2). The test subject was held in a loading apparatus that was designed to restrain the leg and the foot being tested, to support the slave cylinder and platen, and to restrain the subject's torso in order to minimize movement of the imaged volume.

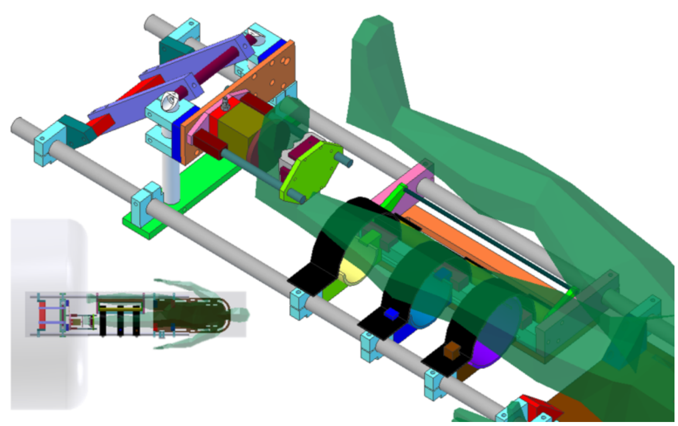

Figure 2: Human loading apparatus.

A gated MRI-protocol, similar to that used in cardiac MRI, was used to obtain 12 static 3D images of the foot while displacement dynamically changed from zero to the patient-specific maximum and then back to zero repeatedly. A signal mimicking that of a peripheral pulse unit (PPU) was generated in custom LabVIEW code and output to the MRI Control and Data Acquisition System (CDAS) to synchronize and trigger the image acquisition. The device measured hydraulic system pressure, actuator displacement, and gating signal output. The force on the foot corresponding to each 3D image obtained was calculated from the hydraulic pressure. Force and deformation data will in the future be input into an inverse finite element analysis (FEA) to calculate the soft tissue material properties.

The test subject was protected from painful loading via a solenoid valve able to release all hydraulic pressure triggered via emergency-stop buttons near the subject and the experiment operator, and via the LabVIEW code detecting a pressure exceeding the patient-specific maximum. A mechanical pressure relief valve ensured system pressure couldn't exceed a patient-specific maximum.

Prior to human subject testing, verification testing was conducted in order to quantify the device's repeatability under different fluid fill/bleed cycles, displacement precision under multiple target displacement amounts, and MRI compatibility. The displacement of the loading platen was measured by a linear variable voltage transducer (LVDT) and the displacement of the actuator by a rotary encoder. A 75 cm^2 piece of silicone gel was loaded by the device to simulate physiologic soft tissue loading.

RESULTS AND DISCUSSION

The repeatability of the displacement of the loading platen under different fill/bleed cycles was ± 0.24 mm at a displacement of 10.8 mm (Fig. 3). The displacement of the platen as a function of displacement of the actuator is non-linear due to the compliance of the hydraulic tubing and residual air bubbles in the fluid. Once a calibration equation was calculated to correlate platen to actuator displacement, the peak displacement of the platen showed an error of less than 3% from the target peak displacement (Table 1). The frequency of the displacement and the root means square (RMS) errors between the displacements of the actuator and platen compared to the target displacement profiles were less than 10% of peak displacement. Human subject data are still being analyzed.

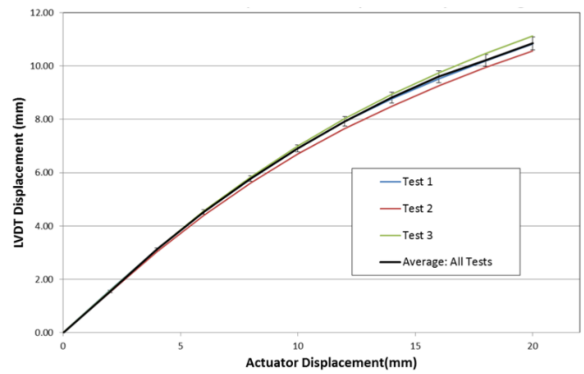

Figure 3: Repeatability of the system displacement under three separate fill/bleed tests.

CONCLUSIONS

The loading system showed repeatable performance during verification testing and a pilot loading study in the MRI was conducted. An inverse FEA will be solved for the material properties of the plantar skin, adipose tissue, and muscle.

REFERENCES

1. Centers for Disease Control and Prevention, *National Diabetes Fact Sheet*, 2007.
2. Pai S., et al. *Journal of Biomechanics*, **43**:1754-60, 2010.
3. Petre M, et al. *Journal of Biomechanics*, **41**:470-4, 2008.

ACKNOWLEDGEMENTS

This work was supported by VA RR&D Grant A6973R.

Table 1: Results of displacement verification testing.

Test #	Displacement (mm) Actuator	Platen Target	Platen Measured	Platen Displacement Frequency (Hz) Target	Measured	RMS Error: Displacement to Target Sine (mm) Actuator	Platen
1	4.072	3.000	3.065 ± 0.003	0.1000	0.1002	0.036	0.324
2	7.625	5.000	5.015 ± 0.005	0.1000	0.0997	0.039	0.361
3	11.943	7.000	7.198 ± 0.047	0.1000	0.0999	0.046	0.658
4	17.974	9.000	9.119 ± 0.117	0.1000	0.0998	0.073	0.869

DIFFERENCES IN REPETITIVE FINGER MOVEMENT BETWEEN THE MOST EFFECTED AND LEAST EFFECTED HAND IN PARKINSON'S DISEASE

[1]Elizabeth Stegemöller, Colum MacKinnon[2], [1]Mark. D. Tillman and [1]Chris J. Hass

[1]University of Florida, Gainesville, FL, USA
[2]Northwestern University, Chicago, IL, USA
email: estegemoller@hhp.ufl.edu

INTRODUCTION

Diagnosis and treatment of Parkinson's disease (PD) is often challenging and is currently dependent on subjective evaluation (by the clinician) of various movement performance tests. As impaired control of repetitive finger movements can significantly impact the performance of daily living activities, such as writing and buttoning clothing in these patients, one such test used to assess the severity, progression, and treatment efficacy in persons with PD is the performance of repetitive finger movements. Clinicians characterize impairments in repetitive finger movements by evaluating slowness, reduced movement amplitude and hesitation or arrests in ongoing movement using a 0-4 ranking scale. Previous work from our team has demonstrated that mild to moderately affected patients with PD when compared to neurologically healthy older adults do not demonstrate these characteristics at movement rates near to and above 2 Hz (2 movements per second). At rates above 2 Hz, movement amplitude significantly decreases and movement rate and phase variability significantly increase [1]. This would suggest that impairments in repetitive finger movements are rate-dependent. However, it remains unknown if rate-dependent impairments differ between the most effected and least effected side in person with PD. Thus, the purpose of this study is examine differences in kinematics between the most effected and least effected hand in persons with PD collected during a repetitive finger movement task.

METHODS

Eight participants (68 ± 11) diagnosed with idiopathic PD completed the study. Testing was completed in the optimal "on" medication state. All participants gave written informed consent. A gonimometer was placed on the second finger between the first and second joints. Subjects sat in a chair with shoulder abducted to 30° and elbow flexed at 90°. The forearm, hand, thumb, and fingers 3-5 were supported by a brace, limiting movement to only the index finger. A periodic auditory tone (50 ms, 500 Hz, 80 dB) was presented at 1.0 Hz for 15 intervals, and then increased by 0.25 Hz every 15 intervals until reaching 3.0 Hz. Participants began moving as soon as the tones were presented, initiating each movement "on the tone" and were instructed to perform an index finger flexion-extension movement from a neutral position to approximately 25 degrees of flexion. No tactile feedback was given. Three trials were completed for both hands.

Movement rate and peak-to-peak amplitude was calculated for each movement and averaged across each tone rate. Movement rate difference was obtained as the difference between movement rate and tone rate. Movement amplitude was normalized to data at 1.0 Hz to allow for comparisons in the relative change in movement amplitude across tone rates and between-subjects since no constraints were placed upon range of motion. It was observed that participants adapted two different strategies when completing the task, either moving slower or faster than the intended tone rate at rates near and above 2 Hz. To account for these differences in performance strategies, the group was divided into a SLOW group (n = 4) and a FAST group (n = 4). The SLOW group was defined as those participants that moved slower than the intended tone rate at rates of 2 Hz and above. The FAST group was defined as those participants that moved faster than the intended tone rate at rates of 2 Hz and above.

For all measures (movement rate difference and movement amplitude), a repeated measures ANOVA was used to compare for differences between hands (most effected vs. least effected) and across conditions (tone rate). Post hoc comparisons were completed and adjusted for multiple comparisons. Level of significance was set at $p < 0.05$.

RESULTS AND DISCUSSION

Results revealed no significant differences between most and least effected hands or for tone rate for both measures of movement amplitude or movement difference. However, once dividing participants into SLOW and FAST groups (Fig. 1), irrespective of hand, results revealed a significant effect for group (SLOW vs. FAST) for movement rate difference ($p = 0.039$). No main effect was found for tone rate. Additionally, no main effects of group or tone rate were found for movement amplitude. Results did reveal an interaction effect for both movement rate difference ($p < 0.001$) and movement amplitude ($p = 0.042$), but post hoc comparisons revealed to further significant differences.

These results suggest that even though persons with PD often demonstrate and more effected side, there is no difference in the performance of repetitive finger movements between sides. Moreover, the adapted movement strategy chosen to complete the task was similar between sides. While these results were not compared to healthy older adults, there is evidence of a change in performance at rates above 2 Hz. This may suggest that the change in movement performance may be due to changes in motor control processes that have a much broader effect on movement performance potentially effecting other rate-dependent movements.

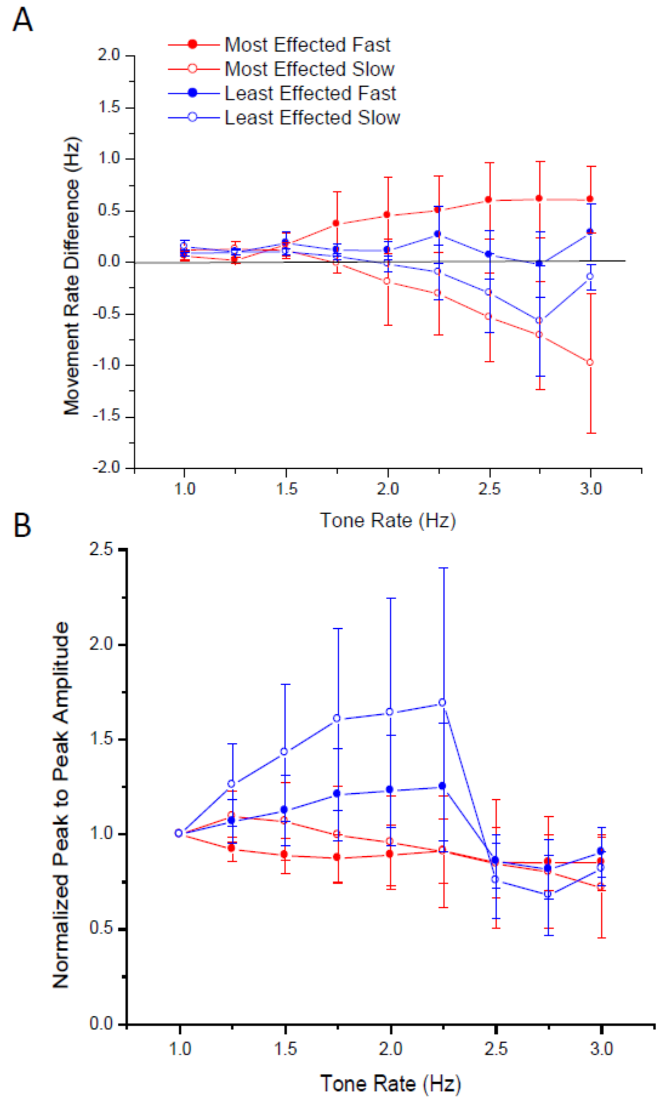

Figure 1: Movement rate difference (A) and movement amplitude (B) across tone rates shown for the most and least effected side and for SLOW and FAST groups.

REFERENCES

1. Stegemöller EL, et al. *Movement Disorders* **24**, 1162-1169, 2009.

MODELING OF HEAD INJURY RESPONSE FOR TRANSLATIONAL AND ROTATIONAL IMPACTS OF VARYING DIRECTIONS AND MAGNITUDES

[1]Joel D. Stitzel, [1]Ashley A. Weaver, and [1]Kerry A. Danelson

[1]Virginia Tech – Wake Forest University Center for Injury Biomechanics, Winston-Salem, NC, USA
email: jstitzel@wakehealth.edu, web: www.wakehealth.edu/cib

INTRODUCTION

An estimated 1.7 million people in the United States sustain a traumatic brain injury (TBI) annually [1]. The Simulated Injury Monitor (SIMon) finite element (FE) model was developed and validated by Takhounts et al. to predict brain injury using a biomechanical injury metric, Cumulative Strain Damage Measure (CSDM) that measures the volume fraction of brain tissue experiencing strains over a certain threshold [2].

Given the potential importance of injury location, one objective was to quantify the differences in model response given specific translations and rotations in different directions. In addition, the effect of increases in input magnitude on these translations and rotations was also investigated. Variations in the model response of the whole-brain and specific regions were explored to understand the biomechanics and occurrence of TBI.

METHODS

To investigate the effects of translational and rotational motions on TBI risk and location, translational and rotational velocities of five magnitudes and 26 different directions were modeled with the SIMon FE brain model in LS-Dyna (Fig 1, Table 1). Translations were applied along the linear direction of the vectors illustrated in Fig. 1 and rotations were applied about each of these vectors using the right-hand rule. The translational and rotational velocities were applied at the model origin, resulting in 130 translational and 130 rotational simulations. CSDM was investigated for the total brain to determine global response [2]. The volume fraction of each individual brain structure exceeding a specific strain threshold was also computed. This volumetric measurement of high strain values is similar to CSDM, and is referred to as the Structure Cumulative Strain Damage Measure (SCSDM).

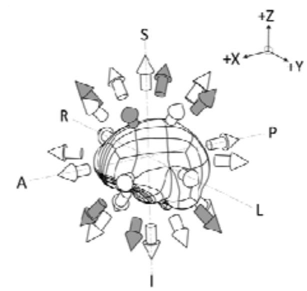

Fig. 1: SIMon with 26 directions illustrated.

RESULTS AND DISCUSSION

Overall, CSDM increased as impact severity increased, varied with the impact direction, and was lower for translational impacts compared to rotational impacts.

Translational Impacts: Strains did not exceed 0.05 in the translational impacts, thus a lower strain threshold of 0.01 was used to compute CSDM and SCSDM values for the translational impacts (Table 1). Greater CSDM(0.01) values were observed in impacts lacking a z-component (no translation in the superior or inferior directions). Differences in CSDM(0.01) ranged from 0.002 to 0.076 when comparing impacts without translation in the superior-inferior direction to impacts with superior or inferior translation.

Translations in the left-right (y) direction resulted in the highest CSDM for the total brain and the highest SCSDM for the cerebrums. Translational applied in the posterior-superior (-x,z) direction resulted in the highest SCSDM values in the brainstem. Translations applied in the posterior-left-inferior (-x,y,-z) and posterior-right-inferior (-x,-y,-z) directions resulted in the highest SCSDM values in the cerebellum.

Rotational Impacts: A strain threshold of 0.10 was used to investigate CSDM and SCSDM for the rotational impacts (Table 1). CSDM(0.10) varied with the direction of rotation (Fig. 2). Simulations with a z-component of rotation (transverse plane rotation) had 0.55-1.7 times larger CSDM(0.10) values compared to those without a z-component of rotation.

Table 1: Velocity magnitudes and CSDM summary (directions for a particular magnitude are grouped to compute the average, min, max, and differential).

	Velocity: Trans (m/s), Rot (rad/s)	Avg	Min	Max	Differential
CSDM(0.01)	T1: 2.46	0.007	0.003	0.012	0.009
	T2: 3.44	0.041	0.016	0.069	0.053
	T3: 4.25	0.103	0.055	0.158	0.103
	T4: 4.87	0.172	0.107	0.249	0.142
	T5: 5.45	0.248	0.162	0.336	0.174
CSDM(0.10)	R1: 12.29	0.102	0.044	0.198	0.154
	R2: 16.12	0.191	0.111	0.323	0.212
	R3: 19.24	0.272	0.188	0.406	0.218
	R4: 21.67	0.335	0.255	0.455	0.200
	R5: 23.93	0.392	0.319	0.495	0.176

Rotations about the inferior-superior (z) axis caused rotation in the transverse plane and resulted in the largest CSDM in the total brain and the largest SCSDM in the cerebrums. Large areas of elevated strain were observed in the lateral cerebrum (Fig. 3). Rotations about the right-left axis in the positive direction (y) caused rotation in the sagittal plane and resulted in the largest CSDM values in the brainstem. Larger strains with a concentrated volume were observed in the superior aspect of the brainstem near the location of the model origin (Fig. 3). Rotations about the anterior-inferior (x,-z) and posterior-superior (-x,z) directions caused medial rotation of the cerebellum and resulted in the largest CSDM in the cerebellum. Elevated strains were seen in the medial-posterior aspect of the cerebellum (Fig. 3).

CONCLUSIONS

CSDM and SCSDM values were orders of magnitude lower for the translational impacts compared to the rotational impacts. CSDM increased as input magnitude increased, varied substantially with the direction of impact, and resulted in global and regional variations in brain injury metrics. This study suggests variations in the geometry and anatomical structures within the brain cause differences in the overall injury response as impact direction is varied, and it may be important to develop or enhance injury criteria to account for directionality of impact.

REFERENCES

1. Faul M, et al. *CDC*, 2010.
2. Takhounts EG, et al. *Stapp Car Crash J* **52**, 1-31, 2008.

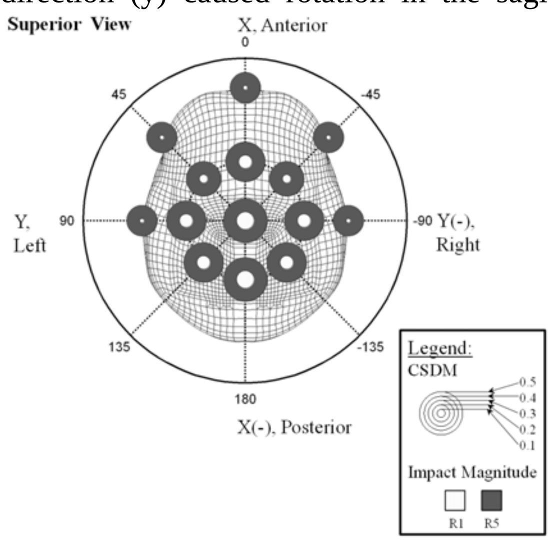

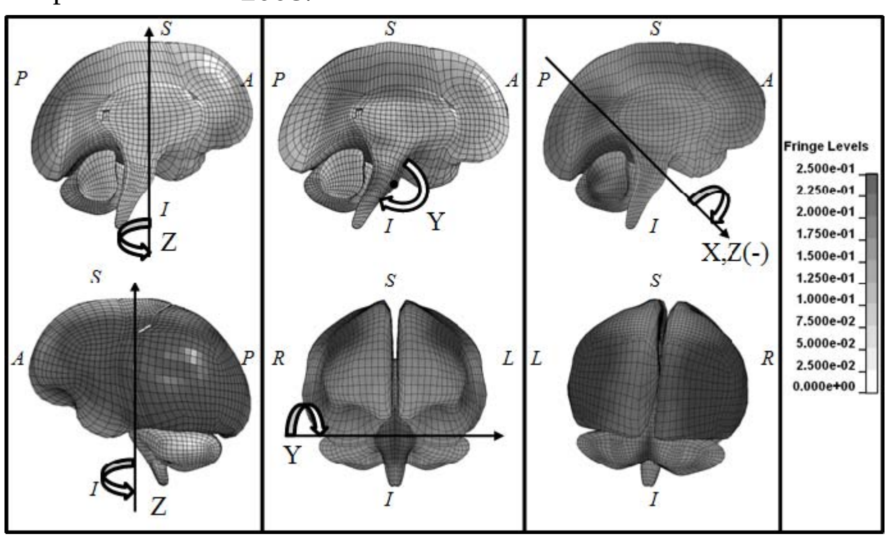

Fig. 2 (left): CSDM(0.10) for the rotational directions at the R1 and R5 magnitudes indicated by circle size. The central point represents isolated transverse plane rotation. The eight medially located points have a positive rotational z-component resulting in some transverse plane rotation. The five points located laterally have no transverse plane rotation. **Fig. 3 (right):** Maximum principal strain for the rotational direction resulting in the largest CSDM(0.10) and SCSDM(0.10) for different brain structures. Left: total brain and cerebrum (z, transverse plane rotation), Center: brainstem (y, sagittal plane rotation), Right: cerebellum (x,-z rotation).

EFFECTS OF FRACTIONAL ANISOTROPY IN THE CORPUS CALLOSUM AS DETERMINED BY DIFFUSION TENSOR IMAGING ON TEMPORAL VARIABILITY IN OLDER ADULTS

[1]Alison L. Sukits, [1]Aaron T. Ledgerwood, [1]Justin M. Haney, [1]April J. Chambers, [1]Rakié Cham, [2]Howard J. Aizenstein and [2]Robert D. Nebes

[1]Human Movement and Balance Laboratory, University of Pittsburgh, Pittsburgh, PA, USA
[2]Department of Psychiatry, University of Pittsburgh, Pittsburgh, PA, USA
email: als110@pitt.edu web: http://www.odar.pitt.edu/hmbl/

INTRODUCTION

With a steadily increasing population of older adults in the United States, falls in the elderly have become a well-known health problem. It has been estimated that one in three community-dwelling adults over the age of 65 experiences a fall at least once a year [1]. In older adults, gait variability has been shown to predict falls and decreased physical function [2,3]. Specifically, increased temporal variability, such as stance time variability, has been associated with a high risk for falling in elderly subjects [1].

Diffusion tensor imaging (DTI) is a magnetic resonance imaging (MRI) technique capable of measuring the restricted diffusion of water along fiber tracts in the brain, also known as fractional anisotropy (FA). FA is the degree of orientational preference within a voxel and can aid in determining the white matter connectivity of the brain. Levels of FA are said to decline with normal aging [4].

Poor gait performance scores within the elderly have been correlated with low FA values in the genu of the corpus callosum [5]. The corpus callosum has previously been linked to gait function [6]. However, no studies have examined the association of gait variability with FA levels using DTI analysis. The objective of this study is to determine if a relationship exists between FA levels in the genu and splenium of the corpus callosum and stance time variability during gait.

METHODS

Thirty-three older adults (19 Female, mean Age 74.9 ± 3.6 years, Height 1.68 ± 0.088 m, Weight 75.47 ± 13.40 kg) were recruited for this study. Participants were asked to walk for 60 seconds at a self-selected pace around an oval track. Motion data were collected at 120 Hz. Stance time variability (ms) and gait speed (m/s) were calculated. Stance time was defined as the time from heel contact to toe off of the same foot. Stance time variability (STV) was determined using the standard deviation across all steps within each trial. Gait speed (GS) was calculated using the average velocity of the sternum marker.

Participants also underwent an MRI scan (3T Siemens TIM TRIO scanner) at the MR Research Center at the University of Pittsburgh. The DTI sequence acquired diffusion images in 12 directions; sequences were averaged over 4 acquisitions. FA levels, normalized to total brain volume, were determined for the genu and splenium of the corpus callosum.

Associations between STV and FA in the genu and splenium of the corpus callosum were investigated. Pearson correlation analyses were run to investigate these possible relationships, with STV as the dependent variable and FA, in the specific brain regions, as the independent variable (A1). This analysis was also performed using GS as a covariate (A2). Statistical significance was set at 0.05.

RESULTS AND DISCUSSION

While a negative relationship was found between FA in both regions of the corpus callosum and STV, they were not found to be significant. Accounting for GS as a covariate strengthened these negative relationships; however it did not change the statistical significance. Figure 1 demonstrates the negative correlation found between FA in the genu of the corpus callosum and STV. Table 1 provides the Pearson correlation coefficients and their corresponding p-values for each region of the brain for A1 while Table 2 provides the same information for A2.

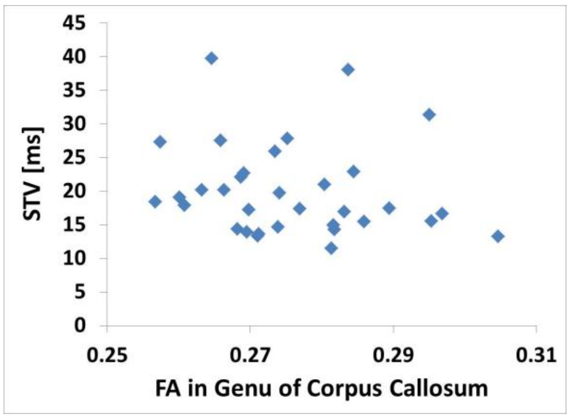

Figure 1. STV [ms] vs. FA in the genu of the corpus callosum. As FA increases, STV decreases.

Table 1. (A1) Pearson correlation coefficients and corresponding p-values for the relationships between FA in the genu and splenium of the corpus callosum and STV

Region	**Pearson Correlation Coefficient**	**p-value**
Genu	-0.158	0.379
Splenium	-0.157	0.384

Table 2. (A2) Pearson correlation coefficients and corresponding p-values for the relationships between FA in the genu and splenium of the corpus callosum and STV

Region	**Pearson Correlation Coefficient**	**p-value**
Genu	-0.183	0.316
Splenium	-0.232	0.202

The findings presented here suggest that STV may not be influenced by levels of FA in the genu or splenium regions of the corpus callosum. While previous literature has noted a significant relationship between FA in the genu of the corpus callosum and gait, the measures used by Bhadelia et al. were subjectively determined measures of gait found using the Performance-Oriented Mobility Assessment scale [5].

All participants were healthy, older adults, screened for neural, orthopedic, and cognitive deficits. Participant characteristics may have generated the small range of FA values, possibly limiting the results found. A greater range of FA values may strengthen the negative relationships found in this work. Additionally, brain regions other than the corpus callosum may have a stronger association with gait variability. Bhadelia et al. suggested that gait is a complex task requiring the integration and coordination of multiple levels of the nervous system [6]. Therefore, investigating other regions of the brain known to be associated with motor or executive function, such as the corticospinal tracts, may produce stronger relationships between FA and gait variability. Future work should include the use of a larger range of FA values and the exploration of additional regions of the brain.

REFERENCES

1. Hausdorff JM, et al. *Arch Phys Med Rehabil*, **82**, 1050-1056, 2001.
2. Hausdorff JM. *Hum Mov Sci*, **26**, 555–589, 2007.
3. Brach JS, et al. *Gait Posture*, **27**, 431–439, 2008.
4. Zahr NM, et al. *Neuroimage* **44**, 1050-1062, 2009.
5. Bhadelia RA. *Stroke*, **40**, 3816-3820, 2009.
6. Ryberg C, et al. *Neurobiol Aging*, **28**, 955-963, 2007.

ACKNOWLEDGEMENTS

Funding Source: NIH/NIA R01 AG030452.
Special thanks to the Geriatric Psychiatry Imaging Laboratory for processing of all MRI data.

The Effects of Whole Body Vibration on the Wingate Test for Anaerobic Power When Applying Individualized Frequencies

[1,2]Rachel K. Surowiec, [1]Henry Wang, [1]Paul Nagelkirk, [1]Jeffrey Frame and [1]D. Clark Dickin

[1]Ball State University, Muncie, IN, USA
[2]Steadman Philippon Research Institute, Vail, CO, USA
email: rksurowiec@bsu.edu

INTRODUCTION

The ability to generate high force in the shortest time possible, also referred to as the rate of force development, is a quality possessed and optimized by elite athletes. Power development has become a primary focus of athletic performance enhancement training programs [1]. Whole-body vibration (WBV) has been proposed as a potential alternative or adjuvant to exercise for power development [2]. More recently individualized frequency (I-Freq) has been introduced with the notion that individuals may elicit a greater reflex response to different levels (Hz) of vibration [3]. As such, the aim of the study was to evaluate acute WBV as a feasible intervention to increase power in trained cyclists. Additionally, we sought to evaluate the efficacy of utilizing I-Freq as an alternative to 30 Hz, a common WBV frequency seen in the literature.

METHODS

Twelve highly-trained, competitive male cyclists (age= 29.9 yrs ± SD 10.0; body height=175.4 cm ± SD 7.8; body mass=77.3 kg ± SD 13.9) participated in the IRB approved study. One subject was excluded due to adherence to the Wingate procedure.

The subject's I-Freq was determined by recording the EMG activity of the vastus lateralis of the dominant leg (DelSys, Boston, MA). The adapted I-Freq protocol included vibrations ranging from 20-55Hz administered randomly in 5Hz increments [3]. Muscle activity was recorded for 10s of no vibration followed by 10s of vibration with four minutes of seated rest between trials. A band-stop filter set at ± 2Hz of the frequency of interest was utilized and averaged root mean square muscular activity was graphed to determine which frequency most exited the muscle of interest resulting in the subject's I-Freq (Figure 1).

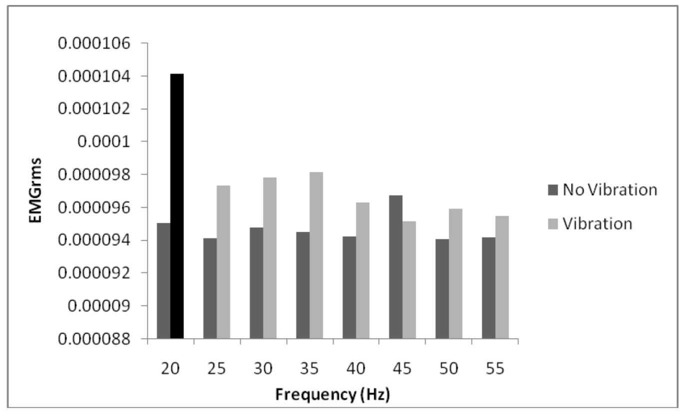

Figure 1: EMG_{rms} of the vastus lateralis for Subject A. The black bar indicates the highest neuromuscular response recorded indicating the participants' I-Freq.

The testing protocol included three conditions; the subject's I-Freq, a fixed frequency of 30 Hz, and a control of no vibration. Each condition was immediately followed by a 30-second Wingate test for anaerobic power where measures of peak power (PP), average power (AP), and rate of fatigue were determined.

The control condition of no vibration was administered on day one of testing. The two vibration conditions, performed on day two, were administered in random order. All vibration conditions were executed on a vibration platform (Pneumex, Sandpoint, ID) (peak to peak amplitude: 2mm) and consisted of 10 series of one minute WBV followed by a one minute pause of no vibration. Immediately following vibration, the Wingate test was administered using a Monark Cycle Ergometer (Monark Exercise, Vansbro, Sweden). The flywheel force was kept at a constant 0.085 kp/kg bodymass within a 0.1-kg resolution of resistance range with the load reflecting the trained nature of the cyclists. PP, AP, and rate of fatigue were calculated by Monark software throughout the 30s test. Immediately following the test the subject pedaled at slow pace (25-100W) for 2-5 minutes as an active recovery phase. To ensure recovery prior to the next test, 20 minutes of passive rest was achieved by the subject in the seated or supine position.

RESULTS AND DISCUSSION

The means and standard deviations of all test variables (PP, AP, and rate of fatigue) are displayed in Table 1. Test variables from the Wingate (i.e., PP, AP, and rate of fatigue) were not impacted differently by the three interventions (control, 30 Hz, and I-Freq). For the measure of PP, no significant effect of vibration ($F=2.54$, $p=0.104$, partial $eta^2=0.202$, observed power=0.358) was observed which indicates that no significant differences between the control, 30 Hz, and I-Freq. Similarly, in response to the vibration treatments, no significant effect was observed for the measure of AP ($F=0.534$, $p=0.589$, partial $eta^2=0.052$, observed power= 0.127). Likewise, as a result of vibration, there was no significant effect in the rate of fatigue ($F=1.966$, $p=0.166$, partial $eta^2=0.164$, observed power= 0.358) as the subjects did not fatigue differently across the three testing conditions regardless of vibration intervention.

Based on the results of the present study, acute WBV did not significantly increase PP, AP or improve rate of fatigue in the trained cyclists. It was also noted that I-Freq was not superior to 30 Hz in that neither vibration intervention was able to elicit an effect on power in the athletes. The literature regarding WBV has been equivocal thus the findings support previous acute WBV data suggesting that WBV may not increase power in highly trained individuals. Up until now WBV studies, specifically ones using I-Freq, have not been tested with a sport specific power measurement such as the Wingate test.

The capacity for improvement for elite athletes in laboratory or field tests is typically small. Although previous vibration studies have elicited a significant increase in power in elite and amateur athletes in other sports (typically measured by the vertical jump), the combination of elite athlete and the sport specific nature of the Wingate test proved to show no significance. This could be due to the stimulus used in the present study as the amount of vibration and length of the protocol prescribed to an athlete remains ambiguous in the literature. Similar findings were reported by Ronnestad et al. supporting recommendations for evaluating greater stimuli for trained individuals [4]. Prospective research endeavors may choose to look at this protocol utilizing greater intensity in vibration amplitude and duration in the event that training status may be a limiting factor for eliciting increases in power following acute WBV.

REFERENCES

1. Cochrane DJ, et al. *European J of Applied Physiology*, **108**:2, 311-319, 2012.
2. Torvinen S, et al. *Medicine & Science in Sports & Exercise*, **34:**9, 1523-1528, 2002.
3. Di Giminiani R, et al. *Journal of Sports Sciences*, **27**:2, 169-177, 2009.
4. Ronnestad BR, et al. *J Strength Cond Res*, **23**(4), 1309-1315, 2009.

Table 1. Wingate test results.

	PP (W)	PP (W/kg^{-1})	AP (W)	AP (W/kg^{-1})	RF (%)
Subjects (n=11)					
Control	945.8 ± 173.8	12.8 ± 2.1	674.7 ± 125.5	9.1 ± 1.2	52.5 ± 6.4
30HZ	907.6 ± 214.9	12.1 ± 1.5	661.8 ± 105.6	8.9 ± 0.7	49.8 ± 5.4
I-Freq	891.2 ± 206.7	11.9 ± 1.5	660.8 ± 117.2	8.8 ± 0.5	49.3 ± 5.2

PP= peak power; AV= average power; RF= rate of fatigue; I-Freq= individualized frequency

MUSCLE ACTIVATIONS IN RESPONSE TO ACHILLES TENDON RUPTURE AND REPAIR

[1]Stephen M. Suydam, [1]Thomas S. Buchanan, [1]Kurt Manal, and [2]Karin Gravare Silbernagel

[1]University of Delaware, Newark, DE, USA
[2]University of the Sciences, Philadelphia, PA, USA
email: suydam@udel.edu

INTRODUCTION

Achilles tendon ruptures are life altering injuries which lead to short term physical deficits and potential long term decreases in strength and physical activity level. Plantar flexion weakness at the end range of motion is still observed more than a year after surgery[1] and the cause of remaining deficits and the optimal treatment for Achilles rupture is currently under debate[2,3]. A solid understanding of the physiologic reaction to a complete rupture and the anatomical variation caused by surgical repair is needed to improve current rehabilitation. The purpose of this study was to relate the lengthening of the Achilles tendon post rupture to muscle activation patterns during walking to discern whether remaining gait abnormalities are due to physical alteration or neural inhibition.

METHODS

EMG data was collected at 1200hz from the medial and lateral gastrocnemius (MG, LG), soleus (SL), and tibialis anterior (TA) muscles during walking from 4 subjects, with an Achilles tendon rupture, at 6 and 12 months post-repair along with 5 healthy control subjects (age: 26.2 ± 6.4yrs, height: 1.76±0.1m, weight: 81.44±20.6kg) using a MA-300 system (Motion Lab Systems, Baton Rouge, LA). Each subject signed an inform constant prior to testing. Bipolar silver/silver chlorides EMG surface electrodes were placed on each of the muscles. Peak EMG values were determined in Visual 3D (C-Motion Inc., Bethesda, MD) by creating a linear envelope using low and high pass filtering, DC offset removal, and full wave rectification. EMG data was normalized to the maximum EMG found during maximum isometric testing.

The Achilles tendon length (ATL) of the injured and uninjured side was measured using a combination of B-mode ultrasound imaging at 10 MHz with a 60mm transducer using a ProSound SSD-5000 (Aloka, Tokyo, Japan) and motion analysis using an 8-camera motion capture system (Qualisys Motion Capture System, Gothenburg, Sweden) collecting motion at 50hz. The tendon was scanned between the calcaneal osteotendinous junction and the musculotendinous junction. The combination of motion capture and the outputted ultrasound files allowed for the length of the Achilles tendon to be determined. Test-retest reliability of this method has found an ICC=0.97 with no significant differences (p=0.889) between the two test occasions.

RESULTS AND DISCUSSION

The Achilles tendon of those patients injured had a significantly increased (p=0.05) ATL compared to the uninjured side at both the 6 and 12 month evaluation with an increase of 3.56±0.75cm and 3.12±0.96cm, respectively (Table 1). There was no significant difference (p=0.05) between the right and the left side in the healthy control group. Six (6) months post-surgery, the peak normalized EMG of the LG during walking on the injured side (0.95) was significantly increased (p=0.05) compared to the EMG of the unaffected side (0.81). The activity of the MG during walking at 12 months was also significantly larger on the injured side (0.91) compared to the uninjured side (0.72). Overall, there was general increase of muscle activity on the injured side of the triceps surae muscles at 6 months post-surgery and an even greater increase of activity at 12 months (Figure 1). Conversely, there was no change in EMG activity of the TA at 6 or 12 months. The healthy controls showed no difference of EMG activity between legs.

The increased muscle activity seen at 6 and 12 months post-surgery indicate, following an Achilles tendon rupture, the calf muscles are not inhibited during gait. Since these patients all had a significantly longer Achilles tendon on the injured side, the gastrocnemii and soleus muscles could instead be contracting more in an attempt to compensate for the increase in tendon slack during walking. The healthy controls had no ATL difference between sides and showed no disparity in peak EMG.

CONCLUSIONS

The increased ATL and EMG signals from the muscles used to stretch the tendon indicate that loss of functionality is primarily caused by anatomical changes in the tendon and the appearance of muscle weakness is due to force transmission from the inhibition. During gait, patients' compensate for an elongated Achilles tendon following surgical repair by greater activation of the gastrocnemii muscles to account for the additional tendon slack before motion is produced at the joint.

REFERENCES

1. Mullaney MJ, et al. *Am J Sport Med.* **34**(7), 1120-1127, 2006.
2. Boyden EM, et al., *Clin Ortho Rel Research.* **317**, 150-158, 1995.
3. Troop RL, et al., *Foot and Ankle International.* **16**(11), 1995.

ACKNOWLEDGEMENTS

The authors would like to acknowledge the Swedish Research Council for its financial support.

Table 1. Mean Achilles tendon lengths of subjects at 6 and 12 months post-Achilles rupture repair and healthy controls. Note: The injured side of the subjects post-surgery is significantly larger than the unaffected side while there is no difference between the left and right sides of the healthy control with the differences in bold.

	6 Months Injured	6 Months Uninjured	Difference at 6 Months	12 Months Injured	12 Months Uninjured	Difference at 12 Months	Healthy Left	Healthy Right	Difference in Healthy
Mean Achilles Length (cm)	24.46	20.90	**3.56**	23.83	20.72	**3.12**	20.33	19.77	**0.56**

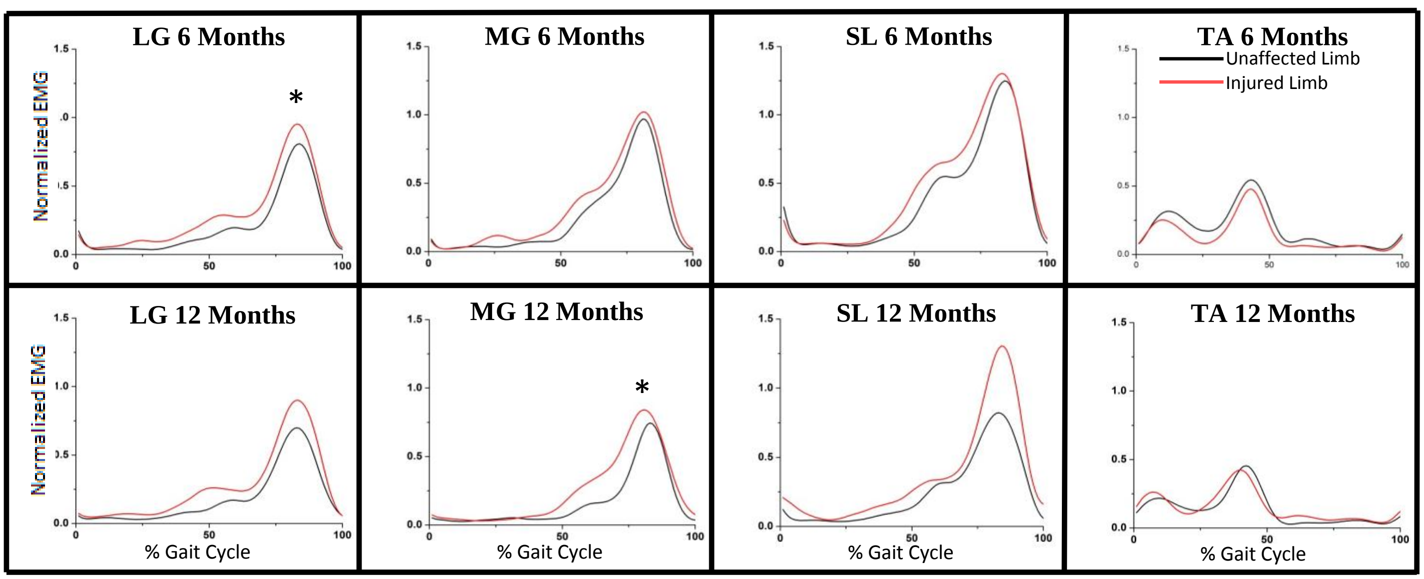

Figure 1. The averaged normalized EMG from the lower leg during one gait cycle of walking from 4 Achilles repaired subjects. The injured limb is graphed in red and the unaffected limb in black for each of the muscles. The astrix (*) represents a significant difference in peak EMG magnitude between limbs.

Asymmetric Morphology of the Hamstring Muscles Following ACL Autografts

[1]Stephen M. Suydam, [1]Kurt Manal, and, [1]Thomas S. Buchanan
[1]University of Delaware, Newark, DE, USA
email: suydam@udel.edu

INTRODUCTION

Common ACL repair techniques include the semitendinosus-gracilis (STG) graft and allografts (ALLO). A STG graft involves a tendon harvest from the semitendinosus (ST) and gracilis muscles, which are then twisted together and attached across the knee to function as the new ACL. The removal of the ST tendon leads to deficits in ST strength which is compensated by the hypertrophy of the synergistic biceps femoris short and long heads (BFS, BFL) and semimembranosus (SM)[1]. Though it is common for the ST tendon to regrow in these patients, regeneration does not always occur[2]. Although overall muscle volume and flexor strength may be compensated by hypertrophic changes of the other hamstring muscles in patients who have had STG autografts, it has not been determined if the volumetric proportion between the medial and lateral hamstrings pre-surgery is maintained post-surgery. Therefore, the purpose of this study was to compare the morphological changes of the lateral and medial hamstrings post-surgery in both the STG and ALLO groups to healthy, unimpaired muscle volumes.

METHODS

Thirty-one previously active (run/cut sports > 50 hrs/yr) subjects who suffered a ruptured ACL (ACLD) were included in this study along with 20 healthy controls. Axial spin, T1-weighted MRIs were taken from the calcaneus to the iliac crest prior to treatment. A 1.5T Signa LX scanner (GE Medical Systems, Milwaukee, WS) captured images with a slice thickness of 10mm (inter-slice gaps of 1.5mm). Twelve ACLD subjects elected for surgical repair; 5 of the subjects received a cadaveric allograft (ALLO) and 7 received a STG graft. Subjects were imaged again 6 month post-op using the same protocol as the pre-op imaging.

The ST, SM, BFS, and BFL were traced on each image using IMOD[3] (University of Colorado, Boulder, CO) and a touch-responsive monitor. After each of the images was traced, the volume of each of the muscles was calculated. For this study, the lateral hamstring volume consists of the sum of the BFS and BFL and the medial hamstring volume consists of the sum of the SM and ST. To determine the medial/lateral difference within the leg, the total volume of the lateral hamstring was subtracted from the total volume of the medial hamstring with the medial being the larger of the two sides in healthy subjects. The medial/lateral differences in hamstring volumes were used to correlate the symmetry between legs. A correlation, with the Y-intercept set to 0, was used to account for the predicted leg symmetry.

RESULTS AND DISCUSSION

The MRI data of the healthy, ACLD, and ALLO cases show strong correlations of the medial/lateral muscle volume difference between legs with R^2 values of 0.89, 0.86, and 0.91, respectively. The STG group, while displaying compensatory morphological changes in each of the hamstring muscles (Fig 1.), shows no correlation of medial/lateral difference between the affected and unaffected legs ($R^2 < 0.01$) (Fig. 2). This finding displays a lack of return to symmetry for the STG case and an unexpected random hypertrophic scenario for the hamstring muscles to recuperate strength loss due to tendon graft harvest, leading to no morphologic similarity between subjects. It is important to note the ACLD leg symmetry was retained post-surgery for the ALLO case, identifying graft type as the cause for this alteration. The shift in medial/lateral hamstring volumes could easily be translated into abnormal forces crossing the knee. Significant force alterations within the knee could lead to additional ligament strains or even the onset of osteoarthritis[4].

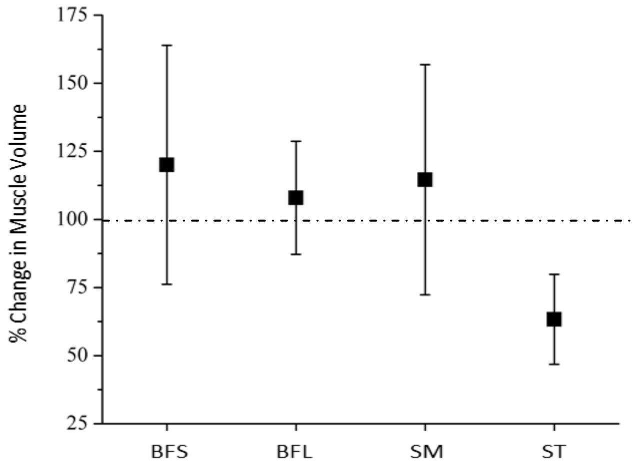

Figure 1. Morphological changes in muscle volume from pre to post surgery for the STG group. The points above the 100% line (-) indicate muscle hypertrophy while the point below indicates muscle atrophy.

The alteration in muscle morphology is observed in the STG group, but not the ALLO group. This later group was observed to have medial to lateral muscle volume ratios that did not substantially change following surgery, i.e., acting just like the healthy subjects. This is very important when considering the potential impact on joint compressive loads. If post-surgery leg muscle volume symmetry is not maintained, the joint loading may be substantially altered. Altering joint compressive loads may lead to joint pain and early onset osteoarthritis. Indeed, osteoarthritis has been shown to be correlated with ACL repair.

The progression and effects of this anatomical asymmetry are unknown. Since this data only include a 6 months post-surgery time step, it is possible that the morphology continues to change, leading to correlated differences in medial and lateral muscle volumes with the unaffected leg. A longitudinal study of ACL reconstructed subjects is necessary to track this phenomenon.

CONCLUSIONS

The muscle morphological changes of the hamstrings in response to the STG graft does not occur in a manner which returns the medial/lateral hamstring volumetric proportions to that of the contralateral limb within 6 months. This could result in abnormal forces within the knee leading to the onset of future pathologies such as osteoarthritis. This observation is not made for the allograft group. It will be important to follow the long-term volumetric growth progression in these muscles to determine if this is a lasting effect.

REFERENCES

1. Simonian PT, et al., *Am J Knee Surg*. **10(**2), 54-59, 1997.
2. Tadokoro K, et al., *Am J Sport Med.* **32(**7**),** 1644-1650, 2004.
3. Kremer JR, et al., *J Struct Biol*. **116**(1), 71-76, 1996.
4. Griffen TM, et al., *Exercise Sport Sci R.* **33**(4), 195-200, 2005.

ACKNOWLEDGEMENTS

The authors would like to acknowledge its financial support from the NIH R01-AR046386.

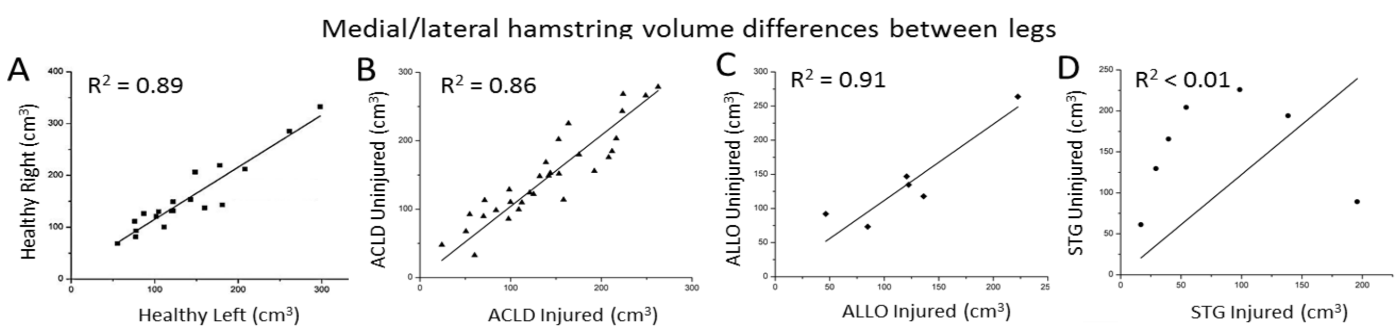

Figure 2. Correlation of leg symmetry defined by the difference of lateral hamstring volume from medial hamstring volume. The comparison of right versus left leg muscle volume differences in healthy subjects (A). The comparison of affected versus unaffected muscle volume differences in ACLD (i.e. pre-surgery) subjects (B), ALLO subjects (C), and STG subjects (D). Note the highly correlated volume differences between legs for the healthy, ACLD, and ALLO cases while the STG group had virtually no correlation between legs. The STG data indicate an unnatural muscle volume apportioning across the knee which may lead to future pathologies.

BREEZING RACEHORSE LIMB KINEMATICS ON DIFFERENT RACE SURFACE MATERIALS

[1,2]Jennifer E. Symons, [2]Tanya C. Garcia and [1,2]Susan M. Stover

[1]Biomedical Engineering Graduate Group, University of California, Davis, CA, USA
[2]J D Wheat Veterinary Orthopedic Research Laboratory, University of California, Davis, CA, USA
email: smstover@ucdavis.edu, web: http://www.vetmed.ucdavis.edu/vorl

INTRODUCTION

Musculoskeletal injury is the leading cause of racehorse fatality and attrition, with the majority of injuries involving the fetlock (metacarpo-, metatarso-phalangeal joints), particularly disruption of structures that support the palmar aspect of the joint and resist fetlock hyperextension[1]. Race surface behavior can be modified through material composition and maintenance. Thus, optimization of surface mechanical behavior may be a viable method to govern limb motion. However, the relationships between equine limb motion and surface mechanical behavior are unknown. The objectives of this study were to characterize, quantify and compare racehorse lower limb kinematics on two disparate race surfaces, dirt and synthetic.

METHODS

Two identical filming corridors were set up at 2 racetracks. The dirt surface was composed of sand, silt, and clay. The synthetic surface was a proprietary blend of wax-coated sand, rubber, and synthetic fibers.

Kinematic markers were applied to the skin over anatomical landmarks for determination of bone positions and joint centers of rotation on the distal half of the left forelimbs and hindlimbs of 5 horses. Hoof markers were applied to extension bars attached to the lateral aspect of the hoof wall to allow visualization of hoof orientation and translation when the hoof was submerged within the surface material. Two high-speed video cameras (500 Hz) recorded a calibration frame and 2D limb kinematics of 5 racehorses at breezing speeds (12-17 m/s) over 3-4 days on each surface.

The positions of kinematic markers during stance were digitized and converted to translational and angular data for distal forelimb and hindlimb joints and hooves. Maximum angular and translational values were quantified and compared using an unbalanced mixed model analysis of variance.

RESULTS AND DISCUSSION

Statistically significant differences were observed in the hind limb fetlock and hoof. Horses breezing on a synthetic surface had a lower degree of maximum hind fetlock hyperextension (dorsiflexion), compared to that observed on a dirt surface. Reduced fetlock hyperextension may contribute to lesser strain of the suspensory apparatus on the palmar side of the fetlock. Lesser strains likely contribute to lower risk for fetlock injuries, the most common site of racehorse musculoskeletal fatalities.

Horses also had a straighter hind fetlock configuration (178º, $\Delta\theta$=14º, p=0.013) at heel strike on a synthetic surface compared to the dirt surface (192º). Humans have been shown to alter leg stiffness in response to differing surface compliance[2], which may explain differences observed between trials on dirt and synthetic surfaces.

Horses running on a synthetic surface also had 40% less horizontal slide of the hind hoof compared to the dirt surface. Differences in the hoof-surface interaction between different surfaces may affect propagation of ground reaction forces applied to the limbs. Further, shoe traction devices may be less warranted on a synthetic surface than on a dirt surface.

CONCLUSIONS

Synthetic surfaces may be effective in reducing the incidence of fetlock injury in racehorses, due to attenuation of fetlock hyperextension during stance. Synthetic surfaces are likely to affect load propagation up the limb, due to differences in the hoof-surface interaction. Shoe traction devices may be less warranted on synthetic surfaces, due to observed reduced horizontal slide.

REFERENCES

1. 2009 Annual Report. CAHFS Postmortem Examination Program.
2. Ferris DP, et al. Running in the real world: adjusting leg stiffness for different surfaces. *Proc Biol Sci* **265**, 989-994, 1998.

ACKNOWLEDGEMENTS

The authors would like to thank Ellen Jackson of Victory Rose Thoroughbreds for the use of her horses, Neil Willits, PhD for statistical assistance, as well as the management and staff of Golden Gate Fields and Alameda County Fairground racetracks for their cooperation in these studies.

KINECT ABNORMAL INVOLUNTARY MOTION ASSESSMENT SYSTEM: INCREASED RELIABILITY OF TESTING FOR TARDIVE DYSKINESIA

[1]Lily Szajnberg, [2]Dustyn Roberts, [3]Daniel Karlin

[1]Interactive Telecommunications Program of New York University, New York, NY, USA
[2]Polytechnic Institute of New York University, Brooklyn, NY, USA
[3]Tufts University Medical Center, Boston, MA, USA
email: lily@lilyszajnberg.com, web: motionassessment.com

INTRODUCTION

The symptoms of patients suffering from Tardive Dyskinesia (TD) include pathological gait, involuntary motions, and trouble with sit to stand and other activities of daily living. TD is a condition that may develop in patients who use metoclopramide [1], a drug sold under brand names such as Reglan in the United States, and prescribed for psychosis and occasionally gastrointestinal issues, particularly in infants. Prolonged use of dopamine receptor blocking prescription drugs such as this, often in high dosages, can result in involuntary, repetitive tic-like movements, primarily in the facial muscles or, less commonly, the limbs, fingers, and toes. The hips and torso may also be affected [2]. The current method of testing for TD is using the Abnormal Involuntary Movement Scale (AIMS), which is a 12 item anchored scale [3]. Though administered by trained clinicians, this method of testing is susceptible to human error and can vary from doctor to doctor. Moreover, it requires doctor/patient time and is costly and time-consuming. As a result, tests are often administered less frequently than is recommended. The best treatment for TD appears to be prevention, either by lowering the dosage of a medication known to cause this condition or switching the patient to a different drug [4]. Thus, decreased reliability and frequency of the test impairs prevention tactics, which is dangerous and costly. Being able to conduct this test more accurately and from the patient's home would significantly improve the accuracy, comfort, and cost of these tests.

By using the inexpensive 3D capabilities of a commercial camera like the Microsoft Kinect to track the coronal, transverse, and sagittal planes of the body, the Kinect Abnormal Motion Assessment System (KAMAS) can conduct this test simply and easily sending the results as electronic medical records for doctors to use.

METHODS

The AIMS scale has five categories of parameters to rate: facial and oral movements, extremity movements, trunk movements, global judgement, and dental status, for a total of 12 parameters. Each of the parameters in the first four categories are judged from 0 (none) to 4 (severe) and the fifth category response is yes or no. Of the nine parameters in the AIMS scale that address physical progress, seven can be tracked using the inexpensive 3D abilities of the Kinect camera (steps 4, 5, 8, 9, 10, 11, and 12). The Kinect can track 16 parts of the human skeleton (head, shoulders, elbows, wrists, torso, hips, knees, ankles) in all three anatomical planes with precision to the millimeter at 30 frames/s [5] (Figure 1). This theoretically provides more precise analysis of the five possible prognoses in the AIMS scale.

Initially, five female control subjects (27.6 +/- 2 years old, 176.8 +/- 12.7 cm tall, 67.91 +/- 15 kg body mass) with no history of musculoskeletal problems participated in the feasibility testing. Their participation was voluntary, and written informed consent was obtained prior to testing.

To assess the feasibility of using KAMAS to test TD patients, the control subjects went through an additional testing session where they were told to voluntarily exhibit some of the behaviors that KAMAS is designed to detect. Through studying AIMS instructional videos, the control subjects were able to mimic the performance of moderate (scoring of three) symptoms in TD for steps four and five of the AIMS scale.

RESULTS AND DISCUSSION

The Kinect was able to correctly identify the joints of the subjects (Figure 1). The control subjects each scored a value of zero on the KAMAS testing, as expected.

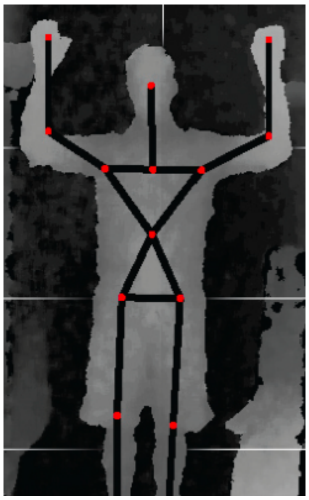

Figure 1: Depth image from the Kinect showing joints in red and limb segments in black

In the subsequent test, the control subjects were able to mimic moderate symptoms, indicated by scores of three using KAMAS (see initial posture for parameter 4 in Figure 2).

Figure 2: KAMAS demonstration of initial posture for evaluation of step four of twelve

Based on initial testing, the Kinect's 3D capabilities can reliably detect the involuntary movement necessary to objectively evaluate TD patients. Out of the relevant nine parameters of the AIMS scale, the Kinect was able to detect seven control levels and two mimicked TD levels. This feasibility study was conducted in advance of TD patient trials that will commence in June 2012 with Dr. Daniel Karlin, MD, PhD at Tufts University. Over the course of one month, four doctors will conduct the AIMS test both visually and electronically (using KAMAS) and compare consistency and reliability between the two. Following testing, statistical analysis will be performed to determine if there are any significant differences between evaluation of TD patients with the AIMS scale both subjectively by clinicians and objectively through KAMAS. Inter-rater reliability will also be performed to confirm the strength of this method. Additionally, two other components of the AIMS scale that rely on facial tracking software, currently in development, will be implemented in the next testing phase if the Kinect tracking proves reliable.

REFERENCES

1. D. Tarsy and G. Indorf, "Tardive Tremor Due to Metoclopramide," *Movement Disorders*, **17**, no. 3, 620–621, Jun. 2002.
2. American Psychiatric Association. Task Force on Tardive Dyskinesia, *Tardive Dyskinesia: A Task Force Report of the American Psychiatric Association*. American Psychiatric Pub, 1992.
3. H. H. Fernandez and J. H. Friedman, "Classification and Treatment of Tardive Syndromes," *The Neurologist*, **9**, no. 1, 16-27, 2003.
4. J. M. Smith, L. T. Kucharski, W. T. Oswald, and Waterman, "A Systematic Investigation of Tardive Dyskinesia in Inpatients," *The American Journal of Psychiatry*, **136**, no. 7, 918, Jul. 1979.
5. G. Borenstein, *Making Things See: 3D vision with Kinect, Processing, Arduino, and MakerBot*. Make: Books, 2012.

NET EFFICIENCY OF THE COMBINED ANKLE-FOOT SYSTEM IN NORMAL GAIT: INSIGHTS FOR PASSIVE AND ACTIVE PROSTHETICS

Kota Z. Takahashi, and Steven J. Stanhope

University of Delaware, Newark, DE, USA
email: ktaka@udel.edu, web: http://www.udel.edu/kaap/research/biomechanicslab.html

INTRODUCTION

With the continuous evolution of lower limb prosthetics, existing designs have diverged into two general categories: 1) *passive* systems composed of elastic materials, and 2) *active* systems composed of motors and inertial sensors [1]. A central goal between these contrasting approaches is to replicate the mechanical energy profiles of the natural ankle-foot system (NAFS) to restore normal gait. The prevalent theory in the field, stemming from the knowledge that the ankle joint musculature produces greater positive work than negative work during stance [2], is that an *active* prosthetic system is required to replicate the work-related efficiency of the NAFS [1]. However, structures like the plantar soft tissue and ligaments deform [3], and the toe joint musculature contracts eccentrically [4], such that these 'distal foot structures' collectively function to remove energy from the system.

As prosthetic ankle-foot systems are intended to restore the functions of *all anatomical structures* within the NAFS, there is a desire to quantify the combined effects of the ankle joint musculature and all distal foot structures in normal gait. Therefore, the purpose of this study was to quantify the *net efficiency* of the NAFS during stance across a full range of walking velocities.

METHODS

Eleven healthy subjects (ages 24.2 ± 2.9yrs, height 1.72 ± 0.08m, and body mass 75.3 ± 21.8kg) participated in a fully-instrumented gait analysis. The subjects walked barefoot at four scaled walking velocities: 0.4, 0.6, 0.8, and 1.0 statures/s (0.8 is considered the normal velocity for a healthy adult [5]). Kinematic data were collected using a six-camera motion capturing system (Motion Analysis Corp., Santa Rosa, CA), and kinetic data were collected from a strain gauge force platforms (AMTI, Watertown, MA). All data were analyzed using Visual3D software (C-Motion Inc., Germantown, MD). The combined ankle-foot power (P_{CAF}), normalized by body mass (W/kg), was quantified by the summation of the ankle joint power (P_{ank}) and the distal foot segmental power (P_{ftd}). P_{ank}, indicative of the total power due to ankle musculature, was quantified using a 6 degree-of-freedom joint model [6]. P_{ftd}, indicative of the total power due to the combined actions of all distal foot structures (e.g., plantar soft tissue, ligaments and intrinsic foot musculatures), was quantified using a deformable foot model [3]. Altogether, P_{CAF} signifies the total power due to the combined effect of *all anatomical structures* within the NAFS.

The total work done by the ankle joint and the combined ankle-foot system were quantified by integrating P_{ank} and P_{CAF}, respectively. The efficiencies of the ankle joint (E_{ank}), and the combined ankle-foot system (E_{CAF}) were calculated as the ratio of positive to negative work. The effect of walking velocity on E_{ank} and E_{CAF} was assessed, using a one-factor repeated measures ANOVA with Bonferroni corrections for pair-wise comparisons (α=0.05).

RESULTS AND DISCUSSION

The ankle joint primarily added energy to the body, while the distal foot structures primarily removed energy from the body (Figure 1). Accounting for the simultaneous influences, the P_{CAF} was generally characterized by a period of negative power from early to mid-stance, followed by a period of positive power (Figure 1).

There was a significant effect of walking velocity for both E_{ank} and E_{CAF} ($p < 0.05$). Across the four walking velocities, E_{ank} values were 1.46 ± 0.37,

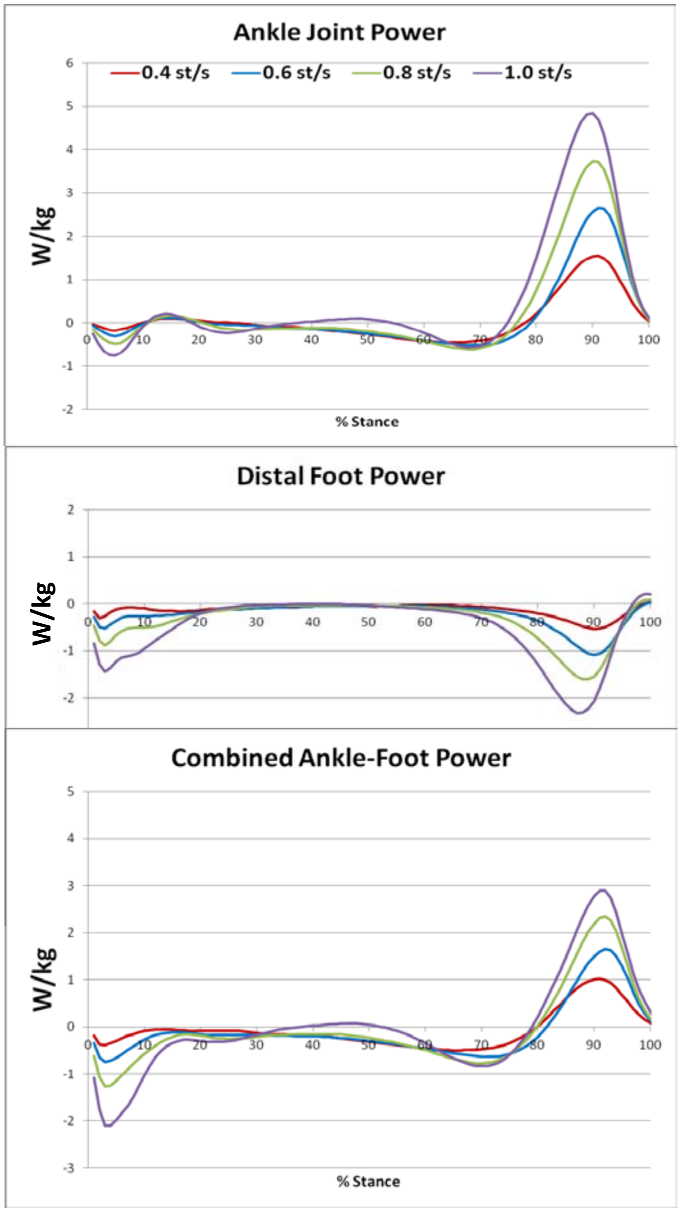

Figure 1: Average data of subjects (n=11) walking at four velocities (0.4, 0.6, 0.8, and 1.0 statures/s). Combined ankle-foot power is quantified by the summation of ankle joint and distal foot power.

1.96 ± 0.67, 2.92 ± 1.25, and 4.40 ± 1.54, while E_{CAF} were 0.65 ± 0.14, 0.69 ± 0.16, 0.87 ± 0.25, and 1.06 ± 0.35 (Figure 2).

As E_{ank} is significantly greater than 1.0 across a full range of walking velocities, an *active* prosthesis would be required to replicate the *isolated effect* of the ankle joint musculature. However, by accounting for the influence of distal foot structures, the E_{CAF} was markedly reduced such that the average efficiencies were less than 1.0 for all but the fastest walking velocity. Therefore, a *passive* prosthetic system that can store and return mechanical energy has the potential to replicate the *combined effect of all anatomical structures* within the NAFS.

CONCLUSIONS

In normal gait, the ankle joint musculature and all distal foot structures collectively function to produce a net negative work during stance over a range of walking velocities. Thus, a *passive* prosthesis might replicate the *net efficiency* of the NAFS during level-ground steady state walking. Future efforts may consider the precise customization of mechanical properties of *passive* prostheses to optimize energy storage and return characteristics.

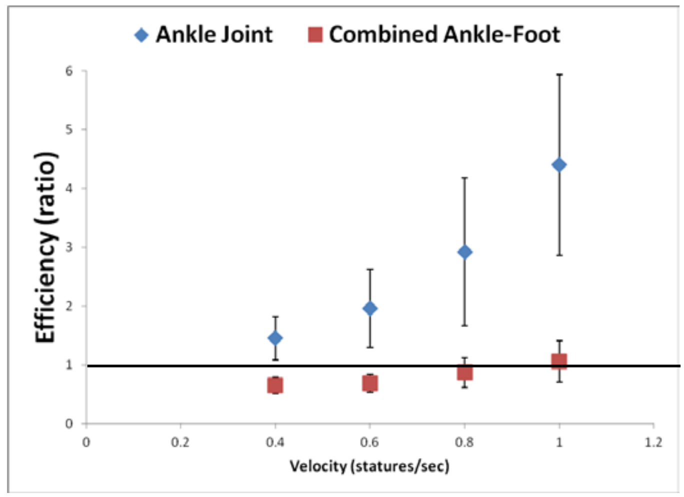

Figure 2: Mean ± std of mechanical efficiencies of ankle joint (blue) and combined ankle-foot system (red). All pair-wise comparisons for ankle joint were significant ($p < 0.05$), except for 0.4 vs 0.6 statures/s. For the combined ankle-foot, pair-wise comparisons between 0.4 vs 1.0, 0.6 vs 0.8, and 0.6 vs 1.0 statures/s were significantly different ($p < 0.05$).

REFERENCES

1. Versluys R, et al. *Disabil Rehabil Assist Technol* **4**, 65-75, 2009.
2. Winter DA. *Clin Orthop Relat Res* **175**, 147-154, 1983.
3. Siegel KL, et al. *J Biomech* **29**, 823-827, 1996
4. MacWilliams BA, et al. *Gait Posture* **17**, 214-224, 2003
5. Rosenrot P, et al. *J Human Movement Stud* **6**, 323-355, 1980
6. Buczek FL, et al. *J Biomech* **27**, 1447-1457, 1994

TRUNK FLEXION ANGLE IS ASSOCIATED WITH PATELLOFEMORAL JOINT STRESS DURING OVERGROUND RUNNING

[1]Hsiang-Ling Sharon Teng and [1]Christopher M Powers
[1]University of Southern California, Los Angeles, CA, USA
email: hsianglt@usc.edu, web: http://pt2.usc.edu/labs/mbrl/

INTRODUCTION

Patellofemoral pain (PFP) is one of the most common lower extremity injuries among runners [1]. A commonly accepted cause of PFP is elevated patellofemoral joint (PFJ) stress [2,3]. As stress is defined as force per unit area, elevated stress could occur as a result of an increase in the PFJ reaction force and/or a decrease in contact area. In turn, an increase in the PFJ reaction force could occur with an increase in the knee flexion angle and/or an increase in the knee extensor moment.

Recent literature suggests that sagittal plane trunk posture is associated with the knee extensor moment and flexion angle during the deceleration phase of landing [4,5]. As such, saggital plane trunk posture may be related to PFJ stress during running. The purpose of this study was to investigate whether an individual's self-selected sagittal plane trunk posture is associated with PFJ stress during overground running.

METHODS

To date, 9 asymptomatic individuals (4 females, 5 males; age: 30.4 ± 3.0 y/o; height: 170.6 ± 9.6 cm; weight: 65.3 ± 10.6 kg) have participated in this on-going study. Three-dimensional trunk and knee kinematics (250 Hz, Qualisys, Gothenburg, Sweden) and ground reaction force data (1500 Hz, AMTI force plate, Watertown, MA) were collected while subjects ran overground with a self-selected trunk posture at a velocity of 3.4 m/s. The trunk segment was defined by markers placed on bilateral acromioclavicular joints and the highest point of the iliac crests. Trunk orientation was calculated relative to the pelvis. Trunk and knee flexion angles as well as knee extensor moment during the stance phase of running were computed using Visual 3D™ software.

A previously described biomechanical model was used to estimate PFJ stress (Figure 1) [2]. The model input variables included subject specific biomechanical parameters (i.e. knee joint kinematics and net knee joint moment) and data from the literature (i.e. knee moment arms, quadriceps force/patella ligament force ratios and joint contact area). The model outputs were PFJ reaction force and PFJ stress. Variables of interest consisted of peak PFJ stress and the PFJ reaction force. In addition, the trunk and knee flexion angles and knee extensor moment at the time of peak PFJ stress were examined. Pearson product-moment correlations were used to evaluate whether the trunk flexion angle was associated with peak PFJ stress and peak PFJ reaction force. In addition, Pearson correlations were run to evaluate the association between the trunk flexion angle and the knee flexion angle and knee extensor moment at the time of peak PFJ stress.

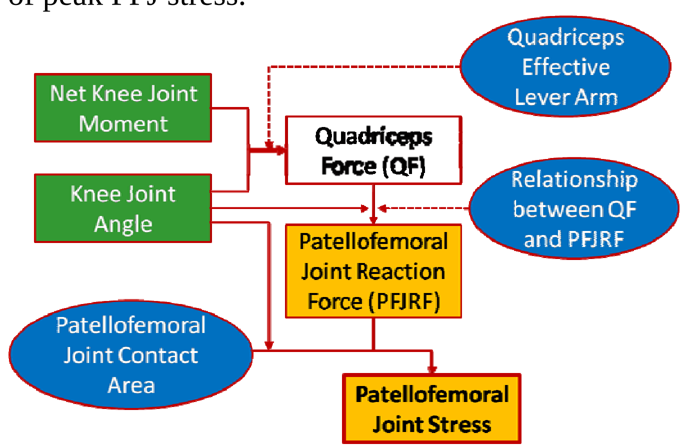

Figure 1: Flow chart of PFJ stress 2D model.

RESULTS AND DISCUSSION

A significant correlation was found between the self-selected trunk flexion angle and peak PFJ stress (r = -0.72, p = 0.03) (Figure 2) as well as the PFJ reaction force (r = -0.78, p = 0.01).

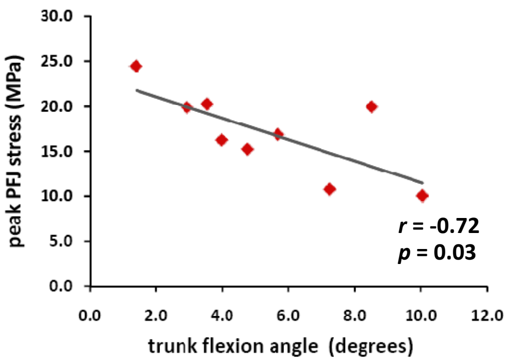

Figure 2: Association between trunk flexion angle and peak PFJ stress (N=9).

In addition, trunk flexion angle was also found to be significantly correlated with knee extensor moment (r = -0.87, p = 0.002) (Figure 3-A). No association was found between trunk posture and knee flexion angle (Figure 3-B).

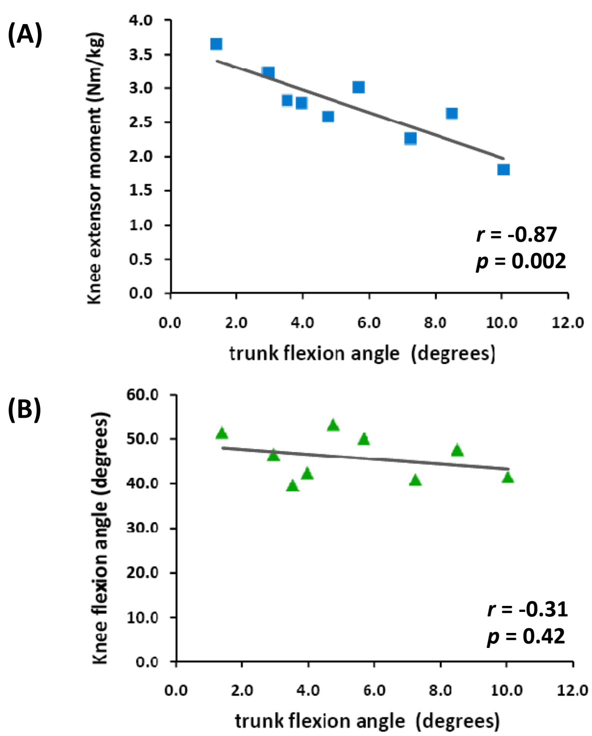

Figure 3: Associations between trunk flexion angle and knee extensor moment (A) and flexion angle (B) (N=9).

Our results indicate that an individual's self-selected trunk flexion angle is negatively correlated with PFJ stress and reaction force during running. More specifically, we found that individuals who run with a more extended trunk posture exhibit higher PFJ stress and therefore, may be predisposed to a higher risk of PFP. Trunk angle appeared to have the largest influence on the knee extensor moment as no association was found between trunk posture and the knee flexion angle.

CONCLUSIONS

Our findings indicate that a more extended trunk forward lean is related to a higher PFJ stress during running. Conversely, a more flexed trunk posture was associated with lower PFJ stress. These findings suggest that trunk posture may contribute to the development of PFP among runners. Future studies are needed to examine whether altering sagittal plane trunk posture can be used as a strategy to lower an individual's PFJ stress and pain during running.

REFERENCES

1.Taunton JE, et al. *Br J Sports Med* **36**, 95-101, 2002.
2.Heino BJ, et al. *Med Sci Sports Exerc* **34**, 1582-93, 2002.
3.Ferrokhi S, et al. *Osteoarthritis Cartilage* **19**, 287-94, 2011.
4.Shimokochi Y, et al. *J Athl Train* **44**,33-8, 2009
5.Blackbourn JT, et al. *Clin Biomech* 2**3**, 313-19, 2008

KNEE KINEMATICS DURING SLOPED WALKING AND RUNNING IN HEALTHY WOMEN WITH KNEE HYPEREXTENSION

P Teran-Yengle, K Bissig, A Paige, A Rogers, HJ Yack

Program in Physical Therapy & Rehabilitation Science, University of Iowa, Iowa, USA
Email: patricia-teranyengle@uiowa.edu

INTRODUCTION

Abnormal knee kinematics can result in excessive loading of structures of the knee joint, such as menisci, ligaments, or cartilage. Associated change to these structures, due to the abnormal stress, can be detrimental to the integrity of the knee joint [1, 2]. Knee hyperextension implies increased stress to the posterior joint capsule of the knee [3] and to the anterior cruciate ligament (ACL) [4]. Studies also point out that there is an increased contact stress on the tibial-femoral joint when the knee joint is extended [5]. Several studies have reported that compared with men, women demonstrated more knee hyperextension [6]. The purpose of this study was to investigate if women with asymptomatic knee hyperextension at rest experience knee hyperextension during level and sloped walking and running.

METHODS

Healthy female recreational runners, 18-39 years of age, with asymptomatic knee hyperextension participated in this study. Knee hyperextension greater than 5° was the designated cut off point since fully extended knee normally positions tibiofemoral joint in 0-5 degrees of extension in the sagittal plane [3]. Participants underwent a physical and gait evaluation. The physical evaluation measured knee extension passive range of motion (PROM), screened muscular strength in each subject's legs using standard techniques, and assessed general joint laxity using the Beighton and Horan Joint Mobility Index (BHJMI). The assessment of walking and running kinematics was conducted on a level, inclined (10%), and declined (-10%) treadmill using a three-dimensional motion analysis system (Optotrak, NDI; Kistler). To reduce inter subject variability, set walking (1.3 m/s) and running (2.7 m/s) velocities were scaled to each subject's leg length using the Froude ratio ($V^2/\sqrt{gL}$) [7,8].

Participants were asked to walk at their scaled speed during 5 minutes to get familiarized with the treadmill. After a 2-3 minutes break, participants were asked to walk on a leveled treadmill for 2 minutes, inclined treadmill for 1 minute, leveled treadmill for 2 minutes, and declined treadmill for 1 minute. After the declined treadmill walking, participants follow the same sequence for the running testing. Fifteen seconds of gait data were collected during level, incline, and decline walking and running tasks. Gait data was processed using Visual 3D software (C-Motion). All statistical testing was performed using SAS 9.3 (SAS Institute Inc., Cary, NC, USA).

RESULTS AND DISCUSSION

Twenty healthy women (mean $\pm$ SD age, 3 $\pm$ 5; mass, 65.4 $\pm$ 8 kg; height, 1.7 $\pm$ 0.1 m) took part in this study.

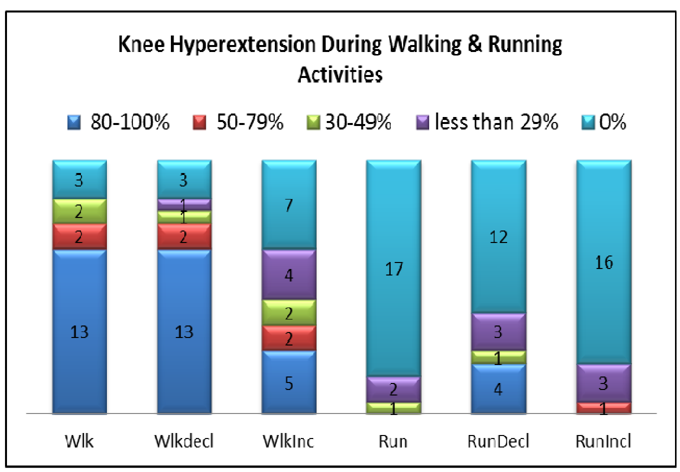

Figure 1: Stacked columns showing the number of subjects who experienced hyperextension (>5°) during level and sloped walking and running.

Mean $\pm$ SD knee passive range of motion was -8.5º $\pm$ 1.8º (range -6° to -13°). Mean knee extension during level, incline, and decline walking was -7.2° + 2.8°, -2.5° + 5.1°, and -5.9° + 5.1°, respectively. Mean knee extension during level, incline, and decline running was 3.3° $\pm$ 4.4°, 6.7° $\pm$ 6°, and -0.9° $\pm$ 5.1°, respectively. As shown in Figure 1, 13 (65%) participants showed knee hyperextension greater than 5° between 80-100% of the 15sec of data collection time during level (Wlk) and declined (Wlkdecl) walking activities. Seventeen (85%) and sixteen (80%) participants showed less than 5° of knee extension during level running (Run) and decline running (RunDecl), respectively (Fig1). During level running (Run), 17 (85%) participants did not show knee extension greater than 5° at all during the 15-second data collection (Fig. 1)

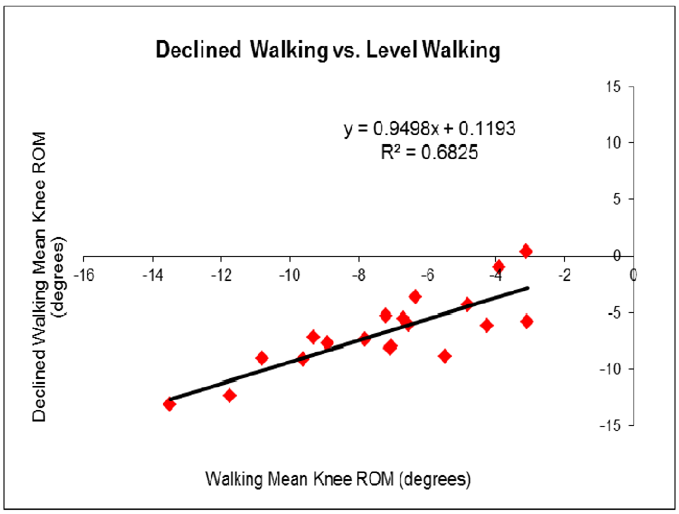

Figure 2: Correlation between decline and level walking in women with knee hyperextension greater than 5° at PROM.

Pearson correlation coefficients showed a very poor correlation between the degree of knee extension at PROM and walking and running. In addition, there was a low correlation between participants' general joint laxity (BHJMI) and PROM. As shown in Figure 2, there was a positive correlation between the degree of knee extension during level and decline walking (R^2 = .68). Figure 3 show a moderate correlation between the degree of knee extension during level and decline running (R^2 =.63).

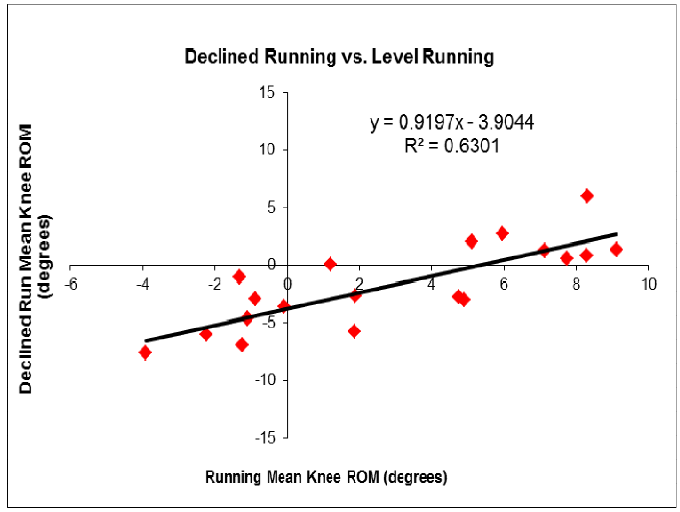

Figure 3: Correlation between decline and level running in women with knee hyperextension greater than 5° at PROM.

CONCLUSIONS

The results of this study show that PROM is poorly correlated with the degree of knee hyperextension during sloped walking and running in women with knee hyperextension greater than 5°. In addition, data suggest a positive correlation between knee extension range of motion during level and declined walking.

REFERENCES

1. Hunter DJ et al. (2009). *Journal of Bone and Joint Surgery* 91(1); p. 85-89.wicki GS. *Proceedings of NACOB'08,* Ann Arbor, MI, USA, 2008.
2. Tanamas S et al. (2009). *Arthritis & Rheumatism* 61(4); p. 459-467
3. Oatis CA. Kinesiology.: *Mechanics & Pathom of human movement* (2004)
4. Senter C et al. (2006). *Sports Medicine* 36(8); p. 635-641.
5. Nisell R et al (1986). *Acta Orthop Scand* 57; p. 41- 46.
6. Medina McKeon J M et al. (2009). *Journal of Athletic Training,* 44(3); p.249-55. olzapfel GA. *Nonlinear Solid Mechanics,* John Wiley & Sons, Ltd., 2000.
7. Moretto P, Bisiaux M, & Lafortune MA. Gait & Posture 25 (40-48), (2007)
8. Delattre N, Lafortune M, & Moretto R. Journal of Biomechanics 42; 312-318, (2008).

COMPARING VISUAL PERTURBATION RESPONSIVENESS IN INDIVIDUALS WITH AND WITHOUT TRANS-TIBIAL AMPUTATION

[1]Kevin Terry, [2]Kathryn A. Faust, [2]Jason M. Wilken, and [1]Jonathan B. Dingwell

[1]Department of Kinesiology, University of Texas at Austin, Austin, TX, USA
[2]Department of Orthopedics and Rehabilitation, Center for the Intrepid,
Brooke Army Medical Center, Ft. Sam Houston, TX, USA
email: kterry@mail.utexas.edu

INTRODUCTION

Reduced sensory feedback caused by lower-limb amputations could lead to increased reliance on vision, increasing susceptibility to visual field disturbances. Inappropriate or excessive responses could diminish gait stability, resulting in trips, stumbles, or falls. However, because of physiological and developmental differences, the degree to which individuals respond to visual perturbations can vary [1, 2]. To assess the effects of visual field disturbances during gait, virtual environments were altered in a controlled manner. Responses to visual perturbations were then quantified using kinematic and temporo-spatial variabilities as in a related study [3]. However, these variabilities may scale with physical characteristics and do not allow for direct comparison between individuals. Therefore, a normalized responsiveness metric was developed to make direct comparisons possible. With that metric, visual responsiveness was quantified in individuals with and without amputation.

METHODS

13 controls and 7 patients with unilateral trans-tibial amputations walked on a treadmill at their normal speed. The virtual environment was produced by the Computer Assisted Rehabilitation ENvironment (CAREN) (Motek, Amsterdam, Netherlands). A 6-min warm-up was followed by five randomized 3-min trials for each perturbation condition: no perturbation (NP), platform (PLAT), or visual (VIS). Movements were tracked by the CAREN's 24-camera Vicon motion analysis system (Oxford Metrics, Oxford, UK). Data analyses were performed using Visual3D (C-Motion Inc., Germantown, MD) and MATLAB (The Mathworks, Natick, MA). Visual perturbations were generated by fixing the center of a path on the horizon while the near field scene translated medio-laterally. Perturbation amplitude, *A(t)*, was calculated as:

$$A_w[\sin(2\pi f_1 t)+0.8\sin(2\pi f_2 t)+1.4\sin(2\pi f_3 t)+0.5\sin(2\pi f_4 t)]$$

where A_w is the weighting factor (0.45 m), t is time (s), and $f_{1\text{-}4}$ are 0.16, 0.21, 0.24, and 0.49 Hz, respectively. Variabilities of center of mass velocity (COM_{vel}) and step width (SW) were used to quantify kinematic (Var) and temporo-spatial (SW_{sd}) effects, respectively. COM_{vel} power spectral density (PSD) was used to decompose Var as follows (Fig. 1):

Var_{xx}: COM_{vel} variance at frequency 0.xx

Var_{stride}: COM_{vel} variance at stride frequency

$Var_{pert} = Var_{16}+Var_{21}+Var_{24}+Var_{49}$

Kinematic variability driven by the perturbation was quantified as a percentage of Var ($Var_{pert}+Var_{stride}$), referred to as the response ratio ($RR = Var_{pert}/Var$).

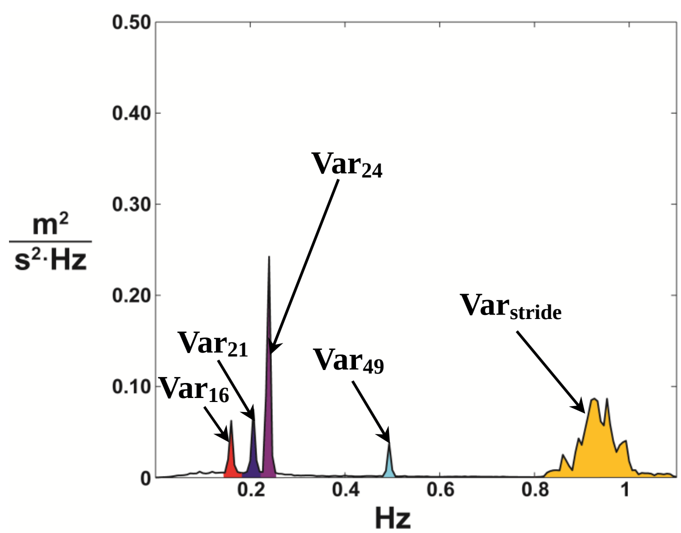

Figure 1. Typical PSD of COM_{vel} recorded during a perturbed gait trial reveals frequency components of variability.

RESULTS AND DISCUSSION

Kinematic variability driven by the perturbation (Var_{pert}) was well-correlated to SW_{sd} (Fig. 2); however, variability associated with stride-to-stride changes (Var_{stride}) was not. As a normalized version of Var_{pert}, RR should be correlated to SW_{sd} and less sensitive to stride-related and physical differences.

Mean RR_{VIS} was not significantly different between controls (0.349±0.193) and patients (0.316±0.166). Likewise, the difference in step width variability increase from the NP to the VIS condition (ΔSW_{sd}) for controls (0.028±0.012 m) versus patients (0.027±0.18 m) was not significant.

For controls, 80% of RR_{VIS} changes were predicted by ΔSW_{sd} (Fig. 3), whereas the regression for patients was not as strong (R^2 = 0.69). The slope for the control group regression was steeper, indicating that for the same RR_{VIS} value, a control participant would have a smaller increase in SW_{sd}.

Finally, patients exhibited a dichotomy of visual responsiveness, with 'responder' $RR_{VIS} \cong 0.4$ and 'non-responder' $RR_{VIS} < 0.2$ groups. Low responsiveness also correlated to smaller ΔSW_{sd} (<0.020 m). Although control group responsiveness was more evenly distributed, this group also included three non-responders.

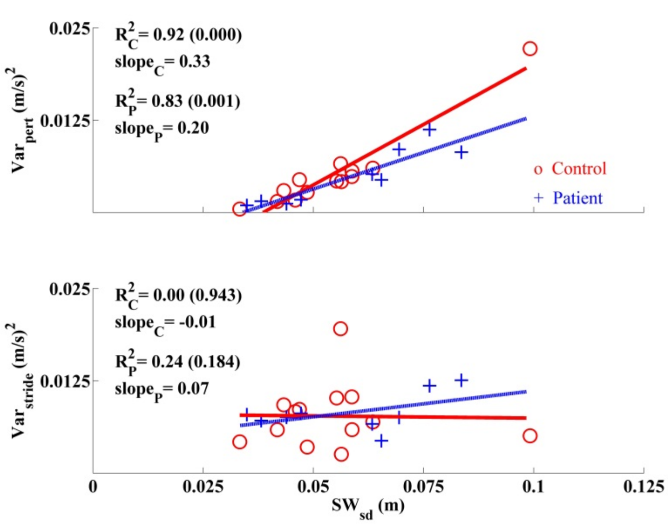

Figure 3. COM_{vel} variance driven by perturbation (Var_{pert}) and stride (Var_{stride}) versus SW_{sd} for visually perturbed gait.

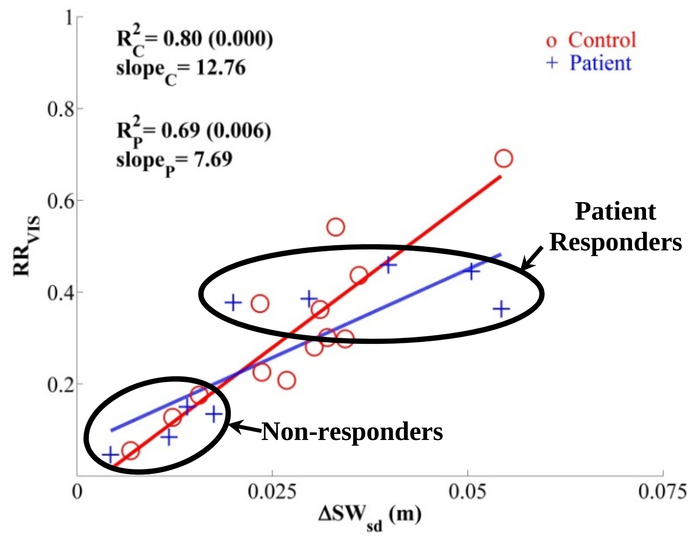

Figure 2. *RR* for visually perturbed gait of both the control (o) and patient (+) groups regressed against the change in step width variability

CONCLUSIONS

The use of RR_{VIS} allowed for direct comparisons of responsiveness using a normalized, bounded measure which indicated that patients with a unilateral trans-tibial amputation did not have higher visual responsiveness. RR_{VIS} also revealed a dichotomy of visual responsiveness in patients not found in the control group. Accurate identification of visual responsiveness in patients could help target rehabilitation to individual needs.

REFERENCES

1. Logan D., et al. *Experimental Brain Research* **206**, 337-350, 2010.
2. Warren, W. H., et al. *Human Perception and Performance* **22(4)**, 818-838, 1996.
3. McAndrew P.M., et al. *Journal of Biomechanics* **43(8)**, 1470-1475, 2010.

ACKNOWLEDGEMENTS

This work was supported by NIH Grant R01-HD059844

The view(s) expressed herein are those of the authors and do not reflect the official policy or position of the Brooke Army Medical Center, U.S. Army Medical Department, U.S. Army Office of the Surgeon General, Department of the Army, Department of Defense, or U.S. Government.

EFFECT OF ACL RECONSTRUCTION ON TIBIOFEMORAL CARTILAGE CONTACT DURING DOWNHILL RUNNING

Eric Thorhauer, William Anderst, Scott Tashman

University of Pittsburgh, Pittsburgh, PA, USA
Corresponding author: edt4@pitt.edu

INTRODUCTION

ACL reconstruction fails to restore normal knee joint kinematics [1]. Changes in kinematics may lead to abnormal loading patterns in the articular cartilage and initiate the onset of osteoarthritis [2]. The purpose of this study was to estimate cartilage-cartilage contact patterns in subjects who have undergone ACL reconstruction during a dynamic, functional activity. We hypothesized that there would be significant differences in the contact patterns of ACL-reconstructed knees compared to subjects' uninjured, contralateral knees.

METHODS

MRI scans (Sagittal SPGR, 0.3125 mm/pixel, 2 mm slice thickness) for 18 ACL patients (32± 11.6 years old at surgery) were collected of both knees 2-8 years after ACL reconstruction surgery in a supine, unloaded position. Tibiofemoral cartilage and bone were segmented using Mimics 14.1 (Materialise) and converted into 3D triangular mesh models.

High-speed biplane radiographic images were collected at 250 frames/s as subjects ran on a treadmill at 2.5m/s at 10° downward slope on the same day as MRI scanning. Tibiofemoral kinematics was derived using previously described methods of registering CT-bone models to the dynamic data with an accuracy of ±0.1 mm or better [3]. MR bone models were coregistered to bone models from segmented CT scans to obtain the MR-to-CT coordinate system transforms. Cartilage models were mapped onto the CT bone models. Cartilage contact centroid paths of the medial and lateral compartments were estimated as the penetration-weighted centroid of the overlapping regions.

Average contact centroids were analyzed during highest joint loading (0 to 0.1 seconds following footstrike). Repeated-measures analysis of variance (SPSS v18 GLM) was used to evaluate overall differences between knees (α=0.05). Post-hoc t-tests were employed where significant interactions were observed to identify direction-specific, intact-vs-reconstructed differences.

RESULTS AND DISCUSSION

Average contact centroid paths are depicted in Figure 1 (scaled and mapped to representative models). The contact paths of the reconstructed knees were shifted posteriorly and medially relative to the uninjured limbs.

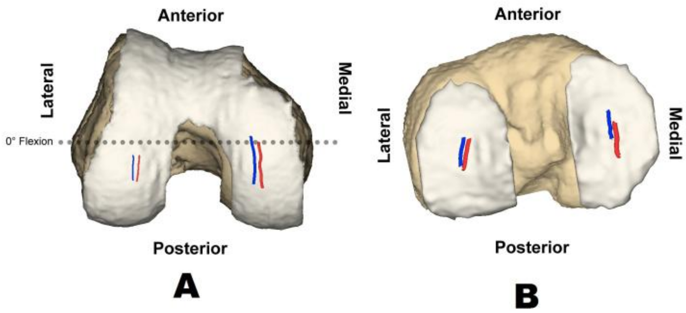

Figure 1: Average contact centroid paths of the femur (A) and tibia (B). Red is reconstructed and blue is uninjured.

In the femur, differences in the medial-lateral location of the contact path were significant in the medial ($p<0.011$) and lateral ($p<0.045$) compartments. Differences in the femur between reconstructed and intact medial-lateral contact location are shown for the medial compartment (Figure 2) and lateral compartment (Figure 3). In the tibia medial compartment, the anterior-posterior shift was significant ($p<0.025$). The interaction between timepoint and limb state (intact or reconstructed) was significant for the medial (p<0.0001) and lateral (p<0.005) tibia, and for the medial femur (p<0.044). Differences in the tibia between reconstructed and intact anterior-posterior contact location are shown for the medial compartment (Figure 4) and lateral compartment (Figure 5). Larger differences were observed in the medial compartment along the anterior-posterior direction after t=0.05s (Figure 4). This time interval typically corresponds to peak loading of the joint.

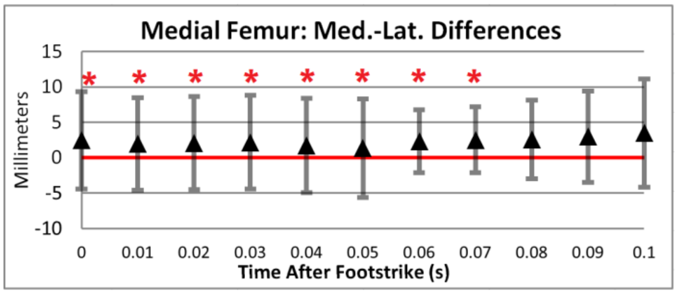

Figure 2: Average medial femur difference in medial-lateral contact location. Error bars are 1 standard deviation. Post-hoc t-tests p<0.05*.

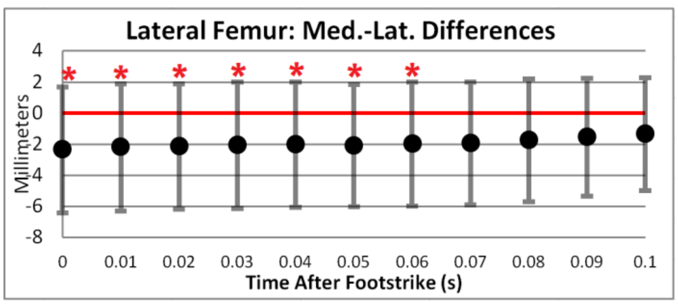

Figure 3: Average lateral femur difference medial-lateral contact location. Error bars are 1 standard deviation. Post-hoc t-tests p<0.05*.

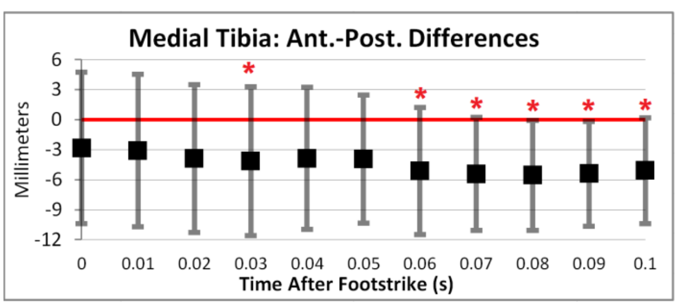

Figure 4: Average medial tibial anterior-posterior contact location. Error bars are 1 standard deviation. Post-hoc t-tests p<0.05*.

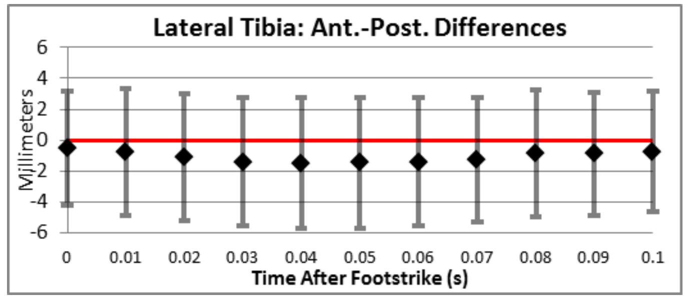

Figure 5: Average lateral tibial anterior-posterior contact location. Error bars are 1 standard deviation.

CONCLUSIONS

The contact centroid paths of the ACL-reconstructed knees were shifted posteriorly and medially relative to the intact, contralateral limbs. Differences in centroid location were much larger for some subjects than the means. Larger anterior-posterior shifts were detected in the medial compartment of the tibia, where osteoarthritis most often occurs after ACL-reconstruction. The differences in contact paths may result from differences in cartilage health or morphology, joint kinematics, or ACL laxity between the reconstructed and uninjured limbs. This study analyzed the cartilage-to-cartilage interaction within the knee joint, during a demanding dynamic activity. The tibiofemoral cartilage interface is where the pathology of osteoarthritis begins; therefore these analyses may offer a more sensitive method for the early detection and progression of the disease following ACL injury and reconstruction.

REFERENCES

1. Tashman S, et al. *Clin Orthop Relat Res* **454**, 66-73, 2007.
2. Andriacchi T, et al. *Annals of Biomedical Engineering* **32**, 417-457, 2004.
3. Tashman S, et al. *J. Biomech. Eng.* **125:2**, 238-245, 2003.

ACKNOWLEDGEMENTS

The data for this study were collected at Henry Ford Health System (Detroit, MI). This study was funded by NIH/NIAMS grant # R01 AR46387

TIBIOFEMORAL CARTILAGE THICKNESS FOLLOWING ACL RECONSTRUCTION

Eric Thorhauer, Scott Tashman

University of Pittsburgh, Pittsburgh, PA, USA
Corresponding author: edt4@pitt.edu

INTRODUCTION

Long term risks following ACL disruption include cartilage degeneration and knee osteoarthritis. Cartilage thinning or thickening as a result of shifting loading patterns after ACL injury in the articular cartilage has been hypothesized as a signal of the onset of osteoarthritis [1]. The objective of this study was to quantify differences in cartilage thickness between ACL-intact and ACL-reconstructed knees at least 24 months after ACL surgery.

METHODS

MRI scans (Sagittal SPGR, 0.3125 mm/pixel, 2 mm slice thickness) for 18 ACL patients (32± 11.6 years old at surgery) were collected of both knees 2-8 years after ACL reconstruction surgery. Tibia and femur cartilage was segmented using LiveWire in Mimics 14.1 (Materialise, Belgium) and converted into 3D triangular mesh models using a marching tetrahedron algorithm. Custom MATLAB (Mathworks, USA) software divided the models into anatomically meaningful subregions (Figure 1) similarly to methods developed by Wirth [2]. Thickness measurement vectors were formed from each triangle centroid of the outer cartilage surface and extended until they intersected a triangle on the opposing inner cartilage surface. Thickness measurement vectors in the tibia were parallel to the anatomical long axis of the tibia. A cylinder was fit to the distal femur, with the cylinder axis matching the medial-lateral anatomical axis of the femur. Femur thickness measurement vectors were radial to the cylinder.

Average thickness within subregions was calculated by averaging thickness values for all triangles within subregions weighted by the triangle areas. Subregions were compared between subjects' ACL-reconstructed and contralateral intact knees using paired t-tests with a significance level of $p<0.05$. Differences in cartilage thickness are reported as the reconstructed thickness minus the intact thickness.

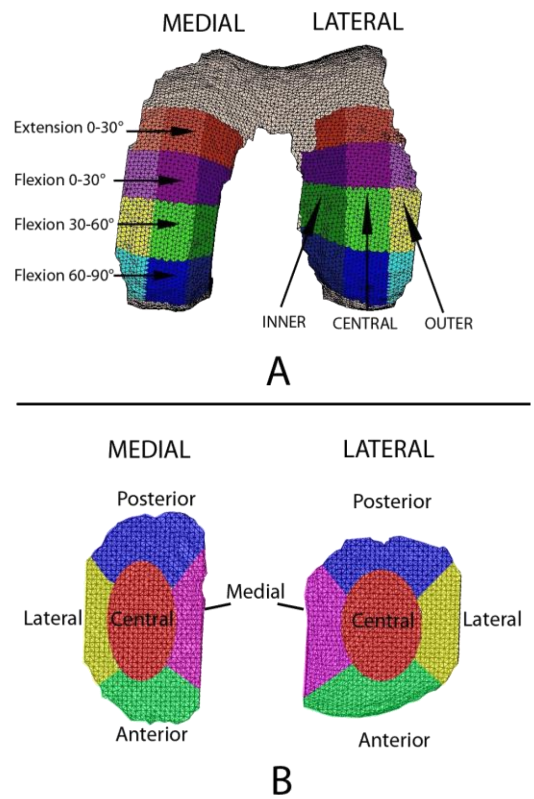

Figure 1: Subdivision of femoral (A) and tibial (B) cartilage into anatomically-based regions of interest.

RESULTS AND DISCUSSION

Significant differences between reconstructed and intact knees were observed in all outer and central regions of the medial femur and in most regions of the lateral femur (Table 1). Both thinning and thickening were observed in the femur, while cartilage thinning predominated in the tibia. This pattern of cartilage thinning in the lateral compartment and thickening in the medial compartment of the femur has been previously reported following ACL disruption [3]. Average thicknesses in the intact femur were 2.52 mm and 2.82 mm for the entire medial and lateral compartments, respectively. In reconstructed femurs, average thicknesses were 2.81 mm for medial and 2.74 mm for lateral compartments. The average difference in all central load bearing regions in the medial femur cartilage of +0.51 mm is a substantial ~20% increase relative to the healthy control knees. The relative cartilage thickening observed in the central regions of the entire medial femur compartment may be indicative of cartilage response to increased load during daily functional activities.

Average tibial intact cartilage thicknesses were 2.32 mm and 2.95 mm for the medial and lateral compartments, respectively. Average reconstructed tibial cartilage thicknesses were 2.21 mm and 2.62 mm for the medial and lateral compartments, respectively. In the lateral tibia, differences in the central, lateral, and anterior subregions were significant (Table 2). In the medial tibia, only differences in the medial aspect were significant. A 5-10% decrease in cartilage thickness was observed in the tibia.

Table 1: Average differences in femur cartilage thickness (mm): Reconstructed minus Intact.

		Medial	Lateral
Angle	**Region**		
0-30° Extension	Outer	0.96 ±0.73**	-1.87 ±1.51**
	Central	0.58 ±0.58**	-0.65 ±0.88**
	Inner	-0.11 ±0.44	0.50 ±0.98**
0-30° Flexion	Outer	0.98 ±0.67**	-0.57 ±0.93*
	Central	0.68 ±0.69**	0.22 ±0.81
	Inner	0.10 ±0.45	0.97 ±1.05**
30-60° Flexion	Outer	0.99 ±0.69**	-0.09 ±0.64
	Central	0.54 ±0.70**	0.57 ±0.91*
	Inner	-0.09 ±0.73	1.27 ±1.21**
60-90° Flexion	Outer	0.73 ±0.64**	-0.63 ±1.01*
	Central	0.26 ±0.46*	-0.52 ±0.90*
	Inner	-0.49 ±1.20	0.36 ±0.54*
*p<0.05 , ** p<0.001			

Table 2: Average differences in tibial cartilage thickness (mm): Reconstructed minus Intact.

Compartment	**Region**	
Medial	Central	-0.04 ± 0.31
	Lateral	-0.04 ± 0.35
	Medial	-0.26 ± 0.36 **
	Anterior	-0.06 ± 0.42
	Posterior	-0.14 ± 0.45
Lateral	Central	-0.26 ± 0.50 *
	Lateral	-0.35 ± 0.35 **
	Medial	-0.19 ± 0.47
	Anterior	-0.46 ± 0.76 *
	Posterior	-0.27 ± 0.83
*p<0.05 , ** p<0.001		

CONCLUSIONS

The observed differences in cartilage thickness may be attributed to altered kinematics following ACL-reconstruction. These changes in kinematics may cause previously unloaded regions of cartilage to become loaded, or vice versa. As a result, the cartilage may respond to these new loading patterns by either thickening to accommodate new joint load patterns, or thinning as the result of degeneration. The results of this study imply structural changes in the tibiofemoral cartilage following ACL injury that are congruent to changes found at the onset of osteoarthritis, and a failure of the reconstructive surgery to restore joint condition to pre-injury conditions.

REFERENCES

1. Andriacchi T, et al. *Annals of Biomedical Engineering* **32**, 417-457, 2004.
2. Wirth W, et al. *IEEE Trans Med Imaging* **27**, 737-744, 2008.
3. Frobell RB. *J Bone Joint Surg Am.* **93**, 1096-1103, 2011.

ACKNOWLEDGEMENTS

The data for this study were collected at Henry Ford Health System (Detroit, MI). This study was funded by NIH/NIAMS grant # R01 AR46387

SCAPULAR AND CLAVICULAR KINEMATICS DURING EMPTY AND FULL CAN EXERCISES IN SUBJECTS WITH SUBACROMIAL IMPINGEMENT SYNDROME

[1,2]Mark Timmons, [2]Molly Grover, [2,3]Andrea Lopes-Albers, [1]Jeffery Ericksen, [2]Lori A Michener
[1]Department of Veterans Affairs-Hunter Holmes McGuire VA Medical Center, Richmond, VA USA,
[2] Virginia Commonwealth University, Richmond, VA USA
[3] Universidade Federal de Sao Paulo, Departamento de Medicina, Sao Paulo, SP, Brazil
email: mktimmons@vcu.edu

INTRODUCTION

The mechanisms that lead to the development of rotator cuff tendinopathy, specifically subacromial impingement syndrome (SAIS) are not well understood due to the complex nature of the disorder. SAIS is theorized to be caused by extrinsic and intrinsic mechanisms. Extrinsically, the rotator cuff tendons are compressed due to narrowing of the subacromial space; intrinsically, the rotator cuff tendinopathy degrade due to factors related to tendon overload, aging, vascularity and changes in tendon histology and mechanical properties.[1]

Treatment of SAIS with exercise has been shown to be helpful in reducing shoulder pain, but not for all patients. Potentially this is because the exercise program does not adequately load the rotator cuff to promote remodeling of the tendon and muscle. An exercise program focused on eccentric loading of the rotator cuff during shoulder external rotation exercises has been shown to reduce shoulder pain.[2] Scapular plane elevation (scaption) exercises are commonly used to strengthen the supraspinatus in rehabilitation. Scaption exercises are performed with the shoulder in internal rotation (empty can) or in external rotation (full can). Both positions have been shown to produce maximal activity of the supraspinatus. A prior study in subjects free from shoulder pain has shown that the empty can elevation exercise produced altered scapular kinematics of decreased scapular posterior tilt and external rotation.[3] These same altered scapular positions have been found in patients with SAIS, and theorized to increase external impingement. The effects of the EC dynamic strengthening exercise has not been examined in patients with shoulder pain, to determine if altered scapular kinematics are present.

Better understanding of the effects of the empty can (EC) as compared to the full can (FC) exercise on scapular kinematics will assist in recommending eccentric strengthening exercises for SAIS. This study characterized scapular kinematics during EC and FC exercises in subjects with SAIS

METHODS

Subjects (n = 28, 10 females, age = 37.9±14.3 years, height = 172.8±11.4cm, mass = 74.1±15.1Kg) participated. All subjects had pain with resisted arm elevation or external rotation, and 3/5 positive SAIS tests: painful arc, pain or weakness with resisted external rotation, Neer, Hawkins, and Jobe tests. All subjects provided informed consent prior participation. The IRB of the Virginia Commonwealth University approved this project.

Three dimensional scapular and clavicular positions were determined using the Polhemus 3Space Fastrak electromagnetic-based motion capture system (Polhemus, Colchester, VT) and Motion Monitor software (Innovative Sports Training, Inc, Chicago, IL) following ISB recommendations.[3] Electromagnetic sensors were placed over the T3 spinous process, posterior acromion and distal humerus. Scapular and clavicular positions data were collected during 5 consecutive arm elevation motions in the plane of the scapula. Scapular upward rotation (UR), scapular internal rotation (IR), and scapular posterior tilt (PT), clavicular elevation (ELE) and clavicular protraction (PRO) were calculated at 30°, 60°, 90° and 120° of humeral elevation.

A three-way repeated measures ANOVA (arm position x arm elevation phase x arm elevation angle) was used to test for statistical differences of the dependent variables between EC and FC arm position, with significance set at $p \leq 0.05$.

RESULTS AND DISCUSSION

Figures 1-5, display the scapular and clavicular position by arm elevation angle. Significant differences were found between EC and FC arm positions and the ascending and descending phases.

During arm elevation in the FC position the scapular was in less UR (p<0.001, mean difference [MD]=2.4°), greater PT (p=0,026, MD=1.9°), the clavicle was less ELE (p<0.001, MD=1.6°) than during elevation in the EC position. The arm position by elevation angle interaction for IR was significant (p<0.001), the scapula experienced an IR rotation during EC and an external rotation during the FC arm elevation. No difference was seen in clavicular PRO (p=0.065) between the EC and FC positions. The scapula was in greater UR (p=0.009, MD=1.3°), IR (p=0.003, MD=1.5°) and PT (p=0.005, MD=2.5°) and the clavicle was in in greater ELE (p=0.001, MD=0.7°) and less PRO (p<0.001, MD=1.67°) during the descending phase than the ascending phase.

In a similar study in subjects without shoulder pain Thigpen et al [3] reported an increase in IR of 1.4° and a decrease in PT of 1.96° during arm elevation in the EC position. In the current study in subjects with SAIS we found that the EC position had a greater effect on scapular and clavicular motion than what was reported by the earlier study in subject without shoulder pain. In the current study subjects with SAIS experienced increased IR during the ascending phase in the EC. This suggests that the use of the EC for eccentric loading the rotator cuff may increase the impingement of the rotator cuff due to the decreased PT and increased IR. Future studies should examine the activity of the scapular stabilizers musculature during EC and FC exercise.

REFERENCES

1. Seitz AL et al, *Clin Biomech* **26**, 1-12, 2011
2. Barnhardsson S, et al., *Clin Rehabil* **25**, 69-78, 2011
3. Thigpen CA, et al. *Am J Sports Med* **34(4)**, 644-652, 2006
4. Wu G, et. al., *J Biomech* May;38(5):981-992, 2005

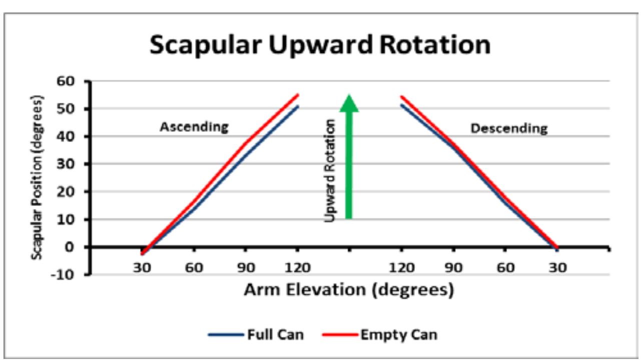

Figure 1. Scapular UR by arm elevation angle during FC (blue) and EC (red) arm elevation, + numbers reflect UR.

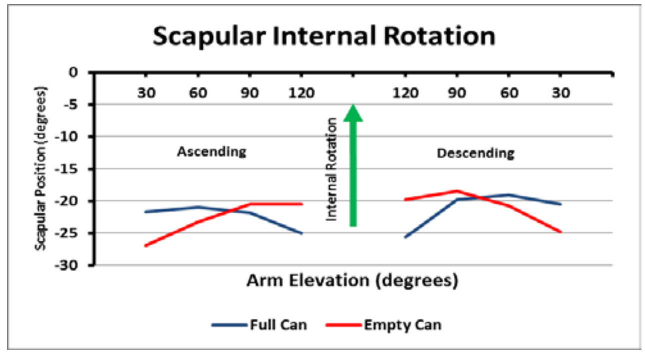

Figure 2. Scapular IR by arm elevation angle during FC (blue) and EC (red) arm elevation, + numbers reflect IR.

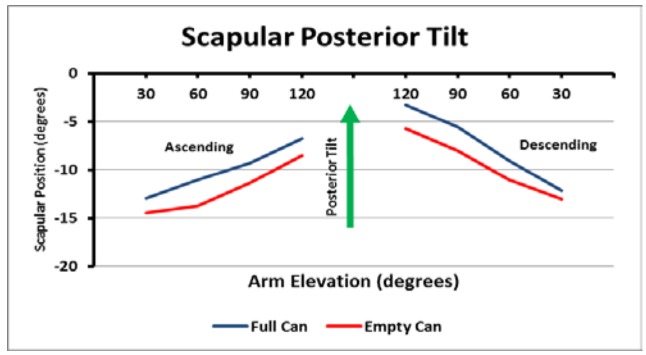

Figure 3. Scapular PT by arm elevation angle during FC (blue) and EC (red) arm elevation, + numbers reflect PT.

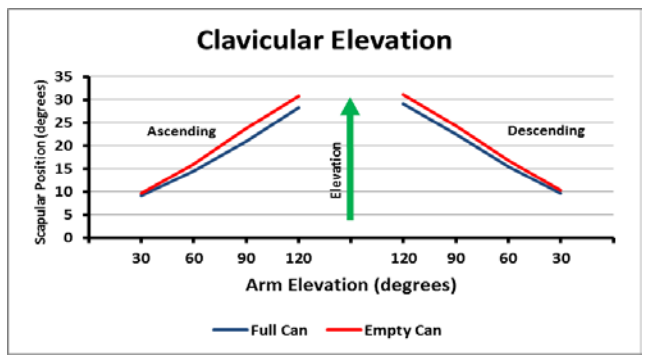

Figure 4. Clavicular ELE by arm elevation angle during FC (blue) and EC (red) arm elevation, + numbers reflect ELE.

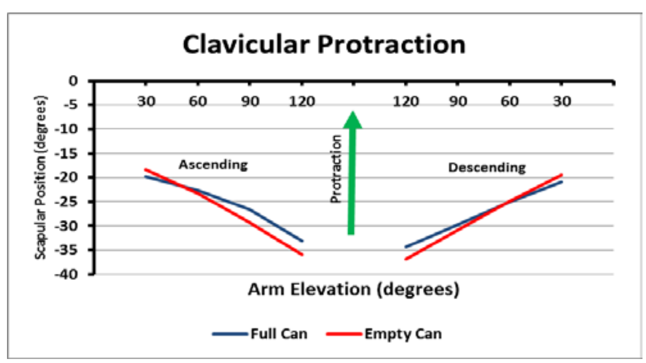

Figure 5. Clavicular PRO by arm elevation angle during FC (blue) and EC (red) arm elevation, + numbers reflect PRO.

Limb Force Variance is Structured to Stabilize the Step-to-Step Transitions of Dynamic Walking

Megan Toney and Young-Hui Chang
Comparative Neuromechanics Laboratory, Georgia Institute of Technology, Atlanta, GA, USA
email: megan.e.toney@gmail.com, web: http://www.ap.gatech.edu/Chang/Lab/CNL/home.html

INTRODUCTION

The dynamic walking model predicts the importance of vertical ground reaction forces (GRF) in accurately redirecting the center of mass (COM) velocity vector between pendular arcs and proposes the mechanical work done in these transition phases accounts for much of the metabolic demands of walking [1-4]. Because vertical forces are important for smooth, repeatable, and energetically optimal walking, we predict that consistent net vertical GRF application during step-to-step transition phases should be an implicit goal of human walking.

An excess of degrees-of-freedom (DOF) within the locomotor system, often termed motor abundance, allows human walkers to select from many equally successful joint and leg coordination strategies. Implicit goals should demonstrate consistent behavior over many steps and at various walking speeds resulting directly from the selection of goal-equivalent limb force combinations. We hypothesized that over many steps, human walkers would generate individual leading and trailing leg forces that would tend to stabilize (i.e., make more consistent) the vertical component of their net ground reaction force (F_v^{net}) during double support.

We predicted the anterior-posterior (AP) component of the net GRF (F_{ap}^{net}) would be modulated to fulfill the additional explicit goal of constant walking speed. Variable F_{ap}^{net} allows inter-step adjustments in propulsive and braking forces to maintain the constant velocity required for treadmill walking. Consistent with previous work in hopping [5], we hypothesized the individual legs would co-vary to destabilize F_{ap}^{net} during transition phases to make step-to-step velocity adjustments, allowing us to test our ability to successfully identify gait goals.

METHODS

Eleven healthy subjects (8 male, mean age 32, mean weight 67.8 kg) gave informed consent and walked on an instrumented split-belt treadmill at 1.0, 1.2, and 1.4m/s. Speed presentation order was randomized and each subject walked for three 30-second trials at each speed. Ground reaction forces were collected independently for each limb as subjects walked on a custom dual-belt instrumented treadmill (1080Hz). Simultaneous kinematics data were captured using a six-camera motion analysis system (120Hz, VICON).

A 2-DOF uncontrolled manifold (UCM) analysis was applied to quantify the structure of inter-step leg force variance to generate consistent (stable) net force values [6]. The inter-step variance of leg GRFs were partitioned into orthogonal components that were goal-equivalent for net force (GEV) and non-goal-equivalent for net force (NGEV). We used the normalized difference between these two variance components, called the index of motor abundance (IMA), to characterize the use of motor abundance to stabilize net force [5].

Separate analyses were conducted and two IMAs calculated for stabilization of F_v^{net} and F_{ap}^{net} at every 1% of the gait cycle. Mean IMA trajectories across all subjects were evaluated for significant differences from zero using a one-tailed Student's t-test (α=0.005). An IMA significantly greater than zero indicates the individual leg forces were coordinated to generate the same net force in each step, which we interpret as purposeful stabilization of an implicit biomechanical goal of walking. An IMA significantly less than zero indicates active destabilization such that the individual limb forces purposefully combined to produce different net forces with each step. We tested two null hypotheses: (1) the IMA for $F_v^{net} \leq 0$ and (2) the IMA for $F_{ap}^{net} \geq 0$.

RESULTS AND DISCUSSION

Total variance per degree of freedom for F_v^{net} remained consistently small during step transitions despite large peaks in individual leg variance, providing evidence of purposeful variance structuring between the two legs to stabilize F_v^{net} by minimizing its inter-step variance. IMAs of F_v^{net} were significantly greater than zero during inter-step transition phases at all walking speeds (**Fig 1**). This result indicates that during step transitions, healthy humans select combinations of individual limb forces that consistently produce the same F_v^{net}. F_v of one leg is coavaried to offset contralateral leg force deviations to maintain consistent values of F_v^{net}. This coordination allows healthy walkers to reliably redirect COM trajectories between successive steps and provides evidence that consistent generation of F_v^{net} during step-to-step transitions is an implicit goal of human walking and may be actively monitored by the nervous system.

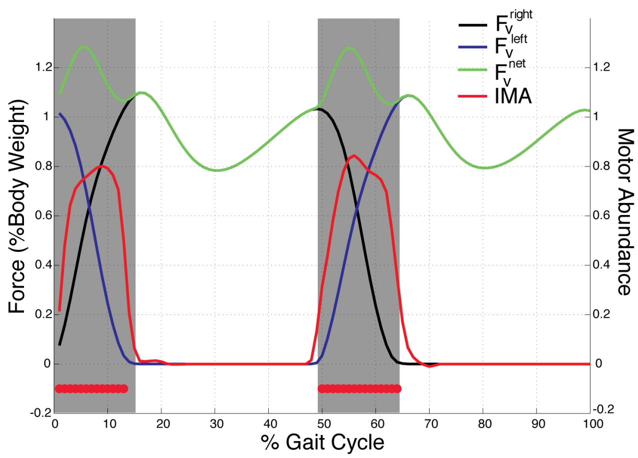

Figure 1: Net vertical GRF is stabilized (IMA>0, red dots) during transition phases (shaded grey) by coordination between the leading and trailing limbs.

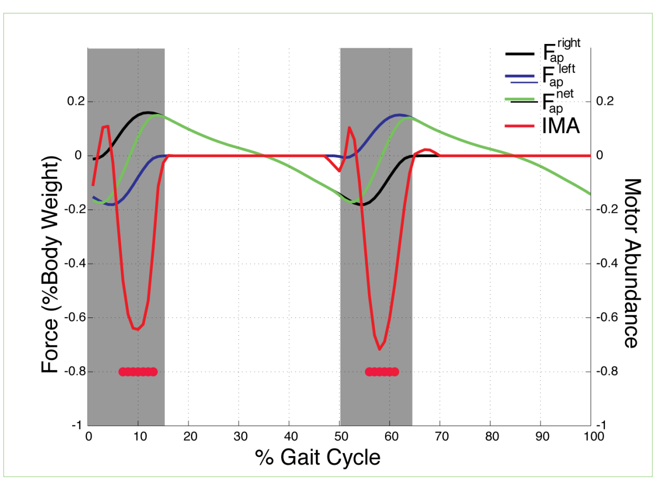

Figure 2: Net anterior-posterior GRF is actively destabilized (IMA<0, red dots) during transition phases (shaded grey).

IMAs of F_{ap}^{net} were significantly less than zero during the step-to-step transitions at all walking speeds (**Fig 2**). Individual AP leg forces were coordinated to purposefully change F_{ap}^{net} with each step. Adjustments to F_{ap}^{net} allow inter-step adjustments to be made for maintaining a constant walking speed. F_{ap}^{net} destabilization represents an explicit goal imposed by walking on a treadmill at a constant speed.

CONCLUSIONS

Consistent performance of F_v^{net} appears to be an implicit task goal of human walking. Humans co-vary vertical limb forces during transition phases to consistently redirect the COM trajectory between the inverted pendular arcs of single limb support.

Walking speed appears to be controlled through the coordination of AP limb forces during step-to-step transitions. Humans select non-goal equivalent combinations of individual leg AP forces so adjustments in propulsive and braking force generation maintain constant walking speeds. Stable net vertical force application during transitions and maintaining constant walking speed are thus critical task goals for successful walking. Identifying the implicit goals of human walking and the inter-limb coordination necessary for their successful achievement will enable more targeted gait rehabilitation protocols and suggests potential control variables for bipedal walking robots.

REFERENCES

1. Donelan JM, Kram R, and Kuo AD. *J Biomec.,* **35**, 117-24, 2002.
2. Kuo, A. *Human Movement Science*, **26**, 617-56, 2007.
3. Kuo, A. *J. Biomech En,* **123**, 113-120, 2002.
4. Ruina A, Bertram JEA, Srinivasan M. *J. Theor Biol* **237**, 170-92, 2005.
5. Yen JT, Auyang AG, Chang YH. *Exp Br Res*, **196**, 439-51, 2009.
6. Scholz JP and Schoner G. *Exp Br Res*, **126**, 289-306, 1999.

ACKNOWLEDGEMENTS

This work was financially supported by NICHD 5T32HD055180 and NINDS

THE EFFECT OF PEDAL CRANK ARM LENGTH ON LOWER LIMB JOINT ANGLES IN AN UPRIGHT CYLING POSITION

Danny Too and Chris Williams

The College at Brockport, NY, USA
email: dtoo@brockport.edu, web: www.brockport.edu

INTRODUCTION

Previous investigations reported that changes in crank arm length (CAL) from 110-265 mm (i.e,, 110, 145, 180, 230, and 265 mm) resulted in significant differences in power production and cycling duration (but not necessarily with adjacent CAL {i.e., 110 vs. 145 vs. 180 vs. 230 vs. 265 mm}) [1,2,3,4]. However, there was no information provided whether changes in CAL also resulted in significant changes in joint angles, and how changes in joint angle may affect cycling performance (based on muscle force-length relationships). Therefore, the purpose of this investigation was to determine whether changes in CAL resulted in significant changes in joint angles, and how these changes are related to changes in cycling performance.

METHODS

Seventeen males participants age 23 ± 6.74 years (mean ± SD) were each tested on a free weight Monark cycle ergometer (Model 814E) at five pedal CAL (110, 145, 180, 215 and 250 mm) using an adjustable pedal shaft mechanism (RangeMaker™). CAL sequence was randomly determined, and seat height was set at 100% of leg length. Each participant pedaled (with pedal toe-clips) at 60 rpm (in cadence to a metronome) with a 3 kg mass applied to the ergometer. Hip, knee and ankle angles (i.e., minimum [Min], maximum [Max], and range of motion [ROM]) were recorded for 10 seconds from the right sides of the body using 3 electrogoniometers (SG150 and SG100 sensors with a K100 amplifier by Biometrics Ltd) connected to a 4 channel analog amplifier. The signal was routed to an A/D box (Noraxon NorBNC), a synchronizing unit, and to a laptop computer.

RESULTS

Nine repeated measures ANOVAs were performed to determine if there were significant differences ($p < 0.01$) in the Min, Max, and ROM of the hip, knee, and ankle. Results indicated a significant change in the Min joint angle and ROM of the hip, knee, and ankle with 35 mm increments in CAL from 110-250 mm (see Table 1). The following trends were found with incrementing CAL: (1) decreasing Min hip and knee angle; (2) increasing Min ankle angle (see Fig 1), (3) increasing ROM of the hip and knee, (4) decreasing ankle angle ROM (see Fig 2) and (5) no apparent trends in the Max hip, knee, and ankle angle (see Fig 3). Significant post-hoc tests ($p < 0.05$) revealed: (1) decrements in the Min hip and knee angle for each 35 mm increment in CAL; (2) increments in the hip and knee ROM for each 35 mm increment in CAL; (3) increments in the Min ankle angle between the 145 mm and 180 mm CAL; and (4) decrements in the ankle angle ROM between the 110 mm and 145 mm CAL, and between the 145 mm and 180 mm CAL.

DISCUSSION

It was expected that increments in CAL would result in decrements in Min joint angles, and increments in joint ROM (if the seat height was controlled). However, the reverse was found for the ankle angle (i.e., increment in Min and decrement in ROM) with increments in CAL. This unexpected trend, in conjunction with a significant increment in the Min ankle angle between the 145 mm and 180 mm CAL (from 87.8 deg [i.e., a dorsiflexed position] to 91.5 degrees [i.e., a plantar flexed position]) may be attributed to: (1) insufficient flexibility of the ankle and/or physical constraints/limitations to dorsiflex (due to the structure of the ankle joint) as the CAL is increased;

(2) greater ankle force production potential (in a more effective portion/range of the force-length curve) as the Min ankle joint angle increases (from a dorsiflexed position to a plantar flexed one); and (3) increased ankle joint angles to a plantar flexed position (with longer CALs) which alters the joint angles to allow the larger hip and knee muscles to more effectively produce force (i.e., changes the length of the hip and knee muscles so it is in a more effective portion of the tension-length curve to produce force). This appears to be supported by the result that a systematic increase of 35 mm in CAL from 110-250 mm did not result in an equivalent systematic decrease in Min knee angle. In fact, with each change in CAL by 35 mm (from 110 to 145 to 180 to 215 to 250 mm), the minimum knee angle decreased 14.5, 13.3, 11.1, and 7.3 degrees, respectively. Further investigations in this area are required to understand the relationship between CAL, joint angles, muscle length, force/torque production and cycling performance.

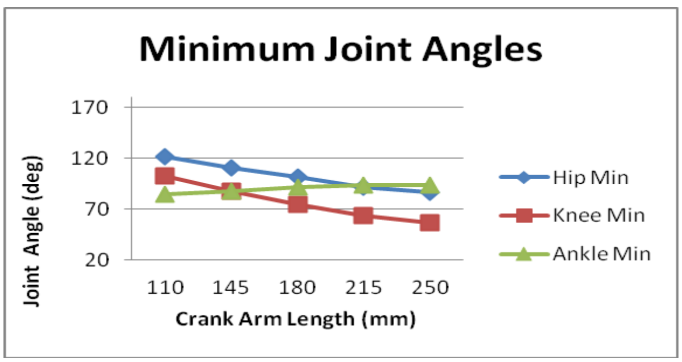

Figure 1: Minimum hip, knee, and ankle angles with changes in pedal crank arm length

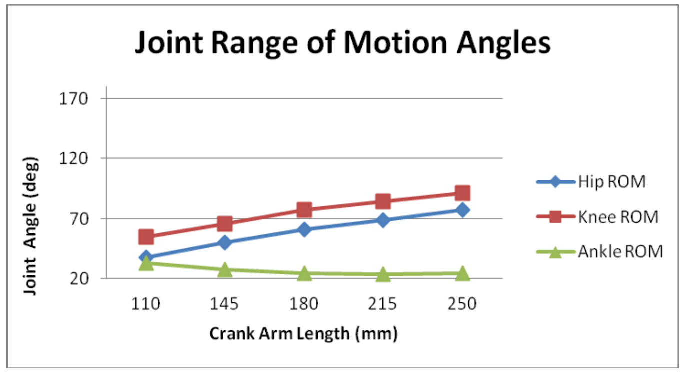

Figure 2: Hip, knee, and ankle range of motion with changes in pedal crank arm length

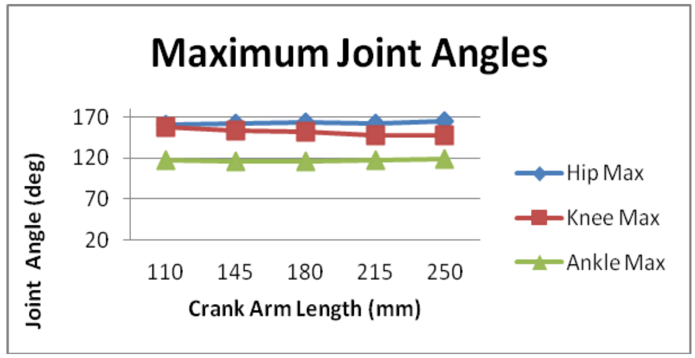

Figure 3: Maximum hip, knee, and ankle angles with changes in pedal crank arm length

REFERENCES

1. Too D, et al. *J Spt Sci* **18**, 153-161, 2000.
2. Too D, et al. *Human Power* **51**, 3-6, 2000.
3. Too D, et al. *Proceedings of NACOB'98*, Waterloo, Ontario, CANADA, 1998.
4. Too D, et al. *ISB'99 Book of Abstracts*, Calgary, Alberta, CANADA, 1999.

Table 1. Main Effect of Hip, Knee, and Ankle Joint Angles at Five Crank Arm Lengths (*p < 0.01)

		Crank Arm Length (mm)				
Angle (deg)	Mean (SE)	110	145	180	215	250
Hip	*Min	121.8 (3.43)	111.0 (3.97)	101.7 (4.68)	91.8 (5.67)	86.9 (6.29)
	Max	160.9 (2.09)	162.4 (2.42)	164.3 (2.17)	161.5 (2.67)	164.7 (2.64)
	*ROM	37.9 (3.61)	50.5 (2.95)	61.4 (4.22)	69.0 (4.81)	77.4 (5.63)
Knee	*Min	102.2 (4.34)	87.7 (4.78)	74.4 (4.93)	63.6 (5..22)	56.3 (5.66)
	Max	157.2 (3.84)	153.5 (3.69)	151.4 (5.41)	147.6 (5.68)	147.9 (6.95)
	*ROM	55.0 (4.28)	65.8 (4.3)	77.1 (5.73)	84.0 (5.94)	91.5 (6.62)
Ankle	*Min	84.3 (2.47)	87.8 (2.13)	91.5 (2.58)	93.2 (2.67)	93.9 (2.47)
	Max	117.2 (3.51)	115.4 (3.62)	115.9 (3.78)	116.8 (3.12)	118.3 (3.71)
	*ROM	32.9 (3.8)	27.5 (3.16)	24.3 (2.76)	23.6 (2.52)	24.4 (2.7)

VISCOELASTIC MODELING OF THE LUMBAR SPINE: THE EFFECT OF PROLONGED FLEXION ON INTERNAL LOADS

Nima Toosizadeh, Maury A. Nussbaum, and Michael L. Madigan

Virginia Tech, Blacksburg, VA, USA
email: nussbaum@vt.edu

INTRODUCTION

Trunk flexion results in viscoelastic deformation of passive tissues and a consequent reduction in trunk stiffness [1]. This decrease in passive stiffness can require a compensatory increase in muscle activation [2], increasing the loads on joints and other soft tissues. *In vivo* methods for measuring such internal loads are invasive and costly [3], and computational modeling is a common alternative. Previous studies have provided fundamental understanding of the time-dependent behavior of trunk tissues and internal load estimation, however new approaches are needed to estimate internal loads during/following flexion exposures. Hence, the purpose of the current study was to develop a viscoelastic torso model and use it to investigate whether prolonged flexion affects internal loads during a functional task. This was done in the context of manual lifting, a common task associated with occupational low back disorders. We hypothesized that peak internal loads during a lifting task would increase following flexion exposure, and that this effect would be influenced by the angle and duration of exposure.

METHODS

A sagittally-symmetric model of the torso was developed, consisting of six deformable lumbar motion segments (i.e., T12/L1 – L5/S1 discs, ligament and facets) and one rigid superior component. Passive muscle components were modeled in the sagittal plane, with 23 local (lumbar extensor) and five global (thorax extensor) muscles. A similar wrapping mechanism as in previous work [4] was used to represent global muscle paths. Axial stiffness of each muscle, and the axial and rotational stiffnesses of each lumbar motion segment, were modeled using Standard Linear Solid (SLS) components. Previous results [5,6] were used to define material properties for each SLS component. Data from a prior study [1] were used to evaluate the viscoelastic behavior of the model.

An inverse dynamics algorithm was used to estimate muscle forces and motion segment loads during a simulated lifting task. The lifting task involved maximum trunk flexion and a 180 N load in the hands, and was performed quasi-statically over 5 sec. Kinematics of the pelvis, trunk, and lumbar motion segments and external kinetics were obtained from a previous study [4]. These were entered into the viscoelastic model to estimate the reactive moment at each level of the spine. Using these moments, a separate algorithm estimated active forces with an objective of minimizing sum of cubed muscle stresses [4]. Estimated internal loads at L4/L5 were converted into intradiscal pressures following established relationships [7], and evaluated in comparison to reported *in vivo* values in several flexed postures [3].

Effects of flexion angle and exposure duration on internal lumbar loads were assessed in 12 combinations of three flexion durations (2, 4, and 16 minutes) and four trunk flexion angles (40, 60, 80, and 100% of the flexion-relaxation (FR) angle). Two lifting tasks were simulated, before and after each exposure. Parameters associated with motion segment failure were estimated during the lifting tasks: peak internal load, peak axial stiffness, and absorbed energy at L5/S1. Changes in these parameters were then compared between the two lifting tasks (after vs. before flexion exposure).

RESULTS AND DISCUSSION

Good agreement between model-based and experimental results was evident both for internal load estimation and viscoelastic behavior (Fig. 1). Estimated internal loads, axial stiffness, and absorbed energy all increased following flexion exposures, and these effects were magnified by increasing flexion angle and duration (Fig. 2). Comparable effects were found after both 4 and 16 minutes of exposure, indicating that most of the moment drop (load-relaxation) occurred within 4 minutes of exposure. A similar duration has been reported using direct measures in response to prolonged flexion [1,5]. For the extreme exposure condition (i.e., 16 minutes and 100% FR), passive moment reduction was ~35% (Fig. 1b), and this caused ~8.9% increase in internal loads. More detailed investigation of load partitioning among passive components indicated that ~0.6 Nm of the total moment drop was caused by load-relaxation in passive muscle components, which is only ~3% of the total moment drop. As such, for angles smaller than FR, the majority of the moment drop resulted from viscoelastic responses of spinal motion segments that led to additional muscle activity.

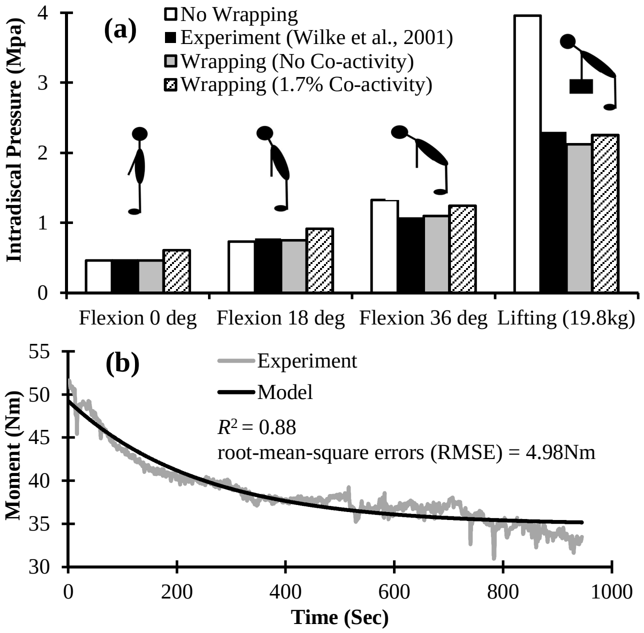

Figure 1: (a): Peak intradiscal pressure at L4/L5 in performing quasi-static tasks from Wilke et al. (2001) and the current model with different configurations. Effects of co-activation were simulated by activating the abdominal muscles at 0 or 1.7% of maximum forces, and with/without wrapping. (b): Predicted load-relaxation responses of the whole trunk from the model and earlier data for 100% FR exposures [1].

There was a limitation in the current model due to inadequate experimental data regarding the nonlinear viscoelastic behavior of passive tissues, which necessitated some assumptions for defining material properties for different muscle groups and different loading magnitudes. To overcome these potential sources of error, additional experimental results are required both for muscles and spinal motion segments at several loading magnitudes.

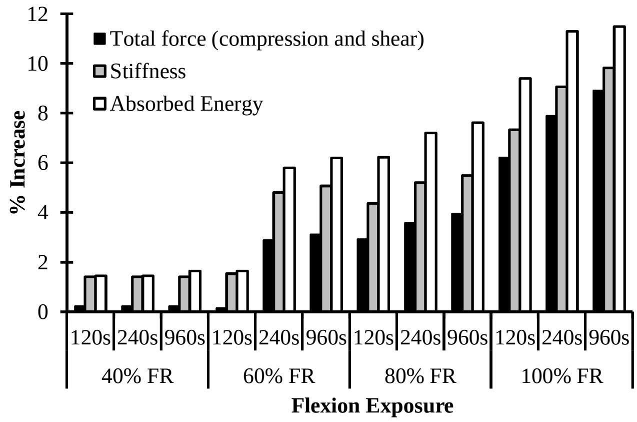

Figure 2: Percentage changes (after vs. before flexion exposure) in L5/S1 peak internal load, peak axial stiffness, and absorbed energy during simulated lifting tasks. Prior to exposure, respective values were 3201N, 708652N/m, and 10.2J.

CONCLUSIONS

Epidemiological evidence indicates an increased risk of low back disorders due to working in environments that require prolonged trunk flexion in combination with repetitive lifting. Current results demonstrated an increased contribution of active components required to complete a lifting task following load-relaxation exposures, consistent with the noted epidemiological evidence.

REFERENCES

1.Hendershot B,et al.*Clin Biomech* **26**, 250–6, 2011.
2.Shin G, et al. *Spine* **34**, 1873-1878, 2009.
3.Wilke HJ, et al.*Clin Biomech* **1**, S111-S126, 2001.
4.Arjmand N, et al. *Clin Biomech* **21**, 668–75, 2006.
5.Adams M, et al.*Clin Biomech* **11**, 194-200, 1995.
6.Best TM, et al. *J Biomech* **27**, 413-419, 1994.
7.Shirazi A,et al. *J Biomech Eng* **110**, 216-22, 1988.

ACKNOWLEDGEMENTS

This work was supported by R01OH008504 from the Centers for Disease Control and Prevention (CDC). The contents are solely the responsibility of the authors and do not necessarily represent the official views of the CDC.

A PROTOCOL TO ASSESS THE CONTRIBUTION OF THE COMPONENTS OF HUMAN ABDOMINAL WALL TO ITS BIOMECHANICAL REPONSE

[1]D. Tran, [1]D. Mitton, [2]D. Voirin, [3]G. Guérin, [3]F. Turquier and [1]P. Beillas

[1]Université de Lyon, F-69622, Lyon; IFSTTAR, LBMC, UMR_T9406, F-69675, Bron; Université Lyon 1, Villeurbanne, France
[2]Clinique de Chirurgie Digestive et de l'Urgence, Hôpital Michallon, CHU Grenoble, France
[3]Covidien, Trévoux, France
email: philippe.beillas@ifsttar.fr, web: http://ifsttar.fr

INTRODUCTION

Abdominal surgical procedures with laparotomy can lead to incisional hernia [1]. A better understanding of the biomechanics of the abdominal wall could help designing better treatments. Past research studies have considered the abdominal wall as homogenous [3, 6, 7, 8] or have characterized isolated components such as abdominal muscles [2, 5] or abdominal fascia [1, 4]. However, the response of isolated components can be difficult to transfer to a complete abdominal wall due to differences in initial strains and tissue loading configurations.
The aim of this study is therefore to develop a protocol to evaluate the contributions of the abdominal wall components to the mechanical response of a complete abdominal wall.

METHODS

The protocol is based on successive dissection techniques. First, a human abdominal wall was excised from the subcostal line to the pubis. It included all layers from skin to peritoneum. It was held in a custom designed fixture (Fig. 1) described in details in [6]. Similarly to a laparoscopic procedure, air pressure (from 0 to 0.03 bar) was applied to the peritoneal surface. The loading was applied successively to 4 abdominal wall states as described in Fig. 2.

A speckle was painted on the peritoneal surface. The surface was filmed by 2 video cameras (SA3 Photron, Tokyo, Japan). Stereocorrelation techniques (Vic-3D, Correlated Solutions Inc, DC, USA) were used to calculate local displacement and strain fields from the videos.

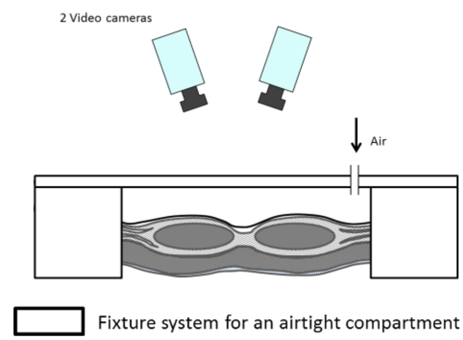

Figure 1: Experimental device for the inflation of the abdominal wall while video recording

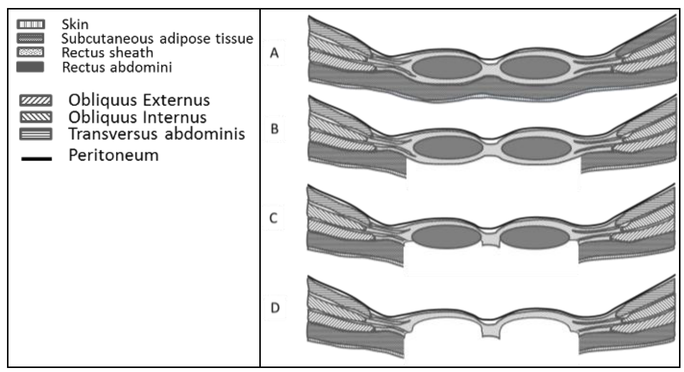

Figure 2: Successive dissection process: states of the abdominal wall. A: intact, B: after dissection of the skin and the subcutaneous adipose tissues, C: after dissection of the anterior rectus sheath, D: after dissection of the rectus abdomini

Echographic and elastographic images (Fig. 3) were collected at 0, 0.02 and 0.03 bar using an Aixplorer ultrasonic scanner (Supersonic imagine, Aix-en-Provence, France). Each acquisition was repeated 3 times. The results were processed to compute the mean thickness and the mean apparent elastic modulus of a muscle and fat layers.

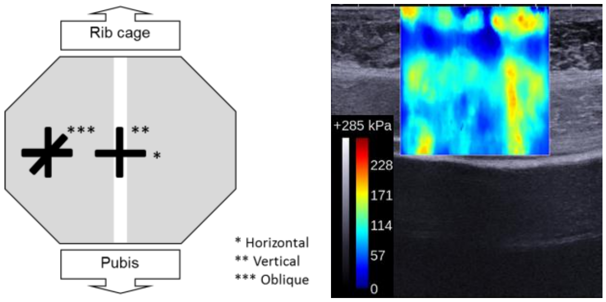

Figure 3: Echographic and elastographic imaging: image location on a bottom view of the fixture (left) and example of result (right). The images were centered on the linea alba in horizontal and vertical directions, and centered on the rectus abdomini in horizontal, oblique and vertical anatomical directions

RESULTS

The protocol was successfully applied to three abdominal walls. Results from one of the tests are summarized hereafter.

Stereo-correlations allowed quantifying the displacements and strain of the peritoneum due to both pressure and dissection. The application of the pressure and dissection lead to a permanent deformation visible even when the wall was only subjected to gravity. An example of deformation between A, B, C and D states of the abdominal wall at zero pressure is provided in Figure 4.

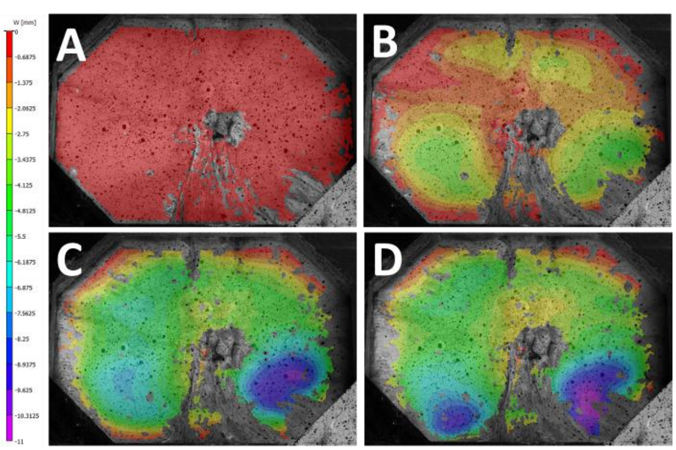

Figure 4: Displacement maps in states A, B, C, and D of the abdominal wall at p = 0.

Pressure and dissection also affected the apparent elastic modulus. Pressure loading seemed to increase the apparent modulus in all configurations, as illustrated in Table 1 for the state B. The apparent modulus also increased between the intact and further states.

Table 1: Mean apparent elastic modulus of the rectus abdomini muscle for abdominal wall state B at 3 pressure levels.

	Modulus (kPa)		
Pressure (bar)	**P = 0**	**P = 0.02**	**P = 0.03**
Horizontal	84.7	105.5	140.2
Oblique	91.8	124.4	141.7
Vertical	130.0	160.9	262.8

DISCUSSION AND CONCLUSIONS

The protocol that was developed was shown to be sensitive to component dissection. It provided both surface and internal metrics (strain field and apparent elastic modulus) during loading. These outputs can give an insight into the abdominal wall behavior and the contribution of its components. However the results are still very preliminary. More tests are ongoing to refine the preliminary trends and assess the specimen to specimen variability.

REFERENCES

1. Bucknall T.E. et al. *Br Med J*, **284,** 931-933, 1982.
2. Förstemann T. et al. *J Biomech* **44 (4)**, 600-606, 2011.
3. Hernández B. et al. *J mechanical behavior of biomedical materials* **4**, 392-404, 2011.
4. Junge K. et al. *Hernia* **5**, 113-118, 2001.
5. Kirilova M. et al. *Medical Engineering & Physics*, **33**, 1-6, 2011.
6. Morrow D.A. et al. *J mechanical behavior of biomedical materials* **3,** 124-129, 2010.
7. Podwojewski F. et al. *Hernia* **14** (Suppl 1), S13-S46, 2010.
8. Podwojewski F. et al. *Hernia*, **15** (Suppl 2), S37-S66, 2011.

COMPRESSIVE LOADING OF THE DISTAL RADIUS IMPROVES BONE STRUCTURE IN YOUNG WOMEN

Karen L. Troy, Varun A. Bhatia, and W. Brent Edwards

University of Illinois at Chicago, Chicago, IL, USA
email: klreed@uic.edu, web: http://www.uic.edu/ahs/biomechanics

INTRODUCTION

Bone is typically well suited for its habitual loading environment because of its ability to adapt. Although bone modeling and remodeling are complicated processes, the resulting adaptive response is understood to be fundamentally "error signal" driven [1]. In theory, application of novel mechanical loads that exceed some threshold elicit a beneficial adaptive response. However, researchers have yet to prospectively link specific strain signals to specific adaptations occurring within the bone of humans. This is, in part, because of challenges associated with noninvasively quantifying bone-specific parameters such as *in vivo* strain. Consequently, indirect measures such as force plate recordings and accelerometers are typically employed when estimating mechanical stimulus exposure in humans. However, individual anatomic variation is considerable; for a particular external force, the strain magnitudes occurring within a bone vary inversely with its stiffness.

Our purposes were to determine the strains occurring in the radius during a novel *in vivo* loading task, in which women apply a force to the distal radius by leaning onto the palm of their hand, and to test whether the task elicited measurable changes to the bone. We hypothesized that regular mechanical loading would increase measures of bone mass and bone strength, and that measures of bone strength would increase more than bone mass.

METHODS

Mechanical Loading Task:

Each subject was instructed to apply an axially-directed force to their wrist by leaning onto the palm of their non-dominant hand. Force was applied 50 cycles per day, three days per week, with each cycle being separated by two seconds. Sound cues assisted subjects in loading at the correct time interval and subjects' hands were placed on a load cell to provide real-time visual feedback about force magnitude. Each subject was given a nominal target force of 300 N. This target load was initially chosen to elicit a radius periosteal surface strain of 1000-2000 $\mu\varepsilon$, to remain consistent with animal loading models.

Subjects:

Eight women (age: 20 ± 1 years, height: 156 ± 6 cm, mass: 58 ± 7 kg) participated in the 28-week mechanical loading regime. An additional seven women (age: 22 ± 2 years, height: 155 ± 4 cm, mass: 63 ± 8 kg) served as controls. Exclusion factors included: pregnancy or breastfeeding during the previous year, upper extremity fracture within the previous four years, and the use of any drugs known to affect bone metabolism during the previous year. All methods were institutionally approved and all subjects provided written informed consent prior to their participation.

Data Collection and Processing:

Load cell data were recorded throughout the intervention to determine the actual load applied by each subject. Quantitative computed tomography (QCT) data were collected on all subjects at weeks 0, 14, and 28 using a single clinical CT scanner (GE Brightspeed, GE Medical, Milwaukee, WI). A calibration phantom was included in each scan so that x-ray attenuation signals could be converted to hydroxyapetite equivalent densities. Each QCT image was aligned and the radius identified. The 45 mm immediately proximal to the subchondral plate was selected for analysis. Cortical, trabecular, and integral (cortical + trabecular) measures of bone volume (BV, cm^3), mineral content (BMC; g), and density (BMD; g/cm^3) were determined. Transverse slice-by-slice moments of inertia (Imin, Imax, Jo; $g*mm^2$) were also determined.

Subject-specific finite element (FE) models were created for each scan to determine peak strain at the periosteal surface and within the enclosed periosteal volume using validated methods [2].

Time by group effects were examined using repeated measures ANOVA, with each variable treated separately. Change in slice-by-slice moments of inertia in the experimental group were compared to a value of zero and also to the change in the control group using Student's t-tests.

RESULTS AND DISCUSSION

The peak load applied by subjects was 326±38 N. This resulted in peak principal compressive, tensile, and von Mises (VM) periosteal strains of -943±579 με, 712±255 με, and 1029±374 με, respectively. Peak principal compressive, tensile, and VM strains for nodes located within the bone volume were -2513±1110 με, 1575±623 με, and 2596±1444 με, respectively. Because the FE models used linear elastic material definitions, the strains for each subject scale linearly with applied force.

All 8 experimental subjects completed all 28 weeks of the intervention. All control subjects returned for the 14 week data collection, and 3 have returned for 28 week follow-up collections at this time. Table 1 shows the 14 and 28 week change in BV, BMC and BMD for each compartment; the experimental group experienced an increase in several measures while there was no significant time effect in the control group. Moments of inertia increased significantly at many locations in the experimental group, and showed no change at any location in the control group. On average, Imin increased by 3.2% in the experimental subjects, which included a single outlier subject whose Imin *decreased* by 5.2%. When this subject was excluded, the mean increase in Imin was 4.4%. In contrast, the average change in the control group was 0.2%. The relative improvements to moments of inertia were similar in magnitude to those of BMC.

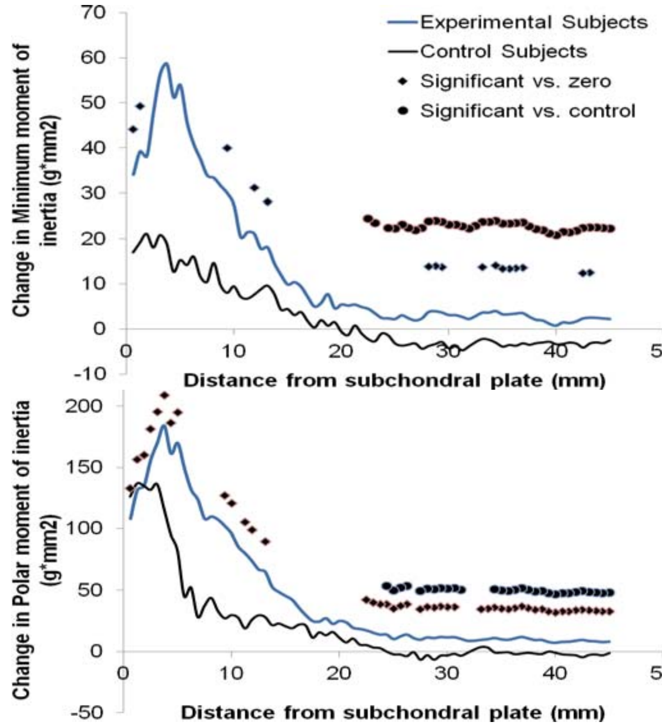

Figure 1 28 week change in slice-by-slice moments of inertia for experimental versus control subjects. Symbols indicate those slices for which the experimental group was different from zero or the control group. The control group was not different from zero at any slice due to widely scattered data.

CONCLUSIONS

A simple mechanical loading task – leaning onto the palm of the hand – elicited significant improvements to radius BMC and moments of inertia. These adaptive changes reflect increased resistance to bending and torsion and may be linked to an improvement in failure load. It is likely that a more vigorous intervention would elicit larger changes that could potentially be linked to specific variables describing the mechanical loading environment.

REFERENCES

1.Lanyon LE, *Bone*, 1996 18(1 Suppl) 37S-43S
2.Edwards WB and Troy KL, *Med. Eng Phys* 2011 (doi: 10.1016/j.medengphy.2011.07.016)

Table 1 Changes in bone parameters in the experimental versus control groups.

		Experimental			Control			
		Baseline	14 week change	28 week change	Baseline	14 week change	28 week change★	p (group *time)
Integral	BV (cm3)	9.29 (0.54)	0.12 (0.15)	0.16 (0.15)•	10.80 (1.30)	-0.01 (0.08)	0.08 (0.11)	0.002
	BMC (mg)	4087 (449)	57 (35)•	57 (35)•	4487 (377)	-36 (34)	-61 (4)	<0.001
	BMD (mg/cm3)	439 (38)	0 (5)	1 (7)	418 (44)	-3 (3)	-8 (3)	0.185
Trabecular	BV (cm3)	6.13 (0.39)	0.10 (0.14)	0.13 (0.16)	7.36 (1.15)	0.03 (0.08)	0.16 (0.14)	0.085
	BMC (mg)	1322 (141)	46 (32)•	29 (41)	1522 (200)	-21 (35)	-7 (21)	<0.001
	BMD (mg/cm3)	223 (29)	4 (1)•	0 (2)	209 (34)	-4 (3)	-5 (0)	<0.001

p≤0.05 for time effect within group • p≤0.05 for change, versus 0 ★ n=3

A TEST OF THE METABOLIC COST OF CUSHIONING HYPOTHESIS IN BAREFOOT AND SHOD RUNNING

Kryztopher D. Tung[1], Jason R. Franz[2] and Rodger Kram[2]

[1]Mechanical Engineering Dept., [2]Integrative Physiology Dept., Univ. of Colorado, Boulder, CO, USA
email: kryztophert@gmail.com, web: http://www.colorado.edu/intphys/research/locomotion.html

INTRODUCTION

Advocates of barefoot running assert that it is more metabolically efficient than shod running. This idea makes sense because wearing shoes adds mass to the feet, and this increases energetic cost. Frederick et al. [2] showed that $\dot{V}O_2$ increases by approximately 1% for each 100 grams of added mass per shoe. Previous studies that controlled for foot/shoe mass suggest that shoe cushioning may provide an energetic advantage over running barefoot [1, 2, 3]. Further, running in lightweight shoes has about the same metabolic cost as running barefoot [1, 4], suggesting that the positive effects of shoe cushioning may counteract the negative effects of added mass (Figure 1).

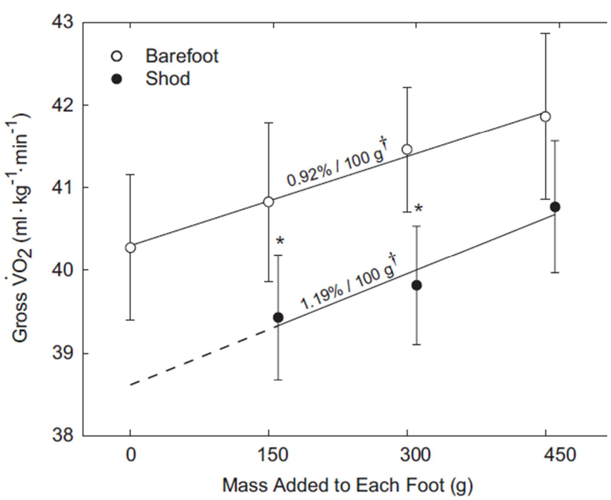

Figure 1. Oxygen consumption data from Franz et al. [1]. When mass is controlled for, other factors make shod running more economical. Asterisks (*) indicate significant difference between barefoot and shod conditions of equal mass. † indicates significant main effect of added mass.

Based on these findings, we hypothesized that: 1) barefoot running would have the same metabolic cost as running with lightweight, cushioned running shoes and 2) the metabolic cost of barefoot running would be less on cushioned surfaces.

METHODS

Ten experienced barefoot runners (mean ± SD, age: 30.2 ± 9.1 yrs) ran at 3.35 m/s with a mid-foot strike pattern on a Quinton 18-60 motorized treadmill modified to have a calibrated digital readout of speed. This classic treadmill has a rigid steel deck. All subjects gave written informed consent as per the Univ. of Colorado IRB. The inclusion criteria were: >18 years of age, mid-foot strike preference both barefoot and with shoes, run at least 25 km/week, including at least 8 km/week barefoot or in minimal running footwear (e.g. Vibram Five Fingers) for at least 3 months out of the last year, injury-free, self-reported ability to sustain 5 min/km (3.3 m/s) running pace for at least 60 minutes, and meeting the criteria of the ACSM for minimal risk of exercise. To verify that subjects preferred a mid-foot strike pattern, they ran at their typical 10 km training pace across a 30m runway equipped with a force platform (AMTI, Watertown, MA) to which a sheet of paper was affixed. To orient foot placement with the force platform origin, we taped small pieces of marker pen felt to each subject’s right foot at 90, 70, and 33% of foot length (measured along the line between the heel and distal end of the second toe). We classified subjects as mid-foot strikers if the center of pressure at initial contact was between 33% and 70% of foot length.

Subjects ran barefoot (BF) and in lightweight cushioned running shoes (SH) (Nike Free 3.0; ~211 g/shoe). Subjects also ran barefoot on the same treadmill with 10 mm and 20 mm thick slabs of ethylene-vinyl acetate (EVA) foam affixed to the treadmill belt (Figure 2). The foam was identical to that used in the running shoes. Prior to testing, subjects completed a 10 minute treadmill acclimation trial. The 4 conditions consisted of: shod, barefoot, barefoot on 10 mm foam, and barefoot on 20 mm foam, performed in random order. A 3-minute rest period separated each of the running trials. We calculated metabolic power (W/kg) from rates of oxygen consumption and carbon dioxide production using the Brockway equation [5]. We calculated stride kinematics from high-speed digital video recordings (210 FPS, Casio EX-FH20).

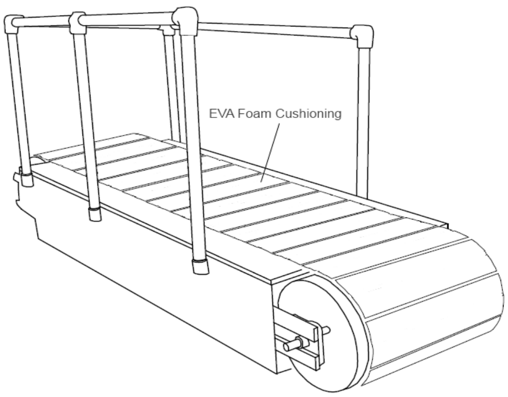

Figure 2. Cushioned treadmill

RESULTS AND DISCUSSION

As hypothesized, on the rigid treadmill surface, metabolic power requirements for running barefoot and in lightweight running shoes were not significantly different (Mean ± SD, BF: 13.65 ± 1.31 W/kg, SH: 13.66 ± 1.15 W/kg; p=0.95). The data (Figure 3) also support our second hypothesis; metabolic cost for barefoot running was 1.91% cheaper on the 10 mm foam compared to the rigid surface (p=0.018). The reduction in metabolic cost on the 20mm thick surface was not statistically significant (1.70%, p=0.056).

Stance times for each of the conditions were: 0.231 ± 0.02 sec (BF), 0.225 ± 0.01 sec (BF 10mm), 0.23 ± 0.015 sec (BF 20mm), and 0.242 ± 0.015 sec (SH). The stride frequencies for each condition were: 1.671 ± 0.14 (BF), 1.666 ± 0.129 (BF 10mm), 1.651 ± 0.136 (BF 20mm), and 1.628 ± 0.124 (SH).

Based on the "1% rule", we would expect that running in 210g shoes to be 2.10% more expensive than barefoot running. However, according to our data, it was essentially the same. 10 mm of foam cushioning (approximately the thickness of the forefoot shoe midsole) afforded a benefit of 1.91%. Thus, it appears that the positive effects of shoe cushioning counteract the negative effects of added mass, resulting in a metabolic cost for shod running approximately equal to that of barefoot running.

Kerdok et al. [3] found that the cost of running on an elastic compliant treadmill steadily decreased with greater compliance. However, we did not find that the metabolic cost of running decreased with thicker cushioning. A possible explanation for this discrepancy is the fact that Kerdok et al.'s treadmill surface acted as a leaf spring, and therefore, provided greater energy return with increased compliance. In contrast, our cushioned treadmill used a material with significant damping.

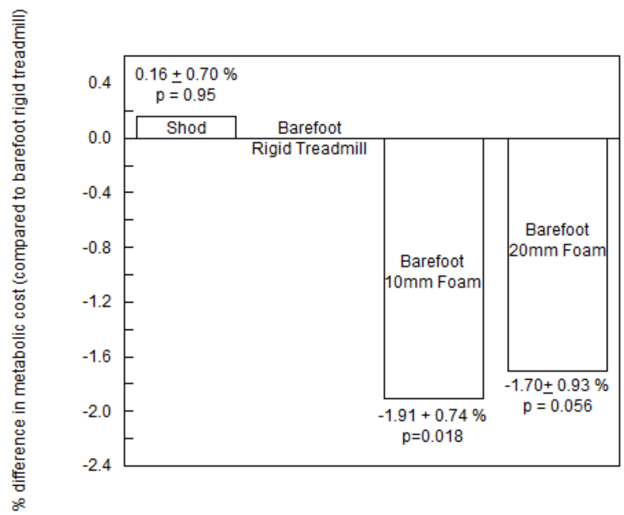

Figure 3. Percent difference (mean ± standard error of the mean) in metabolic power for each running condition with respect to the cost of barefoot running on rigid treadmill surface.

CONCLUSIONS

Cushioning reduces the metabolic cost of running. Further research is needed to identify the metabolically optimal amount of cushioning.

REFERENCES

1. Franz et al., *Med Sci Sports Exerc*, in press.
2. Frederick et al., In: Biomechanical Aspects of Sport Shoes and Playing Surfaces, 1983.
3. Kerdok et al., *J App Physiol*, **92**: 469-78, 2002.
4. Divert et al., *Intl J Sport Med*, **29**, 512-518, 2008.
5. Brockway et al., *Human Nutrition: Clinical Nutrition*, **41C**, 463-471, 1987.

ACKNOWLEDGEMENTS

Thanks to Kelly McKean and Nike Inc. for providing the shoes and EVA foam.

IMPACT OF OBESITY ON THE FUNCTION OF HIP KNEE AND ANKLE DURING TRANSITION BETWEEN LEVEL AND STAIR WALKING

[1]Kyoko Umezaki and [2]Daniel K. Ramsey
[1]Department of Mechanical Engineering, University at Buffalo, NY
[2]Department of Exercise and Nutrition Sciences, University at Buffalo, NY

INTRODUCTION

Obesity is a growing epidemic that is strongly associated with medial compartment Knee Osteoarthritis (OA) onset and disease progression [1, 2]. The increased body mass and consequent high repetitive loading during daily activities exacerbate deterioration of the weight bearing joint structures leading to pain that inhibits knee function [1]. Persons modify their movement strategies in response to chronic pain but the compensatory adaptations have been shown to hasten functional decline [3]. Given the increasing obesity rates, this study examined the influence of increased body mass of young overweight adults as they ambulate over stairs with emphasis on elucidating the mechanics when transitioning between level and stair walking. The research purpose was to identify the biomechanical strategies utilized when adapting to changes in walking environment. The stair movement profile of this population will be used to identify whether they exhibit similar pathomechanics that may predispose them to the same etiologies that mediate Knee OA onset and progression.

METHODS

Ten subjects between the ages of 18 and 30 with a body mass index (BMI) between 25 and 35 kg/m^2 with no history of orthopedic, neurological, or balance problems underwent gait analysis (Table 1). Standard motion capture techniques were used to record lower extremity 3D gait mechanics as persons transitioned from level walking to going up and down a set of instrumented stairs. The stair set-up included 3 steps, each with a height of 18 cm, tread depth of 28 cm, and a width of 60 cm. Two force plates (FP) were utilized, one embedded in the walkway that preceded the 1st step and the other integrated into 1st step. The 3rd step was an extended platform. Kinematic and kinetic data were time normalized to stance, ensemble averaged across trials and conditions, and the means used for statistical analysis. Gait data were analyzed when transitioning from level walking (FP1) to the 1st stair step (FP2) in ascent, and descending from the last stair step (FP2) down to the floor (FP1). Independent t-tests (with appropriate correction for multiple comparisons) were used to assess differences between FP. Statistical significance was accepted at $p<0.05$ and trends defined as $0.05<p<0.10$.

Table 1: Subject Demographics

	Age (yrs)	Height (m)	Weight (kg)	BMI (kg/m^2)
Male n=5	23±3	1.7±0.1	89.8±13.2	30.4±3.3
Female n=5	20±2	1.6±0.1	79.2±11.6	30.0±4.7
Mean	21±3	1.7±0.1	84.5±13.0	30.2±3.8

RESULTS AND DISCUSSION

Distinguishable changes in lower extremity joint kinematics and kinetics were observed during 2nd half of stance when transitioning from level walking (FP1) to stair ascent (FP2) to prepare for the 1st stair step (Fig 1). Significant increase in ground reaction force (GRF) braking impulse (anterior-posterior) was observed on FP1 ($p<0.008$) with concomitant reductions in sagittal knee and ankle range of motion (ROM) to decelerate forward progression of body's center of mass (COM) and to support upper bodyweight ($p<0.05$). Additionally frontal hip ROM decreased ($p<0.05$) in response to the pelvis remaining neutral as the opposite swing limb advanced up and over the 1st stair step. Internal knee extensor moment observed during steady-state level walking was substituted by a small flexor moment during pre-swing (80~100% stance) on the transition step (FP1), which generated power to elevate the ipsilateral limb up to the 2nd stair step. Furthermore, diminished peak internal hip flexor moment and angular impulse ($p<0.008$) that precedes toe-off suggests a reorganization of hip and knee muscular strategy that favors knee flexor activity to clear for the intermediate step as the ipsilateral limb prepares for swing. The highest peak internal hip and knee abductor moments and angular impulses were observed on FP1 ($p<0.008$)

to elevate the pelvis on the opposite side for the swing limb to clear for the 1st stair step.

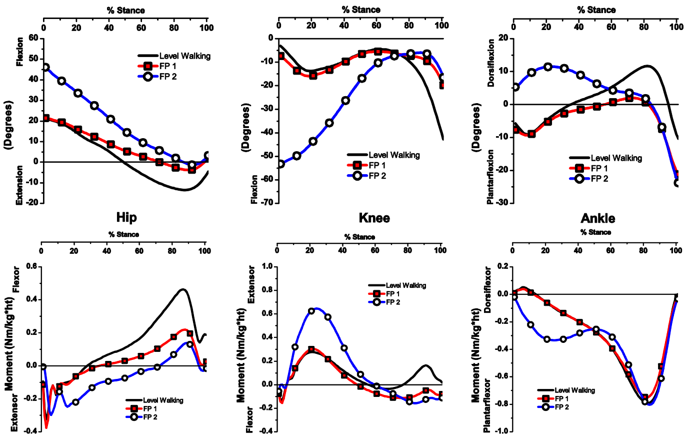

Figure 1: Sagittal hip knee and ankle kinematics and kinetics when approaching stair ascent from level walking.

Similar changes in joint mechanics were evident when transitioning from the last step in stair descent (FP2) to the floor (FP1) (Fig 2). In the sagittal plane, hip, knee and ankle positions at initial contact and kinematic and kinetic patterns through weight acceptance (WA) (0~30% stance) on FP1 were similar to when stepping down to the previous stair step (FP2). Thereafter persons adjusted their motion to transition to level walking. Greater anterior-posterior GRF propulsion impulse was observed ($p<0.008$) to initiate forward progression. Ankle dorsiflexion ROM was significantly reduced ($p<0.017$) on FP1 because downward progression of body's COM was not required to the extent during stair descent. Internal ankle plantarflexor moments during WA absorbed power from foot impact when stepping down. A small internal hip abductor angular impulse was observed during 1st half of stance on FP1 ($p<0.008$) with an internal knee adductor moment throughout stance, which was not evident on the previous stair step (FP2) or during steady-state level walking. It is suggested that persons shift their body's COM over their ipsilateral support limb (lateral trunk displacement) to assist lifting the contralateral side pelvis and swing limb when adjusting motion from stair descent to level walking. Moreover, the femur medially rotates and moves closer to the midline as the hip adducts, causing medial rotation of the knee. Combination of lateral upper body movement with medial shift of the knee would have the greatest potential to translate the GRF vector laterally to the knee joint center, thereby creating and external abduction moment (internal adductor moment).

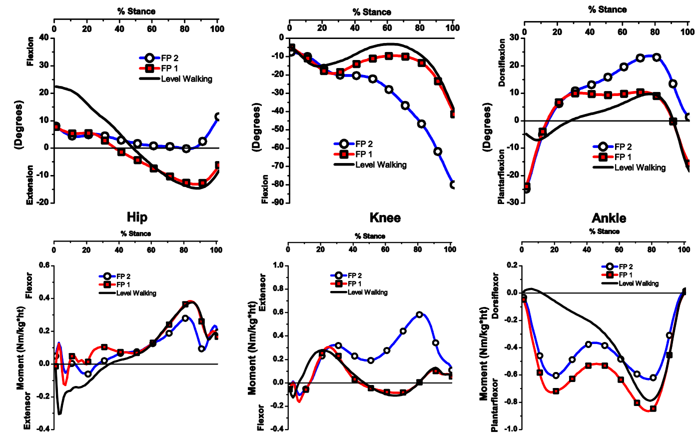

Figure 2: Sagittal hip knee and ankle kinematics and kinetics when approaching the floor from stair descent.

CONCLUSIONS

Negotiating stairs may be the more sensitive measurement to identify subtle functional differences not evident during level walking. The results suggest altered mechanics at the transition steps in both directions of progression to continually adjust the movement of body's COM to successfully negotiate stairs. Persons with orthopedic dysfunctions are known to experience difficulties ambulating over stairs. Given obesity is a significant factor for Knee OA, this profile will be used to ascertain whether the young overweight population exhibit similar compensatory mechanisms seen in older adults with Knee OA.

REFERENCES

1. Russell, E.M. et al. *Lower Extremity Review*, 2010.
2. Messier, S.P. et al. *Arthritis & Rheumatism*, 2005. **52**(7): 2026-2032.
3. Mündermann, A. et al. *Arthritis & Rheumatism*, 2005. **52**(9): 2835-2844.

VALIDATION OF AN ELECTROGONIOMETRY SYSTEM AS A MEASURE OF KNEE KINEMATICS DURING ACTIVITIES OF DAILY LIVING

[1,3]Samuel G. Urwin, [2]Deiary F. Kader, [1,3]Nick Caplan, [1,3]Alan St Clair Gibson, and [1,3]Su Stewart

[1]Department of Sport and Exercise Sciences, Northumbria University, Newcastle upon Tyne, UK
[2]Orthopaedics Department, Queen Elizabeth Hospital, Gateshead, UK
[3]North East Orthopaedic and Sports Injury Research Group, Queen Elizabeth Hospital, Gateshead, UK
Email: samuel.urwin@unn.ac.uk

INTRODUCTION

The use of electrogoniometry (ELG) in the monitoring of sagittal knee joint kinematics can provide an opportunity to measure everyday functional activities [1,2]. This can be undertaken in controlled laboratory environments, or away from clinical observation [3]. ELG is being increasingly used to assess clinical populations, as such, there is a requirement to ascertain the validity of different systems. No authors appear to have assessed the validity of the Biometrics SG150 device in humans across a range of functional activities representative of those undertaken during daily living. The objective of this study was to determine the concurrent validity of the Biometrics SG150 electrogoniometer by comparing intersegmental knee angular displacements to a three dimensional motion analysis system (MA) during walking, stair ascent, stair descent, a sit to stand task, and a stand to sit task.

METHODS

Ten asymptomatic male participants were recruited. Participants had a mean age of 23.1yrs±3.69yrs, height of 1.79m±0.07m, mass of 81.57kg±7.79kg, and body mass index (BMI) of 25.42kg/m^2±2.21kg/m^2 and were free from lower extremity injury.

A 12 camera MA system (Vicon MX, Oxford, UK) was calibrated through a standard dynamic protocol. Participants had 16 retroflective markers placed over anatomical landmarks in line with the lower body Plug in Gait model recommendations (Vicon, Oxford, UK).

A Biometrics SG150 electrogoniometer (Biometrics, Gwent, UK) was placed over the lateral border of the right knee on the anatomical line of the greater trochanter, lateral epicondyle, and lateral malleolus. Electronic foot switches were attached to the forefoot and heel to synchronize the ELG and MA system in analysis.

Participants undertook multiple walking trials until three were collected that coincided with a heel strike on a force plate. Three stair ascent and stair descent trails were performed on a stair rig with a force plate built into the first step. Participants then performed three sit to stand and stand to sit trials onto an orthopaedic stool whilst standing bilaterally on two force plates. Stool height was kept at a consistent height of 560mm during the performance of both sit to stand and stand to sit trials.

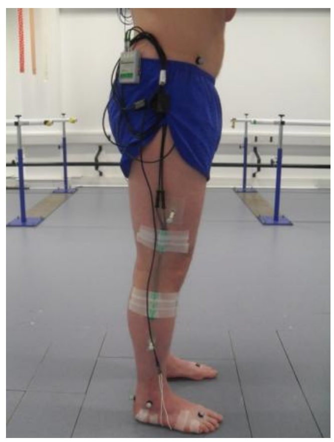

Figure 1: Set-up of the ELG system and retroflective markers required for MA in one participant.

Analysis of validity by linear regression was undertaken. The typical error and Pearson's correlation coefficient *r* were computed for three paired trials between systems for each functional activity.

RESULTS AND DISCUSSION

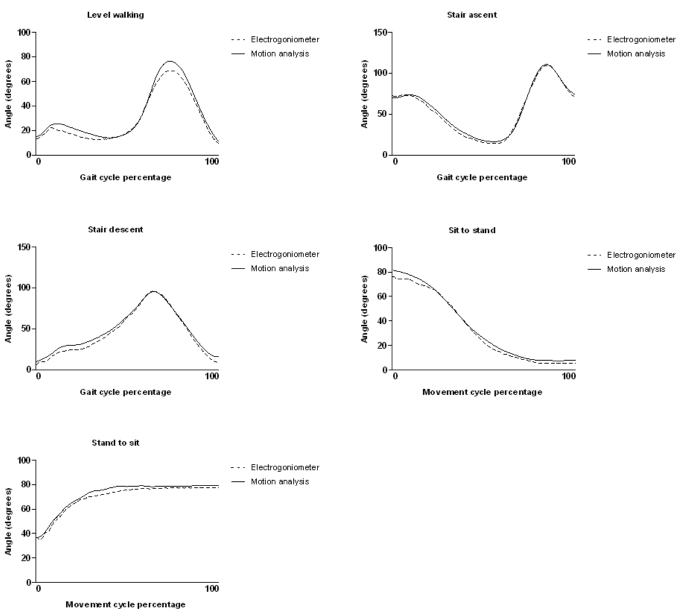

Figure 2: Representative raw data trace of one participant between the ELG and MA systems across walking, stair ascent, stair descent, sit to stand, and stand to sit displacements for the right knee angle.

The mean typical error of estimate, which was the typical magnitude by which the ELG output differed from the MA system output for any given participant over an activity displacement cycle, was found to be 1.87° across walking, stair ascent, stair descent, sit to stand, and stand to sit (Table 1). With 95% statistical confidence, the typical error in this investigation was between 1.74° and 2.04°. Standardisation of this error across all activities produced a 'Trivial' difference of 0.09 between the ELG and MA systems interpreted using a modified Cohen scale.

The mean linear relationship between the ELG and MA system was found to be very high (r = 0.995) across walking, stair ascent, stair descent, sit to stand, and stand to sit (Table 1). This was found to be similar to a previous validation report that described correlations of $r \geq 0.949$ between an ELG and MA system when measuring the knee angle in ten dancing movements [4].

CONCLUSION

ELG is a valid method of measuring the knee angle during activities representative of daily activity. The range is within that suggested to be acceptable for the clinical evaluation of patients with musculoskeletal conditions [2].

ACKNOWLEDGEMENTS

The authors would like to thank De Puy International for funding this investigation.

REFERENCES

1. Van der Linden ML et al. *Clin Biomech* **22**, 292-296, 2007.
2. Rowe PJ et al. *Physiotherapy* **87**, 479 – 488, 2001.
3. Urwin SG et al. *Proceedings of the 2nd International Conference on Ambulatory Monitoring of Physical Activity and Movement*, Glasgow, UK, 2011.
4. Bronner S et al. *JMET* **34**, 232 – 242, 2010.

Table 1: Raw typical error of estimate and Pearson's correlation coefficient *r* between the ELG and MA systems.

	Typical error (°)	95% confidence interval		Pearson's *r*	95% confidence interval	
Walking	2.65	2.43	2.91	0.987	0.983	0.990
Stair ascent	2.24	2.09	2.42	0.996	0.995	0.996
Stair descent	1.93	1.79	2.10	0.996	0.995	0.996
Sit to stand	1.30	1.22	1.41	0.998	0.998	0.998
Stand to sit	1.25	1.17	1.34	0.997	0.996	0.997
Mean	1.87	1.74	2.04	0.995	0.993	0.995
SD	0.60	0.55	0.67	0.004	0.006	0.003

PHYSIOLOGICALLY MODELED SHEAR STRESS AS A FUNCTION OF PULSE FREQUENCY: DRIVING ENDOTHELIAL CELLS TOWARD A QUIESCENT PHENOTYPE

Joseph S. Uzarski and Peter S. McFetridge

University of Florida, Gainesville, FL, USA
email: pmcfetridge@bme.ufl.edu

INTRODUCTION

Endothelial cells (EC) are continuously stimulated by hemodynamic shear stress (SS) that varies spatially throughout the vasculature and temporally with cardiovascular load. Understanding how particular hemodynamic trends affect global EC function will help to elucidate the roles of mechanical cues in various physiological or pathological states. Exposing EC to emulated hemodynamic wave forms *in vitro* has provided invaluable insight into the molecular signaling pathways that participate in mechanotransduction. Here we describe the development of a physiological flow regime that mimics the temporal changes in hemodynamic SS that occur *in vivo*.

METHODS

Computer-controlled peristaltic pumps were used to impose pulsatile SS on human umbilical vein EC monolayers within parallel plate flow chambers. A physiologically modeled perfusion cycle was designed based on transient changes in hemodynamic stresses experienced by EC in vivo. Using primary human umbilical vein EC monolayers, we characterized the phenotypic expression patterns elicited after conditioning with physiological flow by comparison with cells conditioned under steady (fixed-pulse) flow.

RESULTS AND DISCUSSION

Quantitative PCR revealed significant transcriptional differences in expression of genes regulating thrombosis, fibrinolysis, and inflammation between EC conditioned under temporally modulated perfusion conditions. Further, endothelial nitric oxide synthase (eNOS) activity increased (Figure 1) and GFP+ HL-60 leukocyte adhesion decreased (Figure 2) when EC were conditioned under physiological flow compared to steady flow. These phenotypic responses highlight the considerable influence of temporal perfusion conditions on EC gene expression, enzymatic activity, and agonist-induced activation.

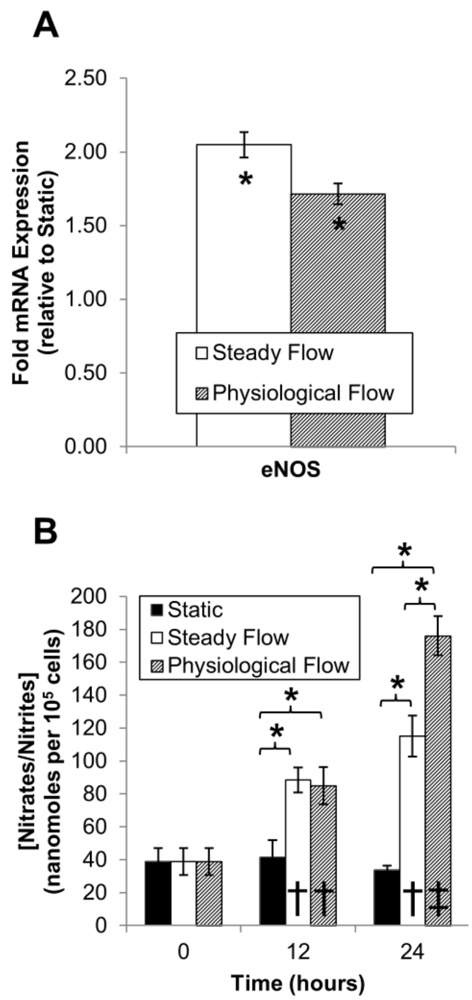

Figure 1. eNOS function in flow-conditioned endothelial cells. A: qPCR revealed upregulation of endothelial nitric oxide synthase (eNOS) in EC conditioned under steady or physiological flow (relative to static culture), though no significance in

expression was observed between flow groups. B: Nitrates/nitrites, stable salt derivatives of NO in conditioned media, were quantified fluorometrically after 0, 12, or 24 hours of static/perfusion culture. Results are displayed as mean ± S.E.M (n = 4-6). One-way ANOVA followed by Tukey-Kramer HSD analyses (significance level: 0.05) were conducted. Asterisks (*) denote significant differences in individual means between groups at each time point. Daggers (†) denotes a significant difference in mean with respect to t=0 hours. Double dagger (‡) denotes significance with respect to t=0 and t=12 hours.

Traditional EC perfusion culture systems have applied continuous or pulsatile flow at a fixed rate; this is not the case, however, *in vivo*. Here we applied an equivalent total magnitude of SS in two distinct perfusion regimes, but varied only the rate at which the shear was applied (fixed pulse vs. temporal modulation). Temporally modulated flow induced dramatic differences in enzymatic activity and inflammatory responses to activation by TNF-α. The steady state flow applied in current culture systems, while useful for close examination of molecular signaling events, may not accurately represent the physiological hemodynamics to which EC are exposed *in vivo*. Physiological time-dependent changes in hemodynamic SS may be important in maintaining endothelial quiescence by influencing gene transcription and/or protein function. Understanding the environmental conditions that regulate EC function and having the capacity to model these appropriately *in vitro* has significant implications for clinical pathologies associated with endothelial dysfunction.

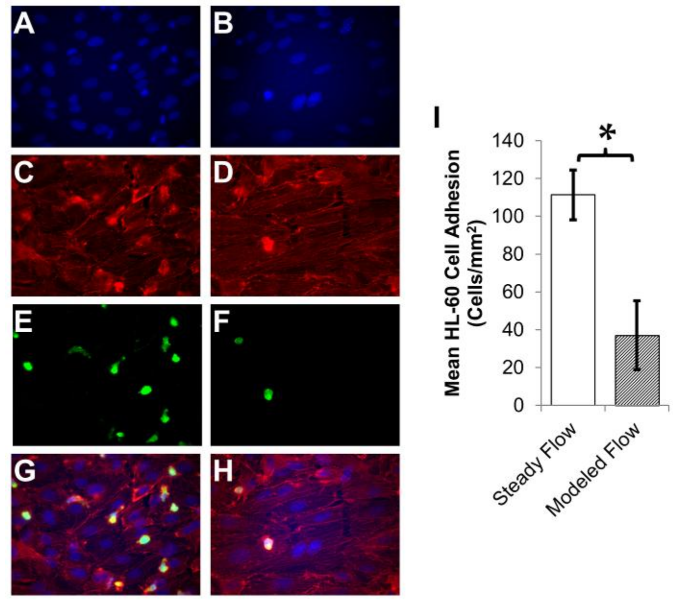

Figure 2. HL-60 cell adhesion to flow-conditioned endothelial cell monolayers. Monolayers of EC were cultured under steady pulsatile flow (left column) or physiological flow (right column) for 24 hours. During the last four hours, HUVEC were activated with 1 U TNF-α. At hour 24, monolayers were removed from flow chambers and incubated for 10 minutes with a bolus of GFP+ HL-60 cells (1000 cells/mm^2), washed, fixed, and stained as indicated (A,B: DAPI; C,D: F-actin; E,F: GFP+ HL-60 cells; G,H: overlay). Scale bar: 20 μm. I: GFP+ HL-60 cells were counted in 12 locations throughout each flow field (10x magnification). Results are displayed as mean ± S.E.M (n = 5). Statistics were conducted as described above.

KINEMATICS AND KINETICS OF STAIR ASCENT WHILE DUAL-TASKING

[1]Srikant Vallabhajosula, [1]Chi Wei Tan, [1]Austin J. Davidson, [1]Mukul Mukherjee, [1,2]Ka-Chun Siu, [1]Jennifer M. Yentes, [1]Denise McGrath and [1]Sara A. Myers

[1]Nebraska Biomechanics Core Facility, University of Nebraska at Omaha, Omaha, NE, USA
[2] College of Public Health, University of Nebraska Medical Center, Omaha, NE, USA
email: svallabhajosula@unomaha.edu, web: nbcf.unomaha.edu

INTRODUCTION

Stair ascent is a common functional and challenging task, particularly for aged populations. Older adults have a greater risk of falling while using stairs as they operate with altered strategies [1,2]. This risk further increases when they ascend stairs while performing multiple tasks like talking (additional cognitive demand) or carrying an object (additional motor task and reduced visual cues). Previous research has focused primarily on evaluating the lower extremity kinematics and kinetics of stair ascent as a single task [3]. During the stance phase of stair ascent, the hip and the knee joints undergo extension while the ankle joint undergoes plantar flexion [3]. Also, the vertical ground reaction force (GRF) profile during stair ascent is characterized by two peaks with the second peak greater than the first peak [3]. Apart from increased attentional demand while ascending stairs while dual tasking [4], it is unknown if and how individuals alter kinematics and kinetics in such situations to successfully ascend stairs. Further, it is unknown if kinematics and kinetics change across multiple steps of the stair ascent. The objective of the current study was to determine the effect of dual-tasking on the joint angles and GRF characteristics during stair ascent. We hypothesized that the joint angles and the GRF characteristics would be altered during dual-tasking and between consecutive steps.

METHODS

Ten healthy young adults (6 males; 23.9±2.8years; 1.76±0.06m; 71.2±8.6kg) ascended a four-step custom-built staircase (angle of staircase rise = 32.73°) under four conditions: stair ascent (control), stair ascent while counting backwards by seven (cognitive), stair ascent while carrying an opaque light-weighted box (motor), and stair ascent while counting backwards by sevens and carrying an opaque light-weighted box (combined), The order of testing conditions was randomized among the subjects. Kinematics (Motion Analysis System; 60 Hz) and kinetics (AMTI; 600 Hz) data were collected. Force platforms were embedded in the first and the third stairs to get data from two consecutive ipsilateral steps. Dependent variables included average speed, peak joint angles, range of motion, the two peak vertical forces, loading rate of the first peak vertical force, minimum force during mid-stance, peak braking and propulsion forces in the antero-posterior direction. The group means for each condition were analyzed through a repeated 2 (steps) by 4 (conditions) ANOVA with Bonferroni post hoc tests when needed ($\alpha = 0.05$). For measures that showed significant differences, a repeated measures ANCOVA was performed with average speed as the covariate.

RESULTS AND DISCUSSION

Step main effects (Table 1): The stance phase during stair ascent can be categorized into weight-acceptance, pull-up and forward continuance phases [3]. During the weight-acceptance phase greater peak hip flexion angle, greater braking force, lesser peak knee flexion angle and lesser loading rate at the first step indicate that the participants adopted a safer and slower strategy. This strategy could have been clearing stair-step through greater hip flexion and slower shock absorption through lesser loading rate. Adopting such a strategy may be due to uncertainty associated with ascending stairs while performing an additional task, resulting in a more tentative approach to the first step (three of the four conditions involved dual-tasking). During the pull-up phase, greater ankle and knee ranges of motion at the second step compared with first step indicate that participants exerted more effort to bring the joints into the extension position. Finally, during the forward continuance phase, where ankle generates the maximum energy, greater ankle plantar flexion and peak anterior propulsion force suggest that participants exerted greater effort to ascend from the second step. Combined, these results suggest that as one ascends higher, greater effort is needed to clear the next step and this effort increases while dual-tasking. *Condition main effects (Table 2)*: During the weight-acceptance and forward continuance phase, greater forces were generated in the control and motor conditions. However, during the pull-up phase, greater forces were generated in the cognitive and combined conditions. Hence, it seems that an additional cognitive task requires an individual to alter their performance of stair ascent task, particularly when the individual prepares to interface with a new step. However, during mid-stance, participants seemed to compensate by exerting greater force during the cognitive and combined conditions. Despite these differences, participants seemed to compensate by perhaps slowing down to produce similar joint angles across the conditions. In fact, participants ascended the stairs slowly in the cognitive and combined conditions and at the second step. When controlled for speed, the dependent measures (Table 2) showed a similar pattern of change. However across all the conditions, the peak ankle dorsiflexion and knee flexion angles became greater when controlled for speed while ascending the first step, indicating that speed played a crucial role in altering the ascent strategy while dual-tasking. Future work should examine how older adults ascend stairs while dual-tasking given that older adults operate closer to their maximal capabilities and ascend more slowly compared to younger adults [2].

CONCLUSIONS

The effect of dual-tasking during stair ascent seemed to vary based on the different phases of stair ascent. Our data suggests that an additional cognitive task has a greater influence on the GRF characteristics during stair ascent than an additional motor task.

REFERENCES

1. Startzell, JK, et al. *J Am Geriatr Soc* **48**, 567-580, 2000
2. Reeves, ND, et al. *J Electromyogr Kinesiol.* **19**, e57-68, 2009
3. McFadyen, BJ, et al. *J Biomech* **21**, 733-744, 1988
4. Ojha, HA, et al. *Phys Ther* **89**, 1080-1088, 2009

ACKNOWLEDGEMENTS

Funding provided by the National Institute on Disability and Rehabilitation research (Grant No. H133G080023), National Institute of Health (Grant No. 1R011AG034995-01A1), and NASA Nebraska Space Grant & EPSCoR (Grant No. NNX11M06A).

Table 1: Mean (SE) of dependent variables that showed significant step main effect; * Significant difference ($P < 0.05$)

Dependent measure	Step 1	Step 2
Peak Ankle Plantar Flexion Angle (°)	14.85 (1.09) *	16.45 (1.21)
Peak Ankle DorsiFlexion Angle (°)	11.57 (1.05) *	14.05 (1.09)
Ankle Range of Motion (°)	26.42 (1.33) *	30.49 (1.23)
Peak Knee Flexion Angle (°)	53.05 (1.71) *	56.84 (1.29)
Knee Range of Motion (°)	45.36 (1.14) *	49.05 (1.23)
Peak Hip Flexion Angle (°)	53.85 (1.01) *	49.44 (1.18)
Loading Rate (N/s*body weight)	4.25 (0.19) *	5.56 (0.28)
Peak Anterior Propulsion Force (/body weight)	0.05 (0.00) *	0.10 (0.01)
Peak Posterior Braking Force (/body weight)	0.13 (0.01) *	0.09 (0.01)

Table 2: Mean (SE) of dependent variables that showed significant condition main effect; * Significant difference between Control and Combined conditions ($P < 0.05$); # Significant difference between Control and Cognitive conditions ($P < 0.05$); ^ Significant difference between Motor and Combined conditions ($P < 0.05$)

Dependent measure	Control	Cognitive	Motor	Combined
First Peak Vertical Force (N/kg)	1.09 (0.02)	1.04 (0.01)	1.09 (0.03)	1.05 (0.01)
Loading Rate (N/kg*s)	5.77 (0.22) #*	4.12 (0.36) #	5.59 (0.31) ^	4.14 (0.35) *^
Vertical Force during midstance (N/kg)	0.69 (0.03)	0.76 (0.02)	0.70 (0.03)	0.75 (0.02)
Second Peak Vertical Force (N/kg)	1.23 (0.04) *	1.14 (0.04)	1.22 (0.03)	1.12 (0.03) *
Peak Anterior Propulsion Force (N/kg)	0.08 (0.01)	0.07 (0.01)	0.08 (0.01)	0.07 (0.01)

EFFECT OF TACTILE PERTUBATION ON BLINDFOLDED CIRCULAR PATH NAVIGATION

[1]Srikant Vallabhajosula, [1]Mukul Mukherjee and [1,2]Nicholas Stergiou

[1]Nebraska Biomechanics Core Facility, University of Nebraska at Omaha, Omaha, NE, USA
[2] College of Public Health, University of Nebraska Medical Center, Omaha, NE, USA
email: svallabhajosula@unomaha.edu, web: nbcf.unomaha.edu

INTRODUCTION

Path integration is the ability to integrate information about perceived self-motion in the absence of external cues. Path integration involves the estimation of one's position with respect to an external frame of reference. This is achieved by integrating information about one's linear and angular velocity and acceleration (inertial navigation) to determine the distances and angles traveled, or by measuring them directly [1]. Particularly, during blindfolded circular path navigation, the estimation of linear and angular components depends on continuous feedback from proprioceptive, vestibular and tactile sensory systems [2]. These afferent sensory inputs are believed to be integrated to form as well as access a cognitive map of the path in the hippocampal region [3]. The objective of this study was to examine the contribution of the tactile system to blindfolded circular path navigation. We hypothesized that perturbing the tactile system will have a greater effect on linear components compared to angular components during blindfolded circular path navigation. This is due to the greater contribution of the proprioceptive and vestibular systems for estimation of angular components during blindfolded circular walking [2].

METHODS

Tactile perturbation was conducted using in-sole underfoot C2 tactors (vibrators) during circular path navigation (Engineering Acoustics, Inc., Casselberry, FL). Nine healthy subjects aged between 19 and 35 years walked once on a 7.2m circular path under four conditions: 1) with eyes open and tactors off (i.e. with all their four sensory systems unperturbed – always performed first to form the cognitive map), 2) with eyes closed and tactors off (i.e. with proprioceptive, tactile and vestibular sensory systems unperturbed), 3) with eyes open and tactors off (i.e. with all their four sensory systems unperturbed – performed to recalibrate the cognitive map), and 4) with eyes closed and tactors on (i.e. with only proprioceptive and vestibular sensory systems unperturbed). Conditions 2 and 4 were randomized among the subjects. Kinematic data (60Hz) was collected using 12 cameras (Motion Analysis Corp., Santa Rosa, CA). Dependent variables included path length, median radius, walking velocity, linear distance between start and end points (linear error), angular distance traversed between start and end points (angular error), heading direction error. All the variables excluding the heading direction error were determined using the sacral marker data. The heading direction error was determined from three markers placed on the front, back and top of the head. Data processing was conducted using Matlab (Mathworks, Natick, MA). A paired samples t-test was performed between conditions 1 and 3 (both conditions: eyes open). If no significant differences were found between conditions 1 and 3, data from condition 1 was compared with data from conditions 2 (eyes-closed and tactors-off) and 4 (eyes-closed and tactors-on). A one-way repeated measure ANOVA was then performed with a Bonferroni post hoc analysis to determine the differences between the conditions. All statistical analyses were performed using the PASW 18.0 (International Business Machines, Armonk, NY) software and α–value equal to 0.05.

RESULTS AND DISCUSSION

There were no significant differences for any dependent measures between the two conditions when the subjects traced the circular path with all their sensory systems unperturbed ($P > 0.05$). The

ANOVA results showed a significant main effect for walking velocity ($P < 0.001$), linear error ($P = 0.003$), angular error ($P = 0.009$) and heading direction error ($P = 0.012$). The path length ($P = 0.177$) and median radius ($P = 0.084$) did not differ significantly. Bonferroni post hoc tests revealed that the subjects walked faster with their eyes open and tactors off (i.e. with all sensory systems unperturbed) compared to both condition 2 (eyes-closed and tactors-off; $P = 0.041$) and condition 4 (eyes-closed and tactors-on; $P = 0.004$). They also produced greater linear error ($P = 0.005$), angular error ($P = 0.009$), and heading direction error ($P = 0.004$) when walking with their eyes closed and tactors on compared to when all the sensory systems were intact. Descriptive statistics of the dependent variables are presented in Table 1. Representative traces are shown in Figures 1a, 1b and 1c.

Results of the current study partially support our hypothesis. Effect of perturbing the tactile sensory system was most evident through reduced walking velocity, where the participants walked the slowest when they had to depend only on their proprioceptive and vestibular systems. Results for estimation of linear and angular error and heading direction showed that though tactile sensory system contributes to path integration, it may not play a dominant role compared to the proprioceptive and vestibular systems combined in accessing the cognitive map. It is also possible that the participants increase their reliance on these systems in the absence of tactile input to perform the task while being blindfolded. Simultaneous perturbation of two of these three sensory systems can highlight the relative contribution of each sensory system for blindfolded circular path navigation.

Table 1: Mean (SE) of dependent variables for the three experimental conditions (n = 9); # Significant difference between Eyes Open – Tactors Off and Eyes Closed – Tactors Off conditions ($P < 0.05$); * Significant difference between Eyes Open – Tactors Off and Eyes Closed – Tactors On conditions ($P < 0.05$)

Dependent Variable	Eyes Open – Tactors Off	Eyes Closed – Tactors Off	Eyes Closed – Tactors On
Path Length (m)	7.50(0.08)	8.38 (0.53)	8.06 (0.41)
Median Radius (m)	1.44 (0.02)	1.59 (0.07)	1.60 (0.07)
Walking Velocity (m/s)	0.72 (0.03) #*	0.60 (0.04) #	0.54 (0.03) *
Linear Error (m)	0.04 (0.01) *	0.81 (0.25)	0.92 (0.19) *
Angular Error (°)	358.76 (0.28) *	337.18 (9.39)	329.75 (6.89) *
Heading Direction Error (°)	1.89 (0.71) *	22.64 (9.49)	27.07 (5.45) *

CONCLUSION

Tactile sensory system contributes to both the linear and angular components of blindfolded circular path navigation.

REFERENCES

1. Berthoz A, et al. *Science*, **269(5220)**, 95-98, 1995.
2. Takei Y, et al. *Exp Brain Res*. **115(2)**, 361-368, 1997.
3. O'Keefe J & Nadel L. *The Hippocampus as a Cognitive Map*, Oxford University Press, 1978.

ACKNOWLEDGEMENTS

Funding provided by the National Institute on Disability and Rehabilitation research (Grant No. H133G080023), National Institute of Health (Grant No. 1R011AG034995-01A1), and the National Aeronautics and Space Administration (Grant No. NNX11AM06A).

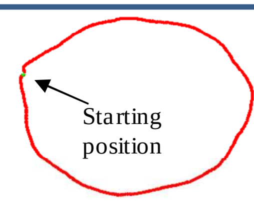

Figure 1a: Representative trace during eyes open and tactors off condition (Condition #1)

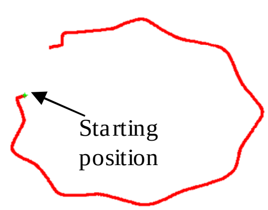

Figure 1b: Representative trace during eyes closed and tactors off condition (Condition #2)

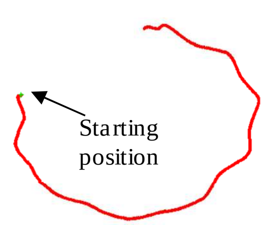

Figure 1c: Representative trace during eyes closed and tactors on condition (Condition #4)

Figure 1: Representative traces in one subject during the three experimental conditions

INFLUENCE OF STEPPING RATE ON STRIDE INTERVAL VARIABILITY OF STAIR-CLIMBING

[1]Srikant Vallabhajosula, [1]Jessica J. Renz, [1]Jung Hung Chien, [1]Nathaniel Hunt and [1,2]Nicholas Stergiou

[1]Nebraska Biomechanics Core Facility, University of Nebraska at Omaha, Omaha, NE, USA
[2]College of Public Health, University of Nebraska Medical Center, Omaha, NE, USA
email: svallabhajosula@unomaha.edu, web: nbcf.unomaha.edu

INTRODUCTION

The temporal structure of gait variability has been shown to exhibit long-range correlations in the stride interval during over-ground walking, treadmill walking and running [1-3]. In fact, it has been shown that these long-range correlations are speed-dependent [2,3]. Particularly, at the preferred walking and running speeds, the strength of these long-range correlations has been shown to be weaker compared to the strength at faster and slower speeds. While previous studies have examined the influence of walking speed on long-range correlations in walking and running, research is limited on other continuous locomotor tasks such as stair-climbing. Stair-climbing is a common activity of daily living that is more demanding. Research on stair-climbing is limited to examining the biomechanics using staircases with limited number of steps. The objective of the current study was to determine how stepping rate influences the stride interval variability during continuous stair-climbing. Based on the walking and running literature [1-3], we hypothesized that the amount of variability would decrease with increasing stepping rate. Also, we hypothesized that the temporal structure of variability would be affected by increasing the stepping rate.

METHODS

Nine healthy participants (5 females; 25.2±4.9years; 1.71±0.10m; 69.1±13.8kg) performed continuous stair climbing on the SC916 Stairmill (StairMaster, Fitness Direct, San Diego, CA) without using the handrails under three randomly presented conditions: at preferred stepping rate (PSR), 110%PSR, and 120%PSR. Stride time intervals of the dominant leg were calculated using the position data of a marker placed on the head of the second metatarsal (60Hz; 12 cameras; Motion Analysis, Santa Rosa, CA). Stride time was defined as the time between two consecutive toe-off events of the dominant leg. All the subjects were right leg dominant. The subjects walked for three minutes during each condition and rested for at least three minutes between each condition testing. A custom Matlab script (Mathworks, Inc., Natick, MA) was used to compute the mean, Standard Deviation (SD) and Coefficient of Variation (CV) of the stride time intervals for each subject under each condition. Additionally, long-range correlations of the stride time intervals were calculated using the Detrended Fluctuation Analysis (DFA) technique [4]. For the current study, the box size range used was $n = 4$ to $N/4$ (=16), where $N = 65$ is the minimum number of stride intervals among all the subjects across all the conditions [2]. This ensured that time series of similar data length were compared. These long-range correlations can be characterized by the slope or scaling factor (α) from DFA. Differences between the group means of the dependent measures (mean, SD, CV, α) for stairmill walking in each of the three conditions were evaluated using a repeated measures one-way ANOVA. Bonferroni post hoc tests were used if the ANOVA yielded a significant result.

RESULTS AND DISCUSSION

The mean stepping rate for the three conditions was: preferred, 52.44 (11.59) steps/min; 100%PSR, 56.67 (12.40) steps/min and 120%PSR, 62.89 (13.81) steps/min. There was a significant main effect of condition for the mean stride time (P < 0.001). The post hoc analysis showed that mean stride time significantly decreased as the stepping rate increased and all the conditions differed significantly with each other (P<0.001; Fig. 1A). In contrast, there were no condition main effects for SD (P=0.182), CV (P=0.228) and alpha (P=0.345). Albeit non-significant, the amount of variability was greater during 110%PSR condition described by both SD and CV values (Fig. 1B & 1C). However, the temporal structure of variability showed the opposite trend with the lowest value at 110%PSR (Fig. 1D). The alpha values of stairmill walking at PSR indicated the presence of white noise and absence of long-range correlations [1]. This was confirmed by surrogation analysis where most subjects exhibited alpha-values that were not significantly different than the randomly shuffled surrogates of the same time series. However, as the stepping rate increases, persistent long-range anti-correlations exist during stairmill walking, implying that, a short stride interval is likely followed by a longer stride interval and vice-versa.

Compared to treadmill walking at different speeds [3], stairmill walking produced greater mean stride interval and CV, but lesser alpha values at all the speeds. However, the pattern of the variation of these variables remained consistent between treadmill and stairmill walking. These results could suggest that performing a more strenuous task like stairmill walking, particularly at a faster pace might place an additional demand on the cardio-vascular and neuro-muscular systems of the body. Perhaps compensation for this additional demand might occur with participants frequently slowing down before picking up the speed. It is also possible that during stairmill walking at PSR, the nervous system considers each step as a new problem to solve and depends minimally on the feedback from the previous step(s). However, as the stepping rate increases, reliance on this feedback probably increases as the problem has to be solved quickly to avoid a fall. We speculate that the range of box size and number of stride intervals used here might also influence the outcomes. Future work should evaluate stairmill walking for longer trials.

CONCLUSIONS

Long range correlations in stride interval were absent during stairmill walking at PSR. However, increase in stepping rate introduces persistent long-range anti-correlations in stride interval. Stepping rate seems to have minimal influence on the amount and structural variability of stride interval.

REFERENCES

[1] Hausdorff J, et al. *J Appl Physiol* **78**, 349-358, 1995

[2] Jordan K, et al. *Gait Posture* **24**, 120-125, 2006

[3] Jordan K, et al. *Gait Posture* **26**, 128-134, 2007

[4] Peng C-K, et al., *Phys Rev E* **49**, 1685-1689, 1994

ACKNOWLEDGEMENTS

Funding provided by the National Institute on Disability and Rehabilitation research (Grant No. H133G080023), National Institute of Health (Grant No. 1R011AG034995-01A1), the NASA Nebraska Space Grant & EPSCoR (Grant No. NNX11AM06A).

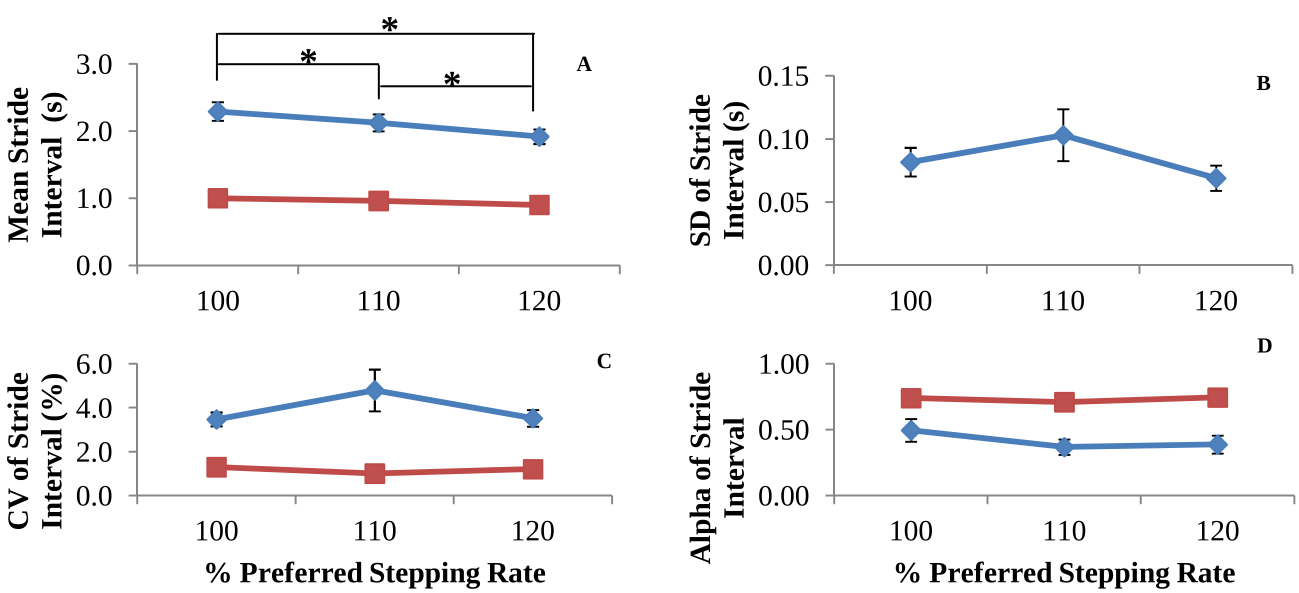

Figure 1: Mean (SE) of dependent variables for the three conditions; blue diamonds – stairmill walking; red squares – treadmill walking from [2] * Significant difference (P<0.05)

INFLUENCE OF TAI CHI ON KINEMATICS DURING MULTI-DIRECTIONAL GAIT INITIATION

[1]Srikant Vallabhajosula, [2]Beverly L. Roberts, [2]Chris J. Hass

[1]University of Nebraska at Omaha, Omaha, NE, USA
[2]University of Florida, Gainesville, FL, USA
email: svallabhajosula@unomaha.edu, web: http://hhp.ufl.edu/apk/ces/affil/nm/index.php

INTRODUCTION

Tai chi intervention has been shown to be effective in improving the balance and reducing the falls among older adults [1]. Tai chi incorporates body movement in different directions, and attentional training to improve posture. Two common activities of daily living with these inherent qualities are gait initiation and turning. Gait initiation is the beginning of locomotion and involves transition from a stationary stable double limb support to a dynamic unstable single limb support. Turning is a motor task that is impaired in the geriatric population. Previous studies reported that older adults exhibit reduced spatio-temporal parameters and alternate strategies during turning while walking [2-3]. However, few studies have investigated the kinematics related to turning while initiating gait. Limited research investigating this multi-directional gait initiation task among older adults is particularly surprising because initiating stepping motion in different directions is a common activity of daily living (for example, walking away after closing the refrigerator door or choosing an aisle in supermarket). The purpose of the current study was to investigate the effect of tai chi on the kinematics of multi-directional gait initiation among older adults. We hypothesized tai chi will enhance performance of older adults in terms of kinematics during multi-directional gait initiation.

METHODS

Seven older adults (6 females; 76±4 years; 1.60±0.06 m; 75.0±18.5 kg) with difficulty walking a quarter mile or climbing a flight of stairs participated in the study. They practiced Yang style short form for one hour, 3 times a week for 16 weeks. They focused on physical relaxation and kinesthetic awareness of the body in space with a slow and relaxed rotation of the torso with shifting of the body weight. Testing was done before and immediately after the tai chi intervention Kinematic data were collected with a seven camera motion capture system using 25 retro-reflective markers (60Hz; Motion Analysis Corp., Santa Rosa, CA). Testing involved participants doing gait initiation in four directions: stepping 45° medially by crossing the swing leg over the stance leg (M45); stepping forward (FWD); stepping laterally 45° (L45); and stepping 90° laterally (L90). The forward stepping was performed first and order of the other directions was randomized. Participants performed three gait initiation trials for each direction at a self-selected pace, maintaining consistent stance-width and using the same self-selected leg to initiate gait. The dependent variables used were: *spatio-temporal parameters* (step length, velocity, time, time to heel-off and toe-off) for both the legs, and *turning-related parameters* (amount of rotation of head, trunk and pelvis at heel-off, toe-off and heel-strike events). All the trials were analyzed from the start of gait initiation. The step length, velocity and time were defined using the movement of the heel marker from the start of the gait initiation to heel-strike event. The head, trunk and pelvic angles were defined in the horizontal plane using the markers placed bilaterally on the temple, acromion process and anterior superior iliac spine respectively. All the dependent variable values were computed using custom MATLAB code (MathWorks Inc., Natick, MA). To assess the effects of tai chi intervention, a 2 (time: pre, post) x 4 (direction: M45, FT, L45, L90) repeated measures ANOVA was performed for the spatio-temporal measures. For the turning-related parameters, a 2 (time: pre, post) x 3 (segment: head, trunk, pelvis) ANOVA was performed for each turning direction.

RESULTS AND DISCUSSION

Spatio-temporal parameters: Significant interaction between time and direction was observed for step velocities of both the legs ($P<=0.03$; Figure 1A and 1B). After tai chi, participants stepped faster with their swing leg (1st stepping leg) in three directions (M45, FWD, and L90) and decreased in L45 direction. Participants also stepped faster with their stance leg (2nd stepping leg) in the M45 and L90 directions but slower in the L45 direction after the intervention. Significant time main effect was found for the time to heel-off and toe-off events of both the legs (P<=0.02; Table 1). Specifically, participants lifted their heel and toe faster after the tai chi intervention. *Turning-related parameters*: In the M45 direction, there was a significant interaction between segment and time at swing leg heel strike. After tai chi, participants reduced their head rotation while increasing their trunk and pelvic rotation (Figure 1C). Also, in the L90 direction, a significant time main effect showed that participants produced an overall lower segmental rotation with heel-off and toe-off events (Table 1).

Overall, the influence of tai chi seemed was dependent on the direction of gait initiation. In the M45 direction, participants completed their steps faster that may reflect a greater confidence in doing the task. Lower head rotation combined with greater trunk and pelvic rotation at the completion of swing leg heel-strike may suggest an alteration strategy with gait initiation. Though eye movement was not tracked, the changes in rotation may reflect lower reliance on visual input and greater kinesthetic awareness of the body segments during the challenging single support phase (on stance leg). Change of strategy was also seen in the L90 direction where the participants stepped faster while decreasing overall segmental rotation after the intervention. Perhaps they were more confident moving into the single stance phase with lower segment rotation. The impact of tai chi was small for gait initiation to the L45 direction. Participants only decreased stepping velocity suggesting a more cautious strategy. Alternatively, they may have perceived initiating gait in this direction as easier and were able to perform it more slowly than in the other directions.

Table 1: Mean (SE) of dependent variables with significant main effects of time*(P<0.05)

Dependent Variable	PRE	POST
Time to Swing Leg Heel-Off (s)	0.58 (0.02) *	0.51 (0.01)
Time to Swing Leg Toe-Off (s)	0.65 (0.02) *	0.57 (0.02)
Time to Stance Leg Heel-Off (s)	1.11 (0.02) *	1.04 (0.03)
Time to Stance Leg Toe-Off (s)	1.32 (0.01) *	1.23 (0.02)
Segment Rotation at Swing Leg Heel-Off in the L90 direction (°)	15.83 (2.87) *	8.24 (1.88)
Segment Rotation at Swing Leg Toe-Off in the L90 direction (°)	18.55 (3.61) *	10.37 (2.46)

CONCLUSIONS

In older adults with mobility disability, tai chi improved performance of multi-directional gait initiation. The extent of this impact was dependent on the direction-of gait initiation.

.

REFERENCES

1. Wolf SL, et al. *J Am Geriatr Soc* **51**, 1794-1803, 2003

2. Paquette MR, et al. *Exp Brain Res* **190**, 1-9, 2008

3. Fuller JR, et al. *Gait Posture* **25**, 393-400, 2007

ACKNOWLEDGEMENTS

Funding provided by the University of Florida Opportunity Grant and the National Institute of Health (Grant No. 5R03HD054594-02).

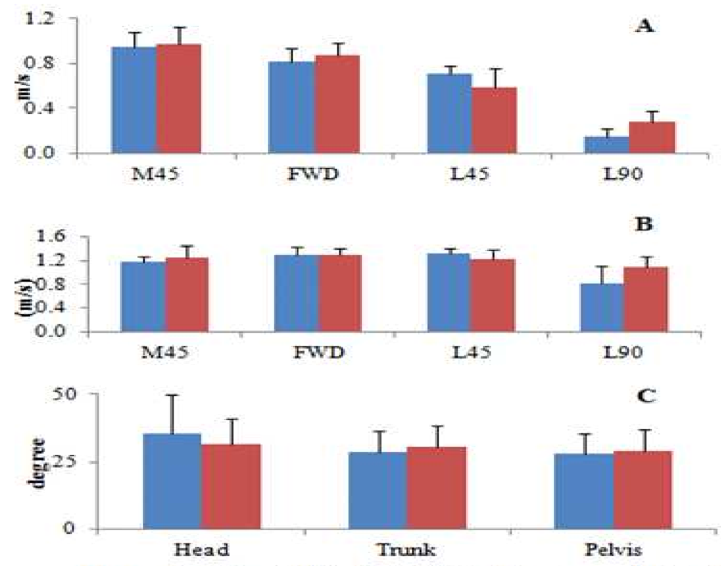

Figure 1: Mean (SE) of A) Swing leg step velocity, B) Stance leg step velocity during four directions of gait initiation, and C) Segmental rotation at swing leg heel-strike (M45 direction); all variables showed significant interaction (P<0.05); Blue – Pre; Red – Post Tai Chi

NON-NEGATIVE MATRIX FACTORIZATION APPLIED TO A FEEDBACK SYSTEM

Keith W. van Antwerp and Thomas J. Burkholder

Georgia Institute of Technology, Atlanta, GA, USA
email: thomas.burkholder@hps.gatech.edu

INTRODUCTION

Both voluntary and involuntary movements exhibit reproducible patterns of coordinated muscle activity, and those patterns may reveal underlying neural structures. Coordinated patterns of muscle activation can be evoked by spinal stimulation (1), suggesting the existence of spinally-defined motor modules or primitives, and these modules can reconstruct reflex behavior (2). Coordinated patterns are also common to diverse voluntary behaviors (3), and non-negative matrix factorization (NMF) seems to be an effective tool for extracting those patterns (4). However, patterns of coordination are also predicted by optimal control theory (5), and may be determined by musculoskeletal structure (6). These observations are based on primarily feedforward contexts in which the nervous system or experimental intervention has free access to the hypothesized, low-dimensional control space.

NMF has begun to be applied in feedback contexts (7), in which the musculoskeletal structure may impose a high degree of covariation among proprioceptive inputs to the feedback controller. In that case, low-dimensional structure in muscle activation patterns may arise from biomechanical structure, from true neural modules, or from some combination. The objective of this work was to determine, in synthetic data, whether NMF can accurately identify neural structure within a data set constrained by mechanical structure.

METHODS

Muscle activations were synthesized from either feedforward or feedback controllers, and NMF performed to extract those controllers. Feedback data sets were generated using a reduced version of our cat hindlimb model (8), containing 31 muscles and 3 degrees of freedom (hip abduction, knee flexion, ankle flexion). There is no redundancy between joint space and Cartesian space, which simplifies the interpretation of mechanical structure.

Feedforward data were used primarily to validate the decomposition evaluation methods and provide a quality-of-fit benchmark. Muscle activations (a) were generated using a modular, non-negative structure:

$$a = W_f * k$$

where each of the 6 columns of W_f represents a module (synergy), and k represents many random weightings of those columns to produce the synthetic muscle activation data set (31 muscles X 1000 samples). The structure of W_f was varied to control the angle, in muscle space, between columns and the mechanical action of the column when projected through the hindlimb model.

Feedback muscle activations were also generated using a non-negative structure:

$$a = W_b * P * \{R^T J^{-1} x\}$$

where P represents a sensory transformation that condenses 31 muscle length changes to the low dimensional control space, R the moment arm matrix, J the endpoint Jacobian, x many random displacements in endpoint space, and {} denote that negative values were set to zero. The structure of W_b was varied to include between 2-9 modules and to vary the angle, in muscle space, between columns.

NMF was performed on each of the resulting activation sets 12 times with different seeds, and the best fit decomposition analyzed further. Extracted factors were matched with corresponding columns of W_f or W_b, and the error in each muscle weighting tabulated.

RESULTS AND DISCUSSION

NMF reconstruction of feedforward controllers was strongly dependent on the sparsity and distribution of the control vectors (fig. 1). Reconstruction becomes more accurate as the angle between individual modules (dispersion) within a controller increases. At dispersion <40º, NMF has difficulty identifying the true number of modules.

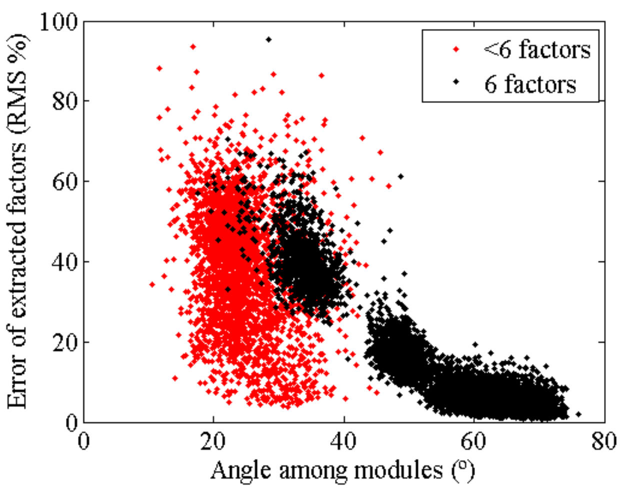

Figure 1. Factor extraction from a 6-module controller improves as modules become more dissimilar.

NMF reconstruction of feedback controllers failed to identify the dimensionality of any control structure containing more than 5 modules (fig. 2). It is noteworthy that the number of extracted factors plateaus at 5-6, while the number of synergies identified in a number of experimental paradigms is frequently 4-6 (7). Endpoint displacements, in 3-D, map into 3-D joint displacements, and result in 6 non-negative dimensions of muscle length change. For W_b with greater than three modules, the extracted factors bore little resemblance to their source modules (Fig. 2). Similar results were obtained for a range of controller structures, including fewer muscles. Mechanical shaping and the random P filter mean that uniform sampling in Cartesian space results in non-uniform sampling in the control space. Thus, the simulated activations do not fully reflect the activation space available to the controller, but include correlations imposed by both the mechanical structure (R^TJ^{-1}) and the sensory transformation (P).

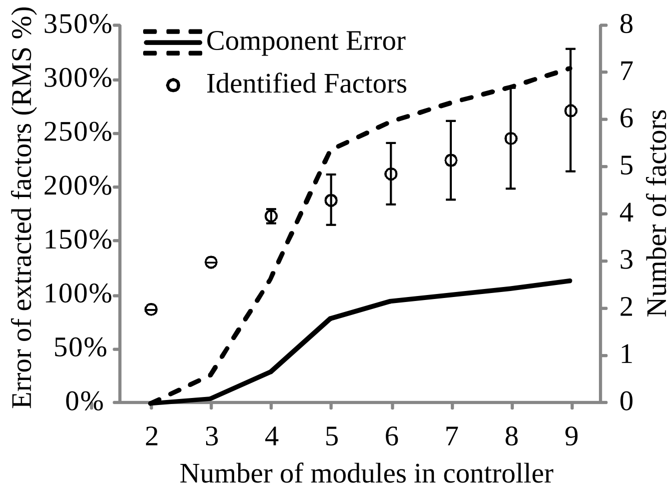

Figure 2. Error of extracted feedback factors (line) increases with controller complexity (70º dispersion). The number of predicted factors is fewer than the true number of factors. Mean ±S.D.

NMF can be a powerful tool for simplifying analysis of complex muscle activation data, but low dimensional structure within that data does not imply neural structure. Mechanical structure can distort existing neural structure, not just in feedback systems, but also in systems where task specifications limit access to the hidden control structure. Although this project focused on NMF, it is likely that these caveats apply to any statistical decomposition technique.

REFERENCES

1. Giszter, et al., *J Neurosci*, **13**, 467-91, 1993
2. d'Avella et al.,*Nat Neurosci*. **6**, 300-8, 2003
3. d'Avella and Bizzi, *PNAS*, **102,** 3076-81, 2005
4. Tresh et al, *J Neurophysiol* **95**, 2199-212, 2006
5. Todorov, *Nat Neurosci*, **7**, 907-915, 2004
6. Berniker et al., *PNAS*, **106**, 7601-8, 2009
7. Ting and Macpherson, *J Neurophysiol*, **93**, 609-13, 2005
8. Bunderson, et al., *J Exp Biol*, **213**, 2131-41, 2010

ACKNOWLEDGEMENTS

Ford Fellowship; HD046922

ASSESSMENT OF FUNCTIONAL REACHING TASKS IN OLDER ADULTS

[1,2]Meghan E. Vidt, [3]Melissa Daly, [2,4]Anthony P. Marsh and [1,2]Katherine R. Saul

[1]Wake Forest School of Medicine, Department of Biomedical Engineering
[2]Virginia Tech – Wake Forest University School of Biomedical Engineering and Sciences
[3]Williams College
[4]Wake Forest University, Department of Health and Exercise Science
email: mvidt@wakehealth.edu, web: http://www.sbes.vt.edu/kholzbau/MoBL/index.html

INTRODUCTION

Sarcopenia and neuromuscular changes are inherent to the aging process [1]. Muscle strength also declines with age, including in the muscles controlling the upper extremity [2]. Together, these age-associated changes may play a role in the performance of daily tasks which are critical for the maintenance of independence in older adults. However, there is a relative paucity of information on upper extremity neuromuscular function in this population. In this study our aim was to characterize changes in kinematics and muscle activations associated with reaching with different loads to different endpoints in a group of healthy older adults. In this study, we isolated the effects of load and endpoint for forward and upward reaches with common household items as external loads.

METHODS

Ten older adults (4M, 6F, mean age 72.4±3.1yrs) participated. Subjects were seated at a table (height=0.68m). Upward reaching tasks were performed with 2 loads: a can of sugar (0.63kg) and a filled 1 gallon jug (3.84kg). Forward reaching tasks were performed with the sugar can, gallon jug, and a dumbbell of the 1 repetition maximum weight (1RM) with which each subject could successfully reach. Reaching tasks started with the object at the end of the table and elbow flexed to 90°. Subjects reached forward so the elbow was flexed 20°; subjects reached upward at 110° to a shelf. To complete the reaching tasks, subjects returned the object to the starting position. During task performance, the locations of 10 retro-reflective anatomical markers were recorded with 7 Hawk motion capture cameras (Motion Analysis Corp., Santa Rosa, CA). Torso and wrist movement were restricted using straps across the chest and a wrist brace. EMG was recorded from the biceps, triceps, and deltoid muscles with 1cm surface electrodes (BIOPAC Systems Inc., Goleta, CA). EMG recordings were normalized to a maximal isometric contraction for each muscle. Post processing of raw data was performed using Cortex (Motion Analysis Corp., Santa Rosa, CA), OpenSim (v.2.4, Stanford University, Palo Alto, CA), and custom Matlab (The Mathworks, Inc., Natick, MA) software.

Shoulder elevation, elevation plane, shoulder rotation, and elbow flexion were investigated. Total range of motion (ROM), peak joint angle, temporal, and joint velocity characteristics were compared for the four degrees of freedom with repeated measures analyses of covariance, with sex as a covariate (SAS, v.9.3, Cary, NC). Mean and standard deviation were calculated for normalized EMG.

RESULTS AND DISCUSSION

<u>Effect of load:</u> In forward and upward reaching tasks, we observed that subjects generally maintained arm posture in the forward flexion plane for a longer portion of the reach and returned to the start position with greater joint velocity when lifting heavier loads (Fig. 1). In upward reaches, ROM increased for shoulder elevation, shoulder rotation, and elbow flexion ($p=0.027$) when moving the jug, but elevation plane ROM decreased as subjects maintained the forward flexion plane. While peak joint angles were increased in forward (elbow flexion $p=0.026$) and upward reaches with the jug, they decreased when reaching with 1RM compared to the can and jug. We identified a temporal delay initiating the return and increased velocity on the return from reaches with heavier loads. For example, there was a delay in return initiation in forward reaches with 1RM compared to the can and jug for shoulder rotation ($p\leq0.002$) and elbow

flexion (p≤0.042). Return velocity from upward reaches with the heavier jug was increased for shoulder rotation and elbow flexion (p≤0.042) and decreased for elevation plane.

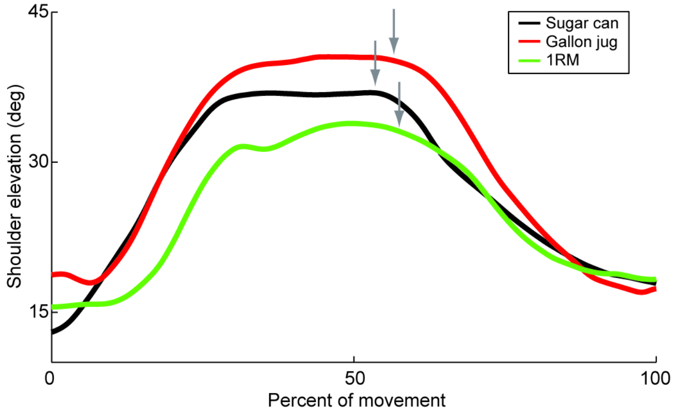

Figure 1: Shoulder elevation angle for forward reach with sugar can (black), jug (red), and 1RM (green). A temporal delay in the return is shown by arrows; a steeper slope during the return indicates a faster velocity.

Effect of endpoint: Similar to our findings for the effect of load, we observed that subjects demonstrated a forward flexed posturing of the arm and greater joint velocity when returning from the upward reach, particularly with a heavier load. Upward reaches required greater ROM (shoulder elevation, shoulder rotation, elbow flexion, p≤0.014) than forward reaches, with increased peak joint angles for reaches with the can (all, p≤0.026) and jug (shoulder elevation, shoulder rotation, elbow flexion, p≤0.001). A temporal delay was seen for the return with both loads from the upward endpoint. Velocity increased during return from the upward reach for the jug compared to the forward reach (shoulder elevation, shoulder rotation, elbow flexion, p<0.005).

Assessment of EMG during these tasks indicated that biceps, triceps, and deltoid muscles were each activated to a greater magnitude when moving heavier loads and when reaching upward. We identified a consistent reaching strategy; deltoid was activated earlier than biceps and triceps to initiate the return portion of the movement, which was more prominent when moving heavier loads and reaching upward. Triceps had notable co-contraction with biceps when moving heavier loads. In the forward reach with 1RM, triceps was activated to a greater magnitude (22% MVC) than the deltoid (18%); triceps had a greater magnitude of activation (24%) than deltoid (18%) and biceps (15%) when reaching upward with the jug.

CONCLUSIONS

In summary, older adults posture the arm in forward flexion and use higher joint velocities during the return with heavier loads and from an upward endpoint, and show increased muscle activation and co-contraction with increased load. Our findings are consistent with previous studies that found anterior (rather than lateral) arm postures provided greater limb stiffness and increased dexterity, in a laboratory setting and during unloaded daily tasks, respectively [3,4]. Our work expands on these studies by exploring freely chosen joint posture in response to real-world tasks.

We conclude that when moving heavier loads to forward and upward endpoints, a stabilization posture is chosen to successfully complete reaching tasks. This could indicate that joint posture and co-contraction are means by which older adults compensate when moving loads that account for a greater proportion of upper limb strength capacity. Further, muscle co-contraction may be a mechanism for increasing upper limb stability during functional tasks. This work establishes normative kinematic patterns for these daily tasks in healthy older adults, which may provide a foundation for comparison and disability risk assessment for special populations of older adults.

REFERENCES

1. Narici MV, Maffulli N. *Br Med Bull* **95,** 139-159, 2010.
2. Vidt ME, et al. *J Biomech* **45**, 334-341, 2012.
3. Trumbower RD, et al. *PLoS ONE* **4** e5411, 2009.
4. Chen W, et al. *Gait Posture* **32**, 475-481, 2010.

ACKNOWLEDGEMENTS

NIH Award # 5R24HD050821-02, Rehabilitation Institute of Chicago, NSF CBET-0828115; Cross campus collaboration research fund; WFU Center for Biomolecular Imaging; WFU Claude Pepper Older Americans Independence Center, National Institutes for Aging P30 AG021332.

AN ADAPTIVE TABU SEARCH OPTIMIZATION ALGORITHM FOR GENERATING FORWARD DYNAMICS SIMULATIONS OF HUMAN MOVEMENT

Arian Vistamehr and Richard R. Neptune

Mechanical Engineering Department, The University of Texas, Austin, TX, USA
email: arian.vistamehr@utexas.edu web: http://www.me.utexas.edu/~neptune

INTRODUCTION

Forward dynamics simulations have become a valuable tool for gaining insight into the biomechanics and neuromotor control of human movement. Quantities that are difficult or impossible to measure, such as individual muscle forces and their contributions to specific movement subtasks, can be estimated using muscle-driven forward dynamics simulations that emulate experimentally collected kinetic and kinematic data [1]. To generate the simulations, dynamic optimization is often used to fine-tune the muscle excitation patterns using an iterative process to produce the desired movement. Typically, an optimal tracking objective function is used to minimize the RMS difference between the simulations and corresponding experimental data. The performance of the optimization algorithm depends on the rate of convergence and how well the objective function is minimized.

The performance of various optimization algorithms (e.g., simulated annealing (SA), gradient-based sequential quadratic programming, and simplex methods) was previously evaluated in solving a pedaling tracking problem, where SA was found to outperform the other algorithms [2]. In the last few decades, tabu search (TS), a metaheuristic memory-based algorithm, has been found to have superior performance in solving combinatorial optimization problems in a number of research domains such as operations research, telecommunications and financial analysis [3].

The purpose of this study was to implement an adaptive TS algorithm to solve a pedaling optimal tracking problem and to compare its performance with a widely used SA algorithm.

METHODS

A previously described musculoskeletal pedaling model was used [1]. The two-legged three degree-of-freedom (crank and two pedal angles) model was driven by 10 muscle groups per leg. Muscle excitations were defined using a modified Gaussian pattern (4 parameters per muscle group). Parameters included amplitude, center point, width and curvature, each referred to as a parameter category in the tabu search. A pedaling simulation of 90 rpm and 265 Watts was generated.

In order to implement the adaptive TS algorithm, the parameter space was discretized within the given bounds of each parameter. Four neighborhood categories were defined, each corresponding to a parameter category. Neighborhoods were generated by perturbing a parameter category in all muscles (± one step size), one muscle at a time. For instance, in neighborhood category one, the amplitude of muscle excitations was perturbed in each muscle. The neighborhood minimum was then calculated and compared to the cost of the incumbent solution. If the cost improved, the solution was accepted and the search was intensified by decreasing the grid size of all the parameters. However, if the cost was not improved, before an uphill solution was accepted, the rest of the parameter categories were perturbed and the neighborhood minimum was accepted as a (downhill or uphill) solution. In the case of an uphill solution acceptance, the search space was expanded within the specified grid size bounds.

Upon solution acceptance, the parameter associated with the accepted move was stored in the tabu memory and was prohibited from repetition for a duration specified by the tabu tenure (TT). Similar to the parameter grid size, TT was also restricted between specified bounds and was used for the search intensification and expansion. If the optimal solution did not improve over five consecutive neighborhoods, as an escape strategy the incumbent solution was replaced with the last optimal solution found. However, to avoid a repeated search, the escape strategy could be used only once after each optimal improvement.

The performance of the TS algorithm was compared to that of SA. The SA algorithm [4] perturbed the parameters randomly, thus a priori insight into the problem was not necessary. Both methods used an identical objective function and initial guess for the excitation parameters. Since TS is deterministic and SA includes stochasticity, the average results from 16 SA optimizations were used for comparison to TS.

RESULTS AND DISCUSSION

In the early stages of the search, TS had a superior performance over SA, improving the solution by over 60% in the first hour (Fig. 1). Despite the initial fast decrease in the cost using TS, both methods converged to similar cost values after 8 hours of search. A similar performance pattern was observed using different starting solutions, except for the case where the starting solution was completely random and the pedaling motion was not completed, in which case the stochasticity in SA was more beneficial in the early stages of the search.

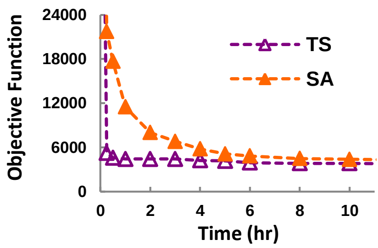

Fig. 1: Objective function value versus elapsed search time. The initial cost (79,500) is not shown.

The quality of the solution obtained by TS after one hour of search was compared to the best SA solution obtained after 49 hours (Fig. 2). The resulting pedal angle, tangential pedal reaction force, crank and joint moments were similar between the different algorithms and were within ±2 SD of the experimental data (Fig. 2).

In summary, an adaptive TS optimization algorithm was designed and implemented in a forward dynamics simulation of pedaling. TS had a superior performance over the SA algorithm in the early stages of the search, although the TS performance was sensitive to appropriate neighborhood and parameter grid size selection. The solution obtained

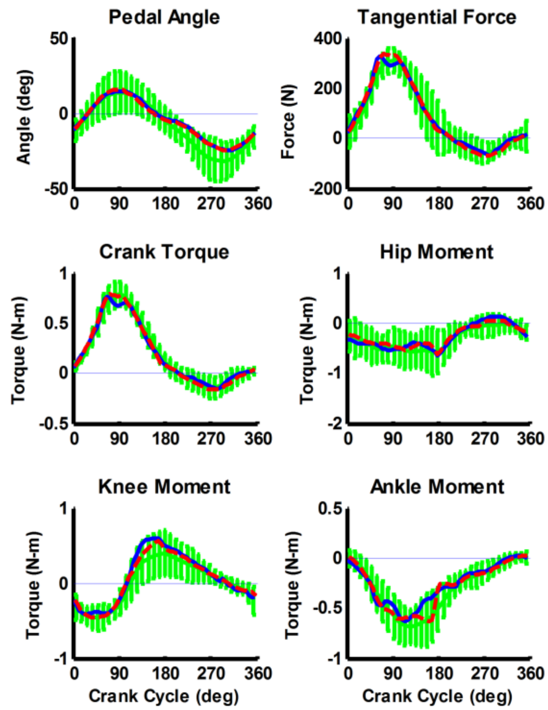

Fig. 2: Experimental data (with error bars representing ±2SD) and simulation data: (--) best optimal solution obtained by SA in 49 hours (cost= 3,150); (—) solution obtained by TS in 1 hour (cost=4,430).

using TS in the first hour of the search tracked well the experimental data. Thus, the TS algorithm is initially computationally more efficient compared to SA, although it is sensitive to the initial parameters. The performance may improve by using a hybrid SA-TS algorithm and/or implementing a reactive TS algorithm [3]. As a future study, we will investigate if adaptive TS will accelerate optimization convergence for other tasks such as walking, which is dynamically more unstable and computationally more intensive than pedaling.

ACKNOWLEDGEMENTS

The authors acknowledge the insightful comments provided by Dr. J Wesley Barnes.

REFERENCES

1. Neptune R.R, and Hull M.L. *J. Biomech. Eng.* **120 (3)**, 334-341, 1998.
2. Neptune R.R. *J. Biomech. Eng.* **121 (2)**, 249-252, 1999.
3. Glover F, and Laguna M. *Tabu Search*, Kluwer Academic Publishers, 1997.
4. Corana A, et al. *ACM T Math Software* **13 (3)**, 262-280, 1987.

THE INFLUENCE OF PEDAL PLATFORM HEIGHT ON MAXIMAL AVERAGE CRANK POWER DURING PEDALING: A SIMULATION STUDY

Arian Vistamehr and Richard R. Neptune

Mechanical Engineering Department, The University of Texas, Austin, TX, USA
email: arian.vistamehr@utexas.edu web: http://www.me.utexas.edu/~neptune

INTRODUCTION

A number of adjustments can be made to the bicycle geometry to influence cycling performance. Previous studies have investigated how chainring shape [1] and seat position influence maximum average crank power [2]. Pedal platform height has the potential to influence pedaling performance by altering how the muscles contribute to the pedal reaction forces. While Hull & Gonzalez [3] investigated the effect of pedal platform height on net joint moments, no study has investigated how pedal platform height influences individual muscle contributions to the pedaling task.

The purpose of this study was to expand on these previous studies by using a muscle-driven forward dynamics simulation analysis to identify how pedal platform height influences maximum crank power.

METHODS

To perform the analysis, a previously developed musculoskeletal model and dynamic optimization framework [1] were used. In the musculoskeletal model, pelvis orientation and seat tube angle were set to the values that were previously found to maximize crank power [1]. Pedal platform height was then systematically varied between -2.0 cm and +6.0 cm about the pedal spindle (Fig. 1). The relative position of the seat with respect to the pedal platform was held constant by adjusting the seat height as the pedal platform height was varied. A simulated annealing optimization algorithm was used to find the muscle excitation patterns that maximized average crank power during steady-state pedaling at 90 rpm at each pedal platform height. To interpret any changes in crank power, the influence of platform height on the net joint moments and individual muscle activity and force generation were quantified. In addition, an induced acceleration analysis was performed to identify how platform height alters the ability of individual muscles to accelerate individual joints and body segments.

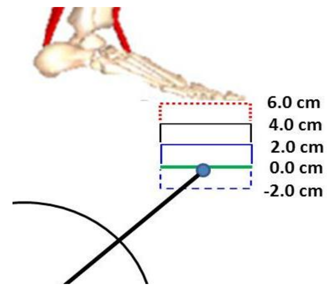

Fig. 1: Schematic of the pedal platform heights used in the simulations (figure not to scale).

RESULTS AND DISCUSSION

Pedal platform height had minimal effect on average crank power, with the maximum power (983W, platform height = 0.0 cm) only 0.21% higher than the minimum value (981W, platform height = +6.0 cm). Similarly, joint angle trajectories were mostly unaffected by the changes in platform height, with the largest change occurring in the peak ankle angle, which was less than 5%.

Although there were no changes in maximum crank power, there were changes in net joint moments and individual muscle quantities. The most pronounced change in the joint moments occurred at the ankle. The absolute average ankle moment was 33% higher for the lowest platform height (-2.0cm) compared to the highest platform height (+6.0cm). The peak plantarflexor moment varied by 18% across platform heights. This was in contrast to a previous inverse dynamics-based analysis that only found a 5% difference when the platform height was varied from -4.0cm to +4.0cm [3]. The difference between studies is most likely due to the fact that pedal reaction force was assumed unchanged with platform height variations [3], which was found to differ between the simulations in the present study. However, the general trend for the change in ankle moment with platform height was consistent between studies.

The changes in the ankle moment were due primarily to differences in the location of the pedal reaction force application at the pedal spindle relative to the ankle joint center. For the case when the pedal platform was below the spindle (-2.0 cm), the tangential component of the pedal reaction force created a dorsiflexor moment about the spindle. Thus, the reaction moment on the ankle was plantarflexor, which increased the net ankle plantarflexor moment during the downstroke (~0-180° crank angle; Fig. 2). For the cases when the platform was above the spindle, the reaction spindle moment on the ankle was dorsiflexor, which reduced the net ankle plantarflexor moment. Consequently, the net ankle moment decreased as the platform height increased.

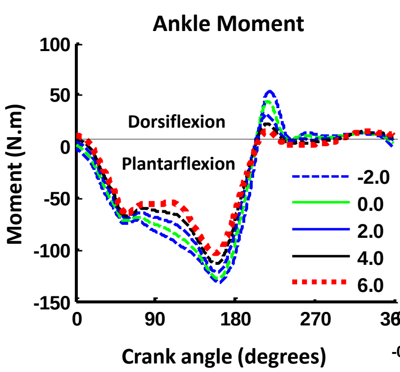

Fig. 2: Net ankle joint moment across pedal platform heights. Zero crank angle denotes top dead center.

Muscle forces remained nearly unchanged for all platform heights, except for the ankle plantarflexor muscles (Fig. 3). For the lowest platform height, soleus (SOL) peak force increased by 15% (compared to the highest platform height) and gastrocnemius (GAS) generated 15% higher force during the second half of the downstroke (~90°-180° crank angle). Plantarflexor fiber lengths and velocities were unaffected by the platform height. However, in the case with the lowest platform height these muscles were activated earlier, resulting in increased muscle forces. These early muscle activations appear necessary to maintain the same (optimal) joint angles for maximizing the crank power [2].

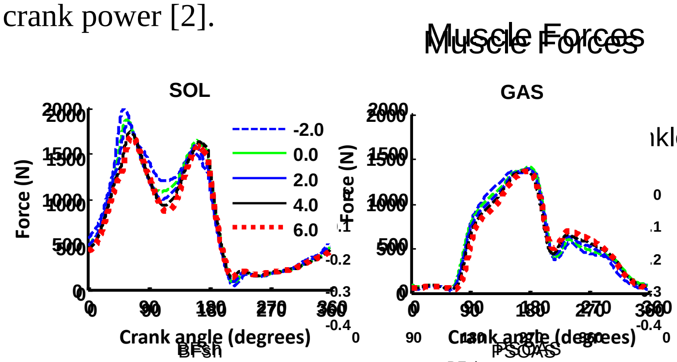

Fig. 3: Muscle forces for various pedal platform heights

The induced acceleration analysis revealed that the plantarflexor contributions to pedal and ankle joint accelerations increased with increasing pedal platform height (Fig. 4). The increased pedal and ankle accelerations, despite a decrease in plantarflexor force (Fig. 3), suggest the ankle is more unstable with increases in platform height.

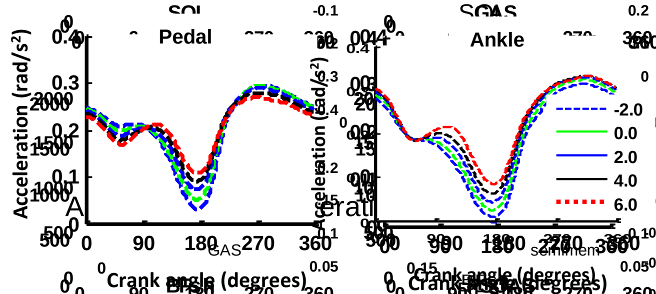

Fig. 4: Soleus induced accelerations per unit force at the pedal and ankle for various pedal platform heights

In summary, increasing pedal platform height had a minimal effect on average maximum crank power. Despite similar power outputs, increasing platform height led to lower plantarflexor force and ankle moment requirements. However, the lower ankle muscle forces led to higher ankle joint and pedal induced accelerations, suggesting higher platform heights are more unstable.

REFERENCES

1. Rankin, J.W., & Neptune, R.R. *J Biomech* **41 (7)**, 1494-1502, 2008.
2. Rankin, J.W., & Neptune, R.R. *J Appl Biomech* **26**, 493-500, 2010.
3. Hull, M.L., & Gonzalez, H.K. *Int'l J Sports Biomech* **6**, 1-17, 1990.

TRAINING INDUCED CHANGES IN QUADRICEPS ACTIVATION DURING MAXIMAL ECCENTRIC CONTRACTIONS

Dimitrios Voukelatos and Matthew T. G. Pain
School of Sport, Health and Exercise Sciences, Loughborough University, Loughborough, UK
email: D.Voukelatos@lboro.ac.uk

INTRODUCTION

Despite full voluntary effort, activation of the quadriceps group of muscles appears inhibited during slow concentric and eccentric contractions. Maximum voluntary eccentric strength (MVC) can be more than 50% lower than the values observed *in vitro* [4]. Pain & Forrester [2] suggested that this apparent reduction could be due to a neural, tension-limiting, mechanism that becomes active during maximal contractions of large skeletal muscles.

Amiridis et al. [1] showed that the difference in force outputs between electrically stimulated and MVC contractions was significantly lower for elite athletes than for sedentary individuals, suggesting that strength training may reduce the inhibitive action of the neural mechanism. The aim of this study was to investigate whether performing a short high velocity eccentric strength training protocol on an isovelocity dynamometer can lead to a decrease in the inhibition during fast eccentric and slow concentric MVC.

METHODS

Six male subjects (age 26.3 ± 2.73 years) took part in the study that consisted of 8 training sessions over a period of 4 weeks. During a pre-training testing session subjects performed five maximal voluntary (MVC) isometric contractions at 15^0, 30^0, 45^0, 60^0 and 75^0 and six maximal voluntary isokinetic knee extensions and flexions at 50, 100, 150, 250, 350 and 450^0/s. Each MVC trial was followed by an electrically stimulated one. The stimulation of the quadriceps muscles was performed transcutaneously via the femoral nerve. A total of 10 isometric and 12 isokinetic contractions were performed. To assess the effects of training the same testing protocol was repeated post-training.

A nine parameter maximum torque-angular velocity-angle function was fitted to the raw, experimental data to obtain the maximum theoretical tetanic torque parameter, T_{ecc}, the maximal voluntary torque parameter, T_{eccmvc}, as well as the minimum level for a differential activation function, a_{min}, that represents the greatest level of neural inhibition. Additionally to assess activation level the interpolated twitch technique was used. To express voluntary activation (VA) as a percentage of theoretical maximal activation of the quadriceps muscle the following formula was employed:

$$\%\text{VA}=\left(1-\frac{\text{superimposed twitch}}{\text{control twitch evoked at rest}}\right)\times 100$$

where the superimposed twitch is the force increment noted during a maximal contraction at the time of stimulation and the control twitch is that evoked in the relaxed muscle [3].

The analysis focused on the comparison of peak eccentric, T_{ecc}, maximal voluntary torque, T_{eccmvc}, the minimun level of muscle activation, a_{min}, parameters as well as the raw peak torque values between pre- and post-training sessions. Student’s paired t-test or, in exceptional cases where data was non-parametric, the Wilcoxon’s test, were used. A statistical level of significance, $p \leq 0.05$, was used throughout the statistical analysis. Data is reported as mean ± SD

RESULTS AND DISCUSSION

On average subjects achieved higher torque outputs during the post-testing session (Fig. 1), however, statistically significant differences were observed only during eccentric contractions at 350^0/s, $p < 0.05$, $t_5 = -2.94$, concentric contractions at 100^0/s,

$p < 0.05$, $t_5 = -2.77$ and isometric contractions, $p < 0.05$, $t_5 = -2.74$. Both T_{ecc} and T_{eccmvc} values were significantly, $p < 0.05$, greater post-training (356 ± 30.9 Nm vs. 313 ± 39.4 Nm; mean ± SD) and (279 ± 31.5 Nm vs. 244 ± 36.9 Nm) respectively. Similarly, the low level differential function, a_{min}, was also significantly greater post-training, $p < 0.05$, (0.62 ± 0.04 vs. 0.67 ± 0.05). The percentage values of voluntary activation (%VA) estimated using the twitch interpolation technique were higher, post-training, for all isovelocities tested, though only the values recorded during eccentric contractions at 50^0/s (67.1 ± 10.4 vs. 76.1 ± 4.36, $t_5 = -2.58$, $p < 0.05$) were significantly higher post-training.

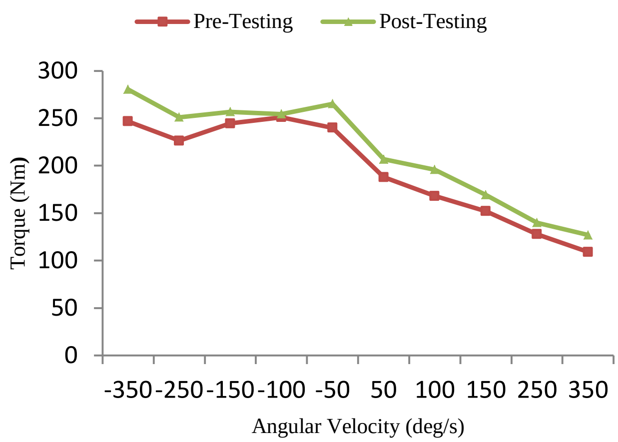

Figure 1: Plot of average raw torque outputs over angular velocities

Raw torque output increased post-training for all angular velocities tested and during both eccentric and concentric contractions with the biggest increases observed during eccentric and concentric contractions at the highest velocities. Moreover, the voluntary activation levels of the quadriceps muscles showed an increase during the post-training testing session, being on average higher than the respective pre-training values

The fitted torque values (Fig. 2) provide a means for comparing and evaluating the raw experimental torque data once it has been processed to remove problems with noise, especially one sided errors due to submaximal voluntary efforts. Both, T_{ecc} and T_{eccmvc} values showed a significant increase post-training which suggests that a greater number of muscle fibres of the quadriceps muscles was recruited during the post-training test. Since 8 sessions of isokinetic training are probably not sufficient to elicit muscle fibre hypertrophy, or some other mechanical change, the increased force output can probably be attributed to neural adaptations. The increase in a_{min} post-training suggests a significant increase in the muscle activation post-training which may be attributed, in part, to the reduced action of the tension limiting mechanism. This is further supported by the increase in the values of %VA post-training.

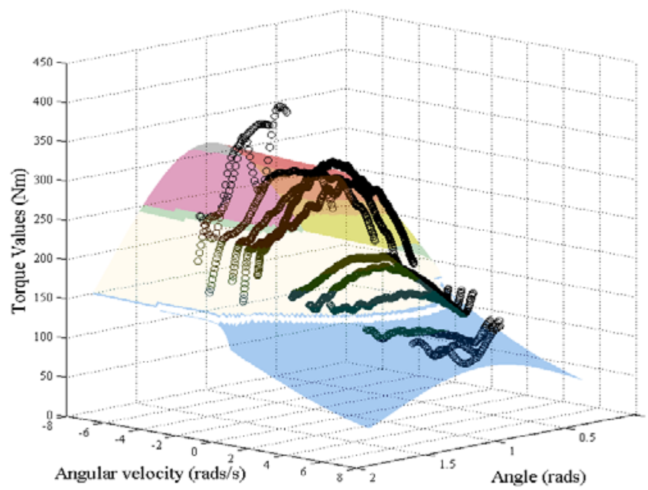

Figure 2: Typical torque–angle–angular velocity raw data (black circles) and fitted surfaces for the quadriceps of one subject.

CONCLUSION

Performing a short, strength training protocol over a range of high angular velocities led to an increase in muscle activation, and, a possible decrease in the inhibitive action of the tension-limiting mechanism.

REFERENCES

1. Amiridis, IG., *European Journal of Applied Physiology Occup Physiol.* **73**, 149-56, 1996
2. Pain, MTG. & Forrester, S., *Journal of Biomechanics*, **42,** 1598-1603, 2009
3. Shield, A., & Zhou, S., *Sports Medicine.* **34,** 253-267, 2004
4. Westing, SH., et al., *Acta Phys. Scand.* **140**, 17-22, 1990

THE EFFECT OF ARM POSITION ON HILL-SACHS ENGAGEMENT: A FINITE ELEMENT STUDY

[1,2] Piyush Walia, [2]Anthony Miniaci, Morgan H. Jones and [3] Stephen D. Fening

[1] Cleveland State University, Cleveland, OH, USA
[2] Cleveland Clinic, Cleveland, OH, USA
[3] Austen BioInnovation Institute, Akron, OH, USA
email: sfening@abiakron.org

INTRODUCTION

Bony lesions of the glenohumeral joint are important risk factors that often lead to recurrent anterior shoulder dislocation. A Hill-Sachs lesion is defined as bone loss from the posterior-superior aspect of the humeral head due to a compression fracture. There exists no clear information about the engagement of the lesion depending on its size and the position of the arm. This may be the reason that sometimes smaller humeral head lesions are left untreated. The aim of this study was to show the theoretical relationship between the engaging Hill-Sachs lesion and the shoulder's anterior instability. This study examined the effects of different sizes of Hill-Sachs lesions at various humero-thoracic abduction and rotation angles of the arm. We hypothesized that the distance to dislocation will decrease with increasing size of the defect and also that the shoulder’s stability would decrease at a higher humero-thoracic abduction angle and greater degree of external rotation of the arm.

METHODS

A computer-based finite element approach was used to model the glenohumeral joint with an intact humerus and glenoid. A generic model was developed for cartilage and bones of the glenoid and humerus, using data available in the literature [4,5]. Bones were assumed to be rigid bodies, and cartilage was modeled with hyperelastic material properties having a Young's modulus (E) of 10 MPa and a Poisson’s ratio (ν) of 0.4 [6]. 3D hexahedral element mesh was used, with 7830 elements for humeral head, and 9280 elements for glenoid mesh. Then different sizes of Hill-Sachs lesions for the humeral head were created, similar to those of Kaar et al. [1]. Lesion sizes were $^1/_8$, $^3/_8$, $^5/_8$, and $^7/_8$ of the humeral head radius (R). The experiments were analyzed using static analysis with displacement control in the anterior inferior direction. A 50-N compressive load was simulated for an intact joint, and the translational distance to dislocation was analyzed. Tests were performed at two different thoracohumeral abduction angles (45° and 90°). At each thoracohumeral abduction angle, a range for arm rotation was chosen between 40° internal to 60° external rotation. For arm to abduct to a humero-thoracic angle of 90º, the glenohumeral joint was rotated 60º. Likewise, thoracohumeral abduction angles of 45º was calculated as the 30º glenohumeral joint rotation.

RESULTS

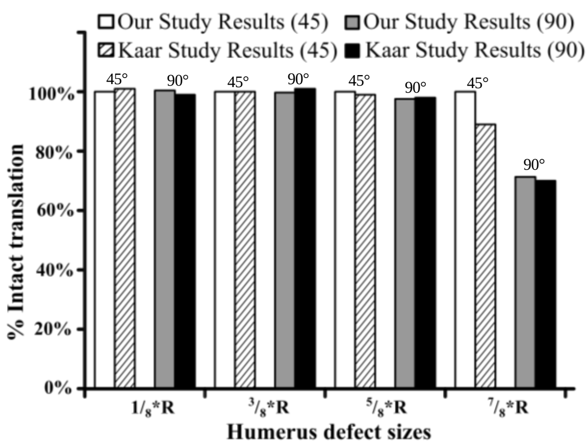

Figure 1: % Intact translation distance comparison for humeral defects in neutral position and humero-thoracic abduction angles of 45° and 90°.

The comparison of percent intact translational distance to dislocation results for four different sizes of Hill-Sachs lesions at neutral rotation with a previous study shows similar patterns [1](Fig. 1). Results showed that for defect size 5/8*R, the gradual decrease in distance to dislocation occurred after external rotation of 30°. But for defect size 7/8*R, the gradual decrease can be seen after 10° of external rotation (Fig. 2). The horizontal and vertical axis represents the angle of rotation of the arm (40° internal to 60° external rotation) and the distance to dislocation (in millimeters), respectively.

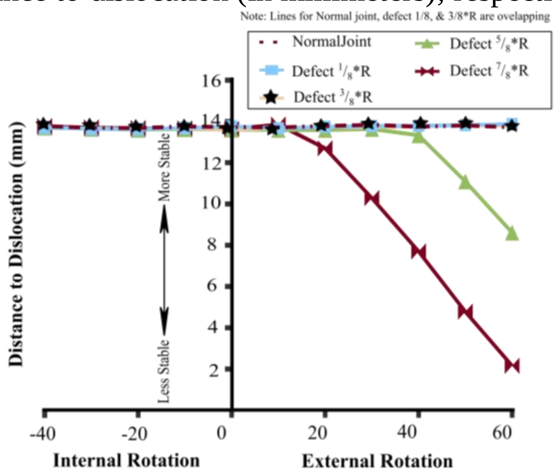

Figure 2: Distance to dislocation (in millimeters) at 45° thoracohumeral abduction.

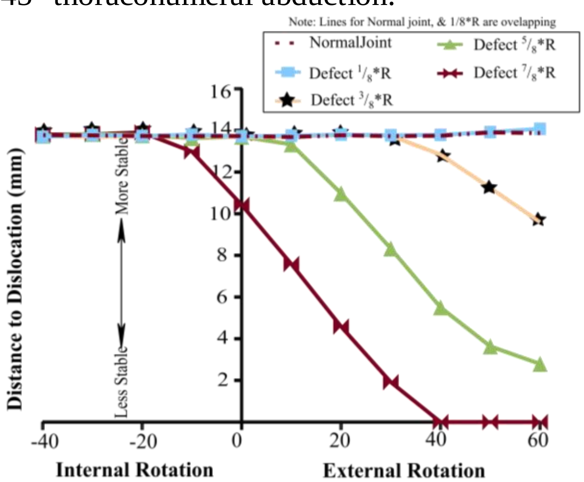

Figure 3: Distance to dislocation (in millimeters) at 90° thoracohumeral abduction.

At a higher abduction angle (90°), the defect size 3/8*R has a reduced distance to dislocation of 9.5 mm during external rotation of 60° (Fig. 3). A decrease in the distance to dislocation for defect sizes 3/8*R , 5/8*R, and 7/8*R occurs at 30° external rotation, 10° external rotation, and 20° internal rotation, respectively.

DISCUSSION

The results from this study were compared to those from the study by Kaar et al. for validation of the model [1]. Results comparison showed similar trend patterns for the reduction of distance to dislocation. The distance to dislocation was reduced to 10.43 mm from 13.73 mm for the largest humerus defect at 90° humero-thoracic abduction and 0° rotation. This signifies that the shoulder becomes unstable with an increase in abduction in the presence of a humeral head defect. Kaar et al. concluded that a defect size of $^{7}/_{8}$*R needs to be treated surgically, with associated soft tissue repairs [1]. But at 45° humero-thoracic abduction, we found that during external rotation of the arm defect size $^{5}/_{8}$*R and $^{7}/_{8}$*R reduces stability rapidly. Whereas, at 90° humero-thoracic abduction, a humerus defect size of $^{3}/_{8}$*R, and $^{5}/_{8}$*R had reduced stability during external rotation. It was interesting to see that defect size $^{7}/_{8}$*R is already engaged at neutral rotation and 90° humero-thoracic abduction, as the distance to dislocation reduced sharply after 20° of internal rotation.

This study predicted that even Hill-Sachs lesions of smaller size can significantly decrease shoulder stability at higher angles of humero-thoracic abduction. Furthermore, we saw the engagement of Hill-Sachs lesion with rotation of the arm. We found that in the presence of a humeral head lesion, shoulder stability decreases with increase in external rotation of the arm. One limitation of this study is that it was based on approximate geometry of the glenohumeral joint and absence of the joint capsule.

CONCLUSIONS

Instability of shoulder increases with increasing size of the humeral head lesions. Smaller size defects are more likely to engage with the arm in greater degrees of abduction and external rotation. These findings may have implication for planning surgical reconstruction for shoulder instability.

REFERENCES

1. Kaar SG et al. *AJSM* **38**,594-599, 2010.
2. Burkhart SS et al. *Arthrosc.* **16**, 677-694, 2000.
3. Soslowsky LJ et al. *CORR* **285**, 181-90, 1992.
4. Iannotti JP et al. *JBJS Am* **74**, 491-500, 1992.
5. Büchler P et al. *Clin Biomech* **17,** 630-639, 2002.

THE EFFECT OF ARM POSITION ON BONY BANKART LESION: A FINITE ELEMENT STUDY

[1,2] Piyush Walia, [2] Anthony Miniaci, Morgan H. Jones and [3] Stephen D. Fening

[1] Cleveland State University, Cleveland, OH, USA
[2] Cleveland Clinic, Cleveland, OH, USA
[3] Austen BioInnovation Institute, Akron, OH, USA
email: sfening@abiakron.org

INTRODUCTION

The shoulder is the most mobile joint of the body, a requirement for performing various activities in daily life and sports. Anterior shoulder instability is a common injury in athletes, and recurrent instability is a difficult problem. Both soft tissue and bony injury can occur at the time of the initial dislocation and lead to recurrent instability. Glenoid bony injuries can predispose to recurrent instability even after operative treatment. These lesions can come from either acute bony Bankart lesions or chronic anterior glenoid erosion. Recent studies have shown that the presence of glenoid bone loss and inferior hyperlaxity led to a 72-75% recurrence rate [1,2].

A better understanding of the relationship between glenoid lesion size and recurrent instability can inform better treatment decisions. So, the aim of our study was to find if there exist a relationship between the bony Bankart lesion size, arm position, and the shoulder's anterior instability. We used a similar protocol to that of Itoi et al. which also helped us to validate our model [3]. Our hypothesis was that the distance to dislocation would decrease with increasing size of the defect and also that shoulder stability would be unaffected by arm position (thoracohumeral abduction angle and external rotation).

METHODS

A computer-based finite element approach was used to model the glenohumeral joint with an intact humerus and glenoid. A generic model was developed for cartilage and bones of the glenoid and humerus, using data available in the literature [4,5]. Bones were assumed to be rigid bodies, and cartilage was modeled with hyperelastic material properties having a Young's modulus (E) of 10 MPa and a Poisson's ratio (ν) of 0.4 [6]. 3D hexahedral element mesh was used, with 7830 elements for humeral head, and 9280 elements for glenoid mesh. Then different sizes of bony Bankart lesions for the glenoid were created at the anterior side similar to those of Itoi et al.3 Lesion sizes were $^1/_4$, $^1/_2$, $^3/_4$, and the full glenoid radius (R) (Fig. 1) [2]. The experiments were analyzed using static analysis with displacement control in the anterior inferior direction. A 50-N compressive load was simulated for an intact joint, and the translational distance to dislocation was analyzed. Tests were performed at two different thoracohumeral abduction angles (45° and 90°). At each thoracohumeral abduction angle, a range for arm rotation was chosen between 40° internal to 60° external rotation. For arm to abduct to a humero-thoracic angle of 90º, the glenohumeral joint was rotated 60º. Likewise, thoracohumeral abduction angles of 45º was calculated as the 30º glenohumeral joint rotation.

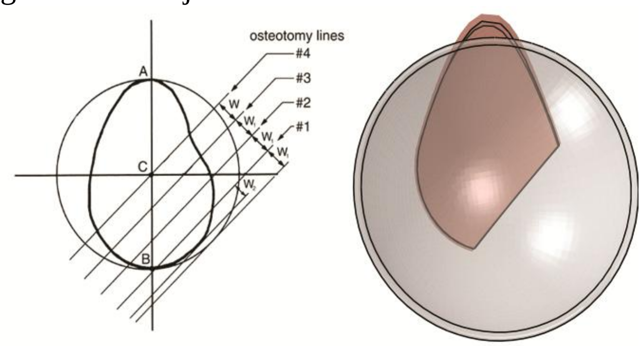

Figure 1: Creation of defects in glenoid, adapted from Itoi et al study (a) [3] and assembly view the joint with glenoid bone loss (b).

RESULTS

Figure 2 shows results for distance to dislocation of a normal joint and a joint with 4 different lesion sizes at a thoracohumeral abduction angle of 45°. The horizontal axis represents the angle of arm rotation (40° internal to 60° external rotation); the vertical axis signifies the distance to dislocation. We saw that in the presence of a small defect in the glenoid, the distance to dislocation defect decreased to 10.2 mm at neutral rotation. It decreased with each successive defect: for defect size $^{1}/_{2}$*R, $^{3}/_{4}$*R, and 1*R, the decrease in distance to dislocation was 6.5 mm, 2.1 mm, and 0.0 mm, respectively. The straight lines signifies that the values are similar at each rotation angle.

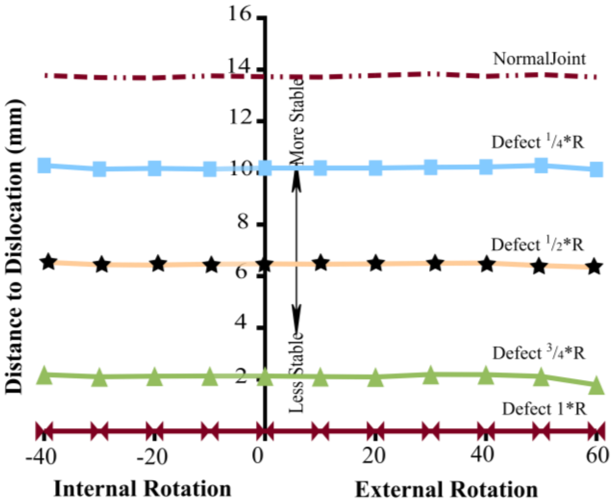

Figure 2: Distance to dislocation at 45° thoracohumeral abduction.

Differences in distance to dislocation of a normal joint and a joint with 4 different bony Bankart lesion sizes at a thoracohumeral abduction angle of 90° are shown in Figure 3. Decreases in the distance to dislocation for defect sizes $^{1}/_{4}$*R , $^{1}/_{2}$*R, $^{3}/_{4}$*R, and 1*R were 10.2 mm, 6.5 mm, 2.1 mm, and 0.0 mm, respectively. The straight lines signify similar stability at all positions.

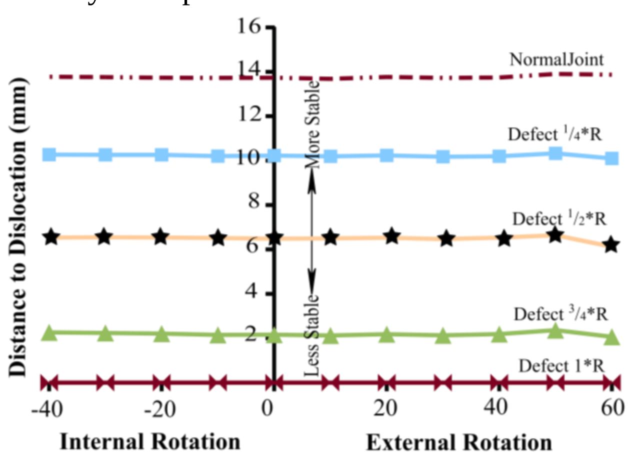

Figure 3: Distance to dislocation (in millimeters) at 90° thoracohumeral abduction.

DISCUSSION

The model was first validated by comparing the reaction force results from our study with those of Itoi et al.; similar trend were seen for decrease in reaction force with increasing size of defect in both cases [3]. Results showed that the distance to dislocation was 13.8 mm for a normal joint, which reduces to 10.2 mm for defect size $^{1}/_{4}$*R and 0.0 mm for largest defect (1*R). This shows that if a person has a glenoid bone loss equivalent to 1*R size of defect then the shoulder's stability will be zero irrespective of the arm position. The straight lines for individual defect at both thoracohumeral abduction at all rotation angles signifies that the shoulder's stability remains unaffected by arm position. We saw from our results that the progression in size of the bony Bankart lesion the shoulder's stability to a great extent. Itoi et al. described that any defect greater than $^{1}/_{4}$*R would need to be surgically treated to restore the glenoid arc and that associated soft tissue would also need repair [3]. We saw from our results that stability drops lower than 50% of normal joint at defect size of $^{1}/_{2}$*R. Results from our finite element model were comparable to those of past studies.

CONCLUSIONS

Instability of shoulder increases with increasing size of the Bankart lesions. We found that bone loss of glenoid equal or greater than the 1*R size can lead to zero stability of joint. Furthermore, instability caused by glenoid bone loss is independent of the position of arm. The limitation of this study is that we used approximate geometry of the glenohumeral joint. But this study helped us to understand how the curvature of the glenoid is important for shoulder stability.

REFERENCES

1. Boileau P et al. *JBJS Am* **88**,1755-63, 2006.
2. Giuseppe Milano et al. *AJSM* **39**, 1870, 2011.
3. Itoi E et al. *JBJS Am* **82**, 35-46, 2000.
4. Soslowsky LJ et al. *CORR* **285**, 181-90, 1992.
5. Iannotti JP et al. *JBJS Am* **74**, 491-500, 1992.
6. Büchler P et al. *Clin Biomech* **17,** 630-639, 2002.

ELECTROMYOGRAPHIC AND KINEMATIC ANALYSIS OF MEDIAL REVERSE SHOULDER ARTHROPLASTIES DURING FUNCTIONAL MOTIONS

+Walker, DR; Struk, AM; Wright, TW; Banks, SA
+Departments of Mechanical & Aerospace Engineering and Orthopaedics and Rehabilitation, University of Florida, Gainesville, Florida
drew208@ufl.edu

INTRODUCTION

Reverse total shoulder arthroplasty (RTSA) increasingly is utilized to restore shoulder function in patients with osteoarthritis and rotator cuff deficiency. However, little is known about post-RTSA shoulder function. We assume that better knowledge of how RTSA affects shoulder function and muscle activation patterns will lead to refinement in the design, utilization and rehabilitation strategies for RTSA. Deltoid muscle activity in the rotator cuff deficient shoulder is of particular interest to determine how patients compensate for lost rotator cuff function with restored glenohumeral stability. The purpose of this study was to evaluate deltoid and upper-trapezius muscle activity between the involved and non-involved side of medial RTSA patients during active shoulder weighted and unweighted abduction weighted and unweighted flexion and external rotation. Motion capture and electromyography (EMG) were used to quantify 3D motion and muscle activation.

METHODS

Fifty subjects participated in this IRB approved study. Subjects who were at least 6 months post RTSA comprised the experimental group. All subjects performed three arm motions in unweighted and weighted (3 lb) conditions: abduction to the side, forward flexion in the sagittal plane and external rotation with the arm at the side. EMG activation of the anterior (AD), Lateral (LD) and posterior (PD) aspects of the deltoid and upper trapezius (UT) muscles were recorded using bipolar surface electrodes (Noraxon USA inc. Scottsdale, AZ). Motion capture using passive reflective markers was used to quantify 3D shoulder motions. Maximal voluntary isometric contractions (MVIC) were used to normalize activity for each muscle. Two-way repeated-measures ANOVA is used to compare groups. Tukey's Honestly Significant Difference was used to perform pair-wise post-hoc comparisons. The level of significance for ANOVA was chosen to be 0.05.

RESULTS AND DISCUSSION

Muscle activation of the lateral deltoid and the upper trapezius was significantly higher in the involved shoulder than non-involved shoulder during abduction (Fig. 1; LD: p=1E-09). This trend is also seen in both weighted and unweighted trials of flexion in the lateral deltoid (Figs. 2&3; AD: p=0.000601). Posterior deltoid activity in all activities averaged less than 20% of MVIC. Maximum posterior deltoid activity of 18% MVIC was observed during external rotation, when the reaction force at the wrist averaged 25N.

The goal of this study was to contrast muscle activation in involved and noninvolved sides of patients with unilateral RTSA during unweighted and weighted activities.

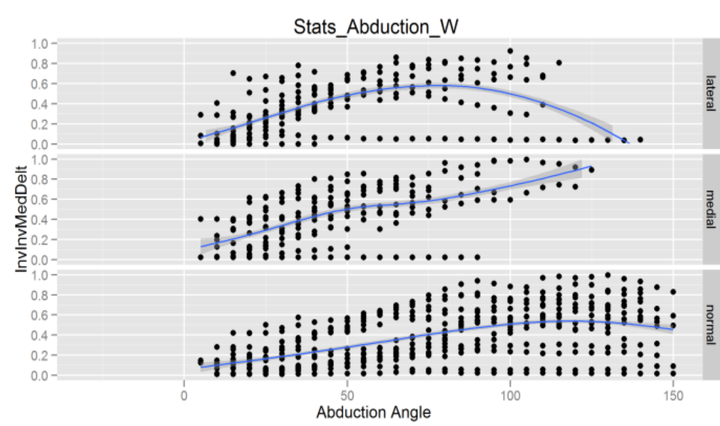

Figure 1: Lateral deltoid activation was greater in involved side RTSA shoulder than the non-involved side during unweighted and weighted abduction .

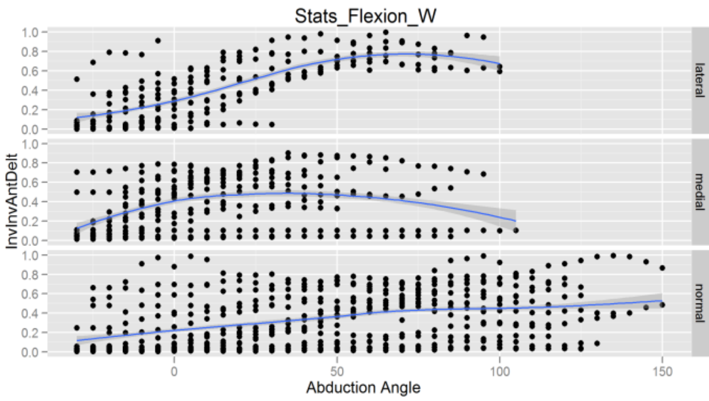

Figure 2: The muscle in the line of action performs at a higher activity in the involved side versus the uninvolved side. The weighted trials have a higher activation than unweighted trials.

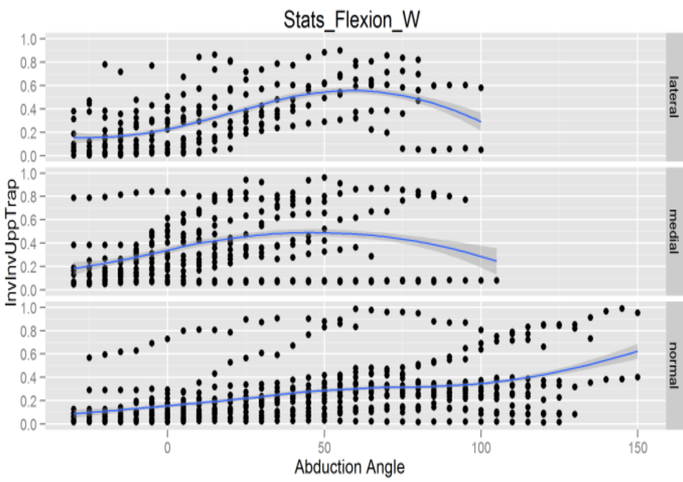

Figure 3: The upper-trapezius activation pattern for both the involved and non-involved sides of the RTSA patients during weighted and unweighted flexion exhibit an activation which steadily increases as a function of angle in attributing to it being said to be the scapular rotator. The weighted trials were significantly higher in activation in the involved side and a lower range of motion.

CONCLUSIONS

Our data suggest RTSA simplifies deltoid muscle activation. We observed high muscle activation in the portion of the deltoid directly in line with the task, but reduced muscle function in the out-of-line portions of the muscle. It appears the intrinsic stability provided by the RTSA allows the out-of-line portions of the muscle to be relatively relaxed, whereas those portions of the muscle in the uninvolved shoulder appear to be actively stabilizing the joint. This is shown in figures 1, 2, and 3 where the muscle activity is significantly greater in the involved side for conditions in which the activated muscle lies along the plane of motion. This is even more pronounced in weighted trials. It was also found that the posterior deltoid was minimally active in all the activities tested. These observations of muscle function in RTSA shoulders improve our understanding of joint function and will inform efforts to improve RTSA implant design, surgical technique and rehabilitation.

SCAPULOHUMERAL RHYTHM OF REVERSE SHOULDER ARTHROPLASTIES DURING WEIGHTED AND UNWEIGHTED SHOULDER ABDUCTION

+Walker, DR; Struk, AM; Wright, TW; Banks, SA

+Departments of Mechanical & Aerospace Engineering and Orthopaedics and Rehabilitation, University of Florida, Gainesville, Florida
drew208@ufl.edu

INTRODUCTION

Reverse total shoulder arthroplasty (RTSA) is increasingly utilized to restore shoulder function in patients with osteoarthritis and rotator cuff deficiency [1]. There is currently little known about shoulder function after RTSA or if differences in surgical technique or implant design affect shoulder performance. The purpose of this study was to quantify scapulohumeral rhythm in patients with RSA during loaded and unloaded shoulder abduction.

METHODS

Seventeen patients with RTSA performed shoulder abduction (elevation and lowering) with and without a handheld 3kg weight during fluoroscopic imaging. Three RTSA designs were included (Figure 1). We used model-image registration techniques to determine the 3D position and orientation of the implants. Cubic curves were fit to the humeral elevation as a function of the scapular elevation over the entire motion. The slope of this curve was used to determine the scapulohumeral rhythm (SHR) [2].Two-way repeated-measures ANOVA was used to compare groups. Tukey's Honestly Significant Difference was used to perform pair-wise post-hoc comparisons. The level of significance for ANOVA was chosen to be 0.05.

RESULTS AND DISCUSSION

For abduction above 40°, shoulders with RTSA exhibited an average SHR of 1.2:1. There was no significant difference in SHR between shoulder abduction with and without 3kg handheld weights (1.6±0.2 unweighted Figure 1 and 3), nor was there a significant difference between elevation and lowering. SHR was highly variable for abduction less than 40°, with SHR ranging from a low of 1 to greater than 10. Differences in implant groups can be seen in figure 3. The lateral group has a significantly lower SHR than the medial group of RTSA shoulders.

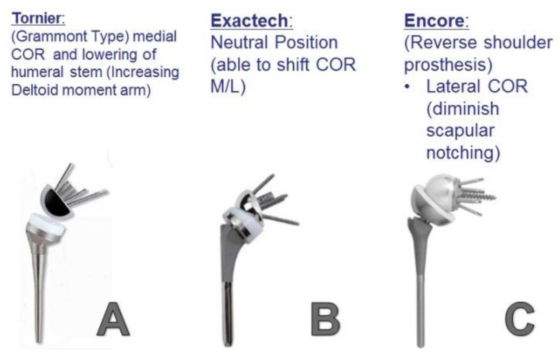

Figure 1: Reverse shoulder types: A. Medial, B. Neutral, and C. Lateral. Note the neutral type is able to shift the rotation to medial or lateral

CONCLUSIONS

At arm elevation angles less than 40°, SHR in RSA shoulders is highly variable and the mean SHR (2-5) with RTSA appears higher than SHR in normal shoulders (2-3) (Figure 2). At higher elevation angles, SHR in shoulders with RTSA (1.5-1.8) is much more consistent and appears lower than SHR in normal shoulders (2-4) (Figure 2). Ongoing analysis of reverse shoulder function with larger cohort sizes will allow us to refine our observations and determine if there are differences in shoulder function due to implant design, preoperative condition and rehabilitation protocols. These insights may lead to improvements in implant design, preoperative planning and rehabilitative strategies for RTSA surgery.

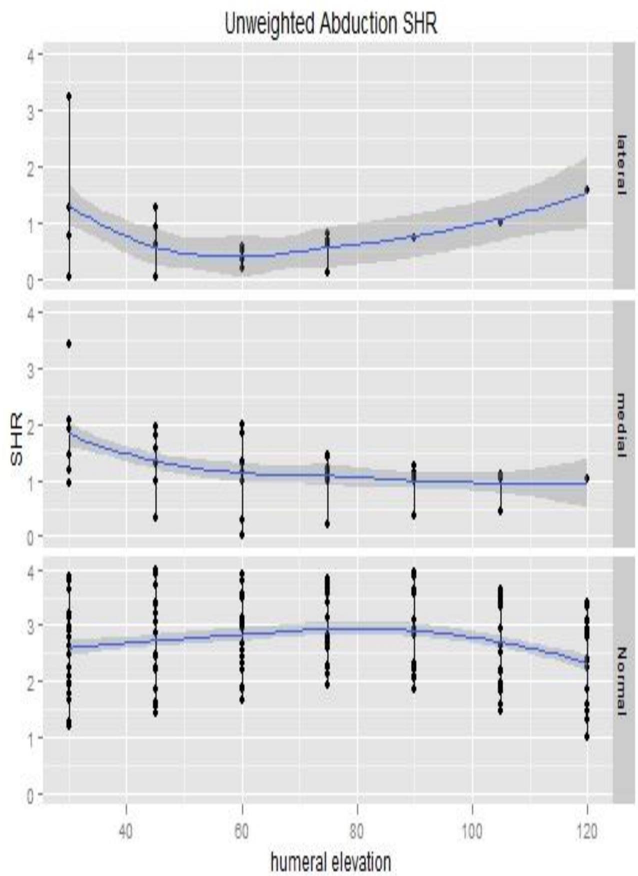

Figure 2: SHR for Lateral, Medial and Normal groups. SHR is found to be lower in RTSA groups than in Normal group.

REFERENCES

1.Boileau P, Watkinson DJ, Hatzidakis AM, Balg F. Grammont reverse prosthesis: design, rationale, and biomechanics. J Shoulder Elbow Surg 2005;14:147S-61.

2. Ebraheim NA, Xu R, Haman SP, Miedler JD, Yeasting RA. Quantitative anatomy of the scapula. Am J Orthop 2000;29:287-92.

3. Frankle M, Siegal S, Pupello D, Saleem A, Mighell M, Vasey M. The reverse shoulder prosthesis for glenohumeral arthritis associated with severe rotator cuff deficiency. A minimum two-year follow- up study of sixty patients. J Bone Joint Surg Am 2005;87:1697-705.

INFLUENCE OF SCALING ASSUMPTIONS ON TENDON STIFFNESS ESTIMATION

Elise H. E. Walker[1,2], Thomas G. Sandercock[1], and Eric J.Perreault[1,2]
[1]Northwestern University, Evanston, IL, USA; [2]SMPP, Rehabilitation Institute of Chicago, Chicago, IL, USA
email: ewalk87@u.northwestern.edu

INTRODUCTION

Muscle-tendon models are a critical component of many biomechanical simulations. An important, but often overlooked part of many such models is the tendon. An ideal tendon model would include parameters specifying all attributes of a tendon, but it is often infeasible to obtain direct measurements for all muscle-tendon units (MTUs) in a complex simulation. Therefore, most models have relied upon judicious simplification. One of the most successful and commonly used tendon models was defined by Zajac [1]. The common implementation of Zajac's tendon model is a generic tendon force-length curve that can be scaled for any individual MTU using two parameters. We shall refer to this model as the *Length Model (LM)*, as it includes only one tendon-specific parameter describing length. The advantage of this scaling model is the ease of applying it to a large number of MTUs, as in [2,3].

The basic *LM* assumes a Young's modulus of 1.2 GPa for tendon, as well as a constant tendon stress of 32 MPa at peak isometric muscle force, implying a constant ratio of muscle to tendon area. These assumptions provide for simple scaling rules, but it is unclear how well the assumptions hold for a wide range of MTUs. For instance, research indicates that tendon geometry and material properties across tendons may vary [4,5]. Thus, a more realistic modeling approach might account for unique tendon geometry while still assuming common material properties, as proposed by Cui et al. [6]. We shall call this the *Area Length Model (ALM)* because it includes parameters for both tendon length and area.

The purpose of this study was to compare these two tendon models across different MTUs from the feline hindlimb. Model predictions were compared to experimental measurements in each MTU, allowing us to assess the errors associated with each model and its underlying assumptions.

METHODS

Measured properties of six feline MTUs were used to estimate tendon stiffness at peak isometric muscle force. At least two specimens were obtained for each of the different MTUs: extensor digitorum longus (EDL), flexor hallucis longus (FHL), tibialis anterior (TA), plantaris (PLA), soleus (SOL), and medial gastrocnemius (MG). Experimental measurements for these specimens are from [6].

Tendon stiffness for the *LM* was calculated as $K^T = 37.5 \cdot \frac{F_o{}^M}{L^T}$, where $F_o{}^M$ is peak isometric muscle force, L^T is tendon length, and *37.5* is a constant derived from the assumed elastic modulus *E* (*1200 MPa*) divided by assumed tendon stress (*32 MPa*) at peak isometric muscle force, as proposed in [1]. Tendon stiffness for the *ALM* was calculated as $K^T = \frac{EA^T}{L^T}$, where A^T is tendon cross-sectional area, L^T is tendon length, and E is defined as 522 MPa, based on [6]. The percent error for each tendon stiffness estimate was computed and normalized using experimental stiffness data from [6].

While comparing estimates of tendon stiffness is useful, the relative performance of the two models is better evaluated by the more functionally relevant short-range stiffness. Short-range stiffness describes how tendon stiffness relates to muscle stiffness, and it represents an upper limit on total MTU stiffness [7], thereby providing a more complete prediction of total MTU behavior. Therefore, we also compared MTU short-range stiffness predictions of each model using the estimates of K^T (see [6] for details of short-range stiffness calculation).

RESULTS AND DISCUSSION

Tendon stiffness errors (Fig. 1) were smaller in magnitude for the *ALM* than for the *LM* in all specimens. Average error across all specimens was significantly less for the *ALM* ($p = 0.0075$). This suggests that a geometric parameter describing tendon area improves model accuracy.

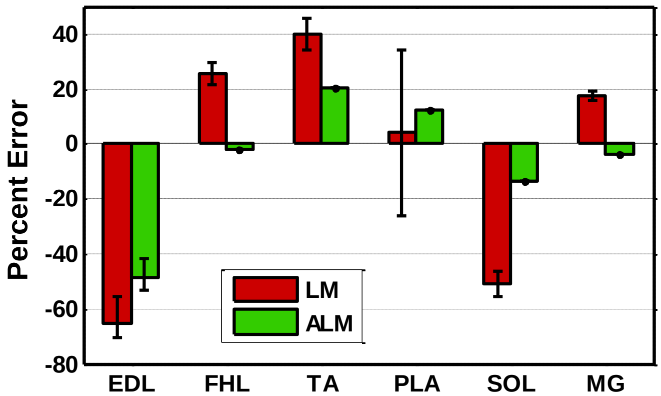

Figure 1: Percent error of tendon stiffness estimates from the *LM* and *ALM*. Error bars specify the range across all MTU specimens.

Predictions of short-range stiffness (Fig. 2) at high forces show differences between the two models that are similar to differences in tendon stiffness estimates, suggesting that tendon stiffness dominates MTU stiffness at these forces. The experimental data is predicted most accurately by the *ALM*, although the *LM* also performs well for a number of these MTUs. Neither model accurately predicts short-range stiffness for EDL, which has

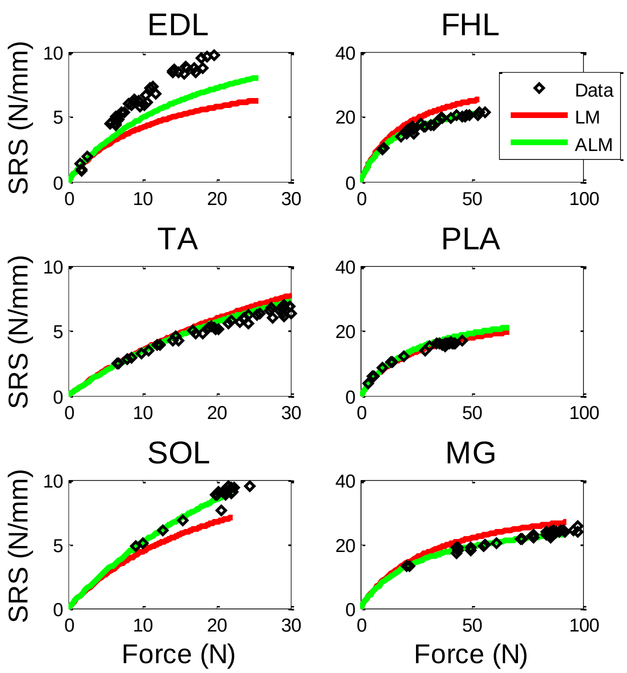

Figure 2: Predictions of short-range stiffness (SRS) for the *LM* and *ALM*. Experimental data points (black) are from [6]. Muscle force ranges from zero to F_o^M.

been shown to have different material properties than the other tested muscles [5].

It is somewhat surprising that the *LM* errors were not larger, if we consider that this model assumes an *E* value that is inaccurate for theses MTUs (according to tendon property measures in [5]). Further investigation reveals that the oversized *E* assumption is nullified by a similarly oversized assumption of tendon stress at F_o^M. Therefore, the *LM* tendon stiffness constant of *37.5* remains relatively accurate for many of these MTUs. This observation allows us to surmise whether the *ALM* is likely to yield improvements over the *LM* for a particular MTU. We can use our best guess of *E* and the stress at F_o^M to approximate the value of *E*/Stress and compare it with the *LM* stiffness constant. The closer this approximation is to *37.5*, the more similar we expect the *LM* and *ALM* models to be. Thus, the values in Table 1 indicate that *ALM* improves stiffness estimates most drastically for EDL and SOL. This is verified in Figure 2.

Table 1: Average ratio of *E*/Stress for each MTU, calculated as $(522\ MPa)/\left(\frac{F_o^M}{A^T}\right)$. Compare to *37.5*.

MTU	*E*/Stress	MTU	*E*/Stress
EDL	55.7	PLA	44.2
FHL	29.2	SOL	66.6
TA	32.4	MG	30.7

CONCLUSION

Tendon models can be improved by using both tendon length and tendon area as model parameters. Estimating the ratio *E*/Stress provides one possible indication of when such a model will yield significant improvements over the *Length Model*. However, EDL demonstrates that tendon material properties can change between MTUs, so caution must be used when assuming a constant *E* value.

REFERENCES

[1] Zajac, *Crit Rev Biomed Eng* **17(4)** 359-411, 1989.
[2] Holzbaur et al. *Ann Biomed Eng* **33(6)** 829-40, 2005.
[3] Delp et al. *Biomed Eng IEEE* **37(8)** 757-67, 1990.
[4] Robinson et al. *Ann Biomed Eng* **32(7)** 924-31, 2004.
[5] Cui et al. *J Biomechanics* **42** 679-85, 2009.
[6] Cui et al. *J Biomechanics* **41** 1945-52, 2008.
[7] Hu et al. *J Neurophysiol* **105** 1633-41, 2011.

THE EFFECTS OF LOAD CARRIAGE AND FATIGUE ON FRONTAL-PLANE KNEE MECHANICS DURING WALKING

[1] He Wang, [1]Jeff Frame, [1]Elicia Ozimek, [2]Daniel Leib, and [2]Eric Dugan,
[1]Ball State University, [2]Boise State University
email: hwang2@bsu.edu

INTRODUCTION

Military personnel are commonly afflicted by lower extremity overuse injuries [1, 2]. Overuse knee conditions are among the most common injuries during basic training [3]. Walking with heavy loads is an inevitable part of the military training, and during the twelve-weeks of basic training, the loaded running and walking distance could exceed 200 miles [1]. Therefore, military personnel have to face physical challenges comprised of load carriage and muscle fatigue.

During walking, the knee joint experiences an external adduction moment [4]. Large varus knee loading leads to cartilage degeneration and medial knee osteoarthritis (OA) [5,6,7]. Thus, the long-term effect of repetitive high varus knee loading could lead to medial knee OA; in the short term, walking with large varus knee loading could result in knee pain.

Load carriage increases vertical ground reaction force (GRF) during walking [8,9]. Walking in a fatigue state also results in increased vertical GRF [10]. It is possible that under the influences of load carriage and muscle fatigue, the knee joint may experience increased internal mechanical loading. However, it is unclear whether load carriage and fatigue result in an increase of varus knee loading during walking.

Analyzing frontal-plane knee mechanics during loaded and fatigued walking will broaden our knowledge on the potential causes of developing lower-extremity overuse injuries such as overuse knee conditions during military training.

The purpose of the study was to investigate the frontal-plane knee mechanics during loaded and fatigued walking. As the vertical GRF is increased during both the loaded and fatigued walking [8,9,10], it was hypothesized that there would be increased internal knee abductor moments during loaded and fatigued walking.

METHODS

Eighteen healthy male subjects (age: 21 ± 2 yr.; body mass: 77.6 ± 9.6 kg; body height: 181 ± 4 cm) participated in the study. Subjects wore military boots and participated in a fatiguing protocol which involved a series of metered step-ups and heel raises while wearing a 16 kg rucksack. Subjects performed the following tasks in sequence: 5-min unloaded walking; 5-min loaded walking with a 32 kg rucksack; Fatiguing protocol; 5-min loaded walking with a 32 kg rucksack under fatigue; 5-min unloaded walking under fatigue. All walking tasks were performed at 1.67 m/s on a force instrumented treadmill (AMTI). A 15-camera system (VICON) was used to track reflective markers placed on the human body at 120 Hz. Ground reaction forces were collected at 2400 Hz. Visual 3D (C-Motion) was used to calculate lower extremity joint mechanics. The following variables were analyzed: peak hip and knee adduction angles, peak hip and knee abductor moments during weight acceptance of walking. Two-way repeated measures ANOVAs were performed. Load carriage and fatigue were the independent factors. $\alpha = 0.05$.

RESULTS AND DISCUSSION

No interactions were found between load carriage and fatigue for all the dependent variables ($P > 0.05$). Load carriage led to significant increases of hip adduction ($P < 0.05$), hip and knee abductor moments ($P < 0.001$) (Table 1). Fatigue did not lead to changes in hip and knee adduction angles and abductor moments ($P > 0.05$) (Table 1).

Frontal-plane knee mechanics is altered during loaded walking. There is a large internal abductor moment introduced at weight acceptance. The increased internal abductor moment may be related to the increased GRF passing through medial side of the knee. As the internal abductor moment increases, medial compartment of the knee is under large compression. Increased stress in medial knee results in cartilage degeneration and onset of medial knee OA [5,6,7]. During a 12-week military training, the accumulated loaded walking/running distance exceeds 200 miles [1], the repetitive large medial knee loading may inflict cartilage damage in medial knee and result in knee pain.

In this study, we also found that the load carriage results in alterations of frontal-plane hip mechanics. There is an increase of hip adduction during weight acceptance of loaded walking. Increasing hip adduction stretches gluteus medius and enhances the muscle's ability to stabilize the pelvis. Indeed, large hip abductor moment is associated with loaded walking. However, increasing hip adduction also stretches tensor fasciae latae on the lateral side of the hip. As load carriage results in increased knee flexion at weight acceptance of walking [8], the friction between the lateral femoral condyle and the illio-tibial band (ITB) could be elevated. Thus, during loaded distance walking, it is possible that increased hip adduction combined with cyclic knee flexion may lead to ITB syndrome.

Interestingly, the effect of fatigue on frontal-plane knee mechanics is insignificant. Although it was reported that there is an increased GRF associated with fatigued walking [10], the increased GRF may be positioned close to the center of the knee. Thus, there is no alteration of the external adduction moment.

In summary, at weight acceptance, load carriage leads to alterations of frontal-plane hip and knee mechanics. The increases of hip adduction and knee abductor moment could be the causes of overuse knee conditions, which are common during military training.

REFERENCES

1.Jones, B.H., et al. *Exercise & Sport Sciences Rev*. **17**: 379-322,1989.
2.Knapik, J. *Military Medicine* **169**: 45-53, 2004.
3.Jones, B.H., et al. *Med. Sci. Sports Exercs.* **25**(2): 197-203, 1993.
4.Rose, J. et al., *Human walking*, 3rd edition. 2006.
5.Morrison, J., *J Biomech* **3**(1): 51-61, 1970.
6.Schipplein, O., et al., *J Orthop Res*. **9**(1): 113-119, 1991.
7.Miyazaki, T., et al., *Ann Rheum Dis* **61**(7): 617-622, 2002.
8.Kinoshita, H., *Ergonomics* **28**: 1347-1362, 1985.
9.Wang, H., et al., *Proceeding of ASB*, Providence, RI. 2010.
10. Wang, H., et al., *Med. Sci. Sports Exerc*. **42**(5) S192, 2010.

ACKNOWLEDGEMENTS

Funding source: US ARMY #W81XWH-08-1-0587

Table 1: Means and SDs of Peak hip and knee adduction angles and abductor moments during weight acceptance of walking.

Variables	Unloaded and Unfatigued	Loaded and Unfatigued	Loaded and Fatigued	Unloaded and Fatigued
Hip adduction angle (deg)*	9.3 (3.2)	10.3 (3.6)	10.2 (3.1)	9.5 (3.2)
Knee adduction angle (deg)	-1.4 (2.9)	-1.1 (2.9)	-1.4 (2.6)	-1.9 (2.9)
Hip abductor moment (Nm/kg)*	1.60 (0.18)	2.18 (0.38)	2.22 (0.35)	1.66 (0.24)
Knee abductor moment (Nm/kg)*	0.84 (0.18)	1.15 (0.32)	1.10 (0.36)	0.83 (0.22)

Note. * indicates significant difference between loaded and unloaded walking conditions ($P < 0.05$).

LOWER LIMB COORDINATION IS ALTERED DURING ASYMMETRIC LOAD CARRYING WHILE WALKING ON A TREADMILL

Wang JS, Roemmich RT and Mark. D. Tillman
University Florida, Gainesville, FL, USA

INTRODUCTION

Bags (backpacks and single sling/messenger bags) have become a daily necessity for individuals of all ages. In particular, messenger bags seem to be increasing in popularity for young people. With the research on numerous types of bags (schoolbags, military bags, and athletic bags) showing that indeed, bags have a direct effect on the movement of the human body, there seems to be a lack of research on other types of bags such as messenger bags. A few researchers have investigated how asymmetric load carrying affects the biomechanics of human movement. For instance, asymmetrical load carriage has been shown to alter joint moments and kinematics of the spine [1,2]. However, few data exist regarding asymmetric load carriage and gait kinematics in terms of coordination patterns of the lower extremities. Therefore, we attempted to evaluate whether carrying a single strap messenger type bag induces abnormal coordination patterns in the lower body while walking. Specifically, the current study aimed to evaluate lower limb coordination in response to different loading conditions in university students during treadmill walking at a self-selected pace.

METHODS

Ten university students (22.6±4.18 yrs, 170.8±10.6cm, 71.7±10.8kg) walked on a treadmill under three different load conditions (Figure 1): "condition 1" (5% of body weight on both shoulders), "condition 2" (10% of body-weight on one shoulder hanging vertically down to the hip) and "condition 3" (10 % of body-weight on one shoulder with the bag draped across the trunk to opposite hip. All participants walked at their preferred pace for five minutes in each condition. A "baseline" (no load with a single strap bags on each shoulder) condition was also tested. Kinematic data were acquired using a Vicon motion analysis system with 7 digital cameras (120Hz). The last sixty seconds of gait data for each condition was recorded and used for analysis.

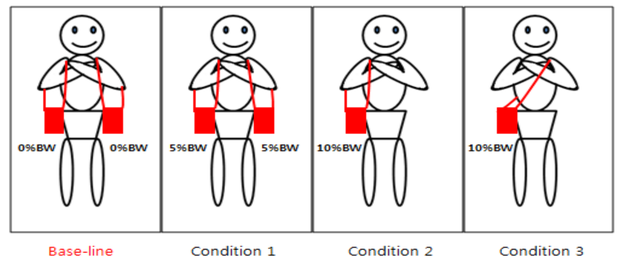

Figure 1. Illustration of three different load conditions and baseline.

Three segmental angles (thigh, shank, and foot), as well as angular velocities were calculated for each limb. Continuous relative phase (CRP) analysis was then performed using a custom Matlab code. CRP measures were conducted for each stride based on marker trajectory profiles. Segmental angular velocities were calculated from segmental angles in the sagittal plane utilizing the central difference method. These data were then used to calculate phase angles from a phase plot, using the arctangent of angular velocity/angular displacement at each data point. CRP was evaluated over three interlimb (thigh-thigh, shank-shank, and foot–foot) and two intralimb couplings (thigh-shank and shank-foot) for each limb during the gait cycle. Coordination patterns were quantified utilizing cross-correlation coefficients (CCC) and root-mean-square (RMS) techniques. CCC and RMS were assessed by comparing the average CRP in each load condition to the average CRP in the no-bag baseline condition on a stride by stride basis for interlimb and intralimb couplings. While CCC measures indicate changes in the spatio-temporal evolution of CRP patterns, RMS measures represent information about the magnitude differences in relative phase between the patterns [3]. A one-way ANOVA with Bonferroni correction was used to analyze the effect of different loading conditions on inter and intralimb coordination parameters ($\alpha < 0.05$).

RESULTS

RMS difference in thigh-shank and shank-foot coupling on the loaded side in condition 3 was significantly higher than condition 1 ($P<0.05$). However, no difference in RMS was observed in thigh-shank and shank-foot parings on the loaded side limb between condition 1 and condition 2. No differences in RMS for the thigh-shank coupling and shank-foot coupling were observed for the limb on the unloaded side. Further, there was no effect of loading condition on cross-correlation at the intralimb level: thigh-shank and shank-foot in both limbs.

RMS changes in interlimb thigh-thigh coupling in condition 2 and condition 3 significantly increased compared to condition 1. No effects on RMS were observed at the other interlimb couplings: shank-shank and foot-foot. However, CCC for thigh-thigh and foot-foot coupling in condition3 was significantly lower than condition 1 ($P<0.05$).

CONCLUSION

The present study of intralimb and interlimb coordination using CRP aimed to evaluate coordinative mechanisms in lower extremity in response to different loading conditions during treadmill walking. RMS difference and CCC were used to quantify differences at the intralimb and interlimb coordination level in three different loading conditions. We evaluated two different asymmetrical loading conditions, which displayed different coordinative patterns at the intralimb and interlimb level, especially for condition 3. Our finding suggested that pronounced differences in coordinative patterns showed when the participant carried a messenger bag on one shoulder with the bag draped across the trunk to the contralateral hip (condition 3) versus when the load was carried with one messenger bag on each shoulder (condition 1). These adaptations were mainly increased RMS (thigh-shank and shank-foot coupling in loaded side) and decreased CCC for thigh-thigh and foot-foot coupling, resulting in coordination instability. One explanation for this observation may be that, because the load was relatively fixed to middle of thigh in the loaded side in condition 3 when compared to condition 2, the load more directly interfered with limb movements in the loaded side.

Therefore, carrying a single strap bag across the trunk appears to disrupt limb coordination to a greater degree than carrying bag vertically. The findings from the current study may prove important because they provide researchers with preliminary knowledge concerning diverse adaptive strategies due to asymmetrical loads. The adaptation in limb coordination due to asymmetrical load carrying should be further investigated, as it may be indicative of acute and chronic joint injury and pain.

REFERENCES

1. DeVita P, Hong D, Hamill J. Effects of asymmetric load carrying on the biomechanics of walking. *J Biomech*. 1991;24(12):1119-1129.

2. Fowler NE, Rodacki ALF, Rodacki CD. Changes in stature and spine kinematics during a loaded walking task. *Gait Posture*. 2006;23(2):133-141.

3**.** Haddad JM, van Emmerik REA, Whittlesey SN, Hamill J. Adaptations in interlimb and intralimb coordination to asymmetrical loading in human walking. *Gait Posture*. 2006;23(4):429-434.

Table 1
Mean RMS difference and Cross-Correlation Coefficient

	RMS Difference (degree) Loading condition			**Cross-Correlation Coefficient Loading condition**		
	Condition 1	**Condition 2**	**Condition 3**	**Condition 1**	**Condition 2**	**Condition 3**
Intralimb coupling						
thigh-shank(loaded)	6.03±2.59	8.08±4.94	8.57±3.99*	0.996±0.004	0.993±0.007	0.992±0.008
shank-foot(loaded)	3.70±1.28	4.29±2.11	5.94±2.63*	0.989±0.012	0.989±0.008	0.982±0.024
thigh-shank(unloaded)	5.81±2.11	8.99±6.45	8.50±4.81	0.997±0.003	0.993±0.011	0.994±0.007
shank-foot(unloaded)	3.08±1.28	4.37±2.51	4.65±2.44	0.997±0.012	0.992±0.010	0.994±0.005
Interlimb coupling						
thigh-thigh	2.49±0.80	4.61±2.43*	4.21±2.33*	0.979±0.013	0.953±0.037	0.944±0.048*
shank-shank	2.24±0.97	3.15±2.20	3.98±2.86	0.983±0.005	0.974±0.018	0.971±0.025
foot-foot	3.08±1.63	3.94±1.77	4.38±2.55	0.975±0.028	0.967±0.018	0.963±0.035*

*Indicates a significant difference compared to condition 1 at $P<0.05$.

PRELIMINARY STUDY OF CHANGES IN TRUNK FORWARD BEND ABERRANT PATTERNS POST CORE STABILIZATION INTERVENTION

Peemongkon Wattananon, Scott Biely, Won Sung, Marco Cannella and Sheri Silfies

Drexel University, Rehabilitation Sciences Spine Research Lab, Philadelphia, PA, USA
email: pw86@drexel.edu web: http://www.drexel.edu/cnhp/rehab_sciences

INTRODUCTION

The aberrant movement patterns observed during a forward bend task are associated with impairments in trunk neuromuscular control and assist in identifying patients with clinical lumbar instability (CLI). Core stabilization exercise aims to restore trunk neuromuscular control during functional tasks. Judder, one type of aberrant pattern, is defined as shaking (sudden deceleration and acceleration), or quick out of plane movements.[1] It causes disruption in sagittal angular velocity. Therefore, judder observed during a forward bending task can be characterized by utilizing a kinematic tracking system in conjunction with the dynamic system approach.[2] The purpose of this study was to investigate the effect of core stabilization exercises on aberrant movement patterns (judder) in patients with CLI.

METHODS

Fifteen healthy subjects (8 women; mean age 37 ± 14; BMI 22.3 ± 1.8) and 6 patients with CLI (5 women; mean age 35 ± 15; BMI 27.5 ± 5.9) were recruited from 2 orthopedic outpatient physical therapy clinics. The patients with CLI demonstrated "judder" during their initial clinical examination and were classified as having CLI. All demonstrated successful outcomes after 8 weeks of core stabilization exercises (50% decrease in Oswestry score and 2-point increase in patient specific functional scale (PSFS)). Kinematic data from the femur, pelvis, lumbar and thoracic segments were recorded utilizing a position tracking system (Polhemus, Inc.) during 2 sets of 3 repetitions of an active forward bend task. Data were recorded pre and post intervention.

All data analysis was performed using custom LabView (National Instrument, Corp.) and SPSS (IBM, Corp.) software programs. Euler angles were derived from the position data and resampled to 100 data points across the task. Intra- and inter-session kinematic pattern consistency (CMC) was .80-.98 and .76-.97 respectively. Kinematic data from 15 healthy control subjects were used to calculate intraclass correlation coefficients ($ICC_{2,2}$) and standard error of the mean (SEM) for each of the 100 data points. These values were used to establish 95% minimal detectable change (MDC_{95}) bands around the control phase plane plot using following formula:

$$MDC\ band = Mean \pm (1.96 \times SEM \times \sqrt{2})$$

$$Where;\quad SEM = SD \times (1 - ICC)$$

The phase plane plots (sagittal angular motion vs. velocity) with MDC_{95} bands for each segment (pelvis, lumbar, thoracic) were created (Fig.1). Each CLI plot was compared against the control. Averaged individual plots were classified as aberrant if they fell outside the MDC_{95} band and/or had sudden fluctuation in instantaneous angular velocity.[2] In addition, pre-post treatment plots were compared to investigate the effect of core stabilization exercises on this aberrant movement pattern.

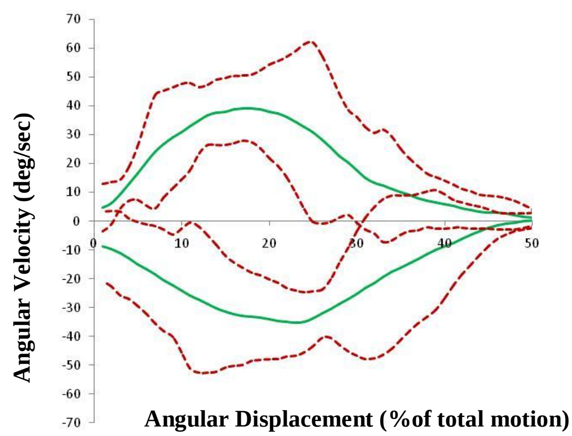

Fig. 1: Example of lumbar phase plane plot with MDC_{95} band. Green solid line represents averaged angular velocity of control group and dotted red line represents MDC_{95} band.

Independent t-tests were performed to compare segment ROM, maximum and mean angular velocity between healthy control and CLI subjects. Paired t-tests were performed between pre and post intervention on the same variables.

RESULTS

Independent t-tests were non-significant ($p > .05$) between control and CLI subjects. Paired t-tests were non-significant ($p > .05$) between pre and post intervention. Pre-post comparisons of movement pattern (judder) are shown in the Table1. Judder was consistently observed in the lumbar phase plane plot.

Table 1: Classification of individual-averaged aberrant movement pattern (judder) pre and post core stabilization exercises based on clinical and kinematic identification of MDC_{95} band and fluctuation.

Subject	Clinical Observation		Lumbar Kinematic Rating				
			MDC_{95}		Fluctuation		
	Pre	Post	Pre	Post	Pre	Post	Note
1	+	-	+	-	+	-	
2	+	-	+	+	-	+	
3	+	+	+	+	-	-	
4	+	-	-	-	+	-	
5	+	+	+	+	+	+	Smoother
6	+	+	-	+	+	+	Smoother

DISCUSSION AND CONCLUSIONS

Both control and CLI subjects performed the task in a comparable manner related to segment ROM and angular velocity. There was no significant effect of the stabilization exercises on segment ROM and angular velocity. Although most of the patients did not change patterns post intervention based on MDC_{95} band, the patterns tended to shift toward the control group as well as increase the smoothness of the phase plane plot (Fig. 2a and 2b). These findings indicate core stabilization exercise may have an effect on the neuromuscular system by enhancing segment control. The fact that there was not a consistent change based on MDC_{95} band may be caused by our averaging of patterns across trials. This preliminary study suggests the smoothness of phase plane plots may provide a better representation of neuromuscular control during trunk forward bend. Further investigations of judder may need to be focused on quantifying the smoothness of the movement patterns. The relationship between the clinical and kinematic findings also requires more exploration.

REFERENCES

1. Hicks GE, et al. *Arch Phys Med Rehabil.* 2005;**86**(9):1753-62.
2. Wattananon P, et al. *Proceedings of the 35th Conference of the American Society of Biomechanics.* 2011; 812-13

ACKNOWLEDGEMENTS

This study was supported by a grant from the National Institutes of Health (NICHD, K01HD53632).

Lumbar Phase Plane Plot with 95% MDC Band

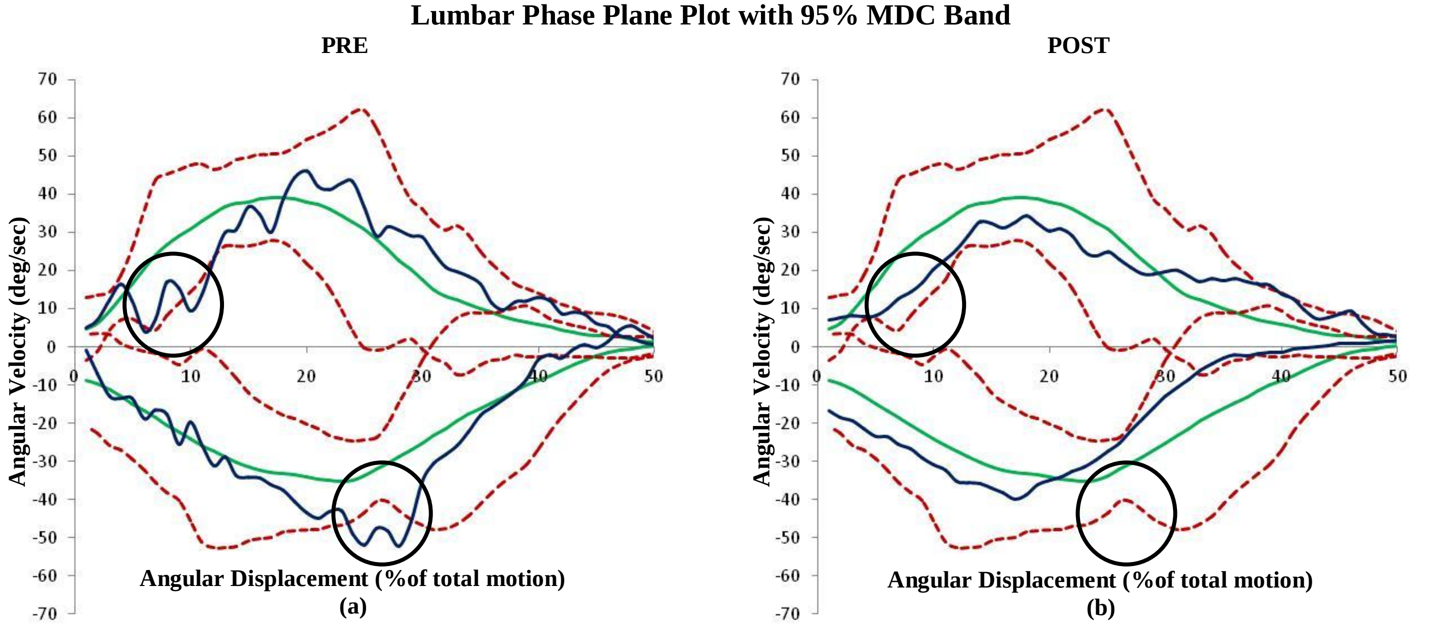

Fig. 2: Phase plane plot (subject 1) pre and post intervention. Green solid line represents averaged angular velocity of control group, dotted red line represents MDC_{95} band, and blue solid line represents a single bend. Phase plane plot had shifted closer to the control group and remained within the MDC_{95} band. The most striking change is the increased control (smoothness) after intervention (circles).

COMPARISON OF HIP MORPHOLOGY IN FEMOROACETABULAR IMPINGEMENT AND NORMAL PATIENTS

[1]Ashley A. Weaver, [1]Laura C. Rucker, [1]Jillian E. Urban, [2]Kanthan Theivendran and [1]Joel D. Stitzel

[1]Virginia Tech – Wake Forest University Center for Injury Biomechanics, Winston-Salem, NC, USA
[2]Royal Orthopedic Hospital, Birmingham, UK
email: asweaver@wakehealth.edu, web: www.wakehealth.edu/cib

INTRODUCTION

Femoroacetabuluar impingement (FAI) is characterized by abnormal hip joint morphology that causes friction between the acetabulum and femur and can lead to osteoarthritis [1]. Hip degradation can be caused by variations in size, shape, and orientation of either the proximal femur or the acetabulum, or a combination of both [1-3]. Types of FAI include cam impingement due to abnormal femoral head shape and pincer impingement characterized by variations in acetabular morphology that result in over coverage of the femur. Previous studies have quantified the 3D morphology of normal hips and compared 3D and 2D hip measures [4-5]. The objective of this study was to quantify the 3D geometry of the acetabulum and femur in FAI and normal hips and determine morphological differences between these two groups.

METHODS

Computed tomography (CT) scans of 48 patients with FAI and 35 normal patients were analyzed. The FAI patients consisted of 24 females and 24 males (mean age: 29) with FAI classified as cam only, pincer only, cam and pincer, or non-cam and non-pincer. The normal patients consisted of 15 females and 20 males (mean age: 33). The acetabulum and femoral head of each hip were segmented using a semi-automated technique and 3D models were created (Figure 1). To calculate acetabular volume, a line was drawn to enclose the acetabulum (Figure 2, left) and the acetabular space occupied by the femoral head was filled (Figure 2, center). The original acetabulum mask was then subtracted to compute the acetabular volume (Figure 2, right).

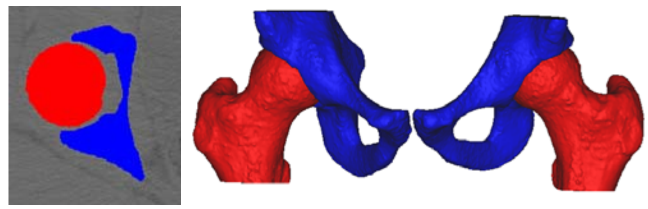

Figure 1: (Left) Axial view of a femur and acetabulum segmented from a CT scan. (Right) 3D models.

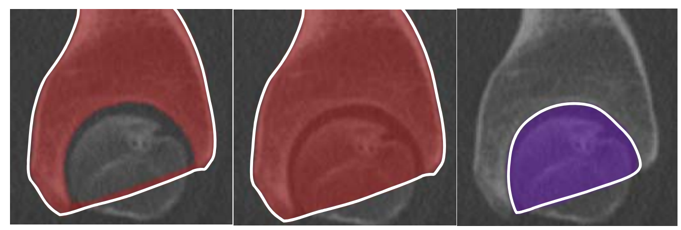

Figure 2: (Left) Line drawn to enclose the acetabulum. (Center) Filled acetabular space occupied by the femoral head. (Right) Acetabular volume.

The following measurements were collected for each hip and used to characterize morphological differences in FAI and normal hips: 1) Acetabular volume, 2) Area of the acetabulum overlapping the femoral head, 3) Area of the femoral head overlapped by acetabulum, and 4) Percentage of the femoral head covered by the acetabulum. The photos in Table 1 illustrate the morphological measurements collected.

RESULTS AND DISCUSSION

Significantly higher acetabular volume, overlapping surface areas, and femoral coverage measurements were found in FAI hips compared to normal hips with a Student's t-test analysis (Table 1). These differences were significant even when gender was controlled, which further suggests the 3D measurements are capturing true differences in FAI and normal hip joint morphology.

A one-way ANOVA analysis was used to investigate morphological differences with differing types of FAI. Significantly higher acetabular volumes and areas of the acetabulum overlapping the femoral head in cam only impingements were found compared to normal hips (*p = 0.0040* for each test).

Larger areas of the femoral head overlapped by acetabulum were found in the cam only and the cam and pincer groups compared to the normal group (*p = 0.0004* and *0.0323*). The area of femoral head overlapped by the acetabulum was also significantly larger in the cam only group compared to the non-cam and non-pincer group (*p = 0.0287).*

Increased percent femoral head coverage was observed in all FAI groups compared to the normal group (*p = <0.0001* for the cam only, pincer only, cam and pincer, and non-cam and non-pincer comparisons). The percent femoral head coverage was also significantly larger in the cam only group compared to the non-cam and non-pincer group (*p = 0.0006*).

The methodology employed in this study can be used to quantify morphological hip pathologies and could provide additional information for borderline FAI and acetabular dysplasia patients. While the method is more time consuming than traditional 2D measures, it eliminates parallax and allows for 3D overlap at the hip joint to be directly measured which is of clinical significance.

CONCLUSIONS

This study presents a systematic method to quantify 3D hip joint morphology from CT scans of FAI and normal patients. Comparisons of acetabular volume, areas of overlap at the acetabular-femoral interface, and percent femoral head coverage found signficantly higher values in FAI hips compared to normal hips.

Significant differences in hip joint morphology between different classifications of FAI and the normal hips were also detected. Overall, results suggest over coverage of the femoral head by the acetabulum in FAI hips compared to normal hips. The methodology and results of this study will assist clinicians in the diagnosis of hip abnormalities such as FAI. Characterization of hip joint morphology also assists surgeons in planning and performing surgeries to correct hip abnormalities such as FAI.

REFERENCES

1. Tannast M, et al. *AJR* **188**, 1540-1552, 2007.
2. Beck M, et al. *JBJS* **87-B**, 1012-1018, 2005.
3. Pfirmann C, et al., *Radiology* **240**, 778-785, 2006.
4. Stubbs AJ, et al. *Hip International* **21(5)**, 549-558, 2011.
5. Weaver AA, et al. *Biomed Sci Instrum* **45**, 155-160, 2009.

Table 1: Results of t-tests comparing means of FAI and normal hip morphological measurements.

	Acetabular volume (cm^3)	**Acetabulum overlapping femoral head (cm^2)**	**Femoral head overlapped by acetabulum (cm^2)**	**Percent femoral head coverage**
FAI (mean)	32.982	38.06	28.66	60.4
Normal (mean)	29.787	35.03	25.41	48.8
p-value	0.0109*	0.0052*	0.0006*	<0.0001*
	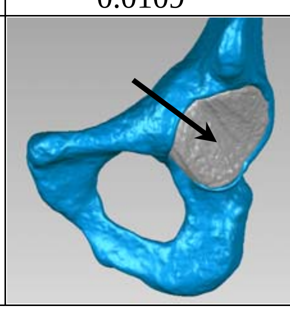	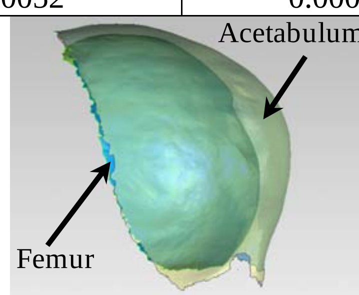		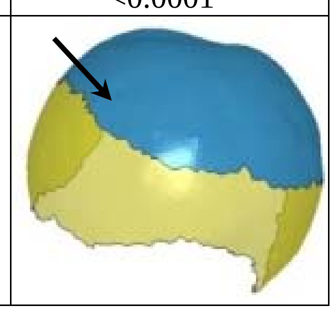

THE ROTATIONAL STIFFNESS OF FOOTBALL SHOES MAY AFFECT THE LOCATION OF A POTENTIAL ANKLE INJURY

[1]Feng Wei, [2]Eric G. Meyer, [1]Jerrod E. Braman, [1]John W. Powell and [1]Roger C. Haut

[1]Michigan State University, East Lansing, MI, USA
[2]Lawrence Technological University, Southfield, MI, USA
Corresponding Email: haut@msu.edu, web: http://www.obl.msu.edu

INTRODUCTION

In young athletes, acute ankle trauma is responsible for 10% to 30% of all sports-related injuries [1]. While medial and high ankle sprains are less common than lateral ankle sprains, they represent a more disabling problem requiring longer recovery and different treatment [2]. The mechanism of injury in medial (anterior deltoid ligament or ADL) and high (anterior tibiofibular ligament or ATiFL) ankle sprains is commonly ascribed to excessive internal rotation of the upper body, while the foot is planted on the playing surface [3]. A recent study by our laboratory showed further that ADL injury occurs during external rotation of the neutral foot, while the ATiFL is typically the site of injury for external rotation of the everted foot [4].

Excessive rotational traction (torque) from shoe-surface interface has been implicated in the high incidence of ankle injuries suffered by athletes [5]. In addition, Livesay et al. [6] showed that differences in rotational stiffness between various shoe-surface combinations are greater than those in peak torque. A recent study by Villwock et al. [7], involving football shoes and various natural and synthetic playing surfaces, suggests that the shoe-surface rotational stiffness may be associated, in part, with the design of a shoe's upper. Yet, the effect of shoe design on patterns of ankle ligament strains during external rotation of the foot has not been directly investigated to date.

METHODS

Four football shoe designs were tested and compared in terms of rotational stiffness. Tests were conducted on a hydraulic, biaxial testing machine (MTS Corp., Eden Prairie, MN). The four football shoe types were Nike Air, Nike Merciless, Adidas Blitz, and Nike Flyposite. A surrogate lower extremity and custom football cleat molds that were made of epoxy resin were used in the tests. After a compressive pre-load of 1500 N and a rotational pre-torque of 2 Nm were applied to a neutral-positioned surrogate ankle, a dynamic torque of 60 Nm was input in load control at a frequency of 1 Hz (0.5 s to peak torque) and repeated two more times for each shoe design. The shoe rotational stiffness, defined as the slope of torque-rotation curve, was calculated in Nm/deg and compared between shoes.

Twelve (six pairs) male cadaveric neutral-positioned ankles were externally rotated 30° using two selected shoe designs. The limbs were transected ~15 cm distal to the center of the knee. Shoes with the highest (rigid) and lowest (flexible) rotational stiffnesses were randomly assigned to the left or right limbs. The same pre-load and pre-torque were used in the cadaveric tests. Internal tibial rotations of 30° were input in position control at a frequency of 1 Hz (0.5 s to peak rotation). Max torques and rotational stiffnesses were reported for each limb.

Motion capture (Vicon, Oxford, UK) was performed to track movement of the talus with a reflective marker array screwed into the bone. These motions, relative to the tibia in three directions, were determined for each limb. A computational ankle model [8] was utilized to input talus motions for estimation of ankle ligament strains. The model was constructed from a generic computer tomography (CT) scan of a cadaveric ankle. CT images were first converted into 3D models in MIMICS (Materialise, Ann Arbor, MI) and then imported into SolidWorks (TriMech Solutions, Columbia, MD) for motion simulation

[9]. Ligament strains, defined in percentage as the relative elongations of ligaments, were estimated from the model. Two-way ANOVA and SNK post hoc tests were used in statistical analysis, with $p<0.05$ considered significant.

RESULTS AND DISCUSSION

Among the four shoe designs, the Air showed the lowest rotational stiffness (21.9 ± 2.8 Nm/deg), while the Flyposite had the highest stiffness (50.0 ± 1.7 Nm/deg). Cadaveric tests demonstrated that torque-rotation responses overall were significantly different between limbs, with the limb in the rigid shoe stiffer than that in the flexible shoe (Fig 1). At 30º of rotation the rigid shoe generated higher ankle joint torque at 46.2 ± 9.3 Nm than the flexible shoe at 35.4 ± 5.7 Nm. While talus rotation was greater in the rigid shoe (15.9 ± 1.6º vs. 12.1 ± 1.0º), the flexible shoe generated more talus eversion (5.6 ± 1.5º vs. 1.2 ± 0.8º). While these talus motions resulted in the same level of ADL strain (~5%) between shoes, likely because of the neutral foot position used in these experiments, there was a significant increase in ATiFL strain (4.5 ± 0.4% vs. 2.3 ± 0.3%) with the flexible versus rigid shoe design (Fig 2).

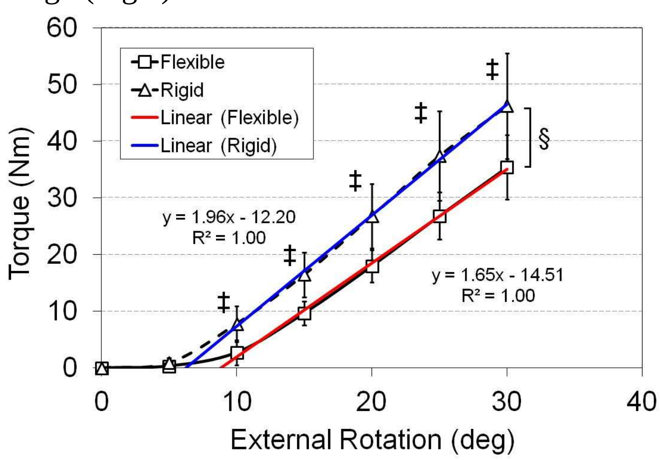

Figure 1: Torque-rotation curves showed a toe region followed by a linear region.

The increase of ATiFL strain was largely due to the increased level of talus eversion noted in the flexible shoe. The study also showed that there was a potential direct relationship between ankle joint torque and the extent of axial talus rotation, and an inverse relationship between ankle joint torque and talus eversion.

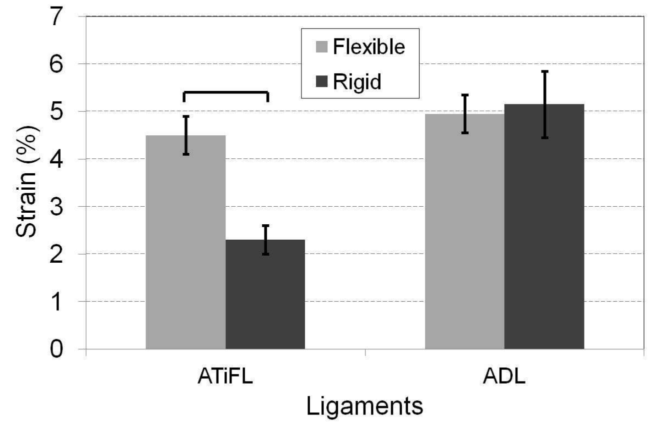

Figure 2: Only two ligaments with the highest strains were reported. ADL strains were statistically greater than ATiFL strains for both shoe designs.

CONCLUSIONS

We externally rotated six pairs of cadaver limbs in two different football shoe designs, a flexible shoe and a rigid shoe, and found that while the torques developed with the more flexible shoe were lower than those with the rigid shoe, more talus eversion resulted in a significant increase in ATiFL strain. This result may suggest an increased risk of high ankle sprains with the more rotationally flexible shoe design during external foot rotation. The study showed that football shoe design may have an effect on the pattern of ankle ligament strains, and potentially the site and severity of ankle sprain resulting from external foot rotation. In future studies these data may be useful in characterizing shoe design parameters and balancing potential ankle injury risks with player performance.

REFERENCES

1. Hootman JM, et al. *J Athl Train* **42**, 311-9, 2007.
2. Waterman BR, et al. *Am J Sports Med* **39**, 992-8, 2011.
3. Guise ER, *Am J Sports Med* **4**, 1-6, 1976.
4. Wei F, et al. *J Orthop Res*, **doi**:10.1002/jor.22085.
5. Nigg BM, et al. *J Sports Sci* **5**, 117-45, 1987.
6. Livesay GA, et al. *Am J Sports Med* **34**, 415-22, 2006.
7. Villwock MR, et al. *Am J Sports Med* **37**, 518-25, 2009.
8. Wei F, et al. *Ann Biomed Eng* **39**, 756-65, 2011.
9. Wei F, et al. *J Biomech* **44**, 2636-41, 2011.

A POTENTIAL ROLE OF EVERSION IN LIMITING MEDIAL AND HIGH ANKLE SPRAINS: A PARAMETRIC STUDY

[1]Feng Wei and [2]Roger C. Haut

[1]Kessler Foundation, West Orange, NJ, USA
Email: weifeng@msu.edu
[2]Michigan State University, East Lansing, MI, USA
Email: haut@msu.edu, web: http://www.obl.msu.edu

INTRODUCTION

Acute injuries that occur to the ankle are among the most frequent musculoskeletal injuries in all levels of sports, and ligament sprains account for 75% of these injuries [1]. As opposed to the most common lateral ankle sprain, medial and high ankle sprains are more problematic due to their potential for a significantly greater time lost and subsequent chronic ankle dysfunction [2]. While lateral ankle sprains are mostly ascribed to excessive foot inversion [3], the mechanisms of injury in medial and high ankle sprains are yet unclear, although clinically they are associated with external foot rotation [4].

We recently conducted biomechanical experiments wherein pairs of cadaver ankles were axially loaded and externally rotated in dorsiflexion with and without 20º foot eversion. The study identified isolated anterior tibiofibular ligament (ATiFL) injury in everted limbs, representing a high ankle sprain, and anterior deltoid ligament (ADL) injury in neutral limbs, representing a medial ankle sprain [5]. Another study examined the influence of a football shoe's rotational stiffness on motion of the talus and corresponding strains in these key ankle ligaments [6]. The study showed that a flexible shoe generated talus eversion and high ATiFL strains under external foot rotation, while a more rigid shoe limited talus eversion but resulted in high ADL strains. The purpose of the current parametric study, using an existing, validated computational ankle model, was to determine if there exists an allowable level of eversion that would help minimize the potential for damaging strains in either the ATiFL or ADL under external foot rotation.

METHODS

Details of model development and validation have been described in previous studies [7,8], thus only a brief description is given here. The ankle model was constructed from a generic computer tomography (CT) scan of a cadaveric ankle, with separations of 0.6 mm between slices. CT images were first converted into 3D models in MIMICS (Materialise, Ann Arbor, MI) and then imported into dynamic rigid-body motion simulation software (SolidWorks, TriMech Solutions, Columbia, MD). The ankle model included 21 ligaments formulated as linear elastic springs with properties adapted from the literature [7].

An axial load of 1500 N (~2X body weight) and a talus dorsiflexion of 20º were applied to the model, as used in the previous cadaveric tests [5]. The talus was successively everted from 0º (neutral) to 15º with an increment of 1º. Following each increment, a constant external rotation of 45º was applied (16 simulations in total). Ligament strains, defined in percentage as the relative elongations of ligaments, were estimated from the computational model.

RESULTS AND DISCUSSION

In all simulations, the highest strain occurred in either the ADL or the ATiFL. For the neutral foot, the ADL reached 20% strain prior to the ATiFL (30º vs. 38º of external rotation). In contrast, the ATiFL strained 20% at 32º while the ADL at 41º for the 15º everted foot (Figure 1). These results were in concert with a previous cadaver study showing that the ankle with a neutral foot failed at smaller input rotations than an everted foot [5]. Up to 15º eversion, there was a negative correlation between eversion and the ADL strain, but the ATiFL strain increased with eversion (Figure 2). External rotation generated higher strains in the ADL than in the ATiFL when eversion was less than 8.5º. The ATiFL strain was the highest with eversion angles between 8.5º and 15º. This threshold of 8.5º did not vary significantly with levels of external rotation (Figure 2 only shows the 30º external rotation case).

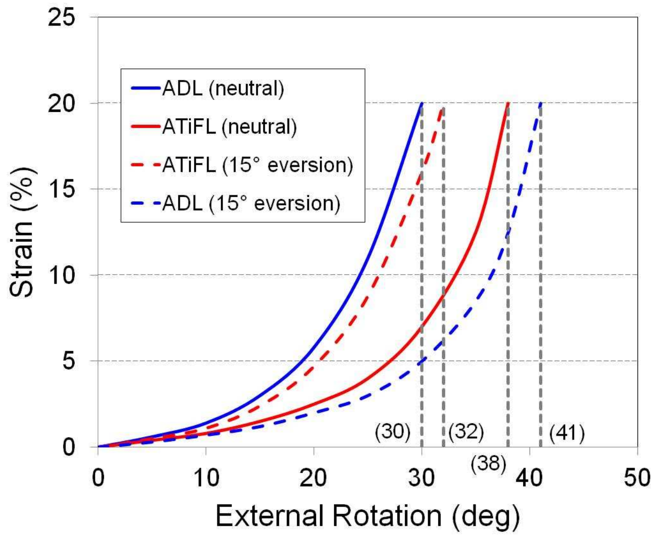

Figure 1: Ligament strain increases non-linearly with external rotation.

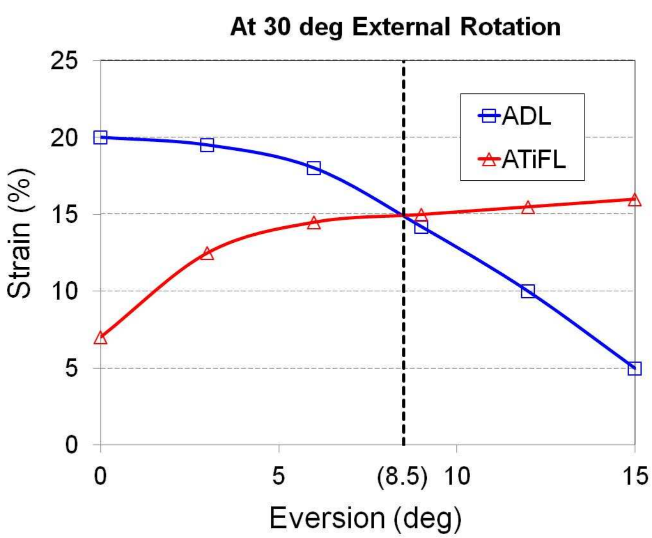

Figure 2: Under a constant external rotation (30º in this case), ADL strain decreased but ATiFL strain increased with an increase of talus pre-eversion. Magnitudes of strain crossed at 8.5º pre-eversion.

A previous study, by others, suggests that ligament strains of 15-20% may result in collagen fiber rupture [9]. These results have recently been supported in a study by our laboratory for ankle ligaments [10]. Results of the current study showed that while eversion up to 8.5° increased ATiFL strains, they were approximately 15% and therefore may not be damaging to the ligament. Thus, this parametric study suggested that, in addition to limiting external rotation, shoe designs or other preventative devices that allow up to ~8.5° ankle eversion may help limit strains in both the ADL and ATiFL to levels that will not generate severe damage to these ankle ligaments.

CONCLUSIONS

With a generic computational model of the ankle we systematically investigated the effects of talus pre-eversion on development of ankle ligament strains during a subsequent external foot rotation. The simulation results implied that excessive external rotation of the foot with 8.5º or less talus pre-eversion may produce injury to the ADL, causing a medial ankle sprain, whereas talus pre-eversion greater than 8.5º may predispose the ATiFL to injury, forming a basis for a high ankle sprain.

The study outcome showing a limiting effect on key ankle ligament strains by allowing a small level of ankle eversion during external foot rotation may provide an avenue for the development of football shoe designs or other protective gear that may help reduce the incidence and/or severity of medial and high ankle sprains on the athletic field.

REFERENCES

1. Barker HB, et al. *Sports Med* **23**, 69-74, 1997.
2. Waterman BR, et al. *Am J Sports Med* **39**, 992-998, 2011.
3. Fong DT, et al. *Sports Med* **37**, 73-94, 2007.
4. Norkus SA, et al. *J Athl Train* **36**, 68-73, 2001.
5. Wei F, et al. *J Orthop Res*, **doi**:10.1002/jor.22085.
6. Wei F, et al. *J Biomech Eng*, **doi**:10.1115/1.4005695.
7. Wei F, et al. *Ann Biomed Eng* **39**, 756-765, 2011.
8. Wei F, et al. *J Biomech* **44**, 2636-2641, 2011.
9. Yahia L, et al. *Matrix* **10**, 58-64, 1990.
10. Button KD, et al. *ASME Summer Bioengineering Conference* 80378, 2012.

ACKNOWLEDGEMENTS

We thank Dr. Seungik Baek for providing MIMICS.

LATERAL HEEL WEDGE AFFECTS THE TIBIOFEMORAL KINEMATICS IN KNEE OA PATIENTS: A PRELIMINARY WEIGHT BEARING MRI STUDY

[1,2]Feng Wei, [1]Jerome Allen, [1]Venkata Gade, [1]Carolyn Stolfi, [3]Jeffrey L. Cole and [1,2]Peter J. Barrance

[1]Kessler Foundation Research Center, West Orange, NJ, USA
[2]University of Medicine and Dentistry of New Jersey, Newark, NJ, USA
[3]Kessler Institute for Rehabilitation, West Orange, NJ, USA
Email: fwei@kesslerfoundation.org

INTRODUCTION

Osteoarthritis (OA) of the knee affects approximately 30% of individuals over the age of 60 in the United States [1]. Lateral, or valgus, wedge orthoses have been proposed as a low-cost, low-risk intervention for medial compartment knee OA, and in many patients produce immediate relief of knee pain [2]. Recently, however, the lack of significant improvement in randomized controlled trials and mixed results from other studies have resulted in recommendation against the use of wedges for management of knee OA [3].

While conventional magnetic resonance imaging (MRI) is commonly used to image the knee when a subject is lying in a supine position, an open, upright MRI system enables *in vivo* measurements of joint kinematic changes by imaging the knee in an actual weight-bearing condition [4]. Combining upright weight-bearing MRI with computer analyses, functional physiological measurements and descriptions of the knee joint may be investigated. Yet, to date, this innovative technique has not been used to study the effects of shoe wedge orthoses on the tibiofemoral joint in patients with knee OA. It was hypothesized that a lateral heel wedge, potentially used as a shoe orthosis for the knee OA patients, will alter the tibiofemoral kinematics under weight-bearing condition. These data would also begin to show the ability of upright MRI technique incorporated with computer-based image analysis in determining biomechanical changes that accompany shoe wedge orthoses, and potentially help develop patient-specific interventions for early treatment of the knee OA.

METHODS

Approval for human subject activities was obtained from Kessler Foundation's Institutional Review Board. Two subjects with diagnosed, primary unilateral or bilateral knee OA underwent physical examinations to eliminate previous injury to the knee, hip, or ankle after obtaining informed consent. MRI scanning was performed in a 0.6 T vertically open scanner (Upright MRI, Fonar, NY) with a 3D protocol. Using high-definition reconstruction, images with 0.483 mm pixel spacing, 0.75 mm slice spacing, and 250 mm field of view were obtained. Time for each scan was 2 m 16 s.

Pairs of custom shoes were used in the study. Each shoe incorporated a moveable heel wedge easily adjusted by investigators to provide neutral (0°) and 5° lateral wedging conditions. For each condition, subjects were positioned at two knee flexion angles, 0° and 20° (4 scans / subject). A fiber-optic motion sensor (Measurand, Canada) was used to measure knee angles and real-time visual feedback was displayed on a TV screen. Subjects were instructed to reach and maintain, in comfort, a target knee flexion angle using the feedback during scanning.

Femoral and tibial bone surfaces, along with medial and lateral compartment cartilage surfaces were digitized for each image using a pen tablet (Wacom, Japan). Custom software was used to project digitized points into 3D coordinates, and images were reconstructed into 3D models. Coordinates for the bones were placed on one scan according to anatomical landmarks, and bone surface matching was used to maintain consistent positioning through the remaining scans [5]. Rotations and translations of the tibia relative to the femur were calculated.

RESULTS AND DISCUSSION

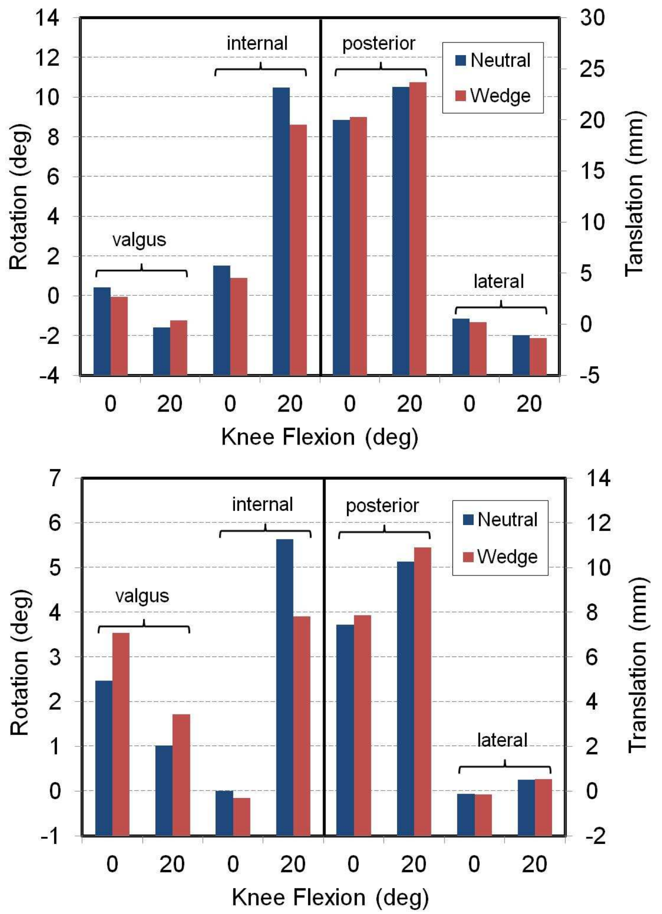

Figure 1: Rotations (left) and translations (right) of the tibia relative to the femur from subject 1 (Top) and 2 (Bottom).

With an increased knee flexion, the tibia exhibited varus (decrease in valgus), internal rotation, and posterior translation for both subjects (Figure 1). Differences in medial-lateral translation of the tibia with flexion were minimal. Lateral heel wedge caused a relative external rotation of the tibia (decrease in internal rotation), which was more pronounced at 20° flexion. Lateral wedging also translated the tibia posteriorly. As expected, the valgus wedge resulted in an increased valgus for both flexion angles in subject 2. Correspondingly, an opening of the medial compartment of the tibiofemoral joint was observed in the computer model (Figure 2). Lateral wedging caused smaller changes in subject 1 which were unexpectedly towards varus for 0° flexion.

Muscle activity in the quadriceps, as well as joint compressive force resulting from weight-bearing, may be desirable to image the knee joint in a physiological loading state. While the current study was limited in that only two subjects were studied at the present stage, and therefore no statistical analysis was performed, it developed a combined upright MRI and computer-based image analysis methodology that may provide a more precise measurement of the knee joint *in vivo* positioning for us and future researchers to better investigate the effectiveness of shoe wedge orthoses as a potential intervention for the knee OA patients.

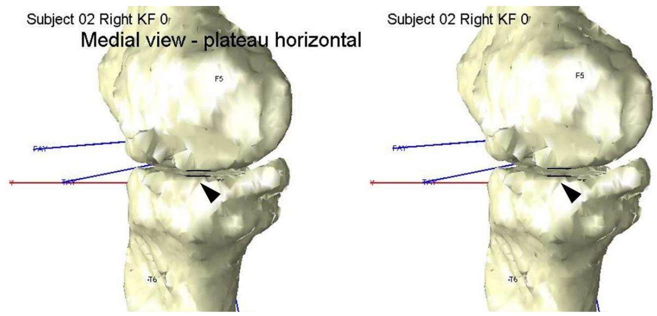

Figure 2: Medial view of the knee joint showing an increased joint space between the tibia and the femur. This was not observed in the lateral compartment.

CONCLUSIONS

Two subjects with diagnosed knee OA wore pairs of custom shoes with and without 5° lateral heel wedges, and underwent upright MRI tests in two knee flexion conditions. The results showed that a lateral heel wedge changed the tibial kinematics for both subjects and may have the potential for reducing the medial compartment loads by separating that compartment. While the current study was indeed limited in scope, it represents a preliminary step in our attempt to apply an innovative concept of weight-bearing MRI to improvement of conservative treatments for knee OA. With more subjects involved in this ongoing study, we believe that future results will be useful in guiding a development of patient-specific interventions for such patients.

REFERENCES

1.Lawrence RC, et al. *Arthritis Rheum* **41**, 778-99, 1998.
2.Hinman RS, et al. *Arthritis Rheum* **59**, 408-15, 2008.
3.Bennell KL, et al. *BMJ* **342**, d2912, 2011.
4.Dubowsky SR, et al. *Orthop Res Soc*, 294, 2010.
5.Barrance PJ, et al. *Am Soc Biomech*, P1-10, 2007.

ACKNOWLEDGEMENTS

This study was supported by Department of Education (NIDRR) grants H133G080136 and H133P070007.

LATISSIMUS DORSI ANTHROPOMETRY AND SWIMMING

[1]Wendi H. Weimar and [2]Brian J. Campbell

[1]Auburn University, Auburn, AL, USA
[2]University of Louisiana, Lafayette, Lafayette, LA, USA
email: weimawh@auburn.edu

INTRODUCTION

The Latissimus dorsi is a large muscle that has attachment sites on the spine, pelvis and humerus. Sometimes referred to as the “swimmer’s muscle”, it is primarily considered a shoulder internal rotator and adductor considering the traditional insertion point. However, due to the origins on the pelvis and spine, its contribution to motion of the trunk and pelvic girdle should not be overlooked. Pilot work on this topic indicated that the Latissimus dorsi produced larger percent maximum volitional isometric contraction (MVIC) during transverse pelvic girdle rotation (origin influence) than during internal rotation of the shoulder (insertion influence). Therefore the purpose of this project was two-fold: (1) to determine if the anthropometry of the Latissimus dorsi correlates well with 100 m freestyle/backstroke swimming times and (2) to determine if anthropometry of the Latissimus dorsi correlates well with its force contribution to transverse pelvic girdle rotation.

METHODS

Participants were 34 highly trained, collegiate swimmers with national and international swimming experience (19 males and 15 females). The personal best times for 100M were within qualifying times for NCAA National competitions. Anthropometric measures were taken such that angles of the line of pull for the Lattisumus dorsi could be calculated. Specifically the following measures were taken: the distance from the posterior, superior iliac crests (PSIC) to the spine (right side and left side); the distance from the acromion to spine (right side and left side) and trunk length, measured as the distance from the height of the PSIC (transposed to the spine) to the prominence of the seventh cervical vertebrae. From these measurements four angles were calculated (Figure 1). The lat angles were defined as the angle between the spine and a ray originating at the fifth lumbar vertebrae and concluding at the acromion, on the respective sides. The left *to* right lat angle is constructed by a ray the length of the trunk, drawn vertically from the left PSIC and a ray that originates on the left PSIC and concludes at the right acromion (this same procedure was employed to calculate the right *to* left lat angle). This unique angle was chosen because of the out of phase timing of the rotation of the pelvis and trunk about the longitudinal axis during the freestyle stroke. It was hypothesized that since the pelvis rotates prior to the upper trunk during the freestyle and rotates synchronous with the upper trunk during the backstroke, that the right *to* left and/or left *to* right lat angle would be highly correlated with the freestyle performance measure and the left and/or right lat angle would be highly correlated for the backstroke performance measure. The author concedes that the acromion is not equivalent to the insertion of the Latissimus dorsi. However, the acromion is a reasonable approximation and provided a reliable landmark for these measurements.

The transverse pelvic girdle rotational force was determined by having the participant assume a prone position and rotate the pelvis against a force transducer. The arms were by the sides of the participants, but the trunk was stabilized to provide for only pelvic girdle rotation. Measurements were taken on both the right and left sides.

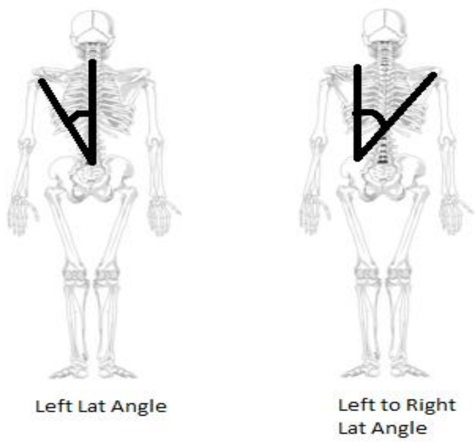

Figure 1: The angles calculated. Only those for the left side are indicated, however the corresponding angles were also calculated for the right side as well.

RESULTS AND DISCUSSION

The transverse pelvic girdle rotation force failed to demonstrate a significant correlation with any of the four angles. In addition, no relationship was noted between the force measures and the personal best performances of the participants.

For this first analysis both strokes were considered together. All four of the Latissimus dorsi angles (left and right angles) demonstrated a significant negative correlation with personal best performances, indicating that the larger the angle the smaller the personal best time. The strongest correlations were between the left side lat angle ($r = -0.628$) and right *to* left lat angle ($r = -0.686$) and the personal best times. Weaker correlations, though significant were noted between the right side lat angle ($r = -0.389$) and left *to* right lat angle ($r = -0.342$) and the personal best times.

Upon closer inspection of the data, the strong correlation remained when the group was broken into freestyle and backstroke groups. The freestyle personal best times were strongly correlated with the right lat angle ($r = -0.487$), left lat angle ($r = -0.757$) and with the right *to* left lat angle ($r = -0.762$). The backstroke personal best times were strongly correlated with the left lat angle ($r = -0.727$) and the right *to* left lat angle ($r = -0.842$).

It was presumed that during the freestyle, the out of phase pelvic girdle rotation would provide for optimal Latissimus dorsi length prior to hand entry by bringing the PSIC closer to the insertion. However, if this was the case, both the left *to* right and the right *to* left lat angles would have demonstrated significance. Significance only in the right *to* left angle may be related to the right hand dominance of all of the swimmers, which also corresponded to a majority of the swimmer's preferred breathing side.

CONCLUSIONS

While previous work has found strong correlations between anthropometric variables and swimming time such as hip and shoulder width [1,2], these variables would seem to have a greater influence on the drag of the swimmer and not the muscle arrangement. This project attempted to determine a relationship between anthropometry in light of muscle line of pull and swim times.

REFERENCES

1. Sprague, H. A. *Research Quarterly* **47**(4), 810-814, 1976.

2. Grimston, SK & Hay, J. *Med. and Sci. in Sports Exerc.* **1**, 60-68, 1986.

HAMSTRINGS WEAKNESS INCREASES ACL LOADING DURING SIDESTEP CUTTING

[1]Joshua T. Weinhandl, [2]Jennifer E. Earl-Boehm, [2]Kyle T. Ebersole, [2]Wendy E. Huddleston, [2]Brian SR Armstrong & [2]Kristian M. O'Connor

[1]Old Dominion University, Norfolk, VA, USA
[2]University of Wisconsin-Milwaukee, Milwaukee, WI, USA
email: jweinhan@odu.edu

INTRODUCTION

Anterior cruciate ligament (ACL) injury is one of the most debilitating and costly lower extremity injuries experience by athletes [1]. It has been shown that 70% of ACL ruptures occur in a noncontact situation, specifically during rapid decelerations of the body's center of mass [2].

Several non-modifiable and modifiable factors have been associated with increased risk of ACL injury. One such modifiable risk factor that has received considerable attention is relative hamstrings to quadriceps muscle strength (H:Q) ratio. *In vitro* studies have demonstrated that a decreased H:Q ratio results in decreased knee joint stability and increased ACL loading [3]. Furthermore, a decreased H:Q ratio has been identified prospectively as a risk factor for ACL injury [4]. Therefore, the purpose of this study was to determine the relationship between H:Q ratio and ACL loading during sidestep cutting using a musculoskeletal modeling approach.

METHODS

Twenty recreationally active females (21 ± 1 years, 61.8 ± 6.4 kg, 1.66 ± 0.05 m) volunteered to perform sidestep cutting maneuvers before (UC) and after (FC) an isokinetic knee flexion fatigue protocol. Three-dimensional joint kinematics of all UC and FC trials were collected using a ten-camera Motion Analysis Eagle system (200 Hz), and force plate data were collected with an AMTI force platform (1000 Hz).

A participant-specific musculoskeletal model was then generated in OpenSim [5] consisting of 21 degrees-of-freedom (*dof*). The left leg was actuated by joint torque actuators, while the right leg and back were actuated by 43 Hill-type muscle actuators. Each muscles maximum isometric force (F_o^m) in the musculoskeletal model was scaled according to each participant's peak isokinetic strength for UC trials. For FC trials, F_o^m of the hamstrings were rescaled according to each participant's peak isokinetic knee flexion strength measured after the fatigue protocol to simulate cutting maneuvers performed with reduced hamstrings strength. Pelvis position and orientation relative to the ground was defined with 6-*dof*. The head, arms and torso were represented as a rigid segment connected with the pelvis by 3-*dof*. Each hip was modeled as a 3-*dof* ball-and-socket joint. The left knee was modeled as a 1-*dof* revolute joint, while the right knee was modeled as a 3-*dof* joint. Both ankles were modeled as 1-*dof* revolute joints. Computed muscle control (CMC) was then implemented to produce forward dynamic simulations for all UC and FC trials generally consistent with the experimentally measured kinematics [6]. Optimal CMC input parameters were found using an optimization algorithm to minimize kinematic errors and residuals [7].

Musculoskeletal model outputs were used in a three-dimensional knee model to calculate ACL force. Dependent t-tests were used to assess differences in ACL force between UC and FC trials. Other variables of interest included timing of peak ACL force, as well as sagittal, frontal and transverse plane ACL loading. Significance for all tests was set at $p < 0.05$.

RESULTS AND DISCUSSION

Reduced hamstrings muscle strength resulted in a 22.8% increase in peak F_{ACL} during sidestep cutting (Figure 1). This increase was primarily due to a 32.4% increase in the sagittal plane ACL loading

(Table 1). Additionally, reduced hamstrings strength resulted in greater frontal plane ACL loading due to an increase in knee abduction moment, although this difference was not significant.

In the sagittal plane, decreased hamstrings force production significantly reduced tibiofemoral contact force despite an increase in vertical ground reaction force and no change in quadriceps force production. This reduction in tibiofemoral contact force would theoretically reduce sagittal plane ACL loading. However, decreased knee flexion angle at peak F_{ACL} caused the hamstrings angle of pull to become more axial with the tibia. This change, coupled with an overall decrease in hamstrings force production resulted in a significantly reduced posteriorly directed hamstrings shear force thereby increasing sagittal plane ACL loading and yielding a net increase in F_{ACL}. The increase in F_{ACL} suggests that injury risk may be subsequently increased in athletes with a decreased H:Q ratio. These results are consistent with the findings of Myer et al. [4] who prospectively identified decreased hamstrings strength as a risk factor for ACL injury.

CONCLUSIONS

Results of the current model suggest that a decreased H:Q ratio significantly increases ACL loading. While the increase in F_{ACL} was not enough to rupture the ligament, it is possible that repeated performance of a high-risk maneuver, such as sidestep cutting, with imbalanced muscle strength may ultimately lead to ligament failure [1]. Furthermore, previous research has shown that the ability to decelerate upon initial ground contact and to control knee loading may be related to a balanced H:Q ratio [8]. Thus, increased balance in hamstrings relative to quadriceps muscle strength may be a mechanism that protects the ACL [4]. Preseason screening programs that monitor H:Q ratio may be warranted to identify female athletes with potential deficits. Targeted neuromuscular interventions that increase relative hamstrings muscle strength may then subsequently decrease injury risk.

Table 1. Effects of fatigue on mean ± stdv peak ACL loading (F_{ACL}), time of peak F_{ACL}, and the planar components of F_{ACL}.

	UC	FC	p-value
Peak F_{ACL} ($N \cdot kg^{-1}$)*	11.02 ± 4.65	13.53 ± 3.53	0.001
Time of peak F_{ACL} (ms)	27 ± 7	27 ± 7	0.988
Planar components at peak F_{ACL} ($N \cdot kg^{-1}$)			
Sagittal*	6.79 ± 3.43	8.99 ± 2.90	<0.001
Frontal	2.89 ± 1.13	3.37 ± 0.93	0.059
Transverse	1.35 ± 1.19	1.18 ± 0.57	0.719

* indicates UC is significantly different from FC (p <0.05).

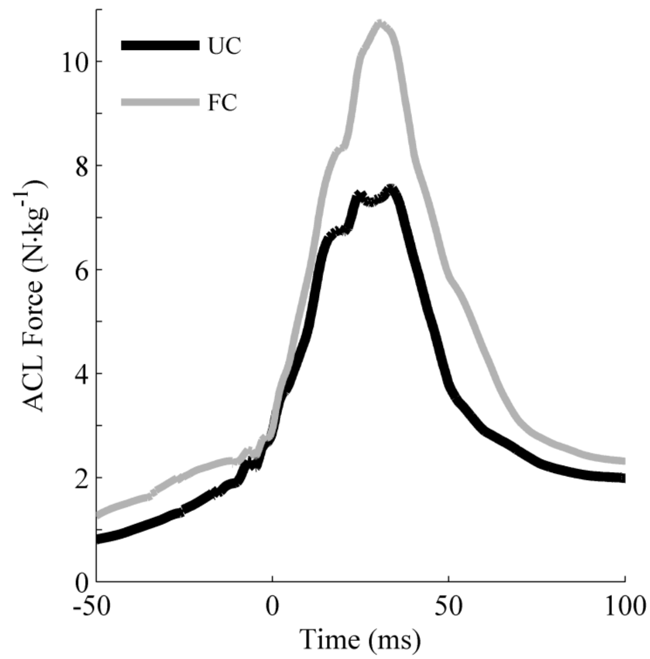

Figure 1. Mean ACL loading during unfatigued (black line), and fatigued (gray line) sidestep cutting.

REFERENCES

1. Hewett TE et al. *AJSM*, **34**, 299-311, 2006.
2. Olsen OE et al. *AJSM*, **32**, 1002-12, 2004.
3. Withrow TJ et al. *JBJS*, **90**, 815-23, 2008.
4. Myer GD et al. *CJSM*, **19**, 3-8, 2009.
5. Delp SL et al. *IEEE TBE*, **54**, 1940-50, 2007.
6. Thelen DG et al. *J Biomech*, **36**, 321-8, 2003.
7. Weinhandl JT et al. *Proceedings of the 35th Annual ASB Meeting*, Long Beach, CA, 2011.
8. Hewett TE et al. *AJSM*, **24**, 765-73, 1996.

ACKNOWLEDGEMENTS

International Society of Biomechanics Dissertation Grant
University of Wisconsin-Milwaukee Dissertation Fellowship
UWM College of Health Sciences Student Research Grant

THE EFFECT OF SEATING SURFACE COMPLIANCE ON TRUNK MOTION

Weiss, K. J., Haggerty, M. C., Heath, J. E. and Wang, H. E.

Ball State University, Muncie, IN, USA
email: hwang2@bsu.edu, web: http://cms.bsu.edu/Academics/CollegesandDepartments/Biomechanics.aspx

INTRODUCTION

There is a high incidence of low back pain which is a major health care concern. Prolonged sitting is a well-known risk factor for low back pain [1]. Lacking low-back movement during sitting on a stable surface (e.g. office chair) may lead to compromised disc nutrition and static loading of the spinal structures as a result of compressive forces caused by the extensor muscles [2]. From an ergonomic standpoint, backrests were assumed to create postural alignment support which would reduce static muscle activity, but it was found that they may also reduce spinal motion which would jeopardize disc nutrition [2]. Introducing subtle motion in the trunk and low back area may reduce low-back tissue tension. Some studies have recognized that dynamic sitting is preferred by individuals sitting for extended periods of time [3]. Although sitting on an unstable surface may result in subtle upper body motion, it is yet to be determined whether using air cushions or stability balls result in increased trunk motion. Stability balls have become a more common alternative to office chairs as a means of reducing low back pain. Despite this fact, little research has been conducted regarding their effectiveness or the effectiveness of an air cushion.

Active sitting is referred to the use of an unstable seating surface that requires the user to engage in more movement to maintain an upright sitting posture. Active sitting can be performed on an extremely compliant surface, such as an exercise ball, or a moderately compliant air cushion placed on the seat of a chair. The following benefits gained from active sitting have been reported: encouraged contraction of core muscles, reduced pressure on the vertebrae, increased control and awareness of body position, better spinal positioning due to the increased forward pelvic tilt, and increased caloric expenditure attributed to increased amplitude of movement [3,9]. In addition, sitting on an exercise ball is also thought to improve balance and posture while decreasing the risk of fall [3, 4]. However, all of these benefits from active sitting have been subjective. To date, there is no quantitative experimental data available to support that active sitting is beneficial to users in decreasing the risk of low back pain.

The purpose of this study was to determine if increased seating surface compliance would result in increased trunk motion during prolonged sitting.

METHODS

Eight healthy females (age = 30.3 ± 12.8 years; height = 163.2 ± 7.2 cm; mass = 62.4 ± 11.2 kg) who sit for an average of eight hours per day were recruited for this study. Participants had a body mass index below 30 kg/m^2, no history of lower back pain, and were able to sit for three, 30-minute sessions while maintaining upright posture. Each participant completed an informed consent document approved by a university Institutional Review Board.

Participants completed three different randomized sitting tasks for a duration of thirty minutes each. Tasks included sitting on an immobile surface, sitting with an Automatic Abs air cushion placed on an immobile surface, and sitting on a stability ball. Participants maintained 90 degree knee flexion with each foot placed on a separate force plate, back erect and hands placed on thighs while looking straight forward.

Sitting position was tracked by using a 12 camera VICON motion capture system at 60 Hz. Ground reaction forces were collected by using two AMTI force plates sampling at 600 Hz. Data were processed using VICON Nexus v1.7 and the biomechanical variables were calculated using Visual 3D v4.9. The average values were calculated for trunk center of mass (Tcom) in the antero-posterior (AP), medio-lateral (ML), and vertical directions, and right and left foot center of pressure (COP) in the AP and ML directions.

A one-way repeated measures MANOVA was used to determine differences between the three sitting conditions. Significance level was set at 0.05.

RESULTS

No significant differences were found for right and left foot COP in any of the sitting conditions ($p>0.05$). Ball condition showed greater Tcom in all directions than both of the cushion and immobile surface conditions (Figure 1, $p<0.05$). Cushion condition showed greater Tcom in the ML direction than the immobile surface condition (Figure 1, $p<0.05$).

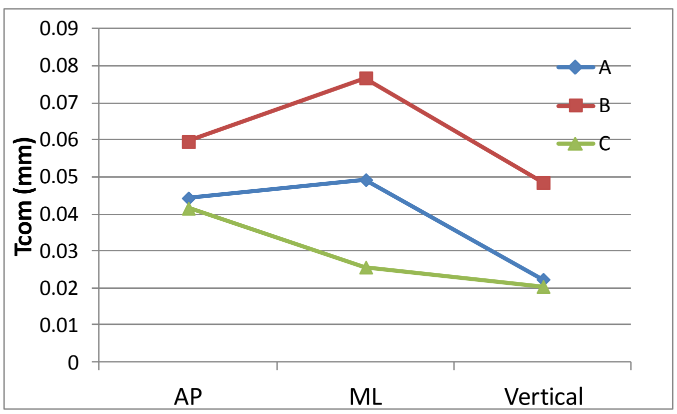

Figure 1: Average values for trunk center of mass trajectories in AP, ML, and vertical directions during the three sitting conditions, the air cushion (A), stability ball (B), and the immobile surface (C).

DISCUSSION AND CONCLUSIONS

The purpose of this study was to determine if increased seating surface compliance would result in increased trunk motion during prolonged sitting. Our findings indicate that trunk center of mass trajectory significantly increased with increased seating surface compliance. In addition, no difference in foot COPs among sitting conditions indicates that foot positioning during sitting has no influence on trunk motion.

With increased surface compliance, greater Tcom trajectory occurred in all three dimensions of spinal motion. The potential benefits of this increased motion include decreasing disc compression, increasing disc nutrition, and better spinal alignment. These findings are in agreement with similar studies [2]. Those individuals looking to offset the risk of low back pain due to prolonged sitting should consider using an unstable seating surface such as an air cushion or a stability ball. Though both surfaces had more significant trunk motion then the chair, the greatest offset to the risk of low back pain was the ball. Future studies may seek to extend the duration of the sitting trials and utilize electromyography for greater understanding of the effects of surface compliance on the trunk.

REFERENCES

1. Lis, A. M., et al., *Eur Spine J*, 2007. **16**, 283-298.
2. O'Sullivan, et al., *Journal of Orthopaedic & Sports Physical Therapy*, 2006. **36**(1), 19-25.
3. Hoy, D., et al., *Research Clinical Rheumatology*, 2010. **24**(6), 769-781.
4. Black, K.M., et al., *Spine*, 1996. **21**(1), 65-70.
5. Callaghan, J.P., et al., *Ergonomics*, 2001. **44**(3), 280-294.
6. McGill, S.M., et al., *Clinical Biomechanics*, 2006. **21**(4), 353-360.
7. Merritt, L.G., et al., *The Journal of the Canadian Chiropractic Association*, 2007. **51**(11), 50-55.
8. Kingma, I., et al., *Applied Ergonomics*, 2009. **40**(2), 199-205.
9. Gregory, D.E., et al., *Human Factors*, 2006. **48**(1), 142-153.

COMPUTATIONAL MODEL OF MAXIMUM-HEIGHT SINGLE-JOINT JUMPING PREDICTS BOUNCING AS AN OPTIMAL STRATEGY

Herman van Werkhoven, Stephen J. Piazza

The Pennsylvania State University, University Park, PA, USA
email: *hxv114@psu.edu*

INTRODUCTION

Because of its unambiguous objective function, maximum-height jumping is especially well suited to simulation-based investigations of musculo-skeletal function and coordination. Previous computational simulations of jumping have increased our understanding of the mechanisms that underlie task performance in a manner that is not always possible using experimental protocols [1]. Multijoint [1] and single joint [2] models of jumping have been employed to study muscle function during maximum-height jumping. Jumping using only the ankles for propulsion has been studied experimentally [2,3] as with simulation [2]. Limiting the task to single joint reduces complexity (eliminating the effects of biarticular muscles, for example) and thereby allows a more focused investigation into the mechanisms of optimal performance. The purposes of this study were to develop a muscle actuated computational simulation of maximum-height, single-joint jumping and to test the model by comparing simulation output with experimental results. This model will be used in future studies to explore the relationship between joint structure and function for various motor tasks.

METHODS

The computational model had two degrees of freedom and consisted of two massless segments (foot and leg) with half body mass positioned atop the leg segment (Fig. 1). The ankle was a revolute joint, as was the connection between the foot and the ground contact, which was located at the position of the MTP joint. Two muscles, a plantar-flexor and a dorsiflexor, acted across the ankle joint. Muscles were modeled as Hill-type actuators with first-order activation dynamics. Muscle architecture properties (optimal fiber length, tendon slack length, maximum isometric force, tendon stiffness, muscle moment arm) were derived using a least squares curve fitting algorithm that gave the best fit between experimental passive and active isometric joint torque curves from the literature [4,5,6] and model-generated joint torque curves. Maximal height jumping was simulated using a forward dynamic optimization approach in the following objective function [7] was maximized:

$$J(t_f, u) = y_c(t_f) + \frac{1}{2g}\dot{y}_c^{\,2}(t_f)$$

The 43 optimization parameters were the muscle excitations u (with 21 nodes for each muscle) and time at takeoff t_f. The vertical position of center of mass is given by y_c. The model was developed using Simulink SimMechanics (MathWorks, Inc.; Natick, MA) and the optimization problem was solved using a combination of gradient- and non-gradient-based algorithms in MATLAB. The jumping strategy used by the model was dictated by setting an upper bound on t_f such that the model had no time for a countermovement; performed a single counter-movement; or "bounced" by performing several successive countermovements (when t_f was unbounded).

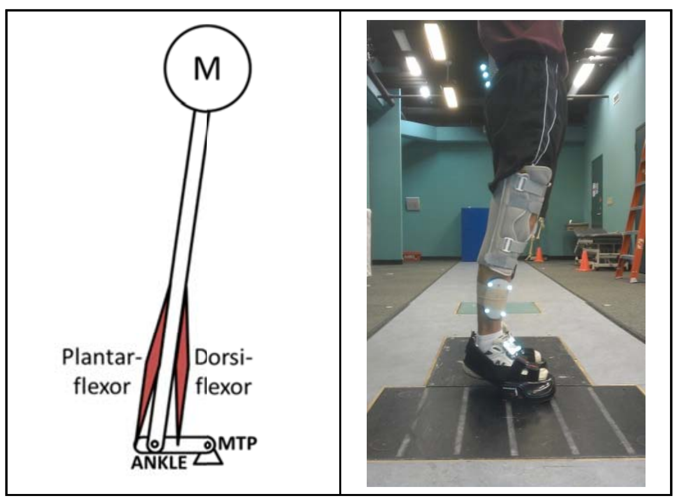

Figure 1: Computational model (*left*) and a subject wearing platform shoes and knee braces (*right*).

`

Eight healthy male subjects performed maximal height jumps using only their ankles for propulsion. The subjects' knees were held immobile by braces and each subject was further instructed not to move his hips, trunk, arms, or head. The arms were folded across each subject's chest. Subjects wore platform shoes (JumpSoles, Metapro; Mountain View, CA) (Fig. 1), which lifted the heel off the ground, allowing the subjects to perform a countermovement (CM) at the ankle. Subjects were instructed to jump as high as possible with no further instruction (CM_{FREE}; 5 trials), with instruction to move down initially (CM_{DOWN}; 5 trials), and with instruction to try bouncing before jumping up (CM_{BOUNCE}; 5 trials). Foot and shank kinematic data were collected to calculate ankle angles and the average peak rise of 4 markers on the pelvis was taken as measure of jump height.

RESULTS AND DISCUSSION

Maximum jump heights were found to be similar between model and experiment (Table 1). The model jumped highest following a series of bounces, and 4 of the 8 subjects also jumped highest when they tried to bounce. For these subjects, the time to takeoff was similar to the time taken by the model and their final bounce was at a similar frequency as the model's predicted final bounce frequency for maximal performance (Table 1).

Humans are known to jump higher when employing a CM during a multijoint jump [8]. During a single joint CM, tendon energy storage has been shown to be enhanced as the muscle fibers act isometrically, allowing subsequent energy release and enhancement of performance [3]. In the present study, the computer simulation and half of the subjects jumped highest after multiple bounces. With each successive bounce the model exhibited more energy storage in the tendon as muscle fibers generated force isometrically (Fig. 2).

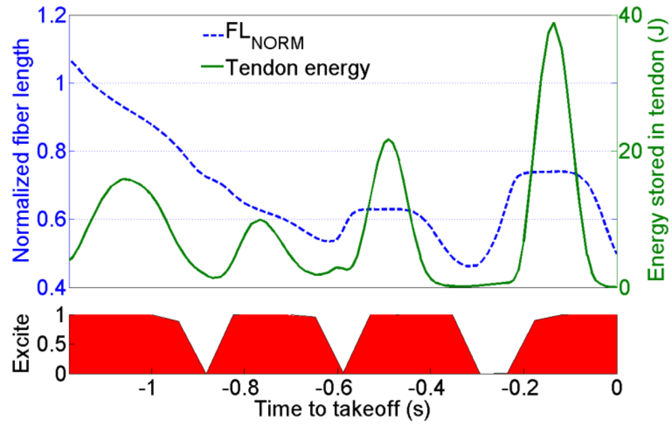

Figure 2: Fiber length and tendon energy versus time to takeoff (*top*). Plantarflexor excitation ($0 \le u \le 1$) versus time to takeoff (*bottom*).

CONCLUSIONS

A computational simulation of single-joint jumping was yielded optimal performance when takeoff was preceded by a series of countermovements, or bouncing. Similar behavior produced the highest jumps in half of the subjects. Simulation output suggests increased elastic energy storage during successive bounces as the mechanism for this performance enhancement. In future studies this computational model will be used to explore how changes in joint structure affect performance in various motor tasks.

REFERENCES

1. Pandy MG, et al. *J Biomech Eng,* **114**, 450-460, 1992.
2. Zajac FE, et al. *J Biomech,* **17**, 513-523, 1984.
3. Kawakami Y, et al. *J Physiol,* **540**, 635-646, 2002.
4. Riener R, et al. *J Biomech,* **32**, 539-544, 1999.
5. Marsh E, et al. *J Appl Physiol,* **51**, 160-167, 1981.
6. Sale D, et al. *J Appl Physiol,* **52**, 1636-1642, 1982.
7. Levine WS, et al. *IEEE T Automat Contr,* **28**, 1008-1016, 1983.
8. Bosco C, et al. *Acta Physiol Scand,* **114**, 557-565, 1982.

Table 1: Comparison of model to subjects (*n* = 4) whose maximum height jumps occurred when bouncing.

	Mass (kg)	**Jump height (cm)**	**Time to jump (s)**	**Bounce freq (Hz)**
MODEL	75.0	13.0	1.2	2.8
SUBJECTS	76.3 ± 7.6	17.3 ± 5.1	1.3 ± 0.3	2.6 ± 0.4

`

Balance Recovery Kinematics after a Lateral Perturbation in Patients with Transfemoral Amputations

[1,2]Kathryn M. Werner, [1]Alison Linberg, [1]Erik J. Wolf

[1]Walter Reed National Military Medical Center, Bethesda, MD, USA
[2]The Henry M. Jackson Foundation for the Advancement of Military Medicine, Rockville, MD, USA
email: kathryn.werner@med.navy.mil

INTRODUCTION

Falls are common for those with lower extremity amputations [1]. Recovery strategies of uninjured subjects include kinematic adjustments of the lower extremities to recover from stumbles [2]. Those with transtibial amputations have been reported to regain dynamic stability as quickly as uninjured subjects after an evoked forward fall from static standing [3]. This suggests that those with lower extremity amputations rely on different recovery strategies than uninjured subjects to regain balance.

The Computer Assisted Rehabilitation Environment (CAREN, Motek Medical, Amsterdam, The Netherlands) can produce lateral perturbations during gait, simulating a loss of balance, while maintaining subject safety with a harness.

The purpose of this research was to compare kinematic and temporal spatial differences between uninjured Service Members and those with transfemoral amputations (TFA), after lateral perturbations during gait. We hypothesized that the primary recovery strategies that would differ would be increased plantar flexion and decreased step length.

METHODS

Eight U.S. Military Service Members with TFA and nine uninjured Service Members were recruited for this study (Table 1). The Walter Reed Army Medical Center institutional review board approved the study and all subjects provided informed, written consent prior to participation.

Table 1: *Test and control subject demographics; Mean (SD).*

Test Subject		Control Subject	
Age (yrs)	**34.1** (6.4)	Age (yrs)	**28.6** (3.4)
Height (cm)	**177.4** (5.6)	Height (cm)	**178.4** (3.7)
Mass (kg)	**94.3** (10.1)	Mass (kg)	**83.8** (9.4)
Amputation (yr)	**4.1** (1.9)		

Subjects experienced lateral perturbations in the CAREN. The CAREN system is a motion platform with an embedded treadmill. Subjects' movements were tracked using a 12 camera motion capture system (Vicon Inc., Oxford UK).

Subjects were required to walk for 4 minutes at a controlled walking speed to acclimate to walking on the CAREN system. The acclimation period was followed by six two-minute trials. During trials, subjects experienced one mediolateral shift of the platform at 0.5 m/s with a magnitude of 5 cm. Perturbations were triggered by toe-off of the contralateral limb and were produced in the direction medial to the limb of interest (i.e. right for the left limb, and left for the right). Three perturbation trials occurred during single limb stance (SLS) on the right limb and three during left SLS. Trials were randomized by the side perturbed, left or right, and the time the perturbation occurred during each 2-minute trial.

Baseline temporal spatial parameters and sagittal kinematics were calculated from the eighteen left and right gait cycles prior to the first perturbation (Visual3D, C-Motion, Germantown, MD). The heel strike immediately before the perturbation marked the beginning of Stride 1 (S1) and the following heel strike began Stride 2 (S2), depicted in Figure 1. Only perturbations to the left limb were included for control subjects.

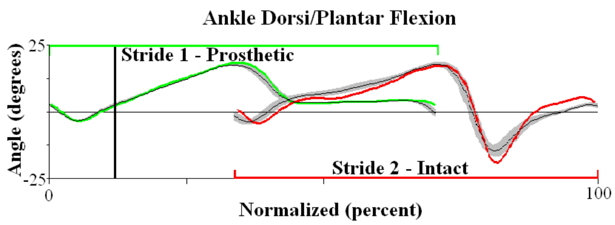

Figure 1: *The gait cycle during which the perturbation (vertical line) occurred (Stride 1) and the contralateral gait cycle (Stride 2). Recovery kinematics were compared to baseline kinematics (gray).*

RESULTS AND DISCUSSION

Temporal spatial parameters and sagittal kinematics before and after the perturbation are shown in Table 2. After perturbations, control subjects decreased step length during S2, while test subjects increased intact S2 step length to compensate for the shorter step taken with the prosthetic side.

Control subjects made slight adjustments to sagittal kinematics during the stride following the perturbation, with the largest change being a 3^{o} increase in knee flexion during stance of S2. By making minimal adjustments with the ankle and knee during S1 and S2, control subjects were able to maintain balance.

After perturbations during prosthetic SLS, the prosthetic limb was not used for recovery as seen by minimal changes in ankle dorsi/plantar flexion and the decreased knee flexion during swing in S1. Increased trunk forward lean during S1 and S2, as well as increased intact knee and hip excursion, allowed subjects to maintain balance.

After perturbations during intact SLS, subjects increased maximum ankle, knee, and trunk angles during S1 with the intact limb, but decreased hip flexion excursion. During S2 with the prosthetic limb, ankle and knee range of motion decreased, while trunk forward lean excursion increased.

CONCLUSIONS

Minor adjustments to sagittal kinematics on the intact side, and decreased prosthetic knee flexion during swing allow transfemoral amputees to maintain balance after lateral perturbations. During the strides after each perturbation, there was little change in prosthetic ankle and knee kinematics; implying that gait corrections were done with the intact limb. This overuse of the intact side could lead to further complications in the future.

REFERENCES

1. Miller WC, et al. *Arch Phys Med Rehab* **82**, 1031-1037, 2001.
2. Grabiner MD, et al. *J Gerontol* **48**, M97-M102, 1992.
3. Curtze C, et al. *Gait Posture* **32**, 336-341, 2010.

ACKNOWLEDGEMENTS

This research was supported by the Military Amputee Research Program and the Center for Rehabilitation Sciences Research.

Table 2: *Effects of lateral perturbations on temporal spatial parameters and sagittal kinematics in those with transfemoral amputations compared to uninjured subjects; Mean (SD).*

	Control Subject				Test Subject					
	Baseline		Perturbation		Baseline		Perturbation to Prosthetic		Perturbation to Intact	
	B L	B R	S1 L	S2 R	B P	B I	S1 P	S2 I	S1 I	S2 P
Step Length (cm)	**68.8** (3.9)	**69.6** (3.4)	**68.8** (3.5)	**68.4** (3.9)	**69.5** (6.5)	**66.2** (3.9)	**68.5** (6.4)	**70.6** (4.5)	**64.6** (5.7)	**67.7** (9.0)
Step Time (s)	**0.6** (0.0)	**0.6** (0.0)	**0.6** (0.6)	**0.6** (0.6)	**0.6** (0.0)	**0.5** (0.0)	**0.6** (0.0)	**0.6** (0.0)	**0.5** (0.0)	**0.6** (0.0)
Stance Percent	**67%** (1.3)	**67%** (1.5)	**67%** (1.3)	**66%** (1.1)	**62%** (0.0)	**69%** (0.0)	**62%** (1.2)	**70%** (1.8)	**70%** (1.6)	**60%** (2.6)
Max Ankle Dorsiflexion (^{0})	**16.8** (3.2)	**16.5** (4.3)	**15.9** (3.6)	**16.8** (4.7)	**14.1** (3.1)	**15.9** (2.8)	**14.7** (3.0)	**14.3** (2.8)	**15.0** (2.9)	**13.9** (3.9)
Max Ankle Plantar flexion (^{0})	**-13.9** (5.9)	**-15.3** (6.0)	**-12.4** (6.2)	**-13.2** (7.5)	**-5.5** (2.8)	**-14.8** (3.3)	**-5.8** (2.4)	**-15.5** (4.0)	**-17.3** (4.9)	**-4.4** (2.8)
Max Knee Flexion during Stance (^{0})	**16.3** (6.5)	**18.4** (7.2)	**16.5** (5.8)	**21.6** (6.9)	**0.3** (5.0)	**25.3** (3.5)	**0.1** (5.3)	**25.6** (5.5)	**25.5** (4.4)	**-1.0** (5.4)
Max Knee Extension during Stance (^{0})	**4.7** (3.4)	**5.0** (3.6)	**4.2** (3.6)	**5.7** (4.8)	**-2.2** (4.5)	**3.4** (3.5)	**-2.2** (4.8)	**5.0** (3.0)	**5.6** (3.4)	**-3.4** (4.5)
Max Knee Flexion during Swing (^{0})	**70.2** (5.0)	**69.8** (5.5)	**72.5** (7.7)	**69.8** (5.7)	**64.2** (6.7)	**69.8** (4.7)	**61.8** (10.2)	**70.2** (5.0)	**71.1** (7.7)	**59.2** (13.0)
Hip Flexion Excursion (^{0})	**43.3** (3.6)	**42.8** (3.5)	**44.5** (7.0)	**42.1** (5.4)	**45.7** (4.1)	**49.3** (3.2)	**46.1** (3.3)	**50.4** (3.1)	**48.4** (5.6)	**42.7** (6.0)
Trunk Forward Lean Excursion (^{0})	**3.1** (0.8)	**3.2** (1.0)	**4.3** (1.6)	**4.6** (1.9)	**5.7** (2.2)	**5.8** (2.3)	**10.0** (6.9)	**8.7** (5.7)	**8.3** (3.5)	**8.1** (4.0)

Key : B - Base, S1 - Stride 1, S2 - Stride 2, L - Left, R - Right, P - Prosthetic, I - Intact

GENDER COMPARISON OF TRUNK AND PELVIS KINEMATICS DURING WALKING AND RUNNING

Carolyn G. Westlake and Brian Noehren

University of Kentucky, Lexington, KY, USA
email: b.noehren@uky.edu

INTRODUCTION

Emerging evidence suggests that pelvis and trunk kinematics play an important role in the development of common conditions such as patellofemoral pain and iliotibal band syndrome [1]. In addition, females are more likely to suffer from these injuries than males [2]. Gender differences in kinematics at the hip, knee and ankle during gait are well defined [3,4]. However, gender differences in trunk and pelvis kinematics during walking and running are unclear. Differences between males and females in trunk and pelvis kinematics could be a factor in the greater incidence of injuries among females. For instance, an increase in the contra-lateral angular displacement of the trunk and pelvis in coronal and transverse planes may result in a larger shift of the center of mass (COM) away from the stance limb. Shifting the COM could alter the demands placed on the tibiofemoral joint and muscles at the knee and hip. In addition, trunk angle relative to the pelvis may indicate overall trunk-pelvis stability.

Differences in trunk and pelvis mechanics between genders could provide further insight into the control strategy used during gait that could be contributing to the higher incidence of injury among females. Unfortunately, differences in trunk and pelvis kinematics between genders during walking and running are unclear. Therefore, the purpose of this study is to compare peak trunk and pelvis kinematics in the coronal and transverse planes between males and females while walking and running. We hypothesized females would have a larger trunk and pelvis angular displacement during the stance phase of walking and running when compared to males. Additionally, we hypothesized females would demonstrate a greater trunk to pelvis angle when compared to males during walking and running.

METHODS

As part of an ongoing study, sixteen healthy runners (8 males and 8 females) between the ages of 18 and 45 participated. First, retroreflective markers were placed on the trunk, pelvis, and bilateral extremities of the participant using previously described methods [1]. Participants then walked at a self-selected speed for 5 minutes on an instrument treadmill (Bertec Corp, Columbus, OH). Marker trajectories and force data were captured using a 15 camera motion capture system (Motion Analysis Corp, Santa Rosa, CA). After the walking trial the participants ran at 3.3 m\s and the data collection was repeated. Data was filtered at 8Hz and 35Hz for marker trajectories and force data. Visual 3D (C-Motion Inc., Germantown, MD) and LabVIEW (National Instruments, Austin, TX) were used to determine heel strike and toe off and to calculate the 3D pelvis angle, trunk angle, and trunk-pelvic angle. For each trial, peak angles were obtained during the first 75% of stance phase per trial and averaged per subject. Because of the preliminary nature of the study, only descriptive statistics, percent differences, and effect sizes were calculated. Effect sizes were defined as large when ≥ 0.8, moderate when between 0.4 and 0.79, and small when ≤ 0.39.

RESULTS

Female participants (height 1.7m ± 0.04, weight 57.3kg ± 4.2, age 24years ± 3.1) ran an average of 47.3km ± 27.0 per week, while males (height 1.7m ± 0.09, weight 73.1kg ± 7.3, age 27years ± 4) ran an average of 35.6km ± 22.7km per week. Average self selected walking speed was similar between males and females (1.3m/s ± 0.12). Peak angles and effect sizes are reported in Table 1. Large effect sizes were associated with clinically meaningful differences between males and females. Peak contra-lateral trunk lean was 43% greater during walking and 44% greater during running in females. Peak contra-lateral pelvis drop was 51% greater during walking and 49% greater during running in females. During running, a 68% greater trunk pelvis angle was observed in females. Peak ipsilateral trunk rotation was 73% greater during walking and 69% greater during running in females. Peak ipsilateral pelvis rotation was 63% greater during walking and 69% greater during running in females. During running, a 68% greater trunk pelvis angle was observed in females compared to males.

DISCUSSION

The purpose of this study was to compare trunk and pelvis kinematics between females and males during walking and running. Females had larger trunk and pelvis angles in the coronal and transverse planes compared to males. The trunk to pelvis angle was also larger in females in both the coronal and transverse plane. All of these differences were associated with a moderate to large effect size.

Larger peak trunk, pelvis, and trunk to pelvis angles in females during walking and running may represent a pattern of decreased proximal stability compared to males. Such a pattern could result in greater shift of the COM, thereby increasing energy expenditure and demands on the proximal hip and trunk muscles such as the gluteus medius, maximus and internal obliques. Increased demands placed on these muscles would hamper their ability to control not only pelvis and trunk movement but hip adduction and internal rotation as well [3,4]. Greater hip adduction and internal rotation angle has been observed in females [5]. These hip angles have also been linked to patellofemoral pain [1] and iliotibial band syndrome [6]. The strategy females use to control the trunk and pelvis could place greater demand on the hip and knee musculature influencing the potential risk for injuries. However, this is speculative at this point and requires further investigation, particularly within injured populations.

In addition, greater contra-lateral pelvis drop may result in larger trunk to pelvis transverse plane rotation towards the stance limb to maintain stability. Rotating the trunk towards the stance limb could decrease the COM excursion, yet increase the compensation demands on the hip. Compensation strategies may then follow at the knee increasing the risk of injury. Thus, investigating the trunk and pelvis coordination may shed light on proximal control strategies among injured populations.

Females experienced a greater change in peak angles during running when compared to walking. With a greater angular displacement of the trunk and pelvis, an increased compensation at other joints could occur. The increased demands placed on females during running may make maintaining trunk control more difficult leading to the greater change in angles seen in females compared to males. This could be a contributing factor to the increased risk of knee injury observed among females during running.

CONCLUSIONS

Females have larger peak trunk, pelvis and trunk to pelvis angles in coronal and transverse planes compared to males. Potentially, females may use the hip to compensate for the larger trunk and pelvis angle displacement. These compensation strategies could increase the risk for injury among females particularly with increasing task demands.

REFERENCES

1. Noehren B, et al. *Clin Biomech,* in press 2012.
2. Boling MC, et al. *Scand J Med Sci Sports* 20, 725-730, 2010.
3. Cho SH, et al. *Clin Biomech* 19, 145-152, 2004.
4. Chumanov ES, et al. *Clin Biomech* 23, 1260-1268, 2008.
5. Ferber R, et al. *Clin Biomech* 18, 350-357, 2003.
6. Ferber R, et al. *J Orthop Sports Phys Ther* 40, 52-58, 2010.

Table 1: Peak trunk and pelvis angles during walking and running. Mean (standard deviation). Note: Coronal plane: negative values indicate contra-lateral trunk lean and pelvis drop. Transverse plane: negative values indicate ipsilateral trunk and pelvis rotation

Joint Angle (degrees)	Males	Females	Effect Size	Males	Females	Effect Size
Walk	**Coronal**			**Transverse**		
Trunk Angle	-1.3 (1.6)	-3.0 (2.5)	0.88	-5.6 (4.6)	-7.7 (5.1)	0.44
Pelvis Angle	-2.9 (1.8)	-5.7 (2.0)	1.49	-2.5 (2.4)	-4.0 (1.8)	0.69
Trunk to Pelvis Angle	3.3 (1.7)	4.4 (2.9)	0.51	-6.7 (4.2)	-10.2 (6.0)	0.69
Run						
Trunk Angle	-1.8 (1.4)	-4.1 (2.2)	1.23	-13.7 (3.3)	-20.0 (2.1)	2.31
Pelvis Angle	-3.2 (1.6)	-6.5 (3.3)	1.33	-6.6 (2.9)	-9.5 (3.0)	1.00
Trunk to Pelvis Angle	6.7 (2.8)	9.8 (3.7)	0.95	-10.8 (4.4)	-15.9 (6.3)	0.97

DYNAMIC CADAVERIC ROBOTIC GAIT SIMULATION OF PES PLANUS

[1]Eric C. Whittaker, [1,2]Grant Roush, and [1,2,3]William R. Ledoux

[1]VA RR&D Center of Excellence for Limb Loss Prevention and Prosthetic Engineering, Seattle, WA
Departments of [2]Mechanical Engineering and [3]Orthopaedics & Sports Medicine
University of Washington, Seattle, WA
Email: wrledoux@u.washington.edu, web: http://www.amputation.research.va.gov/

INTRODUCTION

Pes planus, commonly known as flatfoot (FF), has been explored in a variety of *in vivo* and *in vitro* studies. *In vivo* studies have reported kinematics such as peak angles and range of motion (ROM) of foot bones or segments during gait [1], as well as full sets of kinetic and EMG data. *In vitro* kinematic studies [2,3] have explored the biomechanical effects of flatfoot under static conditions, reporting bone-to-bone orientation at isolated phases of stance and other kinetic variables.

Our group has developed a flatfoot model using cadaveric specimens and performed dynamic gait simulations using the robotic gait simulator (RGS). With the ability to perform reliable gait simulations using a cadaveric flatfoot model, it is possible to use invasive techniques to further understand the biomechanics of pes planus, as well as explore the efficacy of various flatfoot corrective surgeries. The purpose of this study was to demonstrate the fidelity of our flatfoot model using static X-rays and dynamic kinematics and kinetics from stance phase gait simulations.

METHODS

Six neutrally aligned (NA) cadaveric specimens (three pairs) were used in this analysis. All specimens were screened for abnormalities using X-rays. Based on methods by Blackman et al. [3], the ligaments involved in supporting the medial arch were attenuated with cuts every 1-2mm parallel to the longitudinal orientation of the ligament. These included the superomedial and inferior calcaneonavicular, talocalcaneal interosseous, plantar naviculocuneiform, plantar first metatarsocuneiform, and anterior superficial deltoid ligaments. The foot was then cyclically loaded through the tibia up to 35,000 times on a materials testing machine from 10 N to the donor's body weight (BW). A 40˚ wedge was placed under the calcaneus of each specimen during cycling to promote hindfoot eversion. The degree of flattening was measured using 25% BW loaded medial/lateral and anterior/posterior X-rays and the following metrics: lateral talometatarsal angle (LTMA), navicular height (NH), talonavicular coverage angle (TNCA), calcaneal pitch angle (CPA), and calcaneal eversion distance (CED).

The feet were then tested on the RGS, which has been described in detail elsewhere [4,5]. The prescribed tibia-to-ground motion of the 6-degree of freedom RGS and the target vertical ground reaction force was based on average *in vivo* data from 10 symptomatic pes planus subjects collected in our gait lab. Ground reaction forces were scaled to 50% of the donor's BW, and stance phase was simulated in 4.09 sec.

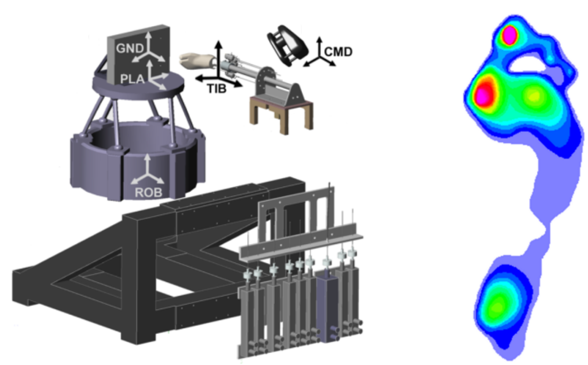

Figure 1: RGS schematic and representative *in vitro* FF pressure data from a dynamic gait simulation trial.

A previously described ten-segment foot model [4] was used to capture individual foot bone motion. Due to their direct relevance to the biomechanics of pes planus, the following kinematic relationships were assessed: calcaneus to tibia (CALC_TIB), first metatarsal to talus (MET1_TAL), and navicular to talus (NAV_TAL). Kinematic data were collected with a six-camera Vicon MX system, and plantar pressure was recorded using a Novel emed-sf pressure plate.

RESULTS AND DISCUSSION

The static X-ray metrics all showed trending towards flattening (Table 1). The LTMA increased significantly, indicating a dorsiflexion of the first metatarsal to a range consistent with mild flatfoot [6]. The navicular height decreased by 3mm, indicating a drop in the medial arch height. The TNCA increased, indicating an abduction of the forefoot consistent with flatfoot [7]. The CPA decreased slightly, although not into a range common for *in vivo* flatfoot [6]. Lastly, the 9.8mm CED indicated an eversion of the hindfoot in a range trending toward flatfoot [7].

Table 1: Static X-ray metrics (mean ± SD) pre- and post-flattening. Pre-flattening values not available for CED. *significant difference from pre to post, paired t-test, p<0.05

Avg ± SD	LTMA* (deg)	NH* (mm)	TNCA* (deg)	CPA* (deg)	CED (mm)
Pre	-1.7 ± 3.9	31.8 ± 7.3	20.4 ± 10.7	25.5 ± 4.9	N/A
Post	5.8 ± 1.8	29.0 ± 7.4	29.4 ± 6.6	23.1 ± 4.2	9.8 ± 4.3

(+) LTMA signifies a more dorsiflexed first metatarsal with respect to talus
(+) TCNA signifies a more abducted navicular
(+) CPA signifies a more dorsiflexed calcaneus

Average plantar pressure data showed peak pressures under the medial forefoot (Figure 1). When compared with pressure data from NA feet [8], there was a medial shift in the pressure distribution under the forefoot (Figure 2), evidenced by the peak pressure under the 1st met (FF) rather than a more evenly distributed pressure across the medial metatarsals (NA). This is indicative of a collapse of the medial arch.

From the kinematic data, range of motion of the bones of the hindfoot and medial arch were compared to data from NA specimens also tested on the RGS [4] (Table 2). For all three angles in all three cardinal planes except for frontal plane MET1_TAL, there were larger ranges of motion for the NA specimens. This is, in general, consistent with *in vivo* flatfoot studies such as Ness et al. [1].

Six of the nine range of motion metrics were significantly different between FF and NA.

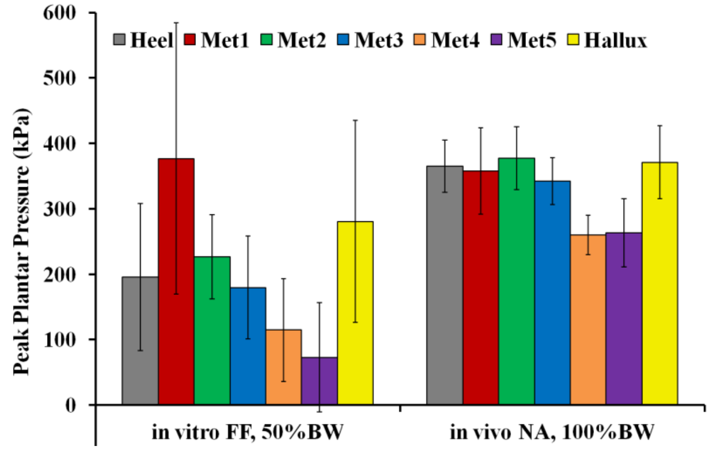

Figure 2: Average *in vitro* FF pressure data (50% BW) from the current study compared to average *in vivo* NA pressure data (100% BW) from Kraszewski et al. [8]

CONCLUSIONS

These data show both static and dynamic evidence that the flatfoot model is in general a robust representation of pes planus. Some limitations include a CPA that does not fall into the common flatfoot range, and a lack of pressure under the medial arch as is seen in many severe flatfoot patients. However, without many years of repetitive loading as would occur *in vivo*, the milder flatfoot created here is a still an acceptable and physiologically sound alternative. Overall, this flatfoot model is a good tool for future exploration of pes planus and its surgical correction.

REFERENCES

1. Ness ME, et al. *Gait Posture.* 27, 2008.
2. Jackson LT, et al. *J Biomech Eng.* 133(5), 2011.
3. Blackman AJ, et al. *J Orthop Res.* 27(12), 2009.
4. Whittaker E, et al. *Gait Posture*. 33(4), 2011.
5. Aubin PM, et al. *IEEE Trans Robot.* 28(1), 2012.
6. Ellis et al. *Foot Ankle Int.* 30(12), 2009.
7. Arangio et al. *Foot Ankle Int.* 30(11), 2009.
8. Kraszewski at el. Abstract, ASB 2010 proceedings.

ACKNOWLEDGEMENTS

This work was funded in part by the VA RR&D grant A6669R.

Table 2: Range of motion (°) (mean ± SD) for six flatfoot (FF) and six neutrally aligned (NA) cadaver specimens [4] during the stance phase of dynamic gait simulation; *significant difference between FF and NA, paired t-test, p<0.05

	CALC_TIB			MET1_TAL			NAV_TAL		
	Frontal	Transverse*	Sagittal	Frontal*	Transverse*	Sagittal*	Frontal*	Transverse*	Sagittal
FF	8.3 ± 2.9	6.5 ± 0.9	21.7 ± 2.3	15.6 ± 4.1	15.3 ± 2.6	15.9 ± 3.8	15.3 ± 3.6	11.5 ± 2.3	8.7 ± 3.6
NA	9.1 ± 3.0	10.7 ± 3.6	23.6 ± 7.0	11.4 ± 4.1	19.5 ± 3.8	22.6 ± 6.4	18.8 ± 4.8	14.9 ± 5.5	9.6 ± 4.6

INERTIAL ESTIMATE ERRORS FOR FEMALE ARMS AND LEGS FROM DIFFERENT BODY MODELS

[1]Jason Wicke and [2]Geneviève A. Dumas

[1]William Paterson University, Wayne, NJ, USA
[2]Queen's University, Kingston, ON, Canada
email: wickej@wpunj.edu

INTRODUCTION

Segment inertial parameters (e.g. mass, center of mass, moment of inertia) are required input parameters for kinetic studies of human motion. Inertial estimates (IE) are derived from indirect methods ranging from cadaver studies to medical imaging devices. IE from dual x-ray absorptiometry (DXA) has been accepted as a standard from which IE computed from specific body segment models can be compared for accuracy [1,3].

Accurate IE for the arms and legs are crucial in open chain movements (e.g. throwing), and where top down models are utilized [2,4]. However, body segment models that are convenient, included in motion analysis software, or most common in the literature are often chosen for IE without knowing the associated errors. For example, many models are specifically derived from male participants, but are still used in female studies and result in large IE errors [1]. The goal of this study was to compare the accuracy of IE of the arm and leg segments of college-age females from different body segment models.

METHODS

Twenty female (height = 59.7 ± 3.8 kg, 1.63 ± 0.04 m) college-aged participants (23.4 ± 4.2 years) were recruited for the study. A full body DXA scan on a Hologic™ fan beam was taken (Figure 1), followed immediately by the required anthropometric measures for the specific body models examined in this study (Table 1).

Inertial estimates for the upper arm, forearm and thigh and lower leg segments from DXA were obtained by interpolating the attenuation elements in the frontal plane into mass elements using an established regression equation [3]. The mass elements were then converted to IE using traditional inertial equations for mass, center of mass location and moment of inertia. Due to the attenuation elements being in the frontal plane, only the moment of inertia at the proximal joint center in the frontal plane (i.e. about the anteroposterior axis) was possible. IE were then calculated using the different body segment models being compared.

The IE mean square errors and their standard deviations were calculated for each measure and model using the DXA values as the criterion. No other statistical analysis was used because the study's goal was to examine the errors in IE associated with a model. Statistical significance is more relevant to the sensitivity of the IE to the output parameters (e.g. kinetic measures) for a specific study.

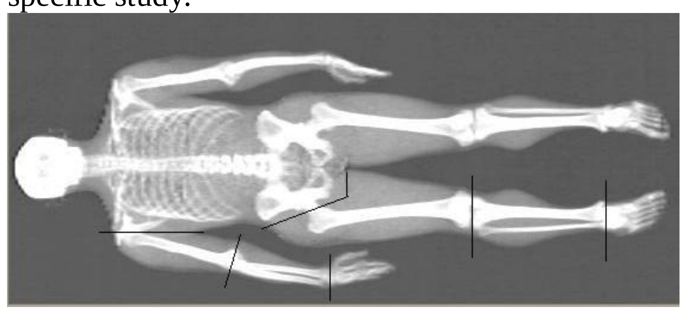

Figure 1: DXA scan with arm and leg segmentation.

RESULTS AND DISCUSSION

No single model performed best across all inertial estimates (IE) for the female arm and leg segment (Table 1). The Clauser model did not provide the most accurate IE for any of the measures. Dempster's model provided the most accurate CM estimates for the forearm and thigh. The Hanavan geometric model yielded the best IE for all shank measures and for the moments of inertia for the forearm and thigh. The thigh moment of inertia estimate from the Hanavan model had a slightly higher percent root mean square error, but the standard deviation was lower, compared to Zatsiorsky (90). The female-specific regression model developed by Zatsiorsky (90) provided the best center of mass (CM) estimates for the upper arm and the best mass estimates for the thigh. The Zatsiorsky male-based regressions with more segment specific anthropometric measures provided the best estimates for both arm mass and the moment of inertia for the upper arm and mass of forearm.

Durkin [1] found similar results in IE errors among females 19 to 30 years old for the Hanavan and Zatsiorsky (90) models. However, this study included the Clauser model which did not provide acceptable IE for college-aged females. The female-based regression model Zatsiorsky (90) provided the best overall IE for females 19-30 years old in the Durkin study. Though not as clear, a similar outcome was found here. Still, large errors in some of the IE from the Zatsiorsky (90) model exist and should be utilized with caution.

Inertial parameters are input variables required to calculate the forces and moments acting across a joint. The sensitivity of these kinetic measures on IE is highly dependent on the research design and the motion being examined. In cases where kinetic measures are calculated using a bottom-up model (through ground reaction forces via force platform), the kinetic measures have minimal sensitivity to IE errors, and therefore differences in IE errors between models may have little or no influence. The same insensitivity was found for lower-velocity movements such as the stance phase in walking [2]. However, analysis of ballistic movements, in top-down models, and where minor changes in IE are to be captured (e.g. female pregnancy), none of the models tested in this study would likely provide appropriate IE for college-aged females.

REFERENCES

1. Durkin JL & Dowling JJ. J. Biomech Eng **125**, 515-522, 2003.
2. Pearsall DJ & Costigan PA. Gait & Posture **9**, 173-183, 1999.
3. Wicke J & Dumas GA. J Appl Biomech **24**,180-184, 2008.
4. Plamondon A et al., J Clin Biomech, **11**, 101-110, 1996.

Table 1: Percent root mean square errors ± SD for inertia estimates (IE). I_{xx} = moment of inertia about the anteroposterior axis at the proximal joint center. Darkened area shows model providing best IE.

		Clauser (69)	Dempster (55)	Hanavan (64)	Zatsiorsky (90)	Zatsiorsky (85)
U. Arm	**Mass**	26.2 ± 6.5	23.9 ± 5.5	54.8 ± 8.2	25.7 ± 1.7	4.9 ± 6.5
	CM	39.6 ± 33.3	27.9 ± 13.7	23.8 ± 14.3	15.5 ± 17.6	16.1 ± 17.3
	I_{xx}	N.A.	N.A.	68.5 ± 9.6	54.9 ± 7.4	20.8 ± 15.1
Forearm	**Mass**	19.8 ± 15.9	31.0 ± 20.0	29.5 ± 20.0	22.7 ± 18.7	19.1 ± 16.0
	CM	103.5 ± 20.9	3.8 ± 5.1	14.9 ± 6.4	5.9 ± 7.8	35.7 ± 7.0
	I_{xx}	N.A.	N.A.	26.3 ± 17.4	67.6 ± 3.6	63.6 ± 7.3
Thigh	**Mass**	9.3 ± 11.4	35.3 ± 4.7	21.6 ± 4.4	6.9 ± 8.3	8.5 ± 10.7
	CM	35.2 ± 8.3	7.4 ± 9.2	38.2 ± 3.5	8.5 ± 10.4	16.0 ± 10.0
	I_{xx}	N.A.	N.A.	14.7 ± 20.1	14.4 ± 26.5	21.0 ± 33.7
Shank	**Mass**	38.6 ± 30.6	17.7 ± 26.2	14.2 ± 22.9	22.9 ± 29.3	32.1 ± 30.1
	CM	14.1 ± 14.9	38.6 ± 19.5	10.4 ± 14.4	21.5 ± 17.7	22.1 ± 16.8
	I_{xx}	N.A.	N.A.	18.3 ± 25.3	19.7 ± 29.2	28.3 ± 32.4

A PASSIVE ELASTIC EXOSKELETON REDUCES THE METABOLIC COST OF WALKING USING CONTROLED ENERGY STORAGE AND RELEASE

Bruce Wiggin, Gregory S. Sawicki
Joint Dept. of Biomedical Engineering, North Carolina State University and University of North Carolina-Chapel Hill, Raleigh, NC, USA Email: Mbwiggin@ncsu.edu

INTRODUCTION

Current exoskeletons fall into two distinct categories- fully-powered [1-4] and purely passive [5]. Fully-powered devices employ motors under high gain force control that can mimic the normal torque output of the lower-limb joints. However, added mass of the hardware most often results in a marked decrease in walking economy during assisted locomotion.

Purely passive devices (e.g. dynamic ankle-foot orthoses (DAFOs)) can store and release elastic energy in rigid, non-hinged frames to assist walking without assistance from motors. This lightweight, simplistic approach has been shown to cause small increases in both walking speed and economy post-stroke [6-8]. However there are downsides to current DAFO designs. First, rigid, non-hinged DAFOs restrict full ankle joint range of motion, allowing only limited rotation in the sagittal plane. Second, and perhaps more crucial- current DAFOs do not allow free ankle rotation during swing, making it difficult to dorsiflex in preparation for heel strike. Inability to dorsiflex freely during swing could impose a significant metabolic penalty, especially in healthy populations [9].

Using a 'hybrid' approach (i.e. controlled energy storage and release) our calculations suggest that a parallel spring of the appropriate stiffness could provide *all* of the torque output of the ankle joint during walking- without an external power source [10]. On the other hand, a recent simple walking model with springy ankles predicts that there is an optimal stiffness (not *too* stiff, not *too* compliant) for reducing the metabolic demands of walking [11]. The purpose of this study was to investigate the influence of the parallel spring stiffness of our passive ankle exoskeleton on the mechanics and energetics of walking.

METHODS

In order to take advantage of the key components from both the purely passive and fully powered assistive devices we developed a portable, passive elastic ankle exoskeleton that uses controlled energy storage and release to provide ankle torque [10]. The device works by controlling elastic energy storage and return of a parallel spring used to produce a large portion of the normal torque output of the ankle joint during walking. This concept is analogous to the elastic 'catapult' mechanism observed in the human ankle during walking [12, 13]. Our device's control system works completely off of mechanical position feedback, using a purely mechanical clutching device.

Three study participants trained with the device over three, thirty minute sessions at 1.25m/s walking speed. Sessions occurred over three separate days each with two days in between. Participants trained with the exoskeleton spring stiffness that stored the most elastic energy at 1.25 m/s. Gas exchange, electromyography, inverse dynamics and exoskeleton spring force data were collected on all days. Following training, participants walked in the exoskeleton at 1.25 m/s, for 7 minutes with 5 spring stiffnesses spanning from 110 N-m/rad to 275 N-m/rad (i.e. 30-75% of normal ankle joint stiffness at 1.25 m/s) in order to determine the optimal stiffness for metabolic economy.

RESULTS and DISCUSSION

Our results indicate that training plays a key role in adaptation to an assistive exoskeleton. By utilizing the dynamic energy storage and return of our exoskeleton, study participants were able to reduce metabolic cost on average by 10% below added mass using a parallel spring stiffness of 110Nm/rad (~35% normal ankle stiffness) after training. Participants were not able to walk comfortably with stiffnesses larger than 275Nm/rad (~75% normal ankle stiffness). The 220Nm/rad stiffness spring stored and returned the most energy, providing 32% of total ankle power. However, mechanical performance (i.e. energy stored/exo contribution) did not predict metabolic savings, emphasizing the importance of the timing of trailing limb push-off on COM dynamics [11].

We are currently building on these preliminary results by adding additional subjects (n=10). Future studies will use that same cohort to examine the interaction between exoskeleton stiffness and walking speed on walking mechanics and energetics.

REFRENCES

1) Herr H, *J Neuroeng Rehabil*, vol. 6, p. 21, 2009.
2) Dollar AM and Herr H, *Ieee T Robot*, vol. 24, pp. 144-158, Feb 2008.
3) Hitt J, et al., *Ieee Int Conf Robot*, pp. 1541-1546, 2007.
4) Kazerooni H, et al., *Int J Robotic Research* vol. 26, pp. 75-89, Jan 2007.
5) Faustini MC, et al., *Ieee T Bio-Med Eng*, vol. 55, pp. 784-790, Feb 2008.
6) Danielsson A and Sunnerhagen KS, *Journal of Rehabilitation Medicine*, vol. 36, pp. 165-168, Jul 2004.
7) Nolan KJ, et al., *NeuroRehabilitation*, vol. 27, pp. 343-50, 2010.
8) Franceschini M, et al., *Clinical Rehabilitation*, vol. 17, pp. 368-372, Jul 2003.
9) Bregman DJ, et al., *Gait Posture*, vol. 35, pp. 148-53, Jan 2012.
10) Wiggin MB, et al., in *Rehabilitation Robotics (ICORR), 2011 IEEE International Conference on*, 2011, pp. 1-5.
11) Bregman DJ, et al., *Clin Biomech (Bristol, Avon)*, vol. 26, pp. 955-61, Nov 2011.
12) Ishikawa M, et al., *J Appl Physiol*, vol. 99, pp. 603-8, Aug 2005.
13) Fukunaga T, et al., *Proceedings of the Royal Society of London: Biological Sciences*, vol. 268, pp. 229-33, Feb 7 2001.

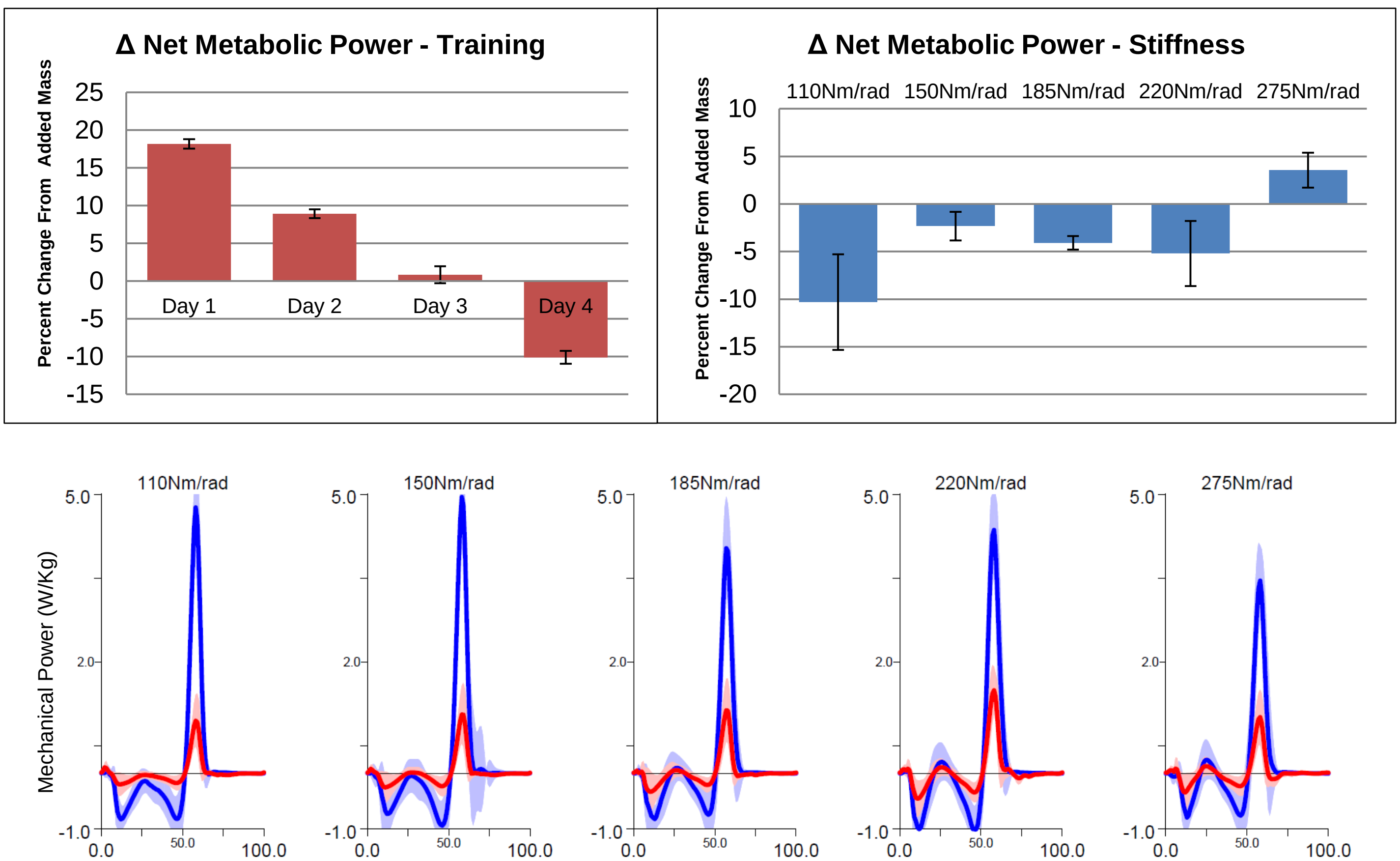

Top Left: Percent change in net metabolic power as a result of training (neg. indicates a metabolic reduction).
Top Right: Percent change in metabolic power on last testing day (Day 4) using 5 different spring stiffnesses at 1.25m/s.
Bottom: Avg. ankle (blue) and exoskeleton (red) mechanical power (W/kg). (N=3, avg. mass = 74.8kg, avg. height=1.72m)

BILATERAL ANALYSIS OF THE SHOULDER INTERNAL ROTATION PASSIVE TORQUE-ANGLE RELATIONSHIP FOR ELITE PITCHERS WITH GLENOHUMERAL INTERNAL ROTATION DEFICIT

[1]Jeff T. Wight, [2]Guy B. Grover, [2]Kelly A. Larkin, [1]Beven P. Livingston and [2]Mark D. Tillman

[1]University of North Florida, Jacksonville, FL, USA
[2]University of Florida, Gainesville, FL, USA
email: j.wight@unf.edu, web: http://www.unf.edu/brooks/movement_science/

INTRODUCTION

It is important to monitor the throwing shoulder's internal rotation (IR) flexibility. Interestingly, pitchers with throwing arm problems often have drastically reduced IR mobility, likely because of excessive shoulder "posterior tightness" [1,2]. This condition is commonly referred to as glenohumeral internal rotation deficit or GIRD. To date, GIRD studies have focused on shoulder range of motion (ROM) only. In this study, we assess the torque that is generated by the shoulder as it is passively internally rotated to the end ROM. The purpose is to conduct a bilateral analysis on a group of pitchers who suffer from GIRD. We hypothesize that the throwing shoulder will have a reduced laxity zone, reduced resistance zone, and increased rotational stiffness. Studying the torque-angle relationship may help to better understand this altered ROM.

METHODS

Eleven college and professional pitchers with GIRD were analyzed. Informed consent was obtained. GIRD was defined as an IR ROM bilateral difference of 15° (the throwing shoulder ROM was reduced).

The torque-angle relationship was assessed using a custom biomechanical device (Figure 1). The forearm was secured to a wheel that was designed to slowly internally rotate the shoulder to the end ROM. The wheel was equipped with a potentiometer to assess angular displacement. A load cell was used to assess the torque required to rotate the shoulder. Testing was completed with the participant laying supine on an athletic training table. The scapula was stabilized.

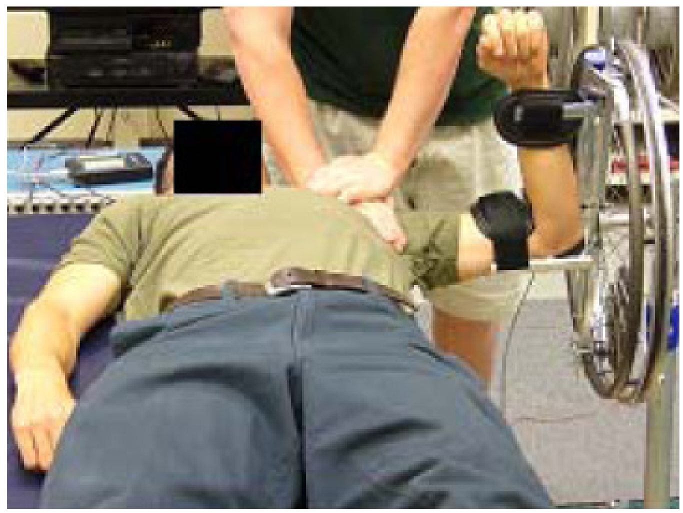

Figure 1. A custom biomechanical device was used to assess the passive torque-angle relationship for shoulder IR.

Arm order was randomized (dominant vs. non-dominant arm). A brief warm-up was completed immediately before the data collection. First, the shoulder was stretched twice for 10 seconds using the custom device. Second, a "practice" repetition was completed to the end ROM. The data collection followed and consisted of three consecutive repetitions to the end ROM.

All data acquisition and analysis was completed using custom programs written in LabVIEW software. The torque-angle data was averaged into 1/2° increments and modeled with a least-squares best-fit line (from the angle where 1N·m of torque was first generated to the end ROM). This worked well for all participants ($R^2 \geq 0.96$). From the best-fit line, the following five torque-angle variables were analyzed: end ROM, laxity zone (from 0° IR to the angle where 1N·m of torque was first achieved), resistance zone (from angle where 1N·m of torque was achieved to the end ROM), rotational stiffness (slope of best-fit line), and the torque needed to internally rotate the shoulder to the end ROM. For each participant, data from the three repetitions were averaged. Dependent t-tests were used to test for bilateral differences. The alpha level was set at 0.05.

RESULTS AND DISCUSSION

Results from the bilateral analysis are presented in Table 1. The mean GIRD for these 11 pitchers was 21°. As hypothesized, the laxity zone was significantly reduced. In fact, the majority of the IR motion loss was attributed to a reduction of the laxity zone. Our data demonstrates that the soft tissues began stretching 17° sooner in the throwing shoulder (compared to the non-throwing shoulder). The resistance zone was also significantly reduced, but the reductions were moderate (approximately 4°). The reduction of the resistance zone is likely related to the throwing shoulder's increased rotational stiffness: the throwing shoulder was 15% stiffer than the non-throwing shoulder.

CONCLUSIONS

In conclusion, the IR torque-angle profile appears to be dramatically altered for the throwing shoulder. Torque is generated much sooner, stiffness increases, and the resistance zone is reduced. These findings support the hypothesis that pitchers with GIRD have increased "posterior tightness".

Studying the torque-angle relationship is the means to thoroughly understanding the flexibility of the throwing shoulder. This study demonstrates that baseball pitching can alter the IR flexibility of the throwing shoulder in complex ways. Future studies should strive to understand the clinical relevance of the torque-angle measures.

REFERENCES

1. Myers JB, et al. *Am J Sports Med.* 34(3), 385-91, 2006.

2. Burkhart SS, et al. *Journal of Arthroscopic and Related Surgery* 19(4): 404-420, 2003.

Table 1: Bilateral shoulder IR flexibility analysis of 11 pitchers with GIRD.

	ROM	**LZ**	**RZ**	**stiffness**	**torque**
Throwing shoulder	77.8° (11.9°)	57.6° (8.6°)	20.1° (6.0°)	0.45 (0.10 N·m/°)	14.1 (3.2 N·m)
Non-throwing shoulder	98.8° (3.2°)	74.7° (9.6°)	24.3° (7.7°)	0.39 (0.07 N·m/°)	14.3 (3.0 N·m)
p-value	$p < 0.01$*	$p < 0.01$*	$p = 0.03$*	$p < 0.01$*	$p = 0.69$

ROM = range of motion; LZ = laxity zone; RZ = resistance zone

DOES THE NUMBER OF REPETITIONS ACHIEVED FOR THE BENCH PRESS PREDICT THE NUMBER OF REPETITIONS ACHIEVED FOR OTHER COMMON RESISTANCE TRAINING EXERCISES?

[1]Jeff T. Wight, [1]Caleb Williams and [1]Peter M. Magyari

[1]University of North Florida, Jacksonville, FL, USA
email: j.wight@unf.edu, web: http://www.unf.edu/brooks/movement_science/

INTRODUCTION

To determine the appropriate load for resistance training, the clinician/trainer often consults published tables [1]. The tables share the recommended load for the desired number of repetitions. Interestingly, these tables were based on 1-repetition maximum (1RM) testing for only 1 exercise (bench press) and generalized to all resistance training exercises [3]. This generalization has not been supported by studies investigating repetitions completed at 60% and 80% of 1RM [2,3]. At these loads, the repetitions clearly vary between the bench press and other exercises. However, it remains unclear if the number of repetitions achieved on the bench press predicts the number of repetitions achieved on other exercises. The purpose of this study was to determine if the number of repetitions achieved for the bench press (at 60% and 80% of 1RM) predicts the number of repetitions achieved on 7 commonly prescribed resistance training exercises. We hypothesize there will be a strong positive correlation between the repetitions achieved on the bench press and the repetitions achieved on the other exercises.

METHODS

The participants were 19 college-aged males (22 ± 4.7 years) with a minimum of 2 months resistance training experience. Informed Consent was obtained and a Health History Questionnaire was completed. Participants completed two exercise testing sessions (≤ 60 minutes).

Session 1. 1RM testing was completed under the supervision of a certified exercise professional (C.W.). The warm-up was 5 minutes of moderate intensity rowing on an ergometer. The following 8 cam mediated variable resistance exercises were assessed: bench press, leg press, shoulder press, pull down, knee extension, knee flexion, elbow flexion, and elbow extension. For each exercise, participants were randomized to perform either 60% or 80% of 1RM. Subjects were instructed to complete as many repetitions as possible, before volitional fatigue, using proper form, through the full range of motion. Rest between exercises was standardized at 2 minutes.

Session 2. Subjects returned for a second exercise testing session to complete testing at the other load. The same protocol (from session 1) was followed. The minimum time between testing sessions was 72 hours to eliminate muscle soreness and fatigue.

For each load (60% and 80% of 1RM), Pearson correlation was used to determine the strength of the relationship between the repetitions achieved on the bench press and the repetitions achieved on the other 7 exercises. The alpha level was set at $p = 0.05$.

RESULTS AND DISCUSSION

Descriptive statistics are presented in Table 1. As expected, for both loads, the number of repetitions achieved was highly variable within and among the exercises.

Correlation results are presented in Table 2. For the lower load (60% 1RM) there was only 1 significant correlation (between bench press and elbow flexion), and the relationship was weak/moderate. For the higher load (80% 1RM) there were significant correlations between bench press and 4 of the 7 exercises (leg press, knee flexion, elbow extension). But the correlations were weak/moderate. The strongest correlation (r = 0.61) is displayed in Figure 1.

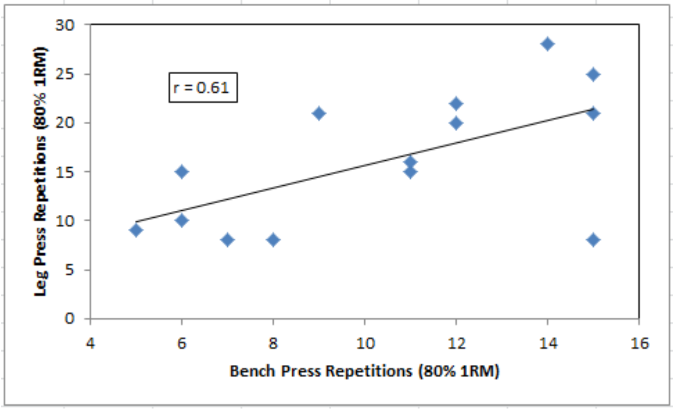

Figure 1: The repetitions achieved on the bench press did not strongly predict the repetitions achieved on other exercises.

CONCLUSIONS

In this study, for all individuals, the repetitions achieved on the 8 exercises varied dramatically. For both loads (60% and 80% 1RM), the bench press had a very limited ability to predict the number of repetitions achieved on other exercises. It was very common for individuals to achieve above average repetitions on the bench press and below average repetitions on other exercises, and vice versa. These results further support the idea that it is inappropriate to use the bench press results to determine expected repetitions for other resistance training exercises; each exercise needs to be assessed independently.

Future studies should focus on 1) determining why the number of repetitions varies so dramatically among exercises at similar loads, 2) determine if the repetitions achieved on "high repetition" exercises (e.g. leg press) predict other high repetition exercises and vice versa 2) establishing exercise-specific load/repetition tables.

REFERENCES

1. Baechle, T.R. and R. W. Earle, Eds. *Essentials of Strength Training and Conditioning.* 3rd Ed. Champaign, IL.: Human Kinetics. 394-398, (2008).

2. Shimano, T., et al. *J. Strength Cond. Res.* 20(4):819-823, 2006.

3. Hoeger W.K., et al. *J. Strength Cond. Res.* 1(1):11-13, (1987).

Table 1: Repetitions achieved (mean ± SD) for each exercise at the 2 loads.

Load	Bench Press	Leg Press	Shoulder Press	Pull Down	Knee Extension	Knee Flexion	Elbow Flexion	Elbow Extension
60% 1RM	20 ± 4.4	30 ± 9.1	11 ± 3.6	22 ± 4.5	21± 5.0	35 ± 12.5	17 ± 3.6	28 ± 11.5
80% 1RM	10 ± 3.4	16 ± 6.5	7 ± 2.5	12 ± 3.6	12 ± 4.1	19 ± 8.7	9 ± 2.6	13 ± 5.9

Table 2: Correlation between repetitions achieved on the bench press and other common exercises.

Load	Leg Press	Shoulder Press	Pull Down	Knee Extension	Knee Flexion	Elbow Flexion	Elbow Extension
60% 1RM	r = 0.01	r = 0.35	r = 0.17	r = 0.16	r = 0.41	r = 0.46*	r = 0.18
80% 1RM	r = 0.61*	r = 0.18	r = 0.02	r = 0.23	r = 0.60*	r = 0.58*	r = 0.51*

*significant correlation ($p \leq 0.05$)

CONCUSSION ALTERS GAIT TERMINATION STRATEGIES

[1]Erik A Wikstrom, [2]Tiffen G. Tapia-Lovler, [2]Barry A Munkasy, and [2]Thomas A Buckley

[1]University of North Carolina at Charlotte, Charlotte, NC, USA
[2]Georgia Southern University, Statesboro, GA, USA
email: ewikstrom@uncc.edu, web: http://kinesiology.uncc.edu

INTRODUCTION

Concussion diagnosis and recovery are hampered by the lack of a truly diagnostic medical tool [1]. Current clinical evaluation is multifaceted and includes self-reported symptoms, assessment of neurocognitive impairments, and postural deficits [1]. However these tools, particularly the postural assessment tools, have been shown to return to baseline values despite the continued presence of concussion symptoms [2]. Thus, it is likely that critical subtle and lingering concussion related deficits in postural control persist long after traditional assessment tools return to their baseline score and that recently concussed athletes may be allowed to return to participation prior to full recovery. Therefore, the purpose of this investigation was to determine if gait termination, a novel and dynamic postural control assessment technique, returned to baseline values as quickly as traditional concussion assessment techniques.

METHODS

Participants included 20 uninjured controls (age: 20.9±1.6 years, height: 164.3±8.0cm, weight: 64.2±10.6kg), and 23 concussed individuals (age: 19.3±1.3 years, height: 174.1±13.2cm, weight: 81.2 ±19.3kg). All subjects completed 2 standard gait and 5 planned gait termination trials at a self-selected pace per test session along a 6.1 meter walkway. Planned gait termination required intended stopping on two adjacent force platforms mounted consecutively in the path of motion and flush with the surrounding floor (Figure 1). Controls were tested once, while concussed individuals were tested daily from the day after their concussion until the day they returned to full unrestricted activity (mean: 12.7±4.4 days).

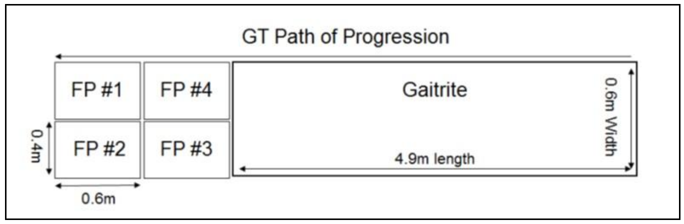

Figure 1: Laboratory set up. Subjects would walk from right to left and terminate on either force plate 4 & 1 (right foot) or 3 & 2 (left foot).

Main outcome measures included maximum propulsive and braking forces from the penultimate and final step of gait termination respectively (Figure 2) as well as gait velocity during gait termination. The forces were then compared with the propulsive and braking forces captured during standard gait trails.

The outcomes were compared to the baseline values at five distinct time points: day one post concussion, on the day that the Standardized Assessment of Concussion (SAC) questionnaire returned to baseline values (1.9±1.3 days), on the day that the Balance Error Scoring System (BESS) returned to baseline values (2.3±1.5 days), the day that all concussive signs and symptoms resolved (4.0±1.8 days), and the day that the concussed athletes was returned to full unrestricted activity.

Independent sample t-tests were used to determine if gait termination outcomes were altered, relative to baseline values, at these time points. Bonferroni adjustments were made to account for the 5 analyses performed per outcome measure. Thus the adjusted alpha level of 0.01.

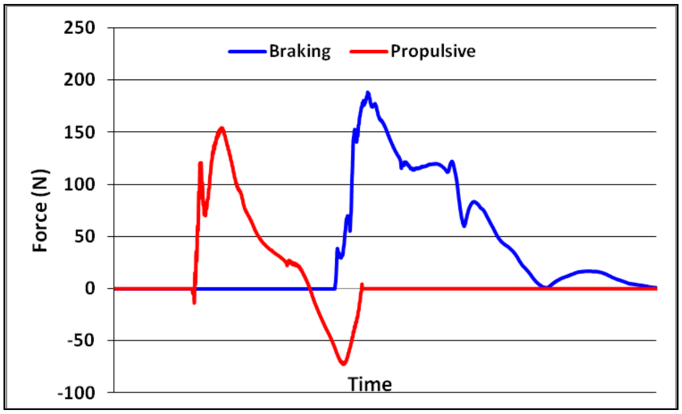

Figure 2: Representative traces of the propulsive and braking forces taken during penultimate and final step of planned gait termination.

RESULTS AND DISCUSSION

Overall, the results indicate that concussed individuals reduced their propulsive forces to a greater extent than uninjured controls (Table 1). Statistically significant differences were noted on the day that the BESS and SAC returned to baseline values and the day that the concussed individuals were allowed to return to full unrestricted activity. Concussed individuals also had smaller braking forces than uninjured controls (Table 1). Statistically significant differences were identified on day one post-concussion, the days that the BESS and SAC returned to baseline values, the day that concussive signs and symptoms resolved, and the day that the concussed individuals were allowed to return to full unrestricted activity. However, no differences were identified with regards to gait velocity regardless of the time point (Table 1).

These results indicate that gait termination outcomes can detect postural control impairments following concussion. More importantly, the results indicate that gait termination outcomes are able to detect lingering postural impairments in concussed individuals after traditional concussion assessment tools indicate the resolution of symptoms.

CONCLUSIONS

Traditional concussion assessment tools may not be sensitive enough to detect lingering postural control deficits following sports related concussions. These results further recent findings [3] which suggest that sophisticated biomechanical analysis can identify lingering postural impairments following a concussion which are not successfully identified by traditional and current assessment techniques.

REFERENCES

1. McCrory P, et al. Consensus statement on concussion in sport: the 3rd International Conference on Concussion in Sport held in Zurich, November 2008. *J Athl Train.* Jul-Aug 2009;44(4):434-448.
2. McCrea M, et al. Acute effects and recovery time following concussion in collegiate football players: the NCAA Concussion Study. *JAMA.* Nov 19 2003;290(19):2556-2563.
3. Slobounov S, et al. Alterations of Postural Responses to Visual Field Motion in Mild Traumatic Brain Injury. *Neurosurgery*. 2006; 58(7): 134–139.

ACKNOWLEDGEMENTS

Supported by: NINDS 1R15NS070744-01A1.

Table 1: Group means and standard deviations for gait termination outcomes at time points of interest.

	Control (n=20)	Concussed Individual Time Points				
		Day 1 (n=14)	SAC (n=18)	BESS (n=16)	Symptoms (n=18)	RTP (n=13)
Propulsive Force Decrease (%)	40.3±10.8	48.9±11.4	49.4±9.2*	52.7±13.0*	49.6±11.7	52.3±10.1*
Braking Force Increase (%)	47.2±23.56	-13.5±19.9*	-10.5±19.6*	-5.6±17.8*	-3.3±20.9*	11.9±26.1*
Gait Velocity (m/s)	1.28±0.11	1.16±0.16	1.27±0.20	1.25±0.19	1.31±0.15	1.38±0.16

* Indicates a statistical difference ($p \leq 0.01$) from the control group.

ELECTROMYOGRAPHIC EFFECTS OF USING A POWERED ANKLE-FOOT PROSTHESIS

[1,3]Matthew R. Williams, [2]Alena Grabowski, [3]Hugh Herr, and [1]Susan D'Andrea

[1]Center for Restorative and Regenerative Medicine, PVAMC, Providence, RI, USA
[2]University of Colorado Boulder, Boulder, CO, USA,
[3]Massachusetts Institute of Technology, Cambridge, MA, USA
email: mrw8@mit.edu

INTRODUCTION

Individuals with a transtibial amputation typically walk 15% slower, have a 25% higher metabolic cost of transport, and exhibit asymmetric gait patterns compared to non-amputees [1]. Over time, individuals with a unilateral leg amputation using current passive-elastic prosthetic feet also have an increased risk of joint and back pain and osteoarthritis likely due to altered gait patterns [2]. Recently, in contrast with passive-elastic prostheses, a novel, powered ankle-foot prosthesis has been shown to lower the metabolic demands of level ground walking, increase preferred walking speed, and restore normative biomechanics in people with unilateral transtibial amputations [3]. Given these changes in amputee gait, it is hypothesized that use of this powered ankle-foot prosthesis would normalize the electromyography (EMG) patterns of people with unilateral transtibial amputations compared to non-amputees.

METHODS

Seven subjects with a unilateral, transtibial leg amputation and an equal number of age-weight-height-sex matched non-amputee subjects were asked to walk across a level 10m walkway while electromyography from the biceps femoris, gluteus maximus, and rectus femoris of both legs was recorded. Subjects walked at five different speeds - 0.75m/s, 1m/s, 1.25m/s, 1.5m/s, and 1.75m/s. Surface EMG was collected at 1 kHz during gait using a wireless EMG system (Delsys Myomonitor, Boston, MA). Prior to walking, each subject's maximum voluntary contraction (MVC) for each muscle was recorded during a 10 second maximum effort, isometric contraction against resistance.

EMG from MVCs and walking trials were processed identically. EMG signal processing consisted of motion artifact identification (any value greater than ±3 standard deviations from the mean) and removal, rectification, and a 2Hz low-pass filter to yield an envelope of the EMG signal. The walking EMG signals for each muscle were then normalized to the corresponding MVCs such that the EMG reported for each muscle is on a 0-100% MVC scale. The EMG for each muscle was then averaged and compared across each speed in non-amputees, subjects using both a powered prosthesis, and conventional prosthesis.

RESULTS AND DISCUSSION

The affected leg of subjects with an amputation had greater biceps femoris muscle activity while using both the powered and passive-elastic prostheses compared to that of non-amputees (21% vs. 8%), (Fig. 1b), particularly during stance phase. The unaffected leg of subjects with an amputation using a passive-elastic prosthesis produced greater biceps femoris muscle activity during the swing phase (13%) compared to that of subjects with an amputation using the powered prosthesis (5%) and to that of non-amputees (5%), (Fig. 1a).

Subjects with an amputation exhibited much lower rectus femoris muscle activity in their affected leg while using the powered prosthesis compared to using a passive-elastic prosthesis (12% vs. 49%), but still greater than the muscle activity of non-amputees (7%), (Fig. 1d). Subjects with an amputation using the powered prosthesis had lower rectus femoris muscle activity in their unaffected leg compared to using a passive-elastic prosthesis (11% vs. 15%), but had greater muscle activity than non-amputees (5%) during stance phase (Fig. 1c). During swing phase, subjects with an amputation using a passive-elastic prosthesis produced greater rectus femoris muscle activity (12%) compared to that while using the powered prosthesis (5%) and to that of non-amputees (6%). There were no differences in rectus femoris muscle activity of the unaffected leg between subjects using the powered prosthesis and non-amputees during swing phase.

Gluteus maximus muscle activity of the affected leg was consistently greater in subjects using a passive-elastic prosthesis (40%) compared to subjects using a powered prosthesis and to non-amputees (25% and 20% respectively from late stance through swing), (Fig. 1f). Gluteus maximus muscle activity of the affected leg was greater in subjects using the powered prosthesis compared to that of non-amputees but follows a similar pattern of activation. Gluteus maximus muscle activity of the unaffected leg was greater in subjects using a passive-elastic prosthesis compared to subjects using the powered prosthesis (58% vs. 34%), (Fig. 1e) and to non-amputees (25%) at lower speeds, with a decreasing amount of difference between conditions with increasing speeds.

Overall the EMG patterns of subjects using the powered prosthesis are more similar to those of non-amputees compared to while using a passive-elastic prosthesis. There is both a reduction in the magnitude of muscle activity as well as activation patterns that are similar to those of non-amputees. However, subjects using the powered prosthesis had greater muscle activity in the biceps femoris compared to non-amputees and similar activity compared to when they used a conventional prosthesis. The increased biceps femoris muscle activity in subjects with an amputation could be due to an increased need to stabilize the body immediately after heel strike. It is also possible that the biceps femoris compensates for the compromised gastrocnemius function in people with a transtibial amputation.

CONCLUSIONS

Passive-elastic prosthetic feet, while enabling individuals to walk, do not allow people with a transtibial amputation to fully replicate the walking patterns of non-amputees. By using a powered prosthesis, people with a transtibial amputation exhibit leg muscle activity that more closely matches that of non-amputees during level-ground walking. This improvement in biomimicry is thought to allow transtibial amputees to walk with a more natural, and therefore healthier gait.

REFERENCES

1. Waters, R. L., Perry, J., Antonelli, D. & Hislop, H. *J Bone Joint Surg Am* **58**, 42–46, 1976.
2. Gailey, R., Allen, K., Castles, J., Kucharik, J. & Roeder, M. *J Rehabil Res Dev* **45**, 15–29, 2008.
3. Herr, H. M. & Grabowski, A. M. *Proc. Biol. Sci.* **279**, 457–464, 2012.

ACKNOWLEDGEMENTS

This work sponsored by a Department of Veterans Affairs Career Development Award to A.M.G. from the RR&D Service, and Providence VAMC CRRM (VA RR&D A3962R).

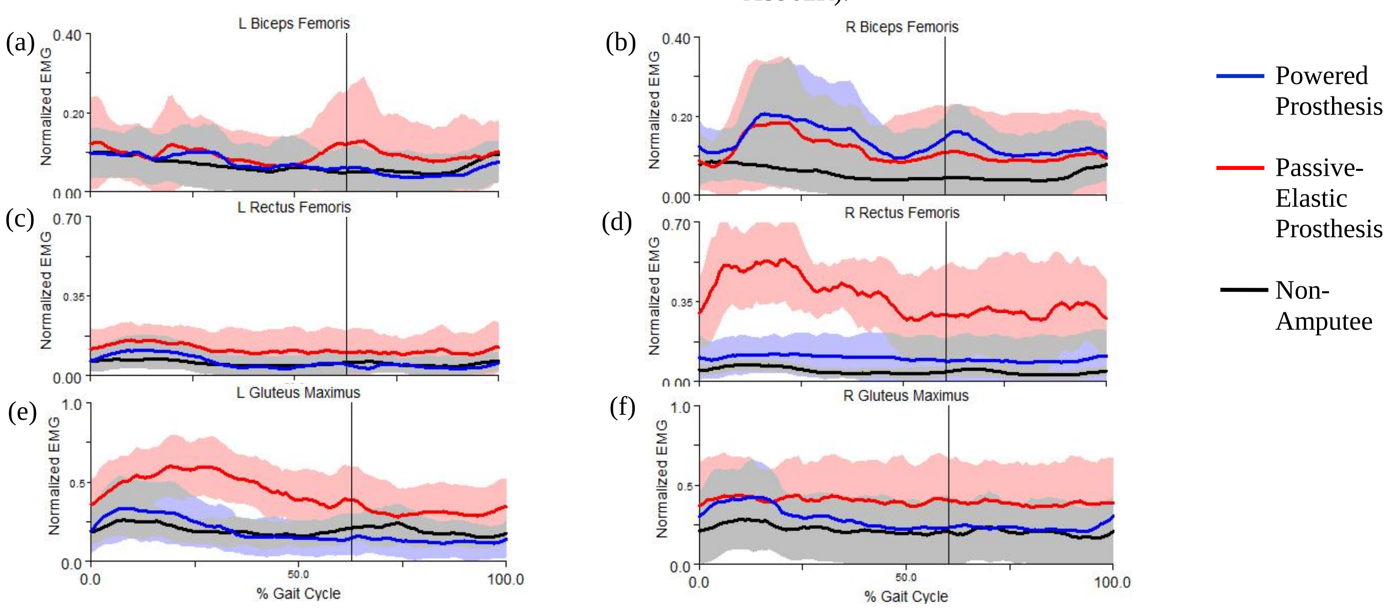

Figure 1: Mean normalized EMG during the gait cycle of three muscles for the unaffected leg (left column) and affected leg (right column), averaged across five speeds. Shaded portions represent ±1 standard deviation. The vertical line in each plot represents the transition from stance to swing phase.

SEX DIFFERENCES IN UNCONSTRAINED TRANSVERSE PLANE KINEMATIC RESPONSE UNDER COMPRESSION AND SIMULATED MUSCLE FORCES

Samuel C. Wordeman[1], Carmen E. Quatman[1], Ata M. Kiapour[2], Richard C. Ditto[2], Vijay K. Goel[2], Constantine K. Demetropoulos[2], Timothy E. Hewett[1,3]

[1]The Ohio State University, Sports Health and Performance Institute
[2]The University of Toledo, Engineering Center for Orthopaedic Research Excellence (ECORE)
[3]Cincinnati Children's Hospital, Sports Medicine Biodynamics Center
Email: Samuel.Wordeman@osumc.edu

INTRODUCTION

In vitro biomechanical experiments provide valuable insight into the responses of biological structures to applied loads and motions. In the human knee, a number of researchers have employed cadaveric techniques to elucidate the roles of passive and active restraints under simple and complex conditions. Several researchers have espoused the theory that increased posterior slope on the medial and lateral tibial plateau in females contributes to increased risk of anterior cruciate ligament injury.[1] However, few *in vitro* biomechanical studies have investigated inherent differences in male and female transverse plane kinematics when selecting specimens and reporting results. The purpose of this study was to examine sex differences in unconstrained kinematic response to simulated muscle forces and compressive loads. We hypothesized that the transverse plane kinematic response between males and females would differ when a compressive load was applied across the knee joint in addition to simulated muscle forces.

METHODS

Sixteen cadaveric limbs (10 female, age 45.7±9.3, 6 male age 41.5±7.1) were sectioned at the mid-femoral shaft and the proximal end of the femur was potted in polyester resin. The potted end was rigidly fixed to a custom 6-axis load cell, inside of a force couple testing system (FCTS). The FCTS was designed to provide 6 degrees of freedom to the tibia, while allowing the application of force couples to apply pure moments to the tibia. Tibiofemoral and patellofemoral rigid body kinematics were captured using an Optotrak 3020 System (Northern Digital, Waterloo, Ontario, Canada) by attaching 3 non-collinear active infrared markers to each bone. Flexion from 0 to 90 degrees was achieved using servo-electric actuators attached to a system of pulleys that applied pure moments about the medial-lateral axis of the knee joint. The neutral alignment of the tibia was determined by the free hanging position of the limb. After capturing the neutral position, a 400 Newton load was applied to the stripped quadriceps' tendon, and a 200 Newton load was applied to the stripped hamstrings tendons (semitendinosus, semimembranosus, biceps femoris). Limbs were tested through 90 degrees of flexion under simulated muscle load, and under simulated muscle load with an added 134 Newton compressive joint force applied.

Differences in transverse plane kinematic data were assessed using a repeated measures mixed model analysis of covariance (ANCOVA). Repeated measures within each specimen were assessed for each knee flexion angle, between specimen effects of sex were assessed, and sex-by-flexion angle interactions were assessed at an *a priori* level of $\alpha=0.05$.

RESULTS

Significant sex by knee flexion angles were observed for both the simulated muscle condition ($p=0.024$) and the simulated muscle + compression condition ($p=0.007$). A within-subject effect of knee flexion angle ($p=0.000$) was also observed. Results are shown in **Figure 1.**

For the isolated simulated muscle loading condition, both males and females started in a relatively neutral transverse plane alignment and moved into greater internal rotation for the first 45 degrees of flexion, replicating the “screw home” mechanism. From 45 to 90 degrees flexion, internal rotation was reduced, with males exhibiting primarily external rotation from 80 to 90 degrees of flexion. Females also moved toward less internal rotation, but the mean rotation angle across specimens never crossed from internal to external rotation.

In the simulated muscle loading + 134 Newton compression condition, males moved from a relatively neutral orientation to greater internal rotation from 0 to 20 degrees of flexion. Subsequently, internal rotation decreased until 50 degrees of flexion at which point external rotation was observed. However, females continued to exhibit greater internal rotation angles until 35 degrees of flexion after which they gradually returned to a neutral rotation angle at 90 degrees of flexion.

DISCUSSION

The current study demonstrates that the unconstrained transverse plane kinematic response differs between sexes under identical loading conditions. Furthermore, this data shows that joint compression and sagittal plane knee angle affect transverse plane response during unconstrained motion. Interestingly, under both loading conditions males reached peak internal rotation at lower flexion and demonstrated less peak internal rotation than females. Given the controlled nature of the loading and motion in the current methodology, only a handful of explanations may be able to account for the observed results. Several studies have reported differences between males and females in medial and lateral tibial plateau slope. However, none of these studies have specifically examined the effects of tibial slope disparities on frontal or transverse plane kinematics. It is also possible that soft tissue structures in the female specimens were smaller, and thus had less structurally robust mechanical properties. [2]

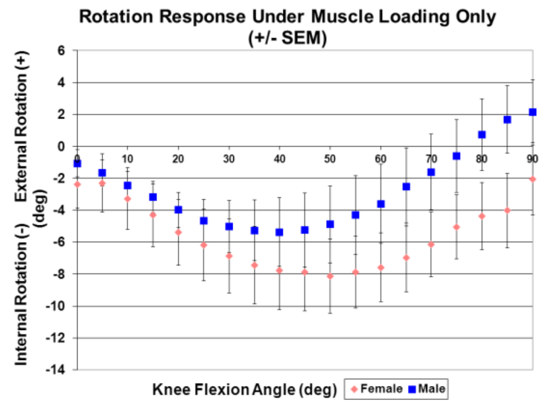

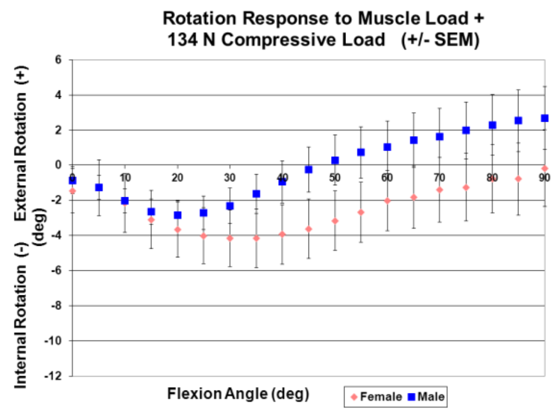

Figure 1: Transverse plane kinematic response of male and female specimens under simulated muscle forces (top) and simulated muscle forces with 134 Newtons of compression added (bottom).

The fact that magnitudes of loading were constant between specimens, not proportional to body weight may potentially explain some of the observed differences.

The interactions observed seem to indicate that translations in the sagittal plane due to increased tibial slope are not the only sex effects to consider when populating an *in vitro* study. Future studies should consider the inherent effects of sex on bony geometry and kinematic response when reporting *in vitro* biomechanical results.

ACKNOWLEDGEMENTS

The work presented in this manuscript was funded by NIH/NIAMS Grant R01-AR056259.

REFERENCES

[1] Musahl et al., 2010 *Knee Surg Sports Traumatol Arthroscopy*
[2] Chandrashekar et al., 2006 *J Biomech*

A HYBRID MODEL SIMULATING HAND GRIPPING ON A CYLINDRICAL HANDLE

*John Z. Wu, Ren G. Dong, Christopher M. Warren, Daniel E. Welcome, and Thomas W. McDowell
National Institute for Occupational Safety and Health, Morgantown, WV, USA. *Email: jwu@cdc.gov

INTRODUCTION

Musculoskeletal disorders of the hand and fingers are associated with occupational activities across all industrial sectors [1]. Since the handle serves as an interface between an operator and a machine or a tool, it is well accepted that an optimized design of the handle can reduce both physical effort and musculoskeletal fatigue, thereby improving comfort and reducing the risk of musculoskeletal disorders. Previous models of hand gripping can be categorized into two groups: multi-body dynamic models [2] and finite element (FE) models [3]. The multi-body dynamic models include muscle forces, but not the effects of the passive soft tissues (i.e., skin and subcutaneous tissues), which play an important role in contact interactions. The traditional FE models do not include multiple finger segments and muscle forces. The goal of the current study is to develop a hybrid FE hand gripping model, which combines the features of conventional FE models and multi-body dynamic models.

METHODS

The gripping model features a finger and a cylindrical handle (Fig. 1A). The model includes three finger segments (distal, middle, and proximal phalanges), three joints [the distal interphalangeal (DIP), proximal interphalangeal (PIP), and metacarpophalangeal (MCP) joint], and contains the major anatomical substructures of the finger (i.e., soft tissues, nail, and bone). The dimensions of the finger segments were scaled to match the average of individual subjects. The simulations were performed in a forward dynamic scheme – the joint moments were applied, whereas the deformation and stress/strain of the soft tissues are predicted.

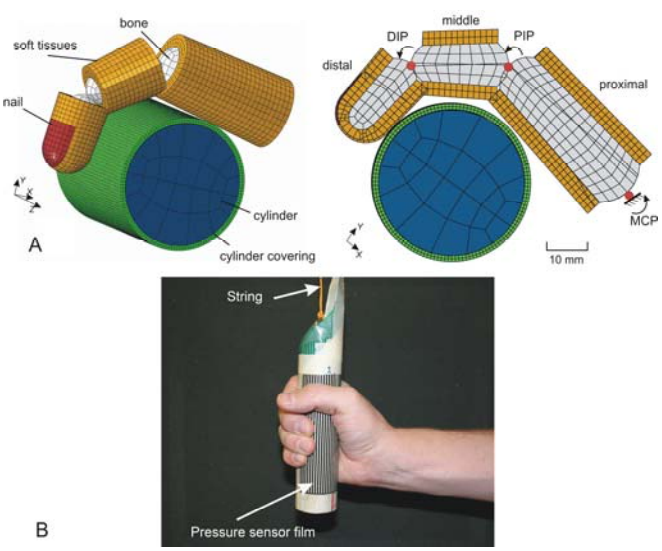

Figure 1. Model and experimental set-up. A: The model of gripping. B: The experimental set-up for the gripping test.

The cylinder was considered of aluminum and covered with materials (thickness 1.5 mm) of different levels of stiffness (Sorbothane thermoplastics with three different hardness values: 30, 50, and 70 on an OO durometer scale). The mechanical properties of the bone, nail, and soft tissues have been described in our previous study [3].

Gripping tests were accomplished by using an instrumented cylindrical handle (Fig. 1B). The distributions of the contact pressure between the fingers and handle were measured by using a pressure sensor film (Model 5076, TekScan) that was wrapped around the surface of the handle.

RESULTS

Our analysis indicated that the best fit of the predicted contact pressure distributions to the experimental data was achieved by applying a joint moment ratio of 1.00:2.63:5.52 at the DIP, PIP, and MCP joints, which is close to the results of multi-body dynamic analysis [4]. The calculated contact pressure distributions are shown in Fig. 2 (right column) in comparison with the corresponding experimental data (left column). The figures show that the calculated pressure distributions match approximately the experimental data throughout the entire loading process. The ratio of the maximal contact pressure at the distal, middle, and proximal segments of the middle finger was observed to be: 1:0.89(SD 0.27):0.72(SD 0.30). Although the contact pressure distributions of the fingers differed from subject to subject, general patterns of the pressure distribution on each segment of a finger

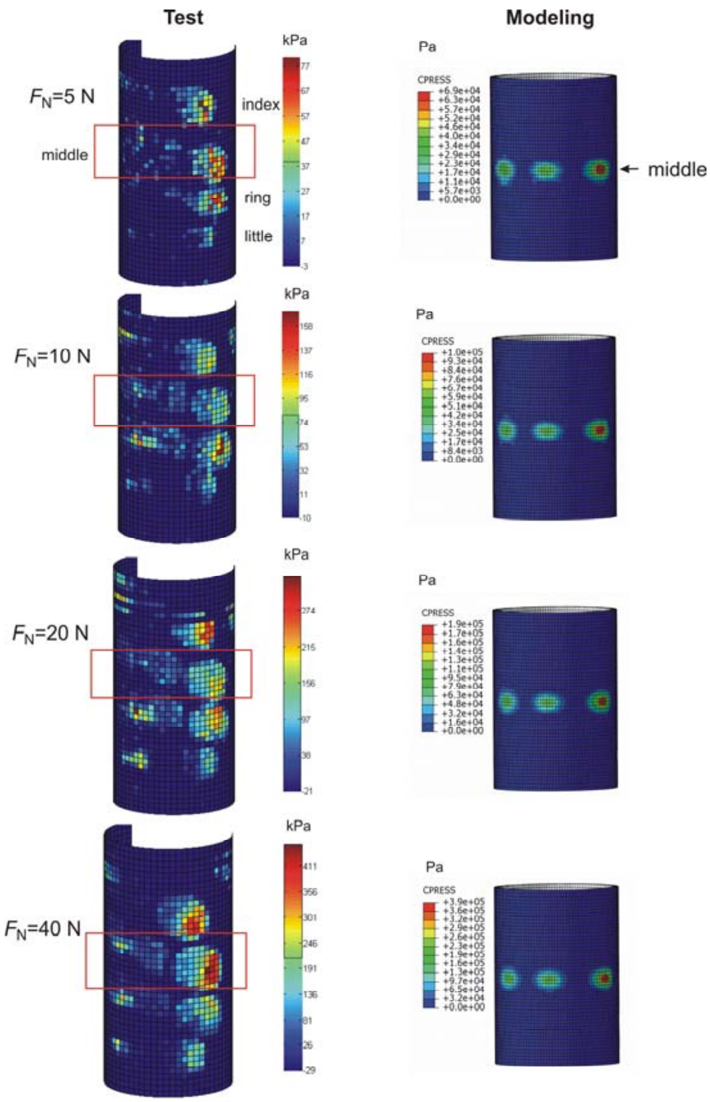

Figure 2. Predicted contact pressures as a function of gripping force (Right column) compared with experimental data (Left column).

were consistent: the contact pressure on the distal segment was substantially greater than those of the middle and proximal segments.

Our simulation results show that, for a given gripping effort, the contact pressure decreased with decreasing stiffness of the covering material (Fig. 3). The maximal contact pressure decreased from 800 kPa to 660 kPa, a reduction of 17.5%, when the covering material varied from "Hard" to "Soft". The change in material stiffness did not alter the pattern of the contact pressure distributions. The maximal contact pressure at the distal finger segment (800 kPa) was approximately the magnitude observed in the experiment with the maximal gripping effort (results not shown).

DISCUSSION AND CONCLUSIONS

The ratio of the maximal contact pressure of the distal, middle, and proximal finger segments (Fig. 2) observed in our study is consistent in trend with results by Chao et al. [5], who measured the ratio of the contact forces applied on the distal, middle, and proximal segments in grip. Because the maximal contact pressure is associated with the contact force on each finger segment, the results of these two studies should be comparable, at least in trend.

Our study suggests that the maximal compressive stress on the skin surface of the middle finger can be reduced by reducing the stiffness of the material covering a cylindrical handle. The current simulation results indicate that the maximal compressive stresses on the distal, middle, and proximal segments were reduced by 24.4%, 10.8%, and 13.9%, respectively, when the stiffness of the covering material decreased from "Hard" to "Soft" (results not shown). Our simulations suggest that an operator's comfort may be effectively modulated by varying the stiffness of the covering materials, since the comfort of a finger may be associated with the responses of the mechanoreceptors that sense the stress/strain states in their surrounding tissues [6]. Our observations may generally support the practice whereby tool handles are often wrapped with a layer of soft materials to improve comfort.

REFERENCES

1. Marras WS, Cutlip RG, Burt SE, Waters TR. *App Ergon*. 40 (1) (2009) 15–22.
2. Freund J, Toivonen R, Takala, EP. *Clin Biomech*. 17 (7) (2002) 515–20.
3. Wu JZ, Welcome DE, Dong RG. *Comput Methods Biomech Biomed Eng*. 9 (1) (2006) 55–63.
4. Wu JZ, Dong RG, McDowell TW, Welcome DE. *Med Eng Phys*. 31(10) (2009) 1214-8.
5. Chao EYS, An KN, Cooney III WP, Linscheid, RL. *Biomechanics of the Hand*. Chapter 5. World Scientific. 1989.
6. Mountcastle V, LaMotte R, Carli G. *J Neurophysiol* 35 (1972) 122–136.

DISCLAIMER

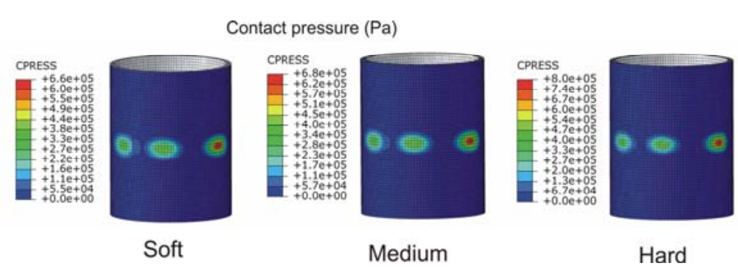

Figure 3: Model prediction of the effects of the contact stiffness on the contact pressure distributions.

MUSCULOSKELETAL LOADING OF THE THUMB DURING PIPETTE OPERATION

[1*]John Z. Wu, [1]Erik W. Sinsel, [1]Justin F. Shroyer, [1]Christopher M. Warren, [1]Daniel E. Welcome, [2]Kristin D. Zhao, [2]Kai-Nan An, [1]Frank L. Buczek

[1] National Institute for Occupational Safety and Health, Morgantown, WV, USA.

[2] Mayo Clinic, Rochester, MN, USA.

*Email: jwu@cdc.gov

INTRODUCTION

Previous studies [1] indicate that the use of mechanical pipettes is strongly associated with musculoskeletal disorders (MSDs) in the hand and shoulder. Almost 90% of pipette users, who continuously used pipettes for more than an hour on a daily basis, reported hand and/or elbow disorders [2]. It was observed that the development of MSDs in the hand could be related to many factors [1,2,3], such as pipetting posture, pace, viscosity of the fluid, pipette design, task precision, etc. These external factors will likely cause variations in the musculoskeletal loading conditions (i.e., muscle/tendon forces and excursions, friction between tendon and sheath), finally leading to MSDs in the hand. The musculoskeletal loading of the thumb during pipetting has not previously been analyzed. The purpose of the current study was to develop a biomechanical model to evaluate the forces in the muscle/tendon units of the thumb during pipetting.

METHODS

A typical thumb-activated pipette was used in the study (Fig. 1A). The pipette is actuated by a thumb-push button to extract and to dispense fluid, whereas there is a separate button to eject the disposable tip. The thumb press force was measured by a force sensor (Type LBS, Capacity 111 N, Interface Inc., Scottsdale, Arizona) installed under the plunger button. The relative displacement of the plunger button was measured via two motion markers placed on the plunger press button and the pipette handle. One female participant was recruited for the study. The subject first pressed the plunger to the first stop, extracted the sample fluid from the container by releasing the plunger, pointed the tip to a second container, and dispensed the fluid by depressing the plunger to the second stop (Fig. 1A). The subject was instructed to repeat the same procedure for one minute in a test session.

Kinematics for the fingers, hand, and forearm were determined using methods previously described [4]. Retro-reflective markers (4 mm diameter hemispheres) were applied individually on the finger/thumb/hand segments using a thin self-adhesive tape (Fig. 1A). The measurement model consists of 12 finger segments (three segments for each of the four fingers), three thumb segments, a hand, and a forearm, with a total of 55 markers

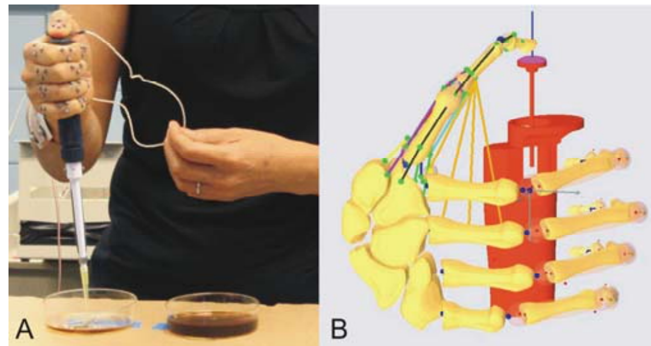

Figure 1. Experimental set-up and model. A: The subject operating the pipette during testing. B: The pipetting model.

being used to obtain pipetting kinematics. A 14-camera Vicon Nexus system (Oxford Metrics Ltd., Oxford England) provided marker trajectories at 100 Hz, with calibration residuals less than 0.5 mm for a control volume approximately 3 m (wide) x 3 m (long) x 2 m (high).

The hand was modeled as a multi-body linkage system and includes four fingers (index, long, ring, and little finger), thumb, and a palm segment (Fig. 1B). Each of the fingers is comprised of a distal, intermediate, and proximal phalanx and a metacarpal. The thumb is comprised of a distal and a proximal phalanx, a metacarpal, and a trapezium. The metacarpals of the four fingers and the trapezium of the thumb were considered to be fixed to the palm segment. Although the model includes the entire hand, we have analyzed only the biomechanics of the thumb because it is the focus of the current study. Nine muscles of the thumb were included in the proposed model: flexor pollicis longus (FPL), extensor pollicis longus (EPL), extensor pollicis brevis (EPB), abductor pollicis longus (APL), flexor pollicis brevis (FPB), abductor pollicis brevis (APB), the transverse head of the adductor pollicis (ADPt), the oblique head of the adductor pollicis (ADPo), and opponens pollicis (OPP). The model was developed using the commercial software package AnyBody (v4.0, AnyBody Technology, Aalborg, Denmark).

RESULTS

Representative plunger displacement and push force as a function of time are illustrated in Fig. 2. The entire work cycle was divided into extraction and dispensing phases. The plunger push force for dispensing is approximately four times that for extraction. The predicted muscle forces as a function of time are shown in Fig. 3. The left column of the figure shows the forces in the four extrinsic muscles (EPB, EPL, APL, and FPL) whereas the right column shows those in the five intrinsic muscles (FPB, ADPo, ADPt, OPP, and APB). Eight muscles (EPB, APB, APL, and APB, FPB, ADPo, ADPt, and OPP) have substantial force output during the pipetting action, whereas the force in EPL is virtually zero. The muscle force for dispensing is about 3-4 times that for extraction at the peaks. The maximal peak forces were found in the OPP and ADPo muscles, in which the peak force values reach approximately 140 N which is about 3.5 times the plunger push force.

Our calculations are consistent with EMG signals measured in a previous study [3], who evaluated activities of four muscles (EPB, APB, APL, and FPL) during pipetting.

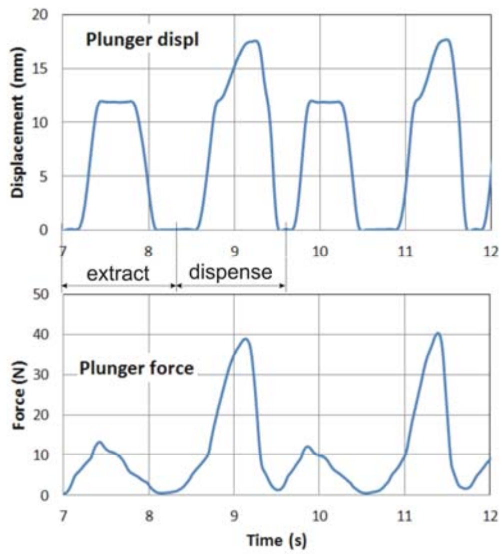

Figure 2. Time histories of the plunger displacement and force measured during the tests.

DISCUSSION AND CONCLUSIONS

The pipetting task is performed in a posture in which the thumb muscles have to generate force to stabilize the grip around the pipette and to press the plunger button. Our results showed that eight of the nine thumb muscles were active and contributed to the pipetting actions, suggesting that the thumb muscles work both as mobilizing and stabilizing structures.

Our results showed that the peak muscle forces are nearly proportional to the peak push force measured at the plunger button. The magnitude of the peak muscle forces is approximately 3.5 times that of the peak button push forces. If muscle force is considered one of the major factors that cause MSDs in the hand, improving the pipette mechanism design to reduce the required button push force may decrease the injury risk associated with pipette use.

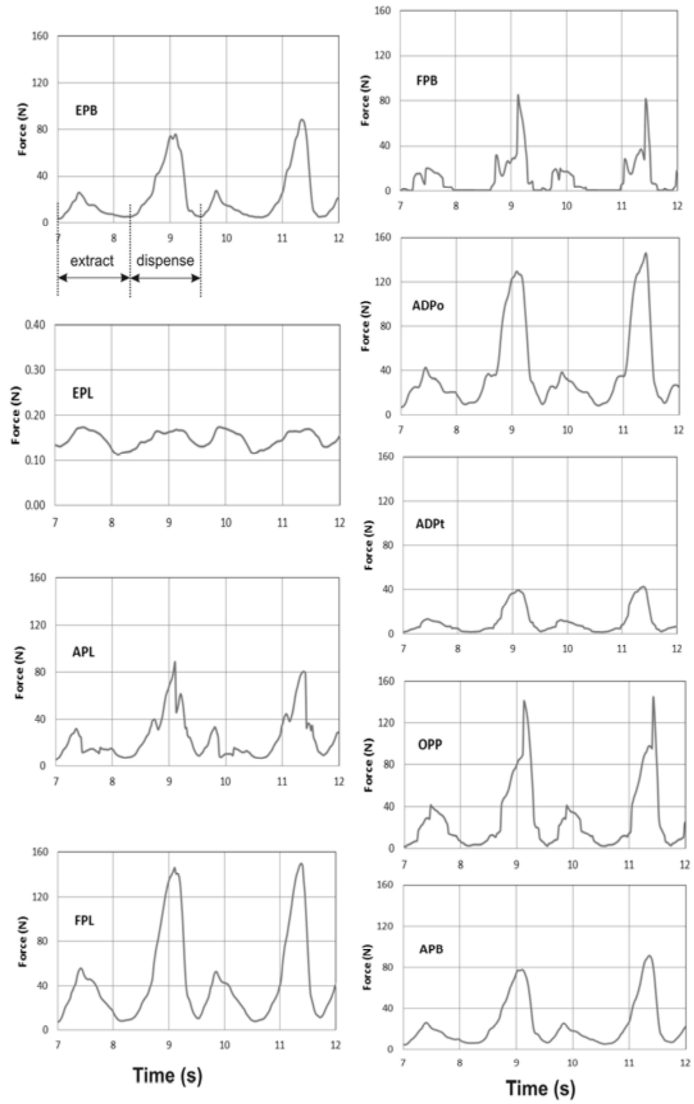

Figure 3: Forces in the thumb muscles as a function of time calculated using the proposed model. Left: extrinsic muscles. Right: intrinsic muscles.

REFERENCES

1. Bjorksten MG, Almby B, Jansson ES. *Appl Ergon* 25 (2) (1994) 88–94.
2. David G, Buckle P. *Appl Ergon* 28 (4) (1997) 257–62.
3. Asundi KR, Bach JM, Rempel DM. *Hum Factors* 47 (1) (2005) 67–76.
4. Buczek FL, Sinsel EW, Gloekler DS, Wimer BM, Warren CM, Wu JZ. *J Biomech* 44(9) (2011) 1805-9.

DISCLAIMER

EFFECT OF ANKLE LOAD ON GAIT PATTERNS DURING TREADMILL WALKING

Jianhua Wu and Toyin Ajisafe
Georgia State University, Atlanta, GA, USA. Email: jwu11@gsu.edu

INTRODUCTION

Ankle load has been used as mechanical loading to perturb the human postural system during walking. It is, however, not clear to what degree additional ankle load influences temporal and kinetic gait variables such as stride time and peak ground reaction forces, respectively. It is also not clear to what extent unilateral ankle load causes differences between the two legs. Further, little is known about the effect of additional ankle load on the long range dependence of these variables. This study investigated the effect of bilateral and unilateral ankle load on kinetic gait pattern and its long range correlation during treadmill walking.

METHODS

Ten male subjects participated in this two-day study (age 24.5±3.7 years, height 1.78±5.1 m, and weight 79.0±7.9 kg). On day 1, ankle load was placed bilaterally on both legs. On day 2, ankle load was placed only on the non-dominant leg (left leg for all the participants). On each day four load conditions were tested in a random order across all the participants. In addition to the no load condition (A0), three different levels of ankle load were used to increase the moment of inertia of the leg by 25%, 50% and 75% (load condition A25, A50 and A75, respectively). An instrumented treadmill was used to collect the vertical ground reaction force during treadmill walking. Each participant's preferred overground walking speed was used to set the respective belt speed of the treadmill. Participants walked on the treadmill for five minutes under each load condition. Adequate rest was provided between conditions.

Force profile collected by the instrumented treadmill was used to calculate gait variables. Temporal variable included step time (StepT). Two peak forces can be identified from each step. Kinetic variables included the first peak force after heel strike (P1) and its loading rate (P1V), and the second peak force before toe off (P2) and its unloading rate (P2V). All the kinetic variables were normalized by the participant's weight. Mean and standard deviation were calculated for both the left and right sides on each gait variable.

Detrended fluctuation analysis (DFA) [1] was used to study the long range dependence of temporal and kinetic variables. The scaling exponent calculated from DFA reveals the structure of variability and the correlation between data points. DFA analysis was conducted for both sides on each gait variable.

A series of ANOVA (2 side x 4 load) with repeated measures was conducted on each gait variable. Significance level was set as $p<0.05$.

RESULTS AND DISCUSSION

Table 1 presents mean and standard deviation of spatial and kinetic variables in the bilateral ankle load condition. A load effect was found for all the variables such that the subjects increased StepT, P1, P1V, P2, and P2V with the increase in ankle load. A side effect was found for P2 only such that the subjects produced a greater P2 on the left side than on the right side. With the bilateral ankle load, the left leg (non-dominant side) consistently showed a higher peak force before toe off to facilitate the initiation of leg swing. The other gait variables showed symmetrical patterns between the two sides as expected.

Table 2 presents mean and standard deviation of spatial and kinetic variables in the unilateral ankle load condition. A load by side interaction was found for StepT and P1V. With the increase of ankle load on the non-dominant (left) side, the subjects increased StepT on the left side and decreased it on the right side. P1V increased with the ankle load on the left side, but no significant change was observed on the right side. Also, a side effect was found on

P2V such that the left side had a significantly greater unloading rate than the right side. However, no side effect was found on both P1 and P2 although both variables increased with the increase of ankle load. With the unilateral ankle load the subjects modified the temporal control of gait and the loading rate after heel strike, but maintained the symmetrical patterns while producing two peak forces during treadmill walking.

Table 3 presents mean and standard deviation of the DFA scaling exponent for each gait variable. Statistical results showed that there was not a side effect or a load effect, nor a side by load interaction for both bilateral and unilateral ankle load conditions. This suggests that the long-range correlation in temporal and kinetic variables is not affected by load condition, level of load intensity, or the combination of both.

CONCLUSIONS

Gait patterns appear to be symmetrical (except P2) during treadmill walking with bilateral ankle load. With unilateral load on the non-dominant leg, step time and loading/unloading rate become asymmetric between the two sides, but not for two peak forces. The DFA scaling exponent is not affected by either bilateral or unilateral ankle load.

REFERENCES

1. Delignieres D., et al. *J Math Psychol*, **50**, 525-544, 2006.

ACKNOWLEDGEMENTS

We would like to thank the funding support from the Jerome Lejeune Foundation.

Table 1: Temporal and kinetic gait variables in the bilateral ankle load condition

	Left				Right				Statistical results
	A0	A25	A50	A75	A0	A25	A50	A75	
StepT	0.52±0.03	0.52±0.03	0.53±0.03	0.54±0.03	0.53±0.03	0.53±0.03	0.53±0.03	0.54±0.03	L
P1	1.00±0.04	1.00±0.03	1.02±0.04	1.03±0.04	1.01±0.04	1.00±0.04	1.03±0.06	1.04±0.05	L
P1V	7.06±1.50	7.04±0.85	7.32±1.02	7.38±0.86	6.90±1.25	7.03±0.99	7.44±1.32	7.46±0.94	L
P2	0.98±0.04	1.00±0.05	1.02±0.06	1.04±0.05	0.96±0.05	0.98±0.04	1.01±0.05	1.03±0.04	L, S
P2V	6.47±0.88	6.63±0.93	6.80±0.91	6.80±0.81	6.39±0.53	6.51±0.72	6.61±0.54	6.59±0.43	L

Note that L, S, and L*S denotes a load effect, a side effect, and a load by side interaction, respectively.

Table 2: Temporal and kinetic gait variables in the unilateral ankle load condition

	Left				Right				Statistical results
	A0	A25	A50	A75	A0	A25	A50	A75	
StepT	0.52±0.03	0.52±0.03	0.53±0.04	0.54±0.03	0.52±0.03	0.52±0.03	0.51±0.03	0.51±0.03	L, S, L*S
P1	0.98±0.05	1.00±0.05	1.02±0.07	1.03±0.06	0.99±0.06	1.00±0.04	1.00±0.06	1.01±0.06	L
P1V	6.76±1.09	7.14±1.30	7.38±1.21	7.46±1.26	6.86±0.99	6.96±1.26	6.90±1.04	6.90±1.33	L, S, L*S
P2	0.97±0.06	0.99±0.04	1.00±0.06	1.02±0.05	0.96±0.05	0.98±0.03	0.99±0.05	1.01±0.04	L
P2V	6.64±1.01	6.69±0.95	6.92±0.93	6.87±0.67	6.46±0.53	6.49±0.54	6.56±0.53	6.59±0.42	S

Table 3: The scaling exponent of temporal and kinetic gait variables

	Bilateral ankle load				Unilateral ankle load			
	A0	A25	A50	A75	A0	A25	A50	A75
StepT	0.64±0.09	0.66±0.10	0.66±0.07	0.69±0.09	0.69±0.11	0.67±0.09	0.70±0.11	0.73±0.13
P1	0.70±0.08	0.70±0.08	0.67±0.11	0.72±0.08	0.67±0.09	0.65±0.09	0.68±0.10	0.69±0.08
P1V	0.65±0.10	0.61±0.08	0.61±0.08	0.63±0.08	0.62±0.11	0.60±0.10	0.64±0.09	0.64±0.09
P2	0.66±0.08	0.70±0.08	0.68±0.09	0.71±0.07	0.69±0.09	0.70±0.10	0.67±0.10	0.70±0.11
P2V	0.62±0.07	0.64±0.06	0.63±0.09	0.65±0.09	0.67±0.13	0.63±0.12	0.68±0.13	0.64±0.08

TRANSTIBIAL AMPUTEE JOINT MOTION HAS LARGER LYAPUNOV EXPONENTS

[1]Shane R. Wurdeman, [1]Sara A. Myers, and [1]Nicholas Stergiou

[1]Nebraska Biomechanics Core Facility, University of Nebraska, Omaha, NE, USA
email: swurdeman@unomaha.edu web: nbcf.unomaha.edu

INTRODUCTION

Previous work revealed a strong, positive relationship between transtibial amputee prosthesis preference and the temporal structure of stride-to-stride fluctuations measured with the largest Lyapunov exponent (LyE) [1]. Amputees had a preference for the prosthesis that produced the smaller LyE from the ankle flexion/extension gait fluctuations.. As a result, the LyE is the first biomechanical measure to strongly correlate with prosthesis preference [2]. However, as noted by the theory of optimal movement variability [3], too low of a LyE reflects a highly predictable, rigid movement and too large of a LyE results from an unpredictable movement with many random stride-to-stride fluctuations occurring. Therefore before initiating the clinical goal of achieving reduced LyE, it is necessary to establish a reference framework with comparisons to non-amputee controls. This will allow us to identify if amputees are ambulating with movements occurring in the highly predictable range or the highly unpredictable, random range. The purpose of this study was to determine the baseline measure of transtibial amputees' joint flexion/extension LyE compared to healthy, non-amputees. Based on our previous work[1], we hypothesized that amputees ambulate with a highly unpredictable, unorganized movement (i.e. greater LyE value) at the prosthetic ankle in particular.

METHODS

Fourteen unilateral, transtibial amputees (age: 48.2 ± 14.8 yrs; ht: 179.6 ± 5.9 cm; mass: 91.9 ± 21.4 kg) and fourteen non-amputee controls (age: 51.6 ± 11.4 yrs; ht: 174.3 ± 7.0 cm; mass: 82.5 ± 12.8 kg) were consented for participation in this study. All amputees were active, community ambulators able to achieve varying cadences. Each subject performed a three minute treadmill walking trial at their self-selected walking speed while three dimensional kinematics for the lower limbs were recorded (60Hz; 8 camera Motion Analysis Corp., Santa Rosa, CA). Custom Matlab software was used to calculate sagittal plane ankle, knee, and hip angle time series. All time series were then cropped to 88 strides, which was the minimum amount of strides any subject was able to achieve in the three minutes. The LyE for each time series was then calculated from the reconstructed state space attractor utilizing the embedding dimension and time lag calculated from false nearest neighbors and average mutual information algorithms [4]. Differences between intact and control legs and prosthetic and control legs were tested for significance through independent t-tests while differences between intact and prosthetic legs were tested with dependent t-tests with alpha equal to 0.05 for significance.

RESULTS AND DISCUSSION

Our hypothesis was correct for three of the six comparisons (Figure 1). The amputees' prosthetic ankle had larger LyE values as compared to the non-amputee controls (p=0.023) and compared to

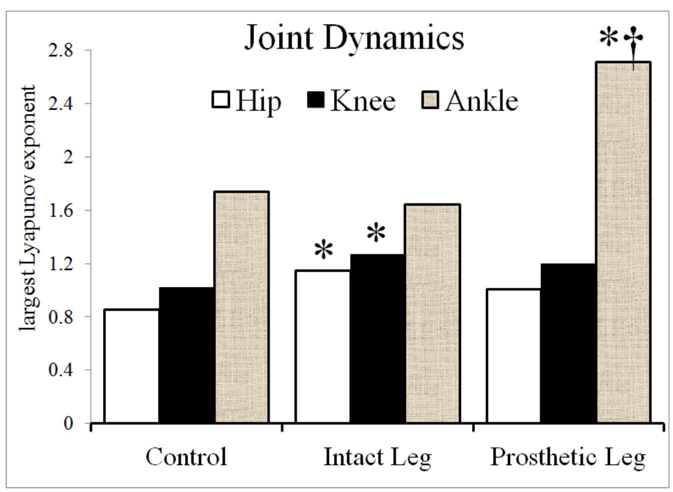

Figure 1: The prosthetic ankle had significantly larger LyE compared to non-amputee controls and the intact ankle. Differences in the intact leg were only found in the hip and knee. Units: bits/s

the amputees' intact ankle (p=0.017). The amputees' intact leg knee (p=0.05) and hip (p=0.013) had larger LyE values compared to the controls. There were no other differences (Table 1).

The movement pattern at each joint that evolves over the course of numerous steps represents the motion of two adjacent segments. In a non-amputee, the neuromuscular system's control over these two segments leads to stride-to-stride fluctuations that are highly organized. Altered neuromuscular control over the two adjacent segments of a joint will cause a change in the movement pattern. The altered movement pattern can be considered to either reflect failure of the neuromuscular system to optimize the movement or an optimized movement pattern given the constraints placed on the neuromuscular system. In either situation, the movement pattern is different from the pattern that is present for a healthy individual and thus should not be considered the ideal movement pattern for safe, efficient locomotion. Transtibial amputees display an altered temporal organization in their stride-to-stride fluctuations of the hip and knee of the intact leg and the prosthetic leg (i.e. larger LyE). The amputees in our study did not have any pathology affecting the neuromuscular system beyond the transtibial amputation. Thus, the increased LyE of the intact leg's hip and knee would seem to be the optimization of the movement based on the constraints on the gait cycle imposed by the contralateral leg's amputation. The increased LyE at the prosthetic ankle is presenting a different situation. Whereas the other five joints of the lower legs in a unilateral transtibial amputee consist of two biological segments, the prosthetic ankle is the sole joint that is the meeting of a biological (remnant shank) and an artificial segment (prosthetic foot). Therefore, the motion about the prosthetic ankle is only partially influenced by the biological system with an additional portion of the motion dictated by the artificial system. The larger LyE at the prosthetic ankle is not a surprise as it represents the inability of the neuromuscular system to fully control the movement patter than evolves. This would align with previous findings that transtibial amputees prefer smaller LyE values at the prosthetic ankle [1] because these LyE values represent a better ability of the neuromuscular system to control the motion about the prosthetic ankle based on the optimal movement variability hypothesis.

CONCLUSIONS

Individuals with unilateral, transtibial amputation ambulate with an altered temporal organization of stride-to-stride fluctuations. The intact leg hip and knee joint motion can be considered as optimization based on constraints on the gait cycle from the contralateral limb's amputation. The prosthetic ankle displays altered stride-to-stride fluctuations presumably as a result of motion at the joint influenced from biological and artificial segments. Clinically, reduced LyE values at the prosthetic ankle should be a goal as this represents less competition between the biological and artificial components and more of a synergistic control of the ankle motion resulting in optimal movement.

REFERENCES

1. Wurdeman SR, et al. *Proceedings of GCMAS*, Grand Rapids, MI, USA, 2012.
2. Hafner BJ, et al. *Clin Biomech* **17**(5), 325-44, 2002.
3. Stergiou N, et al. *Hum Mov Sci* **30**(5), 869-88, 2011.
4. Wolf A, et al. *Physica D* **16**, 285-317, 1985.

ACKNOWLEDGEMENTS

This work was supported in part by a NASA EpSCoR fellowship, NIA 1R01AG034995-01A1, and a NASA mini-grant.

Table 1: Largest Lyapunov exponent.
(mean ± SD) Units: bits/s; *Sig. vs. control p<0.05,†Sig. vs. intact p<0.05

	Control	Intact Leg	Prosthetic Leg
Hip	0.85 ± 0.19	1.15 ± 0.37*	1.01 ± 0.29
Knee	1.02 ± 0.34	1.27 ± 0.28*	1.20 ± 0.24
Ankle	1.74 ± 0.53	1.65 ± 0.54	2.71 ± 1.34*†

BOTH LIMBS IN UNILATERAL TRANSTIBIAL AMPUTEES DISPLAY INCREASED RISK FOR TRIPPING

[1]Shane R. Wurdeman, [1]Jennifer M. Yentes, [1]Sara A. Myers, [2]Adam L. Jacobsen, and [1]Nicholas Stergiou

[1]Nebraska Biomechanics Core Facility, University of Nebraska, Omaha, NE, USA
[2]Department of Prosthetics and Sensory Aids, Veterans Affairs Medical Center, Omaha, NE, USA
email: swurdeman@unomaha.edu web: nbcf.unomaha.edu

INTRODUCTION

Falls are a persistent problem for individuals with lower limb loss, as approximately 52.4% report a fall in the previous year [1]. Trips are a major cause of falls, particularly for amputees. Trips occur when the swing foot fails to clear either an object or the ground [2]. For transtibial amputees in particular, the lack of active plantarflexion and dorsiflexion of the prosthetic leg impairs extension of the stance leg and flexion of the swing foot. This combination may affect the minimum toe clearance (MTC) of the intact and prosthetic leg during swing phase making these individuals more susceptible to tripping. Therefore, the purpose of this study was to determine the differences in MTC occurring after unilateral, transtibial amputation for both the intact and prosthetic leg compared to non-amputee controls. We investigated the average MTC and MTC variability. Increased MTC variability has been suggested as stronger indicator for risk of tripping than average MTC [2]. We hypothesized a decreased average MTC for the prosthetic leg and intact leg as compared to non-amputee controls. We also hypothesized an increased MTC variability of the prosthetic leg as compared to non-amputee controls due to lack of active dorsiflexion to counter the endpoint variability in the kinematic chain. We further hypothesized an increased MTC variability in the prosthetic leg as compared to the intact leg.

METHODS

Twelve unilateral, transtibial amputees (age: 45.8 ± 12.8 years; height: 179.6 ± 5.9 cm; weight: 203.3 ± 49.9 kg) and eleven non-amputee controls (age: 56.2 ± 6.9 years; height: 175.3 ± 7.8 cm; mass: 89.6 ± 19.7 kg) were consented for participation. All subjects ambulated on a treadmill for three minutes at their self-selected walking velocity. Amputees walked in their prescribed prosthesis, which they had worn for longer than one month to assure full adaptation. Three-dimensional marker trajectories were recorded while walking (60Hz; 12 camera Motion Analysis Corp., Santa Rosa, CA). A virtual marker was created to represent the anterior, inferior aspect of the foot (i.e. the lowest anatomical section during swing phase). MTC was calculated as the difference between the virtual toe marker and the contralateral stance foot at the minimum height of the virtual toe marker during swing phase. The first 80 strides were analyzed for each individual, as this was the maximum obtained by the slowest ambulator. MTC variability was quantified through standard deviation (absolute) and coefficient of variation (normalized to the mean). Differences were compared through independent and dependent t-tests ($\alpha=0.05$).

RESULTS AND DISCUSSION

Our results were unexpected. The intact leg in transtibial amputees had increased absolute (i.e. standard deviation) and normalized (i.e. coefficient of variation) MTC variability compared to the non-amputee controls ($p=0.002$ and $p=0.006$, respectively; Table 1). The prosthetic leg had decreased average MTC ($p=0.004$) and increased normalized MTC variability compared to non-amputee controls ($p=0.008$). The prosthetic leg had decreased average MTC and absolute MTC variability compared to the intact leg ($p<0.001$ and $p=0.001$, respectively).

The lack of active dorsiflexion of the prosthetic ankle seems to cause reduced average MTC during the swing phase. This reduced MTC increases the likelihood of unintentionally contacting an object or the ground during the prosthetic leg swing phase and tripping. More interestingly, while transtibial amputees' intact leg swings with similar average MTC as non-amputees, the dispersion of the MTC over many strides is greater, increasing the likelihood that at any point the toe may swing below the bounds of a safe height and a trip would ensue (Figure 1). This is consistent with findings of increased MTC variability in the elderly contributing to increased risk of trips and falls [2,3]. Healthy young adults reflect a "safe" end point control with reduced variability, providing a narrow distribution around the mean [4], consistent with our non-amputee controls.

It is likely that increased MTC standard deviation for the intact leg is due to changes in motor control strategy. Consider that despite altered average MTC for the prosthetic leg, the MTC coefficient of variation of the prosthetic leg is similar to the MTC coefficient of variation of the intact leg. Thus, there appears to be symmetry between limbs in variability normalized to the average MTC. Further work is needed to determine the full implications of this finding.

This study has limitations to consider. The average MTC values we calculated for both groups were greater than those previously reported in the literature for non-amputees [2]. This may be the result of our method of utilizing a virtual representation of the toe rather than a true marker placed on the toe. This prevented a true marker from interfering with the individual's walking during the stance phase. Despite this difference from the literature, the same technique was applied to both groups, so we feel differences measured are true differences in walking performance.

CONCLUSIONS

The prosthetic leg's foot clearance during swing phase is often considered a source of potential falls for amputees [1]. However, in light of these findings, the intact leg is also exhibiting swing phase behavior that is likely to increase their risk for a trip. This knowledge may be utilized to improve limb loss rehabilitation by designing therapies aimed at improving intact limb control during swing phase.

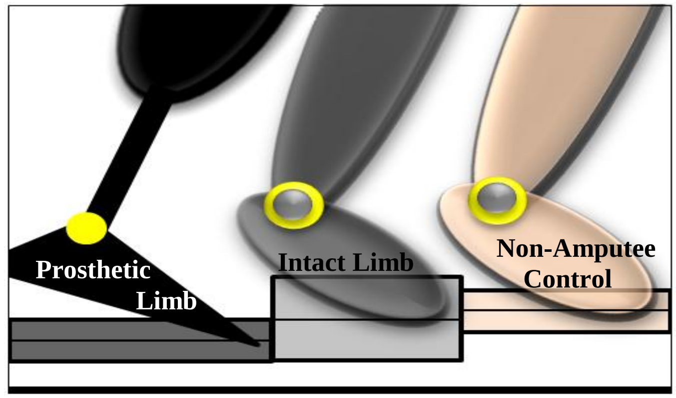

Figure 1: Unilateral transtibial amputee MTC. Left: the prosthetic leg has similar standard deviation as a non-amputee (right) but decreased height of average MTC. Middle: the intact leg has similar height of average MTC as a non-amputee but greater standard deviation. Right: the non-amputee control has optimal average MTC height and standard deviation to prevent tripping. Note: distances are only for illustrative purposes of significant differences.

REFERENCES

1. Miller WC, et al. *Arch Phys Med Rehabil* **82**, 1031-1037, 2001.
2. Mills PM, et al. *Gait Posture* **28**, 101-107, 2008.
3. Barrett RS, et al. *Gait Posture* **32**, 429-435, 2010.
4. Sparrow WA, et al. *Gait Posture* **28**, 563-567, 2008.

Table 1: Average height, standard deviation, and coefficient of variation of minimum toe clearance. MTC: minimum toe clearance. *Sig. vs. control (p<0.05); †Sig. vs. intact (p<0.05).

	Control	Intact Leg	Prosthetic Leg
Average MTC (mm)	39.2 ± 14.5	36.0 ± 8.6	23.3 ± 8.7*†
MTC Standard Deviation (mm)	3.6 ± 1.2	6.2 ± 2.1*	3.9 ± 1.0†
MTC Coefficient of Variation (%)	10.4 ± 5.2	17.4 ± 5.9*	19.0 ± 8.6*

GAIT TRAINING WITH VISUAL AND PROPRIOCEPTIVE FEEDBACK IMPROVES OVERGROUND PROPULSIVE FORCES IN PEOPLE POST-STROKE

Clinton J. Wutzke & Michael D. Lewek

The University of North Carolina at Chapel Hill
email: cwutzke@med.unc.edu

INTRODUCTION

People post-stroke commonly exhibit gait that is slow and asymmetrical [1,2]. While conventional locomotor training programs have improved overground gait speed, additional gait characteristics including step length and stance time asymmetry remain largely unaffected. Spatiotemporal asymmetry may be influenced, in part, by an inability of the paretic limb to produce sufficient propulsive force, thereby relying on the non-paretic limb to advance the body forward. Propulsive impulses have therefore been suggested to be an important factor in gait outcomes for individuals post stroke [3]. By increasing paretic limb propulsion, gait of people post stroke may become more symmetrical.

Our laboratory has developed the Immersive Virtual Environment and Rehabilitation Treadmill (IVERT) system that combines real-time adaptive visual and proprioceptive feedback using a dual-belt treadmill and a virtual environment [4]. The system contains an adaptive algorithm to allow the user to control treadmill speed by manipulating their walking speed. It also provides real-time feedback to make the user aware of spatiotemporal asymmetry [5].

The purpose of this study was to determine if a six week gait training program using the IVERT system influences propulsive force in people post-stroke. We hypothesized that individuals would improve spatiotemporal asymmetry and increase propulsive force of the paretic limb following a six week training program with the IVERT system.

METHODS

All subjects read, understood and signed an institution approved IRB consent form. Seven subjects (4F, 3M, age: 54.3±7.8 years, height: 173.6±10.7 cm; weight: 89.3±20.5 kg, Fugl-Meyer: 22.9±7.2) completed 18 sessions (approx 6 weeks) of gait training using the IVERT system. Assessment of overground spatiotemporal gait characteristics and propulsive force were collected prior to training and 1 week post training. Subjects were trained to improve step length (N=4) or stance time symmetry (N=3), as determined during the pre-training overground gait assessment.

Comfortable gait speed, as well as step length and stance time asymmetry ratios were collected using a 14-foot GAITRite mat. Measures of spatiotemporal inter-limb asymmetry were calculated as ratios (non-paretic to paretic), and inverted, if necessary so that asymmetry ratios ≥ 1.0.

Peak propulsive force ($Prop_{pk}$) and propulsive impulse ($Prop_{imp}$) of the anteriorly directed GRF (i.e. Fy) component were calculated for the paretic and non-paretic limbs from overground walking trials using two Bertec force plates (Bertec Corp., Columbus OH) at a comfortable walking speed.

Paired sample t-tests determined the pre-test and post-test changes in paretic and non-paretic limb measures, while Pearson correlation analyses were used to determine the relationship between propulsion and gait speed/spatiotemporal measures. Significance was determined a priori at α=0.05.

RESULTS AND DISCUSSION

Mean comfortable gait speed increased from 0.64±0.22 m/s to 0.79±0.27 m/s from pre- to post-test assessments ($p<0.001$). Small overall changes in overground spatiotemporal asymmetry following the 6 week IVERT training program were observed. Those trained using step length asymmetry improved from 1.46±0.14 to 1.40±0.14, whereas those trained using stance time asymmetry changed from 1.15±0.04 to 1.13±0.12.

$Prop_{pk}$ during the pre-test was 271.82±147.85 N and increased slightly to 332.87±175.01 N during the post-test assessment (p=0.056). The $Prop_{pk}$ of the non-paretic limb was also not significant between the pre and post test assessments (p=0.091).

The $Prop_{imp}$ of the paretic limb increased significantly between the pre and post training assessments (p=0.014, Figure 1). $Prop_{imp}$ increased from 60.78±35.6 N*sec to 74.62±38.97 N*sec. Non-paretic $Prop_{imp}$ did not significantly change between the pre-test and post-test assessments (p=0.155). $Prop_{pk}$ symmetry ratios improved from 2.18±1.84 (pre-test) to 1.92±1.31 (post-test; p=0.421) whereas $Prop_{imp}$ symmetry ratios improved from 3.65±4.10 (pre) to 2.50±1.71 (post; p=0.284).

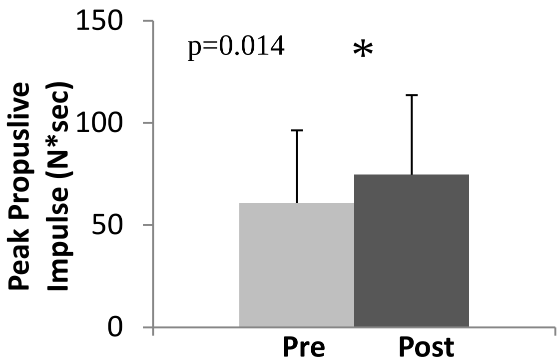

Figure 1: Propulsive Impulse of paretic limb pre (light) and post (dark) IVERT training.

$Prop_{pk}$ and $Prop_{imp}$, increased in 5 of 7 and 7 of 7 subjects respectively. The change in $Prop_{imp}$ of the paretic limb was correlated with the change in comfortable gait speed (R=0.809, p=0.028, Figure 2). Change in propulsive measures were not significantly correlated with change in spatiotemporal asymmetry ratios ($Prop_{peak}$: R=-0.445, p=0.317; $Prop_{imp}$: R=0.132, p=0.778). Change in gait speed was not correlated with change in spatiotemporal asymmetry (R=-0.330, p=0.470).

Our hypothesis that limb propulsive forces would be increased following a 6-week gait training program using visual and proprioceptive feedback was supported by these data.

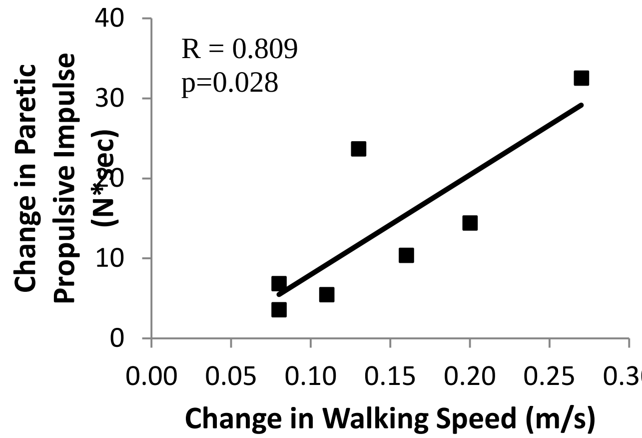

Figure 2: Correlation between change in propulsive impulse and change in walking speed post IVERT training.

The IVERT system provides real-time visual feedback to make subjects aware of spatiotemporal asymmetries. The increased effort to maintain/increase walking speeds with the user controlled algorithm may have influenced the kinetic measures of gait following training. The increased overground gait speed however may have led to the increased propulsive force.

CONCLUSIONS

These results indicate that training with the adaptive user-controlled speed control and feedback regarding spatiotemporal asymmetry may be beneficial to improve propulsive contribution of the paretic limb during overground walking.

REFERENCES

1. Hill, K., et al, *Aust J Physiother*; **43**(3): 173-180, 1997
2. Patterson, K.K., et al., Neurorehabil Neural Repair, **24**(9): p. 783-90, 2010.
3. Bowden, M.G., et al, *Stroke*, **37,** 872-6, 2006.
4. Feasel, J., et al, *IEEE*, **19**(3), 290-7, 2011.
5. Lewek, M.D., et al, Phys Ther, 2012.

LOADING RATE DURING SPINAL MANIPULATION HAS MINIMAL EFFECT ON LUMBAR SPINE PEAK REACTION FORCE AND SPINAL STIFFNESS: A HUMAN SPECIMEN STUDY

[1]Ting Xia, [1]Ram Gudavalli, [2]Yi-Xian Qin, [3]Vijay Goel, [4]Allyson Ianuzzi-Morris, and [1]Joel G. Pickar

[1]Palmer College of Chiropractic, Davenport, IA, USA
[2]Stony Brook University, Stony Brook, NY, USA
[3]University of Toledo, Toledo, OH, USA
[4]Exponent, Philadelphia, PA, USA
email: ting.xia@palmer.edu

INTRODUCTION

Spinal manipulation (SM), a form of manual therapy, is a popular choice for treating low back pain. It is generally believed in chiropractic education and practice that the ability to deliver SM at a faster rate demonstrates a better skill [1]. Biomechanically, viscoelastic structures become stiffer with faster loading rates. Consequently, the same manipulative displacement applied over a shorter duration could result in a higher spinal load. However, it is unclear how such viscoelastic property relates to thrust rates chiropractors deliver manually. The objective of the study was to evaluate lumbar spine peak reaction force and spinal stiffness during simulated SM applied with varying loading rates, directions and anatomic sites of application in human cadaveric lumbar spines.

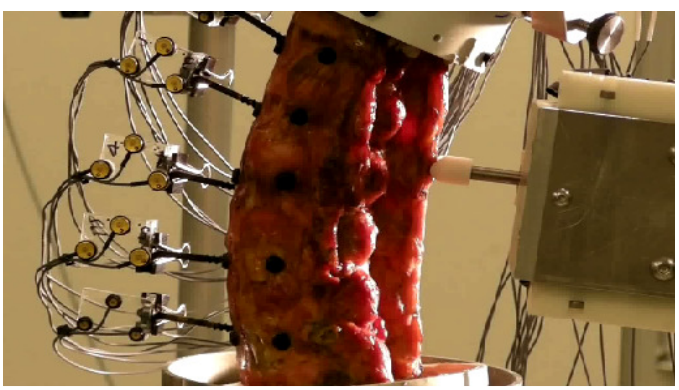

Figure 1: Specimen testing setup to simulate the posterior-anterior spinal manipulation.

METHODS

Human lumbar spine specimens (n = 23; T12 to sacrum) were procured from 10 male and 13 female cadavers with a mean age of 61.6±13.5 years (range 41-82). All specimens were x-rayed and visually inspected to exclude any gross pathology, major trauma, or facet joint capsule abnormality. The specimens were dissected free of musculature to expose the right L2/L3 and right L4/L5 facet joint capsules, then potted at T12 and the sacrum using a quick setting epoxy (Fig. 1). The potted T12 and sacrum were rigidly fixed to a platform. An axially-oriented, rotational preload of 10 Nm was applied to simulate the preparatory phase of a high-velocity, low amplitude, side posture SM.

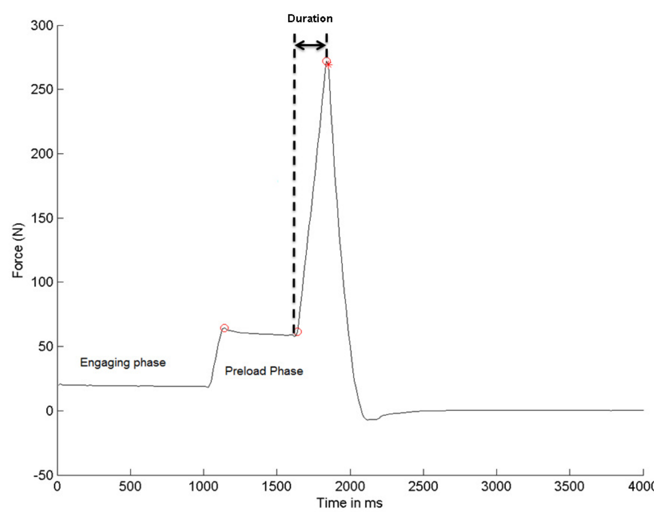

Figure 2: Example lumbar spine reaction force.

The tip of a displacement-driven thruster was placed at either the spinous or the right, superior mammillary process at L2 or L4 level and was used to deliver a simulated SM (Fig. 1). Table 1 summarizes the specimen testing configurations using a factorial study design. The target force level that was monitored using a force transducer was reached by fine tuning the thruster's traveling distance under the 200ms loading duration condition. The loading duration was defined as the rise time from the preload of the preparatory phase to peak load during the thrust (double-headed arrow, Fig. 2). The same traveling distance was used for the 100 and 200ms loading durations. Thus, the 100ms duration manipulation always represented a loading rate twice as fast as the 200ms duration. The spinal stiffness was calculated by dividing the force increment from the end of the preload to the peak reaction force (dashed line, Fig. 2) by the traveling distance during the same period. Due to the exploratory nature of the study, descriptive statistics are reported.

Table 2: Mean (SD) peak reaction forces (N).

Pre/Peak Load (N)	Loading Duration	
	100ms	200ms
200/250	236 (29)	230 (28)
50/250	248 (30)	240 (32)
200/400	396 (53)	388 (50)
50/400	400 (52)	395 (52)

RESULTS AND DISCUSSION

The 100 and 200ms loading durations, as well as the pre and peak loading force levels, were chosen based on our preliminary study with experienced chiropractors who were asked to deliver fast and slow SM (unpublished data). Fig. 2 shows a typical lumbar spine reaction force during a simulated SM. The lumbar spine peak reaction force and spinal stiffness in response to varying loading rates are summarized in Tables 2 and 3, respectively. The 200/250 pre/peak load condition represents the least force increment from the end of preload to peak load while the 50/400 condition represents the largest force increment, or loading rates ranging from 250 to 3500N/s. The data in Tables 2 and 3 demonstrate viscoelastic behavior in the lumbar spine specimens because the faster loading rate (i.e. the 100ms loading duration) led to higher peak reaction forces and higher spinal stiffness compared to the slower loading rate. However, the differences are small.

Table 3: Mean (SD) spinal stiffness (N/mm).

Pre/Peak Load (N)	Loading Duration	
	100ms	200ms
200/250	81.9 (23.9)	76.0 (22.4)
50/250	68.2 (20.2)	66.1 (18.9)
200/400	83.4 (24.0)	81.1 (24.3)
50/400	73.3 (21.8)	71.7 (20.8)

CONCLUSIONS

While the speed with which a spinal manipulation is delivered may be important for its clinical effects, the minimal effect of loading rate on lumbar spine peak reaction force and spinal stiffness suggests that engaging the viscoelastic behavior of spinal tissues may not be part of the therapeutic mechanism.

REFERENCES

1. Herzog, W. *Clinical Biomechanics of Spinal Manipulation,* Churchill Livingstone, 2000.
2. Ianuzzi A, et al. Spine J 4, 141-152, 2004.

ACKNOWLEDGEMENTS

The present study is supported by NIH Award No. 1U19AT004137-01. It was conducted in a facility constructed with support from Research Facilities Improvement Program Grant Number C06 RR15433-01 from the National Center for Research Resources, NIH. We would like to thank Mr. Randall Sozio for specimen preparation and Dr. Robert Vining for X-ray examination.

Table 1: Specimen testing configurations. PA: posterior to anterior direction; LM: lateral to medial direction; IS: PA with 30° inclination in inferior to superior direction; SP: spinous process; MP: mammillary process.

Between-subject factor	**Within-subject factors**			
Loading vector	Segment level	Duration (ms)	Preload (N)	Peak load (N)
PA: middle of SP				
LM: left side of SP	L2	100	50	250
IS: middle of SP	L4	200	200	400
MP: right side, superior MP, PA direction				

FALL DETECTING USING INERTIAL AND ELECTROMYOGRAPHIC SENSORS

Bing-Shiang Yang, Sian-Ting Liao

National Chiao Tung University, Hsinchu, TAIWAN
email: bsyang@mail.nctu.edu.tw, web: http://www.sites.google.com/site/bsyanglab/

INTRODUCTION

Falls are a leading cause of deaths (nearly 15%) from unintentional accidents and the leading cause (more than 25%) of non-fatal injuries treated in hospital emergency departments, and often associated with significant socioeconomic cost, especially in the elderly. Impact absorption devices, such as an airbag, could be used to reduce the force to the human body during a fall, therefore, decrease the severity of injury. One key issue to be solved, for adequately activating the protection mechanism, is how to accurately distinguish falls from activities of daily livings (ADLs) in a short period of time. To detect falls early and accurately is important for reducing fall-related socioeconomic cost. Inertial sensors, such as accelerometers and gyroscopes, have been used to distinguish falls from activities of daily living (ADLs) [e.g. 1, 2]. Using inertial sensors, based on laboratory studies, could detect a fall in 400-400 ms after the fall occurs [3]. However, by using electromyography (EMG), it is possible to reduce this time to 200 ms or less, since there are some unusual EMG signals to be found after subjects unexpectedly lose their balance [4, 5]. In addition, muscle activities could also be used to distinguish active from passive movements, hence improving the accuracy of identifying ADLs. The purpose of this study is to determine the feasibility of combining kinematic variables and EMG recordings for distinguishing falls from ADLs, i.e. to examine the performance of a developing wearable fall detector using combined inertial and EMG sensors.

METHODS

A prototype of the fall detector, combing a tri-axial accelerometer, a tri-axial gyroscope, attached to the dorsal surface of waist, and eight-channel EMG sensors, recording the activities of bilateral deltoid, trapezius, tibial anterior, and gastrocnemius lateralis, was developed. Twenty subjects (23.1±1.0 yrs; 174.8±4.2 cm; 72.1±13.3 kg) without neural or musculoskeletal deficits volunteered to the experiment for evaluating the performance of the fall detector. Each subject performed several activities of daily living (ADLs), such as sit-to-stand, stand-to-sit, normal walking/running, stair ascending/descending, in a mimic living environment. In addition, a few unexpected simulated trips, induced by a custom-made device attached to the ankle, were interspersed among the normal walking trials for each subject. A pre-analysis demonstrated that the peak muscle activities (EMGs) when encountered a trip was significantly larger than those during ADLs (Fig. 1)..

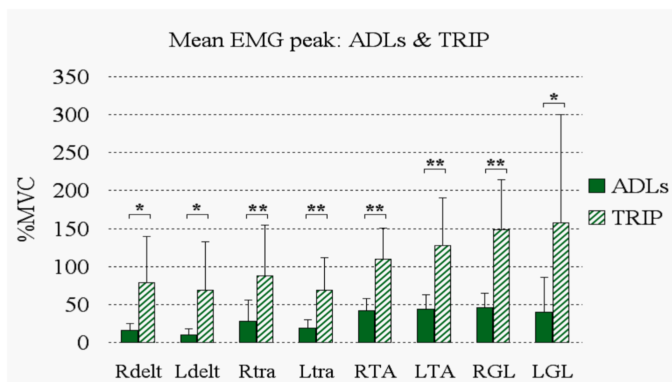

Figure 1: The average of peak EMG during ADLs and simulated 'trip' in different muscles (MVC: Maximal Voluntary Contraction, ADL: activities of daily living, L: left side, R: right side, delt: deltoid, tra: trapezius, TA: tibial anterior, GL: gastrocnemius lateralis. $*p < 0.01$, $**p < 0.001$, paired T-tests.)

A detecting algorithm, written in LabVIEW 8.5 (National Instruments, Texas, USA) platform, was then developed using hybrid thresholds of kinematics and EMGs to distinguish falls (trips) from normal ADLs. The sensitivity (falls correctly identified) and specificity (ADLs correctly distinguished) were quantified to determine the performance of the combined-sensor ‘fall detector’. In addition, Comparisons with using signals of the accelerometer along, the gyroscope alone, and electromyography alone were also performed.

RESULTS AND DISCUSSION

The average lead time (time to impact) of detecting unusual movements, i.e. trip falls, using the combined inertial (either the accelerometer or gyroscope) and EMG sensor, was 265±175 ms, which was significantly longer than the lead time using signals from the accelerometer alone (217±183 ms) or the gyroscope alone (202±185 ms) ($p<0.01$, t-test). In addition, the combined sensors can distinguish falls from normal ADLs before the impact between human body and floor, with sensitivity of 82.2% (falls correctly identified) and specificity of 98.5% (ADLs correctly identified), which were similar to those using accelerations or angular velocities alone (Table 1).

We have demonstrated the possibility of using EMG sensors combined with a tri-axial accelerometer or a tri-axial gyroscope to provide accurate and fast trip-fall detection. This developing system will be used as a base of a monitoring device integrated with fall arresting/protecting mechanism for the elderly and individuals who need long-term care.

REFERENCES

1. Bourke A et al. *Med. Eng. Phys* **30**, 84-90, 2008.
2. Bourke A et al. *Gait Posture* **26**, 194-199, 2007.
3. Wu G. *J Biomech* **33**, 1497-1500, 2000.
4. McIlroy WE et al. *Neurosci Let* **184**, 177-180, 1995.
5. Hughes MA et al. *Clin Biomech* **10**, 318-322, 1995.

ACKNOWLEDGEMENTS

This study was partially supported by Taiwan National Science Council grants NSC 100-2628-E-009-015-MY3 and NSC 100-2218-E-009-001.

Table 1: Sensitivity, specificity and lead time (mean and standard deviation) of fall detection using the accelerometer alone, the gyroscope alone, EMG signals alone, and combined inertial (accelerometer or gyroscope) and EMG signals. Sample size for computing sensitivity is 100; for specificity is 720.

Signal Source \ Performance	Accelerometer	Gyroscope	EMG	Combined
Sensitivity (%)	89.9 (3.7)	88.6 (3.3)	73.9 (5.6)	82.2 (5.1)
Specificity (%)	95.3 (1.2)	98.5 (0.9)	94.2 (1.1)	98.5 (0.6)
Lead Time (ms)	217±183	202±185	241±148	265±175

The Influence of Prophylactic Ankle Braces on Lower Limb Mechanics During a 90° Side-Step Cutting Task

[1]Hyung Suk Yang, [1]Rhonda Boros, [1]Brenda Davies and [1]Jocarol Shields

[1]Texas Tech University, Lubbock, TX, USA
email: hs.yang@ttu.edu web: http://www.depts.ttu.edu/hess/

INTRODUCTION

Ankle sprains are the most frequent injuries in sports and activities of daily living [1]. Over two million people suffer from ankle injuries per year [2], often leading to a long absence from athletic activity when compared to other types of injuries. Jerosch et al. (1996) reported that applying a prophylactic brace can prevent an estimated 30 ankle sprains per 1000 athletic exposures [3]. For that reason, the use of prophylactic ankle bracing in sports has increased greatly in recent years [4].

However, the influence of ankle brace use on the mechanics of other lower extremity joints during ballistic change of direction tasks appears relatively unexplored. The limitation of ankle movement may lead to increased loading on especially the knee joint, which could heighten the potential risk of knee injuries (e.g. anterior cruciate ligament, ACL) during certain athletic activities.

In the current study, knee kinematics and kinetics during 90° side-step cutting commonly seen in sport activities were compared across braced and normal (unbraced) conditions.

METHODS

Nine healthy college students (5 males and 4 females) completed multiple trials of a 90° side-step cutting tasks, both while wearing (Braced) and not wearing (Unbraced) the ankle braces. ASO (Medical Specialties Inc. Charlotte, NC) ankle braces were worn on both ankles, and measures were taken as subjects cut off their dominant limb. The braces have a lace-up closure with figure-eight pattern straps. Brace size for each subject were determined by measuring the circumference spanning the ankle and heel, as per manufacturer guidelines. Each subject performed 90° cutting tasks at their 'game-like' speed, by running forward, planting their dominant foot (e.g. right) fully on the force plate and cutting at a 90 degree angle toward the opposite foot (e.g. left).

For all trials, lower body kinematics and kinetics were obtained using a 6-camera VICON Nexus motion analysis system (VICON, Nexus, Denver, CO) sampling at 300Hz and ground reaction forces (1000Hz) from a force plate (AMTI, Watertown, MA). A 15 marker lower extremity kinematic model (Plug-In-Gait Sacrum) was used to track lower extremity motion. Ground reaction force and kinematic data were time-synched via the VICON system. Five successful trials were collected for each subject. Knee joint moments were calculated utilizing the VICON Nexus software.

Measures that were compared between brace condition included: Peak vertical ground reaction force normalized to body weight (VGRF), time to peak VGRF, knee angle at contact in 3D, peak knee angle in 3D and peak knee moment in 3D. To determine whether average knee joint kinematics and peak knee moments differed between brace conditions and genders, independent sample *t* tests were performed. A repeated measures ANOVA was performed using SPSS statistical software (Chicago, IL). Significance levels were set at $p \leq 0.05$.

RESULTS AND DISCUSSION

Mean (standard deviation) values for measures across brace condition are presented in Table 1. The braced condition demonstrated significantly greater peak knee adduction moments ($p=0.019$) and greater peak knee external rotation moments throughout the contact period ($p=0.032$). Additionally, females demonstrated significantly increased knee flexion at initial contact and decreased peak knee adduction throughout contact when they wore the braces as compared with males. No significant differences were observed in the other variables examined between unbraced and braced conditions ($p>0.05$). Thus, generally ankle brace use in these subjects decreased knee abduction moments which could seen as protective of the ACL. However, this effect may not be consistent across genders.

Post hoc analysis revealed additional statistically significant gender differences (see Table 2). In the unbraced (control) condition, female subjects, compared with males, demonstrated significantly greater knee internal rotation and more knee abduction at initial contact ($p<0.001$). Additionally in the control condition, females when compared with males experienced greater peak values of knee abduction ($p<0.001$), knee internal rotation ($p=0.001$), and knee flexion moment ($p=0.001$) throughout contact. Alternatively, in the braced condition, females demonstrated significantly greater knee internal rotation at initial contact ($p<0.001$), as well as significantly greater peak knee abduction ($p<0.001$) and less peak knee internal rotation ($p=0.001$) throughout contact.

This study assessed the effects of prophylactic bracing on knee joint mechanics during 90° side-step cutting tasks. Previous studies have reported that low knee flexion angles (e.g. relatively extended knee), and the combination of increased knee valgus loading and anterior shear result in increased ACL strains [5]. Our results suggest that the ankle braces forced our female subjects into an abducted knee position at contact, potentially increasing their stress on the ACL in the early stages of landing. Additionally, females when braced, obtained greater knee abduction positions during the contact suggesting the knee could experience an injury during the transition between landing and propulsion phases of the cut. The ankle braces only slightly affected knee mechanics in males, supporting the idea that brace use may have different mechanical effects on the genders.

We conclude that prophylactic ankle brace use does not affect sagittal plane kinematics or kinetics as much as anticipated. However, frontal plane mechanics of the knee may be affected, especially in female athletes, increasing the potential for injury to the ACL during 90° side-step cutting maneuvers. Further research is needed to confirm these results.

REFERENCES

1. Elis E, et al. *Med and Sci in Sports and Exercise*, **33**(12), 1991-1998, 2001.
2. Ivins D. *American Family Physician,* **74**(10), 1714-1720, 2006.
3. Jerosch J, et al. *Orthopedics*, **19**(5), 405-414, 1996.
4. Verhagen E, et al. *Clinical J Sport Med*, **10**(4), 291-296, 2000.
5. Markolf K, et al. *J Orthop Res*, **13**(6), 930-935, 1995.

Table 1: Selected mean (SD) measures across brace condition

Condition	VGRF	APGRF	MLGRF	K_Flx Mom (Nm)	K_Add Mom (Nm)	K_IR Mom (Nm)
Control	2.9 (1.1)	0.8 (0.2)	1.2 (0.5)	2.4 (0.6)	1.5 (0.5)	0.2 (0.1)
Brace	2.7 (0.8)	0.8 (0.3)	1.3 (0.4)	2.4 (0.7)	1.8 (0.6)	0.3 (0.1)
Condition	**K_Flx Con (°)**	**K_Add Con (°)**	**K_IR Con (°)**	**Pk K_Flx (°)**	**Pk K_Abd (°)**	**Pk K_IR (°)**
Brace	25.7 (13.6)	9.1 (10.1)	11.3 (17.7)	60.4 (11.6)	-2.3 (8.4)	-4.9 (11.8)
Brace	26.8 (14.5)	8.6 (11.7)	13.3 (19.4)	57.9 (11.8)	-1.6 (8.4)	-3.2 (11.7)

Table 2. Statistically significant ($p<0.05$) gender comparisons across brace condition. (* notes non-significant)

Gender	Condition	K_Add Con (°)	K_IR Con (°)	Pk K_Add (°)	Pk K_IR (°)	K_Flx Mom (Nm)
Female	Control	0.2 (4.7)	5.1 (15.0)	-8.0 (5.5)	0.8 (10.7)	2.0 (0.5)
Male	Control	16.1 (7.2)	-6.4 (10.2)	2.2 (7.7)	-9.4 (9.2)	2.6 (0.6)
Female	Brace	-1.8 (7.8)	9.8 (16.7)	-8.7 (5.3)	3.0 (11.4)	2.2 (0.7)*
Male	Brace	16.9 (6.6)	-6.4 (10.4)	4.1 (5.5)	-8.1 (9.6)	2.6 (0.7)*

PLANTAR SHEAR STRESS DISTRIBUTIONS IN DIABETIC PATIENTS WITH AND WITHOUT NEUROPATHY

[1]Metin Yavuz, [1]Andrew Franklin, [1]Rebecca McGaha, [1]Vinai Prakash, [1]Jessica Rispoli, [1]Joseph Stuto, [1]Garneisha Torrence, [2]Georgeanne Botek, [3]Danae Lowell, [4]Michael Canales
[1]Ohio College of Podiatric Medicine, Independence, OH, USA
[2]Cleveland Clinic, Cleveland, OH, USA
[3]Louis Stokes VA Medical Center, Cleveland, OH, USA
[4]St Vincent Charity Medical Center, Cleveland, OH, USA
email: myavuz@ocpm.edu, web: http://www.ocpm.edu/yavuz

INTRODUCTION

Diabetic ulcers continue to burden the US Healthcare System with thousands of amputations every year. It is known that in the presence of peripheral neuropathy, a common complication in Diabetes Mellitus, repetitive moderate stresses acting on or under the foot lead to these hard-to-heal sores. The normal component of the plantar stresses (i.e. pressure) has been studied extensively and eventually this factor has been labeled as a “poor tool” in predicting plantar ulcers [1]. Plantar shear stresses are thought to be a major factor in diabetic ulceration; however they were not studied extensively. The purpose of this study was to collect plantar shear stress data using a custom-built stress plate in three subject groups; diabetic neuropathic (DN), diabetic control (DC) and healthy control (HC) and compare the results.

METHODS

The study was approved by the Institutional Review Board. Subjects gave informed consent before participation. Group DN consisted of 12 diabetic neuropathic patients (12M, 65.7±6.9 years, 31.4±5.2 BMI), whereas Group HC included 11 individuals (7F/4M, 65.5±6.0 years, 27.8±5.9 BMI) without diabetes, any foot disorder or major deformities. The third group (DC) served as the diabetic control group and comprised 12 diabetic patients (8F/4M, 51.8±13.3 years, 28.7±7.9 BMI) without neuropathy. Peripheral neuropathy was tested by vibration perception and 5.07 Semmes-Weinstein monofilaments. Each subject walked on the stress plate, which was installed on a 12-ft walkway and set flush, multiple times. Detailed specifications of the device are given elsewhere [2]. Data from three trials were averaged and used in statistical analysis. Data were collected implementing the two-step

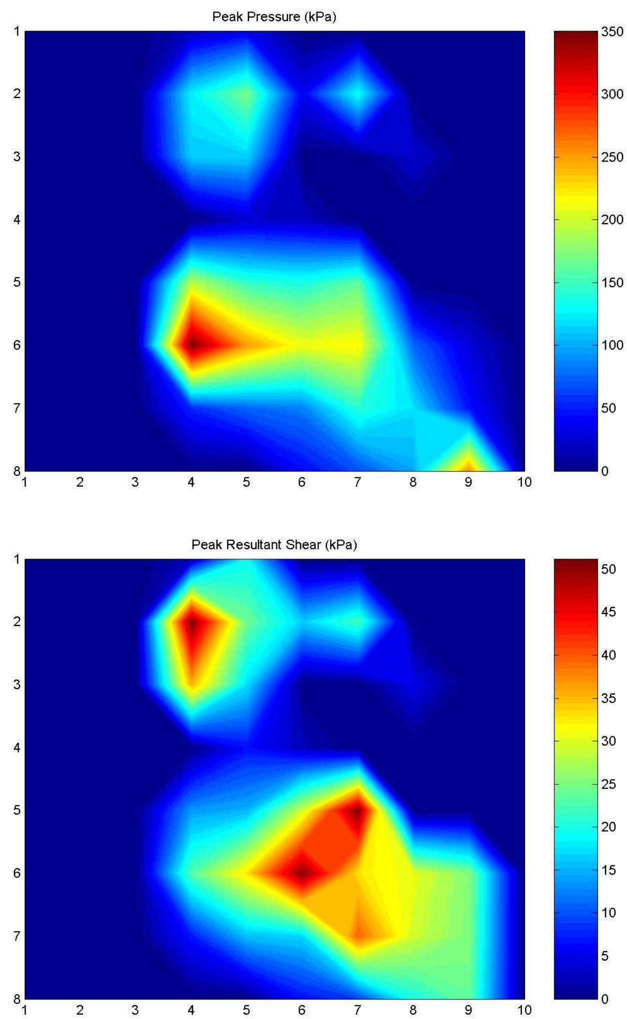

Figure 1: Peak plantar pressure (top) and shear (bottom) profiles of a representative DN subject. Note the difference between the sites of peak pressure (medial forefoot) and peak shear (central forefoot).

method. Four major stress variables were identified in each subject; peak pressure (PP), peak shear (PS), peak pressure-time integral (PTI) and peak shear-time integral (STI). Data analyses were based on global peak values and regional peak values. For the second type of analysis, pressure and shear profiles of the enrollees were masked into five regions by a custom Matlab® script; hallux, lesser toes, medial forefoot, central forefoot and lateral forefoot. Data were analyzed by a General Linear Model. Pair-wise comparisons were conducted via Bonferroni tests. Alpha was set at 0.05.

RESULTS AND DISCUSSION

Global peak pressure and peak shear occurred at different plantar sites in 75%, 50% and 33% of the DN, DC and HC subjects, respectively (Figure 1). This confirms the findings of an earlier report [3].

Global stress analysis: PP was not significantly different across the three groups ($p=.124$), whereas PS ($p=.043$), PTI ($p=.006$) and STI ($p=.006$) were. Table 1 displays the results for each group. Group-wise significant differences were observed in; DN-DC: PTI and STI, DN-HC: PS, PTI and STI, DC-HC: none.

Regional stress analysis: Only a few region-wise significant differences were detected. Peak pressure (PP) and pressure-time integral was significantly higher in the medial forefoot of the DN patients when compared with both control groups. p value in the comparison of PS under the hallux of DN and HC subjects was calculated as borderline (0.052). On the other hand, STI was significantly higher at this region in DN patients ($p=.001$).

It is thought that the results demonstrate the clinical importance of plantar shear in diabetes related foot ulcers. The observation that peak pressure and shear may occur at different anatomical sites of the DN foot may explain why most ulcers do not develop at peak pressure locations [4]. While many previous manuscripts reported significantly higher pressure magnitudes in patients with neuropathy the results of this study revealed non-significant changes, which may be tied to the relatively smaller sample size. It was interesting to observe however that while pressure magnitudes remained similar, shear magnitudes were significantly higher in the diabetic neuropathic group. Comparison of results between the diabetic control and healthy control groups did not disclose significant differences, which indicate that biomechanical alterations in the diabetic foot occur with the onset of neuropathy. To our knowledge, this constitutes the first study that reported on the comparison of plantar shear stresses between diabetic neuropathic patients and a diabetic control group. Also for the first time, this study reported a statistically significant shear stress increase at various anatomical regions of the diabetic neuropathic foot. Further investigation of plantar shear stresses is expected to lead to better understanding of the complication and development of more effective prevention methods.

REFERENCES

1. Lavery LA, et al. *Diabetes Care* **26** (4), 1069-73, 2003.
2. Yavuz M, et al. *J Biomechanics* **41** (3), 556-9, 2008.
3. Yavuz M, et al. *Diabetes Care* **30** (10), 2643-5, 2007.
4. Veves A, et al. *Diabetologia* **35**, 660-3, 1992.

ACKNOWLEDGEMENTS

This study was possible due to funds from the NIH grant 1R15DK082962 - 01A2.

Table 1: Mean (standard deviation) values of global peak pressure and shear stress variables in three groups. * denotes a significant group-wise difference.

	Group DN	**Group DC**	**Group HC**
PP (kPa)	568.2 (74.3)	492.6 (133.6)	481.1 (109.8)
PS (kPa)	91.8* (31.3)	80.7 (24.1)	64.6 (15.7)
PTI (kPa.s)	228.3* (73.1)	164.9 (52.6)	154.0 (32.7)
STI (kPa.s)	34.8* (20.7)	20.5 (4.8)	18.2 (2.8)

PLANTAR SHEAR STRESS AND ITS CLINICAL IMPLICATIONS

Metin Yavuz
Kent State University College of Podiatric Medicine, Independence, OH, USA
email: myavuz@kent.edu

INTRODUCTION

Ground reaction forces (GRF) act in all three dimensions under the foot during locomotion. Many foot disorders, in particular diabetic ulcers, are thought to have a biomechanical pathology. Measurement of the two major components of GRF, vertical (normal) and horizontal (shear) forces is a trivial process that can be accomplished by a force plate. However, since force plates can provide only global GRF data regardless of any plantar region, their clinical value is limited. Plantar stresses, which require surface area information to be calculated, can only be measured using specialized hardware. Among the 3D stresses that act on the plantar surface, vertical stress (pressure) can easily be quantified via commercial pressure measurement systems. Unfortunately, due to technical challenges there is no commercial system that can measure plantar shear stresses, as of today. Thus, scientists were left stuck with only one-dimensional data (i.e., pressure) in assessing lower extremity abnormalities.

While investigators explored plantar pressure in foot complications, they have come to realize that foot pressure alone neither reveals the exact foot function nor explains the etiology of the problem, particularly in diabetic ulceration [1].

Using a custom-built device, we have assessed plantar shear stresses in various complication groups and compared results with that of a healthy control group. This paper will discuss our findings in diabetic neuropathic, rheumatoid and blister-prone feet.

METHODS

The study was approved by the Institutional Review Board. Subjects gave informed consent before participation. A total of 66 subjects were recruited; 15 diabetic neuropathic patients (DN), 9 rheumatoid arthritis patients (RA), 11 athletic individuals prone to foot blisters (FB) and 20 control (AC) subjects. Table 1 provides subject demographics.

Table 1: Demographics of the study subject groups

Groups	n	Gender	Age	BMI
DN	15	3f, 12m	60.5±10.1	29.2±8.0
RA	9	8f, 1m	53.2±12.3	32.3±8.0
FB	11	4f, 7m	32.9±8.7	24.2±2.1
AC	20	8f, 12m	45.8±19.8	24.9±3.4

Each subject walked on the custom-built stress plate multiple times, which was installed on a 12-ft walkway and set flush. Detailed specifications of the device are given elsewhere [2]. Data from three trials were averaged and used in statistical analysis. Data were collected implementing the two-step method. Four major stress variables were identified in each subject; peak pressure (PP), peak shear (PS), peak pressure-time integral (PTI) and peak shear-time integral (STI). Data analyses were based on global peak values. Matlab® scripts were generated to post-process the data. Data were analyzed by a General Linear Model. Pair-wise comparisons were conducted via Bonferroni tests. Alpha was set at 0.05.

RESULTS AND DISCUSSION

These studies, for the first time in literature, have revealed;

(i) A difference in the locations of peak pressure and pressure in subject groups, including diabetic patients
(ii) Elevated shear stress magnitudes in DN, RA and FB patients, when compared with healthy controls
(iii) Shear stress on many plantar regions displays a biphasic character, indicating that shear is twice as repetitive as pressure

(iv) An association between the locations of peak shear-time integral and maximum pain in rheumatoid foot

An earlier prospective study has reported that plantar diabetic ulcers develop at peak plantar pressure locations in only 38% of the patients [3]. A mean distance of approximately one inch between the locations of peak pressure and shear in diabetic feet (Figure 1) may explain why most plantar ulcers do not develop at peak pressure locations.

If the underlying pathology behind diabetic ulceration is fatigue failure of the plantar tissue as indicated by many researchers, then investigators need to focus on shear and its temporal characteristics. Application count of stresses is as important as their magnitudes in fatigue failure of materials. This study has clearly shown that during the stance phase, local plantar tissue experiences shear forces twice, in opposite directions (Figure 2). Due to this characteristic, despite lower magnitudes when compared with pressure, shear stresses are thought to play a major role in tissue breakdown.

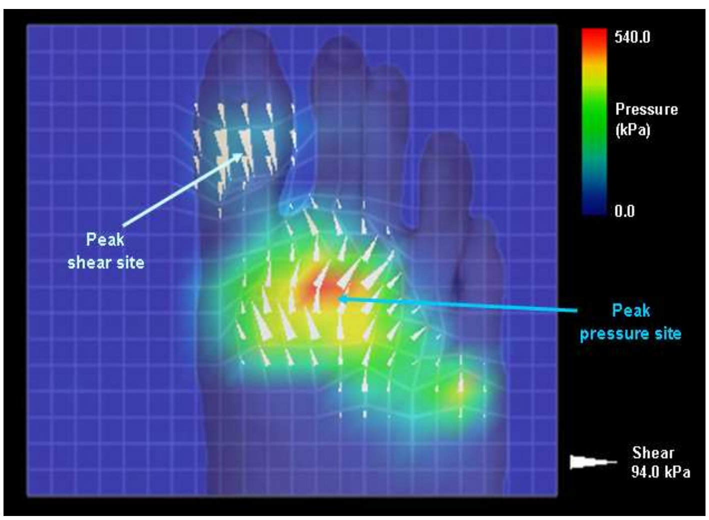

Figure 1: Peak plantar pressure (color) and shear stress (arrows) may occur at different sites in diabetic patients.

Moreover, peak shear stress variables were at least 31% higher in diabetic patients ($p<0.05$) when compared with healthy individuals.

In RA patients, peak shear stress magnitudes were also higher ($p<0.05$). Another interesting finding in this group was that 6 of 7 patients with antalgic gait

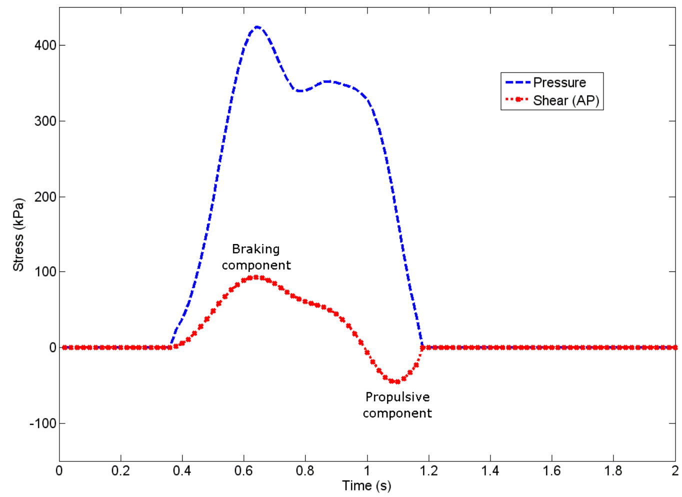

Figure 2: Pressure (blue) and anteroposterior shear (red) stress curves at the first metatarsal head area of a diabetic patient.

experienced maximum foot pain at peak shear-time integral sites. This rate was 5/7 for the peak pressure-time integral variable.

In athletic individuals prone to blistering, shear stresses were again higher ($p<0.05$) when compared with the control group. Moreover, shear magnitudes were seen to be significantly higher ($p<0.05$) at the local level. Friction induced heat generation is also thought to be a major factor in blister formation.

It is thought that further investigation of plantar shear stresses will complete the missing pieces in the complicated 3D puzzle of foot biomechanics and will lead to better understanding and better treatment of foot complications.

REFERENCES

1. Lavery LA, et al. *Diabetes Care* **26** (4), 1069-73, 2003.
2. Yavuz M, et al. *J Biomechanics* **41** (3), 556-9, 2008.
3. Veves A, et al. *Diabetologia* **35**, 660-3, 1992.

ACKNOWLEDGEMENTS

This study was possible due to funds from the NIH grant 2R44DK061164. The author would like to acknowledge Brian L Davis, Vincent J Hetherington and Alan Glaros who have provided support during the course of this study.

WALKING ABNORMALITIES IN PATIENTS WITH COPD

[1]Jennifer M. Yentes, [2]Stephen I. Rennard and [1,2]Nicholas Stergiou

[1]University of Nebraska at Omaha, Omaha, NE, USA
[2]University of Nebraska Medical Center, Omaha, NE, USA
email: jyentes@unomaha.edu, web: http://nbcf.unomaha.edu

INTRODUCTION

Chronic obstructive pulmonary disease (COPD) is currently ranked as the third leading cause of death [1]. Typically thought of as a lung disease, the effects of COPD are not limited to the lung, however. It is known that COPD patients exhibit abnormalities in structure and function of skeletal muscle tissue [2,3]. These include muscle fiber type shifting and decreased mitochondrial density and oxidative capacity [2,3]. It is currently unknown if these muscular abnormalities lead to breakdown in functional mobility in COPD patients. Therefore, the purpose of these series of studies was to investigate walking abnormalities in COPD patients.

METHODS

Seventeen COPD patients (9 male; 66.1$\pm$7.3 years; 86.2$\pm$15.1 kg; 170.8$\pm$12.7 cm) and sixteen healthy controls (11 male; 65.6$\pm$6.8 years; 79.6$\pm$12.4 kg; 173.1$\pm$9.3 cm) participated in these studies.

Study 1 - Rested: Participants were instructed to walk along a 10-meter walkway at their self-selected pace. Three dimensional marker trajectories and ground reaction forces were collected simultaneously. Peak lower extremity joint muscular moments and powers from the ankle, knee, and hip joint sagittal plane of motion were measured from COPD patients and healthy controls. All patients rested one minute between trials to prevent fatigue. Dependent variables were compared using independent t-tests.

Study 2 - Fatigued: COPD patients and healthy controls were asked to walk on a treadmill at their self-selected speed at a 10% incline until the onset of either muscle fatigue or breathlessness. They were immediately removed from the treadmill and asked to complete five walking trials with no rest between trials. A 2-way repeated measures ANOVA (controls/COPD X rested/fatigued) was utilized.

Study 3 – Exercise: COPD patients underwent sixteen sessions of cardiorespiratory and resistance-training exercise. Each session lasted one hour at individual's 60-70% of peak work rate, and the average dosage of training was 2-3 times per week within seven weeks. Biomechanical gait analysis was performed pre- and post-exercise, and both the kinematic and kinetic outcomes were examined using dependent t-tests.

Study 4 – Variability: COPD patients and healthy controls walked at a self-selected speed (0.894$\pm$ 0.52 m/s) on a treadmill for three minutes. From the three-dimensional marker data, the following time series were generated: step width, step length, stride length, swing time, stance time, step time, stride time all from the right leg. Each of these time series were subjected to analysis of central tendency (standard deviation and coefficient of variation) and regularity (approximate entropy; m=2, r=0.2). Means of each dependent variable were compared using independent t-tests.

Study 5 – Speed: The same COPD patients from *Study 4* were then asked to walk on the treadmill at $\pm$ 10% and $\pm$ 20% of their self-selected speed. Data reduction and processing were the same. Condition differences were compared using a repeated measure ANOVA.

RESULTS AND DISCUSSION

Rested: It was found that ankle range of motion was significantly increased (p=0.019) in COPD patients, along with significant decreases in peak ankle plantarflexion moment and peak knee extension moment ($p=0.004$ & $p=0.006$, respectively). The results of this study allowed us to quantify and specifically identify the "altered walking patterns" in COPD patients. Based on the results of our investigation into the NHANES III dataset, it is likely that these biomechanical deficits in walking result from physical inactivity [4].

Fatigued: No main effects for group were found. Significant increases in fatigue condition for peak hip extension moment ($p=0.038$) and peak knee power absorption ($p=0.037$) were found. Speed was significantly decreased in the fatigue condition. It is likely that the findings at the hip and knee are associated with this drop in speed. Another reason for lack of significant differences between the two groups could have been our fatigue protocol. This protocol was modified from a standard fatigue protocol for peripheral arterial disease patients. However, the selection of self-selected pace may not be enough to increase metabolic demand.

Exercise: No significant findings were found between pre- and post-testing. The reason for the failure to discover a pre/post training main effect is thought to be two-fold. First of all, the sample size for our pilot study was limited. However, successful completion of the study in these individuals indicates that COPD patients are capable of performing moderate to high intensity exercise for 30 minutes at a time. Second, it is possible that the length of the study was only 16-sessions. Likely, this is not enough time to elicit changes in walking patterns.

Variability: COPD patients demonstrated significantly increased step time ($p = 0.043$) and stride time ($p = 0.042$) means as compared to controls. No differences were found for standard deviation or coefficient of variation. Results also showed that COPD patients walk with significantly decreased regularity in step length ($p = 0.002$) as compared to healthy controls. Therefore, these data suggest that patients with COPD will alter spatiotemporal gait patterns during walking and further, that the regularity of these steps became disorderly and irregular. This could be of interest as COPD patients are at higher risk for falls [5] and altered gait variability has been associated with fall risk.

Speed: A significant main effect for coefficient of variation of step length ($F_{4,12}$: 4.144, $p = 0.025$) was found. A significant main effect for swing time standard deviation ($F_{4,12}$: 7.229, $p = 0.003$), coefficient of variation ($F_{4,12}$: 5.670, $p = 0.008$) and approximate entropy ($F_{4,12}$: 3.352, $p = 0.046$) was found. The results of this study demonstrate that COPD patients are sensitive to speed perturbations. Future studies should examine the use of speed in rehabilitation protocols.

CONCLUSIONS

Through a series of five studies connected with scientific strong inference, we have been able to demonstrate that COPD patients demonstrate altered walking biomechanics as compared to healthy controls. The lack of significant findings in the *Fatigued* and *Exercise* studies could be due to the small sample size or the insufficient training duration in length. In addition, it is possible that the heterogeneity in manifestations of COPD could also be a cofounding variable. These results have allowed though to adequately power our present studies where we investigate the effect of an adjusted-training exercise on COPD population's abnormal walking patterns.

REFERENCES

1. Miniño A, et al. *Natl Vital Stat Rep* **59,** 2010.
2. Allaire J, et al. *Thorax* **59,** 673-678, 2004.
3. Gosker HR, et al. *Eur Respir* **30,** 73-79, 2007.
4. Yentes JM, et al. *Respir Med* **105,** 80-87, 2011.
5. Beauchamp MK, et al. *Respir Med* **103,** 1885-1891, 2009.

ACKNOWLEDGEMENTS

Funding provided by American Society of Biomechanics Grant-in-Aid, American Alliance for Health, Physical Education, Recreation and Dance Graduate Student Grant-in-Aid, NASA Nebraska Space Grant Fellowship program and Research Support Fund from the Nebraska Medical Center and the University of Nebraska Medical Center, and NIH/NIA 1R011AG034995-01A1.

POSITIVE ANKLE WORK IS AFFECTED BY PERIPHERAL ARTERIAL DISEASE

[1]Jennifer M. Yentes, [1]Shane R. Wurdeman, [2]Iraklis I. Pipinos, [2]Jason M. Johanning, [1]Denise McGrath and [1]Sara A. Myers

[1]University of Nebraska at Omaha, Omaha, NE, USA
[2]University of Nebraska Medical Center, Omaha, NE, USA
email: jyentes@unomaha.edu, web: http://nbcf.unomaha.edu

INTRODUCTION

Peripheral arterial disease (PAD) is the presence of atherosclerotic blockages in the lower extremities leading to pain or discomfort during physical activity, mainly affecting older adults. Compared to healthy controls, patients with PAD have decreased peak powers at the ankle, knee, and hip at unmatched [1,2] and matched velocity [3]. It is not clear how PAD patients are able to ambulate at speeds similar to controls despite decreased peak power output. It is possible that the overall energy output (i.e. work) is similar despite reduced peak powers. The purpose of this study was to investigate positive and negative joint work at the ankle, knee and hip of patients with PAD and compare them to gait-velocity matched controls. Our aim was to identify movement strategies utilized by PAD patients at the joint level that enable them to maintain a gait speed similar to healthy controls.

METHODS

Nineteen patients with PAD and 35 age-, height-, and weight-matched controls provided informed consent prior to participating in this study. Subjects were instructed to walk along a 10-meter walkway at their self-selected pace. Three dimensional marker trajectories and ground reaction forces were collected simultaneously. The right limb was collected for each healthy control and the affected limb of the patients with PAD was collected. Every subject was required to rest a minimum of one minute between trials (pain free condition). This ensured that subjects did not become fatigued or suffer from the onset of pain. A total of five successful trials were collected. After the pain free condition, each PAD patient was then subjected to testing in a pain-induced condition. Using a common clinical protocol to induce pain, subjects were asked to walk on a treadmill at 0.67m/s at 10% incline until the presentation of claudication symptoms [4]. Once the onset of pain occurred, subjects immediately completed five more walking trials without rest. Gait velocity was calculated by differentiating the position of the sacral marker. Healthy controls with a mean velocity $\pm$10% of the pain free mean velocity for patients with PAD were included in the data analysis. Joint power for the ankle, knee and hip was calculated using Visual3D. Positive and negative joint work was calculated by integrating joint power during the stance phase of gait. Two one-way ANOVAs were used to compare controls to PAD pain free and to PAD pain. Dependent t-tests were used to compare PAD pain free to PAD pain conditions. The alpha value was set at 0.05.

RESULTS AND DISCUSSION

Nineteen patients with PAD (67.7$\pm$8.7 years; 172.5$\pm$7.6 cm; 79.0$\pm$12.1 kg; 1.25$\pm$0.14 m/s) and 19 controls (61.6$\pm$8.4 years; 170.9$\pm$6.2 cm; 80.8$\pm$15.1 kg; 1.23$\pm$0.12 m/s) were used for analysis. Results are presented in Table 1.

This study is the first to provide insight into the interplay between phases of positive and negative work walking in patients with PAD. Previous studies have described the gait of patients with PAD as “sluggish and tired” demonstrating the majority of changes at the hip and ankle [2,5]. The data from the present study demonstrate that the ankle is the most affected joint in patients with PAD, followed by the hip joint.

During the pain free condition, patients with PAD were able to maintain a similar work profile as the controls. Under the pain free condition, subjects were given adequate rest between trials to allow for reperfusion of the musculature. However, in the pain condition, there was a marked reduction in positive joint work at the ankle in PAD patients. This highlights a major functional deficit at the level of the ankle, which is consistent with previous studies that have reported reduced ankle joint moments and powers in PAD patients [2,3].

Patients with PAD suffer from muscle weakness, due to myopathy, in the posterior compartment of the shank that may lead to decreased ability to propel the limb forward [2]. However in this study, the fact that there was no difference in ankle joint work between the control group and pain free condition suggests an additional mechanism. Positive joint work at the ankle reduced following a walking protocol that required sustained blood flow to the lower limb muscles and when it could no longer be met, leading to pain. The atherosclerosis hindered adequate blood flow in response to the sustained muscle energy demand during the protocol, resulting in failure of the posterior calf musculature in energy production. This resulted in decreased velocity during the pain condition in patients with PAD. In addition, this decrease in joint work could be related to the patients' level of stenosis. Two main levels of stenosis have been identified: aortoiliac (hip level) and femoropopliteal (knee level). The majority of the patients had femoropopliteal stenosis (n=11), aortoiliac (n=5), both (n=2) and unknown (n=1). Further examination into the association of patients' level may provide insight into the effect a level of stenosis has on gait abnormalities.

In addition to the marked decreases in joint work at the ankle in the pain condition, the hip joint also demonstrated a significant decrease in negative work during the pain condition in patients with PAD as compared to controls. This is consistent with previous findings [2,3] and may be indicative of an adaptive strategy employed in response to reduced positive work generated within the gait cycle.

CONCLUSIONS

Following a pain-inducing protocol, we found decreased positive joint work at the ankle and decreased negative work at the hip, which compliments previous literature. This represents a consistent deficiency at the ankle in patients with PAD, thus limiting their ability to generate propulsive forces during walking. Rehabilitation in patients with PAD should focus on restoring function of the plantarflexors through exercise. Future therapeutic approaches targeting the myopathy in patients with PAD may produce improved gait and reduced impairment. Finally, further research is needed to examine work within different periods in the stance phase to determine how patients can have decreased peak powers but similar work throughout stance.

REFERENCES

1. Koutakis P, et al. *J Vasc Surg* **51**, 80-88, 2010.
2. Koutakis P, et al. *J Vasc Surg* **52**, 340-347, 2010.
3. Wurdeman SR, et al. *Gait Posture* [Accepted].
4. DiBianco R, et al. *Am Heart J* **108**, 1121-1127, 1984.
5. Chen SJ, et al. *J Biomech* **41**, 2506-2514, 2008.

ACKNOWLEDGEMENTS

Funding provided by UNMC Patterson Fellowship, NASA Nebraska Space Grant Fellowship program and NIH/NIA 1R011AG034995.

Table 1: Total positive and negative work at each joint during the stance phase of gait. P-values are listed for each comparison as well. Note: PF=pain free condition, P=pain condition

	Positive Ankle Work	**Negative Ankle Work**	**Positive Knee Work**	**Negative Knee Work**	**Positive Hip Work**	**Negative Hip Work**
Control	0.209(0.056)	-0.159(0.033)	0.081(0.028)	-0.307(0.163)	0.218(0.122)	-0.235(0.085)
PAD PF	0.181(0.039)	-0.165(0.042)	0.083(0.032)	-0.253(0.122)	0.177(0.061)	-0.196(0.081)
PAD P	0.127(0.066)	-0.160(0.057)	0.080(0.051)	-0.242(0.135)	0.157(0.118)	-0.166(0.099)
Control vs PF	0.085	0.594	0.868	0.263	0.204	0.147
Control vs P	<0.001*	0.912	0.907	0.190	0.127	0.026*
PF vs P	0.001*	0.662	0.720	0.356	0.232	0.153

CHILDREN WITH CEREBRAL PALSY MAY NOT BENEFIT FROM STOCHASTIC VIBRATION WHEN DEVELOPING INDEPENDENT SITTING

[1]Yawen Yu, [1]Srikant Vallabhajosula, [1]Joshua L. Haworth, [2]Regina T. Harbourne, and [1,2]Nicholas Stergiou

[1]Nebraska Biomechanics Core Facility, University of Nebraska at Omaha, Omaha, NE, USA
[2]University of Nebraska Medical Center, Omaha, NE, USA
email: yawenyu@unomaha.edu, web: http://nbcf.unomaha.edu/

INTRODUCTION

Dynamic sitting postural control is fundamental for individuals to accomplish functional activities in daily living, such as dining at a table, learning at school, functioning in the workplace, and even watching TV at home. However, the development of independent sitting is commonly delayed in children with cerebral palsy (CP), which affects interaction with the world. Clinical intervention using a perceptual-motor approach, which promotes children's active exploration in the environment, has been shown to be effective when fostering sitting postural control in children with mild CP or at risk of motor developmental delay [1]. In addition, providing stochastic noise through vibrotactile stimulation to the support surface has been used to improve standing postural control in elderly adults by reducing amount of variability in postural sway [2]. In the current study, we sought to investigate the treatment effect of perceptual-motor intervention with the combination of vibrotactile on children with moderate to severe CP.

METHODS

Thirty children with moderate to severe CP between the ages of 1-6 years (Age: 2.3 ± 1.5 years) entered our study when they were just developing the ability to sit. Participants were randomly assigned to receive perceptual-motor intervention twice a week for eight weeks, either with (n=15) or without (n=15) adding stochastic vibration at supporting surface during intervention. Participants were assessed twice: before and 1-month after intervention. Sitting stage was coded as follows: prop sitting as Stage #1, sitting without arm support for 30 seconds as Stage #2, and independent sitting (without arm support over 5 minutes, no falling) as Stage #3 [1, 3]. Sitting postural sway was recorded for three minutes using a force platform (AMTI, Watertown, MA; 200 Hz). Sampling frequency was identified based on our previous work and spectra analysis inspection. For data analysis, three segments were selected using force data combined with video-recording. A segment was defined as the period during which the infant exhibited quiet sitting behavior for at least 10 seconds while being untouched. Postural sway was quantified by calculating the Center of Pressure (COP) data from the force platform which were further analyzed using measures of the amount and the temporal organization of variability present in the COP time series (Table 1 and Figure 1). For statistical analyses, we conducted a 2 (Group: with stochastic vibration vs. without stochastic vibration) x 2 (Time: pre-intervention vs. post-intervention) repeated measures ANOVA on variables derived from the COP data.

RESULTS AND DISCUSSION

Seven infants with stochastic vibration treatment and eight infants without the stochastic vibration treatment showed advancement in sitting stage from pre- to post-intervention. We found a significant main effect of time for LyE in medio-lateral direction (p=0.026). LyE in medio-lateral direction increased significantly, regardless of the utilization of stochastic vibrotactile stimulation (Figure 1). We did not find any significant main effect of Group or an interaction between Group and Time.

Children with moderate to severe CP can benefit from intervention using a perceptual-motor approach with regard to the development of sitting stage and the temporal structure of sitting postural sway, which replicated our previous work [1]. After perceptual-motor intervention, our participants could maintain a better sitting posture as depicted by the improvement of sitting stage. In addition, sitting postural sway in children with CP became less rigid and more flexible as indicated by the increasing value of LyE in medio-lateral direction from the current study.

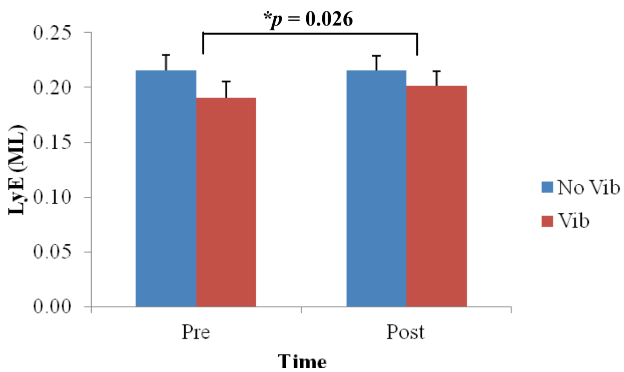

Figure 1: Mean (SE) of Lyapunov's exponent (LyE) in medio-lateral (ML) direction; Vib – With Stochastic Vibration; No Vib – Without stochastic vibration; * Significant Time Main Effect

Compared to the results of our previous work, we did not find significant effect on the other variables derived from COP data. This may due to the fact that different characteristics of population may respond differently to the treatment based on perceptual-motor approach. For the current study, we recruited children with only moderate to severe CP (but not with mild CP); only 33.3% of our participants were able to sit independently (sitting stage 3) at post-assessment.

Adding sub-threshold stochastic vibrotactile stimulus during intervention did not appear to have an effect on the development of sitting skill. Two possible explanations can be drawn here. First, our participants were exposed to the vibrotactile stimulus only during intervention, while elderly adults from previous study were assessed while exposed to vibrating insoles [2]. It can be interpreted that vibrotactile stimulus may not possess a retention effect on the regulation of postural control. Second, the type of vibrotactile signal may play a crucial role in the regulation of posture. Given that a chaotic and flexible structure of postural sway is considered as healthy and better developed [1, 3], to develop postural control in such a direction may not benefit from entrainment to a stochastic signal. Future study is needed to compare the effect of different vibrotactile signals (e.g. stochastic vs. chaotic) on sitting postural control.

CONCLUSIONS

Although both groups made similar progress in sitting stages and the flexibility of the postural sway, the stochastic vibrotactile stimulus did not advance the development of sitting postural control.

REFERENCES

1. Harbourne RT, et al. *Phys Ther* **90**, 1-18, 2010.
2. Priplata AA, et al. *Lancet* **362**, 1123-1124, 2003.
3. Stergiou N, & Decker LM. *HMS* **30**, 869-888, 2011.

ACKNOWLEDGEMENTS

Funding provided by the National Institute of Disability and Rehabilitation Research (H133G080023) and the Nebraska Research Initiative.

Table 1: Mean (SE) of dependent variables across intervention groups (with and without stochastic vibration) and time (pre- and post-intervention); AP – Antero-posterior; ML – Medio-lateral

	Without Stochastic Vibration		**With Stochastic Vibration**	
Dependent Variable	**Pre**	**Post**	**Pre**	**Post**
AP Root Mean Square (mm)	6.64 (1.14)	6.46 (1.06)	6.66 (1.14)	6.64 (1.06)
ML Root Mean Square (mm)	6.43 (2.28)	4.55 (0.80)	7.84 (2.28)	4.53 (0.80)
AP Range (mm)	38.80 (16.78)	35.96 (5.70)	58.47 (16.78)	36.15 (5.70)
ML Range (mm)	35.49 (6.95)	26.53 (5.11)	28.21 (7.19)	25.16 (5.29)
Sway Path (mm)	599.60 (409.25)	611.68 (83.89)	1105.92 (409.25)	540.14 (83.89)
Median Frequency (Hz)	1.28 (0.23)	1.06 (0.15)	1.40 (0.23)	1.17 (0.15)
AP Approximate Entropy	0.43 (0.07)	0.49 (0.09)	0.39 (0.07)	0.46 (0.09)
ML Approximate Entropy	0.45 (0.07)	0.48 (0.08)	0.38 (0.07)	0.37 (0.08)
AP Lyapunov's Exponent	0.22 (0.02)	0.22 (0.01)	0.19 (0.02)	0.20 (0.01)
AP Correlation Dimension	3.03 (0.09)	3.01 (0.07)	2.92 (0.09)	2.91 (0.07)
ML Correlation Dimension	3.07 (0.08)	3.07 (0.07)	2.93 (0.08)	2.97 (0.07)

MECHANISMS DANCERS USE TO MAINTAIN BALANCE AND REGULATE REACTION FORCES WHEN TURNING

[1]Antonia M. Zaferiou and [1,2]Jill L. McNitt-Gray
[1]Departments of Biomedical Engineering and [2]Biological Sciences
University of Southern California, Los Angeles, CA,
Email: zaferiou@usc.edu

INTRODUCTION

Successful performance of a turn requires that the performer rotate his/her body about a vertical axis while maintaining balance on one leg [1,2]. During the turn initiation phase (double leg support), reaction forces of both legs contribute to the linear impulse needed to shift the support of the total body center of mass (CM) from two legs to one leg and the angular impulse needed to rotate the body about the vertical axis. During the turn phase (single leg support), the CM position is controlled relative to the base of support in order to successfully maintain balance throughout the turn.

Theoretical discussion of torque generation in pirouettes have suggested that the number of rotations is related to limitations in balance [3] and increases in torque is achieved by increasing the moment arm of the reaction forces by increasing the distance between feet [4]. In contrast, our recent work related to regulation of body rotation by skilled golfers during golf swing [5], indicates greater torque is essentially scaled by increasing the force magnitude during turn initiation phase without significant modifications in direction [5] or foot position. This evidence has led us to hypothesize that the number of turns in a pirouette would be controlled similarly by regulating the magnitude of the resultant horizontal reaction force at each foot during the initiation of the turn without significant modifications in force direction. found previously in other tasks involving rotation [5], we expected the strategies used to regulate reaction force would be subject-specific.

METHODS

Dancers with various levels of dance experience (professional (S1), intermediate (S2), and recreational (S3)) performed a series of pirouettes requiring varying degrees of rotation. Turns were initiated with each foot supported by a forceplate (Kistler, 1200Hz). Body segment kinematics were captured simultaneously in the frontal, sagittal, and transverse planes. Each dancer used their preferred turning speed, direction, and support leg. The amount of rotation required during each pirouette was progressively increased (0°, 360°, and 720°) to systematically increase the rotation and balance control requirements between turn conditions.

The ground reaction forces, specifically the horizontal component of the resultant reaction force (RFh), were compared across turn conditions to determine how dancers satisfy the linear and angular momentum requirements of the turn during the initiation phase of a pirouette. The net linear impulse generated by the push (PL) and support leg (SL) in the forward (+y) direction (Fig. 1) was used to determine how reaction forces generated by each leg contribute to the shift from double leg stance to single leg stance. The average magnitude of the peak force (peak RFh±10ms) and orientation of the peak RFh on average was used to characterize how RFhs were regulated by each dancer between turn conditions.

RESULTS AND DISCUSSION

During turn initiation, linear effects of the RFhs for each leg tended to act in opposition to each other, resulting in minimal acceleration of the CM (Fig. 1).

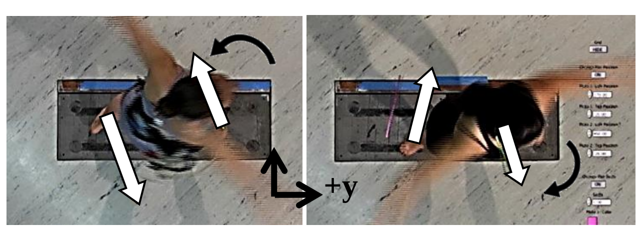

Figure 1: Overhead view of pirouette initiation in for S1 (left, preferred rotation direction to the left) and S2 (right, rotation to right). Arrows represent the resultant horizontal reaction force (RFh) for the push leg (PL) and support leg (SL). RFh arrows originate from the center of pressure of each foot.

The net RFh acting in the forward direction (+y) contributed to the shift in the CM over the stance leg (Fig. 2). The net impulse in the forward direction during the turn initiation phases decreased with increases in turn rotation for the professional dancer yet increased for the recreational dancer (Fig. 2).

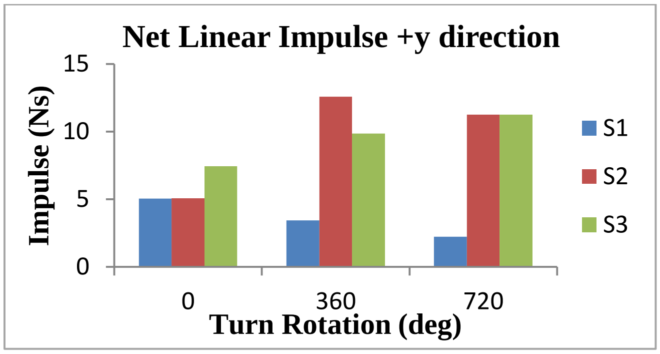

Figure 2: Net linear impulse as rotation increased (subject- preferred trials).

The rotation effects of RFs generated by the PL and SL acted in the direction of the turn (Fig 1). The RFhs acting at each center of pressure (COP) of the turning SL and PL worked together to create a force couple creating total body torque. The role of each leg in generating angular impulse about the vertical axis of the body was found to be subject-specific.

For S1, the RFh of the SL increased in magnitude and shifted in direction with increases in turn rotation. In contrast, S2 and S3 increased the RFh magnitude without significant modifications in RF direction.

The differences in skill level between S2 and S3 may explain the less consistent RFh-angle trajectories observed for S3. For all three subjects, the RFh of the PL increased in magnitude and shifted in direction in the turns requiring greater angular momentum.

Performance of a turn requires that the reaction forces generated at the feet create rotation of the body without a loss in balance. Individuals in this study increased the magnitude *and* in some cases modified the direction of horizontal component of the resultant reaction force of each leg when initiating pirouettes with a greater number of turns. As in golf, the RFhs from both legs were generated in the initial phase of the task to accelerate rotation about the vertical axis. How each leg contributed to the angular impulse required by each turn varied across subjects.

Each participant used a different kinetic mechanism (as well as subject- specific kinematics) during the initiation phase despite the strict aesthetic and mechanical demands of a pirouette. The most consistent control strategy, reflected in the RFh angle curves, was observed for S1, a professional dancer. More subjects are needed before a relationship between experience and consistency can be established.

Future studies involving more subjects will assist in elucidating whether the subject-specific strategies observed in this study are related to dance experience. Reorientation of the legs relative to the reaction forces are also expected to affect the lower extremity joint kinetics and the corresponding muscle activation.

Though pirouettes have a specific mechanical objective much like a golf swing, complexities are expected to arise later in the turn as the feet pivot. Reorienting the feet alters the orientation of the RFh relative to the leg and as a result, is likely to influence which set of muscles are used to generate rotation and which muscles are used to maintain balance during the turn.

REFERENCES

1. Winter DA. *J Biomech*. **13**(11):923-27, (1980).
2. Mathiyakom W, McNitt-Gray JL *J. Rehabil Res Dev* **45**(8):1237-48, (2008).
3. Laws K, Fulkerson L *Kinesiology and medicine for dance*, **15**(1):72-80, (1992).
4. Sugano, A. & Laws, K. *Medical Problems of Performing Artists* **17**, 29-32, (2002).
5. McNitt-Gray, J.L., Munaretto, J.,Requejo, P.S., Zaferiou, A. & Flashner, H. (accepted). *Sport Science.*

THE INFLUENCE OF OCCLUSAL SPLINTING ON THE TRABECULAR MORPHOLOGY IN THE SAGITTAL PLANE OF THE TEMPOROMANDIBULAR JOINT

[1]William Zaylor, [2]Betty Sindelar and [1]John R. Cotton

[1]Mechanical Engineering, Ohio University, Athens, OH 45701
[2]Physical Therapy, Ohio University, Athens, OH 45701
email: cotton@ohio.edu

INTRODUCTION

Temporomandibular joint (TMJ) disorders afflict approximately 10 million Americans. Occlusal splints which reorient the jaw during mastication are a common treatment for this disorder. This reorientation of the jaw presumably alters the loading conditions on the TMJ; however, the effect of the altered loading on the morphological properties of the subchondral bone has not been reported.

Mean intercept length (MIL) is used to measure the anisotropy ratio and principle direction of planar sections of bone. For this study we used samples from micro-CT scans of dried pig mandibles to measure the bone volume fraction (BVF), MIL, and principle direction along the medial-lateral axis.

The dried mandibles are from a previous study by Sindelar et al. [1] where control pigs are compared to two splinted groups. The splinted pigs wore an opening (O) or protruding and opening (PO) occlusal splint for two months. This study showed that splinting altered the soft tissue of the joint. Previous work indicates the joint is primarily loaded superiorly and anteriorly [2].

METHODS

Six pig mandibles (2 control, 2 O, and 2 PO) were micro-CT scanned, and models were rendered with Avizo 7.0 (Visualization Sciences Group, Merignac, France). A three dimensional coordinate system was established with principle directions in the superior-inferior (SI), medial-lateral (ML), and anterior-posterior (AP) directions, a described in a study by Zaylor et al. [3].

Rectangular samples (2 mm x 2 mm x 10 mm) were centered about the origin and harvested from the digital model. The length of the rectangle is along the ML axis as shown in Figure 1. The samples were segmented by thresholding to 5/8 of the maximum HU value.

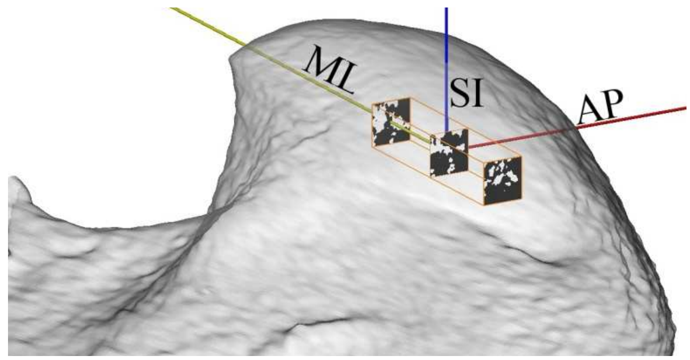

Figure 1: The reconstructed isosurface of the mandibular condyle with the anatomical axes, sample location, and three representative slices.

The segmented samples were exported as a series of 2 mm x 2 mm slices along the ML axis. Those slices were used to measure the BVF, MIL, and principle direction along the sagittal plane. The BVF was measured as the amount of white voxels (representing bone) divided by the total number of voxels in each slice. A custom script (Matlab, Mathworks, Natick, MA) calculated the anisotropy ratio and principle direction for each slice, as described by Odgaard [4]. The principle direction is measured counter-clockwise from the AP axis, about the ML axis as shown in Figure 2.

RESULTS

Samples from 10 of the 12 condyles available were analyzed (3 control, 3 O, and 4 PO). The average results of the BVF, MIL, and principle direction are shown by treatment in Table 1.

One-way ANOVA analysis (PASW Statistics 18 SPSS, Chicago, IL) showed a significant difference in the BVF between O treatment and the PO and control cases. Treatment with an O splint reduced the BVF by 55%. We found no significance in the BVF between the control and the PO treatment.

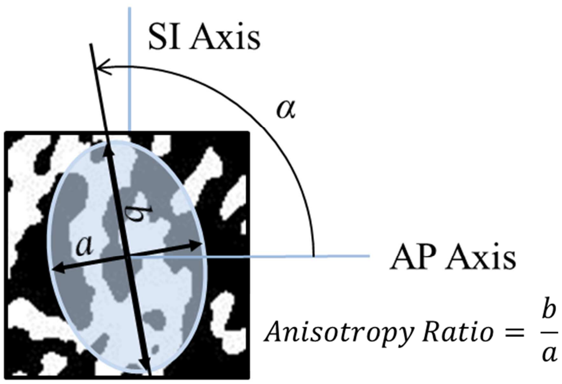

Figure 2: A representative slice showing the anisotropy ratio and the principle direction.

Table 1: The average anisotropy ratio, principle direction, and BVF by treatment

Treatment	*Anisotropy ratio*	*Principle direction (degrees)*	*BVF (%)*
Control	1.24 ±0.12	107.3 ±32.0	59.3 ±11.5
O	1.20 ±0.10	96.3 ±32.0	26.7 ±12.3
PO	1.22 ±0.13	96.3 ±30.5	50.1 ±19.3

A separate analysis did not show significance between the treatment and the anisotropy ratio or principle direction. A plot of representative data can be found in Figure 3. There was no significance between the medial and lateral half of the samples for any of the measured parameters.

CONCLUSION

This study investigated the effect of two different kinds of splints on the morphology of the mandibular condyle in the sagittal plane. Splinting did not show any significant difference in the anisotropy ratio or the principle direction in the sagittal plane, however the O treatment did significantly reduce the BVF. Reduction in BVF indicates that splinting reduces the loading across the ML axis. However the anisotropy ratio and principle direction were not altered by splinting. These two findings indicate that the bone reflects reduced loading parallel to the sagittal plane, but shows no change in the direction of those loads.

REFERENCES

1. Sindelar, B. et al., *Archives of Biochemistry and Biophysics* (2000): 64-70
2. Herring, SW. Ch. 18 *Temporomandibular disorders and related pain conditions* ed. Sessle B. Bryant P. Dionne R. IASP Press (1995).
3. Zaylor W. et al., submitted to *ASME 2012 Summer Bioengineering Conference* (2012)
4. Odgaard, A. Ch. 14, in *Bone Mechanics Hanbook*, ed. Cowin S. CRC Press LLC, 2000.

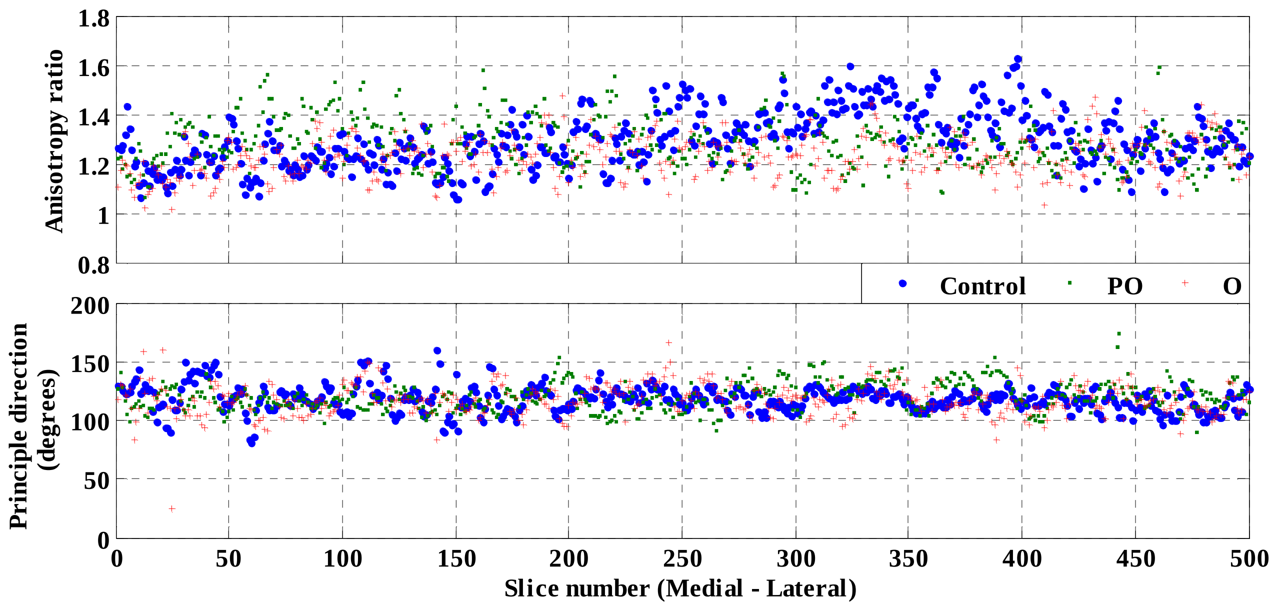

Figure 3: Representative cases of the anisotropy ratio and principle direction plotted by slice from medial (1) to lateral (500) by treatment.

DEVELOPMENT AND VERIFICATION OF AN ELBOW JOINT STIFFNESS TESTER

Sisi Zeng, Charles J. Robinson, and Laurel Kuxhaus

Clarkson University, Potsdam, NY, USA
email: lkuxhaus@clarkson.edu, web: http://people.clarkson.edu/~lkuxhaus/

INTRODUCTION

The measurement of elbow joint stiffness can help diagnose, monitor and treat patients with stiffness problems, but it is complex due to the different models [1] developed. For instance, equilibrium position control [2] and passive joint stiffness [3] use different mathematical models. Accurate measurements of joint stiffness impact the design of artificial limbs and human motor system control and simulation. The long-term research goal is to measure elbow joint stiffness in healthy and impaired subjects and quantify its change with initial elbow joint flexion angles, movement speeds, and with relaxed or contracted forearm muscles. The immediate goal was to verify that measurements made with a modified Stiffness Tester are similar to those previously reported. It was expected that elbow stiffness should increase with muscle contraction and movement speed.

METHODS

A Stiffness Tester, first developed to measure knee joint stiffness [4,5], was adapted for use with the elbow joint (Figures 1 and 2). A torque motor (Model JR24M42CH, PMI, Waltham, MA) was mounted to a steel base to drive the Stiffness Tester. An in-line torque sensor (Model 2121, LeBow Products Inc., Troy, MI) was coupled to the motor's shaft. An aluminum forearm support, also attached to the motor's shaft, rotated in the horizontal plane. An accelerometer (ADXL001, Analog Devices, Norwood, MA) was mounted at the end of the forearm support. Two capacitive rotary position transducers (Model 0603-0001, Transtek, Ellington, CT) provided position feedback and measured the angular displacement of the forearm.

Three healthy subjects (age 22~26, one female) volunteered for the experiment that received IRB approval from Clarkson University. Each subject's

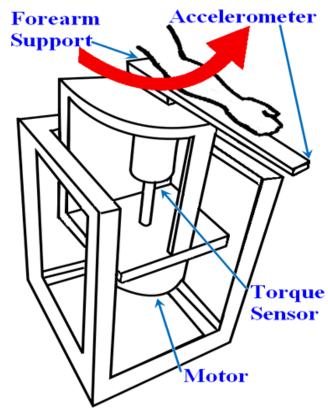

Figure 1: Sketch of the Stiffness Tester.

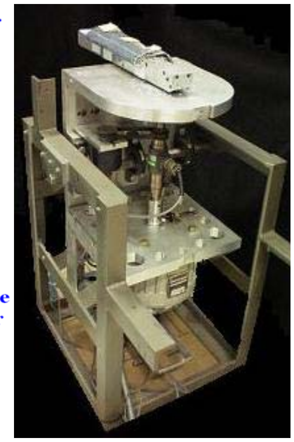

Figure 2: Photo of the Stiffness Tester.

right forearm was securely attached on the support using Velcro™ on a cloth sleeve, with the shoulder abducted 90° and the forearm fully pronated. The center of the elbow joint was aligned with the motor shaft using an axis finder modeled after Hollister et al. [6]. Ramp-and-hold motion was applied to the subject's forearm. The forearm was extended 10° at a constant speed, held for 2 seconds, and returned to the original angular position at the same speed. Measurements were made at two initial elbow joint flexion angles, two constant speeds and two forearm muscle contraction conditions (Table 1). A grip dynamometer was used to measure the maximum grip strength of the subject before the test began. During the tests with muscle contraction, the subject held the dynamometer to maintain a grip force of 20% of his or her maximum grip strength. Each measurement was repeated three times, and there were at least 30s rest between each measurement.

Torque, acceleration, and angular displacement were measured at 500Hz using LabVIEW (NI, Austin, TX). A manually-tuned PID controller controlled the motor based on the LabVIEW-issued command. Output signals from the transducers were scaled via adjustable gain amplifiers before reaching the DAQ card (PCIe-6323, National

Instruments, Austin, TX). The data from the extension movement were analyzed.

The data were digitally filtered using a custom MATLAB (The MathWorks, Natick, MA) program with a second order low-pass Butterworth filter. The cutoff frequency for the torque and angular displacement signals was 100Hz, and 10Hz for the acceleration signal. Elbow joint stiffness, K, was calculated via a nonlinear least squares fit (*nlinfit*) of a mathematical model:

$$T(t) = Ja(t) + Bv(t) + K\theta(t) + C \qquad (1)$$

in which T(t) = torque, J = moment of inertia, a(t) = angular acceleration, B = viscous damping coefficient, v(t) = angular velocity, K = stiffness coefficient, θ(t) = angular displacement, and C = constant torque bias [4]. v(t) was calculated from θ(t) by numerical differentiation after filtering. J, B, K and C were calculated through MATLAB by application of Equation 1. The median values of each type of test are reported here.

RESULTS AND DISCUSSION

The average C is -14.19±0.25 Nm across all subjects and all tests. The small standard deviation verifies that this is a property of the machine itself. Table 1 shows the median values of each subject's elbow joint stiffness, K. In general, K increases with muscle contraction; increases with initial elbow joint flexion angle; and increases noticeably with the rotational speed of the forearm. Elbow joint stiffness values previously reported ranged from 2 to 40 Nm/rad [1,7]. The values measured here at the faster speed are within this range.

With muscle contraction, several two-joint muscles crossing both the elbow and wrist were activated and the elbow joint became stiffer, as seen when comparing the relaxed to contracted states in most cases, particularly with an elbow joint angle of 90°. The variability in the results shown here could be due to the difference in individuals, or they may not have been truly relaxed. When the rotational speed was lower, the elbow joint had more time to receive reflex control from the central nervous system which could have made the joint less stiff.

This marked variability in the stiffness values, particularly at the slower speed, may reflect a need to further refine the PID controller tuning, or a need to provide subjects with feedback about their muscle contraction state. In the future, we will test more subjects with different types of muscular contraction (e.g. to activate brachioradialis, triceps, or the other major movers of the elbow joint) at different joint flexion angles. Electromyography will monitor muscle forces and could be used to stimulate muscles. These studies will further verify this Stiffness Tester in its application to the elbow.

REFERENCES

1. Bennett DJ, et al. *Exp Brain Res* **88**, 433-42, 1992.
2. Kistemaker DA, et al. *Biol Cybern* **96**, 341-350, 2007.
3. Mackay WA, et al. *J Biomech* **19**, 231-238, 1986.
4. Robinson CJ, et al. *Med Biol Eng Comput* **32**, 261-272, 1994.
5. Tai C, et al. *IEEE Trans Rehabil Eng* **7**, 111-115, 1999.
6. Hollister A, et al. *J Orthop Res* **10**, 454-460, 1992.
7. Mussa-Ivaldi FA, et al. *J Neurosci* **5**, 2732-2743, 1985.

ACKNOWLEDGEMENTS

The authors thank Nathan Pepin for designing and manufacturing the axis finder, and Professor James J. Carroll and Doug Leonard for equipment help.

Table 1: Elbow joint stiffness values (Nm/rad).

Initial Angle	60°				90°			
Muscle Contraction	**relaxed**		**contracted**		**relaxed**		**contracted**	
Speed	**10°/s**	**50°/s**	**10°/s**	**50°/s**	**10°/s**	**50°/s**	**10°/s**	**50°/s**
Subject 1	1.69	4.04	1.28	6.97	0.37	10.26	0.69	14.76
Subject 2	0.19	7.45	6.85	6.71	2.13	11.40	2.31	19.20
Subject 3	0.59	2.84	0.18	7.84	0.33	14.36	1.57	10.14

COMPARISONS OF FLIP-FLOP, SANDAL, BAREFOOT AND RUNNING SHOE IN WALKING

[1]Songning Zhang, [2]Xiuli Zhang, and [1]Max R. Paquette

[1]Biomechanics/Sports Medicine Lab, The University of Tennessee, Knoxville, TN, USA
[2]School of Physical Education & Sports Science, South China Normal University, Guangzhou, China
email: szhang@utk.edu, web: web.utk.edu/~sals/resources/biomechanics_laboratory.html

INTRODUCTION

Flip-flops and slip-on sandals have become increasingly popular due to their lightweight, comfort, and convenience. These minimal shoes may promote involvement of intrinsic foot muscles in walking. It has been shown that 2,300 children who wore slippers, sandals, and no shoes had fewer incidents of flat foot compared to those wore closed-toe shoes [3]. However, there are a limited numbers of published research studies on biomechanical characteristics of flip-flops and slippers in gait [1, 2, 5].

A study comparing plantar pressure of flip-flops (FF), barefoot (BF) and running shoe (RS) showed that the peak plantar pressure in FF was significantly higher than RS but smaller than BF [1]. Shroyer et al. [5] showed that FF yielded smaller stride length and stance time, smaller braking impulse but greater ankle angle at contact and during swing compared to shoes. Another study comparing FF with BF and military boot demonstrated increased single support and swing time and decreased total and double support time from BF to FF and a military boot [2]. The review of past research suggest that the results on flip-flips and sandals are far from comprehensive, and differences in methodology and experimental control in these studies prevent from drawing consistent conclusions. Moreover, detailed documentations of ground reaction force (GRF), and ankle kinematic and kinetic data are missing from the literature. Therefore, the main objective of the study was to investigate characteristics of ground reaction force and ankle kinematic and kinetic variables of individuals walking in a thong-style flip-flops, an open-toe sandal (OS), barefoot and a running shoe.

METHODS

Ten healthy males (age: 25.8 ± 4.8 years, mass: 76.4 ± 7.2 kg, and height: 1.77 ± 0.03 m) were recruited from the University of Tennessee campus to participate in this study. Each participant performed 5 successful level walking trials in each of the four shoe conditions at 1.3 m/s (± 5%). A 9-camera motion analysis system (240 Hz, Vicon Motion Analysis) and a force platform (1200 Hz, AMTI) were used to obtain 3D kinematic and ground reaction force data during the walking trials. Anatomical and tracking reflective markers were placed on the pelvis, and the right thigh, leg, and foot (via cutouts in shoe). The shoe conditions were randomized. Visual3D software suite (C-Motion, Inc.) was used to compute 3D kinematic and kinetic variables. Joint moments were computed as internal moments. A right-hand rule was used to establish the 3D kinematics/kinetics conventions. A one-way repeated measures analysis of variance was used to detect any differences between the shoe conditions (18.0, SPSS). Post hoc comparisons were performed using a pairwise comparison. The significance level was set at 0.05.

RESULTS AND DISCUSSION

The stance time was shorter in BF compared to the other shoes, and in SL and FF compared to RS (Table 1). This result is supported by the previous findings [1, 2, 5]. However, the walking speed was controlled at 1.3 m/s in this study whereas the other studies [1, 2, 5] did not control or report walking speeds.

The first and second vertical GRF peaks were not significantly different among the shoes. Sacco et al. reported reduced 1st GRF peak in barefoot walking but at a self-select walking speed [4]. However, the loading rate of 1st GRF (LRate) was higher in BF, OS and FF compared to RS, and in BF compared to OS. The higher loading rate was likely caused by the reduced time to first GRF peak as the time to 1st GRF peak was shorter in BF, OS and FF compared to RS, and in BF compared to OS. These GRF related characteristics have not been reported in the literature. In addition, the braking GRF peak was greater in BF, OS and FF than in RS. This result is in contrast to the smaller braking GRF impulse observed in FF compared to shoes [5], but this previous study did not control or monitor the walking speed.

For the foot and ankle kinematics, the foot contact angle was smaller in BF compared to the other shoes, and in the two sandal shoes compared to RS. The peak ankle dorsiflexion angle in early stance was smaller in BF and two sandal conditions compared to RS and in both OS and FF compared to BF. However, the eversion ROM was not different among the shoe conditions. These unique foot contact position and ankle dorsiflexion motion during early stance may be related to the shorter stance time and greater loading rate observed for the two sandal shoes compared to RS. In addition, the plantarflexion ROM was smaller in BF than in OS and in BF and two sandals than in RS.

The ankle kinetic data showed that peak dorsiflexion moment in early stance was greater in OS than in BF and FF but smaller in BF and two sandals than in RS (Table 1). These kinetic results are in support of the smaller contact foot angle and peak dorsiflexion angle observed in the BF and sandals. The peak plantarflexion moment in late stance did not differ among conditions. Finally, the peak ankle inversion moment was greater in OS and FF compared to BF but it was not different in BF and sandals compared to RS, which suggests greater involvement of ankle muscles in controlling ankle frontal plane motion during initial contact and early stance in the two minimal sandal shoes.

CONCLUSION

Our GRF, kinematic and kinetic results showed that the two sandal shoes tested in this study during walking are different from walking in the running shoe and more similar to walking in barefoot. Kinematic and kinetic differences were found, especially in early stance in FF and OS compared to BF. Finally, only peak ankle dorsiflexion moment was differed during walking in FF and OS. Future studies need to focus on differences between FF and OS, especially on motions within the foot segments.

REFERENCES

1. Carl, T. J., et al. (2008). *J Am Podiat Med Assn,* **98**, 374-378.
2. Majumdar, D., et al. (2006). *Indian J Physiol Pharmacol,* **50**, 33-40.
3. Rao, U. B., et al. (1992). *J Bone Joint Surg Br,* **74**, 525-527.
4. Sacco, I. C., et al. (2010). *BMC Musculoskelet Disord*, **11**, 24.
5. Shroyer, J. F., et al. (2010). *J Am Podiatr Med Assoc*, **100**, 251-257.

Table 1. Selected GRF and ankle kinematic and kinetic variables: mean ± STD.

	Barefoot (BF)	Sandal (OS)	Flip-flops (FF)	Running Shoe (RS)
Stance time (s)	0.698±0.019	0.740±0.022*	0.734±0.019*	0.768±0.026 *#&
1st vertical GRF peak (BW)	1.06±0.04	1.11±0.07	1.10±0.02	1.08±0.042
Time to 1st vertical GRF peak (s)	0.139±0.020	0.166±0.015*	0.162±0.047	0.191±0.012 *#&
LRate (BW/s)	7.96±1.79	7.22±1.54*	7.52±2.61	5.69±0.41 *#&
2nd vertical GRF peak (BW)	1.11±0.04	1.13±0.06	1.11±0.03	1.09±0.05
Braking GRF peak (BW)	0.22±0.03	0.21±0.03	0.22±0.02	0.19±0.02 *#&
Foot contact angle (deg)	19.23 ± 3.4	24.9 ± 3.6*	25.5 ± 3.9*	29.5 ± 4.5*#&
Peak ankle dorsiflex angle (deg)	6.1 ± 4.1	4.6 ± 4.2*	5.2 ± 4.0*	11.3 ± 4.0*#&
Ankle plantarflex ROM (deg)	-8.0 ± 1.9	-9.4 ± 1.7*	-8.7 ± 1.4	-11.8 ± 2.9*#&
Ankle eversion ROM (deg)	-4.9 ± 1.5	-5.1± 2.4	-5.4 ± 2.3	-6.5 ± 3.1
Peak ankle dorsiflex moment (Nm/kg)	0.11 ± 0.04	0.13 ± 0.04*	0.11 ± 0.04#	0.16 ± 0.04*#&
Peak ankle plartarflex moment (Nm/kg)	-1.24±0.21	-1.30±0.13	-1.33±0.13	-1.35±0.09
Peak ankle inversion moment (Nm/kg)	0.29±0.23	0.26±0.22*	0.26±0.22*	0.17±0.10

* significantly different from BF; # significantly different from OS; & significantly different from FF.

PATIENT-SPECIFIC MUSCULOSKELETAL MODELING FOR EVALUATING THE EFFICACY OF MENISCUS TRANSPLANTATION

Liying Zheng, Ameet Aiyangar, Robert Carey, Christopher Lippert, Christopher Harner, and Xudong Zhang
University of Pittsburgh, Pittsburgh, PA, USA
Email: xuz9@pitt.edu

INTRODUCTION

Musculoskeletal modeling and simulation hold tremendous potential to improve patient care and treatment design. A patient-specific musculoskeletal model that incorporates dynamic stereo radiography (DSX)-based kinematics [1] provides more accurate and detailed insights into muscle function and biodynamic responses. It can help identify the fundamental causes of movement aberration and understand the biomechanical consequences of proposed treatment strategies.

The goal of this study is to establish the feasibility of patient-specific musculoskeletal modeling for evaluating the outcome and potentially improving the surgical design of meniscus transplantation.

METHODS

One patient with total lateral meniscectomy on the left knee performed decline walking (15 deg, 1.0 m/s) before and one year after a meniscus allograft transplantation surgery (Fig. 1a). The ground reaction force (GRF) was measured by Bertec force plates embedded in a dual-belt treadmill at 1000 Hz. Electromyographic (EMG) data for seven lower limb muscles—vastus medialis (VM), rectus femoris (RF), vastus lateralis (VL), biceps femoris (BF), semimembranosus (SM), tibialis anterior (TA), and medial gastrocnemius (GA)—were collected at 1000 Hz during the decline walking and prior maximal voluntary contractions (MVC). The whole body kinematics were captured by an 8-camera surface-based motion capture system (VICON) at 100 Hz, while the knee joint kinematics were measured by a DSX system at 100 Hz [2].

A 24-DOF 92-muscle musculoskeletal model was developed in OpenSim [3]. This patient-specific model was scaled from a generic model based on anthropometric measurements and surface marker data from VICON. The knee joint kinematics, both pre- and post-surgery (Fig. 2), were specified as cubic spline functions of knee flexion angle based on the DSX measurement data. Inverse kinematics was performed to derive the full body joint angles based on VICON marker data and DSX-based knee flexion angle. A residual reduction algorithm resolved the dynamic inconsistencies inherent in the model and experimental data. A computed muscle control algorithm was utilized to compute the muscle excitations that drove the model to track the desired joint kinematics in the presence of the external forces (i.e., GRF).

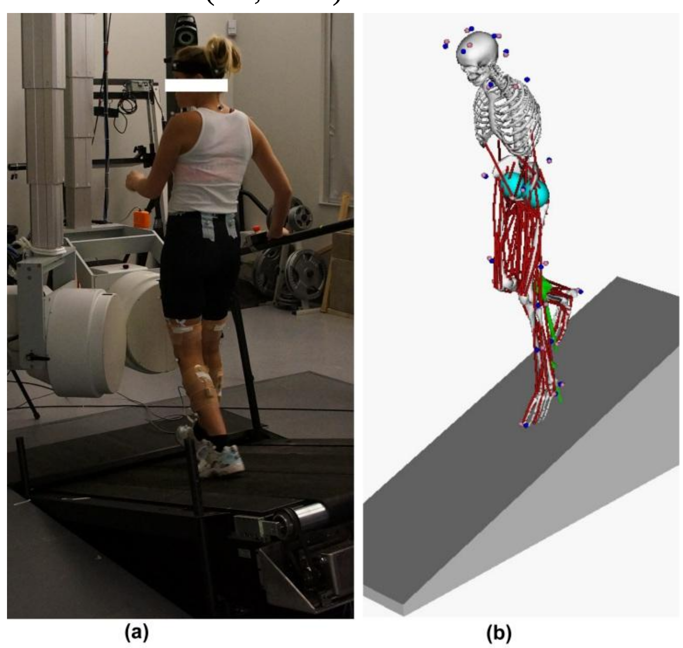

Figure 1: (a) A meniscus transplantation patient performed decline walking, both before and after surgery (performance after surgery shown); (b) The corresponding patient-specific musculoskeletal simulation model developed using OpenSim.

RESULTS AND DISCUSSION

A patient-specific musculoskeletal model was successfully constructed to produce the dynamic simulation of decline walking performed by the patient (Fig. 1b). The model-predicted muscle activations were comparable to the EMG-estimated activations (Fig. 3).

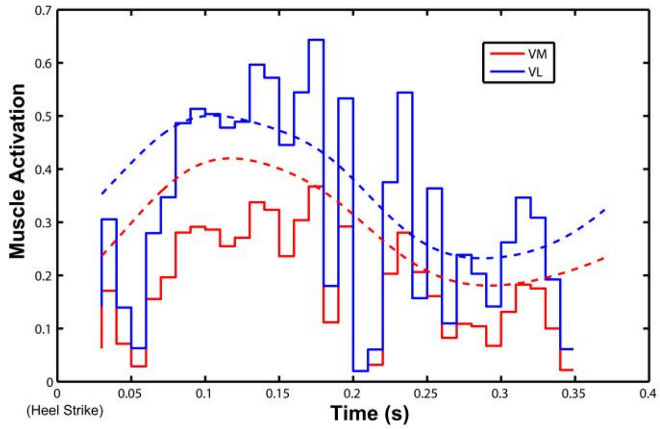

Figure 3: Model-predicted activations (solid lines) vs. EMG-estimated activations (dashed lines) for VM and VL.

A comparison of model-predicted muscle forces between pre- and post-operative decline walking trials indicated greater quadriceps muscle activation post-operatively (Fig. 4). This agreed with the previous report in the literature that weakness in quadriceps was observed after meniscectomy [4]. Because the lower limb muscles play an important role in stabilizing knee joint during gait, the differences found in muscle functions may explain the discrepancy in pre- and post-operative knee joint kinematics (e.g., markedly less lateral translation and less external rotation after meniscus transplantation as seen in Fig. 2).

These preliminary results demonstrate the promise of musculoskeletal modeling as a viable means for assessing the functional outcome of meniscus transplantation surgery. Further integrative analyses of neuromuscular, joint and tissue mechanical responses based on more patients' data may lead to evidence for evaluating and improving the efficacy of meniscus transplantation and guidelines for developing tissue-engineered meniscus constructs.

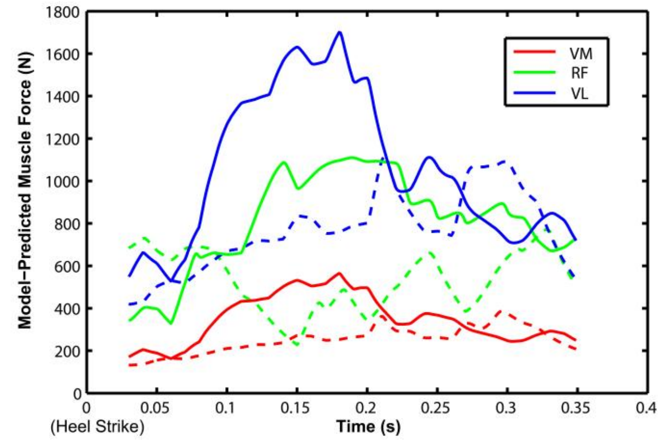

Figure 4: Model-predicted quadriceps forces for pre-operative (dashed lines) and post-operative decline walking (solid lines).

REFERENCES

1. Shetye S., et al., *ASB abstract*, 2011.
2. Anderst W., et al., *Med Eng Phys*, **31**(1), 10-16, 2009.
3. Delp SL., et al., *IEEE*, Transactions on Biomedical Engineering, 2007.
4. Ericsson YB., et al., *Arthritis & Rheumatism*, **55**(6), 946-952, 2006.

ACKNOWLEDGEMENTS

The authors thank Dr. Scott Tashman and Eric Thorhauer for their help with the experiment and post-processing of DSX data, and acknowledge the financial support from the NIH (1R03AR059939) and Musculoskeletal Transplant Foundation (MTF).

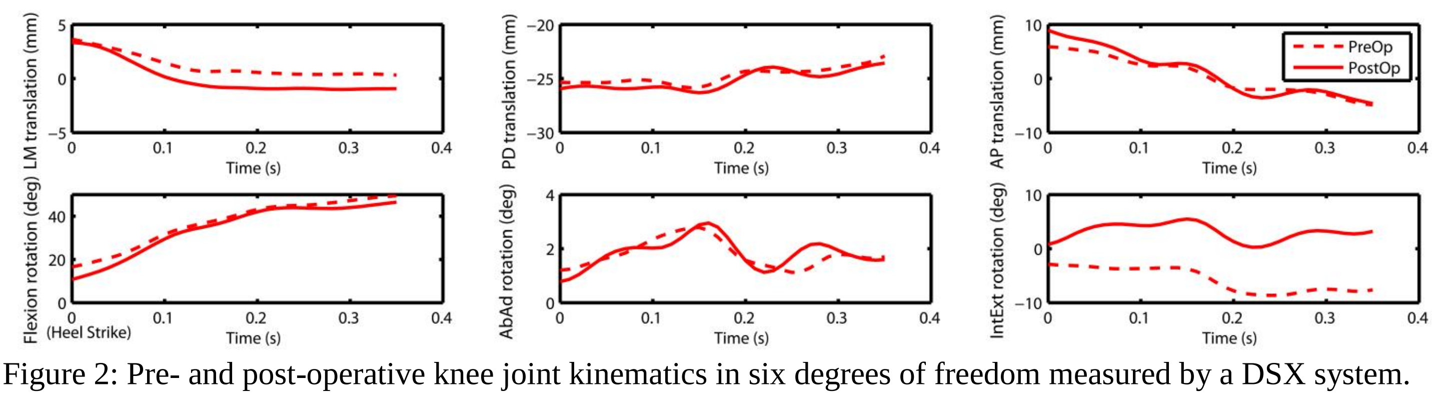

Figure 2: Pre- and post-operative knee joint kinematics in six degrees of freedom measured by a DSX system.

INFLUENCE OF OBJECT SIZE AND HAND POSTURE ON UPPER LIMB JOINT LOADS DURING ONE-HANDED LIFTING EXERTION

[1]Wei Zhou, [1]Thomas J. Armstrong, [2]Diana M. Wegner, and [1]Matthew P. Reed

[1]University of Michigan, Ann Arbor, MI, USA
[2]General Motors, Warren, MI, USA
email: wzhousci@umich.edu

INTRODUCTION

This work aims to collect new information and develop models for design of objects that are held or manipulated with the hand. Examples include, handles that are used to lift and hold containers or support the body, tools, parts and materials. Towards this end, this study examines the effect of object size and posture on upper limb joint loads.

We previously showed that self-selected hand posture used to grasp, hold (approximately eight seconds), and place cylindrical objects is influenced by weight of the object [1]. Subjects reached over and grasped light objects (<1.6 kg) from above using their finger tips more than 50% of the time; for heavier cylinders, reached under and lifted the object with their palm and base of the fingers. As subjects gained control over the cylinder, they shifted to hook grip posture at thigh height or palm grip posture at shoulder height to hold the object. These results are qualitatively consistent with previous findings that grasp posture selection is related to comfort or effort [2-4].

We hypothesize that people will assume posture that reduces relative loads produced on upper limb joints. We compute the moments on the wrist, elbow and shoulder from the load and moment arms. There is not a direct way to compute corresponding moments for the hand because it involves a complex combination of normal and friction forces. Therefore we assume that if the relative loads of wrist, elbow and shoulder all are less than 1, the hand strength is the limiting factor.

METHODS

Twenty right-handed healthy university students (10 males and 10 females, age between 19 and 32 years, mean age 22.0 ± 2.8) were asked to grasp and pull cylindrical handle (D = 3.2 cm and 7 cm) in vertical up direction using three postures (Figure 1), a) an overhand grip in which the load is supported with the tips of the fingers, b) an underhand grip in which the load is supported with the palm and base of the fingers, and c) a hook grip at the side of the body in which the load is supported by hooking the fingers under the handle. They gave written informed consent in accordance with our University IRB regulations. Subjects were asked to “pull the handle in vertical up direction as hard as they can” without jerking it [5] while maintaining the specified posture. There were two repetitions for each size and posture. The order of the trials was randomized for each subject. A break of at least two minutes was given between successive trials. Functional strength tests were then conducted to quantify isolated joint strengths for each subject.

The relative loads were computed as the ratio of the moments produced about the shoulder, elbow and wrist from the lifting test with the corresponding strengths and were expressed as decimal fractions. The moments were calculated as the lifting force multiplied by the moment arms from the handle to joint. The moment arms were computed from marker data obtained using an eight-camera Qualisys motion tracking system (Qualisys Inc., Sweden).

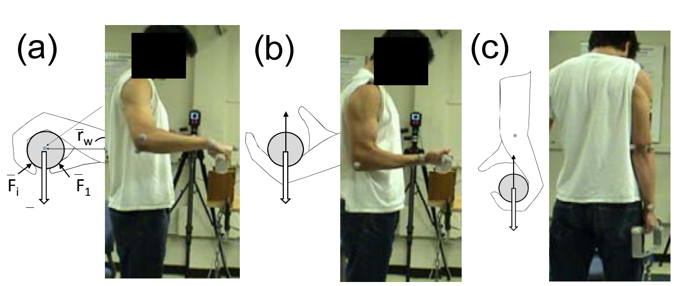

Figure 1: Grasp postures (a) overhand grasp; (b) underhand grasp; (c) hook grip.

Analysis of variance was performed to determine significant factors on the lifting strength data. Model included posture, object diameter, and gender as fixed variables, their second order interactions, and subject as a random variable. Post-hoc Tukey tests were performed on significant main effects and interactions to identify lifting strength differences among conditions.

RESULTS AND DISCUSSION

Maximum voluntary isometric lifting strengths for the three postures and two object sizes are summarized in Table 1. The lifting strength for males was, on average, 2.2 times of the one for females (object diameter and posture pooled, $p<0.01$). The lifting strength for hook grip was 2.2 times of the one for underhand grip (object diameter and gender pooled, $p<0.01$), and 4.3 times of the one for overhand grip (object diameter and gender pooled, $p<0.01$). The lifting strength for the object diameter 3.2 cm was, on average, 56% greater than that of the diameter 7 cm (posture and gender pooled, $p<0.01$). As object diameter increased from 3.2 cm to 7 cm, the lifting strength of overhand grip decreased 32% (gender pooled, $p<0.01$). The lifting strength of underhand grip decreased 9% but was not shown significant difference ($p>0.05$). The lifting strength of hook grip decreased 46% ($p<0.01$).

The relative wrist, elbow, and shoulder moments for the lifting test expressed as decimal fraction of isolated joint strengths are shown in Table 1. The results show that hand strength is the limiting factor for overhand grip because the relative loads for the wrist, elbow, and shoulder all are less than 1 (one-sample t test; $p<0.001$ for the joints and both sizes). Most of the object load is supported by the tips of the fingers and thumb using a complex combination of normal finger flexion forces and friction forces. For underhand grasp, wrist strength is the limiting factor (one-sample t test; $p>0.1$ for both sizes), indicating the finger strength does not limit lifting.

The results support several practical ergonomic applications as well as further research. If possible a 3.2 cm handle size is preferred over 7.0 cm for light weight objects for overhand grasp. Surfaces that enhance friction or geometries that enhance mechanical interference can be used to reduce the effort for overhand grasp. Clearance for underhand grasp should be provided for heavy objects. The results support further studies to develop models that describe grasping behavior and hand-object coupling.

REFERENCES

1.Zhou W, et al, in *Proceedings of Human Factors and Ergonomics Society Annual Meeting*. (2011).
2.Rosenbaum DA, et al. in *Motor control and learning over the lifespan*, M. Latash, F. Lestienne, Eds. Springer, 2006, 9-25.
3.Fischman M. *Percept Mot Skills* **86**, 328, 1998.
4.Lukos J, et al. *J Neurosci* **27**, 3894-3903, 2007.
5.Caldwell LS, et al. *The American Industrial Hygiene Association Journal* **35**, 201-206, 1974.

ACKNOWLEDGEMENTS

This work was supported by General Motors and by the partners of the Human Motion Simulation Laboratory at the University of Michigan.

Table 1: Lifting strengths for two cylindrical handle diameters (3.2 cm, 7 cm) and three grasp postures (overhand grasp, underhand grasp, and hookgrip at the side of body) by gender (mean ± SD). Wrist, elbow, and shoulder joint moments as decimal fraction of respective strengths during maximum voluntary isometric lifting exertions (gender pooled, mean ± SD).

Posture	Object Diameter (cm)	Lifting Strength (N)		Joint moment as fraction of joint strength in maximum lifting exertion (gender pooled)		
		Male	Female	Wrist	Elbow	Shoulder
Overhand grip	3.2	96.1 ± 17.8	48.8 ± 9.4	0.61 ± 0.19	0.58 ± 0.12	0.52 ± 0.09
	7	62.4 ± 12.1	35.7 ± 9.0	0.46 ± 0.16	0.40 ± 0.11	0.38 ± 0.11
Underhand grip	3.2	168.8 ± 49.4	74.9 ± 23.1	0.94 ± 0.20	0.91 ± 0.17	0.68 ± 0.17
	7	152.1 ± 62.1	69.4 ± 21.5	1.06 ± 0.25	0.85 ± 0.16	0.64 ± 0.17
Hook grip	3.2	466.5 ± 103.4	211.9 ± 59.3	-	-	-
	7	256.3 ± 64.8	111.4 ± 38.5	-	-	-

QUANTIFYING THE STIFFNESS OF RUNNING SHOES

[1]Kyle Zobeck, [1]Erick Bodett, [2]Bruce Williams, [1]Craig M. Goehler, [1]Kathleen Sevener
[1]Department of Mechanical Engineering, Valparaiso University, Valparaiso, IN, USA
[2]Breakthrough Podiatry, Merrillville, IN, USA
email: kathleen.sevener@valpo.edu

INTRODUCTION

The aim of a running shoe is to protect a runner's foot from the impacts that occur during the gait cycle. The shoe acts to cushion the impacts and stabilize the foot, preventing lower leg injuries. Hopefully, the number of lower leg injuries will be reduced as material and shoe testing improves, allowing new developments to be made in shoe design. Standard shoe testing today consists of flexion tests used to determine a shoe's stiffness – usually in the forefoot region. Recently, Ballun et al [4] have developed a new method for shoe flexion testing that characterizes not only the forefoot stiffness of a shoe, but also the stiffness in the mid-foot region.

The goal of this study is to further develop an improved flexion test for evaluating and quantifying the stiffness of running shoes over the length of the shoe from the mid-foot to the forefoot section. The results of this experiment will be used to aid shoe design in an attempt to minimize the number of lower leg injuries in runners and walkers alike. This document outlines the experimental setup and method for the improved test, and also presents preliminary data collected for two different shoe architectures.

METHODS

The apparatus used in this study for shoe flexion tests is described elsewhere [4]. The apparatus was designed with an adjustable distance between the loading actuator and the shoe fixture column (Fig. 1). This design permits shoe flexion at various locations along the shoe. Interchangeable supports, mounted to the shoe fixture column, permit a flexible inner support in the shoe (Fig. 2)

Figure 1: Testing apparatus with adjustable base and experimental setup in the MTS machine [4]

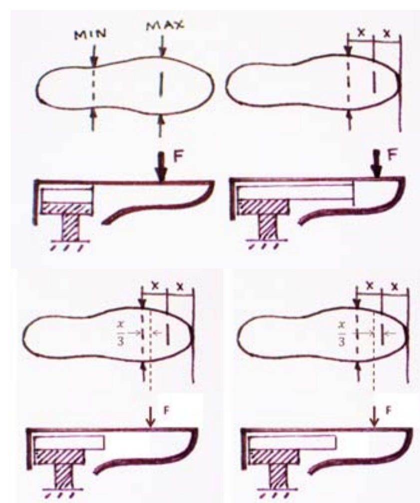

Figure 2: Diagram of shoe inserts, bend locations, and force application points [4]

As in the previous study [4], a cushioned shoe and a stability shoe, with a noticeable tactile difference in stiffness, were chosen for evaluation. Four regions of each shoe sole were tested: the mid-foot, located at the narrowest part of the shoe, the forefoot, located at the widest part, along with two intermediate locations equally spaced between the mid-foot and forefoot. To keep bend lengths proportional to the shoe size, the actuator was positioned at the shoe's maximum width for the mid-foot test and at a distance halfway from maximum width to the end of the shoe for the forefoot test. For the intermediate tests the actuator was equally spaced between the actuator locations for the mid-foot and forefoot tests.

To carry out the flexion test, the testing apparatus was placed in an MTS Q-Test 150 load frame with the desired shoe clamped to the vertical shoe fixture column (Fig. 1). Four supports of differing lengths were used to promote bending at a specific location within the shoe. The actuator was placed in the appropriate location for each test depending on the support being used (Fig. 2). Once in the desired location, the actuator was lowered at a rate of 1 inch per minute until the shoes deflected 1.5 inches. The program controlling the MTS load frame recorded force and displacement data for the actuator. This data was used to calculate the shoe's stiffness at the location of interest. Upon completion of each test, the actuator was raised and the load was removed from the shoe.

Following the same procedure used in the previous study [4], the ground reaction moment was calculated by multiplying the true bend length (d_2) by the true force (Fig. 3). The true force was found using the applied force and bend geometry (y and d_1). The stiffness is plotted versus the bend angle and a value was selected based on where the curve leveled off.

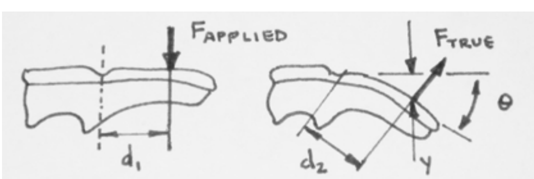

Figure 3: Bend geometry of tested shoes [4]

RESULTS AND DISCUSSION

The results of this study built upon the experimental findings of Ballun et al [4]. In the aforementioned study, the stiffness of two different running shoes was calculated at both the mid-foot and forefoot locations. The results of their earlier test support the tactile difference that was noticed during shoe selection and show that the mid-foot stiffness is higher than the forefoot stiffness for each shoe's architecture. The results also show that the test concepts remain consistent with original test posed by Oleson et al [3].

The results of this flexion test follow the same trends seen in the previous tests. The calculated stiffness is largest at the mid-foot location and decreases down to the forefoot section. Figure 4 illustrates how the stiffness changes through the shoe. The distance, d_1, relates to the location in the shoe. The largest d_1 corresponds to the mid-foot and the smallest d_1 corresponds to the forefoot.

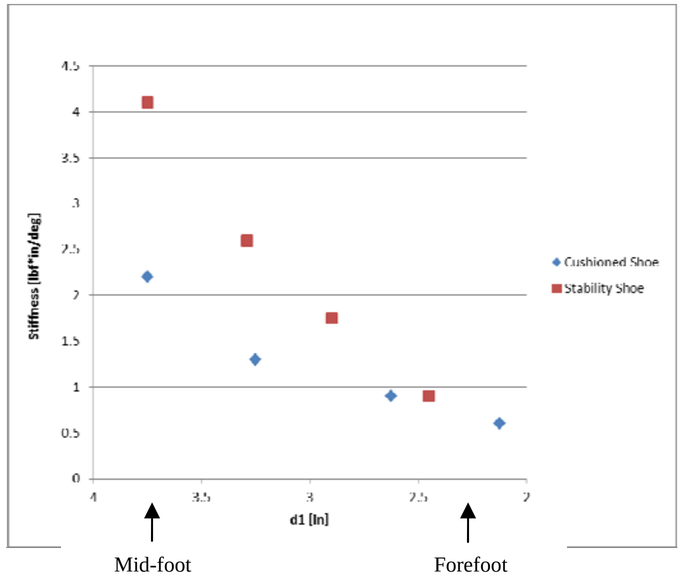

Figure 4: Stiffness values at four locations for a stability and cushioned shoe

Notice that the stability shoe has higher stiffness values than the cushioned shoe at all locations. However, the stiffness values of each shoe approach the same value in regions close to the toe. Further testing will need to take place in order to determine if there is a consistent mathematical relationship governing the trends seen in Figure 4.

REFERENCES

1. Cheskin, M., Fredericksen, R. *Podiatry Management* **24**, 107-118, 2005.

2. Drez, D. *The American Journal of Sports Medicine* **8**, 140-141, 1980.

3. Oleson, M. et al. *Journal of Biomechanics* **38**, 1886–1894, 2005.

4. Ballun, M. et al. *Annual Meeting of ASB 2011*.

THE CORRELATION BETWEEN INTERNAL SKELETAL DIMENSIONS OF TIBIOFEMORAL JOINT AND EXTERNAL BODY MEASUREMENTS

Dequan Zou, Robert H. Deusinger, Melanie Koleini, Kirk E. Smith, Gretchen Hensley, Timothy Machan and Davor Vasiljevic

Washington University School of Medicine, St. Louis, MO, USA
email: zoud@wustl.edu web: http://pt.wustl.edu

INTRODUCTION

Excessive anterior cruciate ligament (ACL) force and distorted joint surface motion (kinematics) are components of tibiofemoral joint (TFJ) mechanics hypothesized to be associated with ACL injury and osteoarthritis (OA) [1]. Quantitative knowledge of the distal femur and proximal tibia morphology depicted by their geometry is critical to understanding ACL injury mechanisms and gender differences in kinematics of anterior tibial translation and tibiofemoral joint surface rolling and sliding during weight bearing and non-weight bearing activities [2]. The geometry of the tibiofemoral joint is complex and asymmetrical within individuals and may also differ between genders [3]. Computed tomography (CT) has been used to obtain reliable measures of internal skeletal dimensions (ISDs) to provide a skeletal framework geometry [3] as the foundation for developing a subject specific 3D computational TFJ model. However, the image capturing and data analysis processes are time-consuming and expensive. A more efficient and less expensive approach may be to predict ISDs from external body dimensions (EBDs) of the subjects. The purpose of the current study is to investigate the correlation between ISDs of the TFJ and EBDs. EBDs highly correlated with ISDs will be used to develop regression equations to predict internal dimensions in future studies.

METHODS

Eighteen healthy adults, 9 men and 9 women, participated in this study (age 27.5±6.5; height 171±9 cm; body mass 78.7±19.3 kg). Before testing, all subjects signed informed-consent forms approved by the Washington University Human Studies Committee. Prior to image acquisition, the following EBDs were recorded for each subject: body height, lower extremity length, femur segment length, tibial segment length and knee width (at joint line).

A CT scan of the right knee of each subject was obtained and analyzed according to an IRB approved research protocol. All CT scans were performed using a research dedicated 64-slice Siemens Somatom Definition CT scanner (Siemens Medical Systems, Inc., Malvern, PA, USA) located within the Center for Clinical Imaging Research (CCIR) at the Mallinckrodt Institute of Radiology following an IRB approved research protocol. Subjects were positioned supine on the CT table and the right knee regions were scanned at 120 kVP, 159 mAs, 1 rotation per second, pitch of 0.65, 32 detectors, detector size of 0.6 mm, 0.75 mm slice thickness, and a 512 x 512 matrix. Conversion of tibiofemoral joint CT image data to triangulated surface models was performed using Materialize Mimics software version 13.1 (Materialize Inc., Belgium). The triangulated surface models were then loaded into Geomagic Studio 12 for landmark identification. Skeletal landmark (SL) location coordinates were used to define ISDs that measure the distal femur and proximal tibia heads.

Fair to good intertester reliability and high intratester reliability were observed for both femoral and tibial ISDs [3]. SLs were used to measure the widths of the femur and tibia and to create planes that define approximate mid-sagittal cross-sections through the medial and lateral femoral condyles. The radii of curvature for the lateral femoral condyle (LFC) and medial femoral condyle (MFC) were calculated based on points along the curves found at the intersection of the surfaces of femoral condyles and the defined planes (red curves in Fig. 1). ISDs measured from CT imaging data were: averaged radii of curvature of the curves at loading regions of the LFC and MFC, respectively, lateral-medial width of distal femoral condyle, LFC anterior-posterior width, MFC anterior-posterior width (Fig. 1), lateral-medial width of tibia, lateral tibial anterior-posterior width, and medial tibial anterior-posterior width. We hypothesized EBDs would strongly correlate with ISDs.

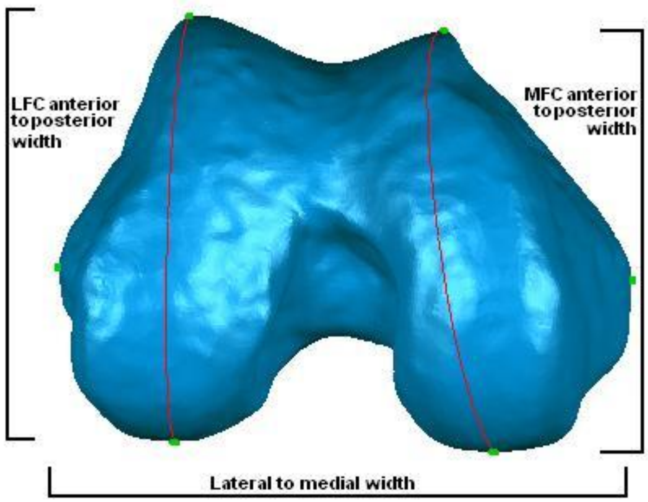

Figure 1. Femur Internal Skeletal Dimensions

RESULTS AND DISCUSSION

High Pearson correlation coefficient values were observed for EBDs of gender (0.544 to 0.878), body height (0.633 to 0.810), and tibial length (.556 to .719) relative to ISDs (Table 1). Surprisingly, EBDs of lower extremity length, femur length, and knee width, were not strongly correlated to the ISDs. Now that we have identified the more relevant potential EBD predictors of ISDs, future studies will use multiple linear regression with a larger sample size to develop regression equations using EBDs to predict ISDs.

CONCLUSIONS

This pilot study demonstrates that the specific EBDs of gender, height, and tibia length are strongly correlated with the ISDs. These results merit further study using a larger sample size to develop regression equations for predicting ISDs from EBDs. This is part of several progressive stages to develop a subject-specific 3D computational TFJ knee model based on CT derived skeletal dimensions.

REFERENCES

1. Wilson DR, et al. *Rheumatic Disease Clinics of North America*, 34, 605-622, 2008.
2. Hollman JH, et al. *Journal of Sport Rehabilitation*, 12, 143-161, 2003.
3. Zou D, Deusinger RH, Smith KE, Koleini M. *Proceedings of IEEE/ICME CME 2011*, Harbin, China, 2011.

ACKNOWLEDGEMENTS

This publication was supported by Grant Number UL1RR024992 from the National Center for Research Resources (NCRR), a component of the National Institutes of Health (NIH), and NIH Roadmap for Medical Research. Its contents are solely the responsibility of the authors and do not necessarily represent the official view of NCRR or NIH

Table 1: Correlation between external body dimensions and TFJ internal skeletal dimensions

Variables	Gender	Height	Lower extremity length	Femur length	Tibia length	Knee width
Lateral Condyle Radius of Curvature	0.544	0.661	0.545	0.438	0.617	0.038
Medial Condyle Radius of Curvature	0.651	0.741	0.556	0.385	0.61	0.029
Femoral Condyle lateral to medial width	0.878	0.779	0.58	0.137	0.647	0.285
Lateral Condyle anterior to posterior width	0.858	0.783	0.635	0.26	0.719	0.297
Medial Condyle anterior to posterior width	0.876	0.810	0.622	0.258	0.707	0.263
Tibial Condyle lateral to medial width	0.872	0.728	0.582	0.202	0.609	0.199
Lateral tibial condyle anterior to posterior width	0.771	0.633	0.562	0.387	0.556	0.121
Medial tibial condyle anterior to posterior width	0.833	0.752	0.551	0.302	0.678	0.419

A Reanalysis of Wrist Jerk During Ergonomic Hand Drive Wheelchair Propulsion

[1]Lisa A. Zukowski, [1]Jaimie A. Roper, [1]Dana Otzel, [1]Patty Hovis, [1]Orit Shechtman, and [1]Mark. D. Tillman

[1]University of Florida, Gainesville, FL, USA
email: zukowski@ufl.edu

INTRODUCTION

Forty-nine to 63% of conventional manual wheelchair (CMW) users suffer from carpal tunnel syndrome (CTS). This wrist pathology is likely induced by a combination of large forces transmitted through the wrist and an extreme wrist range of motion (ROM) that are both typical of CMW propulsion. Boninger et al. [1] determined that median nerve function was most highly related to the rate of rise of the pushrim force, with faster loading resulting in poorer median nerve function. Additionally Keir et al. [2] determined that wrist orientation beyond 48.6° of flexion, 32.7° of extension, 21.8° of radial deviation, and 14.5° of ulnar deviation leads to high carpal tunnel pressure levels (>30 mmHg) which are typical of carpal tunnel syndrome. High carpal tunnel pressure results in paresthesia, reduced median nerve conduction, and an increased probability of nerve impairment.

The ergonomic hand drive mechanism (EHDM) tested in this study utilizes a more neutral wrist orientation. Further, because the EHDM uses continuous contact between the lever and hand, more constant force application and therefore reduced jerk ($\Delta a/\Delta t$) should result.

Previously a similar analysis was conducted in which wrist jerk and angular orientation were evaluated during CMW and EHDM use [3]. The extreme wrist angles used (15° of flexion, 15° of extension, 5° of radial deviation, and 10° of ulnar deviation) were based on more general ergonomic recommendations for hand tools, however. The purpose of this project is to evaluate wrist jerk in relation to angular orientation while using the EHDM with revised wrist angles specific to CTS.

METHODS

Fourteen adult full-time CMW users were recruited to participate in this study (41.3±15.7 yrs, 73.4±16.7 kg, 172.4±12.9 cm). All participants were medically and functionally stable and at least six months post injury.

Motion data were captured by 11 cameras as participants propelled across a length of 8 m. Each participant completed five trials in a CMW and five trials in the same CMW fitted with the EHDM. The EHDM remained attached to the CMW during all ten trials and was rotated to the back of the chair, out of the way, when not in use.

Angular kinematics of the wrist were computed in the planes of flexion/extension and radial/ulnar deviation using Vicon Nexus software. A custom Matlab program was used to further process the data. Jerk was calculated as the third derivative of the wrist position data. At least one push phase was analyzed per trial and all trials were combined to calculate an average push per participant. This average push was then divided into ten consecutive time intervals representing ten percent intervals of the total push. The maximum jerk value (MJV) from each interval was calculated and then the angular orientations of the wrist in both planes of motion at the MJV were compared between the two propulsion style conditions using paired samples t-tests (α=0.05). Additional analyses were performed on these intervals exhibiting statistically different angular orientations that were outside of the neutral range of motion as specified by Keir et al. [2]. The MJV at these extreme ranges of wrist motion were compared between conditions using paired samples t-tests (α=0.05). All statistical procedures were performed using SPSS 17.0.

RESULTS AND DISCUSSION

Use of the EHDM resulted in reduced wrist extension during the first half of the ten intervals ($p<0.05$), during which time CMW wrist orientation was consistently outside of the neutral range of wrist extension (<-32.1°). CMW propulsion resulted in reduced wrist extension during the last four intervals ($p<0.05$). During these last four intervals however, EHDM propulsion utilized a wrist orientation within the neutral range.

During the first interval, CMW propulsion exhibited radial deviation while EHDM propulsion exhibited ulnar deviation, although both were within the neutral ROM. During the last five intervals, however, EHDM propulsion resulted in reduced ulnar deviation, with CMW propulsion consistently outside of the neutral range of ulnar deviation (<-14.5°).

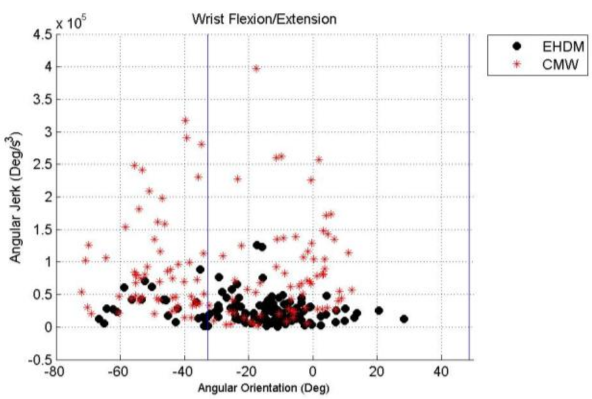

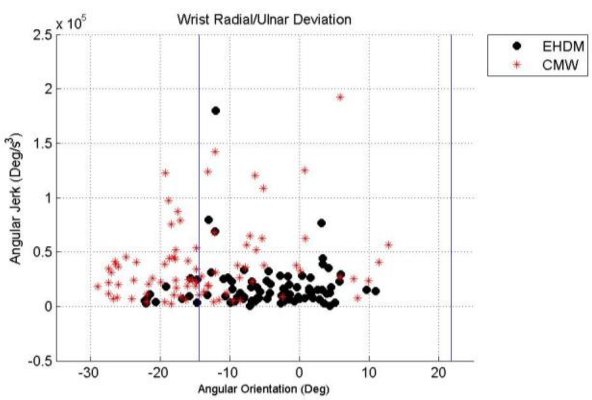

Figure 1. Wrist flexion/extension (negative values) and radial/ulnar deviation (negative values) versus angular jerk of both propulsion styles. The vertical lines represent the limits of a neutral wrist ROM.

After reducing the data to only include orientation and MJV that were significantly different between conditions and outside of the healthy ROM, it was found that EHDM use resulted in more instances of unhealthy range of motion (26 v. 19 for extension, 11 v. 9 for ulnar deviation), but CMW propulsion exhibited larger jerk values at all of these instances in time ($p<0.05$, Figure 1).

CONCLUSIONS

In general EHDM use resulted in reduced extension and ulnar deviation as compared to CMW use throughout the push. Additionally, while EHDM use resulted in more instances of significantly different angular orientations occurring outside of a neutral range of wrist motion, CMW propulsion resulted in consistently higher jerk values at all of these time points. These results evince more constant force application with EHDM use and infer a reduction in wrist joint reaction forces throughout a more neutral ROM, which may lessen both the symptoms as well as the likelihood of developing CTS.

REFERENCES

1. Boninger ML, et al. *Arch Phys Med Rehabil* **80**, 910-915, 1999.
2. Keir PJ, et al. *Hum Factors* **49**, 88-99, 2007.
3. Zukowski LA, et al. *Proceedings of ACSM '12*, San Francisco, CA, USA, 2012.

ACKNOWLEDGEMENTS

Supported by the Clinical and Translational Science Institute Pilot & Collaborative Research Projects (NIH). The hand drive mechanism used in this study is the intellectual property of Shands Healthcare.